IDENTIFICATION AND CHARACTERIZATION OF CONTRASTING GENOTYPES/CULTIVARS TO DISCOVER NOVEL PLAYERS IN CROP RESPONSES TO ABIOTIC/BIOTIC STRESSES

EDITED BY: Raul Antonio Sperotto, Felipe Klein Ricachenevsky, Elizabeth R. Waters, Guihua Bai and Magdalena Arasimowicz-Jelonek

PUBLISHED IN: Frontiers in Plant Science



frontiers Research Topics



frontiers

Frontiers eBook Copyright Statement

The copyright in the text of individual articles in this eBook is the property of their respective authors or their respective institutions or funders. The copyright in graphics and images within each article may be subject to copyright of other parties. In both cases this is subject to a license granted to Frontiers.

The compilation of articles constituting this eBook is the property of Frontiers.

Each article within this eBook, and the eBook itself, are published under the most recent version of the Creative Commons CC-BY licence. The version current at the date of publication of this eBook is CC-BY 4.0. If the CC-BY licence is updated, the licence granted by Frontiers is automatically updated to the new version.

When exercising any right under the CC-BY licence, Frontiers must be attributed as the original publisher of the article or eBook, as applicable.

Authors have the responsibility of ensuring that any graphics or other materials which are the property of others may be included in the CC-BY licence, but this should be checked before relying on the CC-BY licence to reproduce those materials. Any copyright notices relating to those materials must be complied with.

Copyright and source acknowledgement notices may not be removed and must be displayed in any copy, derivative work or partial copy which includes the elements in question.

All copyright, and all rights therein, are protected by national and international copyright laws. The above represents a summary only. For further information please read Frontiers' Conditions for Website Use and Copyright Statement, and the applicable CC-BY licence.

ISSN 1664-8714
ISBN 978-2-88974-009-3
DOI 10.3389/978-2-88974-009-3

About Frontiers

Frontiers is more than just an open-access publisher of scholarly articles: it is a pioneering approach to the world of academia, radically improving the way scholarly research is managed. The grand vision of Frontiers is a world where all people have an equal opportunity to seek, share and generate knowledge. Frontiers provides immediate and permanent online open access to all its publications, but this alone is not enough to realize our grand goals.

Frontiers Journal Series

The Frontiers Journal Series is a multi-tier and interdisciplinary set of open-access, online journals, promising a paradigm shift from the current review, selection and dissemination processes in academic publishing. All Frontiers journals are driven by researchers for researchers; therefore, they constitute a service to the scholarly community. At the same time, the Frontiers Journal Series operates on a revolutionary invention, the tiered publishing system, initially addressing specific communities of scholars, and gradually climbing up to broader public understanding, thus serving the interests of the lay society, too.

Dedication to Quality

Each Frontiers article is a landmark of the highest quality, thanks to genuinely collaborative interactions between authors and review editors, who include some of the world's best academicians. Research must be certified by peers before entering a stream of knowledge that may eventually reach the public - and shape society; therefore, Frontiers only applies the most rigorous and unbiased reviews.
Frontiers revolutionizes research publishing by freely delivering the most outstanding research, evaluated with no bias from both the academic and social point of view. By applying the most advanced information technologies, Frontiers is catapulting scholarly publishing into a new generation.

What are Frontiers Research Topics?

Frontiers Research Topics are very popular trademarks of the Frontiers Journals Series: they are collections of at least ten articles, all centered on a particular subject. With their unique mix of varied contributions from Original Research to Review Articles, Frontiers Research Topics unify the most influential researchers, the latest key findings and historical advances in a hot research area! Find out more on how to host your own Frontiers Research Topic or contribute to one as an author by contacting the Frontiers Editorial Office: frontiersin.org/about/contact

IDENTIFICATION AND CHARACTERIZATION OF CONTRASTING GENOTYPES/CULTIVARS TO DISCOVER NOVEL PLAYERS IN CROP RESPONSES TO ABIOTIC/BIOTIC STRESSES

Topic Editors:
Raul Antonio Sperotto, Universidade do Vale do Taquari - Univates, Brazil
Felipe Klein Ricachenevsky, Federal University of Rio Grande do Sul, Brazil
Elizabeth R. Waters, San Diego State University, United States
Guihua Bai, USDA-ARS Hard Winter Wheat Genetics Research Unit, United States
Magdalena Arasimowicz-Jelonek, Adam Mickiewicz University, Poland

Citation: Sperotto, R. A., Ricachenevsky, F. K., Waters, E. R., Bai, G., Arasimowicz-Jelonek, M., eds. (2021). Identification and Characterization of Contrasting Genotypes/Cultivars to Discover Novel Players in Crop Responses to Abiotic/Biotic Stresses. Lausanne: Frontiers Media SA.
doi: 10.3389/978-2-88974-009-3

Table of Contents

08 ***Editorial: Identification and Characterization of Contrasting Genotypes/Cultivars to Discover Novel Players in Crop Responses to Abiotic/Biotic Stresses***
Raul A. Sperotto, Felipe K. Ricachenevsky, Elizabeth R. Waters, Guihua Bai and Magdalena Arasimowicz-Jelonek

14 ***Overexpression of* CsHMGB *Alleviates Phytotoxicity and Propamocarb Residues in Cucumber***
Shengnan Li, Ming Xin, Jie Luan, Dong Liu, Chunhua Wang, Chunhong Liu, Wenshuo Zhang, Xiuyan Zhou and Zhiwei Qin

34 ***A* Brassica napus *Reductase Gene Dissected by Associative Transcriptomics Enhances Plant Adaption to Freezing Stress***
Yong Huang, Muhammad Azhar Hussain, Dan Luo, Hongzhi Xu, Chuan Zeng, Lenka Havlickova, Ian Bancroft, Zhitao Tian, Xuekun Zhang, Yong Cheng, Xiling Zou, Guangyuan Lu and Yan Lv

49 ***Resilient and Sensitive Key Points of the Photosynthetic Machinery of* Coffea *spp. to the Single and Superimposed Exposure to Severe Drought and Heat Stresses***
Danielly Dubberstein, Fernando C. Lidon, Ana P. Rodrigues, José N. Semedo, Isabel Marques, Weverton P. Rodrigues, Duarte Gouveia, Jean Armengaud, Magda C. Semedo, Sónia Martins, Maria C. Simões-Costa, I. Moura, Isabel P. Pais, Paula Scotti-Campos, Fábio L. Partelli, Eliemar Campostrini, Ana I. Ribeiro-Barros, Fábio M. DaMatta and José C. Ramalho

71 ***Wheat Line "RYNO3936" Is Associated With Delayed Water Stress-Induced Leaf Senescence and Rapid Water-Deficit Stress Recovery***
Marlon-Schylor L. le Roux, N. Francois V. Burger, Maré Vlok, Karl J. Kunert, Christopher A. Cullis and Anna-Maria Botha

92 ***Intraspecific Variation in Drought Response of Three Populations of* Cryptocarya alba *and* Persea lingue*, Two Native Species From Mediterranean Central Chile***
Carolina Alvarez-Maldini, Manuel Acevedo, R. Kasten Dumroese, Marta González and Eduardo Cartes

107 ***An Advanced Lipid Metabolism System Revealed by Transcriptomic and Lipidomic Analyses Plays a Central Role in Peanut Cold Tolerance***
He Zhang, Chunji Jiang, Jingyao Ren, Jiale Dong, Xiaolong Shi, Xinhua Zhao, Xiaoguang Wang, Jing Wang, Chao Zhong, Shuli Zhao, Xibo Liu, Shibo Gao and Haiqiu Yu

125 ***Can Metabolite- and Transcript-Based Selection for Drought Tolerance in* Solanum tuberosum *Replace Selection on Yield in Arid Environments?***
Manuela Haas, Heike Sprenger, Ellen Zuther, Rolf Peters, Sylvia Seddig, Dirk Walther, Joachim Kopka, Dirk K. Hincha and Karin I. Köhl

141 ***Deployment of Genetic and Genomic Tools Toward Gaining a Better Understanding of Rice-*Xanthomonasoryzae *pv.* oryzae *Interactions for Development of Durable Bacterial Blight Resistant Rice***
Anirudh Kumar, Rakesh Kumar, Debashree Sengupta, Subha Narayan Das, Manish K. Pandey, Abhishek Bohra, Naveen K. Sharma, Pragya Sinha, Hajira Sk, Irfan Ahmad Ghazi, Gouri Sankar Laha and Raman Meenakshi Sundaram

164 ***Intra and Inter-specific Variability of Salt Tolerance Mechanisms in* Diospyros *Genus***
Francisco Gil-Muñoz, Juan Gabriel Pérez-Pérez, Ana Quiñones, María del Mar Naval and María Luisa Badenes

180 ***Wheat Cultivars With Contrasting Root System Size Responded Differently to Terminal Drought***
Victoria Figueroa-Bustos, Jairo A. Palta, Yinglong Chen, Katia Stefanova and Kadambot H. M. Siddique

192 ***Mapping Quantitative Trait Loci for Soybean Seedling Shoot and Root Architecture Traits in an Inter-Specific Genetic Population***
Silvas J. Prince, Tri D. Vuong, Xiaolei Wu, Yonghe Bai, Fang Lu, Siva P. Kumpatla, Babu Valliyodan, J. Grover Shannon and Henry T. Nguyen

205 ***Comparative Transcriptome and Proteome Analysis of Salt-Tolerant and Salt-Sensitive Sweet Potato and Overexpression of* IbNAC7 *Confers Salt Tolerance in* Arabidopsis**
Xiaoqing Meng, Siyuan Liu, Tingting Dong, Tao Xu, Daifu Ma, Shenyuan Pan, Zongyun Li and Mingku Zhu

220 ***Comparison of Selection Traits for Effective Popcorn (*Zea mays *L. var. Everta) Breeding Under Water Limiting Conditions***
Samuel Henrique Kamphorst, Antônio Teixeira do Amaral Júnior, Valter Jário de Lima, Pedro Henrique Araújo Diniz Santos, Weverton Pereira Rodrigues, Janieli Maganha Silva Vivas, Gabriel Moreno Bernardo Gonçalves, Katia Fabiane Medeiros Schmitt, Jhean Torres Leite, Marcelo Vivas, Freddy Mora-Poblete, Omar Vergara-Díaz, Jose Luis Araus Ortega, José Cochicho Ramalho and Eliemar Campostrini

238 ***Development and Characterization of Near-Isogenic Lines Revealing Candidate Genes for a Major 7AL QTL Responsible for Heat Tolerance in Wheat***
Lu Lu, Hui Liu, Yu Wu and Guijun Yan

249 ***Physiological and* PIP *Transcriptional Responses to Progressive Soil Water Deficit in Three Mulberry Cultivars***
Xu Cao, Qiudi Shen, Sang Ma, Li Liu and Jialing Cheng

265 ***Tolerance of Combined Drought and Heat Stress Is Associated With Transpiration Maintenance and Water Soluble Carbohydrates in Wheat Grains***
Abdeljalil El Habti, Delphine Fleury, Nathaniel Jewell, Trevor Garnett and Penny J. Tricker

278 ***Comprehensive Genome-Wide Analysis of Thaumatin-Like Gene Family in Four Cotton Species and Functional Identification of* GhTLP19 *Involved in Regulating Tolerance to* Verticillium dahlia *and Drought***
Zhanshuai Li, Xiaoyan Wang, Yupeng Cui, Kaikai Qiao, Longfu Zhu, Shuli Fan and Qifeng Ma

293 ***Endogenous Hormones Inhibit Differentiation of Young Ears in Maize (*Zea mays L.*) Under Heat Stress***
Hui-Qin Wang, Peng Liu, Ji-Wang Zhang, Bin Zhao and Bai-Zhao Ren

308 ***Identification and Characterization of Contrasting Genotypes/Cultivars for Developing Heat Tolerance in Agricultural Crops: Current Status and Prospects***
Shikha Chaudhary, Poonam Devi, Anjali Bhardwaj, Uday Chand Jha, Kamal Dev Sharma, P. V. Vara Prasad, Kadambot H. M. Siddique, H. Bindumadhava, Shiv Kumar and Harsh Nayyar

342 ***Cultivar Variation in Tomato Seed Coat Permeability Is an Important Determinant of Jasmonic Acid Elicited Defenses Against Western Flower Thrips***
Sanae Mouden, Iris F. Kappers, Peter G. L. Klinkhamer and Kirsten A. Leiss

356 ***Tomato Yellow Leaf Curl Virus-Resistant and -Susceptible Tomato Genotypes Similarly Impact the Virus Population Genetics***
Wendy G. Marchant, Saurabh Gautam, Samuel F. Hutton and Rajagopalbabu Srinivasan

373 ***Assessment of Four Portuguese Wheat Landrace Diversity to Cope With Global Warming***
Diana Tomás, Luís Pinto Coelho, José Carlos Rodrigues, Wanda Viegas and Manuela Silva

384 ***Comparative Transcriptome, Metabolome, and Ionome Analysis of Two Contrasting Common Bean Genotypes in Saline Conditions***
Harun Niron, Nazire Barlas, Bekir Salih and Müge Türet

405 ***Linking Leaf Water Potential, Photosynthesis and Chlorophyll Loss With Mechanisms of Photo- and Antioxidant Protection in Juvenile Olive Trees Subjected to Severe Drought***
Sahar Baccari, Olfa Elloumi, Anissa Chaari-Rkhis, Erola Fenollosa, Melanie Morales, Noureddine Drira, Ferjani Ben Abdallah, Lotfi Fki and Sergi Munné-Bosch

419 ***Selecting Aragonez Genotypes Able to Outplay Climate Change–Driven Abiotic Stress***
Luísa Carvalho, Elsa Gonçalves, Sara Amâncio and Antero Martins

433 ***The Effect of Drought on Transcriptome and Hormonal Profiles in Barley Genotypes With Contrasting Drought Tolerance***
Amal Harb, Craig Simpson, Wenbin Guo, Ganesan Govindan, Vijaya Gopal Kakani and Ramanjulu Sunkar

456 ***Genome-Wide Analysis of the GRAS Gene Family and Functional Identification of* GmGRAS37 *in Drought and Salt Tolerance***
Ting-Ting Wang, Tai-Fei Yu, Jin-Dong Fu, Hong-Gang Su, Jun Chen, Yong-Bin Zhou, Ming Chen, Jun Guo, You-Zhi Ma, Wen-Liang Wei and Zhao-Shi Xu

475 ***Grain Inorganic Arsenic Content in Rice Managed Through Targeted Introgressions and Irrigation Management***
Cristina P. Fernández-Baca, Anna M. McClung, Jeremy D. Edwards, Eton E. Codling, Vangimalla R. Reddy and Jinyoung Y. Barnaby

490 ***Drought-Induced Root Pressure in* Sorghum bicolor**
Sarah Tepler Drobnitch, Louise H. Comas, Nora Flynn, Jorge Ibarra Caballero, Ryan W. Barton, Joshua Wenz, Taylor Person, Julie Bushey, Courtney E. Jahn and Sean M. Gleason

505 ***Development of KASP Markers and Identification of a QTL Underlying Powdery Mildew Resistance in Melon (*Cucumis melo L.*) by Bulked Segregant Analysis and RNA-Seq***
Yanyan Cao, Qiannan Diao, Youyuan Chen, Haijun Jin, Yongping Zhang and Hongmei Zhang

516 ***Screening of Onion (*Allium cepa L.*) Genotypes for Drought Tolerance Using Physiological and Yield Based Indices Through Multivariate Analysis***
Pranjali A. Gedam, A. Thangasamy, Dhananjay V. Shirsat, Sourav Ghosh, K. P. Bhagat, Onkar A. Sogam, A. J. Gupta, V. Mahajan, P. S. Soumia, Vanita N. Salunkhe, Yogesh P. Khade, Suresh J. Gawande, P. S. Hanjagi, R. Shiv Ramakrishnan and Major Singh

532 **Oryza sativa *cv. Nipponbare and* Oryza barthii *as Unexpected Tolerance and Susceptibility Sources Against* Schizotetranychus oryzae *(Acari: Tetranychidae) Mite Infestation***
Giseli Buffon, Édina Aparecida dos Reis Blasi, Thainá Inês Lamb, Janete Mariza Adamski, Joséli Schwambach, Felipe Klein Ricachenevsky, Amanda Bertolazi, Vanildo Silveira, Mara Cristina Barbosa Lopes and Raul Antonio Sperotto

547 ***A Comparative Study for Assessing the Drought-Tolerance of Chickpea Under Varying Natural Growth Environments***
Anjuman Arif, Najma Parveen, Muhammad Qandeel Waheed, Rana Muhammad Atif, Irem Waqar and Tariq Mahmud Shah

565 ***Induction of Acquired Tolerance Through Gradual Progression of Drought Is the Key for Maintenance of Spikelet Fertility and Yield in Rice Under Semi-irrigated Aerobic Conditions***
V. S. Lekshmy, Preethi Vijayaraghavareddy, A. N. Nagashree, Vemanna S. Ramu, Venkategowda Ramegowda, Udayakumar Makarla and Sheshshayee Sreeman

579 ***Low Soil Nutrient Tolerance and Mineral Fertilizer Response in White Guinea Yam (*Dioscorea rotundata*) Genotypes***
Ryo Matsumoto, Haruki Ishikawa, Asrat Asfaw and Robert Asiedu

588 ***Responses of Maize Internode to Water Deficit Are Different at the Biochemical and Histological Levels***
Fadi El Hage, Laetitia Virlouvet, Paul-Louis Lopez-Marnet, Yves Griveau, Marie-Pierre Jacquemot, Sylvie Coursol, Valérie Méchin and Matthieu Reymond

599 ***Identification of Candidate Genes Conferring Cold Tolerance to Rice (*Oryza sativa L.*) at the Bud-Bursting Stage Using Bulk Segregant Analysis Sequencing and Linkage Mapping***
Luomiao Yang, Lei Lei, Peng Li, Jingguo Wang, Chao Wang, Fan Yang, Jiahui Chen, HuaLong Liu, Hongliang Zheng, Wei Xin and Detang Zou

611 ***Cadmium-Tolerant and -Sensitive Cultivars Identified by Screening of* Medicago truncatula *Germplasm Display Contrasting Responses to Cadmium Stress***
Vanesa S. García de la Torre, Teodoro Coba de la Peña, José J. Pueyo and M. Mercedes Lucas

628 ***Influence of Rootstock Genotype and Ploidy Level on Common Clementine (*Citrus clementina *Hort. ex Tan) Tolerance to Nutrient Deficiency***
Julie Oustric, Stéphane Herbette, Raphaël Morillon, Jean Giannettini, Liliane Berti and Jérémie Santini

642 ***Acoustic Vulnerability, Hydraulic Capacitance, and Xylem Anatomy Determine Drought Response of Small Grain Cereals***
Szanne Degraeve, Niels J. F. De Baerdemaeker, Maarten Ameye, Olivier Leroux, Geert Jozej Willem Haesaert and Kathy Steppe

654 ***Night Temperature Determines the Interannual Yield Variation in Hybrid and Inbred Rice Widely Used in Central China Through Different Effects on Reproductive Growth***
Liying Huang, Fei Wang, Yi Liu and Yunbo Zhang

666 ***The Resistance of Oilseed Rape Microspore-Derived Embryos to Osmotic Stress Is Associated With the Accumulation of Energy Metabolism Proteins, Redox Homeostasis, Higher Abscisic Acid, and Cytokinin Contents***
Milan O. Urban, Sébastien Planchon, Irena Hoštičková, Radomira Vanková, Peter Dobrev, Jenny Renaut, Miroslav Klíma and Pavel Vítámvás

687 ***Genome Wide Association Mapping of Root Traits in the Andean Genepool of Common Bean (*Phaseolus vulgaris *L.) Grown With and Without Aluminum Toxicity***
Daniel Ambachew and Matthew W. Blair

701 ***Association Analysis Revealed That* TaPYL4 *Genes Are Linked to Plant Growth Related Traits in Multiple Environment***
Yinghong Xue, Jingyi Wang, Xinguo Mao, Chaonan Li, Long Li, Xi Yang, Chenyang Hao, Xiaoping Chang, Runzhi Li and Ruilian Jing

715 ***Laccase Directed Lignification Is One of the Major Processes Associated With the Defense Response Against* Pythium ultimum *Infection in Apple Roots***
Yanmin Zhu, Guanliang Li, Jugpreet Singh, Awais Khan, Gennaro Fazio, Melody Saltzgiver and Rui Xia

frontiers in Plant Science

EDITORIAL
published: 17 November 2021
doi: 10.3389/fpls.2021.784874

Editorial: Identification and Characterization of Contrasting Genotypes/Cultivars to Discover Novel Players in Crop Responses to Abiotic/Biotic Stresses

Raul A. Sperotto[1]*, *Felipe K. Ricachenevsky*[2]*, *Elizabeth R. Waters*[3]*, *Guihua Bai*[4]* and *Magdalena Arasimowicz-Jelonek*[5]*

[1] Graduate Program in Biotechnology, Life Sciences Area, University of Taquari Valley–Univates, Lajeado, Brazil, [2] Graduate Program in Cell and Molecular Biology, Botany Department, Federal University of Rio Grande Do Sul, Porto Alegre, Brazil, [3] Department of Biology, San Diego State University, San Diego, CA, United States, [4] USDA-ARS Hard Winter Wheat Genetics Research Unit, Manhattan, KS, United States, [5] Department of Plant Ecophysiology, Faculty of Biology, Adam Mickiewicz University, Poznań, Poland

Keywords: drought, temperature, salinity, nutrition, toxic metals, biotic factors

OPEN ACCESS

Edited and reviewed by:
Jeremy Astier,
INRA UMR1347 Agroécologie, France

***Correspondence:**
Raul A. Sperotto
rasperotto@univates.br
Felipe K. Ricachenevsky
felipecruzalta@gmail.com
Elizabeth R. Waters
ewaters@sdsu.edu
Guihua Bai
guihua.bai@usda.gov
Magdalena Arasimowicz-Jelonek
arasim@amu.edu.pl

Specialty section:
This article was submitted to Crop and Product Physiology, a section of the journal Frontiers in Plant Science

Received: *28 September 2021*
Accepted: *26 October 2021*
Published: *17 November 2021*

Citation:
Sperotto RA, Ricachenevsky FK, Waters ER, Bai G and Arasimowicz-Jelonek M (2021) Editorial: Identification and Characterization of Contrasting Genotypes/Cultivars to Discover Novel Players in Crop Responses to Abiotic/Biotic Stresses. Front. Plant Sci. 12:784874. doi: 10.3389/fpls.2021.784874

Editorial on the Research Topic

Identification and Characterization of Contrasting Genotypes/Cultivars to Discover Novel Players in Crop Responses to Abiotic/Biotic Stresses

Plants are continuously exposed to several abiotic and biotic stresses that negatively affect crop performance and yield. It is predicted that climate change will enhance the frequency and extent of such negative impacts on crop yield (Chadalavada et al., 2021). Continued greenhouse gas emissions will cause further rise in temperature, leading to increased evapotranspiration and drought severity, soil salinity, and local temperature extremes that reduce plants' capability to defend against insects and pathogenic microorganisms (Baillo et al., 2019). Thus, multifactorial stresses constitute one of the most pressing threats in agricultural areas worldwide (Bai et al., 2018; Saijo and Loo, 2020). This has raised a major challenge for plant scientists to secure global food supply and brought an immediate need to continuously increase the yield of major food crops. Understanding stress-related processes in plants is crucial to develop screening procedures for selecting crop lines that can better adapt to non-optimal conditions. One of the most common strategies used by plant scientists is to identify and characterize genotypes/cultivars with contrasting phenotypes and differential responses to the non-optimal conditions, and find molecular, biochemical and physiological mechanisms involved in crop responses to abiotic and biotic stresses (Nutan et al., 2018; Xu and Bassel, 2020). The elucidation of such mechanisms will facilitate the identification and further characterization of agronomically important genes, alleles, and molecules for creating/engineering new cultivars to improve crop yield under stress. This Research Topic provides an update on recent advances in the plant molecular and physiological mechanisms associated with plant responses to stressful conditions, and provides an overview of different approaches used for improving crop tolerance/resistance. Here, we highlight some of the major points arising from these reports.

ABIOTIC STRESS RESPONSES

Climate change is expected to intensify stressful conditions to most crops, which will limit their yield potential and threaten global food supply (Chadalavada et al., 2021). Several

studies demonstrated that some genotypes are more tolerant to non-optimal conditions than others. However, the mechanisms explaining variation in plant tolerance have not been well-characterized in most crops. In this section, we show that several studies were conducted in different crops to identify new genetic resources and tools for the characterization of the possible mechanisms of plant responses and tolerance to abiotic stresses.

Drought Stress Response

Using artificial mutagenesis, le Roux et al. characterized a wheat mutant line tolerant to drought stress at late booting stage, and found that such mutant line maintained higher relative moisture and photosynthesis rate, besides producing more seeds than its WT progenitor under drought stress. The mutant also showed increased expression of RuBisCO and a set of unique proteins associated with dehydration tolerance, which are probably involved in wheat drought tolerance. Terminal drought is the most significant abiotic stress affecting wheat grain yields worldwide. Figueroa-Bustos et al. investigated the effects of root system size on terminal drought and grain yield by comparing the responses of two genotypes with different root sizes under terminal drought treatments, and found that "Tincurrin" genotype (with smaller root system size) showed less reduction in leaf stomatal conductance, photosynthesis and transpiration rates, and thus higher water use efficiency and grain yield than "Bahatans-87" (with larger root size). Faster phenological development and quick grain filling avoided severe water stress in "Tincurrin". In other cereal crops, Degraeve et al. explored the use of vulnerability to *drought-induced xylem embolism* (DIXE) as a proxy for drought tolerance. The acoustic emissions (AE_{50}) values suggested the wheat cultivar "Excalibur" as the most tolerant, and the triticale cultivar "Dublet" as the most vulnerable to DIXE, though "Dublet" had significantly higher hydraulic capacitances that are essential for internal water storage to temporarily buffer water shortage. In addition, both cultivars have a contrasting trade-off between hydraulic safety and efficiency. They suggested that both AE_{50} and hydraulic capacitances should be considered when evaluating a cultivar's drought responses.

Root pressure has been associated with increased crop production under drought. Drobnitch et al. observed that root pressure was triggered by drought exposure followed by re-watering in *Sorghum bicolor* and was positively associated with fine/coarse root length ratio and shoot biomass. Root allocation may have a possible role in creating root pressure and adaptive benefit of root pressure for shoot biomass production. Through RNA-seq they identified different expression of aquaporins, membrane transporters and ATPases in the plants with root pressure.

To select drought tolerant potato lines, Haas et al. developed a model based on leaf metabolite and transcripts to predict drought tolerance of potato lines in breeding programs. After testing the model in multiple environments, they found that it effectively selected superior drought tolerant genotypes, but not low tolerant or sensitive genotypes. They recommend using the model as an alternative tool to yield-based selection in arid environments by combining with tools that can select against sensitive genotypes.

In soybean, wild relatives may carry novel QTLs for drought avoidance. Prince et al. developed an inter-specific mapping population between cultivated and wild soybean and characterized the population for root architecture traits. Using a high-density SNP map, they identified 11 QTLs for these traits. Two of them on chromosome 7A of wild soybean were significant for total root length (RL) and root surface area (RSA). Four candidate genes were identified for the RL QTLs. The novel QTLs from the wild soybean could be used to improve root system architecture and productivity of elite soybean lines under drought stress.

Kamphorst et al. evaluated the performance of field cultivated popcorn inbred lines under well-watered and water stressed ($\psi_{soil} \geq -1.5$ MPa) conditions. The tolerant lines maintained a stay-green condition (higher SPAD index) until physiological maturity. Besides leaf greenness, traits related to leaf photosynthetic status and stomatal conductance are good indicators of the agronomic performance of popcorn under water constraint.

Cao et al. investigated the drought tolerance mechanisms of mulberry by comparing physiological responses and transcriptional changes of plasma membrane intrinsic proteins (PIPs) in different plant tissues of three cultivars with contrasting drought tolerance under progressive soil water deficit. They found that in the resistant cultivar "Wubu", whole-plant level responses of *PIP* transcription, osmoregulation through proline and soluble proteins, and antioxidative protection are important mechanisms for mulberry to cope with drought stress.

Alvarez-Maldini et al. investigated differences in morpho-physiological traits of native *Cryptocarya alba* and *Persea lingue* from central Chile under water stress and found that the most mesic populations showed more reduction in relative growth rates than the xeric populations in response to water stress in both species. Also, they found that water use efficiency (WUE) in *C. alba* and the two traits (WUE and relative growth rates) in *P. lingue* could further assist in the selection of populations for restoration according to their response to water stress.

Gedam et al. screened 100 onion genotypes for drought tolerance using multivariate analysis. Bulb yield was strongly positively correlated with membrane stability index, relative water content, total chlorophyll content, antioxidant enzyme activity, and leaf area under drought stress. Therefore, the identified tolerant genotypes with drought-adaptive traits may be useful in onion breeding program for drought tolerance and can significantly improve onion productivity in low rainfall areas.

Simulating drought stress in natural field conditions, Arif et al. evaluated the drought tolerance of advanced breeding lines of chickpea. Environment influenced seed yield and number of branches, pods, and seeds, while genotype was the main source of variation in seed weight and plant height. Some genotypes performed well only in non-stressed environments, while others performed consistently well in both environments. Ranks in each environment and genotype selection index will help breeders to select genotypes of their choice for further use as variety or pre-breeding germplasm.

Olive plants growing in the greenhouse were evaluated for drought tolerance under severe stress. Baccari et al. analyzed

growth, plant water status, net photosynthesis rates, chlorophyll contents and the extent of photo- and antioxidant defenses, and concluded that "Zarrazi" and "Chemlali" genotypes showed better performance under severe water stress compared to the other genotypes, which was associated to their ability to trigger a higher antioxidant protection. Also, olive plants were able to continue photosynthesizing under severe stress, which is probably related to increased levels of xanthophyll cycle de-epoxidation and α-tocopherol contents.

Harb et al. evaluated the transcriptomic profile of drought-tolerant "Otis" and drought-sensitive "Baronesse" barley genotypes subjected to drought. "Otis" had better photosynthetic capacity under drought compared to "Baronesse", which could be attributed to the differences in the expression level of photosystem II proteins D1 and D2, both associated with PSII stability. Also, many potential drought tolerance genes such as wax biosynthesis gene (*CER1*), and two *NAC* TFs were uniquely induced in "Otis" under drought stress. Therefore, the overall transcriptional responses were low in "Otis", but the genes that could confer drought tolerance were either specifically induced or greatly upregulated in this genotype.

Mechanisms of lignin distribution regarding cell wall composition and digestibility under contrasted water regimes were studied in maize internodes from a recombinant inbred line (RIL) population grown in field trials (El Hage et al.). Biochemical and histological traits have different response thresholds to water deficit. While histological profiles were only modified under pronounced water deficit, most of the biochemical traits responded whatever the strength of the water deficit. The authors also highlight the potential role of *p*-coumaroylation of maize stem in refining plant agronomic properties and digestibility.

Using high throughput phenomics facility, Lekshmy et al. demonstrated a significant genetic variability in the acquired tolerance to a gradually imposed drought stress protocol among contrasting rice genotypes. Association of free radical production/scavenging with yield attributes showed that genotypes that were able to maintain low levels of free radicals in their cells presented high spikelet fertility and hence grain yield under drought stress, evidencing the importance of assessing genetic variability to improve drought adaptation.

Cold Stress Response

Yang et al. performed high-throughput QTL-sequencing analyses to identify the major QTLs governing cold tolerance at the bud-bursting (CTBB) stage in rice. They found a novel major QTL (*qCTBB9*) on chromosome 9 that controls seed survival rate under low-temperature conditions. Re-sequencing data and local QTL mapping allowed mapping *qCTBB9* to a region containing 58 annotated genes, but only one (Os09g0444200) was strongly induced by cold stress. Therefore, Os09g0444200 is a potential candidate for *qCTBB9* and could be used to improve the cold tolerance of rice varieties by marker-assisted selection.

Zhang et al. found that membrane lipid and fatty acid metabolism may be a significant contributor in peanut cold tolerance. Lipidomic data indicated that photosynthetic damage, resulted from the alteration in fluidity and integrity of photosynthetic membranes under cold stress, were mainly caused by decreased monogalactosyldiacylglycerol levels, and could be relieved by increased digalactosyldiacylglycerol and sulfoquinovosyldiacylglycerol levels, maintaining chloroplast structural integrity and normal photosynthesis. The upregulation of phosphatidate phosphatase and phosphatidate cytidylyltransferase under cold stress inhibited the damage of membrane lipid peroxidation caused by excessive accumulation of phosphatidic acid.

Photosynthetic efficiency is a key determinant and a good indicator of cold tolerance in plants. Huang et al. used associative transcriptomics to identify genetic loci controlling photosynthetic gas exchange parameters in 123 rapeseed (*Brassica napus* L.) accessions. Twenty two candidate genes were identified, and *Cab026133.1* encoding a tropinone reductase (*BnTR1*) was further confirmed to be closely linked to the transpiration rate. Overexpressing *BnTR1* in Arabidopsis plants increased the transpiration rate and the alkaloids content, resulting in enhanced cold tolerance under freezing conditions.

Heat Stress Response

In their study, Wang et al. examined the impact of heat-stress at three developmental stages in two varieties of *Zea mays* contrasting to heat response. It was shown that heat stress has significant impacts on development/morphology in both varieties. However, significant differences among the two varieties were found in hormone pathways. After exposure to heat stress, some but not all hormone pathways respond the same way in the two varieties, such as the upregulation of genes for gibberellic acid and abscisic acid, and the downregulation of those for zeatin and zeatin riboside. In contrast, the genes involved in salicylic acid (SA) and jasmonic acid (JA) pathways are upregulated in the heat-tolerant variety and downregulated in the heat-sensitive variety.

Lu et al. characterized near-isogenic lines (NIL) from two populations of wheat (Cascades X Tevere; Cascades X W165) and identified four pairs of NILs that varied in heat responses. Genotyping identified five single nucleotide polymorphisms (SNPs) in seven candidate genes in a major heat tolerance QTL on chromosome 7A. The genes identified code for the following proteins: a zinc finger domain, an F-box domain, a galactose oxidase, a peroxidase, a sugar transporter, and an HSP-70 protein. In another study of wheat, Tomás et al. examined four Portuguese landraces for heat-tolerant traits. Specifically, they examined the impact of heat on grain yield and protein content. They report that heat stress did impact grain composition, and, importantly, that the impact of heat stress varied across the landraces. This variability supports the use of these genetic resources to increase wheat tolerance to heat stress.

Chaudhary et al. present a review of the traits associated with heat tolerance within a wide range of crop species. The authors distinguish between growth-based parameters, leaf traits, pollen-based traits, biochemical traits, differential gene expression, and yield traits. This analysis provides an opportunity to identify common pathways and processes that control heat tolerance.

Most heat-stress studies examine the impact of daytime stress. This is due to many reasons, including the well-established impact of heat stress on photosynthesis. Huang et al.

make an important contribution by examining the impact of nighttime temperatures on yield in rice. These authors used long-term climate data to evaluate the impact of high nighttime temperatures on both a hybrid cultivar and an inbred cultivar. Notably, this study clearly shows that nighttime temperatures can have significant impacts on yield. Further, they demonstrate that these impacts can vary across genetic backgrounds.

Salt Stress Response

Gil-Muñoz et al. examined salt tolerance in four distinct populations of Persimmon (*Diospyros*). The open-pollinated *D. virginiana* possessed the highest level of salt tolerance. In contrast, the *D. lotus* seedlings had the lowest tolerance to salinity. Principal component analysis of the morphological responses to salinity had the widest distribution in the *D. virginiana* populations and the lowest in the *D. lotus* populations. These data indicate the presence of significant variation within this genus for salinity tolerance. This in turn suggests that future breeding programs have sufficient genetic variation to successfully breed salt-tolerant hybrid persimmon varieties.

The responses to salt stress in two cultivars of sweet potato, Xushu 22 (salt-tolerant) and Xushu 32 (salt-sensitive), were examined by Meng et al.. During stress, the salt-sensitive cultivar differentially expressed twice as many genes as did the tolerant variety. It is also reported that the genes upregulated in the tolerant and sensitive cultivars vary. The more tolerant cultivar upregulated genes associated with the ribosome pathway, as well as genes associated with glucosinolate, and N-Glycan biosynthesis.

Niron et al. examined the response to salt stress in tolerant and susceptible genotypes of common bean (*Phaseolus vulgaris*). The Ispir genotype (tolerant) differentially expressed more genes than did the TR43477 genotype (susceptible). Genes associated with photosynthesis, porphyrin, and chlorophyll were enriched during stress in Ispir but not in TR43477. In addition, sucrose and starch metabolism were enriched in Ispir but declined in TR43477. Ispir was also able to better regulate ion content including sodium (Na^+) compared to TR43477. Finally, amino acid metabolism was normal in Ispir but dysregulated during salt stress in TR43477.

Combined Responses to Abiotic Stresses

Studies focused on abiotic stress responses commonly isolate stresses to understand their physiological and molecular underpinnings. However, these stresses often occur in a combination with the environments, and therefore studies focused in plant responses to combined abiotic stresses are very important. Dubberstein et al. explored how single and combined heat and drought stresses can affect photosynthesis in two genotypes of *Coffea* sp., namely Icatu and CL153. Icatu was clearly more drought-tolerant, while both genotypes were impacted by high temperature and a combination of both stresses. Authors showed that photochemical components are resilient to single and combined stresses, while enzymes involved in photosynthesis are more sensitive, suggesting a pathway for improving *Coffea* sp. tolerance to environmental changes. Other two studies investigated heat and drought responses in wheat plants. El Habti et al. explored how water use and carbohydrate partitioning changed in eight bread wheat (*Triticum aestivum* L.) that vary in stress tolerance. The final grain yield was associated with total water use and aboveground biomass as stresses were more intense. Importantly, glucose and fructose measurements in grains 12 days after anthesis explained more than 40% of the variation in grain weight in the main spike. Authors also found that older wheat varieties increased soluble carbohydrate partitioning from stem to spike when stressed, while modern varieties did not show the same behavior. Moreover, it was clear that maintaining transpiration was key for stress tolerance and productivity, especially when heat and drought were combined. Xue et al. investigated the role of *TaPYL4* gene (involved in plant responses to a variety of stresses) in regulating development of major agronomic traits in wheat under multiple environments (well-watered, drought and heat stress treatments). Functional markers were developed for *TaPYL4-2A* and *TaPYL4-2B* haplotypes, and used to scan a natural population of common wheat accessions for correlation analysis between genotypes and phenotypic traits. *TaPYL4-2A* and *TaPYL4-2B* were identified to be significantly correlated with plant growth-related traits, showing that *TaPYL4* could be a valuable target gene in wheat genetic improvement to develop the ideal plant architecture.

Heat and drought affect grapevine (*Vitis* sp.) cultivation worldwide. Carvalho et al. identified tolerant genotypes within 255 clones of the Aragonez (syn. Trempanillo) variety, commonly grown in Portugal and Spain, using leaf temperature of plants exposed to both stresses. Analyses were performed in 3 years and combined with must characteristics for ranking tolerant genotypes that maintained yield and quality. Selected genotypes with contrasting tolerance/sensitivity to stresses were also evaluated for marker gene expression, identifying selection markers or possible targets for stress tolerance improvement. With that, authors were able to find tolerant clones that maintain must quality.

Wang et al. described the GRAS transcription factor gene family in soybean (*Glycine max*). Authors identified 117 GRAS genes in soybean genome, which were classified in subfamilies and were shown to be regulated by drought, salinity, abscisic acid (ABA) and brassinosteroids (BR). Authors selected *GmGRAS37* for functional characterization. Ectopic expression of *GmGRAS37* in soybean hairy roots leads to up-regulation of several stress-related genes, and to increased salt and drought tolerance. This work provides an excellent candidate gene for soybean improvement and a comprehensive description of the GRAS gene family in this crop.

Nutritional Stress Response

Nutritional stress is a major problem for agricultural systems worldwide. Fertilization is a necessary cost of production, but can lead to environmental pollution, whereas toxic elements found in soils can decrease plant growth or end up in edible organs such as the seeds. Arsenic (As) is a toxic element that can accumulate in rice grains. As accumulation in the segregating population derived from Lemont X TeQing crosses was evaluated by Fernández-Baca et al. when plants were grown under different wetting/drying regimes, a common practice in rice field. It was

found that severe but not mild wetting/drying cycles can reduce inorganic As (the most toxic form) accumulation both in the field and greenhouse conditions. Seven QTLs associated with As accumulation were identified, suggesting that combination of genotypes and water management practices can effectively reduce As in rice grains.

García de la Torre et al. performed a screening on 258 *Medicago truncatula* accessions for cadmium (Cd) tolerance using relative root growth as a proxy to identify tolerant and sensitive genotypes. Cd or other elements concentration in plant tissues were not correlated with tolerance. Authors suggested that NADPH recycling enzymes might be associated with tolerance, while increased expression of enzymes involved in glutathione and phytochelatin synthesis might not be a good marker for Cd tolerance in *M. truncatula*. In another study concerning toxic elements to plants, Ambachew and Blair used a common bean (*Phaseolus vulgaris*) Andean diversity panel composed of 227 genotypes to search for variation in aluminum (Al) tolerance. Genome-wide association using root traits suggested known transporters involved in secretion of malate and citrate as candidate genes, suggesting that increased organic acid secretion is the basis for Al tolerance in this common bean genetic pool.

White Guinea yam (*Discorea rotundata*) tubers are an important crop in West Africa, especially to resource-poor farmers. Matsumoto et al. investigated 20 yam breeding lines and one local variety for their ability to grow in nutrient-poor soils and for responses to added fertilizers. Authors identified tolerant and susceptible genotypes and suggest that biomass vigor may be a marker to select high yield yams. The work provides evidence for genotypic variation for tolerance to low nutrient in yam, which can be used for breeding more resilient varieties. Also focusing on nutritional deficiency, Oustric et al. evaluated combinations of scion and rootstocks of clementine (*Citrus clementina* Hort. ex Tan). Authors identified scion/rootstock combinations that were less affected by nutritional deficiency, but also found that using tetraploid rootstocks does not improve tolerance compared to the same diploid genotype.

Other Stresses Responses

Urban et al. presents the proteome response of two genotypes (Cadeli and Viking) of winter oilseed rape microspore-derived embryos (MDE) to PEG-induced osmotic stress. The approach revealed that osmotic resistance is manifested by the accumulation of proteins engaged in energy metabolism, redox homeostasis, protein destination, and signaling including phospholipases and MAPK4. Additional analysis of hormonal profiles during the stress progression showed that the osmotic resistance noted in cultivar Cadeli was also associated with the time-dependent accumulation of ABA, SA, JA, gibberellin, as well as active cytokinins.

BIOTIC STRESS RESPONSES

Biotic stress causes immense damage to agricultural products worldwide and raises the risk of hunger in many areas (Moustafa-Farag et al., 2019). In this section, we highlight six studies conducted in four different crops (rice, tomato, melon, and apple) that help to elucidate the plant responses and resistance mechanisms to bacteria, fungi, viruses, thrips, and mites.

Kumar et al. summarize the molecular mechanisms associated with the interaction between rice and *Xanthomonas oryzae* pv. *oryzae* responsible for bacterial blight disease. The authors underline that the use of genetic and genomic tools allowed to reveal genetic background of resistance to bacterial blight in rice, and at least 44 genes conferring resistance were identified. Out of these genes, at least 11 have been cloned and characterized favoring molecular breeding, as many resistant rice cultivars and hybrids have been developed and released worldwide. Buffon et al. presented the responses of various rice species/cultivars to *Schizotetranychus oryzae* mite infestation. Surprisingly, the resistant response to phytophagous mites was noted only during *Oryza sativa* cv. Nipponbare-*S. oryzae* interaction, while *Oryza barthii* presented high sensitivity to the mites. Under infested conditions, Nipponbare presented higher protein abundance associated with detoxification, higher levels of proline and a greater abundance of defense-related proteins, such as osmotin, ricin B-like lectin, and protease inhibitors.

Marchant et al. evaluated whether continuous use of tomato yellow leaf curl virus (TYLCV) resistant cultivars promotes overcoming TYLCV resistance and/or affects TYLCV regional diversity. Examination of the full-length genomes of naturally occurring TYLCV isolates from TYLCV-resistant and susceptible tomato genotypes indicated that the genomes did not differentiate with increasing transmission number, as well as no specific mutations were repeatedly observed, and no positive selection was detected. Therefore, tomato resistance might not be exerting selection pressure against TYLCV to facilitate development of resistance-breaking strains. According to Mouden et al., tomato seed treated with JA reduces feeding damage provoked by western flower thrips. Importantly, the effect seems to be cultivar-dependent, and tomato seed coat permeability was indicated as a key factor for effective JA absorption and induction of JA-mediated thrips defense. The results may be particularly valuable for the seed industry to perform pre-treatments on non-responsive cultivars, as well as for tomato breeding programs to select for genetic traits that affect seed permeability.

By the combined application of bulked segregant analysis (BSA) with RNAseq, Cao et al. detected a novel QTL (*qCmPMR-12*) for melon resistance to powdery mildew. Additionally, RNAseq analysis indicated that the *MELO3C002434* gene encoding an ankyrin repeat-containing protein is the most likely candidate gene associated with the resistance to the powdery mildew, caused by *Podosphaera xanthii*. Moreover, the authors developed 15 suitable KASP markers for breeding.

Using six apple rootstock genotypes with contrasting phenotypes to *Pythium ultimum* infection, Zhu et al. identified major miRNA pathways and candidate genes involved in apple root defense activation. Their findings suggest that quick and enhanced lignification of apple roots by the action of laccase may significantly impede pathogen penetration and minimize the disruption of effective defense activation in roots of resistant genotypes.

COMBINED ABIOTIC AND BIOTIC STRESS RESPONSES

In the natural environment, plants are constantly subjected to a combination of abiotic and biotic stresses simultaneously. It is critical to understand how the various response pathways to these stresses interact with one another within the plants, and where the points of crosstalk occur which switch the responses from one pathway to another (Ku et al., 2018). Two articles fall into this category of combined abiotic and biotic stress responses.

Li, Wang et al. performed transcriptome studies proving that *GhTLPs* (thaumatin-like proteins) participate in cotton responses to both stress and developmental stimuli. At physiological level, silencing of *GhTLP19* in cotton was associated with increased content of malondialdehyde and reduced catalase activity, besides increasing the sensitivity to *Verticillium dahliae* and drought. A contrasting response (as higher proline content, thicker and longer trichomes, and higher drought tolerance) was shown by Arabidopsis plants overexpressing *GhTLP19*.

Li, Xin et al. identified a new aspect of pesticide metabolism in cucumber plants, as propamocarb is commonly used to prevent plants against downy mildew. It was found that *CsHMGB* gene contributes to lower propamocarb residue levels in cucumber, and functional analyses revealed that overexpression of *CsHMGB* in D9320 genotype, which naturally accumulates high level of propamocarb, could alleviate the pesticide phytotoxicity. The effect of phytotoxicity mitigation was manifested by an increase in the waxiness of the cuticle and stomatal conductance in the pericarp cells, as well as improved potential of antioxidant system.

FINAL COMMENT

In summary, the work presented here documents recent advances in the plant responses to non-optimal conditions. Now, the challenge is to move forward, to integrate this information and to develop knowledge-driven tolerance/resistance strategies against a diverse range of stressful conditions.

AUTHOR CONTRIBUTIONS

All authors listed have made a substantial, direct and intellectual contribution to the work, and approved it for publication.

REFERENCES

Bai, Y., Kissoudis, C., Yan, Z., Visser, R. G. F., and van der Linden, G. (2018). Plant behaviour under combined stress: tomato responses to combined salinity and pathogen stress. *Plant J.* 93, 781–793. doi: 10.1111/tpj.13800

Baillo, E. H., Kimotho, R. N., Zhang, Z., and Xu, P. (2019). Transcription factors associated with abiotic and biotic stress tolerance and their potential for crops improvement. *Genes* 10:771. doi: 10.3390/genes10100771

Chadalavada, K., Kumari, B. D. R., and Kumar, T. S. (2021). Sorghum mitigates climate variability and change on crop yield and quality. *Planta* 253:113. doi: 10.1007/s00425-021-03631-2

Ku, Y. S., Sintaha, M., Cheung, M. Y., and Lam, H. M. (2018). Plant hormone signaling crosstalks between biotic and abiotic stress responses. *Int. J. Mol. Sci.* 19:3206. doi: 10.3390/ijms19103206

Moustafa-Farag, M., Almoneafy, A., Mahmoud, A., Elkelish, A., Arnao, M. B., Li, L., et al. (2019). Melatonin and its protective role against biotic stress impacts on plants. *Biomolecules* 10:54. doi: 10.3390/biom10010054

Nutan, K. K., Kumar, G., Singla-Pareek, S. L., and Pareek, A. (2018). A salt overly sensitive pathway member from *Brassica juncea* BjSOS3 can functionally complement ΔAtsos3 in arabidopsis. *Curr. Genomics* 19, 60–69. doi: 10.2174/1389202918666170228133621

Saijo, Y., and Loo, E. P. (2020). Plant immunity in signal integration between biotic and abiotic stress responses. *New Phytol.* 225, 87–104. doi: 10.1111/nph.15989

Xu, H., and Bassel, G. W. (2020). Linking genes to shape in plants using morphometrics. *Annu. Rev. Genet.* 54, 417–437. doi: 10.1146/annurev-genet-022620-094553

Conflict of Interest: The authors declare that the research was conducted in the absence of any commercial or financial relationships that could be construed as a potential conflict of interest.

Publisher's Note: All claims expressed in this article are solely those of the authors and do not necessarily represent those of their affiliated organizations, or those of the publisher, the editors and the reviewers. Any product that may be evaluated in this article, or claim that may be made by its manufacturer, is not guaranteed or endorsed by the publisher.

Copyright © 2021 Sperotto, Ricachenevsky, Waters, Bai and Arasimowicz-Jelonek. This is an open-access article distributed under the terms of the Creative Commons Attribution License (CC BY). The use, distribution or reproduction in other forums is permitted, provided the original author(s) and the copyright owner(s) are credited and that the original publication in this journal is cited, in accordance with accepted academic practice. No use, distribution or reproduction is permitted which does not comply with these terms.

frontiers in Plant Science

ORIGINAL RESEARCH
published: 12 June 2020
doi: 10.3389/fpls.2020.00738

Overexpression of *CsHMGB* Alleviates Phytotoxicity and Propamocarb Residues in Cucumber

*Shengnan Li[1], Ming Xin[1], Jie Luan[1], Dong Liu[1], Chunhua Wang[2], Chunhong Liu[1], Wenshuo Zhang[1], Xiuyan Zhou[1] and Zhiwei Qin[1]**

[1] College of Horticulture and Landscape Architecture, Key Laboratory of Biology and Genetic Improvement of Horticultural Crops (Northeast Region), Northeast Agricultural University, Harbin, China, [2] College of Horticulture, Fujian Provincial Key Laboratory of Haixia Applied Plant Systems Biology, Fujian Agriculture and Forestry University, Fuzhou, China

Cucumber (*Cucumis sativus* L.) is one of the most economically important fruits of the Cucurbitaceae family, therefore consideration of potential pesticide residues in the fruit in the context of cucumber breeding and production programs is important. Propamocarb (a pesticide commonly used to prevent downy mildew) is widely used in cucumber cultivation, but the molecular mechanism underlying the degradation and metabolism of propamocarb in cucumber is not well understood. We screened a candidate *CsHMGB* gene (*CsaV3-5G28190*) for response to propamocarb exposure using transcriptome data. The coding region of *CsHMGB* was 624 bp in length and encoded the conserved HMB-box region. *CsHMGB* expression differed significantly between the "D0351" genotype, which accumulated low levels of propamocarb, and the "D9320" genotype, which accumulated high levels of propamocarb. *CsHMGB* expression was positively correlated with propamocarb levels in the cucumber peel. *CsHMGB* expression was upregulated in the fruit peels of the "D0351" genotype following exposure to propamocarb stress for 3–120 h, but no difference was observed in expression between propamocarb treatment and control for the "D9320" genotype. For the "D0351" genotype, *CsHMGB* expression was higher in the fruit peels and leaves than that in female flowers; expression was moderate in the stems and fruit pulps, and weak in male flowers and roots. The CsHMGB protein was targeted to the nucleus in *Arabidopsis* protoplasts and in the epidermis of *Nicotiana benthamiana* leaves. We measured MDA, O_2^-, and H_2O_2 levels in cucumber plants and found that they were likely to accumulate reactive oxygen species (ROS) in response to propamocarb stress. Analysis of antioxidant enzyme activity (SOD, POD, CAT, APX, GPX, GST, and GR) and the ascorbate-glutathione (AsA-GSH) system showed that the resistance of the plants was reduced and the levels of propamocarb residue was increased in CsHMGB-silenced plants in response to propamocarb stress. Conversely, overexpression of *CsHMGB* promoted glutathione-dependent detoxification by AsA-GSH system and improved the antioxidant potential, reduced the accumulation of ROS. Ultimately, the metabolism of propamocarb in cucumber was increased via increase in the wax levels and the stomatal conductance.

Keywords: cucumber, propamocarb residues, *CsHMGB*, antioxidant enzymes, AsA-GSH system

OPEN ACCESS

Edited by:
Raul Antonio Sperotto, Universidade do Vale do Taquari – Univates, Brazil

Reviewed by:
Golam Jalal Ahammed, Henan University of Science and Technology, China
Tse-Min Lee, National Sun Yat-sen University, Taiwan

***Correspondence:**
Zhiwei Qin
qzw303@126.com

Specialty section:
This article was submitted to Plant Abiotic Stress, a section of the journal Frontiers in Plant Science

Received: *20 January 2020*
Accepted: *08 May 2020*
Published: *12 June 2020*

Citation:
Li S, Xin M, Luan J, Liu D, Wang C, Liu C, Zhang W, Zhou X and Qin Z (2020) Overexpression of CsHMGB Alleviates Phytotoxicity and Propamocarb Residues in Cucumber. Front. Plant Sci. 11:738. doi: 10.3389/fpls.2020.00738

INTRODUCTION

Cucumber (*Cucumis sativus* L.) is one of the most economically important fruits in the Cucurbitaceae family and is widely cultivated in greenhouses, where it is susceptible to downy mildew (Liu et al., 2017). Propamocarb is a carbamate fungicide that is used to control downy mildew (Sharma et al., 2016). Most pesticides are heterologous toxic substances, and excessive pesticide application can result in phytotoxicity, increased cell membrane permeability, impaired metabolism, and declined quality and yield (Zhou et al., 2015). Excessive use of pesticides in cultivation leads to lingering residues in cucumber fruit, and can contaminate the fruit and the surrounding environment. Pesticide residue must therefore be carefully considered in the context of cucumber breeding and production programs.

We have previously shown that the magnitude of propamocarb residue accumulation in cucumber is a polygene-regulated quantitative trait. In addition, different genotypes of cucumber differ significantly with respect to residue accumulation (Ma, 2010). Genes involved in propamocarb stress were identified in cucumber through transcriptome analysis, and we screened a candidate high-mobility-group gene (*CsHMGB*) which was upregulated in response to propamocarb stress (Wu et al., 2013). Based on gene function, we speculated that *CsHMGB* may be crucial in mediating the response to propamocarb stress.

High-mobility-group (HMG) protein is a highly abundant non-histone chromosomal protein that is found in eukaryotes. Human diseases, cell damage, trauma-induced stress and necrosis, chronic inflammation, autoimmune diseases, and cancer may all lead to the release of the HMGB1 protein. Extracellular HMGB1 stimulates the inflammatory response and recruits leukocytes by interacting with receptors for advanced glycation end-products (RAGE), toll-like receptor 2 (TLR), and other receptors to protect the organism from disease (Yang et al., 2010; Harris et al., 2012; Venereau et al., 2016). In plants, HMG proteins can be divided into four categories based on their structural characteristics: HMGB type (proHMG-1/-2) protein, containing a characteristic HMG-box domain; ARID-HMG protein, characterized by an A/T-rich binding domain; 3 × HMG protein, containing three HMG-boxes; and SSRP1, a structure-specific recognition protein (Antosch et al., 2012). The HMGB protein is a chromatin structure regulator involved in a variety of stress-tolerance mechanisms in plants. In *Arabidopsis thaliana*, *AtHMGB2* and *AtHMGB3* were significantly downregulated in response to drought and salt stress, but were upregulated in response to cold stress (Kwak et al., 2007; Lildballe et al., 2008). *AtHMGB11* is a nuclear protein that regulates chromatin dynamics and transcription. In *Arabidospsis thaliana*, it interacts with the major groove of other proteins in response to drought stress (Adrita et al., 2016). *AtHMGB15* interacts with the pollen transcription factors, *AtAGL66* and *AtAGL104* to alter pollen germination and growth of the pollen tube (Xia et al., 2014). *AtHMGB3* has been shown to induce the transcription of *AtWRKY33* and *AtFDF1.2*, and to increase the accumulation of corpus callosum (Choi et al., 2016). The HMGB proteins also interact with other proteins, such as histones and transcription factors (Grasser et al., 2007). However, the function of *CsHMGB* in response to propamocarb stress has not been reported in cucumbers.

The detoxification of pesticides [herbicides and chlorothalonil (CHT)] in plants can be divided into four phases: (1) hydrolysis of peroxidase and cytochrome P450s; (2) catalysis of glutathione-*S*-transferase (GST) and glycosyltransferase; (3) transmembrane transport of transporters such as the ABC family; and (4) the hydrolase degradation reaction. The first two steps degrade toxic macromolecular groups into lower levels of toxicity and create poor mobility metabolites, and the latter two steps are responsible for the further hydrolysis and transport of low-toxicity small molecular compounds (Muntane, 2009; Zhou et al., 2015). Additional self-protection mechanisms in plants such as the presence of wax and stomatal action are essential for resisting pesticide stress. In a previous study, we found that the increased opening of stomatal apertures contributes to low levels of pesticide residue (Zhao, 2013). Pesticides can be lost through the stomata during transpiration (Yao and Yang, 2012). Wax is a natural protective screen against plant diseases, insect pests, and external stresses (Yeats and Rose, 2013; Bohinc et al., 2014).

To investigate the mechanisms underlying propamocarb residue accumulation in cucumbers, we identified a putative gene, *CsHMGB*, involved in mediating propamocarb stress. Functional analyses revealed that overexpression of *CsHMGB* could alleviate propamocarb phytotoxicity by increasing the waxiness of the cuticle, increasing the stomatal conductance in the pericarp cells, and activating the antioxidant system.

MATERIALS AND METHODS

Plant Materials

Two cucumber genotypes exhibiting different levels of propamocarb residues in the fruit peel were used: "D0351" (low accumulation of propamocarb residue; 0.014 mg/kg) and "D9320" (high accumulation of propamocarb residue; 0.171 mg/kg). For each genotype, 200 plants were sown in pots containing a mixture of soil and vermiculite (v:v = 1:1) in a solar greenhouse at the Northeast Agricultural University (Harbin, China) (Wu et al., 2013). Plants were grown under a 12 h photoperiod at 28°C/18°C (day/night) and 75% relative humidity.

Propamocarb Treatments

To investigate phytotoxicity in cucumber plants, we sprayed 20 μL propamocarb (400, 800, and 1,200 ppm) onto the leaves of "D0351" and "D9320" plants. Leaves of similar size were selected at 48 h after propamocarb application for further study. MDA content was measured by reacting MDA with thiobarbituric acid (TBA), and MDA-TBA adduct formation was measured based on absorbance at 450, 532, and 600 nm wavelengths (Foyer and Halliwell, 1976).

To determine the accumulation of propamocarb residues in various organs, we applied 50 mL propamocarb (400 ppm) to the entire plant until liquid dripped from the leaves and fruits at 34 days after planting; an equivalent volume of water was

applied as a control. Each plant was sprayed once. Samples were collected from five individual plants at 6, 9, 12, 24, 36, 48, 72, 96, and 120 h after propamocarb application. Fruit were collected from the 10th node. Fruits with the following parameters were selected: length 16–18 cm, diameter 5–6 cm, and weight 160–180 g (Liu et al., 2018; Zhang et al., 2019b). Fruit peels were cut into 2 mm thick samples and fruit pulp sections were cut to 5-mm thickness. Stems and leaves connected to fruits were collected, and female and male flowers in bloom were also collected (**Supplementary Figure S1**). Roots were collected, cleaned, and dried (Liu et al., 2018).

The "D0351" genotype was used for the gene silencing experiment and was planted in an artificial climate incubator (28/18°C, day/night).

The "D9320" genotype was utilized for overexpression studies. T_1 lines of OX2, OX3, and OX5 (each line including five individual plants per biological repeat; three biological repeats) were sown in growth chambers. Plants were treated with propamocarb, and the samples were harvested as previously described.

Determination of Propamocarb Residues

A propamocarb analytical standard was provided by Sigma-Aldrich® (CAS: 24579-73-5) (Merck, United States). Ten grams of homogenized sample were added to a 50 mL colorimetric tube and further homogenized for 5 min. Then, 20 mL acetonitrile and 2.5 g NaCl were added to the sample in the 50 mL colorimetric tube, and mixed for 5 min with shaking at 500 g/min using a mechanical shaker. Samples were allowed to settle for 30 min and then vortex mixed and evaporated until dryness; this step was repeated several times and the resulting material was collected. The sample was then filtered through a polypropylene filter (Merck, United States) (0.22 μm) until no residual particles remained. The levels of propamocarb residue were then analyzed using the Agilent 7890B-5977A gas chromatography system (Agilent Technologies) with a 30 m × 0.25 mm × 0.25 μm capillary column (HP-5MS). The oven temperature was programmed at 40°C 2 min, increased to 200°C at 25°C/min and held for 8 min, sample inlet: 240°C, non-split injection, flow rate of 1.0 mL min^{-1}.

CsHMGB Cloning and Bioinformatic Analysis

The coding sequence for the full-length *CsHMGB* gene was acquired from the cucumber genome database[1]. Fruit peels from cucumber genotype "D9320" were used to clone *CsHMGB* with specific primers (**Supplementary Table S1**). Polymerase chain reactions were performed using the following protocol: 94°C for 2 min; 30 cycles of 94°C for 10 s, 56°C for 15 s, and 72°C for 10 s; and a final extension at 72°C for 5 min. HMGB protein sequences from other species were obtained from the NCBI database[2]. DNAMAN software[3] was used for multiple sequence alignments. MEGA 7.0 software (Poisson model and bootstrap = 1,000) was used to construct a neighbor-joining (NJ) phylogenetic tree (Kumar et al., 2016).

[1]http://www.icugi.org/

[2]http://www.ncbi.nlm.nih.gov/nucleotide/

[3]http://www.lynnon.com/

First-Strand cDNA Synthesis and qRT-PCR Assays

Total RNA was isolated from fruit samples using TRIzol reagent (Invitrogen, Carlsbad, CA, United States). This RNA was then used to synthesize single-stranded cDNA using a reverse transcription kit (Toyobo, Japan), And qRT-PCR was performed in a 20 μL reaction containing 2× Fast qPCR Master Mix (DiNing, China; 10 μL), cDNA template (2 μL), forward and reverse primers (0.5 μL; 10 μmol L^{-1}), and ddH_2O. Cucumber *EF1a* was used as an internal reference gene to calculate the relative expression of the candidate genes (Wan et al., 2010) using the $2^{-\Delta\Delta CT}$ method (Schmittgen and Livak, 2008). The program was run as follows: 95°C for 2 min, then 40 cycles of 95°C for 15 s, 56°C for 15 s, and 72°C for 30 s. The melting curve was generated as per a default application on qTower2.0 (Analytikjena, Germany). All primers used for qRT-PCR are shown in **Supplementary Table S1**. Three biological replicates and three technical replicates were performed.

Subcellular Localization

The full-length sequence of *CsHMGB* (with the exception of TAG) was amplified using PCR. *CsHMGB* was cloned into a green fluorescent protein (GFP) carrier with a super promoter (pSuper-1300) via traditional digestion (*Xba*I and *Bgl*II) and T4 ligation (Invitrogen, Carlsbad, CA, United States) (Li et al., 2018). The empty vector was used as a negative control. Following this process, *A. thaliana* protoplasts were transfected with recombinant CsHMGB-GFP and the empty GFP vector, and were imaged using a confocal spectral microscope with green fluorescence at 488 and 580 nm (Yoo et al., 2007) (Leica, Germany).

The CsHMGB-GFP and empty GFP plasmids were transferred into *Agrobacterium tumefaciens* GV3101 using the freeze-thaw method, and the leaves of 5-week-old *Nicotiana benthamiana* plants were inoculated with the *A. tumefaciens*. The tomato bushy stunt virus gene (*p19*) suppresses the silencing of *CsHMGB* (Grefen et al., 2008). After 2 days, leaf epidermal cells from *N. benthamiana* were observed using a confocal microscopy, as described above.

Silencing of *CsHMGB*

Virus-induced gene silencing (VIGS) for *CsHMGB* was performed in cucumber leaves at 14 days after the seeds were sown (at one-leaf stage). A specific 248 bp fragment of *CsHMGB* was amplified and then cloned into the pTRV2 vector using *Ecor*I with *Bam*HI. Plasmids were used to transform *A. tumefaciens* strain GV3101, which were then cultivated in LB medium containing 50 μg mL^{-1} rifampicin and 50 μg mL^{-1} kanamycin on a rocking platform at 200 rpm and at 28°C for 18 h. Cells were collected and re-suspended in an infiltration buffer supplemented with 200 mM acetosyringone, 10 mM $MgCl_2$, and 10 mM MES (pH 5.6), at a final OD_{600} of approximately 1.2. Culture mixtures primarily contained pTRV2-*CsHMGB* and pTRV1-*CsHMGB*

(v/v, 1:1), or pTRV2 and pTRV1 (negative controls), and were incubated for 3–4 h under 25°C in darkness prior to injection. Silencing of the plant alkene desaturase (PDS) gene causes photobleaching, which can be used to control the efficiency of VIGS (André et al., 2009). In total, there were 30 plants in each combination, which were divided into three groups of 10 plants as biological repeats. Three biological and technical replications were performed.

Cucumber Transformation System

The amplified *CsHMGB* sequence was cloned into the pCXSN-1250 vector harboring the glyphosate resistance gene under a constitutive promoter (Chen et al., 2009). Digestion was performed with *Xcm*I, following which the method followed that described for the TA clone system; the vector was ligated with the *CsHMGB* PCR products using T_4 DNA ligase (Invitrogen, Carlsbad, CA, United States), thus generating the pCXSN-1250-*CsHMGB* overexpression vector. Agrobacteria from the GV3101-mediated method were used to infect the cotyledons of cucumber plants to generate transgenic plants. Cells with over-expression were selected in MS medium supplemented with 1 mg/L glufosinate (Zhang et al., 2014). The generation of T_0 and T_1 cucumber plants was verified via PCR and qRT-PCR. Primer sequences are displayed in **Supplementary Table S1**.

Analysis of Pericarp Cells

The exocarp tissue in the middle of the cucumber fruit peel was sectioned into 2 × 5 mm strips with a double-sided blade. The tissue was then immediately fixed in 2.5% glutaraldehyde (phosphate buffer), immersed in the solution by vacuum pumping, and stored at 4°C for 1.5 h. Samples were then flushed, dehydrated, replaced, and freeze-dried. Conductive tape was glued to the scanning electron microscope table, and the sample surface was coated with a 15 nm metal film using an Emur1010 (HITACHI) ion sputtering coating instrument. Samples were observed and imaged under a Smur3400N scanning electron microscope.

Reactive Oxygen Species Accumulation and Enzymatic Activity Analyses

Samples were collected from five individual plants at 2, 4, 6, 8, and 10 days after propamocarb application (Zhang et al., 2019b). Leaves connected to fruits (approximately 0.5 g leaf weight) were collected in order to measure the physiological index for the leaf tissue.

H_2O_2 content was measured by sulfuric acid peptide oxidation at a 415 nm characteristic absorption. The 0.5 g sample was grinded in the 2 mL pre-cooled acetone in an ice bath followed by centrifugation for 20 min at 10,000 *g* at 4°C, the supernatant was brought to 3 mL. Then, 1 mL extracting solution, 0.1 mL 20% titanic tetrachloride and 0.2 mL concentrated NH_4OH was mixed for 5 min and centrifuged for 15 min at 10,000 *g* at 4°C. The supernatant was discarded and the precipitate was dissolved in 1 mol L^{-1} H_2SO_4, and washed several times with cold acetone, the final volume was made up to 2 mL (Gong et al., 2013).

O_2^- content was assayed using hydroxylamine hydrochloride at 530 nm. The 0.5 g sample added 2 mL phosphoric acid buffer (50 mol L^{-1}, PH = 7.80) with full grinding, and collecting the supernatant after centrifugation at 10,000 *g* for 20 min, then the volume was adjusted to 3 mL. The 0.5 mL extracting solution mixed with 0.5 mL phosphoric acid buffer (50 mol L^{-1}, PH = 7.8) and 1.5 mL hydroxylamine hydrochloride (1 mol L^{-1}), placed at 25°C for 1 h. Then, addition with 2 mL p-aminobenzene sulfonic acid (17 mol L^{-1}) and 2 mL α-naphthylamine (7 mol L^{-1}), the mixture was incubated at 25°C for 20 min (Gong et al., 2013).

The 0.5 g sample was ground to a homogenate with 3 mL pre-cooled potassium phosphate buffer (50 mol L^{-1}, PH = 7.0) in an ice bath followed by centrifugation for 20 min at 10,000 g at 4°C. Extracting solution was used to determine the SOD, POD, CAT, and APX activity. POD activity was determined via the catalytic H_2O_2 oxidation of specific substrates by the guaiacol method at 470 nm (Bradford, 1976). SOD activity was examined by measuring the ability of SOD to inhibit the photochemical reduction of nitro blue tetrazolium at 560 nm (Aebi, 1984). CAT activity was determined via the reduction at 240 nm for H_2O_2 extinction (Giannakoula et al., 2010). APX activity was measured based on the rate of ASA oxidation. 0.1 mL supernatant was mixed with 1 mL extracting solution (50 mol L^{-1} potassium phosphate with pH = 7.0, 750 μmol L^{-1} AsA and 100 mol L^{-1} H_2O_2). The absorbance at 290 nm was measured at every 15 s intervals for 3 min (Durner and Klessig, 1995).

GPX activity was assayed through the oxidation of glutathione by GPX at the absorbance of 412 nm. The 0.5 g sample was ground to a homogenate with 5 mL extracting solution in an ice bath followed by centrifugation for 10 min at 10,000 *g* at 4°C (Anderson and Davis, 2004).

The oxidation rate of ASA measured at 265 nm was used to estimate ASA content. The 0.5 g sample was ground to a homogenate with 5 mL buffer I in an ice bath followed by centrifugation for 20 min at 8,000 *g* at 4°C. A total of 20 μL supernatant was mixed with 160 μL buffer II and 20 μL buffer III from the kit (Solarbio, Beijing).The absorbance at 290 nm was measured at 10 and 130 s; DHA content was calculated from the rate of AsA formation at a wavelength of 265 nm at 10 and 130 s (Solarbio, Beijing).

DHAR and MDHAR activity were analyzed as described by de Pinto et al. (1999). The 0.5 g sample was grinded in the pre-cooled 50 mol L^{-1} phosphoric acid buffer (containing 1 mol L^{-1} EDTA, 2.5% Triton X-100,1 mol L^{-1}ascorbate, and 2% polyvinylpyrolidone) in an ice bath followed by centrifugation for 20 min at 16,000 *g* at 4°C. A total of 0.3 mL extracting solution with 50 mol L^{-1} phosphoric acid buffer (pH = 7.0), 20 mol L^{-1} GSH and 2 mmol L^{-1} DHA up to 3 mL was used to measure DHAR activity at 265 nm. A total of 0.09 mL extracting solution with 50 mol L^{-1} phosphoric acid buffer (pH = 7.0, containing 2 mmol L^{-1} AsA), 2 mmol L^{-1} NADPH and 2 U AAO (pH = 5.6) was used to measure MDHAR activity at 340 nm.

Total glutathione and GSSG content were analyzed as described by Anderson et al. (1992). The 0.5 g sample was ground to a homogenate with 2.5 mL 7% pre-cooled sulfosalicylic acid in an ice bath followed by centrifugation for 20 min at 16,000 g at 4°C. A total of 0.1 mL supernatant was mixed with 0.2 mol L^{-1}

PBS, 0.2 mol L^{-1} NADPH and 1 U GR up to 3 mL. The mixture was incubated at 27°C for 30 min and the absorbance was at 412 nm measured for total glutathione content. The difference between the determination of GSSG and total glutathione was the reaction system containing 0.1 mol L^{-1} 2-vinylpyridine, and the mixture was incubated at 27°C for 1 h for determination of GSSG content. The GSH content was then calculated by subtracting GSSG from total glutathione.

Glutathione-*S*-transferase activity was measured spectrophotometrically using 1-chloro-2,4-dinitrobenzene (CDNB) and 5 mM GSH as standard substrates at a wavelength of 340 nm. The 0.5 g sample was ground to a homogenate with 5 mL 50 mol L^{-1} phosphoric acid buffer (1 mol L^{-1} EDTA, 10 mol L^{-1} KCl, 5 mol L^{-1} DTT, 0.5 mol L^{-1} AEBSF, and PH = 7.5) and polyvinyl-polypyrrolidone (insoluble PVPP), followed by centrifugation for 20 min at 12,000 *g* at 4°C (Anderson and Davis, 2004).

GR activity was detected via the estimation of the dehydrogenation rate of NADPH. The 0.5 g sample was grinded in the reaction mixture (0.1 mol L^{-1} EDTA, 3% Triton X-100, and 50 mol L^{-1} phosphoric acid buffer with 4% polyvinylpyrolidone and PH = 7.5), the volume was adjusted to 4 mL followed by centrifugation for 15 min at 16,000 *g* at 4°C. A total of 0.1 mL supernatant was mixed with 0.1 mM Tris-HCl (PH = 8.0), 1 mol L^{-1} GSSG and 0.5 mM NADPH up to 3 mL with a characteristic absorption peak at 340 nm (Anderson and Davis, 2004).

Statistical Analysis

The statistical significance of differences was calculated by Tukey's tests using Statistical Analysis System (SAS) version 9.21. Data are means (±SE) of three independent experiments each corresponding to at least three replicates. Statistically significant differences were determined by Student's *t* tests ($p < 0.05$ significance level and $p < 0.001$ extremely significant level).

RESULTS

Phytotoxicity of Propamocarb in Cucumber

To determine the phytotoxicity of propamocarb in cucumber, we applied three different concentrations of propamocarb (400, 800, and 1,200 ppm) to the leaves of the "D0351" and "D9320" genotypes. The recommended dose of 400 ppm did not induce phenotypic changes in cucumber. However, excessive use of propamocarb (800 and 1,200 ppm) could induce phytotoxicity, such as yellow speckles on leaves (**Figure 1A**). MDA content was correlated with propamocarb concentration in both of the cucumber genotypes. MDA content was higher in "D9320" than that in "D0351" plants following propamocarb application (**Figure 1B**), indicating that the antioxidative capacity of the cucumber plants was reduced under propamocarb stress.

Propamocarb Residues in Cucumber

We detected the propamocarb residues in "D0351" and "D9320" genotype, results showed that the maximum residue in found in the fruit peels was 2.08-fold higher in "D9320" than that in "D0351" after 2 days of treatment with 400 ppm propamocarb. Dramatic changes in fruit peel propamocarb residue were noted in both "D0351" and "D9320" after application for 3 h to 21 days. Propamocarb residues gradually increased from 12 h to 2 days of propamocarb application and dramatically decreased from 2 to 5 days. However, propamocarb residues rarely decreased between 5 and 21 days of propamocarb application (**Figure 2A**). Detection of propamocarb residues in various tissues revealed that residues in leaves were greater than in fruit peels, and that there were limited residues in the roots, stems, and fruit pulps (**Figure 2B**).

Identification and Cloning of *CsHMGB*

As compared to water as a control, *CsaV3-5G28190* expression significantly changed under propamocarb stress, and the calculated transcript level was consistent with qRT-PCR results. The full-length *CsHMGB* cDNA sequence was cloned through RT-PCR based on the "D0351" genotype total RNA. That genomic coding region was 624 bp in length, including eight exons and seven introns with the start codon of ATG to TAA. The amino acid sequence of *CsHMGB* was obtained from cucumber plants, HMGB proteins were obtained from other Cucurbitaceae crops, and HMGB1/2/7 was obtained from *Arabidopsis* and other plant species. The results indicated that *CsHMGB* from cucumber, CmHMGB7 from melon (*Cucumis melo* L.), MnHMGB7 from bitter gourd (*Momordica charantia* L.), and CpHMGB7 from pepper (*Capsicum annuum* L.) were in the same evolutionary branch, as their genetic relationships were greater than 80%. The alignment of amino acid sequences showed that the *CsHMGB* protein contained the HMB-box conserved region (**Supplementary Figure S2**), and it was therefore placed in the HMGB protein family.

Expression of *CsHMGB* Exhibits Positive Correlation With Propamocarb Residue in Cucumber Fruit

To further investigate the function of *CsHMGB* in response to propamocarb stress, qRT-PCR was carried out to measure the quantity of *CsHMGB* transcripts within each organ. In "D0351" plants under propamocarb stress, the expression of *CsHMGB* was higher in the fruit peels and in the leaves than that in female flowers, moderate in the stems and fruit pulps, and weak in male flowers and in the roots (**Figure 3A**). *CsHMGB* expression was higher in "D0351" leaves and fruit peels than that in "D9320" leaves and fruit peels (**Figure 3B**). There were significant differences between "D0351" and "D9320" in *CsHMGB* mRNA abundance in fruit peels following propamocarb stress for 3, 6, 12, 24, 36, 48, 72, and 120 h. *CsHMGB* expression rapidly increased from 3 to 48 h and was significantly higher in "D0351" plants than in the water control treatment. However, from 72 to 120 h of propamocarb treatment, the expression of *CsHMGB* was reduced (**Figure 3C**). In "D9320" under propamocarb stress, the expression of *CsHMGB* displayed minimal change as compared to the control from 3 to 120 h (**Figure 3D**). In general, *CsHMGB* expression was positively correlated with propamocarb residues in the cucumber fruit peels.

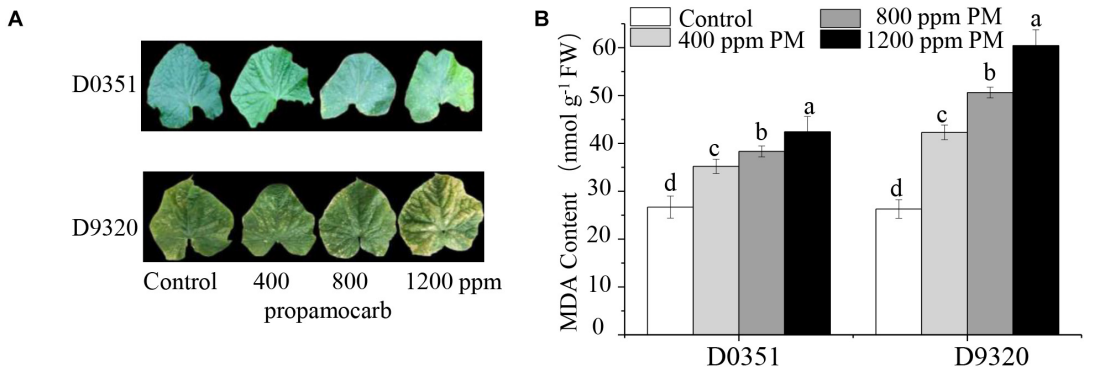


FIGURE 1 | Effects of propamocarb application in cucumbers. **(A)** Phenotype of cucumber leaves following 400, 800, and 1,200 ppm propamocarb applied to "D0351" and "D9320" genotype plants at 2 days after application. **(B)** MDA content in "D0351" and "D9320" genotype plants at 2 days. Data are the means of three replicates with SEs, and different letters indicate a significant difference ($p < 0.05$ by Tukey's test).

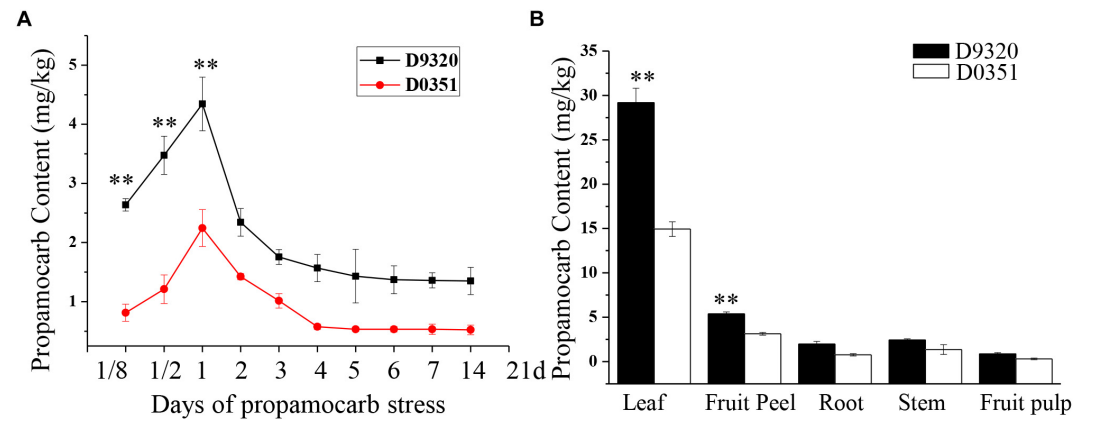


FIGURE 2 | Propamocarb residues in cucumbers. **(A)** Time course of propamocarb residue in cucumber fruit peels of "D0351" and "D9320" plants. **(B)** Propamocarb residues in leaf, stem, root, fruit peel, and fruit pulp of "'D0351" and "D9320." Data are means (±SE) of three independent experiments with three replicates for each. Statistically significant differences were determined by Student's *t*-test ($p < 0.05$).

CsHMGB Is a Nuclear Protein

To determine the subcellular localization of *CsHMGB*, the CsHMGB-GFP protein was constructed and driven by the pSuper promoter. The pSuper, GFP empty vector, and CsHMGB-GFP fusion expression vector were transfected into *Arabidopsis* protoplast and *N. benthamiana* leaf epidermis. Using laser confocal microscopy, we determined that the GFP fluorescence signals were enriched in the nucleus in *Arabidopsis* protoplasts and in the *N. benthamiana* leaf epidermis (**Figures 4A,B**), indicating that *CsHMGB* is a nuclear protein.

Silencing *CsHMGB* Results in Accumulation of More Propamocarb Residues in Cucumber

To verify the function of the *CsHMGB* gene in response to propamocarb stress, the VIGS system was used to silence *CsHMGB* mRNA expression in "D0351" cucumber leaves. pTRV2, TRV2-PDS, TRV2-HMGB, and pTRV1 were mixed, and the mixture was applied to "D0351" cucumber rough leaves according to the *Agrobacterium tumefaciens* strain method. PDS was included as an indicator gene, and the leaves displayed photobleaching at 16 days after inoculation, indicating that *CsHMGB* was momentarily silenced (**Figure 5A**). The mRNA level of *CsHMGB* was markedly lower within *CsHMGB*-silenced leaves than within the TRV2 empty vector group and the control group (**Figure 5B**). Gas chromatography-tandem mass spectrometry revealed propamocarb residues in the control group and TRV2 group (14.94 and 13.85 mg/kg, respectively). However, *CsHMGB*-silenced leaves contained twice accumulations of propamocarb that of the control group (**Figure 5C**). These data demonstrate that *CsHMGB* plays a positive role in response to propamocarb stress.

In the control plants, we observed that the contents of O_2^-, H_2O_2, and MDA were increased in leaves under propamocarb stress, indicating that propamocarb may cause damage to cucumber plants though the accumulation of reactive oxygen species (ROS). In *CsHMGB*-silenced plants, O_2^- and H_2O_2 contents increased by 127 and 125%, respectively, in comparison with the control after 48 h of propamocarb stress

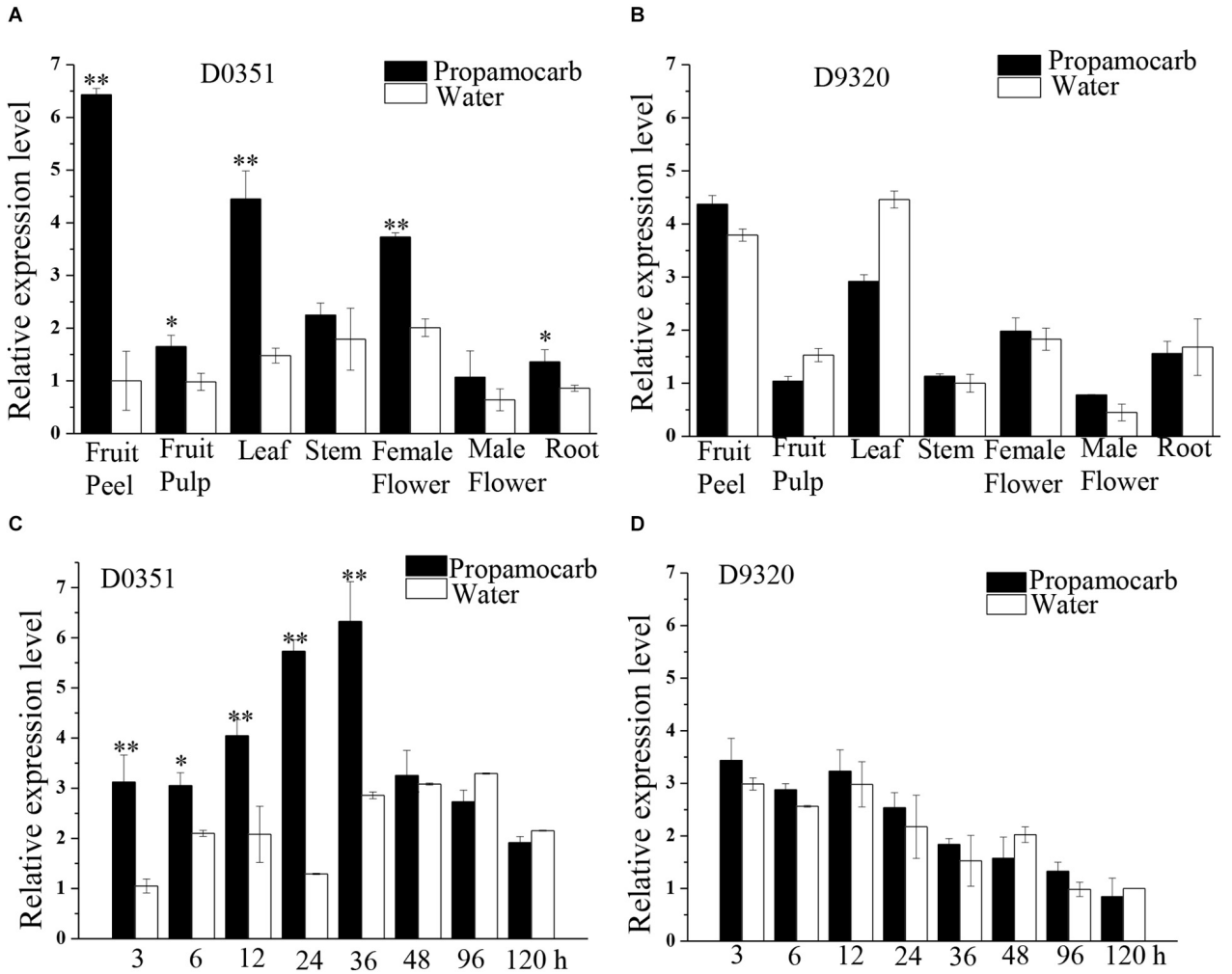


FIGURE 3 | Expression patterns of *CsHMGB* in cucumbers. **(A)** *CsHMGB* levels in various tissues of "D0351" plants under propamocarb stress at 2days after application. **(B)** *CsHMGB* levels in different tissues of "D9320" plants under propamocarb stress at 2 days. **(C)** Time course of *CsHMGB* levels in fruit peels following propamocarb stress in "D0351" plants. **(D)** Time course of *CsHMGB* levels in fruit peels following propamocarb stress in "D9320" plants. *CsEF1a* was used as the reference gene. Significant differences were observed between treatment (*$p < 0.05$ and **$p < 0.01$) by Student's *t*-test.

(**Figures 5D,E**). Similarly, MDA content was higher in *CsHMGB*-silenced plants than in control plants when under propamocarb stress (**Figure 5F**). These results indicate that resistance to propamocarb was reduced in *CsHMGB*-silenced plants under propamocarb stress.

Activities of Antioxidant Enzymes in *CsHMGB*-Silenced Cucumber Plants

The activity levels of antioxidant enzymes were associated with ROS-scavenging. As compared to the water control treatment, the activities of POD (**Figure 6A**), SOD (**Figure 6B**), CAT (**Figure 6C**), APX (**Figure 6D**), and GPX (**Figure 6E**) were enhanced under propamocarb stress. However, the activities of these enzymes were decreased in the *CsHMGB*-silenced plants. Notably, we observed reductions in the activities of detoxification-related enzymes in the ascorbate-glutathione (AsA-GSH) system, such as DHAR (**Figure 7A**), MDHAR (**Figure 7B**), GR (**Figure 7C**), and GST (**Figure 7D**) in the *CsHMGB*-silenced plants under propamocarb stress, as compared to control plants under propamocarb stress. The exchange of ascorbate from DHA to AsA and the regeneration of glutathione were inhibited by the silencing of *CsHMGB*, resulting in the decreased of the redox state of cells. As shown in **Table 1**, AsA, DHA, and total ascorbate contents decreased in *CsHMGB*-silenced plants under propamocarb stress compared to the control treatment with water, as did the redox state of the ascorbate (AsA/DHA). These changes suggested that silencing of *CsHMGB* promoted the conversion of ascorbate from AsA to DHA, leading to the decreased of the redox state of the ascorbate. Total glutathione content did not differ between the control and the *CsHMGB*-silenced plants; however, the ratio of GSH/GSSG was lower in the *CsHMGB*-silenced plants than in the control, indicating that the cucumber plants accelerated GSH

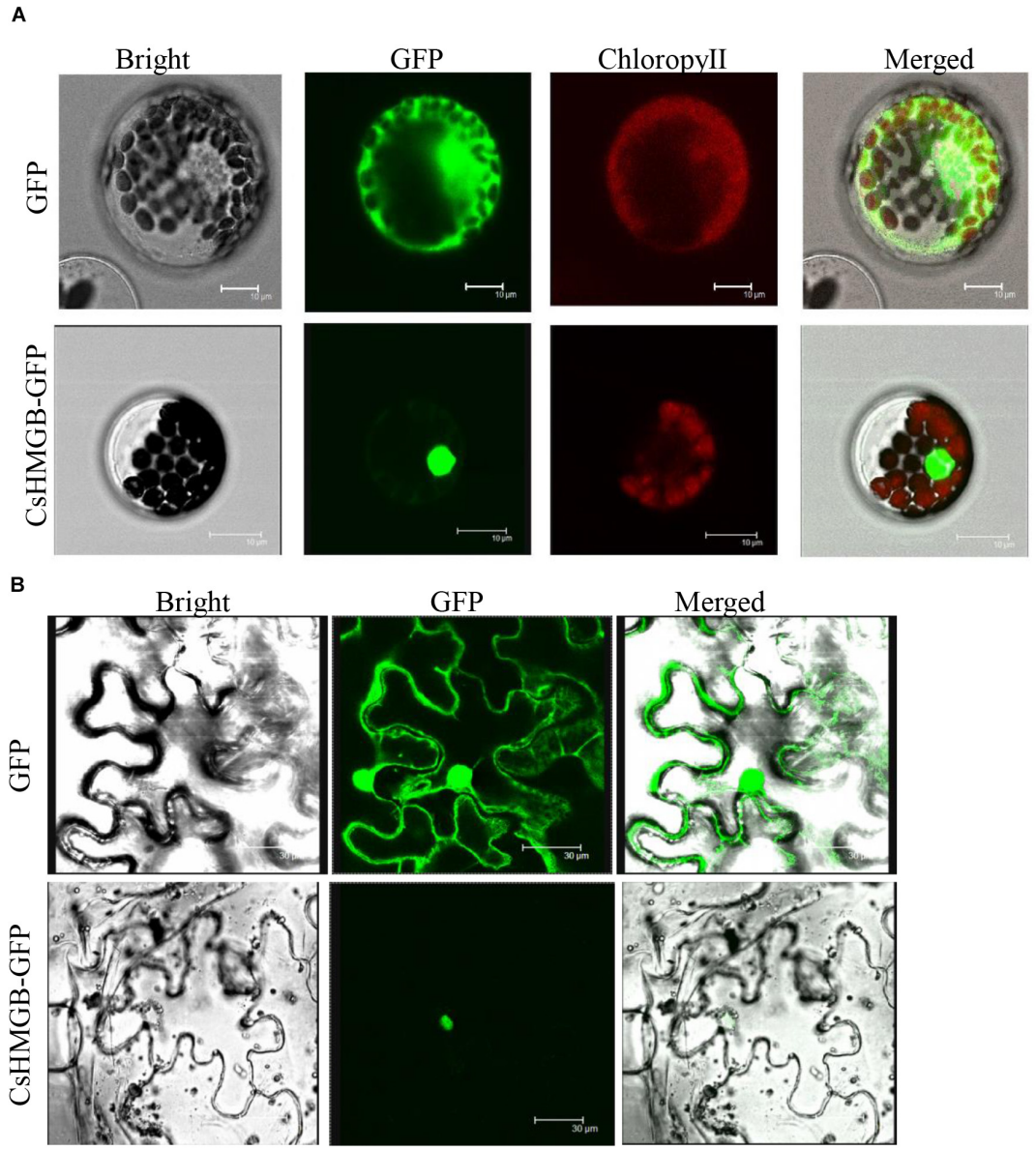


FIGURE 4 | Subcellular localization of *CsHMGB* protein. **(A)** Subcellular localization of the *CsHMGB* protein in *Arabidopsis* protoplasts. The target protein of CsHMGB-GFP and empty plasmids (GFP) were observed with four channels of white light, UV light, and red light to localize the proteins. Bars of 10 μm. **(B)** Subcellular localization of the *CsHMGB* protein in leaf epidermis of *N. benthamiana*. Bars of 30 μm.

consumption in response to propamocarb stress (**Table 1**). Taken together, these results strongly indicate that silencing of *CsHMGB* reduced antioxidation and detoxification in cucumber plants.

Overexpression of *CsHMGB* Alleviates Propamocarb Residues and Phytotoxicity in Cucumber

The overexpressed-vector of *CsHMGB*-PCXSN for transgenic experiments in cucumbers was constructed to assess the biological function of *CsHMGB* under propamocarb stress in cucumber plants, with an empty plasmid as a control group with the 35S promoter. Fifteen *CsHMGB*-overexpressed "D9320" cucumber plants and two empty "D9320" transgenic cucumber plants (as a control) were identified by qPCR through genetic transformation. Three OE lines, which shared the most abundant contents of *CsHMGB* (lines 2, 3, and 5), were harvested from the T_1 generation after self-pollination (**Supplementary Figure S3**).

We sprayed 400 ppm propamocarb on the *CsHMGB*-overexpressed plants and the control plants. We observed no phenotypic differences (such as fruit length and color of fruit peel) between the *CsHMGB*-overexpressed plants and the control plants (**Figures 8A,B**). However, anatomical analysis of fruit peels under a scanning electron microscope revealed distinct

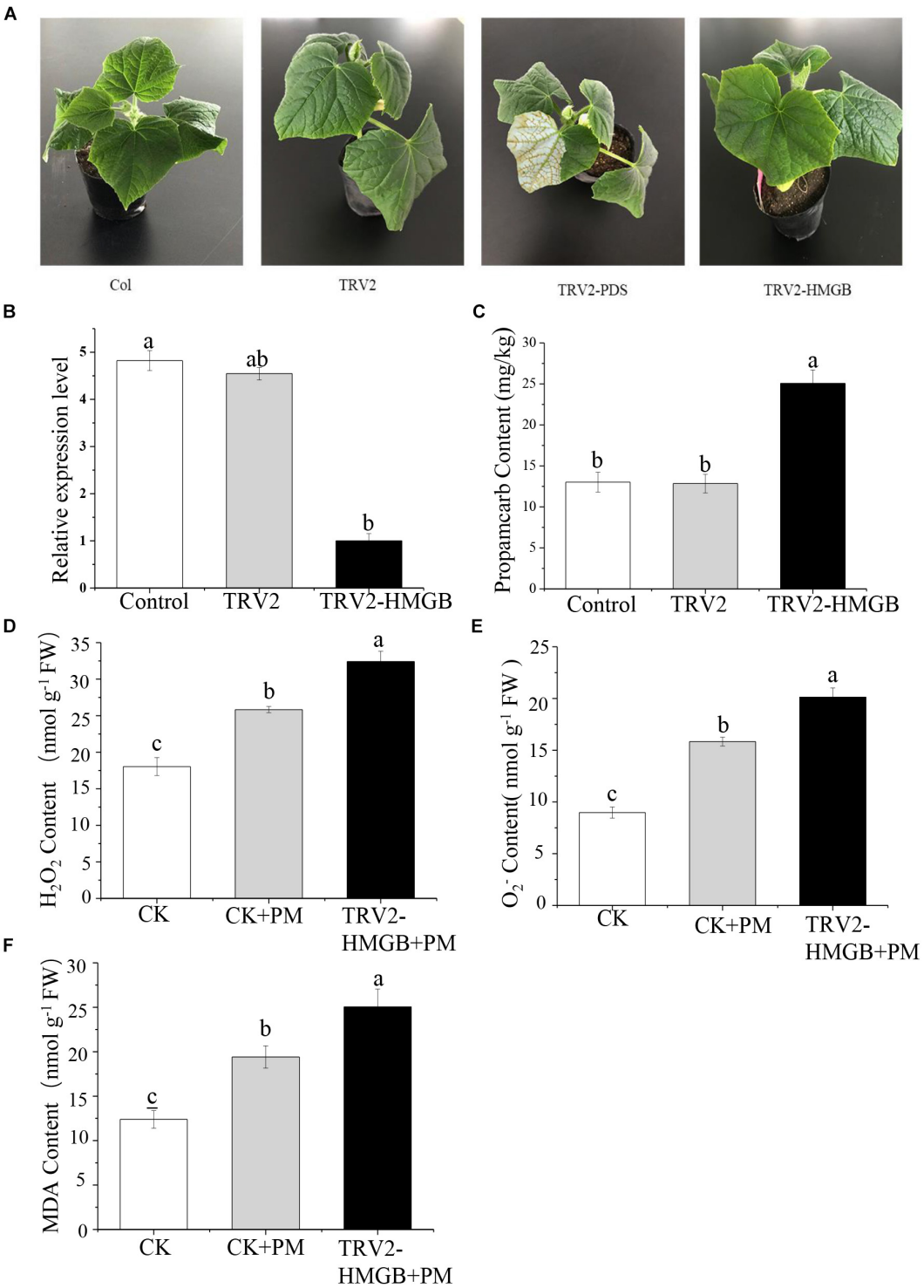


FIGURE 5 | Silencing of CsHMGB in leaves of "D0351" plants. **(A)** Color fading phenotypes via PDS control gene 16 days after inoculation of leaves. **(B)** *CsHMGB* levels in *CsHMGB*-silenced, pTRV2 and control plants. **(C)** Propamocarb contents in leaves of *CsHMGB*-silenced, pTRV2, and control plants at 2 days. **(D)** O_2^- contents in leaves under propamocarb stress. **(E)** H_2O_2 contents in leaves under propamocarb stress. **(F)** MDA contents in leaves under propamocarb stress. Different letters indicate significant differences between genotypes ($p < 0.05$ by Tukey's test). Error bars represent SE.

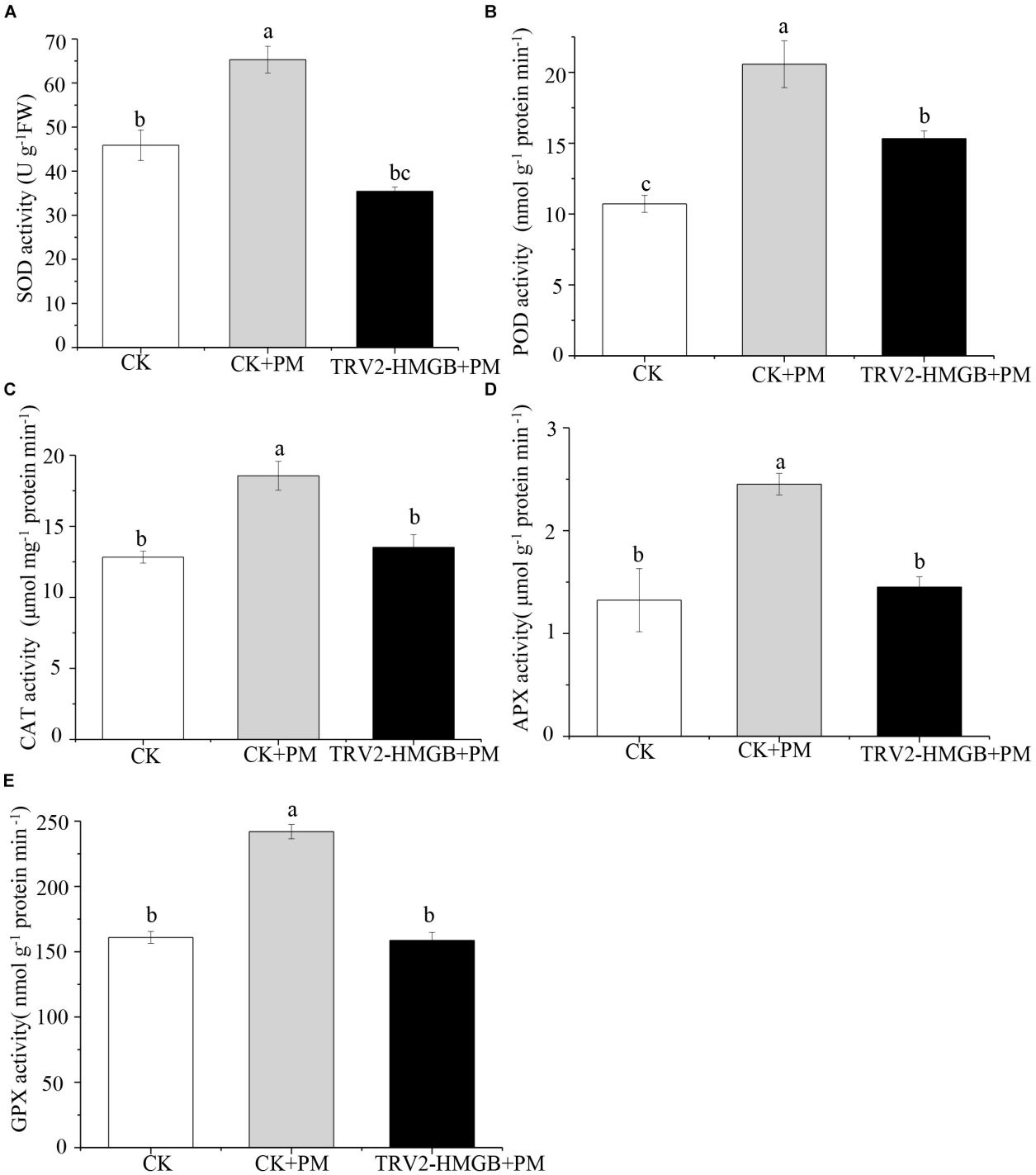


FIGURE 6 | Activity of antioxidant enzymes in *CsHMGB*-silenced leaves of "D0351" plants. **(A)** SOD activity. **(B)** POD activity. **(C)** CAT activity. **(D)** APX activity. **(E)** GPX activity. Data are the means of three replicates with SEs, and different letters indicate a significant difference ($p < 0.05$ by Tukey's test).

differences. With the stomatal opening under the water treatment as a control, the observed increase of the stomatal aperture was larger in *CsHMGB*-overexpressed plants as compared to control plants under propamocarb stress (**Figure 8D**). Waxiness in the fruit peels was notably greater in *CsHMGB*-overexpressed plants, while minimal waxiness was noted in the control plants following application of propamocarb (**Figure 8C**). Changes in propamocarb residues were analogous between *CsHMGB*-overexpressed and control plants, with both increasing from 3 to 48 h and decreasing after 48 h. Residue levels in the

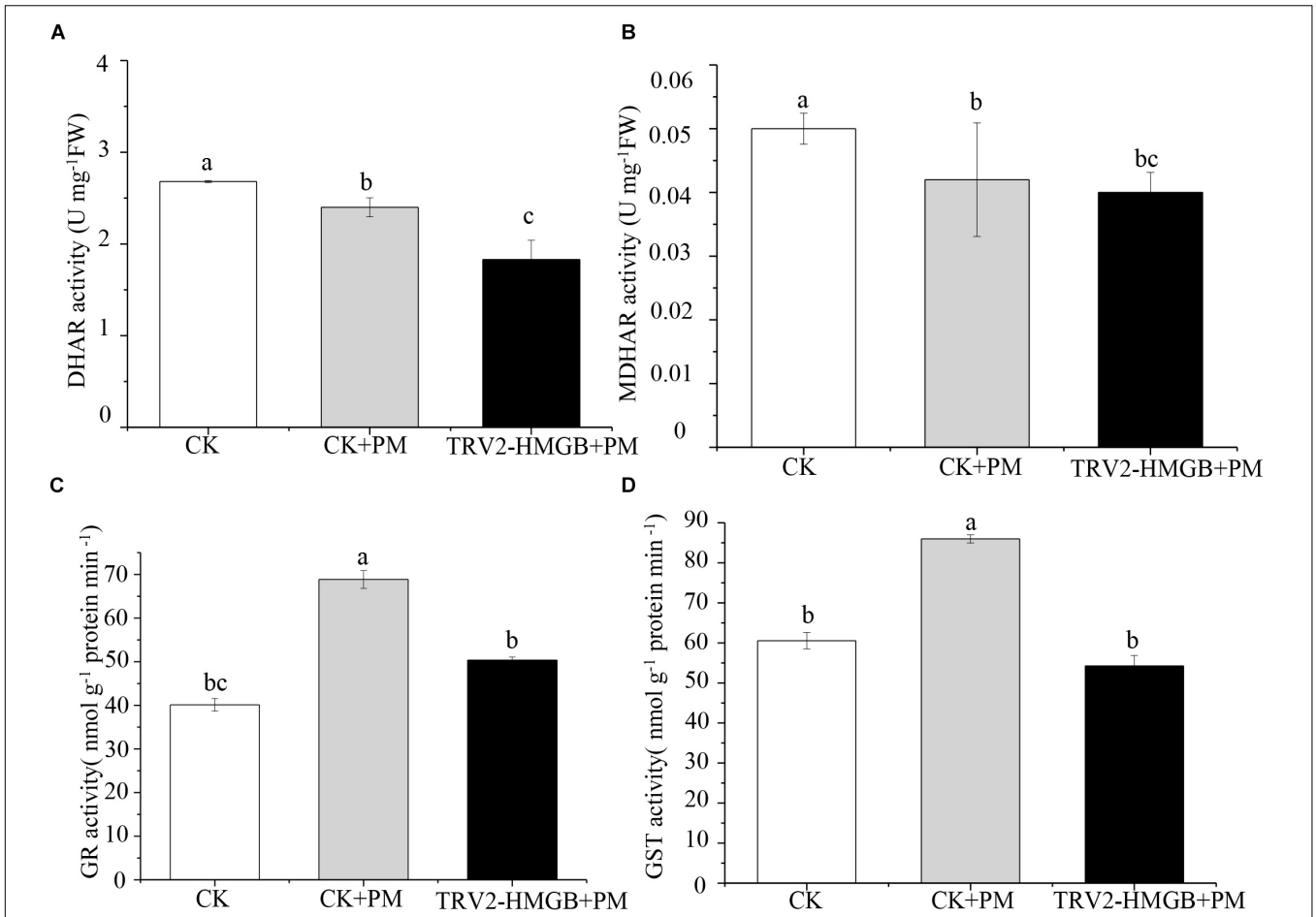


FIGURE 7 | Activity of key enzymes in AsA-GSH system in *CsHMGB*-silenced leaves of "D0351" plants. **(A)** DHAR activity. **(B)** MDHAR activity. **(C)** GST activity. **(D)** GR activity. Data are the means of three replicates with SEs, and different letters indicate a significant difference ($p < 0.05$ by Tukey's test).

TABLE 1 | The ASA-GSH system in *CsHMGB*-silenced leaves from "D0351" genotype under propamocarb stress at 4 days.

Lines	ASA content	DHA content	Total ascorbate	ASA/DHA	GSH content	GSSG content	Total glutathione	GSH/GSSG
Control	0.86^{a}	1.32^{a}	2.18^{a}	0.65^{a}	0.32^{a}	0.23^{b}	0.55^{a}	1.39^{a}
Control + PM	0.52^{b}	0.92^{b}	1.44^{b}	0.57^{b}	0.24^{b}	0.33^{a}	0.57^{a}	0.73^{b}
Slienced-HMGB	$0.45^{b,c}$	0.78^{c}	$1.23^{b,c}$	0.58^{b}	0.21^{b}	0.34^{a}	0.55^{a}	$0.62^{b,c}$

The levels of total glutathione, DHA, ASA, GSH, total ascorbate, and GSSG are presented in the form of mmol g^{-1} FW. The redox states for ascorbate and GSH were determined, respectively, to be the ASA/DHA and GSH/GSSG ratios. Different letters indicate significant differences between genotypes ($p < 0.05$ by Tukey's test). Error bars represent SE.

fruit peels were lower in *CsHMGB*-overexpressed plants than in the control, and decreased by 48.7, 41.0, and 42.1% in the OX2, OX 3, and OX 5 lines at 48 h (**Figure 8E**), respectively. These findings indicate that overexpression of *CsHMGB* alleviates propamocarb residue accumulation through increasing waxiness and the stomatal conductance.

Under propamocarb stress conditions, O_2^- and H_2O_2 contents increased from 2 to 4 days then decreased around 4–10 days in both *CsHMGB*-overexpressed and control plants. O_2^- and H_2O_2 contents were lower in *CsHMGB*-overexpressed plants than in control plants (**Figures 8F–G**). MDA content also decreased in *CsHMGB*-overexpressed plants under propamocarb stress (**Figure 8H**). These results indicate that overexpression of *CsHMGB* enhances the resistance of cucumber plants to propamocarb stress.

Overexpression of *CsHMGB* Enhances the Activities of Antioxidant Enzymes

Compared to the control, the activities of SOD (**Figure 9A**), CAT (**Figure 9C**), APX (**Figure 9D**), and GPX (**Figure 9E**) were increased from 2 to 6 days and then decreased from 6 to 10 days in the *CsHMGB*-overexpressed plants under propamocarb stress. The activity of POD (**Figure 9B**) was

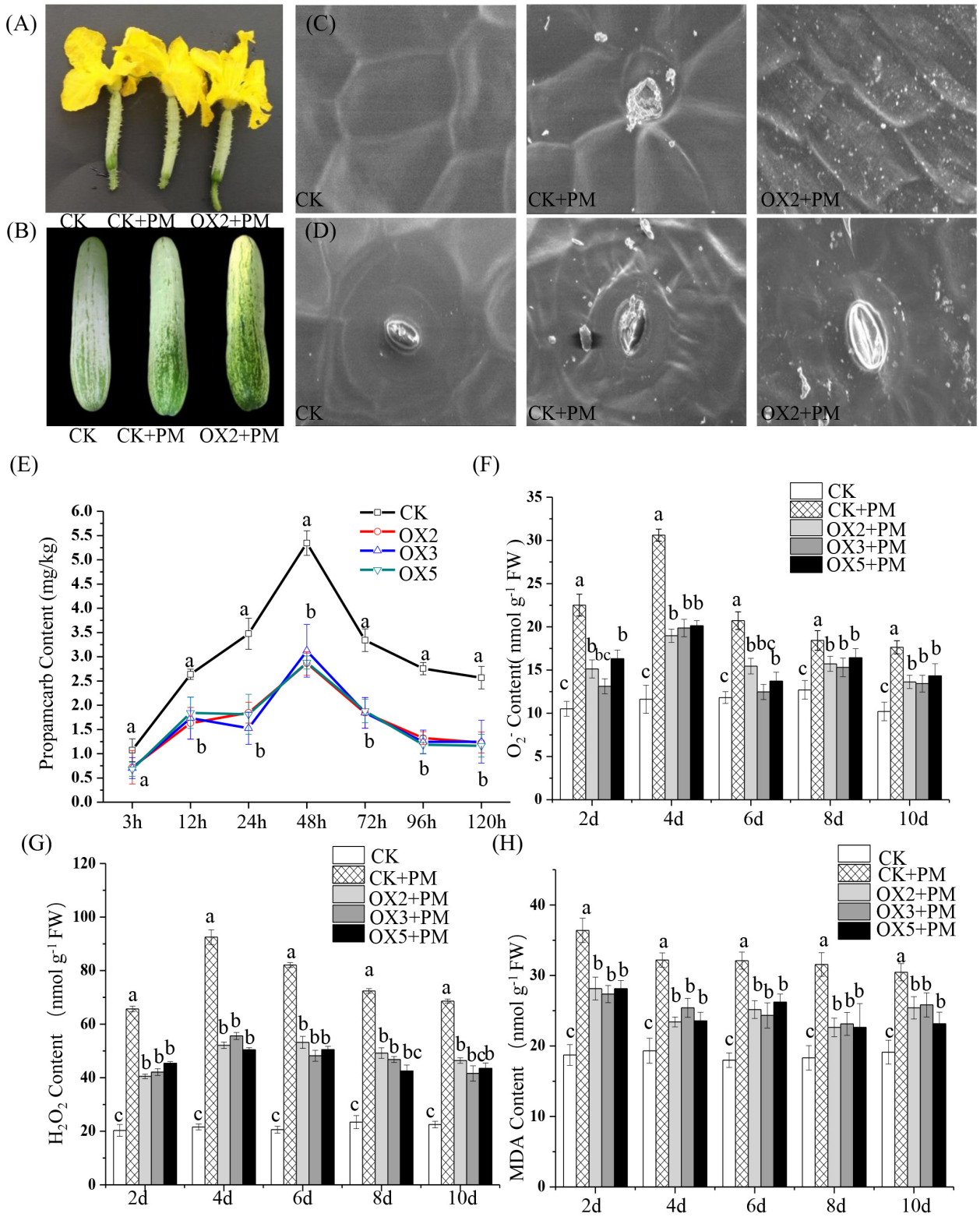


FIGURE 8 | Effects of *CsHMGB* on propamocarb residues and phytotoxicity in "D9320" plants. **(A)** Phenotypes of fruits from the control (Col) and *CsHMGB* overexpressing (OX) plants at 4 days post anthesis (DPA). **(B)** Phenotypes of fruits from Col and OX plants at 12 DPA. **(C)** The accumulation of waxiness on epidermal cells in fruit peels. Bars of 20 μm. **(D)** The opening of the stomatal aperture in fruit peel. Bars of 20 μm. **(E)** Propamocarb contents in fruit peels under propamocarb stress with time course of 3, 12, 24, 48, 72, 96, and 120 h. **(F–H)** O_2^-, H_2O_2, and MDA contents in leaves under propamocarb stress with time course of 2, 4, 6, 8, and 10 days. Data are the means of three replicates with SEs, and different letters indicate a significant difference ($p < 0.05$ by Tukey's test).

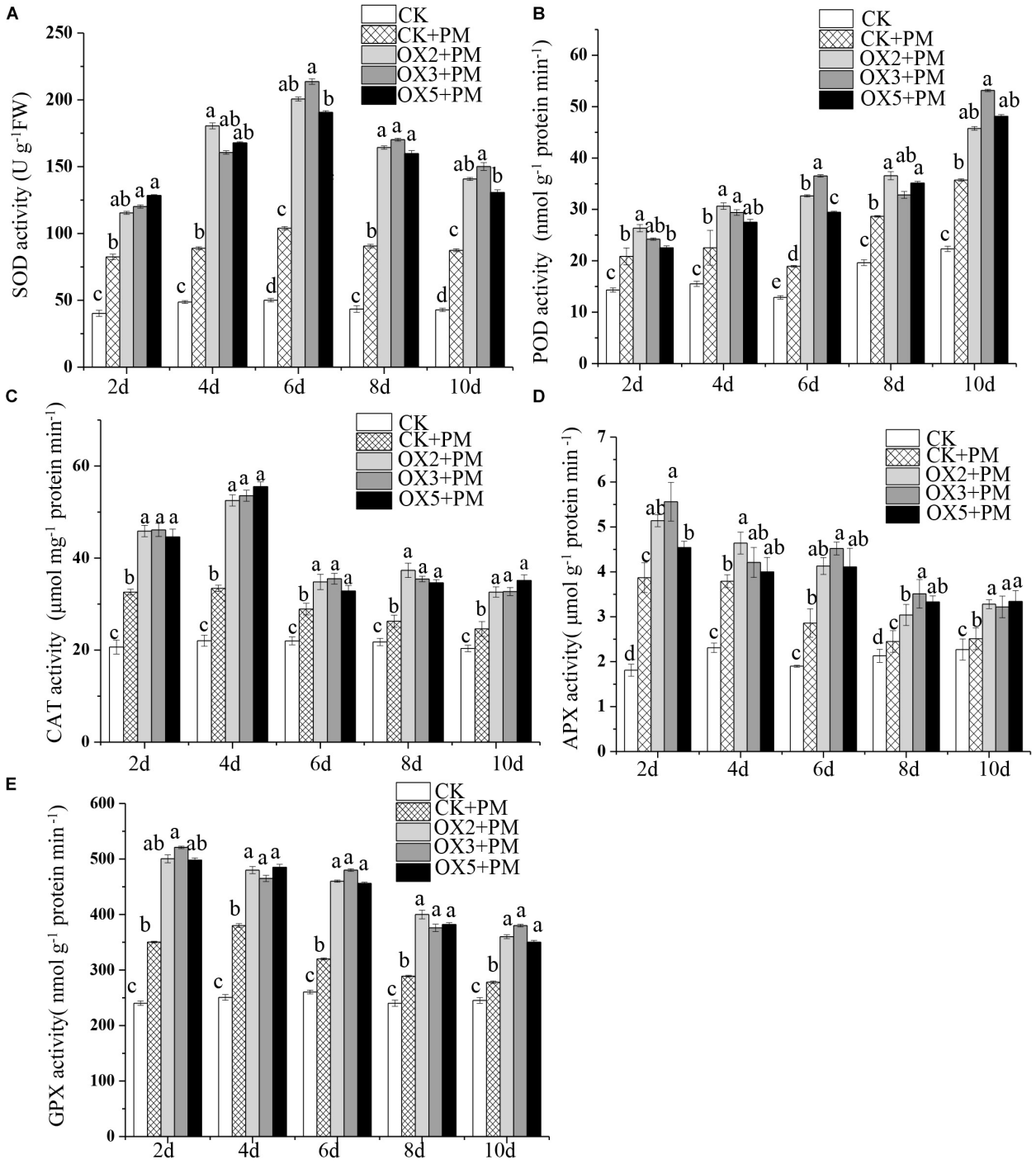


FIGURE 9 | Activity of antioxidant enzymes in *CsHMGB*-overexpressing (OX) leaves of "D9320" plants. **(A)** SOD activity. **(B)** POD activity. **(C)** CAT activity. **(D)** APX activity. **(E)** GPX activity. Data are the means of three replicates with SEs, and different letters indicate a significant difference ($p < 0.05$ by Tukey's test).

more enhanced from 2 to 10 days in the OX2, OX 3, and OX 5 lines than in the control. As shown in **Table 2**, the AsA, DHA, and total ascorbate contents, as well as the redox state of ascorbate (AsA/DHA), were enhanced in the OX2, OX3, and OX5 lines as compared to the control. *CsHMGB* accelerated the transformation of DHA to AsA and improved the antioxidant capacity (**Table 2**). In a surprising finding, there were no notable differences in GSSG, GSH, or total glutathione contents between the *CsHMGB*-overexpressing lines and the control lines under propamocarb treatments. However,

TABLE 2 | The ASA-GSH system in *CsHMGB*-overexpressing leaves from "D9320" genotype under propamocarb stress at 4 days.

Lines	ASA content	DHA content	Total ascorbate	ASA/DHA	GSH content	GSSG content	Total glutathione	GSH/GSSG
CK	1.22^{c}	1.80^{c}	3.02^{d}	0.68^{b}	0.42^{d}	0.33^{a}	0.75^{d}	1.27^{e}
CK + PM	1.61^{b}	2.80^{b}	4.41^{c}	0.58^{c}	0.62^{c}	0.22^{b}	0.84^{c}	2.82^{d}
OX2 + PM	2.45^{a}	3.19^{a}	5.64^{b}	0.77^{a}	0.77^{b}	0.19^{c}	0.96^{b}	4.05^{b}
OX3 + PM	2.78^{a}	3.77^{a}	6.55^{a}	0.74^{a}	0.82^{a}	0.21^{b}	1.03^{a}	3.90^{c}
OX5 + PM	2.62^{a}	3.58^{a}	6.20^{a}	0.73^{a}	0.86^{a}	0.17^{c}	1.03^{a}	5.06^{a}

The levels of total glutathione, DHA, ASA, GSH, total ascorbate, and GSSG are presented in the form of mmol g^{-1} FW. The redox states for ascorbate and GSH were determined, respectively, to be the ASA/DHA and GSH/GSSG ratios. Different letters indicate significant differences between genotypes ($p < 0.05$ by Tukey's test). Error bars represent SE.

the redox state of GSH/GSSG was greater in *CsHMGB*-overexpressing lines as compared to the control lines. It is important to note that overexpression of *CsHMGB* increased the activities of DHAR (**Figure 10A**), MDHAR (**Figure 10B**), GST (**Figure 10C**), and GR (**Figure 10D**). *CsHMGB*-overexpression significantly induced the accumulation of total ascorbate and glutathione following with the exchange of ascorbate from DHA to AsA and the regeneration of glutathione, leading to an enhanced redox state of cells. These findings indicate that overexpression of *CsHMGB* increases key enzymatic activities of AsA-GSH system and promotes propamocarb metabolism in cucumber plants.

Overexpression of *CsHMGB* Induces Increased Key Genes Expression in AsA-GSH System

To investigate the effects of *CsHMGB* on the transcript levels of genes encoding antioxidant enzymes in AsA-GSH, qRT-PCR was carried out to determine the expression levels of key genes. As shown in **Figure 11**, *CsGPX2*, *CsGST1*, and *CsGSH2 CsMDHAR2* were induced by propamocarb stress, *CsGGPase1*, *CsDHAR1*, *CsDHAR2* and *CsMDHAR3* were inhibited by propamocarb stress. Additionally, these genes were significantly up-regulated in the OX2, OX3, and OX5 lines as compared to the control. This result shows that *CsHMGB* induces increased key genes expression in AsA-GSH system.

DISCUSSION

Analyses of mRNA expression and protein localization aid in determining gene functions. A previous study suggested that *CsABCA19*, a membrane transporter protein, was markedly increased in the fruit peels of "D0351" plants under propamocarb stress, but found little change in "D9320" plants (Meng et al., 2016). In addition, mitochondrial proteins of *CsMCF* and glutathione proteins of *CsMAPEG* are up-regulated in the leaves and fruits of propamocarb-stressed "D0351" plants (Zhang et al., 2019a,b). Our results showed that the expression pattern of *CsHMGB* was consistent with those of *CsABCA19*, *CsMCF*, and *CsMAPEG*, which are positively correlated with propamocarb residues in the fruit peels of "D0351" plants and up-regulated in leaves and fruit peels. This indicates that *CsHMGB* is up-regulated in response to propamocarb stress. Eight HMGB proteins have been identified in *A. thaliana*; AtHMGB1, AtHMGB5, AtHMGB6, and AtHMGB14 are primarily located in the nucleus, whereas AtHMGB2 and AtHMGB3 have been reported in both the nucleus and the cytoplasm (Launholt et al., 2006; Grasser et al., 2007; Lildballe et al., 2008; Pedersen et al., 2010). Although AtHMGB12 is unable to bind to DNA, it enables interaction with XPO1a (the nuclear output receptor) and is located in the cytoplasm (Štros et al., 2007). OsHMGB is an OsCML3 target protein, and binds to DNA within the nucleus to regulate intracellular Ca^{2+} (Aumnart et al., 2015). Several studies have shown that HMGB proteins are localized to the nucleus, are able to bind to specific DNA structures, and are involved in a variety of important biological processes (Grasser et al., 2007; Kang et al., 2014). In our study, six HMGB (*CsHMGB* and *CsHMGB*1/2/3/6/14) proteins were identified in cucumbers, and cluster analysis showed that the HMGB proteins were contained in one branch between cucumber and *A. thaliana* (**Supplementary Figure S4**). *CsHMGB* (*CsaV3_5G021890.1*) shared the highest sequence similarity with AtHMGB5 (*AT4G35570.1*) was screened for gene function under propamocarb stress. We found that *CsHMGB* was localized to the nucleus (**Figures 4A,B**), indicating that *CsHMGB* might have a similar function to transcription factors and may specifically bind to DNA or chromatin in response to propamocarb stress.

Several studies have demonstrated that HMGBs play an important regulatory role in responses to abiotic stress (Reeves, 2010). Heterologous expression of *CsHMGB* in *A. thaliana* influences the germination of seeds in the presence of drought and high-salt stress (Jang et al., 2008). In addition, *AtHMGB2* and *AtHMGB3* expression levels are markedly decreased under salt and drought stress. Overexpression of *AtHMGB1* and *AtHMG2* decreases seed germination and inhibits seed growth in the presence of salt stress, and *AtHMGB2*, *AtHMGB3*, and *AtHMGB4* are up-regulated under cold stress (Kwak et al., 2007; Lildballe et al., 2008). In rice, transcriptome data showed that *OsHMGB* was rapidly up-regulated under cold treatment (Yang et al., 2015) and the functional deletion mutant *Oshmgb710* demonstrated high susceptibility to rice bacterial blight; lines overexpressing *OsHMGB710* were significantly more resistant to bacterial blight (Ju, 2017). HMGB1 is also a marker of non-specific and sensitive inflammation in mammals, including humans. HMGB1 can induce the release of cytokines and participate in a variety of pathophysiological processes in higher animals (Harris et al., 2012; Venereau et al., 2016; Mc et al., 2019). In the lungs of rats, HMGB1 abundance was shown to be beneficial following paraquat poisoning. HMGB1

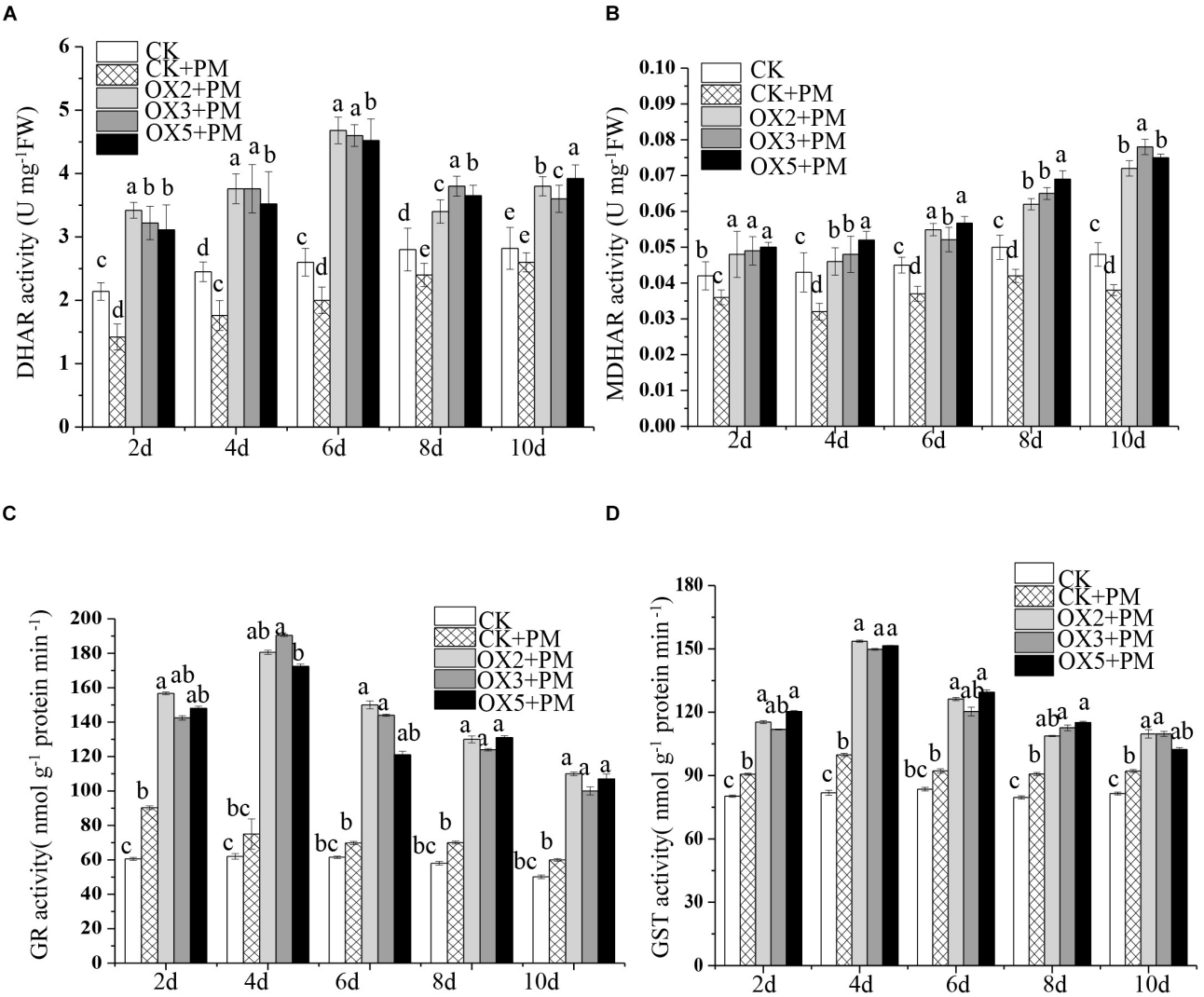


FIGURE 10 | Activity of key enzymes in AsA-GSH system in *CsHMGB*-overexpressing (OX) leaves of "D9320" plants. **(A)** DHAR activity. **(B)** MDHAR activity. **(C)** GST activity. **(D)** GR activity. Data are the means of three replicates with SEs, and different letters indicate a significant difference ($p < 0.05$ by Tukey's test).

is involved in pathophysiological reactions, and changes in its expression reflect the progression of paraquat poisoning (Ju and Zhang, 2019). In the present study, silencing of *CsHMGB* increased the accumulation of propamocarb residues in cucumber plants (**Figure 5C**), while propamocarb residues were significantly decreased in *CsHMGB*-overexpressing cucumber plants (**Figure 8E**). These findings show that *CsHMGB* plays a crucial role in regulating propamocarb residues.

Waxiness of the plant epidermis provides a protective barrier that inhibits non-stomatal water loss and protects plants from diseases and insect pests. In *Arabidopsis*, bryophytes, and soybeans, increased wax content is correlated with drought resistance (Thoenes et al., 2004; Buda et al., 2013; Luo et al., 2013). In cucumbers, the *CsCER1* and *CsWAX2* biosynthesis genes respond to drought stress, light intensity, and other external adverse environmental factors by inducing the accumulation of pericarp wax (Liu et al., 2014; Wang et al., 2015a,b). Notably, stomatal action played a crucial role in the response to plant stress. Low temperature induced increased NO accumulation and decreased stomatal conductance in cucumber plants (Zhang Z. W. et al., 2019). In tomatoes, rapid and increased stomatal closure was co-related with drought tolerance in the *SlWRKY81*-silenced plants (Ahammed et al., 2019). Here, we found that increased wax content and stomatal conductance alleviated propamocarb residue levels in the *CsHMGB*-overexpressed plants (**Figures 8B,C**). These findings show that *CsHMGB* promotes the self-protective mechanisms and propamocarb metabolism in cucumber.

Antioxidant defense plays a crucial role in plant abiotic stress. In cucumber, melatonin has been shown to alleviate iron stress by improving antioxidant defense and reducing the

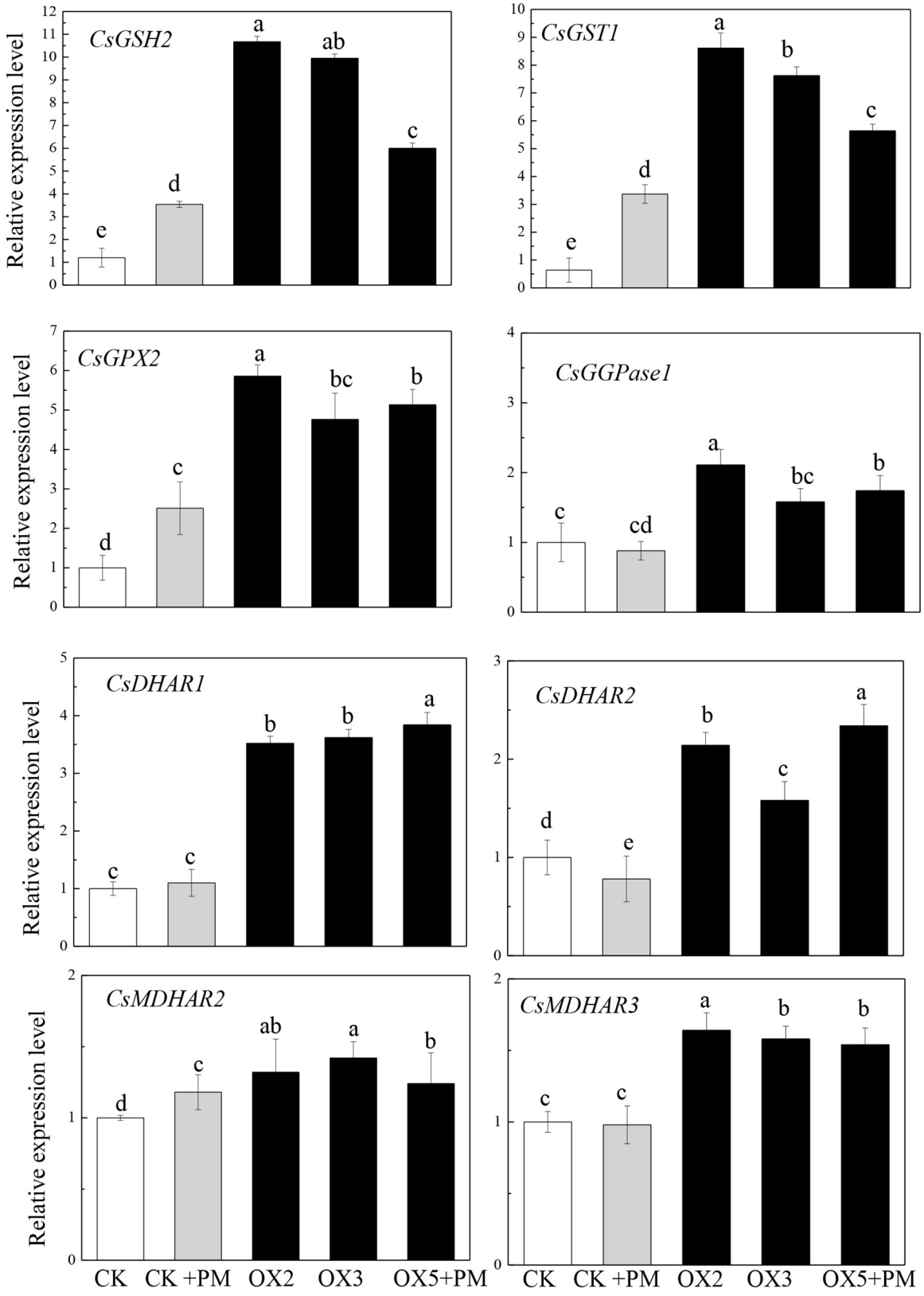


FIGURE 11 | Expression levels of key genes in in AsA-GSH system between the control (Col) and *CsHMGB*-overexpressing (OX) plants. *CsEF1a* was used as the reference gene. Different letters indicate significant differences between genotypes ($p < 0.05$ by Tukey's test). Error bars represent SE.

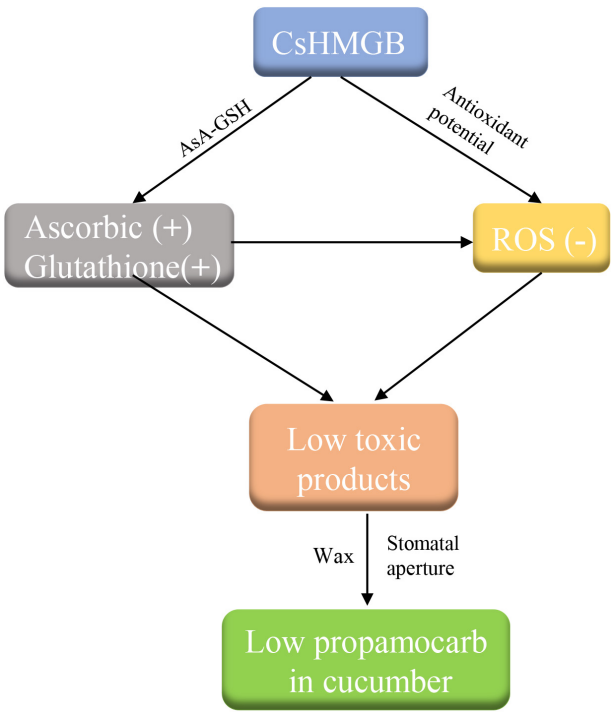


FIGURE 12 | Simple pathway model of propamocarb degradation and metabolism in cucumbers.

accumulation of ROS (Ahammed et al., 2020b). In tomato, melatonin is essential for maintaining the proper antioxidant potential, leading to amelioration of Cd-induced oxidative stress (Hasan et al., 2019). Dopamine alleviated bisphenol A-induced phytotoxicity (an emerging organic pollutant) by enhancing antioxidant and detoxification potential in cucumber (Ahammed et al., 2020a). Silicon improved the activity of antioxidant enzymes and decreased MDA and ROS levels in response to low levels of phosphorus stress in tomato plants (Zhang Y. et al., 2019). Overexpression of *CsMCF* in the presence of propamocarb in cucumbers resulted in enhanced antioxidant enzyme activity and reduced lipid peroxidation levels (Zhang et al., 2019a). Similarly, in the present study, the enhancement of antioxidant enzyme activity induced by overexpressing of *CsHMGB* was also confirmed to involve in detoxification of ROS produced under propamocarb stress in cucumber.

Ascorbate-glutathione cycle acts as an effective antioxidant system for the detoxification of excess ROS and maintaining the redox state of plant cells (Bartoli et al., 2017). Under propamocarb stress, the increasing activity and transcript levels of DHAR and MDHAR positively promoted the AsA regeneration, resulting in the enhancement of the ratio of AsA/DHA and total ascorbic content. Furthermore, the expression of key genes in the glutathione metabolic pathway, *CsGPX2*, *CsGSH2*, and *CsGST1* were induced by overexpression of *CsHMGB* under propamocarb stress, together with the increased activity of GR and GST, accordingly, both the ratio of GSH/GSSG and total glutathione content were significantly increased. These changes contributed to an enhanced redox state of the ascorbate and glutathione for ROS scavenging and propamocarb detoxification (**Figures 9–11** and **Table 2**). In tomatoes, overexpression of CAFFEICACID OMETHYLTRANSFERASE 1 (*COMT1*) and exogenous melatonin alleviated carbendazim phytotoxicity and pesticide residue levels by improving the activity of antioxidant enzymes and activation of the AsA-GSH system and reduction of ROS and MDA levels (Yan et al., 2019). In wheat, the enhanced AsA-GSH system and antioxidant enzyme activities alleviated Cd stress (Qin et al., 2018). Notably, glutathione plays an important role in the detoxification of pesticide residues in plants (Yu et al., 2013). Application of brassinosteroids and silencing of respiratory burst oxidase-1 (*RBOH1*) resulted in H_2O_2-dependent redox homeostasis, glutathione biosynthesis, and increased GST activity to limit CHT residue levels in tomatoes (Zhou et al., 2015). Thus, *CsHMGB* alleviates phytotoxicity and propamocarb residue levels by improving antioxidant potential, ascorbic and glutathione-dependent detoxification.

CONCLUSION

We cloned a 624 bp of *CsHMGB* that contained the conserved HMB-box region. *CsHMGB* expression was positively correlated with propamocarb residue levels in cucumber fruit peels. *CsHMGB* was upregulated in fruit peels of "D0351" genotype plants following exposure to propamocarb stress for 3–120 h. The CsHMGB protein was targeted to the nucleus. In CsHMGB-silenced plants, resistance was reduced and propamocarb residues were increased following increases in MDA content and ROS; reductions in antioxidant enzyme activity (SOD, POD, CAT, APX, GPX, GST, and GR) and the AsA-GSH system were also observed. Overexpression of *CsHMGB* promoted glutathione-dependent detoxification by AsA-GSH system and improved the antioxidant potential, reduced the accumulation of ROS. Ultimately, propamocarb metabolism in cucumber was increased via increase in the wax levels and the stomatal conductance (**Figure 12**). Thus, *CsHMGB* contributes to lower propamocarb residue levels, with possible applications in the production and breeding of cucumbers to achieve lower propamocarb residue levels in fruits.

DATA AVAILABILITY STATEMENT

The datasets generated for this study can be found in the http://www.icugi.org/.

AUTHOR CONTRIBUTIONS

SL and ZQ designed and conceived the research. MX, JL, CW, DL, WZ, and XZ performed the experiments. CW, DL,

CL, and WZ analyzed the sequencing data. SL wrote the entire manuscript. ZQ and XZ edited the manuscript.

FUNDING

This work was funded by the National Key Research and Development Program for Breeding Seven Key Crops (2016YFD0101700), Academic Backbone Project of Northeast Agricultural University (18XG06), and Heilongjiang Postdoctoral Scientific Research Developmental Fund (LBH-Q16021), and National Natural Science Foundation of China (31272158).

ACKNOWLEDGMENTS

We thank Prof. Huazhong Ren (College of Agronomy and Biotechnology, China Agricultural University, Beijing), who graciously provided the methodology for the genetic transformation of cucumbers.

SUPPLEMENTARY MATERIAL

The Supplementary Material for this article can be found online at: https://www.frontiersin.org/articles/10.3389/fpls.2020.00738/full#supplementary-material

FIGURE S1 | Phenotypes of fruits in "D0351" and "D9320" genotype.

FIGURE S2 | Sequence and phylogenetic analysis of *CsHMGB*. **(A)** Analysis of *CsHMGB* sequence. **(B)** Phylogenetic analysis of *CsHMGB* with HMGB proteins in other species; the amino acid sequences of the *CsHMGB* and HMGB proteins were used to construct phylogenetic trees using a neighbor-joining algorithm. Cp, *Cucurbita pelo*; At, *Arabidopsis thaliana*; Cs, *Cucumis sativus*; Pp, *Prunus persica*; Pa, *Populus alba*; Cm, *Cucumis melo*; Mc, *Momordica charantia;* Ns, *Nicotiana Sylvestris*; Nt, *Nicotiana tabacum*; Pt, *Populus trichocarpa*; Vv, *Vitis vinifera*. **(C)** Conservative HMGB-box structure in various species.

FIGURE S3 | *CsHMGB* levels in the control (Col) and *CsHMGB* -overexpressing (OX) plants were screened by qPCR.

FIGURE S4 | Phylogenetic tree of HMG proteins from cucumber (Cs) and Arabidopsis (At).

TABLE S1 | Sequences of the oligo nucleotides used in this study.

REFERENCES

Adrita, R., Arkajyoti, D., Dipan, R., Payel, G., Ritesh, G., Rajiv, K., et al. (2016). Deciphering the role of the AT-rich interaction domain and the HMG-box domain of ARID-HMG proteins of *Arabidopsis thaliana*. *Plant Mol. Biol.* 92, 371–388. doi: 10.1007/s11103-016-0519-y

Aebi, H. (1984). Catalase *in vitro*. *Methods Enzymol.* 105, 121–126.

Ahammed, G. J., Li, X., Yang, Y. X., Liu, C. C., Zhou, G. Z., Wan, H., et al. (2019). Tomato *WRKY81* acts as a negative regulator for drought tolerance by modulating guard cell H2O2-mediated stomatal closure *Environ. Exp. Bot.* 171:103960. doi: 10.1016/j.envexpbot.2019.103960

Ahammed, G. J., Wang, Y. Q., Mao, Q., Wu, M. J., Yan, Y. R., Ren, J., et al. (2020a). Dopamine alleviates bisphenol A-induced phytotoxicity by enhancing antioxidant and detoxification potential in cucumber. *Environ. Pollut.* 259:113957. doi: 10.1016/j.envpol.2020.113957

Ahammed, G. J., Wang, Y. Q., Mao, Q., Wu, M. J., Yan, Y. R., Ren, J., et al. (2020b). Melatonin alleviates iron stress by improving iron homeostasis, antioxidant defense and secondary metabolism in cucumber. *Sci. Hortic.* 265:109205. doi: 10.1016/j.scienta.2020.109205

Anderson, J. V., and Davis, D. G. (2004). Abiotic stress alters transcript profiles and activity of glutathione s-transferase, glutathione peroxidase, and glutathione reductase in euphorbia esula. *Physiol. Plant.* 120, 421–433. doi: 10.1111/j.0031-9317.2004.00249.x

Anderson, J. V., Chevone, B. I., and Hess, J. L. (1992). Seasonal variation in the antioxidant system of eastern white pine needles: evidence for thermal dependence. *Plant Physiol.* 98, 501–508. doi: 10.1104/pp.98.2.501

André, C. V., Chakravarthy, S., and Martin, G. B. (2009). Virus-induced gene silencing (VIGS) in Nicotiana benthamiana and tomato. *J. Vis. Exp.* 28, 1–14.

Antosch, M., Mortensen, S. A., and Grasser, K. D. (2012). Plant proteins containing high mobility group box dna-binding domains modulate different nuclear processes. *Plant Physiol.* 159, 875–883. doi: 10.1104/pp.112.198283

Aumnart, C., Srivilai, P., Mayura, T. C., Qu, L. J., and Buabooch, T. (2015). C-terminal extension of calmodulin-C-terminal extension of calmodulin-like 3 protein from *Oryza sativa* L.: interaction with a high mobility group target protein. *Acta Biochim. Biophys. Sin.* 47, 880–889. doi: 10.1093/abbs/gmv097

Bartoli, C. G., Buet, A., Grozeff, G. G., Galatro, A., and Simontacchi, M. (2017). "Ascorbate-glutathione cycle and abiotic stress tolerance in plants," in *Ascorbic Acid in Plant Growth, Development and Stress Tolerance*, eds M. Hossain, S. Munné-Bosch, D. Burritt, P. Diaz-Vivancos, M. Fujita, and A. Lorence (Cham: Springer), 177–200. doi: 10.1007/978-3-319-74057-7_7

Bohinc, T., Markovic, D., and Trdan, S. (2014). Leaf epicuticular wax as a factor of antixenotic resistance of cabbage to cabbage flea beetles and cabbage stink bugs attack. *Acta Agric. Scand.* 64, 493–500. doi: 10.1080/09064710.2014.926978

Bradford, M. M. (1976). A rapid and sensitive method for the quantitation of microgram quantities of protein using theprinciple of protein-dye binding. *Anal. Biochem.* 72, 248–254. doi: 10.1016/0003-2697(76)90527

Buda, G. J., Barnes, W. J., Fich, E. A., Park, S., and Yeats, T. H. (2013). An ATP binding cassette transporter is required for cuticular wax deposition and desiccation tolerance in the moss physcomitrella patens. *Plant Cell.* 10, 4000–4013. doi: 10.1105/tpc.113.117648

Chen, S., Songkumarn, P., Liu, J., and Wang, G. L. (2009). A versatile zero background T-vector system for gene cloning and functional genomics. *Plant Physiol.* 150, 1111–1121. doi: 10.1104/pp.109.137125

Choi, H. W., Manohar, M., Patricia, M., Tian, M., and Klessig, D. F. (2016). Activation of plant innate immunity by extracellular high mobility group box 3 and its inhibition by salicylic acid. *PLoS Pathog.* 12:e1005518. doi: 10.1371/journal.ppat.1005518

de Pinto, M. C., Francis, D., and De Gara, L. (1999). The redox state of ascorbate-dehydroascorbate pair as a specific sensor of cell division in tobacco TBY-2 cells. *Protoplasma* 209, 90–97. doi: 10.1007/bf01415704

Durner, J., and Klessig, D. F. (1995). Inhibition of ascorbate peroxidase by salicylic acid and 2,6-dichloroisonicotinic acid, two inducers of plant defense responses. *Proc. Natl. Acad. Sci. U.S.A.* 92, 11312–11316. doi: 10.1073/pnas.92.24.11312

Foyer, C. H., and Halliwell, B. (1976). The presence of glutathioneand glutathione reductase in chloroplasts: a proposed role in ascorbic acid metabolism. *Planta* 133, 21–25. doi: 10.1007/BF00386001

Giannakoula, A., Moustakas, M., Syros, T., and Yupsanis, T. (2010). Aluminium stress induces up-regulation of an efficient antioxidant system in the Al-tolerant maize line but not in the Al-sensitive line. *Environ. Exp. Bot.* 67, 487–494. doi: 10.1016/j.envexpbot.2009.07.010

Gong, B., Wen, D., Vandenlangenberg, K., Wei, M., and Yang, F. (2013). Comparative effects of nacl and nahco3 stress on photosynthetic parameters, nutrient metabolism, and the antioxidant system in tomato leaves. *Sci. Hortic.* 157, 1–12. doi: 10.1016/j.scienta.2013.03.032

Grasser, K. D., Launholt, D., and Grasser, M. (2007). High mobility group proteins of the plant HMGB family: dynamic chromatin modulators. *Biochim. Biophys. Acta Gene Struct. Express.* 1769, 346–357. doi: 10.1016/j.bbaexp.2006.12.004

Grefen, C., Katrin, S., Kamil, R., Obrdlik, P., and Jakub, H. (2008). Subcellular localization and in vivo interactions of the *Arabidopsis thaliana* ethylene receptor family members. *Mol. Plant.* 1, 308–320. doi: 10.1093/mp/ssm015

Harris, H. E., Andersson, U., and Pisetsky, D. S. (2012). HMGB1: a multifunctional alarmin driving autoimmune and inflammatory disease. *Nat. Rev. Rheumatol.* 8, 195–202. doi: 10.1038/nrrheum.2011.222

Hasan, M. K., Ahammed, G. J., Sun, S. H., Li, M. Q., Yin, H., Zhou, J., et al. (2019). Melatonin inhibits Cadmium translocation and enhances plant tolerance by regulating Sulfur uptake and assimilation in *Solanum lycopersicum* L. *J. Agric. Food Chem.* 67, 10563–10576. doi: 10.1021/acs.jafc.9b02404

Jang, J. Y., Kwak, K. J., and Kang, H. (2008). Expression of a high mobility group protein isolated from *Cucumis sativus* affects the germination of *Arabidopsis thaliana* under abiotic stress conditions. *J. Integr. Plant Biol.* 50, 593–600. doi: 10.1111/j.1744-7909.2008.00650.x

Ju, F., and Zhang, Y. (2019). Effects of high mobility group protein B1, interleukin-18 and nitric oxide levels on the development and progress of acute paraquat poisoning. *World Clin. Drugs* 40, 565–571.

Ju, Y. (2017). *Functional Analysis of OsHMGB1 Gene in Rice-Xoo Interaction*. Dissertation, ShanDong Agricultural University, Shandong.

Kang, R., Chen, R., Zhang, Q., Hou, W., Wu, S., Cao, L., et al. (2014). HMGB1 in health and disease. *Mol. Aspects Med.* 40, 1–116.

Kumar, S., Stecher, G., and Tamura, K. (2016). MEGA7: molecular evolution-ary genetics analysis version 7.0 for bigger datasets. *Mol. Biol. Evol.* 33, 1870–1874. doi: 10.1093/molbev/msw054

Kwak, K. J., Kim, J. Y., Kim, Y. O. and Kang, H.(2007). Characterization of transgenic *Arabidopsis* plants overexpressing high mobility group B proteins under high salinity, drought or cold stress. *Plant Cell Physiol.* 48, 221–231. doi: 10.1093/pcp/pcl057

Launholt, D., Merkle, T., Houben, A., Schulz, A., and Grasser, K. D. (2006). *Arabidopsis* chromatin-associated HMGA and HMGB use different nuclear targeting signals and display highly dynamic localization within the nucleus[J]. *Plant Cell* 18, 2904–2918. doi: 10.1105/tpc.106.047274

Li, Y., Li, J., Yan, Y., Liu, W., and Zhang, W. (2018). Knock-down of CsNRT2.1, a cucumber nitrate transporter, reduces nitrate uptake, root length, and lateral root number at low external nitrate concentration. *Front. Plant Sci.* 9:722. doi: 10.3389/fpls.2018.00722

Lildballe, L., Pedersen, D. S., Kalamajka, R., Emmersen, J., Houben, K. D., and Grasser, A. (2008). The expression level of the chromatin-associated HMGB1 protein influences growth, stress tolerance, and transcriptome in *Arabidopsis*. *J. Mol. Biol.* 384, 9–21. doi: 10.1016/j.jmb.2008.09.014

Liu, C., Qin, Z., and Zhou, X. (2018). Expression and functional analysis of the propamocarb related gene CsDIR16 in cucumbers. *BMC Plant Biol.* 18:16. doi: 10.1186/s12870-018-1236-2

Liu, D., Xin, M., Zhou, X., Wang, C., Zhang, Y., and Qin, Z. (2017). Expression and functional analysis of transcription factor CsERF004 gene in cucumber. *BMC Plant Biol.* 17:96. doi: 10.1186/s12870-017-1049-8

Liu, J., Li, J., Su, X., and Xia, Z. (2014). Grafting improves drought tolerance by regulating antioxidant enzyme activities and stress-responsive gene expression in tobacco. *Environ. Exp. Bot.* 107, 173–179. doi: 10.1016/j.envexpbot.2014.06.012

Luo, X., Bai, X., Sun, X., Zhu, D., and Liu, B. (2013). Expression of wild soybean *WRKY20* in *Arabidopsis* enhances drought tolerance and regulates ABA signalling. *J Exp Bot.* 8, 2155–2169. doi: 10.1093/jxb/ert073

Ma, B. (2010). Determination of remnant residues in cucumber fruits by gas chromatography. *J. ChangjiangVeg.* 20, 51–53.

Mc, C. L., Connell, Z., Xin, H., Studitsky, V. M., Feofanov, A. V., and Valieva, M. E. (2019). Functional roles of the DNA-binding HMGB domain in the histone chaperone FACT in nucleosome reorganization. *PLoS One* 293:e0216094. doi: 10.1371/journal.pone.0216094

Meng, J., Qin, Z. W., Zhou, Z., and Xin, M. (2016). An Atp-binding cassettetransporter gene from *Cucumis sativus* L., Csabc19, is involved in propamocarb stress in *Arabidopsis thaliana*. *Plant Mol. Biol. Rep.* 34, 947–960. doi: 10.1007/s11105-016-0976-0

Muntane, J. (2009). Regulation of drug metabolism and transporters. *Curr. Drug Metab.* 10, 932–945. doi: 10.2174/138920009790274595

Pedersen, D. S., Merkle, T., Marktl, B., Lildballe, D. L., Antosch, M., Bergmann, T., et al. (2010). Nucleocytoplasmic distribution of the *Arabidopsis* chromatin-associated HMGB2/3 and HMGB4 proteins. *Plant Physiol.* 154, 1831–1841. doi: 10.1104/pp.110.163055

Qin, S. Y., Liu, H. G., Wei, N., Gao, C., Li, Y. H., Lin, Y., et al. (2018). ASA-GSH cycle and antioxidant enzymes play important roles in Cd tolerance of wheat. *Bull. Environ. Contam. Toxicol.* 101, 684–690. doi: 10.1007/s00128-018-2471-9

Reeves, R. (2010). Nuclear functions of the HMG proteins. *Biochim. Biophys. Acta* 1799, 3–14. doi: 10.1016/j.bbagrm.2009.09.001

Schmittgen, T. D., and Livak, K. J. (2008). Analyzing real-time PCR data by the comparative C(T) method. *Nat. Protoc.* 3, 1111–1108. doi: 10.1038/nprot.2008.73

Sharma, K. K., Shukla, V. R., Patel, A. R., Vaghela, K. M., Patel, H. K., Shah, P. G., et al. (2016). Multilocation field trials for risk assessment of a combination fungicide fluopicolide propamocarb in tomato. *Environ. Monit. Assess.* 188:604.

Štros, M., Launholt, D., and Grasser, K. D. (2007). The HMG-box: a versatile protein domain occurring in a wide variety of DNA-binding proteins. *Cell. Mol. Life Sci.* 64:2590. doi: 10.1007/s00018-007-7162-3

Thoenes, E., Dixit, S., Pereira, A., Aharoni, A., Van Rooy, G., and Jetter, R. (2004). The shine clade of ap2 domain transcription factors activates wax biosynthesis, alters cuticle properties, and confers drought tolerance when overexpressed in *Arabidopsis*. *Plant cell* 16, 2463–2480. doi: 10.1105/tpc.104.022897

Venereau, E., De Leo, F., Mezzapelle, R., Careccia, G., Musco, G., and Bianchi, M. E. (2016). HMGB1 as biomarker and drug target. *Pharmacol. Res.* 111, 534–544. doi: 10.1016/j.phrs.2016.06.031

Wan, H., Zhao, Z., Qian, C., Sui, Y., Malik, A. A., and Chen, J. (2010). Selection of appropriate reference genes for gene expression studies by quantitative real-time polymerase chain reaction in cucumber. *Anal. Biochem.* 399, 257–261. doi: 10.1016/j.ab.2009.12.008

Wang, W., Liu, X., Gai, X., Ren, J., Liu, X., Cai, Y., et al. (2015a). *Cucumis sativus* L. WAX2 plays a pivotal role in wax biosynthesis, influencing pollen fertility and plant biotic and abiotic stress responses. *Plant Cell Physiol.* 56, 1339–1354. doi: 10.1093/pcp/pcv052

Wang, W., Zhang, Y., Xu, C., Ren, J., Liu, X., Black, K., et al. (2015b). Cucumber ECERIFERUM1 (CsCER1), which influences the cuticle properties and drought tolerance of cucumber, plays a key role in VLC alkanes biosynthesis. *Plant Mol. Biol.* 87, 219–233. doi: 10.1007/s11103-014-0271-0

Wu, P., Qin, Z., Zhao, W., Zhou, X., Wu, T., and Ming, X. (2013). Transcriptome analysis reveals differentially expressed genes associated with propamocarb response in cucumber (*Cucumis sativus* L.) fruit. *Acta Physiol. Plant.* 35, 2393–2406. doi: 10.1007/s11738-013-1274-1

Xia, C., Wang, Y. J., Liang, Y., Niu, Q. K., and Tan, X. Y. (2014). The ARID-HMG DNA-binding protein AtHMGB15 is required for pollen tube growth in *Arabidopsis thaliana*. *Plant J.* 79, 741–756. doi: 10.1111/tpj.12582

Yan, Y., Sun, S., and Zhao, N. (2019). *COMT1* overexpression resulting in increased melatonin biosynthesis contributes to the alleviation of carbendazim phytotoxicity and residues in tomato plants. *Environ. Pollut.* 253, 51–61. doi: 10.1016/j.envpol.2019.05.052

Yang, H., Hreggvidsdottir, H. S., Palmblad, K., Wang, H., Ochani, M., Li, J., et al. (2010). A critical cysteine is required for hmgb1 binding to toll-like receptor 4 and activation of macrophage cytokine release. *Proc. Natl. Acad. Sci. U.S.A.* 107, 11942–11947. doi: 10.1073/pnas.1003893107

Yang, Y. W., Chen, H. C., Jen, W. F., Liu, L. Y., and Chang, M. C. (2015). Comparative transcriptome analysis of shoots and roots of TNG67 and TCN1 rice seedlings under cold stress and following subsequent recovery: insights into metabolic pathways, phytohormones, and transcription factors. *PLoS One* 10:e0131391. doi: 10.1371/journal.pone.0131391

Yao, A. Q., and Yang, J. (2012). conduction mode of pesticides in plant and pesticide-conduction biology. *China Plant Protect.* 32, 14–18.

Yeats, T. H., and Rose, J. K. C. (2013). The formation and function of plant cuticles. *Plant Physiol.* 163, 5–20. doi: 10.1104/pp.113.222737

Yoo, S. D., Cho, Y. H., and Sheen, J. (2007). *Arabidopsis* mesophyll protoplasts: a versatile cell system for transient gene expression analysis. *Nat. Protoc.* 2, 1565–1572. doi: 10.1038/nprot.2007.199

Yu, G. B., Zhang, Y., Ahammed, G. J., Xia, X. J., and Mao, W. H. (2013). Glutathione biosynthesis and regeneration play an important role in themetabolism of chlorothalonil in tomato. *Chemosphere* 90, 2563–2570. doi: 10.1016/j.chemosphere.2012.10.100

Zhang, F., Qin, Z. W., Zhou, X. Y., Xin, M., Li, S. N., and Luan, J. (2019a). Expression and functional analysis of the propamocarb-related gene *CsMAPEG* in cucumber. *BMC Plant Biol.* 10:371. doi: 10.1186/s12870-019-1971-z

Zhang, F., Xin, M., Yu, S. Q., Liu, D., Zhou, X. Y., and Qin, Z. W. (2019b). Expression and functional analysis of the propamocarb-related gene CsMCF in cucumber. *Front. Plant Sci.* 10:871. doi: 10.3389/fpls.2019.00871

Zhang, Y., Liang, Y., Zhao, X., Jin, X., Hou, L. P., Shi, Y., et al. (2019). Silicon compensates phosphorus deficit-induced growth inhibition by improving photosynthetic capacity, antioxidant potential, and nutrient homeostasis in tomato. *Agronomy* 9:373.

Zhang, Y., Zhang, X., Liu, B., Wang, W., and Liu, X. (2014). *GAMYB* homologue *CsGAMYB1* regulates sex expression of cucumber via an ethylene-independent pathway. *J. Exp. Bot.* 65, 3201–3213. doi: 10.1093/jxb/eru176

Zhang, Z. W., Wu, P., Zhang, W. B., Yang, Z. F., Liu, H. Y., Ahammed, G. J., et al. (2019). Calcium is involved in exogenous NO-induced enhancement of photosynthesis in cucumber (*Cucumis sativus* L.) seedlings under low temperature. *Sci. Hortic.* 261:108953. doi: 10.1016/j.scienta.2019.108953

Zhao, W. (2013). Comparative analysis of anatomical characteristics of pericarp of low pesticide residues in Cucumber. *China Veg.* 20, 32–38.

Zhou, Y., Xia, X., Yu, G., Wang, J., Wu, J., Wang, M., et al. (2015). Brassinosteroids play a critical role in the regulation of pesticide metabolism in crop plants. *Sci. Rep.* 5:9018.

Conflict of Interest: The authors declare that the research was conducted in the absence of any commercial or financial relationships that could be construed as a potential conflict of interest.

Copyright © 2020 Li, Xin, Luan, Liu, Wang, Liu, Zhang, Zhou and Qin. This is an open-access article distributed under the terms of the Creative Commons Attribution License (CC BY). The use, distribution or reproduction in other forums is permitted, provided the original author(s) and the copyright owner(s) are credited and that the original publication in this journal is cited, in accordance with accepted academic practice. No use, distribution or reproduction is permitted which does not comply with these terms.

frontiers in Plant Science

ORIGINAL RESEARCH
published: 26 June 2020
doi: 10.3389/fpls.2020.00971

A *Brassica napus* Reductase Gene Dissected by Associative Transcriptomics Enhances Plant Adaption to Freezing Stress

Yong Huang[1,2†], Muhammad Azhar Hussain[1†], Dan Luo[1], Hongzhi Xu[2], Chuan Zeng[2], Lenka Havlickova[3], Ian Bancroft[3], Zhitao Tian[1], Xuekun Zhang[1], Yong Cheng[1], Xiling Zou[1], Guangyuan Lu[1] and Yan Lv[1*]*

[1] Key Laboratory of Biology and Genetic Improvement of Oil Crops, Ministry of Agriculture, Oil Crops Research Institute of the Chinese Academy of Agricultural Sciences, Wuhan, China, [2] Laboratory of Rapeseed, The Chongqing Three Gorges Academy of Agricultural Sciences, Chongqing, China, [3] Centre for Novel Agricultural Products (CNAP) M119, Department of Biology, University of York, York, United Kingdom

OPEN ACCESS

Edited by:
Raul Antonio Sperotto,
Universidade do Vale do Taquari - Univates, Brazil

Reviewed by:
Liezhao Liu,
Southwest University, China
Harsh Raman,
New South Wales Department of Primary Industries, Australia

***Correspondence:**
Guangyuan Lu
luguangyuan@caas.cn
Yan Lv
lvyan322@163.com

[†]These authors have contributed equally to this work

Specialty section:
This article was submitted to Plant Abiotic Stress, a section of the journal Frontiers in Plant Science

Received: 14 April 2020
Accepted: 15 June 2020
Published: 26 June 2020

Citation:
Huang Y, Hussain MA, Luo D, Xu H, Zeng C, Havlickova L, Bancroft I, Tian Z, Zhang X, Cheng Y, Zou X, Lu G and Lv Y (2020) A Brassica napus Reductase Gene Dissected by Associative Transcriptomics Enhances Plant Adaption to Freezing Stress. Front. Plant Sci. 11:971. doi: 10.3389/fpls.2020.00971

Cold treatment (vernalization) is required for winter crops such as rapeseed (*Brassica napus* L.). However, excessive exposure to low temperature (LT) in winter is also a stress for the semi-winter, early-flowering rapeseed varieties widely cultivated in China. Photosynthetic efficiency is one of the key determinants, and thus a good indicator for LT tolerance in plants. So far, the genetic basis underlying photosynthetic efficiency is poorly understood in rapeseed. Here the current study used Associative Transcriptomics to identify genetic loci controlling photosynthetic gas exchange parameters in a diversity panel comprising 123 accessions. A total of 201 significant Single Nucleotide Polymorphisms (SNPs) and 147 Gene Expression Markers (GEMs) were detected, leading to the identification of 22 candidate genes. Of these, Cab026133.1, an ortholog of the *Arabidopsis* gene AT2G29300.2 encoding a tropinone reductase (*BnTR1*), was further confirmed to be closely linked to transpiration rate. Ectopic expressing *BnTR1* in *Arabidopsis* plants significantly increased the transpiration rate and enhanced LT tolerance under freezing conditions. Also, a much higher level of alkaloids content was observed in the transgenic *Arabidopsis* plants, which could help protect against LT stress. Together, the current study showed that AT is an effective approach for dissecting LT tolerance trait in rapeseed and that *BnTR1* is a good target gene for the genetic improvement of LT tolerance in plant.

Keywords: rapeseed, associative transcriptomics, photosynthetic gas exchange parameter, tropinone reductase, alkaloid

INTRODUCTION

Rapeseed (*Brassica napus* L.) is one of the major oil crops worldwide, with an average annual cropping area of 35.3 million hectares producing 72.8 million tons of seeds in the past five years (http://www.fao.org/faostat/). Meal cake, the byproduct of rapeseed is also an important source of protein-rich feed for livestock (Wanasundara et al., 2016). Due to the agronomic importance of this

oil crop, there is a great interest to boost its yield *via* genetic improvement of major agronomic traits.

The winter type rapeseed is mainly grown in Europe, which requires strong vernalization and is cold tolerant (O'neill et al., 2019). However, the semi-winter type rapeseed grown in China only needs moderate or weak vernalization, and excessive exposure to low temperature (LT) stress in winter will lead to plant damage at vegetative stage and finally cause yield loss (Liao and Guan, 2001; Zhang et al., 2015; O'neill et al., 2019). Yangtze River basin is the major area for growing semi-winter rapeseed, which accounts for at least 80% of the nation's total production (Tian et al., 2018). The rapeseed is usually sown in early October shortly after the harvest of rice in this area (Cong et al., 2019). However, in recent years, the delay of rice harvest usually lead to the postpone of rapeseed sowing until late October or early November, which results in poor germination and seedling establishment due to LT (Luo et al., 2019). The biomass of rapeseed seedling is also significantly reduced at overwintering stage, and thus is more susceptible to LT stresses, i.e. chilling (0–15°C) or freezing (<0°C) (Sage and Kubien, 2007; Zhang et al., 2012; Zhang et al., 2016). Moreover, delay of floral initiation and floral bud differentiation processes (Luo et al., 2018) and decrease of effective pod number, pod length, and seed yield (Ozer, 2003) were observed in the late-sowing rapeseed. To cope with LT stresses, plants have evolved several elaborate regulatory mechanisms; among these, balancing or coordinating the photosynthetic processes could be a critical one (Leister, 2019).

It has been established that light-harvesting complex II (LHCII) proteins in higher plants can facilitate their adaption to external biotic or abiotic environmental stresses such as drought stress or blast fungus infection (Andersson et al., 2003; Ganeteg et al., 2004; Xu et al., 2012; Liu et al., 2019b), and the positive function of LHCBs in abscisic acid (ABA) mediated signaling pathway is repressed by WARY40 (Xu et al., 2012; Liu et al., 2013). LT stress induces the accumulation of transcript encoding heat-shock proteins (HSPs), and the persistence of HSPs can enhance the chilling tolerance of tomato fruit (Sabehat et al., 1996; Ding et al., 2001). In *Arabidopsis*, HSP21 protects the photosynthetic electron transport chain against the deleterious effects imposed by heat stress (Zhong et al., 2013; Bernfur et al., 2017). However, it is unclear whether HSPs function similarly in rapeseed to alleviate injury from LT stress. The other observations have mechanistically described how the photosynthetic organisms maintain their PSII function under stressful conditions with continuing or fluctuating light (Liu et al., 2019a). For instance, the chloroplast protein HHL1 forms a complex with LQY1 to repair and re-assemble PSII, which in turn helps overcome excessive light stress (Jin et al., 2014). In rapeseed, CBF/DREB transcription factors appear to have important roles in maintaining stronger photosynthetic efficiency and higher Calvin circulating enzyme activity under LT conditions (Savitch et al., 2005).

To date, several genetic studies have been reported for quantitative trait loci (QTLs) mapping of photosynthesis (De Miguel et al., 2014; Li et al., 2014; Li et al., 2016; Liu et al., 2017; Oakley et al., 2018; Basu et al., 2019) and LT tolerance in different plant species (Jha et al., 2017). However, very few QTLs have been identified in *Brassica* species (Ge et al., 2012; Yan et al., 2015). The temperature causing 50% of the maximal damage (LT50) has been regarded as a good index for evaluating LT tolerance (Hincha et al., 1987; Steponkus et al., 1990), which is also significantly correlated with net photosynthesis rate (A_n) in rapeseed (Urban et al., 2013). Therefore, photosynthetic gas exchange parameters such as A_n are a suitable index for the evaluation of LT tolerance in rapeseed that can facilitate the follow-up genetic study.

Photosynthesis plays an indispensable role in ensuring adequate energy supply throughout the plant lifecycle. Therefore, enhancing photosynthetic efficiency has been a commonly adopted strategy for crop yield improvement (Long et al., 2006; Lawson et al., 2012; Evans, 2013). In rice, a new photorespiratory bypass was assembled by over-expressing *OsGLO3*, *OsOXO3*, and *OsCATC* genes in the chloroplast, which resulted in obvious increases in photosynthetic efficiency, biomass, and grain yield (Shen et al., 2019). In rapeseed, photosynthetic efficiency has a notable effect on yield, oil content, and fatty acid composition (Ju and Li, 2012; Wang et al., 2015). However, the utilization rate of light energy in rapeseed is only 0.615% to 1.056%, which is much lower than that in rice, wheat or soybean (Zhang et al., 2017a). Therefore, it is possible to further improve the yield by enhancing photosynthetic efficiency in rapeseed.

During the long history of evolution, plants appear to overcome abrupt or mild temperature stresses in winter through a series of changes at molecular, cellular, physiological, and biochemical levels (Zhang et al., 2017b). Alkaloid is one of the major secondary metabolites that is inducible under unfavorable conditions, especially drought stress (Selmar and Kleinwachter, 2013). Heavy metals can also promote the accumulation of alkaloid in *Catharanthus roseus L.* (Srivastava and Srivastava, 2010). The short-chain dehydrogenase/reductase (SDR) protein, which belongs to the NAD(P)-binding Rossmann-fold superfamily, functions in the biosynthesis of benzylisiquinoline alkaloids (i.e. morphine, codeine) and tropane-derived alkaloids such as scopalamine, atropine, and cocaine. Tropinone reductases (TRs) are a group of SDR proteins which play key roles as a branch point in the biosynthesis pathway of tropane alkaloids (Tonfack et al., 2011). Hence, a study on TRs could help understand how alkaloids function in response to different stresses.

Associative transcriptomics (AT) strategy, which combines association mapping and transcriptome, has greatly facilitated the genetic dissection of complex traits (Bazakos et al., 2017). Considerable progress has been achieved by AT in allopolyploidy crops, such as oilseed rape and wheat, which provided a large number of causative genes or functional markers for molecular marker-assisted breeding. For instance, a transcription factor (HAG1) was identified in rapeseed by AT, which plays an indispensable role in the synthesis of aliphatic glucosinolates (Harper et al., 2012). With AT platform, the genetic studies of many other complex traits in rapeseed were also reported, including homeostasis of nitrate, phosphate, and sulfate anions (Koprivova et al., 2014), calcium and magnesium accumulation (Alcock et al., 2017), lodging resistance (Miller et al., 2018),

clubroot resistance (Hejna et al., 2019), erucic acid, and tocopherol (vitamin E) isoform accumulation in seeds (Havlickova et al., 2018), and leaf nutrition concentration (Alcock et al., 2018). Recently, the power of AT was further enhanced by using a much larger panel comprising 383 rapeseed accessions (Havlickova et al., 2018). In bread wheat, two causative genes underlying stem strength variation have also been detected by AT (Miller et al., 2016). Despite the above efforts, the AT approach has not yet been applied to photosynthetic related traits under LT conditions in rapeseed.

The present study aims to identify candidate genes associated with photosynthetic gas exchange parameters including A_n, stomatal conductance to water vapor (G_{sw}), internal CO_2 concentration (C_i) and transpiration rate/evapotranspiration (E) in rapeseed by AT. Twenty-two candidate genes were obtained, and one was functionally validated. Ectopic expressing tropinone reductase (*BnTR1*) in *Arabidopsis* can significantly enhance transpiration rate and LT tolerance, implying its great potential for the genetic improvement of LT tolerance in plant.

MATERIALS AND METHODS

Plant Materials

A panel comprising 123 rapeseed accessions was used for association study, which is available from the John Innes Centre, Norwich, UK (**Supplementary Table S1**) (Havlickova et al., 2018). Within this panel, there are 37 winter type, 32 spring type, 47 semi-winter type, and 7 unclassified rapeseed accessions. The panel was sown on 28th Oct in 2016 in Wuhan (114.30°E, 30.57°N), China. All accessions were planted using a completely randomized block design with three replications. The temperature was recorded during the field experiments (**Supplementary Figure S1**). Compared with those sown on normal occasion (28th Sept in 2016), the late-sown (i.e. 28th Oct) rapeseed seedlings were subjected to LT stress during winter.

Determination of Photosynthetic Gas Exchange Parameters

The fourth true leaf of each of the 123 rapeseed accessions was chosen for the measurement of photosynthetic gas exchange parameters including A_n, G_{sw}, C_i, and E in the open field at the 60-d-old seedling stage. Two independent plants of one accession from each block were measured by LI-6400 photosynthesis equipment (Li-Cor 6400; Li-CorInc, Lincoln, NE, USA) as described previously (Yan et al., 2015). The measurements were performed on a sunny day from 27th December to 30th December with a maximum temperature of 9°C in daytime and the lowest temperature of −1°C at night. The phenotypic data were collected from three blocks as biological replications (**Supplementary Table S2**). Broad-sense heritability was estimated according to a previous study (Kaler and Purcell, 2019).

The photosynthetic gas exchange parameters of *Arabidopsis* wild type (WT) and transgenic seedlings (ecotype Columbia) were measured on the second functional leaf with the light intensity of 800 μmol m^{-2} s^{-1} and CO_2 concentration of 400 μl L^{-1}. All of the *Arabidopsis* plants were grown in the greenhouse (16-h-light/8-h-dark) with the light intensity of 120 μmol m^{-2} s^{-1} at 23°C. Each leaf was measured three times as technical replications, and five independent plants from each line were measured as biological replications (**Supplementary Table S2**).

Genome-Wide Association Study

The association panel and the procedure of AT analysis have been reported in detail previously (Havlickova et al., 2018). In brief, RNA-Seq data were generated from young leaves of the association panel harvested 21 d after sowing under 16-h-light (20°C)/8-h-dark (14°C) glasshouse conditions. The transcriptome data were mapped onto the developed ordered *Brassica* A and C pan-transcriptomes (He et al., 2015) and resulted in a set of 355,536 SNPs and RPKM values for 116,098 CDS models. Following the removal of SNP markers with minor allele frequencies below 0.01, a total of 256,397 SNPs were retained (http://www.yorknowledgebase.info/) and used as marker input for the Associative Transcriptomics analysis as previously described (Harper et al., 2012; Lu et al., 2014). The current study adopted a compressed mixed linear model including both fixed and random effects according to a previous method (Lipka et al., 2012). The *P*-values ($-\log_{10}$ converted) for all SNPs were plotted against their physical position in the "pseudo-molecules" to produce a Manhattan plot. The Bonferroni significance threshold was set as $P = 3.9 \times 10^{-6}$ (1/256397) (Duggal et al., 2008). Allelic effects of all candidate SNPs were calculated according to a previous study (Prado et al., 2017); a positive effect indicates that the allele increases the trait value, whereas a negative effect indicates that the alternative allele increases the trait value.

The transcript level was quantified as reads per kb per million aligned reads (RPKM) across the panel. After filtering (RPKM ≤ 0.4), a total of 53,889 gene expression marker (GEM) was obtained. The GEM was regarded as the dependent variable and trait data as the independent variable (Wood et al., 2017). The fixed effect linear model was performed to assess the relationship between gene expression level and the traits (Alcock et al., 2017). The *P*-value for each GEM was converted ($-\log_{10}P$) and plotted against its physical position to generate a Manhattan plot. The Bonferroni significance threshold was set at $P = 1.85 \times 10^{-5}$ (1/53889).

Growth Conditions and Stress Treatments

To determine the gene function of *BnTR1* on *Arabidopsis* under freezing conditions, the seeds of WT and transgenic *Arabidopsis* plants were germinated on 1/2 MS medium and 1/2 MS medium plus 30 μg/ml hygromycin, respectively. After 1 week growth at 23°C (16-h-light/8-h-dark), healthy seedlings with uniform sizes were transplanted into 8×8 cm pots (four plants per pot). Then, the 21-d-old plants were transferred into a growth chamber at −4°C for 4 h after 24 h of cold acclimation and recover at 23°C (16-h-light/8-h-dark). Six pots from each transgenic line or WT plants were used to investigate the survival rate 3 d after recovery. The leaves were sampled for physiological and biochemical measurements.

To determine the effects of alkaloid on *Arabidopsis* and rapeseed seedlings, WT plants of *Arabidopsis* were firstly grown under the same conditions as above. Before the freezing treatment, a dosage of 0, 10, and 30 nmol alkaloid (atropine) per seedling was added to the soil for *Arabidopsis*, while a dosage of 0, 50, and 150 nmol per seedling was added to the soil for rapeseed accession Zhongshuang 11 (ZS11) according to the previous study (Hara and Kurita, 2014). After inoculation overnight, the 21-d-old *Arabidopsis* plants were transferred into a growth chamber at −4°C for 4 h, the three-leaf-stage rapeseed plants were transferred into the growth chamber at −4°C for 4 h (Yan et al., 2019). The survival rate was investigated in six pots 3 d after recovery (**Supplementary Table S2**).

To investigate the expression of candidate genes under LT stress conditions, six rapeseed accessions showing extreme photosynthetic efficiency (i.e. Sv706118, Kajsa, Callypso, Libritta, Gefion, and Jupiter; **Supplementary Table S1**) were used for expression analysis of candidate genes. The four-leaf seedlings were transferred into the plant growth chamber with −4°C for 4 h (Yan et al., 2019). The leaves were sampled before, and after freezing treatment, and then used for RNA extraction and molecular analysis. The detailed information was listed in **Supplementary Table S2**.

Physiological and Biochemical Measurements

To determine the effects of *BnTR1* on *Arabidopsis* at physiological and biochemical levels under LT stress conditions, the seedlings of transgenic and WT *Arabidopsis* plants were treated under freezing conditions (−4°C for 4 h) and, the leaves of 21-d-old seedlings were sampled at three time-point (i.e. before freezing treatment, after freezing treatment, and recovery for 3 d at 23°C) for measuring physiological and biochemical characteristics, including Fv/Fm, electrolyte leakage, 3,3′-diaminobenzidine (DAB) staining, proline content, soluble sugar content, reactive oxygen species (ROS) scavenging enzymes activity, H_2O_2 content, alkaloid content. All measurements were performed with at least three biological replications; detail information for experimental design and plant materials used was listed in **Supplementary Table S2**.

The Fv/Fm measurement was performed using the second functional leaves before and after the freezing treatment. The leaves were firstly immersed in 1% agarose overnight avoiding of the dark, then the chlorophyll measurement (Fv/Fm) was measured using the modulated chlorophyll fluorescence instrument (PAM-2500; Walz) as previously reported (Lv et al., 2017).

The electrolyte leakage measurement was performed according to the previous study (Lv et al., 2016). Briefly, six leaves from six were cut and immersed in 8 ml of double-distilled H_2O in a 10-ml tube. After shaking overnight, the electrolyte leakage was measured using a model DDS-IIA device (Leici Instrument) as R1; it was measured again and recorded as R2 after boiling at 95°C in a water bath for 15 min and cooling down. The relative electrolyte leakage was calculated as a ratio of R1/R2.

The proline and soluble sugar contents were measured using the kits from Beijing Solarbio Science & Technology as described before (Yan et al., 2019). In brief, 0.1 g fresh tissue was powdered and incubated in 1 ml 3% sulfosalicylic acid (for proline) or ddH_2O (for soluble sugar). After centrifuging, 400 μl supernatant was mix with other reaction buffers and incubated at 95°C in a water bath for 15 min, then the absorbance was measured using MULTISCAN FC (Thermo Scientific).

The ROS scavenging enzymes activity was measured by commercial kits according to the manufacturer's instruction (Beijing Solarbio Science & Technology) with minor modification (Yan et al., 2019). 0.1 g fresh tissue was powdered using 1 ml 0.05 mol/L PBS buffer (pH 7.8). The supernatant was obtained after centrifuging at 8,000*g* for 10 min at 4°C and used for superoxide dismutase (SOD) activity, peroxidase (POD) activity, catalase (CAT) activity measurement using MULTISCAN FC (Thermo Scientific).

DAB staining was performed as previously described (Ning et al., 2010; Zhang et al., 2011). The fourth functional leaf of each plant was sampled and infiltrated in 0.1 mg/ml 3,3′-diaminobenzidine liquid (50 mM Tris-acetate buffer, pH 5.0). After incubation overnight at 25°C in the dark, the stained leaves were photographed after removing the chlorophyll by absolute ethanol. The H_2O_2 content was quantified according to the instruction of the kit (Beijing Solarbio Science & Technology) (Yan et al., 2019).

The total alkaloid was extracted as described previously (Zhang et al., 2004; Chen et al., 2013). The freeze-dried leaves were powdered; 0.1 g powder was homogenized overnight with 1.0 ml 70% aqueous methanol at 4°C. Following centrifugation at 10,000 g for 10 min at 4°C, the extracts were absorbed (CNWBOND Carbon-GCB SPE Cartridge, 250 mg, 3 ml; ANPEL) and filtrated (SCAA-104, 0.22 μm pore size; ANPEL). Next, the total alkaloid content was determined using the alkaloid ELISA kit (Hiton) according to the instructions.

RNA Extraction and Gene Expression Analyses

Total RNA was extracted from the *Arabidopsis* or rapeseed seedlings with TransZol reagent (Trans) and converted to the first-strand cDNA using the EasyScript®One-Step cDNA Synthesis SuperMix (Trans). The Quantitative Real-time PCR (qRT-PCR) was performed using Power SYBR®Green PCR Master Mix according to the manufacturer's instructions on a StepOnePlusReal-Time PCR System (Applied Biosystems). The primers used for expression analysis of candidate genes either detected by AT approach or involved in the known biosynthetic pathway of alkaloid were listed in **Supplementary Table S3**. The relative expression level was determined as previously described (Livak and Schmittgen, 2001).

Vector Construction and Gene Transformation

To generate transgenic lines over-expressing candidate gene (*BnTR1*), the coding sequence (CDS) of *LOC106445422* was amplified from a rapeseed variety ZS11 and ligated into vector pCAMBIA1300 driven by a tobacco cauliflower mosaic virus 35S promoter (CaMV35S). The construct was introduced into

Arabidopsis variety Columbia (Col) by *Agrobacterium*-mediated transformation (Zhang et al., 2006). Three T4 homozygous lines (L1, L3, L5) significantly over-expressing *BnTR1* were obtained by screening at 30 μg/ml hygromycin. The primers used for vector construction were listed in **Supplementary Table S3**.

Statistical Analyses

Statistical analyses were conducted with Microsoft Excel (2003) and SPSS (version 22.0) software using one-way analysis of variance (ANOVA) with Tukey's multiple comparisons test or two-tailed Student's *t*-test. All data were presented as the means ± standard error (SE) based on three replicates. $P<0.05$ and $P<0.01$ were considered statistically significant and highly significant, respectively.

RESULTS

Phenotypic Variation of Photosynthetic Gas Exchange Parameters

A field-grown rapeseed association panel experienced long-term LT stress in winter (**Supplementary Figure S1**). The photosynthetic gas exchange parameters such as A_n, G_{sw}, C_i, and E were measured since they can reflect photosynthetic efficiency for a plant. Substantial variations for the four traits were observed in 123 rapeseed accessions (**Figure 1**). A_n varied from 12.87 to 24.02 with a mean of 19.29 μmol (CO_2) m^{-2} s^{-1}. Similarly, G_{sw} ranged from 245.21 to 383.28 μmol (CO_2) mol^{-1} and E from 0.96 to 3.75 mmol (H_2O) m^{-2} s^{-1}. G_{sw} was the most variable trait since it has the largest coefficient of variation (0.69), with a minimum of 0.16 and a maximum of 2.53 mol (H_2O) m^{-2} s^{-1}; the range of broad-sense heritability varied from 49.49% to 68.91% (**Supplementary Table S4**). Moreover, the four traits in the association panel were positively correlated with each other ($P \leq 0.01$) (**Supplementary Table S5**). For instance, there was a strong correlation between A_n and E ($r = 0.785$, $P<0.01$).

Associative Transcriptomics for Photosynthetic Gas Exchange Parameters

To identify genomic regions controlling photosynthetic related traits, AT was performed in rapeseed. Using the mixed linear model, a total of 201 significant SNPs were detected, which originated from 148 CDSs (**Figure 2**). Unexpectedly, most of the significant CDSs were associated with G_{sw} trait, while only one was related to E trait. The detail results including physical positions, *P*-values, allelic effects were summarized in **Supplementary Table S6**. For GEM analysis, a total of 145 CDSs above the corrected Bonferroni thresholds were identified (**Figure 2**). Of these, a respective of 5, 10, 20, and 110 CDSs were detected for A_n, G_{sw}, C_i, and E. The detailed information,

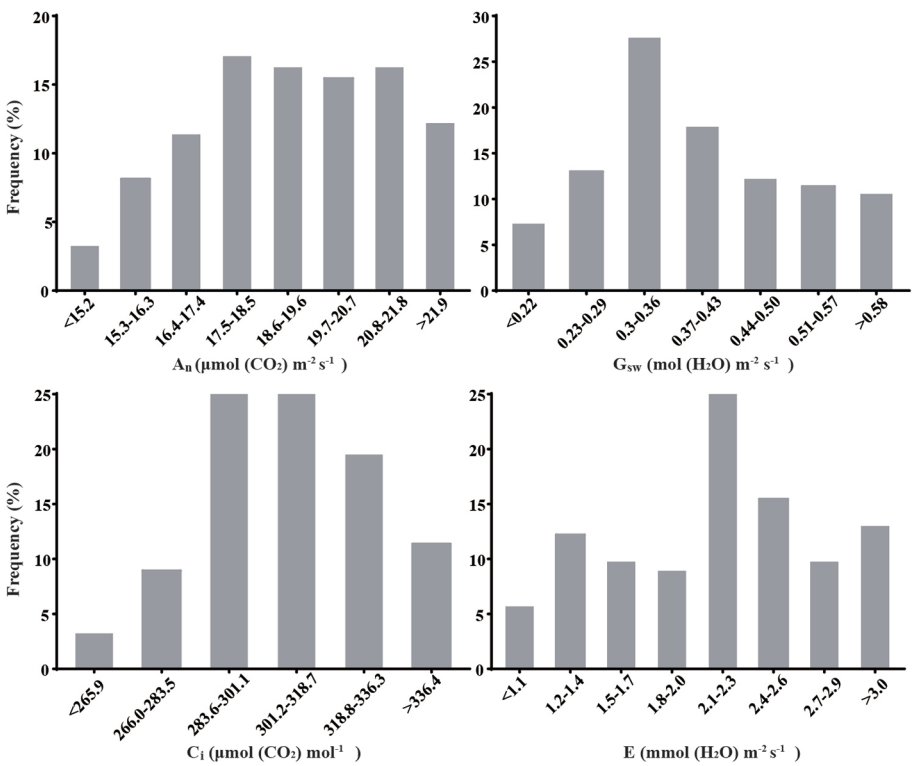


FIGURE 1 | Phenotypic variation of photosynthetic gas exchange parameters in 123 rapeseed accessions. Trait definition: Net photosynthesis rate (A_n), Stomatal conductance to water vapor (G_{sw}), Internal CO_2 concentration (C_i), Transpiration rate (E).

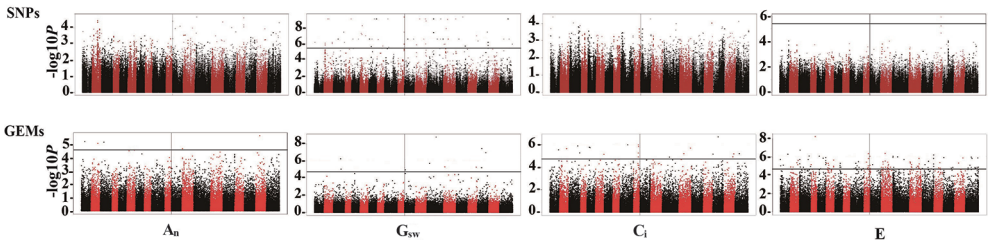


FIGURE 2 | Manhattan plots for AT analysis in 123 rapeseed accessions. Manhattan plots from left to right, represented for A_n, G_{sw}, C_i, and E using SNPs (upper section) and GEMs (bottom section), respectively. The -log10 (*P* values) were plotted against the position of the SNPs or GEMs on 19 chromosomes of *Brassica napus*. The black line represents the -log10 (*P* values) converted Bonferroni significance threshold for SNP (5.41) and GEM (4.73), respectively.

including physical positions and *P* values for all significant GEMs, was listed in **Supplementary Table S7**.

By annotating all the above significant CDS in public database TAIR (https://www.arabidopsis.org/), the present study shortlists the number of candidate genes to only 22 that putatively involved in photosynthesis or LT stress response (**Supplementary Table S8**). To verify their roles in rapeseed with or without LT stress, six accessions from the association panel were selected; Sv706118, Kajsa, and Callypso (Accessions 1–3) exhibited higher photosynthesis efficiency and were tolerant to freezing stress, while Libritta, Gefion, and Jupiter (Accessions 4–6) presented lower photosynthesis efficiency and were sensitive to freezing stress (**Supplementary Table S1**, **Supplementary Figure S2**). The gene expression profiles were investigated by qRT-PCR in the six accessions under freezing conditions. Results showed that all of these genes exhibited a significantly different expression level in the six accessions, suggesting that these genes indeed involved in freezing stress response. *Cab026133.1* seemed to have a much higher expression level in the three tolerant accessions (Accessions 1–3) with or without freezing stress (**Figure 3A**); so did *Cab011968.1*, *Cab022014.2*, and *Cab007526.2*, an ortholog of inorganic carbon transport protein (AT1G70760.1), bZIP transcription factor (AT5G28770.3) and citrate synthase 2 (BnaA10g24440D), respectively. An opposite trend was observed for *Bo5g017460.1* and *Cab008128.1*, an ortholog of F-box family protein (AT2G32560.1) and dehydroascorbate reductase (AT5G16710.1), respectively (**Supplementary Figure S3**).

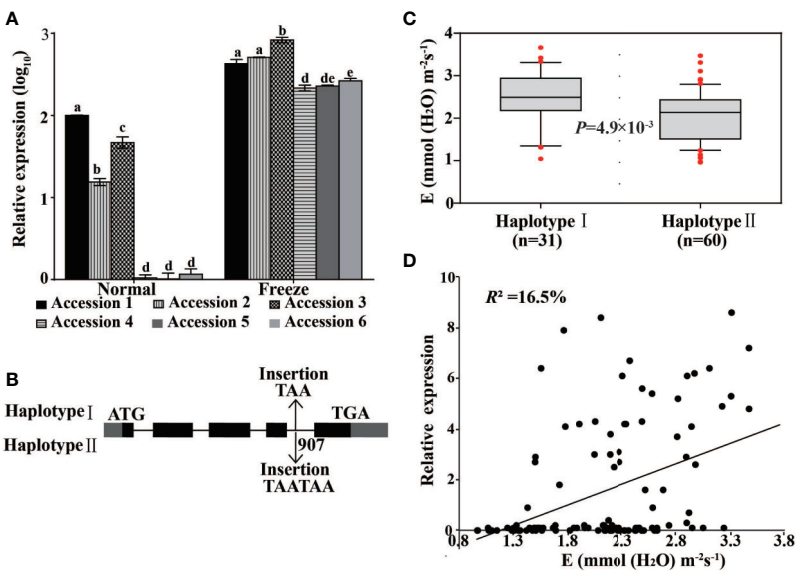


FIGURE 3 | Expression and allelic variation of *BnTR1* in rapeseed. **(A)** Expression analysis of *BnTR1* (homolog of *Cab026133.1*) in six accessions corresponding to Hap 1 and Hap 2 under freezing conditions. The name of accessions 1 to 6 was Sv706118, Kajsa, Callypso, Libritta, Gefion, and Jupiter, respectively. *ACTIN* gene was used as an internal control. Bars indicate the SE of three biological replicates. Different letters indicate significant differences at $P < 0.05$ (one-way ANOVA with Tukey's multiple comparisons test). **(B)** Correlation analysis between Transpiration rate (E) value and expression level of *Cab026133.1* in the association panel (n=123). R^2 indicates the coefficient of determination in linear regression. **(C, D)** Allelic variations at *BnTR1* formed two main haplotypes and their effects on E value.

Selection and Characterization of Candidate Gene

Cab026133.1 was selected for further analysis because it not only exhibited the highest *P*-value (6.33×10^{-9}) for E trait in GEM analysis (**Supplementary Table S8**) but also highly expressed in LT tolerant accessions (**Figure 3A**). Besides, the expression of *Cab026133.1* (presented as RPKM) across the rapeseed panel was positively correlated with E level (r=0.406, $P < 10^{-3}$) and accounted for 16.5% of trait variation (**Figure 3B**). The ortholog of Cab026133.1 in *Arabidopsis* (AT2g29300) encodes an SDR protein involved in the oxidation-reduction process of secondary metabolites, such as phenols, isoprene, and alkaloid (Selmar and Kleinwachter, 2013). SDR proteins are classified into six subfamilies, and the tropinone reductase subfamily belongs to the major route of alkaloid biosynthesis (Tonfack et al., 2011). The alignment of amino acid sequence clearly illustrated that LOC106445422 shared 87.3% similarity with Cab026133.1 and 57% with CoTR, a known tropinone reductase in *Cochlearia officinalis* (Brock et al., 2008). LOC106445422 displayed typical SDRs motifs (Gly-X_3-Gly-X-Gly) and four conserved residues that form the catalytic tetrad NSYK (N127, S155, Y168, K172) (**Supplementary Figure S4**). The current study name LOC106445422 as *BnTR1* and used as the candidate gene for the follow-up studies.

To assess the effect of allelic variation on *BnTR1* in the rapeseed association panel, the genomic region covering the whole gene as well as the 2-kb promoter region was amplified. One TAA/TAATAA insertion was detected in the fourth intron that formed two major haplotypes, i.e. Haplotype I (with TAA insertion) and Haplotype II (with TAATAA insertion) (**Figure 3C**). Haplotype I (n=31) displayed significantly higher E value than Haplotype II (n=60) (P=5.43 × 10^{-4}) (**Figure 3D**). Besides, *the LT tolerant* Accessions 1 to 3 were determined as Haplotype I while sensitive Accessions 4 to 6 as Haplotype II at BnTR1 locus (**Supplementary Table S1**). The expression level of *BnTR1* in Accessions 1 to 3 was also significantly higher than that in accessions 4 to 6 with or without stress treatment (**Figure 3A**). Therefore, it was evident that E variation may be attributed to expression or allelic variation at *BnTR1*, which was expressed almost in all tissues of rapeseed at both vegetative and reproductive stages (**Supplementary Figure S5**).

Ecotopic Expressing *BnTR1* Enhances Freezing Tolerance in *Arabidopsis*

To analyze gene function, three independent *Arabidopsis* lines (L1, L3, L5) ectopic expressing *BnTR1* were generated. All transgenic lines showed an increased expression level of *BnTR1* in comparison to the WT plants (**Figure 4A**). At the seedling stage, E value of the transgenic lines was much higher than that of WT plants (**Figure 4B**), thus confirming that BnTR1 controls transpiration rate. Since photosynthetic gas exchange parameters are significantly correlated with cold tolerance (Urban et al., 2013), it was speculated that BnTR1 also involves in LT stress. To test this hypothesis, seedlings were treated at −4°C for 4 h and then recover at 23°C. All of the transgenic lines were shown to be freezing-tolerant because there was no obvious syndrome, while the WT plants were wrinkled and hydrophanous (**Figure 4C**). After recovery for 3 d at 23°C, all transgenic plants survived, but 62% of the WT plants died (**Figure 4D**). These results strongly suggested that BnTR1 enhanced the freezing tolerance of *Arabidopsis* plants.

To assess whether C-repeat-binding factors (CBFs) contributed to the enhanced freezing tolerance of the transgenic lines, the current study measured the relative expression level of *CBFs* in transgenic and WT plants after freezing stress (**Figures 4E–G**). In the transgenic lines grown under normal conditions, expressions of *CBFs* were much higher than that in WT plants, indicating that they were markedly induced by *BnTR1*. Moreover, the expression of *CBF1* and *CBF3* was significantly up-regulated and *CBF2* down-regulated by *BnTR1* during freezing treatment in comparison with those of normal conditions. The current study further examined the expression level of CBFs-targeted cold-responsive genes (COR genes) (**Figures 4H, I**). As expected, the transcript levels of COR genes (namely *COR15* and *RD29A*) in the transgenic lines were highly induced when compared with that in WT plants. These results indicated that *BnTR1* influences CBF regulon in the stress-signaling pathway to control freezing tolerance.

The chlorophyll fluorescence parameter Fv/Fm, an indicator for the potential maximum photosystem II (PSII) capacity of plants, has been widely used to determine the ability of tolerance to environmental stresses under laboratory conditions (Mishra et al., 2014; Thalhammer et al., 2014). Here, markedly higher Fv/Fm ratio was observed in leaves of the transgenic lines under freezing as well as normal conditions (**Figure 5A**). To further clarify whether the difference of photosynthetic capacity was caused by the excessive expression of *BnTR1*, the current study assessed the expression level of *BnTR1* and other genes involved in photosynthetic processes such as *RCA*, *SBPASE* (for CO_2 fixation or assimilation) and *CAB1-4* (for light-harvesting) (Sun et al., 2017; Basu et al., 2019) (**Figures 5B–H**). Under normal conditions, the expression level of *RCA*, *SPASE,* and *CAB1* were slightly reduced in the transgenic lines compared to WT plants, whereas CAB2, CAB3, and CAB4 were induced. The freezing treatment led to a notable suppression of all genes; however, the expression of genes in the transgenic lines returned to a high level when freezing stress was removed.

BnTR1 Contributes to Cell Membrane Protection and Antioxidants

Altering the osmotic balance to maintain the integrity and stability of cell membrane is proposed to be an efficient way for plants adapting to the changing environments (Morsy et al., 2005; Valerio et al., 2011). To test this hypothesis, physiological and biochemical assays were carried out. Results showed that freezing treatment led to only 40% to 200% increase of proline content in WT plants but as high as 100% to 300% in transgenic plants, indicating that the transgenic plants expressing *BnTR1* could accumulate more proline (**Figure 6A**). The soluble sugar content showed a similar pattern (**Figure 6B**). However, the electrolyte leakage increased more rapidly in WT plants than in transgenic lines (**Figure 6C**). These results implied that BnTR1

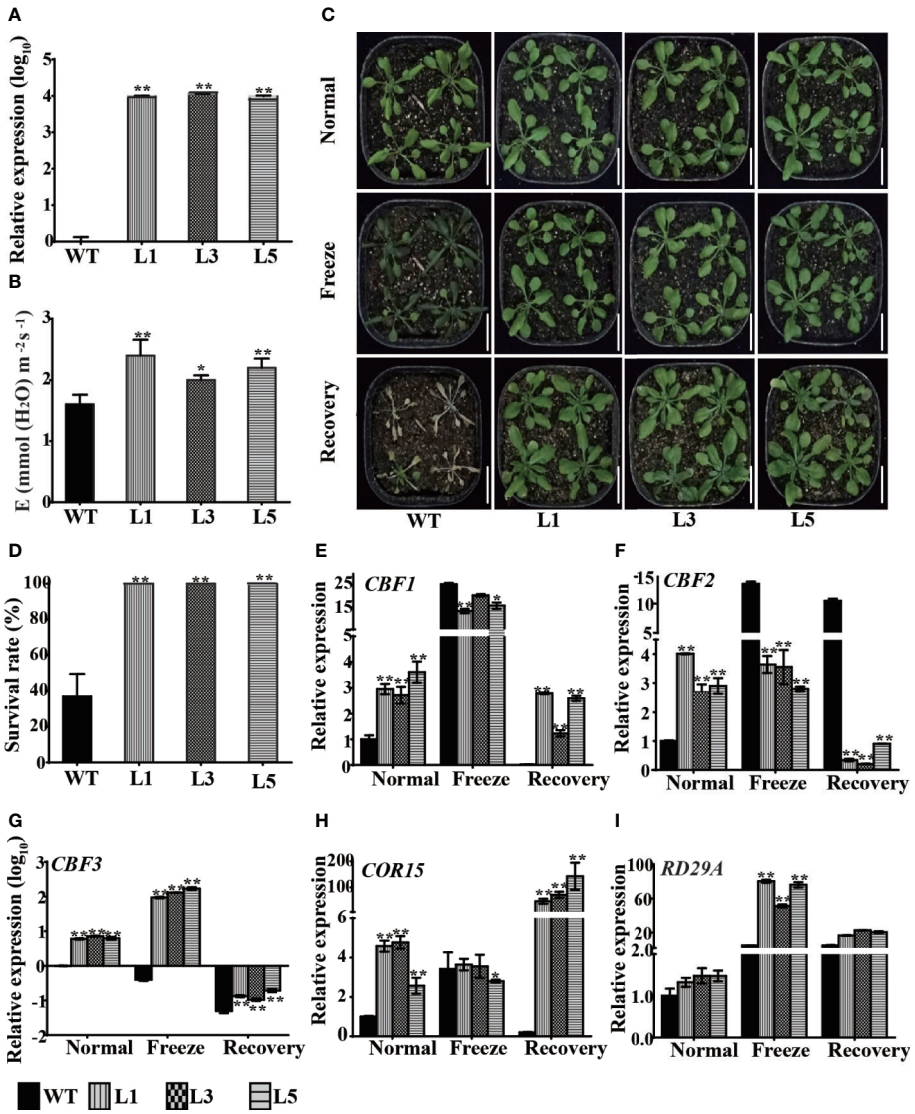


FIGURE 4 | BnTR1 confers freezing tolerance in *Arabidopsis*. **(A)** Expression analysis of the *BnTR1* transgenic plants (L1, L3, L5) and WT plants under normal condition (i.e. 23°C). **(B)** Investigation of transpiration rate **(E)** value in the *BnTR1* transgenic lines and WT plants under normal conditions. **(C)** Performance of the transgenic lines and WT plants before and after freezing treatment (−4°C for 4 h). Scale=2 cm. **(D)** Survival rates of the transgenic lines and WT plants after freezing treatment. **(E–I)** Relative expression levels of *CBF1* **(E)**, *CBF2* **(F)**, *CBF3* **(G)**, *COR15* **(H)**, *RD29A* **(I)** in the transgenic lines and WT plants before and after freezing stress with the *Arabidopsis ACTIN* gene used as an internal control. Normal represents 23°C, freezing treatment represents 4 h at −4°C, recovery represents 3 d of recovery at 23°C. Bars indicate the SE of three biological replicates. Significant differences are determined by Student's *t*-test (*$P < 0.05$, or **$P < 0.01$).

actively responded to freezing stress by maintaining cell membrane stability and osmotic balance.

Antioxidants, which function in scavenging the reactive oxygen species (ROS), are generally considered as another effective element in defending abiotic stresses (Choudhury et al., 2017). To determine whether *BnTR1* affects the antioxidant system, the accumulation of ROS was determined by DAB staining. The brown precipitate (H_2O_2) in WT was much larger than that in the transgenic lines (**Figure 6D**), indicating that WT plants had a higher level of H_2O_2 content than transgenic plants (**Figure 6E**). Oxidoreductases like POD, SOD, and CAT also function in scavenging redundant ROS (Gupta et al., 2016). Here, we found that the transgenic lines exhibited stronger SOD activity than WT (**Figure 6F**), which help plants alleviate oxidation damage from freezing conditions. However, no significant difference was detected for POD and CAT activities. Together, the enhanced freezing adaption for transgenic plants could be attributed to the increased ROS scavenging ability.

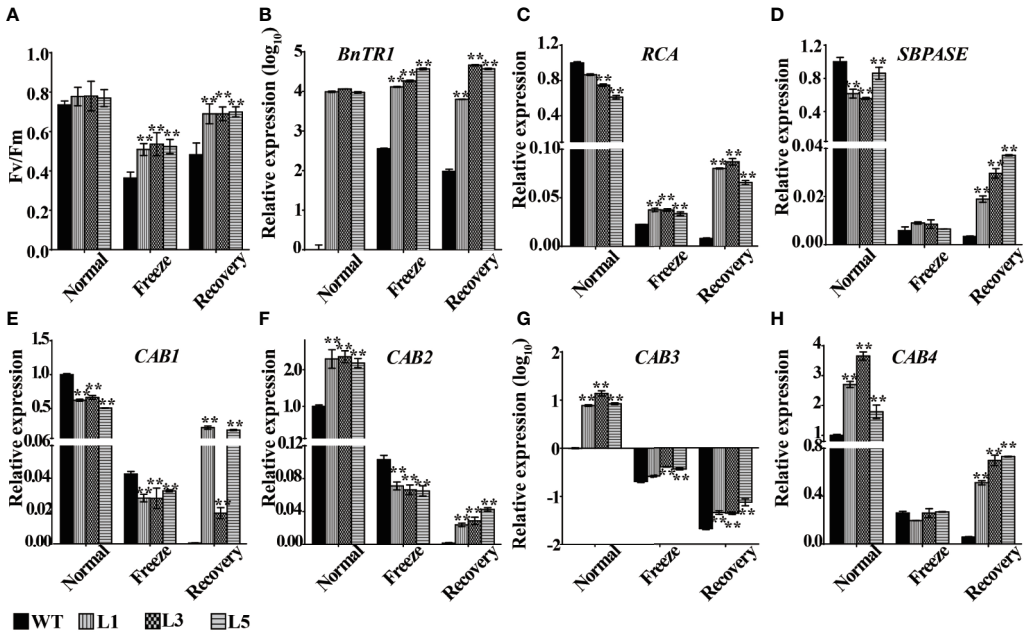


FIGURE 5 | Variation of photosynthetic related traits and genes expression pattern in *BnTR1* transgenic plants. **(A)** Fv/Fm ratio in the transgenic lines and WT plants under freezing stress conditions. **(B–H)** Relative expression levels of *BnTR1* **(B)**, *RCA* **(C)**, *SBPASE* **(D)**, *CAB1* **(E)**, *CAB2* **(F)**, *CAB3* **(G)**, *CAB4* **(H)** in the transgenic lines and WT plants before and after freezing stress treatment with *Arabidopsis ACTIN* gene used as an internal control. L1, L3, L5 represent three independent homozygous lines of *BnTR1* transgenic plants. Bars indicate the SE of three biological replicates. Significant differences are determined by Student's *t*-test (*$P <$ 0.05, or **$P < 0.01$).

BnTR1 Positively Affects Alkaloid Metabolism

BnTR1 (homolog of AT2g29300) is predicted to be a tropinone reductase involved in the biosynthesis of alkaloid (KO00960), which mainly produces atropine. Although all alkaloids (with more than 12,000 different structures) have been well-documented in pharmacology, their roles in abiotic stress remain elusive (Schlager and Drager, 2016). To investigate the specific role of BnTR1 in alkaloid metabolism, the total alkaloids content was quantified. As expected, the transgenic lines led to one- to two-fold increase of alkaloids contents compared with WT plants after freezing stress (**Figure 7A**). To further confirm the effect of alkaloid on stressed plants, exogenous atropine was applied to WT plants, since atropine was considered to be the product of alkaloid metabolism (KO00960) (Hara and Kurita, 2014). Results demonstrated that application of 10 nmol atropine per plant significantly rescued the susceptibility of WT plants, but the protective effect was weakened when dosage increase to 30 nmol (**Figure 7B**). The survival rate increased by three- to four-fold compared with WT plants without atropine treatment (**Figure 7C**).

To further elucidate the protective role of alkaloid in rapeseed, the current study applied exogenous atropine to a widely cultivated rapeseed variety, ZS11, under freezing conditions. Phenotypic analysis showed that the wilting phenotype of ZS11 plants was partially rescued by exogenous atropine application (50 and 150 nmol per plant) (**Figure 7D**), while no significant difference was observed in the survival rate. It was concluded that alkaloids alleviated the damage on plants from extreme LT stress.

DISCUSSION

Power of AT Approach

Brassica napus originated from the hybridization of *Brassica rapa* and *Brassica oleracea* which contribute the A and C genomes, respectively (Cheung et al., 2009). There is only 15% difference in nucleotide structure and 3% difference in transcriptional expression patterns between chromosomes A and C, which limits the development of SNP markers in genome-wide association analysis until the availability of the high throughput next-generation sequencing technology (Adams et al., 2003; Higgins et al., 2012). Over the past years, AT approach based on abundant SNP markers and GEMs, has successfully simplified the complexity of the whole genome (Harper et al., 2012), and has been widely applied in rapeseed, wheat, and other polyploidy crops (Harper et al., 2012; Schuster et al., 2013; Koprivova et al., 2014; Lu et al., 2014; Harper et al., 2016a; Harper et al., 2016b; Miller et al., 2016; Alcock et al., 2017; Havlickova et al., 2018; Miller et al., 2018). However, the genetic basis of photosynthetic-related traits in oil crops remains elusive. Here, the genetic architecture of photosynthetic gas exchange parameters was investigated by AT approach, and a gene termed *BnTR1* was confirmed to be responsible for E trait (**Figure 4**), which might be a promising candidate beneficial to rapeseed in coping with climatic

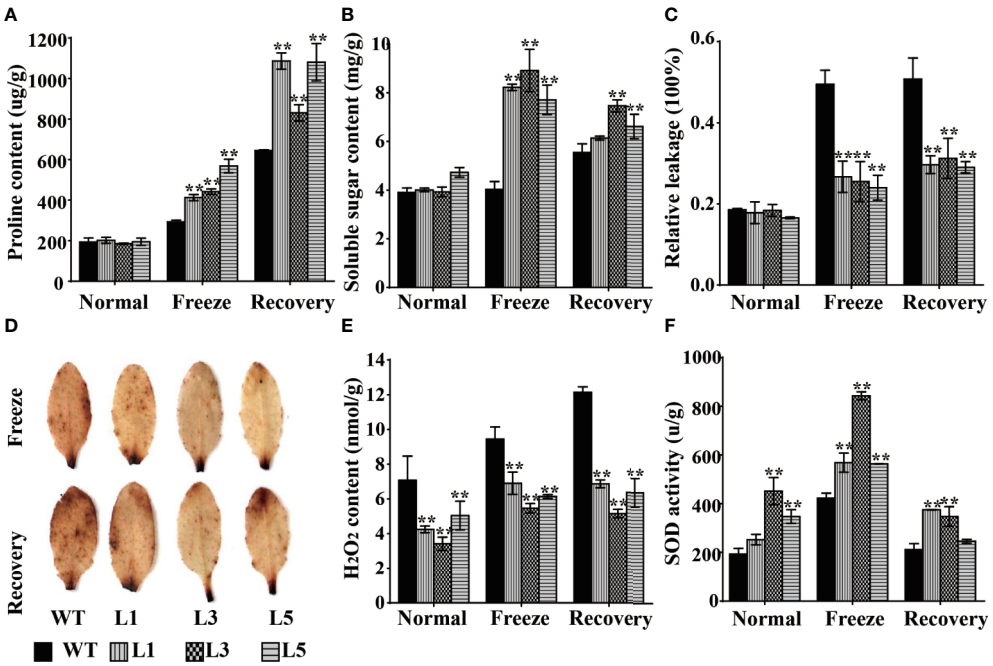


FIGURE 6 | Physiological characterization of *BnTR1* transgenic plants under freezing stress conditions. **(A–F)** Investigation of the proline content **(A)**, soluble sugar content **(B)**, relative leakage **(C)**, DAB staining analysis **(D)**, H_2O_2 content **(E)**, SOD activity **(F)** in the transgenic lines and WT plants under freezing stress conditions. L1, L3, L5 represent three independent homozygous lines of *BnTR1* transgenic *Arabidopsis* plants. Bars indicate the SE of three biological replicates. Significant differences are determined by the Student's *t*-test (*P< 0.05, or **P < 0.01).

changes. Several other interesting candidates were also identified. For instance, Bo5g155110.1 was found to be significantly associated with E traits (P=1.1×10^{-5}), and down-regulated by freezing stress (**Supplementary Figure S3**). The homolog in *Arabidopsis* is Cyclophilin38 (AtCYP38), which functions in the assembly and maintenance of PSII super complex (**Supplementary Table S7**). The loss-of-function mutant of *AtCYP38* shows reduced growth rate and photosynthetic efficiency compared to its wild type. Additionally, the D1 and D2 proteins in PSII reaction center show a short half-life, resulting in susceptibility upon exposure to excessive light (Fu et al., 2007; Sirpio et al., 2008). *Bo3g153100.1* was hit by an SNP marker, with -log10 (P-*value)* value as high as 9.06 (**Supplementary Table S6**), it was also markedly up-regulated by freezing stress (**Supplementary Figure S3**). Bo3g153100.1 was homologs to AT4G37930 in *Arabidopsis*, which has been documented in the photorespiration process (Takahashi et al., 2007). In the knockout mutant of AT4G37930, the photorespiration pathway is destroyed, and the chlorophyll deficiency results in chlorosis (Voll et al., 2006). Therefore, it seems that AT is a powerful tool to identify candidate genes for photosynthesis and LT stress in rapeseed. It is worthy to further study the function of all 22 candidate genes identified here.

The Positive Role of BnTR1 Under LT Conditions

It is generally accepted that photosynthesis is vulnerable to adverse environmental stresses such as extreme temperature, salinity, drought or combined stresses (Sainz et al., 2010; Strzepek et al., 2019). Abiotic stresses lead to photoinhibition as well as excessive generation of ROS, which suppresses the photosynthetic progress and ultimately repress the growth and productivity in plants (Gabriel et al., 2010; Nishiyama et al., 2014). During the long-term evolution, plants have developed a variety of adaptive mechanisms to cope with the stressful conditions (Liu et al., 2019a; Strzepek et al., 2019). The CBF transcription factors in rapeseed are known to be responsible for the photosynthetic performance; CBF5 and CBF17 enhance the energy conversion efficiency under LT conditions (Savitch et al., 2005; Dahal et al., 2012). CBF1-CBF3, also termed dehydration-responsive element-binding factors, have been well-documented in plants. In *Arabidopsis*, CBF2 represents a negative regulator for LT response, while CBF1 and CBF3 are positive regulators (Novillo et al., 2004; Novillo et al., 2012). Interestingly, increased expression of *CBF1* and *CBF3* and repressed expression of *CBF2* were observed in the *BnTR1* transgenic lines (**Figures 4E–G**), indicating that BnTR1 represented a unique influence on CBF members. Both alleviated accumulation of ROS and activated SOD enzyme system was observed in the *BnTR1* transgenic lines (**Figure 6**), suggesting active impacts of BnTR1 on the ROS scavenging system. In addition, ectopic expressing *BnTR1* also promote the expression of the genes associated with plant photosynthesis (**Figure 5**). Specifically, the decrease of *RCA* transcripts leads to lower A_n value, which in turn slows down plant growth (Von Caemmerer et al., 2005; Yin et al., 2010). Moreover, RCA enhances growth and

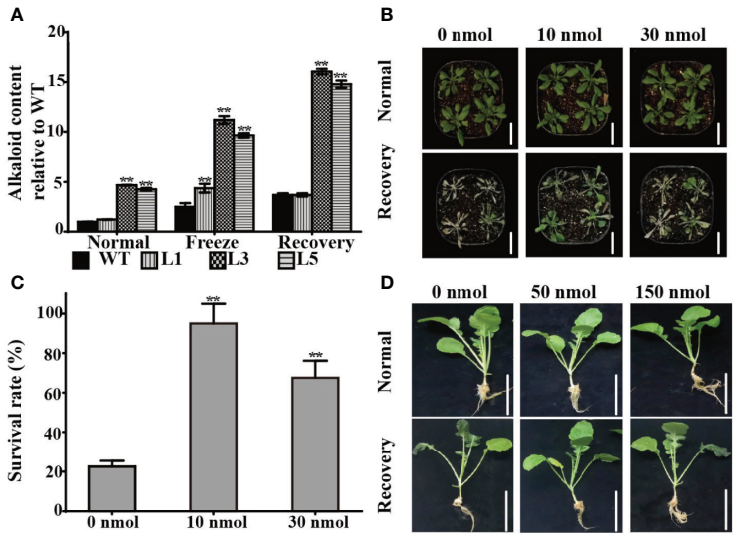


FIGURE 7 | BnTR1 mediates alkaloid accumulation and exogenous atropine application enhances freezing tolerance. **(A)** Total alkaloids accumulation in *BnTR1* transgenic lines and WT plants under freezing stress conditions. L1, L3, L5 represent three independent homozygous lines of *BnTR1* transgenic *Arabidopsis* plants. **(B)** Phenotypes of *Arabidopsis* WT plants with exogenous atropine application (0 nmol per plant, 10 nmol per plant, 30 nmol per plant) under freezing stress conditions. Scale = 2 cm. **(C)** Survival rates of *Arabidopsis* WT plants with exogenous atropine application after the freezing treatment. **(D)** Phenotypes of rapeseed WT plants with exogenous atropine application (0 nmol per plant, 50 nmol per plant, 150 nmol per plant) under LT conditions. Scale=5 cm. Bars indicate the SE of three biological replicates. Significant differences are determined by Student's *t*-test (*$P < 0.05$ or **$P < 0.01$).

photosynthesis under moderate heat stress conditions (Kurek et al., 2007; Kumar et al., 2009). However, overexpression of *SBPASE* improves sugar accumulation and enhanced photosynthesis efficiency (Miyagawa et al., 2001; Feng et al., 2007; De Porcellinis et al., 2018). In the present study, PSII was severely repressed during freezing treatment, whereas the *BnTR1* transgenic *Arabidopsis* plants still exhibited higher Fv/Fm level compared to WT (**Figure 5A**). These observations suggest that BnTR1 triggered a series of responses including the ROS scavenging system, CBF pathway, and photosynthetic processes. However, further work is required to confirm their roles in LT tolerance.

Protective Role of Alkaloids Under LT Conditions

Previous studies have been instrumental in revealing some metabolites underlying stress response mechanisms (Thalmann and Santelia, 2017). So far, definitions of alkaloids are generally focused on strong pharmacological effects, such as antimitotic, antidote, anticancer, and antioxidants (Schlager and Drager, 2016). The concentration of alkaloid compounds is predominantly inducible when plants are subjected to multiple stresses (Srivastava and Srivastava, 2010; Cheng et al., 2018). However, few studies have recognized the positive correlations between alkaloids and stress resistance. Application of sanguinarine for *Arabidopsis* seedlings under heat stress condition could markedly enhance the tolerance, which presumably by promoting the expression of heat shock proteins like HSP70 and HSP90.1S (Hara and Kurita, 2014; Matsuoka et al., 2016). BnTR1 is predicted to encode a tropinone reductase, which is involved in the metabolic pathway of atropine alkaloids. The current study determined the total alkaloids content under stress conditions, which showed an increased level in *BnTR1* transgenic lines under normal and freezing stress conditions compared with WT plants (**Figure 7A**). Moreover, the application of exogenous atropine alleviated the damage caused by extreme temperature in both *Arabidopsis* and rapeseed seedlings (**Figures 7B, D**), which was in agreement with the observations in sanguinarine under heat stress conditions (Schlager and Drager, 2016). However, more studies are still required to confirm that alkaloids could function as a protectant for plants to confer stronger resistance to LT stresses. The current study has compared the expression level of stress-related genes in *Arabidopsis* plants treated with exogenous atropine under freezing conditions (**Supplementary Figure S6**). It was found that atropine could promote the expression of *CBF1*, *CBF3*, *CAB1*, *CAB3*, *CAB4*, *SPASE* before or after freezing treatment, but the extent is much lower than that induced by BnTR1 (**Figures 4** and **5**). Thus the results confirmed at least in part the protective role of atropine for a plant in adaption to LT stress. It is proposed that BnTR1 works as an effecter *via* metabolizing alkaloids accumulation, photosynthesis, CBF/DREB pathways, and ROS scavenging system in stressed *Arabidopsis*, which in turn contributes to the adaptation under LT conditions.

CONCLUSIONS

During overwintering for the semi-winter type rapeseed grown in China, the extremely low temperature has a deleterious impact on plant productivity. Therefore, the identification of genes responsible for stress response is the prime interest of researchers. Despite of limited phenotypic data, our associative transcriptomics approach

has been successfully used to dissect the genetics of photosynthetic-related traits under low temperature conditions. The first short-chain dehydrogenase/reductase, BnTR1 was identified in rapeseed, which improved the transpiration rate and freezing tolerance of *Arabidopsis* plants. Taken together, our findings illustrated the molecular mechanism of plant adaption to low temperature stress. Finally, this work sheds light on the way to increase low temperature tolerance in rapeseed by genetic engineering strategies.

DATA AVAILABILITY STATEMENT

The original contributions presented in the study are included in the article/supplementary material; further inquiries can be directed to the corresponding authors.

AUTHOR CONTRIBUTIONS

Figures, study design: YH, MH. Investigation and data collection: YH, HX, CZ. Data analysis: GL, ZT, LH, IB. Validation: DL. Resources: LH, IB. Writing—original draft: YH, MH. Writing—review and editing: YL, GL. Funding acquisition: XZh, YC, XZ, GL, YL.

FUNDING

This research was financially supported by funds from the National Key Research and Development Program of China (2018YFD0100905), the Oil Crops Research Institution Basal Research Fund of the Chinese Academy of Agricultural Sciences (CAAS), China (1610172018010), the major science and technology project, Ministry of science and technology, China (2018ZX08020001).

SUPPLEMENTARY MATERIAL

The Supplementary Material for this article can be found online at: https://www.frontiersin.org/articles/10.3389/fpls.2020.00971/full#supplementary-material

REFERENCES

Adams, K. L., Cronn, R., Percifield, R., and Wendel, J. F. (2003). Genes duplicated by polyploidy show unequal contributions to the transcriptome and organ-specific reciprocal silencing. *Proc. Natl. Acad. Sci. U. S. A.* 100, 4649–4654. doi: 10.1073/pnas.0630618100.

Alcock, T. D., Havlickova, L., He, Z., Bancroft, I., White, P. J., Broadley, M. R., et al. (2017). Identification of candidate genes for calcium and magnesium accumulation in Brassica napus L. by association genetics. *Front. Plant Sci.* 8, 1968. doi: 10.3389/fpls.2017.01968.

Alcock, T. D., Havlickova, L., He, Z., Wilson, L., Bancroft, I., White, P. J., et al. (2018). Species-wide variation in shoot nitrate concentration, and genetic loci controlling nitrate, phosphorus and potassium accumulation in Brassica napus L. *Front. Plant Sci.* 9, 1487. doi: 10.3389/fpls.2018.01487.

Andersson, J., Wentworth, M., Walters, R. G., Howard, C. A., Ruban, A. V., Horton, P., et al. (2003). Absence of the Lhcb1 and Lhcb2 proteins of the light-harvesting complex of photosystem II—effects on photosynthesis, grana stacking and fitness. *Plant J.* 35, 350–361. doi: 10.1046/j.1365-313x.2003.01811.x.

Basu, U., Bajaj, D., Sharma, A., Malik, N., Daware, A., Narnoliya, L., et al. (2019). Genetic dissection of photosynthetic efficiency traits for enhancing seed yield in chickpea. *Plant Cell Environ.* 42, 158–173. doi: 10.1111/pce.13319.

Bazakos, C., Hanemian, M., Trontin, C., Jimenez-Gomez, J. M., and Loudet, O. (2017). New strategies and tools in quantitative genetics: how to go from the phenotype to the genotype. *Annu. Rev. Plant Biol.* 68, 435–455. doi: 10.1146/annurev-arplant-042916-040820.

Bernfur, K., Rutsdottir, G., and Emanuelsson, C. (2017). The chloroplast-localized small heat shock protein Hsp21 associates with the thylakoid membranes in heat-stressed plants. *Protein Sci.* 26, 1773–1784. doi: 10.1002/pro.3213.

Brock, A., Brandt, W., and Drager, B. (2008). The functional divergence of short-chain dehydrogenases involved in tropinone reduction. *Plant J.* 54, 388–401. doi: 10.1111/j.1365-313X.2008.03422.x.

Chen, W., Gong, L., Guo, Z., Wang, W., Zhang, H., Liu, X., et al. (2013). A novel integrated method for large-scale detection, identification, and quantification of widely targeted metabolites: application in the study of rice metabolomics. *Mol. Plant* 6, 1769–1780. doi: 10.1093/mp/sst080.

Cheng, T., Hu, L., Wang, P., Yang, X., Peng, Y., Lu, Y., et al. (2018). Carbon monoxide potentiates high temperature-induced nicotine biosynthesis in tobacco. *Int. J. Mol. Sci.* 19, 188. doi: 10.3390/ijms19010188.

Cheung, F., Trick, M., Drou, N., Lim, Y. P., Park, J. Y., Kwon, S. J., et al. (2009). Comparative analysis between homoeologous genome segments of Brassica napus and its progenitor species reveals extensive sequence-level divergence. *Plant Cell.* 21, 1912–1928. doi: 10.1105/tpc.108.060376.

Choudhury, F. K., Rivero, R. M., Blumwald, E., and Mittler, R. (2017). Reactive oxygen species, abiotic stress and stress combination. *Plant J.* 90, 856–867. doi: 10.1111/tpj.13299.

Cong, R. H., Zhang, Z., and Lu, J. W. (2019). Climate impacts on yield of winter oilseed rape in different growth regions of the Yangtze River Basin. *Chin. J. Oil Crop Sci.* 41, 894–903. doi: 10.19802/j.issn.1007-9084.2019046

Dahal, K., Gadapati, W., Savitch, L. V., Singh, J., and Huner, N. P. (2012). Cold acclimation and BnCBF17-over-expression enhance photosynthetic performance and energy conversion efficiency during long-term growth of Brassica napus under elevated CO2 conditions. *Planta* 236, 1639–1652. doi: 10.1007/s00425-012-1710-2.

De Miguel, M., Cabezas, J. A., De Maria, N., Sanchez-Gomez, D., Guevara, M. A., Velez, M. D., et al. (2014). Genetic control of functional traits related to photosynthesis and water use efficiency in Pinus pinaster Ait. drought response: integration of genome annotation, allele association and QTL detection for candidate gene identification. *BMC Genomics* 15, 464. doi: 10.1186/1471-2164-15-464.

De Porcellinis, A. J., Norgaard, H., Brey, L. M. F., Erstad, S. M., Jones, P. R., Heazlewood, J. L., et al. (2018). Overexpression of bifunctional fructose-1,6-bisphosphatase/sedoheptulose-1,7-bisphosphatase leads to enhanced photosynthesis and global reprogramming of carbon metabolism in Synechococcus sp. PCC 7002. *Metab. Eng.* 47, 170–183. doi: 10.1016/j.ymben.2018.03.001.

Ding, C.-K., Wang, C. Y., Gross, K. C., and Smith, D. L. (2001). Reduction of chilling injury and transcript accumulation of heat shock proteins in tomato fruit by methyl jasmonate and methyl salicylate. *Plant Sci.* 161, 0–1159. doi: 10.1016/S0168-9452(01)00521-0

Duggal, P., Gillanders, E. M., Holmes, T. N., and Bailey-Wilson, J. E. (2008). Establishing an adjusted p-value threshold to control the family-wide type 1 error in genome wide association studies. *BMC Genomics* 9, 516. doi: 10.1186/1471-2164-9-516.

Evans, J. R. (2013). Improving photosynthesis. *Plant Physiol.* 162, 1780–1793. doi: 10.1104/pp.113.219006.

Feng, L., Wang, K., Li, Y., Tan, Y., Kong, J., Li, H., et al. (2007). Overexpression of SBPase enhances photosynthesis against high temperature stress in transgenic rice plants. *Plant Cell Rep.* 26, 1635–1646. doi: 10.1007/s00299-006-0299-y.

Fu, A., He, Z., Cho, H. S., Lima, A., Buchanan, B. B., and Luan, S. (2007). A chloroplast cyclophilin functions in the assembly and maintenance of photosystem II in Arabidopsis thaliana. *Proc. Natl. Acad. Sci. U. S. A.* 104, 15947–15952. doi: 10.1073/pnas.0707851104.

Gabriel, L. T., Michel, H., and Francois, O. (2010). The chloroplastic lipocalin AtCHL prevents lipid peroxidation and protects Arabidopsis against oxidative stress. *Plant J.* 60, 691–702. doi: 10.1111/j.1365-313X.2009.03991.x.

Ganeteg, U., Kulheim, C., Andersson, J., and Jansson, S. (2004). Is each light-harvesting complex protein important for plant fitness? *Plant Physiol.* 134, 502–509. doi: 10.1104/pp.103.033324.

Ge, Y., Wang, T., Wang, N., Wang, Z., Liang, C., Ramchiary, N., et al. (2012). Genetic mapping and localization of quantitative trait loci for chlorophyll content in Chinese cabbage (Brassica rapa ssp. pekinensis). *Sci. Horticult.* 147, 42–48. doi: 10.1016/j.scienta.2012.09.004.

Gupta, K., Sengupta, A., Chakraborty, M., and Gupta, B. (2016). Hydrogen peroxide and polyamines act as double edged swords in plant abiotic stress responses. *Front. Plant Sci.* 7, 1343. doi: 10.3389/fpls.2016.01343.

Hara, M., and Kurita, I. (2014). The natural alkaloid sanguinarine promotes the expression of heat shock protein genes in Arabidopsis. *Acta Physiol. Plant.* 36, 3337–3343. doi: 10.1007/s11738-014-1681-y.

Harper, A. L., Trick, M., Higgins, J., Fraser, F., Clissold, L., Wells, R., et al. (2012). Associative transcriptomics of traits in the polyploid crop species Brassica napus. *Nat. Biotechnol.* 30, 798–802. doi: 10.1038/nbt.2302.

Harper, A. L., Mckinney, L. V., Nielsen, L. R., Havlickova, L., Li, Y., Trick, M., et al. (2016a). Molecular markers for tolerance of European ash (Fraxinus excelsior) to dieback disease identified using Associative Transcriptomics. *Sci. Rep.* 6, 19335. doi: 10.1038/srep19335.

Harper, A. L., Trick, M., He, Z., Clissold, L., Fellgett, A., Griffiths, S., et al. (2016b). Genome distribution of differential homoeologue contributions to leaf gene expression in bread wheat. *Plant Biotechnol. J.* 14, 1207–1214. doi: 10.1111/pbi.12486.

Havlickova, L., He, Z., Wang, L., Langer, S., Harper, A. L., Kaur, H., et al. (2018). Validation of an updated Associative Transcriptomics platform for the polyploid crop species Brassica napus by dissection of the genetic architecture of erucic acid and tocopherol isoform variation in seeds. *Plant J.* 93, 181–192. doi: 10.1111/tpj.13767.

He, Z., Cheng, F., Li, Y., Wang, X., Parkin, I. A., Chalhoub, B., et al. (2015). Construction of Brassica A and C genome-based ordered pan-transcriptomes for use in rapeseed genomic research. *Data Brief* 4, 357–362. doi: 10.1016/j.dib.2015.06.016.

Hejna, O., Havlickova, L., He, Z., Bancroft, I., and Curn, V. (2019). Analysing the genetic architecture of clubroot resistance variation in Brassica napus by associative transcriptomics. *Mol. Breed.* 39, 112. doi: 10.1007/s11032-019-1021-4.

Higgins, J., Magusin, A., Trick, M., Fraser, F., and Bancroft, I. (2012). Use of mRNA-seq to discriminate contributions to the transcriptome from the constituent genomes of the polyploid crop species Brassica napus. *BMC Genomics* 13, 247. doi: 10.1186/1471-2164-13-247.

Hincha, D. K., Hofner, R., Schwab, K. B., Heber, U., and Schmitt, J. M. (1987). Membrane rupture is the common cause of damage to chloroplast membranes in leaves injured by freezing or excessive wilting. *Plant Physiol.* 83, 251–253. doi: 10.1104/pp.83.2.251.

Jha, U. C., Bohra, A., and Jha, R. (2017). Breeding approaches and genomics technologies to increase crop yield under low-temperature stress. *Plant Cell Rep.* 36, 1–35. doi: 10.1007/s00299-016-2073-0.

Jin, H., Liu, B., Luo, L., Feng, D., Wang, P., Liu, J., et al. (2014). HYPERSENSITIVE TO HIGH LIGHT1 interacts with LOW QUANTUM YIELD OF PHOTOSYSTEM II1 and functions in protection of photosystem II from photodamage in Arabidopsis. *Plant Cell.* 26, 1213–1229. doi: 10.1105/tpc.113.122424.

Ju, X., and Li, Z. (2012). Study of different types of rape (Brassica L.) cultivars (lines) relationship between photosynthetic physiological indices and yield. *J. Anhui Agri. Sci.* 40, 11213–11215. doi: 10.13989/j.cnki.0517-6611.2012.22.106.

Kaler, A. S., and Purcell, L. C. (2019). Estimation of a significance threshold for genome-wide association studies. *BMC Genomics* 20, 20–33. doi: 10.1186/s12864-019-5992-7

Koprivova, A., Harper, A. L., Trick, M., Bancroft, I., and Kopriva, S. (2014). Dissection of the control of anion homeostasis by associative transcriptomics in Brassica napus. *Plant Physiol.* 166, 442–450. doi: 10.1104/pp.114.239947.

Kumar, A., Li, C., and Portis, A. R. Jr. (2009). Arabidopsis thaliana expressing a thermostable chimeric Rubisco activase exhibits enhanced growth and higher rates of photosynthesis at moderately high temperatures. *Photosynth. Res.* 100, 143–153. doi: 10.1007/s11120-009-9438-y.

Kurek, I., Chang, T. K., Bertain, S. M., Madrigal, A., Liu, L., Lassner, M. W., et al. (2007). Enhanced Thermostability of Arabidopsis Rubisco activase improves photosynthesis and growth rates under moderate heat stress. *Plant Cell.* 19, 3230–3241. doi: 10.1105/tpc.107.054171.

Lawson, T., Kramer, D. M., and Raines, C. A. (2012). Improving yield by exploiting mechanisms underlying natural variation of photosynthesis. *Curr. Opin. Biotechnol.* 23, 215–220. doi: 10.1016/j.copbio.2011.12.012.

Leister, D. (2019). Genetic engineering, synthetic biology and the light reactions of photosynthesis. *Plant Physiol.* 179, 778–793. doi: 10.1104/pp.18.00360.

Li, H., Wang, G., Zheng, Q., Li, B., Jing, R., and Li, Z. (2014). Genetic analysis of biomass and photosynthetic parameters in wheat grown in different light intensities. *J. Integr. Plant Biol.* 56, 594–604. doi: 10.1111/jipb.12174.

Li, H., Yang, Y., Zhang, H., Chu, S., Zhang, X., Yin, D., et al. (2016). A Genetic Relationship between Phosphorus Efficiency and Photosynthetic Traits in Soybean As Revealed by QTL Analysis Using a High-Density Genetic Map. *Front. Plant Sci.* 7, 924. doi: 10.3389/fpls.2016.00924.

Liao, G., and Guan, C. (2001). Effect of seeding date on yield characteristics of different rapeseed (Brassica napus) genotypes. *Chin. J. Appl. Ecol.*, 12 (6), 853–858. doi: 10.13287/j.1001-9332.2001.0203

Lipka, A. E., Tian, F., Wang, Q., Peiffer, J., Li, M., Bradbury, P. J., et al. (2012). GAPIT: genome association and prediction integrated tool. *Bioinformatics* 28, 2397–2399. doi: 10.1093/bioinformatics/bts444.

Liu, R., Xu, Y. H., Jiang, S. C., Lu, K., Lu, Y. F., Feng, X. J., et al. (2013). Light-harvesting chlorophyll a/b-binding proteins, positively involved in abscisic acid signalling, require a transcription repressor, WRKY40, to balance their function. *J. Exp. Bot.* 64, 5443–5456. doi: 10.1093/jxb/ert307.

Liu, X., Fan, Y., Mak, M., Babla, M., Holford, P., Wang, F., et al. (2017). QTLs for stomatal and photosynthetic traits related to salinity tolerance in barley. *BMC Genomics* 18, 9. doi: 10.1186/s12864-016-3380-0.

Liu, J., Lu, Y., Hua, W., and Last, R. L. (2019a). A new light on Photosystem II maintenance in oxygenic photosynthesis. *Front. Plant Sci.* 10, 975. doi: 10.3389/fpls.2019.00975.

Liu, M., Zhang, S., Hu, J., Sun, W., Padilla, J., He, Y., et al. (2019b). Phosphorylation-guarded light-harvesting complex II contributes to broad-spectrum blast resistance in rice. *Proc. Natl. Acad. Sci. U. S. A.* 116, 17572–17577. doi: 10.1073/pnas.1905123116.

Livak, K. J., and Schmittgen, T. D. (2001). Analysis of relative gene expression data using real-time quantitative PCR and the 2(-Delta Delta C(T)) Method. *Methods* 25, 402–408. doi: 10.1006/meth.2001.1262.

Long, S. P., Zhu, X. G., Naidu, S. L., and Ort, D. R. (2006). Can improvement in photosynthesis increase crop yields? *Plant Cell Environ.* 29, 315–330. doi: 10.1111/j.1365-3040.2005.01493.x.

Lu, G., Harper, A. L., Trick, M., Morgan, C., Fraser, F., O'neill, C., et al. (2014). Associative transcriptomics study dissects the genetic architecture of seed glucosinolate content in Brassica napus. *DNA Res.* 21, 613–625. doi: 10.1093/dnares/dsu024.

Luo, T., Zhang, J., Khan, M. N., Liu, J., Xu, Z., and Hu, L. (2018). Temperature variation caused by sowing dates significantly affects floral initiation and floral bud differentiation processes in rapeseed (Brassica napus L.). *Plant Sci.* 271, 40–51. doi: 10.1016/j.plantsci.2018.03.004.

Luo, T., Xian, M., Zhang, C., Zhang, C., Hu, L., and Xu, Z. (2019). Associating transcriptional regulation for rapid germination of rapeseed (Brassica napus L.) under low temperature stress through weighted gene co-expression network analysis. *Sci. Rep.* 9, 55–70. doi: 10.1038/s41598-018-37099-0

Lv, Y., Guo, Z., Li, X., Ye, H., Li, X., and Xiong, L. (2016). New insights into the genetic basis of natural chilling and cold shock tolerance in rice by genome-wide association analysis. *Plant Cell Environ.* 39, 556–570. doi: 10.1111/pce.12635.

Lv, Y., Yang, M., Hu, D., Yang, Z., Ma, S., Li, X., et al. (2017). The OsMYB30 Transcription Factor Suppresses Cold Tolerance by Interacting with a JAZ

Protein and Suppressing β-Amylase Expression. *Plant Physiol.* 173, 1475. doi: 10.1104/pp.16.01725.

Matsuoka, E., Matsubara, T., Takahashi, I., Murano, H., and Hara, M. (2016). The isoquinoline alkaloid sanguinarine which inhibits chaperone activity enhances the production of heat shock proteins in Arabidopsis. *Plant Biotechnol. (Tokyo)* 33, 409–413. doi: 10.5511/plantbiotechnology.16.1001a.

Miller, C. N., Harper, A. L., Trick, M., Werner, P., Waldron, K., and Bancroft, I. (2016). Elucidation of the genetic basis of variation for stem strength characteristics in bread wheat by Associative Transcriptomics. *BMC Genomics* 17, 500. doi: 10.1186/s12864-016-2775-2.

Miller, C. N., Harper, A. L., Trick, M., Wellner, N., Werner, P., Waldron, K. W., et al. (2018). Dissecting the complex regulation of lodging resistance in Brassica napus. *Mol. Breed.* 38, 30. doi: 10.1007/s11032-018-0781-6.

Mishra, A., Heyer, A. G., and Mishra, K. B. (2014). Chlorophyll fluorescence emission can screen cold tolerance of cold acclimated Arabidopsis thaliana accessions. *Plant Methods* 10, 38. doi: 10.1186/1746-4811-10-38.

Miyagawa, Y., Tamoi, M., and Shigeoka, S. (2001). Overexpression of a cyanobacterial fructose-1,6-/sedoheptulose-1,7-bisphosphatase in tobacco enhances photosynthesis and growth. *Nat. Biotechnol.* 19, 965–969. doi: 10.1038/nbt1001-965.

Morsy, M. R., Almutairi, A. M., Gibbons, J., Yun, S. J., and De Los Reyes, B. G. (2005). The OsLti6 genes encoding low-molecular-weight membrane proteins are differentially expressed in rice cultivars with contrasting sensitivity to low temperature. *Gene* 344, 171–180. doi: 10.1016/j.gene.2004.09.033.

Ning, J., Li, X., Hicks, L. M., and Xiong, L. (2010). A Raf-like MAPKKK gene DSM1 mediates drought resistance through reactive oxygen species scavenging in rice. *Plant Physiol.* 152, 876–890. doi: 10.1104/pp.109.149856.

Nishiyama, Y., Yamamoto, H., Allakhverdiev, S., Inaba, M., Yokota, A., and Murata, N. (2014). Oxidative stress inhibits the repair of photodamage to the photosynthetic machinery. *EMBO J.* 20, 5587–5594. doi: 10.1093/emboj/20.20.5587.

Novillo, F., Alonso, J. M., Ecker, J. R., and Salinas, J. (2004). CBF2/DREB1C is a negative regulator of CBF1/DREB1B and CBF3/DREB1A expression and plays a central role in stress tolerance in Arabidopsis. *Proc. Natl. Acad. Sci. U. S. A.* 101, 3985–3990. doi: 10.1073/pnas.0303029101.

Novillo, F., Medina, J., Rodriguez-Franco, M., Neuhaus, G., and Salinas, J. (2012). Genetic analysis reveals a complex regulatory network modulating CBF gene expression and Arabidopsis response to abiotic stress. *J. Exp. Bot.* 63, 293–304. doi: 10.1093/jxb/err279.

O'neill, C. M., Lu, X., Calderwood, A., Tudor, E. H., and Penfield, S. (2019). Vernalization and floral transition in autumn drive winter annual life history in oilseed rape. *Curr. Biol.* 29, 4300–4306. doi: 10.1016/j.cub.2019.10.051

Oakley, C. G., Savage, L., Lotz, S., Larson, G. R., Thomashow, M. F., Kramer, D. M., et al. (2018). Genetic basis of photosynthetic responses to cold in two locally adapted populations of Arabidopsis thaliana. *J. Exp. Bot.* 69, 699–709. doi: 10.1093/jxb/erx437.

Ozer, H. (2003). Sowing date and nitrogen rate effects on growth, yield and yield components of two summer rapeseed cultivars. *Eur. J. Agron.* 19, 453–463. doi: 10.1016/S1161-0301(02)00136-3.

Prado, S. A., Cabrera-Bosquet, L., Grau, A., Coupel-Ledru, A., Millet, E. J., Welcker, C., et al. (2017). Phenomics allows identification of genomic regions affecting maize stomatal conductance with conditional effects of water deficit and evaporative demand. *Plant Cell Environ.* 41 (2), 314–326. doi: 10.1111/pce.13083

Sabehat, A., Weiss, D., and Lurie, S. (1996). The correlation between heat-shock protein accumulation and persistence and chilling tolerance in tomato fruit. *Plant Physiol.* 110, 531–537. doi: 10.1104/pp.110.2.531.

Sage, R., and Kubien, D. (2007). The temperature response of C 3 and C 4 photosynthesis. *Plant Cell Environ.* 30, 1086–1106. doi: 10.1111/j.1365-3040.2007.01682.x.

Sainz, M., Diaz, P., Monza, J., and Borsani, O. (2010). Heat stress results in loss of chloroplast Cu/Zn superoxide dismutase and increased damage to Photosystem II in combined drought-heat stressed Lotus japonicus. *Physiol. Plant* 140, 46–56. doi: 10.1111/j.1399-3054.2010.01383.x.

Savitch, L. V., Allard, G., Seki, M., Robert, L. S., Tinker, N. A., Huner, N. P., et al. (2005). The effect of overexpression of two Brassica CBF/DREB1-like transcription factors on photosynthetic capacity and freezing tolerance in Brassica napus. *Plant Cell Physiol.* 46, 1525–1539. doi: 10.1093/pcp/pci165.

Schlager, S., and Drager, B. (2016). Exploiting plant alkaloids. *Curr. Opin. Biotechnol.* 37, 155–164. doi: 10.1016/j.copbio.2015.12.003.

Schuster, T. M., Setaro, S. D., and Kron, K. A. (2013). Age estimates for the buckwheat family Polygonaceae based on sequence data calibrated by fossils and with a focus on the amphi-Pacific Muehlenbeckia. *PloS One* 8, e61261. doi: 10.1371/journal.pone.0061261.

Selmar, D., and Kleinwachter, M. (2013). Stress enhances the synthesis of secondary plant products: the impact of stress-related over-reduction on the accumulation of natural products. *Plant Cell Physiol.* 54, 817–826. doi: 10.1093/pcp/pct054.

Shen, B. R., Wang, L. M., Lin, X. L., Yao, Z., Xu, H. W., Zhu, C. H., et al. (2019). Engineering a new chloroplastic photorespiratory bypass to increase photosynthetic efficiency and productivity in rice. *Mol. Plant* 12, 199–214. doi: 10.1016/j.molp.2018.11.013.

Sirpio, S., Khrouchtchova, A., Allahverdiyeva, Y., Hansson, M., Fristedt, R., Vener, A. V., et al. (2008). AtCYP38 ensures early biogenesis, correct assembly and sustenance of photosystem II. *Plant J.* 55, 639–651. doi: 10.1111/j.1365-313X.2008.03532.x.

Srivastava, N. K., and Srivastava, A. K. (2010). Influence of some heavy metals on growth, alkaloid content and composition in Catharanthus roseus L. *Indian J. Pharm. Sci.* 72, 775–778. doi: 10.4103/0250-474X.84592.

Steponkus, P. L., Lynch, D. V., Uemura, M., Heber, U., and Pearce, R. S. (1990). The Influence of Cold Acclimation on the Lipid Composition and Cryobehaviour of the Plasma Membrane of Isolated Rye Protoplasts [and Discussion]. *Phil. Trans. R. Soc Lond. B.* 326, 571–583. doi: 10.1098/rstb.1990.0032.

Strzepek, R. F., Boyd, P. W., and Sunda, W. G. (2019). Photosynthetic adaptation to low iron, light, and temperature in Southern Ocean phytoplankton. *Proc. Natl. Acad. Sci. U. S. A.* 116, 4388–4393. doi: 10.1073/pnas.1810886116.

Sun, S. N., Wang, Q., Sun, C. C., Liu, F. J., Bi, H. G., and Ai, X. Z. (2017). Response and adaptation of photosynthesis of cucumber seedlings to high temperature stress. *Ying Yong Sheng Tai Xue Bao* 28, 1603–1610. doi: 10.13287/j.1001-9332.201705.009.

Takahashi, S., Bauwe, H., and Badger, M. (2007). Impairment of the photorespiratory pathway accelerates photoinhibition of photosystem II by suppression of repair but not acceleration of damage processes in Arabidopsis. *Plant Physiol.* 144, 487–494. doi: 10.1104/pp.107.097253.

Thalhammer, A., Hincha, D. K., and Zuther, E. (2014). Measuring freezing tolerance: electrolyte leakage and chlorophyll fluorescence assays. *Methods Mol. Biol.* 1166, 15–24. doi: 10.1007/978-1-4939-0844-8_3.

Thalmann, M., and Santelia, D. (2017). Starch as a determinant of plant fitness under abiotic stress. *New Phytol.* 214, 943–951. doi: 10.1111/nph.14491.

Tian, Z., Ji, Y. H., Sun, L. X., Xu, X. L., Fan, D. L., Zhong, H. L., et al. (2018). Changes in production potentials of rapeseed in the Yangtze River Basin of China under climate change: A multi-model ensemble approach. *J. Geogr. Sci.* 28, 1700–1714. doi: 10.1007/s11442-018-1538-1

Tonfack, L., Moummou, H., Latché, A., Youmbi, E., Benichou, M., Pech, J.-C., et al. (2011). The plant SDR superfamily: Involvement in primary and secondary metabolism. *Curr. Top. Plant Biol.* 12, 41–53. doi: 10.1186/1471-2229-12-219.

Urban, M. O., Klima, M., Vitamvas, P., Vasek, J., Hilgert-Delgado, A. A., and Kucera, V. (2013). Significant relationships among frost tolerance and net photosynthetic rate, water use efficiency and dehydrin accumulation in cold-treated winter oilseed rapes. *J. Plant Physiol.* 170, 1600–1608. doi: 10.1016/j.jplph.2013.07.012.

Valerio, C., Costa, A., Marri, L., Issakidis-Bourguet, E., Pupillo, P., Trost, P., et al. (2011). Thioredoxin-regulated beta-amylase (BAM1) triggers diurnal starch degradation in guard cells, and in mesophyll cells under osmotic stress. *J. Exp. Bot.* 62, 545–555. doi: 10.1093/jxb/erq288.

Voll, L. M., Jamai, A., Renne, P., Voll, H., Mcclung, C. R., and Weber, A. P. (2006). The photorespiratory Arabidopsis shm1 mutant is deficient in SHM1. *Plant Physiol.* 140, 59–66. doi: 10.1104/pp.105.071399.

Von Caemmerer, S., Hendrickson, L., Quinn, V., Vella, N., Millgate, A. G., and Furbank, R. T. (2005). Reductions of Rubisco activase by antisense RNA in the C4 plant Flaveria bidentis reduces Rubisco carbamylation and leaf photosynthesis. *Plant Physiol.* 137, 747–755. doi: 10.1104/pp.104.056077.

Wanasundara, P., Mcintosh, T., Perera, S., Withana-Gamage, T., and Mitra, P. (2016). Canola/rapeseed protein-functionality and nutrition. *OCL* 23, D407. doi: 10.1051/ocl/2016028.

Wang, J., Jian, H., Wei, L., Qu, C., Xu, X., Lu, K., et al. (2015). Genome-wide analysis of seed acid detergent lignin (ADL) and hull content in rapeseed (Brassica napus L.). *PloS One* 10, e0145045. doi: 10.1371/journal.pone.0145045.

Wood, I. P., Pearson, B. M., Garcia-Gutierrez, E., Havlickova, L., He, Z., and Harper, A. L. (2017). Carbohydrate microarrays and their use for the identification of molecular markers for plant cell wall composition. *Proc. Natl. Acad. Sci. U. S. A.* 114, 6860–6865. doi: 10.1073/pnas.1619033114.

Xu, Y. H., Liu, R., Yan, L., Liu, Z. Q., Jiang, S. C., Shen, Y. Y., et al. (2012). Light-harvesting chlorophyll a/b-binding proteins are required for stomatal response to abscisic acid in Arabidopsis. *J. Exp. Bot.* 63, 1095–1106. doi: 10.1093/jxb/err315.

Yan, X., Qu, C., Li, J., Chen, L., and Liu, L. (2015). QTL analysis of leaf photosynthesis rate and related physiological traits in in brassica napus. *Sci. Agric. Sin.* 14, 2095–3119. doi: 10.1016/S2095-3119(14)60958-8.

Yan, L., Tariq, S., Cheng, Y., Lü, Y., Zhang, X. K., and Zou, X. L. (2019). Physiological and molecular responses to cold stress in rapeseed (Brassica napus L.). *J. Integr. Agricult.* 18, 2742–2752. doi: 10.1016/S2095-3119(18)62147-1

Yin, Z., Meng, F., Song, H., Wang, X., Xu, X., and Yu, D. (2010). Expression quantitative trait loci analysis of two genes encoding rubisco activase in soybean. *Plant Physiol.* 152, 1625–1637. doi: 10.1104/pp.109.148312.

Zhang, L., Ding, R., Chai, Y., Bonfill, M., Moyano, E., Oksman-Caldentey, K.-M., et al. (2004). Engineering tropane biosynthetic pathway in Hyoscyamus niger hairy root cultures. *Proc. Natl. Acad. Sci. U. S. A.* 101, 6786. doi: 10.1073/pnas.0401391101.

Zhang, X. R., Henriques, R., Lin, S. S., Niu, Q. W., and Chua, N. H. (2006). Agrobacterium-mediated transformation of Arabidopsis thaliana using the floral dip method. *Nat. Protoc.* 1, 641–646. doi: 10.1038/nprot.2006.97.

Zhang, X., Wang, L., Meng, H., Wen, H., Fan, Y., and Zhao, J. (2011). Maize ABP9 enhances tolerance to multiple stresses in transgenic Arabidopsis by modulating ABA signaling and cellular levels of reactive oxygen species. *Plant Mol. Biol.* 75, 365–378. doi: 10.1007/s11103-011-9732-x.

Zhang, S. J., Li, L., and Zhang, C. L. (2012). Effects of sowing date and planting density on the seed yield and oil content of winter oilseed rape. *Ying Yong Sheng Tai Xue Bao* 23, 1326–1332. doi: 10.13287/j.1001-9332.2012.0179.

Zhang, X., Feng, L., Yang, T., Xu, Z., and Hu, L. (2015). Effects of Chilling Stress on Physiological Characteristics of Rapeseed Seedlings in Winter. *Plant Physiol. J.* 51, 737–746. doi: 10.13592/j.cnki.ppj.2014.0411.

Zhang, Y., Zhang, D., Yu, H., Lin, B., Fu, Y., and Hua, S. (2016). Floral Initiation in Response to Planting Date Reveals the Key Role of Floral Meristem Differentiation Prior to Budding in Canola (Brassica napus L.). *Front. Plant Sci.* 7, 1369. doi: 10.3389/fpls.2016.01369.

Zhang, Y., Zhao, X., Guan, Z., Wang, X., Hou, J., and Tian, J. (2017a). A review on photosynthetic physiological research and high photosynthetic efficiency breeding of Brassica napus. *Chin. Agric. Sci. Bull.* 33, 44–54.

Zhang, Z., Li, J., Pan, Y., Li, J., Zhou, L., Shi, H., et al. (2017b). Natural variation in CTB4a enhances rice adaptation to cold habitats. *Nat. Commun.* 8, 14788. doi: 10.1038/ncomms14788.

Zhong, L., Zhou, W., Wang, H., Ding, S., Lu, Q., Wen, X., et al. (2013). Chloroplast small heat shock protein HSP21 interacts with plastid nucleoid protein pTAC5 and is essential for chloroplast development in Arabidopsis under heat stress. *Plant Cell.* 25, 2925–2943. doi: 10.1105/tpc.113.111229.

Conflict of Interest: The authors declare that the research was conducted in the absence of any commercial or financial relationships that could be construed as a potential conflict of interest.

Copyright © 2020 Huang, Hussain, Luo, Xu, Zeng, Havlickova, Bancroft, Tian, Zhang, Cheng, Zou, Lu and Lv. This is an open-access article distributed under the terms of the Creative Commons Attribution License (CC BY). The use, distribution or reproduction in other forums is permitted, provided the original author(s) and the copyright owner(s) are credited and that the original publication in this journal is cited, in accordance with accepted academic practice. No use, distribution or reproduction is permitted which does not comply with these terms.

frontiers in Plant Science

ORIGINAL RESEARCH
published: 09 July 2020
doi: 10.3389/fpls.2020.01049

Check for updates

OPEN ACCESS

Edited by:
Raul Antonio Sperotto, Universidade do Vale do Taquari, Brazil

Reviewed by:
Kun Yan, Yantai Institute of Coastal Zone Research (CAS), China
Marek Zivcak, Slovak University of Agriculture, Slovakia
Tsonko Tsonev, Institute of Plant Physiology and Genetics (BAS), Bulgaria

***Correspondence:**
Ana I. Ribeiro-Barros
aribeiro@isa.ulisboa.pt
Fábio M. DaMatta
fdamatta@ufv.br
José C. Ramalho
cochichor@mail.telepac.pt; cochichor@isa.ulisboa.pt

[†]These authors have contributed equally to this work

Specialty section:
This article was submitted to Plant Abiotic Stress, a section of the journal Frontiers in Plant Science

Received: *28 March 2020*
Accepted: *25 June 2020*
Published: *09 July 2020*

Citation:
Dubberstein D, Lidon FC, Rodrigues AP, Semedo JN, Marques I, Rodrigues WP, Gouveia D, Armengaud J, Semedo MC, Martins S, Simões-Costa MC, Moura I, Pais IP, Scotti-Campos P, Partelli FL, Campostrini E, Ribeiro-Barros AI, DaMatta FM and Ramalho JC (2020) Resilient and Sensitive Key Points of the Photosynthetic Machinery of Coffea spp. to the Single and Superimposed Exposure to Severe Drought and Heat Stresses. Front. Plant Sci. 11:1049. doi: 10.3389/fpls.2020.01049

Resilient and Sensitive Key Points of the Photosynthetic Machinery of *Coffea* spp. to the Single and Superimposed Exposure to Severe Drought and Heat Stresses

Danielly Dubberstein [1,2†], ***Fernando C. Lidon*** [3†], ***Ana P. Rodrigues*** [1†], ***José N. Semedo*** [3,4†], ***Isabel Marques*** [1†], ***Weverton P. Rodrigues*** [5,6], ***Duarte Gouveia*** [7], ***Jean Armengaud*** [7], ***Magda C. Semedo*** [3,8], ***Sónia Martins*** [3,8], ***Maria C. Simões-Costa*** [1], ***I. Moura*** [1], ***Isabel P. Pais*** [3,4], ***Paula Scotti-Campos*** [3,4], ***Fábio L. Partelli*** [2], ***Eliemar Campostrini*** [5], ***Ana I. Ribeiro-Barros*** [1,3*], ***Fábio M. DaMatta*** [9*] ***and José C. Ramalho*** [1,3*]

[1] *PlantStress & Biodiversity Lab, Centro de Estudos Florestais (CEF), Dept. Recursos Naturais, Ambiente e Território (DRAT), Instituto Superior de Agronomia (ISA), Universidade de Lisboa (ULisboa), Lisbon, Portugal,* [2] *Centro Univ. Norte do Espírito Santo (CEUNES), Dept. Ciências Agrárias e Biológicas (DCAB), Univ. Federal Espírito Santo (UFES), São Mateus, Brazil,* [3] *Unidade de Geobiociências, Geoengenharias e Geotecnologias (GeoBioTec), Faculdade de Ciências e Tecnologia (FCT), Universidade NOVA de Lisboa (UNL), Caparica, Portugal,* [4] *Unid. Investigação em Biotecnologia e Recursos Genéticos, Instituto Nacional de Investigação Agrária e Veterinária, I.P. (INIAV), Oeiras, Portugal,* [5] *Setor Fisiologia Vegetal, Centro de Ciências e Tecnologias Agropecuárias, Univ. Estadual Norte Fluminense (UENF), Darcy Ribeiro, Brazil,* [6] *Centro de Ciências Agrárias, Naturais e Letras, Universidade Estadual da Região Tocantina do Maranhão, Estreito, Brazil,* [7] *Laboratoire Innovations technologiques pour la Détection et le Diagnostic (Li2D), Service de Pharmacologie et Immunoanalyse (SPI), CEA, INRA, Bagnols-sur-Cèze, France,* [8] *Área Departamental de Engenharia Química, Instituto Superior de Engenharia de Lisboa, Instituto Politécnico de Lisboa, Lisboa, Portugal,* [9] *Dept. Biologia Vegetal, Univ. Federal Viçosa (UFV), Viçosa, Brazil*

This study unveils the single and combined drought and heat impacts on the photosynthetic performance of *Coffea arabica* cv. Icatu and *C. canephora* cv. Conilon Clone 153 (CL153). Well-watered (WW) potted plants were gradually submitted to severe water deficit (SWD) along 20 days under adequate temperature (25/20°C, day/night), and thereafter exposed to a gradual temperature rise up to 42/30°C, followed by a 14-day water and temperature recovery. Single drought affected all gas exchanges (including A_{max}) and most fluorescence parameters in both genotypes. However, Icatu maintained F_v/F_m and RuBisCO activity, and reinforced electron transport rates, carrier contents, and proton gradient regulation (PGR5) and chloroplast NADH dehydrogenase-like (NDH) complex proteins abundance. This suggested negligible non-stomatal limitations of photosynthesis that were accompanied by a triggering of protective cyclic electron transport (CEF) involving both photosystems (PSs). These findings contrasted with declines in RuBisCO and PSs activities, and cytochromes (b_{559}, f, b_{563}) contents in CL153. Remarkable heat tolerance in potential photosynthetic functioning was detected in WW plants of both genotypes (up to 37/28°C or 39/30°C), likely associated with CEF in Icatu. Yet, at 42/30°C the tolerance limit was exceeded. Reduced A_{max} and increased C_i

values reflected non-stomatal limitations of photosynthesis, agreeing with impairments in energy capture (F_0 rise), PSII photochemical efficiency, and RuBisCO and Ru5PK activities. In contrast to PSs activities and electron carrier contents, enzyme activities were highly heat sensitive. Until 37/28°C, stresses interaction was largely absent, and drought played the major role in constraining photosynthesis functioning. Harsher conditions (SWD, 42/30°C) exacerbated impairments to PSs, enzymes, and electron carriers, but uncontrolled energy dissipation was mitigated by photoprotective mechanisms. Most parameters recovered fully between 4 and 14 days after stress relief in both genotypes, although some aftereffects persisted in SWD plants. Icatu was more drought tolerant, with WW and SWD plants usually showing a faster and/or greater recovery than CL153. Heat affected both genotypes mostly at 42/30°C, especially in SWD and Icatu plants. Overall, photochemical components were highly tolerant to heat and to stress interaction in contrast to enzymes that deserve special attention by breeding programs to increase coffee sustainability in climate change scenarios.

Keywords: acclimation, climate change, coffee, drought, heat, photoinhibition, photosynthesis

INTRODUCTION

The global CO_2 emissions have been increased steadily from the industrial revolution onwards, from around 280 μL CO_2 L^{-1} until a global atmosphere average of 407.4 in 2018 (NOAA, 2019). Further increases might lead to estimated values between 730 and 1,020 μL CO_2 L^{-1} in 2100 accompanied by a global warming up to 4.8°C (IPCC, 2014). In addition, heat waves and altered inter- and intra-annual precipitation patterns, with periods of prolonged drought to extreme rainfall events, have also been predicted (IPCC, 2014; IPCC, 2018).

Heat and drought stresses, which are major environmental constraints to plant growth and crop productivity, have been associated with decreases in both stomatal conductance (g_s) and net CO_2 assimilation rates (P_n) (Long et al., 2006). These decreases predispose leaves to photoinhibitory damage due to decreased energy use through photosynthesis (Baker and Rosenqvist, 2004; Lambers et al., 2008; Haworth et al., 2018), which can be exacerbated when these stresses are superimposed. As a consequence, growth and productivity of agricultural crops are depressed under these conditions to a greater extent than to each single applied stress (Sehgal et al., 2017; Urban et al., 2018). Additionally, the type and magnitude of plant responses to combined stresses usually differ from the responses triggered by single stress exposure (Mittler, 2006; Sehgal et al., 2017). This might be even more relevant for perennial crops such as coffee, which can have a lifespan up to 30 years (Bunn et al., 2015) or even more.

In particular, drought is the major threat to world agricultural production. Water shortage reduces plant growth, nutrient uptake, photosynthesis, and assimilate partitioning, therefore strongly reducing crop yields (Fahad et al., 2017; Lamaoui et al., 2018). Photosynthesis is a major primary process affected by water constraints (Chaves et al., 2009). Under mild drought, the photosynthetic decline is mostly related to stomatal closure that avoids additional water loss through transpiration. However this also reduces the CO_2 supply to ribulose-1,5-bisphosphate carboxylase/oxygenase (RuBisCO), although with limited impact on photochemistry and photosynthetic capacity (A_{max}). Under more prolonged/severe water constraint, non-stomatal limitations will progressively occur with impairments to several photosynthetic components, namely in pigment pools, photosystems (PSs) functioning, and activity of key enzymes such as RuBisCO (Chaves et al., 2003; Ramalho et al., 2014a; Fahad et al., 2017). Limited photochemical energy use can additionally impose a secondary stress related to oxidative conditions due to the uncontrolled generation of reactive species of oxygen (ROS) and chlorophyll, leading to damages to the photosynthetic apparatus (*e.g.*, D1 protein, lipids, electron transport) (Chaves et al., 2009; Osakabe et al., 2014). Therefore, at the cellular level drought tolerance is often associated with the triggering of photoprotective and antioxidative mechanisms. These include cyclic electron flow (CEF) around PSs and antioxidative molecules (*e.g.*, enzymes, carotenoids) (Chu and Chiu, 2016; Ramalho et al., 2018b; Sun et al., 2018).

High temperature can also cause physiological, biochemical and molecular disturbances, affecting all major physiological processes (Long et al., 2006). As regards to the photosynthetic pathway, heat modifies pigment composition (Hasanuzzaman et al., 2013) while reducing electron transport and RuBisCO activity (Crafts-Brandner and Salvucci, 2000; Haldimann and Feller, 2004). Additionally, under heat the chemical bonds are weakened and membrane lipid bilayer becomes more fluid and destabilized (Wahid et al., 2007; Los and Zinchenko, 2009), thus compromising membrane-based events such as chloroplast light energy capture and electron transport (Scotti-Campos et al., 2019). High temperature further alters gas diffusion throughout the mesophyll (Lambers et al., 2008), and stimulates respiration and photorespiration more than photosynthesis. Finally, heat stress alters hormones and primary and secondary metabolite balance (Wahid et al., 2007), causes protein denaturation and

aggregation as well as ROS overproduction and inhibition of transcription and translation (Wahid et al., 2007; Song et al., 2014; Dusenge et al., 2019), thereby further concurring to depress plant growth and crop yields.

Coffee chain of value is supported by *Coffea. arabica* L. and *Coffea canephora* Pierre ex A. Froehner species, which are responsible for nearly 99% of the global coffee production. Coffee is one of the world's most traded agricultural products, being cropped in approximately 80 tropical countries. It supports the livelihoods of *ca*. 25 million smallholder farmers and *ca*. 100-125 million people in its worldwide chain of value (Osorio, 2002; Semedo et al., 2018; Ramalho et al., 2018a; DaMatta et al., 2019).

The estimated increase of air [CO_2] in the coming years could have a positive impact on mineral balance (Martins et al., 2014), C-assimilation (Rodrigues et al., 2016) and even on productivity (DaMatta et al., 2019), helping the preservation of coffee bean quality under supra-optimal temperatures (Ramalho et al., 2018a) if sufficient water is available. However, a growing concern is related to this crop sustainability given that coffee is cultivated in tropical areas, which are predicted to be strongly impacted by climate change (IPCC, 2018). Indeed, inadequate temperature and water availability are known as the most important environmental constraints for the coffee crop (DaMatta et al., 2018; Ramalho et al., 2018b). In addition, coffee is extensively cropped under full sunlight exposure what can further exacerbate both temperature and drought stresses. Climate change, associated with a greater frequency of extreme events of temperature and drought, is expected to reduce crop yield and sustainability, with likely greater impacts in *C. arabica* that is considered more sensitive to heat than *C. canephora* (DaMatta and Ramalho, 2006; DaMatta et al., 2018). Furthermore, predicted future warming may cause the extinction of at least 60% of all coffee species (Davis et al., 2019).

Coffee plants have a common set of response mechanisms allowing them to cope with single stress events, including high irradiance, drought, cold, and heat (Nunes et al., 1993; Pinheiro et al., 2004; Ramalho et al., 2014b; Martins et al., 2019). Under water shortage, drought-tolerant coffee genotypes reduce g_s to avoid excessive transpiration and trigger antioxidant molecules (DaMatta et al., 2003; Pinheiro et al., 2004; Dias et al., 2007). Regarding heat stress, recent studies showed that coffee can maintain photosynthetic performance up to 37°C, well above what was traditionally assumed (DaMatta et al., 2018). Such tolerance has been shown to be supported by the reinforcement of the antioxidant system (Martins et al., 2016; Rodrigues et al., 2016), and adjustments in the lipid profile of chloroplast membranes (Scotti-Campos et al., 2019). However, the predicted scenarios of climate changes point to future greater exposure to the combination of heat and drought stresses. Therefore, the understanding of the underlying mechanisms by which the coffee plant deals with these single and superimposed stresses is of utmost importance for future crop sustainability. In this context, we conducted an in-depth analysis of plant impacts and responses to drought, heat and their interaction on the photosynthetic performance. Morphological (stomata traits), physiological (gas exchanges, chlorophyll *a* fluorescence), and biochemical (thylakoid electron transport and carriers, enzyme activities, and proteins involved in CEF) traits were evaluated. Our findings provide paramount evidence regarding the functioning of the photosynthetic machinery under harsh heat and/or drought conditions, unveiling relevant tolerance/sensitivity points in two cropped genotypes from the most cultivated coffee species. This information should be taken into account in future adaptation/breeding efforts to ongoing climate changes and future harsher environmental scenarios.

MATERIAL AND METHODS

Plant Material and Growth Conditions

Plants of two cultivated genotypes (in Brazil), *C. canephora* Pierre ex A. Froehner cv. Conilon Clone 153 (CL153) and *C. arabica* L. cv. Icatu Vermelho (an introgressed variety resulting from a cross of *C. canephora* and *C. arabica* cv. Bourbon Vermelho, then further crossed with *C. arabica* cv. Mundo Novo), were used. Seven-year-old plants were grown in 80 L pots in walk-in growth chambers (EHHF 10000, ARALAB, Portugal) under controlled temperature (25/20°C, day/night), irradiance (*ca*. 700–800 μmol m^{-2} s^{-1}), relative humidity (70%), photoperiod (12 h), and 380 μL CO_2 L^{-1} air. Plants were maintained without restrictions in water, nutrients (see Ramalho et al., 2013a,b), or root development (as judged by visual examination at the end of the experiment after removing the plants from their pots).

Drought and Temperature Stress Implementation

Water and heat stresses were imposed gradually in order to allow plant acclimation. Initially, watering treatments were established under adequate temperature (25/20°C, day/night), corresponding to control well-watered (WW) or severe water deficit (SWD) conditions, which represented approximately 80 or 10% of maximal pot water availability, respectively (Ramalho et al., 2018b). Drought conditions were imposed along two weeks by partially withholding irrigation (through a partial reposition of water that was lost in each pot) until stability of predawn water potential (Ψ_{pd}) at values below −3.0 MPa for SWD plants, whereas WW plants were maintained at Ψ_{pd} above −0.35 MPa. Water availability conditions were thereafter kept for another five days before the onset of temperature increase.

The temperature rise from 25/20°C up to 42/30°C was imposed on both WW and SWD plants at a rate of 0.5°C day^{-1} (diurnal temperature) with 5 days of stabilization at 31/25, 37/28, and 42/30°C to allow for programmed evaluations. Afterwards, the temperature was readjusted to 25/20°C and the plants from both water treatments were fully irrigated and then monitored over a recovery period of 14 days (Rec14). Overall, the

SWD plants reached the desired Ψ_{pd} within 14 days upon gradual drought imposition, and were maintained at this condition plus 54 days,(49 of which during the temperature rise from 25/20°C to 42/30°C). The entire experiment lasted 82 days.

Determinations were performed on newly matured leaves from the upper third part of 6-8 plants per treatment, usually at 25/20, 31/25, 37/28, 42/30°C, and at Rec14. Additionally, some non-destructive parameters were further monitored at the intermediate temperatures of 28/23, 34/28, 39/30°C, and after 4 days (Rec4) or 7 to 10 (Rec7-10) days of stress relief.

Unless otherwise stated, evaluations or samplings were performed under photosynthetic steady-state conditions after *ca.* 2 h of illumination. For biochemical evaluations, leaf material was collected from 6 to 8 plants of each genotype, flash frozen in liquid nitrogen and stored at −80°C until analysis. Leaf tissue extractions were performed using an ice-cold mortar and pestle, as well as cold homogenizing solutions.

Leaf Water Status

Leaf Ψ_{pd} was determined at predawn immediately after leaf excision (Schölander et al., 1965) using a pressure chamber (Model 1000, PMS Instrument Co., USA). This was performed on 5–6 replicates per treatment, every two or three days, but only the data at the main temperature points for data collection (considering temperature rise, and both heat and drought recoveries) are presented.

Stomatal Traits

Imprints from the leaf abaxial surface were taken from five plants (two leaves per plant, and three different areas per leaf) and observed under an optical light microscope (Ramalho et al., 2013b). Stomatal density (SD) was calculated as the number of stomata per unit of leaf area, and the stomatal index (SI) was calculated as SI = [(stomata)/(total cells + stomata)] x 100. Stomatal area (SA) was measured in 60 randomly selected stomata (using the same leaves) with an ocular micrometer. The area of each individual stoma was calculated as SA = πab, where *a* is 1/2 length and *b* is 1/2 width, thus assuming an elliptical stomata shape.

Leaf Gas Exchanges

The net photosynthesis rate (P_n), stomatal conductance (g_s), transpiration rate (E) rate, and internal [CO_2] (C_i) were obtained using a portable open-system IRGA (Li-Cor 6400, LiCor, USA) with an external [CO_2] supply of *ca.* 400 μL L^{-1}, and *ca.* 650 μmol m^{-2} s^{-1} of irradiance. Instantaneous water use efficiency (*WUE*) was calculated as the P_n/E ratio.

Photosynthetic capacity (A_{max}), representing the photosynthetic rate obtained under saturating light and [CO_2], was measured in 1.86 cm^2 leaf discs through the evolution of O_2 using a Clark-type O_2 electrode (LD2/2; Hansatech, Kings Lynn, UK). A_{max} was obtained at 25°C, *ca.* 7% [CO_2] (supplied by 400 μL 2 M $KHCO_3$), and by exposing the leaf samples to increasing irradiance up to 1,200 μmol m^{-2} s^{-1} using a Björkman lamp (Hansatech) and neutral filters.

Chlorophyll a Fluorescence

Chlorophyll (Chl) *a* fluorescence parameters were determined on the same leaves and conditions used for gas exchange measurements using a PAM-2000 system (H. Walz, Germany), exactly as previously described (Rodrigues et al., 2016). Measurements of the (i) minimal fluorescence from excited Chl *a* molecules from the antennae, before excitation energy migrates to the reaction centers (F_0), (ii) maximal fluorescence, corresponding to the complete reduction of primary photosystem (PS) II acceptors (F_m), and (iii) maximal PSII photochemical efficiency (F_v/F_m) were performed on overnight dark-adapted leaves. F_0 was determined by using a weak light (< 0.5 μmol m^{-2} s^{-1}) beam, while F_m was obtained through a saturation pulse of 0.8 s of *ca.* 7,500 μmol m^{-2} s^{-1} of actinic light.

A second set of parameters were evaluated under photosynthetic steady-state conditions, with 650 μmol m^{-2} s^{-1} of actinic light and superimposed saturating flashes: q_L, $Y_{(II)}$, $Y_{(NPQ)}$, $Y_{(NO)}$, F_v'/F_m' (Kramer et al., 2004; Schreiber, 2004; Klughammer and Schreiber, 2008; Huang et al., 2011) and F_s/F_m' (Stirbet and Govindjee, 2011). F_0', which is required for the quenching calculations, was measured in the dark immediately after the actinic light was switched off and before the first fast phase of the fluorescence relaxation kinetics. F_v'/F_m' expresses the PSII photochemical efficiency of energy conversion under light exposure; q_L is the photochemical quenching based on the concept of interconnected PSII antennae, and represents the proportion of energy captured by open PSII centers and driven to photochemical events; F_s/F_m' is a predictor of the rate constant of PSII inactivation. Estimates of photosynthetic quantum yields of non-cyclic electron transfer ($Y_{(II)}$), photoprotective regulated energy dissipation of *PSII* ($Y_{(NPQ)}$), and non-regulated energy dissipation (heat and fluorescence) of PSII ($Y_{(NO)}$), where ($Y_{(II)}+Y_{(NPQ)}+Y_{(NO)}=1$), were also obtained.

Thylakoid Electron Transport Rates

The sub-chloroplast membrane fractions were obtained from a pool of leaves (*ca.* 5 g FW) from 3 plants (in triplicate), as previously described for coffee leaves (Ramalho et al., 1999). The *in vivo* electron transport rates associated with PSI ($DCPIPH_2 \rightarrow MV$) and PSII, including ($H_2O \rightarrow DCPIP$) or excluding ($DPC \rightarrow DCPIP$) the oxygen-evolving complex (*OEC*), were obtained with an O_2 electrode (LW2, Hansatech) using 1 mL of reaction mixture containing *ca.* 100 mg Chl, at 25°C under *ca.* 3000 μmol m^{-2} s^{-1} irradiance supplied by a Björkman lamp.

Thylakoid Electron Carriers

Chloroplast isolation for cytochrome determinations was performed using a pool of leaves of *ca.* 7 g FW, from 3 plants (in triplicate), following the procedures of Spiller and Terry (1980) with modifications for coffee leaves (Ramalho et al., 1999). The concentrations of cytochromes (Cyt) b_{559LP}, b_{559HP}, b_{563} and *f* were obtained using a spectrophotometer (UV-Vis Shimadzu UV-1800, Japan) with readings at 545 nm, with isosbest wavelengths of 528 and 568 nm for cytochrome b_{559}, and 552 and 572 nm for cytochrome b_{563} (Houchins and Hind, 1984), An extinction coefficient of 20 mmol L^{-1} cm^{-1} was assumed. For Cyt *f* concentration, readings were performed at 554 nm, and an extinction coefficient of 19.7 mmol L^{-1} cm^{-1} was used.

The pool of the redox form of plastoquinone (PQ-9) was determined from sub-chloroplast fractions that were obtained from a pool of leaves of *ca.* 5 g FW, from 3 plants (in triplicate), following Droppa et al. (1987) with minor modifications

(Ramalho et al., 1999). PQ-9 content was determined according to Redfearn and Friend (1962) by measuring the absorption difference between the oxidized and reduced forms of PQ-9 at 255 nm, relative to isosbest wavelengths of 276 and 308 nm. An extinction coefficient of 14.8 mmol L^{-1} cm^{-1} was assumed.

Photosynthetic Enzyme Activities

Activities of ribulose-1,5-bisphosphate carboxylase/oxygenase (RuBisCO; EC 4.1.1.39) (Osório et al., 2006; Tazoe et al., 2008) and ribulose-5-phosphate kinase (Ru5PK; EC 2.7.1.19) (Souza et al., 2005) were adapted for coffee leaves (Ramalho et al., 2003; Ramalho et al., 2013b). In detail, leaf material was finely powdered in liquid nitrogen, and an aliquot of *ca*. 100 mg FW was taken and homogenized in 1 mL extraction buffer consisting of 100 mM Tris-HCl, pH 8, containing 10 mM $MgCl_2$, 15 mM $NaHCO_3$, 10 mM β-mercaptoethanol, 2 mM DTT, 1% (v/v) Triton X-100, 2), 10% (v/v) glycerol and 2% (v/v) "Complete-protease inhibitor cocktail" (Roche, ref. 04693159001), together with 100 mg insoluble PVPP per homogenate. The extracts were centrifuged (16,000 *g*, 15 min, 4°C) and the obtained clean supernatant was used for spectrophotometric assessment of enzyme activities at 25°C, in a final volume of 1 mL.

RuBisCO activities—an assay medium containing 50 mM Tris-HCl buffer, pH 8.0, 15 mM $MgCl_2$, 20 mM $NaHCO_3$, 100 mM phosphocreatine, 10 mM ATP, 0.2 mM NAPH, 20 U mL^{-1} creatine kinase, 15 U mL^{-1}, 3-phosphoglycerate kinase, and 15 U mL^{-1} glyceraldehyde-3-phosphate dehydrogenase was used for determination of initial and total RuBisCO activities. For the initial activity, to the assay medium were added 10 mM RuBP, and then 20 μL of the clean supernatant, followed by immediate reading. For the total activity, to the assay medium were added 20 μL of the clean supernatant, followed by a 20 min incubation period, after which the reaction was started with addition of 10 mM RuBP. In both cases measurements followed the 3-PGA-dependent NADH oxidation at 340 nm (Osório et al., 2006).

Ru5PK activity—the activity was determined according to the method of Souza et al. (2005). Briefly, 20 μL of clean supernatant were added to the spectrophotometer cell with 100 mM Tris-HCl pH 8.0 buffer assay, containing 8 mM $MgCl_2$, 40 mM KCl, 20 mM phosphoenolpyruvate, 5 mM ATP, 1 mM NADH, 20 mM DTT, 8 U pyruvate kinase, 10 U mL^{-1} lactate dehydrogenase and 5 U mL^{-1} phosphoriboisomerase. After a 15 min incubation period, the reaction was started by adding 10 μL of 500 mM ribose-5-phosphate, and NADH oxidation was monitored at 340 nm.

Proteins Associated With Thylakoid Cyclic Electron Flow

Protein Extraction and Trypsin Proteolysis

Protein extraction followed Parkhey et al. (2015) with some modifications. Briefly, *ca*. 200 mg of powdered frozen leaves were suspended in 1.5 mL of TCA (10% w/v in acetone), vortexed and incubated during 30 min at 20°C. After centrifugation (12,300 *g*, 10 min, 4°C) the supernatant was discarded. This washing step was repeated and the pellet was then mixed with 1.5 mL of 0.1 M ammonium acetate in 80% v/v methanol, and left for 30 min. The sample was centrifuged (12,300 *g*, 10 min, 4°C), the dried residue was washed once more and an additional washing step was performed with 80% v/v acetone at the same conditions. The well-dried residue was treated with 500 μL of Tris-saturated phenol pH 8.0 and 500 μL of Tris-HCl-β-mercaptoethanol-SDS buffer (0.1 M Tris-HCl, 5% v/v β-mercaptoethanol, 2% w/v SDS and 30% w/v sucrose, pH 8.0). After 1 h of incubation at room temperature, the mixture was centrifuged (12,300 *g*, 10 min, 4°C) and the upper phenolic phase was removed. To precipitate the proteins, 1.5 mL of 0.1 M ammonium acetate in 80% v/v methanol was added to the phenolic phase collected and left overnight at −20°C. The sample was again centrifuged (12,300 *g*, 10 min, 4°C) to obtain the protein pellet that was then rinsed first with methanol and next with 80% v/v acetone, twice. The protein pellet was briefly air-dried and resuspended in 200 μL Laemmli buffer.

Protein concentration was determined by Coomassie blue dye-binding method using BSA as a standard (Bradford, 1976).

Thereafter, protein samples were diluted with MilliQ water and LDS3X reagent (Invitrogen) to obtain a 30 μL LDS1X solution containing 50 μg of proteins. After heating at 99°C for 5 min, proteins were loaded onto a NuPAGE 4–12% gradient gel (Invitrogen) and subjected to a short electrophoresis of 5 min. The samples were treated and proteolyzed with trypsin Gold (Promega) in presence of ProteaseMax detergent (Invitrogen) as previously described (Hartmann et al., 2014).

Liquid Chromatography and High Resolution Mass Spectrometry

NanoLC-MS/MS analysis of peptides was carried out in data-dependent mode with a Q-Exactive HF mass spectrometer (Thermo Fisher Scientific, USA) coupled to an UltiMate 3000 LC system (Dionex-LC Packings, Thermo Fisher Scientific). The analytical system was operated as described elsewhere (Klein et al., 2016). Peptides (10 μL) were desalted on a reverse-phase C18 PepMap 100 column, and then resolved with a 90 min gradient of CH_3CN, 0.1% formic acid, at a flow rate of 0.2 μL min^{-1}. The gradient was from 4 to 25% solvent B (80% CH_3CN, 19.9% MilliQ water, 0.1% formic acid) against solvent A (99.9% MilliQ water, 0.1% formic acid) for 75 min and then from 25% to 40% for 15 min. Full scan mass spectra were acquired from *m/z* 350 to 1800 with an automatic gain control (AGC) target set at 3×10^6 ions and a resolution of 60,000. The 20 most abundant precursor ions in each scan cycle were sequentially subjected to fragmentation through high-energy collisional dissociation. MS/MS scans were initiated for ions with potential charge states of 2^+ and 3^+ with an AGC target at 10^5 ions and threshold intensity of 83,000. A dynamic exclusion of 10 sec was applied for improving peptide coverage.

Protein Identification and Label Free Quantification

MS/MS spectra were assigned to peptide sequences using the MASCOT Daemon 2.6.1 search algorithm (Matrix Science). A reference database from *C. canephora* (Denoeud et al., 2014) of 25,574 polypeptide sequences totaling 10,251,572 residues was downloaded from Genoscope (http://coffee-genome.org/sites/

coffee-genome.org/files/download/coffea_cds.fna.gz) on July 1st 2019 and used for peptide and protein inference. The following parameters were used in the search: trypsin as proteolytic enzyme, maximum of two missed cleavages, mass tolerances of 5 ppm on the precursor ion and 0.02 Da on the MS/MS, fixed modification of cysteine into carboxyamidomethylated cysteine (+57.0215), and oxidized methionine (+15.9949) as variable modification. All peptide matches with a MASCOT peptide score below a p value of 0.05 were filtered and assigned to a protein. In order to keep the biologically relevant protein isoforms typical from plant proteomes, parsimony was not applied between samples. A protein was validated when at least two different peptide sequences were detected. The false discovery rate for protein identification was estimated through the decoy search option of MASCOT (Matrix Science) to be below 1%. Label-free quantification was based on counts of peptide-to-spectrum matches for each polypeptide.

From our results we searched for proteins that are known to be involved in cyclic electron transport, and four proteins were found: one proton gradient regulation protein PGR5 (*Cc08_g13730 - PGR5-like protein 1A, chloroplastic*) and three chloroplast NADH dehydrogenase-like (NDH) complex proteins (*Cc06_g22880 - Putative NDH-dependent cyclic electron flow 5, Cc04_g05100 - NDH-dependent cyclic electron flow 1, Cc06_g22890 - NDH-dependent cyclic electron flow 1*). The mass spectrometry proteomics data have been deposited to the ProteomeXchange Consortium via the PRIDE partner repository with the dataset identifier PXD019474 and DOI: 10.6019/PXD019474 for *C. arabica* proteome, and the dataset identifier PXD019541 and DOI: 10.6019/PXD019541 for *C. canephora* proteome.

Statistical Analysis

Physiological and biochemical data were analysed using a two-way ANOVA to evaluate the differences between water treatments (WW or SWD), between temperature treatments, and their interaction, followed by a Tukey's test for mean comparisons.

For the proteomic data, a two-way ANOVA was used to evaluate the differences between water treatments, between the several temperatures, and their interaction, followed by a Fisher's LSD test for mean comparisons between each condition and the double control (WW at 25/20°C).

A 95% confidence level was adopted for all tests, which were performed always independently for each genotype.

RESULTS

Leaf Water Status

The Ψ_{pd} was remarkably low (below −3.7 MPa) in SWD plants under control temperature (25/20°C), and tended to reach even lower values, close to −4.40 MPa at the two highest temperatures irrespective of genotype (**Figure 1**).

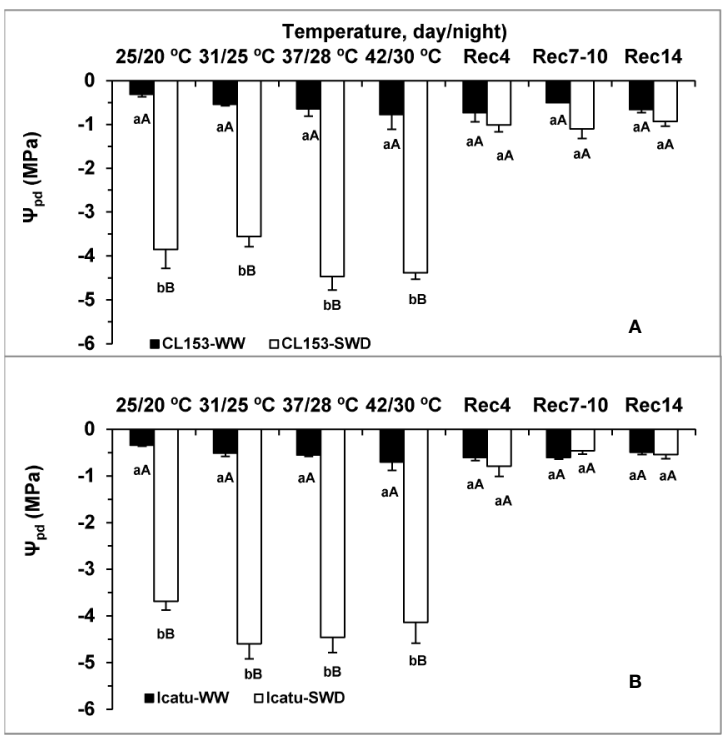


FIGURE 1 | Leaf water potential (Ψ_{pd}) determined at pre-dawn in *Coffea canephora* cv. Conilon Clone 153 (CL153) and *Coffea arabica* cv. Icatu, submitted to well-watered (WW) and severe drought (SWD), and temperature increase from (25/20°C, day/night), to 42/30°C, followed by a recovery of 4 (Rec4), 7 to 10 (Rec7-10) and 14 (Rec14) days. For each parameter, the mean values ± SE (n=5-6) followed by different letters express significant differences between temperature treatments for the same water level **(A, B)**, or between water availability levels for each temperature treatment (a, b), always separately for each genotype.

The single temperature rise did not significantly modify water status, despite the gradual decline tendency of Ψ_{pd} in WW plants from 25/20°C to the highest temperature, *i.e.* from −0.31 to −0.77 MPa in CL153, and from −0.34 to −0.70 MPa in Icatu (**Figure 1**).

Along the recovery period, Ψ_{pd} in SWD plants recovered from 4 days onwards to values close to their respective controls.

Changes in Stomatal Traits Driven by Drought and/or Heat

The stomatal density (SD) was not significantly altered by drought in CL153, but it gradually increased with the imposition of heat, although significantly only at 42/30°C (**Figure 2**). In contrast, SD was reduced in Icatu with the single imposition of either severe drought or heat stress, reaching the lowest values upon stress superimposition (SWD plants at 42/30°C). Two weeks after stress relief the SD values remained similar to those at 42/30°C.

The single exposure to drought (at 25/20°C) reduced the stomata area (SA) in CL153, with an opposite behavior in Icatu, whereas elevated temperature alone (in WW plants) reduced SA in both genotypes from 31/25°C up to 42/30°C (**Figure 2**). The exposure of SWD plants to all supra-optimal temperatures attenuated SA decline in CL153 with no clear impact in Icatu since SA was similar regardless of water treatments, although lower than at 25/20°C.

At the end of the experiment (Rec14), WW and SWD plants showed similar values of SD and SA within each genotype, but a fully recovery to the initial WW values were observed only in Icatu for SA and CL153 for SD.

The stomatal index (SI) was unresponsive to the applied treatments.

Stresses Impact on Leaf Gas Exchanges

Compared to WW plants, single exposure to drought significantly depressed the net photosynthetic rate (P_n) to 18% and 8% in CL153 and Icatu plants, respectively (**Table 1**). Concomitant reductions of stomatal conductance (g_s) (to 25 and 23%), and transpiration rates (E) (to 33 and 40%) were observed, in the same genotype order. Instantaneous water use efficiency (WUE) was also reduced due to a stronger decrease in P_n than in E. In contrast, the internal [CO_2] (C_i) showed an almost doubled value in SWD than in WW plants at 25/20°C. Reductions in photosynthetic capacity (A_{max}) of SWD plants, to 59% (CL153) and 79% (Icatu), were found relative to their respective WW values.

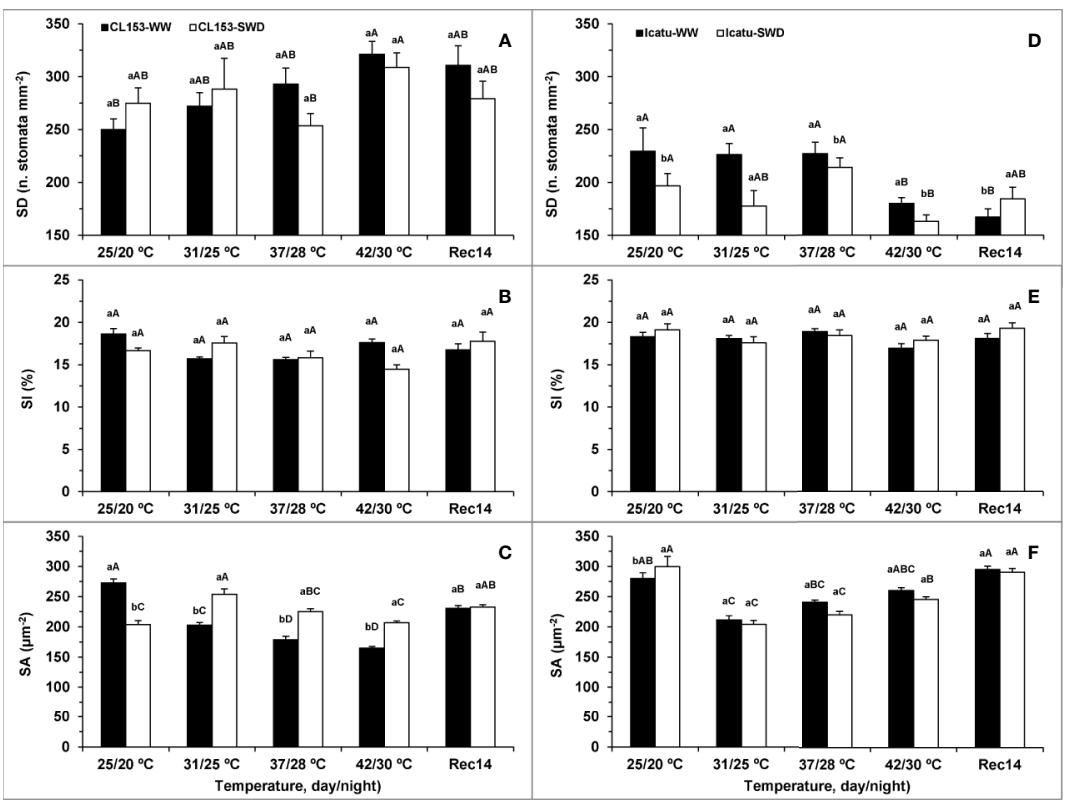


FIGURE 2 | Stomatal density (SD) **(A, D)**, stomatal index (SI) **(B, E)** and stomatal area (SA) **(C, F)** from leaves of *Coffea canephora* cv. Conilon Clone 153 (CL153) and *Coffea arabica* cv. Icatu, submitted to well-watered (WW) and severe drought (SWD), and temperature increase from (25/20°C, day/night), to 42/30°C, followed by a recovery of 14 days (Rec14) days. For each parameter, the mean values ± SE (n=5) followed by different letters express significant differences between temperature treatments for the same water level **(A–D)**, or between water availability levels for each temperature treatment (a, b), always separately for each genotype.

TABLE 1 | Variation in the leaf gas exchange parameters, net photosynthesis (P_n), stomatal conductance to water vapor (g_s), transpiration (E), and photosynthetic capacity (A_{max}) rates, as well as values of internal concentration of CO_2 (C_i), instantaneous water-use efficiency (*WUE*) in *Coffea canephora* cv. Conilon Clone 153 (CL153) and *Coffea arabica* cv. Icatu, submitted to well-watered (WW) and severe drought (SWD), and temperature increase from (25/20°C, day/night), to 42/30°C, followed by a recovery of 4 (Rec4), 7-10 (Rec7-10) and 14 (Rec14) days.

Genotype	Water	Temperature (day/night)								
		25/20°C	28/23°C	31/25°C	34/28°C	37/28°C	39/30°C	42/30°C	Rec4	Rec7-10	Rec14
							P_n (μmol CO_2 m^{-2} s^{-1})				
CL153	WW	5.68 ± 0.48aA	3.85 ± 0.46aAB	3.72 ± 0.25aAB	3.29 ± 0.51aBC	4.20 ± 1.17aAB	1.23 ± 0.18aC	1.24 ± 0.30aC	2.91 ± 0.35aBC	3.11 ± 0.20aBC	4.33 ± 0.10aAB
	SWD	1.01 ± 0.65bA	−0.09 ± 0.16bB	−0.09 ± 0.16bB	0.00 ± 0.25bB	−0.16 ± 0.25bB	−0.25 ± 0.07bB	−0.48 ± 0.18bB	1.51 ± 0.29bB	3.87 ± 0.59aA	4.13 ± 0.54aA
Icatu	WW	5.06 ± 0.40aAB	4.43 ± 0.41aABC	4.16 ± 0.37aABCD	2.77 ± 0.26aCD	2.76 ± 0.36aCD	2.71 ± 0.39aD	2.85 ± 0.41aCD	4.17 ± 0.15aBCD	5.31 ± 0.44aAB	6.12 ± 0.48aA
	SWD	0.41 ± 0.29bCD	0.14 ± 0.26bD	−0.35 ± 0.07bD	−0.01 ± 0.26bD	0.15 ± 0.16bD	−0.13 ± 0.07bD	−0.13 ± 0.15bD	1.87 ± 0.35bC	3.61 ± 0.65bB	5.39 ± 0.46aA
							g_s (mmol H_2O m^{-2} s^{-1})				
CL153	WW	43.3 ± 6.9aAB	52.8 ± 2.6aA	32.7 ± 4.2aAB	32.8 ± 3.2aAB	52.6 ± 11.2aA	27.7 ± 8.5aB	21.3 ± 4.2aB	27.7 ± 3.6aB	36.6 ± 3.6aAB	37.2 ± 3.5aAB
	SWD	10.7 ± 6.8bC	9.7 ± 2.2bC	10.6 ± 1.7bC	7.4 ± 1.1bC	9.0 ± 1.5bC	5.6 ± 0.8bC	7.0 ± 1.0bC	17.0 ± 3.5bBC	50.9 ± 8.3aA	40.0 ± 8.7aAB
Icatu	WW	48.7 ± 5.1aBC	43.5 ± 8.8aC	42.7 ± 8.8aC	28.3 ± 2.9aC	28.6 ± 4.6aC	51.3 ± 8.6aBC	77.4 ± 12.9aAB	57.8 ± 3.6aABC	78.5 ± 12.9aAB	77.7 ± 13.2aAB
	SWD	11.4 ± 2.7bC	6.2 ± 0.8bC	6.6 ± 1.0bC	6.6 ± 1.4bC	4.8 ± 1.2bC	6.3 ± 0.4bC	5.0 ± 0.5bC	19.4 ± 1.8bBC	49.0 ± 6.7bAB	66.8 ± 9.5aA
							C_i (μL L^{-1})				
CL153	WW	160.2 ± 29.1bB	248.3 ± 20.9bA	166.5 ± 18.3bB	250.2 ± 15.0bA	235.0 ± 19.0bAB	257.5 ± 17.0bA	267.2 ± 16.3bA	186.0 ± 5.8aAB	218.7 ± 7.5aAB	155.0 ± 15.4aB
	SWD	312.0 ± 62.9aABCD	352.2 ± 37.9aABC	397.4 ± 23.7aA	341.6 ± 51.5aABC	376.7 ± 42.5aAB	410.4 ± 13.9aA	422.8 ± 30.5aA	218.2 ± 36.3aCD	251.7 ± 11.0 aBCD	184.3 ± 27.2aD
Icatu	WW	166.7 ± 44.1bA	203.0 ± 67.4bA	197.9 ± 29.8bA	220.1 ± 20.3bA	194.7 ± 27.0bA	258.3 ± 5.3bA	267.8 ± 15.3bA	237.2 ± 3.2aA	233.7 ± 12.3aA	204.8 ± 14.7aA
	SWD	317.5 ± 20.6aBCDE	348.4 ± 53.0aABCD	452.4 ± 15.8aA	345.2 ± 47.5aA	274.8 ± 32.2aABCD	378.6 ± 17.7aABC	414.7 ± 21.5aAB	213.5 ± 20.8aE	205.3 ± 17.8aE	253.0 ± 41.6aDE
							E (mmol H_2O m^{-2} s^{-1})				
CL153	WW	0.409 ± 0.066aD	0.835 ± 0.104aBC	0.951 ± 0.053aBCD	1.926 ± 0.462aA	1.818 ± 0.371aAB	1.328 ± 0.287aABC	1.201 ± 0.210aABCD	0.520 ± 0.055aCD	0.567 ± 0.049aCD	0.616 ± 0.064aCD
	SWD	0.136 ± 0.086aA	0.209 ± 0.037bA	0.406 ± 0.065bA	0.310 ± 0.047bA	0.480 ± 0.034bA	0.329 ± 0.033bA	0.479 ± 0.071bA	0.354 ± 0.070aA	0.640 ± 0.076aA	0.549 ± 0.093aA
Icatu	WW	0.362 ± 0.064aD	0.923 ± 0.190 aCD	0.916 ± 0.081aCD	1.134 ± 0.069aC	1.278 ± 0.217aC	2.080 ± 0.237aB	2.938 ± 0.435aA	1.015 ± 0.071aCD	1.003 ± 0.050aCD	0.969 ± 0.080aCD
	SWD	0.145 ± 0.023aB	0.089 ± 0.050bB	0.208 ± 0.034bAB	0.280 ± 0.056bAB	0.245 ± 0.022bAB	0.362 ± 0.022bAB	0.327 ± 0.040bAB	0.401 ± 0.030bAB	0.540 ± 0.084bAB	0.833 ± 0.116aA
							WUE (mmol CO_2 mol^{-1} H_2O)				
CL153	WW	12.10 ± 2.66aA	3.71 ± 0.29aCD	3.98 ± 0.22aBCD	2.18 ± 0.36aCD	2.63 ± 0.57aCD	1.03 ± 0.16aD	0.87 ± 0.19aD	5.54 ± 0.11aBC	5.60 ± 0.28aBC	8.04 ± 1.01aAB
	SWD	4.58 ± 1.74bBC	2.79 ± 1.17aBCD	0.74 ± 0.33bCD	2.80 ± 1.18aBCD	2.23 ± 1.62aBCD	−0.72 ± 0.15aD	0.61 ± 0.05aCD	4.74 ± 1.00aBC	5.85 ± 0.61aAB	9.10 ± 1.80aA
Icatu	WW	15.31 ± 3.19aA	4.53 ± 0.91aB	4.38 ± 0.78aB	2.16 ± 0.23aB	3.05 ± 0.87aB	1.29 ± 0.10aB	1.18 ± 0.19aB	4.18 ± 0.14aB	5.27 ± 0.30aB	6.38 ± 0.22aB
	SWD	3.03 ± 0.95bAB	2.39 ± 1.16aAB	3.42 ± 2.29aAB	3.85 ± 2.06aAB	1.18 ± 0.46aB	0.18 ± 0.09aB	0.13 ± 0.02aB	4.50 ± 0.62aAB	6.85 ± 0.83aA	7.25 ± 0.82aA
							A_{max} (μmol O_2 m^{-2} s^{-1})				
CL153	WW	12.1 ± 1.4aAB	–	13.8 ± 1.9aAB	–	13.5 ± 2.3aAB	–	8.3 ± 0.3aB	9.4 ± 1.8aAB	15.2 ± 2.2aA	12.8 ± 1.1aAB
	SWD	7.1 ± 0.7bAB	–	9.7 ± 2.4bAB	–	8.5 ± 1.1bAB	–	7.6 ± 2.5aAB	8.3 ± 0.9bAB	10.8 ± 0.8bA	10.3 ± 1.7bAB
Icatu	WW	11.1 ± 0.9aBC	–	15.3 ± 2.0aAB	–	10.8 ± 1.7aBC	–	5.4 ± 1.0aD	13.5 ± 1.3aABC	16.4 ± 1.2aA	14.9 ± 1.0aABC
	SWD	8.8 ± 1.2bBC	–	12.0 ± 2.5bAB	–	7.8 ± 1.4bC	–	4.1 ± 0.4aD	10.8 ± 2.0bABC	13.0 ± 0.6bA	10.8 ± 1.8bABC

For each parameter, the mean values ± SE (n=6) followed by different letters express significant differences between temperature treatments for the same water level (A, B, C, D), or between water availability levels for each temperature treatment (a, b), always separately for each genotype.

The single exposure to high temperature (WW plants) caused different impacts between genotypes in these same parameters. P_n was gradually reduced above 25/20°C, significantly only at 39/30 and 42/30°C in CL153, when the values represented only *ca.* 22% of those at 25/20°C. In contrast, Icatu was affected from 34/28°C onwards, but maintained *ca.* 55% of the initial P_n values at these highest temperatures, more than doubling relative to CL153 values. This might have also contributed to an earlier recovery in Icatu from Rec4 onwards, and the partial recovery in CL153 by Rec14, when P_n represented 76% of the control value.

The A_{max} peaked at 31/25°C and decreased afterwards (especially in Icatu), although significantly only at 42/30°C, when it represented 69% and 49% of the values observed at 25/20°C in CL153 and Icatu, respectively.

Stomata opening responded differently to increasing temperatures relative to drought. In fact, g_s suffered some fluctuations until 37/28°C in both genotypes, but above this temperature it was reduced in CL153 (accompanying P_n trend), and increased in Icatu. This was in line with E values, which peaked at 37/28°C in CL153, whereas it increased continuously until 42/30°C in Icatu. At this temperature E values were 193% and 712% higher than those of controls of CL153 and Icatu, respectively. These increases in E, together with P_n declines, led to remarkable *WUE* reductions. Noteworthy is also the fact that C_i increased above 25/20°C, especially at the highest two temperatures, similarly for both genotypes, pointing to an absence of CO_2 limitation to photosynthesis.

Along the recovery period Icatu kept g_s and E values higher than those of control plants (and lower *WUE*), whereas CL153 maintained lowered g_s (as P_n) values until Rec 7-10, although with E and C_i values closer to their control than did Icatu.

The combined stress exposure clearly aggravated most gas exchange impacts. For SWD plants of both genotypes P_n further decreased to negligible (or negative) values from 28/23°C to 42/30°C (**Table 1**), whereas g_s became residual. This strongly reduced the water loss by transpiration as compared to WW plants at each temperature, although E also increased in SWD plants accompanying the temperature rise. In any case,*WUE* values were usually similar to those of WW plants from 28/23 to 42/30°C in CL153 and Icatu plants.

For both genotypes, A_{max} was lower in SWD than in WW plants until 37/28°C (although not differing from values at 25/20°C), suggesting that A_{max} decreases were mostly imposed by drought than by heat until this temperature. However, at 42/30°C A_{max} was further reduced in SWD Icatu plants, but without difference relative to WW plants, thus suggesting that at this extreme temperature heat played a major role for this additional decline of A_{max}.

The greater severity imposed by stress combination was also reflected in the slower recovery of SWD plants, usually until Rec4, but by Rec14 close values of P_n, g_s, C_i, E and *WUE* were observed between WW and SWD plants in both genotypes. Nevertheless, only Icatu showed a complete P_n recovery in SWD plants, as compared to WW at the initial 25/20°C conditions (contrary to WW and SWD plants of CL153), while maintaining significantly higher g_s and E values. Furthermore, only Icatu

SWD plants showed a total recover of A_{max} from Rec4 onwards, although keeping lower values than those of WW plants.

Stress Promoted Alterations in Fluorescence Parameters

In both genotypes, drought (at 25/20°C) did not affect F_0, whereas heat (in WW plants) led to significant increases only at 42/30°C (**Table 2**). Interestingly, at this temperature F_0 was less affected by the combined stress exposure, although a full recovery was faster in WW (Rec4) than in SWD plants (Rec7).

The F_v/F_m was only significantly reduced by the single exposure to drought in CL153. Additionally, WW plants did not show impacts up to 39/30°C, but a large F_v/F_m reduction was observed at 42/30°C (mostly related to the F_0 rise) in both genotypes, although stronger in Icatu. No clear negative stress interaction was evident up to 42/30°C. Indeed, only a tendency to lower F_v/F_m values was observed at 39/30°C in SWD plants of both genotypes, and at 42/30°C the SWD Icatu plants showed even a 32% higher value than their WW counterparts. However, stress interaction was reflected along the recovery period given that SWD plants recovered more slowly and incompletely than WW ones in both genotypes.

The performance of the photosynthetic apparatus was further assessed under steady-state conditions. $Y_{(II)}$ was significantly reduced by single drought (larger in CL153) and 42/30°C (larger in Icatu). Notably, SWD plants tended to somewhat similar (Icatu) or higher (CL153) $Y_{(II)}$ values until 39/20°C, and even at 42/30°C drought seems to be the most important stress driver irrespective of genotype. Also, by Rec4 the SWD plants recovered slightly better than WW plants, but by the end of the experiment $Y_{(II)}$ did not completely recover regardless of genotypes and water conditions. Therefore, the $Y_{(II)}$ values until 42/30°C and in the recovery period did not clearly pointed to a stress interaction.

In both genotypes, F_v'/F_m' was significantly reduced by drought at 25/20°C (40% and 25%), and by 42/30°C (31% and 52%) in CL153 and Icatu, respectively, thus in line with $Y_{(II)}$ and F_v/F_m variations. Additionally, q_L was only significantly reduced by drought (65% in CL153 and 46% in Icatu). However, it is noteworthy that under superimposed stress conditions q_L values did not differ significantly between WW and SWD plants up to 39/30°C in CL153 and 31/25°C in Icatu. Also, at 42/30°C the SWD plants behaved similarly as their SWD counterparts at 25/20°C, again suggesting an absence of stress interaction and that drought was the most important limiting condition. Notably, F_v'/F_m' recovered completely in WW and SWD plants, faster in Icatu (Rec4) than in CL153 (Rec7-10). In turn, q_L showed aftereffects by Rec14 regardless of treatments and genotypes.

A strong reinforcement of photoprotective energy dissipation mechanisms was reflected in $Y_{(NPQ)}$ increases, under the single exposure of either stresses, especially under drought in both genotypes. Notably, the WW plants were not impacted until 39/30°C, but at 42/30°C clear rises (larger in CL153) of $Y_{(NPQ)}$ were observed. With stress superimposition, SWD plants showed significantly higher values of these parameters than the WW plants at 42/30°C, but similar to those of SWD plants at 25/20°C, further pointing to an absence of stress interaction and that drought determined these genotype responses.

Notably, non-regulated energy dissipation processes ($Y_{(NO)}$) were not significantly modified by drought or heat, except for WW Icatu plants at 42/30°C. Furthermore, under stress superimposition $Y_{(NO)}$ tended to lower values in SWD plants than in WW ones at the two highest temperatures, pointing to an absence of aggravated status.

With some fluctuations, $Y_{(NPQ)}$ recovered mostly by Rec7-10, although the SWD plants showed higher values than those of WW ones by the end of the experiment, suggesting that some reinforcement of energy dissipation mechanisms are still needed in place. This was in line with some $Y_{(NO)}$ rise by Rec7-10 (and in WW Icatu plants by Rec14).

PSII inactivation status (estimated as F_s/F_m') nearly followed F_v'/F_m', showing significant increases due to severe drought or heat (only at 42/30°C) conditions. In general, SWD plants from both genotypes maintained higher F_s/F_m' values than those of WW plants up to 42/30°C, although not differing from those at 25/20°C. These results also suggest an absence of stresses interaction.

Along the recovery period the F_s/F_m' values approached those of control, but with higher values even by Rec14. This was in line with the aftereffects in the energy driven to photochemical events ($Y_{(II)}$) (all plants), and with some higher values of $Y_{(NPQ)}$ (SWD plants of both genotypes) or $Y_{(NO)}$ (WW plants of Icatu).

Stresses Impact in Thylakoid Functioning–Electron Transport Rates and Carriers

To unveil specific key impact points at the thylakoid membrane level, we next assessed the potential rates of electron transport involving PSs, and the content of the main carriers involved in electron transport.

In CL153, drought moderately reduced the activities of PSII including (PSII+OEC) or excluding (PSII-OEC) OEC, and of PSI in *ca.* 21, 24, and 18%, respectively (**Figure 3**), thus to a much smaller extent than in $Y_{(II)}$ (**Table 2**) or even A_{max} (**Table 1**). Remarkably, SWD Icatu plants showed significant increases of *ca.* 10% in PSII activity (with or without OEC), whereas that of PSI remained unaffected.

The single exposure to heat did not impair PSs activities until 37/28°C for both genotypes. Furthermore, at the highest temperature no impact at the PSI level was observed in both genotypes, whereas PSII activity was marginally reduced only in CL153, as compared to the WW plants at 25/20°C. Yet, a closer look revealed that CL153 displayed maximum PSII and PSI activities at 37/28°C and 31/25°C, whereas in Icatu this happened at 31/25°C and 37/28°C, respectively. Taking this into account, both genotypes revealed some heat impact at 42/30°C when compared to their respective maxima. These impacts were stronger in Icatu which showed reductions of 16, 32, and 25%, for PSII+OEC, PSII-OEC, and PSI, respectively, against 12, 4, and 5% in CL153, in the same order.

Stress interaction exacerbated the impact on both PSs regardless of genotype, usually at 37/28°C and 42/30°C, when SWD plants presented lower PSs activities relative to (i) WW

TABLE 2 | Variation in the leaf chlorophyll *a* fluorescence parameters in *Coffea canephora* cv. Conilon Clone 153 (CL153) and *Coffea arabica* cv. Icatu, submitted to well-watered (WW) and severe drought (SWD), and temperature increase from (25/20°C, day/night), to 42/30°C, followed by a recovery of 4 (Rec4), 7-10 (Rec7-10) and 14 (Rec14) days.

Genotype	Water	Temperature (day/night)								
		25/20°C	28/23°C	31/25°C	34/28°C	37/28°C	39/30°C	42/30°C	Rec4	Rec7-10	Rec14
							F_o				
CL153	WW	0.210 ± 0.004aB	0.216 ± 0.005aB	0.223 ± 0.007aB	0.195 ± 0.007aB	0.288 ± 0.021aB	0.211 ± 0.006aB	0.499 ± 0.038aA	0.265 ± 0.010bB	0.203 ± 0.011aB	0.248 ± 0.005aB
	SWD	0.233 ± 0.008aABC	0.275 ± 0.016aABC	0.204 ± 0.013aBC	0.182 ± 0.013aC	0.214 ± 0.018aBC	0.232 ± 0.017aABC	0.349 ± 0.020bA	0.353 ± 0.020aA	0.214 ± 0.008aBC	0.312 ± 0.007aAB
Icatu	WW	0.251 ± 0.007aB	0.282 ± 0.007aB	0.265 ± 0.006aB	0.224 ± 0.009aB	0.336 ± 0.016aB	0.214 ± 0.004aB	0.650 ± 0.062aA	0.270 ± 0.007aB	0.206 ± 0.017aB	0.237 ± 0.011aB
	SWD	0.244 ± 0.005aAB	0.241 ± 0.006aAB	0.220 ± 0.009aAB	0.217 ± 0.012aAB	0.226 ± 0.012bAB	0.246 ± 0.010aAB	0.343 ± 0.015bA	0.329 ± 0.009aAB	0.201 ± 0.003aB	0.295 ± 0.007aAB
							F_v/F_m				
CL153	WW	0.770 ± 0.008aAB	0.784 ± 0.005aA	0.794 ± 0.003aA	0.793 ± 0.006aA	0.789 ± 0.007aA	0.765 ± 0.008aAB	0.635 ± 0.025aC	0.728 ± 0.017aB	0.725 ± 0.013aB	0.759 ± 0.009aAB
	SWD	0.705 ± 0.025bAB	0.713 ± 0.026bAB	0.724 ± 0.024bAB	0.769 ± 0.008aA	0.759 ± 0.012aA	0.744 ± 0.015aAB	0.631 ± 0.021aC	0.673 ± 0.014bBC	0.688 ± 0.015bBC	0.718 ± 0.007bAB
Icatu	WW	0.753 ± 0.005aA	0.746 ± 0.006aA	0.766 ± 0.005aA	0.772 ± 0.009aA	0.744 ± 0.009aA	0.782 ± 0.005aA	0.458 ± 0.063bB	0.723 ± 0.011aA	0.736 ± 0.009aA	0.734 ± 0.010aA
	SWD	0.761 ± 0.008aA	0.778 ± 0.009aA	0.785 ± 0.008aA	0.766 ± 0.008aA	0.743 ± 0.004aAB	0.737 ± 0.014aAB	0.671 ± 0.011aB	0.704 ± 0.010aAB	0.718 ± 0.006aAB	0.719 ± 0.007aAB
							$Y_{(II)}$				
CL153	WW	0.358 ± 0.044aABC	0.327 ± 0.033aABC	0.391 ± 0.027aAB	0.325 ± 0.036aABC	0.401 ± 0.013aA	0.279 ± 0.038aBC	0.219 ± 0.019aCD	0.138 ± 0.009aD	0.229 ± 0.051aCD	0.253 ± 0.028aBCD
	SWD	0.065 ± 0.010bB	0.194 ± 0.031bA	0.160 ± 0.030bAB	0.140 ± 0.021bAB	0.157 ± 0.021bAB	0.177 ± 0.036bAB	0.069 ± 0.008bB	0.190 ± 0.018aA	0.177 ± 0.022aAB	0.198 ± 0.012aA
Icatu	WW	0.356 ± 0.029aA	0.305 ± 0.012aABC	0.361 ± 0.014aA	0.301 ± 0.038aABC	0.309 ± 0.019aABC	0.318 ± 0.029aAB	0.085 ± 0.020aD	0.187 ± 0.013aCD	0.203 ± 0.013aBCD	0.265 ± 0.022aABC
	SWD	0.136 ± 0.013bABCD	0.227 ± 0.029aABC	0.206 ± 0.035bABC	0.120 ± 0.018bBCD	0.130 ± 0.019bABCD	0.096 ± 0.019bCD	0.065 ± 0.011aD	0.230 ± 0.027aAB	0.232 ± 0.019aAB	0.252 ± 0.020aA
							$Y_{(NPQ)}$				
CL153	WW	0.245 ± 0.043bA	0.346 ± 0.033bA	0.245 ± 0.037bA	0.345 ± 0.024bA	0.243 ± 0.022bA	0.309 ± 0.056bA	0.476 ± 0.028bA	0.475 ± 0.032aA	0.238 ± 0.060aA	0.331 ± 0.036aA
	SWD	0.615 ± 0.021aAB	0.499 ± 0.033aAB	0.468 ± 0.050aABC	0.511 ± 0.027aAB	0.412 ± 0.047aABC	0.469 ± 0.072aABC	0.633 ± 0.022aA	0.376 ± 0.043aBC	0.225 ± 0.038aC	0.426 ± 0.028aABC
Icatu	WW	0.295 ± 0.034bABC	0.317 ± 0.021bAB	0.241 ± 0.015bBC	0.321 ± 0.034bAB	0.277 ± 0.017bABC	0.316 ± 0.035bAB	0.356 ± 0.039bAB	0.440 ± 0.021aA	0.163 ± 0.049aC	0.191 ± 0.024bC
	SWD	0.585 ± 0.026aAB	0.499 ± 0.034aABC	0.472 ± 0.061aBC	0.558 ± 0.047aABC	0.460 ± 0.045aBC	0.619 ± 0.039aAB	0.649 ± 0.021aA	0.410 ± 0.052aBC	0.114 ± 0.029aD	0.343 ± 0.028aC
							$Y_{(NO)}$				
CL153	WW	0.397 ± 0.015aB	0.327 ± 0.018aB	0.364 ± 0.029aB	0.329 ± 0.016aB	0.356 ± 0.024aB	0.412 ± 0.032aB	0.305 ± 0.017aB	0.388 ± 0.034aB	0.533 ± 0.050aA	0.416 ± 0.025aB
	SWD	0.320 ± 0.026aB	0.306 ± 0.014aB	0.372 ± 0.030aB	0.349 ± 0.015aB	0.432 ± 0.035aB	0.354 ± 0.047aB	0.298 ± 0.019aB	0.434 ± 0.027aB	0.597 ± 0.034aA	0.376 ± 0.022aB
Icatu	WW	0.349 ± 0.018aC	0.378 ± 0.024aC	0.398 ± 0.014aBC	0.378 ± 0.026aC	0.414 ± 0.011aBC	0.366 ± 0.013aC	0.559 ± 0.049aAB	0.374 ± 0.017aC	0.634 ± 0.043aA	0.544 ± 0.026aAB
	SWD	0.280 ± 0.024aB	0.274 ± 0.014bB	0.322 ± 0.029aB	0.322 ± 0.035aB	0.410 ± 0.046aB	0.285 ± 0.028aB	0.287 ± 0.021bB	0.360 ± 0.028aB	0.654 ± 0.027aA	0.405 ± 0.021bB
							q_L				
CL153	WW	0.448 ± 0.066aA	0.302 ± 0.039aABC	0.396 ± 0.030aAB	0.343 ± 0.029aABC	0.359 ± 0.023aABC	0.267 ± 0.055aABC	0.416 ± 0.052aAB	0.191 ± 0.044aC	0.235 ± 0.047aBC	0.237 ± 0.034aBC
	SWD	0.156 ± 0.030bA	0.241 ± 0.026aA	0.241 ± 0.042bA	0.208 ± 0.035bA	0.239 ± 0.032aA	0.309 ± 0.066aA	0.152 ± 0.020bA	0.314 ± 0.035aA	0.195 ± 0.021aA	0.234 ± 0.025aA
Icatu	WW	0.380 ± 0.029aA	0.332 ± 0.043aA	0.288 ± 0.027aA	0.316 ± 0.044aA	0.301 ± 0.033aA	0.371 ± 0.046aA	0.349 ± 0.107aA	0.184 ± 0.009aA	0.195 ± 0.013aA	0.223 ± 0.030aA
	SWD	0.205 ± 0.028bA	0.341 ± 0.042aA	0.286 ± 0.022aA	0.186 ± 0.024bA	0.193 ± 0.025aA	0.191 ± 0.045bA	0.151 ± 0.034bA	0.283 ± 0.033aA	0.240 ± 0.021aA	0.282 ± 0.022aA
							F_v'/F_m'				
CL153	WW	0.595 ± 0.023aAB	0.623 ± 0.036aAB	0.620 ± 0.024aAB	0.581 ± 0.025aAB	0.657 ± 0.015aA	0.614 ± 0.030aAB	0.413 ± 0.028aC	0.495 ± 0.043aBC	0.561 ± 0.038aABC	0.597 ± 0.024aAB
	SWD	0.355 ± 0.037bB	0.474 ± 0.035bAB	0.454 ± 0.039bAB	0.458 ± 0.018bAB	0.447 ± 0.035bAB	0.444 ± 0.056bAB	0.343 ± 0.026bB	0.441 ± 0.011bAB	0.515 ± 0.030bA	0.528 ± 0.025bA
Icatu	WW	0.593 ± 0.022aA	0.585 ± 0.028aA	0.671 ± 0.018aA	0.580 ± 0.031aA	0.608 ± 0.014aA	0.569 ± 0.015aA	0.283 ± 0.051aB	0.553 ± 0.014aA	0.567 ± 0.019aA	0.630 ± 0.018aA
	SWD	0.449 ± 0.020bABC	0.464 ± 0.025bABC	0.455 ± 0.039bABC	0.423 ± 0.035bABC	0.437 ± 0.024bABC	0.393 ± 0.028bBC	0.340 ± 0.023aC	0.508 ± 0.026aAB	0.559 ± 0.019aA	0.544 ± 0.019aA
							F_s/F_m'				
CL153	WW	0.642 ± 0.044bBC	0.673 ± 0.033bBC	0.609 ± 0.027bC	0.675 ± 0.036bBC	0.599 ± 0.013bC	0.721 ± 0.038bABC	0.781 ± 0.019bA	0.862 ± 0.009aA	0.771 ± 0.051aAB	0.747 ± 0.028aABC
	SWD	0.935 ± 0.010aA	0.806 ± 0.031aA	0.840 ± 0.030aA	0.860 ± 0.021aA	0.843 ± 0.021aA	0.823 ± 0.036aA	0.931 ± 0.008aA	0.810 ± 0.018aA	0.823 ± 0.022aA	0.802 ± 0.012aA
Icatu	WW	0.644 ± 0.029bC	0.695 ± 0.012aBC	0.639 ± 0.014bC	0.699 ± 0.038bBC	0.691 ± 0.019bBC	0.682 ± 0.029bBC	0.915 ± 0.020aA	0.813 ± 0.013aAB	0.797 ± 0.013aAB	0.735 ± 0.022aBC
	SWD	0.864 ± 0.013aABC	0.773 ± 0.029aBC	0.794 ± 0.035aBC	0.880 ± 0.018aABC	0.870 ± 0.019aABC	0.904 ± 0.019aAB	0.935 ± 0.011aA	0.770 ± 0.027aB	0.768 ± 0.019aB	0.748 ± 0.020aC

Parameters include the: initial fluorescence (F_o), maximum PSII photochemical efficiency (F_v/F_m), photochemical quenching based on the concept of interconnected PSII antennae (q_L), the actual PSII photochemical efficiency of energy conversion (F_v'/F_m'); and the predictor of the rate constant of PSII inactivation (F_s/F_m'), as well as the estimate of quantum yields of non-cyclic electron transport ($Y_{(II)}$), of regulated energy dissipation in PSII ($Y_{(NPQ)}$), and of non-regulated energy dissipation in PSII (heat and fluorescence) ($Y_{(NO)}$).For each parameter, the mean values ± SE (n=5) followed by different letters express significant differences between temperature treatments for the same water level (A, B, C, D), or between water availability levels for each temperature treatment (a, b), always separately for each genotype.

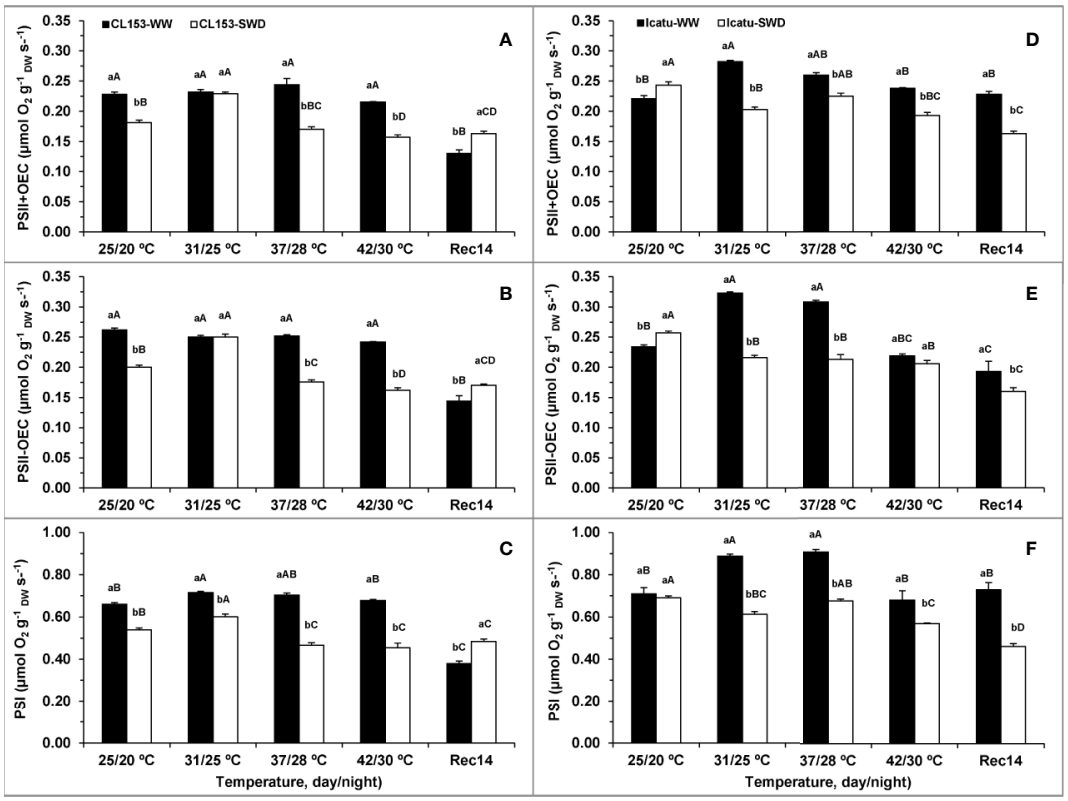


FIGURE 3 | Changes in the potential thylakoid electron transport rates associated with *PSI* **(C, F)**, and *PSII*, with (+OEC) **(A, D)** or without (-OEC) **(B, E)** the oxygen evolving complex participation, in *Coffea canephora* cv. Conilon (CL153) and *Coffea arabica* cv. Icatu, submitted to well-watered (WW) and severe drought (SWD), and temperature increase from (25/20°C, day/night), to 42/30°C, followed by a recovery of 14 days (Rec14) days. For each parameter, the mean values ± SE (n=3) followed by different letters express significant differences between temperature treatments for the same water level **(A–D)**, or between water availability levels for each temperature treatment (a, b), always separately for each genotype.

plants at these temperatures and (ii) SWD plants at 25/20°C. These reductions in SWD plants at 42/30°C reached *ca*. 37% for both PSII and PSI as compared to their maxima, but to a much lower extent than in WW plants at 25/20°C, and still held relevant activity under these very harsh conditions.

Unexpectedly, some of the strongest impacts on electron transport rates at PSs level were found at the end of the recovery period (Rec14). This was the case of WW CL153 plants that showed minimum rates, which were even below those of SWD plants in both PSs. Additionally, SWD plants showed strong aftereffects at the end of the experiment since the rates were maintained (CL153) or even reduced (Icatu) relative to those observed at maximal temperature. In contrast, WW Icatu displayed electron transport rates similar to those at the beginning of the experiment.

As concerns the contents of the thylakoid electron carriers (**Figure 4**), the single exposure to each stress promoted changes in a genotype-dependent manner, which, in most cases, closely followed the patterns of electron transport rates. Single drought increased the content of all cytochromes (Cyt) in Icatu, from 5% in *Cyt* b_{563} (the only non-significant) to 28% in *Cyt f*, whereas *PQ-9* content doubled that of WW plants. In contrast, *PQ-9* was the only carrier to rise (20%) in CL153, whereas Cyt pools significantly declined between 20% (*Cyt f*) and *ca*. 30% (the rest).

At supra-optimal temperatures, the content of all electron carriers significantly increased at 31/25°C and 37/28°C in WW Icatu plants, ranging from *ca*. 30% (all Cyt at 31/25°C) to 83% in *PQ-9* (at 37/28°C). With a further increase to 42/30°C all contents were reduced, but maintaining values close to those at 25/20°C, similarly to what happened with electron transport rates (**Figure 3**). In contrast, the WW CL153 plants maintained Cyt contents at 31/25°C, but showed significant reductions between *ca*. 11–12% (*Cyt f*, *Cyt* b_{563}) and 17–18% (*Cyt* b_{559HP}, *Cyt*b_{559LP}) at 37/28°C. Despite a weak recovery at 42/30°C, significant differences to 25/20°C were still present (except in *Cyt* b_{563}). The *PQ-9* was the only carrier to show large increases over the entire experiment (including 42/30°C), with a maximal 54% rise at 37/30°C.

The simultaneous stress exposure affected the carrier pools in both genotypes. The SWD plants showed lower contents of all carriers than their respective WW plants at 37/28°C and 42/30°C. Still, in CL153 the values were similar to those of SWD plants at 25/20°C, suggesting that the superimposition of stresses did not aggravate the drought impact that was already

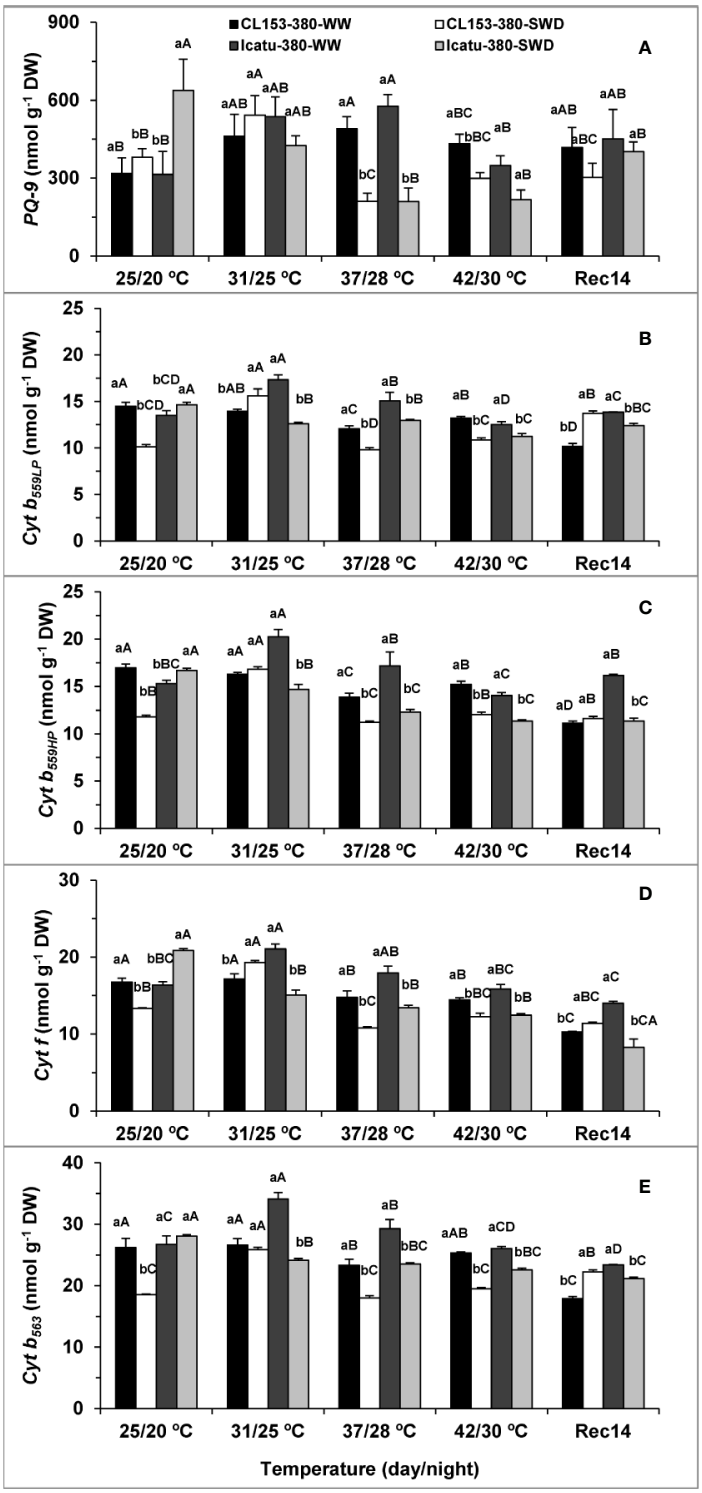


FIGURE 4 | Variation in the contents of the thylakoid electron carriers plastoquinone (*PQ-9*) **(A)**, and cytochromes b_{559LP} **(B)**, b_{559HP} **(C)**; b_{563} **(E)** and *f* **(D)** in *Coffea canephora* cv. Conilon (CL153) and *Coffea arabica* cv. Icatu, submitted to well-watered (WW) and severe drought (SWD), and temperature increase from (25/20°C, day/night), to 42/30°C, followed by a recovery of 14 days (Rec14) days. For each parameter, the mean values ± SE (n=3) followed by different letters express significant differences between temperature treatments for the same water level **(A–D)**, or between water availability levels for each temperature treatment (a, b), always separately for each genotype.

observed at 25/20°C. By opposition, the content of all electron carriers gradually decreased above 25/20°C in SWD Icatu plants, reaching minimum values at either 37/28°C or 42/30°C, thus pointing to an additional negative impact promoted by the stress interaction.

At Rec14, WW Icatu plants completely recovered (except *Cyt* b_{563}) their carriers content, but in SWD plants lower values were still observed for most carriers (*Cyt* b_{559HP}, *Cyt f*, *Cyt* b_{563}), thus confirming the higher impact of stress superimposition. Notably, CL153 plants (WW and SWD) showed an incomplete recovery of all carrier pools (except for *PQ-9*) as compared to those found at 25/20°C. Furthermore, WW CL153 plants tended to lower values of all carriers than at 42/30°C, whereas the SWD plants recovered better than WW ones in some cases (*Cyt* b_{559LP}, *Cyt* b_{563}). These changes followed the same pattern observed for the electron transport rates (incomplete recovery of WW plants and higher values in SWD than WW plants at Rec14), thus further underlining the persistence of aftereffects by the end of the experiment.

Proteins Involved in Cyclic Electron Flow

Under single drought exposure the abundance of PGR5 and NDH (*Cc04_g05100* and *Cc06_g22890*) proteins increased in SWD plants of both genotypes, although to a greater extent and significantly only in Icatu (**Table 3**).

The levels of these three proteins increased by heat exposure in WW plants at 37/28°C, with Icatu showing again a greater responsiveness. However, at 42/30°C, PGR5 declined in both genotypes, whereas NDH (*Cc04_g05100* and *Cc06_g22890*) were mostly maintained in Icatu, and showed a rising tendency in CL153. At this temperature an additional NDH (*Cc06_g22880*) was also detected.

The superimposition of severe water deficit and heat compromised plant responses remarkably. In fact, at 37/28°C the proteins that increased under the single exposure to either stress (PGR5 and NDH, *Cc04_g05100* and *Cc06_g22890*) decreased in SWD plants, both as compared to their values at 25/20°C and to the values of WW plants at 37/28°C. At the highest temperature, abundance of these proteins was usually further reduced in SWD plants, and maintained at lower levels than in their WW counterparts irrespective of genotype.

Notably, two weeks after stresses relief PGR5 and NDH (*Cc04_g05100* and *Cc06_g22890*) protein pools were greater than their control initial values regardless of watering or genotypes.

TABLE 3 | Changes in protein abundance (estimated by MS/MS spectra counts) of the proton gradient regulation protein PGR5 (*Cc08_g13730 - PGR5-like protein 1A, chloroplastic*) and three chloroplast NADH dehydrogenase-like (NDH) complex proteins (*Cc06_g22880 - Putative NDH-dependent cyclic electron flow 5, Cc04_g05100 - NDH-dependent cyclic electron flow 1, Cc06_g22890 - NDH-dependent cyclic electron flow 1*) in plants of *Coffea canephora* cv. Conilon Clone 153 (CL153) and *Coffea arabica* cv. Icatu, submitted to well-watered (WW) and severe drought (SWD), and temperature increase from (25/20°C, day/night), to 42/30°C, followed by a recovery of 14 days (Rec14) days.

Genotype	Water	Temperature (day/night)			
		25/20°C	37/28°C	42/30°C	Rec14
		Cc06_g22880 - Putative NDH-dependent cyclic electron flow 5			
CL153	**WW**	0.00	0.00	2.33	1.33
	SWD	0.00	0.33	1.00	0.00
Icatu	**WW**	0.00	0.00	0.00	0.00
	SWD	0.00	0.00	0.00	0.00
		Cc04_g05100 - NDH-dependent cyclic electron flow 1			
CL153	**WW**	0.33	1.00	2.33*	2.33*
	SWD	1.33	0.67	1.67	1.00
Icatu	**WW**	1.00	3.00*	2.67	2.33
	SWD	3.33*	1.67	1.67	4.00**
		Cc06_g22890 - NDH-dependent cyclic electron flow 1			
CL153	**WW**	2.00	3.00	3.33	4.67
	SWD	3.33	1.33	1.67	3.33
Icatu	**WW**	3.37	6.67	6.33	8.33*
	SWD	9.00**	6.00	4.00	6.67
		Cc08_g13730 - PGR5-like protein 1A, chloroplastic			
CL153	**WW**	0.00	3.67*	1.00	1.33
	SWD	0.33	1.00	0.67	2.00
Icatu	**WW**	3.33	7.67	1.00	4.67
	SWD	9.33*	1.67	0.33	3.67

Relative quantification was obtained by the number of MS/MS spectral counts associated with each protein. For each parameter, the mean values (n=3) followed by asterisks represented significant (< 0.05) or very significant (**< 0.01) differences to the double control (WW plants, at 25/20°C), always separately for each genotype.*

Impact on Key Photosynthetic Enzymes

Drought significantly reduced RuBisCO initial (38%) and total (28%) activities, as well as its activation state (16%) in CL153 plants, whereas Icatu showed marginal reductions of 14, 12, and 1%, in the same order (**Figure 5**). Drought did not significantly affect Ru5PK activity in both genotypes.

The temperature rise up to 37/28°C significantly promoted RuBisCO and Ru5PK activities, while RuBisCO activation was maintained in WW plants of both genotypes. At this temperature, initial RuBisCO activity increased by 55% (CL153) and 38% (Icatu), and its total activity increased by 47% in both genotypes, whereas Ru5PK activity increased by 24% (CL153) or 32% (Icatu). However, these enzymes were particularly affected at 42/30°C irrespective of genotype, to a greater extent than was observed for the photochemical components. In fact, as compared to 25/20°C, the activities of RuBisCO (initial and total) and Ru5PK were nearly halved (or less) in WW plants from both genotypes. These decreases were even greater (*ca.* 65% or even more) when compared to the maximal activities at 37/28°C.

Notably, RuBisCO was mostly unresponsive to stress interaction until 37/28°C, whereas Ru5PK activity decreased significantly at this temperature in the SWD plants of both genotypes as compared to their counterparts at 25/20°C. However, at 42/30°C stress interaction clearly affected both enzymes and genotypes, with SWD plants displaying the lowest activities over the entire experiment. Under these harsh conditions (42/30°C and SWD), drastic reductions (*ca.* 80%) were observed in initial and total RuBisCO activities, as well as in Ru5PK activity in both genotypes, as compared to their controls. Such reductions were even greater if compared to WW plants at 37/28°C. Overall, RuBisCO activation remained unchanged, with a reduction only in WW CL153 plants of at 42/30°C.

At Rec14 enzyme activities recovered remarkably, although some aftereffects remained in RuBisCO (in WW and SWD plants of CL153 for initial activity; in WW Icatu plants for total activity)

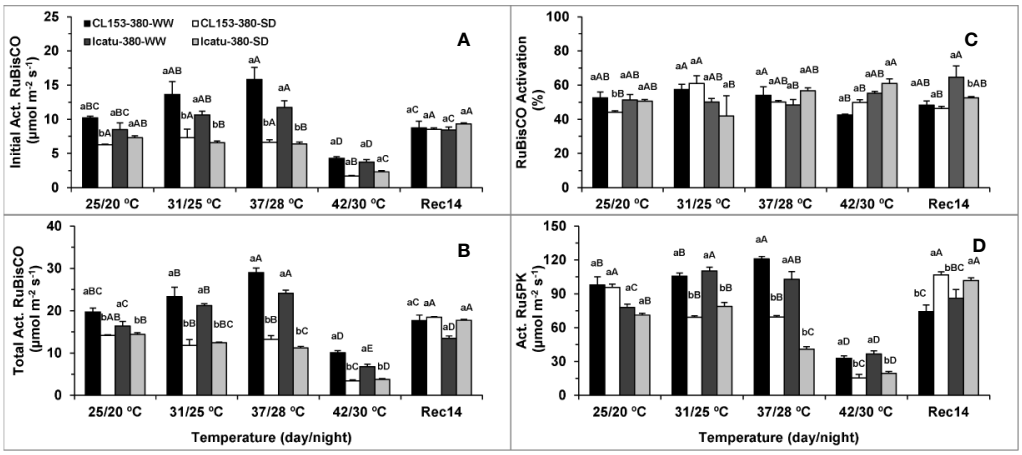


FIGURE 5 | Changes in the Initial and Total Activities of ribulose-1,5-bisphosphate carboxylase oxygenase (RuBisCO), and this enzyme activation status, as well as the maximal activity of ribulose-5-phosphate kinase (Ru5PK), in plants of *Coffea canephora* cv. and *Coffea arabica* cv. Icatu, submitted to well-watered (WW) and severe drought (SWD), and temperature increase from (25/20°C, day/night), to 42/30°C, followed by a recovery of 14 days (Rec14) days. For each parameter, the mean values ± SE (n=5) followed by different letters express significant differences between temperature treatments for the same water level **(A–D)**, or between water availability levels for each temperature treatment (a, b), always separately for each genotype.

and Ru5PK activity (WW CL153 plants). Interestingly, both enzymes recovered completely in SWD Icatu plants, whereas in CL153 that was observed only for Ru5PK.

DISCUSSION

Impact of Severe Drought on the Water Status and Photosynthetic Performance

Severe water restriction was imposed to SWD plants, as judged from the remarkable low Ψ_{pd} (≤ −3.7 MPa) from 25/20°C to 42/30°C. This was below −3.5 MPa, which is considered an extreme water deficit in coffee trees (Pinheiro et al., 2004), or −2.15 MPa, which is low enough to cause leaf wilting (Santos and Mazzafera, 2012).

Water deficit and supra-optimal temperatures altered the stomatal traits SD and SA in a genotype-dependent manner, but not SI which is a reasonably constant trait in coffee (Grisi et al., 2008; Rodrigues et al., 2016). Under drought, Icatu showed reduced SD, similar to findings in droughted plants of *C. arabica* cv. Siriema (Melo et al., 2014), and a rise in SA. In contrast, CL153 presented opposite trends, denoting a different response to water constraints. Overall, decreased g_s is associated with larger stomatal size and lower density for the same total area of stomatal pores, due to a larger diffusion path for water vapor (Franks and Beerling, 2009). Thus, SD and SA changes contributed to reduce g_s in SWD Icatu plants. In CL153 such SD and SA changes would also at a first glance point to a g_s increase.However the marked decreases in g_s imply that the physiological regulation of stomata opening clearly overcomes the contribution of morphological stomatal traits over the control of water loss.

Coffee leaves display intrinsically low g_s values even under optimal growth conditions and thus, stomatal constraints, more than mesophyll or biochemical ones, have been shown to be the major limitations of photosynthesis (DaMatta et al., 2016; DaMatta et al., 2019; Martins et al., 2019). These constraints are believed to be exacerbated due to stomatal closure under soil drought (here shown by the strong Ψ_{pd} decline) or rising leaf-to-air vapor pressure deficit, which in turn usually accompanies increases in air temperature (DaMatta et al., 2018). However, as drought severity progressed, non-stomatal factors dominate the limitations to photosynthesis, as herein shown by the increase in C_i, despite the reduction in g_s. This fact, coupled to reduction of A_{max} (assessed under saturating CO_2 and as such in the absence of diffusion-mediated limitations to photosynthesis) and to the greater decline of P_n than in A_{max}, clearly suggests that both biochemical and mesophyll constraints were the major factors explaining the overall photosynthesis decrease in SWD plants.

Single drought impact was further noted in the SWD plants in PSII photochemical efficiency (F_v/F_m, F_v'/F_m') and inactivation (F_s/F_m'), the energy use to photosynthesis ($Y_{(II)}$, q_L), and the need for thermal energy dissipation ($Y_{(NPQ)}$), with a global lesser impact in Icatu than in CL153, in agreement with the somewhat lower A_{max} impact. Still, in both genotypes, the significant decline of $Y_{(II)}$ reflected a lower use of energy for ATP and NADPH synthesis (Peloso et al., 2017), in line with the very low P_n values. Such lower photochemical use of energy was compensated for by the reinforcement of thermal dissipation mechanisms at the PSII level, reflected in strong $Y_{(NPQ)}$ rise, which protects the coffee leaves from excessive excitation damages (Pompelli et al., 2010; Silva et al., 2015). Besides, $Y_{(NO)}$ tended to lower values, meaning that photoinhibition and deregulated energy dissipation in PSII, related to limitations in photochemical processes ($Y_{(II)}$) and/or insufficiency of photoprotective mechanisms ($Y_{(NPQ)}$) (Kramer et al., 2004; Busch et al., 2009; Huang et al., 2011), did not occur in SWD plants.

Water deficit can cause protein denaturation (Hoekstra et al., 2001), decrease the synthesis of the small RuBisCO units, and increase RuBisCO inhibitors, thus affecting RuBisCO activity (Vu et al., 1999; Fahad et al., 2017). This is in good agreement with the greater drought sensitivity of CL153 plants, which showed stronger negative impacts on RuBisCO activity (and their activation state) (**Figure 5**) and both PSs activity (**Figure 3**), as well as in Cyt contents (**Figure 4**) than did Icatu. In fact, the higher photochemical performance in SWD Icatu plants was likely related to the preservation or reinforcement of those photosynthetic components associated with a strengthened antioxidative system under drought (Ramalho et al., 2018b). Still, PQ-9 increased in both genotypes, especially in Icatu, likely reinforcing the protective mechanisms against drought. In fact, PQ-9 corresponds to the redox form of plastoquinone (PQ) that displays antioxidant properties, capable of suppressing singlet oxygen ($^1O_2$) and inhibiting the oxidation of lipid membranes (Ksas et al., 2018). Furthermore, PQ is also linked to alternative electron flow pathways, among them the CEF involving PSII (with Cyt b_{559}) and PSI (with Cyt b_6/f complex). This is in good agreement with the increase in all Cyts displayed by SWD Icatu plants, in sharp contrast with the reductions found in CL153 plants. In fact, CEF can help to dissipate the excess photon energy and to mitigate PSs photoinhibition (Miyake and Okamura, 2003; Chu and Chiu, 2016; Yamori et al., 2016). For instance, Cyt b_{559} (both LP and HP forms) is not involved in the primary electron transfer pathway in PSII, but can participate in CEF-PSII. This is not accompanied by O_2 evolution, but significantly reduce the excess excitation pressure on PSII (Laisk et al., 2006), thus protecting it against photoinhibition (Shinopoulos and Brudvig, 2012; Chu and Chiu, 2016). Furthermore, the reinforcement of Cyt b_{563} and f in SWD Icatu plants might have additionally promoted a CEF-PSI without accumulation of NADPH, but allowing the transport of H^+ into the thylakoid lumen associated with the Q cycle, thus ultimately contributing to ΔpH formation and ATP synthesis. CEF-PSI further involves proton gradient regulation proteins (PGR5 and PGRL1), which mediate electron transport from ferredoxin to PQ, depending uniquely on the Q cycle of the Cyt b_6/f complex. Additionally, a second CEF-PSI is related to the chloroplast NADH dehydrogenase-like (NDH) complex, which recycles electrons from ferredoxin to PQ and subsequently to PSI, alleviating oxidative pressure in chloroplasts under excessive light energy. Both PGR- and NDH dependent CEF-PSI were reported as essential for photoprotection of PSs under high irradiance and heat (Yamori et al., 2016; Shikanai and Yamamoto, 2017; Sun et al., 2018). Furthermore, the Cyt b_6/f complex is a key control point of photosynthetic flow, and changes in electron transport capacity and C-assimilation are closely related to their content, which is sensitive to changes in environmental disturbances, including drought (Kohzuma et al., 2009; Sanda et al., 2011; Schöttler and Toth, 2014). Altogether, the greater increases in PGR5 and two NDH proteins as well as in all electron carriers observed in Icatu agree with CEF-PSII and CEF-PSI reinforcement, maintenance of PSII photochemical efficiency (F_v/F_m) and both PSs activity in SWD Icatu plants. In contrast, CL153 plants showed significant declines in F_v/F_m, PSs activity, reductions in all Cyt contents in addition to minor changes in PGR5 and NDH proteins. Similar impacts at PSI and PSII levels were associated with drought sensitivity in other plant species (Oukarroum et al., 2009; Chen et al., 2016), and showed that Icatu displayed a greater drought tolerance than CL153.

Impact of Increasing Temperatures at Physiological and Biochemical Levels

Heat impact on photosynthesis was unrelated to leaf dehydration given that Ψ_{pd} (**Figure 1**) was not affected by temperature rise despite the strong E increase (**Table 1**). Therefore, the potential impacts on photosynthetic performance at the imposed temperatures should have been mostly associated with metabolic disturbances or structural damages rather than changed leaf water status.

Temperature rise altered stomatal traits differently from drought, but also in a genotype-dependent manner. Although the SD increase and SA reduction observed in CL153 might have the potential to facilitate leaf cooling through a higher g_s, and in Icatu the SD decrease could have promoted a decreasing g_s trend at 42/30°C, none of these g_s patterns were observed, *i.e.* CL153 showed the lowest, and Icatu the highest, g_s values at 42/30°C. Therefore, as for drought, these findings highlights a greater importance of stomatal opening control, which overrode the contribution of altered stomatal traits in WW plants, confirming previous reports (Rodrigues et al., 2016).

CL153 showed a strong reduction of P_n (and g_s) at 39/30°C onwards, coupled with significant C_i rise and A_{max} reduction, although with a much smaller extent than in P_n. Together this suggests both stomatal and non-stomatal limitations of photosynthesis. In Icatu, the global photosynthetic functioning was even more affected at the highest temperature. Since higher g_s and C_i values were observed, concomitantly with a halved A_{max}, we contend that non-stomatal limitations should have dominated the overall P_n decreases. The dichotomous P_n and E patterns contributed thereafter for the reduction of *WUE* to very low values in both genotypes, as also observed for whole coffee plants subjected to elevated temperatures (Rodrigues et al., 2018).

With the gradual temperature imposition Icatu presented maximal values of PSII activity and Cyt contents at 31/25°C (and for PSI activity and PQ-9 content at 37/28°C), supporting the significant A_{max} rise. For both genotypes, a greater heat tolerance than that observed for severe water restriction was still found until 39/30°C in WW plants. This was reflected in the absence of significant changes in the energy capture in the antennae (F_0), PSII photochemical efficiency (F_v/F_m, F_v'/F_m') and inactivation (F_s/F_m'), photochemical energy use ($Y_{(II)}$, q_L), or even the energy dissipation mechanisms ($Y_{(NPQ)}$, $Y_{(NO)}$). Indeed, maintenance of high values of $Y_{(II)}$ and PSII photochemical efficiency reflect photosynthetic tolerance to stress (Li et al., 2017). This is likely to have been coupled with larger pools of several protective and antioxidative molecules, and the upregulated expression of some genes related to protection mechanisms, as previously demonstrated (Martins et al., 2016). Besides, photochemical quenching (represented by q_L)

is considered an indicator of PSII redox state as well as of energy captured by open PSII centers and used for electron transport (Murchie and Lawson, 2013). The higher the value, the greater the number of open reaction centers, reflecting a greater use of light by the plant, as happened here until 42/30°C in both genotypes.

Notably, at 31/25°C and even at 37/28°C a global rise of all Cyts (only in Icatu) and PQ-9 (both genotypes) was noted. At 37/28°C this was accompanied by higher values of PGR5 and two NDH (*Cc04_g05100* and *Cc06_g22890*), always greater in Icatu, whereas RuBisCO and Ru5PK showed maximal activities (both genotypes). This suggests a global investment in photosynthetic/chloroplast structures, in line with the strong lipid synthesis observed until 37/30°C, particularly in Icatu (Scotti-Campos et al., 2019). Such reinforcement of electron carriers, PGR5 and two NDH proteins, further highlights the presence of photoprotective CEF at PSI (Yamori et al., 2016; Sun et al., 2018) and PSII (Miyake and Okamura, 2003; Chu and Chiu, 2016) levels until 37/28°C, similarly to what was observed for drought conditions in Icatu. This complemented the antioxidative defences (*e.g.*, enzymes such as SOD, and APX, Martins et al., 2016), while maintaining ATP synthesis that can be used, among others, for *de novo* protein synthesis needed for the rapid repair of photodamaged PSII (Murata et al., 2007; Huang et al., 2018). Altogether, these responses would support the maintenance of high PSs performance (Rodrigues et al., 2016) or even an upregulation of the photosynthetic apparatus at 31/25°C (with maximal Cyt and A_{max} values in Icatu) and up to 37/28°C, despite the lower P_n values.

Membrane stability is a crucial feature to drought and heat tolerance (Elbasyoni et al., 2017). Furthermore, thylakoid membranes are considered highly sensitive to heat, and impacts on photochemistry are among the first indicators of sensitivity, with damages occurring at PSII and chloroplast ultrastructure (Mano, 2002). This seemed to occur only at 42/30°C, when most fluorescence parameters were significantly altered in WW plants, usually to a higher extent in Icatu, namely in PSII photochemical efficiency. F_0 rise (accompanied by F_v/F_m decline) may reflected the uncoupling of LHCII from the PSII reaction center (Ruban, 2016). This rise indicates that a threshold for irreversible photoinhibition on the PSII centers have been exceeded (Pastenes and Horton, 1999; Baker and Rosenqvist, 2004), and it has been used to estimate crop tolerance to high temperature. Furthermore, F_0 rise might have been related to an over fluidity of chloroplast membranes (Tovuu et al., 2013) associated with altered membrane properties and loss of fatty acids from 37/28°C to 42/30°C, as previously observed in these genotypes (Scotti-Campos et al., 2019), These impairments found in both genotypes at 42/30°C, are in line with the stronger increase in PSII inactivation (F_s/F_m'), the A_{max} decline, and the increase of non-regulated energy dissipation processes ($Y_{(NO)}$), especially in Icatu (**Tables 1** and **2**). Such $Y_{(NO)}$ increase is usually associated with constraints in the use of incident radiation (Huang et al., 2011), which in turn is largely related to an inability for photochemical energy conversion (reduced $Y_{(II)}$) as found in WW Icatu plants. Finally, this agrees with the rise in the rate constant for PSII inactivation (F_s/F_m') as well as with the lowest values of F_v/F_m and F_v'/F_m' in WW Icatu plants. Overall, these results suggest a higher sensitivity of Icatu than CL153 only under extreme heat. However, PSII activity maintained most of its potential (**Figure 2**), whereas PSs activities (**Figure 3**) and electron carrier contents (**Figure 4**) suffered only minor impacts at the maximal temperature in both genotypes, as compared to their respective controls. This contrasts with reports of heat sensitivity of PSII (namely at D1 protein and OEC level) (Komayama et al., 2007) and PSI (Ivanov et al., 2017; Chovancek et al., 2019) in other species, likely associated with unsuficient photoprotection as well as with heat-induced alterations on the structure, composition, and functional performance. Therefore, these results confirm a notable PSs preservation and a global photochemical functioning in coffee (Rodrigues et al., 2016), thus highlighting that thylakoid membranes function was largely uncompromised. To this would have likely contributed the significant quantitative and qualitative lipid profile adjustments in chloroplast membranes under heat (Scotti-Campos et al., 2019), and the maintenance or reinforcement of the pools of several protective and antioxidative molecules (Martins et al., 2016).

In sharp contrast with the reinforcement up to 37/28°C, RuBisCO and Ru5PK activities suffered the strongest impacts at 42/30°C among the parameters that explore the potential values (A_{max}, PSs activities), with at least a 65% reduction of their maximum activity values, thus reflecting much stronger impacts than those promoted. In contrast to was found up to 37/28°C, RuBisCO and Ru5PK activities were remarkably affected at 42/30°C to a gretear extent than was On the other hand, RuBisCO and Ru5PK activities were remarkably affected from 37/28°C to 42/30°C to a gretear extent than was by single drought exposure. In fact, RuBisCO was found to be the most heat sensitive component in the photosynthetic machinery of *Coffea* spp. (Rodrigues et al., 2016), which agrees with observations of major negative impacts on its activity over a range of abiotic stresses, with direct negative impacts on crop productivity (Galmés et al., 2013).

Impact of the Harsh Conditions of Combined Severe Water Deficit and High Temperature on Photosynthetic Functioning

Stress superimposition did not affect either tissue water status or modify the stomatal SD and SA patterns promoted by temperature. However, some interaction was depicted in P_n which tended to even lower values at 42/30°C than under the single exposure to drought (SWD plants at 25/20°C) or heat (WW plants at 42/30°C) in both genotypes. Since g_s was maintained at very low values, similar to those of SWD plants at 25/20°C, this additional P_n reduction has been likely to be related to further non-stomatal impacts which lead P_n to the minimal values observed over the entire experiment. In fact, severe drought may predispose the leaves to photoinhibitory damage given that a strong stomata closure will impose drastic restriction of CO_2 diffusion into the chloroplast, reducing photochemical energy use and promoting energy overcharge

(Baker and Rosenqvist, 2004; Haworth et al., 2018), with the concurrent need to an increased thermal energy dissipation ($Y_{(NPQ)}$). However, it seems relevant that in some cases at 42/30°C, the SWD plants displayed better values (*e.g.* F_0, $Y_{(NPQ)}$) than the WW plants, in both genotypes, as well also in F_v/F_m, and $Y_{(NO)}$ in Icatu, showing important resilience of these plants to stress combination. In fact, even under the most stressful conditions both genotypes did not show an increased non-regulated energy dissipation in PSII ($Y_{(NO)}$), which is known to rise only under harsh environmental conditions (Busch et al., 2009). Instead, $Y_{(NPQ)}$ reached maximum values, showing that protective mechanisms were still functioning to protect the photosynthetic apparatus from additional damages caused by the excessive excitation (Pompelli et al., 2010; Rodrigues et al., 2016), likely associated with the presence of photoprotective carotenoids (Martins et al., 2016; Ramalho et al., 2018b).

When looking at thylakoid-related photochemical events and components, the exposure to heat aggravated the drought impact (SWD plants) on the PSs activity, electron carriers and the proteins involved in CEF of both genotypes. However, while Icatu showed a negative interaction above 25/20°C, this was not observed in CL153 that showed an impact of drought at 25/20°C but some parameters were mostly insensitive to temperature rise in SWD plants. Electron carriers can be affected under abiotic stress conditions (Nouri et al., 2015) since they are close to the production sites of highly excited molecules of either chlorophyll or oxygen (Logan, 2005). Such oxidative stress conditions can promote the dissociation of the PSII oxygen evolving complex (*OEC*), resulting in greater inhibition of electron transport to the receptor side of PSII (Wang et al., 2018). This was not the case in coffee genotypes, which maintained close PSII activities either including or not the OEC, irrespective of stress conditions (**Figure 3**). In contrast, PSI photoinhibition can be mostly promoted by *ROS* produced on the receptor side of PSI through the Mehler reaction (Sonoike, 2011; Yan et al., 2013). PSI is often considered to be more resistant to photoinhibition through an efficient scavenging of *ROS* produced on the reducing side of PSI (Ozakca, 2013). In any case, under the present experimental conditions, PSI and PSII were affected to a similar extent within each genotype by drought (only CL153), by heat, or even by the stress combination, suggesting that thermal dissipation and/or antioxidative mechanisms protected both PSs indistinctly. In fact, it should be highlighted a high degree of tolerance of SWD plants given that relevant PSs activity and electron carrier contents were preserved under the harshest conditions, even under conditions in which CEF might had a limited role due to PGR5 and NDH proteins reduction at 42/30°C.

Finally, we have demonstrated that the combination of the highest temperature and drought exacerbated the impacts on RuBisCO and Ru5PK activities relative to those promoted by each single stress. In fact, with activity reductions higher than 80%, these enzymes were the most affected photosynthetic components, thus likely limiting the photosynthetic pathway, in good agreement with the minimal A_{max} values. This limiting point in the coffee acclimation to harsh environmental conditions clearly agreed with the estimates pointing that reductions in RuBisCO activity will be one of the main effects caused by climate change, and should be considered in prediction models on future plant productivity (Galmés et al., 2013). Indeed, given that only a few parameters showed an aggravated status under the imposition of both stresses, we contend that the impacts related to the Calvin-Benson cycle enzymes will play a key role in determining the performance of the photosynthetic apparatus irrespective of genotype.

Recovery From Stress Exposure and After Effects

Despite the superior performance of Icatu upon drought, and a relatively better performance of CL153 at the highest temperature, some interesting results were obtained along the recovery period after stress relief, with diverse promptness and extent of recoveries of physiological and biochemical parameters.

An almost full recovery of g_s and Ψ_{pd} was observed in SWD plants from both genotypes, although with a consistent trend to lower water status (*e.g.*, Ψ_{pd} values in CL153 until Rec14). This suggested a considerable tolerance of the hydraulic system under the harsh conditions of combined water deficit and heat.

However, some marked aftereffects persisted in plants submitted to the combined stresses (SWD plants), usually stronger in CL153, namely in A_{max}, $Y_{(NPQ)}$, F_v'/F_m', PSs activity, and *PQ-9* content. In fact, only the SWD CL153 plants were unable to show a full recovery of several parameters (*e.g.*, P_n, $Y_{(II)}$, $Y_{(NPQ)}$) by Rec14, denoting an exacerbated sensitivity to stress interaction. Also, F_s/F_m' was kept at high values by Rec14, in line with lower energy driven to photochemical events ($Y_{(II)}$) (all plants), and with some higher values of $Y_{(NPQ)}$ (SWD plants from both genotypes) or $Y_{(NO)}$ (WW and SWD plants of Icatu).

Several parameters recovered in WW plants of both genotypes (*e.g.*, A_{max}, F_v/F_m, F_v'/F_m', q_L, F_s/F_m', PQ-9 content), but a faster and/or greater recovery was observed in Icatu than in CL153 in WW or SWD plants (P_n, PSs activity, *Cyt f* and b_{563} contents, Ru5PK activity). This denotes lower impairments upon stress exposure and/or greater recovery capability. Overall, our data agree with previous findings for Icatu resilience involving improved antioxidative mechanisms and adjustments of chloroplast membrane lipids, which ultimately minimize oxidative damages under cold and/or drought (Fortunato et al., 2010; Partelli et al., 2011; Ramalho et al., 2014b; Ramalho et al., 2018b).

It was noteworthy that in a few cases the SWD plants recovered better than their WW counterparts (*e.g.*, PSs and Ru5PK activities, *Cyt* b_{559LP} and b_{563} contents in CL153; and RuBisCO and Ru5PK activities in Icatu), suggesting some degree of stress cross-tolerance related to protecting mechanisms of these photosynthetic components. This was likely related, at least partly, to a more effective *ROS* control, as also observed under the combined exposure to cold and drought (Ramalho et al., 2018b).

Finally, some aftereffects were observed by the end of the experiment, particularly in the plants exposed simultaneously to both stresses, thus justifying the plant response to maintain an increased potential for CEF and thermal dissipation mechanisms. Furthermore, most photosynthetic components recovered between Rec4 and Rec14, suggesting that coffee plants present

an interesting resilience to water scarcity and heat, which may help the sustainability of this crop in a scenario of climate variability.

CONCLUSIONS

In the context of ongoing climate changes and extreme weather events, this study thoroughly assessed the impacts of both single and combined drought and heat stressful conditions on the photosynthetic functioning.

Globally, single severe drought significantly affected most gas exchange and fluorescence parameters in both genotypes. This was likely associated with a prevalence of stomata limitations of photosynthesis particularly in Icatu, that showed a better photosynthetic performance and protection of both photosystems, associated with CEF involving PSII and PSI, together with the increase in thermal dissipation mechanisms (the latter in both genotypes). In contrast, in CL153, RuBisCO activities, electron transport rates and Cyt content were reduced, and only minor changes were observed regarding PG5 and NDH proteins. Notably, the reduction of energy use in photochemical events was compensated for by rises in photoprotection and not by uncontrolled energy dissipation in both genotypes, thus reflecting a common triggering of acclimation mechanisms to avoid damages.

A strong photosynthetic heat tolerance was found in WW plants until temperatures well above those considered adequate for the coffee crop. Most parameters related to the photosynthetic potential were barely affected up to 37/28°C or 39/30°C. Notably, CEF around both PSs was also likely involved in the response to heat, particularly in Icatu that showed increased values in all electron carriers, and PG5 and NDH proteins up to 37/28°C. A further increase to 42/30°C impacted most parameters, evidencing that the tolerance threshold in these genotypes was exceeded. At this temperature, g_s was mostly governed by stomata opening control than by stomatal morphological traits. In any case, the simultaneous reduction in A_{max} and increase in C_i indicate the prevalence of non-stomatal limitations of photosynthesis, particularly in RuBisCO and Ru5PK. These enzymes were, by far, the most sensitive components, in sharp contrast with PSs activity and electron carrier contents that were mostly unaffected, even with a reduction of PG5 and NDH proteins from 37/28 to 42/30°C.

Stress interaction was largely absent until 37/28°C, with drought being the main constraint until this temperature. However, the two extreme conditions (SWD plants at 42/30°C) aggravated some single stress impacts, with emphasis on the PSI, PSII, and enzymes activities, and electron carriers, the latter somewhat stronger in Icatu (as also in A_{max}). Noteworthy, even under such harsh conditions uncontrolled energy dissipation did not increase due to reinforcements in energy thermal dissipation.

Strong coffee's resilience to these stress conditions was observed given that most photosynthetic parameters recovered between the 4th and 14th days after stress relief. However, some aftereffects persisted, mostly in SWD plants ($Y_{(NPQ)}$, F_v'/F_m', PSs activity, Cyts) by the end of the experiment, justifying the maintenance of a higher potential for protective mechanisms, reflected in energy thermal dissipation and CEF. Among genotypes, Icatu showed a faster and/or greater recovery in WW or SWD plants in several parameters (P_n, F_v'/F_m', q_N, PSs and enzymes activities, most electron carriers content) than did CL153.

Overall, genotype-related impacts on the photosynthetic performance were observed under the exposure to the two major environmental constraints, and their interaction. Icatu was more tolerant to drought, and displayed a better recovery after stress relief. Both genotypes were clearly tolerant until 37/28°C, but were deeply affected at 42/30°C, with some additional impacts under the stress superimposition (*e.g.*, RuBisCO activity and electron carriers). The photochemical components were highly tolerant to drought (Icatu), heat and stress interaction (both genotypes), in sharp contrast with enzymes (RuBisCO and Ru5PK) that were highly sensitive, thus, deserving special attention in breeding programs regarding these environmental limiting conditions.

DATA AVAILABILITY STATEMENT

The mass spectrometry proteomics data have been deposited to the ProteomeXchange Consortium via the PRIDE partner repository with the dataset identifier PXD019474 and DOI: 10.6019/PXD019474 for *C. arabica* proteome, and the dataset identifier PXD019541 and DOI: 10.6019/PXD019541 for *C. canephora* proteome.

AUTHOR CONTRIBUTIONS

DD: Investigation, formal analysis, writing (original draft). FL: Conceptualization, Investigation, writing (review and editing), project administration. AR: Investigation, validation, formal analysis. JS: Investigation, formal analysis. IMa: Investigation, validation, formal analysis. DG: Investigation, visualization, formal analysis. JA: Investigation, visualization, formal analysis, supervision. MS: Investigation, validation, formal analysis. SM: Investigation, validation, formal analysis. WR: Investigation, formal analysis, writing (review and editing); MS-C: Investigation, validation, formal analysis; IMo: Investigation, validation. formal analysis; IP: Investigation, validation, formal analysis; PS-C: Investigation, validation; FP: Investigation, supervision; EC: Investigation, supervision, writing (review and editing); AR-B: Conceptualization, investigation, formal analysis, supervision, Funding acquisition;. FD: Conceptualization, Data Analysis, writing (review and editing); JR: Conceptualization, investigation, visualization, data analysis, supervision, project administration, funding acquisition, writing (original draft, review and editing).

FUNDING

This work received funding from the European Union's Horizon 2020 research and innovation program under grant agreement No 727934 (project BreedCAFS), and from national funds from

Fundação para a Ciência e a Tecnologia (FCT), Portugal, through the project PTDC/ASP-AGR/31257/2017, and the research units UIDB/00239/2020 (CEF), and UIDP/04035/2020 (GeoBioTec). Funding from Brazil through FAPERJ (grant E-26/202.323/2017, WR) and CNPq (FP, EC, and FD) are also greatly acknowledged.

ACKNOWLEDGMENTS

The authors would like to thank Novadelta – Comércio e Indústria de Cafés Lda., as well as Tech. Paula Alves for technical assistance.

REFERENCES

Baker, N. R., and Rosenqvist, E. (2004). Applications of chlorophyll fluorescence can improve crop production strategies: an examination of future possibilities. *J. Exp. Bot.* 55, 1607–1621. doi: 10.1093/jxb/erh196

Bradford, M. M. (1976). A rapid and sensitive method for the quantitation of microgram quantities of protein utilizing the principle of protein-dye binding. *Anal. Biochem.* 72, 248–254. doi: 10.1006/abio.1976.9999

Bunn, C., Läderach, P., Rivera, O. O., and Kirschke, D. (2015). A bitter cup: climate change profile of global production of Arabica and Robusta coffee. *Clim. Change* 129, 89–101. doi: 10.1007/s10584-014-1306-x

Busch, F., Hunter, N. P. A., and Ensminger, I. (2009). Biochemical constrains limit the potential of the photochemical reflectance index as a predictor of effective quantum efficiency of photosynthesis during the winter-spring transition in Jack pine seedlings. *Funct. Plant Biol.* 36, 1016–1026. doi: 10.1071/FP08043

Chaves, M. M., Maroco, J. P., and Pereira, J. S. (2003). Understanding plant responses to drought – from genes to the whole plant. *Funct. Plant Biol.* 30, 239–264. doi: 10.1071/FP02076

Chaves, M. M., Flexas, J., and Pinheiro, C. (2009). Photosynthesis under drought and salt stress: regulation mechanisms from whole plant to cell. *Ann. Bot.* 103, 551–560. doi: 10.1093/aob/mcn125

Chen, Y.-E., Liu, W.-J., Su, Y.-Q., Cui, J.-M., Zhang, X.-W., Yuan, M., et al. (2016). Different response of photosystem II to short and long-term drought stress in Arabidopsis thaliana. *Physiol. Plant* 158, 225–235. doi: 10.1111/ppl.12438

Chovancek, E., Zivcak, M., Botyanszka, L., Hauptvogel, P., Yang, X., Misheva, D., et al. (2019). Transient heat waves may affect the photosynthetic capacity of susceptible wheat genotypes due to insuficient photosystem I photoprotection. *Plants* 8, 282. doi: 10.3390/plants8080282

Chu, H.-A., and Chiu, Y.-F. (2016). The Roles of cytochrome b_{559} in assembly and photoprotection of Photosystem II revealed by site-directed mutagenesis studies. *Front. Plant Sci.* 6, 1261. doi: 10.3389/fpls.2015.01261

Crafts-Brandner, S. J., and Salvucci, M. E. (2000). Rubisco activase constrains the photosynthetic potential of leaves at high temperature and CO_2. *PNAS* 97, 13430–13435. doi: 10.1073/pnas.230451497

DaMatta, F. M., and Ramalho, J. C. (2006). Impacts of drought and temperature stress on coffee physiology and production: a review. *Braz. J. Plant Physiol.* 18, 55–81. doi: 10.1590/S1677-04202006000100006

DaMatta, F. M., Chaves, A. R. M., Pinheiro, H. A., Ducatti, C., and Loureiro, M. E. (2003). Drought tolerance of two feld-grown clones of *Coffea canephora*. *Plant Sci.* 164, 111–117. doi: 10.1016/S0168-9452(02)00342-4

DaMatta, F. M., Godoy, A. G., Menezes-Silva, P. E., Martins, S. C. V., Sanglard, L. M. V. P., Morais, L. E., et al. (2016). Sustained enhancement of photosynthesis in coffee trees grown under free-air CO_2 enrichment conditions: disentangling the contributions of stomatal, mesophyll, and biochemical limitations. *J. Exp. Bot.* 67, 341–352. doi: 10.1093/jxb/erv463

DaMatta, F. M., Avila, R. T., Cardoso, A. A., Martins, S. C. V., and Ramalho, J. C. (2018). Physiological and agronomic performance of the cofee crop in the context of climate change and global warming: a review. *J. Agric. Food Chem.* 66, 5264–5274. doi: 10.1021/acs.jafc.7b04537

DaMatta, F. M., Rahn, E., Läderach, P., Ghini, R., and Ramalho, J. C. (2019). Why could the coffee crop endure climate change and global warming to a greater extent than previously estimated? *Clim. Change* 152, 167–178. doi: 10.1007/s10584-018-2346-4

Davis, A. P., Chadburn, H., Moat, J., O'Sullivan, R., Hargreaves, S., and Lughadha, E. N. (2019). High extinction risk for wild coffee species and implications for coffee sector sustainability. *Sci. Adv.* 5, eaav3473. doi: 10.1126/sciadv.aav3473

Denoeud, F., Carretero-Paulet, L., Dereeper, A., Droc, G., Guyot, R., Pietrella, M., et al. (2014). The coffee genome provides insight into the convergent evolution of caffeine biosynthesis. *Science* 345, 1181–1184. doi: 10.1126/science.1255274

Dias, P. C., Araujo, W. L., Moraes, G. A. B. K., Barros, R. S., and DaMatta, F. M. (2007). Morphological and physiological responses of two coffee progenies to soil water availability. *J. Plant Physiol.* 164, 1639–1647. doi: 10.1016/j.jplph.2006.12.004

Droppa, M., Masojidek, J., Rózsa, Z., Wolak, A., Horváth, L. I., Farkas, T., et al. (1987). Characteristics of Cu deficiency induced inhibition of photosynthetic electron transport in spinach chloroplasts. *Biochim. Biophys. Acta* 891, 75–84. doi: 10.1016/0005-2728(87)90085-5

Dusenge, M. E., Duarte, A. G., and Way, D. A. (2019). Plant carbon metabolism and climate change: elevated CO_2 and temperature impacts on photosynthesis, photorespiration and respiration. *New Phytol.* 221, 32–49. doi: 10.1111/nph.15283

Elbasyoni, I., Saadalla, M., Baenziger, S., Bockelman, H., and Morsy, S. (2017). Cell membrane stability and association mapping for drought and heat tolerance in a worldwide wheat collection. *Sustainability* 9, 1606. doi: 10.3390/su9091606

Fahad, S., Bajwa, A. A., Nazir, U., Anjum, S. A., Farooq, A., Zohaib, A., et al. (2017). Crop production under drought and heat stress: plant responses and management options. *Front. Plant Sci.* 8, 1147. doi: 10.3389/fpls.2017.01147

Fortunato, A., Lidon, F. C., Batista-Santos, P., Leitão, A. E., Pais, I. P., Ribeiro, A. I., et al. (2010). Biochemical and molecular characterization of the antioxidative system of *Coffea* sp. under cold conditions in genotypes with contrasting tolerance. *J. Plant Physiol.* 167, 333–342. doi: 10.1016/j.jplph.2009.10.013

Franks, P. J., and Beerling, D. J. (2009). Maximum leaf conductance driven by CO_2 effects on stomatal size and density over geologic time. *Proc. Nat. Acad. Sci. U.S.A.* 106, 10343–10347. doi: 10.1073/pnas.0904209106

Galmés, J., Aranjuelo, I., Medrano, H., and Flexas, J. (2013). Variation in Rubisco content and activity under variable climatic factors. *Photosynth. Res.* 117, 73–90. doi: 10.1007/s11120-013-9861-y

Grisi, F. A., Alves, J. D., Castro, E. M., Oliveira, C., Biagiotti, G., and Melo, L. A. (2008). Leaf anatomical evaluations in 'Catuaí' and 'Siriema' coffee seedlings submitted to water stress. *Ciência Agrotec.* 32, 1730–1736. doi: 10.1590/S1413-70542008000600008

Haldimann, P., and Feller, U. (2004). Inhibition of photosynthesis by high temperature in oak (*Quercus pubescens* L.) leaves grown under natural conditions closely correlates with a reversible heat-dependent reduction of the activation state of ribulose-1,5-bisphosphate carboxylase/oxygenase. *Plant Cell Environ.* 27, 1169–1183. doi: 10.1111/j.1365-3040.2004.01222.x

Hartmann, E. M., Allain, F., Gaillard, J. C., Pible, O., and Armengaud, J. (2014). Taking the shortcut for high-throughput shotgun proteomic analysis of bacteria. *Methods Mol. Biol.* 1197, 275–285. doi: 10.1007/978-1-4939-1261-2_16

Hasanuzzaman, M., Nahar, K., Alam, M. M., Roychowdhury, R., and Fujita, M. (2013). Physiological, biochemical, and molecular mechanisms of heat stress tolerance in plants. *Int. J. Mol. Sci.* 14, 9643–9684. doi: 10.3390/ijms14059643

Haworth, M., Marino, G., Brunetti, C., Killi, D., De Carlo, A., and Centritto, M. (2018). The impact of heat stress and water deficit on the photosynthetic and stomatal physiology of olive (*Olea europaea* L.). A case study of the 2017 heat wave. *Plants* 7, pii: E76. doi: 10.3390/plants7040076

Hoekstra, F. A., Golovina, E. A., and Buitink, J. (2001). Mechanisms of plant desiccation tolerance. *Trends Plant Sci.* 6, 431–438. doi: 10.1016/S1360-1385(01)02052-0

Houchins, J. P., and Hind, G. (1984). Concentration and function of membrane-bound cytochromes in cyanobacterial heterocysts. *Plant Physiol.* 76, 456–460. doi: 10.1104/pp.76.2.456

Huang, W., Zhang, S.-B., and Cao, K.-F. (2011). Cyclic electron flow plays an important role in photoprotection of tropical trees illuminated at temporal chilling temperature. *Plant Cell Physiol.* 52, 297–305. doi: 10.1093/pcp/pcq166

Huang, W., Yang, Y.-J., Zhang, S.-B., and Liu, T. (2018). Cyclic electron flow around photosystem I promotes ATP synthesis possibly helping the rapid

repair of photodamaged photosystem II at low light. *Front. Plant Sci.* 9, 239. doi: 10.3389/fpls.2018.00239

IPCC - Intergovernmental Panel on Climate Change (2014). *Climate Change 2014: Mitigation of Climate Change. Contribution of Working Group III to the Fifth Assessment Report of the Intergovernmental Panel on Climate Change*. Eds. O. Edenhofer, R. Pichs-Madruga, Y. Sokona, E. Farahani, S. Kadner, K. Seyboth, A. Adler, I. Baum, S. Brunner, P. Eickemeier, B. Kriemann, J. Savolainen, S. Schlömer, C. Von Stechow, T. Zwickel and J. C. Minx (Cambridge, United Kingdom and New York, NY, USA: Cambridge University Press).

IPCC - Intergovernmental Panel on Climate Change (2018). "Summary for policymakers," in *Global warming of 1.5°C. An IPCC Special Report on the impacts of global warming of 1.5°C above pre -industrial levels and related global greenhouse gas emission pathways, in the context of strengthening the global response to the threat of climate change, sustainable development, and efforts to eradicate poverty*. Eds. V. Masson -Delmotte, P. Zhai, H. O. Pörtner, D. Roberts, J. Skea, P. R. Shukla, A. Pirani, W. Moufouma -Okia, C. Péan, R. Pidcock, S. Connors, J. B. R. Matthews, Y. Chen, X. Zhou, M. I. Gomis, E. Lonnoy, T. Maycock, M. Tignor and T. Waterfield (Switzerland: World Meteorological Organization).

Ivanov, A. G., Velitchkova, M. Y., Allakhverdiev, S. I., and Huner, N. P. A. (2017). Heat stress-induced effects of photosystem I: an overview of structural and functional responses. *Photosynth. Res.* 133, 17–30. doi: 10.1007/s11120-017-0383-x

Klein, G., Mathé, C., Biola-Clier, M., Devineau, S., Drouineau, E., Hatem, E., et al. (2016). RNA-binding proteins are a major target of silica nanoparticles in cell extracts. *Nanotoxicol* 10, 1555–1564. doi: 10.1080/17435390.2016.1244299

Klughammer, C., and Schreiber, U. (2008). Complementary PSII quantum yields calculated from simple fluorescence parameters measured by PAM fluorometry and the Saturation Pulse method. *PAM Appl. Notes* 1, 27–35.

Kohzuma, K., Cruz, J. A., Akashi, K., Hoshiyasu, S., Munekage, Y. N., Yokota, A., et al. (2009). The long-term responses of the photosynthetic proton circuit to drought. *Plant Cell Environ.* 32, 209–219. doi: 10.1111/j.1365-3040.2008.01912.x

Komayama, K., Khatoon, M., Takenaka, D., Horie, J., Yamashita, A., Yoshioka, M., et al. (2007). Quality control of Photosystem II: Cleavage and aggregation of heat-damaged D1 protein in spinach thylakoids. *Biochim. Biophys. Acta* 1767, 838–846. doi: 10.1016/j.bbabio.2007.05.001

Kramer, D. M., Johnson, G., Kiirats, O., and Edwards, G. E. (2004). New flux parameters for the determination of Q_A redox state and excitation fluxes. *Photosynth. Res.* 79, 209–218. doi: 10.1023/B:PRES.0000015391.99477.0d

Ksas, B., Légeret, B., Ferretti, U., Chevalier, A., Pospisil, P., Alric, J., et al. (2018). The plastoquinone pool outside the thylakoid membrane serves in plant photoprotection as a reservoir of singlet oxygen scavengers. *Plant Cell Environ.* 41, 2277–2287. doi: 10.1111/pce.13202

Laisk, A., Eichelmann, H., Oja, V., Rasulov, B., and Rämma, H. (2006). Photosystem II cycle and alternative electron flow in leaves. *Plant Cell Physiol.* 47, 972–983. doi: 10.1093/pcp/pcj070

Lamaoui, M., Jemo, M., Datla, R., and Bekkaoui, F. (2018). Heat and drought stresses in crops and approaches for their mitigation. *Front. Chem.* 6, 26. doi: 10.3389/fchem.2018.00026

Lambers, H., Chapin, F.S. III, and Pons, T. L. (2008). *Plant Physiological Ecology. 2nd Edn.* (New York: Springer-Verlag). doi: 10.1007/978-0-387-78341-3

Li, H., Chang, J., Chen, H., Wang, Z., Gu, X., Wei, C., et al. (2017). Exogenous melatonin confers salt stress tolerance to watermelon by improving photosynthesis and redox homeostasis. *Front. Plant Sci.* 8, 295. doi: 10.3389/fpls.2017.00295

Logan, B. A. (2005). "Reactive Oxygen Species and Photosynthesis Chapter 10," in *Antioxidants and Reactive Oxygen in Plants*. Ed. N. N. Smirnoff (Oxford: Blackwell Publishing), 250–267. doi: 10.1002/9780470988565.ch10

Long, S. P., Ainsworth, E. A., Leakey, A. D. B., Nösberger, J., and Ort, D. R. (2006). Food for thought: lower-than-expected crop yield stimulation with rising CO_2 concentrations. *Science* 312, 1918–1921. doi: 10.1126/science.1114722

Los, D. A., and Zinchenko, V. V. (2009). "Regulatory role of membrane fluidity in gene expression Chapter 15," in *Lipids in Photosynthesis: Essential and Regulatory Functions Series Advances in Photosynthesis and Respiration* Vol. 30. Eds. H. Wada and N. Murata (Dordrecht: Springer Verlag), 329–348. doi: 10.1007/978-90-481-2863-1_15

Mano, J. (2002). "Early events in environmental stresses in plants – induction mechanisms of oxidative stress Chapter 9," in *Oxidative Stress in Plants*. Eds. D. Inzé and M. M. Van Montagu (London: Taylor & Francis), 217–245.

Martins, L. D., Tomaz, M. A., Lidon, F. C., and Ramalho, J. C. (2014). Combined effects of elevated [CO_2] and high temperature on leaf mineral balance in *Coffea* spp. plants. *Clim. Change* 126, 365–379. doi: 10.1007/s10584-014-1236-7

Martins, M. Q., Rodrigues, W. P., Fortunato, A. S., Leitão, A. E., Rodrigues, A. P., Pais, I. P., et al. (2016). Protective response mechanisms to heat stress in interaction with high [CO_2] conditions in *Coffea* spp. *Front. Plant Sci.* 7, 947. doi: 10.3389/fpls.2016.00947

Martins, S. C. V., Sanglard, M. L., Morais, L. E., Menezes-Silva, P. E., Mauri, R., Avila, R. T., et al. (2019). How do coffee trees deal with severe natural droughts? An analysis of hydraulic, diffusive and biochemical components at the leaf level. *Trees* 33, 1679–1693. doi: 10.1007/s00468-019-01889-4

Melo, E. F., Fernandes-Brum, C. N., Pereira, F. J., Castro, E. M., and Chalfun-Júnior, A. (2014). Anatomic and physiological modifications in seedlings of *Coffea arabica* cultivar Siriema under drought conditions. *Ciência Agrotec.* 38, 25–33. doi: 10.1590/S1413-70542014000100003

Mittler, R. (2006). Abiotic stress, the field environment and stress combination. *Trends Plant Sci.* 11, 15–19. doi: 10.1016/j.tplants.2005.11.002

Miyake, C., and Okamura, M. (2003). Cyclic electron flow within PSII protects PSII from its photoinhibition in thylakoid membranes from spinach chloroplasts. *Plant Cell Physiol.* 44, 457–462. doi: 10.1093/pcp/pcg053

Murata, N., Takahashi, S., Nishiyama, Y., and Allakhverdiev, S. I. (2007). Photoinhibition of photosystem II under environmental stress. *Biochim. Biophys. Acta* 1767, 414–421. doi: 10.1016/j.bbabio.2006.11.019

Murchie, E. H., and Lawson, T. (2013). Chlorophyll fluorescence analysis: a guide to good practice and understanding some new applications. *J. Exp. Bot.* 64, 3983–3998. doi: 10.1093/jxb/ert208

NOAA (2019). *Climate change: Atmospheric carbon dioxide*. Climate.gov, USA (Accessed at https://www.climate.gov/news-features/understanding-climate/climate-change-atmospheric-carbon-dioxide, November 2019).

Nouri, M. Z., Moumeni, A., and Komatsu, S. (2015). Abiotic Stresses: Insight into gene regulation and protein expression in photosynthetic pathways of plants. *Int. J. Mol. Sci.* 16, 20392–20416. doi: 10.3390/ijms160920392

Nunes, M. A., Ramalho, J. C., and Dias, M. A. (1993). Effect of nitrogen supply on the photosynthetic performance of leaves from coffee plants exposed to bright light. *J. Exp. Bot.* 44, 893–899. doi: 10.1093/jxb/44.5.893

Osakabe, Y., Osakabe, K., Shinozaki, K., and Tran, L.-S. P. (2014). Response of plants to water stress. *Front. Plant Sci.* 5, 86. doi: 10.3389/fpls.2014.00086

Osório, M. L., Breia, E., Rodrigues, A., Osório, J., Roux, X. L., Daudet, F. A., et al. (2006). Limitations to carbon assimilation by mild drought in nectarine trees growing under field conditions. *Environ. Exp. Bot.* 55, 235–247. doi: 10.1016/j.envexpbot.2004.11.003

Osorio, N. (2002). *The Global Coffee Crisis: A Threat to Sustainable Development* (London: International Coffee Organization).

Oukarroum, A., Schansker, G., and Strasser, R. J. (2009). Drought stress effects on photosystem I content and photosystem II thermotolerance analyzed using Chl a fluorescence kinetics in barley varieties differing in their drought tolerance. *Physiol. Plant* 137, 188–199. doi: 10.1111/j.1399-3054.2009.01273.x

Ozakca, D. U. (2013). "Effect of abiotic stress on photosystem i-related gene transcription in photosynthetic organisms," in *Photosynthesis*. Ed. Z. Dubinsky (London: IntechOpen), 57–85. doi: 10.5772/intechopen.72374

Parkhey, S., Chandrakar, V., Naithani, S. C., and Keshavkant, S. (2015). Efficient extraction of proteins from recalcitrant plant tissue for subsequent analysis by two-dimensional gel electrophoresis. *J. Separation Sci.* 38, 3622–3628. doi: 10.1002/jssc.201500415

Partelli, F. L., Batista-Santos, P., Campos, P. S., Pais, I. P., Quartin, V. L., Vieira, H. D., et al. (2011). Characterization of the main lipid components of chloroplast membranes and cold induced changes in *Coffea* sp. *Environ. Exp. Bot.* 74, 194–204. doi: 10.1016/j.envexpbot.2011.06.001

Pastenes, C., and Horton, H. (1999). Resistance of photosynthesis to high temperature in two bean varieties (*Phaseolus vulgaris* L.). *Photosyn. Res.* 62, 197–203. doi: 10.1023/A:1006391113097

Peloso, A. F., Tatagiba, S. D., Reis, E. F., Pezzopane, J. E. M., and Amaral, J. F. T. (2017). Photosynthetic limitations in leaves of arabic coffee promoted by the water deficit. *Coffee Sci.* 12, 389–399. doi: 10.25186/cs.v12i3.1314

Pinheiro, H. A., DaMatta, F. M., Chaves, A. R. M., Fontes, E. P. B., and Loureiro, M. E. (2004). Drought tolerance in relation to protection against oxidative stress in clones of *Coffea canephora* subjected to long-term drought. *Plant Sci.* 167, 1307–1314. doi: 10.1016/j.plantsci.2004.06.027

Pompelli, M. F., Martins, S. C. V., Antunes, W. C., Chaves, A. R. M., and DaMatta, F. M. (2010). Photosynthesis and photoprotection in coffee leaves is affected by nitrogen and light availabilities in winter conditions. *J. Plant Physiol.* 167, 1052–1060. doi: 10.1016/j.jplph.2010.03.001

Ramalho, J. C., Campos, P. S., Quartin, V. L., Silva, M. J., and Nunes, M. A. (1999). High irradiance impairments on photosynthetic electron transport, ribulose-1,5-bisphosphate carboxilase/oxygenase and N assimilation as a function of N availability in *Coffea arabica* L. plants. *J. Plant Physiol.* 154, 319–326. doi: 10.1016/S0176-1617(99)80174-6

Ramalho, J. C., Quartin, V., Leitão, A. E., Campos, P. S., Carelli, M. L., Fahl, J. I., et al. (2003). Cold acclimation ability of photosynthesis among species of the tropical *Coffea* genus. *Plant Biol.* 5, 631–641. doi: 10.1055/s-2003-44688

Ramalho, J. C., Fortunato, A. S., Goulao, L. F., and Lidon, F. C. (2013a). Cold-induced changes in mineral content in leaves of *Coffea* spp. Identification of descriptors for tolerance assessment. *Biol. Plant* 57, 495–506. doi: 10.1007/s10535-013-0329-x

Ramalho, J. C., Rodrigues, A. P., Semedo, J. N., Pais, I. P., Martins, L. D., Simões-Costa, M. C., et al. (2013b). Sustained photosynthetic performance of *Coffea* spp. under long-term enhanced [CO_2]. *PloS One* 8, e82712. doi: 10.1371/journal.pone.0082712

Ramalho, J. C., Zlatev, Z. S., Leitão, A. E., Pais, I. P., Fortunato, A., and Lidon, F. C. (2014a). Moderate water stress causes differential stomatal and non-stomatal changes on the photosynthetic functioning of *Phaseolus vulgaris* L. genotypes. *Plant Biol.* 16, 133–146. doi: 10.1111/plb.12018

Ramalho, J. C., DaMatta, F. M., Rodrigues, A. P., Scotti-Campos, P., Pais, I., Batista-Santos, P., et al. (2014b). Cold impact and acclimation response of *Coffea* spp. plants. *Theor. Exp. Plant Physiol.* 26, 5–18. doi: 10.1007/s40626-014-0001-7

Ramalho, J. C., Pais, I. P., Leitão, A. E., Guerra, M., Reboredo, F. H., Máguas, C. M., et al. (2018a). Can elevated air [CO_2] conditions mitigate the predicted warming impact on the quality of coffee bean? *Front. Plant Sci.* 9, 287. doi: 10.3389/fpls.2018.00287

Ramalho, J. C., Rodrigues, A. P., Lidon, F. C., Marques, L. M. C., Leitão, A. E., Fortunato, A. F., et al. (2018b). Stress cross-response of the antioxidative system promoted by superimposed drought and cold conditions in *Coffea* spp. *PloS One* 13, e0198694. doi: 10.1371/journal.pone.0198694

Redfearn, E. R., and Friend, J. (1962). Studies on plastoquinone-1. Determination of the concentration and oxidation-reduction state of plastoquinone in isolated chloroplasts. *Phytochem* 1, 147–151. doi: 10.1016/S0031-9422(00)82816-2

Rodrigues, W. P., Martins, M. Q., Fortunato, A. S., Rodrigues, A. P., Semedo, J. N., Simões-Costa, M. C., et al. (2016). Long-term elevated air [CO_2] strengthens photosynthetic functioning and mitigates the impact of supra-optimal temperatures in tropical *Coffea arabica* and *C. canephora* species. *Global Change Biol.* 22, 415–431. doi: 10.1111/gcb.13088

Rodrigues, W. P., Silva, J. R., Ferreira, L. S., Machado Filho, J. A., Figueiredo, F. A., Ferraz, T. M., et al. (2018). Stomatal and photochemical limitations of photosynthesis in *Coffea* sp. plants subjected to elevated temperatures. *Crop Past. Sci.* 69, 317–325. doi: 10.1071/CP17044

Ruban, A. V. (2016). Nonphotochemical chlorophyll fluorescence quenching: Mechanism and effectiveness in protecting plants from photodamage. *Plant Physiol.* 170, 1903–1916. doi: 10.1104/pp.15.01935

Sanda, S., Yoshida, K., Kuwano, M., Kawamura, T., Munekage, Y. N., Akashi, K., et al. (2011). Responses of the photosynthetic electron transport system to excess light energy caused by water deficit in wild watermelon. *Physiol. Plant* 142, 247–264. doi: 10.1111/j.1399-3054.2011.01473.x

Santos, A. B., and Mazzafera, P. (2012). Dehydrins are highly expressed in water stressed plants of two coffee species. *Trop. Plant Biol.* 5, 218–232. doi: 10.1007/s12042-012-9106-9

Schölander, P. F., Hammel, H. T., Bradstreet, E. D., and Hemmingsen, E. A. (1965). Sap pressure in vascular plants. *Science* 148, 339–346. doi: 10.1126/science.148.3668.339

Schöttler, M. A., and Toth, S. Z. (2014). Photosynthetic complex stoichiometry dynamics in higher plants: environmental acclimation and photosynthetic flux control. *Front. Plant Sci.* 5, 188. doi: 10.3389/fpls.2014.00188

Schreiber, U. (2004). "Pulse-Amplitude-Modulation (PAM) fluorometry and saturation pulse method: an overview Chapter 11," in *Chlorophyll a Fluorescence: A Signature of Photosynthesis Advances in Photosynthesis and Respiration*, vol. 19 . Eds. G. C. Papageorgiou and Govindjee, (Dordrecht: Springer), 279–319. doi: 10.1007/978-1-4020-3218-9_11

Scotti-Campos, P., Pais, I. P., Ribeiro-Barros, A. I., Martins, L. D., Tomaz, M. A., Rodrigues, W. P., et al. (2019). Lipid profile adjustments may contribute to warming acclimation and to heat impact mitigation by elevated [CO_2] in *Coffea* spp. *Environ. Exp. Bot.* 167, 103856. doi: 10.1016/j.envexpbot.2019.103856

Sehgal, A., Sita, K., Kumar, J., Kumar, S., Singh, S., Siddique, K. H. M., et al. (2017). Effects of drought, heat and their interaction on the growth, yield and photosynthetic function of lentil (*Lens culinaris* Medikus) genotypes varying in heat and drought sensitivity. *Front. Plant Sci.* 8, 1776. doi: 10.3389/fpls.2017.01776

Semedo, J. N., Rodrigues, W. P., Martins, M. Q., Martins, L. D., Pais, I. P., Rodrigues, A. P., et al. (2018). "Coffee responses to drought, warming and high [CO_2] in a context of future climate change scenarios Chapter 26," in *Theory and Practice of Climate Adaptation Climate Change Management Series*. Eds. F. Alves, W. Leal and U. Azeiteiro (Cham: Springer), 465–477. doi: 10.1007/978-3-319-72874-2

Shikanai, T., and Yamamoto, H. (2017). Contribution of cyclic and pseudo-cyclic electron transport to the formation of proton motive force in chloroplasts. *Mol. Plant* 10, 20–29. doi: 10.1016/j.molp.2016.08.004

Shinopoulos, K. E., and Brudvig, G. W. (2012). Cytochrome b559 and cyclic electron transfer within Photosystem II. *Biochim. Biophys. Acta* 1817, 66–75. doi: 10.1016/j.bbabio.2011.08.002

Silva, V. A., Salgado, S. M. L., Sá, L. A., Reis, A. M., Silveira, H. R. O., Mendes, A. N. G., et al. (2015). Use of physiological characteristics to identify genotypes of arabic coffee tolerant to *Meloidogyne paranaensis*. *Coffee Sci.* 10, 242–250. doi: 10.25186/cs.v10i2.868

Song, Y., Chen, Q., Ci, D., Shao, X., and Zhang, D. (2014). Effects of high temperature on photosynthesis and related gene expression in poplar. *BMC Plant Biol.* 14, 111. doi: 10.1186/1471-2229-14-111

Sonoike, K. (2011). Photoinhibition of photosystem I. *Physiol. Plant* 42, 56–64. doi: 10.1111/j.1399-3054.2010.01437.x

Souza, C. R., Maroco, J., Santos, T. P., Rodrigues, M. L., Lopes, C., Pereira, J. S., et al. (2005). Control of stomatal aperture and carbon uptake by deficit irrigation in two grapevine cultivars. *Agric. Ecosyst. Environ.* 106, 261–274. doi: 10.1016/j.agee.2004.10.014

Spiller, S., and Terry, N. (1980). Limiting factors in photosynthesis. Iron stress diminishes photochemical capacity by reducing the number of photosynthetic units. *Plant Physiol.* 65, 121–125. doi: 10.1104/pp.65.1.121

Stirbet, A., and Govindjee, S. A. (2011). On the relation between the Kautsky effect (chlorophyll a fluorescence induction) and Photosystem II: basics and applications of the OJIP fluorescence transient. *J. Photochem. Photobiol. (B.: Biol.)* 104, 236–257. doi: 10.1016/j.jphotobiol.2010.12.010

Sun, Y., Gao, Y., Wang, H., Yang, X., Zhai, H., and Du, Y. (2018). Stimulation of cyclic electron flow around PSI as a response to the combined stress of high light and high temperature in grape leaves. *Funct. Plant Biol.* 45, 1038–1045. doi: 10.1071/FP17269

Tazoe, Y., Hanba, Y. T., Furumoto, T., Noguchi, K., and Terashima, I. (2008). Relationships between quantum yield for co_2 assimilation, activity of key enzymes and CO_2 leakiness in *Amaranthus cruentus*, a C4 dicot, grown in high or low light. *Plant Cell Physiol.* 49, 19–29. doi: 10.1093/pcp/pcm160

Tovuu, A., Zulfugarov, I. S., and Lee, C. (2013). Correlations between the temperature dependence of chlorophyll fluorescence and the fluidity of thylakoid membranes. *Physiol. Plant* 147 (4), 409–416. doi: 10.1111/j.1399-3054.2012.01700.x

Urban, O., Hlaváčová, M., Klem, K., Novotná, K., Rapantová, B., Smutná, P., et al. (2018). Combined effects of drought and high temperature on photosynthetic characteristics in four winter wheat genotypes. *Field Crops Res.* 223, 137–149. doi: 10.1016/j.fcr.2018.02.029

Vu, J. C. V., Gesch, R. W., Allen, L. H., Boote, K. J., and Bowes, G. (1999). CO_2 enrichment delays a rapid, drought-induced decrease in Rubisco small subunit

transcript abundance. *J. Plant Physiol.* 155, 139–142. doi: 10.1016/S0176-1617(99)80156-4

Wahid, A., Gelani, S., Ashraf, M., and Foolad, M. R. (2007). Heat tolerance in plants: An overview. *Environ. Exp. Bot.* 61, 199–223. doi: 10.1016/j.envexpbot.2007.05.011

Wang, Q.-L., Chen, J.-H., He, N.-Y., and Guo, F.-Q. (2018). Metabolic reprogramming in chloroplasts under heat stress in plants. *Int. J. Mol. Sci.* 19, 849. doi: 10.3390/ijms19030849

Yamori, W., Makino, A., and Shikanai, T. (2016). A physiological role of cyclic electron transport around photosystem I in sustaining photosynthesis under fluctuating light in rice. *Sci. Rep.* 6, 20147. doi: 10.1038/srep20147

Yan, K., Chen, P., Shao, H., Shao, C., Zhao, S., and Bestric, M. (2013). Dissection of photosynthetic electron transport process in sweet sorghum under heat stress. *PloS One* 8, e62100. doi: 10.1371/journal.pone.0062100

Conflict of Interest: The authors declare that the research was conducted in the absence of any commercial or financial relationships that could be construed as a potential conflict of interest.

Copyright © 2020 Dubberstein, Lidon, Rodrigues, Semedo, Marques, Rodrigues, Gouveia, Armengaud, Semedo, Martins, Simões-Costa, Moura, Pais, Scotti-Campos, Partelli, Campostrini, Ribeiro-Barros, DaMatta and Ramalho. This is an open-access article distributed under the terms of the Creative Commons Attribution License (CC BY). The use, distribution or reproduction in other forums is permitted, provided the original author(s) and the copyright owner(s) are credited and that the original publication in this journal is cited, in accordance with accepted academic practice. No use, distribution or reproduction is permitted which does not comply with these terms.

frontiers in Plant Science

ORIGINAL RESEARCH
published: 14 July 2020
doi: 10.3389/fpls.2020.01053

Wheat Line "RYNO3936" Is Associated With Delayed Water Stress-Induced Leaf Senescence and Rapid Water-Deficit Stress Recovery

*Marlon-Schylor L. le Roux[1], N. Francois V. Burger[1], Maré Vlok[2], Karl J. Kunert[3], Christopher A. Cullis[4] and Anna-Maria Botha[1]**

[1] Department of Genetics, University of Stellenbosch, Stellenbosch, South Africa, [2] Proteomics Unit, Central Analytical Facilities, University of Stellenbosch, Stellenbosch, South Africa, [3] Department of Plant and Soil Sciences, Forestry and Agricultural Biotechnology Institute (FABI), University of Pretoria, Pretoria, South Africa, [4] Department of Biology, Case Western Reserve University, Cleveland, OH, United States

OPEN ACCESS

Edited by:
Guihua Bai,
United States Department of Agriculture (USDA), United States

Reviewed by:
Longxing Hu,
Hunan Agricultural University, China
Lyudmila Petrova Simova-Stoilova,
Institute of Plant Physiology and Genetics (BAS), Bulgaria

***Correspondence:**
Anna-Maria Botha
ambo@sun.ac.za

Specialty section:
This article was submitted to Plant Abiotic Stress, a section of the journal Frontiers in Plant Science

Received: *30 December 2019*
Accepted: *25 June 2020*
Published: *14 July 2020*

Citation:
le Roux M-SL, Burger NFV, Vlok M, Kunert KJ, Cullis CA and Botha A-M (2020) Wheat Line "RYNO3936" Is Associated With Delayed Water Stress-Induced Leaf Senescence and Rapid Water-Deficit Stress Recovery. Front. Plant Sci. 11:1053. doi: 10.3389/fpls.2020.01053

Random mutagenesis was applied to produce a new wheat mutant (RYNO3926) with superior characteristics regarding tolerance to water deficit stress induced at late booting stage. The mutant also displays rapid recovery from water stress conditions. Under water stress conditions mutant plants reached maturity faster and produced more seeds than its wild type wheat progenitor. Wild-type Tugela DN plants died within 7 days after induction of water stress induced at late booting stage, while mutant plants survived by maintaining a higher relative moisture content (RMC), increased total chlorophyll, and a higher photosynthesis rate and stomatal conductance. Analysis of the proteome of mutant plants revealed that they better regulate post-translational modification (SUMOylation) and have increased expression of ribulose-1,5-bisphosphate carboxylase/oxygenase (RuBisCO) proteins. Mutant plants also expressed unique proteins associated with dehydration tolerance including abscisic stress-ripening protein, cold induced protein, cold-responsive protein, dehydrin, Group 3 late embryogenesis, and a lipoprotein (LAlv9) belonging to the family of lipocalins. Overall, our results suggest that our new mutant RYNO3936 has a potential for inclusion in future breeding programs to improve drought tolerance under dryland conditions.

Keywords: random mutagenesis, mutant wheat, drought, photosynthesis, chlorophyll fluorescence, RuBisCO, LC-MS/MS

INTRODUCTION

Water deficit caused by drought conditions is a worldwide concern drastically reducing crop yield (Altieri and Nicholls, 2017). This is exacerbated by the increased vulnerability of water deficit-stressed plants to pests resulting in even greater yield loss (Botha et al., 2019). Water deficit stress was proposed as the most important abiotic factor affecting crops, because of its negative effects on both vegetative and reproductive development (Hura et al., 2010; Farooq et al., 2012; Shavrukov et al., 2017). Meteorological literature further suggests that frequency, intensity, and duration of

drought periods will increase in the coming years (Dai, 2011; Schubert et al., 2016; Spinoni et al., 2017; Botha et al., 2019, and references within) and new biotechnological advances are one of the tools required to increase crop productivity (Botha et al., 2019 and references within; Wulff and Dhugga, 2019).

Mutational breeding is a long-known and well-tested technology that increases genetic diversity in a relatively short time span (Muller, 1927; Pacher and Puchta, 2017). Mutagenesis can be induced through exposure to chemicals (e.g., sodium azide, ethylmethanesulfonate [EMS], etc.) or irradiation with X-rays and gamma rays. Effective mutational breeding to select plants for drought tolerance is difficult, as it is a polygenic controlled trait that is heavily regulated by genotype and environment interactions (Vassileva et al., 2011; Simova-Stoilova et al., 2016). In recent years, over 1,500 commercially available cereal varieties are the product of mutagenesis, with most varieties available from rice (828), barley (312) and wheat (282) (FAO/IAEA Mutant Varieties Database, 2018; https://www.iaea.org/resources/databases/mutant-varieties-database). A good example of such a wheat mutant is *tasg1*, developed through EMS, and expressing a "stay-green" phenotype (Tian et al., 2012). The *tasg1* mutant exhibited a distinct delayed senescence under both normal and drought stress conditions, as indicated by slower degradation of chlorophyll and decrease in net photosynthetic rate when compared to its wild type (WT) progenitor. The *tasg1* mutants maintained more integrated chloroplasts and thylakoid ultrastructure than did WT plants under drought stress. The authors suggested that a lower malondialdehyde content and higher antioxidative enzyme activities (ascorbate peroxidase, catalase, peroxidase) in *tasg1* was the casual factor that allowed the plants to perform better under drought stress. However, despite these suggestions, supporting evidence was limited as the observations were mostly based on measuring chlorophyll fluorescence, selected enzymatic activities, and chlorophyll structure using microscopy.

Plants respond to water deficit stress following any combination of four strategies, namely drought avoidance (Franks, 2011); drought tolerance; drought escape and drought recovery. Of particular interest is drought recovery, which defines the plant's ability to recover from dehydration and loss of turgor pressure as a result of the induced water deficit stress, thereby resuming growth and eventually producing seed (Luo, 2010; Fang and Xiong, 2014).

Photosynthetic activity in plants has been shown to be a trait that is highly responsive to water deficit stress (Singh et al., 2014; Serba and Yadav, 2016; Perdomo et al., 2017). In wheat, a direct correlation exists between imposed water-deficit stress and decreases in photosynthetic rate, leading to changes in intercellular CO_2 concentration, stomatal conductance, and transpiration rate (Subrahmanyam et al., 2006; Balla et al., 2014; Sharifi and Mohammadkhani, 2016; Perdomo et al., 2017; Senapati et al., 2018). Water deficit stress negatively affects maximal quantum yield of PSII photochemistry (F_v/F_m) (Tian et al., 2017), and damages the oxygen-evolving complex of PSII and its reaction centers (Aro, 2004; Murata et al., 2007; Tian et al., 2017). Damage to PSII centers are often due to impairment in ATP synthesis as a consequence of a decline in electron transport rate, which leads to a reduction in ATP availability and thus to a concomitant reduction in ribulose-1,5-bisphosphate (RuBP) regeneration (Lawlor and Cornic, 2002; Ma et al., 2006; Perdomo et al., 2017).

Ribulose-1,5-bisphosphate carboxylase/oxygenase (RuBisCO) is the main protein involved in CO_2 assimilation. Reports vary from no changes in the protein (Panković et al., 1999; Pelloux et al., 2001), to significant declines in the enzyme due to water deficit caused by drought conditions (Zhou et al., 2007; Galmés et al., 2011). Collectively, data suggest that RuBisCO levels and activity are influenced by the extent of water deficit stress and appears to be highly species-specific (Tezara, 2002; Bota et al., 2004). Water deficit stress decreased the amount of RuBisCO in maize and rice, but not in wheat (Perdomo et al., 2017). This decline in RuBisCO content subsequently led to a decline in carbon assimilation and an imbalance between photosynthesis and electron availability, with the resultant accumulation of reactive oxygen species (ROS), primarily hydrogen peroxide (Reddy et al., 2004).

Accumulation of ROS due to disturbance of cellular homeostasis can be countered through a unique set of biochemical mechanisms that detoxify ROS (Abid et al., 2016; Foyer et al., 2017; Foyer, 2018; Foyer et al., 2018; Noctor et al., 2018). High concentration of ROS is deemed extremely toxic to cells leading to oxidative bursts and potential cell death (Demidchik, 2015). Proteins involved in oxidative stress are peroxidases (POX), Glutathione S-transferases (GST), ascorbate peroxidases (APX), thylakoidal ascorbate peroxidase (tAPX), copper-zinc superoxide dismutases (SOD), catalases (CAT), and glutathione peroxidases (GPX). These enzymes are often referred to as ROS-scavenging enzymes (Sairam et al., 2005; Asensi-Fabado and Munné-Bosch, 2010). Increase in oxidative signals from photosynthesis and associated redox-sensitive proteome, provide cells with capacity to monitor photosynthetic electron flow and counteract over-reduction or over-oxidation. It further also produces redox regulatory networks that facilitate sensing and response to changes in environmental conditions (Martin and Sies, 2017; Foyer, 2018).

Water deficit stress alters the plants' metabolome (i.e., due to the production of newly synthesized metabolites), which may modify cellular structure, change the plant's metabolism and phenotype (Kosová et al., 2015). Michaletti et al. (2018) demonstrated the fluctuation of major metabolites in two wheat varieties that differ in their sensitivity to water deficit stress. They found that amino acid metabolism correlates to water deficit stress sensitivity after studying nine metabolic pathways. Specifically, N-containing compounds (e.g. betaine, glycine, and proline), and sugars (e.g. sucrose, trehalose, fructans) often accumulate in the cytoplasm as osmoprotectants contributing to water deficit stress tolerance.

Proteomics is a powerful tool to understand plant reactions to drought stimuli especially in a hexaploid crop such as wheat. Comparative proteomics analysis is deemed as an effective strategy to identify crucial proteins, however in crops such as wheat, it becomes very difficult because of the large genome size. Techniques such as Liquid Chromatography with tandem mass spectrometry (LC-MS/MS) provide unique indications of expressed proteins at a given time point. However, it does not

give an indication of the activity of a given protein, and thus, technologies such as LC MS/MS should be combined with activity assays to provide a more holistic demonstration of important proteins and their activities in context of water stress tolerance. Water deficit is known to induce changes in the proteome of plants because of protein breakdown catalyzed by proteases (Vierstra, 1993; Hieng et al., 2004; Simova-Stoilova et al., 2010). Proteases are ubiquitously required for readjustment of a plant's metabolic status, through the method of protein turnover, to remobilize nutrients to counter environmental shifts and maintain developmental processes (Nelson and Millar, 2015). Known protein turnover processes involved in this readjustment include ubiquitination, phosphorylation, and SUMOylation with the latter referring to the post-translational modification of protein substrates through the covalent conjugation with the SUMO (Small Ubiquitin-like Modifier) peptide. This modification is reminiscent of ubiquitination, even though it has its own set of homologous enzymes (Ranieri et al., 2018). The conjugation of SUMO on a protein is reversible (de-SUMOylation) where SUMO proteases (clan cysteine proteases) cleaves SUMO conjugates of the targeted proteins (Guerra et al., 2015; Benlloch and Lois, 2018; Morrell and Sadanandom, 2019 and references within).

Even though water deficit induces major changes in the biochemical processes of plants, drought is often an episodic event. Once soil moisture is restored (i.e., by irrigation or rain fall), plants regain normal physiological functionality (i.e., water transport and turgor pressure, stomatal conductance, photosynthetic activity, etc.) and grow to maturity to produce seed. For plants experiencing prolonged periods of water deficit, this does not happen naturally, and only selected plants display a "recovery" phenotype whereby this can be reversed after severe water deficit (Abid et al., 2018). In order to better understand the underlying genetic mechanisms enabling plants to delay senescence and recover after being completely dehydrated, we compared physiological responses, metabolic and enzymatic activity, and changes in the proteome of a water deficit stress-sensitive wheat line (Tugela DN) with its near-isogenic mutant line (RYNO3936) that express a combination of water deficit stress avoidance and recovery phenotypes. An improved understanding of such a phenotype will ease introducing these traits into breeding programs for enhanced drought-tolerant phenotypes and its future discovery in mutant breeding programs.

MATERIALS AND METHODS

Water-Deficit Treatment, Plant Phenotyping, Plant Biomass, and Soil Relative Moisture Content

Random mutagenesis was performed as previously described (Mbwanjii, 2014; Botha et al., 2017). In brief, mutant RYNO3936 was developed using chemically induced mutagenesis by exposing seed of a red hard winter wheat cultivar, Tugela DN to 1 mM Sodium azide for 2 h, where after the treated seed was planted in trays containing equal amounts of substrate (sand: soil) and grown in a greenhouse at temperatures between 20°C and 26°C. After a month of growth, water was withheld, and plants selected for water deficit tolerance under low nitrogen regimes. The resultant mutant, RYNO3936 was then selfed for six generations to retain the water deficit stress tolerant trait (Mbwanjii, 2014; Botha et al., 2017).

Seeds of the WT parent (Tugela DN) and mutant RYNO3936 were grown in a greenhouse with natural day/night temperature at 23 ± 3°C (Welgevallen Experimental Farm, Stellenbosch University, South Africa). Seeds were planted in pots [dimensions: 25 cm (diameters) × 30 cm (height)] filled with equal amounts of sand and crusher dust (1:1). A total of 30 pots (15 per control and 15 per mutant) arranged in a randomized complete block design was used, with each pot containing 5 seeds. The plants were watered daily using a fully automated system containing nutrients (Multifeed^{TM}, South Africa). All pots were regularly assessed to ensure that a constant gravimetric reading of 80% was maintained, until plants reached the final extension stage (58–65 days after germination) corresponding to phase 45 of Zadoks' scale (Zadoks et al., 1974; Vendruscolo et al., 2007). From this stage onwards, the watering was withheld, and water deficit stress induced. Day 0 measurement was recorded under irrigation (gravimetric reading of 80%). Water was then withheld for 14 consecutive days or until soil moisture reached 21% to 24%, with measurements collected on days 7 and 14. The plants were then subjected to rehydration for 7 days during which a gravimetric reading of 70% was maintained, when the last set of data was collected (i.e., day 21 denoted "re-watered").

Plant growth analysis (i.e., plant height, and flag leaf length and width) were assessed as previously described (Aase, 1977) using a line gauge (unit of measurement in mm). For plant height, all the individual tillers of the plant were measured from the ground to the tip of the tallest tiller of the plant (n = 20). The relative moisture content (RMC) was calculated according to the following formula: RMC (%) = (fresh weight − dry weight)/(turgid weight − dry weight) × 100 (Sade et al., 2014; Sade et al., 2015). The flag leaf was removed and kept in distilled water for ± 4 h to achieve full turgidity. The leaf dry weight was measured after keeping the turgid leaf at 80°C in an oven for 16 h. The RWC was tested at days 0, 7, and 14 after induction of water deficit stress and then 7 days after re-watering (day 21). The RWC was measured using three similar-sized leaves and six replicates for each treatment. Soil samples (n = 3) to 150 mm depth were also collected, and the wet soil mass was determined through drying the soil in an oven at 105°C for 48 h after which the soil was weighed and the gravimetric soil moisture content determined (Black and Power, 1965).

Stomatal Conductance, Chlorophyll Fluorescence, and Chlorophyll Content Measurement

Chlorophyll fluorescence and stomatal conductance were measured at respective time points (days 0, 7, 14, and after re-watering, day 21) as previously described (Le Roux et al., 2019). Stomatal conductance (gsw) was measured at three positions on each leaf using three independent plants (n = 9) with a

porometer (model SC-1, Decagon Devices Inc., Pullman, WA, USA) following the manufacturer's instructions. Rate of photosynthesis was measured according to Strasser et al. (2004) making use of chlorophyll fluorescence induction transients (O-J-I-P), using a hand-held Chlorophyll Fluorometer (model: OS-30P; Manufacturer: Opti-Sciences, Inc., United States). Dark adaptation clips were applied to leaves for 20 min (prior to reading) to achieve a flush out of assimilates. Technical repeats for both instruments were recorded at different places from the tip to the base of the flag leaf to represent the entire leaf surface. All measurements were taken at the onset of the water deficit stress treatment (day 0), then at days 7 and 14 after induction of water deficit stress. At day 14, plants were re-watered and then watered on a daily basis to ensure full recovery. Measurements were then taken on day 21 (denoted "re-watered"). Chlorophyll concentrations were quantified and calculated according to Arnon (1949) using the SmartSpec™ Plus BioRad.

SDS-PAGE Electrophoresis and Western Blot Analysis

Total protein was extracted and separated using the Mini-Protein TGX gradient gel (4%–15%) as previously described (Le Roux et al., 2019). The Bio-Rad protein assay reagents with bovine albumin as the standard (Bio-Rad Laboratories Inc., Hercules, CA) was used for determination of protein concentration (Bradford, 1976), and quantified using a Glomax Spectrophotometer (Promega, Sunnyvale, CA) (Rylutt and Parish, 1982).

Western blot analyses were conducted using a Bio-Rad Trans-Blot® SD semi-dry transfer cell apparatus and polyvinylidene difluoride membranes (Hybond-P, Amersham Biosciences). The membranes were blocked with 3% bovine serum albumin (BSA) and probed with polyclonal large (RbcL) and small (RbcS) RuBisCO Subunits (RbcL and RbcS, 1:50000; Botha and Small, 1987) and human anti-SUMO1 monoclonal antibody (1:2500) (UBPBio, Aurora, USA) diluted in buffered saline containing 3% BSA. Detection employed alkaline phosphatase conjugated Donkey Anti-Mouse (Abcam) (1:2500) or goat anti-rabbit (1:7000) (Sigma-Aldrich, St. Louis, MO, USA) antibodies in conjunction with nitro blue tetrazolium and 5-Bromo-4-chloro-3-indolyl phosphate (Sigma-Aldrich, St. Louis, MO, USA).

Protease Determination

Leaf tissue was ground after being flash frozen in liquid nitrogen; the powder was added to cold 0.1 M citrate-phosphate buffer (pH 5.6) containing 10 mM L-cysteine. A centrifugation step was included at 25,000 × *g* for 20 min at 4°C. The supernatant was electrophoresed using a gradient acrylamide gel (5–15%). The gradient gel was prepared using the Hoefer™ SG Series Gradient Makers system as described by Le Roux et al. (2019). A gel equilibration step was conducted by pre-electrophoresis for 60 min at 50 V in the gel buffer storage condition at 4°C. Samples (80 mg) were loaded with and without addition of the cysteine proteinase inhibitor E64 (Barrett et al., 1982; Matsumoto et al., 1999). Proteins were separated at 15 mA for 2 h. After electrophoresis, the gels were meticulously removed from the glass plates and washed three times in a renatured buffer (5 mM cysteine and 2.5% v/v Triton-X 100) and subsequently incubated in developing buffer (0.5% v/v Triton-X 100, 50 mM Tris–HCl, pH 7.5 and 5 mM $CaCl_2$, 1 mM $ZnCl_2$, 10 mM cysteine) for 24 h. The gels were stained with Coomassie R-250 and de-stained until clear zones were visible against the dark blue background (Le Roux et al., 2019).

Amino Acid Extraction and Quantification

Amino acid extraction and quantification were conducted as previously described (Le Roux et al., 2019). In brief, leaf material was dried out in an oven at 60°C for 24 h, where after samples were ground to a powder and 0.5 ml of 6 M HCl containing norleucine (250 ppm) added as an internal standard. AccQ.Tag derivatives of extracted amino acids were generated using the AccQ.Tag Ultra Derivatization Kit following the manufacturer's instruction (Waters). Derivatized amino acids were analyzed using an Acquity UPLC system equipped with a binary solvent delivery system and an auto sampler. For separation an AccQ.Tag Ultra column (100 9 2.1 mm) (Waters) was used. Derivatized amino acids were detected at 260 nm using a photo diode array detector. Amino acids in the samples were identified by co-elution with amino acid standard H (Pierce) and commercially available individual amino acids (Sigma). Concentration of amino acids in each sample was calculated based on the peak areas and calibration curves generated with commercial standards.

Proteome Analysis

Protein Extraction, Quantification, and Digestion

Leaf protein was extracted using a modified method to that which was previously described (Damerval et al., 1986; Wang et al., 2006; Wang et al., 2007). In brief, after treatment the leaf tissue was ground into fine powder in liquid nitrogen and transferred to a falcon tube. To this, 20 ml of cold (−20°C) extraction buffer (10% w/v TCA/acetone containing 0.07% β-mercaptoethanol (β-ME) was added and homogenized by vortexing vigorously for 20 s. Where after the tube was incubated at −80°C overnight to allow complete precipitation of proteins. This procedure was repeated for each of the treatments. After the overnight incubation, the tubes were centrifuged at 5,200*g* for 30 min at 4°C and the supernatant removed. Three acetone washes were consecutively performed by adding 5 ml of ice-cold acetone (−20°C) containing 0.07% β-ME, vortexing the tube briefly, centrifuging at 5,200*g* for 15 min, and again removing the supernatant. After completing the third wash, the supernatant was removed, and the tube was centrifuged for another 10 min, where after the remaining supernatant was removed using a pipette. The pellet was lyophilized for 2 h. The lyophilized samples were stored at −80°C till further use.

iTRAQ Labeling and SCX Fractionation

Protein Digestion

The iTRAQ-labeling and analyses were conducted as previously described (Wang et al., 2016). In brief, an aliquot containing 100 µg of solubilized protein in 100 mM triethylamonium bicarbonate (TEAB, Sigma) containing 4M Guanidine-HCl, was reduced with tris-carboxyethyl phosphine (TCEP, Sigma) at 60°C prior to cysteine residues being thiomethylated with methane methylthiosulfonate (MMTS, Sigma). The reduced and thiomethylated sample was digested with Trypsin Gold (Promega, Madison, USA) (protein/trypsin = 20:1) after a 10 times dilution at 37°C for 18 h. The peptides dried under vacuum and resuspended for desalting in 2% acetonitrile/water containing 0.1% formic acid. Residual digest reagents were removed using an in-house manufactured C_{18} stage tip (Empore Octadecyl C_{18} extraction discs; Supelco). The 20 µL sample was loaded onto the stage tip after activating the C_{18} membrane with 30 µL methanol (Sigma) and equilibration with 30 µL 2% acetonitrile/water; 0.05% TFA. The bound sample was washed with 30 µL 2% acetonitrile/water; 0.1% FA before elution with 30 µL 50% acetonitrile/water 0.1% FA. The eluate was evaporated to dryness. The dried peptides were dissolved in 20 µL 2% acetonitrile/water; 0.1% FA for LC-MS analysis

LC–ESI-MS/MS Analysis Based on the Thermo Scientific Fusion Tribrid System

Liquid chromatography was performed on a Thermo Scientific Ultimate 3000 RSLC equipped with a 0.5 cm × 300 µm C_{18} trap column and a 35 cm × 75 µm in-house manufactured C_{18} column (Luna C_{18}, 3.6 µm; Phenomenex) analytical column. The solvent system employed was loading: 2% acetonitrile/water; 0.1% FA; Solvent A: 2% acetonitrile/water; 0.1% FA and Solvent B: 100% acetonitrile/water. The samples were loaded onto the trap column using loading solvent at a flow rate of 15 µL/min from a temperature controlled autosampler set at 7°C. Loading was performed for 5 min before the sample was eluted onto the analytical column. Flow rate was set to 500 nl/min and the gradient generated as follows: 2.0% to 10% B over 5 min; 5% to 25% B from 5 to 50 min using Chromeleon non-linear gradient 6, 25% to 45% from 50 to 65 min, using Chromeleon non-linear gradient 6. Chromatography was performed at 50°C and the outflow delivered to the mass spectrometer through a stainless-steel nano-bore emitter.

The Thermo Scientific Fusion mass spectrometer was equipped with a Nanospray Flex ionization source. The sample was introduced through a stainless-steel emitter. Data was collected in positive mode with spray voltage set to 2 kV and ion transfer capillary set to 275°C. Spectra were internally calibrated using polysiloxane ions at m/z = 445.12003 and 371.10024. MS1 scans were performed using the orbitrap detector set at 120 000 resolution over the scan range 350 to 1650 with AGC target at 3 E5 and maximum injection time of 40 ms. Data was acquired in profile mode.

MS2 acquisitions were performed using monoisotopic precursor selection for ion with charges +2-+6 with error tolerance set to ± 0.02 ppm. Precursor ions were excluded from fragmentation once for a period of 30 s. Precursor ions were selected for fragmentation in HCD mode using the quadrupole mass analyzer with HCD energy set to 32.5%. Fragment ions were detected in the orbitrap mass analyzer set to 15 000 resolution. The AGC target was set to 1E4 and the maximum injection time to 45 ms. The data were acquired in centroid mode.

The raw files generated by the mass spectrometer were imported into Proteome Discoverer v1.4 (Thermo Scientific) and processed using the SequestHT algorithm included in Proteome Discoverer. Data analysis was structured to allow for methylthio as fixed modification as well as NQ deamidation (NQ), oxidation (M). Precursor tolerance was set to 10 ppm and fragment ion tolerance to 0.02 Da. The database used was the murine taxonomy database obtained from Uniprot with the sequence of amyloid beta A4 P05067 added. The results files were imported into Scaffold v1.4.4 and identified peptides validated using the X!Tandem search algorithm included in Scaffold. Peptide and protein validation were performed using the Peptide and Protein Prophet algorithms. Protein quantitation was performed by first performing a t-test on the paired data and applying the Hochberg-Benjamini correction (Benjamini and Hochberg, 1995).

Bioinformatics Analysis

When comparing differential expression of peptides between treatments (i.e., days 0, 7, 14, and 21), data obtained were analyzed using Scaffold Viewer 4 proteomics software (http://www.proteomesoftware.com/products/scaffold/; Searle, 2010) by comparing all treatments with each other. The Benjamini-Hochberg multiple testing adjustment was applied in order to control the comparison-wide false discovery rate (Benjamini and Hochberg, 1995). Sequences representing the peptide were subjected to Blast2GO (Conesa et al., 2005) analysis to obtain the representing genes, as well as gene ontologies and functional categories. A *P*-value ≤ 0.05 was used as the threshold to determine the significant enrichments of GO and KEGG pathways.

Clustering and Data Analysis

Resulting peptide intensity signals were first normalized using the Cluster program (Eisen et al., 1998), with mean-centering applying Spearman's rank correlation. A cluster image representing groups of differentially expressed peptides that share similar expression patterns was generated from the normalized data and visualized with Java TreeView (Saldanha, 2004).

Enzyme Measurements and Protein Determination

Extraction of enzymes was performed as described in Botha et al. (2014). All enzyme activity measurements were conducted using three biological repeats (n = 3) and conducted in triplicate (n = 9). Peroxidase activity was determined following a modified method of Zieslin and Ben-Zaken (1993) and expressed as mmol tetraguaiacol min^{-1} mg^{-1} protein. Glutathione S-transferase (GST) enzyme activity was measured as described by Venisse et al. (2001), with the formation of GS-DNB

conjugate measured at 340 nm. GST activity was expressed as mmol GSH min^{-1} mg^{-1} protein.

Statistical Analyses

All data were collected using three biological repeats (n = 3) with measurements done in triplicate (n = 9). Mean values are presented with their standard deviation (SD) and analyzed using Graphpad Prism software version 5.0 (http://www.graphpad.com/scientific-software/prism/) (Motulsky, 2007). Statistical validation and significance ($P \leq 0.05$) were determined with analysis of variance (ANOVA) followed by post-t Dunnett's, or Turkey or Bonferonni tests (Amstrong, 2014).

RESULTS

Plant Phenotypes, Physiological Response, and Reproduction Under Water Deficit

The mutant wheat line RYNO3936 visually displayed a "bushy" phenotype with longer shoots and broader leaves, and more tillers and roots when compared to its WT parent (**Figures 1A, D** and **2**). After induction of water deficit, the WT Tugela DN was visually wilted after 2 days of water deficit stress, and dead after day 7 (**Figures 1B, C**). In contrast, the mutant wheat line RYNO3936 visually displayed signs of stress only after day 7 of induced water deficit stress and lasted much longer than the WT Tugela DN plants (**Figures 1E, F**). Re-watering of the mutant wheat line RYNO3936 after day 14, resulted in partial to full recovery of the mutant plants, but not the control (day 21) (**Figure 1G**).

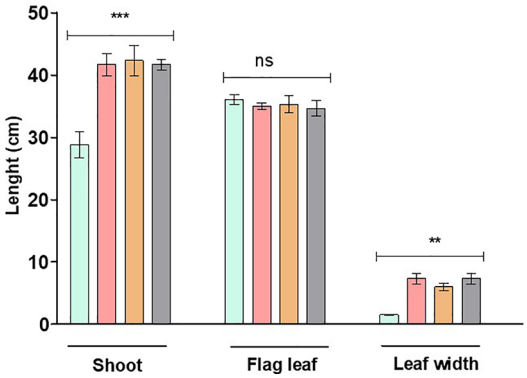


FIGURE 2 | Plant height as well as flag leaf length and width of WT Tugela DN and Mutant RYNO3936 prior to exposure to water stress. Capped bars above means represent ± SD of three replicates. Asterisks above columns means denote the significant differences compared with WT Tugela DN for a single mutant line. **P ≤ 0.01; ***P ≤ 0.05. ns, nonsignificant.

When growth and reproduction of the mutant wheat line RYNO3936 was compared with its WT Tugela DN parent, it took significantly longer (148.0 ± 4.0 *vs.* 100.5 ± 9.5 days) to reach the heading phase under well-watered growth conditions, but headed much sooner (92.0 ± 11.0 days) under water deficit conditions (**Table 1**). Under well-watered growth conditions, mutant wheat line RYNO3936 produced significantly more heads (7.0 ± 2.0) and seeds per plant (120.0 ± 33.0) when compared with its WT parent (heads = 2.0 ± 1.0; seed = 32 ± 10.0). With the induction of water deficit stress, the WT parent

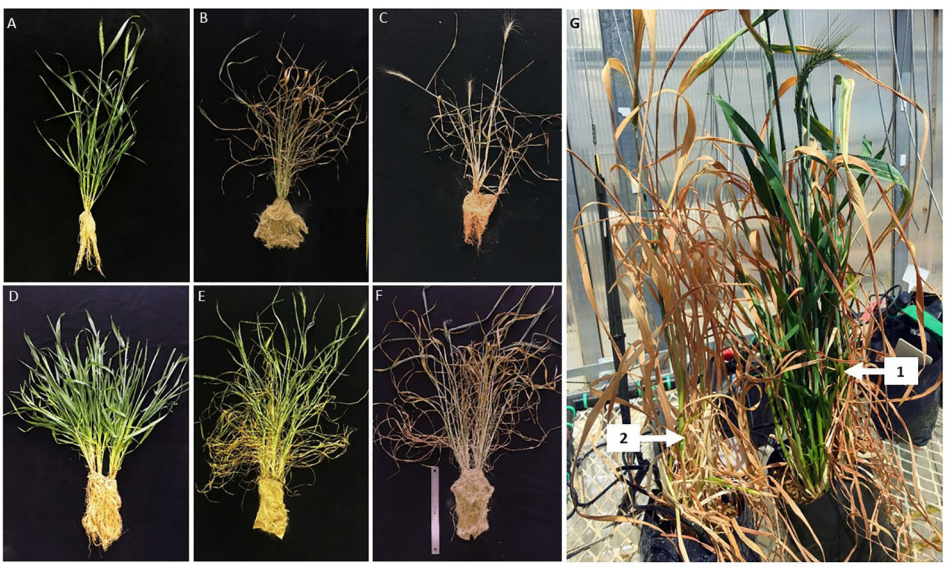


FIGURE 1 | Phenotypic response of WT Tugela DN and Mutant RYNO3936 wheat prior to **(A, D)** and after induction of water stress **(B, C**; **E, F)**. Where **(A–C)** is WT Tugela DN wheat at day 0 **(A)**; day 7 **(B)**; and day 14 **(C)**. While **(D, E)** is Mutant RYNO3936 wheat at day 0 **(D)**; day 7 **(E)**; day 14 **(F)** and re-watering **(G)** the arrow shows initiation of recovery 2 and fully recovery 1.

died after 7 days and failed to reproduce. Under water deficit stress, the mutant wheat line RYNO3936 yielded equivalent to what the WT parent yielded under well-watered growth conditions (**Table 1**).

Even though the relative moisture content (RMC) in the leaves was similar between the mutant and WT plants before the induction of water deficit stress, RMC declined significantly ($P < 0.05$) in WT Tugela DN, but not in the mutants, with the induction of water deficit stress (**Figure 3A**). This decrease in RMC coincided with declines with soil moisture content (**Figure 3A**). At Day 7, the mutant lost nearly 21% of its RMC, whereas the WT lost 65% with both having access to a soil moisture content of ± 24%. After re-watering at day 14, the mutant RYNO3936 took three days to display greening of leaves, with some leaves returning to its natural green color after approximately a week after regaining most of its RMC (± 76%). However, not all leaves could recover in the mutant plants from water stress-induced damage as can be observed in **Figure 1G**.

RMC of the WT Tugela DN plant roots was significantly higher (± 70%) than that of the mutant (± 45%) pre-induction of water deficit stress (day 0) but declined to below 10% after induction of water stress (**Figure 3B**). In contrast, even though the RMC in the roots of mutant RYNO3936 decreased about ±50%, it remained at the ±20% level throughout the water deficit experiment and regained RMC with re-watering to return to pre-water deficit values.

Chlorophyll content decreased in both plants with the WT Tugela DN showing a greater loss in chlorophyll (± 50%) within the 7 days after induction of water deficit, which is much sooner than in the mutant RYNO3936 plants (**Figure 4A**). Chlorophyll content increased with re-watering, while the WT plant suffered a complete loss of chlorophyll with no recovery despite re-watering. A significant ($p < 0.05$) decline in chlorophyll fluorescence, as a measure of PSII efficiency (Schreiber et al., 2003; Strasser et al., 2004), was measured in both the WT Tugela DN and mutant RYNO3936 after induction of water deficit stress (**Figure 4B**). This decrease in chlorophyll fluorescence was less in the mutant wheat line than in its WT parent and recovered in the mutant RYNO3936 wheat line, but not in the WT parent after re-watering of plants after 14 days water deficit treatment. Stomatal conductivity followed similar trends as that measured with chlorophyll fluorescence (**Figure 4B**).

To confirm the observed changes in chlorophyll content and fluorescence in the WT Tugela DN and mutant RYNO3936 lines, the expression of RuBisCO before (day 0) and after induction of water deficit stress (days 7 and 14), and re-watering (day 21) was also analyzed using Western Blot analyses (**Figure 5**). Protein blots probed with anti-LSU (RuBisCO large subunit) and anti-SSU (RuBisCO small subunit) IgGs revealed two cross-reacting peptides for the large subunit (LSU) with sizes of 56 ± 4 kDa and 50 ± 4 kDa (LSU), respectively, and 15 ± 2 kDa for the small subunit, which corresponds to the sizes for the subunits in wheat (Botha and Small, 1987; Le Roux et al., 2019). Interestingly, a smaller form of the LSUs (50 ± 4 kDa) was observed in RYNO3936, but not in the WT, and this form disappears with the induction of water stress (days 7 and 14), but reappears after recovery (day 21, **Figure 5A**).

To further estimate the relative abundance of the RuBisCO subunits, the protein blots were scanned with a laser

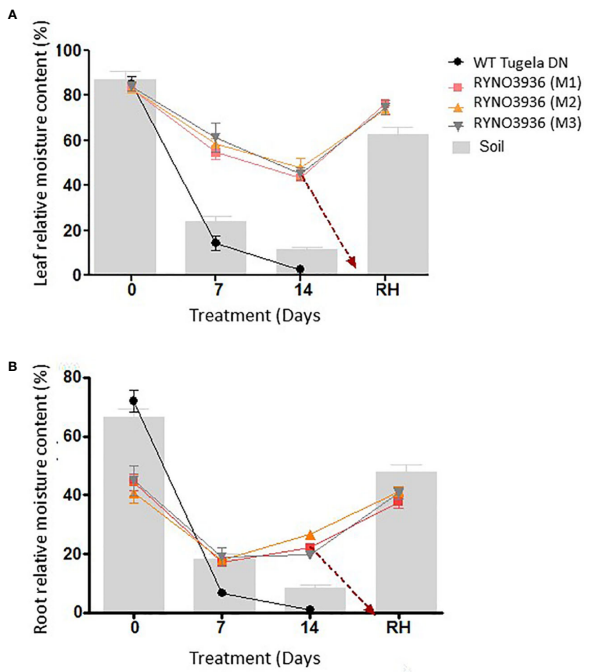


FIGURE 3 | Comparative analysis of relative moisture content (RMC) measured in the leaves **(A)** and roots **(B)** prior to and after induction of water stress. The gravimetric readings of the soil are superimposed against the RMC. Indicated are the RMC of WT Tugela DN and Mutant RYNO3936 emphasizing how they maintain RMC under deficient soil moisture. Error bars indicate SD (n = 9) and significance was set at $p \leq 0.05$.

TABLE 1 | The response of WT Tugela DN and Mutant RYNO3936 to water deficit stress.

Genotype	Treatment (days)	Days to heading (days)	Anthesis from heading date (days)	Heads per plant (number)	Seeds per plant (number)
RYNO3936	Control	148.0 ± 4.0	16.0 ± 4.0	7.0 ± 2.0	120.0 ± 33.0
	Water stressed	92.0 ± 11.0	7.0 ± 2.0	2.5 ± 1.5	34.0 ± 6.0
WT	Control	100.5 ± 9.5	12.5 ± 1.5	2.0 ± 1.0	32.0 ± 10.0
	Water stressed	nd	nd	nd	nd

Indicated are days to heading, days to anthesis, number of heads and seeds produced prior (0 day) and after induction of water deficit stress (days 7 and 14) (± = standard deviation) (n = 3). nd, WT Tugela DN dies prematurely and produced no seed.

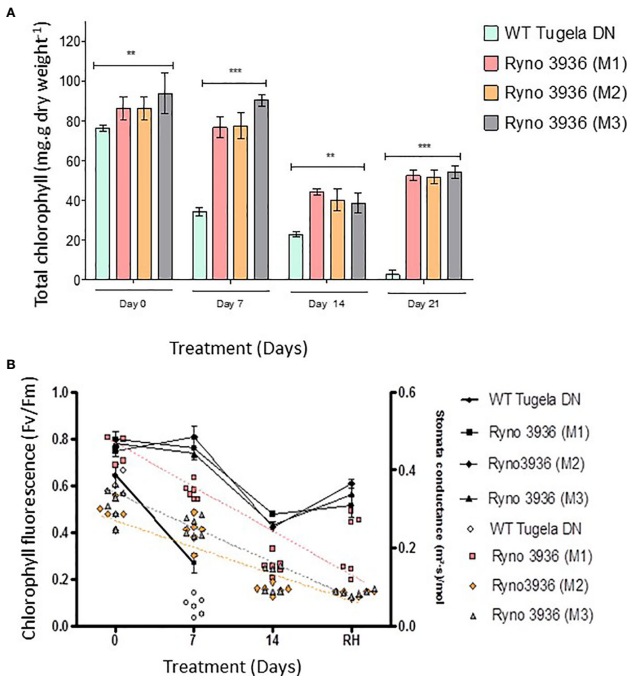


FIGURE 4 | (A) Total chlorophyll measured in the WT Tugela DN and Mutant RYNO3936. prior to (day 0) and after exposure to water stress (days 7 and 14). Capped bars above means represent ± SD of three replicates. Asterisks above columns means denote the significant differences compared with WT Tugela DN for a single mutant line. **P ≤ 0.01; ***P ≤ 0.05. **(B)** Rate of photosynthesis (F_v/F_m) (line graph) and stomatal conductivity (scatter plot) prior to (day 0) and after exposure to water stress (days 7 and 14). Photosynthesis significance was determined by p ≤ 0.005 where n = 6 and error bar indicate SD.

densitometer. Densitometric analyses of the blots revealed a high abundance in LSU in the mutant during irrigation, water stress, and rehydration, when compared to the WT (**Figure 5B**). Both subunits decreased in abundance with the induction of water deficit stress.

Changes in Free Amino Acid Under Water Stress

To access the effect of water deficit on total free amino acid (FAA) the changes thereof were quantified in leaf material before (day 0) and after induction of water stress (days 7 and 14), and after re-watering (day 21; **Table 2**). Before the induction of water stress, the FAA levels between the WT Tugela DN and mutant lines were comparable, with RYNO3936 maintaining slightly lower FAA levels, except for methionine, leucine, and phenylalanine that were present in much higher levels in RYNO3936 ($p < 0.05$). Water deficit (day 7) induced higher amounts of proline, methionine, and phenylalanine in the WT Tugela DN, and higher amounts of serine, aspartate, glutamate, proline, lysine, and isoleucine in the mutant wheat plants. Prolonged water stress (day 14) further increased in all FAA (**Table 2**). Proline was the highest accumulated metabolite, during the water deficit conditions and tends to remain so despite re-watering conditions.

Changes in the Proteome With Water Stress

In order to elucidate the changes in protein expression that was induced in RYNO3936 due to mutagenesis, we next compared the proteome of WT Tugela DN (day 0) with that of RYNO3936 (day 0) (**Figure 6**; **Supplementary Tables S1A, B**). When comparing the top 100 most significantly expressed proteins in WT Tugela DN with that in the mutant RYNO3936, most of the expressed proteins were expressed equally in both lines. However, there were unique proteins only expressed in RYNO3936 that have been previously identified in dehydration-tolerant plants (e.g., abscisic stress-ripening protein, cold induced protein, cold-responsive protein, dehydrin, and Group 3 late embryogenesis abundant protein) (**Supplementary Table S1**). Expressed proteins were grouped into key functional processes (i.e., ribosomal – protein synthesis; energy production – specifically ATP production; photosynthesis; carbon assimilation – specifically respiration; stress – includes host defense; and reactive oxidative stress (ROS) associated) to visualize the mutagenesis-induced differences that enable RYNO3936 to be more tolerant to water deficit than WT Tugela DN (**Figure 6**). RYNO3936 seemingly invests more resources into photosynthesis (e.g., chlorophyll a-b binding protein, Photosystem II CP47 chlorophyll apoprotein, Photosystem I P700 chlorophyll a apoprotein A2, Ribulose bisphosphate carboxylase large chain, Cytochrome b6-f complex iron-sulfur subunit, chloroplastic) and energy production (e.g., ATP synthase subunit alpha, mitochondrial) and less into the production of defense and stress-responsive proteins (e.g., lipoxygenase; glucanases) (**Table 3**).

To better understand the coping mechanisms applied by mutant RYNO3936, we also compared the changes in the proteome of RYNO3936 that occurred before (day 0) and after induction of water stress (days 7, 14), and recovery of the mutant plant (day 21; **Supplementary Tables S1**, **S2**, **S3**). After analysis of the proteins in RYNO3936 across all treatments, we found that 99 proteins were shared among all treatments (**Figure 7**, **Supplementary Table 1S**), with 6 uniquely expressed at day 0 (e.g., thioredoxin, cold responsive proteins), only 1 on day 7 (i.e., LAlv9 family protein), a total of 7 on day 14 (e.g., aldehyde dehydrogenase, lipoxygenase, GTP-binding nuclear protein, heat shock protein 81, 5-methyltetrahydropteroyltriglutamate-homocysteine methyltransferase), and 14 proteins in re-watered, recovered leaf material (day 21) (e.g., alpha gliadin, alpha-amylase/trypsin inhibitor, globulin, gamma gliadin, grain softness protein, high and low molecular weight glutenin subunit proteins, LEA3 protein, dimeric alpha-amylase inhibitor, grain softness protein) (**Figure 8**).

To visualize the observed proteomic changes before (day 0), after induction of water stress (days 7 and 14) and after recovery (day 21), we conducted a cluster analysis (Eisen et al., 1998) and visualized the clusters using TreeView (Saldanha, 2004) (**Supplementary Figure S1**, **Supplementary Table S2**). We obtained two clusters with two major groupings according to protein expression patterns, with unstressed (day 0) and

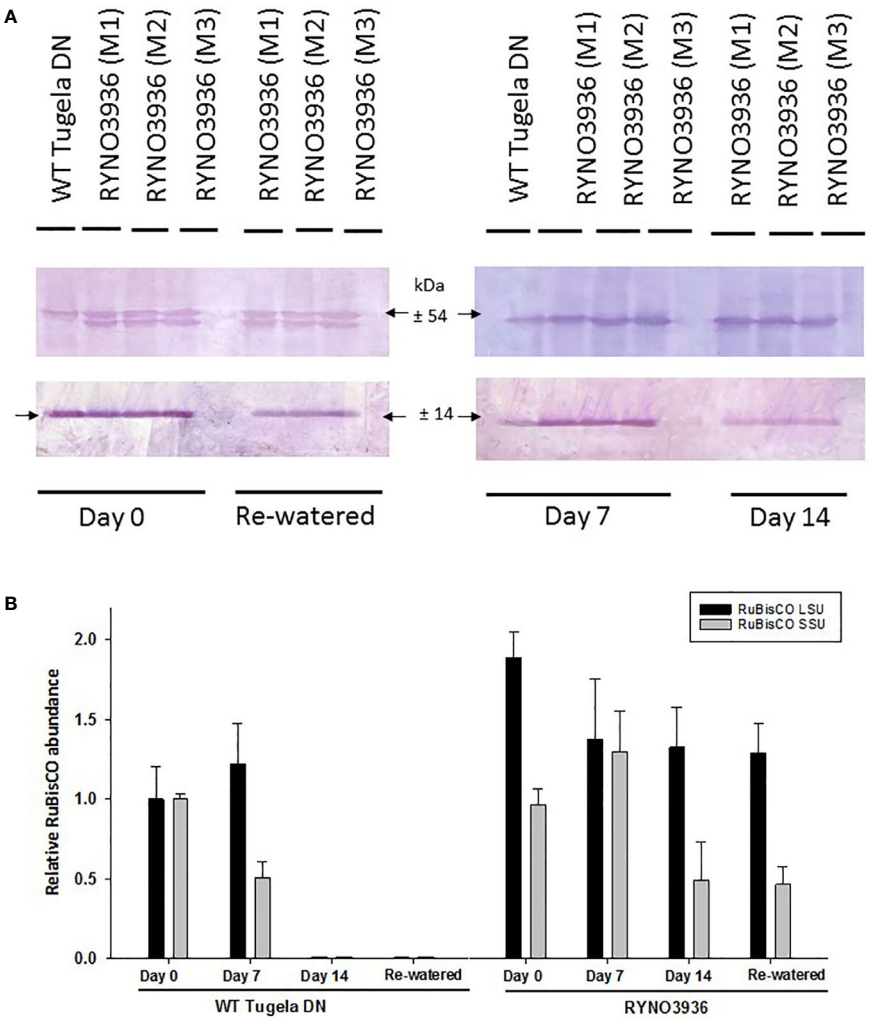


FIGURE 5 | (A) Top: Protein blot of crude extract from WT Tugela DN and Mutant RYNO3936 wheat prior to (day 0) and after exposure (days 7 and 14) to water stress, and re-watered (day 21) probed with anti-Rubisco (LSU) and (SSU) IgG. All lanes were loaded with 20 mg total protein. Blots were probed with a 1:7 000 dilution of the polyclonal IgG against LSU, SSU. The leaf proteins were resolved by 12% (w/v) sodium dodecyl sulfate–polyacrylamide gel electrophoresis prior to transferring to nitrocellulose. Images were cropped for presentation purposes. M1–M3 represents three independent mutant lines. **(B)** Gel densitometric analysis of the protein blot in **(A)** of the rubisco large (LSU, 54 kDa) and small (SSU, 14 kDa) subunits in the leaf crude protein extracts from WT Tugela DN and Mutant RYNO3936 wheat prior to (day 0) and after exposure (days 7 and 14) to water stress, and re-watered. Data are expressed as relative levels of rubisco protein compared with the basic level in control line (mean value of 1.0). Each bar is the mean of three independent values (biological replicates) ± SE.

TABLE 2 | Levels of free amino acids in leaf material of WT Tugela DN and Mutant RYNO3936 measured prior to (day 0) and after induction of water stress (days 7 and 14).

Genotype	Days	Free amino acid content [Concentration in % (m/m) dry solid]															
		his	ser	arg	gly	asp	glu	thr	ala	pro	lys	tyr	met	val	Ile	leu	phe
WT Tugela DN	**0**	0.10	0.33	0.32	0.31	0.55	0.59	0.24	0.39	0.29	0.39	0.21	0.54	0.31	0.18	0.42	0.34
	7	nd	0.20	nd	0.27	nd	0.56	0.31	0.42	0.88	0.50	0.14	2.54	0.14	0.33	0.59	1.65
RYNO3936	**0**	0.10	0.20	0.20	0.16	0.53	0.26	0.10	0.19	0.15	0.17	nd	1.80	0.33	0.09	1.21	1.63
	7	0.17	0.30	0.27	0.29	1.10	0.90	0.19	0.34	1.30	0.39	0.19	0.91	0.39	0.23	0.50	0.46
	14	0.37	0.74	0.75	0.76	1.48	2.55	0.69	0.97	2.87	0.82	0.44	0.28	0.97	0.55	1.15	0.85
	Re-watered	0.37	0.20	0.14	0.18	0.42	0.36	0.10	0.22	0.43	0.23	0.14	0.56	0.23	0.10	0.25	0.79

Measurements were only taken for the WT Tugela DN until day 7, as it suffered irreversible damage and was dead by day 7 (n = 3). nd, not determined.

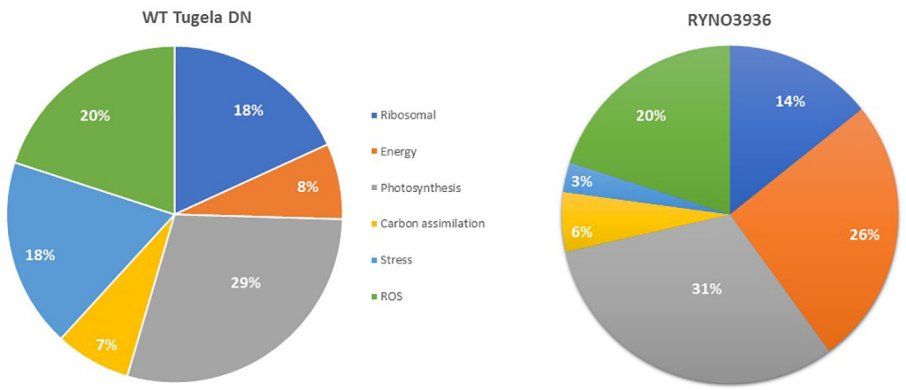


FIGURE 6 | Comparison of the proteins expressed in WT Tugela DN (day 0) and the mutant RYNO3936 (day 0) according by the proportional contributions of functional categories.

recovered plants (day 21) that grouped together, and stressed plants (days 7 and 14) that formed another grouping.

We also assigned the obtained peptides into functional categories (**Supplementary Figure S2**) to confirm their involvement in plant metabolism. Within the biological processes, most of the peptides belonged to cellular metabolic process (18%), while in the cellular component the largest groups belonged to the intracellular (25%) and intercellular (25%) parts. When assigned to the molecular function, most peptides belonged to the ion binding category (38%).

Protein Turnover During Water Deficit

To study the changes in SUMO cysteine proteases, blots of separated crude protein extracts were probed with monoclonal anti-SUMO1 IgG. Several cross-reacting peptides were found ranging in sizes from 150 ± 10 kDa to 10 ± 5 kDa. At day 0, both the WT Tugela DN and mutant RYNO3936 plants had one cross reacting SUMO1 peptide present that was absent in the other line (**Figure 9A**, bottom). At day 7, the WT Tugela DN had two peptides that were absent in the mutant RYNO3936, while the mutant plant had a cross-reacting SUMO1 peptide present that was absent in WT wheat line. When comparing the profile of cross-reacting SUMO1 peptides in RYNO3936 before (day 0) and after induction of water stress (days 7, 14), and after recovery (day 21), more differences in banding patters and intensity of the proteins were observed (**Figure 9A**, bottom).

To further elucidate whether the peptides on the protein blots were cysteine proteases, we included a protease inhibitor E64 specific to cysteine proteases during the protein analysis before separation on gradient zymograms (**Figure 9B**). The WT Tugela DN and mutant RYNO3936 plants differed in protein bands with proteolytic activity. Addition of the cysteine protease inhibitor E64 blocked the activity of three different proteases in each of the plants. A comparison between the profiles of the mutant plant before (day 0) and after induction of water stress (days 7, 14), and after recovery (day 21), revealed three protein bands with proteolytic activity in unstressed and recovered mutant plants, but four protein bands with proteolytic activity in the water stressed plants (days 7 and 14).

Oxidative Defense Enzymes

Mutant RYNO3936 expressed significantly higher POX activity than WT Tugela DN before (day 0) and after water stress (days 7 and 14), with the highest activity on day 7 after induction of water stress (**Figure 10A**). GST activity increased significantly in WT Tugela DN after induction of water deficit stress but did not change significantly in the mutant plant ($P < 0.05$) (**Figure 10B**).

DISCUSSION

Drought tolerance is a polygenic trait that is difficult to attain using conventional breeding. However, chemically induced mutagenesis has already produced excellent results by altering major polygenic traits leading to synergistic effects which increased the quality and yield of wheat (Ahloowalia et al., 2004; Tian et al., 2012). Inducing random mutagenesis in a red hard winter wheat line (Tugela DN), a mutant wheat line RYNO3936 with improved tolerance to water deficit, and the ability to recover fully and reproduce, after being physiologically "dead" (leaves completely dry/dehydrated) was developed. In the current study, we characterized the physiological and biochemical responses of this mutant wheat line RYNO3936 during irrigation and induced water deficit stress.

Our mutant's coping mechanism differs significantly from that of the WT wheat line, as prolonged exposure to water deficit stress seemingly has no influence on the phenotype of the mutant plant, while the WT wheat line suffered various developmental deformities (i.e., leaves are wrinkled or twisted and heads are deformed) and dies. Under non-water deficit conditions, the mutant plants took longer to reach maturity when compared to the control but produced more tillers and 4× more seed. Under water deficit stress, however, our mutant plants matured faster

TABLE 3 | List of proteins expressed in RYNO3936 before (day 0) and after exposure to water stress (days 7 and 14), and recovery after re-watering (day 21) ($p \leq 0.05$).

Identified Proteins (229)	Accession Number	Molecular Weight	ANOVA Test (p-value): *(p < 0.01463)
Oxygen-evolving enhancer protein 1, chloroplastic OS=Triticum urartu GN=TRIUR3_31979 PE=4 SV=1	M8AE10_TRIUA (+1)	34 kDa	<0.00010
ATP synthase delta chain, chloroplastic OS=Aegilops tauschii GN=F775_06392 PE=3 SV=1	N1R5T6_AEGTA	18 kDa	<0.00010
20 kDa chaperonin, chloroplastic OS=Aegilops tauschii GN=F775_32594 PE=3 SV=1	M8AVR4_AEGTA (+2)	26 kDa	<0.00010
Uncharacterized protein OS=Triticum aestivum PE=4 SV=1	W5GFX3_WHEAT (+1)	23 kDa	<0.00010
Stromal 70 kDa heat shock-related protein, chloroplastic OS=Aegilops tauschii GN=F775_29881 PE=3 SV=1	N1QXI7_AEGTA	73 kDa	<0.00010
Adenosylhomocysteinase OS=Triticum urartu GN=TRIUR3_03943 PE=3 SV=1	M7ZAK2_TRIUA (+2)	46 kDa	<0.00010
Alpha-amylase/trypsin inhibitor CM3 OS=Triticum aestivum PE=1 SV=1	IAAC3_WHEAT	18 kDa	<0.00010
Uncharacterized protein OS=Aegilops tauschii GN=F775_27291 PE=4 SV=1	M8CU50_AEGTA	32 kDa	<0.00010
UTP–glucose-1-phosphate uridylyltransferase OS=Triticum urartu GN=TRIUR3_15167 PE=4 SV=1	M7YXN3_TRIUA	51 kDa	<0.00010
40S ribosomal protein S20 OS=Triticum urartu GN=TRIUR3_10578 PE=3 SV=1	M7YRN1_TRIUA (+3)	14 kDa	<0.00010
Gamma-gliadin OS=Triticum dicoccoides GN=ll703 PE=4 SV=1	B6UKJ9_TRIDC (+13)	29 kDa	<0.00010
Aldehyde dehydrogenase 7b OS=Triticum aestivum PE=2 SV=1	D9IFB7_WHEAT (+1)	54 kDa	<0.00010
Uncharacterized protein OS=Triticum aestivum GN=TRAES_3BF028000060CFD_c1 PE=3 SV=1	A0A077S298_WHEAT (+1)	18 kDa	0.00015
Uncharacterized protein OS=Triticum aestivum PE=4 SV=1	W5DYH0_WHEAT	39 kDa	0.0002
Grain softness protein (Fragment) OS=Triticum aestivum GN=Gsp-1D PE=4 SV=1	A0A0A7AA82_WHEAT (+6)	16 kDa	0.00021
Lipoxygenase OS=Triticum aestivum PE=3 SV=1	W5F9D7_WHEAT	97 kDa	0.00023
5-methyltetrahydropteroyltriglutamate–homocysteine methyltransferase OS=Triticum urartu GN=TRIUR3_07672 PE=3 SV=1	M7ZHT1_TRIUA	85 kDa	0.00025
Fructose-bisphosphate aldolase OS=Triticum urartu GN=TRIUR3_24109 PE=3 SV=1	M7ZGS6_TRIUA (+3)	39 kDa	0.00032
ADP,ATP carrier protein, mitochondrial OS=Triticum urartu GN=TRIUR3_11472 PE=3 SV=1	M8A2G0_TRIUA (+3)	41 kDa	0.00032
Uncharacterized protein OS=Triticum aestivum PE=4 SV=1	W5FDV7_WHEAT	25 kDa	0.00037
Uncharacterized protein OS=Triticum aestivum PE=4 SV=1	W5HAX6_WHEAT	15 kDa	0.00037
Uncharacterized protein OS=Triticum aestivum PE=3 SV=1	W5FRF1_WHEAT	34 kDa	0.0004
Uncharacterized protein OS=Triticum aestivum PE=4 SV=1	W5B9F3_WHEAT	27 kDa	0.00054
Uncharacterized protein OS=Triticum aestivum PE=4 SV=1	W5G736_WHEAT	32 kDa	0.00054
Uncharacterized protein OS=Triticum aestivum PE=4 SV=1	W5HCY0_WHEAT	26 kDa	0.00069
Chlorophyll a-b binding protein, chloroplastic OS=Triticum urartu GN=TRIUR3_18701 PE=3 SV=1	M7YH23_TRIUA (+2)	38 kDa	0.00072
GTP-binding nuclear protein OS=Triticum urartu GN=TRIUR3_25734 PE=3 SV=1	M8ACU1_TRIUA (+5)	26 kDa	0.00076
60S acidic ribosomal protein P0 OS=Aegilops tauschii GN=F775_28558 PE=3 SV=1	N1QYE3_AEGTA	35 kDa	0.00086
Oxygen-evolving enhancer protein 3-1, chloroplastic OS=Aegilops tauschii GN=F775_30429 PE=4 SV=1	M8BB25_AEGTA (+3)	18 kDa	0.0013
Actin OS=Triticum aestivum PE=3 SV=1	A0A067YNJ5_WHEAT (+16)	42 kDa	0.0013
Low molecular weight glutenin OS=Triticum aestivum GN=Glu-A3 PE=4 SV=1	C3VN75_WHEAT (+3)	35 kDa	0.0013
Uncharacterized protein OS=Triticum aestivum GN=TRAES_3BF167600010CFD_c1 PE=4 SV=1	W5D1Z1_WHEAT	21 kDa	0.0014
30S ribosomal protein 1, chloroplastic OS=Aegilops tauschii GN=F775_31789 PE=4 SV=1	M8CEC3_AEGTA (+3)	26 kDa	0.0014
Photosystem II CP47 chlorophyll apoprotein OS=Aegilops tauschii GN=F775_04233 PE=4 SV=1	M8CB07_AEGTA	55 kDa	0.0015
70 kDa heat shock protein OS=Triticum aestivum PE=2 SV=1	C7ENF7_WHEAT (+1)	74 kDa	0.0015
Peptidyl-prolyl cis-trans isomerase OS=Triticum aestivum PE=2 SV=1	A7LM55_WHEAT	18 kDa	0.0016
Quinone oxidoreductase-like protein OS=Aegilops tauschii GN=F775_07275 PE=4 SV=1	M8AW52_AEGTA	32 kDa	0.002
Uncharacterized protein OS=Triticum aestivum PE=4 SV=1	W5HLU5_WHEAT (+1)	48 kDa	0.0021
Superoxide dismutase [Cu-Zn] OS=Triticum aestivum GN=SOD1.2 PE=2 SV=1	O24400_WHEAT	20 kDa	0.0022
Single-stranded nucleic acid binding protein OS=Triticum aestivum GN=whGRP-1 PE=2 SV=1	Q41518_WHEAT	16 kDa	0.0022
Low molecular weight glutenin subunit (Fragment) OS=Thinopyrum ponticum x Triticum aestivum PE=4 SV=1	Q5PU42_9POAL	34 kDa	0.0022
Uncharacterized protein OS=Triticum aestivum PE=3 SV=1	W5EHT8_WHEAT	19 kDa	0.0023
Photosystem I P700 chlorophyll a apoprotein A2 OS=Triticum aestivum GN=psaB PE=3 SV=1	PSAB_WHEAT (+1)	83 kDa	0.0026
Uncharacterized protein OS=Triticum urartu GN=TRIUR3_33029 PE=4 SV=1	M7Z7B4_TRIUA	32 kDa	0.0032
Uncharacterized protein OS=Aegilops tauschii GN=F775_04480 PE=4 SV=1	M8BDP7_AEGTA	26 kDa	0.0034
Uncharacterized protein OS=Triticum aestivum PE=3 SV=1	W5E575_WHEAT	35 kDa	0.0034
60S ribosomal protein L4-1 OS=Triticum urartu GN=TRIUR3_35018 PE=4 SV=1	M8A580_TRIUA (+2)	36 kDa	0.0037
Ribulose bisphosphate carboxylase large chain OS=Triticum aestivum GN=rbcL PE=1 SV=2	RBL_WHEAT (+1)	53 kDa	0.0045
Ribosomal protein OS=Triticum urartu GN=TRIUR3_07435 PE=3 SV=1	M7ZM70_TRIUA	18 kDa	0.0047
Cold-responsive protein WCOR14 OS=Aegilops tauschii GN=F775_26151 PE=4 SV=1	C0L981_AEGTA (+2)	14 kDa	0.0049
Putative calcium-binding protein CML7 OS=Triticum urartu GN=TRIUR3_30313 PE=3 SV=1	M7ZNI1_TRIUA	32 kDa	0.0057
Germin-like protein 8-14 OS=Triticum urartu GN=TRIUR3_27105 PE=3 SV=1	M7ZSU0_TRIUA (+2)	22 kDa	0.006
Glyceraldehyde-3-phosphate dehydrogenase OS=Aegilops tauschii GN=F775_07657 PE=3 SV=1	M8C8G6_AEGTA (+1)	37 kDa	0.0061
Uncharacterized protein OS=Triticum aestivum PE=4 SV=1	W5FGX7_WHEAT	41 kDa	0.0076
ATP synthase subunit alpha, mitochondrial OS=Triticum aestivum GN=ATPA PE=3 SV=1	ATPAM_WHEAT (+1)	55 kDa	0.0078

(Continued)

TABLE 3 | Continued

Identified Proteins (229)	Accession Number	Molecular Weight	ANOVA Test (p-value): *(p < 0.01463)
Uncharacterized protein OS=Triticum aestivum PE=3 SV=1	W5G312_WHEAT	82 kDa	0.008
Thioredoxin OS=Triticum urartu GN=TRIUR3_30421 PE=3 SV=1	M8ASF0_TRIUA (+5)	12 kDa	0.008
Uncharacterized protein OS=Triticum aestivum GN=TRAES_3BF092100100CFD_c1 PE=3 SV=1	A0A077S2R7_WHEAT	111 kDa	0.0087
Dimeric alpha-amylase inhibitor OS=Triticum aestivum PE=4 SV=1	I6PZ03_WHEAT (+1)	15 kDa	0.01
Uncharacterized protein OS=Triticum aestivum PE=3 SV=1	W5BD57_WHEAT	102 kDa	0.013
Cytochrome b6-f complex iron-sulfur subunit, chloroplastic OS=Triticum aestivum GN=petC PE=2 SV=1	UCRIA_WHEAT	24 kDa	0.013
Chloroplast inositol phosphatase-like protein OS=Triticum aestivum PE=2 SV=1	Q5XUV3_WHEAT (+1)	32 kDa	0.013
Putative vacuolar defense protein OS=Triticum aestivum GN=PR4e PE=4 SV=1	Q6PWL8_WHEAT (+1)	18 kDa	0.013
14-3-3 protein OS=Triticum aestivum GN=14R2 PE=2 SV=1	L0GED8_WHEAT (+3)	29 kDa	0.014
Globulin 1 OS=Triticum aestivum PE=4 SV=1	Q0Q5D4_WHEAT (+1)	25 kDa	0.014
Uncharacterized protein OS=Aegilops tauschii GN=F775_28677 PE=4 SV=1	R7W586_AEGTA	24 kDa	0.014
Chlorophyll a-b binding protein, chloroplastic OS=Triticum aestivum GN=CBP5 PE=2 SV=1	C1K5B9_WHEAT (+2)	29 kDa	0.015
Uncharacterized protein OS=Triticum aestivum GN=TRAES_3BF068000010CFD_c1 PE=4 SV=1	A0A077RQ49_WHEAT	274 kDa	0.015
ATP-dependent zinc metalloprotease FTSH 1, chloroplastic OS=Triticum urartu GN=TRIUR3_31373 PE=3 SV=1	M8ADT2_TRIUA (+2)	54 kDa	0.015
30S ribosomal protein 2, chloroplastic OS=Aegilops tauschii GN=F775_28246 PE=4 SV=1	M8BN30_AEGTA (+1)	20 kDa	0.015
Fructose-bisphosphate aldolase OS=Triticum aestivum GN=AIDP PE=2 SV=1	C0KTA6_WHEAT (+1)	42 kDa	0.016
Elongation factor Tu OS=Triticum urartu GN=TRIUR3_34609 PE=3 SV=1	M7ZEC4_TRIUA (+2)	46 kDa	0.017
Uncharacterized protein OS=Triticum urartu GN=TRIUR3_27117 PE=3 SV=1	M8AJF1_TRIUA (+3)	26 kDa	0.017
Glyceraldehyde-3-phosphate dehydrogenase OS=Aegilops tauschii GN=F775_05242 PE=3 SV=1	M8C9Y7_AEGTA (+2)	43 kDa	0.018
ATP synthase subunit alpha OS=Triticum urartu GN=atpA PE=3 SV=1	M8AUX6_TRIUA	62 kDa	0.019
Plastocyanin OS=Triticum aestivum PE=3 SV=1	W5DL22_WHEAT	16 kDa	0.02
Peroxisomal (S)-2-hydroxy-acid oxidase GLO1 OS=Triticum urartu GN=TRIUR3_22574 PE=4 SV=1	M7YXL1_TRIUA (+2)	40 kDa	0.021
Ribulose bisphosphate carboxylase small chain OS=Triticum urartu GN=TRIUR3_12281 PE=3 SV=1	M7YCR2_TRIUA (+7)	19 kDa	0.023
Glycine cleavage system H protein, mitochondrial OS=Triticum urartu GN=TRIUR3_12946 PE=3 SV=1	M7Z6F5_TRIUA	17 kDa	0.023
ATP synthase subunit OS=Triticum aestivum PE=2 SV=1	D3K4D8_WHEAT (+1)	40 kDa	0.023
Photosystem II CP43 reaction center protein (Fragment) OS=Triticum timopheevii GN=psbC PE=3 SV=1	A0A090ARF9_TRITI (+3)	54 kDa	0.024
Uncharacterized protein OS=Triticum aestivum PE=4 SV=1	W4ZSM1_WHEAT	15 kDa	0.025
Chlorophyll a-b binding protein, chloroplastic OS=Triticum urartu GN=TRIUR3_20986 PE=3 SV=1	M7ZM86_TRIUA (+3)	23 kDa	0.026
Uncharacterized protein OS=Triticum aestivum PE=4 SV=1	W5F6W2_WHEAT	16 kDa	0.027
LEA3 OS=Triticum turgidum subsp. durum PE=2 SV=1	A0A0M4HM24_TRITD	22 kDa	0.027
Uncharacterized protein OS=Aegilops tauschii GN=F775_29168 PE=4 SV=1	M8BNU5_AEGTA	91 kDa	0.028
Alanine aminotransferase 2 OS=Aegilops tauschii GN=F775_30987 PE=4 SV=1	M8BWQ5_AEGTA (+2)	58 kDa	0.028
Serine hydroxymethyltransferase OS=Triticum aestivum PE=3 SV=1	W5ECJ8_WHEAT	59 kDa	0.029
60S ribosomal protein L23a OS=Triticum urartu GN=TRIUR3_20390 PE=3 SV=1	M8A553_TRIUA (+2)	20 kDa	0.029
Cytochrome f OS=Triticum aestivum GN=petA PE=3 SV=3	CYF_WHEAT (+3)	35 kDa	0.03
High molecular weight glutenin subunit Ax-dp (Fragment) OS=Triticum polonicum PE=4 SV=1	D1MJA1_9POAL	91 kDa	0.03
Ribulose bisphosphate carboxylase small chain OS=Triticum aestivum GN=rbcS PE=3 SV=1	Q9FEE4_WHEAT	19 kDa	0.035
High molecular weight glutenin subunit OS=Triticum aestivum GN=Glu PE=4 SV=1	W6AWK6_WHEAT	67 kDa	0.035
Photosystem 1 subunit 5 OS=Triticum aestivum GN=pssv-1B PE=4 SV=1	Q2L3V4_WHEAT	15 kDa	0.036
Histone H2A OS=Aegilops tauschii GN=F775_29407 PE=3 SV=1	R7WEH7_AEGTA (+1)	16 kDa	0.039
Uncharacterized protein OS=Triticum aestivum PE=3 SV=1	W5B4C8_WHEAT (+1)	29 kDa	0.04
Fructose-bisphosphate aldolase OS=Triticum aestivum PE=3 SV=1	W5G4A2_WHEAT	42 kDa	0.041
Uncharacterized protein OS=Triticum urartu GN=TRIUR3_14987 PE=4 SV=1	M7ZIY8_TRIUA (+1)	27 kDa	0.044
RUBISCO activase alpha (Fragment) OS=Triticum aestivum GN=rca2_alpha PE=4 SV=1	A0A078BQY4_WHEAT (+3)	45 kDa	0.045
Cell division protease ftsH-like protein, chloroplastic OS=Aegilops tauschii GN=F775_28819 PE=3 SV=1	M8BVC8_AEGTA	72 kDa	0.048
PsbP-like protein 1, chloroplastic OS=Aegilops tauschii GN=F775_30938 PE=4 SV=1	R7VZH9_AEGTA (+2)	23 kDa	0.94

Indicated are the significantly regulated peptides, the accession number, molecular weight of the proteins, and P-values.

than WT Tugela DN and produced the same amount of seed than WT Tugela DN under irrigation. This seemingly rapid transition from a vegetative to reproductive stage corresponds to observation in engineered rice (Oryza sativa) expressing the galactinol synthase gene when exposed to water deficit conditions (Selvaraj et al., 2017), which essentially affords the plant the ability to produce seeds before the induced stress becomes lethal for the crop (Kazan and Lyons, 2016; Gol et al., 2017). Interestingly, the mutant RYNO 3936 avoids premature wilting during induced water stress, as demonstrated by its high RMC when compared to WT Tugela DN, which visually wilted within 3 days after water was withheld. Physiologically, the function of wilting is to soften leaves to enable leaf rolling, thus limiting surface area for further water loss by evaporation (Bowne et al., 2012). Mutant RYNO3936 expresses a "slow-wilting phenotype", since it retains a higher RMC during water

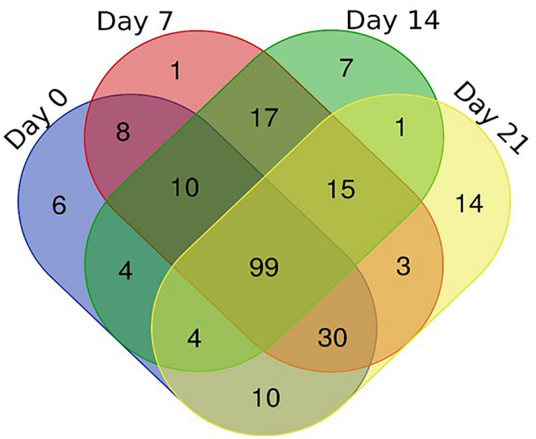


FIGURE 7 | Venn diagram of the shared and unique proteins present in RYNO3936 before (day 0) and after exposure to water stress (days 7 and 14), and recovery after re-watering (day 21).

deficit stress and loses rigidity only with prolonged water stress (day 14). Even though RMC declines in the mutant and the plant shows visual senescence (browning of leaves), the visual browning is less when compared to that of WT Tugela DN. However, after re-watering, the mutant fully recovers as demonstrated by the increase in RMC, suggesting that the mutant can readjust its osmoregulation assuming full turgor pressure and recover to activate its metabolic activity providing whole-plant relief to the water deficit stress (Souza et al., 2004).

When water deficit stress was induced, both WT and mutant plants senesced with their leaves losing their green color which is synonymous to the preferential degradation of chlorophyll over carotenoids (Balazadeh, 2014; Li et al., 2019). The visible de-greening of the leaves, however, took longer in the mutant RYNO3936, as it was evident from its chlorophyll content that remained higher when compared to the WT Tugela DN. This observed "slow-wilting phenotype" is substantiated by the fact that the mutant remained photosynthetically active much longer than the WT Tugela DN (Thomas and Ougham, 2014), before it also senesces. A reduction of chlorophyll during water deficit stress is common in many crop species and largely dependent on the duration and severity of water stress (Brestic et al., 2015; Lakra et al., 2015; Peng et al., 2017).

It is evident that the mutant RYNO3936 could maintain an active metabolic state despite the experienced water deficit stress, as substantiated by the high rate of stomatal conductance and chlorophyll fluorescence during water deficit stress conditions. It is well understood that chlorophyll fluorescence and stomatal conductance are intrinsically coupled under a wide range of environmental conditions (i.e., soil moisture). However, different crop species such as tomatoes, kidney beans, potatoes, rice, and wheat manage the intrinsic relationship differently (Miyashita et al., 2005; Yuan et al., 2015; Ouyang et al., 2017; Wheeler et al., 2019; Wang et al., 2020). Generally, studies suggest that water deficit stress induces a reduction in photosynthesis and stomatal conductance, consequently, restricts the availability of CO2 for carboxylation (Ehonen et al., 2019). The mutant showed a decline in chlorophyll fluorescence and stomatal conductance only after prolonged induced water deficit stress (14 days) and restored to near full functionality with re-watering (Yi et al., 2016). The manner in which the mutant manifest its physiological response to water deficit and re-watering, is consistent with the results reported in maize inbred and hybrid lines (Chen et al., 2016) and two wheat cultivars (Abid et al., 2018), that showed a decrease in chlorophyll fluorescence and stomatal conductance during water deficit stress, but rapid "recovery" in chlorophyll fluorescence and stomatal conductance to normal levels after re-watering. This suggests that

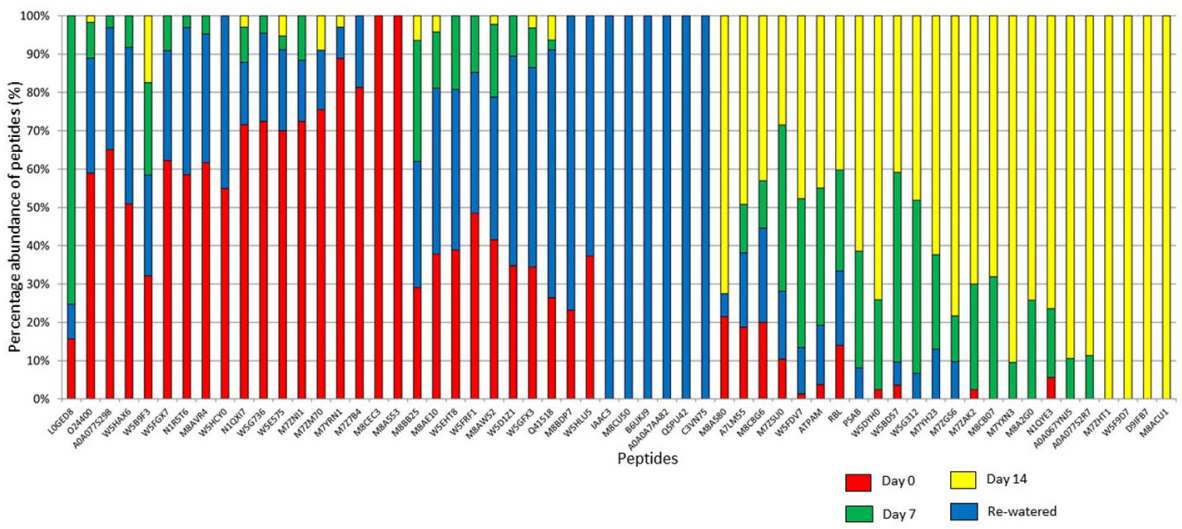


FIGURE 8 | Percentage abundance of the Top 100 peptides expressed in RYNO3936 before (day 0) and after exposure to water stress (days 7 and 14), and recovery after re-watering (day 21).

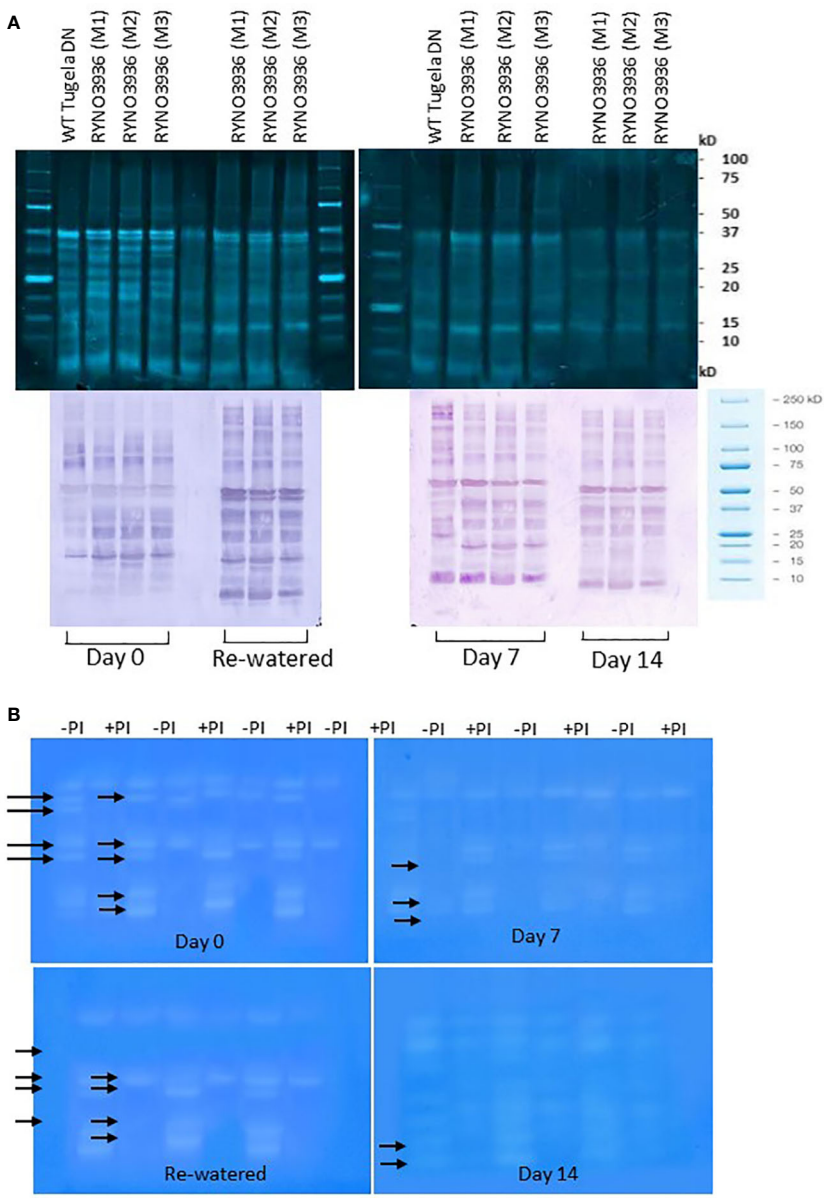


FIGURE 9 | (A) Top: Crude protein separated on a 12.5% SDS-PAGE from WT Tugela DN and Mutant RYNO3936 wheat prior to (day 0) and after exposure to water stress (days 7 and 14). All lanes were loaded with 20 µg total protein. Bottom: WT Tugela DN and Mutant RYNO 3936 wheat prior to (day 0) and after exposure (days 7 and 14) to water stress, probed with anti-SUMO IgG. All lanes were loaded with 20 µg total protein. Blots were probed with a dilution of 1:10 000 dilution of monoclonal IgG against SUMO1. Images were cropped for presentation purposes. M1 to M3 represents three independent Mutants. **(B)** Gradient Zymograms depicting proteolytic activity of WT Tugela DN and Mutant RYNO3936 prior to (day 0) and after exposure to water stress (days 7 and 14). Zymograms (gradient, 5–15%) were cast and in all cases 35 µg protein was loaded. Inclusion of an incubation step with 0.1 mM Cysteine Protease inhibitor (E-64) performed at pH 7, enabled for the identification of cysteine proteases. Lanes with + PI refers to treatment with protease inhibitor; whereas - PI refers to no inhibitor treatment. Arrows indicated bands that were removed after treatment with the 0.1 mM Cysteine Protease inhibitor (E-64). The presented data is representative of two independent experiments. Images were cropped for presentation purposes, and the contrast was adjusted (10%).

the stomatal aperture increased with re-watering thereby facilitating diffusion of CO2 from the atmosphere to the carboxylation site of RuBisCO (Galmés et al., 2011; Kumar et al., 2019).

Water deficit stress is usually associated with the onset of senescence. The process of senescence is associated with modification and/or degradation of photosynthetic proteins making them dysfunctional. Since random mutagenesis was applied to the mutants, it is likely that changes were induced in single/multiple genes, resulting in the expression of more proteins involved in photosynthesis and energy production. *Amaranthus hybridus* is an excellent example where a mutation in a chloroplast protein (i.e., a photosystem II electron transport protein that binds

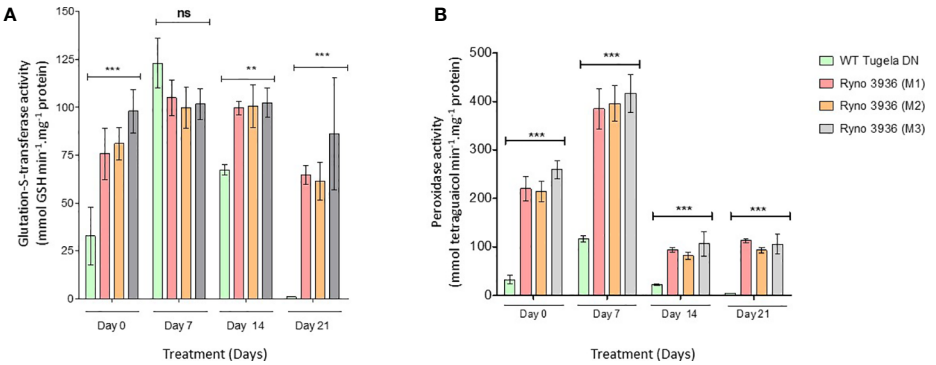


FIGURE 10 | Changes in the peroxidase (POX) **(B)** and glutathione-S-transferase (GST) **(A)** activities measured in WT Tugela DN and Mutant RYNO 3936 wheat prior to (day 0) and after induction of water stress (days 7 and 14). POX activity was measured by the formation of tetraguaiacol monitored at 470 nm while GST activity represents the formation of GS-DNB conjugate at 340 nm. Capped bars above means represent ± SD of three replicates. Asterisks above columns means denote the significant differences compared with WT Tugela DN for a single mutant line. $^{**}P \leq 0.01$; $^{***}P \leq 0.05$. ns, nonsignificant.

the electron carrier plastoquinone) improved tolerance to water deficit (Hirshberg and McIntosh, 1983). The plant also had higher photosynthetic rates when compared to control plants under water deficit conditions (Arntz et al., 2000).

To further our understanding of how the mutant plant manages its photosynthesis, we investigated RuBisCo protein expression. This enzyme is vital for CO_2 fixation and oxygenation. The protein is assembled in the chloroplast from nuclear-encoded genes, cytosol synthesized small subunits (SSU) and plastid encoded genes which synthesis the large subunits (LSU) (Kawashima and Wildman, 1970; Ellis, 1979). Collectively the SSU is responsible for maintaining the form, structure, and activity of RuBisCo, whereas the LSU contain all the active sites (Knight et al., 1990; Andersson and Backlund, 2008). Not only does each subunit's response to water deficit stress differ, the response is also crop dependent. Mutant RYNO 3936 possesses a high abundance of LSU prior to water deficit stress, which only decreases upon the first 7 days of water stress thereafter a slight decline was observed (**Figures 9A, B**). Prolonged water deficit stress (day 14) followed by re-watering resulted in no significant changes in LSU abundance. This unique preservation of LSU could be due to effective control of proteases, which are able to degrade the large subunit of Rubisco (Bushnell et al., 1993). Prins et al. (2008) also found elevated levels of LSU in all tissue types of engineered tobacco (*Nicotiana tabacum* L.) that express a rice cystatin (a family of cysteine proteinases), when compared to WT tobacco. In contrast, the small subunit levels decreased after induction of water stress and never recovered to its pre-stressed state (**Figures 9A, B**) despite full recovery of the plant. Similar findings were also reported for tomato, Arabidopsis, and rice (Bartholomew et al., 1991; Williams et al., 1994; Vu et al., 1999).

Water stress induces senescence processes associated with protein degradation and turnover. We found changes in the mutant's protein profiles after induction of water stress (days 7, 14) and after recovery post-re-watering (day 21) which might also be associated with increased expression of SUMO-proteases with a papain-like proteinase fold (Hickey et al., 2012). In this regard, we found a protein of ± 50 kDa in size highly abundant in the mutant's profile after recovery post-re-watering (**Figure 9A**). Under non-stressed conditions SUMO tags may serve as priming sites essentially preparing our mutant for early stress recognition (Conrath et al., 2002). Many studies have also demonstrated that plants unable to latch SUMO1/2 onto substrate proteins show phenotypes with changes in flowering time (Castro et al., 2018), immune responses (Saleh et al., 2015), growth reduction, and reduced tolerance to salinity, drought, heat, freezing, and phosphate starvation (Roden et al., 2004; Catala et al., 2007; Miura et al., 2007; Li et al., 2019). Although SUMOylation is strongly associated with drought susceptibility (Benlloch and Lois, 2018), a mutated proteome, as in our case, may circumvent the deleterious SUMOylation effects by increasing SUMO-proteases for deSUMOylation influx. In a previous study, we concluded that overexpressing Overly Tolerant to Salt-1 in spring wheat (Gamtoos R) enhances water stress tolerance in the transgenic plants and significantly reduces the effects of SUMOylation (Le Roux et al., 2019). Since SUMO proteins belong to the family of cysteine protease (Botha et al., 2017), we investigated total proteases and cysteine proteases by using the inhibitor E64. Proteases play an important role in programmed cell death, senescence and protein remobilization, and have been shown to be induced by water stress (Liu et al., 2018). RYNO 3936 had fewer and a lower abundance of cysteine proteases during water stress. This also indicates that the mutant has less protein degradation under water deficit stress and therefore senesce less (Botha et al., 2017; Le Roux et al., 2019).

We further found in our study that our mutant plants differ significantly in antioxidative enzyme activities before (day 0) and after induction of water stress (days 7, 14) when compared to WT Tugela DN plants. Water stress generally leads to more ROS signaling linked to ABA production, Ca2+ fluxes and sugar sensing (Cruz de Carvalho, 2008 and references within). In our study, we specifically found expression of an abscisic stress-ripening protein in our mutant plant which was absent from the WT control indicating a greater control to manage increasing ROS production.

The mutant also expressed high levels of POX and GST, in particular 7 days after initiation of water deficit stress. Such

increase in POX was also recently found in two drought-tolerant Chinese wheat varieties when exposed to water stress (Abid et al., 2018), as well as in the tasg1 wheat mutant (Tian et al., 2012). POX catalyzes hydrogen peroxide-dependent oxidation of a wide range of substrates, mainly phenol derivatives (Noctor et al., 2018; Smirnoff and Arnaud, 2019). GST provides a unique intracellular protection and an increase in GST is linked with sustaining cell redox homeostasis and guarding organisms against oxidative stress (Chen et al., 2012; Kumar and Trivedi, 2018). Overall, our findings suggest that there is a significant difference in antioxidative enzyme activities before (day 0) and after induction of water deficit stress (days 7, 14) when compared to WT Tugela DN plants. Water stress generally leads to more ROS signaling linked to ABA production, Ca2+ fluxes, and sugar sensing (Cruz de Carvalho, 2008 and references within). In our study, we specifically found expression of an abscisic stress-ripening protein in our mutant plant which was absent from the WT control indicating a greater control to manage increasing ROS production.

Increases in GST and POX activity further coincided in our study with a higher content of FAA with proline being the highest (**Table 2**), which might suggest that proline also participates in scavenging reactive oxygen species in addition to its role as an osmolyte as previously reported for salt-stressed plants (Hoque et al., 2007; Hossain et al., 2011; Cruz de Carvalho et al., 2013; Rejeb et al., 2014). Proline provides osmo-protection and the amount increases in many plant species, including maize, wheat, and pea, following exposure to water deficit stress (Matysik et al., 2002; Rampino et al., 2006; Charlton et al., 2008; Szabados and Savoure, 2010; Witt et al., 2012; Abid et al., 2018; Le Roux et al., 2019; Verslues and Juenger, 2019). Other FAAs that were much higher in the mutant when compared to the WT Tugela DN include methionine, asparagine, isoleucine, and phenylalanine. Pool sizes of FAAs are important, not only because of their requirement in protein biosynthesis (Good and Zaplachinski, 1994), but also for their additional functions in plant metabolism and signal transduction processes which ultimately may contribute to adequate water stress response. The extended level of amino acids is evident in enhancing stress pliability in our study, since RYNO3936 increases FAA under water deficit stress conditions, but FAA concentrations decrease considerably after re-watering to near well-watered levels (day 0). Abid et al. (2018) demonstrated that drought stress leads to a gradual increase of FAA, but soon decrease to match that of well-watered levels in wheat. This effective management of FAA has been suggested to aid in drought tolerance by protein stabilization, ROS detoxification and osmotic adjustment (Bowne et al., 2012; Rabara et al., 2017; Michaletti et al., 2018; Jia et al., 2019). FAA pool sizes are known to be induced under stress and during senescence (Hildebrandt et al., 2015 and references within). More important in the context of this study, in a recent study by Yadav et al. (2019), a strong genetic association was observed between glasshouse-based RWC, metabolites, and yield gap-based drought tolerance (YDT; the ratio of yield in water-limited versus well-watered conditions) across 18 field environments spanning sites and seasons. Specifically of interest is the observation that 98% of the genetic YDT variance could be explained by drought responses of four metabolites: serine, asparagine, methionine, and lysine ($R2 = 0.98$; $P < 0.01$). More specifically, that higher levels of methionine and lysine were more strongly associated with higher YDT, than the other amino acids, which support our observations in RYNO3638 with enhanced water deficit stress tolerance (Le Roux et al., 2019).

Changes in the transcriptome differs to changes at protein level (Gygi et al., 1999; Bogeat-Triboulot et al., 2006; Morimoto and Yahara, 2018), necessitating studies into the proteome to elucidate the water stress response pathway in crop species (Ford et al., 2011; Budak et al., 2013; Rabello et al., 2014; Liu et al., 2015; Chmielewska et al., 2016). In our study, we also found that our mutant RYNO3936 expressed proteins associated with osmotic stress tolerance (e.g. abscisic stress-ripening protein, cold induced protein, cold-responsive protein, dehydrin, and Group 3 late embryogenesis abundant protein, LEA) more than in the control. Dehydrin and LEA proteins have been long known to increase osmotic stress tolerance in plants (Figueras et al., 2005; Brini et al., 2007). With induction of water stress (day 7), the mutant expressed a LAlv9 family protein belonging to the family of lipocalins. Literature is rather limited regarding functionality of these proteins. In the past, lipocalins have been classified as transport proteins; however, it is now clear that lipocalins are involved in a variety of functions, including regulation of cell homeostasis, modulation of the immune response, programmed cell death (Lee et al., 2007; Kale et al., 2018) and, as carrier proteins, to act in the general clearance of endogenous and exogenous compounds (Flower, 1996 and references within; Kale et al., 2018). In mammals, an ortholog of the lipocalin family (BCL-2) controls cell death primarily by direct binding interactions that regulate mitochondrial outer membrane permeabilization (MOMP) leading to the irreversible release of intermembrane space proteins, subsequent caspase activation, and apoptosis (Kale et al., 2018). While in plants, the AtTIL lipocalin was shown to be functional in modulating tolerance to oxidative stress (Charron et al., 2008), when it was demonstrated that overexpression enhances tolerance to stress caused by freezing, paraquat, and light in Arabidopsis by encoding components of oxidative stress and energy balance. More importantly in the context of the present study, in Arabidopsis AtTIL lipocalin delays flowering and maintains leaf greenness in the latter plant, like our observations in RYNO3936. So lipocalin might partly explain the more water deficit stress tolerance of the mutant. This would be a new and important aspect not found so far for a wheat mutant with improved drought tolerance.

In conclusion, we characterized a new wheat mutant RYNO3936 which is associated with delayed water deficit stress-induced leaf senescence and rapid drought recovery. In particular, when this mutant was exposed to water deficit conditions it displayed higher RWC in its roots and leaves, sustained its chlorophyll fluorescence activity and stomatal conductance, accumulated in a selected set of FAAs associated with drought stress, expressed a unique set of proteins, showed delayed protein degradation and higher antioxidative enzyme activities when compared with its WT

progenitor. Our mutant also uniquely expressed an abscisic stress-ripening protein and a LAlv9 family protein belonging to the family of lipocalins, which are involved in a variety of functions, including regulation of cell homeostasis, modulation of the immune response, and programmed cell death. Overall, our results suggest that our new high yielding wheat mutant RYNO2936 has a potential application in wheat breeding programs to enhance drought tolerance. Additionally, we characterized several of its unique traits (compared to the WT) that will assist future screening of mutant germplasm.

DATA AVAILABILITY STATEMENT

The mass spectrometry proteomics data have been deposited to the ProteomeXchange Consortium *via* the PRIDE (Perez-Riverol et al., 2019; http://www.ebi.ac.uk/pride) partner repository with the dataset identifier PXD019464 and 10.6019/PXD019464.

AUTHOR CONTRIBUTIONS

M-SR and A-MB-O planned the study. M-SR measured the plant phenotypes, analyzed chlorophyll fluorescence and stomatal conductance, as well as protein extractions for gel electrophoresis, and Western blots. A-MB-O conducted the enzyme assays. A-MB-O and M-SR extracted the proteins for MS/MS analysis, while MV conducted the MS/MS analysis. NB assisted with the bioinformatics and cluster analysis. M-SR and A-MB-O wrote the first draft. KK, MV, NB, and CC contributed to the interpretation of data and made editorial inputs.

ACKNOWLEDGMENTS

The authors would like to acknowledge the National Research Foundation of South Africa (NRF Competitive Programme for Rated Researchers (CPRR) Grant: CPR20110615000019459 and NRF Incentive Funding for Rated Researchers Programme (IFR) Grant: IFR201004200013) and the Winter Cereal Trust for provision of funding.

SUPPLEMENTARY MATERIAL

The Supplementary Material for this article can be found online at: https://www.frontiersin.org/articles/10.3389/fpls.2020.01053/full#supplementary-material

TABLE S2 | Blast2GO results from the peptides obtained after LC-ESI-MS/MS analysis of total protein isolated from RYNO3936 before (day 0), and after induction of water stress (days 7 and 14), and after recovery and regrowth (day 21).

TABLE S3 | List of proteins expressed in RYNO3936 before (day 0), and after induction of water stress (days 7 and 14), as well as after recovery and regrowth (day 21). Indicated are the sequence name, protein identity, length and number of hits, number of GO terms, and *e*-value. The cluster numbers correspond to that given in **Figure S2**.

FIGURE S1 | Proportional contribution of proteins expressed in RYNO3936 to the different functional categories, where **(A)** biological processes; **(B)** cellular component; and **(C)** molecular function.

FIGURE S2 | Cluster image generated by Java TreeView (Saldanha, 2004) of the proteins obtained after LC-ESI-MS/MS analysis of total protein isolated from RYNO3936 before (day 0), and after induction of water stress (days 7 and 14), and after recovery and regrowth (day 21). Red bands show up-regulated proteins, whereas green bands show down-regulated proteins.

REFERENCES

Aase, J. K. (1977). Relationship between leaf area and dry matter in winter wheat. *Agron. J. Abst.* 70, 563–565. doi: 10.2134/agronj1978.00021962007000040011x

Abid, M., Tian, Z., Ata-Ul-Karim, S., Liu, Y., Cui, Y., Zahoor, R., et al. (2016). Improved tolerance to post-anthesis drought stress by pre-drought priming at vegetative stages in drought-tolerant and -sensitive wheat cultivars. *Plant Physiol. Biochem.* 106, 218–227. doi: 10.1016/j.plaphy.2016.05.003

Abid, M., Ali, S., Qi, L., Zahoor, R., Tian, Z., Jiang, D., et al. (2018). Physiological and biochemical changes during drought and recovery periods at tillering and jointing stages in wheat (*Triticum aestivum* L). *Sci. Rep.* 8, 4615. doi: 10.1038/s41598-018-21441-7

Ahloowalia, S., Maluszynski, M., and Nichterlein, K. (2004). Global impact of mutation-derived varieties. *Euphytica* 2, 187–204. doi: 10.1023/B:EUPH.0000014914.85465.4f

Altieri, M., and Nicholls, C. (2017). The adaptation and mitigation potential of traditional agriculture in a changing climate. *Climate Change* 140, 33–45. doi: 10.1007/s10584-013-0909-y

Amstrong, R. A. (2014). When to use Bonferonni correction. *Ophthalmic Physiol. Optics* 34, 502–508. doi: 10.1111/opo.12131

Andersson, I., and Backlund, A. (2008). Structure and function of Rubisco. *Plant Physiol. Biochem.* 46, 275–291. doi: 10.1016/j.plaphy.2008.01.001

Arnon, D. I. (1949). Determination of chlorophyll concentration in leaf tissues of plants. *Plant Physiol.* 24, 1–15. doi: 10.1104/pp.24.2.1

Arntz, A., Delucia, E., and Jordan, N. (2000). Fitness effects of a photosynthetic mutation across contrasting environments. *J. Evol. Biol.* 13, 792–803. doi: 10.1046/j.1420-9101.2000.00223.x

Aro, E. (2004). Dynamics of photosystem II, a proteomic approach to thylakoid protein complexes. *J. Exp. Bot.* 56, 347–356. doi: 10.1093/jxb/eri041

Asensi-Fabado, M., and Munné-Bosch, S. (2010). Vitamins in plants, occurrence, biosynthesis and antioxidant function. *Trends Plant Sci.* 15, 582–592. doi: 10.1016/j.tplants.2010.07.003

Balazadeh, S. (2014). Stay-green not always stays green. *Mol. Plant* 7, 1264–1266. doi: 10.1093/mp/ssu076

Balla, K., Bencze, S., Bónis, P., Árendás, T., and Veisz, O. (2014). Changes in the photosynthetic efficiency of winter wheat in response to abiotic stress. *Cent. Eur. J. Biol.* 9, 519–530. doi: 10.2478/s11535-014-0288-z

Barrett, A., Kembhavi, A., Brown, M., Kirschke, H., Knight, C., Tamai, M., et al. (1982). L-trans-epoxysuccinyl-leucylamido(4-guanidino) butane (E-64) and its analogues as inhibitors of cysteine proteinases including cathepsins B. H and L. *Biochem. J.* 201, 189–198. doi: 10.1042/bj2010189

Bartholomew, D., Bartley, G., and Scolnik, P. (1991). Abscisic acid control of *rbcs* and *cab* transcription in tomato leaves. *Plant Physiol.* 96, 291–296. doi: 10.1104/pp.96.1.291

Benjamini, V., and Hochberg, V. (1995). Controlling the false discovery rate: a practical and powerful approach to multiple testing. *J. R. Stat. Soc B.* 57, 289–300. doi: 10.1111/j.2517-6161.1995.tb02031.x

Benlloch, R., and Lois, L. (2018). SUMOylation in plants, mechanistic insights and its role in drought stress. *J. Exp. Bot.* 69, 4539–4554. doi: 10.1093/jxb/ery233

Black, A. L., and Power, J. F. (1965). Effect of chemical and mechanical fallow methods on moisture storage, wheat yields, and soil erodibility 1. *Soil Sci. Soc Am. J.* 29, 465–468. doi: 10.2136/sssaj1965.03615995002900040032x

Bogeat-Triboulot, M., Brosche, M., Renaut, J., Jouve, L., Le Thiec, D., Fayyaz, P., et al. (2006). Gradual soil water depletion results in reversible changes of gene expression, protein profiles, ecophysiology, and growth performance in

Populus euphratica, a poplar growing in arid regions. *Plant Physiol.* 143, 876–892. doi: 10.1104/pp.106.088708

Bota, J., Medrano, H., and Flexas, J. (2004). Is photosynthesis limited by decreased RuBisCO activity and RuBP content under progressive water stress? *New Phytol.* 162, 671–681. doi: 10.1111/j.1469-8137.2004.01056.x

Botha, F. C., and Small, J. C. (1987). Control of ribulose 1, 5-bisphosphate carboxylase synthesis in the cotyledons of *Citrullus lanatus*. *Plant Sci.* 53, 121–129. doi: 10.1016/0168-9452(87)90121-X

Botha, A.-M., Van Eck, L., Burger, N. F. V., and Swanevelder, Z. H. (2014). Near-isogenic lines of *Triticum aestivum* with distinct modes of resistance exhibit dissimilar transcriptional regulation during *Diuraphis noxia* feeding. *Biol. Open* 3, 1116–1126. doi: 10.1242/bio.201410280

Botha, A.-M., Kunert, K. J., and Cullis, C. (2017). Cysteine proteases and wheat (*Triticum aestivum* L) under drought. A still greatly unexplored association. *Plant Cell Environ.* 40, 1679–1690. doi: 10.1111/pce.12998

Botha, A.-M., Kunert, K. J., Malinga, J. M., and Foyer, C. H. (2019). Defining biotechnological solutions for insect control in Sub-Saharan Africa. *Food Ener. Sec.* 9, e191. doi: 10.1002/fes3.191

Bowne, J., Erwin, T., Juttner, J., Schnurbusch, T., Langridge, P., Bacic, A., et al. (2012). Drought responses of leaf tissues from wheat cultivars of differing drought tolerance at the metabolite level. *Mol. Plant* 5, 418–429. doi: 10.1093/mp/ssr114

Bradford, M. M. (1976). A rapid and sensitive method for the quantitation of microgram quantities of protein utilizing the principle of protein-dye binding. *Anal. Biochem.* 72, 248–254. doi: 10.1016/0003-2697(76)90527-3

Brestic, M., Zivcak, M., Kunderlikova, K., Sytar, O., Shao, H., Kalaji, H., et al. (2015). Low PSI content limits the photoprotection of PSI and PSII in early growth stages of chlorophyll b-deficient wheat mutant lines. *Photosynth. Res.* 125, 151–166. doi: 10.1007/s11120-015-0093-1

Brini, F., Hanin, M., Lumbreras, V., Amara, I., Khoudi, H., Hassairi, A., et al. (2007). Overexpression of wheat dehydrin DHN-5 enhances tolerance to salt and osmotic stress in *Arabidopsis thaliana*. *Plant Cell Rep.* 26, 2017–2016. doi: 10.1007/s00299-007-0412-x

Budak, H., Akpinar, B., Unver, T., and Turktas, M. (2013). Proteome changes in wild and modern wheat leaves upon drought stress by two-dimensional electrophoresis and nano LC-ESI–MS/MS. *Plant Mol. Biol.* 83, 89–103. doi: 10.1007/s11103-013-0024-5

Bushnell, T. P., Bushnell, D., and Jagendorf, A. T. (1993). A purified zinc protease of pea chloroplasts, EP1, degrades the large subunit of ribulose-1,5-bisphosphate carboxylase/oxygenase, *Plant Physiol.* 103, 585–591. doi: 10.1104/pp.103.2.585

Castro, P. H., Santos, M., Freitas, S., Cana-Quijada, P., Lourenço, T., Rodrigues, M. A. A., et al. (2018). *Arabidopsis thaliana* SPF1 and SPF2 are nuclear located ULP2-like SUMO proteases that act downstream of SIZ1 in plant development. *J. Exp. Bot.* 69, 4633–4649. doi: 10.1093/jxb/ery265

Catala, R., Ouyang, J., Abreu, I. A., Hu, Y., Seo, H., Zhang, X., et al. (2007). The Arabidopsis E3 SUMO Ligase SIZ1 regulates plant growth and drought responses. *Plant Cell* 19, 2952. doi: 10.1105/tpc.106.049981

Charlton, A. J., Donarski, J. A., Harrison, M., Jones, S. A., Godward, J., Oehlschlager, S., et al. (2008). Responses of the pea (*Pisum sativum* L.) leaf metabolome to drought stress assessed by nuclear magnetic resonance spectroscopy. *Metabolomics* 4, 312. doi: 10.1007/s11306-008-0128-0

Charron, J.-B. F., Ouellet, F., Houde, M., and Sarhan, F. (2008). The plant Apolipoprotein D ortholog protects Arabidopsis against oxidative stress. *BMC Plant Biol.* 8, 86. doi: 10.1186/1471-2229-8-86

Chen, J. H., Jiang, H. W., Hsieh, E. J., Chen, H. Y., Chien, C. T., Hsieh, H. L., et al. (2012). Drought and salt stress tolerance of an Arabidopsis glutathione S-transferase U17 knockout mutant are attributed to the combined effect of glutathione and abscisic acid. *Plant Physiol.* 158, 340–351. doi: 10.1104/pp.111.181875

Chen, D., Wang, S., Cao, B., Cao, D., Leng, G., Li, H., et al. (2016). genotypic variation in growth and physiological response to drought stress and re-watering reveals the critical role of recovery in drought adaptation in maize seedlings. *Front. Plant Sci.* 6, 1241. doi: 10.3389/fpls.2015.01241

Chmielewska, K., Rodziewicz, P., Swarcewicz, B., Sawikowska, A., Krajewski, P., Marczak, Ł., et al. (2016). Analysis of drought-induced proteomic and metabolomic changes in barley (*Hordeum vulgare L*,) leaves and roots unravels some aspects of biochemical mechanisms involved in drought tolerance. *Front. Plant Sci.* 7, 1108. doi: 10.3389/fpls.2016.01108

Conesa, A., Götz, S., García-Gómez, J. M., Terol, J., Talón, M., and Robles, M. (2005). Blast2GO: a universal tool for annotation, visualization and analysis in functional genomics research. *Bioinformatics* 21, 3674–3676. doi: 10.1093/bioinformatics/bti610

Conrath, U., Pieterse, C., and Mauch-Mani, B. (2002). Priming in plant–pathogen interactions. *Trends Plant Sci.* 7, 210–216. doi: 10.1016/S1360-1385(02)02244-6

Cruz de Carvalho, K., de Campos, M. K. F., Domingues, D. S., Pereira, L. F. P., and Vieira, L. G. E. (2013). The accumulation of endogenous proline induces changes in gene expression of several antioxidant enzymes in leaves of transgenic *Swingle citrumelo*. *Mol. Biol. Rep.* 40, 3269–3279. doi: 10.1007/s11033-012-2402-5

Cruz de Carvalho, M. H. (2008). Drought stress and reactive oxygen species. Production, scavenging and signalling. *Plant Signal. Behav.* 3, 156–165. doi: 10.4161/psb.3.3.5536

Dai, A. (2011). Drought under global warming. a review. Wiley Interdisciplinary Reviews. *Climate Change* 2, 45–65. doi: 10.1002/wcc.81

Damerval, C., De Vienne, C., Zivy, M., and Thiellement, H. (1986). The technical improvements in Two-Dimensional Electrophoresis increase the level of genetic variation detected in wheat seedling proteins. *Electrophor* 7, 52–54. doi: 10.1002/elps.1150070108

Demidchik, V. (2015). Mechanisms of oxidative stress in plants. From classical chemistry to cell biology. *Environ. Exp. Bot.* 109, 212–228. doi: 10.1016/j.envexpbot.2014.06.021

Ehonen, S., Yarmolinsky, D., Kollist, H., and Kangasjärvi, J. (2019). Reactive oxygen species, photosynthesis, and environment in the regulation of stomata. *Ant. Redox Signal.* 30, 1220–1237. doi: 10.1089/ars.2017.7455

Eisen, M. B., Spellman, P. T., Brown, P. O., and Botstein, D. (1998). Cluster analysis and display of genome-wide expression patterns. *Proc. Nat. Acad. Sci. U.S.A.* 95, 14863–14868. doi: 10.1073/pnas.95.25.14863

Ellis, R. (1979). The most abundant protein in the world. *Trends Biochem. Sci.* 4, 241–244. doi: 10.1016/0968-0004(79)90212-3

Fang, Y., and Xiong, L. (2014). General mechanisms of drought response and their application in drought resistance improvement in plants. *Cell. Mol. Life Sci.* 72, 673–689. doi: 10.1007/s00018-014-1767-0

Farooq, M., Hussain, M., Wahid, A., and Siddique, K. H. M. (2012). "Drought stress in plants: an overview," in *Plant Responses to Drought Stress*. Ed. R. Aroca (Heidelberg: Springer), 1–33.

Figueras, M., Saleh, J. P., Save, R., Pages, M., and Goday, A. (2005). Maize Rabl7 overexpression in Arabidopsis plants promotes osmotic stress tolerance. *Ann. Appl. Biol.* 144, 251–257. doi: 10.1111/j.1744-7348.2004.tb00341.x

Flower, D. R. (1996). The lipocalin protein family: structure and function. *Biochem. J.* 318, 1–14. doi: 10.1042/bj3180001

Ford, K., Cassin, A., and Bacic, A. (2011). Quantitative proteomic analysis of wheat cultivars with differing drought stress tolerance. *Front. Plant Sci.* 2, 44. doi: 10.3389/fpls.2011.00044

Foyer, C. H., Ruban, A. V., and Noctor, G. (2017). Viewing oxidative stress through the lens of oxidative signalling rather than damage. *Biochem. J.* 474, 877–883. doi: 10.1042/BCJ20160814

Foyer, C. H., Wilson, M., and Wright, M. (2018). Redox regulation of cell proliferation: bioinformatics and redox proteomics approaches to identify redox-sensitive cell cycle regulators. *Free Radic. Biol. Med.* 122, 137–149. doi: 10.1016/j.freeradbiomed.2018.03.047

Foyer, C. H. (2018). Reactive oxygen species, oxidative signaling and the regulation of photosynthesis. *Environ. Exp. Bot.* 154, 134–142. doi: 10.1016/j.envexpbot.2018.05.003

Franks, S. (2011). Plasticity and evolution in drought avoidance and escape in the annual plant *Brassica rapa*. *New Phytol.* 190, 249–257. doi: 10.1111/j.1469-8137.2010.03603.x

Galmés, J., Ribas-Carbo, M., Medrano, H., and Flexas, J. (2011). RuBisCO activity in Mediterranean species is regulated by the chloroplastic CO_2 concentration under water stress. *J. Exp. Bot.* 62, 653–665. doi: 10.1093/jxb/erq303

Gol, L., Tomé, F., and von Korff, M. (2017). Floral transitions in wheat and barley, interactions between photoperiod, abiotic stresses, and nutrient status. *J. Exp. Bot.* 68, 1399–1410. doi: 10.1093/jxb/erx055

Good, A., and Zaplachinski, S. (1994). The effects of drought stress on free amino acid accumulation and protein synthesis in. *Brassica Napus. Physiol. Plant* 90, 9–14. doi: 10.1111/j.1399-3054.1994.tb02185.x

Guerra, D., Crosatti, C., Khoshro, H., Mastrangelo, A., Mica, E., and Mazzucotelli, E. (2015). Post-transcriptional and post-translational regulations of drought

and heat response in plants: a spider's web of mechanisms. *Front. Plant Sci.* 6, 57. doi: 10.3389/fpls.2015.00057

Gygi, S., Rochon, Y., Franza, B., and Aebersold, R. (1999). Correlation between protein and mRNA abundance in yeast. *Mol. Cell. Biol.* 19, 1720–1730. doi: 10.1128/MCB.19.3.1720

Hickey, C. M., Wilson, N. R., and Hochstrasser, M. (2012). Function and regulation of SUMO proteases. *Nat. Rev.* 13, 755–766. doi: 10.1038/nrm3478

Hieng, B., Ugrinović, K., Šuštar-Vozlič, J., and Kidrič, M. (2004). Different classes of proteases are involved in the response to drought of *Phaseolus vulgaris* L. cultivars differing in sensitivity. *J. Plant Physiol.* 161, 519–530. doi: 10.1078/0176-1617-00956

Hildebrandt, T. M., Nesi, A. N., Araujo, W. L., and Braun, H.-P. (2015). Amino acid catabolism. *Mol. Plant* 8, 1563–1579. doi: 10.1016/j.molp.2015.09.005

Hirshberg, J., and McIntosh, L. (1983). Molecular basis of herbicide resistance in *Amaranthus hybridus*. *Science* 222, 1346–1349. doi: 10.1126/science.222.4630.1346

Hoque, M. A., Okuma, E., Banu, M. N., Nakamura, Y., Shimoishi, Y., and Murata, Y. (2007). Exogenous proline mitigates the detrimental effects of salt stress more than exogenous betaine by increasing antioxidant enzyme activities. *J. Plant Physiol.* 164, 553–561. doi: 10.1016/j.jplph.2006.03.010

Hossain, M. A., Hasanuzzaman, M., and Fujita, M. (2011). Coordinate induction of antioxidant defense and glyoxalase system by exogenous proline and glycinebetaine is correlated with salt tolerance in mung bean. *Front. Agric. China* 5, 1–4. doi: 10.1007/s11703-010-1070-2

Hura, T., Hura, K., and Grzesiak, M. (2010). Soil drought applied during the vegetative growth of triticale modifies the physiological and biochemical adaptation to drought during the generative development. *J. Agr. Crop Sci.* 197, 113–123. doi: 10.1111/j.1439-037X.2010.00450.x

Jia, H., Wang, L., Li, J., Sun, P., Lu, M., and Hu, J. (2019). Comparative metabolomics analysis reveals different metabolic responses to drought in tolerant and susceptible poplar species. *Physiol. Plant* 168, 531–546. doi: 10.1111/ppl.13036

Kale, J., Osterlund, E. J., and Andrews, D. W. (2018). BCL-2 family proteins: changing partners in the dance towards death. *Cell Death Differ.* 25, 65–80. doi: 10.1038/cdd.2017.186

Kawashima, N. O., and Wildman, S. G. (1970). Fraction I protein. *Ann. Rev. Plant Physiol.* 21, 325–358. doi: 10.1146/annurev.pp.21.060170.001545

Kazan, K., and Lyons, R. (2016). The link between flowering time and stress tolerance. *J. Exp. Bot.* 67, 47–60. doi: 10.1093/jxb/erv441

Knight, S., Andersson, I., and Brändén, C. (1990). Crystallographic analysis of ribulose 1,5-bisphosphate carboxylase from spinach at 2.4 A resolution. Subunit interactions and active site. *J. Mol. Bio.* 215, 113–160. doi: 10.1016/S0022-2836(05)80100-7

Kosová, K., Vítámvás, P., Urban, M., Klíma, M., Roy, A., and Prášil, I. (2015). Biological networks underlying abiotic stress tolerance in temperate crops—a proteomic perspective. international journal of molecular sciences. *Int. J. Mol. Sci.* 16, 20913–20942. doi: 10.3390/ijms160920913

Kumar, S., and Trivedi, P. (2018). Glutathione S-Transferases, role in combating abiotic stresses including arsenic detoxification in plants. *Front. Plant Sci.* 9, 751. doi: 10.3389/fpls.2018.00751

Kumar, R., Goswami, S., Dubey, K., Singh, K., Singh, J. P., Kumar, A., et al. (2019). RuBisCO activase–a catalytic chaperone involved in modulating the RuBisCO activity and heat stress-tolerance in wheat. *J. Plant Biochem. Biotech.* 28, 63–75. doi: 10.1007/s13562-018-0463-9

Lakra, N., Nutan, K., Das, P., Anwar, K., Singla-Pareek, S., and Pareek, A. (2015). A nuclear-localized histone-gene binding protein from rice (*OsHBP1b*) functions in salinity and drought stress tolerance by maintaining chlorophyll content and improving the antioxidant machinery. *J. Plant Physiol.* 176, 36–46. doi: 10.1016/j.jplph.2014.11.005

Lawlor, D., and Cornic, G. (2002). Photosynthetic carbon assimilation and associated metabolism in relation to water deficits in higher plants. *Plant Cell Environ.* 25, 275–294. doi: 10.1046/j.0016-8025.2001.00814.x

Le Roux, M. L., Van Der Vyver, C., Kunert, K., Cullis, C. A., and Botha, A.-M. (2019). Expression of a small ubiquitin-like modifier protease increases drought tolerance in wheat (*Triticum aestivum* L.). *Front. Plant Sci.* 10, 266. doi: 10.3389/fpls.2019.00266

Lee, S., Lee, J., Kim, S., Park, J.-Y., Lee, W.-H., Mori, K., et al. (2007). A dual role of lipocalin 2 in the apoptosis and deramification of activated microglia. *J. Immunol.* 179, 3231–3241. doi: 10.4049/jimmunol.179.5.3231

Li, Y., Song, H., Zhou, L., Xu, Z., and Zhou, G. (2019). Tracking chlorophyll fluorescence as an indicator of drought and rewatering across the entire leaf lifespan in a maize field. *Agric. Water Manage.* 211, 190–201. doi: 10.1016/j.agwat.2018.09.050

Liu, H., Sultan, M., Liu, X., Zhang, J., Yu, F., and Zhao, H. (2015). Physiological and comparative proteomic analysis reveals different drought responses in roots and leaves of drought-tolerant wild wheat (*Triticum boeoticum*). *PloS One* 10, e0121852. doi: 10.1145/2818302

Liu, H., Hu, M., Wang, Q., Cheng, L., and Zhang, Z. (2018). Role of papain-like cysteine proteases in plant development. *Front. Plant Sci.* 9, 1717. doi: 10.3389/fpls.2018.01717

Luo, L. (2010). Breeding for water-saving and drought-resistance rice (*WDR*) in China. *J. Exp. Bot.* 61, 3509–3517. doi: 10.1093/jxb/erq185

Ma, Q., Wang, W., Li, Y., Li, D., and Zou, Q. (2006). Alleviation of photoinhibition in drought-stressed wheat (*Triticum aestivum*) by foliar-applied glycinebetaine. *J. Plant Physiol.* 163, 165–175. doi: 10.1016/j.jplph.2005.04.023

Martin, W. F., and Sies, H. (2017). Genomic redox footprints. *Nat. Plants* 3, 17071.

Matsumoto, K., Mizoue, K., Kitamura, K., Tse, W. C., Huber, C. P., and Ishida, T. (1999). Structural basis of inhibition of cysteine proteases by E-64 and its derivatives. *Biopolymers* 51, 99–107. doi: 10.1002/(SICI)1097-0282(1999)51:1<99::AID-BIP11>3.0.CO;2-R

Matysik, J., Alia Bhalu, B., and Mohanty, P. (2002). Molecular mechanisms of quenching of reactive oxygen species by proline under stress in plants. *Curr. Sci.* 82, 525–532.

Mbwanjii, K. C. (2014). *Inducing mutations in bread wheat (Tricitum aestivum L.) using chemical treatments. M,Sc, Thesis* (South Africa: Stellenbosch University Library Services), 107.

Michaletti, A., Naghavi, M., Toorchi, M., Zolla, L., and Rinalducci, S. (2018). Metabolomics and proteomics reveal drought-stress responses of leaf tissues from spring-wheat. *Sci. Rep.* 8, 5710. doi: 10.1038/s41598-018-24012-y

Miura, K., Jin, J. B., Lee, J., Yoo, C. Y., Stirm, V., Miura, T., et al. (2007). *SIZ1*-mediated SUMOylation of *ICE1* controls *CBF3/DREB1A* expression and freezing tolerance in Arabidopsis. *Plant Cell* 19, 1403–1414. doi: 10.1105/tpc.106.048397

Miyashita, K., Tanakamaru, S., Maitani, T., and Kimura, K. (2005). Recovery responses of photosynthesis, transpiration, and stomatal conductance in kidney bean following drought stress. *J. Exp. Bot.* 53, 205–214. doi: 10.1016/j.envexpbot.2004.03.015

Morimoto, S., and Yahara, K. (2018). Identification of stress responsive genes by studying specific relationships between mRNA and protein abundance. *Heliyon* 4, 558. doi: 10.1016/j.heliyon.2018.e00558

Morrell, R., and Sadanandom, A. (2019). Plant SUMO proteases lead the way in dealing with environmental stress. *Front. Plant Sci.* 10, 1122. doi: 10.3389/fpls.2019.01122

Motulsky, H. J. (2007). Prism 5 statistics guide. *GraphPad Softw.* 31, 39–42.

Muller, H. (1927). Artificial transmutation of the gene. *Science* 66, 84–87. doi: 10.1126/science.66.1699.84

Murata, N., Takahashi, S., Nishiyama, Y., and Allakhverdiev, S. (2007). Photoinhibition of photosystem II under environmental stress. *Biochim. Biophys. Acta Bioenerg.* 1767, 414–421. doi: 10.1016/j.bbabio.2006.11.019

Nelson, C. J., and Millar, A. H. (2015). Protein turnover in plant biology. *Nat. Plants* 1, 15017. doi: 10.1038/nplants.2015.17

Noctor, G., Reichheld, J., and Foyer, C. (2018). ROS-related redox regulation and signalling in plants. *Sem. Cell Devel. Biol.* 80, 3–12. doi: 10.1016/j.semcdb.2017.07.013

Ouyang, W., Struik, P., Yin, X., and Yang, J. (2017). Stomatal conductance, mesophyll conductance, and transpiration efficiency in relation to leaf anatomy in rice and wheat genotypes under drought. *J. Exp. Bot.* 68, 5191–5205. doi: 10.1093/jxb/erx314

Pacher, M., and Puchta, H. (2017). From classical mutagenesis to nuclease-based breeding - directing natural DNA repair for a natural end-product. *Plant J.* 90, 819–833. doi: 10.1111/tpj.13469

Panković, D., Sakač, Z., Kevrešan, S., and Plesnič, M. (1999). Acclimation to long-term water deficit in the leaves of two sunflower hybrids, photosynthesis, electron transport and carbon metabolism. *J. Exp. Bot.* 50, 127–138. doi: 10.1093/jexbot/50.330.127

Pelloux, J., Jolivet, Y., Fontaine, V., Banvoy, J., and Dizengremel, P. (2001). Changes in RuBisCO and RuBisCO activase gene expression and polypeptide content in *Pinus halepensis* M. subjected to ozone and drought. *Plant Cell Environ.* 24, 123–131. doi: 10.1046/j.1365-3040.2001.00665.x

Peng, Y., Nguy-Robertson, A., Arkebauer, T., and Gitelson, A. (2017). Assessment of canopy chlorophyll content retrieval in maize and soybean, implications of

hysteresis on the development of generic algorithms. *Remote Sens.* 9, 226. doi: 10.3390/rs9030226

Perdomo, J., Capó-Bauçà, S., Carmo-Silva, E., and Galmés, J. (2017). RuBisCO and RuBisCO activase play an important role in the biochemical limitations of photosynthesis in rice, wheat, and maize under high temperature and water deficit. *Front. Plant Sci.* 8, 490. doi: 10.3389/fpls.2017.00490

Perez-Riverol, Y., Csordas, A., Bai, J., Bernal-Llinares, M., Hewapathirana, S., Kundu, D. J., et al. (2019). The PRIDE database and related tools and resources in 2019: improving support for quantification data. *Nucleic Acids Res.* 47 (D1), D442–D450. doi: 10.1093/nar/gky1106

Prins, A., van Heerden, P., Olmos, E., Kunert, K., and Foyer, C. (2008). Cysteine proteinases regulate chloroplast protein content and composition in tobacco leaves: a model for dynamic interactions with ribulose-1,5-bisphosphate carboxylase/oxygenase (Rubisco) vesicular bodies. *J. Exp. Bot.* 59, 1935–1950. doi: 10.1093/jxb/ern086

Rabara, R., Tripathi, P., and Rushton, P. (2017). Comparative metabolome profile between tobacco and soybean grown under water-stressed conditions. *BioMed. Res. Int.* 2017, 1–12. doi: 10.1155/2017/3065251

Rabello, F., Villeth, G., Rabello, A., Rangel, P., Guimarães, C., Huergo, L. F., et al. (2014). Proteomic analysis of upland rice (*Oryza sativa* L.) exposed to intermittent water deficit. *Protein J.* 33, 221–230. doi: 10.1007/s10930-014-9554-1

Rampino, P., Pataleo, S., Gerardi, C., Mita, G., and Perrotta, C. (2006). Drought stress response in wheat: physiological and molecular analysis of resistant and sensitive genotypes. *Plant Cell Environ.* 29, 2143–2152. doi: 10.1111/j.1365-3040.2006.01588.x

Ranieri, M., Vivo, M., De Simone, M., Guerrini, L., Pollice, A., La Mantia, G., et al. (2018). SUMOylation and ubiquitylation crosstalk in the control of ΔNp63α protein stability. *Gene* 645, 34–40. doi: 10.1016/j.gene.2017.12.018

Reddy, A., Chaitanya, K., and Vivekanandan, M. (2004). Drought-induced responses of photosynthesis and antioxidant metabolism in higher plants. *J. Plant Physiol.* 161, 1189–1202. doi: 10.1016/j.jplph.2004.01.013

Rejeb, K. B., Abdelly, C., and Savouré, A. (2014). How reactive oxygen species and proline face stress together. *Plant Physiol. Biochem.* 80, 278–284. doi: 10.1016/j.plaphy.2014.04.007

Roden, J., Eardley, L., Hotson, A., Cao, Y., and Mudgett, M. B. (2004). Characterization of the *Xanthomonas* AvrXv4 effector, a SUMO protease translocated into plant cells. *Mol. Plant-Microbe Interact.* 17, 633–643. doi: 10.1094/MPMI.2004.17.6.633

Rylatt, D. B., and Parish, C. R. (1982). Protein determination on an automatic spectrophotometer. *Anal. Biochem.* 121, 213–214. doi: 10.1016/0003-2697(82)90578-4

Sade, D., Sade, N., Shriki, O., Gebremedhin, A., Karavani, A., Brotman, Y., et al. (2014). Water balance, hormone homeostasis, and sugar signaling are all involved in tomato resistance to tomato yellow leaf curl virus. *Plant Physiol.* 165, 1684–1697. doi: 10.1104/pp.114.243402

Sade, N., Galkin, E., and Moshelion, M. (2015). Measuring Arabidopsis, tomato and barley leaf relative water content (RWC). *BioProtocols* 7, 1451. doi: 10.21769/BioProtoc.1451

Sairam, R., Srivastava, G., Agarwal, S., and Meena, R. (2005). Differences in antioxidant activity in response to salinity stress in tolerant and susceptible wheat genotypes. *Biol. Plant* 49, 85–91. doi: 10.1007/s10535-005-5091-2

Saldanha, A. J. (2004). Java Treeview – extensible visualization of microarray data. *Bioinformatics* 20, 3246–3248. doi: 10.1093/bioinformatics/bth349

Saleh, A., Withers, J., Mohan, R., Marqués, J., Gu, Y., Yan, S., et al. (2015). Posttranslational modifications of the master transcriptional regulator NPR1 enable dynamic but tight control of plant immune responses. *Cell Host. Microbe* 18, 169–182. doi: 10.1016/j.chom.2015.07.005

Schreiber, U., Bilger, W., Hormann, H., and Neubauer, C. (2003). "Chlorophyll fluorescence as a diagnostic tool: basics and some aspects of practical relevance," in *Photosynthesis: A comprehensive treatise*. Ed. A. S. Raghaverdra (Cambridge, UK: Cambridge University Press), pp. 320–335.

Schubert, S. D., Stewart, R. E., Wang, H., Barlow, M., Berbery, E. H., Cai, W., et al. (2016). Global meteorological drought, a synthesis of current understanding with a focus on SST drivers of precipitation deficits. *J. Climate* 29, 3989–4019. doi: 10.1175/JCLI-D-15-0452.1

Searle, B. (2010). Scaffold: A Bioinformatic tool for validating MS/MS-based proteomic studies. *Proteomics* 10, 1265–1269. doi: 10.1002/pmic.200900437

Selvaraj, M., Ishizaki, T., Valencia, M., Ogawa, S., Dedicova, B., Ogata, T., et al. (2017). Overexpression of an *Arabidopsis thaliana* galactinol synthase gene improves drought tolerance in transgenic rice and increased grain yield in the field. *Plant Biotech. J.* 15, 1465–1477. doi: 10.1111/pbi.12731

Senapati, N., Stratonovitch, P., Paul, M., and Semenov, M. (2018). Drought tolerance during reproductive development is important for increasing wheat yield potential under climate change in Europe. *J. Exp. Bot.* 9, 2549–2560.

Serba, D., and Yadav, R. (2016). Genomic tools in pearl millet breeding for drought tolerance, status and prospects. *Front. Plant Sci.* 7, 1724. doi: 10.3389/fpls.2016.01724

Sharifi, P., and Mohammadkhani, N. (2016). Effects of drought stress on photosynthesis factors in wheat genotypes during anthesis. *Cereal Res. Commun.* 44, 229–239. doi: 10.1556/0806.43.2015.054

Shavrukov, Y., Kurishbayev, A., Jatayev, S., Shvidchenko, V., Zotova, L., Koekemoer, F., et al. (2017). Early flowering as a drought escape mechanism in plants, how can it aid wheat production? *Front. Plant Sci.* 8, 1950. doi: 10.3389/fpls.2017.01950

Simova-Stoilova, L., Vaseva, I., Grigorova, B., Demirevska, K., and Feller, U. (2010). Proteolytic activity and cysteine protease expression in wheat leaves under severe soil drought and recovery. *Plant Physiol. Biochem.* 48, 200–206. doi: 10.1016/j.plaphy.2009.11.003

Simova-Stoilova, L., Vassileva, V., and Feller, U. (2016). Selection and breeding of suitable crop genotypes for drought and heat periods in a changing climate, which morphological and physiological properties should be considered? *Agriculture* 6, 26. doi: 10.3390/agriculture6020026

Singh, J., Pandey, P., James, D., Chandrasekhar, K., Achary, V., Kaul, T., et al. (2014). Enhancing C3 photosynthesis, an outlook on feasible interventions for crop improvement. *Plant Biotech. J.* 12, 1217–1230. doi: 10.1111/pbi.12246

Smirnoff, N., and Arnaud, D. (2019). Hydrogen peroxide metabolism and functions in plants. *New Phytol.* 221, 1197–1214. doi: 10.1111/nph.15488

Souza, R., Machado, E., Silva, J., Lagôa, A., and Silveira, J. (2004). Photosynthetic gas exchange, chlorophyll fluorescence and some associated metabolic changes in cowpea (*Vigna unguiculata*) during water stress and recovery. *Environ. Exp. Bot.* 51, 45–56. doi: 10.1016/S0098-8472(03)00059-5

Spinoni, J., Vogt, J., Naumann, G., Barbosa, P., and Dosio, A. (2017). Will drought events become more frequent and severe in Europe? *Int. J. Climatol.* 38, 1718–1736. doi: 10.1002/joc.5291

Strasser, R. J., Tsimilli-Michael, M., and Srivastava, A. (2004). "Analysis of the fluorescence transient," in *Chlorophylla Fluorescence: A signature of photosynthesis*. Eds. G. C. Papageorgiou and Govindjee, (Dordrecht: Springer), 321–362.

Subrahmanyam, D., Subash, N., Haris, A., and Sikka, A. (2006). Influence of water stress on leaf photosynthetic characteristics in wheat cultivars differing in their susceptibility to drought. *Photosynthetica* 44, 125–129. doi: 10.1007/s11099-005-0167-y

Szabados, L., and Savoure, A. (2010). Proline: a multifunctional amino acid. *Trends Plant Sci.* 15, 89–97. doi: 10.1016/j.tplants.2009.11.009

Tezara, W. (2002). Effects of water deficit and its interaction with CO_2 supply on the biochemistry and physiology of photosynthesis in sunflower. *J. Exp. Bot.* 53, 1781–1791. doi: 10.1093/jxb/erf021

Thomas, H., and Ougham, H. (2014). The stay-green trait. *J. Exp. Bot.* 65, 3889–3900. doi: 10.1093/jxb/eru037

Tian, F. X., Gong, J. F., Wang, G. P., Wang, G. K., Fan, Z. Y., and Wang, W. (2012). Improved drought resistance in a wheat stay-green mutant *tasg1* under field conditions. *Biol. Plant* 56, 509–515. doi: 10.1007/s10535-012-0049-7

Tian, Y., Ungerer, P., Zhang, H., and Ruban, A. (2017). Direct impact of the sustained decline in the photosystem II efficiency upon plant productivity at different developmental stages. *J. Plant Physiol.* 212, 45–53. doi: 10.1016/j.jplph.2016.10.017

Vassileva, V., Demirevska, K., Simova-Stoilova, L., Petrova, T., Tsenov, N., and Feller, U. (2011). Long-term field drought affects leaf protein pattern and chloroplast ultrastructure of winter wheat in a cultivar-specific manner. *J. Agr. Crop Sci.* 198, 104–117. doi: 10.1111/j.1439-037X.2011.00492.x

Vendruscolo, E. C. G., Schuster, I., Pilegg, M., Scapim, C. A., Molinari, H. B. C., Marur, C. J., et al. (2007). Stress-induced synthesis of proline confers tolerance to water deficit in transgenic wheat. *J. Plant Physiol.* 164, 1367–1376. doi: 10.1016/j.jplph.2007.05.001

Venisse, J. S., Gullner, G., and Brisset, M. N. (2001). Evidence for the involvement of an oxidative stress in the initiation of infection of pear by *Erwinia amylovora*. *Plant Physiol.* 125, 2164–2172. doi: 10.1104/pp.125.4.2164

Verslues, P., and Juenger, T. (2019). Drought, metabolites, and Arabidopsis natural variation, a promising combination for understanding adaptation to water-limited environments. *Curr. Opin. Plant Biol.* 14, 240–245. doi: 10.1016/j.pbi.2011.04.006

Vierstra, R. (1993). Protein degradation in plants. *Ann. Rev. Plant Physiol. Plant Mol. Biol.* 44, 385–410. doi: 10.1146/annurev.pp.44.060193.002125

Vu, J., Gesch, R., Hartwell Allen, L., Boote, K., and Bowes, G. (1999). $C0_2$ enrichment delays a rapid, drought-induced decrease in RuBisCO small subunit transcript abundance. *J. Plant Physiol.* 155, 139–142. doi: 10.1016/S0176-1617(99)80156-4

Wang, W., Vignani, R., Scali, M., and Cresti, M. (2006). Universal and rapid protocol for protein extraction from recalcitrant plant tissues for proteomic analysis. *Electrophoresis* 27, 2782–2786. doi: 10.1002/elps.200500722

Wang, X. C., Li, X. F., Deng, X., Han, H. P., Shi, W. L., and Li, Y. X. (2007). A protein extraction method compatible with proteomic analysis for the euhalophyte *Salicornia europaea*. *Electrophoresis* 28, 3976–3987. doi: 10.1002/elps.200600805

Wang, X., Shan, X., Wu, Y., Su, S., Li, S., Liu, H., et al. (2016). iTRAQ-based quantitative proteomic analysis reveals new metabolic pathways responding to chilling stress in maize seedlings. *J. Proteomics* 146, 14–24. doi: 10.1016/j.jprot.2016.06.007

Wang, B., Cai, W., Li, J., Wan, Y., Li, Y., Guo, C., et al. (2020). Leaf photosynthesis and stomatal conductance acclimate to elevated [CO2] and temperature thus increasing dry matter productivity in a double rice cropping system. *Field Crops Res.* 248, 107735. doi: 10.1016/j.fcr.2020.107735

Wheeler, R., Fitzpatrick, A., and Tibbitts, T. (2019). Potatoes as a crop for space life support: effect of co2, irradiance, and photoperiod on leaf photosynthesis and stomatal conductance. *Front. Plant Sci.* 10, 1632. doi: 10.3389/fpls.2019.01632

Williams, J., Bulman, M., and Neill, S. (1994). Wilt-induced ABA biosynthesis, gene expression and down-regulation of *rbcS* mRNA levels in. *Arabidopsis Thaliana Physiol. Plant* 91, 177–182. doi: 10.1111/j.1399-3054.1994.tb00416.x

Witt, S., Galicia, L., Lisec, J., Cairns, J., Tiessen, A., Araus, J. L., et al. (2012). Metabolic and phenotypic responses of greenhouse-grown maize hybrids to experimentally controlled drought stress. *Molec. Plant* 5, 401–417. doi: 10.1093/mp/ssr102

Wulff, B., and Dhugga, K. (2019). Wheat–the cereal abandoned by GM. *Am. Ass. Adv. Sci.* 361, 451–452.

Yadav, A. K., Carroll, A. J., Estavillo, G. M., Rebetzke, G. J., and Pogson, B. J. (2019). Wheat drought tolerance in the field is predicted by amino acid responses to glasshouse-imposed drought. *J. Exp. Biol.* 70, 4931–4947. doi: 10.1093/jxb/erz224

Yi, X., Zhang, Y., Yao, H., Luo, H., Gou, L., et al. (2016). Rapid recovery of photosynthetic rate following soil water deficit and re-watering in cotton plants (*Gossypium herbaceum* L.) is related to the stability of the photosystems. *J. Plant Physiol.* 194, 23–34. doi: 10.1016/j.jplph.2016.01.016

Yuan, X., Yang, Z., Li, Y., Liu, Q., and Han, W. (2015). Effects of different levels of water stress on leaf photosynthetic characteristics and antioxidant enzyme activities of greenhouse tomato. *Photosynthetica* 54, 28–39. doi: 10.1007/s11099-015-0122-5

Zadoks, J. C., Chang, T. T., and Konzak, C. F. (1974). A decimal code for the growth stages of cereals. *Weed Res.* 14, 415–421. doi: 10.1111/j.1365-3180.1974.tb01084.x

Zhou, Y., Lam, H., and Zhang, J. (2007). Inhibition of photosynthesis and energy dissipation induced by water and high light stresses in rice. *J. Exp. Bot.* 58, 1207–1217. doi: 10.1093/jxb/erl291

Zieslin, N., and Ben Zaken, R. (1993). Peroxidase activity and presence of phenolic substances in peduncles of rose flowers. *Plant Physiol. Biochem.* 3, 333–339.

Conflict of Interest: The authors declare that the research was conducted in the absence of any commercial or financial relationships that could be construed as a potential conflict of interest.

Copyright © 2020 le Roux, Burger, Vlok, Kunert, Cullis and Botha. This is an open-access article distributed under the terms of the Creative Commons Attribution License (CC BY). The use, distribution or reproduction in other forums is permitted, provided the original author(s) and the copyright owner(s) are credited and that the original publication in this journal is cited, in accordance with accepted academic practice. No use, distribution or reproduction is permitted which does not comply with these terms.

frontiers in Plant Science

ORIGINAL RESEARCH
published: 16 July 2020
doi: 10.3389/fpls.2020.01042

Intraspecific Variation in Drought Response of Three Populations of *Cryptocarya alba* and *Persea lingue*, Two Native Species From Mediterranean Central Chile

Carolina Alvarez-Maldini[1]*, *Manuel Acevedo*[2], *R. Kasten Dumroese*[3], *Marta González*[2] *and Eduardo Cartes*[2]

[1] Institute of Agri-food, Animal and Environmental Sciences (ICA3), Universidad de O Higgins, San Fernando, Chile, [2] Centro Tecnológico de la Planta Forestal, Instituto Forestal, San Pedro de la Paz, Chile, [3] Rocky Mountain Research Station, US Department of Agriculture, Forest Service, Moscow, ID, United States

OPEN ACCESS

Edited by:
Felipe Klein Ricachenevsky, Federal University of Rio Grande, Brazil

Reviewed by:
Enrique Andivia, Complutense University of Madrid, Spain
Juan Pedro Ferrio, Fundacion Agencia Aragonesa para la Investigacion y el Desarrollo, Spain

***Correspondence:**
Carolina Alvarez-Maldini
carolina.alvarez@uoh.cl

Specialty section:
This article was submitted to Plant Abiotic Stress, a section of the journal Frontiers in Plant Science

Received: *27 February 2020*
Accepted: *24 June 2020*
Published: *16 July 2020*

Citation:
Alvarez-Maldini C, Acevedo M, Dumroese RK, González M and Cartes E (2020) Intraspecific Variation in Drought Response of Three Populations of Cryptocarya alba and Persea lingue, Two Native Species From Mediterranean Central Chile. Front. Plant Sci. 11:1042. doi: 10.3389/fpls.2020.01042

An increase in the severity of drought events on Mediterranean climates highlights the need of using plant material adapted to drought during restoration efforts. Thus, we investigated between-population morpho-physiological differences in *Cryptocarya alba* and *Persea lingue*, two native species from Mediterranean central Chile, for traits that could effectively discriminate population performance in response to water restriction (WR) testing. Three populations from each species were subjected to WR treatment and physiological, morphological, and growth parameters were assessed at the beginning and at the end of the experiment. In *C. alba*, the most xeric population displayed smaller plants with mesophyllous leaves and lower photosynthetic rates indicating a resource saving strategy. Moreover, the xeric population performed better during WR than the most mesic populations, exhibiting higher water use efficiency (iWUE) and maintenance of growth rates. All *C. alba* populations responded equally to WR in terms of morphology and biomass partitioning. In contrast, differences among *P. lingue* populations were subtle at the morpho-physiological level with no apparent relation to provenance environmental conditions, and no morphological traits were affected by WR. However, in response to WR application, the most mesic population was, as observed through reduction in relative growth rates, more affected than xeric populations. We attribute such discrete differences between *P. lingue* provenances to the lower distributional range of selected populations. Our results show that relative growth rates in both species, and iWUE only in *C. alba*, exhibited population specific responses upon WR imposition; these results correspond with the environmental conditions found at the origin of each populations. Both traits could further assist in the selection of populations for restoration according to their response to water stress.

Keywords: water deficit, relative growth rate, water use efficiency, gas exchange, population differences, restoration

INTRODUCTION

The world´s forests will need to cope and adapt to changes that are threatening their natural habitats (Allen et al., 2010; Gilliam, 2016). One significant disturbance expected by climate change is an increase in duration and frequency of drought events (Sheffield and Wood, 2008). Most models predict that water will become an even more limiting resource in Mediterranean-type sites under the increasing aridity (Sheffield and Wood, 2008). This is particularly serious for Mediterranean-type climates, already characterized by a dry, 1–5 month summer period with high temperatures imposing a physiological drought (Valladares et al., 2004).

Native ecosystems and their species distributions within the Chilean Mediterranean climate are not exempt from the effects of climate change related to increased drought (Garreaud et al., 2017). This has led to the development of restoration programs in ecosystems with high ecologic value (Bannister et al., 2018). Because knowledge concerning patterns of genetic variability in Chilean native species is scarce, the use of local plant material for restoration has been the customary approach. Concerns about the use of this approach are, however, increasing because of observations of lethal mutations among seedlings of native species, such as in *Cryptocarya alba* and *Persea lingue*, collected from local, but isolated populations (Alvarez et al., 2017). Plants from isolated populations are highly vulnerable to environmental changes because they are characterized by small population sizes, higher levels of inbreeding, and lower individual fitness and genetic variability (Aizen et al., 2002; Angeloni et al., 2011). It is expected that such plant material would have poor performance during drought events and have a lower capacity to adapt to changing climate (Valladares et al., 2007). The use of local plant material for restoration is common (Vander et al., 2010). Moreover, the selection of appropriate propagation stock based on their response to drought is advised, with the objective of replacing sensitive populations with ones that could respond better to forecasted climate change and reduce maladaptation risk (Bolte et al., 2009; Aitken and Whitlock, 2013). This intentional movement of populations to areas were future projected climate matches their current adapted environment (i.e., assisted migration) may be especially important for long-lived species threatened by fragmentation (Dumroese et al., 2015a). Until recently, it was believed that tree species from different populations responded equally to drought (Kawecki, 2008; Banta et al., 2012). However, habitat heterogeneity across species distribution can lead to variability in plant functional traits in response to environmental factors (Linhart and Grant, 1996; Hufford and Mazer, 2003), indicating that populations within a species experiencing different environmental conditions can differ in phenotypic characteristics and genetic structure (Linhart and Grant, 1996). This intraspecific variation in morpho-physiological traits in response to drought has been reported in a large number of tree species from Mediterranean climates (Gratani et al., 2003; Ramírez-Valiente et al., 2010; Kaluthota et al., 2015; Kerr et al., 2015; Ramírez-Valiente and Cavender-Bares, 2017).

Thus, higher degrees of intraspecific variation have been observed in individuals from contrasting environmental conditions. For example, rapid stomatal closure, an increase in water use efficiency (WUE), and a decrease in growth rate are commonly reported in individuals from drier climates (Kerr et al., 2015; Viger et al., 2016; Nguyen et al., 2017), although an opposite relationship between WUE and growth has been reported as well (Fardusi et al., 2016; Peguero-Pina et al., 2016). Such variation in response to drought is strongly associated with water availability in the population of origin and has shown to drive tree population differentiation (Zhang et al., 2004; Marchín et al., 2008; Aletá et al., 2009). This indicates high degrees of local adaptation, where individuals tend to display more relative fitness in their native environments (Savolainen et al., 2007). Local adaptation arises in response to differential selection pressures submitted through variable environmental conditions, especially in widely distributed tree species (Kawecki and Ebert, 2004; Savolainen et al., 2007), and constitutes a strategy to cope with environmental variability.

Hence, research regarding differential adaptive strategies within species and among populations increases the possibilities for selection of appropriate traits suitable for drier climates in future conditions; this is critical for afforestation and conservation purposes (Aitken et al., 2008; Grady et al., 2013). Adaptive responses to drought may be especially important for seedlings because of their susceptibility to water scarcity (Vennetier et al., 2007; Lloret et al., 2009) and because their survival is essential for the success of many restoration programs.

When patterns of genetic variability of species under restoration are unknown, the use of local plant material is advised (Vander et al., 2010). This is no exception for Chile, where the regulation for restoration efforts demands seeds or propagules from the nearest population of the sites to be restored. This approach does not consider plant material adaptation to the local environment, especially under increasing drought conditions of Mediterranean climates. Recent research in Chile suggests that fragmentation of native forests is leading to a possible decrease in genotypic variability (Echeverría et al., 2006), exemplified by an increase in albino-mutant phenotypes in seedlings of *P. lingue* and *C. alba* (Alvarez et al., 2017), increasing the need for research of intraspecific variation of these species under drought condition. Thus, an experiment under common garden conditions was established with three populations of *C. alba* and *P. lingue*. We evaluated physiological, morphological, and growth responses during a cycle of water restriction in both species from each population. We hypothesized that i) populations would display inter-specific differences at both the morphological and physiological levels, with higher differences in the most xeric populations, and ii) that population-specific differences in response to drought treatments would be apparent, especially in physiological parameters, with xeric populations displaying lower water use efficiency due to higher stomatal closure. To test our hypotheses, our objectives were i) to assess inter-population differentiation of morpho-physiological traits of both species and the effect of climate in such differences and ii) to test for morphological and

physiological traits that could effectively differentiate population responses to water restriction.

MATERIALS AND METHODS

Study Species, Sampled Populations, and Growing Conditions

The Chilean endemics *C. alba* and *P. lingue* are sclerophyllous shade tolerant species in the Laureaceae family. They share a large geographic range. *Cryptocarya alba* occurs from Coquimbo (lat 30°S) southward to the La Araucanía region (lat 38°S), while *P. lingue* is distributed from Valparaíso (lat 33°S) to the Los Lagos region (lat 40°S). Both species are highly abundant in the southernmost areas of their distribution (Ezcurra, 2010), usually growing on south-facing slopes or in humid ravines in the Mediterranean climate of central Chile (Niemeyer et al., 2002). We collected seeds from four locations in central Chile (Santiago, Nacimiento, Cayumanque, Santa Juana) that spanned an environmental gradient of xeric to mesic (**Table 1**). Within this gradient and for each species, we selected three populations. The most xeric collections for *C. alba* and *P. lingue* were Santiago and Nacimiento, respectively, whereas the most mesic collections were Cayumanque and Santa Juan, respectively (**Table 1**). The Cayumanque source for both species is especially important because of current restoration efforts; these sites have high levels of endemism and biodiversity but are threatened with severe fragmentation (Muñoz et al., 1996; CONAMA, 2002). We collected plant material from at least 30 mature individuals in all populations. Collections from sites other than Cayumanque were from native forests having a minimum area of 100 hectares and isolation from other sampling areas, with a minimum distance of 20 km between populations.

We collected seeds from February until May of 2016. After collection, seeds were cleaned, placed into plastic bags identified by species and population, and stored at 4°C until sowing. In July of 2016, seeds were sown into an outdoor growing facility at the Centro Tecnológico de la Planta Forestal, Instituto Forestal (lat -36.84°, long -73.13°), Biobío region, Chile. No pre-germination treatment was applied to *C. alba* seeds, while the exocarps and mesocarps of *P. lingue* seeds were removed. Seeds were sowed directly into expanded polystyrene trays (84 cavities per tray, each cavity 14 cm deep, and 130 ml) filled with composted *Pinus radiata* bark medium having total, aeration, and water retention porosity of 49%, 25%, and 24% respectively. Irrigation need was monitored with Decagon (Pullman, WA, USA) soil moisture sensors (ECH_2O EC-5) and data logger (EM-50); sensor values for volumetric water content (m^3m^{-3}) were calibrated with gravimetric mass to estimate the percentage of available water (Dumroese et al., 2015b). During the germination phase until September of 2016, irrigation was applied daily with sprinklers. During the growth phase from October 2016 until December of 2017, irrigation was applied when the substrate lost 50% of the available water and fertigation events (fertilization mixed with water) were alternated with irrigation until the end of the growing phase. During the winter months (from April 2017 until September 2017) no fertilization was added and rainfall provided sufficient irrigation. Fertilization consisted of constant rates of nitrogen, phosphorous, potassium, calcium, magnesium, and sulfur at 300, 150, 180, 100, 80, and 115 mg L^{-1}, respectively, using calcium nitrate ($CaNO_3$), magnesium sulfate ($MgSO_4$), ammonium nitrate (NH_4NO_3), potassium phosphate monobasic (KH_2PO_4), and urea [$CO(NH_2)_2$]. Micronutrients fertilization consisted of constant rates of iron, manganese, copper, and zinc at 6, 4, 0.5, and 6 mg L^{-1}, respectively, using iron sulfate ($FeSO_4$), manganese sulfate ($MnSO_4$), copper sulfate ($CuSO_4$), and zinc sulfate ($ZnSO_4$).

TABLE 1 | Characteristics of the sites where *Cryptocarya alba* and *Persea lingue* populations were collected.

	Population			
	Santa Juana	**Cayumanque**	**Nacimiento**	**Santiago**
Cryptocarya alba	No	Yes	Yes	Yes
Persea lingue	Yes	Yes	Yes	No
Latitude	-37.317847	-36.694929	-37.480583	-33.483321
Longitude	-72.991540	-72.530487	-73.003362	-70.616602
Altitude (m.a.s.l)	333	771	645	716
P_{mean} (mm)	991	593	411	196
T_{max} (°C)	27.2	38.1	32.4	35.1
T_{min} (°C)	0.8	-2.2	-3.9	-5.3
ET (mm $year^{-1}$)	941	1054	1102	1280

P_{mean}, mean annual precipitation; T_{max}, maximum annual temperature; T_{min}, minimum annual temperature; ET, accumulated evapotranspiration (Penman-Monteith).

Water Restriction Experiments

In January 2018, 50 plants from each population and species were transferred to plastic pots of 10 L capacity (29 cm upper diameter and 22 cm height). Each pot was filled with an equal amount of soil from Cayumanque as substrate. The soil is of metamorphic origin and presents an average pH of 6.1 and an organic matter content of 7.9%. Levels of nitrogen and phosphorous are 2.1 and 33.7 mg kg^{-1}, respectively. The experiment was done inside a greenhouse (42 m^2) under semi-controlled conditions. Treatments and populations were assigned randomly within the greenhouse. During the course of the experiment, the minimum and maximum temperature and relative humidity were 7.3–27.8°C and 49%–99%, respectively. Before onset of the water restriction experiments, plants were acclimated to their pots for one month. During this time, pots were irrigated every 2 days to container capacity and we monitored volumetric soil water content (VSWC) (m^3m^{-3}) every 30 min as described above (see evolution of volumetric water content at **Figure S1**, in **Supplementary Material**). Additionally, VSWC (%) was estimated by comparing the weights of pots at container capacity (pot_{wet}) with pots with substrate dried in an oven until constant weight (pot_{dry}) using this equation: $[(pot\text{-}pot_{dry})/(pot_{wet}\text{-}pot_{dry})] \times 100$ (Peuke et al., 2002). After the month of acclimation, plants of each species were divided into two water availability treatments: control and restricted. Control plants (CC) were irrigated regularly to maintain the water content of the substrate at container capacity during the entire experiment. Plants in the water restriction treatment (WR) had irrigation withheld until day 40, at which point VSWC reached 43.0 ± 0.8% and 53.7 ± 1.2% in

C. alba and *P. lingue*, respectively. This VSWC was maintained by weighing the pots every two days and adding water to the substrate to reach desired levels until day 120 (**Figure 1**).

Physiological, Morphological, and Growth Measurements

One month after transplanting, we made an initial measurement of the seedlings. We randomly sampled six seedlings (each seedling was a replicate) from each species (2) and population (3) combination (36 seedlings total) for physiological and morphological traits.

For physiological traits, we measured gas exchange, chlorophyll fluorescence, mid-day water potential, and relative water content. We randomly selected fully developed leaves from the upper third of the stem (i.e., leaves present before onset of the WR treatment). Gas exchange was measured on one leaf per seedling with a LI-6400XT portable photosynthesis system (LI-COR Instruments, Lincoln, NE, USA) having a CO_2 concentration inside the cuvette set to 400 μmol mol^{-1}, leaf temperature maintained at 25 ± 1°C, and leaf illumination of 1500 μmol $m^{-2}s^{-1}$ of photosynthetic photon flux density (PPFD) provided using a mixed red/blue light emitting diode installed on top of the cuvette; measurement duration was 10 to 15 min. Net photosynthesis based on leaf area (A_N), stomatal conductance (gs), intercellular concentration of CO_2 (Ci), and transpiration rate (E) were obtained. Intrinsic water use efficiency (iWUE) was calculated as the ratio between A_N and gs.

We measured chlorophyll fluorescence on one leaf using a pulse-amplitude modulated fluorimeter (FMS2, Hansatech Instruments, Norfolk, England). Leaves were covered with a clamp and adapted to dark for 30 min before fluorescence measurements. The protocol for chlorophyll fluorescence curves was performed according to Alvarez et al. (2012) with slight modifications. The saturating pulses corresponded to the following PPFDs: 14, 35, 86, 167, 562, 888, 1287, and 1824 μmol $m^{-2}s^{-1}$. Maximum efficiency of photosystem II (F_v/F_m) and electron transport rate (ETR) were calculated according to equations 1 and 2, respectively:

$$\frac{F_v}{F_m} = \frac{(F_m - F_o)}{F_m} \quad (1)$$

$$ETR = PFD \times 0.5 \times \Phi PSII \times 0.84 \quad (2)$$

where ΦPSII is the effective quantum yield of PSII, the 0.5 factor assumes that the efficiency between PSI and PSII is equal and that the incident light is equally distributed between them, and the 0.84 factor is the mean value of absorbance for green leaves. The non-photochemical quenching (NPQ) and the photochemical quenching (qP) were calculated according to equations 3 and 4, respectively:

$$NPQ = \frac{(F_m - F_{m'})}{F_{m'}} \quad (3)$$

$$qP = \frac{(F_{m'} - F_s)}{F_{m'} - F_{o'}} \quad (4)$$

After completing the gas exchange and chlorophyll fluorescence measurements, we randomly selected two fully expanded leaves from the upper third of each seedling for mid-day water potential (Ψ_{min}) and two more for relative water content (RWC) assessment (Nguyen et al., 2017). For mid-day water potential, leaves were excised with a razor blade at petiole level between 11:00 PM and 14:00 PM and Ψ_{min} was immediately measured with a Scholander pressure chamber (PMS Instruments, Albany, OR, USA) (Scholander et al., 1965). Harvested leaves were retained to be included in the morphological assessments.

For morphological measurements, plants were removed from pots and separated into leaves, roots, and stems. Roots were gently washed to remove soil. Individual leaves (including those from the physiological tests) were photographed and analyzed using an image analysis software (ImageJ, Rasband/NIH, Bethesda, MD, USA) to obtain total leaf area. Individual leaf area was calculated by dividing total leaf area by the number of leaves of each sample. Stomatal density was determined using the impression approach. The abaxial size of each leaf was cleaned and carefully smeared with fingernail varnish in the area between the leaf margin and the mid-vein. A thin film was peeled off, placed on a glass slide, and covered with a cover slip. The slides were mounted on a microscope (Olympus CX31, Tokyo, Japan) and photographed with Micrometrics SE software v2.7 (Accu-Scope, Commack, NY, USA). Photos were analyzed with the ImageJ software (Rasband/NIH, Berthesda, MD, USA); an area of 100 μm^2 was marked and the total number of stomas inside the area were counted. Each plant component was oven dried at 100°C to constant weight and then root, leaf, and stem dry mass were obtained. Total plant dry mass was calculated as the sum of all plant parts. Specific leaf area (SLA) was calculated as the ratio between leaf area and leaf dry mass, while leaf area ratio (LAR)

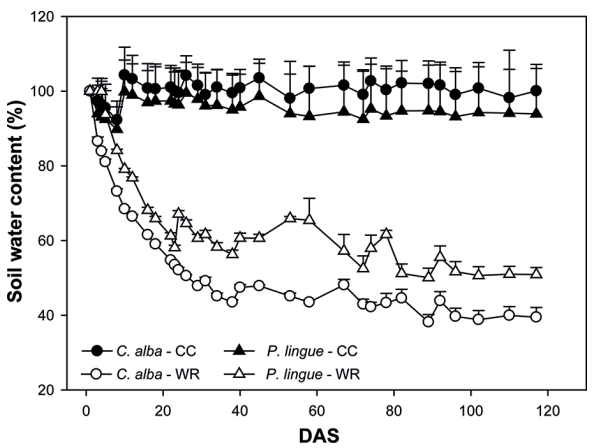


FIGURE 1 | Evolution of soil water content (%) during the water restriction experiment for *Cryptocarya alba* (circles) and *Persea lingue* (triangles) plants at container capacity (CC, black symbols) and in the water restriction (WR, white symbols) treatment. DAS, days after onset of stress treatment. Symbols represent mean + SE.

was calculated as the ratio between leaf area and total dry mass. Also, leaf, root, and stem mass ratio were calculated by dividing the mass of each plant component by total dry mass. Wood density was calculated as oven-dry mass of a 2-cm long segment of the basal part of each plant divided by its green volume (Chave et al., 2009).

At the end of the experiment (120 days after onset of the WR treatment), we randomly selected 6 seedlings from each species (2) x irrigation treatment (2) x population (3) combination (72 plants total) for the final measurement. The same suite of physiological and morphological measurements were completed as described above. For the physiological and stomatal density measurements, we sampled fully expanded leaves that were initiated during the WR treatment.

Changes in morphological traits between the initial (pre-WR treatment) and final (post-WR treatment) measurements allowed us to assess growth. Relative growth rate (RGR) and net assimilation rate (NAR) were calculated with total dry mass (TM) from the initial and final measurement times according to equations 5 and 6 (Galmés et al., 2005):

$$RGR = \frac{log_e TM_2 - log_e TM_1}{t_2 - t_1} \quad (5)$$

$$NAR = \frac{(TM_2 - TM_1) \times (log_e LA_2 - log_e LA_1)}{(t_2 - t_1) \times (LA_2 - LA_1)} \quad (6)$$

where t_1 and t_2 correspond to the initial and final measurement times, respectively.

Data Analysis

Most of the physiological and all of the morphological variables were analyzed by species with a repeated measures model (Kuehl, 2001), modeling the variance and covariance structure with a 95% level of confidence. Statistical differences between means were performed with a Tukey (HSD) test for multiple comparisons, using the PROC MIXED procedure (SAS Institute Inc., Cary, NC, USA). The effect of the different factors was assessed using the following general linear model (GLM):

$$y_{ijkl} = \mu + \alpha_i + \beta_j + \gamma_k + (\alpha\beta)_{ij} + (\alpha\gamma)_{ik} + (\beta\gamma)_{jk} + (\alpha\beta\gamma)_{ijk} + e_{ijkl} \quad (7)$$

where γ_{ijkl} is the value of de dependent variable in plant l measure in time (i=1, 2), in the j population (j=1, 2, 3) in the k irrigation treatment (k=1, 2). μ is the overall mean; α, β, and γ are the fixed effects for time, population, and water restriction treatment respectively; the double and triple terms represent interactions; and e is the error term for the hypothesis $e_{ijkl} \sim N(0, \sigma_e^2)$.

Relative growth rate and net assimilation rate were assessed with two-way analysis of variance (ANOVA) through a PROC GLM procedure (SAS Institute). Differences among means were determined with a Tukey (HSD) test for multiple comparisons.

Chlorophyll fluorescence curves to different PPFD were modeled using the PROC NLIN procedure (SAS Institute Inc.) using the Gauss-Newton method through a derivative-free algorithm. The variables ETR, NPQ, and qP in response to different PPFD were modeled using the Michaelis-Menten model:

$$y = (\beta_1 \times PPFD)/(\beta_2 + PPFD) \quad (8)$$

The variables ΦPSII and qP were modeled using the first-order decay kinetics model:

$$y = \beta_1 \times EXP(-\beta_2 \times PPFD) + \beta_3 \quad (9)$$

The effect of WR was evaluated by population and species to models level using the extra sums of squares principle (Bergerud, 1996). Visualizations were made using SigmaPlot 10 (Systat Software Inc., San Jose, CA, USA).

RESULTS

Gas Exchange and Chlorophyll Fluorescence

In *C. alba*, population and the WR treatment independently affected A_N, gs, and E (**Table 2**). Before the application of the WR treatment, Santiago presented significantly lower A_N than Cayumanque and Nacimiento (2.05 ± 0.19 vs. 6.65 ± 0.58 vs. 6.45 ± 0.64 μmol CO_2 $m^{-2}s^{-1}$, respectively). At the conclusion of the WR treatment, we noted this relationship changed due to a significant interaction between population *x* measurement time; Santiago increased A_N and no significant differences were observed with Cayumanque or Nacimiento (6.42 ± 0.78 vs. 6.16 ± 0.9 vs. 4.23 ± 0.8 μmol CO_2 $m^{-2}s^{-1}$, respectively); gs and E followed the same pattern as A_N. The application of WR significantly decreased A_N compared to CC plants (3.31 ± 0.36 vs. 7.90 ± 0.49 μmol CO_2 $m^{-2}s^{-1}$) in all populations. Similarly, WR decreased gs and E compared to CC plants (0.19 ± 0.03 vs. 0.66 ± 0.05 mol $m^{-2}s^{-1}$ and 0.94 ± 0.07 vs. 0.23 ± 0.04 mmol H_2O $m^{-2}s^{-1}$, respectively). We observed a significant triple interaction between factors that affected iWUE (**Table 2**). Descriptively, no differences were observed between CC plants from both measurement times and populations, but the WR treatment increased iWUE on plants from Nacimiento and Santiago whereas no change was observed for Cayumanque (**Figure 2**).

In *P. lingue*, we observed a significant interaction between measurement time *x* population (**Table 2**) for gs, Ci, and E (data not shown); WR treatment had no significant effect in any variable. Before the WR treatment, Cayumanque displayed higher A_N than Nacimiento and Santa Juana plants (2.12 ± 0.29 vs. 1.22 ± 0.1 vs. 1.20 ± 0.2 μmol CO_2 $m^{-2}s^{-1}$, respectively); the same trend was also observed in gs (0.022 ± 0.004 vs. 0.012 ± 0.002 vs. 0.014 ± 0.001 mmol H_2O $m^{-2}s^{-1}$, respectively). These parameters decreased during the WR treatment, but mainly affected Cayumanque plants. In contrast, a significant triple interaction among measurement time *x* population *x* WR treatment was found for A_N (**Table 2**). Net photosynthesis remained unaffected in Cayumanque plants as measured pre- and post-WR treatment, while it decreased in WR plants from Nacimiento and Santa Juana compared to CC plants (**Figure 3**)

Regarding chlorophyll fluorescence curves, the effect of WR was analyzed separately by population and species. In *C. alba*, WR

TABLE 2 | Summary of three-way repeated measures ANOVA p-values for treatment effects on net photosynthesis (A_N), stomatal conductance (gs), intercellular CO_2 concentration (Ci), transpiration rate (E), and intrinsic water use efficiency (iWUE) in *Cryptocarya alba* and *Persea lingue* plants.

Species	Source of variation	A_N	gs	Ci	E	iWUE
Cryptocarya alba	MT	0.1904	0.5265	**0.0178**	0.0863	**<0.0001**
	P	**0.0003**	**0.0019**	0.1114	**0.0012**	0.2235
	WR	**<0.0001**	**<0.0001**	0.2671	**<0.0001**	**<0.0001**
	P x MT	**<0.0001**	**<0.0001**	0.2839	**<0.0001**	**0.0351**
	MT x WR	**<0.0001**	**<0.0001**	0.2671	**<0.0001**	**<0.0001**
	P x WR	0.9112	0.9383	0.4182	0.9833	0.0918
	P x MT x WR	0.9112	0.9383	0.4182	0.9833	**0.0364**
Persea lingue	MT	**0.0001**	**0.0208**	**<0.0001**	0.0518	**<0.0001**
	P	0.8755	0.1514	0.1857	0.2831	0.8530
	WR	**<0.0001**	0.1537	0.4489	0.1146	0.6613
	P x MT	**<0.0001**	**0.0021**	**0.0001**	**0.0009**	0.1765
	MT x WR	**<0.0001**	0.1691	0.4489	0.1410	0.5740
	P x WR	**0.0308**	0.7302	0.7815	0.5438	0.9761
	P x MT x WR	**0.0308**	0.7471	0.7815	0.5893	0.9609

Significant p-values (p<0.05) are in bold. Each species was analyzed separately. MT, measurement time; P, population; WR, water restriction treatment.

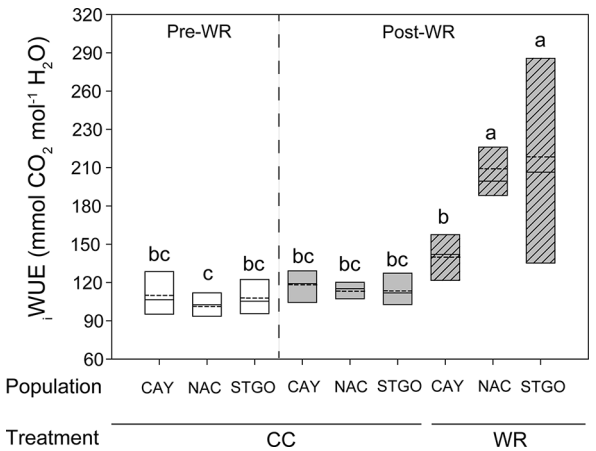


FIGURE 2 | Significant triple interaction between measurement time, population, and water restriction treatment affected intrinsic water use efficiency (iWUE, mmol CO_2 mol^{-1} H_2O) in *Cryptocarya alba* plants. Bottom and top boundaries of the boxes represent the 25th and 75th percentiles, respectively. The solid line in the center of each box represents the mean value and the dashed line represents the median value. Different letters indicate significant differences among measurement time, populations, and water restriction treatment according to Tukey at p<0.05. Pre-WR, measurement before the onset of water restriction; Post-WR, measurement at the end of the experiment; CC, container capacity; WR, water restriction; CAY, Cayumanque; NAC, Nacimiento; STGO, Santiago.

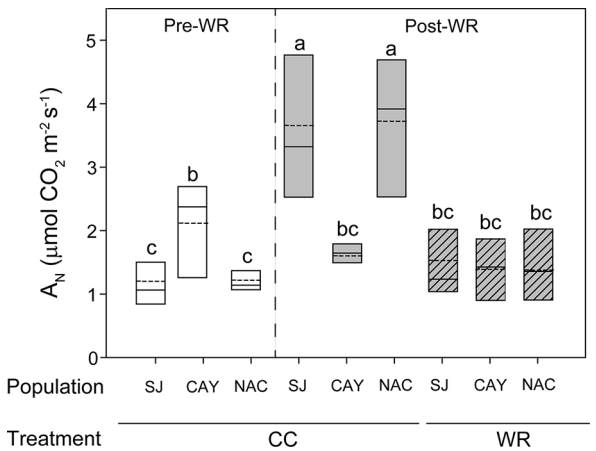


FIGURE 3 | Significant triple interaction between measurement time, population, and water restriction treatment affected net photosynthesis (A_N, µmol CO_2 $m^{-2}s^{-1}$) in *Persea lingue* plants. Bottom and top boundaries of the boxes represent the 25th and 75th percentiles, respectively. The solid line in the center of each box represents the mean value and the dashed line represents the median value. Different letters indicate significant differences among measurement time, populations, and water restriction treatment according to Tukey at p<0.05. Pre-WR, measurement before the onset of water restriction; Post-WR, measurement at end of experiment; CC, container capacity; WR, water restriction; SJ, Santa Juana; CAY, Cayumanque; NAC. Nacimiento.

affected the responses of ETR in Santiago and Nacimiento but not in Cayumanque (p=0.027, p=0.019, and p=0.145, respectively). In Santiago, WR increased ETR compared to CC plants (**Figure 4A**), whereas the opposite was observed in Nacimiento plants (**Figure 4B**). Non-photochemical quenching was affected by WR treatment on Cayumanque (**Figure 4C**) and Nacimiento plants but not on plants from Santiago (p<0.0001, p=0.017, and p=0.157, respectively). Water restriction treatment increased NPQ in Cayumanque and Nacimiento compared to CC plants, although in Nacimiento plants NPQ increased transiently at PPFDs between 167 and 888 µmol photon $m^{-2}s^{-1}$ (**Figure 4D**). Also, ϕPSII decreased in Santiago plants subjected to WR at PPFD between 86 and 1287 µmol photon $m^{-2}s^{-1}$ compared to CC plants, while no effect was observed in Cayumanque or Nacimiento (p=0.036, p=0.256, and p=0.054, respectively). Photochemical quenching was not influenced by WR in any population.

In *P. lingue*, WR significantly affected the responses of ETR, NPQ, ϕPSII, and qP in plants from Cayumanque (p=0.001, p=0.031, p=0.045, and p=0.035, respectively). In Nacimiento only NPQ (p=0.035) was influenced by WR, while

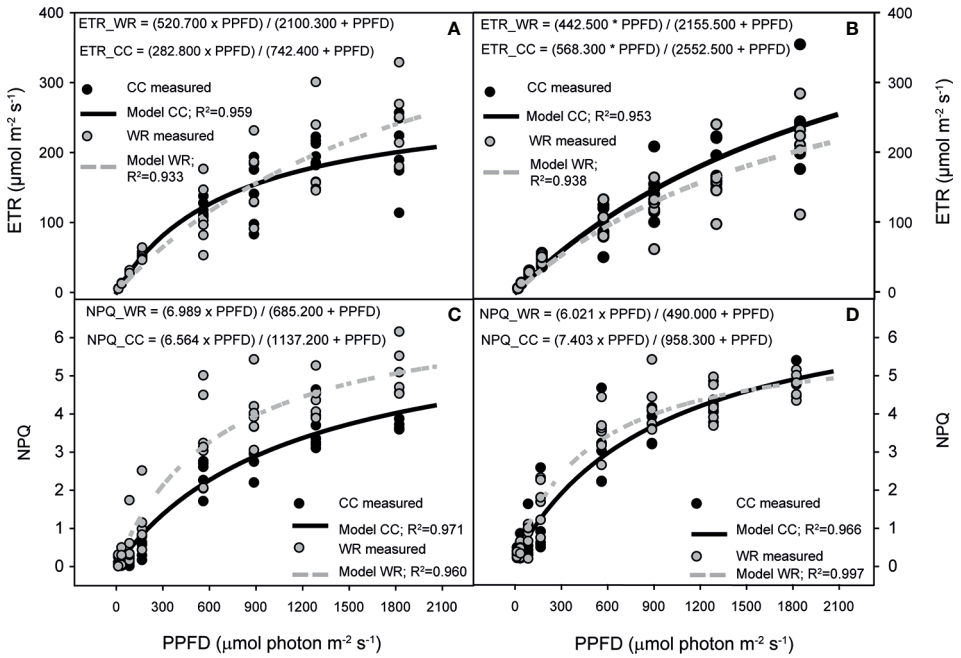


FIGURE 4 | Effect of increasing photosynthetic photon flux density (PPFD, µmol photon $m^{-2}s^{-1}$) on electron transport rate (ETR, µmol $m^{-2}s^{-1}$) **(A**, **B)** and non-photochemical quenching (NPQ) **(C, D)** of *Cryptocarya alba* plants from Santiago **(A)**, Nacimiento **(B, D)** and Cayumanque **(C)** under the water restriction (WR) and container capacity (CC) treatments. Dots indicate measured data (CC in black, WR in gray) and lines indicate modelled data (CC in continuous black line, WR in dashed gray line). Adjusted model for CC and WR treatments for each variable and population are shown on each panel.

photochemistry was not altered by WR in plants from Santa Juana. In plants from Cayumanque, the application of WR decreased ETR, ϕPSII, and qP (**Figures 5A, C, D**) and increased NPQ (**Figure 5B**) compared to CC plants. In contrast, plants from Nacimiento the WR treatment decreased NPQ in comparison to CC plants.

Plant Water Status

In *C. alba*, population and measurement time interacted to affect mid-day water potential (Ψ_{min}; p=0.0094). Before onset of the WR treatment, Ψ_{min} was significantly lower in the Santiago population compared to the Cayumanque and Nacimiento populations (-0.78 ± 0.03 vs. -0.63 ± 0.03 vs. -0.55 ± 0.04 MPa, respectively). At the end of the experiment and independent of population, WR significantly (p<0.0001) decreased Ψ_{min} compared to CC plants (-0.43 ± 0.03 vs. -1.56 ± 0.05 MPa). In *P. lingue*, WR treatment and measurement time interacted to affect Ψ_{min} (p<0.0001). At the beginning of the experiment Ψ_{min} was -0.33 ± 0.03 MPa for all populations and remained relatively constant in CC plants throughout the experiment (-0.34 ± 0.04 MPa), whereas it decreased for WR plants to -1.59 ± 0.04 MPa.

For relative water content in *C. alba*, a small but significant (p=0.0006) variation was observed among populations: Cayumanque was lower than Nacimiento and Santiago (91.2 ± 0.4 vs. 92.6 ± 0.4 vs. 93.5 ± 0.5%, respectively). Similarly in *P. lingue*, relative water content was affected by population (p=0.003), with Nacimiento displaying lower values than Cayumanque and Santa Juana (88.1 ± 0.6 vs. 91.1 ± 0.6 vs. 91.0 ± 0.6%). The WR treatment had no effect on this parameter in either species (p=0.073 in *C. alba*, p=0.914 in *P. lingue*).

Biomass Partitioning, Stomatal Density, and Relative Growth

In *C. alba*, population significantly affected all morphological parameters, including those associated with biomass partitioning, except total leaf area, leaf area ratio, and leaf mass ratio (**Table 3**; see **Supplemental Table 1** for mean morphological values). For these exceptions, we observed high standard deviations around the means (see **Supplemental Table 1**), which resulted in large p-values for the various interactions of population, treatment, and measurement time (**Table 3**). Although a Pearson's correlation analysis revealed no significant correlation between individual leaf area and stomatal density (r=-0.11, p=0.528), we observed significant differences in stomatal density (p=0.0002). Plants under WR had higher stomatal density than CC plants (35.8 ± 1.3 vs. 29.8 ± 0.8 stomas 100 μm^{-2}). Individual leaf area was only significantly affected by population (**Table 3**), higher values were observed in Nacimiento (7.31 ± 1.69 cm^2 $leaf^{-1}$) followed by Cayumanque (5.40 ± 1.46 cm^2 $leaf^{-1}$) and Santiago (3.77 ± 0.83 cm^2 $leaf^{-1}$) Total biomass was significantly higher in Cayumanque and Nacimiento compared to Santiago (**Figure 6A**), while specific leaf area was significantly higher in Nacimiento and Santiago than Cayumanque (**Figure 6C**). In relation to biomass partitioning, we observed no differences in leaf mass ratio and stem mass ratio between populations, but the ratio for root mass

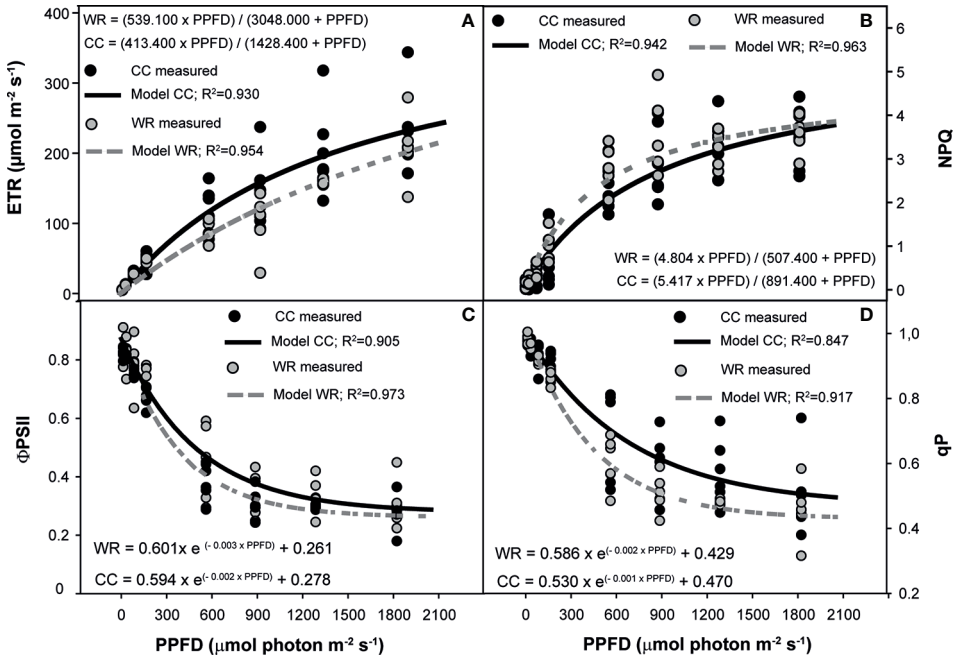


FIGURE 5 | Effect of increasing photosynthetic photon flux density (PPFD, µmol photon $m^{-2}s^{-1}$) on electron transport rate (ETR, µmol $m^{-2}s^{-1}$) **(A)**, non-photochemical quenching (NPQ) **(B)**, photochemical efficiency of PSII (ϕPSII) **(C),** and photochemical quenching (qP) **(D)** of *Persea lingue* plants from Cayumanque under the water restriction (WR) and container capacity (CC) treatments. Dots indicate measured data (CC in black, WR in gray) and lines indicate modelled data (CC in continuous black line, WR in dashed gray line). Adjusted model for CC and WR treatments for each variable and population are shown on each panel.

TABLE 3 | Summary of three-way repeated measures ANOVA p-values for treatment effects on total biomass (TM), leaf dry mass (LDM), shoot dry mass (SDM), root dry mass (RDM), leaf area (LA), individual leaf area (ILA), specific leaf area (SLA), leaf area ratio (LAR), leaf mass per area (LMA), leaf mass ratio (LMR), shoot mass ratio (SMR), root mass ratio (RMR), relative growth rate (RGR), net assimilation rate (NAR), and wood density (WD) in *Cryptocarya alba* and *Persea lingue* plants.

Species	Source of variation	TM	LDM	SDM	RDM	LA	ILA	SLA	LAR	LMA	LMR	SMR	RMR	RGR	NAR	WD
C. alba	MT	**0.0001**	0.2118	**0.0001**	**0.0001**	0.8913	0.8433	**0.0006**	**0.0001**	**0.0002**	**0.001**	0.3774	**0.0001**	—	—	**0.0001**
	P	**0.0001**	**0.0001**	**0.0001**	**0.0001**	0.1718	**0.0001**	**0.007**	0.0856	**0.0133**	0.7854	**0.0001**	**0.0104**	**0.0001**	**0.0001**	**0.0390**
	WR	0.0557	**0.0130**	**0.0199**	0.4781	0.2357	0.1993	0.2257	0.0640	0.2414	0.0743	0.2230	**0.0188**	**0.0002**	**0.0005**	**0.0001**
	P x MT	**0.0001**	**0.0001**	**0.0074**	**0.0043**	0.2079	0.2617	0.2192	0.1201	0.2850	0.2374	0.2757	0.6230	**—**	**—**	0.6778
	MT x WR	0.0557	**0.0130**	**0.0199**	0.4781	0.2357	0.2313	0.2257	0.0640	0.2414	0.1831	0.1217	**0.0188**	—	—	**0.0001**
	P x WR	0.0608	0.0980	**0.0416**	0.1375	0.4346	0.1576	0.9324	0.6262	0.9979	0.3794	0.6557	0.7549	**0.0002**	**0.0005**	0.6091
	P x MT x WR	0.0608	0.0980	**0.0416**	0.1375	0.4346	0.1992	0.9324	0.6262	0.9979	0.5861	0.5040	0.7549	—	—	0.6091
P. lingue	MT	**0.0006**	0.2597	0.0792	**0.0001**	0.5675	0.1662	0.8333	**0.0046**	0.3752	**0.0001**	**0.0002**	**0.0001**	—	—	**0.0003**
	P	**0.0013**	**0.0003**	**0.0001**	**0.0336**	0.2223	**0.0121**	**0.0007**	**0.0017**	**0.0001**	**0.001**	**0.0014**	**0.0001**	**0.0001**	**0.0022**	**0.0026**
	WR	0.2528	0.7143	0.3559	0.086	0.9188	0.8349	0.4164	0.1371	0.7526	0.1270	0.6639	0.0988	**0.0001**	**0.0118**	0.7724
	P x MT	0.3383	0.7411	0.2825	0.1468	0.9637	0.1339	0.1097	0.1539	**0.034**	0.0786	0.4022	0.5485	—	—	0.7846
	MT x WR	0.2528	0.7143	0.3559	0.0860	0.9188	0.8349	0.4164	0.1371	0.7526	0.1270	0.7585	0.0988	—	—	0.783
	P x WR	0.7512	0.8795	0.5293	0.8010	0.9415	0.7518	0.8736	0.7299	0.7711	0.8513	0.4882	0.8622	**0.0001**	0.4646	0.8354
	P x MT x WR	0.7512	0.8795	0.5293	0.8010	0.9415	0.7518	0.8736	0.7299	0.7711	0.8513	0.6958	0.8622	—	—	0.8495

Significant p-values (p<0.05) are in bold. Each species were analyzed separately. MT, measurement time; P, population; WR, water restriction treatment.

was higher in Cayumanque when compared to Nacimiento and Santiago (**Figure 6E**). Compared to CC plants, those under WR increased their root mass ratio (WR = 0.47 ± 0.01 vs. CC = 0.43 ± 0.01 g g^{-1}) and decreased their leaf dry matter (WR = 3.96 ± 0.28 vs. CC = 5.05 ± 0.43 g). A significant interaction between population and WR treatment affected stem dry mass (**Table 3**); Nacimiento and Cayumanque populations had more dry mass in the CC treatment (4.7 ± 0.45 and 2.90 ± 0.30 g, respectively) than those in the WR treatment (3.28 ± 0.34 and 1.76 ± 0.15 g, respectively), but plants from Santiago were unaffected by water supply (WR = 2.75 ± 0.21 g and CC = 2.37 ± 0.22 g).

Wood density in *C. alba* was affected by population and level of water restriction (**Table 3**), with WR plants having a greater density than CC plants (0.60 ± 0.01 vs. 0.49 ± 0.01 g cm^{-3}, respectively) and Cayumanque having greater wood density than Nacimiento and Santiago (0.51 ± 0.01 vs. 0.48 ± 0.02 vs. 0.48 ± 0.02 g cm^{-3}, respectively). A significant interaction between

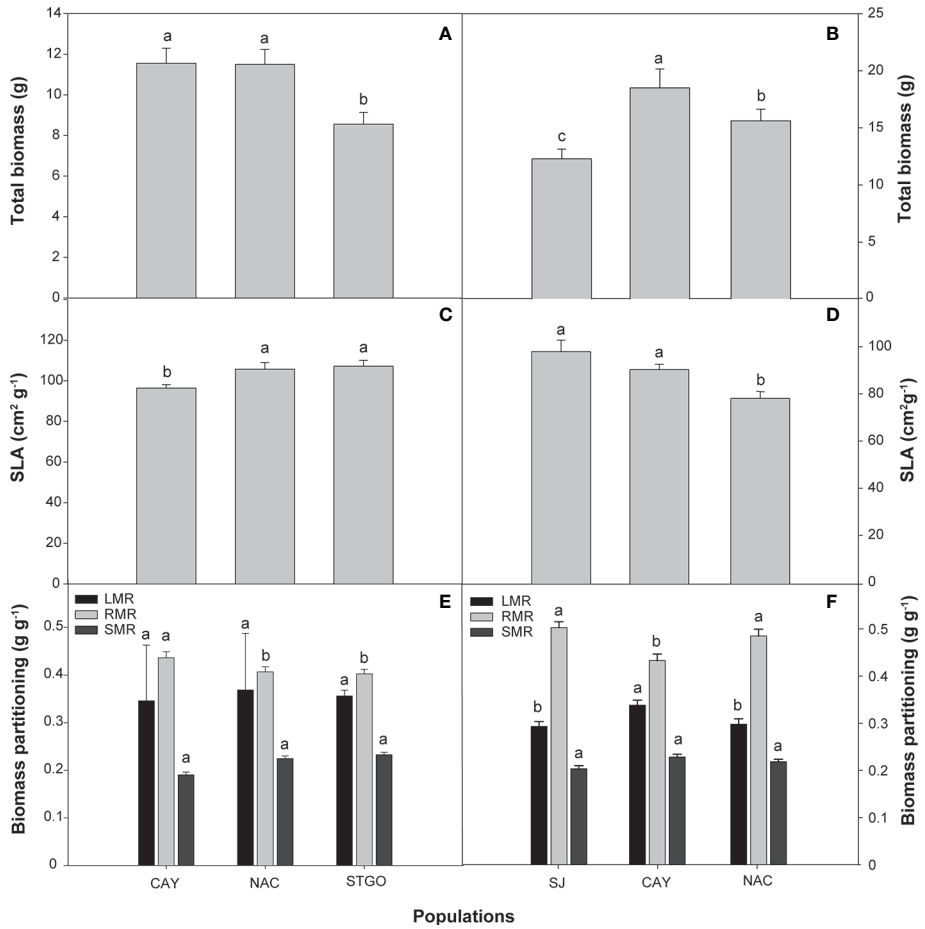


FIGURE 6 | Effect of population on total biomass (g), specific leaf area (SLA, $cm^2 g^{-1}$), and biomass partitioning (g g^{-1}) of *Cryptocarya alba* **(A, C, E)** and *Persea lingue* **(B, D, F)** plants. Bars indicate means + SE. Different letters indicate significant differences according to Tukey at $p<0.05$. CAY, Cayumanque; NAC, Nacimiento; STGO, Santiago; SJ, Santa Juana; LMR, leaf mass ratio; RMR, root mass ratio; SMR, stem mass ratio.

population and WR treatment was found for relative growth rate and net assimilation rate (**Table 3**). The interaction was similar: WR treatment significantly decreased rates in Cayumanque and Nacimiento while Santiago was unaffected (**Figures 7A, C**).

In *P. lingue*, while biomass and biomass partitioning parameters were unaffected by WR treatment, population had a significant effect on all morphological variables except total leaf area (**Table 3**; see **Supplemental Table 1** for means). As with *C. alba*, we again noted high standard deviations around the means (see **Supplemental Table 1**), large p-values for the various interactions of population, treatment, and measurement time (**Table 3**), and no correlation between individual leaf area and stomatal density for any population (Cayumanque r=0.055, p=0.872; Nacimiento r=0.248, p=0.462; Santa Juana r=-0.272, p=0.455). We did, however, observe a significant interaction of population and WR treatment (p=0.0004) on stomatal density. WR significantly increased density in Cayumanque and Nacimiento compared to CC plants but had no effect on Santa Juana (**Figure 8**). Total biomass was significantly higher in Cayumanque than in Nacimiento, followed by Santa Juana (**Figure 6B**), and accordingly, biomass of leaves, stems, and roots followed the same trend as total biomass among populations. Similarly, individual leaf area was significantly higher in Cayumanque (15.19 ± 3.84 cm^2 $leaf^{-1}$) than in Nacimiento and Santa Juana (11.65 ± 2.54 and 12.46 ± 5.30 cm^2 $leaf^{-1}$, respectively). For biomass partitioning, Cayumanque presented significantly higher leaf mass ratio and lower root mass ratio compared to Nacimiento and Santa Juana, while stem mass ratio was unaffected by population (**Figure 6F**). Specific leaf area was also influenced by population, Nacimiento displayed a lower value than Cayumanque and Santa Juana (**Figure 6D**). In contrast, Nacimiento displayed a higher wood density than Cayumanque and Santa Juana (0.49 ± 0.01 vs. 0.46 ± 0.01 vs. 0.47 ± 0.01 g cm^{-3}, respectively). Relative growth rate was significantly affected by a WR treatment and population interaction (**Table 3**); plants from Cayumanque and Nacimiento were unaffected by this treatment but the rate was significantly decreased in plants from Santa Juana (**Figure 7B**). The WR treatment caused a significant (p=0.012) increase in net assimilation rate compared to CC plants (0.217 ± 0.03 vs. 0.127 ±

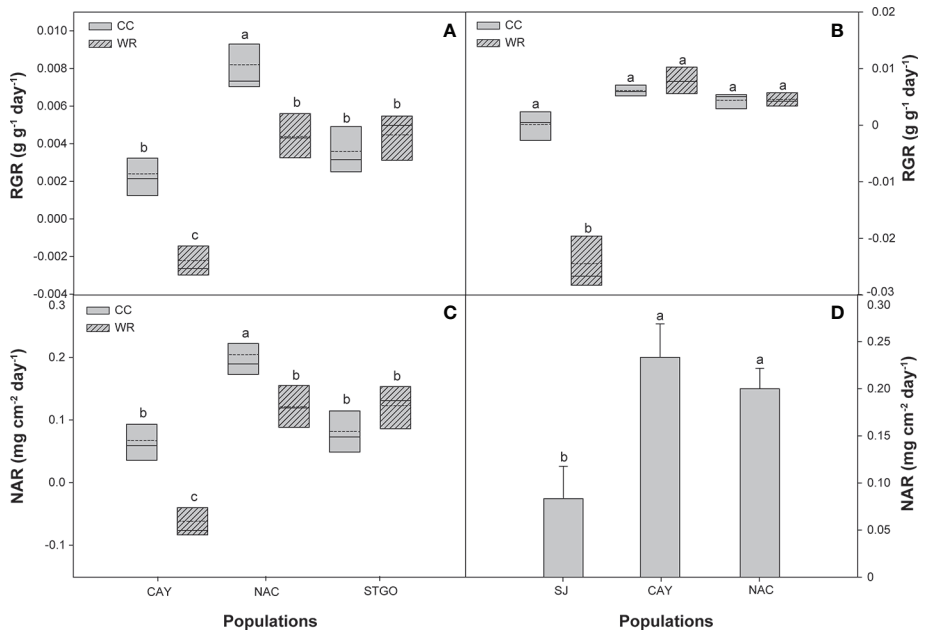


FIGURE 7 | Effect of population and irrigation treatment on relative growth rate (RGR, g g^{-1} day^{-1}) and net assimilation rate (NAR, mg cm^2 day^{-1}) of *Cryptocarya alba* **(A**, **C)** and *Persea lingue* **(B, D)** plants. In panels **(A–C)**, the bottom and top boundaries of the boxes represent the 25th and 75th percentiles, respectively. The solid line in the center of each box represents the mean value and the dashed line represents the median value. Different letters indicate significant differences among populations and irrigation treatments according to Tukey at p<0.05. In panel D, bars indicate means + SE. Different letters indicate significant differences according to Tukey at p < 0.05. CAY, Cayumanque; NAC, Nacimiento; STGO, Santiago; SJ, Santa Juana; WR, water restriction; CC, container capacity.

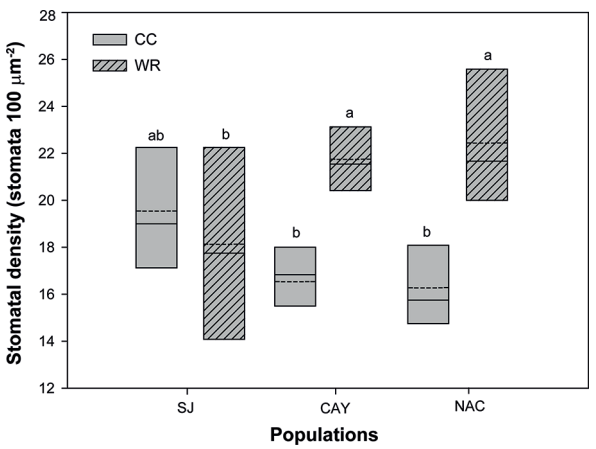


FIGURE 8 | Population and water restriction treatment significantly interacted to affect stomatal density of *Persea lingue* plants. Water restriction (WR) increased stomatal density in plants from Cayumanque (CAY) and Nacimiento (NAC) compared to plants at container capacity (CC), while it had no effect on Santa Juana (SJ). Bottom and top boundaries of the boxes represent the 25th and 75th percentiles, respectively. The solid line in the center of each box represents the mean value and the dashed line represents the median value. Different letters indicate significant differences among populations and the irrigation treatments according to Tukey at p<0.05.

0.03 mg cm^{-2} day^{-1}, respectively), and plants from Cayumanque and Nacimiento showed significantly (p=0.002) higher net assimilation rate than those from Santa Juana (**Figure 7D**).

DISCUSSION

In both species, we found significant differences in plant physiology, morphology, and growth among populations before the application of WR treatment. This was especially pronounced in *C. alba* compared to *P. lingue*; we attribute this to the greater geographic distances between *C. alba* populations compared to *P. lingue*.

In *C. alba*, the most xeric population (Santiago) displayed lower A_N, gs, and E before the WR treatment application, which is in agreement with smaller plants in terms of total biomass, lower relative growth, and net assimilation rates compared to the most mesic population (Cayumanque). Similar differences in size and growth among mesic and xeric populations were observed in species such as *Populus davidiana* (Zhang et al., 2004), *Eucalyptus microtheca* (Li, 2000), and *Pinus ponderosa* (Kerr et al., 2015). Additionally, the most xeric *C. alba* populations displayed higher specific leaf area in contrast to the mesic population. Even though lower specific leaf area is characteristic of tree species with sclerophyllous leaves from xeric sites (Bussotti et al., 2002; Marchín et al., 2008), this trait

carries an increased leaf construction cost (Villar et al., 2006; Vico et al., 2015). Thus, cheaper mesophyllous leaves along with the observed lower wood density could constitute a saving strategy for *C. alba* seedlings in more xeric sites, which concurs with observations in other Mediterranean species (Li, 2000; Zhang et al., 2004; Haramaya et al., 2016; Ramírez-Valiente et al., 2010). Such characteristics in *C. alba* plants from xeric sites, are consistent with a resource-conservative strategy and increased drought tolerance (Wright et al., 2010; Reich, 2014).

In relation to the response of *C. alba* to WR, changes in physiology, morphology, and growth parameters were also observed among populations. A decrease in A_N, gs, and E was observed in all *C. alba* populations under the WR treatment, which has been extensively reported for Mediterranean species (Gulías et al., 2002; Gimeno et al., 2008; Lázaro-Nogal et al., 2013). Thus, the concomitant decrease in gs and E with an increase in stomatal density could be related to a better control of transpiration during drought (Paoletti and Gellini, 1993), as well as a desiccation-avoiding strategy that is coherent with the rapid stomatal closure and maintenance of high relative water content in response to lower water availability observed in *C. alba*. Given that total leaf area was unaffected by the WR treatment, the greater stomatal density we measured on fully expanded leaves at the end of the experiment could be considered an active response to the WR treatment. Although morphological traits were unaffected by the WR treatment, we observed lower individual leaf area (smaller leaves) in plants from the xeric population (Santiago), which is linked to drought resistance and higher WUE (Ackerly et al., 2001). In agreement, we observed a plastic response, seen as the interaction between population *x* irrigation treatment, in iWUE among *C. alba* populations (**Figure 2A**), indicating that iWUE response to the WR treatment is population specific. While an increase in iWUE was observed in plants from xeric populations, which is expected in plants under drought (Gulías et al., 2002; Valladares and Pearcy, 2002; Valladares et al., 2005) and in plants from more xeric climates (Gratani et al., 2003; Figueroa et al., 2010; Kerr et al., 2015; Viger et al., 2016), this was not observed in plants from the most mesic population. Thus, the most xeric population (Santiago) was the least affected by WR with a reduction in A_N and gs of 48% and 68%, respectively. While in Nacimiento the increase in iWUE was mainly due to stronger decrease in gs in the WR treatment, with respect to CC plants (88%). In accordance with iWUE results, we also observed a population specific response to lower water availability for relative growth and net assimilation rates, indicating plasticity in growth among *C. alba* populations. Under the WR treatment, neither relative growth nor net assimilation rates for the most xeric population were affected, in contrast to the less xeric (Nacimiento) and mesic (Cayumanque) populations. For the less xeric and mesic populations, a pronounced decrease in A_N and gs during WR could have limited carbon assimilation, thus negatively affecting growth parameters in both populations. Also, the photosynthetic machinery of the most xeric population was minimally affected by WR with only a transient decrease in ϕPSII and an increment in ETR, results previously observed in Mediterranean tree species in response to drought (Martínez-Ferri et al., 2000; Valladares et al., 2005; Nguyen et al., 2017), suggesting higher tolerance of the primary processes of photosynthesis to WR in populations from xeric climate. Conversely, plants from the mesic population displayed an activation of photoprotective mechanisms as heat dissipation in WR treatment, observed through an increase in NPQ, revealing an impact of WR on photochemistry in this population.

In regard to morphology, including biomass partitioning, all *C. alba* populations responded equally to the WR treatment; this behavior in morphological features with drought has been previously reported for Mediterranean species (Gimeno et al., 2008; Ramírez-Valiente et al., 2010; Ramírez-Valiente and Cavenders-Bares, 2017). According to Gimeno et al. (2008), leaf morphology and biomass partitioning could be more involved in local adaptation, while physiological changes could be plastic enough to cope with changes in water availability. This agrees with results observed in *C. alba*, where population specific responses were observed on physiological traits, such as iWUE. In general, *C. alba* populations responded to reduced water availability with increased root mass ratio and a decrease in leaf biomass. Greater biomass partitioning towards root and a decrease in organs involved in transpiration is a common response to drought for many plant species (Schall et al., 2012). Especially, an increase in root mass ratio is key in coping with drought because more roots in relation to the shoot improve the capacity to explore deeper soil layers for water (Markesteijn and Poorter, 2009; Matías and Jump, 2014), and enhances establishment success during the first drought season. An increase in wood density under WR, which has been previously observed in tree species (Stiller, 2009; Corcuera et al., 2011), could reduce the risk of cavitation under negative pressure imposed by lower water availability (Hacke et al., 2001; Aranda et al., 2015).

Finally, improved iWUE and growth response in plants from the most xeric *C. alba* population could induce an advantage in competition and survival for seedlings as they experience their first summer drought that is characteristic of Mediterranean environments (Gimeno et al., 2008), and could increase resilience and acclimation capacity in future scenarios of increased aridity. In *C. alba*, iWUE and growth rates could be used as possible parameters to differentiate population responses to drought events, while morphological traits could be related to local adaptation.

Similar to *C. alba*, *P. lingue* plants displayed physiological differences among populations before the application of WR. Differences in physiological traits were, however, not related to environmental characteristics of the populations of origin. Thus, higher A_N and gs was observed in Cayumanque plants, which is consistent with bigger plants with higher total biomass. The *P. lingue* plants from the most mesic population (Santa Juana) presented more mesophyllous leaves with higher specific leaf area, which is a common trait in plants from sites with increased rainfall (Fonseca et al., 2000; Bussotti et al., 2002; Marchín et al., 2008). Even though higher photosynthetic rates are expected in such mesophyllous leaves (Wright et al., 2004), Flexas et al. (2014) indicated that a negative correlation between specific leaf area and photosynthesis could be related to changes in Rubisco

carboxylation velocity. Thus, diffusive or biochemical limitations to Rubisco carboxylation velocity could also explain differences among population photosynthesis rates, which is in agreement with lower A_N in Santa Juana plants despite higher Ci compared to the other populations (Gulías et al., 2002; Peña-Rojas et al., 2004). In contrast seedlings from the most xeric population (Nacimiento) presented a lower specific leaf area compared to the more mesic population, which was linked to less leaf biomass and a lower leaf area ratio. These are traits commonly observed in plants from drier climates as a strategy associated to limit water loss through a reduction in transpirational tissue (Poorter and Markesteijn, 2008; Peguero-Pina et al., 2014).

In contrast to *C. alba*, we observed that WR minimally influenced physiological and morphological parameters in *P. lingue*. Only A_N and stomatal density displayed a plastic response among *P. lingue* populations during the WR treatment, while no change was observed on morphological traits. However, as mentioned before, *P. lingue* populations were geographically restricted to the northernmost distribution of the species, so different responses could be found if more broadly distributed populations were included in further analysis. It is worth noticing that *P. lingue* plants reached higher VSWC values in the WR treatment compared to *C. alba* (53.7 ± 1.2% vs. 43.0 ± 0.8%), which could have induced a minor physiological adjustment in response to WR treatment. Also, WR treated *C. alba* plants had higher gs and E than *P. lingue* plants (0.019 ± 0.003 mol $m^{-2}s^{-1}$ and 0.227 ± 0.04 mmol H_2O $m^{-2}s^{-1}$ vs. 0.01 ± 0.005 mol $m^{-2}s^{-1}$ and 0.164 ± 0.12 mmol H_2O $m^{-2}s^{-1}$, respectively); such higher transpiration rates in *C. alba* may have led to lower VSWC than that observed for *P. lingue*. The most xeric populations of *P. lingue* presented an increase in stomatal density, which could contribute to the control of transpiration and iWUE (Nilson and Assmann, 2007; Roussel et al., 2009). This result has, however, no apparent relation with gs, E, or iWUE in this particular species, indicating a poor control of water loss during WR despite a decrease in plant water status (Ψ_{min}) (Sánchez-Vilasand Retuerto, 2007; McDowell et al., 2008; Viger et al., 2016). Nonetheless, we believe our observed changes in stomatal density in response to WR could be considered an active population-specific response, independent of individual leaf area. The most mesic population was negatively affected by WR application, inducing a decrease in A_N and relative growth rate, but with no adjustment in the control of water loss observed through changes on gs, E, or iWUE.

Similar to *C. alba*, fluorescence parameters were slightly affected by WR in *P. lingue*; F_v/F_m was only affected by population (data not shown) but mean values were above 0.8 in all populations. Water restriction affected fluorescence parameters mainly in Cayumanque, a slight decrease in ETR, qP, and ΦPSII was observed in WR plants, indicative of lower capacity of excess energy dissipation through photochemistry, whereas an increase in NPQ indicates activation of photoprotective mechanisms inducing higher energy dissipation as heat. These results regarding the *P. lingue* response to the WR treatment indicate that this species has a drought-tolerant strategy to cope with water scarcity in most xeric populations, which allows plants to maintain physiological function and growth despite a decrease in Ψ_{min} (Martínez-Ferri et al., 2000; Gulías et al., 2002; Meinzer et al., 2014).

Our study revealed that the drought response of *C. alba* and *P. lingue* diverge among populations, in relation to physiological and morphological adjustments. For both species, however, physiological parameters were more responsive to WR treatment than morphological traits, including biomass partitioning. Thus, it seems that physiological adjustments sufficiently plastic to cope with environmental changes imposed in this experiment (Gimeno et al., 2008). Our results indicate that differences between populations in morphological traits are involved in local adaptation processes and can be driven by differences in climate of the original environment (Bussotti et al., 2002; Ramírez-Valiente et al., 2010; Kaluthota et al., 2015; Ramírez-Valiente and Cavender-Bares, 2017). These results concur with Poorter and Nagel (2000) who demonstrated that biomass allocation changes are smaller during water limitation compared to scarcity of other resources such as light and nutrients.

CONCLUSIONS

Our results reveal inter-population differences are evident at the physiological and morphological levels for *C. alba* and *P. lingue*. Differences in morpho-physiological traits in *C. alba* were related to the climatic characteristics of the origin of the populations, indicating that plants from xeric climate present a resource-conservative strategy. In contrast, morpho-physiological differences among *P. lingue* populations were subtle and not clearly linked to climate conditions, which we attribute to the restricted distribution of the populations we selected.

For both species, physiological and growth adjustments were more responsive to the WR treatment than were morphological traits. In response to decreased water availability, the most xeric *C. alba* population performed better under stressful conditions in terms of growth and iWUE. Thus, relative and net assimilation rates with iWUE were effectively capable of differentiate population responses upon WR treatment. Despite that, differences in WR response among *P. lingue* populations were subtle, most xeric populations also performed better under stress, which we observed mainly in relation to relative growth rate response. Growth is an important trait to consider during water stress, as higher growth rates in early life will allow increased survival and establishment success under Mediterranean climates with higher changes of drought events. This research provided evidence regarding different population performances during WR in *C. alba* and *P. lingue* that could assist in the selection of populations with better chances of survival in regions with projected increases in climatic stress. Future research should, however, assess additional populations, aiming to include the complete range of distribution of each species to understand the potential suitability of different populations to be considered for restoration efforts.

While seed transfer should always be considered in restoration efforts, it may be more critical in the face of climate change. Unfortunately, we often lack information on site-adapted ecotypes according to target environment and future climatic patterns, such as an increase in drought events. Our results begin to bridge that information gap, as they suggest that the Santiago population could be a candidate, site-adapted seed source for restoration on more southerly sites. This approach should only be implemented, however, after considering variation in genetic diversity and differentiation (e.g. Hasbún et al., 2016).

DATA AVAILABILITY STATEMENT

The datasets generated for this study are available on request to the corresponding author.

AUTHOR CONTRIBUTIONS

Conceived and designed the experiment: CA-M, MA, MG. Collected plant material from populations: CA-M, MA, MG, EC. Performed experiments: CA-M. Performed data analysis: MA. Wrote the manuscript: CA-M, KD. Revised manuscript language: KD.

FUNDING

Chilean Environmental Ministry and CONICYT research project I786010006.

ACKNOWLEDGMENTS

We thank Prof. Carlos Magni from the Universidad de Chile for kindly providing *C. alba* seeds from the Santiago population for the realization of this research. We appreciate comments and suggestion from reviewers, specially reviewer #2, that helped improve the quality of this manuscript.

SUPPLEMENTARY MATERIAL

The Supplementary Material for this article can be found online at: https://www.frontiersin.org/articles/10.3389/fpls.2020.01042/full#supplementary-material

REFERENCES

Ackerly, D. D., Knight, C. A., Weiss, S. B., Barton, K., and Starmet, K. P. (2001). Leaf size, specific leaf area and microhabitat distribution of chaparral woody plants: contrasting patterns in species level and community level analysis. *Oecologia* 130, 449–457. doi: 10.1007/s004420100805

Aitken, S. N., and Whitlock, M. C. (2013). Assisted gene flow to facilitate local adaptation to climate change. *Annu. Rev. Ecol. Evol. Syst.* 44, 367–388. doi: 10.1146/annurev-ecolsys-110512-135747

Aitken, S. N., Yeaman, S., Holliday, J. A., Wang, T., and Curtis-McLane, S. (2008). Adaptation, migration or extirpation: climate changes outcomes for tree populations. *Evol. Applic.* 1, 95–111. doi: 10.1111/j.1752-4571.2007.00013.x

Aizen, M. A., Ashworth, L., and Galetto, L. (2002). Reproductive success in fragmented habitats: do compatibility systems and pollination specialization matter? *J. Veg. Sci.* 13, 885–892. . doi: 10.1111/j.1654-1103.2002.tb02118.x

Aletá, N., Vilanova, A., Díaz, R., and Voltas, J. (2009). Genetic variation for carbon isotope composition in *Juglans regia* L.: relationships with growth, phenology and climate of origin. *Ann. For. Sci.* 66, 413–424. doi: 10.1051/forest/2009021

Allen, C. D., Macalady, A. K., Chenchouni, H., Bachelet, D., McDowell, N., Vennetier, M., et al. (2010). A global overview of drought and heat-induced tree mortality reveals emerging climate change risk for forests. *For. Ecol. Manage.* 259, 660–684. doi: 10.1016/j.foreco.2009.09.001

Alvarez, C., Sáez, P., Sánchez-Olate, M., and Ríos, D. (2012). Effects of light and ventilation on physiological parameters during *in vitro* acclimatization of *Gevuina avellana* Mol. *Plant Cell Tiss. Org. Cult.* 110, 93–101. doi: 10.1007/s11240-012-0133-x

Alvarez, C., Acevedo, M., González, M., Cartes, E., and Bannister, J. (2017). Detección de albinismo en la regeneración de *Persea lingue* y *Cryptocarya alba* procedentes del cerro Cayumanque, región del Biobío. *Gayana Bot.* 74, 296–198. doi: 10.4067/S0717-66432017000200296

Angeloni, F., Ouborg, N. J., and Leimu, R. (2011). Meta-analysis on the association of population size and life history with inbreeding depression in plants. *Biol. Conserv.* 144, 35–43. doi: 10.1016/j.biocon.2010.08.016

Aranda, I., Cano, F. J., and Gascó, A. (2015). Variation in photosynthetic performance and hydraulic architecture across European beech (*Fagus sylvatica* L.) populations supports the case for local adaptation to water stress. *Tree Physiol.* 35, 34–46. doi: 10.1093/treephys/tpu101

Bannister, J., Vargas-Gaete, R., Ovalle, J. F., Acevedo, M., Fuentes-Ramírez, A., Donoso, J. P., et al. (2018). Major bottlenecks for the restoration of natural forests in Chile. *Rest. Ecol.* 26, 1039–1044. doi: 10.1111/rec.12880

Banta, J. A., Ehrenreich, I. M., Gerard, S., Chou, L., Wilczek, A., Schmitt, J., et al. (2012). Climate envelope modelling reveals intraspecific relationships among flowering phenology, niche breadth and potential range size in *Arabidopsis thaliana*. *Ecol. Lett.* 15, 769–777. doi: 10.1111/j.1461-0248.2012.01796.x

Bergerud, W. A. (1996). *Introduction to Logistic Regression Models: with worked forestry examples* (B.C: Biometrics Information Handbook 7. British Columbia Ministry of Forest Victoria).

Bolte, A., Ammer, C., Löf, M., Madsen, P., Nabuurs, G. J., Schall, P., et al. (2009). Adaptive management in central Europe: climate change impacts strategies and integrative concept. *Scand. J. For. Res.* 24, 471–480. doi: 10.1080/02827580903418224

Bussotti, F., Bettini, D., Grossoni, P., Mansuino, S., Nibbi, R., Soda, C., et al. (2002). Structural and functional traits of *Quercus ilex* in response to water availability. *Environ. Exp. Bot.* 47, 11–23. doi: 10.1016/S0098-8472(01)00111-3

Chave, J., Coomes, D., Jansen, S., Lewis, S. L., Swenson, N. G., and Zanne, A. E. (2009). Towards a worldwide wood economics spectrum. *Ecol. Lett.* 12, 351–366. doi: 10.1111/j.1461-0248.2009.01285.x

CONAMA (Comisión Nacional del Medio Ambiente) (2002). *Estrategia y plan de acción para la conservación de la biodiversidad de la región del Biobio* (Gobierno de Chile: Comisión Nacional del Medio Ambiente).

Corcuera, L., Cochard, H., Gil-Pelegrin, E., and Notivol, E. (2011). Phenotypic plasticity in mesic populations of *Pinus pinaster* improves resistance to xylem embolism (P50) under severe drought. *Trees* 25, 1033–1042. doi: 10.1007/s00468-011-0578-2

Dumroese, R. K., Williams, M.II, Stanturf, J. A., and St. Clair, J. B. (2015a). Considerations for restoring temperate forests of tomorrow: forest restoration, assisted migration, and bioengineering. *New Forest.* 46, 947–964. doi: 10.1007/s11056-015-9504-6

Dumroese, R. K., Montville, M. E., and Pinto, J. R. (2015b). Using container weights to determine irrigation needs: a simple method. *Native Plants J.* 16, 67–71. doi: 10.3368/npj.16.1.67

Echeverría, C., Coomes, D., Salas, J., Rey-Benayas, J. M., Lara, A., and Newton, A. (2006). Rapid deforestation and fragmentation of Chilean temperate forests. *Biol. Conserv.* 30, 481–494. . doi: 10.1016/j.biocon.2006.01.017

Ezcurra, C. (2010). Extensión del límite austral de *Persea lingue* (Lauraceae) al sur de la provincia de Palena, Región de los Lagos, Chile. *Gayana Bot.* 67, 117–119. doi: 10.4067/S0717-66432010000100009

Fardusi, M. J., Ferrio, J. P., Comas, C., Voltas, J., Resco de Dios, V., and Serrano, L. (2016). Intra-specific association between carbon isotope composition and productivity in woody plants: A meta-analysis. *Plant Sci.* 251, 110–118.

Figueroa, J. A., Cabrera, H. M., Queirolo, C., and Hinojosa, L. F. (2010). Variability of water relations and photosynthesis in *Eucryphia cordifolia* Cav. (Cunoniaceae) over the range of its latitudinal and altitudinal distribution in Chile. *Tree Physiol.* 30, 574–585. doi: 10.1093/treephys/tpq016

Flexas, J., Diaz-Espejo, A., Gago, J., Gallé, A., Galmés, J., Gulías, J., et al. (2014). Photosynthetic limitations in Mediterranean plants: a review. *Environ. Exp. Bot.* 103, 12–23. doi: 10.1016/j.envexpbot.2013.09.002

Fonseca, C. R., Overton, J. M., Collins, B., and Westoby, M. (2000). Shifts in trait-combinations along rainfall and phosphorous gradients. *J. Ecol.* 88, 964–977. doi: 10.1046/j.1365-2745.2000.00506.x

Galmés, J., Cifre, J., Medrano, H., and Flexas, J. (2005). Modulation of relative growth rate and its components by water stress in Mediterranean species with different growth forms. *Oecologia* 145, 21–31. doi: 10.1007/s00442-005-0106-4

Garreaud, R. D., Alvarez-Garreton, C., Barichivich, J., Boisier, J. P., Christie, D., Galleguillos, M., et al. (2017). The 2010-2015 megadrought in central Chile: impacts on regional hydroclimate and vegetation. *Hydrol. Earth Syst. Sci.* 21, 6307–6327. doi: 10.5194/hess-21-6307-2017

Gilliam, F. S. (2016). Forests ecosystems of temperate climatic regions: from ancient use to climate change. *New Phytol.* 212, 871–887. doi: 10.1111/nph.14255

Gimeno, T. E., Pias, B., Lemos-Filho, J. P., and Valladares, F. (2008). Plasticity and stress tolerance override local adaptation in responses of Mediterranean holm oak seedlings to drought and cold. *Tree Physiol.* 29, 87–98. doi: 10.1093/treephys/tpn007

Grady, K. C., Laughlin, D. C., Ferrier, S. M., Kolb, T. E., Hart, S. C., Allan, G. J., et al. (2013). Conservative leaf economic traits correlate with fast growth of genotypes of a foundation riparian species near the thermal maximum extent of its geographic range. *Func. Ecol.* 27, 428–438. doi: 10.1111/1365-2435.12060

Gratani, L., Meneghini, M., Pesoli, P., and Crescente, M. F. (2003). Structural and functional plasticity of *Quercus ilex* seedlings of different provenances in Italy. *Trees* 17, 515–521. doi: 10.1007/s00468-003-0269-8

Gulías, J., Flexas, J., Abadía, A., and Medrano, H. (2002). Photosynthetic responses to water deficit in six Mediterranean sclerophyll species: possible factors explaining the declining distribution of *Rhamnus ludovici-salvatoris*, an endemic Balearic species. *Tree Physiol.* 22, 687–697. doi: 10.1093/treephys/22.10.687

Hacke, U. G., Sperry, J. S., Pockman, W. T., Davis, S. D., and McCulloh, K. A. (2001). Trends in wood density and structure are linked to prevention of xylem implosion by negative pressure. *Oecologia* 126, 457–461. doi: 10.1007/s004420100628

Haramaya, H., Ishida, A., and Yoshimura, J. (2016). Overwintering evergreen oaks reverse typical relationships between leaf traits in a species spectrum. *R. Soc Open Sci.* 3, 160276. doi: 10.1098/rsos.160276

Hasbún, R., González, J., Iturra, C., Fuentes, G., Alarcón, D., and Ruiz, E. (2016). Using genome-wide SNP Discovery and genotyping to reveal the main source of population differentiation in *Nothofagus dombeyi* (Mirb.) Oerst. in Chile. *Int. J. Genomics.* doi: 10.1155/2016/3654093

Hufford, K. M., and Mazer, S. J. (2003). Plant ecotypes: genetic differentiation in the age of ecological differentiation. *Trends Ecol. Evol.* 18, 147–155. doi: 10.1016/S0169-5347(03)00002-8

Kaluthota, S., Pearce, D. W., Evans, L. M., Letts, M. G., Whitham, T. G., and Rood, S. B. (2015). Higher photosynthetic capacity from higher latitude: foliar characteristics and gas exchange of southern, central and northern populations of *Populus angustifolia*. *Tree Physiol.* 35, 936–948. doi: 10.1093/treephys/tpv069

Kawecki, T. J., and Ebert, T. (2004). Conceptual issues in local adaptation. *Ecol. Lett.* 7, 1225–1241. doi: 10.1111/j.1461-0248.2004.00684.x

Kawecki, T. J. (2008). Adaptation to marginal habits. *Annu. Rev. Ecol. Syst.* 39, 321–343. doi: 10.1146/annurev.ecolsys.38.091206.095622

Kerr, K. L., Meinzer, F. C., McCulloh, K. A., Woodruff, D. R., and Marias, D. E. (2015). Expression of functional traits during seedling establishment in two populations of *Pinus ponderosa* from contrasting climates. *Tree Physiol.* 35, 535–548. doi: 10.1093/treephys/tpv034

Kuehl, R. O. (2001). Diseño con mediciones repetidas. *Diseño de experimentos: Principios estadísticos de diseño y análisis de investigación* (México DF: Thomson Learning).

Lázaro-Nogal, A., Forner, A., Traveset, T., and Valladares, F. (2013). Contrasting water strategies of two Mediterranean shrubs of limited distribution: uncertain future under a drier climate. *Tree Physiol.* 33, 1284–1295. doi: 10.1093/treephys/tpt103

Li, C. (2000). Population differences in water-use efficiency of *Eucalyptus microtheca* seedlings under different watering regimes. *Physiol. Plant* 108, 134–139. doi: 10.1034/j.1399-3054.2000.108002134.x

Linhart, Y. B., and Grant, M. C. (1996). Evolutionary significance of local genetic differentiation in plants. *Annu. Rev. Ecol. Syst.* 27, 237–277. doi: 10.1146/annurev.ecolsys.27.1.237

Lloret, F., Peñuelas, J., Prieto, P., Llorens, L., and Estiarte, M. (2009). Plant community changes induced by experimental climate change: seedling and adult species composition. *Persp. Plant Ecol. Evol. Syst.* 11, 53–63. doi: 10.1016/j.ppees.2008.09.001

Marchín, R. M., Sage, E. L., and Ward, J. K. (2008). Population-level variation of *Faxinus americana* (white ash) is influenced by precipitation differences across the native range. *Tree Physiol.* 28, 151–159. doi: 10.1093/treephys/28.1.151

Markesteijn, L., and Poorter, L. (2009). Seedling root morphology and biomass allocation of 62 tropical tree species in relation to drought- and shade-tolerance. *J. Ecol.* 97, 311–325. doi: 10.1111/j.1365-2745.2008.01466.x

Martínez-Ferri, E., Balaguer, L., Valladares, F., Chico, J. M., and Manrique, E. (2000). Energy dissipation in drought-avoiding and drought-tolerant tree species at midday during Mediterranean summer. *Tree Physiol.* 20, 131–138. doi: 10.1093/treephys/20.2.131

Matías, L., and Jump, A. S. (2014). Impacts of predicted climate change on recruitment at the geographical limits of Scots pine. *J. Exp. Bot.* 65, 299–310. doi: 10.1093/jxb/ert376

McDowell, N., Pockman, W. T., Allen, C. D., Breshears, D. D., Cobb, N., Kolb, T., et al. (2008). Mechanisms of plant survival and mortality during drought: why do some plants survive while other succumb to drought? *New Phytol.* 178, 719–739. doi: 10.1111/j.1469-8137.2008.02436.x

Meinzer, F. C., Woodruff, D. R., Marias, D. E., McCulloh, K. A., and Sevanto, S. (2014). Dynamics of leaf water relations components in co-occurring iso- and anisohydric conifer species. *Plant Cell Environ.* 3, 2577–2586. doi: 10.1111/pce.12327

Muñoz, S., Nuñez, H., and Yañez, J. (1996). *Libro rojo de los sitios prioritarios para la conservación de la diversidad biológica de Chile* (Santiago, Chile: CONAF).

Nguyen, Q. N., Polle, A., and Pena, R. (2017). Intraspecific variation in drought response and fitness traits of beech (*Fagus sylvatica* L.) seedlings from three provenances differing in annual precipitation. *Trees* 31, 1215–1225. doi: 10.1007/s00468-017-1539-1

Niemeyer, H., Bustamante, R., Simonetti, J. A., Teillier, S., Fuentes, E., and Mella, J. E. (2002). *Historia natural de la Reserva Nacional Rio Clarillo: un especio para aprender ecología* (Santiago: Impresos Socias).

Nilson, S. E., and Assmann, S. M. (2007). The control of transpiration. Insights from *Arabidopsis*. *Plant Physiol.* 143, 19–27. doi: 10.1104/pp.106.093161

Paoletti, E., and Gellini, R. (1993). Stomatal density variation in beech and holm oak leaves collected over the last 200 years. *Acta Oecol.* 14, 173–178.

Peña-Rojas, K., Aranda, X., and Fleck, I. (2004). Stomatal limitation to CO_2 assimilation and down-regulation of photosynthesis in *Quercus ilex* resprouts in response to slowly imposed drought. *Tree Physiol.* 24, 813–822. doi: 10.1093/treephys/24.7.813

Peguero-Pina, J. J., Sancho-Knapik, D., Barrón, E., Camarero, J. J., Vilagrosa, A., and Gil-Pelegrín, E. (2014). Morphological and physiological divergences within *Quercus ilex* support the existence of different ecotypes depending on climate dryness. *Ann. Bot.* 114, 301–313. doi: 10.1093/aob/mcu108

Peguero-Pina, J. J., Sisó, S., Sancho-Knapik, D., Díaz-Espejo, A., Flexas, J., Galmes, J., et al. (2016). Leaf morphological and physiological adaptations of a deciduous oak (Quercus faginea Lam.) to the Mediterranean climate: A comparison with a closely related temperate species (Quercus robur L.). *Tree Physiol.* 36, 287–299.

Peuke, A. D., Schraml, C., Hartung, W., and Rennenberg, H. (2002). Identification of drought-sensitive beech ecotypes by physiological parameters. *New Phytol.* 154, 373–387. doi: 10.1046/j.1469-8137.2002.00400.x

Poorter, L., and Markesteijn, L. (2008). Seedling traits determine drought tolerance of tropical tree species. *Biotropica* 40, 321–331. doi: 10.1111/j.1744-7429.2007.00380.x

Poorter, H., and Nagel, O. (2000). The role of biomass allocation in the growth response of plants to different levels of light, CO_2, nutrients and water: a quantitative review. *Aus. J. Plant Physiol.* 27, 595–607. doi: 10.1071/pp99173_CO

Ramírez-Valiente, J. A., and Cavender-Bares, J. (2017). Evolutionary trade-offs between drought resistance mechanisms across a precipitation gradient in a seasonally dry tropical oak (*Quercus oleoides*). *Tree Physiol.* 37, 889–901. doi: 10.1093/treephys/tpx040

Ramírez-Valiente, J. A., Sánchez-Gómez, D., Aranda, I., and Valladares, F. (2010). Phenotypic plasticity and local adaptation in leaf ecophysiological traits of 13 contrasting cork oak populations under different water availabilities. *Tree Physiol.* 30, 618–627. doi: 10.1093/treephys/tpq013

Reich, P. B. (2014). The world-wide "fast-slow" plant economic spectrum: a traits manifesto. *J. Ecol.* 102, 275–301. doi: 10.1111/1365-2745.12211

Roussel, M., Le Thiec, D., Montpied, P., Ningre, N., Guehl, J.-M., and Brendel, O. (2009). Diversity of water use efficiency among *Quercus robur* genotypes: contribution of related leaf traits. *Ann. For. Sci.* 66, 1–10. doi: 10.1051/forest/2009010

Sánchez-Vilas, J., and Retuerto, R. (2007). *Quercus ilex* shows significant among-population variability in functional and growth traits but maintains invariant scaling relations in biomass allocation. *Int. J. Plant Sci.* 168, 973–983. doi: 10.1086/518943

Savolainen, O., Pyhajarvi, T., and Knurr, T. (2007). Gene flow and local adaptation in trees. *Annu. Rev. Ecol. Syst.* 38, 595–619. doi: 10.1146/annurev.ecolsys.38.091206.095646

Schall, P., Lödige, C., Beck, M., and Ammer, C. (2012). Biomass allocation to roots and shoots is more sensitive to shade and drought in European beech than in Norway spruce seedlings. *For. Ecol. Manage.* 266, 246–253. doi: 10.1016/j.foreco.2011.11.017

Scholander, P. F., Hammel, H. T., Bradstreet, E. D., and Hemmingsen, E. A. (1965). Sap pressure in vascular plants. *Science* 148, 339–346. doi: 10.1126/science.148.3668.339

Sheffield, J., and Wood, E. F. (2008). Global trends and variability in soil moisture and drought characteristics 1950-2000, from observation-driven simulations of the terrestrial hydrologic cycle. *J. Clim.* 21, 432–458. doi: 10.1175/2007JCLI1822.1

Stiller, V. (2009). Soil salinity and drought alter wood density and vulnerability to xylem cavitation of baldcypress (*Taxodium distichum* (L.) Rich.) seedlings. *Botany* 1, 164–171. doi: 10.1016/j.envexpbot.2009.03.012

Valladares, F., and Pearcy, R. (2002). Drought can be more critical in the shade than in the sun: a field study of carbon gain and photoinhibition in a Californian shrub during a dry El Niño year. *Plant Cell Environ.* 25, 749–759. doi: 10.1046/j.1365-3040.2002.00856.x

Valladares, F., Vilagrosa, A., Peñuelas, J., Romá, O., Camarero, J. J., Corcuera, L., et al. (2004). "Estrés hídrico: Ecofisiología y escalas de la sequía," in *Ecología del bosque Mediterráneo en un mundo cambiante*. Ed. F. Valladares (Madrid: Ministerio del Medio Ambiente), 163–190.

Valladares, F., Dobarro, I., Sánchez-Gómez, D., and Pearcy, R. (2005). Photoinhibition and drought in Mediterranean woody saplings: scaling effects and interactions in sun and shade phenotypes. *J. Exp. Bot.* 56, 483–494. doi: 10.1093/jxb/eri037

Valladares, F., Gianoli, E., and Gómez, J. M. (2007). Ecological limits to plant phenotypic plasticity. *New Phytol.* 176, 749–763. doi: 10.1111/j.1469-8137.2007.02275.x

Vander, M. K., Brischoff, A., and Smith, B. (2010). A question of origin: where and how to collect seed for ecological restoration. *Basic Appl. Ecol.* 11, 300–311. doi: 10.1016/j.baae.2009.09.002

Vennetier, M., Vilà, B., Liang, E., Guibal, F., Taahbet, A., and Gabdin-Henry, C. (2007). Impact of climate change on pine forest productivity and on the shift of a bioclimatic limit in Mediterranean area. *Options Méditerr.* 75, 89–97.

Vico, G., Thompson, S. E., Manzoni, S., Molini, A., Albertson, J. D., Almeida-Cortes, J. S., et al. (2015). Climatic, ecophysiological, and phenological controls on plant ecohydrological strategies in seasonally dry ecosystems. *Ecohydrology* 8, 660–681. doi: 10.1002/eco.1533

Viger, M., Smith, K. H., Cohen, D., Dewoody, D., Trewin, H., Steenackers, M., et al. (2016). Adaptive mechanisms and genomic plasticity for drought tolerance identified in European black poplar (*Populus nigra* L.). *Tree Physiol.* 36, 909–928. doi: 10.1093/treephys/tpw017

Villar, R., Robleto, J. R., De Jong, Y., and Poorter, H. (2006). Differences in construction costs and chemical composition between deciduous and evergreen woody species are small as compared to differences among families. *Plant Cell Environ.* 29, 1629–1643. doi: 10.1111/j.1365-3040.2006.01540.x

Wright, I. J., Reich, P. B., Westoby, M., Ackerly, D. D., Baruch, Z., Bongers, F., et al. (2004). The worldwide leaf economics spectrum. *Nature* 42, 821–827. doi: 10.1038/nature02403

Wright, S. J., Kitajima, K., Kraft, N. J., Reich, P. B., Wright, I. J., Bunker, D. E., et al. (2010). Functional traits and the growth-mortality trade-off in tropical trees. *Ecology* 91, 3664–3674. doi: 10.1890/09-2335.1

Zhang, X., Zang, R., and Li, C. (2004). Population differences in physiological and morphological adaptations of *Populus davidiana* seedlings in response to progressive drought stress. *Plant Sci.* 166, 791–797. doi: 10.1016/j.plantsci.2003.11.016

Conflict of Interest: The authors declare that the research was conducted in the absence of any commercial or financial relationships that could be construed as a potential conflict of interest.

Copyright © 2020 Alvarez-Maldini, Acevedo, Dumroese, González and Cartes. This is an open-access article distributed under the terms of the Creative Commons Attribution License (CC BY). The use, distribution or reproduction in other forums is permitted, provided the original author(s) and the copyright owner(s) are credited and that the original publication in this journal is cited, in accordance with accepted academic practice. No use, distribution or reproduction is permitted which does not comply with these terms.

frontiers in Plant Science

ORIGINAL RESEARCH
published: 21 July 2020
doi: 10.3389/fpls.2020.01110

An Advanced Lipid Metabolism System Revealed by Transcriptomic and Lipidomic Analyses Plays a Central Role in Peanut Cold Tolerance

He Zhang, Chunji Jiang, Jingyao Ren, Jiale Dong, Xiaolong Shi, Xinhua Zhao, Xiaoguang Wang, Jing Wang, Chao Zhong, Shuli Zhao, Xibo Liu, Shibo Gao and Haiqiu Yu *

Peanut Research Institute, College of Agronomy, Shenyang Agricultural University, Shenyang, China

OPEN ACCESS

Edited by:
Felipe Klein Ricachenevsky, Federal University of Rio Grande, Brazil

Reviewed by:
Liang Chen, University of Chinese Academy of Sciences, China
Charles L. Guy, University of Florida, United States
Puja Kumari, Hokkaido University, Japan

***Correspondence:**
Haiqiu Yu
yuhaiqiu@syau.edu.cn

Specialty section:
This article was submitted to Plant Abiotic Stress, a section of the journal Frontiers in Plant Science

Received: *26 January 2020*
Accepted: *06 July 2020*
Published: *21 July 2020*

Citation:
Zhang H, Jiang C, Ren J, Dong J, Shi X, Zhao X, Wang X, Wang J, Zhong C, Zhao S, Liu X, Gao S and Yu H (2020) An Advanced Lipid Metabolism System Revealed by Transcriptomic and Lipidomic Analyses Plays a Central Role in Peanut Cold Tolerance. Front. Plant Sci. 11:1110. doi: 10.3389/fpls.2020.01110

Cold stress restricts peanut (*Arachis hypogaea* L.) growth, development, and yield. However, the specific mechanism of cold tolerance in peanut remains unknown. Here, the comparative physiological, transcriptomic, and lipidomic analyses of cold tolerant variety NH5 and cold sensitive variety FH18 at different time points of cold stress were conducted to fill this gap. Transcriptomic analysis revealed lipid metabolism including membrane lipid and fatty acid metabolism may be a significant contributor in peanut cold tolerance, and 59 cold-tolerant genes involved in lipid metabolism were identified. Lipidomic data corroborated the importance of membrane lipid remodeling and fatty acid unsaturation. It indicated that photosynthetic damage, resulted from the alteration in fluidity and integrity of photosynthetic membranes under cold stress, were mainly caused by markedly decreased monogalactosyldiacylglycerol (MGDG) levels and could be relieved by increased digalactosyldiacylglycerol (DGDG) and sulfoquinovosyldiacylglycerol (SQDG) levels. The upregulation of phosphatidate phosphatase (PAP1) and phosphatidate cytidylyltransferase (CDS1) inhibited the excessive accumulation of PA, thus may prevent the peroxidation of membrane lipids. In addition, fatty acid elongation and fatty acid β-oxidation were also worth further studied in peanut cold tolerance. Finally, we constructed a metabolic model for the regulatory mechanism of peanut cold tolerance, in which the advanced lipid metabolism system plays a central role. This study lays the foundation for deeply analyzing the molecular mechanism and realizing the genetic improvement of peanut cold tolerance.

Keywords: peanut, cold tolerance, transcript profiling, lipid metabolism, membrane lipid remodeling, fatty acid metabolism

INTRODUCTION

Peanut (*Arachis hypogaea* L.), one of the most important grain legumes and a source of edible oils and proteins, is cultivated in tropical and subtropical regions of the world (Huang et al., 2019). In recent years, with increasing demand for peanuts, plantings have rapidly expanded in high-latitude areas such as northeast China (Bai et al., 2019). However, the heat condition in northeast China is poor and the extreme climate events such as low temperature caused by global climate change occur frequently, severely restricting peanut growth, development, productivity, and geographical distribution in temperate and high-elevation areas (Xiao and Song, 2011; Chen N. et al., 2014). Improper cold stress can increase the membrane permeability and membrane lipid peroxidation of peanut seedlings, resulting in electrolyte leakage (EL), excessive accumulation of reactive oxygen species (ROS), and substantial metabolic imbalance, especially involving respiration and photosynthesis (Vincent et al., 2018; Chang et al., 2019). In addition to morphological and physiological changes, cold stress can also lead to a series of complex signal transduction and transcriptional rearrangements (Zhang G. H. et al., 2019). These changes eventually incur damages at the whole-plant level, leading to the occurrence of chilling damage. Most temperate or hardy plants have evolved precise mechanisms to survive low temperature. Understanding the specific mechanism of peanut cold tolerance is the critical first step toward providing targets for genetic engineering of cold-tolerant peanut germplasm.

At the physiological level, malondialdehyde (MDA) and EL, the important signs of membrane damage, are negatively correlated with plant cold tolerance and have been used as indices for evaluating cold tolerance (Karami-Moalem et al., 2018). The current model of the signal transduction mechanism of cold tolerance in plants is that cold stress may first be sensed by plasma membrane proteins, such as calcium channels or associated proteins, resulting in calcium influx and leading to membrane fluidity changes and cytoskeleton rearrangement. Then, calcium-responsive protein kinases, including calcium-dependent protein kinases (CDPKs), calcineurin-B-like interacting protein kinases (CIPKs), and calcium-regulated receptor-like kinases (CRLKs), may mediate calcium signals to activate a mitogen-activated protein kinase (MAPK) cascade, which immediately regulates cold-regulated (COR) gene expression and plant cold stress tolerance (Kim et al., 2003; Almadanim et al., 2017; Yuan et al., 2018). COLD1, which regulates G-protein signaling by interacting with G-protein α subunit 1 (RGA1) and may regulate a calcium channel or be a cold-sensing calcium channel, is a transmembrane protein in the plasma membrane and endoplasmic reticulum (ER) and was recently reported to mediate cold stress sensing in rice (Ma et al., 2015). Ding et al. (2015) reported that cold stress can also activate sucrose nonfermenting 1-related protein kinase 2.6 (SnRK2.6)/open stomata 1 (OST1), which could interact with and phosphorylate transcription factors (TFs), such as calmodulin binding transcription activator (CAMTA) and ICE1/2, to activate the dehydration-responsive element-binding protein 1 (DREB1)/C-repeat-binding factors (CBF)-COR gene expression cascade.

However, despite much effort, except for the above conserved feature of cold tolerance in plants, little is known about other cold signal transduction pathways that are associated with gene expression changes. One of the latest discoveries in the field of cold signaling is the formation of the lipid second messenger, phosphatidic acid (PA), which shows to accumulate in suspension-cultured cells within minutes of cold stress (Cantrel et al., 2011; Peppino et al., 2017). In cold-induced signal transduction, PA responses have been mainly attributed to two pathways: the direct product of phospholipase D (PLD), which hydrolyses structural phospholipids such as phosphatidylcholine (PC) and phosphatidylethanolamine (PE), and the secondary product of phospholipase C (PLC) pathway, which first hydrolyzes polyphosphoinositides (PPIs) to diacylglycerol (DAG), and subsequently is phosphorylated to PA by diacylglycerol kinase (DGK) (Arisz et al., 2013; Tan et al., 2018). In addition, PA is the precursor to all phosphoglycerolipids as well as triacylglycerols (TAGs) and galactolipids, and its turnover is crucial in determining lipid metabolic fluxes and membrane compositions (Dubots et al., 2012). Lipid remodeling is another important contributor to cold tolerance, which has been proven in model plant *A. thaliana*, algae, and several crops, while there are specific changes among various plants (Gwak et al., 2014; Barrero-Sicilia et al., 2017; Noblet et al., 2017). In a non-plant system, in addition to PA, temperature stress also causes the generation of various lipid signals, including phosphatidylinositol (PI), sphingolipids, lysophospholipids, oxylipins, N-acylethanolamines, and many others (Suzuki et al., 2016). However, under cold stress, how these specific lipid species are generated and further affect cold tolerance in plants remains elusive.

Despite the evidence from model plants and crops that signal transduction, transcriptional reprogramming and lipid remodeling are essential to plant cold tolerance, there are only a handful of studies related to the cold responses of peanut, and the mechanism underlying peanut cold tolerance is poorly studied. Thus, in this study, we compared the variation in morphological and physiological parameters between tolerant and sensitive peanut varieties, and then identified the differences in gene expression profiles using RNA-seq. Finally, we determined the changes in free fatty acids (FFAs), membrane lipids and storage lipids using an LC-MS-based lipidomic platform and carried out integrated analyses with transcriptomic data. Based on information from multiple studies, we proposed a gene-metabolic network for the regulatory mechanism of peanut cold tolerance.

MATERIALS AND METHODS

Plant Materials, Growth Conditions, and Treatments

Two peanut cultivars with contrasting responses to low temperature were used in this study: the cold-tolerant cultivar Nonghua5 (NH5) and the cold-sensitive cultivar Fuhua18 (FH18). These two cultivars were previously screened out of 68

landraces and cultivars from Northeast China according to their growth and morphological differences at the seedling stage under cold stress. NH5 had less damage than FH18 in response to low temperature, and NH5 can continue to survive normally after 7 d of cold treatment at 6°C, while the growth of FH18 was inhibited severely and the seedlings can hardly survive under cold stress. NH5 is the core parent used for breeding cold-tolerant peanut germplasm in Northeast China. FH18 is a representative peanut variety planted in large areas of northeast China. The seeds used in this study were obtained from the Peanut Research Institute, Shenyang Agricultural University, China.

Peanut seeds were surface sterilized with 3% sodium hypochlorite for 10 min, washed with distilled water five times, soaked in distilled water for 12 h, then placed in Petri dishes with moistened filter papers, and germinated in the dark at 28°C in a growth chamber. After 2 d, the germinated seeds were sown in round plastic pots filled with clean river sand and half strength Hoagland's solution and subsequently transferred to a climate chamber under a 16 h light (28°C)/8 h dark (23°C) cycle, a photosynthetic photon flux density of 700 μmol m^{-2} s^{-1} and a relative humidity of 70%, 10 seeds per plot.

Two-week-old seedlings were grouped into two groups. One group was transferred to another climate chamber maintained under 6°C, a 16 h/8 h cycle (light/dark), a photosynthetic photon flux density of 700 μmol m^{-2} s^{-1}, and a relative humidity of 70%. The other group with the same developmental progression was used as a control and maintained under normal conditions. The second leaves from the treatment and control were collected at 0, 12, 24, 48, 72, 96, and 120 h, respectively, frozen in liquid nitrogen and stored at −80°C for measurements. All treatments were performed in three independent biological replicates.

Morphological Parameters

After 7 d of cold stress, the seedlings under normal and cold conditions were sampled to measure plant height (PH), total leaf area (TLA), shoot (including leaves) fresh weight (SFW), root fresh weight (RFW), shoot dry weight (SDW), and root dry weight (RDW).

Fifteen seedlings for each treatment (5 seedlings per replicate) were selected, and the PH per plant was recorded. The TLA per plant was measured using an electronic area meter (Li-Cor3000, Li-Cor, Lincoln, NE, USA). Then, shoots and roots were separated, and the SFW and RFW were recorded. All plant tissues were dried at 105°C for 15 min and at 80°C for 72 h, and then the SDW and RDW were recorded.

Determination of EL and MDA

The EL was determined using an electrical conductivity meter (DDSJ-308F, Shanghai, China) following Han et al. (2017). Small circular leaf samples were obtained by a 7-mm-diameter hole punch. Then, these circles were rinsed three times with deionized water and dried with filter papers. Twenty circles per replicate were put into a test tube with 20 ml deionized water. The initial electrical conductivity (EC1) of the washing solutions was measured after the samples were incubated at 25°C for 3 h. Then, the tubes were placed in a boiling water bath for 30 min, and the electrical conduction (EC2) was measured again after the solution cooled to room temperature. The EL was calculated using the formula EL = EC1/EC2×100.

The MDA content was determined according to Chen X. et al. (2014). Fresh leaves (0.5 g) were homogenized in 5 ml of 5% (m/v) trichloroacetic acid (TCA) and centrifuged at 12,000 g and 4°C for 10 min. The supernatant (2 ml) was mixed with an equal volume of 0.5% thiobarbituric acid (TBA). The mixture was placed in boiling water for 15 min and then instantly cooled in an ice bath and centrifuged at 10,000 g at 4°C for 10 min. The absorbance of the supernatant was measured at 450, 532, and 600 nm. The MDA content was calculated as follows, where Vt and Vs are the total volume of the extract solution and the volume of the extract solution contained in the reaction mixture, respectively, and m is the mass of the sample: MDA (nmol g^{-1} FW) = [6.45 × (A532-A600) − 0.56 × A450] × Vt/(Vs × m).

Measurement of Photosynthetic Parameters

The net photosynthetic rate (Pn) was measured in the second leaves under cold and normal conditions using a portable photosynthetic system (LI-6400, Li-COR, Lincoln, NE, USA) at 70% relative humidity, a 370 μmol mol^{-1} CO_2 concentration, and a 700 μmolm^{-2}·s^{-1} PPFD (Sui et al., 2018).

The fluorescence parameter Fv/Fm and chlorophyll (Chl) fluorescence images of the second leaves under cold and normal conditions were analyzed after 30 min of dark adaptation using a Chl fluorescence imaging system FluorCam 7 (Photon Systems Instruments, Brno, Czech Republic) (Hantzis et al., 2018).

Chlorophyll (Chl) a, b, (a+b), and (a/b) contents were analyzed as previously described by Lichtenthaler and Wellburn (1983). Fresh leaves (0.1 g) were cut and placed in a 15 ml test tube with a 10 ml mixture of 95% acetone and absolute ethyl alcohol (1:1, v/v). The test tubes were then placed in dark conditions for 48 h until the leaves became white. The absorbance of the supernatant was measured at 663, 646, and 470 nm. The Chl contents were calculated as follows where V is the total volume of the extract solution:

$$\text{Chl a (mg g}^{-1}\text{ FW)} = (12.21 \times A663\text{-}2.81 \times A646) \times V/FW$$

$$\text{Chl b (mg g}^{-1}\text{ FW)} = (20.13 \times A646\text{-}5.03 \times A663) \times V/FW$$

Ultrastructural Observation

Small pieces (approximately 1 mm^2) of fresh leaves after 0 (control) and 24 h of cold stress were fixed in 3% glutaraldehyde in 0.1 M phosphate buffer (pH 7.4) for 24 h at 4°C. Postfixation was conducted in 1% osmium tetroxide for 2 h, and the samples were then washed with phosphate buffer three times. Next, samples were dehydrated with an increasing series of ethanol (50% and 70%) and acetone (80% and 90%) for 15 min each. Then, the samples were dehydrated three times in 100% acetone for 30 min. The samples were soaked in a mix of propylene oxide and SPI-812 embedding medium. Finally, samples were immersed overnight in embedding medium. Ultrathin sections (50 nm) were cut using an ultramicrotome

(Leica EM UC6 ultramicrotome, Japan) and collected on copper grids. Then, the sections were stained with uranyl acetate followed by lead citrate and examined using a transmission electron microscope (TEM, Joel JEM-1230, Japan).

RNA Extraction, RNA-Seq, and Quantitative Real-Time RT-PCR

Total RNA was extracted from the second leaves of peanut seedlings subjected to 0 (control), 12, and 24 h of cold stress, respectively, using TRIzol reagent (Invitrogen). After quality inspection, a total of 20 μg of RNA from each sample was used for library construction. The process started with the synthesis of two cDNA strands, followed by the purification of the double-stranded cDNAs, and finally, the cDNA library was obtained by PCR enrichment. The library integrity was assessed using Qubit 2.0. The insert size was purified (AMPure XP system) and quantified using the Agilent high sensitivity DNA assay of the Agilent Bioanalyzer 2100 system. High-throughput sequencing was performed using the Illumina HiSeq system and was conducted in triplicate for each treatment. The raw data (raw reads) were filtered with the FASTQ_Quality_Filter tool from the FASTX-toolkit. Clean data were used for further analysis. After preprocessing the RNA-seq data, the reads were mapped to the peanut reference genome version Tifrunner.gnm1. ann1. CCJH. The sequence alignment generated by Tophat was then processed by Cufflinks software to assemble the alignments in the sequence alignment/map file into transcript fragments (transfrags).

Quantitative real-time RT-PCR (qRT-PCR) was performed to validate the RNA-seq results. Ten DEGs were randomly selected for qRT-PCR. All primers were designed using Primer 5.0 software (**Table S1**). The peanut actin gene (GenBank accession NC_037620) served as the internal control. The PCR was performed using SYBR Premix Ex Taq™ following the manufacturer's instructions (TaKaRa, Inc., Dalian, China) with a qRT-PCR amplification instrument (ABI 7500, USA). Each 10 μl reaction system contained 3.4 μl ddH2O, 5.0 μl SYBR® Green Master Mix, 0.3 μl each primer, and 1.0 μl cDNA template. The PCR was initiated with a starting step of 95°C/60 s, followed by 40 cycles of 95°C/15 s and 55°C/30 s, and terminated at 72°C for 60 s. Three biological replicates were included in each treatment.

Lipid Extraction

After 24 h of cold stress, the second peanut leaves from five plants in different pots were collected as one replication (the samples growing under normal conditions were used as controls), and the lipidomic analysis was performed with six replicates. Total lipid extraction was conducted according to previously reported methods (Narayanan et al., 2016) with slight modification. The cut peanut samples (approximately 200 mg) were quickly transferred into glass tubes with 3 ml preheated isopropanol [containing 0.01% butylated hydroxytoluene (BHT)] and held in a water bath for 15 min at 75°C. Then, 1.5 ml chloroform and 0.6 ultrapure water were added into the tubes, shaking at 150 g min^{-1} for 1 h. The extracted solution was then transferred into new glass tubes. The lipid extraction was repeated with 4 ml $CHCl_3$/MeOH (2:1, v/v) containing 0.01% BHT at 150 g min^{-1} for 30 min and transferred again. The above steps were repeated until the samples became discolored. Then, the lipid extracts were combined, washed with 1 M KCl (1.0 ml), and centrifuged at 500 g for 5 min, and the water phase was discarded. Next, 2 ml ultrapure water was added to the extract and centrifuged at 500 g for 5 min, and the water phase was discarded. The solvent from the lipid extract was evaporated under a stream of N_2 and stored at –80°C.

Fatty Acid Composition Analysis

The prepared lipids were dissolved in 1 ml benzene/petroleum ether (1:1, v/v) and 1 ml methanol solution containing 0.4 M KOH), then 8 ml deionized water was added and shaken well. The supernatant was analyzed by a gas chromatograph system coupled with a mass spectrometer (GCMS-QP2010 Ultra, SHIMADZU, Japan) with a DB-Wax capillary column (Fan et al., 2017). A 1 μl aliquot of the analyte was injected. The GC conditions were as follows: split ratio of 1:20; injector and flame ionization detector temperature of 240°C; oven temperature programmed at 50°C for 2 min, increased 15°C min^{-1} to 150°C and then increased again at 6°C min^{-1} to 240°C, which was maintained for 4 min; carrier gas (H_2) flow rate of 1 ml min^{-1}. The mass spectrometry data were acquired in scan mode with the m/z range of 33–450 after a solvent delay of 3min.

Lipidomic Analysis

Lipidomic analysis was performed on a 6460 triple quadruple electrospray ionization mass spectrometer (ESI/MS) coupled with a 1290 high-performance liquid chromatograph (Agilent, USA). The specific methods were previously described (Li et al., 2008; Gwak et al., 2014). The detailed method can be found in **Method S1**. For lipidomics analysis, six biological replicates were included. For each biological replicate, lipids were extracted in duplicate for independent LC/MS analysis.

Statistical Analysis

All statistical analyses of physiological and lipidomic data were performed with SPSS 19.0 (SPSS Inc.) using one-way analysis of variance (ANOVA) and Tukey's test. Mean comparisons were performed using the least significant difference (LSD). *P<0.05 and **P<0.01 represent significant difference at the 0.05 and 0.01 level, respectively.

RESULTS

Morphological Differences Between Cold Tolerant and Susceptible Varieties

In a previous study, 14-d-old peanut seedlings were exposed to 6° C for 7 d to examine the cold tolerance of 68 peanut cultivars by observing their phenotypes and measuring their morphological indexes. As shown in **Figure S1**, seedling leaves of FH18 were obviously dehydrated, wilted, and chlorotic, almost can't survive normally, while NH5 were only a little wilted in leaves and can continue to survive at 6°C low temperature. As for morphological characters, the plant height (PH), total leaf area

(TLA), shoot fresh weight (SFW), root fresh weight (RFW), shoot dry weight (SDW), and root dry weight (RDW) of both NH5 and FH18 decreased. However, the magnitude of the decreases of FH18 were greater than those of NH5, especially for SFW, SDW, and RDW, which suggested that peanut cultivar FH18 was more sensitive to 6°C temperature exposure than NH5 and that the leaves and shoots of plants were more susceptible to cold stress than other tissues.

Physiological and Ultrastructural Responses to Cold Stress

The photosynthetic capacity of NH5 and FH18 seedlings after 0, 12, 24, 48, 72, 96, and 120 h of cold stress were estimated by the net photosynthetic rate (Pn), Fv/Fm and Chl content, respectively. After continuous cold stress, the Pn and Fv/Fm were both decreased in the two peanut cultivars, while the levels in NH5 were higher than those in FH18. The differences between NH5 and FH18 reached an extremely significant level after 24 h of cold stress (**Figures 1A–C**). As shown in **Table S2**, Chl a, Chl b, Chl (a+b), and Chl (a/b) also declined continuously under cold stress, which may be the main factor behind leaf discoloration. The decreased Chl (a/b) suggested that Chl a may not be as stable as Chl b and be more easily decomposed and damaged under cold stress. According to the MDA contents and EL, membrane lipid oxidation and permeability also occurred in peanut under cold stress. After 120 h of cold stress, the MDA content in NH5 and FH18 increased by 109.54% and 169.97%, respectively. The EL in NH5 and FH18 increased by 38.41% and 135.65%, respectively. While, the changes of EL and MDA content in NH5 in the early stage of low temperature stress were not significant (**Figures 1D, E**).

These physiological responses indicated that NH5 was relatively stable, but FH18 was more severely damaged during the early stage (24 h) of cold stress. The reason for the decreased photosynthetic capacity, membrane lipid peroxidation and increased membrane permeability may due to damage to the membrane system and chloroplast structure under cold stress. Therefore, the subcellular structure of NH5 and FH18 leaves after 24 h of cold stress was observed. As shown in **Figure 2**, in NH5, the leaf cells, chloroplasts, and membrane system showed no significant changes. However, in FH18, the leaf cells were severely damaged, the cell walls were contorted, and chloroplasts became swollen and twisted, filling the entire cell chamber. Moreover, massive amounts of unknown floccular particles accumulated on the membrane, and severe damage occurred to the plasma membrane and chloroplast membrane structures with low levels of thylakoid stacking and without the typical grana.

Genome-Wide Gene Expression Profiling in Peanut Under Cold Stress

To systematically reveal the specific cold stress responses at the genomic level and the underlying molecular regulatory mechanism, the transcriptional profiling of NH5 and FH18

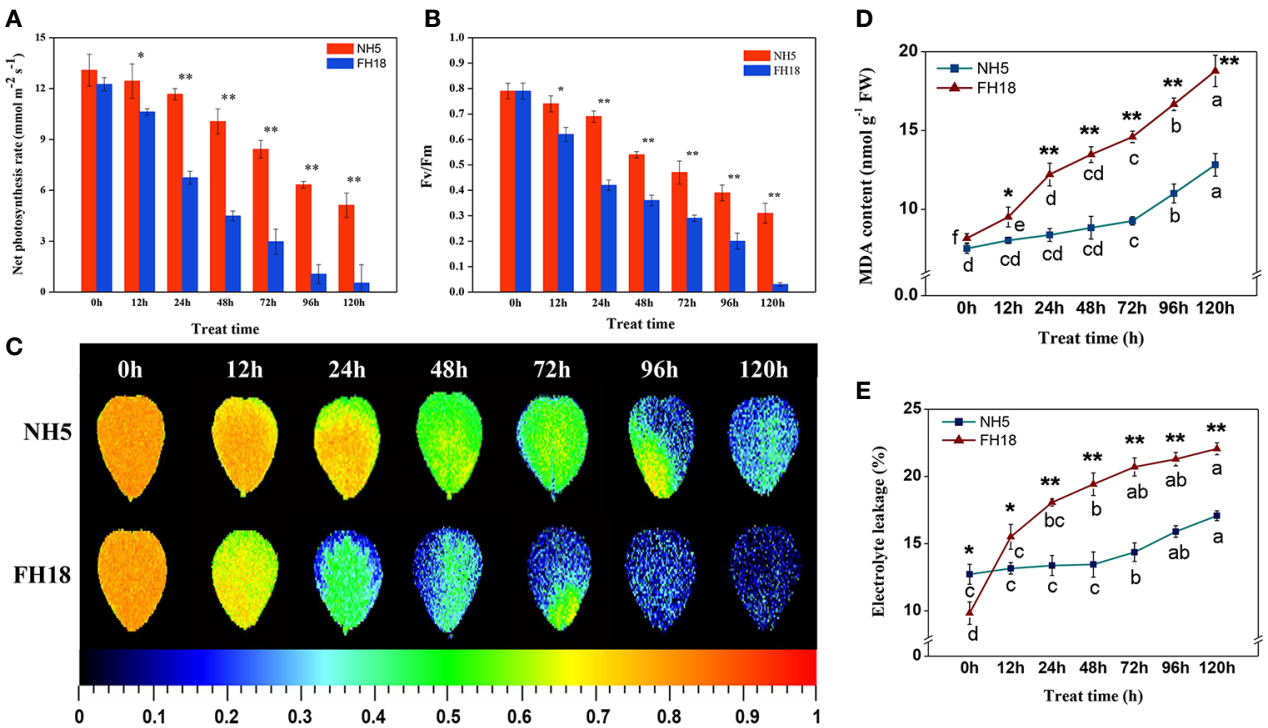


FIGURE 1 | The physiological responses of NH5 and FH18 to continuous cold stress including **(A)** net photosynthetic rate (Pn), **(B, C)** maximum PSII quantum yield (Fv/Fm), **(D)** malondialdehyde (MDA) content, and **(E)** electrolyte leakage (EL). Error bars represent the SD of the means (three replicates). *Asterisk indicates significant difference as determined by the Student's t-test (*P < 0.05; **P < 0.01).

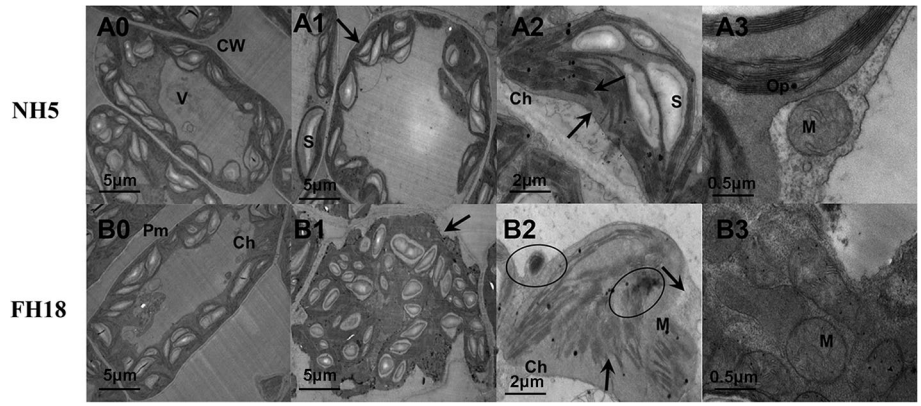


FIGURE 2 | The ultrastructural changes of peanut leaves after 0 and 24 h cold treatments in NH5 (A0-A3) and FH18 (B0–B3). (A0, B0) The leaf cell under 0 h cold treatment. (A1, B1) The leaf cell under 24 h cold treatment. (A2, B2) The chloroplast under 24 h cold treatment. (A3, B3) The mitochondria under 24 h cold treatment. The arrows in (A1) and (B1) indicate the cell membrane. The arrows in (A2) and (B2) indicate the chloroplast membrane and granum. The circles in (B2) indicate the unknown floccular particles. Ch, chloroplast; CW, cell wall; M, mitochondria; Op, osmiophilic granules; Pm, plasma membrane; S, starch grain; V, vacuole. The black lines represent size marker bars.

exposed to 0, 12, and 24 h of cold stress were compared using Illumina RNA-seq (**Table S3**). The RNA-Seq data has been submitted to the online SRA (Sequence Reads Archive) database with the accession number PRJNA602777. A total of 36,944 effectively expressed genes [fragments per kilobase of transcript per million fragments mapped (FPKM) ≥1] were obtained (**Table S4**). Then, based on the statistical test [fold change (FC)≥2 and false discovery rate (FDR)<0.01], the differentially expressed genes (DEGs) in NH5 and FH18 were identified (**Table S5**). Of these, 3910 (2428 showing upregulation and 1482 showing downregulation) and 3702 (2070 upregulation and 1632 downregulation) had ≥ 2-FC in transcription activity relative to that at 28°C at any point, that is, continuously differential expression (CDEGs) during the early stage of cold stress in NH5 and FH18, respectively (**Figure S2**; **Tables S6** and **S7**).

Among all the CDEGs, 569 (277 upregulation and 292 downregulation) were expressed only in NH5 (**Figure S2**; **Table S8**), and 2358 (1534 upregulation and 824 downregulation) were commonly expressed in both cultivars (**Figure S2**; **Table S9**). Moreover, based on the FC values, the differential expression level of 190 (158 upregulation and 32 downregulation) of 2358 CDEGs was significantly higher in NH5 than in FH18 at any point [FC(NH5/FH18) ≥2] (**Table S10**), which comprised the "putative cold tolerance gene set" together with the 569 CDEGs and may play a central role in peanut cold tolerance. These 759 CDEGs were enriched in 39 known GO terms (**Table S11**), and more were classified into the "biological process" category than the "cellular component" or "molecular function" categories (**Figure 3A**). The "metabolic process" in the biological process category was most significantly enriched. The top enriched GO terms in the cellular component category included "cell", "organelle," and "membrane". The top enriched GO terms in the molecular function category included "catalytic activity" and "binding". Furthermore, the biological metabolic process was analyzed in detail by the Kyoto Encyclopedia of Genes and Genomes (KEGG). A total of 147 CDEGs were enriched in 72 KEGG pathways (**Table S12**), of which "fatty acid metabolism", "membrane lipid metabolism", "translation", "carbohydrate metabolism," and "transport and catabolism" had the highest number of CDEGs (**Figure 3B**).

Identification of Key DEGs in Lipid Metabolic Pathways for Cold Tolerance

Transcriptional profiling of two peanut cultivars indicated that lipid metabolism may play a central role in peanut cold tolerance; therefore, we further focused our analyses on the changes in transcription activity of a compiled list of 651 genes involved in lipid metabolism (**Table S13**), which were identified based on a homology search to known lipid metabolism genes in the higher model plant *Arabidopsis thaliana* reported in Aralip website (http://aralip.plantbiology.msu.edu/pathways/pathways). According to the clustering heat map, 111 CDEGs (74 showing upregulation and 37 showing downregulation) contained in clusters I and III were identified (**Figure 4A**; **Table S14**) and categorized into 13 lipid metabolic pathways (**Figure 4B**). The transcriptional profiles of 111 CDEGs in FH18 were significantly different from those in NH5, mainly manifested as smaller quantities and lower expression levels (**Figure 4C**). In NH5, CDEGs involved in "alpha-linolenic acid metabolism", "linoleic acid metabolism", "glycerolipid metabolism", and "glycerophospholipid metabolism" were abundant, and most of them were highly upregulated, while CDEGs involved in "fatty acid elongation" were downregulated.

Of all the 111 CDEGs, 37 were expressed only in NH5, and 22 of 56 CDEGs showed significantly higher expression in NH5 than in FH18 (**Table S14**). We further characterized the functional annotation of these 59 lipid-related CDEGs involved in peanut cold tolerance (**Table S15**). Under cold stress, genes involved in the *de novo* synthesis of the storage lipid TAG were

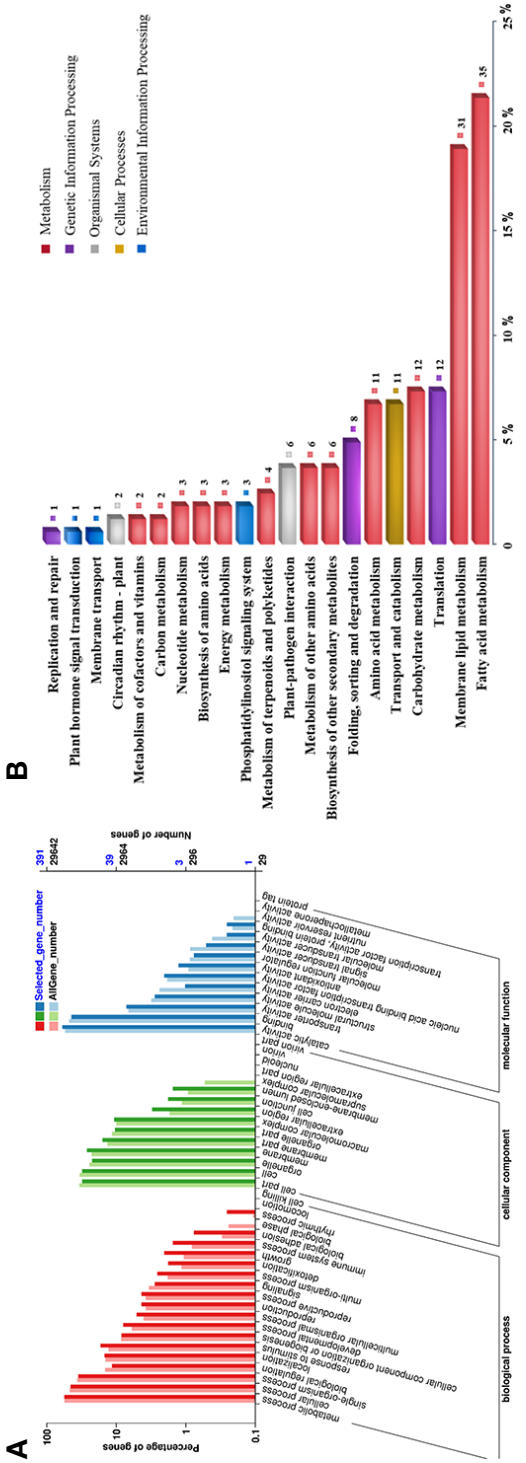


FIGURE 3 | Functional enrichment analysis of 759 continuously differentially expressed genes (CDEGs) in "putative cold tolerance gene set" during the early stage of cold stress. **(A)** Enriched gene ontology (GO) classification. **(B)** Kyoto Encyclopedia of Genes and Genomes (KEGG) classification.

all significantly upregulated, including two glycerol-3-phosphate acyltransferase (*GPAT2*) genes, one lysophosphatidyl acyltransferase (*LPAAT*) gene, two phosphatidate phosphatase (*PAP1*) genes, and one diacylglycerol acyltransferase (*DGAT1*) gene, which may directly lead to the accumulation of DAG and TAG. DAG is a lipid intermediate that is the substrate for membrane lipid synthesis. In membrane-lipid metabolism pathways, genes responsible for the generation of PA, such as *PLDs* (*PLDζ*, *PLDζ1*, and *PLDζ2*) and DGK5, were also upregulated. PA can form CDP-DAG by the catalysis of phosphatidate cytidylyltransferase (*CDS1*) and then produce a small quantity of PI and cardiolipin (CL) by CDP-diacylglycerol–inositol 3-phosphatidyltransferase (*PIS1*) and cardiolipin synthase (*CRLS*), respectively. Here, five genes encoding monogalactosyl diacylglycerol synthase (*MGD*), digalactosyl diacylglycerol synthase (*DGD*), and sulfoquinovosyl diacylglycerol (SQDG) synthase (*SQD*) in galactolipid synthesis pathways were all upregulated. MGD and DGD1 catalyzed the formation of digalactosyldiacylglycerol (DGDG) from monogalactosyldiacylglycerol (MGDG) and *SQD2* catalyzed the formation of SQDG.

Most of the other CDEGs were involved in fatty acid metabolism pathways. Under cold stress, two key genes encoding acyl-CoA oxidase (*ACOX1*) and acetyl-CoA acyltransferase (*ACAA1*) were upregulated and promoted the β-oxidation of fatty acids. Then, acyl CoA with carbon chains of various lengths was hydrolyzed to FFAs by acyl-CoA thioesterase (*ACOT*). The β-oxidation of fatty acids is also the central process in the α-linolenic acid metabolic pathway. With the activation of β-oxidation and the upregulation of other key genes, including six lipoxygenase (*LOX*) genes, four allene oxide synthase (*AOS*) genes, one allene oxide cyclase (*AOC*) gene, and four jasmonate O-methyltransferase (*JMT*) genes, the α-linolenic acid metabolism and jasmonic acid (JA) biosynthesis were significantly activated. In contrast, the genes mapped to the fatty acid elongation pathway, such as 3-ketoacyl-CoA synthase (*KCS*), very-long-chain 3-oxoacyl-CoA reductase (*KCR*), very-long-chain (3R)-3-hydroxyacyl-CoA dehydratase (*HACD*), and very-long-chain enoyl-CoA reductase (*TER*) were all downregulated to inhibit the production of very long-chain fatty acids.

To verify the transcriptomic profile based on gene expression levels, ten CDEGs (*KCS6*, *DGAT1*, *LOX3*, *LOX5*, *PIS1*, *PLDα1*, *PLDδ*, *PLDζ*, *PLDζ1, and PLDζ2*) with differential expression patterns were randomly selected from the putative cold tolerant gene set for quantitative RT-PCR analysis (**Figure 5**). As expected, among all the selected genes, the relative expression levels of *DGAT1*, *LOX3*, *LOX5*, and *PLDζ/ζ1/ζ2* significantly increased in NH5 but were relatively stable in FH18. *PLDδ* was markedly upregulated and KCS6 was downregulated both in NH5 and FH18, which showed the same expression patterns with RNA-Seq analysis.

Quantitative Changes in Lipid Composition Induced by Cold Stress

To investigate whether the differential expression of lipid metabolism genes was reflected in differential lipid abundances,

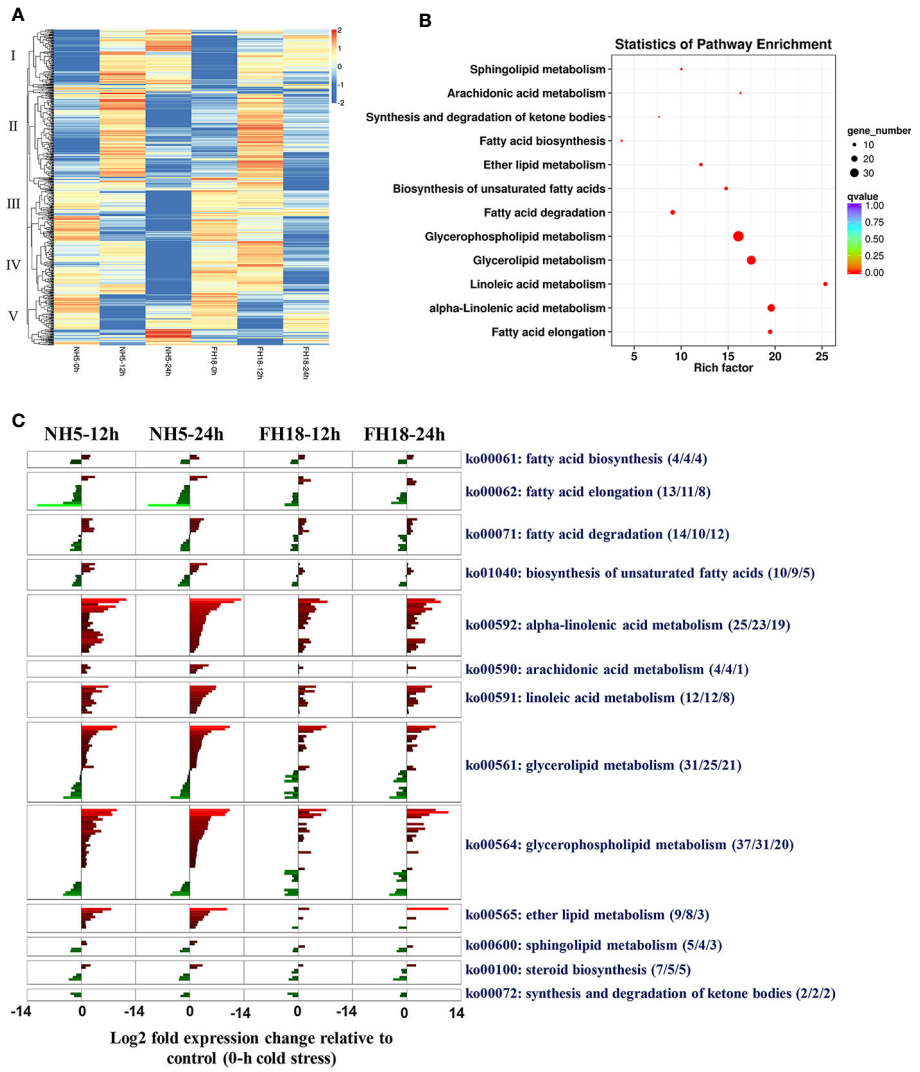


FIGURE 4 | Identification and analyses of CDEGs involved in lipid metabolic pathways during the early stage of cold stress in NH5 and FH18. **(A)** The heat map of expression profiles of 651 genes involved in lipid metabolic pathways under 0, 12, and 24 h cold stress based on the log2–median transformed FPKM averages of three independent biological replications, the expression pattern was categorized into five groups. Red indicates high expression, white indicates intermediate expression, and blue indicates low expression. **(B)** The statistics of KEGG pathway enrichment of 111 CDEGs related to lipid metabolism during the early stage of cold stress. **(C)** The transcriptional changes of 111 CDEGs involved in 13 lipid metabolic pathways during the early stage of cold stress in NH5 and FH18. Aside pathway IDs and descriptions are indicated under the format (X/Y/Z), X indicates the number of CDEGs in the KEGG pathway, Y indicates the number of CDEGs significantly differentially expressed only in NH5 and Z indicates the number of CDEGs differentially expressed only in FH18.

the lipidomes of NH5 and FH18 were compared quantitatively during the early stage of cold stress. Specifically, phospholipids, galactolipids, sphingolipids, diacylglycerols, and TAGs were targeted. In our study, a total of 20 headgroup classes of lipids and 168 molecular lipid species were detected (**Figures 6** and **7**; **Table S16**). The total lipid contents of NH5 and FH18 under control conditions were 219.27 and 237.16 nmol mg^{-1} DW but decreased by 7.32% and 22.14% after cold stress, respectively (**Figure 6A**).

Galactolipids, including MGDG, DGDG, and SQDG, are the main constituents of the chloroplast membranes and photosynthetic complexes, accounting for approximately 70% of the total lipids. The profiling of galactolipids provided consistent data with the transcriptomic analysis that indicated a decrease in the integrity of chloroplast membrane. Indeed, the MGDG contents of both cultivars were significantly decreased, which was mainly caused by the significant reduction in C34:6-(total number of acyl carbon atoms: number of double bounds) and C36:6-MGDG. However, in NH5, almost all molecular species of DGDG and SQDG were significantly increased, which significantly inhibited the reduction of chloroplast membrane lipid and maintained the integrity of the chloroplast membrane to a certain extent, thereby inhibiting the significant reduction in photosynthesis. Besides, the transfer of acyl chains

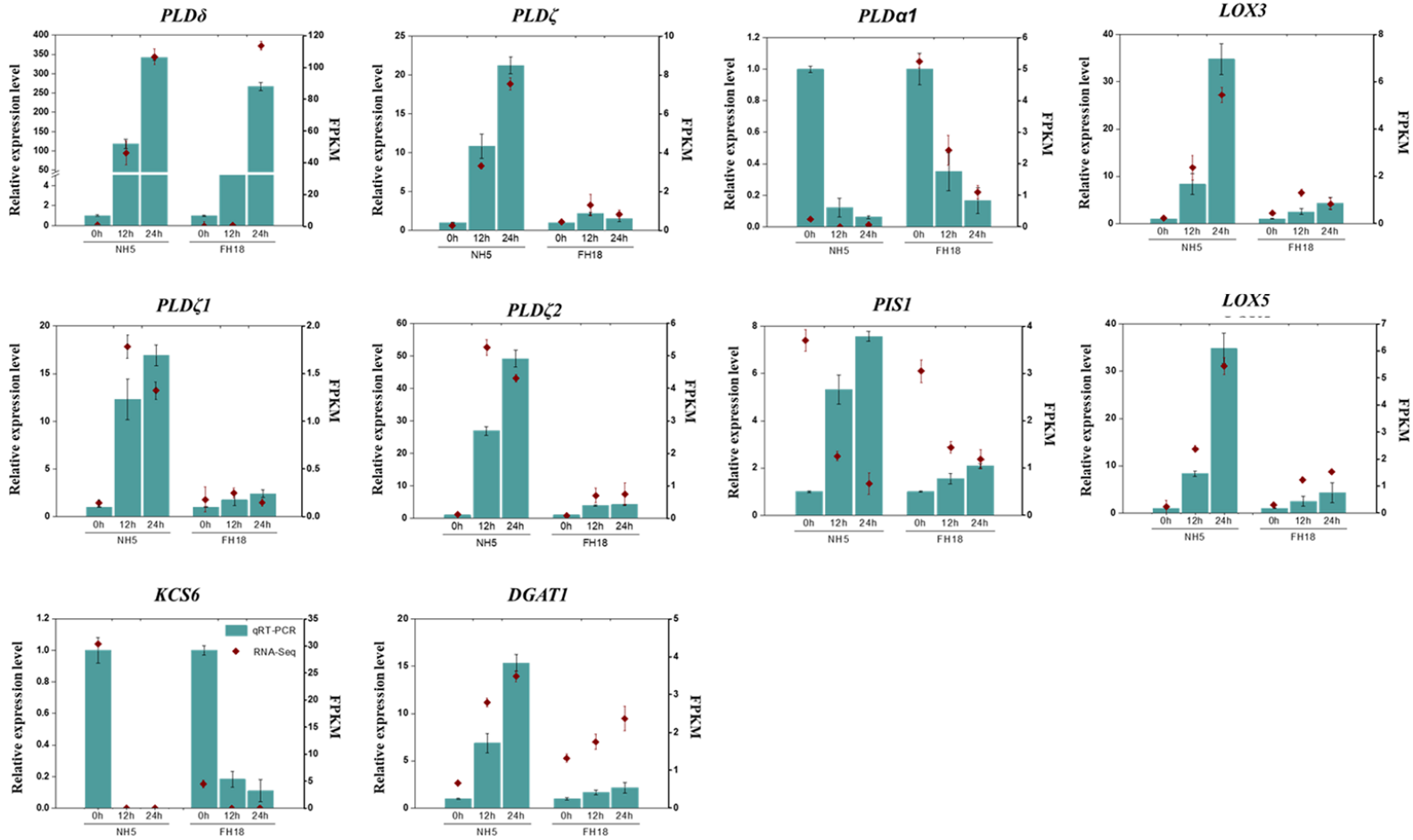


FIGURE 5 | Quantitative real-time PCR (qRT-PCR) validation and RNA-seq data of ten selected DEGs in NH5 and FH18.

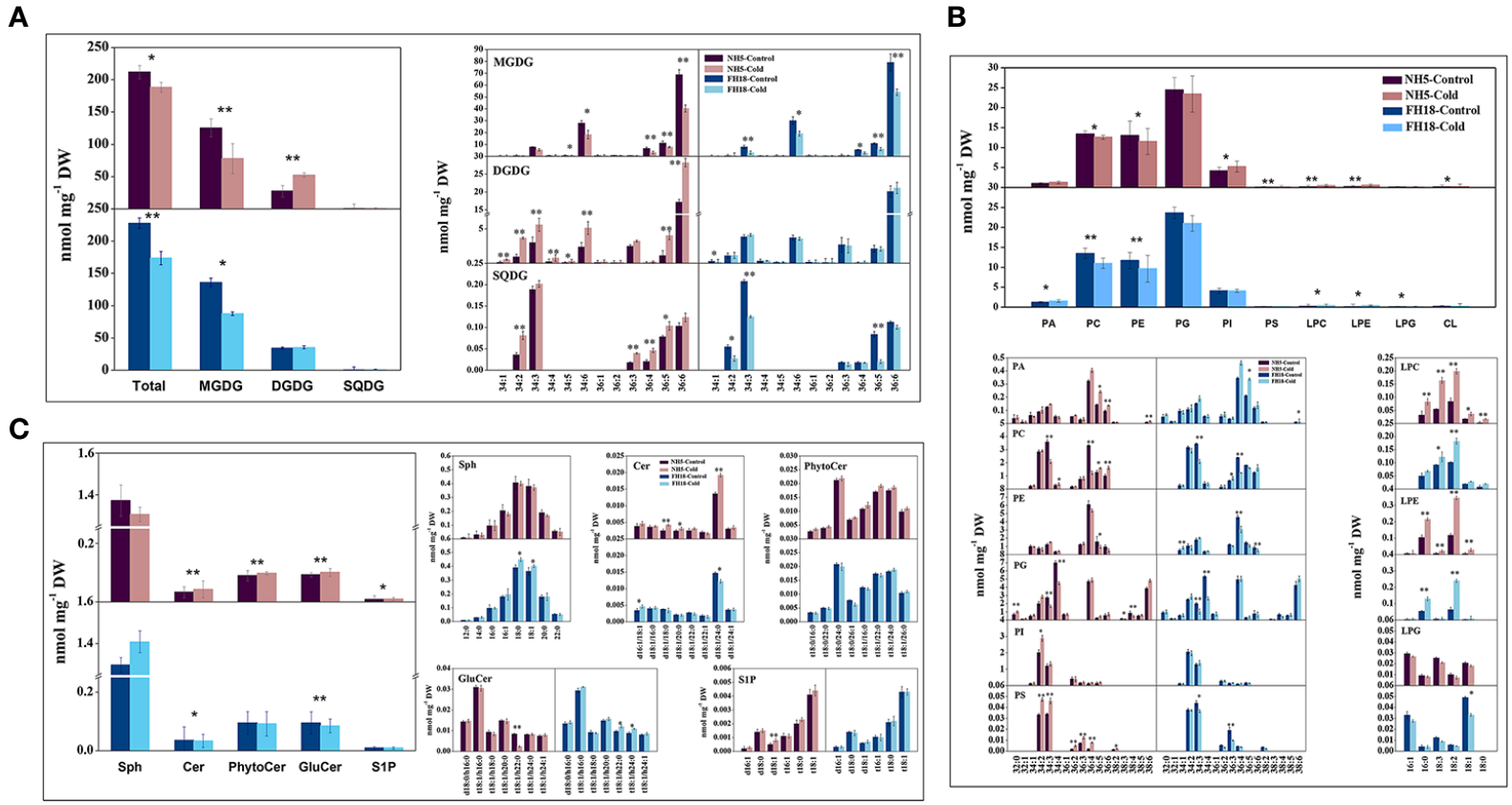


FIGURE 6 | The changes of galactolipid, phospholipid and sphingolipid composition after 0 and 24 h cold treatments in NH5 and FH18. **(A)** The changes of total lipid and galactolipid composition. **(B)** The changes of phospholipid composition. **(C)** The changes of sphingolipid composition. Values are the means ± SD of six independent biological samples. *Asterisk indicates significant difference as determined by the Student's t-test (*$P < 0.05$; **$P < 0.01$). Cer, ceramide; CL, cardiolipin; DGDG, digalactosyldiacylglycerol; GluCer, glucosylceramide; LPC, lyso-phosphatidylcholine; LPE, lyso-phosphatidylethanolamine; LPG, lyso-phosphatidylglycerol; MGDG, monogalactosyldiacylglycerol; PA, phosphatidic acid; PC, phosphatidylcholine; PE, phosphatidylethanolamine; PG, phosphatidylglycerol; PhytoCer, phytoceramide; PI, phosphatidylinositol; PS, phosphatidylserine; Sph, sphingasine; SQDG, sulfoquinovosyl diacylglycerol; S1P, sphingosine-1-phosphate.

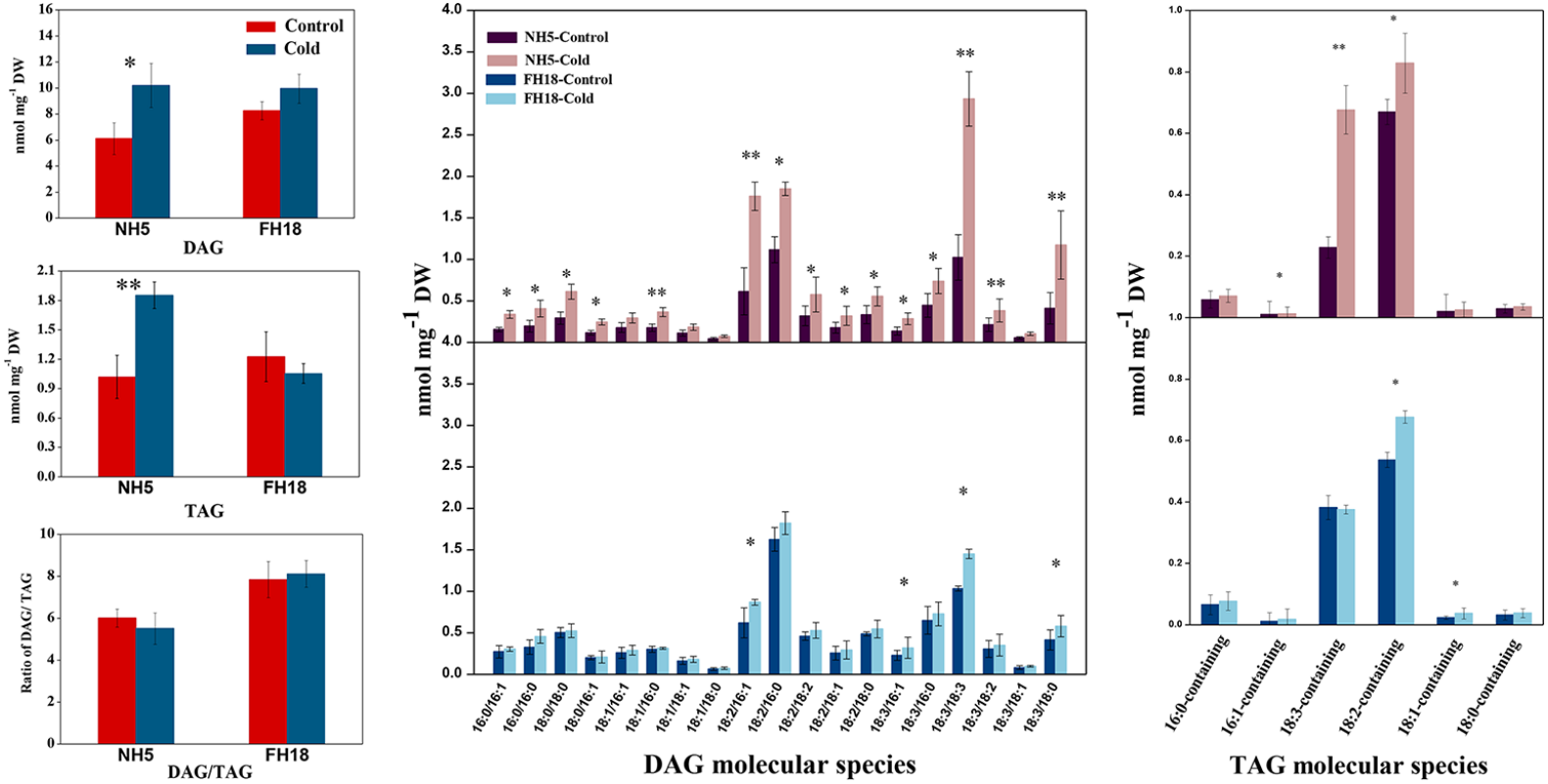


FIGURE 7 | The changes of lipid intermediate and storage lipid composition after 0 and 24 h cold treatments in NH5 and FH18. Values are the means ± SD of six independent biological samples. *Asterisk indicates significant difference as determined by the Student's t-test (*P < 0.05; **P < 0.01). DAG, diacylglycerol; TAG, triacylglycerol.

from C34:6-, C36:5-, and C36:6-MGDG to C34:6-, C36:5-, and C36:6-DGDG was the main reason for decreased MGDG but increased DGDG in NH5 (**Figure 6A**).

Phospholipids, a large family of glycerolipids, accounted for approximately 23–27% of the total lipids. Of which phosphatidyl glycerol (PG), PC, and PE were the most abundant, contributing to approximately 11%, 6%, and 5.5% of the overall lipidome, respectively, but their contents were all reduced, especially in FH18, with the C34:4 and C36:4 species contributing the most to the decline in PC and PE. Conversely, the levels of lyso-phospholipids including lyso-PC (LPC), lyso-phosphatidylethanolamine (LPE), and lyso-phosphatidylglycerol (LPG) significantly increased in both two varieties, suggesting that the increased activities of PLDs (**Figure 5**) promoted the lipid-hydrolytic pathway under cold stress. Other phospholipids, including PA, PI, phosphatidylserine (PS), and CL, were present in minor amounts ranging from 0.03 to 2.6% of the total lipids, and their contents were also increased in NH5. Notably, a significantly higher level of PA in FH18 was observed (**Figure 6B**). Compared with NH5, the PA content in FH18 increased by 1.21 times under cold stress. The major contributors to increased PA were C36:5 and C36:6 in NH5 but C36:4 and C36:5 in FH18.

Sphingolipids were also the main structural lipids, which were composed of five classes in peanut: sphingomyelin (Sph), ceramide (Cer), phytoceramide (PhytoCer), glucosylceramide (GluCer), and sphingosine-1-phosphate (S1P). In response to cold stress, Cer, PhytoCer, and GluCer increased, and Sph and S1P decreased in NH5, while the trends of these five SPL classes in FH18 completely contrasted with those in NH5 (**Figure 6C**). Only a few molecular species changed by cold stress in both two cultivars. d18:1/24:0-Cer was the major component that determined the increase or decrease of Cer. And t18:1/h22:0-GluCer was most affected by cold stress in GluCer in NH5.

In addition to membrane lipids, small amounts of the intermediate lipid DAG and the storage lipid TAG were also detected. There were 19 DAG molecular species in peanut leaves. The contents of DAGs with acyl chains of 18:2/16:1, 18:2/16:0, 18:3/18:3, and 18:3/18:0 were drastically higher in NH5, which were the major contributors to the increased DAG (**Figure 7**). TAG was composed of a few molecular species in peanut leaves, of which 18:2-containing and 18:3-containing TAGs were the main component. The TAG content was increased in NH5 but decreased in FH18, and a decreased DAG-TAG ratio was observed in the cold-tolerant cultivar NH5.

Changes in Membrane Lipid Unsaturation Induced by Cold Stress

The dramatic changes in lipid molecular species may influence the fatty acid classes connected to glycerin molecules, resulting in an alteration of membrane lipid unsaturation. As shown in **Table 1**, the unsaturated double bond index (DBI) of the total membrane lipids increased by 7.92% and decreased by 13.25% in NH5 and FH18, respectively, indicating that NH5 may adapt to cold stress by increasing the membrane lipid unsaturation level. The lower DBI of MGDG was the main reason for the decreased membrane lipid unsaturation. Among all membrane lipid classes, DGDG, PA, PS, SQDG, and PI showed larger relative changes (RC) in DBI ranging from 109.41% to 42.03% and were the major contributors to the increase in total membrane lipid unsaturation, The DBI of sphingolipid classes Sph and GluCer also increased, while sphingolipid was only a minor constituent and contributed little to the DBI of the total membrane lipids.

Changes in Free Fatty Acid Components Induced by Cold Stress

A total of 22 FFA components were detected in peanut leaves (**Table 2**). Although the main FFA classes were similar, there was great diversity in their contents between the two cultivars under cold stress. The total fatty acid (TFA) contents in NH5 and FH18 were increased by 4% and 0.7%, respectively. At the same time,

TABLE 1 | Double-bond index (DBI) of membrane lipids after 0 and 24 h cold treatments in NH5 and FH18.

Lipid class	Double bond index (DBI)				Relative change (RC)	
	NH5-Control	NH5-Cold	FH18-Control	FH18-Cold	NH5	FH18
MGDG	3.3534 ± 0.07^{a}	2.8792 ± 0.13^{a}	3.2965 ± 0.42^{a}	2.2921 ± 0.64^{a}	–0.1414	–0.3047
DGDG	0.6750 ± 0.04^{b}	1.4135 ± 0.09^{a}	0.7822 ± 0.08^{a}	1.0660 ± 1.03^{a}	1.0941	0.3628
SQDG	0.0084 ± 0.00^{b}	0.0125 ± 0.02^{a}	0.0086 ± 0.04^{a}	0.0072 ± 0.01^{a}	0.4881	–0.1628
PA	0.0195 ± 0.01^{b}	0.0339 ± 0.03^{a}	0.0174 ± 0.07^{b}	0.0262 ± 0.02^{a}	0.7385	0.5057
PC	0.2061 ± 0.04^{a}	0.2271 ± 0.05^{a}	0.2183 ± 0.04^{a}	0.2349 ± 0.07^{a}	0.1019	0.0760
PE	0.1911 ± 0.05^{a}	0.1921 ± 0.01^{a}	0.2279 ± 0.02^{a}	0.2179 ± 0.05^{a}	0.0052	–0.0439
PG	0.3981 ± 0.03^{a}	0.4720 ± 0.02^{a}	0.4464 ± 0.03^{a}	0.4824 ± 0.06^{a}	0.1856	0.0806
PI	0.0069 ± 0.01^{b}	0.0098 ± 0.04^{a}	0.0064 ± 0.02^{a}	0.0086 ± 0.02^{a}	0.4203	0.3438
PS	0.0010 ± 0.00^{b}	0.0017 ± 0.00^{a}	0.0013 ± 0.01^{a}	0.0014 ± 0.01^{a}	0.7000	0.0769
CL	0.0109 ± 0.00^{a}	0.0130 ± 0.02^{a}	0.0083 ± 0.03^{a}	0.0117 ± 0.03^{a}	0.1927	0.4096
Sph	0.0024 ± 0.00^{a}	0.0035 ± 0.01^{a}	0.0028 ± 0.01^{a}	0.0030 ± 0.01^{a}	0.4583	0.0714
Cer	0.0002 ± 0.00^{a}	0.0003 ± 0.00^{a}	0.0002 ± 0.00^{a}	0.0003 ± 0.00^{a}	0.2827	0.3074
PhytoCer	0.0003 ± 0.00^{a}	0.0004 ± 0.00^{a}	0.0003 ± 0.00^{a}	0.0004 ± 0.01^{a}	0.3333	0.3333
GluCer	0.0004 ± 0.00^{a}	0.0006 ± 0.00^{a}	0.0004 ± 0.00^{a}	0.0004 ± 0.00^{a}	0.5000	0.0000
S1P	0.0000 ± 0.00^{a}	0.0000 ± 0.00^{a}	0.0000 ± 0.00^{a}	0.0000 ± 0.00^{a}	0.0000	0.0000
Total lipids	4.8736 ± 0.10^{a}	5.2594 ± 0.54^{a}	5.0170 ± 0.31^{a}	4.3524 ± 0.18^{a}	0.0792	–0.1325

DBI = (Σ [N × mol % lipid])/100, N is the total number of double bonds in the two fatty acid chains of each membrane lipid molecule. The DBI is the average number of double bonds in the fatty acid chains of lipid molecular species, a high DBI indicates the presence of more highly unsaturated membrane lipids, and vice versa. Data are the means ± SD of six independent biological samples. Means denoted by the same letter do not differ significantly according to Tukey's test ($p < 0.05$).

TABLE 2 | The changes of fatty acid components after 0 and 24 h cold treatments in NH5 and FH18.

Fatty acid (ng mg $^{-1}$)	NH5		FH18		Relative change	
	Control	Cold	Control	Cold	NH5	FH18
C14:0	0.39 ± 0.01^{a}	0.37 ± 0.05^{a}	0.20 ± 0.01^{b}	0.37 ± 0.06^{a}	–0.10	0.87
C14:1	0.95 ± 0.06^{a}	0.91 ± 0.10^{a}	0.37 ± 0.04^{a}	0.34 ± 0.04^{a}	–0.08	–0.08
C16:0	151.87 ± 9.69^{a}	131.96 ± 11.21^{b}	149.52 ± 10.68^{a}	144.61 ± 12.59^{a}	–0.17	–0.04
C16:1	51.29 ± 3.21^{a}	41.41 ± 5.12^{b}	51.14 ± 2.97^{a}	53.16 ± 6.71^{a}	–0.22	0.03
C18:0	213.37 ± 7.54^{a}	195.57 ± 15.25^{a}	194.53 ± 9.23^{a}	195.45 ± 10.04^{a}	–0.12	0.00
C18:1	59.60 ± 2.48^{a}	51.95 ± 4.63^{b}	58.82 ± 5.59^{a}	58.31 ± 4.97^{a}	–0.16	–0.02
C18:2	83.50 ± 4.44^{b}	117.37 ± 9.13^{a}	79.13 ± 4.67^{b}	99.19 ± 6.42^{a}	0.35	0.24
C18:3	164.18 ± 5.86^{b}	211.32 ± 7.99^{a}	166.05 ± 11.35^{a}	186.73 ± 9.68^{a}	0.24	0.12
C20:0	2.73 ± 0.54^{a}	1.89 ± 0.22^{b}	2.07 ± 0.12^{a}	1.39 ± 0.20^{b}	–0.34	–0.33
C20:1	0.53 ± 0.09^{b}	1.14 ± 0.13^{a}	0.67 ± 0.06^{a}	0.55 ± 0.06^{ab}	1.05	–0.18
C20:2	0.15 ± 0.03^{b}	0.27 ± 0.08^{a}	0.22 ± 0.03^{a}	0.20 ± 0.01^{a}	0.75	–0.09
C20:3	56.72 ± 2.96^{a}	62.60 ± 5.54^{a}	1.08 ± 0.14^{a}	0.80 ± 0.02^{b}	0.06	–0.27
C20:4	81.03 ± 4.17^{a}	84.53 ± 3.69^{a}	65.95 ± 7.26^{a}	33.33 ± 3.68^{b}	0.00	–0.50
C20:5	0.31 ± 0.11^{b}	0.38 ± 0.02^{a}	0.41 ± 0.03^{a}	0.35 ± 0.03^{ab}	0.21	–0.17
C22:0	1.78 ± 0.25^{a}	2.11 ± 0.17^{a}	0.21 ± 0.01^{a}	0.20 ± 0.01^{a}	0.14	–0.05
C22:1	0.34 ± 0.04^{b}	0.55 ± 0.10^{a}	0.43 ± 0.11^{a}	0.42 ± 0.04^{a}	0.55	–0.03
C22:2	0.41 ± 0.06^{a}	0.48 ± 0.06^{a}	0.49 ± 0.06^{a}	0.43 ± 0.10^{a}	0.10	–0.13
C22:4	1.17 ± 0.10^{a}	1.34 ± 0.21^{a}	1.36 ± 0.27^{a}	1.21 ± 0.31^{a}	0.10	–0.12
C22:5	2.53 ± 0.15^{b}	3.04 ± 0.26^{a}	2.97 ± 0.33^{a}	2.64 ± 0.19^{a}	0.15	–0.12
C22:6	2.55 ± 0.08^{a}	2.89 ± 0.14^{a}	2.99 ± 0.16^{a}	2.63 ± 0.12^{a}	0.09	–0.13
C24:0	1.89 ± 0.24^{a}	1.46 ± 0.33^{b}	1.47 ± 0.08^{b}	3.48 ± 0.20^{a}	–0.26	1.35
C24:1	0.63 ± 0.04^{a}	0.72 ± 0.10^{a}	0.67 ± 0.05^{a}	0.60 ± 0.05^{a}	0.10	–0.12
Total	877.90 ± 13.69^{a}	914.26 ± 15.25^{a}	780.77 ± 12.53^{a}	786.40 ± 14.45^{a}	0.04	0.007
PUFA	392.55 ± 13.17^{b}	484.22 ± 6.74^{a}	320.65 ± 11.33^{a}	327.51 ± 7.42^{a}	0.23	0.02
SFA	372.02 ± 10.12^{a}	333.35 ± 3.97^{a}	348.00 ± 9.71^{a}	345.51 ± 4.95^{a}	–0.10	–0.01
PUFA/SFA	1.06 ± 0.12^{b}	1.45 ± 0.14^{a}	0.92 ± 0.06^{a}	0.95 ± 0.05^{a}	0.36	0.03

The 2nd leaf from each peanut seedling after 0 and 24 h cold treatments was harvested for the determination of fatty acid content (ng mg^{-1}). Data are the means ± SD of six independent biological samples. Means denoted by the same letter do not differ significantly according to Tukey's test ($p < 0.05$). PUFA, polyunsaturated fatty acid; SFA, saturated fatty acid.

the content of saturated (SFAs) and monounsaturated fatty acids (MUFAs), including C16:0, C16:1, C18:0, and C18:1, obviously decreased in NH5 but were almost unchanged in FH18. The polyunsaturated fatty acids (PUFAs) C18:2 and C18:3 markedly increased in NH5 but increased more slowly in FH18. In general, NH5 accumulated more PUFAs (increased by 23%) than FH18 (increased by 2%) and exhibited the genetic characteristic of having more PUFAs during the long-term adaptation to low temperature. The main reason for this finding may be that NH5 can increase the ratio of PUFAs to SFAs (increased by 36%) by the rapid synthesis of PUFAs (C18:2 and C18:3).

The Gene-Metabolite Network Revealed the Molecular Regulation Mechanism of Lipids Metabolism in Peanut Cold Tolerance

Based on the results of the transcriptomic and lipidomic analyses, a schematic diagram was proposed to illustrate the gene-metabolite network of lipids in peanut during adapting to cold stress, which clearly demonstrated the molecular regulation mechanism of membrane lipid metabolism in peanut cold tolerance. As illustrated in **Figure 8**, in membrane lipid metabolism, the increased PA induced by cold signal was immediately catalyzed by CDS1/2 and PAP1 to generate the lipid intermediates DAG and CDP-DAG, which inhibited the excessively accumulation of PA. Subsequently, the upregulation of CRLS and PIS1 accelerated the biosynthesis of CL and PI from CDP-DAG. The increased PI can not only increase the DAG level but also activated Ca^{2+} signal transduction pathway through "double messenger system". Moreover, transcriptomic analysis showed the upregulation of SQD2, MGD, and DGD1 that can contribute to the formation of SQDG and DGDG from DAG and CDP-DAG, compensated for the decreased lipid unsaturation caused by the reduced level of MGDG. In fatty acid metabolism, the genes involved in fatty acid elongation all significantly down-regulated and the genes involved in fatty acid β-oxidation all significantly up-regulated, which prevented the formation of very long chain fatty acids (VLCFA) (i.e. fatty acids having at least 20 carbon atoms), and promoted the generation of C16 and C18 fatty acids. The increased level of C18:3 and the significant upregulation of LOX3, AOS1/3, and AOC activated the α-linolenic acid metabolism pathway, which may cause an increase in JA and activate the JA signal transduction pathway. Overall, transcriptional responses of peanut to cold stress were consistent with lipidomic changes, thus indicating the main regulations occurring at the transcriptional level.

DISCUSSION

Cold stress seriously affects the growth, development, yield, and quality of crops, and is a key limiting factor for peanut production at higher altitudes and colder agricultural regions (Zhang H. et al., 2019). It is well known that photosynthesis is very sensitive to cold stress (Peng et al., 2015). In this study, the similar phenomenon had been found that cold-sensitive peanut

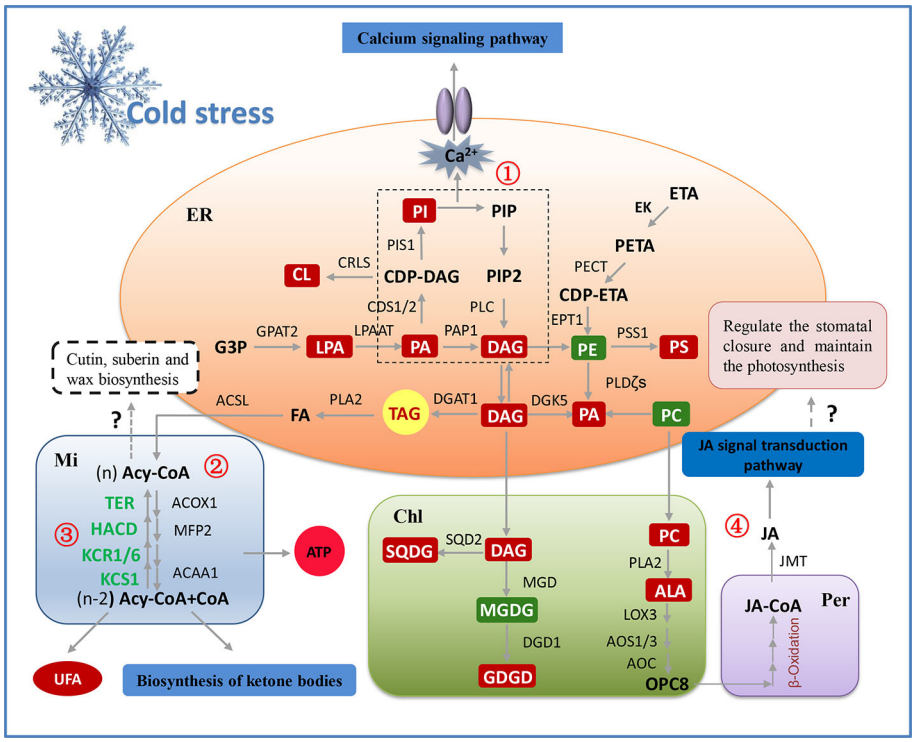


FIGURE 8 | The model illustrating potential regulation mechanism of membrane lipid metabolism in peanut cold tolerance. The glycerolipid, glycerophospholipid and fatty acid metabolic pathways were the significant pathways altering in response to peanut cold tolerance, which were depicted as fully as possible based on the integration of lipidomic and transcriptomic responses. The red boxes represent the increased metabolites and the green boxes represent the decreased metabolites. Except the genes (green words) involved in fatty acid elongation (③), all the genes in this figure were up-regulated. Besides to alter membrane lipid composition and membrane lipid remodeling, lipid classes can also adapt to cold stress through other metabolic processes. For example, accumulated PI can activate the phosphatidylinositol signaling pathway, further increased the concentration of Ca^{2+} and activated the Ca^{2+} channel to regulate the expression of downstream cold-tolerant genes (①). The storage lipid TAG can be hydrolyzed by PLA_2 to produce the FFA and leading to the activation of fatty acid degradation and fatty acid elongation pathways. The fatty acid degradation may provide enough energy for peanut to adapt to cold stress, as well as produce more polyunsaturated short-chain fatty acids to maintain the membrane fluidity (②). The fatty acid elongation may be related to the biosynthesis of plant wax, while the explicit mechanism needs to be further studied (③). Also, the structural lipids may be degraded under cold stress and synthesize the JA through α-linolenic acid metabolism and β-oxidation of fatty acid, then to activate the JA signal transduction that may regulate the stomatal closure and maintain the photosynthesis, but this hypothesis needs to be further validated in peanut (④). ACAA1, acetyl-CoA acyltransferase; ACOX1, acyl-CoA oxidase; ACSL, long-chain acyl-CoA synthetase; Acy-CoA, acyl-coenzyme A; ALA, α-linolenic acid; AOC, allene oxide cyclase; AOS, allene oxide synthase; CDS1/2, phosphatidate cytidylyltransferase; Chl, chloroplast; CL, cardiolipin; CRLS, cardiolipin synthase; DAG, diacylglycerol; DGAT1, diacylglycerol acyltransferase; DGD1, digalactosyl diacylglycerol synthase; DGDG, digalactosyldiacylglycerol; DGK5, diacylglycerol kinase; EK, ethanolamine kinase; EPT1, ethanolamine phosphotransferase; ER, endoplasmic reticulum; ETA, ethanolamine; FA, fatty acid; G3P, glycerol-3-phosphate; GPAT2, glycerol-3-phosphate acyltransferase; HACD, very-long-chain (3R)-3-hydroxyacyl-CoA dehydratase; JA, jasmonic acid; JMT, jasmonate O-methyltransferase; KCR1/6, very-long-chain 3-oxoacyl-CoA reductase; KCS1, 3-ketoacyl-CoA synthase; LOX3, lipoxygenase; LPA, phospholipase A; LPAAT, LPA acyltransferase; MFP2, multifunctional protein; MGD, monogalactosyl diacylglycerol synthase; MGDG, monogalactosyldiacylglycerol; Mi, mitochondria; PA, phosphatidic acid; PAP1, phosphatidate phosphatase; PC, phosphatidylcholine; PE, phosphatidyl ethanolamine; PECT, ethanolamine-phosphate cytidylyltransferase; Per, peroxisome; PETA, phosphoethanolamine; PI, phosphatidylinositol; PIP, polyphosphoinositide; PIP2, phosphatidylinositol 4,5-bisphosphate; PIS1, CDP-diacylglycerol–inositol 3-phosphatidyltransferase; PLC, phospholipase C; PLDζ, phospholipase D; PS, phosphatidylserine; PSS1, CDP-diacylglycerol–serine O-phosphatidyltransferase; SQD2, sulfoquinovosyl diacylglycerol synthase; SQDG, sulfoquinovosyl diacylglycerol; TAG, triacylglycerols; TER, very-long-chain enoyl-CoA reductase; UFA, unsaturated fatty acid.

cultivars experienced pronounced decline in Pn, Fv/Fm, and Chls contents presumably caused by the damaged photosynthetic membrane. This may reduce assimilation products and cause an inhibited growth and a lower yield (Weiszmann et al., 2018). Therefore, it is considered as of the critical importance to elucidate the specific mechanism and promote the genetic improvement of cold tolerance in peanut cultivars. We studied the early changes occurring upon cold stress in the transcriptome and lipidome of peanut, which is so far the best developed gene-metabolite network for peanut adaptation to cold stress.

Comparative Transcriptomic Analysis Revealed Lipid Metabolism May Play a Central Role in Peanut Cold Tolerance

Nowadays, thousands of genes and many signaling pathways have been identified in numerous plants during cold stress (Winfield et al., 2010), however, a clear and comprehensive

relationship between lipid metabolism and cold tolerance has not been established, especially in peanuts. Recent studies suggest that plant hormone signal transduction, photosynthesis, plant-pathogen interaction, and circadian rhythms pathways were essential all play a role in response to cold stress (Li et al., 2019; Ma et al., 2019; Xin et al., 2019). In this study, these responses also were significantly enriched in two peanut cultivars under cold stress. However, lipid metabolism including fatty acid and membrane lipid metabolism pathway was the most significantly enriched in NH5 compared with FH18. It is likely that most of the cold-stress responsive genes have the similar expression patterns in both cold-tolerant and cold-sensitive varieties to cope with the cold stress. However, it is possible that all cold-responsible genes may not contribute to plant cold-tolerance. In fact, several studies have recently shown that membrane lipid remodeling can modulate the lipid composition, fatty acyl group unsaturation, and membrane fluidity, which have been developed as a key strategy for plant to cope with cold stress (Gu et al., 2017; Zuther et al., 2019).

Upregulated Expression of *PAP1* and *CDS1* May Be Important to Prevent the Membrane Peroxidation Caused by Excessive PA Accumulation

In our study, besides the phosphorylation of DAG by DGK5 induced by the upregulated PI and PS, similar to that observed in *A. thaliana* (Hou et al., 2016), PA also largely accumulates through the *de novo* synthesis initiated by two acylations of G3P by GPAT2 and LPAAT, as well as the hydrolysis of PC and PE by PLDζs and PLDδ (**Figure 5**). However, increasing evidence suggests that the excessive PA could generate hydroperoxides and free radicals with a series of enzymes and finally lead to membrane lipid peroxidation (Li et al., 2009), which is consistent with the significantly increased EL and MDA in FH18. In the cold-tolerant cultivar NH5, two *PAP1* and one *CDS1* gene were significantly upregulated, encoding the key enzymes in the PA-DAG and PA-(CDP-DAG) pathways, respectively. The increases in DAG and CDP-DAG may activate a few key genes (*PIS1*, *CRLS*, *EPT1*, *PSS1*, *DGAT1*, *SQD2*, *MGD*, and *DGD1*) encoding lipid synthases to generate complex lipids and inhibit excessive PA accumulation, which may reduce membrane damage to a certain extent and is consistent with the stable EL and MDA content in NH5 during the early stage of cold stress.

Elevated Levels of DGDG and SQDG Ameliorate the Photosynthetic Disorder Induced by Decreased MGDG in Peanut Under Cold Stress

The reduction in MGDG is a common plant response to osmotic stress caused by freezing, drought, or salinity (Gigon et al., 2004; Chen and Thelen, 2013; Omoto et al., 2016), which could result in serious disorder and dysfunction of photosynthetic membranes (Garab et al., 2016). While the decreased MGDG was accompanied by the increased DGDG and SQDG in NH5 because of the upregulated expression of *DGD1* and *SQD2*. In *A. thaliana*, the *dgd1* mutant hindered membrane light-harvesting complex II (LHCII)-macrodomain formation, reduced the stability of PSI, and shortened the lifetime of Chl fluorescence (Klaus et al., 2002). Therefore, the cold-induced upregulation of *DGD1* and increase in DGDG levels are important for maintaining the PSI function by protecting and stabilizing the photosynthetic apparatus in peanut. Furthermore, the increased SQDG is also required for peanut cold tolerance not only because SQDG is closely associated with the photosynthetic apparatus but also because it may play a role in signaling processes in plants. Seigneurin-Berny et al. (2000) showed that SQDG may bind annexin (cellular proteins) in a Ca^{2+}-dependent manner. The family of annexins is considered to play a role in the regulation of membrane organization, membrane fusion, and ion transport across membranes.

Moreover, galactolipids are rich in unsaturated fatty acids. The extremely significant increase of C34:6-, C36:5-, and C36:6-DGDG greatly improved the lipid unsaturation in NH5 (**Figure 6A**; **Table 1**). In addition to being converted to DGDG, the rest of C36:5- and C36:6-MGDG can be also directly hydrolyzed, releasing large amounts of C18:3. The maintenance of polyunsaturated fatty acid levels in chloroplast lipids has been shown to contribute to low temperature survival and the normal formation of chloroplast membranes under cold stress (Li et al., 2015), which might also be responsible for maintaining photosynthesis.

The Essential Role of Fatty Acid Metabolism in Peanut Cold Tolerance

Under cold stress, complex lipids can be further hydrolyzed into FFAs by PLA2 and activate fatty acid metabolic pathways such as fatty acid biosynthesis and degradation. The fatty acid elongation pathway is the key step in fatty acid biosynthesis and is mainly catalyzed by fatty acid elongase complexes (FAEs), including KCS, KCR, HACD, and TER (Haslam and Kunst, 2013). It is noteworthy that all the genes in FAE were significantly downregulated in NH5 and inhibited the elongation of fatty acids. A previous study has shown that changes in the ratio of very long chain (VLCFAs) to short chain fatty acids (SCFAs) can lead to an alteration in membrane fluidity in plants and thus the adaptation to environmental stresses (Rawsthorne, 2002). Under cold stress, the contents of UFAs and C16 and C18 fatty acids were higher, which is because C16 and C18 fatty acids have a lower melting point than C24 fatty acids, allowing membrane lipids to maintain fluidity under cold stress (Upchurch, 2008). Interestingly, KCS1 and KCS6, which are mainly responsible for the synthesis of fatty acids above 24 carbon chain length and involved in cutin, suberine, and wax biosynthesis, catalyze the first step of fatty acid elongation, and were extremely significantly downregulated in NH5 (Hooker et al., 2002). Wax is the first barrier to plant contact with the external environment and plays an important role in adaptation to sudden variations in environmental conditions (Xue et al., 2017; He et al., 2019). The relationship between wax secretion and peanut cold tolerance deserves further study.

Fatty acid β-oxidation is the main form of fatty acid degradation in plants and is catalyzed by a multienzyme complex including ACOX, multifunctional protein (MFP), and ACAA to decrease the carbon chain length of fatty acids

(Yusupov et al., 2010). In the present study, *ACOX1* and *ACAA1* were significantly upregulated in NH5 and activated the β-oxidation pathway of fatty acids under cold stress. Fatty acid β-oxidation is the sole pathway for metabolic breakdown of fatty acids to generate energy and carbon skeletons in plants and plays an important role in plant growth, development and cellular homeostasis (Arent et al., 2010; Jiang et al., 2011). Moreover, fatty acid β-oxidation is also the central part of α-linolenic acid (C18:3) metabolism. Under cold stress, the large amount of accumulated C18:3 caused by the hydrolyzation of C36:5- and C36:6-MGDG in NH5 was sequentially metabolized by LOX, AOS, and AOC into 12-oxo-phytodienoic acid (OPDA) or dinor-OPDA (dnOPDA) and finally underwent three cycles of β-oxidation to yield JA. In *A. thaliana*, JA positively modulates the CBF pathway, leading to the accumulation of cryoprotective compounds and interacting with plant phytohormones to regulate stomatal closure and maintain photosynthesis under cold stress (Verma et al., 2016; Hu et al., 2017). Therefore, we conclude that fatty acid β-oxidation and JA biosynthesis may directly improve peanut cold tolerance through CBF-dependent signaling and plant hormone signal transduction pathways.

In conclusion, the present results revealed that, under cold stress, the cytoplasmic membrane and organellar membrane of peanut plants were severely damaged, the photosynthetic capacity decreased significantly, and the plant growth was inhibited. During the adaptation of peanut plants to cold stress, lipid metabolism including membrane lipid and fatty acid metabolism was the significant contributor. The phospholipid synthesis pathway in ER, and the galactolipid synthesis pathway and the α-linolenic acid metabolism pathway in chloroplast were activated, besides, most of the genes that catalyze these reactions were up-regulated. The upregulation of *PAP1* and *CDS1/2* under cold stress can inhibit the damage of membrane lipid peroxidation caused by excessive accumulation of PA. The upregulation of *MGD*, *DGD1,* and *SQD2* caused the increase of DGDG and SQDG content, which was crucial to the maintenance of chloroplast structural integrity and normal photosynthesis. α-Linolenic acid metabolism and fatty acid β-oxidation may improve peanut cold tolerance by partially modulating the JA signal transduction pathway. This study lays the foundation for deeply analyzing the molecular mechanism and realizing the genetic improvement of peanut cold tolerance.

DATA AVAILABILITY STATEMENT

The datasets generated for this study can be found in the SRA accession number: PRJNA602777.

AUTHOR CONTRIBUTIONS

HZ designed and performed the whole experiment. CJ, JR, and JD identified the cold-tolerant and cold-sensitive peanut varieties and measured the morphological indexes. XS and XZ helped to measure physiological indicators. XW, JW, and CZ helped to conduct the qRT-PCR test. SZ, XL, and SG assisted in data analysis. HY revised the manuscript.

ACKNOWLEDGMENTS

JS kindly revised this manuscript. This study was supported by the China Agricultural Research System (CARS-13) and LiaoNing Revitalization Talents Program (XLYC1902002).

SUPPLEMENTARY MATERIAL

The Supplementary Material for this article can be found online at: https://www.frontiersin.org/articles/10.3389/fpls.2020.01110/full#supplementary-material

REFERENCES

Almadanim, M. C., Alexandre, B. M., Rosa, M. T. G., Sapeta, H., Leitao, A. E., Ramalho, J. C., et al. (2017). Rice calcium-dependent protein kinase OsCPK17 targets plasma membrane intrinsic protein and sucrose-phosphate synthase and is required for a proper cold stress response. *Plant Cell Environ.* 40, 1197–1213. doi: 10.1111/pce.12916

Arent, S., Christensen, C. E., Pye, V. E., Norgaard, A., and Henriksen, A. (2010). The multifunctional protein in peroxisomal beta-oxidation: structure and substrate specificity of the *Arabidopsis thaliana* protein MFP2. *J. Biol. Chem.* 285, 24066–24077. doi: 10.1074/jbc.M110.106005

Arisz, S. A., Wijk, R. V., Roels, W., Zhu, J. K., Haring, M. A., and Munnik, T. (2013). Rapid phosphatidic acid accumulation in response to low temperature stress in Arabidopsis is generated through diacylglycerol kinase. *Front. Plant Sci.* 4, 1. doi: 10.3389/fpls.2013.00001

Bai, H., Zhang, Y., Yu, H., Irfan, M., Huang, Y., Han, M., et al. (2019). Phylogenetic diversity and cross-inoculation of indigenous isolated Bradyrhizobium from nodules of peanut in Liaoning province of China. *Mol. Biol. Res. Commun.* 8, 59–68. doi: 10.22099/mbrc.2019.32983.1392

Barrero-Sicilia, C., Silvestre, S., Haslam, R. P., and Michaelson, L. V. (2017). Lipid remodelling: Unravelling the response to cold stress in Arabidopsis and its extremophile relative Eutrema salsugineum. *Plant Sci.* 263, 194–200. doi: 10.1016/j.plantsci.2017.07.017

Cantrel, C., Vazquez, T., Puyaubert, J., Reze, N., Lesch, M., Kaiser, W. M., et al. (2011). Nitric oxide participates in cold-responsive phosphosphingolipid formation and gene expression in Arabidopsis thaliana. *New Phytol.* 189, 415–427. doi: 10.1111/j.1469-8137.2010.03500.x

Chang, B. W., Zhong, P., Liu, J., Tang, Z. H., Gao, Y. B., Yu, H. J., et al. (2019). Effect of low-temperature stress and gibberellin on seed germination and seedling physiological responses in peanut. *Acta Agronomica Sin.* 45, 118–130. doi: 10.3724/SP.J.1006.2019.84043

Chen, M., and Thelen, J. J. (2013). ACYL-LIPID DESATURASE2 is required for chilling and freezing tolerance in Arabidopsis. *Plant Cell* 25, 1430–1444. doi: 10.1105/tpc.113.111179

Chen, N., Yang, Q. L., Hu, D. Q., Pan, L. J., Chi, X. Y., Chen, M. N., et al. (2014). Gene expression profiling and identification of resistance genes to low temperature in leaves of peanut (Arachis hypogaea L.). *Sci. Hortic.* 169, 214–225. doi: 10.1016/j.scienta.2014.01.043

Chen, X., Song, F., Liu, F., Tian, X., Liu, S., Xu, H., et al. (2014). Effect of different arbuscular mycorrhizal fungi on growth and physiology of maize at ambient and low temperature regimes. *Sci. World J.* 2014, 956141. doi: 10.1155/2014/956141

Ding, Y., Li, H., Zhang, X., Xie, Q., Gong, Z., and Yang, S. (2015). OST1 kinase modulates freezing tolerance by enhancing ICE1 stability in Arabidopsis. *Dev. Cell* 32, 278–289. doi: 10.1016/j.devcel.2014.12.023

Dubots, E., Botte, C., Boudiere, L., Yamaryo, B. Y., Jouhet, J., Marechal, E., et al. (2012). Role of phosphatidic acid in plant galactolipid synthesis. *Biochimie* 94, 86–93. doi: 10.1016/j.biochi.2011.03.012

Fan, J., Yu, L., and Xu, C. (2017). A central role for triacylglycerol in membrane lipid breakdown, fatty acid beta-oxidation, and plant survival under extended darkness. *Plant Physiol.* 174, 1517–1530. doi: 10.1104/pp.17.00653

Garab, G., Ughy, B., and Goss, R. (2016). Role of MGDG and non-bilayer lipid phases in the structure and dynamics of chloroplast thylakoid membranes. *Subcell. Biochem.* 86, 127–157. doi: 10.1007/978-3-319-25979-6_6

Gigon, A., Matos, A. R., Laffray, D., Zuily-Fodil, Y., and Pham-Thi, A. T. (2004). Effect of drought stress on lipid metabolism in the leaves of *Arabidopsis thaliana* (ecotype Columbia). *Ann. Bot.* 94, 345–351. doi: 10.1093/aob/mch150

Gu, Y., He, L., Zhao, C., Wang, F., Yan, B., Gao, Y., et al. (2017). Biochemical and transcriptional regulation of membrane lipid metabolism in maize leaves under low temperature. *Front. Plant Sci.* 8, 2053. doi: 10.3389/fpls.2017.02053

Gwak, Y., Hwang, Y. S., Wang, B., Kim, M., Jeong, J., Lee, C. G., et al. (2014). Comparative analyses of lipidomes and transcriptomes reveal a concerted action of multiple defensive systems against photooxidative stress in Haematococcus pluvialis. *J. Exp. Bot.* 65, 4317–4334. doi: 10.1093/jxb/eru206

Han, Q. H., Huang, B., Ding, C. B., Zhang, Z. W., Chen, Y. E., Hu, C., et al. (2017). Effects of melatonin on anti-oxidative systems and photosystem II in cold-stressed rice seedlings. *Front. Plant Sci.* 8, 785. doi: 10.3389/fpls.2017.00785

Hantzis, L. J., Kroh, G. E., Jahn, C. E., Cantrell, M., Peers, G., Pilon, M., et al. (2018). A program for iron economy during deficiency targets specific Fe proteins. *Plant Physiol.* 176, 596–610. doi: 10.1104/pp.17.01497

Haslam, T. M., and Kunst, L. (2013). Extending the story of very-long-chain fatty acid elongation. *Plant Sci.* 210, 93–107. doi: 10.1016/j.plantsci.2013.05.008

He, J., Tang, S., Yang, D., Chen, Y., Ling, L., Zou, Y., et al. (2019). Chemical and transcriptomic analysis of cuticle lipids under cold Stress in *Thellungiella salsuginea*. *Int. J. Mol. Sci.* 20, 4519. doi: 10.3390/ijms20184519

Hooker, T. S., Millar, A. A., and Kunst, L. (2002). Significance of the expression of the CER6 condensing enzyme for cuticular wax production in Arabidopsis. *Plant Physiol.* 129, 1568–1580. doi: 10.1104/pp.003707

Hou, Q., Ufer, G., and Bartels, D. (2016). Lipid signalling in plant responses to abiotic stress. *Plant Cell Environ.* 39, 1029–1048. doi: 10.1111/pce.12666

Hu, Y., Jiang, Y., Han, X., Wang, H., Pan, J., and Yu, D. (2017). Jasmonate regulates leaf senescence and tolerance to cold stress: crosstalk with other phytohormones. *J. Exp. Bot.* 68, 1361–1369. doi: 10.1093/jxb/erx004

Huang, B., Qi, F., Sun, Z., Miao, L., Zhang, Z., Liu, H., et al. (2019). Marker-assisted backcrossing to improve seed oleic acid content in four elite and popular peanut (*Arachis hypogaea* L.) cultivars with high oil content. *Breed. Sci.* 69, 234–243. doi: 10.1270/jsbbs.18107

Jiang, T., Zhang, X. F., Wang, X. F., and Zhang, D. P. (2011). Arabidopsis 3-ketoacyl-CoA thiolase-2 (KAT2), an enzyme of fatty acid beta-oxidation, is involved in ABA signal transduction. *Plant Cell Physiol.* 52, 528–538. doi: 10.1093/pcp/pcr008

Karami-Moalem, S., Maali-Amiri, R., and Kazemi-Shahandashti, S. S. (2018). Effect of cold stress on oxidative damage and mitochondrial respiratory properties in chickpea. *Plant Physiol. Biochem.* 122, 31–39. doi: 10.1016/j.plaphy.2017.11.011

Kim, K. N., Cheong, Y. H., Grant, J. J., Pandey, G. K., and Luan, S. (2003). CIPK3, a calcium sensor-associated protein kinase that regulates abscisic acid and cold signal transduction in Arabidopsis. *Plant Cell* 15, 411–423. doi: 10.1105/tpc.006858

Klaus, D., Hartel, H., Fitzpatrick, L. M., Froehlich, J. E., Hubert, J., Benning, C., et al. (2002). Digalactosyldiacylglycerol synthesis in chloroplasts of the Arabidopsis *dgd1* mutant. *Plant Physiol.* 128, 885–895. doi: 10.1104/pp.010780

Li, W., Wang, R., Li, M., Li, L., Wang, C., Welti, R., et al. (2008). Differential degradation of extraplastidic and plastidic lipids during freezing and post-freezing recovery in *Arabidopsis thaliana*. *J. Biol. Chem.* 283, 461–468. doi: 10.1074/jbc.M706692200

Li, M., Hong, Y., and Wang, X. (2009). Phospholipase D- and phosphatidic acid-mediated signaling in plants. *Biochim. Biophys. Acta* 1791, 927–935. doi: 10.1016/j.bbalip.2009.02.017

Li, Q., Zheng, Q., Shen, W., Cram, D., Fowler, D. B., Wei, Y., et al. (2015). Understanding the biochemical basis of temperature-induced lipid pathway adjustments in plants. *Plant Cell* 27, 86–103. doi: 10.1105/tpc.114.134338

Li, Y., Wang, X., Ban, Q., Zhu, X., Jiang, C., Wei, C., et al. (2019). Comparative transcriptomic analysis reveals gene expression associated with cold adaptation in the tea plant Camellia sinensis. *BMC Genomics* 20, 624. doi: 10.1186/s12864-019-5988-3

Lichtenthaler, H. K., and Wellburn, A. (1983). Determinations of total carotenoids and chlorophylls a and b of leaf extracts in different solvents. *Biochem. Soc T.* 11, 591–592. doi: 10.1042/bst0110591

Ma, Y., Dai, X., Xu, Y., Luo, W., Zheng, X., Zeng, D., et al. (2015). COLD1 confers chilling tolerance in rice. *Cell* 160, 1209–1221. doi: 10.1016/j.cell.2015.01.046

Ma, L., Coulter, J. A., Liu, L., Zhao, Y., Chang, Y., Pu, Y., et al. (2019). Transcriptome analysis reveals key cold-stress-responsive genes in winter rapeseed (*Brassica rapa* L.). *Int. J. Mol. Sci.* 20, 1071. doi: 10.3390/ijms20051071

Narayanan, S., Prasad, P. V., and Welti, R. (2016). Wheat leaf lipids during heat stress: II. Lipids experiencing coordinated metabolism are detected by analysis of lipid co-occurrence. *Plant Cell Environ.* 39, 608–617. doi: 10.1111/pce.12648

Noblet, A., Leymarie, J., and Bailly, C. (2017). Chilling temperature remodels phospholipidome of Zea mays seeds during imbibition. *Sci. Rep.* 7, 8886. doi: 10.1038/s41598-017-08904-z

Omoto, E., Iwasaki, Y., Miyake, H., and Taniguchi, M. (2016). Salinity induces membrane structure and lipid changes in maize mesophyll and bundle sheath chloroplasts. *Physiol. Plant* 157, 13–23. doi: 10.1111/ppl.12404

Peng, X., Teng, L., Yan, X., Zhao, M., and Shen, S. (2015). The cold responsive mechanism of the paper mulberry: decreased photosynthesis capacity and increased starch accumulation. *BMC Genomics* 16, 898. doi: 10.1186/s12864-015-2047-6

Peppino, M. M., Reyna, M., Meringer, M. V., Racagni, G. E., and Villasuso, A. L. (2017). Lipid signalling mediated by PLD/PA modulates proline and H_2O_2 levels in barley seedlings exposed to short- and long-term chilling stress. *Plant Physiol. Biochem.* 113, 149–160. doi: 10.1016/j.plaphy.2017.02.008

Rawsthorne, S. (2002). Carbon flux and fatty acid synthesis in plants. *Prog. Lipid Res.* 41, 182–196. doi: 10.1016/S0163-7827(01)00023-6

Seigneurin-Berny, D., Rolland, N., Dorne, A. J., and Joyard, J. (2000). Sulfolipid is a potential candidate for annexin binding to the outer surface of chloroplast. *Biochem. Biophys. Res. Commun.* 272, 519–524. doi: 10.1006/bbrc.2000.2805

Sui, N., Wang, Y., Liu, S., Yang, Z., Wang, F., and Wan, S. (2018). Transcriptomic and physiological evidence for the relationship between unsaturated fatty acid and salt stress in peanut. *Front. Plant Sci.* 9, 7. doi: 10.3389/fpls.2018.00007

Suzuki, S., Awai, K., Ishihara, A., and Yamauchi, K. (2016). Cold temperature blocks thyroid hormone-induced changes in lipid and energy metabolism in the liver of Lithobates catesbeianus tadpoles. *Cell Biosci.* 6, 19. doi: 10.1186/s13578-016-0087-5

Tan, W. J., Yang, Y. C., Zhou, Y., Huang, L. P., Xu, L., Chen, Q. F., et al. (2018). DIACYLGLYCEROL ACYLTRANSFERASE and DIACYLGLYCEROL KINASE modulate triacylglycerol and phosphatidic acid production in the plant response to freezing stress. *Plant Physiol.* 177, 1303–1318. doi: 10.1104/pp.18.00402

Upchurch, R. G. (2008). Fatty acid unsaturation, mobilization, and regulation in the response of plants to stress. *Biotechnol. Lett.* 30, 967–977. doi: 10.1007/s10529-008-9639-z

Verma, V., Ravindran, P., and Kumar, P. P. (2016). Plant hormone-mediated regulation of stress responses. *BMC Plant Biol.* 16, 86. doi: 10.1186/s12870-016-0771-y

Vincent, M. V., Zhang, J., Guan, S. Y., Thobela, L. T., Wang, P. W., Wang, X. Z., et al. (2018). Evaluation of groundnut (*Arachis hypogaea* L.) germplasm for chilling tolerance utilizing physiological and biochemical parameters. *J. Peanut Sci.* 47, 13–23.

Weiszmann, J., Furtauer, L., Weckwerth, W., and Nagele, T. (2018). Vacuolar sucrose cleavage prevents limitation of cytosolic carbohydrate metabolism and stabilizes photosynthesis under abiotic stress. *FEBS J.* 285, 4082–4098. doi: 10.1111/febs.14656

Winfield, M. O., Lu, C., Wilson, I. D., Coghill, J. A., and Edwards, K. J. (2010). Plant responses to cold: Transcriptome analysis of wheat. *Plant Biotechnol. J.* 8, 849–871. doi: 10.1111/j.1467-7652.2010.00536.x

Xiao, F., and Song, L. (2011). Analysis of extreme low-temperature events during the warm season in Northeast China. *Nat. Hazards* 58, 1333–1344. doi: 10.1007/s11069-011-9735-6

Xin, H., Xianchao, N., Pan, X., Wei, L., Min, Y., Yu, K., et al. (2019). Comparative transcriptome analyses revealed conserved and novel responses to cold and freezing stress in *Brassica napus* L. *G3 (Bethesda)* 9, 2723–2737. doi: 10.1534/g3.119.400229

Xue, D., Zhang, X., Lu, X., Chen, G., and Chen, Z. H. (2017). Molecular and evolutionary mechanisms of cuticular wax for plant drought tolerance. *Front. Plant Sci.* 8, 621. doi: 10.3389/fpls.2017.00621

Yuan, P., Yang, T., and Poovaiah, B. W. (2018). Calcium signaling-mediated plant response to cold stress. *Int. J. Mol. Sci.* 19, e3896. doi: 10.3390/ijms19123896

Yusupov, R., Finegold, D. N., Naylor, E. W., Sahai, I., Waisbren, S., and Levy, H. L. (2010). Sudden death in medium chain acyl-coenzyme a dehydrogenase deficiency (MCADD) despite newborn screening. *Mol. Genet. Metab.* 101, 33–39. doi: 10.1016/j.ymgme.2010.05.007

Zhang, G. H., Yu, S. T., Wang, H., and Wang, X. D. (2019). Transcriptome profiling of high oleic peanut under low temperature during germination. *Yi Chuan* 41, 1050–1059. doi: 10.16288/j.yczz.19-097

Zhang, H., Dong, J., Zhao, X., Zhang, Y., Ren, J., Xing, L., et al. (2019). Research progress in membrane lipid metabolism and molecular mechanism in peanut cold tolerance. *Front. Plant Sci.* 10, 838. doi: 10.3389/fpls.2019.00838

Zuther, E., Schaarschmidt, S., Fischer, A., Erban, A., Pagter, M., Mubeen, U., et al. (2019). Molecular signatures associated with increased freezing tolerance due to low temperature memory in Arabidopsis. *Plant Cell Environ.* 42, 854–873. doi: 10.1111/pce.13502

Conflict of Interest: The authors declare that the research was conducted in the absence of any commercial or financial relationships that could be construed as a potential conflict of interest.

Copyright © 2020 Zhang, Jiang, Ren, Dong, Shi, Zhao, Wang, Wang, Zhong, Zhao, Liu, Gao and Yu. This is an open-access article distributed under the terms of the Creative Commons Attribution License (CC BY). The use, distribution or reproduction in other forums is permitted, provided the original author(s) and the copyright owner(s) are credited and that the original publication in this journal is cited, in accordance with accepted academic practice. No use, distribution or reproduction is permitted which does not comply with these terms.

frontiers in Plant Science

ORIGINAL RESEARCH
published: 21 July 2020
doi: 10.3389/fpls.2020.01071

Check for updates

OPEN ACCESS

Edited by:
Raul Antonio Sperotto, Universidade do Vale do Taquari - Univates, Brazil

Reviewed by:
Klára Kosová, Crop Research Institute (CRI), Czechia
Benoit Bizimungu, Agriculture and Agri-Food Canada (AAFC), Canada
Sirjan Sapkota, Clemson University, United States
Jagesh Kumar Tiwari, Central Potato Research Institute (ICAR), India

***Correspondence:**
Karin I. Köhl
koehl@mpimp-golm.mpg.de

†Present addresses:
Manuela Haas, Rural Development, Agriculture and Forests, Ministry for Agriculture, Environment and Climate Protection of the State Brandenburg, Potsdam, Germany
Heike Sprenger, Department of Food Safety, German Federal Institute for Risk Assessment, Berlin, Germany

Specialty section:
This article was submitted to Plant Abiotic Stress, a section of the journal Frontiers in Plant Science

Received: *14 January 2020*
Accepted: *30 June 2020*
Published: *21 July 2020*

Citation:
Haas M, Sprenger H, Zuther E, Peters R, Seddig S, Walther D, Kopka J, Hincha DK and Köhl KI (2020) Can Metabolite- and Transcript-Based Selection for Drought Tolerance in Solanum tuberosum Replace Selection on Yield in Arid Environments? Front. Plant Sci. 11:1071. doi: 10.3389/fpls.2020.01071

Can Metabolite- and Transcript-Based Selection for Drought Tolerance in *Solanum tuberosum* Replace Selection on Yield in Arid Environments?

***Manuela Haas*[1†], *Heike Sprenger*[1†], *Ellen Zuther*[1], *Rolf Peters*[2], *Sylvia Seddig*[3], *Dirk Walther*[1], *Joachim Kopka*[1], *Dirk K. Hincha*[1] *and Karin I. Köhl*[1*]**

[1] Max Planck Institute of Molecular Plant Physiology, Potsdam-Golm, Germany, [2] Versuchsstation Dethlingen, Landwirtschaftskammer Niedersachsen, Munster, Germany, [3] Federal Research Centre for Cultivated Plants, Institute for Resistance Research and Stress Tolerance, Julius-Kühn Institut, Sanitz, Germany

Climate models predict an increased likelihood of drought, demanding efficient selection for drought tolerance to maintain yield stability. Classic tolerance breeding relies on selection for yield in arid environments, which depends on yield trials and takes decades. Breeding could be accelerated by marker-assisted selection (MAS). As an alternative to genomic markers, transcript and metabolite markers have been suggested for important crops but also for orphan corps. For potato, we suggested a random-forest-based model that predicts tolerance from leaf metabolite and transcript levels with a precision of more than 90% independent of the agro-environment. To find out how the model based selection compares to yield-based selection in arid environments, we applied this approach to a population of 200 tetraploid *Solanum tuberosum* ssp. *tuberosum* lines segregating for drought tolerance. Twenty-four lines were selected into a phenotypic subpopulation (PP_t) for superior tolerance based on relative tuber starch yield data from three drought stress trials. Two subpopulations with superior (MP_t) and inferior (MP_s) tolerance were selected based on drought tolerance predictions based on leaf metabolite and transcript levels from two sites. The 60 selected lines were phenotyped for yield and drought tolerance in 10 multi-environment drought stress trials representing typical Central European drought scenarios. Neither selection affected development or yield potential. Lines with superior drought tolerance and high yields under stress were over-represented in both populations selected for superior tolerance, with a higher number in PP_t compared to MP_t. However, selection based on leaf metabolites may still be an alternative to yield-based selection in arid environments as it works on leaves sampled in breeder's fields independent of drought trials. As the selection against low tolerance was ineffective, the method is best used in combination with tools that select against sensitive

genotypes. Thus, metabolic and transcript marker-based selection for drought tolerance is a viable alternative to the selection on yield in arid environments.

Keywords: drought tolerance, least absolute shrinkage and selection operator models, marker-assisted selection, metabolite profiling, multi-environment trials, phenotyping, potato, transcript profiling

INTRODUCTION

In the next 30 years, agricultural production must double to ensure global food supply (Stamp and Visser, 2012). Agriculture is predominantly limited by abiotic stresses, in particular drought and unfavorable temperatures, problems that are likely to be aggravated by global climate change (Harrison et al., 2014). In spite of water saving techniques, insufficient water supply will become more frequent because of altered precipitation patterns and an increase of competing water demand by industry and domestic consumption (Monneveux et al., 2012; Monneveux et al., 2013). Combining increased agricultural productivity with sustainable water management thus requires improved selection and phenotyping of drought tolerant or resilient genotypes (Pimentel et al., 1998; Blum, 2013). Drought tolerance in crops is the ability to produce yield with limited water supply (Blum et al., 1989). In wheat, substantial increase in yield under arid conditions has been achieved by selecting for high grain yield potentials (Richards et al., 2014), a concept favored by breeders. However, this approach may have slowed down progress in the breeding of resilient cultivars (Thiry et al., 2016).

Potato (*Solanum tuberosum* L.) is the world's fourth most important food crop and yields more food calories per unit water than cereals (Monneveux et al., 2013; Slater et al., 2016). However, potato drought tolerance is low because of a shallow root system and a low recuperation capacity after drought (van Loon, 1981; Vos and Groenwold, 1986; Anithakumari et al., 2012; Obidiegwu et al., 2015). Lack of water is the most important yield-limiting stress and yield losses due to drought are predicted to increase by 18–32% in the 21st century (Jones et al., 2003). Conventional breeding strategies in potato depend on rather inefficient phenotypic recurrent selection (Slater et al., 2014a; Gopal, 2015). The introgression of drought tolerance genes from wild relatives of potato and South American land races involves a substantial linkage drag introducing undesirable features (Schafleitner et al., 2007; Cabello et al., 2012). However, European *Solanum tuberosum* ssp. tuberosum cultivars vary significantly for drought tolerance thus providing a genetic basis for drought tolerance breeding (Jefferies and Mackerron, 1987; Wishart et al., 2013; Sprenger et al., 2015; Soltys-Kalina et al., 2016; Aliche et al., 2018). Selection for yield stability is challenging as drought tolerance is a highly polygenic trait and heritability of yield decreases under stress (Bolaños et al., 1993; Slater et al., 2014a). Furthermore, a substantial interaction between tolerance traits and environment renders traits favorable in one environment neutral or even negative in another environment (Tardieu, 2012; Parent and Tardieu, 2014). Drought tolerance breeding thus requires laborious testing of a large number of lines in multi-environment trials. The use of marker-assisted selection (MAS), especially in the early breeding cycles could accelerate progress by decreasing the duration of a breeding cycle from ten to four years (Slater et al., 2016). However, efficient genomic MAS for quantitative characteristics requires large effect QTL or a group of markers linked to alleles with smaller effects (Slater et al., 2014a). Presently, most MAS examples successfully introduced into practical breeding are linked to disease resistance (Slater et al., 2014a). Modern methods of genomic selection require detailed genotyping of the germplasm. This information is missing for many orphan crops. As an alternative to genomic selection, metabolite-marker-based selection has been suggested for well-studied crops like maize and rice, but also for understudied crops like *Ipomoea batatas* (Obata and Fernie, 2012; Riedelsheimer et al., 2012; Degenkolbe et al., 2013; Melandri et al., 2020; Price et al., 2020). In a previous publication, we presented a random-forest model that predicted drought tolerance within a panel of German potato cultivars with an accuracy above 90% (Sprenger et al., 2016; Sprenger et al., 2018). The high accuracy and the fact that prediction was independent of the agro-environment, in which the leaves were sampled, was unexpected. Now, we wanted to know whether this approach would efficiently select tolerant genotypes from an independent population and identify genotypes with increased drought tolerance under a range of typical central European drought scenarios. In previous studies on maize, metabolite-based prediction models and SNP-based prediction models showed a similar range of accuracy for the prediction of biomass-related traits (Riedelsheimer et al., 2012). In the present study, we compared metabolite-based and transcript-based selection (Sprenger et al., 2016; Sprenger et al., 2018) to phenotypic selection based on yield data from a limited set of drought stress trials to mimic selection in an arid environment. For this purpose, we generated a population of lines segregating for drought tolerance and phenotyped it for leaf metabolite and transcript levels and for tuber starch yield in

Abbreviations: $2^{-\Delta Ct}$, Gene expression relative to the house-keeping genes; A_t, Tolerant parent A; B2, B4, B6, Big-bag trials 2, 4 and 6; DRYM, Drought tolerance index deviation of the relative yield from the population median; DRYMp, Drought tolerance index deviation of the relative yield from the parent median; E_s, Sensitive parent E; F1 - F8, Field trials 1 to 8; G1, Population of 600 potato lines before selection for above average yield; G2, Population of 200 potato lines selected from G1 for above average yield; GCMS, Gas chromatography mass spectrometry; LASSO, Least absolute shrinkage and selection operator; MAS; Marker assisted selection; MP_s, Sensitive subpopulation selected based on tolerance predicted by model; MP_t, Tolerant subpopulation selected based on tolerance predicted by model; P3, P5, P7, Pot trials 3, 5, and 7; PP_t, Tolerant subpopulation selected based on yield from three stress trials; qRT-PCR, Quantitative reverse-transcription polymerase chain reaction; QTL, Quantitative trait loci; RH, Relative humidity; R_s, Sensitive parent R; SI, Stress index; SSI, Stress susceptibility index; STI, Stress tolerance index; SY, Starch yield; T, Temperature; VPD, Vapour pressure deficit of the air.

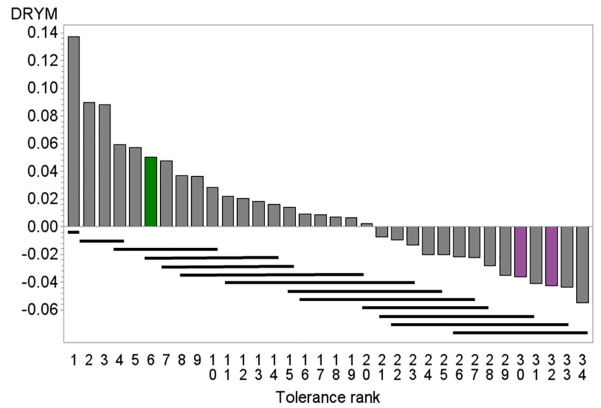


FIGURE 1 | Mean drought tolerance index of 34 potato cultivars depicted against mean tolerance rank, green tolerant cultivar A_t (rank = 6), pink sensitive cultivars E_s (rank = 32) and R_s (rank = 30). Bars indicate significance groups (REGWQ test, alpha = 0.1), cultivars underlined by the same bar are not significant different. Number of replicates 16–22.

drought stress trials. Based on these data, a phenotypic subpopulation was selected for superior tolerance based on yield data from three trials. Two additional populations with lines of superior or inferior tolerance were selected based on tolerance prediction with a least absolute shrinkage and selection operator (LASSO) model (Friedman et al., 2010). To find out, whether the quality of the prediction based on metabolite/transcript markers is similar to the prediction based on starch yield data from a limited set of trials, we characterized the drought tolerance of the selected lines in 10 multi-environment trials representing typical central European drought scenario. An overview of the workflow can be found in **Data Sheet 1**.

MATERIAL AND METHODS

Creation of a Segregating Population

F1-Seeds from crosses between tolerant cultivar A_t (id 2673) and the sensitive cultivars E_s (id 2858) and R_s (id 2880) were obtained from the consortium of potato breeders of the GFPi (German Association for the advancement of plant innovation). The parent cultivars were selected from a range of tetraploid cultivars released in Germany, based on the ranking obtained in previous experiments (see **Figure 1**) and the availability of crosses from the breeders (Sprenger et al., 2015). About 800 seeds were germinated on Murashige and Skoog medium with 2% sucrose. The 600 most vigorous plantlets were micro-propagated under axenic conditions to produce vegetative lines. For each line, three cuttings were cultivated under optimal water supply in 3-liter pots in a polytunnel (FGH) at the Max Planck Institute of Molecular Plant Physiology (MPI-MP) for 98 days in 2013 (Pot trial P1) as described before (Sprenger et al., 2015). Substrates and cultivation procedure were as described below. Further details for all trials can be found in **Table 1**. Lines with aberrant shoot or root development, leaf chlorosis or necrosis were excluded. Tubers from the remaining lines were harvested,

TABLE 1 | Experimental design for pot (Trial-id = P), big-bag (Trial-Id = B), and field (Trial-Id = F) trials.

Trial-Id	Culture-Id	Location	T	n	pl	Number of lines	Start date	Flower date	End date	Water (control)	Water (drought)	SI	Thermal sum	cum VPD end
P1		Golm FGH	1	3	1	549								
B2	67199	Golm FGH	2	3	1	227	16.04.2014	10.06.2014	17.07.2014	54.8	29.2	0.49	1306	120.2
P3	68015	JKI Shelter	2	1	2	195	15.05.2014		01.08.2014	20.9	9.6	0.56	1459	209.7
B4	72247	Golm FGH	2	2	3	60	09.04.2015	05.06.2015	19.07.2015	80.9	38.9	0.60	1489	194.0
P5	72292	JKI Shelter	2	4	2	60	12.05.2015	01.07.2015	10.08.2015	22.5	9.9	0.48	1415	215.1
B6	76240	Golm FGH	2	5	1	60	14.04.2016	06.06.2016	17.07.2016	73.9	40.1	0.54	1460	185.7
P7	76354	JKI Shelter	2	4	2	60	09.05.2016	23.06.2016	11.08.2016	20.2	6.3	0.68	1624	195.6
F1	67516	Golm Field	2	1	5	197	22.04.2014	30.06.2014	28.08.2014	89.4	65.6	0.08	1605	148.4
F2	67518	Groß Lüsewitz	2	1	2	191	28.04.2014		27.08.2014	54.3	4.1	0.56	1165	108.6
F3	72275	Golm Field	2	3	5	60	22.04.2015	30.06.2015	17.08.2015	79.7	27.8	0.73	1488	171.4
F4	72396	Groß Lüsewitz	2	2	6	60	28.04.2015	06.07.2015	04.09.2015	77.5	4.5	0.53	1139	113.3
F5	72482	Dethlingen	3	2	16	60	20.04.2015		31.08.2015	78.2	60.5	0.21	1321	94.4
F6	76219	Golm Field	2	3	8	60	21.04.2016	20.06.2016	09.08.2016	60.0	19.4	0.65	1429	139.1
F7	76529	Groß Lüsewitz	2	2	6	60	02.05.2016	29.06.2016	10.08.2016	62.2	6.8	0.70	1041	94.9
F8	76528	Dethlingen	3	2	16	60	19.04.2016		01.09.2016	99.4	70.8	0.18	1412	103.0

Culture Id = experiment reference Id in the MPI-MP database limsdb2 (Köhl et al., 2008). Location: Golm polytunnel (Golm FGH) and Golm field situated in Potsdam-Golm, Germany (52° 23'55''N13°03'56''E), sandy soil, Julius-Kühn (JKI) Shelter and field Groß Lüsewitz situated in Groß Lüsewitz, Germany (54°04'12''N12°20'19''E) and Dethlingen situated in Dethlingen, Germany (52°57'17''N10°07'33''E), both sandy loam. T= number of treatment levels: 1 optimal, 2 optimal and drought stress treatment, 3 optimal (50% field capacity), reduced irrigation (30% field capacity), and drought stress (no irrigation). n, number of replicate plots or pots per treatment; pl, number of plants per replicate. Number of lines without parent lines. Planting density 440 plants/100 m². Start date, date of planting into final pot size or field; Flower date, start of flowering in the parent cultivars; End date, date of shoot destruction; Water (control), sum of precipitation and irrigation for control treatment in liter per plant. Irrigation/precipitation volume in the field trials was converted from the area based to a plant based volume by dividing the volume per area by the planting density (4.4 plants/m²). Water (drought), sum of precipitation and irrigation for drought treatment; SI, stress index; Thermal sum in °Cdays, cum vpd end, cumulative VPD at the end of the trial in kPa.

weighted, sorted by size, and counted. Tubers were subsequently stored at 5°C to be used as seed tubers in the 2014 field trials.

Microclimate Measurements

Microclimate parameters were measured continuously and logged with a P22 data logger (UP Umweltanalytische Produkte) in the polytunnel and on the managed field sites of the MPI-MP. Air temperature and humidity were measured with HC2-S3 sensors, shielded with a SS3 radiation shield, in 1 min intervals on the field site and 15 min intervals in the polytunnel. Light intensity was measured with a SKP 215 PAR quantum sensor in 1 min intervals. After outlier control, cumulative thermal sums were calculated as the sum of daily thermal sums for each day from the day of planting to haulm destruction. The daily thermal sum (Equation E1) was calculated from the daily minimum (T_{min}) and maximum (T_{max}) temperature, with a base temperature of 6°C and maximum temperatures above 30°C set to 30°C.

$$Thermal\ \ sum = \left(\frac{Tmin + Tmax(30\,^\circ C)}{2}\right) - 6 \qquad \text{(E1)}$$

The vapor pressure deficit (VPD, in kPa) (E2) was calculated by estimating the saturating vapor pressure (vp_{sat}) from the hourly average air temperature T (in °C) and the vapor pressure (vp_{air}) from the hourly average relative humidity RH of the air (in %) as follows (Li6400 manual, Licor).

$$\begin{aligned} VPD &= vp_{sat} - vp_{air} \\ vp_{sat} &= 0.61365 * \tfrac{17.502 * T}{240.97 + T} \\ vp_{air} &= vp_{sat} * \tfrac{RH}{100} \end{aligned} \qquad \text{(E2)}$$

The daily midday VPD was calculated as median VPD in the time interval 10–14 MET and summarized as the cumulative VPD from planting date to the actual day. Original data are available at Edal (Köhl, 2018).

Phenotyping the Segregating Population

Based on the yield data, 225 lines with above-median yield (see results) were selected for preliminary drought tolerance assessment in two container trials (B2, P3) and two field trials (F1, F2) in 2014. For details, see **Table 1**, for field site locations and soil parameters, see heading of **Table 1** and Sprenger et al. (2015), for micrometeorological characterization, see results section "Test environments".

For the big-bag trial B2, micro-propagated cuttings of each line, of the three parent cultivars and the cultivar Desirée (standard cultivar for experiments at the MPI-MP) were pre-cultivated as described above, transferred to 30-liter big-bags filled with a peat-based potato substrate fertilized with 30 g Novatec classic per bag and cultivated in the polytunnel of the MPI-MP. The design was a randomized split-plot design, with one block for optimal water supply (control) and one block for reduced water supply (stress). Plants were irrigated twice to thrice per week with an injector based line-irrigation system (model CNL 8 l/h, combined with arrow dripper system Cobra-LF, Netafim) to maintain optimal soil water content (40–60% of field capacity). Two weeks after transfer, the water supply to the stress block was reduced to 50% of the volume received by the control block, supplied once a week. In experiment P3, plants were cultivated in a randomized split-plot design at the Julius-Kühn Institute (JKI) in Groß Lüsewitz in 5-liter pots as described before (Sprenger et al., 2015).

For the field trials, tubers were planted manually in a split-plot design on the managed field sites of the MPI-MP in Potsdam-Golm (F1) and of the JKI in Groß Lüsewitz (F2) as described before (Sprenger et al., 2015). In F1, each irrigation regime (control, drought treatment) was represented by one block. Plants were drip-irrigated from the top of the ridge with 10 mm water after sunset when turgor loss was visible at noon (control) or in the morning (drought-treatment). In F2, drought stress was applied by stopping watering at the beginning of emergence.

At the end of each trial, shoots were removed (pot experiments) or killed (field experiments). Tubers were counted and weight, and the starch yield measured as described above. Starch content was determined with a starch balance (Type E6100, MEKU). All phenotyping and yield data are available at Edal (Köhl, 2018).

Tuber production is the relevant response parameter with respect to yield potential and stress tolerance of potato. In contrast to cereal grains, the tuber water content is very high and considerably affected by water supply (Yuan et al., 2003). In a drought stress trial, where soil water content differs between treatments, this can lead to systematically lower tuber water contents and thus underestimate yield in drought-treated plants. As water loss of the tuber increases fresh weight-based starch content, we used a parameter that is less affected by the conditions at harvest by calculating the product of fresh weight and starch content, the starch yield. Starch yield was used accordingly as a response parameter to assess performance. Drought tolerance was estimated by calculating the drought tolerance index DRYM (see Equation E3) on the basis of tuber starch yield values.

Leaf samples were taken from each plant of each line under both treatments (control, stress) in experiment B2 (412 pooled samples from 1,250 single plant samples) and P3 (396 pooled samples) after onset of flowering (Sprenger et al., 2016). In preliminary, yet unpublished studies to the experiments published in Sprenger et al. (2016), different sampling strategies with respect to the developmental stage and the time-course of drought had been compared to find the earliest stage in plant development, in which metabolite and transcript levels would correlate to drought tolerance. These tests had shown that sampling during the flowering time results in better genotype differentiation than earlier sampling dates. Metabolite intensities were measured by gas chromatography-mass spectrometry (Sprenger et al., 2016). Original intensities of each metabolite were normalized to the average original intensity (response) of all annotated analytes in a sample and $\log_{10}$-transformed (for data see **Data Sheet 1**). Transcript levels of the 43 genes that are used in the prediction model and the four

reference genes were measured by qRT-PCR (Sprenger et al., 2016; Sprenger et al., 2018). The methodology of gene selection is explained in Sprenger et al. (2018). The primer information is given in **Data Sheet 1**. Gene expression values obtained by qRT-PCR measurements are listed in **Data Sheet 1** as $2^{-\Delta Ct}$ values after correction for the expression levels of reference genes.

Previous cross-validation of the prediction model had shown that the tolerance was predicted independent of the agro-environment (including water supply), in which the samples were taken (Sprenger et al., 2018). Thus, metabolite and transcript data from both treatments (control and stress) were evaluated together.

Selection of Subpopulations

From the segregating population, 60 lines were selected in three subpopulations (details see **Figure 1**) based on the tuber starch yield and metabolite/transcript data from three stress trials. Experiment F1 was excluded from drought tolerance analysis as tuber yield was not significantly affected by the stress treatment as a result of high precipitation during the experiment. Lines with low tuber production (<5 tubers per plant under control conditions) or delayed emergence were excluded from the selection.

For the phenotypic subpopulation PP_t, 20 lines were selected based on the tolerance index DRYM (Sprenger et al., 2015) calculated for each genotype G and experiment E based on the tuber starch yield (SY) as follows:

$$DRYM_{GxEi} = RelSY_{GxEi} - median(relSY_{GxEi})$$

$$RelSy_{GXEi} = starchyield(stress)_{GXEI} / (starchyield(control)_{GXEI})$$

RelSY = relative starch yield

DRYM = deviation of relative starch yield from median

(E3)

Within each experiment, lines were ranked according to their DRYM. Lines that ranked among the best 40 lines in at least two experiments were shortlisted for the phenotypic population PP_t. Lines were removed from this group, when high DRYM values resulted from outliers in tuber yield. Observations were flagged as outliers when the yield value was outside of the mean +/- 3 standard deviations range. The implications of this step are debated in the discussion section "Generation of a segregating population and selection of subpopulations".

For the selection of the MAS population, MP_t and MP_s, predictive models were generated using a LASSO model using the glmnet package version 4.0 (Friedman et al., 2010) in R version 3.6.3 (R Core Team, 2015). The cv.glmnet function was used to run 10-fold cross-validation. Our model predicted the value of the tolerance index DRYM from a linear combination of metabolite level or transcript level values. The LASSO method was used to achieve a minimum number of predictors by applying the 'λmin + 1SE'-rule. Thereby, we achieved a sparse subset of 29 metabolites or 23 transcripts for the general linear model to predict the drought tolerance index. This method avoids the risk of overfitting that arises when the number of independent variables is high compared to the number of observations. Missing values in the metabolite (5.5%) and transcript (2.2%) data were estimated by PCA using the Nipals method from the R-package pcaMethods (Stacklies et al., 2007). The training set included 911 samples for metabolite data originating from five independent field experiments and 202 samples for transcript data from three independent field experiments performed in 2011 and 2012 [Supporting information **Tables S6** and **S7** in (Sprenger et al., 2018)]. The resulting models were used to predict the DRYM of 195 lines from metabolite data (806 samples) and transcript data (803 samples). The predicted DRYM values from both models were ranked and averaged to retrieve the 24 most tolerant (MP_t) and 22 most sensitive (MP_s) lines. The pedigree and rank of the selected lines is shown in **Data Sheet 1** (**Table S1**). The R-scripts for the development of the LASSO model and the prediction of the tolerance index are available at GitHub https://github.com/HeikeSp/trost_select.

Characterization of Subpopulations

The 60 selected lines and their parent cultivars were tested for drought tolerance in four 30-liter big-bag (B4, B6) or 5-liter-pot trials (P5, P7) in 2015 and 2016 at the MPI-MP and the JKI, respectively, as described above. Additionally, all lines were cultivated under optimal and reduced water supply in field trials in 2015 and 2016 at three locations. The design was a randomized split-plot design, with three plots per line and treatment at the site Potsdam-Golm (F3, F6) and two plots per line and treatment at the site Groß Lüsewitz (F4, F7). Plants for the drought stress treatment were cultivated under a rain-out-shelter on both sites.

At the location Dethlingen, lines were cultivated in three blocks with either optimal water supply (control), reduced irrigation and without irrigation (stress). In the optimal and the reduced water supply regime, plants were watered with an irrigation boom when soil water content fell below 50 or 30% field capacity, respectively.

Plants were phenotyped for shoot height and phenological stage in the week when the parent cultivars started flowering. The agricultural standard BBCH scale for potato was used for scoring phenological stages.

Calculation and Statistical Evaluation

Data evaluation was performed in R (3.2.3, RStudio Version 1.0.143, RStudio Inc.; packages knitr, reshape, plyr, dplyr, psych) and in SAS (Version 9.4, SAS Institute). The developmental stages (BBCH) were rank transformed within each experiment, rank = 1 representing the smallest BBCH score. Starch yield (SY) was calculated by multiplying the tuber fresh weight (FW) with the tuber starch content for all tubers harvested from a replicate pot, big-bag, or plot. SY values were processed following the same scheme, both for data in linear as well as logarithmic scale, and normalized with regard to the factors block (B), row (R), and ridge (D). SY values were modelled as a result of a linear effects model associated with the variables B (if two or more blocks were set up in the experiment), R, and D by applying "lm"-function and by treating variables B, R, and D as categorical factors. The obtained model, M, was used to compute normalized SY-values

(SY_{norm}) using the following "predict"-function, where SYM(B, R,D) are the regressed values of SY based on the obtained linear model, M, and adding the median of the raw values to preserve the absolute magnitude of values before and after normalization.

$$SY_{norm} = SY - SYM(B,\ R,\ D) + median(SY) \qquad \text{(E4)}$$

ANOVA (R-function "aov") showed no significant association of the factors B, R, and D after normalization of SY-values, indicating successful normalisation.

The DRYM**p** was calculated by normalizing the relative starch yield of each replicate to the median of the three **p**arent cultivars (E5).

$$DRYM\boldsymbol{p}_{GxEi} = RelSY_{GxEi} - median\left(RelSY_{G=parentEi}\right) \qquad \text{(E5)}$$

The effects of experiment, genotype, subpopulation, treatment, and the interaction between these factors were tested by analysis of variance (ANOVA). Means were compared with TuckeyHSD test and pairwise t-test with Bonferroni p-value adjustment for multiple testing.

For correlation analysis (SAS proc CORR), means of normalized starch yield under control conditions and DRYM**p** were determined for each genotype for the three test systems pot, big-bag, and field.

RESULTS

Selection

The segregating population originated from crosses between the tolerant cultivar A_t and the sensitive cultivars E_s and R_s. These crosses had been chosen from a set of crosses among 34 potato cultivars that had been previously characterized in drought stress trials [**Figure 1** and (Sprenger et al., 2015)]. Among the crosses available from the breeders, cross $A_t \times R_s$ and $E_s \times A_t$ were chosen as A_t ranked among the six most tolerant lines and was significantly more tolerant than the sensitive parent lines E_s and R_s, which ranked among the five least tolerant lines.

The segregating population obtained from both crosses was reduced to 549 lines (population G1) by the first selection against plants with developmental defects. Tuber number [see data at

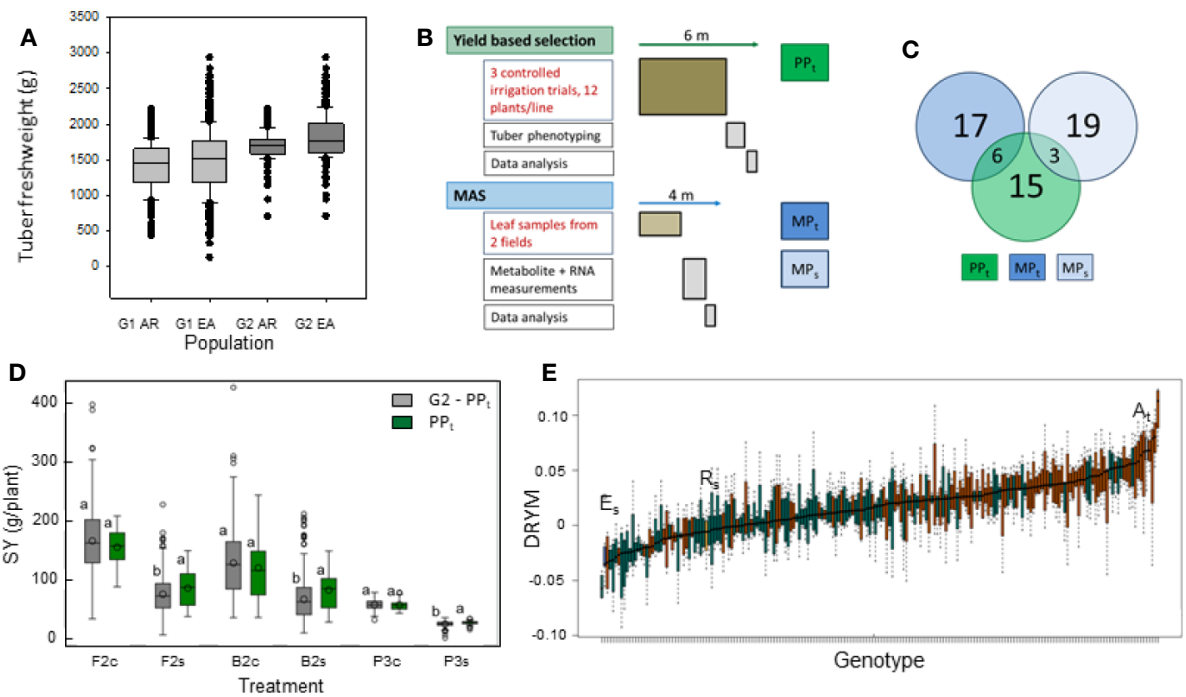


FIGURE 2 | Selection experiment comparing phenotypic selection and MAS from a potato population segregating for drought tolerance. **(A)** Distribution of tuber dry weight in segregating population G1 before selection for above average yield (~600 lines) and population G2 after selection for yield (~200 lines) (experiment P1, yield from three plants, AR = offspring from cross $A_t \times R_s$, EA = offspring from cross $E_s \times A_t$) **(B)** Scheme comparing procedure and timeline for phenotypic, yield-based selection of subpopulation PP_t, and MAS of subpopulations MP_t selected for superior tolerance and MP_s selected for inferior tolerance from 200 G2 lines. Duration of tasked written in red is fixed, duration of those written in black depends on resources. For detailed project plan see **Data Sheet 1**, **Figure S1**. **(C)** Venn diagram showing the number of lines in each subpopulation and the overlap between the subpopulations. There is no overlap between the marker selected populations MP_t and MP_s. **(D)** Tuber starch yield of the phenotypically selected PP_t compared to the remaining lines of G2 grown under optimal (c) and reduced (s) water supply in big-bag/pot (B2, P3) and field trials (F2) with significant water stress. Different letters indicate significant differences between population within an experiment and treatment (REGWQ-Test, $\alpha = 0.05$). **(E)** Drought tolerance predicted from metabolite concentrations for parent cultivars and G2 lines from the crosses $A_t \times R_s$ (red) and $E_s \times A_t$ (green).

Edal (Köhl, 2018)] and fresh weight (**Figure 2A**) were higher in the offspring from the cross $E_s \times A_t$ than in those from the cross $A_t \times R_s$. We selected 200 lines with an above average tuber production [fresh weight and tuber number, population G2 (**Figure 2A**) and (Köhl, 2018)] for drought tolerance assessment in four experiments. One of the experiments was performed in pots, one in big-bags and two under field conditions. In the big-bag system, plants grew in a soil volume similar to that available to a field grown plant and, consequently, produced similar tuber yields. The results from this test environment can thus be expected to be representative of field conditions. Tolerance assessment was based on the starch yield SY under deficit irrigation relative to the starch yield under optimal water supply. Experiment F1 yielded no tolerance data (stress index SI=0.08, no significant effect of treatment, see **Table 1**) because of unusually high precipitation. In the other three experiments, SI ranged between 0.49 and 0.56 with a significant effect of treatment on SY (**Table 1**). Data from these three experiments were used to perform the phenotypic selection based on yield under arid conditions (**Figure 2B**). Yield under arid conditions was normalized by calculating the tolerance index DRYM for each line and each experiment (Equation E3). When calculating this value from a very limited number of replicates per experiment, outliers can result in an extreme DRYM. For example, a very low yield value for a control pot in one of the experiments can result in a very high relative starch yield and thus overestimate the drought tolerance. To obtain a more robust estimate, we used a ranking procedure to select the 24 most drought tolerant lines into subpopulation PP_t. When comparing the starch yield of PP_t with the starch yield of the remaining lines of G2 (G2 minus PP_t), PP_t had a significantly higher starch yield under drought stress, whereas under sufficient water supply, starch yield of PP_t war similar to that of the remaining lines of G2 (**Figure 2D**). The theoretical minimum duration of this selection procedure is six months, including four months for plant cultivation until tuber maturity. The cultivation time cannot be shortened by increased investment of labor or money (**Figure 2B**).

For the MAS, two subpopulations MP_t and MP_s were selected based on the tolerance predicted by the published model (Sprenger et al., 2018) from leaf metabolite (**Figure 2E** and **Data Sheet 1**) and transcript levels (**Data Sheet 1**) measured in two experiments. Lines from the cross A_t x R_s were overrepresented among lines with a high predicted DRYM. Those lines with the highest and the lowest predicted DRYM were selected into MP_t and MP_s, respectively. As some lines were already selected into PP_t, additional lines were chosen for MP_t and MP_s to obtain a total of 60 lines for further testing (**Data Sheet 1**, **Table S1**). As a result, 15 lines were exclusive to PP_t, six were shared with MP_t, and three were shared between PP_t and MP_s (**Figure 2C**) adding up to a total of 24 lines in PP_t. Ten of the PP_t lines originated from the cross E_s x A_t, the remaining 14 lines from the cross A_t x R_s. The lines selected into MP_s predominantly originated from the cross E_s x A_t (21 out of 22 lines). Among the lines selected into MP_t, the majority (20 out of 24) originated from the cross A_t x R_s including the six lines shared between PP_t and MP_t (**Figure 2C**). This overlap was 2.5-fold larger than expected by chance (probability p=0.02; hypergeometric test). The theoretical duration of the MAS procedure is four months with two months being determined by the time the plant requires to reach the optimal sampling stage (BBCH 50–60).

Test Environments

Stress experiments conducted outside controlled environments require monitoring of environmental condition to allow generalization of the results. Thus, soil water content and micro-meteorological parameters were measured continuously [data set available at Edal (Köhl, 2018)]. The cumulative values of VPD (Equation E2) were plotted against the thermal sum (Equation E1) as a measure of developmental time (**Figure 3**). The duration of the experiments conducted in Golm (B2, B4 and B6, F1, F3, and F6) was controlled to achieve a thermal sum of >1400°Cd at the time of haulm destruction. In the big-bag experiments, the cumulative VPD reached about 200 kPA in all experiments except B2, which was conducted in an untypically wet year with high air humidity.

In the big-bag experiments (B2, B4, and B6), where water was supplied twice a week, the curve of the cumulative water supply followed the cumulative VPD curve, except during the time after flowering, when the water demand of potato is highest during tuber filling. The water supply in the big-bag experiments was much higher than in the experiment P3 and P5, which were conducted in 5-liter pots with correspondingly smaller plants. The amount of water used by plants in big-bags was similar to that of field-grown plants (**Table 1**).

In the field experiments, thermal sums at the end of the experiment were between 1,321 and 1,605°Cd at the sites Golm and Dethlingen, respectively, and around 1,100°Cd at the cooler site Groß Lüsewitz. The cumulative VPD was lower than 150 kPa in most experiments and thus considerably lower than in the pot and big-bag experiments. Cumulative VPD were generally highest at the site Golm, reflecting the higher temperatures and lower air humidity. The water supply to the field resulted from irrigation and precipitation for all control treatments and for the stress treatments in F1, F5, and F8, which were conducted without a shelter. These three experiments had only small differences in water supply between control and stress. Those stress treatments that were conducted under a shelter received less than half of the water supplied to the control treatments. In the experiments F2, F4, and F7, plants had access to a considerable water reservoir in the loamy sand soil (about 60 l m^{-2}) in addition to the very low amount of water supplied by irrigation.

Growth and Development

Shoot height and developmental stage were phenotyped when the parent cultivars A_t, E_s, and R_s started flowering (**Figure 4** and **Table 2** for statistics). The parent genotypes showed the developmental characteristics observed for these cultivars in earlier field trials. The tolerant cultivar A_t had shorter shoots and flowered earlier than the sensitive cultivars E_s and R_s. The shoot height of the three subpopulations was intermediate

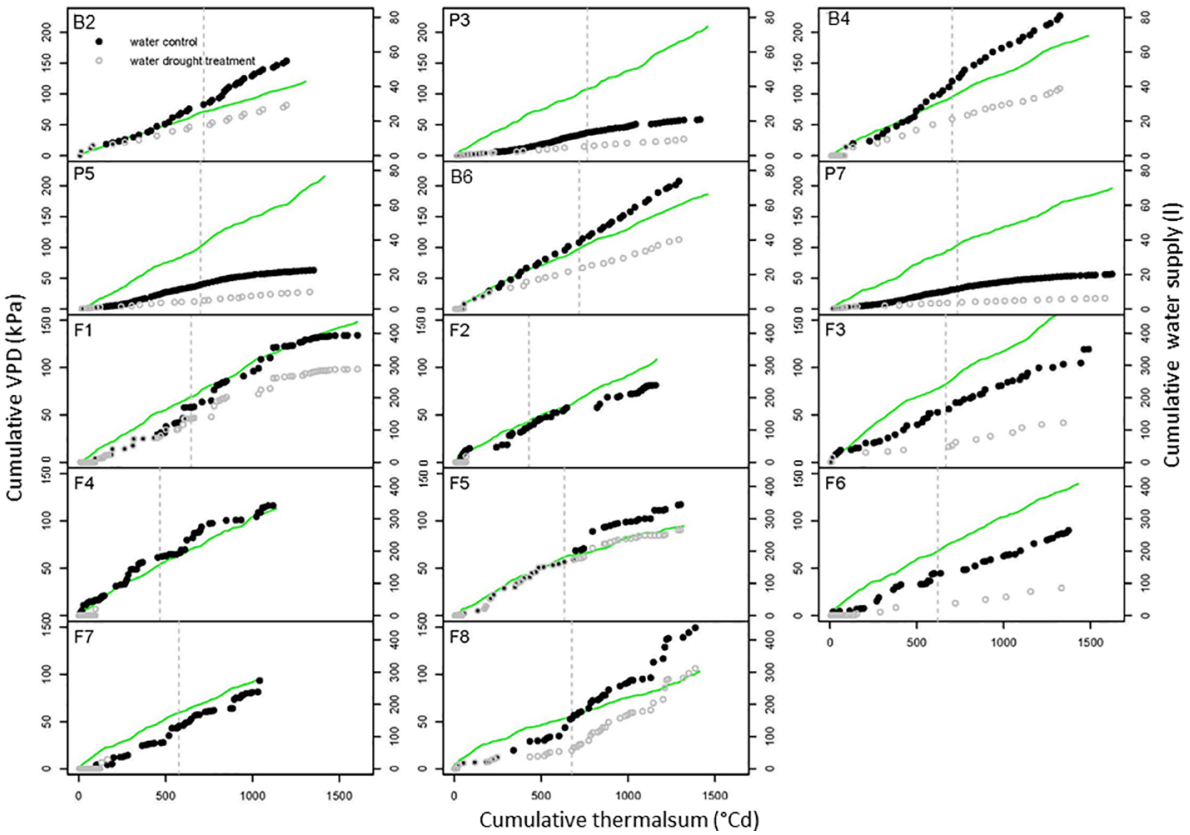


FIGURE 3 | Environmental conditions during drought stress trials. The cumulative vapor pressure deficit (VPD) of the air (green line) and the cumulative water supply to control (closed dots) and drought (open dots) treatments are depicted against the cumulative thermal sum of air temperature for the pot trials P3, P5, and P7, the big-bag trials B2, B4, and B6 and the field trials (F2 to F8). The dotted line indicates the flowering time. Further trial details see **Table 1**.

between the parents with no obvious differences among them. Drought treatment decreased shoot height significantly ($p < 0.05$) in all experiments except F1 (**Table 2**). However, there was only weak interaction between treatment and genotype effects on shoot height and development. Drought stress affected development less consistently than shoot height. Drought stressed plants delayed flowering in several experiments, however, earlier flowering was also observed (P4, F6). The lack of significant interaction effects suggests no significant genetic variation in the response of shoot growth and development to drought stress.

Yield

Tuber fresh weight, starch content, tuber numbers, and their size distribution were analyzed as indicators for yield quality and allocation patterns of the different lines. Tubers were fractionated into the "marketable" medium size fraction (35 to 60 mm), a small and an oversized fraction (**Data Sheet 1**, **Figure S2**). The total tuber number under control conditions was similar in PP_t and MP_s and slightly higher in MP_t. Size distribution was similar in all subpopulations with a slight trend towards less oversized and a higher number of small tubers in MP_t. Drought stress significantly ($p < 0.05$) reduced the number of oversized and medium-sized tubers in all populations, whereas the number of small tubers remained constant.

As a parameter for yield, we analyzed SY (**Figure 5**), which is the product of starch content and tuber fresh weight and equivalent to the dry matter of the tuber. To permit the integration of several experiments, tuber starch yield was normalized to the median tuber starch yield of the parent cultivars grown under optimal water supply. The experiment-wise ANOVA for the effects of drought treatment (E), subpopulation (G), and their interaction (G×E) on normalized starch yield (**Table 3**) indicated a significant treatment effect for all experiments except F1. In most pot and big-bag experiments, normalized starch yield was significantly affected by either G or G×E. In the field experiments, genotype and interaction effects were too small to be significant. To increase the statistical power, we calculated the average normalized starch yield for all lines and the parents for the test systems pot, big-bag and field (**Figure 5**). Under optimal water supply, average tuber starch yield of the subpopulations was similar to that of the three parent cultivars in pot and big-bag experiments, as indicated by the mean value around 1. Under field conditions, the average starch yield of the two sensitive parents E_s and R_s was higher than that of the three subpopulations. Drought treatment reduced normalized starch

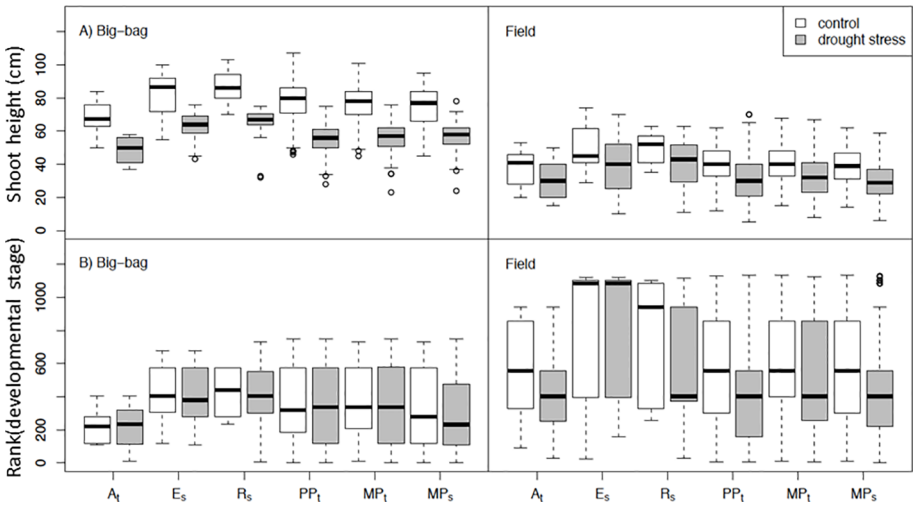


FIGURE 4 | Shoot height and development of subpopulations under control conditions and drought stress. Distribution of shoot height **(A)** and rank-transformed developmental stage **(B)** in subpopulations PP_t, MP_t and MP_s and parents A_t, E_s and R_s under control and drought treatment in two big-bag and two field trials. For the results of ANOVA see **Table 2**.

TABLE 2 | ANOVA on the effect of treatment (E), subpopulation (G), and the treatment × subpopulation interaction (E×G) on shoot height and development in big-bag and field trials.

Trial-Id	Parameter	Df	F(E)	p(E)	F(G)	p (G)	F(E×G)	p(E×G)
B2	Height	322	228.496	<0.0001	2.055	0.130	3.994	0.0193
B4	Height	710	1412.484	<0.0001	3.273	0.038	8.118	0.0003
B6	Height	713	1303.641	<0.0001	0.532	0.587	1.115	0.3280
F1	Height	349	0.287	0.5920	1.029	0.358	1.995	0.1380
F3	Height	1045	696.213	<0.0001	4.49	0.011	2.946	0.0530
F6	Height	1025	495.502	<0.0001	18.766	<0.0001	0.552	0.5760
B2	BBCH	322	9.656	0.0021	0.876	0.417	0.517	0.5966
B4	BBCH	710	6.829	0.0092	13.449	<0.0001	1.128	0.3244
B6	BBCH	713	5.157	0.0234	3.796	0.0229	2.868	0.0574
F1	BBCH	349	0.01	0.9204	0.567	0.5676	2.537	0.0805
F3	BBCH	1052	63.423	<0.0001	13.237	<0.0001	0.149	0.8620
F6	BBCH	1038	45.478	<0.0001	4.103	0.0168	1.800	0.1658

The shoot height was normalized to the median shoot height of the respective experiment. The developmental stage (BBCH) was rank-transformed (rank 1 least developed) within each experiment. The trial-id of big-bag experiments starts with a B, of field experiments with a F. Df, degrees of freedom for the model error; F, F statistic; p, probability. Df(E)= 1, Df(G) = 2, Df(E×G) = 2.

yield to less than 0.5. In pot experiments, average SY under stress was similar in all three subpopulations. In big-bag trials, average stress SY was highest in PP_t, intermediate in MP_t and lowest in MP_s. ANOVA on the normalized starch yield of the subpopulations (**Table 3**) indicated significant G and G×E effects for the big-bag trials and weakly significant G and G×E effects for the field trials. In the big-bag and field experiments, the highest SY measured under stress conditions in PP_t, MP_t and MP_s lines exceeded the highest values measured for the three parent cultivars, suggesting that these populations may contain genotypes with superior drought tolerance, warranting a detailed analysis of the lines.

Drought Tolerance

Drought tolerance was assessed by the deviation of the relative starch yield from the median relative starch yield of the three parent cultivars DRYM**p** (see Material and Methods, Equation E4). Mean DRYM**p** were calculated for each genotype and each experiment and then summarized within the groups parent cultivars and the three subpopulations PP_t, MP_t, and MP_s. **Figure S3** (**Data Sheet 1**) depicts the distribution of DRYM**p** for these groups separately for the three test environments pot, big-bag, and field. **Data Sheet 1 Table S2** (**Data Sheet 1**) lists the descriptive statistics. In all environments, variation of DRYM**p**, estimated by the standard deviation, was highest in the segregating population G2 and lowest in the parent cultivars. The standard deviation of DRYM**p** was substantially smaller in the pot experiments than in the big-bag and field experiments. In pot experiments, mean DRYM**p** of the segregating population G2 was lower than that of the parent cultivars. In contrast, mean and median DRYM**p** of G2 were higher than those of the parent cultivars in big-bag and field experiments, which suggests that the crosses may have yielded

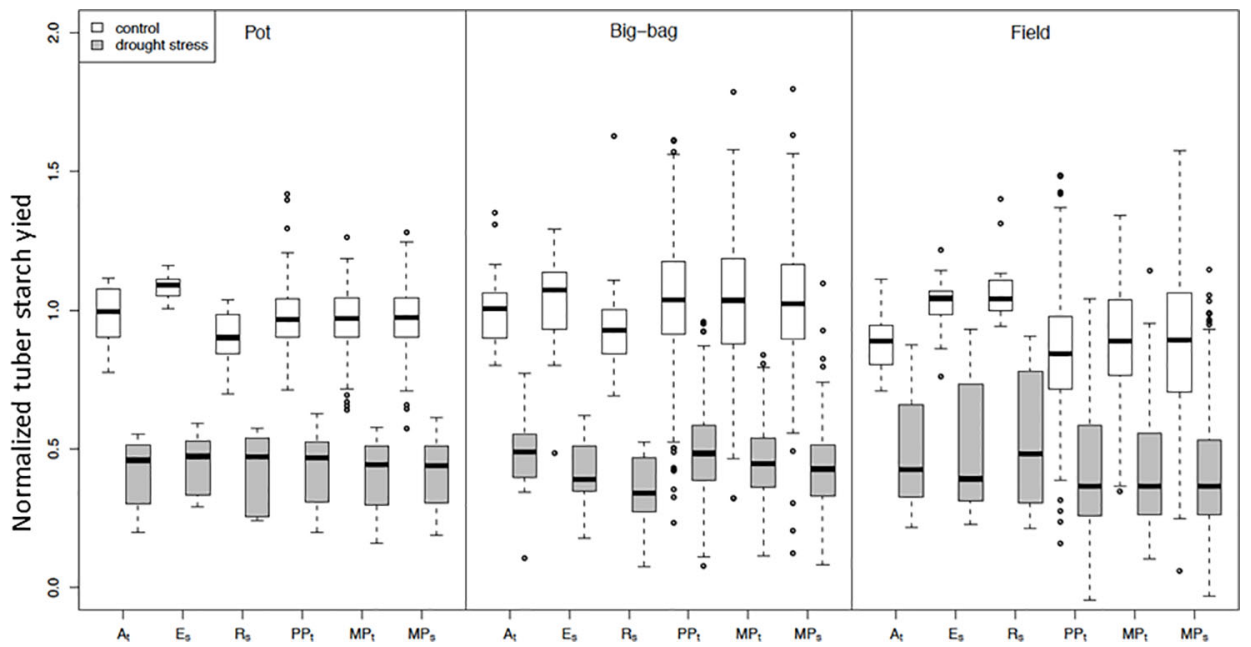


FIGURE 5 | Normalized tuber starch yield of subpopulations PP_t, MP_t and MP_s and parent cultivars A_t, E_s and R_s under control conditions and drought stress. Distribution of normalized mean tuber starch yield under control and stress treatments in pot (P3, P5, P7), big-bag (B2, B4, B6), and field trials (without F1). Starch yield was corrected for spatial effects and normalized to the median of the starch yield of the parent cultivars under control conditions. Result of ANOVA on starch yield in single experiments see **Table 3**.

TABLE 3 | ANOVA on the effect of treatment (E), subpopulation (G), and the treatment x subpopulation interaction (E×G) on normalized tuber starch yield in pot, big-bag and field trials.

Trial-Id	Df	F(E)	p(E)	F(G)	p (G)	F(E×G)	p(E×G)
B2	308	223.822	**<0.0001**	0.34	0.7123	7.892	**0.0005**
P3	231	2105.94	**<0.0001**	1.51	0.2232	5.408	**0.0051**
B4	703	2940.21	**<0.0001**	4.776	**0.0087**	0.249	0.7798
P5	699	8820.39	**<0.0001**	0.933	0.3940	3.153	**0.0433**
B6	705	1842.26	**<0.0001**	6.585	**0.0015**	1.395	0.2486
P7	676	11372.3	**<0.0001**	2.306	0.1000	0.817	0.4420
F1	114	1.917	0.169	0.455	0.6350	0.181	0.8350
F2	227	346.7	**<0.0001**	0.224	0.8000	1.483	0.2290
F3	341	1553.22	**<0.0001**	7.071	**0.0010**	4.635	**0.0103**
F4	221	365.873	**<0.0001**	0.438	0.6460	0.054	0.9480
F5	220	35.313	**<0.0001**	0.184	0.8320	0.579	0.5610
F6	351	1924.41	**<0.0001**	1.725	0.1800	0.919	0.4000
F7	211	1012.94	**<0.0001**	0.452	0.6370	0.624	0.5370
F8	216	43.889	**<0.0001**	3.319	**0.0380**	0.266	0.7670

Df, degrees of freedom for the model error; F, F statistic; p, probability (in bold when p < 0.05).

genotypes of superior drought tolerance compared to the parent cultivars. Analysis of variance on the data set containing the segregating population and the selected subpopulations revealed a significant effect of the population on DRYM**p** in all three test environments (**Table 4**). When comparing the selected populations, PP_t had the highest mean DRYM**p** in pot, big-bag, and field experiments. The MAS populations MP_t and MP_s had lower mean DRYM**p**, which were not significantly different from each other. In all three test environments, the selected populations contained genotypes with a superior DRYM**p** higher than the percentile 90 of the parent cultivars. We therefore analyzed the drought tolerance of each line in relationship to its yield potential.

Relationship Between Yield Potential and Drought Tolerance

The relationship between tolerance and yield is depicted in **Figure 6** (PP_t and MP_t) and **Figure S4** (MP_s) for the three test systems. For each line of the three subpopulations, average and standard error of DRYM**p** are plotted against the average and

TABLE 4 | Result of an analysis of covariance on the effect of population and the covariate cumulative VPD (cum_vpd) on drought tolerance DRYM**p**.

Model	Type	Source	df	F	p
1	pot	error	1096		
1	pot	population	6	8.3	<0.0001
1	pot	cum_vpd	1	48.1	<0.0001
1	big-bag	error	1207		
1	big-bag	population	6	3.9	0.0007
1	big-bag	cum_vpd	1	28.0	<0.0001
1	field	error	1195		
1	field	population	6	2.4	0.0265
1	field	cum_vpd	1	12.2	0.0005
2	pot	error	1057		
2	pot	population	3	13.2	<0.0001
2	pot	cum_vpd	1	51.1	<0.0001
2	big-bag	error	1156		
2	big-bag	population	3	5.7	0.0007
2	big-bag	cum_vpd	1	29.7	<0.0001
2	field	error	1151		
2	field	population	3	3.8	0.0106
2	field	cum_vpd	1	12.8	0.0004

In Model 1, the factor population contains the three subpopulations, the parents, and the population G2 without the lines that were selected into the subpopulations. Model 2 does not contain the data on the parents.

standard error of tuber starch yield under optimal water supply. The median starch yield of the 60 lines was 60, 204, or 240 g plant^{-1} in the pot, big-bag or field experiments, respectively. In all three subpopulations about 50% of the lines had a starch yield above the median starch yield, indicating that the selection did not favor high- or low-yielding lines in any of the populations independent of the test system. The starch yields in the pot system correlated weakly with the starch yield in the big-bag system and the field system (**Table 5**). Furthermore, the correlation between the starch yield in the big-bag and the field system were too weak to be significant (**Table 5**). This suggests a considerable interaction between genotype and the test system on starch yield. The correlation between starch yield and DRYM**p** was significantly negative in the pot and field trials and not significant in the big-bag trials (**Table 5**).

The DRYM**p** was significantly correlated between pot and big-bag experiments (Pearson correlation, $p < 0.0001$), but there was no correlation between the DRYM**p** found in field environments and those in pot and big-bag systems. The number of lines with a DRYM**p** above the confidence interval of the parent's DRYM**p** was 8 (pot), 15 (big-bag), and 11 (field) out of 24 lines in population PP_t. In population MP_t, DRYM**p** was above the parent's confidence interval in 6 (pot), 12 (big-bag), or 6 (field) lines. Two of the six lines that were selected in both populations PP_t and MP_t had very high drought tolerance (mean above 0.025, rank above 55) in pot and big-bag trials. One of the lines selected into PP_t and MP_t. was among the four most tolerant lines under field conditions. Thus, both selection methods identified lines of superior drought tolerance.

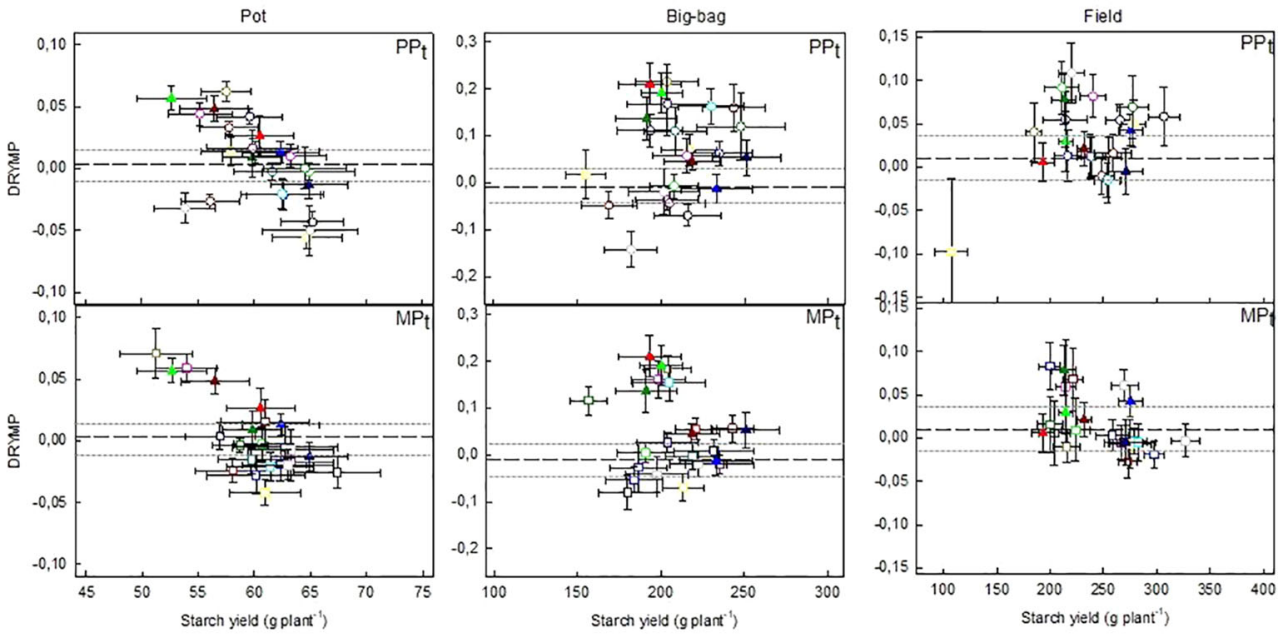


FIGURE 6 | Relationship between drought tolerance (DRYM**p**) and starch yield under optimal water supply in lines selected for superior drought tolerance. Mean and standard error (SE) of DRYM**p** depicted against mean and SE of tuber starch yield of the lines in PP_t and MP_t in pot, big-bag and field trials. Tuber starch yield was normalized to account for the spatial effects in the experiments. The reference lines indicate the mean (dashed line) and 95% confidence interval (dotted line) of DRYM**p** in the respective test system. Lines common in PP_t and MP_t are represented by closed triangles, including three lines with superior performance: AR185 (light green triangle), AR196 (dark green triangle), and AR121 (light red triangle). The outlier in PP_t, field is line AR21. Number of pot trials 3, big-bag trials 3, field trials 7. Data for the lines of MP_s are shown in **Data Sheet 1**, **Figure S4**.

TABLE 5 | Result of Pearson correlation analysis between drought tolerance DRYMp and normalized tuber starch yield under optimal water supply (SY) in pot (P), big-bag (B), and field (F) test environments.

Parameter	DRYMp(P)	SY(P)	DRYMp(B)	SY(B)	DRYMp(F)	SY(F)
DRYM**p(P)**	1	0.0001	0.0001	0.7234	0.8441	0.0001
SY(P)	**-0.6619**	1	0.0228	0.0444	0.2293	0.0112
DRYM**p(B)**	**0.5859**	-0.2961	1	0.4044	0.3826	0.0012
SY(B)	0.0471	0.2627	0.1106	1	0.3399	0.1731
DRYM**p(F)**	0.0262	0.1589	0.1158	-0.126	1	0.0054
SY(F)	**-0.5044**	**0.3279**	**-0.4112**	0.18	**-0.3577**	1

Cells below and left of the diagonal contain the correlation coefficients (bold print indicates $p < 0.05$), cells above the diagonal p-values. N = 59 (outlier line 899484 excluded).

DISCUSSION

Breeding for complex, polygenic traits like yield or drought tolerance (Slater et al., 2014a) based on direct selection for yield requires multi-year, multi-environment field studies on large populations. In consequence, it is slow and expensive. The rapidity of environmental changes predicted by global climate change models requires more efficient breeding. MAS for complex traits has been shown to be rapid and precise when based on large effect QTL, but less successful for polygenic traits without large effect QTL such as yield (Slater et al., 2016). When comparing genomic selection based on SNP markers to phenotypic selection in a limited number of trials on barley, both methods performed equally well in selection for Fusarium head blight resistance, but failed to increase yield significantly (Sallam and Smith, 2016). As an alternative to genomic selection, we suggested a metabolite and transcript marker-based model that predicts drought tolerance with an accuracy of >90% independent of the agro-environment (Sprenger et al., 2018). In the present study, we compared the performance of a selection based on this model to a phenotypic selection based on yield data from a limited set of drought trials.

Generation of a Segregating Population and Selection of Subpopulations

The comparison of selection methods requires a population of genotypes that segregate for the parameter of interest. For that purpose, we chose crosses between one tolerant cultivar (A_t) and two sensitive cultivars (E_s, R_s) based on the cultivar tolerance data gained before in multi-year, multi-environment field trials (Sprenger et al., 2015).

In most crop species, segregating populations are generated by crossing parents of contrasting tolerance and then producing offspring by selfing or by the production of double-haploid lines. As potato is a clonally propagated crop, each seedling yields a vegetative line, which can be maintained *in vitro*. However, as a result of its outbreeding nature, potato is highly heterozygous (Slater et al., 2014a; Gopal, 2015). The narrow genetic base of modern *Solanum tuberosum* cultivars results in acute inbreeding depression (Slater et al., 2014a; Gopal, 2015). Crosses thus produce a high percentage of offspring with inferior performance. Accordingly, the initial seedling population contained a substantial percentage of plants with visual defects or inferior tuber production. Extremely slow growing and low yielding plants may be mistaken for tolerant plants, as they consume less water, thus experiencing higher soil humidity. To avoid this confounding effect, we selected those 200 lines for further characterization that showed tuber yields in the same range as the parent cultivars. The percentage of retained seedlings was within the range of 20 to 50% recommended (Gopal, 2015).

For the selection of the subpopulations, 200 lines from population G2 were cultivated in four drought stress trials. The yield reduction under drought in the three experiments that delivered the data for selection into population PP_t was around 50% and thus is comparable to a selection in an arid agricultural environment. Selection under these conditions is generally selection for maintenance of yield, not for survival. For the MAS populations, the 24 most tolerant and the 22 least tolerant lines were selected into MP_t and MP_s, respectively, based on the tolerance predicted by the LASSO model from transcript and metabolite levels in leaves from two experiments. As some lines selected in PP_t had also been selected in MP_t (6) or MP_s (3), the total number of lines in all three populations was 60. The overlap between the two subpopulations PP_t. and MP_t, selected for superior tolerance was higher than chance.

The percentage of lines selected into a tolerant subpopulation from the segregating G2 population is high (22 to 24 out of 200), resulting in a low selection intensity compared to the intensity applied by breeders. Furthermore, the size of the selected subpopulations is small. While the population size was sufficient to estimate and test for differences in population means, the test power was low when applying contingency table statistics to find out, whether PP_t contains a different number of tolerant lines compared to MP_t. The limiting factors in the selection experiment were the area of the shelters available for the first characterization of the 200 lines and the subsequent phenotyping of the selected populations, the maximum duration of the funding period and the maximum amount of fundable work force. We operated a compromise between the number of replicates per line and the number of lines per experiments based on previous experience with drought tolerance trials in potato (Sprenger et al., 2015; Rudack et al., 2017) and performed joint evaluation of yield and tolerance data from three partners to increase statistical power.

Drought Tolerance Determination in Multi-Environment Trials

Drought tolerance determination in potato in controlled environment pot trials is highly reproducible, but correlates weakly with drought tolerance under field conditions (**Table 5** and (Sprenger et al., 2015). Traits like yield, starch content and drought tolerance show large genotype × environment interaction (Anithakumari, 2011; Slater et al., 2014b; Gopal, 2015). In consequence, traits having beneficial effects on yield in one drought-stress pattern do not necessarily have beneficial effect in another drought stress scenario. This means that the characterization of drought stress experiments by key environmental metadata is a prerequisite for the replication of experiments in phenotyping platforms or managed field trials and the comparison between trials. Furthermore, these metadata are

required for the subsequent generalization of test results to other target environments and the use of the data in modelling approaches using climate change scenarios (Millet et al., 2016).

The three test systems pot, big-bag, and field differed in the size of the soil water capacity available to the plant. In pots, plants rely entirely on the daily water supply as the small substrate volume buffers but a very small amount of water available to the plant. The plant available water is defined by two plant – soil parameters. The permanent wilting point is the lower limit. The upper limit is the maximal soil water content that does not cause damage due to water logging. In the field, however, roots can extract water from a much larger soil volume. This allows to buffer a much larger volume of water. In soils with a large water capacity as in experiments F2, F4, and F7, this permits to maintain the stressed plants on the water stored in the soil without the need for further irrigation. Under these conditions, root parameters, especially rooting depth, affect the amount of water available to a genotype (Puertolas et al., 2014). While in a situation, where the plants depend on the soil water storage, deep rooting enhances performance under drought, this will not be the case in pot grown plants, where water supply rather than the stored water determines the amount of water available to the plant. This may be one of the reasons for the low correlation between drought tolerance determined in pot experiments and field experiments. The correlation was only marginally better when the soil volume was increased by performing the experiment in big-bags.

To characterize the test environments, we used an approach published for maize (Chenu et al., 2011). Maize target production environments were classified based on the relationship between crop water status calculated as water supply/demand ratio versus thermal time pre- and post-flowering. We followed this approach by depicting water supply and the parameter VPD, which governs water demand, against thermal time. The drought stress treatments in the pot and big-bag trials mainly represented the early-terminal (ET) stress pattern, in which drought stress begins early in development and persists until harvests. Stress increases more gradually in pot or big-bag trials with deficit irrigation than in the stress type ET described for European maize environments, where stress increases steeply for the first 400°Cd (Harrison et al., 2014). The gradual increase pattern is found in the field trials conducted under a shelter with deficit irrigation (F3, F6). In contrast, stress increased steeply in those field trials that were conducted under a shelter without further irrigation (F2, F4, F6). However, the stress was mitigated by the comparatively low cumulative VPD at the site of these experiments. The field experiments F5 and F8, which were conducted without a shelter, represent mild late-terminal stress (F5) and late-relieved stress (F8). These stress patterns are typical for the subcontinental part of central Europe, where early terminal stress, late terminal stress and early relieved stress appeared in around 5% of the maize cultivations between 1975 and 2010 (Harrison et al., 2014). In conclusion, the key environmental metadata of our trials suggest that these trials represent common drought stress scenarios in the drought-prone agro-environments of Central Europe.

Drought Tolerance Index

The comparison of drought tolerance information from different trials under non-standardized conditions requires data normalization to account for differences in the degree of stress. Various tolerance indices have been suggested for this purpose, e.g. the stress susceptibility index SSI, the stress tolerance index STI and DRYM (Fischer and Maurer, 1978; Fernandez, 1992; Sprenger et al., 2015). Tests on artificial data sets have shown a superior performance of DRYM with respect to the detection of lines with high tolerance, independent of their yield potential (Sprenger et al., 2015). However, the normalization of DRYM to the median of the relative starch yield of all genotypes means that the relative position of the DRYM changes with the composition of the population. When selecting a population with a higher percentage of tolerant lines, the absolute value of the median will increase and selection for high tolerance will not result in increased DRYM values compared to the original population. This problem also affects the other indices. When the percentage of tolerant lines in a population increases, this will result in a decreased SI under constant stress conditions, thus shifting the median of the SSI and the STI. This is a common problem when comparing populations during selection, which can be solved by using check genotypes that are included in each trial as a basis for normalization. For the determination of drought tolerance, we therefore calculated the DRYM**p**, which was normalized to the median of the parent cultivars, which were used as check cultivars on all sites in this study (see Equation E4). The main disadvantage of this approach is the lower precision of the estimate as the median of the parent cultivars is calculated from a smaller data set than the median of the population. This can be compensated for by increasing the number of replicates for the parent cultivars compared to the tested lines.

Side Effects of Selection

The offspring of crosses may show a wide variation in development, morphology, and yield potential. Developmental variation may interfere with the assessment of drought tolerance, when the developmental stage that is most sensitive to insufficient water supply is reached at different times by different genotypes. In late-terminal stress scenarios, earliness is a trait that allows the crop to avoid water limitations in sensitive intervals such as the anthesis-silking interval in maize and the time between panicle development and anthesis in rice (Fukai and Cooper, 1995; Harrison et al., 2014). In potato, however, there is no consensus as to the timings of the most sensitive period (Carli et al., 2014; Sprenger et al., 2015). Nevertheless, the potential interaction between development and drought tolerance and between growth and drought tolerance requires testing for side effects of selection. We therefore checked whether selection affected development, tuber size distribution, or yield potential. The latter was estimated from the tuber starch yield under optimal water supply. The results indicated that growth and development of the selected genotypes were in the range of the parent cultivars under optimal water supply. There was no effect of selection on tuber starch yield in the pot and big-bag trials. However, under optimal water supply, parent cultivars were

superior in starch yield under field conditions as expected for cultivars that an expert breeder selected for optimal starch yield in field production.

Phenotypic Selection Versus MAS

Estimating drought tolerance based on DRYM**p** for parent cultivars, segregating population G2, and selected subpopulations, we found that all three subpopulations contained lines that were more tolerant than the parent cultivars. Negative correlations between tolerance and tuber starch yield under optimal water supply confirmed the risk of a yield penalty in drought-tolerant potato genotypes, which has been found before in a study on potato cultivars (Sprenger et al., 2015). Generally, high productivity is apparently rarely combined with high stress resilience (Thiry et al., 2016). In rice, yield penalty of drought tolerance results from a linkage between the QTL QDTY1.1 for grain yield under drought with the green revolution gene *sd1*, which was selected against when semi-dwarf types were bred (Vikram et al., 2016). The breeders are thus most interested to know whether the selected populations contained lines with superior drought tolerance and medium to high yield indicating that both selection methods allow identifying lines, which are tolerant without incurring a yield penalty. We thus compared the yield of highly tolerant lines in the subpopulations to the interquartile range of starch yields found in cultivar trials on the test site of the MPI-MP (Sprenger et al., 2015), which was 196–278 g plant^{-1}. In lines AR185 or AR196, which were selected in both, PP_t and MP_t, the starch yield under optimal water supply was 210 or 215 g plant^{-1}, respectively, under field conditions.

The phenotypically selected population PP_t had a significantly higher average DRYM**p** than the parent cultivars. The average DRYM**p** was lower in MP_t and MP_s, which were not significantly different from each other. All three populations contained lines with superior drought tolerance, many of which were selected in both PP_t and one of the MAS populations. The surprise was that the DRYM**p** of the two MAS populations selected for superior (MP_t) or inferior (MP_s) tolerance were not significantly different from each other and both populations contained highly tolerant lines. This unexpected result suggests that our marker model allows selecting for high tolerance, but not against low tolerance. This is a clear limitation of the approach as it does prevent the use of the model to select against drought-sensitive lines during breeding. This result is unexpected as during model validation, both sensitive and tolerant cultivars were classified correctly independent of the agro-environment (Sprenger et al., 2018). The main difference between the population in Sprenger et al. (2018) and this population is its genetic composition. The reliability of genomic prediction decreases when the genetic composition of the population changes (de Roos et al., 2009). It is known that epistatic interactions can skew the evaluation of QTL effects and thus bias the selection procedure (Ribaut and Hoisington, 1998). Our interpretation is that there are several tolerance mechanisms in potato and that additional traits not detected by our marker model became effective when genetic material was recombined. These additional mechanisms could be identified by closer investigation of those lines, in which the observed DRYM**p** is significantly higher than the predicted tolerance level.

The rate-limiting factor in selection is the developmental stage, at which samples can be taken. The time depends on plant development and thus cannot be sped up by increased investments. Yield-based selection requires a complete growth cycle, which is about four months in potato. Leaf samples for the metabolite and transcript based selection can be taken much earlier, ideally, as previous investigations have shown, during flowering. The minimum cultivation time is thus 1.5–2 months. The time required for the subsequent sample analysis depends on the investment in personnel and machinery and can thus be accelerated as needed. As the prediction is independent of the agro-environment (Sprenger et al., 2018), no drought stress trial is required for the metabolite/transcript based selection. Samples could thus be taken from plants grown on farmer's field, taking away the need for managed drought trials in selection. In contrast to yield-based selection, which requires several trials to obtain a reliable estimate, samples from less than five plants from a single field already provide a good prediction for metabolite/transcript based selection (Sprenger et al., 2018). This factor allows increasing the number of tested lines substantially compared to a classic selection based on drought stress trials. Thus, our metabolite/transcript model approach allows the breeder to test more lines in a shorter time compared to yield-based selection in arid environments. The main weakness of the model is the failure to select against drought-sensitive genotypes. Thus, after using the model to select the most tolerant 10% of a segregating population, further selection methods are required to remove sensitive genotypes. In crops like potato, where genomic selection is available, genomic selection during the seedling stage of potato breeding could precede the metabolite-model based selection and remove sensitive genotypes. Phenotypic selection on secondary traits or participatory breeding approaches (Atlin et al., 2001; Lafitte et al., 2003) could follow the transcript/metabolite model based selection in orphan crops.

In conclusion, our selection experiment on a segregating potato population showed that the selection for drought tolerance based on a transcript and metabolite marker model seems to be an efficient alternative to phenotypic selection based on yield measurements in drought-stress trials. As the metabolite/transcript model selection is limited to selection for tolerance, while failing to select against sensitivity, it does not provide a stand-alone solution but may work best in combination with genomic or phenotypic selection.

DATA AVAILABILITY STATEMENT

The data are available at the sources cited in the article, at EDAL, Github, and as **Supplementary Material**.

AUTHOR CONTRIBUTIONS

MH and KK conducted selection and tolerance experiments, evaluated the data, produced the figures, and wrote the manuscript. HS, EZ, DH and JK measured and evaluated the metabolite and transcript levels and designed the prediction model, SS and RP conducted tolerance experiments, DW normalized the starch yield data, SS, RP, DW, EZ, DH, JK, and KK designed the study and supervised the work.

FUNDING

The work was funded by the Fachagentur Nachwachsende Rohstoffe (grant 22010913) and the Gemeinschaft zur Förderung der privaten deutschen Pflanzenzüchtung (GFPi). We thank the breeding companies Böhm-Nordkartoffel-Agrarproduktion GmbH & Co OHG (BNA), NORIKA Nordring-Kartoffelzucht- u. Vermehrungs-GmbH and SaKa Pflanzenzucht GmbH & Co. KG for seeds of cultivar crosses and seed tuber propagation. The donation of the seeds was part of the collaboration funded by GFPi.

ACKNOWLEDGMENTS

We thank Renate Horn (University of Rostock) and Josef Strahwald (SaKa), Bernd Truberg (NORIKA), and Hans-Reinhard Hofferbert (BNA) for valuable discussions and insights into the breeder's perspective. Dirk Zerning, Laura Westphal, Ulrike Seider, Ines Fehrle and Alexander Erban provided valuable technical assistance.

SUPPLEMENTARY MATERIAL

The Supplementary Material for this article can be found online at: https://www.frontiersin.org/articles/10.3389/fpls.2020.01071/full#supplementary-material

DATA SHEET 1 | Presentation 1 - Workflow of the selection experiment; Sup Figures and Sup Table 1 and 2.docx; Data 1 - Corrected normalized metabolome data of trials B2 and P3; Sup Table 3 - Forward and reverse primers for qRT-PCR; Data 2 - List of the expression values of 43 marker genes investigated in the samples used in this study.

REFERENCES

Aliche, E. B., Oortwijn, M., Theeuwen, T. P. J. M., Bachem, C. W. B., Visser, R. G. F., and van der Linden, C. G. (2018). Drought response in field grown potatoes and the interactions between canopy growth and yield. *Agric. Water Manage.* 206, 20–30. doi: 10.1016/j.agwat.2018.04.013

Anithakumari, A. M., Nataraja, K. N., Visser, R. G. F., and van der Linden, C. G. (2012). Genetic dissection of drought tolerance and recovery potential by quantitative trait locus mapping of a diploid potato population. *Mol. Breed.* 30 (3), 1413–1429. doi: 10.1007/s11032-012-9728-5

Anithakumari, A. (2011). *Genetic dissection of drought tolerance in potato. PhD thesis* (Wageningen University).

Atlin, G. N., Cooper, M., and Bjørnstad, Å. (2001). A comparison of formal and participatory breeding approaches using selection theory. *Euphytica* 122 (3), 463–475. doi: 10.1023/a:1017557307800

Blum, A., Shpiler, L., Golan, G., and Mayer, J. (1989). Yield stability and canopy temperature of wheat genotypes under drought-stress. *Field Crops Res.* 22 (4), 289–296. doi: 10.1016/0378-4290(89)90028-2

Blum, A. (2013). The Interdrought conference in perspective. *J. Exp. Bot.* 64 (18), 5773–5774. doi: 10.1093/jxb/err118

Bolaños, J., Edmeades, G. O., and Martinez, L. (1993). Eight cycles of selection for drought tolerance in lowland tropical maize. III. Responses in drought-adaptive physiological and morphological traits. *Field Crops Res.* 31 (3), 269–286. doi: 10.1016/0378-4290(93)90066-V

Cabello, R., De Mendiburu, F., Bonierbale, M., Monneveux, P., Roca, W., and Chujoy, E. (2012). Large-scale evaluation of potato improved varieties, genetic stocks and landraces for drought tolerance. *Am. J. Potato Res.* 89 (5), 400–410. doi: 10.1007/s12230-012-9260-5

Carli, C., Yuldashev, F., Khalikov, D., Condori, B., Mares, V., and Monneveux, P. (2014). Effect of different irrigation regimes on yield, water use efficiency and quality of potato (*Solanum tuberosum* L.) in the lowlands of Tashkent, Uzbekistan: A field and modeling perspective. *Field Crops Res.* 163, 90–99. doi: 10.1016/j.fcr.2014.03.021

Chenu, K., Cooper, M., Hammer, G. L., Mathews, K. L., Dreccer, M. F., and Chapman, S. C. (2011). Environment characterization as an aid to wheat improvement: interpreting genotype–environment interactions by modelling water-deficit patterns in North-Eastern Australia. *J. Exp. Bot.* 62 (6), 1743–1755. doi: 10.1093/jxb/erq459

de Roos, A. P. W., Hayes, B. J., and Goddard, M. E. (2009). Reliability of genomic predictions across multiple populations. *Genetics* 183 (4), 1545–1553. doi: 10.1534/genetics.109.104935

Degenkolbe, T., Do, P. T., Kopka, J., Zuther, E., Hincha, D. K., and Kohl, K. I. (2013). Identification of drought tolerance markers in a diverse population of rice cultivars by expression and metabolite profiling. *PloS One* 8 (5). doi: 10.1371/journal.pone.0063637

Fernandez, G. (1992). "Effective selection criteria for assessing plant stress tolerance," in *Adaptation of food crops to temperature and water stress*. Ed. C. Kuo (Shanhua: Asian Vegetable Research and Development Center).

Fischer, R. A., and Maurer, R. (1978). Drought resistance in spring wheat cultivars I. Grain yield responses. *Aust. J. Agric. Res.* 29, 897–912. doi: 10.1071/AR9780897

Friedman, J., Hastie, T., and Tibshirani, R. (2010). Regularization paths for generalized linear models via coordinate descent. *J. Stat. Software* 33, 1–22. doi: 10.18637/jss.v033.i01

Fukai, S., and Cooper, M. (1995). Development of drought-resistant cultivars using physiomorphological traits in rice. *Field Crops Res.* 40, 67–86. doi: 10.1016/0378-4290(94)00096-U

Gopal, J. (2015). Challenges and way-forward in selection of superior parents, crosses and clones in potato breeding. *Potato Res.* 58 (2), 165–188. doi: 10.1007/s11540-015-9292-6

Harrison, M. T., Tardieu, F., Dong, Z. S., Messina, C. D., and Hammer, G. L. (2014). Characterizing drought stress and trait influence on maize yield under current and future conditions. *Global Change Biol.* 20 (3), 867–878. doi: 10.1111/gcb.12381

Jefferies, R. A., and Mackerron, D. K. L. (1987). Thermal time as a non-destructive method of estimating tuber initiation in potatoes. *J. Agric. Sci.* 108 (1), 249–252. doi: 10.1017/S0021859600064339

Jones, P. D., Lister, D. H., Jaggard, K. W., and Pidgeon, J. D. (2003). Future climate impact on the productivity of sugar beet (*Beta vulgaris* L.) in Europe. *Clim. Change* 58 (1-2), 93–108. doi: 10.1023/a:1023420102432

Köhl, K. I., Basler, G., Luedemann, A., Selbig, J., and Walther, D. (2008). A plant resource and experiment management system based on the Golm Plant Database as a basic tool for omics research. *Plant Methods* 4, 11. doi: 10.1186/1746-4811-4-11

Köhl, K. (2018). *Selection and validation experiment comparing phenotypic and marker-assisted selection for drought tolerance in Solanum tuberosum ssp. tuberosum.* doi: 10.5447/ipk/2020/18

Lafitte, H. R., Blum, A., and Atlin, G. (2003). "Using secondary traits to help identify drought-tolerant genotypes," in *Breeding rice for drought-prone environments*. Eds. K. Fisher, R. Lafitte, S. Fukai, G. Atlin and B. Hardy (Los Banos: IRRI), 37– 48.

Melandri, G., AbdElgawad, H., Riewe, D., Hageman, J. A., Asard, H., Beemster, G. T. S., et al. (2020). Biomarkers for grain yield stability in rice under drought stress. *J. Exp. Bot.* 71 (2), 669–683. doi: 10.1093/jxb/erz221

Millet, E. J., Welcker, C., Kruijer, W., Negro, S., Coupel-Ledru, A., Nicolas, S. D., et al. (2016). Genome-wide analysis of yield in Europe: allelic effects vary with drought and heat scenarios. *Plant Physiol.* 172 (2), 749–764. doi: 10.1104/pp.16.00621

Monneveux, P., Jing, R., and Misra, S. C. (2012). Phenotyping for drought adaptation in wheat using physiological traits. *Front. Physiol.* 3, 429–429. doi: 10.3389/fphys.2012.00429

Monneveux, P., Ramirez, D. A., and Pino, M. T. (2013). Drought tolerance in potato (*S. tuberosum* L.) Can we learn from drought tolerance research in cereals? *Plant Sci.* 205, 76–86. doi: 10.1016/j.plantsci.2013.01.011

Obata, T., and Fernie, A. R. (2012). The use of metabolomics to dissect plant responses to abiotic stresses. *Cell. Mol. Life Sci.* 69 (19), 3225–3243. doi: 10.1007/s00018-012-1091-5

Obidiegwu, J., Bryan, G., Jones, H., and Prashar, A. (2015). Coping with drought: stress and adaptive responses in potato and perspectives for improvement. *Front. Plant Sci.* 6. doi: 10.3389/fpls.2015.00542

Parent, B., and Tardieu, F. (2014). Can current crop models be used in the phenotyping era for predicting the genetic variability of yield of plants subjected to drought or high temperature? *J. Exp. Bot.* 65 (21), 6179–6189. doi: 10.1093/jxb/eru223

Pimentel, D., Houser, J., Preiss, E., White, O., Fang, H., Mesnick, L., et al. (1998). "Water resources: agriculture, the environment and ethics," in *Ecological Sustainability and Integrity*. Eds. J. Lemon, L. Westra and R. Goodland (The Netherlands: Kluwer Academic Publishers), 104–134.

Price, E. J., Drapal, M., Perez-Fons, L., Amah, D., Bhattacharjee, R., Heider, B., et al. (2020). Metabolite database for root, tuber, and banana crops to facilitate modern breeding in understudied crops. *Plant J.* 101 (6), 1258–1268. doi: 10.1111/tpj.14649

Puertolas, J., Ballester, C., Elphinstone, E. D., and Dodd, I. C. (2014). Two potato (*Solanum tuberosum)* varieties differ in drought tolerance due to differences in root growth at depth. *Funct. Plant Biol.* 41 (10-11), 1107–1118. doi: 10.1071/fp14105

R Core Team (2015). *R: A Language and Environment for Statistical Computing* (Vienna, Austria: R Foundation for Statistical Computing).

Ribaut, J.-M., and Hoisington, D. (1998). Marker-assisted selection: new tools and strategies. *Trends Plant Sci.* 3 (6), 236–239. doi: 10.1016/S1360-1385(98)01240-0

Richards, R. A., Hunt, J. R., Kirkegaard, J. A., and Passioura, J. B. (2014). Yield improvement and adaptation of wheat to water-limited environments in Australia - A case study. *Crop Pasture Sci.* 65 (7), 676–689. doi: 10.1071/cp13426

Riedelsheimer, C., Czedik-Eysenberg, A., Grieder, C., Lisec, J., Technow, F., Sulpice, R., et al. (2012). Genomic and metabolic prediction of complex heterotic traits in hybrid maize. *Nat. Genet.* 44 (2), 217–220. doi: 10.1038/ng.1033

Rudack, K., Seddig, S., Sprenger, H., Köhl, K., Uptmoor, R., and Ordon, F. (2017). Drought stress induced changes in starch yield and physiological traits in potato. *J. Agron. Crop Sci.* 203 (6), 494–505. doi: 10.1111/jac.12224

Sallam, A. H., and Smith, K. P. (2016). Genomic selection performs similarly to phenotypic selection in barley. *Crop Sci.* 56 (6), 2871–2881. doi: 10.2135/cropsci2015.09.0557

Schafleitner, R., Rosales, R. O. G., Gaudin, A., Aliaga, C. A. A., Martinez, G. N., Marca, L. R. T., et al. (2007). Capturing candidate drought tolerance traits in two native Andean potato clones by transcription profiling of field grown plants under water stress. *Plant Physiol. Biochem.* 45 (9), 673–690. doi: 10.1016/j.plaphy.2007.06.003

Slater, A. T., Cogan, N. O. I., Hayes, B. J., Schultz, L., Dale, M. F. B., Bryan, G. J., et al. (2014a). Improving breeding efficiency in potato using molecular and quantitative genetics. *Theor. Appl. Genet.* 127 (11), 2279–2292. doi: 10.1007/s00122-014-2386-8

Slater, A. T., Wilson, G. M., Cogan, N. O. I., Forster, J. W., and Hayes, B. J. (2014b). Improving the analysis of low heritability complex traits for enhanced genetic gain in potato. *Theor. Appl. Genet.* 127 (4), 809–820. doi: 10.1007/s00122-013-2258-7

Slater, A. T., Cogan, N. O. I., Forster, J. W., Hayes, B. J., and Daetwyler, H. D. (2016). Improving genetic gain with genomic selection in autotetraploid potato. *Plant Genome* 9 (3). doi: 10.3835/plantgenome2016.02.0021

Soltys-Kalina, D., Plich, J., Strzelczyk-Zyta, D., Sliwka, J., and Marczewski, W. (2016). The effect of drought stress on the leaf relative water content and tuber yield of a half-sib family of 'Katahdin'-derived potato cultivars. *Breed. Sci.* 66 (2), 328–331. doi: 10.1270/jsbbs.66.328

Sprenger, H., Rudack, K., Schudoma, C., Neumann, A., Seddig, S., Peters, R., et al. (2015). Assessment of drought tolerance and its potential yield penalty in potato. *Funct. Plant Biol.* 42 (7), 655–667. doi: 10.1071/FP15013

Sprenger, H., Kurowsky, C., Horn, R., Erban, A., Seddig, S., Rudack, K., et al. (2016). The drought response of potato reference cultivars with contrasting tolerance. *Plant Cell Environ.* 39 (11), 2370–2389. doi: 10.1111/pce.12780

Sprenger, H., Erban, A., Seddig, S., Rudack, K., Thalhammer, A., Le, M. Q., et al. (2018). Metabolite and transcript markers for the prediction of potato drought tolerance. *Plant Biotechnol. J.* 16, 939–950. doi: 10.1111/pbi.12840

Stacklies, W., Redestig, H., Scholz, M., Walther, D., and Selbig, J. (2007). pcaMethods - a Bioconductor package providing PCA methods for incomplete data. *Bioinformatics* 23, 1164–1167. doi: 10.1093/bioinformatics/btm069

Stamp, P., and Visser, R. (2012). The twenty-first century, the century of plant breeding. *Euphytica* 186585-, 591. doi: 10.1007/s10681-012-0743-8

Tardieu, F. (2012). Any trait or trait-related allele can confer drought tolerance: just design the right drought scenario. *J. Exp. Bot.* 63 (1), 25–31. doi: 10.1093/jxb/err269

Thiry, A. A., Dulanto, P. N. C., Reynolds, M. P., and Davies, W. J. (2016). How can we improve crop genotypes to increase stress resilience and productivity in a future climate? A new crop screening method based on productivity and resistance to abiotic stress. *J. Exp. Bot.* 67 (19), 5593–5603. doi: 10.1093/jxb/erw330

van Loon, C. D. (1981). The effect of water stress on potato growth, development, and yield. *Am. Potato J.* 58 (1), 51–69. doi: 10.1007/bf02855380

Vikram, P., Swamy, B. P. M., Dixit, S., Trinidad, J., Cruz, M. T. S., Maturan, P. C., et al. (2016). Linkages and Interactions Analysis of Major Effect Drought Grain Yield QTLs in Rice. *PloS One* 11 (3). doi: 10.1371/journal.pone.0151532

Vos, J., and Groenwold, J. (1986). Root-growth of potato crops on a marine-clay soil. *Plant Soil* 94 (1), 17–33. doi: 10.1007/bf02380587

Wishart, J., George, T. S., Brown, L. K., Ramsay, G., Bradshaw, J. E., White, P. J., et al. (2013). Measuring variation in potato roots in both field and glasshouse: the search for useful yield predictors and a simple screen for root traits. *Plant Soil* 368 (1), 231–249. doi: 10.1007/s11104-012-1483-1

Yuan, B.-Z., Nishiyama, S., and Kang, Y. (2003). Effects of different irrigation regimes on the growth and yield of drip-irrigated potato. *Agric. Water Manage.* 63 (3), 153–167. doi: 10.1016/S0378-3774(03)00174-4

Conflict of Interest: The authors declare that the research was conducted in the absence of any commercial or financial relationships that could be construed as a potential conflict of interest.

Copyright © 2020 Haas, Sprenger, Zuther, Peters, Seddig, Walther, Kopka, Hincha and Köhl. This is an open-access article distributed under the terms of the Creative Commons Attribution License (CC BY). The use, distribution or reproduction in other forums is permitted, provided the original author(s) and the copyright owner(s) are credited and that the original publication in this journal is cited, in accordance with accepted academic practice. No use, distribution or reproduction is permitted which does not comply with these terms.

frontiers in Plant Science

REVIEW
published: 04 August 2020
doi: 10.3389/fpls.2020.01152

Check for updates

Deployment of Genetic and Genomic Tools Toward Gaining a Better Understanding of Rice-*Xanthomonas oryzae* pv. *oryzae* Interactions for Development of Durable Bacterial Blight Resistant Rice

Anirudh Kumar[1], Rakesh Kumar[2], Debashree Sengupta[3], Subha Narayan Das[1], Manish K. Pandey[4†], Abhishek Bohra[5], Naveen K. Sharma[1], Pragya Sinha[4], Hajira Sk[4], Irfan Ahmad Ghazi[3], Gouri Sankar Laha[4] and Raman Meenakshi Sundaram[4]**

[1] Department of Botany, Indira Gandhi National Tribal University (IGNTU), Amarkantak, India, [2] Department of Life Science, Central University of Karnataka, Kalaburagi, India, [3] Department of Plant Sciences, School of Life Sciences, University of Hyderabad (UoH), Hyderabad, India, [4] Department of Biotechnology, ICAR-Indian Institute of Rice Research (IIRR), Hyderabad, India, [5] ICAR-Crop Improvement Division, Indian Institute of Pulses Research (IIPR), Kanpur, India

Rice is the most important food crop worldwide and sustainable rice production is important for ensuring global food security. Biotic stresses limit rice production significantly and among them, bacterial blight (BB) disease caused by *Xanthomonas oryzae* pv. *oryzae* (*Xoo*) is very important. BB reduces rice yields severely in the highly productive irrigated and rainfed lowland ecosystems and in recent years; the disease is spreading fast to other rice growing ecosystems as well. Being a vascular pathogen, *Xoo* interferes with a range of physiological and biochemical exchange processes in rice. The response of rice to *Xoo* involves specific interactions between resistance (R) genes of rice and avirulence (*Avr*) genes of *Xoo*, covering most of the resistance genes except the recessive ones. The genetic basis of resistance to BB in rice has been studied intensively, and at least 44 genes conferring resistance to BB have been identified, and many resistant rice cultivars and hybrids have been developed and released worldwide. However, the existence and emergence of new virulent isolates of *Xoo* in the realm of a rapidly changing climate necessitates identification of novel broad-spectrum resistance genes and intensification of gene-deployment strategies. This review discusses about the origin and occurrence of BB in rice, interactions between *Xoo* and rice, the important roles of resistance genes in plant's defense response, the contribution of rice resistance genes toward development of disease resistance varieties, identification and characterization of

OPEN ACCESS

Edited by:
Elizabeth R. Waters, San Diego State University, United States

Reviewed by:
Gerbert Sylvestre Dossa, Food and Agriculture Organization of the United Nations, Italy
Meng Yuan, Huazhong Agricultural University, China

***Correspondence:**
Raman Meenakshi Sundaram
rms_28@rediffmail.com
Anirudh Kumar
anirudh.kumar@igntu.ac.in

†Present address:
Manish K. Pandey, Research Program-Genetic Gains, International Crops Research Institute for the Semi-Arid Tropics (ICRISAT), Hyderabad, India

Specialty section:
This article was submitted to Plant Pathogen Interactions, a section of the journal Frontiers in Plant Science

Received: *26 May 2020*
Accepted: *15 July 2020*
Published: *04 August 2020*

Citation:
Kumar A, Kumar R, Sengupta D, Das SN, Pandey MK, Bohra A, Sharma NK, Sinha P, Sk H, Ghazi IA, Laha GS and Sundaram RM (2020) Deployment of Genetic and Genomic Tools Toward Gaining a Better Understanding of Rice-Xanthomonas oryzae pv. oryzae Interactions for Development of Durable Bacterial Blight Resistant Rice. Front. Plant Sci. 11:1152. doi: 10.3389/fpls.2020.01152

novel, and broad-spectrum BB resistance genes from wild species of *Oryza* and also presents a perspective on potential strategies to achieve the goal of sustainable disease management.

Keywords: rice, bacterial blight, resistance breeding, marker-assisted selection, genome editing, CRISPR/Cas, plant defense, transcriptome

INTRODUCTION

Rice (O*ryza sativa* L.) is an important staple food crop for more than 3.5 billion people across the world (Khush, 2005), provides 27 percent of the calories and 20 percent of protein required for the global population, and remains a major source of nutrition in developing and underdeveloped countries (FAO, 2004). Notwithstanding the progress witnessed in rice improvement over the last seven decades, the present rate of increase in rice yields are not adequate to keep pace with a rapidly growing population. The global demand of rice is estimated to rise by 26% in next 25 years, demanding an increase in its production from 676 million tones (mt) to 852 mt over the same period across the globe (Khush, 2013). Exacerbating the scenario, this production goal has to be achieved in the face of shrinking agricultural lands, dwindling water resources, declining soil productivity, and, most importantly, increasing cost of labor and other inputs. In parallel, we also need to improve rice production incrementally to combat and overcome the constantly evolving pathogen and pest populations and develop resilience in rice in the realm of rapidly changing climatic conditions.

Biotic stresses such as insect pests (brown plant hoppers, stem borers, etc.) and diseases such as bacterial blight caused by *Xanthomonas oryzae* pv. *oryzae*, rice blast caused by *Magnaporthe oryzae* and sheath blight caused by *Rhizoctonia solani* substantially reduce rice yields globally (Savary et al., 1998). The reduction in rice yield by bacterial blight (BB) is reported to be 50% (Khush et al., 1989), and during severe infection, it can reduce yield up to 81% (Srinivasan and Gnanamanickam, 2005), making it one of the most devastating diseases of rice (Ou, 1985). The conventional remedies recommended for managing BB disease, such as use of chemicals and antibiotics, biological control agents, and cultural practices, have limited utility and remain ineffective, especially when the disease occurs in epidemic proportion (Sundaram et al., 2008; Gnanamanickam, 2009).

Improving host-plant immunity has been considered as one of the best choices available for achieving economical and sustainable management of BB disease in a durable manner (Mundt, 2014; Pradhan et al., 2015). Understanding host resistance mechanisms and immunity against disease-causing pathogens like *Xoo* and their mutual interactions has been a topic of intense research in the past two decades. The evolving tools and techniques of plant molecular biology have been instrumental in getting vital insights into host-pathogen interactions and developing strategies for broad-spectrum, durable resistance. Chen and Ronald (2011) highlighted the nuances associated with innate immunity of rice against diverse pathogen elicitors. Typically, on encountering a biotic stress, the host plant reduces or enhances its susceptibility to a pathogen due to the existence of molecular cross talks between the pathogens themselves and between the pathogens and their host plant (Atkinson and Urwin, 2012). Interactions among pathways associated with response and tolerance/resistance to abiotic and biotic stresses have been established, and new insights have been gained on hormonal signaling pathways associated with antagonistic or synergistic interactions between biotic and abiotic stresses (Denancé et al., 2013; Jain et al., 2017). Therefore, understanding host-pathogen communication has been a longtime pursuit of plant biologists and plant pathologists.

Modern omics approaches like genomics, transcriptomics, proteomics, metabolomics, interactomics, etc. can be helpful in identification of the genes and their products, which are involved in pathogen perception by the host and also the response manifested by the host against the pathogen attack. Several resistance genes from different plant species have been identified, molecular mapped, cloned, and characterized (Sanseverino et al., 2010; Gururani et al., 2012). These genes have been assembled into five classes based on predicted protein domains (Gururani et al., 2012). *Hm1* gene of maize, which encodes a reductase, represents the first class. The HC toxin of *Cochliobolous carbonum* race 1 is inactivated by *Hm1* gene (Johal and Briggs, 1992). *Pto* gene belong to the second class, which encode membrane-associated serine-threonine kinase. It provides resistance to *Pseudomonas syringae* pv. *tomato*. The cytoplasmic receptor kinase protein represents the third class. It includes Rps2 and Rpm1, *N*, *L6*, *Prf*, and *Xa1* gene of *Arabidopsis*, tobacco, flax, tomato, and rice, respectively (Salmeron et al., 1996; Yoshimura et al., 1998). Tomato *Cf* gene represents the fourth class wherein *Cf* gene encodes LRR motifs in extracellular domain and a short C-terminal tail in the intracellular domain (Dixon et al., 1996). The rice *Xa21* represent the fifth class, which encodes a receptor kinase like protein, and it confers broad spectrum resistance to *Xoo* (Song et al., 1995).

In May 2014, the genome sequences of 3,000 strains of rice have been published by a joint effort of Chinese Academy of Agricultural Science (CAAS) and International Rice Research Institute, Philippines (Li et al., 2014). This project undoubtedly will provide the clear insights on utilizing host resistance genes belonging to one or more above mentioned classes of resistance genes for obtaining durable resistance against disease like BB (Li et al., 2014). In this article, we have reviewed the molecular mechanisms that are associated with interaction between rice and *Xoo*, pathways of resistance and susceptibility in rice, and the application of modern biotechnology approaches for breeding durable, broad-spectrum BB resistance rice varieties.

MOLECULAR EVENTS ASSOCIATED WITH INFECTION BY XOO AND RESISTANCE AGAINST THE PATHOGEN

Plant-Pathogen Communication and Symptomatology

Xanthomonas oryzae pv. *oryzae* (*Xoo*) is a gram negative, non-spore forming, rod shaped bacterium, which is motile with a single polar flagellum. Individual cells show a range from around 0.7 to 2.0 μm in length and from 0.4 to 0.7 μm in width and require an optimal temperature between 25 and 30°C for their growth (Bradbury, 1984). Unlike mammals, plants have a complex cell wall and bacteria need to get through this barrier to gain access to nutrients. This is achieved by the bacteria through destruction of the cell wall barrier by means of secreting cell wall degrading enzymes (CDEs) such as lipase/esterase (*LipA*), cellulase (*ClsA*), cellobiosidase (*CbsA*), xylanase (*XynB*), etc., which is one of the most effective virulence strategy adapted by bacterial pathogens (Agrios, 1997; Rajeshwari et al., 2005; Jha et al., 2007; Malukani et al., 2020). However, receptors like WAKL21.2 predict the damage caused by *Xoo* CDEs and recruit the components of immunity (Malukani et al., 2020). *Xoo* gets into rice leaf tissues generally *via* wounds or natural openings such as hydathodes (Ou, 1985). Subsequently, it multiplies and flourishes in the intercellular spaces (apoplast) beneath the epithelial cells. Thereafter, it disseminates to other parts of plants through the xylem vessels (Noda and Kaku, 1999). After few days, xylem vessels are filled by bacteria and its exo-polysacchride (EPS). The bacterial with its exudates can be observed on the leaf surface (**Figures 1** and **2**), as they come out through hydathodes. This is considered as a clear-cut symptom of the disease and most importantly it serves as a source of secondary inoculum (Mew et al., 1993).

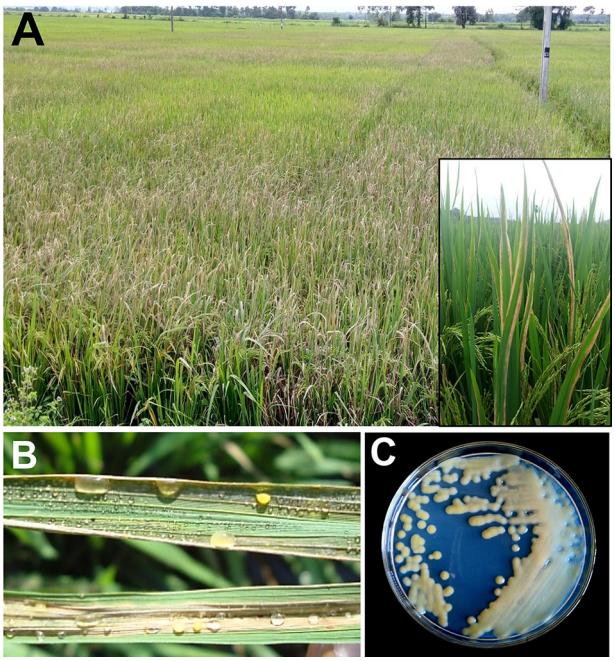


FIGURE 1 | Bacterial blight of rice. **(A)** Closer view of infected plants; **(B)** bacterial ooze on infected leaf; **(C)** *Xanthomonas oryzae* pv. *oryzae* (*Xoo*) colonies on culture plate.

Many plant pathogenic bacteria including *Xoo* use type III secretion system to transport virulence proteins and enzymes to disrupt host signaling and hijacks host metabolism for their growth and development. The proteins secreted by type III secretion system are called effector protein, which includes transcription activator like (TAL) effector and non-TAL effector proteins (White et al., 2009; Scholze and Boch, 2011). TAL effector protein supports the proliferation of *Xoo* and establishment of infection in host plant by altering host transcription machinery through upregulation of selected host genes required for multiplication of the pathogen, whereas non-TAL effector protein promotes virulence through suppression of host innate immunity. Few TAL effectors and their cognate effector (E) genes, viz., *AvrXa10*/*Xa10*, *AvrXa23*/*Xa23*, and *AvrXa27*/*Xa27*, have been cloned from rice (Hopkins et al., 1992; Gu et al., 2005; Tian et al., 2014), and virulence function of others TAL effectors, *TalC*, *pthXo1*, *pthXo2*, *pthXo3*, *pthXo6*, and *pthXo7*, have been studied. The *PthXo1* TAL effector persuades the expression of host susceptibility gene *Os8N3* (*nodulin 3* gene family; renamed as *OsSWEET11*), which encodes a membrane protein associated with sugar transport (Yang B. et al., 2006). In the cultivar Nipponbare, it activates virulence by inducing *Os8N3*/*SWEET11* gene (**Figure 3A**) (Yang S. et al., 2006). It has been reported that the recessive *xa13* resistance allele arose due to mutation in the promoter region of *Os8N3*/*SWEET11* (Chu et al., 2006). Another host susceptibility gene, *SWEET14* is targeted by many TALEs (viz., *AvrXa7*, *PthXo3*, *TalC*, *and TalF*; Oliva et al., 2019) to trigger the release of sugar molecules in the apoplast required by the pathogen as nutrient source (Streubel et al., 2013). Mutation within effector binding element (EBE) of *AvrXa7* in the *Os11N3*/*SWEET14* promoter resulted in disease resistance against *Xoo* (Li T. et al., 2012). Similarly, deletion in the EBE of *Xa7* in wild rice confers broad spectrum resistance to BB (Hutin et al., 2015). Two other TAL effectors *PthXo6* and *PthXo7* promote the transcription of host genes *OsTFX1* and *OsTFIIAγ1*, respectively (Sugio et al., 2007). One more TAL effector gene *pthXo8* (homolog of *pthXo6*) has been found to be involved in manipulation of small RNA pathway of the host (Yang and White, 2004).

Xoo genome also encodes a type II secretion system. Proteins secreted by type II secretion system possess secretion signal at N terminal and are transported to periplasmic space (Voulhoux et al., 2001; Jha et al., 2005). Type II secreted (TIIS) proteins are mostly toxins and enzymes that targets diverse components of the host defense system. In addition, type II secretion system secretes variety of carbohydrate degrading enzymes like cellulases, pectate lyases, xylanases, and polygalacturonases (Cianciotto and White, 2017), thus weakening the cell wall. It has been noted that rice plants perceive type II protein and in response, hypersensitive reaction is inducted (Jha et al., 2005). Mutation in genes encoding type II secretion system diminishes the virulence of *Xoo* in the host, thus clearly demonstrating the importance of TIIS in plant pathogenesis

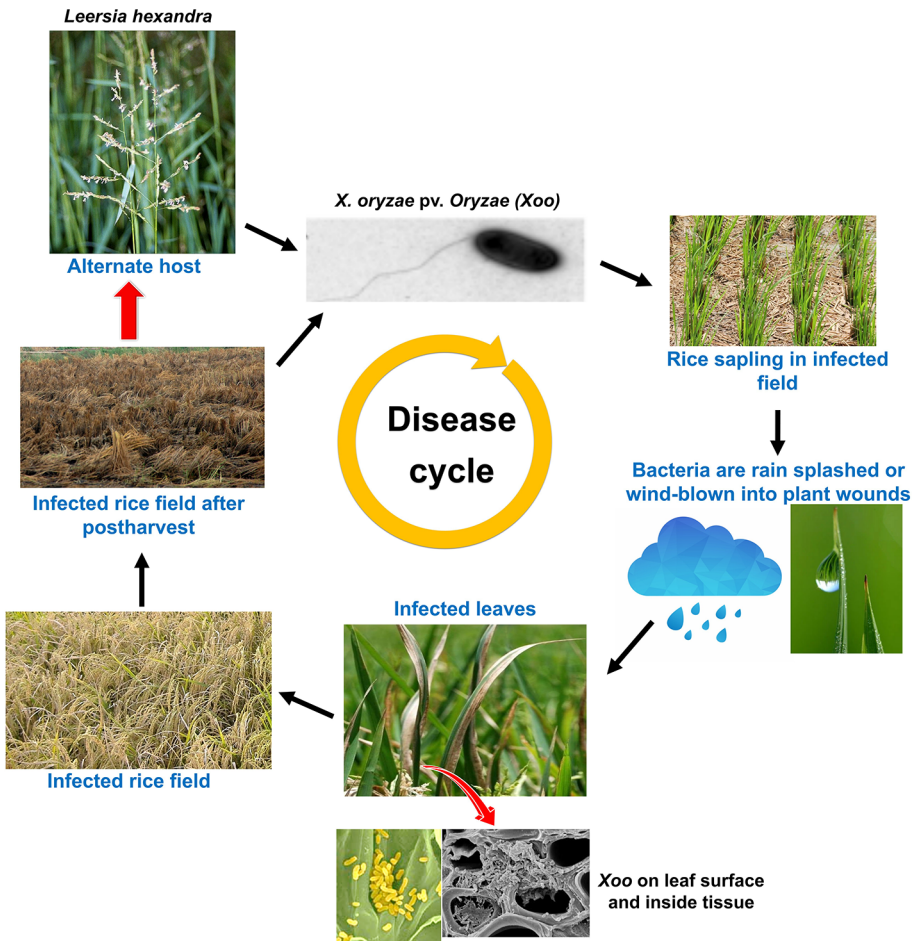


FIGURE 2 | Disease life cycle of the rice bacterial blight caused by bacteria- *Xoo*, including the influence of disease secondary host plant on disease severity.

(Cianciotto and White, 2017). *Xoo* targets and alters different host gene products and TAL effectors to amend the host physiology to have favorable effects on host susceptibility. The ability of plants to detect the adverse effects and speed of response against the pathogen determines the host fate. It has also been found that plants down-regulate the level of auxin in response to pathogen attack for enhancing disease resistance (Navarro et al., 2006). In addition, ABA suppresses the basal defense mechanism of rice against virulent *Xoo* strains and likely to function as virulence factor. An enhanced level of ABA is known to increase susceptibility of rice to *Xoo* by mediating the SA defense mechanism (Xu et al., 2013). *Xoo* also produce autoinducers (hormone like molecule) to detect the local population density (quorum sensing; QS) (Karatan and Watnick, 2009; Pradhan and Chatterjee, 2014). Based on the quorum sensing, bacteria regulate their gene expression pattern to effectively parasitize the plant cells (Karatan and Watnick, 2009). Various signaling molecules engage in QS including *N*-acylhomoserine lactones (AHLs), autoinducers-2 (AI-2), diffusible signal factors (DSFs), and oligopeptides (Deng et al., 2010). Further, the *Xoo* secretes large amount of extracellular polysaccharide (EPS; extra cellular polysaccharide high molecular-weight sugar molecules), which choke the xylem and cause typical wilting symptoms. EPS has an important role to play as it enhances pathogenicity by protecting the bacteria from antimicrobial compounds of the host plants (Leigh and Coplin, 1992; Dharmapuri and Sonti, 1999). All of the above mechanisms contribute together to promote pathogenesis (Leigh and Coplin, 1992). A comprehensive representation of the mode of *Xoo* infection in rice is illustrated in **Figures 1** and **2**.

Host-Mediated Disease Resistance

The pathogen infects by evading or compromising the host defense responses. In doing so, the pathogen escapes the recognition by host receptors, mitigates or inhibits downstream signaling in the host, or takes over the host signaling mechanism to favor establishment of disease. To counter this, plants have also developed several receptors and sensors that interact with microbial components and nullify their effect. A unique strategy has been adopted to improve the immunity in crops by enhancing the recognition spectrum of the host plant's own immune system (Lacombe et al., 2010). It involves the transfer of pathogen-associated molecular pattern (PAMP) like perception system across plant families and provides broad-

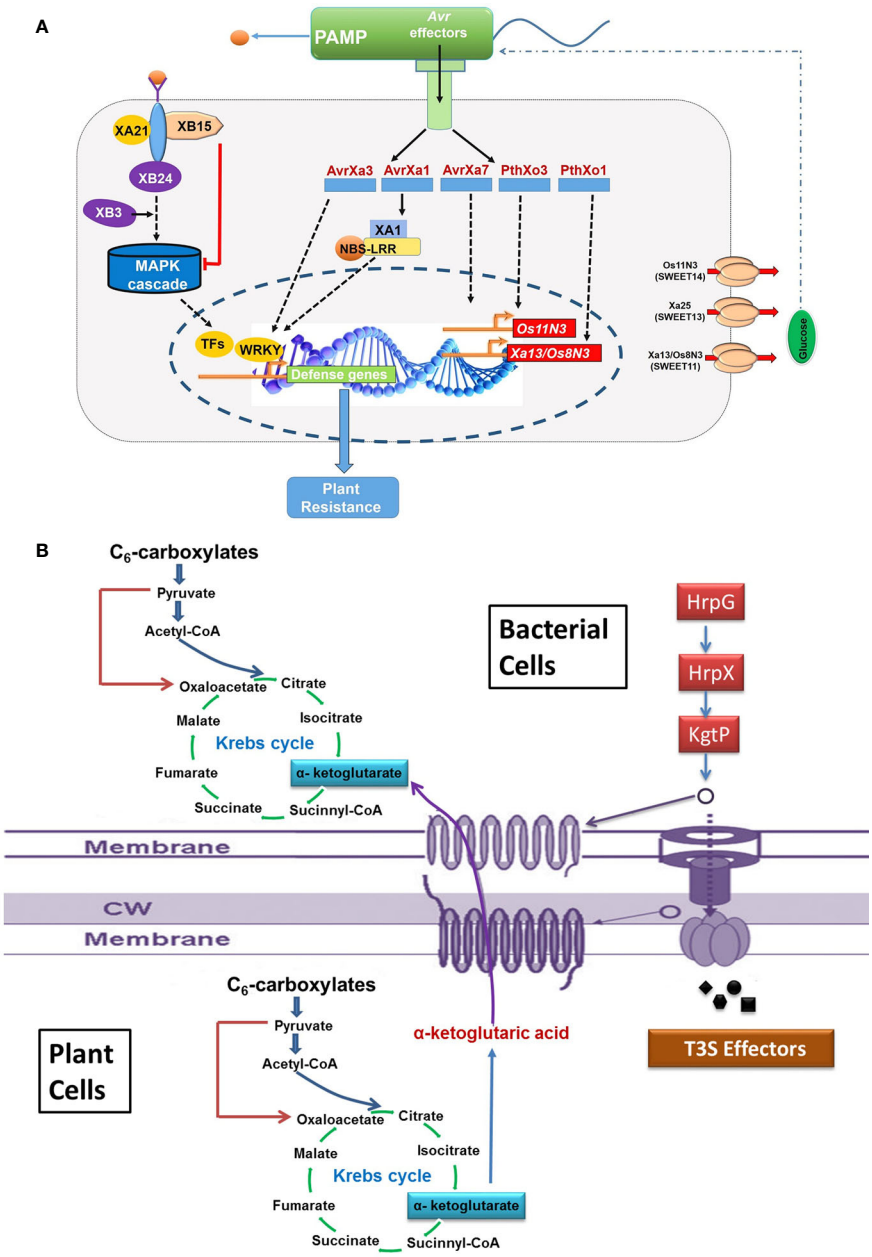


FIGURE 3 | The schematic representation for the molecular signaling involved during host and pathogen interaction. **(A)** Hijacking host key genes (*SWEET11/13/14*) by pathogen; **(B)** utilization of host metabolic resources like Kreb's intermediate by pathogen.

spectrum disease resistance. Plant immunity has been categorized into two levels based on microbial component recognition. The first and second level of immunity is known as basal immunity [PAMPs-triggered immunity (PTI)] and gene-for-gene resistance [effector triggered immunity (ETI)], respectively (Jones and Dangl, 2006; Monaghan and Zipfel, 2012). Both PTI and ETI are mediated by receptor kinase proteins localized in plasma membrane and nucleotide binding (NB) leucine-rich repeat (LRR) proteins and other factors localized in cytoplasm respectively (Jones and Dangl, 2006; Macho and Zipfel, 2014). PTI provides quantitative resistance, and ETI provides qualitative resistance in plant pathogen interaction (Zhang and Wang, 2013). Rice-*Xoo* interaction is an exclusive example of qualitative resistance, i.e., major gene conferred resistance (Zhang and Wang, 2013). The major disease resistance genes of rice, which provide resistance to *Xoo*, fall under either ETI or PTI or may fall under an additional mechanism, different from ETI or PTI (Hu et al., 2017).

One important and unique feature that is typical of qualitative resistance of rice against *Xoo* is that one third of the major disease resistance genes are recessive genetically (Zhang and Wang, 2013;

Hu et al., 2017). Out of the 44 known R-genes, at least 11 have been cloned and characterized (*Xa1*, *Xa3*/*Xa26*, *Xa4*, *xa5*, *Xa10*, *xa13*, *Xa21*, *Xa23*, *xa25*, *Xa27*, and *xa41*) (**Table 1**) (Tian et al., 2014; Wang et al., 2014a; Wang et al., 2014b; Cao et al., 2018). Of the remianing R genes, at least nine have been fine-mapped on different chromosome so far, viz., *Xa2*, *Xa4*, *Xa7*, *Xa22*, *Xa30*, *Xa33*, *Xa38*, *Xa39*, and *Xa40* (http://www.mshigen.nig.ac.jp/rice/oryzabase/gene/list). Interestingly, mutation in rice lines have also produced important R genes/alleles such as *Xa1*, *xa5*, *xa13*, *Xa23*, *xa25*, *Xa26/Xa3*, *Xa27*, and *xa41* (Nakai et al., 1988; Song et al., 1995; Yoshimura et al., 1998; Gao et al., 2002; Lee et al., 2003; Iyer et al., 2004; Sun et al., 2004; Gu et al., 2005; Chu et al., 2006; Liu et al., 2011; Wang et al., 2015; Hutin et al., 2015) (**Table 1**). Different R-genes encodes different types of proteins wherein *Xa1* encodes NB-LRR type protein (Yoshimura et al., 1998) and confers resistance to *Xoo* isolates by recognizing TALEs (Ji et al., 2016). *Xa21* and *Xa3*/*Xa26* encode plasma membrane localized LRR receptor like kinase proteins and confer race specific resistance to *Xoo* (Song et al., 1995; Li et al., 2012). *Xa4* encode cell wall associated protein kinase and boosts resistance to *Xoo* by strengthening the cell wall (Hu et al., 2017). The recessive gene *xa5* encodes gamma subunit of the basal transcription factor IIA 5 (TFIIAγ5) and is a substitution variant of a single amino acid V39E (Iyer and McCouch, 2004; Yuan et al., 2016). The non-variant version of the basal transcription factor is required for survival of *Xoo* in rice. The genes, *xa13*, *xa25*, and *xa41*, encode transmembrane proteins (Chu et al., 2006; Liu et al., 2011; Hutin et al., 2015; Cheng et al., 2017), which are basically sugar transporters, and the dominant alleles of these genes are specifically induced by TALEs produced by the pathogen for establishing infection. *Xa10* encodes an ER membrane protein, which elicits Ca^{2+} depletion in ER membrane inducing host cell death (Tian et al., 2014). *Xa23* is known to be an executor R gene that encodes a protein with 113 amino acid residues. The transcription of *Xa23* is triggered by *AvrXa23*, a TALE from *Xoo* (Wang et al., 2015). *Xa27* encodes apoplast protein, which triggers thickening of the secondary cell wall of the vascular bundle elements (Gu et al., 2004). Both dominant and recessive like *Xa1*, *Xa4*, *Xa21*, *xa5*, and *xa13* confer race specific resistance to *Xoo*, respectively, whereas the recessive alleles of genes such as *xa1*, *xa4*, and *xa21* and dominant alleles of *Xa5* and *Xa13* are susceptible to *Xoo* (Zhang and Wang, 2013). The cloned R genes, its cognate *Avr* genes, and the nature of the resistance of R genes have been summarized in **Table 2**.

INTROGRESSION OF NOVEL BB RESISTANCE GENES FROM WILD RELATIVES OF RICE

The genus *Oryza* includes two cultivated species of rice, i.e., *O. sativa and O. glaberrima* (2n = 24, genome type AA) and 22 wild species (2n = 24, 48) containing an array of genome types, including those belonging to AA, BB, CC, BBCC, CCDD, EE, FF, GG, KKLL, and HHJJ (Goicoechea et al., 2010). The *Oryza*, belonging to wild species are considered as a repository of genetic diversity that can be an asset for crop improvement. Although wild relatives of rice are atrocious to the cultivated varieties in terms of many agronomic traits, they are potential genetic resource with tremendous genetic diversity (Ali et al., 2010). Presence of adaptive traits that are often lacking in cultivars renders them vulnerable to several biotic and abiotic stresses, while a majority of the wild rice can withstand harsh biotic and abiotic environmental conditions. Cultivated rice has been the source of many BB resistance genes, and introgression of these genes into elite varieties/hybrids has been done through conventional breeding or also through marker-assisted breeding (MAB). However, transfer of genes from wild species to cultivated types brings with it a set of challenges such as hybrid sterility, linkage drag, and incompatibility barriers. So far, a handful of BB resistance genes have been identified and introgressed from related wild species of *Oryza* into cultivars (Nino-Liu et al., 2006; Sanchez et al., 2013). With the advent of molecular and genomic tools such as trait-associated DNA markers, high-throughput marker-assisted genotyping rapid identification of BB resistant sources and the process of their introgression into elite cultivars can be accelerated tremendously.

The first BB resistance gene to be cloned and characterized in the rice was *Xa21*. It was originally identified and introgressed from an accession of *O. longistaminata* (AA genome), and the gene encodes a receptor kinase like protein and provides broad-spectrum resistance against BB (Song et al., 1995). *Xa21* has been transferred to several rice cultivars and hybrids through marker-assisted breeding (MAB) (Williams et al., 1996; Singh et al., 2001; Perez et al., 2008; Sundaram et al., 2008; Balachiranjeevi et al., 2018). Additional broad-spectrum BB R-gene *Xa23* (encoding executor R protein) was transferred into Asian cultivated rice from *O. rufipogon* (AA) (Zhang et al., 2001). Various wild species of *Oryza* pertaining to secondary gene pool have also assisted as a source of BB R-genes such as *Xa27* from *O. minuta* (BBCC) and *Xa29(t)* from *O. officinalis* (CC) (Amante-Bordeos et al., 1992; Tan et al., 2004; Gu et al., 2005). Other BB resistance genes isolated from wild relatives and characterized with the help of molecular markers and genomic tools include *Xa10* (Gu et al., 2008; Tian et al., 2014), *Xa30* (*O. rufipogon*) (Jin et al., 2007), *Xa32* (*O. australiensis*) (Zheng et al., 2009), and *xa*32 (*O. meyeriana*) (Ruan et al., 2008), *Xa32t* (*O. australiensis*), *Xa33* (*O. nivara*) (Natrajkumar et al., 2012), *Xa35t* (*O. minuta*), and *Xa38* (*O. nivara*) (Cheema et al., 2008). A novel locus on chromosome 12 of *O. latifolia* (wild allotetraploid rice species) was identified recently, and it confer race specific resistance of *Xoo* strain PXO339 (Angeles-Shim et al., 2020). Based on these developments, it can be inferred that wild relatives of *Oryza* are expected to contribute significantly in developing durable BB resistant rice varieties. Whole genome sequencing of wild rice will expedite identification of resistance genes from the wild relatives of rice and may offer insights about the the pathways associated with the evolution of different resistance genes.

In additional to wild rice resources, it is generally accepted that durable and broad-spectrum resistance against plant dieseases can be enhanced by deployment of quantitative trait loci (QTLs) along with major genes so that both vertical and

TABLE 1 | Genes conferring resistance to bacterial blight pathogens.

S.No.	Gene	Chr. No.	Source	Origin	Resistant to races	Reference
1	*Xa1*	4	Kogyoku	Japan	JR I	Yoshimura et al., 1998
2	*Xa2*	4	Tetep	Vietnam	JR II	He et al., 2006
3	*Xa3/ Xa26*	11	Wase Aikoku3, Java-14, Chugoku-45, Cempocelek	Japan	PR 1,2,4,5 and All JR	Kaku and Ogawa, 2001; Sun et al., 2004
4	*Xa4*	11	TKM 6, IR 20, IR 22	India	PR 1, 4, 5, 7, 8 and 10	Wang et al., 2001
5	*xa5*	5	Aus boro lines (e.g. DZ192), DV85, DV86, DZ78	Bangladesh	PR 1, 2, 3, 5,7, 8, 9,10	Iyer and McCouch, 2004
6	*Xa6*	11	Zenith	USA	PR 1	Sidhu et al., 1978
7	*Xa7*	6	DV85, DV86, DZ78	Bangladesh	PR 1, 2, 3, 5, 7, 8,10	Lee and Khush, 2000; Porter et al., 2003
8	*xa8*	7	PI231128	USA	PR 5, 8	Sidhu et al., 1978; Singh et al., 2002
9	*xa9*	11	Khao Lay Nhay, Sateng	Laos	PRs	Singh et al., 1983; Ogawa, 1988
10	*Xa10*	11	Cas 209	Senegal	PR 2, 5, 7, JR	Yoshimura et al., 1983; Kurata and Yamazaki, 2006
11	*Xa11*	3	IR8, IR944	Philippines	JR IB, II, IIA, V	Mew, 1987
12	*Xa12*	4	Kogyoku,Tetep, Java-14	Japan	IR V	Mew, 1987
13	*xa13*	8	BJ1,Chinsurah Boro II	India	PR 6	Chu et al., 2006
14	*Xa14*	4	TN1	Taiwan	PR 5, 8	Oryzabase, 2006
15	*xa15*	ND	XM41 mutant	ND	JRs	Nakai et al., 1988; Gnanamanickam et al., 1999
16	*Xa16*	ND	Tetep	Vietnam	JI H8581and H8584	Oryzabase, 2006
17	*Xa17*	ND	Asominori	South Korea	JI H8513	Oryzabase, 2006
18	*Xa18*	ND	IR24, Toyonishiki, Miyang23	Philippines, Japan	BI-BM8417and BM8429	Liu et al., 2004; Oryzabase, 2006
19	*xa19*	ND	XM5 (mutant of IR24)	ND	PR 1, 2, 3, 4, 5 and 6	Lee et al., 2003; Oryzabase, 2006
20	*xa20*	ND	XM6 (mutant of IR24)	ND	JI	Taura et al., 1992
21	*Xa21*	11	*O. longistaminata*	Africa, Mali	PR 1, 2, 3, 4,5, 6, 7, 8 and 9	Song et al., 1995
22	*Xa22*	11	Zhachanglong	China	CRs (BSR)	Wang et al., 2003; Sun et al., 2004
23	*Xa23*	11	*O. rufipogon* (CBB23)	China/ Cambodia	All PR, JR, CR, IR	Zhang et al., 1998; Zhang et al., 2001
24	*Xa24(t)*	2	DV85, DV86, Aus 295	Bangaladesh	PR 6, CRs	Khush and Angeles, 1999; Lee and Khush, 2000
25	*xa25/ Xa25(t)*	12	Minghui 63, HX-3	China	PR 1,3 4, and to CR	Amante-Bordeos et al., 1992; Lee et al., 2003
26	*Xa26 (t)*	11	Minghui 63, Nep Bha Bong	China	PRs (BSR)	Yang et al., 2003; Sun et al., 2004
27	*Xa27*	6	*O. minuta* IRGC101141	Philippines	PR 2, 5	Gu et al., 2004; Gu et al., 2005 and Lee et al., 2003
28	*xa28(t)*	ND	Lota Sail	Bangladesh	PR 2, 5	Lee et al., 2003
29	*Xa29(t)*	1	*O. officinalis* (B5)	ND	CRs	Tan et al., 2004
30	*Xa30(t)*	11	*O. rufipogon* (Y238)	India	IR	Tan et al., 2004
31	*Xa31(t)*	4	*Zhachanglong*	China	CRs	Wang et al., 2009
32	*Xa32(t)*	11	O. australiensis	ND	PR PXO339	Chen et al., 2002
33	*xa33(t)/ Xa33 (t)*	6	*Ba7, O. nivara*	Thailand	TRs	Korinsak et al., 2009 Natrajkumar et al., 2012
34	*xa34(t)/Xa34 (t)*	1	Pin Kaset, O. brachyantha	Sri Lanka	TRs	Korinsak et al., 2009; Ram et al., 2010
35	*Xa35(t)*	11	*O. minuta* (Acc.No, 101133)	Philippines	PRs	Guo et al., 2010
36	*Xa36(t)*	11	C4059	China	PR	Miao et al., 2010
37	*Xa37(t)*	ND	Unknown	ND	Unknown	
38	*Xa38*	ND	*O. nivara* IRGC81825	ND	IRs	Cheema et al., 2008 Kaur et al., 2006
39	*Xa39*	11	FF329	ND	CRs, PRs	Zhang et al., 2014
40	*Xa40 (t)*	11	IR65482-7-216-1-2		KRs	Kim et al., 2015
41	*Xa41(t)*	ND	Rice germplasm	ND	Various	Hutin et al., 2015
42	*xa42*	3	XM14 (mutant of IR24)	ND	JRs	Busungu et al., 2016
43	*Xa43(t)*	11	IR36 (P8)	ND	KRs	Kim and Reinke, 2019
44	*xa44 (t)*	11	IR73571-3B-11-3-K3 (P6)	ND	KRs	Kim, 2018

horizontal resistance can be achieved. In the recent past, a few studies highlight the role of QTLs with respect to resistance/ tolerance against BB of rice. Even though few QTLs associated with tolerance/resistance to BB have been reported earlier, most of these QTLs mapped closely to already identify major resistance genes (Li et al., 1999). Five major QTLs were maped on various chromosomes for African resistant *Xoo* strains *Xoo*. Various loci on different chromosomes such as 1, 7, 9, 10, and 11

TABLE 2 | List of cloned rice R genes, cognate *Xanthomonas oryzae* Avr genes, and nature of resistance of R genes (adapted from Jiang et al., 2020).

S.No.	Gene	Chromosome number	Encoded Protein	Cognate *Avr* gene	Encoded Protein	Resistance nature	Reference
1	*Xa1*	4	Nucleotide binding site–leucine rich repeat (*NBS-LRR*)	*PthXo1/Tal4/ Tal9d*	ND	Race specific	Yoshimura et al., 1998; Ji et al., 2016
2	*Xa3/Xa26*	11	Leucine-rich repeat receptor-like protein kinase (LRR-RLK)	*AvrXa3*	ND	Broad spectrum	Sun et al., 2004; Li et al., 2004; Xiang et al., 2006
3	*Xa4*	11	Wall-associated kinase (WAK)	ND	ND	Race specific	Hu et al., 2017
4	*xa5*	5	TFIIAγ5 transcription factor	*Avrxa5/PthXo7*	TAL effector	Race specific	Jiang et al., 2006; Sugio et al., 2007; Zou et al., 2010
5	*Xa10*	11	Executor R protein/	*AvrXa10*	TAL effector	Broad spectrum	Tian et al., 2014
6	*xa13 (OsSWEET11)*	8	SWEET-type protein/nodulin 3 family protein	*PthXo1*	TAL effector	Race specific	Chu et al., 2006; Yang B. et al., 2006; Yuan et al., 2009
7	*Xa21*	11	Leucine-rich repeat receptor-like protein kinase (LRR-RLK)	*RaxX*	ND	Broad spectrum	Song et al., 1995; Pruitt et al., 2015
8	*Xa23*	11	Executor R protein	*AvrXa23*	TAL effector	Broad spectrum	Wang et al., 2014b; Wang et al., 2015
9	*xa25 (OsSWEET13)*	12	SWEET-type protein/nodulin 3 family protein	*PthXo2*	TAL effector	Race specific	Liu et al., 2011; Zhou et al., 2015
10	*Xa27*	6	Executor R protein	*AvrXa27*	TAL effector	Broad spectrum	Gu et al., 2005
11	*xa41 (OsSWEET14)*	11	SWEET-type protein	*AvrXa7/ PthXo3/TalC/ Tal5*	TAL effector	Broad spectrum	Antony et al., 2010; Yu et al., 2011; Hutin et al., 2015; Hutin et al., 2015

TFIIA, transcription factor IIA; SWEET, sugar will eventually be exported transporter; TAL, transcription activator like; ND, not determined.

explained as much as 13%, 37%, 13%, 11% and 15% of phenotypic variation in terms of resistance, respectively (Djedatin et al., 2016). A major *qBBS11* was identified by composite interval mapping of MAGIC population derived from Japonica, and it explained 31.25% of the phenotypic variation (Kim and Reinke, 2019), and this QTL was later renamed as *Xa43(t)*. On closer examination, *xa34(t)* has been identified to co-localize along with *qABB*-1 on rice chromosome 1, which is a resistance QTL induced by the African *Xoo* strain (Chen et al., 2011).

ANALYZING RESISTANCE GENE ANALOGUES (RGAS) AS A NOVEL TOOL TO IDENTIFY BLIGHT RESISTANCE GENE

Resistance genes analogs (RGAs) are a large class of disease resistance associated genes and they can be categorized into two major groups, namely NBS-LRR and transmembrane LRR (TM-LRR) (Hammond-Kosack and Jones, 1997; Sekhwal et al., 2015). Others include pentatricopeptide repeats (PPRs) and apoplastic peroxidases. NBS-LRR class of RGAs targets effector protein of pathogen, thus mediate effector triggered immunity (ETI) in host cell, whereas TM-LRR class of RGAs mediates PTI (Chisholm et al., 2006). NBS-LRR represents the most abundant and best-known family of RGAs contributing to disease resistance in plants (Porter et al., 2009). Analysis of whole genome sequences of japonica Nipponbare and indica 93-11 suggested presence of RGAs in pseudogenes, with 347 RGAs in Nipponbare and 345 in 93-11 as pseudogenes (Luo et al., 2012). Interestingly, most of the identified pseudogenes have strong identity with one or the other NBS protein (Liu et al., 2011). Further, many studies have shown that the RGAs are randomly distributed on chromosome either in large or small clusters (Ghazi et al., 2009), for example, 50% NBS and 74.3% NBS-LRR class of RGAs were found to be clustered in rice (Yang S. et al., 2006). The distribution of RGAs in clustered manner potentially functions like reservoir of genetic variation, which may be responsible for bringing the evolution of new *R* genes (Michelmore and Meyers, 1998; Young, 2000; Zhou et al., 2007). On the long are of chromosome 11, cluster of six *Xa21* like RGAs was reported. The NBS-LRR containing genes cluster was also predicted at 0.6 Mb away from *Xa21*, which indicates the existance of extra NBS-LRR–type genes for activation and expression of the *Xa21* gene (Ghazi et al., 2009). Therefore, from the application point of view, RGAs provide enormous opportunities as they can be used as candidates' genes for R-gene mapping and cloning, co-localization of QTLs, SNP marker development, and for resistance breeding (Liu et al., 2007; Huang et al., 2012).

MODERN APPROACHES FOR DEVELOPMENT OF BB RESISTANT RICE

Molecular Breeding for BB Resistance in Rice

Efforts have been made to improve resistance of rice against BB through conventional and modern breeding techniques. This is achieved through standard crossing and/or backcrossing an elite rice variety/hybrid with the genotype carrying the resistance gene to BB. The practice not only reduces the use of chemical pesticides but also offers a sustainable way for management of

this disease. Presence of several virulent bacterial strains in the rice growing areas throughout the world necesssitates cultivation of such rice varieties, which are endowed with multiple resistance genes as gene-pyramids. To date, identification of 44 R genes conferring resistance to diverse *Xoo* races has been completed (Busungu et al., 2016; Neelam et al., 2019); majority of these identified genes come from *O. sativa* ssp. *indica* or *japonica*. As mentioned earlier, a set of resistance genes have been also identified from wild species of rice such as *O. longistaminata*, *O. rufipogon*, *O. minuta*, and *O. officinalis* (Bhasin et al., 2012; Kumar et al., 2012; Wang et al., 2014a; Zhang et al., 2014; Kim et al., 2015) (**Table 1**).

It is pertinent to note that 14 R-genes (*xa5*, *xa8*, *xa13*, *xa15*, *xa19*, *xa20*, *xa24*, *xa25*, *xa26b*, *xa28*, *xa31*, *xa32*, *xa33*, and *xa34*) out of 44 known R-genes are recessive, while the others are dominant in their inheritance, and *Xa27* has shown both dominant and semi-dominant inheritance in different genetic backgrounds (Gu et al., 2004; Chen et al., 2011; Kim et al., 2015; Cao et al., 2018) (**Table 1**). The incorporation of several resistance (R) genes has been facilitated through marker-assisted backcrossing *(*MABC) or conventional backcross breeding, and resistance breeding has played a significant role in defending rice from the attack by the pathogen (Sundaram et al., 2008; Sundaram et al., 2009; Perumalsamy et al., 2010; Hari et al., 2011; Hari et al., 2013; Pandey et al., 2013; Kim et al., 2015; Balachiranjeevi et al., 2015; Abhilash et al., 2016; Abhilash et al., 2017). A rice derived BB resistance gene *Xa38* was incorporated into a BB susceptible rice variety PB1121 and APMS 6B (a rice maintainer line), either singly or in combination with other BB resistance genes, using a modified MABC approach, and improved lines showed broad spectrum of resistance against different *Xoo* races (Ellur et al., 2016; Yugander et al., 2019). Rice varieties carrying single resistance genes (e.g., *Xa4*) are not recommended for long term cultivation, as acute selection pressure on the pathogen results in rapid evolution of compatibility between *Xoo* and rice (Mew et al., 1992). Harnessing broad-spectrum resistance through pyramiding multiple resistance genes can be helpful to avoid such breakdowns. The probability of breakdown in cases of resistance conferred by two or more genes in a single genotype is much lower than that of a single gene controlling resistance (Mundt, 1990). For instance, R-genes in combination (*Xa4/xa5* and *xa5/Xa21*) offer higher level of resistance compared to both parental level and single gene (Sattari et al., 2014; Pradhan et al., 2016). Huang et al. (1997) developed four-gene pyramid lines comprising *Xa4*, *xa5*, *xa13*, and *Xa21* genes in IR24 cultivar genetic background through MABC, and the gene-pyramid lines showed broad spectrum disease resistance. Several research groups have performed BB gene pyramiding in rice using MABC techniques, e.g., marker-assisted introgression of *xa5*, *xa13*, and *Xa21* in the genetic background of PR106, Samba Mahsuri, Triguna, and Jalmagna (Singh et al., 2001; Sundaram et al., 2008; Sundaram et al., 2009; Pradhan et al., 2015). Similarly, *xa13* and *Xa21*genes pyramiding was carried out in the genetic background of Pusa Basmati 1 (Joseph et al., 2004). **Table 3** offers a comprehensive list of BB resistance genes that have been deployed or in the process of deployment in rice through MAB.

Development of Transgenic Rice Resistant to BB

A potential strategy to control BB disease is the genetic transformation of elite cultivars using cloned resistance genes. Compared to conventional breeding, it is less time-consuming and avoids the problem of linkage drag. The first transgenic line containing *Xa21*, T-309, was developed in *japonica* rice by Wang et al. (1996). Later, *Xa21* was introduced into several varieties such as IR 72, MH 63, and IR 51500 (Datta et al., 2002; Tu et al., 1998; Tu et al., 2000). Similarly, an elite restorer line genetically transformed with *Xa21* has shown marked level of resistance to BB while retaining its original traits (Zhai et al., 2004). Field trials of *Xa21* transgenic rice conducted in India, Philippines, and China led to the identification of BB-resistant lines in transgenic IR 72 (Datta, 2004). Transgenic lines carrying one or the other *Xa* genes were developed for functional characterization of the gene; however, none of these could be commercialized due to regulatory and policy bottlenecks. Hence, conventional breeding combined with marker-assisted breeding or genomics assisted breeding is the preferred strategy for developing resistant lines/varieties to control BB disease.

Mining of Novel Alleles of BB Resistance Genes

Mining superior alleles from different gene pools of any crop provides opportunity to access novel and effective alleles for biotic and abiotic stresses, which can be deployed in plant breeding for cultivar development (Ramkumar et al., 2010). To identify novel or superior allele of the known gene among the population, PCR-based approach is widely used. In this method, PCR amplification of homologs from different wild and cultivated germplasm is performed and analyze the PCR amplicon. This method is known as allele mining, and it has been widely studied for BB resistance genes such as *Xa7* (Utami et al., 2013), *Xa27* (Bimolata et al., 2013), *Xa26*, *Xa21*, *and xa5* (Bimolata et al., 2015), etc. This method will also reveal the degree of conservation among genes and other regulatory regions across the species. As mentioned earlier, fast adaptation of the pathogen races causes the failure of disease resistance in varieties containing single resistance genes and even two genes. Therefore, discovery of novel sources of resistance becomes crucial to match the plasticity of rapidly evolving pathogenic *Xoo* strains (Barry et al., 2007). In this context, surveying the genic/allelic variation available in landraces (Borba et al., 2009), traditional varieties, and wild relatives (Barbier, 1989) of rice will contribute to obtain effective and durable BB resistant varieties. One such example is *Xa7*, which has been used to develop BB resistance rice varieties (Perez et al., 2008; Utami et al., 2010). Allele mining approach was applied in the local rice accessions of Indonesia (Parekaligolara) to isolate resistant alleles of *Xa7* (Utami et al., 2013). Subsequently, these accessions containing variant alleles with respect to *Xa7* have been used as for developing new BB resistant rice lines (Utami et al., 2013). Analysis of variation in

TABLE 3 | Cultivars improved for bacterial blight resistance through breeding/marker-assisted breeding.

S.No.	Resistance genes	Variety/Parental line	References
1.	*Xa21*	Swarna	Reddy et al., 1997
2.	*Xa21*	Minghui63	Chen and Zhang, 2000
3.	*Xa21*	KMR3R	Hari et al., 2011
4.	*Xa33*	Samba Mahsuri	Natrajkumar et al., 2012
5.	*Xa4, xa5*	Angke	Sattari et al., 2014
6.	*xa5*, *xa13*	Triguna	Sundaram et al., 2009
7.	*xa13*, *Xa21*	Pusa Basmati1	Joseph et al., 2004
8.	*Xa7, Xa21*	Minghui63	Zhang et al., 2006
9.	*Xa21, xa13*	Pusa6B, PRR78	Basavaraj et al., 2010
10.	*Xa21, xa13*	Taraori Basmati, Basmati386	Pandey et al., 2013
11.	Xa21, xa13, sd-1	Type 3 Basmati	Rajpurohit et al., 2010
12.	*Xa4*, *xa-5*, *Xa21*	Mangeubyeo	Suh et al., 2013
13.	*Xa4*, *Xa7*, *Xa21*	TGMS1	Perez et al., 2008
14.	*xa5*, *xa13*, *Xa21*	Samba Mahsuri	Sundaram et al., 2008
15.	*xa5*, *xa13*, *Xa21*	Jalmagna	Pradhan et al., 2015
16.	*Xa5*, *xa13*, *Xa21*	ADT43, ASD16	Perumalsamy et al., 2010
17.	*xa5*, *xa13*, *Xa21*	IR65598-112	Sanchez et al., 2000
18.	*xa5*, *xa13*, *Xa21*	PR106	Singh et al., 2001
19.	*xa5*, *xa13*, *Xa21*	IR64	Davierwala et al., 2001
20.	*Xa4*, *xa5*, *Xa7*	IR64	Leung et al., 2004
21.	*Xa21, xa13, Xa38*	Pusa Basmati 121	Ellur et al., 2016
22.	*Xa4*, *xa5, xa13, Xa21*	Lalat, Tapaswini	Dokku et al., 2013
23.	*Xa4*, *xa5*, *xa13*, *Xa21*	IR24	Huang et al., 1997
24.	*Xa4*, *xa5*, *Xa13*, *Xa21*	Mahsuri	Guvvala et al., 2013
25.	*Xa4*, *xa5*, *xa13*, *Xa21*	Swarna, IR64	AICRIP, 2008
26.	*Xa7, Xa21, Xa22, Xa23*	Huahui1035	Huang et al., 2012

amino acid residues between the resistant and susceptible lines has revealed co-linear non-synonymous substitutions of lysine-cysteine-valine to serine-serine-threonine, respectively. Another BB resistance gene, *Xa27* provides resistance to rice against only those strains of *Xoo* harboring the avirulence gene *avrXa27*. Both dominant and recessive alleles of *Xa27* gene code for same protein without any changes in the protein sequence, but polymorphism exists in their promoter sequences. Deletion of three nucleotides AGA at 51st position in the promoter of recessive allele (i.e., non-functional allele) of the gene has been reported (Gu et al., 2005). Twenty-seven alleles of *Xa27* gene have been identified in *O. nivara* and *O. sativa* at both promoter as wel as 5′UTR region. Such nucleotide diversity analysis will certainly help in diversification of gene function and enhancing the intensity of BB resistance (Bimolata et al., 2013). The nucleotide diversity analysis of naturally occurring BB resistance genes (*Xa21*, *Xa26*, and *xa5*) alleles was carried out in diverse cultivars of *Oryza* species and their wild relatives (Bimolata et al., 2013). The highest singleton variable sites (SVS) and nucleotide diversity were reported in *Xa26*, whereas maximum frequency of single nucleotide polymorphisms (SNPs) was observed in *Xa21*. Many substitutions and InDels resulted in nucleotide and amino acid polymorphism at *Xa21* and *Xa26* loci, which also have pathogen recognition LRR domain, and finally resulted in non-functional gene. Transition bias was reported in all the three alleles of *Xa21*, *Xa26*, and *xa5*, where G to A transition was favored more (Bimolata et al., 2015). Functional characterization of the new alleles will help in deciphering their actual roles in resistance against the pathogen. Alternative promising approach is RNA interference (RNAi) technique, which is used to silence molecules involved in regulating resistace genes negatively (Gust et al., 2010; Li C. et al., 2012). The final outcome results as a stronger and durable defense response, which leads to reduce disease manifestation and progression.

Mutagenesis and TILLING

Targeting induced local lesions in genomes (TILLING) is a reverse genetic non-transgenic technique that is exploited to detect induced mutations in the target genes for the improvement of both plant and animal species (Barkley and Wang, 2008). Recently, with the aim to develop disease resistance varieties and creating useful genetic variation for multiple traits, TILLING population have been generated in many economically important plants like wheat (Fitzgerald et al., 2010), barley (Talamè et al., 2008), tomato (Piron et al., 2010), sunflower (Sabetta et al., 2011), and melon (González et al., 2011) by employing either chemical or physical mutagens. In rice, Till and colleagues (2007) could successfully generate a high-density TILLING population (1 mutation/250–300 kb) in Nipponbare variety of rice. Wu et al. (2005) demonstrated the efficacy of TILLING approach for identifying mutant rice lines with enhanced resistance against BB, rice blast and tungro virus, with a frequency ranging from 0.01 to 0.1%. They generated 60,000 IR64 TILLING mutant lines by using chemical and physical mutagens, out of which 38,000 unique lines were advanced to M4 generation for forward and reverse TILLING. In rice, the technique has been employed to isolate various rice mutants by targeting important agro-economical genes such as *OsBZIP* for rice blast resistance (Till et al., 2007); *OsTPS1*c *OsDREB*, *OsSNAC1*, *OsAKT1*, *OsHKT6*, *OsNSCC2*, *OsHAK11*, *OsSOS1*, *OsAHP1*, and *OsPLA1* for abiotic resistance (Till et al., 2007; Suzuki et al., 2008; Casella et al., 2013; Hwang et al., 2016); *OsSD1* for regulating plant height (Casella et al.,

2013); *OsHd1* and *OsSAD* flowering (Suzuki et al., 2008; Casella et al., 2013); *OsACOS12* for fertility (Li et al., 2016); and *OsBADH2* for aroma (Casella et al., 2013).

TILLING population can also be used for forward genetic studies. Screening of 60,000 IR64 (rice *indica* cultivar) mutants led to identification of several loss or gain of resistance mutants of showing resistance or enhanced susceptibility to BB, blast, and tungro diseases (Wu et al., 2005). EMS induced mutant in the genetic background of Nagina 22 rice variety has been developed and utilized for various genetic studies in India (Sevanthi et al., 2018). It may be worthwhile to screen the rice lines for resistance against BB and other biotic stress and identify novel genetic variations. In addition to the above, we have generated a large sized EMS mutagenized population of Samba Mahsuri and screened them for resistance against bacterial blight. Preliminary results show that few of the mutant lines of Samba Mahsuri display enhanced resistance (Ershad Gopi et al., 2017). These mutagenized populations can be shared with researchers or breeders for rapid screening for a range of phenotypes, and the TILLING populations can serve as a public resource for the research community. For instance, IRRI, Philippines has distributed around 15,000 mutant lines of IR64 to researchers worldwide for detection of novel phenotypes, including sensitivity to plant hormones, phytic acid abundance, response to salinity and drought, and non-host resistance (Wu et al., 2005). A public TILLING support tool (http://tilling.ucdavis.edu/index.php/RiceTilling) and rice mutant database (IRIS; http://www.iris.irri.org) have been established in rice.

Sequencing Based High-Throughput Mutation Detection Systems

In rice, NGS based TILLING protocols are well documented (Burkart-Waco et al., 2016) and it is a matter of time before the strategy is widely adopted to identify genes associated with resistance/susceptibility against bacterial blight pathogen in rice. Unlike NGS, where one can obtain the exact information of nucleotide base change and its position caused due to mutagen, high-resolution melting (HRM) identifies the mutation based on the differences in the melting curve of fragments of mutant and wild type. HRM technique is particularly important for analyzing the target genes that consist of multiple exons of smaller lengths. Though NGS and HRM techniques are still costlier, their capacity to generate results within a very short span of time is indeed encouraging. NGS- and HRM-based TILLING or Eco-TILLING strategy could uncover a new set of genes controlling BB resistance, and hence expedite the progress of developing new rice cultivars with greater level of resilience. In this context, it is worthwhile to note that International Rice Research Institute (IRRI), Philippiens along with other collaborators have sequenced ~ 3000 rice accessions and the rice lines can be mined for novel alleles of major, cloned and well characterized genes conferring BB resistance.

Genome Editing

Breeding traits of agronomic significance largely relies upon existing allelic variation and involves repeated cycles of crossing and selection to obtain a crop genotype with desired level of improvements, which may consume considerable time and efforts (Sundaram et al., 2014). These limitations can be overcome by using emerging genome editing technologies. Genome editing based on artificial nucleases is a transformative technology that has the ability to modify plant genomes in an accurate and expectable manner. So far, four sequence-specific nucleases, i.e., transcription activator-like effector nucleases (TALENs) (Christian et al., 2010), zinc finger nucleases (ZFNs) (Kim et al., 1996), meganucleases (Smith et al., 2006) and the CRISPR/Cas (CRISPR-associated) nucleases, have been successfully used in genome editing in many crop plants (Bortesi and Fischer, 2015). In principle, all these technologies can be used for modifying plant traits such as disease resistance. For example, TALEN technology was applied successfully to mutate a BB susceptible gene, *Os11N3/OsSWEET14* promoter in rice. The inability of the effector to bind to the promoter of *OsSWEET14*, ultimately resulted in BB resistance (Li et al., 2012). The *Os11N3* is a sucrose-efflux transporter family gene (i.e., *SWEET* gene) whose expression gets activated by *Xoo* effectors for the pathogen's nutritional needs. By editing the effector-binding element (EBE) of *Os11N3*, the virulence function of effectors produced by *Xoo* was abolished, leading to improved BB resistance (Li et al., 2013). CRISPR/Cas9 mutagenesis of another susceptibility gene encoding sucrose transporter *OsSWEET13* was performed to achieve BB resistance. *Xoo* effector/TALE *PthXo2* induces the expression of *OsSWEET13* in host, which subsequently resulted in establishment of *Xoo* and host susceptibility (Zhou et al., 2015; Borrelli et al., 2018). The expression of *OsSWEET13* gene has been evidenced to be activated by binding of the TALE, *PthXo2* to EBE of its promoter sequence (Xu et al., 2019). Genome edited lines showed significantly higher level of resistance to pathogen strains possessing the TALE. This study exemplified the fact that the technology can be applied to elite rice varieties to edit multiple genes simultaneously or sequentially to provide stronger and durable resistance against majority of BB strains. Furthermore, better understanding of SWEET genes and CRISPR/Cas9-mediated genome editing tool has helped in producing broad spectrum resistance in Kitaake, IR64 and Ciherang-Sub1 rice varieties through genome editing (Oliva et al., 2019; Xu et al., 2019). Recently, CRISPR/Cas9-mediated genome editing in the promoter region EBEs of *OsSWEET14* gene has been demonstrated to confer resistance in Super Basmati rice lines against *Xoo* strain carrying *AvrXa7* TALE (Zafar et al., 2020).

Among the currently available nuclease-based genome editing tools, CRISPR/Cas system is the latest and more popular technology, which relies on RNA-guided engineered nucleases (Jinek et al., 2012). CRISPR/Cas method employed for genome editing consists of a Cas9 endonuclease targeting a specific sequence of the genome defined by a single guide RNA. The CRISPR/Cas technology is simple and efficient, more importantly, has the ability to cleave even methylated DNA (Hsu et al., 2013), and has less or no off-target mutations (Shen et al., 2014). Therefore, CRISPR/Cas system is more versatile for editing plant genomes with highly methylated

CpG sites (Miao et al., 2013) and will the most desirable system for editing sequences of rice susceptibility genes like *OsSWEET11*, *OsSWEET13*, *OsSWEET14*, etc. Broad spectrum resistance against *Xoo* was reported in the transgenic rice lines, in which promoter region EBEs sequence of *OsSWEET11*, *OsSWEET13*, and *OsSWEET14* were edited through CRISPR/Cas9 technology (Xu et al., 2019). Transgenic wheat plants with mutated mildew resistance locus (*MLO*) obtained by CRISPR/Cas9, and TALEN technologies showed improved resistance to powdery mildew (Wang et al., 2014). With constant refinements in the technical aspects with respect to specific targeting of the desired gene sequence with precision, genome editing will certainly be a method of choice for developing disease resistant varieties in rice.

Genomic Selection (GS)

Current crop breeding approach largely depends on the robust phenotyping and deployment of genetic markers. Major limitation of marker-assisted selection in plant breeding is use of biparental mapping population for QTL prediction and its applicability with traits associated with major effect genes but may work for polygenic traits that are controlled by many genes of small-effect, and in general, such traits are crucial for the improvement of new crop varieties (Heffner et al., 2009; Crossa et al., 2017). To improve the crop selection procedure, breeders have now adopting a newer model—a black box approach 'Genomic Selection Model' that does not solely depend on the prior knowledge about the effect or function of individual genetic markers. In fact, GS involves huge set of phenotyping surveillance along with all molecular marker information which avoid biased marker effect estimates; thereby, it can capture more of the variations that appears due to small-effect QTLs (Heffner et al., 2009). Further, GS is an improved form of MAS which concurrently estimates a genomic estimated breeding value for all locus, haplotype, or marker across the entire genome of each genotype. Therefore, genomic selection offers opportunity to increase grain yield and quality by rapid selection of superior genotypes and accelerating breeding cycle in less time. In recent years, GS and genomic-enabled prediction (GP) have been studied in rice for enhancing grain yield by analyzing the genetics and the statistical complexity, which includes environment interaction with genotype that control trait phenotype (Spindel et al., 2015; Xu et al., 2018). The genomic prediction model upon cross validating 363 elite breeding lines from IRRI predicted with an accuracy that ranged from 0.31 to 0.34 for grain yield and 0.63 for flowering time (Spindel et al., 2015). Similarly, Xu et al. (2018) used 575 rice hybrids as a training population, and 362,760 potential hybrids were used to predict agronomic traits such as branch number (primary and secondary) and per panicle grain number and primary branch with accuracy of 36.12, 61.80, and 75.83%, respectively. It can be expected that, in coming years, rice breeding will deploy GS model and GP prediction to rapidly identify novel loci associated with BB resistance and other productivity related traits and quickly use them in breeding programmes.

MOLECULAR OMICS APPROACHES FOR STUDYING RICE-XOO INTERACTION

Transcriptome Analysis

In the last 15 years, more than 70 key genes providing resistance to different plant pathogen have been identified, cloned and characterized from different plant species (Sharma et al., 2009; Sanseverino et al., 2010). Pathogen incursion can alter the transcript levels of various host plant genes (Iqbal et al., 2005), and several techniques have been developed in recent years to study the differential expression pattern of host genes associated with response to pathogen attack and resistance against it. Some of these expression profiling techniques are cDNA microarray (Schena et al., 1995), cDNA- amplified fragment length polymorphisms (AFLP) (Vuylsteke et al., 2007), suppression subtractive hybridization (Diatchenko et al., 1996), serial analysis of gene expression (SAGE) (Velculescu et al., 1995; Mardis, 2008), digital gene expression (DGE) (Audic and Claverie, 1997), qPCR (Mortazavi et al., 2008), etc. Transcriptome analysis helps elucidate key genes and pathways participating in defense signaling during plant pathogen interaction (Glazebrook, 2001).

cDNA microarray study of a transgenic rice (TP309-Xa21)-*Xoo* (P6 and K1avirulent and virulent strain respectively) interaction observed 454 and 498 DEGs in the incompatible and compatible interactions, respectively, of which co-regulated genes were 237 (Li Q. et al., 2006). Ethylene receptor-like protein, ethylene-insensitive protein, protein phosphatase, and ADH were upregulated only in rice-*Xoo* incompatible interaction (Li Q. et al., 2006). A genome-wide identification of defense response genes was performed in *xa13* gene mediated resistance plants wherein 702 unique expressed sequences triggered by *xa13* were identified (Chu et al., 2004). Sequence analysis showed induction of homologs to putative R-genes encoding NBS-LRR and XA21 like protein. There was also induction of gene homologs related to host-pathogen interaction reported in other plant species, such as PR proteins, peroxidases, WRKY transcription factors, GST, RNA helicases, ubiquitins, catalase, ankyrin-like protein, and cytochrome P450 (Chu et al., 2004). Microarray analysis after infection by BXO43 strain of *Xoo* in the resistant variety of rice, Ajaya (IET 8585), and susceptible variety, IR24, has revealed the differential expression of 274 genes between and susceptible genotypes (Grewal et al., 2012). Out of 274 genes, 152 and 122 were reported to be up- and down-regulated, respectively, in IET8585 compared to IR24. Some of the major up-regulated transcripts include chitinase precursor, WRKY69, Hin 1, DREB1B, NB-ARC domain containing protein, glutathione S-transferase (GST), cytochrome P450, harpin-induced protein, lipoxygenase, and flavanoid 3-monooxygenase (Grewal et al., 2012). It was interesting to note that several defense related signaling molecules such as MAPKKK17 (Menges et al., 2008), MAPKKK3 (Zipfel et al., 2004), and PP2C were found to be up-regulated (Grewal et al., 2012). Wen et al. (2002) also conducted an expression profile of 12 defense response genes where they observed constitutive expression of these genes but significantly induced under the influence of *Xoo* and the fungal pathogen

causing blast disease, *Pyricularia grisea*. The RNA-Seq analysis of resistant (CBB23; a rice line carrying *Xa23* gene) and a susceptible (JG30) rice gentotypes led to identify several DEGs post infection by *Xoo* strain PXO99^{A}. Moreover, several of the DEGs were up-regulated in CBB23 were related to immune responses like peroxidase, phytosulfokinase, RLKs, serine/threonine kinase, TFs (WRKY, NAC, MYB, bZIP, AP2/ERF etc.) and phytohormones (SA and ET) (Tariq et al., 2018). In another RNA-Seq analysis, where CBB23 was challenged with PXO99^{A} and its mutant P99M2 exploited 1235 DEGs at defferent time point (Wang et al., 2019). Publicly available *Xoo* infected rice microarray data analysis revealed the importance of mitochondria and chloroplast as an arena for up-regulated and down-regulated genes in response to *Xoo* infection (Kong et al., 2020). Therefore, the genes up-regulated in resistance varieties can be targeted for improvement through molecular breeding and transgenic approaches, and the rice genes that are up-regulated in susceptibility reaction against *Xoo* could be potential targets for silencing or genome editing.

Proteomics Analysis of Products Encoded by Resistance Genes

Completion of sequencing of rice and *Xoo* genomes are significant accomplishments in host-pathogen interaction study. Even though genomes can evolve rapidly because of either transposable elements movement or from epigenetic changes, they are in general contemplated as highly static compared to their extremely dynamic proteomes. Therefore, there has been increased focus on elucidating functional aspect of proteins involved in rice-*Xoo* interaction. Comparative proteomics is emerging as a promising approach to develop a global understanding of protein expression under various conditions including attack by pathogen on the plant host (Agrawal and Rakwal, 2011; Ding et al., 2012). Using proteomic approaches, different biological processes including protein–protein interaction, post-translational modification, protein expression, etc. could be successfully analyzed during plant development, particularly during stress conditions (Hashiguchi et al., 2010). The induction of PR5 protein post nitrogen application was reported in case of *M. grisea* infection (Konishi et al., 2001). Stress related proteins such as superoxide dismutase (SOD), heat shock proteins (HSP), and dehydrins are induced in plant post rice yellow mottle virus (RYMV) inoculation (Ventelon-Debout et al., 2004). Proteomic study of sub-cellular organelles has been performed such as plasma membrane, vacuolar membrane, mitochondria, and chloroplast. Cytosolic and membrane protein study revealed the activation of proteins related to defense such as thaumatin-like protein (TLP) (PR5), probenazole-inducible protein 1 (PBZ10), (SOD), and peroxiredoxin (Mahmood et al., 2006). Transgenic rice lines overexpressing a TLP showed moderate level of resistance. After proteomic analysis, 440 protein spots were detected, where 10 proteins, including TLPs, were differentially expressed (five up-regulated and five down-regulated). TLP, ATP synthase B chain, glycine cleavage H protein, and 2-Cys peroxiredoxin were significantly up-regulated, whereas glycerol aldehyde dehydrogenase, salt induced protein, transketolase, and oxygen evolving enhancer protein 2 were down-regulated. Out of 10 differentially regulated protein spots, two did not show a substantial match with any known proteins (Mahmood et al., 2006). A study on plasma membrane (PM) proteome in rice revealed the involvement of at least eight PM-associated proteins in BB defense out of 20 protein spots induced after *Xoo* infection (Chen et al., 2007). These proteins were H^{+}-ATPase, prohibitin (OsPHB2), hypersensitive-induced response protein (OsHIR1), quinone reductase, zinc finger, universal stress protein (USP), C2 domain protein, HSP, and protein phosphatase. A stable somatic hybrid line SH76 was developed using wild rice *O. meyeriana* and japonica rice cultivar (8411), which proteomic analysis revealed differential expression of 77 proteins including stress related proteins such as putative glutathione S- transferase, ascorbate peroxidase, and mitochondrial chaperonin-60 (Yu et al., 2008). Interestingly, differential induction stress associated proteins have been reported upon *Xoo* challenge, suggesting the likelihood of participation of mutual stress pathways. Some of the important candidate proteins activated in *O. longistaminata* post BB infection include cyclin-dependent kinase C, germin-like protein, putative r40c1, glutathione-dependent dehydroascorbate reductase 1 (GSH-DHAR1), and Ent-isokaur-15-ene synthase (Kumar et al., 2015).

Metabolomics Analysis of Compounds From Resistant Plants

Cell signaling is the first molecular event that occurs during pathogen infection. Plant produces volatile metabolites/hormones such as ethylene, methyl jasmonate, methyl salicylate and nitric oxide as key mediators of host response to pathogen/pest infection and for systemic acquired resistance (Heuberger et al., 2014). These hormones conjugates with other metabolites like jasmonate and isoleucine to provide immunity (Staswick and Tiryaki, 2004). During plant-pathogen interaction, many small size molecules of different class such as homoserine, asparagine, and sphingolipids mediate signaling (Heuberger et al., 2014) and regulated through cross-talk between hormones like ethylene-jasmonate, nitric oxide, and jasmonate (Lorenzo et al., 2003; Jian and Wu, 2005).

Metabolism impacts cellular physiology and plays an essential role in biology. Recent advances in metabolomic analytical tool provides opportunity to dissect the layers of plant metabolic regulation, thus allowing bridging the gap between genome and the phenome (Metallo and Vander-Heiden, 2013). It also aids in identifying signature metabolites linked to agronomic traits, thereby plays dynamic role in crop improvement (Kumar et al., 2017; Sharma et al., 2018). Like other omics approach, metabolomics has the ability to examine the global expression of small metabolites that are involved in signaling, and morphological, physio-chemical responses produced during plant-pathogen interaction. In the past few years, researchers have put an effort to address the diverse mechanisms that rice plants use to adapt its metabolism during infection by *Xoo* and also discuss how metabolic flux alteration can be used to identify central regulatory nodes under pathological cell physiology. A

resistant rice genotype responds to BB pathogenic invasion by increasing carotenoids, total phenolic, and flavonoid contents (Kumar et al., 2013). Boosted levels of flavonoids (cyanidin 3-galactoside, cyanidin 3-glucoside, delphinidin 3-arabinoside, and delphinidin 3-galactoside) in black scented rice protects it from diseases and these compounds are also known to have health promoting effects on human (Asem et al., 2015).

A high resolution metabolite QTL (mQTL) analysis of rice recombinant inbred line (RIL) population revealed ~ 2,800 mQTL associated with 900 metabolites (Gong et al., 2013). A major mQTL for aromatically acylated flavonoids co-located within a 0.5-Mb region on chromosome 10, which consists of one acyltransferase gene *OsAT1* conferring BB resistance in rice by regulating lysophosphatidylcholines, has been identified (Mori et al., 2007; Gong et al., 2013). Leaf samples are excellent source to study the resistance mechanism in rice. Hence, evaluation of susceptible versus resistant mutants, varieties, or genotypes is an ultimate tool to interpret resistance mechanisms and identify defense related metabolites. The leaf metabolome was examined to identify the metabolites that might be responsible for differences between BB susceptible, wild type cultivar, and resistant transgenic rice plant (http://www.agilent.com/cs/library/applications/5989-6234EN.pdf). Studies suggest distinct subsets of metabolites at pre and post-invasion might coordinate during BB infection. For example, 42 metabolites could be predicted to be associated with BB resistance, 22 metabolites were connected to infection response, 25 metabolites could be formed by bacteria or in response to it, and a total of 170 metabolites were identified, which differentially expressed between the two-contrast line (Fisher and Sana, 2007). Recently, seed metabolome of a BB resistant line, C418/Xa23, which was generated through marker assisted breeding, and a transgenic variety C418-Xa21 were compared with the wild type susceptible progenitor (C418) (Wu et al., 2012). The study revealed distinct metabolite pattern in the seed of resistant line with significant decline in few common metabolites: amino acids (alanine, glycine, and tyrosine), organic acids (ferulic acid, succinic acid, and malic acid), and glycerol. Additionally, linoleic acid emerged as specific signature metabolite in the seed of resistant breeding line. Possibly, these metabolites regulate the Kreb's cycle and amine biosynthesis, which drive the metabolic state and cell physiology (**Figure 3B**). There is a possibility to use these metabolites as novel discriminatory metabolites to identify BB resistant rice genotypes.

System Biology Approach to Understand Rice-Xoo Interaction For Developing Strategies For Durable Resistance

Consolidating findings emanating from multiple omics platforms contributes to an improved understanding of metabolic pathways, genes, and gene-interaction networks responsible for the phenotypic changes that accompany plant-microbes interactions. A growing body of literature that integrates metabolomics, transcriptomics, and proteomics analyses suggests that significant metabolic alterations happen during plant-pathogen interactions (Wan et al., 2002; Oksman-Caldentey and Saito, 2005; Hollywood et al., 2006; Figueiredo et al., 2008; Tan et al., 2009; Choi et al., 2010; Sana et al., 2010; Paternain and Campion, 2013). However, similar approach for studying BB resistance in rice is presently lacking. To the best of our knowledge, only one study is conducted in rice to establish correlations between the metabolome and transcriptome (Sana et al., 2010). Examination of the metabolic profile of a resistant rice variety infected with *Xoo* suggested significant up-regulation of compounds such as pigments, rutin, fatty acids, and lipids in the resistant plant. The study compared the differential expression of genes in relation to these metabolite products and the corresponding enzymes, and their regulatory pathways. For instance, the transcriptomics and metabolomics data revealed strong correlation between decreased in glutamate levels with increased expression of *glutamate decarboxylase*, which encodes for an enzyme that catalyzes decarboxylation of glutamate to GABA in the *Xoo* challenged plants. Similarly, the increased expression of *Phenylalanine ammonia lyase* (gene product regulates phenyl propanoid pathway) was in coordination with the elevated level of phenylalanine in the *Xoo* challenged resistant plant. However, the expression of *isocitrate lyase*, *b-1,3-glucanase* and *chitinase* showed negative correlation with the metabolite data in the resistant plant as these genes are involved in degradation of fungal cell wall and provide resistance against fungal pathogen (O'Toole et al., 2001). We anticipate a remarkable increase in the studies that combine different omics platforms to provide better insights into BB resistance in rice.

EPIGENETICS: A NEW WAY TO IMPROVE TRAIT UNDERSTANDING AND MANIPULATION

To evaluate the epigenetic control responsible for resistance against *Xoo*, methylated regions of rice genome were using methylation sensitive amplified polymorphism (MSAP) technique, and cytosine methylation was screened by the bisulfite mapping technique (Akimoto et al., 2007). The rice seed were treated with 5-azadeoxycytidine (inhibitor of DNA methylation), and the progeny were grown in field. Among 1000 seeds treated with 5-azadeoxycytidine, only 35 seedlings survived and, out of that, two showed dwarf phenotypes. In contrast to susceptible wild type, line-2 showed constitutive expression of *Xa21G* and resistance against BB (Akimoto et al., 2007). Normally, the promoter remained at hyper-methylated condition, which silences *Xa21G* gene to cause susceptibility to *Xoo*. Besides DNA methylation, epigenetic regulatory pathways also regulate the initial step of plant-bacteria interaction through small RNAs (sRNAs), such as small interfering RNAs (siRNAs) and micro RNAs (miRNAs) (Carvalho et al., 2016). In *Arabidopsis* and legumes, miR393 is induced during pathogenic infection and confers resistance to associative and endophytic diazotrophic bacteria (AEDB) by attenuation of auxin signaling pathways (Navarro et al., 2006; Subramanian et al., 2008). Similarly, enhanced expression of miR160 in *Arabidopsis* during bacterial

infection indicates its possible involvement in defense response (Fahlgren et al., 2007). In contrast, the down-regulation of miR160 and miR393 in maize caused suppression of defense response (Thiebaut et al., 2014). Genome editing tools such as ZFNs and TALEs were used for targeted epigenetic modifications in plants (Gaj et al., 2013). Presently, the CRISPR/Cas9 technology has become the widely accepted genome editing tool for plant modification including epigenetic modification (Malzahn et al., 2017; Van de Wiel et al., 2017). In mammalian system, targeted enhanced CpG methylation has been successfully demonstrated by using CRISPR/Cas9-DNMT3A as epigenetic modifier (Vojta et al., 2016). In future, such epigenetic modifications are expected to be routinely deployed for targeted methylation for disease resistance.

IMPACT OF CLIMATE ON BB RESISTANCE GENES

The classical concept of Plant Pathology describes a plant disease as the result of interaction of host, pathogen and environment, commonly referred to as 'disease triangle'. Thus, variations in any parameters of environment can remarkably affect the disease consequence. Several studies have shown that the effectiveness of 'R'-gene mediated defense response can be substantially influenced by temperature variation (de Jong et al., 2000; Uauy et al., 2005; Webb et al., 2010; Zhu et al., 2010; Zhao et al., 2016). Webb et al. (2010) reported that near isogenic line IRBB4 owning the BB resistance gene *Xa4* exhibited much longer lesion at higher temperature regime (35:27°C, day:night) than in lower temperature regimes (29:21°C, day:night). Similarly, Dossa et al. (2017) observed that drought stress significantly reduced *Xa4* mediated BB resistance in rice. On the contrary, efficacy of BB resistance gene, *Xa7* was significantly improved at higher temperature (35:31°C, day:night) compared to lower temperature (29:21°C, day:night) in limiting BB severity and *Xoo* population (Webb et al., 2010). In a detailed study, Cohen et al. (2017) found that the level of *Xa7*-mediated BB resistance was comparatively stronger and faster at higher temperature as compared to lower temperature regime. These contrasting scenarios raise concerns about durability of single R gene and different gene combinations in the scenario of a rapidly changing climate. Recently, Dossa et al. (2020) demonstrated that near isogenic line IRBB 67 (owning BB resistance genes *Xa4* and *Xa7*) did not show any difference in lesion length at both lower and higher temperature regimes, indicating that the reduced effectiveness of *Xa4* at higher temperature did not affect the resistance level of IRBB 67.

PERSPECTIVE AND CONCLUSIONS

The research achievements in the recent past have contributed to improved understanding of resistance mechanisms in rice against *Xoo* infection and also the pathways associated with susceptibility. Deploying multiple sets of carefully selected R-genes as gene-pyramids holds promise for developing improved rice cultivars/hybrids with durable and broad-spectrum BB resistance. Identification and utilization of new resistant genes/alleles, tapping the genetic variability in diverse germplasm, and generation novel variation in existing genes through gene-editing will be crucial to achieve sustained production of rice for ever-increasing population. Mapping and characterization of different BB R-genes have made marker-assisted selection a valuable tool to develop durable BB disease resistance in rice. Moreover, strategies for gene discovery based on genomics and proteomics together with transgene validation through genetic transformation are increasingly helping us understand the functional profiles of candidate genes. Research on this aspect has been immensely benefited from the increasing information on structure and function of major BB resistance genes. Although a smaller number of major R-genes have been cloned and characterized as of now, RGAs and DNA markers linked to resistance trait have been routinely deployed in BB resistant genotypes breeding. The possibility to surveil genomic variations and the evolution of virulence-avirulence factors have expanded further with the availability of complete genome sequences of rice and *Xoo*. Domestication of rice has indeed narrowed the genetic diversity particularly with respect to diverse allelic forms of resistance genes that may exist in wild relatives of *Oryza*. Hence, it becomes imperative to conduct large-scale survey of wild rice species to characterize novel BB resistance genes and also novel alleles of known resistance genes so that they can be gainfully used for rice improvements. In our opinion, the need of the hour is to make best possible use of information and resources available not only in rice but also in other related crop species so as to achive durable resistance against BB disease. For example, investigations on how wheat crop avoids infection by *Xoo* or how rice avoids infection by the wheat rust pathogen, *Puccinia gramins fsp. Tritici* may offer clues for developing broad spectrum resistance in rice against multiple pathogens including *Xoo*. Interestingly, the focus of the research is now making a paradigm shift from individual genes to the whole plant systems. We anticipate that a better-coordinated inter-disciplinary research may reduce redundancy and competition in specific area along with dedicating greater attention to previously unexplored research areas.

AUTHOR CONTRIBUTIONS

AK, RK, DS, SD, and AB designed the article. AK, RK, DS, SD, PS, and HS wrote the article. MP, NS, IG, GL, and RS corrected and improved the article. All authors contributed to the article and approved the submitted version.

FUNDING

AK sincerely thanks University Grants Commission (UGC) start-up grant (no. F.30-392/2017 (BSR) and Madhya Pradesh Council of Science and Technology (Endt. no. 3879/CST/R&D/BioSci/2018) for the funding to the laboratory. RK thanks Science and Engineering Research Board (SERB), Department

of Science and Technology (DST) for extending financial support (project #PDF/2016/002758). RS, GL, and PS thank the Indian Council of Agricultural Research, Department of Biotechnology, Department of Science and Technology and Council for Scientific and Industrial Research, Government of India for the generous funding and infrastructural support. SD sincerely thanks University Grants Commission (UGC) for start-up grant (no. F.30-420/2018 (BSR).

REFERENCES

Abhilash, V. A., Balachiranjeevi, C. H., Bhaskar,, Naik, S., Rambabu, R., Rekha, G., Hajira, S. K., et al. (2016). Development of gene-pyramid lines of the elite restorer line, RPHR-1005 possessing durable bacterial blight and blast resistance. *Front. Plant Sci.* 7:1195. doi: 10.3389/fpls.2016.01195

Abhilash, V. A., Balachiranjeevi, C. H., Naik, S. B., Rekha, G., Rambabu, R., Harika, G., et al. (2017). Marker-assisted pyramiding of bacterial blight and gall midge resistance genes into RPHR-1005, the restorer line of the popular rice hybrid DRRH-3. *Mol. Breed.* 37, 86. doi: 10.1007/s11032-017-0687-8

Agrawal, G. K., and Rakwal, R. (2011). Rice proteomics: A move to-ward expanded proteome coverage to comparative and functional proteomics uncovers the mysteries of rice and plant biology. *Proteomics* 11, 1630–1649. doi: 10.1002/pmic.201000696

Agrios, G. N. (1997). *Plant Pathology*. 1(New York, NY, USA: Academic Press).

AICRIP. (2008). *Varietal Improvement. 4th ed.* (Hyderabad, India: All India Coordinated Rice Improvement Project Directorate of Rice Research Rajendranagar). *Vol. 1*,

Akimoto, K., Katakami, H., Kim, H. J., Ogawa, E., Sano, C. M., Wada, Y., et al. (2007). Epigenetic inheritance in rice plants. *Ann. Bot.* 100, 205–217. doi: 10.1093/aob/mcm110

Ali, M. L., Sanchez, P. L., Yu, S. B., Lorieux, M., and Eizenga, G. C. (2010). Chromosome segment substitution lines: a powerful tool for the introgression of valuable genes from Oryza wild species into cultivated rice (O. sativa). *Rice* 3, 218–234. doi: 978-3-319-45021-6_20/s12284-010-9058-3

Amante-Bordeos, A., Sitch, L. A., Nelson, R., Dalmacio, R. D., Oliva, N. P., Aswidinnoor, H., et al. (1992). Transfer of bacterial blight and blast resistance from the tetraploid wild rice Oryza minuta to cultivated rice, Oryza sativa. *Theor. Appl. Genet.* 84, 345–354. doi: 978-3-319-45021-6_20/BF00229493

Angeles-Shim, R. B., Shim, J., Vinarao, R. B., Lapis, R. S., and Singleton, J. J. (2020). A novel locus from the wild allotetraploid rice species Oryza latifolia Desv. confers bacterial blight (Xanthomonas oryzae pv. oryzae) resistance in rice (O. sativa). *PLoS One* 15 (2), e0229155. doi: 10.1371/journal.pone.0229155

Antony, G., Zhou, J., Huang, S., Li, T., Liu, B., White, F., et al. (2010). Rice xa13recessive resistance to bacterial blight is defeated by induction of the disease susceptibility gene Os-11N3. *Plant Cell.* 22, 3864–3876. doi: 10.1105/tpc.110.078964

Asem, I. D., Imotomba, R. K., Mazumder, P. B., and Laishram, J. M. (2015). Anthocyanin content in the black scented rice (Chakhao): its impact on human health and plant defense. *Symbiosis* 66, 47–54. doi: 978-3-319-45021-6_20/s13199-015-0329-z

Atkinson, N. J., and Urwin, P. E. (2012). The interaction of plant biotic and abiotic stresses: from genes to the field. *J. Exp. Bot.* 63, 3523–3543. doi: 10.1093/jxb/ers100

Audic, S., and Claverie, J. M. (1997). The significance of digital gene expression profiles. *Genome Res.* 7, 986–995. doi: 10.1101/gr.7.10.986

Balachiranjeevi, C. H., Bhaskar, N. S., Abhilash, V., Akanksha, S., Viraktamath, B. C., Madhav, M. S., et al. (2015). Marker-assisted introgression of bacterial blight and blast resistance into DRR17B, an elite, fine-grain type maintainer line of rice. *Mol. Breed.* 35, 151. doi: 978-3-319-45021-6_20/s11032-015-0348-8

Balachiranjeevi, C. H., Naik, B., Kumar, A., Harika, G., Mahadev Swamy, H. K., Hajira, Sk., et al. (2018). Marker-assisted pyramiding of two major, broad-spectrum bacterial blight resistance genes, Xa21 and Xa33 into an elite maintainer line of rice, DRR17B. *PLoS One* 13, e0201271. doi: 10.1101/368712

Barbier, P. (1989). Genetic variation and ecotypic differentiation in wild rice Oryza rufipogon: Population differentiation in life-history traits and isozymes. *Jpn. J. Genet.* 64, 259–271. doi: 10.1266/jjg.64.259

Barkley, N. A., and Wang, M. L. (2008). Application of TILLING and EcoTILLING as reverse genetic approaches to elucidate the function of genes in plants and animals. *Curr. Genom.* 9, 212–226. doi: 10.2174/138920208784533656

Barry, M. B., Pham, J. L., Noyer, J. L., Billot, C., Courtois, B., and Ahmadi, N. (2007). Genetic diversity of the two cultivated rice species (O. sativa and O. glaberrima) in maritime Guinea. Evidence for interspecifc recombination. *Euphytica* 154, 127–137. doi: 978-3-319-45021-6_20/s10681-006-9278-1

Basavaraj, S. H., Singh, V. K., Singh, A., and Singh, A. (2010). Singh A. Marker–assisted improvement of bacterial blight resistance in parental lines of Pusa RH10, a superfine grain aromatic rice hybrid. *Mol. Breed.* 26, 293–305. doi: 978-3-319-45021-6_20/s11032-010-9407-3

Bhasin, H., Bhatia, D., Raghuvanshi, S., Lore, J. S., Sahi, G. K., and Kaur, B. (2012). New PCR-based sequence-tagged site marker for bacterial blight resistance gene Xa38 of rice. *Mol. Breed.* 30, 607–611. doi: 978-3-319-45021-6_20/s11032-011-9646-y

Bimolata, W., Kumar, A., Sundaram, R. M., Laha, G. S., Qureshi, I. A., and Reddy, G. A. (2013). Analysis of nucleotide diversity among alleles of the major bacterial blight resistance gene Xa27 in cultivars of rice (Oryza sativa) and its wild relatives. *Planta* 238, 239–305. doi: 978-3-319-45021-6_20/s00425-013-1891-3

Bimolata, W., Kumar, A., Reddy, M. S. K., Sundaram, R. M., Laha, G. S., Qureshi, I. A., et al. (2015). Nucleotide diversity analysis of three major bacterial blight resistance genes in rice. *PLoS One* 10, e0120186. doi: 10.1371/journal.pone.0120186

Borba, T. C., Mendes, C. D., Guimarães, É.P., Brunes, T. O., Fonseca, J. R., Brondani, R. V., et al. (2009). Genetic variability of Brazilian rice landraces determined by SSR markers. *Pesq. Agropec. Bras. Brasília.* 44, 706–712. doi: 10.1590/S0100-204X2009000700009

Borrelli, V. M., Brambilla, V., Rogowsky, P., Marocco, A., and Lanubile, A. (2018). The enhancement of plant disease resistance using CRISPR/Cas9 technology. *Front. Plant Sci.* 9:1245. doi: 10.3389/fpls.2018.01245

Bortesi, L., and Fischer, R. (2015). The CRISPR/Cas9 system for plant genome editing and beyond. *Biotechnol. Adv.* 33, 41–52. doi: 10.1016/j.biotechadv.2014.12.006

Bradbury, J. F. (1984). "Genus II. XanthomonasDowson," in *Bergey"s Manual of Systematic Bacteriology*. Eds. N. R. Krieg and J. G. Holt (Baltimore: Williams & Wilkins), 199–210.

Burkart-Waco, D., Tsai, H., Ngo, K., Henry, I. M., Comai, L., and Tai, T. H. (2016). "Biotechnologies for Plant Mutation Breeding: Protocols," in *Next-Generation Sequencing for Targeted Discovery of Rare Mutations in Rice* Eds. Jankowicz-Cieslak, J., Tai, T. H., Kumlehn, J., and Till, B. J. (Cham, Switzerland: Springer International Publishing), pp, 323–340. doi: 10.1007/978-3-319-45021-6_20

Busungu, C., Taura, S., Sakagami, J. I., and Ichitani, K. (2016). Identification and linkage analysis of a new rice bacterial blight resistance gene from XM14, a mutant line from IR24. *Breed. Sci.* 66, 636–645. doi: 10.1270/jsbbs.16062

Cao, J., Zhang, M., Xiao, J., Li, X., Yuan, M., and Wang, S. (2018). Dominant and Recessive Major R Genes Lead to Different Types of Host Cell Death During Resistance to Xanthomonas oryzae in Rice. *Front. Plant Sci.* 9:1711. doi: 10.3389/fpls.2018.01711

Carvalho, T. L., Ballesteros, H. G., Thiebaut, F., Ferreira, P. C., and Hemerly, A. S. (2016). Nice to meet you: genetic, epigenetic and metabolic controls of plant perception of beneficial associative and endophytic diazotrophic bacteria in non-leguminous plants. *Plant Mol. Biol.* 90, 561–574. doi: 978-3-319-45021-6_20/s11103-016-0435-1

Casella, L., Greco, R., Bruschi, G., Wozniak, B., Dreni, L., Kater, M., et al. (2013). TILLING in European rice: Hunting mutations for crop improvement. *Crop Sci.* 53, 2550–2562. doi: 10.2135/cropsci2012.12.0693

Cheema, K. K., Grewal, N. K., Vikal, Y., Sharma, R., Lore, J. S., Das, A., et al. (2008). A novel bacterial blight resistance gene from Oryza nivara mapped to 38 Kb region on chromosome 4L and transferred to Oryza sativa L. *Genet. Res.* 90, 397–407. doi: 10.1017/S0016672308009786

Chen, H., Wang, S., and Zhang, Q. (2002). New gene for bacterial blight resistance in rice located on chromosome 12 identified from Minghui 63, an elite restorer line. *Phytopathology* 92 (7), 750–754. doi: 10.1094/PHYTO.2002.92.7.750

Chen, X., and Ronald, P. C. (2011). Innate immunity in rice. *Trends Plant Sci.* 16, 451–459. doi: 10.1016/j.tplants.2011.04.003

Chen, S., and Zhang, Q. F. (2000). Improvement of bacterial blight resistance of hybrid rice by molecular marker-assisted selection. *J. Huazhong Agric. Univ.* 19, 183–189.

Chen, F., Yuan, Y., Li, Q., and He, Z. (2007). Proteomic analysis of rice plasma membrane reveals proteins involved in early defense response to bacterial blight. *Proteomics* 7, 1529–1539. doi: 10.1002/pmic.200500765

Chen, S., Liu, X., Zeng, L., Ouyang, D., Yang, J., and Zhu, X. (2011). Genetic analysis and molecular mapping of a novel recessive gene xa34(t) for resistance against Xanthomonas oryzae pv. oryzae. *Theor. Appl. Genet.* 122, 1331–1338. doi: 978-3-319-45021-6_20/s00122-011-1534-7

Cheng, Q., Mao, W., Xie, W., Liu, Q., Cao, J., Yuan, M., et al. (2017). Characterization of a disease susceptibility locus for exploring an efficient way to improve rice resistance against bacterial blight. *Sci. China Life Sci.* 60, 298–306. doi: 978-3-319-45021-6_20/s11427-016-0299-x

Chisholm, S. T., Coaker, G., Day, B., and Staskawicz, B. J. (2006). Host-microbe interactions: shaping the evolution of the plant immune response. *Cell* 124, 803–814. doi: 10.1016/j.cell.2006.02.008

Choi, Y. J., Yun, H. K., Park, K. S., Noh, J. H., Heo, Y. Y., Kim, S. H., et al. (2010). Transcriptional profiling of ESTs responsive to Rhizobium vitis from "Tamnara" grapevines (Vitis sp.). *J. Plant Physiol.* 167, 1084–1092. doi: 10.1016/j.jplph.2010.02.005

Christian, M., Cermak, T., Doyle, E. L., Schmidt, C., Zhang, F., Hummel, A., et al. (2010). Targeting DNA double-strand breaks with TAL effector nucleases. *Genetics* 186, 757–761. doi: 10.1534/genetics.110.120717

Chu, Z., Ouyang, Y., Zhang, J., Yang, H., and Wang, S. (2004). Genome wide analysis of defense responsive genes in bacterial blight resistance of rice mediated by the recessive R gene xa13. *Mol. Genet. Genomics* 271, 111–120. doi: 978-3-319-45021-6_20/s00438-003-0964-6

Chu, Z., Yuan, M., Yao, J., Ge, X., Yuan, B., Xu, C., et al. (2006). Promoter mutations of an essential gene for pollen development result in disease resistance in rice. *Gene Dev.* 20, 1250–1255. doi: 10.1101/gad.1416306

Cianciotto, N. P., and White, R. C. (2017). Expanding role of type II secretion in bacterial pathogenesis and beyond. *Infect. Immun.* 85, e00014–e00017. doi: 10.1128/IAI.00014-17

Cohen, S. P., Liu, H., Argueso, C. T., Pereira, A., Vera Cruz, C., Verdier, V., et al. (2017). RNA-Seq analysis reveals insight into enhanced rice Xa7-mediated bacterial blight resistance at high temperature. *PLoS One* 12 (11), e0187625. . doi: 10.1371/journal.pone.0187625

Crossa, J., Pérez-Rodríguez, P., Cuevas, J., Montesinos-López, O., Jarquín, D., de los Campos, G., et al. (2017). Genomic selection in plant breeding: methods, models, and perspectives. *Trends Plant Sci.* 22, 961–975. doi: 10.1016/j.tplants.2017.08.011

Datta, K., Baisakh, N., Thet, K. M., Tu, J., and Datta, S. (2002). Pyramiding transgenes for multiple resistance in rice against bacterial blight, yellow stem borer and sheath blight. *Theor. Appl. Genet.* 106, 1–8. doi: 978-3-319-45021-6_20/s00122-002-1014-1

Datta, S. K. (2004). Rice Biotechnology: A need for developing countries. *AgBioForum* 7, 31–35.

Davierwala, A. P., Reddy, A. P., Lagu, M. D., Ranjekar, P. K., and Gupta, V. S. (2001). Marker assisted selection of bacterial blight resistance genes in rice. *Biochem. Genet.* 39, 170–183. doi: 10.1023/A:1010282732444

de Jong, C. F., Takken, F. L., Cai, X., de Wit, P. J., and Joosten, M. H. (2000). Attenuation of Cf-mediated defense responses at atelevated temperatures correlates with a decrease in elicitor-binding sites. *Mol. Plant-Microbe Interact.* 15 (10), 1040–1049. doi: 10.1094/MPMI.2002.15.10.1040

Denancé, N., Sánchez-Vallet, A., Goffner, D., and Molina, A. (2013). Disease resistance or growth: the role of plant hormones in balancing immune responses and fitness costs. *Front. Plant Sci.* 4:155. doi: 10.3389/fpls.2013.00155

Deng, Y., Wu, J. E., Tao, F., and Zhang, L. H. (2010). Listening to a new language: DSF-based quorum sensing in Gram-negative bacteria. *Chem. Rev.* 111, 160–173. doi: 10.1021/cr100354f

Dharmapuri, S., and Sonti, R. V. (1999). A transposon insertion in the gumG homologue of *Xanthomonas oryzae pv. oryzae* causes loss of extracellular polysaccharide production and virulence. *FEMS Microbiol. Lett.* 179, 53–59. doi: 10.1111/j.1574-6968.1999.tb08707.x

Diatchenko, L., Lau, Y. F., Campbell, A. P., Chenchik, A., Moqadam, F., Huang, B., et al. (1996). Suppression subtractive hybridization: a method for generating differentially regulated or tissue-specific cDNA probes and libraries. *Proc. Natl. Acad. Sci.* 93, 6025–6030. doi: 10.1073/pnas.93.12.6025

Ding, C., You, J., Wang, S., Liu, Z., Li, G., Wang, Q., et al. (2012). A proteomic approach to analyze nitrogen and cytokinin-responsive proteins in rice roots. *Mol. Biol. Rep.* 39, 1617–1626. doi: 978-3-319-45021-6_20/s11033-011-0901-4

Dixon, M. S., Jones, D. A., Keddie, J. S., Thomas, C. M., Harrison, K., and Jones, J. D. (1996). The tomato Cf-2 disease resistance locus comprises two functional genes encoding leucine-rich repeat proteins. *Cell* 84, 451–459. doi: 10.1016/S0092-8674(00)81290-8

Djedatin, G., Ndjiondjop, M. N., Sanni, A., Lorieux, M., Verdier, V., and Ghesquiere, A. (2016). Identification of novel major and minor QTLsassociated with Xanthomonas oryzae pv. Oryzae (African strains) resistance in rice (Oryza sativaL). *Rice* 9, 18. doi: 10.1186/s12284-016-0090-9

Dokku, P., Das, K. M., and Rao, G. J. N. (2013). Pyramiding of four resistance genes of bacterial blight in Tapaswini, an elite rice cultivar, through marker assisted selection. *Euphytica* 192, 87–96. doi: 978-3-319-45021-6_20/s10681-013-0878-2

Dossa, G. S., Torres, R., Henry, A., Oliva, R., Maiss, E., Vera Cruz, C., et al. (2017). Rice response to simultaneous bacterial blight and drought stress during compatible and incompatible interactions. *Eur. J. Plant Pathol.* 147, 115–127. doi: 978-3-319-45021-6_20/s10658-016-0985-8

Dossa, G. S., Quibod, I., Atienz ana-Grande, G., Olivca, R., Maiss, E., Vera Cruz, C., et al. (2020). Rice pyramided line IRBB67 (Xa4/Xa7)homeostasis under combined stress of high temperature and bacterial blight.*Sci. Rep.* 10, 683. doi: 10.1038/s41598-020-57499-5

Ellur, R. K., Khanna, A., Bhowmick, P. K., Vinod, K. K., Nagarajan, M., Mondal, K. K., et al. (2016). Marker-aided incorporation of Xa38, a novel bacterial blight resistance gene, in PB1121 and comparison of its resistance spectrum with xa13+Xa21. *Sci. Rep.* 6, 29188. doi: 10.1038/srep29188

Ershad, M., Gopi, P., Suneel, B., Laha, G. S., Sundaram, R. M., Padma kumari, A. P., et al. (2017). Identification of Bacterial Blight Resistant Mutant Lines in the Mutagenized Samba Mashuri (BPT 5204) Population. *ICAR-IIRR News Lett.* 15, 234–235.

Fahlgren, N., Howell, M. D., Kasschau, K. D., Chapman, E. J., Sullivan, C. M., and Cumbie, J. S. (2007). High-throughput sequencing of Arabidopsis microRNAs: Evidence for frequent birth and death of miRNA genes. *PLoS One* 2, e219. . doi: 10.1371/journal.pone.0000219

FAO (Food and Agriculture Organization) (2004). *Rice is life* (Italy: FAO International Year of Rice, Rice and Human Nutrition).

Figueiredo, A., Fortes, A. M., Ferreira, S., Sebastiana, M., Choi, Y. H., Sousa, L., et al. (2008). Transcriptional and metabolic profiling of grape (Vitis vinifera L.) leaves unravel possible innate resistance against pathogenic fungi. *J. Exp. Bot.* 59, 3371–3381. doi: 10.1093/jxb/ern187

Fisher, S., and Sana, T. (2007). "," in *Metabolomic profiling of bacterial leaf blight in rice*, vol. 2. (Santa Clara, CA: Agilent Technologies), 16.

Fitzgerald, T. L., Kazan, K., Li, Z., Morell, M. K., and Manners, J. M. (2010). A high-throughput method for the detection of homologous gene deletions in hexaploid wheat. *BMC Plant Biol.* 10, 264. doi: 10.1186/1471-2229-10-264

Gaj, T., Gersbach, C. A., and Barbas, C. F. (2013). ZFN, TALEN and CRISPR/Cas-based methods for genome engineering. *Trends Biotechnol.* 31, 397–405. doi: 10.1016/j.tibtech.2013.04.004

Gao, D. Y., Xu, Z. G., Chen, Z. Y., Sun, L. H., Sun, Q. M., and Lu, F. (2002). Identification of a resistance gene to bacterial blight (Xanthomonas oryzae pv. oryzae) in a somaclonal mutant HX-3 of indica rice. *Yi Chuan Xue Bao* 29, 138–143.

Ghazi, I. A., Srivastava, P. S., Dalal, V., Gaikwad, K., Singh, A. K., and Sharma, T. R. (2009). Physical mapping, expression analysis and polymorphism survey of resistance gene analogues on chromosome 11 of rice. *J. Biosci.* 34, 251–261. doi: 978-3-319-45021-6_20/s12038-009-0029-z

Glazebrook, J. (2001). Genes controlling expression of defense responses in Arabidopsis-status. *Curr. Opin. Plant Biol.* 4, 301–308. doi: 10.1016/S1369-5266(00)00177-1

Gnanamanickam, S. S., Priyadarisini, V. B., Narayanan, N. N., Vasudevan, P., and Kavitha, S. (1999). An overview of bacterial blight disease of rice and strategies for its management. *Curr. Sci.* 77, 1435–1443.

Gnanamanickam, S. S. (2009). "Biological control of bacterial blight of rice," in *Biological control of rice diseases*, vol. 8 . Ed. S. S. Gnanamanickam (New York: Springer), 67–78.

Goicoechea, J. L., Ammiraju, J. S., Marri, P. R., Chen, M., Jackson, S., and Yu, Y. (2010). The future of rice genomics: Sequencing the collective Oryza genome. *Rice* 3, 89–97. doi: 978-3-319-45021-6_20/s12284-010-9052-9

Gong, L., Chen, W., Gao, Y., Liu, X., Zhang, H., and Xu, C. (2013). Genetic analysis of the metabolome exemplified using a rice population. *Proc. Natl. Acad. Sci.* 10, 20320–20325. doi: 10.1073/pnas.1319681110

González, M., Xu, M., Esteras, C., Roig, C., Monforte, A. J., Troadec, C., et al. (2011). Towards a TILLING platform for functional genomics in Piel de Sapo melons. *BMC Res. Notes* 4, 289. doi: 10.1186/1756-0500-4-289

Grewal, R., Gupta, S., and Das, S. (2012). Xanthomonas oryzae pv oryzae triggers immediate transcriptomic modulations in rice. *BMC Genomics* 13, 49. doi: 10.1186/1471-2164-13-49

Gu, K., Tian, D., Yang, F. W., Wu, L., Sreekala, C., Wang, D., et al. (2004). High-resolution genetic mapping of Xa27 (t), a new bacterial blight resistance gene in rice, Oryza sativa L. *Theor. Appl. Genet.* 108, 800–807. doi: 978-3-319-45021-6_20/s00122-003-1491-x

Gu, K., Yang, B., Tian, D., Wu, L., Wang, D., and Sreekala, C. (2005). R gene expression induced by a type-III effector triggers disease resistance in rice. *Nature* 435, 1122–1125. doi: 10.1038/nature03630

Gu, K., Sangha, J. S., Li, Y., and Yin, Z. (2008). High-resolution genetic mapping of bacterial blight resistance gene Xa10. *Theor. Appl. Genet.* 116, 155–163. doi: 978-3-319-45021-6_20/s00122-007-0655-5

Guo, S. B., Zhang, D. P., and Lin, X. H. (2010). Identification and mapping of a novel bacterial blight resistance gene Xa35(t)originated from Oryza minuta. *Sci. Agric. Sin.* 43, 2611–2618.

Gururani, M. A., Venkatesh, J., Upadhyaya, C. P., Nookaraju, A., Pandey, S. K., and Park, S. W. (2012). Plant disease resistance genes: current status and future directions. *Physiol. Mol. Plant Pathol.* 78, 51– 65. doi: 10.1016/j.pmpp.2012.01.002

Gust, A. A., Brunner, F., and Nürnberger, T. (2010). Biotechnological concepts for improving plant innate immunity. *Curr. Opin. Biotechnol.* 21, 204–210. doi: 10.1016/j.copbio.2010.02.004

Guvvala, L. D., Koradi, P., Shenoy, V., and Marella, L. S. (2013). Making an Indian traditional rice variety Mahsuri, bacterial blight resistant using marker-assisted selection. *J. Crop Sci. Biotech.* 16, 111–121. doi: 978-3-319-45021-6_20/s12892-013-0009-6

Hammond-Kosack, K. E., and Jones, J. D. (1997). Plant disease resistance genes. *Annu. Rev. Plant Physiol. Plant Mol. Biol.* 48, 575–607. doi: 10.1146/annurev.arplant.48.1.575

Hari, Y., Srinivasarao, K., Viraktamath, B. C., Hari Prasad, A. S., Laha, G. S., Ahmed, M. I., et al. (2011). Marker-assisted improvement of a stable restorer line, KMR-3R and its derived hybrid KRH2 for bacterial blight resistance and grain quality. *Plant Breed.* 130, 608–616. doi: 10.1111/j.1439-0523.2011.01881.x

Hari, Y., Srinivasarao, K., Viraktamath, B. C., Hari Prasad, A. S., Laha, G. S., Ahmed, M. I., et al. (2013). Marker-assisted introgression of bacterial blight and blast resistance into IR 58025B, an elite maintainer line of rice. *Plant Breed.* 132, 586–594. doi: 10.1111/pbr.12056

Hashiguchi, A., Ahsan, N., and Komatsu, S. (2010). Proteomics application of crops in the context of climatic changes. *Food Res. Int.* 43, 1803–1813. doi: 10.1016/j.foodres.2009.07.033

He, Q., Li, D., Zhu, Y., Tan, M., Zhang, D., and Lin, X. (2006). Fine mapping of Xa2, a bacterial blight resistance gene in rice. *Mol. Breed.* 17, 1–6. doi: 978-3-319-45021-6_20/s11032-005-8698-2

Heffner, L., Sorrells, M. E., and Jannink, J. L. (2009). Genomic selection for crop improvement. *Crop Sci.* 49, 1–12. doi: 10.2135/cropsci2008.08.0512

Heuberger, A. L., Robison, F. M., Lyons, S. M., Broeckling, C. D., and Prenni, J. E. (2014). Evaluating plant immunity using mass spectrometry-based metabolomics workflows. *Front. Plant Sci.* 5:291. doi: 10.3389/fpls.2014.00291

Hollywood, K., Brison, D. R., and Goodacre, R. (2006). Metabolomics: Current technologies and future trends. *Proteomics* 6, 4716–4723. doi: 10.1002/pmic.200600106

Hopkins, C. M., White, F. F., Choi, S. H., Guo, A., and Leach, J. E. (1992). Identification of a family of avirulence genes from Xanthomonas oryzae pv. oryzae. *Mol. Plant Microbe Interact.* 5, 451–459. doi: 10.1094/MPMI-5-451

Hsu, P. D., Scott, D. A., Weinstein, J. A., Ran, F. A., Konermann, S., Agarwala, V., et al. (2013). DNA targeting specificity of RNA-guided Cas9 nucleases. *Nat. Biotechnol.* 31, 827–832. doi: 10.1038/nbt.2647

Hu, K., Cao, J., Zhang, J., Xia, F., Ke, Y., Zhang, H., et al. (2017). Improvement of multiple agronomic traits by a disease resistance gene via cell wall reinforcement. *Nat. Plants* 3, 17009. doi: 10.1038/nplants.2017.9

Huang, N., Angeles, E. R., Domingo, J., Magpantay, G., Singh, S., Zhang, G., et al. (1997). Pyramiding of bacterial blight resistance genes in rice: marker-assisted selection using RFLP and PCR. Theor. *Appl. Genet.* 95, 313–320. doi: 978-3-319-45021-6_20/s001220050565

Huang, B., Xu, J. Y., Hou, M. S., Ali, J., and Mou, T. M. (2012). Introgression of bacterial blight resistance genes Xa7, Xa21, Xa22 and Xa23 into hybrid rice restorer lines by molecular marker-assisted selection. *Euphytica* 187, 449–459. doi: 978-3-319-45021-6_20/s10681-012-0758-1

Hutin, M., Sabot, F., Ghesquière, A., Koebnik, R., and Szurek, B. (2015). A knowledge-based molecular screen uncovers a broad-spectrum Os SWEET 14 resistance allele to bacterial blight from wild rice. *Plant J.* 84, 694–703. doi: 10.1111/tpj.13042

Hwang, J. E., Jang, D. S., Lee, K. J., Ahn, J. W., Kim, S. H., Kang, S. Y., et al. (2016). Identification of gamma ray irradiation-induced mutations in membrane transport genes in a rice population by TILLING. *Genes Genet. Syst.* 91, 245–256. doi: 10.1266/ggs.15-00052

Iqbal, M. J., Yaegashi, S., Ahsan, R., Shopinski, K. L., and Lightfoot, D. A. (2005). Root response to Fusarium solani f. sp. glycines: temporal accumulation of transcripts in partially resistant and susceptible soybean. *Theor. Appl. Genet.* 110, 1429–1438. doi: 978-3-319-45021-6_20/s00122-005-1969-9

Iyer, A. S., and McCouch, S. R. (2004). The rice bacterial blight resistance gene xa5 encodes a novel form of disease resistance. *Mol. Plant Microbe Interact.* 17, 1348–1354. doi: 10.1094/MPMI.2004.17.12.1348

Iyer, A. S., Jiang, H., Huang, L., and McCouch, S. R. (2004). Genetic and functional characterization of the rice bacterial blight disease resistance gene xa5. *Phytopathol* 98, 289–295. doi: 10.1094/PHYTO-98-3-0289

Jain, P., Singh, P. K., Kapoor, R., Khanna, A., Solanke, A. U., Krishnan, S. G., et al. (2017). Understanding host-pathogen interactions with expression profiling of NILs carrying rice-blast resistance Pi9 gene. *Front. Plant Sci.* 8:93. doi: 10.3389/fpls.2017.00093

Jha, G., Rajeshwari, R., and Sonti, R. V. (2005). Bacterial type two secretion system secreted proteins: double-edged swords for plant pathogens. *Mol. Plant-Microbe Interact.* 18, 891–898. doi: 10.1094/MPMI-18-0891

Jha, G., Rajeshwari, R., and Sonti, R. V. (2007). Functional interplay between two *Xanthomonas oryzae* pv. oryzae secretion systems in modulating virulence on rice. *Mol. Plant Microbe Interact.* 20, 31–40. doi: 10.1094/MPMI-20-0031

Ji, Z., Ji, C., Liu, B., Zou, L., Chen, G., and Yang, B. (2016). Interfering TAL effectors of Xanthomonas oryzae neutralize R-gene-mediated plant disease resistance. *Nat. Commun.* 7, 1–9. doi: 10.1038/ncomms13435

Jian, W. W., and Wu, J. Y. (2005). Nitric oxide is involved in methyl jasmonate-induced defense responses and secondary metabolism activities of Taxus cells. *Plant Cell Physiol.* 46, 923–930. doi: 10.1093/pcp/pci098

Jiang, G. H., Xia, Z. H., Zhou, Y. L., Wan, J., Li, D. Y., and Chen, R. S. (2006). Testifying the rice bacterial blight resistance gene xa5 by genetic complementation and further analyzing xa5 (Xa5) in comparison with its homolog TFIIAgamma1. *Mol. Genet. Genomics* 275, 354–366. doi: 978-3-319-45021-6_20/s00438-005-0091-7

Jiang, N., Yan, J., Liang, Y., Shi, Y., He, Z., Wu, Y., et al. (2020). Resistance Genes and their Interactions with Bacterial Blight/Leaf Streak Pathogens (Xanthomonas oryzae) in Rice (Oryza sativa L.)-an Updated Review. *Rice* 13, 1–12. doi: 10.1186/s12284-019-0358-y

Jin, X. W., Wang, C. L., Yang, Q., Jiang, Q. X., Fan, Y. L., Liu, G. C., et al (2007). Breeding of near-isogenic line CBB30 and molecular mapping of Xa30(t), a new resistance gene to bacterial blight in rice. *Sci. Agric. Sin.* 40 (6), 1094–1100.

Jinek, M., Chylinski, K., Fonfara, I., Hauer, M., Doudna, J. A., and Charpentier, E. (2012). A programmable dual-RNA-guided DNA endonuclease in adaptive bacterial immunity. *Science* 337, 816–821. doi: 10.1126/science.1225829

Johal, G. S., and Briggs, S. P. (1992). Reductase activity encoded by the HM1 disease resistance gene in maize. *Science* 258, 985–987. doi: 10.1126/science.1359642

Jones, J. D., and Dangl, J. L. (2006). The plant immune system. *Nature* 444, 323–329. doi: 10.1038/nature05286

Joseph, M., Gopalakrishnan, S., Sharma, R. K., Singh, V. P., Singh, A. K., Singh, N. K., et al. (2004). Combining bacterial blight resistance and basmati quality characteristics by phenotypic and molecular marker-assisted selection in rice. *Mol. Breed.* 13, 377–387. doi: 10.1023/B:MOLB.0000034093.63593.4c

Kaku, H., and Ogawa, T. (2001). Genetic Analysis of the relationship between the browning reaction and bacterial blight resistance gene *Xa3* in rice. *J. Gen. Plant Pathol.* 67, 228–230. doi: 10.1007/PL00013017

Karatan, E., and Watnick, P. (2009). Signals, regulatory networks, and materials that build and break bacterial biofilms. *Microbiol. Mol. Biol. Rev.* 73, 310–347. doi: 10.1128/MMBR.00041-08

Kaur, R., Grewal, N., Das, A., Vikal, Y., Singh, J., Bharaj, T. S., et al. (2005). Inheritance of bacterial blight resistance in two accessions of wild rice, *Oryza nivara*. *Rice Genet. Newsl.* 22, 21.

Khush, G. S., and Angeles, E. R. (1999). A new gene for resistance to race 6 of bacterial blight in rice, Oryza sativa. *Rice Genet. Newsl.* 16, 92– 93.

Khush, G. S., Mackill, D. J., and Sidhu, G. S. (1989). "Breeding rice for resistance to bacterial blight. Bacterial Blight of Rice," in *Proceedings of the International Workshop on Bacterial Blight Rice* (Manila, Philippines: IRRI), 207–217.

Khush, G. S. (2005). What it will take to feed 5.0 billion rice consumers in 2030. *Plant Mol. Biol.* 59, 1–6. doi: 978-3-319-45021-6_20/s11103-005-2159-5

Khush, G. S. (2013). Strategies for increasing the yield potential of cereals: Case of rice as an example. *Plant Breed.* 132, 433–436. doi: 10.1111/pbr.1991

Kim, S. (2018). Identification of novel recessive gene *xa44(t)* conferring resistance to bacterial blight races in rice by QTL linkage analysis using an SNP chip. *Theor. Appl. Genet.* 131, 2733–2743. doi: 10.1007/s00122-018-3187-2

Kim, S.-M., and Reinke, R. F. (2019). A novel resistance gene for bacterial blight in rice Xa43(t) identified by GWAS, confirmed by QTL mapping using a bi-parental population. *PLoS ONE* 14 (2), e0211775. doi: 10.1371/journal.pone.0211775

Kim, Y. G., Cha, J., and Chandrasegaran, S. (1996). Hybrid restriction enzymes: zinc finger fusions to Fok I cleavage domain. *Proc. Natl. Acad. Sci.* 93, 1156–1160. doi: 10.1073/pnas.93.3.1156

Kim, S. M., Suh, J. P., Qin, Y., Noh, T. H., Reinke, R. F., and Jena, K. K. (2015). Identification and fine-mapping of a new resistance gene, Xa40, conferring resistance to bacterial blight races in rice (Oryza sativa L.). *Theor. Appl. Genet.* 128, 1933–1943. doi: 978-3-319-45021-6_20/s00122-015-2557-2

Kong, W., Ding, L., and Xia, X. (2020). Identification and characterization of genes frequently responsive to Xanthomonas oryzae pv. oryzae and Magnaporthe oryzae infections in rice. *BMC Genomics* 21, 21. doi: 10.1186/s12864-019-6438-y

Konishi, H., Ishiguro, K., and Komatsu, S. A. (2001). Proteomics approach towards understanding blast fungus infection of rice grown under different levels of nitrogen fertilization. *Proteomics* 1, 1162–1171. doi: 10.1002/1615-9861(200109)1:9<1162::AID-PROT1162>3.0.CO;2-S

Korinsak, S., Sriprakhon, S., Sirithanya, P., Jairin, J., Vanavichit, A., and Toojinda, T. (2009). Identification of microsatellite markers (SSR) linked to a new bacterial blight resistance gene xa33 (t) in rice cultivar 'Ba7'. Maejo. *Int. J. Sci. Tech.* 3, 235–247.

Kumar, P. N., Sujatha, K., Laha, G. S., Rao, K. S., Mishra, B., Viraktamath, B. C., et al. (2012). Identification and fine-mapping of Xa33 a novel gene for resistance to Xanthomonas oryzae pv. oryzae. *Phytopathol* 102, 222–228. doi: 10.1094/PHYTO-03-11-0075

Kumar, A., Gul, M. Z., Zeeshan, A., Bimolata, W., Qureshi, I. A., and Ghazi, I. A. (2013). Differential antioxidative responses of three different rice genotypes during bacterial blight infection. *Aust. J. Crop Sci.* 7, 1893–1900.

Kumar, A., Bimolata, W., Kannan, M., Kirti, P. B., Qureshi, I. A., and Ghazi, I. A. (2015). Comparative proteomics reveals differential induction of both biotic and abiotic stress response associated proteins in rice during Xanthomonas oryzae pv. oryzae infection. *Funct. Integr. Genomic* 15, 425–437. doi: 978-3-319-45021-6_20/s10142-014-0431-y

Kumar, R., Bohra, A., Pandey, A. K., Pandey, M. K., and Kumar, A. (2017). Metabolomics for plant improvement: status and prospects. *Front. Plant Sci.* 8:1302. doi: 10.3389/fpls.2017.01302

Kurata, N., and Yamazaki, Y. (2006). Oryzabase. An integrated biological and genome information database for rice. *Plant Physiol.* 140, 12–17. doi: 10.1104/pp.105.063008

Lacombe, S., Rougon-Cardoso, A., Sherwood, E., Peeters, N., Dahlbeck, D., Van Esse, H. P., et al. (2010). Interfamily transfer of a plant pattern-recognition receptor confers broad-spectrum bacterial resistance. *Nat. Biotechnol.* 28, 365–369. doi: 10.1038/nbt.1613

Lee, K. S., and Khush, G. S. (2000). Genetic analysis of resistance to bacterial blight, Xanthomonasoryzae pv. oryzae rice. *Rice Genet. Newsl.* 17, 72.

Lee, K. S., Rasabandith, S., Angeles, E. R., and Khush, G. S. (2003). Inheritance of resistance to bacterial blight in 21 cultivars of rice. *Phytopathol* 93, 147–152. doi: 10.1094/PHYTO.2003.93.2.147

Leigh, J. A., and Coplin, D. L. (1992). Exopolysaccharides in plant–bacterial interactions. *Annu. Rev. Microbiol.* 46, 307–346. doi: 10.1146/annurev.mi.46.100192.001515

Leung, H., Wu, J., Liu, B., Bustaman, R., Sridhar, K., Singh, E., et al. (2004). Sustainable disease resistance in rice: currentand future strategies. *Proceedings of the 4th international crop science congress*, Brisbane, Australia, 26 September - 1 October.

Li, Z. K., Luo, L. J., Mei, H. W., Paterson, A. H., Zhao, X. Z., Zhong, D. B., et al. (1999). A "defeated" rice resistance gene acts as a QTL against a virulent strain of Xanthomonas oryzae pv. oryzae. *Mol. Gen. Genet.* 261, 58–63. doi: 978-3-319-45021-6_20/s004380050941

Li, P., Long, J. Y., Huang, Y. C., Zhang, Y., and Wang, J. S. (2004). AvrXa3: a novel member of avrBs3 gene family from Xanthomonas oryzae pv. oryzae has a dual function. *Prog. Nat. Sci.* 14, 767–773. doi: 10.1080/10020070412331344311

Li, Z. K., Arif, M., Zhong, D. B., Fu, B. Y., Xu, J. L., Domingo-Rey, J., et al. (2006). Complex genetic networks underlying the defensive system of rice (Oryza sativa L.) to Xanthomonas oryzae pv. oryzae. *Proc. Natl. Acad. Sci.* 103, 7994–7999. doi: 10.1073/pnas.0507492103

Li, Q., Chen, F., Sun, L., Zhang, Z., Yang, Y., and He, Z. (2006). Expression profiling of rice genes in early defense responses to blast and bacterial blight pathogens using cDNA microarray. *Physiol. Mol. Plant Pathol.* 68, 51–60. doi: 10.1016/j.pmpp.2006.06.002

Li, C., Wei, J., Lin, Y., and Chen, H. (2012). Gene silencing using the recessive rice bacterial blight resistance gene xa13 as a new paradigm in plant breeding. *Plant Cell Rep.* 31, 851–862. doi: 978-3-319-45021-6_20/s00299-011-1206-8

Li, H. J., Li, X. H., Xiao, J. H., Wing, R. A., and Wang, S. P. (2012). Ortholog alleles at Xa3/Xa26 locus confer conserved race-specific resistance against Xanthomonas oryzae in rice. *Mol. Plant* 5, 281–290. doi: 10.1093/mp/ssr079

Li, T., Liu, B., Spalding, M. H., Weeks, D. P., and Yang, B. (2012). High-efficiency TALEN-based gene editing produces disease-resistant rice. *Nat. Biotechnol.* 30, 390–392. doi: 10.1038/nbt.2199

Li, T., Huang, S., Zhou, J., and Yang, B. (2013). Designer TAL effectors induce disease susceptibility and resistance to Xanthomonas oryzae pv. oryzae in rice. *Mol. Plant* 6, 781–789. doi: 10.1093/mp/sst034

Li, J. Y., Wang, J., and Zeigler, R. S. (2014). The 3,000 rice genomes project: new opportunities and challenges for future rice research. *GigaScience* 3, 1–3. doi: 10.1186/2047-217X-3-8

Li, Y., Li, D., Guo, Z., Shi, Q., Xiong, S., Zhang, C., et al. (2016). OsACOS12, an orthologue of Arabidopsisacyl-CoA synthetase5, plays an important role in pollen exine formation and anther development in rice. *BMC Plant Biol.* 16, 256. doi: 10.1186/s12870-016-0943-9

Liu, H. X., Liu, F. Q., Hu, B. S., Yang, W. F., Chen, Z. Y., and Xu, Z. G. (2004). Virulence of Xanthomonas oryzae pv. oryzae on rice near-isogenic lines with single resistance gene and pyramiding lines in China. *Agric. Sci. China* 3, 764–769.

Liu, J., Liu, X., Dai, L., and Wang, G. (2007). Recent progress in elucidating the structure, function and evolution of disease resistance genes in plants. *J. Genet. Genom.* 34, 765–776. doi: 10.1016/S1673-8527(07)60087-3

Liu, Q., Yuan, M., Zhou, Y. A., Li, X., Xiao, J., and Wang, S. (2011). A paralog of the MtN3/saliva family recessively confers race-specific resistance to Xanthomonas oryzae in rice. *Plant Cell Environ.* 34, 1958–1969. doi: 10.1111/j.1365-3040.2011.02391.x

Lorenzo, O., Piqueras, R., Sánchez-Serrano, J. J., and Solano, R. (2003). ETHYLENE RESPONSE FACTOR1 integrates signals from ethylene and jasmonate pathways in plant defense. *Plant Cell* 15, 165–178. doi: 10.1105/tpc.007468

Luo, S., Zhang, Y., Hu, Q., Chen, J., Li, K., Lu, C., et al. (2012). Dynamic nucleotide-binding site and leucine-rich repeat-encoding genes in the grass family. *Plant Physiol.* 159, 197–210. doi: 10.1104/pp.111.192062

Macho, A. P., and Zipfel, C. (2014). Plant PRRs and the activation of innate immune signaling. *Mol. Cell* 54, 263–272. doi: 10.1016/j.molcel.2014.03.028

Mahmood, T., Jan, A., Kakishima, M., and Komatsu, S. (2006). Proteomic analysis of bacterial blight defense-responsive proteins in rice leaf blades. *Proteomics* 6, 6053–6065. doi: 10.1002/pmic.200600470

Malukani, K. K., Ranjan, A., Hota, S. J., Patel, H. K., and Sonti, R. V. (2020). Dual Activities of Receptor-Like KinaseOsWAKL21.2 Induce Immune Responses. *Plant Physiol.* 183 (3), 1345–1363. doi: 10.1104/pp.19.01579

Malzahn, A., Lowder, L., and Qi, Y. (2017). Plant genome editing with TALEN and CRISPR. *Cell Biosci.* 24, 7–21. doi: 10.1186/s13578-017-0148-4

Mardis, E. R. (2008). Next-generation DNA sequencing methods. *Annu. Rev. Genomics Hum. Genet.* 9, 387–402. doi: 10.1146/annurev.genom.9.081307.164359

Menges, M., Dóczi, R., Ökrész, L., Morandini, P., Mizzi, L., Soloviev, M., et al. (2008). Comprehensive gene expression atlas for the Arabidopsis MAP kinase signalling pathways. *New Phytol.* 179, 643–662. doi: 10.1111/j.1469-8137.2008.02552.x

Metallo, C. M., and Vander-Heiden, M. G. (2013). Understanding metabolic regulation and its influence on cell physiology. *Mol. Cell* 49, 388–398. doi: 10.1016/j.molcel.2013.01.018

Mew, T. W., Vera Cruz, C. M., and Medalla, E. S. (1992). Changes in race frequency of Xanthomonas oryzae pv. oryzae in response to rice cultivars planted in the Philippines. *Plant Dis.* 76, 1029–1032. doi: 10.1094/PD-76-1029

Mew, T. W., Alvarez, A. M., Leach, J. E., and Swings, J. (1993). Focus on bacterial blight of rice. *Plant Dis.* 77, 5–12. doi: 10.1094/PD-77-0005

Mew, T. W. (1987). Current status and future prospects of research on bacterial blight of rice. *Ann. Rev. Phytopathol.* 25, 359–382. doi: 10.1146/annurev.py.25.090187.002043

Miao, L., Wang, C., Zheng, C., Che, J., Gao, Y., Wen, Y., et al. (2010). Molecular mapping of a new gene for resistance to rice bacterial blight. *Sci. Agric. Sin.* 43, 3051–3058.

Miao, J., Guo, D., Zhang, J., Huang, Q., Qin, G., Zhang, X., et al. (2013). Targeted mutagenesis in rice using CRISPR-Cas system. *Cell Res.* 23, 1233–1236. doi: 10.1038/cr.2013.123

Michelmore, R. W., and Meyers, B. C. (1998). Clusters of resistance genes in plants evolve by divergent selection and a birth-and-death process. *Genome Res.* 8, 1113–1130. doi: 10.1101/gr.8.11.1113

Monaghan, J., and Zipfel, C. (2012). Plant pattern recognition receptor complexes at the plasma membrane. *Curr. Opin. Plant Biol.* 15, 349–357. doi: 10.1016/j.pbi.2012.05.006

Mori, M., Tomita, C., Sugimoto, K., Hasegawa, M., Hayashi, N., Dubouzet, J. G., et al. (2007). Isolation and molecular characterization of a Spotted leaf 18 mutant by modified activation-tagging in rice. *Plant Mol. Biol.* 63, 847–860. doi: 978-3-319-45021-6_20/s11103-006-9130-y

Mortazavi, A., Williams, B. A., McCue, K., Schaeffer, L., and Wold, B. (2008). Mapping and quantifying mammalian transcriptomes by RNA-seq. *Nat. Methods* 5, 621–628. doi: 10.1038/nmeth.1226

Mundt, C. C. (1990). Probability of mutation to multiple virulence and durability of resistance gene pyramids. *Phytopathol* 80, 221–223. doi: 10.1094/Phyto-80-221

Mundt, C. C. (2014). Durable resistance: a key to sustainable management of pathogens and pests. *Infect. Genet. Evol.* 27, 446–455. doi: 10.1016/j.meegid.2014.01.011

Nakai, H., Nakamura, S., Kuwahara, S., and Saito, M. (1988). Genetic studies of an induced rice mutant resistant to multiple races of bacterial leaf blight. *Rice Genet. Newsl.* 5, 101.

Natrajkumar, P., Sujatha, K., Laha, G. S., Srinivasa Rao, K., Mishra, B., Viraktamath, B. C., et al (2012). Identification and fine-mapping of Xa33, a novel gene for resistance to *Xanthomonas oryzae* pv. *oryzae*. *Phytopathology* 102, 222. doi: 10.1094/PHYTO-03-11-0075

Navarro, L., Dunoyer, P., Jay, F., Arnold, B., Dharmasiri, N., Estelle, M., et al. (2006). A plant miRNA contributes to antibacterial resistance by repressing auxin signaling. *Science* 312, 436–439. doi: 10.1126/science.1126088

Neelam, K., Mahajan, R., Gupta, V., Bhatia, D., Gill, B. K., Komal, R., et al. (2019). High-resolution genetic mapping of a novelbacterial blight resistance gene xa-45 (t) identified from Oryza glaberrima and transferred to Oryzasativa. *Theor. Appl. Genet.* 6, 1–7. doi: 10.1007/s00122-019-03501-2

Nino-Liu, D. O., Ronald, P. C., and Bogdanove, A. J. (2006). Xanthomonas oryzae pathovars: model pathogens of a model crop. *Mol. Plant Pathol.* 7, 303–324. doi: 10.1111/j.1364-3703.2006.00344.x

Noda, T., and Kaku, H. (1999). Growth of Xanthomonas oryzae pv. oryzae in planta and in guttation fluid of rice. *Ann. Phytopathol. Soc Japan* 65, 9–14. doi: 10.3186/jjphytopath.65.9

Ogawa, T. (1988). Near-isogenic lines as international differentials for resistance to bacterial blight of rice. *Rice Genet. Newsl.* 5, 106–109.

Oksman-Caldentey, K. M., and Saito, K. (2005). Integrating genomics and metabolomics for engineering plant metabolic pathways. *Curr. Opin. Biotechnol.* 16, 174–179. doi: 10.1016/j.copbio.2005.02.007

Oliva, R., Ji, C., Atienza-Grande, G., Huguet-Tapia, J. C., Perez-Quintero, A., Li, T., et al. (2019). Broad-spectrum resistance to bacterial blight in rice using genome editing. *Nat. Biotechnol.* 37, 1344–1350. doi: 10.1038/s41587-019-0267-z

O'Toole, J. C., Toenniessen, G. H., Murashige, T., Harris, R. R., and Herdt, R. W. (2001). "The Rockefeller Foundation's international program on rice biotechnology," in *Rice Genetics IV*. Eds. G. S. Khush, (New Delhi: Science Publishers and Los Baños, Philippines: International Rice Research Institute). 39–62.

Oryzabase (2006). *Integrated Rice Science Database*, Japan: National Institute of Genetics and Kyushu University. http://www.shigen.nig.ac.jp/rice/oryzabase/.

Ou, S. H. (1985). *Rice diseases* (Great Britain (UK): Commonwealth Mycological Institute).

Pandey, M. K., Rani, N. S., Sundaram, R. M., Laha, G. S., Madhav, M. S., Rao, K. S., et al. (2013). Improvement of two traditional Basmati rice varieties for bacterial blight resistance and plant stature through morphological and marker-assisted selection. *Mol. Breed.* 31, 239–246. doi: 978-3-319-45021-6_20/s11032-012-9779-7

Paternain, L., and Campion, J. (2013). Metabolomics and transcriptomics of metabolic disorders. *Curr. Nutr. Rep.* 2, 199–206. doi: 978-3-319-45021-6_20/s13668-013-0062-2

Perez, L. M., Redoña, E. D., Mendioro, M. S., Cruz, C. M., and Leung, H. (2008). Introgression of Xa4, Xa7 and Xa21 for resistance to bacterial blight in thermos sensitive genetic male sterile rice (Oryza sativa L.) for the development of two-line hybrids. *Euphytica* 164, 627–636. doi: 978-3-319-45021-6_20/s10681-008-9653-1

Perumalsamy, S., Bharani, M., Sudha, M., Nagarajan, P., Arul, L., Saraswathi, R., et al. (2010). Functional marker-assisted selection forbacterial leaf blight resistance genes in rice (Oryza sativa L.). *Plant Breed.* 129, 400–406. doi: 10.1111/j.1439-0523.2009.01705.x

Piron, F., Nicolai, M., Minoia, S., Piednoir, E., Moretti, A., Salgues, A., et al. (2010). An induced mutation in tomato eIF4E leads to immunity to two potyviruses. *PLoS One* 5, e11313. doi: 10.1371/journal.pone.0011313

Porter, B. W., Chittoor, J. M., Yano, M., Sasaki, T., and White, F. F. (2003). Development and mapping of markers linked to the rice bacterial blight resistance gene Xa7. *Crop Sci.* 43, 1484–1492. doi: 10.2135/cropsci2003.1484

Porter, B. W., Paidi, M., Ming, R., Alam, M., Nishijima, W. T., and Zhu, Y. J. (2009). Genome-wide analysis of Carica papaya reveals a small NBS resistance gene family. *Mol. Genet. Genom.* 281, 609–626. doi: 978-3-319-45021-6_20/s00438-009-0434-x

Pradhan, B. B., and Chatterjee, S. (2014). Reversible non-genetic phenotypic heterogeneity in bacterial quorum sensing. *Mol. Microbiol.* 92, 557–569. doi: 10.1111/mmi.12575

Pradhan, S. K., Nayak, D. K., Mohanty, S., Behera, L., Barik, S. R., Pandit, E., et al. (2015). Pyramiding of three bacterial blight resistance genes for broad-spectrum resistance in deep water rice variety, Jalmagna. *Rice* 8, 51. doi: 10.1186/s12284-015-0051-8

Pradhan, S. K., Nayak, D. K., Pandit, E., Behera, L., Anandan, A., Mukherjee, A. K., et al. (2016). Incorporation of bacterial blight resistance genes into lowland rice cultivars through marker assisted backcross breeding. *Phytopathol* 106, 710–718. doi: 10.1094/PHYTO-09-15-0226-R

Pruitt, R. N., Schwessinger, B., Joe, A., Thomas, N., Liu, F., Albert, M., et al. (2015). The rice immune receptor XA21 recognizes atyrosine-sulfated protein from a gram-negative bacterium. *Sci. Adv.* 1, e1500245. doi: 10.1126/sciadv.1500245

Rajeshwari, R., Jha, G., and Sonti, R. V. (2005). Role of an *in planta* expressed xylanase of *Xanthomonas oryzae* pv. oryzae in promoting virulence on rice. *Mol. Plant-Microbe Interact.* 18, 830–837. doi: 10.1094/MPMI-18-0830

Rajpurohit, D., Kumar, R., Kumar, M., Paul, P., Awasthi, A., Basha, P. O., et al. (2010). Pyramiding of two bacterial blight resistance and a semidwarfing gene

in Type 3 Basmati using marker-assisted selection. *Euphytica* 178, 111–126. doi: 978-3-319-45021-6_20/s10681-010-0279-8

Ram, T., Laha, G. S., Gautam, S. K., Deen, R., Madhav, M. S., Brar, D. S., et al. (2010). Identification of new gene introgressed from Oryza brachyantha with broad-spectrum resistance to bacterial blight of rice in India. *Rice Genet. Newsl.* 25, 57.

Ramkumar, G., Sakthivel, K., Sundaram, R. M., Neeraja, C. N., Balachandran, S. M., Rani, N. S., et al (2010). Allele mining in crops: prospects and potentials. *Biotechnol. Adv.* 28, 451–461. doi: 10.1016/j.biotechadv.2010.02.007

Reddy, J. N., Baraoidan, M. R., Bernardo, M. A., George, M. L. C., and Sridhar, R. (1997). Application of marker-assisted selection in rice for bacterial blight resistance gene, *Xa21*. *Curr. Sci.* 73, 873–875.

Ruan, H. H., Yan, C. Q., An, D. R., Liu, R. H., and Chen, J. P. (2008). Identifying and mapping new gene xa32 (t) for resistance to bacterial blight (*Xanthomonas oryzae* pv. *oryzae, Xoo*) from *Oryzae meyeriana* L. *Acta Agric. Bor. Sin.* 17, 170–174.

Sabetta, W., Alba, V., and Blanco, A. (2011). Montemurro C. sunTILL: a TILLING resource forgene function analysis in sunflower. *Plant Methods* 7, 20. doi: 10.1186/1746-4811-7-20

Salmeron, J. M., Oldroyd, G. E., Rommens, C. M., Scofield, S. R., Kim, H. S., Lavelle, D. T., et al. (1996). Tomato Prf is a member of the leucine-rich repeat class of plant disease resistance genes and lies embedded within the Pto kinase gene cluster. *Cell* 86, 123–133. doi: 10.1016/S0092-8674(00)80083-5

Sana, T. R., Fischer, S., Wohlgemuth, G., Katrekar, A., Jung, K. H., Ronald, P. C., et al. (2010). Metabolomic and transcriptomic analysis of the rice response to the bacterial blight pathogen Xanthomonas oryzae pv. *Oryzae Metabolomics* 6, 451–465. doi: 978-3-319-45021-6_20/s11306-010-0218-7

Sanchez, A. C., Brar, D. S., Huang, N., and Khush, G. S. (2000). Sequence tagged site markers-assisted selection for three bacterial blight resistance genes in rice. *Crop Sci.* 40, 792–797. doi: 10.2135/cropsci2000.403792x

Sanchez, P. L., Wing, R. A., and Brar, D. S. (2013). "The wild relative of rice: genomes and genomics," in *Genetics and genomics of rice, plant gene*. Eds. Q. Zhang and R. A. Wing (New York: Springer), pp 616–626.

Sanseverino, W., Roma, G., De Simone, M., Faino, L., Melito, S., Stupka, E., et al. (2010). PRGdb: a bioinformatics platform for plant resistance gene analysis. *Nucleic Acid Res.* 38, D814–D821. doi: 10.1093/nar/gkp978

Sattari, A., Fakheri, B., Noroozi, M., and Moazami, K. (2014). Leaf blight resistance in rice: a review of breeding and biotechnology. *Int. J. Farm Allied Sci.* 3, 895–902.

Savary, S., Elazegui, F. A., and Teng, P. S. (1998). Assessing the representativeness of data on yield losses due to rice disease in tropical. *Asia Plant Dis.* 84, 357–369. doi: 10.1094/PDIS.2000.84.3.357

Schena, M., Shalon, D., Davis, R. W., and Brown, P. O. (1995). Quantitative monitoring of gene expression patterns with a complementary DNA microarray. *Science* 270, 467–470. doi: 10.1126/science.270.5235.467

Scholze, H., and Boch, J. (2011). TAL effectors are remote controls for gene activation. *Curr. Opin. Microbiol.* 14, 47–53. doi: 10.1016/j.mib.2010.12.001

Sekhwal, M. K., Li, P., Lam, I., Wang, X., Cloutier, S., and You, F. M. (2015). Disease resistance gene analogs (RGAs) in plants. *Int. J. Mol. Sci.* 16, 19248–19290. doi: 10.3390/ijms160819248

Sevanthi, A. M. V., Kandwal, P., Kale, P. B., Prakash, C., Ramkumar, M. K., Yadav, N., et al. (2018). Whole genome characterization of a few EMS-induced mutants of upland rice variety Nagina 22 reveals a staggeringly high frequency of SNPs which show high phenotypic plasticity towards the wild-type. *Front. Plant Sci.* 9:1179 . doi: 10.3389/fpls.2018.01179

Sharma, T. R., Das, A., Kumar, S. P., and Lodha, M. L. (2009). Resistance gene analogues as a tool for rapid identification and cloning of disease resistance genes in plants: A review. *J. Plant Biochem. Biotechnol.* 18, 01–11. doi: 978-3-319-45021-6_20/BF03263289

Sharma, K., Sarma, S., Bohra, A., Mitra, A., Sharma, N. K., and Kumar, A. (2018). "Plant metabolomics: An emerging technology for crop improvement," in *New Visions in Plant Science*, *1st ed.* Ed. O. Çelik (London, UK: IntechOpen), 65–79.

Shen, B., Zhang, W., Zhang, J., Zhou, J., Wang, J., Chen, L., et al. (2014). Efficient genome modification by CRISPR-Cas9 nickase with minimal off-target effects. *Nat. Methods* 11, 399–402. doi: 10.1038/nmeth.2857

Sidhu, G. S., Khush, G. S., and Mew, T. W. (1978). Genetic analysis of bacterial blight resistance in seventy our cultivars of rice, Oryza sativa L. *Theor. Appl. Genet.* 53, 105 –1111. doi: 978-3-319-45021-6_20/BF00272687

Singh, R. J., Khush, G. S., and Mew, T. W. (1983). A new gene for resistance to bacterial blight in rice. *Crop Sci.* 23, 558–560. doi: 10.2135/cropsci1983.0011183X002300030026x

Singh, S., Sidhu, J. S., Huang, N., Vikal, Y., Li, Z., Brar, D. S., et al. (2001). Pyramiding three bacterial blight resistance genes (xa5, xa13 and Xa21) using marker-assisted selection into indica rice cultivar PR106. *Theor. Appl. Genet.* 102, 1011–1015. doi: 978-3-319-45021-6_20/s001220000495

Singh, K., Vikal, Y., Singh, S., Leung, H., Dhaliwal, H. S., and Khush, G. S. (2002). Mapping of bacterial blight resistance gene xa8 using microsatellite markers. *Rice Genet. Newsl.* 19, 94– 97.

Smith, J., Grizot, S., Arnould, S., Duclert, A., Epinat, J. C., Chames, P., et al. (2006). A combinatorial approach to create artificial homing endonucleases cleaving chosen sequences. *Nucleic Acids Res.* 34, e149. doi: 10.1093/nar/gkl720

Song, W. Y., Wang, G. L., Chen, L. L., Kim, H. S., Pi, L. Y., Holsten, T., et al. (1995). A receptor kinase like protein encoded by the rice disease resistance gene Xa21. *Science* 270, 1804–1806. doi: 10.1126/science.270.5243.1804

Spindel, J., Begum, H., Akdemir, D., Virk, P., Collard, B., Redona, E., et al. (2015). Genomic selection and association mapping in rice (Oryza sativa): effect of trait genetic architecture, training population composition, marker number and statistical model on accuracy of rice genomic selection in elite, tropical rice breeding lines. *PLoS Genet.* 11, e1004982. doi: 10.1371/journal.pgen.1004982

Srinivasan, B., and Gnanamanickam, S. (2005). Identification of a new source of resistance in wild rice, Oryza rufipogon to bacterial blight of rice caused by Indian strains of Xanthomonas oryzae pv. oryzae. *Curr. Sci.* 88, 1229–1231.

Staswick, P. E., and Tiryaki, I. (2004). The oxylipin signal jasmonic acid is activated by an enzyme that conjugates it to isoleucine in arabidopsis. *Plant Cell* 16, 2117–2127. doi: 10.1105/tpc.104.023549

Streubel, J., Pesce, C., Hutin, M., Koebnik, R., Boch, J., and Szurek, B. (2013). Five phylogenetically close rice *SWEET* genes confer TAL effector-mediated susceptibility to *Xanthomonas oryzae* pv. *oryzae*. *New Phytol.* 200, 808–819. doi: 10.1111/nph.12411

Subramanian, S., Fu, Y., Sunkar, R., Barbazuk, W. B., Zhu, J. K., and Yu, O. (2008). Novel and nodulation-regulated microRNAs in soybean roots. *BMC Genomics* 9, 160. doi: 10.1186/1471-2164-9-160

Sugio, A., Yang, B., Zhu, T., and White, F. F. (2007). Two type III effector genes of Xanthomonas oryzae pv. oryzae control the induction of the host genes OsTFIIAg1 and OsTFX1 during bacterial blight of rice. *Proc. Nat. Acad. Sci.* 104, 10720–10725. doi: 10.1073/pnas.0701742104

Suh, J. P., Jeung, J. U., Noh, T. H., Cho, Y. C., Park, S. H., Park, H. S., et al. (2013). Development of breeding lines with three pyramided resistance genes that confer broad-spectrum bacterial blight resistance and their molecular analysis in rice. *Rice* 6, 5–12. doi: 10.1186/1939-8433-6-5

Sun, X., Cao, Y., Yang, Z., Xu, C., Li, X., Wang, S., et al. (2004). *Xa26*, a gene conferring resistance to *Xanthomonas oryzae* pv. *oryzae* in rice, encodes an LRR receptor kinase-like protein. *Plant J.* 37, 517–527. doi: 10.1046/j.1365-313X.2003.01976.x

Sundaram, R. M., Vishnupriya, M. R., Biradar, S. K., Laha, G. S., Reddy, G. A., Rani, N. S., et al. (2008). Marker assisted introgression of bacterial blight resistance in Samba Mahsuri, an elite indica rice variety. *Euphytica* 160, 411–422. doi: 978-3-319-45021-6_20/s10681-007-9564-6

Sundaram, R. M., Vishnupriya, M. R., Laha, G. S., Rani, N. S., Rao, P. S., and Balachandran, S. M. (2009). Introduction of bacterial blight resistance into Triguna, a high yielding, mid-early duration rice variety. *Biotechnol. J.* 4, 400–407. doi: 10.1002/biot.200800310

Sundaram, R. M., Chatterjee, S., Oliva, R., Laha, G. S., Cruz, C. V., Leach, J. E., et al. (2014). Update on bacterial blight of rice: Fourth international conference on bacterial blight. *Rice* 7, 12. doi: 10.1186/s12284-014-0012-7

Suzuki, T., Eiguchi, M., Kumamaru, T., Satoh, H., Matsusaka, H., Moriguchi, K., et al. (2008). MNU-induced mutant pools and high-performance TILLING enable finding of any gene mutation in rice. *Mol. Genet. Genomics* 279, 213–223. doi: 978-3-319-45021-6_20/s00438-007-0293-2

Talamè, V., Bovina, R., Sanguineti, M. C., Tuberosa, R., Lundqvist, U., and Salvi, S. (2008). TILLMore, a resource for the discovery of chemically induced mutants in barley. *Plant Biotechnol. J.* 6, 477–485. doi: 10.1111/j.1467-7652.2008.00341.x

Tan, G. X., Ren, X., Weng, Q. M., Shi, Z. Y., Zhu, L. L., and He, G. C. (2004). Mapping of a new resistance gene to bacterial blight in rice line introgressed from Oryza officinalis. *Acta Genet. Sin.* 31, 724–729.

Tan, K. C., Ipcho, S. V., Trengove, R. D., Oliver, R. P., and Solomon, P. S. (2009). Assessing the impact of transcriptomics, proteomics and metabolomics on fungal phytopathology. *Mol. Plant Pathol.* 10, 703–715. doi: 10.1111/j.1364-3703.2009.00565.x

Tariq, R., Wang, C. L., Qin, T. F., Xu, F., Tang, Y., Gao, Y., et al. (2018). Comparative transcriptome profiling of rice near-isogenic line carrying Xa23 under infection of Xanthomonas oryzae pv. Oryzae. *Int. J. Mol. Sci.* 19, 717. doi: 10.3390/ijms19030717

Taura, S., Ogawa, T., Yoshimura, A., Ikeda, R., and Iwata, N. (1992). Identification of a recessive resistance gene to rice bacterial blight of mutant line XM6, *Oryzae sativa* L. Japan. *J. Breed.* 42, 7–13.

Thiebaut, F., Rojas, C. A., Grativol, C., Motta, M. R., Vieira, T., Regulski, M., et al. (2014). Genome-wide identification of microRNA and siRNA responsive to endophytic beneficial diazotrophic bacteria in maize. *BMC Genomics* 15, 766. . doi: 10.1186/1471-2164-15-766

Tian, D., Wang, J., Zeng, X., Gu, K., Qiu, C., Yang, X., et al. (2014). The rice TAL effector-dependent resistance protein Xa10 triggers cell death and calcium depletion in the endoplasmic reticulum. *Plant Cell* 26, 497–515. doi: 10.1105/tpc.113.119255

Till, B. J., Cooper, J., Tai, T. H., Colowit, P., Greene, E. A., Henikoff, S., et al. (2007). Discovery of chemically induced mutations in rice by TILLING. *BMC Plant Biol.* 7, 19. doi: 10.1186/1471-2229-7-19

Tu, J., Ona, I., Zhang, Q., Mew, T. W., Khush, G. S., and Datta, S. K. (1998). Transgenic rice variety IR72 with Xa21 is resistant to bacterial blight. *Theor. Appl. Genet.* 97, 31–36. doi: 978-3-319-45021-6_20/s001220050863

Tu, J., Datta, K., Khush, G. S., Zhang, Q., and Datta, S. K. (2000). Field performance of Xa21 transgenic indica rice (Oryza sativa L.), IR72. *Theor. Appl. Genet.* 101, 15–20. doi: 978-3-319-45021-6_20/s001220051443

Uauy, C., Brevis, J. C., Chen, X., Khan, I., Jackson, L., Chicaiza, O., et al. (2005). High temperature adult-plant (HTAP) stripe rust resistance gene Yr36 from Triticum turgidum ssp. Dicoccoides is closely linked to the grain protein content locus Gpc-B1. *Theor. Appl. Genet.* 112, 97–105. doi: 978-3-319-45021-6_20/s00122-005-0109-x

Utami, D. W., Septiningsih, E. M., Triny, T. S., and Fatimah, Y. (2010). Allele mining of bacterial blight resistance gene, Xa7 on Indonesian local rice germplasm. *J. AgroBiogen.* 6, 1–9. doi: 10.21082/jbio.v6n1.2010.p1-9

Utami, D. W., Lestari, P., and Koerniati, S. (2013). A Relative expression of Xa7 gene controlling bacterial leaf blight resistance in Indonesian local rice population (Oryza sativa L.). *J. Crop Sci. Biotech.* 16, 1–7. doi: 978-3-319-45021-6_20/s12892-012-0091-1

Van de Wiel, C. C., Schaart, J. G., Lotz, L. A., and Smulders, M. J. (2017). New traits in crops produced by genome editing techniques based on deletions. *Plant Biotechnol. Rep.* 11, 1–8. doi: 978-3-319-45021-6_20/s11816-017-0425-z

Velculescu, V. E., Zhang, L., Vogelstein, B., and Kinzler, K. W. (1995). Serial analysis of gene expression. *Science* 270, 484–487. doi: 10.1126/science.270.5235.484

Ventelon-Debout, M., Delalande, F., Brizard, J. P., Diemer, H., Van Dorsselaer, A., and Brugidou, C. (2004). Proteome analysis of cultivar-specific deregulations of Oryza sativaindica and O. sativa japonica cellular suspensions undergoing rice yellow mottle virus infection. *Proteomics* 4, 216–225. doi: 10.1002/pmic.200300502

Vojta, A., Dobrinić, P., Tadić, V., Bočkor, L., Korać, P., Julg, B., et al. (2016). Repurposing the CRISPR-Cas9 system for targeted DNA methylation. *Nucleic Acids Res.* 44, 5615–5628. doi: 10.1093/nar/gkw159

Voulhoux, R., Ball, G., Ize, B., Vasil, M. L., Lazdunski, A., Wu, L. F., et al. (2001). Involvement of the twin-arginine translocation system in protein secretion via the type II pathway. *EMBO J.* 20, 6735–6741. doi: 10.1093/emboj/20.23.6735

Vuylsteke, M., Peleman, J. D., and van-Eijk, M. J. T. (2007). AFLP technology for DNA fingerprinting. *Nat. Protoc.* 2, 1387–1398. doi: 10.1038/nprot.2007.175

Wan, J., Dunning, F. M., and Bent, A. F. (2002). Probing plant-pathogen interactions and downstream defense signaling using DNA microarrays. *Funct. Integr. Genomics* 2, 259–273. doi: 978-3-319-45021-6_20/s10142-002-0080-4

Wang, G. L., Song, W. Y., Ruan, D. L., Sideris, S., and Ronald, P. C. (1996). The cloned gene, Xa21, confers resistance to multiple X. oryzae pv. oryzae isolates in transgenic plants. *Mol. Plant Microbe Interct.* 9, 850–855. doi: 10.1094/MPMI-9-0850

Wang, W., Zhai, W., Luo, M., Jiang, G., Chen, X., Li, X., et al. (2001). Chromosome landing at the bacterial blight resistance gene Xa4 locus using a deep coverage rice BAC library. *Mol. Gen. Genomics* 265, 118–125. doi: 978-3-319-45021-6_20/s004380000382

Wang, C., Tan, M., Xu, X., Wen, G., Zhang, D., and Lin, X. (2003). Localizing the bacterial blight resistance gene, Xa22(t), to a 100-Kilobase bacterial artificial chromosome. *Phytopathol* 93, 1258–1262. doi: 10.1094/PHYTO.2003.93.10.1258

Wang, C., Wen, G., Lin, X., Liu, X., and Zhang, D. (2009). Identification and fine mapping of the new bacterial blight resistance gene, Xa31(t), in rice. *Eur. J. Plant Pathol.* 123, 235–240. doi: 978-3-319-45021-6_20/s10658-008-9356-4

Wang, Y., Cheng, X., Shan, Q., Zhang, Y., Liu, J., Gao, C., et al. (2014). Simultaneous editing of three homoeoalleles in hexaploid bread wheat confers heritable resistance to powdery mildew. *Nat. Biotechnol.* 32, 947–951. doi: 10.1038/nbt.2969

Wang, C., Fan, Y., Zheng, C., Qin, T., Zhang, X., and Zhao, K. (2014a). High-resolution genetic mapping of rice bacterial blight resistance gene Xa23. *Mol. Genet. Genomics* 289, 745–753. doi: 978-3-319-45021-6_20/s00438-014-0848-y

Wang, C., Zhang, X., Fan, Y., Gao, Y., Zhu, Q., Zheng, C., et al. (2014b). XA23 is an executor R protein and confers broad-spectrum disease resistance in rice. *Mol. Plant* 8, 290–302. doi: 10.1016/j.molp.2014.10.010

Wang, C., Zhang, X., Fan, Y., Gao, Y., Zhu, Q., Zheng, C., et al. (2015). XA23 is an executor R protein and confers broad-spectrum disease resistance in rice. *Mol. Plant Pathol.* 8, 290–302. doi: 10.1016/j.molp.2014.10.010

Wang, C., Tariq, R., Ji, Z., Wei, Z., Zheng, K., Mishra, R., et al. (2019). Transcriptome analysis of a rice cultivar reveals the differentially expressed genes in response to wild and mutant strains of Xanthomonas oryzae pv. oryzae. *Sci. Rep.* 9, 3757. doi: 10.1038/s41598-019-39928-2

Webb, K. M., Ona, I., Bai, J., Garrett, K., Mew, T., Cruz, V., et al. (2010). A benefit of high temperature: increased effectiveness of a rice bacterial blight disease resistance gene. *New Phytol.* 185 (2), 568–576. doi: 10.1111/j.1469-8137.2009.03076.x

Wen, J. Q., Oono, K., and Imai, R. (2002). Two novel mitogen-activated protein signaling components, OsMEK1 and OsMAP1, are involved in a moderate low-temperature signaling pathway in rice. *Plant Physiol.* 129, 1880–1891. doi: 10.1104/pp.006072

White, F. F., Potnis, N., Jones, J. B., and Koebnik, R. (2009). The type III effectors of *Xanthomonas*. *Mol. Plant Pathol.* 10, 749–766. doi: 10.1111/j.1364-3703.2009.00590.x

Williams, C. E., Wang, B., Holsten, T. E., Scambray, J., and da Silva, F. D. (1996). Ronald PC. Markers for selection of rice *Xa 21* disease resistance gene. *Theor. Appl. Genet.* 93, 1119–1122. doi: 978-3-319-45021-6_20/BF00230134

Wu, J. L., Wu, C., Lei, C., Baraoidan, M., Bordeos, A., Madamba, M. R., et al. (2005). Chemical- and irradiation-induced mutants of indica rice IR64 for forward and reverse genetics. *Plant Mol. Biol.* 59, 85–97. doi: 978-3-319-45021-6_20/s11103-004-5112-0

Wu, J., Yu, H., Dai, H., Mei, W., Huang, X., Zhu, S., et al. (2012). Metabolite profiles of rice cultivars containing bacterial blight-resistant genes are distinctive from susceptible rice. *Acta Biochim. Biophy. Sin. (Shanghai)* 44, 650–659. doi: 10.1093/abbs/gms043

Xiang, Y., Cao, Y. L., Xu, C. Q., Li, X., and Wang, S. (2006). Xa3, conferring resistance for rice bacterial blight and encoding a receptor kinase-like protein, is the same as Xa26. *Theor. Appl. Genet.* 113, 1347–1355. doi: 978-3-319-45021-6_20/s00122-006-0388-x

Xu, J., Audenaert, K., Hofte, M., and De Vleesschauwer, D. (2013). Abscisic acid promotes susceptibility to therice leaf blight pathogen Xanthomonas oryzae pv. oryzae by suppressing salicylic acid-mediateddefenses. *PLoS One* 8, e67413. doi: 10.1371/journal.pone.0067413

Xu, Y., Wang, X., Ding, X., Zheng, X., Yang, Z., Xu, C., et al. (2018). Genomic selection of agronomic traits in hybrid rice using an NCII population. *Rice* 11, 32. doi: 10.1186/s12284-018-0223-4

Xu, Z., Xu, X., Gong, Q., Li, Z., Li, Y., Wang, S., et al. (2019). Engineering broad-spectrum bacterial blight resistance by simultaneously disrupting variable TALE-binding elements of multiple susceptibility genes in rice. *Mol. Plant* 12 (11), 1434–1446. doi: 10.1016/j.molp.2019.08.006

Yang, B., and White, F. F. (2004). Diverse members of the AvrBs3/PthA family of type III effectors are major virulence determinants in bacterial blight disease of rice. *Mol. Plant-Microbe Interact.* 17, 1192–1200. doi: 10.1094/MPMI.2004.17.11.1192

Yang, Z., Sun, X., Wang, S., and Zhang, Q. (2003). Genetic and physical mapping of a new gene for bacterial blight resistance in rice. *Theor. Appl. Genet.* 106, 1467–1472. doi: 978-3-319-45021-6_20/s00122-003-1205-4

Yang, B., Sugio, A., and White, F. F. (2006). Os8N3 is a host disease susceptibility gene for bacterial blight of rice. *Proc. Natl. Acad. Sci.* 103, 10503–10508. doi: 10.1073/pnas.0604088103

Yang, S., Feng, Z., Zhang, X., Jiang, K., Jin, X., Hang, Y., et al. (2006). Genome-wide investigation on the genetic variations of rice disease resistance genes. *Plant Mol. Biol.* 62, 181–193. doi: 978-3-319-45021-6_20/s11103-006-9012-3

Yoshimura, A., Mew, T. W., Khush, G. S., and Omura, T. (1983). Inheritance of resistance to bacterial blight in rice cultivar Cas 209. *Phytopathology* 73, 1409–1412. doi: 10.1094/Phyto-73-1409

Yoshimura, S., Yamanouchi, U., Katayose, Y., Toki, S., Wang, Z. X., Kono, I., et al. (1998). Expression of Xa1, a bacterial blight-resistance gene in rice, is induced by bacterial inoculation. *Proc. Natl. Acad. Sci.* 95, 1663–1668. doi: 10.1073/pnas.95.4.1663

Young, N. D. (2000). The genetic architecture of resistance. *Curr. Opin. Plant Biol.* 3, 285–290. doi: 10.1016/S1369-5266(00)00081-9

Yu, C. L., Yan, S. P., Wang, C. C., Hu, H. T., Sun, W. N., Yan, C. Q., et al. (2008). Pathogenesis-related proteins in somatic hybrid rice induced by bacterial blight. *Phytochemistry* 69 (10), 1989–1996. doi: 10.1016/j.phytochem.2008.04.006

Yu, Y., Streubel, J., Balzergue, S., Champion, A., Boch, J., and Koebnik, R. (2011). Colonization of rice leaf blades by an African strain of Xanthomonas oryzae pv. oryzae depends on a new TAL effector that induces the rice nodulin-3 Os11N3 gene. *Mol. Plant-Microbe Interact.* 24, 1102–1113. doi: 10.1094/MPMI-11-10-0254

Yuan, M., Chu, Z., Li, X., Xu, C., and Wang, S. (2009). Pathogen-induced expressional loss of function is the key factor in race-specific bacterial resistance conferred by a recessive R gene xa13 in rice. *Plant Cell Physiol.* 50, 947–955. doi: 10.1093/pcp/pcp046

Yuan, M., Ke, Y., Huang, R., Ma, L., Yang, Z., Chu, Z., et al. (2016). A host basal transcription factor is a keycomponent for infection of rice by TALE-carrying bacteria. *eLife* 5, e19605. doi: 10.7554/eLife.19605

Yugander, A., Sundaram, R. M., Singh, K., Prasad, M. S., Prasad, A. H., Madhav, M. S., et al. (2019). Marker assisted introgression of a major bacterial blight resistance gene, Xa38 into a rice maintainer line, APMS 6B. *Indian Phytopathol.* 72, 35–41. doi: 978-3-319-45021-6_20/s42360-018-00111-8

Zafar, K., Khan, M. Z., Amin, I., Mukhtar, Z., Yasmin, S., Arif, M., et al. (2020). Precise CRISPR-Cas9 Mediated Genome Editing in Super Basmati Rice for Resistance Against Bacterial Blight by Targeting the Major Susceptibility Gene. *Front. Plant Sci.* 11:575:575. doi: 10.3389/fpls.2020.00575

Zhai, W., Chen, C., Zhu, X., Chen, X., Zhang, D., Li, X., et al. (2004). Analysis of T-DNA-Xa21 loci and bacterial blight resistance effects of the transgene Xa21 in transgenic rice. *Theor. Appl. Genet.* 109, 534–542. doi: 978-3-319-45021-6_20/s00122-004-1670-4

Zhang, Q., Lin, S. C., Zhao, B. Y., Wang, C. L., Yang, W. C., Zhou, Y. L., et al. (1998). Identification and tagging of a new gene for resistance to bacterial blight (*Xanthomonas oryzae* pv *oryzae*) from *O. rufipogon*. *Rice Genet. Newsl.* 15, 138–142.

Zhang, H., and Wang, S. (2013). Rice versus Xanthomonas oryzae pv. oryzae: a unique pathosystem. *Curr. Opin. Plant Biol.* 16, 188–195. doi: 10.1016/j.pbi.2013.02.008

Zhang, Q., Wang, C. L., Zhao, K. J., Zhao, Y. L., Caslana, V. C., Zhu, X. D., et al. (2001). The effectiveness of advanced rice lines with new resistance gene Xa23 to rice bacterial blight. *Rice Genet. Newsl.* 18, 71–72.

Zhang, J., Li, X., Jiang, G., Xu, Y., and He, Y. (2006). Pyramiding of Xa7 and Xa21 for the improvement of disease resistance to bacterial blight in hybrid rice. *Plant Breed.* 125, 600–605. doi: 10.1111/j.1439-0523.2006.01281.x

Zhang, F., Zhuo, D. L., Zhang, F., Huang, L. Y., Wang, W. S., Xu, J. L., et al. (2014). Xa39, a novel dominant gene conferring broad-spectrum resistance to Xanthomonas oryzae pv. oryzae in rice. *Plant Pathol.* 64, 568–575. doi: 10.1111/ppa.12283

Zhao, F., Li, Y., Chen, L., Zhu, L., Ren, H., Lin, H., et al. (2016). Temperature dependent defence of Nicotiana tabacum against Cucumber mosaic virus and recovery occurs with the formation of dark green islands. *J. Plant Biol.* 59 (3), 293–301. doi: 978-3-319-45021-6_20/s12374-016-0035-2

Zheng, C. K., Wang, C. L., Yu, Y. J., Liang, Y. T., and Zhao, K. J. (2009). Identification and molecular mapping of Xa32(t),a novel resistance ene for bacterial blight (Xanthomonas oryzae pv. oryzae) in rice.*Acta Agron. Sin.* 35, 1173–1180. doi: 10.1016/S1875-2780(08)60089-9

Zhou, B., Dolan, M., Sakai, H., and Wang, G. L. (2007). The genomic dynamics and evolutionary mechanism of the Pi2/9 locus in rice. *Mol. Plant-Microbe Interact.* 20, 63–71. doi: 10.1094/MPMI-20-0063

Zhou, J., Peng, Z., Long, J., Sosso, D., Liu, B., Eom, J. S., et al. (2015). Gene targeting by the TAL effector PthXo2 reveals cryptic resistance gene for bacterial blight of rice. *Plant J.* 82, 632–643. doi: 10.1111/tpj.12838

Zhu, Y., Qian, W., and Hua, J. (2010). Temperature modulates plant defense responses through NB-LRR proteins. *PLoS Pathog.* 6 (4), e1000844. doi: 10.1371/journal.ppat.1000844

Zipfel, C., Robatzek, S., Navarro, L., Oakeley, E. J., Jones, J. D., Felix, G., et al. (2004). Bacterial disease resistance in Arabidopsis through flagellin perception. *Nature* 428, 764–767. doi: 10.1038/nature02485

Zou, H., Zhao, W., Zhang, X., Han, Y., Zou, L., and Chen, G. (2010). Identification of an avirulence gene, avrxa5, from the rice pathogen Xanthomonas oryzae pv. oryzae. *Sci. China Life Sci.* 53, 1440–1449. doi: 978-3-319-45021-6_20/s11427-010-4109-y

Conflict of Interest: The authors declare that the research was conducted in the absence of any commercial or financial relationships that could be construed as a potential conflict of interest.

Copyright © 2020 Kumar, Kumar, Sengupta, Das, Pandey, Bohra, Sharma, Sinha, Sk, Ghazi, Laha and Sundaram. This is an open-access article distributed under the terms of the Creative Commons Attribution License (CC BY). The use, distribution or reproduction in other forums is permitted, provided the original author(s) and the copyright owner(s) are credited and that the original publication in this journal is cited, in accordance with accepted academic practice. No use, distribution or reproduction is permitted which does not comply with these terms.

frontiers in Plant Science

ORIGINAL RESEARCH
published: 07 August 2020
doi: 10.3389/fpls.2020.01132

Intra and Inter-specific Variability of Salt Tolerance Mechanisms in *Diospyros* Genus

*Francisco Gil-Muñoz[1], Juan Gabriel Pérez-Pérez[2], Ana Quiñones[1], María del Mar Naval[1] and María Luisa Badenes[1]**

[1] Centro de Citricultura y Producción Vegetal, Instituto Valenciano de Investigaciones Agrarias (IVIA), Valencia, Spain, [2] Centro de Investigación en Desarrollo de Agricultura Sostenible, Instituto Valenciano de Investigaciones Agrarias (IVIA), Valencia, Spain

Saline stress is one of most important problems that agriculture must face in the context of climate change. In the Mediterranean basin, one of the regions most affected, persimmon production can be compromised by this effect, due to the limited availability of salt tolerant rootstocks. Seedlings coming from four populations from the *Diospyros* genus have been exposed to salt stress in order to identify salt tolerance genotypes within these populations. Morphological, physiological, and transcriptomic approaches have revealed different mechanisms of tolerance among the population studied. An *HKT1-like* gene has been shown to have different root expression related to the salt tolerance phenotypes among and within populations. Additionally, we have observed differences in salt-responsive expression among *PIP* aquaporin genes. Genetic variability for salt tolerance can be generated in Diospyros species through crossings and used for overcome salt stress. Furthermore, differences in water use efficiency (WUE) have been obtained between and within populations. The information gathered at transcriptomic and physiological level demonstrated natural and heritable variability among *Diospyros* genus which is the key for salt-tolerant rootstock breeding programs.

Keywords: *Diospyros*, saline tolerance, rootstock breeding, persimmon, *HKT-1* gene, salt stress

OPEN ACCESS

Edited by:
Magdalena Arasimowicz-Jelonek, Adam Mickiewicz University, Poland

Reviewed by:
Ahmad Arzani, Isfahan University of Technology, Iran
Dong-Ha Oh, Louisiana State University, United States

***Correspondence:**
María Luisa Badenes
badenes_mlu@gva.es

Specialty section:
This article was submitted to Plant Abiotic Stress, a section of the journal Frontiers in Plant Science

Received: *23 March 2020*
Accepted: *13 July 2020*
Published: *07 August 2020*

Citation:
Gil-Muñoz F, Pérez-Pérez JG, Quiñones A, Naval MdM and Badenes ML (2020) Intra and Inter-specific Variability of Salt Tolerance Mechanisms in Diospyros Genus. Front. Plant Sci. 11:1132. doi: 10.3389/fpls.2020.01132

INTRODUCTION

Persimmon (*Diospyros kaki*) production in the Mediterranean has increased by five times in the last 20 years (Perucho, 2018). In fact, it became an important alternative to citrus production and shares the same crop areas. However, in the recent years, cultural practices and climate change have modified rainfall distribution and have increased salt content in the irrigation water (Visconti et al., 2015). In general, there are two major ways to tackle soil salinization problem, irrigation-and-drainage approach and improvement of salinity tolerance in crops. Saline soils are difficult to remediate, for several reasons that have been outlined by Arzani and Ashraf (2016), and thus the use of salinity tolerant varieties is the most effective and widely used approach. In tree crops composed by rootstock and scion, the best approach to overcome soil salinity is to use salt-tolerant rootstocks compatible with the scion (Forner-Giner and Ancillo, 2013). There are three species of *Diospyros* genus used as rootstocks: *D. kaki*, *D. lotus*, and *D. virginiana* (Badenes et al., 2015). *D. lotus* is the most commonly used rootstock in the Mediterranean area due to its tolerance to lime-filled soils,

adaptability, and absence of basal shoots. However, it is high sensitive to salinity (de Paz et al., 2016a; Visconti et al., 2017). *D. virginiana*, is tolerant to salinity and has a good development in lime-filled soils, but it confers too much vigor to the scion and produces basal shoots, both of which are traits that make crop management difficult (Incesu et al., 2014; de Paz et al., 2016b). *D. kaki* is the most used rootstock species around the world, because its compatibility with all the cultivars. This rootstock is not used in the Mediterranean basin because its sensitivity to lime-filled soils and the weak root system developed in those soils that causes pour and slow development (Bellini and Giordani, 2002).

An additional problem for persimmon crop is the origin of the rootstocks; all of them come from seedlings, never from clonal propagation, which implies a high genetic variability among rootstocks. No clonal rootstocks nor clones selected from breeding programs are available, although micropropagation methods have been developed for some genotypes of *D. lotus* and *D. virginiana* (Giordani et al., 2012). Regarding to saline-stress performance, *D. virginiana* has been identified as the most salt-tolerant species and *D. lotus* the most sensitive, being *D. kaki* intermediate (de Paz et al., 2016b; Visconti et al., 2017; Gil-Muñoz et al., 2018a). However, information about the salt tolerance diversity into each rootstock species is not available. To unravel this question is the key for developing genotypes tolerant to salinity. Moreover, to determine the salt tolerance mechanisms among the persimmon rootstock species would allow to define strategies for managing the crop in saline environments and to design interspecific crosses that combined different tolerant mechanisms.

Salt stress tolerance is a polygenic (quantitative) trait highly influenced by environment and genotype-by-environment interaction (Arzani and Ashraf, 2016) (Tiwari et al., 2016). Therefore, discovering the salinity tolerance mechanism or even the genes underlying to the tolerant phenotypes might help to avoid the environment effect in the first steps of a breeding program. Salt stress causes osmotic stress and ion toxicity, leading to cell dehydration, disruption of metabolic processes, nutrient imbalances, membrane dysfunction, and oxidative stress (Essah et al., 2003) (Essah et al., 2003; Arzani, 2008; Munns and Tester, 2008).

Under salinity conditions, osmotic stress causes drought-like effects in the plant. It causes changes in the stomatal aperture of the plant *via* abscisic acid (ABA) route (Fricke et al., 2006). Independently to the water ion profile, this mechanism is activated and might be a drought response effect, as it has been observed that it is regulated by root signals that are also triggered in drought conditions (Termaat et al., 1985; Davies et al., 2005). Photosynthesis of the plant can be severely affected by salinity stress, but the causes are not yet fully known (Gil-Muñoz et al., 2020). Some studies have related salinity stress with an increase in stored carbohydrate (Munns et al., 2000), indicating a reduction in sink demand that may downregulate photosynthesis.

Regulation of water transport, small solutes, and hydric balance through the plant is a mechanism to overcome salinity stress. Maurel et al. (2008) described membrane intrinsic proteins named aquaporins that play a central role in water relations of roots, leaves, and seeds, hence, involved in this regulation. Several studies described changes in aquaporin Plasma membrane intrinsic protein (PIPs) family activity under salt stress (Martínez-Ballesta et al., 2003; Boursiac et al., 2005; López-Pérez et al., 2009) linked to a reduction in hydraulic conductivity (Joly, 1989; Zekri and Parsons, 1989). Furthermore, in citrus rootstocks, it has been observed different aquaporin activity in salt-tolerant genotypes compared to sensitive (Rodríguez-Gamir et al., 2012). Furthermore, experiments on yeast and *Xenopus oocytes* have shown increased Na^+ conductance when overexpressing *AtPIP2;1* from *Arabidopsis thaliana*, suggesting a possible function for Na^+ influx into the plant (Chaumont and Tyerman, 2014).

Several genes have been identified with salt tolerance, mainly with ionic stress overcame by avoiding toxic ion inflow, transport, or by balancing ion homeostasis (Arzani and Ashraf, 2016). The Salt Overly Sensitive (SOS) signaling pathway is responsible of maintaining ion homeostasis during salt stress (Zhu et al., 1998). In this pathway, myristoylated calcium-binding protein CBL4 (SOS3) acts as a sensor to perceive the Na^+-mediated Ca^{2+} spike. After activation, it interacts with a serine/threonine protein kinase (SOS2) (Liu and Zhu, 1998; Halfter, 2000; Liu, 2000; Hrabak et al., 2003) that mediates the activation of the target gene *SOS1* (Shi et al., 2000; Qiu et al., 2002; Quintero et al., 2002; Quan et al., 2007; Quintero et al., 2011), a plasma membrane encoding gene with Na^+/H^+ antiporter activity (Qiu et al., 2003) that mediates the retrieval of Na^+ from the cytosol. However, this pathway has a high demand of energy and can compromise plant growth (Isayenkov and Maathuis, 2019). Other genes related with salt stress tolerance participate in different tolerance mechanisms. Some members of the HKT (High affinity potassium transporter) family have been linked with Na^+ exclusion (Byrt et al., 2007; Munns and Tester, 2008; Almeida et al., 2013; Isayenkov and Maathuis, 2019) showing a higher expression in roots than shoots (Arabbeigi et al., 2018). Also, a member from the Na^+/H^+ exchanger family (NHX) has been liked to salinity tolerance (Apse et al., 1999), possibly *via* a role in stomatal regulation (Barragán et al., 2012). Furthermore, the ALMT (Aluminum-activated Malate Transporter) protein family encodes anion transmembrane channels (Barbier-Brygoo et al., 2011) that have been proposed to have a role in Cl^- and Na^+ sequestration in vacuoles of salt tolerant plants (Baetz et al., 2016).

Plants have developed extensive Na^+ tolerance mechanisms. Therefore, in saline environments Cl^- can become potentially more harmful than Na^+, as Cl^- influx is believed to be mediated by passive mechanisms through anion channels regulated by ABA (Munns and Tester, 2008).

In a previous study, variability of salt tolerance in two *Diospyros* genus species was exploited and studied through interspecific crossings (Gil-Muñoz et al., 2020). However, despite prior works that studied salt stress effect in several *Diospyros* species (Mickelbart and Marler, 1998; Incesu et al., 2014), the mechanisms that regulate the osmotic and ionic stress tolerance within the species used as rootstock in persimmon remain not fully known. Understanding and identifying the mechanisms of salt tolerance present in the natural variability of these species will help to advance in rootstock breeding programs. Screening of physiological parameters and genetic expression of genes involved in tolerance is the strategy proposed

for selecting genetic-dependent salt tolerant individuals. Results will provide insights of the mechanisms of tolerance in the persimmon species used as rootstocks. The discovery of the mechanisms for salt tolerance will provide tools for breeding *Diospyros* rootstocks better adapted to the saline conditions present in the Mediterranean basin environment.

MATERIALS AND METHODS

Plant Material and Salinity Treatment

Four populations were used for the salinity tolerance study: Seedlings from an open pollination family of *D. kaki* (DK), seedlings from open pollination family of *D. virginiana* (DV), seedlings from a half-sibling backcross family between *D. kaki x D. virginiana* (BC) and a population from *D. lotus* (DL), a full sibling family from a cross between two *D. lotus* trees at the IVIA persimmon germplasm bank was added to the study (**Supplementary Figure 1**). At the end of March, seeds were stratified for 30 days in plastic bags filled with perlite in a cold chamber at 4°C. After stratification, seeds were transferred to peat-moss and perlite (4:1 ratio, respectively) and kept in a greenhouse at 18–24°C during 2 months (from April 24 to June 26, 2017).

One hundred and twenty-seven seedlings of each population were transplanted into 1-L pots containing coarse sand to ensure complete drain. The plants were distributed randomly in the greenhouse and watered with a nutrient solution (3% Cristaljisa 18-18-18, soluble fertilizer with micronutrients) until apical meristem growth was observed. The plants were acclimated before exposition to salinity treatment, meaning that they were watered with the nutrient solution until normal growth was observed. After acclimation, plants were submitted to a salinity treatment during 60 days. The treatment consisted in 40 mM NaCl added to the nutrient solution. All the watering of the plants was done three times a day with exclusively nutrient solution with 40 mM NaCl until water leakage to ensure soil washing between waterings. Although this salt concentration may appear to be mild, it was chosen based on our previous findings in persimmon (Gil-Muñoz et al., 2018a). The control plants remained watered with the standard nutrient solution.

Agro-Morphological Data

The parameters total height (cm), leaves (no.), nodes (no.), internodes (cm), and defoliation (1-no. leaves/no. nodes) were measured at days 0, 30, and 45 for all plants (127 of each population). Twenty plants (10 tolerant and 10 sensitive) of each family were selected based on salt tolerance according to the visual and agro-morphological data for further analyses. For the *D. lotus* family only five plants could be selected as tolerant. Ten control plants of each population were randomly selected. At the end of the salinity treatment (day 60), prior parameters were also measured for selected plants. Variables related to growth were calculated as the ratio between initial and final value. Relative growth rate (RGR) was calculated as follows:

$$\mathrm{RGR} = \frac{Ln(Height\quad 2 - Height\quad 1)}{t2 - t1}$$

Based on visual symptoms, salinity injury was rated from 0 to 4: 0, no symptoms; 1, leaf turgor loss; 2, leaf tip necrosis; 3, leaf margin necrosis; 4, defoliated plant (**Supplementary Figure 2**).

Stem Water Potential

Stem water potential (ψ_H, MPa) was measured in three fully expanded leaves of each plant from control and selected plants in a sunny day using a Model 600 Schölander Pressure Chamber (PMS Instrument Company, Albany, OR, USA) at the end of the salinity treatment (day 60). Previously, the leaves was kept in a reflective plastic bag for 30 min to remove water loss (Levin, 2019).

Leaf Gas Exchange Parameters

Leaf net CO_2 assimilation rate (A_{CO2}), stomatal conductance (g_s), leaf transpiration rate (E), and internal CO_2 concentration (C_i) were measured on single attached leaves from selected (tolerant, sensitive, and control) plants. Determinations were performed using three uniform fully expanded leaves from the mid-stem zone. Intrinsic leaf water use efficiency (WUE) was calculated as A_{CO2} and g_s ratio. All measurements were carried out in a sunny day between 9:30 a.m. and 12:30 p.m. at the end of the salt treatment (day 60). Photosynthetically active radiation (PAR) at the leaf surface was adjusted to a photon flux density of 1.000 μmol m^{-2} s^{-1}. A CIRAS-2 Portable Photosynthesis System (PP Systems, Amesbury, Massachusetts, USA) was used for the measurements. Leaf laminae were fully enclosed within a PLC 6 (U) universal leaf autocuvette in a closed-circuit model and kept at 25 ± 0.5°C, with a leaf-to-air vapor deficit of about 1.7 kPa. The air flow rate through the cuvette was 0.5–1.5 L min^{-1}.

Ion Content Analysis

After saline treatment, three leaves from each selected plant (control, tolerant, and sensitive plants) were collected. Sample pre-treatments for ion content measurement were performed as described in Gil-Muñoz et al. (2018b). Chloride concentration (mg ml^{-1}) was determined by silver ion-titration (Gilliam, 1971) with a Corning 926 automatic chloridometer (Corning Ltd. Halstead Essex, UK). Na^+, Ca^{2+}, K^+, Mg^{2+}, P, and S ions were quantified (mg g^{-1} dry w.t.) using a multiple-collector inductively coupled plasma mass spectrometry (MC-ICP MS, Thermo Finnigan Neptune).

Gene Expression Analysis

Young fully expanded leaves and root tip tissue was collected after 60 days of salt treatment and immediately frozen and powdered using liquid nitrogen. Control samples from all populations were also collected and processed. Three biological replicates were collected for each individual. RNA was isolated according to Gambino et al. (2008). DNA was removed with the RNase-Free DNase Set (Qiagen, Valencia, CA, USA), using the RNeasy Plant Mini Kit (Qiagen). Purified RNA (500 ng) was reverse transcribed with PrimeScript RT Reagent Kit (Takara Bio, Otsu, Japan) in a total volume of 10 μl.

Six putative orthologous genes involved in different mechanisms leading to salt tolerance were analyzed *SOS1*, *SOS2*, *SOS3*, *NHX1*, *HKT1*, and *ALMT9* with primers designed from *D. lotus* SRA archive (SRA ID: SRP045872) *cv*. Kunsenshi (Akagi et al., 2014). For the *PIP* aquaporin expression analysis, *Arabidopsis thaliana* PIP genes from the PIP1 and PIP2 families were blasted against the *D. lotus* (SRA ID: SRP045872) *cv*. Kunsenshi (Akagi et al., 2014). The output fragments were manually assembled to complete putative orthologous genes. Specific persimmon primers were designed using the sequences obtained (**Table 1**). For PIP expression analysis, individual biological replicates were mixed into three global biological replicates for each population subset.

The first-strand cDNA was 30-fold diluted, using 1 µl as template in a final volume of 20 µl. Quantitative real-time PCR was performed on a StepOnePlus Real-Time PCR System (Life Technologies, Carlsbad, CA, USA), using SYBR premix Ex Taq (Tli RNaseH plus) (Takara Bio). The PCR protocol consisted of 10 min at 95°C, followed by 40 cycles of 15 s at 95°C, and 1 min at 60°C. The specificity of the reaction was assessed by the presence of a single peak in the dissociation curve and through size estimation of the amplified product by agarose electrophoresis. *DkACT* (Akagi et al., 2009) and *DkTUA* (Wang et al., 2016) were used as reference genes. The normalization factor was calculated by the geometric mean of the values of relative expression of both genes.

TABLE 1 | Primers used for RT-qPCR analysis.

Gene name	Sequence (5'-3')
SOS1-Like	F: GGATTTTCTCTGGAAGGAAAGTGCTA
	R: GGAGATGTAATCAGTTCCTCTTTGACAC
SOS2-Like	F: TTAGAGTTTGTTACTGGAGGGGAACT
	R: CACTCAGTCCAAAGTCAGAAACCTTCA
SOS3-Like	F: GAAGTTGAGGCCTTGTATGAGCTATTT
	R: CCTAATGAACGAACAAATTCTCCAAACTC
HKT1-Like	F: GATTCCTAACCCTGCAGATAAACCCATT
	R: GTTGCAGACACAGAGGTAAAGAACAAG
NHX1-Like	F: CACCAAAGAACTTGACAAGAATGCTG
	R: CCAATAGTAGTGCACGGTACGAG
ALMT9-Like	F: ACTTATGCAAAACTATACCCCACAATG
	R: TAGATAAACATATTCACCACCAAACACAC
PIP1-1-Like	F: CCCCAACAAGTGCTCCAGC
	R: CTTGGTGTAGCCGGAGCTG
PIP1-2-Like	F: TCACCTAGCAAGTGTGCCTCC
	R: CCTTGGTGTAGCCATGCTGC
PIP1-3-Like	F: GGCTCCCAACAAGTGTGCTT
	R: CCTTGGTGTAGCCATGTGCA
PIP1-4-Like	F: TCAGGTCTCCTACCAAGTGTGG
	R: CCCTTGGTATAGCCAGGGTTT
PIP2-1-Like	F: AAGTGAGCGAAGAGGGCCAAAC
	R: GTAGCGACGGTGACGTAGAGG
PIP2-2-Like	F: ATCTGAGCGAGGAAGGCCAAG
	R: GTGGCGACGGTGACGTAGAGA
PIP2-3-Like	F: CCACATTAACCCAGCAGTGACA
	R: CCGATGATCTCAGCTCCGAGT
PIP2-4-Like	F: AGGAAAGTGTCGCTGATCCGG
	R: TTGCTGTAGCCGTGAGCCACCGAA
PIP2-5-Like	F: GAGGAAGGTGTCGCTGATCAGA
	R: TGTTGTAGCCTGACGCCACCTCA
PIP2-6-Like	F: ATTGCTCTTCCTCTACGTCTCAGTG
	R: GCGACACCTTCCTGGCTAACAG

Statistical Analyses and Raw Data

All the data analysis and graphics were made using RStudio v1.1.447 (2018) with packages from the Comprehensive R Archive Network (CRAN). Parameters for all the populations were statistically tested by Kruskal-Wallis test ($P \leq 0.05$) and averages were compared with the Pairwise Wilcoxon-Mann-Whitney test at 95% confidence level ($P \leq 0.05$) using the packages *dplyr* (Wickham et al., 2018), *ggplot2* (Wickham, 2016), *FSA* (Ogle et al., 2018), *DescTools* (Signorell, 2017), *rcompanion* (Mangiafico, 2018), *RColorBrewer* (Neuwirth, 2014), and *multcompView* (Graves et al., 2015). Principal component analysis (PCA) and correlogram were carried out using the packages *ggplot2* (Wickham, 2016), *factoextra* (Kassambara and Mundt, 2017), and *corrplot* (Wei and Simko, 2016). The variables included were the agro-morphological traits measured before the selection. A biplot of individual scores and loadings was obtained. For representation of the RNA expression data, packages *gplots* (Warnes et al., 2016) and *RColorBrewer* (Neuwirth, 2014) were used.

All the raw data has been deposited in https://github.com/fragimuo/Diospyros-salt-tolerance.

RESULTS

Saline Stress Effect Among Populations

Initial morphological parameters from the four populations were measured before salinity treatment began (**Figure 1**). The number of days from sowing to germination showed differences between all the populations. *D. kaki* (DK) population resulted in the smallest plants and *D. lotus* (DL) plants the tallest, backcross (BC), and *D. virginiana* (DV) populations had a similar initial height. No differences were observed in initial node number between DK and BC population and between DL and DV. Interestingly, the highest variability in initial phenotype was found in DV and BC populations compared to DK and DL populations.

After 45 days of saline stress, differences were noticeable among the four populations (**Figure 2**). DV and BC reached higher height than DL and DK populations. The BC population reached the highest internode length compared to other populations, suggesting higher vigor under salinity conditions. Again, more variability was observed among DV and BC populations compared to DK and DL regarding to morphological parameters. Furthermore, some of the plants did not survive to the salt stress treatment. The survival rate after 45 days of saline treatment was 100% for BC, 87% for DV, 89% for DK, and 98% for DL. Comparing the morphological traits before and after the saline treatment, DV and BC populations had less detrimental effects than DK and DL populations that showed significantly reduced height and severe salt stress damage (**Figure 3**).

All the morphological variables measured during the stress treatment were submitted to a Principal Component Analysis (PCA) (**Figure 4**). The first two components explained almost 60% of total variability. The PCA grouped clearly the individuals

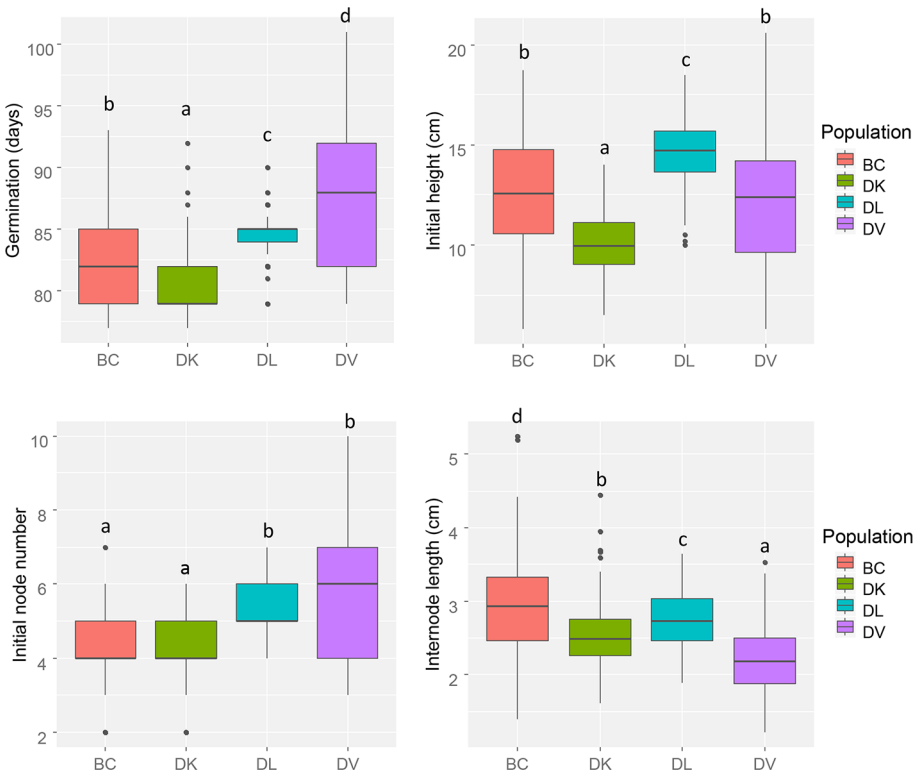


FIGURE 1 | Box and whisker representation of initial morphologic parameters of the four populations (n = 128). Different letters mean statistical differences between populations.

according to the population they belonged, but separated the populations DV, DK, and DL. The backcross population that combines genetic background from *D. kaki* and *D. virginiana* is located at equidistance from DK and DV populations. Furthermore, the DL dispersion was the narrowest. DV, BC, and DK population are separated by the PC1. The variables contributing to the PC1 were final plant height, final number of nodes, and relative final height (**Supplementary Figure 3**). DL population was separated from the other three by variables contributing to the PC2, final internode length, height growth, and defoliation.

Saline Stress Tolerance Variability Within Populations

Using the symptoms and overall plant status, subsets of tolerant and sensitive plants were chosen from each population. The observed symptoms and the scale used are shown on **Supplementary Figure 2**. The tolerant plants were a subset of plants showing less damage caused by salt, and the sensitive ones were the most affected within the population's species. These subsets were submitted to a PCA using the morphological variables, but removing those that showed a high collinearity in the previous PCA (**Figure 5A**). In the four populations sensitive and tolerant plants were grouped apart. DK, BC, and DL were separated on similar directions, according to the PCA variables final height and height growth (**Figure 5B**). DV population showed less clear separation between tolerant and sensitive plants, mainly in the PC2 axis. All the populations showed a coherency in the separation between tolerant and sensitive plants (**Figure 5C**), which implies that the morphological traits used are a useful tool for phenotyping salt tolerance. Due to the higher tolerance to salinity in the DV population, the discrimination by phenotype was weaker.

A correlogram using the morphological variables was done, including the leaf damage symptoms (**Supplementary Figure 4**). The height growth parameter and the relative final height were the variables more correlated with final salt damage symptoms. Differences for both variables were found between tolerant and sensitive individuals in the DK, DL, and BC populations (**Figure 6**). Furthermore, in these populations, the control plants had higher values than both the tolerant and sensitive subsets, except for the DK population in which the control plants were statistical identical to the tolerant subset regarding to height. No significant differences were found within the DV population.

Physiological and Nutritional Effects Related to Salinity Tolerance

In order to elucidate the salinity tolerance mechanisms within each species and population, once the populations were divided

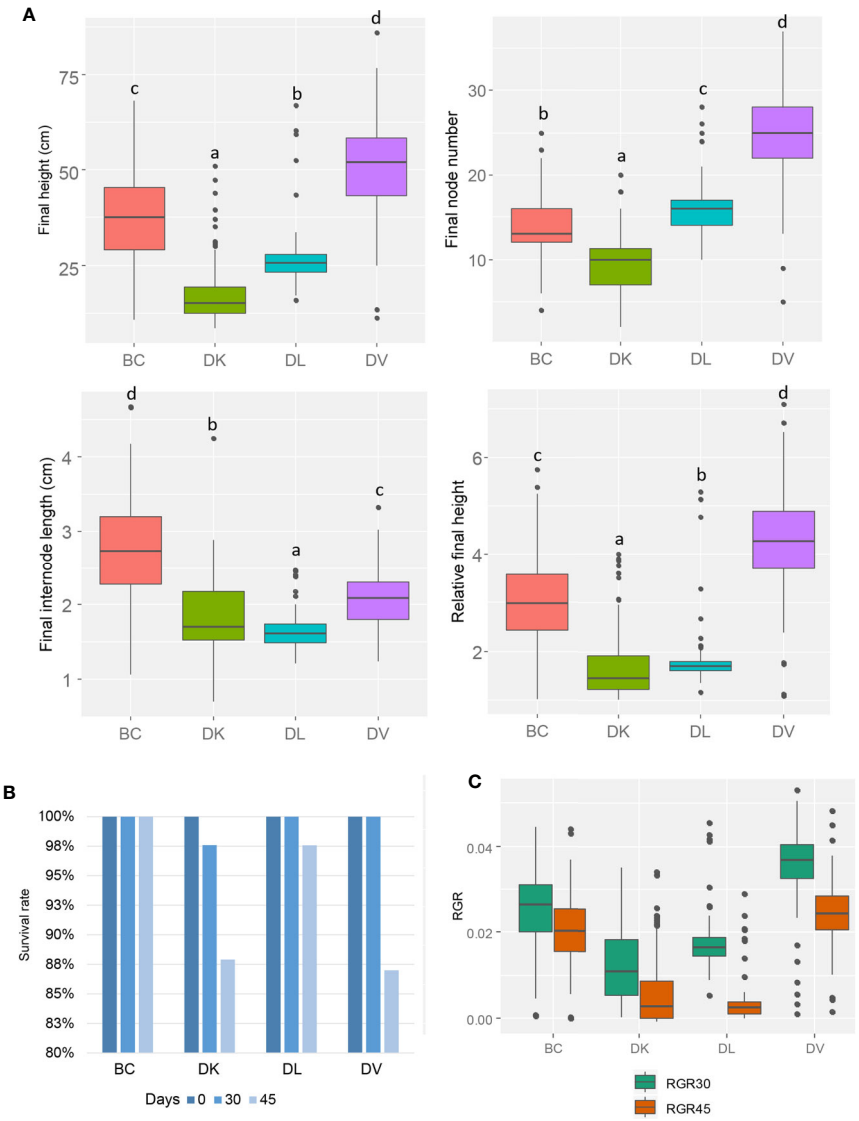


FIGURE 2 | Box and whisker representation of morphologic parameters of the four populations (n = 128) after 45 days of salt treatment **(A)**. Different letters mean statistical differences between populations. Relative final height is the ratio between final and initial height. Percentage of plants that were still alive after 30 and 45 days of treatment **(B)**. Relative growth rate of 0–30 days and 30–45 days **(C)**.

into subsets of tolerant and sensitive plants to saline stress, we analyzed plant water status, leaf gas exchange, and nutritional parameters for each subset after 60 days of saline stress.

Stem water potential was measured to determine differences in plant water status between the different populations. Sensitive plants showed significant better plant water status (higher values of stem water potential) than the tolerant in both DK and DL populations (**Figure 7**). In addition, in these populations, the values of stem water potential from the tolerant subset and the control were statistically identical. Respect to the leaf gas exchange parameters, all tolerant populations maintained similar values of A_{CO2} and g_s than control plants, whereas in sensitive subsets from DK and DL were significantly decreased (**Figures 8A, B**). The C_i were significantly higher in both sensitive and tolerant DK and DL populations than in control plants (**Figure 8C**). In the case of BC populations, C_i were significantly lower in tolerant than in sensitive plants, whereas C_i remained unaltered in DV plants. On the other hand, the DK and DL populations showed significantly lower WUE in both tolerant and sensitive plants than in the control (**Figure 8D**). The BC population had higher WUE in tolerant plants than in sensitive. No differences were observed between any population subset of DV.

Leaf ions content were analyzed to quantify toxic ion accumulation (Cl^- and Na^+) and nutritional imbalances (K^+ and Ca^{2+}) caused by saline stress. Leaf Cl^- accumulation significantly increased in both sensitive and tolerant populations (**Figure 9A**), but in DL populations sensitive plants had higher

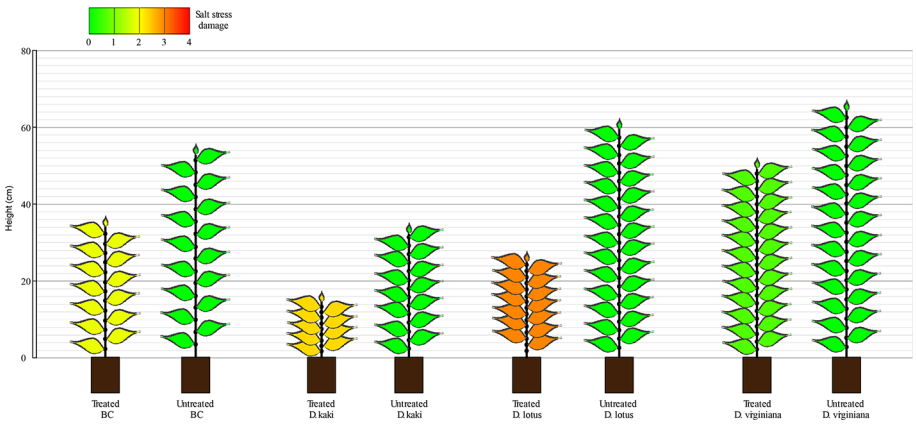


FIGURE 3 | Representation of mean plants from each population with (n = 128) and without salt (control; n = 15 for DK, DV, and BC; n = 4 for DL) after 45 days of treatment (prior to plant selection). Height (cm) number of nodes, defoliation (as missing leaves), and salt stress damage are depicted.

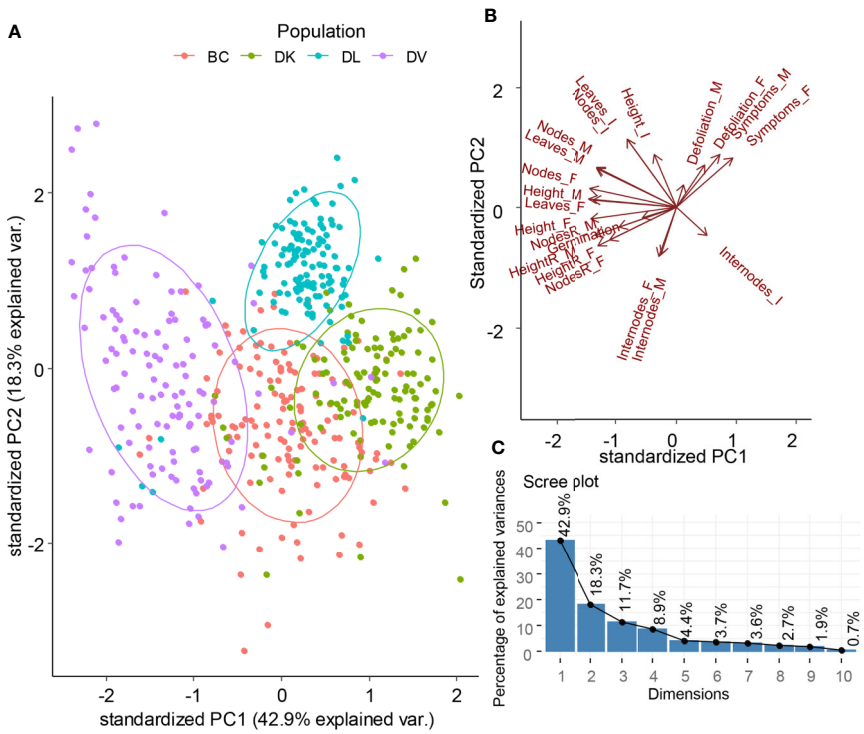


FIGURE 4 | Plot of the first two components from Principal Component Analysis of the morphological variables **(A)**. Projection of the variables on the first two components **(B)**. Scree plot of the dimensions and explained variability for each component **(C)**.

leaf Cl^- content than tolerant plants (**Table 2**). Regarding to leaf Na^+ accumulation, on DV and BC populations, Na^+ foliar content was higher on sensitive than tolerant subsets (**Table 2**; **Figure 9B**), whereas on DK and DL populations no differences were observed between tolerant and sensitive subsets. Comparing leaf Na^+ accumulation between populations, DV showed the lowest values. Control plants had lower Na^+ content in all populations (**Figure 9B**).

Analyzing the nutritional imbalances caused by salinity, the K^+ content in the BC population was higher in tolerant plants than sensitive ones, being both significantly higher than the control plants. However, in the DK a lower K^+ is observed in the control plants compared to the sensitive and tolerant subsets. No significant differences are observed in DL and DV populations (**Table 2**). Regarding to Ca^{2+} content, it was lower in tolerant plants than in control, but without differences with the sensitive

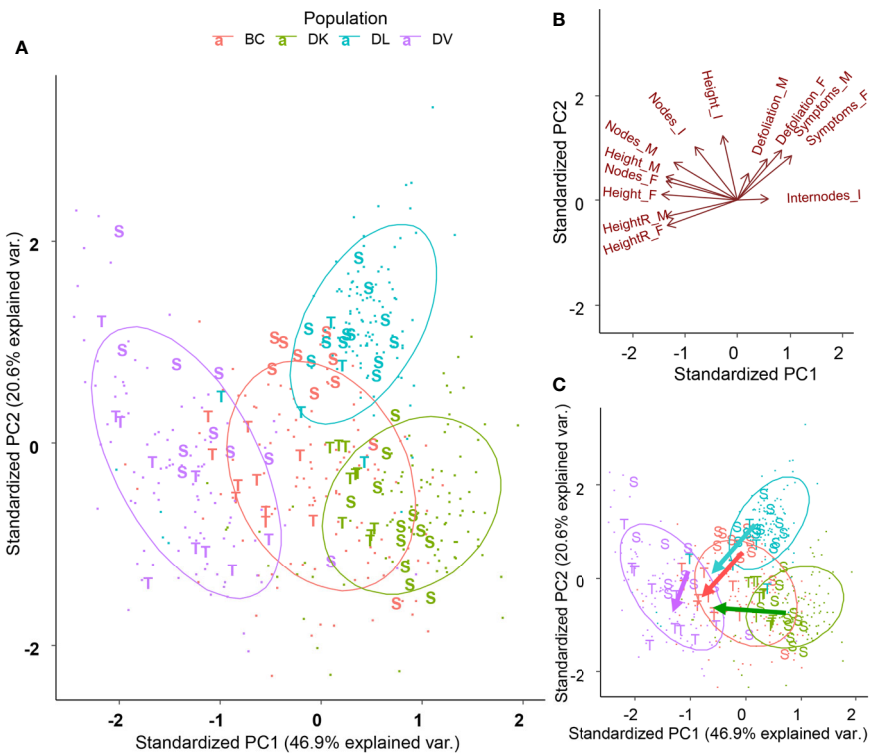


FIGURE 5 | Plot of the first two components from Principal Component (PC) Analysis of the morphological variables after removal of highly collinear variables **(A)**. Plants selected as Tolerant and Sensitive according its phenotype have been represented. Projection of the variables on the first two components **(B)**. Dimensional division between tolerant and sensitive subsets for each population **(C)**.

subset. Nutrient balances were also calculated for Na^+/K^+, Na^+/Ca^{2+}. The Na^+/K^+ balance increased in all salinized plants, but differences between tolerant and sensitive plants were only observed in the BC population (**Figure 9B**). In all populations the control plants had the lowest Na^+/K^+ ratio. Similar results were obtained for Na^+/Ca^{2+}, except that in DV population differences were observed among all subsets.

Differential Expression of Genes Related to Salinity Tolerance

Differential expression of genes related to salt-tolerance was analyzed in leaves and roots of five individuals of each subset at the end of the salt treatment (60 days). Control plants were included in the analysis (**Supplementary Figure 5**). Leaf expression of *SOS1-like*, *SOS2-like* and ALMT9-like was similar among all the populations and different in root tissue. *HKT1-like* expression on leaf was undetectable in all populations, but detectable in roots, being the lowest expression in DL. On the other hand, *NHX1.1-like* highest expression in leaf corresponded to DV population and in roots to BC. In order to compare between tolerant and sensitive subsets, all gene expression was relative to the control plants of each population and a heatmap was constructed using the Log2fold change (**Figure 10**). On leaves, SOS3-like expression was downregulated on both subsets of DK population under salt treatment, whereas an upregulation was observed in the DL population. Interestingly, an upregulation was observed only in the sensitive subset of the BC population on 4/5 plants. Regarding to roots, *SOS2-like* expression was downregulated under salt treatment on the BC population, whereas *SOS3-like* was upregulated. *ALMT9-like* gene expression was upregulated on sensitive BC subset. About *HKT1-like* gene expression, a downregulation has observed in sensitive subset of BC and DL populations, whereas in tolerant DL subset and DV population a higher expression has been observed.

After obtaining the sequences of the putative orthologues of *PIPs* in *Diospyros lotus*, a phylogenetic tree was constructed (**Supplementary Figure 6**). *PIP1-like* family of *D. lotus* was grouped together with the *PIP1 Arabidopsis thaliana* genes, whereas *D. lotus PIP2-like* genes were grouped with the *A. thaliana PIP2* genes. Expression of *PIP1-like* and *PIP2-like* aquaporin families were analyzed and compared between tolerant and sensitive subset bulks for each population. A heat map was constructed using the control bulk for normalizing within populations (**Figure 11**). On the BC population, *PIP2-like 5* showed a four-fold upregulation on leaves from sensitive plants compared to tolerant, Furthermore, *PIP2-like 6* and *PIP1-like 1* showed a downregulation in sensitive plants compared to tolerant in leaves and roots, respectively. For these genes, the tolerant plants had similar levels of expression to the control plants. Regarding to the DK population; comparing sensitive to tolerant leaves, *PIP1-like 1* and *PIP2-like 5* showed a

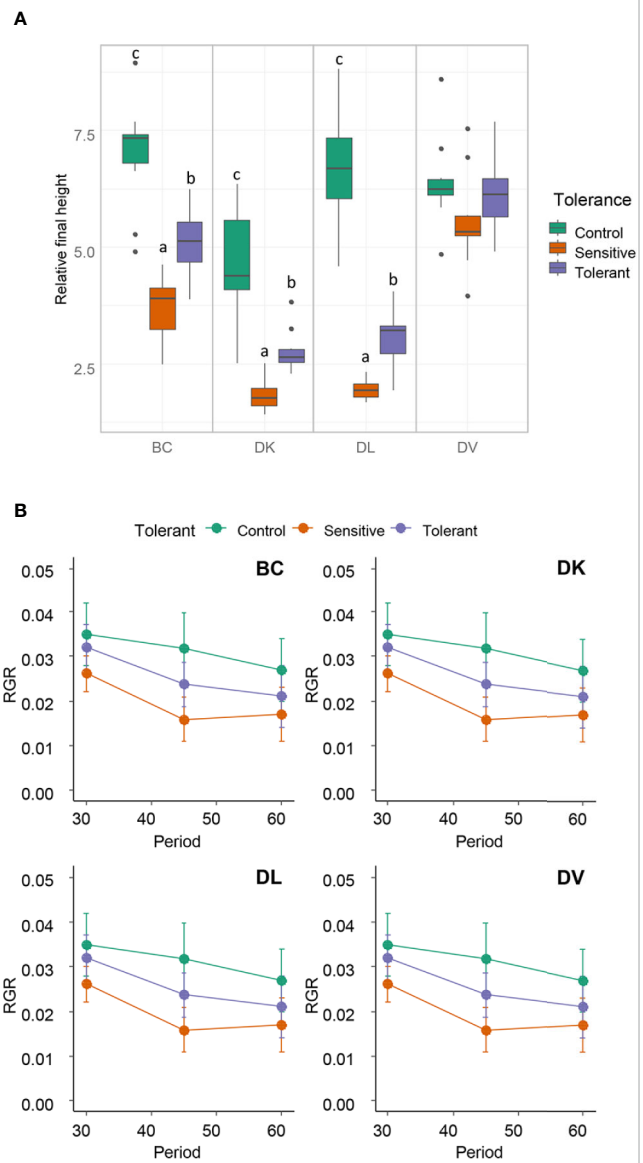


FIGURE 6 | (A) Box and whisker representation of relative final height (ratio between final and initial) of the four populations after 60 days of salt treatment. Individuals from each population were grouped into tolerant and sensitive according to its phenotype as detailed in *Methods*. Control plants were included. Different letters mean statistical differences between populations. **(B)** Representation of the Relative Growth Ratio (RGR) for the subsets of the four populations in the periods of 0–30, 30–45, and 45–60 days. Values are calculated using several biological replicates for control (10, 10, 4, and 10), tolerant (10, 10, 5, and 10), and sensitive (10, 12, 12, and 10) BC, DK, DL, DV, respectively.

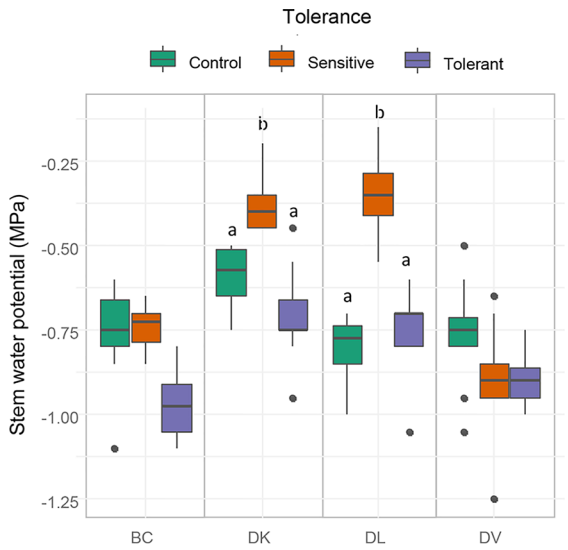


FIGURE 7 | Box and whisker representation of stem water potential of the four populations after 60 days of salt treatment. Genotypes were grouped into tolerant and sensitive according to its phenotype. Control plants were included. Different letters mean statistical differences between populations. Values are calculated using several biological replicates for control (10, 10, 4, and 10), tolerant (10, 10, 5, and 10), and sensitive (10, 12, 12, and 10) BC, DK, DL, DV, respectively.

downregulation, whereas *PIP2-like 3* showed an upregulation. In roots, a strong (32 fold) downregulation was shown in *PIP2-like 6*. Both *PIP1-like 3* and *PIP2-like 3* presented a downregulation in sensitive plants. The DL population showed similar expression differences in roots between tolerant and sensitive to the DK population. In addition, *PIP2-like 5* showed less expression in sensitive roots. In leaves of DV population, the only differential *PIP-like* expression between tolerant and sensitive plants was in *PIP2-like 1*, where the sensitive plants showed a strong upregulation. On roots, *PIP1-like 1*, *PIP2-like 3* and *PIP2-like 5* exhibited lower expression in tolerant plants. Regarding to the salt induction of this genes, *PIP1-like 1* has shown opposite expression patterns in the BC and DK population than the DL and DV populations.

DISCUSSION

Saline Stress Effect Among Populations

The severity of the symptoms in the different populations is coherent with the described differences between these species regarding to salinity tolerance, being *D. virginiana* the most tolerant specie among populations followed by *D. kaki* and *D. lotus* (de Paz et al., 2016b; Visconti et al., 2017; Gil-Muñoz et al., 2018a). The salinity stress results show that the *D. kaki* most compatible rootstock species (*D. kaki*, *D. lotus* and *D. virginiana*) have much lower salt stress tolerance than other *Diospyros* species such as black sapote (*D. digyna*), that even does not show leaf burn when exposed to 16 dS m^{-1} for more than 17 weeks (Mickelbart and Marler, 1998). All the populations exhibited a reduction in the internode length compared to the control. This effect is believed to be caused by the salinity stress response mechanism mediated by DELLA proteins (Achard et al., 2006) as adaption to both saline and osmotic stress *via* ROS detoxification (Achard et al., 2008). The side effect of DELLA expression would be a reduction in bioactive GAs

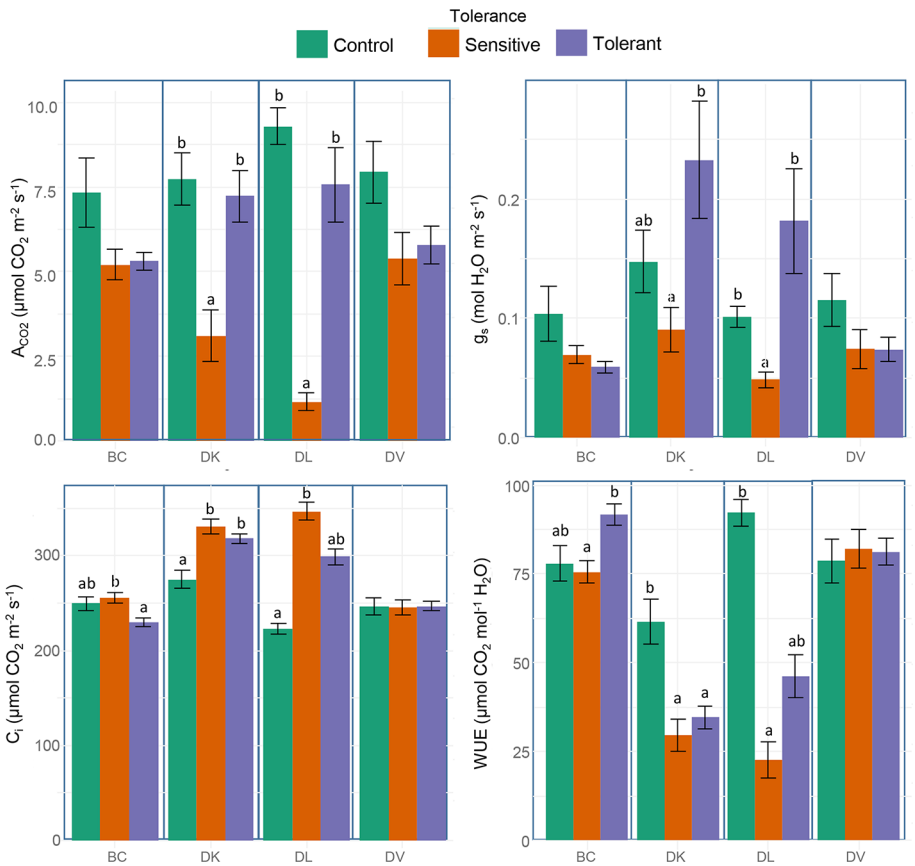


FIGURE 8 | Box and whisker representation of leaf net CO_2 assimilation rate (A_{CO2}), stomatal conductance (g_s), internal CO_2 concentration (C_i), and intrinsic water use efficiency (WUE) of the four populations after 60 days of salt treatment. Genotypes were grouped into tolerant and sensitive according to its phenotype. Control plants were included. Different letters mean statistical differences between populations. Values are calculated using several biological replicates for control (10, 10, 4, and 10), tolerant (10, 9, 5, and 10), and sensitive (10, 12, 11, and 10) BC, DK, DL, DV, respectively.

(Achard et al., 2006; Magome et al., 2008) causing a reduction in the internode length.

Saline Stress Tolerance Variability Within Populations

Differences related to the variability of morphological parameters among the three populations studied were obtained. Furthermore, the Principal Component Analysis (PCA), showed the widest distribution in the DV population, whereas the narrowest corresponded to the DL population. Differences in variability can be explained by the genetic structure of each population; DV population comes from an open pollination family, whereas DL is formed by full siblings. Interestingly, DK population is an open pollination family, but shows narrower variability than DV population. This fact can be explained by the low genetic variability previously described for *D. kaki* (Naval et al., 2010; Parfitt et al., 2015; Gil-Muñoz et al., 2018b). BC population shows an intermediate variability between DV and DK as expected because it combines both genetic backgrounds.

The variability observed in the analyzed parameters is consistent with the population genetic structures. This fact can indicate that a significant percentage of the observed variability might be controlled by genetic traits. The PCA analysis has been also consistent with the genetic structure of the populations, and it can be a useful tool to aid selection during a plant breeding program, as it extracts, compresses, simplifies, and analyzes complex multidimensional datasets (Das et al., 2017). Furthermore, with large datasets, some collinearity is expected to be present among the measured variables. Thus, measurement errors and phenotyping noise can be reduced by PCA projection, providing more precise individual phenotyping. Furthermore, the PCA can provide the importance of easy-measurable variables to the overall desired trait, giving a powerful aid in the selection.

Physiological and Nutritional Effects Related to Salinity Tolerance

Differences in vegetative development between tolerant and sensitive subsets in both DL and DK populations can be explained by the effect of a poor adaption to the osmotic

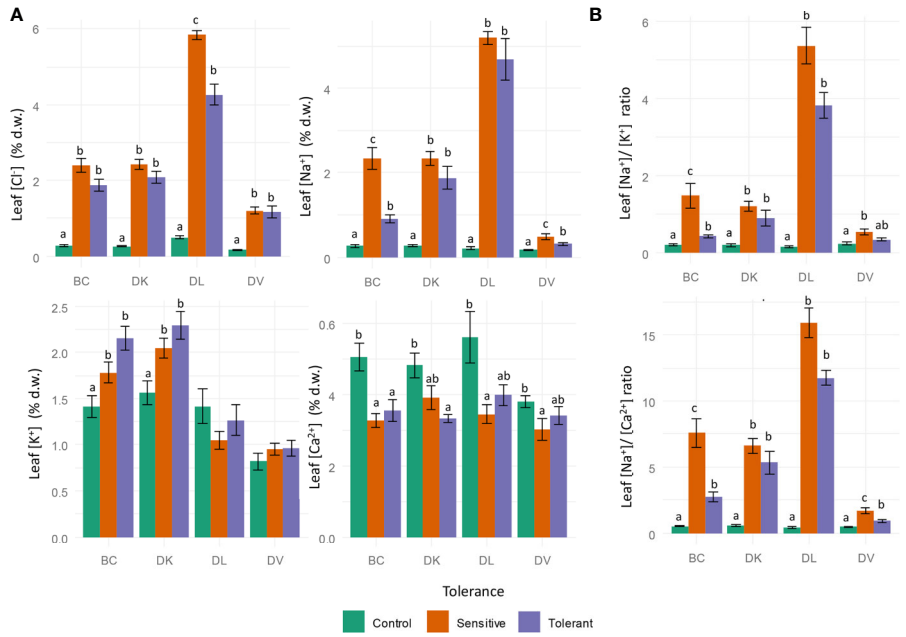


FIGURE 9 | Leaf ion content measurements after 60 days of salinity treatment. Cl^-, Na^+, K^+, and Ca^{2+} **(A)** and Na^+/K^+ and Na^+/Ca^{2+} ratios **(B)**. Genotypes were grouped into tolerant and sensitive according to its phenotype. Control plants were included. Different letters mean statistical differences between populations. Values are calculated using several biological replicates for control (10, 10, 4, and 10), tolerant (9, 9, 5, and 10), and sensitive (10, 10, 12, and 9) BC, DK, DL, DV, respectively.

TABLE 2 | Relative ionic content of each tolerant and sensitive populations compared to control.

	BC		***D. kaki***		***D. lotus***		***D. virginiana***	
	Tolerant	**Sensitive**	**Tolerant**	**Sensitive**	**Tolerant**	**Sensitive**	**Tolerant**	**Sensitive**
Cl^-	+	+	+	+	+	++	+	+
Na^+	+	++	+	+	+	+	+	++
K^+	++	+	+	+	=	=	=	=
Ca^{2+}	–	–	–	=	=	–	=	–

Two signs refer to statistically different concentrations between tolerant and sensitive.

stress, as shown by changes in plant water status and the lower photosynthesis rate. However, which one is the cause and which one the effect is not yet known (Munns and Tester, 2008). Nevertheless, ABA contributes to stress tolerance by regulating water balance and stomatal closure (Lim et al., 2015). However, our results show higher stomatal closure in sensitive than in tolerant plants, indicating that the sensitive populations have suffered higher saline stress. On the other hand, differences in photosynthesis, stomatal aperture, or water relations between tolerant and control plants are not observed, indicating that the tolerant subsets had a better response to the osmotic stress than the sensitive subsets in both populations. Furthermore, differences were neither observed between tolerant and control final internode relative length, discarding DELLA response as a mechanism effect. All facts indicate that the observed differences in growth rate and relative final height between tolerant and control plants must be mainly related to ionic stress, which affects growth in a different way than osmotic stress (Munns and Tester, 2008). Respect to the BC population, no differences in parameters as relative growth and growth rate, photosynthesis, stomatal aperture, or water relations were obtained in the analyzed subsets. This may indicate that both tolerant and sensitive plants are not strongly affected by the osmotic stress but rather the ionic stress and differences between these groups might be related to ion exclusion. The DV population has proven to be highly tolerant to saline stress as previously described (de Paz et al., 2016b; Gil-Muñoz et al., 2018a). The similar growth rates and relative final weight among the subsets while maintaining photosynthesis, stomatal aperture, and plant water status indicate the presence of highly efficient mechanisms to overcome osmotic and saline stress.

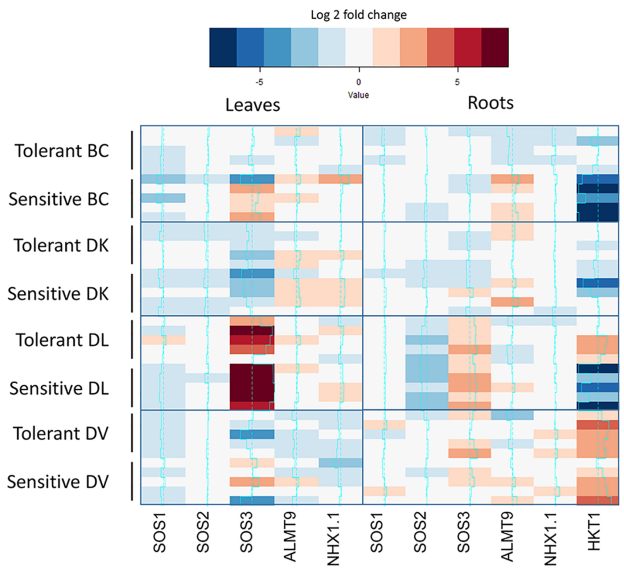


FIGURE 10 | Expression analysis of salt tolerance related-like genes from control and treated subsets of tolerant and sensitive plants from each population. Expression is mean value of three biological replicates of each individual. Only significant differences between control and treated subsets are show in color.

As foliar contents of Na^+ and Cl^- have been analyzed, other mechanisms such as vacuolar sequestration have not been detected that could further explain the differences observed. Our aim has been to study intake and root to shoot exclusion mechanisms taking into account the background objective of breeding rootstock plant, as different scions might have different responses mechanisms of vacuolar ion sequestration. Variability in osmotic stress tolerance is present within DK, DL, and BC populations and in Cl^- uptake within DL population. The differences for Na^+ exclusion observed within BC population but not in DV and DK populations indicate that DV and DK populations have different Na^+ exclusion mechanisms, being the DV mechanism more efficient. Further crosses between DL and DV might reveal variability in Cl^- exclusion mechanisms that might help to untangle the salt tolerance mechanisms present in *Diospyros* genus.

Differential Expression of Genes Related to Salinity Tolerance

Regarding to salt tolerance-related genes expression, a strong upregulation of *SOS3-like* gene has been observed in the DL population on both tolerant and sensitive plants. This gene is responsible for activating the SOS salinity response mechanism when a low Ca^{2+} concentration is detected in the cell (Gong et al., 2004). Interestingly, DL population showed similar Na^+ accumulation on leaves from control plants than leaves from the end of the salinity experiment. This population presented the highest Na^+ concentration in leaves and both the highest Na^+/K^+ and Na^+/Ca^{2+}. Furthermore, the higher *SOS3-like* expression present in the sensitive plants leaves of the BC population, but not in the DK in despite of similar Na^+, Ca^{2+} and Na^+/Ca^{2+} levels are observed in the DK population and BC sensitive plants. Surprisingly, differences in *SOS3-like* response are present even though 75% of the BC population genome comes from DK population. *SOS3-like* expression level is upregulated on plants where it can be a response caused by the toxic Na^+ concentrations in leaves and not a direct indicator of salinity tolerance, s. BC population might have inherited the more sensitive SOS response mechanism present on DV population, whose response has not been observed due to the low levels of Na^+ in leaves. On the other hand, *HKT1-like* gene expression differences on roots observed

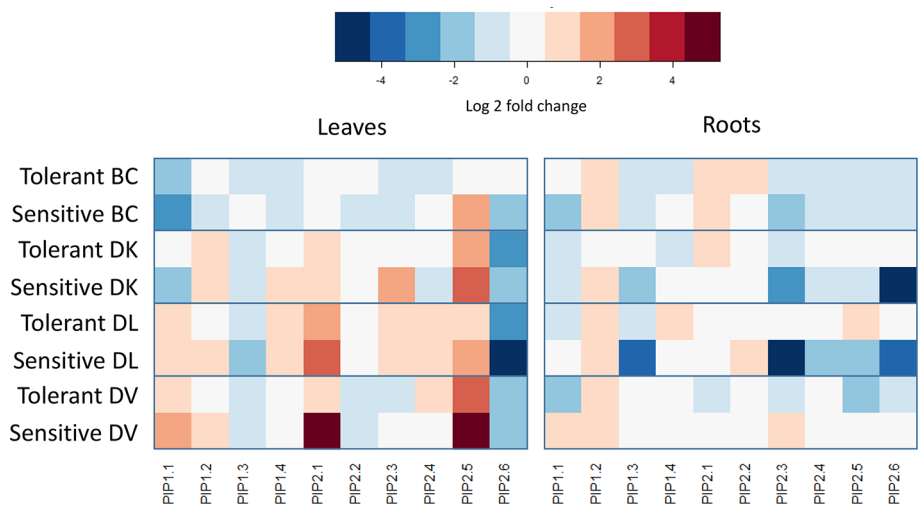


FIGURE 11 | PIP aquaporin-like genes expression changes between control and treated subsets of tolerant and sensitive plants from each population. Expression values were calculated using three biological replicates from each group. Only significant differences between control and treated subsets are colored.

between tolerant and sensitive subsets in BC population were consequent with the tolerant/sensitive phenotype similarly to the observations made in other species (Arabbeigi et al., 2018). *HKT1* higher expression could contribute to the salinity tolerance, as this gene is responsible to avoid Na^+ translocation from roots to shoot *via* xylem transport (Hanin et al., 2016). PIP gene expression has been linked to an increase in osmotic stress tolerance (Katsuhara et al., 2014; Afzal et al., 2016; Alavilli et al., 2016). In our study, a downregulation in several PIPs has been observed in roots of sensitive subsets of both DL and DK populations where lower stem water potential values were measured. Furthermore, a strong upregulation was observed in some *PIP2-like* family members on leaves of the sensitive DV subset. In Arabidopsis, the AtPIP2.1 gene has been described to act as a Na^+ gate to the leaves (Chaumont and Tyerman, 2014).

To sum up, in DK population, we have not observed variability in active Na^+ or Cl^- exclusion mechanisms, but they are present for osmotic stress tolerance *via* water balance regulation. Regarding to the DL population, we have observed the lowest basal expressions of *SOS1-like* gene and *HKT1-like* in roots compared to the other populations. Also, this population has poor ability to exclude Na^+ ions and therefore prevent toxic concentrations. However, variability in both osmotic stress tolerance *via* water balance regulation is present. Cl^- exclusion variability in this population has been observed, but the mechanism is yet unknown. The DV population tolerance to salinity has been also linked to higher *SOS1-like* basal expression and *HKT1-like* upregulation in roots. In other species, the role of this gene is linked to avoid Na^+ translocation from roots to shoot *via* xylem transport (Hanin et al., 2016) to the prevention of. Furthermore, in a previous study we observed a higher root expression of HKT1-like gene in a salt-tolerant subset of a *Diospyros* population (Gil-Muñoz et al., 2020). In addition, variability in the indicators used in this work to identify mechanisms related to salt stress tolerance are not observed within this population.

Conclusions

Among the different populations studied, different mechanism of tolerance could be hypothesized, providing different strategies for breeding for salinity tolerance.

BC Tolerant Population

The mechanism of tolerance to osmotic stress found was based in the water use efficiency (WUE). BC tolerant population has shown to have better tolerance to saline stress than sensitive BC through a higher WUE, which agrees with previous results on *Diospyrus* genus (Gil-Muñoz et al., 2020). Since the lack of variability for this character in the DV and DK populations, we can conclude the variability into BC has been generated through crossing. We have generated a tolerant population by back crossing in which the water use efficiency is higher than in DV population, which might be a sign of transgressive segregation through expressing the DV higher tolerance under the DK genetic background. Concerning to ionic stress, the Na^+ accumulation was higher in the BC than in the DV population, indicating other factors involved in Na^+ absorption. The expression of the genes analyzed resulted in a high expression of *HKT1-like* in roots of DV population; this gene is being involved in Na^+ exclusion, which might be a mechanism of preventing Na^+ translocation to the higher parts of the plant in *D. virginiana* species.

DK Population

Little variability was found within the DK population regarding to salinity tolerance, neither by ion leaf content nor salt tolerance gene expression. In this case, the observed differences between tolerant and sensitive subsets might be explained by differences in osmotic stress tolerance, but not in ionic stress. In this population, the tolerance might be based only in plant water regulation *via* stomatal aperture and water flow.

DL Population

Similarly, to the DK population, the tolerance observed in DL population for Na^+ might be based in passive mechanisms through water regulation. In despite of DL population was the most susceptible to salinity, is the only population that has shown differences in Cl^- accumulation. However, with the analyzed data we cannot provide a hypothesis that can explain this fact, as water flow differences were similar than the observed in DK population and this differences in Cl^- accumulation were not detected. Also, the expression analysis revealed high expression of *HKT1-like* in roots of the tolerant subset despite of it cannot be linked to lower Na^+ leaf content.

DV Population

In this population, variability for saline tolerance was low, most of the plants showed high saline tolerance. Significant Na^+ accumulation might be related to the higher *PIP2-like* family expression in leaves, acting as a gate of Na^+ influx into the leaves.

As a result of the comparison between physiological parameters, transcriptomic analysis and phenotypes under saline conditions, we can conclude that interspecific crosses of *D. virginiana* can be an option for breeding persimmon rootstocks tolerant to salinity. Crosses with *D. kaki* can provide better rootstock-scion compatibility with varieties than genotypes from *D. virginiana*. However, further selection of agronomic traits that improve crop management would be most necessary.

DATA AVAILABILITY STATEMENT

All datasets generated for this study are included in the article/ **Supplementary Material**.

AUTHOR CONTRIBUTIONS

MB and MN contributed conception and design of study. FG-M performed the experiments, and data analysis. AQ contributed to the data. JP-P and MB contributed to data analysis and interpretation. MB provided supplies and facilities. FG-M

wrote the first draft of the manuscript. MB and JP-P revised the manuscript. All authors contributed to the article and approved the submitted version.

FUNDING

JP-P gratefully acknowledges the postdoctoral contract "Ramón y Cajal" program (RYC-2015-17726), supplied by the Spanish Ministry of Economy, Industry and Competitiveness (MINECO).

FG-M acknowledges the support granted with the PhD fellowship co-financed by the European Social Fund and the Generalitat Valenciana ACIF/2016/115). The project was partially funded by the IVIA grant 51914 and FEDER funds.

ACKNOWLEDGMENTS

We acknowledge the technical support provided by M.A. Forner-Giner and M.A. Primo-Capella in the Chloride quantification, hydric pressure measurements, and assay assessment. We also acknowledge Lidia López-Serrano for the assessment in measuring leaf gas exchange parameters.

SUPPLEMENTARY MATERIAL

The Supplementary Material for this article can be found online at: https://www.frontiersin.org/articles/10.3389/fpls.2020.01132/full#supplementary-material

REFERENCES

Achard, P., Cheng, H., De Grauwe, L., Decat, J., Schoutteten, H., Moritz, T., et al. (2006). Integration of plant responses to environmentally activated phytohormonal signals. *Science* 311 (5757), 91–94. doi: 10.1126/science.1118642

Achard, P., Renou, J. P., Berthomé, R., Harberd, N. P., and Genschik, P. (2008). Plant DELLAs restrain growth and promote survival of adversity by reducing the levels of reactive oxygen species. *Curr. Biol.* 18, 656–660. doi: 10.1016/j.cub.2008.04.034

Afzal, Z., Howton, T. C., Sun, Y., and Mukhtar, M. S. (2016). The roles of aquaporins in plant stress responses. *J. Dev. Biol.* 4 (1), 9. doi: 10.3390/jdb4010009

Akagi, T., Ikegami, A., Tsujimoto, T., Kobayashi, S., Sato, A., Kono, A., et al. (2009). DkMyb4 is a Myb transcription factor involved in proanthocyanidin biosynthesis in persimmon fruit. *Plant Physiol.* 151, 2028–2045. doi: 10.1104/pp.109.146985

Akagi, T., Henry, I. M., Tao, R., and Comai, L. (2014). A y-chromosome-encoded small RNA acts as a sex determinant in persimmons. *Science* 346 (6209), 646–650. doi: 10.1126/science.1257225

Alavilli, H., Awasthi, J. P., Rout, G. R., Sahoo, L., Lee, B. H., and Panda, S. K. (2016). Overexpression of a Barley aquaporin gene, HvPIP2;5 confers salt and osmotic stress tolerance in yeast and plants. *Front. Plant Sci.* 7, 1566. doi: 10.3389/fpls.2016.01566

Almeida, P., Katschnig, D., and de Boer, A. H. (2013). HKT transporters-state of the art. *Int. J. Mol. Sci.* 14, 20359–20385. doi: 10.3390/ijms141020359

Apse, M. P., Aharon, G. S., Snedden, W. A., and Blumwald, E. (1999). Salt tolerance conferred by overexpression of a vacuolar Na+/H+ antiport in Arabidopsis. *Science* 285 (5431), 1256–1258. doi: 10.1126/science.285.5431.1256

Arabbeigi, M., Arzani, A., Majidi, M. M., Sayed-Tabatabaei, B. E., and Saha, P. (2018). Expression pattern of salt tolerance-related genes in Aegilops cylindrica. *Physiol. Mol. Biol. Plants.* 24 (1), 1–73. doi: 10.1007/s12298-017-0483-2

Arzani, A., and Ashraf, M. (2016). Smart engineering of genetic resources for enhanced salinity tolerance in crop plants. *CRC. Crit. Rev. Plant Sci.* 35 (3), 146–189. doi: 10.1080/07352689.2016.1245056

Arzani, A. (2008). Improving salinity tolerance in crop plants: a biotechnological view. *Vitr. Cell. Dev. Biol. - Plant.* 44, 373–383. doi: 10.1007/s11627-008-9157-7

Badenes, M. L., Naval, M. M., Martínez-Calvo, J., and Giordani, E. (2015). "Material Vegetal y Mejora Genetica," in *El cultivo del caqui*. Eds. M. L. Badenes, D. Intrigliolo, A. Salvador and A. Vicent (Valencia, Spain: Generalitat Valenciana), 58–80.

Baetz, U., Eisenach, C., Tohge, T., Martinoia, E., and De Angeli, A. (2016). Vacuolar chloride fluxes impact ion content and distribution during early salinity stress. *Plant Physiol.* 172, 1167–1181. doi: 10.1104/pp.16.00183

Barbier-Brygoo, H., De Angeli, A., Filleur, S., Frachisse, J.-M., Gambale, F., Thomine, S., et al. (2011). Anion channels/transporters in plants: from molecular bases to regulatory networks. *Annu. Rev. Plant Biol.* 62, 25–51. doi: 10.1146/annurev-arplant-042110-103741

Barragán, V., Leidi, E. O., Andrés, Z., Rubio, L., de Luca, A., Fernández, J. A., et al. (2012). Ion exchangers NHX1 and NHX2 mediate active potassium uptake into vacuoles to regulate cell turgor and stomatal function in arabidopsis. *Plant Cell* 24, 1127–1142. doi: 10.1105/tpc.111.095273

Bellini, E., and Giordani, E. (2002). Cultural practices for persimmon production. *CIHEAM Options Mediterr.* 51, 39–52.

Boursiac, Y., Chen, S., Luu, D. T., Sorieul, M., Van Den Dries, N., and Maurel, C. (2005). Early effects of salinity on water transport in Arabidopsis roots. Molecular and cellular features of aquaporin expression. *Plant Physiol.* 139, 790–805. doi: 10.1104/pp.105.065029

Byrt, C. S., Platten, J. D., Spielmeyer, W., James, R. A., Lagudah, E. S., Dennis, E. S., et al. (2007). HKT1;5-like cation transporters linked to Na+ exclusion loci in wheat, Nax2 and Kna1. *Plant Physiol.* 143, 1918–1928. doi: 10.1104/pp.106.093476

Chaumont, F., and Tyerman, S. D. (2014). Aquaporins: highly regulated channels controlling plant water relations. *Plant Physiol.* 164, 1600–1618. doi: 10.1104/pp.113.233791

Das, S., Debojit, S., Chakraborti, I., Roy, N., and Das, S. S. (2017). Principal component analysis in plant breeding. *Biomol. Rep.*

Davies, W. J., Kudoyarova, G., and Hartung, W. (2005). Long-distance ABA signaling and its relation to other signaling pathways in the detection of soil drying and the mediation of the plant's response to drought. *J. Plant Growth Regul.* 24, 285–295. doi: 10.1007/s00344-005-0103-1

de Paz, J. M., Visconti, F., Chiaravalle, M., and Quiñones, A. (2016a). Determination of persimmon leaf chloride contents using near-infrared spectroscopy (NIRS). *Anal. Bioanal. Chem.* 408, 3537–3545. doi: 10.1007/s00216-016-9430-2

de Paz, J. M., Visconti, F., Tudela, L., Quiñones Oliver, A., Intrigliolo, D., Jordà, M., et al. (2016b). La fitotoxicidad por cloruro en el cultivo del caqui: descripción del problema. *Agrícola Vergel: Fruticultura, Horticultura* 391, 91–96.

Essah, P. A., Davenport, R., and Tester, M. (2003). Sodium influx and accumulation in arabidopsis. *Plant Physiol.* 133, 307–318. doi: 10.1104/pp.103.022178

Forner-Giner, M. A., and Ancillo, G. (2013). "Breeding salinity tolerance in citrus using rootstocks," in *Salt stress in plants: signalling, omics and adaptations*. (Berlin, Germany: Springer), 355–376. doi: 10.1007/978-1-4614-6108-1_14

Fricke, W., Akhiyarova, G., Wei, W., Alexandersson, E., Miller, A., Kjellbom, P. O., et al. (2006). The short-term growth response to salt of the developing barley leaf. *J. Exp. Bot.* 57 (5), 1079–1095. doi: 10.1093/jxb/erj095

Gambino, G., Perrone, I., and Gribaudo, I. (2008). A rapid and effective method for RNA extraction from different tissues of grapevine and other woody plants. *Phytochem. Anal.* 19, 520–525. doi: 10.1002/pca.1078

Gilliam, J. W. (1971). Rapid measurement of chlorine in plant materials. *Soil Sci. Soc. Am. J.* 35, 512. doi: 10.2136/sssaj1971.03615995003500030051x

Gil-Muñoz, F., Peche, P. M., Climent, J., Forner, M. A., Naval, M. M., and Badenes, M. L. (2018a). Breeding and screening persimmon rootstocks for saline stress tolerance. *Acta Hortic.* 1195, 105–110. doi: 10.17660/ActaHortic.2018.1195.18

Gil-Muñoz, F., Zuriaga, E., Badenes, M. L., and Naval, M. M. (2018b). Analysis of genetic diversity among a set of accessions from the IVIA's persimmon collection. *Acta Hortic.* 1195, 43–50. doi: 10.17660/ActaHortic.2018.1195.7

Gil-Muñoz, F., Pérez-Pérez, J. G., Quiñones, A., Primo-Capella, A., Cebolla, J., Ángeles Forner-Giner, M., et al. (2020). A cross population between D. Kaki, and D. Virginiana shows high variability for saline tolerance and improved salt stress tolerance. *PLoS One* 15, e0229023. doi: 10.1371/journal.pone.0229023

Giordani, E., Naval, M., and Benelli, C. (2012). In vitro propagation of Persimmon (Diospyros kaki Thunb.). *Methods Mol. Biol. (Clifton, N.J.)* 11013, 89–98. doi: 10.1007/978-1-62703-074-8_7

Gong, D., Guo, Y., Schumaker, K. S., and Zhu, J. K. (2004). The SOS3 family of calcium sensors and SOS2 family of protein kinases in arabidopsis. *Plant Physiol.* 134, 919–926. doi: 10.1104/pp.103.037440

Graves, S., Piepho, H.-P., Selzer With Help From Sundar, L., Maintainer, D.-R., and Selzer, L. (2015). *Package "multcompView" Visualizations of Paired Comparisons. R Packag.* http://CRAN.R-project.org/package=multcompView

Halfter, U. (2000). The Arabidopsis SOS2 protein kinase physically interacts with and is activated by the calcium-binding protein SOS3. *Proc. Natl. Acad. Sci.* 97, 3735–3740. doi: 10.1073/pnas.040577697

Hanin, M., Ebel, C., Ngom, M., Laplaze, L., and Masmoudi, K. (2016). New insights on plant salt tolerance mechanisms and their potential use for breeding. *Front. Plant Sci.* 7, 1787. doi: 10.3389/fpls.2016.01787

Hrabak, E. M., Chan, C. W. M., Gribskov, M., Harper, J. F., Choi, J. H., Halford, N., et al. (2003). The Arabidopsis CDPK-SnRK superfamily of protein kinases. *Plant Physiol.* 132, 666–680. doi: 10.1104/pp.102.011999

Incesu, M., Cimen, B., Yesiloglu, T., and Yilmaz, B. (2014). Growth and photosynthetic response of two persimmon rootstocks (Diospyros kaki and D. virginiana) under different salinity levels. *Not. Bot. Horti. Agrobot. Cluj-Napoca* 42, 386–391. doi: 10.1583/nbha4229471

Isayenkov, S. V., and Maathuis, F. J. M. (2019). Plant salinity stress: many unanswered questions remain. *Front. Plant Sci.* 10, 80. doi: 10.3389/fpls.2019.00080

Joly, R. J. (1989). Effects of sodium chloride on the hydraulic conductivity of soybean root systems. *Plant Physiol.* 91, 1262–1265. doi: 10.1104/pp.91.4.1262

Kassambara, A., and Mundt, F. (2017). *Package "factoextra" for R: Extract and Visualize the Results of Multivariate Data Analyses. R Packag. version.*

Katsuhara, M., Tsuji, N., Shibasaka, M., and Panda, S. K. (2014). Osmotic stress decreases PIP aquaporin transcripts in barley roots but H2O2 is not involved in this process. *J. Plant Res.* 127, 787–792. doi: 10.1007/s10265-014-0662-y

Levin, A. D. (2019). Re-evaluating pressure chamber methods of water status determination in field-grown grapevine (Vitis spp.). *Agric. Water Manage.* 221, 422–429. doi: 10.1016/j.agwat.2019.03.026

Lim, C. W., Baek, W., Jung, J., Kim, J. H., and Lee, S. C. (2015). Function of ABA in stomatal defense against biotic and drought stresses. *Int. J. Mol. Sci.* 16, 15251–15270. doi: 10.3390/ijms160715251

Liu, J., and Zhu, J. K. (1998). A calcium sensor homolog required for plant salt tolerance. *Science* 280 (5371), 1943–1945. doi: 10.1126/science.280.5371.1943

Liu, J. (2000). The Arabidopsis thaliana SOS2 gene encodes a protein kinase that is required for salt tolerance. *Proc. Natl. Acad. Sci.* 97, 3730–3734. doi: 10.1073/pnas.060034197

López-Pérez, L., Martínez-Ballesta, M., del, C., Maurel, C., and Carvajal, M. (2009). Changes in plasma membrane lipids, aquaporins and proton pump of broccoli roots, as an adaptation mechanism to salinity. *Phytochemistry* 70, 492–500. doi: 10.1016/j.phytochem.2009.01.014

Magome, H., Yamaguchi, S., Hanada, A., Kamiya, Y., and Oda, K. (2008). The DDF1 transcriptional activator upregulates expression of a gibberellin-deactivating gene, GA2ox7, under high-salinity stress in Arabidopsis. *Plant J.* 56, 613–626. doi: 10.1111/j.1365-313X.2008.03627.x

Mangiafico, S. (2018). *rcompanion: Functions to Support Extension Education Program Evaluation*. Available at: http://rcompanion.org

Martínez-Ballesta, M. C., Aparicio, F., Pallás, V., Martínez, V., and Carvajal, M. (2003). Influence of saline stress on root hydraulic conductance and PIP expression in Arabidopsis. *J. Plant Physiol.* 160, 689–697. doi: 10.1078/0176-1617-00861

Maurel, C., Verdoucq, L., Luu, D. -T., and Santoni, V.. (2008). Plant aquaporins: membrane channels with multiple integrated functions. *Annu. Rev. Plant Biol.* 59, 595–624. doi: 10.1146/annurev.arplant.59.032607.092734

Mickelbart, M. V., and Marler, T. E. (1998). Growth, gas exchange, and mineral relations of black sapote (Diospyros digyna Jacq.) as influenced by salinity. *Sci. Hortic. (Amsterdam)* 72 (2), 103–110. doi: 10.1016/S0304-4238(97)00095-2

Munns, R., and Tester, M. (2008). Mechanisms of Salinity Tolerance. *Annu. Rev. Plant Biol.* 59, 651–681. doi: 10.1146/annurev.arplant.59.032607.092911

Munns, R., Guo, J., Passioura, J. B., and Cramer, G. R. (2000). Leaf water status controls day-time but not daily rates of leaf expansion in salt-treated barley. *Aust. J. Plant Physiol.* 27, 949–957. doi: 10.1071/pp99193

Naval, M., del, M., Zuriaga, E., Pecchioli, S., Llácer, G., Giordani, E., et al. (2010). Analysis of genetic diversity among persimmon cultivars using microsatellite markers. *Tree Genet. Genomes* 6, 677–687. doi: 10.1007/s11295-010-0283-0

Neuwirth, E. (2014). *RColorBrewer: ColorBrewer palettes. R Packag. version 1.1-2.* https://cran.R-project.org/package=RColorBrewer. Available at: https://cran.r-project.org/web/packages/RColorBrewer/index.html.

Ogle, D. H., Wheeler, P., and Dinno, A. (2018). *FSA: Fisheries Stock Analysis. R package version 0.8.22*. Available at: https://github.com/droglenc/FSA

Parfitt, D. E., Yonemori, K., Honsho, C., Nozaka, M., Kanzaki, S., Sato, A., et al. (2015). Relationships among Asian persimmon cultivars, astringent and non-astringent types. *Real-Time Syst.* 51, 1–9. doi: 10.1007/s11295-015-0848-z

Perucho, R. (2018). "Evolution of production of the 'Rojo Brillante' cultivar in Spain and its impact on markets," in *Acta Horticulturae* (Leuven, Belgium: International Society for Horticultural Science (ISHS)), 1–8. doi: 10.17660/ActaHortic.2018.1195.1

Qiu, Q. S., Guo, Y., Dietrich, M. A., Schumaker, K. S., and Zhu, J. K. (2002). Regulation of SOS1, a plasma membrane Na+/H+ exchanger in Arabidopsis thaliana, by SOS2 and SOS3. *Proc. Natl. Acad. Sci. U. S. A.* 99, 8436–8441. doi: 10.1073/pnas.122224699

Qiu, Q. S., Barkla, B. J., Vera-Estrella, R., Zhu, J. K., and Schumaker, K. S. (2003). Na+/H+ exchange activity in the plasma membrane of Arabidopsis. *Plant Physiol.* 132, 1041–1052. doi: 10.1104/pp.102.010421

Quan, R., Lin, H., Mendoza, I., Zhang, Y., Cao, W., Yang, Y., et al. (2007). SCABP8/CBL10, a putative calcium sensor, interacts with the protein kinase SOS2 to protect Arabidopsis shoots from salt stress. *Plant Cell* 19, 1415–1431. doi: 10.1105/tpc.106.042291

Quintero, F. J., Ohta, M., Shi, H., Zhu, J. K., and Pardo, J. M. (2002). Reconstitution in yeast of the Arabidopsis SOS signaling pathway for Na+ homeostasis. *Proc. Natl. Acad. Sci. U. S. A.* 99, 9061–9066. doi: 10.1073/pnas.132092099

Quintero, F. J., Martinez-Atienza, J., Villalta, I., Jiang, X., Kim, W. Y., Ali, Z., et al. (2011). Activation of the plasma membrane Na/H antiporter salt-overly-sensitive 1 (SOS1) by phosphorylation of an auto-inhibitory C-terminal domain. *Proc. Natl. Acad. Sci. U. S. A.* 108, 2611–2616. doi: 10.1073/pnas.1018921108

Rodríguez-Gamir, J., Ancillo, G., Legaz, F., Primo-Millo, E., and Forner-Giner, M. A. (2012). Influence of salinity on pip gene expression in citrus roots and its relationship with root hydraulic conductance, transpiration and chloride exclusion from leaves. *Environ. Exp. Bot.* 78, 163–166. doi: 10.1016/j.envexpbot.2011.12.027

Shi, H., Ishitani, M., Kim, C., and Zhu, J. K. (2000). The Arabidopsis thaliana salt tolerance gene SOS1 encodes a putative Na+/H+ antiporter. *Proc. Natl. Acad. Sci. U. S. A.* 97, 6896–6901. doi: 10.1073/pnas.120170197

Signorell, A. (2017). *DescTools: Tools for descriptive statistics. R package version 0.99.20. CRAN.* doi: 10.1016/j.foreco.2014.09.033

Termaat, A., Passioura, J. B., and Munns, R. (1985). Shoot Turgor Does Not Limit Shoot Growth of NaCl-Affected Wheat and Barley. *Plant Physiol.* 77, 869–872. doi: 10.1104/pp.77.4.869

Tiwari, S., Sl, K., Kumar, V., Singh, B., Rao, A. R., Sv, A. M., et al. (2016). Mapping QTLs for salt tolerance in rice (Oryza sativa L.) by bulked segregant analysis of recombinant inbred lines using 50K SNP chip. *PLoS One* 11, e0153610. doi: 10.1371/journal.pone.0153610

Visconti, F., de Paz, J. M., Bonet, L., Jordà, M., Quiñones, A., and Intrigliolo, D. S. (2015). Effects of a commercial calcium protein hydrolysate on the salt tolerance of Diospyros kaki L. cv. "Rojo Brillante" grafted on Diospyros lotus L. *Sci. Hortic. (Amsterdam)* 185, 129–138. doi: 10.1016/j.scienta.2015.01.028

Visconti, F., Intrigliolo, D. S., Quiñones, A., Tudela, L., Bonet, L., and de Paz, J. M. (2017). Differences in specific chloride toxicity to Diospyros kaki cv. "Rojo Brillante" grafted on D. lotus, and D. virginiana. *Sci. Hortic. (Amsterdam)* 214, 83–90. doi: 10.1016/j.scienta.2016.11.025

Wang, P., Xiong, A., Gao, Z., Yu, X., Li, M., Hou, Y., et al. (2016). Selection of suitable reference genes for RTqPCR normalization under abiotic stresses and hormone stimulation in persimmon (Diospyros kaki Thunb). *PLoS One* 11 (8), e160885. doi: 10.1371/journal.pone.0160885

Warnes, G. R., Bolker, B., Bonebakker, L., Gentleman, R., Liaw, W. H. A., Lumley, T., et al. (2016). *Package "gplots": various R programming tools for plotting data. R Packag. version 2.17.0.* doi: 10.1111/j.0022-3646.1997.00569.x

Wei, T., and Simko, V. (2016). *Visualization of a Correlation Matrix: Package "corrplot." CRAN Comprehensive R Archive Network* 1–17. Available at: https://cran.r-project.org/package=corrplot

Wickham, H., François, R., Henry, L., and Müller, K. (2018). *Package "dplyr."*

Wickham, H. (2016). *ggplot2 Elegant Graphics for Data Analysis*. (Berlin, Germany: Springer). doi: 10.1007/978-3-319-24277-4

Zekri, M., and Parsons, L. R. (1989). Growth and root hydraulic conductivity of several citrus rootstocks under salt and polyethylene glycol stresses. *Physiol. Plant* 77, 99–106. doi: 10.1111/j.1399-3054.1989.tb05984.x

Zhu, J. K., Liu, J., Xiong, L., and Santoni, V. (1998). Genetic analysis of salt tolerance in arabidopsis: evidence for a critical role of potassium nutrition. *Plant Cell* 10, 1181–1191. doi: 10.1105/tpc.10.7.1181

Conflict of Interest: The authors declare that the research was conducted in the absence of any commercial or financial relationships that could be construed as a potential conflict of interest.

Copyright © 2020 Gil-Muñoz, Pérez-Pérez, Quiñones, Naval and Badenes. This is an open-access article distributed under the terms of the Creative Commons Attribution License (CC BY). The use, distribution or reproduction in other forums is permitted, provided the original author(s) and the copyright owner(s) are credited and that the original publication in this journal is cited, in accordance with accepted academic practice. No use, distribution or reproduction is permitted which does not comply with these terms.

frontiers in Plant Science

ORIGINAL RESEARCH
published: 19 August 2020
doi: 10.3389/fpls.2020.01285

Wheat Cultivars With Contrasting Root System Size Responded Differently to Terminal Drought

Victoria Figueroa-Bustos[1]*, *Jairo A. Palta*[1,2], *Yinglong Chen*[1], *Katia Stefanova*[1] and *Kadambot H. M. Siddique*[1]

[1] The UWA Institute of Agriculture, and UWA School of Agriculture and Environment, The University of Western Australia, Perth, WA, Australia, [2] CSIRO Agriculture & Food, Wembley, WA, Australia

In the Mediterranean-type environment of Australia and other parts of the world, end-of-season or terminal drought is the most significant abiotic stress affecting wheat grain yields. This study examined the response of two wheat cultivars with contrasting root system size to terminal drought and the effect of terminal drought on grain yield and yield components. The cultivars were grown in 1.0 m deep PVC columns filled with soil in a glasshouse under well-watered conditions until the onset of ear emergence (Z51) when well-watered and terminal drought treatments were imposed. Terminal drought reduced stomatal conductance, leaf photosynthesis, and transpiration rates faster in Bahatans-87 (larger root system size) than Tincurrin (smaller root system size). Terminal drought reduced grain yield in both cultivars, more so in Bahatans-87 (80%) with the large root system than Tincurrin (67%) with the small root system, which was mainly due to a reduction in grain number and grain size in Bahatans-87 and grain size in Tincurrin. In the terminal drought treatment, Bahatans-87 had 59% lower water use efficiency than Tincurrin, as Bahatans-87 used 39% more water and reduced grain yield more than Tincurrin. The lesser reduction in grain yield in Tincurrin was associated with slower water extraction by the small root system and slower decline in stomatal conductance, leaf photosynthesis, and transpiration rates, but more importantly to faster phenological development, which enabled grain filling to be completed before the severe effects of water stress.

Keywords: terminal drought, root system size, water use efficiency, water use, wheat

OPEN ACCESS

Edited by:
Raul Antonio Sperotto, Universidade do Vale do Taquari – Univates, Brazil

Reviewed by:
Roger David Armstrong, Grains Innovation Park, Horsham, Australia
Alexandro Cagliari, Universidade Estadual do Rio Grande do Sul, Brazil

***Correspondence:**
Victoria Figueroa-Bustos
victoria.figueroabustos@research.uwa.edu.au

Specialty section:
This article was submitted to Crop and Product Physiology, a section of the journal Frontiers in Plant Science

Received: *27 April 2020*
Accepted: *06 August 2020*
Published: *19 August 2020*

Citation:
Figueroa-Bustos V, Palta JA, Chen Y, Stefanova K and Siddique KHM (2020) Wheat Cultivars With Contrasting Root System Size Responded Differently to Terminal Drought. Front. Plant Sci. 11:1285. doi: 10.3389/fpls.2020.01285

INTRODUCTION

In the Australian grainbelt, annual rainfall declined from 1900 to 2009 by up to 20% and a further 10% reduction is estimated by 2070, threatening wheat production (Asseng and Pannell, 2013). This change in annual rainfall has followed a declining linear trend with annual wheat yield losses (up to 1.5%) in the Australian grainbelt from 1981 to 2018 (Ababaei and Chenu, 2019). End-of-season drought or terminal drought occurs in most Australian wheat-growing areas (Chenu et al., 2013), particularly in Mediterranean-type environments, where crops are usually sown on the first major rainfall between mid-April and the end of June. In this region, 80% of annual rainfall is received between May and

October and soil water losses by deep drainage below the root zone can occur during early winter in deep sands when the crop is small (Scanlon and Doncon, 2020). Conversely, water deficits develop after flowering when rainfall decreases and evaporation increases (Turner and Nicolas, 1987). Terminal drought reduces grain yield mainly because it reduces photosynthesis and the duration of grain filling (Fabian et al., 2011; Saeidi and Abdoli, 2015; Christopher et al., 2016; Yu et al., 2016). Under terminal drought, every millimeter of extra soil water extracted by the root system is critical for maintaining grain filling and improving water use efficiency (Passioura, 1983).

The root system plays a key role in the uptake of soil water and regulation of leaf senescence and leaf photosynthesis rate during grain filling (Kong et al., 2013). A deeper root system can prevent a severe water deficit from developing by accessing soil water at depth during terminal drought (Palta and Watt, 2009). Root length and root biomass are positively correlated with water use (Abdolshahi et al., 2015). However, a compact, deeper, and uniform root system should reduce water use early in the season increasing water availability from deeper soil layers post-anthesis (Palta and Turner, 2018). This is because conservative water use during vegetative growth will increase available soil water at flowering and during grain filling, and thus increase harvest index and grain yield (Araus et al., 2002; Ahmed et al., 2018). In contrast, large and shallow root systems can extract water from the top layers of the soil profile during vegetative growth, when rainfall is plentiful in the winter season (Manschadi et al., 2006). Cultivars with larger root systems had greater grain yield than cultivars with smaller root systems in rain-fed experiments in Central Europe (Motzo et al., 1993; Středa et al., 2012). Early season drought reduced grain yield less in Bahatans-87 (larger root system size) than Tincurrin (smaller root system size) due to slow phenology that allows better recovery in leaf area and shoot biomass at anthesis (Figueroa-Bustos et al., 2019). However, it is not clear whether a strategy of higher water use (higher biomass production and transpiration rate) of the cultivar with larger root system size or the saving water strategy (lower water use combined with a lower leaf area) of cultivar with smaller root system size are superior under terminal drought. This study examined whether differences in root system size are associated with differences in tolerance to terminal drought. It was hypothesized that root system size (in terms of root length and biomass) at anthesis in a wheat cultivar with a large root system increase water use, water use efficiency, and grain yield relative to cultivars with smaller root system size, under terminal drought. To test this hypothesis, two wheat cultivars with different-sized root systems were exposed to terminal drought. Differences in shoot and root traits were analyzed before starting the water treatment and at final harvest.

MATERIALS AND METHODS

Plant Material and Growing Conditions

Two wheat (*Triticum aestivum* L.) cultivars—Bahatans-87 (large root system size) and Tincurrin (small root system size)—were selected from a phenotyping study characterizing root trait variability in 184 genotypes using a semi-hydroponic phenotyping platform (Chen et al., 2020), and further validated in a rhizobox experiment (Figueroa-Bustos et al., 2018). The root system size were categorized, following the definition of Hamblin and Tennant (1987); Palta and Watt (2009); Palta et al. (2011) and was based on total root length and root biomass. The selection of these two cultivars was based on previous studies (Figueroa-Bustos et al., 2018; Chen et al., 2020). Growth and development of the two cultivars with contrasting root system size were characterized in a previous study under well-watered conditions (Figueroa-Bustos et al., 2018) and the differences in root system size between the two cultivars were correlated with leaf area, tiller number, leaf biomass, and phenological development. The two cultivars are not near isogenic lines, and they do not have common parents or the same phenological development. Previous studies showed that tall and semi-dwarf isogenic lines with same phenology had similar root biomass, and root: shoot ratio and this is because there are a strong association between phenology and root system size (Siddique et al., 1990a). Bahatans-87 is an old bread wheat released in 1924 in Algeria and Tincurrin is a biscuit wheat released in 1978 in Australia. The two cultivars were grown in PVC columns (0.15 m diameter, 1.0 m deep) with a long sleeve clear plastic bag (150 μm thick with 24 small holes in the bottom) inserted into each column for the ease of root recovery at harvest. The pots (0.15 m diameter and 1.0 m deep) contained 26 kg of soil (volume 0.01766 m3). Several studies have reported that the above volume of soil and particularly depth (1 m) did not show root development restrictions in wheat (Aziz et al., 2016; Saradadevi et al., 2017; Figueroa-Bustos et al., 2019; Pooniya et al., 2019). In addition, Turner (2018) suggested that large tall pots better simulate water extraction and root development similar to field conditions than smaller pots. In our experiment, the size of the pot simulated a similar rate of decline of soil water content (**Figure 1**) that observed under field conditions in Western Australia. Small holes at the bottom of the plastic bag to facilitate drainage from the plastic bag to the PVC pot, which had fixed bottom lid and short plastic tubes connected to a bottle to collect any drainage. Drainage was minimized by manually watering each pot. Each column was filled with soil at a bulk density of 1.47 g cm^{-3} over a 5-cm layer of gravel at the bottom to facilitate drainage. The soil was a reddish-brown sandy clay loam (Red Calcic Dermosal) (Isbell, 1993), obtained from the top 0 to 15 cm of a field site at Cunderdin (31°64' S, 117°24' E), Western Australia. The soil consisted of 63.5% brown sand, 8.3% silt, and 28.3% clay with a pH 6.0 (measured in a 1:5 suspension of soil in 0.01 M $CaCl_2$). Air-dried soil was sieved to 2 mm and mixed with coarse river sand (200–2000 μm particle size) in a 4:1 ratio by weight using a cement mixer for uniformity (Aziz et al., 2016; Figueroa-Bustos et al., 2018). Fertilizer equivalent to 60 kg ha^{-1} N, 77 kg ha^{-1} P, 71 kg ha^{-1} K, and trace amounts of micronutrients (S, Cu, Zn, Mo, and Mn) was mixed homogeneously into the top 0.1 m soil layer in each column the day before sowing. The fertilizer dose at sowing corresponded to the optimal nutrient supply for wheat crops in

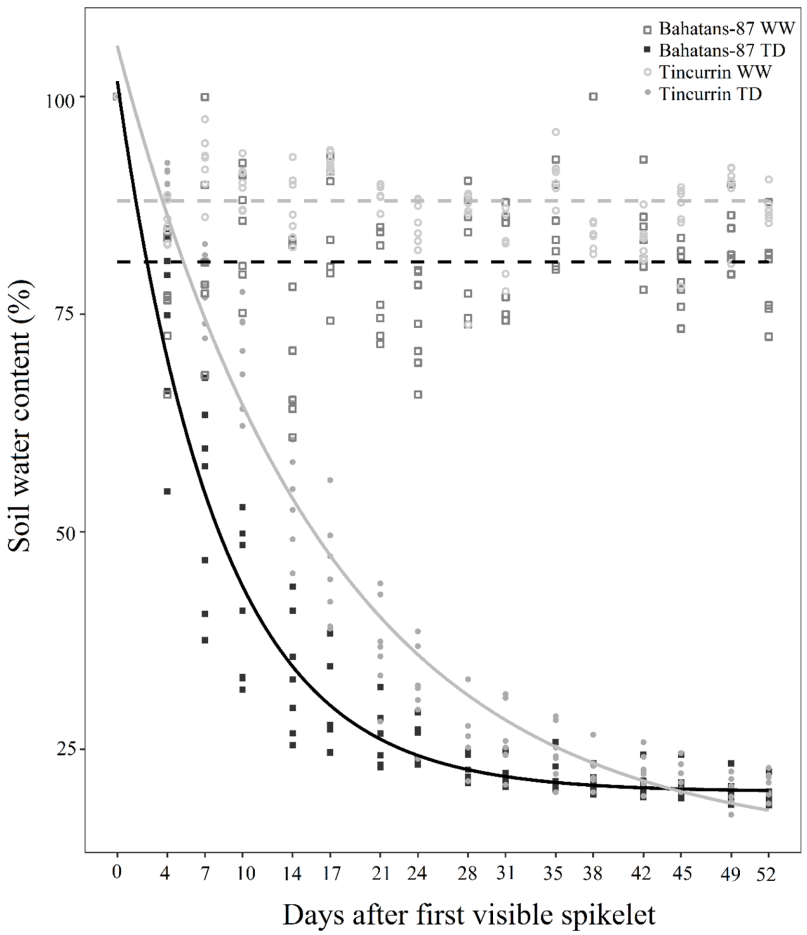


FIGURE 1 | Change with time in soil water content (%) after the first spikelet on the main stem ear was visible (Z51) in Bahatans-87 (large root system) and Tincurrin (small root system) under well-watered (WW) and terminal drought conditions (TD). Points represent the data of each replicate individually. Broken lines represent soil water content in WW treatment. Solid lines represent the best exponential fitted model for soil water content over days after booting stage TD.

the Cunderdin district in Western Australia, from where the soil was collected for the experiment (Flower et al., 2012). Five seeds per column were sown on 14 May 2020 and thinned to two plants per pot at the 1 to 2 leaf stage. At tillering (Z23) (Zadoks et al. (1974), 2.5 cm layer of plastic beads was uniformly spread on the top of the soil in each pot to prevent the soil water losses from evaporation. A water soluble fertilizer (Scott Peter excel) with 15% nitrogen, 2.2% phosphorus, 12.4% potassium, and other micronutrients was supplied through irrigation at 34, 49, and 65 DAS to prevent any nutrient deficiencies.

Plants were grown in an evaporative cooled glasshouse at The University of Western Australia, Perth, Australia (31°93' S, 115° 83' E) from May to November 2019, with an average air temperature of 17°C (range, 9–27°C), relative humidity of 60% and natural daylight (photoperiod) of 11 to 12 h. From sowing to ear emergence, before the terminal drought was induced, all plants in each cultivar were watered twice a week to maintain the pot soil water capacity close to 80%. On each occasion, pots were weighed, and the amount of water supplied was based on amount of water transpired.

Experimental Design and Treatments

A randomized complete block design was used with two factors and seven replicates per treatment, for a total of 28 columns (experimental units). Twelve extra columns (six columns per cultivar) were grown for measurements of root and shoot traits at the time when the first spikelet on the main stem ear was visible in each cultivar (Z51), just before the watering treatments were imposed. Five of the six replicates were used as controls. The layout of the experimental units in the glasshouse consisted of four columns by ten rows. One replicate consisted of two columns by two rows. The two watering treatments were imposed when the tip of the ear was just visible in the main stem of 50% of the plants (Z51; start of ear emergence). Water deficit was induced by withholding water from 14 columns (seven per cultivar) in the terminal drought treatment. A

second group of seven columns per cultivar were well watered twice weekly to maintain above 80% of column water holding capacity (WW) until physiological maturity (Z91). The column water holding capacity was 4.6 L.

Measurements

Phenological development was monitored regularly using the scale of Zadoks et al. (1974). Days after sowing (DAS) to boot swollen (Z51), anthesis (Z61), and physiological maturity (Z91) were recorded. Apparent duration of grain filling was calculated as the difference between days to physiological maturity and anthesis.

When the first spikelet on the main stem ear was visible in each genotype (Z51), just before inducing terminal drought, five columns from each cultivar were randomly selected and harvested. Plants were harvested by cutting the shoots from the roots at the crown, the number of tillers recorded, and stems and leaves separated for measurements of leaf area, leaf biomass, and specific leaf area (leaf area per unit leaf weight, SLA). Leaf area was measured using a portable leaf area meter (LI-3000, Li-COR Bioscience, Lincoln, NE, USA). Stems and leaves were dried separately in an oven at 60°C for 48 h and then weighed for shoot biomass.

Immediately after harvesting the shoots, the plastic bag inside each column was pulled out from the column and opened to recover the roots. The soil profile was sampled in 0.2 m sections from the top by cutting the soil with a carbon steel blade. The roots in each 0.2 m section were recovered from the soil by washing through a 1.4 mm sieve to produce a clean sample (Palta and Fillery, 1993). The recovered roots from each 0.2 m soil section were placed in plastic bags at 4°C until being scanned at 400 dpi per mm (Epson Perfection V800, Long Beach, CA, USA) to measure root length. The root samples were dried after scanning as per the shoot samples to measure root biomass and specific root length (root length per unit of biomass; SRL). Root images were analyzed using WinRHIZO Pro Software (v2009, Regent Instrument, Quebec, QC, Canada) (Chen et al., 2016). Specific root length, an indirect measure of the thickness of the root system, was estimated as total root length divided by total root biomass (Liao et al., 2006; Aziz et al., 2016).

From the time the first spikelet on the main stem ear was visible in each genotype (Z51) until the flag leaf in plants under terminal drought conditions had dried and rolled, measurements of stomatal conductance (g_s), leaf net photosynthesis rate (P_n), and transpiration (Tr) were made at 3- to 4-day intervals. Measurements were made on the top fully expanded leaf of the main stem on seven replicate plants between 10:00 AM and 1:00 PM on days with clear sky using a LI-COR gas-exchanged system (LI-6400, LI-COR Bioscience, Lincoln, NE, USA) with LED light source on the leaf chamber. In the LI-COR cuvette, CO_2 concentration was set to 380 μmol mol^{-1} and LED light intensity 900 μmol m^{-2} s^{-1}, which is the average saturation intensity for photosynthesis in wheat (Austin, 1990).

The amount of water applied to each column at watering was recorded. Pre-ear emergence water use was calculated as the sum of water applied until ear emergence (Z51). After the well-watered and terminal drought treatments had commenced, the columns in both treatments were weighed twice a week. After weighing the columns, the soil in the well-watered treatment was slowly watered to keep the soil close to full capacity, while the columns in the terminal drought treatment were not watered. Post-ear-emergence water use was calculated as the difference in weight of individual columns at ear emergence (Z51) and at maturity plus the water applied in-between. Total water use was calculated as the sum of pre- and post-ear-emergence water use. The ratio pre-to post-anthesis water use was calculated. Water use efficiency (WUE_{grain}) was calculated as grain yield per unit total water used. Soil water content (SWC) was calculated as

$$[1 - (W_c - W_n)/(W_c - W_d))]*100$$

where W_c is the initial column weight at saturation, W_n is the weight of the column on the day of measurements, and W_d is the weight of the column with dry soil.

Final pot weight of the droughted plants, when the plants were permanently wilted (w_f), was recorded before harvest to calculate fraction of transpirable soil water (FTSW) $(w_n - w_f)/(w_i - w_f)$, where w_n is the weight of the pot on the day of measurement, and w_i is the initial pot weight at saturation (Sinclair and Ludlow, 1986).

At final harvest, the number of tillers and spikes per plant was counted. Spikes were separated from shoots, oven dried at 60°C for 48 h before being hand-threshed. The number and weight of grains per plant were recorded. Harvest index (HI) was calculated as the ratio of grain yield to shoot biomass.

Statistical Analysis

One-way ANOVA was used for the analysis of growth parameters collected at the beginning of ear emergence before the water treatments were imposed. The analysis aimed to compare the two cultivars at growth stage.

Two-way ANOVA was undertaken for the following response variables: days to anthesis, physiological maturity, growth and yield parameters at final harvest. The main effects of "cultivar," "water treatment," and their interaction were fitted in the model. The predicted means for the significant terms in the model were compared using least significant difference (LSD) at 5%.

Both ANOVA models accounted for the blocking structure, presented here as a replicate.

Measurements of stomatal conductance (g_s), leaf net photosynthesis rate (P_n) and transpiration (T_r) were taken at days 7, 10, 14, 21 and 24 after the drought treatment started. The data were analyzed in two ways addressing two questions of interest. First, repeated measures techniques were used to assess the significance of the main effects of cultivar, water treatment, and their interaction along with fitting an unstructured model to account for the correlation of the observations measured on the same experimental unit for each of the 7 days. The second model modeled the dynamics of g_s, P_n, and T_r in time for the four cultivar and water treatment combinations. An exponential curve of type $y=a+br^x$ was fitted for each of the response variables, where a, b, and r are the shift, scale, and rate parameters, respectively, and x is the numbers of days. The same type of exponential curve was used to model the soil water content (SWC).

The data were analyzed using the statistical software Genstat statistical 20th edition (VSI International, Hemel Hemstead, UK, 2019).

RESULTS

Phenology

The first visible spikelet on the main stem ear (Z51) appeared 29 days earlier in Tincurrin than Bahatans-87 ($P< 0.01$; **Table 1**). Regardless of water treatment, anthesis in Tincurrin occurred 13 days earlier than Bahatans-87. Terminal drought accelerated physiological maturity by 17 days ($P< 0.01$; **Table 1**) in both cultivars. Regardless of water treatment, grain filling took around 14 days longer in Tincurrin than Bahatans-87 ($P< 0.01$; **Table 1**). Terminal drought conditions shortened grain filling by 15 days in Bahatans-87 and 17 days in Tincurrin ($P< 0.01$; **Table 1**). The non-significant interaction between cultivar and treatment indicates that cultivars responded similarly to terminal drought.

Soil Drying, Stomatal Conductance, Leaf Rate Photosynthesis and Transpiration Rate

In the first 52 days of treatments, soil water content in the well-watered treatment was maintained at about 81% in Bahatans-87 and 88% in Tincurrin (**Figure 1**). The fitted curve of the soil water content model under terminal drought explained 96% of the variance ($P<0.001$). The fitted curve is presented as $SWC = 20.15 + 81.62 \times 0.88^{day}$ for Bahatans-87 and $SWC = 13.86 + 91.97 \times 0.94^{day}$ for Tincurrin (**Figure 1**). The dynamic of the curve showed that the soil water content under Bahatans-87 decreased faster than Tincurrin when water was withheld completely from ear emergence (Z51) ($P< 0.001$). The soil water content rate decreased 7% faster in Bahatans-87 than in Tincurrin (**Figure 1**) from the commencement of water stress treatment (ear emergence Z51) to physiological maturity. Three-gas exchange parameters measured in the study declined with increase in water stress. There was no difference between the cultivars in their gas exchange response to water stress (**Figure S1**).

Under well-watered conditions, stomatal conductance (g_s) ranged from 290 to 481 mmol m^{-2} s^{-1} in Bahatans-87 and 398 to 641 mmol m^{-2} s^{-1} in Tincurrin (**Figure 2A**). Under terminal drought, g_s decreased from 346 to 17 mmol m^{-2} s^{-1} in Bahatans-87 and 607 to 56.3 mmol m^{-2} s^{-1} in Tincurrin in the first 24 days after the start of the treatment. The reduction in g_s under terminal drought was faster in Bahatans-87 than Tincurrin, with g_s decreasing by 90% in Bahatans-87 and 24 days in Tincurrin after 14 days of withholding watering ($P<0.001$). The best-fitted model explained 86% of the variance ($P<0.001$). The curves generated by the model for well-watered conditions followed the equations: $g_s = 334.6 + 1682 \times 0.717^{day}$ for Bahatans-87 and $g_s = 427.3 + 20391 \times 0.527^{day}$ and for Tincurrin. The curves for terminal drought conditions followed the equations: $g_s = 18.8 + 7014 \times 0.6551^{day}$ for Bahatans-87 and $g_s = -255 + 1297 \times 0.9438^{day}$ for Tincurrin, indicating that g_s in Bahatans-87 declined 31% faster than Tincurrin under terminal drought.

The leaf photosynthesis rate (P_n) under well-watered conditions ranged from 15 to 17 μmol m^{-2} s^{-1} in Bahatans-87 and 13 to 17 μmol m^{-2} s^{-1} in Tincurrin (**Figure 2B**), while under terminal drought it decreased from 14 to 2 μmol m^{-2} s^{-1} in Bahatans-87 and 16 to 5 μmol m^{-2} s^{-1} in Tincurrin (**Figure 2B**). The best-fitted model explained 75% of the variance ($P<0.001$). The curves for well-watered conditions followed the equations: $P_n = 17.27 - 0.27 \times 1.096^{day}$ for Bahatans-87 and $P_n = 13.98 + 11.2 \times 0.857^{day}$ for Tincurrin, indicating that Bahatans-87 had a 22% higher photosynthetic rate than Tincurrin. The curves for terminal drought followed the equations: $P_n = 2.321 + 100.9 \times 0.7465^{day}$ for Bahatans-87 and $P_n = 19.71 - 1.4 \times 1.1023^{day}$ for Tincurrin, indicating that Bahatans-87 growth rate declined 32% faster than Tincurrin.

The transpiration rate (T_r) under well-watered conditions ranged from 3.5 to 5.5 mmol m^{-2} s^{-1} in both cultivars (**Figure 2C**). However, under terminal drought, the transpiration rate declined in Bahatans-87 from 3.4 to 0.3 mmol m^{-2} s^{-1} and Tincurrin from 5.1 to 1.1 mmol m^{-2} s^{-1} in Tincurrin (**Figure 2C**). The best-fitted model explained 81% of the variance ($P<0.001$). Under well-watered conditions, the T_r of Tincurrin increased 14% faster than Bahatans-87, while under terminal drought, the Tr of Bahatans-87 declined 41% faster than Tincurrin.

TABLE 1 | Number of days to the first visible spikelet on the main stem ear (Z51), anthesis (Z61), physiological maturity (Z91), and duration of the grain filling in Bahatans-87 (large root system) and Tincurrin (small root system) under well-watered (WW) and terminal drought conditions (TD) from the time the first spikelet on the main stem ear was visible.

Cultivar	Treatment	First visible main steam spikelet (DAS)	Anthesis (DAS)	Physiological maturity(DAS)	Grain filling duration (Days)
Bahatans-87	TD	101a	109a	131c	22c
	WW	100a	109a	147a	37b
Tincurrin	TD	72b	86b	121d	35b
	WW	72b	86b	138b	52a
P value (LSD)					
Cultivar		***(2)	***(2)	***(2)	***(2)
Treatment		NS	NS	***(2)	***(2)
Cultivar × treatment		NS	NS	NS	NS

*Means followed by different letters differ significantly (LSD test). *** significant at P < 0.001. NS, not significant P > 0.05.*

Plant Growth

At the first spikelet on the main stem ear appeared, just before terminal drought was induced, Bahatans-87 had 28% more leaf area than Tincurrin ($P<0.05$; **Figure 3A**) and lower specific leaf area (235 cm^2 g^{-1}) than Tincurrin (299 cm^2 g^{-1}) ($P<0.01$; **Figure 3B**). The specific leaf area provides the leaf thickness values. The higher specific leaf area of Tincurrin indicates its thinner leaves than Bahatans-87. Thinner leaves of Tincurrin can be an advantageous in terms of higher photosynthetic efficiency per unit of leaf area; however Bahatans-87 compensated with a larger

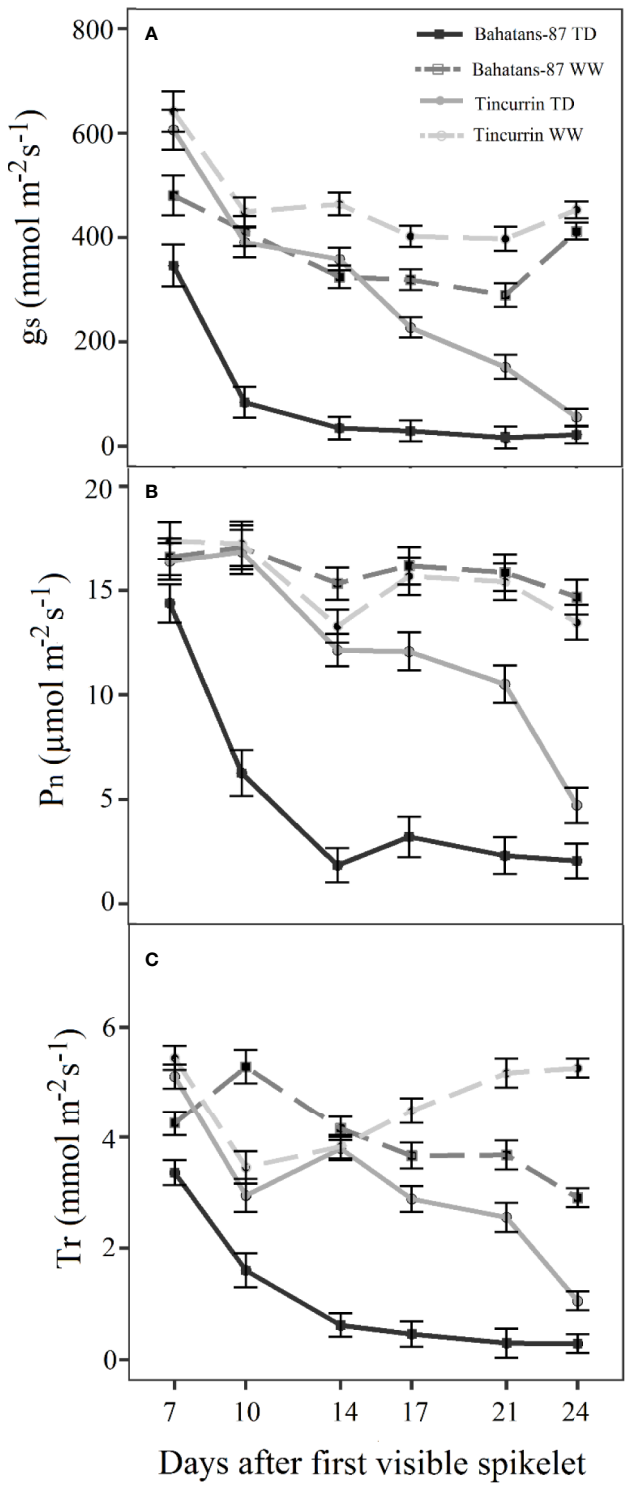


FIGURE 2 | Change with time in **(A)** stomatal conductance (g_s), **(B)** leaf photosynthesis rate (P_n) and **(C)** transpiration rate (T_r) after the first spikelet on the main stem ear was visible (Z51) in Bahatans-87 (large root system) and Tincurrin (small root system) under well-watered (WW) and terminal drought conditions (TD). Error bars represent standard errors of means (s.e.m.) (n=7).

leaf area. Bahatans-87 also had 81%, 70%, and 47% higher root biomass, root length, and root: shoot ratio than Tincurrin ($P<0.05$; **Figure 4**), but Tincurrin had 40% higher specific root length than Bahatans-87 ($P<0.01$; **Figure 4C**), indicating that Tincurrin had a thinner root system than Bahatans-87.

Shoot biomass, before terminal drought was induced, was 63% higher in Bahatans-87 than Tincurrin ($P<0.001$; **Figure 5A**). At final harvest, Bahatans-87 had 31% more shoot biomass under well-watered conditions than Tincurrin ($P<0.001$; **Figure 5B**) and 42% more shoot biomass under terminal drought conditions than Tincurrin ($P<0.001$; **Figure 5B**). Terminal drought reduced shoot biomass more in Tincurrin (47%) than in Bahatans-87 (36%) ($P<0.001$; **Figure 5B**). Tiller number, before terminal drought was induced, was higher in Bahatans-87 (five more tillers) than Tincurrin ($P<0.01$; **Figure 5C**). At final harvest, Bahatans-87 had seven more tillers than Tincurrin, irrespective of water treatment ($P<0.001$; **Figure 5D**). Terminal drought had no effect on tiller number in either cultivar ($P>0.05$), mainly because it was induced at ear emergence.

Water Use and Water Use Efficiency

Under well-watered conditions, Bahatans-87 had 45% and 33% greater pre-and post-ear emergence water use than Tincurrin, respectively ($P<0.01$; **Table 2**). Across the whole experiment, under well-watered conditions, Bahatans-87 used 39% more water than Tincurrin. Under terminal drought, post-ear emergence water use decreased by 82% in Bahatans-87 and 49% in Tincurrin, compared with their respective well-watered treatment ($P<0.01$; **Table 2**). Across the whole experiment, under terminal drought, Bahatans-87 used 39% more water than Tincurrin ($P<0.01$; **Table 2**). Terminal drought reduced total water use by 37% in both cultivars ($P<0.01$). The ratio of pre-and post-ear emergence water use was comparable in both cultivars under well-watered conditions, but it almost doubled under terminal drought ($P<0.001$). Tincurrin had 36% and 59% higher WUE_{grain} than Bahatans-87 under well-watered and terminal drought conditions, respectively ($P<0.001$; **Table 2**). Under terminal drought, WUE_{grain} declined by 67% in Bahatans-87 and 49% in Tincurrin ($P<0.001$; **Table 2**).

Grain Yield

Under well-watered conditions, Bahatans-87 and Tincurrin had similar grain numbers and grain yields, despite Bahatans-87 producing five more spikes than Tincurrin ($P<0.05$; **Table 3**). Tincurrin had 30% more grains per spike than Bahatans-87 ($P<0.001$; **Table 3**). Under terminal drought, Tincurrin produced 36% higher grain yield than Bahatans-87 ($P<0.001$). Terminal drought reduced grain yield by 67% in Tincurrin and 80% in Bahatans-87 ($P<0.001$). Under terminal drought, Tincurrin had 33% more grains per spike than Bahatans-87 ($P<0.001$). Terminal drought reduced grain number by 30% in Tincurrin and 57% in Bahatans-87 ($P<0.001$). Under terminal drought, both species had similar spike numbers, despite terminal drought reducing spike number per plant by five in Bahatans-87 and one in Tincurrin ($P<0.05$). Tincurrin produced 30% more grains per

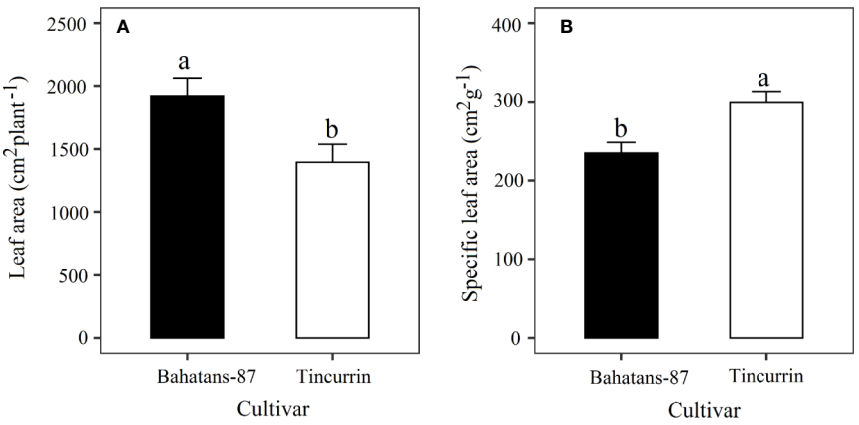


FIGURE 3 | (A) Leaf area and **(B)** specific leaf area after the first spikelet on the main stem ear was visible (Z51) in Bahatans-87 (large root system) and Tincurrin (small root system), just before terminal drought was induced. Means followed by different letters differ significantly ($P < 0.05$). Vertical error bars represent s.e.m (n= 5).

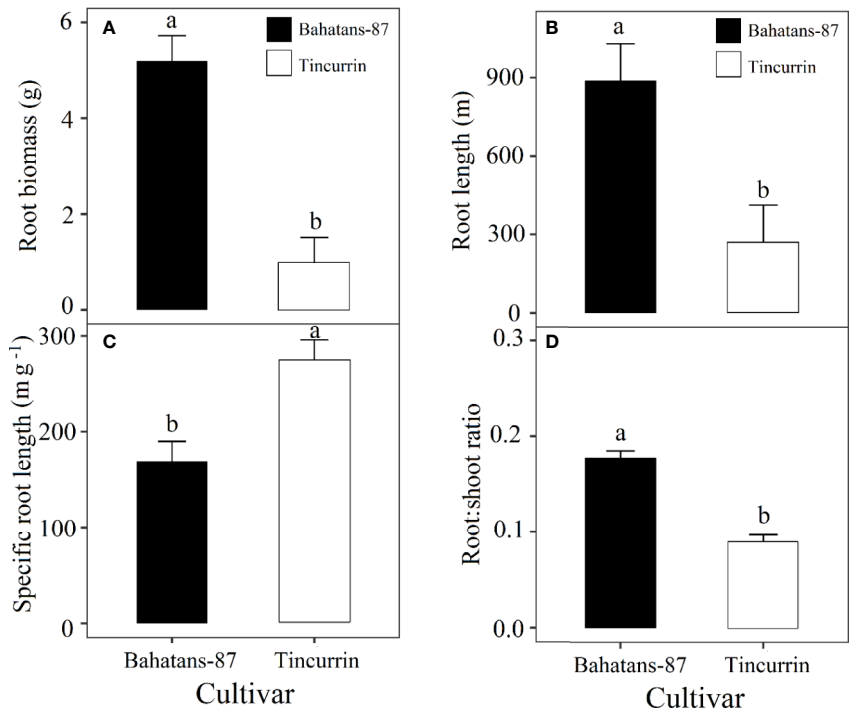


FIGURE 4 | (A) Root biomass, **(B)** root length, **(C)** specific root length, and **(D)** root/shoot ratio in Bahatans-87 (large root system) Tincurrin (small root system) after the first spikelet on the main stem ear was visible (Z51), just before terminal drought was induced. Means followed by different letters differ significantly ($P< 0.05$). Vertical error bars represent s.e.m (n= 5).

spike than Bahatans-87 under well-watered conditions ($P<0.001$). Under terminal drought, Bahatans-87 produced 43% more grains per spike than Tincurrin ($P<0.001$). Terminal drought reduced grain number per spike by 31% in Bahatans-87 and 15% in Tincurrin ($P<0.001$). Both cultivars had similar 1000-grain weights (~ 41 g) under well-watered conditions. Terminal drought reduced 1000-grain weight in both cultivars by about 53% (~19 g; $P<0.001$). Under well-watered conditions, Tincurrin had 28% higher HI than Bahatans-87 ($P<0.001$; **Table 3**), which increased to 61% higher under terminal drought ($P<0.001$). Terminal drought reduced HI by 67% in Bahatans-87 and 39% in Tincurrin ($P<0.001$).

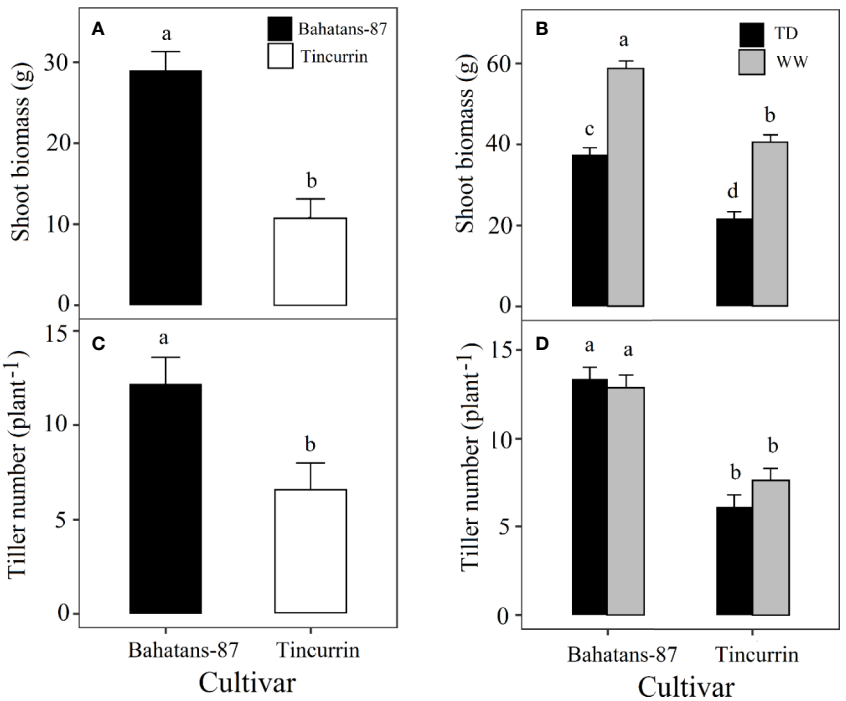


FIGURE 5 | Shoot biomass **(A)**, before the watering treatments were applied and **(B)** at final harvest, and tiller number **(C)** just before terminal drought was induced and **(D)** at final harvest in Bahatans-87 (large root system) and Tincurrin (small root system) under well-watered (WW) and terminal drought conditions (TD) from the time the first spikelet on the main stem ear was visible. Means followed by different letters differ significantly ($P < 0.05$). Vertical error bars represent s.e.m (n= 7).

TABLE 2 | Pre- and post-ear emergence water use, total water use, ratio of pre-ear to post-ear emergence water use, and water use efficiency (WUE_{grain}), in Bahatans-87 (large root system) and Tincurrin (small root system) under well-watered (WW) and terminal drought conditions (TD) from the time the first spikelet on the main stem ear was visible.

Cultivar	Treatment	Pre-ear emergence water use (L plant^{-1})	Post-ear emergence water use (L plant^{-1})	Total water use (L plant^{-1})	Pre-ear/post-ear emergence water use	WUE_{grain} (g grain L^{-1})
Bahatans-87	TD	12.0a	1.8c	13.8b	6.6a	0.29d
	WW	12.1a	10.2a	22.2a	1.3c	0.88b
Tincurrin	TD	6.6b	1.8c	8.5c	3.5b	0.71c
	WW	6.6b	6.8b	13.5b	1.0d	1.38a
P-value (LSD)						
Cultivar		***(0.13)	**(1.0)	***(1.1)	***(0.12)	***(0.097)
Treatment		NS	***(1.0)	***(1.1)	***(0.12)	***(0.097)
Cultivar × treatment		NS	**(1.4)	**(1.5)	***(0.16)	NS

*Means followed by different letters differ significantly (LSD test). **, *** significant at P < 0.01 and P<0.001, respectively. NS, not significant P > 0.05.*

DISCUSSION

Cultivar With Large Root System Size Depleted Soil Water Faster Than Cultivar With Small Root System Size

Before the watering treatments were imposed at ear emergence, the cultivar with the larger root system size (Bahatans-87) had higher leaf area and shoot biomass than the cultivar with smaller root system size (Tincurrin), confirming that the size of the root system in wheat is positively correlated with leaf area and shoot biomass (Liao et al., 2006; Aziz et al., 2016). In near isogenic lines of durum wheat with large root system had great leaf area and biomass at anthesis than the small root system line (Pooniya et al., 2019). Since leaf area and shoot biomass are positively associated with transpiration (Araya et al., 2019), it was expected that Bahatans-87 would deplete available soil water faster than Tincurrin. Indeed, withholding watering from when the first spikelet was visible rapidly reduced soil water content in Bahatans-87 (large root system) 17 days earlier than Tincurrin (small root system), which reflected the faster reduction in stomatal conductance and leaf net photosynthesis. Stomatal conductance dropped below 200 mm m^{-2} s^{-1} within 10 days of withholding water in Bahatans-87, while Tincurrin reached a similar value within 17 days of withholding water, indicating that

TABLE 3 | Grain yield, grain number, spike number, grains per spike, 1000-grain weight, and harvest index (HI) in Bahatans-87 (large root system) and Tincurrin (small root system) under well-watered (WW) and terminal drought conditions (TD) from the time the first spikelet on the main stem ear was visible.

Cultivar	Treatment	Grain yield (g plant^{-1})	Grains plant^{-1}	Spikes plant^{-1}	Grains spike^{-1}	1000 grain weight (g)	Harvestindex
Bahatans-87	TD	3.9c	209c	7.9b	26.5d	19.5b	0.11d
	WW	19.4a	484a	12.8a	38.2c	40.3a	0.33b
Tincurrin	TD	6.1b	312b	6.9b	46.2b	19.3b	0.28c
	WW	18.6a	443a	8.1b	54.5a	42.0a	0.46a
P value (LSD)							
Cultivar		NS	NS	***(1.4)	***(4.6)	NS	***(0.03)
Treatment		***(1.6)	***(48)	***(1.4)	***(4.6)	***(2.4)	***(0.03)
Cultivar × treatment		NS	**(67)	*(1.9)	NS	NS	NS

*Means followed by different letters differ significantly (LSD test). *, **, *** significant at P < 0.05, P < 0.01 and P < 0.001, respectively. NS, not significant P > 0.05.*

the cultivar with the large root system size closed the stomata and developed plant water deficit earlier than cultivar with small root system.

Water Use Higher in the Cultivar With Larger Root System Size

The higher pre-ear emergence water use in Bahatans-87 could be related to a higher demand for water due to its higher leaf area and shoot biomass and slower phenological development. Bahatans-87 (large root system) reached anthesis 23 days after Tincurrin (small root system), confirming that there is a correlation between time to anthesis and root system size in wheat (Aziz et al., 2016; Figueroa-Bustos et al., 2018). In wheat roots reach maximum biomass by anthesis (Gregory et al., 1978). In our experiment, terminal drought stress was imposed at heading when the root system size was fully developed. We did not observe differences in the root system size within a cultivar under the water treatment (well-watered and terminal drought treatment). It is likely that wheat cultivars with longer time to anthesis have more time for root system growth, since the allocation of daily photosynthates to roots decreased abruptly from 42% to 18% at floral initiation (double ridge, Z31) and to 4% by booting (Z47) (Gregory and Atwell, 1991; Palta and Gregory, 1997). The 33% higher post-ear emergence water use in Bahatans-87 than Tincurrin are directly associated with its shoot biomass and higher leaf area, since leaf area and water transpired are linearly correlated (Ritchie, 1974).

Cultivar With Larger Root System Had Higher Reduction in Grain Yield Than Cultivar With Smaller Root System Under Terminal Drought

The wheat cultivars with contrasting root system size in this study had no significant difference in grain yield under well-watered conditions. Despite both cultivars having similar grain numbers per plant and thousand grain weights, Bahatans-87 had more spikes per plant than Tincurrin. Tincurrin compensated for the lower number of spikes by producing more grains per spike. Bahatans-87 is an old cultivar released in 1924, while Tincurrin was released 54 years later (Figueroa-Bustos et al., 2018). Old cultivars produced more tillers than newer cultivars (Siddique et al., 1989; Fang et al., 2017). However, in dryland environments, many of these tillers die before producing a spike (Duggan et al., 2000). Modern cultivars have more grains per spike than older cultivars (Álvaro et al., 2008; Fang et al., 2017; Qin et al., 2018). Hence, modern cultivars like Tincurrin produce similar grain yields to old cultivars like Bahatans-87 by increasing grain numbers per spike under well-watered conditions.

Terminal drought reduced grain yield in both cultivars, with the differences reflected in phenological development. Bahatans-87 had slower phenological development allowing root and shoot growth to continue for longer (Figueroa-Bustos et al., 2019). Early flowering allows grain filling to be completed before the onset of severe water stress (Shavrukov et al., 2017). In Mediterranean environments cultivars with slower phenological development had higher pre-anthesis water use and less soil water available for reproductive stages (Siddique et al., 1990b). Post-anthesis water use is directly used for grain filling, such that cultivars that used more water during vegetative stages end up with grain yield penalties (Fischer and Wood, 1979). Hence, the faster phenology, lower ratio of pre-to post-ear emergence water use, and lower total water use in Tincurrin under terminal drought might explain its smaller reduction in grain yield, relative to Bahatans-87.

Grain Number Affected Yield in Cultivar With Larger Root System Size Under Terminal Drought

The critical period for grain set in wheat is from the appearance of the penultimate leaf (Z33) to the beginning of grain filling 10 days after anthesis (Z65) (Zadoks et al., 1974; Fischer, 2008). Soil water content at 10 days after flowering, when grain number was already set, was 27% in Bahatans-87 and 34% in Tincurrin, indicating that Bahatans-87 depleted most of the available soil water before grain number was determined. Since terminal drought reduced photosynthesis in Bahatans-87 earlier and faster than Tincurrin, grain number declined significantly in Bahatans-87, presumably as current photosynthate is essential for maintaining grain number during the critical period for grain set in wheat (Kirby, 1988). It is also likely that reduction in photosynthesis induces floret abortion, reduction in grain number, and grain filling (Rajala et al., 2009).

Cultivar With Smaller Root System Size Had Better Grain Water Use Efficiency

The higher water use efficiency of the cultivar with smaller root system size (Tincurrin) was associated with its low ratio of pre-to post-ear emergence water use, longer grain filling duration, and higher harvest index than the cultivar with the larger root

system size (Bahatans-87). Selection for high yield in wheat has also lowered the ratio of pre- to post-anthesis water use, indicating that modern wheat cultivars use proportionally less water during vegetative stages, conserving water in the soil for reproductive stages (Siddique et al., 1990b). The lower ratio of pre- to post-anthesis water use and lower total water use in Tincurrin is likely due to its early anthesis and lower shoot biomass than Bahatans-87. Tincurrin is a semi-dwarf cultivar with lower stem weight that could increase harvest index (Siddique et al., 1989; Acreche et al., 2008; Friedli et al., 2019). Increases in harvest index are associated with increases in grain yield (Perry and D'Antuono, 1989; Richards et al., 2014).

Breeding programs for improving wheat grain yield in dry environments and dry seasons have mainly focused on improving tolerance to terminal drought (Siddique et al., 1990a; Asseng and van Herwaarden, 2003; Golabadi et al., 2010; Senapati et al., 2018) by selecting for early vigor and early flowering to minimize frost damage and escape the effects of terminal drought (Perry and D'Antuono, 1989; Rebetzke and Richards, 1999; Richards et al., 2014). This advantage seems to diminish when cultivars selected for early anthesis experience early season drought, which main effect is to delays phenology, particularly time to anthesis (Figueroa-Bustos et al., 2019). With the slow onset of climate change, early winter rainfall in the Mediterranean-type climate of Australia has been decreasing; as a result, more than 82% of wheat growers are dry sowing their crops (Fletcher et al., 2015). Wheat crops sown into dry soil will germinate on the first rainfall, potentially leaving crops vulnerable to 20-32 days of drought after emergence, called early season drought (French and Palta, 2014).

Despite the fact that several studies indicated that increasing root length and root biomass could associate with drought tolerance on field conditions (Heřmanská et al., 2015; Palta and Turner, 2018); the five decades of breeding and selection for yield showed a reduction in root length and root biomass in modern wheat compared to older cultivars (Siddique et al., 1990a; Aziz et al., 2016; Fang et al., 2017). This is due to the strong positive association between root system size, leaf biomass, and phenology that increases water use which in turn reduces water use efficiency and yield in plants under terminal drought.

This study was conducted in a controlled environment with two wheat cultivars differ in root system size. To validate our findings further studies with more cultivars are required under field conditions. Differences in root system size measured in the glasshouse also needs validation under field conditions; since the growth of the root system in wheat depends on a number of factors and their interaction, such as such as soil type (clay vs. sand), soil physical and chemical characteristics, and the soil water content that, in turn, is influenced by the amount and distribution of rainfall. Root models such as ROOTMAP (Diggle, 1988) and OpenSimRoot (Postma et al., 2017) provide useful tool to not only to validate root traits and root system architecture, but also allow to compute root acquisition of water and nutrients (Chen et al., 2011; Chen et al., 2013). The modeling simulation has the potential to elucidate the role of the root system in conferring tolerance to terminal drought (Dunbabin et al., 2013).

CONCLUSION

Differences in grain yield between wheat cultivars with contrasting root system size under terminal drought, were mainly related to water use, particularly post-ear emergence water use. Bahatans-87 (larger root system) depleted the available soil water faster than Tincurrin (smaller root system) due to higher leaf area and shoot biomass. Under well-watered conditions, both cultivars had similar grain yields, despite, Tincurrin having higher water use efficiency. Under terminal drought, leaf net photosynthesis rate during the first 10 days after anthesis sharply declined in Bahatans-87, which significantly affected grain number per plant, while the slow reduction in soil water content and photosynthesis in Tincurrin resulted in smaller reductions in grain number per plant. Terminal drought reduced grain yield in both cultivars, more so in Bahatans-87 than Tincurrin. The strong association between root system size and phenology, leaf area, and shoot biomass, determined cultivar performance under terminal drought. Further studies to improve grain yield in water-limited environments should consider that association.

DATA AVAILABILITY STATEMENT

The original contributions presented in the study are included in the article or supplementary material; further inquiries can be directed to the corresponding author.

AUTHOR CONTRIBUTIONS

VF-B, JP, YC, and KHMS conceived and designed the experiments. VF-B performed the experiments along the supervisions of JAP, YC, and KHMS. VF-B and KS analyzed the data. VF-B wrote the manuscript. JP, YC, and KHMS revised the manuscript.

FUNDING

VF-B acknowledges The National Commission for Scientific and Technological Research of Chile (CONICYT) and The University of Western Australia's Institute of Agriculture and School of Agriculture and Environment for funding this research.

SUPPLEMENTARY MATERIAL

The Supplementary Material for this article can be found online at: https://www.frontiersin.org/articles/10.3389/fpls.2020.01285/full#supplementary-material

FIGURE S1 | Relationship between fraction of transpirable soil water and the ratio of water stressed to well-watered for **(A)** stomatal conductance, **(B)** photosynthesis rate, and **(C)** transpiration rate in two wheat cultivars Bahatans-87 and Tincurrin.

REFERENCES

Ababaei, B., and Chenu, K. (2019). Recent trends in drought, heat and frost-induced yield losses across the Australian wheatbelt. *Proceedings* 36, 5. doi: 10.3390/proceedings2019036005

Abdolshahi, R., Nazari, M., Safarian, A., Sadathossini, T. S., Salarpour, M., and Amiri, H. (2015). Integrated selection criteria for drought tolerance in wheat (*Triticum aestivum* L.) breeding programs using discriminant analysis. *Field Crops Res.* 174, 20–29. doi: 10.1016/j.fcr.2015.01.009

Acreche, M. M., Briceño-Félix, G., Sánchez, J. A. M., and Slafer, G. A. (2008). Physiological bases of genetic gains in Mediterranean bread wheat yield in Spain. *Europ. J. Agron.* 28, 162–170. doi: 10.1016/j.eja.2007.07.001

Ahmed, M. A., Passioura, J., and Carminati, A. (2018). Hydraulic processes in roots and the rhizosphere pertinent to increasing yield of water-limited grain crops: a critical review. *J. Exp. Bot.* 69, 3255–3265. doi: 10.1093/jxb/ery183

Álvaro, F., Isidro, J., Villegas, D., García del Moral, L. F., and Royo, C. (2008). Old and modern durum wheat varieties from Italy and Spain differ in main spike components. *Field Crops Res.* 106, 86–93. doi: 10.1016/j.fcr.2007.11.003

Araus, J. L., Slafer, G. A., Reynolds, M. P., and Royo, C. (2002). Plant breeding and drought in C3 cereals: what should we breed for? *Ann. Bot.* 85, 925–940. doi: 10.1093/aob/mcf049

Araya, A., Prasad, P. V. V., Gowda, P. H., Kisekka, I., and Foster, A. J. (2019). Yield and water productivity of winter wheat under various irrigation capacities. *J. Am. Water Resour. As.* 55, 24–37. doi: 10.1111/1752-1688.12721

Asseng, S., and Pannell, D. J. (2013). Adapting dryland agriculture to climate change: Farming implications and research and development needs in Western Australia. *Clim. Change* 118, 167–181. doi: 10.1007/s10584-012-0623-1

Asseng, S., and van Herwaarden, A. F. (2003). Analysis of the benefits to wheat yield from assimilates stored prior to grain filling in a range of environments. *Plant Soil* 256, 217–229. doi: 10.1023/A:1026231904221

Austin, R. B. (1990). "Prospects for genetically increasing the photosynthetic capacity of crops," in *Perspectives in biochemical and genetic regulation of photosynthesis*. Ed. I. Zelitch (New York: Alan R. Liss Inc).

Aziz, M. M., Palta, J. A., Siddique, K. H. M., and Sadras, V. O. (2016). Five decades of selection for yield reduced root length density and increased nitrogen uptake per unit root length in Australian wheat varieties. *Plant Soil* 413, 181–192. doi: 10.1007/s11104-016-3059-y

Chen, Y. L., Dunbabin, V. M., Postma, J. A., Diggle, A. J., Palta, J. A., Lynch, J. P., et al. (2011). Phenotypic variability and modelling of root structure of wild *Lupinus angustifolius* genotypes. *Plant Soil* 348, 345–364. doi: 10.1007/s11104-011-0939-z

Chen, Y. L., Dunbabin, V. M., Postma, J. A., Diggle, A. J., Siddique, K. H. M., and Rengel, Z. (2013). Modelling root plasticity and response of narrow-leafed lupin to heterogeneous phosphorus supply. *Plant Soil* 372, 319–337. doi: 10.1007/s11104-013-1741-x

Chen, Y., Ghanem, M., and Siddique, K. H. M. (2016). Characterising root trait variability in chickpea (*Cicer arietinum* L.) germplasm. *J. Exp. Bot.* 68 (8), 1987–1999. doi: 10.1093/jxb/erw368

Chen, Y., Palta, J. A., Prasad, V., and Siddique, K. H. M. (2020). Phenotypic variability in bread wheat root systems at the early vegetative stage. *BMC Plant Biol.* 20, 185. doi: 10.1186/s12870-020-02390-8

Chenu, K., Deihimfard, R., and Chapman, S. C. (2013). Large-scale characterization of drought pattern: a continent-wide modelling approach applied to the Australian wheatbelt–spatial and temporal trends. *New Phytol.* 198, 801–820. doi: 10.1111/nph.12192

Christopher, J. T., Christopher, M. J., Borrell, A. K., Fletcher, S., and Chenu, K. (2016). Stay-green traits to improve wheat adaptation in well-watered and water-limited environments. *J. Exp. Bot.* 67, 5159–5172. doi: 10.1093/jxb/erw276

Diggle, A. J. (1988). ROOTMAP—a model in three-dimensional coordinates of the growth and structure of fibrous root systems. *Plant Soil* 105, 169–178. doi: 10.1007/BF02376780

Duggan, B. L., Domitruk, D. R., and Fowler, D. B. (2000). Yield component variation in winter wheat grown under drought stress. *Can. J. Plant Sci.* 80, 739–745. doi: 10.4141/P00-006

Dunbabin, V. M., Postma, J. A., Schnepf, A., Pagès, L., Javaux, M., Wu, L., et al. (2013). Modelling root–soil interactions using three–dimensional models of root growth, architecture and function. *Plant Soil* 372, 93–124. doi: 10.1007/s11104-013-1769-y

Fabian, A., Jager, K., Rakszegi, M., and Barnabas, B. (2011). Embryo and endosperm development in wheat (Triticum aestivum L.) kernels subjected to drought stress. *Plant Cell Rep.* 30, 551–563. doi: 10.1007/s00299-010-0966-x

Fang, Y., Du, Y., Wang, J., Wu, A., Qiao, S., Xu, B., et al. (2017). Moderate drought stress affected root growth and grain yield in old, modern and newly released cultivars of winter wheat. *Front. Plant Sci.* 8, 672. doi: 10.3389/fpls.2017.00672

Figueroa-Bustos, V., Palta, J., Chen, Y., and Siddique, K. H. M. (2018). Characterization of root and shoot traits in wheat cultivars with putative differences in root system size. *Agronomy* 8, 109. doi: 10.3390/agronomy8070109

Figueroa-Bustos, V., Palta, J. A., Chen, Y., and Siddique, K. H. M. (2019). Early season drought largely reduces grain yield in wheat cultivars with smaller root systems. *Plants* 8, 305. doi: 10.3390/plants8090305

Fischer, R. A., and Wood, J. T. (1979). Drought resistance in spring wheat cultivars. III.* Yield associations with morpho-physiological traits. *Aust. J. Agric. Res.* 30, 1001–1020. doi: 10.1071/AR9791001

Fischer, R. A. (2008). The importance of grain or kernel number in wheat: A reply to Sinclair and Jamieson. *Field Crops Res.* 105, 15–21. doi: 10.1016/j.fcr.2007.04.002

Fletcher, A. L., Robertson, M. J., Abrecht, D. G., Sharma, D. L., and Holzworth, D. P. (2015). Dry sowing increases farm level wheat yields but not production risks in a Mediterranean environment. *Agric. Syst.* 136, 114–124. doi: 10.1016/j.agsy.2015.03.004

Flower, K. C., Cordingley, N., Ward, P. R., and Weeks, C. (2012). Nitrogen, weed management and economics with cover crops in conservation agriculture in a Mediterranean climate. *Field Crops Res.* 132, 63–75. doi: 10.1016/j.fcr.2011.09.011

French, B., and Palta, J. A. (2014). Early vigour avoids drought stress. *GRDC Ground Cover* 112, 71–74.

Friedli, C. N., Abiven, S., Fossati, D., and Hund, A. (2019). Modern wheat semi-dwarfs root deep on demand: response of rooting depth to drought in a set of Swiss era wheats covering 100 years of breeding. *Euphytica* 215, 4. doi: 10.1007/s10681-019-2404-7

Golabadi, M., Arzani, A., Mirmohammadi Maibody, S. A. M., Sayed Tabatabaei, B. E., and Mohammadi, S. A. (2010). Identification of microsatellite markers linked with yield components under drought stress at terminal growth stages in durum wheat. *Euphytica* 177, 207–221. doi: 10.1007/s10681-010-0242-8

Gregory, P. J., and Atwell, B. J. (1991). The fate of carbon in pulse-labelled crops of barley and wheat. *Plant Soil* 136, 205–213. doi: 10.1007/BF02150051

Gregory, P. J., McGowan, M., Biscoe, P. V., and Hunter, B. (1978). Water relations of winter wheat: 1. Growth of the root system. *J. Agric. Sci.* 91, 91–102. doi: 10.1017/s0021859600056653

Hamblin, A., and Tennant, D. (1987). Root length density and water uptake in cereals and grain legumes: how well are they correlated? *Aust. J. Agric. Res.* 38, 513–527. doi: 10.1071/AR9870513

Heřmanská, A., Středa, T., and Chloupek, O. (2015). Improved wheat grain yield by a new method of root selection. *Agron. Sustain. Dev.* 35, 195–202. doi: 10.1007/s13593-014-0227-4

Isbell, R. F. (1993). *A classification system for Australian soils (third approximation). Technical Report 2/1993* (Australia: CSIRO).

Kirby, E. J. M. (1988). Analysis of leaf, stem and ear growth in wheat from terminal spikelet stage to anthesis. *Field Crops Res.* 18, 127–140. doi: 10.1016/0378-4290(88)90004-4

Kong, L., Si, J., Sun, M., Feng, B., Zhang, B., Li, S., et al. (2013). Deep roots are pivotal for regulating post-anthesis leaf senescence in wheat (*Triticum aestivum* L.). *J. Agron. Crop Sci.* 199, 209–216. doi: 10.1111/jac.12007

Liao, M., Palta, J. A., and Fillery, I. R. P. (2006). Root characteristics of vigorous wheat improve early nitrogen uptake. *Aust. J. Agric. Res.* 57, 1097–1107. doi: 10.1071/ar05439

Manschadi, A. M., Christopher, J., de Voil, P., and Hammer, G. L. (2006). The role of root architectural traits in adaptation of wheat to water-limited environments. *Funct. Plant Biol.* 33, 823–837. doi: 10.1071/fp06055

Motzo, R., Attene, G., and Deidda, M. (1993). Genotypic variation in durum wheat root systems at different stages of development in a Mediterranean environment. *Euphytica* 66, 197–206. doi: 10.1007/BF00025303

Palta, J. A., and Fillery, I. R. (1993). Nitrogen accumulation and remobilisation in wheat of 15~-urea applied to a duplex soil at seeding. *Aust. J. Exp. Agric.* 33, 233–238. doi: 10.1071/EA9920995

Palta, J. A., and Gregory, P. J. (1997). Drought affects the fluxes of carbon to roots and soil in 13C pulse-labelled plants of wheat *Soil Biol. Biochem.* 29 (9/10), 1395–1403. doi: 10.1016/S0038-0717(97)00050-3

Palta, J. A., and Turner, N. C. (2018). Crop root system traits cannot be seen as a silver bullet delivering drought resistance. *Plant Soil* 439, 31–43. doi: 10.1007/s11104-018-3864-6

Palta, J. A., and Watt, M. (2009). "Vigorous crop root systems: form and function for improving the capture of water and nutrients," in *Crop physiology. Applications for genetic improvement and agronomy*. Eds. V. Sadras and D. Calderini (New York: Elservier), 309–325.

Palta, J. A., Chen, X., Milroy, S. P., Rebetzke, G. J., Dreccer, M. F., and Watt, M. (2011). Large root systems: Are they useful in adapting wheat to dry environments? *Funct. Plant Biol.* 38, 347–354. doi: 10.1071/fp11031

Passioura, J. B. (1983). Roots and drought resistance. *Agric. Water Manage.* 7, 265–280. doi: 10.1016/0378-3774(83)90089-6

Perry, M. W., and D'Antuono, M. F. (1989). Yield improvement and associated characteristics of some Australian spring wheat cultivars introduced between 1860 and 1982. *Aust. J. Agric. Res.* 40, 457–472. doi: 10.1071/AR9890457

Pooniya, V., Palta, J. A., Chen, Y., Delhaize, E., and Siddique, K. H. M. (2019). Impact of the TaMATE1B gene on above and below-ground growth of durum wheat grown on an acid and Al3+-toxic soil. *Plant Soil* 447, 73–84. doi: 10.1007/s11104-019-04231-6

Postma, J. A., Kuppe, C., Owen, M. R., Mellor, N., Griffiths, M., Bennett, M. J., et al. (2017). OpenSimRoot: widening the scope and application of root architectural models. *New Phytol.* 215, 1274–1286. doi: 10.1111/nph.14641

Qin, X., Feng, F., Wen, X., Siddique, K. H. M., and Liao, Y. (2018). Historical genetic responses of yield and root traits in winter wheat in the yellow-Huai-Hai River valley region of China due to modern breeding, (1948–2012). *Plant Soil* 439, 7–18. doi: 10.1007/s11104-018-3832-1

Rajala, A., Hakala, K., Mäkelä, P., Muurinen, S., and Peltonen-Sainio, P. (2009). Spring wheat response to timing of water deficit through sink and grain filling capacity. *Field Crops Res.* 114, 263–271. doi: 10.1016/j.fcr.2009.08.007

Rebetzke, G. J., and Richards, R. A. (1999). Genetic improvement of early vigour in wheat. *Aust. J. Agric. Res.* 50, 291–301. doi: 10.1071/A98125

Richards, R. A., Hunt, J. R., Kirkegaard, J. A., and Passioura, J. B. (2014). Yield improvement and adaptation of wheat to water-limited environments in Australia—a case study. *Crop Pasture Sci.* 65, 676–689. doi: 10.1071/cp13426

Ritchie, J. T. (1974). Atmospheric and soil water influences on the plant water balance. *Agric. Meteorol.* 14, 183–198. doi: 10.1007/bf02180050

Saeidi, M., and Abdoli, M. (2015). Effect of drought stress during grain filling on yield and its components, gas exchange variables, and some physiological traits of wheat cultivars. *J. Agr. Sci. Tech.* 17, 885–898.

Saradadevi, R., Bramley, H., Palta, J. A., and Siddique, K. H. M. (2017). Stomatal behaviour under terminal drought affects post-anthesis water use in wheat. *Funct. Plant Biol.* 44, 279–289. doi: 10.1071/fp16078

Scanlon, T. T., and Doncon, G. (2020). Rain, rain, gone away: decreased growing-season rainfall for the dryland cropping region of the south-west of Western Australia. *Crop Pasture Sci.* 71, 128–133. doi: 10.1071/cp19294

Senapati, N., Stratonovitch, P., Paul, M. J., and Semenov, M. A. (2018). Drought tolerance during reproductive development is important for increasing wheat yield potential under climate change in Europe. *J. Exp. Bot.* 70, 2549–2560. doi: 10.1093/jxb/ery226

Shavrukov, Y., Kurishbayev, A., Jatayev, S., Shvidchenko, V., Zotova, L., Koekemoer, F., et al. (2017). Early flowering as a drought escape mechanism in plants: how can it aid wheat production? *Front. Plant Sci.* 8, 1950. doi: 10.3389/fpls.2017.01950

Siddique, K. H. M., Belford, R. K., Perry, M. W., and Tennant, D. (1989). Growth, development and light interception of old and modern wheat cultivars in a Mediterranean-type environment. *Aust. J. Agric. Res.* 40, 473–487. doi: 10.1071/AR9890473

Siddique, K. H. M., Belford, R. K., and Tennant, D. (1990a). Root:shoot ratios of old and modern, tall and semi-dwarf wheats in a Mediterranean environment. *Plant Soil* 121, 89–98. doi: 10.1007/BF00013101

Siddique, K. H. M., Tennant, D., Perry, M. W., and Belford, R. K. (1990b). Water use and water use efficiency of old and modern wheat cultivars in a Mediterranean-type environment. *Aust. J. Agric. Res.* 41, 431–447. doi: 10.1071/AR9900431

Sinclair, T., and Ludlow, M. (1986). Influence of soil water supply on the plant water balance of four tropical grain legumes. *Funct. Plant Biol.* 13, 329–341. doi: 10.1071/PP9860329

Středa, T., Dostál, V., Horáková, V., and Chloupek, O. (2012). Effective use of water by wheat varieties with different root system sizes in rain-fed experiments in Central Europe. *Agr. Water Manage.* 104, 203–209. doi: 10.1016/j.agwat.2011.12.018

Turner, N. C., and Nicolas, M. E. (1987). "Drought resistance of wheat for light-textured soils in the mediterranean climate," in *Drought Tolerance in Winter Cereals*. Eds. J. P. Srivastava, E. Porceddu, E. Acevedo and S. Varma (Capri, Italy: John Wiley & Sons), 203–216.

Turner, N. C. (2018). Imposing and maintaining soil water deficits in drought studies in pots. *Plant Soil* 439, 45–55. doi: 10.1007/s11104-018-3893-1

Yu, X., Li, B., Wang, L., Chen, X., Wang, W., Gu, Y., et al. (2016). Effect of drought stress on the development of endosperm starch granules and the composition and physicochemical properties of starches from soft and hard wheat. *J. Sci. Food Agric.* 96, 2746–2754. doi: 10.1002/jsfa.7439

Zadoks, J. C., Chang, T. T., and Konzak, C. F. (1974). A decimal code for the growth stages of cereals. *Weed Res.* 14, 415–421. doi: 10.1111/j.1365-3180.1974.tb01084.x

Conflict of Interest: The authors declare that the research was conducted in the absence of any commercial or financial relationships that could be construed as a potential conflict of interest.

Copyright © 2020 Figueroa-Bustos, Palta, Chen, Stefanova and Siddique. This is an open-access article distributed under the terms of the Creative Commons Attribution License (CC BY). The use, distribution or reproduction in other forums is permitted, provided the original author(s) and the copyright owner(s) are credited and that the original publication in this journal is cited, in accordance with accepted academic practice. No use, distribution or reproduction is permitted which does not comply with these terms.

frontiers in Plant Science

ORIGINAL RESEARCH
published: 19 August 2020
doi: 10.3389/fpls.2020.01284

Mapping Quantitative Trait Loci for Soybean Seedling Shoot and Root Architecture Traits in an Inter-Specific Genetic Population

Silvas J. Prince[1,2], *Tri D. Vuong*[1], *Xiaolei Wu*[3], *Yonghe Bai*[4], *Fang Lu*[5], *Siva P. Kumpatla*[6], *Babu Valliyodan*[1,7], *J. Grover Shannon*[1] *and Henry T. Nguyen*[1]*

[1] Division of Plant Sciences, University of Missouri, Columbia, MO, United States, [2] Plant Biology Division, Noble Research Institute, LLC, Ardmore, OK, United States, [3] BASF Agricultural Solutions, Morrisville, NC, United States, [4] Nuseed Americas, Woodland, CA, United States, [5] Amgen Inc., Thousand Oaks, CA, United States, [6] Corteva Agriscience™, Johnston, IA, United States, [7] Department of Agriculture and Environmental Sciences, Lincoln University, Jefferson City, MO, United States

OPEN ACCESS

Edited by:
Guihua Bai,
United States Department of Agriculture (USDA), United States

Reviewed by:
Dawei Xin,
Northeast Agricultural University, China
Marta Silva Lopes,
Institute of Agrifood Research and Technology (IRTA), Spain

***Correspondence:**
Henry T. Nguyen
nguyenhenry@missouri.edu

Specialty section:
This article was submitted to Plant Abiotic Stress, a section of the journal Frontiers in Plant Science

Received: 09 March 2020
Accepted: 06 August 2020
Published: 19 August 2020

Citation:
Prince SJ, Vuong TD, Wu X, Bai Y, Lu F, Kumpatla SP, Valliyodan B, Shannon JG and Nguyen HT (2020) Mapping Quantitative Trait Loci for Soybean Seedling Shoot and Root Architecture Traits in an Inter-Specific Genetic Population. Front. Plant Sci. 11:1284. doi: 10.3389/fpls.2020.01284

Wild soybean species (*Glycine soja* Siebold & Zucc.) comprise a unique resource to widen the genetic base of cultivated soybean [*Glycine max* (L.) Merr.] for various agronomic traits. An inter-specific mapping population derived from a cross of cultivar Williams 82 and PI 483460B, a wild soybean accession, was utilized for genetic characterization of root architecture traits. The objectives of this study were to identify and characterize quantitative trait loci (QTL) for seedling shoot and root architecture traits, as well as to determine additive/epistatic interaction effects of identified QTLs. A total of 16,469 single nucleotide polymorphisms (SNPs) developed for the Illumina beadchip genotyping platform were used to construct a high resolution genetic linkage map. Among the 11 putative QTLs identified, two significant QTLs on chromosome 7 were determined to be associated with total root length (RL) and root surface area (RSA) with favorable alleles from the wild soybean parent. These seedling root traits, RL (BARC_020495_04641 ~ BARC_023101_03769) and RSA (SNP02285 ~ SNP18129_Magellan), could be potential targets for introgression into cultivated soybean background to improve both tap and lateral roots. The RL QTL region harbors four candidate genes with higher expression in root tissues: Phosphofructokinase (Glyma.07g126400), Snf7 protein (Glyma.07g127300), unknown functional gene (Glyma.07g127900), and Leucine Rich-Repeat protein (Glyma.07g127100). The novel alleles inherited from the wild soybean accession could be used as molecular markers to improve root system architecture and productivity in elite soybean lines.

Keywords: soybean (*Glycine max*), quantitative trait loci (QTL), shoot and root architecture, inter-specific genetic population, molecular markers, single nucleotide polymorphism, KASP assay

HIGHLIGHTS

Wild soybeans are useful genetic resources to improve drought avoidance in cultivated soybean by improving shoot and root architectural traits.

INTRODUCTION

Soybean [*Glycine max* (L.) Merr.] is a major oil crop that plays a key role in food and industrial production (Tran and Mochida, 2010). In terms of global production, USA ranks first with 84.2 million metric tons (33% of total global production) of soybean produced followed by Brazil (29%) and Argentina (19%) (www.soystats.com). Cultivated soybean, *Glycine max*, was domesticated from wild soybean (*Glycine soja* Siebold & Zucc.) more than 5,000 years ago in China (Carter et al., 2004) and underwent two rounds of whole genome duplication (Schmutz et al., 2010). Although the breeding process within cultivated soybean has accelerated genetic gain, it has also narrowed the genetic pool (Carter et al., 2004; Hyten et al., 2006). The reduction in genetic diversity among U.S. cultivars poses a threat to future food security due to anticipated pest incidence and disease outbreaks (Hyten et al., 2006).

Wild soybeans represent a significant genetic resource with many rare alleles that are not present in cultivated soybean accessions (Lee et al., 2008; Mammadov et al., 2018). Advancements in next-generation sequencing (NGS) technologies helped researchers to tap into the valuable wild soybean genome for novel haplotypes (Kim et al., 2012; Joshi et al., 2013). Roots are known to be smaller in wild soybean accessions (Liang et al., 2014; Manavalan et al., 2015; Prince et al., 2015). The present study was aimed at identifying wild soybean alleles that could be utilized to widen the genetic base and improve stress resilience in cultivated soybean. Previous studies using 397 diverse soybean accessions with maturity groups, III to IV (Prince et al., 2018) and III to VI (Prince et al., 2019), revealed that constitutive seedling traits, like total root length, root surface area, and lateral root number, are linked to grain yield under water limitation. Field studies in two different soil types that represent most of the U.S. soybean growing target environments also validated the association of root traits to grain yield under stress (Prince et al., 2016; Prince et al., 2019).

Research that uses a crop's wild relative was first demonstrated in tomato through identification of a major fruit weight QTL of 2.2 in green- and red-fruited wild tomato species, explaining a phenotypic variation of 30% and 47% and increased fruit size (Alpert et al., 1995; Frary et al., 2000). Introgression of yield-enhancing quantitative trait locus (QTL) from *Glycine soja* in cultivated soybean through a marker-assisted backcross breeding approach increased seed yield (Concibido et al., 2003; Li et al., 2008). Similar introductions of wild species haplotypes into cultivated cereal crops were also proven successful for various agronomic traits (Guo et al., 2013; Placido et al., 2013).

Soybean-growing target environments have been severely affected by drought and flooding stresses, and key physiological and biochemical pathways are the basis of adaptation to these stresses (Valliyodan et al., 2014). Deeper root systems enable soybean to acquire water and result in higher yields under drought condition (Hudak and Patterson, 1995). However, biomass allocation to produce robust root systems under non-stress condition was shown to affect final crop productivity (Boyer and Westgate, 2004). In soybean, specific root morphological and anatomical traits have been reported as adaptive mechanisms that enhance plant performance and productivity under drought (Prince et al., 2016; Prince et al., 2017; Prince et al., 2019) and flooding (Valliyodan et al., 2014) stresses. The association of different root traits and their contributions to drought avoidance are well-established in several crops, including rice (Nguyen et al., 1997; Suji et al., 2012), maize (Tuberosa et al., 2011), wheat (Wasson et al., 2012), common bean (Sponchiado et al., 1989), chickpea (Varshney et al., 2011), and soybean (Hufstetler et al., 2007; Prince et al., 2016; Prince et al., 2017; Prince et al., 2019). In comparison to cereal crops, the information on mapped root QTL in legumes is highly limited. Although many rice root QTLs were mapped, there have been few successful cases of their application in marker-assisted breeding programs (Steele et al., 2006; Suji et al., 2012). However, a major QTL controlling root growth angle was cloned, and the gene "*Dro1*" was identified that could be used in the genetic improvement of drought avoidance in rice (Uga et al., 2013). Identifying rare alleles for root growth and development and understanding the regulation of quantitative trait loci (QTL) governing root traits are essential to improving abiotic stress tolerance in soybean.

Previously in soybean breeding programs, selection of root traits under field conditions is hindered by several practical constraints (Pantalone et al., 1996; Myers et al., 2007). The establishment of associations between seedling root traits like total root length, root surface area, lateral root number, and field root response (narrow root angle and fibrous root score) under water limitation is promising (Prince et al., 2016). A gel-based seedling root imaging platform was built to select for these proxy root traits to predict field root response and hasten large-scale germplasm characterization (Prince et al., 2018). Mapping root QTL and identifying markers associated with root traits will facilitate root trait introgression in breeding programs (Coudert et al., 2010). In the last five years, considerable progress has been made toward mapping QTL for soybean root traits in greenhouse (Rong et al., 2011; Prince et al., 2013; Liang et al., 2014; Manavalan et al., 2015; Prince et al., 2015) and field conditions (Abdel-Haleem et al., 2011). Increase in availability of genomic sequences also enabled researchers to link genes associated with different root architectural traits and identify soybean accessions adaptable to water-limited environments (Prince et al., 2017; Prince et al., 2019). In soybean, most of the root QTL mapping studies have utilized genetic diversity within cultivated soybeans. Recently, our group has successfully identified and mapped QTL for root traits using two inter-specific soybean mapping populations (Manavalan et al., 2015; Prince et al., 2015) and could successfully map wild soybean alleles from PI 407162 that improve root traits in cultivated soybean. This was the first effort to map root QTL in an inter-specific mapping population, and

further exploration of novel alleles from wild soybeans is needed to improve drought avoidance in soybean.

In this study, we used an inter-specific mapping population developed from a cross between cv. "Williams 82" and "PI 483460B," a wild soybean accession, to map novel haplotypes for root architectural trait and identify SNPs associated with major root QTLs towards the crop improvement. The objectives of this study were to identify significant genomic regions for seedling shoot and root architecture traits, identify genes underlying major QTLs and identify potential SNPs as molecular markers for root trait breeding.

MATERIALS AND METHODS

Plant Materials

This study used two soybean accessions: cultivar Williams 82 (Bernard and Cremeens, 1988), which is widely used as a reference genome (Schmutz et al., 2010) in various genetic studies, and PI 483460B, a wild soybean accession originating from China with desirable traits for seed composition, such as high protein content (48%) and high linolenic acid (21%) (http://www.ars-grin.gov). Williams 82 has a long and robust root system in comparison to PI 483460B, which has smaller roots. These parental genotypes significantly differ in shoot traits, root architecture, and many other morphological traits. The phenotypic descriptors of the parental lines are presented in **Table 1**. An inter-specific mapping population was developed from a Williams 82 × PI 483460B cross made at the University of Missouri (MU)'s Delta Research Center in Portageville, Missouri. Following the verification of F_1 true hybridization, F_2 seed generation was advanced in the soybean nursery in Costa Rica. One hundred eighty-four $F_{7:8}$ recombinant inbred lines (RIL) were generated using the single seed descent method. These RILs were grown in the Bradford Research and Education Center (BREC) at MU in Columbia, Missouri, in the summer of 2012.

Phenotyping of RILs

Parental lines (Williams 82 and PI 483460B) and the 184 $F_{7:8}$ RILs were grown in a cone system and replicated five times in a completely randomized block design using DL60L cones and D20 supporting racks (Stuwe and Sons, Oregon, USA). Each replication was conducted separately in the Sears Greenhouse Facility at MU from January 2014 to July 2015 in 20 experimental batches, each comprising 50 genotypes. Turface (Turface Athletics, Illinois, USA) and sand were mixed in a 1:1 ratio as a growing medium.

In the greenhouse, the day and night temperatures were maintained at 29°C and 21°C, respectively. The 12 h photoperiod in the greenhouse was maintained using overhead 400 W metal halide lamps that generated a photosynthetic photon flux density of approximately 1620 μmol m^{-2} s^{-1}. The seedlings were grown up to V1 growth stage (approximately 14 days after sowing), and the intact seedlings from the cones were collected to analyze shoot and root traits.

DNA Extraction

Genomic DNA samples were isolated from pooled leaf tissues of five seedlings of each $F_{7:8}$ RIL and their parents using an automated Autogen 960 system and the CTAB protocol (AutoGen Inc., Holliston, MA) with minor modifications as previously described (Vuong et al., 2010). Briefly, ground leaf tissue was mixed with CTAB extraction buffer, followed by an incubation period at 65°C for 1.5 h. Chloroform was then added to the suspension, followed by agitation and centrifugation. The aqueous layer was collected and treated with RNase enzyme. Following DNA precipitation, DNA pellets were washed with ethanol and dissolved in TE (Tris-HCl-EDTA, pH 8.0) buffer. Subsequently, DNA was quantified and checked for quality.

SNP Development, Genotyping, and Analysis

A total of 16,469 single nucleotide polymorphism (SNP) markers were included in the final Illumina Infinium BeadChip for genotyping. This SNP set included 7,113 SNPs developed at the Soybean Genomics and Improvement Laboratory at USDA-ARS in Beltsville, Maryland, and 9,356 SNPs developed at the National Center for Soybean Biotechnology (NCSB) in Missouri. DNA samples were quantified by PicoGreen and about 200 to 400 ng DNA/sample were analyzed using the Illumina Infinium assays, following the protocol described by Illumina Inc. (San Diego, CA). SNP calling was automated using the Genome Studio program, with manual modifications when needed. (Infinium® II Assay Workflow, Pub. No. 370-2006-027 07Dec06).

Construction of Genetic Linkage Map

A genetic linkage map was constructed for the Williams 82 × PI 483460B population (Patil et al., 2018) using the software MSTmap as previously described (Wu et al., 2008). Based on the population size and the number of markers in a genotypic data set, the parameters specified for the MSTmap software were as follows: Kosambi, *p* value cutoff: 1.0E-13 for Genetic mapping function; 2 for No mapping size threshold; 10 cM for No mapping distance threshold; and 0.4 for No mapping missing threshold. The map quality was manually improved by removing markers with significant segregation distortion and misplaced 373 markers compared to the physical map of the Williams 82 reference genome (**Supplementary Table S1**). Out of 9,356 SNPs in the Infimum chips, more than 6,000 markers were found to be polymorphic between the two parents and were incorporated into linkage analysis. The total genetic linkage map distance was 2,925 cM. The number of SNP markers and length of each chromosome are presented in **Supplementary Table S2**.

Shoot and Root Traits Phenotyping

The mapping population of 184 RILs along with two parental lines of each replication, one normal seedling at the growth stage V1 was collected to manually measure shoot root traits, such as shoot length (SL), plant height (PH), and tap root length (TRL), with a ruler. For other root traits, including total root length (RL), root surface area (RSA), root volume (RV), and distribution of root length (RD_L), root surface area (RD_S), and thickness (RD_T) in

diameter class of 1.0 to 1.5 mm, were evaluated using an Epson Scanner 10000XL (Epson America Inc., CA, USA) and analyzed using WinRhizo software (Regent Instruments Inc., Canada). The detailed information of root diameter distribution is critical to understand the root system architecture and its implication in soil function (Blouin et al., 2007). The measurements of shoot- and root-related traits were averaged for further analysis in this study as described in **Table 1**. The phenotypic data generated for the above said traits are provided in **Supplementary Table S3**.

Gene Expression Data

To gain further insight into the expression of genes underlying root trait QTLs we used the publicly available differential gene expression data of Williams 82, a parental line used in developing this inter-specific mapping population. Gene expressions across diverse soybean genetic backgrounds were obtained from Array express (https://www.ebi.ac.uk/arrayexpress/) and RNA-sequencing datasets (Ithal et al., 2007; Libault et al., 2010; Gong et al., 2014; Kour et al., 2014; Leisner et al., 2014; Lin et al., 2014; Shen et al., 2014; Valdés-López et al., 2014; Wu et al., 2014; Zabala and Vodkin, 2014; Aghamirzaie et al., 2015; Brown and Hudson, 2015; Devi et al., 2015; Huang and Schiefelbein, 2015; Jones et al., 2015; Lambirth et al., 2015; Lanubile et al., 2015; Okamoto et al., 2015; Shin et al., 2015; Whaley et al., 2015; Bellieny-Rabelo et al., 2016; Song et al., 2016; Cho et al., 2017; Dastmalchi et al., 2017; Huang et al., 2017; Waters et al., 2018; Adhikari et al., 2019; Li et al., 2019; Liu et al., 2019; Neupane et al., 2019; Wang et al., 2019) integrated into Genevestigator database, www.genevestigator.com (Zimmermann et al., 2014). The transcriptome data of the wild soybean parental line, PI 483460B used in this study is not available. Thus to mine tissue-specific gene-expression of genes underlying major QTLs, the study used a public transcriptome generated with a *Glycine max*, A81-356022 with introgression of genomic fragments from another wild soybean accession from the same province of China, PI 468916 available in SoyBase (Severin et al., 2010).

Data Analysis

Statistical Analysis

Shoot and root traits among the $F_{7:8}$ RILs and parental lines evaluated were tested for normality using the PROC UNIVARIATE procedure of SAS 9.1 (SAS Institute, Cary, NY, USA) and the Shapiro–Wilk (w) test. Pearson correlation coefficients among the traits were estimated using the SAS PROC CORR procedure. Broad-sense heritability (Nyquist and Baker, 1991) for each trait was estimated based on the expected mean squares (EMS) derived from an analysis of variance (ANOVA) with the SAS PROC GLM procedure. The chromosome numbers (Chr.) were assigned to the soybean genetic linkage groups (LGs) as enumerated in SoyBase (http://www.soybase.org).

TABLE 1 | List of soybean shoot and root architecture traits evaluated in the soybean mapping population (Williams 82/PI483460B).

Trait Abbreviation	Description (units)
SL	Shoot length (cm) measured from soil level to cotyledons
PH	Plant height (cm) measured from soil level to shoot tip
TRL	Tap root length (cm)
RL	Root length (cm)
RSA	Root surface area (cm^2)
RV	Root volume (cm^3)
RD_L	Distribution of root length in diameter class (1.0–1.5 mm)
RD_S	Distribution of root surface area in diameter class (1.0–1.5 mm)
RD_T	Distribution of root thickness in diameter class (1.0–1.5 mm)

QTL Mapping

A comprehensive approach for QTL analysis, including interval mapping (IM), cofactor selection, genome-wide permutation test, and multi-QTL method (MQM), to detect and map significant QTL was performed using the program MapQTL 5.0 (Van Ooijen and Voorrips, 2001) as previously described (Vuong et al., 2010). A permutation test (Churchill and Doerge, 1994) was performed with 1,000 runs to determine the P = 0.05 genome-wide significance level for declaring a QTL significant. A LOD threshold of 3.4 was determined using a genome-wide permutation test (P = 0.05) for the traits studied and the root trait QTLs detected are shown in **Figure 1**.

A multivariate ANOVA model in SAS (SAS Institute, Cary, NY, USA) was used to estimate the total phenotypic variation explained by the significant QTL. The chromosomes with LOD plots were subsequently created using the MapChart 2.2 program (Voorrips, 2002) based on the outputs from MapQTL 5.0. The prediction of epistatic interactions between significant QTL was performed using the computer program QTLNetwork 2.0 (Yang et al., 2007) with a mixed-model based composite interval mapping (MCIM). For MCIM, critical F-value was assessed by permutation test using 1,000 permutations. QTL effects were estimated using Markov chain Monte Carlo method. Candidate interval selection, epistatic effects, and putative QTL detection were calculated with an experimental-wise type I error of α = 0.05, α = 0.001, and α = 0.001, respectively.

RESULTS

Phenotypic Variation of Shoot and Root Architecture Traits

The parental genotypes, Williams 82 and PI 483460B, showed significant variation (p value= 0.05) for shoot and root traits measured (**Table 2**). Williams 82 is an adapted cultivar with robust root architecture relative to that of the wild soybean parent, PI 483460B. The RIL mapping population developed from a cross of these parental lines showed a transgressive segregation for shoot-related traits (SL, PH) and root traits like TRL (**Table 2**; **Figure 2**). The RILs had longer or shorter shoot and root morphology compared to the *G. max* (Williams 82) and wild parent (PI 483460B), respectively (**Table 2**), for example: TRL (**Figure 2**) and RL. A Shapiro–Wilk test showed that the frequency distributions of the traits followed

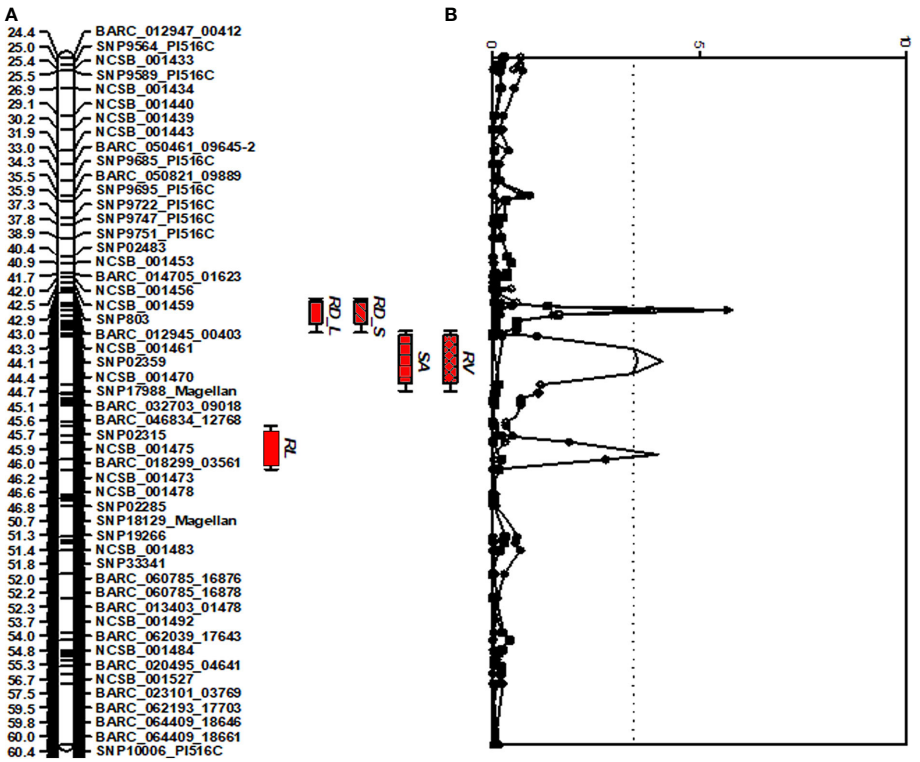


FIGURE 1 | Distribution of QTLs for seedling traits identified in the interspecific soybean mapping population (Williams 82/PI483460B) **(A)** QTLs associated with root traits identified on chromosome 7 with positive allele from wild soybean parent, PI 483460B. **(B)** QTLs with an Likelihood of Odds (LOD) score exceeding the genome-wide LOD of 3.4 were declared as significant QTLs. QTL for root length (RL), root distribution based on length in diameter (1.0–1.5 mm) (RD_L), root distribution based on surface area in diameter (1.0–1.5 mm) (RD_S), root surface area (RSA); and root volume (RV).

approximately normal distribution. The heritability of measured traits was calculated based on the analysis of variance of family means. Heritability values ranged from 0.47 to 0.80 for shoot- and root-related traits (**Table 2**). In this mapping population, the significant negative relationship between SL and root traits like TRL and RL showed more allocation of seed reserves to shoot growth and formation of fine roots in contrast to thicker roots, which is evident with its positive association with RD_T (**Table 3**). Even at later stages of shoot development, the trait PH showed a positive relation with RD_T, representing biomass allocation to formation of fine roots. Among root-related traits, TRL is the only trait that showed significant positive correlation with all other root-related traits measured in our study, while RD_T showed positive correlations with TRL and RD_L (**Table 3**). This positive correlation facilitates the selection of longer taproot and robust root system with finer roots, which would enhance both water and nutrients uptake, respectively.

TABLE 2 | Descriptive statistics of different shoot and root traits in mapping population derived from Williams 82 X PI 483460B cross.

Trait (†)	Parents		RIL population			Variance	SE*	Skewness	Kurtosis	W-test	*P*-value	Heritability (broad-sense)
	Williams 82	PI 483460B	Mean	Min	Max							
SL	12.48	2.95	7.01	2.80	20.10	9.17	0.11	2.11	9.20	0.8613	<0.0001	0.79
PH	7.28	1.98	4.77	1.68	15.65	10.83	0.12	4.99	42.78	0.6500	<0.0001	0.79
TRL	37.18	27.00	34.08	20.40	41.50	40.37	0.24	−0.72	−0.08	0.9518	<0.0001	0.58
RL	823.73	236.95	451.33	127.61	839.41	30611.63	6.48	0.27	−0.16	0.9914	0.0003	0.80
RSA	130.75	23.52	59.07	16.81	102.56	727.20	1.09	5.19	77.53	0.7730	<0.0001	0.77
RV	1.72	0.20	0.61	0.17	1.19	0.06	0.01	1.00	5.63	0.9537	<0.0001	0.73
RD_L	271.00	55.82	209.20	29.89	382.94	9345.32	3.58	0.18	−0.36	0.9910	0.0002	0.67
RD_S	24.74	5.88	20.14	5.57	34.53	78.21	0.33	0.63	0.89	0.9777	<0.0001	0.64
RD_T	247.75	66.75	148.13	14.25	350.25	10036.33	3.70	1.55	3.30	0.8832	0.000	0.47

*(†), trait descriptions were described in **Table 1**, *S.E, Standard Error.*

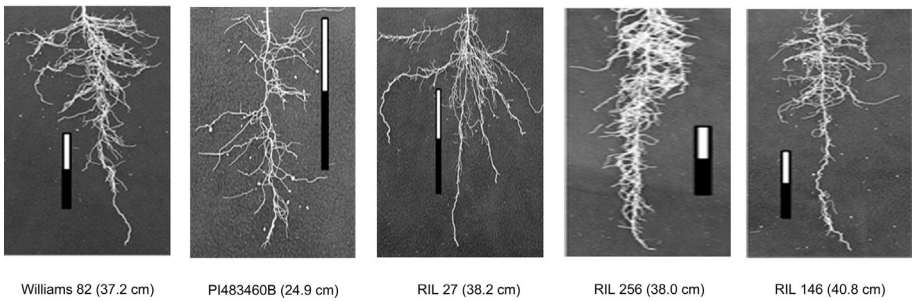


FIGURE 2 | Transgressive segregation pattern for Tap Root Length (TRL) among recombinant inbred lines of the interspecific mapping population. The TRL (in cm) phenotypic values of parental and progenies are provided within the parenthesis.

QTL for Seedling Shoot and Root Traits

For shoot-related traits, two significant QTLs for SL and PH were detected and mapped to the same regions of chromosomes (Chr.) 3 and 7 with high LOD values of 8.1 and 4.4, explaining a total percent phenotypic variation of 23.6% and 19.8% (**Table 4**). The positive allele for the SL trait on Chr. 3 was provided by the wild soybean parent, PI 438460B, whereas the cultivated soybean, Williams 82, contributed the positive allele for QTL on Chr.7. However, none of the root architectural traits was mapped in the confidence intervals of these shoot-related traits. Two QTLs for TRL were mapped on Chrs. 8 and 20, with LOD values greater than 3, explaining a phenotypic variation of 6.4% and 7.9%, respectively. Similar to the SL QTL, the wild soybean parent contributed the positive allele for PH QTL on Chr. 3. Two SNP markers, NCSB_000550 and SNP5617_Magellan, flanked QTL for RL and RD_L on Chr. 3 and explained more than 7% of phenotypic variation for both traits. Another QTL for RD_L was detected on Chr. 7 (**Figure 1**), which explained a large effect in phenotypic variation of 12.4%, with the positive allele from the wild soybean. The SNP markers, SNP02285 and SNP18129_Magellan, flank the QTL for RSA and RV with the explained phenotypic variation of about 8.9% and 9.9%, respectively, with the positive allele contributed by the wild soybean. Two QTLs for RSA were mapped on Chrs. 3 and 7, with positive allele contributed from both cultivated and wild soybeans, respectively. On Chr. 14, a QTL for RD_T was mapped within a NCSB_003319 ~ SNP21671_PI516C marker interval, explaining a phenotypic variation of 7.3% and with a positive allele from the wild soybean parent. No epistatic interaction was detected between either of the QTL on Chrs. 3 and 7 for SL, PH, TRL, and RV, or other QTL regions mapped on Chrs. 14 and 20. The traits, SL, RL, and RD_L showed inconsistency with their magnitude of additive effects, and phenotypic variation observed might be explained by the nature of gene inheritance and their interactions as explained previously with root (maximum root length) and shoot trait (hypocotyl weight) in soybean seedlings (Liang et al., 2014).

TABLE 3 | Pearson correlation coefficients among shoot and root traits evaluated in soybean mapping population.

Trait (†)	SL	PH	TRL	RL	RSA	RV	RD_L	RD_S	RD_T
SL	1	**0.89**	**–0.07**	**–0.11**	**–0.05**	**0.03**	**–0.11**	**–0.11**	**0.06**
		<.0001	*0.052*	*0.003*	*0.192*	*0.477*	*0.003*	*0.005*	*0.123*
PH		1	**–0.06**	**–0.12**	**–0.07**	**–0.01**	**–0.12**	**–0.13**	**0.08**
			0.091	*0.001*	*0.081*	*0.764*	*0.001*	*0.001*	*0.040*
TRL			1	**0.23**	**0.23**	**0.18**	**0.28**	**0.22**	**0.15**
				<.0001	*<.0001*	*<.0001*	*<.0001*	*<.0001*	*<.0001*
RL				1	**0.95**	**0.80**	**0.72**	**0.85**	**–0.08**
					<.0001	*<.0001*	*<.0001*	*<.0001*	*0.027*
RSA					1	**0.95**	**0.74**	**0.82**	**–0.05**
						<.0001	*<.0001*	*<.0001*	*0.200*
RV						1	**0.68**	**0.71**	**0.02**
							<.0001	*<.0001*	*0.558*
RD_L							1	**0.77**	**0.19**
								<.0001	*<.0001*
RD_S								1	**0.00**
									0.938
RD_T									1

*(†): trait descriptions were described in **Table 1**. The respective p-value for each trait measured are shown as italicized values.*
The + and - bold values represent the positive and negative association between traits.

TABLE 4 | Quantitative trait loci (QTL) for soybean shoot and root traits were detected with multiple-QTL method in an inter-specific mapping population.

Trait[(a)]	Chr. No[†]	Marker interval	Map position (cM)[‡]	Confidence interval (cM)[§]	LOD score[#]	R^2 (%)	Additive effect[††]	Total PVE (%)[‡‡]
SL	3	BARC_038823_07340 ~ NCSB_000710	96.6	95.5_97.2	8.1	17.1	−1.00	23.6
	7	NCSB_001434 ~ NCSB_001439	29.1	26.8_30.2	4.1	8.1	0.68	
PH	3	BARC_038823_07340 ~ NCSB_000710	96.6	95.5_97.2	4.4	9.2	−0.69	19.8
	7	NCSB_001434 ~ NCSB_001439	29.1	26.8_30.2	4.2	9.4	0.70	
TRL	8	BARC_040339_07714 ~ SNP11199_PI516C	50.8	50.5_51.8	3.0	6.4	1.09	16.2
	20	SNP06258 ~ NCSB_004833	82.6	81.8_83.6	3.6	7.9	1.23	
RL	3	NCSB_000550 ~ SNP5617_Magellan	14.4	13.0_15.4	3.4	7.5	35.84	16.2
	7	BARC_020495_04641 ~ BARC_023101_03769	56.7	55.3_57.5	4.0	9.0	−39.60	
RSA	7	SNP02285 ~ SNP18129_Magellan	48.8	46.7_50.6	3.5	8.9	−5.43	
RV	7	SNP02285 ~ SNP18129_Magellan	48.8	46.7_50.6	4.0	9.9	−0.05	
RD_L	3	NCSB_000550 ~ SNP5617_Magellan	14.4	13.0_16.4	3.7	7.9	19.14	18.7
	7	SNP02359 ~ BARC_032703_09018	44.7	44.1_45.1	5.7	12.4	−24.26	
RD_S	3	NCSB_000550 ~ SNP5617_Magellan	14.4	13.0_16.4	4.3	9.5	1.89	16.7
	7	SNP02359 ~ BARC_032703_09018	44.7	44.1_45.1	3.8	8.3	−1.75	
RD_T	14	NCSB_003319 ~ SNP21671_PI516C	138.8	137.6_139.4	3.0	7.3	−17.06	

[†]*Chromosome.*
[‡]*The QTL position was determined based on genetic linkage map constructed in the present study.*
[§]*Confidence interval for QTL location was estimated using a 2-LOD support interval value as described by van Ooijen (1992).*
[#]*LOD, logarithm of the odds.*
[††]*Positive sign indicates alleles from cv. Williams 82 and negative sign indicates alleles from PI 483460B.*
[‡‡]*PVE, phenotypic variation explained.*
[(a)]*Trait descriptions were described in* ***Table 1***.

Candidate Genes Within Shoot-Related QTL

Generally, wild soybeans are short-statured plants with smaller shoot and root systems as well as smaller leaves and seeds. However, in our study, positive alleles influencing both SL and RL were identified in PI 483460B. Moreover, this wild soybean genotype was found to contribute positive alleles on the Chr. 3 for SL QTL region flanked by BARC_038823_07340 and NCSB_000710 SNP markers, which explained a higher phenotypic variation of 17%. Another QTL for SL was identified on Chr. 7 with the positive alleles from the cultivated soybean, Williams 82 flanked by NCSB_001434 (49,59,463 Mb) - NCSB_001439 (55,22,767 Mb) harbors 65 candidate genes with expression data available for 45 genes in the SoyBase transcriptome database (http://www.soybase.org). Among these genes, four genes expressed higher (more than 50 fold) in leaf tissues with highest expression of protein of unknown function (Glyma.07g060700; 492 fold), followed by 60S ribosomal proteins (Glyma.07g060000; 71 fold and Glyma.07g059900; 61 fold), and core histone protein (Glyma.07g057300; 55 fold).

Root Trait QTLs With Positive Alleles From Wild Soybean

Four strong effective QTLs were mapped on Chr. 7 for RL, RSA, and RV, RD_L and one QTL for RD_T on Chr. 14. These QTLs were identified with the positive alleles from wild soybean accession. Despite the fact that a small root system is predominant among wild soybeans, the wild soybean accession, PI 483460B, was found to possess positive alleles. These alleles could positively affect total root system architecture, enabling us to effectively mine these QTL regions for candidate genes. These QTLs were flanked by several SNPs: RL (BARC_020495_04641; 14.9 Mb - BARC-023101-03769; 15.3 Mb), both RSA and RV QTL (SNP02285; 0.9 Mb -SNP18129; 10.1 Mb) and RD_L QTL (SNP02359; 88.5 Mb-BARC_032703_09018; 89.3 Mb). The SNPs on Chr. 14 NCSB_003319 (48.2 Mb) - SNP21671_PI516C (48.3 Mb) flank the QTL for RD_T. Based on the major QTL confidence interval flanked by SNPs, genes underlying major QTLs associated with the root phenotypes were identified.

Mining of RL QTL revealed the presence of 27 genes within the confidence interval. Four genes showed higher expression (< 100 fold change) in root tissues: Phosphofructokinase (Glyma.07g126400; 750 fold), Snf7 protein (Glyma.07g127300; 130 fold), unknown functional gene (Glyma.07g127900; 127 fold) and Leucine Rich-Repeat protein (Glyma.07g127100; 219 fold) were identified in the SoyBase transcriptome database (http://www.soybase.org). Mining of whole genome sequence information of parental line PI483460B (Zhou et al., 2015; Patil et al., 2018) within RL QTL interval revealed the wild soybean to have a nonsynonymous SNP in Snf7 protein (Glyma07.G127000) that alters the amino acid from Glutamic acid to Lysine. This gene does not show expression in any of the tissues. However, it has a role in DNA methylation, which is known to alter other gene expression levels (Schmitz et al., 2013). Further, genome mining of the RL QTL region across 106 diverse (landraces and elite) lines sequenced at 17× depth with 10 million SNPs (Valliyodan et al., 2016) revealed two highly expressed genes in root tissues, Phosphofructokinase (Glyma.07g126400) and Leucine Rich-Repeat protein (Glyma.07g127100), harbor non-Synonymous SNP variation that alters amino acid content (**Table 5**). The KASP (competitive allele-specific PCR) assays to genotype these variations are detailed in **Table 5**.

TABLE 5 | Details on genes underlying root length (RL) genomic region with non-synonymous SNP variation and KASP assay to genotype sequence level variation.

Gene ID	SNP Position (Mb)	Reference/ Alternate allele	Amino acid change	KASP marker assay designed†
Glyma.07g126400	15079572	T/A	Aspartic to valine	ATGTCAATTTTAATTGGTTATTTATGAATTGATTTTTAAGTAATTAGGGA **[A/T]** GGTTTGATGGTACTTCTTCATTAAGGTGGTGCTGCATCTCCATTGCTAA
Glyma.07g126400	15079581	A/G	Isoleucine to threonine	TTTAATTGGTTATTTATGAATTGATTTTTAAGTAATTAGGGATGGGTTTG **[A/G]**TGGTACTTCTTCATTAAGGTGGTGCTGCATCTCCATTGCTAAGTATGGAC
Glyma.07g126400	15079825	T/G	Threonine to proline	TCTACCTACCTTAATTTACCCGTCATTTATTTCCATTTTGTTCTGACTTA **[T/G]**GACAGGTCGTTGTTCACAAAGATGGTGCAAGAGGGGTACATTTTAGGCGT
Glyma.07g126400	15079828	G/A	Proline to leucine	CTACCTTAATTTACCCGTCATTTATTTCCATTTTGTTCTGACTTATGACA **[G/A]**GTCGTTGTTCACAAAGATGGTGCAAGAGGGGTACATTTTAGGCGTGCCGG
Glyma.07g127100	15225989	G/C	Isoleucine to methionine	AAGTTGACAATTGACCCATTGTTTTGTTTTCCGACCCTGTTGCCAAGAAA **[G/C]**TATCTTTGGACAATATGCATAGCCATAGCCACCGATATGAAACATCATCA
Glyma.07g127100	15228832	C/T	Glutamic acid to lysine	CACGTTGAGGTATGCCCTGATATAATAGACCTAAAGATGTTTATTTCAAG **[C/T]**CACGTTGAGGTATGCCCTGATATAATAGACCTAAAGATGTTTATTTCAAG
Glyma.07g127100	15230096	G/A	Alanine to valine	AGATGTCTCATGTTTGCAGATGGAAATTCACATTGCTTGAGTTGGAAAAG **[G/A]**AGAATACAGATAGCAATCGATGCTGCAGAGGGTCAGTATAACTTCATTTT
Glyma.07g127100	15230407	A/T	Asparagine to lysine	TACTCAAAAATTTTATGGATTGTTTAAACCAGTCTAAGGGCATGTTTTAT **[A/T]**TTTTTCAACCATGATTATGTTACCATGACTAATAACTTGTTGCCCTGTAA
Glyma.07g127100	15230658	G/T	Leucine to isoleucine	GAAGACTTAGAAGCCAAGATAGCAGATTTTGGCCTCTCCAGGGAGTTTAG **[G/T]**ACAGATAACCAAGATCAACAATCTCAAGTGATTCACAGTGATGCTACAAA

†*The non-synonymous SNP allele variation between Williams 82 and PI483460B is shown as bold letter within parenthesis and 50-bp sequence on either side of the SNP variation is provided to facilitate the design of KASP marker assay.*

Array-based transcriptome of diverse soybean genotypes from 31 gene expressions experiments on 28 anatomical tissues revealed that the four genes mentioned above show higher expression in root tissues (**Figure 3**) compared to non-root tissues. The co-location of root QTL for RSA and RV on the same region of Chr. 7 suggests the possibility to improve both traits by identifying key genes underlying the QTL. In comparison to the QTL region on Chr. 7, the QTL confidence interval on Chr. 14 was smaller and observed to possess only 15 genes, of which lysine decarboxylase (Glyma.14g218100; 39 fold)

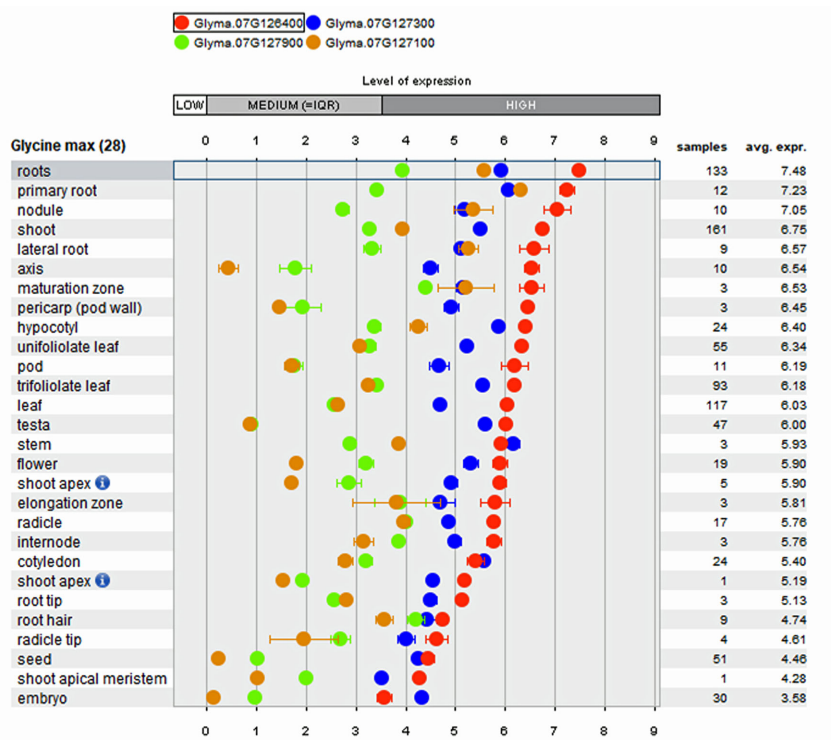


FIGURE 3 | Tissue specific expression pattern of genes within major Root Length (RL) QTL derived from public Affymetrix and RNA-transcriptome experiments integrated into the Genevestigator software.

has been reported as expressed specifically higher in root tissues. The biological role of these genes in regulating the roots, main tap, and finer roots warrants further investigation.

DISCUSSION

Phenotypic Variation for Shoot and Root Traits

Two parental lines and RILs of the mapping population showed a wide range of phenotypic variation for the shoot and root traits measured along with higher heritability. Cultivar Williams 82 possesses a better developed, robust root system compared to the wild soybean parental line, PI483460B. The recombination of chromosomal regions in the progenies of William 82 and PI 483460B showed higher phenotypic value that exceeded the better parent, William 82 (**Figure 2**). A similar effect was observed in lines of inter-specific mapping populations for root traits, which enabled the identification of novel alleles to improve root system architecture (Manavalan et al., 2015; Prince et al., 2015).

Field-based selection of root traits, root angle, and fibrous root score are proven to contribute to yield protection under stress in soybeans (Fenta et al., 2011; Prince et al., 2016; Prince et al., 2019). The seedlings traits, like total root length, root surface area, lateral root number, were reported to improve root angle and fibrous root score (Prince et al., 2016), which impacted soybean yield under water limitation. In spite of narrow genetic base, intra-specific soybean mapping populations were used to map root QTLs in soybean (Rong et al., 2011; Brensha et al., 2012; Liang et al., 2014). Recent inter-specific mapping studies identified large effect root QTL with positive alleles from wild/semi-wild soybeans (Liang et al., 2014; Manavalan et al., 2015; Prince et al., 2015). Recently, the soybean cultivar USDA-N7004 was successfully developed with 25% exotic germplasm from the Japanese cultivar Tamahikari (PI 423897) and had improved seed protein and yield on par with check cultivars (McNeece et al., 2020). McCouch et al., 2007 reviewed the use of wild rice, *Oryza rufipogan*, as donors of yield-enhancing alleles to enhance the performance of elite *O. sativa* cultivars.

In this study, we identified nine unique genomic regions significantly associated with shoot and root traits involving two (Chr. 3 and 7) and five chromosomal regions (Chr.3, 7, 8, 14, and 20), respectively. Most of the root-related QTLs with large effects, the positive alleles were contributed by a wild soybean accession, PI 438460B, with a range of phenotypic variation explained from 7.3% to 12.4% for finer root QTL. Interestingly, the TRL QTL on chromosome 8 mapped in this study with a positive allele from Williams 82 collocates with shoot and root weight (fresh and dry) QTLs reported in an intra-specific soybean population (Brensha et al., 2012). This region also collocates with leaf morphology (Kim et al., 2005), internode length (Alcivar et al., 2007), plant height (Lee et al., 1996), and pod number (Zhang et al., 2010) in soybean. The QTL RD_S associated with finer roots collocates with plant height (Guzman et al., 2007), leaf morphology (Orf et al., 1999), and seed yield QTL in soybean (Du et al., 2009).

The root traits of this study showed higher broad-sense heritability, indicating that the major contribution of the phenotypic variation observed was due to largely due to genetic effects. The lines exhibited an especially large phenotypic variation for RL with heritability of 0.8. In soybean, total root length is positively correlated with photosynthetic efficiency at vegetative growth stages and to lateral and fibrous rooting ability as well as canopy temperature during the reproductive growth stage under water-limited conditions in clay soil (Prince et al., 2016). This root trait has been correlated to rooting angle in multiple crop species (Kato et al., 2006; Singh et al., 2011; Kashiwagi et al., 2015) and ultimately cuts down the carbon resources required for the plant to acquire resources in deeper soil horizons in areas with limited rainfall (Wasson et al., 2012).

On chromosome 7, a QTL associated with RSA and RV was identified with a positive allele from wild soybean that explains a higher phenotypic variation. Similar root traits with a positive allele contribution by an inferior parental line in soybean have been reported (Liang et al., 2014; Prince et al., 2015). Rare alleles from wild soybean germplasm (Hajjar and Hodgkin, 2007) have been employed to improve various agronomic traits, like domestication-related traits (Liu et al., 2007), stress tolerance (Carter et al., 2004; Chen et al., 2006; Tuyen et al., 2010), seed compositional traits (Kanamaru et al., 2006), and seed yield (Concibido et al., 2003; Li et al., 2008).

Based on the results obtained, SNPs associated with total root length (RL) on chromosomes 3 (NCSB_000550 ~ SNP5617_Magellan) and 7 (BARC_020495_04641 ~ BARC_023101_03769) and root surface area (RSA) on chromosome 7 (SNP02285 ~ SNP18129_Magellan) are candidates for KASP marker development for use in soybean breeding. Soybean seedling root traits, such as RL and RV are highly associated with stress tolerant (drought and aluminum stress) indices (Liu et al., 2005; Yang et al., 2005; Liu et al., 2007). RL influences the deep rooting ability of soybean, which ultimately improves drought tolerance and is positively associated with yield under drought (Hudak and Patterson, 1995) and rice (Bengough et al., 2011; Suji et al., 2012). Soybean genotypes with deep rooting ability (Taylor et al., 1978; Cortes and Sinclair, 1986) and more fibrous roots (Myers et al., 2007) are supposed to offer effective acquisition of water resources. Root-related traits, such as RL and RSA, facilitate foraging and phosphorus accumulation (Liang et al., 2014) and improve shoot growth (Bates and Lynch, 2001).

Candidate Genes Underlying QTL

Mining genes that underlie promising QTL with strong effects enable the plant research community to fine-map genes and to identify causal genes responsible for modulating a trait of interest (Pradeepa et al., 2012). Further development in sequencing technologies enables researchers to look for allelic variants among causal genes and to develop functional DNA markers for use in marker-assisted selection (MAS) processes. Similar variants were observed for root traits, such as meristem and cell length in *Arabidopsis* (Meijón et al., 2014), lateral roots in rice (Lyu et al., 2013), soybean (Prince et al., 2019), and root angle in

rice (Uga et al., 2013). Most QTL mapping studies in soybean reveal that root traits are polygenic in nature (Liang et al., 2014) and interactions among them (Prince et al., 2015). In this study, we used an inter-specific mapping population in combination with whole-genome transcriptome and Affymetrix gene expression data to identify genes associated with key root traits and to investigate their difference in tissue-specific expression. The Leucine Rich-Repeat class of proteins within RL QTL was found to have large effect on other root traits, like lateral root number and root volume in soybean, on chromosome 7 (Prince et al., 2019). Two SNF proteins identified within this QTL interval with no (Glyma07.G127000) and 130-fold (Glyma.07g127300) expression in root tissues need more detailed analysis to elucidate their roles in root growth and development. In this study, the function of Glyma.07g060700, a gene with unknown function underlying SL QTL on Chr.7, showed a higher level of expression and its interaction with the other genes, Glyma.07g057300, Glyma.07g057200, and Glyma.07g059800 needs to be elucidated to understand the plant stature difference between wild and cultivated soybean species. Further studies on genes underlying the root trait QTLs, RSA, and RL, would enhance the understanding of root growth and development in soybean. The novel wild alleles for these traits could help us to improve root system architecture in cultivated soybean.

CONCLUSIONS

In the present study, we detected and genetically mapped strong effect QTLs for SL and several root-related traits, e.g., root volume and finer root distribution, using an inter-specific mapping population. The QTL region on Chr. 7 governs both RSA and RV with the positive alleles from a wild soybean accession, PI 483460B. These QTL could be potential targets for introgression into cultivated soybean genetic background to improve the root system. Characterizing candidate genes underlying the SL and root traits will enhance understanding of the molecular mechanisms involved in root and shoot growth maintenance. The novel alleles inherited from the wild soybean accession could be potentially used to improve RSA trait in elite, high yielding soybean lines.

DATA AVAILABILITY STATEMENT

All datasets generated for this study are included in the article/ **Supplementary Material**.

AUTHOR CONTRIBUTIONS

SP conceived and designed the experiment; phenotypic data generation conducted statistical and QTL mapping analysis; and drafted, wrote, and revised the manuscript. TV performed QTL mapping analysis and edited the manuscript. XW selected a SNP panel and constructed a genetic map. YB, FL, and SK conducted bioinformatics analysis of SNP sequences; designed SNP assays for Infinium beadchips; and performed genotyping analysis. BV, JS, and HN edited the manuscript and provided valuable suggestions.

ACKNOWLEDGMENTS

This research was supported by the Missouri Soybean Merchandizing Council (project 220), and the National Center for Soybean Biotechnology (USDA-CSREES Award No. 2008-34555-19305). The authors would like to thank Mrs. Theresa Musket for coordinating professional English editing and Dr. Heng Ye for making suggestions on the manuscript.

SUPPLEMENTARY MATERIAL

The Supplementary Material for this article can be found online at: https://www.frontiersin.org/articles/10.3389/fpls.2020.01284/full#supplementary-material

REFERENCES

Abdel-Haleem, H., Lee, G.-J., and Boerma, R. H. (2011). Identification of QTL for increased fibrous roots in soybean. *Theor. Appl. Genet.* 122, 935–946. doi: 10.1007/s00122-010-1500-9

Adhikari, S., Damodaran, S., and Subramanian, S. (2019). Lateral Root and Nodule Transcriptomes of Soybean. *Data* 4, 64. doi: 10.3390/data4020064

Aghamirzaie, D., Batra, D., Heath, L. S., Schneider, A., Grene, R., and Collakova, E. (2015). Transcriptome-wide functional characterization reveals novel relationships among differentially expressed transcripts in developing soybean embryos. *BMC Genomics* 16, 928. doi: 10.1186/s12864-015-2108-x

Alcivar, A., Jacobson, J., Rainho, J., Meksem, K., Lightfoot, D., and Kassem, M. (2007). Genetic analysis of soybean plant height, hypocotyl and internode lengths. *J. Agric. Food Environ. Sci.* 1, 1–20.

Alpert, K., Grandillo, S., and Tanksley, S. (1995). fw 2.2: a major QTL controlling fruit weight is common to both red-and green-fruited tomato species. *Theor. Appl. Genet.* 91, 994–1000. doi: 10.1007/BF00223911

Bates, T. R., and Lynch, J. P. (2001). Root hairs confer a competitive advantage under low phosphorus availability. *Plant Soil* 236, 243–250. doi: 10.1023/A:1012791706800

Bellieny-Rabelo, D., De Oliveira, E., Da Silva Ribeiro, E., Costa, E. P., Oliveira, A. E. A., and Venancio, T. M. (2016). Transcriptome analysis uncovers key regulatory and metabolic aspects of soybean embryonic axes during germination. *Sci. Rep.* 6, 36009. doi: 10.1038/srep36009

Bengough, A. G., Mckenzie, B., Hallett, P., and Valentine, T. (2011). Root elongation, water stress, and mechanical impedance: a review of limiting stresses and beneficial root tip traits. *J. Exp. Bot.* 62, 59–68. doi: 10.1093/jxb/erq350

Bernard, R., and Cremeens, C. (1988). Registration of 'Williams 82'soybean. *Crop Sci.* 28, 1027–1028. doi: 10.2135/cropsci1988.0011183X002800060049x

Blouin, M., Barot, S., and Roumet, C. (2007). A quick method to determine root biomass distribution in diameter classes. *Plant Soil* 290, 371–381. doi: 10.1007/s11104-006-9169-1

Boyer, J., and Westgate, M. (2004). Grain yields with limited water. *J. Exp. Bot.* 55, 2385–2394. doi: 10.1093/jxb/erh219

Brensha, W. B., Kantartzi, S. K., Meksem, K., Grier, I., Robert, L., Barakat, A., et al. (2012). Genetic analysis of root and shoot traits in the 'Essex'by 'Forrest'recombinant inbred line (RIL) population of soybean [Glycine max (L.) Merr.]. *J. Plant Genome Sci.* 1, 1–9. doi: 10.5147/jpgs.2012.0051

Brown, A. V., and Hudson, K. A. (2015). Developmental profiling of gene expression in soybean trifoliate leaves and cotyledons. *BMC Plant Biol.* 15, 169. doi: 10.1186/s12870-015-0553-y

Carter, T. E., Nelson, R. L., Sneller, C. H., and Cui, Z. (2004). "Genetic diversity in soybean. Soybeans: Improvement, production, and uses", in *Agronomy Monographs*. 303–416. doi: 10.2134/agronmonogr16.3ed.c8

Chen, Y., Chen, P., and De Los Reyes, B. G. (2006). Differential responses of the cultivated and wild species of soybean to dehydration stress. *Crop Sci.* 46, 2041–2046. doi: 10.2135/cropsci2005.12.0466

Cho, Y. B., Jones, S. I., and Vodkin, L. O. (2017). Mutations in Argonaute5 illuminate epistatic interactions of the K1 and I loci leading to saddle seed color patterns in Glycine max. *Plant Cell* 29, 708–725. doi: 10.1105/tpc.17.00162

Churchill, G. A., and Doerge, R. W. (1994). Empirical threshold values for quantitative trait mapping. *Genetics* 138, 963–971.

Concibido, V., La Vallee, B., Mclaird, P., Pineda, N., Meyer, J., Hummel, L., et al. (2003). Introgression of a quantitative trait locus for yield from Glycine soja into commercial soybean cultivars. *Theor. Appl. Genet.* 106, 575–582. doi: 10.1007/s00122-002-1071-5

Cortes, P., and Sinclair, T. (1986). Water Relations of Field-Grown Soybean under Drought 1. *Crop Sci.* 26, 993–998. doi: 10.2135/cropsci1986.0011183X002600050031x

Coudert, Y., Périn, C., Courtois, B., Khong, N. G., and Gantet, P. (2010). Genetic control of root development in rice, the model cereal. *Trends Plant Sci.* 15, 219–226. doi: 10.1016/j.tplants.2010.01.008

Dastmalchi, M., Chapman, P., Yu, J., Austin, R. S., and Dhaubhadel, S. (2017). Transcriptomic evidence for the control of soybean root isoflavonoid content by regulation of overlapping phenylpropanoid pathways. *BMC Genomics* 18, 70. doi: 10.1186/s12864-016-3463-y

Devi, M. J., Sinclair, T. R., and Taliercio, E. (2015). Comparisons of the effects of elevated vapor pressure deficit on gene expression in leaves among two fast-wilting and a slow-wilting soybean. *PLoS One* 10, e0139134. doi: 10.1371/journal.pone.0139134

Du, W., Wang, M., Fu, S., and Yu, D. (2009). Mapping QTLs for seed yield and drought susceptibility index in soybean (Glycine max L.) across different environments. *J. Genet. Genomics* 36, 721–731. doi: 10.1016/S1673-8527(08)60165-4

Fenta, B. A., Schluter, U., Garcia, B. M., Duplessis, M., Foyer, C. H., and Kunert, K. J. (2011). Identification and application of phenotypic and molecular markers for abiotic stress tolerance in soybean. *Soybean—Genetics and Novel Techniques for Yield Enhancement*. (nTechOpen), pp. 181–200.

Frary, A., Nesbitt, T. C., Frary, A., Grandillo, S., Van Der Knaap, E., Cong, B., et al. (2000). fw2. 2: a quantitative trait locus key to the evolution of tomato fruit size. *Science* 289, 85–88. doi: 10.1126/science.289.5476.85

Gong, W., Qi, P., Du, J., Sun, X., Wu, X., Song, C., et al. (2014). Transcriptome analysis of shade-induced inhibition on leaf size in relay intercropped soybean. *PLoS One* 9, e98465. doi: 10.1371/journal.pone.0098465

Guo, S.-B., Yu, W., Li, X.-Q., Liu, K.-Q., Huang, F.-K., Chen, C.-H., et al. (2013). Development and identification of introgression lines from cross of Oryza sativa and Oryza minuta. *Rice Sci.* 20, 95–102. doi: 10.1016/S1672-6308(13)60111-0

Guzman, P. S., Diers, B., Neece, D., St Martin, S., Leroy, A., Grau, C., et al. (2007). QTL associated with yield in three backcross-derived populations of soybean. *Crop Sci.* 47, 111–122. doi: 10.2135/cropsci2006.01.0003

Hajjar, R., and Hodgkin, T. (2007). The use of wild relatives in crop improvement: a survey of developments over the last 20 years. *Euphytica* 156, 1–13. doi: 10.1007/s10681-007-9363-0

Huang, L., and Schiefelbein, J. (2015). Conserved gene expression programs in developing roots from diverse plants. *Plant Cell* 27, 2119–2132. doi: 10.1105/tpc.15.00328

Huang, L., Shi, X., Wang, W., Ryu, K. H., and Schiefelbein, J. (2017). Diversification of root hair development genes in vascular plants. *Plant Physiol.* 174, 1697–1712. doi: 10.1104/pp.17.00374

Hudak, C., and Patterson, R. (1995). Vegetative growth analysis of a drought-resistant soybean plant introduction. *Crop Sci.* 35, 464–471. doi: 10.2135/cropsci1995.0011183X003500020031x

Hufstetler, E. V., Boerma, H. R., Carter, T. E., and Earl, H. J. (2007). Genotypic variation for three physiological traits affecting drought tolerance in soybean. *Crop Sci.* 47, 25–35. doi: 10.2135/cropsci2006.04.0243

Hyten, D. L., Song, Q., Zhu, Y., Choi, I.-Y., Nelson, R. L., Costa, J. M., et al. (2006). Impacts of genetic bottlenecks on soybean genome diversity. *Proc. Natl. Acad. Sci.* 103, 16666–16671. doi: 10.1073/pnas.0604379103

Ithal, N., Recknor, J., Nettleton, D., Maier, T., Baum, T. J., and Mitchum, M. G. (2007). Developmental transcript profiling of cyst nematode feeding cells in soybean roots. *Mol. Plant-Microbe Interact.* 20, 510–525. doi: 10.1094/MPMI-20-5-0510

Jones, S. I., Tan, Y., Shamimuzzaman, M., George, S., Cunningham, B. T., and Vodkin, L. (2015). Direct detection of transcription factors in cotyledons during seedling development using sensitive silicon-substrate photonic crystal protein arrays. *Plant Physiol.* 167, 639–649. doi: 10.1104/pp.114.253666

Joshi, T., Valliyodan, B., Wu, J., Lee, S., Xu, D., and Nguyen, H. T. (2013). Genomic differences between cultivated soybean, G. max and its wild relative G. soja. *BMC Genomics* 14, S5.

Kanamaru, K., Wang, S., Abe, J., Yamada, T., and Kitamura, K. (2006). Identification and characterization of wild soybean (Glycine soja Sieb. et Zecc.) strains with high lutein content. *Breed. Sci.* 56, 231–234. doi: 10.1270/jsbbs.56.231

Kashiwagi, J., Krishnamurthy, L., Purushothaman, R., Upadhyaya, H., Gaur, P., Gowda, C., et al. (2015). Scope for improvement of yield under drought through the root traits in chickpea (Cicer arietinum L.). *Field Crops Res.* 170, 47–54. doi: 10.1016/j.fcr.2014.10.003

Kato, Y., Abe, J., Kamoshita, A., and Yamagishi, J. (2006). Genotypic variation in root growth angle in rice (Oryza sativa L.) and its association with deep root development in upland fields with different water regimes. *Plant Soil* 287, 117–129. doi: 10.1007/s11104-006-9008-4

Kim, H., Kang, S., and Suh, D. (2005). Analysis of quantitative trait loci associated with leaflet types in two recombinant inbred lines of soybean. *Plant Breed.* 124, 582–589. doi: 10.1111/j.1439-0523.2005.01152.x

Kim, K. S., Diers, B. W., Hyten, D. L., Roufmian, M. A., Shannon, J. G., and Nelson, R. L. (2012). Identification of positive yield QTL alleles from exotic soybean germplasm in two backcross populations. *Theor. Appl. Genet.* 125, 1353–1369.

Kour, A., Boone, A. M., and Vodkin, L. O. (2014). RNA-Seq profiling of a defective seed coat mutation in Glycine max reveals differential expression of proline-rich and other cell wall protein transcripts. *PLoS One* 9, e96342. doi: 10.1371/journal.pone.0096342

Lambirth, K. C., Whaley, A. M., Blakley, I. C., Schlueter, J. A., Bost, K. L., Loraine, A. E., et al. (2015). A comparison of transgenic and wild type soybean seeds: analysis of transcriptome profiles using RNA-Seq. *BMC Biotechnol.* 15, 89. doi: 10.1186/s12896-015-0207-z

Lanubile, A., Muppirala, U. K., Severin, A. J., Marocco, A., and Munkvold, G. P. (2015). Transcriptome profiling of soybean (Glycine max) roots challenged with pathogenic and non-pathogenic isolates of Fusarium oxysporum. *BMC Genomics* 16, 1089. doi: 10.1186/s12864-015-2318-2

Lee, S., Bailey, M., Mian, M., Carter, T., Ashley, D., Hussey, R., et al. (1996). Molecular markers associated with soybean plant height, lodging, and maturity across locations. *Crop Sci.* 36, 728–735. doi: 10.2135/cropsci1996.0011183X003600030035x

Lee, J.-D., Yu, J.-K., Hwang, Y.-H., Blake, S., So, Y.-S., Lee, G.-J., et al. (2008). Genetic diversity of wild soybean (Glycine soja Sieb. and Zucc.) accessions from South Korea and other countries. *Crop Sci.* 48, 606–616. doi: 10.2135/cropsci2007.05.0257

Leisner, C. P., Ming, R., and Ainsworth, E. A. (2014). Distinct transcriptional profiles of ozone stress in soybean (Glycine max) flowers and pods. *BMC Plant Biol.* 14, 335. doi: 10.1186/s12870-014-0335-y

Li, D., Pfeiffer, T., and Cornelius, P. (2008). Soybean QTL for yield and yield components associated with Glycine soja alleles. *Crop Sci.* 48, 571–581. doi: 10.2135/cropsci2007.06.0361

Li, M., Cao, L., Mwimba, M., Zhou, Y., Li, L., Zhou, M., et al. (2019). Comprehensive mapping of abiotic stress inputs into the soybean circadian clock. *Proc. Natl. Acad. Sci.* 116, 23840–23849. doi: 10.1073/pnas.1708508116

Liang, H., Yu, Y., Yang, H., Xu, L., Dong, W., Du, H., et al. (2014). Inheritance and QTL mapping of related root traits in soybean at the seedling stage. *Theor. Appl. Genet.* 127, 2127–2137. doi: 10.1007/s00122-014-2366-z

Libault, M., Farmer, A., Joshi, T., Takahashi, K., Langley, R. J., Franklin, L. D., et al. (2010). An integrated transcriptome atlas of the crop model Glycine max, and its use in comparative analyses in plants. *Plant J.* 63, 86–99. doi: 10.1111/j.1365-313X.2010.04222.x

Lin, F., Zhao, M., Baumann, D. D., Ping, J., Sun, L., Liu, Y., et al. (2014). Molecular response to the pathogen Phytophthora sojae among ten soybean near isogenic lines revealed by comparative transcriptomics. *BMC Genomics* 15, 18. doi: 10.1186/1471-2164-15-18

Liu, Y., Gai, J., and Lu, H. (2005). Identification of rhizosphere abiotic stress tolerance and related root traits in soybean [Glycine max(L.) Merr.]. *Zuo wu xue bao* 31, 1132–1137.

Liu, B., Fujita, T., Yan, Z.-H., Sakamoto, S., Xu, D., and Abe, J. (2007). QTL mapping of domestication-related traits in soybean (Glycine max). *Ann. Bot.* 100, 1027–1038. doi: 10.1093/aob/mcm149

Liu, A., Xiao, Z., Li, M. W., Wong, F. L., Yung, W. S., Ku, Y. S., et al. (2019). Transcriptomic reprogramming in soybean seedlings under salt stress. *Plant Cell Environ.* 42, 98–114. doi: 10.1111/pce.13186

Lyu, J., Zhang, S., Dong, Y., He, W., Zhang, J., Deng, X., et al. (2013). Analysis of elite variety tag SNPs reveals an important allele in upland rice. *Nat. Commun.* 4, 2138. doi: 10.1038/ncomms3138

Mammadov, J., Buyyarapu, R., Guttikonda, S. K., Parliament, K., Abdurakhmonov, I., and Kumpatla, S. P. (2018). Wild relatives of maize, rice, cotton, and soybean: treasure troves for tolerance to biotic and abiotic stresses. *Front. Plant Sci.* 9:886. doi: 10.3389/fpls.2018.00886

Manavalan, L. P., Prince, S. J., Musket, T. A., Chaky, J., Deshmukh, R., Vuong, T. D., et al. (2015). Identification of novel QTL governing root architectural traits in an interspecific soybean population. *PLoS One* 10, e0120490. doi: 10.1371/journal.pone.0120490

McCouch, S. R., Sweeney, M., Li, J., Jiang, H., Thomson, M., Septiningsih, E., et al. (2007). Through the genetic bottleneck: O. rufipogon as a source of trait-enhancing alleles for O. sativa. *Euphytica* 154, 317–339. doi: 10.1007/s10681-006-9210-8

McNeece, B. T., Bagherzadi, L., Carter, T. E.Jr., and Mian, M. (2020). Registration of USDA-N7004 soybean germplasm with good yield, elevated seed protein, and 25% exotic pedigree from Tamahikari. *J. Plant Regist.*, 1–6. doi: 10.1002/plr2.20039

Meijón, M., Satbhai, S. B., Tsuchimatsu, T., and Busch, W. (2014). Genome-wide association study using cellular traits identifies a new regulator of root development in Arabidopsis. *Nat. Genet.* 46, 77–81. doi: 10.1038/ng.2824

Myers, D. B., Kitchen, N. R., Sudduth, K. A., Sharp, R. E., and Miles, R. J. (2007). Soybean root distribution related to claypan soil properties and apparent soil electrical conductivity. *Crop Sci.* 47, 1498–1509. doi: 10.2135/cropsci2006.07.0460

Neupane, S., Mathew, F. M., Varenhorst, A. J., and Nepal, M. P. (2019). Transcriptome profiling of interaction effects of soybean cyst nematodes and soybean aphids on soybean. *Sci. Data* 6, 1–8. doi: 10.1038/s41597-019-0140-4

Nguyen, H. T., Babu, R. C., and Blum, A. (1997). Breeding for drought resistance in rice: physiology and molecular genetics considerations. *Crop Sci.* 37, 1426–1434. doi: 10.2135/cropsci1997.0011183X003700050002x

Nyquist, W. E., and Baker, R. (1991). Estimation of heritability and prediction of selection response in plant populations. *Crit. Rev. Plant Sci.* 10, 235–322. doi: 10.1080/07352689109382313

Okamoto, S., Suzuki, T., Kawaguchi, M., Higashiyama, T., and Matsubayashi, Y. (2015). A comprehensive strategy for identifying long-distance mobile peptides in xylem sap. *Plant J.* 84, 611–620. doi: 10.1111/tpj.13015

Orf, J., Chase, K., Jarvik, T., Mansur, L., Cregan, P., Adler, F., et al. (1999). Genetics of soybean agronomic traits: I. Comparison of three related recombinant inbred populations. *Crop Sci.* 39, 1642–1651. doi: 10.2135/cropsci1999.3961642x

Pantalone, V., Rebetzke, G., Burton, J., and Carter, T. (1996). Phenotypic evaluation of root traits in soybean and applicability to plant breeding. *Crop Sci.* 36, 456–459. doi: 10.2135/cropsci1996.0011183X003600020039x

Patil, G., Vuong, T. D., Kale, S., Valliyodan, B., Deshmukh, R., Zhu, C., et al. (2018). Dissecting genomic hotspots underlying seed protein, oil, and sucrose content in an interspecific mapping population of soybean using high-density linkage mapping. *Plant Biotechnol. J.* 16 (11), 1939–1953. doi: 10.1111/pbi.12929

Placido, D. F., Campbell, M., Jin, J., Cui, X., Kruger, G. R., Baenziger, P. S., et al. (2013). Introgression of novel traits from a wild wheat relative improves drought adaptation in wheat (*Triticum aestivum*). *Plant Physiol.* 161, 1806–1819. doi: 10.1104/pp.113.214262

Pradeepa, N., Priya, P. S., Prince, K. S. J., Kavitha, S., Poornima, R., Prabhakar, M. S., et al. (2012). In Silico analysis of a consensus QTL for drought resistance in rice. *Online J. Bioinf.* 13, 1–13.

Prince, S. J., Mutava, R. N., Pegoraro, C., De Oliveira, A. C., and Nguyen, H. T. (2013). Root characters. *Genomics and Breeding for Climate-Resilient Crops* (Springer), 67–131. doi: 10.1007/978-3-642-37048-9

Prince, S. J., Song, L., Qiu, D., Dos Santos, J. V. M., Chai, C., Joshi, T., et al. (2015). Genetic variants in root architecture-related genes in a Glycine soja accession, a potential resource to improve cultivated soybean. *BMC Genomics* 16, 132. doi: 10.1186/s12864-015-1334-6

Prince, S. J., Murphy, M., Mutava, R. N., Zhang, Z., Nguyen, N., Kim, Y. H., et al. (2016). Evaluation of high yielding soybean germplasm under water limitation. *J. Integr. Plant Biol.* 58, 475–491. doi: 10.1111/jipb.12378

Prince, S. J., Murphy, M., Mutava, R. N., Durnell, L. A., Valliyodan, B., Shannon, J. G., et al. (2017). Root xylem plasticity to improve water use and yield in water-stressed soybean. *J. Exp. Bot.* 68, 2027–2036. doi: 10.1093/jxb/erw472

Prince, S., Das, K., Tushar, N., Murphy, M., Valliyodan, B., Desouza, G. N., et al. (2018). Prediction of Soybean Root Response in the Field Using Nondestructive Seedling Three-Dimensional Root Features. *Plant Phenome J.* 1, 1–15. doi: 10.2135/tppj2018.04.0003

Prince, S. J., Valliyodan, B., Ye, H., Yang, M., Tai, S., Hu, W., et al. (2019). Understanding genetic control of root system architecture in soybean: Insights into the genetic basis of lateral root number. *Plant Cell Environ.* 42, 212–229. doi: 10.1111/pce.13333

Rong, Z., Hai-Feng, C., Xian-Zhi, W., Bao-Duo, W., Shui-Lian, C., Zhang, X.-J., et al. (2011). Analysis of QTLs for root traits at seedling stage in soybean. *Acta Agronom. Sin.* 37, 1151–1158. doi: 10.1016/S1875-2780(11)60032-1

Schmitz, R. J., He, Y., Valdés-López, O., Khan, S. M., Joshi, T., Urich, M. A., et al. (2013). Epigenome-wide inheritance of cytosine methylation variants in a recombinant inbred population. *Genome Res.* 23, 1663–1674. doi: 10.1101/gr.152538.112

Schmutz, J., Cannon, S. B., Schlueter, J., Ma, J., Mitros, T., Nelson, W., et al. (2010). Genome sequence of the palaeopolyploid soybean. *Nature* 463, 178. doi: 10.1038/nature08670

Severin, A. J., Woody, J. L., Bolon, Y.-T., Joseph, B., Diers, B. W., Farmer, A. D., et al. (2010). RNA-Seq Atlas of Glycine max: a guide to the soybean transcriptome. *BMC Plant Biol.* 10, 160. doi: 10.1186/1471-2229-10-160

Shen, Y., Zhou, Z., Wang, Z., Li, W., Fang, C., Wu, M., et al. (2014). Global dissection of alternative splicing in paleopolyploid soybean. *Plant Cell* 26, 996–1008. doi: 10.1105/tpc.114.122739

Shin, J. H., Vaughn, J. N., Abdel-Haleem, H., Chavarro, C., Abernathy, B., Do Kim, K., et al. (2015). Transcriptomic changes due to water deficit define a general soybean response and accession-specific pathways for drought avoidance. *BMC Plant Biol.* 15, 26. doi: 10.1186/s12870-015-0422-8

Singh, V., Van Oosterom, E. J., Jordan, D. R., Hunt, C. H., and Hammer, G. L. (2011). Genetic variability and control of nodal root angle in sorghum. *Crop Sci.* 51, 2011–2020. doi: 10.2135/cropsci2011.01.0038

Song, B., An, L., Han, Y., Gao, H., Ren, H., Zhao, X., et al. (2016). Transcriptome profile of near-isogenic soybean lines for β-conglycinin α-subunit deficiency during seed maturation. *PLoS One* 11, e0159723. doi: 10.1371/journal.pone.0159723

Sponchiado, B., White, J., Castillo, J., and Jones, P. (1989). Root growth of four common bean cultivars in relation to drought tolerance in environments with contrasting soil types. *Exp. Agric.* 25, 249–257. doi: 10.1017/S0014479700016756

Steele, K. A., Price, A. H., Shashidhar, H. E., and Witcombe, J. R. (2006). Marker-assisted selection to introgress rice QTLs controlling root traits and aroma into an Indian upland rice variety. *Theor. Appl. Genet.* 112, 208–221.

Suji, K., Prince, K. S. J., Mankhar, P. S., Kanagaraj, P., Poornima, R., Amutha, K., et al. (2012). Evaluation of rice (Oryza sativa L.) near iso-genic lines with root QTLs for plant production and root traits in rainfed target populations of environment. *Field Crops Res.* 137, 89–96. doi: 10.1016/j.fcr.2012.08.006

Taylor, H., Burnett, E., and Booth, G. (1978). Taproot elongation rates of soybeans. *Z. fuer Acker und Pflanzenbau.* 146 (1), 33–39.

Tran, L.-S. P., and Mochida, K. (2010). Functional genomics of soybean for improvement of productivity in adverse conditions. *Funct. Integr. Genomics* 10, 447–462. doi: 10.1007/s10142-010-0178-z

Tuberosa, R., Salvi, S., Giuliani, S., Sanguineti, M. C., Frascaroli, E., Conti, S., et al. (2011). Genomics of root architecture and functions in maize. *Root genomics*. (Springer), 179–204.

Tuyen, D., Lal, S., and Xu, D. (2010). Identification of a major QTL allele from wild soybean (Glycine soja Sieb. & Zucc.) for increasing alkaline salt tolerance in soybean. *Theor. Appl. Genet.* 121, 229–236. doi: 10.1007/s00122-010-1304-y

Uga, Y., Sugimoto, K., Ogawa, S., Rane, J., Ishitani, M., Hara, N., et al. (2013). Control of root system architecture by DEEPER ROOTING 1 increases rice yield under drought conditions. *Nat. Genet.* 45, 1097–1102. doi: 10.1038/ng.2725

Valdés-López, O., Khan, S. M., Schmitz, R. J., Cui, S., Qiu, J., Joshi, T., et al. (2014). Genotypic variation of gene expression during the soybean innate immunity response. *Plant Genet. Resour.* 12, S27–S30. doi: 10.1017/S1479262114000197

Valliyodan, B., Van Toai, T. T., Alves, J. D., De Fátima P Goulart, P., Lee, J. D., Fritschi, F. B., et al. (2014). Expression of root-related transcription factors associated with flooding tolerance of soybean (Glycine max). *Int. J. Mol. Sci.* 15, 17622–17643. doi: 10.3390/ijms151017622

Valliyodan, B., Qiu, D., Patil, G., Zeng, P., Huang, J., Dai, L., et al. (2016). Landscape of genomic diversity and trait discovery in soybean. *Sci. Rep.* 6, 23598. doi: 10.1038/srep23598

Van Ooijen, J. W., and Voorrips, R. (2001). *JoinMap® 3.0, Software for the calculation of genetic linkage maps* (The Netherlands: Plant Research International, Wageningen), 1–51.

Varshney, R. K., Pazhamala, L., Kashiwagi, J., Gaur, P. M., Krishnamurthy, L., and Hoisington, D. (2011). "Genomics and physiological approaches for root trait breeding to improve drought tolerance in chickpea (*Cicer arietinum* L.)," in *Root genomics*. (Springer), 233–250.

Voorrips, R. (2002). MapChart: software for the graphical presentation of linkage maps and QTLs. *J. Heredity* 93, 77–78. doi: 10.1093/jhered/93.1.77

Vuong, T. D., Sleper, D. A., Shannon, J. G., and Nguyen, H. T. (2010). Novel quantitative trait loci for broad-based resistance to soybean cyst nematode (Heterodera glycines Ichinohe) in soybean PI 567516C. *Theor. Appl. Genet.* 121, 1253–1266. doi: 10.1007/s00122-010-1385-7

Wang, J., Hossain, M. S., Lyu, Z., Schmutz, J., Stacey, G., Xu, D., et al. (2019). SoyCSN: Soybean context-specific network analysis and prediction based on tissue-specific transcriptome data. *Plant Direct* 3, e00167. doi: 10.1002/pld3.167

Wasson, A. P., Richards, R., Chatrath, R., Misra, S., Prasad, S. S., Rebetzke, G., et al. (2012). Traits and selection strategies to improve root systems and water uptake in water-limited wheat crops. *J. Exp. Bot.* 63, 3485–3498. doi: 10.1093/jxb/ers111

Waters, B. M., Amundsen, K., and Graef, G. (2018). Gene expression profiling of iron deficiency chlorosis sensitive and tolerant soybean indicates key roles for phenylpropanoids under alkalinity stress. *Front. Plant Sci.* 9:10. doi: 10.3389/fpls.2018.00010

Whaley, A., Sheridan, J., Safari, S., Burton, A., Burkey, K., and Schlueter, J. (2015). RNA-seq analysis reveals genetic response and tolerance mechanisms to ozone exposure in soybean. *BMC Genomics* 16, 426. doi: 10.1186/s12864-015-1637-7

Wu, Y., Bhat, P. R., Close, T. J., and Lonardi, S. (2008). Efficient and accurate construction of genetic linkage maps from the minimum spanning tree of a graph. *PLoS Genet.* 4, e1000212. doi: 10.1371/journal.pgen.1000212

Wu, F., Price, B. W., Haider, W., Seufferheld, G., Nelson, R., and Hanzawa, Y. (2014). Functional and evolutionary characterization of the CONSTANS gene family in short-day photoperiodic flowering in soybean. *PLoS One* 9, e85754. doi: 10.1371/journal.pone.0085754

Yang, S., Chen, J., He, X., Yu, D., and Gai, J. (2005). Inheritance of drought tolerance and root traits of seedling in soybeans. *Soybean Sci.* 24, 275–280.

Yang, J., Zhu, J., and Williams, R. W. (2007). Mapping the genetic architecture of complex traits in experimental populations. *Bioinformatics* 23, 1527–1536. doi: 10.1093/bioinformatics/btm143

Zabala, G., and Vodkin, L. O. (2014). Methylation affects transposition and splicing of a large CACTA transposon from a MYB transcription factor regulating anthocyanin synthase genes in soybean seed coats. *PLoS One* 9, e111959. doi: 10.1371/journal.pone.0111959

Zhang, D., Cheng, H., Wang, H., Zhang, H., Liu, C., and Yu, D. (2010). Identification of genomic regions determining flower and pod numbers development in soybean (Glycine max L.). *J. Genet. Genomics* 37, 545–556. doi: 10.1016/S1673-8527(09)60074-6

Zhou, Z., Jiang, Y., Wang, Z., Gou, Z., Lyu, J., Li, W., et al. (2015). Resequencing 302 wild and cultivated accessions identifies genes related to domestication and improvement in soybean. *Nat. Biotechnol.* 33, 408–414. doi: 10.1038/nbt.3096

Zimmermann, P., Bleuler, S., Laule, O., Martin, F., Ivanov, N. V., Campanoni, P., et al. (2014). ExpressionData-A public resource of high quality curated datasets representing gene expression across anatomy, development and experimental conditions. *BioData Min.* 7, 18. doi: 10.1186/1756-0381-7-18

Conflict of Interest: Author SP was employed by the company Noble Research Institute, LLC. XW was employed by Bayer Crop Science. YB was employed by Nuseed Americas. FL was employed by Amgen. SK was employed by Corteva Agriscience.

The remaining authors declare that the research was conducted in the absence of any commercial or financial relationships that could be construed as a potential conflict of interest.

Copyright © 2020 Prince, Vuong, Wu, Bai, Lu, Kumpatla, Valliyodan, Shannon and Nguyen. This is an open-access article distributed under the terms of the Creative Commons Attribution License (CC BY). The use, distribution or reproduction in other forums is permitted, provided the original author(s) and the copyright owner(s) are credited and that the original publication in this journal is cited, in accordance with accepted academic practice. No use, distribution or reproduction is permitted which does not comply with these terms.

frontiers in Plant Science

ORIGINAL RESEARCH
published: 27 August 2020
doi: 10.3389/fpls.2020.572540

Comparative Transcriptome and Proteome Analysis of Salt-Tolerant and Salt-Sensitive Sweet Potato and Overexpression of *IbNAC7* Confers Salt Tolerance in *Arabidopsis*

Xiaoqing Meng[1,2], *Siyuan Liu*[1,2], *Tingting Dong*[1,2], *Tao Xu*[1,2], *Daifu Ma*[1,3], *Shenyuan Pan*[1,2], *Zongyun Li*[1,2]* and *Mingku Zhu*[1,2]*

[1] *Institute of Integrative Plant Biology, School of Life Sciences, Jiangsu Normal University, Xuzhou, China,* [2] *Jiangsu Key Laboratory of Phylogenomics & Comparative Genomics, School of Life Science, Jiangsu Normal University, Xuzhou, China,* [3] *Jiangsu Xuzhou Sweet Potato Research Center, Chinese Academy of Agricultural Sciences (CAAS), Xuzhou, China*

OPEN ACCESS

Edited by:
Raul Antonio Sperotto, Universidade do Vale do Taquari-Univates, Brazil

Reviewed by:
Sang-Soo Kwak, Korea Research Institute of Bioscience and Biotechnology (KRIBB), South Korea
Fei Gao, Montpellier SupAgro, France

***Correspondence:**
Zongyun Li
zongyunli@jsnu.edu.cn
Mingku Zhu
mingkuzhu007@126.com

Specialty section:
This article was submitted to Plant Abiotic Stress, a section of the journal Frontiers in Plant Science

Received: *14 June 2020*
Accepted: *14 August 2020*
Published: *27 August 2020*

Citation:
Meng X, Liu S, Dong T, Xu T, Ma D, Pan S, Li Z and Zhu M (2020) Comparative Transcriptome and Proteome Analysis of Salt-Tolerant and Salt-Sensitive Sweet Potato and Overexpression of IbNAC7 Confers Salt Tolerance in Arabidopsis. Front. Plant Sci. 11:572540. doi: 10.3389/fpls.2020.572540

Salt stress is one of the major devastating factors affecting the growth and yield of almost all crops, including the crucial staple food crop sweet potato. To understand their molecular responses to salt stress, comparative transcriptome and proteome analysis of salt-tolerant cultivar Xushu 22 and salt-sensitive cultivar Xushu 32 were investigated. The results showed the two genotypes had distinct differences at the transcription level and translation level even without salt stress, while inconsistent expression between the transcriptome and proteome data was observed. A total of 16,396 differentially expressed genes (DEGs) and 727 differentially expressed proteins (DEPs) were identified. Wherein, 1,764 DEGs and 93 DEPs were specifically expressed in the tolerant genotype. Furthermore, the results revealed that the significantly upregulated genes were mainly related to the regulation of ion accumulation, stress signaling, transcriptional regulation, redox reactions, plant hormone signal transduction, and secondary metabolite accumulation, which may be involved in the response of sweet potato to salt stress and/or may determine the salt tolerance difference between the two genotypes. In addition, 1,618 differentially expressed regulatory genes were identified, including bZIP, bHLH, ERF, MYB, NAC, and WRKY. Strikingly, transgenic *Arabidopsis* overexpressing *IbNAC7* displayed enhanced salt tolerance compared to WT plants, and higher catalase (CAT) activity, chlorophyll and proline contents, and lower malondialdehyde (MDA) content and reactive oxygen species (ROS) accumulation were detected in transgenic plants compared with that of WT under salt stress. Furthermore, RNA-seq and qRT-PCR analysis displayed that the expression of many stress-related genes was upregulated in transgenic plants. Collectively, these findings provide revealing insights into sweet potato molecular response to salt stress and underlie the complex salt tolerance mechanisms between genotypes, and *IbNAC7* was shown as a promising candidate gene to enhance salt tolerance of sweet potato.

Keywords: differentially expressed genes, IbNAC7, salt stress, sweet potato, transcriptome and proteome analysis

INTRODUCTION

Plants are often permanently exposed to a variety of abiotic stresses, such as salinity, drought, heat, and cold. Among them, salt stress is the major devastating factor affecting crop growth and productivity (Parida and Das, 2005). About 9 billion hm^2 of land worldwide is affected by salt stress, accounting for at least 6% of the total land area, and 50% of irrigated land is facing salinity problems (Flowers, 2004; Acosta-Motos et al., 2015; Kumar et al., 2017). Therefore, salt stress is a widespread and common feature of massive lands, and plants have evolved various mechanisms to tolerate salt stress. Presently, a great deal of documents have identified and characterized the components of the salt stress signaling network. For instance, the first established plant abiotic stress signaling pathway, the SOS pathway, is a calcium-dependent protein kinase pathway that plants use for salt stress signaling and Na^+ resistance (Zhu, 2002; Zhu, 2016). However, the specific physiological and molecular mechanisms of salt tolerance remain largely unknown in plants.

Plants' response to salt stress involves sophisticated and diverse tolerance mechanisms that are activated and integrated by the transcription of thousands of genes with enormous biological roles (Kant et al., 2007; Zhu, 2016). Transcription factors (TFs) are pivotal because they are involved in the regulation of signal transduction and the transcription of many stress-related genes, such as bZIP, MYB, WRKY, AP2/ERF, and NAC proteins (Erpen et al., 2018; Zhu et al., 2018; Li et al., 2019; Yang et al., 2019). NACs are one of the largest plant-specific TFs, and have been widely isolated from various species, such as *Arabidopsis* and rice (Nuruzzaman et al., 2010), potato (Singh et al., 2013), tomato (Jin et al., 2020) and maize (Wang et al., 2020). Typically, NACs have an N-terminal NAC domain consisting of approximately 150 conserved amino acids involved in DNA or protein binding, and the NAC domain can be divided into five sub-domains (A–E). Studies have shown that the diverse C-terminal is considered as a transcription regulatory region that can activate or repress gene expression (Puranik et al., 2012; Mohanta et al., 2020).

Significant progress has critically demonstrated that numerous NACs in various plant species are involved in diverse biological processes, especially in response to biotic and abiotic stress, such as drought, salt, and cold (Puranik et al., 2012; Mathew and Agarwal, 2018). A large number of documents showed that transgenic plants overexpressing a NAC gene have enhanced stress tolerance, illustrating that NACs are promising candidate factors for genetic engineering of crops under adverse conditions (Tran et al., 2010; Marques et al., 2017). For example, the over accumulation of *Arabidopsis ANAC019*, *ANAC055*, and *ANAC072* resulted in improved drought tolerance and modulated the transcription of numerous stress- and ABA-related genes (Tran et al., 2004). Transgenic rice that overexpressed *SNAC1* or *SNAC2* genes displayed obviously improved tolerance to drought and salt, and the expression of lots of stress-related genes was upregulated in *SNAC2*-overexpressing plants (Hu et al., 2006; Nakashima et al., 2007). Presently, Hou et al. (2020) find that overexpression of *CaNAC064* confers cold tolerance, while down-regulation of *CaNAC064* displays the opposite performance in transgenic pepper (Hou et al., 2020). Furthermore, plenty of studies have suggested that NACs respond to various abiotic stresses *via* the downstream actions of hormones including ABA and ethylene. For instance, overexpression of multiple NACs results in altered ABA sensitivity in transgenic plants (Marques et al., 2017; He et al., 2019). And multiple NAC TFs function directly to the ABA biosynthesis-related genes, such as both *Arabidopsis* ATAF1 and rice OsNAC2 can directly bind to the promoter of *NCED3* gene (Jensen et al., 2013; Mao et al., 2017).

Sweet potato (*Ipomoea batatas* L.) is the only crop with starch storage roots in the Convolvulaceae family (Liu, 2017; Arisha et al., 2020), and is one of the most important food crops, ranking seventh in the world and fourth in China (Meng et al., 2018). Sweet potato is widely applied for human food, animal feed, and for manufacturing starch and alcohol. Because of its ability to adapt various agro-ecological conditions, sweet potato has ensured food supply and safety in many developing countries, but its yield is still reduced by many biotic and abiotic stresses (Liu, 2017). Presently, many stress-related genes have been identified in sweet potato. For example, IbABF4 TF confers drought and salt tolerance in transgenic sweet potato and *Arabidopsis* (Wang W. et al., 2019), and IbMYB116 TF improves drought tolerance in transgenic *Arabidopsis* (Zhou et al., 2019). Our previous study also displayed that overexpression of a AP2/ERF gene, *IbCBF3*, increased the cold and drought tolerance in transgenic sweet potato (Jin et al., 2017). However, the roles of most stress-responsive genes in sweet potato remain largely unknown. At the same time, although extensive reports have largely revealed the importance of transcriptional regulations under salt stress, few studies have studied the regulation of translation level. In this study, transcriptome and proteome analysis were simultaneously performed in two contrasting sweet potato cultivars Xushu 22 (salt-tolerant, abbreviated as Xu22) and Xushu 32 (salt-sensitive, abbreviated as Xu32) we previously identified (Yu et al., 2016) under control and salt-exposed conditions. We found that overexpression of *IbNAC7* obviously enhanced the salt tolerance of transgenic *Arabidopsis*. This study identified crucial genes/proteins and pathways between the two contrasting cultivars under salt stress, and provided fundamental insights into the molecular mechanisms underlying sweet potato stress tolerance.

MATERIALS AND METHODS

Plant Materials and Cultural Conditions

The tuberous roots of two contrasting sweet potato cultivars Xu22 and Xu32 with different salt tolerance (Yu et al., 2016) were placed in the greenhouse, and then the shoots with functional leaves were cut and hydroponic culture in 1/4 Hoagland solutions in a plant growth chamber timed for 16 h days (25°C) and 8 h nights (20°C). Hoagland solution was replaced every three days, afterwards

uniform seedlings of both cultivars with five to six functional leaves and 8 to 10 cm fibrous roots were exposed to 150 mM NaCl for 24 h, and fibrous roots before and after salt stress were harvested for transcriptome analysis. All the samples were immediately immersed in liquid nitrogen and stored at −70°C.

Transcriptome Analysis

The fibrous roots of Xu22 and Xu32 were harvested from six different plants for transcriptome analysis of each set with three biological replicates. 1 μg RNA from each sample was employed as input material, and 12 samples were transferred to Biomarker technology Co. Ltd. (Beijing, China) for transcriptome sequencing and assembly. Clean reads were achieved by removing reads containing adapters, poly-N and low-quality reads from raw reads, and then the filtered sequences were used for downstream analysis. Hisat2 was used to map with the sweet potato reference genome (https://ipomoea-genome.org/). Gene expression was estimated by read counts, and genes with adjusted P-values (false discovery rate, FDR) < 0.05 detected by DESeq (Anders and Huber, 2010) and |log2 (fold change)| >1 were considered as DEGs. GO enrichment analysis was implemented by GOseq (Young et al., 2010), and the statistical enrichment of KEGG pathways were tested by KOBAS (Mao et al., 2005).

Proteome Analysis

The iTRAQ analysis of the proteome was carried out by Biomarker technology Co. Ltd. (Beijing, China) as described in our previous report (Dong et al., 2019). Briefly, total proteins were extracted from 12 samples, and their purity was detected by 10% SDS-PAGE. The peptides were dried by vacuum centrifugation after trypsin digestion, and then labeled using iTRAQ® Reagent-8PLEX Multiplex Kit (Sigma). About 600 μg of the labeled peptide mix was fractionated by a C18 column on Rigol L3000 HPLC. The obtained spectra were searched against the sweet potato reference genome using the PD 2.2 (Thermo). The protein quantitation was estimated by the Mann-Whitney test, and fold change >1.2 was applied to screen the differential proteins. GO and InterPro (IPR) analysis were carried out by the InterProScan-5 against multiple protein databases, such as Pfam, SMART and ProSiteProfiles, and KEGG database was employed to analyze the protein pathways.

Construction of Overexpression Vector and *Arabidopsis* Transformation

The coding region of *IbNAC7* was inserted into the pBI121 binary vector driven by the CaMV 35S promoter using the primers *Ov-IbNAC7*-F/R (**Supplementary Table S1**). The vector was then transferred into *A. tumefaciens* GV3101, and transgenic *Arabidopsis thaliana* (Columbia-0) were produced and further to obtain homozygous T3 seeds according to the methods described by Zhang et al. (2006). The expression of *IbNAC7* in transgenic plants was confirmed by qRT-PCR using the CFX96™ Real-Time System (Bio-Rad, USA) as described in our previous report (Meng et al., 2019). The relative expression was normalized to *EF1α* (**Supplementary Table S1**), and the transcription was further calibrated using the transgenic line with the lowest *IbNAC7* expression.

Assays for NaCl Stress Tolerance of Transgenic *Arabidopsis*

For germination greening rate assay, seeds of WT and T3 transgenic lines were sterilized with 1% NaClO for 10 min, and then sown on 1/2 MS medium with 0 (as a control) and NaCl (100 and 150 mM). About 180 seeds per line were used in each assay, and the germination greening rate was calculated after 10 d. For root length assay, 4-d-old seedlings of WT and transgenic lines were selected based on the consistency of root length, and were vertically cultured on 1/2 MS medium with 0 (as a control) and 120 mM NaCl in a growth chamber. The length of the primary roots was measured after 10 d. For salt stress in soil, 7 d-old seedlings of WT and transgenic lines obtained on 1/2 MS medium were transferred to pots in a greenhouse; two weeks later, plants were randomly selected for salt tolerance assay. One group was watered normally as a control, and the other group was irrigated with 200 mM NaCl solution from the bottom of pots every 3 d. Pictures were taken 15 d later to record the phenotype.

RNA-Seq Analysis and Salt Tolerance Evaluation of Transgenic *Arabidopsis*

The 10-d-old seedlings of WT and transgenic line 8, which were vertically cultured on 1/2 MS medium, were soaked in liquid 1/2 MS medium containing 100 mM NaCl solution for 6 h, and then the whole plants before and after NaCl treatment were collected and used for RNA-seq analysis as described above, except that clean reads were mapped to the *Arabidopsis* reference genome (https://www.arabidopsis.org/).

In addition, the leaves of WT and transgenic plants in the soil under normal and salt stress for 15 d were used to determine stress-related physiological indicators. Chlorophyll, proline and malondialdehyde (MDA) contents, and catalase (CAT) activity were detected using corresponding test kits (for plant) purchased from Nanjing Jiancheng Bioengineering Institute (Nanjing, China) according to the manufacturer's protocols. Superoxide radicals were histochemically detected using the nitroblue tetrazolium (NBT) and dead cells were visualized by trypan blue (TB) staining according to the procedures described by Lee et al. (2012).

RNA Extraction and qRT-PCR Analysis

Total RNA was isolated from all samples using an RNA extraction kit (TianGen, Beijing, China) according to the manufacturer's instructions. 2 μg RNA was reverse-transcribed using PrimeScript reverse transcriptase with gDNA Eraser (TaKaRa, Dalian, China) using the mix of Oligo dT Primer and Random 6 mers. qRT-PCR experiments were carried out on a CFX96™ Real-Time System (Bio-Rad, USA) as described in our previous report (Meng et al., 2019). The *Arabidopsis EF1α* gene was selected as the internal standard. All qRT-PCR primers are listed in **Supplementary Table S1**, and each gene was performed with three independent biological replicates, and three technical replicates for each biological replicate.

Statistical Analyses

The data were analyzed by one-way analysis of variance (ANOVA) and means different were significant by a Dunnett's test at $P < 0.05$. Statistical analyses were conducted with SPSS software 20 version (IBM Corp., USA).

RESULTS

Enrichment Analysis of the DEGs (Differentially Expressed Genes) Between Xu22 and Xu32 Under Salt Stress

Our previous studies have shown that better ion homeostasis and nitrogen metabolism make Xu22 more salt tolerant than Xu32 (Yu et al., 2016). To further understand the molecular mechanism underlying the two contrasting sweet potato cultivars with different salt tolerance, their fibrous roots from control and salt-exposed conditions (total 12 samples) were collected for transcriptome sequencing using the Illumina HiSeq 2500 platform. A total of 40,767,744 to 55,915,888 clean reads were generated, of which 73.73% to 75.21% clean reads were mapped to the sweet potato genome, and less than 3.98% of the reads were mapped to multiple sites (**Supplementary Table S2**). The RNA data in the three biological replicates showed high expression correlation ($R^2 \geq 0.897$) except Xu22-CR2 ($R^2 \leq 0.738$, **Supplementary Figure S1**), thus these assembled sequences except Xu22-CR2 are appropriately employed for downstream analysis.

The read counts value was calculated to profile the transcription level of genes. A total of 16,396 DEGs were identified from the fibrous root libraries under normal and salt-treated conditions based on the FDR < 0.05, and |log2 (fold change)| > 1 (**Supplementary Figure S2**, **Supplementary Table S3**). Among them, 4,460 and 6,150 DEGs were from Xu22-SR vs Xu22-CR and Xu32-SR vs Xu32-CR, respectively, 8,128 DEGs were from Xu22 vs Xu32 without salt stress, and 8,525 DEGs were from Xu22 vs Xu32 under salt stress. Interestingly, the total number of salt-responsive genes in Xu32 was larger than in Xu22 under salt stress (both upregulated and downregulated genes) (**Figure 1A**). Venn analysis showed that many DEGs identified were salt stress-responsive and/or genotype-specific. Among them, 1,764 and 3,454 DEGs were specifically expressed in Xu22 and Xu32 under salt stress, respectively, and 2,696 DEGs were expressed in both libraries (**Figure 1B**).

Functional annotations showed that a large number of salt-responsive genes identified in the roots of Xu22 and Xu32 under salt stress are involved in the regulation of ion accumulation, stress signaling, redox reactions, plant hormone signal transduction, and accumulation of secondary metabolites (**Supplementary Table S3**). These pathways have been shown to play pivotal roles in the salt tolerance of many plants (Zhang et al., 2019), and thus may represent the core genes related to salt stress response, despite the differential levels of salt tolerance in sweet potato. Especially, compared to samples from salt-sensitive Xu32, we found that many DEGs encode stress-related proteins/factors, such as NAC TF, zinc finger protein, F-box protein, MAPKKK, DEAD-box RNA helicase, plasma membrane ATPase, calmodulin-binding protein, and cytochrome P450 were uniquely expressed in salt-tolerant Xu22. Furthermore, the expression levels of many DEGs related to WRKY TF, ERF TF, PPR protein, F-box protein, zinc finger protein, ABA-induced protein, potassium transporter, methyltransferase, homeobox protein, cytochrome P450 were also significantly upregulated in Xu22 compare to that in Xu32 under salt stress (**Supplementary Table S3**).

GO annotations of the DEGs showed that over 50 functional terms of the four sets of data were classified (**Supplementary Table S4**). The first seven most enriched functional terms are similar between Xu22 and Xu32 under salt stress. Among them, "catalytic activity" term (ranging from 1,765 to 2,539 DEGs) in molecular function and "metabolic process" term (ranging from 1,640 to 2,731 DEGs) in biological process were the two most common categories in both Xu22 and Xu32 under salt stress

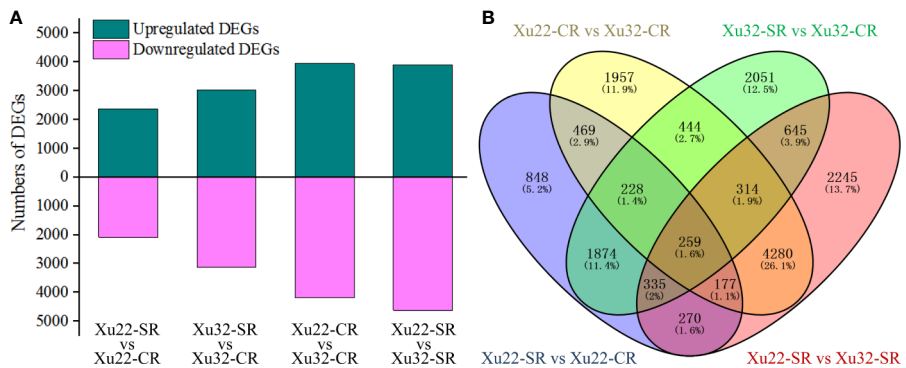


FIGURE 1 | Overview and Venn diagram of upregulated or downregulated genes in fibrous roots of two sweet potato genotypes under normal and salt-treated conditions at a level of |log2 (fold change)| > 1 and FDR < 0.05. **(A)** The total number of differentially expressed genes (DEGs) found in the fibrous roots of Xu22 and Xu32 under control and salt-treated conditions. **(B)** The four-way Venn diagram in Xu22 and Xu32 suggests that the DEGs were genotype-specific and salt-responsive. Overlapping regions indicate co-expressed DEGs among different data sets, and numbers in only one circle represent DEGs expressed in only one library.

(**Figure 2A**, **Supplementary Figure S3A**). The results indicated that the response of sweet potato to salt stress involves intensive metabolic activity and catalytic activity. Strikingly, lots of DEGs were involved in multiple crucial GO terms which are known to be related to plant salt tolerance, such as "antioxidant activity," "transcription factor activity," and "response to stimulus." Moreover, GO analysis also displayed apparent genotype-specific enrichment, suggesting that many important biological process, cellular component and molecular function occurred differently between Xu22 and Xu32 under salt stress (**Supplementary Table S4**).

Besides, KEGG-based DEGs enrichment analysis showed that most KEGG pathways were enriched in both genotypes under salt stress. The most enriched categories are "phenylpropanoid biosynthesis" in both Xu22 (106 DEGs) and Xu32 (143 DEGs) under salt stress, and "ribosome" in Xu22 vs Xu32 under salt stress (137 DEGs) and Xu22 vs Xu32 without salt stress (133 DEGs) (**Figure 2B**, **Supplementary Figure S3B**). Common

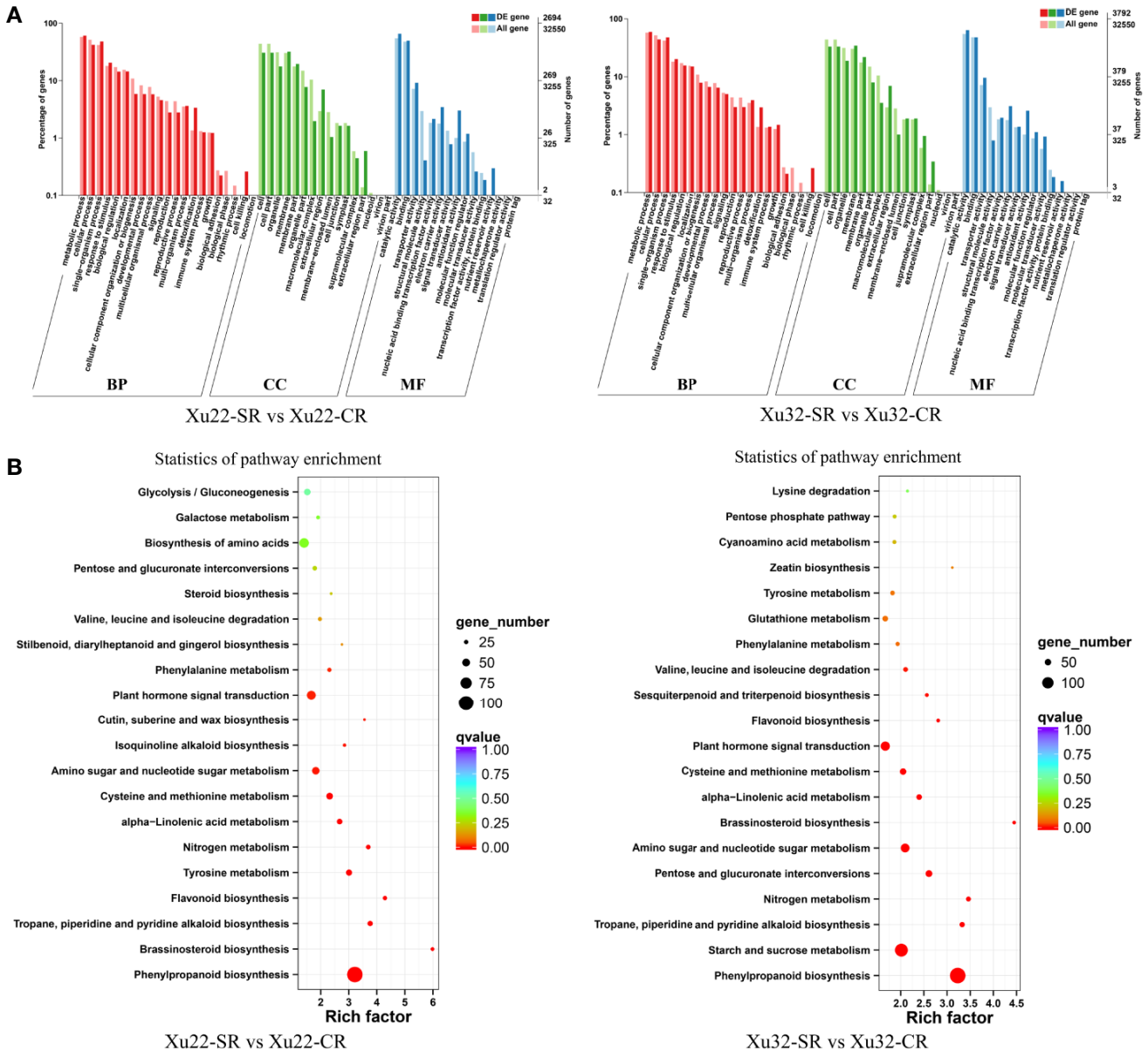


FIGURE 2 | GO classifications and KEGG pathways of the DEGs in the fibrous roots of Xu22 and Xu32 under salt stress. **(A)** GO classifications of the annotated DEGs. The left Y-axis indicates the percentage of DEGs identified, and the right Y-axis indicates the number of DEGs. The DEGs were categorized based on the annotations of GO, and the numbers are displayed according to the biological process (BP), cellular component (CC), and molecular function (MF). **(B)** Enriched KEGG pathways of the DEGs in Xu22 and Xu32 under salt stress. X-axis and Y-axis represent the GeneRatio and the terms of pathways, respectively. Coloring correlates with the q-value. The lower the q-value, the more significant the enrichment. Point size correlates with the numbers of DEGs.

categories of high enrichment also included "starch and sucrose metabolism," "carbon metabolism," "plant hormone signal transduction," "biosynthesis of amino acids." However, the "ribosome" pathway in Xu22 was significantly upregulated compared to Xu32 under salt stress (**Supplementary Figure S4**). In particular, several categories were uniquely enriched in Xu22, such as "N-Glycan biosynthesis" and "glucosinolate biosynthesis" (**Supplementary Table S5**). Overall, the data provide valuable knowledge for further understanding the complicated molecular mechanisms of sweet potato responses to salt stress.

Proteome Analysis and Transcriptome-Proteome Matching Analysis

In many cases, changes in transcription level are not always accompanied by changes in protein abundance, thus comparative proteome analysis was conducted using the same samples as the transcriptome by the iTRAQ. A total of 3,123 proteins were identified in the four sets of data, while the proteome data in the three biological replicates showed a very low expression correlation (each ≤ 0.69) (**Supplementary Figure S5**). Among these proteins, 86.5% (2701), 70.3% (2,196) and 44.7% (1,395) were annotated in the COG, GO, and KEGG databases, respectively (**Supplementary Table S6**). The comparison between different samples showed that a total of 727 DEPs (differentially expressed proteins) were identified, wherein, 124 DEPs (59 upregulated and 66 downregulated) in Xu22, and 262 DEPs (119 upregulated and 143 downregulated) in Xu32 under salt stress were identified. And 93 and 231 DEPs were uniquely expressed in Xu22 and Xu32 under salt stress, respectively. 216 DEPs were from Xu32 vs Xu22 under salt stress, and 125 DEPs were from Xu32 vs Xu22 without salt stress (**Supplementary Figures S6** and **S7**). Commonly upregulated proteins of the two genotypes under salt stress included peroxidase, elongation factor, phosphoglycerate kinase, glycine-rich RNA-binding protein, plasma membrane ATPase, and NADH dehydrogenase. Some DEPs, such as cytochrome P450, cinnamic acid 4-hydroxylase, lipoxygenase, and DNA repair protein, were uniquely upregulated in Xu22 under salt stress. In addition, 104 upregulated and 112 downregulated DEPs were identified in Xu32 compared with Xu22 under salt stress. Among them, the expression of many proteins, such as elongation factor, catalase, DEAD-box ATP-dependent RNA helicase, rubisco activase, glutamate dehydrogenase, and ATP-citrate synthase was upregulated in Xu22 vs Xu32 under salt stress (**Supplementary Table S7**).

GO annotations of the DEPs displayed that there were multiple categories such as "glutamine biosynthetic process," "single-organism catabolic process," and "cellular catabolic process" in Xu22; "photosynthesis, light reaction" and "protein localization to vacuole" in Xu32 were remarkably enriched under the biological process after exposure to salt stress. And "photosynthesis," "response to oxidative stress," and "cellular metabolic compound salvage" were significantly enriched in Xu32 vs Xu22 under salt stress (**Figure 3A**). As for the celelular components, multiple terms were downregulated in Xu32 compared with Xu22 under salt stress, such as "respiratory chain," "late endosome membrane," and "membrane-enclosed lumen" (**Figure 3B**). It is interesting to note that many terms in the molecular function category were prominently enriched in Xu22, while only several terms were enriched in Xu32 under salt stress (**Figure 3C**). In addition, the enrichment analysis of DEPs based on KEGG database showed that many categories, including "citrate cycle"; "alanine, aspartate, and glutamate metabolism"; "microbial metabolism in diverse environments"; and "Alzheimer's disease" were remarkably enriched in Xu22 under salt stress. However, only "photosynthesis-antenna proteins" was enriched in Xu32 under salt stress. In addition, "arginine biosynthesis" and "citrate cycle" were significantly downregulated in Xu32 compared with Xu22 under salt stress (**Figure 3D**).

To obtain more information on response changes under salt stress, the identified proteins were matched with the genes from RNA-seq analysis. Of the 3,123 identified proteins, 1,113 had corresponding genes in the RNA-seq data (**Supplementary Table S8**). The results showed that the correlation between gene and protein expression was very weak, only a few genes and their corresponding proteins have consistent expression profiles. For instance, 8 and 11 DEGs showed consistent expression between the transcription level and translation level in Xu22 and Xu32 under salt stress, respectively. And the encoding products of common upregulated genes between transcriptome and proteome analysis included aldehyde dehydrogenase, glutamate dehydrogenase, and glutamine synthetase in Xu22 compared with Xu32 under salt stress (**Supplementary Table S9**). However, 68 and 144 proteins was differentially expressed in Xu22 and Xu32 under salt stress, respectively, but no changes in the expression of their corresponding genes were detected. 126 and 77 proteins were differentially expressed in Xu32 vs Xu22 under salt stress and Xu32 vs Xu22 without salt stress, respectively, while no changes in their gene expression were observed. Similarly, 20 and 30 DEGs was detected in Xu22 and Xu32 under salt stress, respectively, while no corresponding DEPs were identified (**Supplementary Table S9**).

Identification of Salt-Responsive TFs in Sweet Potato and Overexpression of *IbNAC7* Improved Salt Tolerance in Transgenic *Arabidopsis*

The identification and characterization of stress-responsive TFs is crucial for the development of transgenic crops with improved stress tolerance. In this study, a total of 1,618 differentially expressed TFs were identified with FDR < 0.01 and |log2 (fold change)| > 1 (**Supplementary Table S10**). Representative differentially expressed TFs were shown in **Table 1**, including various salt tolerance/stress-related bZIP, bHLH, ERF, MYB, NAC, and WRKY TFs, and their diverse transcription profiles suggest their pivotal regulatory roles in salt stress response. Wherein, MYB (98 members), WRKY (95 members) and NAC (74 members) are the three TF families with the largest number of differential expression. Interestingly, the amount of

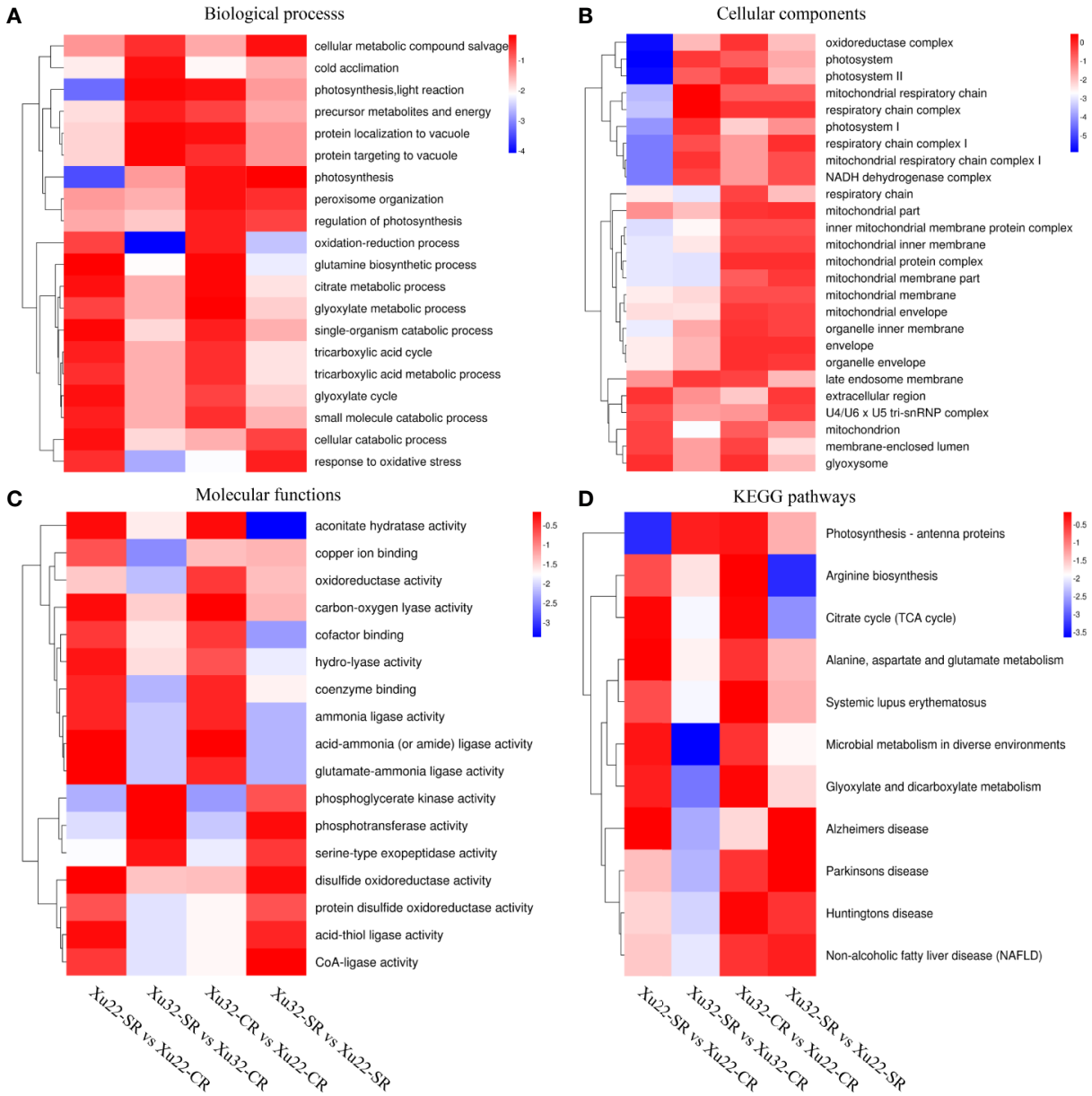


FIGURE 3 | Heatmaps of the enriched GO classifications and KEGG pathways of differentially expressed proteins (DEPs) in Xu22 and Xu32 in proteome analysis. **(A–C)** The biological process (BP, **A**), cellular component (CC, **B**), and molecular function (MF, **C**) of the GO classifications of the annotated DEPs. **(D)** Enriched KEGG pathways of the DEPs in Xu22 and Xu32. The color scales at right indicate the relative expression. Red and blue shading indicate the relative high or low expression levels, respectively.

upregulated expressed TFs detected in salt-tolerant Xu22 was significantly lower than that in salt-sensitive Xu32 under salt stress (**Table 1**), the specifically upregulated TFs in Xu22 may make a positive contribution to its salt tolerance. Previously, 12 stress-responsive *IbNAC* genes were selected based on the present RNA-seq data. Among them, the transcription of *IbNAC7* (one of the 74 NACs) was remarkably upregulated by multiple abiotic stresses and hormones, such as salt, cold, ABA, and ACC (Meng et al., 2018), indicating that *IbNAC7* may be involved in the stress response of sweet potato.

Subsequently, eight transgenic *Arabidopsis* lines overexpressing the *IbNAC7* gene were obtained, and the results displayed that all the transgenic lines showed remarkably higher transcription of *IbNAC7* than that in WT plants (**Supplementary Figure S8**). Three T3 homozygous lines with high expression of *IbNAC7* were selected for salt tolerance test. Firstly, the salt tolerance of transgenic lines was examined at the germination and post-germination stages. No obvious differences in germination greening rates on 1/2 MS medium with 0 and 100 mM NaCl between transgenic and WT seeds were observed. However, the germination greening rates of

TABLE 1 | Representative salt stress-responsive TFs under salt stress in sweet potato transcriptome analysis.

Name	Total No.	Xu22-SR vs Xu22-CR		Xu32-SR vs Xu32-CR		Xu22-CR vs Xu32-CR		Xu22-SR vs Xu32-SR	
		Upregulated	Downregulated	Upregulated	Downregulated	Upregulated	Downregulated	Upregulated	Downregulated
ARF	22	6	4	6	3	3	10	1	5
bHLH	34	5	10	6	9	5	9	2	12
bZIP	15	2	0	5	3	3	3	2	3
ERF	32	12	4	13	2	6	8	4	14
HSF	25	7	3	16	2	4	3	0	5
MADS	16	3	1	2	3	4	6	2	7
MYB	98	34	19	35	22	14	19	5	22
NAC	74	36	1	39	4	10	13	11	21
GRAS	17	4	1	5	3	2	5	2	6
SBP	4	0	0	1	0	0	2	1	2
TCP	9	3	3	0	2	0	3	1	1
Trihelix	6	1	0	1	0	1	2	1	3
Whirly	3	0	0	0	0	2	1	1	1
WRKY	95	43	9	44	10	9	16	20	23
zinc finger	49	3	7	7	14	10	12	5	18

CR, control fibrous roots; SR, salt-treated fibrous roots.

transgenic lines were notably higher than that of WT plants under 150 mM NaCl conditions (**Figures 4A, B**). And the transgenic and WT seedlings showed similar growth on control medium, while the transgenic lines provided remarkably longer roots than that of WT under 120 mM NaCl stress (**Figures 4C, D**). The results showed that *IbNAC7* conferred salt tolerance during the germination and post-germination stages of *Arabidopsis*.

Performance of Transgenic *IbNAC7* Plants Under Salt Stress in Soil and Salt Tolerance Evaluation

The performance of transgenic lines under NaCl stress was further tested in soil, 20-d-old WT and transgenic lines were irrigated with 200 mM NaCl every 3 d. Under control conditions, normal morphological phenotypes were observed in WT and transgenic lines. Nevertheless, transgenic lines displayed better growth after salt stress, such as delayed leaf necrosis and yellowing at 15 d post-treatment (**Figure 5A**). To characterize the salt tolerance of the transgenic lines, several stress-related physiological parameters were detected. No significant differences in the physiological analysis between WT and transgenic lines were observed under normal conditions. After 15 d of salt stress, the CAT and SOD activity and chlorophyll content of transgenic plants were markedly higher than those of WT. In contrast, transgenic plants accumulated less MDA than the WT plants (**Figure 5B**). Besides, biochemical staining was analyzed by NBT and TB using the detached leaves. In the absence of salt stress, transgenic and WT plants displayed similar basal levels of ROS and cell death. After exposure to salt stress for 15 d, transgenic lines accumulated much less ROS and dead cells

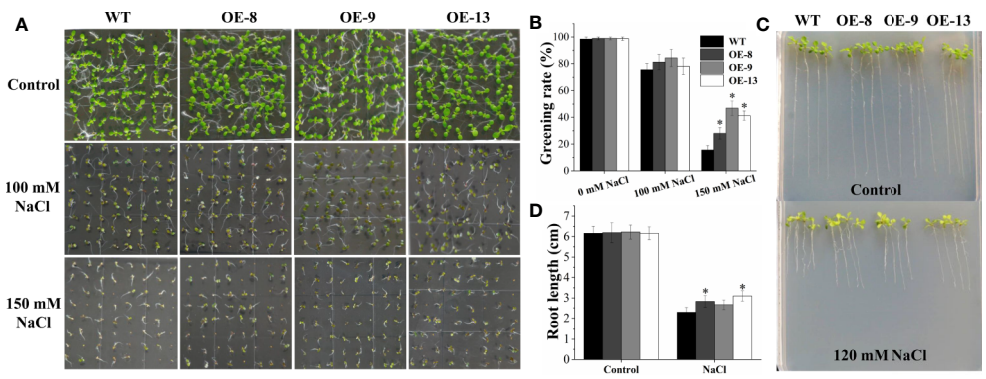


FIGURE 4 | The germination greening rate and root length of transgenic plants overexpressing *IbNAC7* were improved under salt stress. **(A, B)** Comparisons of germination phenotype **(A)** and germination greening rate **(B)** between WT and transgenic seeds (n ≥ 60 each) grown on 1/2 MS medium containing 0, 100, and 150 mM NaCl for 10 d. **(C, D)** Comparisons of growth phenotype **(C)** and root length **(D)** between WT and transgenic seedlings (n ≥ 20 each) grown on 1/2 MS medium with or without NaCl for 10 d. Data are the means ± SE of three independent biological experiments. Asterisks indicate statistical significance (*P < 0.05) between the WT and transgenic plants.

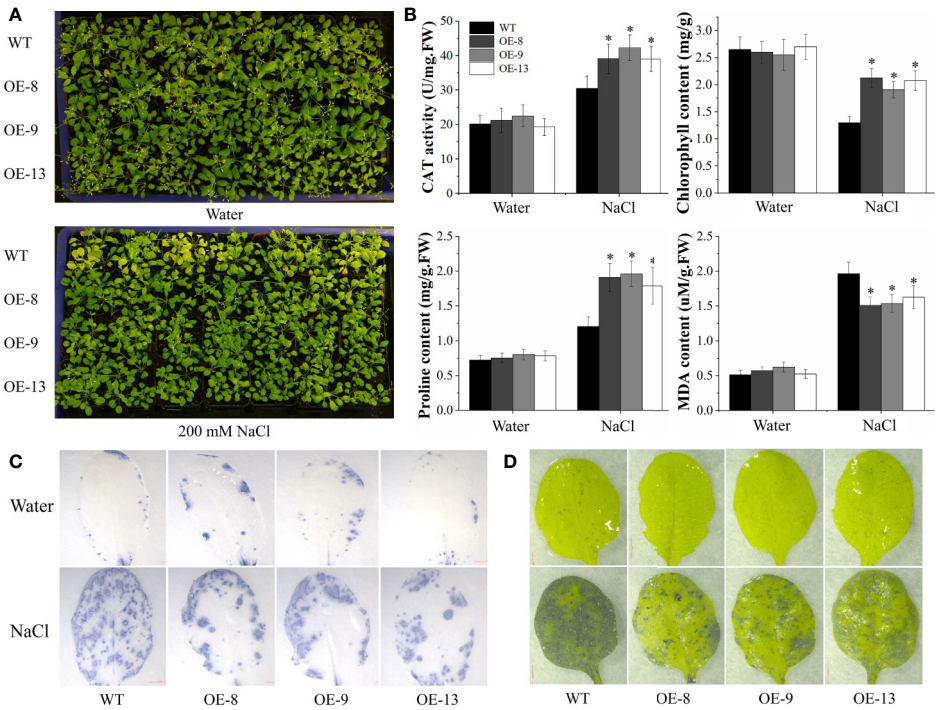


FIGURE 5 | Comparisons of WT and transgenic plants overexpressing *IbNAC7* treated with water or salt stress in soil. **(A)** Phenotype comparison of WT and transgenic plants exposed to salinity stress in soil. 20-d-old plants were randomly selected for the salt tolerance assay by irrigating with 200 mM NaCl solution every 3 d from the bottom of pots. 15 plants from each line were employed for one experiment, and three independent experiments were conducted. **(B)** Comparisons of CAT activity, chlorophyll, proline and MDA content between WT and transgenic plants under normal and salt stress conditions. Data are the means ± SE of three independent biological experiments. Asterisks indicate statistical significance (*P < 0.05) between the WT and transgenic plants. **(C, D)** Histochemical staining of TB **(C)** and NBT **(D)** of transgenic *Arabidopsis* plants under under normal and salt treatment for 15 d.

than that of WT plants (**Figures 5C, D**). These results suggested that transgenic *Arabidopsis* overexpressing *IbNAC7* had significantly improved salt tolerance compared to the WT plants.

IbNAC7 Affect Multiple Groups of Biotic- and Abiotic Stress-Related Genes Under Salt Stress

To clarify the potential mechanism of salt tolerance modulated by IbNAC7, RNA-seq was used to detect the gene expression differences of transgenic plants (line 8) under NaCl stress. A summary of the sequencing assembly is shown in **Supplementary Table S11**. At least 94.31% of the genes in each library were mapped to the *Arabidopsis* genome, and the RNA data displayed a strong expression correlation ($R^2 \geq 0.791$). Venn diagram showed that 2,441 and 943 DEGs were specifically expressed in transgenic and WT plants under salt stress, respectively, and 2,484 DEGs were expressed in both plants (**Figures 6A, B**). A total of 1016 DEGs, including 774 upregulated and 242 downregulated genes, were detected in the transgenic lines compared with those in WT plants under salt stress (**Figure 6C**, **Supplementary Table S12**). Representative upregulated DEGs included 306 salt tolerance/stress-related TFs, such as AP2/ERF, bHLH, MYB, NAC, WRKY, and Zinc finger protein, indicating their vital roles under salt stress. In addition, the upregulated genes are also associated with diverse stress response. For instance, multiple upregulated genes encoded ABC transporter family proteins, LEA proteins, pathogenesis-related proteins, peroxidases, and PPR proteins (**Supplementary Table S12**).

When the DEGs were analysed for GO annotations, multiple stress-related GO terms were found, such as the peroxidase activity, antioxidant activity, defense response, and response to biotic stimulus (**Supplementary Figure S9A**). And multiple terms including response to stress, response to oxidative stress, response to biotic stimulus were significantly upregulated in transgenic lines compared with WT plants under salt stress (**Figure 6D**). Moreover, DEG-associated KEGG pathways were also identified. The results showed that the pathways related to ribosome, carbon metabolism, and starch and sucrose metabolism were significantly enriched in transgenic plants compared with those in WT plants under salt stress (**Supplementary Figure S9B**). And the pathways related to ribosome, plant-pathogen interaction, and phenylpropanoid biosynthesis were remarkably upregulated in transgenic plants (**Figure 6E**). Taken together, these results suggested that IbNAC7 is involved in the regulation of numerous and diverse stress-related genes in response to salt stress in *Arabidopsis*.

To validate the DEGs obtained from RNA-seq data, the expression levels of eight genes were detected by qRT-PCR. The upregulated DEGs were selected being representative of

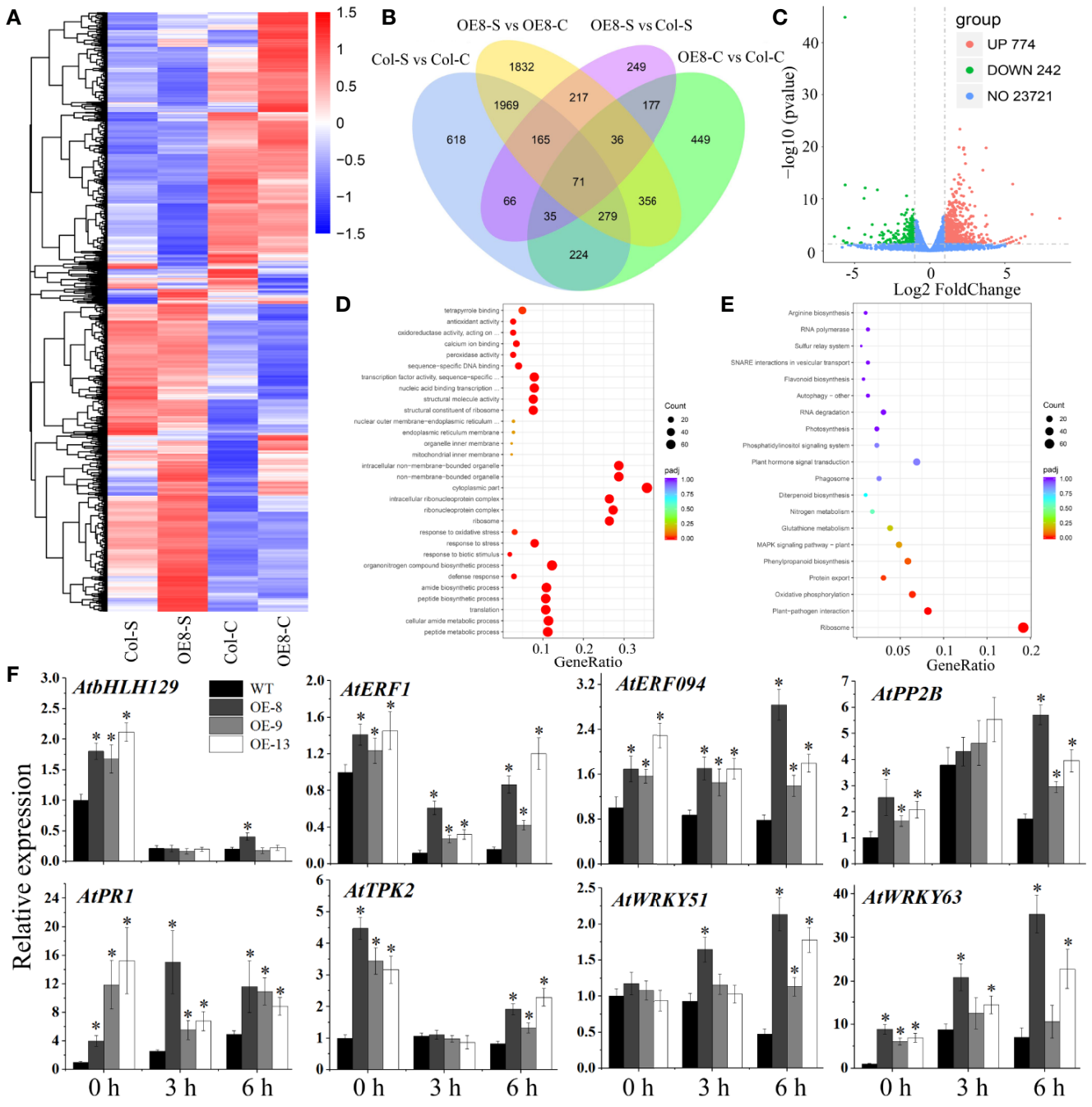


FIGURE 6 | RNA-seq analysis of stress-related genes affected by IbNAC7 under salt stress. **(A)** The DEGs were hierarchically clustered according to the Log_{10} (FPKM+1) values. The red and blue bands represent induced and repressed DEGs, respectively. **(B)** Venn diagrams between WT and transgenic plants suggested specific DEGs and shared DEGs under control and salt stress conditions. Overlapping region indicates co-expressed DEGs between WT and transgenic plants. The numbers only in one circle represent DEGs expressed only in WT or transgenic plants. **(C)** Volcano plot of DEGs in OE-8 vs WT plants after salt treatment. The red and green dots represent the upregulated and downregulated DEGs, respectively, and the blue dots represent non-DEGs. **(D, E)** GO classifications **(D)** and KEGG pathways **(E)** of annotated upregulated genes in OE-8 vs WT plants under salt stress. X-axis and Y-axis represent the GeneRatio and the category names, respectively. Coloring correlates with the padj. The lower the padj, the more significant the enrichment. The point size correlates with the number of DEGs. **(F)** Validation of the expression of selected stress-related genes by qRT-PCR between WT and transgenic plants under normal and salt stress conditions. 10-d-old plants were soaked in liquid 1/2 MS medium containing 100 mM NaCl solution for 3 and 6 h, and then the whole plants before and after NaCl treatment were collected. The relative expression levels were normalized to 1 in WT plants at 0 h. Data are the means ± SE of three independent biological experiments. Asterisks indicate statistical significance (*$P < 0.05$) between the WT and transgenic plants.

important genes in stress response. For instance, TF encoding genes *AtbHLH129* (Tian et al., 2015), *AtERF1* (Lorenzo et al., 2003), *AtERF094* (Zarei et al., 2011), *AtWRKY51* (Yan et al., 2018) and *AtWRKY63* (Ren et al., 2010), K^+ channel protein encoding gene *AtTPK2* (Isayenkov and Maathuis, 2013), stress-related F-box protein encoding gene *AtPP2B2* (Stefanowicz, 2015) and pathogenesis-related gene *AtPR1* (Pecenkova et al., 2017). Our results showed that the expression of almost all the selected genes was significantly upregulated in transgenic lines compared to that of WT under both control and salt conditions, which was consistent with that obtained by RNA-seq analysis, although there were variations in fold changes among the transgenic lines (**Figure 6F**). Therefore, these results demonstrated that IbNAC7 may affect the transcription of multiple groups of stress-related genes under salt stress.

DISCUSSION

pt?>Cultivating salt tolerant and high-yielding crop varieties is the most effective way to reduce crop yield losses. Therefore, it is critical to understand the salt stress response and tolerance mechanism of plants, which will help us to improve the stress tolerance of plants through molecular breeding and transgenic approaches. Genome-wide detection of specific stress-responsive genes based on transcriptome analysis in many crops with different characteristics has been increasingly conducted under various stresses. For instance, the gene expression dynamics of two contrasting genotypes, such as rice, sesame, cotton, and maize, under salt-treated and normal conditions were examined, and large numbers of diverse stress-related genes were identified (Guo et al., 2015; Li et al., 2018; Wang M. et al., 2019; Zhang et al., 2019). However, there is a lack of research on sweet potato, a hexaploid heterozygous non-model crop, responses to salt stress, and the regulations at translational levels have been rarely studied. In addition to RNA-seq analysis, proteome analysis is also critically necessary for understanding the change in translational regulation during stress responses. In this study, comparative transcriptome and proteome analysis of two contrasting sweet potato cultivars with different salt tolerance were investigated, which will provide a unique opportunity to gain insights into the candidate genes and proteins involved in salt stress response in this important crop. To our knowledge, this is the first comparison of salt stress-responsive transcriptome and proteome in sweet potato with contrasting genotypes.

In the present study, distinct differences were detected in transcription and translation levels between the two sweet potato genotypes even without salt stress. A total of 16,396 DEGs and 724 DEPs were identified under normal and salt-treated conditions, suggesting that transcription and translation regulations play a crucial role in the response of sweet potato to salt stress. The results showed that the correlation between gene and protein expression of both genotypes was very weak. Similar to our previous report (Dong et al., 2019) and multiple other studies (Bogeat-Triboulot et al., 2007; Liu et al., 2016; Li et al., 2018), the results showed that not all mRNA: protein ratios reflected the corresponding changes in transcription and protein levels (Haider and Pal, 2013). This may be due to the technical limitations of the proteome method or the possible occurrence of posttranscriptional regulation during salt stress response in sweet potato, making it difficult to compare with RNA-seq data. In view of this, we mainly focus on the discussion of transcriptome data between the two genotypes. Transcriptome data showed that many significantly enriched functional GO and KEGG terms of DEGs are consistent between Xu22 and Xu32 under salt stress, indicating that the main salt stress response pathways between the two cultivars may be similar. However, the "ribosome" and "glutathione metabolism" pathways in Xu22 were significantly upregulated compared to Xu32, and "N-Glycan biosynthesis" and "glucosinolate biosynthesis" were only enriched under salt stress in Xu22. These pathways be involved in the regulation of the salt tolerance of Xu22. Differently, the methionine metabolism pathway was previously shown as a primary contributor to the salt-tolerant jute (Yang et al., 2017). In addition, in proteome analysis, we also found that many proteins were common upregulated in the two genotypes under salt stress, such as peroxidase, elongation factor, phosphoglycerate kinase, plasma membrane ATPase, and NADH dehydrogenase. However, multiple proteins such as cytochrome P450, cinnamic acid 4-hydroxylase, and lipoxygenase were uniquely upregulated in Xu22 under salt stress, suggesting that these specific proteins may affect the contrasting salt tolerance between the two genotypes. Besides, previous reports showed that the numbers of upregulated genes of salt-tolerant varieties were higher than that of salt-sensitive varieties under salt stress (Geng et al., 2019; Zhang et al., 2019). However, our current RNA-seq data showed that the numbers of upregulated and downregulated genes in salt-sensitive Xu32 were more than that in salt-tolerant Xu22. And 1,764 and 3,454 DEGs were specifically detected in Xu22 and Xu32 under salt stress, respectively. Especially, many genes encoding stress-related proteins/factors, including NAC TF, WRKY TF, ERF TF, PPR protein, F-box protein, zinc finger protein, potassium transporter, methyltransferase, cytochrome P450 were uniquely expressed or significantly upregulated in salt-tolerant Xu22 under salt stress. Therefore, these differential genes and pathways may contribute to the difference in salt tolerance between the two contrasting genotypes, and the salt tolerance of Xu22 could be enhanced by high expression of some genotype-specific genes.

Salt stress has primary osmotic shock and ion-toxicity effects, while secondary effects are complex, including reactive oxygen species (ROS) burst, cell component damages, and metabolic dysfunctions in plant cells (Munns and Tester, 2008; Zhu, 2016). During the initial phase, cell expansion, cell wall and protein biosynthesis, and photosynthetic activity of plant cells are all inhibited, and many plants can accumulate compatible solutes and ABA to preserve the osmotic pressure (Apel and Hirt, 2004). At the same time, the ratios of Na^+/K^+ and Na^+/Ca^{2+} are also altered (Apse and Blumwald, 2007). In this context, increased expression of many genes related to cell division, amino acid metabolism, sucrose synthesis, photosynthetic activity, ABA signaling as well as potassium and potassium transport were observed in Xu22 and Xu32 under salt stress. This is consistent with the previous observations on salt-induced accumulations of special metabolites in multiple plants such as rice, sesame, and sugar beet (Wang et al., 2018; Geng et al., 2019; Zhang et al., 2019). Accordingly, KEGG enrichment analysis of the DEGs showed that

"phenylpropanoid biosynthesis," "starch and sucrose metabolism," "biosynthesis of amino acids," "flavonoid biosynthesis," and "plant hormone signal transduction" categories were significantly enriched. Similar metabolism enrichment was also enhanced in salt-tolerant sesame (Zhang et al., 2019). Enhanced synthesis of polyphenols, such as phenolic acids and flavonoids are detected under multiple abiotic stresses, and they have the potential to scavenge ROS, which can help plants respond to environmental stimuli (Sharma et al., 2019). Plant hormones including ABA, SA, JA, and ethylene play critical roles in regulating plant response to extensively biotic and abiotic stresses (Bari and Jones, 2009). Besides, amino acids can function as compatible solutes and the precursors of secondary metabolites can protect plants from various stresses, suggesting that amino acid metabolisms play a pivotal role in plant response to stress (Stepansky and Galili, 2003; Haeusler et al., 2014). The results suggested that many functional classifications of DEGs were similar between salt-tolerant Xu22 and salt-sensitive Xu32. Particularly, several categories were preferably enriched in Xu22, such as "N-Glycan biosynthesis" and "glucosinolate biosynthesis," indicating that these categories might play a role in the differential salt tolerance between Xu22 and Xu32. The later phase is mainly associated with ROS, and the imbalance between ROS production and ROS scavenging will lead to subsequent oxidative stress (Xu et al., 2018). To maintain ROS homeostasis under adverse stress, plants have evolved multiple antioxidant mechanisms, including a ROS scavenging system. In our present study, the data revealed that numerous DEGs in both Xu22 and Xu32 were associated with antioxidant activity and peroxisome under salt stress, implying that ROS scavenging-related antioxidant metabolisms are vital tolerance mechanisms for sweet potato adaptive response to salinity stress. Therefore, our data strongly suggested that salt-induced accumulations of these pivotal metabolites through biosynthesis or metabolism pathways may contribute to enhancing salt tolerance of sweet potato.

TFs are critical components that regulate plant signal transduction and gene expression in response to various biotic and abiotic stresses (Erpen et al., 2018; Zhu et al., 2018; Li et al., 2019). In our transcriptome data, a total of 1,618 differentially expressed TFs were examined, including bZIP, bHLH, ERF, MYB, NAC, and WRKY, suggesting their important roles in regulating the salt tolerance of sweet potato. Interestingly, the amount of upregulated TFs detected in salt-tolerant Xu22 was lower than that in salt-sensitive Xu32 under salt stress. Besides, the differential expression of TFs of the same family suggests that different members may have distinct biological functions or regulatory mechanisms in sweet potato response to salt stress. NACs are promising candidate factors for genetic engineering to improve crop tolerance, which have been extensively demonstrated by numerous stress-responsive NACs in various plant species (Mohanta et al., 2020). A total of 74 NACs were differentially expressed in the two phenotypes under salt stress, and the transcription of *IbNAC7* (one of the 74 NACs) was remarkably induced by salt, cold, ABA, and ACC treatments (Meng et al., 2018), suggesting that *IbNAC7* may be involved in the response to environmental cues. Subsequently, salt tolerance test of transgenic *Arabidopsis* overexpressing *IbNAC7* suggested this gene played important roles in salt tolerance. Similarly, numerous transgenic plants achieved by overexpression of *OsNAC6* (Nakashima et al., 2007), *ONAC022* (Hong et al., 2016), and *ThNAC13* (Wang et al., 2017b) displayed significantly improved salt tolerance. Our previous reports also showed that *SlNAC4* and *SlNAC11* participated in the regulation of tomato salt and drought tolerance (Zhu et al., 2014; Wang et al., 2017a). The transgenic *Arabidopsis* overexpressing *IbNAC7* not only displayed morphological advantages in germination greening rate and root length, but also displayed higher CAT activity, chlorophyll, and proline contents than that of WT under salt stress. CAT is the key antioxidant enzyme involved in ROS scavenging (Gill and Tuteja, 2010). Chlorophyll, the main pigment of plant photosynthesis, was reported that its content is positively correlated with salt tolerance (Zhu et al., 2018). Proline functions as a regulator of antioxidant system to stabilize proteins (Hong et al., 2016). In addition, the reduced MDA content and histochemical staining suggested that ROS accumulation in transgenic plants was less than than that in WT. Similarly, previous reports showed that overexpression of *NAC57* and *OsNAC2* could preclude excess ROS accumulations and improve salt tolerance in *Arabidopsis* (Mao et al., 2018; Yao et al., 2018). These results suggest that transgenic plants may have more robust photosynthetic capacity and less oxidative damage than WT plants, thus helping them to enhance tolerance to salt stress.

Besides, the improved salt tolerance of transgenic plants was also characterized by the upregulated expression of numerous and diverse types of downstream stress regulators compared to that in WT plants. A total of 1016 DEGs were detected by RNA-seq in transgenic plants compared with those in WT plants under salt stress. GO annotations of the DEGs showed that multiple terms, such as response to stress, response to oxidative stress, response to biotic stimulus were significantly upregulated in transgenic lines compared with WT plants under salt stress. qRT-PCR validation analysis showed that the expression of multiple stress-related genes in transgenic lines was indeed upregulated. For instance, the TF encoding genes *AtbHLH129*, *AtERF1*, *AtERF094*, *AtWRKY51*, and *AtWRKY63*. Wherein, *AtWRKY63* plays an important role in the response of *Arabidopsis* to ABA and drought stress (Ren et al., 2010) and *AtERF1* integrates signals from ethylene and jasmonate pathways in plant defense (Lorenzo et al., 2003). In addition, pathogenesis-related AtPR1 is an important defense protein in *Arabidopsis* (Pecenkova et al., 2017) and K^+ channel protein AtTPK2 was reported to complement the K^+ uptake deficient *E. coli* mutant (Isayenkov and Maathuis, 2013), both of their expression was significantly upregulated in transgenic plants. The enhanced expression of these genes may lead to alterations in biochemical and physiological pathways, which are important for *Arabidopsis* to adapt to salt stress. Taken together, these results suggested that IbNAC7 may be involved in the regulation of numerous and diverse stress-related genes in *Arabidopsis* responses to salt stress.

Collectively, in this study, comparative transcriptome and proteome analyses were simultaneously conducted to investigate the salt tolerance mechanisms between salt-tolerant Xu22 and salt-sensitive Xu32. We have shown that the tolerant and sensitive sweet potato genotypes response differently to salt stress, and large

amounts of DEGs and DEPs have been detected in the two cultivars, suggesting that transcription and translation regulations play a crucial role in the response of sweet potato salt stress. Importantly, our results showed that overexpression of *IbNAC7* remarkably enhanced salt tolerance in *Arabidopsis* mainly by deterring the accumulation of ROS. In addition, the data also provide numerous valuable candidate genes that may facilitate the functional characterization of the salt-responsive genes, and many of which can be used to breed salt-tolerant sweet potato cultivars. Overall, these results provide a revealing insight into sweet potato molecular response to salt stress and underlie the complex salt tolerance mechanisms between genotypes, and *IbNAC7* has been shown as a promising candidate gene to enhance the salt tolerance of sweet potato.

DATA AVAILABILITY STATEMENT

The datasets generated for this study can be found in the NCBI database under the bioproject PRJNA631585 and PRJNA649852. The proteomics data can be found in FigShare https://doi.org/10.6084/m9.figshare.12758444.v1.

AUTHOR CONTRIBUTIONS

MZ and ZL designed the experiments. MZ and XM analyzed the data and wrote the manuscript. XM, SL, TD, and TX performed the experiments. DM and SP analyzed the data and improved the manuscript. All authors contributed to the article and approved the submitted version.

FUNDING

This work was supported by National Natural Science Foundation of China (31700226), China Agriculture Research System (CARS-10-B3), and the Priority Academic Program Development of Jiangsu Higher Education Institutions (PAPD).

SUPPLEMENTARY MATERIAL

The Supplementary Material for this article can be found online at: https://www.frontiersin.org/articles/10.3389/fpls.2020.572540/full#supplementary-material

REFERENCES

Acosta-Motos, J. R., Diaz-Vivancos, P., Álvarez, S., Fernández-García, N., Sánchez-Blanco, M. J., and Hernández, J. A. (2015). NaCl-induced physiological and biochemical adaptative mechanisms in the ornamental *Myrtus communis* L. plants. *J. Plant Physiol.* 183, 41–51. doi: 10.1016/j.jplph.2015.05.005

Anders, S., and Huber, W. (2010). Differential expression analysis for sequence count data. *Genome Biol.* 11, R106. doi: 10.1186/gb-2010-11-10-r106

Apel, K., and Hirt, H. (2004). Reactive oxygen species: Metabolism, oxidative stress, and signal transduction. *Annu. Rev. Plant Biol.* 55, 373–399. doi: 10.1146/annurev.arplant.55.031903.141701

Apse, M. P., and Blumwald, E. (2007). Na+ transport in plants. *FEBS Lett.* 581, 2247–2254. doi: 10.1016/j.febslet.2007.04.014

Arisha, M. H., Aboelnasr, H., Ahmad, M. Q., Liu, Y., Tang, W., Gao, R., et al. (2020). Transcriptome sequencing and whole genome expression profiling of hexaploid sweetpotato under salt stress. *BMC Genomics* 21, 18. doi: 10.1186/s12864-020-6524-1

Bari, R., and Jones, J. D. (2009). Role of plant hormones in plant defence responses. *Plant Mol. Biol.* 69, 473–488. doi: 10.1007/s11103-008-9435-0

Bogeat-Triboulot, M.-B., Brosche, M., Renaut, J., Jouve, L., Le Thiec, D., Fayyaz, P., et al. (2007). Gradual soil water depletion results in reversible changes of gene expression, protein profiles, ecophysiology, and growth performance in *Populus euphratica*, a poplar growing in arid regions. *Plant Physiol.* 143, 876–892. doi: 10.1104/pp.106.088708

Dong, T., Zhu, M., Yu, J., Han, R., Tang, C., Xu, T., et al. (2019). RNA-seq and iTRAQ reveal multiple pathways involved in storage root formation and development in sweet potato (Ipomoea batatas L.). *BMC Plant Biol.* 19, 136. doi: 10.1186/s12870-019-1731-0

Erpen, L., Devi, H. S., Grosser, J. W., and Dutt, M. (2018). Potential use of the DREB/ERF, MYB, NAC and WRKY transcription factors to improve abiotic and biotic stress in transgenic plants. *Plant Cell Tissue Organ Cult.* 132, 1–25. doi: 10.1007/s11240-017-1320-6

Flowers, T. J. (2004). Improving crop salt tolerance. *J. Exp. Bot.* 55, 307–319. doi: 10.1093/jxb/erh003

Geng, G., Lv, C., Stevanato, P., Li, R., Liu, H., Yu, L., et al. (2019). Transcriptome analysis of salt-sensitive and tolerant genotypes reveals salt-tolerance metabolic pathways in sugar beet. *Int. J. Mol. Sci.* 20, 19. doi: 10.3390/ijms20235910

Gill, S. S., and Tuteja, N. (2010). Reactive oxygen species and antioxidant machinery in abiotic stress tolerance in crop plants. *Plant Physiol. Biochem.* 48, 909–930. doi: 10.1016/j.plaphy.2010.08.016

Guo, J., Shi, G., Guo, X., Zhang, L., Xu, W., Wang, Y., et al. (2015). Transcriptome analysis reveals that distinct metabolic pathways operate in salt-tolerant and salt-sensitive upland cotton varieties subjected to salinity stress. *Plant Sci.* 238, 33–45. doi: 10.1016/j.plantsci.2015.05.013

Haeusler, R. E., Ludewig, F., and Krueger, S. (2014). Amino acids - A life between metabolism and signaling. *Plant Sci.* 229, 225–237. doi: 10.1016/j.plantsci.2014.09.011

Haider, S., and Pal, R. (2013). Integrated analysis of transcriptomic and proteomic data. *Curr. Genomics* 14, 91–110. doi: 10.2174/1389202911314020003

He, L., Bian, J., Xu, J., and Yang, K. (2019). Novel maize NAC transcriptional repressor ZmNAC071 confers enhanced sensitivity to ABA and osmotic stress by downregulating stress-responsive genes in transgenic *Arabidopsis*. *J. Agric. Food Chem.* 67, 8905–8918 doi: 10.1021/acs.jafc.9b02331

Hong, Y., Zhang, H., Huang, L., Li, D., and Song, F. (2016). Overexpression of a stress-responsive NAC transcription factor gene *ONAC022* improves drought and salt tolerance in rice. *Front. Plant Sci.* 7, 4. doi: 10.3389/fpls.2016.00004

Hou, X.-M., Zhang, H.-F., Liu, S.-Y., Wang, X.-K., Zhang, Y.-M., Meng, Y.-C., et al. (2020). The NAC transcription factor CaNAC064 is a regulator of cold stress tolerance in peppers. *Plant Sci.* 291, 10. doi: 10.1016/j.plantsci.2019.110346

Hu, H., Dai, M., Yao, J., Xiao, B., Li, X., Zhang, Q., et al. (2006). Overexpressing a NAM, ATAF, and CUC (NAC) transcription factor enhances drought resistance and salt tolerance in rice. *Proc. Natl. Acad. Sci.* 103, 12987–12992. doi: 10.1073/pnas.0604882103

Isayenkov, S., and Maathuis, F. J. (2013). *Arabidopsis thaliana* vacuolar TPK channels form functional K^+ uptake pathways in *Escherichia coli*. *Plant Signaling Behav.* 8, e24665. doi: 10.4161/psb.24665

Jensen, M. K., Lindemose, S., Masi, F. D., Reimer, J. J., Nielsen, M., Perera, V., et al. (2013). ATAF1 transcription factor directly regulates abscisic acid biosynthetic gene *NCED3* in *Arabidopsis thaliana*. *FEBS Open Bio* 3, 321–327. doi: 10.1016/j.fob.2013.07.006

Jin, R., Kim, B. H., Ji, C. Y., Kim, H. S., Li, H. M., Ma, D. F., et al. (2017). Overexpressing *IbCBF3* increases low temperature and drought stress tolerance in transgenic sweetpotato. *Plant Physiol. Biochem.* 118, 45–54. doi: 10.1016/j.plaphy.2017.06.002

Jin, J. F., Wang, Z. Q., He, Q. Y., Wang, J. Y., Li, P. F., Xu, J. M., et al. (2020). Genome-wide identification and expression analysis of the NAC transcription factor family in tomato (*Solanum lycopersicum*) during aluminum stress. *BMC Genomics* 21, 14. doi: 10.1186/s12864-020-6689-7

Kant, P., Kant, S., Gordon, M., Shaked, R., and Barak, S. (2007). STRESS RESPONSE SUPPRESSOR1 and STRESS RESPONSE SUPPRESSOR2, two DEAD-box RNA helicases that attenuate *Arabidopsis* responses to multiple abiotic stresses. *Plant Physiol.* 145, 814–830. doi: 10.1104/pp.107.099895

Kumar, J., Singh, S., Singh, M., Srivastava, P. K., Mishra, R. K., Singh, V. P., et al. (2017). Transcriptional regulation of salinity stress in plants: A short review. *Plant Gene* 11, 160–169. doi: 10.1016/j.plgene.2017.04.001

Lee, S., Seo, P. J., Lee, H.-J., and Park, C.-M. (2012). A NAC transcription factor NTL4 promotes reactive oxygen species production during drought-induced leaf senescence in *Arabidopsis*. *Plant J.* 70, 831–844. doi: 10.1111/j.1365-313X.2012.04932.x

Li, Y.-F., Zheng, Y., Vemireddy, L. R., Panda, S. K., Jose, S., Ranjan, A., et al. (2018). Comparative transcriptome and translatome analysis in contrasting rice genotypes reveals differential mRNA translation in salt-tolerant Pokkali under salt stress. *BMC Genomics* 19, 19. doi: 10.1186/s12864-018-5279-4

Li, Y., Zhang, L., Zhu, P., Cao, Q., Sun, J., Li, Z., et al. (2019). Genome-wide identification, characterisation and functional evaluation of WRKY genes in the sweet potato wild ancestor *Ipomoea trifida* (HBK) G. Don. under abiotic stresses. *BMC Genet.* 20, 15. doi: 10.1186/s12863-019-0789-x

Liu, Y., Beyer, A., and Aebersold, R. (2016). On the dependency of cellular protein levels on mRNA abundance. *Cell* 165, 535–550. doi: 10.1016/j.cell.2016.03.014

Liu, Q. (2017). Improvement for agronomically important traits by gene engineering in sweetpotato. *Breed. Sci.* 67, 15–26. doi: 10.1270/jsbbs.16126

Lorenzo, O., Piqueras, R., Sanchez-Serrano, J. J., and Solano, R. (2003). ETHYLENE RESPONSE FACTOR1 integrates signals from ethylene and jasmonate pathways in plant defense. *Plant Cell* 15, 165–178. doi: 10.1105/tpc.007468

Mao, X., Cai, T., Olyarchuk, J. G., and Wei, L. (2005). Automated genome annotation and pathway identification using the KEGG Orthology (KO) as a controlled vocabulary. *Bioinformatics* 21, 3787–3793. doi: 10.1093/bioinformatics/bti430

Mao, C., Lu, S., Lv, B., Zhang, B., Shen, J., He, J., et al. (2017). A rice NAC transcription factor promotes leaf senescence via ABA biosynthesis. *Plant Physiol.* 174, 1747–1763. doi: 10.1104/pp.17.00542

Mao, C., Ding, J., Zhang, B., Xi, D., and Ming, F. (2018). OsNAC2 positively affects salt-induced cell death and binds to the *OsAP37* and *OsCOX11* promoters. *Plant J.* 94, 454–468. doi: 10.1111/tpj.13867

Marques, D. N., Reis, S. P. D., and Souza, C. R. B. D. (2017). Plant NAC transcription factors responsive to abiotic stresses. *Plant Gene* 11, 170–179. doi: 10.1016/j.plgene.2017.06.003

Mathew, I. E., and Agarwal, P. (2018). May the fittest protein evolve: favoring the plant-specific origin and expansion of NAC transcription factors. *Bioessays* 40, 19. doi: 10.1002/bies.201800018

Meng, X., Li, G., Yu, J., Cai, J., Dong, T., Sun, J., et al. (2018). Isolation, expression analysis, and function evaluation of 12 novel stress-responsive genes of NAC transcription factors in sweetpotato. *Crop Sci.* 58, 1328–1341. doi: 10.1007/s00344-019-10025-y

Meng, X., Li, G., Gu, L., Sun, Y., Li, Z., Liu, J., et al. (2019). Comparative metabolomic and transcriptome analysis reveal distinct flavonoid biosynthesis regulation between petals of white and purple *phalaenopsis amabilis*. *J. Plant Growth Regul.* 39, 823–840. doi: 10.2135/cropsci2017.12.0738

Mohanta, T. K., Yadav, D., Khan, A., Hashem, A., Tabassum, B., Khan, A. L., et al. (2020). Genomics, molecular and evolutionary perspective of NAC transcription factors. *PLoS One* 15, e0231425–e0231425. doi: 10.1371/journal.pone.0231425

Munns, R., and Tester, M. (2008). Mechanisms of salinity tolerance. *Annu. Rev. Plant Biol.* 59, 651–681. doi: 10.1146/annurev.arplant.59.032607.092911

Nakashima, K., Tran, L. S. P., Van Nguyen, D., Fujita, M., Maruyama, K., Todaka, D., et al. (2007). Functional analysis of a NAC-type transcription factor OsNAC6 involved in abiotic and biotic stress-responsive gene expression in rice. *Plant J.* 51, 617–630. doi: 10.1111/j.1365-313X.2007.03168.x

Nuruzzaman, M., Manimekalai, R., Sharoni, A. M., Satoh, K., Kondoh, H., Ooka, H., et al. (2010). Genome-wide analysis of NAC transcription factor family in rice. *Gene* 465, 30–44. doi: 10.1016/j.gene.2010.06.008

Parida, A. K., and Das, A. B. (2005). Salt tolerance and salinity effects on plants: a review. *Ecotoxicol. Environ. Saf.* 60, 324–349. doi: 10.1016/j.ecoenv.2004.06.010

Pecenkova, T., Pleskot, R., and Zarsky, V. (2017). Subcellular localization of *Arabidopsis* pathogenesis-related 1 (PR1) protein. *Int. J. Mol. Sci.* 18, 825. doi: 10.3390/ijms18040825

Puranik, S., Sahu, P. P., Srivastava, P. S., and Prasad, M. (2012). NAC proteins: regulation and role in stress tolerance. *Trends Plant Sci.* 17, 369–381. doi: 10.1016/j.tplants.2012.02.004

Ren, X., Chen, Z., Liu, Y., Zhang, H., Zhang, M., Liu, Q., et al. (2010). ABO3, a WRKY transcription factor, mediates plant responses to abscisic acid and drought tolerance in *Arabidopsis*. *Plant J.* 63, 417–429. doi: 10.1111/j.1365-313X.2010.04248.x

Sharma, A., Shahzad, B., Rehman, A., Bhardwaj, R., Landi, M., and Zheng, B. (2019). Response of phenylpropanoid pathway and the role of polyphenols in plants under abiotic stress. *Molecules* 24, 2452. doi: 10.3390/molecules24132452

Singh, A. K., Sharma, V., Pal, A. K., Acharya, V., and Ahuja, P. S. (2013). Genome-wide organization and expression profiling of the NAC transcription factor family in potato (*Solanum tuberosum* L.). *DNA Res.* 20, 403–423. doi: 10.1093/dnares/dst019

Stefanowicz, K. (2015). *Involvement of a carbohydrate-binding F-box-Nictaba protein from Arabidopsis thaliana in plant stress responses*. PhD thesis (Ghent: Ghent University).

Stepansky, A., and Galili, G. (2003). Synthesis of the *Arabidopsis* bifunctional lysine-ketoglutarate reductase/saccharopine dehydrogenase enzyme of lysine catabolism is concertedly regulated by metabolic and stress-associated signals. *Plant Physiol.* 133, 1407–1415. doi: 10.1104/pp.103.026294

Tian, H., Guo, H., Dai, X., Cheng, Y., Zheng, K., Wang, X., et al. (2015). An ABA down-regulated bHLH transcription repressor gene, *bHLH129* regulates root elongation and ABA response when overexpressed in *Arabidopsis*. *Sci. Rep.* 5, 11. doi: 10.1038/srep17587

Tran, L. S. P., Nakashima, K., Sakuma, Y., Simpson, S. D., Fujita, Y., Maruyama, K., et al. (2004). Isolation and functional analysis of *Arabidopsis* stress-inducible NAC transcription factors that bind to a drought-responsive cis-element in the early responsive to dehydration stress 1 promoter. *Plant Cell* 16, 2481–2498. doi: 10.1105/tpc.104.022699

Tran, L. S. P., Nishiyama, R., Yamaguchi-Shinozaki, K., and Shinozaki, K. (2010). Potential utilization of NAC transcription factors to enhance abiotic stress tolerance in plants by biotechnological approach. *GM Crops* 1, 32–39. doi: 10.4161/gmcr.1.1.10569

Wang, L., Hu, Z., Zhu, M., Zhu, Z., Hu, J., Qanmber, G., et al. (2017a). The abiotic stress-responsive NAC transcription factor SlNAC11 is involved in drought and salt response in tomato (*Solanum lycopersicum* L.). *Plant Cell Tissue Organ Cult.* 129, 161–174.

Wang, L., Li, Z., Lu, M., and Wang, Y. (2017b). ThNAC13, a NAC transcription factor from *Tamarix hispida*, confers salt and osmotic stress tolerance to transgenic tamarix and *Arabidopsis*. *Front. Plant Sci.* 8, 13. doi: 10.3389/fpls.2017.00635

Wang, J., Zhu, J., Zhang, Y., Fan, F., Li, W., Wang, F., et al. (2018). Comparative transcriptome analysis reveals molecular response to salinity stress of salt-tolerant and sensitive genotypes of indica rice at seedling stage. *Sci. Rep.* 8, 13. doi: 10.1038/s41598-018-19984-w

Wang, M., Wang, Y., Zhang, Y., Li, C., Gong, S., Yan, S., et al. (2019). Comparative transcriptome analysis of salt-sensitive and salt-tolerant maize reveals potential mechanisms to enhance salt resistance. *Genes Genomics* 41, 781–801. doi: 10.1007/s13258-019-00793-y

Wang, W., Qiu, X., Yang, Y., Kim, H. S., Jia, X., Yu, H., et al. (2019). Sweetpotato bZIP transcription factor IbABF4 confers tolerance to multiple abiotic stresses. *Front. Plant Sci.* 10, 15. doi: 10.3389/fpls.2019.00630

Wang, G., Yuan, Z., Zhang, P., Liu, Z., Wang, T., and Wei, L. (2020). Genome-wide analysis of NAC transcription factor family in maize under drought stress and rewatering. *Physiol. Mol. Biol. Plants* 26, 705–717. doi: 10.1007/s12298-020-00770-w

Xu, N., Chu, Y., Chen, H., Li, X., Wu, Q., Jin, L., et al. (2018). Rice transcription factor OsMADS25 modulates root growth and confers salinity tolerance via the ABA–mediated regulatory pathway and ROS scavenging. *PLoS Genet.* 14, e1007662. doi: 10.1371/journal.pgen.1007662

Yan, C., Fan, M., Yang, M., Zhao, J., Zhang, W., Su, Y., et al. (2018). Injury activates Ca^{2+}/calmodulin-dependent phosphorylation of JAV1-JAZ8-WRKY51 complex for jasmonate biosynthesis. *Mol. Cell* 70, 136–149. doi: 10.1016/j.molcel.2018.03.013

Yang, Z., Lu, R., Dai, Z., Yan, A., Tang, Q., Cheng, C., et al. (2017). Salt-stress response mechanisms using de novo transcriptome sequencing of salt-tolerant and sensitive corchorus spp. genotypes. *Genes* 8, 15. doi: 10.3390/genes8090226

Yang, Z., Sun, J., Chen, Y., Zhu, P., Zhang, L., Wu, S., et al. (2019). Genome-wide identification, structural and gene expression analysis of the bZIP transcription factor family in sweet potato wild relative *Ipomoea trifida*. *BMC Genet.* 20, 41. doi: 10.1186/s12863-019-0743-y

Yao, W., Zhao, K., Cheng, Z., Li, X., Zhou, B., and Jiang, T. (2018). Transcriptome analysis of poplar under salt stress and over-expression of transcription factor *NAC57* gene confers salt tolerance in transgenic *Arabidopsis*. *Front. Plant Sci.* 9, 10. doi: 10.3389/fpls.2018.01121

Young, M. D., Wakefield, M. J., Smyth, G. K., and Oshlack, A. (2010). Gene ontology analysis for RNA-seq: accounting for selection bias. *Genome Biol.* 11, R14. doi: 10.1186/gb-2010-11-2-r14

Yu, Y., Xu, T., Li, X., Tang, J., Ma, D., Li, Z., et al. (2016). NaCl-induced changes of ion homeostasis and nitrogen metabolism in two sweet potato (*Ipomoea batatas* L.) cultivars exhibit different salt tolerance at adventitious root stage. *Environ. Exp. Bot.* 129, 23–36. doi: 10.1016/j.envexpbot.2015.12.006

Zarei, A., Körbes, A. P., Younessi, P., Montiel, G., Champion, A., and Memelink, J. (2011). Two GCC boxes and AP2/ERF-domain transcription factor ORA59 in jasmonate/ethylene-mediated activation of the *PDF1.2* promoter in *Arabidopsis*. *Plant Mol. Biol.* 75, 321–331. doi: 10.1007/s11103-010-9728-y

Zhang, X., Henriques, R., Lin, S.-S., Niu, Q.-W., and Chua, N.-H. (2006). Agrobacterium-mediated transformation of *Arabidopsis thaliana* using the floral dip method. *Nat. Protoc.* 1, 641–646. doi: 10.1038/nprot.2006.97

Zhang, Y., Li, D., Zhou, R., Wang, X., Dossa, K., Wang, L., et al. (2019). Transcriptome and metabolome analyses of two contrasting sesame genotypes reveal the crucial biological pathways involved in rapid adaptive response to salt stress. *BMC Plant Biol.* 19, 14. doi: 10.1186/s12870-019-1665-6

Zhou, Y., Zhu, H., He, S., Zhai, H., Zhao, N., Xing, S., et al. (2019). A novel sweetpotato transcription factor gene *IbMYB116* enhances drought tolerance in transgenic *Arabidopsis*. *Front. Plant Sci.* 10, 12. doi: 10.3389/fpls.2019.01025

Zhu, M., Chen, G., Zhang, J., Zhang, Y., Xie, Q., Zhao, Z., et al. (2014). The abiotic stress-responsive NAC-type transcription factor SlNAC4 regulates salt and drought tolerance and stress-related genes in tomato (*Solanum lycopersicum*). *Plant Cell Rep.* 33, 1851–1863. doi: 10.1007/s00299-014-1662-z

Zhu, M., Meng, X., Cai, J., Li, G., Dong, T., and Li, Z. (2018). Basic leucine zipper transcription factor SlbZIP1 mediates salt and drought stress tolerance in tomato. *BMC Plant Biol.* 18, 83. doi: 10.1186/s12870-018-1299-0

Zhu, J. K. (2002). Salt and drought stress signal transduction in plants. *Annu. Rev. Plant Biol.* 53, 247. doi: 10.1146/annurev.arplant.53.091401.143329

Zhu, J. K. (2016). Abiotic stress signaling and responses in plants. *Cell* 167, 313–324. doi: 10.1016/j.cell.2016.08.029

Conflict of Interest: The authors declare that the research was conducted in the absence of any commercial or financial relationships that could be construed as a potential conflict of interest.

The reviewer SK declared a past co-authorship with several of the authors ZL and DM to the handling editor.

Copyright © 2020 Meng, Liu, Dong, Xu, Ma, Pan, Li and Zhu. This is an open-access article distributed under the terms of the Creative Commons Attribution License (CC BY). The use, distribution or reproduction in other forums is permitted, provided the original author(s) and the copyright owner(s) are credited and that the original publication in this journal is cited, in accordance with accepted academic practice. No use, distribution or reproduction is permitted which does not comply with these terms.

frontiers in Plant Science

ORIGINAL RESEARCH
published: 27 August 2020
doi: 10.3389/fpls.2020.01289

Comparison of Selection Traits for Effective Popcorn (*Zea mays* L. var. Everta) Breeding Under Water Limiting Conditions

Samuel Henrique Kamphorst[1], Antônio Teixeira do Amaral Júnior[1], Valter Jário de Lima[1], Pedro Henrique Araújo Diniz Santos[1], Weverton Pereira Rodrigues[2], Janieli Maganha Silva Vivas[1], Gabriel Moreno Bernardo Gonçalves[1], Katia Fabiane Medeiros Schmitt[1], Jhean Torres Leite[1], Marcelo Vivas[1], Freddy Mora-Poblete[3], Omar Vergara-Díaz[4,5], Jose Luis Araus Ortega[4,5], José Cochicho Ramalho[6,7] and Eliemar Campostrini[1]**

[1] Laboratório de Melhoramento Genético Vegetal, Centro de Ciências e Tecnologias Agropecuárias, Universidade Estadual Norte Fluminense Darcy Ribeiro (UENF), Rio de Janeiro, Brazil, [2] Centro de Ciências Agrárias, Naturais e Letras, Universidade Estadual da Região Tocantina do Maranhão, Estreito, Brazil, [3] Instituto de Ciencias Biológicas, Universidad de Talca, Talca, Chile, [4] Unitat de Fisiologia Vegetal, Facultat de Biologia, Universitat de Barcelona, Barcelona, Spain, [5] AGROTECNIO (Center of Research in Agrotechnology), Lleida, Spain, [6] PlantStress & Biodiversity Lab, Centro de Estudos Florestais (CEF), Departamento de Recursos Naturais, Ambiente e Território, Instituto Superior de Agronomia, Universidade de Lisboa, Oeiras, Portugal, [7] Unidade de Geobiociências, Geoengenharias e Geotecnologias (GeoBioTec), Faculdade de Ciências e Tecnologia (FCT), Universidade NOVA de Lisboa (UNL), Monte de Caparica, Portugal

OPEN ACCESS

Edited by:
Raul Antonio Sperotto, Universidade do Vale do Taquari-Univates, Brazil

Reviewed by:
Mukhtar Ahmed, Swedish University of Agricultural Sciences, Sweden
Bipin Kumar Pandey, University of Nottingham, United Kingdom

***Correspondence:**
Samuel Henrique Kamphorst
samuelkampho@hotmail.com
Eliemar Campostrini
campostenator@gmail.com

Specialty section:
This article was submitted to Crop and Product Physiology, a section of the journal Frontiers in Plant Science

Received: 24 June 2020
Accepted: 07 August 2020
Published: 27 August 2020

Citation:
Kamphorst SH, Amaral Júnior ATd, de Lima VJ, Santos PHAD, Rodrigues WP, Vivas JMS, Gonçalves GMB, Schmitt KFM, Leite JT, Vivas M, Mora-Poblete F, Vergara-Díaz O, Araus Ortega JL, Ramalho JC and Campostrini E (2020) Comparison of Selection Traits for Effective Popcorn (Zea mays L. var. Everta) Breeding Under Water Limiting Conditions. Front. Plant Sci. 11:1289. doi: 10.3389/fpls.2020.01289

Climate change is expected to intensify water restriction to crops, impacting on the yield potential of crops such as popcorn. This work aimed to evaluate the performance of 10 field cultivated popcorn inbred lines during two growing seasons, under well-watered (WW) and water stressed (WS) ($\psi_{soil} \geq -1.5$ MPa) conditions. Water stress was applied by withholding irrigation in the phenological phase of male pre-anthesis. Additionally, two contrasting inbred lines, P7 (superior line) and L75 (low performer) were compared for grain yield (GY) and expanded popcorn volume (EPV), selected from previous studies, were tested under greenhouse conditions. In the field, no genotype x water condition x crop season (G×WC×CS) interaction was observed, whereas GY (–51%), EPV (–55%) and leaf greenness (SPAD index) measured 17 days after anthesis (DAA) (> –10%) were highly affected by water limitation. In general, root traits (angles, number, and density) presented G×WC×CS interaction, which did not support their use as selection parameters. In relation to leaf senescence, for both WS and WW conditions, the superior inbred lines maintained a stay-green condition (higher SPAD index) until physiological maturity, but maximum SPAD index values were observed later in WW (48.7 by 14 DAA) than in WS (43.9 by 7 DAA). Under both water conditions, negative associations were observed between SPAD index values 15 and 8 days before anthesis DBA), and GY and EPV ($r \geq -0.69$), as well as between SPAD index 7, 17, and 22 DAA, and angles of brace root (AB), number of crown roots (NC) and crown root density (CD), in WS ($r \geq -0.69$), and AB and CD, in WW ($r \geq -0.70$). Lower NC and CD values may allow

further root deepening in WS conditions. Under WS P7 maintained higher net photosynthesis values, stomatal conductance, and transpiration, than L75. Additionally, L75 exhibited a lower (i.e., more negative) carbon isotope composition value than P7 under WS, confirming a lower stomatal aperture in L75. In summary, besides leaf greenness, traits related to leaf photosynthetic status, and stomatal conductance were shown to be good indicators of the agronomic performance of popcorn under water constraint.

Keywords: carbon isotope composition ($\delta^{13}C$), drought, leaf gas exchanges, popcorn yield, water use efficiency

INTRODUCTION

Since the pre-industrial period, anthropogenic activities mainly associated with increased greenhouse gas emissions, have caused an increase of about 1°C in the average global temperature. Depending on future emissions, this increase may reach up to 1.5°C between 2030 and 2052, which tends to aggravate the frequency of extreme droughts and rainfall events worldwide (IPCC, 2019). This will have severe impacts on world agribusiness (Awange et al., 2016; Van Loon et al., 2016), particularly for Brazil, whose economy relies on large-scale agricultural activities. Thus, global environmental changes may increase plant stress levels, requiring specific plant breeding expertise to overcome these challenging conditions (Blum, 2011).

Popcorn sales are worth approximately one hundred million dollars annually in the USA, and there is also a high demand in Brazil for this product (Kist et al., 2019). The seed market offers cultivars with high-yield potential for environments with optimal water supply but, to date, there are no cultivars adapted to water deficit conditions, with droughts being one of the most limiting abiotic factors for the productivity of this crop (Kamphorst et al., 2019; Lima et al., 2019). Thus, it is essential to obtain genotypes which are more efficient regarding water use and identifying plant traits for genotypic selection under drought conditions.

The initial step is the evaluation of germplasm with identification of predictor characteristics for drought adaptation. Traditionally, secondary characteristics associated with higher grain yield are considered, such as a shorter interval between male and female anthesis (Câmara et al., 2007; Teixeira et al., 2010), late leaf senescence (Câmara et al., 2007; Costa et al., 2008), higher prolificity (Li et al., 2003; Câmara et al., 2007), and fewer tassel branches (Durães et al., 2004; Câmara et al., 2007). Technological advances associated with the use of remote sensing techniques present the opportunity for using new approaches such as canopy temperature measurements (Romano et al., 2011; Zia et al., 2013), leaf senescence estimated by NDVI (Cabrera-Bosquet et al., 2011; Adebayo et al., 2014), leaf greenness, obtained by SPAD index (Cairns et al., 2012), and RGB images (Araus et al., 2018).

Photosynthesis is the process responsible for increasing plant biomass and productivity, while stomatal conductance is responsible for controlling water loss to the atmosphere, however reducing stomatal opening also decreases CO_2 availability to the RuBisCO carboxylation sites, and thus C-assimilation (Farquhar and Sharkey, 1982; Buckley, 2019). Therefore, gas exchange measurements can be used to distinguishing tolerant/susceptible genotypes to drought (Flexas et al., 2018), however this requires a high number of evaluations under field conditions in breeding programs (Earl and Tollenaar, 1999). Additionally, the characteristics derived from leaf spectral indices associated with canopy temperature, cell and leaf water content, and the composition of photosynthetic leaf pigments, allows the use of thermal and multispectral imaging as feasible options to understand biological phenomena and select plants under stress (Fernández-Calleja et al., 2020). Another option is the isotopic signature obtained from C^{13} quantification, which indicates water use efficiency (Araus et al., 2010; Chairi et al., 2016). The deployment of these high-performance phenotyping techniques is known as physiological breeding (Reynolds and Langridge, 2016).

Some of the high-performance phenotyping techniques use multispectral analyses associated with photosynthetic leaf pigment (NDVI, PRI) and chlorophyll concentrations (SPAD index) (Araus et al., 2018). The analysis of these characteristics has been efficiently used to select drought tolerant genotypes (Khanna et al., 2019), associated with the fact that genotypes which are more susceptible to soil water limitation, present increased leaf senescence (Romano et al., 2011; Araus et al., 2012; Zia et al., 2013). Both leaf and canopy studies of leaf senescence can generate information to improve the ability to estimate grain yield (Echarte et al., 2008; Escobar-Gutiérrez and Combe, 2012). Stay-green maize genotypes are the most productive and considered more adapted to drought conditions. However, the efficient use of phenotyping methodologies partly depend on the ability to use them accurately at critical grain production stages (Cairns et al., 2012; Adebayo et al., 2014; Araus et al., 2018).

Maize plants under water stress have less crown roots, increasing water acquisition through other roots located in

Abbreviations: 100GW, 100-grain weight; A, net photosynthetic rate; AB, angles of brace roots; AC, angles of crown roots; CS, crop seasons; DA, branching density of adventitious roots; DAA, days after anthesis; DAS, days after sowing; DB, branching density of brace roots; DC, branching density of crown roots; E, transpiration rate; ED, ear diameter; EL, ear length; EPV, expanded popcorn volume; FC, field capacity; G, genotype; GNR, grain number per row; g_s, stomatal conductance; GY, grain yield; LA, leaf area; NA, number of adventitious roots; NB, number of brace roots; NC, number of crown roots; PE, popping expansion; rg, genotypic correlation coefficient; RNE, row number per ear; RWD, root weight density; SB, shoot dry biomass; SLA, specific leaf area; SPAD, soil plant analyzer development; WC, water condition; WS, water-stressed; WUE_{agron}, agronomic water use efficiency; $WUE_{instant}$, instantaneous water use efficiency; $WUE_{intrinsic}$, intrinsic water use efficiency; WW, well-watered.

deeper soil layers (Gao and Lynch, 2016), since a deeper root system can allow access to water in additional soil layers (Hund et al., 2009). Therefore, in cases of soil water restriction, an efficient root architecture associated with a deeper root system, is essential to delay leaf senescence, maintaining a high photosynthetic performance to sustain growth and productivity (Lynch, 1995). In this context, the objective of this study was to evaluate the field performance of agronomic and root characteristics and the SPAD index of a group of popcorn inbred lines cultivated under contrasting soil water conditions during male pre-anthesis: well-watered (WW) and water-stressed (WS). Furthermore, this study evaluated the use of possible players (selection traits) in the selection of contrasting grain yield (GY) and expanded popcorn volume (EPV) genotypes cultivated under greenhouse conditions.

MATERIALS AND METHODS

Field Experiment Conditions

Plant Material

This study evaluated ten popcorn inbred lines (S_7), whose genealogy is derived from germplasm adapted to tropical (L61, L63, L65, and L71 from the BRS-Angela population) and temperate/tropical conditions (P7, from the commercial hybrid Zélia; P2 and P3, from the compound CMS-42; P6, from the commercial hybrid IAC-112; L54, L55, and L75 and L76, from the Barão de Viçosa population) (Kamphorst et al., 2019).

Experimental Design, Cultural Treatments, and Water Conditions

The experiments were conducted at the Experimental Station of the Antônio Sarlo Agricultural State College in Campos dos Goytacazes, RJ, Brazil (Latitude 21°42′48″ S, Longitude 41°20′38″ W; altitude 14 m), in the crop seasons (CS) of 2016 and 2018, during the dry seasons (April and August).

The experimental design was completely randomized blocks with three repetitions for both well-watered (WW) and water-stressed (WS) conditions. The plots comprised two 4.40-m lines, spaced 0.20 m between plants and 0.80 m between lines (44 plants per plot).

The plants were irrigated using a drip system, using a Katif dripper for each plant at a flow rate of 2.3 mm h^{-1}. Soil water was monitored using three Decagon MPS-6 sensors (Decagon, USA) installed at a depth of 0.20 m in the planting line between two plants. The WW condition received irrigation at soil field capacity (−0.01 MPa), whereas in WS conditions, irrigation was withheld 15 days before male anthesis (June 22nd to June 26th during both years). Under WS, the soil reached permanent wilting point (−1.5 MPa) 77 days after sowing (DAS) (grain filling stage) in the 2016 experiment, and at 68 DAS (male anthesis) and 90 DAS (grain filling stage) in the 2018 experiment (due to a rainfall episode between these two periods) (**Supplementary Table 1**). During the experimental period, total rainfall was 133 and 148 mm in 2016 and 2018, respectively (**Supplementary Table 1**, **Figure 1**).

During the crop cycle, in the 2016 and 2018 harvests, the average temperature was 22.6°C and 21.6°C and the relative humidity was 69.7% and 78.5%, respectively. The average solar

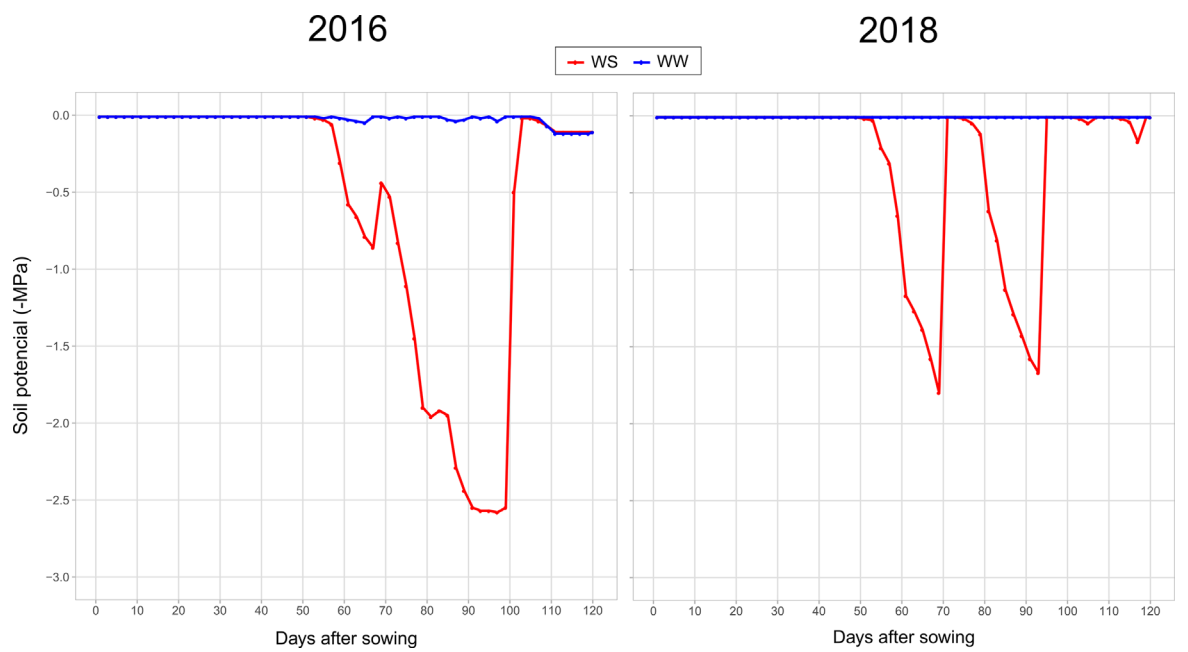


FIGURE 1 | Soil water potential (MPa) in days after sowing for experiments performed during the 2016 and 2018 harvests with popcorn inbred lines in water stressed (WS, in red) and well-watered (WW, in blue) conditions.

radiation was ≅1,100 and 1,200 μmol m^{-2} s^{-1} in 2016 and 2018, respectively (**Figure 2**). Weather conditions were recorded at a National Institute of Meteorology (INMET) weather station located near the experimental area.

Planting fertilization included 30 kg ha^{-1} N (urea), 60 kg ha^{-1} P_2O_5 (triple superphosphate), and 60 kg ha^{-1} K_2O (potassium chloride). Cover fertilization (30 DAS) included 100 kg ha^{-1} N (urea).

Agronomic and Root System Traits and the SPAD Index

The 100-grain weight (100GW) was determined by averaging the weight (g) of two samples of 100 grains per plot. Popping expansion (PE) was measured by the mass of 30 g of grains placed in a microwave oven in a kraft bag for 2 min, with the volume of popcorn quantified in a 2000-ml beaker and the ratio of the popped volume being divided by 30 g and expressed in ml g^{-1}. Grain yield (GY) was obtained after threshing the ears of each plot, which were corrected to 13% humidity (kg ha^{-1}). The EPV was obtained by multiplying GY and PE (m^3 ha^{-1}). The row number per ear (RNE) and grain number per row (GNR) were determined by counting, ear diameter (ED) was estimated with a Vernier caliper (mm), and ear length (EL) was measured with a ruler (cm). The characteristics 100GW, PE, GY, and EPV were measured in all plants in the plot. GNR, RNE, ED, and EL were measured using a random sample of six plants per plot.

Root architecture was evaluated based on the methods used by Trachsel et al. (2011) with some modifications. The root systems of two plants per plot, one from each row, were removed in a 40 cm diameter soil cylinder with a depth of 25 cm to allow the following measurements: angles (°) of brace (AB) and crown roots (AC) [using a protractor and expressed in relation to the soil]; number (N) of adventitious (NA), of brace (NB), and of crown roots (NC) [by counting these structures]; and branching density (D) of adventitious (DA), of brace (DB), and of crown roots (DC) [using the diagrammatic scale proposed by Trachsel et al. (2011)]. Root density values ranging from 1 to 9, with higher counts indicating higher density.

Leaf greenness (SPAD index) was estimated using three readings from the middle third of the leaf counted from the apex and below the flag leaf using a portable SPAD-502 chlorophyll meter (Minolta, Japan). The SPAD index was measured on eight different dates according to male anthesis: 15 (S1) and 8 (S2) days before anthesis (DBA), during male anthesis (S3), and 7 (S4), 17 (S5), 22 (S6), 35 (S7), and 42 (S8) days after anthesis (DAA). SPAD index was evaluated in six plants per plot, with three readings per plant.

Statistical Analysis

Analysis of variance was performed for each water treatment and year considering the linear model: $y_{ij} = \mu + g_i + b_j + e_{ij}$, where mean (μ) and genotype effect (g) were considered fixed and block (b) and error (e) were considered random.

The experiments were then jointly analyzed considering different water treatments and years using the following mathematical model: $y_{ijk} = \mu + (b/l)/wc_{jkm} + g_i + cs_j + wc_k + g_{aij} + gw_{cik} + csw_{cjk} + gcswc_{ijk} + e_{ijk}$, where the mean (μ), the effect of genotype (G), crop (CS), water condition (WC), G × CS interaction (gcs), G × WC interaction (gwc), CS × WC (cswc) interaction, and G × CS × WC interaction (gcswc) were considered fixed and the block within WC (b/l) and error (e) were considered random.

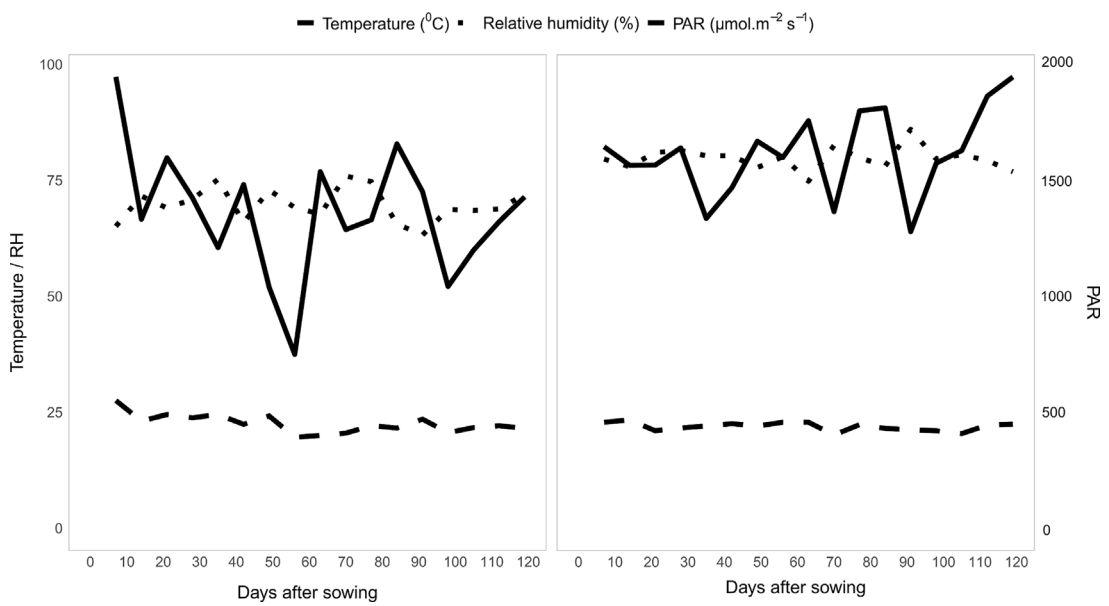


FIGURE 2 | Weekly average values on DAS of temperature (°C), relative humidity (%) and solar radiation (μmol $m^{-2}s^{-1}$) throughout the growing period of the experiments with popcorn inbred lines during the 2016 and 2018 crop seasons.

The variables that showed significant differences between genotypes with at least 5% probability from the F-test were analyzed with the Tukey's test at the same level of significance.

Regression analysis was performed for the SPAD index variable after analysis of variance using the quadratic model and considering significance at 5% probability from the F-test.

Subsequently, genotypic correlation coefficient (*rg*) estimates were calculated according to Mode and Robinson (1959), and tested at 5% and 1% probability levels using the *t*-test.

Greenhouse Experiments

Genotypes and Growth Conditions

This experiment was conducted from early May to mid-July 2019 (spring-summer), in a greenhouse at the Faculty of Biology, University of Barcelona, Spain, using two inbred lines (P7 and L75) identified as drought tolerant and sensitive, respectively, in the 2016 and 2018 field experiments in Brazil. Three seeds from each lineage were germinated in substrate in PVC tubes of 14 cm diameter and 150 cm length, which were kept at field capacity (FC). The substrate consisted of 80% perlite and 20% peat with the addition of a slow-release fertilizer, which in absolute values corresponded to 144.7 kg N ha^{-1}, 36.2 kg P ha^{-1}, and 57.8 kg K ha^{-1}.

The tubes were longitudinally divided into two halves held together with adhesive tape. The lower part of the tube was tied with wire and closed with a vase of the same diameter, with eight holes to avoid loss of substrate. In addition, the tubes were covered with plastic to reduce evapotranspiration.

Thinning was performed 15 days after germination, retaining one plant per tube. The experiment was arranged in completely randomized blocks under the two water conditions, with three repetitions each. The plants were cultivated under a rain shelter that allowed the control of water availability. The temperature and humidity inside the greenhouse followed a seasonal pattern as shown in **Figure 3**.

For field capacity evaluation the tubes were fully irrigated before plant sowing, and left for 72 h to drain the excess irrigation water. After this time, the cylinders were weighed. Field capacity was calculated from the weight difference between the dry substrate and after draining excess water.

In the WW condition, the tubes were kept at FC until the time of the evaluations, which were conducted during the pre-anthesis period. For this, every 2 to 3 days before irrigation, the tubes were weighed and received the corresponding amount of water to return to FC. In the WS condition, limited irrigation was imposed 15 days

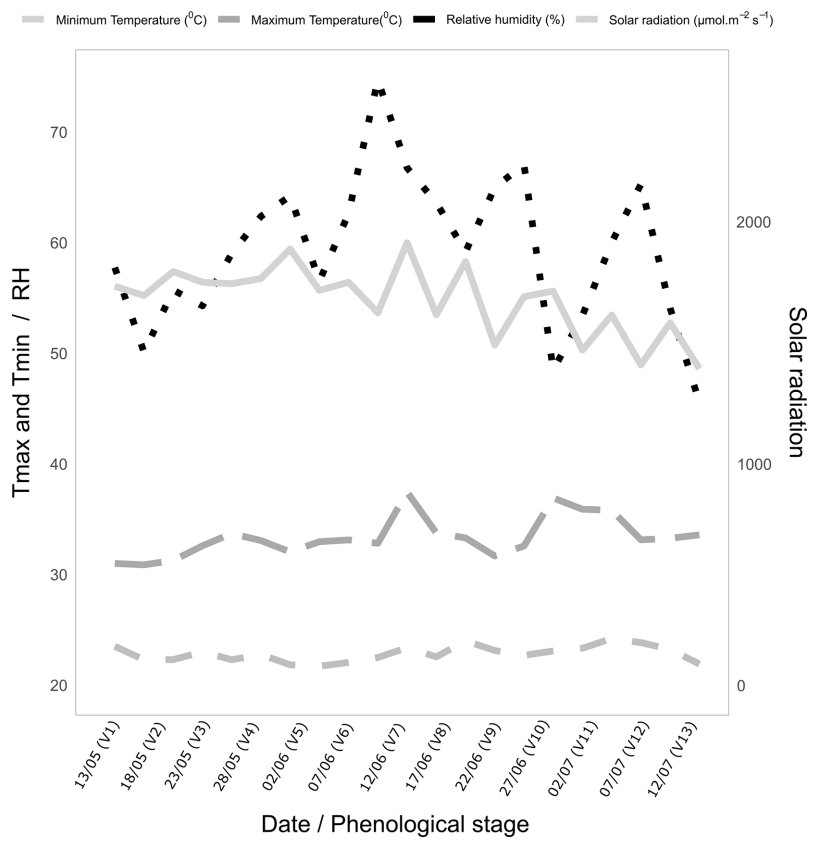


FIGURE 3 | Average minimum (Tmin) and maximum (Tmax) air temperatures (°C), relative humidity (RH, %), and photosynthetically active radiation (PAR, µmol m^2 s^1) as a function of the phenological stages (V) during the growing period of popcorn plants.

after the emergence of seedlings. The amount of water available in the tubes gradually reduced according to plant consumption, until reaching 35% of FC (40 DAS); thereafter, they were maintained for 15 days until harvest. The decrease in moisture in the tubes was homogeneous as the plants that consumed the most water received the precise amount of irrigation to return to the substrate water conditions of the plants that consumed the least. In both WCs, the weight of the plants was disregarded for the calculation of the water capacity of the tubes.

Morphological Characteristics, Stomata and Epidermal Cell Density, and Foliar Pigments

After harvest, plants were collected and dried (70°C, 72 h) to determine shoot biomass (SB; g). The specific leaf area (SLA) was calculated using the leaf area (cm^2) to dry leaf mass ($cm^2\ g^{-1}$) ratio. For this, of 1.65 cm diameter leaf discs were collected from the last developed leaf of each plant and dry mass determined as above.

The leaf area (m^2) was calculated from photographs of each individual plant. The images were acquired with a Sony α6000 DSLR (Sony Corporation, Japan), 24.5-megapixel resolution camera with a 23.5 x 15.6 mm sensor size, native resolution of 6,000 × 4,000 pixels and equipped with a 35-mm focal length lens. The pixel size was calculated using the Ground Sample Distance (GSD) calculator tool developed by Pix4D (https://support.pix4d.com/hc/en-us/articles/202559809-Ground-sampling-distance-GSD). We have used the following equation: $D = \frac{(Sw \,.\, H.100)}{(Fr \,.\, imW)}$, where GSD represent the distance between two consecutive pixel centers, Sw denotes the sensor width of the camera (mm), H is the height distance between the camera and the object (m), Fr is the real focal length of the camera (mm) and imW is the image width (pixels). In our case, Sw = 23.2 mm, the height average was H = 1.95 m, Fr = 18 mm and the imW = 4608 pixels. Therefore, images with GSD = 0.054 cm/pixel were analyzed using ImageJ software (Schneider et al., 2012).

For the evaluation of stomatal morphological traits, the adaxial and abaxial epidermal sides of the last developed leaf (2nd or 3rd leaf counted from the apex specifically between the central vein and the extremity), were coated with a colorless nail base coat. After drying for 10 min, the dried coat layer was removed with adhesive tape and transferred to a glass slide. The number of stomata (s) and epidermal cells (e) were counted at ×40 magnification. Each foliar replica (adaxial and abaxial) was counted in three microscope fields, according to the methodology described by Radoglou and Jarvis (1990).

The stomatal and epidermal cell densities were calculated using the following equations: $SD = \frac{s}{0.152}$ and $ECD = \frac{e}{0.152}$, where SD is stoma density (mm^{-2}), ECD is epidermal cell density (mm^{-2}), and 0.152 mm^{-2} is the surface area of the microscope (0.22 mm radius).

The stomatal index (SI, %) of each leaf face was calculated using the following equation: $SI = 100 \cdot (\frac{SD}{ECD})$.

Foliar chlorophyll, flavonoid, and anthocyanin epidermal levels and the nitrogen balance index were evaluated from the middle third of the last leaf developed at the time of harvest, using a portable Dualex® meter (FORCE-A, Orsay, France).

Foliar Gas Exchange and Fluorescence Measurements, Relative Foliar Water Content, and C Isotope Discrimination

One day before harvest, between 11:00 AM and 2:00 PM, gas exchanges were evaluated using an infrared gas analyzer, model LI-6400 (LI-COR, Lincoln, NE, USA), equipped with a light source (6400-40 LCF, LI-COR). During the evaluations, the PAR was set to 1500 μmol $m^{-2}\ s^{-1}$, CO_2 concentration to 400 μmol mol^{-1}, relative humidity to between 55% and 60%, and temperature to 25°C. Net photosynthetic rate (A), stomatal conductance (g_s), and transpiration rate (E) were evaluated from the last developed leaf of each plant. The instantaneous ($WUE_{instant}$ = A/E) and intrinsic ($WUE_{intrinsic}$ = A/g_s) water use efficiencies were also calculated.

The agronomic water use efficiency was calculated using the equation $WUE_{agron} = \frac{SB}{T_{cum}}$, where SB is the shoot dry biomass, and T_{cum} is the total amount of transpired water of each plant (T_{cum}, $dm^3\ plant^{-1}$). Irrigation was controlled during the whole growth cycle, which allowed estimation of the T_{cum} values.

The stable carbon (^{13}C:^{12}C) isotope ratio was measured in leaf dry matter using an elemental analyzer (Flash 1112 EA; Thermo Finnigan, Bremen, Germany) coupled to an isotope ratio mass spectrometer (Delta C IRMS, Thermo Finnigan) operating in a continuous flow mode. Samples of 0.7–0.8 mg of leaf dry matter from each plant, together with reference materials were weighed and sealed into tin capsules. Measurements were performed at the Scientific Facilities of the University of Barcelona. Isotopic values were expressed in composition notation (δ) as follows: $\delta^{13}C$ = [($^{13}C/^{12}C$) sample/($^{13}C/^{12}C$) standard]–1, where "sample" refers to plant material and "standard" to international secondary standards of known ^{13}C:^{12}C ratios (IAEA CH7 polyethylene foil, IAEA CH6 sucrose, and USGS 40 L-glutamic acid) calibrated against Vienna Pee Dee Belemnite calcium carbonate with analytical precision (standard deviation) of 0.15‰. The last fully developed leaf of each plant was used.

Before harvesting, leaf discs (1.65 cm in diameter) were collected from the same leaves as those used for gas exchange evaluation to obtain the relative water content according to the methodology proposed by González and González-Vilar (2001).

Root Traits

After harvesting the shoots, the roots were also collected, being abundantly washed with water to remove perlite and peat, rinsed with distilled water and superficially dried with paper towels. Finally, the root material was cut into five equal sections, each 0.30 m long, obtained from the upper surface of the tubes to the lower end, in the following layers: 0–30 cm (a), 30–60 cm (b), 60–90 cm (c), 90–120 cm (d), and 120–150 cm (e).

The root sections were stored separately in a paper envelope and dried (70°C, 72 h). Afterward, the ratio between the dry biomass of the aerial parts and the roots was calculated.

The root weight density in each section of soil (RWD_{sec}, g m^{-3}) was estimated by: $RWD_{sec} = RB_{sec}/(\pi * R^2 * L)$ where RB_{sec} is the dry biomass of the roots in the soil section (g); R is the tube radius (0.07 m), and L is the length of the section (0.30 m long) (Elazab et al., 2012).

Statistical Analysis

Analysis of variance was performed for each water condition (WS and WW) and for the interaction genotype by WC. The analysis followed the statistical model: $Y_{ijk} = \mu + G_i + B/WC_{jk} + WC + WC_{ij} + \epsilon_{ijk}$,, where: Y_{ijk} = observation of the i-th genotype in the j-th environment in the k-th block; μ = general constant; Gi = fixed effect of i-th genotype; B / WC_{jk} = random effect of the k-th block within WCj; WC_j = fixed effect of the j-th environment; GWC_{ij} = fixed effect of the interaction between the i-th genotype and the j-th WC; and ϵ_{ijk} = random error. Then, the effects of the inbred lines were estimated for each trait along with the estimates of the genotypic correlation coefficient.

RESULTS

Field Study

Genetic Variability in Different Water Conditions and Cropped Years

The inbred lines showed significantly different agronomic characteristics in both WCs and CS, except for 100GW in WW-2018. Comparing WCs, expressive reductions (> 20%) occurred in 100GW (23.39), PE (29.31), GY (56.70), and EPV (68.27) in CS 2016 and in GY (44.58), EPV (50.61), and GNR (26.15) in CS 2018. There were significant differences between CS (except for PE), WC, and G. The CS × WC interactions for the variables GNR and ED, as well as the CS × G interactions for the variables GY, ED, and EL and the WC× G interactions for the variables 100GW, RNE, GNR, ED, and EL were not significant. The CS × WC × G interaction was significant only for PE (**Table 1**).

Most of the inbred lines presented significantly different SPAD index values in both WCs and CS. In the evaluations conducted in 2018, the variables S1 and S3 in WS and WW, as well as S5 in WS, presented no significant differences. Comparing the WS and WW conditions, significant reductions (> 10%) occurred for S5 (11.26), S6 (18.33), S7 (28.23), and S8 (50.85) in 2016; and S2 (14.85), S3 (17.41), S4 (13.72), S7 (13.26), and S8 (21.59) in 2018. There were significant differences for CS, WC, and G when considering the SPAD variable for all evaluation dates. The CS × WC interactions for SPAD in the evaluations at S1 and S5, as well as the CS × G interactions at S4 and S7 and WC × G interactions at S1, S2, S3, S4, S5, S7, and S8 were not significant ($p > 0.05$). The CS × WC × G interaction was significant only for S7 ($p < 0.01$) (**Table 1**).

In CS 2016, the inbred lines presented significant differences in all the root characteristics and in both WCs. In 2018, the variables AC, NA, DA, DB, and DC under WS conditions, and AB and AC under WW conditions, expressed significant differences between genotypes. Comparing the WS and WW conditions, significant increases were

TABLE 1 | Summary of variance analysis, general means, interactions by joint analysis for agronomic variables, SPAD index, and root architecture in popcorn inbred lines under well-watered (WW) and water stress (WS) conditions, in the 2016 and 2018 crop seasons (CS).

Traits		WS				WW				Joint analysis						
		2016		2018		2016		2018		CS	WC	G	CS*WC	CS*G	WC*G	CS*WC*G
Agronomic	100-grain weight (g)	10.10	**	13.40	**	13.20	*	14.0	ns	***	***	***	***	**	ns	ns
	Popping expansion (g ml^{-1})	19.63	**	23.17	**	27.77	*	25.65	**	ns	***	***	***	***	*	*
	Grain yield (kg ha^{-1})	1089.0	**	1010.4	**	2515.2	**	1823.2	**	***	***	***	***	ns	***	ns
	Expanded popcorn volume (m^3 ha^{-1})	21.88	**	22.49	**	68.96	**	45.54	**	***	***	***	***	*	**	ns
	Row number per ear	12.92	**	10.48	*	13.41	*	12.08	**	***	***	***	*	*	ns	ns
	Grain number per row	19.88	**	14.29	**	24.68	**	19.34	**	***	***	***	ns	**	ns	ns
	Ear diameter (mm)	27.61	**	25.58	**	29.35	**	28.29	**	***	***	***	ns	ns	ns	ns
	Ear length (cm)	12.40	**	9.51	**	12.31	**	10.77	**	***	**	***	**	ns	ns	ns
SPAD index	S1 (15DFA)	41.90	**	41.13	ns	40.54	**	39.10	ns	*	**	***	ns	***	ns	ns
	S2 (8DFA)	40.56	**	34.47	*	41.38	**	40.48	**	***	***	***	***	***	ns	ns
	S3 (Anthesis)	44.46	**	32.71	ns	47.30	**	39.60	ns	***	***	***	**	*	ns	ns
	S4 (7DAA)	46.98	**	34.45	*	50.29	**	39.93	**	***	***	***	*	ns	ns	ns
	S5 (17DAA)	43.90	**	37.53	ns	49.47	**	41.24	**	***	***	***	ns	*	ns	ns
	S6 (22DAA)	40.53	**	37.07	**	49.62	**	40.05	**	***	***	***	***	**	*	ns
	S7 (35DAA)	33.24	**	30.92	**	46.32	**	35.65	**	***	***	***	***	ns	ns	**
	S8 (42DAA)	19.62	**	24.65	**	39.91	**	31.44	**	*	***	***	***	***	ns	ns
Roots	Angles of brace roots (°)	52.03	**	62.00	ns	39.68	**	59.08	*	***	***	***	***	***	**	ns
	Angles of crown roots (°)	54.05	**	71.25	*	44.49	**	68.75	*	***	***	***	***	**	*	**
	Number of adventitious roots	10.91	**	12.45	*	10.93	**	12.02	ns	**	ns	***	ns	ns	*	*
	Number of brace roots	8.75	**	7.73	ns	8.43	**	7.73	ns	***	ns	***	ns	ns	***	**
	Number of crown roots	16.38	**	13.92	ns	15.83	**	14.67	ns	***	ns	***	*	ns	*	ns
	Density of adventitious roots	6.73	**	4.42	**	6.23	**	5.23	ns	***	ns	***	***	**	*	**
	Density of brace roots	6.39	**	4.35	**	5.33	**	4.93	ns	***	ns	***	***	***	***	*
	Density of crown roots	5.78	**	3.45	**	3.91	**	3.77	ns	***	***	***	***	***	***	ns

*Levels of signification: *p < 0.05; **p < 0.01; ***p < 0.001; ns, not significant. SPAD index, expressed in days before (DBA) and after (DAA) anthesis.*

observed in the variables AB (31.13), AC (21.48), DB (19.83), and DC (47.90) in 2016, and decreases in DA (15.61) and DB (11.82) in 2018.

Root variables presented significant differences for CS and G. The absence of significant differences for WC was observed in NA, NB, NC, and DB. The CS × WC interactions for NA and NB, as well as the CS × G interactions for NA, NB, and NC were not significant ($p > 0.05$). All root variables had significant WC × G interactions. The CS × WC × G interaction was significant for AC, NA, NB, DA, and DB ($p < 0.01$) (**Table 1**).

Agronomic and Root Traits Performance

Under WS and WW conditions for CS evaluated in relation to 100GW, L65 presented the highest mean estimates. The inbred lines L71, L76, P6, and P7 had the highest means for PE in CS 2016 and L61, L71, P6, and P7 in CS 2018. The highest GY and EPV means, at the same time for different WCs and CS, were obtained for P2, P3, P6, and P7 (**Figure 4**).

The highest mean values for RNE, occurring simultaneously in different WCs and CS, and were expressed by L61, L71, L76, and P2; for GNR by P2 and P7; for ED by L76, P2, and P3; and for EL by P2 and P7 (**Figure 5**).

Unlike L61, L65, and L75, the P2, P6, and P7 inbred lines expressed better agronomic performance for GY and EPV in both WCs and CS. In greenhouse studies and with a greater number of physiological traits, the genotype P7 was notable as being superior and L75 as inferior.

Considering the different WCs and CS together, L61, L65, and L76 showed the highest estimates for AB, whereas L61, L75, and L76 were notable with the highest means for AC (**Figure 6**). Superiority of NA was identified for P2 and P6 (**Figure 6**), whereas that of NC was identified in L76. The variables related to root density showed the supremacy of L75 (**Figure 7**).

SPAD Index in the Phenological Stages From Pre-Anthesis to Physiological Maturation

The evaluation of S7 was removed from the analysis because the CS × WC × G interaction effect was significant ($p < 0.01$) (**Table 1**). For the

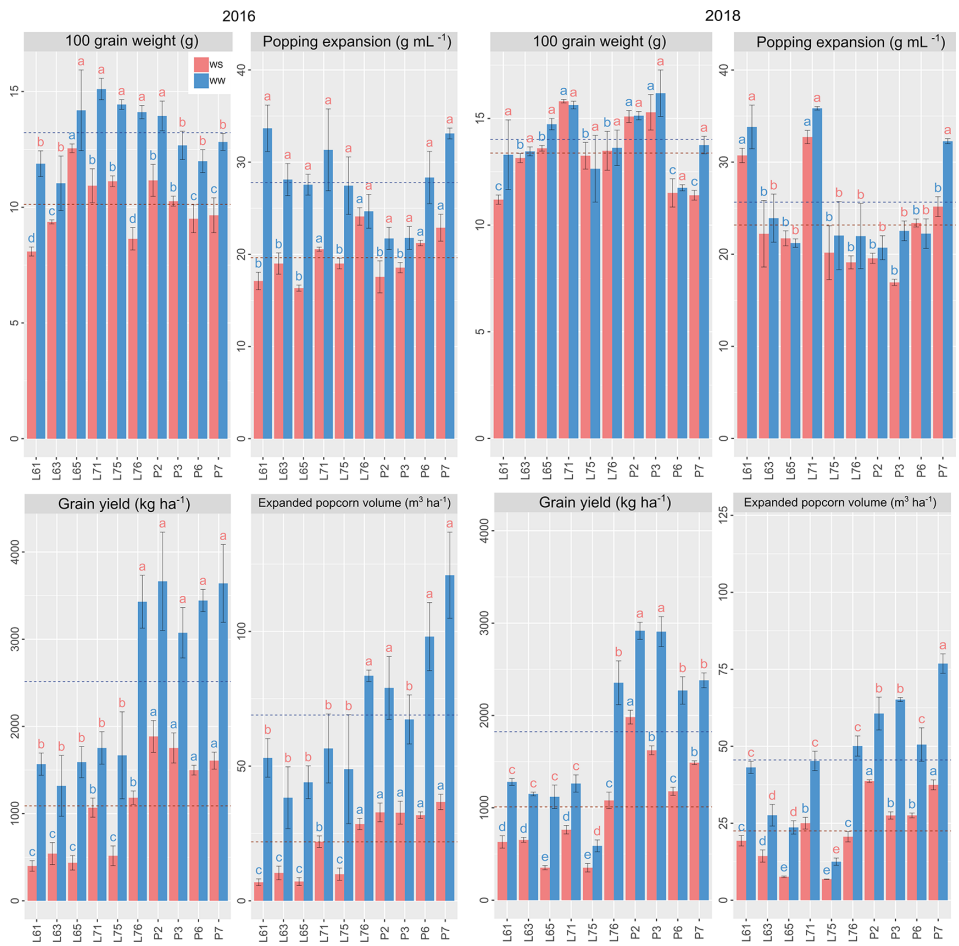


FIGURE 4 | Agronomic potential of popcorn inbred lines under WS and WW conditions in 2016 and 2018. Mean genotypes, red (WS) and blue (WW), followed by the same letter do not differ using the Scott and Knott test at 5%. The bars denote the standard error.

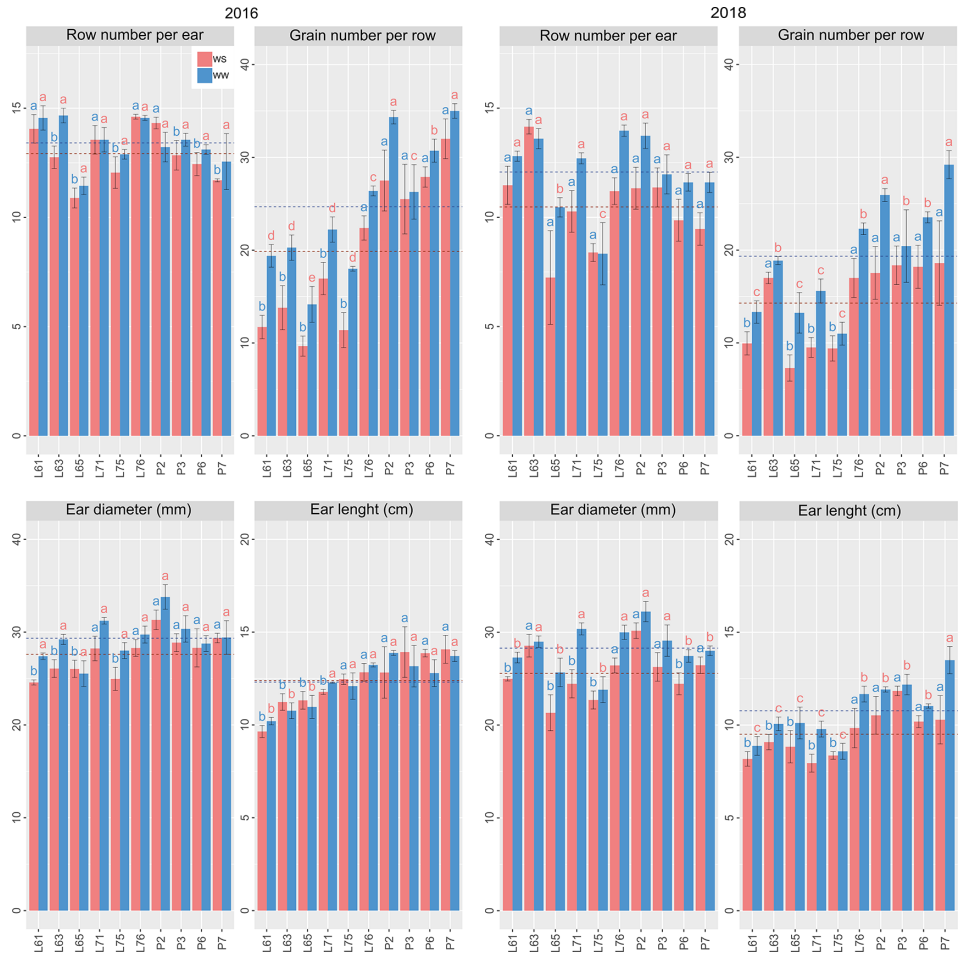


FIGURE 5 | Agronomic potential of popcorn inbred lines under WS and WW conditions in 2016 and 2018. Mean genotypes, red (WS) and blue (WW), followed by the same letter do not differ using the Scott and Knott test at 5%. The bars denote the standard error.

other SPAD index evaluations, the means of the variable in both CS were used. The quadratic model was the best fit to the response of the SPAD index with the number of days before and after male anthesis in the different WCs (**Figure 8**). In addition, **Figure 8** shows the regressions of SPAD index values over the days before and after male anthesis as that of three groups: superior (P2, P6, and P7), inferior (L61, L65, and L75), and evaluation of all inbred lines.

Considering the inbred lines evaluated jointly (all), the value corresponding to the starting point (β_0), date of occurrence of the male anthesis, was 41.36 in WS and 44.17 in WW. In WS, the maximum value of the SPAD index was 41.39, verified at both DAA. Whereas in WW, the maximum value observed was 45.32, verified at 11 DAA (**Figure 8**). At S8, the SPAD index values were 23.35 and 36.08 in WS and WW, respectively.

The superior genotypes had values of 41.31 in WS and of 46.26 in WW corresponding to β_0. In WS, the maximum value of the SPAD index was 43.18, reached at seven DAA. Whereas in WW, the maximum value observed was 48.71, found at 14 DAA (**Figure 8**). At S8, the SPAD index values were 25.70 and 39.60 in WS and WW, respectively.

The inferior genotypes had values of 41.31 in WS and 43.66 in WW corresponding to β_0. In WS, the maximum value of the SPAD index was 41.66 at six DAA. Whereas in WW, the maximum point was 43.74 at four DAA (**Figure 8**). At S8, the SPAD reading values were 22.39 and 34.61 in WS and WW, respectively.

Relations Between Agronomic and Root Characteristics and SPAD Readings

The variables PE, S7, AC, NA, NB, DA, and DB, which showed significant CS × WC × G interaction (**Table 1**), were eliminated from the genetic correlation analysis (*rg*).

In the WS condition, for the main characteristics of agronomic interest, GY and EPV, there were positive estimates for the GY × EPV, GY × GNR, GY × ED, GY × EL, EPV × GNR, EVP × ED, and EPV × EL pairs. Among the SPAD index evaluations, the most expressive *rg* were in the pairs S1 × S2, S1 × S3, S3 × S4, S3 × S5, S3 × S6, S4 × S5, S4 × S6, and S5 × S6, all also positive. Although with positive estimates, no significant *rg* was observed for root variables (**Figure 9**).

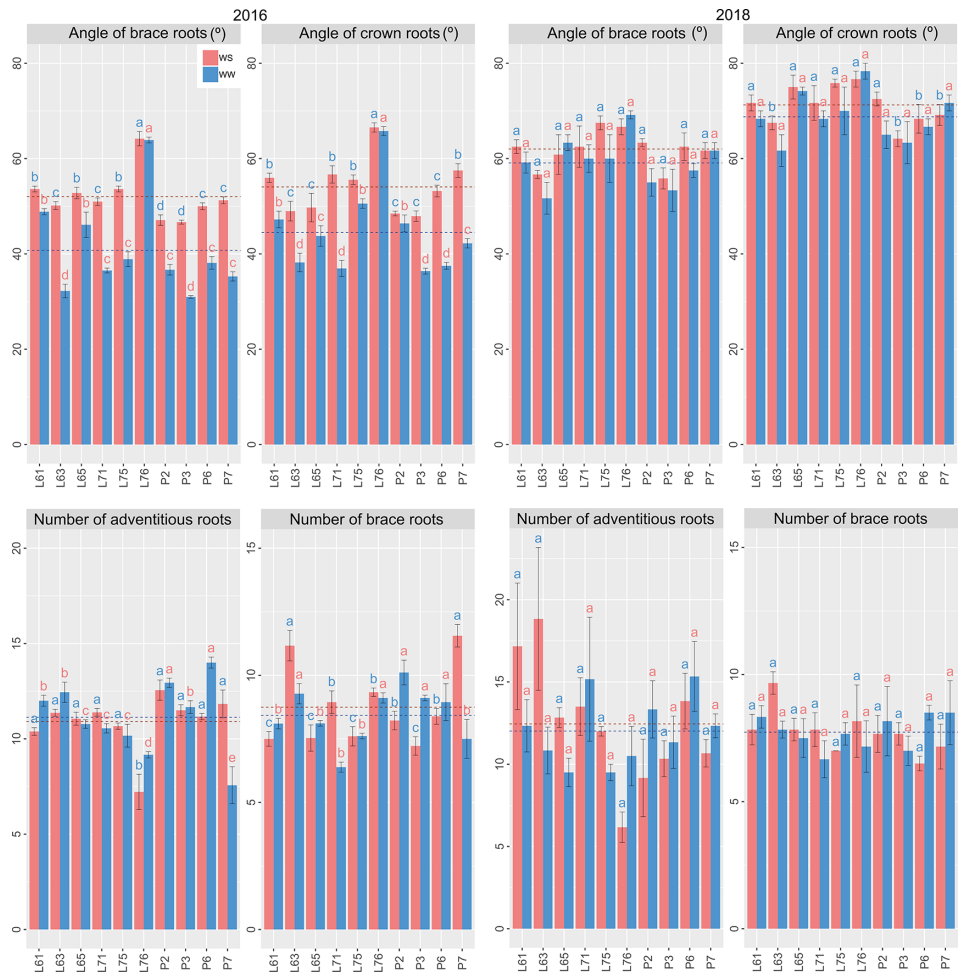


FIGURE 6 | Root traits of popcorn inbred lines under WS and WW conditions in CS 2016 and 2018. Mean genotypes, red (WS) and blue (WW), followed by the same letter do not differ using the Scott and Knott test at 5%. The bars denote the standard error.

Analyzing the most significant *rg* in the WS condition, the notable pairs between agronomic characteristics and the SPAD index were 100GW × S1 (positive); GY × S1, EPV × S1, RNE × S1, GNR × S1, and ED × S1 (negative); 100GW × S2 (positive); GY × S2, EPV × S2, RNE × S2, GNR × S2, ED × S2, and EL × S2 (negative); 100GW × S3 (positive); RNE × S3 (negative); GY × S5, EPV × S5, EL × S5, and RNE × S8 (positive). No significant positive *rg* were observed between agronomic and root variables, although there was a tendency for negative correlations between them. Among the different SPAD reading dates, the following negative *rg* were observed for the root variables: S4 × AB, S4 × NC, S4 × DC, S5 × AB, S5 × NC, S5 × DC, S6 × AB, S6 × NC, and S6 × DC (**Figure 9**).

In the WW condition, a positive *rg* was observed between GY × EPV, GY × GNR, GY × ED, GY × EL, EPV × GNR, EPV × ED, and EPV × EL. Among the SPAD index evaluations, there were significant and positive *rg* between S1 × S2, S3 × S4, S3 × S5, S3 × S6, S3 × S8, S4 × S5, S4 × S6, S4 × S8, S5 × S6, S5 × S8, and S6 × S8. No significant *rg* was observed for root variables, although positive *rg* occurred among them (**Figure 9**).

Analyzing the *rg* between agronomic traits and SPAD index in the WW condition, the associations GY × S1, EPV × S1, RNE × S1, GNR × S1, ED × S1, GY × S2, EPV × S2, RNE × S2, and GNR × S2 were negative, and the associations 100GW × S3 and 100GW × S4 were positive. A significant and positive *rg* was observed between the agronomic variable RNE and the root variable NC. In general, there was a tendency toward negative *rg* between the root variables AB and DC and agronomic variables. The following negative *rg* were observed between different SPAD index evaluation dates for the root variables, S3 × AB, S4 × AB, S5 × AB, S6 × AB, S8 × AB, S3 × DC, S4 × DC, S5 × DC, and S6 × DC (**Figure 9**).

Greenhouse Study

Phenotyping of Contrasting Genotypes

Morphological Characteristics and Foliar Pigments

In the WS condition, SB was 72.40 and 49.30 g for P7 and L75, respectively; and in the WW condition, P7 and L75 presented SB of 113.67 and 79.21 g, respectively. In the different WCs, there was a significant difference between means, with a proportional variation

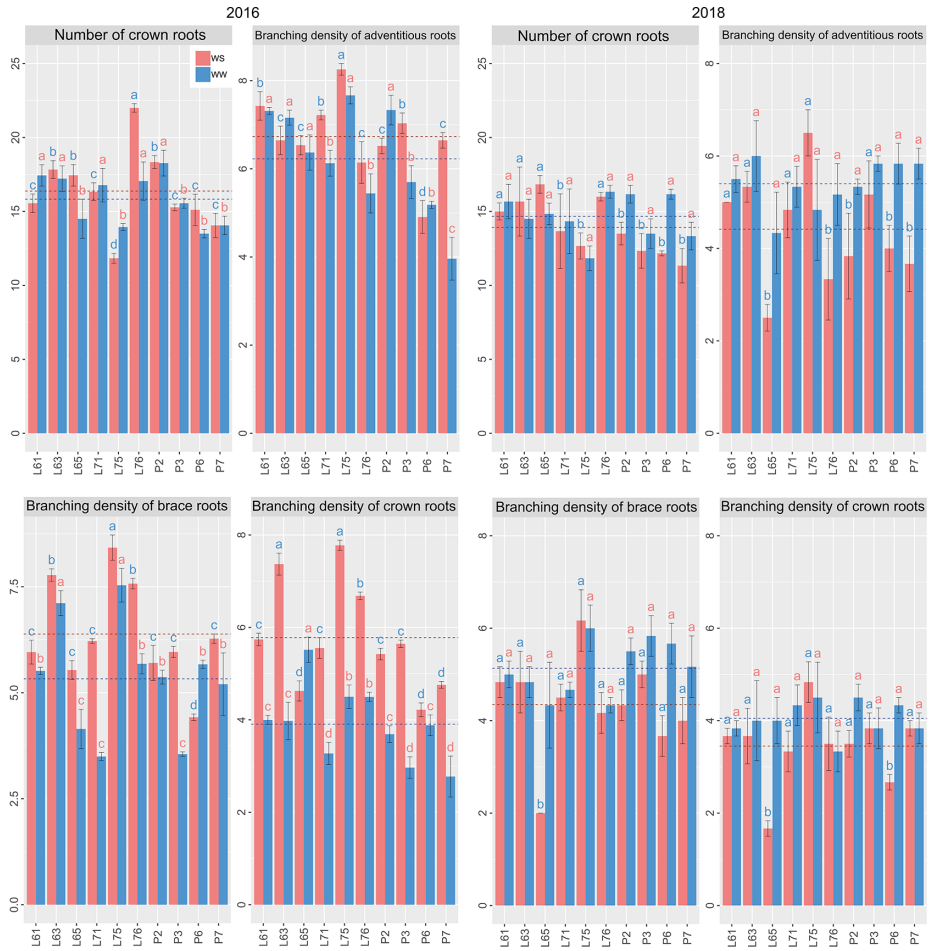


FIGURE 7 | Root traits of popcorn inbred lines under WS and WW conditions in CS 2016 and 2018. Mean genotypes, red (WS) and blue (WW), followed by the same letter do not differ using the Scott and Knott test at 5%. The bars denote the standard error.

of approximately 37.0%. Regardless of WC, P7 tended to have a lower SLA (but without achieving significance) in relation to L75. There was a mean SLA increase of approximately 21.8% when comparing WS with WW. The leaf area (LA), independently of WC, was higher in P7, with values of 0.51 m^2 and 0.63 m^2 in WS and WW, respectively. In both WCs there was a difference in the comparison between means. L75 had a greater decrease in LA, corresponding to 32.5% (**Table 2**). The joint analysis of the variables studied here presented significant differences between G and WC, without significant G × WC interaction (**Table 2**).

Among the variables related to stomatal characteristics, significant differences were observed between adaxial stomatal density and abaxial stomatal density, in both WCs; and for abaxial stomatal density only in WW. The comparison between WCs, in general, showed increases for P7 and decreases for L75 when considering these variables. The joint analysis showed neither statistical differences between G and WS nor significant G × WC interactions (**Table 2**).

In foliar pigments, statistical differences were observed only in chlorophyll and NBI in the WW condition. Chlorophyll and NBI decreased under WW compared with WS conditions, being more pronounced for P7. However, there was also a slight increase of anthocyanin in the same lineage. The joint analysis for both WC showed statistical differences only for chlorophyll and NBI (**Table 2**).

Gas Exchange and Water Status

In WW, no statistical differences were observed between genotypes in A, g_s, and E (**Table 2**). However, under WS the P7 plants showed A, g_s, and E values of 27.50 μmol m^{-2} s^{-1}, 0.13 mol m^{-2} s^{-1}, and 3.50 mmol m^{-2} s^{-1}, respectively, which were significantly greater than the 9.80 μmol m^{-2} s^{-1}, 0.09 mol m^{-2} s^{-1}, and 2.55 mmol m^{-2} s^{-1} observed in L75 plants, respectively. Furthermore, P7 presented smaller proportional decreases between WCs than L75.

RWC, $WUE_{instant}$, $WUE_{intrinsic}$, and WUE_{agron} did not show significant differences between water conditions in P7 and L75 plants, with the exception of WUE_{agron}, which varied in a similar way in both lines (**Table 2**).

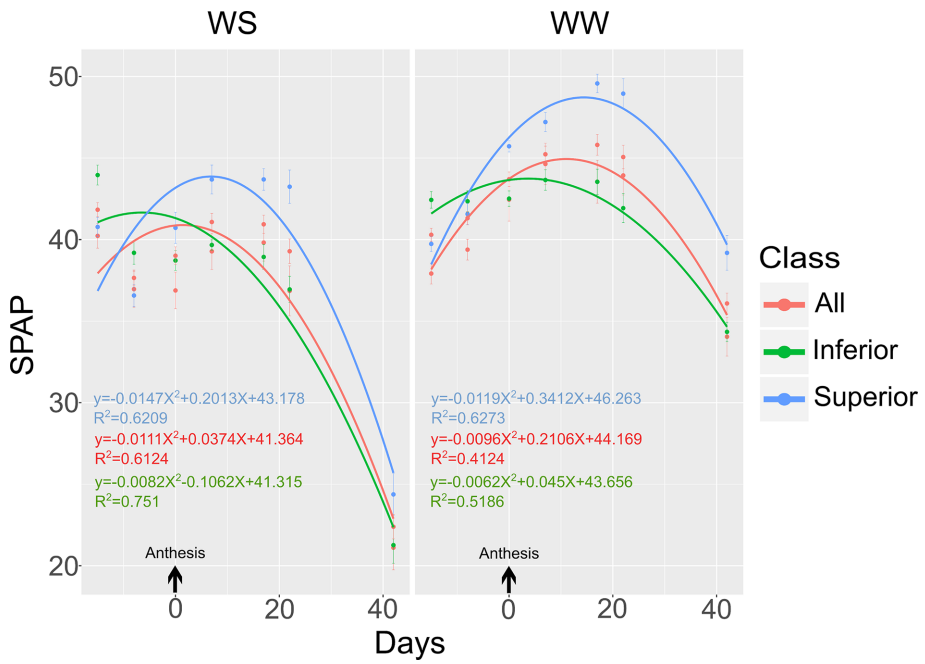


FIGURE 8 | SPAD index evaluated in ten popcorn inbred lines (all) with contrasting performance groups, i.e., superior and inferior, measured at different dates from the male pre-anthesis period until physiological maturity. SPAD index: S1 (15 DBA), S2 (8 DBA), S3 (anthesis), S4 (7 DAA), S5 (17 DAA), S6 (22 DAA), S7 (35 DAA), and S8 (42 DAA).

In WS, the stable isotope carbon composition ($\delta^{13}C$) of biomass was −13.16‰ for P7, and −13.75‰ for L75 (significant), which were slight lower values than the −12.18‰ and −12.37‰ observed in their respective WW plants (not significant) (**Table 2**). In the joint analysis, significant differences were observed between G and WC, as well as in the G × WC interaction (**Table 2**).

Root Characteristics

Regardless of water condition, P7 plants had higher RWD values in the different soil strata. Significant difference between inbred lines for RWDa in both WCs and for RWDb and RWDc in WS, as well as for RWDe in WW was observed. Considering the comparison between WCs, a mean RWD decrease was observed in the different strata, being 53.4% for P7 and 57.20% for L75.

The shoot/root ratio of dry biomass increased from 3.80 to 4.93 when comparing the WW to WS condition, without significant differences between these inbred lines.

In general, root characteristics in the joint analysis showed significant differences within G and WC. However, there was no significant G × WC interaction.

DISCUSSION

Field Studies of the Effect of Soil Water Limitation on Evaluated Characteristics and Implications for Plant Improvement

Soil water limitation most affected GY and EPV yield components. Water limitation implemented during pre-anthesis and grain filling reduced the yield covariates to a lesser extent. Under dry conditions, the reduction in the number of grains per ground area has been indicated as being responsible for GY reduction in common maize (Cairns et al., 2012). Pollen viability and zygote formation are drought-sensitive processes (Zinselmeier et al., 1995), leading to a reduction in the number of grains produced under water limiting conditions. This effect may have occurred in 2018, where WS was evaluated earlier (before anthesis), affecting the GNR. However, in 2016, where the water limitation occurred later, the main effect was noticed in 100GW (but not for the variables related to grain quantity), which also affected GY. Water stress may shorten the period of grain filling, decrease photosynthetic activity, accelerate ABA-mediated leaf senescence and reduce the activity of enzymes involved in sucrose metabolism and starch synthesis, which altogether can contribute to a lower grain weight (Yang and Zhang, 2006; Sehgal et al., 2018; Yang et al., 2019).

The variables of economic interest, i.e., PE, GY, and EPV, had a significant WC × G interaction, which pointed to different responses among the evaluated genotypes in the different implemented WCs. Interactions of this nature interfere with selection gains and cultivar recommendation for specific environments (Hallauer et al., 2010). In these cases, indirect selection variables that are determinants of the expression of the main characteristics and that do not present significant WC × G but are associated in a significant and positive way can be identified (Kamphorst et al., 2019). The absence of significant WC × G interaction in relation to 100GW, RNE, GNR, ED, and

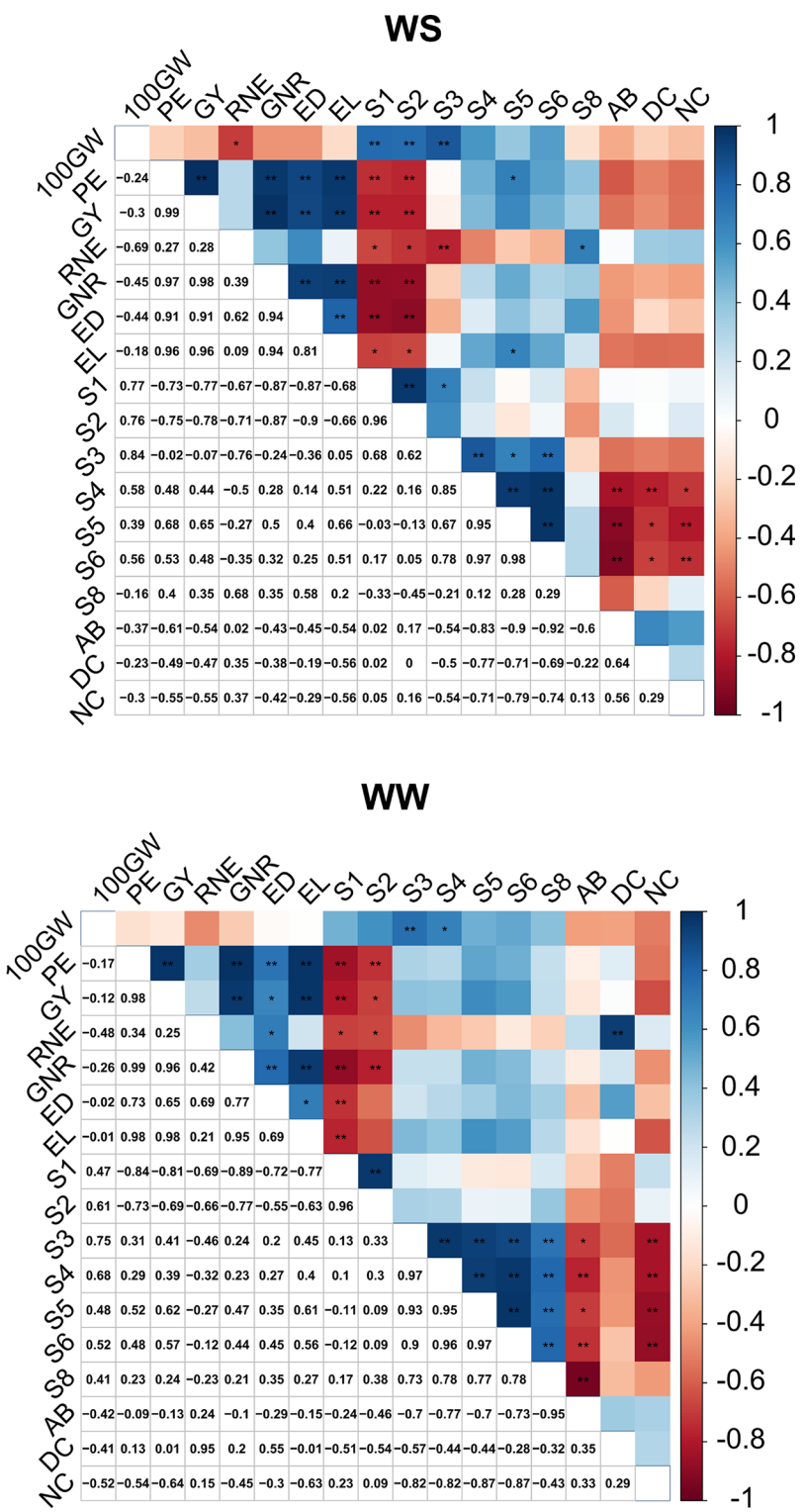


FIGURE 9 | Estimates of the genotypic correlation coefficient between agronomic, root traits, and different dates of SPAD reading in popcorn inbred lines evaluated under different water conditions. 100GW: 100-grain weight, GY: grain yield, EPV: expanded popcorn volume, RNE: row number per row, GNR, grain number per row; ED, ear diameter; EL, ear length. SPAD index: S1 (15 DBA), S2 (8 DBA), S3 (anthesis), S4 (7 DAA), S5 (17 DAA), S6 (22 DAA), S8 (42 DAA). AB, angles of brace roots; NC, number of crown roots; DC, branching density of crown roots.

TABLE 2 | Mean values of morphological characteristics, foliar pigments, gas exchange measurements, C isotope discrimination, and root variables in popcorn inbred lines contrasting with drought under different water conditions.

Traits	WS			WW			Joint analysis		
	P7	L75	Prob.	P7	L75	Prob.	G	WC	G*WC
Shoot biomass (g)	72.40	49.30	***	113.67	79.21	*	**	**	ns
Specific leaf area ($cm^2\ g^{-1}$)	199.33	228.38	ns	163.56	187.63	ns	*	**	ns
Leaf area (m^2)	0.51	0.37	**	0.63	0.54	*	**	**	ns
Stomatal density adaxial (stomata mm^{-2})	80.17	106.36	**	74.56	96.49	*	**	ns	ns
Stomatal index adaxial (%)	21.00	21.27	ns	20.88	22.26	ns	ns	ns	ns
Stomatal density abaxial (stomata mm^{-2})	106.73	105.26	ns	83.33	116.23	**	ns	ns	ns
Stomatal index abaxial (%)	27.47	22.85	**	22.39	27.71	**	ns	ns	**
Chlorophyll content (SPAD index) (arbitrary units)	27.93	30.75	ns	42.15	34.45	*	ns	*	ns
Flavonoid content (arbitrary units)	0.97	0.97	ns	0.96	1.05	ns	ns	ns	ns
Anthocyanin content (arbitrary units)	0.20	0.18	ns	0.18	0.19	ns	ns	ns	ns
Nitrogen balance index (arbitrary units)	29.08	31.90	ns	44.96	34.67	**	ns	**	ns
Net photosynthetic rate (A, μmol $CO_2\ m^{-2}\ s^{-1}$)	27.50	19.80	**	30.13	32.33	ns>	*	**	*
Stomatal conductance (g_s, mol $H_2O\ m^{-2}s^{-1}$)	0.13	0.09	*	0.17	0.19	ns	ns	**	*
Transpiration rate (E, mmol $H_2O\ m^{-2}s^{-1}$)	3.50	2.55	*	4.56	4.96	ns	ns	**	*
Relative water content (%)	89.92	90.64	ns	92.44	92.04	ns	ns	ns	ns
$WUE_{Instantaneous}$ (μmol CO_2 mmol H_2O^{-1})	7.86	7.92	ns	6.64	6.56	ns	ns	**	ns
$WUE_{intrinsic}$ (μmol CO_2 mol H_2O^{-1})	218.52	213.16	ns	183.63	179.29	ns	ns	**	ns
$WUE_{agronomic}$ (g kg^{-1} DM)	6.06	5.81	ns	5.40	6.33	ns	ns	ns	ns
Stable carbon isotope composition ($\delta^{13}C$) (‰)	−13.16	−13.75	*	−12.18	−12.37	ns	**	***	*
RWDa (g m^{-3})	117.53	75.78	*	193.21	155.22	*	**	**	ns
RWDb (g m^{-3})	44.38	27.60	*	65.21	55.73	ns	*	**	ns
RWDc (g m^{-3})	25.31	18.16	*	59.60	55.58	ns	ns	**	ns
RWDd (g m^{-3})	13.46	13.46	ns	51.94	33.29	ns	*	**	*
RWDe (g m^{-3})	21.06	17.05	ns	58.61	40.04	*	*	**	ns
Shoot/root biomass dry ratio	4.96	4.90	ns	4.06	3.53	ns	ns	*	ns

*Prob.: Differences between inbred lines in each water treatment (WS, water stress; WW, well-watered) were separated by genotype effects. Levels of significance: *p < 0.05; **p < 0.01; ***p < 0.001; ns, not significant. WUE, water use efficiency; RWD, root weight density, where RWD a, b, c, d, and e refer to the depth of each soil section. G, genotypes; G*WC, genotype × water condition interaction.*

EL allowed us to infer that selection in any WC can be effective in obtaining simultaneous genetic gains for these characteristics.

The SPAD index can be used for the indirect selection of the most productive plants in the WS condition, as there was no significant WC × G or CS × WC × G interaction, whereas a positive association with GY and EPV was found (**Table 1**). The use of the SPAD index may allow for the reliable selection of productive genotypes both under adequate and reduced water availability environments, with "stay-green" cultivars being the best option for the latter (Joshi et al., 2006; Costa et al., 2008).

Root systems had phenotypic plasticity in different WCs, which implies significant WC × G and CS × WC × G interactions. Therefore, in addition to the difficulty in measuring root traits, the occurrence of interactions is an obstacle to improving the use of root characteristics in plant breeding (Lynch, 2015), which is reinforced by their low heritability estimates (Trachsel et al., 2011). The phenotypic plasticity of root systems was observed when there was an increase in the angles and density of the supporting roots and the crown in 2016 only. In fact, root angle increases are considered an adaptive response to water stress (Trachsel et al., 2011; Kamphorst et al., 2019).

Dynamics of Foliar Senescence Between Contrasting Genotypes

To understand the physiological traits inherent to the most productive lines under water limiting conditions, the genotypes were grouped using on the best results for GY and EPV. Soil water depletion reduced the SPAD index regardless of genotypic groups. Foliar senescence induction is a plant response to water deficit conditions (Ghannoum, 2008; Araus et al., 2018), being coordinated by the reproductive stage of plants, but also strongly influenced by the environment (Combe and Escobar-Gutiérrez, 2009). A portable chlorophyll meter (SPAD) can be an interesting tool for plant stress diagnosis (Romano et al., 2011; Araus et al., 2012; Zia et al., 2013; De Castro et al., 2014). In fact, spectrometric methods can be used to efficiently evaluate different WCs and assess the agronomic performance of cereals (Yousfi et al., 2019).

Regardless of the phenotypic class, the maximum SPAD index values were attained later (11 DAA) in WW than in WS (2 DAA) condition. Furthermore, the genotypes with greater productivity were more stay-green (higher SPAD index values), as shown by the higher SPAD values recorded during grain filling. In contrast, genotypes with lower productivity reached higher SPAD index values earlier, irrespective of water conditions, thus reflecting an association between higher SPAD index values and higher yield values. These finding were in line with reports that higher SPAD index values, together with a senescence delay, are likely to contribute to the maintenance of C-assimilation and the mobilization of photoassimilates to the reproductive organs, therefore, increasing agricultural productivity (Gregersen et al., 2008).

Implications of Genetic Associations Between Agronomic and Root Characteristics and the Different SPAD Measurement Dates

The GNR, ED, and EL components are important selection characteristics for yield and EPV increments, especially in popcorn plants under adequate water availability (Cabral et al., 2016; de Lima et al., 2016; do Amaral Júnior et al., 2016) and during droughts (Kamphorst et al., 2019). A disadvantage of using these characteristics is the need to wait until the end of the crop cycle to obtain results. An ideal scenario is the possibility of predicting higher yields through the use of characteristics and methods that can be evaluated early using non-destructive procedures, such as remote sensing (Araus et al., 2018).

The choice of an appropriate phenological stage for SPAD index measurements is crucial, since phenotyping methodologies should be used in critical stages associated with grain production (Cairns et al., 2012). In this study, the range of 17 to 22 DAA was adequate for these measurements, allowing us to obtain highly positive correlations to yield estimates (and its components). Under WS, maize genotypes with delayed leaf senescence are often more productive, showing selection advantages for water limiting conditions (Cairns et al., 2012; Adebayo et al., 2014). It is important to mention that among the popcorn varieties evaluated, the inbred lines that had high SPAD index values before anthesis were not the most productive. Regardless of water availability level, the high SPAD index values found at 15 and 8 DBA were negatively correlated with GY and EPV. As stated, late leaf senescence produces photoassimilates and remobilizes nutrients at the appropriate time of grain filling, thus sustaining higher yields (Jordan et al., 2012), but late remobilization can also decrease grain filling (Sehgal et al., 2018).

A root system adapted to specific abiotic soil stress conditions represents an agronomic advantage with positive impact on yield (Trachsel et al., 2011). Notably, no significant correlations were found between GY and its covariables for the evaluated root characteristics. An explanation for this can be the phenotypic plasticity of the root response, which resulted in significant WC × G interaction. However, there is a tendency for negative correlations between agronomic and root characteristics, especially with NC and DC. In fact, it was previously reported that a reduced NC led to a deeper root system and resulted in better soil water acquisition, which in turn increased carbon gain, growth and plant productivity (Gao and Lynch, 2016). An optimal number of crown roots can also interact with other characteristics to which they are associated, and this will increase deeper soil exploration (increases tolerance to water deficit), such as the greater root angle in relation to the soil surface and reduced lateral branching (Trachsel et al., 2013; Zhan and Lynch, 2015; Zhan et al., 2015).

The highest SPAD values at 7, 17, and 22 DAA were associated with the lowest root values for the variables AB and DC, regardless of water availability. As for the NC variable in WS, there was a negative association with the same SPAD measurement dates (7, 17, and 22 DAA). In fact, the lowest NC value, as well as the decreased branching density of the lateral root, may have improved the water absorption capacity in the soil, which was indirectly reflected in a better leaf status and therefore higher SPAD values. Notably, the most productive genotypes under lower water availability are expected to have steeper angles to the soil horizon (Gao and Lynch, 2016), which was not observed in our study.

Phenotyping of Contrasting Genotypes Under Greenhouse Conditions

When comparing the two water availability levels, the superior genotype (P7) showed higher SB and LA values, and a smaller proportional LA decrease under WS when compared to WW. Higher biomass accumulation before flowering and increased leaf size may result in a larger photosynthesizing area, which would increase C-assimilation (Tollenaar et al., 2004). SLA showed significant and positive correlations with water use efficiency, expressed by the ratio of plant dry matter to water used (Zhang et al., 2015). These authors showed that there was an increase in SLA values in maize plants at the seedling stage, while in the booting and tasseling phases, SLA decreased, coinciding with the translocation of photoassimilates to the stem and reproductive organs. In our study, the plants under both water regimes showed a significant and positive correlation of SLA with the agronomic efficiency for water use (**Supplementary Figure 1**). However, this did not contribute to the differentiation of the tested genotypes, but only the water conditions.

Water regime did not affect stomatal density or index of the abaxial and adaxial leaf sides. However, following WS, P7 had lower stomatal density than L75 on the adaxial face. As a response to water stress, the stomatal density and the stomatal index decreased in L75, considered the most sensitive line. Stomatal density and index in combination with the stomatal opening can determine the maximum diffusive conductivity of the leaf to CO_2 (Brodribb et al., 2013; Zhao et al., 2015). In maize plants, decreased soil water availability was observed to significantly increase stomatal density, together with a reduction of stomatal size and opening (Zhao et al., 2015). However, our results indicate higher net photosynthetic rate (A) and transpiration rates in leaves exhibiting a lower density and stomata index, which may be associated with the compensatory effect of stomata size (i.e., larger stomata area, which was not measured in this study). It is important to note that g_s is considered a key trait for the detection of a WS effect (Hetherington and Woodward, 2003). In fact, Zhao et al. (2015) also reported that photosynthetic rate and transpiration were negatively correlated with stomatal density in maize plants. However, under WS, P7 plants showed higher A values and transpiration than L75, associated to a higher g_s value (**Table 2**). Gas exchange measurements differentiate inbred lines in WS, where P7 presented higher A, g_s, and E values. Also, limited water in the soil caused a reduction of only 9% in A for P7, reflecting a minor impact in the functioning of the photosynthetic apparatus. The maintenance of higher A values for P7 than L75 in WS conditions, might have been supported by maintaining chlorophyll pigment concentration (Busch et al., 2009). Thus, the superiority of P7 is explained by the higher SB and LA accumulation.

P7 plants maintained the highest g_s value, even with lower adaxial stomatal density, showing a greater ability to obtain water from the soil to maintain water status under WS, as suggested by the higher RWD values in layers a, b, and c. Roots play an important role in plant adaptation to dry environments, and genotypes that have a more developed root system can provide higher GY (Ali et al., 2016). Lambers et al. (2002) reported that the metabolic cost of the root system for soil exploration under dry conditions is high, which can exceed the plant's daily photosynthetic rate by 50%. Thus, higher A values in P7 plants might have supported the costs for this larger root system.

Under soil water limitation conditions, amongst other strategies, tolerant genotypes can maintain a higher RWC than more sensitive ones, associated to larger and more efficient root systems (increasing water removal from the soil) or by osmotic adjustment (Blum, 2011). The higher RWC results in improved cellular homeostasis and greater stomatal opening, which collectively allows the photosynthetic metabolism to be maintained to some extent (Blum, 2011). However, the ability to keep the stomata open can increase water loss *via* transpiration, so that RWC is reduced. In fact, there was a weak negative correlation between g_s, E, and RWC in the WS condition (**Supplementary Figure 1**). Even so, A and g_s had positive correlation with several root traits under WS, but not under WW conditions. Interestingly, A and g_s had significant and positive correlation in WS but did not show the same result in WW. These results indicate an adjustment associated mainly with stomatal density in the WS condition, as observed by the strong negative correlation between g_s and SDA (**Supplementary Figure 1**). Both $WUE_{instant}$ and $WUE_{intrinsic}$ increased equally among the inbred lines under WS. This finding indicates that the lower stomatal conductance and transpiration rates influenced the use of H_2O in the same manner. However, $WUE_{instant}$ and $WUE_{intrinsic}$ did not have a positive or significant correlation with A and g_s in WS but presented a negative correlation in the WW condition.

$WUE_{intrinsic}$ and $WUE_{instant}$, together with WUE_{agron} and RWC, did not help to differentiate the evaluated inbred lines. In fact, $WUE_{instant}$ and $WUE_{intrinsic}$ are leaf scale characteristics mainly associated with transpiration. Therefore, an increase in these variables can be associated with reduced g_s, which in turn can reduce photosynthesis, growth, and productivity (Blum, 2009). Therefore, WUE_{agron} has been suggested to be a variable more associated with the effective use of water (Blum, 2009). However, this variable was also not efficient in differentiating the inbred lines studied here.

In addition, as a response to WS, L75 presented lower values, i.e., more negative of $\delta^{13}C$ (carbon isotope composition) than P7, indicating that L75 stomata were more frequently closed throughout the crop development (Farquhar et al., 1989; Cabrera-Bosquet et al., 2009; Araus et al., 2010; Cabrera-Bosquet et al., 2017), showing that L75 was more susceptible to water stress than P7.

New Players

This study was conducted in two parts. Firstly, field experiments (in 2016 and 2018) were designed to understand which secondary characteristics were most important to explain the higher yield and EPV values (main characteristics). As a result, we identified GNR, ED, and EL, as adequate traits for plant selection. With the same objective, we sought to identify important root characteristics. Among these, at the 25 cm depth evaluated, it was not possible to diagnose root characteristics that could be indicative of satisfactory agronomic performance. The high root plasticity response to different WCs may have been responsible for this finding. There was an association between the highest SPAD index values and the highest yield values, favoring the use of this characteristic for indirect selection. Second, complementing the field experiments, two contrasting inbred lines were studied under greenhouse conditions. Under WS at the end of the experiment, P7 maintained higher values of leaf net photosynthetic rates, stomatal conductance, and transpiration than L75. Thus, single-leaf gas exchange measurements shortly before the harvest proved to be adequate indicators for the evaluation the agronomic performance of popcorn under soil water limitation conditions. However, gas exchange measurements are not amenable for high throughput phenotyping when a large number of genotypes are evaluated. In that case, a trait which can be used to evaluate stomatal conductance throught the crop cycle, such as the stable carbon isotope composition on dry leaf matter, was shown to indicate that L75 maintained the stomata closed for longer periods (i.e. exhibited more negative value $\delta^{13}C$) under water stress than P7.

DATA AVAILABILITY STATEMENT

The raw data supporting the conclusions of this article will be made available by the authors, without undue reservation.

AUTHOR CONTRIBUTIONS

Conceptualization: SHK. Methodology and investigation: SHK, VJL, PHADS, WPR, JMSV, GMBG, KFMS, JTL, MV, FM-P, and OV-D. Software: VJL and PHADS. Resources: SHK, ATAJ, and JCR. Writing—original draft preparation: SHK, ATAJ, WPR, JLAO, JCR, and EC. Supervision: ATAJ, JLAO, and EC. Critical review of final manuscript version: JLAO and JCR.

FUNDING

This study was financed in part by the Coordenação de Aperfeiçoamento de Pessoal de Nível Superior – Brasil (CAPES) – Finance Code 001. Funding was also provided by FAPERJ, with the project E26/201.813/2017 to SK and E26/202.761/2017 to AA. Funding to JR by Fundação para a Ciência e a Tecnologia (FCT), Portugal, through the research units UID/UIDB/00239/2020 (CEF), and UIDP/04035/2020 (GeoBioTec) is also greatly acknowledged. JA acknowledges the support of Catalan Institution for Research and Advanced Studies (ICREA, Generalitat de Catalunya, Spain), through the ICREA Academia Program.

ACKNOWLEDGMENTS

The authors thank Fundação Carlos Chagas de Apoio à Pesquisa do Estado do Rio de Janeiro - FAPERJ (grants E-26/010.100972/2018 EC), CNPq (fellowships awarded 303166/2019-3, EC) and PVS 00583/20, EC [FAPEMA (Fundação de Amparo à Pesquisa e ao Desenvolvimento Científico e Tecnológico do Maranhão). We thank Joseph Matas, Experimental Field Facilities of the Faculty of Biology, UB, and Geraldo Francisco de Carvalho, Colégio Estadual Agrícola Antônio Sarlo, UENF, for the support provided in the experiments. We also thank Professor Richard Ian Samuels (State University of Northern Fluminense Darcy Ribeiro) for English-language review.

SUPPLEMENTARY MATERIAL

The Supplementary Material for this article can be found online at: https://www.frontiersin.org/articles/10.3389/fpls.2020.01289/full#supplementary-material

SUPPLEMENTARY TABLE 1 | Precipitation records and irrigation (mm) applied to popcorn inbred lines for experiments conducted during 2016 and 2018 in WS and WW conditions in relation to days after sowing (DAS).

SUPPLEMENTARY FIGURE 1 | Correlation coefficients between morphological traits (SB, SLA, LA, SDAd, SIAd, SDAb, and SIAb), foliar pigments (Chl, Flav, Anth, NBI), gas exchange measurements (A, g_s, and E), water status traits (RWC, $WUE_{instant}$, WUE_{intrin}, and WUE_{agron}), C isotope composition ($\delta^{13}C$) and root variables (RWDa-b-c-d-e and Shot root).

REFERENCES

Adebayo, M. A., Menkir, A., Blay, E., Gracen, V., Danquah, E., and Hearne, S. (2014). Genetic analysis of drought tolerance in adapted × exotic crosses of maize inbred lines under managed stress conditions. *Euphytica* 196, 261–270. doi: 10.1007/s10681-013-1029-5

Ali, M. L., Luetchens, J., Singh, A., Shaver, T. M., Kruger, G. R., and Lorenz, A. J. (2016). Greenhouse screening of maize genotypes for deep root mass and related root traits and their association with grain yield under water-deficit conditions in the field. *Euphytica* 207, 79–94. doi: 10.1007/s10681-015-1533-x

Araus, J. L., Sánchez, C., and Cabrera-Bosquet, L. (2010). Is heterosis in maize mediated through better water use? *New Phytol.* 187, 392–406. doi: 10.1111/j.1469-8137.2010.03276.x

Araus, J. L., Serret, M. D., and Edmeades, G. O. (2012). Phenotyping maize for adaptation to drought. *Front. Physiol.* 3, 305. doi: 10.3389/fphys.2012.00305

Araus, J. L., Kefauver, S. C., Zaman-Allah, M., Olsen, M. S., and Cairns, J. E. (2018). Translating High-Throughput Phenotyping into Genetic Gain. *Trends Plant Sci.* 23, 451–466. doi: 10.1016/j.tplants.2018.02.001

Awange, J. L., Mpelasoka, F., and Goncalves, R. M. (2016). When every drop counts: Analysis of Droughts in Brazil for the 1901-2013 period. *Sci. Total Environ.* 566–567, 1472–1488. doi: 10.1016/j.scitotenv.2016.06.031

Blum, A. (2009). Effective use of water (EUW) and not water-use efficiency (WUE) is the target of crop yield improvement under drought stress. *F. Crop Res.* 112, 119–123. doi: 10.1016/j.fcr.2009.03.009

Blum, A. (2011). *Plant Breeding for Water-Limited Environments* (New York, NY: Springer New York). doi: 10.1007/978-1-4419-7491-4

Brodribb, T. J., Jordan, G. J., and Carpenter, R. J. (2013). Unified changes in cell size permit coordinated leaf evolution. *New Phytol.* 199, 559–570. doi: 10.1111/nph.12300

Buckley, T. N. (2019). How do stomata respond to water status? *New Phytol.* 224, 21–36. doi: 10.1111/nph.15899

Busch, F., Hüner, N. P. A., and Ensminger, I. (2009). Biochemical constrains limit the potential of the photochemical reflectance index as a predictor of effective quantum efficiency of photosynthesis during the winter spring transition in Jack pine seedlings. *Funct. Plant Biol.* 36, 1016. doi: 10.1071/FP08043

Cabral, P. D. S., do Amaral Júnior, A. T., de J. Freitas, I. L., Ribeiro, R. M., and da C Silva, T. R. (2016). Cause and effect of quantitative characteristics on grain expansion capacity in popcorn. *Rev. Ciec. Agron.* 47, 108–117. doi: 10.5935/1806-6690.20160013

Cabrera-Bosquet, L., Sánchez, C., and Araus, J. L. (2009). Oxygen isotope enrichment (Δ 18 O) reflects yield potential and drought resistance in maize. *Plant Cell Environ.* 32, 1487–1499. doi: 10.1111/j.1365-3040.2009.02013.x

Cabrera-Bosquet, L., Molero, G., Stellacci, A., Bort, J., Nogués, S., and Araus, J. (2011). NDVI as a potential tool for predicting biomass, plant nitrogen content and growth in wheat genotypes subjected to different water and nitrogen conditions. *Cereal Res. Commun.* 39, 147–159. doi: 10.1556/CRC.39.2011.1.15

Cabrera-Bosquet, L., Grieder, C., Alvarez Prado, S., Sánchez, C., and Araus, J. L. (2017). Kernel $\delta^{18}O$ reflects changes in apical dominance and plant transpiration in tropical maize. *J. Agron. Crop Sci.* 203, 277–285. doi: 10.1111/jac.12196

Cairns, J. E., Sanchez, C., Vargas, M., Ordoñez, R., and Araus, J. L. (2012). Dissecting Maize Productivity: Ideotypes Associated with Grain Yield under Drought Stress and Well-watered Conditions. *J. Integr. Plant Biol.* 54, 1007–1020. doi: 10.1111/j.1744-7909.2012.01156.x

Câmara, T. M. M., Bento, D. A. V., Alves, G. F., Santos, M. F., Moreira, J. U. V., and Souza Júnior, C. L. (2007). Parâmetros genéticos de caracteres relacionados à tolerância à deficiência hídrica em milho tropical. *Bragantia* 66, 595–603. doi: 10.1590/S0006-87052007000400009

Chairi, F., Elazab, A., Sanchez-Bragado, R., Araus, J. L., and Serret, M. D. (2016). Heterosis for water status in maize seedlings. *Agric. Water Manage.* 164, 100–109. doi: 10.1016/j.agwat.2015.08.005

Combe, L., and Escobar-Gutiérrez, A. J. (2009). Sénescence d'un pied de maïs : évolution de la floraison à la récolte. *Botany* 87, 1036–1053. doi: 10.1139/B09-066

Costa, E. F. N., Santos, M. F., Moro, G. V., Alves, G. F., and de Souza Júnior, C. L. (2008). Herança da senescência retardada em milho. *Pesqui. Agropecuária Bras.* 43, 207–213. doi: 10.1590/S0100-204X2008000200008

De Castro, F. A., Campostrini, E., Netto, A. T., De Menezes De Assis Gomes, M., Ferraz, T. M., and Glenn, D. M. (2014). Portable chlorophyll meter (PCM-502) values are related to total chlorophyll concentration and photosynthetic capacity in papaya (Carica papaya L.). *Theor. Exp. Plant Physiol.* 26, 201–210. doi: 10.1007/s40626-014-0018-y

de Lima, V. J., do Amaral Junior, A. T., Kamphorst, S. H., Pena, G. F., Leite, J. T., Schmitt, K. F., et al. (2016). Combining ability of S_3 progenies for key agronomic traits in popcorn: comparison of testers in top-crosses. *Genet. Mol. Res.* 15, 1–14. doi: 10.4238/gmr15049319

do Amaral Júnior, A. T., dos Santos, A., Gerhardt, I. F. S., Kurosawa, R. N. F., Moreira, N. F., Pereira, M. G., et al. (2016). Proposal of a super trait for the optimum selection of popcorn progenies based on path analysis. *Genet. Mol. Res.* 15, 1–9. doi: 10.4238/gmr15049309

Durães, F. O. M., dos Santos, M. X., Gama, E. E. G. E., Magalhães, P. C., Albuquerque, P. E. P., and Guimarães, C. T. (2004). Fenotipagem Associada a Tolerância a Seca em Milho para Uso em Melhoramento, Estudos Genômicos e Seleção Assistida por Marcadores. *Embrapa Milho e Sorgo-Circular Técnica (INFOTECA-E)* 39, 18. https://www.infoteca.cnptia.embrapa.br/bitstream/doc/487708/1/Circ39.pdf.

Earl, H., and Tollenaar, M. (1999). Using chlorophyll fluorometry to compare photosynthetic performance of commercial maize (Zea mays L.) hybrids in the field. *F. Crop Res.* 61, 201–210. doi: 10.1016/S0378-4290(98)00162-2

Echarte, L., Rothstein, S., and Tollenaar, M. (2008). The Response of Leaf Photosynthesis and Dry Matter Accumulation to Nitrogen Supply in an Older and a Newer Maize Hybrid. *Crop Sci.* 48, 656–665. doi: 10.2135/cropsci2007.06.0366

Elazab, A., Molero, G., Serret, M. D., and Araus, J. L. (2012). Root traits and δ13C and δ18O of durum wheat under different water regimes. *Funct. Plant Biol.* 39, 379. doi: 10.1071/FP11237

Escobar-Gutiérrez, A. J., and Combe, L. (2012). Senescence in field-grown maize: From flowering to harvest. *F. Crop Res.* 134, 47–58. doi: 10.1016/j.fcr.2012.04.013

Farquhar, G. D., and Sharkey, T. D. (1982). Stomatal conductance and photosynthesis. *Annu. Rev. Plant Physiol.* 33, 317–345. doi: 10.1146/annurev.pp.33.060182.001533

Farquhar, G. D., Hubick, K. T., Condon, A. G., and Richards, R. A. (1989). "Carbon isotope fractionation and plant water-use efficiency," in *Stable isotopes in ecological research*, vol. 21–40. (New York, NY: Springer).

Fernández-Calleja, M., Monteagudo, A., Casas, A. M., Boutin, C., Pin, P. A., Morales, F., et al. (2020). Rapid On-Site Phenotyping via Field Fluorimeter Detects Differences in Photosynthetic Performance in a Hybrid—Parent Barley Germplasm Set. *Sensors* 20, 1486. doi: 10.3390/s20051486

Flexas, J., Carriquí, M., and Nadal, M. (2018). Gas exchange and hydraulics during drought in crops: who drives whom? *J. Exp. Bot.* 69, 3791–3795. doi: 10.1093/jxb/ery235

Gao, Y., and Lynch, J. P. (2016). Reduced crown root number improves water acquisition under water deficit stress in maize (Zea mays L.). *J. Exp. Bot.* 67, 4545–4557. doi: 10.1093/jxb/erw243

Ghannoum, O. (2008). C4 photosynthesis and water stress. *Ann. Bot.* 103, 635–644. doi: 10.1093/aob/mcn093

González, L., and González-Vilar, M. (2001). "Determination of Relative Water Content," in *Handbook of Plant Ecophysiology Techniques*. Ed. M. J. Reigosa Roger (Dordrecht: Springer).

Gregersen, P. L., Holm, P. B., and Krupinska, K. (2008). Leaf senescence and nutrient remobilisation in barley and wheat. *Plant Biol.* 10, 37–49. doi: 10.1111/j.1438-8677.2008.00114.x

Hallauer, A. R., Carena, M. J., and Miranda Filho, J. B. (2010). *Quantitative Genetics in Maize Breeding* (New York, NY: Springer).

Hetherington, A. M., and Woodward, F.II (2003). The role of stomata in sensing and driving environmental change. *Nature* 424, 901–908. doi: 10.1038/nature01843

Hund, A., Ruta, N., and Liedgens, M. (2009). Rooting depth and water use efficiency of tropical maize inbred lines, differing in drought tolerance. *Plant Soil* 318, 311–325. doi: 10.1007/s11104-008-9843-6

IPCC - Intergovernmental Panel on Climate Change (2019). *The physical science basis* (Cambridge: Cambridge University press, Cambrigde, UK).

Jordan, D. R., Hunt, C. H., Cruickshank, A. W., Borrell, A. K., and Henzell, R. G. (2012). The Relationship Between the Stay-Green Trait and Grain Yield in Elite Sorghum Hybrids Grown in a Range of Environments. *Crop Sci.* 52, 1153–1161. doi: 10.2135/cropsci2011.06.0326

Joshi, A. K., Kumari, M., Singh, V. P., Reddy, C. M., Kumar, S., Rane, J., et al. (2006). Stay green trait: variation, inheritance and its association with spot blotch resistance in spring wheat (Triticum aestivum L.). *Euphytica* 153, 59–71. doi: 10.1007/s10681-006-9235-z

Kamphorst, S. H., do Amaral Júnior, A. T., de Lima, V. J., Guimarães, L. J. M., Schmitt, K. F. M., Leite, J. T., et al. (2019). Can Genetic Progress for Drought Tolerance in Popcorn Be Achieved by Indirect Selection? *Agronomy* 9, 792. doi: 10.3390/agronomy9120792

Khanna, R., Schmid, L., Walter, A., Nieto, J., Siegwart, R., and Liebisch, F. (2019). A spatio temporal spectral framework for plant stress phenotyping. *Plant Methods* 15:13. doi: 10.1186/s13007-019-0398-8

Kist, B. B., de Carvalho, C., and Beling, R. R. (2019). *Anuário brasileiro do milho 2019*. Ed. R. R. (Beling Santa Cruz do Sul: Editora Gazeta).

Lambers, H., Atkin, O., and Millenaar, F. (2002). "Respiratory Patterns in Roots in Relation to Their Functioning," in *Plant Roots* (New York: CRC Press), 521–552. doi: 10.1201/9780203909423.pt6

Li, X.-H., Liu, X.-D., Li, M.-S., and Zhang, S.-H. (2003). Identification of quantitative trait loci for anthesis-silking interval and yield components under drought stress in maize. *Acta Bot. Sin.* 45, 852–857.

Lima, V.J.de, do Amaral Júnior, A. T., Kamphorst, S. H., Bispo, R. B., Leite, J. T., de O. Santos, T., et al. (2019). Combined Dominance and Additive Gene Effects in Trait Inheritance of Drought-Stressed and Full Irrigated Popcorn. *Agronomy* 9:782. doi: 10.3390/agronomy9120782

Lynch, J. (1995). Root Architecture and Plant Productivity. *Plant Physiol.* 109, 7–13. doi: 10.1104/pp.109.1.7

Lynch, J. P. (2015). Root phenes that reduce the metabolic costs of soil exploration: opportunities for 21st century agriculture. *Plant Cell Environ.* 38, 1775–1784. doi: 10.1111/pce.12451

Mode, C. J., and Robinson, H. F. (1959). Pleiotropism and the genetic variance and covariance. *Biometrics* 15, 518–537. doi: 10.2307/2527650

Radoglou, K. M., and Jarvis, P. G. (1990). Effects of CO2 Enrichment on Four Poplar Clones. I. Growth and Leaf Anatomy. *Ann. Bot.* 65, 617–626. doi: 10.1093/oxfordjournals.aob.a087978

Reynolds, M., and Langridge, P. (2016). Physiological breeding. *Curr. Opin. Plant Biol.* 31, 162–171. doi: 10.1016/j.pbi.2016.04.005

Romano, G., Zia, S., Spreer, W., Sanchez, C., Cairns, J., Luis, J., et al. (2011). Use of thermography for high throughput phenotyping of tropical maize adaptation in water stress. *Comput. Electron. Agric.* 79, 67–74. doi: 10.1016/j.compag.2011.08.011

Schneider, C. A., Rasband, W. S., and Eliceiri, K. W. (2012). NIH Image to ImageJ: 25 years of image analysis. *Nat. Methods* 9, 671–675. doi: 10.1038/nmeth.2089

Sehgal, A., Sita, K., Siddique, K. H. M., Kumar, R., Bhogireddy, S., Varshney, R. K., et al. (2018). Drought or/and Heat-Stress Effects on Seed Filling in Food Crops: Impacts on Functional Biochemistry, Seed Yields, and Nutritional Quality. *Front. Plant Sci.* 9 (1705), 1–19. doi: 10.3389/fpls.2018.01705

Teixeira, F. F., Gomide, R. L., de Albuquerque, P. E. P., de Andrade, C. L. T., Leite, C. E. P., Parentoni, S. N., et al. (2010). Evaluation of maize core collection for drought tolerance. *Crop Breed. Appl. Biotechnol.* 10, 312–320. doi: 10.1590/S1984-70332010000400005

Tollenaar, M., Ahmadzadeh, A., and Lee, E. A. (2004). Physiological Basis of Heterosis for Grain Yield in Maize. *Crop Sci.* 44, 2086. doi: 10.2135/cropsci2004.2086

Trachsel, S., Kaeppler, S. M., Brown, K. M., and Lynch, J. P. (2011). Shovelomics: high throughput phenotyping of maize (Zea mays L.) root architecture in the field. *Plant Soil* 341, 75–87. doi: 10.1007/s11104-010-0623-8

Trachsel, S., Kaeppler, S. M., Brown, K. M., and Lynch, J. P. (2013). Maize root growth angles become steeper under low N conditions. *F. Crop Res.* 140, 18–31. doi: 10.1016/j.fcr.2012.09.010

Van Loon, A. F., Gleeson, T., Clark, J., Van Dijk, A.II, Stahl, K., Hannaford, J., et al. (2016). Drought in the Anthropocene. *Nat. Geosci.* 9, 89–91. doi: 10.1038/ngeo2646

Yang, J., and Zhang, J. (2006). Grain filling of cereals under soil drying. *New Phytol.* 169, 223–236. doi: 10.1111/j.1469-8137.2005.01597.x

Yang, H., Gu, X., Ding, M., Lu, W., and Lu, D. (2019). Activities of starch synthetic enzymes and contents of endogenous hormones in waxy maize grains subjected to post-silking water deficit. *Sci. Rep.* 9, 7059. doi: 10.1038/s41598-019-43484-0

Yousfi, S., Gracia-Romero, A., Kellas, N., Kaddour, M., Chadouli, A., Karrou, M., et al. (2019). Combined Use of Low-Cost Remote Sensing Techniques and δ13C to Assess Bread Wheat Grain Yield under Different Water and Nitrogen Conditions. *Agronomy* 9, 285. doi: 10.3390/agronomy9060285

Zhan, A., and Lynch, J. P. (2015). Reduced frequency of lateral root branching improves N capture from low-N soils in maize. *J. Exp. Bot.* 66, 2055–2065. doi: 10.1093/jxb/erv007

Zhan, A., Schneider, H., and Lynch, J. P. (2015). Reduced Lateral Root Branching Density Improves Drought Tolerance in Maize. *Plant Physiol.* 168, 1603–1615. doi: 10.1104/pp.15.00187

Zhang, C., Zhang, J., Zhang, H., Zhao, J., Wu, Q., Zhao, Z., et al. (2015). Mechanisms for the relationships between water-use efficiency and carbon isotope composition and specific leaf area of maize (Zea mays L.) under water stress. *Plant Growth Regul.* 77, 233–243. doi: 10.1007/s10725-015-0056-8

Zhao, W., Sun, Y., Kjelgren, R., and Liu, X. (2015). Response of stomatal density and bound gas exchange in leaves of maize to soil water deficit. *Acta Physiol. Plant* 37, 1704. doi: 10.1007/s11738-014-1704-8

Zia, S., Romano, G., Spreer, W., Sanchez, C., Cairns, J., Araus, J. L., et al. (2013). Infrared Thermal Imaging as a Rapid Tool for Identifying Water-Stress Tolerant Maize Genotypes of Different Phenology. *J. Agron. Crop Sci.* 199, 75–84. doi: 10.1111/j.1439-037X.2012.00537.x

Zinselmeier, S. A., Lauer, M. J., and Boyer, J. S. (1995). Reversing Drought-Induced Losses in Grain Yield: Sucrose Maintains Embryo Growth in Maize. *Crop Sci.* 35, 1390. doi: 10.2135/cropsci1995.0011183X003500050022x

Conflict of Interest: The authors declare that the research was conducted in the absence of any commercial or financial relationships that could be construed as a potential conflict of interest.

Copyright © 2020 Kamphorst, Amaral Júnior, de Lima, Santos, Rodrigues, Vivas, Gonçalves, Schmitt, Leite, Vivas, Mora-Poblete, Vergara-Díaz, Araus Ortega, Ramalho and Campostrini. This is an open-access article distributed under the terms of the Creative Commons Attribution License (CC BY). The use, distribution or reproduction in other forums is permitted, provided the original author(s) and the copyright owner(s) are credited and that the original publication in this journal is cited, in accordance with accepted academic practice. No use, distribution or reproduction is permitted which does not comply with these terms.

frontiers in Plant Science

ORIGINAL RESEARCH
published: 28 August 2020
doi: 10.3389/fpls.2020.01316

Development and Characterization of Near-Isogenic Lines Revealing Candidate Genes for a Major 7AL QTL Responsible for Heat Tolerance in Wheat

Lu Lu[1,2,3], *Hui Liu*[1,2*], *Yu Wu*[3] *and Guijun Yan*[1,2*]

[1] Faculty of Science, UWA School of Agriculture and Environment, The University of Western Australia, Perth, WA, Australia, [2] The UWA Institute of Agriculture, The University of Western Australia, Perth, WA, Australia, [3] Chengdu Institute of Biology, Chinese Academy of Sciences, Chengdu, China

OPEN ACCESS

Edited by:
Felipe Klein Ricachenevsky, Federal University of Rio Grande, Brazil

Reviewed by:
Marta Silva Lopes, Institute of Agrifood Research and Technology (IRTA), Spain
Dawei Xin, Northeast Agricultural University, China

***Correspondence:**
Hui Liu
hui.liu@uwa.edu.au
Guijun Yan
guijun.yan@uwa.edu.au

Specialty section:
This article was submitted to Plant Abiotic Stress, a section of the journal Frontiers in Plant Science

Received: 11 May 2020
Accepted: 11 August 2020
Published: 28 August 2020

Citation:
Lu L, Liu H, Wu Y and Yan G (2020) Development and Characterization of Near-Isogenic Lines Revealing Candidate Genes for a Major 7AL QTL Responsible for Heat Tolerance in Wheat. Front. Plant Sci. 11:1316. doi: 10.3389/fpls.2020.01316

Wheat is one of the most important food crops in the world, but as a cool-season crop, it is more prone to heat stress, which severely affects crop production and grain quality. Heat tolerance in wheat is a quantitative trait, and the genes underlying reported quantitative trait loci (QTL) have rarely been identified. Near-isogenic lines (NILs) with a common genetic background but differing at a particular locus could turn quantitative traits into a Mendelian factor; therefore, they are suitable material for identifying candidate genes for targeted locus/loci. In this study, we developed and characterized NILs from two populations Cascades × Tevere and Cascades × W156 targeting a major 7AL QTL responsible for heat tolerance. Molecular marker screening and phenotyping for SPAD chlorophyll content and grain-yield-related traits confirmed four pairs of wheat NILs that contrasted for heat-stress responses. Genotyping the NILs using a 90K Infinium iSelect SNP array revealed five single nucleotide polymorphism (SNP) markers within the QTL interval that were distinguishable between the isolines. Seven candidate genes linked to the SNPs were identified as related to heat tolerance, and involved in important processes and pathways in response to heat stress. The confirmed multiple pairs of NILs and identified candidate genes in this study are valuable resources and information for further fine-mapping to clone major genes for heat tolerance.

Keywords: heat tolerance, near-isogenic lines, 7AL, quantitative trait loci, single nucleotide polymorphism assay, candidate genes, wheat

INTRODUCTION

Crop growth and productivity are often limited by abiotic stresses, especially heat and drought (Priya et al., 2019). Wheat is one of the most important food grain crops in the world, but being a cool-season crop, it often experiences heat stress. Each 1°C rise in temperature above the optimum can cause a 3–5% reduction in single grain weight under controlled environments (Dawson and Wardlaw, 1989) or field conditions (Wiegand and Cuellar, 1981). Phenology is known to confound

crop responses to heat; therefore, the effect of heat stress depends on its timing, duration, and frequency (Rezaei et al., 2015; Balla et al., 2019). While conventional breeding has developed some heat-tolerant lines, it is a time-consuming process, and the genetic and physiological basis of the improvements remain unclear (Driedonks et al., 2016). Understanding the underlying mechanism of heat tolerance and identifying candidate genes will help to accelerate the breeding of heat-stress-resilient genotypes (Budak et al., 2015).

Heat tolerance is a quantitative trait (Moffatt et al., 1990a; Yang et al., 2002) that involves complex genetic, physiological, and biochemical controls and is affected by environmental factors. Numerous heat tolerance QTL have been identified; for example, Yang et al. (2002) found QTL on the short arms of chromosomes 1B and 5A linked to grain filling duration; Mason et al. (2010, 2011) reported several QTL for heat susceptibility indices and yield traits on chromosomes 1A, 1B, 2A, 2B, 3B, 5A, and 6D; Paliwal et al. (2012) reported QTL on chromosomes 2B, 7B, and 7D for thousand-grain weight, grain fill duration, and canopy temperature depression, respectively; Vijayalakshmi et al. (2010) reported QTL on chromosomes 2A, 3A, 4A, 6A, 6B, and 7A with significant effects on grain yield, grain weight, grain filling, stay green, and senescence-associated traits under post-anthesis high-temperature stress in wheat. Most of these reported QTL have been based on mapping using low-density simple sequence repeat (SSR) markers and/or amplified fragment length polymorphism (AFLP) markers. Talukder et al. (2014) increased the marker density to 972 molecular markers and identified QTL associated with different traits related to heat tolerance in wheat. They found that QTL QHtscc.ksu-7A on chromosome 7A was consistently identified for traits thylakoid membrane damage (TMD), plasma membrane damage (PMD), and SPAD chlorophyll content (SCC), with high logarithm of odds (LOD) values ranging from 4.15 to 6.95 and explaining high phenotypic variations ranging from 18.9 to 33.5%. This major QTL QHtscc.ksu-7A, with flanking markers Xbarc121 and Xbarc49, was chosen as the target locus for developing NILs in this study.

It remains challenging to use QTL markers directly in breeding programs due to the large genomic intervals of the most identified QTL (Mia et al., 2019). One solution for identifying candidate genes and closely linked markers is to develop NILs, which turn quantitative traits into Mendelian factors (Liu et al., 2006). NILs are pairs of lines that have the same genetic background between isolines, except for the targeted locus (Dorweiler et al., 1993). NILs make it easier to study phenotypic impacts attributable to a specific gene or locus (Pumphrey et al., 2007). Characterizing NILs through genotype–phenotype association analyses can lead to the identification of candidate genes (Mirdita et al., 2008; Liu et al., 2010; Mia et al., 2019; Wang et al., 2019). Traditionally, NILs development has been considered time-consuming and tedious (Tuinstra et al., 1997). By combining a fast generation cycling system (FGCS) (Zheng et al., 2013) with heterogeneous inbred family (HIF) method and repeated DNA marker-assisted selection (MAS) (Tuinstra et al., 1997), the NIL development process can be shortened to about six generations per year (Yan et al., 2017).

Single nucleotide polymorphism (SNP) markers are high-density DNA markers widely used in genetic studies, including genetic diversity, phylogenetic relationships, and marker-trait associations, such as genome-wide association study (GWAS) or QTL mapping (Wang et al., 2014; Cabral et al., 2018). The 90k SNP array, developed from hexaploid wheat and *Aegilops tauschii* sequences (Wang et al., 2014) with dense coverage of the wheat genome, has been extensively harnessed for genetic research (Cavanagh et al., 2013; Avni et al., 2014; Colasuonno et al., 2014; Russo et al., 2014; Sukumaran et al., 2015). Due to its efficiency of characterizing genetic resources and discriminating between closely related lines (Rimbert et al., 2018), 90k SNP genotyping was used in this study to characterize the developed NILs, in combination with phenotyping under controlled environments.

The objectives of this study were to 1) develop and confirm NILs targeting the major heat tolerance QTL on chromosome 7A, 2) identify candidate gene(s) underlying the 7A QTL responsible for heat tolerance by genotypic and phenotypic characterization of the NILs, and 3) shed light on the genetic mechanism of heat tolerance in wheat by inspecting this major genomic region and investigating its underlying candidate genes.

MATERIALS AND METHODS

Plant Materials and Selection of Crossing Parents

In a previous study, 499 wheat genotypes from a variety of sources were screened and evaluated for heat-stress responses (Hameed, 2015). Among them, cultivars Tevere and W156 showed heat tolerance at both the seedling and reproductive stages with high yield, whereas Cascades (Aroona//Tadorna/Inia 66) was sensitive at both stages (unpublished data). Cascades and Tevere are two common wheat cultivars and W156 is a landrace, which originated from Australia, Italy, and India, respectively. When the flanking marker Xbarc49 of the targeted 7A QTL was used for genotyping the three cultivars, heat-tolerant Tevere and W156 showed the tolerance allele at 216 bp, and heat-susceptible Cascades showed the susceptibility allele at 203 bp. The three cultivars were therefore used to establish two cross populations, Cascades/W156 and Cascades/Tevere, for the development of NILs targeting the 7A locus.

Development of NILs

NILs were developed from the two populations using the HIF method (Tuinstra et al., 1997) in combination with embryo-culture-based FGCS (Zheng et al., 2013; Yan et al., 2017), following a similar procedure as described in Wang et al. (2019). Specifically, MAS started from the second generation of progenies (F2) (**Figure 1A**) where genomic DNA was isolated from two-week-old seedlings of each plant using a modified CTAB method (Murray and Thompson, 1980). Xbarc49 (**Figure 1B**), the flanking marker of QHtscc.ksu-7A (Talukder et al., 2014), was used to identify heterozygous progenies (Rr) from the two cross populations (**Figure 1C**). PCR reactions were performed, and amplified products viewed following the

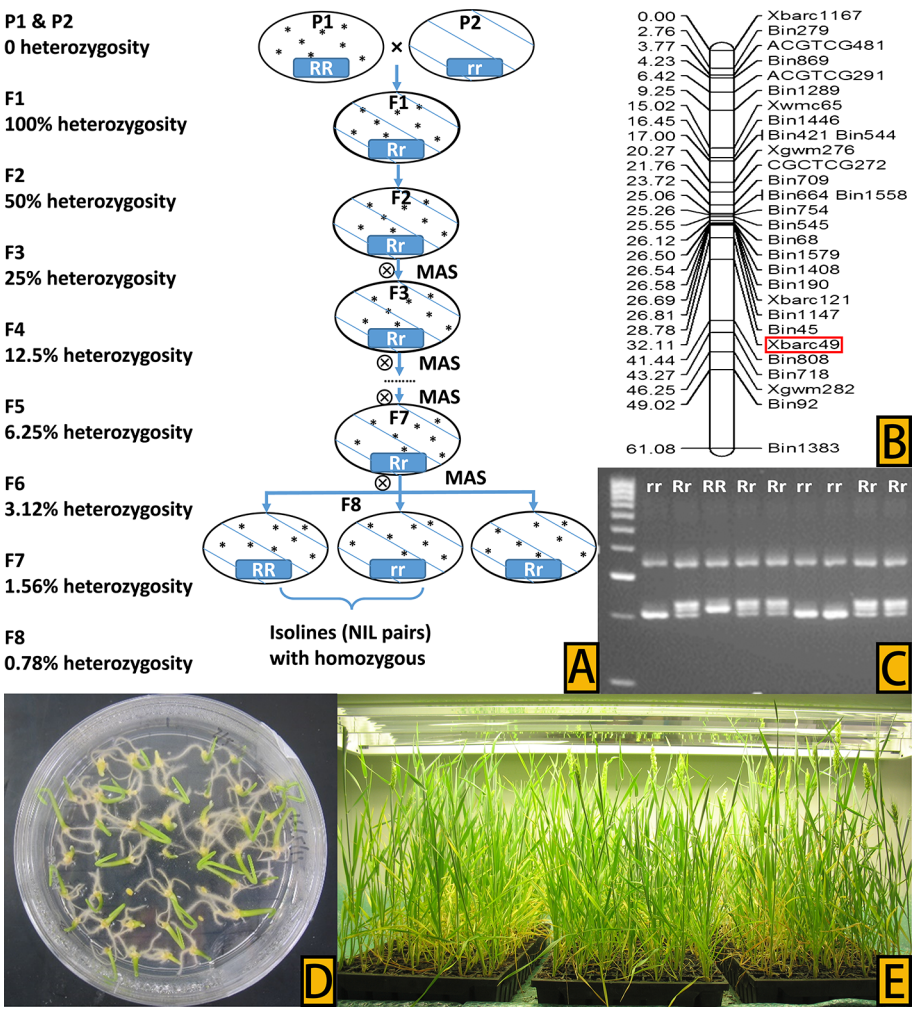


FIGURE 1 | (A) Process of the HIF method to develop NIL pairs, with percentage heterozygosity in each generation shown on the left of the flow chart. **(B)** QTL hotspot in wheat chromosome 7A and the marker (in the box) used for selection, adapted from Talukder et al., 2014. **(C)** Marker-assisted selection of different progeny types, with tolerance progeny, susceptible progeny, and heterozygous progeny marked RR, rr, and Rr, respectively, on the top of the gel bands. **(D)** Culture of young embryos on Petri plates in a sterile medium. **(E)** Seedlings from embryo culture growing in the plant growth chamber.

protocol described in Wang et al. (2018). MAS of heterozygous progenies, together with embryo-culture-based FGCS (**Figures 1D, E**), continued until the eighth generation of progenies (F8); at F8, only those homozygous progenies from single seed descent with the tolerance allele (RR/+) from either W156 or Tevere and those with susceptibility allele (rr/–) from Cascades were selected as pairs of candidate NILs. Thirteen pairs of F8 NILs, numbered from NIL1 to NIL13, developed from the two populations were used as putative NIL pairs to screen their phenotypes for performance under heat stress.

Plant Growth Conditions and Heat Treatments

The seeds of all isolines were germinated in water on Petri dishes, before sowing one plant per pot (8 cm × 8 cm × 16 cm) containing soil media (5:2:3 compost:peat:sand, pH 6.0) (Mia et al., 2019). For each isoline, six pots (three replicates each for the control and the heat-stress treatment) were grown in a naturally lit glasshouse at The University of Western Australia, Crawley, Western Australia (31°59' S, 115°49'E). The plants were fertilized fortnightly with 'Diamond Red' (Campbells Fertilisers Australasia Pty Ltd, Australia) from four weeks after sowing until the end of the grain-filling period. The glasshouse environment (temperature, relative humidity, and light intensity) is detailed in **Supplementary Table S1**. The experiment was arranged in a completely randomized block design.

Anthesis date, as Zadoks' growth scale Z60 (Zadoks, 1974), of each plant was recorded by tagging each plant on the wheat head where the first anther appeared. The time point to start the heat treatment, treatment temperature, and other settings were as per previous studies (Pradhan et al., 2012; Talukder et al., 2014; Shirdelmoghanloo et al., 2016a). Specifically, on the 10th day after anthesis (DAA), the three treatment pots were moved into a growth chamber set to 37/27°C (day/night), 14-h photoperiod,

and 420 μmol m^{-2} s^{-1} light intensity for the 3-day heat treatment. Enough water was given to the plants to ensure there was no drought stress, only heat stress. The pots were returned to the glasshouse after the heat treatment.

Phenotype Screening

Chlorophyll contents were measured on flag leaves using a handheld portable chlorophyll meter (SPAD-502Plus; Konica Minolta, Osaka) for both the control and heat-stressed plants. Time points for measurements followed the procedures described in Pradhan et al. (2012). Changes in SPAD chlorophyll contents (ΔSCC) in flag leaves were calculated based on differences in chlorophyll contents before (as 'Chl10' at 10 DAA) and after (as 'Chl13' at 13 DAA) treatment, as follows: ΔSCC = mean of Chl10 – mean of Chl13 (Shirdelmoghanloo et al., 2016b). Measurements and calculations were the same for controls.

Agronomic traits (grain number and grain yield per plant) were measured after harvest for plants in the control and heat-stressed treatments. The performance differences in final yield between isoline pairs were determined by subtracting mean values in the control from those in the heat treatment.

Statistical analyses were undertaken using t-tests to compare phenotypic variation in the NIL pairs. True NILs were confirmed if significant differences existed in the performance of tested traits between isolines, and their resistant and susceptible phenotypes matched their genotypes of Xbarc49's RR/+ and rr/ – alleles, respectively.

Genotyping by 90k Infinium iSelect SNP Array

The 90K SNP array was used for genotyping, with genotype–phenotype associations used to identify candidate gene(s) (Alaux et al., 2018). Specifically, genomic DNA samples of the confirmed NILs were genotyped using the Wheat 90K Illumina iSelect Array (Wang et al., 2014). SNP clustering and genotype calling were performed using GenomeStudio 2.0 software (Illumina). SNPs with a call frequency <0.8 (i.e., missing data points >20%), minor allele frequency (MAF) <0.05 or heterozygous calls >0.25 were removed. SNP sequences that differed between NIL pairs were used to perform a BLAST search against the wheat reference genome (IWGSC, 2018). SNPs located on the 7AL chromosome arm, especially those within the marker interval of QHtscc.ksu-7A (Talukder et al., 2014), were scrutinized using JBrowse (http://www.wheatgenome.org/Tools-and-Resources/Sequences) for candidate gene discovery.

RESULTS

Four NIL Pairs Confirmed With Significant Differences in Chlorophyll Content

After comparing the ΔSCC data for NIL pairs, no significant differences were observed among the 13 putative NIL pairs grown in the non-stressed (control) treatment, whereas the isolines of four NIL pairs significantly differed in the heat-stressed treatment. Of these, the isolines with positive alleles (+NILs) had smaller reductions in SPAD chlorophyll content than isolines with negative alleles (–NILs). The isolines of NILs 5, 10, and 13 differed significantly at $P < 0.05$, and NIL 9 differed significantly at $P < 0.01$ (**Table 1**).

Tolerant Isolines Performed Better Than Susceptible Isolines on Other Agronomic Traits in the Confirmed NILs

Further investigation showed that significant differences existed between most of the treated isolines and their corresponding controls for yield-related traits. The differences or gaps in grain number per pot and yield per pot between the control and heat-stressed treatments are shown in **Figure 2** to compare yield performance in tolerant and susceptible isolines. For grain number, three of the four +NILs (5, 9, and 10) had smaller gaps than –NILs. For yield, all four +NILs had smaller gaps between non-stressed and stressed treatments than their counterparts. Generally, heat stress had smaller negative effects on grain number and yield in +NILs than –NILs.

Five SNP Markers With Consistent Contrasting Genotypes in the Confirmed NIL Pairs

Of the 81,587 SNPs on the array, 53,052 were analyzed across the 21 chromosomes after removing those that did not meet the

TABLE 1 | Reduction of SPAD chlorophyll content (ΔSCC) in the confirmed NIL pairs.

NIL name	Population	ΔSCC (Chl10–Chl13)			
		Control		Treatment	
		Mean	P-value	Mean	P-value
NIL5(+)	Cascade/Tevere	–0.4	ns	0.53	*
NIL5(–)		–0.8		7.13	
NIL9(+)	Cascade/W156	1.1	ns	4.57	**
NIL9(–)		5.05		7.97	
NIL10(+)	Cascade/W156	0.67	ns	1.7	*
NIL10(–)		0.6		12.23	
NIL13(+)	Cascade/Tevere	0.15	ns	1.7	*
NIL13 (–)		1.27		6.7	

*ns = non-significant at P ≤ 0.05; * = significant at P ≤ 0.05; ** = significant at P ≤ 0.01. The statistics was done using t-test. (+) indicates isolines with resistance allele from W156 or Tevere; (–) indicates isolines with susceptibility allele from Cascades.*

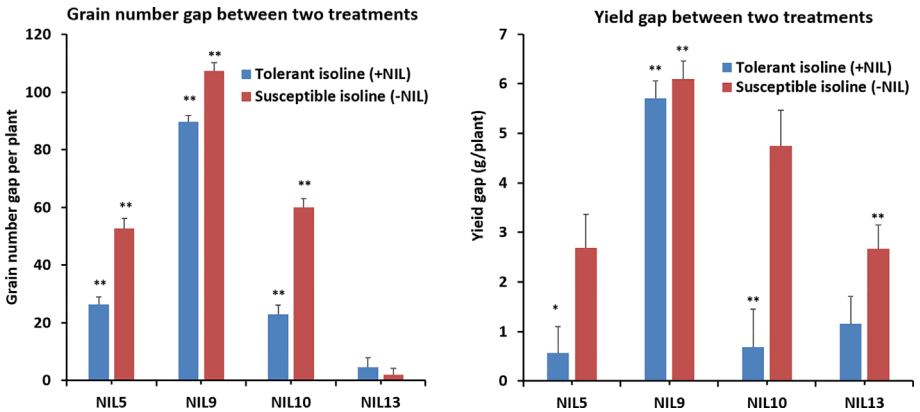


FIGURE 2 | Differences in agronomic trait gaps between the confirmed isolines of tolerant and susceptible alleles. Three replicates each for the control (naturally lit glasshouse with conditions described in detail in **Table S1**) and the heat-stressed treatment (growth chamber set at 37/27°C day/night) were used for statistical analysis. The column indicates trait gaps between the treatment and control, with error bar on top. * indicates significant difference at $P \leq 0.05$; ** indicates significant difference at $P \leq 0.01$. Statistics done using t-test.

selection criteria. Analyzing the SNPs among the four confirmed pairs of isolines identified five SNPs within the 7AL QTL region with consistent contrasting genotypes between the resistant and susceptible isolines (**Table 2**).

Candidate Genes Identified by Blasting the Wheat Reference Genome

Seven candidate genes were identified within the QHtscc.ksu-7A region by blasting the above five SNP markers with wheat reference genome RefV1.0. The annotations for high and low confidence genes of RefV1.0 were used, with various databases compared, including NCBI (https://www.ncbi.nlm.nih.gov) and InterMine (http://www.wheatgenome.org/Tools-and-Resources/Sequences), to determine possible gene functions (**Table 3**).

Markers BS00071558_51 and wsnp_Ku_c5160_9203226 were co-located on gene *TraesCS7A01G612600LC*, with their SNP variations in the intron and untranslated region (UTR), respectively (**Figure 3**). Markers wsnp_Ku_rep_c113718_96236830 and wsnp_RFL_Contig2864_2688208 were co-located on gene *TraesCS7A01G432000* and *TraesCS7A01G431600*, respectively, with their SNP variations in the UTR and exon regions. Although no gene was co-located on wsnp_Ra_c26491_36054023, the marker was located close to genes *TraesCS7A01G428200* (15,752 bp away) and *TraesCS7A01G428400* (273,590 bp away), both of which function as peroxidase.

Blasting the sequence of *TraesCS7A01G612600LC* in NCBI identified five ESTs related to plant biotic or abiotic stress responses (Manickavelu et al., 2012). Genes *TraesCS7A01G432000* and *TraesCS7A01G431600* were involved in important biochemistry or molecular functions, such as protein binding, Zinc finger, F-box domain, Kelch motif, and Per-Arnt-Sim (PAS) domain, all of which are involved in various pathways of plant responses and reactions to external stimulus (Craig and Tyers, 1999; Adams et al., 2000; Prag and Adams, 2003; Hefti et al., 2004; van den Burg et al., 2008; Hennig et al., 2009; Moglich et al., 2009; Peng et al., 2012; Liu et al., 2015).

Apart from these genes, two other noteworthy genes—*TraesCS7A01G430500*, which functions as a sugar transporter family protein, and *TraesCS7A01G430600*, which functions as a heat shock protein (HSP)—were located in the interval between marker wsnp_Ra_c26491_36054023 and wsnp_RFL_Contig2864_2688208.

DISCUSSION

In this study, we reported the development of 13 putative NIL pairs targeting a major locus for heat tolerance. Among them, four pairs were confirmed as true NILs by genotype–phenotype association analysis. The confirmed NILs showed differential responses under non-stressed and heat-stressed conditions. NILs with alleles from the heat-tolerant parents (Tevere and W156) performed better than their counterparts in terms of physiological and agronomical traits, such as chlorophyll content, grain number, and grain yield. Characterization of these NIL pairs revealed that the presence of the tolerance allele significantly increased heat tolerance in the

TABLE 2 | SNPs showing consistent contrast callings in the confirmed four pairs of NILs.

No.	Marker Name	SNP	Physical location
1	BS00071558_51	[T/C]	chr7A:626897156.626897256
2	wsnp_Ku_c5160_9203226	[T/C]	chr7A:626897816.626898016
3	wsnp_Ku_rep_c113718_96236830	[A/G]	chr7A:625739519.625739719
4	wsnp_Ra_c26491_36054023	[A/G]	chr7A:621582917.621583094
5	wsnp_RFL_Contig2864_2688208	[T/C]	chr7A:625640069.625640169

TABLE 3 | Function annotations of candidate genes.

Gene	Physical position	Database	Identifier	Description
TraesCS7A01G612600LC	626894752.626898021	EMBL-EBI	BQ245642	Yield improvement under stress
			HX055146	response to blast fungus
			HX055177	wheat responses to fungi infections
			CJ956871	response to powdery mildew infection
			CJ945027	responses to fungi infections
TraesCS7A01G432000	625737761.625740656	Interpros	IPR013083	Zinc finger, RING/FYVE/PHD-type
TraesCS7A01G431600	625635655.625640991	GOs	GO:0005515	Molecular Function: protein binding
		Interpros	IPR001810	F-box domain
			IPR015915	Kelch-type beta propeller
			IPR000014	PAS domain
			IPR011498	Kelch-repeat type 2
		Pfams	PF13426	PAS domain
			PF13415	Galactose oxidase, central domain
			PF07646	Kelch motif
			PF13418	Galactose oxidase, central domain
			PF12937	F-box-like
TraesCS7A01G428200	621564527.621567165	GOs	GO:0020037	MF: heme binding
			GO:0055114	BP: oxidation-reduction process
			GO:0004601	MF: peroxidase activity
			GO:0006979	BP: response to oxidative stress
		Interpros	IPR000823	Plant peroxidase
			IPR002016	Haem peroxidase, plant/fungal/bacterial
			IPR010255	Haem peroxidase
			IPR019793	Peroxidases heam-ligand binding site
			IPR019794	Peroxidase, active site
		Pfams	PF00141	Peroxidase
TraesCS7A01G428400	621856684.621857860			Similar function as gene *TraesCS7A01G428200*
TraesCS7A01G430500	624959655.624961254	GOs	GO:0016021	CC: integral component of membrane
			GO:0016020	CC: membrane
			GO:0055085	BP: transmembrane transport
			GO:0005215	MF: transporter activity
			GO:0022857	MF: transmembrane transporter activity
			GO:0022891	MF: substrate-specific transmembrane transporter activity
			IPR020846	Major facilitator superfamily domain
		Interpros	IPR003663	Sugar/inositol transporter
			IPR005828	Major facilitator, sugar transporter-like
			IPR005829	Sugar transporter, conserved site
		Pfams	PF00083	Sugar (and other) transporter
TraesCS7A01G430600	624965100.624967076	Interpros	IPR013126	Heat shock protein 70 family
			IPR029047	Heat shock protein 70kD, peptide-binding domain
			IPR029048	Heat shock protein 70kD, C-terminal domain
			IPR018181	Heat shock protein 70, conserved site
		Pfams	PF00012	Hsp70 protein

plants. One reason for the higher grain yield and grain number in the heat-tolerant NILs may be the positive correlation between chlorophyll content and gas exchange parameters reported in several studies (Chen et al., 2016; Wang et al., 2016).

Many physiological traits have been closely associated with heat response, such as canopy temperature, leaf senescence, night respiration, chlorophyll fluorescence, and cell membrane thermo-stability (Narayanan, 2018). The original QTL targeted in this study was associated with multiple traits, including thylakoid membrane damage (TMD), plasma membrane damage (PMD), and SPAD chlorophyll content (SCC) (Talukder et al., 2014). Membrane thermostability has a strong genetic correlation with grain yield in wheat (Reynolds et al., 1994; Fokar et al., 1998). Loss of chlorophyll content during grain filling has been associated with reduced yield under field conditions (Reynolds et al., 1994). TMD and PMD have also been associated with grain yield (Moffatt et al., 1990b; Saadall et al., 1990; Reynolds et al., 1994; Araus et al., 1998; Marcum, 1998; Blum et al., 2001; Wahid and Shabbir, 2005). Strong correlations among these traits suggest that these traits are under pleiotropic genetic control.

Leaf chlorophyll content is a major indicator of the photosynthetic capability of plant tissues (Rao et al., 2001; Pietrini et al., 2017). Some studies that focused on yield and photosynthetic traits (Raven and Griffiths, 2015; Gaju et al., 2016; Merchuk-Ovnat et al., 2016) have shown that the photosynthetic function duration of leaves is closely correlated to grain yield in wheat. Furthermore, spectral characteristics measured by SPAD are a good indicator for evaluating crop responses to high

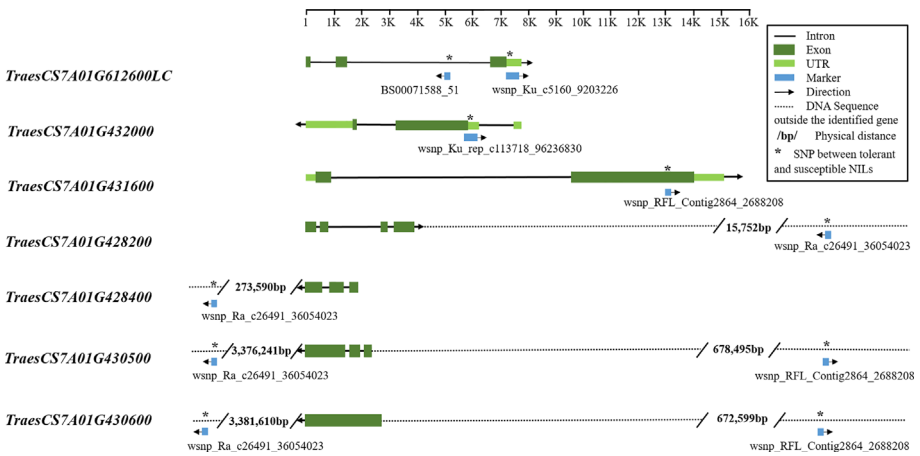


FIGURE 3 | Candidate gene structures and SNPs between tolerant and susceptible NILs. The structural information of genes and SNP markers was extracted from the wheat genome database (https://urgi.versailles.inra.fr/jbrowseiwgsc/gmod_jbrowse). The SNP positions between tolerant and susceptible NILs are marked with an asterisk. For the first three genes, SNPs distinguishing tolerant and susceptible NILs were within the identified genes, either exon, intron, or untranslated region (UTR); for the other four genes, SNPs were outside the candidate genes and their physical distances to the genes are labeled.

temperature (Talukder et al., 2014; Tao et al., 2016). Due to its correlation with yield and other performance indicators under heat stress, chlorophyll content measured by SPAD could be used as an easy and reasonable morphological marker for assessing heat tolerance, especially at the initial mass screening stage. The smaller the reduction in SPAD chlorophyll content (ΔSCC), the more tolerant the plant should be to heat stress. SPAD meters have been used to estimate leaf chlorophyll content in research and agricultural practices because it is a quick, simple and non-destructive method (Novichonok et al., 2016; Padilla et al., 2018; Zhao et al., 2018; de Souza et al., 2019; Galanti et al., 2019; Zhang et al., 2019). Here, agronomic traits such as grain number and grain yield were also measured to further confirm the true NIL pairs, which are valuable material for further studies of post-anthesis heat tolerance in wheat.

Except for the report by Talukder et al. (2014), the major QTL QHtscc.ksu-7A targeted in this study has been identified as responsible for heat tolerance in other studies. Vijayalakshmi et al. (2010) reported a 7A QTL linked to marker Xbarc121 for heat-tolerance traits, including Fv/Fm and time to maximum rate of senescence. Talukder et al. (2014) revealed that several ESTs, located in the same wheat deletion bin as Xbarc49, were related to stress response in different studies; therefore, the authors proposed that the major QTL QHtscc.ksu-7A was a genomic region rich in genes related to stress response. Dixit et al. (2015) hypothesized that multiple genes underpinned large-effect QTL. In this study, seven candidate genes within the targeted major 7AL QTL were identified as responsible for heat tolerance post-anthesis. The gene *TraesCS7A01G612600LC* is a homologous gene to *TraesCS7A01G612600L*; blasting *TraesCS7A01G612600L* by Blastx (translated nucleotide to protein) on NCBI with criteria of percentage identity ≥50% and e-value of <1e-5 revealed its origin from *Triticum urartu*, and it has been up-regulated at 24 h osmotic stress in the ABA-dependent signaling pathway (Li et al., 2019). Therefore, the gene *TraesCS7A01G612600LC* identified in this study supposedly has a similar function as its homologous gene. Abscisic acid (ABA) is generally considered as a stress signaling hormone, and the expression of stress-responsive genes in plants is primarily regulated by ABA-dependent and ABA-independent pathways (Agarwal and Jha, 2010; Yoshida et al., 2014). The ABA-dependent pathway is central to osmotic-stress responses in plants (Li et al., 2019). Moreover, five expression sequence tag (EST) markers associated with *TraesCS7A01G612600LC* were related to plant biotic or abiotic stress responses. Among these EST markers, HX055146, HX055177, CJ956871, and CJ945027 were related to wheat responses to fungi infections, including Fusarium head blight and powdery mildew (Manickavelu et al., 2012), while BQ245642 encoded a polypeptide useful for yield improvement by improving plant growth and development under at least one stress condition (Kovalic et al., 2007).

The annotation of genes *TraesCS7A01G432000* and *TraesCS7A01G431600* revealed their involvement in some important biochemistry or molecular functions, such as protein binding, Zinc finger, F-box domain, Kelch motif, PAS domain, and galactose oxidase. F-box domain genes are related to plant resistance, while F-box proteins are associated with cellular functions, such as signal transduction and regulation of the cell cycle during plant vegetative and reproductive growth and development (Craig and Tyers, 1999). For example, F-box protein FOA1 plays a role in ABA signaling involved in seed germination (Peng et al., 2012), ACRE189/ACIF1 regulates cell defense and death when tomato and tobacco are attacked by pathogens (van den Burg et al., 2008), Kelch motifs and kelch-repeat β-propellers undergo a variety of binding interactions with other molecules (Adams et al., 2000; Prag and Adams, 2003), and a PAS domain acts as a molecular sensor (Hennig et al., 2009; Moglich et al., 2009; Liu et al., 2015) and has been deemed as the key structural motif involved in protein-protein interactions during physiological reactions (Hefti et al.,

2004). In summary, all these biological structures are extensively involved in various pathways of plant responses and reactions to external stimuli such that we can deduce that genes *TraesCS7A01G432000* and *TraesCS7A01G431600* regulate heat tolerance by controlling protein structures and protein binding on the biological structures mentioned above to achieve signal transduction, which is the key part in the pathway of heat tolerance.

The remaining four genes *TraesCS7A01G428200*, *TraesCS7A01G428400*, *TraesCS7A01G430500*, and *TraesCS7A01G430600* have functions as peroxidase, peroxidase, sugar transporter family protein, and HSP, respectively. The sugar transporter family protein is related to yield as sugar transport is one of the most important processes for plant development and their responses to biotic and abiotic factors (Lalonde et al., 2004; Lemoine et al., 2013). Tolerance to heat stress is frequently associated with maintaining sugar content in source leaves (Vasseur et al., 2011; Zhou et al., 2017). For example, a heat-tolerant tomato (*Solanum lycopersicum*) genotype had significantly higher fructose and sucrose contents in mature leaves than a heat-sensitive genotype under heat stress (Zhou et al., 2017). Peroxidase is related to stress tolerance—peroxidase activities increased significantly in a heat-tolerant wheat genotype in response to heat treatment (Sairam et al., 1998). Exposure to heat stress often leads to the generation of destructive ROS (reactive oxygen species), but plants have antioxidant mechanisms to escape excessive ROS. Several studies have shown that peroxidase plays an important role in antioxidant mechanisms and ameliorates the effects of heat stress in wheat (Suzuki et al., 2011; Caverzan et al., 2016). HSPs play a pivotal role as chaperones in conferring biotic and abiotic stress tolerance (Baniwal et al., 2004). The expression of HSP genes induced by high temperature can preserve the stability and function of intracellular proteins and protect them from denaturation through protein folding. They enhance membrane stability and detoxify ROS by positively regulating the antioxidant enzyme system. Additionally, HSP genes use ROS as a signal to molecules to induce HSP production. HSP also enhances plant immunity by accumulating and stabilizing pathogenesis-related proteins under various biotic stresses (Haq et al., 2019). Genotypes generating HSPs can withstand heat stress as they protect proteins from heat-induced damage (Farooq et al., 2011).

The gene structure analysis (**Figure 3**) identified several SNPs distinguishing tolerant and susceptible NILs located within the candidate genes, in which one marker wsnp_RFL-Contig2864_2688208 falls in the exon region. These markers can be used as functional markers, because not only does the exon encodes protein functional units but also noncoding DNA including intron and UTR has played significant roles in many studies (Cobb et al., 2008; Khurana et al., 2013; Lu et al., 2015; Grünewald et al., 2015). SNPs outside the identified candidate genes can still be used in marker-assisted selection for genetic and breeding research. Aharon et al. (2016) explored how far SNPs can be from the affected genes using a pathway-based approach and found that affected genes were often up to 2 Mbps from the associated SNP and not necessarily the closest to the SNP.

The molecular mechanisms underlying heat tolerance in wheat remain unclear. A schematic network, proposed to explain the mechanism of heat tolerance in legumes, suggested that signalling and metabolic pathways, involving a series of physiochemical processes and important molecules such as HSPs, antioxidants, metabolites, and hormones, play key roles in regulating the legume response to heat stress (Liu et al., 2019). The candidate genes identified in this study are consistent, to a large extent, with their proposed network. Therefore, we hypothesize that such a pathway might exist in wheat, where many key genes collaboratively regulate the crop's response to heat stress (**Figure 4**).

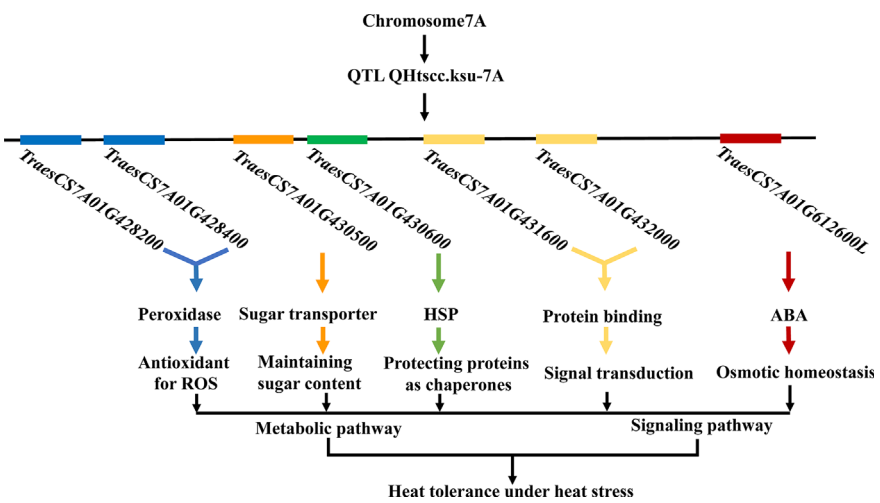


FIGURE 4 | Postulated pathway based on the findings of this study showing a collaborative regulation network of multiple genes in wheat in response to heat stress. Signaling pathway and metabolic pathway involving a series of physiochemical processes and important molecules, including HSPs, antioxidants, metabolites, and hormones.

CONCLUSIONS

The NILs developed and validated in this study confirmed that the 7AL QTL, QHtscc.ksu-7A, is a major locus responsible for heat tolerance in wheat. The confirmed NILs and identified candidate genes are valuable resources for future studies in fine mapping and functional analyses of the chromosome region to clone the underlying gene(s).

DATA AVAILABILITY STATEMENT

All datasets presented in this study are included in the article/supplementary material.

AUTHOR CONTRIBUTIONS

LL, HL, and GY conceived and designed the study. HL developed NIL populations, and LL conducted the experiments in the plant growth chambers and greenhouse. LL collected the relevant data and performed the analysis with guidance from GY and HL. LL prepared the manuscripts with inputs from YW, HL, and GY. All authors contributed to the article and approved the submitted version.

FUNDING

This research was funded by the Global Innovation Linkages Project (GIL53853) from the Australian Department of Industry, Innovation, and Science. The first author acknowledges the Research Training Program Scholarship from the Australian Government for sponsoring her Ph.D. study. The University of Western Australia provided funds for the open access publication fee.

ACKNOWLEDGMENTS

The authors would like to thank Professor Jacqueline Batley and Dr. Aneeta Pradhan for assistance in the 90k SNP array genotyping. The authors also thank Dr. Christine Davies at Tweak Editing for correcting English language errors.

SUPPLEMENTARY MATERIAL

The Supplementary Material for this article can be found online at: https://www.frontiersin.org/articles/10.3389/fpls.2020.01316/full#supplementary-material.

REFERENCES

Adams, J., Kelso, R., and Cooley, L. (2000). The kelch-repeat superfamily of proteins: propellers of cell function. *Trends Cell Biol.* 10 (1), 17–24. doi: 10.1016/S0962-8924(99)01673-6

Agarwal, P. K., and Jha, B. (2010). Transcription factors in plants and ABA dependent and independent abiotic stress signalling. *Biol. Plant* 54 (2), 201–212. doi: 10.1007/s10535-010-0038-7

Aharon, B., Johnathan, R. A., and Yanay, O. (2016). How far from the SNP may the causative genes be? *Nucleic Acids Res.* 44 (13), 6046–6054. doi: 10.1093/nar/gkw500

Alaux, M., Rogers, J., Letellier, T., Flores, R., Alfama, F., Pommier, C., et al. (2018). Linking the International Wheat Genome Sequencing Consortium bread wheat reference genome sequence to wheat genetic and phenomic data. *Genome Biol.* 19 (1), 111. doi: 10.1186/s13059-018-1491-4

Alsamadany, H. (2015). Diversity and genetic studies of heat tolerance in wheat. [Ph.D. thesis]. (Perth (WA): The University of Western Australia).

Araus, J. L., Amaro, T., Voltas, J., Nakkoul, H., and Nachit, M. M. (1998). Chlorophyll fluorescence as a selection criterion for grain yield in durum wheat under Mediterranean conditions. *Field Crop Res.* 55 (3), 209–223. doi: 10.1016/S0378-4290(97)00079-8

Avni, R., Nave, M., Eilam, T., Sela, H., Alekperov, C., Peleg, Z., et al. (2014). Ultra-dense genetic map of durum wheat × wild emmer wheat developed using the 90K iSelect SNP genotyping assay. *Mol. Breed.* 34 (4), 1549–1562. doi: 10.1007/s11032-014-0176-2

Balla, K., Karsai, I., Bónis, P., Kiss, T., Berki, Z., Horváth, Á., et al. (2019). Heat stress responses in a large set of winter wheat cultivars (*Triticum aestivum* L.) depend on the timing and duration of stress. *PloS One* 14 (9), e0222639. doi: 10.1371/journal.pone.0222639

Baniwal, S. K., Bharti, K., Chan, K. Y., Fauth, M., Ganguli, A., Kotak, S., et al. (2004). Heat stress response in plants: a complex game with chaperones and more than twenty heat stress transcription factors. *J. Biosci.* 29, 471–487. doi: 10.1007/BF02712120

Blum, A., Klueva, N., and Nguyen, H. T. (2001). Wheat cellular thermotolerance is related to yield under heat stress. *Euphytica* 117 (2), 117–123. doi: 10.1023/A:1004083305905

Budak, H., Kantar, M., Bulut, R., and Akpinar, B. A. (2015). Stress responsive miRNAs and isomiRs in cereals. *Plant Sci.* 235, 1–13. doi: 10.1016/j.plantsci.2015.02.008

Cabral, A. L., Jordan, M. C., Larson, G., Somers, D. J., Humphreys, D. G., and McCartney, C. A. (2018). Relationship between QTL for grain shape, grain weight, test weight, milling yield, and plant height in the spring wheat cross RL4452/'ACDomain'. *PloS One* 13 (1), 1–32. doi: 10.1371/journal.pone.0190681

Cavanagh, C. R., Chao, S. M., Wang, S. C., Huang, B. E., Stephen, S., Kiani, S., et al. (2013). Genome-wide comparative diversity uncovers multiple targets of selection for improvement in hexaploid wheat landraces and cultivars. *Proc. Natl. Acad. Sci. U.S.A.* 110 (20), 8057–8062. doi: 10.1073/pnas.1217133110

Caverzan, A., Casassola, A., and Brammer, S. P. (2016). Antioxidant responses of wheat plants under stress. *Genet. Mol. Biol.* 39 (1), 1–6. doi: 10.1590/1678-4685-GMB-2015-0109

Chen, D. Q., Wang, S. W., Cao, B. B., Cao, D., Leng, G. H., Li, H. B., et al. (2016). Genotypic variation in growth and physiological response to drought stress and re-watering reveals the critical role of recovery in drought adaptation in maize seedlings. *Front. Plant Sci.* 6, 1241. doi: 10.3389/fpls.2015.01241

Cobb, J., Büsst, C., Petrou, S., Harrap, S., and Ellis, J. (2008). Searching for functional genetic variants in non-coding DNA. *Clin. Exp. Pharmacol. Physiol.* 35 (4), 372–375. doi: 10.1111/j.1440-1681.2008.04880.x

Colasuonno, P., Gadaleta, A., Giancaspro, A., Nigro, D., Giove, S., Incerti, O., et al. (2014). Development of a high-density SNP-based linkage map and detection of yellow pigment content QTLs in durum wheat. *Mol. Breed.* 34 (4), 1563–1578. doi: 10.1007/s11032-014-0183-3

Craig, K. L., and Tyers, M. (1999). The F-box: a new motif for ubiquitin dependent proteolysis in cell cycle regulation and signal transduction. *Prog. Biophys. Mol. Biol.* 72 (3), 299–328. doi: 10.1016/S0079-6107(99)00010-3

Dawson, I. A., and Wardlaw, I. F. (1989). The tolerance of wheat to high-temperatures during reproductive growth. 3. Booting to anthesis. *Aust. J. Agric. Res.* 40 (5), 965–980. doi: 10.1071/Ar9890965

de Souza, R., Pena-Fleitas, M. T., Thompson, R. B., Gallardo, M., Grasso, R., and Padilla, F. M. (2019). The use of chlorophyll meters to assess crop N status and derivation of sufficiency values for sweet pepper. *Sensors* 19 (13), 1–20. doi: 10.3390/s19132949

Dixit, S., Kumar, B. A., Min, A., Henry, A., Oane, R. H., Raorane, M. L., et al. (2015). Action of multiple intra-QTL genes concerted around a co-localized transcription factor underpins a large effect QTL. *Sci. Rep.* 5, 15183–15183. doi: 10.1038/srep15183

Dorweiler, J., Stec, A., Kermicle, J., and Doebley, J. (1993). Teosinte-glume-architecture-1- a genetic-locus controlling a key step in maize evolution. *Science* 262 (5131), 233–235. doi: 10.1126/science.262.5131.233

Driedonks, N., Rieu, I., and Vriezen, W. H. (2016). Breeding for plant heat tolerance at vegetative and reproductive stages. *Plant Reprod.* 29, 67–79. doi: 10.1007/s00497-016-0275-9

Farooq, M., Bramley, H., Palta, J. A., and Siddique, K. H. M. (2011). Heat stress in wheat during reproductive and grain-filling phases. *Crit. Rev. Plant Sci.* 30 (6), 491–507. doi: 10.1080/07352689.2011.615687

Fokar, M., Nguyen, H. T., and Blum, A. (1998). Heat tolerance in spring wheat. I. Estimating cellular thermotolerance and its heritability. *Euphytica* 104 (1), 1–8. doi: 10.1023/A:1018346901363

Gaju, O., DeSilva, J., Carvalho, P., Hawkesford, M. J., Griffiths, S., Greenland, A., et al. (2016). Leaf photosynthesis and associations with grain yield, biomass and nitrogen-use efficiency in landraces, synthetic-derived lines and cultivars in wheat. *Field Crop Res.* 193, 1–15. doi: 10.1016/j.fcr.2016.04.018

Galanti, R., Cho, A., Ahmad, A., and Mollinedo, J. (2019). Use of a chlorophyll meter for nondestructive and rapid estimation of leaf tissue nitrogen in macadamia. *HortTechnology* 29 (3), 308–313. doi: 10.21273/Horttech04276-19

Grünewald, T. G., Bernard, V., Gilardi-Hebenstreit, P., Raynal, V., Surdez, D., Aynaud, M. M., et al. (2015). Chimeric EWSR1-FLI1 regulates the Ewing sarcoma susceptibility gene EGR2 via a GGAA microsatellite. *Nat. Genet.* 47 (9), 1073–1078. doi: 10.1038/ng.3363

Haq, U. S., Khan, A., Ali, M., Khattak, A. M., Gai, W. X., Zhang, H. X., et al. (2019). Heat shock proteins: dynamic biomolecules to counter plant biotic and abiotic stresses. *Int. J. Mol. Sci.* 20:5321. doi: 10.3390/ijms20215321

Hefti, M. H., Francoijs, K. J., de Vries, S. C., Dixon, R., and Vervoort, J. (2004). The PAS fold-A redefinition of the PAS domain based upon structural prediction. *Eur. J. Biochem.* 271 (6), 1198–1208. doi: 10.1111/j.1432-1033.2004.04023.x

Hennig, S., Strauss, H. M., Vanselow, K., Yildiz, O., Schulze, S., Arens, J., et al. (2009). Structural and functional analyses of PAS domain interactions of the clock proteins drosophila period and mouse period2. *PloS Biol.* 7 (4), 836–853. doi: 10.1371/journal.pbio.1000094

IWGSC (2018). Shifting the limits in wheat research and breeding using a fully annotated reference genome. *Science* 361:7191. doi: 10.1126/science.aar7191

Khurana, E., Fu, Y., Colonna, V., Mu, X. J., Kang, H. M., Lappalainen, T., et al. (2013). Integrative annotation of variants from 1092 humans: application to cancer genomics. *Science* 342 (6154), 1235587. doi: 10.1126/science.1235587

Kovalic, D. K., Andersen, S. E., Byrum, J. R., Conner, T. W., Masucci, J. D., and Zhou, Y. (2007). *Nucleic acid molecules and other molecules associated with plants and uses thereof for plant improvement* (Washington, DC: U.S. Patent and Trademark Office).

Lalonde, S., Wipf, D., and Frommer, W. B. (2004). Transport mechanisms for organic forms of carbon and nitrogen between source and sink. *Annu. Rev. Plant Biol.* 55, 341–372. doi: 10.1146/annurev.arplant.55.031903.141758

Lemoine, R., La Camera, S., Atanassova, R., Deedaldeechamp, F., Allario, T., Pourtau, N., et al. (2013). Source-to-sink transport of sugar and regulation by environmental factors. *Front. Plant Sci.* 4, 272. doi: 10.3389/fpls.2013.00272

Li, C., Zhang, W., Yuan, M., Jiang, L., Sun, B., Zhang, D., et al. (2019). Transcriptome analysis of osmotic-responsive genes in ABA-dependent and -independent pathways in wheat (*Triticum aestivum L.*) roots. *PeerJ* 7:6519. doi: 10.7717/peerj.6519

Liu, S., Zhang, X., Pumphrey, M. O., Stack, R. W., Gill, B. S., and Anderson, J. A. (2006). Complex microcolinearity among wheat, rice, and barley revealed by fine mapping of the genomic region harboring a major QTL for resistance to Fusarium head blight in wheat. *Funct. Integr. Genomics* 6 (2), 83–89. doi: 10.1007/s10142-005-0007-y

Liu, Y. X., Yang, X. M., Ma, J., Wei, Y. M., Zheng, Y. L., Ma, H. X., et al. (2010). Plant height affects fusarium crown rot severity in wheat. *Phytopathology* 100 (12), 1276–1281. doi: 10.1094/Phyto-05-10-0142

Liu, Y. C., Machuca, M. A., Beckham, S. A., Gunzburg, M. J., and Roujeinikova, A. (2015). Structural basis for amino-acid recognition and transmembrane signalling by tandem Per-Arnt-Sim (tandem PAS) chemoreceptor sensory domains. *Acta Crystallogr. Sect. D-Struct. Biol.* 71, 2127–2136. doi: 10.1107/S139900471501384X

Liu, Y., Li, J., Zhu, Y., Jones, A., Ray, J. R., and Song, Y. (2019). Heat stress in legume seed setting: effects, causes, and future prospects. *Front. Plant Sci.* 10, 1–12. doi: 10.3389/fpls.2019.00938

Lu, Y. F., Mauger, D. M., Goldstein, D. B., Urban, T. J., Weeks, K. M., and Bradrick, S. S. (2015). IFNL3 mRNA structure is remodeled by a functional non-coding polymorphism associated with hepatitis C virus clearance. *Sci. Rep.* 5:16037. doi: 10.1038/srep16037

Manickavelu, A., Kawaura, K., Oishi, K., Shin-I, T., Kohara, Y., Yahiaoui, N., et al. (2012). Comprehensive functional analyses of expressed sequence tags in common wheat (*Triticum aestivum*). *DNA Res.* 19 (2), 165–177. doi: 10.1093/dnares/dss001

Marcum, K. B. (1998). Cell membrane thermostability and whole-plant heat tolerance of Kentucky bluegrass. *Crop Sci.* 38 (5), 1214–1218. doi: 10.2135/cropsci1998.0011183X003800050017x

Mason, R. E., Mondal, S., Beecher, F. W., Pacheco, A., Jampala, B., Ibrahim, A. M. H., et al. (2010). QTL associated with heat susceptibility index in wheat (*Triticum aestivum* L.) under short-term reproductive stage heat stress. *Euphytica* 174 (3), 423–436. doi: 10.1007/s10681-010-0151-x

Mason, R. E., Mondal, S., Beecher, F. W., and Hays, D. B. (2011). Genetic loci linking improved heat tolerance in wheat (*Triticum aestivum* L.) to lower leaf and spike temperatures under controlled conditions. *Euphytica* 180 (2), 181–194. doi: 10.1007/s10681-011-0349-6

Merchuk-Ovnat, L., Fahima, T., Krugman, T., and Saranga, Y. (2016). Ancestral QTL alleles from wild emmer wheat improve grain yield, biomass and photosynthesis across envirоinments in modern wheat. *Plant Sci.* 251, 23–34. doi: 10.1016/j.plantsci.2016.05.003

Mia, M. S., Liu, H., Wang, X. Y., and Yan, G. J. (2019). Multiple near-isogenic lines targeting a QTL hotspot of drought tolerance showed contrasting performance under post-anthesis water stress. *Front. Plant Sci.* 10, 271. doi: 10.3389/fpls.2019.00271

Mirdita, V., Dhillon, B. S., Geiger, H. H., and Miedaner, T. (2008). Genetic variation for resistance to ergot (*Claviceps purpurea* [Fr.] Tul.) among full-sib families of five populations of winter rye (*Secale cereale* L.). *Theor. Appl. Genet.* 118 (1), 85–90. doi: 10.1007/s00122-008-0878-0

Moffatt, J. M., Sears, R. G., Cox, T. S., and Paulsen, G. M. (1990a). Wheat high-temperature tolerance during reproductive growth. II. genetic-analysis of chlorophyll fluorescence. *Crop Sci.* 30 (4), 886–889. doi: 10.2135/cropsci1990.0011183X003000040025x

Moffatt, J. M., Sears, R. G., and Paulsen, G. M. (1990b). Wheat high temperature tolerance during reproductive growth. I. Evaluation by chlorophyll fluorescence. *Crop Sci.* 30, 881–885. doi: 10.2135/cropsci1990.0011183X003000040024x

Moglich, A., Ayers, R. A., and Moffat, K. (2009). Structure and signaling mechanism of Per-ARNT-Sim domains. *Structure* 17 (10), 1282–1294. doi: 10.1016/j.str.2009.08.011

Murray, M. G., and Thompson, W. F. (1980). Rapid isolation of high molecular-weight plant DNA. *Nucleic Acids Res.* 8 (19), 4321–4325. doi: 10.1093/nar/8.19.4321

Narayanan, S. (2018). Effects of high temperature stress and traits associated with tolerance in wheat. *Open Access J. Sci.* 2 (3), 177–186. doi: 10.15406/oajs.2018.02.00067

Novichonok, E. V., Novichonok, A. O., Kurbatova, J. A., and Markovskaya, E. F. (2016). Use of the atLEAF plus chlorophyll meter for a nondestructive estimate of chlorophyll content. *Photosynthetica* 54 (1), 130–137. doi: 10.1007/s11099-015-0172-8

Padilla, F. M., de Souza, R., Pena-Fleitas, M. T., Gallardo, M., Gimenez, C., and Thompson, R. B. (2018). Different responses of various chlorophyll meters to increasing nitrogen supply in sweet pepper. *Front. Plant Sci.* 9 (1752), 1–14. doi: 10.3389/fpls.2018.01752

Paliwal, R., Roder, M. S., Kumar, U., Srivastava, J. P., and Joshi, A. K. (2012). QTL mapping of terminal heat tolerance in hexaploid wheat (*T. aestivum* L.). *Theor. Appl. Genet.* 125 (3), 561–575. doi: 10.1007/s00122-012-1853-3

Peng, J., Yu, D. S., Wang, L. Q., Xie, M. M., Yuan, C. Y., Wang, Y., et al. (2012). Arabidopsis F-box gene FOA1 involved in ABA signaling. *Sci. China Life Sci.* 55 (6), 497–506. doi: 10.1007/s11427-012-4332-9

Pietrini, F., Baccio, D. D., Iori, V., Veliksar, S., Lemanova, N., Juškaitė, L., et al. (2017). Investigation onmetal tolerance and phytoremoval activity in the poplar hybrid clone "Monviso" under Cu-spiked water: Potential use for wastewater treatment. *Sci. Total Environ.* 592, 412–418. doi: 10.1016/j.scitotenv.2017.03.101

Pradhan, G. P., Prasad, P. V. V., Fritz, A. K., Kirkham, M. B., and Gill, B. S. (2012). Effects of drought and high temperature stress on synthetic hexaploid wheat. *Func. Plant Biol.* 39 (3), 190–198. doi: 10.1071/Fp11245

Prag, S., and Adams, J. C. (2003). Molecular phylogeny of the kelch-repeat superfamily reveals an expansion of BTB/kelch proteins in animals. *BMC Bioinform.* 4:42. doi: 10.1186/1471-2105-4-42

Priya, M., Dhanker, O. P., Siddique, K. H. M., HanumanthaRao, B., Nair, R. M., Pandey, S., et al. (2019). Drought and heat stress-related proteins: an update about their functional relevance in imparting stress tolerance in agricultural crops. *Theor. Appl. Genet.* 132 (6), 1607–1638. doi: 10.1007/s00122-019-03331-2

Pumphrey, M. O., Bernardo, R., and Anderson, J. A. (2007). Validating the Fhb1 QTL for fusarium head blight resistance in near-isogenic wheat lines developed from breeding populations. *Crop Sci.* 47 (1), 200–206. doi: 10.2135/cropsci2006.03.0206

Rao, R. C. N., Talwar, H. S., and Wright, G. C. (2001). Rapid assessment of specific leaf area and leaf nitrogen in peanut (*Arachis hypogaea* L.) using a chlorophyll meter. *J. Agron. Crop Sci.* 186 (3), 175–182. doi: 10.1046/j.1439-037X.2001.00472.x

Raven, J. A., and Griffiths, H. (2015). Photosynthesis in reproductive structures: costs and benefits. *J. Exp. Bot.* 66 (7), 1699–1705. doi: 10.1093/jxb/erv009

Reynolds, M. P., Balota, M., Delgado, M.II, Amani, I., and Fischer, R. A. (1994). Physiological and morphological traits associated with spring wheat yield under hot, irrigated conditions. *Aust. J. Plant Physiol.* 21 (6), 717–730. doi: 10.1071/Pp9940717

Rezaei, E. E., Siebert, S., and Ewert, F. (2015). Intensity of heat stress in winter wheat—phenology compensates for the adverse effect of global warming. *Environ. Res. Lett.* 10:24012. doi: 10.1088/1748-9326/10/2/024012/meta

Rimbert, H., Darrier, B., Navarro, J., Kitt, J., Choulet, F., Leveugle, M., et al. (2018). High throughput SNP discovery and genotyping in hexaploid wheat. *PloS One* 13 (1), e0186329. doi: 10.1371/journal.pone.0186329

Russo, M. A., Ficco, D. B. M., Laido, G., Marone, D., Papa, R., Blanco, A., et al. (2014). A dense durum wheat x T-dicoccum linkage map based on SNP markers for the study of seed morphology. *Mol. Breed.* 34 (4), 1579–1597. doi: 10.1007/s11032-014-0181-5

Saadall, M. M., Quick, J. S., and Shanahan, J. F. (1990). Heat tolerance in winter wheat: II. membrane thermostability and field performance. *Crop Sci.* 30 (6), 1248–1251. doi: 10.2135/cropsci1990.0011183X003000060018x

Sairam, R. K., Deshmukh, P. S., and Saxena, D. C. (1998). Role of antioxidant systems in wheat genotypes tolerance to water stress. *Biol. Plant* 41, 387–394. doi: 10.1023/A:1001898310321

Shirdelmoghanloo, H., Taylor, J. D., Lohraseb, I., Rabie, H., Brien, C., Timmins, A., et al. (2016a). A QTL on the short arm of wheat (*Triticum aestivum* L.) chromosome 3B affects the stability of grain weight in plants exposed to a brief heat shock early in grain filling. *BMC Plant Biol.* 16, 100. doi: 10.1186/s12870-016-0784-6

Shirdelmoghanloo, H., Lohraseb, I., Rabie, H., Brien, C., and Timmins, A. (2016b). Heat susceptibility of grain filling in wheat (*Triticum aestivum* L.) linked with rapid chlorophyll loss during a 3-day heat treatment. *Acta Physiol. Plant* 38:208. doi: 10.1007/s11738-016-2208-5

Sukumaran, S., Dreisigacker, S., Lopes, M., Chavez, P., and Reynolds, M. P. (2015). Genome-wide association study for grain yield and related traits in an elite spring wheat population grown in temperate irrigated environments. *Theor. Appl. Genet.* 128 (2), 353–363. doi: 10.1007/s00122-014-2435-3

Suzuki, N., Miller, G., Morales, J., Shulaev, V., Torres, M. A., and Mittler, R. (2011). Respiratory burst oxidases: the engines of ROS signaling. *Curr. Opin. Plant Biol.* 14 (6), 691–699. doi: 10.1016/j.pbi.2011.07.014

Talukder, S. K., Babar, M. A., Vijayalakshmi, K., Poland, J., Prasad, P. V., Bowden, R., et al. (2014). Mapping QTL for the traits associated with heat tolerance in wheat (*Triticum aestivum* L.). *BMC Genet.* 15:97. doi: 10.1186/s12863-014-0097-4

Tao, Z. Q., Chen, Y. Q., Zou, J. X., Li, C., Yuan, S. F., Yan, P., et al. (2016). Spectral characteristics of spring maize varieties with different heat tolerance to high temperature. *Spectrosc. Spectr. Anal.* 36 (2), 520–526. doi: 10.3964/j.issn.1000-0593(2016)02-0520-07

Tuinstra, M. R., Ejeta, G., and Goldsbrough, P. B. (1997). Heterogeneous inbred family (HIF) analysis: a method for developing near-isogenic lines that differ at quantitative trait loci. *Theor. Appl. Genet.* 95 (5–6), 1005–1011. doi: 10.1007/s001220050654

van den Burg, H. A., Tsitsigiannis, D.II, Rowland, O., Lo, J., Rallapalli, G., MacLean, D., et al. (2008). The F-box protein ACRE189/ACIF1 regulates cell death and defense responses activated during pathogen recognition in tobacco and tomato. *Plant Cell* 20 (3), 697–719. doi: 10.1105/tpc.107.056978

Vasseur, F., Pantin, F., and Vile, D. (2011). Changes in light intensity reveal a major role for carbon balance in Arabidopsis responses to high temperature. *Plant Cell Environ.* 34 (9), 1563–1576. doi: 10.1111/j.1365-3040.2011.02353.x

Vijayalakshmi, K., Fritz, A. K., Paulsen, G. M., Bai, G. H., Pandravada, S., and Gill, B. S. (2010). Modeling and mapping QTL for senescence-related traits in winter wheat under high temperature. *Mol. Breed.* 26 (2), 163–175. doi: 10.1007/s11032-009-9366-8

Wahid, A., and Shabbir, A. (2005). Induction of heat stress tolerance in barley seedlings by pre-sowing seed treatment with glycinebetaine. *Plant Growth Regul.* 46 (2), 133–141. doi: 10.1007/s10725-005-8379-5

Wang, S. C., Wong, D. B., Forrest, K., Allen, A., Chao, S. M., Huang, B. E., et al. (2014). Characterization of polyploid wheat genomic diversity using a high-density 90 000 single nucleotide polymorphism array. *Plant Biotechnol.* 12 (6), 787–796. doi: 10.1111/pbi.12183

Wang, X. B., Wang, L. F., and Shangguan, Z. (2016). Leaf gas exchange and fluorescence of two winter wheat varieties in response to drought stress and nitrogen supply. *PloS One* 11 (11), ARTN e0165733. doi: 10.1371/journal.pone.0165733

Wang, X., Liu, H., Mia, M. S., Siddique, K. H. M., and Yan, G. J. (2018). Development of near-isogenic lines targeting a major QTL on 3AL for pre-harvest sprouting resistance in bread wheat. *Crop Pasture Sci.* 69, 864–872. doi: 10.1071/CP17423

Wang, X., Liu, H., Liu, G., Mia, M. S., Siddique, K. H. M., and Yan, G. J. (2019). Phenotypic and genotypic characterization of near-isogenic lines targeting a major 4BL QTL responsible for pre-harvest sprouting in wheat. *BMC Plant Biol.* 19, 348. doi: 10.1186/s12870-019-1961-1

Wiegand, C. L., and Cuellar, J. A. (1981). Duration of grain filling and kernel weight of wheat as affected by temperature. *Crop Sci.* 21 (1), 95–101. doi: 10.2135/cropsci1981.0011183X001100010027x

Yan, G. J., Liu, H., Wang, H. B., Lu, Z. Y., Wang, Y. X., Mullan, D., et al. (2017). Accelerated generation of selfed pure line plants for gene identification and crop breeding. *Front. Plant Sci.* 8, 1–14. doi: 10.3389/fpls.2017.01786

Yang, J., Sears, R. G., Gill, B. S., and Paulsen, G. M. (2002). Growth and senescence characteristics associated with tolerance of wheat-alien amphiploids to high temperature under controlled conditions. *Euphytica* 126 (2), 185–193. doi: 10.1023/A:1016365728633

Yoshida, T., Mogami, J., and Yamaguchi-Shinozaki, K. (2014). ABA-dependent and ABA-independent signaling in response to osmotic stress in plants. *Curr. Opin. Plant Biol.* 21, 133–139. doi: 10.1016/j.pbi.2014.07.009

Zadoks, J. C. (1974). A decimal code for the growth stages of cereals. *Weed Res.* 14, 415–421. doi: 10.1111/j.1365-3180.1974.tb01084.x

Zhang, K., Liu, X. J., Ata-Ul-Karim, S. T., Lu, J. S., Krienke, B., Li, S. Y., et al. (2019). Development of chlorophyll-meter-index-based dynamic models for evaluation of high-yield japonica rice production in Yangtze River reaches. *Agronomy-Basel* 9 (2), 1–17. doi: 10.3390/agronomy9020106

Zhao, B., Ata-Ul-Karim, S. T., Liu, Z. D., Zhang, J. Y., Xiao, J. F., Liu, Z. G., et al. (2018). Simple assessment of nitrogen nutrition index in summer maize by using chlorophyll meter readings. *Front. Plant Sci.* 9 (11), 1–13. doi: 10.3389/fpls.2018.00011

Zheng, Z., Wang, H. B., Chen, G. D., Yan, G. J., and Liu, C. J. (2013). A procedure allowing up to eight generations of wheat and nine generations of barley per annum. *Euphytica* 191 (2), 311–316. doi: 10.1007/s10681-013-0909-z

Zhou, R., Kjaer, K. H., Rosenqvist, E., Yu, X., Wu, Z., and Ottosen, C. O. (2017). Physiological response to heat stress during seedling and anthesis stage in tomato genotypes differing in heat tolerance. *J. Agron. Crop Sci.* 203 (1), 68–80. doi: 10.1111/jac.12166

Conflict of Interest: The authors declare that the research was conducted in the absence of any commercial or financial relationships that could be construed as a potential conflict of interest.

Copyright © 2020 Lu, Liu, Wu and Yan. This is an open-access article distributed under the terms of the Creative Commons Attribution License (CC BY). The use, distribution or reproduction in other forums is permitted, provided the original author(s) and the copyright owner(s) are credited and that the original publication in this journal is cited, in accordance with accepted academic practice. No use, distribution or reproduction is permitted which does not comply with these terms.

frontiers in Plant Science

ORIGINAL RESEARCH
published: 28 August 2020
doi: 10.3389/fpls.2020.01310

Physiological and *PIP* Transcriptional Responses to Progressive Soil Water Deficit in Three Mulberry Cultivars

Xu Cao[1,2], *Qiudi Shen*[1,2], *Sang Ma*[1,2], *Li Liu*[1,2] *and Jialing Cheng*[1,2*]

[1] College of Biotechnology, Jiangsu University of Science and Technology, Zhenjiang, China, [2] Key Laboratory of Silkworm and Mulberry Genetic Improvement, Ministry of Agricultural and Rural Areas, Sericultural Research Institute, Chinese Academy of Agricultural Sciences, Zhenjiang, China

OPEN ACCESS

Edited by:
Raul Antonio Sperotto, Universidade do Vale do Taquari—Univates, Brazil

Reviewed by:
Hayssam M. Ali, King Saud University, Saudi Arabia
Suriyan Cha-um, National Science and Technology Development Agency (NSTDA), Thailand
Yordan Muhovski, Walloon Agricultural Research Centre, Belgium

***Correspondence:**
Jialing Cheng
chengjialing1@yeah.net

Specialty section:
This article was submitted to Crop and Product Physiology, a section of the journal Frontiers in Plant Science

Received: 21 June 2020
Accepted: 11 August 2020
Published: 28 August 2020

Citation:
Cao X, Shen Q, Ma S, Liu L and Cheng J (2020) Physiological and PIP Transcriptional Responses to Progressive Soil Water Deficit in Three Mulberry Cultivars. Front. Plant Sci. 11:1310. doi: 10.3389/fpls.2020.01310

Although mulberry cultivars Wubu, Yu711, and 7307 display distinct anatomical, morphological, and agronomic characteristics under natural conditions, it remains unclear if they differ in drought tolerance. To address this question and elucidate the underlying regulatory mechanisms at the whole-plant level, 2-month old saplings of the three mulberry cultivars were exposed to progressive soil water deficit for 5 days. The physiological responses and transcriptional changes of *PIPs* in different plant tissues were analyzed. Drought stress led to reduced leaf relative water content (RWC) and tissue water contents, differentially expressed *PIPs*, decreased chlorophyll and starch, increased soluble sugars and free proline, and enhanced activities of antioxidant enzymes in all plant parts of the three cultivars. Concentrations of hydrogen peroxide (H_2O_2), superoxide anion ($O_2^{\bullet-}$), and malonaldehyde (MDA) were significantly declined in roots, stimulated in leaves but unaltered in wood and bark. In contrast, except the roots of 7307, soluble proteins were repressed in roots and leaves but induced in wood and bark of the three cultivars in response to progressive water deficit. These results revealed tissue-specific drought stress responses in mulberry. Comparing to cultivar Yu711 and 7307, Wubu showed generally slighter changes in leaf RWC and tissue water contents at day 2, corresponding well to the steady *PIP* transcript levels, foliar concentrations of chlorophyll, $O_2^{\bullet-}$, MDA, and free proline. At day 5, Wubu sustained higher tissue water contents in green tissues, displayed stronger responsiveness of *PIP* transcription, lower concentrations of soluble sugars and starch, lower foliar MDA, higher proline and soluble proteins, higher ROS accumulation and enhanced activities of several antioxidant enzymes. Our results indicate that whole-plant level responses of *PIP* transcription, osmoregulation through proline and soluble proteins and antioxidative protection are important mechanisms for mulberry to cope with drought stress. These traits play significant roles in conferring the relatively higher drought tolerance of cultivar Wubu and could be potentially useful for future mulberry improvement programmes.

Keywords: drought stress, wood, bark, osmoregulatory substance, antioxidant enzyme, plasma membrane intrinsic proteins, *Morus*

INTRODUCTION

Drought is one of the most detrimental environmental stresses well known for impairing plant growth and inhibiting productivity (Peng et al., 2011). In the context of global climate change, increasing frequency and severity of drought scenarios, accompanied by heat waves, have posed great threats to tree growth (Jia et al., 2016; Jia et al., 2017) and are closely associated with multiple forest mortality events around the world (Allen et al., 2010; Kharuk et al., 2017). To this end, it is of huge significance to better understand the responses of trees to drought stress in order to screen drought tolerant species, cultivars, or genotypes that can well adapt to future climate change.

Mulberry leaves are the sole food source for domestic silkworm (*Bombyx mori* L.), which endows mulberry an economically important tree species in sericulture industry (Cao et al., 2018). *Morus* genus consists of 68 species worldwide, covering a wide range of geographical range from temperate to tropical areas, among which over one-third occur naturally in China (Sarkar et al., 2017). Besides its traditional use in silkworm raising, mulberry is also considered a promising pioneer tree species in marginal lands (Lu et al., 2009) and a potential energy crop for biofuel generation (Velazquez-Marti et al., 2013; Wang et al., 2018). The rapid growth of mulberry trees depends upon a high consumption of water, which is one of the major reasons why large-scale mulberry plantations are traditionally established in humid areas in China. To meet the increasing economic and ecological demands, new mulberry plantations are expanding to areas where water is limited. Drought events occurred either seasonally or regionally in these plantations which can lead to decreased yield and deteriorated quality of mulberry trees (Reddy et al., 2017; Cao et al., 2020). Given this, it is crucial to characterize the physiological and transcriptional responses of mulberry species/cultivars/genotypes to drought stress.

Plant can cope with the adverse effects of soil water deficit through a suite of complex physiological and molecular mechanisms. Water uptake from soil to roots and the subsequent movement to shoot are critical steps limiting water use efficiency. This water transport is primarily facilitated by aquaporins residing on different biological membranes (Maurel et al., 2008). A plethora of studies have focused on the identification and characterization of the aquaporin gene family in various plant species such as Arabidopsis (Johanson et al., 2001), rice (Sakurai et al., 2005), maize (Chaumont et al., 2000), and poplar (Gupta and Sankararamakrishnan, 2009). Plasma membrane intrinsic proteins (PIPs) is a subfamily of aquaporin that are abundantly presented on the plasma membrane, acting as the most crucial barrier and exchange platform of water as well as some uncharged small molecules in and out of plant cells (Alexandersson et al., 2005). PIP isoforms transporting water are relevant to osmotic hydraulic conductance, whereas members transporting CO_2 regulate stomatal and mesophyll conductance (Pawlowicz and Masajada, 2019). *PIP* genes are associated with the abilities to tolerate several stress conditions such as salt, cold, and dehydration (Kayum et al., 2017; Sun et al., 2017). Different PIPs can either play positive or negative roles in drought tolerance (Hussain et al., 2020). Transgenic *Arabidopsis thaliana* overexpressing *GsPIP2;1* of *Glycine soja* exhibited depressed tolerance to drought probably by regulating water potential (Wang et al., 2015). Otherwise overexpression of a maize *PIP1;1* gene increased PEG-induced osmotic tolerance in Arabidopsis (Zhou L. et al., 2019). It was estimated that xylem PIPs could contribute up to 79–85% of root hydraulic conductivity in rice (Grondin et al., 2016), and therefore play an important role in recovery from xylem embolism under soil water deficit (Secchi and Zwieniecki, 2014). Recently, a genome-wide analysis of the aquaporin gene family reveals that mulberry (*Morus notabilis*) had 36 aquaporin members, seven of them were *PIP* genes that can be divided into two subgroups, PIP1 and PIP2 (Baranwal and Khurana, 2017). Reddy et al. (2017) found that aquaporin expression was highly associated with the genotypic variations in drought tolerance in mulberry. Nevertheless, it is still largely unexplored how *PIPs* respond to acute drought stress in contrasting mulberry cultivars, especially in tissues such as wood and bark that have long received meager attention.

Soil water deficit leads to reduced CO_2 uptake from the leaf stomata and disturbs photosynthesis and starch metabolism (Thalmann and Santelia, 2017). The gradual depletion of plant carbon pool or dysfunction of sugar transport and allocation under drought stress, namely carbon starvation, causes failures in basic carbon maintenance (Malone, 2017) and even tree death (Mitchell et al., 2013). Starch is the predominate form of nonstructural carbon storage pool, the interconversion of starch–sugar can facilitate adaptive changes for protection against environmental stresses (Dong and Beckles, 2019). Drought can inactivate AGPase and starch synthase (Hu et al., 2020) or activate starch-degrading enzymes (Zanella et al., 2016); both can result in decreased starch and increased sugar levels. It is suggested that accelerated starch degradation might be correlated with higher tolerance. A drought-resistant variety of broad bean (*Phaseolus vulgaris*) degraded more starch than a drought-sensitive variety under drought (Gonzalez-Cruz and Pastenes, 2012). The released sugars can function as osmo-regulators to mitigate the adversities of abiotic stresses (Krasensky and Jonak, 2012). Noteworthily, starch accumulation in cereal grain is also often reported to increase primarily because of enhanced source to sink remobilization (from leaf to rice grain) under drought stress (Prathap et al., 2019). This phenomenon of starch accumulation was also observed in Arabidopsis mutant under mild water deficit which can activate the key enzymes for sucrose-to-starch pathway (Prasch et al., 2015).

Overproduction of compatible solutes is one of the most well documented stress responses of plants under drought stress (Naser et al., 2010). Soluble proteins, soluble sugars, and proline are important osmoregulation substances in plants. Their accumulation can reduce water potential of cells and enhance the water holding capacity, thereby alleviating drought damage (Abid et al., 2018). Furthermore, soluble sugars are also acknowledged to be important regulatory molecules with both signaling and reactive oxygen species (ROS) quenching functions against oxidative stress (Regier et al., 2009; Keunen et al., 2013). Total soluble sugars were less affected in drought tolerant rice variety than the drought sensitive variety under drought conditions (Dien et al., 2019). Proline is also a widely detected metabolite in response to

drought stress. Similarly, drought tolerant rice variety expressed higher ability in accumulation of proline than susceptible varieties (Dien et al., 2019). It is assumed that soluble sugars and proline might be useful index of drought stress in citrus trees (Zaher-Ara et al., 2016). Additionally, photosynthetic pigments and photosystem II function (Menezes-Silva et al., 2017; Liu et al., 2019a), antioxidant enzymes (Cuk et al., 2010), and secondary metabolites (Liu et al., 2019b) are also important components involved in drought stress responses in plants.

Although enormous studies have investigated the above-mentioned responses to drought in a long list of economic tree species at different levels from species (Zaher-Ara et al., 2016), population (Kreyling et al., 2008) to ecosystems (Golinski et al., 2008; Itter et al., 2019), our understanding of the physiological and transcriptional responses in mulberry, a relatively less mainstream tree species, is still limited compared to its counterparts such as the model tree poplar. Mulberry generally shows strong endurance to various environmental stresses, and large variations in drought tolerance exist among different mulberry species/cultivars (Sharma and Zote, 2010; Vijayan et al., 2011). Comparing the differences in drought responses of these species/cultivars is an important approach to reveal the underlying mechanisms of drought tolerance, which can hopefully aid the breeding, evaluation, and selection of mulberry cultivars or genotypes with desirable drought tolerance in the future.

In our previous studies, it was found that mulberry cultivars Wubu, Yu711, and 7307 had distinct anatomical traits in the stem xylem and leaf blade (Cao et al., 2020). They also had different field performance in terms of leaf and shoot growth and spring yield (Cao et al., 2019). These findings render us to hypothesize that these cultivars are contrasting in drought tolerance. To test this hypothesis and elucidate the underlying mechanisms, we compared the short-term physiological responses of 2-month old saplings of these cultivars under progressive soil drought stress for 5 days. Measurements of leaf relative water content (RWC), tissue water contents, chlorophylls, soluble sugars and starch, reactive oxygen species (ROS), osmoregulatory substances, antioxidant enzymes, and *PIP* transcript levels known to be important for drought responses were comprehensively conducted in roots, wood, bark, and leaves. Specifically, we aim to address the following questions: (1) Do the physiological regulation responses of the three cultivars display different patterns to progressive drought? and (2) By which physiological mechanisms does mulberry respond to progressive drought? This study is the first attempt to explore the drought stress mechanisms in mulberry from the perspective of the whole-plant level, and the results can provide references for breeding of drought-tolerant cultivars.

MATERIALS AND METHODS

Plant Cultivation, Drought Treatment and Harvests

Healthy and dormant hardwood cuttings (12 cm in length) of mulberry cultivars Wubu, Yu711, and 7307 were collected from the National Mulberry Germplasm Resource Bank (Zhenjiang, China). The cuttings were artificially induced to root (Du et al., 2016) and planted in an 8 L plastic pot filled with 3 kg substrate of equal volume of clay and sand, with one cutting per pot. The rooted cuttings were cultivated in a greenhouse for two months with natural light until they reached an average height of 60 cm. Subsequently, 18 saplings with relatively uniform growth for each cultivar were selected as experimental materials and were evenly distributed under half-controlled environment. The day/night temperature was maintained at 25/36°C, the relative air humidity was 70%, and the maximum light intensity was 200 μmol m^{-2} s^{-1}. Saplings were subjected to a short period of water deficit by withholding water for 5 days; soil volume moisture was measured every day using a WET sensor (WET-2, Delta-T devices Ltd, Cambridge, UK). Harvests were performed after 0 (0 d), 2 (2 d), and 5 days (5 d) from the start of the drought treatment, and six plants were sampled randomly at each sampling time point. When harvesting, each individual plant was separated into roots, wood, bark, and leaves. These samples were wrapped with tinfoil and fast-frozen in liquid nitrogen. Frozen samples were ground into fine powder in liquid nitrogen with a mortar and a pestle and stored at −80°C. Equal amounts of fine powder from the same tissue of two saplings at each time point were combined into a pooled sample for physiological analysis.

Evaluation of Plant Water Status

Harvested fresh leaves were gently brushed to remove any contaminants on the surface. Leaf discs (diameter = 6.6 mm) were excised from the middle (1 cm to the main vein) of the harvested leaves and weighed immediately for fresh weight (Fw). The discs were then immersed in distilled water in the dark until reaching turgid weight (Tw). Afterwards, the leaf discs were oven-dried at 70°C for 72 h for dry weight (Dw). Leaf relative water content (RWC) was calculated as: (Fw – Dw)/(Tw – Dw) × 100 (%). To determine the water content in different plant parts, fresh subsamples (about 0.5 g) from roots, bark, wood, and leaves per plant were dried at 70°C for 72 h, and the water content was computed as: (Fw – Dw)/Fw × 100 (%). To exclude the effects of variations in plant water status on the physiological parameters, all the calculations were based on dry weight if not particularly noted.

Analysis of Chlorophyll, Soluble Sugars and Starch

About 40 mg fine powder of fresh leaf or bark samples was extracted in 10 ml of 80% acetone overnight in darkness until the sample became white. The contents of chlorophyll a (chla) and chlorophyll b (chlb) in the extracts were determined spectrophotometrically as suggested previously (Wellburn, 1994).

The concentrations of total soluble sugars and starch in roots, wood, bark, and leaves were determined using the anthrone method as described (Yemm and Willis, 1954). Specifically, about 100 mg of fine powder was extracted by 80% ethanol in an 80°C water bath for 30 min and then centrifuged at 6,000 rpm for 10 min. After collecting the supernatant, the sediment was extracted again as mentioned above. The two supernatants were combined and reacted with 2 ml of anthrone reagent in boiling water for 7 min. The absorbance of the mixture was recorded spectrophotometrically at 620 nm. The standard curve was generated by a serial of diluted glucose solutions.

The sediment retained after the extraction of soluble sugars was further extracted by $HClO_4$ to determine starch concentrations. The sediment was gelatinized in 2 ml distilled water in a boiling water bath for 15 min. After cooling down to room temperature, it was mixed with 0.5 ml of 9.2 M $HClO_4$ and 2 ml distilled water for degradation. The homogenate was further centrifuged at 6,500 rpm for 10 min. The first supernatant was collected, and the sediment was extracted again by $HClO_4$ as mentioned above. The two supernatants were combined for starch quantification, expressed as glucose equivalents.

Determination of H_2O_2, $O_2^{\bullet-}$, MDA, and Proline

Concentrations of peroxide hydrogen (H_2O_2) were determined spectrophotometrically at 410 nm according to Shang et al. (2019). Concentrations of the superoxide anion ($O_2^{\bullet-}$) in plant materials were measured by monitoring the nitrite formation from hydroxylamine as described by Shi et al. (2015). In short, the fine powder of fresh tissues (about 100 mg) was homogenized in 2 ml of 50 mM sodium phosphate buffer (pH 7.8) and centrifuged (10,000 rpm, 23°C, 10 min) twice. The supernatant was incubated with 10 mM hydroxylamine hydrochloride at 25°C for 20 min and further reacted with 17 mM p-aminobenzene sulfonic acid and 7 mM α-naphthylamine at 30°C for 30 min. The absorbance of the mixture was recorded spectrophotometrically at 530 nm. The standard curve was generated by a serial of diluted $NaNO_2$ solutions.

The malonaldehyde (MDA) concentrations were analyzed as previously described (Lei et al., 2007). Briefly, about 100 mg fine powder of frozen samples was homogenized in 3 ml of 5% trichloroacetic acid (TCA). After centrifugation of 8,000 rpm at 4°C for 20 min, 2 ml of the supernatant was reacted with 2 ml of 0.6% thiobarbituric acid (TBA) in 5% TCA in boiling water for 15 min. Then, the reaction mixture was cooled down in an ice bath, and the absorbance at 450, 532, and 600 nm was recorded for calculation of MDA concentrations.

Concentrations of proline were determined following the method described by Jia et al. (2016). Briefly, frozen plant powder (about 100 mg) was extracted in 1.5 ml of 3% sulfosalicylic acid in a water bath at 100°C for 15 min. After centrifugation (6,000 rpm, 23°C, 15 min), the supernatant was mixed with 1 ml glacial acetic acid and 1 ml ninhydrin reagent. The mixture was reacted at 100°C for 30 min. The absorbance of the mixture was recorded spectrophotometrically at 520 nm after cooling to room temperature. The standard curve was produced by a serial of diluted proline solutions.

Assay of Antioxidant Enzyme Activities

To quantify the activities of antioxidant enzymes on the protein basis, soluble proteins were extracted from 200 mg frozen homogenized samples in 2 ml of 50 mM phosphate buffer (pH 7.0). The concentrations of soluble proteins were determined spectrophotometrically at 595 nm by color reaction of Coomassie brilliant blue G-250 (Loffler and Kunze, 1989). The standard curve was generated by a serial of diluted BSA solutions. The activities of peroxidase (POD, EC 1.11.1.7), catalase (CAT, EC 1.11.1.6), ascorbate peroxidase (APX, EC 1.11.1.11), and glutathione reductase (GR, EC 1.8.1.7) were assayed by monitoring the changes of absorbance at 470, 240, 290, and 340 nm, respectively, as reported previously (He et al., 2011). The method to determine the activity of superoxide dismutase (SOD, EC 1.15.1.1) was adopted from Morina et al. (2010). One unit of activity was defined as the amount of enzyme that caused a 50% decrease in the SOD-inhibited nitroblue tetrazolium reduction at 560 nm.

Analysis of *PIP* Transcript Levels

The frozen powder of plant materials (about 50 mg) was used for total RNA extraction with a plant RNA extraction kit (R6827, Omega Bio-Tek, Norcross, GA). The quality and concentration of the isolated RNA were measured using a NanoDrop 2000 spectrophotometer (Therom Scientific, Wilmington, DE, USA). The integrity of total RNA was evaluated by an Agilent 2100 Bioanalyzer (Agilent Technologies, Santa Clara, CA, USA). Trace genomic DNA in the total RNA extract was digested by DNase I (E1091; Omega Bio-Tek) attached to the RNA extraction kit. The absence of trace genomic DNA in the total RNA was verified by a control PCR using total RNA as templates. Depending on plant tissue, the first-strand cDNA was synthesized from aliquots of 0.5–1 μg of total RNA with a PrimeScript™ RT reagent kit (RR047A, Takara, Japan) following the enclosed protocol. The procedure for real time qPCR (RT-qPCT) was performed as described previously (Du et al., 2017). The 20 μl reaction mixture contained 0.8 μl of cDNA, 0.6 μl of each primer (10 μM), 10 μl of 2 × TB Green Premix Ex Taq II (RR820A, Takara, Japan). Three technical replicates for each cDNA were performed on an ABI Prism 7300 Real-Time PCR System (Applied Biosystems, MA, USA). Primers of *PIP*s were designed by the online tool on NCBI (Primer-Blast, https://www.ncbi.nlm.nih.gov/tools/primer-blast/). Mulberry actin gene was used as the internal reference gene (Pan and Lou, 2008). Sequences of primers, annealing temperature and amplicon size were shown in **Table S1**; the *PIP* genes were named after a previous report (Baranwal and Khurana, 2017). To ensure the specificity of the primers, PCR products were sequenced and aligned with the homologs in *Morus notabilis*.

Statistical Analysis

Statistical tests were carried out in SPSS statistics 22 (IBM, NY, USA). Before statistical analysis, all data were checked for normality. To examine the effects of cultivars and drought duration on experimental variables, two-way ANONAs were used with cultivar (C) and time (T) as two main factors. Differences between means were considered significant when the P-value of F-test was less than 0.05. The Ct values obtained after RT-qPCR were used to calculate the relative expression levels of the genes by the $2^{-\Delta\Delta Ct}$ method. The heatmap was graphed by MeV4.9 (MeV4.9, Boston, MA).

RESULTS

Plant Water Conditions and Transcript Levels of *PIP*s

After the onset of withholding water, the daily soil moisture dramatically decreased from 33.2 to 9.4% at day 2 and further dropped to 3.3% at day 5 (**Figure S1**), indicating a progressive

and abrupt drought stress that the plants were subjected. Leaf RWC decreased as drought proceeded in all the studied cultivars, while cultivar Wubu had relatively higher RWC than the other two cultivars (**Figure S2**). Drought stress led to significant reduction in water content in different tissues (**Figure 1**). In leaves, water content decreased significantly in the three cultivars with stress level increasing, among which cultivar 7307 had the lowest water content (**Figure 1A**). Marked decrease was only found in wood of Wubu and bark of Yu711 and 7307 at day 5 compared to day 0 (**Figures 1B, C**). In leaves of Wubu and Yu711, water content showed no significant changes at day 2 but sharply dropped at day 5, whereas consistent decline was found in 7307 (**Figure 1D**).

Sequence alignment showed that PIPs in the three examined mulberry cultivars had high similarities to these in *Morus notabilis* at both cDNA and amino acid levels (**Figure S3**). The transcriptional levels of *PIP* genes greatly varied in roots, wood, bark, and leaves among the three cultivars under progressive drought stress (**Figure 2**). Globally, *PIP*s were induced in roots and bark, inhibited in leaves, while they displayed larger variations in wood. Except that *PIP1.1* in roots of Wubu was downregulated, transcript levels of *PIP1;1* and *PIP2;3* were elevated in roots of the three cultivars at day 2 compared with those at day 0 (**Figure 2A**). On the contrary, transcriptions of *PIP1;1* and *PIP2;3* were holistically inhibited in the cultivars, apart from *PIP2;3* in 7307. The overall transcript levels of *PIP1;2*, *PIP1;3*, *PIP2;1*, and *PIP2;4* were enhanced after the onset of progressive drought stress. The only detected continuous downregulations were found for *PIP2;4* in roots of 7307. Particularly, *PIP1;2* in all the cultivars, *PIP2;1* in Yu711 and 7307, and *PIP2;4* in Wubu were upregulated continuously as drought stress proceeded. However, transcript levels of *PIP1;3* in Yu711 and 7307, *PIP2;1* and *PIP2;4* in Yu711, declined at day 5 compared to day 2.

As the cluster analysis has shown, changes of *PIP1;1*, *PIP1;3*, and *PIP2;3* transcript levels in wood were similar in all cultivars after the onset of progressive drought, which exhibited continuous downregulations except *PIP1.3* in Yu711 (**Figure 2B**). The transcript levels of *PIP2;1* were elevated in Yu711 and 7307 at day 2, while *PIP2;1* transcript abundance in Wubu only began to rise at day 5. The mRNA levels of *PIP1;2* and *PIP2;4* were continuously increased in Wubu, Yu711, and 7307 except for *PIP1.2* in Yu711.

In bark, *PIP1;3* and *PIP2;3* transcript levels were generally increased at day 2 but decreased at day 5 in all the cultivars (**Figure 2C**). The transcript abundances of *PIP2;1 PIP1;1*, *PIP1;2*, and *PIP2;4* were elevated with the increasing stress duration regardless of cultivars. Notably, the responsiveness of these genes was stronger at day 5 than at day 2 for cultivars Wubu and 7307, whereas the opposite was true for Yu711.

In general, Wubu and Yu711 had stronger *PIP* responses in leaves than 7307 (**Figure 2D**). The expression levels of *PIP1;3* and *PIP2;3* in leaves of the three cultivars were gradually increased as the duration of drought stress increased, except for Wubu at day 2. Transcript levels of *PIP1;2*, *PIP2;1*, and *PIP2;4* in Wubu declined with stress time increasing, whereas these genes were induced firstly at day 2 and repressed at day 5 relative to day 2. *PIP1;1* level in the three cultivars showed a similar pattern to those of *PIP2;4* in Yu711 and 7307.

Concentrations of Chlorophyll, Soluble Sugars and Starch

Among the three mulberry cultivars, only Wubu presented a significant increase of chlorophyll a at day 2, whereas the other cultivars showed a slightly descending trend (**Figure 3A**). In leaves of Wubu, chlorophyll a content at day 2 was comparable to day 0, but it remarkably declined at day 5. In contrast, the chlorophyll a content in leaves of Yu711 and 7307 significantly rose at day 2 and then decreased at day 5 (**Figure 3B**). The variations of chlorophyll b content in bark and leaves of the three mulberry cultivars resembled those of chlorophyll a (**Figures 3C, D**).

The concentrations of soluble sugars displayed an overall increase in roots, wood, and bark as the drought stress proceeded from mild to severe, except for those in leaves of the three mulberry cultivars (**Figures 4A–D**). At day 2, the concentrations of soluble sugars were higher in roots, bark, and leaves of cultivar Yu711 than the other cultivars. Similarly, concentrations of soluble sugars were higher in roots and leaves of 7307, and wood and bark in Yu711 than the rest of the cultivars at day 5. Although progressive drought led to significant changes of starch in different tissues, only remarkable differences were detected in

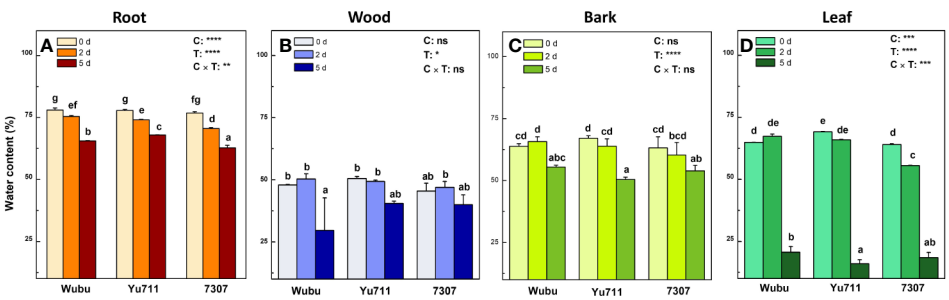


FIGURE 1 | Water contents in roots **(A)**, wood **(B)**, bark **(C)**, and leaves **(D)** of mulberry cultivar Wubu, Yu711, and 7307 exposed to progressive drought stress for 0, 2, and 5 days (denoted as 0 d, 2 d, and 5 d), respectively. The bar indicates mean ± SE (n = 6). Different letters on the bars indicate significant difference. ANOVAS of cultivars (C), time (T), and their interaction (C × T) are also indicated. *$P < 0.05$; **$P < 0.01$; ***$P < 0.001$; ****$P < 0.0001$; ns, not significant.

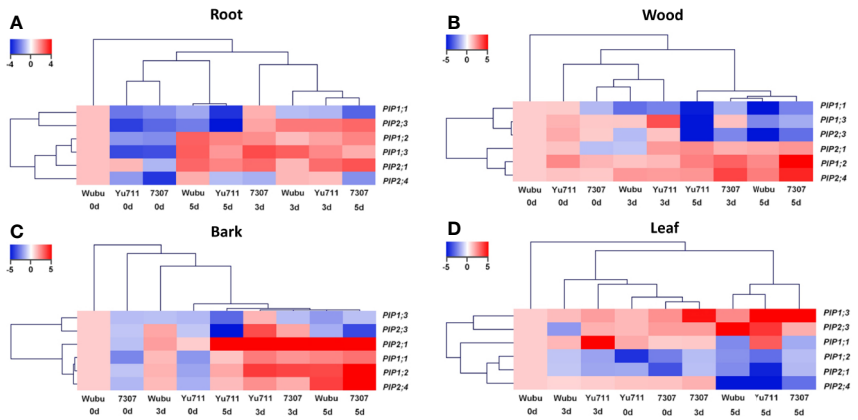


FIGURE 2 | Fold changes of transcript levels of *PIPs* in roots **(A)**, wood **(B)**, bark **(C)** and leaves **(D)** of mulberry cultivar Wubu, Yu711, and 7307 exposed to progressive drought stress for 0, 2, and 5 days (denoted as 0 d, 2 d, and 5 d), respectively. Fold changes of transcript levels of *PIPs* in roots, wood, bark or leaves of Wubu at day 0 were defined to be 1.

roots between the three cultivars (**Figures 4E–H**). Starch concentrations were lower in roots of Wubu than those in other cultivars on either time point during the treatment (**Figure 4E**). The concentrations of starch in wood and bark increased at day 2 and decreased at day 5 compared to those at day 0 (**Figures 4F, G**), whereas gradual declines were found in leaves of the three cultivars (**Figure 4H**).

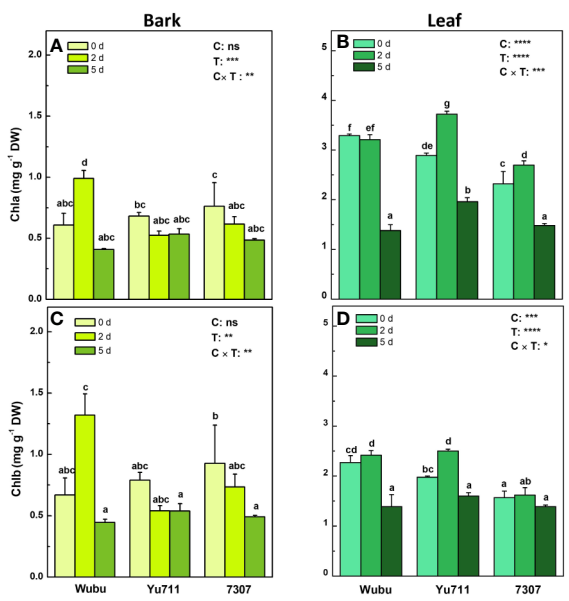


FIGURE 3 | Concentrations of chlorophylls a **(A, B)** and b **(C, D)** in bark and leaves of mulberry cultivar Wubu, Yu711, and 7307 exposed to progressive drought stress for 0, 2, and 5 days (denoted as 0 d, 2 d, and 5 d), respectively. The bar indicates mean ± SE (n = 6). Different letters on the bars indicate significant difference. ANOVAS of cultivars (C), time (T), and their interaction (C × T) are also indicated. *$P < 0.05$; **$P < 0.01$; ***$P < 0.001$; ****$P < 0.0001$; ns, not significant.

H_2O_2, $O_2^{\bullet-}$, and MDA

Pronounced responses were found in the concentrations of H_2O_2 in roots and leaves (**Figures 5A, D**). In contrast, no dramatic changes of H_2O_2 were observed in wood and bark of the three cultivars under progressive drought, although there was a slight tendency of increase (**Figures 5B, C**). The concentrations of H_2O_2 markedly decreased in roots of Wubu and 7307 at day 2 but increased in roots of 7307 at day 5 compared to day 0. Wubu always had higher H_2O_2 concentrations in roots that the other cultivars (**Figure 5A**). The concentrations of H_2O_2 in leaves were generally elevated as the drought persisted. Yu711 appeared to have higher H_2O_2 than the other cultivars (**Figure 5D**).

In roots, $O_2^{\bullet-}$ concentrations were significantly decreased in all the tested cultivars in response to gradual water depletion, among which Wubu constantly showed higher $O_2^{\bullet-}$ production than the other cultivars (**Figure 5E**). No significant responses of $O_2^{\bullet-}$ were detected in wood and bark of the tested cultivars (**Figures 5F, G**). In leaves, significantly higher $O_2^{\bullet-}$ concentrations were found upon the onset of drought stress. Among the tested cultivars, Yu711 and 7307 had significantly higher $O_2^{\bullet-}$ accumulation within the first 2 days, whereas Wubu did not respond significantly until at day 5 (**Figure 5H**).

There were no cultivar effects on MDA concentrations in roots, wood, and bark under drought stress, except for the leaves (**Figures 5I–L**). Progressive drought led to decreased MDA concentrations in roots, while no strong variations were displayed in wood and bark of the tested cultivars (**Figures 5I–K**). The MDA concentrations in leaves increased as drought proceeded in the three cultivars, among which Wubu exhibited the lowest concentrations at each time point (**Figure 5L**).

Free Proline and Soluble Proteins

Upon drought stress, concentrations of free proline in different tissues were significantly altered in the three cultivars (**Figures 6A–D**). At day 2, concentrations of free proline remarkedly increased in roots, wood, bark, and leaves of cultivar 7307, but

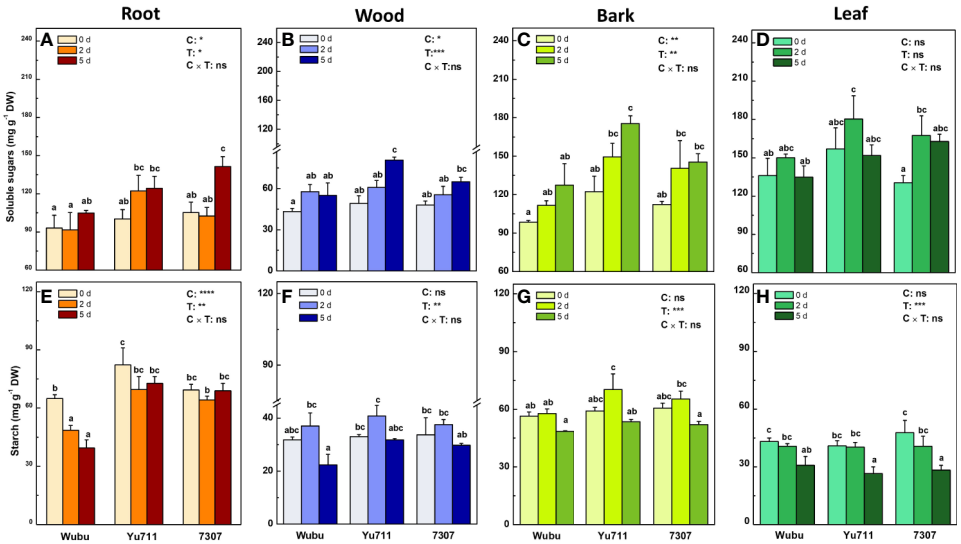


FIGURE 4 | Concentrations of soluble sugars **(A–D)** and starch **(E–H)** in roots, wood, bark, and leaves of mulberry cultivar Wubu, Yu711, and 7307 exposed to progressive drought stress for 0, 2, and 5 days (denoted as 0 d, 2 d, and 5 d), respectively. The bar indicates mean ± SE (n = 6). Different letters on the bars indicate significant difference. ANOVAS of cultivars (C), time (T) and their interaction (C × T) are also indicated. *$P < 0.05$; **$P < 0.01$; ***$P < 0.001$; ****$P < 0.0001$; ns, not significant.

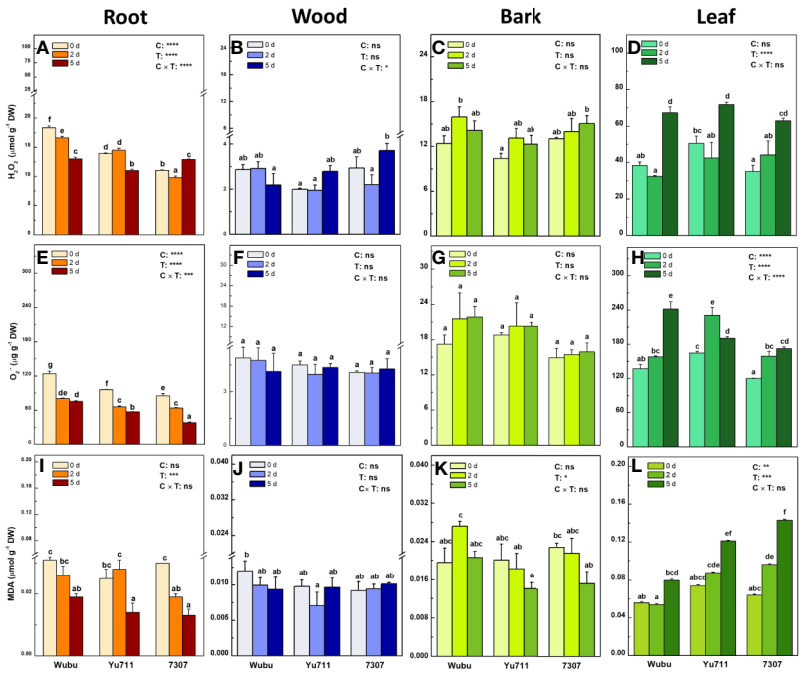


FIGURE 5 | Concentrations of H_2O_2 **(A–D)**, $O_2^{\bullet-}$ **(E–H)** and MDA **(I–L)** in roots, wood, bark, and leaves of mulberry cultivar Wubu, Yu711, and 7307 exposed to progressive drought stress for 0, 2, and 5 days (denoted as 0 d, 2 d, and 5 d), respectively. The bar indicates mean ± SE (n = 6). Different letters on the bars indicate significant difference. ANOVAS of cultivars (C), time (T) and their interaction (C × T) are also indicated. *$P < 0.05$; **$P < 0.01$; ***$P < 0.001$; ****$P < 0.0001$; ns, not significant.

did not change significantly in wood, bark, and leaves of the other cultivars in comparison with day 0. However, comparing to day 0, the concentrations of free proline at day 5 were dramatically elevated by an average of about 10-, 25-, 50-, and 8-fold in roots, wood, bark, and leaves of the three cultivars, respectively. Notably, 7307 had relatively higher free proline levels when drought stress was moderate (day 2), whereas Wubu had higher accumulation of free proline as drought became severe (day 5).

In general, soluble proteins in roots and leaves were at higher levels than those in wood and bark and exhibited stronger responsiveness as well (**Figure 6E–H**). In roots, the concentrations of soluble proteins declined significantly in Wubu and Yu711 but increased greatly in 7307 as drought stress proceeded (**Figure 6E**). However, concentrations of soluble protein were elevated significantly in wood and bark until at day 5 compared to day 0, except for those in wood of Yu711 (**Figures 6F, G**). In leaves of Yu711 and 7307, reduced levels of soluble proteins were found as drought stress persisted (**Figure 6H**). It is noteworthy that cultivar Wubu had higher levels of soluble proteins in roots and wood under either time point than the other cultivars, and it also displayed relatively more soluble proteins in leaves under drought stress (**Figures 6E, F, H**).

Enzyme Activities

The activities of POD in roots, wood, and leaves of all cultivars were inhibited as the stress time prolonged, except those in roots and bark of Yu711 and wood of 7307 (**Figures 7A–D**). Remarkably, Wubu had generally higher activities of POD in drought conditions than the other two cultivars. The activities of SOD were enhanced in roots of Wubu and Yu711, wood of all the three cultivars, and leaves of Yu711 and 7307 upon drought stress (**Figures 7E–H**). In contrast, SOD activities were progressively decreased in roots of 7307 and bark of Wubu (**Figure 7E, G**). The activities of APX were increased in roots, wood, and bark of Wubu and Yu711 in comparison with those at day 0 (**Figures 7I–K**). However, the levels of APX declined significantly in roots and bark and remained relatively unchanged in wood of 7307 as drought stress level increased. Interestingly, APX activities in leaves of Yu711 and 7307 were significantly elevating under moderate drought but declining under severe drought; the opposite tendency was found for Wubu (**Figure 7L**). The activities of CAT were decreased in roots and bark, increased in wood, and unaltered in leaves of Wubu under progressive drought (**Figures 7M–P**). Unlike Wubu, cultivar Yu711 exhibited increased CAT activities in roots, wood, and leaves, except in bark in response to drought stress (**Figures 7M–P**). As for 7307, enhanced activities of CAT were only shown in roots upon stress exposure (**Figure 7M**). Among the analyzed cultivars, strong responsiveness of the GR activities was found in bark and leaves than in roots and wood (**Figures 7Q–T**). In the bark of the three cultivars, considerable variations in GR activities were detected as early as day 2, among which GR levels were rapidly decreased in Wubu but increased in Yu711 and 7307 (**Figure 7S**). Inversely, GR activities did not show significant increase in leaves of Wubu and Yu711 until day 5. However, GR activities declined acutely in leaves of 7307 once the drought stress started (**Figure 7T**).

DISCUSSION

Variations in Responses to Progressive Drought Among the Three Cultivars

Among the three examined mulberry cultivars, Wubu is mainly cultivated in northwest China where it experiences relatively drier climate. Anatomical analysis found that this cultivar had smaller vessels in the stem xylem (Cao et al., 2020), smaller leaf area, higher foliar stable carbon isotope composition ($\delta^{13}C$) compared to the other two cultivars under natural conditions (Cao et al., 2019). These are beneficial characteristics to reduce xylem embolism and increase water use efficiency under drought stress, thereby potentially conferring higher tolerance. Yu711 and 7307 are popular high-yield cultivars in southeast China where rainfall is abundant during growth season. However, Yu711

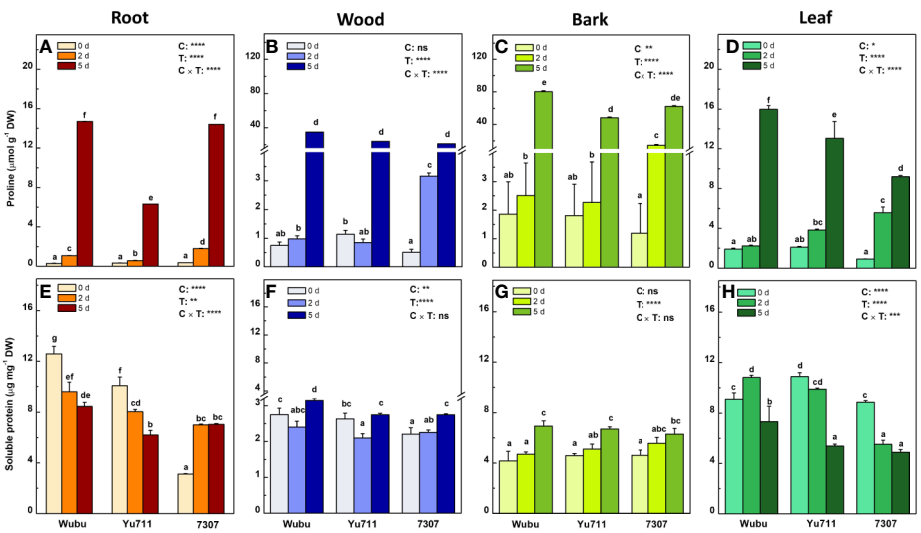


FIGURE 6 | Concentrations of free prolien **(A–D)** and soluble proteins **(E–H)** in roots, wood, bark, and leaves of mulberry cultivar Wubu, Yu711, and 7307 exposed to progressive drought stress for 0, 2, and 5 days (denoted as 0 d, 2 d, and 5 d), respectively. The bar indicates mean ± SE (n = 6). Different letters on the bars indicate significant difference. ANOVAS of cultivars (C), time (T) and their interaction (C × T) are also indicated. *$P < 0.05$; **$P < 0.01$; ***$P < 0.001$; ****$P < 0.0001$; ns, not significant.

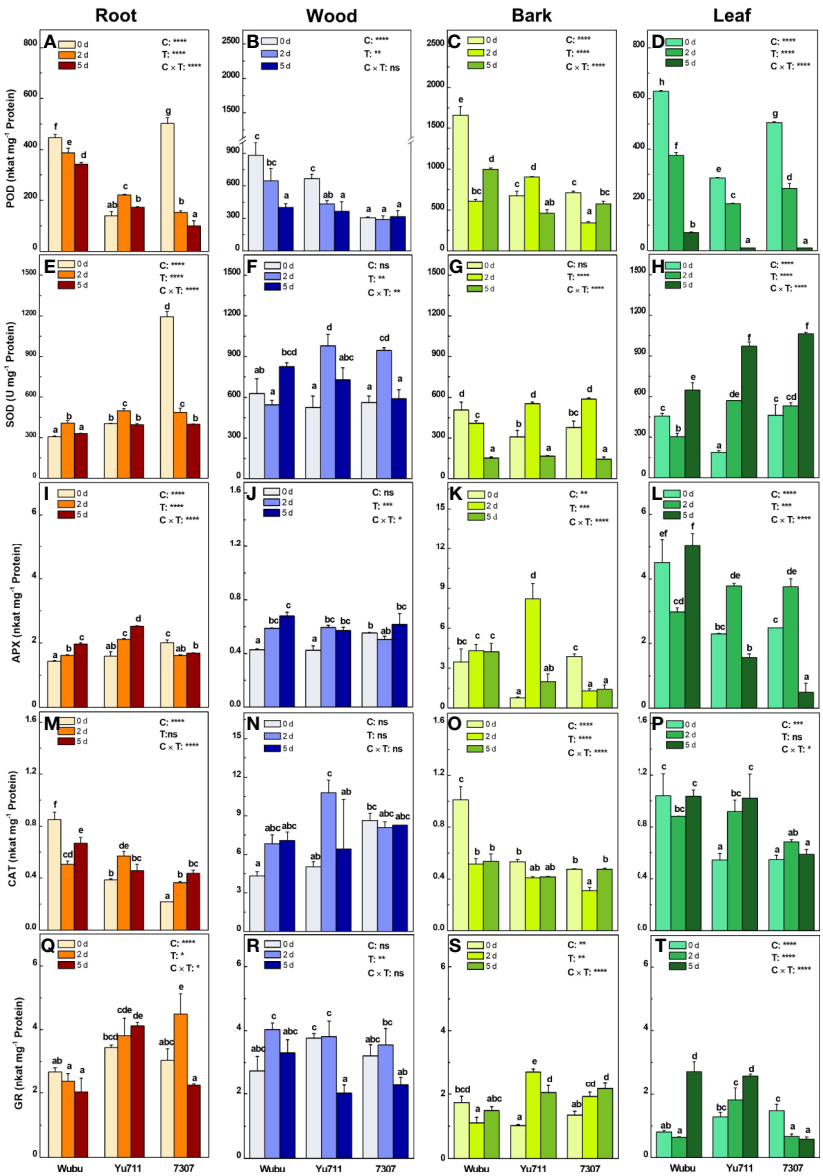


FIGURE 7 | Activities of POD **(A–D)**, SOD **(E–H)**, APX **(I–L)**, CAT **(M–P)** and GR **(Q–T)** in roots, wood, bark, and leaves of mulberry cultivar Wubu, Yu711, and 7307 exposed to progressive drought stress for 0, 2, and 5 days (denoted as 0 d, 2 d, and 5 d), respectively. The bar indicates mean ± SE (n = 6). Different letters on the bars indicate significant difference. ANOVAS of cultivars (C), time (T) and their interaction (C × T) are also indicated. *$P < 0.05$; **$P < 0.01$; ***$P < 0.001$; ****$P < 0.0001$; ns, not significant.

had larger leaf size, smaller specific leaf area, and higher foliar $\delta^{13}C$ than 7307 (Cao et al., 2019). Therefore, these two cultivars could be different in drought tolerance. As shown in this study, the three cultivars responded differently to progressive soil water depletion. Wubu showed the highest leaf RWC and water content in the root, bark, and leaves at day 2 and in the bark and leaves at day 5, whereas 7307 displayed earlier (day 2) and greater water loss as soil water moisture rapidly decreased. Notably, Wubu always had relatively higher water content in the green photosynthetic tissues including the bark and leaf under drought. Since tissue free water content reflects plants' metabolic capacity under drought stress (Kumar and Sharma, 2010; Soltys-Kalina et al., 2016; Kalandyk et al., 2017), it is anticipated that the capacity to sustain water conservation among the examined cultivars decreases in the order Wubu > Yu711 > 7307, and the differences might be associated with their distinct physiological and transcriptional regulation in response to progressive drought stress.

PIPs are the major facilitators controlling cell water uptake and transport under changeable water availability (Maurel et al., 2015). Under well-watered condition, the transcript levels of *PIPs* were globally highest in Wubu and lowest in 7307, indicating that they have different ability in transcellular water transport.

Under drought stress, Wubu still maintained generally higher transcript levels of *PIPs* in the roots and bark at day 5 than the other cultivars, partially corresponding to its higher water contents in these tissues. The relative levels of *PIP* genes and/or PIP proteins are suggested to be positively correlated with drought tolerance (Tsuchihira et al., 2010). This coincides with our assumption that Wubu is better acclimated to severe drought by adjusting to water absorption and transport than the other two cultivars. Not surprisingly, we found the three cultivars displayed different responsiveness to progressive drought stress. *PIP* expressions in the roots, wood, and bark of Wubu and Yu711 displayed a slighter responsiveness to progressive drought in comparison with those in 7307, which echoed their smaller variations in tissue water contents. Conversely, transcript levels of *PIPs* in the leaves of Wubu displayed stronger modulation than Yu711 and 7307, especially at day 5 when drought became severe. Previous studies also presented different degrees of transcriptional changes between drought sensitive and drought tolerant genotypes, such as in grapevine (Vandeleur et al., 2009), poplar (Almeida-Rodriguez et al., 2010), and citrus (Wei et al., 2019). Additionally, it is noticeable that several *PIP* genes were cultivar- and tissue-specific expressed under drought stress. For instance, only *PIP2;4* in the roots of 7307 was transcriptionally downregulated when that of the other two cultivars was upregulated, which could probably lead to decreased water absorption from the soil. The mRNA level of *PIP1;2* in the wood was inhibited in Yu711 but stimulated in Wubu and 7307, which partly corresponded to the findings in wood of pear trees (Paudel et al., 2019). *PIP1;3* abundance in the root and bark was depressed in Wubu but increased in Yu711 and 7307. These results demonstrate that different mulberry cultivars can differentially regulate gene expression of *PIPs* to acclimate to changes in soil water availability.

In response to water shortage, osmotic regulation is a physiological mechanism that facilitates the acclimation to drought. Soluble sugars act as osmolytes and signaling molecules under various abiotic stresses, which can contribute to differences in drought tolerance in plants (Naser et al., 2010). In this study, Wubu remained relatively unchanged at low levels of soluble sugars in all the tissues. In contrast, significantly higher increases of soluble sugars were observed in the wood and bark in Yu711, and in the roots of 7307 at day 5 of drought stress. A study on rice found that soluble sugars only significantly increased in the roots and leaves of susceptible rice variety but unchanged in tolerant variety (Dien et al., 2019). Our results, however, indicated that the changes of soluble sugars under drought stress conditions could depend on the characteristics of the different cultivars. Apart from soluble sugars, proline is also one of the most important components in osmoregulatory machinery to acclimate to environmental stresses (Singh et al., 2015). Many plants accumulate proline as a response to drought stress (Hare et al., 1998). Interestingly, Wubu and Yu711 did not respond to mild drought at day 2 in any tissues except the roots, whereas Wubu accumulated the highest levels of free prolines at day 5 in all the tissues, especially in the bark and leaves. This superior whole-plant level osmoregulation mediated by proline in Wubu could greatly contribute to its higher tissue water contents under drought stress. Similarly, Man et al. (2011) also found that leaf proline in drought-tolerant turfgrass (*Festuca arundinacea*) cultivar was 32% higher relative to the sensitive one. The reason for the difference of proline levels between cultivars might be associated with higher proline catabolism in the sensitive cultivar as reported in peanut plants (Furlan et al., 2020). In terms of soluble proteins which also play roles in osmotic adjustment, Wubu had higher soluble protein concentrations in all the living tissues regardless of water availability in comparison with the other two cultivars. In olive (*Olea europaea* L.) trees, it was suggested that higher levels of soluble proteins may reflect higher activities of oxidative enzymes and represent a reserve for post stress recovery (Bacelar et al., 2009). Hence, the superior whole-plant level osmoregulation in Wubu is a vital mechanism to maximally sustain tissue water conservation under severe drought, among which proline probably plays the most predominate role.

Enhanced ROS production is one of the inevitable outcomes of drought stress, which is however kept under tight control by versatile and cooperative antioxidant enzymes (Cruz de Carvalho, 2008). We found that Wubu always had higher H_2O_2 in the roots and $O_2^{\bullet-}$ in the roots and leaves compared with the other two cultivars regardless of soil water moisture. Accordingly, higher activities of root POD and CAT, and foliar SOD, APX, and CAT were observed, which can diminish the oxidative damage of ROS to cell structures and macromolecules (Boaretto et al., 2014). ROS can also act as signaling molecules linking to ABA, Ca^{2+} fluxes and sugar sensing under drought stress (Cruz de Carvalho, 2008). So, it is inferred that the higher ROS levels are required in Wubu to activate multiple drought signaling pathways and thereby subsequent physiological responses to confront drought stress. As was expected, Wubu consistently exhibited the lowest concentrations of MDA in the leaves compared to the other two cultivars, and it maintained relatively stable as drought intensified, indicating that Wubu has stronger ability to adjust activities of antioxidant enzymes to alleviate cellular membrane lipid peroxidation and protect plants from drought-induced oxidative stress.

Collectively, it appears that the physiological and transcriptional reactions of Wubu were not evoked until the stress level intensified, thereby presenting a delayed responsiveness compared to the other cultivars. Higher leaf RWC and tissue water contents, stronger responsiveness of transcriptional regulations of *PIPs*, higher proline and soluble proteins, lower MDA production, and higher activities of antioxidant enzymes in cultivar Wubu in comparison with those in Yu711 and 7307 contribute to the different physiological response patterns of the three cultivars under short-term progressive drought stress.

Common Regulatory Mechanisms in Mulberry in Response to Progressive Drought

Numerous studies have investigated the expression patterns of individual aquaporin genes to uncover their roles in plant water relations either when water is abundant or scarce (Hu et al., 2016; Kayum et al., 2017; Sun et al., 2017; Lu et al., 2018). However, no

information is available up to date on the transcriptional expression patterns of *PIPs* in mulberry under drought stress, taking all plant parts into consideration. Existing data are commonly based on the roots and leaves that show either upregulation, downexpression, or no changes of the transcript levels of *PIPs* under drought conditions (Aroca et al., 2006; Mahdieh et al., 2008; Šurbanovski et al., 2013). In the current study, a complex pattern of *PIP* expression was exposed, with transcription levels diverged more among *PIP* members and tissues than among cultivars, implying that *PIPs* in mulberry could function differently depending on the organ types. Specifically, most of the detected *PIP* genes were gradually upregulated in the roots and bark, and slowly downregulated in the leaves, whereas comparable numbers of up- and downregulated *PIP* genes were found in wood under progressive drought. More commonly, drought stress can lead to reduced transcripts of *PIP* genes in the roots and elevated expression in the leaves (Jang et al., 2004; Porcel et al., 2006). Upregulation of *PIPs* is considered to increase membrane permeability to water transport (Paudel et al., 2017), whereas downregulation may improve water conservation under drought stress (Almeida-Rodriguez and Hacke, 2012). Thus, it is plausible that enhanced expressions of *PIP1;2*, *1;3*, *2;1* and *2;4* in the roots might be a direct response to drying substrate. In fact, similar upregulation of *PIPs* was also observed in roots of *Phaseolus vulgaris* plants exposed to water deprivation for 4 days, which then decreased with subsequent re-watering (Aroca et al., 2006). The accompanied elevated root water uptake was proven to be essential to keep higher water content in above-ground parts in plants under drought (Hu et al., 2016). Conversely, repressed transcript levels of *PIPs* in leaves can reduce water loss from transpiration at leaf level (Alexandersson et al., 2005). Merlaen et al. (2019) also found downregulated *PIP* expressions in leaves of two contrasting *Fragaria* × *ananassa* Duch. cultivars exposed to progressive drought, which is well in line with our results.

Additionally, several studies have revealed that PIPs in the xylem participate the refilling of embolized conduits and adjusting root/stem hydraulic conductance (Secchi and Zwieniecki, 2010; Perrone et al., 2012). The increased transcription of *PIP1;2*, *2;1*, and *2;4* in the wood in this study is consistent to a previous report on hybrid poplar (Leng et al., 2013). The elevated PIPs can work together with root pressure to refill drought-induced embolized vessels, playing important roles in maintaining long-distance water transport from the roots to the aboveground tissues. Of special interest was bark tissue where several same *PIPs* displayed opposite expression pattern compared to leaves in response to drought stress. Bark, as a photosynthetic tissue besides leaves, has seldom been valued in studying drought responses (Cernusak et al., 2001; Cernusak and Cheesman, 2015; Vandegehuchte et al., 2015). In the current study, the dramatic responsiveness of *PIPs* in the bark highlights the importance of bark in acclimation to drought. One possible explanation for the increased mRNA levels of most *PIPs* in the bark might be enhanced assimilate transport accompanied by water transport in the phloem, in order to maximumly sustain basic carbon metabolism in other sink organs under severe drought conditions. These results highlight the importance of PIPs in wood and bark for acclimation to drought stress in mulberry. The overall complexity of *PIP* transcriptional regulation demonstrates that maintenance of an appropriate water status within individual plant under drought stress requires a coordinated regulation of *PIP*-facilitated increase or decrease in water transport in different tissues as proposed previously (Jang et al., 2004).

Soluble sugars and starch are important nonstructural carbohydrates (NSCs) in plants for adaptation to drought stress (Piper and Paula, 2020). Previous studies often present opposite trends in NSC changes in different organs under drought stress (Zaher-Ara et al., 2016; Dien et al., 2019; Camison et al., 2020). In this study, the concentrations of total soluble sugars showed a trend to increase, while starch tends to decrease in the three tested cultivars with prolonged drought duration. These are frequently observed responses in plants under drought stress, as evidenced by a recent meta-analysis on 52 tree species from 47 drought experiments, which also discovered such a universal pattern in different tree organs (He et al., 2020). The tendency of starch degradation is suggested to provide energy and carbon when photosynthesis is compromised under drought stress (Siaut et al., 2011). On the other hand, the released soluble sugars from starch degradation can also act as osmolytes contributing to increasing osmoregulation (Krasensky and Jonak, 2012). Notably, we found that soluble sugars were more responsive in the stem (*i.e.* wood and bark), while starch responded most significantly in the bark and leaves, indicating organ-level differences in response to drought stress.

Proline accumulation generally improves osmotic stress tolerance in plants (Hanif et al., 2020). In this study, we detected dramatic increases of free proline in all the tissues across the three mulberry cultivars under drought stress, and that longer duration of drought stress resulted in higher proline accumulation. This correlation between proline accumulation and drought intensity is widely reported in other plants (Szabados and Savouré, 2010). Surprisingly, wood and bark displayed an averagely much higher fold-change (25–30) than the root and leaves (8–10), indicating the important roles mulberry stem could play in response to drought stress. In contrast, soluble proteins appeared to respond in an organ-specific manner. The concentrations of soluble proteins were generally higher in the roots and leaves than in the wood and bark, where they exhibited opposite patterns of changes. The increases of soluble proteins in the wood and bark are speculated to be an osmotic response (Regier et al., 2009). Conversely, the decreases in roots and leaves could be a typical symptom of oxidative stress, either resulted from elevated activity of some catabolic enzymes (*e.g.* protease) under drought stress or ascribed to ROS induced protein fragmentation (Palma et al., 2002). This phenomenon has also been observed in other drought stressed plants such as chickpea (*Cicer arietinum*) (Mafakheri et al., 2011), sorghum (*Sorghum bicolor*) (Chen et al., 2015), and wheat (*Triticum aestivum* L.) (Abid et al., 2018). It appears that progressive drought stress had higher effects on proline and soluble proteins relative to soluble sugars among the three cultivars. Nevertheless, these tissue-specific responses indicate the multilayer coordination of osmoregulatory machinery in mulberry trees to cope with intensified drought stress at whole-plant level.

Drought stress can disturb the homeostasis of ROS production and scavenging, often resulting in ROS overaccumulation in plants (Zhang et al., 2019; Zhang et al., 2020), but decreases are also documented (Keunen et al., 2013; Cao et al., 2014). In the current study, ROS levels in stem tissues were much lower than those in roots and leaves and exhibited hardly any changes under drought stress, suggesting mulberry roots and leaves are the major sources of ROS production in response to drought. It appears that H_2O_2, $O_2^{\bullet-}$, and MDA were more prone to be overproduced in the leaves but tend to decrease in the roots as the stress intensified. Zhou R. et al. (2019) also observed sharp increases in concentrations of H_2O_2, $O_2^{\bullet-}$, and MDA after 6 days of water cessation in leaves of tomato saplings. This augmentation corresponded well to the increased activities of SOD and GR in leaves. In alfalfa, concurrently induced mRNA levels of SOD and ROS-generating enzyme were also reported under gradual drought stress (Kang and Udvardi, 2012). The decreased levels of ROS in the roots somehow are contradictory to previous studies (You and Chan, 2015; Nxele et al., 2017), but it corresponded to the repressed activities of SOD and POD. Although the reason for lower accumulation of ROS in the roots is not clear, it is explicit that oxidative defense presents a complex picture in different

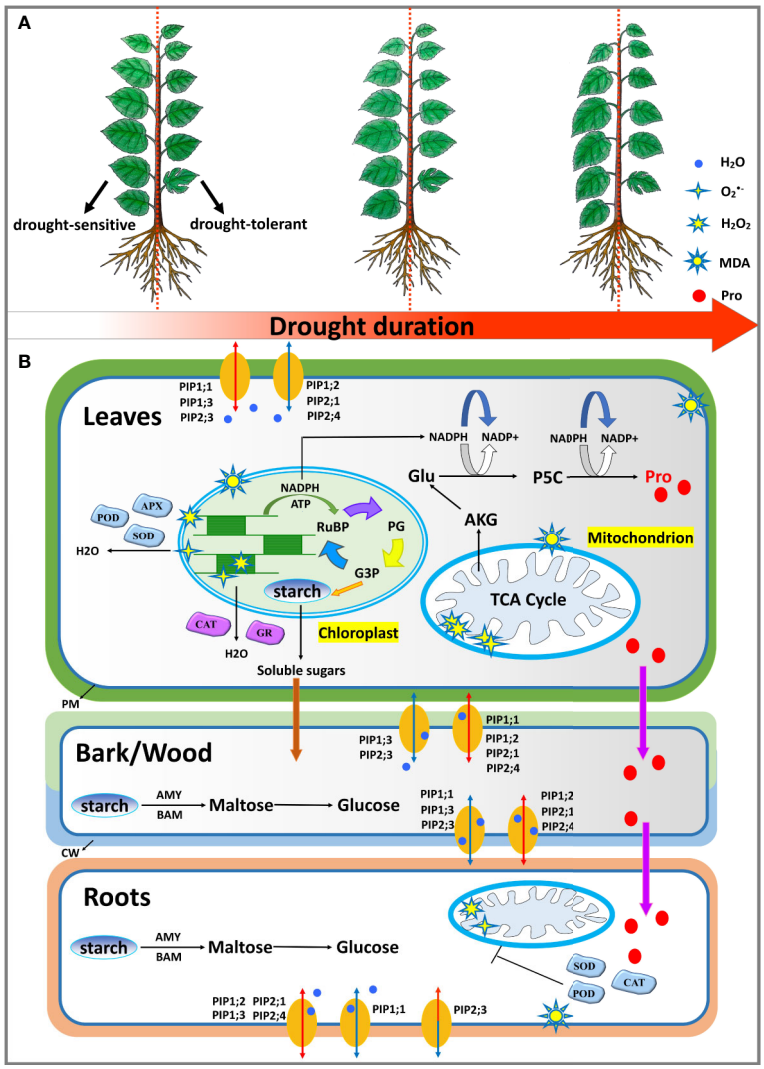


FIGURE 8 | A schematic model of the morphological **(A)** and physiological **(B)** responses to progressive soil water deficit in mulberry. Drought tolerant cultivar Wubu generally displayed delayed stress responses in comparison with drought sensitive cultivars, *i.e.* 7307. When the stress level was relatively mild, Wubu exhibited no or slight responsiveness in plant water contents, *PIP* expression regulation, leaf chlorophyll concentrations, soluble sugars, MDA production, free proline accumulation, but displayed strong changes in chlorophyll in bark, starch, and ROS in roots and activities of antioxidant enzymes. However, all these responses were dramatically intensified as the stress level became severe. All the examined cultivars demonstrated differentially expressed patterns of *PIPs*, decreased starch concentrations, increased osmoregulatory substances, shifted ROS production and scavenging under progressive drought stress. AKG α-ketoglutaric acid; AMY, α-amylase; APX, ascorbate peroxidase; BAM, β-amylase; CAT, catalase; Glu, glutamic acid; G3P, glyceraldehyde 3-phosphate; GR, Glutathione reductase; P5C, 1-pyrroline-5-carboxylic acid; PG, phosphoglycerate; POD, peroxidase; RuBP, ribulose-1,5-bisphosphate; SOD, superoxide dismutase.

tissues in mulberry, by which a new ROS homeostasis might have been established in acclimation to severe drought.

As discussed above, mulberry can adapt to gradual soil water deprivation by changes of transcriptional modulations of *PIPs*, enhanced osmoregulation, decreased starch accumulation, and shifted balance of ROS production and scavenging. And importantly, it not only depends on the leaves and roots, but involves a whole-plant level collaboration for better acclimation to drought stress.

CONCLUSIONS

In this study, we explored the underlying mechanisms of drought tolerance by comparative analysis of three contrasting mulberry cultivars. In general, drought-tolerant cultivar Wubu sustained higher plant water contents and a delayed stress response to progressive drought stress (**Figure 8A**). When the stress level was relatively mild, Wubu exhibited no or slight responsiveness in tissue water contents, *PIPs* expression regulation, leaf chlorophyll, soluble sugars, MDA production, and proline accumulation, but displayed strong changes in chlorophyll in the bark, starch, and ROS in the roots and activities of antioxidant enzymes. However, all these responses were dramatically augmented as the stress intensified. In contrast, drought-sensitive cultivar 7307 displayed faster and higher tissue water loss, earlier and stronger transcriptional regulation of *PIPs*, lower ROS production and higher MDA, earlier but lower proline and soluble proteins. All the examined cultivars demonstrated differentially expressed *PIPs*, decreased starch concentrations, increased osmoregulatory substances, and shifted ROS production and scavenging under progressive drought stress. Meanwhile, organ-specific responses were observed, suggesting coordinated whole-plant level defenses against drought stress in mulberry (**Figure 8B**). Based on the above physiological and transcriptional defense mechanisms, it is concluded that cultivar Wubu showed better performance under progressive drought, and these traits are potentially useful for future mulberry improvement programs.

DATA AVAILABILITY STATEMENT

The original contributions presented in the study are included in the article/supplementary material; further inquiries can be directed to the corresponding author.

AUTHOR CONTRIBUTIONS

XC and JC conceived and designed the experiment. XC, QS, LL, and JC performed the experiments. XC, QS, SM, analyzed the data and prepared the figures. XC wrote the paper. JC revised the paper. All authors contributed to the article and approved the submitted version.

FUNDING

This work was jointly supported by the National Natural Science Foundation of China (Grant No. 31700527 and 31670306) and China Agriculture Research System (Grant No. CARS-18).

SUPPLEMENTARY MATERIAL

The Supplementary Material for this article can be found online at: https://www.frontiersin.org/articles/10.3389/fpls.2020.01310/full#supplementary-material

REFERENCES

Abid, M., Ali, S., Qi, L. K., Zahoor, R., Tian, Z. W., Jiang, D., et al. (2018). Physiological and biochemical changes during drought and recovery periods at tillering and jointing stages in wheat (*Triticum aestivum* L.). *Sci. Rep.* 8, 4615. doi: 10.1038/s41598-018-21441-7

Alexandersson, E., Fraysse, L., Sjovall-Larsen, S., Gustavsson, S., Fellert, M., Karlsson, M., et al. (2005). Whole gene family expression and drought stress regulation of aquaporins. *Plant Mol. Biol.* 59 (3), 469–484. doi: 10.1007/s11103-005-0352-1

Allen, C. D., Macalady, A. K., Chenchouni, H., Bachelet, D., McDowell, N., Vennetier, M., et al. (2010). A global overview of drought and heat-induced tree mortality reveals emerging climate change risks for forests. *For. Ecol. Manage.* 259 (4), 660–684. doi: 10.1016/j.foreco.2009.09.001

Almeida-Rodriguez, A. M., and Hacke, U. G. (2012). Cellular localization of aquaporin mRNA in hybrid poplar stems. *Amer. J. Bot.* 99 (7), 1249–1254. doi: 10.3732/ajb.1200088

Almeida-Rodriguez, A. M., Cooke, J. E. K., Yeh, F., and Zwiazek, J. J. (2010). Functional characterization of drought-responsive aquaporins in *Populus balsamifera* and *Populus simonii* × *balsamifera* clones with different drought resistance strategies. *Physiol. Plant* 140 (4), 321–333. doi: 10.1111/j.1399-3054.2010.01405.x

Aroca, R., Ferrante, A., Vernieri, P., and Chrispeels, M. J. (2006). Drought, abscisic acid and transpiration rate effects on the regulation of *PIP* aquaporin gene expression and abundance in *Phaseolus vulgaris* plants. *Ann. Bot.* 98 (6), 1301–1310. doi: 10.1093/aob/mcl219

Bacelar, E. A., Moutinho-Pereira, J. M., Goncalves, B. C., Lopes, J. I., and Correia, C. M. (2009). Physiological responses of different olive genotypes to drought conditions. *Acta Physiol. Plant* 31 (3), 611–621. doi: 10.1007/s11738-009-0272-9

Baranwal, V. K., and Khurana, P. (2017). Major intrinsic proteins repertoire of *Morus notabilis* and their expression profiles in different species. *Plant Physiol. Bioch.* 111, 304–317. doi: 10.1016/j.plaphy.2016.12.007

Boaretto, L. F., Carvalho, G., Borgo, L., Creste, S., Landell, M. G., Mazzafera, P., et al. (2014). Water stress reveals differential antioxidant responses of tolerant and non-tolerant sugarcane genotypes. *Plant Physiol. Biochem.* 74, 165–175. doi: 10.1016/j.plaphy.2013.11.016

Camison, A., Martin, M. A., Dorado, F. J., Moreno, G., and Solla, A. (2020). Changes in carbohydrates induced by drought and waterlogging in *Castanea sativa*. *Trees-Struct. Funct.* 34 (2), 579–591. doi: 10.1007/s00468-019-01939-x

Cao, X., Jia, J., Zhang, C., Li, H., Liu, T., Jiang, X., et al. (2014). Anatomical, physiological and transcriptional responses of two contrasting poplar genotypes to drought and re-watering. *Physiol. Plant* 151 (4), 480–494. doi: 10.1111/ppl.12138

Cao, X., Du, W., Shang, C., Shen, Q., Liu, L., and Cheng, J. (2018). Comparative transcriptome reveals circadian and hormonal control of adventitious rooting in mulberry hardwood cuttings. *Acta Physiol. Plant* 40 (11), 197. doi: 10.1007/s11738-018-2772-y

Cao, X., Shen, Q., Shang, C., Yang, H., Liu, L., and Cheng, J. (2019). Determinants of shoot biomass production in mulberry: combined selection with leaf morphological and physiological Traits. *Plants* 8 (5), 118. doi: 10.3390/plants8050118

Cao, X., Shen, Q., Liu, L., and Cheng, J. (2020). Relationships of growth, stable carbon isotope composition and anatomical properties of leaf and xylem in seven mulberry cultivars: a hint towards drought tolerance. *Plant Biol.* 22 (2), 287–297. doi: 10.1111/plb.13067

Cernusak, L. A., and Cheesman, A. W. (2015). The benefits of recycling: how photosynthetic bark can increase drought tolerance. *New Phytol.* 208 (4), 995–997. doi: 10.1111/nph.13723

Cernusak, L. A., Marshall, J. D., Comstock, J. P., and Balster, N. J. (2001). Carbon isotope discrimination in photosynthetic bark. *Oecologia* 128 (1), 24–35. doi: 10.1007/s004420100629

Chaumont, F., Barrieu, F., Jung, R., and Chrispeels, M. J. (2000). Plasma membrane intrinsic proteins from maize cluster in two sequence subgroups with differential aquaporin activity. *Plant Physiol.* 122 (4), 1025–1034. doi: 10.1104/pp.122.4.1025

Chen, D., Wang, S., Xiong, B., Cao, B., and Deng, X. (2015). Carbon/nitrogen imbalance associated with drought-induced leaf senescence in *Sorghum bicolor*. *PloS One* 10 (8), e0137026. doi: 10.1371/journal.pone.0137026

Cruz de Carvalho, M. H. (2008). Drought stress and reactive oxygen species: Production, scavenging and signaling. *Plant Signal. Behav.* 3 (3), 156–165. doi: 10.4161/psb.3.3.5536

Cuk, K., Gogala, M., Tkalec, M., and Vidakovic-Cifrek, Z. (2010). Transgenerational stress memory in *Arabidopsis thaliana* (L.) Heynh.: antioxidative enzymes and HSP70. *Acta Bot. Croat.* 69 (2), 183–197.

Dien, D. C., Mochizuki, T., and Yamakawa, T. (2019). Effect of various drought stresses and subsequent recovery on proline, total soluble sugar and starch metabolisms in rice (*Oryza sativa* L.) varieties. *Plant Prod. Sci.* 22 (4), 530–545. doi: 10.1080/1343943x.2019.1647787

Dong, S. Y., and Beckles, D. M. (2019). Dynamic changes in the starch-sugar interconversion within plant source and sink tissues promote a better abiotic stress response. *J. Plant Physiol.* 234, 80–93. doi: 10.1016/j.jplph.2019.01.007

Du, W., Ban, Y., Nie, H., Tang, Z., Du, X., and Cheng, J. (2016). A comparative transcriptome analysis leads to new insights into the molecular events governing root formation in mulberry softwood cuttings. *Plant Mol. Biol. Rep.* 34 (2), 365–373. doi: 10.1007/s11105-015-0927-1

Du, X. L., Cao, X., Yin, C. R., Tang, Z., Du, W., Ban, Y. Y., et al. (2017). Comprehensive analysis of R2R3-MYB genes during adventitious root formation in cuttings of *Morus alba*. *J. Plant Growth Regul.* 36 (2), 290–299. doi: 10.1007/s00344-016-9639-5

Furlan, A. L., Bianucci, E., Giordano, W., Castro, S., and Becker, D. F. (2020). Proline metabolic dynamics and implications in drought tolerance of peanut plants. *Plant Physiol. Biochem.* 151, 566–578. doi: 10.1016/j.plaphy.2020.04.010

Golinski, M., Bauch, C., and Arland, M. (2008). The effects of endogenous ecological memory on population stability and resilience in a variable environment. *Ecol. Model.* 212 (3-4), 334–341. doi: 10.1016/j.ecolmodel.2007.11.005

Gonzalez-Cruz, J., and Pastenes, C. (2012). Water-stress-induced thermotolerance of photosynthesis in bean (*Phaseolus vulgaris* L.) plants: The possible involvement of lipid composition and xanthophyll cycle pigments. *Environ. Exp. Bot.* 77, 127–140. doi: 10.1016/j.envexpbot.2011.11.004

Grondin, A., Mauleon, R., Vadez, V., and Henry, A. (2016). Root aquaporins contribute to whole plant water fluxes under drought stress in rice (*Oryza sativa* L.). *Plant Cell Environ.* 39 (2), 347–365. doi: 10.1111/pce.12616

Gupta, A., and Sankararamakrishnan, R. (2009). Genome-wide analysis of major intrinsic proteins in the tree plant *Populus trichocarpa*: Characterization of XIP subfamily of aquaporins from evolutionary perspective. *BMC Plant Biol.* 9 (1), 134. doi: 10.1186/1471-2229-9-134

Hanif, S., Saleem, M. F., Sarwar, M., Irshad, M., Shakoor, A., Wahid, M. A., et al. (2020). Biochemically triggered heat and drought stress tolerance in rice by proline application. *J. Plant Growth Regul.* doi: 10.1007/s00344-020-10095-3

Hare, P. D., Cress, W. A., and Van Staden, J. (1998). Dissecting the roles of osmolyte accumulation during stress. *Plant Cell Environ.* 21 (6), 535–553. doi: 10.1046/j.1365-3040.1998.00309.x

He, J., Qin, J., Long, L., Ma, Y., Li, H., Li, K., et al. (2011). Net cadmium flux and accumulation reveal tissue-specific oxidative stress and detoxification in *Populus* × *canescens*. *Physiol. Plant* 143 (1), 50–63. doi: 10.1111/j.1399-3054.2011.01487.x

He, W., Liu, H., Qi, Y., Liu, F., and Zhu, X. (2020). Patterns in nonstructural carbohydrate contents at the tree organ level in response to drought duration. *Global Change Biol.* 26 (6), 3627–3638. doi: 10.1111/gcb.15078

Hu, S. B., Zhou, Q., An, J., and Yu, B. J. (2016). Cloning *PIP* genes in drought-tolerant vetiver grass and responses of transgenic Vz*PIP2;1* soybean plants to water stress. *Biol. Plant* 60 (4), 655–666. doi: 10.1007/s10535-016-0631-5

Hu, W., Huang, Y., Loka, D. A., Bai, H., Liu, Y., Wang, S., et al. (2020). Drought-induced disturbance of carbohydrate metabolism in anthers and male abortion of two *Gossypium hirsutum* cultivars differing in drought tolerance. *Plant Cell Rep.* 39 (2), 195–206. doi: 10.1007/s00299-019-02483-1

Hussain, A., Tanveer, R., Mustafa, G., Farooq, M., Amin, I., and Mansoor, S. (2020). Comparative phylogenetic analysis of aquaporins provides insight into the gene family expansion and evolution in plants and their role in drought tolerant and susceptible chickpea cultivars. *Genomics* 112 (1), 263–275. doi: 10.1016/j.ygeno.2019.02.005

Itter, M. S., D'Orangeville, L., Dawson, A., Kneeshaw, D., Duchesne, L., and Finley, A. O. (2019). Boreal tree growth exhibits decadal-scale ecological memory to drought and insect defoliation, but no negative response to their interaction. *J. Ecol.* 107 (3), 1288–1301. doi: 10.1111/1365-2745.13087

Jang, J. Y., Kim, D. G., Kim, Y. O., Kim, J. S., and Kang, H. (2004). An expression analysis of a gene family encoding plasma membrane aquaporins in response to abiotic stresses in *Arabidopsis thaliana*. *Plant Mol. Biol.* 54 (5), 713–725. doi: 10.1023/B:PLAN.0000040900.61345.a6

Jia, J., Li, S., Cao, X., Li, H., Shi, W., Polle, A., et al. (2016). Physiological and transcriptional regulation in poplar roots and leaves during acclimation to high temperature and drought. *Physiol. Plant* 157 (1), 38–53. doi: 10.1111/ppl.12400

Jia, J., Zhou, J., Shi, W., Cao, X., Luo, J., Polle, A., et al. (2017). Comparative transcriptomic analysis reveals the roles of overlapping heat-/drought-responsive genes in poplars exposed to high temperature and drought. *Sci. Rep.* 7:43215. doi: 10.1038/srep43215

Johanson, U., Karlsson, M., Johansson, I., Gustavsson, S., Sjövall, S., Fraysse, L., et al. (2001). The complete set of genes encoding major intrinsic proteins in arabidopsis provides a framework for a new nomenclature for major intrinsic proteins in plants. *Plant Physiol.* 126 (4), 1358–1369. doi: 10.1104/pp.126.4.1358

Kalandyk, A., Waligorski, P., and Dubert, F. (2017). Role of the maternal effect phenomena in improving water stress tolerance in narrow-leafed lupine (*Lupinus angustifolius*). *Plant Breed.* 136 (2), 167–173. doi: 10.1111/pbr.12457

Kang, Y., and Udvardi, M. (2012). Global regulation of reactive oxygen species scavenging genes in alfalfa root and shoot under gradual drought stress and recovery. *Plant Signal. Behav.* 7 (5), 539–543. doi: 10.4161/psb.19780

Kayum, M. A., Park, J. I., Nath, U. K., Biswas, M. K., Kim, H. T., and Nou, I. S. (2017). Genome-wide expression profiling of aquaporin genes confer responses to abiotic and biotic stresses in *Brassica rapa*. *BMC Plant Biol.* 17, 23. doi: 10.1186/s12870-017-0979-5

Keunen, E., Peshev, D., Vangronsveld, J., Wim, V. D. E., and Cuypers, A. (2013). Plant sugars are crucial players in the oxidative challenge during abiotic stress: extending the traditional concept. *Plant Cell. Environ.* 36 (7), 1242–1255. doi: 10.1111/pce.12061

Kharuk, V. I., Im, S. T., Petrov, I. A., Golyukov, A. S., Ranson, K. J., and Yagunov, M. N. (2017). Climate-induced mortality of Siberian pine and fir in the Lake Baikal Watershed, Siberia. *For. Ecol. Manage.* 384, 191–199. doi: 10.1016/j.foreco.2016.10.050

Krasensky, J., and Jonak, C. (2012). Drought, salt, and temperature stress-induced metabolic rearrangements and regulatory networks. *J. Exp. Bot.* 63 (4), 1593–1608. doi: 10.1093/jxb/err460

Kreyling, J., Wenigmann, M., Beierkuhnlein, C., and Jentsch, A. (2008). Effects of extreme weather events on plant productivity and tissue die-back are modified by community composition. *Ecosystems* 11 (5), 752–763. doi: 10.1007/s10021-008-9157-9

Kumar, A., and Sharma, K. D. (2010). Leaf water content-a simple indicator of drought tolerance in crop plants. *Indian J. Agric. Sci.* 80 (12), 1095–1097.

Lei, Y., Korpelainen, H., and Li, C. (2007). Physiological and biochemical responses to high Mn concentrations in two contrasting *Populus cathayana* populations. *Chemosphere* 68 (4), 686–694. doi: 10.1016/j.chemosphere.2007.01.066

Leng, H., Lu, M., and Wan, X. (2013). Variation in embolism occurrence and repair along thestemin drought-stressed and re-watered seedlings of a poplar clone. *Physiol. Plant* 147 (3), 329–339. doi: 10.1111/j.1399-3054.2012.01665.x

Liu, X., Zhang, H., Wang, J., Wu, X., Ma, S., Xu, Z., et al. (2019a). Increased CO_2 concentrations increasing water use efficiency and improvement PSII function

of mulberry seedling leaves under drought stress. *J. Plant Interact.* 14 (1), 213–223. doi: 10.1080/17429145.2019.1603405

Liu, X., Challabathula, D., Quan, W., and Bartels, D. (2019b). Transcriptional and metabolic changes in the desiccation tolerant plant *Craterostigma plantagineum* during recurrent exposures to dehydration. *Planta* 249 (4), 1017–1035. doi: 10.1007/s00425-018-3058-8

Loffler, B. M., and Kunze, H. (1989). Refinement of the Coomassie brilliant blue G assay for quantitative protein determination. *Anal. Biochem.* 177 (1), 101–102.

Lu, L., Tang, Y., Xie, J.-s., and Yuan, Y.-l. (2009). The role of marginal agricultural land-based mulberry planting in biomass energy production. *Renew. Energ.* 34 (7), 1789–1794. doi: 10.1016/j.renene.2008.12.017

Lu, L. H., Dong, C. H., Liu, R. F., Zhou, B., Wang, C., and Shou, H. X. (2018). Roles of soybean plasma membrane intrinsic protein GmPIP2;9 in drought tolerance and seed development. *Front. Plant Sci.* 9, 530. doi: 10.3389/fpls.2018.00530

Mafakheri, A., Siosemardeh, A., Bahramnejad, B., Struik, P. C., and Sohrabi, Y. (2011). Effect of drought stress and subsequent recovery on protein, carbohydrate contents, catalase and peroxidase activities in three chickpea (*Cicer arietinum*) cultivars. *Aust. J. Crop Sci.* 5 (10), 1255–1260.

Mahdieh, M., Mostajeran, A., Horie, T., and Katsuhara, M. (2008). Drought stress alters water relations and expression of *PIP*-type aquaporin genes in *Nicotiana tabacum* plants. *Plant Cell Physiol.* 49 (5), 801–813. doi: 10.1093/pcp/pcn054

Malone, S. L. (2017). Monitoring changes in water use efficiency to understand drought induced tree mortality. *Forests* 8 (10), 365. doi: 10.3390/f8100365

Man, D., Bao, Y.-X., Han, L. B., and Zhang, X. (2011). Drought tolerance associated with proline and hormone metabolism in two tall fescue cultivars. *Hortscience* 46 (7), 1027–1032. doi: 10.21273/hortsci.46.7.1027

Maurel, C., Verdoucq, L., Luu, D.-T., and Santoni, V. (2008). Plant aquaporins: membrane channels with multiple integrated functions. *Annu. Rev. Plant Biol.* 59, 595–624. doi: 10.1146/annurev.arplant.59.032607.092734

Maurel, C., Boursiac, Y., Luu, D. T., Santoni, V., Shahzad, Z., and Verdoucq, L. (2015). Aquaporins in plants. *Physiol. Rev.* 95 (4), 1321–1358. doi: 10.1152/physrev.00008.2015

Menezes-Silva, P. E., Sanglard, L. M. V. P., Avila, R. T., Morais, L. E., Martins, S. C. V., Nobres, P., et al. (2017). Photosynthetic and metabolic acclimation to repeated drought events play key roles in drought tolerance in coffee. *J. Exp. Bot.* 68 (15), 4309–4322. doi: 10.1093/jxb/erx211

Merlaen, B., De Keyser, E., Ding, L., Leroux, O., Chaumont, F., and Van Labeke, M. C. (2019). Physiological responses and aquaporin expression upon drought and osmotic stress in a conservative vs prodigal *Fragaria* × *ananassa* cultivar. *Plant Physiol. Biochem.* 145, 95–106. doi: 10.1016/j.plaphy.2019.10.030

Mitchell, P. J., O'Grady, A. P., Tissue, D. T., White, D. A., Ottenschlaeger, M. L., and Pinkard, E. A. (2013). Drought response strategies define the relative contributions of hydraulic dysfunction and carbohydrate depletion during tree mortality. *New Phytol.* 197 (3), 862–872. doi: 10.1111/nph.12064

Morina, F., Jovanovic, L., Mojovic, M., Vidovic, M., Pankovic, D., and Veljovic Jovanovic, S. (2010). Zinc-induced oxidative stress in *Verbascum thapsus* is caused by an accumulation of reactive oxygen species and quinhydrone in the cell wall. *Physiol. Plant* 140 (3), 209–224. doi: 10.1111/j.1399-3054.2010.01399.x

Naser, L., Kourosh, V., Bahman, K., and Reza, A. (2010). Soluble sugars and proline accumulation play a role as effective indices for drought tolerance screening in Persian walnut (*Juglans regia* L.) during germination. *Fruits* 65 (2), 97–112. doi: 10.1051/fruits/20010005

Nxele, X., Klein, A., and Ndimba, B. K. (2017). Drought and salinity stress alters ROS accumulation, water retention, and osmolyte content in sorghum plants. *S. Afr. J. Bot.* 108, 261–266. doi: 10.1016/j.sajb.2016.11.003

Palma, J. M., Sandalio, L. M., Javier Corpas, F., Romero-Puertas, M. C., McCarthy, I., and del Río, L. A. (2002). Plant proteases, protein degradation, and oxidative stress: role of peroxisomes. *Plant Physiol. Biochem.* 40 (6), 521–530. doi: 10.1016/S0981-9428(02)01404-3

Pan, G., and Lou, C. (2008). Isolation of an 1-aminocyclopropane-1-carboxylate oxidase gene from mulberry (*Morus alba* L.) and analysis of the function of this gene in plant development and stresses response. *J. Plant Physiol.* 165 (11), 1204–1213. doi: 10.1016/j.jplph.2007.02.012

Paudel, I., Cohen, S., Shlizerman, L., Jaiswal, A. K., Shaviv, A., and Sadka, A. (2017). Reductions in root hydraulic conductivity in response to clay soil and treated waste water are related to *PIPs* down-regulation in *Citrus*. *Sci. Rep.* 7 (1), 15429. doi: 10.1038/s41598-017-15762-2

Paudel, I., Gerbi, H., Zisovich, A., Sapir, G., Ben-Dor, S., Brumfeld, V., et al. (2019). Drought tolerance mechanisms and aquaporin expression of wild vs. cultivated pear tree species in the field. *Environ. Exp. Bot.* 167:103832. doi: 10.1016/j.envexpbot.2019.103832

Pawlowicz, I., and Masajada, K. (2019). Aquaporins as a link between water relations and photosynthetic pathway in abiotic stress tolerance in plants. *Gene* 687, 166–172. doi: 10.1016/j.gene.2018.11.031

Peng, C., Ma, Z., Lei, X., Zhu, Q., Chen, H., Wang, W., et al. (2011). A drought-induced pervasive increase in tree mortality across Canada's boreal forests. *Nat. Clim. Change* 1 (9), 467–471. doi: 10.1038/nclimate1293

Perrone, I., Gambino, G., Chitarra, W., Vitali, M., Pagliarani, C., Riccomagno, N., et al. (2012). The grapevine root-specific aquaporin VvPIP2;4N controls root hydraulic conductance and leaf gas exchange under well-watered conditions but not under water stress. *Plant Physiol.* 160 (2), 965–977. doi: 10.1104/pp.112.203455

Piper, F. I., and Paula, S. (2020). The role of nonstructural carbohydrates storage in forest resilience under climate change. *Curr. For. Rep.* 6 (1), 1–13. doi: 10.1007/s40725-019-00109-z

Porcel, R., Aroca, R., Azcón, R., and Ruiz-Lozano, J. M. (2006). *PIP* aquaporin gene expression in arbuscular mycorrhizal *Glycine max* and *Lactuca sativa* plants in relation to drought stress tolerance. *Plant Mol. Biol.* 60 (3), 389–404. doi: 10.1007/s11103-005-4210-y

Prasch, C. M., Ott, K. V., Bauer, H., Ache, P., Hedrich, R., and Sonnewald, U. (2015). β-amylase1 mutant Arabidopsis plants show improved drought tolerance due to reduced starch breakdown in guard cells. *J. Exp. Bot.* 66 (19), 6059–6067. doi: 10.1093/jxb/erv323

Prathap, V., Ali, K., Singh, A., Vishwakarma, C., Krishnan, V., Chinnusamy, V., et al. (2019). Starch accumulation in rice grains subjected to drought during grain filling stage. *Plant Physiol. Biochem.* 142, 440–451. doi: 10.1016/j.plaphy.2019.07.027

Reddy, K. S., Sekhar, K. M., and Reddy, A. R. (2017). Genotypic variation in tolerance to drought stress is highly coordinated with hydraulic conductivity-photosynthesis interplay and aquaporin expression in field-grown mulberry (*Morus* spp.). *Tree Physiol.* 37 (7), 926–937. doi: 10.1093/treephys/tpx051

Regier, N., Streb, S., Cocozza, C., Schaub, M., Cherubini, P., Zeeman, S. C., et al. (2009). Drought tolerance of two black poplar (*Populus nigra* L.) clones: contribution of carbohydrates and oxidative stress defence. *Plant Cell Environ.* 32 (12), 1724–1736. doi: 10.1111/j.1365-3040.2009.02030.x

Sakurai, J., Ishikawa, F., Yamaguchi, T., Uemura, M., and Maeshima, M. (2005). Identification of 33 rice aquaporin genes and analysis of their expression and function. *Plant Cell Physiol.* 46 (9), 1568–1577. doi: 10.1093/pcp/pci172

Sarkar, T., Mogili, T., and Sivaprasad, V. (2017). Improvement of abiotic stress adaptive traits in mulberry (*Morus* spp.): an update on biotechnological interventions. *3 Biotech.* 7, 214–228. doi: 10.1007/s13205-017-0829-z

Secchi, F., and Zwieniecki, M. A. (2010). Patterns of *PIP* gene expression in *Populus trichocarpa* during recovery from xylem embolism suggest a major role for the *PIP1* aquaporin subfamily as moderators of refilling process. *Plant Cell Environ.* 33 (8), 1285–1297. doi: 10.1111/j.1365-3040.2010.02147.x

Secchi, F., and Zwieniecki, M. A. (2014). Down-regulation of plasma intrinsic protein1 aquaporin in poplar trees is detrimental to recovery from embolism. *Plant Physiol.* 164 (4), 1789–1799. doi: 10.1104/pp.114.237511

Shang, C., Yang, H., Ma, S., Shen, Q., Liu, L., Hou, C., et al. (2019). Physiological and transcriptomic changes during the early phases of adventitious root formation in mulberry stem hardwood cuttings. *Int. J. Mol. Sci.* 20 (15), 3707. doi: 10.3390/ijms20153707

Sharma, S. K., and Zote, K. K. (2010). MULBERRY - A multi purpose tree species for varied climate. *Range Manage. Agrofor.* 31 (2), 97–101.

Shi, W. G., Li, H., Liu, T. X., Polle, A., Peng, C.-H., and Luo, Z. B. (2015). Exogenous abscisic acid alleviates zinc uptake and accumulation in *Populus* × *canescens* exposed to excess zinc. *Plant Cell Environ.* 38 (1), 207–223. doi: 10.1111/pce.12434

Siaut, M., Cuine, S., Cagnon, C., Fessler, B., Nguyen, M., Carrier, P., et al. (2011). Oil accumulation in the model green alga *Chlamydomonas reinhardtii*: characterization, variability between common laboratory strains and relationship with starch reserves. *BMC Biotechnol.* 11:7. doi: 10.1186/1472-6750-11-7

Singh, M., Kumar, J., Singh, S., Singh, V. P., and Prasad, S. M. (2015). Roles of osmoprotectants in improving salinity and drought tolerance in plants: a review. *Rev. Environ. Sci. Biotechnol.* 14 (3), 407–426. doi: 10.1007/s11157-015-9372-8

Soltys-Kalina, D., Plich, J., Strzelczyk-Zyta, D., Sliwka, J., and Marczewski, W. (2016). The effect of drought stress on the leaf relative water content and tuber

yield of a half-sib family of 'Katahdin'-derived potato cultivars. *Breed. Sci.* 66 (2), 328–331. doi: 10.1270/jsbbs.66.328

Sun, H. Y., Li, C., Lou, Y. F., Zhao, H. S., Yang, Y. H., Wang, S. N., et al. (2017). The bamboo aquaporin gene *PeTIP4;1-1* confers drought and salinity tolerance in transgenic Arabidopsis. *Plant Cell Rep.* 36 (4), 597–609. doi: 10.1007/s00299-017-2106-3

Šurbanovski, N., Sargent, D. J., Else, M. A., Simpson, D. W., Zhang, H., and Grant, O. M. (2013). Expression of *Fragaria vesca* PIP aquaporins in response to drought stress: PIP down-regulation correlates with the decline in substrate moisture content. *PloS One* 8 (9), e74945. doi: 10.1371/journal.pone.0074945

Szabados, L., and Savouré, A. (2010). Proline: a multifunctional amino acid. *Trends Plant Sci.* 15 (2), 89–97. doi: 10.1016/j.tplants.2009.11.009

Thalmann, M., and Santelia, D. (2017). Starch as a determinant of plant fitness under abiotic stress. *New Phytol.* 214 (3), 943–951. doi: 10.1111/nph.14491

Tsuchihira, A., Hanba, Y. T., Kato, N., Doi, T., Kawazu, T., and Maeshima, M. (2010). Effect of overexpression of radish plasma membrane aquaporins on water-use efficiency, photosynthesis and growth of *Eucalyptus* trees. *Tree Physiol.* 30 (3), 417–430. doi: 10.1093/treephys/tpp127

Vandegehuchte, M. W., Bloemen, J., Vergeynst, L. L., and Steppe, K. (2015). Woody tissue photosynthesis in trees: salve on the wounds of drought? *New Phytol.* 208 (4), 998–1002. doi: 10.1111/nph.13599

Vandeleur, R. K., Mayo, G., Shelden, M. C., Gilliham, M., Kaiser, B. N., and Tyerman, S. D. (2009). The role of plasma membrane intrinsic protein aquaporins in water transport through roots: diurnal and drought stress responses reveal different strategies between isohydric and anisohydric cultivars of grapevine. *Plant Physiol.* 149 (1), 445–460. doi: 10.1104/pp.108.128645

Velazquez-Marti, B., Sajdak, M., and Lopez-Cortes, I. (2013). Available residual biomass obtained from pruning *Morus alba* L. trees cultivated in urban forest. *Renew. Energ.* 60, 27–33. doi: 10.1016/j.renene.2013.04.001

Vijayan, K., Srivastava, P. P., Raghunath, M. K., and Saratchandra, B. (2011). Enhancement of stress tolerance in mulberry. *Sci. Hortic.* 129 (4), 511–519. doi: 10.1016/j.scienta.2011.04.018

Wang, X., Cai, H., Li, Y., Zhu, Y., Ji, W., Bai, X., et al. (2015). Ectopic overexpression of a novel *Glycine soja* stress-induced plasma membrane intrinsic protein increases sensitivity to salt and dehydration in transgenic *Arabidopsis thaliana* plants. *J. Plant Res.* 128 (1), 103–113. doi: 10.1007/s10265-014-0674-7

Wang, Y., Wu, K., Zhen, Z., Shi, Z., Yang, H., Zhang, J., et al. (2018). Combined pretreatment with NaOH and fenton of mulberry wood to enhance enzymatic digestibility for biofuels. *J. Biobased Mater. Bio.* 12 (1), 65–75. doi: 10.1166/jbmb.2018.1734

Wei, Q., Ma, Q., Ma, Z., Zhou, G., Feng, F., Le, S., et al. (2019). Genome-wide identification and characterization of sweet orange (*Citrus sinensis*) aquaporin genes and their expression in two citrus cultivars differing in drought tolerance. *Tree Genet. Genomes* 15 (2), 17. doi: 10.1007/s11295-019-1321-1

Wellburn, A. R. (1994). The spectral determiantion of chlorophyll-a and chlorophyll-b, as well as total carotenoids, using various solvents with spectrophotometers of different resolution. *J. Plant Physiol.* 144, 307–313. doi: 10.1016/S0176-1617(11)81192-2

Yemm, E. W., and Willis, A. J. (1954). The estimation of carbohydrates in plant extracts by anthrone. *Biochem. J.* 57 (3), 508–514. doi: 10.1042/bj0570508

You, J., and Chan, Z. (2015). ROS regulation during abiotic stress responses in crop plants. *Front. Plant Sci.* 6:1092. doi: 10.3389/fpls.2015.01092

Zaher-Ara, T., Boroomand, N., and Sadat-Hosseini, M. (2016). Physiological and morphological response to drought stress in seedlings of ten citrus. *Trees-Struct. Funct.* 30 (3), 985–993. doi: 10.1007/s00468-016-1372-y

Zanella, M., Borghi, G. L., Pirone, C., Thalmann, M., Pazmino, D., Costa, A., et al. (2016). β-amylase 1 (BAM1) degrades transitory starch to sustain proline biosynthesis during drought stress. *J. Exp. Bot.* 67 (6), 1819–1826. doi: 10.1093/jxb/erv572

Zhang, Z., Cao, B., Gao, S., and Xu, K. (2019). Grafting improves tomato drought tolerance through enhancing photosynthetic capacity and reducing ROS accumulation. *Protoplasma* 256 (4), 1013–1024. doi: 10.1007/s00709-019-01357-3

Zhang, H. H., Xu, N., Li, X., Han, Y., Ren, J. W., Li, M. B., et al. (2020). Effects of exogenous abscisic acid on the photosynthetic function and reactive oxygen species metabolism of tobacco leaves under drought stress. *Photosynthetica* 58 (2), 585–594. doi: 10.32615/ps.2019.143

Zhou, L., Zhou, J., Xiong, Y., Liu, C., Wang, J., Wang, G., et al. (2019). Overexpression of a maize plasma membrane intrinsic protein ZmPIP1;1 confers drought and salt tolerance in Arabidopsis. *PloS One* 14 (6), e0198639. doi: 10.1371/journal.pone.0218234

Zhou, R., Kong, L., Yu, X., Ottosen, C.-O., Zhao, T., Jiang, F., et al. (2019). Oxidative damage and antioxidant mechanism in tomatoes responding to drought and heat stress. *Acta Physiol. Plant* 41 (2), 20. doi: 10.1007/s11738-019-2805-1

Conflict of Interest: The authors declare that the research was conducted in the absence of any commercial or financial relationships that could be construed as a potential conflict of interest.

Copyright © 2020 Cao, Shen, Ma, Liu and Cheng. This is an open-access article distributed under the terms of the Creative Commons Attribution License (CC BY). The use, distribution or reproduction in other forums is permitted, provided the original author(s) and the copyright owner(s) are credited and that the original publication in this journal is cited, in accordance with accepted academic practice. No use, distribution or reproduction is permitted which does not comply with these terms.

frontiers in Plant Science

ORIGINAL RESEARCH
published: 15 October 2020
doi: 10.3389/fpls.2020.568693

Tolerance of Combined Drought and Heat Stress Is Associated With Transpiration Maintenance and Water Soluble Carbohydrates in Wheat Grains

Abdeljalil El Habti[1], Delphine Fleury[1], Nathaniel Jewell[1,2], Trevor Garnett[1,2†] and Penny J. Tricker[1]*

[1] School of Agriculture, Food and Wine, The University of Adelaide, Adelaide, SA, Australia, [2] Australian Plant Phenomics Facility, The Plant Accelerator, School of Agriculture, Food & Wine, The University of Adelaide, Adelaide, SA, Australia

OPEN ACCESS

Edited by:
Raul Antonio Sperotto, Universidade do Vale do Taquari (Univates), Brazil

Reviewed by:
Dejan Bogdan Dejan, Maize Research Institute Zemun Polje, Serbia
Alejandro Del Pozo, University of Talca, Chile
Yin-Gang Hu, Northwest A&F University, China

***Correspondence:**
Abdeljalil El Habti
abdeljalil.elhabti@adelaide.edu.au

†Present address:
Trevor Garnett, Grains Research and Development Corporation, Dulwich, SA, Australia

Specialty section:
This article was submitted to Plant Abiotic Stress, a section of the journal Frontiers in Plant Science

Received: *01 June 2020*
Accepted: *22 September 2020*
Published: *15 October 2020*

Citation:
El Habti A, Fleury D, Jewell N, Garnett T and Tricker PJ (2020) Tolerance of Combined Drought and Heat Stress Is Associated With Transpiration Maintenance and Water Soluble Carbohydrates in Wheat Grains. Front. Plant Sci. 11:568693. doi: 10.3389/fpls.2020.568693

Wheat (*Triticum aestivum L.*) production is increasingly challenged by simultaneous drought and heatwaves. We assessed the effect of both stresses combined on whole plant water use and carbohydrate partitioning in eight bread wheat genotypes that showed contrasting tolerance. Plant water use was monitored throughout growth, and water-soluble carbohydrates (WSC) and starch were measured following a 3-day heat treatment during drought. Final grain yield was increasingly associated with aboveground biomass and total water use with increasing stress intensity. Combined drought and heat stress immediately reduced daily water use in some genotypes and altered transpiration response to vapor pressure deficit during grain filling, compared to drought only. In grains, glucose and fructose concentrations measured 12 days after anthesis explained 43 and 40% of variation in final grain weight in the main spike, respectively. Starch concentrations in grains offset the reduction in WSC following drought or combined drought and heat stress in some genotypes, while in other genotypes both stresses altered the balance between WSC and starch concentrations. WSC were predominantly allocated to the spike in modern Australian varieties (28–50% of total WSC in the main stem), whereas the stem contained most WSC in older genotypes (67–87%). Drought and combined drought and heat stress increased WSC partitioning to the spike in older genotypes but not in the modern varieties. Ability to maintain transpiration, especially following combined drought and heat stress, appears essential for maintaining wheat productivity.

Keywords: crops, water use, carbohydrate partitioning, *Triticum aestivum*, drought and heat stress

INTRODUCTION

Recent decades have witnessed severe drought and heatwaves worldwide, including in major wheat producing regions such as India, the United States, Russia, Western Europe, and Australia. These climatic conditions have a significant impact on global wheat production, with dramatic social and economic consequences (Van Dijk et al., 2013). Current climate projections predict drought and heatwaves will become more common and more intense in the future (Rosenzweig et al., 2014). One way to limit the impact of weather variability on productivity is to develop wheat varieties

better adapted to the changing climate. This can be assisted by understanding the mechanisms underlying plants' responses to complex stresses so as to identify the traits that characterize stress tolerant varieties for breeding. A small number of studies document the impact of combined drought and high temperature on wheat productivity and biological processes, especially during the reproductive developmental stage. The effect of combined stresses is more detrimental than the effect of an individual stress (Mittler, 2006). Both drought and high temperatures reduce expansive growth, accelerate flowering and shorten grain filling duration, resulting in a low grain set, size and weight (Asana and Williams, 1965; Pradhan et al., 2012). In combination, drought and high temperature impair the photosynthetic system, reduce stomatal conductance and gas exchange, and disrupt plants' water relations (Machado and Paulsen, 2001; Shah and Paulsen, 2003). These additive alterations of morphological, physiological and cellular processes result in severe reductions in final grain weight. Although the major impact of combined drought and high temperature on wheat productivity is well-described, there is scarce information on the mechanisms that determine the ability to maintain grain weight in these unfavorable environments (also called tolerance).

Wheat harvested grain mass consists of 85% carbohydrates, of which ∼80% is starch (Stone and Morell, 2009). During grain filling, water-soluble carbohydrates (WSC) are delivered to grains either from current photosynthesis in photosynthesizing organs or from remobilization of WSC stored during the vegetative stage (Borrell et al., 1989; Schnyder, 1993). Abiotic stress after anthesis can limit gas exchange and damage the photosynthetic system, in which case stored carbohydrates become a major source of carbon for grain filling (Blum, 1998). In addition to the contribution from stem reserves, spike organs, especially awns, are thought to contribute to the grain filling process due to their active photosynthesis, especially in dry environments (Evans et al., 1972; Rebetzke et al., 2016). Carbohydrate synthesis and transport are closely related to water movements in plants. Open stomata are necessary for carbon capture and plants trade-off between maximizing carbon assimilation and limiting water loss through transpiration under adverse conditions such as drought. Carbohydrate transport via the phloem and distribution throughout the plant rely on water exchange with adjacent xylem (Hölttä et al., 2009), and the impact of water shortage on xylem water transport also impairs phloem function (Sevanto, 2018). Soluble carbohydrates also play an important role during drought by acting as compatible osmolytes to maintain cell turgor and favorable plant water status, thereby sustaining biological processes and soil water uptake (Blum, 2017). Maintaining plant hydration and enhancing carbohydrate remobilization to grains are considered key factors for crop productivity in limiting environments (Blum, 2006), and the interplay between plant water relations and carbohydrate metabolism and distribution highlights the importance of studying both mechanisms together.

Wheat genetic diversity is a valuable resource for the identification of new stress-adaptive mechanisms to environmental stress (Lopes et al., 2015). In this work, we describe the impact of combined drought and heat stress on whole plant water use and carbohydrate partitioning during grain filling in diverse wheat genotypes. We hypothesized that the combination of both stresses would alter plant water use and carbohydrate partitioning in the stem and spike, and that WSC availability would be a limiting factor for optimal grain weight under combined drought and heat stress.

MATERIALS AND METHODS

Experiment 1

Genetic Material and Growth Conditions

Eight bread wheat (*Triticum aestivum L.*) genotypes were selected from a diverse panel of 534 wheat accessions from 44 countries described in Garcia et al. (2019). The diversity panel was previously subjected to post-anthesis drought and combined drought and heat stress in a pilot experiment and evaluated for plant total grain weight (yield) at harvest (data not shown). The selected genotypes contrasted for grain weight following drought or combined drought and heat stress, and consisted of three Australian older varieties (Currawa, Koda, Mendos), three Australian modern commercial varieties (Frame, Young, Gladius), one synthetic line from CIMMYT (Synthetic W7984) and one landrace from Ethiopia (Odessa ES19565) (**Supplementary Table S1**). The selected genotypes were released between 1912 and 2007. In this study, Frame, Gladius, and Young were considered as modern genotypes; the remaining genotypes were considered as older genotypes. Single seeds were sown in 40 cm × 15 cm round pots containing 8.2 kg of a mixture of 1:1:1 (v/v/v) clay/loam:UC Davis mix:cocopeat mix. Seeds were sown on 11 August 2016, late winter in the southern hemisphere. From 13 days after sowing (DAS) until the end of the experiment, plants were grown in a glasshouse (34°58′17.8″ S, 138°38′23.4″ E) on a gravimetric platform (Droughtspotter, Phenospex, Heerlen, Netherlands) that automatically irrigated to the pre-defined pot weight and recorded weights and water added (details in Water use and transpiration below). The 168 pots (6–7 pots per genotype and per treatment) were randomized to 168 Droughtspotter cells using a factorial, randomized complete block design, such that each block comprised one replicate of each Genotype–Treatment combination, except in three blocks that contained one empty pot each to estimate soil evaporation. The three treatment groups comprised well-watered (WW), drought (D) and combined drought & heat stress (D&H). In particular, all plants were well-watered [soil water potential = −0.3 MPa, gravimetric soil water content = 20% (g/g)] and grown in temperate conditions (22°C/15°C day/night) until anthesis of the main spike. Anthesis date was the first day anthers were observed on the main spike. One third of the plants (WW) were maintained in well-watered, cool conditions until harvest. The remaining plants (D, D&H) were subject to a 6 days drought treatment [soil water potential = −0.6 MPa, gravimetric soil water content = 12% (g/g)] starting 3 days after anthesis on the main spike of each individual; this was followed, in half of these plants (D&H), by a 3 days heat treatment at 37°C/27°C day/night (n = 7 for each accession in each treatment). Heat treatment was imposed in an adjacent glasshouse where plants were watered to weight manually. Drought was maintained until

harvest in the D and D&H groups. LED lights (400 $\mu E/m^2/s$) were installed above plants to minimize variations due to light intensity. A graphical representation of the experimental design is shown in **Supplementary Figure S1**. Environmental data are shown in **Supplementary Figure S2**.

Water Use and Transpiration

The gravimetric platform was configured to weigh each pot at regular time intervals. All weight and water values were automatically logged and water usage estimated hourly for each pot throughout the experiment. During the heat treatment in an adjacent glasshouse, plants were watered to weight manually at similar times as the drought treatment and weights recorded. Pots were watered at least six times daily (6 and 10 am, 12, 2, 4, and 10 pm). Pots containing soil only were weighed to estimate non-transpirational water loss under WW, D, and D&H treatments. The water usage is a combination of plant transpiration and evaporation from the soil surface, which was negligible in all treatments as estimated from pots containing soil only.

Carbohydrates Quantification

The main stem and spike of three plants per genotype per treatment were sampled 12 days after anthesis (DAA), i.e., 1 day after heat treatment in drought and heat stressed plants, and stored at −80°C for further analysis. Measurements were conducted separately on the stem, flag leaf sheath, covered peduncle, exposed peduncle, rachis, grains, palea, lemma, awns, and glumes. Dry weight was obtained by weighing the samples after freeze-drying. Total WSC in each tissue were determined using the anthrone method (Yemm and Willis, 1954) with some modifications: soluble sugars were extracted with 80% ethanol at 80°C for 1 h, then extracted with distilled water at 60°C for 1 h. The extraction was repeated as many times as needed until no coloration was observed. Supernatants were combined in the same tube for colorimetric assay. Starch content in grains was measured using the Megazyme Total Starch HK (K-TSHK 08/18, Megazyme, Bray, Ireland) according to the manufacturer's instructions. Individual WSC measurements in grains were performed in four genotypes (Frame, Odessa, Synthetic, and Young). As plant morphology and grain number varied greatly between the genotypes, WSC and starch contents were expressed as g/g DW to allow for comparison between genotypes. Glucose, fructose and sucrose were analyzed in the same samples used for total WSC analysis using high performance anion exchange chromatography with pulsed amperometric detection HPAEC-PAD (Dionex ICS-5000; Thermo Fisher Scientific, Sunnyvale, United States). Separations were performed at 30°C and the flow rate was 0.5 mL/min. A 25 µL sample was injected on a Guard CarboPac PA20 (3 mm × 30 mm) in series with an analytical CarboPac PA20 (3 mm × 150 mm). The elution program consisted of 0.1M NaOH from 0 to 2 min, followed by increasing 1M sodium acetate concentration up to 20% from 2 min to 35 min, followed by increasing 1M sodium acetate concentration up to 100% from 35 to 36.5 min, a steady concentration from 36.5 to 37.5 min, followed by a 0.1M NaOH wash until return to equilibrium. Glucose, fructose and sucrose were identified based on glucose, fructose and sucrose standards. Fructans were identified by acid hydrolysis. Two WSC samples from the stem and awns were incubated with 0.2M trifluoroacetic acid (TFA) at 80°C for 30 min together with untreated samples. Treated and untreated samples were analyzed using HPAEC-PAD as described above. Glucose, fructose, and sucrose were quantified using external standards and peak areas determined using the instrument's Chromeleon software. Fructans were quantified using peak areas.

Harvest Data at Maturity

Four plants per genotype per treatment were harvested at maturity to measure grain yield components. Total grain weight was determined for the main spike and for the whole plant. Seed number was counted using an automatic seed counter (Contador, Pfeuffer GmbH, Germany). Biomass weight included tillers, leaves and spikes but excluded grains. Plant height was measured from the base of the main stem to the top of the highest spike excluding awns. Biomass water use efficiency (bWUE) was calculated as the ratio of total aboveground biomass to total water use per plant. Grain water use efficiency (gWUE) was calculated as the ratio of total grain weight to total water use per plant.

Experiment 2

In order to test the reproducibility of water use results, the 2016 experiment described above was replicated in an independent experiment with four genotypes (Currawa, Synthetic W7984, Mendos, and Young) in 2017 with the same settings used for plant growth and treatments, except that plants were sown 1 month earlier. Plant water use was recorded using the gravimetric platform and three plants per genotype and per treatment were harvested at maturity and measured as before.

Statistical Analyses

The data were analyzed by two-way ANOVA with genotype and treatment as fixed factors for all measured yield component and biomass traits and for the analysis of carbohydrates within each tissue. Treatment means within genotypes were compared using Tukey's HSD (honestly significant difference) test at $p = < 0.1$. Statistical analyses (ANOVA, Tukey's tests, regression analyses) and graphical representation were performed using R software (version 3.4.4, R Core Team, 2019) and ASReml-R (Butler et al., 2009).

The recorded water use data were used to identify genotype and treatment effects on hourly transpiration rate (TR, mL/hr) and specific transpiration rate (STR, mL/hr/g biomass), with the proviso that soil evaporation and plant transpiration water losses were indistinguishable.

VPD was computed hourly from vapor capacity (VC, kPa) using the following formula:

$$VC = 0.611 \exp(17.62\ T/(T + 243))$$

$$VPD = (1 - RH/100)\ VC$$

where T is temperature and RH is relative humidity. It was further decided to model TR or STR (henceforth denoted y) as a simple linear function of VPD with (a) genotype × treatment interaction

incorporated into the VPD slope and intercept parameters, and (b) error variance modeled as a function of treatment (but not genotype). The resulting model comprises 2 × 8 × 3 = 48 fixed effects of interest (i.e., slope and intercept parameters) and 3 variance estimates, represented symbolically as

$$y_{ij} = Pot_i + spatial_i + Gen_i \times Tr_i + VPD_j \times Gen_i \times Tr_i + \sigma^2_{Tr}$$

where (a) *yij* is the TR or STR value for Pot *i* on hour *j*, (b) Pot*i* is a random-effects term for variation between pots, and (c) spatial comprises fixed-effects terms for spatial variation within the greenhouse. The model was fitted separately to each of TR and STR using the R package ASReml-R4 (Butler et al., 2017). Analysis of the effect of 3 days heat stress on transpiration was narrowed to 30 days [0 to 30 days after treatment (DAT)] after heat stress, while all genotypes were still using water in the well-watered treatment, to limit the effects of intrinsic differences of grain-filling duration on transpiration and distinguish the effects of treatments.

RESULTS

Combined Drought and Heat Stress Differentially Reduced Total Grain Weight at Harvest

The effect of drought and combined drought and heat stress (D&H) on total grain weight per plant at harvest (per plant yield) depended on genotype (**Table 1**). Drought reduced per plant yield in Currawa, Odessa, Frame, Young, and Gladius (**Figure 1A**). Interaction of drought with high temperature further reduced per plant yield in Odessa, Mendos, and Young. In contrast, heat stress did not exacerbate the effect of drought on yield in Currawa, Frame, and Gladius. Per plant yield in Koda was not sensitive to either drought or D&H stress. Overall, the combination of drought and high temperature was more detrimental to per plant yield in some genotypes, but not all (**Figure 1A**). In order to assess the impact of drought and combined D&H on grain filling, grain dry weight in the main spike was measured at 12 days after anthesis (DAA) and at harvest. At 12 DAA, total grain weight in the main spike was different among genotypes (**Figure 1B**) but there was no effect of the treatments or genotype × treatment interaction (**Table 1**). At harvest, total grain weight in the main spike was reduced by drought in Gladius, and reduced by combined D&H in Odessa, Koda, Mendos, and Frame (**Figure 1C**). There was no effect of drought or combined D&H on the main spike total grain weight at harvest in Currawa, Synthetic W7984 and Young.

TABLE 1 | Analysis of variance (ANOVA) showing the statistical significance of the traits measured for genotype, treatment and interaction between genotype and treatment.

Traits	Genotype	Treatment	Interaction
Total grain weight per plant	***	***	**
Total grain weight in the main spike at 12 DAA	***	ns	ns
Total grain weight in the main spike at harvest	***	***	ns
Total grain weight in tillers	***	***	*
Grain number per plant	***	***	**
Grain number in the main spike	***	ns	ns
Grain number in tillers	***	***	*
Aboveground biomass (excluding grains)	***	***	ns
Number of spikes	***	ns	ns
Plant height	***	ns	ns
Harvest index	***	***	***
Single grain weight	***	***	**
Total water use	***	***	ns
Water use after treatment	**	**	ns
biomass WUE	***	***	*
grain WUE	***	***	***
WSC concentration in grains	***	***	**
Starch concentration in grains	***	***	***
Total carbohydrates concentration in grains	***	**	*

*$p < 0.1$; **$p < 0.01$; ***$p < 0.001$. ns, not significant.*

The Correlation Between Aboveground Biomass, Water Use and Plant Yield Increased With Increasing Stress Intensity

There was a significant interaction between genotype and treatment for both harvest index (grain weight/biomass) and water productivity (grain weight/water used) (**Table 1**). Plant yield was associated with aboveground vegetative biomass and total water use to different degrees depending on treatments (**Figure 2**). Total grain weight was linearly related to aboveground biomass and total water used by the plant throughout the experiment; these coefficients increased with stress intensity from $r^2 = 0.2$ and $r^2 = 0.31$ in well-watered conditions (WW), to $r^2 = 0.35$ and $r^2 = 0.56$ under drought, and $r^2 = 0.46$ and $r^2 = 0.67$ under combined D&H, respectively (**Figure 2C**). This dependence of plant yield on total water use and interaction with treatment was confirmed in a repeated experiment (**Supplementary Figure S3**). During the 3 days heat treatment, plants generally used similar amounts of water as compared to well-watered conditions (**Figure 3**), although soil water potential was halved. When comparing modern Australian genotypes (Frame, Young, and Gladius) to older genotypes (Currawa, Odessa, Koda, Mendos, and Synthetic W7984), the relationship between per plant yield and aboveground biomass was similar in both groups ($r^2 = 0.48$ and $r^2 = 0.46$, $p < 0.001$, respectively). Despite this, the slope of the regression for modern varieties, i.e., harvest index, was higher compared to older genotypes ($a = 0.8$ and $a = 0.3$, respectively, **Figure 2A**). The higher slope for modern genotypes was explained by the lower biomass required to produce similar grain weight compared to older genotypes under well-watered conditions and reflects the high harvest index of modern genotypes in favorable conditions. The dependence of plant yield on total water used was higher in modern genotypes

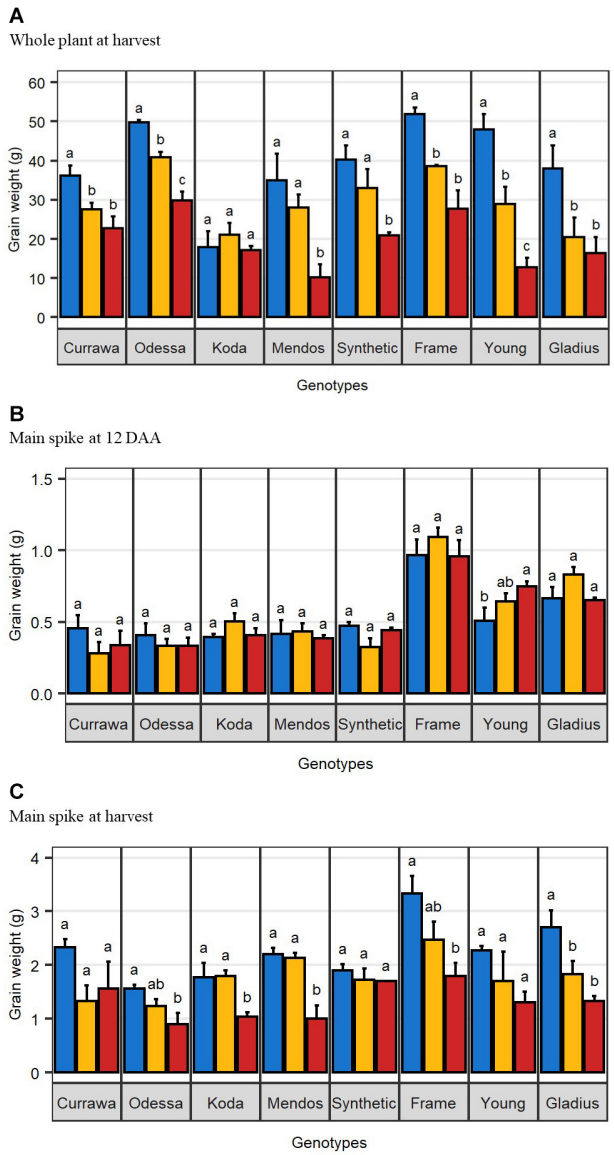
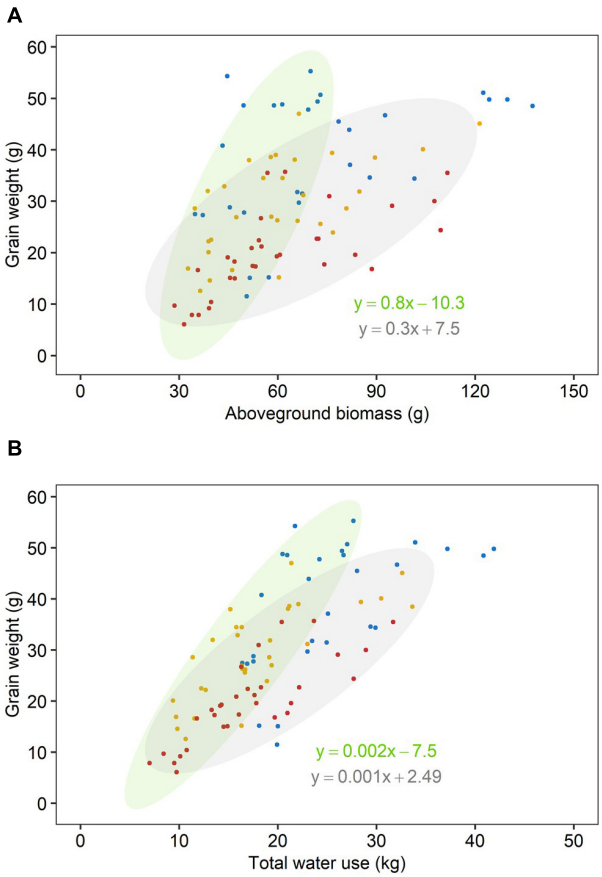


FIGURE 1 | Combined drought and heat stress differentially reduced final grain weight. **(A)** Mean total grain weight per plant at harvest (n = 4). **(B)** Mean total grain weight in the main spike at 12 days after anthesis (n = 3). **(C)** Mean total grain weight in the main spike at harvest (n = 4). Error bars are standard error. Letters indicate the results of Tukey's test comparing treatment effect within each genotype ($p < 0.1$). Plants were grown under well-watered conditions (blue), drought (orange), or combined drought and heat (red).



C

	Aboveground biomass		Total water use	
	r^2	p	r^2	p
Well-watered	0.2	*	0.31	**
Drought	0.35	*	0.56	***
Drought and heat	0.46	*	0.67	***
Modern genotypes	0.48	***	0.8	***
Older genotypes	0.46	***	0.63	***

* p < 0.1; ** p < 0.01; *** p < 0.001

FIGURE 2 | Aboveground biomass and water use explained more of the variation in grain weight under increasing stress intensity than in well-watered conditions. Relationships between final grain weight per plant and **(A)** final aboveground biomass excluding grains, **(B)** total water use. Each point represents one plant, grown under well-watered conditions (blue), drought (orange) or combined drought and heat stress (red). Ellipses circle modern genotypes (in green) and older genotypes (in gray). Linear regression equations correspond to linear regression for modern genotypes (in green) and older genotypes (in gray). **(C)** Table shows r^2 and p-value of linear regressions ($^*p < 0.1$, $^{**}p < 0.01$, $^{***}p < 0.001$) for each treatment (well-watered, drought, combined drought, and heat stress) and genotype group (modern, older).

compared to older genotypes (r^2 = 0.80 and r^2 = 0.63, $p < 0.001$, respectively).

Although in modern genotypes, spikes were longer and grain number was higher compared to older genotypes in all treatments, single grain weight was higher in older genotypes (**Figure 4A**). The difference in HI between modern and older types was reduced by the drought treatment and disappeared in the combined drought and heat treatment (**Figure 4B**). This was due to a greater reduction in single grain weight from developing tillers, post-anthesis of the main spike, in more modern types that were more sensitive to reduction in biomass and particularly water use (**Figure 2C**). There was little genotypic difference in biomass water-use efficiency (bWUE, **Figure 4C**) as most of biomass was produced before treatment in WW conditions and water use was highly dependent on biomass (**Supplementary Figure S4**). bWUE averaged 4.4 mg/g water in WW conditions, 5.1 mg/g water under drought and 4.7 mg/g water under

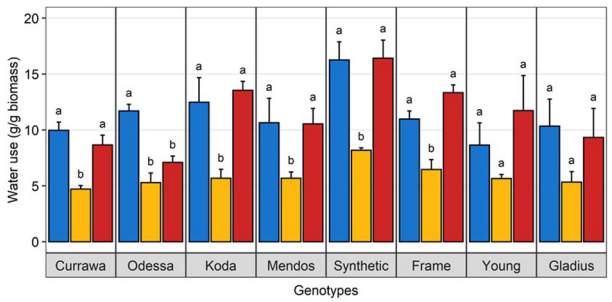


FIGURE 3 | Water use under heat stress was similar to well-watered plants. Water use per plant during the 3-day heat treatment, normalized to aboveground biomass. Plants grown in well-watered conditions (blue), drought (orange) or combined drought and heat stress (blue). Values are means and standard error of four replicates (n = 4). Data were subjected to two-way ANOVA. Letters indicate the results of Tukey's test comparing treatment effect within each genotype ($p < 0.1$).

combined D&H. In contrast, there was high genotypic variation in grain water-use efficiency (gWUE) under WW conditions, modern genotypes having the highest gWUE (**Figure 4D**). The difference in gWUE was reduced by the drought treatment and disappeared in the combined drought and heat treatment.

Combined Drought and Heat Stress Differentially Reduced Transpiration Response to Vapor Pressure Deficit

As total water use was strongly dependent on plant biomass, water use was normalized to the final aboveground biomass and expressed as unit of water per unit of biomass to allow for comparison between plants. Water use differed between genotypes following combined D&H when all treated plants (D and D&H replicates) were in the same droughted conditions (**Figure 5A**). Interaction of drought and 3 days high temperature reduced daily water use in Odessa, Koda, Mendos, and Young for the subsequent 30 days, whereas daily water use following combined D&H was similar to D alone in Currawa, Frame, Synthetic W7984, and Gladius. Plant water use is the summation of transpiration, which is driven by changes in vapor pressure deficit (VPD). Transpiration response to VPD was differentially altered by the 3 day high temperature treatment depending on genotype over the same grain-filling period when D and D&H plants were in the same droughted conditions (**Figure 5B**). For both transpiration rate (TR) and specific transpiration rate (STR), statistical significance was confirmed ($p < 0.05$) for the genotype × treatment interaction component of the VPD slope parameter. That is, the VPD effect on transpiration exhibited genotype × treatment interaction both before and after normalization to final aboveground biomass. Heat stress reduced subsequent transpiration rate at VPD > 0.5 kPa in Odessa, at VPD > 0.7 kPa in Young and at VPD > 1.0 kPa in Koda and Mendos (**Figure 5B**). In contrast, transpiration response to VPD was not altered following combined D&H stress in Currawa, Frame, Synthetic W7984, and Gladius. Transpiration response to VPD was affected in the same genotypes where daily water use was reduced by combined D&H. During drought, Young had the highest transpiration rate at VPD > 1.5 kPa whereas Currawa and Frame had the lowest transpiration rates. Following combined D&H, Synthetic W7984 had the highest transpiration rate at VPD > 1.5 kPa whereas Currawa and Odessa had the lowest transpiration rates (**Supplementary Figure S5B**).

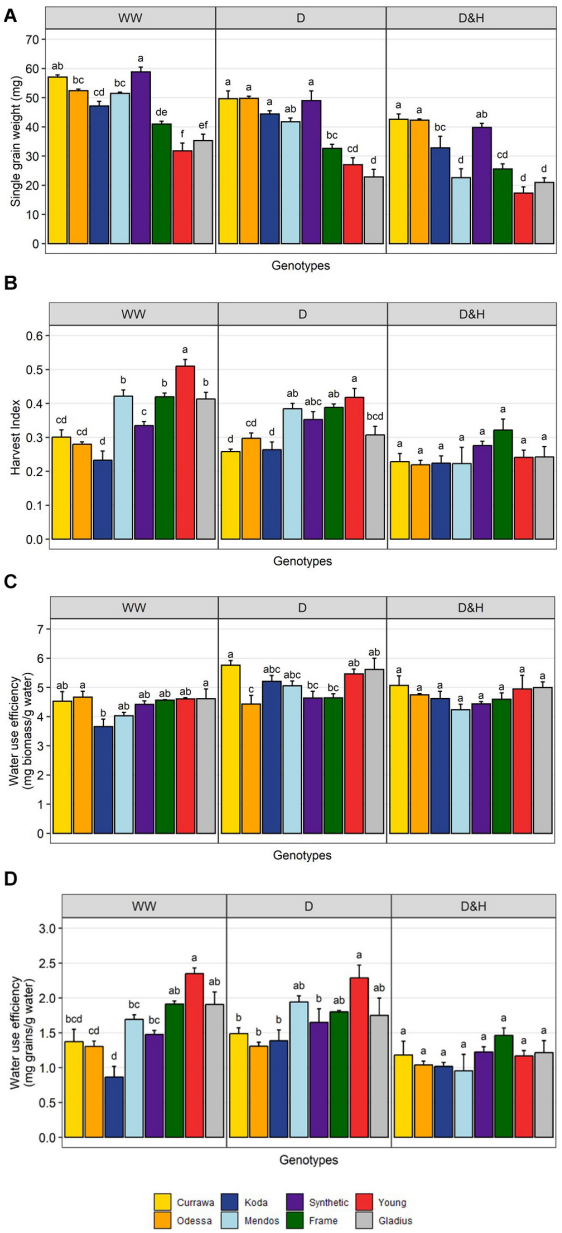


FIGURE 4 | Reduction in yield per plant was due to reduction in grain weight post-anthesis. Genotypic differences in single grain weight **(A)**, harvest index **(B)**, biomass water-use efficiency **(C)**, and grain water-use efficiency **(D)**. Plants grown in well-watered conditions (WW), drought (D), or combined drought and heat stress (D&H). Values are means and standard error of four replicates (n = 4). Values represent average per plant. Data were subjected to two-way ANOVA. Letters indicate the results of Tukey's test comparing genotype effect within each treatment ($p < 0.1$).

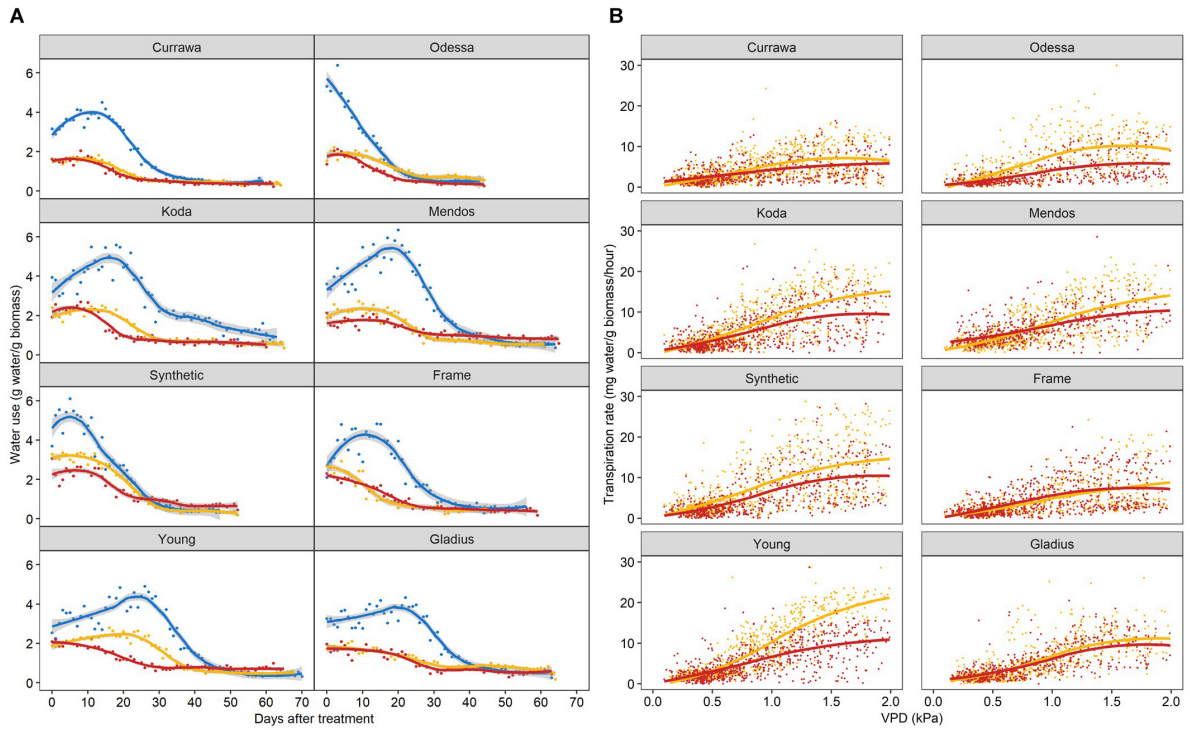


FIGURE 5 | Interaction of high temperature and drought differentially reduced daily water use and transpiration response to vapor pressure deficit. **(A)** Daily water use per plant estimated as total irrigation per day, normalized to aboveground biomass. Plants grown in well-watered conditions (blue), drought (orange), or in drought following 3-day heat stress (red). 0 DAT is the first day post-heat treatment (12 days after anthesis). Trend lines are loess regressions. Values are means of four replicates (n = 4). The confidence interval (0.95) is displayed around smoothed regressions in gray. **(B)** Hourly transpiration rate response to VPD normalized to aboveground biomass. Plants grown in drought (orange) or in drought following 3-day heat stress (red). Graphs include data from 0 to 30 DAT. Trend lines are smooth regression lines.

Drought and Combined Drought and Heat Stress Altered WSC and Starch Balance in Grains

In order to quantify WSC availability for starch synthesis, WSC and starch concentrations were measured in grains 12 DAA, immediately following D&H treatments. There was a significant interaction between genotype and treatment for WSC and starch concentrations in grains (**Table 1**). Drought significantly reduced WSC concentration in grains in the Synthetic type and heat stress did not exacerbate the effect of drought (**Figure 6**). WSC concentration in grains was reduced by combined D&H in Odessa and Koda compared to WW and was specifically reduced by combined D&H in Currawa, Young, and Gladius. Starch concentrations offset the reduction in WSC concentration in Currawa, Odessa and Synthetic W7984, resulting in a similar total non-structural carbohydrates (NSC) concentration in grains in all conditions. The balance between WSC and starch concentrations was altered in Koda, Young, and Gladius (**Figure 6**). Total NSC concentration was reduced under drought in Koda and Young, and combined D&H reduced total NSC in Gladius. There was no significant effect of drought and combined D&H on total NSC concentration in grains in Currawa, Odessa, Mendos, and Frame. Overall, there was a significant interaction between genotypes and treatments for total carbohydrates concentration in grains (**Table 1**) that was mainly driven by interaction between genotypes and treatments for WSC concentration.

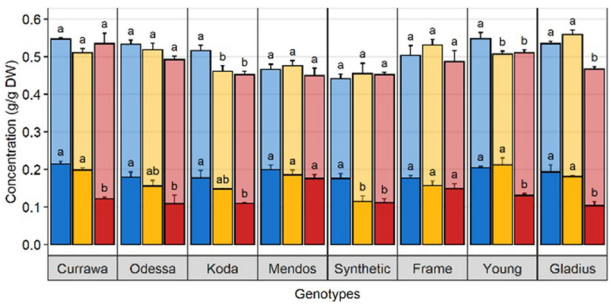


FIGURE 6 | Drought and combined drought and heat stress altered WSC and starch balance in grains at 12 DAA. Water-soluble carbohydrates (solid) and starch (transparent) concentration in grains at 12 DAA from plants grown under well-watered conditions (blue), drought (orange), or combined drought and heat stress (red). The sum of WSC and starch concentrations constitutes the non-structural carbohydrate (NSC). Values are means of three replicates (± SE). Letters (top: NSC, bottom: WSC) indicate the results of Tukey's test comparing treatment effects within each genotype ($p < 0.1$).

TABLE 2 | r^2 and *p*-values of linear regressions between individual carbohydrates' concentrations in different plant organs at 12 DAA and final grain weight per plant, in modern or older genotypes.

		Modern		Old	
Carbohydrate	**Plant tissue**	r^2	*p*	r^2	*p*
WSC	Grains	0.13	0.33	0.41	**0.01**
	Awns	0.06	0.54	0.85	**0.01***
	Stem	0.53	**0.03**	0.1	0.26
Glucose	Grains	0.47	0.13	0.00	0.9
	Awns	0.14	0.33	0.84	**0.1**
	Stem	0.34	**0.1**	0.01	0.73
Fructose	Grains	0.54	**0.09**	0.06	0.63
	Awns	0.11	0.39	0.81	**0.01**
	Stem	0.08	0.45	0.31	**0.03**
Sucrose	Grains	0.44	0.15	0.05	0.66
	Awns	0.07	0.49	0.67	**0.05**
	Stem	0.56	**0.02**	0.13	0.18
Fructan1	Grains	0.04	0.7	0.08	0.6
	Awns	0.47	**0.04**	0.35	0.22
	Stem	0.17	0.27	0.1	0.25
Fructan2	Grains	0.47	0.13	0.24	0.32
	Awns	0.05	0.56	0.44	0.15
	Stem	0.73	**0.003**	0.23	**0.07**
Starch	Grains	0.08	0.46	0.14	0.18

**Only two older genotypes were awned. In bold: $p < 0.1$.*

The Relationships Between WSC Concentrations and Plant Yield Depended on Plant Organ, Individual Carbohydrate and the Date of Release of the Variety

The relationship between WSC concentration at 12 DAA and plant yield depended on tissue and date of variety release. Total WSC concentration in grains at 12 DAA was positively related with plant yield in older genotypes ($r^2 = 0.41$) whereas there was no relationship in modern genotypes ($r^2 = 0.13$) (**Table 2** and **Figure 7A**). Similarly, total WSC concentration in awns at 12 DAA was positively related with plant yield in the two, awned older genotypes ($r^2 = 0.85$) whereas there was no relationship in modern genotypes ($r^2 = 0.06$, **Figure 7B**). In contrast, total WSC concentration in the stem at 12 DAA was positively related with per plant yield in modern genotypes ($r^2 = 0.53$) whereas there was no significant regression observed in older genotypes ($r^2 = 0.1$) (**Table 2** and **Figure 7C**). To determine whether individual WSC varied similarly to total WSC, we quantified glucose, fructose and sucrose concentrations in the stem, awns and grains. In grains, glucose and fructose concentrations were positively related with total grain weight at harvest ($r^2 = 0.43$ and 0.40, respectively – **Figure 7A**). Sucrose concentrations at 12 DAA were low compared to glucose and fructose concentrations (**Figure 7A**). There was no relationship between starch concentrations at 12 DAA and plant yield (**Figure 7A**). In awns, glucose, fructose and sucrose concentrations at 12 DAA were each negatively related with plant yield in the two, awned older genotypes ($r^2 = 0.84$, 0.81, and 0.67, respectively) but there were no significant relationships between these sugars and plant yield in more modern types (**Table 2** and **Figure 7B**). In the stem, a similar contrast was observed for individual WSC between older and modern varieties as was observed for total WSC (**Table 2** and **Figure 7C**). Glucose and sucrose concentrations in the stem at 12 DAA were positively related with plant yield in modern varieties ($r^2 = 0.34$ and 0.56, respectively). Stem fructose concentrations at 12 DAA were negatively related to plant yield in older varieties ($r^2 = 0.31$). Two (unknown) fructans also appeared important for plant yield in modern varieties: fructan 1 in awns ($r^2 = 0.47$) and fructan 2 in the stem ($r^2 = 0.73$). In contrast with other sugars in the awns, fructan 1 concentrations at 12 DAA and yield per plant were positively related.

Combined Drought and Heat Stress Increased WSC Partitioning to the Spike in Old Genotypes, but Not in Modern Varieties

Water-soluble carbohydrates were quantified in the main stem and the spike tissues following all treatments 12 DAA, i.e., immediately following the heat stress for the D&H replicates. There was a clear contrast between older genotypes (Currawa, Odessa, Koda, Mendos, Synthetic W7984) and more modern varieties (Frame, Young, Gladius) for WSC partitioning (defined as the percentage of the total WSC content) in stem parts compared with the main spike (**Figure 8**). In well-watered conditions, stem parts contained 67–87% of total WSC in older wheat genotypes compared to 28–50% in modern varieties. The spike tissues (excluding grains) contained 49–71% of total WSC in modern varieties, whereas WSC in the spike were 12–33% of total WSC in older genotypes. Drought and combined D&H differentially affected WSC distribution in the main stem and spike depending on genotype (**Figure 8**). Drought significantly increased WSC partitioning into the spike in Currawa and Odessa and reduced the WSC fraction in the stem in Frame (**Supplementary Table S2**). Combined D&H significantly increased WSC partitioning into the spike in older genotypes, whereas there was no change in WSC partitioning in modern varieties in both treatments. Changes in WSC allocation to the spike following combined drought and heat stress did not affect WSC partitioning to grains, except in the Synthetic genotype where WSC partitioning to grains was significantly increased by combined D&H compared to drought only.

DISCUSSION

Higher Water Use and Responsiveness to Evaporative Demand Are Indicators of Higher Yield Under Combined Drought and Heat Stress

In this study, the impact of drought and combined D&H on total grain weight at harvest was assessed in eight diverse wheat

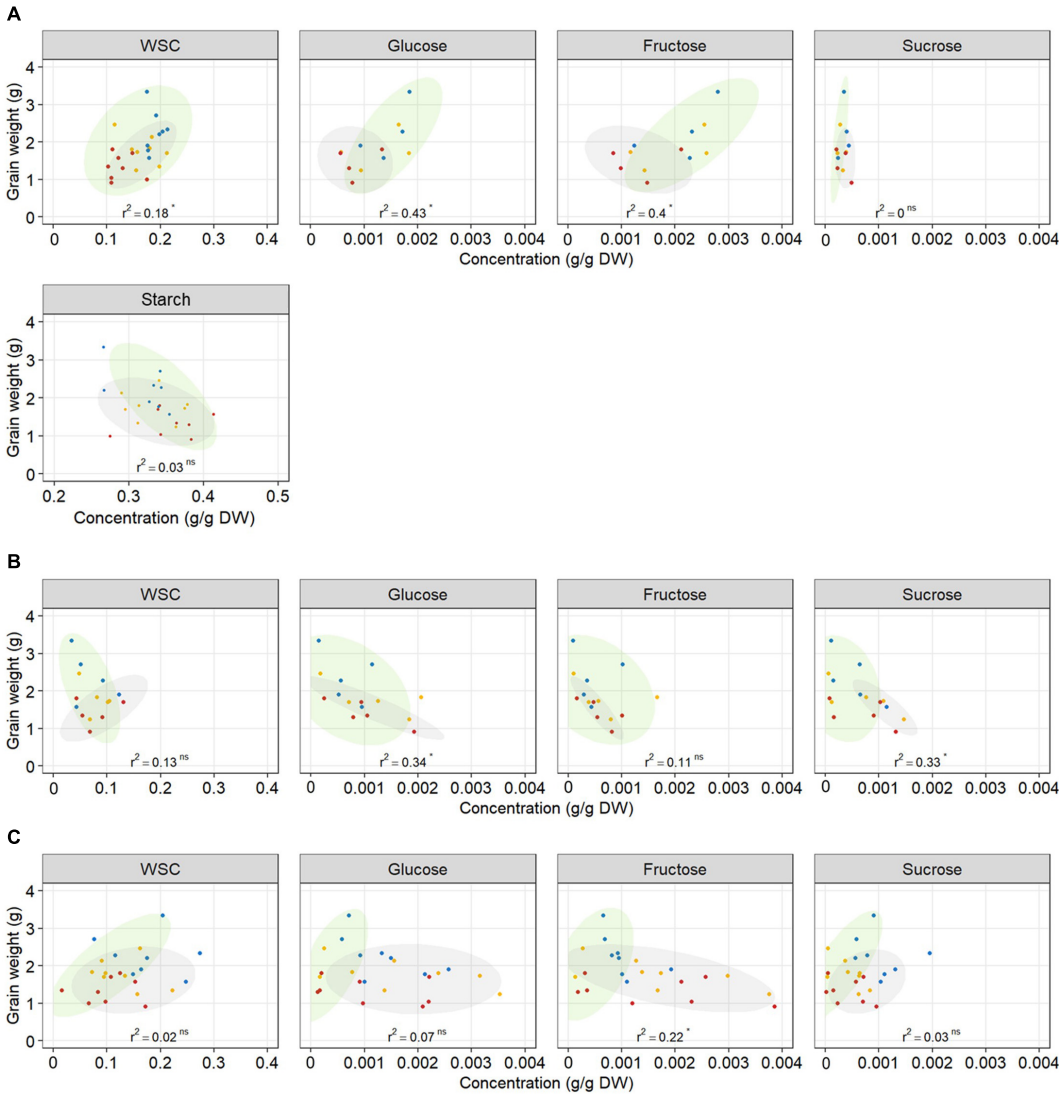


FIGURE 7 | Relationship between total WSC, glucose, fructose, sucrose, and starch concentrations in **(A)** grains, **(B)** awns, **(C)** the stem at 12 DAA, and final grain weight per plant. Each point represents an average of carbohydrate concentration ($n = 3$) in the main tiller for one genotype and one treatment. Each regression line includes the whole dataset. r^2 and p-value of linear regressions ('ns' not significant, $^*p < 0.05$) are indicated. Ellipses circle old genotypes (gray) and modern genotypes (green). Plants grown under well-watered conditions (blue), drought (orange), or combined drought and heat stress (red).

genotypes released between 1912 and 2007. The detrimental effect of heat stress combined with drought depended on genotype, illustrating genetic variation in grain weight response to combined D&H in wheat. Per plant yield was increasingly dependent on both aboveground biomass and total water use with increasing stress intensity (drought, then additional heat stress) (**Figure 2**), highlighting the important relationships between biomass, water use and grain weight under stress previously reported (Reynolds et al., 2006; Blum, 2009; Reynolds and Langridge, 2016). Biomass and water use are linearly related (de Wit, 1958) and mutually dependent during the plant's lifecycle. During the vegetative stage, transpiration drives biomass accumulation, which in turn results in high water use during grain filling when water is available. The maintenance of water use ensures the favorable water status of plant tissues and assimilate transport to grains. We observed a high association between per plant yield and total water used in two independent experiments (**Figure 2B** and **Supplementary Figure S3**) regardless of transpiration sensitivity to heat stress: the higher the water use, the higher the total grain weight at harvest. This indicated that maintaining transpiration following heat stress was a desirable trait in our conditions, confirming the strong relationship between plant transpiration and yield (de Wit, 1958; Fischer and Turner, 1978; Sinclair et al., 2005). The amount of water used in transpiration is driven by the evaporative demand in the atmosphere (Grantz, 1990). Our work illustrated the genetic variation in transpiration response to VPD previously observed in diverse wheat genotypes grown

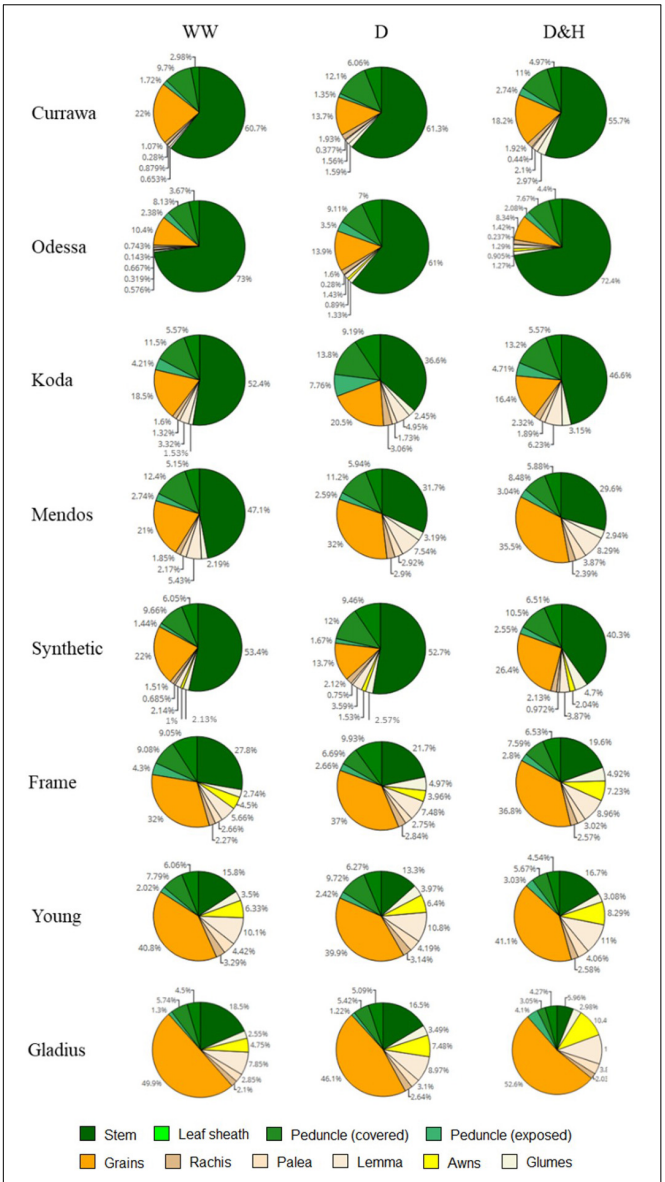


FIGURE 8 | Combined drought and heat stress increased WSC partitioning to the spike in old genotypes, not in modern varieties. Genotypes are shown in order of date of release (top – bottom, oldest = Currawa to newest = Gladius). Total water-soluble carbohydrates (WSC) in different organs of plants as a percentage of total WSC (n = 3). Plant organs are color-coded as shown in the legend.

under well-watered and water-limited conditions (Schoppach and Sadok, 2012; Schoppach et al., 2016; Medina et al., 2019). In addition, we identified genetic variation in transpiration response to combined D&H (**Figure 5B**). A 3-day heat treatment altered transpiration response to VPD in the subsequent drought-only treatment in some genotypes. As transpiration largely depends on green leaf area, the dynamics of senescence in response to heat stress could potentially have explained genotypic differences in transpiration response to heat stress; water use would be quickly reduced in genotypes with faster heat-induced senescence compared to genotypes with slower senescence rate following heat stress. However, no significant differences or genetic variation for drought and heat stress-induced chlorophyll content (greenness) in comparison with drought were found in these genotypes in repeated experiments (Schmidt et al., 2020). The combination of high evaporative demand and water scarcity can lead to the disruption of the water column in the xylem and cause cavitation. Cavitation damage might explain the lack of recovery in water use following heat stress observed in some genotypes in our experiments.

Wheat yield potential in water-limited environments is driven by water use, water use efficiency and harvest index (Passioura, 1977) with the theoretical possibility that, if genetic variation for each of these factors is independent from the others, yield may be increased by selection of favorable genotypes for any one factor (Reynolds and Tuberosa, 2008). The transpiration driven water use changes observed here following heat stress during grain-filling, when plants were all subjected to drought, influenced final grain weight. This trait – ability to maintain transpiration following heat stress under drought – separated more from less tolerant types. Tolerant genotypes may use more water by opening stomata at cooler times of the day or be more resistant to xylem cavitation, allowing continuous water flow through the plant and more favorable water status under stress.

In contrast, there was no clear genetic variation within the limited number of genotypes used in our experiments for either whole plant water-use efficiency or harvest index following the heat stress while under drought. There were interactions between treatments and genotypes for both biomass WUE and grain WUE, but no significant differences between genotypes once heat stress was applied. Despite the limited number of genotypes, in well-watered conditions we observed clear increased grain weight per unit of biomass, as well as per unit of water, in more modern compared with older genotypes reflecting the improved yield driven by the higher harvest index of modern types. Although harvest index was generally still higher in modern than in older genotypes under drought, this was not the case following heat stress which abolished harvest index difference between modern, semi-dwarf types compared with older, tall types. These results suggest that the responses of WUE and harvest index under combined drought and heat stress are independent from the water use response and that their contributions may be limited by the relative sensitivity of modern types to stress-induced decrease in biomass following heat stress.

WSC Availability in Grains Rather Than Grain Capacity Limited Grain Weight Under Stress

Starch is the main component of final grain mass. It is synthesized from stored WSC or produced from current photosynthesis. Drought and heat stress alter WSC supply to grains, either by limiting carbon assimilation through photosynthesis or by interrupting assimilate remobilization. Thus WSC availability in grains might be a limiting factor for starch synthesis and grain filling (Jurgens et al., 1978). In a field study on wheat genotypes grown in well-watered conditions, Fahy et al. (2018) quantified WSC and starch content and key starch biosynthesis enzyme activity in grains at different grain developmental stages. They

did not find any correlation between carbohydrate content in grains and final grain yield, suggesting that assimilate availability for starch synthesis is not a limiting factor for grain filling in wheat in favorable growing conditions. These findings are in accordance with our results in well-watered conditions where there was no relationship between WSC and starch content and plant yield. However, WSC concentration was reduced with increased stress intensity, and grains with relatively higher WSC concentrations at 12 DAA had higher yield (**Figure 7A**). Glucose and fructose are the first substrates in the starch biosynthesis pathway (Emes et al., 2003). Genotypes with higher glucose and fructose concentrations in grains at 12 DAA had higher yield, implying that shortage in glucose and fructose might have limited starch biosynthesis later during grain filling and consequently final grain weight. Accelerated starch biosynthesis under stress depleted glucose and fructose in grains without any increase in sucrose content, indicating that insufficient sucrose supply to grains probably limited starch biosynthesis under stress. Many studies propose sink strength (grain capacity) is the limiting factor for starch accumulation and grain filling in favorable environments (Borrás et al., 2004; Borrill et al., 2015; Fahy et al., 2018). In our study, genotypes with higher grain capacity, represented by grain dry weight at 12 DAA, had a higher yield in the well-watered treatment (**Figures 1A,B**) suggesting that grain sink strength was a major determinant of grain weight at harvest when conditions were favorable. With D&H stress, however, genotypes with higher grain capacity did not have higher yield, suggesting that high grain capacity was not sufficient to determine grain weight at harvest under stress, as has also been observed in barley (Savin and Nicolas, 1996). In our experiments, drought and combined D&H did not immediately reduce grain weight at 12 DAA. Reduction in grain filling occurred after 12 DAA, which corresponds to the end of cell enlargement and beginning of carbohydrate accumulation (Emes et al., 2003). Reduced grain weight under stress was due to altered grain filling, probably as a consequence of limited WSC supply to grains.

The Spike Is the Main Storage Tissue for WSC in the More Modern Wheat Varieties

Excess assimilates that are not used for growth and defence may be stored for further use during reproductive stages. The stem is considered an important source of stored WSC for grain filling, and the ability to store and remobilize stem reserves is regarded as a beneficial trait for wheat productivity under stress (Bidinger et al., 1977; Blum, 1998; Rebetzke et al., 2008). At 12 DAA, WSC content in the stem is at its peak (Zhang et al., 2015; Shirdelmoghanloo et al., 2016). Our results showed that the stem was the main storage organ for WSC in tall genotypes in which the stem was the largest organ by weight, but not in more modern varieties where stems are much shorter as a consequence of the introduction of semi-dwarfing Rht genes (Borrell et al., 1993). More recent varieties partitioned more of the biomass to spikes, and the reproductive organ was also the major store of WSC in modern varieties (**Figure 8**). Interestingly, in our experiment, a positive relationship between WSC concentration in the stem and total grain weight in the main spike at harvest was only observed in modern genotypes, which suggests that the important contribution of WSC content stored in the stem to grain filling may be a consequence of the introduction of semi-dwarfing genes (Richards, 1992; Miralles et al., 1998). Alternatively, it might suggest that plant breeders have selected for varieties that partition more of their WSC to spike tissues in the hot and dry conditions of South Eastern Australia, the origin of the more modern varieties. Older genotypes had large reserves of WSC in the stem for a limited sink in the spike (lower grain number), which could explain the absence of a relationship between both traits as stored WSC in the stem may not have been used (Borrell et al., 1993). In contrast with older types, more modern varieties had relatively low WSC concentration in the stem, indicating an opportunity to increase stem capacity for WSC storage in modern varieties. Dreccer et al. (2014) demonstrated in a recombinant inbred line population that proportionately high stem WSC types were also proportionately high spike WSC types. They also showed that these WSC were associated with higher grain weight and recently fixed carbon under heat stress, i.e., high WSC types (stem and spike) remobilized proportionately more WSC. Recently, Liu et al. (2020) showed a gradient of WSC and remobilization efficiency along the stem toward the spike under drought stress, contributing to grain filling. Taken together, these results suggest that there could be capacity to increase stem WSC in future varieties that would be remobilized to increase stress tolerance.

CONCLUSION

Drought and heat stress have rarely been studied together, despite their co-occurrence being a common scenario in wheat-growing regions. This work illustrated the effect of morphological changes introduced in wheat over a century on plant water use and carbohydrates partitioning. Results showed that heat stress occurring during grain filling, while plants were suffering from water stress, changed subsequent water use immediately so that some genotypes were unable to recover. Sensitivity to increased stress intensity was associated with low transpiration response to high VPD following heat stress and to genetic variation in transpiration. Reduced availability of WSC in grains following combined D&H was also identified and important for final grain weight. This suggested that measurements of transpiration and WSC content in grains following heat stress might be used to identify genetic variation for tolerance of combined drought and heat stress.

DATA AVAILABILITY STATEMENT

All datasets generated for this study are included in the article/**Supplementary Material**.

AUTHOR CONTRIBUTIONS

AE, DF, TG, and PT conceived and designed the experiments. AE performed the experiments, analyzed and interpreted

the data. NJ analyzed and interpreted data. All authors drafted the manuscript.

FUNDING

This work was supported by the Australian Research Council Industrial Transformation Research Hub for wheat in a hot and dry climate (IH130200027).

ACKNOWLEDGMENTS

We thank and acknowledge the use of the facilities and scientific and technical assistance of the Australian Plant Phenomics Facility, which is supported by the Australian Government's National Collaborative Research Infrastructure Strategy (NCRIS). In particular, we thank Chris Brien of the APPF for his constructive comments and advise on analysis of these data. We thank Priyanka Kalambettu, Coline de l'Hommeau, and Pauline Perrodin for technical assistance. We acknowledge and thank Vincent Bulone, Helen Collins and Jelle Lahnstein for helpful comments and assistance with the carbohydrates analysis.

SUPPLEMENTARY MATERIAL

The Supplementary Material for this article can be found online at: https://www.frontiersin.org/articles/10.3389/fpls.2020.568693/full#supplementary-material

REFERENCES

Asana, R., and Williams, R. (1965). The effect of temperature stress on grain development in wheat. *Austr. J. Agric. Res.* 16, 1–13. doi: 10.1071/AR9650001

Bidinger, F., Musgrave, R. B., and Fischer, R. A. (1977). Contribution of stored pre-anthesis assimilate to grain yield in wheat and barley. *Nature* 270, 431–433. doi: 10.1038/270431a0

Blum, A. (1998). Improving wheat grain filling under stress by stem reserve mobilisation. *Euphytica* 100, 77–83. doi: 10.1023/a:1018303922482

Blum, A. (2006). "Drought adaptation in cereal crops: a prologue," in *Drought Adaptation in Cereals*, ed. J. M. Ribaut (Binghamton: Food Products Press), 21–42.

Blum, A. (2009). Effective use of water (EUW) and not water-use efficiency (WUE) is the target of crop yield improvement under drought stress. *Field Crops Res.* 112, 119–123. doi: 10.1016/j.fcr.2009.03.009

Blum, A. (2017). Osmotic adjustment is a prime drought stress adaptive engine in support of plant production. *Plant Cell Environ.* 40, 4–10. doi: 10.1111/pce.12800

Borrás, L., Slafer, G. A., and Otegui, M. A. E. (2004). Seed dry weight response to source-sink manipulations in wheat, maize and soybean: a quantitative reappraisal. *Field Crops Res.* 86, 131–146. doi: 10.1016/j.fcr.2003.08.002

Borrell, A. K., Incoll, L. D., and Dalling, M. J. (1993). The influence of the Rht1 and Rht2 alleles on the deposition and use of stem reserves in wheat. *Ann. Bot.* 71, 317–326. doi: 10.1006/anbo.1993.1041

Borrell, A. K., Incoll, L. D., Simpson, R. J., and Dalling, M. J. (1989). Partitioning of dry matter and the deposition and use of stem reserves in a semi-dwarf wheat crop. *Ann. Bot.* 63, 527–539. doi: 10.1093/oxfordjournals.aob.a087778

Borrill, P., Fahy, B., Smith, A. M., and Uauy, C. (2015). Wheat grain filling is limited by grain filling capacity rather than the duration of flag leaf photosynthesis: a case study using NAM RNAi plants. *PLoS One* 10:e0134947. doi: 10.1371/journal.pone.0134947

Butler, D. G., Cullis, B. R., Gilmour, A. R., Gogel, B. G., and Thompson, R. (2017). *ASReml-R Reference Manual Version 4*. Hemel Hempstead: VSN International Ltd.

Butler, D. G., Cullis, B. R., Gilmour, A. R., and Gogel, B. J. (2009). *ASReml-R Reference Manual*. Brisbane: DPI Publications.

de Wit, C. T. (1958). *Transpiration and Crop Yields: Agricultural Research Reports 64.6*. Wageningen: PUDOC.

Dreccer, M. F., Wockner, K. B., Palta, J. A., McIntyre, C. L., Borgognone, M. G., Bourgault, M., et al. (2014). More fertile florets and grains per spike can be achieved at higher temperature in wheat lines with high spike biomass and sugar content at booting. *Funct. Plant Biol.* 41, 482–495. doi: 10.1071/FP13232

Emes, M. J., Bowsher, C. G., Hedley, C., Burrell, M. M., Scrase-Field, E. S. F., and Tetlow, I. J. (2003). Starch synthesis and carbon partitioning in developing endosperm. *J. Exper. Bot.* 54, 569–575. doi: 10.1093/jxb/erg089

Evans, L. T., Bingham, J., Jackson, P., and Sutherland, J. (1972). Effect of awns and drought on the supply of photosynthate and its distribution within wheat ears. *Ann. Appl. Biol.* 70, 67–76. doi: 10.1111/j.1744-7348.1972.tb04689.x

Fahy, B., Siddiqui, H., David, L. C., Powers, S. J., Borrill, P., Uauy, C., et al. (2018). Final grain weight is not limited by the activity of key starch-synthesising enzymes during grain filling in wheat. *J. Exper. Bot.* 69, 5461–5475. doi: 10.1093/jxb/ery314

Fischer, R. A., and Turner, N. C. (1978). Plant productivity in the arid and semiarid zones. *Annu. Rev. Plant Physiol.* 29, 277–317. doi: 10.1146/annurev.pp.29.060178.001425

Garcia, M., Eckermann, P., Haefele, S., Satija, S., Sznajder, B., Timmins, A., et al. (2019). Genome-wide association mapping of grain yield in a diverse collection of spring wheat (*Triticum aestivum* L.) evaluated in southern Australia. *PLoS One* 14:e0211730. doi: 10.1371/journal.pone.0211730

Grantz, D. A. (1990). Plant response to atmospheric humidity. *Plant Cell Environ.* 13, 667–679. doi: 10.1111/j.1365-3040.1990.tb01082.x

Hölttä, T., Mencuccini, M., and Nikinmaa, E. (2009). Linking phloem function to structure: analysis with a coupled xylem-phloem transport model. *J. Theoret. Biol.* 259, 325–337. doi: 10.1016/j.jtbi.2009.03.039

Jurgens, S. K., Johnson, R. R., and Boyer, J. S. (1978). Dry matter production and translocation in maize subjected to drought during grain fill. *Agron. J.* 70, 678–682. doi: 10.2134/agronj1978.00021962007000040036x

Liu, Y., Zhang, P., Li, M., Chang, L., Cheng, H., Chai, S., et al. (2020). Dynamic responses of accumulation and remobilization of water soluble carbohydrates in wheat stem to drought stress. *Plant Physiol. Biochem.* 155, 262–270. doi: 10.1016/j.plaphy.2020.07.024

Lopes, M. S., El-Basyoni, I., Baenziger, P. S., Singh, S., Royo, C., Ozbek, K., et al. (2015). Exploiting genetic diversity from landraces in wheat breeding for adaptation to climate change. *J. Exper. Bot.* 66, 3477–3486. doi: 10.1093/jxb/erv122

Machado, S., and Paulsen, G. M. (2001). Combined effects of drought and high temperature on water relations of wheat and sorghum. *Plant Soil* 233, 179–187. doi: 10.1023/a:1010346601643

Medina, S., Vicente, R., Nieto-Taladriz, M. T., Aparicio, N., Chairi, F., Vergara-Diaz, O., et al. (2019). The plant-transpiration response to vapor pressure deficit (VPD) in durum wheat is associated with differential yield performance and specific expression of genes involved in primary metabolism and water transport. *Front. Plant Sci.* 9:1994. doi: 10.3389/fpls.2018.01994

Miralles, D. J., Katz, S. D., Colloca, A., and Slafer, G. A. (1998). Floret development in near isogenic wheat lines differing in plant height. *Field Crops Res.* 59, 21–30. doi: 10.1016/S0378-4290(98)00103-8

Mittler, R. (2006). Abiotic stress, the field environment and stress combination. *Trends Plant Sci.* 11, 15–19. doi: 10.1016/j.tplants.2005.11.002

Passioura, J. B. (1977). Grain yield, harvest index and water use of wheat. *J. Austr. Instit. Agric. Sci.* 43, 117–120.

Pradhan, G. P., Prasad, P. V. V., Fritz, A. K., Kirkham, M. B., and Gill, B. S. (2012). Effects of drought and high temperature stress on synthetic hexaploid wheat. *Funct. Plant Biol.* 39, 190–198. doi: 10.1071/FP11245

R Core Team (2019). *R: A Language and Environment for Statistical Computing*. Vienna: R Foundation for Statistical Computing.

Rebetzke, G. J., Bonnett, D. G., and Reynolds, M. P. (2016). Awns reduce grain number to increase grain size and harvestable yield in irrigated and rainfed spring wheat. *J. Exper. Bot.* 67, 2573–2586. doi: 10.1093/jxb/erw081

Rebetzke, G. J., Van Herwaarden, A. F., Jenkins, C., Weiss, M., Lewis, D., Ruuska, S., et al. (2008). Quantitative trait loci for water-soluble carbohydrates and associations with agronomic traits in wheat. *Austr. J. Agric. Res.* 59, 891–905. doi: 10.1071/AR08067

Reynolds, M., Dreccer, F., and Trethowan, R. (2006). Drought-adaptive traits derived from wheat wild relatives and landraces. *J. Exper. Bot.* 58, 177–186. doi: 10.1093/jxb/erl250

Reynolds, M., and Langridge, P. (2016). Physiological breeding. *Curr. Opin. Plant Biol.* 31, 162–171. doi: 10.1016/j.pbi.2016.04.005

Reynolds, M., and Tuberosa, R. (2008). Translational research impacting on crop productivity in drought-prone environments. *Curr. Opin. Plant Biol.* 11, 171–179. doi: 10.1016/j.pbi.2008.02.005

Richards, R. (1992). The effect of dwarfing genes in spring wheat in dry environments. I. Agronomic characteristics. *Austr. J. Agric. Res.* 43, 517–527. doi: 10.1071/AR9920517

Rosenzweig, C., Elliott, J., Deryng, D., Ruane, A. C., Müller, C., Arneth, A., et al. (2014). Assessing agricultural risks of climate change in the 21st century in a global gridded crop model intercomparison. *Proc. Natl. Acad. Sci.* 111, 3268–3273. doi: 10.1073/pnas.1222463110

Savin, R., and Nicolas, M. E. (1996). Effects of short periods of drought and high temperature on grain growth and starch accumulation of two malting barley cultivars. *Funct. Plant Biol.* 23, 201–210. doi: 10.1071/PP9960201

Schmidt, J., Tricker, P. J., Eckermann, P., Kalambettu, P., Garcia, M., and Fleury, D. (2020). Novel alleles for combined drought and heat stress tolerance in wheat. *Front. Plant Sci.* 10:1800. doi: 10.3389/fpls.2019.01800

Schnyder, H. (1993). The role of carbohydrate storage and redistribution in the source-sink relations of wheat and barley during grain filling — a review. *New Phytol.* 123, 233–245. doi: 10.1111/j.1469-8137.1993.tb03731.x

Schoppach, R., and Sadok, W. (2012). Differential sensitivities of transpiration to evaporative demand and soil water deficit among wheat elite cultivars indicate different strategies for drought tolerance. *Environ. Exper. Bot.* 84, 1–10. doi: 10.1016/j.envexpbot.2012.04.016

Schoppach, R., Taylor, J. D., Majerus, E., Claverie, E., Baumann, U., Suchecki, R., et al. (2016). High resolution mapping of traits related to whole-plant transpiration under increasing evaporative demand in wheat. *J. Exper. Bot.* 67, 2847–2860. doi: 10.1093/jxb/erw125

Sevanto, S. (2018). Drought impacts on phloem transport. *Curr. Opin. Plant Biol.* 43, 76–81. doi: 10.1016/j.pbi.2018.01.002

Shah, N. H., and Paulsen, G. M. (2003). Interaction of drought and high temperature on photosynthesis and grain-filling of wheat. *Plant Soil* 257, 219–226. doi: 10.1023/A:1026237816578

Shirdelmoghanloo, H., Cozzolino, D., Lohraseb, I., and Collins, N. C. (2016). Truncation of grain filling in wheat (*Triticum aestivum*) triggered by brief heat stress during early grain filling: association with senescence responses and reductions in stem reserves. *Funct. Plant Biol.* 43, 919–930. doi: 10.1071/FP15384

Sinclair, T. R., Hammer, G. L., and Van Oosterom, E. J. (2005). Potential yield and water-use efficiency benefits in sorghum from limited maximum transpiration rate. *Funct. Plant Biol.* 32, 945–952. doi: 10.1071/FP05047

Stone, B., and Morell, M. K. (2009). "Carbohydrates," in *Wheat*, 4 Edn, eds K. Khan and P. R. Shewry (London: AACC International Press), 299–362. doi: 10.1016/B978-1-891127-55-7.50016-1

Van Dijk, A. I. J. M., Beck, H. E., Crosbie, R. S., De Jeu, R. A. M., Liu, Y. Y., Podger, G. M., et al. (2013). The millennium drought in southeast australia (2001-2009): natural and human causes and implications for water resources, ecosystems, economy, and society. *Water Resour. Res.* 49, 1040–1057. doi: 10.1002/wrcr.20123

Yemm, E. W., and Willis, A. J. (1954). The estimation of carbohydrates in plant extracts by anthrone. *Biochem. J.* 57, 508–514. doi: 10.1042/bj0570508

Zhang, J., Chen, W., Dell, B., Vergauwen, R., Zhang, X., Mayer, J. E., et al. (2015). Wheat genotypic variation in dynamic fluxes of WSC components in different stem segments under drought during grain filling. *Front. Plant Sci.* 6:624. doi: 10.3389/fpls.2015.00624

Conflict of Interest: The authors declare that the research was conducted in the absence of any commercial or financial relationships that could be construed as a potential conflict of interest.

Copyright © 2020 El Habti, Fleury, Jewell, Garnett and Tricker. This is an open-access article distributed under the terms of the Creative Commons Attribution License (CC BY). The use, distribution or reproduction in other forums is permitted, provided the original author(s) and the copyright owner(s) are credited and that the original publication in this journal is cited, in accordance with accepted academic practice. No use, distribution or reproduction is permitted which does not comply with these terms.

frontiers in Plant Science

ORIGINAL RESEARCH
published: 20 October 2020
doi: 10.3389/fpls.2020.575015

Comprehensive Genome-Wide Analysis of Thaumatin-Like Gene Family in Four Cotton Species and Functional Identification of *GhTLP19* Involved in Regulating Tolerance to *Verticillium dahlia* and Drought

Zhanshuai Li[1,2], Xiaoyan Wang[3], Yupeng Cui[3], Kaikai Qiao[1], Longfu Zhu[2], Shuli Fan[1,2] and Qifeng Ma[1]**

[1] State Key Laboratory of Cotton Biology, Institute of Cotton Research of Chinese Academy of Agricultural Sciences, Anyang, China, [2] National Key Laboratory of Crop Genetic Improvement, Huazhong Agricultural University, Wuhan, China, [3] College of Biology and Food Engineering, Anyang Institute of Technology, Anyang, China

OPEN ACCESS

Edited by:
Guihua Bai,
United States Department of Agriculture (USDA), United States

Reviewed by:
Yunqing Yu,
Donald Danforth Plant Science Center, United States
Anthony Guihur,
University of Lausanne, Switzerland

***Correspondence:**
Shuli Fan
fsl427@126.com
Qifeng Ma
13837240176@163.com

Specialty section:
This article was submitted to Plant Abiotic Stress, a section of the journal Frontiers in Plant Science

Received: 22 June 2020
Accepted: 28 September 2020
Published: 20 October 2020

Citation:
Li Z, Wang X, Cui Y, Qiao K, Zhu L, Fan S and Ma Q (2020) Comprehensive Genome-Wide Analysis of Thaumatin-Like Gene Family in Four Cotton Species and Functional Identification of GhTLP19 Involved in Regulating Tolerance to Verticillium dahlia and Drought. Front. Plant Sci. 11:575015. doi: 10.3389/fpls.2020.575015

Thaumatin-like proteins (*TLP*s) present in the form of large multigene families play important roles in biotic stress and abiotic stress. However, there has been no systematic analysis of the *TLP*s in cotton. In this study, comprehensive identification and evolutionary analysis of *TLP*s in four species of cotton were conducted. In total, 50, 48, 91, and 90 homologous sequences were identified in *Gossypium raimondii*, *G. arboreum*, *G. barbadense*, and *G. hirsutum*, respectively. Gene structure, protein motifs, and gene expression were further investigated. Transcriptome and quantitative real-time PCR analysis indicated that *GhTLP*s participate in abiotic, biotic stress and cotton fiber development. *GhTLP19* on chromosome At05 was selected as a candidate gene for further study. When *GhTLP19* was silenced by virus-induced gene silencing (VIGS) in cotton, with the increase of malondialdehyde (MDA) content and the decrease of catalase (CAT) content, and as the increase of disease index (DI) and hyphae accumulation, the plants were more sensitive to drought and *Verticillium dahliae*. Furthermore, the *GhTLP19* overexpressing *Arabidopsis* transgenic lines exhibited higher proline content, thicker and longer trichomes and more tolerance to drought when compared to wild type. This study will provide a basis and reference for future research on their roles in stress tolerance and fiber development.

Keywords: cotton, thaumatin-like protein, expression patterns, *Verticillium dahliae*, drought, trichome

INTRODUCTION

Terrestrial plants are constantly threatened by various pathogens (Li et al., 2016; Xin et al., 2016). Plants have evolved sophisticated defense mechanisms to effectively protect against pathogens (Gimenez-Ibanez and Solano, 2013; Kazan and Lyons, 2014). Recognition receptors for plasma membrane-localized interact with pathogen- and damage-associated molecular patterns

or extracellular effectors, and the interaction of intracellular recognition receptors and effectors from the corresponding pathogens is the main strategy to fight against the pathogen (Li et al., 2017; Xu et al., 2017). Pathogen-related (PR) proteins, which are induced in response to pathogen invasion, are the main plant defense factors against pathogens (Dubey and Singh, 2018). PR5, also known as thaumatin-like protein, is a member of the 17 PR families (Zhao and Su, 2010). Most TLPs contain structures that are thought to their specific receptor binding for antifungal activity: the highly conserved G-x-[GF]-x-C-x-T-[GA]-D-C-x(1,2)-[GQ]-x(2,3)-C sequence, a REDDD (arginine, glutamic acid, and three aspartic acid residues) structure and sixteen or ten cysteine residues that form eight or five disulfide bonds to maintain the stability of protein structure (Hu and Reddy, 1997; Liu et al., 2010a, 2020). The antifungal activity of the TLPs might be related to their ability to penetrate the fungal membrane and cause perforation through enzyme activity (Liu et al., 2010a; Jiao et al., 2018). Related studies have also shown that the TLPs have strong glucanase activity to hydrolyze β-D-glucan, which is the major cell wall component of oomycetes (Latijnhouwers et al., 2003; Singh et al., 2017).

The *TLP*s play an important role in the defense system of plants against various biotic and abiotic stresses (Petre et al., 2011). The *ClTLP27* gene in watermelon could significantly inhibit the growth of various fungal pathogens, such as *Fusarium verticillioides* and *Didymella bryoniae* (Zhang et al., 2018). Overexpression of an *Ocimum basilicum PR5* family member (*ObTLP1*) in *Arabidopsis* not only increased the tolerance of transgenic plants to *Sclerotinia sclerotiorum* and *Botrytis cinerea* but also enhanced the resistance to methyl jasmonate (Misra et al., 2016). Overexpression of *AsPR5* from garlic could significantly improve the resistance of garlic and *Arabidopsis* to *B. cinerea* (Rout et al., 2016). Overexpression of *GbTLP1*, which is involved in cotton fiber secondary cell wall development, increased the resistance to *V. dahlia*, salt and drought in transgenic tobacco (Munis et al., 2010). A grape *VqTLP29* gene enhanced the stomatal closure immune response of transgenic lines in response to pathogen-related molecular patterns, increased the resistance of transgenic *Arabidopsis* to powdery mildew and *Pseudomonas syringae*, and might also play a role in the signaling pathways of jasmonic acid, salicylic acid and ethylene (Yan et al., 2017). *Di19* combined with the TACA (A/G) fragment of the *PR5* promoter to increase the expression level of *PR5* and thus enhance the drought resistance of *Arabidopsis* (Liu et al., 2013). In addition, *TLP* could improve plant resistance to abiotic stress and played a role in growth and development processes, such as floral organ formation (Neale et al., 1990) and seed germination (Seo et al., 2008).

Although there have been some relevant studies on the *TLP*s in plants, further research on these genes is still needed, especially in cotton. As an important industrial crop, cotton plays an important supporting role in the economy and textile industry. Among the cotton species, tetraploid *Gossypium hirsutum* and *G. barbadense* cultivated in agricultural production were formed by interspecific hybridization between A genomic variety *G. arboreum* and D genomic variety *G. raimondii* during the evolutionary process (Wendel et al., 2009). Cotton is widely cultivated around the world, with high production of *G. hirsutum*, accounting for 90% of total cotton produced in the world; *G. barbadense* is of high quality but low yield, accounting for only 5–8%; *G. arboreum* and *G. raimondii* are rarely cultivated (Zhang et al., 2015). *V. dahliae* is the main pathogen of cotton, and the disease resistance of most commercial varieties is poor, which seriously affects fiber quality and yield (Gong et al., 2017; Zhang et al., 2017; Ma et al., 2018, 2019b). However, little is known about the *TLP*s and their roles in tolerance to *V. dahliae* and fiber development in cotton. In this study, we identified and characterized the *TLP* gene family in sequenced cotton species. Then, we analyzed their gene structures, phylogenetic relationships, and expression patterns in various tissues and under *V. dahliae*, salt, PEG and cold stress; the *cis*-elements in the putative promoters; and transcription factor binding sites of the *TLP*s.

To further identify the *TLP*s function in cotton, *GhTLP19* was identified and cloned for study. We found that when *GhTLP19* was silenced by VIGS, the tolerance of plants to *V. dahliae* and drought decreased. Moreover, the transgenic *Arabidopsis* lines of overexpressing *GhTLP19* were more drought-tolerant and had thicker and longer trichomes. This study aimed to provide important and useful information for further studies on the interaction between cotton and fungal invasion, other abiotic stresses and developmental processes.

MATERIALS AND METHODS

Member Identification and Sequence Analysis

The hidden Markov model (HMM) profile of the conserved thaumatin (THN) domain (PF00314) was downloaded from the Pfam database (Finn et al., 2016)[1]. The four cotton genomic data (*Gossypium arboreum*, JGI; *G. raimondii*, CRI; *G. hirsutum*, ZJU; *G. barbadense*, ZJU) were downloaded from the Cotton Functional Genomics Database (CottonFGD)[2] (Zhu et al., 2017). The genomic data of other species were obtained from the Phytozome v12.1[3]. HMMER 3.0 and BLASTP were used to search the *TLP* genes in four genomes of cotton and other species. Then, we eliminated the redundant genes from the HMM and BLASTP searches. The remaining genes were further identified using the normal mode of the SMART database[4] (Letunic et al., 2015). The basic information of the four cotton *TLP* genes was collected from CottonFGD (see footnote). The signal peptides and transmembrane (TM) domains were predicted with SignalP 5.0[5] (Petersen et al., 2011), and TMHMM 2.0[6] (Krogh et al., 2001), respectively. The subcellular localization of the *TLP* genes was predicted by using the CELLO v.2.5 server[7].

[1]http://pfam.xfam.org
[2]https://cottonfgd.org/
[3]http://www.phytozome.net
[4]http://smart.embl-heidelberg.de/
[5]http://www.cbs.dtu.dk/services/SignalP/
[6]http://www.cbs.dtu.dk/services/TMHMM/
[7]http://cello.life.nctu.edu.tw

Gene Structure, Phylogenetic Tree, and Conserved Motif Analysis

The gene exon/intron structure information of the cotton *TLP* family was retrieved from CottonFGD, and the gene structures were graphically visualized using the GSDS2.0 web server[8] (Hu et al., 2015). The conserved motifs of cotton *TLP* protein sequences were analyzed using the MEME program. All the identified *TLP* protein sequences from four *Gossypium* species, *Theobroma cacao*, *Arabidopsis*, and *Oryza sativa,* were aligned using ClustalX 2.0. The maximum likelihood (ML) and JTT method of MEGA 7.0 was used to construct the phylogenetic tree with the p-distance model and 1,000 bootstrap replications (Tamura et al., 2013).

Cis-Elements and TFBSs Analysis

The 2,000 bp predicted upstream region of the initiation codon (ATG) of all *TLP*s was determined, and then, all the sequences were submitted to the PlantCARE database to identify the *cis*-elements (Lescot, 2002). The putative transcription factor binding sites (TFBSs) of the *GhTLP* gene promoter regions were predicted using the Binding Site Prediction tool in the PlantTFDB 5.0 server[9], with a strict criterion: threshold $p \leq 1 \times 10^{-6}$.

Transcriptome Data and qRT-PCR Analysis

Raw RNA-seq data of *G. hirsutum* acc. TM-1 were downloaded from the NCBI Sequence Read Archive (PRJNA248163). TopHat (Kim et al., 2013) and Cufflinks (Trapnell et al., 2012) were used for mapping reads and analyzing gene expression levels, and the value of the gene expression levels was normalized by fragments per kilobase million (FPKM).

The cultivated cotton lines CCRI36 (upland cotton with weak resistance to *V. dahliae*) and Hai7124 (sea-island cotton with strong resistance to *V. dahliae*) were grown in a greenhouse free of *V. dahliae*. The root dip method was used to inoculate two true-leaf stage cotton seedlings with *V. dahliae* (V991) at 2×10^7 spores per ml. The roots of seedlings were collected from each sample at 0, 6, and 12 h after inoculation. Control plants were treated in the same way with sterile water. Fiber samples were taken from normally growing CCRI36 and Hai7124 plants at 5, 10 and 15 days after flowering. All samples collected were immediately flash-frozen with liquid nitrogen and stored in a −80°C freezer for RNA isolation. The total RNA of all samples was isolated by the RNAprep Pure Plant kit (Tiangen, Beijing, China), and the RNA was reverse transcribed to cDNA by the PrimerScript 1st Strand cDNA synthesis kit (TaKaRa, Dalian, China). qRT-PCR analysis of the *TLP*s was conducted using the SYBR Premix Ex Taq Kit (TaKaRa) and the ABI 7500 real-time PCR System (Applied Biosystems, Foster City, CA, United States), and the data were normalized using cotton ubiquitin 7 (*UBQ7*) as an internal control. The relative expression levels of the *TLP*s were calculated by the $2^{-\Delta\Delta Ct}$ method (Livak and Schmittgen, 2001; Wang et al., 2017). Genesis software[10] was used to draw the heat-map. The color represents *TLP* expression profiles: Log2 (expression levels). Three biological replicates were obtained using 40 plants grown at a uniform growth stage. For each biological replicate, three technical replicates of each qRT-PCR reaction were applied.

Cloning of *GhTLP19* and Transformation of *Arabidopsis*

The complete ORF of *GhTLP19* was cloned from cDNA of mixed samples of CCRI36 tissues. The ORF of *GhTLP19* was cloned into *pBI121* vector containing 35S promoter to construct 35S:*GhTLP19*. The 35S:*GhTLP19* vector was transferred to *Arabidopsis* (Colombia-0; WT) by *Agrobacterium*-mediated floral dip method (Clough and Bent, 1998). The positive transgenic lines were screened on 1/2 MS medium containing 50 ng/μl kanamycin. The mutant *atpr5* (*At1g75040*;SALK_052587C) was purchased from AraShare[11]. *Arabidopsis* seeds were sterilized with commercially diluted (1:1, V/V) sodium hypochlorite and then rinsed several times with sterile water. Germination was carried out on sterile 1/2 MS medium. The seedlings were transferred to soil and grown at 22°C under long-day conditions (16 h light and 8 h dark) after 7 days. The trichome of *Arabidopsis* leaves (WT, *atpr5,* and 35S:*GhTLP19*) was observed and photographed in real-time using an OLYMPUS BX53 microscope, and the diameter and length of the trichome were measured in real-time using the measurement tool of cellSens Standard software.

VIGS and Stresses Treatment

A 313bp fragment of *GhTLP19* ORF was amplified and cloned into the pCLCrVA vector. The vectors (CLCrV:*GhTLP19*, empty vector CLCrV:*00* and CLCrVB) were transformed into *A. tumefaciens* strain LBA4404. The OD_{600} of activated agrobacterium was adjusted to 1.5 with the infiltration buffer (10 mM $MgCl_2$, 10 mM MES, and 200 μM acetosyringone). We mixed CLCrV:*GhTLP19* and CLCrVB, CLCrV:*00* and CLCrVB, CLCrV:*GhPDS* and CLCrVB in a 1:1 ratio, then agroinfiltrated into fully unfolded cotton cotyledons of CCRI36 (Hu et al., 2018). After a night of darkness, the plants were transferred to a greenhouse at 25℃ with a 16 h light/8 h dark photoperiod. When CLCrV:*GhPDS* plants showed phenotype, CLCrV:*GhTLP19* and CLCrV:*00* plants were treated with drought and *V. dahliae*, respectively. VIGS plants were irrigated with 15% PEG6000 to simulate drought treatment. The transgenic *Arabidopsis* and WT plants were also irrigated with 15% PEG6000 to simulate the drought environment. The *V. dahliae* (V991) was grown on PDA medium for 6 days at 25℃. Some mycelia were selected and cultured in Czapek's liquid medium at 150 rpm in a shaking at 25℃ for about 5 days. Finally, VIGS plants were infected with *V. dahliae* spore suspension with concentration of 2×10^7 by root dip method (Miao et al., 2019). The contents of MDA and CAT were determined using Malondialdehyde (MDA) Assay Kit and Micro Catalase (CAT) Assay Kit (Solarbio, Beijing, China), respectively. At least 30 strains of each treatment were

[8]http://www.bioinfogenome.net/piece/

[9]http://planttfdb.cbi.pku.edu.cn/

[10]http://www.gsoft.com.au/

[11]http://www.arashare.cn/

investigated for disease index. Three independent biological replicates were included for each sample in the experiment.

RESULTS

Member Identification, Sequence Analysis and Phylogenetic Tree of *TLP*s

We identified 90, 91, 48, and 50 full-length putative *TLP*s in *G. hirsutum*, *G. barbadense*, *G. arboretum*, and *G. raimondii*, respectively. Based on their locations on the chromosomes, the *TLP* family members of the four cotton species were renamed *GhTLP1* to *GhTLP90*, *GbTLP1* to *GbTLP91*, *GaTLP1* to *GaTLP48,* and *GrTLP1* to *GTLP50*. The subcellular localization results showed that most of the TLP proteins were mainly located in the extracellular space, just a few were located in the periplasmic and outer-membrane. Most TLPs contained an N-terminal signal peptide. The prediction results of the TM domains showed that half of the TLPs possessed one or two TM domains, while only GhTLP12 possessed four TM domains, and GhTLP55 and GbTLP53 possessed three TM domains. The molecular weight (MW), isoelectric point (pI) and grand average of hydropathicity (GRAVY) of the *TLP*s of the four cotton species were analyzed and are shown in **Supplementary Table S1**.

Through multiple sequence analysis, we found that most TLP members contained conserved cysteine residues (**Figure 1** and **Supplementary Figure S1**). Highly conserved REDDD amino acids and typical thaumatin family signature, which are essential for the antifungal and structural stability of the proteins under extreme environmental conditions (Fierens et al., 2009), also exist in most TLP family members. To study the evolutionary relationship of the *TLP*s, we collected *TLP* protein sequences from *G. raimondii*, *G. arboreum*, *G. hirsutum*, *G. barbadense*, *A. thaliana*, *T. cacao,* and *O. sativa* to construct a phylogenetic tree. On the basis of previous *AtTLP* and *CmTLP* family studies (Liu et al., 2010a, 2020), the phylogenetic tree was divided into 10 groups (**Figure 2**). All members of Group10 were derived from dicotyledonous plants, while the other nine groups included members of both dicotyledonous and monocotyledonous plants. The distribution of the cotton *TLP* members in all groups was relatively uneven. Group7 had 58 members, making it the largest group. Group6 is the smallest group, with only sixteen members.

To further elucidate the structural diversity of *TLP*s in cotton, we first analyzed the intron/exon structure and phylogenetics of the *GhTLP*s (**Supplementary Figures S2A,B**). The results showed that the number of introns in the *GhTLP*s was small, which is similar to results in *Solanum nigrum* and *Cucumis melo* (Jami et al., 2007; Liu et al., 2020). These individual genes with multiple exons contained other domains (such as PF11891 and PF00069) in addition to the THN domain. The conserved region of a protein determines its function. Therefore, the conserved motifs of *GhTLP*s were also predicted (**Supplementary Figure S2C**). A total of 10 highly conserved motifs were discovered, and most *GhTLP*s contained them. Each motif was located on 80% or more of the *GhTLP*s. Motif 5, 6, and 8, for example, existed on all *GhTLP*s. Members of the same group had nearly identical motifs, suggesting that they may be functionally identical or similar. We also analyzed the gene structure and motifs of all cotton *TLP*s (**Supplementary Figure S3**). The results showed that the *TLP*s were significantly conserved in cotton.

Analysis of *Cis*-Acting Elements and TFBS

Transcription factors (TFs) are protein molecules that bind to specific sequences of a gene promoter (mainly *cis*-acting elements) to ensure specific temporal and spatial expression of the target gene at a specific intensity. To further elucidate the regulatory mechanism of *TLP* expression, we identified all *cis*-acting elements within 2000 bp upstream of the start codons of the *TLP*s (**Supplementary Figures S4, S5** and **Supplementary Table S2**) and predicted the corresponding TFs of the *GhTLP*s (**Supplementary Table S3**). We found that the different *cis*-acting elements in the *TLP* gene promoters had the same proportion among the four cotton varieties (**Supplementary Figure S4A**), suggesting that the *TLP*s had similar expression regulatory patterns among these species. The statistical results showed that the sum of different *cis*-acting elements in tetraploid cotton (*G. hirsutum* and *G. barbadense*) was twice that in diploid cotton (*G. raimondii* and *G. arboreum*) (**Supplementary Figure S4B**), which supported the evolutionary theory that chromosome doubling resulted in tetraploid formation of the two diploid cotton species by hybridization. Since the number and category of *cis*-acting elements in the two tetraploid cotton species were basically the same and were twice as many as those in the two diploid cottons, we only performed the distribution map of the *cis*-acting elements in the *GhTLP* promoters (**Supplementary Figure S5**). Various plant hormone-related elements, such as ABRE (ABA), CGTAC-motif (MeJA), ERE (ethylene), TGA-element (auxin), and TATC-box (gibberellin), and stress-related elements, such as LTR (cold), MBS (drought), ARE (anaerobic), TC-rich (defense and stress), as-1, and WUN-motif, were identified. Among the plant hormone-related components, ERE components had the highest number and can respond to ethylene, disease and insect damage. There were also large numbers of SA elements, and the synthesis of SA can improve the resistance of cotton to *V. dahliae*. As an important component for the response to damage and pathogens, the W-box is necessary for the response of the *TLP* gene promoter to fungal elicitors, as well as many *GhTLP* promoters. These results suggested that *TLP*s might be involved in the resistance of cotton to pests and diseases. The binding sites of MYB and MYC-like TFs on various antistress gene promoters were abundant on the *TLP* promoters. There were also tissue-specific components, such as the RY-element, O2-site, and CCGTCC motif.

The TFBS results showed that a total of 308 TFs belonging to 40 families might combine with 90 promoter regions of *GhTLP*s (**Supplementary Table S3**). There are many plant-specific TF families, such as TCP, Dof, BBR-BPC, NAC, and B3. Some TF families, such as the MYB, ERF, and C2H2 families, are found not only in plants but also in animals,

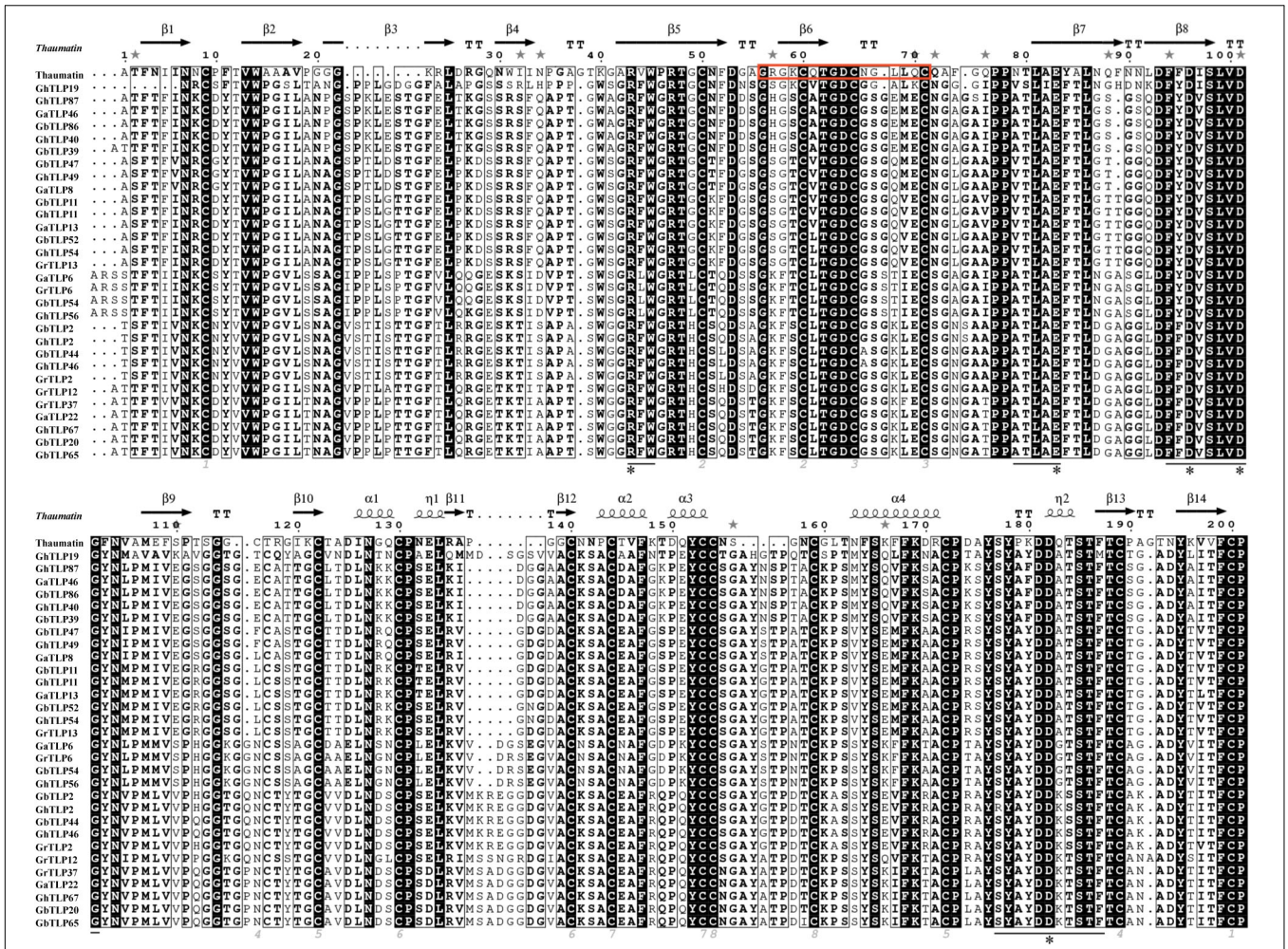


FIGURE 1 | Thaumatin sequence alignment of partial *TLP*s in cotton. The *TLP* family signature in thaumatin is framed with a red border. The conserved residues are indicated by gray numbers. Conserved positions of five amino acids are labeled with a black asterisk. The black line shows the amino acids forming the bottom of the acidic cleft.

yeast and bacteria. These TFs interact with *cis*-acting elements on the promoter to regulate biological processes, including biotic/abiotic stress, plant growth and development. For example, ERF can bind to the *cis*-acting elements LTRE and DRE to respond to low temperature, drought and high salt stress. bZIP can interact with the *cis*-acting elements ABRE and as-1 in response to wounding, ABA, and MeJA. In addition, we analyzed the GO annotation information of the transcription factors of the *GhTLP*s (**Supplementary Figure S6**). The results showed that these TF families were mainly involved in biological processes and molecular functions, while fewer TF families were involved in cellular components. The main biological processes involving in these TFs were cellular process, metabolic process, biological regulation, and regulation of biological process. Among the molecular functions, binding and nucleic acid binding transcription factor activity are involved in the regulatory processes of these transcription factors. The number of TFs and *cis*-acting elements of the *TLP*s was very high; these elements might not only participate in cotton resistance to biotic stress (such as *V. dahliae*) and abiotic stress (drought, salt, and cold, etc.) but also might affect the growth and development process.

Expression Patterns During Growth and Development

Analyzing gene expression patterns is a key method for exploring gene function. To explore the spatio-temporal expression patterns of *TLP* genes, the RNA-seq, and qRT-PCR data from different tissues and developmental stages were used to generate heat-maps. The expression pattern of each *TLP* gene was significantly different across different tissues and developmental stages (**Figures 3A**, **4C,D, Supplementary Figure S7** and **Supplementary Table S4**). Some genes were specifically expressed in the reproductive organs (**Figure 3A**). *GhTLP7*, *GhTLP40,* and *GhTLP46* exhibited preferential gene expression in the petals, *GhTLP25* and *GhTLP58* were specifically expressed in the calycles, and *GhTLP46* showed strong expression

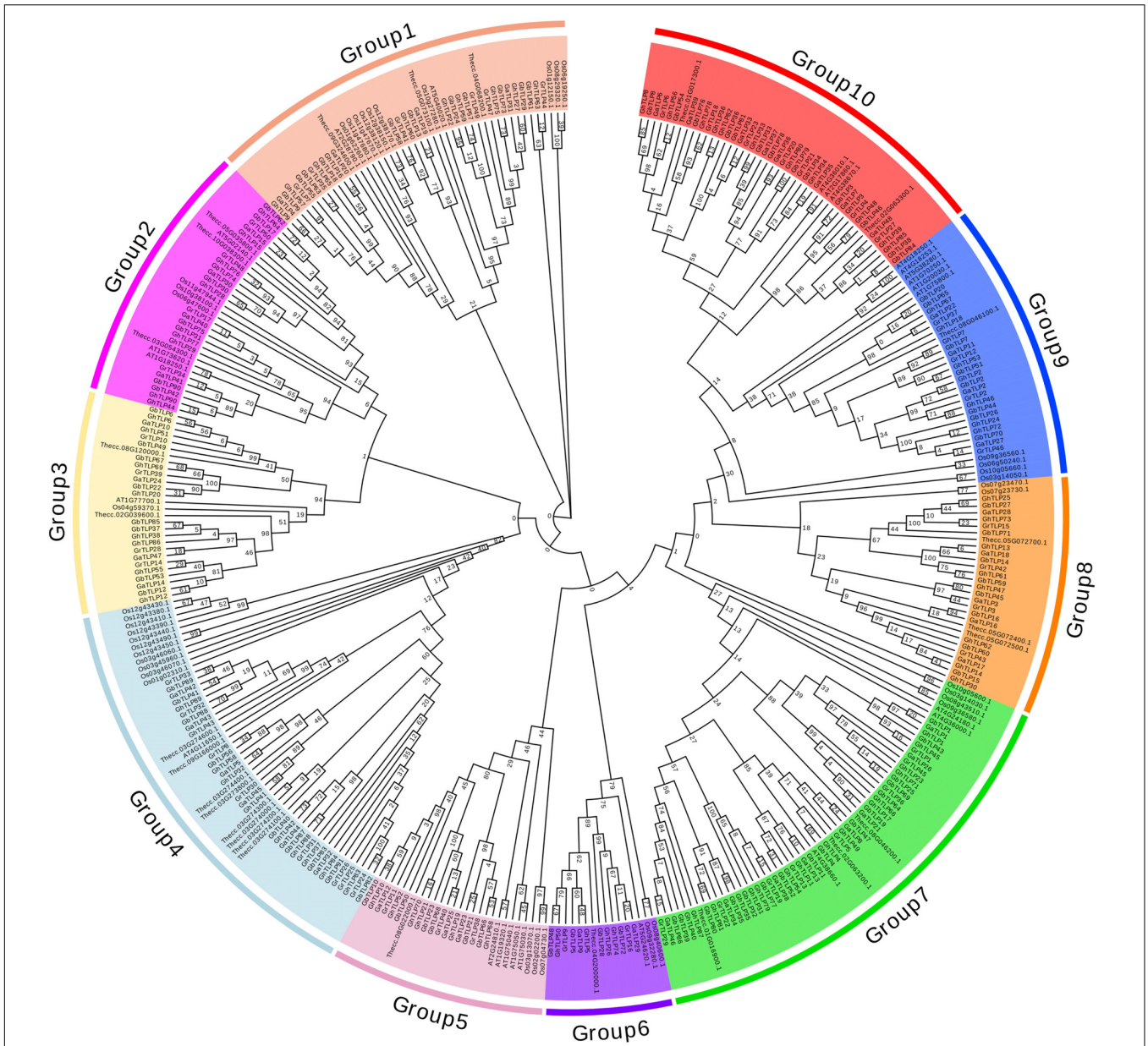


FIGURE 2 | Phylogenetic tree of Thaumatin-like proteins. All predicted protein sequences from *G. raimondii*, *G. arboreum*, *G. hirsutum*, *G. barbadense*, *Arabidopsis*, *T. cacao,* and *O. sativa* were aligned with ClustalX 2.0, and the maximum likelihood (ML) and JTT method of MEGA 7.0 was used to construct the phylogenetic tree with the p-distance model and 1,000 bootstrap replications. Ten groups were indicated using different background colors.

in the stamens. Four genes (*GhTLP29*, *GhTLP77*, *GhTLP16,* and *GhTLP65*) were highly expressed continuously and specifically during ovule development. *GhTLP84* was highly expressed only in ovules 20 days post-anthesis (dpa). These genes might be involved in the development of cotton reproductive organs. These results indicated that these five genes played a corresponding role in ovule development. Fiber is an important indicator of cotton yield and quality, and it is very important to analyze gene expression in fiber development. *GhTLP72* exhibited preferential gene expression in fiber_5 dpa and then gradually decreased, indicating that this gene might be involved in the fiber elongation stage of development. *GhTLP19*, *GhTLP68,* and *GhTLP44* showed the strongest gene expression in fiber at 20 and 25 dpa, suggesting that these genes played a role in the development of the fiber secondary cell wall.

GbTLP1 has been reported to be involved in the development of fibers (Munis et al., 2010). To further confirm the role of *TLP*s in fiber elongation and secondary wall thickening, we collected fiber samples of upland and sea-island cotton 5, 10, and 15 days after flowering and then analyzed the *TLP* expression patterns by qRT-PCR (**Figures 4C,D** and **Supplementary Tables**

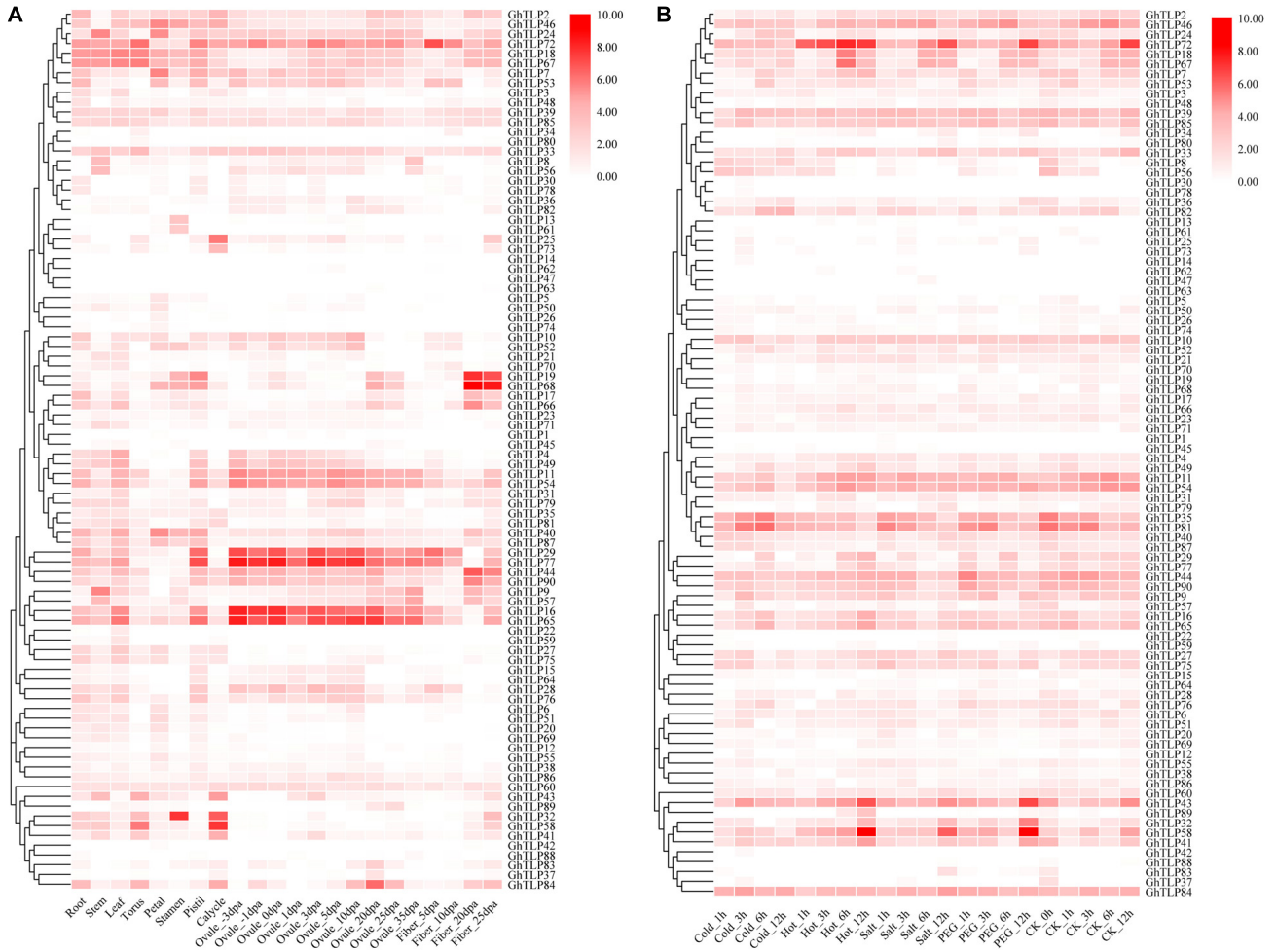


FIGURE 3 | Expression profiles of the *GhTLP*s in different tissues **(A)** and in response to different stresses **(B)** of TM-1. The raw data for RNA-Seq of *G. hirsutum* acc. TM-1 was downloaded and used to analyze the expression patterns of *ChTLP* genes. The color bar represents the expression values in log2 of fragments per kilobase per million reads (FPKMs).

S4, S6). In upland cotton (**Figure 4C**), *GhTLP19*, *GhTLP68*, *GhTLP17*, *GhTLP44*, *GhTLP90*, *GhTLP9,* and *GhTLP84* were specifically expressed at high levels in fiber_15 dpa. There were also many *GhTLP*s, such as *GhTLP65*, *GhTLP16*, *GhTLP29,* and *GhTLP77,* specifically and highly expressed during the fiber_5 dpa period. This finding was consistent with the results of public data transcripts (**Figure 3A**). In sea-island cotton (**Figure 4D**), genes such as *GbTLP55*, *GbTLP42*, *GbTLP21,* and *GbTLP66* were highly expressed during the fiber_15 dpa period, while the expression levels of *GbTLP63*, *GbTLP18*, *GbTLP75,* and *GbTLP31* were significantly upregulated during the fiber 5 dpa period. These results suggested that the *TLP*s might play a role in cotton fiber elongation and secondary wall development.

In addition, the expression levels of some genes (such as *GhTLP41*, *GhTLP43,* and *GhTLP89*) increased significantly during seed germination and in the roots but decreased gradually with cotyledon development (**Supplementary Figure S7**). There were also some genes (such as *GhTLP16* and *GhTLP65*) whose expression levels decreased with root development (**Supplementary Figure S7**). *GhTLP9* and *GhTLP24* were specifically expressed in the stems (**Figure 3A**). The results suggested that these genes played a role in cottonseed germination and seedling growth.

Expression Patterns Under Biotic/Abiotic Stresses

It was found in plants that *TLP*s had a certain response to abiotic stress in many plants (Hiroyuki and Terauchi, 2008; Tachi et al., 2009; Goel et al., 2010; Munis et al., 2010; Misra et al., 2016). Therefore, we also used public RNA-seq and qRT-PCR data to analyze the expression patterns of the *GhTLP*s under abiotic and biotic stress (**Figures 3B**, **4A,B**). Several genes showed increased expression levels under different stresses (**Figure 3B**). For example, *GhTLP35* and *GhTLP81* showed a tendency to increase and then decrease under salt, cold and PEG conditions. However, both *GhTLP58* and *GhTLP43* increased to the highest

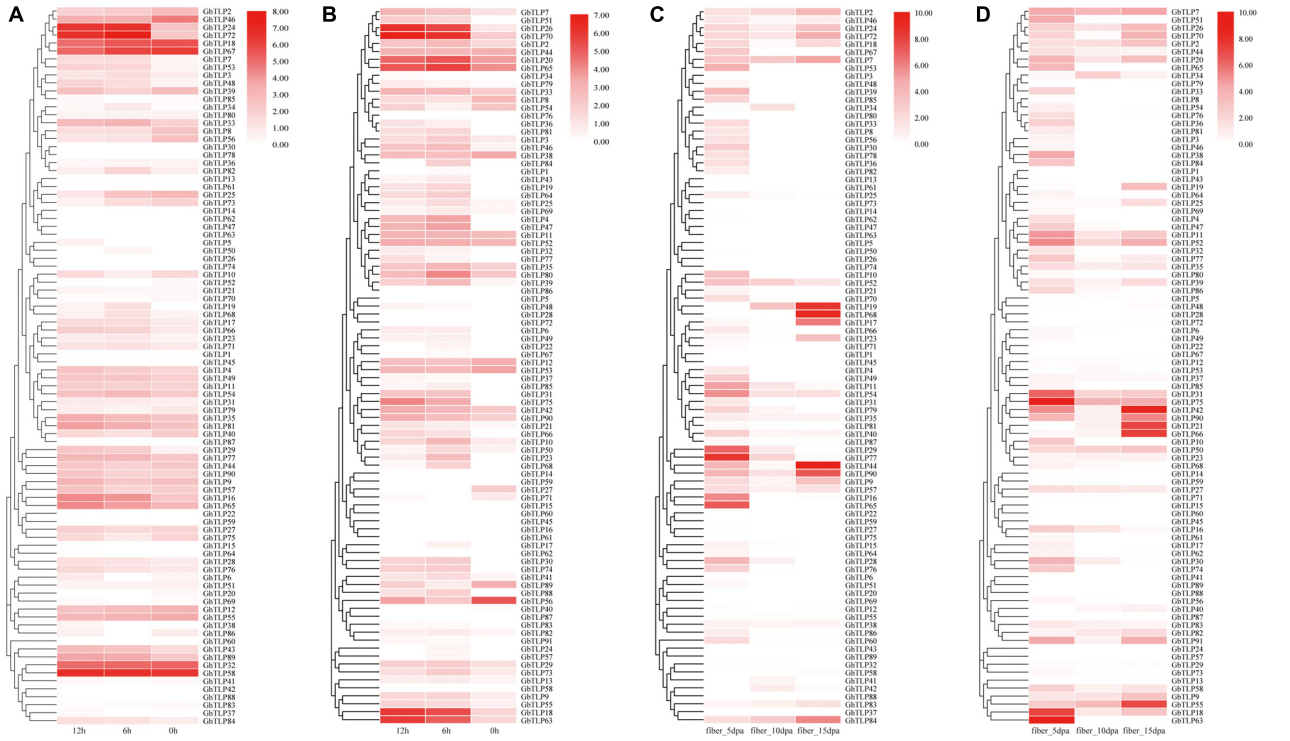


FIGURE 4 | The expression patterns of the *TLP*s under *V. dahliae* treatment and during fiber development via qRT-PCR. **(A,B)** Show the expression patterns of the *TLP*s at 0, 6, and 12 h after CCRI36 and Hai7124 were inoculated with *V. dahliae*, respectively. **(C,D)** Show the expression profiles of the *TLP*s in 5 dpa, 10 dpa and 15 dpa fibers of CCRI36 and Hai7124 after flowering, respectively. The color represents *TLP* expression profiles: Log2 (expression levels). Three independent biological replicates and three technical replicates for each PCR reaction were included.

level after 12 h of salt and PEG treatment. The results showed that these genes could respond to different abiotic stresses to different degrees. Other *GhTLP*s also showed changes in expression levels under different abiotic stresses.

*TLP*s have been reported to play an important role in plant resistance to pathogen infection (Yan et al., 2017). To further explore the function of the *TLP*s in cotton resistance to *V. dahliae*, the expression patterns of the *TLP*s in CCRI35 and Hai7124 after *V. dahliae* inoculation were analyzed by qRT-PCR (**Figures 4A,B** and **Supplementary Table S6**). The results showed that many *TLP*s of CCRI36 and Hai7124 were rapidly upregulated under the induction of *V. dahlia*. In upland cotton (**Figure 4A**), *GhTLP24* and *GhTLP72* were most significantly upregulated. Some genes, such as *GhTLP84*, *GHTLP33*, *GhTLP19*, *GhTLP66*, *GhTLP16*, *GhTLP65*, *GhTLP43,* and *GhTLP89*, were also upregulated to some extent. There were also some genes whose expression was downregulated, such as *GhTLP46* and *GhTLP25*, and some whose expression levels were unchanged, such as *GhTLP32* and *GhTLP58*. In sea-island cotton (**Figure 4B**), most *TLP*s were upregulated under the induction of *V. dahlia*. For instance, the upregulation of *GbTLP18*, *GbTLP63*, *GbTLP26*, *GbTLP70*, *GbTLP20,* and *GbTLP65* was the most obvious. *GbTLP51*, *GbTLP4*, *GbTLP47*, *GbTLP75,* and *GbTLP74* were barely expressed at 0 h, but the expression levels were significantly upregulated after *V. dahlia* infection. These results indicated that many *TLP*s might participate in the resistance of cotton to *V. dahlia*.

Ectopic Expression of *GhTLP19* Promotes the Development of Trichome and Resistance to Drought in *Arabidopsis*

Tissue expression patterns showed that *GhTLP19* was specifically highly expressed during fiber_15, 20, 25 dpa period. Due to the similar regulatory mechanism of cotton fiber and *Arabidopsis* trichome (Wang et al., 2004; Guan et al., 2014), *GhTLP19* was overexpressed in *Arabidopsis* to further explore its function in fiber development. Then, the relatively high expression of *GhTLP19* was selected from T3 generation transgenic lines to observe the trichome development (**Figures 5A,B,D**). At the same time, *Arabidopsis* T-DNA insertion mutant *atpr5* (*At1g75040*; SALK_052587C) of *GhTLP19* homologous gene was recruited to analyze the phenotype (**Figures 5A–C**). It was indicated that the leaf trichome of transgenic lines was thicker than that of WT, but the difference was not significant, and the mutant was obviously the thinnest. What is more obvious is that the branching length and diameter of leaf trichome of transgenic lines increased significantly compared with that of WT and mutants (**Figure 5B** and **Table 1**). The results showed that the ectopic expression of *GhTLP19* significantly

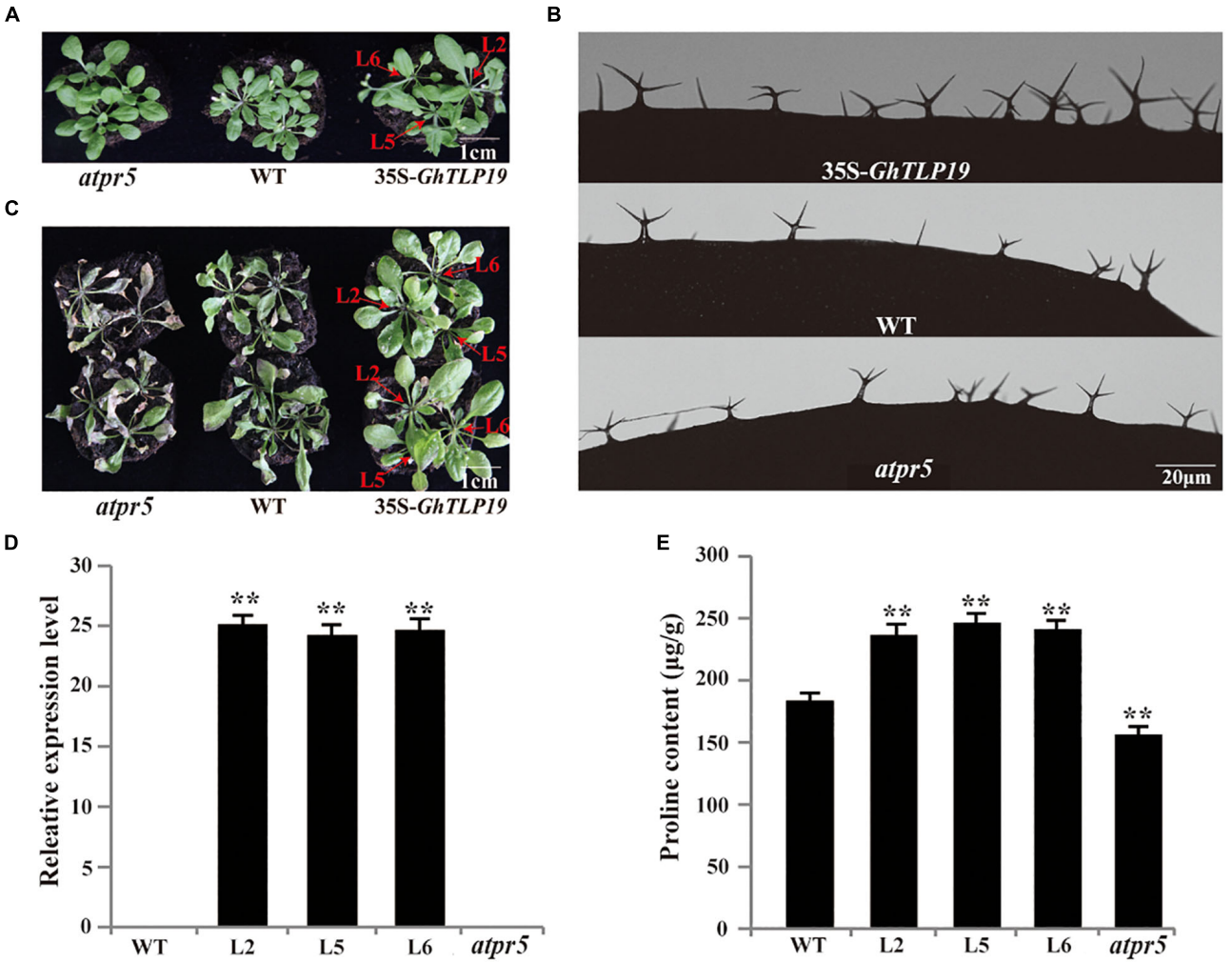


FIGURE 5 | *GhTLP19* overexpression promotes the trichome development and confers tolerance to drought in *Arabidopsis*. **(A)** Normal growth of *Arabidopsis* transgenic lines overexpressing *GhTLP19*, WT and *atpr5*. **(B)** The morphology of trichome in *Arabidopsis* transgenic lines overexpressing *GhTLP19*, WT and *atpr5* under normal growth conditions. **(C)** *GhTLP19* overexpression improved tolerance to drought in *Arabidopsis*. The plants were treated with 15% PEG6000 for 10 days. **(D)** Identification of *Arabidopsis* transgenic lines overexpressing *GhTLP19*. **(E)** The proline contents of *Arabidopsis* transgenic lines overexpressing *GhTLP19*, WT and *atpr5* under drought stress. L2, L5, L6 represent CLCrV:*GhTLP19*-2, -5, -6 lines, respectively. The bars represent the means ± SEs from three independent experiments. **indicates statistical significance at the 0.01 probability level. Three biological replicates were used, one of which is represented. In each biological replicate, more than 20 plants were used.

TABLE 1 | Compare the length and diameter of trichome.

Genotype	Length of trichome main stem/μm	Diameter of trichome main stem/μm	Length of trichome branch/μm	Diameter of trichome branch/μm	n
35S-*GhTLP19*	6.98 ± 2.15	2.56 ± 0.47	16.25 ± 4.13**	1.07 ± 0.08*	26
WT	5.34 ± 1.83	2.07 ± 0.31	10.58 ± 1.86	0.91 ± 0.06	27
Mutant	4.99 ± 0.95	1.01 ± 0.01*	5.98 ± 0.47**	0.65 ± 0.06**	23

*Values represent the means and standard deviations of three biological replicates. *Indicates a significant difference from WT ($p < 0.05$). **Indicates a significant difference from WT ($p < 0.01$). Data are presented as the mean ± SD.*

promoted the development of *Arabidopsis* trichome. Cotton fiber and *Arabidopsis* trichome are both composed of single cells, and their development patterns are also very similar, so it is speculated that *GhTLP19* might participate in the development of cotton fiber.

The well-growing *GhTLP19* transgenic lines, WT and mutant were irrigated with 15% PEG6000 to observe their response to the drought conditions. After irrigating with 15% PEG6000 for 10 days, the results of the determination of proline content showed that the proline content of *GhTLP19* overexpressed lines

was significantly higher than that of WT, while the proline content of mutant strains was significantly lower than that of WT (**Figure 5E**). The wilting phenomenon of WT leaves was obvious, and that of mutant leaves was the most serious, while the growth of *GhTLP19* overexpressed plants was relatively good (**Figure 5C**). Thus, overexpression of *GhTLP19* in *Arabidopsis* could improve the drought resistance of transgenic lines.

Silencing *GhTLP19* Reduced Tolerance to Stress in Cotton

VIGS technology was used to reduce the expression level of *GhTLP19* to identify its role in cotton plant response to drought (**Figure 6A**) and *V. dahlia* (**Figure 6B**). The expression levels of *GhTLP19* in young leaves of control (CLCrV:*00*) and CLCrV:*GhTLP19* lines were measured after albino plaques appeared in the true leaves of plants inoculated with CLCrV:*PDS*-expressing agrobacteria, the results showed that the expression level of *GhTLP19* decreased significantly after VIGS (**Figures 6D,G**). The VIGS lines of CLCrV:*GhTLP19* (Line 1, 2, and 3) and CLCrV:*00* lines were treated with drought. Treated with 15% PEG6000 irrigation a week later, leaves of CLCrV:*GhTLP19* lines appeared obvious wilting phenotype, compared with the CLCrV:*00* (**Figure 6A**). Then we measured the contents of MDA and CAT in VIGS and control lines, and it was found that MDA content in VIGS lines was significantly higher than that in control lines (**Figure 6E**), while CAT content was significantly lower (**Figure 6F**). The results showed that silencing *GhTLP19* reduced cotton's tolerance to drought.

qRT-PCR results showed that the expression level of *GhTLP19* was significantly up-regulated after CCRI36 was infected with *V. dahlia* (**Figure 4A**). VIGS technology was also used to silence the expression level of *GhTLP19* (Line 11, 12, and 13) to further identify its role in cotton response to *V. dahlia* (**Figures 6B,C,G**). After being infected with *V. dahlia*, CLCrV:*GhTLP19* lines showed obvious necrosis, yellowish and leaf shedding, while this phenomenon of the control lines was less severe (**Figure 6B**). Furthermore, the accumulation of mycelia in the stem of VIGS lines was significantly higher than that of the control lines (**Figure 6C**). The disease index (DI) of CLCrV:*GhTLP19* lines was significantly higher than that of control lines (**Figure 6H**). These data indicated that silencing *GhTLP19* could reduce cotton resistance to *V. dahlia*.

DISCUSSION

Our understanding of the genetic function of cotton, an economically important crop that can provide a large amount of industrial raw materials such as fiber, is limited (Ma et al., 2019a). As an important factor for plant resistance to biotic and abiotic stresses, *TLP*s may have a critical role in the regulation of the expression of many genes involved in the defense system (Wang et al., 2011; Singh et al., 2013; Zhang et al., 2018). However, there have been few reports on *TLP*s of cotton. In this study, we performed a systematic and comprehensive analysis of *TLP*s, and studied the function of *GhTLP19*.

Characterization of the *TLP*s in Cotton

With the evolution of plants and the expansion of various gene families, plants have gradually increased their tolerance to various kinds of environmental stresses (Kohler et al., 2008). *TLP*s, found in many plants, are a gene family that resists both biotic and abiotic stress. Allotetraploid cotton species descended from interspecific hybridization events between their ancestors *G. raimondii* and *G. arboretum* (Wendel et al., 2009), and the number of *TLP*s in upland and island cotton should be equal to the sum of the *TLP*s in *G. raimondii* and *G. arboreum*. However, the actual number of *TLP*s in allotetraploids (*G. hirsutum* 90 and *G. barbadense* 91) was less than the sum of those in the two diploids (*G. raimondii* 50 and *G. arboreum* 48) (**Supplementary Table S1**), indicating that, the doubling of chromosomes and the rapid sequence arrangement of the genome would result in different degrees of gene loss in the process of polyploidization (Paterson et al., 2004). Sequence analysis results showed that most of the cotton TLPs contained highly conserved cysteine residues, typical thaumatin family signature, and REDDD amino acids, as well as signal peptides and transmembrane domains (**Figure 1**, **Supplementary Figure S1**, and **Supplementary Table S1**). The 16 cysteine residues form eight disulfide bonds that increase the protein stability and resistance to pH, proteases, and heat-induced denaturation (Ghosh and Chakrabarti, 2008; Fierens et al., 2009). The N-terminal signal peptides and transmembrane domains of the TLPs allow mature proteins to enter the secretory pathway and secrete extracellular proteins to participate in the defense response (Wang et al., 2011; Singh et al., 2013). The acid cleft domain composed of the conserved REDDD amino acids was thought to have antifungal activity after binding to specific receptors (Min et al., 2004). These sequential structural characteristics indicated that the *TLP*s in cotton might be involved in resistance to biotic stress, such as *V. dahliae*.

Evolutionary tree analysis showed that the *TLP*s from several species were divided into 10 groups, and the distribution of the *TLP*s was relatively dispersed in each subgroup (**Figure 2**), which was consistent with the distribution in melon and *Arabidopsis* (Liu et al., 2010a, 2020). The sequence characteristics of *TLP*s indicate that its family members should be paraphyletic and originate from 10 common ancestors before the differentiation of monocotyledons and dicotyledons (Shatters et al., 2006; Kohler et al., 2008; Liu et al., 2010b). The TLP motifs in cotton were highly conserved, basically containing 10 conservative motifs (**Supplementary Figures S2, S3**). In terms of gene structure, the *TLP*s have a relatively small number of introns, similar to those in melon (Liu et al., 2020) and black nightshade (Jami et al., 2007), except for a few genes containing other domains. These differences in the structure of individual genes might be related to the polyploidy of cotton chromosomes and the diversity of gene functions (Rogozin et al., 2003; Yang et al., 2008).

Potential Regulatory Mechanisms and Functions of *TLP*s

As gene families expand and adapt to changes in the environment, members of a gene family might evolve new functions or increase/decrease the strength of old ones. By

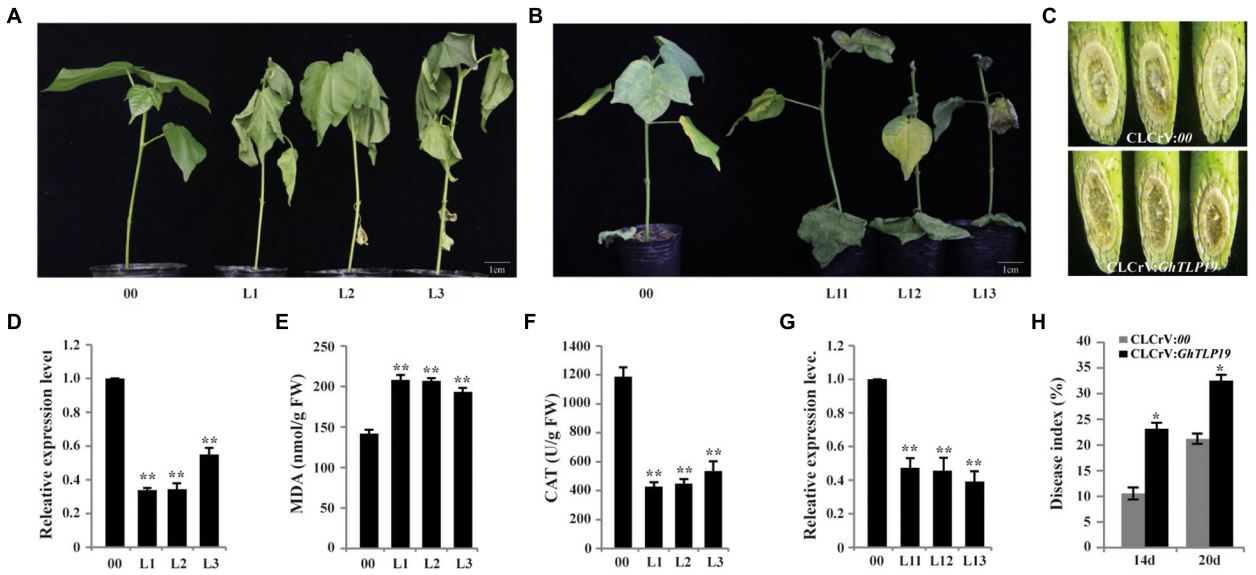


FIGURE 6 | Silencing *GhTLP19* via VIGS increased sensitivity to drought and *V. dahliae* in cotton. **(A)** Phenotype of empty control and VIGS plants under 15% PEG6000 treatment. **(B)** Phenotype of empty control and VIGS plants under *V. dahliae* treatment. **(C)** V991 hyphal accumulation in WT and VIGS plants after inoculation. **(D)** The expression level of *GhTLP19* in empty control and VIGS plants to drought treat. **(E)** The MDA content of empty control and VIGS plants under drought stress. **(F)** The CAT content of empty control and VIGS plants under drought stress. **(G)** The expression level of *GhTLP19* in empty control and VIGS plants to *V. dahliae* treat. **(H)** Disease indices of CLCrV:*00* and CLCrV:*GhTLP19* plants were determined after inoculation with *V. dahliae*. L1, L2, L3, L11, L12, L13 represent CLCrV:*GhTLP19*-1, -2, -3, -11, -12, -13 lines, respectively. The bars represent the means ± SEs from three independent experiments. **and *indicate statistical significance at the 0.01 and 0.05 probability levels, respectively.

analyzing the expression patterns and regulatory relationships of family members, we further elucidated the potential functions of the *TLP* family in cotton. Our results suggested that the function of the *TLP*s in cotton might be not only related to resistance to biotic stress but also involved in abiotic stress, and plant growth and development.

For instance, studies have shown that *GbTLP1* was specifically expressed during the secondary wall development of cotton fiber (Munis et al., 2010), while we found that some genes, such as *GhTLP19*, *GhTLP68*, *GbTLP21*, and *GbTLP66* were specifically expressed in this period, and the expression levels were particularly high (fiber_15,20, and 25 dpa) (**Figures 3A**, **4C,D**). In their promoter regions, all of these genes contained ERE regulatory elements (**Supplementary Figures S4B, S5** and **Supplementary Table S2**) that could bind to ethylene transcription factors and regulate fiber development (Gou et al., 2007), and there were also many ERE-related TFs found in the TFBS analysis (**Supplementary Table S3**). *Cis*-elements (such as ABRE, TGA-element) and TFs (such as WRKY and Dof) can respond to ABA, IAA, and GA (Rushton et al., 2010) and participate in the growth and developmental processes of plants (Lijavetzky et al., 2003). The analysis of *cis*-element and TFBS revealed many specific elements that might be related to the development of seeds (RY-elements), endosperm (GCN4_motif) and TFs (**Supplementary Figures S4B, S5** and **Supplementary Tables S2, S3**). Specific genes were also highly expressed in seeds (*GhTLP56* and *GhTLP82*) and roots (*GhTLP16* and *GhTLP65*) during seedling germination (**Supplementary Figure S7**). These results further suggested that the *TLP*s might be involved in the growth and development of cotton, especially reproductive and fiber development.

*TLP*s have also been found to respond to various biotic/abiotic stresses in other plants. Recently, study found that all *PR-5* genes might play a particular role in the defense system of soybean plants, especially leaves, against high salt stress (Tachi et al., 2009). *Arabidopsis* Di19, as a transcription factor, regulates the expression of *PR5* in response to drought stress (Liu et al., 2013). Overexpression of the osmotin gene increased the tolerance of transgenic tomato plants to salt and drought (Goel et al., 2010). In our expression profile of abiotic stress (**Figure 3B**), we found that *GhTLP35* and *GhTLP81* showed first increase then decrease trend under salt, cold and PEG conditions. Both *GhTLP58* and *GhTLP43* reached their highest expression levels after 12 h of heat, salt or PEG treatment (**Figure 3B**).

Moreover, study showed that ectopic expression of *ObTLP1* in *Arabidopsis* enhanced the tolerance to *S. sclerotiorum* and *B. cinerea* infection, as well as to dehydration and salt stress (Misra et al., 2016). Resistance to *V. dahliae* and *F. oxysporum* was significantly enhanced in transgenic plants overexpressing *GbTLP1*, and tolerance to salt and drought stress was also enhanced (Munis et al., 2010). As an important antimicrobial-related protein, *Rtlp1* can be induced by rice blast fungus, salicylic acid (SA) and methyl jasmonate (MeJA), and the W-box is an essential *cis*-acting element of the *Rtlp1* promoter in response to fungal elicitors (Hiroyuki and Terauchi, 2008; Miao et al., 2019). In our study, various elements that respond to SA (TCA-element), MeJA (CGTCA-motif, TGACG-motif) and the W-box were also found in the promoter regions of most *TLP*s and were

necessary components for plants for induction of *TLP* expression by fungal elicitors. We also found that most *TLP* gene promoter regions in cotton contain *cis*-acting elements that respond to low temperature (LTR) and drought (MYC, DRE). In the TFBS analysis results (**Supplementary Table S3** and **Supplementary Figure S6**), various transcription factors interacting with *TLP*s were related to plant resistance to biotic/abiotic stress. For example, the AP2 transcription factor could not only withstand abiotic stress such as drought and salt but also interacted with pathogen-related protein promoters to resist pathogen invasion (Park et al., 2001; Mizoi et al., 2012). ERF is also an important transcription factor in the response to important ethylene signals and pathogen invasion in plants (Licausi et al., 2010). The bZIP and C2H2 zinc finger protein transcription factors play a key role in the transcriptional regulation of plants in response to extreme temperature, salinity, drought and oxidative stress (Agarwal et al., 2019; Joo et al., 2019; Wang et al., 2019). The analysis results of these regulatory mechanisms indicate that *TLP*s might be involved in the process of cotton environmental stress.

Our qRT-PCR results showed that many *TLP*s (such as *GhTLP24*, *GhTLP72*, *GbTLP20,* and *GbTLP65*) were significantly upregulated in upland and sea-island cotton after *V. dahliae* infection (**Figures 4A,B**). Our experimental data showed that *Arabidopsis* with overexpression of *GhTLP19* was more drought-resistant, and cotton with silencing of *GhTLP19* gene was more sensitive to drought and *V. dahliae*. The above results indicated that the *TLP*s should participate in biotic/abiotic stress processes in cotton.

Function of *GhTLP19* in *Arabidopsis* and Cotton

The development mechanism of cotton fiber and leaf trichome of *Arabidopsis* share many similarities (Lee et al., 2007). MiR828 and miR858 regulate the function of *MYB2* in *Arabidopsis* and cotton, respectively, to affect the development of trichome and fiber (Guan et al., 2014). Overexpression of *GhCLASP2* in *Arabidopsis* increased the number of trichome branches and restored the trichome phenotype of *clasp-1* mutant (Zhu et al., 2018). In our study, by overexpressing *GhTLP19* in *Arabidopsis*, the branches of the trichome are significantly longer than those of the WT. At the same time, the diameter of the trichome of the overexpressed *GhTLP19* lines was thicker than that of WT (**Figure 5B** and **Table 1**). We also found that the leaves of mutant and overexpressed lines were larger than those of wild-type. These results suggested that *GhTLP19* may play a role in the development of cotton fiber.

As previously mentioned, a large number of studies have shown that *PR* proteins play an important role in plant environmental stress (Munis et al., 2010; Misra et al., 2016). As a member of *PR* proteins, *GhTLP19* should also have certain resistance to environmental stress. In the current study, the overexpression lines and WT were irrigated with 15% PEG6000, and the results showed that the tolerance of the overexpressed lines to drought stress was significantly higher than that of WT, and the content of proline was also significantly increased (**Figures 5C,E**). Due to factors such as long time and low efficiency of cotton transgene, we chose short experimental period, simple operation method, low cost and high-efficiency VIGS technology to silence *GhTLP19* to study its functions (Gu et al., 2018). Thus we silenced *GhTLP19* in cotton with VIGS strategy and irrigated them with 15% PEG6000. The results showed that the silenced plants showed significant wilting than the control plants, and the content changes of MDA and CAT also reached a significant difference (**Figures 6A,D,E,F**). In order to identify the role of *GhTLP19* in the corresponding *V. dahliae* invasion of cotton, 2×10^7 *V. dahliae* were used to infect VIGS and control plants (**Figures 6B,G,H**). The results showed that the resistance of VIGS plants to *V. dahliae* was weaker than that of control plants, the disease index and mycelia accumulation in the stems of VIGS plants were significantly higher than that of the control plants. This research is consistent with the research results of *GbTLP1* (Munis et al., 2010). Therefore, *GhTLP19* was also resistant to drought and *V. dahliae*. Further, *GhTLP19* co-expression network analysis found that a total of 26 genes were co-expressed with *GhTLP19* (**Supplementary Figure S8**). Through functional annotation (**Supplementary Table S6**), we found that the gene *Gh_A07G1075* (*CIPK1*)encoding serine-threonine protein kinase may improve the response of plants to environmental stress such as drought, high salt, wounding and abscisic acid (Pan et al., 2018). *Gh_D12G1855* and *Gh_A12G1694* (*CEP1*) may be involved in controlling late epidermal cell death, limiting growth, and increasing resistance to pathogen (Höwing et al., 2014). These genes may be co-expressed with *GhTLP19* and participate in the response to environmental stress (**Figures 5**, **6**).

CONCLUSION

In this study, we identified the *TLP*s in four different cotton varieties. Segmental and tandem duplication were the main mechanisms of gene expansion in the *TLP*s during evolution. The structural characteristics, evolutionary relationships, and conserved domains of these genes were also analyzed. In addition, we predicted and analyzed the potential molecular regulatory mechanisms and functions of the *TLP*s, as well as their expression patterns after the cotton species were infected with *V. dahliae*, during the fiber development period and in environmental conditions. The overexpression of *GhTLP19* in *Arabidopsis* and the VIGS experiment in cotton showed that *GhTLP19* could enhance plant resistance to drought and *V. dahliae*, and promote the development of *Arabidopsis* trichome and likely cotton fiber. These genes might be precisely regulated by transcription factors and various plant hormone signals in the external environment. Their functions are diverse; they not only respond to various biotic/abiotic stresses and hormone signaling pathways but also participate in some growth and development processes, such as fiber development.

DATA AVAILABILITY STATEMENT

The datasets presented in this study can be found in online repositories. The names of the repository/repositories

and accession number(s) can be found in the article/ **Supplementary Material**.

AUTHOR CONTRIBUTIONS

QM and SF conceived and designed the experiments. KQ and XW prepared the figures and tables. LZ and YC analyzed and interpreted the data. ZL prepared the manuscript and participated in all experiments. KQ constructed the vector. LZ and QM treated and adjusted of traits. LZ and XW revised the manuscript. All authors have read and agreed to the published version of the manuscript.

FUNDING

The research was supported by grants from the National Natural Science Foundation of China (31701474).

ACKNOWLEDGMENTS

We thank Edanz Group (www.liwenbianji.cn/ac), for editing the English text of a draft of this manuscript.

SUPPLEMENTARY MATERIAL

The Supplementary Material for this article can be found online at: https://www.frontiersin.org/articles/10.3389/fpls.2020.575015/full#supplementary-material

Supplementary Figure 1 | Thaumatin sequence alignment of all the *TLP* genes in cotton. The *TLP* family signature in thaumatin is framed with a black border. The conserved residues are indicated by cyan numbers. Conserved positions of five amino acids are labeled with a red asterisk. The black line shows the amino acids forming the bottom of the acidic cleft.

Supplementary Figure 2 | Phylogenetic relationships, gene structure and motif analysis of the *GhTLP*s. **(A)** Phylogenetic relationships of the *GhTLP*s. **(B)** Gene structures of the *GhTLP*s. **(C)** The conserved motifs of the *GhTLP*s.

Supplementary Figure 3 | Phylogenetic relationships, gene structures and motif analysis of the cotton *TLP*s. **(A)** Phylogenetic relationships and gene structures of the cotton *TLP*s. **(B)** The conserved motifs of the *TLP*s.

Supplementary Figure 4 | Distribution characteristics of *cis*-acting elements in the promoter regions of *TLP*s. **(A)** The proportion of each *cis*-acting element in four different cotton species. **(B)** The number of *cis*-acting elements in each of the four cotton species.

Supplementary Figure 5 | Distribution characteristics of the *cis*-acting elements in the promoter regions of the *GhTLP*s. Different *cis*-acting elements are represented by different color boxes.

Supplementary Figure 6 | Gene Ontology (GO) annotation of the TFs binding to the *GhTLP* genes' putative promoter regions based on their cellular component, molecular function, and biological process.

Supplementary Figure 7 | Expression profile of the *GhTLP*s at the seed germination and seedling stages. The tissues are shown at the opening, genes are shown on the periphery, and the phylogenetic relationships are shown in the inner region. The color represents TLP expression profiles: Log2 (FPKM).

Supplementary Figure 8 | Co-expression network of *GhTLP19*. Nodes representing individual genes and edges indicate significant co-expression between genes. The pink lines represent protein's own interaction and positive co-expression relationship with the target protein. The blue lines represent protein's own interaction and negative co-expression relationship with the target protein. The orange line represents protein own interaction and protein-protein relationship with the target protein. Prediction and analysis of co-expression networks, as well as gene function annotation, were performed on ccNET (http://structuralbiology.cau.edu.cn/gossypium/).

Supplementary Table 1 | Details of the *TLP*s in four *Gossypium* species.

Supplementary Table 2 | Distribution of the major *cis*-elements in the promoter regions of the *TLP*s. The locations of these *cis*-elements were confirmed using the PlantCARE database.

Supplementary Table 3 | List of the identified TFBSs in the putative promoter regions of the *GhTLP* gene family using PlantTFDB 4.0.

Supplementary Table 4 | The expression levels of the *TLP*s under *V. dahliae* treatment and during fiber development via qRT-PCR. The expression levels of each target gene were calculated by the cycle threshold $(CT)^{2-\Delta\Delta Ct}$ method.

Supplementary Table 5 | Primers for qRT-PCR in this study.

Supplementary Table 6 | The annotation of *GhTLP19* co-expression genes.

REFERENCES

Agarwal, P., Baranwal, V. K., and Khurana, P. (2019). Genome-wide Analysis of bZIP Transcription Factors in wheat and Functional Characterization of a TabZIP under Abiotic Stress. *Sci. Rep.* 9:4608. doi: 10.1038/s41598-019-40659-7

Clough, S. J., and Bent, A. F. (1998). Floral dip: a simplified method for Agrobacterium-mediated transformation of *Arabidopsis thaliana*. *Plant J.* 16, 735–743. doi: 10.1046/j.1365-313x.1998.00343.x

Dubey, N., and Singh, K. (2018). "Role of NBS-LRR proteins in plant defense," in *Molecular Aspects of Plant-Pathogen Interaction*, eds A. Singh and I. Singh (Singapore: Springer), 115–138. doi: 10.1007/978-981-10-7371-7_5

Fierens, E., Gebruers, K., Voet, A. R. D., De Maeyer, M., Courtin, C. M., and Delcour, J. A. (2009). Biochemical and structural characterization of TLXI, the Triticum aestivum L. thaumatin-like xylanase inhibitor. *J. Enzyme Inhib. Med. Chem.* 24, 646–654. doi: 10.1080/14756360802321831

Finn, R. D., Coggill, P., Eberhardt, R. Y., Eddy, S. R., Mistry, J., Mitchell, A. L., et al. (2016). The Pfam protein families database: towards a more sustainable future. *Nucleic Acids Res.* 44, D279–D285. doi: 10.1093/nar/gkv1344

Ghosh, R., and Chakrabarti, C. (2008). Crystal structure analysis of NP24-I: a thaumatin-like protein. *Planta* 228, 883. doi: 10.1007/s00425-008-0790-5

Gimenez-Ibanez, S., and Solano, R. (2013). Nuclear jasmonate and salicylate signaling and crosstalk in defense against pathogens. *Front. Plant Sci.* 4:72. doi: 10.3389/fpls.2013.00072

Goel, D., Singh, A. K., Yadav, V., Babbar, S. B., and Bansal, K. C. (2010). Overexpression of osmotin gene confers tolerance to salt and drought stresses in transgenic tomato (*Solanum lycopersicum* L.). *Protoplasma* 245, 133–141. doi: 10.1007/s00709-010-0158-0

Gong, Q., Yang, Z., Wang, X., Butt, H. I., Chen, E., He, S., et al. (2017). Salicylic acid-related cotton (*Gossypium arboreum*) ribosomal protein GaRPL18 contributes to resistance to *Verticillium dahliae*. *BMC Plant Biol.* 17:59. doi: 10.1186/s12870-017-1007-5

Gou, J. Y., Wang, L. J., Chen, S. P., Hu, W. L., and Chen, X. Y. (2007). Gene expression and metabolite profiles of cotton fiber during cell elongation and secondary cell wall synthesis. *Cell Res.* 17, 422–434. doi: 10.1038/sj.cr.7310150

Gu, L., Wang, H., Wei, H., Sun, H., Li, L., Chen, P., et al. (2018). Identification, expression, and functional analysis of the group iid wrky subfamily in upland cotton (*Gossypium hirsutum* l.). *Front. Plant Sci.* 871:1684. doi: 10.3389/fpls.2018.01684

Guan, X., Pang, M., Nah, G., Shi, X., Ye, W., Stelly, D. M., et al. (2014). MiR828 and miR858 regulate homoeologous *MYB2* gene functions in *Arabidopsis* trichome and cotton fibre development. *Nat. Commun.* 5:3050. doi: 10.1038/ncomms4050

Hiroyuki, K., and Terauchi, R. (2008). Regulation of expression of rice thaumatin-like protein: inducibility by elicitor requires promoter W-box elements. *Plant Cell Rep.* 27, 1521–1528. doi: 10.1007/s00299-008-0536-7

Höwing, T., Huesmann, C., Hoefle, C., Nagel, M. K., Isono, E., Hückelhoven, R., et al. (2014). Endoplasmic reticulum KDEL-tailed cysteine endopeptidase 1 of Arabidopsis (AtCEP1) is involved in pathogen defense. *Front. Plant Sci.* 5:58. doi: 10.3389/fpls.2014.00058

Hu, B., Jin, J., Guo, A. Y., Zhang, H., Luo, J., and Gao, G. (2015). GSDS 2.0: an upgraded gene feature visualization server. *Bioinformatics* 31, 1296–1297. doi: 10.1093/bioinformatics/btu817

Hu, Q., Zhu, L., Zhang, X., Guan, Q., Xiao, S., Min, L., et al. (2018). GhCPK33 negatively regulates defense against *Verticillium dahliae* by phosphorylating GhOPR3. *Plant Physiol.* 178, 876–889. doi: 10.1104/pp.18.00737

Hu, X., and Reddy, A. S. N. (1997). Cloning and expression of a PR5-like protein from Arabidopsis: inhibition of fungal growth by bacterially expressed protein. *Plant Mol. Biol.* 34, 949–959. doi: 10.1023/A:1005893119263

Jami, S. K., Swathi Anuradha, T., Guruprasad, L., and Kirti, P. B. (2007). Molecular, biochemical and structural characterization of osmotin-like protein from black nightshade (*Solanum nigrum*). *J. Plant Physiol.* 164, 238–252. doi: 10.1016/j.jplph.2006.01.006

Jiao, W., Li, X., Zhao, H., Cao, J., and Jiang, W. (2018). Antifungal activity of an abundant thaumatin-like protein from banana against penicillium expansum, and its possible mechanisms of action. *Molecules* 23:1442. doi: 10.3390/molecules23061442

Joo, H., Lim, C. W., and Lee, S. C. (2019). Roles of pepper bZIP transcription factor CaATBZ1 and its interacting partner RING-type E3 ligase CaASRF1 in modulation of ABA signalling and drought tolerance. *Plant J.* 100, 399–410. doi: 10.1111/tpj.14451

Kazan, K., and Lyons, R. (2014). Intervention of phytohormone pathways by pathogen effectors. *Plant Cell* 26, 2285–2309. doi: 10.1105/tpc.114.125419

Kim, D., Pertea, G., Trapnell, C., Pimentel, H., Kelley, R., and Salzberg, S. L. (2013). TopHat2: accurate alignment of transcriptomes in the presence of insertions, deletions and gene fusions. *Genome Biol.* 14:R36. doi: 10.1186/gb-2013-14-4-r36

Kohler, A., Rinaldi, C., Duplessis, S., Baucher, M., Geelen, D., Duchaussoy, F., et al. (2008). Genome-wide identification of NBS resistance genes in Populus trichocarpa. *Plant Mol. Biol.* 66, 619–636. doi: 10.1007/s11103-008-9293-9

Krogh, A., Larsson, B., Von Heijne, G., and Sonnhammer, E. L. L. (2001). Predicting transmembrane protein topology with a hidden Markov model: application to complete genomes. *J. Mol. Biol.* 305, 567–580. doi: 10.1006/jmbi.2000.4315

Latijnhouwers, M., De Wit, P. J. G. M., and Govers, F. (2003). Oomycetes and fungi: similar weaponry to attack plants. *Trends Microbiol.* 11, 462–469. doi: 10.1016/j.tim.2003.08.002

Lee, J. J., Woodward, A. W., and Chen, Z. J. (2007). Gene expression changes and early events in cotton fibre development. *Ann. Bot.* 100, 1391–1401. doi: 10.1093/aob/mcm232

Lescot, M. (2002). PlantCARE, a database of plant cis-acting regulatory elements and a portal to tools for in silico analysis of promoter sequences. *Nucleic Acids Res.* 30, 325–327. doi: 10.1093/nar/30.1.325

Letunic, I., Doerks, T., and Bork, P. (2015). SMART: recent updates, new developments and status in 2015. *Nucleic Acids Res.* 43, D257–D260. doi: 10.1093/nar/gku949

Li, B., Meng, X., Shan, L., and He, P. (2016). Transcriptional regulation of pattern-triggered immunity in plants. *Cell Host Microbe* 19, 641–650. doi: 10.1016/j.chom.2016.04.011

Li, W., Zhu, Z., Chern, M., Yin, J., Yang, C., Ran, L., et al. (2017). A natural allele of a transcription factor in rice confers broad-spectrum blast resistance. *Cell* 170, 114–126.e15. doi: 10.1016/j.cell.2017.06.008

Licausi, F., Giorgi, F. M., Zenoni, S., Osti, F., Pezzotti, M., and Perata, P. (2010). Genomic and transcriptomic analysis of the AP2/ERF superfamily inVitis vinifera. *BMC Genomics* 11:719. doi: 10.1186/1471-2164-11-719

Lijavetzky, D., Carbonero, P., and Vicente-Carbajosa, J. (2003). Genome-wide comparative phylogenetic analysis of the rice and Arabidopsis Dof gene families. *BMC Evol. Biol.* 3:17. doi: 10.1186/1471-2148-3-17

Liu, J. J., Sturrock, R., and Ekramoddoullah, A. K. M. (2010a). The superfamily of thaumatin-like proteins: its origin, evolution, and expression towards biological function. *Plant Cell Rep.* 29, 419–436. doi: 10.1007/s00299-010-0826-8

Liu, J. J., Zamani, A., and Ekramoddoullah, A. K. M. (2010b). Expression profiling of a complex thaumatin-like protein family in western white pine. *Planta* 231, 637–651. doi: 10.1007/s00425-009-1068-2

Liu, W. X., Zhang, F. C., Zhang, W. Z., Song, L. F., Wu, W. H., and Chen, Y. F. (2013). Arabidopsis Di19 functions as a transcription factor and modulates PR1, PR2, and PR5 expression in response to drought stress. *Mol. Plant* 6, 1487–1502. doi: 10.1093/mp/sst031

Liu, Y., Cui, J., Zhou, X., Luan, Y., and Luan, F. (2020). Genome-wide identification, characterization and expression analysis of the TLP gene family in melon (*Cucumis melo* L.). *Genomics* 112, 2499–2509. doi: 10.1016/j.ygeno.2020.02.001

Livak, K. J., and Schmittgen, T. D. (2001). Analysis of relative gene expression data using real-time quantitative PCR and the 2-ΔΔCT method. *Methods* 25, 402–408. doi: 10.1006/meth.2001.1262

Ma, J., Geng, Y., Pei, W., Wu, M., Li, X., Liu, G., et al. (2018). Genetic variation of dynamic fiber elongation and developmental quantitative trait locus mapping of fiber length in upland cotton (*Gossypium hirsutum* L.). *BMC Genomics* 19:882. doi: 10.1186/s12864-018-5309-2

Ma, J., Liu, J., Pei, W., Ma, Q., Wang, N., Zhang, X., et al. (2019a). Genome-wide association study of the oil content in upland cotton (*Gossypium hirsutum* L.) and identification of *GhPRXR*1, a candidate gene for a stable QTLqOC-Dt5-1. *Plant Sci.* 286, 89–97. doi: 10.1016/j.plantsci.2019.05.019

Ma, J., Pei, W., Ma, Q., Geng, Y., Liu, G., Liu, J., et al. (2019b). QTL analysis and candidate gene identification for plant height in cotton based on an interspecific backcross inbred line population of *Gossypium hirsutum* × *Gossypium barbadense*. *Theor. Appl. Genet.* 132, 2663–2676. doi: 10.1007/s00122-019-03380-7

Miao, Y., Xu, L., He, X., Zhang, L., Shaban, M., Zhang, X., et al. (2019). Suppression of tryptophan synthase activates cotton immunity by triggering cell death via promoting SA synthesis. *Plant J.* 98, 329–345. doi: 10.1111/tpj.14222

Min, K., Ha, S. C., Hasegawa, P. M., Bressan, R. A., Yun, D. J., and Kim, K. K. (2004). Crystal structure of Osmotin, a plant antifungal protein. *Proteins Struct. Funct. Genet.* 54, 170–173. doi: 10.1002/prot.10571

Misra, R. C., Sandeep, Kamthan, M., Kumar, S., and Ghosh, S. (2016). A thaumatin-like protein of *Ocimum basilicum* confers tolerance to fungal pathogen and abiotic stress in transgenic Arabidopsis. *Sci. Rep.* 6:25340. doi: 10.1038/srep25340

Mizoi, J., Shinozaki, K., and Yamaguchi-Shinozaki, K. (2012). AP2/ERF family transcription factors in plant abiotic stress responses. *Biochim. Biophys. Acta* 1819, 86–96. doi: 10.1016/j.bbagrm.2011.08.004

Munis, M. F. H., Tu, L., Deng, F., Tan, J., Xu, L., Xu, S., et al. (2010). A thaumatin-like protein gene involved in cotton fiber secondary cell wall development enhances resistance against *Verticillium dahliae* and other stresses in transgenic tobacco. *Biochem. Biophys. Res. Commun.* 393, 38–44. doi: 10.1016/j.bbrc.2010.01.069

Neale, A. D., Wahleithner, J. A., Lund, M., Bonnett, H. T., Kelly, A., Meeks-Wagner, D. R., et al. (1990). Chitinase, β-1,3-glucanase, osmotin, and extensin are expressed in tobacco explants during flower formation. *Plant Cell* 2, 673–684. doi: 10.2307/3869130

Pan, W., Shen, J., Zheng, Z., Yan, X., Shou, J., Wang, W., et al. (2018). Overexpression of the Tibetan Plateau annual wild barley (*Hordeum spontaneum*) HsCIPKs enhances rice tolerance to heavy metal toxicities and other abiotic stresses. *Rice* 11:51. doi: 10.1186/s12284-018-0242-1

Park, J. M., Park, C. J., Lee, S. B., Ham, B. K., Shin, R., and Paek, K. H. (2001). Overexpression of the tobacco Tsi1 gene encoding an EREBP/AP2-type

transcription factor enhances resistance against pathogen attack and osmotic stress in tobacco. *Plant Cell* 13, 1035–1046. doi: 10.1105/tpc.13.5.1035

Paterson, A. H., Bowers, J. E., and Chapman, B. A. (2004). Ancient polyploidization predating divergence of the cereals, and its consequences for comparative genomics. *Proc. Natl. Acad. Sci. U.S.A.* 101, 9903–9908. doi: 10.1073/pnas.0307901101

Petersen, T. N., Brunak, S., Von Heijne, G., and Nielsen, H. (2011). SignalP 4.0: discriminating signal peptides from transmembrane regions. *Nat. Methods* 8, 785–786. doi: 10.1038/nmeth.1701

Petre, B., Major, I., Rouhier, N., and Duplessis, S. (2011). Genome-wide analysis of eukaryote thaumatin-like proteins (TLPs) with an emphasis on poplar. *BMC Plant Biol.* 11:33. doi: 10.1186/1471-2229-11-33

Rogozin, I. B., Wolf, Y. I., Sorokin, A. V., Mirkin, B. G., and Koonin, E. V. (2003). Remarkable interkingdom conservation of intron positions and massive, lineage-specific intron loss and gain in eukaryotic evolution. *Curr. Biol.* 13, 1512–1517. doi: 10.1016/S0960-9822(03)00558-X

Rout, E., Nanda, S., and Joshi, R. K. (2016). Molecular characterization and heterologous expression of a pathogen induced PR5 gene from garlic (*Allium sativum* L.) conferring enhanced resistance to necrotrophic fungi. *Eur. J. Plant Pathol.* 144, 345–360. doi: 10.1007/s10658-015-0772-y

Rushton, P. J., Somssich, I. E., Ringler, P., and Shen, Q. J. (2010). WRKY transcription factors. *Trends Plant Sci.* 15, 247–258. doi: 10.1016/j.tplants.2010.02.006

Seo, P. J., Lee, A. K., Xiang, F., and Park, C. M. (2008). Molecular and functional profiling of Arabidopsis pathogenesis-related genes: insights into their roles in salt response of seed germination. *Plant Cell Physiol.* 49, 334–344. doi: 10.1093/pcp/pcn011

Shatters, R. G., Boykin, L. M., Lapointe, S. L., Hunter, W. B., and Weathersbee, A. A. (2006). Phylogenetic and structural relationships of the PR5 gene family reveal an ancient multigene family conserved in plants and select animal taxa. *J. Mol. Evol.* 63, 12–29. doi: 10.1007/s00239-005-0053-z

Singh, N. K., Kumar, K. R. R., Kumar, D., Shukla, P., and Kirti, P. B. (2013). Characterization of a pathogen induced thaumatin-like protein gene AdTLP from *Arachis diogoi*, a wild peanut. *PLoS One* 8:e83963. doi: 10.1371/journal.pone.0083963

Singh, S., Tripathi, R. K., Lemaux, P. G., Buchanan, B. B., and Singh, J. (2017). Redox-dependent interaction between thaumatin-like protein and β-glucan influences malting quality of barley. *Proc. Natl. Acad. Sci. U.S.A.* 114, 7725–7730. doi: 10.1073/pnas.1701824114

Tachi, H., Fukuda-Yamada, K., Kojima, T., Shiraiwa, M., and Takahara, H. (2009). Molecular characterization of a novel soybean gene encoding a neutral PR-5 protein induced by high-salt stress. *Plant Physiol. Biochem.* 47, 73–79. doi: 10.1016/j.plaphy.2008.09.012

Tamura, K., Stecher, G., Peterson, D., Filipski, A., and Kumar, S. (2013). MEGA6: molecular evolutionary genetics analysis version 6.0. *Mol. Biol. Evol.* 30, 2725–2729. doi: 10.1093/molbev/mst197

Trapnell, C., Roberts, A., Goff, L., Pertea, G., Kim, D., Kelley, D. R., et al. (2012). Differential gene and transcript expression analysis of RNA-seq experiments with TopHat and Cufflinks. *Nat. Protoc.* 7, 562–578. doi: 10.1038/nprot.2012.016

Wang, K., Ding, Y., Cai, C., Chen, Z., and Zhu, C. (2019). The role of C2H2 zinc finger proteins in plant responses to abiotic stresses. *Physiol. Plant.* 165, 690–700. doi: 10.1111/ppl.12728

Wang, Q., Li, F., Zhang, X., Zhang, Y., Hou, Y., Zhang, S., et al. (2011). Purification and characterization of a CkTLP protein from Cynanchum komarovii seeds that confers antifungal activity. *PLoS One* 6:e16930. doi: 10.1371/journal.pone.0016930

Wang, S., Wang, J. W., Yu, N., Li, C. H., Luo, B., Gou, J. Y., et al. (2004). Control of plant trichome development by a cotton fiber MYB gene. *Plant Cell* 16, 2323–2334. doi: 10.1105/tpc.104.024844

Wang, W., Zhang, X., Deng, F., Yuan, R., and Shen, F. (2017). Genome-wide characterization and expression analyses of superoxide dismutase (SOD) genes in *Gossypium hirsutum*. *BMC Genomics* 18:376. doi: 10.1186/s12864-017-3768-5

Wendel, J. F., Brubaker, C., Alvarez, I., Cronn, R., and Stewart, J. M. (2009). "Evolution and natural history of the cotton genus," in *Genetics and Genomics of Cotton*, ed. A. H. Paterson (New York, NY: Springer), 3–22. doi: 10.1007/978-0-387-70810-2_1

Xin, X. F., Nomura, K., Aung, K., Velásquez, A. C., Yao, J., Boutrot, F., et al. (2016). Bacteria establish an aqueous living space in plants crucial for virulence. *Nature* 539, 524–529. doi: 10.1038/nature20166

Xu, G., Yuan, M., Ai, C., Liu, L., Zhuang, E., Karapetyan, S., et al. (2017). UORF-mediated translation allows engineered plant disease resistance without fitness costs. *Nature* 545, 491–494. doi: 10.1038/nature22372

Yan, X., Qiao, H., Zhang, X., Guo, C., Wang, M., Wang, Y., et al. (2017). Analysis of the grape (*Vitis vinifera* L.) thaumatin-like protein (TLP) gene family and demonstration that TLP29 contributes to disease resistance. *Sci. Rep.* 7:4269. doi: 10.1038/s41598-017-04105-w

Yang, Z., Zhou, Y., Wang, X., Gu, S., Yu, J., Liang, G., et al. (2008). Genomewide comparative phylogenetic and molecular evolutionary analysis of tubby-like protein family in Arabidopsis, rice, and poplar. *Genomics* 92, 246–253. doi: 10.1016/j.ygeno.2008.06.001

Zhang, L., Zhao, H. K., Dong, Q. L., Zhang, Y. Y., Wang, Y. M., Li, H. Y., et al. (2015). Genome-wide analysis and expression profiling under heat and drought treatments of HSP70 gene family in soybean (*Glycine max* L.). *Front. Plant Sci.* 6:773. doi: 10.3389/fpls.2015.00773

Zhang, M., Xu, J., Liu, G., and Yang, X. (2018). Antifungal properties of a thaumatin-like protein from watermelon. *Acta Physiol. Plant.* 40:186. doi: 10.1007/s11738-018-2759-8

Zhang, Y., Wang, X., Rong, W., Yang, J., Li, Z., Wu, L., et al. (2017). Histochemical analyses reveal that stronger intrinsic defenses in *Gossypium barbadense* than in *G. hirsutum* are associated with resistance to verticillium dahliae. *Mol. Plant Microbe Interact.* 30, 984–996. doi: 10.1094/MPMI-03-17-0067-R

Zhao, J. P., and Su, X. H. (2010). Patterns of molecular evolution and predicted function in thaumatin-like proteins of *Populus trichocarpa*. *Planta* 232, 949–962. doi: 10.1007/s00425-010-1218-6

Zhu, S. H., Xue, F., Li, Y. J., Liu, F., Zhang, X. Y., Zhao, L. J., et al. (2018). Identification and functional characterization of a microtubule-associated protein, GhCLASP2, from upland cotton (*Gossypium hirsutum* L.). *Front. Plant Sci.* 9, 882. doi: 10.3389/fpls.2018.00882

Zhu, T., Liang, C., Meng, Z., Sun, G., Meng, Z., Guo, S., et al. (2017). CottonFGD: an integrated functional genomics database for cotton. *BMC Plant Biol.* 17:101. doi: 10.1186/s12870-017-1039-x

Conflict of Interest: The authors declare that the research was conducted in the absence of any commercial or financial relationships that could be construed as a potential conflict of interest.

Copyright © 2020 Li, Wang, Cui, Qiao, Zhu, Fan and Ma. This is an open-access article distributed under the terms of the Creative Commons Attribution License (CC BY). The use, distribution or reproduction in other forums is permitted, provided the original author(s) and the copyright owner(s) are credited and that the original publication in this journal is cited, in accordance with accepted academic practice. No use, distribution or reproduction is permitted which does not comply with these terms.

frontiers in Plant Science

ORIGINAL RESEARCH
published: 22 October 2020
doi: 10.3389/fpls.2020.533046

Endogenous Hormones Inhibit Differentiation of Young Ears in Maize (*Zea mays L.*) Under Heat Stress

Hui-Qin Wang, Peng Liu, Ji-Wang Zhang, Bin Zhao and Bai-Zhao Ren*

State Key Laboratory of Crop Biology, Agronomy College of Shandong Agricultural University, Tai'an, China

Global warming frequently leads to extreme temperatures, which pose a serious threat to the growth, development, and yield formation of crops such as maize. This study aimed to deeply explore the molecular mechanisms of young ear development under heat stress. We selected the heat-tolerant maize variety Zhengdan 958 (T) and heat-sensitive maize variety Xianyu 335 (S), and subjected them to heat stress in the V9 (9th leaf), V12 (12th leaf), and VT (tasseling) growth stages. We combined analysis of the maize phenotype with omics technology and physiological indicators to compare the differences in young ear morphology, total number of florets, floret fertilization rate, grain abortion rate, number of grains, and main metabolic pathways between plants subjected to heat stress and those left to develop normally. The results showed that after heat stress, the length and diameter of young ears, total number of florets, floret fertilization rate, and number of grains all decreased significantly, whereas the length of the undeveloped part at the top of the ear and grain abortion rate increased significantly. In addition, the differentially expressed genes (DEGs) in young ears were significantly enriched in the hormone signaling pathways. The endogenous hormone content in young ears exhibited different changes: zeatin (ZT) and zeatin riboside (ZR) decreased significantly, but gibberellin acid$_3$ (GA_3), gibberellin acid$_4$ (GA_4), and abscisic acid (ABA) increased significantly, in ears subjected to heat stress. In the heat-tolerant maize variety, the salicylic acid (SA), and jasmonic acid (JA) content in the vegetative growth stage also increased in ears subjected to heat stress, whereas the opposite effect was observed for the heat-sensitive variety. The changes in endogenous hormone content of young ears that were subjected to heat stress significantly affected ear development, resulting in a reduction in the number of differentiated florets, fertilized florets and grains, which ultimately reduced the maize yield.

Keywords: high temperature, ear development, transcriptomic, floret, hormones

OPEN ACCESS

Edited by:
Felipe Klein Ricachenevsky, Federal University of Rio Grande, Brazil

Reviewed by:
Fangmin Cheng, Zhejiang University, China
Muhammad Hamayun, Abdul Wali Khan University Mardan, Pakistan

****Correspondence:***
Peng Liu
liupengsdau@126.com

Specialty section:
This article was submitted to Plant Abiotic Stress, a section of the journal Frontiers in Plant Science

Received: *06 February 2020*
Accepted: *06 October 2020*
Published: *22 October 2020*

Citation:
Wang H-Q, Liu P, Zhang J-W, Zhao B and Ren B-Z (2020) Endogenous Hormones Inhibit Differentiation of Young Ears in Maize (Zea mays L.) Under Heat Stress. Front. Plant Sci. 11:533046. doi: 10.3389/fpls.2020.533046

INTRODUCTION

In many parts of the world, temperatures hit record highs in 2019. Concentrations of greenhouse gases are rising, making 2015–2019 the warmest 5 years on record. In 2016, the global surface temperature reached a new high of 14.84°C and global temperature records were broken for three consecutive years (Sun et al., 2017). The "greenhouse effect" is becoming more intense, and rising

temperatures have become a global problem affecting crop growth and yield. In recent years, frequent extreme weather and meteorological disasters have become the main factors restricting crop production (Högy et al., 2019). It has been predicted that the global temperature will increase by 1.5–6°C in the future (Müller et al., 2017), causing the expectation that heat stress will become the main abiotic stress factor for crop production in times to come. Previous research has shown that heat stress has a major impact on crop yield: for every 1°C increase in global temperature over the appropriate temperature needed to grow crops, the crop yield decreases by 2.5–16% (Battisti and Naylor, 2009). According to a USDA report, the world produced 10.34 and 11.23 million tons of maize in 2017 and 2018, while global maize consumption was 10.62 and 11.34 million tons, respectively. In 2022, the global maize consumption is expected to exceed 13 million tons. Furthermore, the FAO estimates that by 2050 the world will need 70–110% more food than today for meeting the projected population growth, and this increase would need to be realized largely by improving the efficiency of the production process without increasing the finite area of land currently assigned to agriculture (Ravic and Sandy, 2016). Due to the increasing gap between the supply and demand for maize, maintaining the total maize yield is a priority. This requires clarification of the molecular mechanisms involved in responses of maize to heat stress, improving its thermotolerance, and increasing the yield per unit area.

Maize is very sensitive to heat stress, especially during the critical stage when young ears differentiate. Observations show heat stress responses including reductions in the growth rate of young ears, duration of ear differentiation, and number of floret differentiations leading to anomalies such as reduced ear size and increased floret abortion, and eventually, to a significant reduction in the number of grains per spike (Cicchino et al., 2010; Hossain and Teixeira, 2012; Sobol et al., 2014). Of all the stages in the life cycle of maize, anthesis shows the highest sensitivity to heat stress. The optimum temperature for tasseling is 26–27°C, and exposure to temperatures above 30°C results in a drop in production (Lobell et al., 2011). The main reasons for production loss due to heat stress are a reduced number of filaments, delayed silking time, and decreased silking rate and filament viability. These changes in ear development ultimately result in reduced florescence, insufficient pollination and fertilization, and significantly decreased grain numbers (Wu C. et al., 2019). For rice, the most damaging heat stress responses occur at either the anthesis stage or the gametogenesis stage and include inhibited pollen viability and pollen tube growth, which result in a higher spikelet sterility rate (Jagadish et al., 2010, 2013). For heat-sensitive rice varieties, the main reason for decreases in grain yield is a decrease in spikelet fertility (Wu et al., 2016). In general, the harm done by heat stress during the reproductive growth stage is much more severe than that done during the vegetative growth stage, and the harm done during the reproductive organ differentiation stage is irreversible (Obata et al., 2015).

About 18% of the gene expression of *Sorghum bicolor* is altered in response to heat stress (Johnson et al., 2014). In heat-tolerant genotypes, gene expression is mainly up-regulated, but in heat-sensitive genotypes it is mainly down-regulated (Craita et al., 2011). Over half of the differentially expressed genes (DEGs) are involved in endoplasmic reticulum protein processing, metabolic pathways, and biosynthesis of secondary metabolites (Liu et al., 2014). Transcriptome data shows that there is a broad interaction between plant thermotolerance and cytokinin signaling (Černý et al., 2014). Understanding the dynamic changes in gene expression will be helpful in revealing the signaling pathways involved in the response of young ears to heat stress. However, relatively few transcriptome studies, which consider different heat-resistant maize varieties, technology have been carried out, using RNA sequencing (RNA-seq), on ear responses to heat stress during multiple growth stages. In this study, we used RNA-seq based on the Illumina sequencing platform for the transcriptome analysis of ears subjected to heat stress. We aimed to identify the molecular mechanisms carrying the signals involved in heat stress responses during the development of young ears at various growth stages for different heat-resistant maize varieties. The results will contribute to the research data in the field.

Hormones, which play an important role in plant development, are capable of regulating various life processes efficiently, even at extremely low concentrations. When external stress disrupts a plant's homeostasis, hormones enable plants to perceive these unfavorable changes in the external environment and counter them to maintain homeostasis (Wu et al., 2018). A single hormone might regulate many physiological processes, and a single physiological process might need the synergistic action of many hormones. This gives rise to a complex regulatory network of hormones that collectively regulate life processes such as differentiation and grain development in young ears (Wolters and Jürgens, 2009). For example, cytokinins can regulate the ear size and thermotolerance of rice (Wu et al., 2017). A decrease in cytokinin content, induced by heat stress, has been shown to lead to inhibited ear differentiation, floret fertility, pollen viability, and anther cracking, as well as a smaller grain size, none of which are conducive to yield formation (Sobol et al., 2014; Wu et al., 2016). Heat stress causes the abscisic acid (ABA) content in anthers and grains to increase and gibberellin content to decrease, which in turn leads to floret abortion. Spraying cytokinin can protect the floret primordia, allowing them to develop normally (Sobol et al., 2014). A high gibberellin acid$_3$ content in young panicles is conducive to the differentiation of spikelets in wheat, and a high content of zeatin promotes the development of florets, but a high ABA content during the booting stage inhibits the development of florets (Sheng et al., 2001). Spraying brassinolide during panicle differentiation can increase the number of spikelets, which ultimately increases the number of grains per panicle (Chen et al., 2019). Spraying cytokinins can also mitigate heat-stress-related damage to heat-sensitive rice varieties (Wu et al., 2016). Salicylic acid (SA) and jasmonic acid (JA) are considered to be important signaling substances with respect to plant stress responses, especially those responses that improve the thermotolerance of a crop (Clarke et al., 2009; Lu et al., 2009; Keykha et al., 2014). The content of endogenous SA and JA in plants increases under heat stress (Escandón et al., 2016; Scalabrin et al., 2016). Nevertheless, the relationship between the changes in endogenous hormone content and development of young ears in maize under heat stress is still unclear. To fill this

gap, our study aimed to systematically integrate the phenotype, physiology, and omics of maize under heat stress.

Previous studies on maize responses to heat stress mainly focused on ear traits, yield, ZR, GA, and ABA content in a single growth stage. The missing element is a comprehensive analysis of the effects of heat stress response of maize on young ear development, omics, and endogenous hormones, in different heat-resistant maize varieties, during different growth stages. The current study combined the analysis of phenotypical and physiological changes with transcriptome analysis, and deeply explored the molecular mechanism of ear development under heat stress, providing strong scientific and technological support for mitigating crop disasters, stabilizing yields, improving thermotolerance, and breeding stress-resistant maize varieties.

MATERIALS AND METHODS

Plant Materials and Growth Condition

The experiments were carried out during the summer maize growing season in 2018 and 2019 at Shandong Agricultural University Farm, Tai'an, SD, China (36° 09′ N, 117° 09′ E). After applying a screening process, we selected and planted two hybrid varieties of summer maize with different heat tolerance capacities: Zhengdan 958 (T), which represents the heat-tolerant variety, and Xianyu 335 (S), which represents the heat-sensitive variety. Pot experiments were set, and a basal fertilizer of 4.80 *g* N, 1.92 *g* P_2O_5, and 3.84 *g* K_2O was applied per pot before sowing. All plants were sown in plastic pots (40 cm length × 40 cm width × 50 cm depth). To ensure that moisture, diseases, pests and weeds did not restrict plant growth, additional management measures developed for high-yield cultivation were adopted.

Heat Stress Treatment and Sampling

While not being subjected to heat stress, the plants were left to grow in a natural environment, in this case the ambient environment at the research station. When the plants entered the V9 (9th leaf), V12 (12th leaf), or VT (tasseling) stage in their development, all plants in the test groups that were required to be subjected to heat stress during that stage were moved to transparent plastic sheds (12 m length × 6 m width, with a light transmittance of 92%), which featured automatic electric heaters used to control the temperature. Inside the sheds, the test groups were exposed to a heat-stressed environment with a day-time temperature of 40°C and night-time temperature of 30°C. The sheds had 60 cm air vents on all sides to ensure proper ventilation and establish identical concentrations of carbon dioxide and air humidity on the inside and outside. The temperature and humidity were recorded using a thermohygrograph, GSP-6 (Jingchuang Instruments Co., Ltd; **Figure 1**). Plants that were grown only in a natural environment were considered the controls (L), the experiment included 12 treatments: T-H-V9, T-L-V9, T-H-V12, T-L-V12, T-H-VT, T-L-VT, S-H-V9, S-L-V9, S-H-V12, S-L-V12, S-H-VT, and S-L-VT, where T and S denote the heat-tolerant maize variety Zhengdan 958 and heat-sensitive maize variety Xianyu 335, respectively, H denotes a heat stress group, L denotes a control group, and V9, V12, and VT denote the growth stages during which the plants in the corresponding heat stress test group were subjected to heat stress.

After subjecting the plants in the relevant test groups to heat stress for 10 days, we collected 10 young ears from plants in each group and immediately froze them in liquid nitrogen, then stored them at −80°C for quantifying endogenous hormones and RNA-seq analysis, each group had three replicates. We also collected 10 young ears that were used to characterize the ear morphology, as described in the next section. After completing the sampling process, the remaining plants in the test groups were removed from the shed and returned to the natural environment, where they were left to grow naturally until harvest time.

Ear Characterization

To analyze the 10 young ears collected for the purpose of ear characterization, we measured the length of the ear, the length of the undeveloped part at the top of the ear, and the ear diameter with a ruler.

Floret Differentiation

Before the silking stage set in, we selected 15 representative plants in each treatment for labeling, according to the method of Cui et al. (2014). After pollination finished, we peeled the bracts from the ear and counted the total number of differentiated florets. The count was divided into three parts: first, after shaking gently, we counted the number of filaments that were shed and the number of filaments that were not shed but were wilted at the base and added these counts to obtain the number of fertilized florets; second, the number of fresh filaments that were not shed was taken to represent the number of unfertilized florets; and third, the number of filaments that were not drawn out was taken to represent the number of degenerated florets. We then calculated the floret fertilization rate and grain abortion rate, using the following formulae:

Floret fertilization rate (%) = (number of fertilized florets/number of total florets) × 100

Grain abortion rate (%) = (number of fertilized florets – grain numbers) × 100/number of fertilized florets

RNA Extraction and Sequencing

Total RNA was isolated from the ears using a TRIzol reagent according to manufacturer's instructions (Invitrogen). An additional DNase I digestion step was performed to ensure that the samples were not contaminated with genomic DNA. RNA purity was assessed using the Nanodrop-2000. Each RNA sample had an A260:A280 ratio above 1.8 and A260:A230 ratio above 2.

The methods for library preparation and sequencing were modified from those described by Garzón-Martínez et al. (2012). The paired-end (PE) RNA-seq libraries were prepared following Illumina's protocols and sequenced on the Illumina HiSeq^{TM} X Ten platform. Data analysis and base calling were performed using the Illumina instrument software. High throughput sequencing was performed at Ori-Gene Science and Technology Co., Ltd. (Beijing, China).

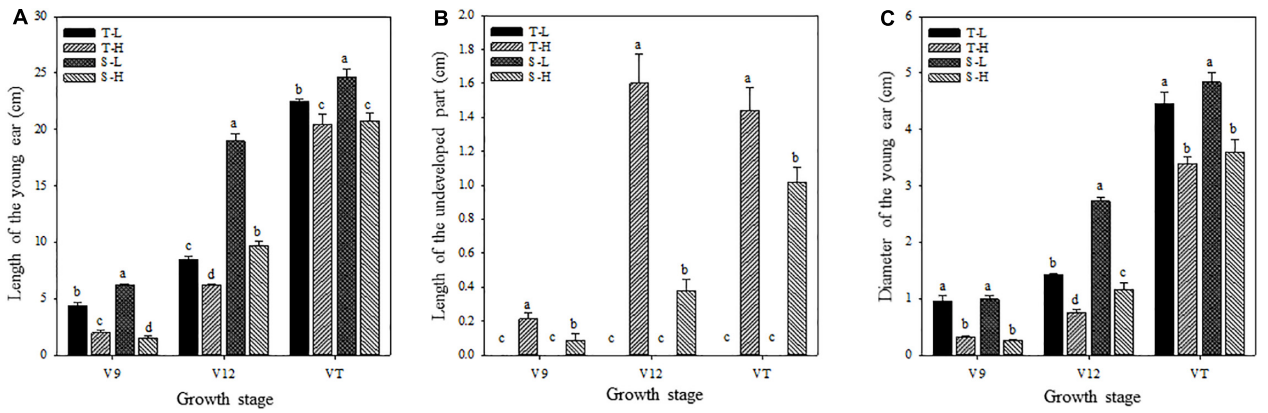


FIGURE 1 | Effects of heat stress on the length of the young ear **(A)**, the length of the undeveloped part at the top of the ear **(B)**, and the ear diameter **(C)**. T and S represent the heat-tolerant variety and the heat-sensitive variety, respectively. L represents the natural environment and H represents the heat-stressed environment. V9, V12, and VT represent the 9th leaf, 12th leaf, and tasseling stages. Vertical bars represent ± SD of the mean. a, b, c, and d indicate significant difference among different treatments ($n = 3$, $P < 0.05$).

RNA-seq Quality Pre-processing and Analysis Results

The RNA-seq results were qualified by the Q20 standard, which showed that the sequencing quality was acceptable. Raw reads from sequencing machines contain dirty reads that include adapters, as well as unknown or low-quality bases, which would negatively affect any bioinformatics analysis. Therefore, dirty raw reads (i.e., reads with adapters, reads with an unknown nucleotides ratio larger than 5%, and low-quality reads) were discarded. After filtering the raw reads, *de novo* assembly of the transcriptome was carried out with Trinity, a short reads assembly program. Trinity connected the contigs and obtained sequences defined as unigenes. The generated unigenes were used for BLASTX and annotation against a protein database, such as the KEGG database, with a cut-off *E*-value of 0.00001. KEGG is a major public pathway-related database that can analyze a gene product during metabolic processes and related gene functions in cellular processes. With the help of the KEGG database, we could further study the complex biological behaviors of genes, and through KEGG annotation we could obtain pathway annotation for unigenes. KEGG pathway annotation was performed using the Blastall software against the KEGG database.

Quantitative Real Time (qRT)-PCR Analysis

The quantitative real time (qRT-PCR) analysis was carried out for the further verification of RNA–Seq data using gene–specific primer sets (**Supplementary Table 1**). The cDNA was synthesized with a Goldenstar^{TM} RT6 cDNA Synthesis Kit Ver 2 (TsingKe Biotech Co., Ltd, Beijing, China). Using LineGene 9600 Plus (Bioer, Hangzhou, China) and SYBR Green I Mixture (TsingKe) for amplification, detection, and data analysis. The specific primers used for qRT-PCR were designed from National Center for Biotechnology Information (NCBI) and those were synthesized by TsingKe Biotech Co., Ltd (Beijing, China). GAPDH (Zm00001d049641) was used as the reference gene (Magneschi et al., 2009). The fluorescence was measured at the end of each cycle for quantification, and three technical replicates were performed. Relative expression levels were calculated using the $2^{-\Delta\Delta Ct}$ method.

Availability of Supporting Data

All sequences were deposited in the NCBI and can be accessed in the Short Read Archive (SRA) under accession number: SRP250388.

Extraction and Determination of Endogenous Hormones

The methods for extraction and purification of ABA, JA, SA, ZR, ZT, GA_3, and GA_4 were modified from those described by Engelberth et al. (2003). Endogenous hormones were analyzed using a triple quadrupole mass spectrometer (ACQUITY UPLC I-Class/Xevo TQ-S, Waters, Milford, MA, United States) equipped with an electrospray ion source (ESI). The LC separation was performed on a reversed-phase C18 column (ACQUITY UPLC BEH, 1.7 μm, 2.1 mm × 100.0 mm, Waters, Milford, MA, United States) using a binary solvent system composed of water with 0.1% acetonitrile, 0.1% formic acid (mobile phase A), and MeOH (mobile phase B) at a flow rate of 0.4 mL min^{-1}. Standard ABA, JA, ZR, ZT, GA_3, GA_4, and isotopically labeled internal standards including D-JA, D-ABA, D-GA_4, and D-ZT were purchased from OlChemIm Ltd. (OlChemIm Ltd., Olomouc, Czech Republic), and standard SA was purchased from Sigma. Methanol, acetonitrile, and formic acid were purchased from Fisher (Thermo Fisher Scientific, Waltham, MA, United States).

Statistical Analysis

Statistical analyses were performed using the analysis of variance (ANOVA) algorithm from the General Linear Model procedure of the SPSS software, version 26.0 (SPSS Inc). Unless indicated otherwise, significant differences among different plants were

given at $p \leq 0.05$. The values of the mean, among treatments, were compared using the Tukey Honestly Significant Difference test. Figures were plotted using the SigmaPlot 14.0 program.

RESULTS

Characteristics of Young Maize Ears

After being subjected to heat stress at any of the stages included in the experiment, the length and diameter of young ears was significantly reduced, and the proportion of the undeveloped part at the top of the ear was significantly increased. The average ear length for the heat-tolerant maize variety after heat stress application during the V9, V12, and VT stage was 54.44, 26.54, and 8.89% lower than that of the control groups, respectively, and for the heat-sensitive maize variety, it was 75.97, 48.89, and 15.6% lower. For the ear diameter, the heat-tolerant maize variety was 66.39, 46.49, and 23.63% lower than that of the control in the V9, V12, and VT stage, respectively, and the heat-sensitive maize variety was 74.44, 57.25, and 25.62% lower (**Figure 1**). In addition, the growth stage of the ear was delayed, and during the VT stage, severe abortion of the upper and base grains was observed, while morphologies of the control ears were better and their grains were fully developed (**Figure 2**).

Total Number of Florets and Floret Fertilization Rate

The total number of florets in young ears decreased significantly after heat stress in 2 years. 2018 for example, despite having a different capacity for heat tolerance, both maize varieties showed that the most significant decrease happened during the V9 stage, for which the decrease reached 21.07% for the heat-tolerant variety and 12.06% for the heat-sensitive variety. When heat stress was applied during the V12 or VT stage, the total number of florets showed a greater decrease in the heat-sensitive maize variety (**Figure 3A**). Heat stress also affected the process of floret fertilization. The floret fertilization rates of the heat-tolerant and heat-sensitive maize varieties were only 9.51% and 4.14%, respectively, after heat stress application during the VT stage, and compared with the control group, the floret fertilization rates were 89.26% and 95.68% lower. After heat stress application during the V12 stage, the floret fertilization rate in the heat-tolerant and heat-sensitive varieties was 56.38% and 78.11% lower than that for the control groups, respectively. Although the effect of heat stress application during the V9 stage, on the floret fertilization rate, was significantly less than that of heat stress application during the V12 and VT stages, the floret fertilization rate was still significantly lower than that of the control groups (**Figure 3B**).

Grain Numbers and Abortion Rate

After being subjected to heat stress during any of the stages included in the experiment, the grain numbers for both varieties were significantly reduced and reduction was greater for the heat-sensitive maize variety than that for the heat-tolerant variety. Number of grains decreased the most when the heat stress occurred during the VT stage. According to the data for 2018, the grain number for the heat-tolerant maize variety after heat stress application during the V9 or V12 stage was 40.12% and 82.42% lower than that for the control groups, respectively, and for the heat-sensitive maize variety it was 50.68% and 92.89% lower (**Figure 4A**).

After being subjected to heat stress, the grain abortion rate for the heat-sensitive maize variety was always higher than that for the heat-tolerant maize variety. The abortion rate for both varieties was the highest after heat stress application during the VT stage, followed by the V12 stage; it was the lowest after heat stress application during the V9 stage. Indeed, in 2018, after applying heat stress during the VT stage, the grain abortion rate for both the heat-tolerant and the heat-sensitive maize variety was 100%. When heat stress was applied during the V9 or V12 stage, the grain abortion rate was 19.09% and 60.53% for the heat-tolerant variety, and 35.90% and 69.84% for the heat-sensitive variety, respectively (**Figure 4B**).

As shown in **Table 1**, the length of the young ear, the length of the undeveloped part at the top of the ear, the ear diameter and the grain abortion rate exhibited extremely significant differences between varieties, temperatures, stages

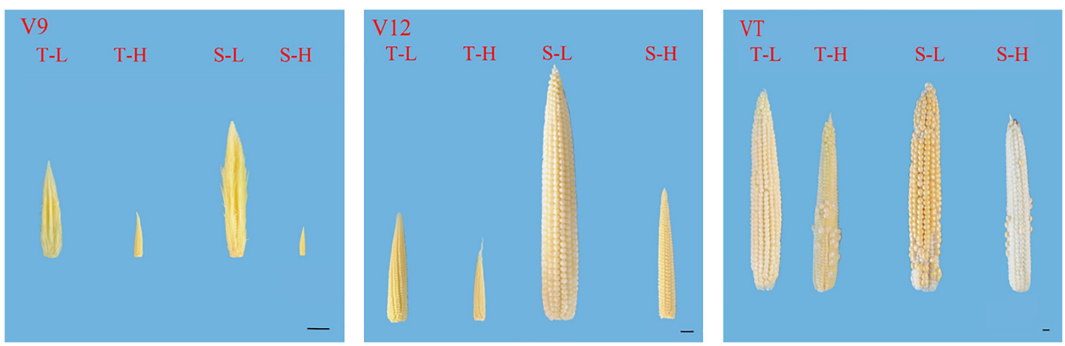


FIGURE 2 | Effects of heat stress on the morphology of young ears of two varieties of summer maize with a different capacity for heat tolerance. T and S represent the heat-tolerant variety and the heat-sensitive variety, respectively. L represents the natural environment and H represent the heat-stressed environment. V9, V12, and VT represent the 9th leaf, 12th leaf, and tasseling stages. The length of the ruler is 1 cm.

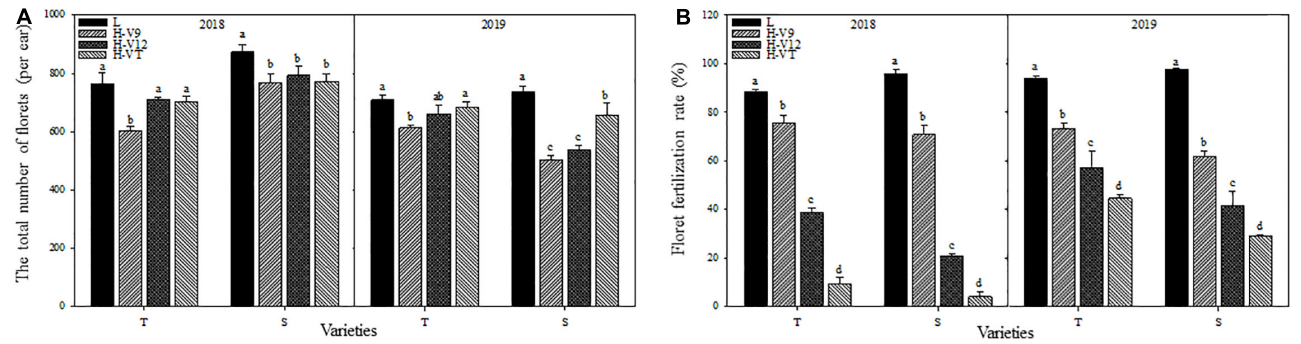


FIGURE 3 | Effect of heat stress on the total number of differentiated florets in the ear **(A)** and the floret fertilization rate **(B)**. T and S represent the heat-tolerant variety and the heat-sensitive variety, respectively. L represents the natural environment and H represents the heat-stressed environment. V9, V12, and VT represent the 9th leaf, 12th leaf, and tasseling stages. Vertical bars represent ± SD of the mean. a, b, c, and d indicate significant difference among different treatments ($n = 3$, $P < 0.05$).

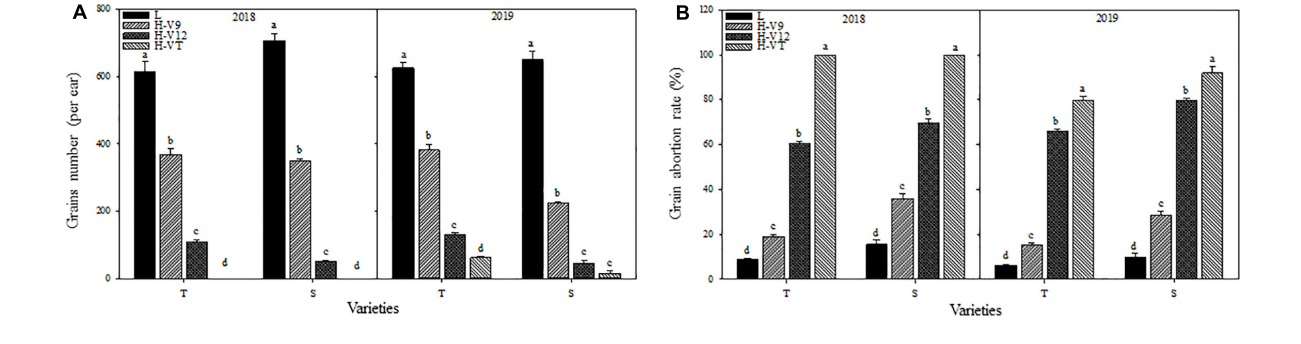


FIGURE 4 | Effect of heat stress on the grains number **(A)** and grain abortion rate **(B)**. T and S represent the heat-tolerant variety and the heat-sensitive variety, respectively. L represents the natural environment and H represents the heat-stressed environment. V9, V12, and VT represent the 9th leaf, 12th leaf, and tasseling stages. Vertical bars represent ± SD of the mean. a, b, c, and d indicate significant difference among different treatments ($n = 3$, $P < 0.05$).

TABLE 1 | ANOVA (*F* value) of the effects of heat stress applied during different growth stages on the differentiation of young ear in maize varieties with different capacities for heat tolerance.

Source of variation	Variable					
	The number of total florets	Floret fertilization rate	Grain abortion rate	Length of the young ear	Length of the undeveloped part	Diameter of the young ear
Variety	127.99**	2.19^{ns}	299.53**	349.17**	153.29**	87.88**
Temperature	94.39**	6788.58**	13715.59**	663.73**	1108.97**	596.02**
Stage	4.44*	834.07**	2225.28**	4669.03**	190.33**	2643.78**
Variety × Temperature	0.05^{ns}	149.90**	5.35*	139.01**	153.29**	24.35**
Variety × Stage				161.68**	47.46**	40.59**
Temperature × Stage				29.79**	190.33**	13.60**
Variety × Temperature × Stage	2.47^{ns}	9.72**	30.02**	27.21**	47.46**	9.95**

**Significant at $P < 0.05$ ($n = 3$); **Significant at $P < 0.01$ ($n = 3$); and ^{ns}non-significant.*

during which heat stress occurred, and the interactions between various factors. As for the total number of florets, there were significant or extremely significant differences between varieties, temperatures and growth stages during which heat stress was applied, but no significant differences between the types of interactions. In addition, there was no significant difference in the floret fertilization rate between varieties, but there were significant differences between temperatures, heat stages during which heat stress occurred, and the interactions of various factors.

Analysis of Gene Expression and Differentially Expressed Genes

In the heat-tolerant maize variety, there were 49256, 50029, and 53197 genes expressed in the V9, V12, and VT stage, respectively.

TABLE 2 | Summary of genes expressed for different treatments.

Control VS Case	All_gene	All_DEG	UP	DOWN
T-L-V9 VS T-H-V9	49256	1489	680	809
T-L-V12 VS T-H-V12	50029	676	271	405
T-L-VT VS T-H-VT	53197	340	192	148
S-L-V9 VS S-H-V9	50776	61	44	17
S-L-V12 VS S-H-V12	52985	2174	1606	568
S-L-VT VS S-H-VT	53950	216	69	147

All_gene represent the total number of genes expressed under heat stress, all_DEG represent the number of differently expressed genes, UP, and DOWN represent the number of genes that are up-regulated and down-regulated under heat stress, respectively. T and S represent the heat-tolerant variety and the heat-sensitive variety, respectively. L represents the natural environment and H represents the heat-stressed environment. V9, V12, and VT represent the 9th leaf, 12th leaf, and tasseling stages.

The highest number of DEGs (p value < 0.05 and $|\log_2$ fold change$| \geq 1$), which was observed in the V9 stage, was 1489; among these genes, 680 were up-regulated, and 809 were down-regulated. In the heat-sensitive maize variety, there were 50776, 52985, and 53950 genes expressed in the V9, V12, and VT stage, respectively. The highest number of DEGs, which was observed in the V12 stage, was 2174; among these genes, 1606 were up-regulated and 568 were down-regulated (**Table 2**).

KEGG Pathway Analysis of DEGs

To explore the biological and signal transduction pathways associated with DEGs involved in young ear development under heat stress, a KEGG pathway analysis of the DEGs was conducted. After heat stress, DEGs associated mainly with biosynthesis, primary and secondary metabolism, and signal transduction pathways were enriched, and the pathways related to plant hormones were ubiquitous. In the heat-tolerant maize variety, most of the DEGs were clustered around plant hormone signal transduction, zeatin biosynthesis and brassinosteroid biosynthesis pathways (**Figures 5A–C**). The heat-sensitive maize variety also showed significant expression in pathways associated with plant hormone signal transduction and zeatin biosynthesis (**Figures 5D–F**). Therefore, we speculate that endogenous plant hormones might play an important role in responses to heat stress.

Genes Related to Hormones and Heat Stress

We further analyzed the genes associated with hormones and heat shock after heat stress. The results showed that the expression of genes related to ZT biosynthesis (Zm00001d002989, Zm00001d010689, Zm00001d012641, Zm00001d032664, and Zm00001d050371) was down-regulated. The expression

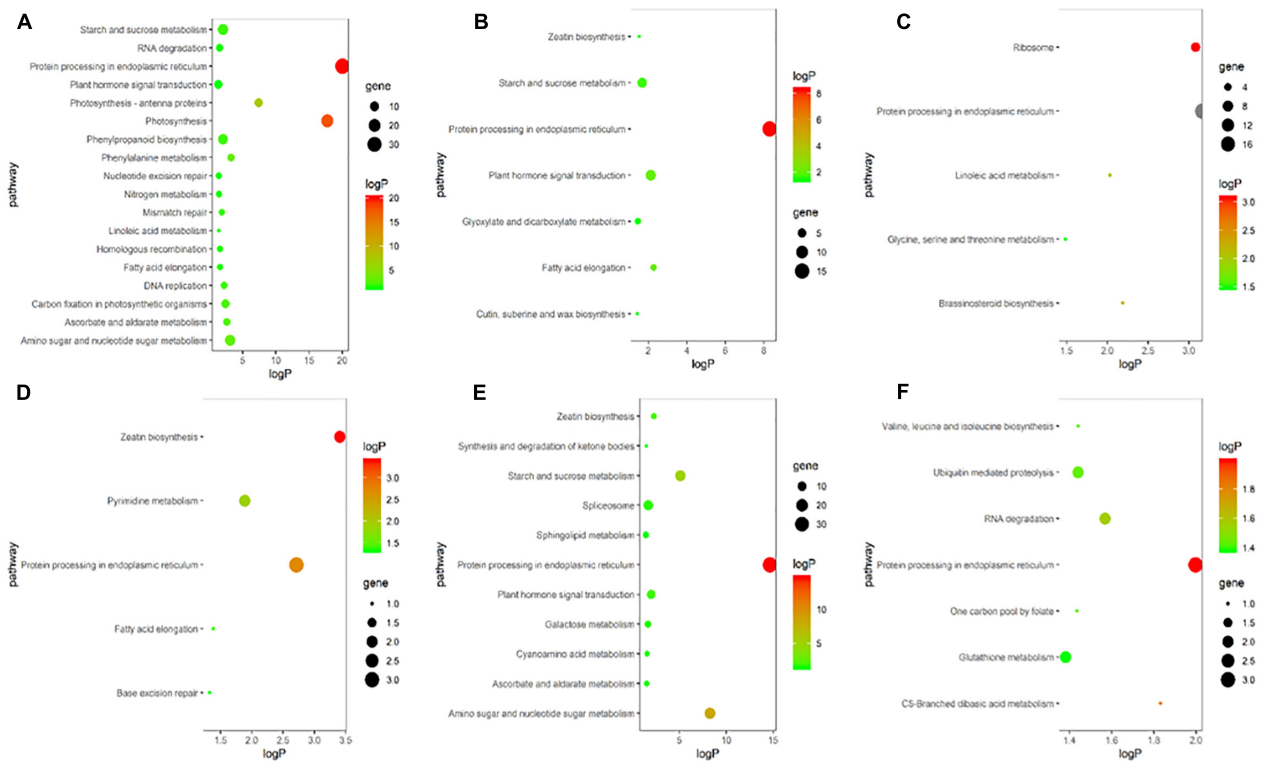


FIGURE 5 | KEGG enrichment bubble chart of differentially expressed genes in ears under heat stress. **(A–C)** represent T in V9, V12, and VT stage, respectively. **(D–F)** represent S in V9, V12, and VT stage, respectively. The *X*-axis is the enrichment factor (enriched to the differentially expressed genes in these pathway/background genes in this pathway), the *Y*-axis is the description of the corresponding pathway, the size of bubble represents the number of differentially expressed genes, and the color of bubble represent the *P* value.

of genes related to GA biosynthesis (Zm00001d012296, Zm00001d014863, Zm00001d040423, Zm00001d018045, and Zm00001d038695), ABA (Zm00001d020717, Zm00001d043180, Zm00001d046471, Zm00001d047582, and Zm00001d048667), and heat shock protein (Zm00001d008841, Zm00001d024903, Zm00001d028408, Zm00001d039933, and Zm00001d039936), and heat shock transcription factor (Zm00001d052738, Zm00001d016255, Zm00001d031736, Zm00001d032923, and Zm00001d033987) was up-regulated. The expression of genes in response to SA (Zm00001d020492, Zm00001d021677, Zm00001d034186, Zm00001d040426, and Zm00001d045685) and JA (Zm00001d008251, Zm00001d009261, Zm00001d009715, Zm00001d009714, and Zm00001d052868) was up-regulated in heat-tolerant maize variety; however, the heat-sensitive maize variety showed the opposite trend (**Figure 6**). There were no significant differences in the gene expression related to auxin and ethylene in each treatment.

Validation of RNA-seq Data Using qRT-PCR

To further verify the expression of genes obtained by RNA-seq, 10 genes related to hormones and heat shock were selected for qRT-PCR. We compared the relative gene expression levels obtained from qRT-PCR with those generated from the RNA-seq analyses related to the 12 treatments. The qRT-PCR results (**Figure 7**) confirmed that almost all 10 DEGs displayed expression patterns consistent with the expression levels obtained from RNA-seq analyses.

Endogenous Hormones

The endogenous hormone content showed the same trend in the two-year data and in the detailed analysis based on 2018. The ZT and ZR content decreased after heat stress application, except in the heat-tolerant maize variety during the V12 stage. The largest response in terms of ZT and ZR content was observed in ears that were subjected to heat stress during the VT stage, followed by those subjected to heat stress during the V9 stage. Moreover, after heat stress application during the V9 stage, the decrease in ZT and ZR content for the heat-sensitive maize variety was greater than that for the heat-tolerant maize variety, whereas the opposite results were found after applying heat stress in the V12 or VT stage (**Figures 8A,B**).

For the heat-tolerant maize variety, the SA content of young ears increased after applying heat stress at any of the experimental stages. The highest increase, which was 75.21% over the control group, occurred after applying heat stress during the V9 stage. In contrast, the content of SA in the heat-sensitive maize variety showed a decreasing trend after heat stress, and the largest decrease, which was 83.69% below the control group, occurred after applying heat stress during the V12 stage. Furthermore, when applying heat stress during the V9 or V12 stages, the SA content in young ears showed greater variations for the heat-tolerant maize variety, but when heat stress was applied during the VT stage, the opposite trend was observed (**Figure 8C**). The JA content in young ears of the heat-tolerant maize subjected to heat stress during the V9 and V12 stages was 89.17% and 207.04% higher than for the control group, respectively, but it was 65.48% lower than the control group if the heat stress was applied during the VT stage. The heat-sensitive maize variety showed the opposite trend. Despite having different capacities for heat tolerance, both varieties were more sensitive to heat stress application during the V12 stage, and for the heat-tolerant maize variety, the variations were consistently greater than those for the heat-sensitive variety (**Figure 8D**).

GA_3, GA_4, and ABA content in the young ears of both maize varieties increased under heat stress. The greatest increase in GA_3 content, which was observed after heat stress application during

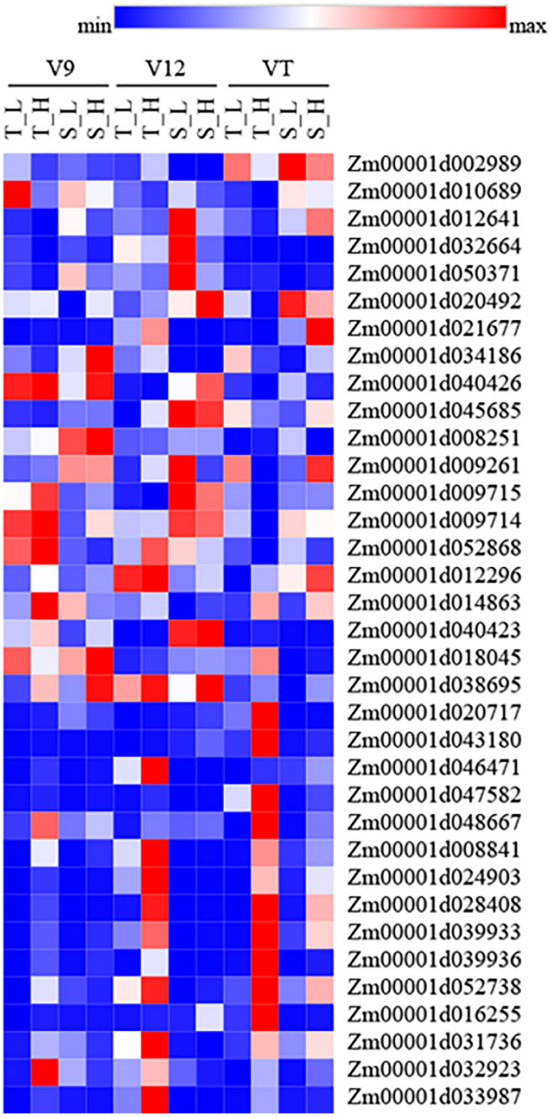


FIGURE 6 | Heatmap of genes which related to hormones and heat shock under heat stress. Red represent up-regulated, and blue represent down-regulated. T and S represent the heat-tolerant variety and the heat-sensitive variety, respectively. L represents the natural environment and H represents the heat-stressed environment. V9, V12, and VT represent the 9th leaf, 12th leaf, and tasseling stages.

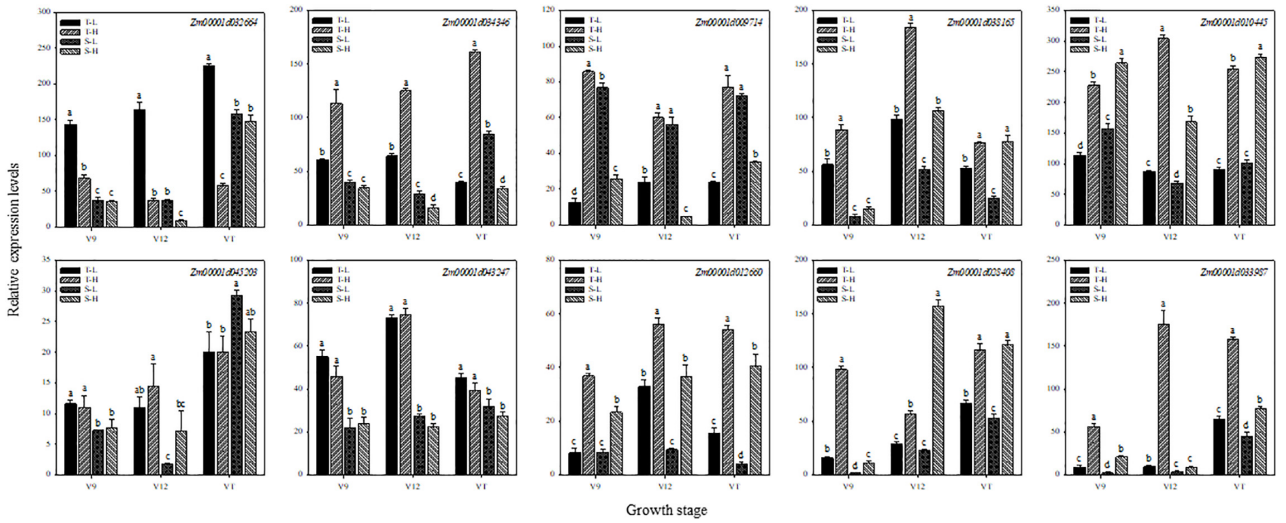


FIGURE 7 | Validation of differential expression of 10 universal genes using qRT-PCR. These genes are related to zeatin (Zm00001d032664), salicylic acid (Zm00001d034346), jasmonic acid (Zm00001d009714), gibberellin (Zm00001d038165), abscisic acid (Zm00001d010445), auxin (Zm00001d045203), ethylene (Zm00001d043247), hormone signal transduction (Zm00001d012660), heat shock protein (Zm00001d028408), and heat shock transcription factor (Zm00001d033987), respectively. T and S represent the heat-tolerant variety and the heat-sensitive variety, respectively. L represents the natural environment and H represents the heat-stressed environment. V9, V12, and VT represent the 9th leaf, 12th leaf, and tasseling stages. Vertical bars represent ± SD of the mean. a, b, c, and d indicate significant difference among different treatments (n = 3, P < 0.05).

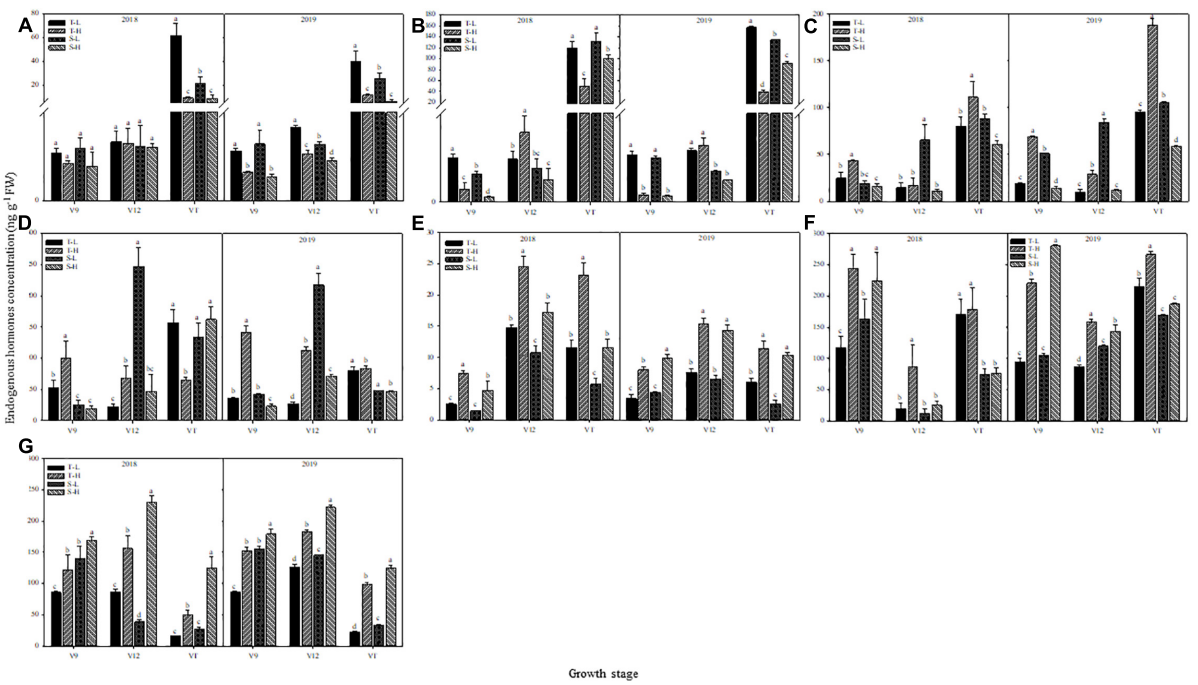


FIGURE 8 | Effect of heat stress on the concentration of zeatin **(A)**, zeatin riboside **(B)**, salicylic acid **(C)**, jasmonic acid **(D)**, gibberellin acid$_3$ **(E)**, gibberellin acid$_4$ **(F)**, and abscisic acid **(G)** in ears. T and S represent the heat-tolerant variety and the heat-sensitive variety, respectively. L represents the natural environment and H represents the heat-stressed environment. V9, V12, and VT represent the 9th leaf, 12th leaf, and tasseling stages. Vertical bars represent ± SD of the mean. a, b, c, and d indicate significant difference among different treatments (n = 3, P < 0.05).

the V9 stage, were 196.54% higher than the control group for the heat-tolerant variety, and 228.00% higher than the control group for the heat-sensitive variety (**Figure 8E**). In addition, the greatest increase in GA_4 content, which was observed after applying heat stress during the V12 stage, was 337.64% higher than the control group, for the heat-tolerant variety, and 102.26% higher than

the control group, for the heat-sensitive variety (**Figure 8F**). For ABA content, the greatest increase was 212.63% higher than the control group, and this, occurred in the heat-tolerant maize variety after heat stress application during the VT stage. In the heat-sensitive maize variety, however, the greatest increase, which occurred after the application of heat stress during the V12 stage, was 417.97% higher than the control group (**Figure 8G**).

In **Table 3**, the contents of ZT, ZR, JA, and ABA show significant differences between maize varieties, temperatures, and the stages during which heat stress occurred, as well as their interactions. There was no significant difference in SA content between varieties or temperatures, but there was an extremely significant difference between the stages during which heat-stress occurred, as well as in the interactions between various factors. The GA_3 and GA_4 content was also extremely significantly affected by the variety, temperature, and stage associated with heat stress occurrence.

Correlation Analysis of Plant Endogenous Hormones With Ear Characteristics

Endogenous hormones are an important signaling substance for regulating plant characteristics that facilitate tolerance to external stress. As shown in **Table 4**, the correlation between ZT and ZR content and the characteristics of young ears after the application of heat stress were consistent. Except for the ZR content of heat-tolerant maize after heat stress application during the V12 stage, the hormone content of plants subjected to any other treatment was positively correlated with the length of young ears, ear diameter, total floret number, and floret fertilization rate, and negatively correlated with the length of the undeveloped part of young ears and the grain abortion rate. The correlations were significant or extremely significant, except for those related to the ZT content of heat-sensitive maize after heat stress application during the V12 stage. The correlations between SA and the observed ear characteristics were similar to those for JA. The SA and JA content of the heat-tolerant variety were negatively correlated with the length of young ears, ear diameter, total floret number, and floret fertilization rate and positively correlated with the grain abortion rate, except for the JA content after heat stress application during the VT stage. For the heat-sensitive maize variety, however, the trend was reversed. Except for the SA content after heat stress application during the V12 stage, the correlation between the hormone level and the ear characteristics all reached significant or extremely significant levels. Similarly, the correlation between the GA_3 content and the young ear characteristics was similar to that for GA_4 and ABA. Except for the GA_4 content of the heat-tolerant maize variety after heat stress application during the VT stage, the GA_3, GA_4, and ABA content was negatively correlated with the length of the young ears, ear diameter, total floret number, and floret fertilization rate and positively correlated with the length of the undeveloped part and the grain abortion rate. With respect to the heat-sensitive maize variety, however, the GA_4 content was not significantly correlated with any ear trait.

DISCUSSION

In this study, we aimed to identify the signaling mechanisms involved in heat stress responses during the development of young ears at three different growth stages for heat-tolerant and heat-sensitive maize varieties (**Figure 9**). We found that heat stress decreased maize production, even in the heat-tolerant variety, and this will affect maize yields in a warmer world. Deploying increased planting densities may seem like an obvious technique to achieve high maize yields in the future, but there is a decrease in grain number as the density of plantation is increased. Increased planting densities also lead to canopy closure and a reduced tolerance to adversity (Xu et al., 2017), especially to heat stress (Cicchino et al., 2010; Ordóñez et al., 2015). The number of grains is the most significant factor affecting yield, and thus, reducing the heat-stress-induced reduction in grain numbers is the key to obtaining high and stable yield (Prasad et al., 2011). The grain number depends on the total number of florets, number of fertilized florets, and effective number of grains that develop from a fertilized floret (Dong et al., 2010). In plants under heat stress, the floret abortion rate, pollen viability, and ability to germinate are decreased; moreover, the silking time is delayed and filament viability is decreased. As a result, the pollination and fertilization processes are blocked, which decreases the fertilization rate,

TABLE 3 | ANOVA (*F* value) of the effects of heat stress in different stages on the concentration of endogenous hormones in maize varieties with different capacities for heat tolerance.

Source of variation	Variable						
	ZT	ZR	SA	JA	GA_3	GA_4	ABA
Variety	26.32**	82.10**	3.41^{ns}	34.47**	187.82**	41.88**	1250.05**
Temperature	124.44**	378.20**	1.47^{ns}	86.62**	312.76**	56.75**	4815.57**
Stage	214.95**	3387.49**	237.50**	110.15**	369.05**4	158.51**	1316.52**
Variety × Temperature	31.34**	18.40**	111.86**	63.70**	20.43**4	19.81**	1060.96**
Variety × Stage	27.12**	175.13**	20.16**	118.57**	25.026**	28.61**	77.76**
Temperature × Stage	103.03**	308.33**	16.69**	70.36**	13.45**	4.37*	635.63**
Variety × Temperature × Stage	34.68**	61.63**	4.66*	227.58**	2.31^{ns}	1.50^{ns}	136.96**

*ZT, ZR, SA, JA, GA_3, GA_4, and ABA represent the zeatin, zeatin riboside, salicylic acid, jasmonic acid, gibberellin acid$_3$, gibberellin acid$_4$, and abscisic acid, respectively. *Significant at $P < 0.05$ ($n = 3$); **Significant at $P < 0.01$ ($n = 3$); and ^{ns}non-significant.*

TABLE 4 | Correlation coefficients of endogenous hormones and ear phenotype in maize varieties with different capacities for heat tolerance.

		T						S					
		Length of the young ear	**Length of the undeveloped part**	**Diameter of the young ear**	**Total number of florets**	**Floret fertilization rate**	**Grain abortion rate**	**Length of the young ear**	**Length of the undeveloped part**	**Diameter of the young ear**	**Total number of florets**	**Floret fertilization rate**	**Grain abortion rate**
ZT	V9	0.96**	−0.95**	0.95**	0.91*	0.93**	−0.98**	0.91*	−0.86*	0.92**	0.84*	0.89*	−0.87*
	V12	0.92**	−0.94**	0.95**	0.68^{ns}	0.93**	−0.93**	0.73^{ns}	-0.66^{ns}	0.65^{ns}	0.42^{ns}	0.68^{ns}	-0.69^{ns}
	VT	0.88*	−0.97**	0.94**	0.85*	0.98**	−0.98**	0.91*	−0.86*	0.86*	0.70^{ns}	0.85*	−0.83*
ZR	V9	0.96**	−0.95**	0.97**	0.95**	0.92*	−0.97**	1.00**	−0.91*	0.99**	0.90*	0.98**	−0.99**
	V12	-0.79^{ns}	0.89*	-0.80^{ns}	-0.62^{ns}	−0.84*	0.83*	1.00**	−0.97**	0.98**	0.88*	0.99**	−1.00**
	VT	0.88*	−0.96**	0.88*	0.75^{ns}	0.94**	−0.94**	0.60^{ns}	-0.76^{ns}	0.62^{ns}	0.86*	0.73^{ns}	-0.76^{ns}
SA	V9	−0.91*	0.90*	−0.96**	−0.98**	−0.85*	0.87*	0.92**	-0.80^{ns}	0.91*	0.86*	0.91*	−0.88*
	V12	-0.71^{ns}	0.80^{ns}	-0.70^{ns}	-0.57^{ns}	-0.75^{ns}	0.74^{ns}	0.98**	−0.94**	0.94**	0.78^{ns}	0.96**	−0.97**
	VT	−0.85*	0.84*	−0.83*	-0.60^{ns}	−0.87*	0.88*	0.90*	−0.93**	0.96**	0.84*	0.96**	−0.95**
JA	V9	−0.83*	0.89*	−0.85*	-0.79^{ns}	−0.85*	0.85*	0.83*	-0.77^{ns}	0.83*	0.65^{ns}	0.85*	-0.71^{ns}
	V12	−0.99**	0.99**	−0.99**	-0.79^{ns}	−0.99**	0.99**	1.00**	−0.97**	0.99**	0.83*	1.00**	−1.00**
	VT	0.86*	−0.96**	0.99**	0.86**	0.97**	−0.97**	−0.95**	0.91*	−0.85*	−0.83*	−0.89*	0.89*
GA_3	V9	−0.98**	0.99**	−0.98**	−0.95**	−0.94**	0.97**	−0.87*	0.87*	−0.89*	−0.95**	-0.81^{ns}	0.94**
	V12	−0.97**	0.95**	−0.98**	-0.68^{ns}	−0.98**	0.98**	−0.94**	0.98**	−0.95**	−0.95**	−0.95**	0.96**
	VT	−0.93**	0.99**	−0.95**	-0.70^{ns}	−0.97**	0.97**	−0.85*	0.93**	−0.95**	−0.85*	−0.95**	0.95**
GA_4	V9	−0.99**	0.97**	−0.98**	−0.98**	−0.95**	0.97**	-0.61^{ns}	0.77^{ns}	-0.62^{ns}	−0.82*	-0.50^{ns}	0.69^{ns}
	V12	−0.95**	0.98**	−0.96**	-0.74^{ns}	−0.96**	0.96**	-0.74^{ns}	0.70^{ns}	-0.72^{ns}	-0.46^{ns}	-0.78^{ns}	0.74^{ns}
	VT	0.89*	-0.78^{ns}	0.83*	0.94**	0.75^{ns}	-0.77^{ns}	-0.33^{ns}	0.53^{ns}	-0.58^{ns}	-0.53^{ns}	-0.57^{ns}	0.59^{ns}
ABA	V9	−0.96**	0.95**	−0.95**	−0.91**	−0.90*	1.00**	−0.98**	0.96**	−0.97**	−0.96**	−0.95**	0.99**
	V12	−1.00**	0.99**	−0.99**	-0.78^{ns}	−1.00**	−1.00**	−1.00**	0.98**	−0.99**	−0.86*	−1.00**	1.00**
	VT	−0.91*	0.98**	−0.96**	-0.77^{ns}	−0.99**	0.99**	−0.96**	0.10**	−0.96**	−0.93**	−1.00**	1.00**

*ZT, ZR, SA, JA, GA_3, GA_4, and ABA represent the zeatin, zeatin riboside, salicylic acid, jasmonic acid, gibberellin $acid_3$, gibberellin $acid_4$, and abscisic acid, respectively. T and S represent the heat-tolerant variety and heat-sensitive variety, respectively. L represents the natural environment and H represents the heat-stressed environment. V9, V12, and VT represent the 9th leaf, 12th leaf, and tasseling stages. *Significant at $P < 0.05$ ($n = 3$); **Significant at $P < 0.01$ ($n = 3$); and ^{ns}non-significant.*

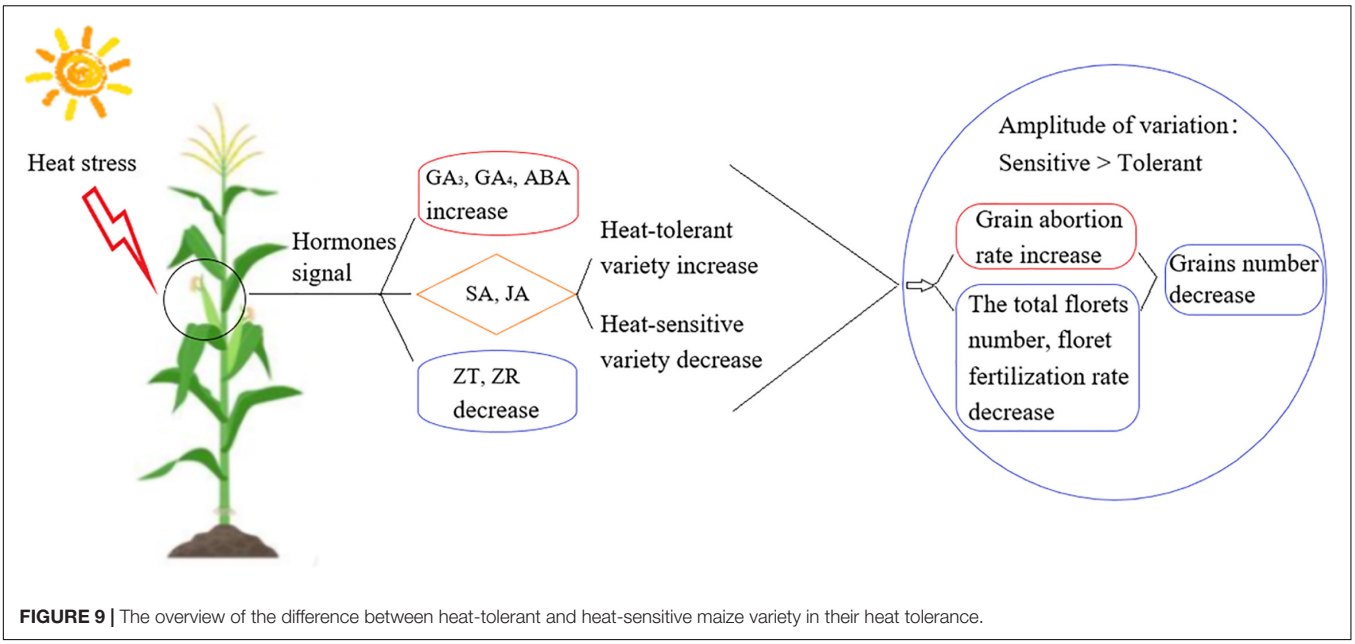


FIGURE 9 | The overview of the difference between heat-tolerant and heat-sensitive maize variety in their heat tolerance.

increases the abortion rate, and ultimately reduces the grain number (Dreccer et al., 2014; Prasad and Djanaguiraman, 2014). The spikelet and floret differentiation stages are key stages in the young ear differentiation process. During these stages, the ear length, ear diameter, floret number and grain abortion rate are the key factors that determine the grain number (Mohammed and Tarpley, 2011). Our results showed that when heat stress occurred during the V9, V12, or VT stage, the length of the young ear was 8.88–75.97% shorter than in the control group and the ear diameter was 23.63–74.44% smaller. The greatest impact occurred in plants subjected to heat stress during the V9 stage. At this stage, the ear is in the growth cone extension phase, and heat stress significantly inhibits the longitudinal and transverse elongation of the ear. At the same time, it renders the top of the ear dysplastic, thus suppressing its capability to form normal florets. Moreover, heat stress causes the growth stage to be delayed, the filaments to appear later, the florescence to be insufficient, and the fertilization process of filaments to be seriously impaired, especially for those filaments that grow at the top and the base of the ear. Finally, an increased grain abortion rate ultimately results in a significant reduction in the number of grains. This effect is more obvious for the heat-sensitive maize variety than for the heat-tolerant variety, indicating that the young ear differentiation process is sensitive to heat stress.

About 5% of the genes in the plants were up-regulated more than twice after the plants were subjected to heat stress (Finka et al., 2011). In the current study, the transcriptome analysis revealed that in the heat-tolerant maize variety, the DEGs that were induced by heat stress accounted for 0.64–3.02% of the total number of expressed genes, and that most genes were down-regulated. In the heat-sensitive maize variety, the DEGs that were induced by heat stress accounted for 0.12–4.10% of the total number of expressed genes, and most genes were up-regulated. Evidently, maize varieties with different capacities for heat tolerance exhibit different regulation patterns for gene expression when subjected to heat stress. When plants were under heat stress, the expression of many heat-resistant genes changed, such as those encoding hormones, heat shock proteins, and heat shock transcription factor, among others (Liu and Chen, 2015). Interestingly, although there were complicated interactions between different genes, GA might induce a gene associated with heat-tolerance (Ko et al., 2007). It is reported that ABA and SA are also connected with heat signal transduction under heat stress (Kotak et al., 2007). Furthermore, heat shock proteins, can be induced as a stress protein by many adversities, including temperature, water, and saltinity, which could alleviate the damage caused by stress and repair the plant in the meantime (Grigorova et al., 2011). Transcriptome analyses have shown that different crops exhibit different pathways in their response to heat stress; moreover, they have shown that most of these pathways are hormone signal transduction pathways (Larkindale et al., 2005; Qin et al., 2008). This observation indicates that, as important signaling molecules in response to heat stress, hormones play an irreplaceable role in the perception and conduction of heat signals. According to the results of our study, the enriched DEGs were related to pathways associated with hormone biosynthesis and signal transduction. The genes related to ZT were down-regulated after heat stress, while genes related to GA, ABA, heat shock proteins and heat shock transcription factor were up-regulated. Gene related to SA and JA were up-regulated in the heat-tolerant maize variety but down-regulated in the heat-sensitive maize variety. The qRT-PCR data supported the data obtained from RNA-seq, proving that our approach of finding the differences between endogenous hormone levels in ears subjected to heat stress is a valid approach for exploring the response of maize varieties with different heat tolerance to heat stress.

Endogenous plant hormones are closely related to plant growth, development, and yield formation, and their existence

and relative content can be used as an indicator of the physiological state of a plant, particularly as heat stress has the greatest influence on a plant's hormonal state (Scalabrin et al., 2016). Abiotic stress usually causes an increase in ABA content, which is one of the fastest ways to obtain heat tolerance (Yamaguchi-Shinozaki and Shinozaki, 2006; Raghavendra et al., 2010). In sweet maize, the expression of genes related to ZT biosynthesis is down-regulated in heat-tolerant variety under heat stress, so as to maintain a low growth level (Shi et al., 2017). Similarly, in grains, heat stress causes the ZT and ZR content to decrease in maize, rice, and wheat, but it causes the ABA and GA_3 content to increase (Sobol et al., 2014; Yang et al., 2014; Wu et al., 2016). Spraying ABA and GA also significantly increases grain weight and thermotolerance (Yang et al., 2011; Mo et al., 2018). Our results showed that the ZT and ZR content of maize ears decreased under heat stress and that the decrease in the heat-tolerant maize variety was greater when heat stress occurred in the V12 or VT stage. The GA_3, GA_4, and ABA content of young ears increased under heat stress, and the increase in ABA was greater for the heat-sensitive maize variety. The changes in the ZT, ZR, GA_3, GA_4, and ABA content of young ears under heat stress were significantly or extremely significantly correlated to the length of the young ear, ear diameter, length of the undeveloped part at the top of the ear, total floret number, floret fertilization rate, and grain abortion rate. The results showed that these hormones were all involved in the heat stress response of young ears and that they had a significant adverse effect on their development. As signaling substances in response to biological and abiotic stresses (Clarke et al., 2009), SA and JA play key roles in the establishment of thermotolerance (Zhou et al., 2010). The SA content increases rapidly during the first 30 min of heat stress application and subsequently decreases sharply, indicating that SA can quickly transmit heat signals. Moreover, the SA content in the leaves of heat-tolerant maize increases under heat stress, while it decreases in heat-sensitive maize (Dinler et al., 2014). The results from our study showed that the SA and JA content of young ears in the heat-tolerant maize variety increased under heat stress and that the trend was reversed for ears of the heat-sensitive maize variety. Moreover, the hormone content of ears of the heat-sensitive maize variety were positively correlated with the total floret number and the floret fertilization rate and negatively correlated with the grain abortion rate. Therefore, the decreases in SA and JA content under heat stress might be an important reason for the low thermotolerance and poor development of young ears of the heat-sensitive maize variety. Taken together, heat stress caused changes in the hormone levels in young ears, and inhibited their development, which was the main reason for the decrease in grain numbers under heat stress. Nevertheless, the content of both GA and ABA increased in maize ear under heat stress, although they are antagonistic hormones (Yang et al., 2017). In addition, a similar GA and ABA increase under temperature or water stress has been described in wheat, rice and Arabidopsis (Van et al., 2009; Yang et al., 2014; Wu H. et al., 2019). Therefore, a set of complex physiological reaction mechanisms must exist, which we will take exploring them as the focus of our further research.

CONCLUSION

Transcriptome analysis, of a heat-sensitive and a heat-tolerant maize variety subjected to heat stress, showed that the DEGs in the heat-sensitive maize variety were up-regulated rather than down-regulate under heat stress, and that the heat-tolerant maize variety had the opposite response. A KEGG analysis showed that the DEGs were mostly enriched in pathways associated with hormone signaling in response to heat stress. After applying heat stress, the ZT and ZR content decreased, and the GA_3, GA_4, and ABA content increased, which resulted in the floret number, floret fertilization rate, and grain number decreasing and the grain abortion rate increasing. Furthermore, there was evidence that heat- stress-induced increases in SA and JA content were the key reasons for high thermotolerance of the heat-tolerant maize variety.

DATA AVAILABILITY STATEMENT

All sequences were deposited in the National Center for Biotechnology Information (NCBI) and can be accessed in the Short Read Archive (SRA) under accession number: SRP250388.

AUTHOR CONTRIBUTIONS

PL and H-QW initiated and designed the research. H-QW analyzed the data, and wrote the manuscript. J-WZ, BZ, and B-ZR provided advice on the experiments. All authors contributed to the article and approved the submitted version.

FUNDING

We are grateful for grants from National Basic Research Program of China (2016YFD0300106), National Natural Science Foundation of China (31771713 and 31371576), and Shandong Province Key Agricultural Project for Application Technology Innovation (SDAIT02-08).

SUPPLEMENTARY MATERIAL

The Supplementary Material for this article can be found online at: https://www.frontiersin.org/articles/10.3389/fpls.2020.533046/full#supplementary-material

Supplementary Figure 1 | Diurnal changes of mean temperature **(A)** and mean relative humidity **(B)** in heat-stressed and natural environments. The heat-stressed and natural environments represent the temperature or relative humidity inside and outside the sheds. The hourly value is the average of 10 days' measurements.

Supplementary Table 1 | Primer design for quantitative real-time PCR (qRT-PCR) of commonly expressed genes from RNA sequencing data.

REFERENCES

Battisti, D. S., and Naylor, R. L. (2009). Historical warnings of future food insecurity with unprecedented seasonal heat. *Science* 323, 240–244. doi: 10.1126/science.1164363

Černý, M., Jedelskı, P. L., Novák, J., Schlosser, A., and Brzobohatı, B. (2014). Cytokinin modulates proteomic, transcriptomic and growth responses to temperature shocks in *Arabidopsis*. *Plant Cell Environ.* 37, 1641–1655. doi: 10.1111/pce.12270

Chen, Y., Wang, Y., Zhu, D., Shi, Q., Chen, H., Xiang, J., et al. (2019). Mechanism of exogenous brassinolide in alleviating high temperature injury at panicle initiation stage in rice. *Chinese J. Rice Sci.* 33, 457–466. doi: 10.16819/j.1001-7216.2019.9036

Cicchino, M., Edreira, J. I. R., Uribelarrea, M., and Otegui, M. E. (2010). Heat stress in field-grown maize: response of physiological determinants of grain yield. *Crop Sci.* 50, 1438–1448. doi: 10.2135/cropsci2009.10.0574

Clarke, S. M., Cristescu, S. M., Miersch, O., Harren, F. J. M., Wasternack, C., and Mur, L. A. (2009). Jasmonates act with salicylic acid to confer basal thermotolerance in *Arabidopsis thaliana*. *New Phytol.* 182, 175–187. doi: 10.1111/j.1469-8137.2008.02735.x

Craita, E. B., Sara, Z., Wim, H. V., Celestina, M., Mario, P., and Tom, G. (2011). Temperature stress differentially modulates transcription in meiotic anthers of heat-tolerant and heat-sensitive tomato plants. *BMC Genomics* 12:384. doi: 10.1186/1471-2164-12-384

Cui, H., Jin, L., Li, B., Dong, S., Liu, P., Zhao, B., et al. (2014). Effects of shading on endogenous hormones regulation in kernel development of summer maize in the field. *Chinese J. Appl. Ecol.* 25, 1373–1379. doi: 10.13287/j.1001-9332.2014.0021

Dinler, B. S., Demir, E., and Kompe, Y. O. (2014). Regulation of auxin, abscisic acid and salicylic acid levels by ascorbate application under heat stress in sensitive and tolerant maize leaves. *Acta Biol. Hung.* 65, 469–480. doi: 10.1556/ABiol.65.2014.4.10

Dong, H., Li, H., Li, A., and Yan, X. (2010). Relationships between spike and stem growth and female spike differentiation under different densities. *J. Maize Sci.* 18, 65–75. doi: 10.13597/j.cnki.maize.science.2010.05.018

Dreccer, M. F., Wockner, K. B., Palta, J. A., McIntyre, C. L., Borgognone, M. G., Bourgault, M., et al. (2014). More fertile florets and grains per spike can be achieved at higher temperature in wheat lines with high spike biomass and sugar content at booting. *Funct. Plant Biol.* 41, 482–495. doi: 10.1071/FP13232

Engelberth, J., Schmelz, E. A., Alborn, H. T., Cardoza, Y. J., Huang, J., and Tumlinson, J. H. (2003). Simultaneous quantification of jasmonic acid and salicylic acid in plants by vapor-phase extraction and gas chromatography-chemical ionization-mass spectrometry. *Anal. Biochem.* 312, 242–250. doi: 10.1016/S0003-2697(02)00466-9

Escandón, M., Cañal, M. J., Pascual, J., Pinto, G., Correia, B., Amaral, J., et al. (2016). Integrated physiological and hormonal profile of heat-induced thermotolerance in pinus radiate. *Tree Physiol.* 36, 63–77. doi: 10.1093/treephys/tpv127

Finka, A., Mattoo, R. U. H., and Goloubinoff, P. (2011). Meta-analysis of heat- and chemically upregulated chaperone genes in plant and human cells [J]. *Cell Stress Chaperones* 2011, 15–31. doi: 10.1007/s12192-010-0216-8

Garzón-Martínez, G. A., Zhu, Z. I., Landsman, D., Barrero, L. S., and Mariño-Ramírez, L. (2012). The *Physalis peruviana* leaf transcriptome: assembly, annotation and gene model prediction. *BMC Genomics* 13:151. doi: 10.1186/1471-2164-13-151

Grigorova, B., Vaseva, I. I., Demirevska, K., and Feller, U. (2011). Expression of selected heat shock proteins after individually applied and combined drought and heat stress. *Acta Physiol. Plant.* 33, 2041–2049. doi: 10.1007/s11738-011-0733-9

Högy, P., Kottmann, L., Schmid, I., and Fangmeier, A. (2019). Heat, wheat and CO2: the relevance of timing and the mode of temperature stress on biomass and yield. *J. Agron. Crop Sci.* 205, 608–615. doi: 10.1111/jac.12345

Hossain, A., and Teixeira, D. (2012). Phenology, growth and yield of three wheat (*Triticum aestivum* L.) varieties as affected by high temperature stress. *Notulae Sci. Biol.* 4, 97–109. doi: 10.15835/nsb437879

Jagadish, K. S. V., Craufurd, P. Q., Shi, W., and Oane, R. (2013). A phenotypic marker for quantifying heat stress impact during microsporogenesis in rice (*Oryza sativa* L.). *Funct. Plant Biol.* 41, 48–55. doi: 10.1071/FP13086

Jagadish, K. S. V., Muthurajan, R., Oane, R., Wheeler, T. R., Heuer, S., Bennett, J., et al. (2010). Physiological and proteomic approaches to address heat tolerance during anthesis in rice (*Oryza sativa* L.). *J. Exp. Bot.* 61, 143–156. doi: 10.1093/jxb/erp289

Johnson, S. M., Lim, F. L., Finkler, A., Fromm, H., Slabas, A. R., and Knight, M. R. (2014). Transcriptomic analysis of sorghum bicolor responding to combined heat and drought stress. *BMC Genomics* 15:456. doi: 10.1186/1471-2164-15-456

Keykha, M., Ganjali, H. R., and Mobasser, H. R. (2014). Effect of salicylic acid and gibberellic acid on some characteristics in mungbean (*Vigna radiata*). *Int. J. Biosci.* 5, 70–75. doi: 10.12692/ijb/5.11.70-75

Ko, C. B., Woo, Y. M., Lee, D. J., Lee, M. C., and Kim, C. S. (2007). Enhanced tolerance to heat stress in transgenic plants expressing the GASA4 gene. *Plant Physiol. Biochem.* 45, 722–728. doi: 10.1016/j.plaphy.2007.07.010

Kotak, S., Larkindale, J., Lee, U., Koskull-Döring, P. V., Vierling, E., and Scharf, K. D. (2007). Complexity of the heat stress response in plants. *Curr. Opin. Plant Biol.* 10, 310–316. doi: 10.1016/j.pbi.2007.04.011

Larkindale, J., Hall, J. D., Knight, M. R., and Vierling, E. (2005). Heat stress phenotypes of *Arabidopsis* mutants implicate multiple signaling pathways in the acquisition of thermotolerance. *Plant Physiol.* 138, 882–897. doi: 10.1104/pp.105.062257

Liu, F., Wang, W., Sun, X., Liang, Z., and Wang, F. (2014). RNA-Seq revealed complex response to heat stress on transcriptomic level in *Saccharina japonica* (Laminariales, Phaeophyta). *J. Appl. Phycol.* 26, 1585–1596. doi: 10.1007/s10811-013-0188-z

Liu, K., and Chen, W. (2015). Recent advances in plant heat-related genes. *J. Plant Genet. Resourc.* 16, 127–132. doi: 10.13430/j.cnki.jpgr.2015.01.018

Lobell, D. B., Bänzige, M., Magorokosho, C., and Vivek, B. (2011). Nonlinear heat effects on African maize as evidenced by historical yield trials. *Nat. Clim. Change* 1, 42–45. doi: 10.1038/nclimate1043

Lu, J., Zhang, R., Zong, X., Wang, S., and He, G. (2009). Effect of salicylic acid on heat resistance of rice seedling under heat stress. *Chinese J. Eco Agric.* 17, 1168–1171. doi: 10.3724/sp.j.1011.2009.01168

Magneschi, L., Kudahettige, R. L., Alpi, A., and Perata, P. (2009). Expansin gene expression and anoxic coleoptiles elongation in rice cultivars. *J. Plant Physiol.* 166, 1576–1580. doi: 10.1016/j.jplph.2009.03.008

Mo, X., Wen, Q., Qin, L., Mo, Y., and Lan, Q. (2018). Improving heat-resistance of rhododendron hybridum by using salicylic acid combined with abscisic acid during high temperature stress. *Northern Horticult.* 13, 87–94. doi: 10.11937/bfyy.20174127

Mohammed, A. R., and Tarpley, L. (2011). Effects of night temperature, spikelet position and salicylic acid on yield and yield-related parameters of rice (*Oryza sativa* L.) plants. *J. Agron. Crop Sci.* 197, 40–49. doi: 10.1111/j.1439-037X.2010.00439.x

Müller, L. L. B., Albach, D. C., and Zotz, G. (2017). 'Are 3°C too much?': thermal niche breadth in bromeliaceae and global warming. *J. Ecol.* 105, 507–516. doi: 10.1111/1365-2745.12681

Obata, T., Witt, S., Lisec, J., Palacios-Rojas, N., Florez-Sarasa, I., Yousfi, S., et al. (2015). Metabolite profiles of maize leaves in drought, heat, and combined stress field trials reveal the relationship between metabolism and grain yield. *Plant Physiol.* 169, 2665–2683. doi: 10.1104/pp.15.01164

Ordóñez, R. A., Savin, R., Cossani, C. M., and Slafer, G. A. (2015). Yield response to heat stress as affected by nitrogen availability in maize. *Field Crops Res.* 183, 184–203. doi: 10.1016/j.fcr.2015.07.010

Prasad, P. V. V., and Djanaguiraman, M. (2014). Response of floret fertility and individual grain weight of wheat to high temperature stress: sensitive stages and thresholds for temperature and duration. *Funct. Plant Biol.* 41, 1261–1269. doi: 10.1071/FP14061

Prasad, P. V. V., Pisipati, S. R., and Momèiloviæ, I. Z. (2011). Independent and combined effects of high temperature and drought stress during grain filling on plant yield and chloroplast EF-Tu expression in spring wheat. *J. Agron. Crop Sci.* 197, 430–441. doi: 10.1111/j.1439-037X.2011.00477.x

Qin, D., Wu, H., Peng, H., Yao, Y., Ni, Z., Li, Z., et al. (2008). Heat stress-responsive transcriptome analysis in heat susceptible and tolerant wheat (*Triticum aestivum* L.) by using wheat genome array. *BMC Genomics* 9:432. doi: 10.1186/1471-2164-9-432

Raghavendra, A. S., Gonugunta, V. K., Christmann, A., and Grill, E. (2010). ABA perception and signalling. *Trends Plant Sci.* 15, 395–401. doi: 10.1016/j.tplants.2010.04.006

Ravic, P. N., and Sandy, J. A. (2016). Regional suitability for agricultural intensification: a spatial analysis of the southern agricultural growth corridor of tanzania. *Int. J. Agric. Sustainab.* 14, 231–247. doi: 10.1080/14735903.2015.1071548

Scalabrin, E., Radaelli, M., and Capodaglio, G. (2016). Simultaneous determination of shikimic acid, salicylic acid and jasmonic acid in wild and transgenic nicotiana langsdorffii plants exposed to abiotic stresses. *Plant Physiol. Biochem.* 103, 53–60. doi: 10.1016/j.plaphy.2016.02.040

Sheng, J., Feng, C., Guo, W., Li, C., Zhang, Y., and Peng, Y. (2001). Relation of endogenous hormone contents in spikes to floret development of wheat. *Jiangsu Agricult. Res.* 22, 5–8. doi: 10.16872/j.cnki.1671-4652.2001.04.002

Shi, J., Yan, B., Lou, X., Ma, H., and Ruan, S. (2017). Comparative transcriptome analysis reveals the transcriptional alterations in heat-resistant and heat-sensitive sweet maize (*Zea mays* L.) varieties under heat stress. *BMC Plant Biol.* 17:26. doi: 10.1186/s12870-017-0973-y

Sobol, S., Chayut, N., Nave, N., Kafle, D., Hegele, M., Kaminetsky, R., et al. (2014). Genetic variation in yield under hot ambient temperatures spotlights a role for cytokinin in protection of developing floral primordia. *Plant Cell Environ.* 37, 643–657. doi: 10.1111/pce.12184

Sun, S., Li, D., Liu, L., Wang, Z., and Yin, Y. (2017). Global major weather and climate events in 2016 and the possible causes. *Meteorol. Monthly* 43, 477–485. doi: 10.7519/j.issn.1000-0526.2017.04.010

Van, Z. M., Voesenek, L. A., Peeters, A. J., and Millenaar, F. F. (2009). Hormone-and light-mediated regulation of heat-induced differential petiole growth in *Arabidopsis*. *Plant Physiol.* 151, 1446–1458. doi: 10.1104/pp.109.144386

Wolters, H., and Jürgens, G. (2009). Survival of the flexible: hormonal growth control and adaptation in plant development. *Nat. Rev. Genet.* 10, 305–317. doi: 10.1038/nrg2558

Wu, C., Cui, K., Hu, Q., Wang, W., Nie, L., Huang, J., et al. (2019). Enclosed stigma contributes to higher spikelet fertility for rice (*Oryza sativa* L.) subjected to heat stress. *Crop J.* 7, 335–349. doi: 10.1016/j.cj.2018.11.011

Wu, H., Chen, H., Zhang, Y., Zhang, Y., Zhu, D., and Xiang, J. (2019). Effects of 1-aminocyclopropane-1-carboxylate and paclobutrazol on the endogenous hormones of two contrasting rice varieties under submergence stress. *Plant Growth Regul.* 87, 109–121. doi: 10.1007/s10725-018-0457-6

Wu, C., Cui, K., Wang, W., Li, Q., Fahad, S., Hu, Q., et al. (2016). Heat-induced phytohormone changes are associated with disrupted early reproductive development and reduced yield in rice. *Sci. Rep.* 6:34978. doi: 10.1038/srep34978

Wu, C., Cui, K., Wang, W., Li, Q., Fahad, S., Hu, Q., et al. (2017). Heat-induced cytokinin transportation and degradation are associated with reduced panicle cytokinin expression and fewer spikelets per panicle in rice. *Front. Plant Sci.* 8:371. doi: 10.3389/fpls.2017.00371

Wu, H., Li, Y., and Xie, C. (2018). Research advances on physiological basis and gene discovery for thermal tolerance in crops. *Crops* 5, 1–9. doi: 10.16035/j.issn.1001-7283.2018.05.001

Xu, W., Liu, C., Wang, K., Xie, R., Ming, B., Wang, Y., et al. (2017). Adjusting maize plant density to different climatic conditions across a large longitudinal distance in China. *Field Crops Res.* 212, 126–134. doi: 10.1016/j.fcr.2017.05.006

Yamaguchi-Shinozaki, K., and Shinozaki, K. (2006). Transcriptional regulatory networks in cellular responses and tolerance to dehydration and cold stresses. *Annu. Rev. Plant Biol.* 57, 781–803. doi: 10.1146/annurev.arplant.57.032905.105444

Yang, D., Wang, Z., Ni, Y., Yin, Y., Cai, T., Yang, W., et al. (2014). Effect of high temperature stress and spraying exogenous ABA post- anthesis on grain filling and grain yield in different types of stay-green wheat. *Sci. Agric. Sin.* 47, 2109–2125. doi: 10.3864/j.issn.0578-1752.2014.11.005

Yang, H., Shen, X., Ding, M., Lu, D., and Lu, W. (2017). Effects of high temperature after pollination on grain development and endogenous hormone contents of waxy maize. *J. Maize Sci.* 25, 55–60. doi: 10.13597/j.cnki.maize.science.20170210

Yang, W., Wang, Z., Yin, Y., Li, W., Li, Y., Chen, X., et al. (2011). Effects of spraying exogenous ABA or GA on the endogenous hormones concentration and filling of wheat grains. *Sci. Agric. Sin.* 44, 2673–2682. doi: 10.3864/j.issn.0578-1752.2011.13.005

Zhou, B., Tang, X., and Wang, Y. (2010). Salicylic acid and heat acclimation pretreatment protects *Laminaria japonica* sporophyte (Phaeophyceae) from heat stress. *Chinese J. Oceanol. Limnol.* 28, 924–932. doi: 10.1007/s00343-010-9049-7

Conflict of Interest: The authors declare that the research was conducted in the absence of any commercial or financial relationships that could be construed as a potential conflict of interest.

Copyright © 2020 Wang, Liu, Zhang, Zhao and Ren. This is an open-access article distributed under the terms of the Creative Commons Attribution License (CC BY). The use, distribution or reproduction in other forums is permitted, provided the original author(s) and the copyright owner(s) are credited and that the original publication in this journal is cited, in accordance with accepted academic practice. No use, distribution or reproduction is permitted which does not comply with these terms.

frontiers in Plant Science

REVIEW
published: 22 October 2020
doi: 10.3389/fpls.2020.587264

Identification and Characterization of Contrasting Genotypes/Cultivars for Developing Heat Tolerance in Agricultural Crops: Current Status and Prospects

*Shikha Chaudhary[1], Poonam Devi[1], Anjali Bhardwaj[1], Uday Chand Jha[2], Kamal Dev Sharma[3], P. V. Vara Prasad[4], Kadambot H. M. Siddique[5], H. Bindumadhava[6], Shiv Kumar[7] and Harsh Nayyar[1]**

[1] Department of Botany, Panjab University, Chandigarh, India, [2] Indian Institute of Pulses Research, Kanpur, India, [3] Department of Agricultural Biotechnology, Chaudhary Sarwan Kumar Himachal Pradesh (CSK HP) Agricultural University, Palampur, India, [4] Kansas State University, Manhattan, KS, United States, [5] The UWA Institute of Agriculture, The University of Western Australia, Perth, WA, Australia, [6] World Vegetable Center, International Crops Research Institute for the Semi-Arid Tropics (ICRISAT), Hyderabad, India, [7] International Center for Agriculture Research in the Dry Areas (ICARDA), Rabat, Morocco

OPEN ACCESS

Edited by:
Raul Antonio Sperotto, Universidade do Vale do Taquari - Univates, Brazil

Reviewed by:
Daniel Kean Yuen Tan, The University of Sydney, Australia
Paul Kiprotich Kimurto, Egerton University, Kenya
Rebecca Janette Thistlethwaite, The University of Sydney, Australia

***Correspondence:**
Harsh Nayyar
harshnayyar@hotmail.com

Specialty section:
This article was submitted to Crop and Product Physiology, a section of the journal Frontiers in Plant Science

Received: 25 July 2020
Accepted: 14 September 2020
Published: 22 October 2020

Citation:
Chaudhary S, Devi P, Bhardwaj A, Jha UC, Sharma KD, Prasad PVV, Siddique KHM, Bindumadhava H, Kumar S and Nayyar H (2020) Identification and Characterization of Contrasting Genotypes/Cultivars for Developing Heat Tolerance in Agricultural Crops: Current Status and Prospects. Front. Plant Sci. 11:587264. doi: 10.3389/fpls.2020.587264

Rising global temperatures due to climate change are affecting crop performance in several regions of the world. High temperatures affect plants at various organizational levels, primarily accelerating phenology to limit biomass production and shortening reproductive phase to curtail flower and fruit numbers, thus resulting in severe yield losses. Besides, heat stress also disrupts normal growth, development, cellular metabolism, and gene expression, which alters shoot and root structures, branching patterns, leaf surface and orientation, and anatomical, structural, and functional aspects of leaves and flowers. The reproductive growth stage is crucial in plants' life cycle, and susceptible to high temperatures, as reproductive processes are negatively impacted thus reducing crop yield. Genetic variation exists among genotypes of various crops to resist impacts of heat stress. Several screening studies have successfully phenotyped large populations of various crops to distinguish heat-tolerant and heat-sensitive genotypes using various traits, related to shoots (including leaves), flowers, fruits (pods, spikes, spikelets), and seeds (or grains), which have led to direct release of heat-tolerant cultivars in some cases (such as chickpea). In the present review, we discuss examples of contrasting genotypes for heat tolerance in different crops, involving many traits related to thermotolerance in leaves (membrane thermostability, photosynthetic efficiency, chlorophyll content, chlorophyll fluorescence, stomatal activity), flowers (pollen viability, pollen germination, fertilization, ovule viability), roots (architecture), biomolecules (antioxidants, osmolytes, phytohormones, heat-shock proteins, other stress proteins), and "omics" (phenomics, transcriptomics, genomics) approaches. The traits linked to heat tolerance can be introgressed into high yielding but heat-sensitive genotypes of crops to enhance their thermotolerance. Involving these traits will be useful for screening

contrasting genotypes and would pave the way for characterizing the underlying molecular mechanisms, which could be valuable for engineering plants with enhanced thermotolerance. Wherever possible, we discussed breeding and biotechnological approaches for using these traits to develop heat-tolerant genotypes of various food crops.

Keywords: heat-stress, crops, tolerance, agriculture, physiology

INTRODUCTION

The Earth's increasing average surface temperature due to climate change is proving to be stressful for all phases of plant growth and development, particularly in tropical and subtropical countries (Li B. et al., 2018). Among abiotic stresses, high temperature stress is a major factor disrupting plants' performance (Wahid et al., 2007). Each plant species has its own maximum, optimum and minimum temperatures, known as cardinal temperatures. Temperatures below or above these thresholds causes stress (Wahid et al., 2007). Above optimum (high-temperatures) affect plant's morphological, physiological, biochemical and molecular traits, which ultimately leads to poor growth and yields (Hasanuzzaman et al., 2013). The impact of high-temperature (heat) stress depends on intensity, timing, duration of stress and type of plant species (Wahid et al., 2007). Although all stages of plant development can be negatively impacted by heat stress, reproductive stages of crop are relatively more sensitive than vegetative stages (Prasad et al., 2008b, 2017). Heat stress during seed germination reduces germination percentage, seedling emergence, and radicle and plumule growth in germinated seedlings, resulting in abnormal seedlings with poor seedling vigor (Hasanuzzaman et al., 2013). At later vegetative stages, heat stress adversely affects photosynthesis, leaf area development leading to lower biomass production; whereas, stress during reproductive stages of development results in lower seed numbers and decrease seed size resulting in lower yields (Bita and Gerats, 2013; Prasad et al., 2017). Different crops and their genotypes vary in their heat sensitivity, the response is generally stage-and trait-specific, which can reveal mechanisms related to heat tolerance (Bita and Gerats, 2013; Prasad et al., 2017). Thus, genotypes having contrasting heat sensitivity have been identified in several crops (detailed below), that yielded vital information on various traits controlling heat tolerance (**Figure 1**).

IMPACT OF HEAT STRESS

Heat stress can have damaging effects (direct and indirect) on all stages of plant growth and development (Kaushal et al., 2016). Phenological stages differ in their sensitivity to heat stress, and vary between species and genotypes of same species. Various plant tissue injuries have been observed under heat stress, such as leaf and twig scorching, leaf, branch and stem chlorosis and necrosis, leaf senescence and abscission, root and shoot growth inhibition, flower drop, and fruitdamage, which consequently reduce plant productivity (Vollenweider and Günthardt-Goerg, 2005). Heat stress primarily affects the stability of plasma membranes, several proteins, cytoskeleton organization, and the efficiency of cell enzymatic reactions and creating metabolic disparity (Xu et al., 2006). Heat-stress-induced oxidative stress causes peroxidation of membrane lipids, proteins, and nucleic acids (Mittler et al., 2004). Due to reduced membrane stability, electrolyte leakage increases, which intensifies the membrane injuries (Wahid et al., 2007). Physiological processes, such as photosynthetic activity and sucrose metabolism, are highly sensitive to heat stress (Berry and Bjorkman, 1980). At the subcellular level, disruption of structural organization of thylakoids and loss of grana stacking in chloroplasts are the primary sites of heat injury (Sharkey, 2005), which lead to changes in electron transport to PSII (Lu and Zhang, 2000). Heat stress also damages PSII and inhibits its repair due to the generation of reactive oxygen species (ROS) (Allakhverdiev et al., 2008). Heat stress affects enzymes in Calvin cycle, including RuBisCo and RuBisCo activase (Camejo et al., 2005; HanumanthaRao et al., 2016; Bindumadhava et al., 2018), which hampers photosynthesis and photorespiration. Heat stress during reproductive stages adversely affects seed-set and yield in many food legumes, such as chickpea (*Cicer arietinum*) (Kaushal et al., 2013), mungbean (*Vigna radiata*) (Kaur et al., 2015; HanumanthaRao et al., 2016), peanut (*Arachis hypogaea*) (Prasad et al., 1999a,b) and lentil (*Lens culinaris*) (Bhandari et al., 2016) and cereals, such as wheat (Wahid et al., 2007; Prasad and Djanaguiraman, 2014), sorghum (*Sorghum bicolor*) (Prasad et al., 2015), barley (*Hordeum vulgare*) (Barnabás et al., 2008), and maize (*Zea mays*) (Kumar et al., 2012). During the reproductive stage, gametogenesis and fertilization are highly sensitive to heat stress, which impairs meiosis in both male and female organs, affects pollen germination and pollen tube growth, reduces ovule viability and ovule size, alters stigmatic and style positions, reduces stigma receptivity, disturbs fertilization processes, affects embryo fertilization, and impedes endosperm growth (Farooq et al., 2017; Prasad et al., 2017). Heat stress hastens the rate of grain filling, but reduces the duration of grain filling, as reported in wheat (Prasad et al., 2008a; Farooq et al., 2011), which may be due to direct effects of heat stress on the source–sink relationship that reduce photoassimilate supply to developing seeds (Calderini et al., 2006). The detrimental effects of heat stress can be alleviated by developing crop varieties with improved heat tolerance. The most popular approach used by many plant researchers has been screening a large population to identify contrasting genotypes for elucidating physiological, biochemical, and molecular mechanisms governing heat

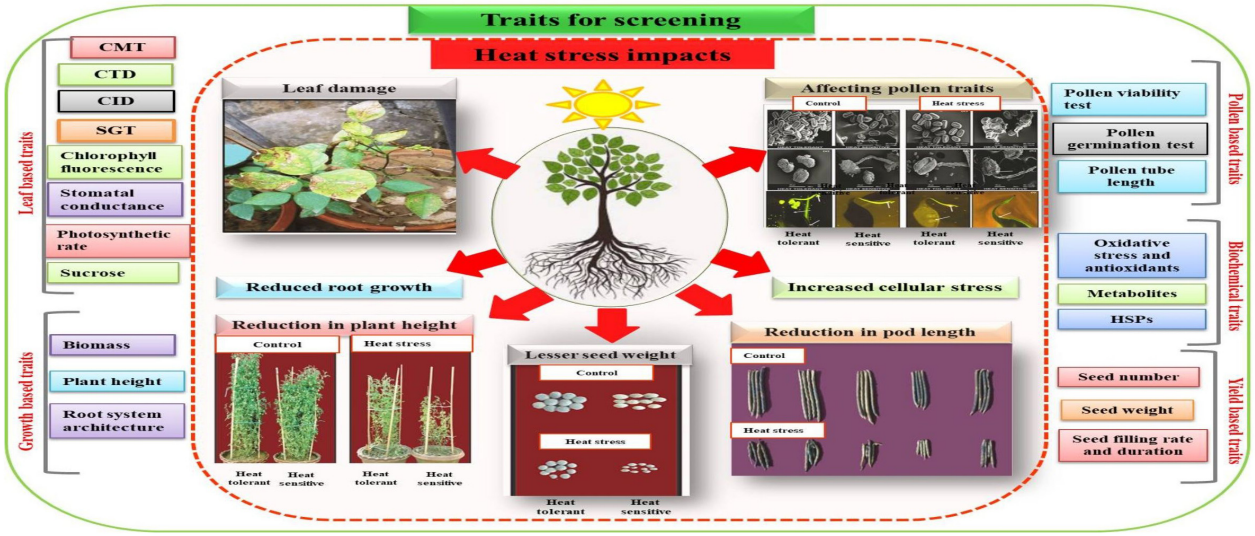


FIGURE 1 | Screening traits for developing heat tolerant genotypes. Different traits based on leaf, growth, pollen grains biochemical and yield can be used for the selection of genotypes. Cell membrane thermostability (CMT), canopy temperature depression (CTD), carbon isotope discrimination (CID), stay green trait (SGT), chlorophyll fluorescence, stomatal conductance, photosynthetic rate and sucrose are the traits that can be assessed from leaves. However growth pattern such as plant biomass, plant height, and RSA of different genotypes can also be compared for selection of contrasting genotypes. Similarly, reproductive wellness of genotypes can be checked by using pollen based traits such as pollen viability test, pollen germination test and pollen tube length. The mitigation of cellular stress by genotypes can be compared by analysis of oxidative stress damage (production of free radicals) and production of antioxidants, metabolites and heat shock proteins (HSPs) whereas yield based traits such as seed number, seed weight, seed filling rate and duration can also be employed for selection purpose.

tolerance. Understanding such mechanisms will pave the way for improving crop genotypes under heat stress. Here, we discuss how heat stress impacts traits related to stress tolerance in contrasting genotypes of various crops to provide further clues for breeders and agronomists for improving the selection of heat-tolerant genotypes across crop species. Heat stress is often accompanied by drought stress; the impacts of heat stress are worsened in drought-stressed plants, which are manifested in various organizational changes in plants (Sehgal et al., 2017), hence, wherever possible, we have also included some examples where genotypes of crops have been screened against combined heat and drought stress situations.

MECHANISMS GOVERNING THERMOTOLERANCE

Plants can endure two types of mechanisms to cope with heat stress: (1) basal thermotolerance (inherent ability of plant) and (2) acquired thermotolerance (induced by pre-exposure to higher but non-lethal temperatures) (Bokszczanin and Fragkostefanakis, 2013). Acquired thermotolerance has an important role to play in plant survival (Kotak et al., 2007). Hence, the heat stress response is a genetically controlled process that can be stimulated by mild or sub-lethal temperatures and further trigger the onset of heat-stress response in plants (Charng et al., 2006). The heat-stress response in plants is mainly conserved via cellular compartments and regulatory networks (Wahid et al., 2007). Plants have evolved various short-term acclimation mechanisms and long-term adaptations in response to heat stress. Short-term acclimation mechanisms include leaf orientation, transpirational cooling, and changes in membrane lipid composition (Wahid et al., 2007). For longer term adaptations, plants activate heat-stress tolerance mechanisms, such as heat stress sensing through various sensors and regulating downstream signal transduction pathways (e.g., lipidome, metabolome, transcriptome, and proteome) to modify gene expression to ensure survival (Sung et al., 2003; Bokszczanin and Fragkostefanakis, 2013; Dang et al., 2013).

Major adaptive mechanisms that induce thermotolerance in plants include amplified production of thermoprotectants, such as secondary metabolites, compatible solutes, ROS scavenging mechanisms, and heat-shock proteins (HSPs) (Nakamoto and Hiyama, 1999; Sakamoto and Murata, 2002; Wahid et al., 2007; Mittler et al., 2012). During severe heat stress, ROS generated as a byproduct of aerobic metabolism negatively affect cellular metabolism, such as peroxidation of lipid membranes and damage to nucleic acids and proteins (Bita and Gerats, 2013). Plants activate enzymatic and non-enzymatic ROS scavenging systems to defend this ROS production. The main ROS scavenging enzymes are superoxide dismutase (SOD), catalase (CAT), peroxidase (POX), ascorbate peroxidase (APX), and glutathione reductase (GR), and the non-enzymatic systems include ascorbic acid (ASC) and glutathione (GSH) (Suzuki et al., 2012). Elevated levels of these antioxidants are crucial for imparting thermotolerance in plants (Awasthi et al., 2015). Thus, to cope with heat stress, plants synthesize and accumulate more stress proteins, including HSPs, which are well-defined molecular chaperones involved in protein folding, and proper aggregation, translocation, and degradation under normal and stress conditions, and essential for sustaining cellular stability

(Vierling, 1991). Five major families of HSPs/chaperones are HSP60, HSP70, HSP90, HSP100, and the small HSP (sHSP) family (Wang et al., 2004), which play an important role in the mitigation of heat-stress effects, especially protecting native proteins from denaturation. The accumulation of secondary metabolites, such as carotenoids, isoprenoids, and flavonoids, augments high-temperature stress tolerance by preventing peroxidase activity (Havaux, 1998; Loreto et al., 1998; Rivero et al., 2004). The accumulation of compatible solutes, *viz.* sugars (trehalose), sugar alcohols (polyols), proline, glycine betaine, tertiary, and quaternary ammonium compounds, also provides heat-stress tolerance in plants (Sakamoto and Murata, 2002). Due to their low molecular weight, these molecules can buffer the cellular redox potential under heat stress. Phytohormones, such as salicylic acid, abscisic acid, brassinosteroids, and polyamines, also play a significant role in providing thermotolerance to plants (Ahammed and Yu, 2016; Sharma et al., 2020).

GROWTH-BASED PARAMETERS

Most studies on contrasting genotypes have measured biomass, plant height, and root growth, with significant variations identified in various crops subjected to heat stress, either in laboratory or field experiments, which has resulted in using these traits to quantify the impact of heat stress. Some examples of the impacts of heat stress on these traits are described below.

Plant Height

Vegetative growth can be assessed as plant height to distinguish heat-stress tolerant genotypes (Debnath et al., 2016). In *Brassica juncea* L., high temperature (34°C) after the induction of flowering significantly affected plant height when grown in the field, declining by 18.9–30.5% (mean 22.3%), relative to the control. Genotypes BPR-538-10, NRCDR-2, RH-0216 had lower heat susceptibility, based on plant height, than genotypes RGN193, NPJ112 and SKM531 (Chauhan et al., 2009). Heat stress (>40°C) reduced plant height in 20 maize genotypes in the field (Debnath et al., 2016), with the most heat-tolerant genotype (DTPYC9F119) declining by 2.31% compared with a 72.2% reduction in the most heat-sensitive genotype LM13. Assessment of five potato cultivars (L1: 84.194.30; L2:86.61.26; L3: 87HW13.7, L4: DG81-68, and L5: Desiree) under controlled environment of combined heat (30 + 1°C) and drought stress (PEG 8000) for 21 days revealed severe effects all the cultivars on plant height, when both the stresses were together, except L2 and L3 (Handayani and Watanabe, 2020).

Seedling growth could be a potentially useful trait for early screening against heat stress. For instance, in some tropical parts of Africa, surface temperatures of tropical soils at planting time can exceed 50°C for hours to restrict the germination and seedling growth (Setimela et al., 2007). Hence, seedling heat tolerance is critical for adequate crop establishment in the semi-arid tropics. In a study carried out on sorghum (*Sorghum bicolor*) in Zimbabwe, seedling tolerance was estimated as heat tolerance index (HTI; defined as a ratio of resumed coleoptile growth after a controlled heat shock, compared to normal growth). Genetic parameters of HTI were assessed by crossing four sorghum lines having varying HTI, with three tester lines, and deriving F1, F2, F3, BC1, and BC11 families for generation means analysis. HTI was found to be highest (0.71) in Line IS20969 from Egypt, while an experimental line (290R), from the University of Nebraska, had the lowest at 0.51. The study revealed that additive and dominance effects contributed to coleoptile elongation under normal conditions, but only additive effects were significant in recovery growth. Epistatic effects were observed in both normal and heat-stressed environment. General combining ability (GCA) effects for HTI were highly marked in both conditions, but specific combining ability (SCA) effects were negligible. These results showed that it is achievable to enhance seedling heat tolerance and, thus, improve plant populations of sorghum in tropical areas where hot soil temperatures occur.

Root System Architecture

The structure, spatial, and temporal configuration of the plant root system is called root system architecture (RSA) (de Dorlodot et al., 2007). The organization of primary and secondary roots is determined by RSA at the macroscale (Smith and De Smet, 2012). Root microstructure, such as fine root hairs, root tips and their interactions with soil and soil microorganisms responsible for water and mineral uptake, is determined by RSA at the microscale (Wu et al., 2018). Most resources are heterogeneously distributed in the soil, and the spatial and temporal distribution of roots determines the crop's ability to exploit resources (Brussaard et al., 2007). Better understanding of RSA allows us to determine the impact of environmental conditions and management practices on crops, which can help to reduce the difference between genetic potential and actual average yields (Garnett et al., 2009; Judd et al., 2015; Ryan et al., 2016). RSA has a vital role in plant–soil–microbe interactions and resolves the crosstalk with beneficial soil microbes in the rhizosphere (Ryan et al., 2016).

Across fluctuating environments, RSA is an important characteristic for adaptability. Therefore, we can improve crop performance in terms of increased root traits, such as allocation, morphological, anatomical, or developmental plasticity (Sultan, 2000). There is a direct relationship between individual RSA plasticity and yield, which is related to more stable plant performance across changing environments in various species (Sadras, 2009; Niones et al., 2012, 2013). Root branching is important for improving the root surface area, enabling the plant to reach more distant reserves of water and nutrients and improve soil anchorage. In plants, heat stress generally reduces primary root length, lateral root density (number of lateral roots per unit primary root length) and angle of emergence of lateral roots from the primary root, but has little effect on average lateral root length (McMichael and Quisenberry, 1993; Nagel et al., 2009). Root growth has a lower optimal growing temperature than shoot growth and is thus more sensitive to rising temperatures (Huang and Gao, 2000; Xu and Huang, 2000). Plant heat tolerance is directly influenced by root morphological features. Among Kentucky bluegrass (*Poa pratensis)* cultivars, increased root number and root length contributed to variations in heat tolerance (Lehman and Engelke, 1993). Root phenotyping of 577 common bean (*Phaseolus vulgaris* L.) genotypes in

variable environments of heat, drought, and nutrient deficiency revealed significant relationships between seed yield and seedling basal root number, seedling adventitious root abundance, and seedling taproot length. Under heat stress, adventitious root number had a positive relationship (13%) with seed yield. Mesoamerican genotypes of common bean yielded higher than Andean genotypes under heat stress (Strock et al., 2019). In canola, heat stress reduced stem diameter by 8.4%, cross-sectional area by 17.3%, and aboveground biomass by 11.5% in two genotypes; genotype 13C204 (heat-sensitive) had smaller stem diameter, cross-sectional area, root length, root surface area, root biomass, and root volume than Invigor 5440 (heat-tolerant) (Wu et al., 2017). In another study, heat stress reduced lateral root elongation (–38%), number of axile roots (–30%), elongation rate of primary root (–26%), root dry weight (–39%), leaf water potential (–59%) and leaf area (19%) in heat-sensitive maize lines K64R, Ac7643, and Ac7729TZSRW when the temperature increased from 28 to 37°C. The heat-tolerant lines H16, CML444, and SC-Malawi were least affected by high temperature (Trachsel et al., 2010). In maize, screening of 10 genotypes for combined heat and drought stress (40°C/60%) revealed DK 6789, NT 6621 as tolerant and genotypes FH 988 and FH 1137 as sensitive on the basis of root tolerance indices (Ayub et al., 2020).

Biomass

Wheat seedlings grown for 7 days under normal conditions and then subjected to heat stress (42°C for 2 h) in a growth chamber revealed growth differences between genotypes (Gupta et al., 2013). In general, heat stress reduced growth (shoot/root dry weight and shoot/root length). Heat-tolerant genotypes (Raj-4037 and PBW590) retained more shoot and root length and dry weight than heat-sensitive genotypes (PBW502, DBW16, DBW17, WH1021, and PBW550) (Gupta et al., 2013). In a field experiment, heat stress (30/20°C) reduced wheat biomass, relative to optimum conditions (25/15°C), but heat-tolerant genotypes (MW-8, BW-4, and BW-3) maintained more biomass than heat-sensitive genotypes (MW-7, MW-6, and BW-5) (Rahman et al., 2009). Heat stress (>32/20°C) significantly reduced chickpea biomass by 22–30%, relative to those grown under normal temperatures; heat stress had a smaller effect on the biomass of heat-tolerant genotypes (ICC15614 and ICCV92944) than heat-sensitive genotypes (ICC5912, ICC10685) (Kaushal et al., 2013). Similarly, in a field experiment on alfalfa (*Medicago sativa*), heat stress (38/35°C) reduced plant biomass, relative to the control (25°C), more so in heat-sensitive Wl712 than heat-tolerant Bara310SC (Wassie et al., 2019). Field studies on lentil revealed that heat stress (>32/20°C) significantly reduced plant biomass, relative to the control (Sita et al., 2017a); genotypes IG3263, IG2507, IG3297, IG3312, IGG3327, IG3330, IG3546, IG3745, IG4258, and FLIP2009 retained more biomass (termed heat-tolerant) than genotypes IG2519, IG2802, IG2506, IG2849, IG2821, IG2878, IG3326, IG3290, IG3973, IG3964, IG4242, DPL15, DP315, IG4221, and IG3568 (termed heat-sensitive). Likewise, heat stress (>40/28°C) significantly reduced mungbean biomass (up to 76%), relative to the control (34/16°C) in the field, due to the inhibition of vegetative growth and acceleration in reproductive growth. Genotypes EC693357, EC693358, EC693369, Harsha, and ML 1299 produced more biomass under heat stress (heat-tolerant) than genotypes EC693363, EC693361, KPS1, EC693370, and IPM02-3 (heat-sensitive) (Sharma et al., 2016). A study on potato (*Solanum tuberosum*) revealed that warmer temperatures (31/29°C) severely affected plant biomass in two genotypes—Norchip (heat-tolerant) and Up-to-date (heat-sensitive)—grown in controlled environment chambers (Lafta and Lorenzen, 1995). Both genotypes had similar total dry mass under controlled conditions (19/17°C), but heat stress (31/29°C) reduced total dry mass by up to 44% in Norchip and 72% in Up-to-date. Leaf, stem, shoot, and tuber dry and fresh weights followed the same trend under high temperature in both genotypes. At Niger, West Africa (ICRISAT Sahelian Centre research farm (13° 29« N, 2° 10« E; 221 m above sea level), field experiments were performed to evaluate heat tolerance of groundnut (*Arachis hypogaea* L.) using physiological traits identified in a yield model [crop growth rate (C), reproductive duration (Dr) and partitioning (p)]. After screening 625 diverse groundnut genotypes, under irrigation during the hottest months (February to May), 16 contrasting genotypes, selected on the basis of combination of high pod yield and partitioning coefficient, revealed that crop growth rate was a powerful factor affecting pod yield. Pod yield of most genotypes decreased by more than 50% because of heat stress (40°C) at the time of flowering and pod formation. The findings showed that estimates of p would be vital as a dependable selection criterion, compared to yield, for identification of heat tolerant genotypes. The breeders should explore strategies to maximize the crop growth rate and partitioning in genotypes growing under warm environments (Ntare et al., 2001). Under combined heat and drought (36/26°C without irrigation) stresses, Biomass was used as a trait for evaluation of 3 tomato cultivars (Arvento and two heat tolerant; LA1994 and LA2093) (Zhou et al., 2017) resulting in identification of "Areventro" cultivar as more tolerant than "LA1994" and "LA2093" genotypes (Zhou et al., 2017).

LEAF-BASED TRAITS

Heat stress causes serious leaf injuries, yellowing of leaves (chlorosis), tissue death (necrosis), especially tips and margins, wilting, and drying, resulting in severe loss of functionality (Wahid et al., 2007). Various traits have been used to assess heat damage, with genotypes contrasting for heat tolerance identified based on these traits.

Tissue Damage

Tissue damage can be assessed by measuring membrane damage based on electrolyte leakage, which is a reliable indicator of heat sensitivity in several crop species. The primary target of environmental stress is the cell membrane (Chen et al., 2014; Sita et al., 2017b). Heat stress loosens chemical bonds within the molecules of biological membranes by accelerating the kinetic energy and movement of molecules across membranes, which results in membrane fluidity by protein denaturation or increased unsaturated fatty acids (Savchenko et al., 2002). Under high temperature, protein denaturation, increased membrane

fluidity, and enzyme inactivation decreases protein synthesis and degradation, and alters membrane integrity (Howarth, 2005). The tertiary and quaternary structure of membrane proteins changes with heat stress and enhances membrane permeability, as evident from increased ionic leakage, which is an indicator of decreased cell membrane thermostability (CMT) (Wahid et al., 2007). Damage to leaf membranes occurs due to the direct effects of high temperature, photo-oxidation of chlorophyll pigments, impaired electron flow, inhibition of carbon fixation, and water loss from leaves. Damage to membranes impairs photo-assimilate production in leaves (Prasad et al., 2017). Under high temperature, the relationship between CMT and crop yield varies from plant to plant. CMT has been used as an indirect measure of heat stress tolerance in plant species, such as sorghum (Sullivan, 1997; Marcum, 1998), soybean (Martineau et al., 1979), potato and tomato (Chen et al., 1982), sorghum, wheat (Blum et al., 2001), cotton (Ashraf et al., 1994; Cottee et al., 2010), lentil (Sita et al., 2017a), chickpea (Kaushal et al., 2013), mungbean (Sharma et al., 2016), and barley (Wahid and Shabbir, 2005). Abro et al. (2015) identified several heat-tolerant cotton genotypes with high membrane thermostability at 50°C in the laboratory environment, which could be used for breeding purposes to develop heat-tolerant genotypes. During the late developmental phase of plants, membrane stability tends to decrease (Ahmad and Prasad, 2011). For breeding purposes, significant variations in membrane thermostability among genotypes could be used to improve selection (Hemantaranjan et al., 2014).

In wheat grown under high temperatures (45°C for 2 h), genotypes (Raj4037, PBW373) with high CMT (58.20, 55.43) during grain filling performed better than those (Raj4083, DBW16, PBW550) with low membrane thermostability (48.15, 50, 51.96). Under controlled conditions, membrane thermostability was maximum in WH1021 (64.13) and minimum in DBW16 (51.11) (Gupta et al., 2013). Similarly, CMT was markedly higher in heat-tolerant (56.83%) than heat-sensitive (31.43%) wheat genotypes during grain filling. Based on CMT, Bala and Sikder (2017) identified heat-tolerant wheat genotypes BAW-1143, BARI Gom-25, BARI Gom-26, and Prodip. At the seedling stage in wheat, CMT had a positive correlation with grain yield, grain weight (Saadalla et al., 1990), and biomass (Blum et al., 2001), indicating the effectiveness of this trait for assessing heat tolerance. In rice at 40°C, thermostability was closely related to crop yield potential (Maavimani and Saraswathi, 2014). In a comparative study of rice and maize grown under controlled high temperatures (40/35°C and 45/40°C), the rice genotypes (PR116, PR118) had greater electrolyte leakage (27.4–40.2%) than the maize genotypes (PMH1, PMH2) (19.2–26.2%) (Kumar et al., 2012). Similarly, among three rice cultivars, F60 and F733 were more heat-susceptible than F473 when grown at 40°C, with greater electrolyte leakage (20 and 15%) (Sanchez-Reinoso et al., 2014). Likewise, Yadav et al. (2014) used CMT as an effective screening parameters for selecting heat tolerant lines in Pearl millet. From the same study, the authors also identified H77/29-2 × CVJ-2-5-3-1-3 hybrid as heat tolerance based on seedling thermotolerance index. Under combined stresses (drought-42–45% of irrigated conditions) and heat (> 32/20°C), the drought tolerant chickpea genotypes were found to tolerate the two stresses more effectively than heat tolerant genotypes. For instance, genotypes ICC1356 (drought-tolerant) showed less damage to membranes than genotype ICC3776 (drought-sensitive), when subjected to both the stresses (Awasthi et al., 2017).

In legumes, a few studies have identified heat-tolerant and heat-sensitive genotypes. Based on the membrane stability test, chickpea was most sensitive to heat stress, relative to other legumes such as pigeon pea, groundnut, and soybean (Devasirvatham et al., 2012). Contrasting chickpea genotypes exposed to high temperatures (40/30°C and 45/35°C) varied markedly, with heat-tolerant genotypes (ICCV07110, ICCV92944) showing less membrane damage (22.6, 20.6%) than heat-sensitive genotypes (ICC14183, ICC5912) (30.4, 33.3%) (Kumar et al., 2013). A similar test conducted at 37/27°C reported up to 25% electrolyte leakage in chickpea seedlings (Pareek et al., 2019). A heat-tolerant genotype (ICC1205) had low electrolyte leakage (13–14%), indicating better cell membrane integrity. Screening of cowpea genotypes exposed to heat stress also revealed less leaf electrolyte leakage (35.8–36.7%) in heat-tolerant genotypes (H36, H8-9, DLS99) during flowering and pod set than heat-susceptible genotypes (CB5, CB3, DLS127) (66.2–79%) (Ismail and Hall, 1999). In lentil, heat tolerance was related to less membrane damage (<20%) in heat-tolerant genotypes (IG2507, IG3263, IG3745, IG4258, and FLIP2009) than heat-sensitive genotypes (IG2821, IG2849, IG4242, IG3973, IG3964) (> 30%) at 38/28°C and 40/30°C in a controlled environment (Sita et al., 2017a). In another study, lentil genotypes (Ranjan, Moitree, 14-4-1, IC201710, and IC208329) were reported as heat-tolerant based on cell membrane stability under field and growth chamber studies at 34°C (Choudhury et al., 2012). Barghi et al. (2013) reported the highest CMT in genotype Qazvin (98.13%) and regarded it as heat-tolerant, whereas genotype B4400 (33.19%) had the lowest CMT (heat-sensitive). Under high temperature (38/35°C), screening of 15 *Medicago* cultivars for CMT identified Bara310SC and WL712 as heat-tolerant (24.07%) and heat-sensitive (53.2%) cultivars, respectively, having minimum and maximum electrolyte leakage, respectively (Wassie et al., 2019).

Cotton displays heat sensitivity at various growth stages. Cotton genotypes grown in a controlled environment under optimal conditions (35/21 ± 2°C) for 30 days and then exposed to high temperature (46/30 ± 2°C) at the reproductive stage, by gradually increasing temperature by 2°C per day, were screened for CMT—cultivars FH-900, MNH-552, CRIS-19, and Karishma emerged as relatively heat-tolerant (thermostable) and FH-634, CIM-448, HR109-RT, and CIM-443 as heat-susceptible (Rahman et al., 2004). In a similar study at > 32°C, cotton genotypes B557 and NIAB-78 showed minimum electrolyte leakage (<40%) and were regarded as tolerant compared to genotypes MNH-554, FH682 and FH900 which showed maximum electrolyte leakage (>50%) (Rana et al., 2011). Abro et al. (2015) reported cotton varieties NIA-80, NIA-81, NIA-83, NIA-84, NIA-M-30, NIA-M31, NIA-HM-48, NIA-HM-327, NIA-H-32, NIA-HM-2-1, NIA-Bt1, NIA-Bt2, NIA-Perkh, CRIS-342, CRIS-134, and

NIAB-111 and check variety Sadori as heat-tolerant using CMT as a screening parameter in both heat-stressed (44°C) and non-stressed (32°C) temperature regimes. Other similar studies where cotton genotypes were differentiated by CMT into heat-tolerant and heat-sensitive were conducted by Karademir et al. (2012); 15 genotypes; > 40°C) and Singh K. et al. (2018); 37 genotypes; > 40°C).

Likewise, in cucumber, contrasting genotypes were identified based on membrane stability under heat stress (40/32°C)—L3466 and Desi cucumber as heat-tolerant and Suyo Long and Poinsett as heat-sensitive (Ali et al., 2019). In tomato, 2 h exposure to high temperature (45°C) altered CMT more in heat-sensitive variety Campbell-28 (> 45%) than heat-tolerant variety Nagcarlang (<20%) (Camejo et al., 2005). In another study on 44 tomato lines, exposure to 44°C for 4 h after 1 week of vegetative stage increased electrolyte leakage in heat-sensitive genotypes (32.92 μmhos/cm) more than heat-tolerant genotypes (22.2 μmhos/cm) (Hameed et al., 2015). Similar studies have screened tomato genotypes for heat tolerance using membrane thermostability (Sangu et al., 2015; Alsamir et al., 2017). Thus, CMT is an effective trait for identifying stable and heat-tolerant genotypes.

Canopy Temperature Depression

At the whole crop level, leaf temperatures decrease below air temperature when water evaporates. Canopy temperature depression (CTD)—the difference between air temperature (T_a) and canopy temperature (T_c)—acts as an indirect measure of transpiration (Reynolds et al., 2001) and plant water status (Araus et al., 2003). A positive CTD value is observed when the canopy is cooler than the air (CTD = T_a–T_c) (Balota et al., 2008). CTD is a heritable trait that can be measured on cloudless days with an infrared thermometer (Reynolds et al., 1998). Plants transpire through open stomata to maintain canopy temperature in a metabolically comfortable range. Under stress, plants close their stomata for some period, which increases the canopy temperature (Kashiwagi et al., 2008). Canopy temperature is affected by soil water status, wind, evapotranspiration, cloudiness, conduction systems, plant metabolism, air temperature, relative humidity, and continuous radiation (Reynolds et al., 2001). To assess heat tolerance, many traits can be used as selection criteria, but, CTD is considered to be best as a single reading integrates scores of leaves (Reynolds et al., 1994, 1998; Fischer et al., 1998). Yield potential and the metabolic fitness of crop plants under specific environmental conditions are determined by CTD (Kumari et al., 2013). A study on barley revealed a strong link between epicuticular leaf wax QTL and CTD, and that wax load influences plant canopy temperature (Awika et al., 2017). Based on phenotypic variation, CTD can act as a desirable criterion for heat-tolerant genotype selection (Mason and Singh, 2014). CTD is a mechanism of heat escape and has a strong genetic correlation with yield (Reynolds et al., 2001). Heat-tolerant genotypes of wheat had higher CTD than heat-sensitive genotypes, indicating their greater ability to maintain a cooler canopy environment (Gare et al., 2018). In another study, the CTD value in wheat was correlated with heat resilience (Pradhan et al., 2012). In 102 durum wheat genotypes tested under late-sown conditions, CTD had a strong positive correlation with days to maturity (Gautam et al., 2015), confirming that CTD is an effective selection criterion in plant breeding (Seema et al., 2014). Leaf area having more greenness and CTD are strongly interrelated in wheat and with grain yield, grain-filling duration, and biomass (Kumari et al., 2013). Stay-green genotypes have high CTD values due to transpirational cooling, resulting in lower canopy temperatures (Reynolds et al., 1994; Fischer et al., 1998). In stay-green lines, low CTD values delayed senescence (Kumari et al., 2013). Leaf width in wheat had a high correlation with canopy temperature under heat stress (Mohammadi et al., 2012). In durum wheat, CTD had a positive correlation with biological yield and spike number/m^2 at first spikelet emergence and 50% inflorescence stages. At three growth stages (first spikelet emergence, 50% inflorescence, and completion of anthesis), harvest index had a negative correlation with CTD (Bahar et al., 2008). Screening of Indian and CIMMYT wheat germplasm for the stay-green trait and CTD revealed higher CTD values in the stay-green genotypes due to transpirational cooling and lower canopy temperatures (Kumari et al., 2013). In wheat *(Triticum aestivum),* heat stress reduced CTD by 39.7% at the grain-filling stage (Joshi et al., 2016). Timely sown wheat had higher CTD than late-sown wheat (Saxena et al., 2016), with genotypes HD2932, HD2864, HD3095, HI8703, and HUW234 identified as heat-tolerant due to their higher net photosynthesis, relative water content, membrane stability index and CTD than the other tested genotypes (Saxena et al., 2016). Additional management factors, such as the use of farmyard manure and NPK, improved physiological traits (light interception, CTD, and flag leaf chlorophyll content) in wheat (Badaruddin et al., 1999). In seven rice varieties, CTD was closely related to stomatal conductance and leaf photosynthetic rate (Takai et al., 2010). Rice varieties Takanari and TUAT1-5-6a had lower leaf temperatures and higher stomatal conductance and leaf photosynthetic rates than the other varieties tested under cloudy conditions. Infrared thermography, as a simple method of evaluating varietal differences in stomatal conductance via CTD, is feasible even under cloudy conditions. In chickpea, water potential, osmotic pressure, relative leaf water content, and seed yield had a negative correlation with CTD (Sharma D. K. et al., 2015). Heat-tolerant chickpea genotypes ICCVs 95311, 98902, 07109, and 92944 had higher CTD than sensitive genotypes ICCVs 07116, 07117, and 14592, which had negative CTD values (Devasirvatham et al., 2015). In mungbean, CTD had a significant positive correlation with seed yield, and a negative correlation with root traits, such as lateral branch number and dry root weight (Raina et al., 2019). Greater pod number and pod to node ratio was associated with CTD in pea (Tafesse et al., 2019). In cotton, the involvement of CTD in heat tolerance was indicated (Cornish et al., 1991), with additive, dominance, and epistatic components involved in its inheritance (Khan et al., 2014). In another study on cotton, crop development stage had no effect on CTD, which was significantly correlated with seed yield (Karademir et al., 2018). Canopy temperature in cotton increased under combined heat and drought stress treatment (>36°C and 35% irrigation) (Carmo-Silva et al., 2012), as compared to control. Low canopy temperature was noticed in cotton cultivar Pima S-6 (S6),

which was reported as tolerant, unlike high canopy temperature in Monseratt Sea Island (MS), termed as sensitive, under combined stress.

Stomatal Conductance

Under heat stress, regulating the transpirational mechanisms is a possible strategy for selecting heat-tolerant varieties (Condon et al., 2007). As leaves open their stomata, the rate of gaseous exchange may create differences in stomatal behavior that can be recorded by a leaf porometer (Chandra et al., 2017; Priya et al., 2018). Fully opened stomata increase the diffusion of CO_2 and, at the same time, increase transpiration and photosynthetic efficiency in wheat (Condon et al., 2007). Consequently, stomatal regulation is an important factor that governs plant growth and survival. Therefore, stomatal conductance (g_S) is a useful trait for determining photosynthetic and transpiration rates. Stomatal conductance increases with rising temperature (Urban et al., 2017). Crawford et al. (2012) suggested that plants acclimatize to high temperatures by evaporating more water, thereby keeping their canopies cool despite the presence of fewer stomata. Similarly, semi-dwarf spring wheat cultivars had strong positive correlations between g_S and photosynthetic rate, cooler canopies and yield (Fischer et al., 1998). Heat-tolerant advanced cotton lines (e.g., Pima S-6) developed by Cornish et al. (1991) had higher stomatal conductance and photosynthetic rates under heat stress, which was possibly due to cooling effect of plants through stomata. The stomatal conductance of 50 cotton genotypes was measured under high temperature (45–50°C/20–30°C day/night) in a glasshouse, and identified five heat-tolerant genotypes (NIAB-111/2, BH-160, MNH-554, N-313, BH-163, Mutant-94) (Khan et al., 2008). Similarly, 41 wheat lines of different origin were screened for higher g_S, which was associated with heat tolerance (36/30°C for 1 week) (Sharma K. D. et al., 2015). Heat-tolerant genotypes with high g_S also had higher photosynthetic efficiency under severe heat stress; therefore, this trait acts as a useful genetic tool for developing heat tolerance. Stomatal conductance increased in heat-stressed tomato plants, relative to control conditions (Camejo et al., 2005). In another study, heat-tolerant tomato genotypes maintained higher stomatal conductance under stressed conditions (36/28°C), relative to the control (26/18°C). Further, heat stress severely affected stomatal anatomy and stomatal number in heat-sensitive genotypes, relative to heat-tolerant genotypes (Zhou et al., 2015).

Multiple screening parameters, including stomatal conductance, were used to screen 15 common bean genotypes for heat tolerance in a greenhouse chamber (Traub et al., 2018). Five genotypes—SB761, SB776, SB781, Jaguar, and TB1—were screened at three temperature regimes (35/30, 40/35, 45/40°C). Stomatal conductance increased with increasing temperature until 40/35°C—after which, it declined—genotype TB1 had the highest values for stomatal conductance. In mungbean genotypes, g_S increased up to 40/30°C but declined significantly under heat stress at 43/30°C and 45/32°C, contributing to a rise in leaf temperature (Kaur et al., 2015). In another study on mungbean, g_S was used to differentiate between heat-tolerant and heat-sensitive genotypes (Sharma et al., 2016). Using a similar approach, Sita et al. (2017a) identified heat-tolerant lentil genotypes (IG2507, IG3263, IG3745, IG4258, and FLIP2009) on the basis of stomatal conductance, with g_S increasing with increasing temperature up to 38/28°C in heat-tolerant genotypes. Heat-tolerant genotypes also had higher g_S values under late-sown than normal-sown conditions; in contrast, heat-sensitive genotypes were unable to maintain higher g_S under heat stress. In chickpea, heat-tolerant (ICC1356, ICC15614) and heat-sensitive genotypes (ICC4567, ICC5912) genotypes were selected on the basis of leaf and seed traits (Awasthi et al., 2014)—heat-tolerant genotypes maintained higher stomatal conductance and photosynthetic function than heat-sensitive genotypes under similar conditions and produced more seed yield. Evaluation of three varieties of tomato (Nagcarlang, Hybrid 61 and Moskvich) against combined heat and drought stresses (25–45°C; 20% irrigation; 2 days), revealed that genotype Hybrid 61 performed better by maintaining higher stomatal conductance and having lower leaf temperature than other two varieties (Nankishore and Farrell, 2016), suggesting this trait to be useful even under stress combinations.

Carbon Isotope Discrimination (CID, $\Delta^{13}C$)

Carbon isotope discrimination has become an important tool for interpreting photosynthetic rate and water use efficiency (WUE) in plant species (Sheshshayee et al., 2003; Bindumadhava et al., 2011). ^{12}C (98.89%) and ^{13}C (1.11%) are the two stable carbon isotopes (non-radioactive) in the global carbon pool. Small but significant amount of ^{13}C (heavy isotope) incorporated in the organic and inorganic matter during CO_2 fixation by carboxylating enzymes. These small differences in ^{13}C abundance are expressed as Carbon isotope ratio and analyzed with isotope ratio mass spectrometer (IRMS) (Farquhar et al., 1989). Composition of carbon isotopes in plant tissue samples show photosynthetic ability governed by RuBisCO in mesophyll tissues (Bindumadhava et al., 2005, 2011, Impa et al., 2005). Lower values of CID represent lower stomatal conductance (limited diffusion of CO_2) and vice versa (Bindumadhava et al., 2011). Further, under high temperature, leaf water status declines due to reduced root hydraulic conductivity, resulting in stomatal closure (Hairat and Khurana, 2016). Therefore, lower CID values at high temperature can be ascribed to indicate declined root absorption and stomatal closure. In barley, carbon-13 discrimination is a useful indicator of high yield (Craufurd et al., 1999), and could be a sound screening parameter for identifying heat-tolerant genotypes. Heat-tolerant (C306, K7903) and heat-sensitive (HD2329) wheat genotypes were identified from CID values and other physiological traits. The heat-tolerant genotypes had higher mean CID values at high temperature (42°C) than the heat-sensitive genotypes. This study demonstrated that the heat-tolerant genotype maintained stomatal opening by accumulating osmolytes, such as proline, to maintain osmotic pressure for water absorption (Hairat and Khurana, 2016).

Photosynthetic Pigments

Heat stress negatively affects photosynthesis by decreasing leaf pigment content and damaging leaf ultrastructure. Chloroplasts

play a vital role in photosynthesis as one of the most heat-sensitive organelles (Krause and Santarius, 1975; Ogweno et al., 2008; Abdelmageed and Gruda, 2009). Decreases in total chlorophyll content and changes in the chlorophyll a/b ratio have been correlated with reductions in photosynthesis during heat stress, due to reduced "antenna (pigment units)" size and thus reduced light-harvesting (Blum, 1986; Harding et al., 1990; Shanmugam et al., 2013). The stay-green (SGR) trait, or delayed leaf senescence, is a crucial trait that allows plants to retain leaves in an active photosynthetic state under high temperature to maintain the assimilation process and increase crop yield (Gregersen et al., 2013; Kumari et al., 2013). Stay-green rice genotypes exhibited high photosynthetic activities under heat stress, resulting in high yields (Jagadish et al., 2015).

Chlorophyll content is an integrative trait that is correlated with stomatal conductance, photosynthetic rate, and transpiration (Del Blanco et al., 2000; Netto et al., 2005), and considered a good criterion for screening for heat-stress tolerance. In the current era of global climate change, introduction of the SGR trait is vital for developing heat-resistant cultivars (Kumari et al., 2013). The SGR trait has been linked to increased yield production in many crops under heat stress, including wheat, barley, rice, maize, and cowpea (Kumari et al., 2007; Borrell et al., 2014; Kobata et al., 2015; Gous et al., 2016; Abdelrahman et al., 2017). The stay-green trait has helped to identify heat-tolerant wheat cultivars that maintain yields at high temperatures (Vijayalakshmi et al., 2010). A significant correlation was detected between heat tolerance and the stay-green trait in 936 elite wheat genotypes (Kumari et al., 2007), suggesting that delayed senescence is an essential selection criterion for heat adaptability. The stay-green characteristic of wheat cultivar Mairaj-2008 was correlated with higher grain yield under heat stress than other lines that lacked the stay-green trait (Nawaz et al., 2013). Genotypes with delayed leaf senescence or stay-green traits have been associated with thermotolerance, due to the longer grain-filling period and thus higher yields, relative to genotypes lacking these traits (Reynolds et al., 1997; Vijayalakshmi et al., 2010). Delayed leaf senescence enhances the transpiration use efficiency, resulting in higher yields. Thus, the stay-green trait is beneficial for retaining active photosynthesis under heat stress (Bavei et al., 2011).

The stay-green trait was used to identify three promising heat-tolerant wheat genotypes [CB-367 (BB#2/PT//CC/INIA/3/ALD"S"), CB-333 (WL 711/3/KAL/BB//ALD "S"), and CB-335 (WL711/CROW "S"//ALD#1/CMH 77A] based on maximum grain development and survival under heat stress (32°C for 4 weeks) (Rehman et al., 2009). Two recombinant inbred lines (RILs) of wheat, SB062 and SB003, were exposed to 7-day heat shocks (32.7/21.6°C day/night) in a growth chamber during the vegetative or reproductive stage. SB062 maintained leaf greenness for longer than SB003 under heat stress and identified as heat-tolerant; in addition, delayed leaf senescence appeared to play a role in maintaining grain size in SB062 under heat stress (Ullah and Chenu, 2019). Lu et al. (1997) suggested that higher stomatal conductance and photosynthetic rate are functionally important for higher heat tolerance and yields. A high temperature (38/28°C) treatment for 6 days under controlled conditions in a greenhouse modified chlorophyll content in two contrasting maize genotypes; DTPYC9F119 maintained higher leaf chlorophyll content (identified as heat-stress tolerant) than K64R (identified as heat-stress susceptible) (Debnath et al., 2016; Singh et al., 2020). In another study, 12 barley genotypes were exposed to heat stress (> 40°C) for 107–119 days in the field—genotypes L3, L6, L8, and L10 had longer stay-green duration and higher yields under heat stress than the other genotypes. Fifteen cotton genotypes were screened for thermotolerance (40°C) in the field—genotypes AGC375 and AGC208 were identified as heat-tolerant based on their chlorophyll content (Karademir et al., 2012). In a similar study, cotton genotype Sicot 53 had higher thermotolerance than Sicala 45 (Cottee et al., 2007). In rice, cultivar N44 was identified as heat-tolerant (exposed to 38°C for 25 days in the field during the reproductive stage), with its higher chlorophyll content under heat stress than N-22 (Bahuguna et al., 2015).

Chlorophyll content was used to screen for heat tolerance in several lentil genotypes after exposure to heat stress (>32/20°C) in a growth chamber at the vegetative and reproductive stage. Heat-tolerant genotypes IG3263 and IG2507 had more chlorophyll than heat-sensitive genotypes IG4242 and IG3964, which was positively correlated with yield (Sita et al., 2017a). In chickpea, genotypes were selected for heat tolerance based on the SGR trait; plants were exposed to gradual increasing temperatures (2°C per day) from 27/18°C to 42/25°C day/night for 8 days in a growth chamber; at which time, genotype ICC16374 (heat-sensitive) had lower leaf chlorophyll content than JG14 (heat-tolerant) (Parankusam et al., 2017). Likewise, Kaushal et al. (2013) identified two heat-tolerant (ICC15614, ICCV92944) and two heat-sensitive (ICC10685, ICC5912) chickpea genotypes based on chlorophyll content, after exposure to heat stress (>32°C/20°C) in the field during reproductive development. The stay-green trait could be used as a morphological indicator for thermotolerance in tomato, as in wheat (Sharma D. K. et al., 2015; Zhou et al., 2015). The stay-green trait contributes to high yield in tomato exposed to heat stress (Zhou et al., 2015). Tomato's ability to stay-green and maintain photosynthesis during heat stress at different developmental stages, especially anthesis, could be vital for reproductive growth and yield (Zhou et al., 2017). Heat-sensitive tomato genotypes do not stay-green under heat stress due to the decline in chlorophyll and carotenoid contents, and show early chlorosis and withered leaves (Vijayalakshmi et al., 2010; Zhou et al., 2015).

Chlorophyll Fluorescence

Chlorophyll fluorescence (F_v/F_m ratio) is a relatively sensitive indicator of direct or indirect effects of abiotic stress on photosynthesis (Schreiber and Bilger, 1993). The relationships between primary photosynthetic reactions and chlorophyll fluorescence are crucial as they provide information on the plant's photosynthetic capability and its acclimation capacity under stressful environmental conditions (Lichtenthaler, 1987; Kalaji et al., 2018). Of the photosynthetic apparatus, photosystem II (PSII) is the most heat-labile cell structure (Vacha et al., 2007). As damage to PSII is often the first response when plants are

subjected to heat stress, PSII response studies can reveal the primary effects of heat stress on plants (Mathur et al., 2011; Van der Tol et al., 2014); measuring chlorophyll *a* fluorescence is an effective and non-invasive technique to identify damage to PSII efficiency (Baker and Rosenqvist, 2004; Baker, 2008). The ratio between variable fluorescence (F_v) and maximum fluorescence (F_m), or F_v/F_m, reflects the maximum quantum efficiency of PSII (Butler, 1978), and is one of the most heat-affected fluorescence parameters. A decline in F_v/F_m is frequently observed when plants are subjected to abiotic stress, including heat (Willits and Peet, 2001; Molina-Bravo et al., 2011; Sharma et al., 2012). There is a negative linear correlation between F_v/F_m and the maximum quantum yield of photosynthesis, when measured as O_2 evolution (Demmig and Björkman, 1987; Kao and Forseth, 1992) and CO_2 fixation (Ogren and Sjostrom, 1990). Screening methodologies using chlorophyll fluorescence to detect and quantify damage in photosystem II (PSII) and thylakoid membranes in response to temperature stress have been used in several cereal crops, including barley (Rizza et al., 2011), wheat (Balouchi, 2010), maize (Sinsawat et al., 2004), legume crops [chickpea, groundnut, pigeon pea (*Cajnus cajan*), and soybean] (Srinivasan et al., 1996; Herzog and Chai-Arree, 2012), and horticultural crops, including strawberry (*Fragaria ananassa*) (Ledesma et al., 2004; Kadir et al., 2006), tomato (Willits and Peet, 2001), grapes (*Vitis vinifera*) (Kadir et al., 2007), and various tropical and subtropical fruits (Yamada et al., 1996; Weng and Lai, 2005). Therefore, chlorophyll fluorescence is a promising tool for detecting stress-induced injuries and thermotolerance (Méthy et al., 1994) but its successful implementation in crop breeding programs requires careful selection of suitable fluorescence parameters (Malaspina et al., 2014).

Heat-tolerant wheat lines with tolerance to high temperatures during grain filling had greater F_v/F_m ratios than heat-sensitive lines in warmer irrigated environments, which were linked to higher grain yield (Shefazadeh et al., 2012). The physiological state of thylakoid membranes, as determined by chlorophyll *a* fluorescence, identified heat-tolerant wheat cultivars with high chlorophyll fluorescence (Ristic et al., 2007). Various wheat lines were exposed to heat stress for 3 days at 40°C in controlled conditions; the lines having high chlorophyll fluorescence (F_v/F_m 0.836)—830, 1313, 1039, 1223—were less sensitive to heat in terms of growth and photosynthesis than the other lines, and were identified as heat-tolerant (Sharma et al., 2014). Similarly, genotypic variation for chlorophyll fluorescence parameters exists in rice under heat stress (29°C for 25 days at anthesis) in a growth chamber; N22 genotype maintained high F_v/F_m (0.75) under heat stress, and was identified as heat-tolerant, relative to the low F_v/F_m (0.70) in Vandana (Sailaja et al., 2015). Modified chlorophyll fluorescence imaging was used to screen 20 wild barley (*Hordeum spontaneum*) genotypes exposed to heat stress (45°C, 1 h) in growth chambers, and identified HOR10478 as the most heat-sensitive and HOR12818 as the most heat-tolerant genotypes (Jedmowski and Brüggemann, 2015). Oukarroum et al. (2016) also differentiated heat tolerance in 10 varieties of barley. After 2 weeks of growth, detached leaves were exposed to a short-term heat treatment at 45°C for 10 min in a growth chamber, which decreased chlorophyll fluorescence; notably, varieties Ig, Im, and Tz had high chlorophyll fluorescence (heat-tolerant) and Ma, Ra and I_{gr} had low chlorophyll fluorescence (heat-sensitive).

In many legumes, chlorophyll fluorescence has been used to identify genotypes that tolerate heat stress. In lentil, photosynthetic efficiency was measured as PSII function (F_v/F_m ratio) in a natural environment by exposing plants to heat stress (above 32/20°C) during the reproductive stage. Heat-tolerant genotypes—IG2507, IG3263, IG3297, IG3312, IG3327, IG3546, IG3330, IG3745, IG4258, and FLIP2009—maintained high chlorophyll fluorescence (F_v/F_m 0.71) under heat stress, relative to heat-sensitive genotypes—IG2821, IG2849, IG4242, IG3973, IG3964—which had the lowest F_v/F_m values (0.58) (Sita et al., 2017a). Nine common bean lines were measured for changes in chlorophyll fluorescence under heat stress at flowering (2 h at 45°C) in a greenhouse; thermotolerant lines 83201007 and RRR46 had higher F_v/F_m values under heat stress than the heat-sensitive line Secuntsa (Petkova et al., 2009). In another study, 12 varieties and lines of common bean were exposed to 42°C in the field during the reproductive period; two genotypes (Ranit and Nerine) maintained F_v/F_m values at 42°C, relative to the controls at 26°C, and were considered heat-tolerant. These two genotypes also showed good productivity and quality and can be used as parental lines in bean breeding programs (Petkova et al., 2007). Likewise, 41 mungbean lines were grown outdoors and exposed to high temperatures (>40/28°C) during the reproductive stage; several promising heat-tolerant lines (EC693358, EC693357, EC693369, Harsha, and ML1299) were identified, with high F_v/F_m ratios (0.73–0.75 units) compared to sensitive lines (0.61–0.67 units), which would not only serve as useful donor/s for breeding programs, but also as suitable base plant source to gain insight into heat-stress-induced effects in cell metabolism (Sharma et al., 2016). In chickpea, heat stress (>30°C) in the field during the reproductive stage reduced F_v/F_m more (0.48, 0.41) in two heat-sensitive genotypes ICC10685 and ICC5912, than in two heat-tolerant genotypes ICC15614 and ICCV92944 (0.64, 0.60) (Kaushal et al., 2013; Awasthi et al., 2014). A field experiment conducted in two winter seasons at three locations with known differences in temperature in NE South Africa, involving four chickpea genotypes, showed. that two genotypes, which were tolerant to heat stress had chlorophyll fluorescence (Fv/Fm) of 0.83–0.85 at the warmer site, while the two sensitive genotypes showed lower Fv/Fm of 0.78–0.80; these values correlated positively with grain yield. The two tolerant genotypes had higher photosynthetic rates, starch, sucrose and grain yield than the sensitive genotypes at the warmer site. The observation revealed that chlorophyll fluorescence and leaf carbohydrates are suitable tools for selection of heat tolerant chickpea genotypes under field conditions (Makonya et al., 2019). Screening of 15 alfalfa (*Medicago sativa* L.) genotypes by exposing seedlings to 38/35°C day/night for 7 days in a growth chamber identified Bara310SC (F_v/F_m 0.79) and WL712 (F_v/F_m < 0.79) as heat-tolerant and heat-sensitive cultivars, respectively (Wassie et al., 2019), showing that F_v/F_m is an effective tool for phenotyping contrasting genotypes for heat tolerance.

The heat susceptibilities of 67 tomato genotypes were evaluated in a climate chamber—the genotypes with higher F_v/F_m under heat stress (36/28°C for 4 days or 40°C for 7 h),

maintained their physiological status, relative to genotypes with lower F_v/F_m (Zhou et al., 2015). The two genotypes with the highest F_v/F_m ratios (heat-tolerant group; T1, T2; 0.82, 0.80 units) and two with the lowest F_v/F_m ratios (heat-sensitive group; S1 and S2; 0.74, 0.77 units) were selected for further study (Zhou et al., 2015). Another study screened wild genotypes and cultivars of tomato in a growth chamber at 33°C—wild tomato varieties Pe and Pr1 had the highest temperature stress tolerance with high F_v/F_m ratios (0.56, 0.58), while the cultivated species were more sensitive to temperature stress with lower F_v/F_m ratios (0. 28, 0.38) (Zhou et al., 2018).

Chlorophyll fluorescence was used to screen cotton landraces—6-week-old cotton plants were subjected to heat stress at 45°C in a growth chamber to determine thermotolerance in terms of photosynthetic ability, independent of agronomic yield and productivity. Three genotypes (TX2287, TX2285, and TX761) maintained high photosynthetic efficiency (F_v/F_m 0.57), relative to sensitive genotype (F_v/F_m 0.46) (Wu et al., 2014). In another growth chamber study, a commercial set of eight cotton genotypes was screened for heat tolerance by subjecting to heat stress (>35°C); four genotypes (SG215BR, ST474, and DP444BG/RR) had relatively high F_v/F_m indicating that they suffered less from stress, while Sphinx and Acala Riata had low F_v/F_m, indicating temperature sensitivity (Bibi et al., 2004). In a related study, screening of 15 cotton genotypes for thermotolerance (40°C) in the field identified genotypes AGC375 and AGC208 as heat-tolerant, based on their superior chlorophyll fluorescence (Karademir et al., 2012). Imposing combined drought and heat stress significantly affected the photosynthetic efficiency of chickpea (*Cicer arietinum*) genotypes, in a study conducted in outdoor conditions at two different sowing times [November (<32–20°C at the time of reproductive stage; control) and in February (>32–20°C at the time of reproductive stage; heat stress during pod filling)], while drought was applied during both sowing times during pod filling (at ∼75% podding) by withholding water until maturity. The photosynthetic efficiency (Fv/Fm) of the leaves decreased more in plants subjected to drought stress (54–74%) than to heat stress alone (9–46%) and the combined heat + drought stress treatment showed the greatest reduction in photosynthetic efficiency (68–83%), with the smallest reduction occurring in the drought-tolerant genotype (ICC8950), compared to drought-and heat sensitive genotypes (Awasthi et al., 2017).

Photosynthetic Rate

Heat stress affects plant characteristics such as the stay-green trait, chlorophyll content, and chlorophyll fluorescence, which influences the photosynthetic rate (Sharkey, 2005). Hence, photosynthetic rate can be used as a screening parameter for the selection of heat-tolerant genotypes. Variation in photosynthetic rate among plant species in response to heat stress has been well-documented. For example, a heat-shock treatment (45°C for 2 h at the fourth true leaf stage) reduced the net photosynthetic rate (P_n) of two tomato cultivars, more so in Campbell-28 (heat-sensitive) than wild Nagcarlang (heat-tolerant) (Camejo et al., 2005). High temperature deactivates RuBisCo, which could be involved in reducing photosynthetic rate (Sharkey, 2005). Another study on tomato compared the P_n of one cultivated (Ly from *Solanum lycopersicum*) and six wild (Ha from *S. habrochaites*, Pe from *S. pennellii*, Pi1 and Pi2 from *S. pimpinellifolium*, Pr1 and Pr2 from *S. peruvianum*) genotypes grown at high temperature (33°C) in a growth chamber—Ly, Ha, Pi1, and Pi2 had lower P_n than the control, while Pe, Pr1, and Pr2 showed higher P_n indicating their heat tolerance (Zhou et al., 2018). Plants of the tomato cultivar "Liaoyuanduoli" grown in greenhouse exposed to heat stress (35°C after 15 DAS led to a significant change in photosynthetic apparatus as damage of chloroplast membrane and at the same time, the thylakoids loosely distributed with lesser grana, thus, changed chloroplast ultrastructure might have declined the P_n (Zhang et al., 2014). In rice, heat tolerant genotype (N22) could maintain photosynthetic activity for a longer time after anthesis and thus could produce higher grain weights, compared to heat-sensitive genotypes (IR20, IR53, IR46) (Gesch et al., 2003).

Soybean cultivars (IA3023 and KS4694) and PI lines (PI393540 and PI588026A) expressed heat tolerance and susceptibility with high and low P_n, respectively (Djanaguiraman et al., 2019). The soybean cultivars had less thylakoid membrane damage than the PI lines. In an earlier study on soybean genotype K03−2897, high-temperature stress (38/28°C) for 14 days at the flowering stage significantly decreased leaf P_n, due to anatomical and structural changes (increased thickness of palisade and spongy layers and lower epidermis) in cells and cell organelles, particularly damage to chloroplasts and mitochondria (Djanaguiraman and Prasad, 2010). Two heat-tolerant chickpea genotypes (Acc#RR-3, Acc#7) had higher P_n than two heat-sensitive genotypes (Acc#2, Acc#8) at high temperature (35/30°C), which may have been due to increased RuBisCo activity (Makonya et al., 2019). In another chickpea study, 56 genotypes were exposed to high temperatures in the field from the flowering stage to crop maturity (maximum temperatures 25–40°C)—the tolerant genotypes (PUSA1103, PUSA1003, KWR108, BGM408, BG240, PG95333, JG14, BG) had higher Pn than the sensitive genotypes (ICC1882, PUSA372, PUSA2024) (Kumar et al., 2017). Similarly, the response of four chickpea genotypes to a natural temperature gradient in the field at the flowering stage identified two heat-tolerant genotypes (Acc#RR-3, Acc#7) with high P_n and two heat-sensitive genotypes (Acc#2, Acc#8) with lower P_n; these results were validated in a climate chamber experiment set at 30/25°C and 35/30°C (Makonya et al., 2019). Improvement of heat stress tolerance by stabilizing PSII system through introducing *IbOr* gene in transgenic potato (Goo et al., 2015), sweet potato (Kang et al., 2017), and in alfalfa (Wang et al., 2015) is worth mentioning. Heat, drought and their combination limited the Photosynthetic rate of lentil (*Lens culinaris* Medikus), particularly during reproductive growth and seed filling. In recent study eight lentil genotypes two drought-tolerant (DT; DPL53 and JL1), two drought-sensitive (DS; ILL 2150 and ILL 4345), two heat-tolerant (HT; 1G 2507 and 1G 4258) and two heat-sensitive (HS; 1G 3973 and 1G 3964) sown at the normal time (November), at the time of seed filling (30/20°C), or sown late (February) to impose heat stress (> 30/20°C (day/night) and drought maintained by water withheld (50% of field capacity) from the start of

seed filling to maturity. The photosynthetic rate (Pn) decreased significantly more under drought stress (33.4–56.6%) than heat stress (13.3–43%), as compared to the control plants. Under the combined stress, Pn declined more (57–82% reduction), less so in the heat and drought tolerant genotypes compared to sensitive (Sehgal et al., 2017).

Sucrose

Leaf photosynthates are largely transported to sink organs in the form of sucrose, and sucrose synthase (SS) is a key enzyme for sucrose to enter a variety of metabolic pathways (Lu et al., 2005). Down-regulation of SS indirectly inhibits carbohydrate production, eventually reducing yield and quality. Maintaining sucrose levels is vital during stressed conditions, which depend on its synthesis and hydrolysis. Heat-stressed plants had significant reductions in the activity of key enzymes—sucrose phosphate synthase (SPS) and SS—involved in sucrose synthesis. The availability of sucrose to reproductive organs is crucial for sustaining their function (Kaushal et al., 2013). Heat-tolerant genotypes are expected to stabilize the photosynthetic process better than heat-sensitive genotypes. Measuring sucrose concentrations reveals the photosynthetic status of plants under heat stress (Awasthi et al., 2014). A large core-collection of chickpea genotypes screened or heat tolerance (32/20°C) in a natural environment identified two heat-tolerant (ICC15614, ICCV92944) and two heat-sensitive (ICC10685, ICC5912) genotypes. The heat-sensitive genotypes had significantly greater inhibition of RuBisCo (carbon-fixing enzyme), SPS, and SS than the heat-tolerant genotypes, and thus produced less sucrose than the tolerant genotypes (Kaushal et al., 2013). Heat-sensitive genotypes produced far less leaf sucrose than heat-tolerant genotypes, which impaired its supply to developing reproductive organs (flowers, pods, and seeds) in sorghum (Prasad and Djanaguiraman, 2011), tomato (Li et al., 2012), and chickpea (Kaushal et al., 2013).

In wheat, heat-tolerant genotypes (PBW343 and C306) exposed to heat stress (>25°C) in the field had higher SS activity and thus higher sucrose contents in grain than heat-sensitive genotypes (PBW521, PBW522) (Bavita et al., 2012). Limitations in sucrose supply may disrupt the development and function of reproductive organs (Prasad and Djanaguiraman, 2011; Snider et al., 2011). In lentil, sucrose production is vital for leaf and anther function, and has been correlated with SPS activity in natural high-temperature environments (> 32/20°C). Heat-tolerant lentil genotypes (IG2507, IG3263, IG3297, IG3312, IG3327, IG3546, IG3330, IG3745, IG4258, and FLIP2009) produced more sucrose in their leaves (65–73%) and anthers (35–78%), than heat-sensitive genotypes (IG2821, IG2849, IG4242, IG3973, IG3964), which was associated with superior reproductive function and nodulation in tolerant genotypes (Sita et al., 2017a). Thus, heat stress negatively affects sucrose metabolism due to the inhibition of carbon fixation and assimilation (Awasthi et al., 2014). Sucrose concentrations in leaves and anthers and SS and SPS activities declined significantly in two mungbean genotypes (SML832 and SML668) exposed to heat stress (>40/25°C day/night) outdoors and in a controlled environment, more so in SML668 (heat-tolerant) than SML832 (heat-susceptible) (Kaur et al., 2015). Tomato cultivars exposed to heat stress in growth chambers (31/25°C day/night) or greenhouses (32/26°C day/night) revealed four genotypes (FLA7516, Hazera3018, Hazera3042, and Saladate) as heat-tolerant with high sucrose contents in the mature pollen grains, and three genotypes (Grace, NC8288, and Hazera3017) as heat-sensitive, with 50% less sucrose than the tolerant genotypes (Firon et al., 2006).

Expression of the sucrose transporter gene, OsSUT1, is important for maintaining photo-assimilate supply to grains. In rice exposed to high-temperature stress (31/26°C) in a glasshouse, cultivar Genkitsukushi (heat-tolerant) had higher expression of OsSUT1 in stems than Tsukushiroman (heat-sensitive), indicating that sugar transport is more effective in Genkitsukushi than Tsukushiroman under heat stress, which improves grain quality (Miyazaki et al., 2013).

BIOCHEMICAL TRAITS

Heat sensitivity is linked to the expression of several cellular molecules, including antioxidants (Wilson et al., 2014), HSPs (Xu et al., 2011) osmolytes (Bita and Gerats, 2013), and phytohormones (Sharma et al., 2020). These molecules assist cells to adapt, repair, and survive in adverse temperature environments; hence, measuring the extent of their expression in contrasting genotypes grown under heat stress might reveal mechanisms regulating the heat response.

Oxidative Stress and Antioxidants

Heat stress negatively affects cellular metabolism due to extensive ROS production that can severely damage lipids, proteins, and nucleic acids (Bita and Gerats, 2013). Plants protect themselves from ROS production by activating enzymatic and non-enzymatic processes (Bita and Gerats, 2013). The main ROS-scavenging enzymes are superoxide dismutase (SOD), catalase (CAT), peroxidase (POD), ascorbate peroxidase (APX), and glutathione reductase (GR), and the non-enzymatic system includes ascorbic acid (ASC) and glutathione (GSH) (Suzuki et al., 2012). Genotypes can be selected based on their enzyme expression level, with more prominent activities among heat-tolerant than heat-sensitive genotypes (Kumar et al., 2013). Genotypes respond differently to heat stress due to variation in their antioxidant systems. Hence, this trait is useful for identifying heat-tolerant genotypes.

Two tomato cultivars differing in heat sensitivity (Sufen14, Jinlingmeiyu) were raised in a greenhouse in optimum temperature (26/18°C) and heat-stressed (38/30°C for 6 days with 2 days recovery). Jinlingmeiyu had lower activities of SOD, POD, APX, and MDA (malondialdehyde) and lower proline content than Sufen14, suggesting the involvement of these enzymes in imparting heat tolerance in Sufen14 (Zhou et al., 2019). Categorization of 50 *Brassica juncea* genotypes into tolerant, moderately tolerant and susceptible genotypes after exposure to 45°C was based on oxidative damage tolerant genotypes had less lipid peroxidation and higher POD, CAT, and GR activities than moderately tolerant and susceptible

genotypes (Wilson et al., 2014). In contrast, *Brassica juncea* seedlings grown under optimum (25°C) and high (45°C) temperatures had higher MDA and lipoxygenase (LOX) activities of antioxidants (SOD, CAT, POX, APX, and GR) in the thermosensitive genotype (NPJ-119) than the thermotolerant genotype (NRCDR-02) suggesting variations in the response of antioxidatnts, which might be stage-or plant-specific (Rani et al., 2012). Wheat genotypes were differentiated into heat-tolerant (C306), intermediate heat-tolerant (HD2285), and heat-sensitive genotype (HD2329) by subjecting them to heat stress (8 and 23 days after anthesis) by delaying the sowing time: C306 had higher relative water content, ASC, APO, CAT, and SOD and lower lipid peroxidation and H_2O_2 content than HD2285 and HD2329 (Sairam and Srivastava, 2000).

In chickpea plants raised under natural conditions and heat stressed at 50% flowering (30/20, 35/25, 40/30, and 45/35°C) in growth chambers, tolerant genotypes (ICCV07110, ICCV92944) had lower MDA concentration and H_2O_2 content than sensitive genotypes (ICC14183, ICC5912), which was attributed to their higher activity levels of APX, GR, and ASC (Kumar et al., 2013). Forty-one mungbean genotypes exposed to heat stress (>40/28°C) in the field revealed that heat-tolerant genotypes (EC693357, EC693358, EC693369, Harsha, and ML1299) suffered less oxidative damage (1.52–2.0-fold increase MDA; 1.59–1.96-fold increase H_2O_2) than sensitive genotypes (2.2–2.4-fold increase MDA; 2.21–2.93-fold H_2O_2) (Sharma et al., 2016). The heat-tolerant genotypes also significantly increased APX activity (by 1.48–1.77-fold), relative to susceptible genotypes (1.27–1.37-fold) and similar response was observed for GR activity. However, heat-tolerant and heat-sensitive genotypes had similar increases in CAT activity. Similarly, 38 lentil accessions screened for heat tolerance (>35/20°C) during the reproductive stage revealed less oxidative damage (MDA and H_2O_2 contents increased) and higher SOD, CAT, APX, and GR activities—involved in detoxification—in heat-tolerant genotypes (IG2507, IG3263, IG3745, IG4258 and FLIP2009) than heat-sensitive genotypes (IG2821, IG2849, IG4242, IG3973, IG3964 (Sita et al., 2017a). Concurrence of heat and drought stress will do more damage at the biochemical level. Oxidative damage and antioxidant mechanisms responding toward combined stress were reported in tomato cultivars. Two cultivars of tomato (CV1; Sufen14 and CV2; Jinlingmeiyu) were raised in green house conditions to compare the cultivar difference. Treatment (Heat stress-38/30°C, and drought stress-no irrigation) were given to 28 days old seedlings for six days. Significant increase in ROS such as H_2O_2 and O^{2-} were reported in both the cultivars than control (26/18°C). Their studies showed that CV2 had lower activity of enzymes-peroxidase, ascrobate peroxidase, superoxide dismutase, malondialdehyde (MDA) and proline content than CV1, under combined stress on day 6, clearly depicting cultivar differences with respect to antioxidant activity (Zhou et al., 2019).

Metabolites

Plant metabolites are low molecular weight compounds involved in stress tolerance. They play a crucial role in maintaining the redox homeostasis of cells and stabilizing cell membranes and proteins (Wahid et al., 2007) through various intermediate/precursor compounds, such as compatible solutes, signaling agents, and antioxidants (Kaplan et al., 2004). Metabolites are categorized into primary and secondary metabolites. Primary metabolites that are specifically upregulated in response to abiotic stress are amino acids (proline), polyamines (spermidine, spermine, putrescine), carbohydrates (sucrose, hexoses, polyhydric alcohols), and glycine betaine. Similarly, secondary metabolites include phenolic compounds (flavonoids, isoflavonoids, anthocyanins), terpenoids (saponins, tocopherols), and nitrogen-containing metabolites (alkaloids and glucosinolates) (Rodziewicz et al., 2014). Under heat stress, plants restructure their metabolites to help the cells to maintain homeostasis via the production of stress-induced compounds (Serrano et al., 2019). Activation of heat-shock factors, such as HSFA2 and HSFA3, increases the level of metabolites such as galactinol and its derivatives in response to heat stress (Song et al., 2016). Therefore, metabolites may serve as a useful tool for selecting heat-tolerant varieties under high-temperature stress. Comparing heat-tolerant and heat-sensitive genotypes can identify metabolite markers that are constitutively expressed and allow selection of superior germplasm.

Seed metabolomic analysis performed on contrasting soybean genotypes (PI587982A, heat-tolerant; A5279 and DP3478, heat-sensitive) revealed 25 metabolites that differed between genotypes, including tocopherol isoforms, ascorbate precursors, flavonoids, two amino acids, and amino acid derivatives (Chebrolu et al., 2016). At 36°C, 10 flavonoids were more abundant in the seeds of the heat-tolerant genotype than the heat-sensitive genotypes, along with several tocopherols (major antioxidants). Moreover, the heat-tolerant genotype had higher levels of a precursor of L-ascorbic acid biosynthesis—gulono-1,4-lactone—than the heat-tolerant genotypes. Overexpression of these stress-induced compounds provides thermotolerance to soybean seeds, which ultimately perform better in terms of seed vigor, seed germination, seed weight, and oil content. Metabolomic analysis of rice spikelets in a heat-tolerant (N22) and heat-sensitive (Moroberekan) genotype revealed that N22 accumulated more metabolites than Moroberekan, including carbohydrates (glucose 6-phosphate, fructose 6-phosphate, glucose, maltose, and other sugars), compatible solutes, and amino acids (leucine, isoleucine, and valine). N22 had lower levels of trehalose, sugar phosphatases, malic acid, and galactaric acid than Moroberekan under heat stress (Li X. et al., 2015). In wheat, a comparative analysis of metabolites in transgenic wheat (PC_{27} and PC_5) and its wild type (varying in heat sensitivity), exposed to heat stress (40°C for 4 h) during heading revealed 25 metabolites that were highly expressed in transgenic wheat, including proline, three sugar alcohols (inositol, mannitol, and xylitol), pyruvic acid, and other amino acids (glycine, alanine, serine, valine, and tyrosine) (Qi et al., 2017). The metabolite profiling approach is an effective way to accurately screen and select the best-performing genotypes.

Proline is a multifunctional amino acid with diverse roles in maintaining cellular redox balance by dissipating excess of reducing potential (Rivero et al., 2004). Proline levels are upregulated under stress conditions as its biosynthesis is an adaptive response to reduce excess NADPH produced in response

to the halt in CO_2 fixation in the Calvin cycle due to stomatal closure (Berry and Bjorkman, 1980). Moreover, under stress conditions, proline is involved in osmotic adjustment, ROS scavenging, and as an energy source. Therefore, high proline contents under high-temperature stress can be used to screen heat-tolerant genotypes. Twenty wheat genotypes were screened for heat tolerance by exposing them to 25 or 35°C, and measuring proline content and membrane damage (Ahmed and Hasan, 2011). Heat-tolerant genotypes (Bijoy, Sufi, Kanchan, Fang 60, BAW 1059, BL 1883, BL 1022, IVT 7, IVT 8, IVT 9, IVT 10, and BAW 917) had higher proline contents (>200%) and less membrane damage (<50%) than heat-sensitive genotypes (Shatabdi, PRODIP, BAW 1064, Gourab, Pavon 76, Sonara, Kalyansona, and IVT 6). Thirty-five-day-old seedlings of different cabbage cultivars, including Chinese cabbage and their hybrids, were exposed to two temperature regimes (25 or 35°C) at the flower bud stage and assessed for heat tolerance based on proline contents in stalks, flower buds, and leaves—heat-tolerant cultivars (Yoshin, Kenshin, and full white) had higher proline levels than heat-sensitive cultivars (YR Kinshun, Chihiri 70, and Large leaf) (Hossain et al., 1995). Six cotton cultivars (Sicala, Acala 1517-88, Molopo, Alpha, Delta Pine Acala90, and OR19) were tested for genetic variability against combined heat and drought stress. Stress treatment (Heat stress; 40°C without irrigation for 15 days) were imposed on 3 weeks old seedlings. Stress treatment were increased the proline content in all the genotypes but the accumulation was more in tolerant genotypes (Alpha, Delta Pine Acala90, and OR19) compared to sensitive genotypes (Sicala, Acala 1517-88, Molopo) (De Ronde et al., 2000).

Heat-Shock Proteins

During rapid heat stress, plants synthesize and accumulate specific proteins called heat-shock proteins (HSPs) (Howarth, 1991); this is a universal response to high-temperature stress in all organisms (Vierling, 1991). Heat-shock genes are upregulated during stress to encode HSPs which are vital for plant survival under such conditions (Chang et al., 2007). Three classes of HSPs are distinguished, according to molecular weight—HSP90, HSP70, and low molecular weight proteins. HSPs provide stress-related chaperone functions in plants under stress conditions (Reddy et al., 2010, 2016). Chaperones have a role in protein synthesis, maturation, targeting, degradation, renaturation, and membrane stabilization (Reddy et al., 2014, 2016). HSPs are located in the cytoplasm, nucleus, mitochondria, chloroplasts, and endoplasmic reticulum (Waters et al., 1996). Heat-stress transcription factors (HSFs), located in the cytoplasm in an inactive state, control HSP gene transcription and play a vital role in plant thermotolerance. Specific HSPs have been identified in response to high temperature, including HSP68 in the mitochondria of potato, maize, soybean, and barley (Neumann et al., 1994). The expression profiles of HSPs have been compared in plant species/genotypes contrasting in heat sensitivity. For instance, the higher heat tolerance of maize than wheat and rye at 42°C is correlated with the expression of five mitochondrial low molecular weight HSPs (28, 23, 22, 20, and 19 kDa), as opposed to only 20 kDa in wheat and rye (Korotaeva et al., 2001). According to Sharma-Natu et al. (2010), HSP18 was upregulated in developing grains of heat-tolerant wheat exposed to 3.2–3.6°C higher temperatures than normal. In other studies, HSP100 increased with heat stress in a tolerant wheat variety (Sumesh et al., 2008). Similarly, HSP26 increased in heat-tolerant wheat genotypes (K7903, C306) at 42°C, relative to heat-sensitive genotypes (PBW343, HD2329) (Hairat and Khurana, 2016). At 42°C, the expression levels of five Hsps—Hsp26.7, Hsp23.2, Hsp17.9A, Hsp17.4, and Hsp16.9A—were upregulated in the heat-tolerant rice cultivar Co39, relative to the heat-sensitive rice cultivar Azucena, and regarded as biomarkers for screening rice cultivars for heat tolerance (Chen et al., 2014). At 40°C, potato cultivar Norchip synthesized small (sm) Hsps for longer than other cultivars. In Norchip and Desiree, an 18 kDa small (sm)HSP increased for up to 24 h, while in cultivars Russet Burbank and Atlantic, the levels started to decline after 4 and 12 h respectively (Ahn et al., 2004). Anthers of a heat-tolerant tomato cultivar had higher constitutive levels of HSP100 than a heat-sensitive cultivar (Pressman et al., 2007). In chickpea, HSP levels increased in genotype JG14 (heat-tolerant) more than genotype ICC16374 (Heat-sensitive) when exposed to 42/25°C at anthesis (Parankusam et al., 2017). Likewise, in peanut, the best-characterized aspect of acquired thermotolerance is HSP production, with ICGS76, COC038, and COC068 selected as heat-tolerant genotypes and COC812, COC166, Tamrun OL 02, and Spanco selected as heat-sensitive (Selvaraj et al., 2011). In another study, heat-tolerant peanut genotype ICGS 44 showed higher HSP expression throughout the stress period than heat-sensitive genotypes AK 159 and DRG 1 (Chakraborty et al., 2018). Comparison of expression of heat shock proteins in wheat cultivars (Katya and Sadovo) under combined heat and drought stress (40°C/56%) reported 100% elevation of HSP100 and HSP70 as compared to 60 and 10% elevation under individual drought and heat stress in tolerant cultivar Katya (Grigorova et al., 2011).

GENE/S EXPRESSION

Relatively few studies have been undertaken on changes in gene expression in contrasting genotypes under heat stress, but vital information has been garnered. In wheat, two contrasting genotypes—Chinese spring (heat-sensitive) and TAM107 (heat-tolerant)—were analyzed for changes in gene expression upon exposure to heat stress (40°C), using Affymetrix Barley 1 GeneChip, and expressed sequence tags. The analysis identified 6550 heat-responsive probe sets, accounting for 11% of the total probe sets (Qin et al., 2008). Heat-tolerant genotype (2199 probe set) had more heat-responsive probe sets than the heat-sensitive genotype (2084 probe set), which mainly belonged to HSPs, transcription factors, calcium and sugar signaling pathways, phytohormones biosynthesis and signaling, ribosomal proteins, RNA metabolism, and primary and secondary metabolites (Qin et al., 2008). In rice, contrasting genotypes N2219379 (heat-tolerant) and IR64 and N226264 (heat-susceptible) were compared for their heat response at 38°C using reproductive function and molecular

approaches (González-Schain et al., 2016). Heat stress impaired reproductive functions, such as pollen production, pollen number, anther dehiscence, pollen germination, and stigma receptivity, more so in the sensitive genotypes than the tolerant genotype (Devasirvatham et al., 2012). Eighteen heat-responsive genes, such as HSFA2a, OsFKBP62b, and OsHSP17.9A had higher upregulation in tolerant genotypes than sensitive genotype. Under heat stress, the expression of HSFA2a increased 268-, 15-, and 3.2-fold in N2219379 (heat-tolerant), N226264 (heat-sensitive), and IR64 (heat-sensitive), respectively and that of OsFKBP62b increased by 108-, 10-, and 3-fold in N2219379, N226264, and IR64, respectively (González-Schain et al., 2016). A study was conducted on 197 spring wheat genotypes from ICARDA at two different locations, one in Sudan (Wad Medani) and another one in Egypt (Sids), to identify single nucleotide polymorphism (SNP) markers association mapping. The study detected 111 significant marker-trait associations; the wsnp_Ex_c12812_20324622 marker on chromosome 4A was significantly correlated with yield at both locations. Wheat genotypes carrying the cytosine base at the wsnp_Ex_c12812_20324622 and wsnp_Ex_c2526_4715978 markers produced more yield, compared to those carrying the alternative bases, by 15%, indicating the significance of involving these markers for marker-assisted selection in breeding programs to increase yield under heat stress. The best performing 20 high-yielding as well as heat-tolerant wheat genotypes, found in this study, have been distributed across Central and West Asia and North Africa (CWANA) and sub-Saharan Africa (SSA) for potential direct release and/or use as parents after local adaptation trials (Tadesse et al., 2019).

DNA methylation is one of the mechanisms of epigenetic modifications that plays a crucial role in imparting stress tolerance for various environmental stresses (Lukens and Zhan, 2007). A study on heat-tolerant (Huyou 2) and heat-sensitive (Fengyou 1) *Brassica napus* seedlings exposed to 45°C measured changes in DNA methylation levels and the cytosine methylation pattern using Methylation Sensitive Amplification Polymorphism (MSAP) analysis and RT-PCR (Gao et al., 2014). Under heat stress, percentage of methylated bands was 10.7% in Fengyou 1 (heat-sensitive) and 0.6% in Huyou 2 (heat-tolerant) (Gao et al., 2014). The cytosine methylation was also higher in the heat-sensitive genotype than the heat-tolerant genotype suggesting involvement of methylation to heat stress sensitivity. It has already been reported that superior crop genotypes avoid the methylation process (Gao et al., 2014). The effects of combined heat and drought stress on the gene expression in durum wheat (*Triticum turgidum subsp. durum*) cultivar "ofanto" were evaluated (Rampino et al., 2012). Plants were raised in the growth chamber and stress conditions were introduced at booting stage; heat stress- 30/22°C for 2 days, then raised to 34/24°C for following 2 days, 40/32°C for next one day and 42°C for last day and collected samples after 6 h of heat treatment, however, drought conditions were maintained at 28% field capacity. Gene expressions, analyzed through cDNA-AFLP studies, showed that combined stress down-regulated 92 genes and up-regulated 132 genes. Many of these genes reported to control the expression level of HSPs and dehydrins.

POLLEN-BASED TRAITS

In most plant species, reproductive tissues, mainly male gametophytes, are more sensitive to heat stress than female gametophytes (Djanaguiraman et al., 2018a), and the threshold temperature for imposing damage in these tissues is lower than that for vegetative tissues. Damage imposed by heat stress can occur pre- or post-pollination, which impair fertilization and ultimately reduce seed set (Prasad et al., 2008a, 2017; Prasad and Djanaguiraman, 2014; Sage et al., 2015). Pre-pollination events that are highly susceptible to high temperature are (1) meiosis I and meiosis II of the microspore mother cell (Young et al., 2004), (2) development and subsequent dissolution of the tapetum layer (Farooq et al., 2011), and (3) exine and intine formation (Nahar et al., 2016). Post-pollination events that are highly susceptible to heat stress are (1) pollen load (Prasad et al., 1999b, 2006), (2) pollen germination (Prasad et al., 2001), (3) pollen tube growth (Prasad et al., 2001), and (4) fertilization (Prasad et al., 2001; Barnabás et al., 2008; Hedhly, 2011; Sita et al., 2017b). The development of male gametophyte under high temperature is more susceptible than female gametophyte (Djanaguiraman et al., 2018a; Liu et al., 2019). However, in peal millet (*Pennisetum glaucum*), the female gametophyte was more sensitive than male gameophyte (Djanaguiraman et al., 2018b). Several effects of heat stress on reproductive function have been reported. For instance, it reduced the fertility of the microgametophyte in *Brassica* (Rao et al., 1992), and impaired meiosis in the male gametophyte in tomato (*Lycopersicon esculentum*), which affected pollen germination and pollen tube growth (Firon et al., 2006). Shriveled pollen grains under high temperature may be why heat stress prevents starch accumulation in anther walls and pollen grains by disturbing the source–sink relationship that subsequently leads to lower levels of soluble sugars for their development (Pressman et al., 2002; Djanaguiraman et al., 2018a). Variation in contrasting genotypes of various pollen traits; could be used to identify and screen genotypes tolerant to high-temperature stress. For instance, 12 field-grown cultivars of *Brassica napus* L. were screened for heat tolerance based on pollen traits—pollen viability, pollen germination and pollen tube length—at 33.7°C (Singh et al., 2008). Pollen grains were placed on a germinating medium in Petri plates and artificially incubated by raising the temperature by 5°C at 5-hourly intervals from 10 to 35°C for 30 h before measuring the three pollen traits. As a result, the *Brassica* cultivars were divided into four groups—heat-tolerant (Kadore, ARC98007, NPZ0591RR, and DSV06200), moderately heat-tolerant (Plainsman, Kronos and DSV05102), moderately heat-susceptible (DSV05101 and KS4085), and heat-susceptible (KS4002, Ceres and KS3077). Thirty-four tomato genotypes were tested under field conditions in a normal (27.1/15.5°C) and summer (39.2/24.4°C) season for heat tolerance, which identified three heat-tolerant genotypes (Pusa Sadabahar, FLA-7171, and NDTVR-60) with high pollen germination and pollen viability, relative to the heat-susceptible genotypes (Floradade and H-86) (Srivastava et al., 2012). In another study, 17 tomato genotypes were evaluated under heat stress (32/26°C) for thermotolerance on the basis of pollen traits (Paupière et al., 2017). The tomato plants were raised in a greenhouse (25/19°C), before being

moved to climate chambers when the first flower appeared for the subsequent heat treatment (32/26°C). Thermotolerant genotypes (LA2854, LA1478, and LA0417) had higher pollen viability and pollen numbers than thermosensitive genotypes (LA1719, LA1580, and SWEET4). Similarly, 18 rice (*Oryza sativa*) genotypes varying in heat sensitivity were raised in a greenhouse before being transferred to growth cabinets for high-temperature exposure during anthesis—30°C (control), and 35 and 38°C (heat stress) In this study, two experiments were conducted in two successive years, 1st year experiment involved 30°C (control), and 35°C and 38°C (heat stress) for 2h on the onset of anthesis while 2nd year experiment involved the same set of conditions but heat stress exposure was raised to 6 h (Jagadish et al., 2008). A lower fertility percentage was noticed at 38°C for 6 h compared to 2 h. Genotype N22 had the highest spikelet fertility (86%) and was selected as highly tolerant, while Azucena and Moroberekan had <10% spikelet fertility, thus being the most susceptible genotypes (IR64, CG14); the observations correlated with superior pollen performance at high temperature (Jagadish et al., 2008). *In vitro* pollen germination and pollen tube growth were used to screen 14 cotton cultivars for heat tolerance by raising the temperature by 10°C at 5-hourly intervals from 10 to 50°C for 24 h under controlled environment (Liu et al., 2006). The study revealed that boll retention and boll number per plant were strongly correlated with pollen germination and pollen tube length. The genotypes were categorized into heat-tolerant (Sumian 16 and HLY11), moderately tolerant (JC108, Simian 3, Simian 4, and Lumian 584), moderately susceptible (Zhongmiansuo 12, Zhongmiansuo 41, Zhongmiansuo 9409, Xinyoumian 68, and Sumian 12), and susceptible (TS18, HLY15, and NuCOTN33B).

In legumes, heat stress exposure (47°C) to 44 soybean genotypes identified heat-tolerant (DG 5630RR), heat-intermediate (PI 471938), and heat-sensitive (Stewart III) genotypes based on pollen germination and pollen tube length (Salem et al., 2007). Similarly, heat-tolerant and heat-sensitive mungbean genotypes were identified based on pollen stainability (Suzuki et al., 2001). The plants were exposed to high temperatures (38/28°C) for 24 h in a growth chamber, with pollen stainability recorded on flowers that opened 8–11 days after heat treatment. The heat-tolerant genotype (Haibushi) had higher pollen stainability (60%) than heat-sensitive genotypes (<20%; Kentucky Wonder, Oregon, and Okinawa Local). Heat stress (43/30°C and 45/32°C) in mungbean affected pollen viability, pollen germination, and pollen tube length, more so in the heat-tolerant genotype (SML832) than the heat-sensitive genotype (SML668) in outdoor and controlled conditions (Kaur et al., 2015; Bindumadhava et al., 2018). Exposure of 45 mungbean genotypes to high temperature (42°C) during flowering in the field produced fewer and more shriveled pollen grains, and identified heat-tolerant genotypes (C693357, EC693358, EC693369, Harsha, and ML1299) with superior pollen traits (pollen germination, pollen viability) (Sharma et al., 2016). In chickpea, reproductive traits such as pollen viability, pollen germination, and pollen tube length were used to screen a large number of chickpea genotypes for heat tolerance by delaying sowing to expose plants to temperatures > 32/20°C (day/night); a few tolerant (ICC15614, ICCV92944) and sensitive (ICC10685, ICC5912) genotypes were identified (Kaushal et al., 2013). Another study identified heat-tolerant and heat-sensitive chickpea genotypes using reproductive traits (Devasirvatham et al., 2013) by exposing plants to high temperature (≥35°C). Pollen grains were more sensitive to high temperature than stigmas in both controlled and field conditions. Genotype ICC1205 was identified as heat-tolerant and ICC4567 as heat-sensitive, with a positive correlation between reproductive and yield traits. Lentil is sensitive to heat stress (>35°C), which adversely impairs pollen development and function, resulting in poor pod yields. Based on pollen traits, Kumar et al. (2016) identified heat-tolerant genotypes (FLIP2009-55L, IG2507, and IG4258) after screening 334 lentil accessions for heat tolerance under field conditions (>35/25°C), with a positive correlation between pollen viability and filled pods/plant. In another field study, heat stress (>35/25°C) reduced pollen viability in lentil by up to 78–83% (Sita et al., 2017b), with heat-tolerant genotypes (IG2507, IG3263, IG3745, IG4258, and FLIP2009) maintaining higher pollen germination (48–50%) than heat-sensitive genotypes (28–33%), which was positively correlated with yield. In soybean, exposure of cultivars (i.e., IA3023 and KS4694) and plant introduction lines (PI) lines (i.e., PI393540 and PI588026A) to heat stress (36.5–38.6°C) between gametogenesis and full bloom, as compared to control treatment (29.5–31.6°C; optimum temperature) revealed that the cultivars were more heat tolerant because of greater pollen germination and less distortion in pollen shapes (Djanaguiraman et al., 2019). Combined stress treatment damages the reproductive stages mainly pollen grains to a larger extent (Sehgal et al., 2017). Genetic variations among 38 cotton cultivars for heat and drought were assessed using reproductive and physiological traits. Among reproductive traits, pollen germination as well as pollen viability were tested at two temperature regimes (30 and 38°C) and cumulative heat and drought stress response (CHDSRI) using photosynthetic and reproductive traits was calculated. Based upon CHDSRI, 12 genotypes were categorized as heat and drought sensitive, 20 as intermediate and 6 genotypes as heat and drought tolerant (CT12214, MON11R124B2R2, UA48, MON11R112B2R2, PHY367WRF, and PX53221 1WRF) (Singh K. et al., 2018), which could be potentially used for breeding programs.

YIELD-BASED PARAMETERS

Heat stress adversely affects the reproductive and seed-filling stages, leading to severe reductions in crop yield and quality (Sehgal et al., 2018). Various studies have confirmed that the relative performance of plants in terms of yield under heat stress was suitable for selecting genotypes with heat-tolerance mechanisms/traits that can be used for crop improvement. Various traits linked to yield have been used to identify genotypes contrasting for heat tolerance.

Seed formation and seed filling is the last phase in the life cycle of seed plants. Heat stress drastically affects seed development and seed filling in many crop species, which consequently

increases the fraction of abnormal and shriveled seeds. Seed development starts from cell division; when seed cells are fully formed, storage reserves start to accumulate in the seed (Egli, 1998). The direct effect of heat stress is reportedly on the division and size of endosperm cells (Commuri and Jones, 1999), such that lower amounts of carbohydrates, proteins, lipids, and starch accumulate in developing seeds. Heat stress also accelerates the rate and duration of seed filling, resulting in more abnormal seeds, which reduces crop yield. Heat stress reduces seed yield by (i) reducing seed number, (ii) reducing seed weight, and (iii) accelerating the seed filling rate (Farooq et al., 2017; Prasad et al., 2017).

Seed Filling Rate and Duration

Heat stress hastens the seed filling rate and reduces the duration of seed filling. In cowpea, raising the temperature from 15.5 to 26.6°C shortened the seed filling duration by 14–21 days (Nielsen and Hall, 1985). Heat stress impaired the growth of the cotyledons, and reduced the number of endosperm cells and cell expansion in the embryo, which had a negative effect on photosynthate translocation in developing seeds and resulted in shriveled seeds in maize (Jones et al., 1985; Munier-Jolain and Ney, 1998). A heat-stressed environment (>32/20°C) during seed development increased the seed filling rate in six chickpea genotypes, relative to the optimum temperature (Awasthi et al., 2014). The same study revealed that heat stress decreased the duration of seed filling more in heat-sensitive (ICC 4567) than heat-tolerant (ICC1356, ICC15614) genotypes. High temperature (25/20°C) reduced the duration of grain filling by 30% and increased the grain-filling rate by 20% in six wheat genotypes (G1, G2, G3, G4, G5, G6), relative to the control (20/15°C), more so in heat-sensitive (G6) than heat-tolerant (G4) genotypes (Yin et al., 2009).

Seed Number

Heat stress leads to poor pollination and fertilization, which reduces seed number. In faba bean (*Vicia faba* L), seed number declined with increasing temperature (Bishop et al., 2016). In mungbean, heat-tolerant genotype (SML 832) produced more seeds than heat-sensitive genotype (SML 668) under high temperature (45/32°C) in the field (Kaur et al., 2015). While testing 24 genotypes of common bean in the greenhouse under different temperature regimes (24/21°C, 27/24°C, 30/27°C, 33/30°C), 33/30°C was the most damaging to plants with respect to seed number and seeds/pod, with the reductions more prominent in heat-sensitive genotypes (–66%; A55, Labrador, Majestic, IJR) than heat-tolerant genotypes (–31%; Brio, Carson, G122, HB1880, HT38, Venture) (Rainey and Griffiths, 2005). Heat stress (36/27°C) reduced seed number/pod in 46 of 48 lines of cowpea (*Vigna unguiculata*) evaluated for heat tolerance in a greenhouse; two heat-tolerant lines (B89-600 and TN88-63) did not exhibit reduced seed numbers/pod (Ehlers and Hall, 1998). The average number of seeds/pod varied in the heat-sensitive genotypes (e.g., 3.3 in IT82E-60, 2.9 in Bambey 21 and 3.6 in IT84S-2049), while those of the heat-tolerant genotypes had 6.3 in B89-600 and 8.1 in TN88-63 compared to control values (e.g., 11 in IT84S-2049, 9.6 in IT82E-60, 7.4 in B89-600 and 6.4 in TN88-63).

Seed Weight

Seed weight represents the ultimate yield of the crop; hence it has been reliably used as a trait to screen for heat tolerance (Sehgal et al., 2018). Chickpea yields declined when genotypes were exposed to various temperature ranges (35/25°C, 40/30°C, and 45/35°C) in a growth chamber, relative to the control (30/20°C) (Kumar et al., 2013). At 40/30°C, the seed weight of heat-sensitive genotypes (ICC14183, ICC5912) declined by 37–45% compared with heat-tolerant genotypes (ICCV07110, ICCV92944). At 45/35°C, heat-tolerant genotypes also experienced a decline in seed weight but heat-sensitive genotypes did not set any pods. Similarly, mungbean genotypes grown outdoors in April, with high temperatures (45/32°C) coinciding with reproductive phase, reduced seed weight by 48.3% in the heat-sensitive genotype (SML668) and 35.1% in the heat-tolerant genotype (SML832), relative to control (Sharma et al., 2016). Likewise, seed weight of lentil grown at high temperature (>32/20°C) in field declined drastically compared to control plants (Bhandari et al., 2016), more so in heat-sensitive genotypes (–50%; LL699 and LL1122) than the heat-tolerant genotype (–33%; LL931). In common bean, heat stress (33/30°C) under field conditions was significant for the selection of heat-tolerant (Brio, Carson, G122, HB1880, HT38, Venture) and heat-sensitive genotypes (A55, Labrador, Majestic, IJR), based on seed weight. At this temperature, seed weight declined by 47% across genotypes, more so in heat-sensitive genotypes (–88%) than heat-tolerant genotypes (–25%) (Rainey and Griffiths, 2005). In cowpea, studies at two locations with varying temperatures (Coachella (41/25°C) and Riverside (36/17°C) assessed the effect of high temperature on the yield of contrasting genotypes (Ismail and Hall, 1999). Yield parameters such as seed weight and seeds/pod reduced drastically, as the temperature increased, however, heat-tolerant genotypes (H36, H8-9, DLS99) at higher temperature (41/25°C) retained more seed weight (193 mg/seed) than heat-sensitive genotypes (CB5, CB3, DLS127), which had smaller seeds with an average weight of 168 mg. Screening experiments on Pearl millet, conducted over a period of 3–4 years (2009–2012) at ICRISAT, India, involving 221 hybrid parental lines (both B- and R-lines), 53 germplasm accessions and 4 improved populations over 4-year period showed large genetic variability in seed set at daily maximum air-temperature of $\geq$ 42 °C during flowering. Five hybrid seed parents (ICMB 92777, ICMB 05666, ICMB 00333, ICMB 02333, and ICMB 03555) and a germplasm accession IP 19877 with 61–69% seed set as compared to 71% seed set in a heat tolerant commercial hybrid 9444 (used as a control) was identified. A comparative study on 23 hybrids and their parents for seed set at high air temperature (>42°C) showed heat tolerance as a dominant trait, indicating that heat tolerance in one parent would be ample to generate heat tolerant hybrids in pearl millet (Gupta et al., 2015). In sub-Saharan Africa, 24 elite durum wheat breeding lines and cultivars were tested for adaptation to warm environments at two stations: Kaedi, Mauritania and Fanaye, Senegal. Top grain yield was recorded at 5,330 kg ha^{-1} and the average yield at 2,484 kg ha^{-1}. Biomass and spike

fertility (i.e., number of seeds produced per spike) were found to be the most vital adaptive traits to warm environments. The study showed three genotypes ("Bani Suef 5," "DAWRyT118," and "DAWRyT123") as the most stable and high yielding; while the last two genotypes were the best performers (Sall et al., 2018).

Combined drought and heat stress were found to be greatly detrimental for production potential of crops. Thus, lentil genotypes were evaluated for their response to impacts of combined drought and heat stress (drought tolerant: DPL53 and drought sensitive: LL699) (Sehgal et al., 2019). The heat and drought (33/28°C with 50% field capacity) treatments were imposed to determine to effects on yield traits (seed filling duration, seed filling rate, seed number/plant, and seed weight/plant). Under combined stress, a decline in seed filling duration by 5.4–8.9 days, seed growth rate by 44–60.2%, seed number/plant by 35–48.7%, seed weight/plant by 47–59% compared to control. This reduction pattern was more drastic in heat sensitive genotype than heat tolerant genotype. A field experiment on 300 maize inbred lines test-crossed to CML539 was conducted at multiple locations (Tlaltizapán, México (18°41′ N, 99°07′ W, and 940 m asl), Kiboko, Kenya (2°21′ S, 37°72′ E, and 975 m asl), Chiredzi, Zimbabwe (21°01′ S, 31°34′ E, and 430 m asl), at the Nakhonsawan Field Crops Research Center in Takfa, Thailand (15°21′ N, 100°30′ E, and 87 m asl), and at the ICRISAT experimental station in Hyderabad, India) to evaluate their response to reproductive stage drought stress, heat stress, and combined drought and heat stress. The study identified few lines (notably La posta Sequia C7-F64-2-6-2-2 and DTpYC9-F46-1-2-1-2) having higher tolerance to drought and combined drought and heat stress. The findings indicated that tolerance to individual stresses was genetically distinct from tolerance to combined stresses. The assessment indicated that most of the current drought donors and key inbreds used in widely grown African hybrids were sensitive combined drought and heat stresses. The identified lines, as mentioned above, need to be introduced into breeding programs for maize (Cairns et al., 2013).

BREEDING FOR HEAT TOLERANCE INVOLVING CONTRASTING GENOTYPES

Breeding techniques remain one of the inexpensive and viable approaches for developing heat stress tolerance in crop plants (Priya et al., 2018). Field-based screening of crop gene pool and landraces for yield and heat stress tolerance in targeted environments is a way to develop heat tolerant genotypes in various crop plants (Craufurd et al., 1998; Hede et al., 1999; Ntare et al., 2001; Jagadish et al., 2008; Scafaro et al., 2010; Krishnamurthy et al., 2011; Dhanda and Munjal, 2012; Pradhan et al., 2012). The breeders also focus toward yield and yield-related traits under heat stress so that genotypes/progeny lines with higher yield under heat stress can be selected. Varieties possessing heat stress tolerance as well as higher yields will ensure adequate food to the world's burgeoning population under global warming. To develop heat tolerant crop varieties, contrasting donor parents are crossed, progenies advanced using various crop breeding strategies and desirable heat tolerant segregants are selected. Finally, heat tolerant homozygous lines are evaluated for yield and other useful agronomic traits under appropriate environments followed by possible release as a variety/ies. For transfer of heat tolerance to high yielding but heat sensitive mega crop varieties (varieties that occupy large area) from heat tolerant landraces or wild relatives, backcross breeding with recurrent parent remains an effective strategy as it allows for the recovery of the genome of recurrent parent, thereby traits of mega variety, with an addition of heat tolerance. To broaden the genetic base for heat tolerance, next generation breeding schemes viz., development of Multiparents Advanced Generation Intercross (MAGIC) and Nested Association Mapping (NAM) population are also receiving wider attention (Li H. et al., 2018).

Morpho-physiological and phenological traits could play an important role in contributing toward heat stress adaptation as these could act as surrogate traits for selecting heat tolerance (Reynolds et al., 2007). These physiological traits range from early phenology (Gaur et al., 2015), canopy temperature (Kumar et al., 2012; Mondal et al., 2013), chlorophyll fluorescence, chlorophyll content (Ristic et al., 2007; Kumar et al., 2013), cell membrane stability (Blum and Ebercon, 1981), stay green trait or delayed senescence (Thomas and Howarth, 2000; Ristic et al., 2007), pollen and pollen related traits (Devasirvatham et al., 2010; Kaushal et al., 2013; Djanaguiraman et al., 2018, Djanaguiraman et al., 2019) to water soluble carbohydrates in stem (Schittenhelm et al., 2020). The physiological trait-breeding has gained great attention for improving plant adaptation to heat stress in various crop plants especially in wheat (Reynolds et al., 2007; Reynolds and Langridge, 2016). A focus on selection of physiological traits that are correlated with yield either directly or indirectly could increase chances of accumulation of yield contributing genes thereby ensuring higher plant yield under heat stress (Reynolds and Langridge, 2016). In developing heat tolerance in wheat, the cross-species gene transfer system was used wherein three heat-tolerant accessions of *Aegilops tauschii* (wild genotype) were crossed with bread wheat (*Triticum aestivum* L.) cultivar "PBW 550" (Sehgal et al., 2011). The BC_1F_4 lines derived from these crosses that possessed improved cell membrane stability, TTC and chlorophyll retention under heat stress were selected (Sehgal et al., 2011). For winter sown crops, early phenology allows plants to escape heat stress (Bueckert et al., 2015). For such crops, selection for earliness could be an important option to develop crop varieties that escape heat stress thereby escaping the damage caused by heat. As reproductive processes are most vulnerable to heat stress, physiological screening of genotypes for two reproductive traits, i.e., better pollen viability and pollen germination under heat stress could lead to the identification of heat tolerant genotypes as stability of these two traits under heat stress will ensure better fertilization, adequate seed set and improved grain yield (Devasirvatham et al., 2013; Poli et al., 2013). Relying on higher pollen germination and better seed setting capability Nguyen et al. (2013) identified two sorghum R9403463–2-1 and IS8525 genotypes from a set of diverse sorghum genotypes originated from United States, Australia, Africa and Asia. Likewise, several promising genotypes viz., PI609489, AQL33/QL36; CCH2; IS

8525 (Singh V. et al., 2015) due to their better seed setting ability and Macia, BTx378, SC155 (Sunoj et al., 2017) having better pollen germination capability and maintaining high grain yield under heat stress were identified. Given the field screening of large set of germplasm and hybrid parental lines of Pearl millet under high temperature stress, a wide range of genetic variability for seed setting was noted in under high temperature stress (Gupta et al., 2015). Several parental lines viz., ICMB 92777, ICMB 05666, ICMB 00333 along with IP 19877 germplasm accession exhibited better seed setting under heat stress and thus could be used in developing heat tolerant hybrid Pearl millet (Gupta et al., 2015). Likewise, Jukanti et al. (2017) underscored the importance of CZH 233, CZP 9603, CZI 2011/5, and CZMS 21A genotypes due to their better seed setting higher capability of grain yield for developing superior Pearl millet genotypes under heat stress. Likewise, the potentiality of "Norchip" and "Désirée" potato cultivars in potato breeding program for improving genetic gain because of their better photo-assimilate transport from leaf to tuber under heat stress has been discussed (Basu and Minhas, 1991; Ahn et al., 2004).

Heat stress tolerance is a polygenic trait. Classical genetics was earlier used to identify the genetic bases of heat tolerance in various field and vegetable crops (Patel and Hall, 1988; Marfo and Hall, 1992; Gupta et al., 2015; Jha et al., 2019), this approach, however, could not completely explain the genetic nature of heat stress tolerance because of its multigenic nature (Upadhyaya et al., 2011). Subsequent advances in molecular marker technology has allowed identification and precise mapping of genes/QTLs governing heat stress tolerance several crops such as rice (Gui-lian et al., 2009; Lei et al., 2013; Wei et al., 2013; Li M. et al., 2018), maize (Inghelandt et al., 2019), wheat (Mason et al., 2010; Pinto et al., 2010; Paliwal et al., 2012; Lopes-Caitar et al., 2013; Sharma et al., 2017), chickpea (Paul et al., 2018), cowpea (Pottorff et al., 2014), *Brassica* (Branham et al., 2017) and tomato (Wen et al., 2019). Marker assisted selection can be used to transfer heat tolerant QTLs/genomic region to the elite but heat stress sensitive genotypes if genetic maps with sufficient marker density are available (see Jha et al., 2014). The approach has been successfully employed in rice (Ye et al., 2012; Shirasawa et al., 2013), wheat (Pinto et al., 2010; Bennett et al., 2012; Bonneau et al., 2013) and tomato (Grilli et al., 2007) to transfer QTLs governing heat tolerance. Considering potato, Trapero-Mozos et al. (2017) discussed the scope of introgression of *HSc70* allelic variant contributing toward enhancing yield under heat stress into high yielding potato cultivars through marker assisted breeding for improving heat tolerance in potato. Advent of improved sequencing technologies that allow faster sequencing of genomes at lower costs led to generation of profuse SNP markers that enabled genome-wide association studies (GWAS) for elucidating novel genomic regions controlling heat stress tolerance. GWAS for identifying heat stress tolerance genomic regions have been conducted in rice (Lafarge et al., 2017), maize (Yuan et al., 2019), wheat (Maulana et al., 2018), barley (Cantalapiedra et al., 2017), pea (Tafesse et al., 2020), chickpea (Thudi et al., 2014; Jha et al., 2018; Varshney et al., 2019), and in *Brassica* (Rahaman et al., 2018).

TRANSCRIPTOMICS

Previously cDNA-AFLP and microarrays were employed for identifying heat tolerance genes in various crop plants (Bita et al., 2011; Johnson et al., 2014). After the advent of crop-specific gene chips, microarrays became the method of choice for estimating changes in gene expression upon exposure to abiotic stress e.g., Gene Chip wheat genome array in wheat (Qin et al., 2008), Affymetrix GeneChip® Tomato Genome Array in tomato (Frank et al., 2009), Affymetrix 22K Barley 1 Gene Chip microarray in barley (Mangelsen et al., 2011) and *Brassica* 95k EST microarray in *Brassica* (Yu et al., 2014). Microarray-based analysis by Johnson et al. (2014) provided insights into various genes involved in heat tolerance in sorghum. Major revolution in our understanding of genes involved in heat stress tolerance occurred after the advent of modern DNA sequencing technologies that allowed sequencing of whole transcriptomes, a technique called transcriptomics/transcriptome sequencing/whole genome transcriptome sequencing/whole genome expression profiling. Transcriptomics allowed identification of various heat tolerant candidate genes with greater precision in rice (González-Schain et al., 2016; Mangrauthia et al., 2016; Fang et al., 2018), wheat (Liu et al., 2015), maize (Shi et al., 2017), chickpea (Agarwal et al., 2016), and soybean (Gillman et al., 2019). Transcriptome analysis of contrasting heat tolerant and sensitive lines led to identification of 35 differentially expressed transcripts between the contrasting rice lines, 21 of which were functionally validated (Liao et al., 2015). The study suggested involvement in oxidation-reduction, metabolic activity, defense response and photosynthesis activity in heat tolerance (Liao et al., 2015). Zhao et al. (2018) explored several *Hsp20* family genes involved in heat stress response across the whole genome in potato. A total of 14 *Hsp20* genes displaying up-regulatory role under heat stress in potato was confirmed through real-time quantitative PCR. RNA-seq analysis of maize seedling treated with heat stress unveiled myriads of up and down regulated genes related to photosynthesis, protein synthesis and biosynthesis of various metabolites including zeatin, brassinosteroids (Frey et al., 2015; Shi et al., 2017). Further, Zhao et al. (2019) unearthed the involvement of 5,400 non-additive genes specific to heat stress through transcriptome analysis of parental lines and F_1 hybrid maize seedlings under heat stress conditions. RNA-seq technology not only identified the genes for heat tolerance but also the non-coding RNAs that were involved in regulating heat stress responses in various crops (Wang et al., 2011; Xin et al., 2011; Yu et al., 2013; Mangrauthia et al., 2017).

PROTEOMICS

Gene expression enhanced our understanding of mechanisms of heat stress tolerance significantly, however, gene transcripts do not directly influence plants' responses to stresses. Instead the proteins/enzymes, the gene products, modify plants' metabolite pool in response to external stimulus. To understand better, the mechanisms of stress tolerance, studies of the proteome, i.e., entire set of proteins in a cell or organ were initiated. Prior to

TABLE 1 | Few selective heat-tolerant genotypes identified for various crops involving various traits (details in the text).

Crop	Traits used	Screening method	Promising heat-tolerant genotypes	Country	References
1. Cereals					
Barley (*Hordeum vulgare L.*)	Stay green trait	Field experiments (> 40°C)	L6 and L8 and L3 and L10	Iran	Bavei et al., 2011
	Chlorophyll fluorescence	Growth chamber (45°C)	Ig, Im, and Tz	North Africa	Oukarroum et al., 2016
Wheat (*Tritium aestivum L.*)	Stay green trait	Field experiments (32°C)	CB367(BB#2/PT//CC/INIA/3/ALD"S," CB = 333(WL711/3/KAL/BB//ALD"S"and CB335(WL711/CROW"S"//ALD#1/CMH77A.917/3/HI666PVN"S")	Pakistan	Rehman et al., 2009
	Canopy temperature depression	Field experiment (41°C)	HD 2932, HD 2864, HD 3095, HI 8703, HUW 234	India	Saxena et al., 2016
Rice (*Oryza sativa* L.**)**	Pollen-based	Growth cabinets (35°C, 38°C)	N22	United Kingdom	Jagadish et al., 2008
	Cell membrane thermostability	Phytotron (40°C)	F473	America	Sanchez-Reinoso et al., 2014
Maize (*Zea mays* L.)	Plant height	Field experiments (>40°C)	DTPYC9F119	India	Debnath et al., 2016
	Root system architecture	Growth chamber (37°C)	H16, CML444, SC-Malavi	United States	Trachsel et al., 2010
2. Legumes					
Chickpea (*Cicer arietinum*)	Photosynthetic rate	Field environment (25 to 40°C)	Pusa 1103, Pusa 1003, KWR 108, BGM 408, BG 240, PG 95333, JG 14, BG	India	Kumar et al., 2017
	Cell membrane thermostability	Growth chamber (40–45°C)	ICCV07110, ICCV92944, ICC1205	India	Kumar et al., 2013
Lentil (*Lens culinaris* Medik.)	Biomass Stomatal conductance Chlorophyll fluorescence Chlorophyll content Sucrose Oxidative stress and antioxidants	Field study (>32/20°C)	IG2507, IG3263, IG3745, IG4258, and FLIP2009	India	Sita et al., 2017a
	Cell membrane thermostability	Growth chamber (34°C)	FLIP2009, Ranjan, Moitree, 14-4-1, IC201710, IC208329	India	Choudhury et al., 2012
Mungbean (*Vigna radiata* L.)	Pollen-based Biomass Chlorophyll fluorescence Oxidative stress and antioxidants	Field experiments (>40/28°C)	EC693357, EC693358, EC693369, Harsha, and ML 1299	India	Sharma et al., 2016
Common bean (*Phaseolus vulgaris* L.),	Chlorophyll fluorescence	Growth chamber (42°C)	*Ranit* and *Nerine RS*	Bulgaria	Petkova et al., 2007
	Seed weight Seed number	Field conditions (27/24°C, 30/27°C, and 33/30°C)	Brio, Carson, G122, HB1880, HT38, Venture	Switzerland	Rainey and Griffiths, 2005
Alfalfa (*Medicago sativa*)	Biomass Chlorophyll fluorescence Cell membrane thermostability	Greenhouse and growth incubators (38/35°C)	Bara310SC	China	Wassie et al., 2019
Soybeans (*Glycine max* L. Merr.)	Photosynthetic rate	Field experiments (36.5–38.6°C)	IA3023 and KS4694	United States	Djanaguiraman et al., 2019
	Metabolites	Lab experiments (36°C/24°C; 46/26°C)	PI587982A	South America	Chebrolu et al., 2016
Cowpea (*Vigna unguiculate* L. Walp)	Seed weight	Field studies (41/25°C)	H36, H8-9, DLS99	United States	Ismail and Hall, 1999
	Seed number	Greenhouse conditions, (36/27°C)	B89-600 and TN88-63	United States	Ehlers and Hall, 1998
3. Oil seed crops					
Indian Mustard (*Brassica juncea* L)	Plant height	Field conditions (34°C)	BPR-538-10, NRCDR-2, RH-0216	India	Chauhan et al., 2009
Canola (*Brassica napus*)	Pollen-based	Field studies (10–35°C)	Kadore, ARC98007, NPZ0591RR, and DSV06200	United States	Singh et al., 2008
	Root system architecture	Growth chamber (32°C)	Invigor 5440	Canada	Wu et al., 2017
Peanut (*Arachis hypogaea* L.),	Carbon isotope discrimination	Polytunnels (40/28°C)	Spanish botanical type	United Kingdom	Craufurd et al., 1999
Peanut (*Arachis hypogea*)	Heat shock proteins	Controlled environment (50°C)	ICGS 76, COC038, COC068, COC050, COC041	United States	Selvaraj et al., 2011

(Continued)

TABLE 1 | Continued

Crop	Traits used	Screening method	Promising heat-tolerant genotypes	Country	References
Cotton (*Gossypium hirsutum* L.)	Cell membrane thermostability	Field conditions (>44°C)	NIA-80, NIA-81, NIA-83, NIA-84, NIA-M-30, NIA-M31, NIA-HM-48, NIA-HM-327, NIA-H-32, NIA-HM-2-1, NIA-Bt1, NIA-Bt2, NIA-Perkh, CRIS-342, CRIS-134, NIAB-111 and check variety Sadori	Pakistan	Abro et al., 2015
	Chlorophyll fluorescence	Green house (30 and 40°C)	DP393, VH260 and DP 210 B2RF	Africa	Van der Westhuizen et al., 2020
4. Vegetable crops					
Potato (*Solanum tuberosum* L.)	Heat shock proteins	Growth chamber (40°C)	Norchip, Desiree	Baltimore	Ahn et al., 2004
Tomato (*Solanum lycopersicum* L.)	Pollen-based	Field conditions (39.24/24.42°C)	Pusa Sadabahar, FLA-7171, NDTVR-60	Japan	Srivastava et al., 2012
	Sucrose	Growth chambers (31/25°C) or Greenhouses (32/26°C)	FLA 7516, Hazera 3018, Hazera 3042, and Saladate	Israel/United States	Firon et al., 2006
Cabbage (*Brassica* species)	Metabolites	Control environment (25–35°C)	Yoshin, Kenshin and full white	Japan	Hossain et al., 1995
Cucumber (*Cucumis sativus* L.)	Cell membrane thermostability	Growth room (40/32°C)	L-3466, Desi Cucumber	Pakistan	Ali et al., 2019

proteomics, proteins suspected to play role in heat tolerance were analyzed by MALDI TOF MS/MS analysis, e.g., rice (Han et al., 2009; Jagadish et al., 2010; Liao et al., 2014). Further advances in proteomics strengthen our understanding of identification of the proteins that confer thermotolerance in plants. Proteomics analysis of two contrasting rice genotypes, N22 (tolerant) and Gharib (sensitive), showed that heat tolerance of N22 was due to higher capability of mediating renaturation of stress damaged proteins, higher efficiency in repairing ribosomal protein, higher upregulation of proteins involved in calcium signaling and phytohormone synthesis and protein modifications under high night temperature at early grain filling stage (Shi et al., 2013). The functional role of proteins that contribute to heat tolerance ranges from oxidation-reduction, cellular metabolic activity to defense responses (Lu et al., 2017; Zhang et al., 2017). In this context, Zhang et al. (2017) identified various proteins by analysis of grains of contrasting heat tolerant rice lines by employing isobaric tags for relative and absolute quantitation (iTRAQ) methods (Zhang et al., 2017). Similarly, by employing iTRAQ technique, Lu et al. (2017) identified 258 heat responsive proteins from wheat leaf, most of which were involved in chlorophyll synthesis, carbon fixation and redox regulation under heat stress. Various proteins such as HSP, those related to anti-oxidant mechanism, and glycolysis were involved in adaption of grape to heat stress as revealed through iTRAQ analysis (Liu et al., 2014). Proteomics analysis of ethylene pre-treated tomato pollen by LC-MS/MS suggested that various proteins help in protecting pollen development and function through higher abundance of protein synthesis and upregulating stress protecting proteins that maintain cellular redox state under heat stress (Jegadeesan et al., 2018). Proteomics analysis by 2-DE technique allowed identification of important heat shock proteins viz., HSP26, HSP16.9, and unknown HSP/Chaperonin contributing to heat stress tolerance in maize (Abou-Deif et al., 2019). Considering contributory role of proteins adapting roots under heat stress, Valdes-Lopez et al. (2016) reported the involvement of both up and down regulatory proteins contributing to heat tolerance in soybean root. Recently, proteomics analysis deduced that protein phosphorylation and protein acetylation could regulate heat tolerance by modulating photosynthesis protein in grape (Liu et al., 2019). The proteins involved in heat tolerance elucidated through proteomics analysis could serve as biomarkers for identifying heat tolerant cultivars in various crop plants. Participatory role of miR156 targeting SPL transcription factor in *A. thaliana* (Stief et al., 2014), miRl60, miRl66, and miRl67 in wheat and barley (Xin et al., 2010), IbmiR397 targeting *laccase gene* in sweet potato (Yu et al., 2020) controlling heat stress response are worth mentioning.

METABOLOMICS

Metabolomics, the study of metabolites in a cell or organ, enhance our understanding of novel metabolites that contribute to plant adaptation to heat stress (Bokszczanin and Fragkostefanakis, 2013). Metabolomics have unraveled the key metabolites ranging from sugars, proteins and lipids participating in key biological processes to anti-oxidants and defense molecules in response to heat stress (Li T. et al., 2015; Chebrolu et al., 2016; Muhlemann et al., 2018; Salvi et al., 2018). Metabolomics at specific plant stages viz., seed germination, vegetative, reproductive, grain formation and grain filling have broadened our understanding of metabolites involved in heat stress responses at different development stages (Wang et al., 2015; Mangrauthia et al., 2016; Spicher et al., 2016; Templer et al., 2017; Muhlemann et al., 2018; Qu et al., 2018; Thomason et al., 2018). Metabolomics

provided novel insights into the role of various lipids viz., plastidic glycerolipids, oxidized glycerolipids in regulating heat stress responses in wheat leaves (Narayanan et al., 2016), that of α-tocopherol and plastoquinone in maintaining the photosynthesis apparatus in tomato under heat stress (Spicher et al., 2016) and that of galactinol in minimizing excessive ROS activity in chickpea under heat stress (Salvi et al., 2018). Metabolomics also emphasized the role of sugars in anthers such as glucose−6−P, fructose−6−P, glucose, maltose and *myo*−inositol in improving heat stress acclimation in N22 (heat-tolerant) rice genotype (Li X. et al., 2015). Likewise, the ameliorative role of various anti-oxidant phenolic compounds viz., flavonoids, flavonols, tocopherols in heat tolerance by preventing ROS mediated negative effect on pollen tube germination in tomato (Muhlemann et al., 2018) and also during seed development in soybean (Chebrolu et al., 2016) are other examples of the use of metabolomics in improving knowledge of heat stress tolerance mechanisms. At post anthesis stage, metabolites viz., drummondol, anthranilate appear to regulate heat stress response in wheat flag leaves (Thomason et al., 2018). The studies pinpoint that metabolomics along with system biology approaches could significantly enhance significantly our understanding of various metabolites produced in response to heat stress (Janni et al., 2020) and would be a vital tool to develop heat tolerant crops in agriculture.

CONCLUSION AND FUTURE PERSPECTIVES

The past few decades have seen considerable developments in genetics, biochemical, genomics, transcriptomics, proteomics and metabolomics approaches to enhance the understanding of heat stress tolerance. However, basal thermotolerance remains the major tool to develop agronomically superior heat tolerant cultivars for agricultural crops. Basal thermotolerance is primarily evaluated by exposing small or large sets of germplasm (accessions, cultivars, wild relatives) under controlled (laboratory, screen/greenhouse) or natural field environments to stressful temperatures. These tests have identified several sources of heat tolerance in various crop gene pools and landraces, which may act as potential candidates/donors of heat stress tolerance for developing heat tolerant cultivars using conventional or modern breeding approaches (**Table 1**). In some instances, heat tolerant genotypes have been directly released as cultivars (as in Chickpea) owing to their agronomic superiority. In addition to heat stress tolerance, contrasting genotypes are also being evaluated for diverse traits related to phenology, growth, physiology and biochemistry, genes, and reproductive biology. Of the several traits being evaluated for heat stress tolerance in crops, the majority of studies have indicated pollen function to be highly sensitive to heat stress, thus making it one of the vital selection traits for heat tolerance. Evaluation of thousands of germplasm or progeny lines for several traits associated with heat tolerance in a short span of time is needed to fasten the breeding for heat tolerance. High-throughput phenotyping that allows choosing important traits as selection criteria for heat tolerance can facilitate identification of genotypes for heat stress tolerance as well as other desirable agronomic traits in a short span of time but high throughput phenotyping requires high investment and is available with only a few laboratories around the world. In addition to it, remote sensing tools (UAVs with spectral and thermal imaging camera) can be effectively deployed under realistic field environments to screen thousands of germplasm or progeny lines.

Plant heat tolerance being a quantitative trait is highly influenced by G × E interactions and genetic inheritance of heat tolerance remains challenging. Large scale DNA-based marker development during the last decade led to mapping of QTLs linked to heat tolerance in various crops (Jha et al., 2014; Janni et al., 2020). Advances in sequencing technologies especially, next generation sequencing (NGS), genotyping by sequencing (GBS), and other high throughput genotyping platforms have facilitated narrowing down of the heat tolerance QTL regions for analysis of candidate genes (Xu et al., 2017; Kilasi et al., 2018; Inghelandt et al., 2019; Tadesse et al., 2019). Given the huge number of novel SNPs developed recently and GWAS in large set of global crop germplasm, it became possible to identify novel haplotypes/genomic regions controlling heat tolerance (Paul et al., 2018; Varshney et al., 2019; Khan et al., 2020; Weckwerth et al., 2020) and allowed for the assessment of genetic diversity at nucleotide-scale. High throughput phenotyping coupled with advanced imaging devices, unmanned vehicles and machine learning, deep learning approaches and molecular genetics tools can further enhance the accuracy of selection of genomic regions associated with heat tolerance. The developments in marker and sequencing technologies are expected to allow genome wide marker profiling facilitating genomic selection for heat tolerance (Tricker et al., 2018; Inghelandt et al., 2019) and thus, rapid breeding for the development of varieties with novel genetic combinations. Similarly, advances in proteomics, transcriptomics and metabolomics will further unravel the complexity of heat stress tolerance in crops by identifying missing links in the current information. A combination of these approaches could allow for the quantifying of plant heat stress responses, spatially and temporally, at a large scale, thus narrowing the "genotype-phenotype gap" (Fahlgren et al., 2015; Singh A. et al., 2015; Singh A. K. et al., 2018; Pinto et al., 2016). Corresponding to breeding approaches, current developments in the spatial and temporal expressions of engineered genes or pathway engineering by the targeted editing of genomes using CRISPR–Cas technology can be used for development of heat tolerant designer crops. A better knowledge of plant cellular mechanisms associated with heat tolerance and increased yields would be vital to drive essential gains in crop improvement, which can be greatly assisted by exploring the genetic diversity in heat tolerance, and put into practice by genome-scale breeding, precisely done gene engineering and better agronomic management practices.

AUTHOR CONTRIBUTIONS

HN conceived the outline. All authors contributed in preparing various sections of this manuscript.

ACKNOWLEDGMENTS

Contribution no. 21-068-J from Kansas Agricultural Experiment Station. HN is thankful to DST (India; PURSE grant), DBT (India), CSIR (India), World Vegetable Center (at ICRISAT), University of Western Australia, Australia, International Center for Agricultural Research in Dry Areas (ICARDA), Morocco, for supporting the research by funding, Indian Institute of Pulses Research, Kanpur, Punjab Agricultural University, Ludhiana, for providing the germplasm from time to time. PD is thankful to CSIR (India) for fellowship during the course of this study.

REFERENCES

Abdelmageed, A. H. A., and Gruda, N. (2009). Influence of high temperatures on gas exchange rate and growth of eight tomato cultivars under controlled heat stress conditions. *Eur. J. Hortic. Sci.* 74, 152–159.

Abdelrahman, M., El-Sayed, M., Jogaiah, S., Burritt, D. J., and Tran, L. S. P. (2017). The "STAY-GREEN" trait and phytohormone signalling networks in plants under heat stress. *Plant Cell Rep.* 36, 1009–1025. doi: 10.1007/s00299-017-2119-y

Abou-Deif, M. H., Rashed, M. A., Khalil, K. M., and Mahmoud, F. E. S. (2019). Proteomic analysis of heat shock proteins in maize (*Zea mays* L.). *Bull Natl Res Cent.* 43, 1–9. doi: 10.1186/s42269-019-0251-2

Abro, S., Rajput, M. T., Khan, M. A., Sial, M. A., and Tahir, S. S. (2015). Screening of cotton (*Gossypium hirsutum* L.) genotypes for heat tolerance. *Pak. J. Bot.* 47, 2085–2091.

Agarwal, G., Garg, V., Kudapa, H., Doddamani, D., Pazhamala, L. T., Khan, A. W., et al. (2016). Genome-wide dissection of AP2/ ERF and HSP90 gene families in five legumes and expression profiles in chickpea and pigeonpea. *Plant Biotechnol. J.* 14, 1563–1577. doi: 10.1111/pbi.12520

Ahammed, G. J., and Yu, J. Q. (2016). *Plant Hormones Under Challenging Environmental Factors*. Berlin: Springer, 1–269. doi: 10.1007/978-94-017-7758-7752

Ahmad, P., and Prasad, M. N. V. (eds) (2011). *Environmental Adaptations and Stress Tolerance of Plants in the Era of Climate Change*. Berlin: Springer Science & Business Media.

Ahmed, J., and Hasan, M. (2011). Evaluation of seedling proline content of wheat genotypes in relation to heat tolerance. *Bangladesh J. Bot.* 40, 17–22. doi: 10.3329/bjb.v40i1.7991

Ahn, Y. J., Claussen, K., and Zimmerman, J. L. (2004). Genotypic differences in the heat-shock response and thermotolerance in four potato cultivars. *Plant Sci.* 166, 901–911. doi: 10.1016/j.plantsci.2003.11.027

Ali, M., Ayyub, C. M., Amjad, M., and Ahmad, R. (2019). Evaluation of thermotolerance potential in cucumber genotypes under heat stress. *Pak. J. Agric. Sci.* 56, 53–61. doi: 10.21162/PAKJAS/19.7519

Allakhverdiev, S. I., Kreslavski, V. D., Klimov, V. V., Los, D. A., Carpentier, R., and Mohanty, P. (2008). Heat stress: an overview of molecular responses in photosynthesis. *Photosynth. Res.* 98, 541–550. doi: 10.1007/s11120-008-9331-9330

Alsamir, M., Ahmad, N. M., Keitel, C., Mahmood, T., and Trethowan, R. (2017). Identification of high temperature tolerant and agronomically viable tomato (*S. lycopersicum*) genotypes from a diverse germplasm collection. *Adv. Crop Sci. Tech.* 5:110. doi: 10.4172/2329-8863.1000299

Araus, J. L., Bort, J., Steduto, P., Villegas, D., and Royo, C. (2003). Breeding cereals for Mediterranean conditions: ecophysiological clues for biotechnology application. *Ann. Appl. Biol.* 142, 129–141. doi: 10.1111/j.1744-7348.2003.tb00238.x

Ashraf, M., Saeed, M. M., and Qureshi, M. J. (1994). Tolerance to high temperature in cotton (*Gossypium hirsutum* L.) at initial growth stages. *Environ. Exp. Bot.* 34, 275–283. doi: 10.1016/0098-8472(94)90048-5

Awasthi, R., Bhandari, K., and Nayyar, H. (2015). Temperature stress and redox homeostasis in agricultural crops. *Front. Environ. Sci.* 3:11. doi: 10.3389/fenvs.2015.00011

Awasthi, R., Gaur, P., Turner, N. C., Vadez, V., Siddique, K. H., and Nayyar, H. (2017). Effects of individual and combined heat and drought stress during seed filling on the oxidative metabolism and yield of chickpea (*Cicer arietinum*) genotypes differing in heat and drought tolerance. *Crop Pasture Sci.* 68, 823–841. doi: 10.1071/CP17028

Awasthi, R., Kaushal, N., Vadez, V., Turner, N. C., Berger, J., Siddique, K. H. M., et al. (2014). Individual and combined effects of transient drought and heat stress on carbon assimilation and seed filling in chickpea. *Funct. Plant Biol.* 41, 1148–1167. doi: 10.1071/FP13340

Awika, H. O., Hays, D. B., Mullet, J. E., Rooney, W. L., and Weers, B. D. (2017). QTL mapping and loci dissection for leaf epicuticular wax load and canopy temperature depression and their association with QTL for staygreen in *Sorghum bicolor* under stress. *Euphytica* 213, 1–22. doi: 10.1007/s10681-017-1990-5

Ayub, M., Ashraf, M. Y., Kausar, A., Saleem, S., Anwar, S., Altay, V., et al. (2020). Growth and physio-biochemical responses of maize (*Zea mays* L.) to drought and heat stresses. *Plant Biosyst. Int. J. Deal. all Aspects Plant Biol.* 2020:1762785. doi: 10.1080/11263504.2020.1762785

Badaruddin, M., Reynolds, M. P., and Ageeb, O. A. (1999). Wheat management in warm environments: effect of organic and inorganic fertilizers, irrigation frequency, and mulching. *Agron. J.* 91, 975–983. doi: 10.2134/agronj1999.916975x

Bahar, B., Yildirim, M., Barutcular, C., and Ibrahim, G. E. N. C. (2008). Effect of canopy temperature depression on grain yield and yield components in bread and durum wheat. *Not. Bot. Horti. Agrobo.* 36, 34–37. doi: 10.15835/nbha36187

Bahuguna, R. N., Jha, J., Pal, M., Shah, D., Lawas, L. M., Khetarpal, S., et al. (2015). Physiological and biochemical characterization of NERICA-L-44: a novel source of heat tolerance at the vegetative and reproductive stages in rice. *Physiol. Plant.* 154, 543–559. doi: 10.1111/ppl.12299

Baker, N. R. (2008). Chlorophyll fluorescence: a probe of photosynthesis in vivo. *Annu. Rev. Plant Biol.* 59, 89–113. doi: 10.1146/annurev.arplant.59.032607.092759

Baker, N. R., and Rosenqvist, E. (2004). Applications of chlorophyll fluorescence can improve crop production strategies: an examination of future possibilities. *J. Exp. Bot.* 55, 1607–1621. doi: 10.1093/jxb/erh196

Bala, P., and Sikder, S. (2017). Evaluation of heat tolerance of wheat genotypes through membrane thermostability test. *J. Agr. Sci.* 2, 1–6.

Balota, M., Payne, W. A., Evett, S. R., and Peters, T. R. (2008). Morphological and physiological traits associated with canopy temperature depression in three closely related wheat lines. *Crop Sci.* 48, 1897–1910. doi: 10.2135/cropsci2007.06.0317

Balouchi, H. R. (2010). Screening wheat parents of mapping population for heat and drought tolerance, detection of wheat genetic variation. *Int. J. Biol. Life Sci.* 4, 63–73.

Barghi, S. S., Mostafaii, H., Peighami, F., Zakaria, R. A., and Nejhad, R. F. (2013). Response of in vitro pollen germination and cell membrane thermostabilty of lentil genotypes to high temperature. *Int. J. Agric. Res.* 3, 13–20.

Barnabás, B., Jäger, K., and Fehér, A. (2008). The effect of drought and heat stress on reproductive processes in cereals. *Plant Cell Environ.* 31, 11–38. doi: 10.1111/j.1365-3040.2007.01727.x

Basu, P. S., and Minhas, J. S. (1991). Heat tolerance and assimilate transport in different potato genotypes. *J. Exp. Bot.* 42, 861–866. doi: 10.1093/jxb/42.7.861

Bavei, V., Vaezi, B., Abdipour, M., Jalal Kamali, M. R., and Roustaii, R. (2011). Screening of tolerant spring barleys for terminal heat stress: different importance of yield components in barleys with different row type. *Int. J. Plant Breed. Genet.* 5, 175–193. doi: 10.3923ijpbg.2011.175.193

Bavita, A., Puneet, K. R., Navtej, S. B., and Virinder, S. S. (2012). Genotypic variation for high temperature tolerance in relation to carbon partitioning and grain sink activity in wheat. *Am. J. Plant Sci.* 3, 1–10. doi: 10.4236/ajps.2012.33046

Bennett, D., Reynolds, M., Mullan, D., Izanloo, A., Kuchel, H., Langridge, P., et al. (2012). Detection of two major grain yield QTL in bread wheat (*Triticum aestivum* L.) under heat, drought and high yield potential environments. *Theor. Appl. Genet.* 125, 1473–1485. doi: 10.1007/s00122-012-1927-2

Berry, J., and Bjorkman, O. (1980). Photosynthetic response and adaptation to temperature in higher plants. *Annu. Rev. Plant Physiol.* 31, 491–543. doi: 10.1146/annurev.pp.31.060180.002423

Bhandari, K., Siddique, K. H. M., Turner, N. C., Kaur, J., Singh, S., Agrawal, S. K., et al. (2016). Heat stress at reproductive stage disrupts leaf carbohydrate

metabolism, impairs reproductive function, and severely reduces seed yield in lentil. *J. Crop Improv.* 30, 118–151. doi: 10.1080/15427528.2015.1134744

Bibi, A. C., Oosterhuis, D. M., Gonias, E. D., and Bourland, F. M. (2004). Screening a diverse set of cotton cultivars for high temperature tolerance. *Summaries Arkansas Cotton Res.* 533, 39–43.

Bindumadhava, H., Prasad, T. G., and Sharma, N. (2011). *Plant Isotope Signatures: For Plant Traits*. Germary: LAP Lambert Academic Publications.

Bindumadhava, H., Sharma, L., Nair, R. M., Nayyar, H., Riley, J. J., and Easdown, W. (2018). High temperature-tolerant mungbean (*Vigna radiata* L.) lines produce better yields when exposed to higher CO2 levels. *J. Crop Improv*. 2018:1439132. doi: 10.1080/15427528.2018.1439132

Bindumadhava, H., Sheshshayee, M. S., Prasad, T. G., and Udaya Kumar, M. (2005). The Ratio of Carbon and Oxygen Stable Isotopic Composition ((13C/(18O) Describes the Variability in Leaf Intrinsic Carboxylation Efficiency in Plants. *Curr Sci.* 89, 1256–1258.

Bishop, J., Potts, S. G., and Jones, H. E. (2016). Susceptibility of faba bean (*Vicia faba* L.) to heat stress during floral development and anthesis. *J. Agron. Crop Sci.* 202, 508–517. doi: 10.1111/jac.12172

Bita, C. E., and Gerats, T. (2013). Plant tolerance to high temperature in a changing environment: scientific fundamentals and production of heat stress-tolerant crops. *Front. Plant Sci.* 4:273. doi: 10.3389/fpls.2013.00273

Bita, C. E., Zenoni, S., Vriezen, W. H., Mariani, C., Pezzotti, M., and Gerats, T. (2011). Temperature stress differentially modulates transcription in meiotic anthers of heat-tolerant and heat-sensitive tomato plants. *BMC Genom.* 12:384. doi: 10.1186/1471-2164-12-384

Blum, A. (1986). The effect of heat stress on wheat leaf and ear photosynthesis. *J. Exp. Bot.* 37, 111–118. doi: 10.1093/jxb/37.1.111

Blum, A., and Ebercon, A. (1981). Cell membrane stability as a measure of drought and heat tolerance in wheat. *Crop Sci.* 21, 43–47. doi: 10.2135/cropsci1981.0011183X002100010013x

Blum, A., Klueva, N., and Nguyen, H. T. (2001). Wheat cellular thermotolerance is related to yield under heat stress. *Euphytica* 117, 117–123. doi: 10.1023/A:1004083305905

Bokszczanin, K. L., and Fragkostefanakis, S. (2013). Perspectives on deciphering mechanisms underlying plant heat stress response and thermotolerance. *Front. Plant Sci.* 4:315. doi: 10.3389/fpls.2013.00315

Bonneau, J., Taylor, J., Parent, B., Bennett, D., Reynolds, M., Feuillet, C., et al. (2013). Multi-environment analysis and improved mapping of a yield-related QTL on chromosome 3B of wheat. *Theor. Appl. Genet.* 126, 747–761. doi: 10.1007/s00122-012-2015-3

Borrell, A. K., van Oosterom, E. J., Mullet, J. E., George-Jaeggli, B., Jordan, D. R., Klein, P. E., et al. (2014). Stay-green alleles individually enhance grain yield in sorghum under drought by modifying canopy development and water uptake patterns. *New Phytol.* 203, 817–830. doi: 10.1111/nph.12869

Branham, S. E., Stansell, Z. J., Couillard, D. M., and Farnham, M. W. (2017). Quantitative trait loci mapping of heat tolerance in broccoli (*Brassica oleracea* var. italica) using genotyping-by-sequencing. *Theor. Appl. Genet.* 130, 529–538. doi: 10.1007/s00122-016-2832-x

Brussaard, L., De Ruiter, P. C., and Brown, G. G. (2007). Soil biodiversity for agricultural sustainability. *Agr. Ecosyst. Environ.* 121, 233–244. doi: 10.1016/j.agee.2006.12.013

Bueckert, R. A., Wagenhoffer, S., Hnatowich, G., and Warkentin, T. D. (2015). Effect of heat and precipitation on pea yield and reproductive performance in the field. *Can. J. Plant Sci.* 95, 629–639. doi: 10.4141/cjps-2014-342

Butler, W. L. (1978). Energy distribution in the photochemical apparatus of photosynthesis. *Annu. Rev. Plant Physiol.* 29, 345–378. doi: 10.1146/annurev.pp.29.060178.002021

Cairns, J. E., Crossa, J., Zaidi, P. H., Grudloyma, P., Sanchez, C., Araus, J. L., et al. (2013). Identification of drought, heat, and combined drought and heat tolerant donors in maize (*Zea mays* L.). *Crop Sci.* 53, 1335–1346. doi: 10.2135/cropsci2012.09.0545

Calderini, D. F., Reynolds, M. P., and Slafer, G. A. (2006). Source-sink effects on grain weight of bread wheat, durum wheat, and triticale at different locations. *Aust. J. Agric. Res.* 57, 227–233. doi: 10.1071/AR05107

Camejo, D., Rodríguez, P., Morales, M. A., Dell'Amico, J. M., Torrecillas, A., and Alarcón, J. J. (2005). High temperature effects on photosynthetic activity of two tomato cultivars with different heat susceptibility. *J. Plant Physiol.* 162, 281–289. doi: 10.1016/j.jplph.2004.07.014

Cantalapiedra, C. P., García-Pereira, M. J., Gracia, M. P., Igartua, E., Casas, A. M., and Contreras-Moreira, B. (2017). Large differences in gene expression responses to drought and heat stress between elite barley cultivar scarlett and a spanish landrace. *Front. Plant Sci.* 8:647. doi: 10.3389/fpls.2017.00647

Carmo-Silva, A. E., Gore, M. A., Andrade-Sanchez, P., French, A. N., Hunsaker, D. J., and Salvucci, M. E. (2012). Decreased CO2 availability and inactivation of Rubisco limit photosynthesis in cotton plants under heat and drought stress in the field. *Environ. Exp.* 83, 1–11. doi: 10.1016/j.envexpbot.2012.04.001

Chakraborty, K., Bishi, S. K., Singh, A. L., Zala, P. V., Mahatma, M. K., Kalariya, K. A., et al. (2018). Rapid induction of small heat shock proteins improves physiological adaptation to high temperature stress in peanut. *J. Agron. Crop Sci.* 204, 285–297. doi: 10.1111/jac.12260

Chandra, K., Prasad, R., Thakur, P., Madhukar, K., and Prasad, L. C. (2017). Heat tolerance in wheat - A key strategy to combat climate change through molecular markers. *Int. J. Curr. Microbiol. Appl. Sci.* 6, 662–675. doi: 10.20546/ijcmas.2017.603.077

Chang, P. F. L., Jinn, T. L., Huang, W. K., Chen, Y., Chang, H. M., and Wang, C. W. (2007). Induction of a cDNA clone from rice encoding a class II small heat shock protein by heat stress, mechanical injury, and salicylic acid. *Plant Sci.* 172, 64–75. doi: 10.1016/j.plantsci.2006.07.017

Charng, Y. Y., Liu, H. C., Liu, N. Y., Hsu, F. C., and Ko, S. S. (2006). Arabidopsis Hsa32, a novel heat shock protein, is essential for acquired thermotolerance during long recovery after acclimation. *Plant Physiol.* 140, 1297–1305. doi: 10.1104/pp.105.074898

Chauhan, J. S., Meena, M. L., Saini, M., Meena, D. R., Singh, M., Meena, S. S., et al. (2009). "Heat stress effects on morpho-physiological characters of Indian mustard (*Brassica juncea* L.)," in *Proceedings of the 16thAustralian Research Assembly on Brassicas*, Ballarat Victoria.

Chebrolu, K. K., Fritschi, F. B., Ye, S., Krishnan, H. B., Smith, J. R., and Gillman, J. D. (2016). Impact of heat stress during seed development on soybean seed metabolome. *Metabolomics* 12, 1–14. doi: 10.1007/s11306-015-0941-941

Chen, H. H., Shen, Z. Y., and Li, P. H. (1982). Adaptability of crop plants to high temperatures stress 1. *Crop Sci.* 22, 719–725. doi: 10.2135/cropsci1982.0011183X002200040006x

Chen, X., Lin, S., Liu, Q., Huang, J., Zhang, W., Lin, J., et al. (2014). Expression and interaction of small heat shock proteins (sHsps) in rice in response to heat stress. *BBA-Proteins Proteom.* 1844, 818–828. doi: 10.1016/j.bbapap.2014.02.010

Choudhury, D. R., Tarafdar, S., Das, M., and Kundagrami, S. (2012). Screening lentil (*Lens culinaris* Medik.) germplasms for heat tolerance. *Trends Biosci.* 5, 143–146.

Commuri, P. D., and Jones, R. J. (1999). Ultrastructural characterization of maize (*Zea mays* L.) kernels exposed to high temperature during endosperm cell division. *Plant Cell Environ.* 22, 375–385. doi: 10.1046/j.1365-3040.1999.00424.x

Condon, A. G., Reynolds, M. P., Rebetzke, G. J., Ginkel, M., van, Richards, R. A., et al. (2007). "Using stomatal aperture-related traits to select for high yield potential in bread wheat," in *Proceedings of the 7th International Wheat Conference*, Mar del Plata, 617–624. doi: 10.1007/1-4020-5497-1_74

Cornish, K., Radin, J. W., Turcotte, E. L., Lu, Z., and Zeiger, E. (1991). Enhanced photosynthesis and stomatal conductance of pima cotton (*Gossypium barbadense* L.) bred for increased yield. *Plant Physiol.* 97, 484–489. doi: 10.1104/pp.97.2.484

Cottee, N. S., Tan, D. K. Y., Bange, M. P., Cothren, J. T., and Campbell, L. C. (2010). Multi-level determination of heat tolerance in cotton (*Gossypium hirsutum* L.) under field conditions. *Crop Sci.* 50, 2553–2564. doi: 10.2135/cropsci2010.03.0182

Cottee, N. S., Tan, D. K. Y., Cothren, J. T., Bange, M. P., and Campbell, L. C. (2007). "Screening cotton cultivars for thermotolerance under field conditions," in *Proceedings of the 4th World Cotton Research Conference*, Lubbock, TX.

Craufurd, P. Q., Qi, A., Ellis, R. H., Summerfield, R. J., Roberts, E. H., and Mahalakshmi, V. (1998). Effect of temperature on time to panicle initiation and leaf appearance in sorghum. *Crop Sci.* 38, 942–947. doi: 10.2135/cropsci1998.0011183X003800040011x

Craufurd, P. Q., Wheeler, T. R., Ellis, R. H., Summerfield, R. J., and Williams, J. H. (1999). Effect of temperature and water deficit on water-use efficiency, carbon isotope discrimination, and specific leaf area in peanut. *Crop Sci.* 39, 136–142. doi: 10.2135/cropsci1999.0011183X003900010022x

Crawford, A. J., McLachlan, D. H., Hetherington, A. M., and Franklin, K. A. (2012). High temperature exposure increases plant cooling capacity. *Curr. Biol.* 22, R396–R397. doi: 10.1016/j.cub.2012.03.044

Dang, F. F., Wang, Y. N., Yu, L., Eulgem, T., Lai, Y., Liu, Z. Q., et al. (2013). CaWRKY40, a WRKY protein of pepper, plays an important role in the regulation of tolerance to heat stress and resistance to *Ralstonia solanacearum* infection. *Plant Cell Environ.* 36, 757–774. doi: 10.1111/pce.12011

de Dorlodot, S., Forster, B., Pagès, L., Price, A., Tuberosa, R., and Draye, X. (2007). Root system architecture: opportunities and constraints for genetic improvement of crops. *Trends Plant Sci.* 12, 474–481. doi: 10.1016/j.tplants.2007.08.012

De Ronde, J. A., Van Der Mescht, A., and Steyn, H. S. F. (2000). Proline accumulation in response to drought and heat stress in cotton. *Afr Crop Sci J.* 8, 85–92.

Debnath, S., Gazal, A., Yadava, P., and Singh, I. (2016). Identification of contrasting genotypes under heat stress in maize (*Zea mays* L.). *Maize J.* 5, 14–24.

Del Blanco, I. A., Rajaram, S., Kronstad, W. E., and Reynolds, M. P. (2000). Physiological performance of synthetic hexaploid wheat-derived populations. *Crop Sci.* 40, 1257–1263. doi: 10.2135/cropsci2000.4051257x

Demmig, B., and Björkman, O. (1987). Comparison of the effect of excessive light on chlorophyll fluorescence (77K) and photon yield of O2 evolution in leaves of higher plants. *Planta* 171, 171–184. doi: 10.1007/BF00391092

Devasirvatham, V., Gaur, P. M., Mallikarjuna, N., Raju, T. N., Trethowan, R. M., and Tan, D. K. Y. (2013). Reproductive biology of chickpea response to heat stress in the field is associated with the performance in controlled environments. *Field Crops Res.* 142, 9–19. doi: 10.1016/j.fcr.2012.11.011

Devasirvatham, V., Gaur, P. M., Raju, T. N., Trethowan, R. M., and Tan, D. K. Y. (2015). Field response of chickpea (*Cicer arietinum* L.) to high temperature. *Field Crops Res.* 172, 59–71. doi: 10.1016/j.fcr.2014.11.017

Devasirvatham, V., Tan, D. K. Y., Gaur, P. M., Raju, T. N., and Trethowan, R. M. (2012). High temperature tolerance in chickpea and its implications for plant improvement. *Crop Pasture Sci.* 63, 419–428. doi: 10.1071/CP11218

Devasirvatham, V., Tan, D. K. Y., Trethowan, R. M., Gaur, P. M., and Mallikarjuna, N. (2010). "Impact of high temperature on the reproductive stage of chickpea," in *Proceedings of the 15th Australian Society of Agronomy conference: Food security from Sustainable Agriculture*, Lincoln.

Dhanda, S. S., and Munjal, R. (2012). Heat tolerance in relation to acquired thermotolerance for membrane lipids in bread wheat. *Field Crops Res.* 135, 30–37. doi: 10.1016/j.fcr.2012.06.009

Djanaguiraman, M., Perumal, R., Ciampitti, I. A., Gupta, S. K., and Prasad, P. V. V. (2018a). Quantifying pearl millet response to high temperature stress: thresholds, sensitive stages, genetic variability and relative sensitivity of pollen and pistil. *Plant Cell Environ.* 41, 993–1007. doi: 10.1111/pce.12931

Djanaguiraman, M., Perumal, R., Jagadish, S. V. K., Ciampitti, I. A., Welti, R., and Prasad, P. V. V. (2018b). Sensitivity of sorghum pollen and pistil to high temperature stress. *Plant Cell Environ.* 41, 1065–1082. doi: 10.1111/pce.13089

Djanaguiraman, M., and Prasad, P. V. V. (2010). Ethylene production under high temperature stress causes premature leaf senescence in soybean. *Funct. Plant Biol.* 37, 1071–1084. doi: 10.1071/fp10089

Djanaguiraman, M., Schapaugh, W., Fritschi, F., Nguyen, H., and Prasad, P. V. (2019). Reproductive success of soybean (*Glycine max* L. Merril) cultivars and exotic lines under high daytime temperature. *Plant Cell Environ.* 42, 321–336. doi: 10.1111/pce.13421

Egli, D. B. (1998). *Seed Biology and the Yield of Grain Crops*. Wallingford: CAB international.

Ehlers, J. D., and Hall, A. E. (1998). Heat tolerance of contrasting cowpea lines in short and long days. *Field Crops Res.* 55, 11–21. doi: 10.1016/S0378-4290(97)00055-55

Fahlgren, N., Gehan, M. A., and Baxter, I. (2015). Lights, camera, action: high throughput plant phenotyping is ready for a close-up. *Curr. Opin. Plant Biol.* 24, 93–99. doi: 10.1016/j.pbi.2015.02.006

Fang, C., Dou, L., Liu, Y., Yu, J., and Tu, J. (2018). Heat stress-responsive transcriptome analysis in heat susceptible and tolerant rice by high-throughput sequencing. *Ecol. Genet. Genomics* 6, 33–40. doi: 10.1016/j.egg.2017.12.001

Farooq, M., Bramley, H., Palta, J. A., and Siddique, K. H. M. (2011). Heat stress in wheat during reproductive and grain-filling phases. *CRC. Crit. Rev. Plant Sci.* 30, 491–507. doi: 10.1080/07352689.2011.615687

Farooq, M., Nadeem, F., Gogoi, N., Ullah, A., Alghamdi, S. S., Nayyar, H., et al. (2017). Heat stress in grain legumes during reproductive and grain-filling phases. *Crop Pasture Sci.* 68, 985–1005. doi: 10.1071/CP17012

Farquhar, G. D., Ehleringer, J. R., and Hubick, K. T. (1989). Carbon isotope discrimination and photosynthesis. *Annu. Rev. Plant Physiol. Plant Mol. Biol.* 40, 503–537. doi: 10.1146/annurev.pp.40.060189.002443

Firon, N., Shaked, R., Peet, M. M., Pharr, D. M., Zamski, E., Rosenfeld, K., et al. (2006). Pollen grains of heat tolerant tomato cultivars retain higher carbohydrate concentration under heat stress conditions. *Sci. Hortic.* 109, 212–217. doi: 10.1016/j.scienta.2006.03.007

Fischer, R. A., Rees, D., Sayre, K. D., Lu, Z. M., Condon, A. G., and Larque Saavedra, A. (1998). Wheat yield progress associated with higher stomatal conductance and photosynthetic rate, and cooler canopies. *Crop Sci.* 38, 1467–1475. doi: 10.2135/cropsci1998.0011183X003800060011x

Frank, G., Pressman, E., Ophir, R., Althan, L., Shaked, R., Freedman, M., et al. (2009). Transcriptional profiling of maturing tomato (*Solanum lycopersicum* L.) microspores reveals the involvement of heat shock proteins, ROS scavengers, hormones, and sugars in the heat stress response. *J. Exp. Bot.* 60, 3891–3908. doi: 10.1093/jxb/erp234

Frey, F. P., Urbany, C., Hüttel, B., Reinhardt, R., and Stich, B. (2015). Genome-wide expression profiling and phenotypic evaluation of European maize inbreds at seedling stage in response to heat stress. *BMC Genom.* 16:123. doi: 10.1186/s12864-015-1282-1

Gao, G., Li, J., Li, H., Li, F., Xu, K., Yan, G., et al. (2014). Comparison of the heat stress induced variations in DNA methylation between heat-tolerant and heat-sensitive rapeseed seedlings. *Breed. Sci.* 64, 125–133. doi: 10.1270/jsbbs.64.125

Gare, S., Wagh, R. S., Ingle, A. U., and Soni, N. (2018). Effect of temperature on stem reserve mobilization for grain development in wheat. *J. Agric. Res. Technol.* 43, 334–341.

Garnett, T., Conn, V., and Kaiser, B. N. (2009). Root based approaches to improving nitrogen use efficiency in plants. *Plant Cell Environ.* 32, 1272–1283. doi: 10.1111/j.1365-3040.2009.02011.x

Gaur, P. M., Samineni, S., Krishnamurthy, L., Kumar, S., Ghanem, M. E., Beebe, S., et al. (2015). High temperature tolerance in grain legumes. *Legume Perspect.* 7, 23–24. doi: 10.3389/fphys.2012.00179

Gautam, A., Prasad, S. S., Jajoo, A., and Ambati, D. (2015). Canopy temperature as a selection parameter for grain yield and its components in durum wheat under terminal heat stress in late sown conditions. *Agric. Res. J.* 4, 238–244. doi: 10.1007/s40003-015-0174-6

Gesch, R. W., Kang, I. H., Gallo-Meagher, M., Vu, J. C. V., Boote, K. J., Allen, L. H., et al. (2003). Rubsico expression in rice leaves is related to genotypic variation of photosynthesis under elevated growth CO2 and temperature. *Plant Cell Environ.* 26, 1941–1950. doi: 10.1046/j.1365-3040.2003.01110.x

Gillman, J. D., Biever, J. J., Ye, S., Spollen, W. G., Givan, S. A., Lyu, Z., et al. (2019). A seed germination transcriptomic study contrasting two soybean genotypes that differ in terms of their tolerance to the deleterious impacts of elevated temperatures during seed fill. *BMC Res. Notes* 12:522. doi: 10.1186/s13104-019-4559-7

González-Schain, N., Dreni, L., Lawas, L. M. F., Galbiati, M., Colombo, L., Heuer, S., et al. (2016). Genome-wide transcriptome analysis during anthesis reveals new insights into the molecular basis of heat stress responses in tolerant and sensitive rice varieties. *Plant Cell Physiol.* 57, 57–68. doi: 10.1093/pcp/pcv174

Goo, Y. M., Han, E. H., Jeong, J. C., Kwak, S. S., Yu, J., Kim, Y. H., et al. (2015). Overexpression of the sweet potato IbOr gene results in the increased accumulation of carotenoid and confers tolerance to environmental stresses in transgenic potato. *C. R. Biol.* 338, 12–20. doi: 10.1016/j.crvi.2014 10.006

Gous, P. W., Hickey, L., Christopher, J. T., Franckowiak, J., and Fox, G. P. (2016). Discovery of QTL for stay-green and heat-stress in barley (*Hordeum vulgare*) grown under simulated abiotic stress conditions. *Euphytica* 207, 305–317. doi: 10.1007/s10681-015-1542-1549

Gregersen, P. L., Culetic, A., Boschian, L., and Krupinska, K. (2013). Plant senescence and crop productivity. *Plant Mol. Biol.* 82, 603–622. doi: 10.1007/s11103-013-0013-8

Grigorova, B., Vaseva, I. I., Demirevska, K., and Feller, U. (2011). Expression of selected heat shock proteins after individually applied and combined drought and heat stress. *Acta Physiol. Plant.* 33, 2041–2049. doi: 10.1007/s11738-011-0733-739

Grilli, G. V. G., Braz, L. T., and Lemos, E. G. M. (2007). QTL identification for tolerance to fruit set in tomato by fAFLP markers. *Crop Breed. Appl. Biotechnol.* 7, 234–241. doi: 10.12702/1984-7033.V07N03A02

Gui-lian, Z., Li-yun, C., Guo-yang, X., Ying-hui, X., Xin-bo, C., and Shun-tang, Z. (2009). Bulked segregant analysis to detect QTL related to heat tolerance in rice (*Oryza sativa* L.) using SSR markers. *Agric. Sci. China.* 8, 482–487. doi: 10.1016/S1671-2927(08)60235-7

Gupta, N. K., Agarwal, S., Agarwal, V. P., Nathawat, N. S., Gupta, S., and Singh, G. (2013). Effect of short-term heat stress on growth, physiology and antioxidative defence system in wheat seedlings. *Acta Physiol. Plant.* 35, 1837–1842. doi: 10.1007/s11738-013-1221-1221

Gupta, S., Rai, K., Singh, P., Ameta, V., Gupta, S. K., Jayalekha, A., et al. (2015). Seed set variability under high temperatures during flowering period in pearl millet (*Pennisetum glaucum* L.(R.) Br.). *Field Crops Res.* 171, 41–53. doi: 10.1016/j.fcr.2014.11.005

Hairat, S., and Khurana, P. (2016). Photosynthetic efficiency, temperature induction response, carbon isotope discrimination correlate with expression profiling in Indian wheat cultivars. *Plant Signal. Behav.* 11, 1–11. doi: 10.1080/15592324.2016.1179416

Hameed, M., Keitel, C., Ahmad, N., Mahmood, T., and Trethowan, R. (2015). Screening of tomatoes germplasm for heat stress tolerance under controlled conditions. *Proc. Environ. Sci.* 29, 173–174. doi: 10.1016/j.proenv.2015.07.245

Han, F., Chen, H., Li, X. J., Yang, M. F., Liu, G. S., and Shen, S. H. (2009). A comparative proteomic analysis of rice seedlings under various high-temperature stresses. *Biochim. Biophys. Acta* 1794, 1625–1634. doi: 10.1016/j.bbapap.2009.07.013

Handayani, T., and Watanabe, K. (2020). The combination of drought and heat stress has a greater effect on potato plants than single stresses. *Plant Soil Environ.* 66, 175–182. doi: 10.17221/126/2020-PSE

HanumanthaRao, B., Nair, R. M., and Nayyar, H. (2016). Salinity and High Temperature Tolerance in Mungbean [*Vigna radiata* (L.) Wilczek] from a Physiological Perspective. *Front. Plant Sci.* 7:957. doi: 10.3389/fpls.2016.00957

Harding, S. A., Guikema, J. A., and Paulsen, G. M. (1990). Photosynthetic decline from high temperature stress during maturation of wheat: I. Interaction with senescence processes. *Plant Physiol.* 92, 648–653. doi: 10.1104/pp.92.3.648

Hasanuzzaman, M., Nahar, K., Alam, M. M., Roychowdhury, R., and Fujita, M. (2013). Physiological, biochemical, and molecular mechanisms of heat stress tolerance in plants. *Int. J. Mol. Sci.* 14, 9643–9684. doi: 10.3390/ijms14059643

Havaux, M. (1998). Carotenoids as membrane stabilizers in chloroplasts. *Trends Plant Sci.* 3, 147–151. doi: 10.1016/S1360-1385(98)01200-X

Hede, A. R., Skovmand, B., Reynolds, M. P., Crossa, J., Vilhelmsen, A. L., and Stølen, O. (1999). Evaluating genetic diversity for heat tolerance traits in Mexican wheat landraces. *Genet. Resour. Crop Evol.* 46, 37–45. doi: 10.1023/A:1008684615643

Hedhly, A. (2011). Sensitivity of flowering plant gametophytes to temperature fluctuations. *Environ. Exp. Bot.* 74, 9–16. doi: 10.1016/j.envexpbot.2011.03.016

Hemantaranjan, A., Nishant Bhanu, A., Singh, M. N., Yadav, D. K., and Patel, P. K. (2014). Heat stress responses and thermotolerance. *Adv. Plants Agric. Res.* 1, 1–10.

Herzog, H., and Chai-Arree, W. (2012). Gas exchange of five warm-season grain legumes and their susceptibility to heat stress. *J. Agron. Crop Sci.* 198, 466–474. doi: 10.1111/j.1439-037X.2012.00517.x

Hossain, M. M., Takeda, H., and Senboku, T. (1995). Proline content in Brassica under high temperature stress. *Jarq.-Jpn. Agr. Res. Q.* 2, 87–93.

Howarth, C. J. (1991). Molecular responses of plants to an increased incidence of heat shock. *Plant Cell Environ.* 14, 831–841. doi: 10.1111/j.1365-3040.1991.tb01446.x

Howarth, C. J. (2005). ""Genetic Improvements of Tolerance to High Temperature"," in *Abiotic stresses: Plant Resistance through Breeding and Molecular Approaches*, eds M. Ashraf, and P. J. C. Harris (New York, NY: Haworth Press Inc).

Huang, B., and Gao, H. (2000). Growth and carbohydrate metabolism of creeping bentgrass cultivars in response to increasing temperatures. *Crop Sci.* 40, 1115–1120. doi: 10.2135/cropsci2000.4041115x

Impa, S. M., Nadaradjan, S., Boominathan, P., Shashidhar, G., Bindumadhava, H., and Sheshshayee, M. S. (2005). Carbon isotope discrimination accurately reflects variability in WUE measured at a whole plant level in Rice. *Crop Sci.* 45, 2517–2522. doi: 10.2135/cropsci2005.0119

Inghelandt, D. V., Frey, F. P., Ries, D., and Stich, B. (2019). QTL mapping and genome-wide prediction of heat tolerance in multiple connected populations of temperate maize. *Sci. Rep.* 9, 1–16. doi: 10.1038/s41598-019-50853-2

Ismail, A. M., and Hall, A. E. (1999). Reproductive-stage heat tolerance, leaf membrane thermostability and plant morphology in cowpea. *Crop Sci.* 39, 1762–1768. doi: 10.2135/cropsci1999.3961762x

Jagadish, S. V. K., Craufurd, P. Q., and Wheeler, T. R. (2008). Phenotyping parents of mapping populations of rice for heat tolerance during anthesis. *Crop Sci.* 48, 1140–1146. doi: 10.2135/cropsci2007.10.0559

Jagadish, S. V. K., Murty, M. V. R., and Quick, W. P. (2015). Rice responses to rising temperatures-challenges, perspectives and future directions. *Plant Cell Environ.* 38, 1686–1698. doi: 10.1111/pce.12430

Jagadish, S. V. K., Muthurajan, R., Oane, R., Wheeler, T. R., Heuer, S., Bennette, J., et al. (2010). Physiological and proteomic approaches to address heat tolerance during anthesis in rice (*Oryza sativa* L.). *J. Exp. Bot.* 61, 143–156. doi: 10.1093/jxb/erp289

Janni, M., Mariolina, G., Maestri, E., Marmiroli, M., Valliyodan, B., Nguyen, H. T., et al. (2020). Molecular and genetic bases of heat stress response in crop plants for increased resilience and productivity. *J. Exp. Bot.* 71, 1–23. doi: 10.1093/jxb/eraa034

Jedmowski, C., and Brüggemann, W. (2015). Imaging of fast chlorophyll fluorescence induction curve (OJIP) parameters, applied in a screening study with wild barley (*Hordeum spontaneum*) genotypes under heat stress. *J. Photochem. Photobiol.* 151, 153–160. doi: 10.1016/j.jphotobiol.2015.07.020

Jegadeesan, S., Chaturvedi, P., Ghatak, A., Pressman, E., Meir, S., Faigenboim, A., et al. (2018). Proteomics of heat-stress and ethylene-mediated thermotolerance mechanisms in tomato pollen grains. *Front. Plant Sci.* 9:1558. doi: 10.3389/fpls.2018.01558

Jha, U. C., Bohra, A., and Singh, N. P. (2014). Heat stress in crop plants: its nature, impacts and integrated breeding strategies to improve heat tolerance. *Plant Breed.* 133, 679–701. doi: 10.1111/pbr.12217

Jha, U. C., Jha, R., Bohra, A., Parida, S. K., Kole, P. C., Thakro, V., et al. (2018). Population structure and association analysis of heat stress relevant traits in chickpea (*Cicer arietinum* L.). *3 Biotech* 8, 1–14. doi: 10.1007/s13205-017-1057-2

Jha, U. C., Kole, P. C., and Singh, N. P. (2019). Nature of gene action and combining ability analysis of yield and yield related traits in chickpea (*Cicer arietinum* L.) under heat stress. *Indian J. Agric. Sci.* 89, 500–508.

Johnson, S. M., Lim, F. L., Finkler, A., Fromm, H., Slabas, A. R., and Knight, M. R. (2014). Transcriptomic analysis of *Sorghum bicolor* responding to combined heat and drought stress. *BMC Genom.* 15:456. doi: 10.1186/1471-2164-15-456

Jones, R. J., Roessler, J. A., and Ouattar, S. (1985). Thermal environment during endosperm cell division in maize: effect on number of endosperm cells and starch granules. *Crop Sci.* 25, 830–834. doi: 10.2135/cropsci1985.0011183X002500050025x

Joshi, M. A., Faridullah, S., and Kumar, A. (2016). Effect of heat stress on crop phenology, yield and seed quality attributes of wheat (*Triticum aestivum* L.). *J. Agrometeorol.* 18, 206–215.

Judd, L. A., Jackson, B. E., and Fonteno, W. C. (2015). Advancements in root growth measurement technologies and observation capabilities for container-grown plants. *Plants* 4, 369–392. doi: 10.3390/plants4030369

Jukanti, A. K., Manga, V. K., Bhatt, R. K., and Pathak, R. (2017). Differential response of pearl millet genotypes to high temperature stress at flowering. *J. Environ. Biol.* 38:791. doi: 10.22438/jeb/38/5/mrn-432

Kadir, S., Sidhu, G., and Al-Khatib, K. (2006). Strawberry (*Fragaria ananassa* Duch.) growth and productivity as affected by temperature. *Hort. Sci.* 41, 1423–1430. doi: 10.21273/HORTSCI.41.6.1423

Kadir, S., Von Weihe, M., and Al-Khatib, K. (2007). Photochemical efficiency and recovery of photosystem II in grapes after exposure to sudden and gradual heat stress. *J. Am. Soc. Horict. Sci.* 132, 764–769. doi: 10.21273/JASHS.132.6.764

Kalaji, H. M., Rastogi, A., Živèák, M., Brestic, M., Daszkowska-Golec, A., Sitko, K., et al. (2018). Prompt chlorophyll fluorescence as a tool for crop phenotyping: an example of barley landraces exposed to various abiotic stress factors. *Photosynthetica* 56, 953–961. doi: 10.1007/s11099-018-0766-z

Kang, L., Kim, H. S., Kwon, Y. S., Ke, Q., Ji, C. Y., Park, S.-C., et al. (2017). IbOr Regulates Photosynthesis under Heat Stress by Stabilizing IbPsbP in Sweetpotato. *Front. Plant Sci.* 8:989. doi: 10.3389/fpls.2017.00989

Kao, W. Y., and Forseth, I. N. (1992). Dirunal leaf movement, chlorophyll fluorescence and carbon assimilation in soybean grown under different nitrogen and water availabilities. *Plant Cell Environ.* 15, 703–710. doi: 10.1111/j.1365-3040.1992.tb01012.x

Kaplan, F., Kopka, J., Haskell, D. W., Zhao, W., Schiller, K. C., Gatzke, N., et al. (2004). Exploring the temperature-stress metabolome. *Plant Physiol.* 136, 4159–4168. doi: 10.1104/pp.104.052142.1

Karademir, E., Karademir, Ç, Ekinci, R., Basbag, S., and Başal, H. (2012). Screening cotton varieties (*Gossypium hirsutum* L.) for heat tolerance under field conditions. *Afr. J. Agric. Res.* 7, 6335–6342. doi: 10.5897/AJAR12.1868

Karademir, E., Karademir, Ç, Sevilmiş, U., and Başal, H. (2018). Correlations between canopy temperature, chlorophyll content and yield in heat tolerant cotton (*Gossypium hirsutum* L.) genotypes. *Fresenius Environ. Bull.* 27, 5230–5237.

Kashiwagi, J., Krishnamurthy, L., Upadhyaya, H. D., and Gaur, P. M. (2008). Rapid screening technique for canopy temperature status and its relevance to drought tolerance improvement in chickpea. *J. SAT Agric. Res.* 6, 1–4. doi: 10.9734/ijpss/2018/47090

Kaur, R., Bains, T. S., Bindumadhava, H., and Nayyar, H. (2015). Responses of mungbean (*Vigna radiata* L.) genotypes to heat stress: effects on reproductive biology, leaf function and yield traits. *Sci. Hortic.* 197, 527–541. doi: 10.1016/j.scienta.2015.10.015

Kaushal, N., Awasthi, R., Gupta, K., Gaur, P., Siddique, K. H. M., and Nayyar, H. (2013). Heat-stress-induced reproductive failures in chickpea (*Cicer arietinum*) are associated with impaired sucrose metabolism in leaves and anthers. *Funct. Plant Biol.* 40, 1334–1349. doi: 10.1071/FP13082

Kaushal, N., Bhandari, K., Siddique, K. H. M., and Nayyar, H. (2016). Food crops face rising temperatures: an overview of responses, adaptive mechanisms, and approaches to improve heat tolerance. *Cogent Food Agric.* 2, 1–42. doi: 10.1080/23311932.2015.1134380

Khan, A. I., Khan, I. A., and Sadaqat, H. A. (2008). Heat tolerance is variable in cotton (*Gossypium hirsutum* l.) and can be exploited for breeding of better yielding cultivars under high temperature regimes. *Pak. J. Bot.* 40, 2053–2058.

Khan, A. W., Garg, V., Roorkiwal, M., Golicz, A. A., Edwards, D., and Varshney, R. K. (2020). Super-pangenome by integrating the wild-side of a species for accelerated crop improvement. *Trends Plant Sci.* 25, 148–158. doi: 10.1016/j.tplants.2019.10.012

Khan, N., Azhar, F. M., Khan, A. A., and Ahmad, R. (2014). Measurement of canopy temperature for heat tolerance in Upland cotton: variability and its genetic basis. *Pak. J. Agric. Sci.* 51, 359–365.

Kilasi, N. L., Singh, J., Vallejos, C. E., Ye, C., Jagadish, S. V. K., Kusolwa, P., et al. (2018). Heat stress tolerance in rice (*Oryza sativa* L.): identification of Quantitative Trait Loci and Candidate Genes for Seedling Growth Under Heat Stress. *Front. Plant Sci.* 9:1578. doi: 10.3389/fpls.2018.01578

Kobata, T., Shinonaga, M., Yoshida, H., Tomisaka, K., and Akai, K. (2015). Stay-green trait assessment using the leaf incubation method to examine the maintenance of assimilation rates under high temperature conditions during the grain-filling period in rice. *Plant Prod. Sci.* 18, 54–266. doi: 10.1626/pps.18.254

Korotaeva, N. E., Antipina, A. I., Grabelnykh, O. I., Varakina, N. N., Borovskii, G. B., and Voinikov, V. K. (2001). Mitochondrial low-molecular-weight heat-shock proteins and the tolerance of cereal mitochondria to hyperthermia. *Russ. J. Plant Physl.* 48, 798–803. doi: 10.1023/A:1012516826835

Kotak, S., Larkindale, J., Lee, U., von Koskull-Döring, P., Vierling, E., and Scharf, K. D. (2007). Complexity of the heat stress response in plants. *Curr. Opin. Plant Biol.* 10, 310–316. doi: 10.1016/j.pbi.2007.04.011

Krause, G. H., and Santarius, K. A. (1975). Relative thermostability of the chloroplast envelope. *Planta* 127, 285–299. doi: 10.1007/BF00380726

Krishnamurthy, L., Gaur, P. M., Basu, P. S., Chaturvedi, S. K., Tripathi, S., Vadez, V., et al. (2011). Large genetic variation for heat tolerance in the reference collection of chickpea (*Cicer arietinum* L.) germplasm. *Plant Genet. Resour.* 9, 59–69. doi: 10.1017/S1479262110000407

Kumar, J., Kant, R., Kumar, S., Basu, P. S., Sarker, A., and Singh, N. P. (2016). Heat tolerance in lentil under field conditions. *Legume Genomics Genet.* 7, 1–11. doi: 10.5376/lgg.2016.07.0001

Kumar, P., Shah, D., and Singh, M. P. (2017). Evaluation of chickpea (*Cicer arietinum* L.) genotypes for heat tolerance: a physiological assessment. *Indian J. Plant Physiol.* 22, 164–177. doi: 10.1007/s40502-017-0301-4

Kumar, S., Gupta, D., and Nayyar, H. (2012). Comparative response of maize and rice genotypes to heat stress: status of oxidative stress and antioxidants. *Acta Physiol. Plant.* 34, 75–86. doi: 10.1007/s11738-011-0806-809

Kumar, S., Thakur, P., Kaushal, N., Malik, J. A., Gaur, P., and Nayyar, H. (2013). Effect of varying high temperatures during reproductive growth on reproductive function, oxidative stress and seed yield in chickpea genotypes differing in heat sensitivity. *Arch. Agron. Soil Sci.* 59, 823–843. doi: 10.1080/03650340.2012.683424

Kumari, M., Pudake, R. N., Singh, V. P., and Joshi, A. K. (2013). Association of staygreen trait with canopy temperature depression and yield traits under terminal heat stress in wheat (*Triticum aestivum* L.). *Euphytica* 190, 87–97. doi: 10.1007/s10681-012-0780-783

Kumari, M., Singh, V. P., Tripathi, R., and Joshi, A. K. (2007). "Variation for stay green trait and its association with canopy temperature depression and yield traits under terminal heat stress in wheat," in *Wheat Production in Stressed Environments*, eds H. T. Buck, J. E. Nisi, and N. Salomón (Dordrecht: Springer), 357–363. doi: 10.1007/1-4020-5497-1_44

Lafarge, T., Bueno, C., Frouin, J., Jacquin, L., Courtois, B., and Ahmadi, N. (2017). Genome-wide association analysis for heat tolerance at flowering detected a large set of genes involved in adaptation to thermal and other stresses. *PLoS One* 12, 1–27. doi: 10.1371/journal.pone.0171254

Lafta, A. M., and Lorenzen, J. H. (1995). Effect of high temperature on plant growth and carbohydrate metabolism in potato. *Plant Physiol.* 109, 637–643. doi: 10.1104/pp.109.2.637

Ledesma, N. A., Kawabata, S., and Sugiyama, N. (2004). Effect of high temperature on protein expression in strawberry plants. *Biol. Plant.* 48, 73–79. doi: 10.1023/B:BIOP.0000024278.62419.ee

Lehman, V. G., and Engelke, M. C. (1993). Heat resistance and rooting potential of Kentucky bluegrass cultivars. *Internat. Turfgrass Soc. Res. J.* 7, 775–779.

Lei, C., Hao, K., Yang, Y., Ma, J., Wang, S., Wang, J., et al. (2013). Identification and fine mapping of two blast resistance genes in rice cultivar 93-11. *Crop J.* 1, 2–14. doi: 10.1016/j.cj.2013.07.007

Li, B., Gao, K., Ren, H., and Tang, W. (2018). Molecular mechanisms governing plant responses to high temperatures. *J. Integr. Plant Biol.* 60, 757–779. doi: 10.1111/jipb.12701

Li, H., Rasheed, A., Hickey, L. T., and He, Z. (2018). Fast-forwarding genetic gain. *Trends Plant Sci.* 23, 183–186. doi: 10.1016/j.tplants.2018.01.007

Li, M., Li, X., Yu, L., Wu, J., Li, H., Liu, J., et al. (2018). Identification of QTLs associated with heat tolerance at the heading and flowering stage in rice (*Oryza sativa* L.). *Euphytica* 214, 1–11. doi: 10.1007/s10681-018-2136-2130

Li, T., Xu, X., Li, Y., Wang, H., Li, Z., and Li, Z. (2015). Comparative transcriptome analysis reveals differential transcription in heat-susceptible and heat-tolerant pepper (*Capsicum annum* L.) cultivars under heat stress. *J. Plant Biol.* 58, 411–424. doi: 10.1007/s12374-015-0423-z

Li, X., Lawas, L. M. F., Malo, R., Glaubitz, U., Erban, A., Mauleon, R., et al. (2015). Metabolic and transcriptomic signatures of rice floral organs reveal sugar starvation as a factor in reproductive failure under heat and drought stress. *Plant, Cell Environ.* 38, 2171–2192. doi: 10.1111/pce.12545

Li, Z., Palmer, W. M., Martin, A. P., Wang, R., Rainsford, F., Jin, Y., et al. (2012). High invertase activity in tomato reproductive organs correlates with enhanced sucrose import into, and heat tolerance of, young fruit. *J. Exp. Bot.* 63, 1155–1166. doi: 10.1093/jxb/err329

Liao, J. L., Zhou, H. W., Peng, Q., Zhong, P. A., Zhang, H.-Y., He, C., et al. (2015). Transcriptome changes in rice (*Oryza sativa* L.) in response to high night temperature stress at the early milky stage. *BMC Genomics* 16:18. doi: 10.1186/s12864-015-1222-0

Liao, J.-L., Zhou, H.-W., Zhang, H.-Y., Zhong, P.-A., and Huang, Y.-J. (2014). Comparative proteomic analysis of differentially expressed proteins in the early milky stage of rice grains during high temperature stress. *J. Expt. Bot.* 65, 655–671. doi: 10.1093/jxb/ert435

Lichtenthaler, H. K. (1987). "Chlorophylls and carotenoids: pigments of photosynthetic biomembranes," in *Methods in Enzymology*, ed J. A. Cotruvo (Amsterdam: Elsevier), 350–382. doi: 10.1016/0076-6879(87)48036-1

Liu, G. T., Jiang, J. F., Liu, X. N., Jiang, J. Z., Sun, L., Duan, W., et al. (2019). New insights into the heat responses of grape leaves via combined phosphoproteomic and acetylproteomic analyses. *Hort. Res.* 6, 1–15. doi: 10.1038/s41438-019-0183-x

Liu, G. T., Ma, L., Duan, W., Wang, B. C., Li, J. H., Xu, H. G., et al. (2014). Differential proteomic analysis of grapevine leaves by iTRAQ reveals responses to heat stress and subsequent recovery. *BMC Plant Biol.* 14:110. doi: 10.1186/1471-2229-14-110

Liu, Z., Xin, M., Qin, J., Peng, H., Ni, Z., Yao, Y., et al. (2015). Temporal transcriptome profiling reveals expression partitioning of homeologous genes contributing to heat and drought acclimation in wheat (*Triticum aestivum* L.). *BMC Plant Biol.* 15:152. doi: 10.1186/s12870-015-0511-8

Liu, Z., Yuan, Y. L., Liu, S. Q., Yu, X. N., and Rao, L. Q. (2006). Screening for high-temperature tolerant cotton cultivars by testing in vitro pollen germination, pollen tube growth and boll retention. *J. Integr. Plant Biol.* 48, 706–714. doi: 10.1111/j.1744-7909.2006.00276.x

Lopes-Caitar, V. S., de Carvalho, M. C. C. G., Darben, L. M., Kuwahara, M. K., Nepomuceno, A. L., Dias, W. P., et al. (2013). Genome-wide analysis of the Hsp20 gene family in soybean: comprehensive sequence, genomic organization and expression profile analysis under abiotic and biotic stresses. *BMC Genom.* 14:577. doi: 10.1186/1471-2164-14-577

Loreto, F., Förster, A., Dürr, M., Csiky, O., and Seufert, G. (1998). On the monoterpene emission under heat stress and on the increased thermotolerance of leaves of *Quercus ilex* L. fumigated with selected monoterpenes. *Plant Cell Environ.* 21, 101–107. doi: 10.1046/j.1365-3040.1998.00268.x

Lu, C. M., and Zhang, J. H. (2000). Heat-induced multiple effects on PSII in wheat plants. *J. Plant Physiol.* 156, 259–265. doi: 10.1016/S0176-1617(00)80315-80316

Lu, H., Shen, F., Liu, L., and Sun, W. (2005). Recent advances in study on plant sucrose synthase. *Chin. Agri. Sci. Bull.* 21, 34–37.

Lu, Y., Li, R., Wang, R., Wang, X., Zheng, W., Sun, Q., et al. (2017). Comparative proteomic analysis of flag leaves reveals new insight into wheat heat adaptation. *Front. Plant Sci.* 8:1086. doi: 10.3389/fpls.2017.01086

Lu, Z., Chen, J., Percy, R. G., and Zeiger, E. (1997). Photosynthetic rate, stomatal conductance and leaf area in two cotton species (*Gossypium barbadense* and *Gossypium hirsutum*) and their relation with heat resistance and yield. *Funct. Plant Biol.* 24, 693–700. doi: 10.1071/PP97056

Lukens, L. N., and Zhan, S. (2007). The plant genome's methylation status and response to stress: implications for plant improvement. *Curr. Opin. Plant Biol.* 10, 317–322. doi: 10.1016/j.pbi.2007.04.012

Maavimani, M., and Saraswathi, R. (2014). Anther characteristics and spikelet fertility in rice (*Oryza sativa* L.) under high temperature stress at anthesis. *Indian J. Genet.* 74, 300–308. doi: 10.5958/0975-6906.2014.00847.5

Makonya, G. M., Ogola, J. B., Muasya, A. M., Crespo, O., Maseko, S., Valentine, A. J., et al. (2019). Chlorophyll fluorescence and carbohydrate concentration as field selection traits for heat tolerant chickpea genotypes. *Plant Physiol. Biochem.* 141, 172–182. doi: 10.1016/j.plaphy.2019.05.031

Malaspina, P., Giordani, P., Faimali, M., Garaventa, F., and Modenesi, P. (2014). Assessing photosynthetic biomarkers in lichen transplants exposed under different light regimes. *Ecol. Indic.* 43, 126–131. doi: 10.1016/j.ecolind.2014.02.034

Mangelsen, E., Kilian, J., Harter, K., Jansson, C., Wanke, D., and Sundberg, E. (2011). Transcriptome analysis of high-temperature stress in developing barley caryopses: early stress responses and effects on storage compound biosynthesis. *Mol. Plant.* 4, 97–115. doi: 10.1093/mp/ssq058

Mangrauthia, S. K., Agarwal, S., Sailaja, B., Sarla, N., and Voleti, S. R. (2016). Transcriptome analysis of *Oryza sativa* (Rice) seed germination at high temperature shows dynamics of genome expression associated with hormones signalling and abiotic stress pathways. *Trop. Plant Biol.* 9, 215–228. doi: 10.1007/s12042-016-9170-7

Mangrauthia, S. K., Bhogireddy, S., Agarwal, S., Prasanth, V. V., Voleti, S. R., Neelamraju, S., et al. (2017). Genome-wide changes in microRNA expression during short and prolonged heat stress and recovery in contrasting rice cultivars. *J. Exp. Bot.* 6, 2399–2412. doi: 10.1093/jxb/erx111

Marcum, K. B. (1998). Cell membrane thermostability and whole-plant heat tolerance of Kentucky bluegrass. *Crop Sci.* 38, 1214–1218. doi: 10.2135/cropsci1998.0011183X003800050017x

Marfo, K. O., and Hall, A. E. (1992). Inheritance of heat tolerance during pod set in cowpea. *Crop Sci.* 32, 912–918. doi: 10.2135/cropsci1992.0011183X003200040015x

Martineau, J. R., Specht, J. E., Williams, J. H., and Sullivan, C. Y. (1979). Temperature tolerance in soybeans. I. Evaluation of a technique for assessing cellular membrane thermostability. *Crop Sci.* 19, 75–78. doi: 10.2135/cropsci1979.0011183X001900010017x

Mason, R. E., Mondal, S., Beecher, F., and Hays, D. (2010). QTL associated with heat susceptibility index in wheat (*Triticum aestivum* L.) under short-term reproductive stage heat stress. *Euphytica* 174, 423–436. doi: 10.1007/s10681-010-0151-x

Mason, R. E., and Singh, R. P. (2014). Considerations when deploying canopy temperature to select high yielding wheat breeding lines under drought and heat stress. *Agron. J.* 4, 191–201. doi: 10.3390/agronomy4020191

Mathur, S., Jajoo, A., Mehta, P., and Bharti, S. (2011). Analysis of elevated temperature-induced inhibition of photosystem II using chlorophyll a fluorescence induction kinetics in wheat leaves (*Triticum aestivum*). *Plant Biol.* 13, 1–6. doi: 10.1111/j.1438-8677.2009 00319.x

Maulana, F., Ayalew, H., Anderson, J. D., Kumssa, T. T., Huang, W., and Ma, X.-F. (2018). Genome-wide association mapping of seedling heat tolerance in winter wheat. *Front. Plant Sci.* 9:1272. doi: 10.3389/fpls.2018.01272

McMichael, B. L., and Quisenberry, J. E. (1993). The impact of the soil environment on the growth of root systems. *Environ. Exp. Bot.* 33, 53–61. doi: 10.1016/0098-8472(93)90055-K

Méthy, M., Olioso, A., and Trabaud, L. (1994). Chlorophyll fluorescence as a tool for management of plant resources. *Remote Sens. Environ.* 47, 2–9. doi: 10.1016/0034-4257(94)90121-X

Mittler, R., Finka, A., and Goloubinoff, P. (2012). How do plants feel the heat? *Trends Biochem. Sci.* 37, 118–125. doi: 10.1016/j.tibs.2011.11.007

Mittler, R., Vanderauwera, S., Gollery, M., and Van Breusegem, F. (2004). Reactive oxygen gene network of plants. *Trends Plant Sci.* 9, 490–498. doi: 10.1016/j.tplants.2004.08.009

Miyazaki, M., Araki, M., Okamura, K., Ishibashi, Y., Yuasa, T., and Iwaya-Inoue, M. (2013). Assimilate translocation and expression of sucrose transporter, OsSUT1, contribute to high-performance ripening under heat stress in the heat-tolerant rice cultivar Genkitsukushi. *J. Plant Physiol.* 170, 1579–1584. doi: 10.1016/j.jplph.2013.06.011

Mohammadi, R., Armion, M., Kahrizi, D., and Amri, A. (2012). Efficiency of screening techniques for evaluating durum wheat genotypes under mild drought conditions. *Int. J. Plant Prod.* 4, 11–24. doi: 10.22069/ijpp.2012.677

Molina-Bravo, R., Arellano, C., Sosinski, B. R., and Fernandez, G. E. (2011). A protocol to assess heat tolerance in a segregating population of raspberry using chlorophyll fluorescence. *Sci. Hortic.* 130, 524–530. doi: 10.1016/j.scienta.2011.07.022

Mondal, S., Singh, R. P., Crossa, J., Huerta-Espino, J., Sharma, I., Chatrath, R., et al. (2013). Earliness in wheat: a key to adaptation under terminal and continual high temperature stress in South Asia. *Field Crops Res.* 151, 19–26. doi: 10.1016/j.fcr.2013.06.015

Muhlemann, J. K., Younts, T. L. B., and Muday, G. K. (2018). Flavonols control pollen tube growth and integrity by regulating ROS homeostasis during high-temperature stress. *Proc. Natl. Acad. Sci. U.S.A.* 115, E11188–E11197. doi: 10.1073/pnas.1811492115

Munier-Jolain, N. G., and Ney, B. (1998). Seed growth rate in grain legumes II. Seed growth rate depends on cotyledon cell number. *J. Exp. Bot.* 49, 1971–1976. doi: 10.1093/jxb/49.329.1971

Nagel, K. A., Kastenholz, B., Jahnke, S., Van Dusschoten, D., Aach, T., Mühlich, M., et al. (2009). Temperature responses of roots: impact on growth, root system architecture and implications for phenotyping. *Funct. Plant Biol.* 36, 947–959. doi: 10.1071/FP09184

Nahar, K., Hasanuzzaman, M., and Fujita, M. (2016). "Heat stress responses and thermotolerance in soybean," in *Abiotic and Biotic Stresses in Soybean Production*, Ed. M. Miransari (Cambridge, MA: Academic Press), 261–284. doi: 10.1016/B978-0-12-801536-0.00012-8

Nakamoto, H., and Hiyama, T. (1999). "Heat-shock proteins and temperature stress," in *Handbook of Plant and Crop Stress*, Ed. M. Pessarakli (New York, NY: Marcel Dekker), 399–416.

Nankishore, A., and Farrell, A. D. (2016). The response of contrasting tomato genotypes to combined heat and drought stress. *J. Plant Physiol.* 202, 75–82. doi: 10.1016/j.jplph.2016.07.006

Narayanan, S., Prasad, P. V., and Welti, R. (2016). Wheat leaf lipids during heat stress: II. Lipids experiencing coordinated metabolism are detected by analysis of lipid co-occurrence. *Plant Cell Environ.* 39, 608–617. doi: 10.1111/pce.12648

Nawaz, A., Farooq, M., Cheema, S. A., and Wahid, A. (2013). Differential response of wheat cultivars to terminal heat stress. *Int. J. Agric. Biol.* 15, 1354–1358.

Netto, A. T., Campostrini, E., de Oliveira, J. G., and Bressan-Smith, R. E. (2005). Photosynthetic pigments, nitrogen, chlorophyll a fluorescence and SPAD-502 readings in coffee leaves. *Sci. Hortic.* 104, 199–209. doi: 10.1016/j.scienta.2004.08.013

Neumann, D., Lichtenberger, O., Günther, D., Tschiersch, K., and Nover, L. (1994). Heat-shock proteins induce heavy-metal tolerance in higher plants. *Planta* 194, 360–367. doi: 10.1007/BF00197536

Nguyen, C. T., Singh, V., van Oosterom, E. J., Chapman, S. C., Jordan, D. R., and Hammer, G. L. (2013). Genetic variability in high temperature effects on seed-set in sorghum. *Funct. Plant Biol.* 40, 439–448. doi: 10.1071/FP12264

Nielsen, C. L., and Hall, A. E. (1985). Responses of cowpea (*Vigna unguiculata* (L.) Walp) in the field to high night air temperature during flowering. *Field Crops Res.* 10, 181–196. doi: 10.1016/0378-4290(85)90025-5

Niones, J. M., Suralta, R. R., Inukai, Y., and Yamauchi, A. (2012). Field evaluation on functional roles of root plastic responses on dry matter production and grain yield of rice under cycles of transient soil moisture stresses using chromosome segment substitution lines. *Plant Soil.* 359, 107–120. doi: 10.1007/s11104-012-1178-7

Niones, J. M., Suralta, R. R., Inukai, Y., and Yamauchi, A. (2013). Roles of root aerenchyma development and its associated QTL in dry matter production under transient moisture stress in rice. *Plant Prod. Sci.* 16, 205–216. doi: 10.1626/pps.16.205

Ntare, B. R., Williams, J. H., and Dougbedji, J. (2001). Evaluation of groundnut genotypes for heat tolerance under field conditions in a Sahelian environment using a simple physiological model for yield. *J. Agricult. Sci.* 136, 81–88. doi: 10.1017/s0021859600008583

Ogren, E., and Sjostrom, M. (1990). Estimation of the effect of photoinhibition on the carbon gain in leaves of a willow canopy. *Planta* 181, 560–567. doi: 10.1007/BF00193011

Ogweno, J. O., Song, X. S., Shi, K., Hu, W. H., Mao, W. H., Zhou, Y. H., et al. (2008). Brassinosteroids alleviate heat-induced inhibition of photosynthesis by increasing carboxylation efficiency and enhancing antioxidant systems in *Lycopersicon esculentum*. *J. Plant Growth Regul.* 27, 49–57. doi: 10.1007/s00344-007-9030-7

Oukarroum, A., El Madidi, S., and Strasser, R. J. (2016). Differential heat sensitivity index in barley cultivars (*Hordeum vulgare* L.) monitored by chlorophyll a fluorescence OKJIP. *Plant Physiol. Biochem.* 105, 102–108. doi: 10.1016/j.plaphy.2016.04.015

Paliwal, R., Röder, M. S., Kumar, U., Srivastava, J. P., and Joshi, A. K. (2012). QTL mapping of terminal heat tolerance in hexaploid wheat (*T. aestivum* L.). *Theor. Appl. Genet.* 125, 561–575. doi: 10.1007/s00122-012-1853-3

Parankusam, S., Bhatnagar-Mathur, P., and Sharma, K. K. (2017). Heat responsive proteome changes reveal molecular mechanisms underlying heat tolerance in chickpea. *Environ. Exp. Bot.* 141, 132–144. doi: 10.1016/j.envexpbot.2017.07.007

Pareek, A., Rathi, D., Mishra, D., Chakraborty, S., and Chakraborty, N. (2019). Physiological plasticity to high temperature stress in chickpea: adaptive responses and variable tolerance. *Plant Sci.* 289, 1–12. doi: 10.1016/j.plantsci.2019.110258

Patel, P. N., and Hall, A. E. (1988). Inheritance of heat-induced brown discoloration in seed coats of cowpea. *Crop Sci.* 28, 929–932. doi: 10.2135/cropsci1988.0011183X002800060011x

Paul, P. J., Samineni, S., Sajja, S. B., Rathore, A., Das, R. R., Chaturvedi, S. K., et al. (2018). Capturing genetic variability and selection of traits for heat tolerance in a chickpea recombinant inbred line (RIL) population under field conditions. *Euphytica* 214, 1–14. doi: 10:1007/s10681-018-2112-8

Paupière, M. J., van Haperen, P., Rieu, I., Visser, R. G. F., Tikunov, Y. M., and Bovy, A. G. (2017). Screening for pollen tolerance to high temperatures in tomato. *Euphytica* 213, 1–8. doi: 10.1007/s10681-017-1927-z

Petkova, V., Denev, I., and Stefanov, D. (2009). Resistance to high temperature stress of various bean (*Phaseolus vulgaris* L.) cultivars and lines. *Gen. Appl. Plant Physiol.* 35, 117–121.

Petkova, V., Denev, I. D., Cholakov, D., and Porjazov, I. (2007). Field screening for heat tolerant common bean cultivars (*Phaseolus vulgaris* L.) by measuring of chlorophyll fluorescence induction parameters. *Sci. Hortic.* 111, 101–106. doi: 10.1016/j.scienta.2006.10.005

Pinto, F., Damm, A., Schickling, A., Panigada, C., Cogliati, S., Muller-Linow, M., et al. (2016). Sun-induced chlorophyll fluorescence from high-resolution imaging spectroscopy data to quantify spatio-temporal patterns of photosynthetic function in crop canopies. *Plant Cell Environ.* 39, 1500–1512. doi: 10.1111/pce.12710

Pinto, R. S., Reynolds, M. P., Mathews, K. L., McIntyre, C. L., Olivares-Villegas, J. J., and Chapman, S. C. (2010). Heat and drought adaptive QTL in a wheat population designed to minimize confounding agronomic effects. *Theor. Appl. Genet.* 121, 1001–1021. doi: 10.1007/s00122-010-1351-4

Poli, Y., Basava, R. K., Panigrahy, M., Vinukonda, V. P., Dokula, N. R., Voleti, S. R., et al. (2013). Characterization of a Nagina22 rice mutant for heat tolerance and mapping of yield traits. *Rice* 6, 1–9. doi: 10.1186/1939-8433-6-36

Pottorff, M., Roberts, P. A., Close, T. J., Lonardi, S., Wanamaker, S., and Ehlers, J. D. (2014). Identification of candidate genes and molecular markers for heat-induced brown discoloration of seed coats in cowpea (*Vigna unguiculata* (L.) Walp). *BMC Genom.* 15:328. doi: 10.1186/1471-2164-15-328

Pradhan, G. P., Prasad, P. V. V., Fritz, A. K., Kirkham, M. B., and Gill, B. S. (2012). Effects of drought and high temperature stress on synthetic hexaploid wheat. *Funct. Plant Biol.* 39, 190–198. doi: 10.1071/FP11245

Prasad, P. V., Boote, K. J., and Allen, L. H. Jr. (2006). Adverse high temperature effects on pollen viability, seed-set, seed yield and harvest index of grain-sorghum [*Sorghum bicolor* (L.) Moench] are more severe at elevated carbon dioxide due to higher tissue temperatures. *Agr. Forest Meteorol.* 139, 237–251. doi: 10.1016/j.agrformet.2006.07.003

Prasad, P. V. V., Bheemanahalli, R., and Jagadish, S. K. (2017). Field crops and the fear of heat stress—opportunities, challenges and future directions. *Field Crops Res.* 200, 114–121. doi: 10.1016/j.fcr.2016.09.024

Prasad, P. V. V., Craufurd, P. Q., Kakani, V. G., Wheeler, T. R., and Boote, K. J. (2001). Influence of high temperature during pre- and post-anthesis stages of floral development on fruit-set and pollen germination in peanut. *Aust. J. Plant Physiol.* 28, 233–240. doi: 10.1071/PP00127

Prasad, P. V. V., Craufurd, P. Q., and Summerfield, R. J. (1999a). Fruit number in relation to pollen production and viability in groundnut exposed to short episodes of heat stress. *Ann. Bot.* 84, 381–386. doi: 10.1006/anbo.1999.0926

Prasad, P. V. V., Craufurd, P. Q., and Summerfield, R. J. (1999b). Sensitivity of peanut to timing of heat stress during reproductive development. *Crop Sci.* 39, 1352–1357. doi: 10.2135/cropsci1999.3951352x

Prasad, P. V. V., and Djanaguiraman, M. (2011). High night temperature decreases leaf photosynthesis and pollen function in grain sorghum. *Funct. Plant Biol.* 38, 993–1003. doi: 10.1071/FP11035

Prasad, P. V. V., and Djanaguiraman, M. (2014). Response of floret fertility and individual grain weight of wheat to high temperature stress: sensitive stages and thresholds for temperature and duration. *Funct. Plant Biol.* 41, 1261–1269. doi: 10.1071/FP14061

Prasad, P. V. V., Djanaguiraman, M., Perumal, R., and Ciampitti, I. A. (2015). Impact of high temperature stress on floret fertility and individual grain weight of grain sorghum: sensitive stages and thresholds for temperature and duration. *Front. Plant Sci.* 6:820. doi: 10.3389/fpls.2015.00820

Prasad, P. V. V., Pisipati, S. R., Ristic, Z., Bukovnik, U., and Fritz, A. (2008a). Impact of nighttime temperature on physiology and growth of spring wheat. *Crop Sci.* 48, 2372–2380. doi: 10.2135/cropsci2007.12.0717

Prasad, P. V. V., Staggenborg, S. A., and Ristic, Z. (2008b). "Impact of drought and heat stress on physiological, growth and yield processes," in *modeling Water Stress Effects on Plant Growth Processes*, eds L.H. Ahuja, and S.A. Saseendran (Madison, WI: ASA - CSSA), doi: 10.2134/advagricsystmodel1.c11

Pressman, E., Peet, M. M., and Pharr, D. M. (2002). The effect of heat stress on tomato pollen characteristics is associated with changes in carbohydrate concentration in the developing anthers. *Ann. Bot.* 90, 631–636. doi: 10.1093/aob/mcf240

Pressman, E., Shaked, R., and Firon, N. (2007). Tomato (*Lycopersicon esculentum*) response to heat stress: focus on pollen grains. *Plant Stress* 1, 216–227.

Priya, M., Siddique, K. H. M., Dhankhar, O. P., Prasad, P. V. V., Rao, B. H., Nair, R. M., et al. (2018). Molecular breeding approaches involving physiological and reproductive traits for heat tolerance in food crops. *Indian J. Plant Physiol.* 23, 697–720. doi: 10.1007/s40502-018-0427-z

Qi, X., Xu, W., Zhang, J., Guo, R., Zhao, M., Hu, L., et al. (2017). Physiological characteristics and metabolomics of transgenic wheat containing the maize C4 phosphoenolpyruvate carboxylase (PEPC) gene under high temperature stress. *Protoplasma* 254, 1017–1030. doi: 10.1007/s00709-016-1010-y

Qin, D., Wu, H., Peng, H., Yao, Y., Ni, Z., Li, Z., et al. (2008). Heat stress-responsive transcriptome analysis in heat susceptible and tolerant wheat (*Triticum aestivum* L.) by using Wheat Genome Array. *BMC Genomics* 9:432. doi: 10.1186/1471-2164-9-432

Qu, M., Chen, G., Bunce, J. A., Zhu, X., and Sicher, R. C. (2018). Systematic biology analysis on photosynthetic carbon metabolism of maize leaf following sudden heat shock under elevated CO 2. *Sci. Rep.* 8, 1–11. doi: 10.1038/s41598-018-26283-x

Rahaman, M., Mamidi, S., and Rahman, M. (2018). Genome-wide association study of heat stress-tolerance traits in spring-type *Brassica napus* L. under controlled conditions. *Crop J.* 6, 115–125. doi: 10.1016/j.cj.2017.08.003

Rahman, M. A., Chikushi, J., Yoshida, S., and Karim, A. J. M. S. (2009). Growth and yield components of wheat genotypes exposed to high temperature stress under control environment. *Bangladesh J. Agr. Res.* 34, 360–372. doi: 10.3329/bjar.v34i3.3961

Raina, S. K., Rane, J., Raskar, N., Singh, A. K., Govindasamy, V., Kumar, M., et al. (2019). Physiological traits reveal potential for identification of drought tolerant mungbean [*Vigna radiata* (L.) Wilczek] genotypes under moderate soil-moisture deficit. *Indian J. Genet.* 7, 427–437. doi: 10.31742/IJGPB.79.2.6

Rainey, K. M., and Griffiths, P. D. (2005). Differential response of common bean genotypes to high temperature. *J. Am. Soc. Hort. Sci.* 130, 18–23. doi: 10.21273/JASHS.130.1.18

Rampino, P., Mita, G., Fasano, P., Borrelli, G. M., Aprile, A., Dalessandro, G., et al. (2012). Novel durum wheat genes up-regulated in response to a combination of heat and drought stress. *Plant Physiol. Biochem.* 56, 72–78. doi: 10.1016/j.plaphy.2012.04.006

Rana, R. M., Khan, S. H., Ali, Z., Khan, A. I., and Khan, I. A. (2011). Elucidation of thermotolerance diversity in cotton (*Gossypium hirsutum* L.) using physio-molecular approaches. *Genet. Mol. Res.* 10, 1156–1167. doi: 10.4238/vol10-2gmr1180

Rani, B., Jain, V., Chhabra, M. L., Dhawan, K., Kumari, N., and Yadav, P. (2012). Oxidative stress and antioxidative system in *Brassica juncea* (L.) under high temperature stress. *Ann. Biol.* 28, 110–115.

Rao, G. U., Jain, A., and Shivanna, K. R. (1992). Effects of high temperature stress on Brassica pollen: viability, germination and ability to set fruits and seeds. *Ann. Bot.* 69, 193–198. doi: 10.1093/oxfordjournals.aob.a088329

Reddy, P. S., Chakradhar, T., Reddy, R. A., Nitnavare, R. B., Mahanty, S., and Reddy, M. K. (2016). Role of heat shock proteins in improving heat stress tolerance in crop plants. *Heat Shock Proteins Plants* 10, 283–307. doi: 10.1007/978-3-319-46340-7_14

Reddy, P. S., Kishor, P. B. K., Seiler, C., Kuhlmann, M., Eschen-Lippold, L., Lee, J., et al. (2014). Unraveling regulation of the small heat shock proteins by the heat shock factor HvHsfB2c in barley: its implications in drought stress response and seed development. *PLoS One* 9:e89125. doi: 10.1371/journal.pone.0089125

Reddy, P. S., Mallikarjuna, G., Kaul, T., Chakradhar, T., Mishra, R. N., Sopory, S. K., et al. (2010). Molecular cloning and characterization of gene encoding for cytoplasmic Hsc70 from *Pennisetum glaucum* may play a protective role against abiotic stresses. *Mol. Genet. Genomic* 283, 243–254. doi: 10.1007/s00438-010-0518-7

Rehman, A., Habib, I., Ahmad, N., Hussain, M., Khan, M. A., Farooq, J., et al. (2009). Screening wheat germplasm for heat tolerance at terminal growth stage. *Plant Omics* 2, 9–19.

Reynolds, M., and Langridge, P. (2016). Physiological breeding. *Curr. Opin. Plant Biol.* 31, 162–172.

Reynolds, M. P., Balota, M., Delgado, M. I. B., Amani, I., and Fischer, R. A. (1994). Physiological and morphological traits associated with spring wheat yield under hot, irrigated conditions. *Funct. Plant Biol.* 21, 717–730. doi: 10.1071/PP9940717

Reynolds, M. P., Nagarajan, S., Razzaque, M. A., and Ageeb, O. A. A. (2001). "Heat tolerance," in *Application of Physiology in Wheat Breeding*, eds M. P. Reynolds, and A. McNab (Mexico: CIMMYT), 124–135.

Reynolds, M. P., Nagarayan, S., Razzaue, M. A., and Ageeb, O. A. A. (1997). *Using Canopy Temperature Depression to Select for Yield Potential of Wheat in Heat-Stressed Environments*. Wheat Special Rep. No. 42. (Mexico: CIMMYT).

Reynolds, M. P., Pierre, C. S., Saad, A. S., Vargas, M., and Condon, A. G. (2007). Evaluating potential genetic gains in wheat associated with stress-adaptive trait expression in elite genetic resources under drought and heat stress. *Crop Sci.* 47, S–172–S–189. doi: 10.2135/cropsci2007.10.0022IPBS

Reynolds, M. P., Singh, R. P., Ibrahim, A., Ageeb, O. A. A., Larque-Saavedra, A., and Quick, J. S. (1998). Evaluating physiological traits to complement empirical selection for wheat in warm environments. *Euphytica* 100, 85–94. doi: 10.1023/A:1018355906553

Ristic, Z., Bukovnik, U., and Prasad, P. V. V. (2007). Correlation between heat stability of thylakoid membranes and loss of chlorophyll in winter wheat under heat stress. *Crop Sci.* 47, 2067–2073. doi: 10.2135/cropsci2006.10.0674

Rivero, R. M., Ruiz, J. M., and Romero, L. M. (2004). Importance of N source on heat stress tolerance due to the accumulation of proline and quaternary ammonium compounds in tomato plants. *Plant Biol.* 6, 702–707. doi: 10.1055/s-2004-821293

Rizza, F., Pagani, D., Gut, M., Prasil, I. T., Lago, C., Tondelli, A., et al. (2011). Diversity in the response to low temperature in representative barley genotypes cultivated in Europe. *Crop Sci.* 51, 2759–2779. doi: 10.2135/cropsci2011.01.0005

Rodziewicz, P., Swarcewicz, B., Chmielewska, K., Wojakowska, A., and Stobiecki, M. (2014). Influence of abiotic stresses on plant proteome and metabolome changes. *Acta Physiol. Plant.* 36, 1–19. doi: 10.1007/s11738-013-1402-y

Ryan, P. R., Delhaize, E., Watt, M., and Richardson, A. E. (2016). Plant roots: understanding structure and function in an ocean of complexity. *Ann. Bot.* 118, 555–559. doi: 10.1093/aob/mcw192

Saadalla, M. M., Quick, J. S., and Shanahan, J. F. (1990). Heat tolerance in winter wheat: II. Membrane thermostability and field performance. *Crop Sci.* 30, 1248–1251. doi: 10.2135/cropsci1990.0011183X003000060018x

Sadras, V. O. (2009). Does partial root-zone drying improve irrigation water productivity in the field? A meta-analysis. *Irrigat. Sci.* 27, 183–190. doi: 10.1007/s00271-008-0141-0

Sage, T. L., Bagha, S., Lundsgaard-Nielsen, V., Branch, H. A., Sultmanis, S., and Sage, R. F. (2015). The effect of high temperature stress on male and female reproduction in plants. *Field Crop. Res.* 182, 30–42. doi: 10.1016/j.fcr.2015.06.011

Sailaja, B., Subrahmanyam, D., Neelamraju, S., Vishnukiran, T., Rao, Y. V., Vijayalakshmi, P., et al. (2015). Integrated physiological, biochemical, and molecular analysis identifies important traits and mechanisms associated with differential response of rice genotypes to elevated temperature. *Front. Plant. Sci.* 6:1044. doi: 10.3389/fpls.2015.01044

Sairam, R. K., and Srivastava, G. C. (2000). Induction of oxidative stress and antioxidant activity by hydrogen peroxide treatment in tolerant and susceptible wheat genotypes. *Biol. Plant.* 43, 381–386. doi: 10.1023/A:1026730008917

Sakamoto, A., and Murata, N. (2002). The role of glycine betaine in the protection of plants from stress: clues from transgenic plants. *Plant Cell Environ.* 25, 163–171. doi: 10.1046/j.0016-8025.2001.00790.x

Salem, M. A., Kakani, V. G., Koti, S., and Reddy, K. R. (2007). Pollen-based screening of soybean genotypes for high temperatures. *Crop Sci.* 47, 219–231. doi: 10.2135/cropsci2006.07.0443

Sall, A. T., Kabbaj, H., Cisse, M., Gueye, H., Ndoye, I., Maltouf, A. F., et al. (2018). Heat tolerance of durum wheat (*tritcum durum* desf.) elite germplasm tested along the senegal river. *J. Agric. Sci.* 10:217. doi: 10.5539/jas.v10n2p217

Salvi, P., Kamble, N. U., and Majee, M. (2018). Stress-inducible galactinol synthase of chickpea (CaGolS) is implicated in heat and oxidative stress

tolerance through reducing stress-induced excessive reactive oxygen species accumulation. *Plant Cell Physiol.* 59, 155–166. doi: 10.1093/pcp/pcx170

Sanchez-Reinoso, A. D., Garces-Varon, G., and Restrepo-Diaz, H. (2014). Biochemical and physiological characterization of three rice cultivars under different daytime temperature conditions. *Chil. J. Agric. Res.* 74, 373–379. doi: 10.4067/S0718-58392014000400001

Sangu, E., Tibazarwa, F. I., Nyomora, A., and Symonds, R. C. (2015). Expression of genes for the biosynthesis of compatible solutes during pollen development under heat stress in tomato (*Solanum lycopersicum*). *J. Plant Physiol.* 178, 10–16. doi: 10.1016/j.jplph.2015.02.002

Savchenko, G. E., Klyuchareva, E. A., Abramchik, L. M., and Serdyuchenko, E. V. (2002). Effect of periodic heat shock on the inner membrane system of etioplasts. *Russ. J. Plant Physiol.* 49, 349–359. doi: 10.1023/A:1015592902659

Saxena, D. C., Prasad, S. S., Parashar, R., and Rathi, I. (2016). Phenotypic characterization of specific adaptive physiological traits for heat tolerance in wheat. *Indian J. Plant Physiol.* 21, 318–322. doi: 10.1007/s40502-016-0241-4

Scafaro, A. P., Haynes, P. A., and Atwell, B. J. (2010). Physiological and molecular changes in *Oryza meridionalis* Ng., a heat-tolerant species of wild rice. *J. Exp. Bot.* 61, 191–202. doi: 10.1093/jxb/erp294

Schittenhelm, S., Langkamp-Wedde, T., Kraft, M., Kottmann, L., and Matschiner, K. (2020). Effect of two-week heat stress during grain filling on stem reserves, senescence, and grain yield of European winter wheat cultivars. *J Agro Crop Sci.* 2020, 1–12. doi: 10.1111/jac.12410

Schreiber, U., and Bilger, W. (1993). "Progress in chlorophyll fluorescence research: major developments during the past years in retrospect," in *Progress in Botany/Fortschritte der Botanik*, eds H. D. Behnke, U. Lüttge, K. Esser, J. W. Kadereit, and M. Runge (Berlin: Springer). doi: 10.1201/9780203752647-1

Seema, N., Oad, F. C., Khan, I. A., Keerio, M. I., and Tunio, S. (2014). Performance of sugarcane somaclones under different irrigation and fertilizers doses. *Pak. J. Bot.* 46, 227–232.

Sehgal, A., Sita, K., Bhandari, K., Kumar, S., Kumar, J., Vara Prasad, P. V., et al. (2019). Influence of drought and heat stress, applied independently or in combination during seed development, on qualitative and quantitative aspects of seeds of lentil (*Lens culinaris* Medikus) genotypes, differing in drought sensitivity. *Plant Cell Environ* 42, 198–211. doi: 10.1111/pce.13328

Sehgal, A., Sita, K., Kumar, J., Kumar, S., Singh, S., Siddique, K. H., et al. (2017). Effects of drought, heat and their interaction on the growth, yield and photosynthetic function of lentil (*Lens culinaris* Medikus) genotypes varying in heat and drought sensitivity. *Front. Plant Sci.* 8:1776. doi: 10.3389/fpls.2017.01776

Sehgal, A., Sita, K., Siddique, K. H. M., Kumar, R., Bhogireddy, S., Varshney, R. K., et al. (2018). Drought or/and heat-stress effects on seed filling in food crops: impacts on functional biochemistry, seed yields, and nutritional quality. *Front. Plant Sci.* 871:1705. doi: 10.3389/fpls.2018.01705

Sehgal, S. K., Kaur, S., Gupta, S., Sharma, A., Kaur, A., and Bains, N. S. (2011). A direct hybridization approach to gene transfer from *Aegilops tauschii* Coss. to *Triticum aestivum* L. *Plant Breed.* 130, 98–100. doi: 10.1111/j.1439-0523.2010.01817.x

Selvaraj, M. G., Burow, G., Burke, J. J., Belamkar, V., Puppala, N., and Burow, M. D. (2011). Heat stress screening of peanut (*Arachis hypogaea* L.) seedlings for acquired thermotolerance. *Plant Growth Regul.* 65, 83–91. doi: 10.1007/s10725-011-9577-y

Serrano, N., Ling, Y., Bahieldin, A., and Mahfouz, M. M. (2019). Thermopriming reprograms metabolic homeostasis to confer heat tolerance. *Sci. Rep.* 9, 1–14. doi: 10.1038/s41598-018-36484-z

Setimela, P. S., Andrews, D. J., Eskridge, K. M., and Partridge, J. (2007). Genetic evaluation of seedling heat tolerance in sorghum. *Afr. Crop Sci. J.* 15, 33–42.

Shanmugam, S., Kjær, K. H., Ottosen, C. O., Rosenqvist, E., Sharma, K. D., and Wollenweber, B. (2013). The alleviating effect of elevated CO2 on heat stress susceptibility of two wheat (*Triticum aestivum* L.) cultivars. *J. Agron. Crop Sci.* 199, 340–350. doi: 10.1111/jac.12023

Sharkey, T. D. (2005). Effects of moderate heat stress on photosynthesis: importance of thylakoid reactions, rubisco deactivation, reactive oxygen species, and thermotolerance provided by isoprene. *Plant Cell Environ.* 28, 269–277. doi: 10.1111/j.1365-3040.2005.01324.x

Sharma, D. K., Andersen, S. B., Ottosen, C. O., and Rosenqvist, E. (2012). Phenotyping of wheat cultivars for heat tolerance using chlorophyll a fluorescence. *Funct. Plant Biol.* 39, 936–947. doi: 10.1071/FP12100

Sharma, D. K., Andersen, S. B., Ottosen, C. O., and Rosenqvist, E. (2015). Wheat cultivars selected for high Fv/Fm under heat stress maintain high photosynthesis, total chlorophyll, stomatal conductance, transpiration and dry matter. *Physiol. Plant.* 153, 284–298.

Sharma, K. D., Boora, K. S., and Kumar, N. (2015). Plant water status, canopy temperature and chlorophyll fluorescence in relation to yield improvement in chickpea (*Cicer arietinum* L.) under soil moisture stress environments. *J. Agrometeorol.* 17, 11–16.

Sharma, D. K., Fernández, J. O., Rosenqvist, E., Ottosen, C. O., and Andersen, S. B. (2014). Genotypic response of detached leaves versus intact plants for chlorophyll fluorescence parameters under high temperature stress in wheat. *J. Plant Physiol.* 171, 576–586. doi: 10.1016/j.jplph.2013.09.025

Sharma, D. K., Torp, A. M., Rosenqvist, E., Ottosen, C. O., and Andersen, S. B. (2017). QTLs and potential candidate genes for heat stress tolerance identified from the mapping populations specifically segregating for Fv/Fm in wheat. *Front. Plant Sci.* 8:1668. doi: 10.3389/fpls.2017.01668

Sharma, L., Priya, M., Bindumadhava, H., Nair, R. M., and Nayyar, H. (2016). Influence of high temperature stress on growth, phenology and yield performance of mungbean [*Vigna radiata* (L.) Wilczek] under managed growth conditions. *Sci. Hortic.* 213, 379–391. doi: 10.1016/j.scienta.2016.10.033

Sharma, L., Priya, M., Kaushal, N., Bhandhari, K., Chaudhary, S., Dhankher, O. P., et al. (2020). Plant growth-regulating molecules as thermoprotectants: functional relevance and prospects for improving heat tolerance in food crops. *J. Exp. Bot.* 71, 569–594. doi: 10.1093/jxb/erz333

Sharma-Natu, P., Sumesh, K. V., and Ghildiyal, M. C. (2010). Heat shock protein in developing grains in relation to thermotolerance for grain growth in wheat. *J. Agron. Crop Sci.* 196, 76–80. doi: 10.1111/j.1439-037X.2009.00390.x

Shefazadeh, M. K., Mohammadi, M., and Karimizadeh, R. (2012). Genotypic difference for heat tolerance traits under real field conditions. *J. Food, Agric. Environ.* 10, 484–487.

Sheshshayee, M. S., Bindumadhava, H., Shankar, A. G., Prasad, T. G., and Udaya Kumar, M. (2003). Breeding strategies to exploit Water Use Efficiency for crop improvement. *J. Plant Biol.* 30, 253–268.

Shi, J., Yan, B., Lou, X., Ma, H., and Ruan, S. (2017). Comparative transcriptome analysis reveals the transcriptional alterations in heat-resistant and heat-sensitive sweet maize (*Zea mays* L.) varieties under heat stress. *BMC Plant Biol.* 17:973. doi: 10.1186/s12870-017-0973-y

Shi, W., Muthurajan, R., Rahman, H., Selvam, J., Peng, S., Zou, Y., et al. (2013). Source-sink dynamics and proteomic reprogramming under elevated night temperature and their impact on rice yield and grain quality. *New Phytol.* 197, 825–837. doi: 10.1111/nph.12088

Shirasawa, K., Sekii, T., Ogihara, Y., Yamada, T., Shirasawa, S., Kishitani, S., et al. (2013). Identification of the chromosomal region responsible for high-temperature stress tolerance during the grain-filling period in rice. *Mol. Breed.* 32, 223–232. doi: 10.1007/s11032-013-9864-6

Singh, A., Ganapathysubramanian, B., Singh, A. K., and Sarkar, S. (2015). Machine learning for high-throughput stress phenotyping in plants. *Trends Plant Sci.* 21, 110–124. doi: 10.1016/j.tplants.2015.10.015

Singh, V., Nguyen, C. T., van Oosterom, E. J., Chapman, S. C., Jordan, D. R., and Hammer, G. L. (2015). Sorghum genotypes differ in high temperature responses for seed set. *Field Crop. Res.* 171, 32–40. doi: 10.1016/j.fcr.2014.11.003

Singh, A. K., Ganapathysubramanian, B., Sarkar, S., and Singh, A. (2018). Deep learning for plant stress phenotyping: trends and future perspectives. *Trends Plant Sci.* 23, 883–898. doi: 10.1016/j.tplants.2018.07.004

Singh, K., Wijewardana, C., Gajanayake, B., Lokhande, S., Wallace, T., Jones, D., et al. (2018). Genotypic variability among cotton cultivars for heat and drought tolerance using reproductive and physiological traits. *Euphytica* 214, 1–22. doi: 10.1007/s10681-018-2135-1

Singh, I., Debnath, S., Gautam, A., and Yadava, P. (2020). Characterization of contrasting genotypes reveals general physiological and molecular mechanisms of heat-stress adaptation in maize (*Zea mays* L.). *Physiol. Mol. Biol. Plants.* 26, 921–929. doi: 10.1007/s12298-020-00801-6

Singh, S. K., Kakani, V. G., Brand, D., Baldwin, B., and Reddy, K. R. (2008). Assessment of cold and heat tolerance of winter-grown canola (*Brassica napus* L.) cultivars by pollen-based parameters. *J. Agron. Crop Sci.* 194, 225–236. doi: 10.1111/j.1439-037X.2008.00309.x

Sinsawat, V., Leipner, J., Stamp, P., and Fracheboud, Y. (2004). Effect of heat stress on the photosynthetic apparatus in maize (*Zea mays* L.) grown at control or high temperature. *Environ. Exp. Bot.* 52:129. doi: 10.1016/j.envexpbot.2004.01.010

Sita, K., Sehgal, A., HanumanthaRao, B., Nair, R. M., Prasad, P. V. V., Kumar, S., et al. (2017a). Food legumes and rising temperatures: effects, adaptive functional mechanisms specific to reproductive growth stage and strategies to improve heat tolerance. *Front. Plant Sci.* 8:1658. doi: 10.3389/fpls.2017.01658

Sita, K., Sehgal, A., Kumar, J., Kumar, S., Singh, S., Siddique, K. H. M., et al. (2017b). Identification of high-temperature tolerant lentil (*Lens culinaris* Medik.) genotypes through leaf and pollen traits. *Front. Plant Sci.* 8:744. doi: 10.3389/fpls.2017.00744

Smith, S., and De Smet, I. (2012). Root system architecture: insights from *Arabidopsis* and cereal crops. *Philos. Trans. R. Soc. B.* 367, 1441–1452. doi: 10.1098/rstb.2011.0234

Snider, J. L., Oosterhuis, D. M., Loka, D. A., and Kawakami, E. M. (2011). High temperature limits in vivo pollen tube growth rates by altering diurnal carbohydrate balance in field-grown *Gossypium hirsutum* pistils. *J. Plant Physiol.* 168, 1168–1175. doi: 10.1016/j.jplph.2010.12.011

Song, C., Chung, W. S., and Lim, C. O. (2016). Overexpression of heat shock factor gene HsfA3 increases galactinol levels and oxidative stress tolerance in *Arabidopsis*. *Mol. Cells* 39, 477–483. doi: 10.14348/molcells.2016.0027

Spicher, L., Glauser, G., and Kessler, F. (2016). Lipid antioxidant and galactolipid remodeling under temperature stress in tomato plants. *Front. Plant Sci.* 7:167. doi: 10.3389/fpls.2016.00167

Srinivasan, A., Takeda, H., and Senboku, T. (1996). Heat tolerance in food legumes as evaluated by cell membrane thermostability and chlorophyll fluorescence techniques. *Euphytica* 88, 35–45. doi: 10.1007/BF00029263

Srivastava, K., Kumar, S., Kumar, S., Prakash, P., and Vaishampayan, A. (2012). Screening of tomato genotypes for reproductive characters under high temperature stress conditions. *Sabrao J. Breed. Genet.* 44, 263–276.

Stief, A., Altmann, S., Homann, K., Pant, B. D., Scheible, W. R., and Baurle, I. (2014). Arabidopsis miR156 regulates tolerance to recurring environmental stress through SPL transcription factors. *Plant Cell* 26, 1792–1807. doi: 10.1105/tpc.114.123851

Strock, C. F., Burridge, J., Massas, A. S., Beaver, J., Beebe, S., Camilo, S. A., et al. (2019). Seedling root architecture and its relationship with seed yield across diverse environments in *Phaseolus vulgaris*. *Field Crops Res.* 237, 53–64. doi: 10.1016/j.fcr.2019.04.012

Sullivan, C. (1997). "Selection for drought and heat resistance in grain sorghum," in *Stress Physiology in Crop Plants*, eds H. W. Mussell, and R. C. Staples (California: Wiley), 263–281.

Sultan, S. E. (2000). Phenotypic plasticity for plant development, function and life history. *Trends Plant Sci.* 5, 537–542. doi: 10.1016/S1360-1385(00)01797-0

Sumesh, K. V., Sharma-Natu, P., and Ghildiyal, M. C. (2008). Starch synthase activity and heat shock protein in relation to thermal tolerance of developing wheat grains. *Biol. Plantarum* 52, 749–753. doi: 10.1007/s10535-008-0145-x

Sung, D. Y., Kaplan, F., Lee, K. J., and Guy, C. L. (2003). Acquired tolerance to temperature extremes. *Trends Plant Sci.* 8, 179–187. doi: 10.1016/S1360-1385(03)00047-45

Sunoj, V. J., Somayanda, I. M., Chiluwal, A., Perumal, R., Prasad, P. V., and Jagadish, S. K. (2017). Resilience of pollen and post-flowering response in diverse sorghum genotypes exposed to heat stress under field conditions. *Crop Sci.* 57, 1658–1669. doi: 10.2135/cropsci2016.08.0706

Suzuki, K., Tsukaguchi, T., Takeda, H., and Egawa, Y. (2001). Decrease of pollen stainability of green bean at high temperatures and relationship to heat tolerance. *J. Am. Soc. Hortic. Sci.* 126, 571–574. doi: 10.21273/jashs.126.5.571

Suzuki, N., Koussevitzky, S., Mittler, R., and Miller, G. (2012). ROS and redox signalling in the response of plants to abiotic stress. *Plant Cell Environ.* 35, 259–270. doi: 10.1111/j.1365-3040.2011.02336.x

Tadesse, W., Suleiman, S., Tahir, I., Sanchez-Garcia, M., Jighly, A., Hagras, A., et al. (2019). Heat-tolerant QTLs associated with grain yield and its components in spring bread wheat under heat-stressed environments of Sudan and Egypt. *Crop Sci.* 59, 199–211. doi: 10.2135/cropsci2018.06.0389

Tafesse, E. G., Gali, K. K., Lachagari, V. B., Bueckert, R., and Warkentin, T. D. (2020). Genome-wide association mapping for heat stress responsive traits in field pea. *Inter. J. Mol. Sci.* 21, 1–26. doi: 10.3390/ijms21062043

Tafesse, E. G., Warkentin, T. D., and Bueckert, R. A. (2019). Canopy architecture and leaf type as traits of heat resistance in pea. *Field Crops Res.* 241, 1–11. doi: 10.1016/j.fcr.2019.107561

Takai, T., Yano, M., and Yamamoto, T. (2010). Canopy temperature on clear and cloudy days can be used to estimate varietal differences in stomatal conductance in rice. *Field Crops Res.* 115, 165–170. doi: 10.1016/j.fcr.2009.10.019

Templer, S. E., Ammon, A., Pscheidt, D., Ciobotea, O., Schuy, C., McCollum, C., et al. (2017). Metabolite profiling of barley flag leaves under drought and combined heat and drought stress reveals metabolic QTLs for metabolites associated with antioxidant defense. *J. Exp. Bot.* 68, 1697–1713. doi: 10.1093/jxb/erx038

Thomas, H., and Howarth, C. J. (2000). Five ways to stay green. *J. Exp. Bot.* 51, 329–337. doi: 10.1093/jexbot/51.suppl_1.329

Thomason, K., Babar, M. A., Erickson, J. E., Mulvaney, M., Beecher, C., and MacDonald, G. (2018). Comparative physiological and metabolomics analysis of wheat (*Triticum aestivum* L.) following post-anthesis heat stress. *PLoS One* 13:e197919. doi: 10.1371/journal.pone.0197919

Thudi, M., Upadhyaya, H. D., Rathore, A., Gaur, P. M., Krishnamurthy, L., Roorkiwal, M., et al. (2014). Genetic dissection of drought and heat tolerance in chickpea through genome-wide and candidate gene-based association mapping approaches. *PLoS One* 9:e96758. doi: 10.1371/journal.pone.0096758

Trachsel, S., Stamp, P., and Hund, A. (2010). Effect of high temperatures, drought and aluminum toxicity on root growth of tropical maize (*Zea mays* L.) seedlings. *Maydica* 55, 249–260.

Trapero-Mozos, A., Morris, W. L., Ducreux, L. J., McLean, K., Stephens, J., Torrance, L., et al. (2017). Engineering heat tolerance in potato by temperature-dependent expression of a specific allele of HEAT SHOCK COGNATE 70. *Plant Biotech. J.* 16, 197–207. doi: 10.1111/pbi.12760

Traub, J., Porch, T., Naeem, M., Urrea, C. A., Austic, G., Kelly, J. D., et al. (2018). Screening for heat tolerance in *Phaseolus* spp. using multiple methods. *Crop Sci.* 58, 2459–2469. doi: 10.2135/cropsci2018.04.0275

Tricker, P. J., ElHabti, A., Schmidt, J., and Fleury, D. (2018). The physiological and genetic basis of combined drought and heat tolerance in wheat. *J. Exp. Bot.* 69, 3195–3210. doi: 10.1093/jxb/ery081

Ullah, N., and Chenu, K. (2019). "Impact of post-flowering heat stress on stay-green and grain development in wheat," in *Proceedings of the Australian Agronomy Conference*, Wagga Wagga, 1–4.

Upadhyaya, H. D., Dronavalli, N., Gowda, C. L. L., and Singh, S. (2011). Identification and evaluation of chickpea germplasm for tolerance to heat stress. *Crop Sci.* 51, 2079–2094. doi: 10.2135/cropsci2011.01.0018

Rahman, H., Malik, S. A., and Saleem, M. (2004). Heat tolerance of upland cotton during the fruiting stage evaluated using cellular membrane thermostability. *Field Crops Res.* 85, 149–158. doi: 10.1016/S0378-4290(03)00159-X

Urban, J., Ingwers, M., McGuire, M. A., and Teskey, R. O. (2017). Stomatal conductance increases with rising temperature. *Plant Signal. Behav.* 12, 21–24. doi: 10.1080/15592324.2017.1356534

Vacha, F., Adamec, F., Valenta, J., and Vacha, M. (2007). Spatial location of photosystem pigment-protein complexes in thylakoid membranes of chloroplasts of *Pisum sativum* studied by chlorophyll fluorescence. *J. Luminesc.* 122, 301–303. doi: 10.1016/j.jlumin.2006.01.148

Valdes-Lopez, O., Batek, J., Gomez-hernandez, N., Nguyen, C. T., Isidra-arellano, M. C., Zhang, N., et al. (2016). Soybean roots grown under heat stress show global changes in their transcriptional and proteomic profiles. *Front. Plant Sci.* 7:517. doi: 10.3389/fpls.2016.00517

Van der Tol, C., Berry, J. A., Campbell, P. K. E., and Rascher, U. (2014). Models of fluorescence and photosynthesis for interpreting measurements of solar-induced chlorophyll fluorescence. *J. Geophys. Res. Biogeosci.* 119, 2312–2327. doi: 10.1002/2014JG002713

Van der Westhuizen, M. M., Oosterhuis, D. M., Berner, J. M., and Boogaers, N. (2020). Chlorophyll a fluorescence as an indicator of heat stress in cotton (*Gossypium hirsutum* L.). *S. Afr. J. Plant Soil.* 37, 116–119. doi: 10.1080/02571862.2019.1665721

Varshney, R. K., Thudi, M., Roorkiwal, M., He, W., Upadhyaya, H. D., Yang, W., et al. (2019). Resequencing of 429 chickpea accessions from 45 countries provides insights into genome diversity, domestication and agronomic traits. *Nat. Genet.* 51, 857–864. doi: 10.1038/s41588-019-0401-3

Vierling, E. (1991). The roles of heat shock proteins in plants. *Annu. Rev. Plant Physiol. Plant Mol. Biol.* 42, 579–620. doi: 10.1146/annurev.pp.42.060191.003051

Vijayalakshmi, K., Fritz, A. K., Paulsen, G. M., Bai, G., Pandravada, S., and Gill, B. S. (2010). Modeling and mapping QTL for senescence-related traits in winter wheat under high temperature. *Mol. Breed.* 26, 163–175. doi: 10.1007/s11032-009-9366-8

Vollenweider, P., and Günthardt-Goerg, M. S. (2005). Diagnosis of abiotic and biotic stress factors using the visible symptoms in foliage. *Environ. Pollut.* 137, 455–465. doi: 10.1016/j.envpol.2005.01.032

Wahid, A., Gelani, S., Ashraf, M., and Foolad, M. R. (2007). Heat tolerance in plants: an overview. *Environ. Exp. Bot.* 61, 199–223. doi: 10.1016/j.envexpbot.2007.05.011

Wahid, A., and Shabbir, A. (2005). Induction of heat stress tolerance in barley seedlings by pre-sowing seed treatment with glycinebetaine. *Plant Growth Regul.* 46, 133–141. doi: 10.1007/s10725-005-8379-5

Wang, L., Yu, X., Wang, H., Lu, Y. Z., de Ruiter, M., Prins, M., et al. (2011). A novel class of heat-responsive small RNAs derived from the chloroplast genome of Chinese cabbage (*Brassica rapa*). *BMC Genom.* 12:289. doi: 10.1186/1471-2164-12-289

Wang, W., Vinocur, B., Shoseyov, O., and Altman, A. (2004). Role of plant heat-shock proteins and molecular chaperones in the abiotic stress response. *Trends Plant Sci.* 9, 244–252. doi: 10.1016/j.tplants.2004.03.006

Wang, Z., Ke, Q., Kim, M. D., Kim, S. H., Ji, C. Y., Jeong, J. C., et al. (2015). Transgenic alfalfa plants expressing the sweetpotato Orange gene exhibit enhanced abiotic stress tolerance. *PLoS One* 10:e0126050. doi: 10.1371/journal.pone.0126050

Wassie, M., Zhang, W., Zhang, Q., Ji, K., and Chen, L. (2019). Effect of heat stress on growth and physiological traits of alfalfa (*Medicago sativa* L .) and a comprehensive evaluation for heat tolerance. *Agron.* 9, 1–20. doi: 10.3390/agronomy9100597

Waters, E. R., Lee, G. J., and Vierling, E. (1996). Evolution, structure and function of the small heat shock proteins in plants. *J. Exp. Bot.* 47, 325–338. doi: 10.1093/jxb/47.3.325

Weckwerth, W., Ghatak, A., Bellaire, A., Chaturvedi, P., and Varshney, R. K. (2020). Panomics meets germplasm. *Plant Biotechnol. J.* 18, 1507–1525. doi: 10.1111/pbi.13372

Wei, H., Liu, J., Wang, Y., Huang, N., Zhang, X., Wang, L., et al. (2013). A Dominant major locus in chromosome 9 of rice (*Oryza sativa* L) confers tolerance to 48°C high temperature at seedling stage. *J. Hered.* 104, 287–294. doi: 10.1093/jhered/ess103

Wen, J., Jiang, F., Weng, Y., Sun, M., Shi, X., Zhou, Y., et al. (2019). Identification of heat-tolerance QTLs and high-temperature stress-responsive genes through conventional QTL mapping, QTL-seq and RNA-seq in tomato. *BMC Plant Biol.* 19:398. doi: 10.1186/s12870-019-2008-3

Weng, J. H., and Lai, M. F. (2005). Estimating heat tolerance among plant species by two chlorophyll fluorescence parameters. *Photosynthetica* 43, 439–444. doi: 10.1007/s11099-005-0070-6

Willits, D. H., and Peet, M. M. (2001). Measurement of chlorophyll fluorescence as a heat stress indicator in tomato: laboratory and greenhouse comparisons. *J. Am. Soc. Hortic. Sci.* 126, 188–194. doi: 10.21273/JASHS.126.2.188

Wilson, R. A., Sangha, M. K., Banga, S. S., Atwal, A. K., and Gupta, S. (2014). Heat stress tolerance in relation to oxidative stress and antioxidants in *Brassica juncea*. *J. Environ. Biol.* 35, 383–387.

Wu, T., Weaver, D. B., Locy, R. D., McElroy, S., and van Santen, E. (2014). Identification of vegetative heat-tolerant upland cotton (*Gossypium hirsutum* L.) germplasm utilizing chlorophyll fluorescence measurement during heat stress. *Plant Breed.* 133, 250–255. doi: 10.1111/pbr.12139

Wu, W., Duncan, R. W., and Ma, B. L. (2017). Quantification of canola root morphological traits under heat and drought stresses with electrical measurements. *Plant Soil* 415, 229–244. doi: 10.1007/s11104-016-3155-z

Wu, W., Ma, B. L., and Whalen, J. K. (2018). Enhancing rapeseed tolerance to heat and drought stresses in a changing climate: perspectives for stress adaptation from root system architecture. *Adv. Agron.* 151, 87–157. doi: 10.1016/bs.agron.2018.05.002

Xin, M., Wang, Y., Yao, Y., Song, N., Hu, Z., Qin, D., et al. (2011). Identification and characterization of wheat long non-protein coding RNAs responsive to powdery mildew infection and heat stress by using microarray analysis and SBS sequencing. *BMC Plant Biol.* 11:61. doi: 10.1186/1471-2229-11-61

Xin, M., Wang, Y., Yao, Y., Xie, C., Peng, H., Ni, Z., et al. (2010). Diverse set of microRNAs are responsive to powdery mildew infection and heat stress in wheat (*Triticum aestivum* L.). *BMC Plant Biol.* 10:123. doi: 10.1186/1471-2229-10-123

Xu, J., Driedonks, N., Rutten, M. J. M., Vriezen, W. H., de Boer, G. J., and Rieu, I. (2017). Mapping quantitative trait loci for heat tolerance of reproductive traits in tomato (*Solanum lycopersicum*). *Mol Breed* 37.

Xu, Q., and Huang, B. (2000). Effects of differential air and soil temperature on carbohydrate metabolism in creeping bentgrass. *Crop Sci.* 40, 1368–1374. doi: 10.2135/cropsci2000.4051368x

Xu, S., Li, J., Zhang, X., Wei, H., and Cui, L. (2006). Effects of heat acclimation pretreatment on changes of membrane lipid peroxidation, antioxidant metabolites, and ultrastructure of chloroplasts in two cool-season turfgrass species under heat stress. *Environ. Exp. Bot.* 56, 274–285. doi: 10.1016/j.envexpbot.2005.03.002

Xu, Y., Zhan, C., and Huang, B. (2011). Heat shock proteins in association with heat tolerance in grasses. *Int. J. Proteomics.* 2011, 1–11. doi: 10.1155/2011/529648

Yadav, A. K., Arya, R. K., and Narwal, M. S. (2014). Screening of pearl millet F1 hybrids for heat tolerance at early seedling stage. *Adv. Agric.* 2014:231301.

Yamada, M., Hidaka, T., and Fukamachi, H. (1996). Heat tolerance in leaves of tropical fruit crops as measured by chlorophyll fluorescence. *Sci. Hortic.* 67, 39–48. doi: 10.1016/S0304-4238(96)00931-4

Ye, C., Argayoso, M. A., Redoña, E. D., Sierra, S. N., Laza, M. A., Dilla, C. J., et al. (2012). Mapping QTL for heat tolerance at flowering stage in rice using SNP markers. *Plant Breed.* 131, 33–41. doi: 10.1111/j.1439-0523.2011.01924.x

Yin, X., Guo, W., and Spiertz, J. H. (2009). A quantitative approach to characterize sink-source relationships during grain filling in contrasting wheat genotypes. *Field Crop. Res.* 114, 119–126. doi: 10.1016/j.fcr.2009.07.013

Young, L. W., Wilen, R. W., and Bonham-Smith, P. C. (2004). High temperature stress of Brassica napus during flowering reduces micro- and megagametophyte fertility, induces fruit abortion, and disrupts seed production. *J. Exp. Bot.* 55, 485–495. doi: 10.1093/jxb/erh038

Yu, E., Fan, C., Yang, Q., Li, X., Wan, B., Dong, Y., et al. (2014). Identification of heat responsive genes in *Brassica napus* siliques at the seed-filling stage through transcriptional profiling. *PLoS One* 9:e101714. doi: 10.1371/journal.pone.0101914

Yu, J., Su, D., Yang, D., Dong, T., Tang, Z., Li, H., et al. (2020). Chilling and heat stress-induced physiological changes and MicroRNA-Related Mechanism in Sweetpotato (*Ipomoea batatas* L.). *Front. Plant Sci.* 11:687. doi: 10.3389/fpls.2020.00687

Yu, X., Yang, J., Li, X., Liu, X., Sun, C., Wu, F., et al. (2013). Global analysis of cis-natural antisense transcripts and their heat-responsive nat-siRNAs in *Brassica rapa*. *BMC Plant Biol.* 13:208. doi: 10.1186/1471-2229-13-208

Yuan, Y., Cairns, J. E., Babu, R., Gowda, M., Makumbi, D., Magorokosho, C., et al. (2019). Genome-wide association mapping and genomic prediction analyses reveal the genetic architecture of grain yield and flowering time under drought and heat stress conditions in maize. *Front. Plant Sci.* 9:1919. doi: 10.3389/fpls.2018.01919

Zhang, H.-Y., Lei, G., Zhou, H. W., He, C., Liao, J. L., and Huang, Y. J. (2017). Quantitative iTRAQ-based proteomic analysis of rice grains to assess high night temperature stress. *Proteomics* 17:1600365. doi: 10.1002/pmic.201600365

Zhang, J., Jiang, X. D., Li, T. L., and Cao, X. J. (2014). Photosynthesis and ultrastructure of photosynthetic apparatus in tomato leaves under elevated temperature. *Photosynthetica* 52, 430–436. doi: 10.1007/s11099-014-0051-8

Zhao, P., Wang, D., Wang, R., Kong, N., Zhang, C., Yang, C., et al. (2018). Genome-wide analysis of the potato Hsp20gene family: identification, genomic organization and expression profiles in response to heat stress. *BMC Genomics* 19:61. doi: 10.1186/s12864-018-4443-1

Zhao, Y., Hu, F., Zhang, X., Wei, Q., Dong, J., Bo, C., et al. (2019). Comparative transcriptome analysis reveals important roles of nonadditive genes in maize hybrid An'nong 591 under heat stress. *BMC Plant Biol.* 19:273. doi: 10.1186/s12870-019-1878-8

Zhou, R., Kjaer, K. H., Rosenqvist, E., Yu, X., Wu, Z., and Ottosen, C. O. (2017). Physiological response to heat stress during seedling and anthesis stage in

tomato genotypes differing in heat tolerance. *J. Agron. Crop Sci.* 203, 68–80. doi: 10.1111/jac.12166

Zhou, R., Kong, L., Yu, X., Ottosen, C. O., Zhao, T., Jiang, F., et al. (2019). Oxidative damage and antioxidant mechanism in tomatoes responding to drought and heat stress. *Acta Physiol. Plant.* 41, 1–11. doi: 10.1007/s11738-019-2805-2801

Zhou, R., Wu, Z., Wang, X., Rosenqvist, E., Wang, Y., Zhao, T., et al. (2018). Evaluation of temperature stress tolerance in cultivated and wild tomatoes using photosynthesis and chlorophyll fluorescence. *Hortic. Environ. Biotech.* 59, 499–509. doi: 10.1007/s13580-018-0050-y

Zhou, R., Yu, X., Kjær, K. H., Rosenqvist, E., Ottosen, C. O., and Wu, Z. (2015). Screening and validation of tomato genotypes under heat stress using Fv/Fm to reveal the physiological mechanism of heat tolerance. *Environ. Exp. Bot.* 118, 1–11. doi: 10.1016/j.envexpbot.2015.05.006

Conflict of Interest: The authors declare that the research was conducted in the absence of any commercial or financial relationships that could be construed as a potential conflict of interest.

The reviewer PK declared a past co-authorship with one of the authors KS to the handling editor.

Copyright © 2020 Chaudhary, Devi, Bhardwaj, Jha, Sharma, Prasad, Siddique, Bindumadhava, Kumar and Nayyar. This is an open-access article distributed under the terms of the Creative Commons Attribution License (CC BY). The use, distribution or reproduction in other forums is permitted, provided the original author(s) and the copyright owner(s) are credited and that the original publication in this journal is cited, in accordance with accepted academic practice. No use, distribution or reproduction is permitted which does not comply with these terms.

frontiers in Plant Science

ORIGINAL RESEARCH
published: 11 November 2020
doi: 10.3389/fpls.2020.576505

Cultivar Variation in Tomato Seed Coat Permeability Is an Important Determinant of Jasmonic Acid Elicited Defenses Against Western Flower Thrips

Sanae Mouden[1,2], Iris F. Kappers[3], Peter G. L. Klinkhamer[1] and Kirsten A. Leiss[3]*

[1] Plant Science and Natural Products, Institute of Biology, Leiden University, Leiden, Netherlands, [2] Business Unit Horticulture, Wageningen University and Research, Bleiswijk, Netherlands, [3] Laboratory of Plant Physiology, Wageningen University and Research, Wageningen, Netherlands

Induction of defenses is one of the most widely accepted eco-friendly approaches for management of pests and diseases. Seeds are receptive to resistance-inducing chemicals and could offer broad-spectrum protection at the early stages of development. However, seed treatment with elicitors has previously been shown to differentially influence induced defense responses among cultivars and thus, could hamper commercial exploitation. In this context, the objective of the present study was to evaluate the genotype-dependent ability of jasmonic acid (JA) to induce resistance against western flower thrips (WFT) at the seed stage. We examined the variation in inducibility of resistance in eight commercial tomato cultivars. Causal factors accounting for discrepancies in JA-induced responses at the seed stage were phenotypically and biochemically evaluated. Seed receptivity to exogenous JA appeared to be cultivar dependent. Thrips associated silver damage was only reduced in JA seed-treated plants of cultivar Carousel. Enhancement of resistance, was not associated with activation of defense-related traits such as polyphenol oxidase activity (PPO), trichomes or volatiles. Sulfuric acid scarification, prior to JA seed incubation, significantly augmented the embryonic responsiveness to JA in cv. Moneymaker without an adverse effect on growth. Hence, these results support the hypothesis that seed coat permeability is a key factor for successfully inducing JA mediated thrips defenses. The outcome of our study is of translational value as it creates opportunities for the seed industry to perform pre-treatments on non-responsive cultivars as well as for tomato breeding programs to select for genetic traits that affect seed permeability.

Keywords: induced resistance, seed receptivity, elicitor, *Frankliniella occidentalis*, scarification, *Solanum lycopersicum*

OPEN ACCESS

Edited by:
Guihua Bai,
United States Department of Agriculture (USDA), United States

Reviewed by:
Isabel Diaz,
Polytechnic University of Madrid, Spain
Arafat Abdel Hamed Abdel Latef,
South Valley University, Egypt

****Correspondence:***
Sanae Mouden
sanae.mouden@wur.nl;
samouden@yahoo.com

Specialty section:
This article was submitted to Plant Abiotic Stress, a section of the journal Frontiers in Plant Science

Received: *26 June 2020*
Accepted: *14 October 2020*
Published: *11 November 2020*

Citation:
Mouden S, Kappers IF, Klinkhamer PGL and Leiss KA (2020) Cultivar Variation in Tomato Seed Coat Permeability Is an Important Determinant of Jasmonic Acid Elicited Defenses Against Western Flower Thrips. Front. Plant Sci. 11:576505. doi: 10.3389/fpls.2020.576505

INTRODUCTION

Plants are continuously under attack by a variety of pests and pathogens. Besides constitutive defenses, plants may also deploy inducible defenses that are activated in response to an attack. The expression of inducible defenses is primarily mediated by endogenous signaling molecules, among which the phytohormone jasmonic acid (JA) plays a key role in resistance against herbivorous

arthropods and necrotrophic pathogens (Howe and Jander, 2008; Pieterse et al., 2012). For several decades it is known that activation of the JA signaling pathway is characterized by induction of multiple defensive traits including secondary metabolites (Bennett and Wallsgrove, 1994; War et al., 2012), proteins (Farmer and Ryan, 1990; Thaler et al., 1996), leaf trichomes (Boughton et al., 2005) as well as indirect induction mechanisms such as the production of plant volatiles (Ament et al., 2004; Arimura et al., 2005). Plant signals responsible for inducing resistance are highly conserved among plant species. Accordingly, artificial manipulation of these JA-associated defenses by natural or synthetic elicitors has proven to confer enhanced resistance against multiple insects and diseases and is, therefore, regarded as a valuable component in pest management programs (Thaler, 1999; Vallad and Goodman, 2004; Walters et al., 2013; Steenbergen et al., 2018).

Despite the long-standing importance of jasmonates in plant resistance, commercial applications have up to date met with rather limited success, as induced defenses are often associated with yield penalties (Cipollini et al., 2003; Walters and Heil, 2007). However, JA application does not necessarily lead to direct activation of defense mechanisms, as it may also condition a plant for boosted responses to future attacks, a phenomenon commonly known as priming (Conrath et al., 2006; Martinez-Medina et al., 2016; Mauch-Mani et al., 2017). The prospects of broad-spectrum enhanced resistance provided by priming has led to increased interest in the development of agents which can mimic natural inducers of resistance, particularly because priming is expected to cause a positive cost-benefit balance in times of stress (Van Hulten et al., 2006).

The vast majority of studies on JA induction focused on foliar application and root drenches, whereas the use of elicitors in seed treatments has been investigated less vigorously despite the fact that seedlings and young juvenile plants can be particularly more vulnerable to herbivory (Moles and Westoby, 2004; Barton and Hanley, 2013; Ochoa-López et al., 2015). Worrall et al. (2012) demonstrated that tomato seeds are receptive to plant defense activators and, thus, are able to activate herbivore resistance responses by stimulating the plant's own defense mechanisms. Plants grown from JA-treated seeds exhibited long-lasting increased resistance against herbivores of multiple arthropod taxa, persisting over 8 weeks, without concurrent impact on plant growth. These findings were corroborated by Paudel et al. (2014) and Strapasson et al. (2014), who demonstrated that seed soaking of tomato cultivars Micro-Tom and Santa-Clara with methyl jasmonate (MeJA) induced durable resistance against herbivory by *Helicoverpa zea* and *Tuta absoluta*, respectively. Hence, seed treatments can be particularly useful in activation of induced resistance, especially for crops which are likely to face pest and pathogen attack early in the growing season. Intriguingly, JA seed treatment of the tomato cultivar " Moneymaker" failed to induce resistance against *Tetranychus urticae*, whereas a significant reduction in oviposition on JA-seed treated plants was observed in the tomato cultivar " Carousel" (Smart et al., 2013). Whilst the mechanisms behind these differential responses remain unclear, differences in the availability of inducible defense genes have been suggested to play an important role. The phenomenon of genetic variation in inducibility of resistance has been demonstrated in numerous studies, however, the majority of these considered variation in plant responsiveness caused by pests and pathogens rather than variation in defense responses elicited by chemicals (Degen et al., 2004; Sharma et al., 2010; Bruce, 2014). Alternatively, genetic factors underpinning seed coat permeability may also explain variations in elicitor induced responses across cultivars. The existence of a semi-permeable layer has been extensively reported in several species, including tomato, yet its importance for seed treatments has rarely been addressed (Salanenka and Taylor, 2011). Seed uptake of JA is pivotal and insufficient penetration into the seed would fail to activate defenses. For potential inclusion of elicitors in integrated pest management (IPM) programs it is, therefore, of importance to understand how these factors potentially affect plant resistance mechanisms.

To date, little is known about differences in elicitor-mediated induced resistance during the seed stage. This prompted us to evaluate several key questions concerning the inducibility of resistance against western flower thrips (WFT; *Frankliniella occidentalis*) by exogenous application of JA at the seed stage. Western flower thrips is one of the most economically important pest insects worldwide (Mouden et al., 2017). This polyphagous insect causes extensive damage in agriculture through feeding, oviposition as well as through the transmission of tospoviruses. Artificial induction of JA-mediated defenses has been reported to increase resistance to thrips in cotton (Omer et al., 2001), Chinese cabbage (Abe et al., 2009), and tomato (Escobar-Bravo et al., 2017).

In the present study, we addressed the following questions: (i) can tomato seed treatments with JA confer resistance to WFT? (ii) if so, are the defense responses against thrips elicited by JA seed soaking cultivar dependent? (iii) what mechanisms underlie this elicitor-mediated resistance? and (iv) can tomato seed scarification, prior to exogenous JA seed treatment, augment thrips resistance in cultivars that are non-responsive?

MATERIALS AND METHODS

Seed Treatments and Growth Conditions

Seed treatments were performed as previously described by Worrall et al. (2012) with slight modifications. Briefly, a jasmonic acid stock solution (0.476 M) was purchased from Cayman Chemical Company (United States) containing 1 g JA in 10 ml absolute ethanol which was diluted to appropriate concentrations prior to use. Tomato seeds were soaked in an excess amount of freshly prepared dilutions of the JA stock solvent and incubated at 4°C in a rotary shaker for 24 h to facilitate the penetration of JA into the seeds. Control seeds were soaked in a mock solution consisting of aqueous ethanol under the same conditions. Following incubation, seeds were thoroughly washed in aqueous ethanol followed by sterilized MilliQ water. Subsequently, seeds were randomly sown in plastic trays filled with potting soil (Horticoop, Lentse Potgrond, Netherlands) and placed in a climate room provided with 113.6 μmol photons m^{-2} s^{-1} of photosynthetically active radiation (PAR) and a

photoperiod of 16/8 h light/dark, at 20°C and 70% RH. 10 days later, seedlings were transplanted into individual plastic pots (11 × 11 × 12 cm) and grown under the same conditions for a period of 4 weeks. Pots were watered when needed.

Non-choice Whole Plant Thrips Bioassay

A non-choice whole plant bioassay was used to evaluate tomato resistance against WFT (Leiss et al., 2009). Four-week old tomato plants were individually placed in thrips-proof cages consisting of a perspex cylinder (50 cm height, 20 cm diameter) closed at one end with a displaceable ring of nylon gauze of 120 μm mesh size. Plants were randomly placed in a climate-controlled growth chamber at a constant temperature of 25°C, a photoperiod of 16L:8D and 70% RH. For thrips infestation 20 adult thrips (18 females and 2 males) were collected using a mouth-operated aspirator and were then released inside the cage. Western flower thrips were obtained from a colony reared on chrysanthemum flowers (cultivar Euro Sunny) maintained in a climate room at 25°C and 70% RH. Seven days after infestation, thrips feeding damage, hereafter referred to as "silver damage" was evaluated by visually scoring all leaves. Silver damage was expressed as total damaged leaf area in mm^2.

Comparison of JA Seed and Foliar Treatments

To explore the potential of JA as an active inducer of systemic resistance at the seed stage, we aimed to determine its capacity to induce resistance to WFT and the consequent implication onproduction of defensive response markers (i.e., polyphenol oxidase) in tomato. For this, the systemic nature of JA-induced protection against WFT was evaluated by comparing the efficacy of two application methods namely: foliar spray and seed soaking. Seeds of the tomato cultivar Virona (provided by Incotec International BV, Enkhuizen, Netherlands) were immersed in JA solutions at concentrations ranging from 0.1 to 5 mM JA, under the same conditions as described above. Seeds treated with aqueous ethanol were used as controls. For foliar application, treatment concentrations and controls were equal to those used in seed treatments. To avoid direct toxic effects of foliar applied JA, 2 ml aliquots were uniformly sprayed 72 h prior to thrips infestation. Four weeks old plants were subjected to a non-choice whole plant thrips bioassay (n = 10). Plant growth parameters were measured prior to infestation, to evaluate potential growth effects. Furthermore, we explored plant defense responses triggered upon JA treatments by measuring the activity of the defense-related marker protein polyphenol-oxidase in non-infested plants (PPO; n = 4).

Genotypic Variation in JA Seed Receptivity

To determine responsiveness of tomato seeds to JA induced defenses against WFT, an additional eight different cultivars were evaluated. Tomato cultivars, Carousel, 72-323, Mahitos untreated, Mahitos commercial (hydro-primed seeds), Brioso, Trovanzo and Raymos were kindly provided by Rijk Zwaan (de Lier, Netherlands), whereas cv. Moneymaker was obtained from Pieterpikzonen BV (Luinjeberd, Netherlands). The selected commercial tomato cultivars varied in fruit type, with the majority of cultivars producing classic round tomatoes. Brioso, on the other hand, was characterized as cocktail-type whereas, Mahitos produces beef tomatoes. Four weeks old plants, grown from JA (3 mM) or mock treated seeds, were subjected to a non-choice whole plant thrips bioassay (n = 10) or sampled for polyphenol oxidase (PPO) activity analysis (n = 7–8).

Differences in Water Permeability Among Seeds of Different Cultivars

To explore whether permeability differences among cultivars contribute to the variability in JA responsiveness, an imbibition test was carried out by monitoring the fresh seed mass increase in the eight selected cultivars. Hundred seeds, separated into four replicates of 25 seeds each, were used for this test and weighed to the nearest 0.0001 g. Seeds were fully submerged in a freshly prepared solution of 3 mM jasmonic acid and kept at 4°C. The seeds were blotted and weighed at indicated time intervals for 24 h. The percentage mass increase (fresh mass basis) for each interval was calculated as % increase in mass = $[(W_i - W_d)/W_d] \times 100$, where W_i = mass of imbibed and W_d = mass of dry seeds (Baskin et al., 2004).

Improvement of JA Seed Receptivity by Scarification

With the aim to explore whether seed scarification could augment JA receptivity at the seed stage, we evaluated the effect of scarification on JA-induced defenses against WFT, using tomato seeds of one of the non-responsive tomato cultivars. Initially, three scarification methods were evaluated in cultivar Virona. For mechanical scarification, seeds were individually scarified by a razor blade. Chemical scarification was performed with 10% sulfuric acid. A non-specified commercial scarification method was carried out by the seed company Incotec International BV (Enkhuizen, Netherlands). Non scarified seeds served as control. Preliminary experimental results demonstrated that chemical scarification with sulfuric acid, prior to JA soaking, was the most potential method to improve thrips resistance in cv. Virona. In a follow-up experiment, seeds of the unresponsive tomato cultivar Moneymaker and the JA-seed receptive cultivar Carousel were used to study the effect of scarification on JA-inducibility. Tomato seeds were chemically scarified with 10% sulfuric acid (H_2SO_4) for 5 min and shaken on a platform shaker at slow to moderate speed. After exposure, seeds were thoroughly washed with distilled water to remove residual sulfuric acid and subjected to JA (3 mM) soaking as previously described. Four weeks old plants were evaluated for thrips silver damage 7 days after infestation using a non-choice bioassay.

PPO Activity

Polyphenol oxidase (PPO) activity was determined in non-infested plants by sampling one leaflet taken from the third leaf from the bottom, following the protocol described in Stout et al. (1998). In brief, 150 mg of fresh leaf material was flash frozen in liquid nitrogen and stored at −80°C until analysis

for PPO activity. The enzyme was extracted by homogenizing ground plant material in 1.25 ml ice-cold potassium phosphate buffer (0.1 M, pH 6.8) containing 7% polyvinyl polypyrolidine, and 400 µl of 10% Triton X-100. Extracts were vortexed for 2 min and centrifuged at 11,000 × g for 10 min at 4°C. The supernatant was then collected as the crude enzyme extract. PPO activity was measured immediately after the extract was obtained. Activity was assayed by measuring the oxidation of chlorogenic acid as substrate in a reaction mixture containing 5 µl of the enzyme extract and 1 ml of 2.92 mM chlorogenic acid prepared in 0.1 M potassium phosphate buffer at pH 8.0. The increase in absorbance at 470 nm was measured spectrophotometrically (UV-1800 UV-VIS spectrophotometer, Shimadzu Europe GmbH, Duisburg, Germany) for 1 min. PPO activity was expressed as changes in absorbance values per min per gram of fresh weight.

Determination of Type VI Glandular Trichome Density

In tomato, foliar application of JA or its volatile derivative methyl jasmonate has been reported to induce the production of type-VI leaf glandular trichomes (Escobar-Bravo et al., 2017; Chen et al., 2018). To investigate whether exogenous JA seed treatment also influenced physical leaf properties, we measured the density of type-VI glandular trichomes following the methodology described by Chen et al. (2018). The second terminal leaflet from the third youngest and fully expanded leaf was sampled in 4 weeks old plants grown from mock- and JA-treated seeds. A Leica stereomicroscope (MZ16, Leica Microsystems, Wetzlar Germany) equipped with a Leica DFC420 digital camera was used to take pictures on the adaxial surface at both sides of the main vein in the middle section of the leaflet. Trichomes were counted in an area of 12 mm^2 using Fiji ImageJ software[1] and expressed as the number of type-VI trichomes per centimeter square.

GC-MS Analysis of Terpenes

Artificial induction of type-VI glandular trichomes and their associated volatiles has been related to increased levels of resistance against diverse herbivorous arthropods (Kang et al., 2010; Tian et al., 2012; Escobar-Bravo et al., 2017) Terpene production from type-VI trichome-derived leaf exudates was evaluated using the leaf dip method. This protocol was chosen because the terpenoid profile detected in individually collected type VI glands has been shown to be nearly identical to that observed with the leaf dip procedure (Kang et al., 2010, 2014). Four weeks after initial seed treatment, two leaflets belonging to the same leaf used for trichome density measurement, were sampled and leaf fresh weight was measured before extraction. Leaf exudates were obtained by dipping the leaf tissue in 2 ml of pentane. Following an incubation period of 2 min with gentle shaking, leaflets were discarded, and the extracts were analyzed by gas chromatography-mass spectrometry (Kappers et al., 2011). Two microliter of pentane extracts were splitless analyzed on a Hewlett–Packard GC-MS system consisting of a gas chromatograph (5,890 series II, Hewlett–Packard) equipped with DB-5MS column (30 m × 0.25 mm, 0.25 µm film thickness) and a mass-selective detector (model 5972A, Hewlett–Packard). Compounds were identified by comparing retention times and mass spectra with those of authentic standards and reported in Adams (2007). The area under the curve of selected compounds was calculated to be representative for the concentration.

[1]http://fiji.sc/Fiji

Statistical Analysis

Normal distributions were tested by Shapiro-Wilk tests and homogeneity of variances were determined by Levene's tests. Means were analyzed using one-way ANOVA followed by Fisher's least significance difference (LSD) *post hoc* test. When assumptions were violated, data transformations were performed or differences in means were compared using the nonparametric Kruskal-Wallis-test or Welch's ANOVA. Data on number of leaves were analyzed by Kruskal-Wallis followed by Dunn's test with Bonferroni correction for multiple comparisons. The effect of foliar JA application on silver damage and PPO activity were analyzed by Welch Anova followed by Games-Howell *post-hoc*. Generalized Linear Models (GLM) using linear distribution and identity link functions were used to analyze the effect of cultivar, seed treatment and their interaction on silver damage, PPO activity, number of trichomes, volatile emission and dry mass. Data on silver damage obtained from the scarification experiment were square root transformed and subsequently analyzed by GLM. Differences among groups were tested by Fisher's LSD *post-hoc* test. All statistical analyses were conducted with SPSS v. 24 software (IBM; SPSS Inc., Chicago, IL, United States).

RESULTS

Effect of Elicitor Application on Thrips Feeding Damage

To explore the potential of JA as an active inducer of systemic resistance at the seed stage, we firstly compared seed responsiveness to foliar applied JA in tomato cv. Virona. Foliar application of JA caused a marked reduction in silver damage compared to mock-treated Virona plants (Welch's $F_{(5,24.27)} = 7.53$, $p \leq 0.001$). With the exception of 0.1 mM JA, significant reductions in damage were observed, ranging between 53 and 97% (**Figure 1A**). The pattern of responses to thrips damage mirrored the induction of PPO (**Figure 1C**). Levels of PPO were greatly enhanced in response to foliar application of JA, showing a dose-dependent trend (Welch's $F_{(5,7.34)} = 44.23$, $p \leq 0.001$). Next, we compared the efficacy of foliar applied JA in suppressing silver damage with the efficacy of seed applied JA (**Figures 1A,B**, respectively). In contrast to foliar application, exogenous application of different JA doses to the seed did not affect total silver damage ($H(5) = 4.839$, $p = 0.436$). The lack of increased resistance levels to thrips corresponded with the measured PPO levels (**Figure 1D**). PPO activity was not increased in JA seed treated plants ($F_{(5,18)} = 0.295$, $p = 0.909$). Costs of foliar or seed JA treatment related to yield were investigated. The impact of seed soaking on plant performance were minimal. Whereas seed exposure to 5 mM JA adversely affected tomato growth, seeds pre-treated with intermediate concentrations of JA

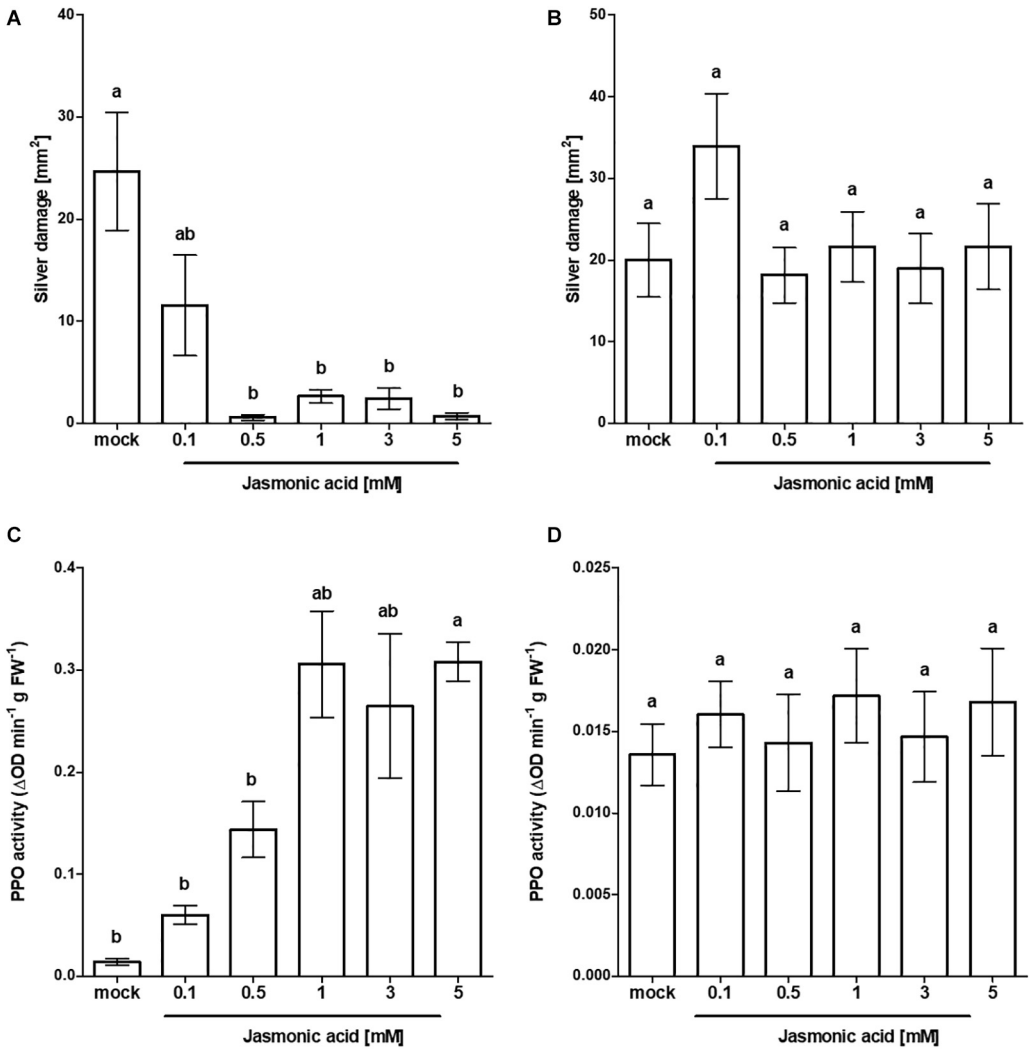


FIGURE 1 | Effect of exogenous JA treatment on tomato resistance to WFT and JA-associated responses. Silver damage symptoms in tomato plants (cv. Virona) following **(A)** foliar application of JA or **(B)** JA seed treatment at different concentrations (n = 10). Four-week old plants were infested with WFT for 1 week or sampled for polyphenol oxidase (PPO) activity. PPO activity (n = 4) was measured in the third leaf from the bottom in **(C)** JA foliar treated plants or in **(D)** JA-seed treated plants. Data are presented as mean ± SEM. Different letters indicate significant differences among treatments (Welch ANOVA followed by Games–Howell at $P < 0.05$).

(1 and 3 mM) surprisingly caused a stimulatory effect on plant dry mass (**Supplementary Table S1**).

Exploring JA Seed Receptivity Among Tomato Cultivars

In the previous experiment, seed applied JA had no effect on silver damage in tomato cultivar Virona. Yet, application of JA as a seed soaking treatment in cultivar Carousel was capable of improving resistance against WFT (**Supplementary Figure S1**). Thus, we further examined variation among cultivars in the efficacy of thrips resistance induced by seed application of JA. Concomitantly, we evaluated whether seed applied JA affected the induction of the JA-associated marker polyphenol oxidase. Four weeks old plants of eight different tomato cultivars, grown from JA or mock treated seeds, were challenged with WFT (**Figure 2A**). Overall, JA seed treatment had no significant effect on silver damage, but symptoms were affected by plant genotype (GLM: Wald $\chi^2 = 38.94$, $p < 0.001$ for cultivar; Wald $\chi^2 = 0.60$, $p = 0.438$ for treatment and Wald $\chi^2 = 11.87$, $p = 0.105$ for the interaction). However, as in our preliminary experiment with Carousel, a strong reduction in silver damage symptoms was observed in JA seed treated Carousel plants. Such a reduction was absent in the remaining other seven cultivars. Silver damage symptoms of plants grown from untreated seeds, revealed that the eight cultivars varied inherently in susceptibility, from cultivar Raymos being moderately resistant with 40.6 ± 7.4 mm2 silver damage to cultivars Moneymaker and Carousel being highly susceptible with 123.1 ± 23.9 and 123.9 ± 20.1 mm^2 damage, respectively. Furthermore, we observed that the seed treatment was not

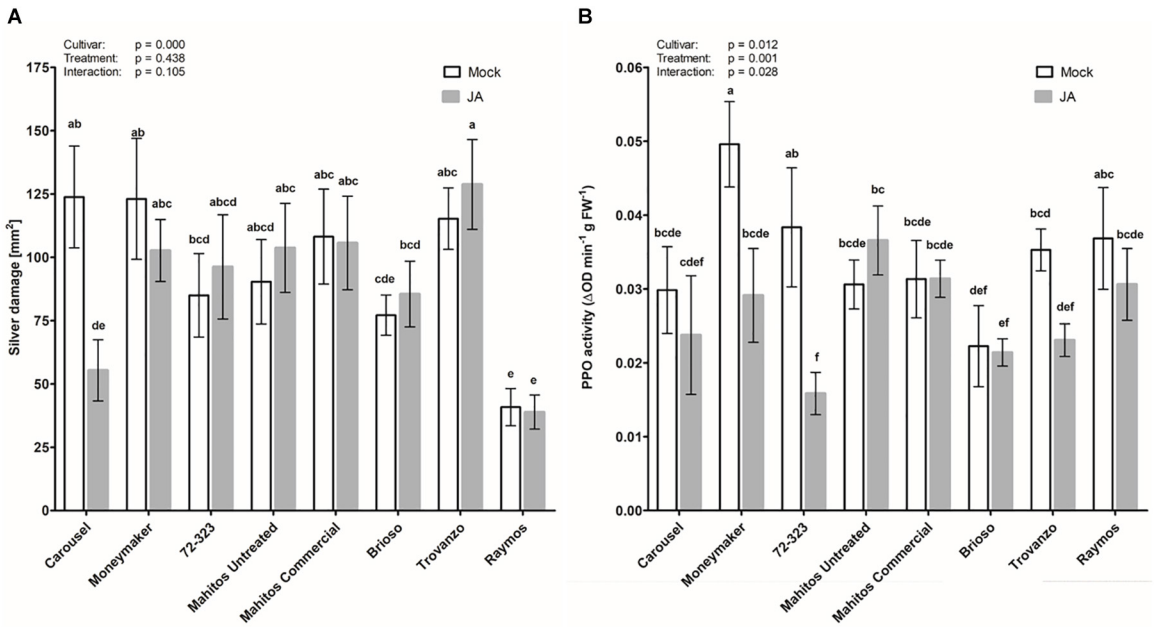


FIGURE 2 | Effect of exogenous JA treatment on tomato resistance to WFT and JA-associated responses. Silver damage symptoms **(A)** and PPO activity **(B)** were measured in 8 tomato cultivars: Moneymaker, Carousel, 72-323, Mahitos untreated, Mahitos commercial, Brioso, Trovanzo and Raymos. Plants were subjected to mock or jasmonic acid (3 mM) seed treatment. When 4 weeks old, plants were exposed to a non-choice whole plant bioassay and infested with 20 adult thrips (n = 10). Silver damage symptoms were visually scored after 7 days of thrips infestation. **(B)** Polyphenol oxidase activity was measured in non-infested plants taking the third leaf from the bottom (n = 7–8). Data are presented as mean ± SEM. Different letters denote significant differences among groups as determined by GLM followed by Fisher's LSD test ($P < 0.05$). The overall effects of cultivar, treatment and their interaction are indicated in each graph.

associated with a reduction in vegetative growth (**Supplementary Figure S2**). Cultivar, on the other hand, affected dry mass of seed treated plants (GLM: Wald χ^2 = 89.44, $p < 0.001$ for cultivar; Wald χ^2 = 0.175, p = 0.676 for treatment and Wald χ^2 = 3.86, p = 0.795 for the interaction). To evaluate whether reductions in thrips feeding damage were associated with the JA signaling pathway, we measured PPO activities in JA-seed elicited plants and control plants in the absence of thrips. Seed applied JA had a significant effect on PPO levels (GLM: Wald χ^2 = 18.09, p = 0.012 for cultivar; Wald χ^2 = 10.86, p = 0.01 for treatment and Wald χ^2 = 15.67, p = 0.028 for the interaction).the enhanced resistance following JA seed application in "Carousel" plants, however, was not associated with direct induction of plant defenses (**Figure 2B**).

Differences Among Cultivars in Water Permeability

To better understand the underlying mechanisms responsible for the differences in JA seed induced responses, we examined the eight tomato cultivars in relation to mass increase (**Figure 3**). The water imbibition pattern of Moneymaker showed a slightly curved pattern, while other cultivars had a more linear pattern. Within 1 h, water absorption differed strikingly among tomato cultivars ($F_{(7,16)}$ = 5.376, p = 0.03). Moneymaker absorbed significantly higher amounts of water during this period in comparison to the other cultivars. However, no significant differences in final water uptake (i.e., after24 h) were observed between tomato cultivars (Welch's $F_{(7,6\cdot66)}$ = 1.11, p = 0.452). Nevertheless, Carousel, together with Raymos seeds hydrated at the slowest rate. Carousel gained only 39% by weight over the initial seed weight after 24 h soaking. The tomato cultivar Moneymaker, on the other hand, hydrated most rapidly and imbibed 10% more water than Carousel seeds in this time period (49.73 ± 2.35 vs. Carousel 39.02 ± 2.15). Moreover, we evaluated whether hydro-priming of commercial Mahitos seeds influenced subsequent water permeability. Seed priming is a commercially used pre-sowing technique which involves the uptake of water by the seed followed by drying to trigger pre-germinative events without protrusion of the radical through the seed coat. Such achieved physiological state enables seeds to germinate more efficiently (Taylor et al., 1992). Hydropriming of seeds had no significant effect on water imbibition percentage (46.30 ± 3.08 commercial vs. untreated i.e., unprimed Mahitos 58.02 ± 3.37).

Phenotypic Characterization of Seed Receptivity

Based on the above results, Moneymaker and Carousel were chosen as "non-responsive" and "highly responsive" to JA seed soaking, respectively. With the aim to explore underlying differences in JA seed receptivity, vegetative plants resulting from JA soaked seeds from both cultivars were phenotypically characterized based on morphological and chemical criteria (**Figure 4**). Type-VI trichome density was significantly affected by cultivar (GLM; Wald χ^2 = 22.260, $p \leq 0.001$) but not by

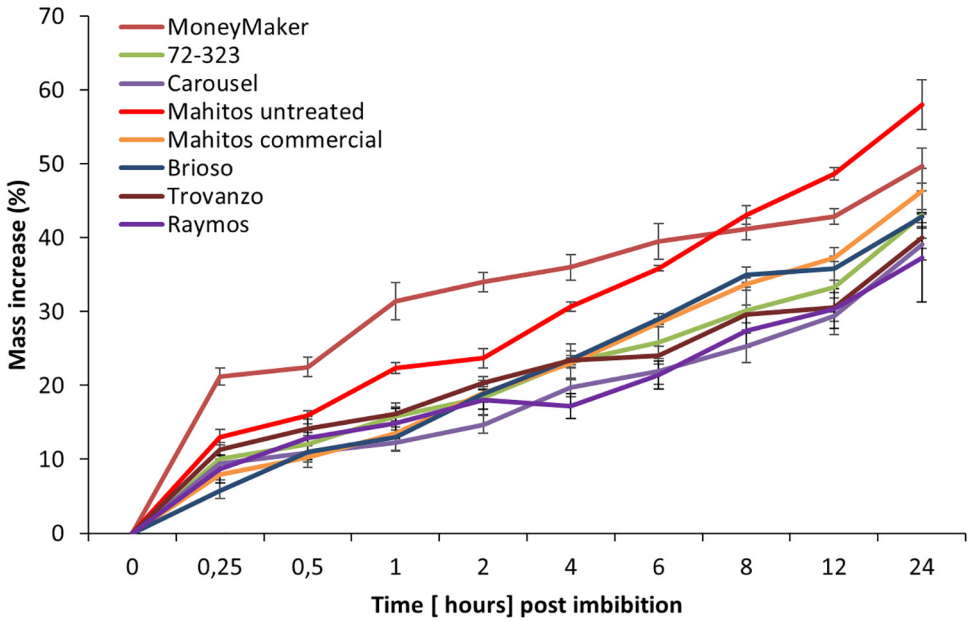


FIGURE 3 | Imbibition curves of eight different tomato cultivars. The percentage of mass increase in weight was used as a measure of water imbibition. Different line colors correspond to different cultivars. Red, orange, green, blue, gray, brown yellow and purple correspond to the following cultivars; "Mahitos untreated," "Moneymaker," "Mahitos commercial," "Brioso," "72-323," "Trovanzo," "Carousel," and "Raymos," respectively.

treatment (GLM; Wald $\chi^2 = 2.576$, $p = 0.108$). The cultivar by treatment interaction was not significant (GLM: Wald $\chi^2 = 1.990$, $p = 0.158$). The number of glandular trichomes in Carousel plants was 2.2-fold lower than in Moneymaker (**Figure 4A**). On the contrary, Carousel plants displayed significantly higher terpene content than Moneymaker plants (**Figure 4B**; GLM; Wald $\chi^2 = 9.682$, $p = 0.002$ for cultivar, Wald $\chi^2 = 0.547$, $p = 0.460$ for treatment and Wald $\chi^2 = 3.778$, $p = 0.052$ for interaction). Analysis of volatiles in leaf exudates revealed that cultivars differed in relative abundance of monoterpenes whereas no significant effect of treatment was observed (**Figures 4C–E**). Carousel plants produced significantly more α-terpinolene, β-phellandrene in comparison to Moneymaker plants (**Figures 4C–E**). Moreover, the results of the interactions suggested that seed treatment affected the emissions of α-terpinolene and β-phellandrene (GLM; Wald $\chi^2 = 7.677$, $p = 0.006$ and Wald $\chi^2 = 4.711$, $p = 0.003$ for interaction, respectively). Whilst upon JA seed soaking the monoterpenes α-terpinolene and β-phellandrene significantly decreased in Carousel, no significant effect was observed for JA seed treated Moneymaker plants (**Figures 4C,D**). Furthermore, no difference was observed for the sesquiterpene and β-caryophyllene (**Figure 4F**).

Improvement of JA seed Receptivity by Scarification

Systemic compounds must be able to permeate the seed coat and diffuse to the embryo in order to exert efficacy. To further demonstrate the importance of the seed coat several scarification methods were explored, prior to JA seed soaking, to determine whether embryonic responsiveness to JA could be augmented. Preliminary experimental results in one of the non-responsive tomato cultivars (Virona) demonstrated that chemical scarification with 10% sulfuric acid was the most potential method to improve JA seed receptivity with no adverse effects on the embryo and subsequent growth (**Supplementary Figure S3**). Therefore, acid scarification was applied to increase seed coat permeability of the non-responsive cultivar Moneymaker. The effect was compared with the highly responsive cultivar Carousel (**Figure 5**). The response to JA elicitation varied depending on cultivar, scarification and treatment (GLM; Wald $\chi^2 = 3.896$, $p = 0.048$ for three-way interaction). Seed applied JA reduced silver damage symptoms in Carousel plants, independent of acid scarification. Interestingly, acid scarification prior to JA seed treatment augmented seed receptivity in Moneymaker plants. Following JA soaking of Moneymaker seeds, whole plant silver damage was significantly reduced by 60% as compared to the acid-scarified mock treated control (**Figure 5A**). Whilst no negative effects of seed pre-treatments on dry mass were observed in Moneymaker, acid scarification significantly reduced dry mass in JA-seed treated Carousel plants (**Figure 5B**).

DISCUSSION

In the past decades, elicitor-mediated induced resistance has become one of the most challenging research areas in plant herbivory. Recent studies have shown that seeds are receptive to direct application of exogenous phytohormones without being constrained by the inherent costs of defense (Rajjou et al., 2006; Worrall et al., 2012; Haas et al., 2018). However, research on the beneficial effects of JA seed treatments are restricted to one

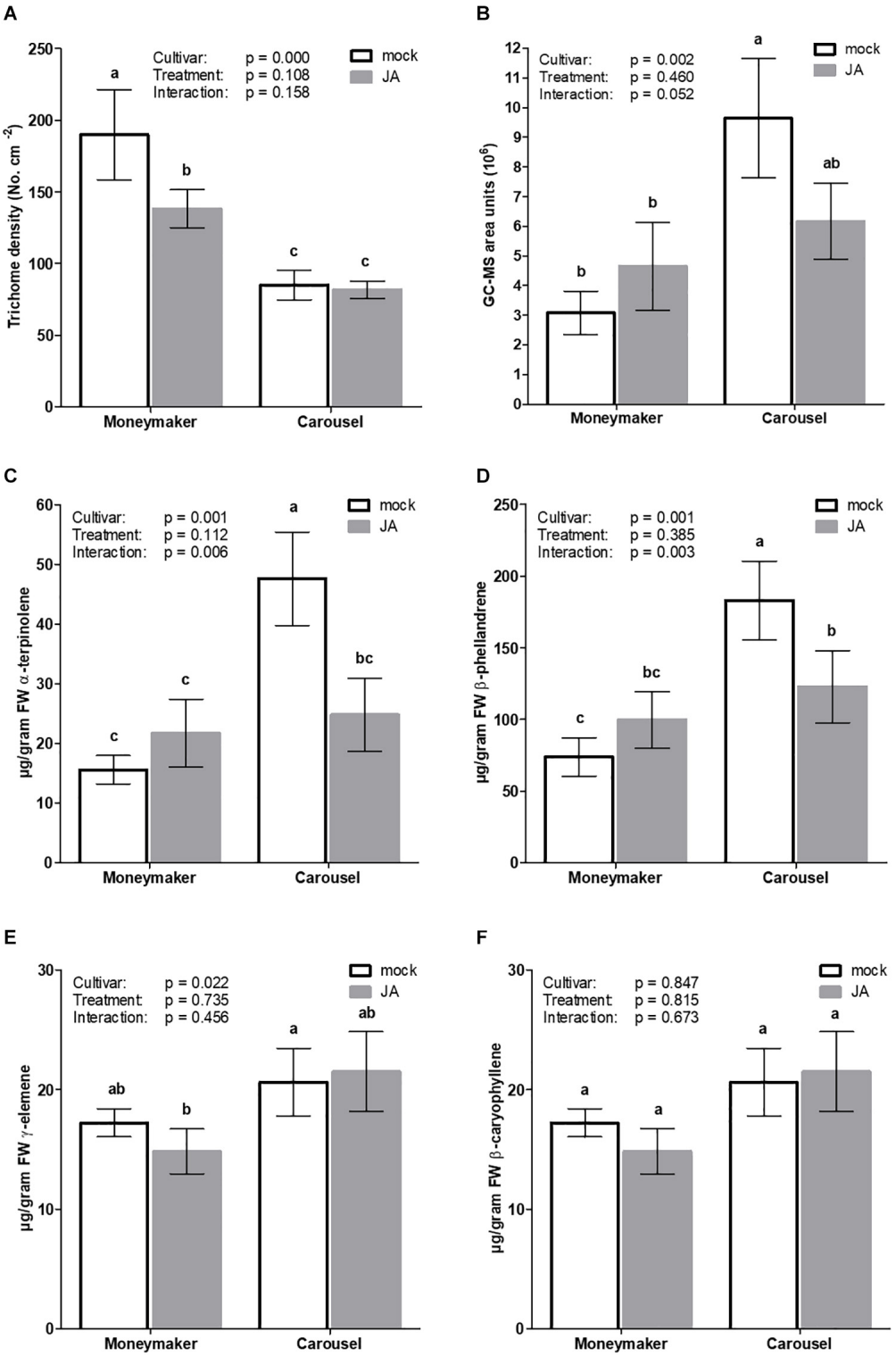


FIGURE 4 | Effect of exogenous JA seed treatment on type-VI trichome density and trichome derived volatiles in uninfested tomato plants. Seeds of cultivar Moneymaker and Carousel were soaked in mock or 3 mM JA for 24 h. Four weeks after initial treatments, **(A)** type VI glandular trichome density (n = 10) was evaluated on the adaxial leafside of leaflets from the third youngest leaf. **(B)** total terpene content and content of monoterpenes **(C)** α-terpinolene, **(D)** β-phellandrene and sesquiterpenes **(E)** γ-elemene and **(F)** β-caryophyllene derived from leaf exudates of mock and JA-seed treated tomato plants (n = 5). Bars represent mean ± SEM. Different letters denote significant differences among groups as determined by GLM followed by Fisher's LSD test ($P < 0.05$). The overall effects of cultivar, treatment and their interaction are indicated in each panel.

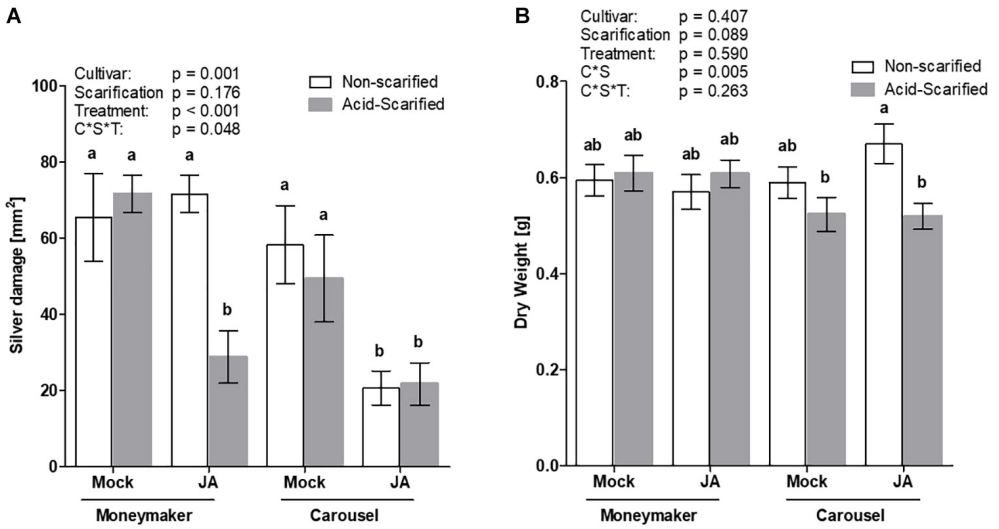


FIGURE 5 | The effect of acid scarification on JA seed receptivity in Moneymaker and Carousel was measured by evaluating whole plant silver damage **(A)** and dry mass **(B)**. Seeds of the cultivar Moneymaker and Carousel were scarified with 10% sulfuric acid prior to seed treatments. Acid scarified seeds were soaked in 3 mM JA or 0.5% ethanol mock for 24 h. Bars represent mean ± SEM of 10 individual plants. Different letters denote significant differences among groups as determined by GLM followed by Fisher's LSD test ($P < 0.05$). The overall effects of cultivar, treatment and the three way interaction are indicated in the graph. Two-way interactions were not significant except the interacting effect of cultivar * scarification on dry mass.

or only few tomato cultivars (Smart et al., 2013). To further explore the potential of JA as an active inducer of systemic resistance, it was of interest to investigate whether its' application at the seed stage could confer resistance against the economically important pest insect species WFT. Here, we show that in the tomato cultivar Carousel, JA seed treatment induced defenses against WFT. This result is in line with previous studies on other arthropod herbivores (Worrall et al., 2012; Smart et al., 2013). In addition, across eight tomato cultivars we demonstrated that seed receptivity of Carousel seeds appeared to be an exception, rather than the rule. Preliminary experiments with Moneymaker demonstrated that seeds of this cultivar were not receptive to JA-mediated defenses (**Supplementary Figure S4**). This is line with earlier findings obtained by Smart et al. (2013), who reported that Moneymaker plants lacked systemic induction of defense against the two-spotted spider mite *Tetranychus urticae* in response to JA seed treatment. These observations prompted us to investigate the differential seed receptivity responses of several commercial tomato cultivars.

Foliar JA-mediated herbivore resistance is a regulated at transcriptional and translational level. To this end, we first studied the influence of JA on elicitation of defense responses in tomato (cv. Virona) by comparing the efficacy of JA seed treatment with foliar application. Thrips resistance was differently affected by treatments. In contrast to foliar application of JA, which significantly reduced silver damage and caused a dose-dependent induction of the defensive enzyme polyphenol oxidase (PPO), JA seed treated plants failed to enhance resistance to thrips consistent with its inability to induce PPO activity. Interestingly, when we evaluated the tomato cultivar Carousel, JA seed treatment led to durable thrips resistance (**Supplementary Figure S1**). The question naturally arises as to "what features contribute to Carousels' uniqueness?" A number of hypotheses have been put forth to account for differences in seed receptivity. Among these, genetic variation may play a major role in how plants respond to elicitor induced resistance (Sharma et al., 2010; Walters et al., 2013; Bruce et al., 2017; Goodwin et al., 2017, 2018). To the best of our knowledge, no studies have so far explored the underlying mechanisms accountable for variable JA induced responses at the seed stage. Subsequently, we decided to expand our range of cultivars to study variation in response to JA seed applied induced defenses. We observed that cultivar was a major factor in determining the efficacy of JA (**Figure 2**). Among the eight tomato cultivars, only Carousel seed-treated plants showed a significant decrease in silver damage without concurrent impact on vegetative growth compared to the mock control. Silver damage symptoms in mock-seed treated Carousel plants were, however, for an unknown reason twice as high as in the first experiment (**Supplementary Figure S1** vs. **Figure 2**). Nonetheless, the percentage of symptom reduction was in both experiments approximately 50%. Increased resistance to WFT in JA seed-treated Carousel plants, however, was not associated with induction of PPO activities. Surprisingly, in the non-responsive cv. Moneymaker PPO levels were significantly reduced upon JA seed treatment suggesting that it may also exert also important physiological roles in addition to defenses. In contrast, readily measurable PPO activities were observed in foliar treated Carousel plants when JA was applied 3 days before thrips challenge (**Supplementary Figure S1**). One possible explanation for the lack of PPO induction is the time gap following JA seed treatment and PPO measurements. Following induction treatment, there is usually a set period of time required for the establishment of induced resistance. PPO activities may have increased after this lag period with a slow decrease

thereafter. Furthermore, induced plant responses often decline with age and, in addition, are markedly influenced by leaf developmental stage (Cipollini and Redman, 1999; Chen et al., 2018). Perhaps, 4 weeks post treatment, when PPO activity was measured, induction of defense related enzyms, in the absence of thrips, might thus not be measurable anymore. Nonetheless, Paudel et al. (2014) demonstrated that the induction of plant defense against *Helicoverpa zea*, following MeJA seed treatment of tomato cultivar Micro-Tom, was correlated with increased PPO activity. Moreover, the effect of seed treatment was described to be considerably long lasting as 25- and 50-days old plants displayed significant increases in PPO levels. Rather than direct induction of defenses, it is plausible that JA seed treatments primed for enhanced defense reactions although this was not addressed by our experiments. So far, it remains inconclusive whether priming of JA responses functions as control mechanism underlying induced resistance in seed-treated Carousel plants. In addition to PPO activity, future experiments evaluating spatiotemporal distributions of JA marker genes following JA seed soaking could provide helpful information here.

Seed Coat and Compound Characteristics

Seed coat permeability has also been postulated to contribute to discrepancies in JA-induced host responses (Smart et al., 2013). Tomato seeds are classified as having selectively permeable seed coat characteristics (Taylor and Salanenka, 2012). This semi-permeable layer, composed of suberin, is an important structure for restricting or impeding the penetration of some solutes into embryos during imbibition, while being permeable to water and gases (Beresniewicz et al., 1995b). To better understand the underlying mechanisms responsible for variable JA seed induced responses, we measured imbibition rates as a proxy to characterize seed coat permeability. In contrast to our expectations, water absorption characteristics did not strikingly differ among cultivars (**Figure 3**) while JA application had a significant effect on PPO. Intriguingly, Carousel seeds were shown to hydrate at the slowest rate and imbibed among the least amount of water after a soaking period of 24 h. contrast, the non-responsive cultivar Moneymaker hydrated most rapidly. Although not significant, Moneymaker imbibed more water than Carousel seeds. This suggests that discrepancies in JA induced responses at the seed stage are not directly explained by differences in seed coat permeability. The results of this experiment, however, must be interpreted in the context of a number of potential limitations. Firstly, the possible diagnostic value of seed coat permeability was assessed by comparing the water uptake which, by itself, does necessarily reflect uptake characteristics and subsequent bioavailability of JA. Jasmonic acid uptake by seeds is pivotal and insufficient penetration into the seed would fail to prime or induce defenses. Dissection and separation of seed tissues, followed by chemical extractions and quantification are a prerequisite to adequately evaluate whether induced host response variations arose from differences in JA uptake. We suggest follow-up studies to evaluate the uptake and metabolic fate of seed applied JA. Moreover, it is generally known that differences in seed coat anatomy play an important role in the process of water imbibition and that these differences relate to permeability (Koizumi et al., 2008). Physical properties of seeds such as surface area, sphericity and seed size, however, were not evaluated in the present study. In addition to structural differences, chemical compositions of seed covering layers may also provide a biochemical rationale for variations in uptake and bioavailability (Beresniewicz et al., 1995a; Vu et al., 2014). Comparison of soybean varieties, for example, revealed that the outer cuticle of non-permeable varieties contained disproportionally more hydroxylated fatty acids than permeable varieties (Shao et al., 2007; Qutob et al., 2008). The relative contribution of structural and chemical properties of the seed surface to understanding the seed responsiveness requires more in-depth analysis. Furthermore, seed coat compositions may differ from that of the embryo and, thus, can affect both permeability and affinity for a compound. Retention by the seed coat could result in suboptimal concentrations reaching the embryo which consequently, is unable to activate defense-related processes. Finally, a central question related to such differential embryonic responses is whether, and to what extent, seeds are transcriptionally or translationally responsive to exogenous plant hormones (Walker-Simmons, 1990; Liao et al., 2020).

Moreover, the physicochemical nature of JA in relation to seed coat permeability of different tomato cultivars could shed light on the lack of a systemic induced response to thrips. Non-ionic compounds that are moderately lipophilic in nature should be able to diffuse through the semi-permeable seed coat of tomato, whereas ionic compounds are blocked (Salanenka and Taylor, 2011). At a pH significantly below the pKa of the ionisable carboxylic center (pKa = 4.71; predicted by ChemAxon, Cambridge, MA, United States), the majority of JA occurs in its protonated or unionized form, whereas at a pH above the pKa, the ionized form predominates. It can be expected that a large proportion of JA, at a concentration of 3 mM, occurs in in a non-dissociated form and thus, theoretically could diffuse through tomato seed coats. Apart from the electrical charge, lipophilicity, measured by the octanol-water partition coefficient (Log Kow or Log P), forms another key determinant for the ability of a compound to penetrate the seed coat as it describes the affinity of compounds for the lipid phase of plant tissue (e.g., plasma membrane, waxes, cutin, suberin, etc.) (Braumann, 1986). Translocation of JA, a derivative of the fatty acid linolenic acid, could potentially be limited by the presence of suberin, which in general is well known to adsorb lipophilic compounds. The lipophilic behavior of JA is most dominant when the carboxylic group is unionized, as it becomes more soluble in the immiscible lipophilic solvent. Recently, Yang et al. (2017, 2018) studied the uptake and distribution of a series of nonionic fluorescent piperonyl amides in relation to their chemical lipophilicity (Log Kow) in permeable soybean and semi-permeable tomato and corn seeds. Contrasting trends in uptake between seed tissues were observed for soybean. In tomato, as in corn, the overall uptake pattern for seed covering layers was similar to that of the internal tissues (Yang et al., 2017). The maximum uptake for non-ionic compounds to diffuse to the embryo of tomato ranged between Log Kow 3–4. Interestingly, at optimal Log Kow <5%

of the applied compound was measured in the embryo of tomato seeds. The predicted log P or Log Kow for JA is 2.41 (ChemAxon). This value lies in the lower range of permeability, and as such, the uptake efficiency in the embryo may, theoretically, even be <5%. Nonetheless, uptake efficiencies clearly varied among the three evaluated tomato varieties (Yang et al., 2017). Seed applied products with a high potency (i.e., require a lower effective concentration EC_{50}) could, therefore, potentially compensate for their low permeability.

Effect of JA Seed Treatment on Physicochemical Leaf Properties

We further investigated whether the enhancement of thrips resistance in the responsive cultivar Carousel was associated with induction of physical and chemical leaf properties. Type-VI glandular trichomes are controlled by the JA-pathway (Boughton et al., 2005; Maes and Goossens, 2010) and provide physical and chemical barriers which are known to produce and secrete diverse compounds affecting survival (Frelichowski and Juvik, 2001), growth (Kang et al., 2010) and fecundity (Bleeker et al., 2012) of many herbivorous arthropods. In tomato, artificial application of JA or its volatile derivative methyl jasmonate (MeJA) has been reported to induce the production of type-VI leaf glandular trichomes and volatile emissions (Escobar-Bravo et al., 2017; Chen et al., 2018). Carousel plants contained significantly less type-VI glandular trichomes than Moneymaker, however, we observed no significant effect of seed treatment on trichome densities. Intriguingly, total terpene content was significantly higher in mock seed treated Carousel plants, suggesting a relative decrease in terpene production per trichome in JA-seed treated plants. Furthermore, JA seed treatments markedly decreased the emission of the monoterpenes α-terpinolene and β-phellandrene in Carousel whereas, no significant effects were observed in JA seed treated Moneymaker plants. These findings are in agreement with Strapasson et al. (2014), who reported that MeJA seed treatment of cultivar Micro-Tom decreased volatile emissions, including that of β-phellandrene, in uninfested tomato plants. Consequently, manipulation of plant volatile emissions could contribute to the control of insect pests as herbivores rely on volatile cues for host location. Reduced levels of emitted volatile compounds involved in volatile-mediated foraging may lead to a decrease in host finding efficiency and, ultimately a lower number of offspring (Bruce et al., 2005; Proffit et al., 2011). On the contrary, foliar applications of JA or MeJA differentially affect volatile emissions. Significant increases in the emission of terpinolene and β-phellandrene were reported in cultivated (cv. Moneymaker) and wild-type (Castlemart) tomato plants and could potentially reinforce defenses as a result of their direct toxic or repellent potency (Bleeker et al., 2009; Escobar-Bravo et al., 2017; Chen et al., 2018). These intriguing findings suggests that indirect defenses can have opposite ontogenic trends.

Acid Scarification Augments JA Seed Responsiveness

The phenotypical and bio-chemical analyses discussed above did not provide a causal explanation for the underlying characteristic low receptivity of tomato cultivar Moneymaker. Acid scarification prior to JA seed treatment was, therefore, evaluated to further demonstrate the importance of the seed coat permeability. Our results show that pre-treatment with 10% sulfuric acid significantly augmented receptivity in JA-seed treated Moneymaker plants and, hence suggest that the lack of defense induction was likely caused by seed coat impermeability. The observed enhancement in resistance is encouraging. It demonstrates the possibility to manipulate seed coat characteristics of non-responsive cultivars without the need of difficult and time-consuming breeding techniques. Further evidence that the lack of induced resistance to thrips was caused by impermeability comes from extended seed treatment experiments. Extended soaking (i.e., 6 days) of germinating tomato seeds (cv. Moneymaker) in JA solutions bypasses the limitations of reduced permeability of the tomato seed coat and increased the effectiveness of induced resistance. However, this approach is not without risk as prolonged soaking can cause serious negative effects on seed viability (Chen et al., unpublished). Luna et al. (2016) reported similar findings in Moneymaker using 1 mM β-aminobutyric acid (BABA) for durable induced resistance to *Botrytis cinera*. After a 7-days incubation period of seeds in BABA, lesion size was significantly reduced in 4 weeks old tomato plants although they found that the relative growth rate was not negatively affected.

CONCLUDING REMARKS

Seed applied JA reduced feeding damage by western flower thrips but, among the eight evaluated tomato cultivars, silver damage symptoms were only reduced in JA-seed treated plants of the cultivar Carousel. The observed variability in responsiveness constitutes a major obstacle, because one of the foremost conditions for successful commercialization of elicitors is consistent efficacy. The variability among different cultivars clearly demonstrates the necessity to include multiple cultivars as a biological test system to establish consistent statements concerning compound efficacy. This is particularly important because, in scientific literature, Moneymaker along with tomato cultivars Aisla Craig, Micro-Tom and Castlemart are frequently used to represent tomato as a plant model system. Notably, we demonstrated that acid scarification significantly augmented responsiveness to seed applied JA in the non-responsive cultivar Moneymaker. This observation lends added support to the contention that permeability is an important factor for facilitation of JA absorption (i.e., bioavailability) and its' exerted effect on defense responses. We conclude that future experiments focusing on seed structural properties, compound uptake as well as early transcriptional responses could provide explanations underlying the genotype dependent differences in seed permeability and, ultimately its importance in priming JA anti-thrips defenses. Nonetheless, the outcome of our work creates opportunities for tomato breeding programs to select for genetic traits that affect seed permeability as well as for private seed companies to pre-treat and manipulate nonresponsive cultivars.

DATA AVAILABILITY STATEMENT

The raw data supporting the conclusions of this article will be made available by the authors, without undue reservation.

AUTHOR CONTRIBUTIONS

SM, KL, and PK designed the experimental research. SM performed hormone seed and plant treatments and insect experiments. SM and IK performed (bio)-chemical analysis and interpretation. SM drafted the manuscript with critical review of all authors. All authors approved the final version of the manuscript.

FUNDING

This work was supported by the Technology Foundation TTW (formerly STW), project "Green Defense against Pests" (GAP) (Ref. 13553); we thank the companies involved in the GAP project: Rijk Zwaan, Dümmen Orange, Dekker Chrysanten, Deliflor Chrysanten, and Incotec International for their financial support.

ACKNOWLEDGMENTS

We thank Karin van der Veen-van Wijk for technical assistance.

SUPPLEMENTARY MATERIAL

The Supplementary Material for this article can be found online at: https://www.frontiersin.org/articles/10.3389/fpls.2020.576505/full#supplementary-material

Supplementary Figure 1 | Effect of exogenous JA treatment on tomato resistance against WFT and JA-associated responses. **(A)** Silver damage symptoms in tomato plants (n = 12) following JA or mock treatment applied at the seed stage or as foliar spray 4 days prior to thrips infestation. Four weeks old tomato plants, variety Carousel, were subjected to a non-choice whole plant bioassay and infested with 20 adult thrips. Silver damage symptoms were visually scored after 7 days of infestation. **(B)** Polyphenol oxidase activity was measured in non-infested plants taking the third leaf from the bottom (n = 6–8). Data are presented as mean ± SEM. Different letters denote significant differences among groups as determined by GLM followed by Fisher's LSD test ($P < 0.05$). The overall effects of application, treatment and their interaction are indicated in each graph.

Supplementary Figure 2 | Effect of seed applied JA on dry mass of tomato plants. Dry mass was measured for 8 tomato cultivars; "Moneymaker," "Carousel," "72-323," "Mahitos untreated," "Mahitos Commercial," "Brioso," "Trovanzo," and "Raymos" plants that were subjected to mock or jasmonic acid (3 mM) seed treatment. Data are means (+SEM) of 10 individual plants and different letters indicate significant differences among groups as determined by GLM followed by Fisher's LSD test ($P < 0.05$). The overall effects of cultivar, treatment and their interaction are indicated in the graph.

Supplementary Figure 3 | Effect of different pre-treatments on JA-induced defenses against WFT on silver damage and plant growth. Seeds were mechanically (razor blade), chemically (10% sulfuric acid) or commercially scarified prior to JA or mock seed treatment. Control seeds were non-scarified. **(A)** Total silver damage was evaluated in 4 weeks old tomato plants (cv. Virona) after 7 days of thrips infestation. **(B)** Dry mass was assessed as a measure of plant performance. Data are presented as mean ± SEM, n = 12. Different letters indicate significant differences among groups as determined by GLM followed by Fisher's LSD test ($P < 0.05$). The overall effects of scarification method, treatment and their interaction are indicated in the graph.

Supplementary Figure 4 | Effect of seed applied JA on tomato resistance against Wester Flower Thrips (*Frankliniella occidentalis*). Four weeks after seed treatment "Moneymaker" plants were subjected to a non-choice whole plant bioassay and infested with 20 adult thrips. Silver damage symptoms were visually scored after 7 days of infestation. Data are presented as mean ± SEM, n = 8. There was no statistically significant effect among treatments on silver damage symptoms [Welch's $F_{(3,15.19)} = 0.36$, $p = 0.781$].

Supplementary Table 1 | Effect of jasmonic acid foliar application and seed soaking on plant growth parameters of tomato (cv. Virona). Data are expressed as mean ± SEM (n = 10).

REFERENCES

Abe, H., Shimoda, T., Ohnishi, J., Kugimiya, S., Narusaka, M., Seo, S., et al. (2009). Jasmonate-dependent plant defense restricts thrips performance and preference. *BMC Plant Biol.* 9:97. doi: 10.1186/1471-2229-9-97

Adams, R. P. (2007). *Identification of Essential Oil Components by Gas Chromatography/Mass Spectrometry*. Carol Stream, IL: Allured Publishing Corporation.

Ament, K., Kant, M. R., Sabelis, M. W., Haring, M. A., and Schuurink, R. C. (2004). Jasmonic acid is a key regulator of spider mite-induced volatile terpenoid and methyl salicylate emission in tomato. *Plant Physiol.* 135, 1–13. doi: 10.1104/pp.103.038315

Arimura, G., Kost, C., and Boland, W. (2005). Herbivore-induced, indirect plant defenses. *Biochem. Biol. Phys. Acta* 1734, 91–111. doi: 10.1016/j.bbalip.2005.03.001

Barton, K. E., and Hanley, M. E. (2013). Seedling–herbivore interactions: insights into plant defence and regeneration patterns. *Ann. Bot.* 112, 643–650. doi: 10.1093/aob/mct139

Baskin, J. M., Davis, B. H., Baskin, C. C., Gleason, S. M., and Cordell, S. (2004). Physical dormancy in seeds of *Dodonaea viscosa* (*Sapindales, Sapindaceae*) from Hawaii. *Seed Sci. Res.* 14, 81–90. doi: 10.1079/SSR2003157

Bennett, R. N., and Wallsgrove, R. M. (1994). Secondary metabolites in plant defence mechanisms. *New Phytol.* 127, 617–633. doi: 10.1111/j.1469-8137.1994.tb02968.x

Beresniewicz, M. M., Taylor, A. G., Goffinet, M. C., and Koeller, W. D. (1995a). Chemical nature of a semipermeable layer in seed coats of leek, onion (Liliaceae), tomato and pepper (Solanaceae). *Seed Sci. Technol.* 23, 135–145.

Beresniewicz, M. M., Taylor, A. G., Goffinet, M. C., and Terhune, B. T. (1995b). Characterization and location of a semipermeable layer in seed coats of leek and onion (*Liliaceae*), tomato and pepper (*Solanaceae*). *Seed Sci. Technol.* 23, 123–134.

Bleeker, P. M., Diergaarde, P. J., Ament, K., Guerra, J., Weidner, M., Schütz, S., et al. (2009). The role of specific tomato volatiles in tomato–whitefly interaction. *Plant Physiol.* 151, 925–935. doi: 10.1104/pp.109.142661

Bleeker, P. M., Mirabella, R., Diergaarde, P. J., Van Doorn, A., Tissier, A., Kant, M., et al. (2012). Improved herbivore resistance in cultivated tomato with the sesquiterpene biosynthetic pathway from a wild relative. *Proc. Natl. Acad. Sci. U.S.A.* 109, 20124–20129. doi: 10.1073/pnas.1208756109

Boughton, A. J., Hoover, K., and Felton, G. W. (2005). Methyl jasmonate application induces increased densities of glandular trichomes on tomato, *Lycopersicon esculentum*. *J. Chem. Ecol.* 31, 2211–2216. doi: 10.1007/s10886-005-6228-7

Braumann, T. (1986). Determination of hydrophobic parameters by reversed-phase liquid chromatography: theory, experimental techniques, and application

in studies on quantitative structure-activity relationships. *J. Chromatogr. A* 373, 191–225. doi: 10.1016/s0021-9673(00)80213-7

Bruce, T. J. (2014). Variation in plant responsiveness to defense elicitors caused by genotype and environment. *Front. Plant Sci.* 5:349. doi: 10.3389/fpls.2014.00349

Bruce, T. J., Smart, L. E., Birch, A. N. E., Blok, V. C., MacKenzie, K., Guerrieri, E., et al. (2017). Prospects for plant defence activators and biocontrol in IPM–Concepts and lessons learnt so far. *Crop Prot.* 97, 128–134. doi: 10.1016/j.cropro.2016.10.003

Bruce, T. J. A., Birkett, M. A., Blande, J., Hooper, A. M., Martin, J. L., Khambay, B., et al. (2005). Response of economically important aphids to components of *Hemizygia petiolata* essential oil. *Pest Manag. Sci.* 61, 1115–1121. doi: 10.1002/ps.1102

Chen, G., Klinkhamer, P. G. L., Escobar-Bravo, R., and Leiss, K. A. (2018). Type VI glandular trichome density and their derived volatiles are differently induced by jasmonic acid in developing and fully developed tomato leaves: implications for thrips resistance. *Plant Sci.* 276, 87–98. doi: 10.1016/j.plantsci.2018.08.007

Cipollini, D., Purrington, C. B., and Bergelson, J. (2003). Costs of induced responses in plants. *Basic Appl. Ecol.* 4, 79–89. doi: 10.1078/1439-1791-00134

Cipollini, D. F., and Redman, A. M. (1999). Age-dependent effects of jasmonic acid treatment and wind exposure on foliar oxidase activity and insect resistance in Tomato. *J. Chem. Ecol.* 25, 271–281. doi: 10.1023/A:1020842712349

Conrath, U., Beckers, G. J. M., Flors, V., García-Agustín, P., Jakab, G., Mauch, F., et al. (2006). Priming: getting ready for battle. *Mol. Plant Microbe Interact.* 19, 1062–1071. doi: 10.1094/MPMI-19-1062

Degen, T., Dillmann, C., Marion-Poll, F., and Turlings, T. C. (2004). High genetic variability of herbivore-induced volatile emission within a broad range of maize inbred lines. *Plant Physiol.* 135, 1928–1938. doi: 10.1104/pp.104.039891

Escobar-Bravo, R., Klinkhamer, P. G. L., and Leiss, K. A. (2017). Induction of jasmonic acid-associated defenses by thrips alters host suitability for conspecifics and correlates with increased trichome densities in tomato. *Plant Cell Physiol.* 58, 622–634. doi: 10.1093/pcp/pcx014

Farmer, E. E., and Ryan, C. A. (1990). Interplant communication: airborne methyl jasmonate induces synthesis of proteinase inhibitors in plant leaves. *Proc. Natl. Acad. Sci. U.S.A.* 87, 7713–7716. doi: 10.1073/pnas.87.19.7713

Frelichowski, J. E. Jr., and Juvik, J. A. (2001). Sesquiterpene carboxylic acids from a wild tomato species affect larval feeding behavior and survival of *Helicoverpa zea* and *Spodoptera exigua* (Lepidoptera: Noctuidae). *J. Econ. Entomol.* 94, 1249–1259. doi: 10.1603/0022-0493-94.5.1249

Goodwin, P. H., Trueman, C. L., Loewen, S. A., and Tazhoor, R. (2017). Variation in the response of tomato (*Solanum lycopersicum*) breeding lines to the effects of benzo (1, 2, 3) thiadiazole-7-carbothioic acid S-methyl ester (BTH) on systemic acquired resistance and seed germination. *J. Phytopathol.* 165, 670–680. doi: 10.1111/jph.12606

Goodwin, P. H., Trueman, C. L., Loewen, S. A., and Tazhoor, R. (2018). Variation in the responsiveness of induced resistance against *Pseudomonas syringae* pv. tomato by *Solanum lycopersicum* treated with para-aminobenzoic acid. *Physiol. Mol. Plant Pathol.* 10, 31–39. doi: 10.1016/j.pmpp.2018.08.007

Haas, J., Lozano, E. R., Haida, K. S., Mazaro, S. M., de Souza Vismara, E., and Poppy, G. M. (2018). Getting ready for battle: do cabbage seeds treated with jasmonic acid and chitosan affect chewing and sap-feeding insects? *Entomol. Exp. Appl.* 166, 412–419. doi: 10.1111/eea.12678

Howe, G. A., and Jander, G. (2008). Plant immunity to insect herbivores. *Annu. Rev. Plant Biol.* 59, 41–66. doi: 10.1146/annurev.arplant.59.032607.092825

Kang, J. H., McRoberts, J., Shi, F., Moreno, J. E., Jones, A. D., and Howe, G. A. (2014). The flavonoid biosynthetic enzyme chalcone isomerase modulates terpenoid production in glandular trichomes of tomato. *Plant Physiol.* 164, 1161–1174. doi: 10.1104/pp.113.233395

Kang, J. H., Shi, F., Jones, A. D., Marks, M. D., and Howe, G. A. (2010). Distortion of trichome morphology by the hairless mutation of tomato affects leaf surface chemistry. *J. Exp. Bot.* 61, 1053–1064. doi: 10.1093/jxb/erp370

Kappers, I. F., Hoogerbrugge, H., Bouwmeester, H. J., and Dicke, M. (2011). Variation in herbivory-induced volatiles among cucumber (*Cucumis sativus* l.) varieties has consequences for the attraction of carnivorous natural enemies. *J. Chem. Ecol.* 37, 150–160. doi: 10.1007/s10886-011-9906-7

Koizumi, M. K., Kikuchi, K., Isobe, S., Ishida, N., Naito, S., and Kano, H. (2008). Role of seed coat in imbibing soybean seeds observed by micro-magnetic resonance imaging. *Ann. Bot.* 102, 343–352. doi: 10.1093/aob/mcn095

Leiss, K. A., Maltese, F., Choi, Y. H., Verpoorte, R., and Klinkhamer, P. G. L. (2009). Identification of chlorogenic acid as a resistance factor for thrips in chrysanthemum. *Plant Physiol.* 150, 1567–1575. doi: 10.1104/pp.109.138131

Liao, P., Woodfield, H. K., Harwood, J. L., Chye, M. L., and Scofield, S. (2020). Erratum comparative transcriptomics analysis of *Brassica napus* L. during seed maturation reveals dynamic changes in gene expression between embryos and seed coats and distinct expression profiles of Acyl-CoA-binding proteins for lipid accumulation. *Plant Cell Physiol.* 61, 2812–2825. doi: 10.1093/pcp/pcz220

Luna, E., Beardon, E., Ravnskov, S., Scholes, J., and Ton, J. (2016). Optimizing chemically induced resistance in tomato against *Botrytis cinerea*. *Plant Dis.* 100, 704–710. doi: 10.1094/PDIS-03-15-0347-RE

Maes, L., and Goossens, A. (2010). Hormone-mediated promotion of trichome initiation in plants is conserved but utilizes species and trichome-specific regulatory mechanisms. *Plant Signal. Behav.* 5, 205–207. doi: 10.4161/psb.5.2.11214

Martinez-Medina, A., Flors, V., Heil, M., Mauch-Mani, B., Pieterse, and Conrath, U. (2016). Recognizing plant defense priming. *Trends Plant Sci.* 21, 818–822. doi: 10.1016/j.tplants.2016.07.009

Mauch-Mani, B., Baccelli, I., Luna, E., and Flors, V. (2017). Defense priming: an adaptive part of induced resistance. *Annu. Rev. Plant Biol.* 68, 485–512. doi: 10.1146/annurev-arplant-042916-041132

Moles, A. T., and Westoby, M. (2004). What do seedlings die from and what are the implications for evolution of seed size? *Oikos* 106, 193–199. doi: 10.1111/j.0030-1299.2004.13101.x

Mouden, S., Sarmiento, K. F., Klinkhamer, P. G. L., and Leiss, K. A. (2017). Integrated pest management in western flower thrips: past, present and future. *Pest Manag. Sci.* 75, 813–822. doi: 10.1002/ps.4531

Ochoa-López, S., Villamil, N., Zedillo-Avelleyra, P., and Boege, K. (2015). Plant defence as a complex and changing phenotype throughout ontogeny. *Ann. Bot.* 116, 797–806. doi: 10.1093/aob/mcv113

Omer, A. D., Granett, J., Karban, R., and Villa, E. M. (2001). Chemically-induced resistance against multiple pests in cotton. *Intl. J. Pest Manag.* 47, 49–54. doi: 10.1080/09670870150215595

Paudel, S., Rajotte, E. G., and Felton, G. W. (2014). Benefits and costs of tomato seed treatment with plant defense elicitors for insect resistance. *Arthropod. Plant Interact.* 8, 539–545. doi: 10.1007/s11829-014-9335-y

Pieterse, C. M., Van Der Does, D., Zamioudis, C., Leon-Reyes, A., and Van Wees, S. C. (2012). Hormonal modulation of plant immunity. *Annu. Rev. Cell Dev. Biol.* 28, 489–521. doi: 10.1146/annurev-cellbio-092910-154055

Proffit, M., Birgersson, G., Bengtsson, M., Reis, R. Jr., Witzgall, P., and Lima, E. (2011). Attraction and oviposition of *Tuta absoluta* females in response to tomato leaf volatiles. *J. Chem. Ecol.* 37, 565–574. doi: 10.1007/s10886-011-9961-0

Qutob, D., Ma, F., Peterson, C. A., Bernards, M. A., and Gijzen, M. (2008). Structural and permeability properties of the soybean seed coat. *Botany* 86, 219–227. doi: 10.1139/B08-002

Rajjou, L., Belghazi, M., Huguet, R., Robin, C., Moreau, A., Job, C., et al. (2006). Proteomic effect of salicylic acid on arabidopsis seed germination and establishment of early defense mechanisms. *Plant Physiol.* 141, 910–923. doi: 10.1104/pp.106.082057

Salanenka, Y. A., and Taylor, A. G. (2011). Seedcoat permeability: uptake and post-germination transport of applied model tracer compounds. *HortScience* 46, 622–626. doi: 10.21273/HORTSCI.46.4.622

Shao, S., Meyer, C. J., Ma, F., Peterson, C. A., and Bernards, M. A. (2007). The outermost cuticle of soybean seeds: chemical composition and function during imbibition. *J. Exp. Bot.* 58, 1071–1082. doi: 10.1093/jxb/erl268

Sharma, K., Butz, A. F., and Finckh, M. R. (2010). Effects of host and pathogen genotypes on inducibility of resistance in tomato (*Solanum lycopersicum*) to *Phytophthora infestans*. *Plant Pathol.* 59, 1062–1071. doi: 10.1111/j.1365-3059.2010.02341.x

Smart, L. E., Martin, J. L., Limpalaër, M., Bruce, T. J., and Pickett, J. A. (2013). Responses of herbivore and predatory mites to tomato plants exposed to jasmonic acid seed treatment. *J. Chem. Ecol.* 39, 1297–1300. doi: 10.1007/s10886-013-0345-5

Steenbergen, M., Abd-el-Haliem, A., Bleeker, P., Dicke, M., Escobar-Bravo, R., Cheng, G., et al. (2018). Thrips advisor: exploiting thrips-induced defences to combat pests on crops. *J. Exp. Bot.* 69, 1837–1848. doi: 10.1093/jxb/ery060

Stout, M. J., Brovont, R. A., and Duffey, S. S. (1998). Effect of nitrogen availability on expression of constitutive and inducible chemical defenses in tomato, *Lycopersicon esculentum*. *J. Chem. Ecol.* 24, 945–963. doi: 10.1023/A:1022350100718

Strapasson, P., Pinto-Zevallos, D. M., Paudel, S., Rajotte, E. G., Felton, G. W., and Zarbin, P. H. (2014). Enhancing plant resistance at the seed stage: low concentrations of methyl jasmonate reduce the performance of the leaf miner *Tuta absoluta* but do not alter the behavior of its predator *Chrysoperla externa*. *J. Chem. Ecol.* 40, 1090–1098. doi: 10.1007/s10886-014-0503-4

Taylor, A. G., Prusinski, J., Hill, H. J., and Dickson, M. D. (1992). Influence of seed hydration on seedling performance. *HortTechnology* 2, 336–344. doi: 10.21273/HORTTECH.2.3.336

Taylor, A. G., and Salanenka, Y. A. (2012). Seed treatments: phytotoxicity amelioration and tracer uptake. *Seed Sci. Res.* 22, S86–S90. doi: 10.1017/S0960258511000389

Thaler, J. S. (1999). Induced resistance in agricultural crops: effects of jasmonic acid on herbivory and yield in tomato plants. *Environ. Entomol.* 28, 30–37. doi: 10.1093/ee/28.1.30

Thaler, J. S., Stout, M. J., Karban, R., and Duffey, S. S. (1996). Exogenous jasmonates simulate insect wounding in tomato plants (*Lycopersicon esculentum*) in the laboratory and field. *J. Chem. Ecol.* 22, 1767–1781. doi: 10.1007/BF02028503

Tian, D., Tooker, J., Peiffer, M., Chung, S. H., and Felton, G. W. (2012). Role of trichomes in defense against herbivores: comparison of herbivore response to woolly and hairless trichome mutants in tomato (*Solanum lycopersicum*). *Planta* 236, 1053–1066. doi: 10.1007/s00425-012-1651-9

Vallad, G. E., and Goodman, R. M. (2004). Systemic acquired resistance and induced systemic resistance in conventional agriculture. *Crop Sci.* 44, 1920–1934. doi: 10.2135/cropsci2004.1920

Van Hulten, M., Pelser, M., van Loon, L. C., Pieterse, C. M. J., and Ton, J. (2006). Costs and benefits of priming for defense in *Arabidopsis*. *Proc. Natl. Acad. Sci. U.S.A.* 103, 5602–5607. doi: 10.1073/pnas.0510213103

Vu, D. T., Velusamy, V. I. J., and Park, E. U. (2014). Structure and chemical composition of wild soybean seed coat related to its permeability. *Pak. J. Bot.* 46, 1847–1857.

Walker-Simmons, M. (1990). *Dormancy in Cereals—Levels of and Response to Abscisic Acid. in Plant Growth Substances 1988*. Berlin: Springer, 400–406.

Walters, D., and Heil, M. (2007). Costs and trade-offs associated with induced resistance. *Physiol. Mol. Plant Pathol.* 71, 3–17. doi: 10.1016/j.pmpp.2007.09.008

Walters, D. R., Ratsep, J., and Havis, N. D. (2013). Controlling crop diseases using induced resistance: challenges for the future. *J. Exp. Bot.* 64, 1263–1280. doi: 10.1093/jxb/ert026

War, A. R., Paulraj, M. G., Ahmad, T., Buhroo, A. A., Hussain, B., Ignacimuthu, S., et al. (2012). Mechanisms of plant defense against insect herbivores. *Plant Signal. Behav.* 7, 1306–1320. doi: 10.4161/psb.21663

Worrall, D., Holroyd, G. H., Moore, J. P., Glowacz, M., Croft, P., Taylor, J. E., et al. (2012). Treating seeds with activators of plant defence generates long-lasting priming of resistance to pests and pathogens. *New Phytol.* 193, 770–778. doi: 10.1111/j.1469-8137.2011.03987.x

Yang, D., Donovan, S., Black, B. C., Cheng, L., and Taylor, A. G. (2018). Relationship between compound lipophilicity on seed coat permeability and embryo uptake by soybean and corn. *Seed Sci.* 28, 229–223. doi: 10.1017/S096025851800017X

Yang, D., Mayton, H. S., Amirkhani, M., and Taylor, A. G. (2017). "Compound lipophilicity and implications for seed treatment efficacy," in *Proceedongs of the 32nd Annual Tomato Disease Workshop*, Tampa, FL. doi: 10.1017/s096025851800017x

Conflict of Interest: The authors declare that the research was conducted in the absence of any commercial or financial relationships that could be construed as a potential conflict of interest.

Copyright © 2020 Mouden, Kappers, Klinkhamer and Leiss. This is an open-access article distributed under the terms of the Creative Commons Attribution License (CC BY). The use, distribution or reproduction in other forums is permitted, provided the original author(s) and the copyright owner(s) are credited and that the original publication in this journal is cited, in accordance with accepted academic practice. No use, distribution or reproduction is permitted which does not comply with these terms.

frontiers in Plant Science

ORIGINAL RESEARCH
published: 07 December 2020
doi: 10.3389/fpls.2020.599697

Tomato Yellow Leaf Curl Virus-Resistant and -Susceptible Tomato Genotypes Similarly Impact the Virus Population Genetics

Wendy G. Marchant[1], *Saurabh Gautam*[2], *Samuel F. Hutton*[3] *and Rajagopalbabu Srinivasan*[2]*

[1] Department of Entomology, University of Georgia, Tifton, GA, United States, [2] Department of Entomology, University of Georgia, Griffin, GA, United States, [3] Horticulture Sciences Department, University of Florida, Wimauma, FL, United States

Tomato yellow leaf curl virus is a species in the genus *Begomovirus* and family *Geminiviridae*. Tomato yellow leaf curl virus (TYLCV) infection induces severe symptoms on tomato plants and causes serious yield losses worldwide. TYLCV is persistently transmitted by the sweetpotato whitefly, *Bemisia tabaci* (Gennadius). Cultivars and hybrids with a single or few genes conferring resistance against TYLCV are often planted to mitigate TYLCV-induced losses. These resistant genotypes (cultivars or hybrids) are not immune to TYLCV. They typically develop systemic infection, display mild symptoms, and produce more marketable tomatoes than susceptible genotypes under TYLCV pressure. In several pathosystems, extensive use of resistant cultivars with single dominant resistance-conferring gene has led to intense selection pressure on the virus, development of highly virulent strains, and resistance breakdown. This study assessed differences in TYLCV genomes isolated from susceptible and resistant genotypes in Florida and Georgia. Phylogenetic analyses indicated that Florida and Georgia isolates were distinct from each other. Population genetics analyses with genomes field-collected from resistant and susceptible genotypes from Florida and/or Georgia provided no evidence of a genetic structure between the resistant and susceptible genotypes. No codons in TYLCV genomes from TYLCV-resistant or susceptible genotypes were under positive selection, suggesting that highly virulent or resistance-breaking TYLCV strains might not be common in tomato farmscapes in Florida and Georgia. With TYLCV-resistant genotypes usage increasing recently and multiple tomato crops being planted during a calendar year, host resistance-induced selection pressure on the virus remains a critical issue. To address the same, a greenhouse selection experiment with one TYLCV-resistant and susceptible genotype was conducted. Each genotype was challenged with TYLCV through whitefly-mediated transmission serially 10 times (T_1-T_{10}). Population genetics parameters at the genome level were assessed at T_1, T_5, and T_{10}. Results indicated that genomes from resistant and susceptible genotypes did not differentiate with increasing transmission number, no specific mutations were repeatedly observed,

OPEN ACCESS

Edited by:
Magdalena Arasimowicz-Jelonek, Adam Mickiewicz University, Poland

Reviewed by:
Enrique Moriones, University of Málaga, Spanish Council of Scientific Research (IHSM-UMA-CSIC), Spain
Pedro Gomez Lopez, Spanish National Research Council, Spain

***Correspondence:**
Rajagopalbabu Srinivasan
babusri@uga.edu

Specialty section:
This article was submitted to Crop and Product Physiology, a section of the journal Frontiers in Plant Science

Received: *27 August 2020*
Accepted: *13 November 2020*
Published: *07 December 2020*

Citation:
Marchant WG, Gautam S, Hutton SF and Srinivasan R (2020) Tomato Yellow Leaf Curl Virus-Resistant and -Susceptible Tomato Genotypes Similarly Impact the Virus Population Genetics. Front. Plant Sci. 11:599697. doi: 10.3389/fpls.2020.599697

and no positive selection was detected. These results reiterate that resistance in tomato might not be exerting selection pressure against TYLCV to facilitate development of resistance-breaking strains. TYLCV populations rather seem to be shaped by purifying selection and/or population expansion.

Keywords: whitefly, tomato, TYLCV, host resistance, selection

INTRODUCTION

Tomato yellow leaf curl virus (TYLCV) infects tomato and causes substantial yield losses in the southeastern United States and in many parts of the world (Czosnek and Laterrot, 1997; Momol et al., 1999; Polston et al., 1999; Moriones and Navas-Castillo, 2000; Pappu et al., 2000; Varma and Malathi, 2003). Symptoms of TYLCV infection in tomato plants include stunted growth, chlorosis, curling of leaves, and reduced fruit yield (Cohen and Nitzany, 1966; Cohen and Antignus, 1994; Picó et al., 1996). *Tomato yellow leaf curl virus* is a species in the genus *Begomovirus* and in the family *Geminiviridae*. TYLCV is a monopartite DNA virus with circular genome that contains six genes with two genes on the viral strand (V1–V2) and four genes on the complementary sense strand (C1–C4) (Gronenborn, 2007). The virus is phloem limited in its hosts, and it is transmitted exclusively by the sweetpotato whitefly, *Bemisia tabaci* (Gennadius), in a persistent and circulative manner (Cohen and Harpaz, 1964; Cohen and Nitzany, 1966; Ghanim and Medina, 2007; Czosnek, 2008).

Resistance to TYLCV has been incorporated from wild solanum species into tetraploid cultivated tomato (Lapidot et al., 1997; Lapidot and Friedmann, 2002; Yan et al., 2018). TYLCV-resistant tomato cultivars and hybrids (hereafter referred to as genotypes) have proven to be effective in managing the virus (Lapidot et al., 1997; Gilreath et al., 2000; Lapidot and Friedmann, 2002). TYLCV-resistant tomato genotypes are not immune to the virus, and do not completely stop the replication of TYLCV. TYLCV-resistant genotypes are systemically infected, often exhibit milder symptoms, and suffer reduced yield loss than susceptible genotypes (**Figure 1**). Resistant genotypes also accumulate lower levels of the virus compared with susceptible genotypes (Lapidot et al., 2001; Legarrea et al., 2015). Consequently, whiteflies acquire reduced amounts of virus from TYLCV-infected resistant genotypes than susceptible genotypes, suggesting that resistant genotypes might not function as effective inoculum sources in comparison with susceptible genotypes (Lapidot et al., 2001; Legarrea et al., 2015). Resistance to TYLCV was initiated largely by exploitation of the *Ty*-1 semi-dominant gene (Zamir et al., 1994). In addition to *Ty*-1 gene, more recently developed resistant stocks contain *Ty*-2, *Ty*-3, *Ty*-4, *ty*-5, and *Ty*-6 genes (Hanson et al., 2000; Ji et al., 2007, 2009; Anbinder et al., 2009; Hutton et al., 2012). Recent studies have shed light on mechanisms of resistance for these resistance-conferring genes. *Ty*-1and *Ty*-3 have been identified as RNA-dependent RNA polymerases (Verlaan et al., 2013). *Ty*-2 has been identified as a nucleotide binding domain containing leucine rich repeat gene (NB-LRR) (Yamaguchi et al., 2018). *Ty*-4 has been identified as a partial dominant gene (Ji et al., 2009; Kadirvel et al., 2013), and the *ty*-5 gene encodes a mRNA surveillance factor Pelota (Lapidot et al., 2015). Most recently, *Ty*-6 has been characterized as the incomplete dominance gene (Gill et al., 2019).

TYLCV-resistant genotypes were not initially preferred in the southeastern United States due to the reduced fruit size, poor taste, and non-uniform ripening qualities (Ozores-Hampton et al., 2010; Srinivasan et al., 2012). However, horticultural traits have substantially improved in recently available TYLCV genotypes, and resistant genotypes are increasingly planted (Riley and Srinivasan, 2019). Tomato also is grown nearly year-round in Florida and Georgia, thereby providing numerous opportunities for positive selection against TYLCV. TYLCV mutates at a very high rate. The rate of mutation for the full-length TYLCV genome is 2.88×10^{-4} substitutions/site/year, and it is comparable to RNA viruses (Duffy and Holmes, 2008). This high mutation rate combined with selection pressure from continued use of resistant cultivars could lead to the emergence of resistance-breaking TYLCV strains.

Numerous examples of resistance-breaking virus strains have been documented in other pathosystems. Beet necrotic yellow vein virus (BNYVV), an RNA virus, has overcome the *Rz1*-resistance gene in sugar beet in northwestern Europe due to mutations in the pathogenicity gene P25 (Bornemann et al., 2015). Tomato spotted wilt orthotospovirus (TSWV), also an RNA virus, has overcome resistance genes *Tsw* and *Sw5* in pepper and tomato, respectively. *Tsw* and *Sw5* resistance breakdown has been documented in Asia, Europe, and in the Americas (Latham and Jones, 1998; Roggero et al., 2002; Aramburu and Marti, 2003; Ciuffo et al., 2005; Sharman and Persley, 2006; Deligoz et al., 2014; Almási et al., 2015; Debreczeni et al., 2015; Ferrand et al., 2015; Jiang et al., 2016; Batuman et al., 2017). Another RNA virus, cotton leafroll dwarf virus (CLRDV), in Brazil overcame resistance in cotton accessions that were originally resistant (da Silva et al., 2015).

No instances of TYLCV overcoming *Ty*-induced resistance through positive selection in the field have been documented yet. However, an experiment in the lab led to the development of a resistance-breaking strain of TYLCV (Ohnishi et al., 2016). The tomato cultivar H24 was homozygous for the *Ty*-2 gene, and it was resistant to the TYLCV-IL strain but not the TYLCV-Mld strain. A virus chimera created in lab with the C4 and C1 genes from the Mld strain and the remainder of the genome from the IL strain led to resistance breakdown (Ohnishi et al., 2016). Similarly, if a natural recombination event occurred, resistance-breaking TYLCV strains could emerge under field situations. This was witnessed in southern Morocco with the recombinant TYLCV-IS76 that outcompeted its parents TYLCV-IL and tomato yellow leaf curl Sardinia virus (TYLCSV-ES) in tomato genotypes with the *Ty*-1 resistance gene (Belabess et al., 2016).



FIGURE 1 | (A) Photograph representing differences in TYLCV infection symptoms on a TYLCV-resistant and -susceptible tomato genotype under intense TYLCV pressure. Both genotypes were planted at the same time. Photograph was taken ∼2 months after planting. **(B)** Photograph representing typical size and quality of tomato fruits obtained from TYLCV-resistant (left) and -susceptible (right) genotypes.

This recombinant is now the prevalent TYLCV present in the region. Extensive use of TYLCV-resistant cultivars can also displace certain begomoviruses and/or their strains in favor of others. A survey in Spain found that susceptible genotypes in tomato fields were more often infected with TYLCSV-ES, while resistant genotypes with the *Ty*-1 gene in tomato fields were more often infected with TYLCV (García-Andrés et al., 2009).

This study attempted to examine if there is evidence for continuous use of TYLCV resistant cultivars resulting in TYLCV overcoming resistance and/or affecting TYLCV diversity in Florida and Georgia in southeastern United States. This was accomplished by examining the full-length genomes of naturally occurring TYLCV isolates from TYLCV-resistant and susceptible tomato genotypes from Florida and Georgia. Through a simulated greenhouse experiment, this study also attempted to determine if whitefly-mediated serial transmission of TYLCV involving a resistant genotype would lead to increased selection on the virus and development of resistance-breaking strains.

MATERIALS AND METHODS

Maintenance of Whiteflies and TYLCV

The sweetpotato whitefly, *B. tabaci* Middle East-Asia Minor 1 (MEAM1) cryptic species (GenBank accession number MN970031), was first collected in Tifton, Georgia, USA in 2009. The whiteflies since then were maintained on 15 to 20 cm tall cotton plants in 45L × 45W × 90H cm^3 whitefly-proof cages (Megaview Science Co., Taichung, Taiwan) in a greenhouse at 25–30°C with a 14 h L:10 h D photoperiod. The TYLCV isolate (GenBank accession number KY965880) was collected from a TYLCV-infected tomato plant in Montezuma, Georgia, USA in 2009. The virus has since been maintained in tomato (cultivar Florida 47, Seminis Vegetable Seeds, MO, USA) through whitefly-mediated transmission in the greenhouse at above-stated conditions.

Isolation of TYLCV From Field-Collected TYLCV-Resistant and -Susceptible Tomato Genotypes

Leaf tissue was collected from symptomatic tomato plants in agricultural fields with TYLCV-resistant and -susceptible genotypes from Tifton, Georgia in 2015 and 2016 and from Immokalee, Florida, USA in 2015. Detailed sample information is included in **Table 1**. Whole genome sequences obtained from those leaf tissue samples were deposited in the GenBank with accession numbers KY971320–KY971372.

TABLE 1 | Details of TYLCV isolates field-collected from susceptible and resistant tomato genotypes.

Sample name	Collection date	Location	Host plant	TYLCV-susceptibility of host plant	Accession no.	Resistant gene*
Florida_1.2	Mar-2015	USA: Immokalee, Florida	*Solanum lycopersicum* cv. FL47 (Seminis)	Susceptible	KY971320	None[#]
Florida_11.1_R	Apr-2015	USA: Immokalee, Florida	*Solanum lycopersicum* cv. Skyway 687 (Enza Zaden)	Resistant	KY971321	*Ty3Ty6*[$]
Florida_11.2_R	Apr-2015	USA: Immokalee, Florida	*Solanum lycopersicum* cv. Skyway 687 (Enza Zaden)	Resistant	KY971322	*Ty3Ty6*
Florida_11.3_R	Apr-2015	USA: Immokalee, Florida	*Solanum lycopersicum* cv. Skyway 687 (Enza Zaden)	Resistant	KY971323	*Ty3Ty6*
Florida_17.1	Jun-2015	USA: Immokalee, Florida	*Solanum lycopersicum* cv. Suddath's Strain (Nature and Nuture Seeds)	Susceptible	KY971324	None
Florida_18.1	Jun-2015	USA: Immokalee, Florida	*Solanum lycopersicum* cv. Orange Strawberry (Baker Creek Heirloom Seeds)	Susceptible	KY971325	None
Florida_19.1	Jun-2015	USA: Immokalee, Florida	*Solanum lycopersicum* cv. Legend (Tomato Growers)	Susceptible	KY971326	None
Florida_2.1	Apr-2015	USA: Immokalee, Florida	*Solanum lycopersicum* cv. Plum Regal (Bejo Seeds)	Susceptible	KY971327	None
Florida_3.1	Apr-2015	USA: Immokalee, Florida	*Solanum lycopersicum* cv. BHN 685 (Siegers Seed Company)	Susceptible	KY971328	None
Florida_4.2_R	Apr-2015	USA: Immokalee, Florida	*Solanum lycopersicum* cv. HM 8845 (Harris Moran Seed Company)	Resistant	KY971329	Unk.[^]
Florida_4.4_R	Apr-2015	USA: Immokalee, Florida	*Solanum lycopersicum* cv. HM 8845 (Harris Moran Seed Company)	Resistant	KY971330	Unk.
Florida_5.1	Apr-2015	USA: Immokalee, Florida	*Solanum lycopersicum* cv. Juliet (Johnny's Selected Seeds)	Susceptible	KY971331	None
Florida_6.5	Apr-2015	USA: Immokalee, Florida	*Solanum lycopersicum* cv. Gator (Bejo Seeds)	Susceptible	KY971332	None
Florida_7.1	Apr-2015	USA: Immokalee, Florida	*Solanum lycopersicum* cv. yellow pear heirloom (Tomato Growers)	Susceptible	KY971333	None
Florida_7.2	Apr-2015	USA: Immokalee, Florida	*Solanum lycopersicum* cv. yellow pear heirloom (Tomato Growers)	Susceptible	KY971334	None
Florida_7.3	Apr-2015	USA: Immokalee, Florida	*Solanum lycopersicum* cv. yellow pear heirloom (Tomato Growers)	Susceptible	KY971335	None
Florida_7.5	Apr-2015	USA: Immokalee, Florida	*Solanum lycopersicum* cv. yellow pear heirloom (Tomato Growers)	Susceptible	KY971336	None
Florida_8.4	Apr-2015	USA: Immokalee, Florida	*Solanum lycopersicum* cv. Brickyard (Syngenta)	Susceptible	KY971337	None
Georgia_107.2	Sep-2016	USA: Tifton, Georgia	*Solanum lycopersicum* cv. Lanai (lab cultivar)	Susceptible	KY971338	None
Georgia_108.1	Sep-2016	USA: Tifton, Georgia	*Solanum lycopersicum* cv. FL47 (Seminis)	Susceptible	KY971339	None
Georgia_108.2	Sep-2016	USA: Tifton, Georgia	*Solanum lycopersicum* cv. FL47 (Seminis)	Susceptible	KY971340	None
Georgia_112.1	Sep-2016	USA: Tifton, Georgia	*Solanum lycopersicum* cv. FL47 (Seminis)	Susceptible	KY971341	None
Georgia_118.1_R	Sep-2016	USA: Tifton, Georgia	*Solanum lycopersicum* cv. Security (Harris Seeds Company)	Resistant	KY971342	*Ty1ty1*[&]
Georgia_122.2_R	Sep-2016	USA: Tifton, Georgia	*Solanum lycopersicum* cv. Security (Harris Seeds Company)	Resistant	KY971343	*Ty1ty1*
Georgia_124.3_R	Sep-2016	USA: Tifton, Georgia	*Solanum lycopersicum* cv. Inbar (Hazera Genetics)	Resistant	KY971344	*Ty1/3Ty6*[$]
Georgia_127.1_R	Sep-2016	USA: Tifton, Georgia	*Solanum lycopersicum* cv. Inbar (Hazera Genetics)	Resistant	KY971345	*Ty1/3Ty6*
Georgia_130.1_R	Sep-2016	USA: Tifton, Georgia	*Solanum lycopersicum* cv. Shanty (Hazera Genetics)	Resistant	KY971346	*Ty1-*[%]
Georgia_130.2_R	Sep-2016	USA: Tifton, Georgia	*Solanum lycopersicum* cv. Shanty (Hazera Genetics)	Resistant	KY971347	*Ty1-*
Georgia_132.1_R	Sep-2016	USA: Tifton, Georgia	*Solanum lycopersicum* cv. Shanty (Hazera Genetics)	Resistant	KY971348	*Ty1-*

(Continued)

TABLE 1 | Continued

Sample name	Collection date	Location	Host plant	TYLCV-susceptibility of host plant	Accession no.	Resistant gene*
Georgia_133.1_R	Sep-2016	USA: Tifton, Georgia	*Solanum lycopersicum* cv. Tygress (Seminis)	Resistant	KY971349	*Ty1ty1*[&]
Georgia_133.2_R	Sep-2016	USA: Tifton, Georgia	*Solanum lycopersicum* cv. Tygress (Seminis)	Resistant	KY971350	*Ty1ty1*
Georgia_135.1_R	Sep-2016	USA: Tifton, Georgia	*Solanum lycopersicum* cv. Tygress (Seminis)	Resistant	KY971351	*Ty1ty1*
Georgia_135.2_R	Sep-2016	USA: Tifton, Georgia	*Solanum lycopersicum* cv. Tygress (Seminis)	Resistant	KY971352	*Ty1ty1*
Georgia_25.1_R	Sep-2015	USA: Tifton, Georgia	*Solanum lycopersicum* cv. Security (Harris Seeds Company)	Resistant	KY971353	*Ty1ty1*
Georgia_30.1_R	Sep-2015	USA: Tifton, Georgia	*Solanum lycopersicum* cv. Shanty (Hazera Genetics)	Resistant	KY971354	*Ty1-*
Georgia_35.1	Sep-2015	USA: Tifton, Georgia	*Solanum lycopersicum* cv. FL47 (Seminis)	Susceptible	KY971355	None
Georgia_40.2_R	Oct-2015	USA: Tifton, Georgia	*Solanum lycopersicum* cv. Shanty (Hazera Genetics)	Resistant	KY971356	*Ty1-*
Georgia_47.1_R	Oct-2015	USA: Tifton, Georgia	*Solanum lycopersicum* cv. Tygress (Seminis)	Resistant	KY971357	*Ty1ty1*
Georgia_50.1_R	Oct-2015	USA: Tifton, Georgia	*Solanum lycopersicum* cv. Security (Harris Seeds Company)	Resistant	KY971358	*Ty1ty1*
Georgia_57.1	Oct-2015	USA: Tifton, Georgia	*Solanum lycopersicum* cv. FL47 (Seminis)	Susceptible	KY971359	None
Georgia_58.1	Oct-2015	USA: Tifton, Georgia	*Solanum lycopersicum* cv. Red Bounty (Harris Seeds Company)	Susceptible	KY971360	None
Georgia_58.2	Oct-2015	USA: Tifton, Georgia	*Solanum lycopersicum* cv. Red Bounty (Harris Seeds Company)	Susceptible	KY971361	None
Georgia_59.1	Oct-2015	USA: Tifton, Georgia	*Solanum lycopersicum* cv. FL47 (Seminis)	Susceptible	KY971362	None
Georgia_59.3	Oct-2015	USA: Tifton, Georgia	*Solanum lycopersicum* cv. FL47 (Seminis)	Susceptible	KY971363	None
Georgia_63.1_R	Oct-2015	USA: Tifton, Georgia	*Solanum lycopersicum* cv. Tygress (Seminis)	Resistant	KY971364	*Ty1ty1*
Georgia_67.2_R	Oct-2015	USA: Tifton, Georgia	*Solanum lycopersicum* cv. Tygress (Seminis)	Resistant	KY971365	*Ty1ty1*
Georgia_72.1_R	Oct-2015	USA: Tifton, Georgia	*Solanum lycopersicum* cv. Shanty (Hazera Genetics)	Resistant	KY971366	*Ty1-*
Georgia_76.2_R	Oct-2015	USA: Tifton, Georgia	*Solanum lycopersicum* cv. Security (Harris Seeds Company)	Resistant	KY971367	*Ty1ty1*
Georgia_81.3_R	Oct-2015	USA: Tifton, Georgia	*Solanum lycopersicum* cv. Security (Harris Seeds Company)	Resistant	KY971368	*Ty1ty1*
Georgia_9.10	Jan-2015	USA: Tifton, Georgia	*Solanum lycopersicum* cv. FL47 (Seminis)	Susceptible	KY971369	None
Georgia_9.9	Jan-2015	USA: Tifton, Georgia	*Solanum lycopersicum* cv. FL47 (Seminis)	Susceptible	KY971370	None
Georgia_92.1_R	Nov-2015	USA: Tifton, Georgia	*Solanum lycopersicum* cv. Security (Harris Seeds Company)	Resistant	KY971371	*Ty1ty1*
Georgia_99.1	Sep-2016	USA: Tifton, Georgia	*Solanum lycopersicum* cv. Lanai (lab cultivar)	Susceptible	KY971372	None

[*] *Heterozygous nature of Ty resistance genes in tomato cultivars and hybrids are indicated.*
[#] *None- implies that susceptible cultivars/hybrids did not carry a TYLCV resistant gene.*
[^] *Unknown- implies information not publicly available/experimentally determined yet.*
[&] *Ji et al. (2007).*
[$] *Genotyped for this study.*
[%] *Gelbart et al. (2020).*

Cloning and Sequencing of TYLCV Genomes

DNA from leaf tissue was extracted using GeneJET Plant Genomic DNA Purification Kit (Thermo Scientific, Waltham, MA). TYLCV DNA from susceptible tomato genotypes was amplified with rolling circle amplification. TYLCV DNA from resistant cultivars did not amplify optimally with rolling circle amplification, probably because resistant genotypes typically accumulated reduced levels of viral DNA than susceptible genotypes (Legarrea et al., 2015). Consequently, a PCR-based cloning method was employed to amplify TYLCV DNA from resistant genotypes. TYLCV DNA from susceptible genotypes was amplified using the TempliPhi (GE Healthcare, Chicago, IL) kit and the protocol outlined by Inoue-Nagata

et al. (2004). Amplified DNA was digested with SacI (Fisher BioReagents, Pittsburgh, Pennsylvania). To purify the DNA, a gel extraction was performed on the SacI-digested DNA using crystal violet (Fisher Chemical, Fair Lawn, NJ) as the DNA-visualizing agent. The DNA was then ligated into the vector pGEM-3Z (Promega Corporation, Madison, WI) and a transformation was performed into One Shot TOP10 Chemically Competent *E. coli* (Invitrogen, Carlsbad, CA). Colonies were screened for TYLCV inserts via PCR with primers T7F (5′-TAATACGACTCACTATAGGG-3′) and M13R (5′- CAGGAAACAGCTATGACC-3′), and purified plasmids were sequenced (Eurofins Genomics, Louisville, KY) using the following primers: 5370F (5′-TTCGCTATTACGCCAGCT-3′), 2941R (5′-CCCAGGCTTTACACTTTATGCTTCC-3′), 710F (5′-TCTTATATCTGTTGTAAGGGCCCGT-3′), and 1400F (5′-ACGAGAACCATACTGAAAACGCCTT-3′).

TYLCV DNA from resistant genotypes was amplified using PCR with three different primer sets to cover the full-length of the TYLCV genome. The first segment was amplified with primers 1470R (5′-TGCATACACTGGATTAGAGGCATG-3′) and 2243F (5′-GAAACATAAACTTCTAAAGGAGGAC-3′), and a PCR program with an initial 95°C denaturation step for 3 min followed by 35 cycles of 95°C for 30s, 56°C for 30 s, and 72°C for 1 min, and a final extension step of 72°C for 5 min. The PCR mixture for each sample was 10 μl comprising 5 μl of GoTaq® Green Master Mix (Promega Corporation, Madison, WI), 2 μl of water, 0.5 μl of each primer at 10 μM concentration, and 2 μl of DNA extract. The second segment was amplified with primers C2R (5′-CCAATAAGGCGTAAGCGTGT-3′) and 1371F (5′-AACTTATAATCATCAGGAGGCAGCC-3′), and the third segment was amplified with C2F (5′-GCAGTGATGAGTTCCCCTGT-3′) and 2326R (5′-GAGGCCCTCAATATATTAAAAGA-3′). Both the second and third segments were amplified with a PCR program with an initial denaturation step of 95°C for 3 min followed by 35 cycles of 95°C for 30 s, 55°C for 30 s, and 72°C for 50 s, and a final extension step of 72°C for 5 min. The three segments were cloned using CloneJET PCR Cloning Kit (Thermo Scientific, Waltham, MA). Ligated vectors were transformed into One Shot TOP10 Chemically Competent *E. coli* (Invitrogen, Carlsbad, CA). Colonies were screened via PCR to verify the ligation of expected-length inserts into plasmids. Five colonies that contained inserts of the proper length were chosen from each sample. Purified plasmids were then sequenced (Eurofins Genomics, Louisville, KY) using primers pJET1.2F (5′-CGACTCACTATAGGGAGAGCGGC-3′) and pJET1.2R (5′-AAGAACATCGATTTTCCATGGCAG-3′). Vector sequences were manually excised from TYLCV sequences, and the reads were assembled into full-length genomes using Geneious Pro v. 8.1.9 (Drummond et al., 2011).

Whitefly-Mediated Serial Transmission of TYLCV to TYLCV-Resistant and -Susceptible Genotypes

Five tomato plants at the ten-leaf stage (∼8 weeks old) of either the TYLCV-susceptible cultivar, Florida Lanai, or the TYLCV-resistant hybrid (*Ty1/3-Ty6*), Inbar (Hazera Genetics, Berurim M.P Shikmim, Israel), were individually caged in the greenhouse at the above-stated conditions. Viruliferous whiteflies were obtained by providing whiteflies with a 48 h acquisition access period (AAP) on TYLCV (KY965880)-infected tomato plant. The tomato plants were inoculated by clip-caging twenty viruliferous whiteflies to a fully expanded leaf at the upper portion of each plant. After a 48 h inoculation access period (IAP), the whiteflies were removed. The tomato plants were allowed to develop infection for 3 weeks and tested for TYLCV infection by PCR using the primers C2-1201 (5′- CATGATCCACTGCTCTGATTACA−3′) and C2-1800V2 (5′-TCATTGATGACGTAGACCCG-3′), which targeted a 695-nucleotide region of the TYLCV genome encompassing the entire C2 gene. The PCR mixture for each sample was 10 μl comprising 5 μl of GoTaq® Green Master Mix, 2 μl of water, 0.5 μl of each primer at 10 μM concentration, and 2 μl of DNA extract. The PCR program had an initial denaturation step at 94°C for 2 min, followed by 30 cycles of 94°C for 30 s, 52°C for 30 s, and 72°C for 1 min, and a final extension at 72°C for 5 min. After 3 weeks, non-viruliferous whiteflies (20/plant) were then clip-caged to the upper leaves of TYLCV-infected plants (T_1) and given a 48 h AAP. These whiteflies were subsequently transferred to non-infected plants of the same cultivar/hybrid (T_2) for a 48 h IAP. The inoculated plants were maintained for 3 weeks, and TYLCV was again transmitted by whiteflies to non-infected plants. This process was repeated until whitefly-mediated transmission to tomato plants was completed 10 times (T_1-T_{10}). Leaf tissue samples were taken from each plant post first (T_1), fifth (T_5), and tenth (T_{10}) transmission for DNA extraction. Three full-length TYLCV genomes were sequenced from all five replicates (plants) belonging to resistant and susceptible genotypes. Full-length genomes were cloned and sequenced as described earlier and deposited in GenBank (accession numbers KY965834 - KY965923).

TYLCV Quantitation in Resistant and Susceptible Genotypes Following Whitefly-Mediated Serial Transmission

To assess if whitefly-mediated serial transmission over 10 passages affected TYLCV accumulation/TYLCV load differently in TYLCV-resistant genotypes and TYLCV-susceptible genotypes, DNA extracted from both susceptible and resistant genotypes at T_1, T_5, and T_{10} were subjected to absolute quantitation using real time PCR following the protocol outlined by Legarrea et al. (2015). Primers targeting a 102-bp region of the TYLCV C2 gene were used for this purpose (Legarrea et al., 2015). Plasmids with C2 gene inserts were used for generating a standard curve for absolute quantitation (Legarrea et al., 2015). DNA from 100 mg leaf tissue/plant corresponding to 10 to 15 resistant and susceptible genotypes at T_1, T_5, and T_{10} were used for absolute quantitation. A duplicate was included for all samples for the real time PCR runs. The virus copy numbers were analyzed using R Version 3.4.2 (R Core Team, 2019). Data were analyzed using a mixed-effect model in the "Lme4" package (Bates et al., 2015). Time intervals were considered as fixed effects and replications were as considered random effects. To meet the assumptions of normality and homoscedasticity of

variance, virus copy numbers were log transformed. Differences in virus accumulation in susceptible and resistant genotypes leaf tissues independently were analyzed using one-way repeated-measures ANOVA, and treatment means were separated in the "emmeans" package with the default Tukey's honest significant difference (Tukey HSD) *post-hoc* test. To compare TYLCV copy numbers or virus loads in leaf tissues of resistant vs. susceptible genotypes a two-way analysis of variance was used. For this analyses, susceptibility/resistant status and transmission number were considered as fixed effects, replication was considered as random effect. Differences in virus loads between resistant and susceptible genotypes' leaf tissues at each transmission T_1, T_5, and T_{10} were assessed using the Tukey's honest significant difference (Tukey HSD) *post-hoc* test.

Phylogenetic Analysis

A maximum-likelihood phylogenetic tree was constructed in MEGA X (Kumar et al., 2018). Fifty-three TYLCV genome sequences from samples collected from Florida and Georgia were used for phylogenetic analysis. Sequences were aligned in MUSCLE. The best-fitting nucleotide substitution model (Jukes-Cantor model) was determined by relying on the Akaike Information Criterion (AIC) in jMODELTEST (Darriba et al., 2012). The support for each individual branch was assessed via 1,000 bootstrap replications. For phylogenetic analyses involving comparison of genomes of Florida and Georgia isolates, a TYLCV genome sequence available from the GenBank (accession AY530931 from Florida) was also added to the data set. Representative genome sequences from each of the seven TYLCV strains viz., TYLCV-IL (GenBank accession number X15656), TYLCV-Bou (GenBank accession number GU076454), TYLCV-IR (GenBank accession number AJ132711), TYLCV-Kah (GenBank accession number EU635776), TYLCV-Ker (GenBank accession number GU076442), TYLCV-Mld (GenBank accession number X76319), and TYLCV-OM (GenBank accession number FJ956700) were included as outgroup taxa. Tomato yellow leaf curl China virus (TYLCCV) (GenBank accession number NC_004044) and TYLCSV (GenBank accession number GU951759) genome sequences were also included in the analyses.

Nucleotide/Haplotype Diversity and Gene Flow and Genetic Differentiation

Nucleotide diversity (π), haplotype diversity, population mutation rate (θ), substitutions, and indels were calculated using the software DnaSP v5.10.01 (Librado and Rozas, 2009). To determine if TYLCV isolates obtained from TYLCV-resistant and -susceptible genotypes in Florida and/or Georgia differentiated from one another, nucleotide sequence-based Ks, Kst, Snn, Z, and Fst statistics were calculated using the Gene Flow and Genetic Differentiation tool in DnaSP (Hudson et al., 1992). To test for level of significance, a permutation test with 1,000 replications was performed. Values were considered significant if p-values were <0.05.

Positive Selection

All six genes of TYLCV genomes were analyzed for positive selection using the HyPhy tool (Pond and Muse, 2005) in MEGA 7.0.21 (Kumar et al., 2016). The HyPhy tool determined non-synonymous (dN) and synonymous (dS) nucleotide substitutions for each codon. The Tamura-Nei model was selected as the substitution model (Tamura and Nei, 1993). Codons with a dN greater than dS and a $p < 0.05$ were considered to be under positive selection.

Population Neutrality

To test for neutrality among TYLCV isolates (populations) from TYLCV-resistant and susceptible genotypes, Tajima's D (Tajima, 1989) was computed in DnaSP using the Tajima's Test tool. Tajima's D statistic was determined by the average number of nucleotide pair-wise differences and the number of segregating sites among all sequences.

Fu and Li's D and F statistics (Fu and Li, 1993) were also calculated using DnaSP. The D statistic is calculated based on the number of mutations appearing just once and the total number of mutations. The F statistic is calculated based the number of mutations appearing just once and the average pairwise differences between sequences.

RESULTS

TYLCV Isolates Field-Collected From TYLCV-Resistant and -Susceptible Genotypes

Twenty-seven TYLCV genomes from isolates of resistant genotypes and 26 TYLCV genomes from isolates of susceptible genotypes were sequenced and compared (**Table 1**). All TYLCV genomes isolated from resistant and susceptible genotypes were closely related to the TYLCV-IL strain than the other six TYLCV strains known. The nucleotide identities of isolated genomes ranged from of 96.61 to 98.25% in comparison with

TABLE 2 | Nucleotide and haplotype diversity associated with TYLCV genomes isolated from resistant and susceptible tomato genotypes from Florida and Georgia.

Populations analyzed	π^v	θ^w	Hap^x	Substitutions^y	Indel sites^z
Florida-R	0.012	0.014	3.00	91.00	3.00
Florida-S	0.011	0.017	3.00	148.00	3.00
Georgia-R	0.006	0.012	3.00	114.00	3.00
Georgia-S	0.007	0.012	2.00	102.00	2.00
Florida- R & S combined	0.011	0.019	4.00	156.00	6.00
Georgia- R & S combined	0.005	0.012	3.00	130.00	4.00

R, Represents genomes from resistant genotypes.
S, Represents genomes from susceptible genotypes.
[v] π Represents nucleotide diversity.
[w] Population mutation rate.
[x] Number of haplotypes.
[y] Number of substitutions.
[z] InDel sites.
Reference sequence TYLCV-IL(X15656) was used in determining substitutions and indel sites.

the TYLCV-IL strain genome (GenBank accession number X15656). The nucleotide identities of TYLCV genomes from resistant and susceptible genotypes in Florida ranged from 97.98 to 99.16%. The number of haplotypes were the same. However, the number of substitutions were higher in the TYLCV genomes isolated from susceptible than resistant Florida genotypes (**Table 2**). The nucleotide identities of TYLCV genomes from resistant and susceptible genotypes in Georgia ranged from 99.49 to 99.89%. The number of haplotypes was slightly higher in TYLCV genomes isolated from resistant genotypes than susceptible genotypes in Georgia. The number of substitutions and indels were also slightly higher in TYLCV genomes isolated from resistant genotypes than susceptible genotypes in Georgia (**Table 2**). The mutations in all genomes were more concentrated on the non-coding region (1–285 nucleotides) and on the viral strand genes (V1 and V2) than on the complementary strand genes (C1 through C4) (**Figure 2**).

The average pairwise nucleotide differences (Kt) between genomes of TYLCV isolates from resistant vs. susceptible genotypes from Florida was 2.36 times higher than that from Georgia (**Table 3**). The nucleotide-based population differentiation statistics Ks, Kst, and Z values calculated were determined by the permutation test to be not significantly different between genomes of TYLCV isolates from resistant and susceptible genotypes from either Georgia or Florida (**Table 3**). On the contrary, the *p*-value indicated associated with another differentiation statistic Snn was significantly different between genomes of TYLCV isolates from resistant and susceptible Florida genotypes. However, the associated Fst between the genomes of TYLCV isolates from resistant and susceptible genotypes from Florida indicated a high level of similarity. When genomes of TYLCV isolates from resistant and susceptible genotypes from both states were combined, significant differences for Ks, Kst, Snn, and Z between were observed (**Table 3**). Overall, the Fst values were low when the genomes of TYLCV isolates from resistant and susceptible genotypes from Florida and/or Georgia were compared, indicating a high level of similarity between TYLCV isolates present in resistant and susceptible genotypes.

Positive selection on all six genes of Florida and Georgia TYLCV isolates from resistant and susceptible genotypes was assessed using the HyPhy codon selection test. No codon was determined to be under positive selection at a statistically significant level for any of the six genes (**Supplementary Material 1**).

Population neutrality statistics Fu and Li's D and F statistics and Tajima's D were calculated using the TYLCV genomes obtained from TYLCV-resistant and/or susceptible genotypes in Florida and/or Georgia. These statistics examined the frequency of segregating sites across the genome. Positive values for all three statistics were noticed in the case of genomes of TYLCV isolates from resistant genotypes from Florida, but the corresponding *p*-values indicated no statistical significance (**Table 4**). On the contrary, a significant *p*-value was accompanied by negative values for Fu and Li's D and F statistics in the case of genomes of TYLCV isolates from resistant genotypes in Georgia (**Table 4**). Negative values and insignificant *p*-values for all three statistics were obtained for genomes of TYLCV isolates from susceptible genotypes from either Florida or Georgia (**Table 4**). Similar results were obtained when genomes of TYLCV isolates from resistant genotypes from Florida and Georgia, and genomes of TYLCV isolates from susceptible genotypes from both Florida and Georgia were examined (**Table 4**). When the genomes of TYLCV isolates from resistant and susceptible genotypes from both states were combined, significant results for Fu and Li's F and D statistics were identified (**Table 4**). However, negative values for Fu and Li's D and F statistics reiterated evidence for either a recent population expansion or purifying selection.

TYLCV Isolates Field-Collected From Florida and Georgia

The genomes of TYLCV isolates were divided based on the state they were collected from and regardless of the genotype resistance status. The nucleotide identities for TYLCV genomes between Florida and Georgia isolates ranged from 98.62 to 99.20%. The number of haplotypes were higher in TYLCV genomes isolated from Florida than Georgia regardless of resistant status of genotypes. The number of substitutions and indels were also higher in TYLCV genomes isolated from Florida than Georgia regardless of resistant status of genotypes (**Table 2**). The mutations in all genomes were more concentrated on the non-coding region (1–285 nucleotides) and on the viral strand (V1 and V2) genes than on the complementary strand genes (C1 through C4) (**Figure 2**).

The nucleotide-based genetic differentiation statistics Ks, Kst, Snn, and Z statistics with their corresponding permutation tests revealed differences between two populations (**Table 3**).

All six genes from the Florida, Georgia, and combined populations were tested with the HyPhy codon selection test. No codon was under positive selection at a statistically significant level (**Supplementary Material 1**).

The genomes of Florida and Georgia isolates regardless of the genotype resistance status were tested for neutrality with Fu and Li's D and F and Tajima's D statistics. The Florida and Georgia populations both had negative values for all three statistics, and they were not at a statistically significant level (**Table 4**). The combined population had statistically significant values for Fu and Li's D and F statistics but not for Tajima's D. The negative values of the Fu and Li's D and F statistics once again indicated evidence for either population expansion or purifying selection.

The maximum likelihood tree showed the Florida and Georgia TYLCV isolates clearly parsed from one another into separate clades (**Figure 3**). The Georgia clade/s appeared to emerge from the Florida population. This could indicate that the Georgia TYLCV populations arose from an introduction into Florida. The TYLCV samples from resistant and susceptible genotypes did not parse with one another. There does not appear to be any phylogenetic relationship between TYLCV

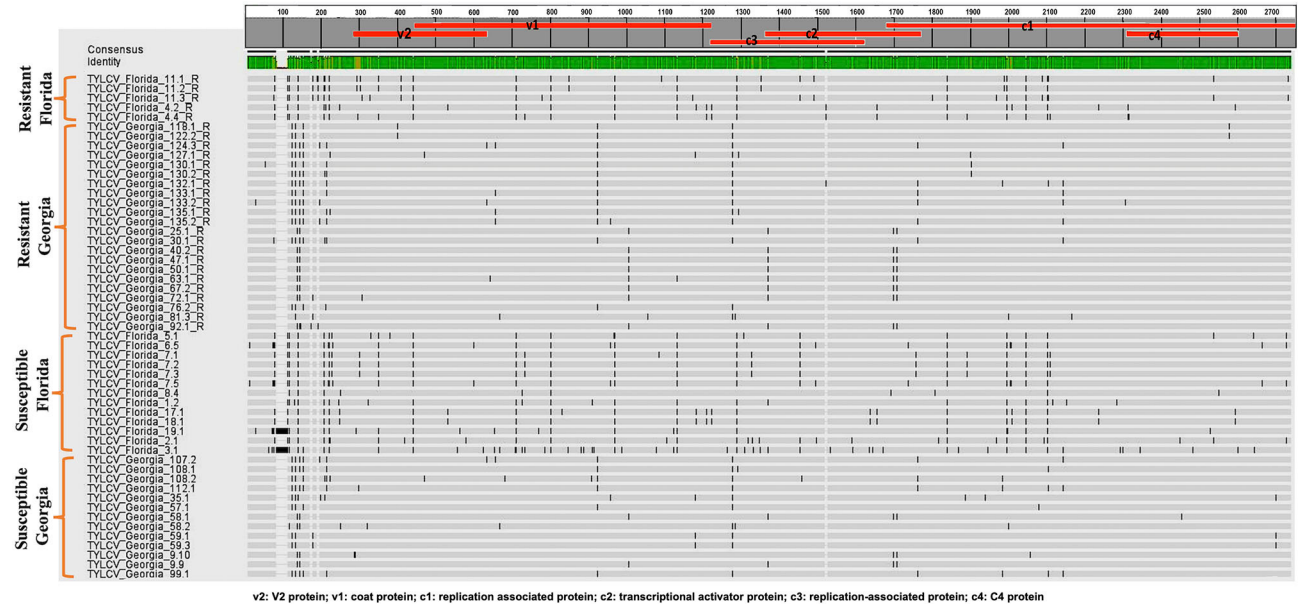


FIGURE 2 | An alignment of full length TYLCV genomes corresponding to TYLCV-resistant and susceptible genotypes from Florida and Georgia with a single consensus sequence and mutations markings.

TABLE 3 | Genetic differentiation statistics with genomes of TYLCV isolates field-collected from TYLCV-resistant and -susceptible tomato genotypes from Florida and Georgia.

Populations analyzed	Kt[x]	Ks[y]	Kst[y]	*p*-value of Ks and Kst	Snn[y]	*p*-value of Snn	Z[y]	*p*-value of Z	Fst[z]
Florida_R vs. Florida_S	26.332	25.583	0.028	0.079	0.889	**0.011**	72.165	0.107	0.067
Georgia_R vs. Georgia_S	11.826	11.880	−0.004	0.487	0.588	0.193	299.427	0.577	−0.009
Resistant vs. Susceptible	24.620	23.861	0.031	**0.017**	0.680	**0.004**	670.422	**0.034**	0.059
Florida vs. Georgia	24.869	16.346	0.342	**0.000**	0.981	**0.000**	455.610	**0.000**	0.497

[x] *Kt is the average number of pairwise nucleotide differences across genomes in both populations.*

[y] *Ks, Kst, Snn, and Z are nucleotide sequence-based genetic differentiation statistics.*

[z] *Fst is a population differentiation statistic. Values range from 0 to 1. Low Fst values indicate a high level of similarity between populations while high Fst values indicate genetically distinct groups. Bold values indicate statistical significance.*

genomes and the resistance status of the genotypes they were collected from.

Whitefly-Mediated Serial Transmission of TYLCV to TYLCV-Resistant and -Susceptible Genotypes

TYLCV was successfully serially transmitted 10 times (T_1-T_{10}) via whiteflies to both TYLCV-resistant and susceptible genotypes. TYLCV genomes from both resistant and/or susceptible genotypes at T_1, T_5, and T_{10} were assessed to determine if TYLCV populations from the susceptible and/or resistant genotypes differentiated from one another. The nucleotide identities of TYLCV genomes isolated from resistant and susceptible genotypes following serial transfer ranged from 99.35 to 99.75%. The number of haplotypes were higher in TYLCV genomes isolated from the resistant genotype than the susceptible genotype (**Table 5**). The number of substitutions and indels were also higher in TYLCV genomes isolated from the resistant genotype than the susceptible genotype (**Table 5**). The mutations were more concentrated on the non-coding region (1–285 nucleotides) and on the viral strand (V1 and V2) genes than on the complementary strand genes (C1 through C4) (**Figures 4A,B**).

With the TYLCV susceptible genotype, the nucleotide sequence-based genetic differentiation statistics Ks, Kst, Snn, and Z showed a statistically significant differentiation occurring at T_5, and T_{10}, but not T_1 (**Table 6**). But the Fst values were low indicating lack of differentiation with increasing transmission number. Similar results were also obtained with the resistant genotype, indicating no evidence of population differentiation with increasing transmission number (**Table 6**). When the TYLCV genomes from the resistant genotype were compared with TYLCV genomes from susceptible genotype, genetic differentiation statistics Ks, Kst, Snn, and Z were statistically significant at T_5, and T_{10}, but not T_1 (**Table 6**). Nevertheless, the Fst values were still low and indicated no genetic differentiation in TYLCV genomes between resistant and susceptible genotypes following serial transfer.

TABLE 4 | Tests of neutrality with genomes of TYLCV isolates field-collected from TYLCV-resistant and -susceptible tomato genotypes from Florida and Georgia.

Population analyzed	Fu and Li's D[a]	*p*-value	Fu and Li's F[a]	*p*-value	Tajima's D[a]	*p*-value
Florida_R	0.177	$p > 0.10$	0.177	$p > 0.10$	0.279	$p > 0.10$
Florida_S	−1.586	$p > 0.10$	−1.835	$p > 0.10$	−1.599	$0.10 > p > 0.05$
Georgia_R	−2.527	$\mathbf{p < 0.05}$	−2.55	$\mathbf{p < 0.05}$	−1.053	$p > 0.10$
Georgia_S	−1.200	$p > 0.10$	−1.294	$p > 0.10$	−0.788	$p > 0.10$
Florida_R and Georgia_R	−1.186	$p > 0.10$	−1.32671	$p > 0.10$	−0.998	$p > 0.10$
Florida_S and Georgia_S	−2.158	$0.10 > p > 0.05$	−2.248	$0.10 > p > 0.05$	−1.383	$p > 0.10$
Florida	−1.92670	$p > 0.10$	−2.18758	$0.10 > p > 0.05$	−1.76221	$0.10 > p > 0.05$
Georgia	−2.14999	$0.10 > p > 0.05$	−2.12725	$0.10 > p > 0.05$	−1.10892	$p > 0.10$
Combined	−3.23971	$\mathbf{p < 0.05}$	−3.15494	$\mathbf{p < 0.05}$	−1.66634	$0.10 > p > 0.05$

[a]*Negative Fu and Li's D and F values and Tajima's D values indicate population expansion or purifying selection. Bold values indicate statistical significance.*

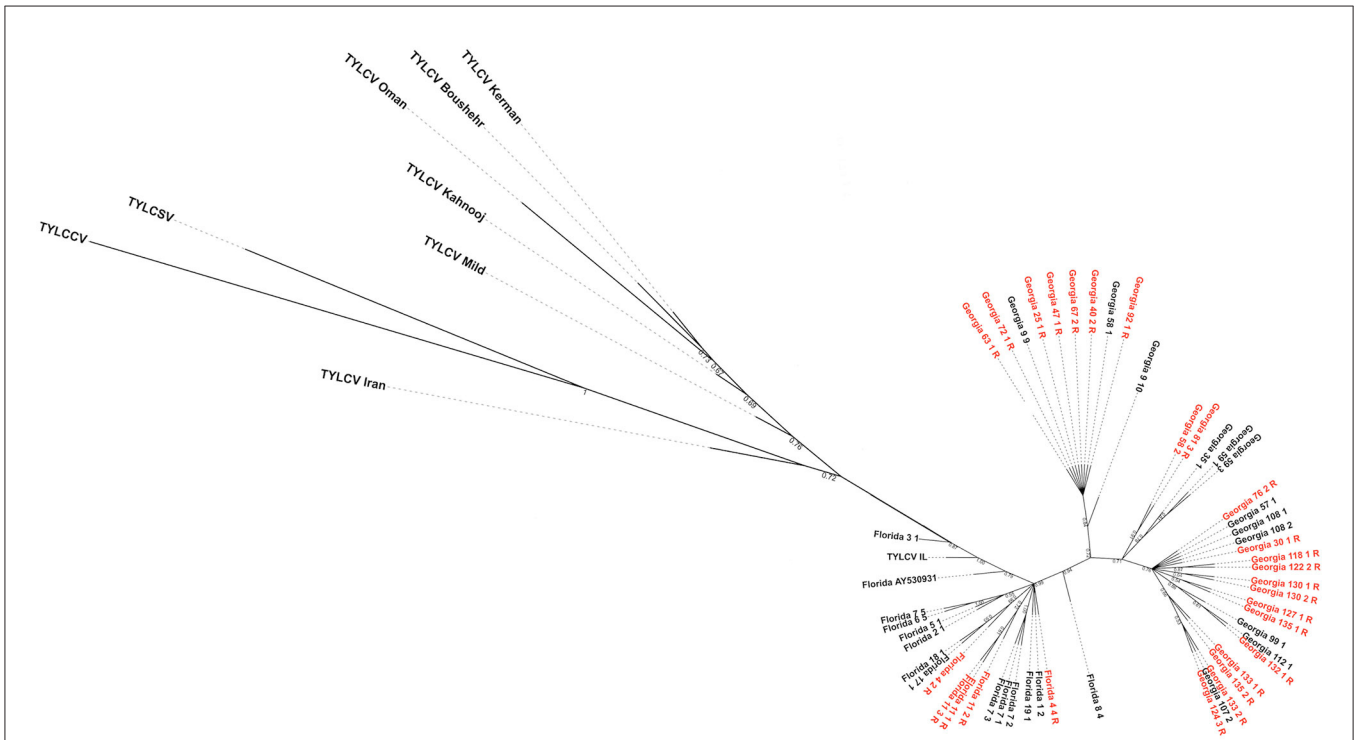


FIGURE 3 | Maximum-likelihood phylogenetic tree constructed with field-collected TYLCV genomes from Florida and Georgia. Samples with a "R" at the end of their name and labeled in red were isolated from a resistant genotype. All other TYLCV genomes were isolated from a susceptible genotype, except "Florida GenBank accession# AY530931" whose TYLCV susceptibility status is unknown. Representative genome sequences from each of the seven TYLCV strains viz., TYLCV-IL, TYLCV-Boushehr, TYLCV-Iran, TYLCV-Kahnooj, TYLCV-Kerman, TYLCV-Mild, and TYLCV-Oman were included as outgroup taxa. Tomato yellow leaf curl China virus and tomato yellow leaf curl Sardinia virus genome sequences were also included in the analyses.

All six genes were tested for positive selection by determining the non-synonymous to synonymous substitution ratio (dN/dS) for each codon. TYLCV genome sequences from resistant and susceptible genotypes were tested both separately and together at T_1, T_5, and T_{10}. No statistically significant ($p < 0.05$) positive selection of any of the codons was detected (**Supplementary Material 1**).

Fu and Li's F and D statistics and Tajima's D were calculated for TYLCV genomes from TYLCV- resistant and -susceptible genotypes at T_1, T_5, and T_{10}. Fu and Li's F and D statistics and Tajima's D were only significant for the genomes from the resistant genotype at T_1 (**Table 7**). However, Fu and Li's F and D statistics and Tajima's D were all negative for TYLCV genomes from both susceptible and resistant genotypes at T_1, T_5, and T_{10} (**Table 7**). Again, these statistics provided evidence for purifying selection and/or population expansion than positive selection.

TYLCV Quantitation in Resistant and Susceptible Genotypes Following Whitefly-Mediated Serial Transmission

TYLCV-induced symptoms were more prominent in the susceptible genotype and quite subdued in the resistant genotype.

TABLE 5 | Nucleotide and haplotype diversity associated with TYLCV genomes isolated from a TYLCV-resistant and susceptible tomato genotype following serial transmission of TYLCV.

Populations analyzed	π^v	θ^w	Hap^x	Substitutions^y	Indel sites^z
Serial transmission R T_1-T_{10}	0.007	0.021	8.00	229.00	8.00
Serial transmission S T_1-T_{10}	0.004	0.012	4.00	142.00	4.00

R, Represents genomes from the resistant genotype following 10 serial transmissions (T_1-T_{10}).
S, Represents genomes from susceptible genotypes.
$^v\pi$ Represents nucleotide diversity.
^{w}Population mutation rate.
^{x}Number of haplotypes.
^{y}Number of substitutions.
^{z}InDel sites.
Reference sequence TYLCV-IL(X15656) was used in determining substitutions and indel sites.

The symptom severity did not change in either the susceptible or resistant genotype with increasing transmission number. TYLCV virus loads from leaf tissue corresponding to resistant genotype plants did not differ with transmission number [T_1-T_5: $F_{(1, 28)} = 2.01$, $p = 0.337$; T_1-T_{10}: $F_{(1, 25)} = 0.44$, $p = 0.997$; T_5-T_{10}: $F_{(1,25)} = 1.51$, $p = 0.624$] (**Figure 5**). Similarly, TYLCV virus loads from leaf tissue corresponding to susceptible genotype plants did not differ with transmission number [T_1-T_5: $F_{(1, 27)} = 0.13$, $p= 0.999$; T_1-T_{10}: $F_{(1, 23)} = 1.160$, $p = 0.855$; T_5-T_{10}: $F_{(1, 23)} = -1.291$, $p = 0.790$] (**Figure 5**). However, TYLCV loads between susceptible and resistant plants varied significantly at T_1 [$F_{(1,28)} = 5.23$, $p < 0.001$], T_5 [$F_{(1, 27)} = 3.42$, $p = 0.004$] and T_{10} [$F_{(1,20)} = 6.14$, $p < 0.001$] (**Figure 5**). TYLCV loads were higher in the susceptible genotype than in the resistant genotype at T_1, T_5, and T_{10}.

DISCUSSION

High incidences of TYLCV are becoming the norm in the southeastern United States and in many other tomato-producing parts of the world. TYLCV-resistant genotypes are considered as the most effective management tool in the fight against TYLCV and are increasingly being used. This study attempted to assess whether the increased use of TYLCV-resistant genotypes can lead to selection pressure on the virus. Also, with multiple tomato crops grown in a calendar year in many locations, continuous planting of resistant genotypes could exert selection pressure on the virus. Positive selection against the virus could in turn lead to development of resistance-breaking strains of TYLCV. However, results in this study provided scant evidence to suggest that TYLCV is currently facing positive selection pressure stemming from the use of TYLCV-resistant genotypes in Florida and Georgia. Nevertheless, genetic differentiation was observed between TYLCV populations found in Florida and Georgia. The serial transmission assays also did not provide evidence for positive selection against TYLCV after 10 transfers (T_1-T_{10}). Overall, the TYLCV populations examined in this study seem to be shaped by purifying selection and/or population expansion than positive selection.

The genome sequences obtained from TYLCV-resistant and susceptible genotypes in both states were >97.5% similar in nucleotide identity. The phylogenetic analysis reveals that all the genome sequences from this study were closely related to the TYLCV-IL strain. The begomovirus strain demarcation limit is 94% nucleotide identity, and seven different TYLCV strains have been recognized thus far (Brown et al., 2015). TYLCV-IL seems to be only predominant strain in the southeastern United States despite evidence for multiple introductions of TYLCV (Duffy and Holmes, 2007). In spite of the high nucleotide sequence similarity among the genomes sequenced in this study, the phylogenetic analysis indicated that the Florida and Georgia samples parsed out into distinct clades. The phylogenetic tree hinted that the Georgia TYLCV population may be derived from an introduction from the Florida population. TYLCV was initially introduced into the Southeastern United States in Florida in 1996 or 1997 (Polston et al., 1999). In 1998, TYLCV was reported from South Georgia (Momol et al., 1999), therefore it seems likely that the Georgia population originated from a northern spread of the TYLCV population that first entered Florida. The absence of evidence of selection forces both in Florida and in Georgia suggests that the observed genetic differentiation between the two populations is shaped by population expansion and/or purifying selection aided by differences in introduction history, host availability, weather patterns, and agricultural practices that occur between the two states.

Mutations in TYLCV genomes predominantly included substitutions and fewer insertions and/or deletions. Mutations were at times higher in resistant genotypes and were generally higher in all genotypes from Florida. The Increased mutations from resistant genotypes than susceptible genotypes should be cautiously interpreted, as the genomes were sequenced using three sets of primers as opposed to RCA. This exercise could have inadvertently accounted for some of the observed mutations. However, no genetic differentiation was observed between genomes isolated from susceptible and resistant genotypes. The lack of significant results from the hypothesis testing using phylogenies (HyPhy) suggested absence of adaptive evolution or significant positive selection currently acting at the codon level. Positive selection pressure has been responsible for resistance breakdown against several viruses such as BNYVV and TSWV (Roggero et al., 2002; Aramburu and Marti, 2003; Ciuffo et al., 2005; Bornemann et al., 2015; Ferrand et al., 2015; Jiang et al., 2016; Batuman et al., 2017). The results in this study reiterated that the TYLCV populations in resistant and susceptible genotypes are being shaped by purifying selection and/or population expansion. There are several differences between *Ty*-mediated resistance and other dominant gene conferred resistance. Unlike the hypersensitive response observed in the case of *Sw5* and *Tsw* governed resistance against TSWV in tomato and pepper, respectively, *Ty*-mediated resistance results in systemic infection of the plant with mild to moderate symptoms and virus accumulation is typically at a reduced level than susceptible genotypes (Lapidot et al., 2001;

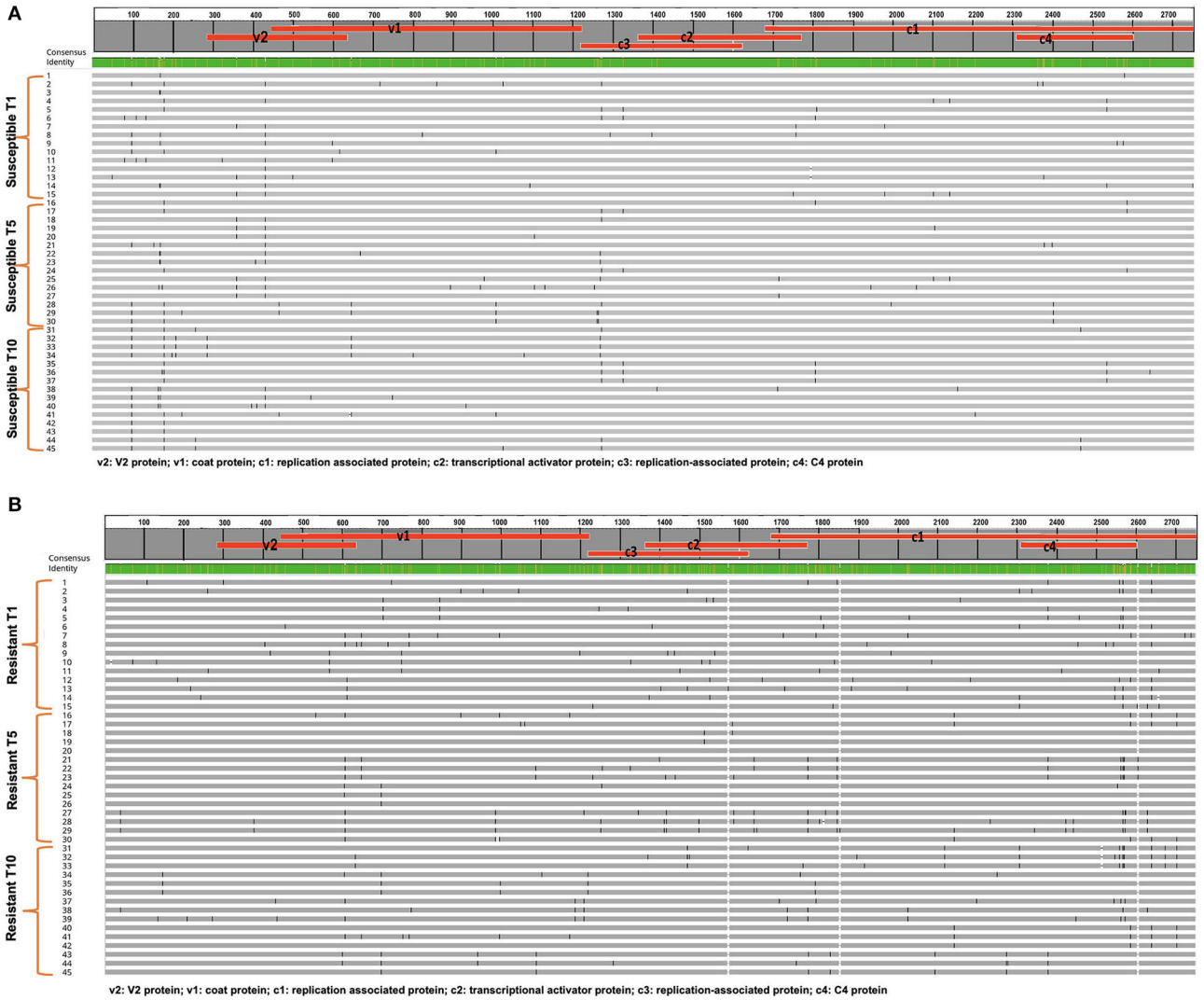


FIGURE 4 | (A) An alignment of full length TYLCV genomes corresponding to the TYLCV-susceptible genotype Lanai following whitefly mediated serial transmission. Fifteen genomes from transmission 1 (T1), transmission 5 (T5), and transmission (10) are included along with a consensus sequence. Mutations in each genome are tracked. **(B)** An alignment of full length TYLCV genomes corresponding to the TYLCV-resistant genotype Inbar following whitefly mediated serial transmission. Fifteen genomes from transmission 1 (T1), transmission 5 (T5), and transmission (10) are included along with a consensus sequence. Mutations in each genome are tracked.

Legarrea et al., 2015). Similar results were observed with TSWV-resistant peanut cultivars, which do not exhibit hypersensitive response, get systemically infected, and display mild to moderate symptoms upon infection (Shrestha et al., 2013; Sundaraj et al., 2014). Positive selection pressure was not observed in the case of TSWV-resistant peanut genotypes either (Sundaraj et al., 2014). The *Ty*1-6 resistance conferring genes vary in their biochemistry and differ in their mode of action (Ji et al., 2009; Verlaan et al., 2013; Lapidot et al., 2015; Yamaguchi et al., 2018; Gill et al., 2019). Of all the *Ty* gene combinations in the sampled genotypes, Ty1 seems to be the most common. The Ty1 gene belongs to the plant class of RNA dependent RNA polymerase (RDRPγ type) (Verlaan et al., 2013). Plant RDRPs are capable of targeting uncommon RNA molecules such as viruses and silencing them through the RNA interference mechanism (Ahlquist, 2002; Schwach et al., 2005; Díaz-Pendón et al., 2010; Garcia-Ruiz et al., 2010). In addition, many resistant genotypes seem to contain more than one *Ty* gene. These factors together could be contributing to reduction in selection pressure against the virus.

The whitefly-mediated TYLCV serial transmission experiment conducted to simulate continuous exposure of TYLCV, indicated that genetic differentiation in TYLCV genomes did not increase with serial transmission number, and was not different between the resistant and susceptible genotype. The dN/dS ratios calculated by the HyPhy codon selection test did not detect positive selection on any of the codons in the six TYLCV genes from genomes of the resistant or the susceptible

TABLE 6 | Genetic differentiation statistics with genomes of TYLCV isolates from a TYLCV-resistant and -susceptible genotype at different stages of whitefly-mediated serial transmission.

Populations analyzed	Kt[x]	Ks[y]	Kst[y]	*p*-value of Ks and Kst	Snn[y]	*p*-value of Snn	Z[y]	*p*-value of Z	Fst[z]
S1 vs. S5	8.718	8.685	0.003	0.310	0.712	**0.005**	216.623	0.395	0.007
S1 vs. S10	8.595	8.076	0.060	**0.001**	0.827	**0.000**	196.785	**0.001**	0.110
S5 vs. S10	8.834	8.400	0.049	**0.001**	0.900	**0.000**	203.333	**0.005**	0.090
R1 vs. R5	15.480	14.971	0.032	**0.007**	0.600	0.126	215.297	0.250	0.061
R1 vs. R10	15.790	15.428	0.022	**0.014**	0.813	**0.000**	210.557	0.055	0.043
R5 vs. R10	15.082	14.647	0.028	**0.024**	0.833	**0.000**	212.542	0.108	0.054
R1 vs. S1	11.820	11.790	0.002	0.331	0.467	0.640	214.121	0.161	0.005
R5 vs. S5	12.071	11.400	0.055	**0.001**	0.933	**0.000**	202.683	**0.002**	0.102
R10 vs. S10	12.429	11.380	0.084	**0.000**	0.933	**0.000**	188.652	**0.000**	0.151

[x] *Kt is the average number of pairwise nucleotide differences across genomes in both populations.*

[y] *Ks, Kst, Snn, and Z are nucleotide sequence-based genetic differentiation statistics.*

[z] *Fst is a genetic differentiation statistic. Values range from 0 to 1. Low Fst values indicate a high-level similarity between populations while high Fst values indicate genetically distinct groups. Bold values indicate statistical significance.*

TABLE 7 | Tests of neutrality with genomes of TYLCV isolates from a TYLCV-resistant and -susceptible genotype at different stages of whitefly-mediated serial transmission.

Population analyzed	Fu and Li's D[a]	*p*-value	Fu and Li's F[a]	*p*-value	Tajima's D[a]	*p*-value
Transmission 1 (T_1)-Resistant	−2.39208	$p < 0.05$	−2.59396	$p < 0.05$	−1.88472	$p < 0.05$
Transmission 5 (T_5)-Resistant	−0.63476	$p > 0.10$	−0.78389	$p > 0.10$	−0.79782	$p > 0.10$
Transmission 10 (T_{10})-Resistant	−0.91053	$p > 0.10$	−1.12974	$p > 0.10$	−1.15968	$p > 0.10$
Transmission 1 (T_1)-Susceptible	−1.22645	$p > 0.10$	−1.45762	$p > 0.10$	−1.36701	$p > 0.10$
Transmission 5 (T_5)-Susceptible	−1.10155	$p > 0.10$	−1.28177	$p > 0.10$	−1.14230	$p > 0.10$
Transmission 10 (T_{10})-Susceptible	−1.06583	$p > 0.10$	−1.20065	$p > 0.10$	−0.98299	$p > 0.10$

[a] *Negative Fu and Li's D and F values and Tajima's D values indicate population expansion or purifying selection. Bold values indicate statistical significance.*

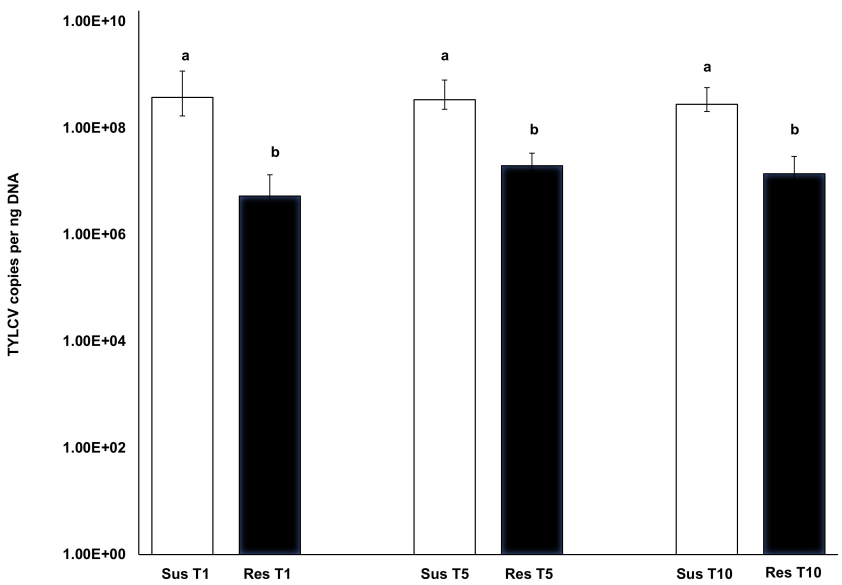


FIGURE 5 | Absolute quantitation of TYLCV loads in the susceptible genotype (Lanai) and resistant genotype (Inbar) following serial transmission at T_1, T_5, and T_{10}. DNA extracted from both susceptible and resistant genotypes at T_1, T_5, and T_{10} were subjected to absolute quantitation using real time PCR. Differences in virus loads between resistant and susceptible genotypes' leaf tissues at each transmission T_1, T_5, and T_{10} were assessed using the Tukey's honest significant difference (Tukey HSD) *post-hoc* test. Differences in mean separation letters indicate differences in TYLCV loads between the susceptible and resistant genotypes at each serial transfer.

genotype (**Supplementary Material 1**). The serial transmission experiment in this study lasted ∼210 days. It is possible that with more time, the resistant and susceptible populations might have further differentiated, and positive selection may have eventually occurred. With another begomovirus, tomato yellow leaf curl China virus (TYLCCV), Ge et al. (2007) observed variation in the population structure following natural inoculation in tomato and experimental TYLCCV clone inoculation in *Nicotiana benthamiana* Domin. plants. Mutations in TYLCCV genomes did not vary between 60 and 120-days post inoculation. The observed mutations did not deviate much from progenitor sequences with a mutation rate of $\sim 10^{-4}$, suggesting that TYLCCV was resembling a quasispecies and its mutation rate was similar to an RNA virus aided by purifying selection and population differentiation (Ge et al., 2007). Ge et al. (2007) also stated that TYLCCV mutation was responsible for its diversification, but it was somehow constrained. Similarly, in the current study, there seems to be evidence for the quasispecies nature of TYLCV and population diversification in general regardless of the susceptibility status of the host genotype or the geography. The lack of positive selection and hot spots in genomes analyzed in this study also point to constrained diversity driven by purifying selection and/or population expansion. Of course, the caveats in this study pertaining to the sampling size and sampling locations deserve further scrutiny. Another reason for the lack of significant population differentiation and/or selection could include the fact that the resistant genotype (Inbar) had multiple resistant genes viz., *Ty*-1/3 and *Ty*-6 with ability to confer at least two modes of resistance. In addition, all TYLCV genomes from Inbar were assembled using three PCR primer sets, this could have inadvertently accounted for an artifactual increase of substitutions and/or indels. Inadvertent introduction of mutations could be influenced by the presence of multiple isolates in the inoculum source. However, the original inoculum source used in this study was a susceptible genotype (Lanai), and RCA amplifications from that genotype only revealed the presence of a single isolate. Therefore, it is possible that the mutations observed in the resistant genotype Inbar may not be artificially introduced. The TYLCV-susceptible (Lanai) and TYLCV resistant (Inbar) are not near isogenic lines, the innate differences in their genetic background, besides *Ty* genes, could have also influenced the increased mutations in the resistant genotype. TYLCV resistant genotypes typically display less severe symptoms than susceptible genotypes, and they accumulate less virus than susceptible cultivars (Lapidot et al., 2001; Legarrea et al., 2015). Virus symptoms were less severe in the resistant genotype Inbar and did not change with serial transmission. The virus loads, as determined by qPCR in this study, was lower in the resistant genotype than the susceptible genotype at T_1, T_5, and T_{10}. Virus loads also did not increase with transmission number in either the susceptible or resistant genotype. There was no evidence of development of a highly virulent or resistance-breaking strain characterized by enhanced symptom severity and/or increased virus load following serial transmission in the resistant genotype.

Recombination can play a major role in the evolution of begomoviruses (Navas-Castillo et al., 2000; García-Andrés et al., 2007; Moriones et al., 2007; Belabess et al., 2016). Recombinants of begomovirus species occur in nature especially aided by mixed infection and recombinants could also increase in frequency with time (García-Andrés et al., 2007). Resulting recombinants could produce a phenotype in infected hosts that is more pathogenic than the parental strains/species as seen in the case of TYLCSV and TYLCV in Spain (Monci et al., 2002). Also, begomovirus recombinants can outcompete parental virus strains in resistant cultivars as seen in southern Morocco and produce a more severe phenotype than parental virus strains (Belabess et al., 2016). It is possible that recombination could be occurring among TYLCV isolates used in this study, but the genomes of TYLCV isolates were very similar to one another within the two geographic regions and between the TYLCV-resistant and -susceptible genotypes, therefore making it impossible to detect recombination. Another tomato-infecting begomovirus, tomato mottle virus (ToMoV), is present in Florida, but it has not been recorded in Georgia (Akad et al., 2007). TYLCV is monopartite, whereas ToMoV is bipartite. TYLCV and ToMoV have been documented to co-infect individual tomato plants in Florida (Akad et al., 2007), but there is no indication that these two viruses could recombine. Elsewhere, TYLCV has been documented to recombine with several monopartite begomoviruses (Bananej et al., 2004; Idris and Brown, 2005; Guo et al., 2009; Kim et al., 2011; Park et al., 2011; Urbino et al., 2013). Introduction of a new begomovirus, specifically a monopartite species or a different strain of TYLCV, could offer more opportunities for recombination in the southeastern United States. Seven different strains of TYLCV have been identified thus far worldwide (Brown et al., 2015). In the southeastern United States, as shown in this study, TYLCV-IL seems to be only strain. Nevertheless, that scenario could change.

The availability of TYLCV-resistant cultivars/hybrids with improved horticultural traits and substantial whitefly pressure becoming the pattern, resistant genotypes have become a rather obvious choice for tomato growers in the southeastern United States. Currently, TYLCV resistant genotypes are planted in ∼40% of the production acreage in Florida and Georgia (Ozores-Hampton et al., 2010; Srinivasan et al., 2012; Riley and Srinivasan, 2019). Based on information obtained in this study, the use of TYLCV-resistant tomato genotypes has not led to the development of resistance-breaking strains. However, positive selection and/or recombination with newly introduced TYLCV strains could change this scenario. Certain cropping strategies can be employed to reduce the risks of emergence of resistance-breaking strains (Fabre et al., 2012). One strategy is to plant a mixture of resistant and susceptible genotypes of tomato in order to reduce the overall selection pressure on the virus from the resistant genotype. This might already be unwillingly happening in the southeastern United States. The other strategy is to plant only resistant varieties on a landscape level. This strategy could help reduce the overall inoculum level in the landscape over time, as resistant genotypes typically accumulate less virus than susceptible genotypes (Lapidot et al., 2001; Legarrea et al., 2015). Resistant cultivars are an invaluable tool for growing tomatoes in TYLCV-affected areas and measures should be taken to preserve their usefulness.

CONCLUSION

Virus-host interactions influenced by resistance-conferring dominant genes in several instances have placed substantial selection pressure on viruses. The resultant evolution of resistance-breaking strains has jeopardized the usefulness of resistant genotypes, wherein in many instances, rendering the only viable management option ineffective. With increasing whitefly and virus pressure in many tomato growing areas worldwide, reliance on TYLCV-resistant cultivars/hybrids is rising. Nevertheless, implications of usage of resistant genotypes under field conditions on rapid evolution of highly virulent or resistance-breaking TYLCV strains have been sparsely explored. This study made a preliminary attempt to examine the possibility of evolution of hot spots in the virus genome isolated from resistant genotypes that could trigger evolution of resistance-breaking strains. The lack of hypersensitive response to TYLCV as in the case of infection of several RNA viruses and the permissive replication due to systemic infection of TYLCV in resistant genotypes could be pivotal in preventing positive selection. However, introduction of other TYLCV strains and ensuing recombination events could alter that scenario. The TYLCV population structure in the southeastern United States at this moment seems to be determined by purifying selection and/or population expansion despite the use of resistant genotypes. Adoption of risk reduction strategies as outlined above could limit the development of resistance-breaking strains and facilitate the sustainable long-term usage of TYLCV-resistant genotypes.

DATA AVAILABILITY STATEMENT

The datasets presented in this study can be found in online repositories. The names of the repository/repositories and accession number(s) can be found in the article/**Supplementary Material**.

AUTHOR CONTRIBUTIONS

WM and RS designed the experiments. WM conducted the experiments and prepared the original draft of the manuscript. RS supervised the project. WM, SH, and SG performed the data analyses. All authors reviewed and approved the final version of the manuscript.

FUNDING

This study was supported by funds from by the USDA Hatch Grant awarded to RS # GEO 00671, Georgia Commodity Commission for vegetables, and the USDA-UGA Cooperative Agreement #6080-22000-027-18-S.

ACKNOWLEDGMENTS

We thank Dr. Jane Polston for guidance on the rolling circle amplification and for providing tomato cultivar Florida Lanai seeds. We extend our sincere gratitude to Dr. Monica Ozores-Hampton for providing us with TYLCV samples from Florida. We also acknowledge the technical help rendered by Mr. Simeon McKeown and Ms. Sheran Thompson during the course of this study.

SUPPLEMENTARY MATERIAL

The Supplementary Material for this article can be found online at: https://www.frontiersin.org/articles/10.3389/fpls.2020.599697/full#supplementary-material

REFERENCES

Ahlquist, P. (2002). RNA-dependent RNA polymerases, viruses, and RNA silencing. *Science* 296,1270–1273. doi: 10.1126/science.1069132

Akad, F., Jacobi, J. C., and Polston, J. E. (2007). Identification of Tomato yellow leaf curl virus and tomato mottle virus in two counties in Alabama. *Plant Dis.* 91:906. doi: 10.1094/PDIS-91-7-0906C

Almási, A., Csilléry, G., Csömör, Z., Nemes, K., Palkovics, L., Salánki, K., et al. (2015). Phylogenetic analysis of Tomato spotted wilt virus (TSWV) NSs protein demonstrates the isolated emergence of resistance-breaking strains in pepper. *Virus Genes* 50, 71–78. doi: 10.1007/s11262-014-1131-3

Anbinder, I., Reuveni, M., Azari, R., Paran, I., Nahon, S., Shlomo, H., et al. (2009). Molecular dissection of Tomato leaf curl virus resistance in tomato line TY172 derived from *Solanum peruvianum*. *Theor. Appl. Genet.* 119, 519–530. doi: 10.1007/s00122-009-1060-z

Aramburu, J., and Marti, M. (2003). The occurrence in north-east Spain of a variant of Tomato spotted wilt virus (TSWV) that breaks resistance in tomato (*Lycopersicon esculentum*) containing the Sw-5 gene. *Pl. Pathol.* 52:407. doi: 10.1046/j.1365-3059.2003.00829.x

Bananej, K., Kheyr-Pour, A., Salekdeh, G. H., and Ahoonmanesh, A. (2004). Complete nucleotide sequence of Iranian tomato yellow leaf curl virus isolate: further evidence for natural recombination amongst begomoviruses. *Arch. Virol.* 149, 1435–1443. doi: 10.1007/s00705-004-0308-9

Bates, D., Mächler, M., Bolker, B., and Walker, S. (2015). Fitting linear mixed-effects models using lme4. *J. Stat. Softw.* 67, 1–48. doi: 10.18637/jss.v067.i01

Batuman, O., Turini, T. A., Oliveira, P. V., Rojas, M. R., Macedo, M., Mellinger, H. C., et al. (2017). First report of a resistance-breaking strain of tomato spotted wilt virus infecting tomatoes with the Sw-5 tospovirus-resistance gene in California. *Plant Dis.* 10:637. doi: 10.1094/PDIS-09-16-1371-PDN

Belabess, Z., Peterschmitt, M., Granier, M., Tahiri, A., Blenzar, A., and Urbino, C. (2016). The non-canonical tomato yellow leaf curl virus recombinant that displaced its parental viruses in southern Morocco exhibits a high selective advantage in experimental conditions. *J. Gen. Virol.* 97, 3433–3445. doi: 10.1099/jgv.0.000633

Bornemann, K., Hanse, B., Varrelmann, M., and Stevens, M. (2015). Occurrence of resistance-breaking strains of beet necrotic yellow vein virus in sugar beet in northwestern Europe and identification of a new variant of the viral pathogenicity factor P25. *Plant Pathol.* 64, 25–34. doi: 10.1111/ppa.12249

Brown, J. K., Zerbini, F. M., Navas-Castillo, J., Moriones, E., Ramos-Sobrinho, R., Silva, J. C. F., et al. (2015). Revision of Begomovirus taxonomy based on pairwise sequence comparisons. *Arch. Virol.* 160, 1593–1619. doi: 10.1007/s00705-015-2398-y

Ciuffo, M., Finetti-Sialer, M. M., Gallitelli, D., and Turina, M. (2005). First report in Italy of a resistance-breaking strain of tomato spotted wilt virus infecting tomato cultivars carrying the Sw5 resistance gene. *Plant Path.* 54:564. doi: 10.1111/j.1365-3059.2005.01203.x

Cohen, S., and Antignus,. Y. (1994). Tomato yellow leaf curl virus, a whitefly-borne Geminivirus of tomatoes. *Adv. Dis. Vector Res.* 10, 259–288. doi: 10.1007/978-1-4612-2590-4_10

Cohen, S., and Harpaz,. I. (1964). Periodic, rather than continual acquisition of a new tomato virus by its vector, the tobacco whitefly (*Bemisia tabaci Gennadius*). *Entomol. Exp. Appl.* 7, 155–160. doi: 10.1111/j.1570-7458.1964.tb02435.x

Cohen, S., and Nitzany, F. E. (1966). Transmission and host range of the tomato yellow leaf curl virus. *Phtyopathology* 56, 1127–1131.

Czosnek, H. (2008). "Tomato yellow leaf curl virus" in *Encylopedia of Virology*, eds B.W. J. Mahy and M. H. V. van Regenmortel (Oxford: Academic Press; Elsevier Ltd), 138–145.

Czosnek, H., and Laterrot, H. (1997). A worldwide survey of tomato yellow leaf curl viruses. *Arch. Virol.* 142, 1391–1406. doi: 10.1007/s007050050168

da Silva, A. K. F., Romanel, E., Silva, T. D. F., Castilhos, Y., Schrago, C. G., Galbieri, R., et al. (2015). Complete genome sequences of two new virus isolates associated with cotton blue disease resistance breaking in Brazil. *Arch. Virol.* 160, 1371–1374. doi: 10.1007/s00705-015-2380-8

Darriba, D., Taboada, G. L., Doallo, R., and Posada, D. (2012). jModelTest 2: more models, new heuristics and parallel computing. *Nat. Methods* 9:772. doi: 10.1038/nmeth.2109

Debreczeni, D. E., López, C., Aramburu, J., Darós, J. A., Soler, S., Galipienso, L., et al. (2015). Complete sequence of three different biotypes of tomato spotted wilt virus (wild type, tomato Sw-5 resistance-breaking and pepper Tsw resistance-breaking) from Spain. *Arch. Virol.* 160, 2117–2123. doi: 10.1007/s00705-015-2453-8

Deligoz, I., Sokmen, M. A., and Sari, S. (2014). First report of resistance breaking strain of tomato spotted wilt virus (*Tospovirus*; *Bunyaviridae*) on resistant sweet pepper cultivars in Turkey. *New Dis. Rep.* 30:26. doi: 10.5197/j.2044-0588.2014.030.026

Díaz-Pendón, J. A., Cañizares, M. C., Moriones, E., Bejarano, E. R., Czosnek, H., and Navas-Castillo, J. (2010). Tomato yellow leaf curl viruses: ménage à trois between the virus complex, the plant and the whitefly vector. *Mol. Plant Pathol.* 11, 441–450. doi: 10.1111/j.1364-3703.2010.00618.x

Drummond, A. J., Ashton, B., Buxton, S., Cheung, M., Cooper, A., Duran, C., et al. (2011). *Geneious, version 5.4*.

Duffy, S., and Holmes, E. C. (2007). Multiple introductions of the old world begomovirus tomato yellow leaf curl virus into the new world. *Appl. Environ. Microbiol.* 73, 7114–7117. doi: 10.1128/AEM.01150-07

Duffy, S., and Holmes, E. C. (2008). Phylogenetic evidence for rapid rates of molecular evolution in the single-stranded DNA begomovirus tomato yellow leaf curl virus. *J. Virol.* 82, 957–965. doi: 10.1128/JVI.01929-07

Fabre, F., Rousseau, E., Mailleret, L., and Moury, B. (2012). Durable strategies to deploy plant resistance in agricultural landscapes. *New Phytol.* 193, 1064–1075. doi: 10.1111/j.1469-8137.2011.04019.x

Ferrand, L., García, M., Resende, R., Balatti, P., and Dal, B.ó, E. (2015). First report of a resistance-breaking isolate of tomato spotted wilt virus infecting sweet pepper harboring the Tsw gene in Argentina. *Plant Dis.* 99, 1869–1870. doi: 10.1094/PDIS-02-15-0207-PDN

Fu, Y. X., and Li, W. H. (1993). Statistical tests of neutrality of mutations. *Genetics* 133, 693–709.

García-Andrés, S., Tomás, D., Navas-Castillo, J., and Moriones, E. (2009). Resistance-driven selection of begomoviruses associated with the tomato yellow leaf curl disease. *Virus Res.* 146, 66–72. doi: 10.1016/j.virusres.2009.08.012

García-Andrés, S., Tomás, D. M., Sánchez-Campos, S., Navas-Castillo, J., and Moriones,. E. (2007). Frequent occurrence of recombinants in mixed infections of tomato yellow leaf curl disease-associated begomoviruses. *Virology* 365, 210–219. doi: 10.1016/j.virol.2007.03.045

Garcia-Ruiz, H., Takeda, A., Chapman, E. J., Sullivan, C. M., Fahlgren, N., et al. (2010). Arabidopsis RNA-dependent RNA polymerases and dicer-like proteins in antiviral defense and small interfering RNA biogenesis during turnip mosaic virus infection. *Plant Cell Online* 22, 481–496. doi: 10.1105/tpc.109.073056

Ge, L., Zhang, J., Zhou, X., and Li, H. (2007). Genetic structure and population variability of tomato yellow leaf curl China virus. *J. Virol.* 81, 5902–5907. doi: 10.1128/JVI.02431-06

Gelbart, D., Chen, L., Alon, T., Dobrinin, S., Levin, I., and Lapidot, M. (2020). The recent association of a DNA betasatellite with tomato yellow leaf curl virus in Israel – a new threat to tomato production. *Crop Protect.* 128:104995. doi: 10.1016/j.cropro.2019.104995

Ghanim, M., and Medina, V. (2007). "Localization of tomato yellow leaf curl virus in its whitefly vector Bemisia tabaci," in *Tomato Yellow Leaf Curl Virus Disease*, ed H. Czosnek (Dordrecht: Springer), 171–183.

Gill, U., Scott, J. W., Shekasteband, R., Ogundiwin, E., Schuit, C., Francis, D. M., et al. (2019). Ty-6, a major begomovirus resistance gene on chromosome 10, is effective against tomato yellow leaf curl virus and tomato mottle virus. *Theor. Appl. Genet.* 132, 1543–1554. doi: 10.1007/s00122-019-03298-0

Gilreath, P., Shuler, K., Polston, J., Sherwood, T., McAvoy, G., Stansly, P., et al. (2000). Tomato yellow leaf curl virus resistant tomato variety trials. *Proc. Fla. State Hort. Soc.* 113, 190–193. Available online at: https://fshs.org/access-fshs-proceedings/

Gronenborn, B. (2007). "The tomato yellow leaf curl virus genome and function of its proteins," in *Tomato Yellow Leaf Curl Virus Disease,* ed H. Czosnek (Dordrecht: Springer), 67–84.

Guo, W., Yang, X., Xie, Y., Cui, X., and Zhou, X. (2009). Tomato yellow leaf curl Thailand virus-[Y72] from Yunnan is a monopartite begomovirus associated with DNAβ. *Virus Genes* 38, 328–333. doi: 10.1007/s11262-009-0327-4

Hanson, P. M., Bernacchi, D., Green, S., Tanksley, S. D., Muniyappa, V., Padmaja, A. S., et al. (2000). Mapping a wild tomato introgression associated with tomato yellow leaf curl virus resistance in a cultivated tomato line. *J. Am. Soc. Hortic. Sci.* 125, 15–20. doi: 10.21273/JASHS.125.1.15

Hudson, R. R., Slatkin, M., and Maddison, W. P. (1992). Estimation of levels of gene flow from DNA sequence data. *Genetics* 132, 583–589.

Hutton, S. F., Scott, J. W., and Schuster, D. J. (2012). Recessive resistance to tomato yellow leaf curl virus from the tomato cultivar Tyking is located in the same region as Ty-5 on chromosome 4. *HortScience* 47, 324–327. doi: 10.21273/HORTSCI.47.3.324

Idris, A., and Brown, J. (2005). Evidence for interspecific-recombination for three monopartite begomoviral genomes associated with the tomato leaf curl disease from central Sudan. *Arch. Virol.* 150, 1003–1012. doi: 10.1007/s00705-004-0484-7

Inoue-Nagata, A. K., Albuquerque, L. C., Rocha, W. B., and Nagata, T. (2004). A simple method for cloning the complete begomovirus genome using the bacteriophage ϕ29 DNA polymerase. *J. Virol. Methods.* 116, 209–211. doi: 10.1016/j.jviromet.2003.11.015

Ji, Y., Schuster, D. J., and Scott, J. W. (2007). Ty-3, a begomovirus resistance locus near the tomato yellow leaf curl virus resistance locus Ty-1 on chromosome 6 of tomato. *Mol. Breed.* 20, 271–284. doi: 10.1007/s11032-007-9089-7

Ji, Y., Scott, J. W., Schuster, D. J., and Maxwell, D. P. (2009). Molecular mapping of Ty-4, a new tomato yellow leaf curl virus resistance locus on chromosome 3 of tomato. *J. Am. Soc. Hortic. Sci.* 134, 281–288. doi: 10.21273/JASHS.134.2.281

Jiang, L., Huang, Y., Sun, L., Wang, B., Zhu, M., Li, J., et al. (2016). Occurrence and diversity of tomato spotted wilt virus isolates breaking the Tsw resistance gene of Capsicum chinense in Yunnan, southwest China. *Plant Pathol.* 66, 980–989. doi: 10.1111/ppa.12645

Kadirvel, P., de la Peña, R., Schafleitner, R., Huang, S., Geethanjali, S., Kenyon, L., et al. (2013). Mapping of QTLs in tomato line FLA456 associated with resistance to a virus causing tomato yellow leaf curl disease. *Euphytica* 190, 297–308. doi: 10.1007/s10681-012-0848-0

Kim, S. H., Oh, S., Oh, T., Park, J. S., Kim, S. C. S., Kim, H., et al. (2011). Genetic diversity of tomato-infecting tomato yellow leaf curl virus (TYLCV) isolates in Korea. *Virus Genes* 42, 117–127. doi: 10.1007/s11262-010-0541-0

Kumar, S., Stecher, G., Li, M., Knyaz, C., and Tamura, K. (2018). MEGA X: molecular evolutionary genetics analysis across computing platforms. *Mol. Biol. Evol.* 35, 1547–1549. doi: 10.1093/molbev/msy096

Kumar, S., Stecher, G., and Tamura, K. (2016). MEGA7: molecular evolutionary genetics analysis version 7.0 for bigger datasets. *Mol. Biol. Evol.* 33, 1870–1874. doi: 10.1093/molbev/msw054

Lapidot, M., and Friedmann, M. (2002). Breeding for resistance to whitefly-transmitted geminiviruses. *Ann. Appl. Biol.* 140, 109–127. doi: 10.1111/j.1744-7348.2002.tb00163.x

Lapidot, M., Friedmann, M., Lachman, O., Yehezkel, A., Nahon, S., Cohen, S., et al. (1997). Comparison of resistance level to tomato yellow leaf curl virus

among commercial cultivars and breeding lines. *Plant Dis*. 81, 1425–1428. doi: 10.1094/PDIS.1997.81.12.1425

Lapidot, M., Friedmann, M., Pilowsky, M., Ben-Joseph, R., and Cohen, S. (2001). Effect of host plant resistance to tomato yellow leaf curl virus (TYLCV) on virus acquisition and transmission by its whitefly vector. *Phytopathology* 91, 1209–1213. doi: 10.1094/PHYTO.2001.91.12.1209

Lapidot, M., Karniel, U., Gelbart, D., Fogel, D., Evenor, D., Kutsher, Y., et al. (2015). A novel route controlling begomovirus resistance by the messenger RNA surveillance factor pelota. *PLoS Genet*. 11:e1005538. doi: 10.1371/journal.pgen.1005538

Latham, L. J., and Jones, R. A. C. (1998). Selection of overcoming strains of tomato spotted wilt tospovirus. *Ann. Appl. Biol*. 133, 385–402. doi: 10.1111/j.1744-7348.1998.tb05838.x

Legarrea, S., Barman, A., Marchant, W., Diffie, S., and Srinivasan, R. (2015). Temporal effects of a Begomovirus infection and host plant resistance on the preference and development of an insect vector, Bemisia tabaci, and implications for epidemics. *PLoS ONE* 10:e0142114. doi: 10.1371/journal.pone.0142114

Librado, P., and Rozas, J. (2009). DnaSP v5: a software for comprehensive analysis of DNA polymorphism data. *Bioinformatics* 25, 1451–1452. doi: 10.1093/bioinformatics/btp187

Momol, M., Simone, G., Dankers, W., Sprenkel, R., Olson, S., Momol, E., et al. (1999). First report of tomato yellow leaf curl virus in tomato in South Georgia. *Plant Dis*. 83, 487–487. doi: 10.1094/PDIS.1999.83.5.487C

Monci, F., Sánchez-Campos, S., Navas-Castillo, J., and Moriones, E. (2002). A natural recombinant between the geminiviruses tomato yellow leaf curl Sardinia virus and tomato yellow leaf curl virus exhibits a novel pathogenic phenotype and is becoming prevalent in Spanish populations. *Virology* 303, 317–326. doi: 10.1006/viro.2002.1633

Moriones, E., García-Andrés, S., and Navas-Castillo, J. (2007). "Recombination in the TYLCV complex: a mechanism to increase genetic diversity implications for plant resistance development" in *Tomato Yellow Leaf Curl Virus Disease*, ed H. Czosnek (Dordrecht: Springer), 119–138.

Moriones, E., and Navas-Castillo, J. (2000). Tomato yellow leaf curl virus, an emerging virus complex causing epidemics worldwide. *Virus Res*. 71, 123–134. doi: 10.1016/S0168-1702(00)00193-3

Navas-Castillo, J., Sánchez-Campos, S., Noris, E., Louro, D., Accotto, G., and Moriones, E. (2000). Natural recombination between tomato yellow leaf curl virus-is and tomato leaf curl virus. *J. Gen. Virol*. 81, 2797–2801. doi: 10.1099/0022-1317-81-11-2797

Ohnishi, J., Yamaguchi, H., and Saito, A. (2016). Analysis of the mild strain of tomato yellow leaf curl virus, which overcomes Ty-2 gene-mediated resistance in tomato line H24. *Arch. Virol*. 161, 2207–2217. doi: 10.1007/s00705-016-2898-4

Ozores-Hampton, M., McAvoy, E., Sargent, S., and Roberts, P. (2010). Evaluation of tomato yellow leaf curl virus (TYLCV) resistant and fusarium crown rot (FCr) resistant tomato variety under commercial conditions in southwest Florida," in *Proceedings, Florida Tomato Institute, 8 September 2010, Naples, FL, University of Florida, IFAS Extension* (Gainesville, FL), 11–15.

Pappu, S. S., Pappu, H. R., Langston, D. B. Jr., Flanders, J. T., Riley, D. G., et al. (2000). Outbreak of tomato yellow leaf curl virus (Family *Geminiviridae*) in Georgia. *Plant Dis*. 84:370. doi: 10.1094/PDIS.2000.84.3.370C

Park, J., Lee, H., Kim, M., Kwak, H., Auh, C., Lee, K., et al. (2011). Phylogenetic lineage of tobacco leaf curl virus in Korea and estimation of recombination events implicated in their sequence variation. *Virus Res*. 159, 124–131. doi: 10.1016/j.virusres.2011.04.017

Picó, B., Diez, M. J., and Nuez, F. (1996). Viral diseases causing the greatest economic losses in tomato crop. Part II: the tomato yellow leaf curl virus- a review. *Sci. Horticul*. 67, 151–196. doi: 10.1016/S0304-4238(96)00945-4

Polston, J., McGovern, R., and Brown, L. (1999). Introduction of tomato yellow leaf curl virus in Florida and implications for the spread of this and other geminiviruses of tomato. *Plant Dis*. 83, 984–988. doi: 10.1094/PDIS.1999.83.11.984

Pond, S. L. K., and Muse, S. V. (2005). "HyPhy: hypothesis testing using phylogenies," in *Statistical Methods in Molecular Evolution*, ed R. Nielsen (New York, NY: Springer), 125–181.

R Core Team (2019). *R: A Language, and Environment for Statistical Computing*. Vienna: R Foundation for Statistical Computing.

Riley, D. G., and Srinivasan, R. (2019). Integrated management of tomato yellow leaf curl virus and its whitefly vector in tomato. *J. Econ. Ent*. 112, 1526–1540. doi: 10.1093/jee/toz051

Roggero, P., Masenga, V., and Tavella, L. (2002). Field isolates of tomato spotted wilt virus overcoming resistance in pepper and their spread to other hosts in Italy. *Plant Dis*. 86, 950–954. doi: 10.1094/PDIS.2002.86.9.950

Schwach, F., Vaistij, F. E., Jones, L., and Baulcombe, D. C. (2005). An RNA-dependent RNA polymerase prevents meristem invasion by potato virus x and is required for the activity but not the production of a systemic silencing signal. *Plant Physiol*. 138: 1842–1852. doi: 10.1104/pp.105.063537

Sharman, M., and Persley, D. (2006). Field isolates of tomato spotted wilt virus overcoming resistance in capsicum in Australia. *Australas. Plant Pathol*. 35, 123–128. doi: 10.1071/AP06014

Shrestha, A., Srinivasan, R., Sundaraj, S., Culbreath, A., and Riley, D. (2013). Second generation peanut genotypes resistant to thrips-transmitted Tomato spotted wilt virus exhibit tolerance rather than true resistance and differentially affect thrips fitness. *J. Econ. Entomol*. 106, 587–596. doi: 10.1603/EC12430

Srinivasan, R., Riley, D., Diffie, S., Sparks, A., and Adkins,. S. (2012). Whitefly population dynamics and evaluation of whitefly-transmitted tomato yellow leaf curl virus (TYLCV)-resistant tomato genotypes as whitefly and TYLCV reservoirs. *J. Econ. Ent*. 105, 1447–1456. doi: 10.1603/EC11402

Sundaraj, S., Srinivasan, R., Culbreath, A. K., Riley, D. G., and Pappu, H. R. (2014). Host plant resistance against Tomato spotted wilt virus in peanut (*Arachis hypogaea*) and its impact on susceptibility to the virus, virus population genetics, and vector feeding behavior and survival. *Phytopathology* 104, 202–210. doi: 10.1094/PHYTO-04-13-0107-R

Tajima, F. (1989). The effect of change in population size on DNA polymorphism. *Genetics* 123, 597–601.

Tamura, K., and Nei, M. (1993). Estimation of the number of nucleotide substitutions in the control region of mitochondrial DNA in humans and chimpanzees. *Mol. Biol. Evol*. 10, 512–526.

Urbino, C., Gutiérrez, S., Antolik, A., Bouazza, N., Doumayrou, J., Granier, M., et al. (2013). Within-host dynamics of the emergence of tomato yellow leaf curl virus recombinants. *PLoS ONE* 8:e58375. doi: 10.1371/journal.pone.0058375

Varma, A., and Malathi, V. G. (2003). Emerging geminivirus problems. a serious threat to crop production. *Ann. Appl. Biol*. 142, 145–164. doi: 10.1111/j.1744-7348.2003.tb00240.x

Verlaan, M. G., Hutton, S. F., Ibrahem, R. M., Kormelink, R., Visser, R. G., Scott, J. W., et al. (2013). The tomato yellow leaf curl virus resistance genes Ty-1 and Ty-3 are allelic and code for DFDGD-class RNA–dependent RNA polymerases. *PLoS Genet*. 9:e1003399. doi: 10.1371/journal.pgen.1003399

Yamaguchi, H., Ohnishi, J., Saito, A., Ohyama, A., Nunome, T., Miyatake, K., et al. (2018). An NB-LRR gene, TYNBS1, is responsible for resistance mediated by the Ty-2 Begomovirus resistance locus of tomato. *Theor Appl Genet*. 131, 1345–1362. doi: 10.1007/s00122-018-3082-x

Yan, Z., Pérez-de-Castro, A., Díez, M. J., Hutton, S. F., Visser, R. G. F., Wolters, A. M. A., et al. (2018). Resistance to tomato yellow leaf curl virus in tomato germplasm. *Front. Plant Sci*. 9:1198. doi: 10.3389/fpls.2018.01198

Zamir, D., Ekstein-Michelson, I., Zakay, Y., Navot, N., Zeidan, M., Sarfatti, M., et al. (1994). Mapping and introgression of a tomato yellow leaf curl virus tolerance gene, Ty-1. *Theor. Appl. Genet*. 88, 141–146. doi: 10.1007/BF00225889

Conflict of Interest: The authors declare that the research was conducted in the absence of any commercial or financial relationships that could be construed as a potential conflict of interest.

Copyright © 2020 Marchant, Gautam, Hutton and Srinivasan. This is an open-access article distributed under the terms of the Creative Commons Attribution License (CC BY). The use, distribution or reproduction in other forums is permitted, provided the original author(s) and the copyright owner(s) are credited and that the original publication in this journal is cited, in accordance with accepted academic practice. No use, distribution or reproduction is permitted which does not comply with these terms.

frontiers in Plant Science

ORIGINAL RESEARCH
published: 09 December 2020
doi: 10.3389/fpls.2020.594977

Assessment of Four Portuguese Wheat Landrace Diversity to Cope With Global Warming

*Diana Tomás[1], Luís Pinto Coelho[1], José Carlos Rodrigues[2], Wanda Viegas[1] and Manuela Silva[1]**

[1] Linking Landscape, Environment, Agriculture and Food, Instituto Superior de Agronomia, Universidade de Lisboa, Lisbon, Portugal, [2] Centro de Estudos Florestais, Instituto Superior de Agronomia, Universidade de Lisboa, Lisbon, Portugal

OPEN ACCESS

Edited by:
Raul Antonio Sperotto, Universidade do Vale do Taquari - Univates, Brazil

Reviewed by:
Dejan Bogdan Dejan, Maize Research Institute Zemun Polje, Serbia
Dolors Villegas, Institute of Agrifood Research and Technology (IRTA), Spain
Jirui Wang, Sichuan Agricultural University, China

***Correspondence:**
Manuela Silva
manuelasilva@isa.ulisboa.pt

Specialty section:
This article was submitted to Plant Abiotic Stress, a section of the journal Frontiers in Plant Science

Received: *14 August 2020*
Accepted: *27 October 2020*
Published: *09 December 2020*

Citation:
Tomás D, Coelho LP, Rodrigues JC, Viegas W and Silva M (2020) Assessment of Four Portuguese Wheat Landrace Diversity to Cope With Global Warming. Front. Plant Sci. 11:594977. doi: 10.3389/fpls.2020.594977

Wheat is a dietary staple consumed worldwide strongly responsible for proteins and carbohydrate population intake. However, wheat production and quality will scarcely fulfill forward demands, which are compounded by high-temperature (HT) events as heatwaves, increasingly common in Portugal. Thus, landraces assume crucial importance as potential reservoirs of useful traits for wheat breeding and may be pre-adapted to extreme environmental conditions. This work evaluates four Portuguese landrace yield and grain composition through attenuated total reflection Fourier transform infrared (ATR-FTIR) spectroscopy, particularly protein content, and their responses to HT treatment mimicking a heatwave. Landraces showed distinct yield traits, especially plant height and first spike grain number, and a similar pattern in FTIR spectra, although revealing differences in grain components' proportions. Comparison between spectra band intensity indicates that Ardito has the highest protein-related peaks, contrary to Magueija, which appears to be the landrace with higher lipid content. In plants submitted to 1 week of HT treatment 10 days after anthesis, the first spike grain size and weight were markedly reduced in all landraces. Additionally, it was observed that a general increase in grain protein content in the four landraces, being the increment observed in Ardito and Grécia, is statistically significant. The comparative assessment of control and HT average FTIR spectra denoted also the occurrence of alterations in grain polysaccharide composition. An integrated assessment of the evaluations performed revealed that Ardito and Magueija landraces presented diverse yield-related characteristics and distinct responses to cope with HT. In fact, the former landrace revealed considerable grain yield diminution along with an increase in grain protein proportion after HT, while the latter showed a significant increase in spikes and grain number, with grain quality detriment. These results reinforce the relevance of scrutinizing old genotype diversity seeking for useful characteristics, particularly considering HT impact on grain production and quality.

Keywords: bread wheat, landraces, heatwave, yield, grain composition, protein content

INTRODUCTION

Wheat (*Triticum aestivum* L.) is a major cereal consumed worldwide on a daily basis (FAO, 2017). However, the global mean growth rate of wheat is not sufficient to cover the production predicted to be necessary in 2050 (Ray et al., 2013), and one of this limitation causes is the progressive global warming (Gaupp et al., 2019). In fact, the increase in mean temperature during wheat development was predicted to reduce grain production (Asseng et al., 2014; Wang et al., 2019).

Major effects of high temperature (HT) on wheat plants include decrease in pollen viability, plant cycle shortening, as well as deterioration of chlorophyll and reduction of photochemical efficiency with consequent grain number diminution and kernel shrinkage (reviewed in Akter and Islam, 2017). Temperatures above 30°C after anthesis, in the early stages of grain filling, accelerate plant development leading to smaller and shrunken grains (Altenbach et al., 2002, 2003). This reduction in grain development time caused by heat decreases starch and protein deposition, affecting grain composition and final quality (reviewed in Farooq et al., 2011). Several reports suggested that a HT induces higher grain protein content as kernel size is smaller, and this augment seems to be more pronounced when HTs are imposed in early stages of grain filling (Corbellini et al., 1998; Daniel and Triboi, 2001; Castro et al., 2007). However, distinct stress responses were registered in different wheat genotypes commercially available with a reduction in both kernel weight and protein content in some varieties (Tomás et al., 2020a). In this context, it is particularly relevant to comparatively assess the variability of distinct commercial varieties (Pradhan et al., 2019) and also, more importantly, the old and traditional landraces, considering the eroded genetic pool of commercial varieties that resulted from decades of homogenization through breeding.

Landraces provided notable successes in crop improvement (reviewed in Dwivedi et al., 2016). Wheat landraces, defined as a traditional varieties with potential higher tolerance to biotic and abiotic stresses, present better yield stability under low input agricultural system (Zeven, 1998). Thus, landraces may constitute extremely valuable agrobiodiversity pools assuming a prominent role in the actual unpredictable weather conditions (Lopes et al., 2015; Alipour et al., 2017).

The effects of extreme heat events particularly frequent in Portugal, like heatwaves (Cardoso et al., 2019), defined as five or more consecutive days of heat in which the daily maximum temperature is at least 5°C higher than the average maximum temperature (WMO, 2015), have been studied in wheat commercial varieties. Those reports showed that HT treatments mimetizing heatwaves during grain filling leads to lower intervarietal diversity in transcription levels of genes related to grain quality and in the proportions of distinct protein fractions (Tomás et al., 2020b), as well as in grain polysaccharide composition and global protein content (Tomás et al., 2020a). Thus, it is crucial to assess the biodiversity enclosed in landraces to cope with a broad range of environmental conditions. The objective of this work was to assess the effect of a short period of HT during grain filling in distinct Portuguese landraces on grain yield and composition with special focus on protein content as one of the most determinant parameters of grain quality. Our results revealed distinct responses to HT treatment concerning most yield parameters, except grain weight, and a concordant general increase in protein content and reduction in starch amount. Additionally, landraces presenting distinct responses to HT treatment imposed during grain filling were identified.

MATERIALS AND METHODS

Plant Material

Bread wheat (*T. aestivum* L., 2n = 6 × = 42, AABBDD) old Portuguese landraces from Vasconcellos collection, established in the 1930s of the last century (Vasconcellos, 1933), were used in this work—Ardito, Grécia, Magueija e Ruivo. These landraces were selected considering a previous study of photosynthetic rate and thousand grain weight (Scotti-Campos et al., 2011). The seeds used were obtained after 2 years of controlled propagation under equal environmental conditions of material gently supplied by EAN Germplasm Bank (Oeiras, Portugal, PRT005). Twenty seeds from each landrace were simultaneously germinated and grown in controlled conditions—8 h of dark at 20°C followed by 16 h of light period divided into 6 h increasing to 25°C, 4 h at 25°C, and 6 h decreasing to 20°C. Three weeks after germination, plants in the growth stage between 1.3 and 1.4 Zadoks code (Zadoks et al., 1974) were transferred individually to 7-L soil pots and maintained in greenhouse conditions.

When the first anther was observed in the first spike (anthesis), plants were transferred to growth chambers with the previously described conditions. A HT regime with a daily plateau of 40°C maximum temperature (**Supplementary Figure 1**) was imposed to subsets of 10 plants (independent biological replicates) of each landrace, 10 days after anthesis beginning–anthesis complete (Zadoks decimal code 61) (Zadoks et al., 1974) in each plant, thus occurring in distinct dates (flowering times presented in **Supplementary Table 1**) for each wheat landrace/plant evaluated.

After treatments, plants were kept in the greenhouse until the end of the lifecycle. All yield and grain composition analyses were performed exclusively in seeds from the first spike to guarantee identical developmental stages during HT treatments. For grain composition analyses through ATR-FTIR spectroscopy and elemental analysis, the embryo was removed from each kernel, simulating germen industrial removal procedure for flour production.

Yield Evaluations

Yield parameters were evaluated in all plants of all varieties in both control and treatment conditions after the plants reached harvest maturity, corresponding to at least eight independent biological replicates for each genotype/condition. The parameters evaluated per plant were height, area, and number of spikes; and in the first spike were length, number of grains, and grain weight. The average weight of 10 grains (g/10 kernels) was deduced from the two later data.

Plant area was calculated through the analysis of mature plant images (**Supplementary Figure 2**). At the end of the growing cycle, the plant shoot system was photographed with a

Nikon D90 camera using a black background for easier software segmentation, with constant light conditions and image capture parameters (exposure time, aperture, and ISO speed). Raw images were quantified using ImageJ software (United States) with Fiji platform (Schindelin et al., 2012).

ATR-FTIR Spectroscopy

For attenuated total reflection Fourier transform infrared (ATR-FTIR) spectra acquisition, four grains of the first spike were pooled from each plant, and a minimum of eight independent biological replicates per variety and per condition (control and HT treated) were evaluated. Grains were ball-milled in a Cryomill (Retsch GmbH, Haan, Germany) after embryo removal, and all samples obtained were lyophilized overnight. Flours ATR-FTIR spectra were recorded with a Bruker-P Alpha spectrometer (Bruker, Ettlingen, Germany) equipped with a single-reflection diamond ATR (attenuated total reflection) accessory. The spectra were obtained between 4,000 and 400 cm^{-1} with a resolution of 4 cm^{-1}, and each spectrum was the average of 24 scans corresponding to technical replicates. Processing of the spectra was performed with OPUS software Vsn. 8.0 (Bruker Optics, Ettlingen, Germany). The average spectra were calculated per landrace and condition and subsequently Min–Max normalized between the minimum at 1,800 cm^{-1} and the maximum between 1,800 and 895 cm^{-1}. For the nitrogen (N) prediction model, the partial least square (PLS) regression model obtained previously (Tomás et al., 2020a) was used to predict the landrace samples. After prediction, 10 samples covering the obtained N range were selected for nitrogen content quantification by elemental analysis. The spectra and values obtained (**Supplementary Table 2**) were included in the model, and a new model (further on referred as adjusted model) was obtained and further used to predict N content, which was then used to calculate protein content using the conversion factor of 5.7x (Caporaso et al., 2018).

Elemental Analysis

The nitrogen content was quantified in flour of 10 samples (obtained as described for ATR-FTIR analysis) at the REQUIMTE@UCIBIO-FCT-UNL analytical laboratory using a Flash EA1112 CHNS analyzer (Thermo Finnigan CE Instruments, Italy) equipped with a gas chromatography column and a thermal conductivity detector.

Data Analysis

To compare the yield parameters and protein content between varieties, values were fitted to a linear model (*ANOVA* with one factor with fixed effects) and analyzed through multiple means comparison test (*Tukey test*). The individual effect of HT treatment in comparison with control condition for each variety was tested using *t-test*, and χ^2 test was used to compare frequency distributions. Models were fitted in R using *aov* and *Tukey.HSD* (*agricolae* package) and *chisq.test* functions, respectively.

The principal component analysis (PCA) and clustering analysis (dendrogram) were made based on yield quantification data in RStudio using *prcomp* and *HCPC* functions, and *FactoMineR* and *factoextra* packages.

RESULTS

In this work, plants of landraces Ardito, Grécia, Magueija, and Ruivo were submitted to HT treatment simulating a heatwave for 1 week during grain filling stage. Yield parameters were comparatively evaluated in the end of the lifecycle in these plants and in plants kept in control conditions. The results obtained were used to compare between landraces in each condition and to evaluate the HT effects on each landrace.

Landraces Revealed Different Responses to HT Treatment in Yield Parameters

The yield parameters considered are the following: (i) per plant—height, area, and spike number; (ii) in the first spike—length, grain number, grain weight, and 10 grains weight. The results obtained are summarized in **Figure 1**.

Plant height and area, often used as predictor of the plant biomass (Armoniené et al., 2018), calculated for control condition, revealed that Ardito was the landrace with significant lower average values in both parameters (103.42 and 549.94 cm^2, respectively) in comparison with the other landraces (**Figure 1A**). However, only plant height values are significantly different among all landraces. On the other hand, HT treatment influenced significantly Ardito and Ruivo plant height, although in inverse ways. Ardito HT treated plants are 6.9% taller (110.52 cm), and Ruivo plants are 8.3% shorter (145.42 cm). Magueija HT treated plants showed an average area significantly higher (31%) than the control ones and the comparison between landraces submitted to HT conditions indicates that this value (1,166.37 cm^2) is significantly higher than other landrace plant areas (**Figure 1A**).

Considering the average number of spikes per plant kept in control conditions, Magueija and Ruivo presented the lowest average values (6.9 and 6.5, respectively), significantly different than the highest average number (9.6) shown by Grécia (**Figure 1B**). The comparison of the average number of spikes between control and HT-treated plants revealed a significant difference only in Magueija, with a remarkable increase of 72%, (from 6.9 to 11.9). Also, the comparison between landraces submitted to HT treatment revealed that Magueija plants showed a significantly higher number of spikes in comparison with all other genotypes (**Figure 1B**). The number of spikes was moreover influenced by the appearance of new tillers after the HT treatment period, during ripening, with subsequent additional spikes (**Figure 2A**). These late spikes were observed in all landraces, although not in all plants, and their average number per plant as well as the percentage of plants with late spikes are presented in **Figure 2B**. In control conditions, the average number of late spikes per plant observed ranged between 2 in Ardito and 1 in Ruivo, but no significant differences were observed between landraces. On the other hand, Ardito was the landrace in which we detected a lower percentage of control plants with late spikes (20%), and Magueija was the landrace with higher percentage (50%) (**Figure 2B**). In HT-treated plants, only Magueija landrace presented a significant increase in the average number of late spikes per plant compared with the

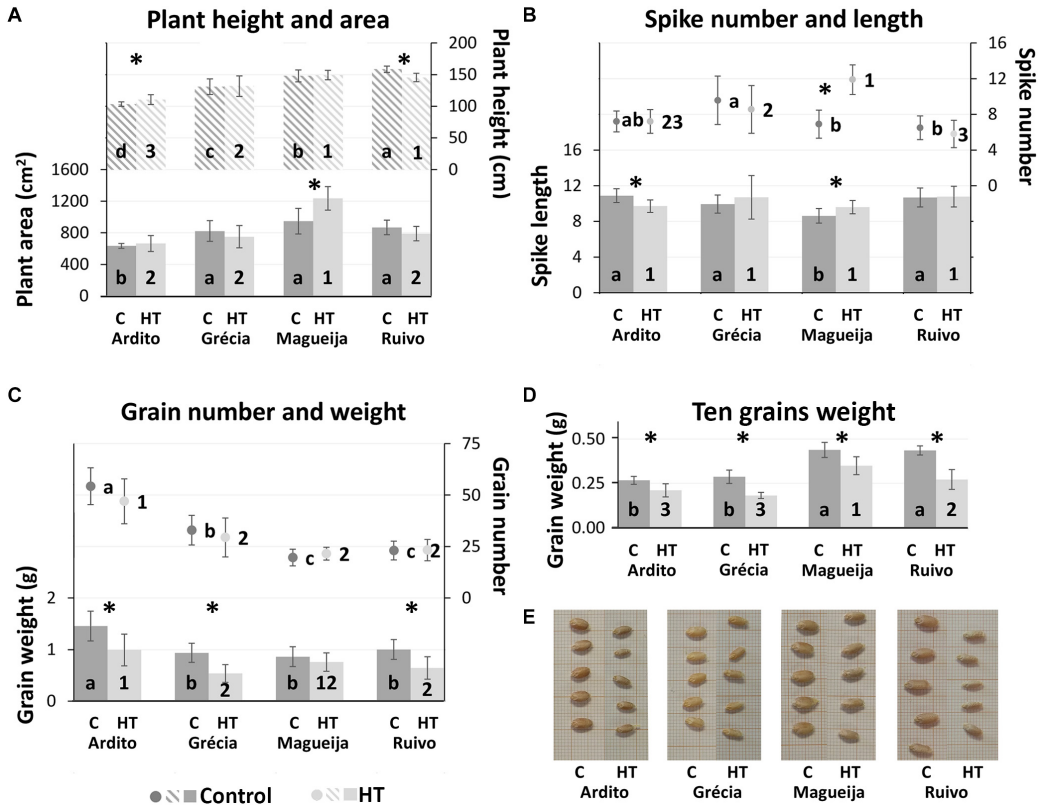


FIGURE 1 | Yield parameter evaluation. **(A)** plant height (listed columns) and area (full columns). **(B)** Number of spikes per plant (dots) and first spike length (columns). **(C)** First spike number of grains (dots) and grain weight (columns). **(D)** First spike 10-grain weight. Mean values of plants kept in control conditions (dark gray) and high temperature (HT) treatment (light gray) ± standard deviation (represented as bars). Different letters and numbers indicate *ANOVA* significant differences between varieties, in control and high-temperature (HT) conditions, respectively. **t-test* statistical differences between control and treatment in each variety ($p < 0.05$). **(E)** Grains from the four landraces' plants kept in control conditions or HT treated.

control ones, from 1.6 to 3.6. Regarding the percentage of plants with late spikes, it was observed a significant increase in all the landraces except Grécia and all HT treated Magueija plants presented late spikes.

Spike length and grain parameters (number and weight) were measured only in the first spike. Magueija plants kept in control conditions revealed to have the smallest spike with an average length of 8.6 cm, significantly lower than the other three landraces (**Figure 1B**), though it was the only landrace revealing a significantly larger spike in HT-treated plants in comparison with the control ones. Ardito HT-treated plants, on the other hand, showed a significant decrease in average spike length in comparison with the control plants. HT-induced alterations reduced the intervarietal variability observed regarding spike length since no significant differences were observed between landraces after HT treatment.

In accordance with the spike length, both grain number and grain weight/spike were also lower in Magueija plants maintained in control conditions (19.7 and 0.86 g, respectively) comparative to the other landraces (**Figure 1C**). On the other hand, Ardito was the landrace with significantly higher values in these two parameters (54.3 and 1.46 g). Although HT treatment showed no significant effect in grain number, it induced a grain weight/spike decrease in all the varieties that was statistically significant in all landraces except in Magueija. The comparison between landraces submitted to HT treatment showed that Ardito has the significantly higher number of grains/spike of all landraces (47) and a higher grain weight/spike (0.99 g) than Grécia and Ruivo. Ten grain weight (**Figure 1D**) allows a more accurate assessment of the distinct developmental conditions' effects in plants' yield. In plants kept in control conditions, Magueija and Ruivo have higher values (0.44 g) in comparison with Ardito (0.27 g) and Grécia (0.29 g). This yield parameter was significantly lower in HT-treated plants of the four landraces (between 0.17 g in Ruivo and 0.06 g in Ardito), and Magueija remains the variety with significantly higher ten grain weight in plants submitted to HT treatment. This result is clearly illustrated by the comparison of grain size presented in **Figure 1E** since grains from treated plants are smaller in all the landraces.

HT Impact in Grain Composition Revealed by Attenuated Total Reflection Fourier Transform Infrared Spectra

The spectra in the wavenumber region between 4,000 and 400 cm^{-1} obtained for the four landraces studied in each

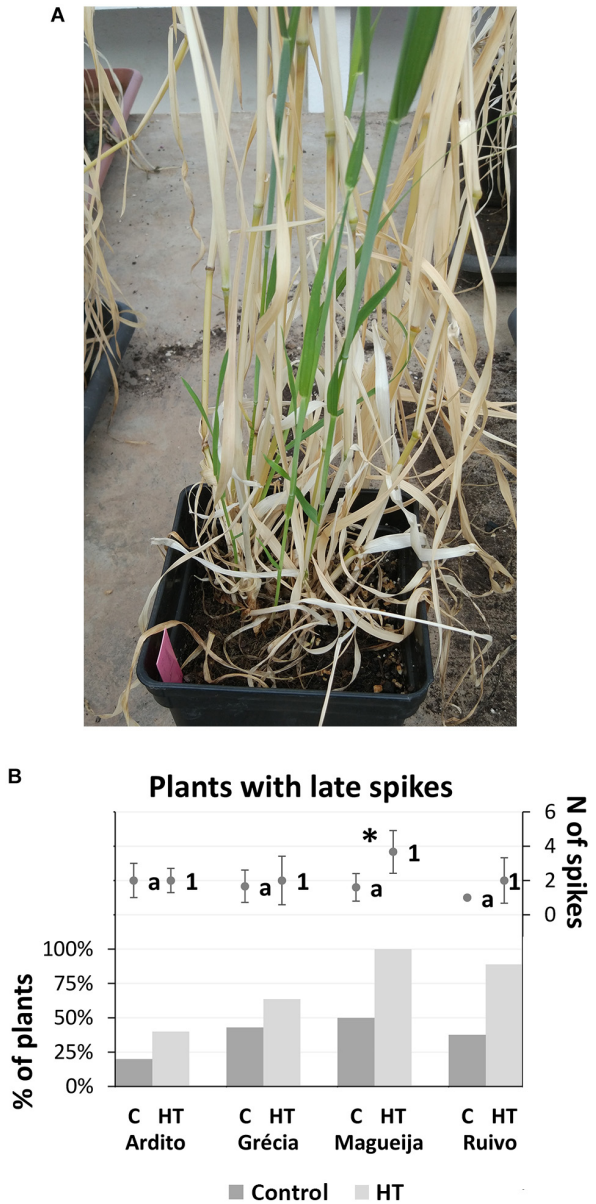


FIGURE 2 | Late spike evaluation. **(A)** HT-treated plant of Magueija landrace presenting four late spikes. **(B)** Mean number of late spikes per plant in control (dark gray dots) and HT treated (light gray dots) plants ± standard deviation (represented as bars) and percentage of plants with late spikes in control (dark gray columns) and high temperature (HT) conditions (light gray columns). Different letters and numbers next to dots indicate *ANOVA* significant differences between landraces in both control and treatment conditions, respectively, and *indicates *t-test* statistical differences between control and treatment in each variety ($p < 0.05$).

condition show no evident pattern differences, but the same bands presented intensity variations (**Figure 3**). The most intense bands in the region of 1,150 and 800 cm^{-1} are mainly from starch, including the most intense band of the spectra, with a maximum close to 997 cm^{-1}. The band with a maximum at 2,927 cm^{-1} assigned to the stretch vibration of CH_2 is also essentially from starch with a small contribution from proteins and lipids. The protein contribution, the second most important component of wheat grain, is clearly seen as two bands with maxima close to 1,648 and 1,532 cm^{-1} from Amide I and II, respectively. The broad band with maximum close to 3,294 cm^{-1} from O–H stretching of the starch polymer masks completely the NH band from proteins. A very weak band, in some cases only a shoulder, located at 1,745 cm^{-1}, could be from C = O stretching from lipids that if present at all would be in a very small percentage.

The comparison between landraces' min–max normalized spectra obtained for control conditions, regarding the maxima intensity at selected wavenumber bands, was performed (**Figure 3A**). This analysis unravels that Ardito has a more intense spectra than Magueija and Ruivo in half of the selected bands, including the band with maximum at 3,294 cm^{-1} assigned to starch polymer and Amides I and II bands. On the contrary, the average spectrum of grains from Magueija control plants was the most intense at the 1,745 cm^{-1} band (probably related with fat), and 2,927, 929, and 848 cm^{-1} starch-related bands. Globally, only for the Amide I, the four spectra are clearly separated, while for the other selected bands, at least two spectra have similar absorbance intensities.

The comparison of maximum intensity at selected wavenumber between the average spectra of grains from control and HT = treated plants, after min-max normalization is shown in **Table 1**. Overall, the spectra of grains from HT-treated plants are more intense than the ones obtained from grains of control plants for all four landraces. The only exceptions to these were the more intense Grécia and Magueija control spectra in the band with a maximum at 3,294 cm^{-1}, mainly assigned to O–H stretching from the starch polymer. Amide I and II proteins bands are the ones that revealed more relevant differences between control and HT. In fact, the intensity of HT Ardito and Grécia spectra is much higher than the control ones in both Amide bands, as well as in Ruivo regarding Amide I band. This increase in protein content is expected to be associated with a proportional reduction in starch grain content, as these are the main components of wheat grain, and the spectra normalization was done by the more intense band at 997 cm^{-1}, associated with starch. Although Ardito HT spectrum is also quite more intense than the control one in bands with a maximum at 1,149 and 1,077 cm^{-1}, and Grécia presented a greater difference between the control and HT spectra in 1,077 and 929 cm^{-1} bands, in both cases, the bands are associated with starch. These alterations suggest that the proportions of distinct polysaccharides may also be altered after HT treatment. Last, based on the 1,745-cm^{-1} band, the lipid fraction increases slightly in grains from HT-treated plants of Ardito, Grécia, and Ruivo.

Intensity differences between spectra obtained from grains of HT-treated plants are presented in **Figure 3B** and showed that Ardito spectra are the most intense in all wavenumber range, except for the 929-cm^{-1} band. In the wavenumber region most related to fat with a peak at 1,745 cm^{-1} as well as two other regions more related to starch with peaks at 2,927 and 997 cm^{-1}, the intensities are similar for all landraces. As for control conditions, Magueija is the landrace with lower intensity in eight

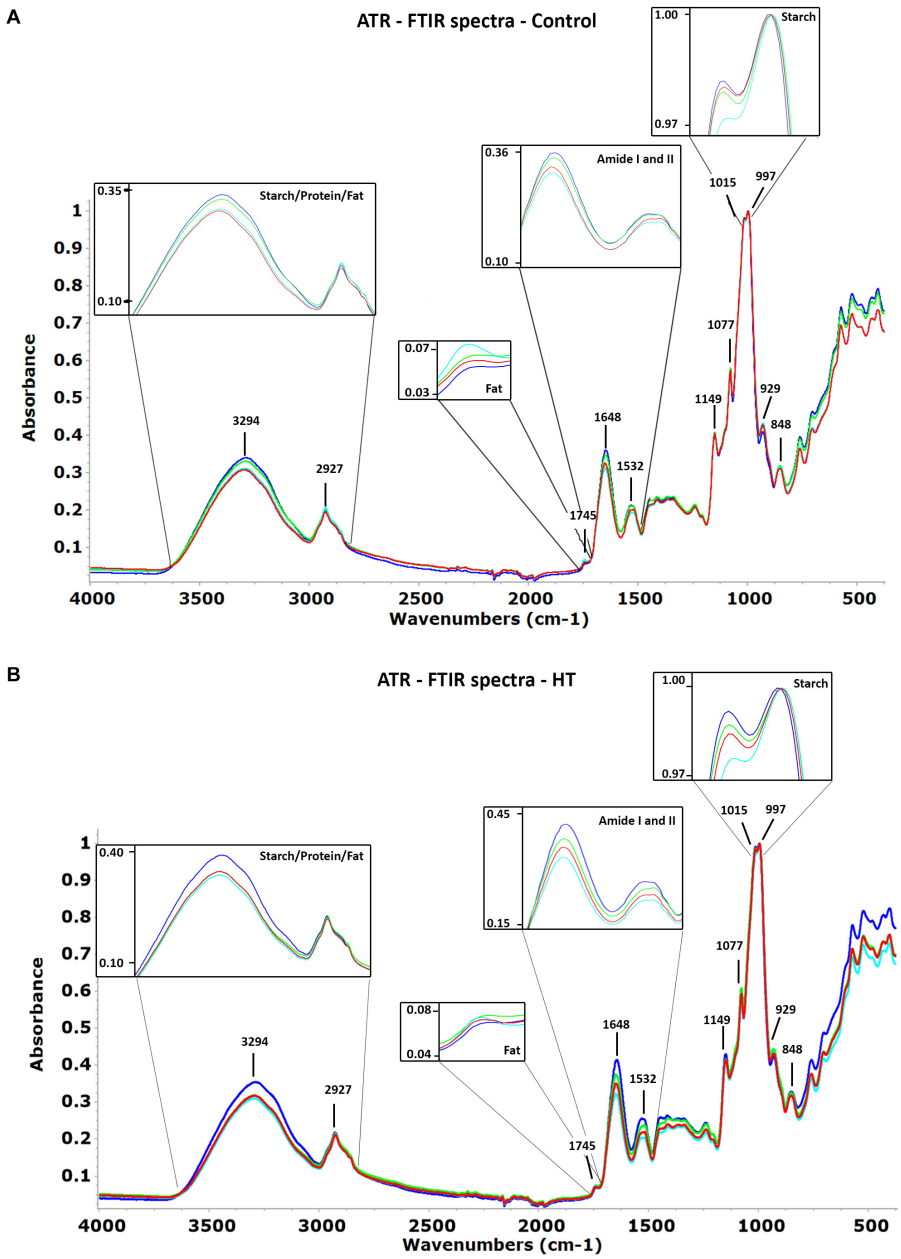


FIGURE 3 | Attenuated total reflection Fourier transform infrared (ATR-FTIR) average spectra of Ardito (dark blue), Grécia (green), Magueija (light blue), and Ruivo (red) **(A)** control and **(B)** HT samples with the assignment of relevant bands. Insets magnify peaks related with starch, protein, and fat showing differences between landraces in each condition.

of the selected spectra bands. Compared with the control, it is possible to observe more differences between the spectra of grains obtained from HT-treated plants, indicating more dissimilarities between landraces under this abiotic stress condition.

Grain Protein Content Increase Is a Common Response to HT Treatment

Protein content was predicted using spectra acquired from grain of control and HT-treated plants of the four landraces using the model calibrated in Tomás et al. (2020a) adjusted with N content values of landrace grains (**Supplementary Table 2**). The adjusted model to predict nitrogen content had very good statistics (R^2 = 0.92, RMSECV = 0.14), and the predicted nitrogen values for all control and HT samples ranged from 1.8 to 4.5% (mg of N/100 mg of flour). These values were used to infer protein content using a conversion factor of 5.7× (Caporaso et al., 2018). The average protein content of grains from control and HT-treated plants of the four landraces studied are summarized in **Figure 4**.

TABLE 1 | Comparison between peaks' high of average spectra of grains from control and treated landraces plants after min–max normalization.

Landrace	Condition	Wavelength (cm^{-1})											
		Starch/proteins	Starch/fat	Fat	Proteins			Starch					
		OH, NH ~3,294	CH ~2,927	C = O ~1,745	Amide I ~1,648	Amide II ~1,532	C-O_C ~1,149	1,077	1,015	997	929	848
Ardito	C	–	–	–	–	–	–	–	–	=1	–	–
	HT	+	+	+	‡	‡	‡	‡	+	=1	+	+
Grécia	C	+	–	–	–	–	–	–	–	=1	–	–
	HT	–	+	+	‡	‡	+	‡	+	=1	‡	+
Magueija	C	+	–	–	–	–	–	–	–	=1	–	–
	HT	–	+	+	+	+	+	+	+	=1	+	+
Ruivo	C	–	–	–	–	–	–	–	–	=1	–	–
	HT	+	+	+	‡	+	+	+	+	=1	+	+

C, control plants, HT, high-temperature-treated plants. (+) and (-), higher and lower intensity, respectively, (=1) maximum at which the spectra were normalized.

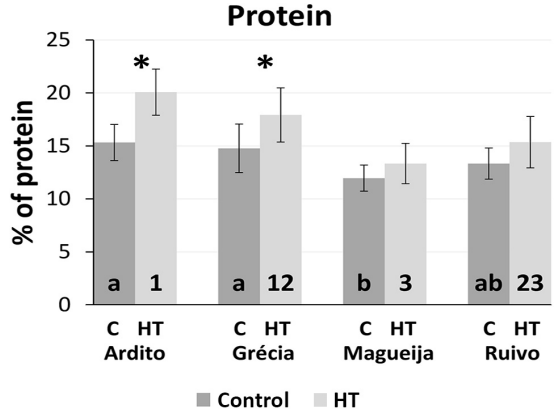


FIGURE 4 | Mean protein content of plants kept in control conditions (dark gray) and HT-treated (light gray) and respective standard deviations (represented as bars). Different letters and numbers inside columns indicate *ANOVA* significant differences between varieties in control and treatment conditions (HT), respectively. **t-test* statistical differences between control and treatment in each variety ($p < 0.05$).

Considering the values obtained from plants kept in control conditions for each landrace, Magueija samples are the ones with the lower mean protein content (12%), significantly different from Ardito and Grécia with 15.3 and 14.8%, respectively (**Figure 4**). Grains of HT-treated plants showed higher protein content in all landraces analyzed in comparison with control being this augment significant in Ardito (20.1%) and Grécia (17.9%). The comparison between landraces of mean protein content obtained in HT-treated plants showed a higher value in Ardito, which is significantly different from those of Ruivo (15.4%) and Magueija (13.3%) (**Figure 4**).

A global perspective of protein content in all analyzed samples is presented in **Figure 5** that represents the division by classes of protein content of all individual samples from control or HT-treated plants analyzed (dark and light bars, respectively), independently of the genotype. It shows that control grains presented a lower number of classes (nine classes with values ranging between 10.3 and 19.7%) than HT-treated samples (13 classes, with values ranging between 10.2 and 25.4%). Likewise, this result representation substantiates the lower average protein content of the control samples (13.8%) in comparison to the average value of the treatment samples (16.8%).

On the other hand, an integrated assessment of the four landraces studied can be performed through the PCA of all yield parameters and protein quantification presented in **Figure 6**. In this PCA, the two represented dimensions explain 63% of the variation found between samples. The first, that clearly separates Ardito and Magueija, is defined by five of the eight parameters used (plant area, spike length, grain number, grain weight, and protein content). On its turn, Ardito responds to HT privileging plant growth, increasing plant height, but reducing grain yield, with spike length, and both grain number and weight reduced in treated plants. Concerning grain composition, a significant increase in protein content was observed and, allied

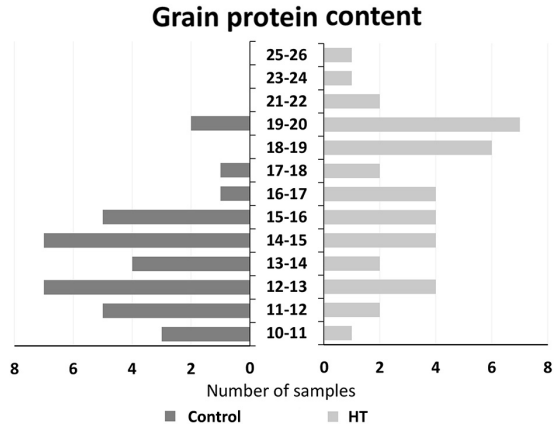


FIGURE 5 | Grain protein content. Distribution of all grain samples protein content from control (dark gray) and HT-treated (light gray) plants of the four landraces studied.

to the reduction in grain size and weight, foresee a reduction in grain starch amount. Also, in Magueija, the responses to HT increase plant biomass, spikes in both number and length, and grain quantity.

DISCUSSION

Landrace variability may assume special relevance due to commercial varieties reduced genetic diversity, constituting valuable agrobiodiversity pools potentially more adapted to local conditions where they have been cultivated for long periods (Alipour et al., 2017). Facing a global warming scenario, these advantages are even more relevant for essential crops like bread wheat considering the projections of insufficient cereal production to meet the demand in a few decades (Ray et al., 2013; Gaupp et al., 2019). In this context, the invaluable resource encompassed in the wheat old traditional landraces collected in the 1930s of the last century by Vasconcellos (1933) in Portugal fields assume special relevance. In this work, we studied four of these bread wheat landraces evaluating their yield and grain quality modulation by a HT treatment mimicking a heatwave during grain filling. This particular extreme heat event was predicted to be intensified onward especially in Portugal (Cardoso et al., 2019). Yield parameters and grain composition were comparatively evaluated in landrace plants kept in control conditions and HT treated.

The evaluation of the four landraces showed considerable intervariety diversity since significant differences were detected in all yield parameters analyzed in control plants, especially in the number of spikes, grain number, and plant height, the latter being significantly different between all the landraces. The variability disclosed in the number of grains per spike contrasts with the complete homogeneity observed in this parameter of grain yield observed in bread wheat commercial varieties (Tomás et al., 2020a). On the other hand, the diversity disclosed in the number of spikes contrasts also with the lack of diversity reported in commercial genotypes (Khan and Naqvi, 2011). Ardito landrace stands out as the one with the lower plant height and area along with the higher grain number and weight in the first spike, characteristics close to the desired for commercial varieties (Khush, 1999). Globally, the yield parameters are similar to other European landraces previously studied (Dotlaèil et al., 2003). Unexpectedly, two landraces (Magueija and Grécia) 10 grain weight was higher (0.44 g) than the higher value reported for commercial varieties recommended to be used in Portugal (0.38 g) assessed in similar assays (Tomás et al., 2020a). Concerning the average protein content, the values obtained in the landraces studied, ranging from 10.3 to 19.7% (control condition), were similar to the ones assessed in commercial varieties through the same methodology (between 9.5 and 21.4%, Tomás et al., 2020a). It is relevant that although these landraces were not submitted to breeding programs, their values of protein content are very acceptable and similar to the ones reported for commercial varieties. Recently, the screening of Pakistani wheat landraces also found several traditional genotypes with high storage protein concentration, pointing out their potential to improve the nutritional quality of modern wheat commercial genotypes (Mughal et al., 2020).

On the other hand, different landraces studied in our work revealed distinct responses to HT traduced even in opposite effects in most yield parameters evaluated. The evaluation of the plant height of Ardito and Ruivo, and the area of Magueija revealed significant differences between the control and HT plants. As plant area is often used as plant biomass predictor (Armoniené et al., 2018), our results indicate that Magueija increase in biomass may compromise grain filling, as in this plant development phase, all plant resources should be directed to grain. Both number of spikes per plant and first spike length showed a significant difference between the control and HT plants in Ardito and Magueija, although HT induced differences in the first spike length in opposite ways in these two landraces. Additionally, the increase in Magueija number of spikes induced by HT treatment was mainly due to the appearance of new tillers with spike during ripening. The appearance of these late tillers was observed in all the landraces, in both control and HT-treated plants. It must be emphasized that late spikes were never observed in commercial varieties previously assayed in similar conditions (Tomás et al., 2020a). Moreover, extemporaneous tiller appearance was described in some wheat varieties but only until the beginning of stem elongation (Bowden et al., 2007). We speculate that this phenomenon can constitute a strategy to assure descendance in extreme conditions.

The less affected yield parameter was grain number since it was the only one that did not reveal significant differences between the control and HT-treated plants in any of the genotypes assessed, in opposition to 10-grain weight, which was significantly lower in HT-treated plants of all four landraces. This is in accordance with some previous works that reported that grain number is mostly affected by HT treatments imposed before fertilization, while elevated temperature occurring during grain filling is known to shorten developing period and lead to shrunken grains (Stone and Nicolas, 1995; Farooq et al., 2011; Talukder et al., 2014; Tao et al., 2018). Although an increase

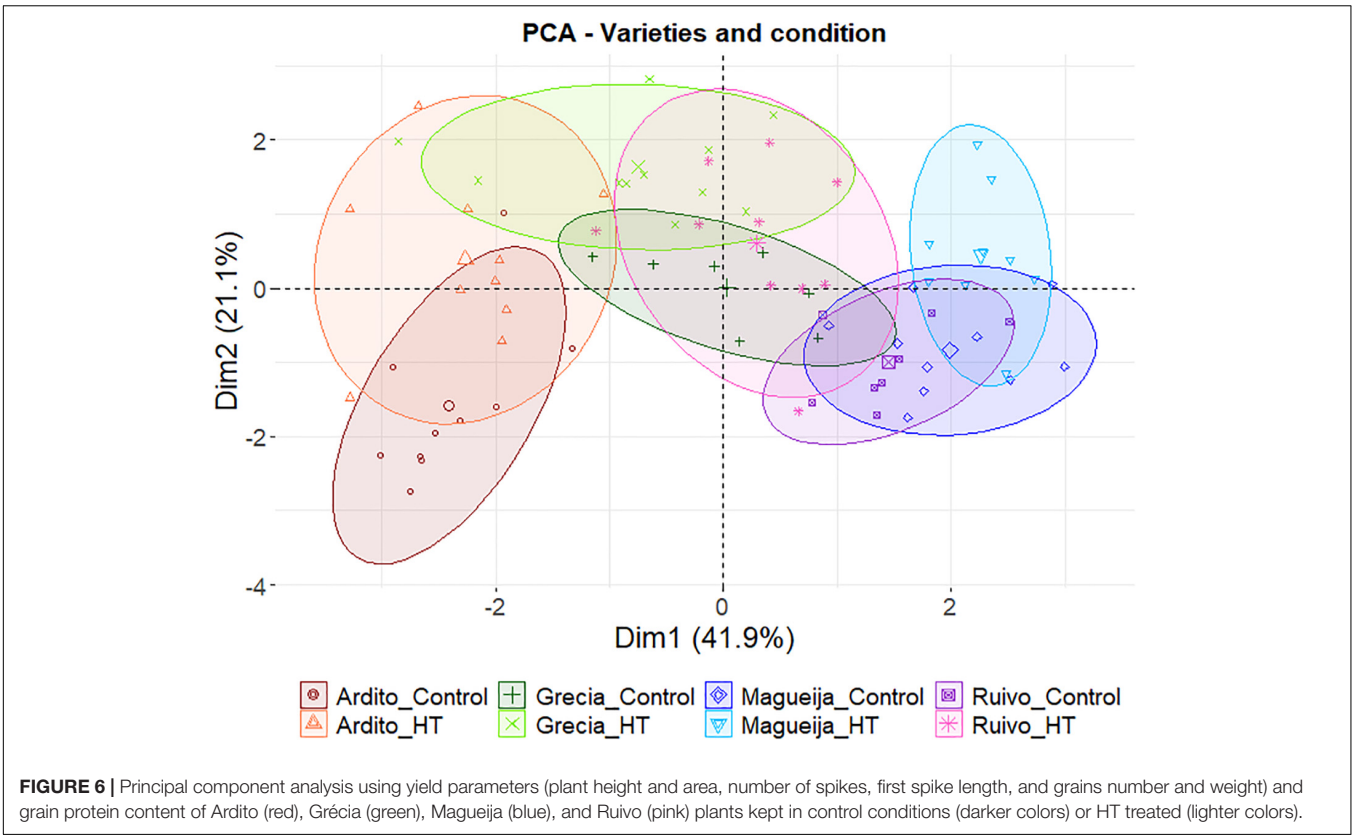


FIGURE 6 | Principal component analysis using yield parameters (plant height and area, number of spikes, first spike length, and grains number and weight) and grain protein content of Ardito (red), Grécia (green), Magueija (blue), and Ruivo (pink) plants kept in control conditions (darker colors) or HT treated (lighter colors).

in assimilate supply was reported in this phase, it was not sufficient to fully compensate the shorter duration of grain filling period (Lobell et al., 2012). Contrary to this uniform effect on grain weight observed in all landraces analyzed, some previous works revealed different HT effects in grain weight between distinct genotypes (Scotti-Campos et al., 2011; Tomás et al., 2020a). Globally, the comparative evaluation of yield-related traits between genotypes in the control and HT treatment plants showed that parameters determinant for grain yield like spike number and 10-grain weight presented high variability in both developmental conditions assayed.

Concerning grain composition evaluated by ATR-FTIR, all spectra here obtained were similar to the ones already described in Tomás et al. (2020a) for commercial wheat varieties and were concordant with the main components of wheat grain—starch and proteins (Shewry, 2009). The balance between starch and the other components suggests that grains from Ardito plants have higher protein content than the other four landraces, especially due to the contribution of Amide I (1,648 cm^{-1}). Lipid fraction constitutes only 3–4% of the whole grain (Wrigley et al., 2009), and in our work, it is negligible as the embryo, which is responsible for one-third of the wheat grain lipid fraction that was removed before grain milling. Nevertheless, the comparison between average spectra shows that Magueija grains have the higher fat amount.

Overall, spectra from HT-treated samples were more intense than the control ones in all the landraces, indicating an increase in protein content and a decrease in starch. These results are in accordance with model predicted protein content, which shows a significant increase in Ardito and Grécia grains from HT-treated plants and with previous works (DuPont et al., 2006; Zhang et al., 2017; Tao et al., 2018). Also, an increase in protein content should be related with a decrease in starch content and this is in accordance with the decrease in 10-grain weight and grain size previously observed and with other studies showing that HTs affect the starch synthesis in wheat grain (Hurkman et al., 2003; Tomás et al., 2020b). A shift between landrace spectra in bands mainly assigned to starch suggests that also the proportions of different polysaccharides are altered as the effect of HT treatment. This effect was also observed in commercial genotypes submitted to similar HT treatments (Tomás et al., 2020a).

After HT treatment, the significant increase in Ardito protein amount was also reflected in the greater distance between this landrace and the other ones regarding maximum intensity at Amide I and II bands. Also, the range of maxima intensity values in each spectra band is bigger indicating differences between landraces in HT-treated plants not observed in control ones. This is also corroborated by the increased dispersion of HT sample protein values as shown in **Figure 5**. In fact, associated with the global increase in protein content induced by HT treatment, a higher range of protein content values was obtained after HT (15%) in comparison to control samples (9%). Even more important was the increase in protein observed in HT-treated plants that corroborate the relevance of identifying variable wheat genotypes more adapted to global warming, particularly concerning the major determinant of grain quality—protein

content (Asseng et al., 2019). Additionally, the comparison of protein content range in grains from plants submitted to heatwave like the treatment here observed in landraces (10.2–25.4%) and reported in commercial genotypes (10.1–17.6%, Tomás et al., 2020a). This diversity, together with the higher average protein content observed in landraces after HT treatment, supports the relevance of old traditional genotypes as a source of useful variability breeding focused in wheat nutrimental quality.

Altogether, the four landraces studied presented clear distinct pathways in HT response testifying once again the diversity enclosed in the old varieties studied. Grécia and Ruivo are both affected in vegetative growth and yield, with a reduction, although not always significant, in almost all the parameters. The other two landraces—Magueija and Ardito—showed opposite behaviors, as unraveled by the PCA of all yield parameters and protein quantification (**Figure 6**). Magueija plants seem to be less affected by heatwave-like treatment in terms of yield as after HT, 10-grain weight is higher even when compared with commercial varieties. However, no significant increase in grain protein content was induced by HT, suggesting that the increase in tillers' number may reduce the allocation of resources to the grain filling per spike, ultimately resulting in worst flour quality (Li et al., 2016; Yang et al., 2019). On the other hand, Ardito not only revealed the higher protein content in the control condition but also disclosed a significant increase in this grain quality parameter after HT treatment. Moreover, Ardito is the earlier landrace (**Supplementary Table 1**), with a number of days from germinations to flowering similar to the ones previously observed (not published) in commercial varieties studied in Tomás et al. (2020a), which may be determinant to avoid heat stress conditions.

The overall diverse outcomes induced by a heatwave-like treatment in distinct landraces contrasts with the reduced diversity observed in wheat commercial varieties submitted to a similar treatment previously reported (Tomás et al., 2020a,b). This superior variability, unraveled under extreme thermal conditions, highlights the potential usefulness of the biodiversity enclosed in old traditional wheat genotypes facing climate changes already sensed. Moreover, the integrative assessment of this work outcomes suggests that both Magueija and Ardito genotypes should be further evaluated seeking for attractive genotypes for wheat breeding plans.

DATA AVAILABILITY STATEMENT

The original contributions presented in the study are included in the article/**Supplementary Material**. Further inquiries can be directed to the corresponding author/s.

AUTHOR CONTRIBUTIONS

DT and MS conceptualized and validated the study. DT, JR, and MS were in charge of the methodology. DT and JR made the formal analysis. DT and LC took part in the investigation. DT wrote and prepared the original draft and was in charge of the visualization. JR, WV, and MS wrote, reviewed, and edited the manuscript. MS supervised the study, was in charge of the project administration, and acquired the funding for the study. All authors contributed to the article and approved the submitted version.

FUNDING

DT was funded by a Fundação para a Ciência e a Tecnologia, Portugal (FCT) doctoral scholarship (SFRH/BD/93156/2013), MS by the FCT Investigator Program (IF/00834/2014), and the research work was financed by FCT research project IF/00834/2014/CP1219/CT0003, LEAF Unit (Linking Landscape, Environment, Agriculture and Food) (UID/AGR/04129/2020), and CEF Unit (Forest Research Centre, UIDB/00239/2020).

ACKNOWLEDGMENTS

We would like to thank Eng. Manuela Veloso (PRT005: EAN Germplasm Bank, Oeiras) for the landrace accessions studied in the present study. We would like to acknowledge the support of Ana Alves from Forest Research Centre, ISA-Ulisboa, on ATR-FTIR spectra acquisition.

SUPPLEMENTARY MATERIAL

The Supplementary Material for this article can be found online at: https://www.frontiersin.org/articles/10.3389/fpls.2020.594977/full#supplementary-material

REFERENCES

Akter, N., and Islam, M. R. (2017). Heat stress effects and management in wheat. a review. *Agron. Sustain. Dev.* 37:37. doi: 10.1007/s13593-017-0443-9

Alipour, H., Bihamta, M. R., Mohammadi, V., Peyghambari, S. A., Bai, G., and Zhang, G. (2017). Genotyping-by-sequencing (GBS) revealed molecular genetic diversity of iranian wheat landraces and cultivars. *Front. Plant Sci.* 8:1293. doi: 10.3389/fpls.2017.01293

Altenbach, S. B., DuPont, F. M., Kothari, K. M., Chan, R., Johnson, E. L., and Lieu, D. (2003). Temperature, water and fertilizer influence the timing of key events during grain development in a US spring wheat. *J. Cereal Sci.* 37, 9–20. doi: 10.1006/jcrs.2002.0483

Altenbach, S. B., Kothari, K. M., and Lieu, D. (2002). Environmental conditions during wheat grain development alter temporal regulation of major gluten protein genes. *Cereal Chem.* 79, 279–285. doi: 10.1094/CCHEM.2002.79.2.279

Armonieńe, R., Odilbekov, F., Vivekanand, V., and Chawade, A. (2018). Affordable imaging lab for noninvasive analysis of biomass and early vigour in cereal crops. *Biomed. Res. Int.* 2018:5713158. doi: 10.1155/2018/5713158

Asseng, S., Ewert, F., Martre, P., Rötter, R. P., Lobell, D. B., Cammarano, D., et al. (2014). Rising temperatures reduce global wheat production. *Nat. Clim. Chang.* 5, 143–147. doi: 10.1038/nclimate2470

Asseng, S., Martre, P., Maiorano, A., Rötter, R. P., O'Leary, G. J., Fitzgerald, G. J., et al. (2019). Climate change impact and adaptation for wheat protein. *Glob. Chang. Biol.* 25, 155–173. doi: 10.1111/gcb.14481

Bowden, P., Edwards, J., Fergson, N., McNee, T., Manning, B., Raoberts, K., et al. (2007). *Wheat Growth & Development*, eds J. White and J. Edwards Orange, NSW: NSW Department of Primary Industries.

Caporaso, N., Whitworth, M. B., and Fisk, I. D. (2018). Protein content prediction in single wheat kernels using hyperspectral imaging. *Food Chem.* 240, 32–42. doi: 10.1016/j.foodchem.2017.07.048

Cardoso, R. M., Soares, P. M. M., Lima, D. C. A., and Miranda, P. M. A. (2019). Mean and extreme temperatures in a warming climate: EURO CORDEX and WRF regional climate high-resolution projections for Portugal. *Clim. Dyn.* 52, 129–157. doi: 10.1007/s00382-018-4124-4

Castro, M., Peterson, C. J., Rizza, M. D., Dellavalle, P. D., Vázquez, D., IbáÑez, V., et al. (2007). "Influence of heat stress on wheat grain characteristics and protein molecular weight distribution," in *Wheat Production in Stressed Environments. Developments in Plant Breeding*, Vol. 12, eds H. T. Buck, J. E. Nisi, and N. Salomón (Dordrecht: Springer), 365–371. doi: 10.1007/1-4020-5497-1_45

Corbellini, M., Mazza, L., Ciaffi, M., Lafiandra, D., and Borghi, B. (1998). Effect of heat shock during grain filling on protein composition and technological quality of wheats. *Euphytica* 100, 147–154.

Daniel, C., and Triboi, E. (2001). Effects of temperature and nitrogen nutrition on the accumulation of gliadins analysed by RP-HPLC. *Funct. Plant Biol.* 28, 1197–1205. doi: 10.1071/PP00142

Dotlaèil, L., Hermuth, J., and Stehno, Z. (2003). Earliness, spike productivity and protein content in European winter wheat landraces and obsolete cultivars. *Plant Soil Environ.* 49, 67–74. doi: 10.17221/4092-pse

DuPont, F. M., Hurkman, W. J., Vensel, W. H., Chan, R., Lopez, R., Tanaka, C., et al. (2006). Differential accumulation of sulfur-rich and sulfur-poor wheat flour proteins is affected by temperature and mineral nutrition during grain development. *J. Cereal Sci.* 44, 101–112. doi: 10.1016/J.JCS.2006.04.003

Dwivedi, S. L., Ceccarelli, S., Blair, M. W., Upadhyaya, H. D., Are, A. K., and Ortiz, R. (2016). Landrace germplasm for improving yield and abiotic stress adaptation. *Trends Plant Sci.* 21, 31–42. doi: 10.1016/j.tplants.2015.10.012

FAO (2017). *FAOSTAT. Food Balances. New Food Balances*. Available online at: http://www.fao.org/faostat/en/#data/FBS (accessed September 9, 2019).

Farooq, M., Bramley, H., Palta, J. A., and Siddique, K. H. M. (2011). Heat stress in wheat during reproductive and grain-filling phases. CRC. *Crit. Rev. Plant Sci.* 30, 491–507. doi: 10.1080/07352689.2011.615687

Gaupp, F., Hall, J., Mitchell, D., and Dadson, S. (2019). Increasing risks of multiple breadbasket failure under 1.5 and 2 °C global warming. *Agric. Syst.* 175, 34–45. doi: 10.1016/j.agsy.2019.05.010

Hurkman, W. J., McCue, K. F., Altenbach, S. B., Korn, A., Tanaka, C. K., Kothari, K. M., et al. (2003). Effect of temperature on expression of genes encoding enzymes for starch biosynthesis in developing wheat endosperm. *Plant Sci.* 164, 873–881. doi: 10.1016/S0168-9452(03)00076-1

Khan, N., and Naqvi, F. N. (2011). Effect of water stress on grain weight in bread wheat. *Curr. Res. J. Biol. Sci.* 3, 487–498.

Khush, G. S. (1999). Green revolution: preparing for the 21st century. *Genome (Natl. Res. Council Canada)* 42, 646–655. doi: 10.1139/g99-044

Li, Y., Cui, Z., Ni, Y., Zheng, M., Yang, D., Jin, M., et al. (2016). Plant density effect on grain number and weight of two winter wheat cultivars at different spikelet and grain positions. *PLoS One* 11:e0155351. doi: 10.1371/journal.pone.0155351

Lobell, D. B., Sibley, A., and Ivan Ortiz-Monasterio, J. (2012). Extreme heat effects on wheat senescence in India. *Nat. Clim. Chang.* 2, 186–189. doi: 10.1038/nclimate1356

Lopes, M. S., El-Basyoni, I., Baenziger, P. S., Singh, S., Royo, C., Ozbek, K., et al. (2015). Exploiting genetic diversity from landraces in wheat breeding for adaptation to climate change. *J. Exp. Bot.* 66, 3477–3486. doi: 10.1093/jxb/erv122

Mughal, I., Shah, Y., Tahir, S., Haider, W., Fayyaz, M., Yasmin, T., et al. (2020). Protein quantification and enzyme activity estimation of Pakistani wheat landraces. *PLoS One* 15:e0239375. doi: 10.1371/journal.pone.0239375

Pradhan, S., Babar, M. A., Robbins, K., Bai, G., Mason, R. E., Khan, J., et al. (2019). Understanding the genetic basis of spike fertility to improve grain number, harvest index, and grain yield in wheat under high temperature stress environments. *Front. Plant Sci.* 10:1481. doi: 10.3389/fpls.2019.01481

Ray, D. K., Mueller, N. D., West, P. C., and Foley, J. A. (2013). Yield trends are insufficient to double global crop production by 2050. *PLoS One* 8:e66428. doi: 10.1371/journal.pone.0066428

Schindelin, J., Arganda-Carreras, I., Frise, E., Kaynig, V., Longair, M., Pietzsch, T., et al. (2012). Fiji-an open source platform for biological image analysis. *Nat. Methods* 9, 676–682. doi: 10.1038/nmeth.2019

Scotti-Campos, P., Semedo, J. N., Pais, I., Oliveira, M. M., and Passarinho, J. (2011). Alguns indicadores fisiológicos de tolerância ao calor em trigo mole. *Agrorrural Contrib. Cient* 939–946.

Shewry, P. R. (2009). Wheat. *J. Exp. Bot.* 60, 1537–1553. doi: 10.1093/jxb/erp058

Stone, P. J., and Nicolas, M. E. (1995). A survey of the effects of high temperature during grain filling on yield and quality of 75 wheat cultivars. *Aust. J. Agric. Res.* 46, 475–492. doi: 10.1071/AR9950475

Talukder, A. S. M. H. M., McDonald, G. K., and Gill, G. S. (2014). Effect of short-term heat stress prior to flowering and early grain set on the grain yield of wheat. *Field Crop. Res.* 160, 54–63. doi: 10.1016/J.FCR.2014.01.013

Tao, Z., Wang, D., Chang, X., Wang, Y., Yang, Y., and Zhao, G. (2018). Effects of zinc fertilizer and short-term high temperature stress on wheat grain production and wheat flour proteins. *J. Integr. Agric.* 17, 1979–1990. doi: 10.1016/S2095-3119(18)61911-2

Tomás, D., Rodrigues, J. C., Viegas, W., and Silva, M. (2020a). Assessment of high temperature effects on grain yield and composition in bread wheat commercial varieties. *Agronomy* 10:499. doi: 10.3390/agronomy10040499

Tomás, D., Viegas, W., and Silva, M. (2020b). Effects of post-anthesis heat waves on the grain quality of seven european wheat varieties. *Agronomy* 10:268. doi: 10.3390/agronomy10020268

Vasconcellos, J. C. (1933). Trigos portuguêses ou de há muito cultivados no País. Subsídios para o seu estudo botânico. *Bol. Agric.* 1, 2, 1–150.

Wang, P., Deng, X., and Jiang, S. (2019). Global warming, grain production and its efficiency: case study of major grain production region. *Ecol. Indic.* 105, 563–570. doi: 10.1016/j.ecolind.2018.05.022

WMO (2015). *Guidelines on the Definition and Monitoring of Extreme Weather and Climate Events - Draft Version – First Review By TT-DEWCE*. Available online at: http://www.wmo.int/pages/prog/wcp/ccl/opace/opace2/documents/DraftversionoftheGuidelinesontheDefinitionandMonitoringofExtremeWeatherandClimateEvents.pdf (accessed October 24, 2019).

Wrigley, C., Asenstorfer, R., Batey, I., Cornish, G., Day, L., Mares, D., et al. (2009). "The biochemical and molecular basis of wheat quality," in *Wheat Science and Trade Wiley Online Books*, ed. B. F. Carver, 495–520. doi: 10.1002/9780813818832.ch21

Yang, D., Cai, T., Luo, Y., and Wang, Z. (2019). Optimizing plant density and nitrogen application to manipulate tiller growth and increase grain yield and nitrogen-use efficiency in winter wheat. *PeerJ* 7:e6484. doi: 10.7717/peerj.6484

Zadoks, J. C., Chang, T. T., and Konzak, C. F. (1974). A decimal code for the growth stages of cereals. *Weed Res.* 14, 415–421. doi: 10.1111/j.1365-3180.1974.tb01084.x

Zeven, A. C. (1998). Landraces: a review of definitions and classifications. *Euphytica* 104, 127–139. doi: 10.1023/A:1018683119237

Zhang, Y., Pan, J., Huang, X., Guo, D., Lou, H., Hou, Z., et al. (2017). Differential effects of a post-anthesis heat stress on wheat (*Triticum aestivum* L.) grain proteome determined by iTRAQ. *Sci. Rep.* 7, 1–11. doi: 10.1038/s41598-017-03860-0

Conflict of Interest: The authors declare that the research was conducted in the absence of any commercial or financial relationships that could be construed as a potential conflict of interest.

Copyright © 2020 Tomás, Coelho, Rodrigues, Viegas and Silva. This is an open-access article distributed under the terms of the Creative Commons Attribution License (CC BY). The use, distribution or reproduction in other forums is permitted, provided the original author(s) and the copyright owner(s) are credited and that the original publication in this journal is cited, in accordance with accepted academic practice. No use, distribution or reproduction is permitted which does not comply with these terms.

frontiers in Plant Science

ORIGINAL RESEARCH
published: 10 December 2020
doi: 10.3389/fpls.2020.599501

Comparative Transcriptome, Metabolome, and Ionome Analysis of Two Contrasting Common Bean Genotypes in Saline Conditions

Harun Niron[1], Nazire Barlas[2], Bekir Salih[2] and Müge Türet[1]*

[1] Department of Molecular Biology and Genetics, Bogazici University, Istanbul, Turkey, [2] Department of Chemistry, Hacettepe University, Ankara, Turkey

Soil salinity is a major abiotic stress factor that limits agricultural productivity worldwide, and this problem is expected to grow in the future. Common bean is an important protein source in developing countries however highly susceptible to salt stress. To understand the underlying mechanism of salt stress responses, transcriptomics, metabolomics, and ion content analysis were performed on both salt-tolerant and susceptible common bean genotypes in saline conditions. Transcriptomics has demonstrated increased photosynthesis in saline conditions for tolerant genotype while the susceptible genotype acted in contrast. Transcriptome also displayed active carbon and amino-acid metabolism for the tolerant genotype. Analysis of metabolites with GC-MS demonstrated the boosted carbohydrate metabolism in the tolerant genotype with increased sugar content as well as better amino-acid metabolism. Accumulation of lysine, valine, and isoleucine in the roots of the susceptible genotype suggested a halted stress response. According to ion content comparison, the tolerant genotype managed to block accumulation of Na^+ in the leaves while accumulating significantly less Na^+ in the roots compared to susceptible genotype. K^+ levels increased in the leaves of both genotype and the roots of the susceptible one but dropped in the roots of the tolerant genotype. Additionally, Zn^{+2} and Mn^{+2} levels were dropped in the tolerant roots, while Mo^{+2} levels were significantly higher in all tissues in both control and saline conditions for tolerant genotype. The results of the presented study have demonstrated the differences in contrasting genotypes and thus provide valuable information on the pivotal molecular mechanisms underlying salt tolerance.

Keywords: common bean, metabolome, *Phaseolus vulgaris* L., salt-stress, tolerance, transcriptome

OPEN ACCESS

Edited by:
Felipe Klein Ricachenevsky, Federal University of Rio Grande, Brazil

Reviewed by:
Linhai Wang, Oil Crops Research Institute, Chinese Academy of Agricultural Sciences, China
Ashwani Pareek, Jawaharlal Nehru University, India

****Correspondence:***
Harun Niron
harun.niron@boun.edu.tr

Specialty section:
This article was submitted to Plant Abiotic Stress, a section of the journal Frontiers in Plant Science

Received: *27 August 2020*
Accepted: *23 November 2020*
Published: *10 December 2020*

Citation:
Niron H, Barlas N, Salih B and Türet M (2020) Comparative Transcriptome, Metabolome, and Ionome Analysis of Two Contrasting Common Bean Genotypes in Saline Conditions. Front. Plant Sci. 11:599501. doi: 10.3389/fpls.2020.599501

INTRODUCTION

Salt accumulation has become one of the most imminent agricultural threats in the recent years. It is estimated that nearly 20% of cultivated and 33% of irrigated farmland has been affected by salt globally (Munns and Tester, 2008). These percentages are expected to increase annually through diverse causes such as excessive evaporation, improper irrigation, or inadequate precipitation, which are related to the global climate change. At the current rate of salt accumulation, 50% of

arable farmlands may become salt-affected by 2050 (Jamil et al., 2011). Most of the economically significant crops such as rice, maize, potato, tomato, and legumes are rather susceptible to salinity (Muchate et al., 2016). Production of these and other crops will have to increase up to 70% to cope up with the steadily growing human population, which is predicted to surpass 9 billion by 2050 (Davies and Bowman, 2016). These global challenges call for urgent but sustainable solutions, which can be found in more-salt tolerant varieties of cultivated plants. The genetic program for salt tolerance can be transferred to salt-sensitive crops with otherwise valuable agronomical traits using conventional breeding or transgenic methods (Hanin et al., 2016). Therefore, identification of genes responsible for the superior salt tolerance, their functional characterization, and understanding of the associated metabolic processes are essential for sustainable agriculture in the era of overpopulation and climate change.

A soil is considered saline if it contains enough soluble salt to have detrimental effects on the growth of crop plants. Saline soil is roughly defined as a soil with electrical conductivity of saturated extract (ECe) equal or higher than 4 dS m-1 (Shrivastava and Kumar, 2015); but the majority of common crop yields display reduction even at lower ECes (Munns, 2005; Jamil et al., 2011). Although various salts contribute to soil salinity, sodium chloride (NaCl) is the most predominant form. Elevated NaCl disrupts diverse systems necessary for consistent plant growth and development (Munns and Tester, 2008; Shahzad et al., 2013). It leads to two types of generalized stress for plants: osmotic and ionic stress. Osmotic stress arouses from the decreased water potential and water availability for the plant. Ionic stress, on the other hand, is caused by the toxic ion accumulation over time (R. Munns, 2002). These stress factors create a network of restraints on survival, not just with ion toxicity and water retention, but also with nutrient and metabolic imbalance that collectively become a physiological response (Tester and Davenport, 2003).

Understanding this response is a laborious task and requires a comprehensive strategy against these stress factors. Essentially, plants employ water homeostasis control and adjustment of osmotic balance, salt exclusion, sequestration, oxidative protection, regulation of potassium exchange, biochemical responses, and growth regulation to cope with salt stress (Tester and Davenport, 2003; Munns, 2005; Munns and Tester, 2008; Shabala and Cuin, 2008). As there is a complex network of connections between these systems, tolerance to salt may involve the regulation of thousands of genes (Monforte et al., 1997; Foolad, 2004). This complexity can be reduced by making a comparison among species and varieties of plants that have evolved distinct mechanisms to deal more successfully with salinity. Although tolerant and susceptible plants use very similar strategies, differential regulation of the responses can indicate the key points of the salt tolerance mechanisms (Nilsen et al., 1996).

Common bean (*Phaseolus vulgaris* L.) is a grain legume with substantial agricultural importance. As a rich source of vitamins, minerals, and dietary proteins it is an essential nutrient for human consumption. It represents approximately half of the produced and consumed grain legumes in the world (Broughton et al., 2003). With its high phytochemical content and high antioxidant capacity, it supports the human immune system against disorders like obesity, cancer, and cardiovascular diseases (Pinheiro et al., 2010). Moreover, it is integral to sustainable agriculture as it supplements the soil with nitrogen through symbiotic associations (Broughton et al., 2003). However, common bean is fairly susceptible to salt. This crop can suffer nearly 20% yield loss even in slightly saline soil with 1 dS m-1 ECe (Chinnusamy et al., 2005). This inconvenience can be mitigated through somewhat salt tolerant genotypes of common bean cultivars such as Ispir, but this solution may not be sustainable against the increasing soil salt content. To expand the tolerance capacity in such superior varieties, it is necessary to understand the existing mechanisms, so that potential paths to further improvement become unveiled.

A phenotype is the product of dynamic interplay between various factors such as DNA, RNA, proteins, and metabolites together with the influence of the environment. Therefore genome- and transcriptome-based approaches demand studies from complementary fields such as proteomics and metabolomics to establish accurate genotype–phenotype relationships (Arbona et al., 2013). While gene and protein expression exhibit capacity and inclination of a plant in response to environmental conditions, metabolite content forms the link between expression and environment (Arbona et al., 2013).

In this study, we have compared two genotypes of *P. vulgaris* L. that contrast in their response to salt stress, namely Ispir (tolerant) and TR43477 (susceptible) (Dasgan and Koc, 2009). This comparative analysis facilitates an in-depth understanding of salt stress tolerance mechanisms by combining transcriptomics, metabolomics and ionomics data under salinity conditions. Our results indicated differentially regulated transcripts that can be further functionally characterized by mutagenesis-based approaches. Our data also revealed the enriched and depleted metabolic pathways and their disparity in these genotypes. We believe, this study will also provide insights into the genetic programs and the regulation of other abiotic stress responses, since they are known to share mechanisms (Zhu, 2016).

MATERIALS AND METHODS

Plant Growth, Salt-Stress Application, and Sample Collection

Ispir (salt-tolerant) and TR43477 (salt-susceptible) varieties of common bean (*Phaseolus vulgaris* L.) were grown and salt-treated in hydroponic conditions to collect tissue samples. The seeds were sterilized in 5% hypochlorite solution. Germination was performed in vermiculite containing plug trays under a 16-h light/8-h dark photoperiod at 24°C/20°C cycle with 50–70% relative humidity. Trays were irrigated daily with 1X Hoagland nutrient solution (Hoagland and Arnon, 1950) until the plants got fully expanded foliage (Nine days for Ispir and eight days for TR43477 after sowing). Seedlings from each genotype were transferred to hydroponics system. Salt treatments were carried out in the same conditions as in our earlier transcriptome study

Hiz et al. (2014). Gradual step acclimation method was employed to prevent osmotic shock (Sanchez et al., 2008). Five days post transfer, the plants were subjected to gradual NaCl treatment starting with 50 mM first day, increased to 100 mM on the second day, and set to 125 mM on the third day. In total, the plants were grown under 125 mM NaCl for three days before they were sacrificed for tissue sample collection.

RNA-Sequencing and Transcriptome Analysis

Total RNA extractions from the leaf and root tissues of three plants as biological replicates for control and salt-treatment conditions separately, were performed with RNeasy Plant RNA extraction kit (QIAGEN, United States). Sample qualities were inspected with Agilent 2100 Bioanalyzer system by measuring the RNA integrity number (Schroeder et al., 2006). Poly(A +) enrichment and cDNA library construction were performed with Truseq Stranded mRNA kit (Illumina, United States). The obtained paired-end library was sequenced using NovaSeq 6000 system. Raw data quality control was performed with FastQC tool (Andrews and Babraham Bioinformatics, 2010) and Trimmomatic software (Bolger et al., 2014) was employed for raw-read trimming. Genome indexing and paired read alignment were performed with HISAT2 tool (Kim et al., 2015) using *Phaseolus vulgaris* genome v.2.1 (phytozome.org) as reference. Read counts, determined with Seqmonk v.1.44.0 tool[1], were harnessed with EdgeR (McCarthy et al., 2012) for differential expression analysis. Differentially expressed genes (DEGs) were selected among all genes with a filter of $|\log_2$ fold change$| > 1$ and FDR < 0.01. DEGs from different genotypes were further subjected to intensity difference filter of Seqmonk v.1.44.0 tool, which compares the datasets and detects the differences with lowest variability, to discover the genes that displayed highly reliable and sharp changes in response to salt treatment.

[1]bioinformatics.babraham.ac.uk/projects/seqmonk/

Verification of Expressional Levels With qRT-PCR Analysis

Ten genes were selected for the qRT-PCR analysis: The procedure was carried out with 10 ng of cDNA from the roots of each variety per reaction. Three technical replicates were performed for each of the three-biological replicates. PikoReal 96 Real-time PCR system (Thermo Fisher Scientific, DE) was utilized for the experiment. *Actin-11* (GenBank: CV529679.1) and *insulin-degrading enzyme* (GenBank: FE702602.1) genes of common bean were used as the reference genes as they were reported to have stable expression under salt treatment in common bean (Borges et al., 2012). Relative expression levels were calculated by $2^{\Delta\Delta}$ Ct method (Livak and Schmittgen, 2001). The correlation between RNA-Seq and qRT-PCR results was assessed with Pearson correlation coefficient. Primers that were used in this study can be found in **Table 1**.

Gene Ontology (GO) and KEGG Pathway Enrichment Analyses

Gene ontology IDs for the transcripts were obtained from the Biomart (Smedley et al., 2015). GO enrichment analysis was performed with the GO-IDs of DEGs via AgriGO v2.0 tool (Tian et al., 2017). KEGG pathway enrichment analysis

TABLE 1 | qRT-PCR primers used for RNA-seq validation.

Sequence	Transcript ID	Amplicon size	Annealing T. (°C)
TCTTGCCTTGATCTTCGG	Phvul.001G195700	172	53
AGGTTTGAATAGAGGATGTG			
ACTCCAACAAACTCGAAACA	Phvul.002G027900	234	55
CACATACCACTCGGACCA			
TGATCCCATTGCAAATCC	Phvul.008G170800	151	53
TCCCCCCATAAAACCAAC			
CTCCACCTTTTCCACCAAC	Phvul.009G105300	157	56
CTTCCCACTACTCCTATTCC			
GCTATGGTTCCAGCTTTT	Phvul.006G159600	120	54
AGTTATTGGGGTTGGGTT			
CTCCTTTATCGCCTTCCT	Phvul.001G083000	230	54
ACTTCCGCATTACCAACA			
GCCTTCTCTTTTACCTTCT	Phvul.004G117100	102	53
ACACCACCATAATCCTCA			
GCTAGCTGTTCCATTTACGCAGAGT	Phvul.003G229500	100	60
AGCTGCCGTAGAGTTTGATTGCACC			
GCAGCTCCCAACCACTGACTAC	Phvul.001G181100	186	58
CCATCCAACCAAAGATCAACGCCCA			
AACCATGCCTTCACCAGCTTCAAAT	Phvul.005G051600	107	60
AGGTTGTGGGAGAAGAAGATGTGGA			
TGCATACGTTGGTGATGAGG	Phvul.008G011000(Actin-11)	190	58
AGCCTTGGGGTTAAGAGGAG			

was performed with the transcript IDs via ShinyGo v.0.61 (Ge et al., 2020). In both enrichment analyses, the enriched terms were subjected to multi-test adjustment with Benjamini-Hochberg method (Benjamini and Hochberg, 1995) and terms with FDR < 0.05 were selected.

Untargeted Metabolomics

Extraction of Metabolites

The metabolite extraction procedure for the leaf and root tissues of five biological replicates for control and salt-treatment conditions separately, was performed as described by Lisec et al. (2006). 100 mg of flash-frozen ground tissue samples were mixed with 60 μl of water containing ribitol as internal standard. The samples were mixed with 0.3 ml of methanol and 0.1 ml of chloroform and vortexed for 5 min followed by incubation at 70°C for 10 min. After centrifugation, supernatants were collected to be dried in a vacuum-dryer system. Following desiccation, each sample was incubated for 2 h at 37°C with 80 μl of methoxamine hydrochloride. Derivatization for gas-chromatography was performed with 1% trimethylchlorosilane (TMCS) in N-Methyl-N-(trimethylsilyl)-trifluoroacetamide (MSTFA) (100 μl) at 70°C for 1 h (Lisec et al., 2006).

Gas Chromatography-Coupled Mass-Spectrometry

Untargeted metabolomics analysis was carried out with Gas Chromatography system (Agilent technologies 6890 N Network GC system, United States) and Mass Spectrometry system (Agilent technologies 5973 inert mass selective detector, United States) equipped with automatic injector (Agilent Technologies 7683 series, United States). For the ionization of the compounds, Electron Impact (EI) ionization source was used in positive ion mode at 70 electron-volts. Al the parameters for GC-MS system used in this study are given in **Table 2**.

TABLE 2 | Conditions for GC-MS measurements.

Gas Chromatography		Mass Spectrometry	
Parameter	**Type and Set Value**	**Parameter**	**Set Value**
Column Name	HP-5MS	Solvent delay	2.5 min.
Split ratio	01:25	Low mass (amu)	70
Carrier gas	He	High mass (amu)	600
Actual length (m)	30	Aux. temperature (°C)	250
Internal diameter (mm)	250	Acquisition mode	Scan
Film thickness (mm)	0.25	Electron multiplier voltage (V)	2282
Inlet temperature (°C)	230	Ion Source temperature (°C)	180
Inject volume (ml)	1	Quadrupole temperature (°C)	230
Temperature programming	Start with 80°C and set 2 min, up to 300°C with 15°C/min ramp and then set 10 min. at 300°C. Total run time for each sample is ∼ 27 min.	Mass tuning compound	Perfluorotributylamine (PFTBA)

GC-MS Data Analysis

In-house MassHunter WorkStation with MSD ChemStation DA software (Agilent, United States) was utilized for GC-MS data processing such as transformation of the retention time, chromatogram alignment, peak extraction, normalization, and annotation. Wiley7n, Nist98, and W9N11 libraries were utilized for compound identification. Similarity ratio of 90% was taken into consideration for software-suggested annotations and final compound annotations were selected under manual curation. Data normalization was performed with the default options of the software. Principal component analysis for dimensionality reduction of the normalized data was implemented with XLSTAT software (Addinsoft Corporation, United States) (Addinsoft, 2019). Differentially accumulated/depleted metabolites (DADMs) were determined by statistical significance ($p < 0.05$) according to univariate analysis (two-sample *t*-test).

Extraction of Heavy Metals and Ionomics

Flash-frozen ground leaf and root tissue samples of five biological replicates for control and saline conditions were dried in oven at 80°C and 100 mg was mixed with 10 ml HNO_3 and 5 ml H_2O_2 in 50 ml Falcon tubes. The digestion was implemented by heating the samples 10 min at 100°C, then 15 min at 150°C, and finally 15 min at 180°C. The solutions were completed to 25 ml with dH_2O. Concentrations of six ions (B, Mn, Fe, Cu, Zn, Mo) were measured by inductively coupled plasma mass spectrometry (Agilent 7700 Series ICP-MS, Agilent, United States) and concentrations of other four ions (Na, K, Mg, Ca) were measured by inductively coupled atomic emission spectrometry (Agilent 700 Series ICP-OES, Agilent, United States). Differentially accumulated/depleted ions were determined by statistical significance ($p < 0.05$) according to two-sample t-test. Statistical significance of distinction between the responses of the genotypes was measured by two-way ANOVA with replication ($p < 0.05$) with Excel Analysis ToolPak add-inn (Microsoft, 2019).

Omics Data Merge and Pathway Analysis

Transcriptomics, metabolomics, and ionomics data for differentially expressed genes, regulated metabolites, and ions in Ispir and TR43477 varieties were integrated via KEGG Mapper (Kanehisa and Goto, 2000). KEGG pathways were used for a pathway-based integration to generate a representative map of carbon and amino acid biosynthesis metabolisms.

Chlorophyll Content Measurement

Chlorophyll contents of the leaves of five biological replicates were determined as described by Warren, 2008. Specific absorbance values of methanol extracted pigments were used in equations (Ritchie, 2006) to estimate chlorophyll a, chlorophyll b, and carotenoid contents of the leaves.

RESULTS

Transcriptome Analysis Signifies the Whole-Plant and Tissue-Specific Differences Upon Salt-Stress Treatment

Overview of RNA-Sequencing Results

After adapter removal, reads had presented an average Q30 of 95.14%, with the lowest being 94.34%. On average, the mapping has produced the 89.05% concordant alignment and the 96.28% overall alignment to the reference (**Table 3**). The greatest number of DEGs was observed in Ispir leaves (IL) with 3072 genes, while roots of the TR43477 (TR) displayed the lowest number of DEGs, with 910 genes (**Figures 1A,B**). On the other hand, roots of Ispir (IR) and leaves of TR43477 (TL) displayed similar numbers of 2700 and 2750 DEGs, respectively.

Comparison of the DEG lists has shown that 71 genes were differentially expressed in all tissues and both varieties upon salt treatment (**Figure 1A**). 3090 DEGs were specific to Ispir with 247 DEGs expressed in both above-ground and under-ground tissues. On the other hand, TR43477 displayed 1892 specific DEGs, only 61 of which were shared between tissues (**Figure 1A**). Regarding the number of upregulated and downregulated DEGs, IL displayed the highest number in both categories among all samples, while the lowest numbers in both categories were associated with TR (**Figure 1B**). Examination of upregulated and downregulated DEGs according to the tissue type demonstrated that leaves of the two genotypes shared 260 upregulated and 286 downregulated DEGs, whereas 248 genes displayed contrasting patterns (**Figure 1C**). The root tissues exhibited similar numbers of shared upregulated and downregulated DEGs, with 287 and 210 DEGs, respectively, but only six DEGs displayed contrasting pattern in roots (**Figure 1D**).

To check the reliability of RNA-Seq data, expression analysis of 10 genes was performed with qRT-PCR for the roots of both varieties. The results indicated high correlation levels with Pearson r values of 0.87 and 0.84 for the resistant (**Supplementary Figure 1A**) and the susceptible genotype, respectively (**Supplementary Figure 1B**).

TABLE 3 | Statistics for raw read alignment to refence genome with HISAT2 tool.

			Paired read count	Concordant alignment (%)	Overall alignment (%)
ISPIR	LEAF	Control_1	15492583	92.1	97.99
		Control_2	24501307	89.49	97.34
		Control_3	24519671	92.88	97.92
		Treatment_1	14073496	91.15	97.25
		Treatment_2	22721821	90.4	97.52
		Treatment_3	14335336	92.2	97.85
	ROOT	Control_1	15713485	87.87	96.25
		Control_2	15019777	89.31	95.87
		Control_3	16496524	89.15	96.94
		Treatment_1	14253723	85.57	96.5
		Treatment_2	16537801	90.26	96.95
		Treatment_3	15648266	90.55	97.33
TR43477	LEAF	Control_1	15753609	88.56	95.54
		Control_2	15196921	90.44	96.38
		Control_3	17281002	88.51	96.04
		Treatment_1	14931185	88.20	95.71
		Treatment_2	18796243	88.77	95.67
		Treatment_3	17793700	88.73	95.66
	ROOT	Control_1	15559453	87.59	95.64
		Control_2	20006512	87.48	95.5
		Control_3	17229757	86.48	93.65
		Treatment_1	17897796	87.2	95.25
		Treatment_2	31045673	86.69	94.3
		Treatment_3	26924512	87.62	95.72

GO and KEGG Pathway Enrichment Analysis of DEGs in Response to Salt-Stress

Comparative GO and KEGG pathway enrichment analyses of DEGs (**Figures 2**, **3**, **Additional Files 1, 2**) demonstrated distinct responses of these two genotypes against salinity stress. Photosynthesis-related terms were enriched in IL but depleted in TL according to both databases. KEGG results also indicated a similar trend for porphyrin and chlorophyll metabolism. This result was in concert with the leaf chlorophyll contents for IL and TL (**Figure 4A**): While IL *chl* b content has displayed a significant increase, TL *chl* b content decreased and the difference between the change was highly significant. Genes of photosystem II and photosynthetic e^- transport modules have demonstrated a strong contrast in salinity responsive regulation for those genotypes (**Figure 4B**; **Additional File 3**). Furthermore, *ATP synthase delta* subunit (Phvul.003G211100) was upregulated in IL but it was downregulated together with *ATP synthase gamma* subunit (Phvul.006G149700) in TL which implicated a disrupted proton conduction for the susceptible genotype together with decreased chlorophyll content (**Figure 4A**; **Additional File 3**).

TL was depleted in GO terms for polysaccharide metabolic process and KEGG terms for carbon fixation, whereas carbon fixation related GO terms and KEGG pathways were enriched in IL (**Figures 2A**, **3B**). Sucrose and starch metabolism and glyoxylate and dicarboxylate metabolism displayed a similar result in KEGG pathway analysis: enriched in IL, depleted in TL (**Figure 3A**). Especially, Phvul.004G029100 (*Starch synthase*), Phvul.008G210100 (β-*D-glucan exohydrolase*) and Phvul.011G107700 (β-*amylase 5*) genes have stood out in IL for sucrose and starch metabolism in intensity difference analysis (**Additional File 4**). IL was depleted in GO terms related to transcription, translation, and post-translational modification, while transcriptional, expressional regulation, and functional modification-related GO terms were enriched in TL. In relation, TL displayed enrichment and depletion patterns for various amino acids together with a decrease in DNA synthesis and ribosome biogenesis-related terms. Cell wall and cytoplasm (cellular components)-related GO terms were enriched in IL, while GO terms related to manufacture of cell wall components were depleted in TL. IL displayed a complex response; diminished cell wall organization together with increased pectinesterase activity for cell-wall modification in GO analysis, while TL

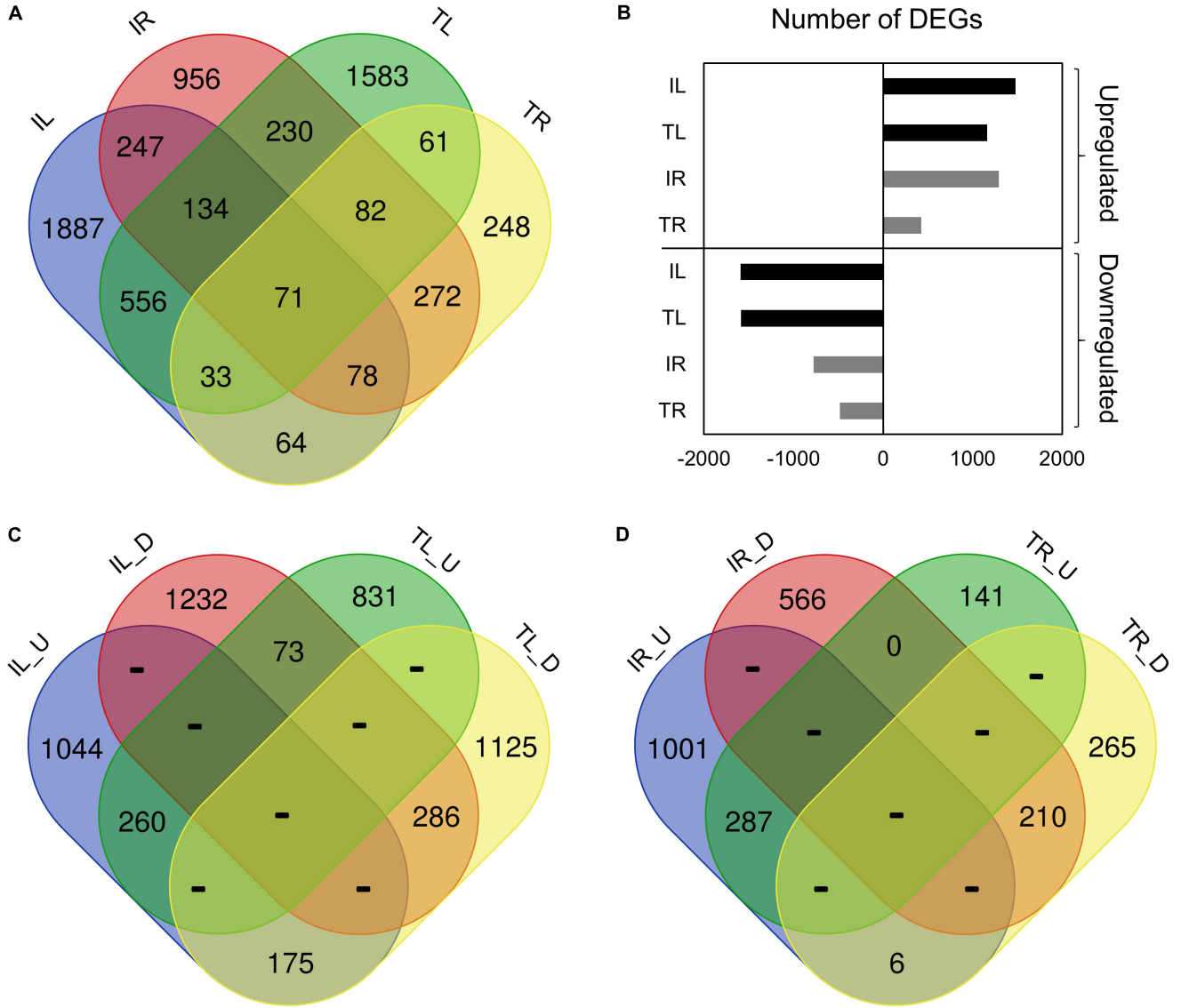


FIGURE 1 | Venn diagram representation of the tissue- and genotype-specific DEGs distribution. IL_U: Ispir Leaf Upregulated; IL_D: Ispir Leaf Downregulated; TL_U: TR43477 Leaf Upregulated; TL_D: TR43477 Leaf Downregulated; IR_U: Ispir Root Upregularted; IR_D: Ispir Root Downregulated; TR_U: TR43477 Root Upregulated; TR_D: TR43477 Root Downregulated.

had diminished cell-wall organization (**Figure 2A**). Notably, IL displayed eight separate upregulated pectinesterase-related genes (**Additional File 3**). KEGG analysis indicated that both IL and TL were enriched in cutin, suberine, and wax biosynthesis. IL was enriched in protein folding activity and cofactor/coenzyme metabolism-related GO terms. TL, on the other hand, displayed diminished proteolysis and peptidase activities. Both IL and TL were enriched in KEGG terms for protein processing in endoplasmic reticulum (**Figures 2A**, **3A**).

The responses of roots were limited compared to leaves: While TR was enriched in GO terms for transcriptional regulation, IR had enriched functional modification terms in GO and protein processing in endoplasmic reticulum pathway terms in KEGG. Indeed, five different heat shock family genes (Phvul.003G154800, Phvul.004G107700, Phvul.004G129400, Phvul.008G112700, and Phvul.009G080200) that are part of KEGG 'Protein processing in endoplasmic reticulum' pathway displayed intense upregulation patterns in IR tissue (**Additional File 4**) which hints the significant activity of unfolded or misfolded protein response. Moreover, IR had decreased helicase activity-related GO terms, probably an indication of halted DNA replication and modification, together with diminished GO nitrogen compound metabolic process terms, which is a sign of decreased translational activity. Although KEGG pathway results demonstrated that nitrogen metabolism was depleted in both IR and TL, IR was also depleted in biosynthesis

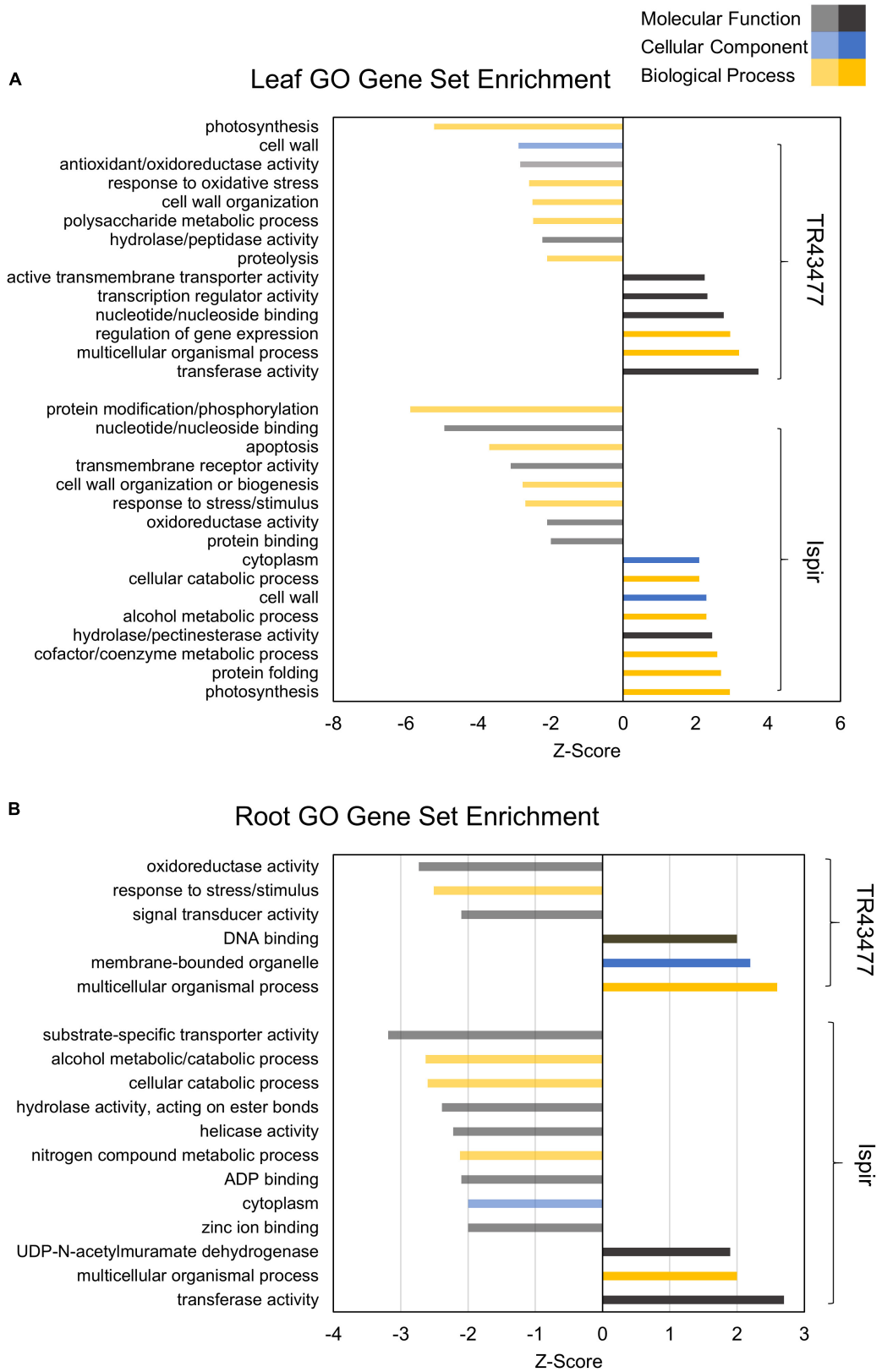


FIGURE 2 | Parametric GO gene set enrichment of leaf **(A)** and root **(B)** DEGs. The Z-Score was derived from the number of DEGs and their log_2FC. Performed for at least five genes in a gene set (adjusted *p*-value < 0.05).

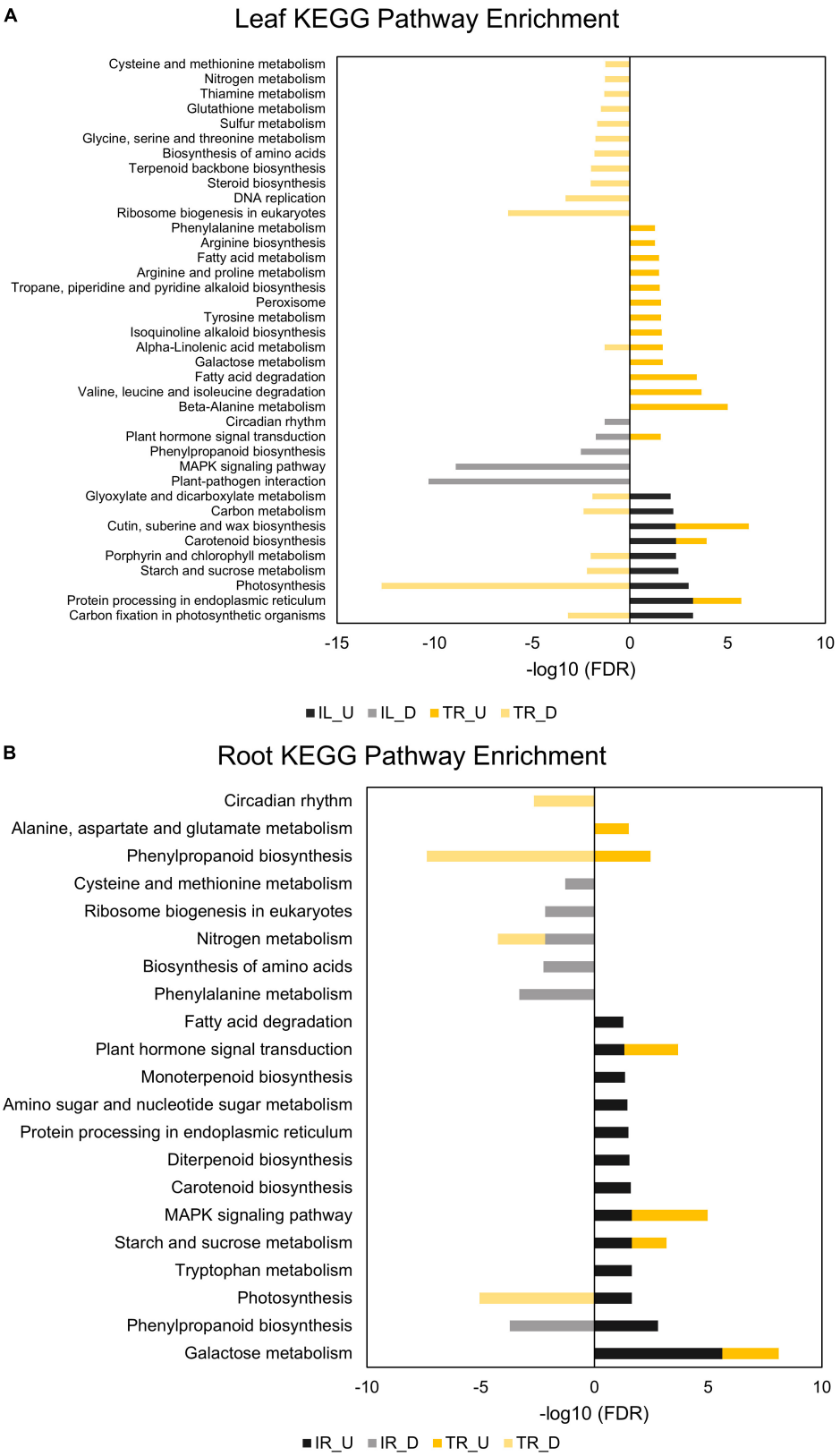


FIGURE 3 | KEGG pathway enrichment analyses of leaf **(A)** and root **(B)** DEGs. "U" depicts upregulated and "D" depicts downregulated DEGs in the legends of KEGG graphs. Performed for at least five genes in a pathway (adjusted p-value < 0.05).

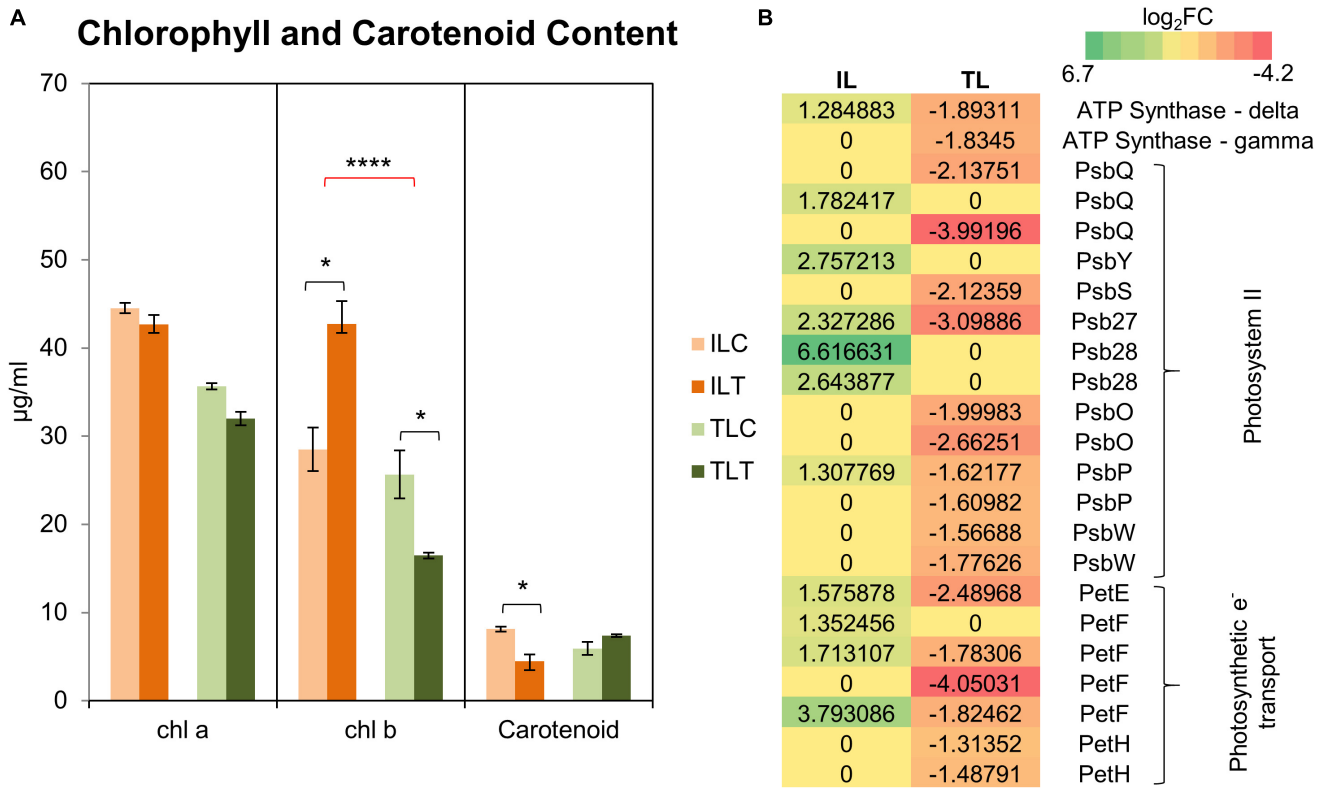


FIGURE 4 | Chlorophyll and carotenoid content changes in the leaf tissues **(A)**. "C" depicts control condition and "T" depicts treatment condition. Heatmap with log_2-fold changes of photosynthesis-related transcripts in KEGG pathways **(B)**. A more comprehensive table can be found at **Additional File 3**. * indicates significance and quantity of * displays the level of significance. (*$p < 0.05$; **$p < 0.01$; ***$p < 0.005$; ****$p < 0.001$).

of amino acids and ribosome biogenesis (**Figures 2B**, **3B**). Concerning that, intensity difference filtering pointed out the downregulation of a *nicotinate phosphoribosyltransferase* homolog (Phvul.002G017800) that is part of GO 'nitrogen compound metabolic process' and 'NAD metabolic process' terms, together with the downregulation of a putative helix-loop-helix transcription factor (Phvul.001G126400) in IR (**Additional File 4**) which may be key constituents of difference in response between these genotypes.

Metabolic Characteristics of the Tolerant and Susceptible Genotype Under Salt Stress

Untargeted GC-MS analysis has detected 79 different metabolites; 32 of which were Ispir-specific, and only 13 of which were TR43477-specific, while 34 metabolites were detected in both genotypes (**Additional Files 5, 6**). Principle component analysis (F1 and F2 represented a total of 50.3% of all data) of genotypes and tissues has clearly distinguished the behavior of leaf and root tissues from each other (**Figure 5A**; **Additional File 7**). The close projection of biological replicates indicated a reliable correlation for replicas. For both leaf and root tissues, Ispir has displayed a greater difference between control and stress-treated components compared to TR43477 (**Figure 5A**).

Although all the samples had similar numbers of differentially accumulated/decreased metabolites (DADMs), IL had the highest number of accumulated metabolites (17 metabolites) and TL had the highest number of decreased metabolites (19 metabolites). The number of accumulated and decreased metabolites were roughly even for both root tissues. Out of total 52 DADMs (number of metabolites significantly accumulated/decreased in at least one of the samples), only three (L-proline, L-serine, and myo-Inositol; all were accumulated) were found in all tissues and genotypes and 22 were unique to specific tissues and genotypes (**Figure 5B**).

Hierarchical clustering of DADMs displayed the distinction between the responses of different genotypes to salt treatment. The algorithm placed the root and leaf tissues of genotypes in the same clade and diverged the tissues of contrasting genotypes (**Figure 5C**). This analysis also demonstrated the difference of metabolic response patterns of tissues and genotypes; while IL has accumulated nine separate carbohydrates in response to salt, TL managed to accumulate only one and displayed decreased amounts for other three. A similar imbalance was also evident in the root tissues, as IR had six accumulated and two decreased carbohydrates, while TR displayed two accumulated and one diminished metabolite identified as a carbohydrate. (**Figure 5C**; **Supplementary Figure 2**). All tissues mainly increased their amino acid contents, but this

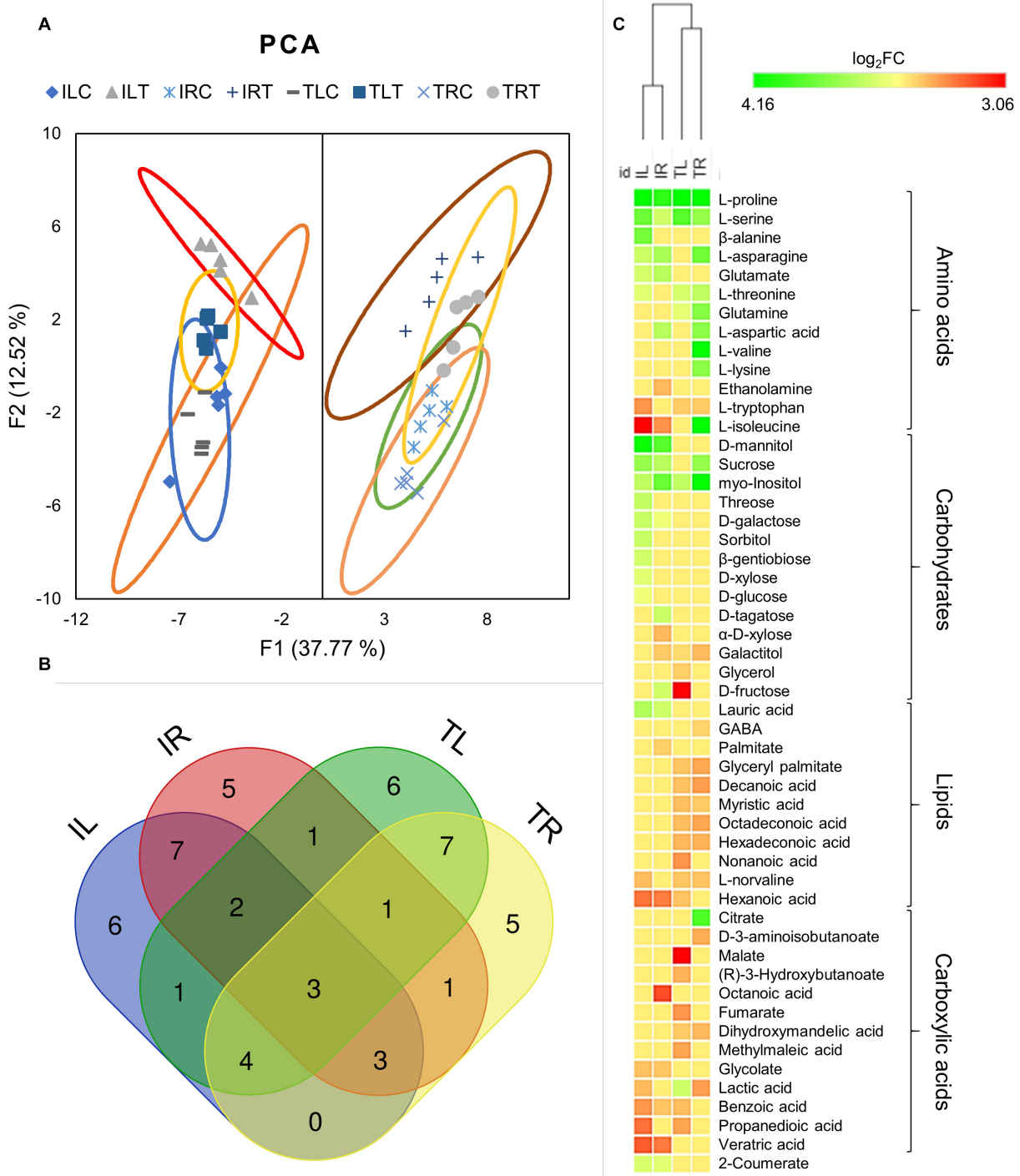


FIGURE 5 | Principal component analysis was employed to visualize the distinction of metabolic responses in different tissues and conditions **(A)**. Venn diagram displays the distribution of DADMs among tissues in salt stress **(B)**. Hierarchical clustering analysis of DADMs demonstrated the differential reaction of the two genotypes **(C)**.

increase was particularly noteworthy for TR as it displayed nine DADMs for the amino acid class. The lipid contents (mainly structural derivatives of a fatty acid, decanoic acid) of both root and leaf tissues of TR43477 were significantly decreased compared to tissues of Ispir. Carboxylic acid contents appeared to decrease in both tissues and both genotypes in

response to salt stress. Also, accumulation of 2-coumerate was detected in both leaves and roots of Ispir (**Figure 5C**; **Supplementary Figure 2**).

Transcriptional and Metabolic Changes in the Carbon and Amino Acid Metabolism

The DEGs and DADMs were mapped to the common bean biological pathways in the KEGG online database. As the untargeted metabolome mainly detected the primary metabolites such as amino acids and carbohydrates, the analysis was focused on the carbon and amino acid metabolism and their connections to relevant carbohydrates (**Figure 6**). Comparison of the leaf tissues demonstrated the escalated feeding of citrate cycle in Ispir leaves through upregulated genes in Fructose-6P – PEP – Oxaloacetate and Fructose-6P – PEP – Pyruvate – Acetyl CoA pathways. Both malate and fumarate levels are drastically decreased in TL (p-value < 0.01; $\log_2$FC > 1). On the other hand, their levels were stable in Ispir. Carbohydrates were mainly accumulated in IL, but there is no significant change for many in TL tissues (**Supplementary Figure 2**). Particularly accumulation of sucrose and glucose in Ispir leaf tissues reflects the sustained carbon fixation – glycolysis cycle, which is also implied by enriched photosynthesis (**Figures 2**, **3A**, **4**).

Glutamate - Glutamine/2-Oxogluterate reaction pathway is enriched in leaf tissues of both varieties (**Figure 6**; **Additional File 3**). In turn, IL accumulated glutamate, TL accumulated glutamine; this indicates inequality in the direction of reaction between the genotypes. IL displayed an increased asparagine production with accumulated asparagine and an upregulated asparagine biosynthesis-related gene -Phvul. 006G069300-, while a homolog of that gene -Phvul.001G252200- was downregulated in TL (**Additional file 3**).

In the root tissues, genes related to glycolysis and citric acid cycle were more inclined to downregulation in the IR compared to TR, which displayed a more stable carbon pathway (**Figure 6**; **Additional File 3**). Especially downregulations on Fructose-6P – PEP – Oxaloacetate pathway genes and upregulations on Oxaloacetate to PEP and Pyruvate to PEP conversions indicated a decelerated energy metabolism in IR compared to TR (**Figure 6**; **Additional File 3**). While both genotypes accumulated sucrose, IR managed to accumulate fructose, mannitol, galactose, and tagatose as well (**Supplementary Figure 2**). In connection, the intensity difference analysis have pointed out a *sucrose-phosphate synthase* homolog Phvul.005G002600 (**Additional File 4**), that might have a role in accumulation of these carbohydrates in IR. Sucrose to glucose/fructose-6P conversions were in complex regulation in the roots of both genotypes with various up- and downregulated genes. IR accumulated glutamate but was depleted in isoleucine; TR on the other hand accumulated isoleucine, valine, threonine, glutamine, and lysine but were depleted in tryptophan in contrast to IR. Intensity difference analysis has displayed IR specific upregulation of a putative *2-oxoisovalerate dehydrogenase*, Phvul.009G132900, which is part of 'valine, leucine and isoleucine degradation' pathway in KEGG; increase of this enzyme in IR might have been crucial for the content difference for the related amino acids (**Additional File 4**). Both varieties accumulated proline, asparagine, aspartate, and serine amino acids. Serine appeared to be accumulated in both root tissues, yet TR had higher accumulation ($\log_2$FC < 1.82) compared to IR ($\log_2$FC < 0.94). The genes related to production of serine from fructose-6P and conversion of it to threonine/isoleucine were downregulated in IR together with a decrease in isoleucine levels. In contrast, this pathway turned out to be mainly unaffected in TR with the accumulation of serine, threonine, and isoleucine. Alternatively, IR serine accumulation might be the result of serine biosynthesis through glycolate as both IR and TR displayed a '*serine-glyoxylate transaminase*' annotated gene (Phvul.006G029100) that plays role in serine production through glycolate. Yet glycolate levels were significantly decreased in IR (**Figure 6**; **Additional File 3**; **Supplementary Figure 2**).

Ion Contents and Regulation of Ion-Transport Related Transcripts

Examination of tissue ion contents (**Additional File 8**) in salt-stress generated both expected and unexpected results. While the most important differences were detected in Na^+ and K^+ contents, there were changes in Mg^{+2}, Mn^{+2}, Cu^{+2}, B^{+3}, and Zn^{+2} contents as well (**Figure 7A**; **Supplementary Figures 3**, **4**). In the root tissues of both varieties, Na^+ ion levels were drastically increased upon salt-stress as expected, but Ispir gave a much better performance: Not only did it manage to keep the Na^+ upsurge at significantly lower levels in the roots compared to TR43477 (**Figure 7D**), but also managed to keep the leaf Na^+ levels unchanged, unlike the TR43477. Notably, Na^+ levels were much higher in IL (3200.56 μg/g) compared to TL (955.9 μg/g) in control conditions; but in saline conditions, TL Na^+ content drastically increased (4536.4 μg/g), while IL Na^+ content did not demonstrate a significant change if not a decrease (2630.8 μg/g) (**Figure 7C**; **Supplementary Figure 3**). Two Na^+/H^+ antiporter-annotated genes were found as DEG in IR; one upregulated and one downregulated, while no Na^+ -related transporter was differentially regulated in TR. Two Na^+ symporter-annotated genes were uniquely found as DEGs in IL (**Additional File 3**) which might indicate their possible roles in pre-stress and stress leaf Na^+ homeostasis in IL.

K^+ levels significantly decreased in the salt-stress tolerant Ispir roots, while its content slightly increased in TR in salt stress conditions (**Figure 6B**). TR displayed four separate downregulated K^+-transport-related DEGs; IR displayed one unique upregulated and three downregulated K^+-transport-related DEGs. While three K^+-transport-related DEGs were common to both IR and TR, leaves of both genotypes activated/deactivated completely different sets of genes related to the same term. However, leaf K^+ levels were significantly boosted in both genotypes. Cu^{+2} levels dropped in IL together with five downregulated DEGs related to Cu^{+2} transport. Separately, TL Mn^{+2} content displayed a somewhat significant decrease in salinity. IL Mn + 2 content did not show a significant change upon salt stress, but in both control and treatment conditions,

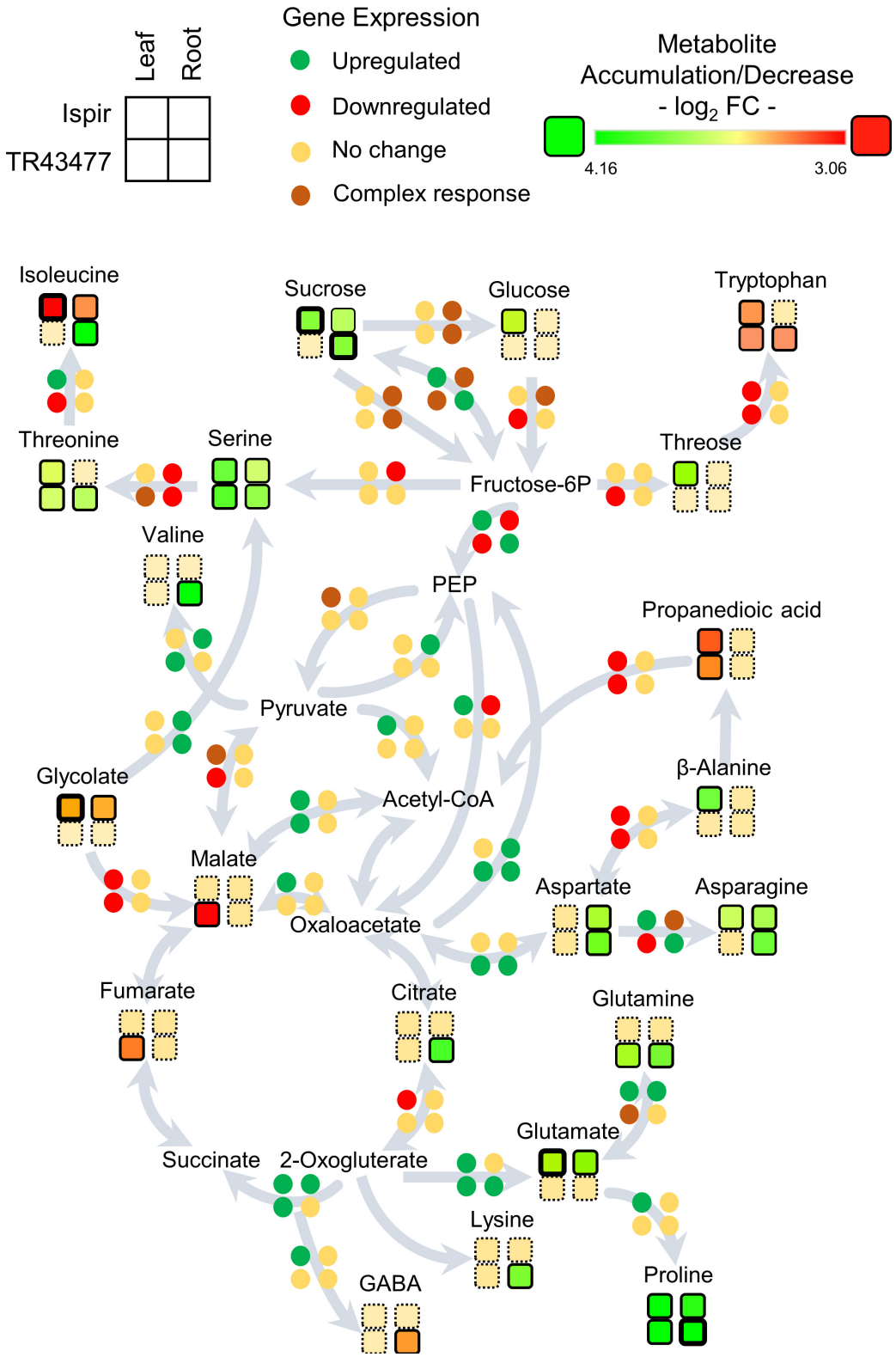


FIGURE 6 | Representation of the transcript and metabolite changes in carbon and amino-acid metabolism in root and leaf tissues of both genotypes in saline conditions. The pathway map was derived from KEGG database. Disk units for gene expression represent one or more genes depending on the pathway: Detailed list of the relevant genes can be found in **Additional file 3**; Primary Metabolism tab. Rows represent genotypes and columns represent tissues. Bold outlines indicate high significance with a p-value < 0.01.

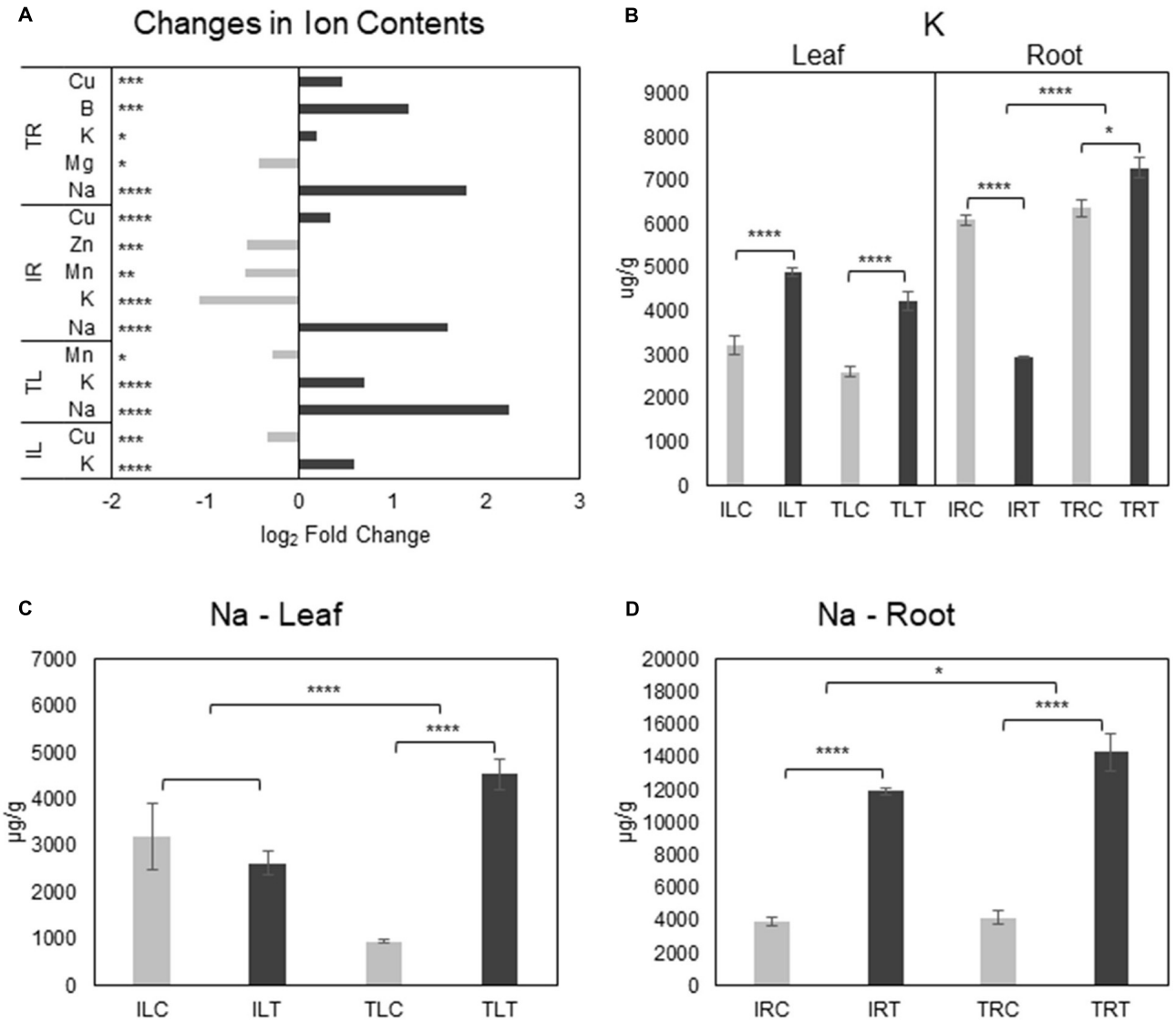


FIGURE 7 | Salt responsive ion content changes for tissues and genotypes **(A)**. K^+ **(B)** and Na^+ **(C,D)** content changes were also displayed separately to emphasize the difference in changes between genotypes (C, control; T, salt treatment). Comparison of other ions can be found in **Supplementary Figures 3, 4**. * indicates significance and quantity of * displays the level of significance. (*$p < 0.05$; **$p < 0.01$; ***$p < 0.005$; ****$p < 0.001$).

it was approximately 2-fold higher for IL compared to TL (**Supplementary Figure 3**). A similar scenario was observed for Zn^{+2} as well, with TL accumulating 3-fold higher than IL in both control and treatment conditions (**Supplementary Figure 3**).

Cu^{+2} levels displayed a highly significant increase in both root tissues of Ispir and TR43477 (**Figure 7A**; **Supplementary Figure 4**), but TR did not present any DEGs related to transport of this ion. In contrast, IR displayed three down- and two upregulated genes (**Additional File 3**). TR also accumulated B^{+3} and had a slight decrease of Mg^{+2}. IR, on the other hand, displayed significant reductions in Mn^{+2} and Zn^{+2} contents together with mostly downregulated transporter genes related to both ions (**Additional File 3**). But Zn^{+2} levels were already significantly higher for IR in control conditions compared to TR (approx. 1.4 fold difference) (**Supplementary Figure 4**) and salt-treatment only reduced Zn^{+2} content of IR similar to the Zn^{+2} level in TR in treatment conditions. Interestingly, Mo^{+2} content was exceptionally higher (**Supplementary Figure 4**) in the tissues of Ispir in both conditions, although it did not change significantly in salt-stress condition.

DISCUSSION

Rise of salt content in arable lands coupled with yield drop in salt-sensitive crops has become one of the most urgent problems in the developing world. Although several effects of salinity-induced dehydration and ionic imbalance on the plant growth

and development are known, many aspects of this process remain to be elucidated. Thus, it is important to decipher molecular mechanisms of salt-stress response and tolerance for the generation of salt-tolerant crops. Our study has focused on the transcriptomic, metabolomic, and ionic differences of two contrasting common bean genotypes under salinity stress to unravel the tolerance-related genes, metabolites, ions, and the pathways that connect them.

The exposure of root tissues to elevated salt levels stimulates signaling cascades that initially regulate ionic balance with Na^+ influx restriction and root-to-shoot Na^+ translocation. Subsequently, mechanisms that result in scavenging of toxic ions to vacuoles are activated to protect the cytoplasmic activities. The robustness of this systemic response, rather than a qualitative distinction, constitutes the main factor for the difference in tolerance between glycophytes and halophytes (Flowers and Colmer, 2008, 2015; Maathuis et al., 2014). Moreover, excessive salt in the environment results in an impasse as it both generates water stress and provide the cheap osmolytes to maintain the water potential. As this condition persists, with the accumulation of ions, escalating imbalance disrupts the molecular mechanisms in salt-susceptible species. Differential success in alleviating this stress is observed among different genotypes, which may help us understand the molecular basis and define better tolerance mechanisms.

Carbon Fixation With Osmotic and Ionic Balance

Our ion analysis demonstrated high Na^+ accumulation in root tissues of both genotypes upon salt stress, but IR managed to keep it at significantly lower levels than TR (**Figures 7A–D**). A more striking difference was observed at the leaf tissues: IL maintained the level of Na^+ after salt treatment while there was a large-scale Na^+ accumulation in TL. This implies a better Na^+ exclusion ability for IR that was not due to root-to-leaf translocation of excess Na^+ as implied by the stable IL Na^+ levels. The much higher control condition Na^+ level of IL compared to TL (3.3-fold, p-value < 0.05) (**Supplementary Figure 3A**) might also be an effective strategy against stress-driven Na^+ influx to the leaves. In either case, this distinction might be one of the focal points explaining the high endurance of Ispir genotype.

On the other hand, the situation is different with K^+ levels: The K^+ decrease in roots of Ispir can be expected since it is a glycophyte, even though a relatively salt-tolerant genotype. The decrease in cellular K^+ levels was observed previously both in glycophytes (Kronzucker et al., 2006; C.-M. Wang et al., 2009) and in halophytes (S. Wang et al., 2005; S.-M. Wang et al., 2007; C.-M. Wang et al., 2009). However, the roots of the susceptible TR43477 increased its K^+ levels (**Figures 7A,B**). Since much of the Na^+ entry to the root cells is through K^+ channels (Amtmann and Sanders, 1998; Laurie et al., 2002; Garciadeblás et al., 2003; R. A. James et al., 2011), it is possible that Ispir roots prevent the excessive Na^+ influx via closure of K^+ channels, which as a trade-off, may result in lower K^+ levels. A less successful approach adopted by TR43477 evidently allows for high Na^+ accumulation both in leaf and in root tissues together with K^+. Potentially better vacuole sequestration in roots on top of better exclusion ability might mitigate the negative effect of slightly lower K^+/Na^+ ratio in the Ispir roots. Another important aspect of this distinction might be the ability to achieve a much favorable K^+/Na^+ ratio in the leaves of the Ispir genotype. IL has managed to increase its K^+/Na^+ ratio by 1.8-fold while the same ratio decreased by 2.9-fold in TL under salt stress. This asymmetry, on the other hand, could be a vital element for the observed contrast in photosynthetic capacities of these genotypes.

Salt stress builds a major constraint on the photosynthetic capacity (Munns et al., 2006). Na^+ accumulation in chloroplasts affects growth mainly by disrupting the photosynthetic electron transport (Boyer, 1976; Kirst, 1990) and inhibiting the PSII activity (Mishra et al., 1991; Everard et al., 1994; Kao et al., 2003; Parida et al., 2003). Moreover, it decreases chlorophyll content in susceptible plants such as potato (Abdullah and Ahmad, 1990), tomato (Moghaieb et al., 2001), pea (Hamada and El-Enany, 1994), as well as common bean (Seemann and Critchley, 1985). However, Ispir, unlike TR43477, displayed a boosted carbon fixation metabolism with enriched GO terms and KEGG pathways (**Figures 2**, **3**) and an active chlorophyll content regulation (**Figure 4A**). Photosynthesis capacity is firmly connected to stomata, which control water loss/photosynthesis balance (Jones, 1998). As a major stomatal guard cell osmoregulator (Talbott and Zeiger, 1996; Hedrich, 2012), K^+ coordinates the gas exchange and transpiration rates (Kim et al., 2010), which can be heavily affected by salt-stress (Liu et al., 2017). Accumulated Na^+ competes with K^+ for the regulation of stomata, which causes considerable side effects such as deregulation through ABA and CO_2 (Jaschke et al., 1997; Fricke et al., 2004). Since salt-tolerant plants are known to have more efficient regulation of stomata compared to sensitive ones (Hedrich and Shabala, 2018), superior stomatal regulation through a higher K^+/Na^+ ratio for Ispir leaves may be the essence of its enhanced photosynthetic capacity. This connection is further implied by the decreased glycolate production in Ispir leaf tissues, which is an indication of reduced photorespiration, a metabolism that consumes ATP together with the reducing power of the photosynthetic electron transport system and reduces the efficiency of CO_2 fixation (Keys et al., 1986). As photosynthesis/photorespiration rate depends mainly on the CO_2/O_2 levels which on the other hand depends on stomatal density and conductance (Hetherington and Woodward, 2003; Chen et al., 2017; Zhao et al., 2019), Ispir potentially is a better stomatal regulator compared to TR43477 under salt stress. An enrichment of pectinesterase related terms and genes in Ispir leaves (**Figure 2A**, **Additional File 3**) further supports this hypothesis: Amsbury et al. (2016) have demonstrated that the guard cells in Arabidopsis have high content of un-esterified pectins. The guard-cell pectins were shown to be esterified in an Arabidopsis mutant deficient for a potent *pectinesterase* (*PME6*). The lack of this enzyme resulted in a decreased guard cell dynamic motility and, in turn, crippled the stomatal function causing susceptibility to low-water conditions. Indeed, one of the pectinesterase genes (Phvul.001G209400) that displayed an upregulation in IL is a somewhat close homolog (%43 similarity) of Arabidopsis *PME6;* thus, might be

playing a similar role in common bean. A decreased glycolate content and enriched pectinesterase-related terms along with the enriched photosynthesis pathway genes, increased chlorophyll content, and highly upregulated genes that were annotated as *Rubisco* (**Additional File 3**), are good indicators of an increased photosynthesis/lower photorespiration rate and a better stomatal regulatory system in Ispir genotype.

The improved photosynthetic capacity and enriched carbon fixation (**Figures 2A**, **3A**, **4**) in IL have conceivably yielded accumulation of various carbohydrates (nine types including sucrose and glucose- **Figure 5**) and enrichment in sucrose and starch metabolism (**Figure 3A**). Notably, intense upregulation of a *starch synthase* (Phvul.004G029100) together with a β-*amylase* (Phvul.011G107700), which is involved in starch breakdown (Scheidig et al., 2002), in IL also implied an enriched starch metabolism (**Additional File 4**). In turn, TL was depleted in such metabolites and exhibited a decrease in polysaccharide metabolic processes (**Figure 2A**). The augmented carbohydrate metabolism and soluble sugar contents in Ispir point to a superior tolerance mechanism in this genotype as carbohydrates provide osmoprotection, membrane stability, and turgor maintenance under osmotic stress (Ende and Peshev, 2013). Soluble carbohydrates are also known to be a metabolic source of energy, act as signaling molecules in plant growth regulation (Jang and Sheen, 1994; Pego et al., 2000) and to have roles in plant-stress response regulation (Ho et al., 2001; Chinnusamy et al., 2004). The variation in the resulting carbohydrate quantity might also explain the difference between the carbohydrate levels of the root systems (**Figure 5**; **Supplementary Figure 2**). Specifically, accumulation of mannitol (log_2FC – 2.76; p-value < 0.01), which is a well-known osmoprotectant (Tarczynski et al., 1993; Thomas et al., 1995; Shen et al., 1997; Abebe et al., 2003) and hydroxyl radical quencher (Smirnoff and Cumbes, 1989; Shen et al., 1997) may be important for the tolerance of Ispir roots to the excessive ion uptake (Stoop et al., 1996) and osmoregulation (Hellebusi, 1976).

Another implication of ionic balance regulation difference between the roots of these two genotypes is the significant reductions in IR Mn^{+2} and Zn^{+2} levels (**Figure 7A**). Especially Zn^{+2} was demonstrated to have positive effects on abiotic stress tolerance (Bagci et al., 2007; Ahmad et al., 2017). In our study, salt treatment caused a significant reduction of Zn^{+2} level in IR (from 1674.8 μg/g to 1143.4 μg/g). In TR, however, the control-condition level was already low (1.3-fold compared to IR, p-value < 0.005) and remained almost unchanged after the exposure to salt stress (a decrease from 1214.12 μg/g to 1184.2 μg/g) (**Supplementary Figures 4C,D**). It is intriguing to further explore this difference to understand if the higher initial content of Zn^{+2} contributes to the salt tolerance. One possibility is that Zn^{+2} normally accumulated in IR was incorporated into Zn-containing metalloproteins (McCall et al., 2000) required for an efficient response such as *alcohol dehydrogenase* (Shi et al., 2017), *carbonic anhydrase* (Yu et al., 2007), and *superoxide dismutase* (Bowler et al., 1992). As TR roots did not have such a pool of Zn^{+2} they might have failed to address the stress condition as efficiently as IR due to the lower activity/availability of such metalloproteins. On the other hand, salt-treatment caused Mn^{+2} decrease in IR may be due to allocation of the ion to the leaf tissues for protection of relatively high leaf Mn^{+2} content in Ispir (1.9-fold higher in control conditions compared to TL – **Supplementary Figures 3C,D**) while already low TL Mn^{+2} content displayed a significant reduction in treatment conditions. Since Mn^{+2} is an essential element for photosystem II to function and its scarcity disrupts the photosynthetic efficiency and stability (Gavalas and Clark, 1971; Husted et al., 2009; Schmidt et al., 2015), this allocation pattern might be a crucial aspect of tolerance as well.

However, together with significant reductions in Mn^{+2} and K^{+} contents (while only Mg^{+2} content displayed a slightly significant decrease in TR43477), Ispir roots displayed a distinct pattern (**Figure 7A**). A pattern that might also suggest regulation of ionic balance by lowering the concentration of necessary cations in the root system to a bare minimum to counteract the effects of toxic levels of Na^{+} ions. Evidently, Ispir genotype manages to not only preserve, if not boost, its energy metabolism but also to increase its photosynthesis intensity, which is a basic tolerance mechanism in low-water conditions (Santos and Pimentel, 2009; Loutfy et al., 2012). This is most probably feasible for the Ispir leaves as the stable Na^{+} level throughout stress did not affect any enzymatic activity and did not disrupt the osmotic and ionic balance.

Protein and Amino Acid Metabolism

Natural variation in salinity-tolerance is very high in the plant kingdom, even within the same species, which is reflected in different growth responses of different genotypes (Munns and Tester, 2008). Under the condition of salt-stress, IL displayed diminished protein production and modification but enriched protein protection-related terms (**Figure 2**). It is possible that keeping translation to a minimum is an efficient way to protect the proteome from oxidative stress associated with salinity conditions. On the other hand, the response of TL was less conservative: Terms for transcription were increased but translation and proteolysis terms were decreased (**Figure 2A**). The allocation of energy and valuable elements to transcription under conditions where normal levels of translation are harmful or not possible may be one of the weak points of the salt-sensitive genotype. Root systems were different in their response too: IR displayed a reduction in growth and production-related terms, while TR was only depleted in nitrogen metabolism (**Figure 3B**). Keeping the root smaller under salinity conditions may be one of the ways to limit the exposure of the nutrient-uptake interface to saline environment. Curiously, TR accumulated the highest number of amino acids among tissues and genotypes (valine, isoleucine and lysine were unique to TR). Although accumulation of amino acids is generally assumed as representation of tolerance (see review (Batista-Silva et al., 2019), catabolism of lysine, valine, isoleucine, and leucine were recognized as important pathways for osmotic stress tolerance in Arabidopsis (Pires et al., 2016). Pointedly, IR did not accumulate valine and had decreased amount of isoleucine in response to salt stress (**Figures 5C**, **6**) and this might be due to upregulation of a *2-oxoisovalerate dehydrogenase* homolog, Phvul.009G132900 (**Additional File 4**), which was demonstrated to have a major role in branched-chain amino acid catabolism (Fujiki et al., 2002). Increase in lysine

content in TR deserves special attention, since, as mentioned above, it may be considered as a tolerance mechanism as lysine accumulates in some drought-tolerant plant ecotypes (Yadav et al., 2019; You et al., 2019). But lysine catabolism, especially SACPATH pathway, a highly stress-responsive protective system (Markovitz and Chuang, 1987; Arruda et al., 2000; Azevedo et al., 2003; Moulin et al., 2006; Kiyota et al., 2015; Michaletti et al., 2018; Yadav et al., 2019; You et al., 2019), appeared to be inactive in the TR43477 compared to Ispir: The latter genotype has two upregulated SACPATH pathway genes in the genome (**Additional File 3**) including the only gene annotated as *lysine-ketoglutarate reductase/saccharopine dehydrogenase*. SACPATH pathway can lead to production of proline via glutamate or α-aminoadipate (Lawrence and Grant, 1964; Sodek and Wilson, 1970; Brandt, 1975). Although the proline levels were increased in both tissues and genotypes, glutamate was only accumulated in Ispir tissues (**Figures 5C**, **6**; **Supplementary Figure 2**). Thus the elevated lysine level in TR may be simply the result of more intensive proteolysis associated with stress (for a review, see Hildebrandt et al., 2015).

The difference in glutamate/glutamine biosynthesis also deserves attention as glutamate-glutamine/2-oxogluterate reaction is enriched in both varieties but glutamate/glutamine conversion pathway is mainly activated in Ispir tissues (**Figure 6**; **Additional File 3**). While both tissues of Ispir accumulated glutamate, TR43477 tissues accumulated glutamine, which indicates an inequality in the reaction direction for these varieties. Glutamate is essential for stress tolerance as it was demonstrated to support amino-acid synthesis under osmotic stress (Ramos et al., 2005), activate stress tolerance pathways via H_2O_2 burst (Lei et al., 2017), act as a signaling molecule for stress response pathways (Kan et al., 2017) and regulate the stomatal aperture under low-water conditions (Yoshida et al., 2016; Qiu et al., 2020). Glutamate is also necessary for biosynthesis of glutathione, an active compound of antioxidant defense system (Lu, 2013). Glutamine has also been implicated in stress-responses, acting as a regulator of a transcription factor (Kan et al., 2015). Overexpression of the enzyme necessary for its production, glutamine synthase, yields better abiotic stress tolerance in several species (Lee et al., 2013; D. James et al., 2018). Still, glutamate appears to be a hub for stress response patterns.

Moreover, the imbalance of regulation in glutamate/glutamine cycle genes (**Figure 6**; **Additional File 3**) may be another indication of the difference in stress-responsive nitrogen metabolism for these genotypes (Masclaux-Daubresse et al., 2006; Zhang et al., 2017) as implied by the KEGG pathway analysis (**Figures 3A,B**). Concerning that, asparagine biosynthesis and content were also differentially regulated between genotypes and tissues. Asp was mainly accumulated in the root tissues of both genotypes, but also displayed low but significant accumulation in the leaves of Ispir (**Figures 5C**, **6**; **Supplementary Figure 2**). An "*asparagine synthase-1*" annotated gene (Phvul.006G069300) was upregulated in all tissues except TL, where a different member of this gene family annotated as "*asparagine synthase-3*" (Phvul.001G252200) was downregulated. If the elevated Asp levels in TR were high mainly due to increased proteolysis as discussed above, the high accumulation of this amino acid in both tissues of Ispir may indicate the better nitrogen storage capacity of this genotype, since asparagine is known to be a good nitrogen reserve molecule (Pate, 1980; Lea et al., 2007). As salinity declines nitrogen assimilation and acquisition capacity of plants (Gouia et al., 1994; Debouba et al., 2006), and nitrogen is a necessary building block for amino acids, hormones such as auxin and other important amine-compounds, nitrogen withholding may be another key aspect of Ispir's salt tolerance.

Other Aspects of Tolerance

Certainly, salt tolerance is a complex feature that cannot be attributed to only a few biological processes such as carbon fixation and amino acid biosynthesis of primary metabolism (Munns and Tester, 2008; Gupta and Huang, 2014). Secondary metabolism is also known to be highly responsive to environmental factors including salt stress (Gupta and Huang, 2014; Sytar et al., 2018). Our previous study on Ispir in salt stress has displayed the enrichment of secondary metabolism genes in response to salt in both leaves and roots (Hiz et al., 2014). The present comparative study demonstrated that the roots of Ispir were differentially enriched in KEGG terms related to terpenoid metabolism (**Figure 3B**), a type of metabolism that involves volatile unsaturated hydrocarbon compounds with high structural diversity (Degenhardt et al., 2009). Other studies have reported terpenoids to upsurge in response to saline conditions and to be involved in tolerance responses (Harborne, 1999; Bourgaud et al., 2001; Sytar et al., 2018). A recent study in maize demonstrated the accumulation of phytoalexin terpenoids in roots as a key feature of an abiotic stress response and hormonal regulation under stress conditions (Vaughan et al., 2015). Terpenoid biosynthesis has been associated with photosynthetic machinery, especially chloroplasts, in non-stressed plants before (Loreto et al., 1996; Sharkey et al., 1996) and the impairment of terpenoid production in drought stress conditions was related to a decrease in levels of available substrates due to disrupted photosynthesis (Peñuelas et al., 2009; Šimpraga et al., 2011; Kleine and Müller, 2014; Nogués et al., 2015). The photosynthetic machinery in Ispir, compared to TR43477, displayed a rather boosted response in salt-stress conditions, thus enabling the production of new terpenoids in the roots. Moreover, IR was diminished in esterase and alcohol catabolism-related GO terms (**Figure 2B**), which indicates improved conservation of secondary metabolites such as terpenoids (Isah, 2019).

The prevention of salinity-induced reduction of photosynthetic activity in Ispir might also had a positive outcome for respiratory metabolism. Since salt stress does not affect cellular O_2 levels, the respiration rate mainly depends on the supply of substrate and biochemical regulation. Thus, the negative effect of salt stress on the respiratory machinery can be attributed to lower carbon fixation (Seemann and Critchley, 1985; Centritto et al., 2003) and disruption of electron transport chain due to high accumulation of ions (T. J. Flowers, 1974). Although there is no concrete evidence for the effect of increased or decreased respiration rates on salt-tolerance (Jacoby et al., 2011), respiratory homeostasis was correlated with better tolerance responses in a few species (Kasai et al., 1998; Jacoby et al., 2011). In this regard, the elevated levels of lactic acid in TL (log_2FC – 0.97; p-value < 0.01) (**Figure 5C**; **Supplementary Figure 2**) might be an indicator of perturbed

mitochondrial and increased anaerobic respiration. In contrast, lactic acid levels in IL have slightly decreased in response to salt stress (log_2FC – −0.64; p-value < 0.05), which might also be related to higher intensity of alcohol metabolism in IL. Out of five homologs of *alcohol dehydrogenase 1* (*ADH1*), one (Phvul.001G067300) was significantly upregulated in IL, while the others were not regulated in either genotype. The activity of this gene might have been sufficient for the reduction of toxic acetaldehyde (Bondy, 1992; M. Zhang et al., 1997) to ethanol, thus preventing the accumulation of lactic acid in IL. Additionally, *ADH1* upregulation might have had other positive effects since this gene is known to respond to abiotic-stresses and is essential for tolerance to osmotic and salt stresses (Conley et al., 1999; Shi et al., 2017; Yi et al., 2017).

Like other cellular activities, lipid metabolism is also affected by salt stress (Parida and Das, 2005). Indeed, in our study, the lipid content was low in TR43477 tissues (**Figure 5C**), which may be an indicator of susceptibility, as reported before in drought stress conditions. (Yordanov et al., 2000; Alpaslan et al., 2001).

Finally, besides the salt-caused differences, the constitutive 55- to 177-fold difference in Mo content between Ispir and TR43477 tissues under both conditions (**Supplementary Figures 3E,F, 4E,F**) can be important for salt tolerance in Ispir. Mo has been reported in many studies to improve abiotic stress tolerance in drought, salinity and low temperature conditions (Sun et al., 2009, 2014; Zhang et al., 2012; Wu et al., 2014). In saline conditions, Mo was demonstrated to regulate the antioxidant machinery and osmotic balance in Chinese cabbage (Zhang et al., 2012). Furthermore, it was reported to increase chlorophyll and carotene contents together with photosynthesis rate and have a positive effect on ionic balance regulation in the same species (Zhang et al., 2014). Thus, it is conceivable that the higher accumulation of Mo in Ispir contributes to its superior salt tolerance.

CONCLUSION

To understand the molecular basis of differential response to salt stress in two common bean genotypes, we performed comprehensive analyses of transcript levels, abundance of different metabolites, and ionic content in the root and leaf tissues of these genotypes. Our data suggest that the preservation of photosynthetic machinery via the control of Na^+ accumulation in leaves and the efficient sequestration of K^+ in roots may be vital for the stability of carbohydrate and energy metabolisms under saline conditions. Together with the resulting osmoprotection and higher substrate availability, a better regulation of amino acid metabolism, the remarkable shift in the ratio between glutamine and glutamate, the maintenance of ionic balance and the higher accumulation capacity for certain ions, such as Mo and Mn in roots and leaves and Zn in roots, might be the fundamentals of salt-tolerance in Ispir genotype of common bean. Functional studies on candidate genes and pathways highlighted in this study will improve our understanding of salt-tolerance and facilitate the generation of salt-tolerant plants.

DATA AVAILABILITY STATEMENT

High-throughput sequencing data generated in this study have been deposited to the NCBI GEO Datasets and can be accessed by GEO accession number: GSE156113.

AUTHOR CONTRIBUTIONS

HN and MT conceived and designed the experiment. HN conducted plant growth, stress treatments, RNA isolation, and metabolite extraction. mRNA library preparation and RNA-Seq was conducted by Macrogen, Inc. (S. Korea). HN performed the RNA-Seq raw data analysis. BS and NB performed the GC-MS measurements, data collection and metabolite identification. ICP-MS and ICP-OES measurements were conducted by Yildiz Technical University Merklab. (Turkey/Istanbul). Statistical and bioinformatics analyses for transcriptome, metabolome and ionome data were performed by HN. HN and MT wrote the manuscript with valuable contributions from all authors.

FUNDING

This work was financially supported by Bogazici University Research Funds [BAP 14925]. The funder had no role in study design, data collection, and analysis, decision to publish, or preparation of the manuscript.

ACKNOWLEDGMENTS

We wish to thank Dr. Igor Kryvoruchko for his valuable suggestions and editing the manuscript.

SUPPLEMENTARY MATERIAL

The Supplementary Material for this article can be found online at: https://www.frontiersin.org/articles/10.3389/fpls.2020.599501/full#supplementary-material

Supplementary Figure 1 | qRT-PCR verification of RNA-Seq Data. RNAseq and qPCR results (log_2 fold change (FC)) of 10 genes from Ispir **(A)** and TR43477 **(B)** root tissues were compared to each other. "r" depicts Pearson's r.

Supplementary Figure 2 | Graph representation of significantly accumulated and decreased metabolites in saline conditions. Highly significant (p-value < 0.01) changes were pointed out with asterisk. *p < 0.05; **p < 0.01; ***p < 0.005; ****p < 0.001.

Supplementary Figure 3 | Comparison of leaf ion contents in control and saline conditions. **(A,B)** Display the macroelement content comparisons for control and treatment conditions respectively. **(C–F)** Display the microelement content comparisosn for control and treatment conditions respectively. *p < 0.05; **p < 0.01; ***p < 0.005; ****p < 0.001.

Supplementary Figure 4 | Comparison of root ion contents in control and saline conditions. **(A,B)** Display the macroelement content comparisons for control and treatment conditions respectively. **(C–F)** Display the microelement content comparisosn for control and treatment conditions respectively. *p < 0.05; **p < 0.01; ***p < 0.005; ****p < 0.001.

REFERENCES

Abdullah, Z., and Ahmad, R. (1990). Effect of Pre- and Post-Kinetin Treatments on Salt Tolerance of Different Potato Cultivars Growing on Saline Soils. *J. Agron. Crop Sci.* 165, 94–102. doi: 10.1111/j.1439-037X.1990.tb00839.x

Abebe, T., Guenzi, A. C., Martin, B., and Cushman, J. C. (2003). Tolerance of Mannitol-Accumulating Transgenic Wheat to Water Stress and Salinity. *Plant Physiol.* 131, 1748–1755. doi: 10.1104/pp.102.003616

Addinsoft (2019). *XLSTAT statistical and data analysis solution*. New York, NY: Addinsoft. Available Online at: https://www.xlstat.com

Ahmad, P., Ahanger, M. A., Alyemeni, M. N., Wijaya, L., Egamberdieva, D., Bhardwaj, R., et al. (2017). Zinc application mitigates the adverse effects of NaCl stress on mustard (*Brassica juncea* (L.) Czern & Coss) through modulating compatible organic solutes, antioxidant enzymes, and flavonoid content. *J. Plant Interact.* 12, 429–437. doi: 10.1080/17429145.2017.1385867

Alpaslan, M., Boydak, E., Hayta, M., Gerçek, S., and Simsek, M. (2001). Effect of row space and irrigation on seed composition of Turkish sesame (*Sesamum indicum* L.). *Journal of the American Oil Chemists'. Society* 78, 933–935. doi: 10.1007/s11746-001-0366-0

Amsbury, S., Hunt, L., Elhaddad, N., Baillie, A., Lundgren, M., Verhertbruggen, Y., et al. (2016). Stomatal Function Requires Pectin De-methyl-esterification of the Guard Cell Wall. *Curr. Biol.* 26, 2899–2906. doi: 10.1016/j.cub.2016.08.021

Amtmann, A., and Sanders, D. (1998). "Mechanisms of Na^+ Uptake by Plant Cells," in *Advances in Botanical Research*, ed. J. A. Callow (Cambridge: Academic Press), 75–112. doi: 10.1016/S0065-2296(08)60310-9

Andrews, S., and Babraham Bioinformatics. (2010). *FastQC: A quality control tool for high throughput sequence data*. Burlington, MA: ScienceOpen, Inc.

Arbona, V., Manzi, M., Ollas, C., and Gómez-Cadenas, A. (2013). Metabolomics as a Tool to Investigate Abiotic Stress Tolerance in Plants. *Int. J. Mol. Sci.* 14, 4885–4911. doi: 10.3390/ijms14034885

Arruda, P., Kemper, E. L., Papes, F., and Leite, A. (2000). Regulation of lysine catabolism in higher plants. *Trends Plant Sci.* 5, 324–330. doi: 10.1016/S1360-1385(00)01688-5

Azevedo, R. A., Damerval, C., Landry, J., Lea, P. J., Bellato, C. M., Meinhardt, L. W., et al. (2003). Regulation of maize lysine metabolism and endosperm protein synthesis by opaque and floury mutations. *Eur. J. Biochem.* 270, 4898–4908. doi: 10.1111/j.1432-1033.2003.03890.x

Bagci, S. A., Ekiz, H., Yilmaz, A., and Cakmak, I. (2007). Effects of Zinc Deficiency and Drought on Grain Yield of Field-grown Wheat Cultivars in Central Anatolia. *J. Agron. Crop Sci.* 193, 198–206. doi: 10.1111/j.1439-037X.2007.00256.x

Batista-Silva, W., Heinemann, B., Rugen, N., Nunes-Nesi, A., Araújo, W. L., Braun, H.-P., et al. (2019). The role of amino acid metabolism during abiotic stress release. *Plant Cell Environ.* 42, 1630–1644. doi: 10.1111/pce.13518

Benjamini, Y., and Hochberg, Y. (1995). Controlling the False Discovery Rate: A Practical and Powerful Approach to Multiple Testing. *J. R. Statist. Soc.* 57, 289–300. doi: 10.2307/2346101

Bolger, A. M., Lohse, M., and Usadel, B. (2014). Trimmomatic: A flexible trimmer for Illumina sequence data. *Bioinformatics* 30, 2114–2120. doi: 10.1093/bioinformatics/btu170

Bondy, S. C. (1992). Ethanol toxicity and oxidative stress. *Toxicol. Lett.* 63, 231–241. doi: 10.1016/0378-4274(92)90086-Y

Borges, A., Tsai, S. M., and Caldas, D. G. G. (2012). Validation of reference genes for RT-qPCR normalization in common bean during biotic and abiotic stresses. *Plant Cell Rep.* 31, 827–838. doi: 10.1007/s00299-011-1204-x

Bourgaud, F., Gravot, A., Milesi, S., and Gontier, E. (2001). Production of plant secondary metabolites: A historical perspective. *Plant Sci.* 161, 839–851. doi: 10.1016/S0168-9452(01)00490-3

Bowler, C., Montagu, M. V., and Inze, D. (1992). Superoxide Dismutase and Stress Tolerance. *Annu. Rev. Plant Physiol. Plant Mol. Biol.* 43, 83–116. doi: 10.1146/annurev.pp.43.060192.000503

Boyer, J. S. (1976). "Water Deficits and Photosynthesis," in *Soil Water Measurement, Plant Responses, and Breeding for Drought Resistance*, ed. T. T. Kozlowski (Cambridge, CA: Academic Press), 153–190. doi: 10.1016/B978-0-12-424154-1.50010-3

Brandt, A. B. (1975). In vivo incorporation of [^{14}C] lysine into the endosperm proteins of wild type and high-lysine barley. *FEBS Lett.* 52, 288–291. doi: 10.1016/0014-5793(75)80827-1

Broughton, W. J., Hernández, G., Blair, M., Beebe, S., Gepts, P., and Vanderleyden, J. (2003). Beans (Phaseolus spp.) – model food legumes. *Plant Soil* 252, 55–128. doi: 10.1023/A:1024146710611

Centritto, M., Loreto, F., and Chartzoulakis, K. (2003). The use of low [CO_2] to estimate diffusional and non-diffusional limitations of photosynthetic capacity of salt-stressed olive saplings. *Plant Cell Environ.* 26, 585–594. doi: 10.1046/j.1365-3040.2003.00993.x

Chen, Z.-H., Chen, G., Dai, F., Wang, Y., Hills, A., Ruan, Y.-L., et al. (2017). Molecular Evolution of Grass Stomata. *Trends Plant Sci.* 22, 124–139. doi: 10.1016/j.tplants.2016.09.005

Chinnusamy, V., Jagendorf, A., and Zhu, J.-K. (2005). Understanding and Improving Salt Tolerance in Plants. *Crop Sci.* 45:437. doi: 10.2135/cropsci2005.0437

Chinnusamy, V., Schumaker, K., and Zhu, J.-K. (2004). Molecular genetic perspectives on cross-talk and specificity in abiotic stress signalling in plants. *J. Exp. Bot.* 55, 225–236. doi: 10.1093/jxb/erh005

Conley, T. R., Peng, H.-P., and Shih, M.-C. (1999). Mutations Affecting Induction of Glycolytic and Fermentative Genes during Germination and Environmental Stresses in Arabidopsis. *Plant Physiol.* 119, 599–608. doi: 10.1104/pp.119.2.599

Dasgan, Y., and Koc, S. (2009). Evaluation of salt tolerance in common bean genotypes by ion regulation and searching for screening parameters. *J. Food Agricult. Environ.* 77, 363–372.

Davies, F. T., and Bowman, J. E. (2016). Horticulture, food security, and the challenge of feeding the world. *Acta Horticult.* 1128, 1–6. doi: 10.17660/ActaHortic.2016.1128.1

Debouba, M., Gouia, H., Suzuki, A., and Ghorbel, M. H. (2006). NaCl stress effects on enzymes involved in nitrogen assimilation pathway in tomato "*Lycopersicon esculentum*" seedlings. *J. Plant Physiol.* 163, 1247–1258. doi: 10.1016/j.jplph.2005.09.012

Degenhardt, J., Köllner, T. G., and Gershenzon, J. (2009). Monoterpene and sesquiterpene synthases and the origin of terpene skeletal diversity in plants. *Phytochemistry* 70, 1621–1637. doi: 10.1016/j.phytochem.2009.07.030

Ende, W. V., and Peshev, D. (2013). "Sugars as Antioxidants in Plants," in *Crop Improvement Under Adverse Conditions*, eds N. Tuteja and S. S. Gill (New York: Springer), 285–307. doi: 10.1007/978-1-4614-4633-0_13

Everard, J. D., Gucci, R., Kann, S. C., Flore, J. A., and Loescher, W. H. (1994). Gas Exchange and Carbon Partitioning in the Leaves of Celery (*Apium graveolens* L.) at Various Levels of Root Zone Salinity. *Plant Physiol.* 106, 281–292. doi: 10.1104/pp.106.1.281

Flowers, T. J. (1974). Salt tolerance in *Suaeda maritima* (L.) DumA: Comparison of mitochondria isolated from green tissues of suaeda and pisum. *J. Exp. Bot.* 25, 101–110. doi: 10.1093/jxb/25.1.101

Flowers, T. J., and Colmer, T. D. (2008). Salinity tolerance in halophytes. *N. Phytol.* 179, 945–963. doi: 10.1111/j.1469-8137.2008.02531.x

Flowers, Timothy, J., and Colmer, T. D. (2015). Plant salt tolerance: Adaptations in halophytes. *Ann. Bot.* 115, 327–331. doi: 10.1093/aob/mcu267

Foolad, M. R. (2004). Recent advances in genetics of salt tolerance in tomato. *Plant Cell Tissue Organ Cult.* 76, 101–119. doi: 10.1023/b:ticu.0000007308.47608.88

Fricke, W., Akhiyarova, G., Veselov, D., and Kudoyarova, G. (2004). Rapid and tissue-specific changes in ABA and in growth rate in response to salinity in barley leaves. *J. Exp. Bot.* 55, 1115–1123. doi: 10.1093/jxb/erh117

Fujiki, Y., Ito, M., Itoh, T., Nishida, I., and Watanabe, A. (2002). Activation of the Promoters of Arabidopsis Genes for the Branched-Chain α-Keto Acid Dehydrogenase Complex in Transgenic Tobacco BY-2 Cells under Sugar Starvation. *Plant Cell Physiol.* 43, 275–280. doi: 10.1093/pcp/pcf032

Garciadeblás, B., Senn, M. E., Bañuelos, M. A., and Rodríguez-Navarro, A. (2003). Sodium transport and HKT transporters: The rice model. *Plant J.* 34, 788–801. doi: 10.1046/j.1365-313X.2003.01764.x

Gavalas, N. A., and Clark, H. E. (1971). On the Role of Manganese in Photosynthesis: Kinetics of Photoinhibition in Manganese-deficent and 3-(4-Chlorophenyl)-1, 1-dimethylurea-inhibited *Euglena gracilis*. *Plant Physiol.* 47, 139–143. doi: 10.1104/pp.47.1.139

Ge, S. X., Jung, D., and Yao, R. (2020). ShinyGO: A graphical gene-set enrichment tool for animals and plants. *Bioinformatics* 36, 2628–2629. doi: 10.1093/bioinformatics/btz931

Gouia, H., Ghorbal, M. H., and Touraine, B. (1994). Effects of NaCl on Flows of N and Mineral Ions and on NO_3- Reduction Rate within Whole Plants of Salt-Sensitive Bean and Salt-Tolerant Cotton. *Plant Physiol.* 105, 1409–1418. doi: 10.1104/pp.105.4.1409

Gupta, B., and Huang, B. (2014). Mechanism of Salinity Tolerance in Plants: Physiological. Biochemical, and Molecular Characterization. *Int. J. Genomics* 2014, 1–18. doi: 10.1155/2014/701596

Hamada, A. M., and El-Enany, A. E. (1994). Effect of NaCl salinity on growth, pigment and mineral element contents, and gas exchange of broad bean and pea plants. *Biol. Plantarum* 36, 75–81. doi: 10.1007/BF029 21273

Hanin, M., Ebel, C., Ngom, M., Laplaze, L., and Masmoudi, K. (2016). New Insights on Plant Salt Tolerance Mechanisms and Their Potential Use for Breeding. *Front. Plant Sci.* 7:1787. doi: 10.3389/fpls.2016.01787

Harborne, J. B. (1999). "Classes and Functions of Secondary Products from Plants," in *Chemicals from Plants*, eds N. J. Walton and D. E. Brown (London: Imperial College Press), 1–25. doi: 10.1142/9789812817273_0001

Hedrich, R. (2012). Ion Channels in Plants. *Physiol. Rev.* 92, 1777–1811. doi: 10.1152/physrev.00038.2011

Hedrich, R., and Shabala, S. (2018). Stomata in a saline world. *Curr. Opin. Plant Biol.* 46, 87–95. doi: 10.1016/j.pbi.2018.07.015

Hellebusi, J. A. (1976). Osmoregulation. *Annu. Rev. Plant Physiol.* 27, 485–505. doi: 10.1146/annurev.pp.27.060176.002413

Hetherington, A. M., and Woodward, F. I. (2003). The role of stomata in sensing and driving environmental change. *Nature* 424, 901–908. doi: 10.1038/nature01843

Hildebrandt, T. M., Nunes Nesi, A., Araújo, W. L., and Braun, H.-P. (2015). Amino Acid Catabolism in Plants. *Mol. Plant* 8, 1563–1579. doi: 10.1016/j.molp.2015.09.005

Hiz, M. C., Canher, B., Niron, H., and Turet, M. (2014). Transcriptome Analysis of Salt Tolerant Common Bean (*Phaseolus vulgaris* L.) under Saline Conditions. *PLoS One* 9:e92598. doi: 10.1371/journal.pone.0092598

Ho, S.-L., Chao, Y.-C., Tong, W.-F., and Yu, S.-M. (2001). Sugar Coordinately and Differentially Regulates Growth- and Stress-Related Gene Expression via a Complex Signal Transduction Network and Multiple Control Mechanisms. *Plant Physiol.* 125, 877–890. doi: 10.1104/pp.125.2.877

Hoagland, D. R., and Arnon, D. I. (1950). *The water-culture method for growing plants without soil. Circular*. California: University of California.

Husted, S., Laursen, K. H., Hebbern, C. A., Schmidt, S. B., Pedas, P., Haldrup, A., et al. (2009). Manganese Deficiency Leads to Genotype-Specific Changes in Fluorescence Induction Kinetics and State Transitions. *Plant Physiol.* 150, 825–833. doi: 10.1104/pp.108.134601

Isah, T. (2019). Stress and defense responses in plant secondary metabolites production. *Biol. Res.* 52:39. doi: 10.1186/s40659-019-0246-3

Jacoby, R. P., Taylor, N. L., and Millar, A. H. (2011). The role of mitochondrial respiration in salinity tolerance. *Trends Plant Sci.* 16, 614–623. doi: 10.1016/j.tplants.2011.08.002

James, D., Borphukan, B., Fartyal, D., Ram, B., Singh, J., Manna, M., et al. (2018). Concurrent Overexpression of OsGS1;1 and OsGS2 Genes in Transgenic Rice (*Oryza sativa* L.): Impact on Tolerance to Abiotic Stresses. *Front. Plant Sci.* 9:786. doi: 10.3389/fpls.2018.00786

James, R. A., Blake, C., Byrt, C. S., and Munns, R. (2011). Major genes for Na+ exclusion, Nax1 and Nax2 (wheat HKT1;4 and HKT1;5), decrease Na+ accumulation in bread wheat leaves under saline and waterlogged conditions. *J. Exp. Bot.* 62, 2939–2947. doi: 10.1093/jxb/err003

Jamil, A., Riaz, S., Ashraf, M., and Foolad, M. R. (2011). *Gene expression profiling of plants under salt stress*, Vol. 30. Abingdon: Taylor & Francis Group, doi: 10.1080/07352689.2011.605739

Jang, J. C., and Sheen, J. (1994). Sugar sensing in higher plants. *Plant Cell* 6, 1665–1679. doi: 10.1105/tpc.6.11.1665

Jaschke, W. D., Peuke, A. D., Pate, J. S., and Hartung, W. (1997). Transport, synthesis and catabolism of abscisic acid (ABA) in intact plants of castor bean (*Ricinus communis* L.) under phosphate deficiency and moderate salinity. *J. Exp. Bot.* 48, 1737–1747. doi: 10.1093/jxb/48.9.1737

Jones, H. G. (1998). Stomatal control of photosynthesis and transpiration. *J. Exp. Bot.* 49, 387–398. doi: 10.1093/jxb/49.Special_Issue.387

Kan, C.-C., Chung, T.-Y., Juo, Y.-A., and Hsieh, M.-H. (2015). Glutamine rapidly induces the expression of key transcription factor genes involved in nitrogen and stress responses in rice roots. *BMC Genomics* 16:731. doi: 10.1186/s12864-015-1892-7

Kan, C.-C., Chung, T.-Y., Wu, H.-Y., Juo, Y.-A., and Hsieh, M.-H. (2017). Exogenous glutamate rapidly induces the expression of genes involved in metabolism and defense responses in rice roots. *BMC Genomics* 18:186. doi: 10.1186/s12864-017-3588-7

Kanehisa, M., and Goto, S. (2000). KEGG: Kyoto Encyclopedia of Genes and Genomes. *Nucl. Acids Res.* 28, 27–30. doi: 10.1093/nar/28.1.27

Kao, W.-Y., Tsai, T.-T., and Shih, C.-N. (2003). Photosynthetic Gas Exchange and Chlorophyll a Fluorescence of Three Wild Soybean Species in Response to NaCl Treatments. *Photosynthetica* 41, 415–419. doi: 10.1023/B:PHOT.0000015466.22288.23

Kasai, K., Fukayama, H., Uchida, N., Mori, N., Yasuda, T., Oji, Y., et al. (1998). Salinity tolerance in *Triticum aestivum-Lophopyrum elongatum* amphiploid and 5E disomic addition line evaluated by NaCl effects on photosynthesis and respiration. *Cereal Res. Commun.* 26, 281–287. doi: 10.1007/BF035 43501

Keys, A. J., Ellis, R. J., and Gray, J. C. (1986). Rubisco: Its role in photorespiration. *Philosoph. Trans. R. Soc. London B Biol. Sci.* 313, 325–336. doi: 10.1098/rstb.1986.0040

Kim, D., Langmead, B., and Salzberg, S. L. (2015). HISAT: A fast spliced aligner with low memory requirements. *Nat. Methods* 12, 357–360. doi: 10.1038/nmeth.3317

Kim, T.-H., Böhmer, M., Hu, H., Nishimura, N., and Schroeder, J. I. (2010). Guard Cell Signal Transduction Network: Advances in Understanding Abscisic Acid, CO_2, and Ca^{2+} Signaling. *Annu. Rev. Plant Biol.* 61, 561–591. doi: 10.1146/annurev-arplant-042809-112226

Kirst, G. O. (1990). Salinity Tolerance of Eukaryotic Marine Algae. *Annu. Rev. Plant Physiol. Plant Mol. Biol.* 41, 21–53. doi: 10.1146/annurev.pp.41.060190.000321

Kiyota, E., Pena, I. A., and Arruda, P. (2015). The saccharopine pathway in seed development and stress response of maize. *Plant Cell Environ.* 38, 2450–2461. doi: 10.1111/pce.12563

Kleine, S., and Müller, C. (2014). Drought Stress and Leaf Herbivory Affect Root Terpenoid Concentrations and Growth of *Tanacetum vulgare*. *J. Chem. Ecol.* 40, 1115–1125. doi: 10.1007/s10886-014-0505-2

Kronzucker, H. J., Szczerba, M. W., Moazami-Goudarzi, M., and Britto, D. T. (2006). The cytosolic Na^+: K^+ ratio does not explain salinity-induced growth impairment in barley: a dual-tracer study using $^{42}K^+$ and $^{24}Na^+$. *Plant Cell Environ.* 29, 2228–2237. doi: 10.1111/j.1365-3040.2006.01597.x

Laurie, S., Feeney, K. A., Maathuis, F. J. M., Heard, P. J., Brown, S. J., and Leigh, R. A. (2002). A role for *HKT1* in sodium uptake by wheat roots. *Plant J.* 32, 139–149. doi: 10.1046/j.1365-313X.2002.01410.x

Lawrence, J. M., and Grant, D. R. (1964). Incorporation of lysine-C^{14} into the developing grain of wheat. *Arch. Biochem. Biophys.* 104, 73–78. doi: 10.1016/S0003-9861(64)80036-9

Lea, P. J., Sodek, L., Parry, M. A. J., Shewry, P. R., and Halford, N. G. (2007). Asparagine in plants. *Ann. Appl. Biol.* 150, 1–26. doi: 10.1111/j.1744-7348.2006.00104.x

Lee, H. J., Abdula, S. E., Jang, D. W., Park, S.-H., Yoon, U.-H., Jung, Y. J., et al. (2013). Overexpression of the glutamine synthetase gene modulates oxidative stress response in rice after exposure to cadmium stress. *Plant Cell Rep.* 32, 1521–1529. doi: 10.1007/s00299-013-1464-8

Lei, P., Pang, X., Feng, X., Li, S., Chi, B., Wang, R., et al. (2017). The microbe-secreted isopeptide poly-γ-glutamic acid induces stress tolerance in Brassica napus L. seedlings by activating crosstalk between H_2O_2 and Ca^{2+}. *Sci. Rep.* 7:41618. doi: 10.1038/srep41618

Lisec, J., Schauer, N., Kopka, J., Willmitzer, L., and Fernie, A. R. (2006). Gas chromatography mass spectrometry–based metabolite profiling in plants. *Nat. Protocols* 1, 387–396. doi: 10.1038/nprot.2006.59

Liu, X., Fan, Y., Mak, M., Babla, M., Holford, P., Wang, F., et al. (2017). QTLs for stomatal and photosynthetic traits related to salinity tolerance in barley. *BMC Genomics* 18:9. doi: 10.1186/s12864-016-3380-0

Livak, K. J., and Schmittgen, T. D. (2001). Analysis of relative gene expression data using real-time quantitative PCR and the $2^{-\Delta\Delta CT}$ method. *Methods* 25, 402–408. doi: 10.1006/meth.2001.1262

Loreto, F., Ciccioli, P., Cecinato, A., Brancaleoni, E., Frattoni, M., Fabozzi, C., et al. (1996). Evidence of the Photosynthetic Origin of Monoterpenes Emitted

by *Quercus ilex* L. Leaves by 13^C Labeling. *Plant Physiol.* 110, 1317–1322. doi: 10.1104/pp.110.4.1317

Loutfy, N., El-Tayeb, M. A., Hassanen, A. M., Moustafa, M. F. M., Sakuma, Y., and Inouhe, M. (2012). Changes in the water status and osmotic solute contents in response to drought and salicylic acid treatments in four different cultivars of wheat (*Triticum aestivum*). *J. Plant Res.* 125, 173–184. doi: 10.1007/s10265-011-0419-9

Lu, S. C. (2013). Glutathione synthesis. *Biochimica Biophysica Acta* 1830, 3143–3153. doi: 10.1016/j.bbagen.2012.09.008

Maathuis, F. J. M., Ahmad, I., and Patishtan, J. (2014). Regulation of Na^+ fluxes in plants. *Front. Plant Sci.* 5:467. doi: 10.3389/fpls.2014.00467

Markovitz, P. J., and Chuang, D. T. (1987). The bifunctional aminoadipic semialdehyde synthase in lysine degradation. Separation of reductase and dehydrogenase domains by limited proteolysis and column chromatography. *J. Biol. Chem.* 262, 9353–9358.

Masclaux-Daubresse, C., Reisdorf-Cren, M., Pageau, K., Lelandais, M., Grandjean, O., Kronenberger, et al. (2006). Glutamine Synthetase-Glutamate Synthase Pathway and Glutamate Dehydrogenase Play Distinct Roles in the Sink-Source Nitrogen Cycle in Tobacco. *Plant Physiol.* 140, 444–456. doi: 10.1104/pp.105.071910

McCall, K. A., Huang, C., and Fierke, C. A. (2000). Function and Mechanism of Zinc Metalloenzymes. *J. Nutrit.* 130, 1437S–1446S. doi: 10.1093/jn/130.5.1437S

McCarthy, D. J., Chen, Y., and Smyth, G. K. (2012). Differential expression analysis of multifactor RNA-Seq experiments with respect to biological variation. *Nucl. Acids Res.* 40, 4288–4297. doi: 10.1093/nar/gks042

Michaletti, A., Naghavi, M. R., Toorchi, M., Zolla, L., and Rinalducci, S. (2018). Metabolomics and proteomics reveal drought-stress responses of leaf tissues from spring-wheat. *Sci. Rep.* 8:5710. doi: 10.1038/s41598-018-24012-y

Microsoft (2019). *Analysis ToolPak—Complex Data Analysis*. New Mexico: Microsoft.

Mishra, S. K., Subrahmanyam, D., and Singhal, G. S. (1991). Interrelationship between Salt and Light Stress on Primary Processes of Photosynthesis. *J. Plant Physiol.* 138, 92–96. doi: 10.1016/S0176-1617(11)80736-4

Moghaieb, R. E. A., Saneoka, H., Ito, J., and Fujita, K. (2001). Characterization of salt tolerance in tomato plant in terms of photosynthesis and water relations. *Soil Sci. Plant Nutrit.* 47, 377–385. doi: 10.1080/00380768.2001.10408400

Monforte, A. J., Asíns, M. J., and Carbonell, E. A. (1997). Salt tolerance in Lycopersicon species VI. Genotype-by-salinity interaction in quantitative trait loci detection: Constitutive and response QTLs. *TAG Theoret. Appl. Genet.* 95, 706–713. doi: 10.1007/s001220050616

Moulin, M., Deleu, C., Larher, F., and Bouchereau, A. (2006). The lysine-ketoglutarate reductase–saccharopine dehydrogenase is involved in the osmo-induced synthesis of pipecolic acid in rapeseed leaf tissues. *Plant Physiol. Biochem.* 44, 474–482. doi: 10.1016/j.plaphy.2006.08.005

Muchate, N. S., Nikalje, G. C., Rajurkar, N. S., Suprasanna, P., and Nikam, T. D. (2016). Plant Salt Stress: Adaptive Responses, Tolerance Mechanism and Bioengineering for Salt Tolerance. *Botanic. Rev.* 82, 371–406. doi: 10.1007/s12229-016-9173-y

Munns, R. (2002). Comparative physiology of salt and water stress. *Plant Cell Environ.* 25, 239–250. doi: 10.1046/j.0016-8025.2001.00808.x

Munns, R. (2005). Genes and salt tolerance: Bringing them together. *N. Phytol.* 167, 645–663. doi: 10.1111/j.1469-8137.2005.01487.x

Munns, R., and Tester, M. (2008). Mechanisms of Salinity Tolerance. *Annu. Rev. Plant Biol.* 59, 651–681. doi: 10.1146/annurev.arplant.59.032607.092911

Munns, R., James, R. A., and Läuchli, A. (2006). Approaches to increasing the salt tolerance of wheat and other cereals. *J. Exp. Bot.* 57, 1025–1043. doi: 10.1093/jxb/erj100

Nilsen, E. T., Orcutt, D. M., and Hale, M. G. (1996). "The Physiology of Plants Under Stress: Soil and Biotic Factors," in *The physiology of plants under stress*, eds D. M. Orcutt and E. T. Nilsen (New Jersey: Wiley).

Nogués, I., Medori, M., and Calfapietra, C. (2015). Limitations of monoterpene emissions and their antioxidant role in Cistus sp. Under mild and severe treatments of drought and warming. *Environ. Exp. Bot.* 119, 76–86. doi: 10.1016/j.envexpbot.2015.06.001

Parida, A. K., and Das, A. B. (2005). Salt tolerance and salinity effects on plants: A review. *Ecotoxicol. Environ. Safety* 60, 324–349. doi: 10.1016/J.ECOENV.2004.06.010

Parida, A. K., Das, A. B., and Mittra, B. (2003). Effects of NaCl Stress on the Structure, Pigment Complex Composition, and Photosynthetic Activity of Mangrove *Bruguiera parviflora* Chloroplasts. *Photosynthetica* 41:191. doi: 10.1023/B:PHOT.0000011951.37231.69

Pate, J. S. (1980). Transport and Partitioning of Nitrogenous Solutes. *Annu. Rev. Plant Physiol.* 31, 313–340. doi: 10.1146/annurev.pp.31.060180.001525

Pego, J. V., Kortstee, A. J., Huijser, C., and Smeekens, S. C. M. (2000). Photosynthesis, sugars and the regulation of gene expression. *J. Exp. Bot.* 51(Suppl._1), 407–416. doi: 10.1093/jexbot/51.suppl_1.407

Peñuelas, J., Filella, I., Seco, R., and Llusià, J. (2009). Increase in isoprene and monoterpene emissions after re-watering of droughted *Quercus ilex* seedlings. *Biol. Plantarum* 53, 351–354. doi: 10.1007/s10535-009-0065-4

Pinheiro, C., Baeta, J. P., Pereira, A. M., Domingues, H., and Ricardo, C. P. (2010). Diversity of seed mineral composition of *Phaseolus vulgaris* L. germplasm. *J. Food Composit. Anal.* 23, 319–325. doi: 10.1016/j.jfca.2010.01.005

Pires, M. V., Júnior, A. A. P., Medeiros, D. B., Daloso, D. M., Pham, P. A., Barros, K. A., et al. (2016). The influence of alternative pathways of respiration that utilize branched-chain amino acids following water shortage in Arabidopsis. *Plant Cell Environ.* 39, 1304–1319. doi: 10.1111/pce.12682

Qiu, X.-M., Sun, Y.-Y., Ye, X.-Y., and Li, Z.-G. (2020). Signaling Role of Glutamate in Plants. *Front. Plant Sci.* 10:1743. doi: 10.3389/fpls.2019.01743

Ramos, M. L. G., Parsons, R., and Sprent, J. I. (2005). Differences in ureide and amino acid content of water stressed soybean inoculated with *Bradyrhizobium japonicum* and *B. elkanii*. *Pesquisa Agropecuária Brasileira* 40, 453–458. doi: 10.1590/S0100-204X2005000500005

Ritchie, R. J. (2006). Consistent Sets of Spectrophotometric Chlorophyll Equations for Acetone. Methanol and Ethanol Solvents. *Photosynth. Res.* 89, 27–41. doi: 10.1007/s11120-006-9065-9

Sanchez, D. H., Lippold, F., Redestig, H., Hannah, M. A., Erban, A., Krämer, U., et al. (2008). Integrative functional genomics of salt acclimatization in the model legume *Lotus japonicus*. *Plant J.* 53, 973–987. doi: 10.1111/j.1365-313X.2007.03381.x

Santos, M. G., and Pimentel, C. (2009). Daily balance of leaf sugars and amino acids as indicators of common bean (*Phaseolus vulgaris* L.) metabolic response and drought intensity. *Physiol. Mol. Biol. Plants* 15, 23–30. doi: 10.1007/s12298-009-0002-1

Scheidig, A., Fröhlich, A., Schulze, S., Lloyd, J. R., and Kossmann, J. (2002). Downregulation of a chloroplast-targeted β-*amylase* leads to a starch-excess phenotype in leaves. *Plant J.* 30, 581–591. doi: 10.1046/j.1365-313X.2002.01317.x

Schmidt, S. B., Persson, D. P., Powikrowska, M., Frydenvang, J., Schjoerring, J. K., Jensen, P. E., et al. (2015). Metal Binding in Photosystem II Super- and Subcomplexes from Barley Thylakoids. *Plant Physiol.* 168, 1490–1502. doi: 10.1104/pp.15.00559

Schroeder, A., Mueller, O., Stocker, S., Salowsky, R., Leiber, M., Gassmann, M., et al. (2006). The RIN: An RNA integrity number for assigning integrity values to RNA measurements. *BMC Mol. Biol.* 7:3. doi: 10.1186/1471-2199-7-3

Seemann, J. R., and Critchley, C. (1985). Effects of salt stress on the growth, ion content, stomatal behaviour and photosynthetic capacity of a salt-sensitive species. *Phaseolus vulgaris* L. *Planta* 164, 151–162. doi: 10.1007/BF00396077

Shabala, S., and Cuin, T. A. (2008). Potassium transport and plant salt tolerance. *Physiol. Plantarum* 133, 651–669. doi: 10.1111/j.1399-3054.2007.01008.x

Shahzad, M., Zörb, C., Geilfus, C.-M., and Mühling, K. H. (2013). Apoplastic Na^+ in *Vicia faba* Leaves Rises After Short-Term Salt Stress and is Remedied by Silicon. *J. Agron. Crop Sci.* 199, 161–170. doi: 10.1111/jac.12003

Sharkey, T. D., Singsaas, E. L., Vanderveer, P. J., and Geron, C. (1996). Field measurements of isoprene emission from trees in response to temperature and light. *Tree Physiol.* 16, 649–654. doi: 10.1093/treephys/16.7.649

Shen, B., Jensen, R. G., and Bohnert, H. J. (1997). Increased Resistance to Oxidative Stress in Transgenic Plants by Targeting Mannitol Biosynthesis to Chloroplasts. *Plant Physiol.* 113, 1177–1183. doi: 10.1104/pp.113.4.1177

Shi, H., Liu, W., Yao, Y., Wei, Y., and Chan, Z. (2017). *Alcohol dehydrogenase 1* (*ADH1*) confers both abiotic and biotic stress resistance in Arabidopsis. *Plant Sci.* 262, 24–31. doi: 10.1016/j.plantsci.2017.05.013

Shrivastava, P., and Kumar, R. (2015). Soil salinity: A serious environmental issue and plant growth promoting bacteria as one of the tools for its alleviation. *Saudi J. Biol. Sci.* 22, 123–131. doi: 10.1016/j.sjbs.2014.12.001

Šimpraga, M., Verbeeck, H., Demarcke, M., Joó, É, Pokorska, O., Amelynck, C., et al. (2011). Clear link between drought stress, photosynthesis and biogenic volatile organic compounds in *Fagus sylvatica* L. *Atmospher. Environ.* 45, 5254–5259. doi: 10.1016/j.atmosenv.2011.06.075

Smedley, D., Haider, S., Durinck, S., Pandini, L., Provero, P., Allen, et al. (2015). The BioMart community portal: An innovative alternative to large, centralized data repositories. *Nucl. Acids Res.* 43, W589–W598. doi: 10.1093/nar/gkv350

Smirnoff, N., and Cumbes, Q. J. (1989). Hydroxyl radical scavenging activity of compatible solutes. *Phytochemistry* 28, 1057–1060. doi: 10.1016/0031-9422(89)80182-7

Sodek, L., and Wilson, C. M. (1970). Incorporation of leucine-^{14}C and lysine-^{14}C into protein in the developing endosperm of nomal and opaque-2 corn. *Arch. Biochem. Biophys.* 140, 29–38. doi: 10.1016/0003-9861(70)90006-8

Stoop, J. M. H., Williamson, J. D., and Mason Pharr, D. (1996). Mannitol metabolism in plants: A method for coping with stress. *Trends Plant Sci.* 1, 139–144. doi: 10.1016/S1360-1385(96)80048-3

Sun, X., Hu, C., Tan, Q., Liu, J., and Liu, H. (2009). Effects of molybdenum on expression of cold-responsive genes in abscisic acid (ABA)-dependent and ABA-independent pathways in winter wheat under low-temperature stress. *Ann. Bot.* 104, 345–356. doi: 10.1093/aob/mcp133

Sun, X., Tan, Q., Nie, Z., Hu, C., and An, Y. (2014). Differential Expression of Proteins in Response to Molybdenum Deficiency in Winter Wheat Leaves Under Low-Temperature Stress. *Plant Mol. Biol. Reporter* 32, 1057–1069. doi: 10.1007/s11105-014-0713-5

Sytar, O., Mbarki, S., Zivcak, M., and Brestic, M. (2018). "The Involvement of Different Secondary Metabolites in Salinity Tolerance of Crops," in *Salinity Responses and Tolerance in Plants, Volume 2: Exploring RNAi, Genome Editing and Systems Biology*, eds V. Kumar, S. H. Wani, P. Suprasanna, and L.-S. P. Tran (switzerland: Springer International Publishing), 21–48. doi: 10.1007/978-3-319-90318-7_2

Talbott, L. D., and Zeiger, E. (1996). Central Roles for Potassium and Sucrose in Guard-Cell Osmoregulation. *Plant Physiol.* 111, 1051–1057. doi: 10.1104/pp.111.4.1051

Tarczynski, M. C., Jensen, R. G., and Bohnert, H. J. (1993). Stress Protection of Transgenic Tobacco by Production of the Osmolyte Mannitol. *Science* 259, 508–510. doi: 10.1126/science.259.5094.508

Tester, M., and Davenport, R. (2003). Na^+ tolerance and Na^+ transport in higher plants. *Ann. Bot.* 91, 503–527. doi: 10.1093/aob/mcg058

Thomas, J. C., Sepahi, M., Arendall, B., and Bohnert, H. J. (1995). Enhancement of seed germination in high salinity by engineering mannitol expression in Arabidopsis thaliana. *Plant Cell Environ.* 18, 801–806. doi: 10.1111/j.1365-3040.1995.tb00584.x

Tian, T., Liu, Y., Yan, H., You, Q., Yi, X., Du, Z., et al. (2017). AgriGO v2.0: A GO analysis toolkit for the agricultural community, 2017 update. *Nucl. Acids Res.* 45, W122–W129. doi: 10.1093/nar/gkx382

Vaughan, M. M., Christensen, S., Schmelz, E. A., Huffaker, A., Mcauslane, H. J., Alborn, et al. (2015). Accumulation of terpenoid phytoalexins in maize roots is associated with drought tolerance. *Plant Cell Environ.* 38, 2195–2207. doi: 10.1111/pce.12482

Wang, C.-M., Zhang, J.-L., Liu, X.-S., Li, Z., Wu, G.-Q., Cai, J.-Y., et al. (2009). Puccinellia tenuiflora maintains a low Na^+ level under salinity by limiting unidirectional Na+ influx resulting in a high selectivity for K^+ over Na^+. *Plant Cell Environ.* 32, 486–496. doi: 10.1111/j.1365-3040.2009.01942.x

Wang, S., Zhao, G., Gao, Y., Tang, Z., and Zhang, C. (2005). *Puccinellia tenuiflora* Exhibits Stronger Selectivity for K^+ over Na^+ than Wheat. *J. Plant Nutrit.* 27, 1841–1857. doi: 10.1081/PLN-200026435

Wang, S.-M., Zhang, J.-L., and Flowers, T. J. (2007). Low-Affinity Na^+ Uptake in the Halophyte *Suaeda maritima*. *Plant Physiol.* 145, 559–571. doi: 10.1104/pp.107.104315

Warren, C. R. (2008). Rapid Measurement of Chlorophylls with a Microplate Reader. *J. Plant Nutrit.* 31, 1321–1332. doi: 10.1080/01904160802135092

Wu, S., Hu, C., Tan, Q., Nie, Z., and Sun, X. (2014). Effects of molybdenum on water utilization, antioxidative defense system and osmotic-adjustment ability in winter wheat (*Triticum aestivum*) under drought stress. *Plant Physiol. Biochem.* 83, 365–374. doi: 10.1016/j.plaphy.2014.08.022

Yadav, A. K., Carroll, A. J., Estavillo, G. M., Rebetzke, G. J., and Pogson, B. J. (2019). Wheat drought tolerance in the field is predicted by amino acid responses to glasshouse-imposed drought. *J. Exp. Bot.* 70, 4931–4948. doi: 10.1093/jxb/erz224

Yi, S. Y., Ku, S. S., Sim, H.-J., et al. (2017). An Alcohol Dehydrogenase Gene from Synechocystis sp. Confers Salt Tolerance in Transgenic Tobacco. *Front. Plant Sci.* 8:1965. doi: 10.3389/fpls.2017.01965

Yordanov, I., Velikova, V., and Tsonev, T. (2000). Plant Responses to Drought. Acclimation, and Stress Tolerance. *Photosynthetica* 38, 171–186. doi: 10.1023/A:1007201411474

Yoshida, R., Mori, I. C., Kamizono, N., Shichiri, Y., Shimatani, T., Miyata, F., et al. (2016). Glutamate functions in stomatal closure in Arabidopsis and fava bean. *J. Plant Res.* 129, 39–49. doi: 10.1007/s10265-015-0757-0

You, J., Zhang, Y., Liu, A., Li, D., Wang, X., Dossa, K., et al. (2019). Transcriptomic and metabolomic profiling of drought-tolerant and susceptible sesame genotypes in response to drought stress. *BMC Plant Biol.* 19:267. doi: 10.1186/s12870-019-1880-1

Yu, S., Zhang, X., Guan, Q., Takano, T., and Liu, S. (2007). Expression of a carbonic anhydrase gene is induced by environmental stresses in Rice (*Oryza sativa* L.). *Biotechnol. Lett.* 29, 89–94. doi: 10.1007/s10529-006-9199-z

Zhang, M., Hu, C., Sun, X., Zhao, X., Tan, et al. (2014). Molybdenum Affects Photosynthesis and Ionic Homeostasis of Chinese Cabbage under Salinity Stress. *Commun. Soil Sci. Plant Anal.* 45, 2660–2672. doi: 10.1080/00103624.2014.941855

Zhang, M., Hu, C., Zhao, X., Tan, Q., Sun, X., et al. (2012). Molybdenum improves antioxidant and osmotic-adjustment ability against salt stress in Chinese cabbage (*Brassica campestris* L. ssp. *Pekinensis*). *Plant Soil* 355, 375–383. doi: 10.1007/s11104-011-1109-z

Zhang, M., Nagata, S., Miyazawa, K., Kikuchi, H., and Esashi, Y. (1997). A Competitive Enzyme-Linked Immunosorbent Assay to Quantify Acetaldehyde-Protein Adducts That Accumulate in Dry Seeds during Aging. *Plant Physiol.* 113, 397–402. doi: 10.1104/pp.113.2.397

Zhang, Z., Xiong, S., Wei, Y., Meng, X., Wang, X., and Ma, X. (2017). The role of glutamine synthetase isozymes in enhancing nitrogen use efficiency of N-efficient winter wheat. *Sci. Rep.* 7:1000. doi: 10.1038/s41598-017-01071-1

Zhao, C., Wang, Y., Chan, K. X., Marchant, D. B., Franks, P. J., Randall, D., et al. (2019). Evolution of chloroplast retrograde signaling facilitates green plant adaptation to land. *Proc. Natl. Acad. Sci.* 116, 5015–5020. doi: 10.1073/pnas.1812092116

Zhu, J.-K. (2016). Abiotic Stress Signaling and Responses in Plants. *Cell* 167, 313–324. doi: 10.1016/J.CELL.2016.08.029

Conflict of Interest: The authors declare that the research was conducted in the absence of any commercial or financial relationships that could be construed as a potential conflict of interest.

Copyright © 2020 Niron, Barlas, Salih and Türet. This is an open-access article distributed under the terms of the Creative Commons Attribution License (CC BY). The use, distribution or reproduction in other forums is permitted, provided the original author(s) and the copyright owner(s) are credited and that the original publication in this journal is cited, in accordance with accepted academic practice. No use, distribution or reproduction is permitted which does not comply with these terms.

frontiers in Plant Science

ORIGINAL RESEARCH
published: 11 December 2020
doi: 10.3389/fpls.2020.614144

Linking Leaf Water Potential, Photosynthesis and Chlorophyll Loss With Mechanisms of Photo- and Antioxidant Protection in Juvenile Olive Trees Subjected to Severe Drought

*Sahar Baccari[1,2], Olfa Elloumi[1], Anissa Chaari-Rkhis[1], Erola Fenollosa[3], Melanie Morales[3], Noureddine Drira[2], Ferjani Ben Abdallah[4], Lotfi Fki[2] and Sergi Munné-Bosch[3]**

[1] Laboratoire LR16IO01, Institut de l'Olivier (IO), University of Sfax, Sfax, Tunisia, [2] Laboratory of Plant Biotechnology (LR01ES21), Faculty of Sciences of Sfax, University of Sfax, Sfax, Tunisia, [3] Department of Evolutionary Biology, Ecology and Environmental Sciences, Faculty of Biology, University of Barcelona, Barcelona, Spain, [4] Laboratory of Plant Biodiversity and Dynamics of Ecosystems in Arid Area, Faculty of Sciences of Sfax, University of Sfax, Sfax, Tunisia

OPEN ACCESS

Edited by:
Felipe Klein Ricachenevsky, Federal University of Rio Grande, Brazil

Reviewed by:
José Manuel Moutinho-Pereira, University of Trás-os-Montes and Alto Douro, Portugal
José Cochicho Ramalho, University of Lisbon, Portugal

***Correspondence:**
Sergi Munné-Bosch
smunne@ub.edu

Specialty section:
This article was submitted to Plant Abiotic Stress, a section of the journal Frontiers in Plant Science

Received: *05 October 2020*
Accepted: *23 November 2020*
Published: *11 December 2020*

Citation:
Baccari S, Elloumi O, Chaari-Rkhis A, Fenollosa E, Morales M, Drira N, Ben Abdallah F, Fki L and Munné-Bosch S (2020) Linking Leaf Water Potential, Photosynthesis and Chlorophyll Loss With Mechanisms of Photo- and Antioxidant Protection in Juvenile Olive Trees Subjected to Severe Drought. Front. Plant Sci. 11:614144. doi: 10.3389/fpls.2020.614144

The identification of drought-tolerant olive tree genotypes has become an urgent requirement to develop sustainable agriculture in dry lands. However, physiological markers linking drought tolerance with mechanistic effects operating at the cellular level are still lacking, in particular under severe stress, despite the urgent need to develop these tools in the current frame of global change. In this context, 1-year-old olive plants growing in the greenhouse and with a high intra-specific variability (using various genotypes obtained either from cuttings or seeds) were evaluated for drought tolerance under severe stress. Growth, plant water status, net photosynthesis rates, chlorophyll contents and the extent of photo- and antioxidant defenses (including the de-epoxidation state of the xanthophyll cycle, and the contents of carotenoids and vitamin E) were evaluated under well-watered conditions and severe stress (by withholding water for 60 days). Plants were able to continue photosynthesizing under severe stress, even at very low leaf water potential of −4 to −6 MPa. This ability was achieved, at least in part, by the activation of photo- and antioxidant mechanisms, including not only increased xanthophyll cycle de-epoxidation, but also enhanced α-tocopherol contents. "Zarrazi" (obtained from seeds) and "Chemlali" (obtained from cuttings) showed better performance under severe water stress compared to the other genotypes, which was associated to their ability to trigger a higher antioxidant protection. It is concluded that (i) drought tolerance among the various genotypes tested is associated with antioxidant protection in olive trees, (ii) the extent of xanthophyll cycle de-epoxidation is strongly inversely related to photosynthetic rates, and (iii) vitamin E accumulation is sharply induced upon severe chlorophyll degradation.

Keywords: drought tolerance, olive germplasm, photoprotection, α-tocopherol, xanthophyll cycle

INTRODUCTION

Olive tree (*Olea europaea* L.) is one of the most widespread crops in Mediterranean-type agroecosystems, with high economic and social importance. In semi-arid areas of the Mediterranean basin, the scarcity of precipitation combined with extreme climatic conditions such as high temperatures increase water stress in olive trees. It is particularly in this context that serious concerns have been raised about the impact of climate change on olive agricultural productivity. According to De Ollas et al. (2019), the Mediterranean region is expected to witness a decrease in the total amount of precipitation and an increase of the spread and intensity of drought. Among various countries from the Mediterranean basin, Tunisia is considered to be one of countries most exposed to climate change. During the drought episode of 1999–2002, the decrease of olive production reached 90%, which adversely affected farmers income (Gargouri et al., 2012). Considering this situation, much attention has recently been drawn to the valorization and conservation of plant genetic resources to achieve relatively high yields under severe drought. New approaches including the selection of drought-tolerant cultivars and rootstocks have been considered to reduce the effects of water stress. Several researchers have demonstrated that combinations of rootstocks and scions decrease the depressive effects of water stress and increase resistance to drought (Trifilo et al., 2007; Therios, 2009).

Understanding the mechanisms that olive trees have evolved to withstand drought stress is important for selecting drought-tolerant genotypes and improving olive yield and oil quality (Sofo et al., 2004). Under water stress conditions, olive trees regulate leaf water status by morphological, anatomical and physiological adaptations (Guerfel et al., 2009). Indeed, water deficit affects leaf water relations and gas exchange mechanisms of olive cultivars (Trabelsi et al., 2019). Some authors attributed the decrease of photosynthetic rate in response to water stress to stomatal conductance limitation (Perez-Martin et al., 2014; Ben Hamed et al., 2016). Stomatal control is an effective mechanism that decreases water loss through transpiration in drought conditions (Perez-Martin et al., 2014). When environmental stress factors become severe for plants, the mesophyll conductance and biochemical limitations further contribute to the decrease of photosynthetic activity (Flexas and Medrano, 2002).

The limitation of CO_2 assimilation in water-stressed olive trees leads to an over-reduction of the photosynthetic electron chain (Sofo et al., 2004). Since chloroplasts cannot dissipate the excess light energy, there is a redirection of photon energy into processes that favor the production of reactive oxygen species (ROS) (Hasanuzzaman et al., 2017). High ROS concentration can seriously disrupt the metabolism of the plant causing enzyme inhibition, protein oxidation and membrane lipid peroxidation, and plants are endowed with antioxidant defense systems to protect the photosynthetic apparatus against oxidative damage (Sircelj et al., 2007). Several researchers have been interested in the enzymatic activity against oxidative stress in olive trees (Sofo et al., 2004; Ben Ahmed et al., 2009, Ben Abdallah et al., 2017), but little is known about the role of non-enzymatic antioxidants on the tolerance of olive trees under drought stress conditions. Among them, carotenoids and tocopherols constitute the main protection system against ROS, including their role in quenching the singlet oxygen ($^1O_2$) and in the case of tocopherols additionally preventing lipid peroxidation in thylakoid membranes (Muñoz and Munné-Bosch, 2019). The increase in carotenoids contents is one of the mechanisms evolved by the olive tree to protect the photosynthetic apparatus against photooxidation (Bacelar et al., 2007; Ben Abdallah et al., 2017). However, the identification of particular carotenoids involved in photo- and antioxidant protection under water deficit conditions in olive trees has been poorly investigated to date. The excess excitation energy is harmlessly dissipated in the antennae complexes of PSII as heat through a process which involves the xanthophyll cycle (Demmig-Adams and Adams III , 1996). Likewise, enhanced non-enzymatic antioxidant defense systems have been reported to improve plant abiotic stress tolerance in different studies (Munné-Bosch and Alegre, 2000; Hasanuzzaman et al., 2017). Some non-enzymatic antioxidant mechanisms, such as the increase in the content of phenolic compounds and glutathione, have been described to play a role in olive trees subjected to contrasting water availability regimes (Bacelar et al., 2006, 2007; Petridis et al., 2012), but to our knowledge no studies have been performed at the level of the xanthophyll cycle and α-tocopherol in olive trees, and even less these photo- and antioxidant mechanisms tested for their potential use in genotype selection.

Tunisian olive germplasm is characterized by a large number of varieties with about 200 cultivars. The main olive cultivars in Tunisia are Chemlali in the south and the center of the country and Chetoui in the north. These varieties account for 95% of the total olive trees and contribute more than 90% of the national production of olive oil. Chemlali is well known for its ability to cope with arid conditions (rainfall <200 mm per year). By taking advantage of the variability associated to the genotypic diversity of various young olive trees, we aimed here to unravel the link, if any, between leaf water potential, photosynthesis rates and chlorophyll loss with mechanisms of photo- and antioxidant protection in juvenile olive trees subjected to severe drought. Furthermore, it is discussed how the development of new photo- and antioxidant markers may be useful in order to select and develop new drought-tolerant olive tree cultivars for oil production in semi-arid regions. Due to the difficulty of performing studies in mature olive trees in field trials, we used here trees at an early stage of development. The juvenile phase of trees usually represents the most abiotic stress sensitive stage in woody plants (Shannon et al., 1994); therefore, young genotypes represented here may be considered a proper and valuable material for the detection of drought-tolerant genotypes. Furthermore, another important goal of our study was to establish new photo- and antioxidant markers that may be useful in order to select and develop new drought-tolerant olive tree cultivars in semi-arid regions. Selection methods including field trials testing several genotypes are generally limited, more

Abbreviations: Ψ_L, leaf water potential; $^1O_2$, singlet oxygen; A_n, net photosynthesis rate; Chl, chlorophyll; DPS, de-epoxidation state of the xanthophyll cycle; DW, dry weight; LPR, leaf production rate; PSII, photosystem II; ROS, reactive oxygen species; SGR, stem growth rate; VZA, xanthophyll cycle pool.

specifically comparing rooted cutting with seedlings obtained from seeds (Laczko and Aghazarm, 2009). We aimed to fill this knowledge gap by testing the drought stress response of several olive trees at the juvenile stage under semi-controlled conditions to offer a rapid alternative (in comparison to field trials) in genotype selection for crop improvement.

MATERIALS AND METHODS

Plant Material and Drought Stress Conditions

One-year-old olive trees (*Olea europaea* L.) were grown under natural daylight conditions with a mean maximum daily photosynthetically active radiation (PAR) of 1017 $\mu mol\ m^{-2}\ s^{-1}$ in a plastic greenhouse at the Olive Tree Institute of Sfax. Plants were obtained from cuttings and/or from germination of seeds. Rooted cuttings were obtained from the two main Tunisian olive cultivars "Chemlali" and "Chetoui," while seedlings were regenerated from the seeds of wild olive tree "Oleaster" and from three olive cultivars "Chetoui," "Chemlali" and "Zarrazi" which are cultivated, respectively, in the north, the center and the south of Tunisia. All seeds were collected from the experimental station "Taous" of the Olive Tree Institute (central Tunisia, 34°56′38″N, 10°36′50″E), except for the wild olive tree "Oleaster," whose seeds were collected from the National Park of Ichkeul (north Tunisia, 37°10′00″N, 9°40′00″E).

After germination, seedlings were selected for homogeneity and grown for 3 months on an MS medium (Murashigue and Skoog, 1962) supplemented with 8 $g{\cdot}L^{-1}$ agar and 30 $g{\cdot}L^{-1}$ sucrose. Both seedlings and rooted cuttings were transplanted in 1-L plastic pots filled with sand and peat (2:1, v/v) and then irrigated twice a week with half-strength Hoagland"s solution (Hoagland and Arnon, 1950) for 8 months. During this period, mean daily maximum and minimum temperatures and relative humidity in the greenhouse ranged from 20 to 30°C, and between 40 and 50%, respectively. Before stress application, soil field capacity was calculated. Indeed, all the plants were saturated with water and left to drain freely until drainage became negligible. After 24 h, the weight recorded for each individual pot (W1) was considered as the soil field capacity. Soil water content was monitored by weighing all the pots every 2 days (W2) and the amount of water transpired was determined and restored by irrigation. The weight difference (W1–W2) allowed a calculation of the amount of water lost by transpiration and used for irrigation. Drought stress was imposed by a gradual reduction of 20% of the total transpired water every 2 days until full irrigation withdrawal. Well-watered (control) plants were irrigated with 100% of soil field capacity throughout the experiment.

Plants were arranged in two completely randomized blocks design. Each block represents a water regime: irrigated and stressed. A total number of 24 seedlings and 3 plants per cultivar were selected for the irrigated water regime. For the contrasting water regime, a total number of 50 seedlings and 8 plants per cultivar were used. Measurements were performed on plants exposed to severe stress after 60 days of starting treatments, including leaf water potential, leaf gas exchange and mechanisms of photo- and antioxidant protection. Growth parameters were estimated both after 30 and 60 days of starting treatments, For biochemical analyses, fully-expanded young leaves exposed to sunlight were sampled between 10 a.m. and 11 a.m. (local time), immediately frozen in liquid nitrogen and stored at −20°C until analyses.

Growth Parameters

Stem elongation (cm) and the number of leaves per plant were measured for each plant at the beginning of stress (H_i, L_i), at 30 days (H_{30}, L_{30}) and at 60 days (H_{60}, L_{60}) of drought. Stem growth rate (SGR) and leaf production rate (LPR) were estimated from these parameters according to the equations described by Sun et al. (2019) and Rodrigues de Lima et al. (2019).

Leaf Water Potential and Leaf Gas Exchange

Leaf water potential (Ψ_L) was measured using a Scholander pressure chamber model SKPM 1400 (Skye Instruments, Powys, United Kingdom) between 9:00 and 11:00 local time. Net photosynthesis rate (A_n), stomatal conductance (gs), transpiration (E), water use efficiency (A/E) and intercellular to ambient carbon dioxide concentration ratio (Ci/Ca) were determined between 9:00 and 11:00 using a portable gas exchange system (Cl-340 Handheld Photosynthesis System). During leaf gas exchange measurements, photosynthetically-active radiation was set at 1250 $\mu mol{\cdot}m^{-2}{\cdot}s^{-1}$, leaf temperature at 35°C, CO_2 concentration at 430 ppm and vapor pressure deficit at 5 KPa. All measurements were carried out on fully-expanded young leaves taken from the median part of the shoot. Leaf water potential determination was performed using the whole leaf with the petiole, taking care the latter remained intact during measurements.

Chlorophyll Contents and Extent of Photo- and Antioxidant Protection

The extraction and HPLC analysis of chlorophylls and carotenoids were performed as described by Munné-Bosch and Alegre (2000). In short, leaves were ground in liquid nitrogen and pigments extracted with cold methanol using ultrasonication. After centrifuging at 1000 × *g* for 10 min at 4°C, the supernatant was collected, and the pellet re-extracted with the same solvent until it turned colorless. Then, supernatants were pooled and filtered with a 0.22-μm pore size. Pigments were separated by high-performance liquid chromatography (HPLC) on a Dupont non-end capped Zorbax ODS-5-μm column (250 mm long, 4.6 mm i.d.; 20% carbon, Teknokroma, Sant Cugat, Spain) at 30°C at a flow rate of 1 $ml{\cdot}min^{-1}$ for 38 min. The solvent mixture for the gradient, detection at 445 nm (diode array detector, HP1100 Series HPLC System, Agilent Technologies, Santa Clara, CA, United States) and calculation of pmol/are ratios for quantification of chlorophyll a, chlorophyll b, neoxanthin, violaxanthin, antheraxanthin, zeaxanthin, lutein, and β-carotene were performed as described by Munné-Bosch and Alegre (2000). The de-epoxidation state of the xanthophyll cycle (DPS) was calculated as DPS = (Z + 0.5A)/(V + Z + A),

where V, A, and Z are violaxanthin, antheraxanthin and zeaxanthin, respectively.

The same methanolic extract was used for the determination of tocopherols, which were separated isocratically on a normal-phase HPLC system (JASCO, Tokyo, Japan) and quantified using a fluorescent detector as described by Amaral et al. (2005). Detection was carried out at an excitation of 295 nm and emission at 330 nm. α-Tocopherol was quantified by co-elution with an authentic standard (Sigma–Aldrich, Steinheim, Germany) and quantified using a calibration curve. From all vitamin E homologs measured (α-, β-, γ-, and δ-tocopherol), only the α-tocopherol form accumulated in olive tree leaves.

Statistical Analysis

Statistical analyses were carried out with the SPSS Base 20.0 software (Chicago, IL, United States). A two-way analysis of variance (ANOVA) was used to examine cultivar and treatment effects. Duncan"s multiple range tests were used for mean comparison at $p \leq 0.05$. Correlation between variables was determined according to Pearson tests.

RESULTS

Impact of Drought on Growth, Leaf Water Potential and Photosynthesis

Drought and cultivar effects on growth were observed (**Figure 1A**). Leaf production rate (LPR) dropped severely in all olive trees exposed to drought stress, with the seedlings "Chemlali" ("Chemlali S") and "Oleaster" ("Oleaster S") being the most affected already at 30 days of drought (**Figure 1B**). Increasing drought stress up to 60 days resulted in a further leaf production decrease with a response that depended on the cultivar, as evidenced by a strong cultivar × water regime interaction ($p < 0.001$) (**Figure 1B**).

In irrigated conditions, Ψ_L showed the lowest values (−1.4 MPa) in both "Chetoui" rooted cuttings and seedlings, which significantly differ to other genotypes except "Chemlali" (**Figure 2A**). The highest values (−0.8 MPa) were observed for "Zarrazi" seedlings. For the stressed treatment, Ψ_L decreased significantly ($p < 0.001$) in all olive trees compared to control plants (**Figure 2A**). The response to water stress depended on the cultivar as evidenced by cultivar × water regime interaction ($p < 0.001$). The reduction of Ψ_L ranged from 71 to 88%.

A_n decreased significantly after 60 days of drought stress in all genotypes, irrespective of whether the plants were obtained from cuttings or seeds (**Figure 2B**). As compared to the control plants, "Zarrazi" seedlings ("Zarrazi S"), followed by "Chemlali" rooted cuttings, were the less affected by water deficit. For the rest of olive trees, more severe reductions due to water deficit were observed, ranging from 87 to 93% relative to their respective controls.

Except for "Oleaster" seedlings, the high decrease of A_n coincided with the decrease in gs and E. Stressed olive plants exhibited severe decreases in gs and E, as compared to well-watered plants. However, for the "Oleaster S," despite the decrease in photosynthetic activity (more than 92%), no significant difference was observed in gs and E between irrigated and stressed plants (**Figures 2C,D**). Water use efficiency (calculated as A/E) did not show significant differences between irrigated and stressed olive trees, with the exception of "Oleaster S," which showed a severe reduction in this stress marker. By contrast, "Zarrazi S" was the most efficient in water use (**Figure 2E**). The intercellular to ambient carbon dioxide concentration ratio (Ci/Ca) kept nearly constant in response to drought with values close to 1 for all genotypes (**Figure 2F**).

Impact of Drought Stress on Photo- and Antioxidant Protection

A significant interaction between cultivar and water regime ($p = 0.001$) was recorded on leaf chlorophyll (Chl a + b) content after 60 days of drought stress (**Table 1**). Compared to control plants, withholding irrigation induced a significant decrease in Chl a + b, with the exception of "Zarrazi S" and both rooted cuttings "Chemlali" and "Chetoui" in which no significant changes were observed. The highest decrease of Chl a + b was recorded in "Oleaster S" which was about 36.4%. Also, no significant change in terms of chlorophyll a/b ratio (Chl a/b) was observed between irrigated and stressed olive trees, with the exception of "Chemlali S" and "Chetoui" rooted cuttings for which significant decreases of 12.2 and 10.2%, respectively, were obtained (**Table 1**).

Drought stress increased significantly the xanthophyll cycle pool expressed per unit of chlorophyll (VZA/Chl) and the de-epoxidation state of the xanthophyll cycle (DPS) in olive trees compared to control plants ($p < 0.001$). The increase in VZA/Chl ranged in all genotypes between 1.3 and 1.9-fold in stressed plants compared to their respective controls. The highest VZA/Chl ratio was recorded in "Zarrazi S," followed by "Chemlali" rooted cuttings, whereas the lowest one was obtained for "Oleaster S" (**Table 1**). An effect of water regime, but not of cultivar, was also observed in DPS ($p < 0.001$). The stress-related increase in DPS ranged between 1.2 and 1.5-fold relative to controls, respectively, in "Chetoui" seedlings ("Chetoui S") and "Zarrazi S." In contrast, the β-carotene per unit of chlorophyll (β-car/Chl) decreased significantly under stress conditions in all olive trees with "Zarrazi S" showing the lowest decrease (27.2%). However, the lutein to Chl ratio (Lut/Chl) increased significantly with stress in "Chemlali S "and remained unchanged in the rest of the olive trees compared to control plants (**Table 1**).

Under water stress conditions, α-tocopherol per unit of chlorophyll (α-Toc/Chl) increased significantly in stressed olive trees compared to control plants, with the exception of "Chemlali S," "Oleaster S" and "Chetoui" rooted cuttings, in which no significant changes were observed (**Table 1**). This increase ranged between 2 and 6-fold relative to controls in "Chemlali" rooted cuttings and "Chetoui S," respectively.

De-epoxidation state of the xanthophyll cycle and VZA levels were closely related to leaf water potential (**Figure 3**), photosynthetic activity (**Figure 4**) and leaf chlorophyll content (**Figure 5**). In fact, results showed negative correlations between either DPS or VZA with Ψ_L ($r = -0.85$ and $r = -0.74$, respectively), A_n ($r = -0.73$ and $r = -0.62$, respectively), Chl a + b ($r = -0.46$ and $r = -0.43$, respectively). It appears that

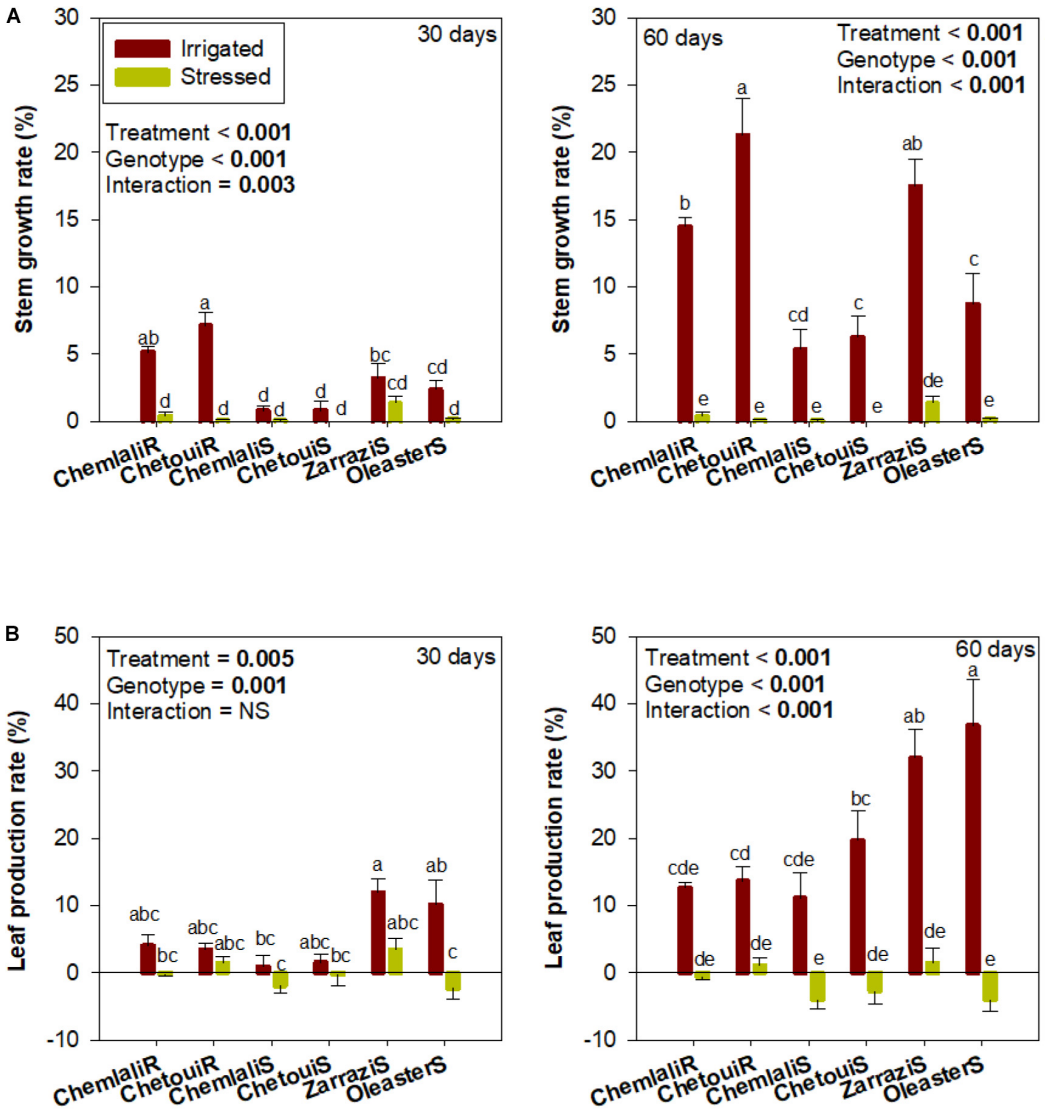


FIGURE 1 | Stem and leaf growth in olive trees subjected to mild and severe drought stress. Effects of drought stress periods (30 and 60 days after start of treatments) on **(A)** stem growth and **(B)** leaf production rate in olive trees obtained from cuttings (cv. "Chemlali" and "Chetoui") and obtained from seeds ("Chemlali S," "Chetoui S," "Zarrazi S" and "Oleaster S"). Values represent means ± S.E. of $n \geq 3$ for irrigated plants and $n \geq 8$ for water-stressed plants. A two-way analysis of variance (ANOVA) was used to examine if the effects of treatment (water regime) and genotype (cultivar) were statistically significant and to look at the significance of interaction effects. Different letters indicate significant differences between genotypes in each condition using Duncan *post hoc* tests ($p \leq 0.05$).

a linear and significant increase of DPS and VZA levels occurred when the Ψ_L decreased below −4 MPa and A_n was reduced below 5 μmol $CO_2 \cdot m^{-2} \cdot s^{-1}$. Moreover, a significant correlation was observed between Ψ_L and α-Toc/Chl, and between Chl a + b and α-Toc/Chl ($r = -0.51$ and $r = -0.48$, respectively, **Figures 3–5**).

DISCUSSION

The effects of water stress on growth may be considered the first line of defense, as it has been previously reported on olive trees (Trabelsi et al., 2019). This is essentially due to the inhibition of cell elongation by the interruption of water flow from the xylem to the surrounding cells (Nonami, 1998) and serves to reduce the amount to total water transpired by the plant under drought conditions. In the present study, growth measurements revealed genotypic variability in response to drought stress. Using stem and leaf growth parameters as indicators of tolerance, "Chemlali" rooted cuttings and "Zarrazi S" can be considered the genotypes more tolerant to drought. In contrast, "Chemlali S," "Oleaster S" and "Chetoui S" can be considered the most susceptible to drought stress because these seedlings showed the highest reduction in LPR. The superior performance of "Zarrazi S" to drought stress could be explained by the genotypic adaptation to the local environment of this variety, which is natural from Medenine

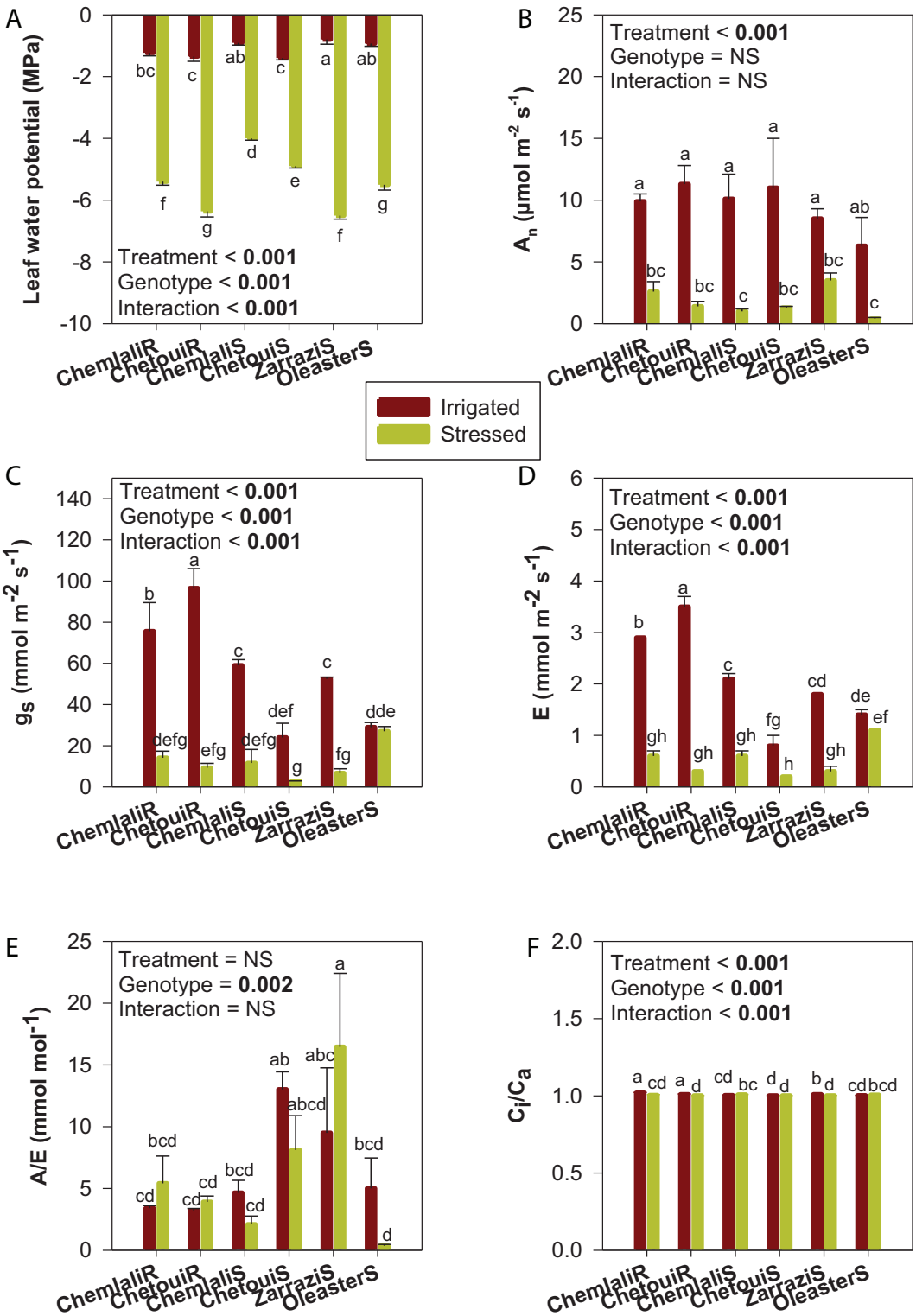


FIGURE 2 | Water status and leaf gas exchange in olive trees subjected to severe drought stress. **(A)** Leaf water potential (Ψ_L), **(B)** net photosynthesis rate (An), **(C)** stomatal conductance (gs), **(D)** transpiration (E), **(E)** water use efficiency (A/E) and **(F)** intercellular to ambient carbon dioxide concentration ratio (Ci/Ca) in olive trees obtained from cuttings (cv. "Chemlali" and "Chetoui") and obtained from seeds ("Chemlali S," "Chetoui S," "Zarrazi S" and "Oleaster S") after 60 days of drought stress. Values represent means ± S.E. of $n = 3$. A two-way analysis of variance (ANOVA) was used to examine if the effects of treatment (water regime) and genotype (cultivar) were statistically significant and to look at the significance of water regime × cultivar interaction effects. Means having the same letter are not significantly different according to Duncan *post hoc* test at $p \leq 0.05$.

TABLE 1 | Contents of chlorophyll (Chl a + b mg·g^{-1} DW), chlorophyll a/b ratio (Chl a/b), xanthophyll cycle pool per unit of Chl (VZA/Chl mmol·mol^{-1}), de-epoxidation state of the xanthophyll cycle (DPS), lutein per Chl ratio (Lut/Chl mmol·mol^{-1}), β-carotene per Chl ratio (β-car/Chl mmol·mol^{-1}), and α-tocopherol per unit of Chl (α-Toc/Chl mmol·mol^{-1}) in olive trees under irrigated and water stress conditions for 60 days.

			Chla + b	Chl a/b	VZA/Chl	DPS	Lut/Chl	β-car/Chl	α-Toc/Chl
Cuttings	"Chemlali"	Irrigated	5.5 ± 0.5^{de}	1.9 ± 0.02^{ab}	269.7 ± 21.3^{cde}	0.48 ± 0.01^{b}	573.3 ± 28.2^{bc}	193.8 ± 9.5^{ab}	40.0 ± 1.4^{bc}
		Stressed	4.6 ± 0.0^{ef}	1.8 ± 0.05^{bcd}	383.0 ± 26.6^{a}	0.65 ± 0.00^{a}	565.9 ± 18.8^{bc}	109.7 ± 28.8^{c}	82.5 ± 6.6^{a}
	"Chetoui"	Irrigated	4.8 ± 0.1^{ef}	2.0 ± 0.02^{a}	204.2 ± 7.2^{e}	0.50 ± 0.02^{b}	460.3 ± 5.0^{d}	182.1 ± 11.9^{b}	60.6 ± 8.5^{ab}
		Stressed	4.0 ± 0.1^{f}	1.8 ± 0.03^{bcd}	324.0 ± 39.2^{abc}	0.66 ± 0.02^{a}	531.6 ± 14.4^{bcd}	52.5 ± 10.9^{c}	85.9 ± 26.4^{a}
Seedlings	"Chemlali S"	Irrigated	8.9 ± 0.7^{b}	1.8 ± 0.01^{bcd}	200.2 ± 19.8^{e}	0.45 ± 0.04^{b}	562.0 ± 41.0^{bc}	217 ± 25.5^{ab}	14.9 ± 0.6^{def}
		Stressed	5.8 ± 0.1^{de}	1.6 ± 0.04^{e}	366.9 ± 37.3^{ab}	0.65 ± 0.00^{a}	678.6 ± 38.0^{a}	105.7 ± 10.8^{c}	25.4 ± 10.9^{cde}
	"Chetoui S"	Irrigated	8.7 ± 0.5^{b}	1.9 ± 0.01^{ab}	217.2 ± 18.4^{e}	0.49 ± 0.02^{b}	512.5 ± 24.4^{cd}	204.2 ± 19.3^{ab}	9.41 ± 1.7^{ef}
		Stressed	6.1 ± 0.4^{de}	1.9 ± 0.10^{abc}	332.9 ± 22.1^{abc}	0.61 ± 0.01^{a}	604.0 ± 16.8^{abc}	110.7 ± 39.9^{c}	57.1 ± 17.8^{ab}
	"Zarrazi S"	Irrigated	7.7 ± 0.6^{bc}	1.9 ± 0.04^{abc}	256.8 ± 21.3^{cde}	0.45 ± 0.03^{b}	621.3 ± 50.6^{ab}	247.9 ± 14.2^{a}	11.4 ± 2.8^{ef}
		Stressed	6.5 ± 0.5^{cd}	1.8 ± 0.06^{bcd}	399.0 ± 19.9^{a}	0.66 ± 0.00^{a}	616.5 ± 26.3^{ab}	180.2 ± 9.7^{b}	35.0 ± 5.1^{bcd}
	"Oleaster S"	Irrigated	12.9 ± 0.5^{a}	1.7 ± 0.05^{cde}	227.7 ± 7.23^{de}	0.48 ± 0.01^{b}	532.3 ± 24.7^{bcd}	172.3 ± 8.1^{b}	5.5 ± 0.6^{f}
		Stressed	8.2 ± 0.4^{b}	1.7 ± 0.06^{de}	302.3 ± 34.6^{bcd}	0.62 ± 0.01^{a}	576.0 ± 12.6^{bc}	71.2 ± 16.5^{c}	15.0 ± 2.8^{def}
	Treatment		$p < 0.001$	$p < 0.001$	$p < 0.001$	$p < 0.001$	**0.003**	$p < 0.001$	0.907
	Genotype		$p < 0.001$	**0.001**	**0.032**	0.668	**0.001**	$p < 0.001$	$P < 0.001$
	Interaction		**0.001**	0.242	0.58	0.353	0.173	0.697	0.931

Values represent means ± S.E. of n = 4. A two-way analysis of variance (ANOVA) was used to examine if the effects of treatment (water regime) and genotype (cultivar) were statistically significant and to look at the significance of interaction effects. Means on the same column having a same letter are not significantly different according to Duncan post hoc test at $p \leq 0.05$. Bold values show significant differences.

- southern Tunisia, in which the average annual rainfall does not exceed 180 mm. In our study, two irrigation treatments and 60 days of drought stress were selected for measurements of leaf water potential, net photosynthesis and photo- and antioxidant protection, which due to the high tolerance of some of the genotypes tested led to an adequate comparison between genotypes under well-watered and severe water deficit conditions. No information is available in the literature on selection methods including photoprotection and chloroplastic antioxidant markers such as carotenoids and tocopherols, and even less comparing olive tree rooted cuttings with seedlings (obtained from seeds). We filled here this knowledge gap by testing the drought stress response of several olive trees at the juvenile stage under semi-controlled conditions to offer a rapid alternative (in comparison to field trials) in genotype selection for crop improvement. Furthermore, found a link between both water potential and net photosynthesis rates with various photo- and antioxidant markers in olive trees subjected to severe water deficit, which helps us better understand the response of a very tolerant xerophyte plant, such as olive trees, to severe drought.

Plant growth decrease is mainly due to the loss of turgor pressure (Nonami, 1998). Indeed, exposure of plants to severe drought stress (60 days without irrigation) decreased significantly the olive trees water status attaining leaf water potential values between −6 and −4 MPa, thus indicating severe water deficit. For olive trees (cv. Koroneiki), 30 days without watering decreased significantly the Ψ_L to achieve −6.5 MPa (Boussadia et al., 2008). Similarly, for pistachio, Behboudian et al. (1986) revealed very low leaf water potential (−6 MPa), which is not completely unusual for woody plants growing under severe drought conditions. Furthermore, our results indicated that Ψ_L were differently affected by drought stress depending on the cultivar. Contrary to "Zarrazi S," "Chetoui S" showed the less reduction rate (71.4%) of Ψ_L. This difference is probably associated with the different mechanisms of osmotic adjustment adopted by the olive trees under water stress conditions, as previously reported by Dichio et al. (2005). In olive trees, damage caused by drought stress is mainly associated with a decrease of photosynthesis activity. The net photosynthesis rate showed a significant decrease (between 58 and 93%) after a long period of drought stress (60 days). These differences in gas exchange responses between olive trees could be used as a selection factor for olive trees grown under drought conditions (Ben Ahmed et al., 2009; Guerfel et al., 2009). In fact, the lowest decrease of A_n was recorded in "Zarrazi S" and, in a second degree, in "Chemlali" rooted cuttings, which allows them to withstand water stress more effectively than the other tested olive trees. These results are in accordance with those found by Guerfel et al. (2009), who have indicated a small decrease in A_n in "Chemlali" classified as a drought-tolerant cultivar. However, "Oleaster S" can be considered the most sensitive to water stress as they showed the highest depressive effect of water stress on A_n (92.8% reduction compared to control). In susceptibility to water stress, "Oleaster S" was followed by "Chemlali S," "Chetoui S" and "Chetoui" rooted cuttings with a mean of 88.4% reduction on A_n compared to its respective control. Moreover, the increase in water use efficiency (calculated here as the A/E ratio) could be considered as a drought tolerance index (Jimenez et al., 2013; Santana-Vieira et al., 2016). As compared to the rest of olive trees, "Zarrazi S" were able to maintain the highest A_n value even with a minimum Ψ_L of about −6.5 MPa and was more efficient in water use under severe drought conditions. Plants with a high A/E ratio may be suitable for cultivation in semi-arid regions (Santana-Vieira et al., 2016). It should be noted that cultivated varieties "Chemlali"

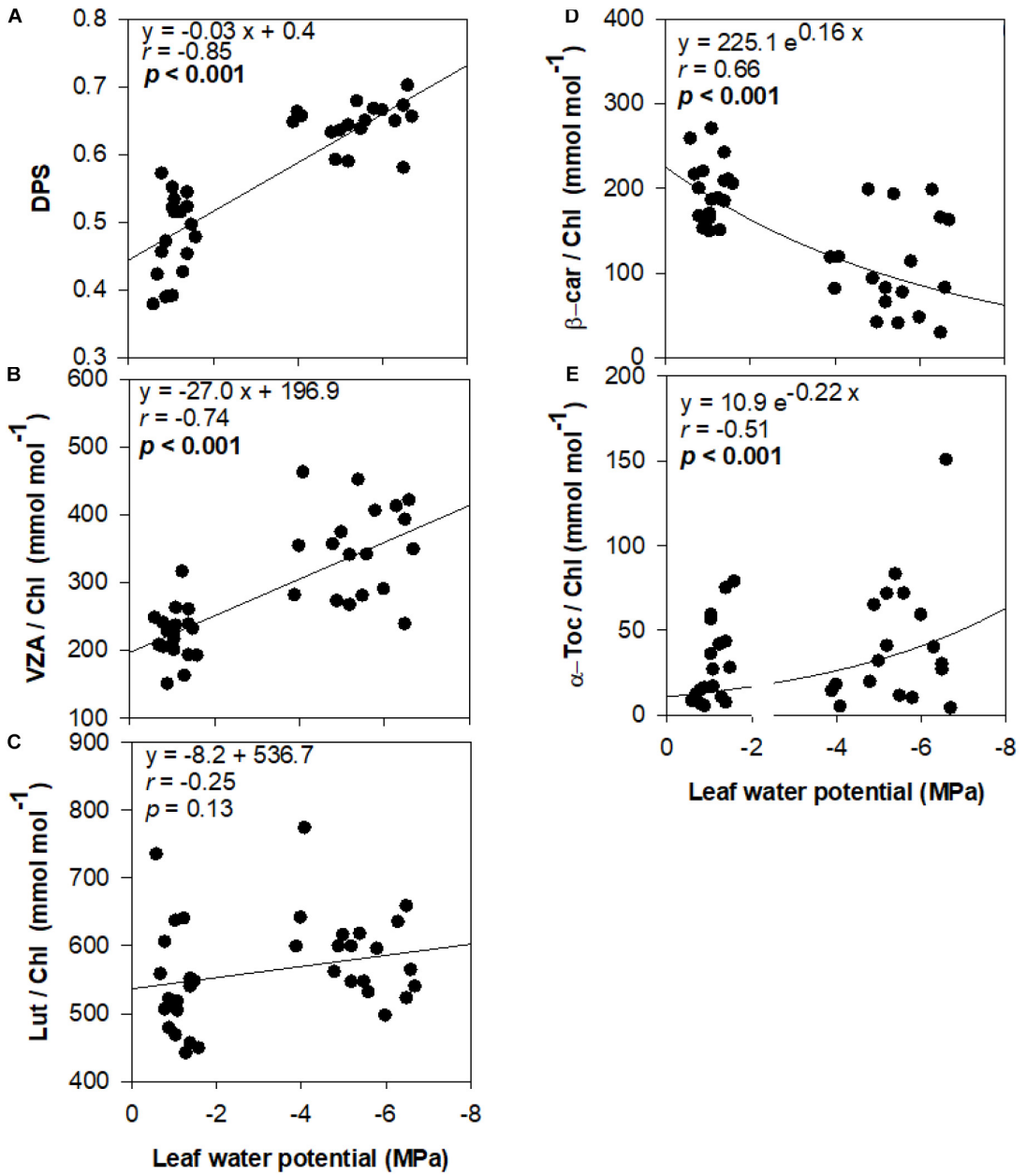


FIGURE 3 | Relationship between leaf water status and photo- and antioxidant protection in olive trees. Relationship between leaf water potential and the de-epoxidation state of the xanthophyll cycle **(A)**, the contents of the xanthophyll cycle pool **(B)**, lutein **(C)**, β-carotene **(D)**, and α-tocopherol **(E)** per unit of chlorophyll of olive trees after 60 days of treatments. Correlation was determined according to Pearson test. *p* values and corresponding correlation coefficient (*r*) are shown.

and "Chetoui" are at the origin of selected genotypes propagated vegetatively. The "Chemlali" variety is known for its tolerance to drought, hence the predominance of its cultivation in central and southern Tunisia in arid and semi-arid conditions, whereas the "Chetoui" variety with less pronounced tolerance to drought predominates in the north with climatic conditions where rainfalls are more abundant.

It is interesting to note that despite the very low values of −6 MPa achieved, some photosynthetic activity was maintained in some cultivars of olive trees. At leaf water potentials below −4 MPa, net photosynthesis rate ranged between 0.45 and 3.57 μmol $CO_2 \cdot m^{-2} \cdot s^{-1}$. The ability to maintain some photosynthetic activity at very low leaf water potential was reported in other fruity tree species such as pistachio (Behboudian et al., 1986). Indeed, these authors showed that although photosynthesis declined with decreasing leaf water potential, plants continued to photosynthesize until a leaf water potential of as low as −5 MPa was reached which is a typical response of xerophytic plants. Likewise, in the case of olive tree (cv. Koroneiki), Boussadia et al. (2008)

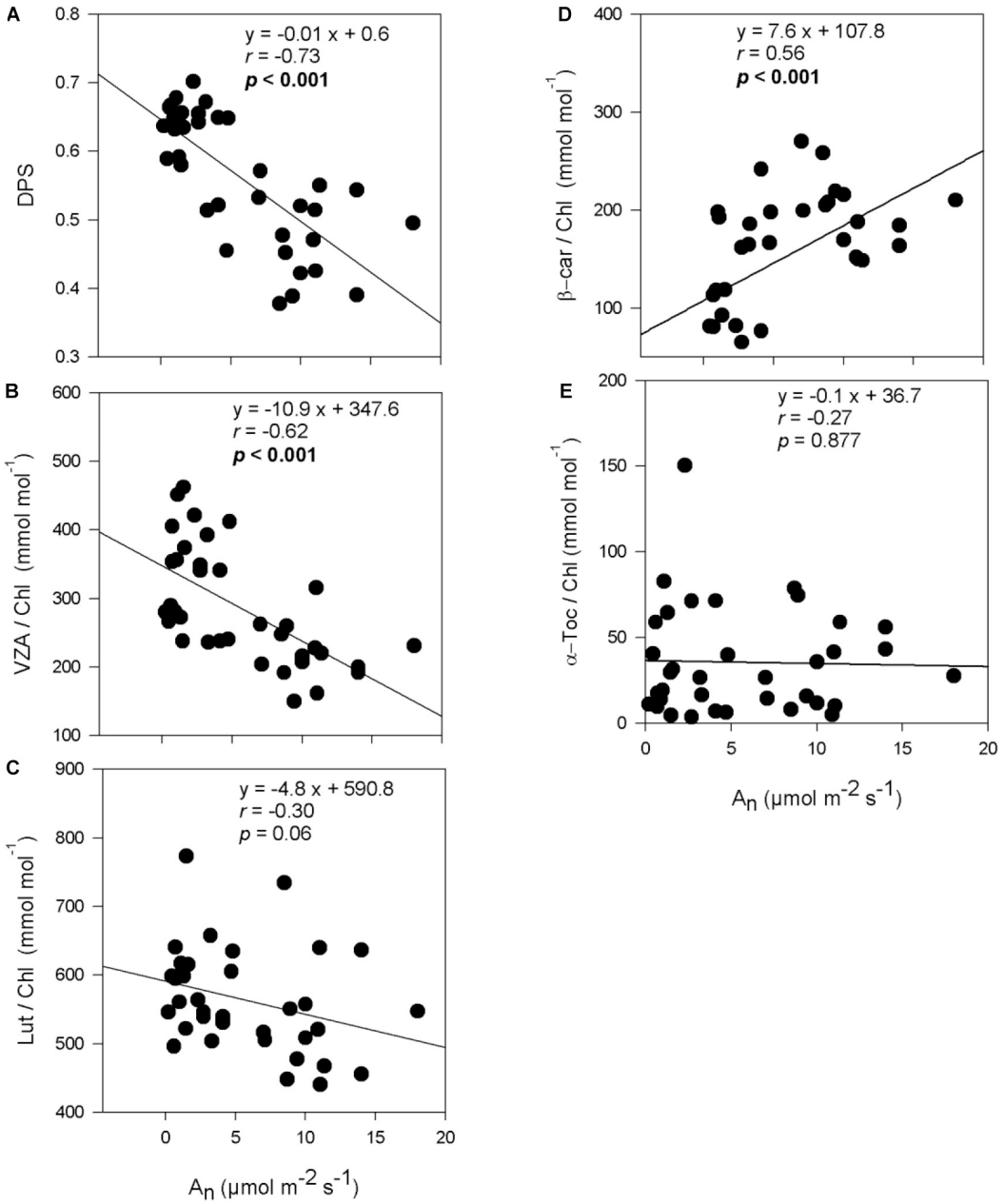


FIGURE 4 | Relationship between photosynthesis and photo- and antioxidant protection in olive trees. Relationship between net photosynthesis rates and the de-epoxidation state of the xanthophyll cycle **(A)**, the contents of the xanthophyll cycle pool **(B)**, lutein **(C)**, β-carotene **(D)**, and α-tocopherol **(E)** per unit of chlorophyll of olive trees after 60 days of treatments. Correlation was determined according to Pearson test. *p* values and corresponding correlation coefficient (r) are shown.

recorded a net CO_2 assimilation rate of 1 µmol $CO_2 \cdot m^{-2} \cdot s^{-1}$ under severe drought stress in which the leaf water potential dropped to very low values of −6.5 MPa. It appears from the present study that stressed young olive plants maintained some photosynthetic activity at low leaf water potential, which might allow them help surviving the severe water stress conditions. It is noteworthy that conditions imposed to plants during leaf gas exchange measurements were very severe, including high temperatures (35°C) and a high vapor pressure deficit (5 KPa), which explains the low stomatal conductance and photosynthesis rates together with the high Ci/Ca values observed in well-watered plants. Similar stomatal conductance, net photosynthesis rates and Ci/Ca ratios were observed for anti-sense Rubisco transgenic tobacco plants (Von Caemmerer et al., 2004). Leaf gas exchange results obtained in our study suggest that there was a stomatal and non-stomatal limitation of photosynthesis under well-watered conditions, and that both of them increased under severe water deficit, given that

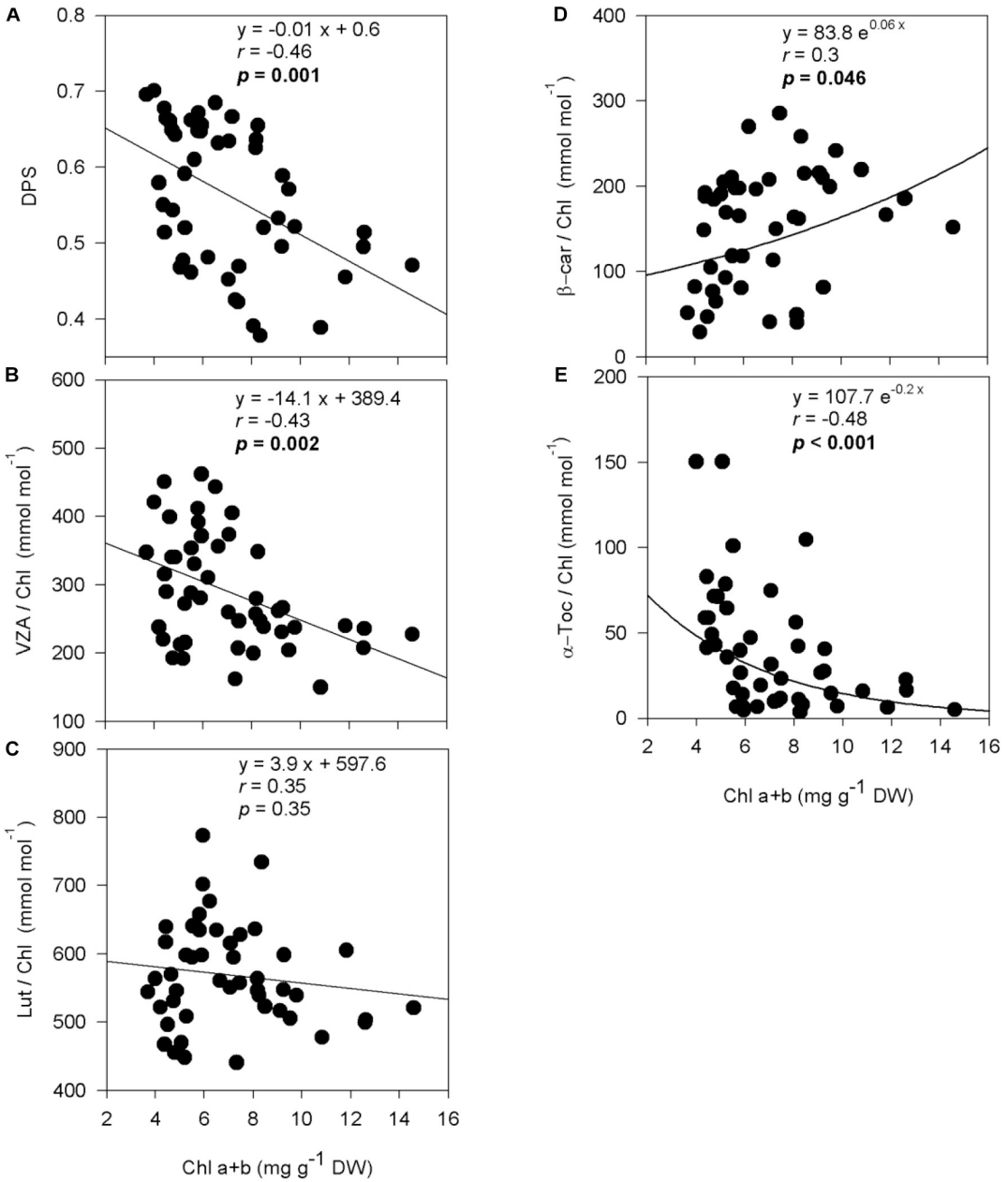


FIGURE 5 | Relationship between chlorophyll loss and photo- and antioxidant protection in olive trees. Relationship between chlorophyll contents and the de-epoxidation state of the xanthophyll cycle **(A)**, the contents of the xanthophyll cycle pool **(B)**, lutein **(C)**, β-carotene **(D)**, and α-tocopherol **(E)** per unit of chlorophyll of olive trees after 60 days of treatments. Correlation was determined according to Pearson test. *p* values and corresponding correlation coefficient (r) are shown.

not only stomatal conductance and net photosynthesis were reduced but also the Ci/Ca ratio kept constant in water-stressed plants. It is very likely that the severe stomatal closure in severely water-stressed plants did not result in an increased Ci/Ca ratio because Rubisco and non-stomatal limitations of photosynthesis impaired the correct functioning of the Calvin cycle, which might indeed led to a oversaturation of the photosynthetic electron transport and excess excitation energy in chloroplasts. To avoid the potential deleterious effects of oxidative damage induced by water stress, plants have evolved both enzymatic and non-enzymatic antioxidant defense systems. The role of photosynthetic pigments (total carotenoids) and enzymatic antioxidant systems as mechanisms of water stress tolerance in olive trees have been already investigated previously (Sofo et al., 2005, 2008; Bacelar et al., 2006, 2007; Brito et al., 2009; Ben Abdallah et al., 2017; reviewed by Brito et al., 2019). Hence, we focused here on the study of specific photosynthetic pigments with a function in photoprotection

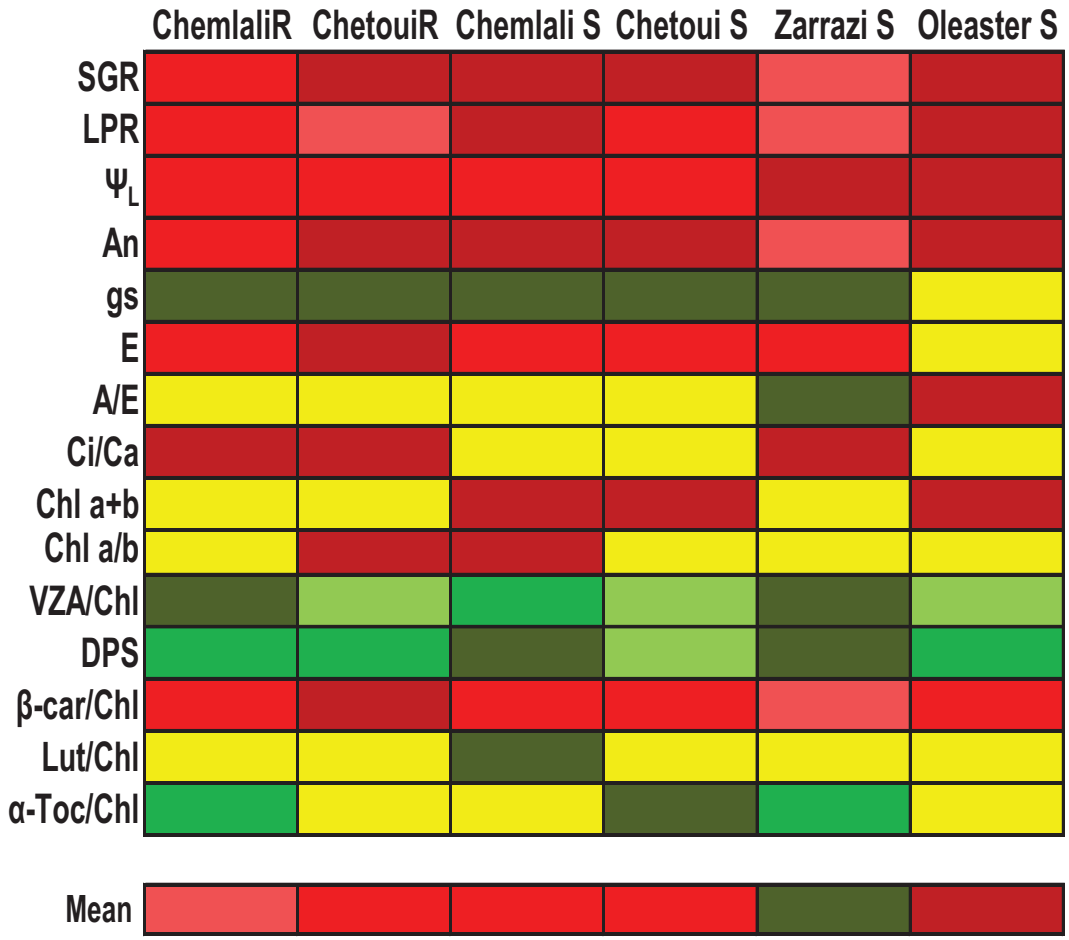


FIGURE 6 | Tolerance to severe water stress of olive genotypes. The color gradation ranges from dark red to dark green to indicate progressively increased stress tolerance. Three levels of susceptibility and three levels of tolerance were given for each of the parameters in red and green, respectively, and the mean of tolerance was then calculated considering all parameters measured after 60 days of treatments. SGR, Stem growth rate; LPR, Leaf production rate; Ψ_L, Leaf water potential; A_n, Net photosynthesis rate; gs, stomatal conductance; E, transpiration; A/E, water use efficiency; Ci/Ca, intercellular to air carbon dioxide concentration ratio; Chl a + b, Total chlorophyll; Chl a/b, chlorophyll a/b ratio; VZA/Chl, xanthophyll cycle pool per unit of Chl; DPS, de-epoxidation state of the xanthophyll cycle; Lut/Chl, lutein per Chl ratio; β-car/Chl, β-carotene per Chl ratio; α-Toc/Chl, α-tocopherol per unit of Chl. Genotypes: Rooted cuttings, "Chemlali" and "Chetoui"; Seedlings, "Chemlali S," "Chetoui S," "Zarrazi S" and "Oleaster S."

(such as individual xanthophylls and carotenes) and other non-enzymatic chloroplastic antioxidants (such as tocopherols) Among those molecules, carotenoids and tocopherols are well known to play an important role in preventing photo-oxidative stress in several species, including other xerophytes such as rosemary plants (Munné-Bosch and Alegre, 2000). Our results showed an increase in the xanthophyll cycle pool (VZA) and the de-epoxidation state of the xanthophyll cycle (DPS) levels in stressed olive trees. The contribution of VZA to olive drought tolerance mechanisms is clearly demonstrated in "Zarrazi S" and "Chemlali" rooted cuttings that accumulated the largest amount of VZA/Chl (399 and 383 mmol·mol^{-1}, respectively). The lowest VZA/Chl level (302 mmol·mol^{-1}) was recorded in "Oleaster S." Indeed, water stress is known to induce the activation of the xanthophyll cycle, in which violaxanthin is de-epoxidized to antheraxanthin and then zeaxanthin, enabling excess light energy to be dissipated as heat (Demmig-Adams and Adams III , 1996). The increase observed in DPS and VZA/Chl levels was associated with the decrease in Ψ_L and A_n (**Figures 3**, **4**). It appears therefore that the antioxidant defense mechanisms can be efficiently developed even when the Ψ_L decreased below −4 MPa and A_n turned less than 5 μmol $CO_2 \cdot m^{-2} \cdot s^{-1}$. Indeed, loss of leaf turgor and photosynthetic limitation might be involved in triggering the activation of photoprotective mechanisms in young olive trees under severe water stress. β-carotene/Chl ratio was significantly decreased under drought conditions. A similar response was reported by Sircelj et al. (1999), who described an increase in the zeaxanthin level at the expense of β-carotene in field-grown apple trees subjected to water stress. Reduced β-carotene associated with increased zeaxanthin contents, as occurred in our study, may be indicative of an enhanced conversion of β-carotene to xanthophyll cycle components for excess energy dissipation, as well as an increased oxidation of β-carotene

by singlet oxygen in light harvesting complexes and thylakoid membranes (Burton and Ingold, 1984; D'Alessandro and Havaux, 2019). Furthermore, changes in α-tocopherol content under water stress conditions were also observed. In fact, Ψ_L decreases paralleled an accumulation of α-Toc/Chl in leaves in all studied cultivars, although significantly only for "Chemlali" rooted cuttings, "Chetoui S" and "Zarrazi S." Differences observed in α-Toc/Chl level could be related to genotypic differences in antioxidant capacity among olive trees. α-Tocopherol is involved in the elimination of $^1O_2$ (Fahrenholtz et al., 1974; Muñoz and Munné-Bosch, 2019) and among other functions, α-tocopherol is known to inhibit the propagation of lipid peroxidation in thylakoid membranes by reducing the accumulation of lipid peroxyl radicals in chloroplasts (Munné-Bosch and Alegre, 2002; Muñoz and Munné-Bosch, 2019). α-Toc/Chl ratio was also associated with the decrease in Chl a + b, which may be related to the fact that this antioxidant can be synthesized using the phytol recycling pathway from chlorophyll degradation (in the so-called phytol recycling pathway, see Muñoz and Munné-Bosch, 2019). The accumulation of photoprotective molecules together with a reduction in chlorophyll content may be an effective strategy to survive severe drought conditions, as it has been observed in other highly drought-tolerant plants (Kyparissis et al., 2000; Munné-Bosch and Alegre, 2000).

A summary of the differences in the response to severe water stress among olive trees are shown in **Figure 6**. Our data suggest that "Zarrazi S" may cope better with drought conditions which exhibited a lower decrease in growth and net photosynthesis rates, as well as a higher accumulation of photoprotective molecules. "Chemlali" rooted cuttings showed an acclimation response close to that of "Zarrazi S." "Oleaster S" can be considered the most sensitive to these water stress conditions as it was the genotype showing the highest depressive effect of water stress on growth and net photosynthesis rates and lower photoprotective capacity. In susceptibility to water stress, "Oleaster S" were followed by "Chemlali S," "Chetoui S" and "Chetoui" rooted cuttings (**Figure 6**). To our knowledge, this is the first time in which the activation of photo- and antioxidant protection mechanisms is linked to leaf water status, net photosynthetic rates and chlorophyll loss in olive trees, showing that mechanisms of photo- and antioxidant protection can still be active at very low water potentials in this plant species and that the better adapted genotypes show their photo- and antioxidant protection capacity intact, despite suffering from severe drought. In general, "Chemlali" rooted cuttings were more drought tolerant than "Chemlali S", and "Chetoui" root cuttings and seedlings did respond similarly, thus indicating that vegetative propagation in these two genotypes, and most particularly in Chemlali, may be effective in large-scale propagation for field cultivation in arid or semi-arid areas. Further research is, however, needed to unravel whether the same occurs in "Zarrazi" genotype, which was the genotype showing the highest drought stress tolerance among all the genotypes tested.

In conclusion, withholding irrigation for 60 days induced a considerable decrease in growth, leaf water potential and net photosynthesis rates in 1-year-old olive trees. This might lead to the activation of photoprotective mechanisms, including, increases in xanthophyll cycle de-epoxidation, and accumulation of α-tocopherol as chlorophyll loss progressed in severely stressed plants. These increases may contribute to the survival of young olive trees under severe water stress conditions. The study also revealed that "Zarrazi" seedlings may serve as drought-tolerant rootstock which exhibited a lower decrease in growth and net photosynthesis rate, as well as a higher antioxidant activity. "Oleaster," "Chemlali" and "Chetoui" seedlings could be comparatively considered in this order as more drought-sensitive rootstocks. "Chemlali" rooted cuttings showed the tolerance behavior closer to that of "Zarrazi" seedlings, thus, "Chemlali" rooted cuttings are interesting to create vegetatively propagated drought-tolerant rootstocks and/or cultivars used for breeding programs.

DATA AVAILABILITY STATEMENT

The raw data supporting the conclusions of this article will be made available by the authors, without undue reservation.

AUTHOR CONTRIBUTIONS

SB, AC-R, and SM-B conceived and designed the study. SB, EF, and MM performed the experiments. SB, OE, and SM-B analyzed the data and wrote the manuscript, while other authors performed a critical revision of the manuscript. AC-R, FBA, LF, and SM-B supervised the work. All authors approved the final manuscript.

FUNDING

This research was financially supported by the Tunisian Ministry of Higher Education and Scientific Research and the Tunisian Ministry of Agriculture (grant number L22019204063).

ACKNOWLEDGMENTS

We are thankful to Mrs. Zina Ben Salem, Mrs. Hajera Chatti, and Mr. Fouad Labidi for their technical assistance.

REFERENCES

Amaral, J. S., Casal, S., Torres, D., Seabra, R. M., and Oliveira, B. P. P. (2005). Simultaneous determination of tocopherols and tocotrienols in hazelnuts by a normal phase liquid chromatographic method. *Anal. Sci.* 21, 1545–1548. doi: 10.2116/analsci.21.1545

Bacelar, E. A., Santos, D. L., Moutinho-Pereira, J. M., Gonçalves, B. C., Ferreira, H. F., and Correia, C. M. (2006). Immediate responses and adaptative strategies of three olive cultivars under contrasting water availability regimes: changes on

structure and chemical composition of foliage and oxidative damage. *Plant Sci.* 170, 596–605. doi: 10.1016/j.plantsci.2005.10.014

Bacelar, E. A., Santos, D. L., Moutinho-Pereira, J. M., Lopes, J. L., Goncalves, B. C., Ferreira, T. C., et al. (2007). Physiological behaviour, oxidative damage and antioxidative protection of olive trees grown under different irrigation regimes. *Plant Soil* 292:1. doi: 10.1007/s11104-006-9088-1

Behboudian, M. H., Walker, R. R., and Törökfalvy, E. (1986). Effects of water stress and salinity on photosynthesis of pistachio. *Sci. Hort.* 29, 251–261. doi: 10.1016/0304-4238(86)90068-3

Ben Abdallah, M., Methenni, K., Nouairi, I., Zarrouk, M., and BenYoussef, N. (2017). Drought priming improves subsequent more severe drought in a drought-sensitive cultivar of olive cv. *Chétoui. Sci. Hort.* 221, 43–52. doi: 10.1016/j.scienta.2017.04.021

Ben Ahmed, Ch, Ben Rouina, B., Sensoy, S., Boukhris, M., and Ben Abdallah, F. (2009). Changes in gas exchange, proline accumulation and antioxidative enzyme activities in three olive cultivars under severe water availability stress. *Environ. Exp. Bot.* 67, 345–352. doi: 10.1016/j.envexpbot.2009.07.006

Ben Hamed, S., Lefi, E., and Chaieb, M. (2016). Physiological responses of *Pistacia vera* L. versus *Pistacia atlantica* Desf. to water stress conditions under arid bioclimate in Tunisia. *Sci. Hort.* 203, 224–230. doi: 10.1016/j.scienta.2016.03.019

Boussadia, O., Ben Mariem, F., Mechri, B., Boussetta, W., Braham, M., and Ben El Hadj, S. (2008). Response to drought of two olive tree cultivars (cv Koroneki and Meski). *Sci. Hort.* 116, 388–393. doi: 10.1016/j.scienta.2008.02.016

Brito, C., Dinis, L.-T., Moutinho-Pereira, J., and Correia, C. M. (2019). Drought stress effects and olive tree acclimation under a changing climate. *Plants* 8:232. doi: 10.3390/plants8070232

Brito, G., Costa, A., Coelho, C., and Santos, C. (2009). Large-scale field acclimatization of *Olea maderensis* micropropagated plants: morphological and physiological survey. *Trees* 23, 1019–1031. doi: 10.1007/s00468-009-0344-x

Burton, G. W., and Ingold, K. U. (1984). beta-Carotene: an unusual type of lipid antioxidant. *Science* 224, 569–573. doi: 10.1126/science.6710156

D'Alessandro, S., and Havaux, M. (2019). Sensing β-carotene oxidation in photosystem II to master plant stress tolerance. *New Phytol.* 223, 1776–1783. doi: 10.1111/nph.15924

De Ollas, C., Morillón, R., Fotopoulos, V., Puértolas, J., Ollitrault, P., Gómez-Cadenas, A., et al. (2019). Facing climate change: biotechnology of iconic Mediterranean woody crops. *Front. Plant Sci.* 10:427. doi: 10.3389/fpls.2019.00427

Demmig-Adams, B., and Adams III, W. W. (1996). Xanthophyll cycle and light stress in nature: uniform response to excess direct sunlight among higher plant species. *Planta* 198, 460–470. doi: 10.1007/BF00620064

Dichio, B., Xiloyannis, C., Sofo, A., and Montanaro, G. (2005). Osmotic regulation in leaves and roots of olive trees during a water deficit and rewatering. *Tree Physiol.* 26, 179–185. doi: 10.1093/treephys/26.2.179

Fahrenholtz, S. R., Doleiden, F. H., Trozzolo, A. M., and Lamola, A. A. (1974). On the quenching of singlet oxygen by alpha-tocopherol. *Photo. Chem. Photobiol.* 20, 505–509. doi: 10.1111/j.1751-1097.1974.tb06610.x

Flexas, J., and Medrano, H. (2002). Drought-inhibition of photosynthesis in C3 plants: stomatal and non-stomatal limitations revisited. *Ann. Bot.* 89, 183–189. doi: 10.1093/aob/mcf027

Gargouri, K., Bentaher, H., and Rhouma, A. (2012). A novel method to assess drought stress of olive tree. *Agron. Sustain. Dev.* 32, 735–745. doi: 10.1007/s13593-011-0078-1

Guerfel, M., Baccouri, O., Boujnah, D., Chaïbi, W., and Zarrouk, M. (2009). Impacts of water stress on gas exchange, water relations, chlorophyll content and leaf structure in the two main Tunisian olive (*Olea europaea* L.) cultivars. *Sci. Hort.* 119, 257–263. doi: 10.1016/j.scienta.2008.08.006

Hasanuzzaman, M., Nahar, K., Hossain, M. S., Al Mahmud, J., Rahman, A., Inafuku, M., et al. (2017). Coordinated actions of glyoxalase and antioxidant defense systems in conferring abiotic stress tolerance in plants. *Int. J. Mol. Sci.* 8:200. doi: 10.3390/ijms18010200

Hoagland, D. R., and Arnon, D. I. (1950). *The Water Culture Method for Growing Plants Without Soil*. Berkeley, CA: California Agricultural Experiment Station Circular, 347.

Jimenez, S., Dridi, J., Gutiérrez, D., Moret, D., Irigoyen, J. J., Moreno, M. A., et al. (2013). Physiological, biochemical and molecular responses in four *Prunus* rootstocks submitted to drought stress. *Tree Physiol.* 33, 1061–1075. doi: 10.1093/treephys/tpt074

Kyparissis, A., Drilias, P., and Manetas, Y. (2000). Seasonal fluctuations in photoprotective (xanthophyll cycle) and photoselective (chlorophylls) capacity in eight Mediterranean plant species belonging to two different growth forms. *Aust. J. Plant Physiol.* 27, 265–272. doi: 10.1071/PP99037

Laczko, F., and Aghazarm, C. (2009). *Migration, Environment and Climate Change: Assessing the Evidence*. Grand-Saconnex: International Organization for Migration.

Munné-Bosch, S., and Alegre, L. (2000). Changes in carotenoids, tocopherols and diterpenes during drought and recovery, and the biological significance of chlorophyll loss in *Rosmarinus officinalis* plants. *Planta* 210, 925–931. doi: 10.1007/s004250050699

Munné-Bosch, S., and Alegre, L. (2002). Interplay between ascorbic acid and lipophilic antioxidant defences in chloroplasts of water-stressed *Arabidopsis* plants. *FEBS Lett.* 524, 145–148. doi: 10.1016/S0014-5793(02)03041-7

Muñoz, P., and Munné-Bosch, S. (2019). Vitamin E in plants: biosynthesis, transport, and function. *Trends Plant Sci.* 24, 1040–1051. doi: 10.1016/j.tplants.2019.08.006

Murashigue, T., and Skoog, F. (1962). A revised medium for rapid growth and bioassays with tobacco tissue cultures. *Physiol. Plant* 15, 473–479. doi: 10.1111/j.1399-3054.1962.tb08052.x

Nonami, H. (1998). Plant water relations and control of cell elongation at low water potentials. *J. Plant Res.* 111, 373–382. doi: 10.1007/BF02507801

Perez-Martin, A., Michelazzo, C., Torres-Ruiz, J. M., Flexas, J., Fernández, J. E., Sebastiani, L., et al. (2014). Regulation of photosynthesis and stomatal and mesophyll conductance under water stress and recovery in olive trees: correlation with gene expression of carbonic anhydrase and aquaporins. *J. Exp. Bot.* 65, 3143–3156. doi: 10.1093/jxb/eru160

Petridis, A., Therios, I., Samouris, G., Koundouras, S., and Giannakoula, A. (2012). Effect of water deficit on leaf phenolic composition, gas exchange, oxidative damage and antioxidant activity of four Greek olive (*Olea europaea* L.) cultivars. *Plant Physiol. Biochem.* 60, 1–11. doi: 10.1016/j.plaphy.2012.07.014

Rodrigues de Lima, K., Brandão de Carvalho, C. A., Vidal Azevedo, F. H., de Campos, F. P., et al. (2019). Morphogenesis and forage accumulation of *Urochloa ruziziensis* under nitrogen and potassium fertilization management. *Semina Ciências Agrárias* 40, 1605–1618. doi: 10.5433/1679-0359.2019v40n4p1605

Santana-Vieira, D. D. S., Freschi, L., Almeida, L. A., Moraes, D. H., Neves, D. M., Santos, L. M., et al. (2016). Survival strategies of *citrus* rootstocks subjected to drought. *Sci. Rep.* 6:38775. doi: 10.1038/srep38775

Shannon, M. C., Grieve, C. M., and Francois, L. E. (1994). "Whole-plant response to salinity," in *Plant–Environment Interactions*, ed. R. E. Wilkinson (New York, NY: Marcel Dekker), 199–244.

Sircelj, H., Batic, F., and Stampar, F. (1999). Effects of drought stress on pigment, ascorbic acid and free amino acids content in leaves of two apple tree cultivars. *Phyton* 39, 97–100.

Sircelj, H., Tausz, M., Grill, D., and Batic, F. (2007). Detecting different levels of drought stress in apple trees (*Malus domestica* Borkh.) with selected biochemical and physiological parameters. *Sci. Hort.* 113, 362–369. doi: 10.1016/j.scienta.2007.04.012

Sofo, A., Dichio, B., Xiloyannis, C., and Masia, A. (2004). Lipoxygenase activity and proline accumulation in leaves and roots of olive trees in response to drought stress. *Physiol. Plant* 121, 58–65. doi: 10.1111/j.0031-9317.2004.00294.x

Sofo, A., Dichio, B., Xiloyannis, C., and Masia, A. (2005). Antioxidant defences in olive trees during drought stress: changes in activity of some antioxidant enzymes. *Func. Plant Biol.* 32, 45–53. doi: 10.1071/FP04003

Sofo, A., Manfreda, S., Fiorentino, M., and Dichio, B. (2008). The olive tree: a paradigm for drought tolerance in Mediterranean climates. *Hydrol. Earth Syst. Sci.* 12, 293–301. doi: 10.5194/hess-12-293-2008

Sun, J., Wang, M., Lyu, M., Niklas, K. J., Zhong, Q., Li, M., et al. (2019). Stem and leaf growth rates define the leaf size vs. number trade-off. *AoB Plants* 11:plz063. doi: 10.1093/aobpla/plz063

Therios, I. N. (2009). *Olives, Crop Production Science in Horticulture 18*. Wallingford: CABI Publishing.

Trabelsi, L., Gargouri, K., Ben Hassena, A., Mbadra, C., Ghrab, M., Ncubec, B., et al. (2019). Impact of drought and salinity on olive water status and physiological

performance in an arid climate. *Agric. Water Manag.* 213, 749–759. doi: 10.1016/j.agwat.2018.11.025

Trifilo, P., Lo Gullo, M. A., Nardini, A., Pernice, F., and Salleo, S. (2007). Rootstock effects on xylem conduit dimensions and vulnerability to cavitation of *Olea europaea* L. *Trees* 21, 549–556. doi: 10.1007/s00468-007-0148-9

Von Caemmerer, S., Lawson, T., Oxborough, T., Baker, N. R., Andrews, T. J., and Raines, C. A. (2004). Stomatal conductance does not correlate with photosynthetic capacity in transgenic tobacco with reduced amounts of Rubisco. *J. Exp. Bot.* 55, 1157–1166. doi: 10.1093/jxb/erh128

Conflict of Interest: The authors declare that the research was conducted in the absence of any commercial or financial relationships that could be construed as a potential conflict of interest.

Copyright © 2020 Baccari, Elloumi, Chaari-Rkhis, Fenollosa, Morales, Drira, Ben Abdallah, Fki and Munné-Bosch. This is an open-access article distributed under the terms of the Creative Commons Attribution License (CC BY). The use, distribution or reproduction in other forums is permitted, provided the original author(s) and the copyright owner(s) are credited and that the original publication in this journal is cited, in accordance with accepted academic practice. No use, distribution or reproduction is permitted which does not comply with these terms.

frontiers in Plant Science

ORIGINAL RESEARCH
published: 17 December 2020
doi: 10.3389/fpls.2020.599230

Selecting Aragonez Genotypes Able to Outplay Climate Change–Driven Abiotic Stress

Luísa Carvalho†, Elsa Gonçalves†, Sara Amâncio and Antero Martins*

LEAF- Linking Landscape, Environment, Agriculture and Food, Instituto Superior de Agronomia, Universidade de Lisboa, Lisbon, Portugal

OPEN ACCESS

Edited by:
Raul Antonio Sperotto, Universidade do Vale do Taquari - Univates, Brazil

Reviewed by:
Sangram Keshari Lenka, TERI Deakin Nanobiotechnology Centre, India
Junhong Zhang, Huazhong Agricultural University, China

***Correspondence:**
Luísa Carvalho
lcarvalho@isa.ulisboa.pt

†*These authors have contributed equally to this work*

Specialty section:
This article was submitted to Plant Abiotic Stress, a section of the journal Frontiers in Plant Science

Received: *26 August 2020*
Accepted: *17 November 2020*
Published: *17 December 2020*

Citation:
Carvalho L, Gonçalves E, Amâncio S and Martins A (2020) Selecting Aragonez Genotypes Able to Outplay Climate Change–Driven Abiotic Stress. Front. Plant Sci. 11:599230. doi: 10.3389/fpls.2020.599230

High temperatures and extreme drought are increasingly more frequent in Portugal, which represents a strong threat to viticulture in certain regions of the country. These multifactorial abiotic stresses are threatening viticultural areas worldwide, and the problem can hardly be overcome only by changing cultural practices. This scenario has raised a major challenge for plant scientists to find ways to adapt existing varieties to the new conditions without loss of their characteristic flavors, yield, and associated varietal character of wines. Aragonez (syn. Tempranillo) is one such variety, widely cultivated in Portugal and Spain, with specific characteristics associated with *terroir*. In this context, insight into intravarietal variability to enable its exploitation for selection becomes an important tool to mitigate the effect of multifactorial stresses driven by climate changes. The present work describes an innovative selection approach: selection for abiotic stress tolerance, measured by the leaf temperature of clones under environmental conditions of drought and extreme heat. This evaluation was complemented with values of yield and quality characteristics of the must (pH, acidity, °Brix, and anthocyanins). The application of this methodology was done in an experimental population of 255 clones of Tempranillo for 3 years. The genotypes were then ranked according to their level of tolerance to abiotic stress without loss of yield/quality. To understand the differences at the transcription level that could account for such variability, several of the most tolerant and most sensitive genotypes were analyzed for key genes using reverse transcriptase–quantitative polymerase chain reaction. The results enabled the selection of a group of genotypes with increased tolerance to stress, in relation to the average of the variety, which maintained the typical must quality of Aragonez. In parallel, several transcripts previously acknowledged as markers for abiotic stress tolerance were identified in several clones and are possible targets for plant breeding and genetic modification and/or to develop screening procedures to select genotypes better adapted to the abiotic stress driven by climate change.

Keywords: abiotic stress tolerance, empirical best linear unbiased predictors (EBLUP of genotypic effects), polyclonal selection, quality of the must, RT-qPCR

INTRODUCTION

Grapevine is one of the most economically important crop species in Portugal. Its main product, grapes, feeds the wine sector, highly significant for the national economy and a major export. In 2018, Portugal was the fifth wine producer in the European Union, and the 11th worldwide (International Organisation of Vine and Wine [OIV], 2018). Viticulture is highly dependent upon climatic conditions during the growing season, and thus wine production is being affected by climate change. Return on investment is driven by yield and its quality; thus, it is relevant to study the impact of climate change, namely, the implications of changes in temperature levels and patterns, radiation, and water availability on those parameters. Portugal is extremely rich in autochthonous grapevine varieties with more than 250 already known and with a high level of intravarietal variability (Martins and Gonçalves, 2015).

Intravarietal diversity has ensured stable behavior of the varieties over time and constitutes today the raw material for carrying out the selection with high genetic and economic gains of different relevant characteristics. Polyclonal selection consists in the selection of a top-ranked set of genotypes concerning target traits in an experimental population containing a representative sample of the intravarietal variability, and the genetic gains of selection are predicted as the average of the empirical best linear unbiased predictors (EBLUPs) of the genotypic effects of those traits in the set of selected genotypes (Martins and Gonçalves, 2015). Theoretical developments about the most suitable experimental designs and statistical models for the quantification of intravarietal diversity and prediction of genetic gains of polyclonal selection have been developed in the past years (Gonçalves et al., 2010, 2013). Specifically for selection purposes, the multivariate mixed-model approach proposed by Gonçalves et al. (2016) was shown to provide greater accuracy and precision in selection. Actually, the exploitation of intravarietal genetic variability became a crucial strategy to face future challenges (climate change, biotic and abiotic stresses, consumer demands, etc.), and its importance was recently recognized by the OIV through the adoption of Resolution OIV-VITI 564B-2019 (2019).

Vine phenology, that is, the date on which bud break, flowering, *véraison*, and maturation occur, is driven by temperature. This relation is so strong that vine phenology can be predicted by models based on temperature alone (Parker et al., 2011). During ripening, sugar accumulation increases with temperature, but certain secondary metabolites, such as anthocyanins, are negatively affected by high temperature (van Leeuwen and Darriet, 2016). Grape acidity, in particular, malic acid content, decreases in high temperature (van Leeuwen and Darriet, 2016).

Limited vine water availability affects photosynthesis and leaf transpiration (Chaves et al., 2010), shoot (Carvalho et al., 2016), and root development (Dry et al., 2000), and leaf and berry mineral nutrition (Gonzalez-Dugo et al., 2010). Stomatal control of leaf transpiration is a physiological drought avoiding mechanism that enables the optimization of crop water use while preventing embolism events (Lovisolo et al., 2010). The severity of a drought and its timing and duration impair final berry size and composition (Deloire et al., 2004). Generally, moderate water stress during the ripening period is favorable for sugar accumulation (van Leeuwen et al., 2009) and increases the anthocyanin and tannin contents in berries (van Leeuwen and Darriet, 2016). In temperate climates, conditions of water deficit are favorable for producing high-quality red wines (van Leeuwen et al., 2009).

Grapevine varieties demonstrate significant variability in their hydraulic behavior (Schultz, 2003), a feature reflected in the variety-specific responses to water deficit (Carvalho et al., 2016). Differences in drought tolerance between varieties (Carvalho et al., 2016; Carvalho et al., 2017) are likely due to differences in root-to-shoot signaling and differential hydraulic regulation between those varieties (Vandeleur et al., 2009; Zarrouk et al., 2016).

In the wine industry, the distinct and recognizable characteristics of wine are usually attributed to differences in the chemical composition of flavonoid compounds, as a varietal "signature" (Downey et al., 2006). Phenylalanine-derived polyphenols accumulate mainly in the skin of grape berries, during the course of fruit development, and comprise mainly flavonols, flavan-3-ols (flavanols), and anthocyanins (Downey et al., 2006). Their accumulation in berries varies among varieties, developmental stages, growing regions, and viticultural practices in relation to irradiation, nutrient, and temperature changes (Downey et al., 2006). In fact, there is differential regulation in the berry polyphenol metabolism in drought-prone environments (Degu et al., 2014). Nevertheless, flavonoid synthesis and degradation in response to heat waves and in respect to intravarietal variability are yet to be elucidated. Identifying genotypes (clones) showing higher stress tolerance or better performance under high temperatures and drought is a major objective of present-day grapevine selection.

As a reference variety for the intravarietal diversity analysis, we selected a major wine variety in Portugal, known as Aragonez in Alentejo and Tinta Roriz in Douro and internationally known as Tempranillo. Vegetative multiplication of this variety for centuries has originated the accumulation of somatic mutations that have been the base for its adaptation to current growing conditions in different wine-making regions of the world and could also be useful for adaptation to climate change. Any genetic variation identified in screenings for abiotic stress could immediately be used to select clones with improved stress adaptive traits.

An innovative approach was chosen because of the importance of developing a method to quantify the plant's response to changes in the environment that can be expedited and is reproducible and non-invasive, to accurately scan a large population in real time. Surface leaf temperature (SLT), measured with a portable infrared thermometer, is a parameter that sets the boundary condition for the latent and sensible heat transport through vegetation, soil, and atmosphere, depending on the availability of moisture at the interface soil atmosphere (Fuchs, 1990), giving an estimate of the response of a leaf to the environmental parameters affecting it at any time (air temperature, relative humidity, solar radiation, leaf resistance, and boundary layer resistance) (Udompetaikul et al., 2011).

By utilizing appropriate measurement devices, the relationship between these parameters can be studied. A plant is able to keep an SLT lower than ambient temperature by controlling stomatal aperture and thus gas and water vapor exchanges through stomata. The capacity to control stomata opening and thus CO_2 intake for photosynthesis regardless of high air temperature allows identifying the clones tolerant to face impending climate change without loss of productivity and quality of their grapes.

In previous works, we thoroughly characterized the different and contrasting responses of the varieties Touriga Nacional (TN) and Trincadeira (TR) to abiotic stresses (Carvalho et al., 2015a,b; Rocheta et al., 2016), showing that TN is a variety that can withstand severe levels of stress without being much affected, whereas TR is more sensitive. We have also proven that 49 of the DEGs (differentially expressed genes) identified by Rocheta et al. (2016) can be used as "abiotic stress markers" to characterize stress tolerance of grapevine varieties and as indicators of the major kind of stress the plant is subjected to (drought, heat, or excess light) (Carvalho et al., 2017). With the objective of studying the variability of tolerance to abiotic stress within varieties, we chose the red variety Aragonez (syn. Tempranillo), a variety that is known to have high variability regarding yield and quality traits (Gonçalves et al., 2007; Gonçalves and Martins, 2019).

Under the hypothesis that abiotic stress-tolerant clones show lower average SLT, a large collection of Aragonez clones in a field trial was evaluated. In this selection assay, established in Alentejo, in Reguengos de Monsaraz, 255 genotypes of this variety were used for stress tolerance monitoring based on the identification of clones with lower SLT together with analyses of berry trait variation. SLT was used as a non-invasive and expedite indicator of abiotic stress tolerance. These clones were subjected to a detailed analysis during 2014, 2015, and 2016 seasons to identify clones tolerant to stress, regardless of environmental conditions, and among those, the ones that gave rise to musts with good-quality traits for wine production. Taking advantage of this analysis, randomly chosen clones from the tolerant and sensitive ranking groups were scanned using quantitative polymerase chain reaction (qPCR) for the expression of the transcripts previously identified.

MATERIALS AND METHODS

Experimental Design and Location of the Field Trial

The evaluations were performed in an experimental population of clones of the Aragonez variety, containing representative samples of the intravarietal diversity in different growing regions of Portugal (Alentejo and Douro) and Spain (Rioja and Valdepeñas). This field trial is located in Reguengos de Monsaraz (Alentejo, Portugal) and was established in 1996, according to a balanced randomized complete block design (255 genotypes × three plants per plot × five blocks). As control of heterogeneity within complete blocks is best accomplished with a row–column arrangement within each complete block, the plots (experimental unit with three plants) were located on a grid of columns by rows. All plants were grafted on the same clone of 1103P rootstock and were free from grapevine leafroll associated virus type 3 and grapevine fanleaf virus. The training system was a vertical shoot position, and the pruning system was a bilateral Royat Cordon system.

Abiotic Stress and Quality Traits Evaluation

The evaluations were conducted in 2014, 2015, and 2016 seasons. The field was drip irrigated, but *circa* 2 weeks before the first SLT quantifications, irrigation was upheld and resumed only after the measurements were finished. Water stress conditions were quantified through the measurement of predawn leaf water potential (pressure chamber; Model 600, PMS Instruments Company, Albany, OR, United States) in the field. The average values obtained were of moderate stress in 2014 (−0.55 MPa) and severe stress in 2015 (−0.73 MPa) and 2016 (−0.7 MPa).

For SLT evaluation, the original experimental design was updated to control as strictly as possible the environmental effects (namely, the effects of the day and time of the evaluation). Each complete block was evaluated per day and in a day the plants of the plots of each column were measured in the shortest time possible. As a consequence, a resolvable incomplete block experimental design was adopted: (1) each complete block comprised the effect of the original experimental design and the effect of the day; (2) each column within each complete block, with approximately 13 plots, constituted an incomplete block, which comprised the effect of the time of day. In each plot, three measurements were performed in three different leaves with 10 technical replicates. Measurements were taken on peak heat hours on leaves exposed to the sun using a non-contact IR thermometer (Scan Temp 440).

Berry quality traits (soluble solids, acidity, pH, anthocyanins, and total phenols) were analyzed in the must, as well as berry weight. Berry collection was performed for all genotypes in three complete blocks. A sample of 60 berries per plot (experimental unit) was collected the day before the harvest. In laboratory, the berries from each plot were counted and weighted, and grape must was obtained from berries by applying the sample preparation procedure described by Carbonneau and Champagnol (1993). The analyses of the must were performed by standard methods: soluble solids by refractometry (probable alcohol by conversion), acidity by titration, and anthocyanins and total phenolics by spectrophotometric method described by Somers and Evans (1977).

Data Analysis

A preliminary univariate analysis for each trait and year was conducted to verify the quality of the data obtained in each year and the existence of significant genetic variability ($P < 0.05$) for the studied traits. For the analysis of SLT data, a linear mixed model was fitted, considering fixed effects for complete blocks and random effects for genotype, incomplete block within replicate (complete block), and leaf (within plot). For data analysis of berry weight and quality traits of the must, a linear mixed model was fitted for each trait, considering fixed effects for complete blocks and random effects for genotype. In

these models, random effects and random error were assumed independent and identically distributed normal random variables with expected value zero and the respective variance.

The variance parameters were estimated by the restricted maximum likelihood method (Patterson and Thompson, 1971) using the average information algorithm (Gilmour et al., 1995). The variance components were tested using a residual maximum likelihood ratio test. Because the null hypothesis was on the boundary of the parameter space, the *P*-value of the test was assumed to be half of the reported *P*-value from the χ^2 distribution with one degree of freedom (Self and Liang, 1987; Stram and Lee, 1994).

For selection purposes, the multivariate mixed-model approach proposed by Gonçalves et al. (2016) was adopted. For SLT, three response variables ("traits") were considered (SLT2014, SLT2015, and SLT2016); for berry traits, for each year, six response variables were included (soluble solids, pH, acidity, anthocyanins, total phenols, and berry weight). For both analyses, an unstructured covariance matrix was assumed between traits. From this methodology, quantitative genetic analysis was implemented through the indicators described as follows: (1) a generalized measure of heritability for each trait was obtained, based on prediction error variance and genotypic variance component estimates (Gonçalves et al., 2013); (2) for each multivariate model, genetic correlations between pairs of traits were obtained; (3) the EBLUPs of the genotypic effects of the studied traits were obtained through mixed-model equations (Henderson, 1975); the predicted genotypic values (PGVs) were computed, and both were ranked to characterize the more tolerant genotypes (rank for SLT) and for quality traits of the berries; (4) for each year, the Pearson correlation coefficient between the PGVs of SLT and each berry trait was calculated.

Data analysis was carried out with R (R Core Team, 2018; The R Foundation for Statistical Computing Platform). Linear mixed models were fitted using ASREML-R software (Butler et al., 2018).

Polyclonal Selection

The EBLUPs of genotypic effects for the studied traits provide information about the genetic component affecting those traits, and selection should be performed based on those values. Thus, the EBLUPs of the genotypic effects of the studied traits and the PGVs were ranked to characterize the more tolerant genotypes (rank for SLT). A set of 12 genotypes out of the 30 with lower SLT and that are present simultaneously in 2 or 3 years of evaluation were selected (when present simultaneously only in 2 years, in the third year, the genotype was, in the worst scenario, on the average, i.e., with EBLUP of genotypic effect near zero). Their behavior for the other evaluated traits was then analyzed. The yield data obtained in previous evaluations (Gonçalves et al., 2007) were also considered for the characterization of the final selected group. The predicted genetic gains for SLT, quality traits, and yield for the group of tolerant genotypes were computed as the average of the EBLUPs of the genotypic effects of each of the traits in the selected group of genotypes.

RNA Extraction

Samples were collected in 2015, under the same conditions as the measurements of SLT, and kept at −80°C. For gene expression analysis, three replicates of five clones within the best ranking clones for SLT in 2014 and five clones within the worst ranking ones in the same year were used. Samples were ground in the presence of liquid nitrogen with a mortar and pestle. Total RNA was extracted with the Spectrum™ Plant Total RNA kit (Sigma–Aldrich, St. Louis, MO, United States). In all samples, nucleic acid concentration was quantified by spectrophotometry using the software Gen5 1.09 (Synergy HT; BioTek Instruments, Winooski, VT, United States). The quality of the extracted RNA was evaluated using A260/A280 and A260/A230. To be used, samples had to have ratios A260/A280 between 1.8 and 2.1 and A260/A230 between 2.0 and 2.2. Total RNA integrity was assessed through 1% agarose gel electrophoresis under denaturing conditions.

cDNA Synthesis for qPCR

RNA samples were treated with RQ1 RNase-Free DNase (Promega, Madison, WI, United States). cDNA was synthesized from 2 μg of total RNA using oligo$(dT)_{20}$ in a 20-μL reaction volume using RevertAid Reverse Transcriptase (Fermentas Life Science, Helsingborg, Sweden) according to the manufacturer's recommendations. cDNA was tested for gDNA contamination in PCRs using intron spanning primers that yield a 229-bp amplicon in cDNA and a 547 amplicon in gDNA. Amplicon sizes were compared in 2% agarose gels together with the molecular weight marker 1 Kb+ (Invitrogen), and no gDNA contamination was detected. cDNA was stored at −20°C until further use.

Quantitative Polymerase Chain Reaction (qPCR)

Primers were designed using the software Beacon Designer (Premier Biosoft) using a primer length of 20 ± 2 bp, melting temperature of 60°C ± 2°C, a guanine–cytosine content of circa 50% and an expected amplicon size of 180–280 bp. Sequences were the same as in Carvalho et al. (2017). The real-time qPCR was performed in 96-well white reaction plates (Bio-Rad, Hercules, CA, United States), using an IQ5 Real Time PCR (Bio-Rad) with five biological replicates. The 20-μL reaction mixture was composed of 1 μL cDNA diluted 50-fold, 0.5 μM of each gene-specific primer, and 10 μL master mix (SsoFast_EvaGreen Supermix; Bio-Rad). Amplification of PCR products was monitored via intercalation of Eva-Green (included in the master mix). The following program was applied: initial polymerase activation, 95°C, 3 min, and then 40 cycles at 94°C 10 s (denaturation), 60°C 20 s (annealing), and 72°C 15 s (extension), followed by a melting curve analysis to confirm the correct amplification of target gene fragments and the lack of primer dimers. The PCR products were run on 2% agarose gels to make sure that there was only one amplicon of the expected size. PCRs with each primer pair were also performed on samples lacking cDNA template, in triplicate (no template controls). To assess amplification efficiency of the candidate genes, identical volumes of cDNA samples were diluted and used to generate

five-point standard curves based on a fivefold dilution series (1, 1:5, 1:25, 1:125, 1:625), in triplicate. Amplification efficiency (E) is calculated as $E = 10(-1/a) - 1$, "a" being the slope of the linear regression curve [$y = a \log(x) + b$] fitted over the log-transformed data of the input cDNA dilution (y) plotted against the respective quantification cycle (Cq) values (x). E-values of the target genes were considered comparable when they did not exceed 100 ± 10%, corresponding to a standard curve slope of 3.3 ± 0.33. All cDNA samples were diluted 50-fold and were amplified in duplicate in two independent PCR runs.

To generate a baseline-subtracted plot of the logarithmic increase in fluorescence signal (ΔRn) versus cycle number, baseline data were collected between cycles 5 and 17. All amplification plots were analyzed with an Rn threshold of 0.2 at the beginning of the region of exponential amplification, to obtain Cq (quantification cycle), and the data obtained were exported into an MS Excel workbook (Microsoft Inc., United States) for analysis. Reference genes used were ACT, TIF, and TIF-GTP (Coito et al., 2012).

Statistical Analysis of Gene Expression

For the relation between the expressions of the selected genes and the reference genes, the relative quantity values were transformed into log2 (thus rendering them parametric) and tested through analysis of variance (ANOVA) in the program SAS 9 (for Windows; SAS Institute Inc., Cary, NC, United States). When the P-value of the ANOVA was lower than 0.05, a Tukey test was performed, and statistically significant differences were accepted for $P < 0.05$.

RESULTS

SLT Analysis

The quantification of genetic variability within the variety for each trait was assessed by the estimate of the genetic variance component. From the results obtained from the univariate analysis (**Table 1**), it was possible to verify that there is significant genetic variability within the variety for the trait SLT ($P < 0.001$). The other variance components associated with the experimental design were all significant ($P < 0.001$), as well as the fixed-effects factor (complete block).

Empirical best linear unbiased predictors (EBLUPs) of genotypic effects and PGVs for SLT in 2014, 2015, and 2016 for all studied genotypes are provided in **Supplementary Tables 1**, **2**, respectively, as well as the rank for tolerance to abiotic stress. The differences between the EBLUP of genotypic effect of the more and the less tolerant clones and the PGVs for SLT in 2014, 2015, and 2016 are shown in **Table 2**. On average, there is a genetic quantifiable difference of 4°C between the coolest and warmest of the 255 clones measured in each of the three consecutive seasons. The values obtained for generalized broad sense heritability were moderate (ranging between 0.44 and 0.54), but very interesting given the nature of the trait assessed. This quantitative genetic parameter is particularly useful to complement the genetic analysis as it reflects the relationship between the true and predicted genotypic effects and, consequently, is an indicator of the success of genetic selection. Genetic correlations for SLT between the 3 years were low, which indicates the existence of genotype × environment interaction. That is, the rank of the most tolerant clones changed over the years, although it was possible to select a group of clones consistently identified as the most tolerant in all evaluated seasons.

Must Quality Versus SLT Analysis

The results of the characterization of must quality traits within the Aragonez collection are shown in **Table 3**. These traits also showed the existence of significant genetic variability (for any usual significance level). For acidity, the values obtained for heritability were lower, and for anthocyanins, total phenols, and berry weight, they were similar to those obtained for SLT. Genetic correlations estimates between traits obtained with the fitting of the multivariate linear mixed model for berry traits in 2014, 2015, and 2016 were low, except the correlation between anthocyanins and total phenols in 2015 (**Supplementary Table 3**).

For each year, genetic correlations between PGV of SLT and berry traits are described in **Table 4**. All the correlations were not significantly different from zero. This means that by exploring the genetic variability within the variety, several genotypes satisfying several criteria can be selected. For example, it is possible to select genotypes that are simultaneously more tolerant to stress and with berry traits above or near the mean of the population studied.

For the polyclonal selection, the 255 genotypes were then ranked according to the EBLUP genotypic effects and PGVs for SLT. Additionally, the results of the average values of all years for berry traits were used (those with higher values of heritability). EBLUPs of genotypic effects and PGVs for berry traits for all studied genotypes are provided in **Supplementary Tables 4**, **5**, respectively, as well as the rank for each trait. A set of 12 genotypes out of the 30 with lower SLT present simultaneously in 2 or 3 years of evaluation were selected. The features of selected

TABLE 1 | Variance components estimates and respective standard errors, obtained with the fitting of the univariate linear mixed model for SLT in 2014, 2015, and 2016, and the P-value of the likelihood ratio test for variance components (testing the null hypothesis if the variance component is zero).

Year	Variance component	Estimate (*SE*)	*P*
2014	Genotypic	0.664 (0.108)	<0.001
	Incomplete block within complete block	6.157 (0.970)	<0.001
	Leaf (within plot)	7.034 (0.176)	<0.001
	Error	0.606 (0.005)	
2015	Genotypic	0.725 (0.104)	<0.001
	Incomplete block within complete block	6.910 (1.081)	<0.001
	Leaf (within plot)	5.609 (0.140)	<0.001
	Error	0.441 (0.003)	
2016	Genotypic	0.766 (0.115)	<0.001
	Incomplete block within complete block	4.308 (0.687)	<0.001
	Leaf (within plot)	6.623 (0.165)	<0.001
	Error	0.365 (0.003)	

For the fixed-effects factor of the experimental design (complete block), the effect was significant in the 3 years ($P < 0.01$).

TABLE 2 | Differences between empirical best linear unbiased predictors (EBLUPs) of genotypic effects for SLT between the most sensitive and most tolerant genotypes and the predicted genotypic value (PGV) of the more and the less tolerant clones for SLT in 2014, 2015, and 2016; broad sense heritability; and genetic correlations for SLT between the years (and respective standard error, SE), obtained with the fitting of the multivariate linear mixed model.

Year	EBLUPs of genotypic effects for SLT		PGV for SLT		Broad sense heritability	Genetic correlation estimate (SE)	
	Most sensitive	Most tolerant	Most sensitive	Most tolerant			
2014	+1.7°C	−1.5°C	33.3°C	30.1°C	0.44	SLT2014, SLT2015	0.084 (0.108)
2015	+2.3°C	−1.8°C	36.3°C	32.2°C	0.52	SLT2015, SLT2016	0.239 (0.100)
2016	+2.3°C	−2.2°C	34.1°C	29.6°C	0.54	SLT2014, SLT2016	0.285 (0.104)

TABLE 3 | Genotypic variance component estimates and respective standard errors, obtained with the fitting of the univariate linear mixed model for berry traits in 2014, 2015, and 2016, and average values of all seasons, the *P*-value of the likelihood ratio test for genotypic variance component, and broad sense heritability for all traits in all years obtained with the fitting of the multivariate linear mixed model.

Trait	Year	Overall mean	Genotypic variance component estimate (*SE*)	*P*	Broad sense heritability
Soluble solids (°Brix)	2014	25.76	1.788 (0.249)	<0.001	0.663
	2015	22.54	1.064 (0.171)	<0.001	0.615
	2016	22.07	0.725 (0.159)	<0.001	0.453
	Average	23.47	0.831 (0.106)	<0.001	0.710
pH	2014	4.25	0.007 (0.001)	<0.001	0.568
	2015	4.36	0.008 (0.002)	<0.001	0.543
	2016	4.36	0.004 (0.001)	<0.001	0.513
	Average	4.32	0.005 (0.001)	<0.001	0.644
Acidity (tartaric acid, g L^{-1})	2014	2.68	0.025 (0.008)	<0.001	0.307
	2015	2.71	0.010 (0.004)	0.003	0.299
	2016	2.43	0.013 (0.005)	0.003	0.262
	Average	2.61	0.009 (0.002)	<0.001	0.380
Anthocyanins (mg L^{-1})	2015	443.14	4439.622 (976.912)	<0.001	0.473
	2016	425.26	4385.909 (732.043)	<0.001	0.573
	Average	434.31	2754.188 (497.936)	<0.001	0.511
Total phenols	2015	34.69	37.646 (8.351)	<0.001	0.462
	2016	43.67	43.230 (8.107)	<0.001	0.514
	Average	39.21	25.169 (4.784)	<0.001	0.476
Berry weight (g)	2015	1.29	0.016 (0.004)	<0.001	0.455
	2016	1.33	0.008 (0.002)	<0.001	0.455
	Average	1.31	0.009 (0.002)	<0.001	0.417

TABLE 4 | Pearson correlation coefficient between the predicted genotypic values (PGVs) of SLT and each berry trait in 2014, 2015, and 2016.

Traits	Year	Pearson correlation coefficient†
SLT/°Brix	2014	0.034
	2015	−0.008
	2016	−0.114
SLT/pH	2014	0.120
	2015	−0.023
	2016	0.052
SLT/acidity	2014	−0.033
	2015	0.077
	2016	0.030
SLT/anthocyanins	2015	0.003
	2016	−0.009
SLT/total phenols	2015	0.022
	2016	−0.004
SLT/berry weight	2015	0.030
	2016	−0.042

†*Non-significant for all cases (P > 0.05).*

TABLE 5 | Characterization of the selected group of 12 genotypes (polyclonal selection) for abiotic stress.

Year	Predicted genotypic value for SLT	Decreasing in SLT comparing to the mean of the population	Predicted genetic gain (as percentage of the mean of the population)	Decreasing in SLT comparing to the most sensitive genotype
2014	30.6°C	−1.0°C	−3.2%	−2.7°C
2015	33.1°C	−0.9°C	−2.6%	−3.2°C
2016	30.8°C	−1.0°C	−3.2%	−3.3°C

polyclonal group are described in **Tables 5**, **6**. Compared to the mean of the population, on average the SLT of the selected group decreased 1°C, corresponding to a predicted genetic gain of about 3% (as percentage of the mean of the population) in decrease of SLT. It must be emphasized that, on average, there is a genetic quantifiable difference of 3°C between this tolerant selected group and the highest value measured among the 255 clones in each of the three seasons (**Table 5**).

The behavior of the selected group for the other evaluated traits is shown in **Table 6**. The yield data obtained in previous evaluations were also considered for the characterization of the final selected group. A group of genotypes simultaneously tolerant and with higher yield was selected, ensuring a mean overall performance for berry traits. In fact, the predicted genetic gains for quality traits and berry weight were around zero, which means that, for the considered traits, the behavior of the selected group is around the mean of the variety. However, as a predicted

TABLE 6 | Predicted genetic gains of the selected group of 12 genotypes (polyclonal selection) for abiotic stress concerning other traits.

Trait	Predicted genetic gain (as percentage of the mean of the population)
Soluble solids (°Brix)	0.0%
pH	−0.2%
Acidity (tartaric acid, g L^{-1})	+0.5%
Anthocyanins (mg L^{-1})	+0.7%
Total phenols	−0.4%
Berry weight (g)	0.0%
Yield (kg $plant^{-1}$)	+14.1%

genetic gain of yield of +14.1% was observed, a tendency of more tolerant genotypes to show a yield performance above the mean of the population can be considered.

According to the results obtained in 2014 for SLT (**Supplementary Tables 1**, **2**), 10 genotypes were selected for gene expression analysis: five tolerant (RZ1124, RZ1338, RZ6210, RZ1502, and RZ1703) and five sensitive (RZ0703, RZ1243, RZ8207, RZ3710, and RZ3408).

Abiotic Stress Array in the 10 Tolerant and Sensitive Clones

As indicated above, for gene expression analysis clones were chosen as sensitive or tolerant according to SLT results of 2014. However, after the global 3-year PGV of SLT analysis, a third group emerged of clones highly affected by genotype × environment interaction, thus changing their rank each season. These were kept in the analysis, as it is also important to identify these highly variable genotypes. Thus, the three-group analysis comprised as tolerant, the clones RZ1124, RZ1338, and RZ6210; as sensitive, the clones RZ3408 and RZ3710; as variable, the clones RZ0703, RZ1243 RZ1502, RZ1703, and RZ8207. As samples for gene expression were taken in 2015, comparisons with SLT were made using values of that same season.

The DEGs used and their respective regulation is described in Carvalho et al. (2017). In **Figure 1**, the distribution of expression of down-regulated (A) and up-regulated (B) DEGs is represented by whisker–box plots, for the clones analyzed. The classification through SLT analysis of tolerance/sensitivity is indicated by the clone's code in green (tolerant), red (sensitive), or black (variable). In all clones, the expression of down- and up-regulated genes was consistent with their expected regulation tendency. Thus, this global gene analysis confirmed the expected regulation of the markers, as a whole. However, it is possible to verify that the stability of expression of both down-regulated and up-regulated genes was higher in sensitive and "variable" clones than in tolerant ones.

When allocating the significantly regulated DEGs in each clone to functional categories, some changes in regulation emerged (**Figure 2**); namely, the down-regulated category protein metabolism and modification became up-regulated in all clones but RZ8207, whereas secondary metabolism was up-regulated in all but RZ0703 and RZ6210 (**Figure 2A**). Conversely, the expected up-regulated ankyrin domain was down-regulated in all clones but RZ1703 and RZ0703, whereas leucine domain was down-regulated in all clones but RZ1502 and RZ6210 (**Figure 2B**). With these exceptions, all other functional categories followed the expected regulation in all clones.

Chosen clones were ranked as sensitive/tolerant/variable to abiotic stress in the field by using SLT analysis. The gene expression of the array in the chosen 10 clones was analyzed relative to individual stresses (heat, light, and water stress), using the values of expression of the chosen up- and down-regulated DEGs that were associated with each stress (see Carvalho et al., 2017). The results obtained were compared with those of the reference tolerant variety (TN) and the reference sensitive variety (TR) as described in Carvalho et al. (2017). Thus, a "stress matrix" for light, heat, and water stress was obtained (**Figure 3**). The clones studied were subjected to high levels of stress, as described in Section "Materials and Methods" and consistent with a typical Mediterranean summer. As a result, there was no irresponsive clone in DEG expression analysis (only one value of expression lower than 3-fold was observed in the variable clone RZ1243 in the response to heat stress).

On the whole, RZ0703, RZ6210, and RZ8207 were the clones that showed higher increases of expression of the stress-associated DEGs. In the season 2015, the variable response clones RZ0703 and RZ8207 ranked as tolerant through analysis of PGV of SLT, and thus, this response was consistent with SLT ranking. The genotype RZ1243 was the one with a lower level of response to stress. Sensitive ranked clones through PGV of SLT analysis were also classified as weakly responsive to stress by the stress matrix (RZ3408 and RZ3710).

Correlation Between DEG Stress Markers and SLT

Gene expression was quantified in samples taken on the season 2015; therefore, the correlation between values obtained for the stress matrix was compared with PGV of SLT only of the 2015 analysis (**Figure 4**). The correlation with the overall stress indicators is quite high. When correlating SLT values with the individual stress markers, it was possible to find better correlations with the "sensitive" markers for heat and water stress and with the "tolerant" only for light stress, an indication that, overall, the variety Aragonez is fairly sensitive to heat and water stress and tolerant to excess light (**Figure 4B**). Also, the clones with the lowest PGV of SLT in 2015 (RZ0703 and RZ6210) are also the ones ranking as tolerant in the stress matrix indicators. Ranking fairly well in these indicators is clone RZ8207, which does not rank as good in overall SLT analysis because it is prone to high genotype × environment interaction. Nevertheless, in the specific season analysis, it was moderately tolerant, thus justifying a high level of response to stress, as seen by the stress matrix result (**Figure 3**).

Relative gene expression ratios were calculated in relation to control plants of the sensitive control (left) and the tolerant control (right) for antioxidative stress response DEGs (**Figure 5**), and for DEGs characterizing each individual stress (Heat, Light, and Water), as in Carvalho et al. (2017) (**Figure 6**). In **Figures 5**, **6**, individual DEG expression of genes that

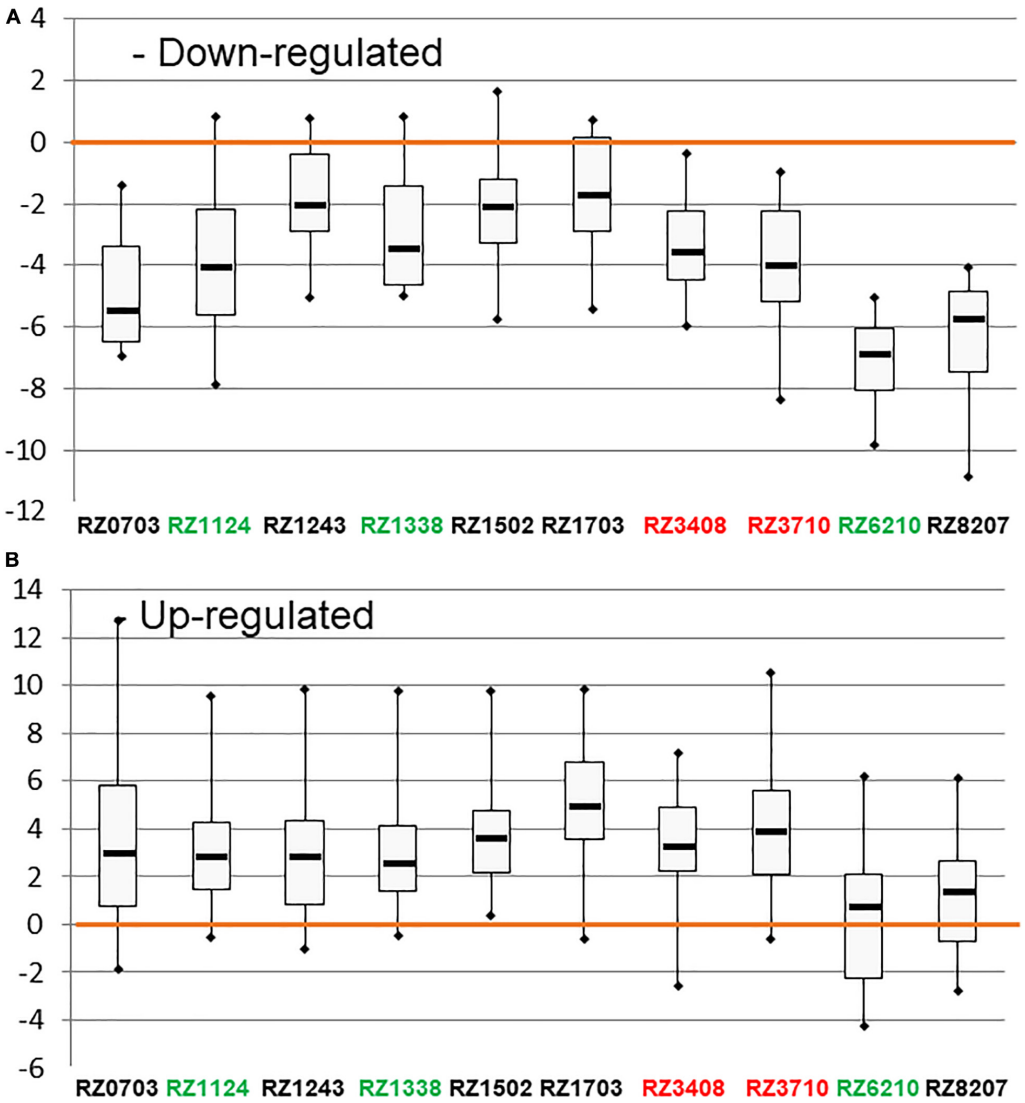


FIGURE 1 | Box plots representing the distribution of the expression of down-regulated **(A)** and up-regulated **(B)** DEGs (as in **Supplementary Table 6**) in [$\log_{2\,(geneexpressionratio)}$] in the 10 chosen Aragonez clones. The color code of the varieties' names, according to the overall SLT analysis, is the following: red: sensitive, green: tolerant, black: variable.

were expected to be up- or down-regulated according to each individual stress is shown (as in **Supplementary Table 6**). The levels of individual expression of the array of stress DEGs correlated better with the expected patterns in the sensitive control than in the tolerant one. This can be explained because the variety Aragonez is more similar in its response to stress to TR (the sensitive control) than to TN (the tolerant one). In fact, water stress in the tolerant control represented a challenge, as some DEGs had to be removed (Carvalho et al., 2017). The expression of the remaining ones was quantified, but clustering was not significant with so few genes, and therefore, only the comparison with the sensitive control is shown for water stress (**Figure 6E**). The expression of up- and down-regulated DEGs clustered with the expected patterns in all clones and the levels of expression allowed the characterization of the clones regarding individual abiotic stress: the overall tolerant RZ6204 emerged as tolerant to heat and drought and moderately sensitive to light and all individual stresses; the variable clone RZ8207 was tolerant to all individual stresses in the season of 2015; and RZ0703, another variable clone but tolerant in 2015 through PGV of SLT analysis was tolerant to water and light and moderately sensitive to heat. The stress that affected the sensitive genotypes RZ3408 and RZ3710 to a larger extent was drought.

DISCUSSION

Currently, as climate changes impose a new order into Mediterranean vegetation, high-value crops begin feeling the pressure to move to higher latitudes and altitudes. However,

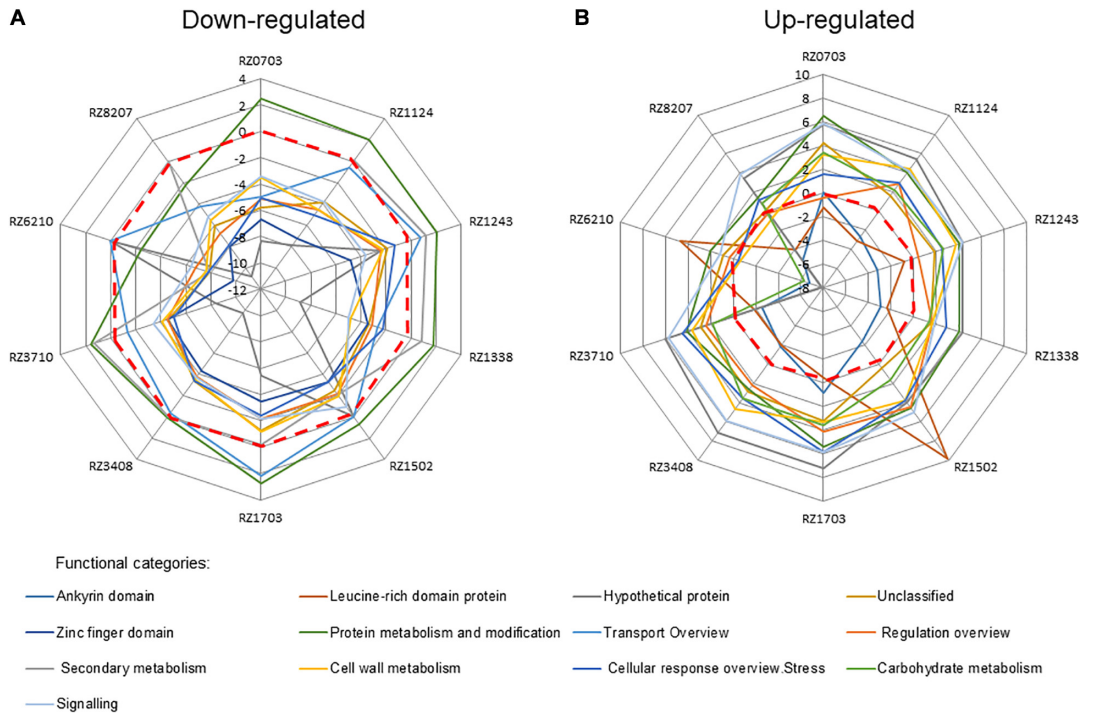


FIGURE 2 | Relative relevance of functional categories of down-regulated **(A)** and up-regulated **(B)** DEGs (as in **Supplementary Table 6**) in 10 chosen Aragonez clones, by MapMan analysis. Values correspond to the average $\log_{2\,(geneexpressionratio)}$ of all DEGs in the mentioned functional category.

	RZ0703	RZ1124	RZ1243	RZ1338	RZ1502	RZ1703	RZ3408	RZ3710	RZ6210	RZ8207
Tol-HS	5,21	4,15	2,34	3,82	5,06	3,81	3,89	5,85	6,50	6,53
Sens-HS	6,09	4,73	4,41	4,23	4,26	4,55	3,56	4,37	5,94	5,43
Tol-LS	6,59	4,81	4,37	4,14	3,71	4,94	3,81	3,77	6,11	5,42
Sens-LS	5,97	5,37	4,03	4,78	4,36	4,22	5,60	5,77	7,30	6,14
Tol-WS	4,17	5,78	5,31	4,39	4,62	7,33	4,68	5,28	4,32	4,47
Sens-WS	4,93	4,32	4,44	4,36	5,78	5,36	4,58	5,63	6,30	5,03

0-1.5
1.5-3.0
3.0-4.5
4.5-6.0
6.0-7.0
>7.0

FIGURE 3 | Stress matrix built using the average of the $|\log_{2\,(geneexpressionratio)}|$ of HS/LS/WS DEGs (as in **Supplementary Table 6**) that yielded a significant value ($|>1.5|$) of the expected regulation (down-/up-). Expression in relation to Tol, tolerant; Sens, sensitive; HS, heat stress; LS, light stress; WS, water stress.

crops whose economic revenue is closely linked with region, soil type, and characteristic genotypes are not so easy to move. One such species is grapevine, with high-value wine production closely associated with the *terroir* concept and also being subject to very strict region-specific regulations. Thus, it is not possible to change the geographical location of many high-value varieties to accommodate climate conditions. In Portugal, grapevine selection has evolved enormously in the last decades, with innovative methods developed that help increase quality and productivity in ancient varieties while at the same time preserving genetic variability (Martins and Gonçalves, 2015). This careful and exhaustive search for as many as possible different genotypes within each variety has led to the gathering of raw material for selection based on any desirable trait, provided that the adequate experimental setup is used in the establishment of the trials and that the right tools to scan an enormous amount of plant material in the field are available.

Clonal Selection for Abiotic Stress

With this in mind, we set up to establish a non-destructive, easy-to-use, reproducible, and fast method to scan a grapevine selection experimental field for abiotic stress. The method chosen was the measurement of SLT. This parameter is highly influenced by the environment; thus, to obtain accurate and reproductive results, measurements must be made in an experimental field with a specific layout, in days with specific light, temperature, and wind conditions and in the hottest hours of the day and following a carefully established order. In fact, only an efficient experimental design allows to control the effects of the environment and, most importantly, to quantify the contribution of the genetic component through broad sense

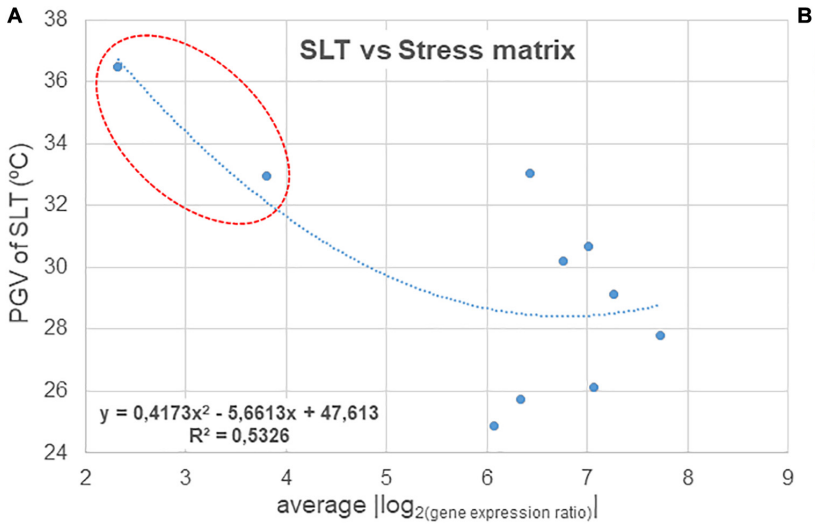


FIGURE 4 | (A) Correlation between the stress matrix values and SLT values measured at the same time as the sampling for gene expression analysis. **(B)** Coefficient of determination for the correlations between SLT values and the stress matrix values for individual stresses in the tolerant and sensitive controls. Tol, tolerant; Sens, sensitive; HS, heat stress; LS, light stress; WS, water stress.

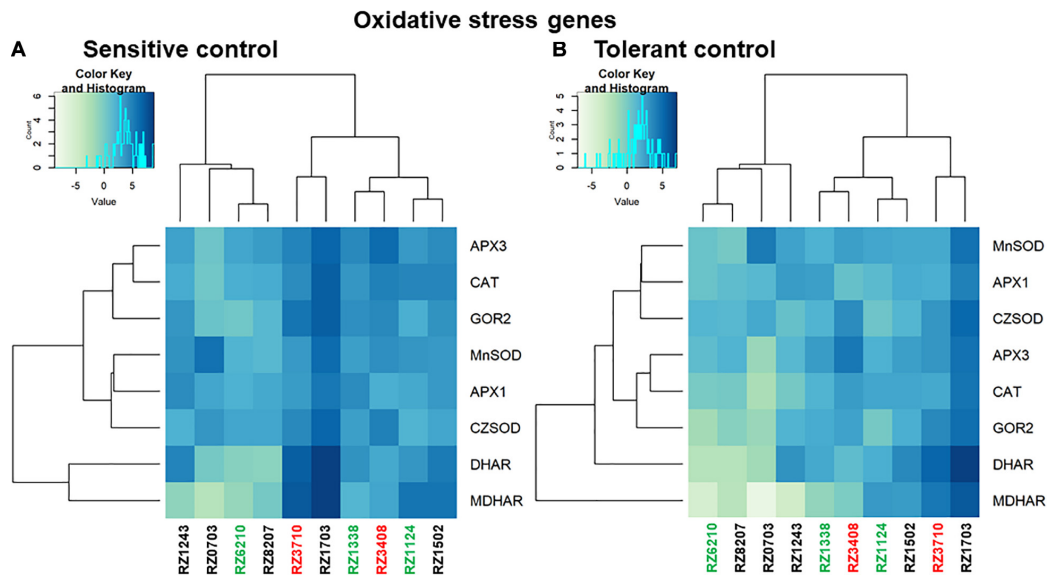


FIGURE 5 | Relative gene expression ratios obtained by reverse transcriptase–qPCR of antioxidative stress response genes (as in **Supplementary Table 6**) in relation to control plants of the sensitive control **(A)** and the tolerant control **(B)**. Values were normalized with respect to *translation initiation factor eIF-3 subunit 4 (TIF)*, *translation initiation factor eIF-2B alpha subunit* (*TIF-GTP*) and *actin 2 (act)* mRNA. The data correspond to $\log_{2\,(geneexpressionratio)}$ of three independent samples measured in duplicate.

heritability and EBLUPs of genotypic effects. This process is time- and space-consuming and expensive. Hundreds of genotypes under evaluation in several repetitions occupy a large area (usually between 1.0 and 2.0 ha); an efficient control of the field installation cannot use ready-made grafted plants, and evaluations can only begin after at least 4 years of field occupation. Additionally, repetitions in different seasons must also be made to assess the genotype × environment interaction. Therefore, trials such as these are only feasible for economically important and traditional/regional varieties. Nevertheless, they are of paramount relevance for the preservation and evaluation of the intravarietal diversity of those varieties.

In this study, sources of variation such as seasonal fluctuations in environmental conditions put in evidence the importance of the adopted experimental design and the need to account for those variations in the model for SLT data analysis. In the results of the fitted model, the significant effects of the complete blocks reflect the control of spatial variation among complete

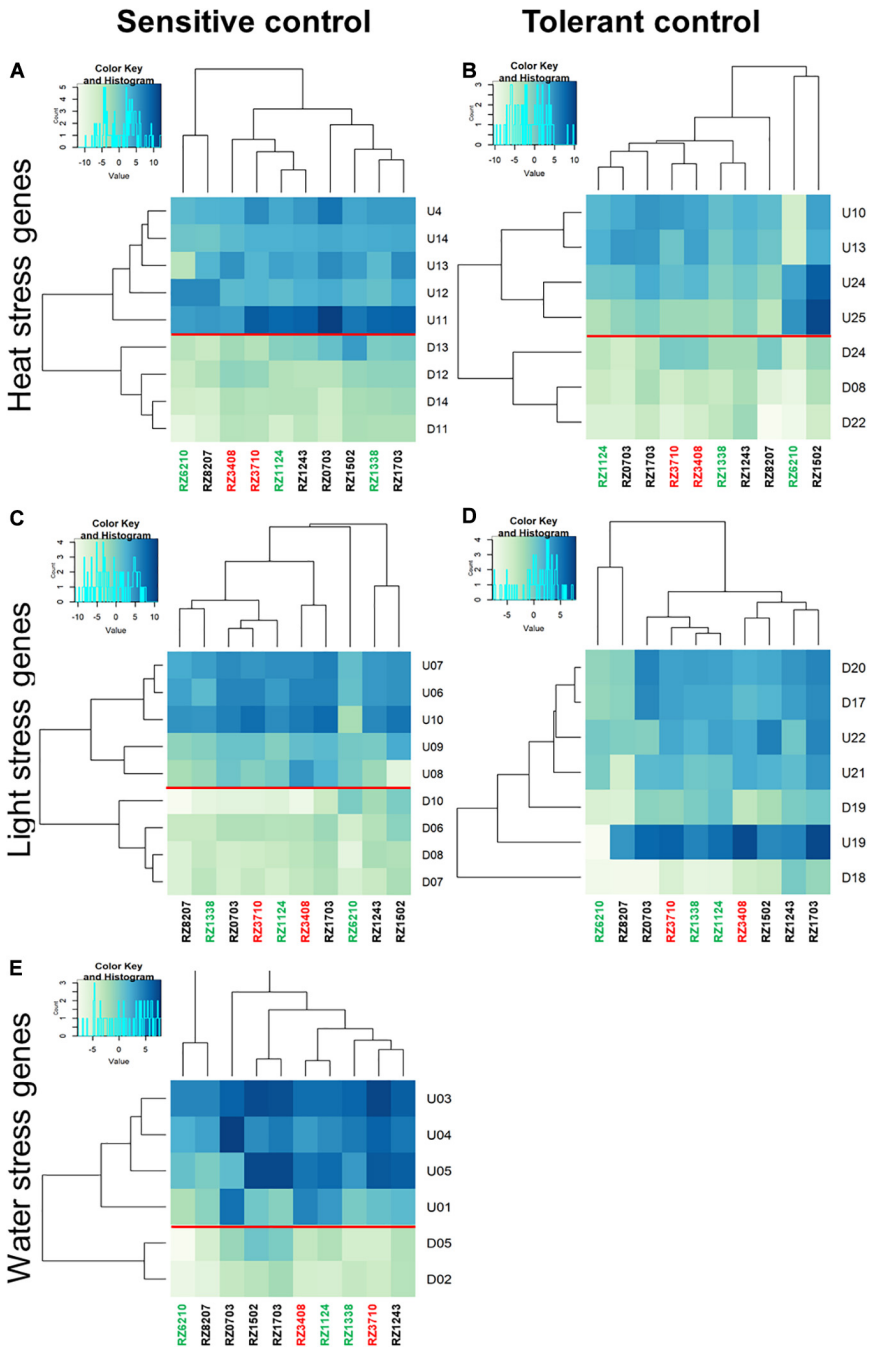


FIGURE 6 | Relative gene expression ratios obtained by reverse transcriptase–qPCR of the stress matrix DEGs (as in **Supplementary Table 6**) quantified in the 10 chosen Aragonez clones. Relative expressions in relation to control plants of the sensitive control (left) and the tolerant control (right) were calculated for each individual stress (heat: **A,B**; light: **C,D**; and water: **E**). Values were normalized with respect to *translation initiation factor eIF-3 subunit 4 (TIF)*, *translation initiation factor eIF-2B alpha subunit* (*TIF-GTP*) and *actin 2 (act)* mRNA. The data correspond to $\log_{2\,(geneexpressionratio)}$ of three independent samples measured in duplicate.

blocks and the differences in air temperatures among the days of the measurements; the significant variance of incomplete blocks within complete block reveals the importance of taking into account the differences in air temperatures in each measurement interval (accounting for the time of day of the measurements); the significant variance of leaf within plot is associated with the control of the differences among plants in the same plot and to the exposition deviations of the measured leaves.

Results showed that there was significant genetic variability within the variety for SLT in the three seasons. However, in the season with moderate stress (2014, average $\Psi_{pd} = -0.55$), the range of values obtained for the EBLUPs of genotypic effects for

SLT between sensitive and tolerant genotypes was lower than in the two seasons with severe stress. This was also reflected by the lower value obtained for broad sense heritability in 2014.

Although genetic variability among clones was found for SLT in all evaluated years, there were clones that maintained the same tendency for lower or higher SLT over the years, whereas others had more unstable performance. The latter ones correspond to genotypes that are more sensitive to genotype × environment interaction. This phenomenon occurs for any quantitative trait, as is the case of SLT. Therefore, when selecting clones, an important criterion is the selection of those with lower sensitivity to genotype × environment interaction for the evaluated traits. For this reason, the classification of clones selected in just 1 year (2014) for gene expression analysis was changed when performing the final selection of genotypes, in which the sensitivity to genotype × environment interaction was also taken into account.

Integration of the Evaluated Traits

As the selection of genotypes of well-established high-value varieties only makes sense in the context of high-quality and good levels of production, genotypes were also monitored for quality of the must, even if those genotypes had already been subject to selection for those traits (Gonçalves and Martins, 2019). Quality traits showed the existence of significant genetic variability (for any usual significance level). For acidity, anthocyanins, total phenols, and berry weight, the values obtained for heritability were similar to those obtained for SLT. This represents a relevant result for SLT because, theoretically, this trait should be subject to higher environmental variability than anthocyanins, total phenols, and berry weight. Therefore, such result confirms that a good experimental design and an adequate model were applied to study SLT. Also, according to previous works (Gonçalves et al., 2013), higher estimates for heritability were consistently obtained when using the average of years because, for each clone, a convergence of the phenotypic values to the true genotypic value is expected.

Genetic correlations between SLT and quality traits estimated for each season were approximately zero. This result indicates that, when exploring the genetic variability within the variety, several genotypes satisfying several criteria, for example, simultaneously more tolerant to stress and with quality traits above the mean of the population studied, can be selected. This indicates that quality will not be lost when selecting for stress tolerance. In general, the low genetic correlations observed between traits are in agreement with the findings of previous studies on selection in grapevine ancient varieties (Gonçalves et al., 2016).

The DEGs used in this analysis were described as being able to characterize tolerance/sensitivity to stress in grapevine varieties (Carvalho et al., 2017). Because of the enormous plasticity of the grapevine transcriptome (Dal Santo et al., 2013) and the fact that Aragonez is a variety with high intravarietal variability (Gonçalves et al., 2007; Gonçalves and Martins, 2019), it was expected that differences in gene expression between the clones of the experiment would emerge. In fact, the analysis of the "stress array" identified the clones as sensitive or tolerant to stress, in the same pattern as the SLT analysis of that single season. However, SLT analysis in successive years showed that some of those initially regarded as tolerant or sensitive in fact belonged to a yet unidentified group of highly variable genotypes with contradictory results in successive years. It must be emphasized that gene expression analysis of these clones in one single year could yield false results, as they will respond differently from season to season.

Physiological Aspects of Tolerance/Sensitivity

The foundation for SLT analysis is that a plant that can keep its leaf temperature lower will only be able to do so if it has a good control of stomatal opening and thus of its transpiration. This will be associated with a better modulation of gas exchange and thus higher levels of CO_2 uptake. These plants will be able to produce more photoassimilates that will be available for berry production. These conditions during the plant's life cycle contribute to better growth rates, higher level of photoassimilate storage for winter and thus higher number of productive flowers that will lead to higher yield in the following season. In fact, as a predicted genetic gain of yield of +14.1% was observed, this tendency of more tolerant genotypes to show a yield performance above the mean of the population was confirmed.

Oxidative stress response genes were not present in the original array (Carvalho et al., 2017), but as they are key players in abiotic stress response in general and specifically in grapevine (Terrier et al., 2005; Carvalho et al., 2015a), they were included in this study. All the genes were up-regulated, especially in RZ1703 and RZ3710, an indication of these clones' sensitivity to stress. The three clones that behaved as tolerant in the year chosen, RZ6210, RZ8207, and RZ0703, were the less affected by oxidative stress. In these clones, hydrogen peroxide scavenging through CAT and APX was predominant, while in more sensitive genotypes, the whole asc-glut cycle was up-regulated, with higher levels of expression of GOR and DHAR (for review, see Carvalho et al., 2015b). Regarding the comparison with the individual stress markers, all the Aragonez clones studied clustered better with the sensitive control in all stresses, confirming previous results of sensitivity to water stress (Martorell et al., 2015) in the variety as a whole.

CONCLUSION

It was possible to identify intravarietal genetic variability for the several traits analyzed in the field trial of Aragonez accessions, including for SLT. This variation could be useful in the improvement of genotypes of this variety to withstand stress conditions and to better adapt to climate change.

To sum up, the selection of a group of genotypes tolerant to abiotic stress was performed, with an increase of the mean yield and maintaining the behavior for quality traits.

DATA AVAILABILITY STATEMENT

The original contributions generated for this study are included in the article/**Supplementary Materials**, further inquiries can be directed to the corresponding author.

AUTHOR CONTRIBUTIONS

EG, LC, and AM conceived the ideas and the overall study design. LC and EG designed the methodology and collected the data. LC and EG analyzed the data. LC and EG wrote the manuscript. SA and AM revised it. All authors contributed with reagents, materials, and analysis tools. All authors contributed critically to the drafts and gave final approval for publication.

FUNDING

This research was funded by Fundação para a Ciência e Tecnologia (FCT) through LEAF funding (UID/AGR/04129/2020) and DL57/2016/CP1382/CT0024 to LC. This work also benefited from the networking activities within the European project KBBE InnoVine (ref. 311775).

ACKNOWLEDGMENTS

Authors would like to acknowledge Associação Portuguesa para a Diversidade da Videira (PORVID) for its support in data collection, the colleagues of "National Network for Grapevine Selection" for their assistance in SLT data collection in 2014, and José Maria da Fonseca S.A. company for the maintenance of the field trial of Aragonez.

SUPPLEMENTARY MATERIAL

The Supplementary Material for this article can be found online at: https://www.frontiersin.org/articles/10.3389/fpls.2020.599230/full#supplementary-material

REFERENCES

Butler, D. G., Cullis, B. R., Gilmour, A. R., Gogel, B. J., and Thompson, R. (2018). *ASReml-R Reference Manual, Version 4*. Wollongong, NSW: University of Wollongong.

Carbonneau, A., and Champagnol, F. (1993). *Nouveaux Systemes de Culture Integre du Vignoble. Programme AIR-3-CT*. 93.

Carvalho, L. C., Coito, J. L., Colaço, S., Sangiogo, M., and Amâncio, S. (2015a). Heat stress in grapevine: the pros and cons of acclimation. *Plant Cell Environ.* 38, 777–789. doi: 10.1111/pce.12445

Carvalho, L. C., Coito, J. L., Gonçalves, E. F., Chaves, M. M., and Amâncio, S. (2016). . *Plant Biol.* 18, 101–111. doi: 10.1111/plb.12410

Carvalho, L. C., Silva, M., Coito, J. L., Rocheta, M. P., and Amâncio, S. (2017). Design of a custom RT-qPCR array for assignment of abiotic stress tolerance in traditional Portuguese grapevine varieties. *Front. Plant Sci.* 8:1835. doi: 10.3389/fpls.2017.01835

Carvalho, L. C., Vidigal, P., and Amâncio, S. (2015b). Oxidative stress mediated signaling and homeostasis in grapevine (*Vitis vinifera* L.). *Front. Environ. Sci.* 3:20. doi: 10.3389/fenvs.2015.00020

Chaves, M. M., Zarrouk, O., Francisco, R., Costa, J. M., Santos, T., Regalado, A. P., et al. (2010). Grapevine under deficit irrigation: hints from physiological and molecular data. *Ann. Bot.* 105, 661–676. doi: 10.1093/aob/mcq030

Coito, J., Rocheta, R., Carvalho, L. C., and Amâncio, S. (2012). Microarray-based uncovering reference genes for quantitative real time PCR in grapevine under abiotic stress. *BMC Res. Notes* 5:220. doi: 10.1186/1756-0500-5-220

Dal Santo, S., Tornielli, G. B., Zenoni, S., Fasoli, M., Farina, L., Anesi, A., et al. (2013). The plasticity of the grapevine berry transcriptome. *Genome Biol.* 14:r54. doi: 10.1186/gb-2013-14-6-r54

Degu, A., Hochberg, U., Sikron, N., Venturini, L., Buson, G., Ghan, R., et al. (2014). Metabolite and transcript profiling of berry skin during fruit development elucidates differential regulation between Cabernet Sauvignon and Shiraz cultivars at branching points in the polyphenol pathway. *BMC Plant Biol.* 14:188. doi: 10.1186/s12870-014-0188-4

Deloire, A., Carbonneau, A., Wang, Z., and Ojeda, H. (2004). Vine and water, a short review. *J. Int. Sci. Vigne Vin* 38, 1–13. doi: 10.20870/oeno-one.2004.38.1.93218

Downey, M. O., Dokoozlian, N. K., and Krstic, M. P. (2006). Cultural practice and environmental impacts on the flavonoid composition of grapes and wine: a review of recent research. *Am. J. Enol. Vitic.* 57, 257–268.

Dry, P. R., Loveys, B. R., and Düring, H. (2000). Partial drying of the rootzone of grape. II. Changes in the pattern of root development. *Vitis* 39, 9–12.

Fuchs, M. (1990). Infrared measurement of canopy temperature and detection of plant water stress. *Theor. Appl. Climatol.* 42, 253–261. doi: 10.1007/BF00865986

Gilmour, A., Thompson, R., and Cullis, B. (1995). Average information REML: an efficient algorithm for variance parameter estimation in linear mixed models. *Biometrics* 51, 1440–1450. doi: 10.2307/2533274

Gonçalves, E., Carrasquinho, I., Almeida, R., Pedroso, V., and Martins, A. (2016). Genetic correlations in grapevine and their effects on selection. *Aust. J. Grape Wine Res.* 22, 52–63. doi: 10.1111/ajgw.12164

Gonçalves, E., Carrasquinho, I., St. Aubyn, A., and Martins, A. (2013). Broad-sense heritability in the context of mixed models for grapevine initial selection trials. *Euphytica* 189, 379–391. doi: 10.1007/s10681-012-0787-9

Gonçalves, E., and Martins, A. (2019). Genetic gains of selection in ancient grapevine cultivars. *Acta Hortic.* 1248, 47–54. doi: 10.17660/ActaHortic.2019.1248.7

Gonçalves, E., St. Aubyn, A., and Martins, A. (2007). Mixed spatial models for data analysis of yield on large grapevine selection field trials. *Theor. Appl. Genet.* 115, 653–663. doi: 10.1007/s00122-007-0596-z

Gonçalves, E., St. Aubyn, A., and Martins, A. (2010). Experimental designs for evaluation of genetic variability and selection of ancient grapevine varieties: a simulation study. *Heredity* 104, 552–562. doi: 10.1038/hdy.2009.153

Gonzalez-Dugo, V., Durand, J.-L., and Gastal, F. (2010). Water deficit and nitrogen nutrition of crops. A review. *Agron. Sustain. Dev.* 30, 529–544. doi: 10.1051/agro/2009059

Henderson, C. (1975). Best linear unbiased estimation and prediction under a selection model. *Biometrics* 31, 423–447. doi: 10.2307/2529430

International Organisation of Vine and Wine [OIV]. (2018). *World Vitiviniculture Situation OIV Statistical Report on World Vitiviniculture*. Paris: OIV.

Lovisolo, C., Perrone, I., Carra, A., Ferrandino, A., Flexas, J., Medrano, H., et al. (2010). Drought-induced changes in development and function of grapevine (*Vitis* spp.) organs and in their hydraulic and non-hydraulic interactions at the whole-plant level: a physiological update. *Func. Plant Biol.* 37, 98–116. doi: 10.1071/FP09191

Martins, A., and Gonçalves, E. (2015). "Grapevine breeding programmes in Portugal," in *Grapevine Breeding Programs for the Wine Industry: Traditional and Molecular Techniques*, ed. A. G. Reynolds (Sawston: Woodhead Publishing), 159–182. doi: 10.1016/b978-1-78242-075-0.00008-9

Martorell, S., Diaz-Espejo, A., Tomàs, M., Pou, A., El Aou-ouad, H., Escalona, J. M., et al. (2015). Differences in water-use-efficiency between two *Vitis vinifera* cultivars (Grenache and Tempranillo) explained by the combined response of stomata to hydraulic and chemical signals during water stress. *Agric. Water Manag.* 156, 1–9. doi: 10.1016/j.agwat.2015.03.011

Parker, A., de Cortazar Atauri, G., van Leeuwen, C., and Chuine, I. (2011). General phenological model to characterise the timing of flowering and véraison of *Vitis vinifera* L. *Aust. J. Grape Wine Res.* 17, 206–216. doi: 10.1111/j.1755-0238.2011.00140.x

Patterson, H. D., and Thompson, R. (1971). Recovery of inter-block information when block sizes are unequal. *Biometrika* 58, 545–554. doi: 10.2307/2334389

R Core Team (2018). *R: A Language and Environment for Statistical Computing*. Vienna: R Foundation for Statistical Computing.

Resolution OIV-VITI 564B-2019. (2019). OIV Process for the Recovery and Conservation of the Intra-varietal Diversity and the Polyclonal Selection in Grape Varieties with Wide Genetic Variability. Available online at: http://www.oiv.int/en/technical-standards-and-documents/resolutions-of-the-oiv/viticulture-resolutions

Rocheta, M., Coito, J. L., Ramos, M., Carvalho, L. C., Becker, J. D., Carbonell-Bejerano, P., et al. (2016). Transcriptomic comparison between two *Vitis vinifera* L. varieties (Trincadeira and Touriga Nacional) in abiotic stress conditions. *BMC Plant Biol.* 2016:224. doi: 10.1186/s12870-016-0911-4

Schultz, H. (2003). Differences in hydraulic architecture account for near-isohydric and anisohydric behaviour of two field-grown *Vitis vinifera* L. cultivars during drought. *Plant Cell Environ.* 26, 1393–1405. doi: 10.1046/j.1365-3040.2003.01064.x

Self, S. G., and Liang, K. Y. (1987). Asymptotic properties of maximum likelihood estimators and likelihood ratio tests under nonstandard conditions. *J. Am. Stat. Assoc.* 82, 605–610. doi: 10.1080/01621459.1987.10478472

Somers, T. C., and Evans, M. E. (1977). Spectral evaluation of young red wines: anthocyanin equilibria, total phenolics, free and molecular so2, "chemical age". *J. Sci. Food Agric.* 28, 279–287. doi: 10.1002/jsfa.2740280311

Stram, D. O., and Lee, J. W. (1994). Variance components testing in the longitudinal mixed effects model. *Biometrics* 50, 1171–1177. doi: 10.2307/2533455

Terrier, N., Glissant, D., Grimplet, J., Barrieu, F., Abbal, P., Couture, C., et al. (2005). Isogene specific oligo arrays reveal multifaceted changes in gene expression during grape berry (*Vitis vinifera* L.) development. *Planta* 222, 832–847. doi: 10.1007/s00425-005-0017-y

Udompetaikul, V., Upadhyaya, S. K., Slaughter, D., Lampinen, B., and Shackel, K. (2011). *Plant Water Stress Detection Using Leaf Temperature and Microclimatic Information.* ASABE Paper No 1111555. St. Joseph, MI: ASABE, doi: 10.13031/trans.57.10319

van Leeuwen, C., and Darriet, P. (2016). The impact of climate change on viticulture and wine quality. *J. Wine Econ.* 11, 150–167. doi: 10.1017/jwe.2015.21

van Leeuwen, C., Trégoat, O., Choné, X., Bois, B., Pernet, D., and Gaudillère, J.-P. (2009). Vine water status is a key factor in grape ripening and vintage quality for red Bordeaux wine. How can it be assessed for vineyard management purposes? *J. Int. Sci. Vigne Vin* 43, 121–134. doi: 10.20870/oeno-one.2009.43.3.798

Vandeleur, R. K., Mayo, G., Shelden, M. C., Gilliham, M., Kaiser, B. N., and Tyerman, S. D. (2009). The role of plasma membrane intrinsic protein aquaporins in water transport through roots: diurnal and drought stress responses reveal different strategies between isohydric and anisohydric cultivars of grapevine. *Plant Physiol.* 149, 445–460. doi: 10.1104/pp.108.128645

Zarrouk, O., Garcia-Tejero, I., Pinto, C., Genebra, T., Sabir, F., Prista, C., et al. (2016). Aquaporins isoforms in cv. Touriga Nacional grapevine under water stress and recovery—regulation of expression in leaves and roots. *Agric. Water Manag.* 164, 167–175. doi: 10.1016/j.agwat.2015.08.013

Conflict of Interest: The authors declare that the research was conducted in the absence of any commercial or financial relationships that could be construed as a potential conflict of interest.

Copyright © 2020 Carvalho, Gonçalves, Amâncio and Martins. This is an open-access article distributed under the terms of the Creative Commons Attribution License (CC BY). The use, distribution or reproduction in other forums is permitted, provided the original author(s) and the copyright owner(s) are credited and that the original publication in this journal is cited, in accordance with accepted academic practice. No use, distribution or reproduction is permitted which does not comply with these terms.

frontiers in Plant Science

ORIGINAL RESEARCH
published: 23 December 2020
doi: 10.3389/fpls.2020.618491

The Effect of Drought on Transcriptome and Hormonal Profiles in Barley Genotypes With Contrasting Drought Tolerance

Amal Harb[1,2*], *Craig Simpson*[3], *Wenbin Guo*[4], *Ganesan Govindan*[1], *Vijaya Gopal Kakani*[5] *and Ramanjulu Sunkar*[1*]

[1] Department of Biochemistry and Molecular Biology, Oklahoma State University, Stillwater, OK, United States, [2] Department of Biological Sciences, Faculty of Science, Yarmouk University, Irbid, Jordan, [3] Cell and Molecular Sciences, The James Hutton Institute, Dundee, United Kingdom, [4] Informatics and Computational Sciences, The James Hutton Institute, Dundee, United Kingdom, [5] Department of Plant and Soil Science, Oklahoma State University, Stillwater, OK, United States

OPEN ACCESS

Edited by:
Raul Antonio Sperotto, Universidade do Vale do Taquari - Univates, Brazil

Reviewed by:
Viswanathan Chinnusamy, Indian Agricultural Research Institute (ICAR), India
Nikolai Borisjuk, Huaiyin Normal University, China

***Correspondence:**
Amal Harb
aharb@yu.edu.jo;
harbhope78@gmail.com
Ramanjulu Sunkar
ramanjulu.sunkar@okstate.edu

Specialty section:
This article was submitted to Plant Abiotic Stress, a section of the journal Frontiers in Plant Science

Received: 17 October 2020
Accepted: 27 November 2020
Published: 23 December 2020

Citation:
Harb A, Simpson C, Guo W, Govindan G, Kakani VG and Sunkar R (2020) The Effect of Drought on Transcriptome and Hormonal Profiles in Barley Genotypes With Contrasting Drought Tolerance. Front. Plant Sci. 11:618491. doi: 10.3389/fpls.2020.618491

Like many cereal crops, barley is also negatively affected by drought stress. However, due to its simple genome as well as enhanced stress resilient nature compared to rice and wheat, barley has been considered as a model to decipher drought tolerance in cereals. In the present study, transcriptomic and hormonal profiles along with several biochemical features were compared between drought-tolerant (Otis) and drought-sensitive (Baronesse) barley genotypes subjected to drought to identify molecular and biochemical differences between the genotypes. The drought-induced decrease in the leaf relative water content, net photosynthesis, and biomass accumulation was relatively low in Otis compared to Baronesse. The hormonal profiles did not reveal significant differences for majority of the compounds other than the GA20 and the cis-zeatin-o-glucoside (c-ZOG), whose levels were greatly increased in Otis compared to Baronesse under drought. The major differences that emerged from the transcriptome analysis are; (1), the overall number of differentially expressed genes was relatively low in drought-tolerant Otis compared to drought-sensitive Baronesse; (2), a wax biosynthesis gene (CER1), and NAC transcription factors were specifically induced in Otis but not in Baronesse; (3), the degree of upregulation of betaine aldehyde dehydrogenase and a homeobox transcription factor (genes with proven roles in imparting drought tolerance), was greater in Otis compared to Baronesse; (4) the extent of downregulation of gene expression profiles for proteins of the reaction center photosystem II (PSII) (D1 and D2) was low in Otis compared to Baronesse; and, (5), alternative splicing (AS) was also found to differ between the genotypes under drought. Taken together, the overall transcriptional responses were low in drought-tolerant Otis but the genes that could confer drought tolerance were either specifically induced or greatly upregulated in the tolerant genotype and these differences could be important for drought tolerance in barley.

Keywords: drought tolerance, barley, photosynthesis, proline, RNA-Seq, differential gene expression, alternative splicing

INTRODUCTION

Drought negatively impacts the growth and productivity of many important crops (Bartels and Sunkar, 2005; Kim et al., 2019). Future predictions indicate that drought will worsen, challenging worldwide food security and the needs of an increasing human population (Meza et al., 2020). Indeed, hunger, famine, and malnutrition are expected due to climate change and drought, in addition to other social and political factors (Lobell et al., 2011; Lesk et al., 2016; Cafiero et al., 2018).

Drought is known to disrupt the hormonal balance in plants, which plays an important role in stress tolerance (Peleg and Blumwald, 2011; Bielach et al., 2017; Ullah et al., 2018). The enhanced accumulation of Abscisic acid (ABA) is a hallmark of plant response to drought, which in turn controls the stomatal closure to decrease the transpiration under drought (Munemasa et al., 2015; Ullah et al., 2018). Auxins regulate root growth in response to abiotic stresses including drought (Korver et al., 2018). Similarly, the Gibberellin (GA) mediates many responses to drought. GA concentration is reduced, and the DELLA regulators accumulate, which could be attributed to the retarded growth under drought (Colebrook et al., 2014). Cytokinins (CKs) and their metabolism are important in plants' adaptation to different abiotic stresses including drought (Ha et al., 2012; Pavlu et al., 2018). Both positive and negative effects of CKs on drought tolerance were reported (Zwack and Rashotte, 2015). These observations suggest that the fine-tuned hormonal homeostasis during stress conditions plays an important role in plant's response to abiotic stresses.

Barley (*Hordeum vulgare* L.) is the fourth most important crop plant in terms of production and harvested area (Giraldo et al., 2019). It is a relatively drought resistant crop and is cultivated globally in more than 100 countries (Hiei et al., 2014; Giraldo et al., 2019). Barley is considered as an important model system for dissecting drought tolerance in cereals because of its ability to tolerate drought better than the cereals such as rice and wheat. Moreover, it has a reliable genetic and molecular infrastructure (Dawson et al., 2015).

Barley subjected to drought stress has been investigated previously (Ozturk et al., 2002; Diab et al., 2004; Talamé et al., 2007; Guo et al., 2009; de Mezer et al., 2014; Sallam et al., 2019). Drought significantly reduced the net photosynthetic rate, stomatal conductance, and transpiration in barley (Harb and Samarah, 2015; Mejri et al., 2016; Schmid et al., 2016; Hasanuzzaman et al., 2019). Tibetan barley genotypes subjected to drought revealed the importance of ABA-dependent and ABA-independent signaling pathways during drought, while genes linked to photosynthesis appears to be important during recovery from drought (Zeng et al., 2016). Comparison of barley spikelets' responses in drought-sensitive and drought-tolerant lines revealed a role for a set of more recently evolved genes in the tolerant lines (Hübner et al., 2015). A drought-resistant line exposed to drought stress over 30 days showed acclimation to the stress while the gene expression profiles in this genotype did not differ compared to a drought-sensitive cultivar (Cantalapiedra et al., 2017). Studies also indicated that maintaining a low background expression of drought tolerance related genes under mild stress allows barley to respond more quickly with the onset of the drought stress (Janiak et al., 2019). Furthermore, recent studies underscored the importance of AS in drought-responsive gene expression in barley (Cantalapiedra et al., 2017). By and large, these reports reveal a complex interaction between multiple mechanisms and processes that differ between genotypes/landraces, tissue analyzed and duration of the stress (Hübner et al., 2015; Zeng et al., 2016; Cantalapiedra et al., 2017; Wang et al., 2018). They also highlight the importance of analyzing additional contrasting genotypes to better understand the drought tolerance processes in barley. Deep large-scale transcriptome sequencing allows expression at an individual gene transcript level to be monitored. New quasi-mapping programs (kallisto, salmon) facilitate rapid and highly accurate measurement of transcript level expression but require a comprehensive and accurate reference transcriptome. A first version reference transcript dataset for barley (BaRTv1.0) has recently been established that facilitates measurement of dynamic reprogramming of gene expression in barley and captures post-transcriptional regulation (Rapazote-Flores et al., 2019). In this study, drought-tolerant (Otis) has been compared with drought-sensitive (Baronesse) to identify biochemical and molecular differences associated with differential sensitivities. The drought-responsive RNA-Seq analysis revealed a greater number of differentially expressed genes in Baronesse than in Otis. Interestingly, several genes with proven roles in drought tolerance such as NAC genes, wax biosynthesis gene (CER1), a beta-expansin, and Armadillo (ARM) repeat superfamily were only induced in Otis but not in Baronesse. By contrast, the degree of inhibition of genes associated with PSII (D1 and D2) was much stronger in Baronesse. Furthermore, AS was also found to differ between the genotypes under drought.

MATERIALS AND METHODS

Plant Material

Seeds of Otis and Baronesse genotypes were obtained from Dr. Harold Bockelman, National Small Grains Collection (NSGC), U.S. Department of Agriculture - Agricultural Research Service, Aberdeen, Idaho, USA. Otis is a two-rowed, spring feed barley with high growth and yield in drylands (Mornhinweg et al., 2009). This genotype was developed for growth in dry environments and released by Colorado State University in 1951. Baronesse is a two-rowed, spring, feed barley cultivar that was donated by Peterson Seed Company Incorporation to the NSGC in 1993.

Growth and Relative Water Content Measurements

Barley seeds were germinated on moist papers and kept in darkness at 24°C. After 3 days, seedlings were transferred to 19 × 13.5 × 17 cm plastic pots filled with BM1 potting medium (peat moss (75–85%), vermiculite, perlite and wetting agent) (Berger, Canada). To ensure both genotypes experienced the same level of drought stress during the treatment, two seedlings of each genotype were transferred to the same pot. The plants were grown in a growth chamber maintained at 25/17°C (day/night temperature), 14/10 h (day/night cycle), 400 μmole m^{-1} s^{-1} light intensity and 50% humidity. Barely plants were fertilized twice

(first fertilization was 2 days after seedling transfer to pots, and the second was 10 days after the first fertilization) with Miracle-Gro® Water-Soluble All-Purpose Plant Food (Scotts Miracle Gro, USA). Drought treatment was initiated at the tillering stage Z21 (Zadoks scale) (Zadoks et al., 1974) at which the pots were divided into two groups: the control (well-watered) group and the drought-treated group. For the control group, plants were watered every other day. For imposing drought, watering was withheld, and plants were allowed to experience progressive drought (pDr). For the determination of growth, only main shoot (the shoot that appeared before the tillering stage) was chosen because the differences in the number of tillers among the individual plants of the same genotype varied. After 7 days of pDr, the leaf relative water content (LRWC) was calculated as described (Schonfeld et al., 1988) LRWC% = (Fresh weight-Dry weight)/ (Turgid weight-Dry weight) X 100.

Gas Exchange Measurements

For assessing photosynthesis-associated parameters, after 5 days of pDr (initial wilting), net photosynthetic rate, stomatal conductance, internal CO_2 concentration, and transpiration rate of the control and the drought-treated plants were measured on the youngest fully expanded leaf of the control and drought-treated plants (8 plants of each genotype per treatment) using LICOR 6400XT (LI-COR Inc., NE, USA). The following conditions were set for LICOR measurements: flow rate of 300 mmol s^{-1}, CO_2 at 400 mmol, leaf temperature 25°C, and relative humidity of 50%.

Proline Content

Proline was analyzed according to Carillo and Gibon (2011). Fresh samples from the youngest fully expanded leaf were homogenized using one ml extraction solution (70 ethanol: 30 water). Then, a volume of 100 µl of the extract was added to 200 µl of the reaction mixture (1% (w/v) ninhydrin, 60% (v/v) acetic acid, and 20% (v/v) ethanol). The reaction was kept in a boiling water bath for 20 min, and then kept on ice for stopping the reaction. The absorbance of the reaction mixture was measured at 520 nm.

Malondialdehyde Accumulation

Oxidative stress was determined by quantification of the malondialdehyde (MDA) levels (Heath and Packer, 1968) with some modifications. Samples of known fresh weight of the youngest fully expanded leaf were collected and snap frozen in liquid nitrogen. The samples were homogenized in 1 ml of 0.1% (w/v) trichloroacetic acid (TCA). Then, they were centrifuged at 4,100 rpm for 10 min. About 100 µl of the supernatant was added to 400 µl of 0.5% (w/v) thiobarbituric acid in 20% (w/v) TCA and the homogenates were boiled at 95°C for 30 min and the reaction was stopped by cooling the tubes on ice. The reaction mixture was centrifuged, and the absorbance was read at 532 nm and 600 nm. After subtracting the non-specific absorbance at 600 nm, the MDA concentration was determined by its extinction coefficient of 155 mM^{-1} cm^{-1}.

Hormonal Profiling

After 5 days of pDr (the initial wilting stage), three biological replicates (ten leaves from 10 different plants were used for each biological replicate) of the youngest fully expanded leaves of the control and the drought-treated plants were collected, snap frozen in liquid nitrogen and kept at −80°C. The frozen samples were lyophilized and used for hormonal analysis. The levels of major hormones and their metabolites were quantified using UPLC ESI-MS/MS by the National Research Council of Canada (Saskatchewan, Canada). The analyzed hormones and metabolites are: cis-abscisic acid (ABA), abscisic acid glucose ester (ABAGE), dihydrophaseic acid (DPA), phaseic acid (PA), 7'-hydroxy-abscisic acid (7'OH-ABA), neo-phaseic acid (neo-PA), trans-abscisic acid (t-ABA), gibberellin 1 (GA1), GA3, GA4, GA7, GA8, GA9, GA19, GA20, GA24, GA29, GA34, GA44, GA51, GA53, indole-3-acetic acid (IAA), N-(indole-3-yl-acetyl)-aspartic acid (IAA-Asp), N-(indole-3-yl-acetyl)-glutamic acid (IAA-Glu), N-(indole-3-yl-acetyl)-alanine (IAA-Ala), N-(indole-3-yl-acetyl)-leucine (IAA-Leu), indole-3-butyric acid (IBA), (trans) zeatin-O-glucoside (t-ZOG), (cis) zeatin-O-glucoside (c-ZOG), (trans) zeatin (t-Z), (cis) zeatin (c-Z), dihydrozeatin (dhZ), (trans) zeatin riboside (t-ZR), (cis) zeatin riboside (c-ZR), dihydrozeatin riboside (dhZR), isopentenyladenine (iP), isopentenyladenosine (iPR), and kinetin (KIN).

Statistical Analysis

The morphological, physiological, and biochemical data were analyzed using Student's *t*-test, 2-tailed distribution, and type 3 (2-sample unequal variance) (Excel, Microsoft, USA). A difference in means at value < 0.05 was considered significant.

RNA Sequencing

Three biological samples per genotype per treatment were collected from the youngest fully expanded leaf of 10 plants/sample from the control and the drought treated plants after 5 days of drought (initial wilting stage). The total RNA was extracted following the standard TRIzol method. The RNA integrity was checked with Agilent Technologies 2100 Bioanalyzer (Agilent Technologies, California, USA). Poly(A) tail-containing mRNAs were purified using oligo-(dT) magnetic beads with two rounds of purification. The purified poly(A) RNA was fragmented, and the library was constructed by synthesizing first strand cDNA, followed by second strand cDNA with dUTP, end repair, 3' adenylation, adaptor ligation, Uracil-DNA-Glycosylase (UDG) treatment, and PCR. Quality analysis and quantification of the sequencing library were performed using Agilent Technologies 2100 Bioanalyzer High Sensitivity DNA Chip. Paired-ended sequencing was performed on Illumina's NovaSeq 6000 sequencing system (LC Sciences, TX, USA). To remove the reads that contained adaptor contamination, low quality bases and undetermined bases in the sequenced RNA-seq libraries, Cutadapt (Martin, 2011) and perl scripts developed in house were used. Then, sequence quality was verified using FastQC (http://www.bioinformatics.babraham.ac.uk/projects/fastqc/).

Differential Expression and Differential Alternative Splicing Analyses

The RNA-seq data had 4 treatment groups: Otis, drought treatment (OD) Otis, watered treatment (OW); Baronesse drought treatment (BD) and Baronesse, watered treatment (BW) and each had 3 biological replicates (12 samples in total). Transcript quantifications were generated using Salmon (Patro et al., 2017) and the Barley transcriptome BARTv1.0-QUASI (https://ics.hutton.ac.uk/barleyrtd/index.html) (Rapazote-Flores et al., 2019). The 3D RNA-seq analysis App was used for differential expression (DE) and differential alternative splicing (DAS) analysis (Calixto et al., 2018; Guo et al., 2019). In the pipeline, expressed transcripts were identified when found in $\geq$ 2 of the 12 samples with count per million reads (CPM) $\geq$ 1, which provided an optimal mean-variance trend of the read count distribution. The Trimmed Mean of M-values (TMM) method was used to normalize the gene and transcript read counts to log_2-CPM (Bullard et al., 2010). Limma-VoomWeights method was used for DE and DAS (Law et al., 2014; Ritchie et al., 2015). To compare the expression changes between conditions of experimental design, the contrast groups were set as OD-OW, BD-BW, OW-BW, OD-BD. For DE genes, the log_2 fold change (L_2FC) of gene abundance were calculated based on contrast groups and p-values of multiple testing were adjusted with Benjamini–Hochberg (BH) to correct for false discovery rate (FDR) (Benjamini and Yekutieli, 2001). A gene was significantly DE in a contrast group if it had adjusted $p < 0.01$ and $L_2FC \geq 1$. For DAS genes, each individual transcript L_2FC were compared to gene level L_2FC, which was calculated as the weighted average of L_2FCs of all transcripts of the gene. Then p-values of individual transcript comparison were summarized to a single gene level p-value with an F-test. A gene was significantly DAS in a contrast group if it had an adjusted $p < 0.01$ and any of its transcripts had a Δ Percent Spliced (ΔPS) ratio $\geq$ 0.1 (see **Supplementary Report**).

Functional Analysis of the DE Genes

The Venn diagram generator of the Bioinformatics and Evolutionary Genomics lab at Ghent University and VIB, Belgium was used to find the unique and the common DE genes in the four contrast groups (http://bioinformatics.psb.ugent.be/webtools/Venn/).

Gene Ontology Tags were applied to the BaRT transcripts using Protein Annotation with Z-score (PANNZER) (Törönen et al., 2018) to produce GO annotations for 25,906 BaRT genes. GO functional enrichment analysis of the DE genes was done using g:profiler (https://biit.cs.ut.ee/gprofiler/gost) (Raudvere et al., 2019) with reference GO annotation dataset file BART_V_1.gmt (https://ics.hutton.ac.uk/barleyrtd/GO_enrichment.html).

The analysis of transcription factors (TFs) and kinases were performed using iTAK online (Zheng et al., 2016). First, the HORV annotation was retrieved for each of DE BaRT genes. Then, BioMart from Ensembl plants was used to get the protein sequence for each gene using Ensembl plants 47 as the database and *Horduem vulgare* genes (IBSC V2) as the dataset (https://plants.ensembl.org/biomart/martview/31c188c3a5aff85045c3cceb489e5597). Protein sequences of the DE genes were the input for the transcription factor and kinase analysis by iTAK online.

Quantitative Real-Time (qRT) PCR Analysis

Total RNA was used for cDNA conversion and the qRT PCR reactions were performed using the Light Cycler 96 system (Roche). Each PCR reaction was performed on two independent biological samples with two technical replicates. The relative expression levels of the target genes were calculated using the formula 2-$\Delta\Delta$Ct (Livak and Schmittgen, 2001). Fold change was calculated for the drought treated plants relative to the well-watered control, but for cellulose synthase and phenylalanine ammonia lyase the fold change was also calculated for Otis control relative to Baronesse control. Cyclophilin A (BART1_0-p42566) was used as reference gene for data normalization (Burton et al., 2004). **Supplementary Table 1** shows the list of primers used.

RESULTS

Morphological and Physiological Changes in Barley Genotypes Under Drought

Two barley genotypes with expected differences in resistance to drought were deprived of water to examine morphological and physiological differences between the two genotypes. The morphology of Otis and Baronesse after 7 days of drought is shown in **Figure 1A**. At this stage of drought, the leaves of both genotypes were severe wilting, and yellowing. The fresh weight of the main shoot of Baronesse was reduced by 49.4% of the control compared to 30.6% reduction in Otis (**Figure 1B**). The dry weight of the main shoot of Baronesse was significantly reduced by 18.7% compared to 0% reduction in Otis (**Figure 1C**).

In response to drought, the LRWC was significantly reduced in Baronesse compared to Otis (43.9 and 50.2% compared to 95.1 and 88.4% of the control, respectively). At this level of drought, LRWC was 58% of the control in Otis, and 46.2% in Baronesse (**Figure 2A**). In general, the two genotypes showed a significant decrease in the photosynthetic characteristics [CO_2 assimilation rate (P_N), stomatal conductance (gs), and transpiration rate (E)] under drought stress (**Figures 2B–D**). Under drought, P_N was 63% and 56% of the control in Otis and Baronesse, respectively. A similar trend was observed for gs and E (**Figures 2C,D**). In the drought-treated Otis, the gs and E showed 24 and 27% of the control, respectively, whereas these were 19 and 21% of the control, respectively, in Baronesse. Under well-watered conditions, Otis showed significantly less gs and E (0.092 and 2.31 mmol m^{-2} S^{-1}) than Baronesse (0.148 and 3.72 mmol m^{-2} S^{-1}). Both morphological and physiological tests show that both genotypes respond to the loss of water, but Otis shows greater endurance under these conditions.

Biochemical and Hormonal Changes in Barley Genotypes Under Drought

The differential responses between the barley genotypes were further assessed using biochemical and hormonal profiles. Proline accumulation was frequently observed in plants subjected to drought. Drought stress significantly increased proline content

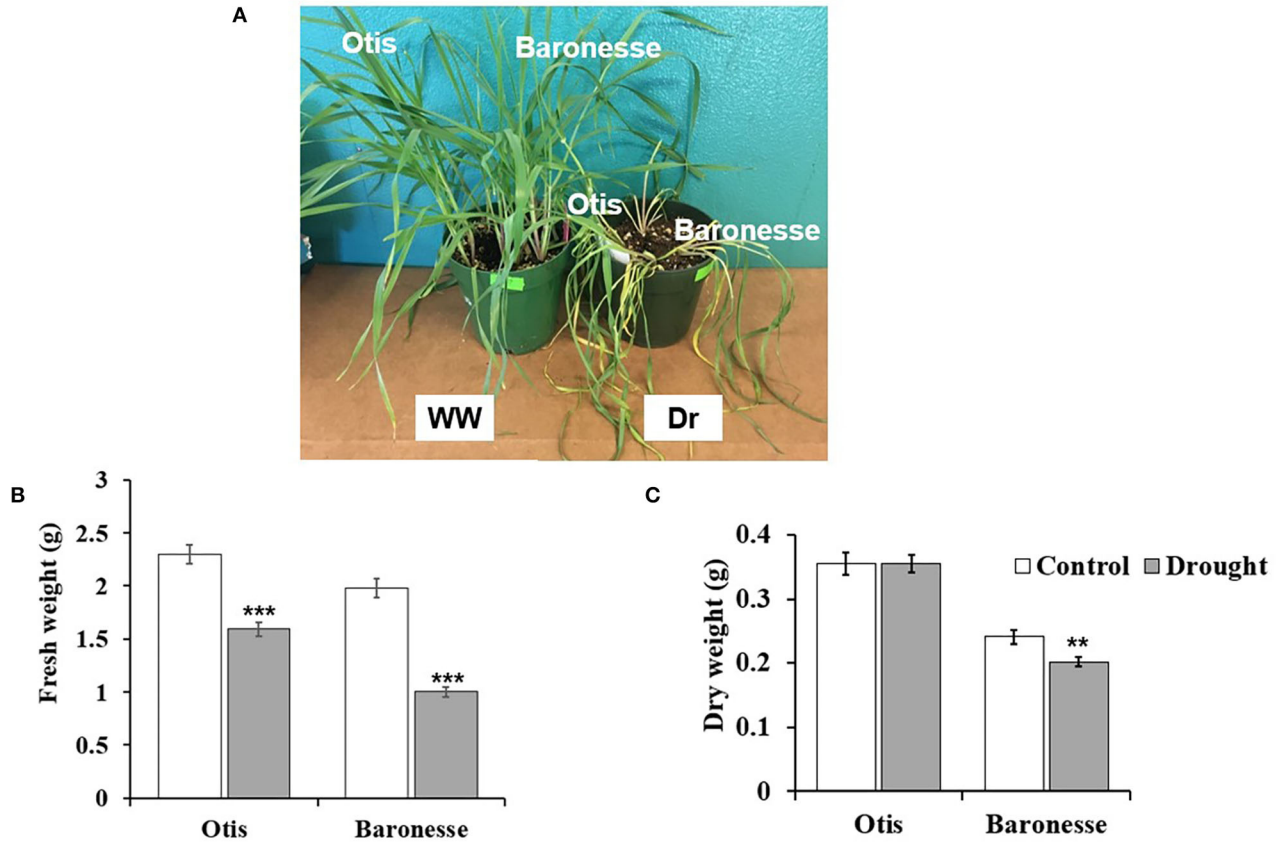


FIGURE 1 | Morphological changes between Otis and Baronesse under drought stress. **(A)** Barley plants of Otis and Baronesse under well-watered (WW) and drought (Dr) conditions. **(B)** Fresh weight (FW) of the main shoot (g). **(C)** Dry weight (DW) of the main shoot (g). Bars represent standard errors of the means. $N = 10$ plants. $^{**}P < 0.01$ and $^{***}P < 0.001$.

in the leaves of both genotypes. However, the accumulation found to be higher in Otis (86.94 μmol g-1 FW) compared to Baronesse (43.27 μmol g-1) (**Figure 3A**). Differential gene expression analysis of proline synthesis and turnover pathway genes further support the accumulation of proline in the leaves under water deficit stress (**Supplementary Figure 1**). The amount of lipid peroxidation (quantified as MDA) has been often correlated with the degree of stress-induced injury. The concentration of MDA was increased in both the genotypes, although the increase was significant only in the case of Baronesse (**Figure 3B**).

Changes in the major hormonal groups (ABA, auxins, cytokinins, and GAs) and their metabolites were analyzed in Otis and Baronessse at the initial wilting stage of pDr. The levels of ABA and its metabolites such as DPA, ABGE, and PA were significantly increased in the drought-treated Otis and Baronesse compared to their respective well-watered controls (**Figure 3C**). The concentration of ABA and its metabolites such as 7'OH ABA, neo-PA, and t-ABA was not significantly different between the genotypes under both conditions. In the drought-treated Otis, the concentration of ABA, 7'OH ABA, neo-PA, and t-ABA was 1,528.71, 61.82, 50.69, and 18.22 ng g-1 dry weight (DW), respectively, while their concentration in the drought-treated Baronesse was 1,882.68, 80.96, 60.82, and 22.54 ng g-1 DW, respectively.

The analysis of 14 GAs including GA19 did not reveal significant differences between the genotypes both under well-watered and drought conditions (**Figure 3D**). However, GA20 was only detected in the drought-treated Otis but not in Baronesse. This observation indicates that the GA20 is specifically induced under drought in drought-tolerant Otis.

Among the auxins, the IAA was detected in both the genotypes under well-watered as well as drought conditions. However, no significant differences were observed between the genotypes under both the conditions (**Figure 3D**).

The response of cytokinins, specifically t-ZOG accumulation under drought did not reveal significant differences between the genotypes compared to their respective controls (**Figure 3D**). However, the c-ZOG was significantly increased in the drought-treated Otis but not in Baronesse (**Figure 3D**). The concentration of c-ZOG was 496.85, and 177.22 ng g-1 DW in the drought-treated and the control plants of Otis genotype, respectively. Similarly, the iPR levels were increased in both the genotypes under drought but the degree of increase was higher in Otis

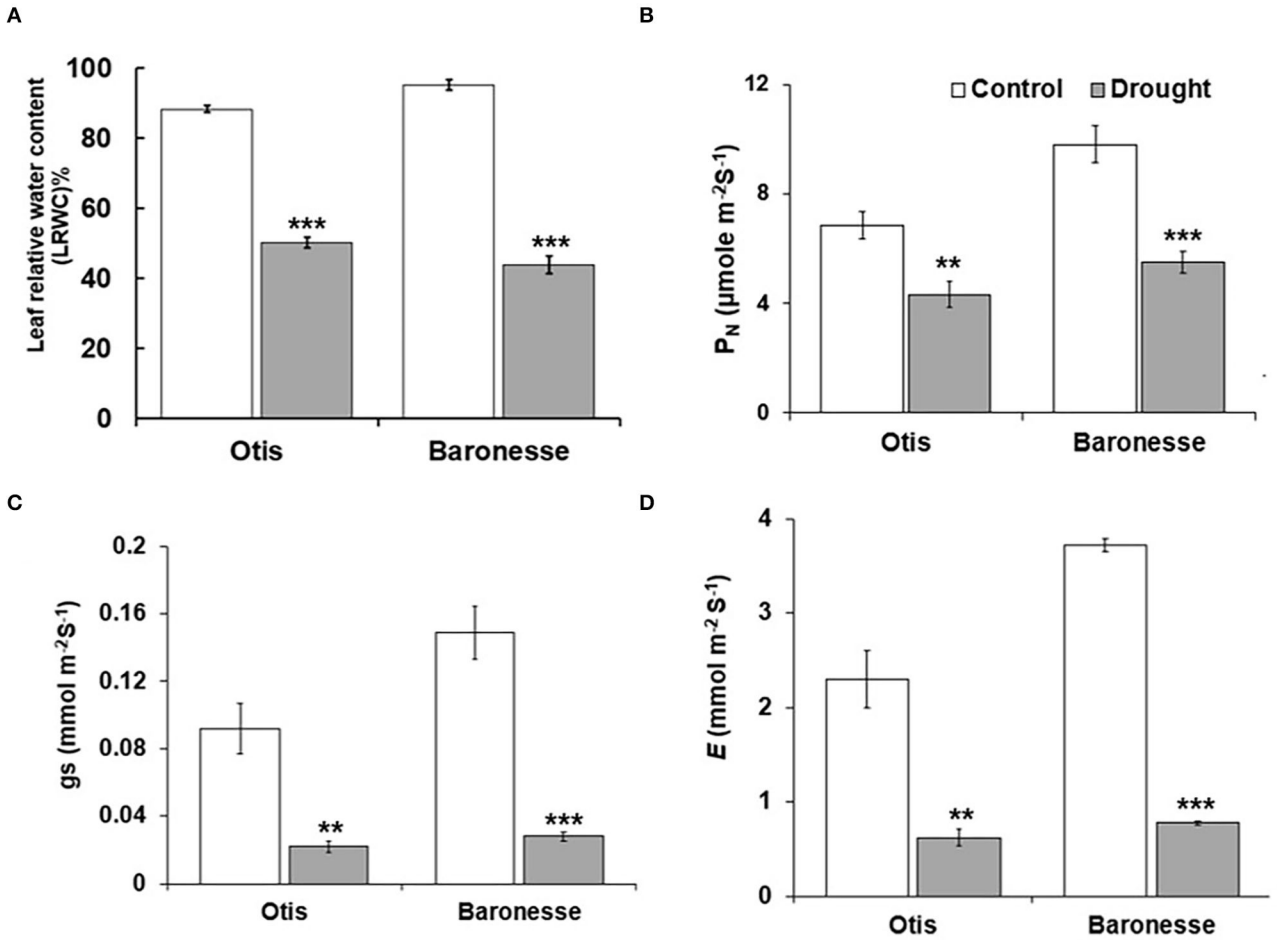


FIGURE 2 | Physiological changes in Otis and Baroness under drought. **(A)** LRWC. **(B)** Net photosynthetic rate (P_N). **(C)** Stomatal conductance (gs). **(D)** Transpiration rate (*E*). Values are the means of 10 plants for LRWC and 6 plants for photosynthesis measurements. Bars represent standard errors of the means. $^{**}P < 0.01$ and $^{***}P < 0.001$.

than in Baronesse (3.32 and 2.25 ng g-1 DW in the drought-treated and 1.58 and 1.92 ng g-1 DW in the controls of Otis and Baronesse, respectively).

Overview of the RNA-Seq Analysis of Drought Response in Two Barley Genotypes

RNA sequencing resulted in at least 40 million paired end reads per sample. The abundance of RNA transcripts in each Otis and Baronesse replicated samples were determined using Salmon and the reference transcript dataset BaRTv1.0. The raw RNA-Seq data has 176,343 transcripts and 59,930 genes After data processing to remove poorly expressed transcripts, there were 57,971 expressed transcripts and 23,970 genes. Principal Component Analysis (PCA) was performed using gene level $\log_2$ CPM values of the data to visualize RNA-seq data variation between the samples and replicates. The PCA scatter plot shows that replicates of the watered samples of Otis and Baronesse form distinct groups highlighting differences between the two genotypes. The watered samples were also distinct from the water deprived samples which showed less distinct grouping due to some variation between the replicates but both drought treated genotypes remained distinct (**Figure 4**). Differential gene expression analysis was calculated for four contrast groups (OD-OW, BD-BW, OW-BW, and OD-BD) to compare the differences in gene expression between genotypes Otis and Baronesse (O and B, respectively), and between drought (D) and watered (W) treatments in each of the genotypes. Expression analysis across all the contrast groups revealed a total number of 3,330 significant differentially expressed (DE) genes [adjusted $p = <$ 0.01; >2 fold change ($\log_2$ FC >1)]; 3,221 genes were regulated at the transcription level (DE), 314 genes were regulated by DAS (adjusted $p = < 0.01$; >10% change in alternative splicing) and 109 genes were regulated by both DE and DAS (**Figure 5A**). The BD-BW contrast group showed the highest total of DE genes (1,203 up-regulated and 786 down-regulated), and OD-BD showed the lowest number of DE genes (396 up-regulated and 292 down-regulated), indicating that Baronesse showed the

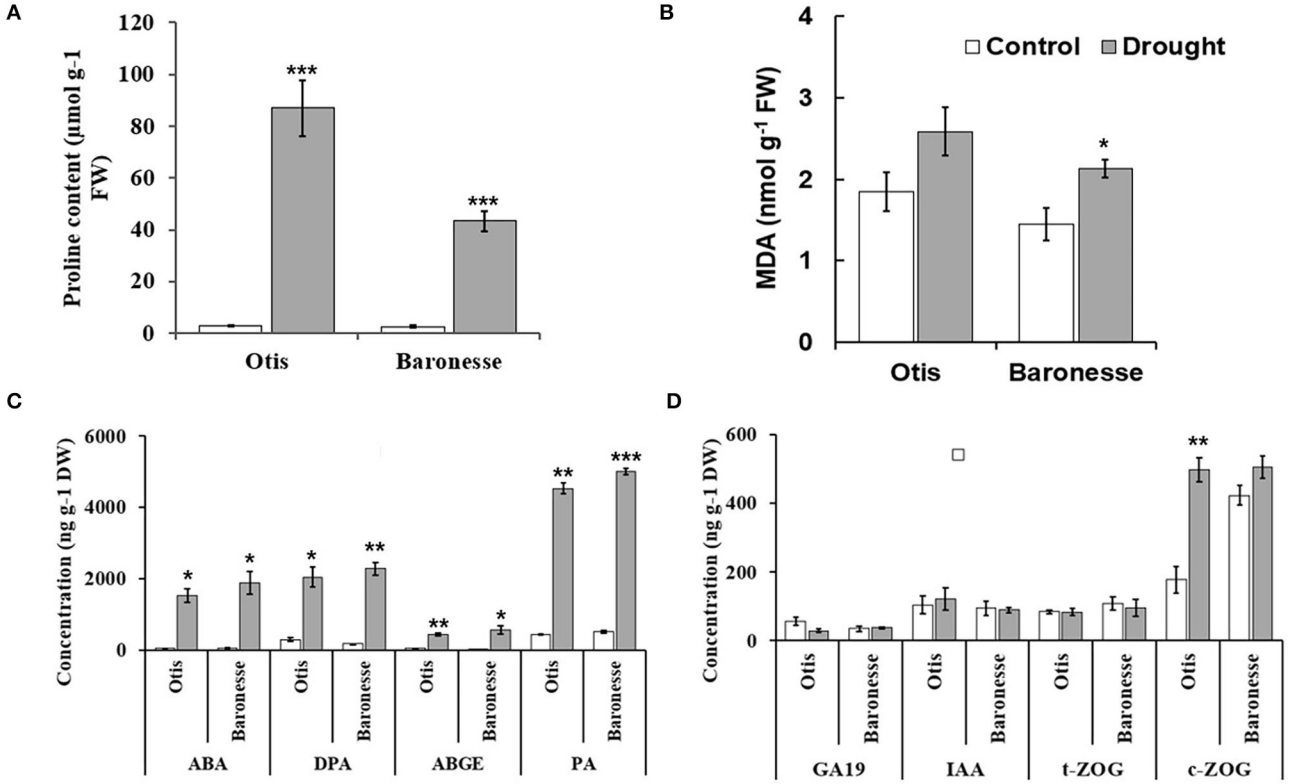


FIGURE 3 | Biochemical and hormonal profiles in Otis and Baronesse under drought stress. **(A)** Proline content. **(B)** Malondialdehyde (MDA) content. **(C)** Concentration of ABA and some of its metabolites (DPA, ABGE, and PA). **(D)** Concentration of Gibberellin 19 (GA19), Indole-3-acetic acid (IAA), trans-zeatin-O-glucoside (t-ZOG), and cis- zeatin-O-glucoside (c-ZOG). Hormones concentrations are the means of 3 biological replicates (each biological replicate is a pool of 10 plants). Bars represent standard errors of the means. $^{*}P < 0.05$, $^{**}P < 0.01$, and $^{***}P < 0.001$.

greatest transcriptional response to 5 days of drought. Some genes showed a similar up (286 genes) and downregulated (171 genes) expression response in both genotypes to the water deprived conditions (**Table 1**; **Figure 5B**). However, both genotypes responded differently to the drought conditions and there were 675 Baronesse genes and 126 Otis genes that were uniquely regulated in each genotype contributing to a different response by these two genotypes to the condition (**Figures 5C,D**). In addition, each genotype showed differentially expressed genes despite application of the condition (contrast groups OW-BW and OD-BD). These gene expression differences highlight common responses to the deprived water condition but also show that these genotypes differ substantially from each other, which supports the morphological and physiological variation found. **Supplementary Tables 2–7** show the detailed results of RNA Seq and gene expression.

Differentially Expressed Genes in Otis and Baronesse Under Drought

The categories of genes enriched in response to water deprivation were determined by performing a GO-enrichment analysis. The top three functional groups that were enriched in the common up-regulated genes between Otis and Baronesse were: response to water deprivation (GO:0009414), cation binding (GO:0043169), and raffinose alpha-galactosidase activity (GO:0052692) (**Table 2**). The unique up-regulated genes in Otis showed no significantly enriched processes. Whereas, the unique up-regulated genes of Baronesse were significantly enriched for cytosolic part (GO:0044445) and structural constituent of ribosome (GO:0003735) (**Table 2**).

The common down-regulated genes between the genotypes under water deprivation were found to be enriched for peptidyl-tyrosine modification (GO:0018212) (**Table 2**). The uniquely down-regulated genes of Otis (OD-OW) showed no significantly enriched processes. The top four processes that were enriched in the unique down-regulated genes of Baronesse (BD-BW) are: protein phosphorylation (GO:0006468), ATP binding (GO:0005524), plasma membrane (GO:0005886), and protein kinase activity (GO:0004672).

The BARTV1.0 and HORVU annotations of the 21 genes under the GO term response to water deprivation (GO:0009414) are shown in **Table 3**. The common up-regulated genes showed known stress responsive genes such as chaperones, annexin, signaling genes (kinases and phosphatases), aquaporin, and transcription factors. The expression level of most of these genes in the drought treated plants of the two genotypes

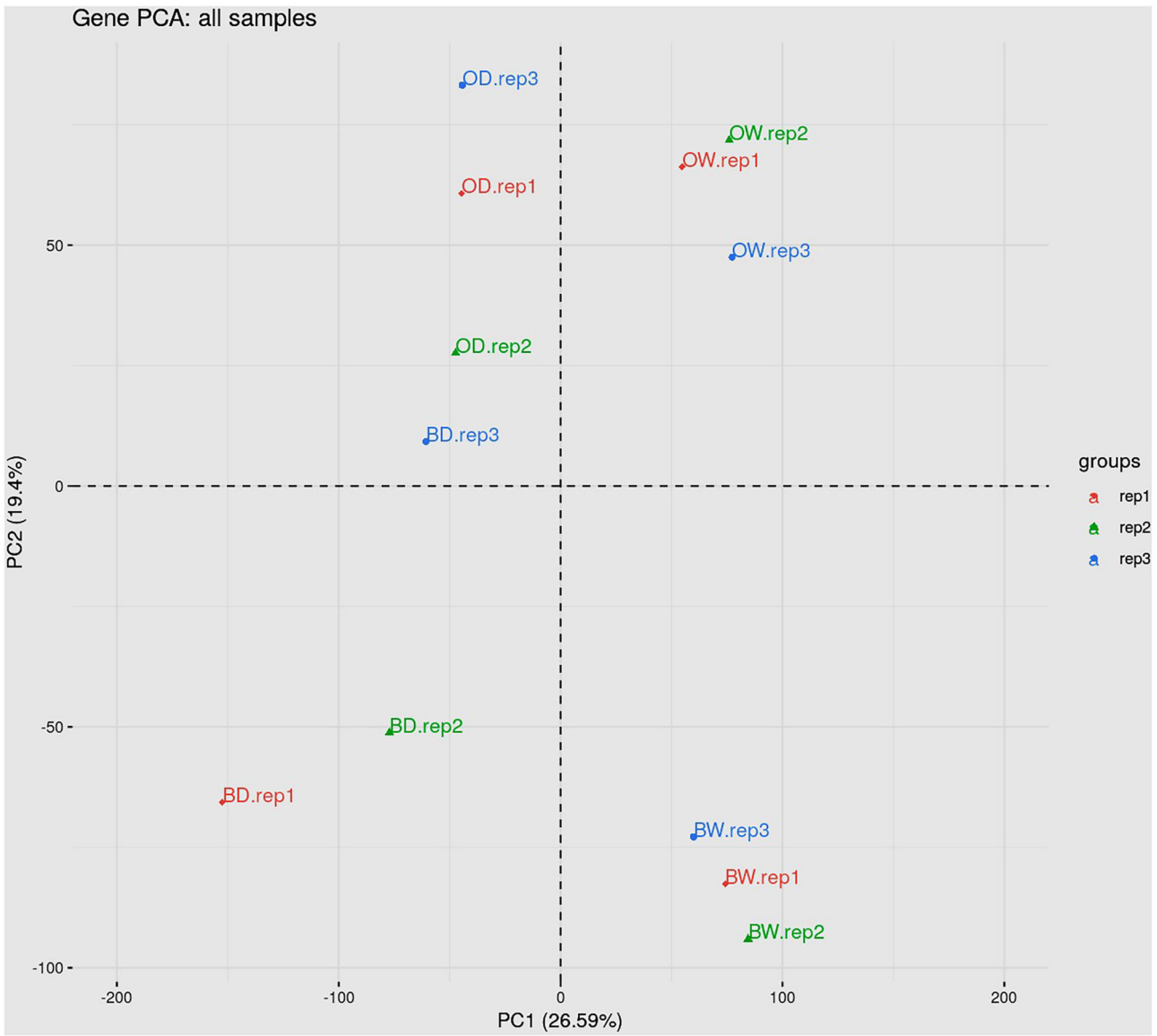


FIGURE 4 | Principal component analysis of the data showing the variation due to genotype and treatment.

TABLE 1 | Number of genes that are regulated by differential expression and/or by differential alternative splicing (DAS) in the different contrast groups.

Contrast	DE genes	DE only	DE and DAS	DAS only
OD-OW	774	773	1	36
BD-BW	1,809	1,806	3	61
OW-BW	1,328	1,280	48	260
OD-BD	688	669	19	131

is almost the same, except for a few genes. For example, the $\log_2$ FC of homeobox-leucine zipper protein ATHB-6 is 3.83 and 4.89 in the drought treated Otis and Baronesse plants, respectively. And the $\log_2$ FC of betaine aldehyde dehydrogenase was 2.43 and 1.52 in the drought treated Otis and Baronesse, respectively.

The common down regulated genes between Otis and Baronesse were enriched for peptidyl-tyrosine modification (GO:0018212). Under this process 13 genes were down regulated under drought compared to the control. The BART and HORVU annotations of these genes are shown in **Table 4**. In general, the common-down regulated genes are groups of kinases such as cysteine-rich receptor like protein kinase 5, leucine-rich receptor-like protein kinase family protein isoform 2, and serine/threonine protein kinase. A number of these kinase genes show a much greater down-regulation in expression

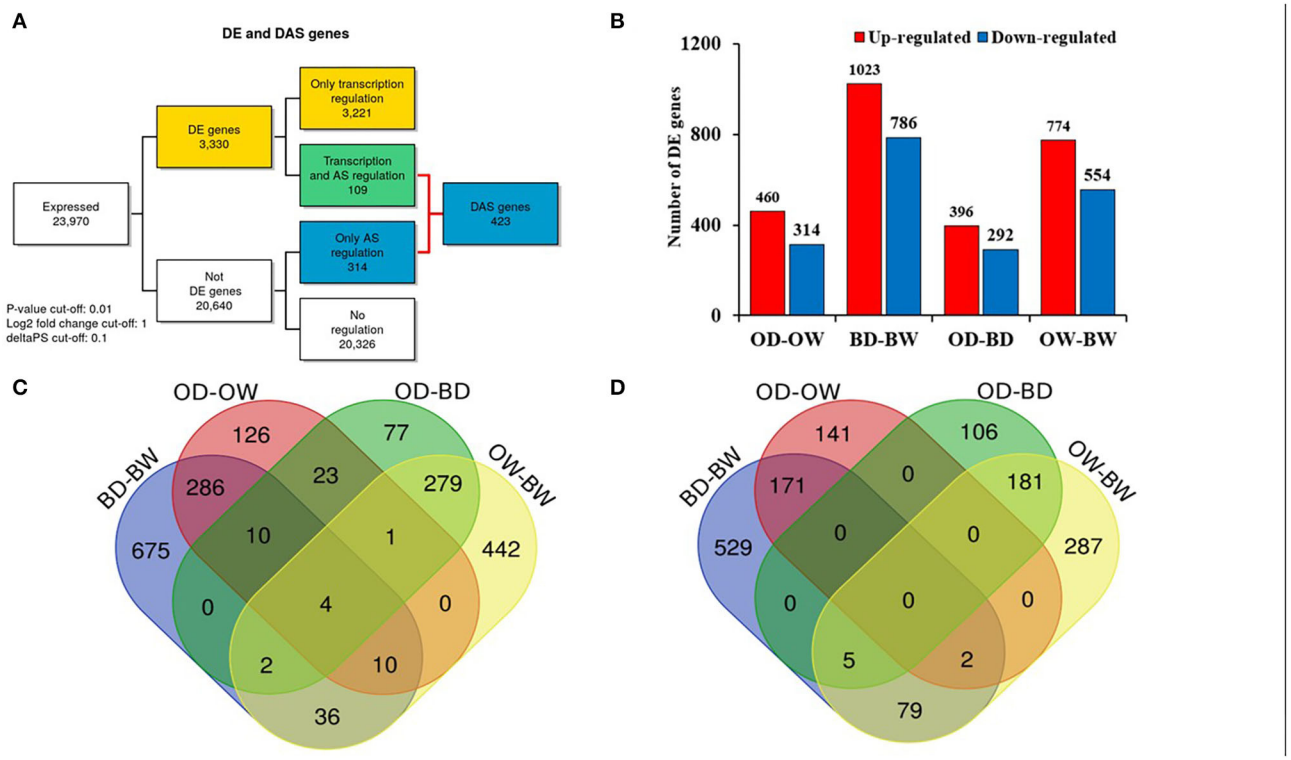


FIGURE 5 | Differential gene and alternative splicing analysis in two barley genotypes under progressive drought. **(A)** Number of genes regulated only by transcription (DE), only by alternative splicing (DAS) and by both transcription and alternative splicing (DE+DAS) across barley contrast groups (OD-OW, BD-BW, OW-BW, and BD-OD). **(B)** Number of up- and down-regulated DE genes in the different contrast groups. **(C)** Venn diagram of the up-regulated genes of the different contrast groups (OD-OW, BD-BW, OD-BD, and OW-BW). **(D)** Venn diagram of the down-regulated genes of the different contrast groups (OD-OW, BD-BW, OD-BD, and OW-BW).

TABLE 2 | GO enrichment of the differentially expressed genes in Otis and Baronesse under drought compared to well-watered control (OD-OW and BD-BW).

Commonly up-regulated genes between Otis and Baronesse under drought (OD-OW and BD-BW)					
Term name	**Term ID**	**Adjusted *P*-value**	**Term size**	**Query size**	**Intersection size**
Response to water deprivation	GO:0009414	1.42E-07	399	240	21
Cation binding	GO:0043169	0.000373003	75	240	8
Raffinose alpha-galactosidase activity	GO:0052692	0.000416886	33	240	6
Metabolic process	GO:0008152	0.01750248	37	240	5
Commonly down-regulated genes between Otis and Baronesse under drought (OD-OW and BD-BW)					
Peptidyl-tyrosine modification	GO:0018212	0.007915027	507	145	13
Uniquely up-regulated genes BD-BW					
Cytosolic part	GO:0044445	0.00131172	146	507	14
Structural constituent of ribosome	GO:0003735	0.006559518	1,094	507	44
Uniquely down-regulated genes BD-BW					
Protein phosphorylation	GO:0006468	9.99E-12	3,331	422	113
ATP binding	GO:0005524	1.30E-07	6,392	422	163
Plasma membrane	GO:0005886	3.88E-07	3,249	422	99
Protein kinase activity	GO:0004672	1.35272E-05	2,578	422	80

TABLE 3 | The BART and HORVU annotations of the commonly up-regulated genes under drought.

BART gene ID	BART annotation	HORVU gene ID	HORVU annotation	Log_2 FC OD-OW	Log_2 FC BD-BW
BART1_0-P29927	2C-type protein phosphatase protein	HORVU4Hr1G060370	Protein phosphatase 2C family protein	3.41	3.33
BART1_0-P34164	Molecular chaperone HtpG	HORVU5Hr1G027910	Chaperone protein htpG family protein	1.55	1.44
BART1_0-p07678	Aquaporin protein	HORVU2Hr1G010990	Aquaporin-like superfamily protein	3.11	2.58
BART1_0-P51213	Low quality protein: annexin D2	HORVU7Hr1G037080	Annexin 1	3.08	3.57
BART1_0-P39278	Cold-regulated plasma membrane protein 2	HORVU5Hr1G098190	Cold acclimation protein WCOR413 family	1.69	2.59
BART1_0-P07561	Putative ATP-binding cassette subfamily C member 8	HORVU2Hr1G009580	ABC transporter C family member 14	2.58	2.08
BART1_0-P50224	Leucine-rich repeat, cysteine-containing subtype	HORVU7Hr1G023610	F-box protein MAX2	2.15	1.44
BART1_0-P45680	Homeobox-leucine zipper protein ATHB-6	HORVU6Hr1G061390	Homeobox-leucine zipper protein family	3.83	4.89
BART1_0-P36679	Non-specific serine/threonine kinase protein kinase	HORVU5Hr1G065350	Serine/threonine protein kinase 1	1.78	1.32
BART1_0-P35808	RNA recognition motif domain	HORVU5Hr1G053230	RNA-binding protein 1	1.32	1.17
BART1_0-P47576	Betaine aldehyde dehydrogenase	HORVU2Hr1G070680	Betaine aldehyde dehydrogenase 2	2.43	1.52
BART1_0-P13794	Abscisic stress-ripening protein 2	HORVU2Hr1G092710	Homeobox-leucine zipper protein family	3.17	1.75
BART1_0-P47022	Class I homeodomain-leucine zipper protein 22	HORVU6Hr1G080670	bZIP transcription factor 27	1.49	1.31
BART1_0-P12382	G-box-binding factor 4	HORVU2Hr1G074770	Abscisic stress-ripening protein 3	3.49	3.60
BART1_0-P46765	Signal transduction response regulator	HORVU6Hr1G077070	Histidine kinase 3	1.28	1.15
BART1_0-P37103	Molecular chaperone HtpG	HORVU5Hr1G070720	Chaperone protein htpG family protein	1.65	1.79
BART1_0-P29183	Sucrose synthase	HORVU4Hr1G049500	Sucrose synthase 3	1.28	1.15
BART1_0-P29382	Hexosyltransferase	HORVU4Hr1G052450	Hexosyltransferase	2.79	2.17
BART1_0-P21831	2C-type protein phosphatase protein	HORVU3Hr1G067380	Protein phosphatase 2C family protein	2.98	3.27
BART1_0-P15058	Putative zeaxanthin epoxidase	HORVU2Hr1G106880	Chloroplastic lipocalin	1.18	1.21
BART1_0-P29181	Sucrose synthase	HORVU4Hr1G049500	Sucrose synthase 3	2.03	2.02

in Baronesse compared to Otis (**Table 4**). For example, the Log_2 FC of LRR receptor-like serine/threonine-protein kinase EFR (BART1_0-p15086) is −1.94 in Otis and −3.18 in Baronesse.

The Most Highly Regulated Genes Under Drought in Genotype-Dependent Manner

Differential gene expression analysis of the RNA-seq data identified highly induced or reduced genes as a response to drought. Both genotypes showed a different gene responding highly to the condition. In Otis, CER1 protein (BART1_0-p02677), Triticum beta-expansin (BART1_0-p22302), multidrug/pheromone exporter, ABC superfamily (BART1_0-p46064), Armadillo (ARM) repeat superfamily protein (BART1_0-p34106), STAM-binding protein (BART1_0-p13576), jasmonate induced protein (BART1_0-p25925), and NAC-type transcription factor (BART1_0-p58823) showed an expression level of $>$ 5 Log_2 FC. In Baronesse, the top

TABLE 4 | The BART and HORVU annotations of the common down-regulated genes in barley plants under drought stress.

BART gene ID	BART annotation	HORVU gene ID	HORVU annotation	Log_2FC OD-OW	Log_2FC BD-BW
BART1_0-p16694	Cysteine-rich receptor-like protein kinase 5 (Fragment)	HORVU2Hr1G041380	receptor kinase 1	−2.77	−3.62
BART1_0-p22957	Leucine-rich receptor-like protein kinase family protein isoform 2	HORVU3Hr1G081600	Leucine-rich repeat receptor-like protein kinase family protein	−2.66	−3.33
BART1_0-p16935	Serine-threonine/tyrosine-protein kinase catalytic domain-containing protein	HORVU3Hr1G000350	Protein kinase superfamily protein	−2.14	−3.32
BART1_0-p41113	Serine/threonine-protein kinase	HORVU5Hr1G120420	Receptor serine/threonine kinase, putative	−1.98	−3.25
BART1_0-p15086	LRR receptor-like serine/threonine-protein kinase EFR	HORVU2Hr1G107180	Leucine-rich receptor-like protein kinase family protein	−1.94	−3.18
BART1_0-p10197	Protein serine/threonine kinase	HORVU2Hr1G042210	Serine/threonine-protein kinase	−1.68	−2.24
BART1_0-p16723	ATP binding protein	HORVU2Hr1G124530	Protein kinase superfamily protein	−1.66	−2.12
BART1_0-p38965	Serine/threonine-protein kinase HT1	HORVU5Hr1G094510	Protein kinase superfamily protein	−1.60	−1.49
BART1_0-p10214	Protein serine/threonine kinase	HORVU2Hr1G042220	Serine/threonine-protein kinase	−1.58	−1.47
BART1_0-p45360	LRR receptor-like serine/threonine-protein kinase EFRprotein	HORVU6Hr1G057240	Leucine-rich repeat receptor-like protein kinase family	−1.37	−1.22
BART1_0-p16670	Protein kinase	HORVU2Hr1G125210	Receptor kinase 1	−0.133	−1.21
BART1_0-p13090	Inactive LRR receptor-like serine/threonine-protein kinase BIR2	HORVU2Hr1G084260	Receptor-like protein kinase 4	−1.23	−1.07
BART1_0-p51631	Transmembrane receptor protein serine/threonine kinase	HORVU7Hr1G043150	Protein kinase superfamily protein	−1.14	−1.04

up-regulated genes with Log_2 FC > 7.5 were: peptidyl-prolyl cis-trans isomerase (BART1_0-p44951), monooxygenase (BART1_0-p00176), late embryogenesis abundant protein-like (BART1_0-p38756), dehydrin (BART1_0-p23589), late embryogenesis abundant (BART1_0-p47280), rRNA N-glycosylase (BART1_0-p31866), late embryogenesis abundant protein (BART1_0-p48484), and asparagine synthetase [glutamine-hydrolyzing] (BART1_0-p35535) (**Supplementary Table 8**).

The most significant down-regulated genes in Otis were catalytic genes such as NADPH-hemoprotein reductase (BART1_0-p22029), myrcene synthase, chloroplastic (BART1_0-p56454), glucan endo-1,3-beta-glucosidase 13 (BART1_0-p06463), peroxidase (BART1_0-p08311), and O-acyltransferase WSD1 (BART1_0-p05934). In Baronesse, 6 of the most significant down-regulated genes were kinases such as L-type lectin-domain containing receptor kinase IX.1 (BART1_0-p48873), putative receptor protein kinase ZmPK1 (BART1_0-p21390), and Cysteine-rich receptor-like protein kinase 25 (BART1_0-p06472). Interestingly, aquaporin (BART1_0-p57239), transcription factor MYB4 (BART1_0-p45446), and nicotianamine synthase (BART1_0-p47748) are among the most highly down-regulated genes in Baronesse (see **Supplementary Table 9**).

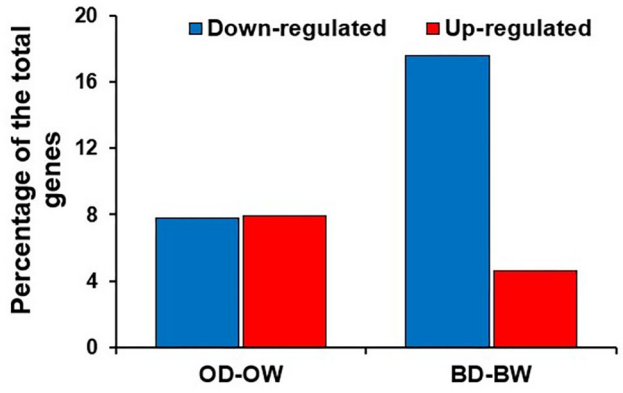


FIGURE 6 | Percentage of DEGs encoding kinases in Otis and Baronesse under drought.

Photosynthesis Genes Were Repressed Under Drought

The expression levels of several photosynthesis related genes were significantly down regulated in both the genotypes, indicating a general suppression of photosynthesis under drought. In drought-treated Otis, the expression level of photosystem II protein D1 (BART1_0-p16339), NAD(P)H-quinone oxidoreductase subunit 2, chloroplastic (BART1_0-p59777), ferredoxin-dependent glutamate synthase, chloroplastic-like (BART1_0-p10355), ATPase subunit IV (BART1_0-p59370), and proton-transporting ATP synthase activity (BART1_0-p26862) were significantly downregulated. Likewise in Baronesse, the abundances of PSII protein D1 (Fragment) (BART1_0-p60027), PSII D2 protein (Fragment) (BART1_0-p16337), NAD(P)H-quinone oxidoreductase subunit 2, chloroplastic (BART1_0-p44871), photosynthetic NDH subunit of subcomplex B (BART1_0-p46676), NADH-plastoquinone oxidoreductase subunit 5 (BART1_0-p03209), and ATP synthase CF1 alpha subunit, chloroplastic (BART1_0-p60215) were significantly down regulated under drought.

The Differentially Expressed Kinases in the Two Genotypes Under Drought

In plants, the kinases represent one of the largest category of genes which play significant roles in response to stress conditions. Differential gene expression analysis revealed that the kinases are the highest number of down-regulated genes in Baronesse under drought (**Figure 6**). Kinases account for 17.6 and 4.6% of down- and up-regulated genes in Baronesse, respectively, while the differentially regulated kinases represent 8% each for the upregulated and downregulated categories in Otis.

The DE kinases in the two genotypes are shown in **Table 5**; **Supplementary Tables 10–13**. In the down-regulated group of genes from Baronesse, the dominant family-subfamily was receptor like kinase-Pelle (RLK-Pelle). In this family/subfamily, 14 types of kinases were significantly down regulated more than 2-fold, including 10 RLK-Pelle-DLSV, 8 RLK-Pelle-WAK, 8 RLK-Pelle-L-LEC, and 7 RLK-Pelle-SD-2b. Baronesse also showed 7 RLK-Pelle genes up-regulated more than 2-fold. Otis showed 12 categories of kinases regulated under reduced water. For example, two Ca2+/calmodulin-dependent protein kinases (CAMK) (OST1L and CAMKL-CHK1) were significantly down-regulated while CAMK-CAMKL-CHK1 was uniquely up-regulated in Otis. In addition, two different categories of plant specific tyrosine kinase like (TLK) genes were significantly up regulated in the two genotypes under drought conditions.

Differentially Expressed Transcription Factors in the Two Genotypes Under Drought

Transcription factors (TFs) are key regulatory genes that coordinate regulation of plant development and conditional responses to a variety of stresses including drought. The number of differentially expressed TFs was higher in Baronesse (52 genes) compared to Otis (8 genes) (**Supplementary Tables 14–17**). In Otis, two bZIP and one NAC TFs were significantly down-regulated while mainly NAC TFs were up-regulated. In Baronesse plants under drought stress, 4 out of 21 down-regulated TFs were WRKY, 3 MYB and 3 bZIP domain TFs were down-regulated too. The up-regulated TFs in drought-stressed Baronesse were 3 GATA, 2 NAC domain, 2 bZIP, 2 MYB, nuclear factor Y subunit B, PLATZ, trihelix, and ethylene-responsive transcription factor 5 TFs.

Altered Expression of Chromatin Remodeling and Epigenetics-Associated Genes Under Drought

Epigenetic mechanisms are involved in the plant's transcriptional response to environmental stresses such as drought. Baronesse showed the greatest transcriptional response to water depravation and showed regulation of chromatin remodeling genes. One histone methyl transferase (SET) (BART1_0-p53128) and 2 Snf2-family ATPases (SNF2 chromatin remodeler) (BART1_0-p18056, BART1_0-p51557) were significantly down regulated while two SET (BART1_0-p38488, and BART1_0-p46523) and 1 GCN5-related N-terminal acetyltransferase (GNAT) (BART1_0-p31567) genes were up-regulated.

Differential Alternative Splicing Under Drought Stress

Serine and arginine-rich (SR) proteins are a group of highly conserved alternative splicing factors that have a role in regulating AS, changing the proportions of gene transcript isoforms under different plant stresses (Duque, 2011). Differential gene expression analysis identified barley orthologs of splicing factor RS31 (BART1_0-p31971; HORVU4Hr1G088790) and SC35-like splicing factor SCL30 (BART1_0-p26316; HORVU1Hr1G043200) genes that were up-regulated in response to water deprivation. RS31 showed a 2.7-fold increase in Otis and 3.6-fold in Baroness, while SCL30 showed a 1.7-fold increase in Otis and 2.5-fold increase in Baronesse in response to the drought stress (**Figure 7A**). Gene expression analysis using the barley reference transcript dataset allowed quantification of individual transcript isoforms and

TABLE 5 | The differentially expressed kinases in Otis and Baronesse under drought stress.

OD-OW Down	OD-OW Up	BD-BW Down	BD-BW Up
CAMK (Ca2+/calmodulin-dependent protein kinase) _OST1L (Open stomata-like kinase)	CAMK_CDPK (calcium-dependent protein kinases)	CAMK_CAMKL-CHK1	CAMK_CDPK
CAMK_CAMKL-CHK1 (CAMK-Like, Checkpoint Kinase 1)	CAMK_CAMKL-CHK1	WNK_NRBP [With No Lysine (K)' kinases and nuclear receptor binding protein (NRBP)]	RLK-Pelle_RLCK-VIIa-1
RLK-Pelle_RLCK-VIIa-2 (Receptor Like Cytoplasmic Kinase-VIIa-2)	CMGC_MAPK	PEK_GCN2 (Pancreatic eukaryotic initiation factor-2alpha kinase, general control non-derepressible)	RLK-Pelle_DLSV
RLK-Pelle_WAK (Wall Associated Kinase)	RLK-Pelle_DLSV (DUF26, SD-1, LRR-VIII and VWA, a moss-specific new RLK subfamily)	ULK_ULK4 (Unc-51 Like Kinase 4)	RLK-Pelle_CrRLK1L-1 (Catharanthus roseus RLK1-like)
RLK-Pelle_LRR-XI-2 (Leucine-rich repeat-XI-2)	RLK-Pelle_WAK	NEK [Mitotic Kinase family, also known as NRK (NimA-Related Kinase, based on Aspergillus NimA)]	RLK-Pelle_RLCK-Os
	RLK-Pelle_LRR-V	RLK-Pelle_WAK	RLK-Pelle_RLCK-V
	TKL-PI-4 (Tyrosine kinase like Plant-specific 4)	RLK-Pelle_SD-2b (S Domain 2b)	RLK-Pelle_L-LEC
		RLK-Pelle_LRR-Xa	RLK-Pelle_PERK-1 (Plant External Response Like Kinase 1)
		RLK-Pelle_LRR-VIII-1	TKL_Gdt (growth-differentiation transition)
		RLK-Pelle_L-LEC (L-type lectin)	
		RLK-Pelle_LRR-XII-1 (Leucine-rich repeat-XII-1)	
		RLK-Pelle_RLCK-Os (Receptor Like Cytoplasmic Kinase-Os)	
		RLK-Pelle_LRR-Xb-1	
		RLK-Pelle_LRK10L-2 (LRK10-like kinase type 2)	
		RLK-Pelle_DLSV	

to determine significant DAS events using the 3D RNA-seq App (Rapazote-Flores et al., 2019). To identify significant DAS genes, expression changes of a log2 fold change between gene transcripts were determined along with an adjusted $p < 0.01$ and a minimum 0.1 (10%) change in the proportion of spliced transcripts (Δ Percent Spliced – ΔPS). Across the two genotypes under watered and drought conditions 423 genes were detected that showed significant changes in transcript isoforms across the different genotypes and conditions and 109 of these genes were regulated by both transcription and AS such that 314 genes were uniquely regulated by AS, with no overall significant change in gene expression (**Figure 5A**). Pair-wise comparisons of Otis and Baronesse's response to drought stress showed only 37 and 61 significant DAS genes, respectively, and only 6 genes were common between the two genotypes (**Table 1**; **Supplementary Figure 2**; **Supplementary Tables 18–22**). Of the 6 genes showing significant changes in AS in both genotypes, BART1_0-u33753 (HORVU5Hr1G021770) has similarity to unc-93 homolog A, a positive regulator of abiotic stress tolerance in Arabidopsis (Xiang et al., 2018). This showed a complete reversal of the most abundant transcript BART1_0-u33753.005 in the watered samples of both genotypes to the BART1_0-u33753.001 transcript which was most abundant in drought samples (**Figure 7B**). This complete switch in transcript processing does not affect the protein coding sequence but results in the retention of an intron in the 3'UTR. GO enrichment analysis did not find any enrichment of GO terms, due to the broad range of different types of genes affected by AS genes and low number of AS genes found. These studies suggest that alternative splicing is less frequently affected under drought compared to other abiotic stresses. The results here also show genotype-specific differences in DAS responses under drought.

Validation of the RNA-Seq Profiles Using RT-qPCR

We used qRT-PCR and validated the gene expression profiles of several genes (**Figure 8**). For example, the cytokinin-o-glucosyltransferase 2 (BART_0-p11824) was up-regulated under drought stress in both the genotypes (OD-OW and BD-BW showed 1.69- and 1.30-fold change (RNA Seq) and 2.23

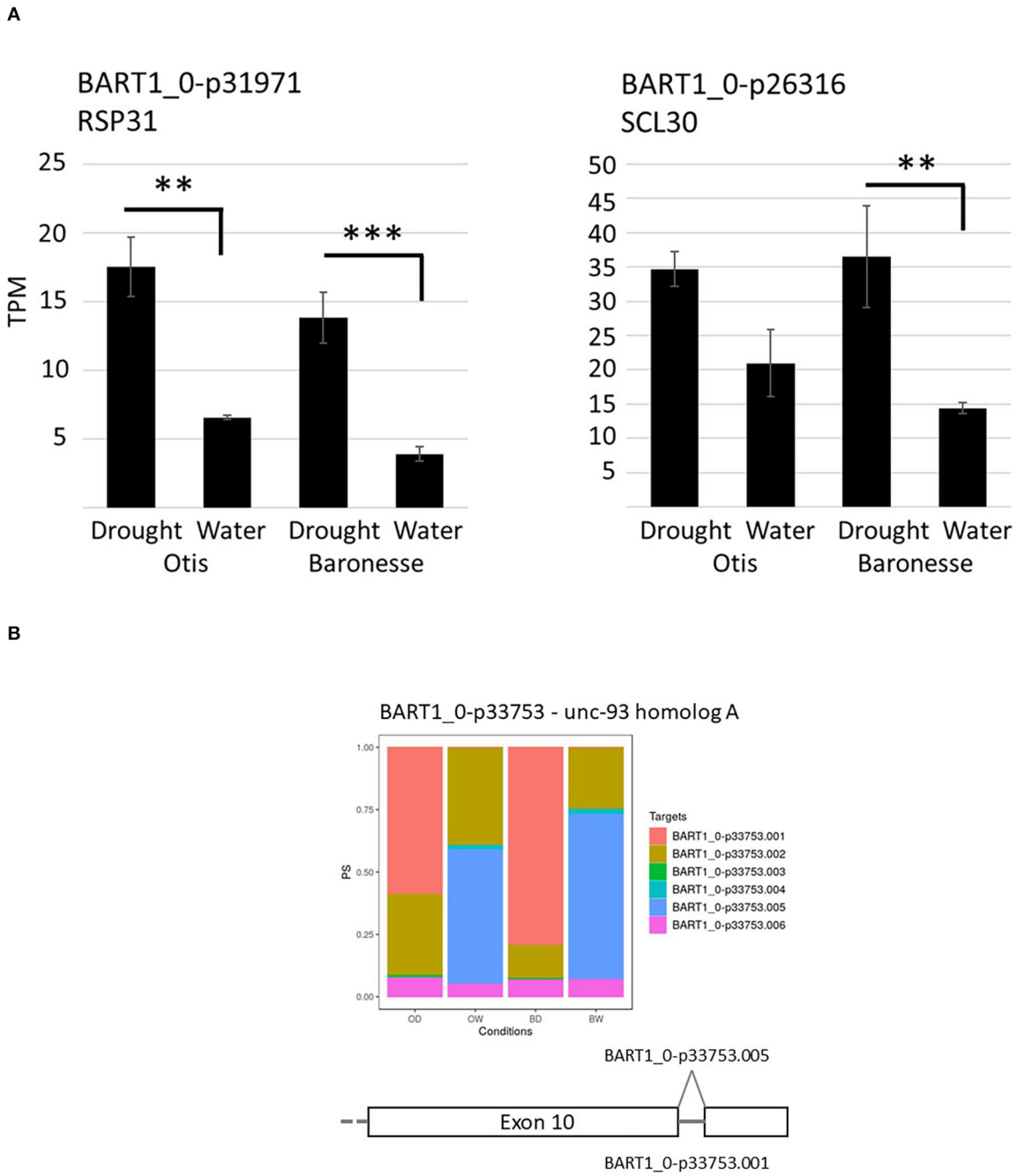


FIGURE 7 | Expression analysis of AS associated genes. **(A)** Mean differential gene expression of barley orthologs of SR splicing factors, RS31 and SCL30. Histograms show expression levels in transcripts per million (TPM) for watered and drought-treated Otis and Baronesse. Standard errors are the result of three biological repeats. Adjusted *p* values on $\log_2$ FC: ** < 0.005; *** < 0.001. **(B)** Expression analysis of UNC93-A AS transcripts. Each gene transcript is represented by a different color. Each histogram bar represents an individual genotype under a specific condition. From left to right is Otis drought (OD), Otis watered (OW), Baronesse drought (BD) and Baronesse watered (BW).

and 6.81 (qPCR), respectively). Tryptophan aminotransferase related 2 (BART1_0-p18317) was down-regulated in Baronesse under drought (-2.67 (RNA Seq) and 0.24-fold change (qPCR). Cellulose synthase was downregulated in Otis plants under control conditions compared to Baronesse plants [-2.99 (RNA Seq) and−19.87 (qPCR]. But it was up regulated in Otis under drought stress compared to Baronesse. Phenylalanine ammonia lyase was down-regulated in Otis plants under control conditions

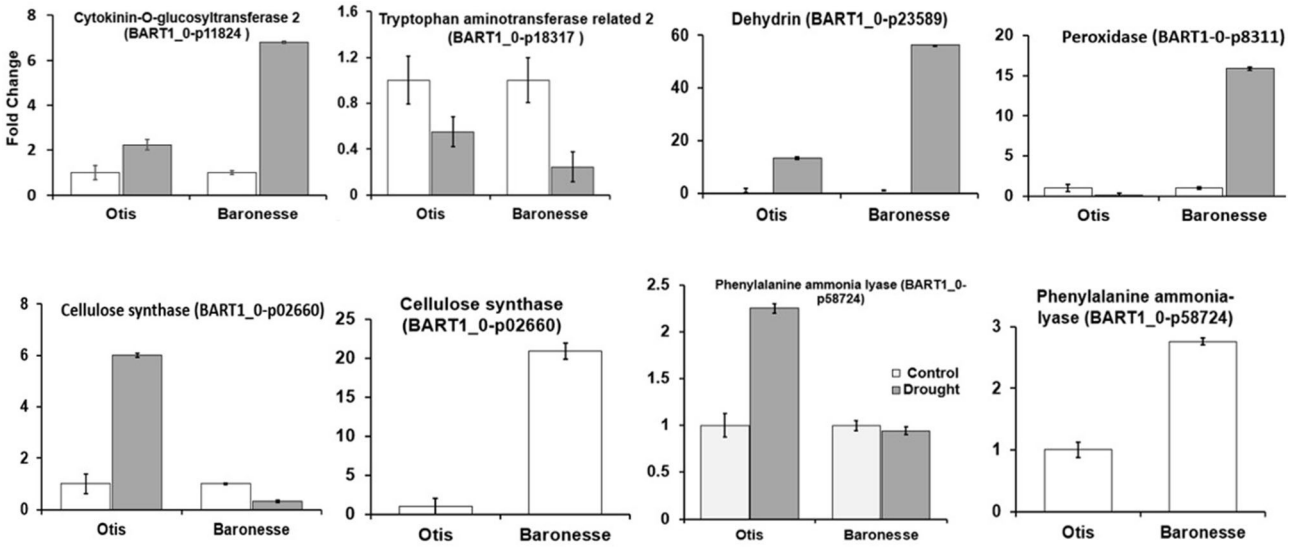


FIGURE 8 | Quantitative real-time PCR validation of RNA-seq data for selected genes.

compared to Baronesse plants [-1.16 (RNA Seq) and −1.76 (qPCR)]. But it was up regulated in Otis under drought stress compared to Baronesse.

DISCUSSION

When compared with Otis, Baronesse was found to be more sensitive to drought as revealed by the biomass, leaf relative water content, proline accumulation, and the parameters associated with photosynthesis. Although significant decrease in the net photosynthetic rate (PN), stomatal conductance (gs), and the transpiration rate (E) was observed in both the barley genotypes under drought, but the degree of inhibition was less in the Otis compared to Baronesse. Indeed, this difference between the genotypes was supported by the RNA-Seq analysis that revealed a greater down regulation of several photosynthesis-related genes (genes for D1 protein (PsbA) and D2 protein (PsbD) in Baronesse compared to Otis. PSII (both D1 and D2 proteins are needed for assembly of a stable PSII complex) plays an important role in response to environmental stresses (Baker, 1991). In wheat genotypes, drought resulted in different degrees of repression of PsbA and PsbD genes, however, less repression of both genes (especially the PsbD gene) in the drought tolerant genotype (Liu et al., 2006).

Under well-watered conditions, Otis plants showed significantly less gs and E than Baronesse. This suggests that Otis might have lower stomatal density compared to Baronesse, which could be one player in drought tolerance of Otis. In line with this, the overexpression of epidermal patterning factor (EPF) (*HvEPF1*) in barley resulted in a significant reduction in stomatal density without adverse effects on the normal growth of the overexpression lines (Hughes et al., 2017). In addition, the overexpression lines showed less gs than the wild type under well-watered conditions. And under drought stress, they have higher water use efficiency and drought tolerance compared to the wild type. In drought tolerant rice and wheat genotypes, transpiration efficiency (TE) was enhanced by maximizing mesophyll conductance (gm) and minimizing stomatal conductance (gs) (Ouyang et al., 2017). Indeed, the drought tolerant rice and wheat showed low stomatal density, and thick mesophyll with thin cell walls.

Correlations Between the Gene Expression Profiles of Proline and Glycine Betaine and Their Accumulation and Relative Water Content

Proline content was increased in both genotypes under drought, but the increase was significantly higher in Otis plants. Proline is an imino acid that acts as an osmoprotectant, a metal chelator, an antioxidative molecule, and a signaling molecule that enhances drought tolerance by maintaining the osmotic balance of the cells (Blum, 2009; Hayat et al., 2012). The LRWC of the two genotypes was significantly reduced, but drought treated Otis plants showed less reduction in their LRWC (**Figure 2A**). This response highlights one aspect of several mechanisms that could be used by Otis to tolerate drought better compared to Baronesse. High proline accumulation in the leaves of barley plants under severe osmotic stress leads to less membrane injury (Bandurska, 2001). In wild barley high proline accumulation in the leaves increased drought tolerance compared to cultivated barley (Bandurska and Stroihski, 2003). Indeed, in many major crop plants such as wheat, barley, and maize, osmotic adjustment was positively correlated with stress resistance (Blum, 2017). The expression of proline biosynthesis and turnover genes reflect this enhanced production of proline in both genotypes under drought. Pyrroline-5-carboxylate

synthase (P5CS), pyrroline-5-carboxylate reductase, pyrroline-5-carboxylate dehydrogenase and Orn-δ-aminotransferase were all significantly induced in drought conditions. Only the proline turnover gene proline dehydrogenase expression was reduced under drought conditions. Although differences between the genotypes were not significant under reduced water conditions, the trend showed larger levels of expression in Otis (**Supplementary Figure 1**).

Glycine betaine (GB) is another important osmolyte and is known to accumulate in response to abiotic stresses in a variety of plant species (Ashraf and Foolad, 2007). GB is produced from choline via choline monooxygenase (CMO) and betaine aldehyde dehydrogenase (BADH). In barley, BADH1 and BADH2 genes were significantly induced under drought and salinity (Nakamura et al., 2001). Our results reveal that BADH (BART1_0-p47576, HORVU2Hr1G070680) was induced in both genotypes under drought. However, its expression was higher in Otis compared to Baronesse.

Hormonal Profiles

Among the hormones, ABA is the most important hormone regarding its role in plant drought tolerance (Daszkowska-Golec, 2016; Sah et al., 2016; Vishwakarma et al., 2017). In this study, both genotypes accumulated ABA as well as several ABA-related metabolites under drought but the accumulation levels did not differ greatly between the genotypes. Likewise, the response of auxin levels was hardly differed between the genotypes under drought.

Cytokinins (CKs) and their metabolism is important in plants' adaptation to different abiotic stresses including drought (Ha et al., 2012; Pavlu et al., 2018). Drought stress caused a significant increase in the cytokinin, cZOG in Otis compared to Baronesse, suggesting a potential role for cZOG in the drought tolerance. Conjugation of O-glucose to cZ CKs (O-glucosylation) results in the formation of O-glucosides, and it is a reversible modification and the O-glucosides such as c-ZOG are storage forms of cZ CKs (Schäfer et al., 2015). A role for cis-Zeatin (cZ) CKs in plant growth and development has been reported (Kudo et al., 2012; Schäfer et al., 2015). It was also suggested that cZ CKs could be important for maintaining minimum CK activity for cell survival under stress conditions (Gajdošová et al., 2011).

With over 100 identified GAs, only a few are bioactive: GA1, GA3, and GA4 (Yamaguchi, 2008). The levels of GAs were found to be decreased under drought stress, and this could be associated with the retarded plant growth under stress (Nelissen et al., 2018). In small cereals (Tef and finger millet), the inhibition of GA biosynthesis resulted in an enhanced tolerance to osmotic stress (Plaza-Wüthrich et al., 2016). It was further reported that the reduction of GAs enhanced drought tolerance by osmotic adjustment and maintenance of leaf turgor of tomato (Omena-Garcia et al., 2019). Remarkably, GA20 levels were only increased in the drought-treated Otis. GA20 is an intermediate of GA1 and GA3, which is converted to GA1 by GA 3-oxidase (GA3ox) (Yamaguchi, 2008). This conversion was shown to be inhibited by heat, dehydration, and salinity (Colebrook et al., 2014). The increase in GA20 in the drought-treated Otis suggests a less conversion of this gibberellin to the bioactive forms of GA.

For hormonal profiling, samples of barley leaves were taken at the initial wilting stage of drought (5 days of drought). At this stage, no significant changes were observed for shoot length or biomass in the two genotypes under drought stress compared to the control. This might explain the observed small number of differences regarding hormonal profiles under drought in the genotypes.

General Transcriptional Responses Greatly Differed Between the Genotypes

The drought sensitive genotype Baronesse showed higher number of differentially expressed genes (DEGs) under drought (1,023, and 786 up and down-regulated, respectively), compared to Otis (460, and 314 up and down-regulated genes, respectively), in the drought-tolerant Otis indicating that the transcriptional changes were far greater in sensitive genotype. Indeed, previous studies have reported a greater number of stress-regulated genes in the sensitive genotypes compared to the tolerant genotypes subjected to stress treatments (Silveira et al., 2015; Cantalapiedra et al., 2017; Janiak et al., 2019; Ereful et al., 2020).

The Shared Responses Between Otis and Baronesse as Revealed by the Differentially Expressed Genes

In this study, several differentially regulated genes (signaling genes (kinases and phosphatases), transcription factors, chaperones, annexins, and aquaporins) that showed almost similar level of regulation in both the genotypes under drought have been identified and these could be important for maintaining cellular homeostasis under stress.

Chaperones have been shown to stabilize membranes and proteins by assisting with folding, association, translocation, and degradation of proteins under stress (Priya et al., 2019). The chaperone gene BART1_0-p34164 (HORVU5Hr1G027910) was up regulated in the drought-treated Otis and Baronesse (Log2 FC is 1.55 and 1.44, respectively). The ortholog of this gene in Arabidopsis was shown to be induced under drought stress (Gupta and Senthil-Kuma, 2017).

Aquaporins (AQPs) are pore forming proteins belonging to the major intrinsic proteins (MIP) superfamily which transport water and other small neutral compounds across the membrane. The upregulation of AQPs in response to abiotic stresses is known in plants (Quigley et al., 2001; Scharwies, 2017; Kapilan et al., 2018). The aquaporin, BART1_0-p07678, HORVU2Hr1G010990 was significantly induced in both the genotypes under drought stress. The rice ortholog (OsPIP2.6) of this gene (LOC_Os04g16450), has shown to be induced in the drought tolerant parent and the inbred lines but repressed in the drought sensitive parent (Baghyalakshmi et al., 2020).

Annexins are a diverse, multigene family of calcium-dependent, membrane-binding proteins that serve as targets for

Ca2+ in most eukaryotic cells (Clark et al., 2001). An annexin gene (BART1_0-p51213, HORVU7Hr1G037080) was one among the commonly up regulated genes in Otis and Baronesse under drought stress (Log2 FC is 3.08 and 3.57, respectively). The orthologous gene in rice (LOC_Os06g11800) was shown to be upregulated under drought stress (Gorantla et al., 2005). The Arabidopsis ortholog of Annexin 1 (AT1G35720) was also induced by drought and its overexpression confers enhanced drought tolerance (Konopka-Postupolska et al., 2009). A possible mode of Annexin 1 in drought tolerance include the alleviation of the oxidation of the membrane's lipids and proteins (Jami et al., 2008).

A Gene for Wax Biosynthesis was Uniquely and Highly Induced in Otis Genotype Under Drought

ECERIFERUM1 (*CER1*) gene [CER1 from fatty acid hydrolase superfamily (BART1_0-p02677)] involved in wax biosynthesis was highly upregulated in Otis under drought. The Arabidopsis and rice orthologs of this gene are *CER1* (AT1G02205) and WAX2 (LOC_Os10g33250), respectively. In drought treated Arabidopsis plants, the expression of *CER1* gene was up regulated, along with a significant increase in the very long chain (VLC) alkanes in the cuticle (Kosma et al., 2009). The Arabidopsis *CER1* gene codes for an important enzyme involved in the biosynthesis of VLC alkanes of the cuticle (Bourdenx et al., 2011). The cuticle is a hydrocarbon epidermal extension, that acts as a protective barrier against water loss under drought stress. Indeed, the overexpression of *CER1* in Arabidopsis conferred drought tolerance due to reduced water loss (Bourdenx et al., 2011). In Brachypodium, eight homologs of *CER1* were identified (Wu et al., 2019). *BdCER1-8* was highly expressed in the leaves, and it was significantly induced by drought and osmotic stress. Moreover, *BdCER1-8* rescued the biosynthesis of the VLC alkanes in cer1 Arabidopsis mutant (Wu et al., 2009). The overexpression of the transcription factor *TaSHN1* in wheat resulted in reduced stomatal density and leaf water loss, and thereby improved drought tolerance of the transgenic lines (Bi et al., 2018). In addition, the analysis of the cuticle composition of *TaSHN1*overexpression lines revealed a significant increase in the alkanes under control and drought conditions. The overexpression of *TaSHN1* also resulted in more than 10-fold upregulation of the cuticle biosynthetic genes such as: *ATT1/CYP86*, *CER4-6*, *KCS1*, and *LACS3*. This indicates that one mechanism of the improved drought tolerance in the *TaSHN1* overexpression lines is through changes in the cuticle composition both at the molecular and biochemical levels. The induction of CER1 in the drought-treated Otis is one of the few major differences of supporting drought tolerant nature of Otis compared to Baronesse. This might explain the less reduction in the leaf relative water content in Otis under drought stress. Indeed, a detailed analysis of the cuticle composition of Otis and Baronesse under drought and control conditions will shed more light on drought tolerance in barley.

A Beta-Expansin Gene was Uniquely and Highly Induced in Otis Genotype Under Drought

Expansin gene family is one group of cell wall modifying genes (Cosgrove, 2000). Expansin genes are important players in cell growth through loosening of the cell wall (Cosgrove, 2015). Phylogenetically, expansin genes are divided into two major families: EXPA (α-expansins) and EXPB (β-expansins) (Cosgrove, 2015). In barley, a total of 34 expansin genes (14 EXPA, 17 EXPB, and 3 EXPLA) were identified (Lombardi, 2012). The expression of the barley expansin genes showed specific expression profile for each tissue, organ, and developmental stage. Previous studies showed the involvement of expansin genes in many growth and developmental processes (Choi et al., 2003; Marowa et al., 2016). Moreover, expansin genes were found to be differentially expressed under different abiotic stresses (Wu et al., 2001; Bray, 2004; Harb et al., 2010; Marowa et al., 2016). The overexpression of TaEXPA2 in tobacco and wheat enhanced drought tolerance in the transgenic plants (Chen et al., 2016; Yang et al., 2020). Moreover, improved tolerance to salinity and drought was also shown in tobacco plants overexpressing the tobacco EXPA4 (Chen et al., 2018). In barley, HvEXPB7 improved the growth of barley root hairs under drought in the drought tolerant Tibetan wild barley genotype (He et al., 2015). The beta expansin gene (BART1_0-p22302) was highly induced in the drought stressed Otis (Log2 FC is 6). The Arabidopsis and rice orthologs of this gene are AT1G65680 (AtEXPB2), and LOC_Os03g01270 (OsEXPB7). The rice gene was significantly repressed under dehydration conditions (Zhou et al., 2007; Ray et al., 2011; Shaik and Ramakrishna, 2012). In these studies, the changes in gene expression were tested in one genotype of rice under dehydration stress, which is considered as a shock stress to plants. Whereas, in this study, two barley genotypes with contrasting drought tolerance were exposed to progressive drought for 5 days. Indeed, a low correlation between gene expression under dehydration shock and that under progressive (gradual) drought was shown in barley (Talamé et al., 2007).

An Armadillo (ARM) Repeat Gene is Highly Upregulated in Otis Genotype Under Drought

Armadillo (ARM) repeat gene family has the ARM repeat domain, which is composed of one short and two relatively longer α-helices (Mudgil et al., 2004; Sharma and Pandey, 2016). It includes members of diverse functions such as: signal transduction, nuclear transport, cell adhesion, and protein degradation (Sharma et al., 2014). The most common protein arrangement of ARM family is U-box/ARM (PUB/ARM), which suggests a role in protein ubiquitination (Sharma and Pandey, 2016). This will result in higher plasticity in response to the changing environments. The Armadillo gene was among the drought responsive genes in the drought tolerant potato genotype (Pieczynski et al., 2018). In rice plants, 36 OsARM genes were differentially expressed under different abiotic stresses (drought, salt, and cold) (26 up-regulated and 10 down-regulated) (Sharma et al., 2014). Out of the 26 up-regulated genes 7 were uniquely

drought induced genes, and 4 out of 10 were uniquely drought repressed genes. In barley, 5 PUB/ARM genes [class II U-box E3 ubiquitin ligases (HvPUB7, HvPUB9, HvPUB15, HvPUB16, HvPUB21, and HvPUB22)] were significantly induced, and one gene (HvPUB18) was repressed under dehydration stress (Ryu et al., 2019). The ARM repeat gene (BART1_0-p34106) was highly induced in Otis drought stressed plants (Log2 FC 5.88). This gene is not a member of the U-box E3 ubiquitin ligase family in barley (Ryu et al., 2019). This suggests that it might function in drought tolerance of Otis via mechanism (s) other than protein ubiquitination and degradation.

Kinases are Predominantly Down Regulated in Baronesse Plants Under Drought

Genes encoding protein kinases (Pks) were overrepresented among the down regulated genes in drought-treated Baronesse. Most of these kinases are receptor like kinase-Pelle (RLK-Pelle). Receptor like kinase-Pelle is the largest gene family in Arabidopsis and rice, which are responsive to different abiotic and biotic stresses (Lehti-Shiu et al., 2009). In rice, receptor-like cytoplasmic kinase GROWTH UNDER DROUGHT KINASE (GUDK) was shown to improve drought tolerance through the activation of the transcription factor APETALA2/ETHYLENE RESPONSE FACTOR OsAP37 (Ramegowda et al., 2014). The overexpression of poplar leucine-rich repeat (LRR) receptor-like kinase in Arabidopsis enhanced water use efficiency (Xing et al., 2011). The general down regulation of many kinases in Baronesse relative to Otis could be one of the factors associated with drought sensitivity.

Transcription Factors

Transcription factors (TFs) are regulatory proteins that play an important role in almost all plant processes including adaptation to biotic and abiotic stresses (Nakashima et al., 2014; Joshi et al., 2016). TF genes such as AP2/EREBP, bZIP, MYB/MYC, NAC, WRKY have been implicated in drought stress responses (Gahluat et al., 2016). The number of DEGs encoding TFs were more in the drought-stressed Baronesse than in Otis.

NAC genes are plant-specific transcription factors involved in growth and development and stress responses. Overexpression of several NAC genes from Arabidopsis, rice, and soybean increased the tolerance of transgenic plants to abiotic stresses including drought (Nakashima et al., 2007; Hao et al., 2011; Wang and Dane, 2013; Shim et al., 2018). In drought stressed Otis, two NAC genes were up regulated, while one NAC gene was down regulated. The overexpression of wheat NAC TF improved tolerance to drought and salt stress in Arabidopsis (Huang et al., 2015).

One of the induced NAC genes in Otis genotype is BART1_0-p58823 (HORVU0Hr1G017490), which has Log2FC of 5.33. The rice ortholog of this gene is LOC_Os02g56600, which was induced in the salt-tolerant rice genotype but repressed in the salt-sensitive genotype (García-Morales et al., 2014). The other NAC gene that was induced specifically in the Otis genotype is BART1_0-p12809 (HORVU2Hr1G080460), which has Log2FC of 2.95. The ortholog of this gene in rice is LOC_Os04g38720 (OsNAC2), which was also induced by salt stress (Narsai et al., 2013). The one NAC gene that was uniquely repressed (Log2FC of−2.09) in Otis under drought is BART1_0-p22840 (HORVU3Hr1G080100). The rice ortholog of this gene is OsNAC4 (LOC_Os01g60020), which was induced in the dehydrated wild rice (*Oryza rufipogon*) (Zhang et al., 2017). Another study showed this gene was highly induced in the drought tolerant rice genotype than the sensitive genotype after 3 hours of dehydration (Borah et al., 2017). In the two previous studies, rice plants were exposed to a dehydration shock rather than a progressive drought treatment.

The rice ortholog of BART1_0-p13794 gene is OsHOX22 (LOC_Os04g45810), which was induced by desiccation, salinity, cold, and osmotic stresses (Bhattacharjee et al., 2016). Moreover, it was among the drought expressed genes in rice in the co-expression analysis of different transcriptome datasets (Lv et al., 2019). The expression level of this gene greatly differed between Otis and Baronesse (3.17 and 1.75 Log2FC, Otis and Baronesse, respectively). The higher induction of this gene in Otis might be important for drought tolerance in this genotype.

Tryptophan-arginine-tyrosine (WRKY) proteins are one of the largest families of transcription factors specific to plants (Zhang and Wang, 2005). Many WRKY genes have been shown to be induced by abiotic stresses including drought (Chen et al., 2011). Their overexpression resulted in improved drought tolerance in different plant species (Wu et al., 2009; Cai et al., 2014; Xu et al., 2014; Ding et al., 2016). In this study, 4 out of the 21 drought-repressed TFs in the Baronesse plants were WRKY TFs with Log2 FC ≤ -2. These WRKY genes are: BART1_0-p09203 (HORVU2Hr1G029450), BART1_0-p23505 (HORVU3Hr1G088200), BART1_0-p01968 (HORVU1Hr1G027700), and BART1_0-p21247 (HORVU3Hr1G059210) with Log2FC−3.22,−2.31,−2.82, and−2.95, respectively. The rice orthologs of these genes are: OsWRKY69 (LOC_Os08g29660), OsWRKY24 (LOC_Os01g61080), OsWRKY67 (LOC_Os05g09020), and OsWRKY15 (LOC_Os01g46800). OsWRKY69 was up regulated in the leaves and root of drought tolerant rice genotype (Silveira et al., 2015; Baldoni et al., 2016). Whereas, OsWRKY24, OsWRKY67, and OsWRKY15 were found to play a role in tolerance of phosphorus deficiency, bacterial resistance, and cold tolerance, respectively (Yang et al., 2015; Deng et al., 2018; Liu Q. et al., 2018).

Alternative Splicing

Alternative splicing (AS) is an important posttranscriptional mechanism in which different combinations of exons of a primary transcript are joined to produce diverse messenger RNA (mRNA) isoforms. Interestingly, the abiotic stresses were shown to alter the AS pattern in plants (Reddy et al., 2013; Laloum et al., 2018). In this study only a relatively small number of AS genes (37 genes in Otis and 61 genes in Baronesse) were identified in barley genotypes exposed to drought (**Table 1**). It was reported previously that the DAS events were relatively smaller under drought compared to other abiotic stresses. For example, in

wheat, only 200 genes undergoing DAS under drought while this number is rather high (3,576 genes) under heat stress (Liu Z. et al., 2018). In Cassava, only 1,025 genes showed DAS in response to drought stress compared to 3,292 genes in response to cold stress (Li et al., 2020). In maize, 1,045 and 985 genes showed DAS under heat and cold stresses, respectively, while only 281 and 204 genes showed DAS during drought stress in ovary and leaf, respectively, and only 14 of these DAS genes were common to both tissues indicating a tissue-specific differences (Mei et al., 2017). These studies suggest that alternative splicing is less frequently used under drought compared to other abiotic stresses. The results here also show genotype-specific differences in DAS responses under drought.

Interestingly, the proteins involved in splicing were also modulated by stress conditions (Ali and Reddy, 2008). In the present study, we found that the levels of two splicing factors (RS31 and SCL30) were significantly upregulated in drought-stressed Otis and Baronesse (**Figure 7A**). Arabidopsis orthologs of these genes have been found to regulate plant splice site selection and it is possible that changes in their expression will also lead to DAS in barley (Lopato et al., 1996; Yan et al., 2017). Remarkably, most DAS events were genotype-specific in this study indicating differences in AS between the two barley genotypes. Some of these transcript changes led to a switch from one major abundant isoform to an alternative transcript, which became the abundant transcript isoform under drought stress (**Figure 7B**; **Supplementary Figure 2**). Such large changes in AS transcript abundances have been described previously in human cancers and were considered as post-transcriptional biological markers of the condition (Climente-González et al., 2017). We found drought induced AS events affecting exon skipping and changes in the selection of alternative 5' and 3' splice sites. But many stress changes led to transcripts that show intron retention. In some cases, the switched transcript under drought led to a transcript with an intron retention (**Figure 7B** is one example). Intron retentions alters the length of the 3'UTR and may affect transcript stability or transport from the nucleus (Kalyna et al., 2012; Göhring et al., 2014). Overall, DAS affects a small number of genes in the two genotypes under drought stress but alters the abundance of the gene transcripts in a highly significant manner and it remains to be determined the importance of such changes.

CONCLUSIONS

Drought tolerance is a complex process involving several thousands of genes associated with various biochemical and physiological processes. In this study, two barley genotypes differing in their drought tolerance (Otis and Baronesse) were compared for their molecular, hormonal, and physiological differences under drought. Otis had better photosynthetic capacity under drought compared to Baronesse, which could be attributed to the differences in gene expression (D1 and D2) associated with PSII stability. The hormone analysis revealed that both genotypes showed significant induction of ABA under stress conditions. Similarly, at the molecular level, many stress responsive genes such as chaperones, aquaporins, and annexins were found to be regulated at similar levels in both genotypes under drought stress. However, a few genes such as BADH and homeobox TF were highly induced in Otis compared to Baronesse. Importantly, many potential drought tolerance genes such as wax biosynthesis gene (CER1), and two NAC TFs were uniquely induced in Otis under drought stress. On the other hand, genes for WRKY TFs, and PKs were highly down-regulated in the drought-stressed Baronesse. Taken together, the overall transcriptional responses were low in drought-tolerant Otis but the genes that could confer drought tolerance were either specifically induced or greatly upregulated in the tolerant genotype and these differences could be important for drought tolerance in barley.

DATA AVAILABILITY STATEMENT

The datasets generated for this study can be found in online repositories. The names of the repository/repositories and accession number(s) can be found at: European Nucleotide Archive (ENA) at EMBL-EBI under accession number PRJEB40905.

AUTHOR CONTRIBUTIONS

AH and RS conceived the idea. AH conducted the drought treatments and harvested samples as well as estimation of biochemical parameters. CS and WG performed the bioinformatics analysis of RNA-Seq datasets. VGK assisted with measurements of photosynthesis-related parameters. GG performed qPCR analysis. AH prepared the manuscript with contributions from WG and CS. RS, CS, and AH refined and finalized the draft. All authors reviewed and approved the final manuscript.

FUNDING

This research was supported in part by the NSF-EPSCoR award 1826836 and NSF-IOS award 1849708 to RS. CS and WG were supported by Scottish Government Rural and Environment Science and Analytical Services division (RESAS).

ACKNOWLEDGMENTS

Special thanks to Fulbright for giving AH Jordanian Fulbright Scholar Research Award (2019/2020). The authors are also thankful to Dr. Dolores Mornhinweg (USDA-ARS Plant Science and Water Conservation Research Laboratory Stillwater, Oklahoma, USA) for providing the barley seeds used in this study.

SUPPLEMENTARY MATERIAL

The Supplementary Material for this article can be found online at: https://www.frontiersin.org/articles/10.3389/fpls.2020.618491/full#supplementary-material

REFERENCES

Ali, G. S., and Reddy, A. S. N. (2008). "Regulation of alternative splicing of pre-mRNAs by stresses," in *Nuclear pre-mRNA Processing in Plants. Current Topics in Microbiology and Immunology*, eds A. S. N. Reddy and M. Golovkin. (Berlin: Springer Berlin Heidelberg), 257–275.

Ashraf, M., and Foolad, M. R. (2007). Roles of glycine betaine and proline in improving plant abiotic stress resistance. *Environ. Exp. Bot.* 59, 206–216. doi: 10.1016/j.envexpbot.2005.12.006

Baghyalakshmi, K., Ramchander, S., Raveendran, M., and Jeyaprakash, P. (2020). Unravelling of osmotic genes involved in, drought tolerance in Backcross inbred lines of rice (*Oryza sativa L.*) cultivars. *Res. J. Biotech.* 15, 52–60. Available online at: https://www.researchgate.net/profile/Ramchander_Selvaraj2/publication/342623213_Unravelling_of_Osmotic_genes_involved_in_Drought_tolerance_in_Backcross_inbred_lines_of_rice_Oryzasativa_L_cultivars/links/5efd58a7458515505084919d/Unravelling-of-Osmotic-genes-involved-in-Drought-tolerance-in-Backcross-inbred-lines-of-rice-Oryzasativa-L-cultivars.pdf

Baker, N. (1991). A possible role for photosystem II in environmental perturbations of photosynthesis. *Physiol. Plant.* 81, 563–570. doi: 10.1111/j.1399-3054.1991.tb05101.x

Baldoni, E., Bagnaresi, P., Locatelli, F., Mattana, M., and Genga, A. (2016). Comparative leaf and root transcriptomic analysis of two rice Japonica cultivars reveals major differences in the root early response to osmotic stress. *Rice* 9, 25–45. doi: 10.1186/s12284-016-0098-1

Bandurska, H. (2001). Does proline accumulated in leaves of water deficit stressed barley plants confine cell membrane injuries? II. Proline accumulation during hardening and its involvement in reducing membrane injuries in leaves subjected to severe osmotic stress. *Acta Physiol. Plant.* 23, 483–490. doi: 10.1007/s11738-001-0059-0

Bandurska, H., and Stroihski, A. (2003). ABA and proline accumulation in leaves and roots of wild (*Hordeum spontaneum*) and cultivated (*Hordeum vulgate 'Maresi'*) barley genotypes under water deficit conditions. *Acta Physiol. Plant* 25, 55–61. doi: 10.1007/s11738-003-0036-x

Bartels, D., and Sunkar, R. (2005). Drought and salt tolerance in plants. *Crit. Rev. Plant Sci.* 24, 23–58. doi: 10.1080/07352680590910410

Benjamini, Y., and Yekutieli, D. (2001). The control of the false discovery rate in multiple testing under dependency. *Ann. Statist.* 29, 1165–1188. doi: 10.1214/aos/1013699998

Bhattacharjee, A., Khurana, J. P., and Jain, M. (2016). Characterization of rice homeobox genes, OsHOX22 and OsHOX24, and over-expression of OsHOX24 in transgenic Arabidopsis suggest their role in abiotic stress response. *Front. Plant Sci.* 7:627. doi: 10.3389/fpls.2016.00627

Bi, H., Shi, J., Kovalchuk, N., Luang, S., Bazanova, N., Chirkova, L., et al. (2018). Overexpression of the *TaSHN1* transcription factor in bread wheat leads to leaf surface modifications, improved drought tolerance, and no yield penalty under controlled growth conditions. *Plant Cell Environ.* 41, 2549–2566. doi: 10.1111/pce.13339

Bielach, A., Hrtyan, M., and Tognetti, V. (2017). Plants under stress: involvement of auxin and cytokinin. *Int. J. Mol. Sci.* 18, 1427–1456. doi: 10.3390/ijms18071427

Blum, A. (2009). Effective use of water (EUW) and not water-use efficiency (WUE) is the target of crop yield improvement under drought stress. *Field Crops Res.* 112, 119–123. doi: 10.1016/j.fcr.2009.03.009

Blum, A. (2017). Osmotic adjustment is a prime drought stress adaptive engine in support of plant production. *Plant Cell Environ.* 40, 4–10. doi: 10.1111/pce.12800

Borah, P., Sharma, E., Kaur, A., Chandel, G., Mohapatra, T., Kapoor, S., et al. (2017). Analysis of drought-responsive signalling network in two contrasting rice cultivars using transcriptome-based approach. *Sci. Rep.* 7:42131. doi: 10.1038/srep42131

Bourdenx, B., Bernard, A., Domergue, F., Pascal, S., Le'ger, A., Roby, D., et al. (2011). Overexpression of Arabidopsis ECERIFERUM1 promotes wax very-long-chain alkane biosynthesis and influences plant response to biotic and abiotic stresses. *Plant Physiol.* 156, 29–45. doi: 10.1104/pp.111.172320

Bray, E. A. (2004). Genes commonly regulated by water-deficit stress in *Arabidopsis thaliana*. *J. Exp. Bot.* 55, 2331–2341. doi: 10.1093/jxb/erh270

Bullard, J. H., Purdom, E., Hansen, K. D., and Dudoit, S. (2010). Evaluation of statistical methods for normalization and differential expression in mRNA-Seq experiments. *BMC Bioinformatics* 11, 94–107. doi: 10.1186/1471-2105-11-94

Burton, R., Shirley, N., King, B., Harvey, A., and Fincher, G. (2004). The CesA. quantitative analysis of transcripts reveals two groups of co-expressed genes. *Plant Physiol.* 134, 224–236. doi: 10.1104/pp.103.032904

Cafiero, C., Viviani, S., and Nord, M. (2018). Food security measurement in a global context: the food insecurity experience scale. *Measurement* 116, 146–152. doi: 10.1016/j.measurement.2017.10.065

Cai, R., Zhao, Y., Wang, Y., Lin, Y., Peng, X., Li, Q., et al. (2014). Overexpression of a maize WRKY58 gene enhances drought and salt tolerance in transgenic rice. *Plant Cell Tissue Organ Cult.* 119, 565–577. doi: 10.1007/s11240-014-0556-7

Calixto, C. P. G., Guo, W., James, A. B., Tzioutziou, N. A., Entizne, J. C., Panter, P. E., et al. (2018). Rapid and dynamic alternative splicing impacts the arabidopsis cold response transcriptome. *Plant Cell* 30, 1424–1444. doi: 10.1105/tpc.18.00177

Cantalapiedra, C. P., García-Pereira, M. J., Gracia, M. P., Igartua, E., Casas, A. M., and Contreras-Moreira, B. (2017). Large differences in gene expression responses to drought and heat stress between elite barley cultivar Scarlett and a Spanish landrace. *Front. Plant Sci.* 8:647. doi: 10.3389/fpls.2017.00647

Carillo, P., and Gibon, Y. (2011). *Protocol: Extraction and Determination of Proline*. Available online at: http://prometheuswiki.org/tiki-index.php?page=Extraction+and+determination+of+proline (accessed December 6, 2019).

Chen, L., Song, Y., Li, S., Zhang, L., Zou, C., and Yu, D. (2011). The role of WRKY transcription factors in plant abiotic stresses. *Biochim. Biophys. Acta.* 1819, 120–128. doi: 10.1016/j.bbagrm.2011.09.002

Chen, L. J., Zou, W. S., Fei, C. Y., Wu, G., Li, X. Y., Lin, H. H., et al. (2018). α-expansin *EXPA4* positively regulates abiotic stress tolerance but negatively regulates pathogen resistance in *Nicotiana tabacum*. *Plant Cell Physiol.* 59, 2317–2330. doi: 10.1093/pcp/pcy155

Chen, Y., Han, Y., Zhang, M., Zhou, S., Kong, X., and Wang, W. (2016). Overexpression of the wheat expansin gene *TaEXPA2* improved seed production and drought tolerance in transgenic tobacco plants. *PLoS ONE* 11:e0153494. doi: 10.1371/journal.pone.0153494

Choi, D., Lee, Y., Cho, H. T., and Kende, H. (2003). Regulation of expansin gene expression affects growth and development in transgenic rice plants. *Plant Cell* 15, 1386–1398. doi: 10.1105/tpc.011965

Clark, G. B., Sessions, A., Eastburn, D. J., and Roux, S. J. (2001). Differential expression of members of the annexin multigene family in *Arabidopsis*. *Plant Physiol.* 126, 1072–1084. doi: 10.1104/pp.126.3.1072

Climente-González, H., Porta-Pardo, E., Godzik, A., and Eyras, E. (2017). The functional impact of alternative splicing in cancer. *Cell Rep.* 20, 2215–2226. doi: 10.1016/j.celrep.2017.08.012

Colebrook, E., Thomas, S., Philips, A., and Hedden, P. (2014). The role of gibberellin signalling in plant responses to abiotic stress. *J. Exp. Bot.* 217, 67–75. doi: 10.1242/jeb.089938

Cosgrove, D. (2000). Expansive growth of plant cell walls. *Plant Physiol. Biochem. 38, 109*—124. doi: 10.1016/S0981-9428(00)00164-9

Cosgrove, D. (2015). Plant expansins: diversity and interactions with plant cell walls. *Curr. Opin. Plant Biol.* 25, 162–172. doi: 10.1016/j.pbi.2015.05.014

Daszkowska-Golec, A. (2016). "The role of abscisic acid in drought stress: how ABA helps plants to cope with drought stress," in *Drought Stress Tolerance in Plants, Vol 2*, eds M. Hossain, S. Wani, S. Bhattacharjee, D. Burritt, L. S. Tran. (Cham: Springer), 123–151. doi: 10.1007/978-3-319-32423-4_5

Dawson, I., Russell, J., Powell, W., Steffenson, B., Thomas, W., and Waugh, R. (2015). Barley: a translational model for adaptation to climate change. *New Phytol.* 206, 913–931. doi: 10.1111/nph.13266

de Mezer, M., Turska-Taraska, A., Kaczmarek, Z., Glowacka, K., Swarcewicz, B., and Rorat, T. (2014). Differential physiological and molecular response of barley genotypes to water deficit. *Plant Physiol. Biochem.* 80, 234–248. doi: 10.1016/j.plaphy.2014.03.025

Deng, Q., Luo, X., Chen, Y., Zhou, Y., Zhou, Y., and Zhang, F. (2018). Transcriptome analysis of phosphorus stress responsiveness in the seedlings of Dongxiang wild rice (*Oryza rufpogon Grif.*). *Biol. Res.* 51, 7–19. doi: 10.1186/s40659-018-0155-x

Diab, A., Teulat-Merah, B., This, D., Ozturk, N. Z., Benscher, D., and Sorrells, M. E. (2004). Identification of drought-inducible genes and differentially

expressed sequence tags in barley. *Theor. Appl. Genet*. 109, 1417–1425. doi: 10.1007/s00122-004-1755-0

Ding, W. W., Fang, W. B., Shi, S. Y., Zhao, Y. Y., Li, X. J., and Xiao, K. (2016). Wheat WRKY type transcription factor gene TaWRKY1 is essential in mediating drought tolerance associated with an ABA-dependent pathway. *Plant Mol. Biol. Rep*. 34, 1111–1126. doi: 10.1007/s11105-016-0991-1

Duque, P. (2011). A role for SR proteins in plant stress responses. *Plant Signal. Behav*. 6, 49–54. doi: 10.4161/psb.6.1.14063

Ereful, N. C., Liu, L., Greenland, A., Powell, W., Mackay, I., and Leung, H. (2020). RNA-seq reveals differentially expressed genes between two indica inbred rice genotypes associated with drought-yield QTLs. *Agron* 10, 621–640. doi: 10.3390/agronomy10050621

Gahluat, V., Jaiswal, V., Kumar, A., and Gupta, P. K. (2016). Transcription factors involved in drought tolerance and their possible role in developing drought tolerant cultivars with emphasis on wheat (*Triticum aestivum* L.). *Theor. Appl. Genet*. 129, 2019–2042. doi: 10.1007/s00122-016-2794-z

Gajdošová, S., Spíchal, L., Kamínek, M., Hoyerová, K., Novák, O., Dobrev, P., et al. (2011). Distribution, biological activities, metabolism, and the conceivable function of cis-zeatin-type cytokinins in plants. *J. Exp. Bot*. 62, 2827–2840. doi: 10.1093/jxb/erq457

García-Morales, S., Gómez-Merino, F., and Trejo-Téllez, L. (2014). NAC transcription factor expression, amino acid *concentration* and growth of elite rice cultivars upon salt stress. *Acta Physiol. Plant*. 36, 1927–1936. doi: 10.1007/s11738-014-1569-x

Giraldo, P., Benavente, E., Manzano-Agugliaro, F., and Gimenez, E. (2019). Worldwide research trends on wheat and barley: a bibliometric comparative analysis. *Agron* 9, 352–370. doi: 10.3390/agronomy9070352

Göhring, J., Jacak, J., and Barta, A. (2014). Imaging of endogenous messenger RNA splice variants in living cells reveals nuclear retention of transcripts inaccessible to nonsense-mediated decay in Arabidopsis. *Plant Cell* 26, 754–764. doi: 10.1105/tpc.113.118075

Gorantla, M., Babu, P. R., Lachagari, V. B. R., Feltus, F. A., Paterson, A. H., and Reddy, A. R. (2005). Functional genomics of drought-stress response in rice: transcript mapping of annotated unigenes of an indica rice (*Oryza sativa L.* cv. Nagina 22). *Curr. Sci*. 89, 496–514. Available online at: http://www.iisc.ernet.in/currsci/aug102005/496.pdf

Guo, P., Baum, M., Grando, S., Ceccarelli, S., Bai, G., Li, R., et al. (2009). Differentially expressed genes between drought-tolerant and drought-sensitive barley genotypes in response to drought stress during the reproductive stage. *J. Exp. Bot*. 60, 3531–3544. doi: 10.1093/jxb/erp194

Guo, Y., Ping, W., Chen, J., Zhu, L., Zhao, Y., Guo, J., et al. (2019). Meta-analysis of the effects of overexpression of WRKY transcription factors on plant responses to drought stress. *BMC Genetics* 20, 63–77. doi: 10.1186/s12863-019-0766-4

Gupta, A., and Senthil-Kuma, M. (2017). Transcriptome changes in *Arabidopsis thaliana* infected with *Pseudomonas syringae* during drought recovery. *Sci. Rep*. 7:9124. doi: 10.1038/s41598-017-09135-y

Ha, S., Vankova, R., KazukoYamaguchi-Shinozaki, K., Shinozaki, K., and Tran, L. S. (2012). Cytokinins: metabolism and function in plant adaptation to environmental stresses. *Trends Plant Sci*. 17, 172–179. doi: 10.1016/j.tplants.2011.12.005

Hao, Y. J., Wei, W., Song, Q. X., Chen, H. W., Zhang, Y. Q., Wang, F., et al. (2011). Soybean NAC transcription factors promote abiotic stress tolerance and lateral root formation in transgenic plants. *Plant J*. 68, 302–313. doi: 10.1111/j.1365-313X.2011.04687.x

Harb, A., Krishnan, A., Ambavaram, M. M., and Pereira, A. (2010). Molecular and physiological analysis of drought stress in *Arabidopsis* reveals early responses leading to acclimation in plant growth. *Plant Physiol*. 54, 1254–1271. doi: 10.1104/pp.110.161752

Harb, A., and Samarah, N. (2015). Physiological and molecular responses to controlled severe drought in two barley (*Hordeum Vulgare* L.) genotypes. *J. Crop Improv*. 29, 82–94. doi: 10.1080/15427528.2014.976802

Hasanuzzaman, M., Shabala, L., Brodribb, T., Zhou, M., and Shabala, S. (2019). Understanding physiological and morphological traits contributing to drought tolerance in barley. *J. Agron. Crop Sci*. 205, 129–140. doi: 10.1111/jac.12307

Hayat, S., Hayat, Q., Alyemeni, M. N., Wani, A., Pichtel, J., and Ahmad, A. (2012). Role of proline under changing environments. *Plant Signal. Behav*. 7, 1456–1466. doi: 10.4161/psb.21949

He, X., Zeng, J., Cao, F., Ahmed, I. M., Zhang, G., Vincze, E., et al. (2015). HvEXPB7, a novel β-expansin gene revealed by the root hair transcriptome of Tibetan wild barley, improves root hair growth under drought stress. *J. Exp. Bot*. 66, 7405–7749. doi: 10.1093/jxb/erv436

Heath, R., and Packer, L. (1968). Photoperoxidation in isolated chloroplasts. I. Kinetics and stoichiometry of fatty acid peroxidation. *Arch. Biochem. Biophys*. 125, 189–198. doi: 10.1016/0003-9861(68)90654-1

Hiei, Y., Ishida, Y., and Komari, T. (2014). Progress of cereal transformation technology mediated by *Agrobacterium tumefaciens*. *Front. Plant Sci*. 5, 628–640. doi: 10.3389/fpls.2014.00628

Huang, Q., Wang, Y., Li, B., Chang, J., Chen, M., and Li, K. (2015). TaNAC29, a NAC transcription factor from wheat, enhances salt and drought tolerance in transgenic Arabidopsis. *BMC Plant Biol*. 15, 268–283. doi: 10.1186/s12870-015-0644-9

Hübner, S., Korol, A. B., and Schmid, K. J. (2015). RNA-Seq analysis identifies genes associated with differential reproductive success under drought-stress in accessions of wild barley *Hordeum spontaneum*. *BMC Plant Biol*. 5, 134–148. doi: 10.1186/s12870-015-0528-z

Hughes, J., Hepworth, C., Dutton, C., Dunn, J., Hunt, L., Stephens, J., et al. (2017). Reducing stomatal density in barley improves drought tolerance without impacting on yield. *Plant Physiol*. 174, 776–787. doi: 10.1104/pp.16.01844

Jami, S. K., Clark, G. B., Turlapati, S. A., Handley, C. A., Roux, S. J., and Kirti, P. B. (2008). Ectopic expression of an annexin from Brassica juncea confers tolerance to abiotic and biotic stress treatments in transgenic tobacco. *Plant Physiol. Biochem*. 46, 1019–1030. doi: 10.1016/j.plaphy.2008.07.006

Janiak, A., Kwasniewski, M., Sowa, M., Kuczyńska, A., Mikołajczak, K., Ogrodowicz, P., et al. (2019). Insights into barley root transcriptome under mild drought stress with an emphasis on gene expression regulatory mechanisms. *Int. J. Mol. Sci*. 20, 6139–6164. doi: 10.3390/ijms20246139

Joshi, R., Wani, S. H., Singh, B., Bohra, A., Dar, Z. A., Lone, A. A., et al. (2016). Transcription factors and plants response to drought stress: current understanding and future directions. *Front. Plant Sci*. 7, 1029–1044. doi: 10.3389/fpls.2016.01029

Kalyna, M., Simpson, C. G., Syed, N. H., Lewandowska, D., Marquez, Y., Kusenda, B., et al. (2012). Alternative splicing and nonsense-mediated decay modulate expression of important regulatory genes in *Arabidopsis*. *Nucleic Acids Res*. 40, 2454–2469. doi: 10.1093/nar/gkr932

Kapilan, R., Vaziri, M., and Zwiazek, J. J. (2018). Regulation of aquaporins in plants under stress. *Biol. Res*. 51, 4–16. doi: 10.1186/s40659-018-0152-0

Kim, W., Iizumi, T., and Nishimori, M. (2019). Global patterns of crop production losses associated with droughts from 1983 to 2009. *J. Appl. Meteorol. Climatol*. 58, 1233–1244. doi: 10.1175/JAMC-D-18-0174.1

Konopka-Postupolska, D., Clark, G., Goch, G., Debski, J., Floras, K., Cantero, A., et al. (2009). The role of annexin 1 in drought stress in Arabidopsis. *Plant Physiol*. 150, 1394–1410. doi: 10.1104/pp.109.135228

Korver, R. A., Koevoets, I. T., and Testerink, C. (2018). Out of shape during stress: a key role for auxin. *Trends Plant Sci*. 23, 783–793. doi: 10.1016/j.tplants.2018.05.011

Kosma, D., Bourdenx, B., Bernard, A., Parsons, E., Lü, S., Joubès, J., et al. (2009). The impact of water deficiency on leaf cuticle lipids of Arabidopsis. *Plant Physiol*. 151, 918–1929. doi: 10.1104/pp.109.141911

Kudo, T., Makita, N., Kojima, M., Tokunaga, H., and Sakakibara, H. (2012). Cytokinin activity of cis-Zeatin and phenotypic alterations induced by overexpression of putative cis-Zeatin-O-glucosyltransferase in rice. *Plant Physiol*.160, 319–331. doi: 10.1104/pp.112.196733

Laloum, T., Martín, G., and Duque, P. (2018). Alternative splicing control of abiotic stress responses. *Trends Plant Sci*. 23, 140–150. doi: 10.1016/j.tplants.2017.09.019

Law, C., Chen, Y., Shi, W., and Smyth, G. (2014). voom: precision weights unlock linear model analysis tools for RNA-seq read counts. *Genome Biol*. 15:R29. doi: 10.1186/gb-2014-15-2-r29

Lehti-Shiu, M., Zou, C., Hanada, K., and Shiu, S. H. (2009). Evolutionary history and stress regulation of plant receptor-like kinase/pelle genes. *Plant Physiol*. 150, 12–26. doi: 10.1104/pp.108.134353

Lesk, C., Rowhani, P., and Ramankutty, N. (2016). Influence of extreme weather disasters on global crop production. *Nature* 529, 84–87. doi: 10.1038/nature16467

Li, S., Yu, X., Cheng, Z., Zeng, C., Li, W., Zhang, L., et al. (2020). Large-scale analysis of the cassava transcriptome reveals the impact of cold stress on alternative splicing. *J. Exp. Bot*. 71, 422–434. doi: 10.1093/jxb/erz444

Liu, Q., Li, X., Yan, S., Yu, T., Yang, J., Dong, J., et al. (2018). OsWRKY67 positively regulates blast and bacteria blight resistance by direct activation of PR genes in rice. *BMC Plant Biol*. 18, 257–270. doi: 10.1186/s12870-018-1479-y

Liu, W. J., Yuan, S., Zhang, N. H., Lei, T., Duan, H. G., and Liang, H. G. (2006). Effect of water stress on photosystem 2 in two wheat cultivars. *Physiol. Plant*. 50, 597–602. doi: 10.1007/s10535-006-0094-1

Liu, Z., Qin, J., Tian, X., Xu, S., Wang, Y., Li, H., et al. (2018). Global profiling of alternative splicing landscape responsive to drought, heat and their combination in wheat (*Triticum aestivum* L.). *Plant Biotechnol. J*. 16, 714–726. doi: 10.1111/pbi.12822

Livak, K., and Schmittgen, T. (2001). Analysis of relative gene expression data using real-time quantitative PCR and the 2−ΔΔCT method. *Methods* 25, 402–408. doi: 10.1006/meth.2001.1262

Lobell, D. B., Schlenker, W., and Costa-Roberts, J. (2011). Climate trends and global crop production since 1980. *Science* 333, 616–620. doi: 10.1126/science.1204531

Lombardi, M. (2012). *The barley expansin family*. (Ph.D. dissertation). University of Adelaide, Waite, MN.

Lopato, S., Waigmann, E., and Barta, A. (1996). Characterization of a novel arginine/serine-rich splicing factor in Arabidopsis. *Plant Cell* 8, 2255–2264. doi: 10.1105/tpc.8.12.2255

Lv, Y., Xu, L., Dossa, K., Zhou, K., Zhu, M., Xie, H., et al. (2019). Identification of putative drought-responsive genes in rice using gene co-expression analysis. *Bioinformation* 15, 480–489. doi: 10.6026/97320630015480

Marowa, P., Ding, A., and Kong, Y. (2016). Expansins: roles in plant growth and potential applications in crop improvement. *Plant Cell Rep*. 35, 949–965. doi: 10.1007/s00299-016-1948-4

Martin, M. (2011). Cutadapt removes adapter sequences from high-throughput sequencing reads. *EMBnet J*. 17, 10–12. doi: 10.14806/ej.17.1.200

Mei, W., Liu, S., Schnable, J. C., Yeh, C. T., Springer, N. M., Schnable, P. S., et al. (2017). A comprehensive analysis of alternative splicing in paleopolyploid maize. *Front. Plant Sci*. 8:694. doi: 10.3389/fpls.2017.00694

Mejri, M., Siddique, K., Saif, T., Abdelly, C., and Hessini, K. (2016). Comparative effect of drought duration on growth, photosynthesis, water relations, and solute accumulation in wild and cultivated barley species. *J. Plant Nutr. Soil Sci.* 179, 327–335. doi: 10.1002/jpln.201500547

Meza, I., Siebert, S., Döll, P., Kusche, J., Herbert, C., Rezaei, E., et al. (2020). Global-scale drought risk assessment for agricultural systems. *Nat. Hazards Earth Syst. Sci*. 20, 695–712. doi: 10.5194/nhess-20-695-2020

Mornhinweg, D. W., Bregitzer, P. P., Porter, D. R., Peairs, F. B., Baltensperger, D. D., Hein, G. L., et al. (2009). Registration of Sidney Spring feed barley resistant to Russian wheat aphid. *J. Plant Regist*. 3, 214–218. doi: 10.3198/jpr2009.04.0205crc

Mudgil, Y., Shiu, S. H., Stone, S., Salt, J., and Goring, J. (2004). A Large complement of the predicted Arabidopsis ARM repeat proteins are members of the U-Box E3 ubiquitin ligase family. *Plant Physiol*. 134, 59–66. doi: 10.1104/pp.103.029553

Munemasa, S., Hauser, F., Park, J., Waadt, R., Brandt, B., and Schroeder, J. (2015). Mechanisms of abscisic acid-mediated control of stomatal Aperture. *Curr. Opin. Plant Biol*. 28, 154–162. doi: 10.1016/j.pbi.2015.10.010

Nakamura, T., Nomura, M., Jagendorf, A., Ueda, A., and Takabe, T. (2001). An isozyme of betaine aldehyde dehydrogenase in barley. *Plant Cell Physiol*. 42, 1088–1092. doi: 10.1093/pcp/pce136

Nakashima, K., Tran, L. S., Nguyen, D. V., Fujita, M., Maruyama, K., Todaka, D., et al. (2007). Functional analysis of a NAC-type transcription factor OsNAC6 involved in abiotic and biotic stress-responsive gene expression in rice. *Plant J*. 51, 617–630. doi: 10.1111/j.1365-313X.2007.03168.x

Nakashima, K., Yamaguchi-Shinozaki, K., and Shinozaki, K. (2014). The transcriptional regulatory network in the drought response and its crosstalk in abiotic stress responses including drought, cold, and heat. *Front. Plant Sci*. 5:170. doi: 10.3389/fpls.2014.00170

Narsai, R., Wang, C., Chen, J., Wu, J., Shou, H., Whelan, J., et al. (2013). Antagonistic, overlapping and distinct responses to biotic stress in rice (*Oryza sativa*) and interactions with abiotic stress. *BMC Genomics* 14, 93–114. doi: 10.1186/1471-2164-14-93

Nelissen, H., Sun, X. H., Rymen, B., Jukumaru, Y., Kojima, M., and Takebayashi, Y. (2018). The reduction in maize leaf growth under mild drought affects the transition between cell division and cell expansion and cannot be restored by elevated gibberellic acid levels. *Plant Biotechnol. J*. 16, 615–627. doi: 10.1111/pbi.12801

Omena-Garcia, R. P., Martins, A. O., Medeiros, D. B., Vallarino, J. G., Ribeiro, D. M., and Fernie, A. R. (2019). Growth and metabolic adjustments in response to gibberellin deficiency in drought stressed tomato plants. *Environ. Exp. Bot*. 159, 95–107. doi: 10.1016/j.envexpbot.2018.12.011

Ouyang, W., Struik, P., Yin, X., and Yang, J. (2017). Stomatal conductance, mesophyll conductance, and transpiration efficiency in relation to leaf anatomy in rice and wheat genotypes under drought. *J. Exp. Bot*. 68, 5191–5205. doi: 10.1093/jxb/erx314

Ozturk, N. Z., Talamè, V., Deyholos, M., Michalowski, C., Galbraith, D., Gozukirmizi, N., et al. (2002). Monitoring large-scale changes in transcript abundance in drought- and salt-stressed barley. *Plant Mol. Biol*. 48, 551–573. doi: 10.1023/A:1014875215580

Patro, R., Duggal, G., Love, M. I., Irizarry, R. A., and Kingsford, C. (2017). Salmon provides fast and bias-aware quantification of transcript expression. *Nat. Methods*. 14, 417–419. doi: 10.1038/nmeth.4197

Pavlu, J., Novák, J., Koukalová, V., Luklová, M., and Brzobohatý, B., Cerný, M. (2018). Cytokinin at the crossroads of abiotic stress signalling pathways. *Int. J. Mol. Sci*. 19, 2450–2486. doi: 10.3390/ijms19082450

Peleg, Z., and Blumwald, E. (2011). Hormone balance and abiotic stress tolerance in crop plants. *Curr. Opin. Plant Biol.* 14, 290–295. doi: 10.1016/j.pbi.2011.02.001

Pieczynski, M., Wyrzykowska, A., Milanowska, K., Boguszewska-Mankowska, D., Zagdanska, B., Karlowski, W., et al. (2018). Genome wide identification of genes involved in the potato response to drought indicates functional evolutionary conservation with Arabidopsis plants. *Plant Biotechnol. J*. 16, 603–614. doi: 10.1111/pbi.12800

Plaza-Wüthrich, S., Blösch, R., Rindisbacher, A., Cannarozzi, G., and Tadele, Z. (2016). Gibberellin deficiency confers both lodging and drought tolerance in small cereals. *Front. Plant Sci*. 7:643. doi: 10.3389/fpls.2016.00643

Priya, M., Dhanker, O., Siddique, K. H. M., HanumanthaRao, B., Nair, R., Pandey, S., et al. (2019). Drought and heat stress-related proteins: an update about their functional relevance in imparting stress tolerance in agricultural crops. *Theor. Appl. Genet*. 132, 1607–1638. doi: 10.1007/s00122-019-03331-2

Quigley, F., Rosenberg, J. M., Shachar-Hill, Y., and Bohnert, H. (2001). From genome to function: the *Arabidopsis aquaporins*. *Genome Biol.* 3:research0001. doi: 10.1186/gb-2001-3-1-research0001

Ramegowda, V., Krishnan, A., and Pereira, A. (2014). Rice GROWTH UNDER DROUGHT KINASE is required for drought tolerance and grain yield under normal and drought stress conditions. *Plant Physiol*. 166, 1634–1645. doi: 10.1104/pp.114.248203

Rapazote-Flores, P., Bayer, M., Milne, L., Mayer, C. D., Fuller, J., Guo, W., et al. (2019). BaRTv1.0: an improved barley reference transcript dataset to determine accurate changes in the barley transcriptome using RNA-seq. *BMC Genomics* 20, 968–985. doi: 10.1186/s12864-019-6243-7

Raudvere, U., Kolberg, L., Kuzmin, I., Arak, T., Adler, P., Peterson, H., et al. (2019). g: Profiler: a web server for functional enrichment analysis and conversions of gene lists (2019 update). *Nucl. Acid. Res*. 47, W191–W198. doi: 10.1093/nar/gkz369

Ray, S., Dansana, P. K., Giri, J., Deveshwar, P., Arora, R., et al. (2011). Modulation of transcription factor and metabolic pathway genes in response to water-deficit stress in rice. *Funct. Integr. Genomic*. 11, 157–178. doi: 10.1007/s10142-010-0187-y

Reddy, A. S. N., Marquez, Y., Kalyna, M., and Barta, A. (2013). Complexity of the alternative splicing landscape in plants. *Plant Cell* 25, 3657–3683. doi: 10.1105/tpc.113.117523

Ritchie, M. E., Phipson, B., Wu, D., Hu, Y., Law, C. W., Shi, W., et al. (2015). Limma powers differential expression analyses for RNA-sequencing and microarray studies. *Nucleic Acids Res*. 43:e47. doi: 10.1093/nar/gkv007

Ryu, M., Cho, S. K., Hong, Y., Kim, J., Kim, J. H., Kim, G. M., et al. (2019). Classification of barley U-box E3 ligases and their expression patterns in response to drought and pathogen stresses. *BMC Genomics* 20, 326–341. doi: 10.1186/s12864-019-5696-z

Sah, S. K., Reddy, K. R., and Li, J. (2016). *Abscisic acid and abiotic stress tolerance in crop* plants. *Front. Plant Sci.* 7:571. doi: 10.3389/fpls.2016.00571

Sallam, A., Alqudah, A., Dawood, M., Baenziger, P., and Börner, A. (2019). Drought stress tolerance in wheat and barley: advances in physiology, breeding and genetics research. *Int. J. Mol. Sci*. 20, 3137–3175. doi: 10.3390/ijms20133137

Schäfer, M., Brütting, C., Meza-Canales, I., Großkinsky, D., Vankova, R., and Baldwin, I. (2015). The role of cis-zeatin-type cytokinins in plant growth regulation and mediating responses to environmental interactions. *J. Exp. Bot*. 66, 4873–4884. doi: 10.1093/jxb/erv214

Scharwies, J. D. (2017). *The role of aquaporins in plant responses to drought*. (Ph.D. dissertation). The University of Adelaide, Waite, MN.

Schmid, I., Franzaring, J., Müller, M., Brohon, N., Calvo, O. C., Högy, P., et al. (2016). Drought stress effects of CO_2 enrichment and drought on photosynthesis, growth and yield of an old and a modern barley cultivar. *J. Agron. Crop Sci*. 202, 81–95.

Schonfeld, M. A., Johnson, R. C., Carver, B. F., and Mornhinweg, D. W. (1988). Water relations in winter wheat as drought resistance indicator. *Crop Sci.* 28, 526–531.

Shaik, R., and Ramakrishna, W. (2012). Bioinformatic analysis of epigenetic and microRNA mediated regulation of drought responsive genes in rice. *PLoS ONE* 7:e49331. doi: 10.1371/journal.pone.0049331

Sharma, M., and Pandey, G. K. (2016). Expansion and function of repeat domain proteins during stress and development in plants. *Front. Plant Sci*. 6:1218. doi: 10.3389/fpls.2015.01218

Sharma, M., Singh, A., Shankar, A., Pandey, A., Baranwal, V., Kapoor, S., et al. (2014). Comprehensive expression analysis of rice Armadillo gene family during abiotic stress and development. *DNA Res*. 21, 267–283. doi: 10.1093/dnares/dst056

Shim, J. S., Oh, N., Chung, P. J., Kim, Y. S., Choi, Y. D., and Kim, J. K. (2018). Overexpression of OsNAC14 improves drought tolerance in rice. *Front. Plant Sci*. 9:310. doi: 10.3389/fpls.2018.00310

Silveira, R. D. D., Abreu, F. R. M., Mamidi, S., McClean, P. E., Vianello, R. P., Lanna, A. C., et al. (2015). Expression of drought tolerance genes in tropical upland rice cultivars (*Oryza sativa*). *Genet. Mol. Res*. 14, 8181–8200. doi: 10.4238/2015.July.27.6

Talamé, V., Ozturk, N. Z., Bohnert, H., and Tuberosa, R. (2007). Barley transcript profiles under dehydration shock and drought stress treatments: a comparative analysis. *J. Exp. Bot*. 58, 229–240. doi: 10.1093/jxb/erl163

Törönen, P., Medlar, A., and Holm, L. (2018). PANNZER2: a rapid functional annotation web server. *Nucl. Acid Res*. 46, W84–W88. doi: 10.1093/nar/gky350

Ullah, A., Manghwar, H., Shaban, M., Khan, A., Akbar, A., Ali, U., et al. (2018). Phytohormones enhanced drought tolerance in plants: a coping strategy. *Environ. Sci. Pollut. Res*. 25, 33103–33118. doi: 10.1007/s11356-018-3364-5

Vishwakarma, K., Upadhyay, N., Kumar, N., Yadav, G., Singh, J., and Mishra, R. K. (2017). Abscisic acid signaling and abiotic stress tolerance in plants: a review on current knowledge and prospects. *Front. Plant Sci*. 8, 161–173. doi: 10.3389/fpls.2017.00161

Wang, X., Chen, Z. H., Yang, C., Zhang, X., and Jin, G., Chen, G., et al. (2018). Genomic adaptation to drought in wild barley is driven by edaphic natural selection at the Tabigha evolution slope. *Proc. Natl. Acad. Sci. U.S.A*. 115, 5223–5228. doi: 10.1073/pnas.1721749115

Wang, Z., and Dane, F. (2013). NAC (NAM/ATAF/CUC) transcription factors in different stresses and their signaling pathway. *Acta Physiol. Plant* 35, 1397–1408. doi: 10.1007/s11738-012-1195-4

Wu, H., Shi, S., Lu, X., Li, T., Wang, J., Liu, T., et al. (2019). Expression analysis and functional characterization of CER1 family genes involved in very-long-chain alkanes biosynthesis in *Brachypodium distachyon*. *Front. Plant. Sci*. 10:1389. doi: 10.3389/fpls.2019.01389

Wu, X. L., Shiroto, Y., Kishitani, S., Ito, Y., and Toriyama, K. (2009). Enhanced heat and drought tolerance in transgenic rice seedlings overexpressing *OsWRKY11* under the control of HSP101 promoter. *Plant Cell Rep*. 28, 21–30. doi: 10.1007/s00299-008-0614-x

Wu, Y., Thorne, E. T., Sharp, R. E., and Cosgrove, D. (2001). Modification of expansin transcript levels in the maize primary root at lower water potentials. *Plant Physiol*. 126, 1471–1479. doi: 10.1104/pp.126.4.1471

Xiang, J., Zhou, X., Zhang, X., Liu, A., Xiang, Y., Yan, M., et al. (2018). The Arabidopsis AtUNC-93 acts as a positive regulator of abiotic stress tolerance and plant growth via modulation of ABA signaling and K(+) homeostasis. *Front. Plant Sci*. 9,718–733. doi: 10.3389/fpls.2018.00718

Xing, H. T., Guo, P., Xia, X. L., and Yin, W. L. (2011). PdERECTA, a leucine-rich repeat receptor-like kinase of poplar, confers enhanced water use efficiency in Arabidopsis. *Planta* 234, 229–241. doi: 10.1007/s00425-011-1389-9

Xu, Q., Feng, W. J., Peng, H. R., Ni, Z. F., and Sun, Q. X. (2014). TaWRKY71, a WRKY transcription factor from wheat, enhances tolerance to abiotic stress in transgenic *Arabidopsis thaliana*. *Cereal Res. Commun*. 42, 47–57. doi: 10.1556/CRC.2013.0051

Yamaguchi, S. (2008). Gibberellin metabolism and its regulation. *Annu. Rev. Plant Biol*. 59, 225–251. doi: 10.1146/annurev.arplant.59.032607.092804

Yan, Q., Xia, X., Sun, Z., and Fang, Y. (2017). Depletion of Arabidopsis SC35 and SC35-like serine/arginine-rich proteins affects the transcription and splicing of a subset of genes. *PLoS Genet*. 13:e1006663. doi: 10.1371/journal.pgen.1006663

Yang, J., Zhang, G., An, J., Li, Q., Chen, Y., and Zhao, X. (2020). Expansin gene TaEXPA2 positively regulates drought tolerance in transgenic wheat (*Triticum aestivum* L.). *Plant Sci*. 298, doi: 10.1016/j.plantsci.2020.110596

Yang, Y. W., Chen, H. C., Jen, W. F., Liu, L. Y., and Chang, M. C. (2015). Comparative transcriptome analysis of shoots and roots of TNG67 and TCN1 rice seedlings under cold stress and following subsequent recovery: insights into metabolic pathways, phytohormones, and transcription factors. *PLoS ONE* 10:e0131391. doi: 10.1371/journal.pone.0131391

Zadoks, C. J., Chang, T. T., and Konzak, C. F. (1974). A decimal code for the growth stages of cereals. *Weed Res*. 14, 415–421. doi: 10.1111/j.1365-3180.1974.tb01084.x

Zeng, X., Bai, L., Wei,1, Z., Yuan, H., and Wang, Y., Xu, Q., et al. (2016). Transcriptome analysis revealed the drought-responsive genes in Tibetan hulless barley. *BMC Genomics* 17, 386–398. doi: 10.1186/s12864-016-2685-3

Zhang, F., Zhou, Y., Zhang, M., Luo, X., and Xie, J. (2017). Effects of drought stress on global gene expression profile in leaf and root samples of Dongxiang wild rice (*Oryza rufipogon*). *Biosci. Rep*. 37:BSR20160509. doi: 10.1042/BSR20160509

Zhang, Y., and Wang, L. (2005). The WRKY transcription factor superfamily: its origin in eukaryotes and expansion in plants. *BMC Evol. Biol*. 5:1.

Zheng, Y., Jiao, C., Sun, H., Rosli, H. G., Pombo, M. A., Zhang, P., et al. (2016). iTAK: a program for genome-wide prediction and classification of plant transcription factors, transcriptional regulators, and protein kinases. *Mol. Plant* 9,1667–1670. doi: 10.1016/j.molp.2016.09.014

Zhou, J., Wang, X., Jiao, Y., Qin, Y., Liu, X., et al. (2007). Global genome expression analysis of rice in response to drought and high-salinity stresses in shoot, flag leaf, and panicle. Plant *Mol. Biol*. 63, 591–608. doi: 10.1007/s11103-006-9111-1

Zwack, P., and Rashotte, A. (2015). Interactions between cytokinin signalling and abiotic stress responses. *J. Exp. Bot*. 66, 4863–4871. doi: 10.1093/jxb/erv172

Conflict of Interest: The authors declare that the research was conducted in the absence of any commercial or financial relationships that could be construed as a potential conflict of interest.

Copyright © 2020 Harb, Simpson, Guo, Govindan, Kakani and Sunkar. This is an open-access article distributed under the terms of the Creative Commons Attribution License (CC BY). The use, distribution or reproduction in other forums is permitted, provided the original author(s) and the copyright owner(s) are credited and that the original publication in this journal is cited, in accordance with accepted academic practice. No use, distribution or reproduction is permitted which does not comply with these terms.

frontiers in Plant Science

ORIGINAL RESEARCH
published: 23 December 2020
doi: 10.3389/fpls.2020.604690

Genome-Wide Analysis of the GRAS Gene Family and Functional Identification of *GmGRAS37* in Drought and Salt Tolerance

Ting-Ting Wang[1,2,3,4†], Tai-Fei Yu[4†], Jin-Dong Fu[5†], Hong-Gang Su[4], Jun Chen[4], Yong-Bin Zhou[4], Ming Chen[4], Jun Guo[6], You-Zhi Ma[4], Wen-Liang Wei[1,2,3] and Zhao-Shi Xu[4*]*

[1]College of Agriculture, Yangtze University, Jingzhou, China, [2]Hubei Collaborative Innovation Center for Grain Industry, Yangtze University, Jingzhou, China, [3]Engineering Research Center of Ecology and Agricultural Use of Wetland, Ministry of Education, Yangtze University, Jingzhou, China, [4]Institute of Crop Science, Chinese Academy of Agricultural Sciences (CAAS)/National Key Facility for Crop Gene Resources and Genetic Improvement, Key Laboratory of Biology and Genetic Improvement of Triticeae Crops, Ministry of Agriculture, Beijing, China, [5]Institute of Urban Agriculture, Chinese Academy of Agricultural Sciences, Chengdu, China, [6]State Key Laboratory of Crop Stress Biology for Arid Areas, College of Plant Protection, Northwest A&F University, Yangling, China

OPEN ACCESS

Edited by:
Magdalena Arasimowicz-Jelonek, Adam Mickiewicz University, Poland

Reviewed by:
Qibin Ma, South China Agricultural University, China
Marcelo Nogueira Do Amaral, Federal University of Pelotas, Brazil

***Correspondence:**
Zhao-Shi Xu
xuzhaoshi@caas.cn
Wen-Liang Wei
whwenliang@163.com

†These authors have contributed equally to this work

Specialty section:
This article was submitted to Plant Abiotic Stress, a section of the journal Frontiers in Plant Science

Received: *10 September 2020*
Accepted: *23 November 2020*
Published: *23 December 2020*

Citation:
Wang T-T, Yu T-F, Fu J-D, Su H-G, Chen J, Zhou Y-B, Chen M, Guo J, Ma Y-Z, Wei W-L and Xu Z-S (2020) Genome-Wide Analysis of the GRAS Gene Family and Functional Identification of GmGRAS37 in Drought and Salt Tolerance. Front. Plant Sci. 11:604690. doi: 10.3389/fpls.2020.604690

GRAS genes, which form a plant-specific transcription factor family, play an important role in plant growth and development and stress responses. However, the functions of *GRAS* genes in soybean (*Glycine max*) remain largely unknown. Here, 117 *GRAS* genes distributed on 20 chromosomes were identified in the soybean genome and were classified into 11 subfamilies. Of the soybean *GRAS* genes, 80.34% did not have intron insertions, and 54 pairs of genes accounted for 88.52% of duplication events (61 pairs). RNA-seq analysis demonstrated that most *GmGRASs* were expressed in 14 different soybean tissues examined and responded to multiple abiotic stresses. Results from quantitative real-time PCR analysis of six selected *GmGRASs* suggested that *GmGRAS37* was significantly upregulated under drought and salt stress conditions and abscisic acid and brassinosteroid treatment; therefore, this gene was selected for further study. Subcellular localization analysis revealed that the GmGRAS37 protein was located in the plasma membrane, nucleus, and cytosol. Soybean hairy roots overexpressing *GmGRAS37* had improved resistance to drought and salt stresses. In addition, these roots showed increased transcript levels of several drought- and salt-related genes. The results of this study provide the basis for comprehensive analysis of *GRAS* genes and insight into the abiotic stress response mechanism in soybean.

Keywords: GRAS protein, genome-wide analysis, abiotic stress, hairy root assay, soybean

INTRODUCTION

Abiotic stresses, such as drought, heat, cold, and salt, seriously affect plant growth and development. Some transcription factors respond to adverse conditions by binding to specific DNA sequences in target promoters to regulate the transcription level of the target genes (Riano-Pachon et al., 2007; Liu et al., 2018; Song et al., 2019). Studying plant transcription

factors can help us understand the regulatory network underlying various biological processes. The GRAS group, which is named from the three initially determined members, *GIBBERELLIN-ACID INSENSITIVE* (*GAI*), *REPRESSOR of GA1* (*RGA*), and *SCARECROW* (*SCR*; Di Laurenzio et al., 1996; Peng et al., 1997; Silverstone et al., 1998).

The C-terminal region of GRAS proteins is highly conserved and is commonly referred to as the GRAS domain (Pysh et al., 1999). GRAS transcription factors usually have only one GRAS domain, but a few GRAS proteins have two GRAS domains or one GRAS domain and another functional domain. The GRAS domain can be divided into five units: Leucine heptad repeat I (LHRI), Leucine heptad repeat II (LHRII), VHIID, PFYRE, and SAW (Bolle, 2004). However, the N-terminal amino acid sequences of GRAS proteins are highly variable and may determine the specificity of these regulatory proteins (Tian et al., 2004).

GRAS family members have been identified in multiple plants, and the family classification is slightly different between species (Liu and Widmer, 2014). For example, 47 *GRAS* genes of Tartary buckwheat were divided into 10 subfamilies: DELLA, DLT, HAM, PAT1, LAS, LISCL, SCR, SCL3, SHR, and SCL4/7 (Liu et al., 2019). However, 150 *GRAS* genes in upland cotton have been classified into 14 subfamilies, namely DLT, DELLA, HAM, PAT1, LAS, SHR, LISCL, SCR, SCL3, SCL4/7, Os19, Os4, OS43, and G_GRAS (Zhang et al., 2018). In tomato, 53 *GRAS* genes were divided into 13 subfamilies: PAT1, SHR, SCL9, Os4, GRAS37, Pt20, DELLA, SCR, Os19, SCL28, SCL4/7, LAS, and HAM (Huang et al., 2015). These studies indicate that this gene family diversified substantially in different species plants. The classification of members of the *GRAS* gene family reflects its evolutionary history.

Different subfamilies may have different functions during plant growth. According to previous reports, GRAS family members are essential for physiological processes such as gibberellic acid signal transduction, stem cell maintenance, axillary meristem initiation, light signaling, phytochrome signaling, male gametogenesis, and detoxification (Dill et al., 2001; Stuurman et al., 2002; Greb et al., 2003; Li et al., 2003; Lee et al., 2008). For example, the DELLA subfamily participates in gibberellin signaling in *Arabidopsis* (Peng et al., 1997); the AtLAS subfamily in axillary meristem development of tomato (Schumacher et al., 1999); the HAM subfamily in shoot meristem sustention in petunia (Stuurman et al., 2002); the AtPAT1 subfamily in phytochrome A signaling in *Arabidopsis* (Bolle et al., 2000); the LISCL subfamily in transcriptional regulation during microsporogenesis of lily (Morohashi et al., 2003); and the DLT subfamily in BR signaling in rice (Tong et al., 2009). AtSHR and AtSCR subfamily members participate in root radial patterning and growth in *Arabidopsis* by forming a SCR/SHR complex, while AtSCL3 subfamily members integrate multiple signals during root cell elongation (Di Laurenzio et al., 1996; Helariutta et al., 2000; Heo et al., 2011).

A large number of *GRAS* genes are associated with responses to abiotic stresses. For example, *SCL14* activates a general detoxification network in *Arabidopsis* in response to xenobiotics (Fode et al., 2008). *GRAS1* participates in signal transduction pathways in tobacco and increases the level of reactive oxygen species under various stress conditions (Mayrose et al., 2006; Fode et al., 2008). Overexpression of *PAT1*, a GRAS member from wild grape, enhances abiotic stress tolerance in *Arabidopsis* (Czikkel and Maxwell, 2007). The SCL4/7 subfamily members in rapeseed appear to be involved in enhancing drought and salt tolerance (Yuan et al., 2016). *GRAS6*-silenced tomato plants have reduced tolerance to drought stress (Mayrose et al., 2006). *GRAS23* is involved in drought resistance and oxidative stress tolerance as well as decreased hydrogen peroxide (H_2O_2) accumulation *via* regulation of stress-related gene expression in rice (Xu et al., 2015). In tomato, the *GRAS40* gene is essential for the activation of abiotic stress-inducible promoters and auxin and gibberellin signaling (Liu et al., 2017).

Although previous research has revealed the role of *GRAS* genes in responses to abiotic stresses, up to now, there have been few reports of *GRAS* genes involved in abiotic stress in soybean (*Glycine max*). In this study, we performed a comprehensive genome-wide analysis of the *GRAS* gene family in soybean and surveyed the characteristics of 117 *GRAS* genes. *GmGRAS37*, which was significantly upregulated under drought and salt stress conditions and abscisic acid (ABA) and brassinosteroid (BR) treatments, was chosen for further analysis. Overexpression of *GmGRAS37* improved soybean tolerance to drought and salt stress, indicating the importance of the *GmGRAS37* gene in abiotic stress responses.

MATERIALS AND METHODS

Identification of *GRAS* Genes in Soybean

GmGRAS protein sequences were obtained from Phytozome (Zhang et al., 2012). The Hidden Markov Model (HMM) profile corresponding to the GRAS domain (PF03514; Lu et al., 2015) from the Pfam protein family database was used to scan the predicted proteins in the soybean genome (*G. max* Wm82. a2.v1) using HMMERv3 (Prince and Pickett, 2002). The soybean GRAS protein sequences were aligned using the HMM model in HMMERv3. The putative GRAS gene core sequences were verified by performing searches against the Pfam and SMART databases to confirm the presence of the GRAS conserved domain. The *Arabidopsis GRAS* gene family protein sequences and annotation information were downloaded from TAIR (Liu and Widmer, 2014), and the protein sequences of maize and rice were obtained from previous studies (Liu and Widmer, 2014; Guo et al., 2017). Molecular weight and isoelectric point information for GmGRASs were obtained from the ExPASy online website (**Supplementary Table S1**).

Chromosomal Location and Phylogenetic Analysis

The physical locations of *GRAS* genes on soybean chromosomes were extracted from the soybean genomic database in Phytozome. All *GmGRASs* were mapped onto the 20 chromosomes of soybean.

The amino acid sequences of *Arabidopsis*, maize, rice, and soybean GRASs were aligned using ClustalW. A phylogenetic tree was constructed in MEGA version 7.0 (Kumar et al., 2016)

using the maximum likelihood (ML) method with 1,000 bootstrap replications.

The amino acid sequence of nine GRAS proteins from tomato, rice, *Brassica rapa*, and soybean aligned using DNAMAN.

Analysis of Gene Structure and the GRAS Motif

The intron insertion sites in the *GRAS* genes were identified by comparing the coding sequence with the corresponding full-length sequence using the Gene Structure Display Server (Guo et al., 2007). The conserved GRAS motifs were analyzed using the MEME online program; the maximum number of motifs was set to 15 (Bailey et al., 2009).

Gene Duplication

BLASTp (*E*-value > $1e^{-10}$) was used to search all GRAS proteins of soybean. Duplicated genes were identified as described in a previous study; for each gene pair, when the alignment covered >80% of the longer gene and the aligned region had >80% identity at the nucleotide level, the pair was defined as duplicated genes (Fan et al., 2019). Tandem duplication events were determined by comparing the chromosomal position each duplicated gene. TBtools software was used to obtain and visualize the related syntenic blocks and duplicate gene pairs in soybean (**Supplementary Table S2**).

Expression Patterns of *GRAS* Genes

The RNA-seq data for soybean *GRAS* genes in distinct tissues at different developmental stages under normal conditions were extracted from SoyBase (Du et al., 2018). The transcriptome data for various abiotic stresses were obtained in our previous study (Shi et al., 2018). TBtools software was used to visualize the expression levels of *GmGRASs*. The RNA-seq data are provided in **Supplementary Tables S3–S7**.

Promoter Sequence Analysis

The promoter sequences (the 1,500 bp region upstream of the ATG start codon) of the *GmGRAS* genes were obtained from the Phytozome database and analyzed using the PlantCARE database (Lescot et al., 2002).

Plant Materials and Stress Treatments

Soybean variety, Williams 82, was used for gene expression pattern analysis. The seeds were cultivated for 15 days in pots containing mixed soil (1:1 vermiculite/humus). For drought treatment, the soybean seedlings were placed on filter paper for 0, 0.5, 1, 2, 4, 8, 12, and 24 h. For the NaCl, ABA, and BR treatments, the soybean seedlings were immersed in 250 mM NaCl, 100 μM ABA, and 150 μM BR solution, respectively, for 0, 0.5, 1, 2, 4, 8, 12, and 24 h. After treatment, leaves were submerged immediately in liquid nitrogen and then stored at −80°C for further analysis (Zhang et al., 2019).

RNA Extraction and qRT-PCR

Total RNA was isolated from soybean leaves with Trizol according to the manufacturer's protocol (TIANGEN, Beijing, China). The cDNA was synthesized using the PrimeScriptTM RT Reagent Kit (TaKaRa, Shiga, Japan) according to the manufacturer's protocol (Gao et al., 2019). The primers were designed using Primer Premier 5.0. The soybean Actin (*U60506*) gene was used as the internal control. Three biological replicates were used for quantitative real-time PCR (qRT-PCR) analysis (Le et al., 2011). All primers are listed in **Supplementary Table S8**.

Subcellular Localization Analysis

The full-length cDNA sequence of *GmGRAS37* was fused to the N-terminus of the *hGFP* gene with expression driven by the CaMV 35S promoter. The 35S::GmGRAS37-hGFP fusion construct was transformed into *Arabidopsis* protoplasts by PEG4000-mediated transformation (Yoo et al., 2007). GFP expression in different subcellular compartments was detected by laser scanning confocal microscopy after 16 h at 22°C in darkness, as described elsewhere (Liu et al., 2013). Three biological replicates were performed in this experiment.

Agrobacterium Rhizogenes-Mediated Transformation of Soybean Hairy Roots

Soybean Williams 82 was used for *Agrobacterium rhizogenes*-mediated transformation to generate *GmGRAS37*-overexpressing (*GmGRAS37*-OE) soybean hairy roots. The cDNA of *GmGRAS37* was ligated into the plant transformation vector pCAMBIA3301 under the control of the CaMV *35S* promoter. For the *GmGRAS37* RNA interference (*GmGRAS37*-RNAi) construct, a 586 bp fragment consisting of a 220 bp *GmGRAS37* fragment and its antisense sequence and a 146 bp maize alcohol dehydrogenase gene as connection between the repeats was synthesized (Augct, China) and inserted into pCAMBIA3301. The recombinant constructs and empty pCAMBIA3301 vector (CK) were transferred into *A. rhizogenes* strain K599 and then injected into hypocotyls following the protocol described previously (Kereszt et al., 2007; Du et al., 2018). The injected plants were placed in a greenhouse and kept at high humidity until hairy roots were generated at the infection site and had grown to about 5 cm in length. Remove the hypocotyl below 1 cm of the infected site. Seedlings were transplanted into mixed soil (1:1 vermiculite/humus) and cultured normally in the greenhouse for 7 days (25°C 16 h light/8 h dark photoperiod). After verification, positive soybean hair roots were used for abiotic stress assays, with six biological replicates of each stress treatment. For drought treatment, the soybean plants were grown without watering for 7 days, and for the NaCl treatment, the soybean plants were treated with 250 mM NaCl for 3 days. The primers used for cloning are listed in **Supplementary Table S8**.

Measurement of Physiological Indicators

The leaves of drought- and salt-treated *GmGRAS37*-RNAi, EV-Control, and *GmGRAS37*-OE seedlings were obtained for measuring physiological indicators. The catalase (CAT), peroxidase (POD), and superoxide dismutase (SOD) activities and the malonaldehyde (MDA) content of leaves were determined using the corresponding assay kits (Cominbio, Suzhou, China) based on the manufacturer's protocols. The measurement of

chlorophyll content and determination of relative electrical conductivity (REC) were carried out as described previously (Sharp et al., 1990). All measurements were from three biological replicates.

Trypan Blue and Nitroblue Tetrazolium Staining

The leaves of *GmGRAS37*-RNAi, EV-Control, and *GmGRAS37*-OE seedlings subjected to drought or NaCl treatment were soaked in 0.5% trypan blue (BioDee, China) and nitroblue tetrazolium (NBT; Creek Huizhi, China) solution for 12 h and then in 75% ethanol for decoloration until the samples became white (Du et al., 2018). Images were taken with a Canon 50D (Canon, Japan) camera. Each experiment was performed in triplicate.

RESULTS

Identification of *GRAS* Genes in the Soybean Genome

A total of 118 *GRAS* genes were discovered in the soybean genome. All of the encoded GRAS proteins were checked for the presence of the GRAS domain using the SMART and Pfam databases; 117 genes contained a GRAS domain. The 117 *GRAS* genes were named *GmGRAS1* to *GmGRAS117* according to their chromosomal positions (**Supplementary Table S1**). The protein lengths, molecular weights, and isoelectric points are provided in **Supplementary Table S1**. Of the 117 GmGRAS proteins, the protein length of GmGRAS from 168 (GmGRAS56) amino acids to 842 amino acids (GmGRAS112). The smallest protein Mw is 18975.84 Da (GmGRAS56), and the largest protein Mw is 91543.91 Da (GmGRAS112). The pI from 4.76 (GmGRAS34) to 9.21 (GmGRAS56).

Chromosomal Distribution, Phylogenetic Analysis, and Multiple Sequence Alignment

The physical location map of the *GmGRASs* was drawn based on the physical location information of the soybean genome. The 117 *GRAS* genes were widely and irregularly distributed on the 20 soybean chromosomes (**Figure 1**). Chromosome 11 harbored the most *GmGRAS* genes (16 genes), followed Chromosome 12 and Chromosome 13 (11 genes each). Chromosome 19 contained the fewest *GRAS* genes (two genes). In addition, we found that the number of *GRASs* distributed in the middle of the 20 chromosomes in soybean was relatively small, and its distribution on chromosomes was similar to *AtGRASs* and *OsGRASs* (Tian et al., 2004).

To explore the phylogenetic relationships of *GRAS* genes in different plant species, we built phylogenetic trees from the alignment of 286 GRAS domain amino acid sequences from soybean (117), *Arabidopsis* (33), maize (86), and rice (50) using the ML method in MEGA7.0 (**Figure 2**). In the resulting tree, the *GRAS* genes were divided into 12 subfamilies, in which 11 contained soybean *GRAS* genes: DELLA, DLT, HAM, AtPAT1, LISCL, AtSCR, AtSCL3, AtSHR, AtSCL4/7, Os19, Os4, and AtLAS. These subfamilies were designated following previous studies (Liu and Widmer, 2014; Guo et al., 2017). The HAM and LISCL groups were the two largest subfamilies. In general, members of most of the GRAS subfamilies were found in all four species. However, the soybean GRAS family does not include the AtLAS subfamily, and Os4 and Os19 subfamilies did not contain any *Arabidopsis* genes, which indicating that lineage-specific gene loss had occurred in soybean and *Arabidopsis*. The lineage-specific genes may represent genes with major diversity in the function of a particular species, genes that may have been highly specialized, or genes that have been lost from other species.

To explore the conservation between the GmGRAS proteins and BrLAS, OsGRAS23, and SlGRAS40, which have been reported to be involved in stress tolerance (Xu et al., 2015; Liu et al., 2017; Li et al., 2018), and GmGRAS27, GmGRAS37, GmGRAS66, GmGRAS72, GmGRAS94, and GmGRAS115, which are expressed at high levels in the two transcriptome databases of soybean drought and salt, were selected for multiple sequence alignment. The alignment of the C-terminal regions of these nine proteins indicated that the GRAS proteins were relatively highly conserved (**Figure 3**). All nine proteins contained the SAW motif (**Figure 3**), which is characterized by three pairs of absolutely conserved residues: R-E, W-G, and W-W (Pysh et al., 1999). Additionally, we constructed a phylogenetic tree to reveal the relationship between the nine proteins and GmGRASs are more closely related to each other. The closer the relationship between proteins, the higher the protein sequence similarity (**Supplementary Figure S1**).

Gene Structure and Motif Composition of Soybean *GRAS* Genes

To identify differences in gene structure, the exon and intron structures of the 117 soybean *GRAS* genes were compared; this analysis provided useful evidence for the evolution of structural diversity in the GRAS family. Almost all *GRAS* genes contained very few or no introns (**Figure 4** and **Supplementary Table S1**); 80.34% of the *GRAS* genes was free of introns, which is similar to the lack of introns in members of this family in other species. For example, 88, 83.3, and 80.23% of *GRAS* genes in grapevine, Chinese cabbage, and maize, respectively, have no introns (Song et al., 2014; Guo et al., 2017). Four and six introns were found in *GmGRAS29* and *GmGRAS95*, respectively.

Conservation of motifs in the 117 *GmGRAS* proteins was analyzed using the MEME website (**Figure 5**). A total of 15 different conserved motifs were discovered. Because the structures and functions of the GRASs are not known, the motifs were defined based on sequence conservation. The C-terminal regions contained a highly conserved domain (motif 5), and the sequence ZGCLLLGWKGRPLIAASAWR was found in most GRAS proteins (**Supplementary Figure S2**). Six proteins did not contain this conserved motif, namely *GmGRAS92*, *GmGRAS29*, *GmGRAS56*, *GmGRAS62*, *GmGRAS64*, and *GmGRAS39*, which may be because the C-terminal regions of these GRAS proteins are truncated and missing a part of the GRAS domain.

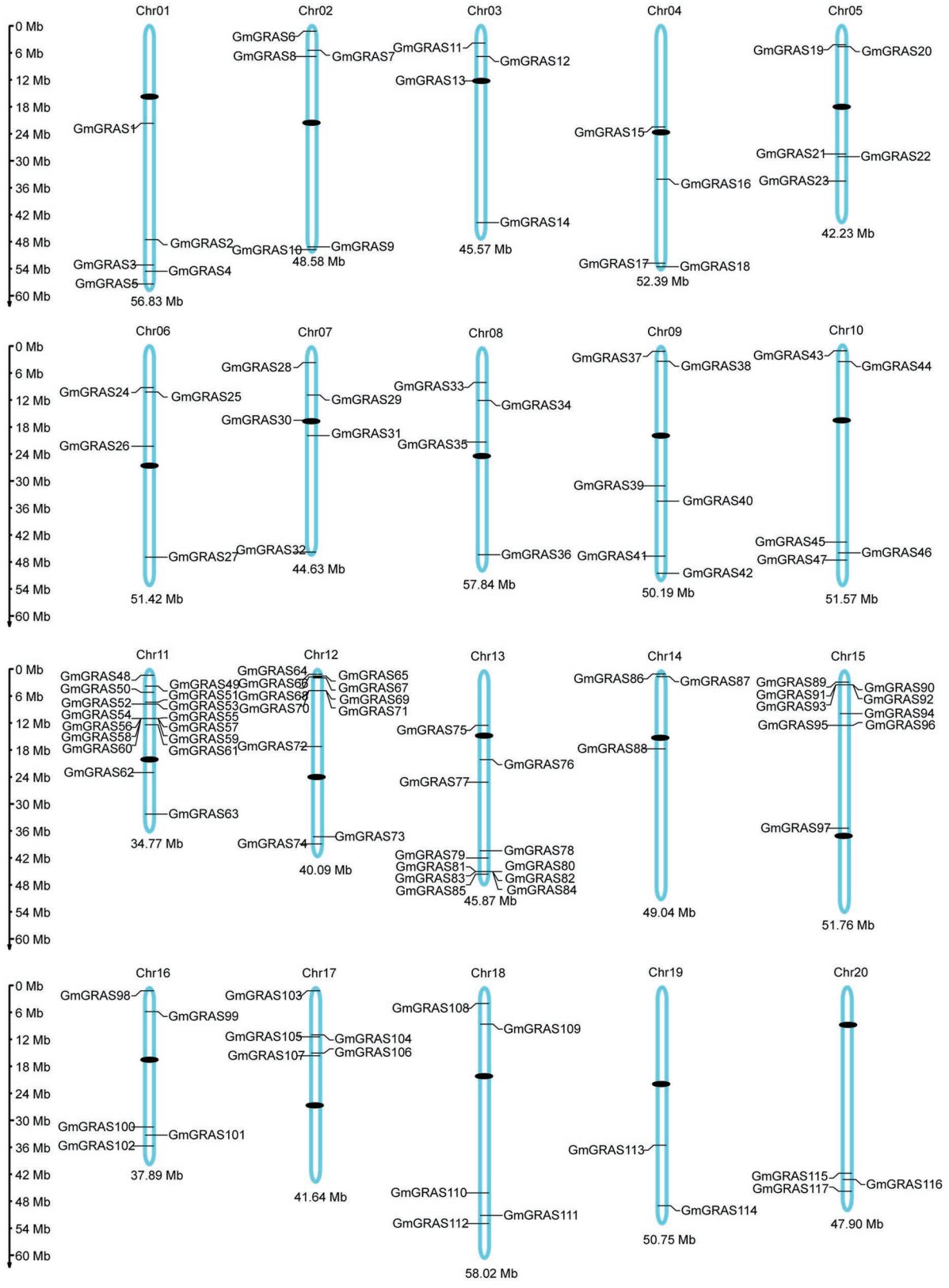


FIGURE 1 | Chromosomal distribution of 117 *GRAS* genes in soybean. The scale bar on the left indicates the size of the chromosomes.

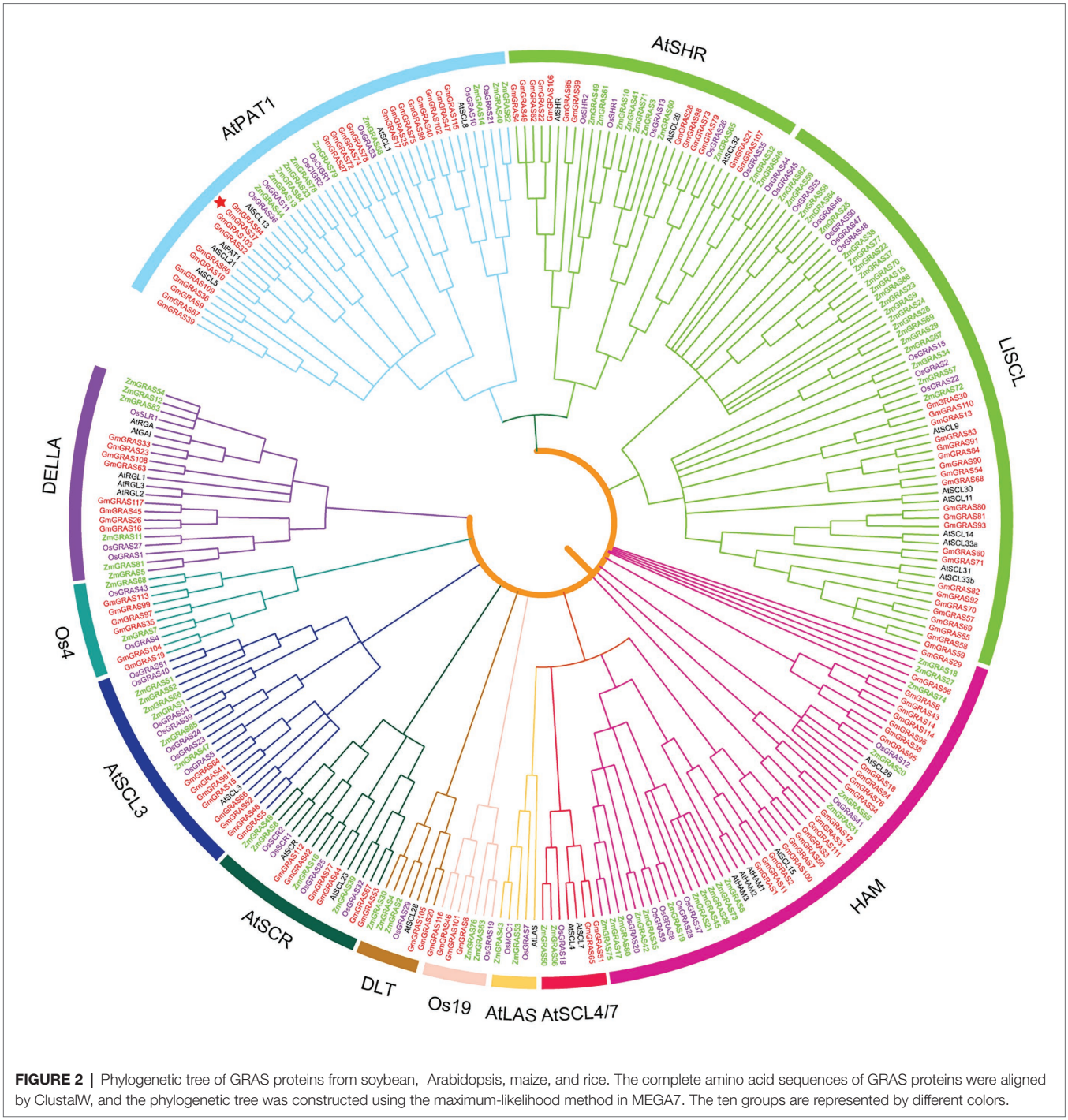


FIGURE 2 | Phylogenetic tree of GRAS proteins from soybean, Arabidopsis, maize, and rice. The complete amino acid sequences of GRAS proteins were aligned by ClustalW, and the phylogenetic tree was constructed using the maximum-likelihood method in MEGA7. The ten groups are represented by different colors.

Duplication and Divergence Rate of Soybean *GRAS* Genes

We analyzed the duplication events giving rise to *GmGRAS* genes because gene duplication plays an important role in the amplification of gene families and their subsequent evolution. When two or more genes were located within a 200 kb chromosomal region, they were deemed to have arisen from tandem duplication events (Holub, 2001). Among the *GmGRASs*, six genes were clustered into seven tandem duplicated regions on soybean chromosomes 11 and 12, and 54 pairs of segmentally duplicated genes were detected; these segmental duplicates were found on all 20 chromosomes. (**Figure 6** and **Supplementary Table S2**). The results showed that gene segmental duplication events may have been the main driving force behind *GRAS* gene evolution in soybean.

We estimated the synonymous (Ks) and nonsynonymous (Ka) substitution rates (Ka/Ks) of 61 segmentally duplicated pairs (**Figure 7** and **Supplementary Table S2**). The Ka/Ks ratios for segmentally duplicated gene pairs ranged from 0.06

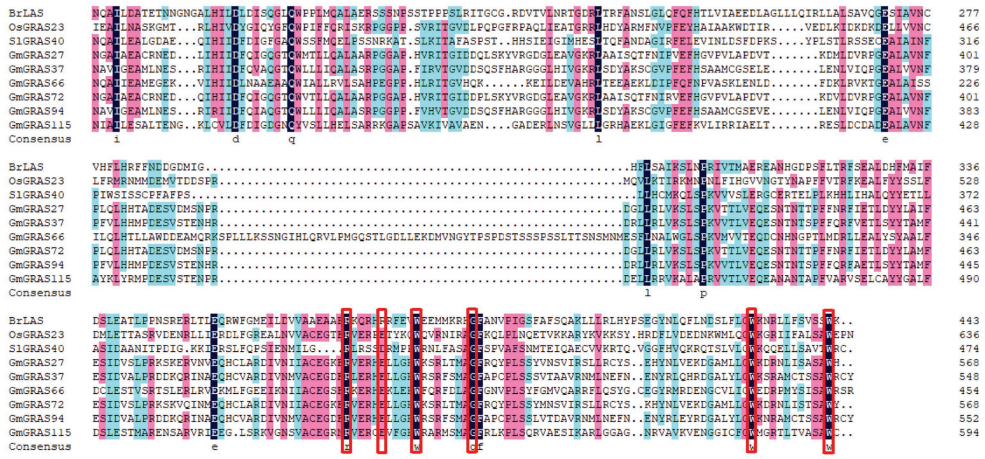


FIGURE 3 | Multiple sequence alignment of nine GRAS proteins from tomato, rice, *Brassica rapa*, and soybean. Amino acid sequences were aligned using DNAMAN. Black shading represents 100% amino acid similarity, blue shading represents >75% similarity, and pink shading represents >50% similarity. The red rectangles indicate residues R-E, W-G, and W-W.

to 0.62 with an average of 0.26. Furthermore, the frequency distribution of the Ka/Ks ratios showed that more than 60% of duplicated gene pairs had ratios ranging from 0.1 and 0.3. The fact that these duplicated *GRAS* genes have Ka/Ks ratios lower than 1 indicates that they are under purifying selection.

Expression Patterns of *GRAS* Genes

To investigate the expression profiles of the soybean *GRAS* members in different tissues, we used publicly available RNA-seq data from the SoyBase database, including young leaves, flowers, 1-cm pods, pod shells at different developmental stages, roots, and nodules. The expression levels of different *GRAS* genes varied widely in the same tissue (**Figure 8** and **Supplementary Table S3**). Of the 117 *GRAS* genes, about one-fifth were not expressed. As shown in **Figure 8**, *GRAS24* and *GRAS70* showed extremely high expression levels in all tissues, suggesting that these *GRAS* genes are regulators of various processes of soybean growth and development. Also, we analyzed the expression levels of several duplicated genes of *GmGRASs* to understand the functional redundancy and homologous gene pairs (**Figure 8**). As a result, several duplicated genes pairs had similar expression levels (*GmGRAS37/94*, *GmGRAS85/89*, and *GmGRAS53/67*); however, *GmGRAS73/79*, *GmGRAS4/49*, and *GmGRAS92/82* displayed different or antipodal expression levels, which indicated that they may have experienced functional differences.

Previous research has indicated that *GRAS* genes can be induced by various abiotic stresses (Mayrose et al., 2006; Xu et al., 2015; Liu et al., 2017). Analysis of RNA-seq data for soybean seedlings subjected to drought, NaCl, ABA, and BR treatments (Shi et al., 2018) revealed that 52, 54, 54, and 52 *GmGRAS* genes responded to drought, NaCl, ABA, and BR treatments, respectively (**Figure 9** and **Supplementary Tables S4**–**S7**). Of these genes, 65.4% (34 out of 52), 64.8% (35 out of 54), 64.8% (35 out of 54), and 71.1% (37 out of 52) were upregulated under the drought, NaCl, ABA, and BR treatments, respectively. *GmGRAS27*, *GmGRAS37*, *GmGRAS66*, *GmGRAS72*, *GmGRAS94*, and *GmGRAS115* were all upregulated under all four conditions, so these six candidate genes were used for *cis*-elements and qRT-PCR analysis. Most duplicated gene pairs had similar expression levels, such as *GmGRAS27/72* and *GmGRAS37/94* under drought stress, *GmGRAS27/72* under salt stress, and *GmGRAS37/94* under exogenous ABA and BR treatments, which suggested that they might perform similar physiological functions.

Cis-Elements Analysis

To investigate the biological functions of *GmGRAS* genes, six genes that have high transcription levels under drought, salt, ABA, and BR treatments according to the results of RNA-seq (*GmGRAS27*, *GmGRAS37*, *GmGRAS66*, *GmGRAS72*, *GmGRAS94*, and *GmGRAS115*) were selected for *cis*-elements analysis. The 1.5 kb region upstream of the start codon in promoter of each gene was isolated. A series of important *cis*-elements were identified (**Table 1**), including the ABRE (ABA-responsive element), MYB (drought responsive), MYC (drought and cold responsive), MBS (MYB-site), ERE (ethylene-responsive element), TCA-element (salicylic-responsive element), and GT-1 (salt induced). Moreover, these six genes had many MYB, MYC, and ABRE *cis*-elements, which suggested that these genes might respond to abiotic stresses, such as drought, ABA, and cold.

GmGRAS Genes Are Involved in the Response to Abiotic Stresses

The transcription levels of the six *GmGRAS*s under abiotic stress were further confirmed by qRT-PCR (**Figure 10**). The expression patterns determined by qRT-PCR corresponded to those from RNA-seq data. All six genes showed the same expression patterns under drought treatment and were upregulated by salt stress. In addition, the expression levels of

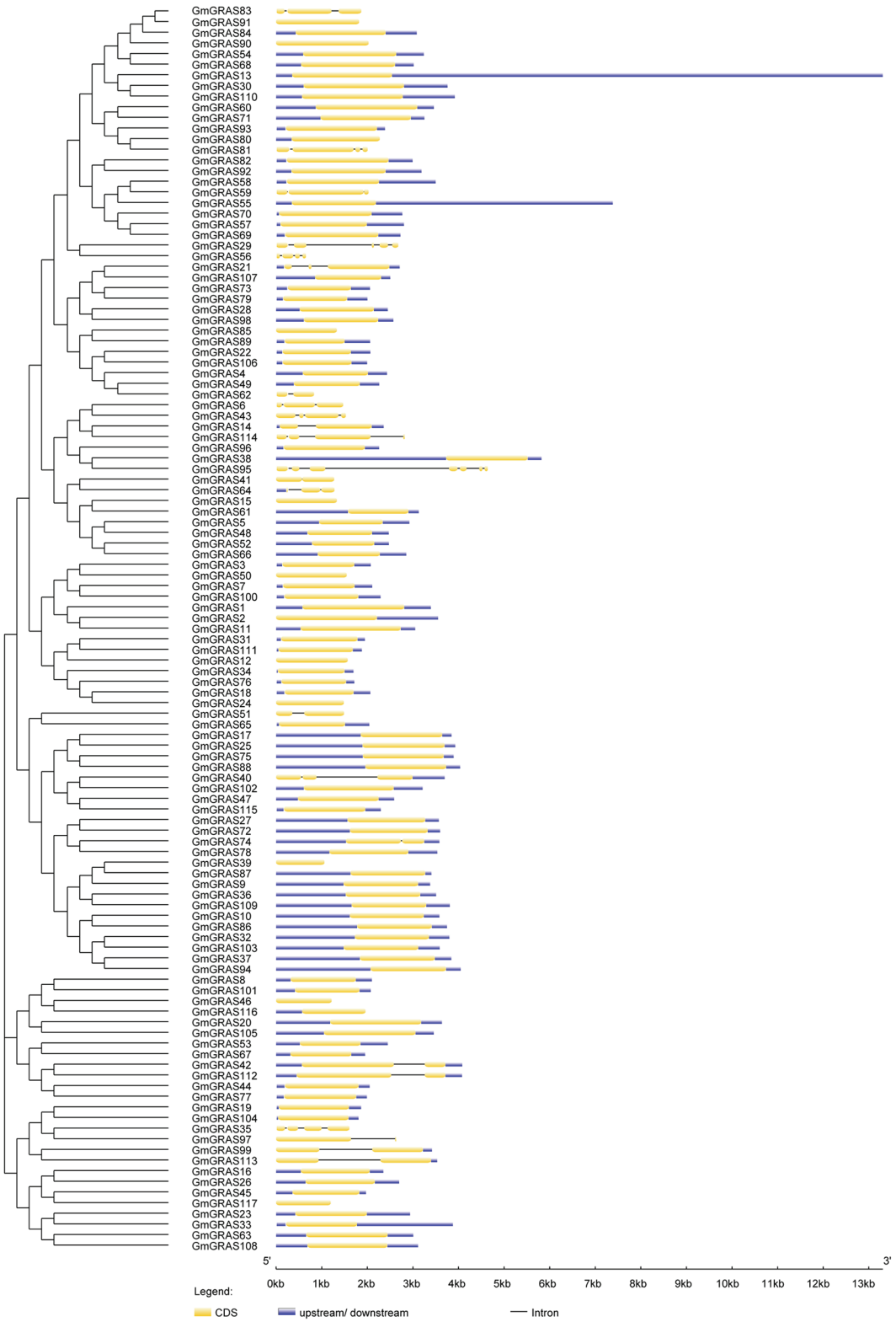


FIGURE 4 | Phylogenetic relationships and structures of the 117 GmGRAS proteins. The phylogenetic tree was constructed using MEGA7.0 software; the different classes of GRAS proteins make up separate clades. The schematic diagram indicates the gene structure. Introns and exons are indicated by black lines and yellow boxes, respectively. The lengths of introns and exons of each gene are displayed proportionally.

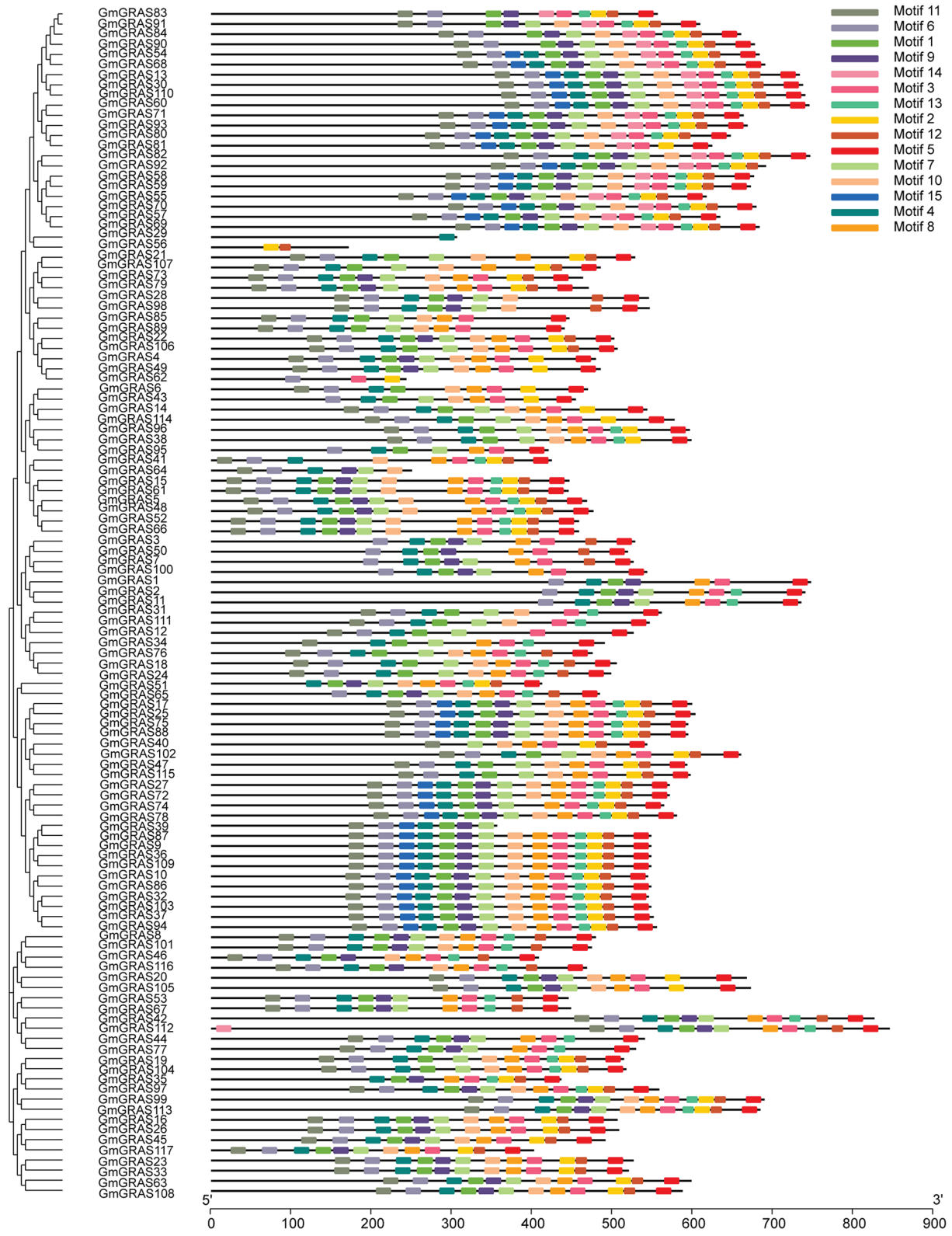


FIGURE 5 | Putative motifs in each GmGRAS protein. Conserved motifs were identified using MEME and TBtools software. Ten putative motifs are indicated by colored boxes. The length of each protein can be estimated using the scale at the bottom.

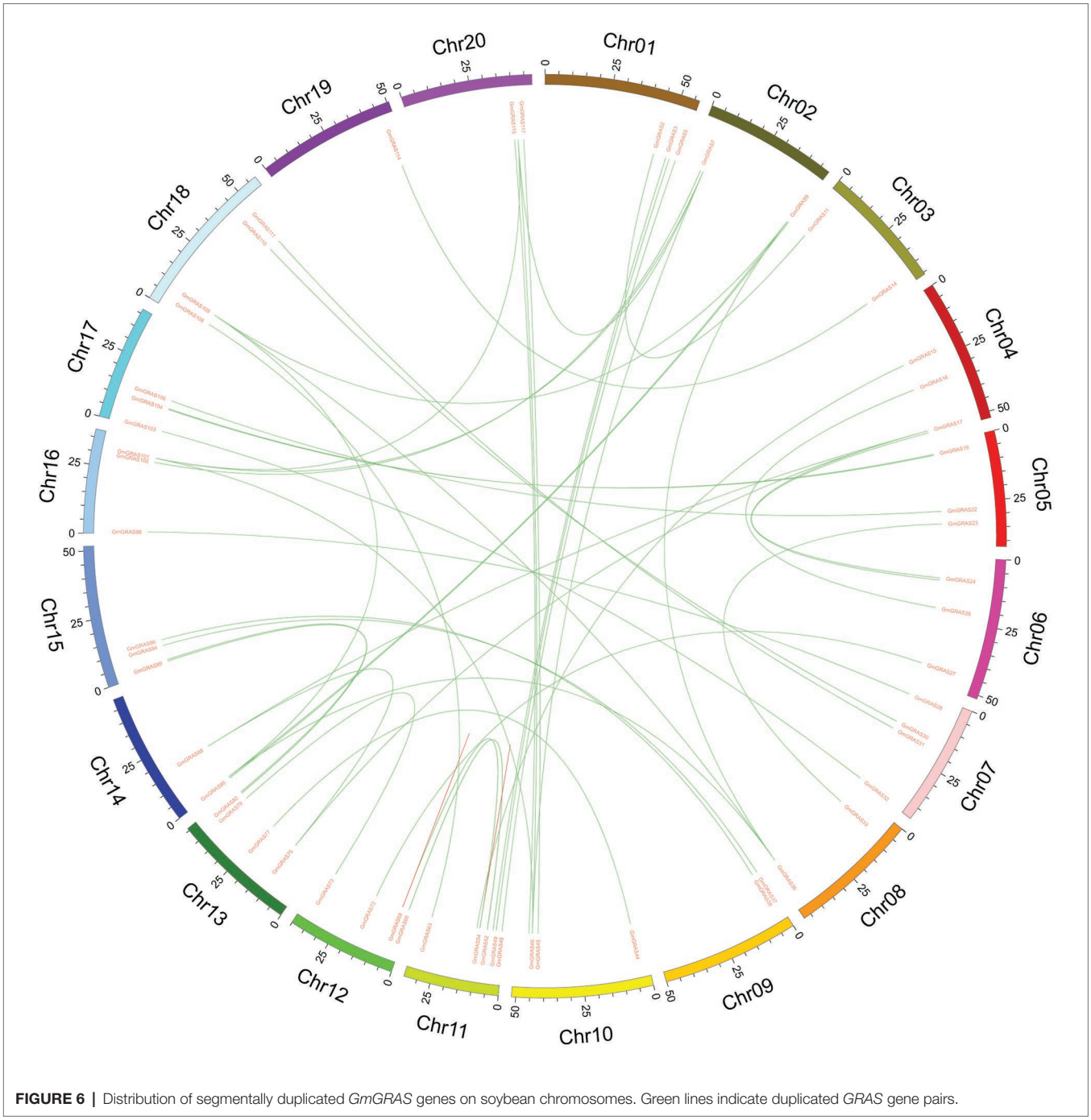


FIGURE 6 | Distribution of segmentally duplicated *GmGRAS* genes on soybean chromosomes. Green lines indicate duplicated *GRAS* gene pairs.

these six genes were induced by ABA and BR. For example, *GmGRAS37*, which was highly expressed in the drought, NaCl, ABA, and BR RNA-seq datasets, displayed high expression under these conditions in qRT-PCR analysis. In addition the expression level of *GmGRAS37* was highest under salt (8 h), ABA (2 h), and BR (1 h) treatment than other genes, so *GmGRAS37* were selected for the further analysis. The expression patterns of these stress-induced *GmGRASs* provide useful information for further understanding their functions in coping with abiotic stresses.

GmGRAS37 Is Localized in the Plasma Membrane, Nucleus, and Cytosol

GmGRAS37 was selected for further analysis because it was significantly upregulated under all tested treatment conditions. To analyze the subcellular localization of GmGRAS37, the cDNA of *GmGRAS37* lacking the stop codon was fused to the N-terminus of the *hGFP* reporter gene and ligated into an expression vector under the control of the CaMV 35S promoter. The vector was transformed into *Arabidopsis* protoplasts and observed under a confocal microscope. The control hGFP

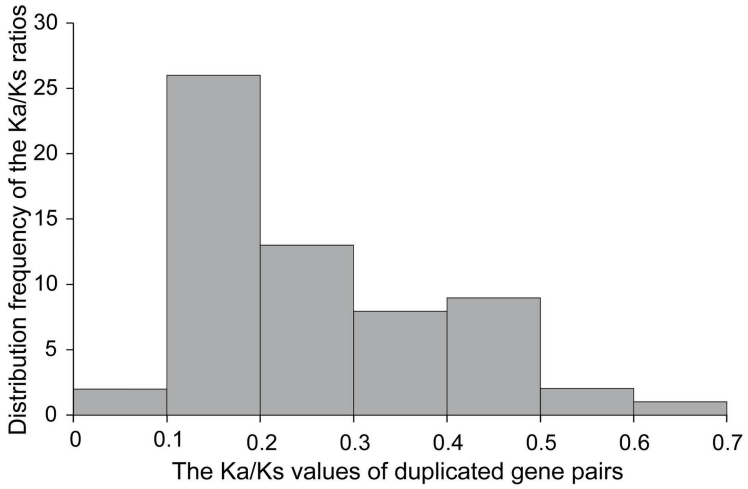


FIGURE 7 | Histogram of distribution frequency of pairwise Ka/Ks ratios for pairs of homologous genes.

and GmGRAS37-16318hGFP fusion proteins both localized to the plasma membrane, nucleus, and cytosol (**Figure 11**). These results indicated that GmGRAS37 may function throughout the cell.

Overexpression of *GmGRAS37* Improves Drought and Salt Tolerance in Soybean Hairy Roots

To further verify the physiological function of *GmGRAS37 in vivo*, *GmGRAS37*-OE, EV-transformed control, and *GmGRAS37*-RNAi hairy roots were generated using *A. rhizogenes*-mediated transformation (Gao et al., 2019). qRT-PCR analysis showed that the level of *GmGRAS37* expression in OE transgenic hairy roots was much higher than that in the EV-transformed control, and the level of *GmGRAS37* expression in RNAi transgenic hairy roots was lower than that in the EV-transformed control (**Supplementary Figure S3**). Under normal growth conditions, the *GmGRAS37*-OE transgenic plants displayed almost the same growth pattern as the *GmGRAS37*-RNAi and EV-Control plants (**Figure 12A**). However, under drought and salt stress conditions, there were obvious differences in the growth patterns of the *GmGRAS37*-RNAi, EV-Control, and *GmGRAS37*-OE plants (**Figures 12B,C**). Severely dehydrated leaves were observed on *GmGRAS37*-RNAi plants after drought and salt treatment, and wilted leaves appeared in EV-Control plants. However, the *GmGRAS37*-OE seedlings showed delayed and less leaf rolling during drought stress. There were no considerable differences between the *GmGRAS37*-RNAi, EV-Control, and *GmGRAS37*-OE roots under normal growth conditions (**Figure 12D**), but the *GmGRAS37*-OE roots were longer than EV-Control roots and the roots of *GmGRAS37*-RNAi were shorter than those of the EV-Control under drought and salt treatment conditions (**Figures 12E,F**).

Trypan blue was used to observe cell activity in *GmGRAS37*-RNAi, EV-Control, and *GmGRAS37*-OE leaves. Under normal growth conditions, there was no significant difference in trypan blue staining (**Supplementary Figure S4A**). Under drought and salt treatment conditions, less staining was observed in *GmGRAS37*-OE than in the EV-Control. In contrast, more intense staining was observed in *GmGRAS37*-RNAi leaves compared with EV-Control leaves (**Figures 12G,I**). These results suggested that the cell membrane integrity and stability in the *GmGRAS37*-OE plants leaves were better than those in the EV-Control and *GmGRAS37*-RNAi leaves. NBT was used to assess the level of superoxide anions (O_2^-), which affect plant growth and development. No difference was observed between the *GmGRAS37*-RNAi, EV-Control, and *GmGRAS37*-OE leaves under normal growth conditions (**Supplementary Figure S4B**). Under drought and salt treatment conditions, the amount of NBT staining was lower in *GmGRAS37*-OE leaves than in EV-Control leaves. However, significantly darker staining was observed in *GmGRAS37*-RNAi leaves than in EV-Control leaves (**Figures 12H,J**). These results indicated that the content of O_2^- in *GmGRAS37*-OE was lower than that in EV-Control plants; however, the content of O_2^- in *GmGRAS37*-RNAi was greater than that in EV-Control plants.

We found that the CAT, POD, and SOD activities and chlorophyll content of *GmGRAS37*-OE plants under drought and salt treatment conditions were all greater than those in EV-Control plants but lower in *GmGRAS37*-RNAi plants than in EV-Control plants (**Figures 12K–N**). In contrast, the MDA content in *GmGRAS37*-OE plants was lower than that in EV-Control plants, and the content in *GmGRAS37*-RNAi plants was greater than that in EV-Control plants (**Figure 12O**). Compared with EV-Control plants, the aerial tissue and root biomasses of *GmGRAS37*-OE plants were higher under drought and salt stresses, while those of *GmGRAS37*-RNAi plants were lower (**Figures 12P,Q**). Under drought and salt stresses, *GmGRAS37*-RNAi had a higher REC than EV-Control plants, and *GmGRAS37*-OE the lowest value (**Figure 12R**).

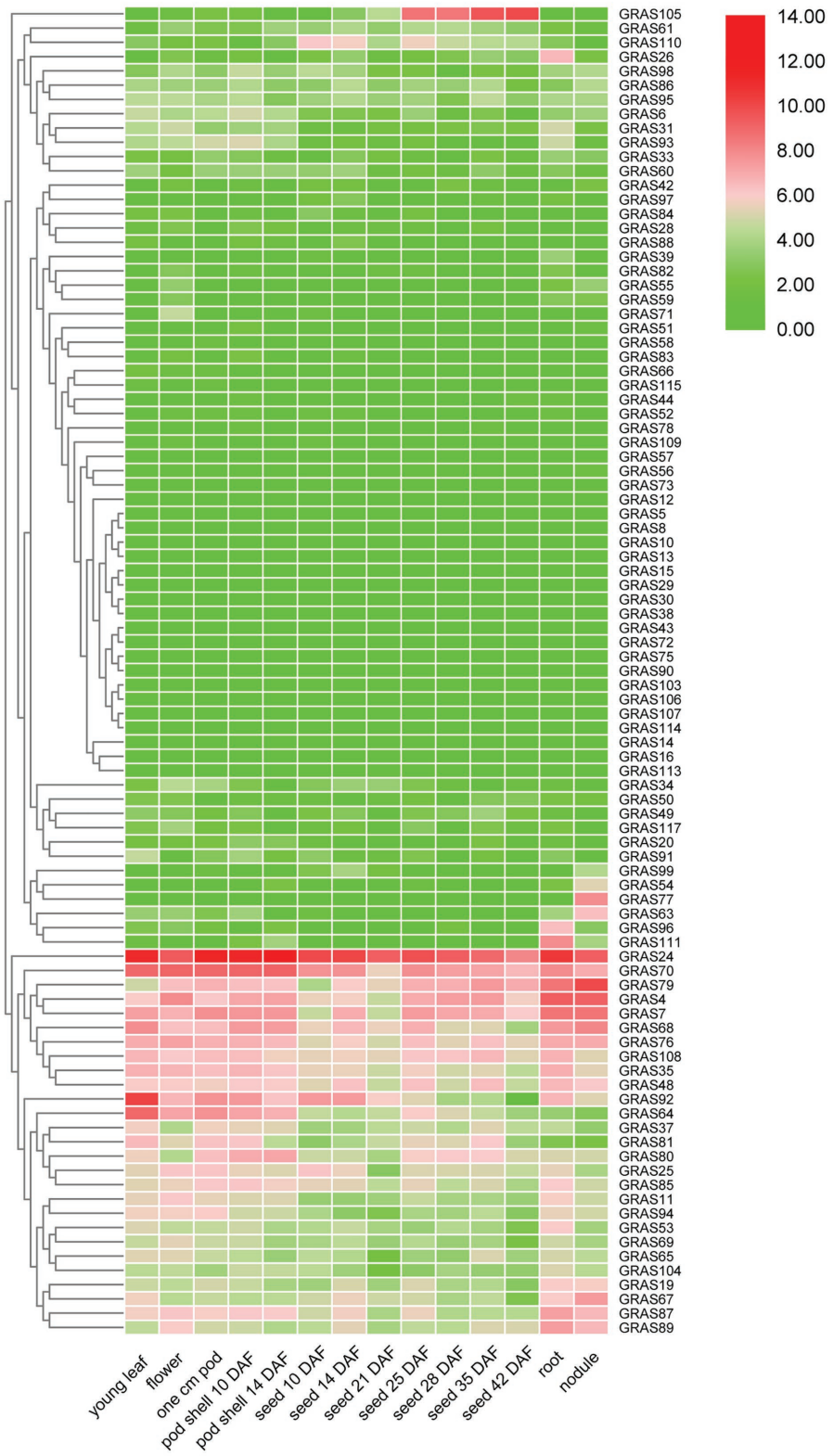


FIGURE 8 | Heat map of the expression profiles of all *GmGRAS* genes in different soybean tissues. The expression abundance (in log10-based FPKM) of each transcript is represented by the color: red, higher expression; green, lower expression. Expression levels in 14 different tissues are shown: young leaves, flowers, one cm pods, pod shells at different days after flowering (DAF), roots, and nodules.

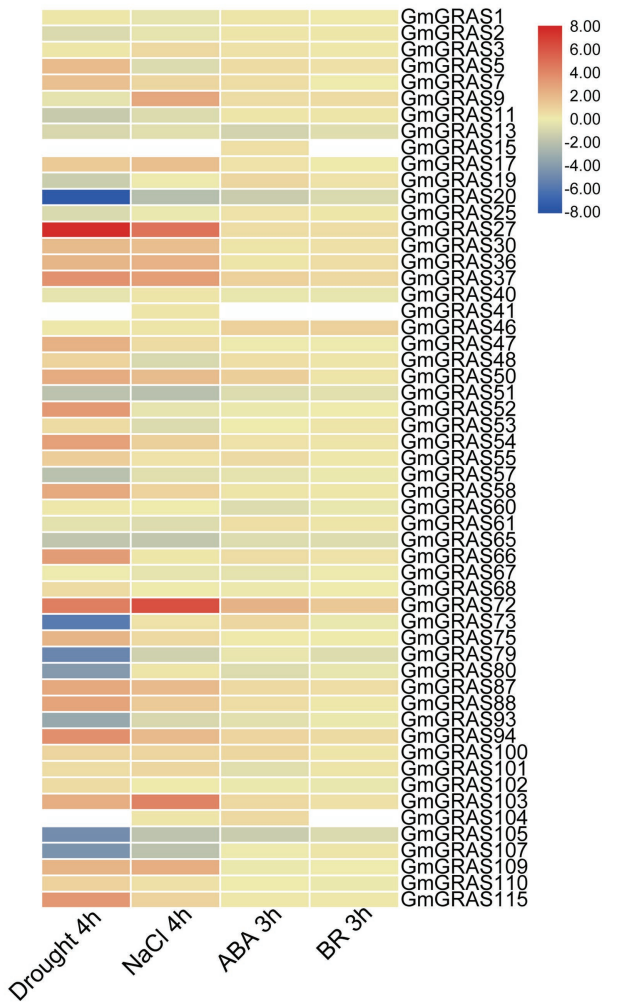


FIGURE 9 | Heat map of expression profiles of all *GmGRAS* genes under different abiotic stresses. The expression abundance of each transcript (in log10-based FPKM) is represented by the color: red, higher expression; blue, lower expression; white, miss value.

Analysis of the Mechanism of *GmGRAS37*-Mediated Resistance in Soybean

To analyze the possible resistance mechanisms regulated by *GmGRAS37* during multiple stress responses, *GmGRAS37*-OE, EV-Control, and *GmGRAS37*-RNAi hairy roots treated with or without stresses were used for investigating the expression changes of six genes (*GmDREB1*, *GmNCED3*, *GmCLC1*, *GmSOS1*, *GmSOD1*, and *GmSOD2*) that were reported to be involved in abiotic stress responses (Kidokoro et al., 2015; Wei et al., 2016; Cao et al., 2018; Li et al., 2019; Yadav et al., 2019) and identified as being upregulated in response to stress in our analysis of *de novo* transcriptomic sequences of soybean. The results of qRT-PCR analysis (**Figure 13**) showed that under normal growth conditions, the transcript levels of these genes in *GmGRAS37*-OE plants were higher than those in EV-Control plants; however, the transcript levels were lower in *GmGRAS37*-RNAi plants than in EV-Control plants. Similarly, the transcript levels of these six genes in *GmGRAS37*-OE plants were dramatically upregulated under drought and salt stresses compared with the EV-Control plants; however, the transcript levels of these genes in *GmGRAS37*-RNAi plants were lower than those in EV-Control plants. These results showed that *GmGRAS37* may activate the transcription of drought- or salt-responsive genes to meditate stress responses.

DISCUSSION

GRAS proteins, which are plant-specific transcription factors, play vital roles in various processes of tissue or organ development. The previous study about soybean GRAS family had been reported and identified 117 *GRAS* member genes (Wang et al., 2020). However, in our study, we found a new GRAS family member gene Glyma.07G105100 by scanning the whole soybean genome, and further analysis showed soybean Glyma.U013800 gene was not found on a total of 20 typical soybean chromosomes, so it was deleted. Therefore, 117 *GRAS* genes were identified in the soybean genome

TABLE 1 | Distribution and numbers of *cis*-acting elements in the promoters of soybean *GRAS* genes.

Genes	*GmRAS27*	*GmGRAS37*	*GmGRAS66*	*GmGRAS72*	*GmGRAS94*	*GmGRAS115*
ABRE	3	5	3	4	3	4
ARE	5	6	4	2	3	4
Box4	2	1	1	3	1	4
CGTCA-motif	5	4	0	3	0	4
ERE	1	1	4	1	0	2
G-Box	5	4	3	6	4	3
GT1-motif	3	1	2	3	0	4
LTR	2	1	0	1	1	4
MBS	2	2	1	1	2	0
MYB	8	3	8	16	7	4
MYC	5	6	7	9	6	1
P-box	0	2	4	1	2	0
TC-rich repeats	0	2	1	0	2	0
TCA-element	0	3	1	0	2	0
WUN-motif	0	0	2	0	0	1

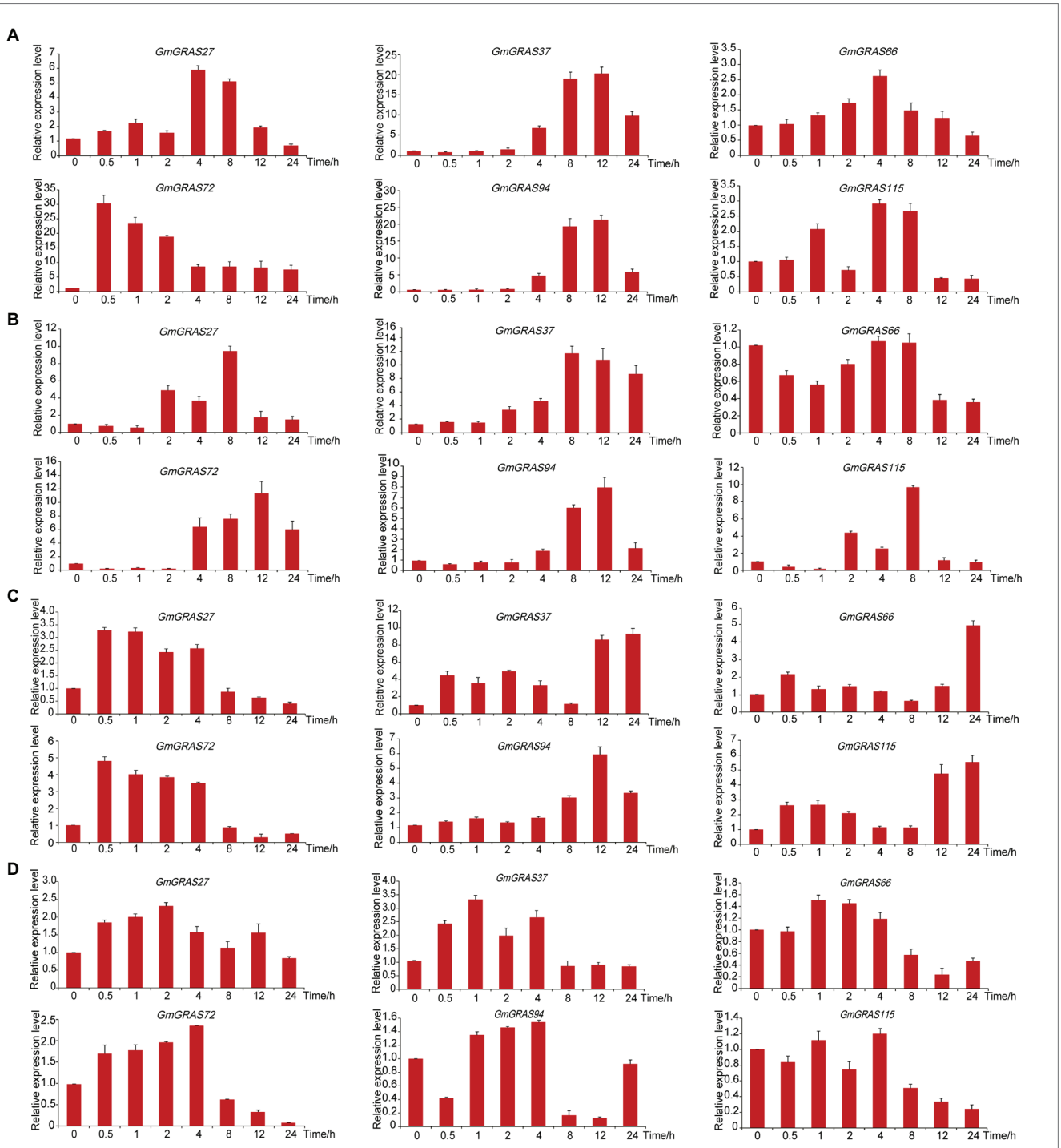


FIGURE 10 | Expression patterns of *GmGRAS* genes under drought, salt, abscisic acid (ABA), and brassinosteroid (BR) treatment. **(A–D)** Expression levels of six *GmGRAS* genes, as measured using quantitative real-time PCR (qRT-PCR), under drought **(A)**, NaCl **(B)**, ABA **(C)**, and BR **(D)** treatment applied for 0, 0.5, 1, 2, 4, 8, 12, and 24 h. qRT-PCR data were normalized using the soybean Actin gene (U60506) and are displayed relative to 0 h. The *x*-axes show the duration of treatment and *y*-axes depict relative expression level (error bars indicate SD). The data are shown as means of three biology repeats ± SD.

and used to system analysis in our study. One hundred and seventeen soybean genes were divided into nine subfamilies in the previous study (Wang et al., 2020); however, *GRAS* genes were classified into 12 subfamilies by introducing maize and rice *GRAS* genes, and among these 12 subfamilies, 11 contained soybean *GRAS* genes. By analyzing the intron-exon structure of *GmGRAS* genes, we found that the majority of these genes were free of introns, which was similar to

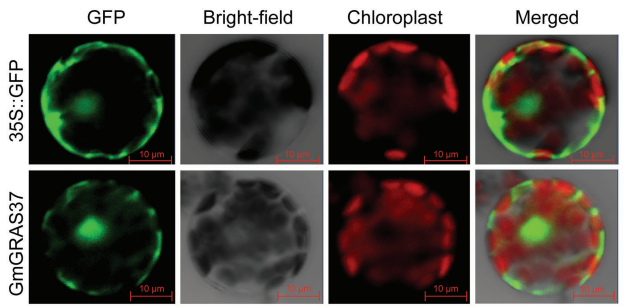


FIGURE 11 | Subcellular localization of GmGRAS37-16318hGFP fusion protein. 35S::GFP was used as a control. The scale bar indicates 10 μm.

the observed lack of introns in *Arabidopsis* and rice *GRAS* genes (Tian et al., 2004). A previous study showed that ancestors of each eukaryote had intron-rich genes and that extensive loss and insertion of introns from most genes may have occurred due to selective pressure, with gene duplication accelerating this process (Roy and Penny, 2007; Rogozin et al., 2012). Nevertheless, some *GRAS* genes have evolved different exon-intron structures, indicating that they likely evolved new specialized functions to adapt their environment. Previous research has indicated that the plant *GRAS* gene family originated from a prokaryotic genome through horizontal gene transfer, followed by duplication events (Zhang et al., 2012). Accordingly, the variation in the number of *GRAS* genes between species may be related to gene duplication events. In our study, we identified seven pairs of tandem duplicated *GmGRASs* and 54 pairs of segmentally duplicated *GmGRASs* (**Figure 6** and **Supplementary Table S2**). These results further validate the notion that duplication plays a vital role in the expansion of the *GRAS* gene family and show that segmental duplication contributed more to the expansion of the soybean *GRAS* family than tandem duplication. Protein structure analysis showed that the GmGRAS27, GmGRAS37, GmGRAS72, GmGRAS94, and GmGRAS115 proteins all have the SAW motif, which is a highly conserved C-terminal region (**Figure 3**), and we found that these five GmGRAS proteins are in the same subfamily and have the same gene structure and motifs, which suggests that these *GmGRAS* genes may have similar functions.

Cis-acting elements analysis showed that there are many stress-related *cis*-acting elements in six *GmGRAS* genes with high transcription levels under drought, salt, ABA, and BR treatments (**Table 1**). Among these stress-related *cis*-acting elements, the ABRE is an important component in the ABA pathway and has been shown to be bound by transcription factors in response to ABA-mediated osmotic stress signals. Through qRT-PCR analysis (**Figure 10**), all six *GmGRAS* genes, which contain the ABRE, were upregulated by ABA. Further analysis found that the expression levels of these six *GmGRAS* genes were upregulated under drought and salt stress conditions. Therefore, it is speculated that these genes may be involved in abiotic stress response and participate in the regulation of ABA signaling. Our analysis showed that *GmGRAS37* was highly expressed under multiple stress conditions (**Figure 10**); therefore, this gene was selected for further analysis. Previous research has indicated that GRAS proteins, such as BrLAS, OsGRAS23, and SlGRAS40, play a significant role in growth and development and abiotic stress response in plants (Xu et al., 2015; Liu et al., 2017; Li et al., 2018). Protein structure analysis showed that the GmGRAS37 protein shared functional domains with these three stress response proteins. Further analysis revealed that drought and salt treatments resulted in significant differences in growth and physiology of *GmGRAS37*-RNAi, EV-Control, and *GmGRAS37*-OE plants. In particular, *GmGRAS37*-OE plants had significantly delayed leaf wilting; longer roots; higher CAT, POD, and SOD activities, chlorophyll content, and biomass; lower MDA content, REC, and H_2O_2 and O_2^- levels; and fewer dead cells. The above results suggested that *GRAS37* may play a role in decreasing H_2O_2 accumulation *via* regulation of stress-related gene expression (Xu et al., 2015). Therefore, *GmGRAS37*-OE had increased stress resistance, whereas *GmGRAS37*-RNAi had impaired stress resistance.

Previous research indicated that several genes play an important role in drought and salt stresses. *GmDREB1*, DREB-type transcription factor, was reported to be strongly induced by multiple stresses, such as cold, drought, high salt, and heat. The GmDREB1 protein activates transcription by binding to dehydration-responsive elements (DREs). The *GmDREB1* gene can induce the expression of ABA receptor family genes. Previous studies have shown that *GmDREB1* can improve the drought tolerance of wheat (Kidokoro et al., 2015; Zhou et al., 2020). 9-*cis*-epoxycarotenoid dioxygenase (NCED) is considered to be an important contributor to ABA synthesis during drought and salt stress. Previous studies have indicated that seedlings overexpressing *OsNCED3* have increased drought stress tolerance (Hwang et al., 2010; Li et al., 2019). The chloride channel protein family mediates the transport of Cl^-, which is important for plant nutrient supply, stomatal movement, hormone signal recognition and transduction, Cl^- homeostasis, and abiotic and biotic stress tolerance. *GmCLC1* enhances salt tolerance by reducing Cl^- accumulation to reduce the negative impact of salt stress (Wei et al., 2016). *GmSOS1* improves the salt tolerance of plants. Previous studies suggested that *GmSOS1* may play a role in the extrusion of Na^+ from the roots and the regulation of long-distance Na^+ transport from roots to shoots (Cao et al., 2018). *AtSODs* have been reported to improve tolerance to abiotic stresses such as salinity, cold, and drought stress; these stresses limit plant growth by causing an imbalance between the generation and metabolism of various reactive oxygen species. As a main component of the first line of defense, SOD converts O_2^- into H_2O_2 and O_2. SODs act as signals in various signal transduction pathways of plants and participate in various plant developmental processes (Yadav et al., 2019). Under drought and salt treatment conditions, these six genes were upregulated in *GmGRAS37*-OE plants, indicating that they are regulated by *GmGRAS37* in response to abiotic stress.

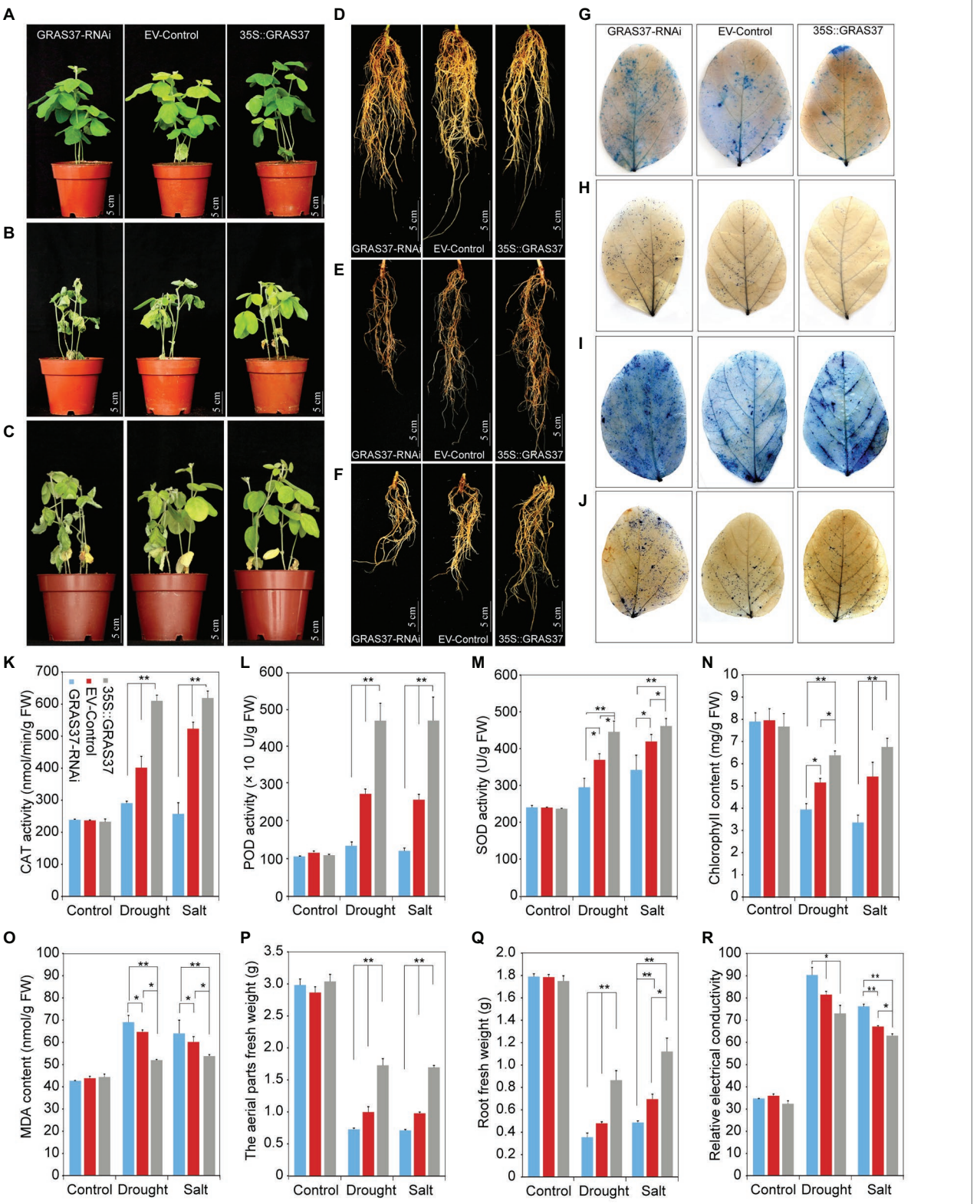


FIGURE 12 | Analysis of the function of soybean *GmGRAS37* under normal conditions and drought and salt stresses. **(A–C)** Phenotypes of transgenic soybean hairy root composite *GRAS37*-RNAi, EV-Control (expressing the pCAMBIA3301 empty vector), and *GmGRAS37*-overexpression (*35S::GRAS37*) plants under

(Continued)

FIGURE 12 | normal conditions **(A)**, drought stress **(B)**, and salt stress **(C)**. **(D–F)** The roots of transgenic soybean hairy root composite *GRAS37*-RNAi, EV-Control, and *35S: GRAS37* plants under normal conditions **(A)**, drought stress **(B)**, and salt stress **(C)**. **(G,I)** Trypan blue staining of leaves of transgenic soybean hairy root composite *GRAS37*-RNAi, EV-Control, and *35S: GRAS37* plants under drought **(G)** and salt stress **(I)**; the dead cells can be strained, but living cells cannot. **(H,J)** Nitroblue tetrazolium (NBT) staining of the leaves of transgenic soybean hairy root composite *GRAS37*-RNAi, EV-Control, and *35S: GRAS37* plants under drought **(H)** and salt stress **(J)**. The intensity of color indicates the concentration of O_2^- in the leaves. **(K–M)** CAT **(K)**, POD **(L)**, and SOD **(M)** activities of transgenic soybean hairy root composite *GRAS37*-RNAi, EV-Control, and *35S: GRAS37* plants under drought conditions. **(N,O)** Chlorophyll content **(N)** and MDA content **(O)** of transgenic soybean hairy root composite *GRAS37*-RNAi, EV-Control, and *35S: GRAS37* plants under drought conditions. **(P,Q)** The fresh weights of the aerial parts **(P)** and roots **(Q)** of transgenic soybean hairy root composite *GRAS37*-RNAi, EV-Control, and *35S: GRAS37* plants under drought conditions. **(R)** Relative electrical conductivity of transgenic soybean hairy root composite *GRAS37*-RNAi, EV-Control, and *35S: GRAS37* plants under drought conditions. Vertical bars indicate ±SD of three replicates. * ($p < 0.05$) and ** ($p < 0.01$) indicate significant differences determined by Student's *t*-test.

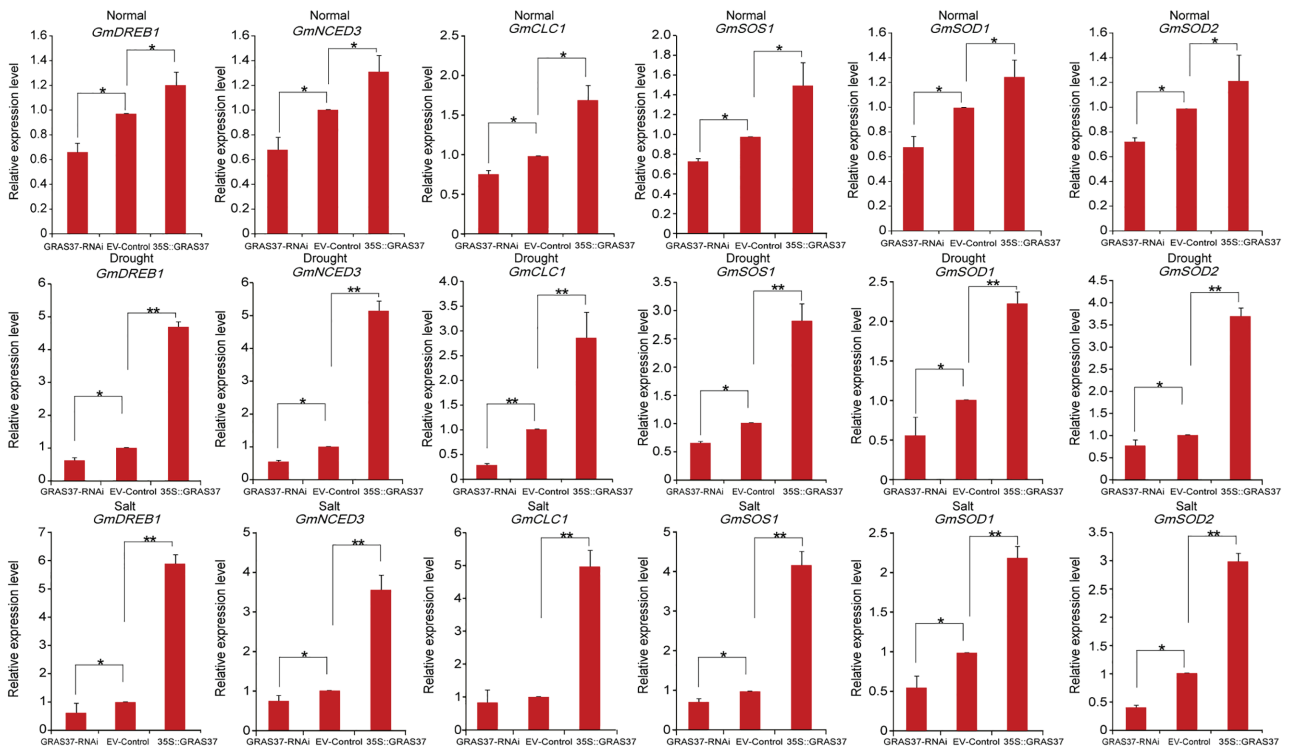


FIGURE 13 | Expression levels of six stress-responsive genes in transgenic *GmGRAS37* soybean hairy root plants under normal conditions, drought stress, and 250 mM NaCl treatment determined by qRT-PCR. Vertical bars indicate ±SD of three replicates. * ($p < 0.05$) and ** ($p < 0.01$) indicate significant differences determined by Student's *t*-test.

CONCLUSION

A total of 117 soybean *GRAS* genes were identified and phylogenetically divided into 11 subfamilies. Six *GRAS* genes, including *GmGRAS37*, were induced by drought, salt, ABA, and BR treatments. *GmGRAS37* enhanced drought and salt tolerance in transgenic plants by activating the expression of *GmDREB1*, *GmNCED3*, *GmCLC1*, *GmSOS1*, *GmSOD1*, and *GmSOD2*. Our study provides a basis for further research on the functions of GRAS family members in abiotic stress tolerance.

DATA AVAILABILITY STATEMENT

The datasets presented in this study can be found in online repositories. The names of the repository/repositories and accession number(s) can be found in the article/**Supplementary Material**.

AUTHOR CONTRIBUTIONS

Z-SX coordinated the project, conceived and designed experiments, and edited the manuscript. T-TW performed experiments and wrote the first draft. T-FY revised the manuscript. H-GS, JC, Y-BZ, and MC contributed to data analysis and managed reagents. J-DF, W-LW, JG, and Y-ZM contributed with valuable discussions. All authors reviewed and approved the final manuscript.

FUNDING

This research was financially supported by the National Natural Science Foundation of China (31871624), the National Transgenic Key Project of the Ministry of Agriculture of China (2020ZX08009-15B), China Postdoctoral Science Foundation (2019M660886), and Fundamental Research Funds for Central

Non-Profit of Institute of Crop Sciences, Chinese Academy of Agricultural Sciences.

ACKNOWLEDGMENTS

We are grateful to Lijuan Qiu and Tianfu Han of the Institute of Crop Science, Chinese Academy of Agricultural Sciences (CAAS) for kindly providing soybean seeds. Also, we are grateful to Wensheng Hou and Hui Zhang of the Institute of Crop Science, CAAS for kindly providing vectors and procedure of high-efficiency *Agrobacterium rhizogenes*-mediated transformation, respectively.

SUPPLEMENTARY MATERIAL

The Supplementary Material for this article can be found online at: https://www.frontiersin.org/articles/10.3389/fpls.2020.604690/full#supplementary-material

REFERENCES

Bailey, T. L., Boden, M., Buske, F. A., Frith, M., Grant, C. E., Clementi, L., et al. (2009). MEME SUITE: tools for motif discovery and searching. *Nucleic Acids Res.* 37, W202–W208. doi: 10.1093/nar/gkp335

Bolle, C. (2004). The role of GRAS proteins in plant signal transduction and development. *Planta* 218, 683–692. doi: 10.1007/s00425-004-1203-z

Bolle, C., Koncz, C., and Chua, N. H. (2000). PAT1, a new member of the GRAS family, is involved in phytochrome A signal transduction. *Genes Dev.* 14, 1269–1278. doi: 10.1101/gad.14.10.1269

Cao, D., Li, Y., Liu, B., Kong, F., and Tran, L. -S. P. (2018). Adaptive mechanisms of soybean grown on salt-affected soils. *Land Degrad. Dev.* 29, 1054–1064. doi: 10.1002/ldr.2754

Czikkel, B. E., and Maxwell, D. P. (2007). NtGRAS1, a novel stress-induced member of the GRAS family in tobacco, localizes to the nucleus. *J. Plant Physiol.* 164, 1220–1230. doi: 10.1016/j.jplph.2006.07.010

Di Laurenzio, L., Wysocka-Diller, J., Malamy, J. E., Pysh, L., Helariutta, Y., Freshour, G., et al. (1996). The SCARECROW gene regulates an asymmetric cell division that is essential for generating the radial organization of the *Arabidopsis* root. *Cell* 86, 423–433. doi: 10.1016/s0092-8674(00)80115-4

Dill, A., Jung, H. S., and Sun, T. P. (2001). The DELLA motif is essential for gibberellin-induced degradation of RGA. *Proc. Natl. Acad. Sci. U. S. A.* 98, 14162–14167. doi: 10.1073/pnas.251534098

Du, Y. T., Zhao, M. J., Wang, C. T., Gao, Y., Wang, Y. X., Liu, Y. W., et al. (2018). Identification and characterization of GmMYB118 responses to drought and salt stress. *BMC Plant Biol.* 18:320. doi: 10.1186/s12870-018-1551-7

Fan, K., Yuan, S., Chen, J., Chen, Y., Li, Z., Lin, W., et al. (2019). Molecular evolution and lineage-specific expansion of the PP2C family in *Zea mays*. *Planta* 250, 1521–1538. doi: 10.1007/s00425-019-03243-x

Fode, B., Siemsen, T., Thurow, C., Weigel, R., and Gatz, C. (2008). The *Arabidopsis* GRAS protein SCL14 interacts with class II TGA transcription factors and is essential for the activation of stress-inducible promoters. *Plant Cell* 20, 3122–3135. doi: 10.1105/tpc.108.058974

Gao, Y., Ma, J., Zheng, J. C., Chen, J., Chen, M., Zhou, Y. B., et al. (2019). The elongation factor GmEF4 is involved in the response to drought and salt tolerance in soybean. *Int. J. Mol. Sci.* 20:3001. doi: 10.3390/ijms20123001

Greb, T., Clarenz, O., Schafer, E., Muller, D., Herrero, R., Schmitz, G., et al. (2003). Molecular analysis of the LATERAL SUPPRESSOR gene in *Arabidopsis* reveals a conserved control mechanism for axillary meristem formation. *Genes Dev.* 17, 1175–1187. doi: 10.1101/gad.260703

Guo, Y., Wu, H., Li, X., Li, Q., Zhao, X., Duan, X., et al. (2017). Identification and expression of *GRAS* family genes in maize (*Zea mays* L.). *PLoS One* 12:e0185418. doi: 10.1371/journal.pone.0185418

Guo, A. Y., Zhu, Q. H., Chen, X., and Luo, J. C. (2007). GSDS: a gene structure display server. *Yi Chuan* 29, 1023–1026. doi: 10.1360/yc-007-1023

Helariutta, Y., Fukaki, H., Wysocka-Diller, J., Nakajima, K., Jung, J., Sena, G., et al. (2000). The SHORT-ROOT gene controls radial patterning of the *Arabidopsis* root through radial signaling. *Cell* 101, 555–567. doi: 10.1016/s0092-8674(00)80865-x

Heo, J. O., Chang, K. S., Kim, I. A., Lee, M. H., Lee, S. A., Song, S. K., et al. (2011). Funneling of gibberellin signaling by the GRAS transcription regulator scarecrow-like 3 in the *Arabidopsis* root. *Proc. Natl. Acad. Sci. U. S. A.* 108, 2166–2171. doi: 10.1073/pnas.1012215108

Holub, E. B. (2001). The arms race is ancient history in *Arabidopsis*, the wildflower. *Nat. Rev. Genet.* 2, 516–527. doi: 10.1038/35080508

Huang, W., Xian, Z., Kang, X., Tang, N., and Li, Z. (2015). Genome-wide identification, phylogeny and expression analysis of GRAS gene family in tomato. *BMC Plant Biol.* 15:209. doi: 10.1186/s12870-015-0590-6

Hwang, S. G., Chen, H. C., Huang, W. Y., Chu, Y. C., Shii, C. T., and Cheng, W. H. (2010). Ectopic expression of rice OsNCED3 in *Arabidopsis* increases ABA level and alters leaf morphology. *Plant Sci.* 178, 12–22. doi: 10.1016/j.plantsci.2009.09.014

Kereszt, A., Li, D., Indrasumunar, A., Nguyen, C. D., Nontachaiyapoom, S., Kinkema, M., et al. (2007). *Agrobacterium rhizogenes*-mediated transformation of soybean to study root biology. *Nat. Protoc.* 2, 948–952. doi: 10.1038/nprot.2007.141

Kidokoro, S., Watanabe, K., Ohori, T., Moriwaki, T., Maruyama, K., Mizoi, J., et al. (2015). Soybean DREB1/CBF-type transcription factors function in heat and drought as well as cold stress-responsive gene expression. *Plant J.* 81, 505–518. doi: 10.1111/tpj.12746

Kumar, S., Stecher, G., and Tamura, K. (2016). MEGA7: molecular evolutionary genetics analysis version 7.0 for bigger datasets. *Mol. Biol. Evol.* 33, 1870–1874. doi: 10.1093/molbev/msw054

Le, D. T., Nishiyama, R., Watanabe, Y., Mochida, K., Yamaguchi-Shinozaki, K., Shinozaki, K., et al. (2011). Genome-wide expression profiling of soybean two-component system genes in soybean root and shoot tissues under dehydration stress. *DNA Res.* 18, 17–29. doi: 10.1093/dnares/dsq032

Lee, M. H., Kim, B., Song, S. K., Heo, J. O., Yu, N. I., Lee, S. A., et al. (2008). Large-scale analysis of the GRAS gene family in *Arabidopsis thaliana*. *Plant Mol. Biol.* 67, 659–670. doi: 10.1007/s11103-008-9345-1

Lescot, M., Dehais, P., Thijs, G., Marchal, K., Moreau, Y., Van de Peer, Y., et al. (2002). PlantCARE, a database of plant cis-acting regulatory elements and a portal to tools for in silico analysis of promoter sequences. *Nucleic Acids Res.* 30, 325–327. doi: 10.1093/nar/30.1.325

Li, X., Qian, Q., Fu, Z., Wang, Y., Xiong, G., Zeng, D., et al. (2003). Control of tillering in rice. *Nature* 422, 618–621. doi: 10.1038/nature01518

Li, S., Wang, N., Ji, D., Zhang, W., Wang, Y., Yu, Y., et al. (2019). A GmSIN1/GmNCED3s/GmRbohBs feed-forward loop acts as a signal amplifier that regulates root growth in soybean exposed to salt stress. *Plant Cell* 31, 2107–2130. doi: 10.1105/tpc.18.00662

Li, P., Zhang, B., Su, T., Li, P., Xin, X., Wang, W., et al. (2018). BrLAS, a GRAS transcription factor from *Brassica rapa*, is involved in drought stress tolerance in transgenic *Arabidopsis*. *Front. Plant Sci.* 9:1792. doi: 10.3389/fpls.2018.01792

Liu, M., Huang, L., Ma, Z., Sun, W., Wu, Q., Tang, Z., et al. (2019). Genome-wide identification, expression analysis and functional study of the GRAS gene family in Tartary buckwheat (*Fagopyrum tataricum*). *BMC Plant Biol.* 19:342. doi: 10.1186/s12870-019-1951-3

Liu, Y., Huang, W., Xian, Z., Hu, N., Lin, D., Ren, H., et al. (2017). Overexpression of SlGRAS40 in tomato enhances tolerance to abiotic stresses and influences auxin and gibberellin signaling. *Front. Plant Sci.* 8:1659. doi: 10.3389/fpls.2017.01659

Liu, B., Sun, Y., Xue, J., Jia, X., and Li, R. (2018). Genome-wide characterization and expression analysis of GRAS gene family in pepper (*Capsicum annuum* L.). *PeerJ* 6:e4796. doi: 10.7717/peerj.4796

Liu, X., and Widmer, A. (2014). Genome-wide comparative analysis of the GRAS gene family in populus, *Arabidopsis* and rice. *Plant Mol. Biol. Report.* 32, 1129–1145. doi: 10.1007/s11105-014-0721-5

Liu, P., Xu, Z. S., Pan-Pan, L., Hu, D., Chen, M., Li, L. C., et al. (2013). A wheat PI4K gene whose product possesses threonine autophophorylation activity confers tolerance to drought and salt in *Arabidopsis*. *J. Exp. Bot.* 64, 2915–2927. doi: 10.1093/jxb/ert133

Lu, J., Wang, T., Xu, Z., Sun, L., and Zhang, Q. (2015). Genome-wide analysis of the GRAS gene family in *Prunus mume*. *Mol. Gen. Genomics.* 290, 303–317. doi: 10.1007/s00438-014-0918-1

Mayrose, M., Ekengren, S. K., Melech-Bonfil, S., Martin, G. B., and Sessa, G. (2006). A novel link between tomato *GRAS* genes, plant disease resistance and mechanical stress response. *Mol. Plant Pathol.* 7, 593–604. doi: 10.1111/j.1364-3703.2006.00364.x

Morohashi, K., Minami, M., Takase, H., Hotta, Y., and Hiratsuka, K. (2003). Isolation and characterization of a novel *GRAS* gene that regulates meiosis-associated gene expression. *J. Biol. Chem.* 278, 20865–20873. doi: 10.1074/jbc.M301712200

Peng, J., Carol, P., Richards, D. E., King, K. E., Cowling, R. J., Murphy, G. P., et al. (1997). The *Arabidopsis* GAI gene defines a signaling pathway that negatively regulates gibberellin responses. *Genes Dev.* 11, 3194–3205. doi: 10.1101/gad.11.23.3194

Prince, V. E., and Pickett, F. B. (2002). Splitting pairs: the diverging fates of duplicated genes. *Nat. Rev. Genet.* 3, 827–837. doi: 10.1038/nrg928

Pysh, L. D., Wysocka-Diller, J. W., Camilleri, C., Bouchez, D., and Benfey, P. N. (1999). The GRAS gene family in *Arabidopsis*: sequence characterization and basic expression analysis of the SCARECROW-LIKE genes. *Plant J.* 18, 111–119. doi: 10.1046/j.1365-313x.1999.00431.x

Riano-Pachon, D. M., Ruzicic, S., Dreyer, I., and Mueller-Roeber, B. (2007). PlnTFDB: an integrative plant transcription factor database. *BMC Bioinformatics* 8:42. doi: 10.1186/1471-2105-8-42

Rogozin, I. B., Carmel, L., Csuros, M., and Koonin, E. V. (2012). Origin and evolution of spliceosomal introns. *Biol. Direct* 7:11. doi: 10.1186/1745-6150-7-11

Roy, S. W., and Penny, D. (2007). Patterns of intron loss and gain in plants: intron loss-dominated evolution and genome-wide comparison of O. sativa and *A. thaliana*. *Mol. Biol. Evol.* 24, 171–181. doi: 10.1093/molbev/msl159

Schumacher, K., Schmitt, T., Rossberg, M., Schmitz, G., and Theres, K. (1999). The lateral suppressor (Ls) gene of tomato encodes a new member of the VHIID protein family. *Proc. Natl. Acad. Sci. U. S. A.* 96, 290–295. doi: 10.1073/pnas.96.1.290

Sharp, R. E., Hsiao, T. C., and Silk, W. K. (1990). Growth of the maize primary root at low water potentials: II. Role of growth and deposition of hexose and potassium in osmotic adjustment. *Plant Physiol.* 93, 1337–1346. doi: 10.1104/pp.93.4.1337

Shi, W. Y., Du, Y. T., Ma, J., Min, D. H., Jin, L. G., Chen, J., et al. (2018). The WRKY transcription factor GmWRKY12 confers drought and salt tolerance in soybean. *Int. J. Mol. Sci.* 19:4087. doi: 10.3390/ijms19124087

Silverstone, A. L., Ciampaglio, C. N., and Sun, T. (1998). The *Arabidopsis* RGA gene encodes a transcriptional regulator repressing the gibberellin signal transduction pathway. *Plant Cell* 10, 155–169. doi: 10.1105/tpc.10.2.155

Song, X. M., Liu, T. K., Duan, W. K., Ma, Q. H., Ren, J., Wang, Z., et al. (2014). Genome-wide analysis of the GRAS gene family in Chinese cabbage (*Brassica rapa ssp. pekinensis*). *Genomics* 103, 135–146. doi: 10.1016/j.ygeno.2013.12.004

Song, Y., Xuan, A., Bu, C., Ci, D., Tian, M., and Zhang, D. (2019). Osmotic stress-responsive promoter upstream transcripts (PROMPTs) act as carriers of MYB transcription factors to induce the expression of target genes in *Populus simonii*. *Plant Biotechnol. J.* 17, 164–177. doi: 10.1111/pbi.12955

Stuurman, J., Jaggi, F., and Kuhlemeier, C. (2002). Shoot meristem maintenance is controlled by a *GRAS*-gene mediated signal from differentiating cells. *Genes Dev.* 16, 2213–2218. doi: 10.1101/gad.230702

Tian, C., Wan, P., Sun, S., Li, J., and Chen, M. (2004). Genome-wide analysis of the GRAS gene family in rice and *Arabidopsis*. *Plant Mol. Biol.* 54, 519–532. doi: 10.1023/B:PLAN.0000038256.89809.57

Tong, H., Jin, Y., Liu, W., Li, F., Fang, J., Yin, Y., et al. (2009). DWARF AND LOW-TILLERING, a new member of the GRAS family, plays positive roles in brassinosteroid signaling in rice. *Plant J.* 58, 803–816. doi: 10.1111/j.1365-313X.2009.03825.x

Wang, L., Ding, X. L., Gao, Y. Q., and Yang, S. P. (2020). Genome-wide identification and characterization of *GRAS* genes in soybean (*Glycine max*). *BMC Plant Biol.* 20:415. doi: 10.1186/s12870-020-02636-5

Wei, P., Wang, L., Liu, A., Yu, B., and Lam, H. M. (2016). GmCLC1 confers enhanced salt tolerance through regulating chloride accumulation in soybean. *Front. Plant Sci.* 7:1082. doi: 10.3389/fpls.2016.01082

Xu, K., Chen, S., Li, T., Ma, X., Liang, X., Ding, X., et al. (2015). OsGRAS23, a rice GRAS transcription factor gene, is involved in drought stress response through regulating expression of stress-responsive genes. *BMC Plant Biol.* 15:141. doi: 10.1186/s12870-015-0532-3

Yadav, S., Gill, S. S., Passricha, N., Gill, R., Badhwar, P., Anjum, N. A., et al. (2019). Genome-wide analysis and transcriptional expression pattern-assessment of superoxide dismutase (SOD) in rice and *Arabidopsis* under abiotic stresses. *Plant Gene.* 17:100165. doi: 10.1016/j.plgene.2018.10.001

Yoo, S. D., Cho, Y. H., and Sheen, J. (2007). *Arabidopsis* mesophyll protoplasts: a versatile cell system for transient gene expression analysis. *Nat. Protoc.* 2, 1565–1572. doi: 10.1038/nprot.2007.199

Yuan, Y., Fang, L., Karungo, S. K., Zhang, L., Gao, Y., Li, S., et al. (2016). Overexpression of VaPAT1, a GRAS transcription factor from *Vitis amurensis*, confers abiotic stress tolerance in *Arabidopsis*. *Plant Cell Rep.* 35, 655–666. doi: 10.1007/s00299-015-1910-x

Zhang, D., Iyer, L. M., and Aravind, L. (2012). Bacterial GRAS domain proteins throw new light on gibberellic acid response mechanisms. *Bioinformatics* 28, 2407–2411. doi: 10.1093/bioinformatics/bts464

Zhang, B., Liu, J., Yang, Z. E., Chen, E. Y., Zhang, C. J., Zhang, X. Y., et al. (2018). Genome-wide analysis of GRAS transcription factor gene family in *Gossypium hirsutum* L. *BMC Genomics* 19:348. doi: 10.1186/s12864-018-4722-x

Zhang, X. Z., Zheng, W. J., Cao, X. Y., Cui, X. Y., Zhao, S. P., Yu, T. F., et al. (2019). Genomic analysis of stress associated proteins in soybean and the role of GmSAP16 in abiotic stress responses in *Arabidopsis* and soybean. *Front. Plant Sci.* 10:1453. doi: 10.3389/fpls.2019.01453

Zhou, Y., Chen, M., Guo, J., Wang, Y., Min, D., Jiang, Q., et al. (2020). Overexpression of soybean DREB1 enhances drought stress tolerance of transgenic wheat in the field. *J. Exp. Bot.* 71, 1842–1857. doi: 10.1093/jxb/erz569

Conflict of Interest: The authors declare that the research was conducted in the absence of any commercial or financial relationships that could be construed as a potential conflict of interest.

Copyright © 2020 Wang, Yu, Fu, Su, Chen, Zhou, Chen, Guo, Ma, Wei and Xu. This is an open-access article distributed under the terms of the Creative Commons Attribution License (CC BY). The use, distribution or reproduction in other forums is permitted, provided the original author(s) and the copyright owner(s) are credited and that the original publication in this journal is cited, in accordance with accepted academic practice. No use, distribution or reproduction is permitted which does not comply with these terms.

frontiers in Plant Science

ORIGINAL RESEARCH
published: 25 January 2021
doi: 10.3389/fpls.2020.612054

Grain Inorganic Arsenic Content in Rice Managed Through Targeted Introgressions and Irrigation Management

*Cristina P. Fernández-Baca[1], Anna M. McClung[1], Jeremy D. Edwards[1], Eton E. Codling[2], Vangimalla R. Reddy[2] and Jinyoung Y. Barnaby[1]**

[1] United States Department of Agriculture, Agricultural Research Service, Dale Bumpers National Rice Research Center, Stuttgart, AR, United States, [2] Adaptive Cropping Systems Laboratory, United States Department of Agriculture, Agricultural Research Service, Beltsville Agricultural Research Center, Beltsville, MD, United States

Arsenic (As) accumulation in rice grain is a significant public health concern. Inorganic As (iAs) is of particular concern because it has increased toxicity as compared to organic As. Irrigation management practices, such as alternate wetting and drying (AWD), as well as genotypic differences between cultivars, have been shown to influence As accumulation in rice grain. A 2 year field study using a Lemont × TeQing backcross introgression line (TIL) mapping population examined the impact of genotype and AWD severity on iAs grain concentrations. The "Safe"-AWD [35–40% soil volumetric water content (VWC)] treatment did not reduce grain iAs levels, whereas the more severe AWD30 (25–30% VWC) consistently reduced iAs concentrations across all genotypes. The TILs displayed a range of iAs concentrations by genotype, from less than 10 to up to 46 $\mu g\ kg^{-1}$ under AWD30 and from 28 to 104 $\mu g\ kg^{-1}$ under Safe-AWD. TIL grain iAs concentrations for flood treatments across both years ranged from 26 to 127 $\mu g\ kg^{-1}$. Additionally, seven quantitative trait loci (QTLs) were identified in the mapping population associated with grain iAs. A subset of eight TILs and their parents were grown to confirm field-identified grain iAs QTLs in a controlled greenhouse environment. Greenhouse results confirmed the genotypic grain iAs patterns observed in the field; however, iAs concentrations were higher under greenhouse conditions as compared to the field. In the greenhouse, the number of days under AWD was negatively correlated with grain iAs concentrations. Thus, longer drying periods to meet the same soil VWC resulted in lower grain iAs levels. Both the number and combinations of iAs-affecting QTLs significantly impacted grain iAs concentrations. Therefore, identifying more grain iAs-affecting QTLs could be important to inform future breeding efforts for low iAs rice varieties. Our study suggests that coupling AWD practices targeting a soil VWC of less than or equal to 30% coupled with the use of cultivars developed to possess multiple QTLs that negatively regulate grain iAs concentrations will be helpful in mitigating exposure of iAs from rice consumption.

Keywords: inorganic As, alternate wetting and drying, chromosome segment substitution line, soil volumetric water content, rice, quantitative trait loci

OPEN ACCESS

Edited by:
Raul Antonio Sperotto, Universidade do Vale do Taquari–Univates, Brazil

Reviewed by:
Satoru Ishikawa, National Agriculture and Food Research Organization (NARO), Japan
Gian Attilio Sacchi, University of Milan, Italy

***Correspondence:**
Jinyoung Y. Barnaby
Jinyoung.barnaby@usda.gov

Specialty section:
This article was submitted to Crop and Product Physiology, a section of the journal Frontiers in Plant Science

Received: *30 September 2020*
Accepted: *23 December 2020*
Published: *25 January 2021*

Citation:
Fernández-Baca CP, McClung AM, Edwards JD, Codling EE, Reddy VR and Barnaby JY (2021) Grain Inorganic Arsenic Content in Rice Managed Through Targeted Introgressions and Irrigation Management. Front. Plant Sci. 11:612054. doi: 10.3389/fpls.2020.612054

INTRODUCTION

Arsenic (As) exposure from rice consumption is a serious and growing concern as rice is a staple dietary crop for half of the world's population and is cultivated worldwide. Rice has been identified as a major As exposure route for humans and is often the principal source of As where drinking water As concentrations are low (Kile et al., 2007; Meharg et al., 2009). Consumption of rice containing high levels of As is linked to adverse health impacts including cancer (Zhao et al., 2010; Banerjee et al., 2013).

As is naturally present in soil but can be exacerbated by the use of contaminated irrigation water or anthropogenic sources (e.g., mining activities, use of arsenical pesticides, etc.) (Zhao et al., 2010; Kumarathilaka et al., 2018). Paddy rice accumulates As at a higher rate than other cereal crops (e.g., wheat or barley) for two principal reasons (Williams et al., 2007). First, rice is traditionally grown in flooded fields, which creates anoxic soil conditions leading to As mobilization, in the form of arsenite, in the soil solution (Takahashi et al., 2004; Yamaguchi et al., 2011). Second, arsenite, a form of inorganic As (iAs), is taken up through silicic acid transporters in rice (Ma et al., 2008; Norton et al., 2010). Arsenic accumulates throughout rice plant tissues, but in the grain the predominant forms are organic dimethylarsinic acid (DMA) and inorganic arsenite, a class 1 carcinogen (International Agency for Research on Cancer [IARC], 2004; Williams et al., 2006).

Concern over iAs is increasing in rice markets because of its potentially high concentrations in the grain (Schoof et al., 1999). While both polished and brown rice contain As, brown rice tends to have higher As concentrations because As accumulates in the bran layer (Meharg et al., 2008; Sun et al., 2008). Restrictions have been placed on iAs concentrations in rice by FAO/CODEX, with a limit of 200 $\mu g\ kg^{-1}$ for polished rice and 350 $\mu g\ kg^{-1}$ for husked (brown) rice products (Codex Alimentarius, 2017), and in the United States, the Food and Drug Administration (FDA) has set a limit of 100 $\mu g\ kg^{-1}$ for rice used in infant food products (Gray et al., 2012).

Many studies have shown that rice grain As accumulation can be mitigated by implementing one or more periods of soil drying during the growing season. Alternate wetting and drying (AWD), a water saving irrigation management method, can reduce grain As accumulation; however, the extent of grain As reduction appears to be highly dependent on the severity and timing of the soil dry-down period (Carrijo et al., 2018, 2019; Li et al., 2019). A meta-analysis of AWD studies by Carrijo et al. (2017) found a loss of yield has been observed with too severe of a drying period, whereas AWD cycles that are too mild can fail to reduce grain iAs at all (Carrijo et al., 2017). In practice, it is difficult to impose and hold a uniform soil volumetric water content (VWC) across a non-flooded field and is particularly difficult with unpredictable rain events. Moreover, to protect against yield loss or a reduction in milling quality, rice farmers will implement "Safe"-AWD practices, which try to minimize crop stress while maximizing irrigation savings (Carrijo et al., 2018). Thus, it is important to develop rice varieties that have low As accumulation in the grain and also perform well with reduced irrigation practices.

Multiple studies have established that rice cultivars vary in As accumulation rates; however, the genetics that influence accumulation or exclusion of As are not as well understood. Using mapping populations such as chromosome segment substitution lines (CSSLs) to study grain As accumulation can facilitate identification of As-affecting quantitative trait loci (QTLs). Previous studies have identified QTLs for total As accumulation in shoots and roots after applying an iAs treatment (Murugaiyan et al., 2019), as well as total As (Dasgupta et al., 2004; Zhang et al., 2007, 2014; Norton et al., 2010, 2012, 2014) and organic As accumulation (DMA) in the grain (Kuramata et al., 2013). However, identification of QTLs specifically affecting grain iAs, as opposed to total or organic As fractions, has not been previously reported in the literature. Identifying QTLs affecting iAs accumulation in rice grain can inform breeding efforts toward developing low iAs accumulating varieties. Additionally, understanding how the combined effect of irrigation management practices and QTL presence impact the accumulation of grain iAs is important for producing low As cultivars. The objective of this research is threefold: to identify genomic regions (i.e., QTLs) controlling iAs accumulation in rice grain, to understand how specific QTLs and their combinations influence grain iAs concentrations, and to understand changes in grain iAs levels resulting from QTL combinations in response to irrigation management practices. Ultimately, the goal of this research is to inform future marker-assisted breeding toward As excluding varieties to mitigate human exposure to As from rice consumption.

MATERIALS AND METHODS

Field Experiment

A set of 123 CSSLs, developed from backcrossing "Lemont" (tropical Japonica) as the recurrent parent and "Teqing" (*indica*) as the donor as described by Pinson et al. (2012), was used in this study. Seeds were obtained from the USDA-ARS Genetic Stocks Oryza (GSOR) collection[1]. The experiment was conducted at the Dale Bumpers National Rice Research Center in Stuttgart, AR, during the summer of 2013 and 2014. The soil at the site is described as a Dewitt silt loam (fine, smectitic, thermic, Typic Albaqualfs) with a total C content of 0.67% and a total N content of 0.085%. The naturally occurring As content of this soil has previously been reported to be between 5.5 and 6.8 mg kg^{-1} (Somenahally et al., 2011a,b). A soil analysis was performed prior to planting each year followed by 100 and 56 kg ha^{-1} phosphorous ($P_2 0_5$) applied in 2013 and 2014, respectively, along with 100 kg ha^{-1} potassium (K_2O) and 11 kg ha^{-1} zinc. Pre-emergent herbicide was applied, and additional pesticide treatments were applied as needed throughout the growing season according to local recommendations. The study consisted of 117 and 121 TeQing-into-Lemont backcross introgression lines (TILs) (genotypes) in 2013 and 2014, respectively, along

[1]www.ars.usda.gov/GSOR

with six repeated check plots of the two parents, evaluated under two irrigation regimes. Each irrigation treatment was conducted in separate adjacent fields. Within each irrigation regime, the TILs were arranged as a randomized complete-block design with four replications; however, only one field replication was used for the grain As analysis (see below).

The studies were planted on May 30, 2013, and June 5, 2014, and the TILs were sown in hill plots with a Hege 1000 plot planter (Wintersteiger Inc., Salt Lake City, UT), with each experimental unit consisting of 10 plants having approximately 30 cm between plants. All fields were irrigated after planting to ensure uniform germination and stand establishment. Approximately 2 weeks after emergence, 56 kg N ha^{-1} was applied as urea, followed by flood irrigation. For the remainder of the season, the flood treatment was sustained, whereas the AWD treatment was allowed to dry until the target soil VWC was reached (see below for VWC targets). The field was then flooded for 3 days, drained, and allowed to dry to the target VWC again; cycles were repeated a total of four times during the season (**Table 1**). A POGO Pro (Stevens Water Monitoring Systems Inc., Portland, OR, United States) was used to monitor soil moisture at a depth of 5 cm on about half of the experimental units to determine when to irrigate the AWD treatment. In 2013, a Safe-AWD treatment was implemented with a target soil VWC range of 35–40%. No plant stress symptoms were observed in 2013; thus, in 2014, the severity of the AWD cycles was increased to a target range of 25–30% VWC (hereafter referred to as AWD30) (**Table 1**). Soil VWC measurements are reported for the specific experimental units analyzed for grain iAs in this study. Temperature and rain data were collected on site by the USDA-ARS weather station[2].

Two plants per experimental unit were monitored for days to heading and were harvested individually at maturity for collection of all agronomic data for each of the four field replications. The plants were dried to approximately 12% moisture, threshed individually, and agronomic traits were determined as an average of the two plants per experimental unit, across the four field replications. The paddy rice samples were stored at 4°C prior to further analysis.

Analysis of Grain iAs

Rough rice from one of the harvested plants for each experimental unit in one field replication per irrigation treatment was shelled using the Testing Husker (Satake Engineering Co., Uino Taito-Ku, Tokyo) to produce between 3 and 10 g of whole-grain brown rice in 2013 and 2014. Because of low yields, in some cases both of the plants per experimental unit were combined prior to shelling to reach a minimum of 3 g of brown rice per genotype. The grain samples were ground to a fine powder using a UDY Cyclone Sample Mill (Fort Collins, CO, United States) with a 0.8 mm screen. Ground samples were stored at 4°C for later analysis. iAs was measured following the protocol described in Chaney et al. (2018); all reagents were trace metal grade. Briefly, 0.7 g (dry weight) rice flour was weighed into 50 mL polyethylene tubes. Samples were extracted using the standard hot block method (Gray et al., 2012) with 10 mL of 0.28 M HNO_3 for 90 min at 95°C. At the end of extraction, tubes were removed from the hot block and allowed to reach room temperature before filtering the extracts through Whatman Grade 40 filter paper into new 50 mL polyethylene tubes. Filters were rinsed twice with 0.28 M HNO_3, and the filtrate was diluted to 20 mL with 0.28 M HNO_3.

iAs in filtered extracts was measured by inductively coupled plasma atomic emission spectroscopy using a hydride generation flow injection method (Musil et al., 2014; Pétursdóttir et al., 2014). Technical replicates of the NIST (National Institute of Standards and Technology) standard reference for rice flour 1568b (certified values for total As of 285 ± 14 μg kg^{-1}, iAs of 92 ± 10 μg kg^{-1}, DMA of 180 ± 12 μg kg^{-1} and monomethylarsonic acid of 11.6 ± 3.5 μg kg^{-1}) and in-house standards were run for quality assurance. Additionally, control blank, spiked samples, and random technical replicates of samples were also analyzed. In this study, the mean measured iAs for the NIST 1568b standard was 99 ± 2 μg kg^{-1}, which is within 1 standard deviation of the certified value of 92 ± 10 μg kg^{-1}.

QTL Analysis and TIL Selection

Grain iAs results from the 2013 and 2014 field study of the TILs and their parental lines were used in QTL mapping using IciMapping 4.1[3] (Meng et al., 2015). Genotypic data were obtained from next-generation sequencing according to Elshire et al. (2011) and processed using the Tassel 5 GBS v2 Pipeline (Glaubitz et al., 2014). The stepwise regression method (RSTEP-LTR) of IciMapping was used to identify QTLs. The threshold for the log-of-odds to declare significant QTLs was calculated via a 1,000 permutation test to ensure genome-wide type 1 error rate to be ≤ 0.05. The identified QTLs and grain iAs concentrations were used to select eight TILs from the mapping population. The selected TILs represent a span of low to high grain iAs accumulating phenotypes and differ in number and combinations of the seven identified QTLs. Additionally, the subset was selected to have heading days within 2 weeks to ensure developmental stages were similar within the selected set. Four genotypes were selected to represent each of the grain iAs excluder and grain iAs accumulator groups.

Greenhouse Study

In 2019, the eight selected TILs and their parents (Lemont and TeQing) were grown concurrently in two adjacent greenhouses at the USDA-ARS, Beltsville Area Research Center in Beltsville, MD. Sterilized seeds were germinated and then planted in 72-cell trays in potting soil. Approximately 2 weeks later, a single seedling was transplanted to a 19-l bucket made of high-density polyethylene filled with soil collected from the plow layer of a field used in the 2013/2014 field study at the Dale Bumpers National Rice Research Center in Stuttgart, AR. The buckets were filled with soil to a depth of 27 cm, leaving approximately 10 cm above the soil surface to allow for watering.

[2]https://www.ars.usda.gov/southeast-area/stuttgart-ar/dale-bumpers-national-rice-research-center/docs/weather-stations/

[3]http://www.isbreeding.net/

TABLE 1 | Severity of alternate wetting and drying (AWD) treatment and mean soil volumetric water content (VWC, %) at the end of each AWD cycle by experiment.

Site	Year	AWD severity	Grow location	Mean soil VWC (%) at the end of AWD			
				1st AWD	2nd AWD	3rd AWD	4th AWD
Dale Bumpers National Rice Research Center, Stuttgart, AR	2013	Safe-AWD	Field	43	40	34	44
	2014	AWD30	Field	37	25	28	23
Beltsville Agricultural Research Center, Beltsville, MD	2019	AWD20	Greenhouse 1	20	20	—	—
			Greenhouse 2	19	20	—	—

The eight TILs and two parents were grown in four biological replicates per greenhouse and evaluated using two water treatments (10 genotypes × 4 replications × 2 water treatments × 2 greenhouses). Pots were arranged in two randomized complete blocks per bench, with four benches per greenhouse. All pots on a bench were subjected to the same water treatment and treatments alternated by bench (e.g., AWD on bench 1, flood on bench 2, etc.), for a total of two AWD and two flood benches per greenhouse. Benches in the two greenhouses differed in distance from the cooling pad, and for this reason, the order of treatments alternated between the greenhouses (e.g., bench 1 nearest the cooling pad was AWD in greenhouse 1 but was flood in greenhouse 2).

Two water management treatments were used: flood (continuously flooded control) and AWD during which two cycles of wetting and drying were completed (**Table 1**). The target soil VWC for drying was 20% (AWD20) in 2019, which was more severe than that used in the field studies. Beginning 2 weeks after transplanting, all pots were grown under flooded conditions until the AWD treatment was started approximately 4 weeks prior to panicle initiation. Flooding was held at a water depth of approximately 10 cm above the soil surface. Urea (80 kg N ha^{-1}) was applied as N fertilizer in a three-way split during the 2 months following transplanting.

Soil VWC was monitored continuously using TDR probes (CS650 s from Campbell Scientific, Logan, Utah; and Acclima 310 s from Acclima, Meridian, Idaho) for each individual pot in the AWD treatment. Probes were installed to measure soil VWC at a depth of 0–10 cm. Soil VWC was monitored in one flood control pot per greenhouse. For AWD treatments, pots were drained, and when the soil in a pot reached the target VWC (± 1%), it was reflooded. Thus, each pot was reflooded based on their individually measured VWC, and reflooding dates varied by pot, which is in contrast to field conditions where average field VWC was used to decide when to reflood the entire field. The flooded state was held for 8–10 days to ensure soil water saturation before draining and starting the second AWD cycle. The two AWD cycles were completed prior to heading stage after which pots were reflooded until harvest. Soil samples from the greenhouse were also analyzed for total As. The samples were analyzed using the Niton XL3t XRF Analyzer (Thermo Fisher Scientific, Waltham, MA, United States) and measured 7.1 ± 1.3 mg kg^{-1}.

Plants were harvested at maturity, and grain samples for each biological replicate (n = 8 across the two greenhouses) were processed for iAs analysis as described above. Additional agronomic traits including tiller and mature panicle number, shoot biomass without panicles, and total grain yield were determined for each plant at harvest. Temperature, humidity, and light measurements were also recorded for each greenhouse.

Statistical Analysis

All data analyses were conducted in R (version 3.6.1) (R Core Team, 2013) and IciMapping 4.1[4]. Differences in grain iAs accumulation between genotypes or number of QTLs were determined using analysis of variance (ANOVA) with a $p < 0.05$ and using Tukey HSD for multiple mean comparisons using a $p < 0.05$. Individual genotype comparisons between treatments (flood and AWD) were tested for significance using Welch t-tests.

RESULTS

Field Study 2013 and 2014 Grain iAs

In 2013, the targeted average soil VWC was achieved at 40%, which is near saturation (termed Safe-AWD) for this soil type. There was little rainfall prior to heading, which occurred during the week prior to the fourth AWD cycle, but more rainfall occurred during the later grain fill stage (**Supplementary Figure 1A**). Because no plant stress was observed in 2013, the goal in 2014 was to decrease the soil VWC to a target of 25–30%. At an average of 28.3% across the four AWD cycles, this target was achieved in 2014 despite the more frequent rainfall observed prior to heading, which occurred during the week following the fourth AWD cycle (**Supplementary Figure 1B**).

The frequency distribution of brown rice iAs concentrations varied by water treatment and year (**Supplementary Figure 2**). In 2013, the AWD was less severe (Safe-AWD) than in 2014 (AWD30), resulting in little to no difference in grain iAs accumulation between AWD and flood treatments. In 2014, the more severe drying cycles resulted in a marked decrease in grain iAs by AWD as compared to flood for the TILs and both parents.

QTL Identification and Impact on Grain iAs Levels

No QTLs were identified by irrigation treatment when data were pooled across years because of the large environmental variation between the 2013 and 2014 field seasons. Thus, data were grouped by each year and treatment combination for QTL identification. Seven QTLs affecting grain iAs accumulation were identified in the TIL mapping population corresponding to chromosomes 4, 5, 8, 9, 11, and 12 (**Figure 1**, detailed information

[4]http://www.isbreeding.net

on QTLs in **Supplementary Table 1**). Two QTLs affecting grain iAs were identified from the 2013 flood treatment, five QTLs were identified from the 2014 flood treatment, and one QTL from the 2013 Safe-AWD was also identified from the 2013 flood condition (C9_18034390). Two TeQing introgression QTLs were associated with decreased grain iAs levels (C4_2481896 and C11_2659978), whereas the other five QTLs (C4_27292997, C5_19872059, C8_5186967, C9_18034390, C12_824609) were associated with increased grain iAs levels. No genotype-by-management (G × M) QTLs affecting iAs levels were found.

To examine which of the identified QTLs are most abundant in the TILs, we calculated the percent of lines containing each QTL among four grain iAs groups defined by different ranges in iAs concentrations (**Figure 2**). Groups were determined for the two treatment-year datasets (**Figure 2A**, flood 2013 and 2014; **Figure 2B**, Safe-AWD in 2013) by ranking the measured grain iAs concentrations and dividing the resulting range into four groups where each group represents a quarter of the full range of concentrations (e.g., 0–25% represent those samples whose concentrations are less than 25% of the maximum observed iAs for that experiment). Within each iAs group, we calculated the percent of genotypes containing each identified QTL. In general, the genotypes in the top 75% of grain iAs concentrations had a higher percentage of each of the five QTLs identified that are associated with increased iAs (C4_27292997, C5_19872059, C8_5186967, C9_18034390, C12_824609) when compared to the other lower iAs groups. Furthermore, the two QTLs (C4_2481896 and C11_2659978) having the opposite effect were more abundant in the low iAs group. The high iAs concentration group (75–100%) tends to have a higher number of positive iAs-associated QTLs and is more likely to have C4_27292997, C5_19872059, and C9_18034390 than those in the lower iAs groups.

To examine whether the presence of other TeQing background introgressions, not specifically identified as iAs affecting QTLs, was influencing the observed grain iAs concentrations, the effect of TeQing kinship (i.e., the fraction of a TIL's genome coming from TeQing introgressions) was explored. However, there was no correlation between iAs accumulation and how closely related a TIL is to TeQing (**Supplementary Figure 3**). Thus, there is no intrinsic bias in the TIL population as a whole for grain iAs as a result of TeQing background introgressions.

QTL Impact on Grain iAs Accumulation

Grain iAs levels increase concomitantly with an increasing number of identified QTLs in both the AWD and flood field management treatments across the entire mapping population (**Supplementary Figure 4**), which was stronger under flood conditions than AWD conditions. The eight TILs and two parents grown across all experiments (see *TIL Selection for Greenhouse Study*) were examined separately, and a similar pattern was observed where grain iAs levels increased with increasing number of QTLs identified. The relationship was again more apparent under flood and the 2013 Safe-AWD treatments as compared to the more severe 2014 AWD30 (**Figure 3**).

TIL Selection for Greenhouse Study

The eight TILs selected based on iAs grain concentrations and number and combination of QTLs represent a set of low and high As accumulators (**Table 2**), which may allow for further investigation of genetic influence on grain iAs accumulation. Both TIL596.11 and TIL643 have no identified grain iAs QTLs and were chosen for comparison to Lemont as all TILs in the population have some level of random background TeQing introgressions (Pinson et al., 2012).

Greenhouse 2019 Grain iAs Accumulation and QTL Impact

The eight selected TILs and their parents grown in the greenhouse (greenhouse environmental conditions are summarized in **Supplementary Figure 5**) showed significant ($p < 0.05$ for all) reductions in grain iAs accumulation under AWD20 as compared to flood management practices (**Figure 4** and **Table 3**). Indeed, most TILs with the exception of two high iAs accumulators (TIL 634 and TeQing) meet the FDA limit of 100 $\mu g\ kg^{-1}$ when grown under AWD20 practice with only 2 dry down cycles completed before heading stage. Analysis of variance indicated that there was no significant genotype × irrigation treatment effect on any trait measured (data not shown).

Containing any single QTL alone did not appear to impact differences in grain iAs accumulation in the greenhouse study (**Supplementary Figure 6**) as much as the number and type (i.e., positive or negative) of QTL contained by the genotype (**Supplementary Figure 7**). TILs containing QTLs negatively affecting iAs levels in the 2013 and 2014 field study (C11_265997 or C4_248189) represent the lowest mean grain iAs concentrations in the greenhouse data (**Figure 3** and **Supplementary Figure 7**).

Comparison of Field vs. Greenhouse Studies

There is a noticeable increase in grain iAs concentrations in greenhouse-grown rice as compared to field-grown rice, particularly under the flooded treatment (**Figure 4**). Lack of replication in the field study for grain iAs prohibits any statistical comparisons. However, there was replication of the parents, Lemont and TeQing, which show a statistically significant higher grain iAs accumulation between the 2014 field and the 2019 greenhouse results under flooded ($p < 0.001$, **Table 3**).

Genotype differences in mean grain iAs levels within treatments were also examined, and some were found to be significant under flood (greenhouse 1) and AWD (greenhouse 2) (data not shown); however, the most significant differences were observed between the AWD and flood treatments. To compare iAs reductions between treatments, we calculated the percent change in grain iAs accumulation between flood and AWD in all studies (**Table 3**). The four cycles of Safe-AWD used in 2013 were not effective in reducing grain iAs (ranging from a reduction of 30% to an increase of 101%), whereas the more severe AWD30 used in 2014 did result in consistent reductions across all eight TILs and their parents (ranging from a reduction of 56–96%).

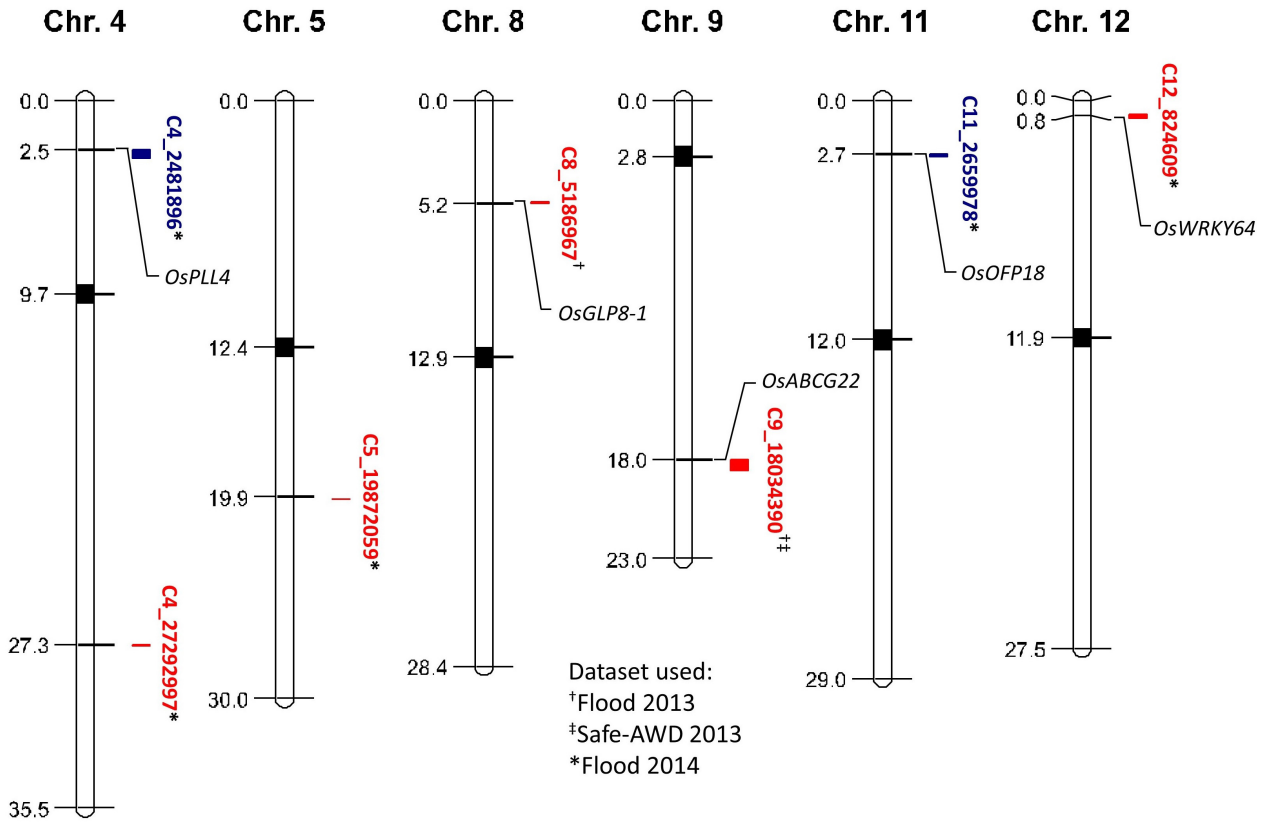


FIGURE 1 | Map of quantitative trait loci (QTLs) affecting brown rice grain inorganic As concentrations and candidate gene locations. Red and blue indicate positive and negative QTL effects on grain iAs levels, respectively. Datasets used to identify QTLs are shown with symbols following the QTL identifier, flood 2013 (†), Safe-AWD 2013 (‡), flood 2014 (*). Approximate locations of genes colocalized with the identified iAs affecting QTLs are depicted with italicized gene names.

Similarly, in 2019, under the more severe two-cycle AWD20 in the greenhouse study, all TILs and their parents had significantly reduced iAs in the rice grain (**Table 3**). In 2019, reductions by AWD in grain iAs were generally 40% or greater ($p < 0.05$ for both greenhouses) across almost all genotypes, with TIL634, a high iAs accumulator, in greenhouse 1, the only exception having a reduction of 36% in grain iAs concentrations under AWD. TIL634 had some of the lowest reductions in grain iAs from flood to AWD treatments overall. In contrast, the low iAs accumulator TIL455 had some of the greatest iAs reductions from flood to AWD with a mean reduction across both greenhouses in 2019 of 61%. In 2014 under AWD30, four TILs, 552, 596.11, 604.11, and 381.1, reduced grain iAs accumulation by at least 80%, whereas under the more severe AWD20 in 2019, the same TILs on average reduced iAs by markedly less, ranging from 49 to 64% on average across two greenhouses.

Impact of Days Under AWD on Grain iAs Accumulation

In the greenhouse study, grain iAs accumulation was significantly negatively correlated to the total number of days a plant was under AWD to achieve the target soil VWC of 20% (i.e., the sum of days under AWD for the first and second AWD cycles) (**Figure 5**). In general, plants in greenhouse 1 had faster AWD drying cycles as compared to plants in greenhouse 2. Total days of AWD under the faster AWD of greenhouse 1 ranged from 16 to 41 days vs. 24 to 53 days under the slower AWD in greenhouse 2. Thus, it took approximately 10 more days under the slow AWD to achieve the same target soil VWC as the fast AWD. Additionally, the grain iAs levels were reduced to a greater extent under slow AWD as compared to fast AWD. The range of grain iAs levels under fast AWD was 32–138 $\mu g\ kg^{-1}$ as compared to 31–110 $\mu g\ kg^{-1}$ under slow AWD.

Pot distance from the cooling pad (**Supplementary Figure 8**) influenced the soil drying time. Because greenhouse cooling pads created a temperature gradient in each greenhouse, we chose to alternate AWD and flood treatment benches by greenhouse. In greenhouse 1, a flood treatment was imposed on the first bench nearest the cooling pad, whereas in greenhouse 2, the first bench nearest the cooling pad was an AWD treatment. The greenhouse temperature gradient affected drying time by pot distance to the cooling pad. In greenhouse 1 the plants that were farther from the cooling pad (7.6–8.8 m) dried faster than those closer to the cooling pad (4.0–5.2 m), with a similar trend apparent in greenhouse 2. This suggests there was a temperature gradient in the greenhouses, and the gradient in greenhouse 1 was stronger than that of greenhouse 2, which ultimately affected the total days under AWD.

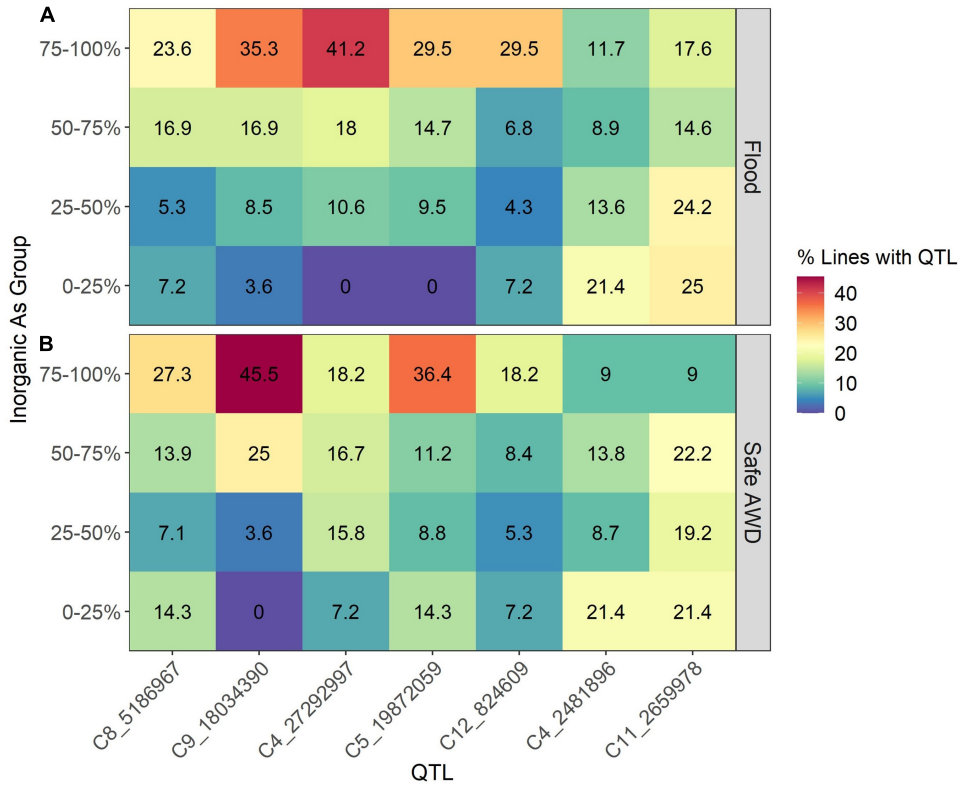


FIGURE 2 | Percent of lines containing each of the identified QTLs among groups based on the range of inorganic arsenic observed in each experiment (e.g., 0–25% represent those samples whose concentrations are < 25% of the maximum observed inorganic As for that experiment). **(A)** Flood 2013 and 2014; **(B)** Safe-AWD in 2013.

Agronomic Traits

In general, there was a decrease in grain yield under the more severe AWD30 and AWD20. However, only 1 of the 10 genotypes had a statistically significant decrease in total yield due to irrigation treatment; TIL 381.11 in greenhouse 2 had a 30% reduction ($p = 0.029$) in yield under AWD as compared to flood (**Supplementary Table 2**).

In the greenhouse study, there was a trend for genotypes with increasing number of As accumulating QTLs to have higher mean total yield (**Supplementary Figure 9**), mature panicle number (**Supplementary Figure 10**), and tiller number (**Supplementary Figure 11**); however, this increase was only significant for mature panicle number and total yield ($p < 0.05$).

A significant, strong correlation was found between grain iAs accumulation and total yield in the greenhouse AWD treatment (**Figure 6**) but was only significant and moderately strong in the field for the 2014 flood treatment (**Supplementary Figure 12**). Mature panicle number had no clear relationship with grain iAs concentrations (**Supplementary Figure 13**), and no strong correlations were found between tiller number (**Supplementary Figure 14**) or days to heading (**Supplementary Figure 15**) and grain iAs accumulation from the field experiments.

DISCUSSION

Inorganic As Reductions by AWD

Mitigation of As accumulation in rice is dependent on the severity of AWD cycles. Several studies have shown that the more severe the AWD, the greater the reduction in both total As (Hu et al., 2013; Linquist et al., 2015) and iAs in rice grain (Carrijo et al., 2019; Li et al., 2019). In 2013, the Safe-AWD with a target soil VWC of 35–40% was not severe enough to reduce iAs concentrations. In fact, in this study, iAs was the same or even increased for some TILs under the Safe-AWD in 2013 as compared to flood, whereas in 2014, the more severe AWD30 led to consistent reductions in grain iAs across all TILs. These results are similar to those reported by Carrijo et al. (2019). In our field study, it is likely that the soil did not become fully aerobic during the Safe-AWD of 2013 as the soil VWC did not drop sufficiently below saturation (saturated soil VWC in the field is slightly above 40%). Thus, microbial processes that oxidize As making it less bioavailable could not occur, allowing As to be present in the soil solution as the reduced arsenite form, which is easily taken up by rice (Ma et al., 2008; Norton et al., 2010; Zhao et al., 2010). In comparison, in both the field 2014 and the greenhouse study, the imposed AWD cycles were severe enough to make the soil fully aerobic, allowing for geochemical and microbial

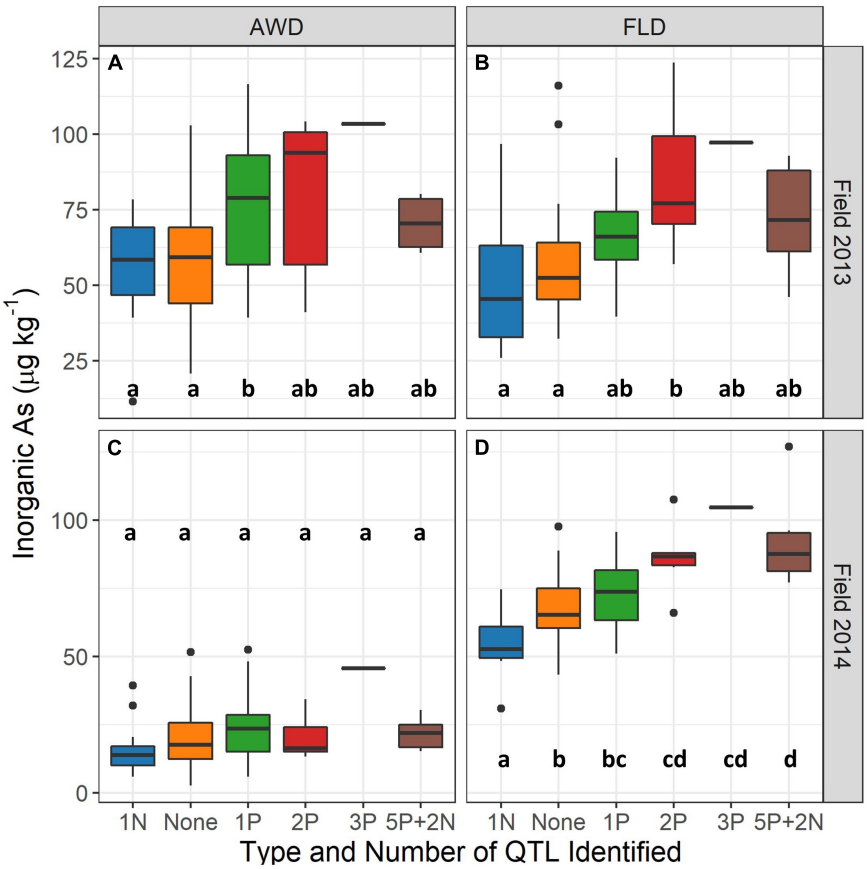


FIGURE 3 | Brown rice inorganic As concentrations (μg kg^{-1}) in field 2013 under alternate wetting and drying (AWD) **(A)** and flooded (FLD) **(B)** and 2014 AWD **(C)** and flood **(D)** irrigation management treatments by number of quantitative trait loci (QTLs) in eight TILs and two parents. Safe-AWD was used in 2013, and AWD30 was used in 2014. Only one biological replication of the genotype containing three positive iAs affecting QTLs was grown in 2013 and 2014; all other QTL groups have a minimum of six biological replicates. Letters indicate significant differences within each treatment and year ($p < 0.05$).

TABLE 2 | Genotypes selected for the greenhouse study including parents, Lemont and TeQing, and eight TILs.

Selected lines	Number and type of QTLs	Grain iAs phenotype	Allele at identified QTLs affecting grain inorganic arsenic content						
			C4_2481896*	C4_27292997*	C5_19872059*	C8_5186967†	C9_18034390†‡	C11_2659978*	C12_824609*
Lemont	None	Parent	L	L	L	L	L	L	L
TeQing	5P + 2N	Parent	**T**	**T**	**T**	**T**	**T**	**T**	**T**
634	3P	High	L	**T**	**T**	L	**T**	L	L
381.11	2P	High	L	**T**	L	**T**	L	L	L
604.11	2P	High	L	L	L	L	**T**	L	**T**
389	1P	High	L	L	L	L	**T**	L	L
455	1N	Low	**T**	L	L	L	L	L	L
552	1N	Low	L	L	L	L	L	**T**	L
596.11	None	Low	L	L	L	L	L	L	L
643	None	Low	L	L	L	L	L	L	L

*Datasets used to identify QTLs are denoted by symbols: †Flood 2013, ‡Safe-AWD 2013, *Flood 2014. The number and type of identified QTLs are shown for each line with the notation chromosome number, followed by position in bp (e.g., chromosome 8 position 5,186,967 bp is C8_5186967), with L and T representing Lemont or TeQing alleles. Letters P and N indicate the number of TeQing QTL introgressions that are either positively (P) or negatively (N) affecting grain iAs. Letters within a QTL column indicate the presence of the TeQing introgressed allele (T) or the Lemont recurrent parent allele (L). Red and blue highlights indicate the TeQing allele increases or decreases grain inorganic arsenic, respectively. No highlight indicates Lemont was the segment present in the identified QTL region.*

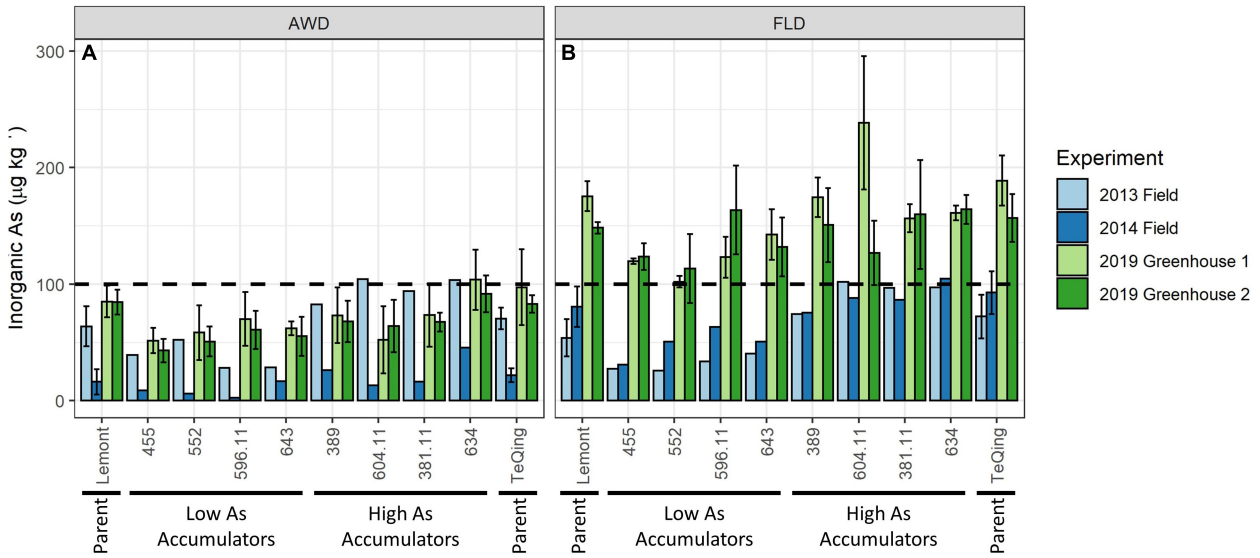


FIGURE 4 | Comparison of brown rice inorganic arsenic concentrations for eight TILs and their parents. Genotypes were grown in the field in 2013 and 2014 and in two greenhouse studies (Greenhouse 1 and Greenhouse 2) in 2019 under alternate wetting and drying (AWD) **(A)** and flooded **(B)** irrigation management practices. Error bars represent standard deviation of biological replicates (n = 4 in 2019 for each greenhouse, and n = 6 in 2013 and 2014 for parents only). Dotted line represents FDA limit of 100 µg kg^{-1} for inorganic arsenic in rice-based infant food.

TABLE 3 | Percent change in brown rice inorganic arsenic of eight TILs and their parents from AWD to flood treatments in studies conducted in the field and greenhouse.

Type	Name	Observed grain iAs phenotype	Percent change in grain inorganic As between AWD to flood treatments				
			Field 2013	Field 2014	Greenhouse 1	Greenhouse 2	Average of greenhouse studies
Parent	Lemont	Parent	**+ 18**	**−80***	**−51.5**	**−42.9**	**−47.2**
TIL	455	Low	*+ 43*	*−71.2*	**−56.9**	**−65.3**	**−61.1**
TIL	552	Low	*+ 101*	*−88.2*	**−42.7**	**−55.2**	**−48.9**
TIL	596.11	Low	*−16.7*	*−95.9*	**−43.0**	**−62.9**	**−53.0**
TIL	643	Low	*−29.6*	*−67.4*	**−56.5**	**−58.1**	**−57.3**
TIL	389	High	*+ 10.9*	*−65.4*	**−58.0**	**−54.8**	**−56.4**
TIL	604.11	High	*+ 2.3*	*−85.0*	**−78.1**	**−49.5**	**−63.8**
TIL	381.11	High	*−3*	*−81.4*	**−53.1**	**−57.8**	**−55.4**
TIL	634	High	*+ 6.5*	*−56.5*	**−35.5**	**−44.2**	**−39.9**
Parent	TeQing	Parent	**−2.3**	**−76.6***	**−48.5**	**−47.0**	**−47.7**

Percent change values in bold font indicate significant differences in mean inorganic As levels between flood and AWD treatments based on Welch t-test ($p < 0.05$). Italics indicate no test of significance was performed because of lack of replication. Biological replicates were used in calculations, n = 4 in 2019 for each greenhouse, n = 6 in 2013 and 2014 for parents Lemont and TeQing, and n = 1 for the TILs in 2013 and 2014). Asterisk (*) indicates significant difference based on Welch t-test ($p < 0.05$) for grain inorganic As concentrations between field 2014 and average greenhouse 2019 results.

processes to oxidize As, resulting in sequestration into iron and manganese oxides (Takahashi et al., 2004; Zecchin et al., 2017; Maguffin et al., 2020).

The AWD implemented in the greenhouse pots was more severe (20% VWC) and controlled than that realized in the field (30–40% VWC). Additionally, the measurement depth for soil VWC in the greenhouse (10 cm) as compared to the field (5 cm) likely compounded the difference in severity of the AWD cycles experienced by the plants in the greenhouse vs. those in the field. In fact, Maguffin et al. (2020) demonstrated that even when severe AWD cycles were implemented in field soil at the Stuttgart, Arkansas, location and low soil VWC was achieved at soil depths of 10 cm, there was only a small decrease in soil moisture at the 25 cm depth. Because a shallower depth was used for VWC measurements in the field, it was assumed that the AWD cycles would be even less severe in the field compared to those in the greenhouse. However, although only two cycles of AWD20 were used in the greenhouse, the net reductions in grain iAs were significant but lower in magnitude than those observed with the four-cycle AWD30 used in the field (mean reduction under AWD20 in the greenhouse was 53% as compared to 77% for AWD30 in the field). When averaged over the two greenhouse experiments, the two-cycle AWD20 effectively reduced iAs across the 10 genotypes with a minimum grain iAs reduction of 40%

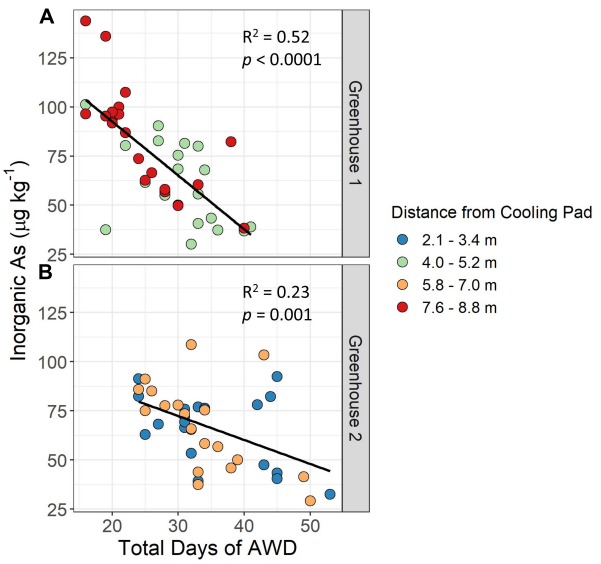


FIGURE 5 | Impact of days under AWD on grain inorganic As levels. Brown rice inorganic As accumulation in response to the total number of days to achieve the target soil volumetric water content (VWC) using alternate wetting and drying (AWD) cycles (e.g., sum of the total days under AWD for cycles 1 and 2) and distance of experimental units from the greenhouse cooling pad. In greenhouse 1 **(A)** the AWD tables were farther from the cooling pad than in greenhouse 2 **(B)**.

from flood to AWD (**Table 3**). The consistent reduction in grain iAs across the years regardless of severity in the field (AWD30) or in the greenhouse (AWD20) is evident; however, future studies implementing AWD in the field will need to monitor VWC levels at a greater soil depth to be comparable to the AWD treatment achieved in this greenhouse study.

AWD severity is the driving factor reducing grain As; however, the timing of AWD cycles is an important factor for yield and may also play a role in grain As reduction. A handful of studies have examined how the number and timing of AWD cycles impact total and iAs reduction. A study by Linquist et al. (2015) found that one AWD cycle followed by sustained flooding after plants reached the reproductive stage resulted in higher total As concentrations as compared to those that underwent repeated AWD cycles of the same severity (Linquist et al., 2015). This suggests the success of AWD in reducing grain total As accumulation is tied to both the number and, importantly, the timing of AWD cycles. However, reductions in grain total As due to AWD do not necessarily result in a concomitant reduction in grain iAs. Indeed, several studies have found low severity AWD can reduce total As by reducing the organic As fraction, while the inorganic fraction remains unchanged, whereas a more severe AWD or aerobic growth can reduce both (Xu et al., 2008; Carrijo et al., 2019; Li et al., 2019). Carrijo et al. (2019) found that severe soil drying late in the growing season (either at booting or heading stage) was needed to decrease iAs concentration in rice grain compared to flooded treatments (Carrijo et al., 2019). In our greenhouse study, the first AWD cycle began prior to panicle initiation, and the second AWD cycle was completed around the onset of heading stage; all cycles were completed before grain fill. In 2014, the AWD cycles began earlier in the plants' development and were ongoing during booting stage, but the majority of plants were heading after the fourth AWD cycle. Thus, optimal timing for completion of AWD cycles appears to be before plants reach the grain fill stage. In our study, we cannot decouple the severity of AWD from the timing of AWD; future studies should focus on imposing moderate to severe AWD cycles before plants reach the grain fill stage to confirm the trend observed here.

Interestingly, we found a significant correlation ($p < 0.0001$ for greenhouse 1 and $p = 0.001$ for greenhouse 2) between the

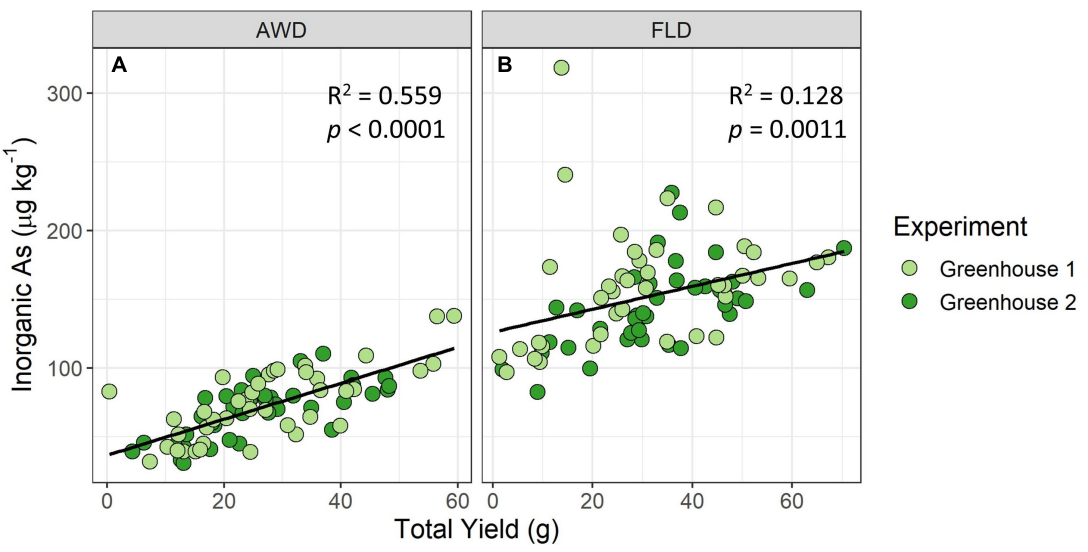


FIGURE 6 | Brown rice inorganic As accumulation vs. total grain yield in greenhouse experiment under AWD20 (AWD) **(A)** and flood (FLD) **(B)** treatments. A significant positive correlation is seen between total grain yield and grain inorganic As concentrations in the greenhouses.

number of days under AWD and grain iAs accumulation, even though all plants were subjected to the same AWD severity. This relationship was stronger in greenhouse 1 where the AWD was faster (R^2 = 0.52) compared to greenhouse 2 (R^2 = 0.23) where the AWD was slower, likely in part because the AWD tables in greenhouse 1 were farther from the cooling pad than in greenhouse 2 (**Supplementary Figure 8**), leading to shorter drying cycles. The correlation between days under AWD and iAs accumulation suggests that the duration of the AWD cycle could be as important as the severity of drying. It is possible that a less severe AWD held for a longer period may reduce grain iAs concentrations more than a relatively fast AWD cycle targeting the same water stress level. Under drying conditions, as the soil VWC drops, the soil redox potential concomitantly begins to increase, creating favorable conditions for iAs to be oxidized and adsorbed to iron and manganese oxides (Maguffin et al., 2020). We measured redox potential in a subset of pots in the greenhouses and confirmed that those under flooded conditions had low redox potential (approximately -400 mV), and as they dried, their redox potential increased rapidly (up to approximately +375 mV) (Fernández-Baca et al., in preparation). This indicates conditions in the pots became favorable for iAs oxidation, likely leading to iAs adsorption, reducing its bioavailability. Previous studies have shown that rice grown under aerobic conditions has lower grain iAs concentrations (Xu et al., 2008). However, aerobic growth can negatively impact yield, whereas multiple studies have shown that AWD can reduce grain iAs without decreasing yield (Das et al., 2016; Honma et al., 2016; Yang et al., 2019), and there is evidence it may even increase yield (Norton et al., 2017). Indeed, Honma et al. (2016) found that increasing the number of AWD drying days from 1 to 5 days significantly reduced grain iAs by 60% with no reduction in yield. Similarly, we found increased days under AWD reduced grain iAs (**Figure 5**), and only one genotype (TIL381.11) had a significant reduction in yield under AWD (**Supplementary Table 2**).

Genotype and Environmental Impact on iAs Accumulation

A number of studies have shown that rice genotypic differences influence grain As accumulation and speciation (Williams et al., 2005; Zavala et al., 2008; Jia et al., 2014). Williams et al. (2005) measured total As, organic As, and iAs in 36 rice varieties grown in pots and found that the proportion of iAs in the grain is significantly dependent on the rice genotype (Williams et al., 2005). Our study focused on iAs because of its higher toxicity to humans compared to organic As (Schoof et al., 1999; International Agency for Research on Cancer [IARC], 2004) and evaluated brown rice samples where iAs is concentrated in the bran (Meharg et al., 2008; Sun et al., 2008). We found genotypic differences in grain iAs contents among a large set of CSSLs, which ranged from less than 10 up to 46 $\mu g\ kg^{-1}$ under AWD30 and 28 up to 104 $\mu g\ kg^{-1}$ under Safe-AWD (**Supplementary Figure 2**). Concentrations for flood treatment in the field study ranged from 31 to 127 $\mu g\ kg^{-1}$ in 2013 and 26 to 124 $\mu g\ kg^{-1}$ in 2014 (**Supplementary Figure 2**). Within the CSSL mapping population, some TIL offspring displayed more extreme (i.e., higher or lower) iAs grain phenotypes than either parent, regardless of treatment (**Supplementary Figure 2**). This is characteristic of transgressive segregation in which offspring display a phenotype outside of the parental range. Indeed, transgressive phenotypes are more likely to occur when two parents have a wider genetic diversity as in our study (de los Reyes, 2019). In our greenhouse study, the transgressive phenotype was most apparent when comparing the low iAs accumulator TIL455 (mean grain iAs concentrations of 27.2 $\mu g\ kg^{-1}$ under AWD and 34.1 $\mu g\ kg^{-1}$ under flood) to the low iAs accumulator parent, Lemont (mean grain iAs levels of 34.7 $\mu g\ kg^{-1}$ under AWD and 46.4 $\mu g\ kg^{-1}$ under flood). Genotypic differences were also observed within the TIL population, with TIL455 and TIL634 displaying a mean difference of 40 $\mu g\ kg^{-1}$ under flood and 50 $\mu g\ kg^{-1}$ under AWD, respectively.

The 10 genotypes, two parents and eight TILs, grown across all experiments showed consistent patterns (i.e., high accumulators had high grain iAs concentrations, and low accumulators had low grain iAs concentrations) across both field years and greenhouses under flood and AWD conditions (**Figure 4**). However, the magnitude of grain iAs accumulation differed notably between the field and greenhouse studies. This could be a result of differences in biomass traits between field and greenhouse-grown plants (Barnaby et al., unpublished). We found mature panicle and tiller numbers, proxies for total plant biomass, were both higher in the field compared to the greenhouse (**Supplementary Figures 12, 13**, respectively).

Root biomass, physiology, and aeration capacity are also known to impact total and iAs accumulation in rice grain (Wu et al., 2011, 2012; Jia et al., 2014). Jia et al. (2014) compared As uptake in two rice cultivars with differing soil oxygenation rates. They found that the genotype with greater oxygenation capacity had lower As uptake overall compared to the genotype with lower oxygenation capacity likely because the higher oxygenation rate allowed for aerobic microbial processes to oxidize As, making it unavailable for rice uptake (Jia et al., 2014). Although we did not measure root biomass in this study, it has been shown that root biomass and oxygenation rates differ by genotype (Wu et al., 2012; Barnaby et al., 2019) and environment (i.e., greenhouse vs. field) (Barnaby et al., unpublished), and it is likely that similar genetic and environmental differences may have impacted grain iAs differences observed between field and greenhouse-grown rice.

Interestingly, we saw a strong, positive correlation between yield and grain iAs concentrations in the greenhouse study under AWD (**Figure 6**). Norton et al. (2009) found a similar positive correlation between yield and grain total As concentrations for rice grown at two field sites (Norton et al., 2009). However, our field results showed no clear relationship between yield and grain iAs concentrations (**Supplementary Figure 12**). The controlled greenhouse experiment, where each pot was monitored to precisely meet the AWD20 target, contrasted with field conditions, where heterogeneity across a large field can result in plants experiencing very different soil VWCs under AWD and in turn impacting both yield and grain iAs. Thus, although the greenhouse study is not necessarily indicative of what may happen in the field, it did underscore the relationship between grain yield and iAs concentrations previously identified

by Norton et al., which was particularly strong under AWD conditions in this study.

QTL Impacts on Grain iAs Content

We identified seven QTLs in the TIL mapping population using the grain iAs data from the field 2013 and 2014 flood treatments (**Figure 1**). One of these QTLs (C9_18034390) was also identified in the 2013 Safe-AWD data, but none were identified from the 2014 AWD30 experiment. However, for the Safe-AWD in 2013, the soil was dried to a target VWC between 35 and 40%, which is only slightly below field saturation; thus, it is not surprising that the QTL identified under this treatment was also found in the flooded field studies. Similar to the QTL identification in our study, Zhang et al. (2014) found more significant QTLs associated with grain total As levels under flooded conditions than under non-flooded conditions (Zhang et al., 2014). This suggests the identified QTLs lack stability across years, which is not uncommon as previous studies have found QTLs can be unstable for several reasons including variations in flowering time or yield by year (Norton et al., 2014, 2019). However, one QTL (C9_18034390) was found in both flood and Safe-AWD treatments, which suggests this QTL is more stable. It has been suggested that even small-effect loci that are environmentally variable may be used to breed low iAs lines through genomic selection as opposed to traditional marker assisted selection (Norton et al., 2019). Thus, identifying putative iAs affecting QTLs regardless of the size of their effect has the potential to inform future breeding efforts.

Wang et al. (2020) found that several QTLs for total As in the grain were associated with those controlling As in the straw and that there was a positive relationship with straw and grain total As contents. Although no straw iAs measurements were made in this study, this may suggest that limiting uptake of As in the vegetative portion of the plant may be one means of decreasing grain accumulation. However, identification of QTLs related to sequestration of As in vegetative tissue may be another means of increasing the effectiveness of breeding efforts (Heuschele et al., 2017).

The TILs selected for the greenhouse study represent genotypes with low to high levels of grain iAs accumulation and contained differing numbers and combinations of QTLs. Although the identified QTLs did not overlap between the 2013 flood and 2014 flood datasets, we were still able to confirm that TILs harboring these QTLs, regardless of the treatment or year they were identified in, resulted in differences in grain iAs levels in the greenhouse study. These results support our finding from the field data that the identified QTLs are indeed affecting grain iAs.

QTLs affecting grain total As accumulation have previously been identified in the TIL mapping population and other cultivars; however, to the authors' knowledge, no previous study has identified QTLs affecting the more toxic iAs in rice grain (Norton et al., 2014; Zhang et al., 2014; Pinson et al., 2015). The total As QTLs previously identified have some overlap with the iAs QTLs identified in this study. Thus, we further explored these regions for genes that may be responsible for iAs uptake and incorporation. We found five candidate genes within the identified QTL regions (**Figure 1**). Candidate genes are genes that are suspected of being causal based on their annotated function; however, the QTL regions are large and contain many other potentially causal genes. *OsABCG22* (*LOC_Os09g29660*), an ATP-binding cassette (ABC) transporter gene, was identified in the region of QTL C9_18034390. This gene belongs to the ABCG-WBC cluster, which has been shown to be upregulated by submergence (i.e., flooding) and high concentrations of As (Nguyen et al., 2014). Genes involved in panicle and seed development were colocalized with grain iAs-affecting QTLs on chromosomes 4 and 11, respectively. The *OsPLL4* gene (*LOC_Os04g05050*), a pectate lyase-like gene colocated with QTL C4_2481896, is highly expressed during panicle development (Zheng et al., 2018), whereas *OsOFP18* (*LOC_Os11g05770*), colocated with QTL C11_2659978, is expressed both during seed development and during the young root stage (Yu et al., 2015) and thus could be involved in both the uptake and storage of As. Two genes related to stress tolerance were also found. The germin-like protein (GLP) gene *OsGLP8-1* (*LOC_Os08g08920*) was identified within the QTL region of C8_5186967; GLPs have been shown to colocate with other QTLs associated with drought and blast resistance (Mahmood et al., 2007; Davidson et al., 2010). *OsWRKY64* (*LOC_Os12g02450*) has been found to be upregulated under conditions of iron excess/toxicity and is thought to regulate root elongation as well as shoot growth under stress (Berri et al., 2009; Viana et al., 2017). The colocalization of transporter genes, plant development genes, and stress response genes with the identified iAs-affecting QTLs suggests that grain iAs accumulation is a result of many mechanisms spread across the rice genome.

Across both field and greenhouse experiments, grain iAs accumulation was impacted by the presence or absence of specific QTLs with positive or negative additive effects and specific QTL combinations. The two TILs selected for the greenhouse study that contained no QTLs, TIL596.11 and TIL643, did not differ in grain iAs concentrations from Lemont, which likewise lacked any of the identified iAs-affecting QTLs. This indicates that any additional background TeQing introgressions in the two TILs did not impact grain iAs accumulation. Two QTLs from TeQing introgressions, C11_2659978 and C4_2481896, result in low grain iAs phenotypes, and the other five QTLs result in high iAs phenotypes. Genotypes that contained C9_18034390 had higher mean iAs concentrations as compared to those without (**Supplementary Figure 7**). Greater than 30% of the highest iAs accumulating group contained C9_18034390 across the field study years and treatments (**Figure 2**). The QTL combination affecting grain iAs concentrations is most evident when comparing Lemont to TIL455 and TIL552. TIL455 and TIL552 each possess one of the two QTLs that negatively affect grain iAs (C11_2659978 and C4_2481896, respectively), resulting in lower mean grain iAs concentration under both flood and AWD treatments in the greenhouse study as compared to Lemont. The other six TILs possessing QTLs positively affecting iAs levels had mean grain iAs concentrations greater than either TIL455 or TIL552 regardless of irrigation treatment.

We also observed a cumulative effect on grain iAs concentrations regardless of the specific QTL or QTL

combination, particularly under flood conditions (**Figure 3**). This suggests individual QTL effects on iAs grain concentrations may be small compared to the additive effect of containing a combination of several QTLs. Additionally, TILs in the lowest 0–25% of grain iAs concentrations contained fewer of the positive iAs regulating QTLs overall and were more likely to have the negative iAs regulating QTL C11_2659978 and C4_2481896 (**Figure 2**). In contrast, the percent of genotypes containing a positive iAs regulating QTL in the highest iAs group (75–100%) was greater when compared to the lower iAs groups (<75%). Thus, although we did observe that specific QTLs affect grain iAs accumulation, our results indicate that the cumulative impact of several QTL introgressions associated with an increase in grain iAs can outweigh the impact of any individual QTL.

In contrast to previous studies that have primarily compared varieties that are genetically diverse, our study used a CSSL mapping population generated by backcrossing an F1 hybrid, TeQing, with the recurrent parent, Lemont, leading to targeted TeQing introgressions across the population. The common genetic background of the CSSL population allowed us to identify introgressions on six chromosomes that impact grain iAs concentrations. The fact that QTLs were identified across several chromosomes in this CSSL population indicates that genetic control of this trait is not by one or a few genes but is more widely dispersed throughout the rice genome. Indeed, these results suggest that multiple small-effect QTLs contribute to grain As accumulation, making them difficult to uncover particularly in the case of environmental variability. However, although identifying more iAs affecting QTLs could be beneficial to inform future selective breeding for grain iAs mitigation, we have identified seven QTLs in this CSSL population that can be used as selectable markers to produce new cultivars with low grain iAs content.

Both TIL552 and TIL455 each contained one of the negative iAs regulating QTLs (C11_2659978 and C4_2481896, respectively), resulting in consistently lower grain iAs concentrations when introgressed into Lemont, which has a moderately low iAs grain phenotype. Additionally, neither TIL had significantly reduced yield under AWD20. However, yields for TIL455 were higher under AWD (greenhouse mean of 35 g) compared to TIL 552 (greenhouse mean of 13 g), indicating TIL455 may hold promise for future studies focused on breeding low iAs varieties that are robust to severe AWD treatments.

CONCLUSION

Grain iAs accumulation is dependent on both irrigation management practices and genotypic differences. While a severe AWD will reliably reduce grain iAs accumulation, incorporation of selected QTLs can ensure genetic mitigation of iAs, which is particularly important under field production conditions where soil moisture conditions may vary because of management systems or weather conditions. Ultimately, coupling AWD, or other water-saving irrigation management practices, with the deployment of low iAs accumulating cultivars is key to reducing rice iAs exposure while maintaining crop productivity.

DATA AVAILABILITY STATEMENT

The original contributions presented in the study are included in the article/**Supplementary Material**, further inquiries can be directed to the corresponding author/s.

AUTHOR CONTRIBUTIONS

CF-B, JB, and AM conceived and designed the experiments. CF-B and JB performed the experiments. CF-B, JB, JE, and AM analyzed the data. JB, AM, EC, and VR provided the financial and technical assistance. CF-B wrote the initial manuscript. CF-B, AM, JE, EC, VR, and JB approved the manuscript for publication. All authors contributed to the article and approved the submitted version.

ACKNOWLEDGMENTS

This research used facilities and assistance provided by the USDA Agricultural Research Service Dale Bumpers National Rice Research Center. We acknowledge Dr. Neal Teaster, Dr. John Bernhardt, Laduska Sells, Tiffany Sookaserm, Nick Murphy, Jeremy Kite, Kesha Wicklund, and Angela Hunter for conducting the field experiments and collecting the agronomic data, Lorie Bernhardt for compiling weather data and Dr. Carrie Green, Darryl Baxam, Melisa Feng, and Juanita Carballeira-Martínez for their technical assistance with inorganic arsenic measurements, and Dr. Shannon Pinson for intellectual feedback.

SUPPLEMENTARY MATERIAL

The Supplementary Material for this article can be found online at: https://www.frontiersin.org/articles/10.3389/fpls.2020.612054/full#supplementary-material

REFERENCES

Banerjee, M., Banerjee, N., Bhattacharjee, P., Mondal, D., Lythgoe, P. R., Martínez, M., et al. (2013). High arsenic in rice is associated with elevated genotoxic effects in humans. *Sci. Rep.* 3:2195. doi: 10.1038/srep02195

Barnaby, J. Y., Pinson, S. R. M., Chun, J., and Bui, L. T. (2019). Covariation among root biomass, shoot biomass, and tiller number in three rice populations. *Crop Sci.* 59, 1516–1530. doi: 10.2135/cropsci2018.09.0595

Berri, S., Abbruscato, P., Faivre-Rampant, O., Brasileiro, A. C. M., Fumasoni, I., Satoh, K., et al. (2009). Characterization of WRKY co-regulatory networks in rice and *Arabidopsis*. *BMC Plant Biol.* 9:120. doi: 10.1186/1471-2229-9-120

Carrijo, D. R., Akbar, N., Reis, A. F. B., Li, C., Gaudin, A. C. M., Parikh, S. J., et al. (2018). Impacts of variable soil drying in alternate wetting and drying rice systems on yields, grain arsenic concentration and soil moisture dynamics. *Field Crops Res.* 222, 101–110. doi: 10.1016/J.FCR.2018.02.026

Carrijo, D. R., Li, C., Parikh, S. J., and Linquist, B. A. (2019). Irrigation management for arsenic mitigation in rice grain: timing and severity of a single soil drying. *Sci. Total Environ.* 649, 300–307. doi: 10.1016/J.SCITOTENV.2018.08.216

Carrijo, D. R., Lundy, M. E., and Linquist, B. A. (2017). Rice yields and water use under alternate wetting and drying irrigation: a meta-analysis. *Field Crops Res.* 203, 173–180. doi: 10.1016/j.fcr.2016.12.002

Chaney, R. L., Green, C. E., and Lehotay, S. J. (2018). Inter-laboratory validation of an inexpensive streamlined method to measure inorganic arsenic in rice grain. *Anal. Bioanal. Chem.* 410, 5703–5710. doi: 10.1007/s00216-018-1075-x

Codex Alimentarius, (2017). *General Standard for Contaminants and Toxins in Food and Feed*. Rome: Codex Alimentarius.

Das, S., Chou, M.-L., Jean, J.-S., Liu, C.-C., and Yang, H.-J. (2016). Water management impacts on arsenic behavior and rhizosphere bacterial communities and activities in a rice agro-ecosystem. *Sci. Total Environ.* 542, 642–652. doi: 10.1016/J.SCITOTENV.2015.10.122

Dasgupta, T., Hossain, S. A., Meharg, A. A., and Price, A. H. (2004). An arsenate tolerance gene on chromosome 6 of rice. *New Phytol.* 163, 45–49. doi: 10.1111/j.1469-8137.2004.01109.x

Davidson, R. M., Manosalva, P. M., Snelling, J., Bruce, M., Leung, H., and Leach, J. E. (2010). Rice germin-like proteins: allelic diversity and relationships to early stress responses. *Rice* 3, 43–55. doi: 10.1007/s12284-010-9038-7

de los Reyes, B. G. (2019). Genomic and epigenomic bases of transgressive segregation – New breeding paradigm for novel plant phenotypes. *Plant Sci.* 288:110213. doi: 10.1016/j.plantsci.2019.110213

Elshire, R. J., Glaubitz, J. C., Sun, Q., Poland, J. A., Kawamoto, K., Buckler, E. S., et al. (2011). A robust, simple genotyping-by-sequencing (GBS) approach for high diversity species. *PLoS One* 6:e19379. doi: 10.1371/journal.pone.0019379

Glaubitz, J. C., Casstevens, T. M., Lu, F., Harriman, J., Elshire, R. J., Sun, Q., et al. (2014). TASSEL-GBS: a high capacity genotyping by sequencing analysis pipeline. *PLoS One* 9:e90346. doi: 10.1371/journal.pone.0090346

Gray, P. J., Mindak, W. R., and Cheng, J. (2012). *Elemental Analysis Manual*. Silver Spring, MD: FDA.

Heuschele, D. J., Pinson, S. R., and Smith, A. P. (2017). Metabolic responses to arsenite in rice seedlings that differed in grain arsenic concentration. *Crop Sci.* 57, 2671–2687. doi: 10.2135/cropsci2016.06.0493

Honma, T., Ohba, H., Kaneko-Kadokura, A., Makino, T., Nakamura, K., and Katou, H. (2016). Optimal Soil Eh, pH, and Water Management for Simultaneously Minimizing Arsenic and Cadmium Concentrations in Rice Grains. *Environ. Sci. Technol.* 50, 4178–4185. doi: 10.1021/acs.est.5b05424

Hu, P., Li, Z., Yuan, C., Ouyang, Y., Zhou, L., Huang, J., et al. (2013). Effect of water management on cadmium and arsenic accumulation by rice (Oryza sativa L.) with different metal accumulation capacities. *J. Soils Sediments* 13, 916–924. doi: 10.1007/s11368-013-0658-6

International Agency for Research on Cancer [IARC], (2004). *Some Drinking-water Disinfectants and Contaminants, including Arsenic - NCBI Bookshelf*. Geneva: WHO.

Jia, Y., Huang, H., Chen, Z., and Zhu, Y.-G. (2014). Arsenic uptake by rice is influenced by microbe-mediated arsenic redox changes in the rhizosphere. *Environ. Sci. Technol.* 48, 1001–1007. doi: 10.1021/es403877s

Kile, M. L., Houseman, E. A., Breton, C. V., Smith, T., Quamruzzaman, Q., Rahman, M., et al. (2007). Dietary arsenic exposure in Bangladesh. *Environ. Health Perspect.* 115, 889–893. doi: 10.1289/ehp.9462

Kumarathilaka, P., Seneweera, S., Meharg, A., and Bundschuh, J. (2018). Arsenic speciation dynamics in paddy rice soil-water environment: sources, physico-chemical, and biological factors - a review. *Water Res.* 140, 403–414. doi: 10.1016/j.watres.2018.04.034

Kuramata, M., Abe, T., Kawasaki, A., Ebana, K., Shibaya, T., Yano, M., et al. (2013). Genetic diversity of arsenic accumulation in rice and QTL analysis of methylated arsenic in rice grains. *Rice* 6:3. doi: 10.1186/1939-8433-6-3

Li, C., Carrijo, D. R., Nakayama, Y., Linquist, B. A., Green, P. G., and Parikh, S. J. (2019). Impact of alternate wetting and drying irrigation on arsenic uptake and speciation in flooded rice systems. *Agricul. Ecosystems Environ.* 272, 188–198. doi: 10.1016/j.agee.2018.11.009

Linquist, B. A., Anders, M. M., Adviento-Borbe, M. A. A., Chaney, R. L., Nalley, L. L., da Rosa, E. F. F., et al. (2015). Reducing greenhouse gas emissions, water use, and grain arsenic levels in rice systems. *Global Change Biol.* 21, 407–417. doi: 10.1111/gcb.12701

Ma, J. F., Yamaji, N., Mitani, N., Xu, X.-Y., Su, Y.-H., McGrath, S. P., et al. (2008). Transporters of arsenite in rice and their role in arsenic accumulation in rice grain. *Proc. Natl. Acad. Sci. U S A.* 105, 9931–9935. doi: 10.1073/PNAS.0802361105

Maguffin, S. C., Abu-Ali, L., Tappero, R. V., Pena, J., Rohila, J. S., McClung, A. M., et al. (2020). Influence of manganese abundances on iron and arsenic solubility in rice paddy soils. *Geochimica et Cosmochimica Acta* 276, 50–69. doi: 10.1016/j.gca.2020.02.012

Mahmood, T., Zeeshan Hyder, M., and Saqlan Naqvi, S. M. (2007). Cloning and sequence analysis of germin-like protein gene 2 promoter from *Oryza sativa* L. ssp. indica. *DNA Sequence* 18, 26–32. doi: 10.1080/10425170600986688

Meharg, A. A., Lombi, E., Williams, P. N., Scheckel, K. G., Feldmann, J., Raab, A., et al. (2008). Speciation and localization of arsenic in white and brown rice grains. *Environ. Sci. Technol.* 42, 1051–1057. doi: 10.1021/es702212p

Meharg, A. A., Williams, P. N., Adomako, E., Lawgali, Y. Y., Deacon, C., Villada, A., et al. (2009). Geographical variation in total and inorganic arsenic content of polished (white) rice. *Environ. Sci. Technol.* 43, 1612–1617. doi: 10.1021/es802612a

Meng, L., Li, H., Zhang, L., and Wang, J. (2015). QTL IciMapping: integrated software for genetic linkage map construction and quantitative trait locus mapping in biparental populations. *Crop J.* 3, 269–283. doi: 10.1016/j.cj.2015.01.001

Murugaiyan, V., Ali, J., Mahender, A., Aslam, U. M., Jewel, Z. A., Pang, Y., et al. (2019). Mapping of genomic regions associated with arsenic toxicity stress in a backcross breeding populations of rice (*Oryza sativa* L.). *Rice (N. Y)* 12:61. doi: 10.1186/s12284-019-0321-y

Musil, S., Pétursdóttir, ÁH., Raab, A., Gunnlaugsdóttir, H., Krupp, E., and Feldmann, J. (2014). Speciation without chromatography using selective hydride generation: inorganic arsenic in rice and samples of marine origin. *Anal. Chem.* 86, 993–999. doi: 10.1021/ac403438c

Nguyen, V. N. T., Moon, S., and Jung, K. H. (2014). Genome-wide expression analysis of rice ABC transporter family across spatio-temporal samples and in response to abiotic stresses. *J. Plant Physiol.* 171, 1276–1288. doi: 10.1016/j.jplph.2014.05.006

Norton, G. J., Deacon, C. M., Xiong, L., Huang, S., Meharg, A. A., and Price, A. H. (2010). Genetic mapping of the rice ionome in leaves and grain: identification of QTLs for 17 elements including arsenic, cadmium, iron and selenium. *Plant Soil* 329, 139–153. doi: 10.1007/s11104-009-0141-8

Norton, G. J., Douglas, A., Lahner, B., Yakubova, E., Guerinot, M. Lou, Pinson, S. R. M., et al. (2014). Genome wide association mapping of grain arsenic, copper, molybdenum and zinc in rice (*Oryza sativa* L.) grown at four international field sites. *PLoS One* 9:e89685. doi: 10.1371/journal.pone.0089685

Norton, G. J., Duan, G. L., Lei, M., Zhu, Y.-G., Meharg, A. A., and Price, A. H. (2012). Identification of quantitative trait loci for rice grain element composition on an arsenic impacted soil: influence of flowering time on genetic loci. *Annals Appl. Biol.* 161, 46–56. doi: 10.1111/j.1744-7348.2012.00549.x

Norton, G. J., Islam, M. R., Deacon, C. M., Zhao, F. J., Stroud, J. L., Mcgrath, S. P., et al. (2009). Identification of low inorganic and total grain arsenic rice cultivars from Bangladesh. *Environ. Sci. Technol.* 43, 6070–6075. doi: 10.1021/es901121j

Norton, G. J., Shafaei, M., Travis, A. J., Deacon, C. M., Danku, J., Pond, D., et al. (2017). Impact of alternate wetting and drying on rice physiology, grain production, and grain quality. *Field Crops Res.* 205, 1–13. doi: 10.1016/j.fcr.2017.01.016

Norton, G. J., Travis, A. J., Talukdar, P., Hossain, M., Islam, M. R., Douglas, A., et al. (2019). Genetic loci regulating arsenic content in rice grains when grown flooded or under alternative wetting and drying irrigation. *Rice* 12:54. doi: 10.1186/s12284-019-0307-9

Pétursdóttir, ÁH., Friedrich, N., Musil, S., Raab, A., Gunnlaugsdóttir, H., Krupp, E. M., et al. (2014). Hydride generation ICP-MS as a simple method for determination of inorganic arsenic in rice for routine biomonitoring. *Anal. Methods* 6, 5392–5396. doi: 10.1039/c4ay00423j

Pinson, S. R. M., Liu, G., Jia, M. H., Jia, Y., Fjellstrom, R. G., Sharma, A., et al. (2012). Registration of a rice gene-mapping population consisting of

'TeQing'-into-'Lemont' backcross introgression lines. *J. Plant Registrat.* 6, 128–135. doi: 10.3198/jpr2011.02.0066crmp

Pinson, S. R. M., Tarpley, L., Yan, W., Yeater, K., Lahner, B., Yakubova, E., et al. (2015). Worldwide genetic diversity for mineral element concentrations in rice grain. *Crop Sci.* 55, 294–311. doi: 10.2135/cropsci2013.10.0656

R Core Team, (2013). *R: A Language and Environment for Statistical Computing.* Vienna: R Foundation for Statistical Computing.

Schoof, R. A., Yost, L. J., Eickhoff, J., Crecelius, E. A., Cragin, D. W., Meacher, D. M., et al. (1999). A market basket survey of inorganic arsenic in food. *Food Chem. Toxicol.* 37, 839–846. doi: 10.1016/S0278-6915(99)00073-3

Somenahally, A. C., Hollister, E. B., Loeppert, R. H., Yan, W., and Gentry, T. J. (2011a). Microbial communities in rice rhizosphere altered by intermittent and continuous flooding in fields with long-term arsenic application. *Soil Biol. Biochem.* 43, 1220–1228. doi: 10.1016/J.SOILBIO.2011.02.011

Somenahally, A. C., Hollister, E. B., Yan, W., Gentry, T. J., and Loeppert, R. H. (2011b). Water management impacts on arsenic speciation and iron-reducing bacteria in contrasting rice-rhizosphere compartments. *Environ. Sci. Technol.* 45, 8328–8335. doi: 10.1021/es2012403

Sun, G. X., Williams, P. N., Carey, A. M., Zhu, Y. G., Deacon, C., Raab, A., et al. (2008). Inorganic arsenic in rice bran and its products are an order of magnitude higher than in bulk grain. *Environ. Sci. Technol.* 42, 7542–7546. doi: 10.1021/es801238p

Takahashi, Y., Minamikawa, R., Hattori, K. H., Kurishima, K., Kihou, N., and Yuita, K. (2004). Arsenic behavior in paddy fields during the cycle of flooded and non-flooded periods. *Environ. Sci. Technol.* 38, 1038–1044. doi: 10.1021/es034383n

Viana, V. E., Marini, N., Finatto, T., Ezquer, I., Busanello, C., dos Santos, R. S., et al. (2017). Iron excess in rice: from phenotypic changes to functional genomics of WRKY transcription factors. *Genet. Mol. Res.* 16:gmr16039694. doi: 10.4238/gmr16039694

Wang, C., Tang, Z., Zhuang, J. Y., Tang, Z., Huang, X. Y., and Zhao, F. J. (2020). Genetic mapping of ionomic quantitative trait loci in rice grain and straw reveals OsMOT1; 1 as the putative causal gene for a molybdenum QTL qMo8. *Mol. Genet. Genom.* 295, 391–407.

Williams, P. N., Islam, M. R., Adomako, E. E., Raab, A., Hossain, S. A., Zhu, Y. G., et al. (2006). Increase in rice grain arsenic for regions of Bangladesh irrigating paddies with elevated arsenic in groundwaters. *Environ. Sci. Technol.* 40, 4903–4908. doi: 10.1021/es060222i

Williams, P. N., Price, A. H., Raab, A., Hossain, S. A., Feldmann, J., and Meharg, A. A. (2005). Variation in arsenic speciation and concentration in paddy rice related to dietary exposure. *Environ. Sci. Technol.* 39, 5531–5540. doi: 10.1021/es0502324

Williams, P. N., Villada, A., Deacon, C., Raab, A., Figuerola, J., Green, A. J., et al. (2007). Greatly enhanced arsenic shoot assimilation in rice leads to elevated grain levels compared to wheat and barley. *Environ. Sci. Technol.* 41, 6854–6859. doi: 10.1021/es070627i

Wu, C., Ye, Z., Li, H., Wu, S., Deng, D., Zhu, Y., et al. (2012). Do radial oxygen loss and external aeration affect iron plaque formation and arsenic accumulation and speciation in rice? *J. Exp. Botany* 63, 2961–2970. doi: 10.1093/jxb/ers017

Wu, C., Ye, Z., Shu, W., Zhu, Y., and Wong, M. (2011). Arsenic accumulation and speciation in rice are affected by root aeration and variation of genotypes. *J. Exp. Botany* 62, 2889–2898. doi: 10.1093/jxb/erq462

Xu, X. Y., McGrath, S. P., Meharg, A. A., and Zhao, F. J. (2008). Growing rice aerobically markedly decreases arsenic accumulation. *Environ. Sci. Technol.* 42, 5574–5579. doi: 10.1021/es800324u

Yamaguchi, N., Nakamura, T., Dong, D., Takahashi, Y., Amachi, S., and Makino, T. (2011). Arsenic release from flooded paddy soils is influenced by speciation. Eh, pH, and iron dissolution. *Chemosphere* 83, 925–932. doi: 10.1016/j.chemosphere.2011.02.044

Yang, Y., Hu, H., Fu, Q., Zhu, J., and Huang, G. (2019). Water management of alternate wetting and drying reduces the accumulation of arsenic in brown rice - as dynamic study from rhizosphere soil to rice. *Ecotoxicol. Environ. Safety* 185:109711. doi: 10.1016/j.ecoenv.2019.109711

Yu, H., Jiang, W., Liu, Q., Zhang, H., Piao, M., Chen, Z., et al. (2015). Expression pattern and subcellular localization of the ovate protein family in rice. *PLoS One* 10:e0118966. doi: 10.1371/journal.pone.0118966

Zavala, Y. J., Gerads, R., Gürleyük, H., and Duxbury, J. M. (2008). Arsenic in rice: II. arsenic speciation in USA grain and implications for human health. *Environ. Sci. Technol.* 42, 3861–3866. doi: 10.1021/es702748q

Zecchin, S., Corsini, A., Martin, M., Romani, M., Beone, G. M., Zanchi, R., et al. (2017). Rhizospheric iron and arsenic bacteria affected by water regime: implications for metalloid uptake by rice. *Soil Biol. Biochem.* 106, 129–137. doi: 10.1016/J.SOILBIO.2016.12.021

Zhang, J., Zhu, Y.-G., Zeng, D.-L., Cheng, W.-D., Qian, Q., and Duan, G.-L. (2007). Mapping quantitative trait loci associated with arsenic accumulation in rice (*Oryza sativa*). *New Phytol.* 177, 350–355. doi: 10.1111/j.1469-8137.2007.02267.x

Zhang, M., Pinson, S. R. M., Tarpley, L., Huang, X. Y., Lahner, B., Yakubova, E., et al. (2014). Mapping and validation of quantitative trait loci associated with concentrations of 16 elements in unmilled rice grain. *Theoret. Appl. Genet.* 127, 137–165. doi: 10.1007/s00122-013-2207-5

Zhao, F.-J., McGrath, S. P., and Meharg, A. A. (2010). Arsenic as a food chain contaminant: mechanisms of plant uptake and metabolism and mitigation strategies. *Ann. Rev. Plant Biol.* 61, 535–559. doi: 10.1146/annurev-arplant-042809-112152

Zheng, Y., Yan, J., Wang, S., Xu, M., Huang, K., Chen, G., et al. (2018). Genome-wide identification of the pectate lyase-like (PLL) gene family and functional analysis of two PLL genes in rice. *Mol. Genet. Genom.* 293, 1317–1331. doi: 10.1007/s00438-018-1466-x

Conflict of Interest: The authors declare that the research was conducted in the absence of any commercial or financial relationships that could be construed as a potential conflict of interest.

Copyright © 2021 Fernández-Baca, McClung, Edwards, Codling, Reddy and Barnaby. This is an open-access article distributed under the terms of the Creative Commons Attribution License (CC BY). The use, distribution or reproduction in other forums is permitted, provided the original author(s) and the copyright owner(s) are credited and that the original publication in this journal is cited, in accordance with accepted academic practice. No use, distribution or reproduction is permitted which does not comply with these terms.

frontiers in Plant Science

ORIGINAL RESEARCH
published: 03 February 2021
doi: 10.3389/fpls.2021.571072

Drought-Induced Root Pressure in *Sorghum bicolor*

Sarah Tepler Drobnitch[1], Louise H. Comas[2], Nora Flynn[2], Jorge Ibarra Caballero[3], Ryan W. Barton[2], Joshua Wenz[2], Taylor Person[3], Julie Bushey[2], Courtney E. Jahn[3] and Sean M. Gleason[2]*

[1] Department of Soil and Crop Sciences, Colorado State University, Fort Collins, CO, United States, [2] Water Management Research Unit, Agricultural Research Service, USDA, Ft. Collins, CO, United States, [3] Department of Agricultural Biology, Colorado State University, Fort Collins, CO, United States

Root pressure, also manifested as profusive sap flowing from cut stems, is a phenomenon in some species that has perplexed biologists for much of the last century. It is associated with increased crop production under drought, but its function and regulation remain largely unknown. In this study, we investigated the initiation, mechanisms, and possible adaptive function of root pressure in six genotypes of *Sorghum bicolor* during a drought experiment in the greenhouse. We observed that root pressure was induced in plants exposed to drought followed by re-watering but possibly inhibited by 100% re-watering in some genotypes. We found that root pressure in drought stressed and re-watered plants was associated with greater ratio of fine: coarse root length and shoot biomass production, indicating a possible role of root allocation in creating root pressure and adaptive benefit of root pressure for shoot biomass production. Using RNA-Seq, we identified gene transcripts that were up- and down-regulated in plants with root pressure expression, focusing on genes for aquaporins, membrane transporters, and ATPases that could regulate inter- and intra-cellular transport of water and ions to generate positive xylem pressure in root tissue.

Keywords: water relations, xylem transport, root pressure, RNA-Seq, agriculture, transporter, aquaporin

OPEN ACCESS

Edited by:
Felipe Klein Ricachenevsky, Federal University of Rio Grande, Brazil

Reviewed by:
Raju Bheemanahalli Rangappa, Mississippi State University, United States
Mozhgan Sepehri, Shiraz University, Iran

****Correspondence:***
Sarah Tepler Drobnitch
s.k.tepler@gmail.com

Specialty section:
This article was submitted to Plant Abiotic Stress, a section of the journal Frontiers in Plant Science

Received: *09 June 2020*
Accepted: *08 January 2021*
Published: *03 February 2021*

Citation:
Drobnitch ST, Comas LH, Flynn N, Ibarra Caballero J, Barton RW, Wenz J, Person T, Bushey J, Jahn CE and Gleason SM (2021) Drought-Induced Root Pressure in Sorghum bicolor. Front. Plant Sci. 12:571072. doi: 10.3389/fpls.2021.571072

INTRODUCTION

Root pressure is a phenomenon that has long puzzled plant scientists (Hales, 1727; Priestley, 1920; Pickard, 2003; Wegner, 2014; Singh, 2016). It is observed in the xylem of a paraphyletic array of woody and herbaceous dicots and monocots, from *Acer* sp. to kiwifruit to *Zea mays* (O'Leary, 1965; Fisher et al., 1997; Enns et al., 2000; Ewers et al., 2001; Clearwater et al., 2007). It is difficult to measure *in vivo*, particularly for herbaceous plants but with high variability among species, genotypes within species and temporally, is intriguing to better understand (Grossenbacher, 1938; Fisher et al., 1997; McCully, 1999; Ewers et al., 2001; Sperry et al., 2008; Gleason et al., 2017; Comas et al., under review). Despite numerous observations and manipulative experiments, the molecular mechanism(s) generating positive pressure in a xylem hydraulic system dominated by negative tension remain unknown (Fiscus and Kramer, 1975; Schenk et al., 2021). Among several hypotheses, one posits that root pressure is generated by xylem parenchyma acting as an osmometer, structuring the osmotic potential of cell compartments to passively pull water into the mature xylem from the apoplast or bulk medium (Enns et al., 2000). Another suggests a hydraulic pressure scenario driving water into vessels via membrane asymmetry and compartmentalization of

forces (Pickard, 2003). Yet another suggests a "futile cycling" system in which water molecules are repeatedly scavenged from the apoplast back into the symplastic xylem parenchyma and pumped into the mature xylem, requiring energy expense (Pickard, 2003; Wegner, 2014). All of these mechanisms are in stark opposition to the mechanism of xylem water flow during transpiration, in which water is drawn through the xylem apoplast along a hydrostatic pressure gradient (Steudle, 2000). Importantly, generation of root pressure also must involve a mechanism for preventing leakage of water out of the xylem into the bulk medium (soil) during times of positive pressure. This process may be a combination of regulation across mechanical barriers (e.g. the Casparian strip) or the abovementioned "futile cycling" in which water is scavenged from the apoplast back into the symplast (Lee et al., 2004; Wegner, 2014).

There is also considerable debate as to whether root pressure is an evolutionary positive or neutral trait. A potential positive adaptive function of root pressure may be to refill xylem embolisms in water- or salt-stressed plants under drought, and after freezing events. Indeed, embolism refilling has been correlated with root pressure in multiple systems, including ferns (Holmlund et al., 2020), poplar (Secchi and Zwieniecki, 2014), birch (Hölttä et al., 2018), grapevine (Barrios-Masias et al., 2015; Knipfer et al., 2015), and maize (Tyree et al., 2008; Gleason et al., 2017). However, embolism refilling has also been observed in the absence of root pressure (Stiller et al., 2005; Choat et al., 2015; Knipfer et al., 2016) and attributed to other mechanisms such as biomechanical capillary action (Rolland et al., 2015). Historically, most researchers have assumed that both root pressure and embolism refilling occur at night, when most plants have low or no transpiration. During this time xylem is under little to no tension, and the generation of even slight positive pressure could potentially refill embolized conduits. However, embolism refilling has also been observed in the early afternoon, easily the most stressful part of the day in *Zea mays* (McCully, 1999). Root pressure may be diurnally constitutive but simply masked during the day by the magnitude of negative hydrostatic forces.

Most work on root pressure to date has focused on establishing the presence or absence of root pressure in species of interest, with some functional studies using various inhibitors to regulate root pressure magnitude in plants subjected to osmotic stress (Heindl et al., 1982; Ranathunge et al., 2003; Wright et al., 2004). While these plant physiological studies are important, transcriptomic tools represent another approach to identifying the mechanisms of root pressure. Using RNA-seq, researchers have been able to observe differential expression of both known and unknown genes during the activation of plant functions in response to stress (Buchanan et al., 2005; Johnson et al., 2014; Reddy et al., 2015; Kadam et al., 2017). A transcriptomic approach to identify the molecular mechanisms of root pressure generation is certainly exploratory but can be focused on the regulation of genes responsible for osmotic adjustment and transmembrane transport. Of particular interest are aquaporins, a class of proteins facilitating water transport across cellular membranes that is already known to be involved in hydraulic regulation (Henzler et al., 1999; McElrone et al., 2007; Vandeleur et al., 2009; Secchi et al., 2011; Meng et al., 2016; Shi et al., 2016).

The causal dynamics of the relationship between drought stress, drought recovery and root pressure are largely unknown. If root pressure ameliorates embolism in drought stressed plants, is it initiated by drought or constitutively present in well-watered plants as well? Do plants with greater root pressure have greater stem or leaf hydraulic conductance due to reduced embolism and higher parenchymal turgor? Does greater root pressure under drought support less negative leaf water potentials and better photosynthetic function? If root pressure is generated by root tissues, do biometric root traits correlate with root pressure? Is root pressure generated by a certain root class, such as fine roots, which have a lesser degree of suberization and barriers to apoplastic water movement (Guo et al., 2008; McCormack et al., 2015)? Finally, of utmost importance—do plants or species with robust root pressure show empirically greater survivorship, growth, or yield under drought conditions than counterparts with lower or no root pressure?

To investigate the mechanism and function of root pressure, we carried out a drought experiment in the greenhouse using *Sorghum bicolor*. *S. bicolor* is an important drought tolerant grain traditionally cultivated in Africa and Asia, with subspecies and varieties used for silage, biofuels, and human consumption (Rosenow et al., 1983; Doggett, 1988; Hariprasanna and Patil, 2015). As rising temperatures, unpredictable precipitation regimes, and drought intensify as the result of climate change, drought-tolerant *S. bicolor* is of great interest to plant breeders (Boyer, 1982). As an important global crop, its annotated genome is readily available, aiding in transcriptomic studies (Buchanan et al., 2005; McCormick et al., 2018). Finally, a wide range of cultivars are available within *S. bicolor*, providing marked differences in habit, physiology, and drought-tolerance (Turner et al., 2016; Miller, 2018).

We grew six genotypes of *S. bicolor*, three drought tolerant and three susceptible, under well-watered conditions, and then subjected a subset of the plants to a 2-week drought period. To understand the relationship between root pressure magnitude and plant physiological traits, we destructively harvested plants after drought and re-watering treatment to measure root pressure, leaf water potential, leaf vascular embolism, and root/shoot biometric traits. Finally, we explored molecular mechanisms of root pressure by sampling the root transcriptome of drought stressed and control plants immediately preceding root pressure measurement. Using differential expression analysis, we searched for genes that could be involved in inter- and intra-cellular transport of water and ions to generate positive xylem pressure in root tissue.

METHODS

Location and Dates of Study

The study was carried out in the greenhouse at the USDA Crops Research Laboratory in Fort Collins, CO. Germinated seedlings were planted into experimental pots on January 30, 2018, and destructively harvested during the week of April 1, when most plants had 5-6 fully expanded leaves.

Selection of *S. bicolor* Varieties

Six diploid lines of grain *S. bicolor* (bred for grain yield) were selected to span a broad range of variation in morphology, grain yield, and drought tolerance (Rosenow et al., 1983; Dahlberg, 2000; Evans et al., 2013; Miller, 2018). Rtx430 (Feterita x Zerazera: Sudan/Ethiopia), BTx623 (Kafir: Southern Africa), and Tx7000 (Durra: Sudan/Ethiopia/Egypt) are pre-flowering drought tolerant; BTx642 (Caudatum: North-central Africa), IS3620C (Guinea: West Africa), and SC56 (Caudatum) are pre-flowering drought susceptible. Susceptibility/tolerance are inferred from the effect of pre-flowering drought on final grain yield. RTx430, BTx623, and Tx7000 have the highest water use efficiency (WUE), followed by BTx642 and IS3620C, with SC56 having the lowest WUE (Turner et al., 2016).

Seed Germination

Seeds of the six genotypes were germinated (25°C, dark) in Petri dishes on filter paper with fungicide solution (Maxim XL, Syngenta) for 1 week prior to transplanting to pots. When seedling shoots and roots were each 2 cm long, they were transplanted into 7.57 L black polypropylene pots filled with fritted clay (Profile® Greens Grade™ in Emerald, PROFILE Products, LLC., Buffalo Grove, IL, USA). Fritted clay is a non-nutritive substrate with excellent water retention that detaches easily from plant material when dried, making it ideal for studies of root biomass and morphology.

Experimental Setup

The 7.57 L pots were arranged into two rows with nine groups of six pots with randomized placement of each genotype within each group (**Supplementary Figure 1**). Two groups of four pots were added to both ends of the bench to provide buffer. Four groups of the genotypes ended up missing two genotypes when seedlings failed after transplanting and thus were lost replicates. These plants were replaced with extra seedlings of an available genotype and treated as an additional buffer plant (**Figure 1**). Pots were irrigated by polypropylene irrigation lines that delivered fertigated water via an inline Dosatron (model D14, Dosatron Inc., Clearwater, FL) to 3.8 L/min emitters (one emitter per pot). A closed 227 L drum of concentrated fertilized irrigation water was prepared using municipal water, Gro-Mor fertilizer (Gro-Mor Plant Food Co., Inc., Leola, PA), and $CaNO_3$ each month to supply the Dosatron. After the initiation of the deficit treatment, control blocks were watered by hand.

Initial Growth Conditions

Experimental plants were established and grown in well-watered, nutrient replete conditions for 8 weeks (**Supplementary Figure 2**). Pots were fertigated with 80 ppm nitrogen (N) solution to holding capacity each afternoon at 1,600 h. Plants were given a 14/10 h day/night regime using banks of LED lights emitting ∼300 μmol photons/m^2/s. During natural daytime, sunlight increased ambient irradiance to a maximum of 1,000 μmol photons/m^2/s. The greenhouse air temperature was maintained at 28°C (day) and 17°C (night), and relative humidity was observed to be between 40 and 50% during the day and 60–70% at night.

Growth Conditions During Deficit Treatments

After 8 weeks of growth at 100% replenishment of daily evapotranspiration (ET), water deficit treatments were established on March 19, 2018 (**Supplementary Figure 2**). Five blocks were established as controls, continuing to receive 100% ET and 80 ppm N via hand watering (Control). Control plants were weighed daily to track mean ET as it increased with plant size and for calculations of deficit watering amounts. The remaining 8 blocks were watered at 30% of control ET and 80 ppm N (Deficit). These experimental treatments were implemented for 2 weeks, after which plants were destructively measured.

Non-destructive Measurements During Deficit Treatment

Non-destructive plant biometrics (leaf length, number of leaves, tiller length, and tiller count) were measured at the start of deficit treatments (after 8 weeks of growth) and at final harvest (after 10 weeks of growth).

Gas exchange measurements were taken during week 9 of the experiment from the following subset of treatments: 3 control blocks, 4 deficit + high N blocks, and 4 deficit + low N blocks. Measurements were made between 0800 and 1,100 h, the period when leaves were most photosynthetically active. From each plant, the 3rd collared leaf from the top was placed into a gas exchange cuvette (LI-6400–40, LI-COR Biosciences, Lincoln, Nebraska, USA), avoiding the midrib. Leaves were permitted to acclimate to conditions in the cuvette (1,200 PAR, 25°C T_{leaf}, 400 ppm CO_2, and 70% RH) for 10 min or more until the rate of photosynthesis remained constant, at which point an instantaneous measurement of maximal photosynthetic rate (A_{max}) was made. Temperature and relative humidity were kept between 24.6–30.2°C and 45–86%, respectively, for all measurements.

Re-watering Treatment and Assessment of Hydraulic Traits

Following the 2-week drought period, a subset of 72 plants was re-watered to 100% ET (19 control plants, 16 deficit plants), 50% ET (17 deficit plants), or kept dry (six control plants, six deficit plants). All 72 plants were then individually wrapped in 1 × 1.5 m bags made of reflective Mylar plastic, which excluded all light and retained all moisture, to down-regulate photosynthesis and close stomata (Holbrook, 2001). The internal pressure of the plants was allowed to equilibrate to a steady state for 1 h while covered by Mylar.

Leaf Water Potential Determination

After the 1 h equilibration under Mylar, the Ψ_L of each plant was determined. One upper leaf (generally the 2nd collared leaf from the top) was cut from the plant, wrapped with a damp cloth, trimmed along the midrib so the midrib could be inserted through the chamber lid and transferred immediately to a Scholander pressure chamber (Model 3005, Soil Moisture Equipment Corp, Santa Barbara, CA, USA) to determine Ψ_L.

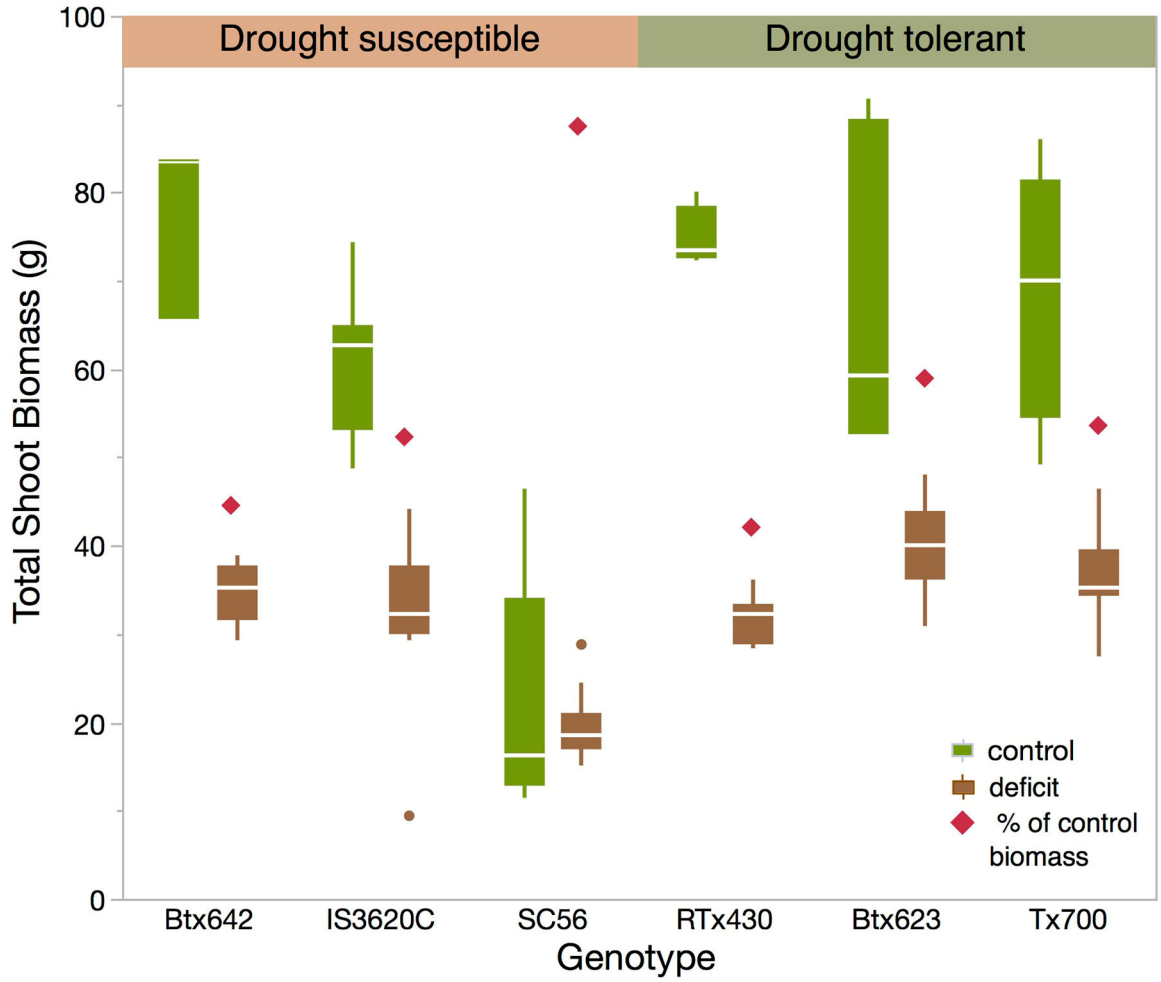


FIGURE 1 | Boxplot of total shoot biomass achieved before harvest by each genotype grown either under control or deficit conditions, as well as percent deficit shoot biomass for each genotype.

Leaf Embolism Determination

Simultaneously another leaf (generally the first collared leaf from the top) was sampled to measure incidence of leaf embolisms. The leaf was cut with a sharp pair of scissors. Adhesive was immediately applied to the cut surfaces (Loctite Liquid, Henkel, Corp., Westlake, OH, USA) to reduce air entry. Leaves were placed in sealed plastic bags and kept in a dark insulated box until Ψ_L could be measured, generally within 1 h of collection. Bagged leaves were taken to the x-ray micro-computed tomography (μCT) facility (The CSU Flint Animal Cancer Center, Colorado State University, Fort Collins, CO, USA) and scanned at ∼5-μm pixel^{-1} resolution through the leaf tissue and midribs (VivaCT 80, Scanco Medical AG, Bruttisellen, Switzerland). Leaves were bundled together and scanned in one run.

Embolized vessels were clearly identifiable in the images, whereas water-filled vessels were indistinguishable from the hydrated tissues surrounding them. Sample μCT images are provided in the **Supplementary Figure 3**. The total number of meta- xylem vessels in each scanned leaf was determined from stained (0.01% safranin-o, Fisher Scientific, Nazareth, NJ, USA) and photographed sections taken on the same leaf sections using a Nikon SMZ-U dissecting microscope (Nikon, Tokyo, Japan). The fraction of total conductance lost was assumed equal to the number of gas-filled meta-xylem vessels (from μCT), relative to the total number of meta-xylem vessels (from photographs).

Root Tissue Sampling for Transcriptomic Analysis

Finally, after leaf sampling, fine roots were sampled for transcriptomic analysis. An hour after re-watering, a 10 × 5 cm window was cut into the bottom third of the polypropylene pot and a large clump of fine roots extracted with sterile forceps. Fine roots were quickly rinsed to remove soil and mineral precipitates, blotted dry with a sterile Kimwipe (Kimberley-Clark Corporation, Irving, TX), and chopped roughly into 0.5 cm lengths with a sterile razor blade. Chopped roots were immediately transferred to 10 mL vials containing RNALater stabilization solution (Invitrogen, Carlsbad, CA), refrigerated

for 24 h, and subsequently frozen at −80°C until extraction and sequencing. A subset of roots was reserved and frozen for assessment of root viability in dry vials.

Root Pressure Measurements

Directly following internal plant pressure equilibration and leaf/root sampling, plants were moved to a dark room, uncovered, and the shoot removed 3 cm above the brace roots. Immediately after each shoot was removed from the plant, a pre-weighed cotton pad was placed on the cut surface of the stem to absorb root flow (sap driven by root pressure). Cotton pads were removed after 10 min and re-weighed to calculate the quantity of sap pushed out of the root system through the cut stem ("root flow rate") (Zhang et al., 1995). Directly after measuring root flow rate, the decapitated shoot base was capped with nested sections (∼2 cm) of polypropylene tubing and sealed with Loctite adhesive. The cap terminated in a 0–0.21 MPa pressure transducer (model PX26-030DV, Omega Engineering, Inc., Stamford, CT, USA) (Sperry, 1983). Root pressure measured by this transducer was then recorded for 24–48 h in total darkness via a data-logger (CR1000, Campbell Scientific, Inc., Logan, UT, USA) and the maximum pressure documented during this time was used for analyses. We note that our measured root flow rates likely overestimate the flow rates that would occur in entire intact plants because they do not include resistances associated with xylem conduits as well as extra-xylary resistances in stems and leaves.

Plant Biomass Measurement

After all destructive measurements were performed, intact roots were removed from pots, thoroughly rinsed and collected through a 2 mm sieve to remove all soil particles. Leaves, with the exception of the leaf section used for microCT, were scanned with a LI-3100C leaf area meter (LI-COR Biosciences, Lincoln, Nebraska, USA). All plant material was dried at 60°C and weighed. Root systems were then rehydrated for 24 h and separated into coarse (> 0.15 mm in diameter) and fine roots, a subset of which was scanned and analyzed in WinRHIZO (Regent Instruments, Inc., Canada), dried and reweighted to quantify specific and total root length of each class.

Transcriptomic Analysis of Root Tissue

After root pressure data was analyzed, samples from two genotypes, both watering treatments, and three ranges of root pressure magnitude were chosen to be processed for transcriptomic analysis. Three groups were established to carry out differential expression analysis: Control, Low (consistently watered control plants with root pressure expression < 5.0 KPa), Deficit, Low (deficit-grown plants with root pressure expression < 5.0 KPa), and Deficit, Mid (deficit-grown plants with root pressure expression between 5.0 and 10.0 KPa). Three individual plant samples were sequenced for each treatment except Control, Low, for which we only took two samples.

RNA from root tissue was extracted and sequenced by Amaryllis Nucleics (Oakland, CA) using the protocol of Townsley et al. (2015). RNA-Seq libraries were prepared using a high-throughput Illumina RNA-Seq library extraction protocol (Kumar et al., 2012). The enriched libraries were then quantified on an Analyst Plate Reader (LJL Biosystems) using SYBR Green I reagent (Invitrogen). Once the concentration of libraries was determined, a single pool of all the RNA-Seq libraries within each block was made. The pooled libraries were run on a Bioanalyzer (Agilent, Santa Clara) to determine the average product size for each pool. Each pool was adjusted to a final concentration of 20 nM and sequenced on a single lane on an Illumina Hi-Seq 2000 flow cell as 50 bp single-end reads. Any failed samples from the five blocks were run on two additional lanes.

Analysis

Statistical analysis of plant trait responses to imposed treatments was carried out in JMP 13 (SAS Institute Inc., Cary, North Carolina USA) and in R. The dataset was split into subsets (see **Table 1** notes) to evaluate specific hypotheses given the available sample sizes. Distributions of trait residuals were assessed for non-normality and transformed as needed. Traits for each ANOVA were examined for unequal variances within each treatment factor combination and the validity of differences between means with unequal variances were checked using Welch's ANOVA and, when necessary, non-parametric pair-wise comparisons using Wilcoxon's method. In all cases, non-parametric tests supported the results of initial ANOVA analyses; thus, for simplicity, the ANOVA results are reported. Finally, to visualize which traits strongly covary with root pressure, we performed a Principal Component Analysis (PCA) in R using the prcomp() function. We chose the following seven variables for the PCA based on cluster analysis (Proc VARCLUS, SAS Institute Inc., Cary, North Carolina USA) and a priori hypotheses of which traits might contribute to different drought-adaptive strategies: root pressure, green shoot biomass, number of tillers, mean tiller height, leaf water potential, ratio of fine: coarse root length and root mass fraction. Mean tiller height is a proxy for total plant height, with which it was strongly correlated in the cluster analysis.

Preprocessing of the Illumina RNASeq raw reads was done using fastp (Chen et al., 2018). Quality of the reads before and after the fastp processing was assessed using fastqc (Andrews, 2010). Reads were mapped to the *S. bicolor* genome (v.3.1.1) from the Joint Genome Institute (McCormick et al., 2018). Assembly of the transcriptome was performed using the Tuxedo Protocol (Trapnell et al., 2012). The included versions of Bowtie, TopHat and Cufflinks were 2-2.3.4.2, 2.1.1, and 2.2.1, respectively. Default parameters were used, with the exception of the following: min-intron-length 4 and max-intron-length 1,900. Intron length was chosen based on Panahi et al. (2014). Functional annotation was obtained for a subset of the transcriptome by BLASTing annotated *S. bicolor* genes to all members of the Poaceae in the NCBI Gene Database. To assess the similarity of transcriptomes within treatments, and thus the validity of choosing those treatments for differential expression analysis, we performed a PCA in the DESeq package in R on raw counts (**Supplementary Figure 4**). Based on this PCA, 2 outliers were removed (one each from the Deficit, Low, and Deficit, Mid treatments). Differential analysis was then performed using DESeq on the remaining six samples (two in each treatment).

TABLE 1 | ANOVA of total biomass, leaf water potential, and root pressure magnitude by genotype, drought treatment, re-watering treatment, major root type, and interactions.

Response variable	Explanatory variable	Nparm	DF	Sum of Squares	F Ratio	Prob > F	Dataset notes
Total biomass	GENOTYPE	5	5	39436.089	30.9788	<0.0001	
Total biomass	H20_TREAT	1	1	17746.743	69.7043	<0.0001	
Total biomass	GENOTYPE*H20_TREAT	5	5	5796.321	4.5533	0.0009	
Leaf water potential	GENOTYPE	5	5	22.167734	1.8494	0.1206	Re-watered plants only
Leaf water potential	H20_TREAT	1	1	7.786381	3.248	0.0777	Re-watered plants only
Leaf water potential	H20_TREAT*GENOTYPE	5	5	7.132211	0.595	0.7038	Re-watered plants only
sqrt(Root pressure)	H20_TREAT	1	1	11.631048	3.6098	0.0657	100% and 0% rewatering levels only
sqrt(Root pressure)	REWATER(H20_TREAT)	1	1	66.425874	10.3079	0.0003	100% and 0% rewatering levels only
Root pressure (KPa)	REWATER	1	1	959.3009	6.983	0.0152	Deficit plants only
Root pressure (KPa)	GENOTYPE	5	5	1528.3695	2.2251	0.0898	Deficit plants only
Root pressure (KPa)	GENOTYPE*REWATER	5	5	4053.8495	5.9018	0.0015	Deficit plants only

We observed significant differential expression between the three treatments and subsequently searched this subset of genes for functions with possible relevance to the creation of and maintenance of elevated root pressure. We searched our functional annotation for aquaporins, membrane-bound transporters in the plasma or vacuolar membrane, enzymes involved in carbohydrate metabolism, osmotic regulation, or vascular transport, and ATPases (necessary for aquaporin gating). We further carried out a Gene Ontology (GO) enrichment analysis using topGO in R on our annotated subset of genes to illuminate broader physiological trends differentiating the three treatments.

RESULTS

Genotype Response to Deficit Conditions

The six *S. bicolor* genotypes demonstrated distinct morphologies and growth potential in both control (well-watered) and drought treatments. Final total biomass varied significantly as a function of watering treatment and genotype with significant interaction between these effects (ANOVA, **Table 1**). All five genotypes other than SC56 produced significantly greater biomass under control conditions (88.6–115.8 g mean dry weight) than deficit conditions but did not differ significantly among one another within the control treatment (**Figure 1**, Tukey's HSD). SC56 under control conditions produced a mean total biomass of 33.6 ± 7.1 g, not statistically different from its total biomass under deficit (37.8 ± 4.3 g). Under deficit conditions, Tx700 (a "drought-tolerant" genotype) produced the greatest mean total biomass (79.9 ± 4.0 g), significantly >SC56 and IS3620C (58.0 ± 4.3 g, both "drought susceptible" genotypes), but not statistically different from other genotypes of intermediate performance (BTx642 = 78.1 ± 4.8 g, "susceptible"; BTx623 = 76.2 ± 4.3 g, "tolerant"; RTx430 = 62.0 ± 5.0 g, "tolerant").

The six genotypes did not significantly vary in Ψ_L after re-watering (**Table 1**). Plants that received any level of re-watering (30–100% of daily ET) recovered to a statistically similar mean Ψ_L (−0.28 to −0.42 MPa), which was significantly less negative than either control plants with zero re-watering (−0.64 ± 0.053 MPa) and deficit plants with zero re-watering (−1.45 + 0.084 MPa, nested ANOVA, re-watering level nested within deficit treatment, $p < 0.0001$).

Induction of Root Pressure by Drought

As observed in previous studies, generation of root pressure depended on the presence of ambient soil water content (Kramer, 2006; Gleason et al., 2017); thus, root pressure was only observed in plants that were re-watered prior to measurement (ANOVA, **Table 1**, **Figure 2**). *S. bicolor* grown in the well-watered (control) treatment either generated no root pressure or very little (similar to pressures observed in deficit plants that were not re-watered, up to 4.72 kPa). Plants grown in the water deficit treatment generated a range of high root pressures after re-watering (mean pressure 22.25 ± 3.21 kPa, ANOVA, **Table 1**, **Figure 2**).

Within the deficit treatments there was high variation in individual root pressure measurements, unexplained by either genotype or re-watering level (50 vs. 100% of daily ET, ANOVA, **Table 1**, **Figure 3**). There was, however, a significant interaction between genotypes and the degree of re-watering on root pressure, with each genotype showing a significantly different response to the degree of re-watering (ANOVA, $p = 0.0015$, **Table 1**, **Figure 3**). Two of the three drought tolerant genotypes showed lower root pressure generation under 100% re-watering than under 50% re-watering.

Relating Root Pressure to Other Plant Traits

Two principal components accounted for 62% of the total variation among seven traits in a PCA across deficit plants of all genotypes that had been re-watered (the group in which the root pressure was mainly observed). Among these components, there was a general association of greater root pressure, greater proportional investment in fine root length (greater ratio of fine:coarse root length), and larger green shoot biomass (**Figure 4**).

Among individual correlations with this same data, greater root pressure was correlated with greater green

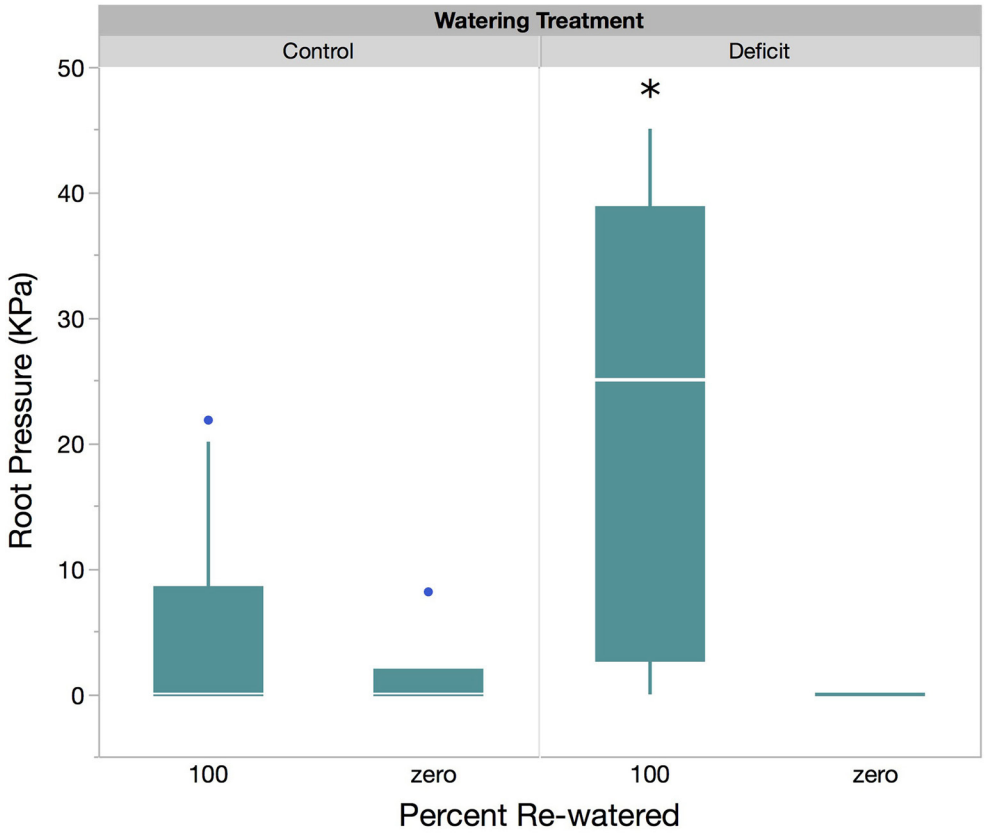


FIGURE 2 | Boxplot of root pressure (KPa) measured in control plants vs. deficit plants. Directly before measurements, sample plants were re-watered with 100% of their daily evapotranspiration loss, or not re-watered at all.

shoot biomass, total shoot biomass, and total plant biomass (**Supplementary Figure 5**). There was no general individual correlation between root pressure and total root biomass, coarse or fine root biomass, Ψ_L, photosynthetic rate, or number of leaf emboli (**Supplementary Figure 5**).

Root pressure was also correlated with root flow, the measure of the overall mass of sap exuded in the first 10 min after de-topping. Root flow was correlated with total root and coarse root biomass, total leaf area, green and total shoot biomass, and total plant biomass (**Supplementary Figure 5**).

Among genotypes there were qualitatively different relationships between root pressure and the proportion of fine root investment (**Figure 5**). Interestingly, Btx642 and IS3620C, which are both drought-susceptible genotypes from mesic central Africa, had a slight negative relationship between root pressure and proportion of fine root investment, whereas the drought-tolerant genotypes generally displayed greater root pressure with greater fine root investment (**Figure 5**).

Transcriptomic Profiling of Root Pressure Expression

After screening for data quality, we retained an average of 24.6 million reads per sample for use in transcriptome profiling. RNA sequencing provided a rich dataset of both unknown and annotated expressed genes. The data discussed in this publication were deposited in NCBI's Gene Expression Omnibus (Edgar et al., 2002) and are accessible through GEO Series accession number GSE152143 (https://www.ncbi.nlm.nih.gov/geo/query/acc.cgi?acc=GSE152143). Of 91,978 total transcripts, 47,122 were annotated in the *S. bicolor* genome. Further functional annotation using known genes in the greater Poaceae was obtained to add context to differentially expressed genes between treatments. There were 278 differentially expressed genes between deficit low and control low, 158 of which were down-regulated. 422 genes were differentially expressed between deficit mid and control low, 298 of which were down-regulated. Finally, 684 genes were differentially expressed between deficit mid and deficit low treatments, 417 of which were down-regulated. Differential expression tables are available in supplemental information (**Supplementary Tables 1–3**). Of these many genes, only seven genes of interest were identified: XP_002445047.2 aquaporin NIP3-2, XP_021314143.1 beta-galactosidase 4 isoform X1, WAT1-related protein At2g40900, XP_021316558.1 salt stress-induced protein, XP_015614593.1 beta-amylase 3, XP_002453072.1 aquaporin PIP1-5, and XP_002452133.1 plasmodesmata callose-binding protein 2 (**Figures 6A–G**). The top ten GO enrichment terms are available for each treatment comparison in **Supplementary Tables 4–6**. Other than general

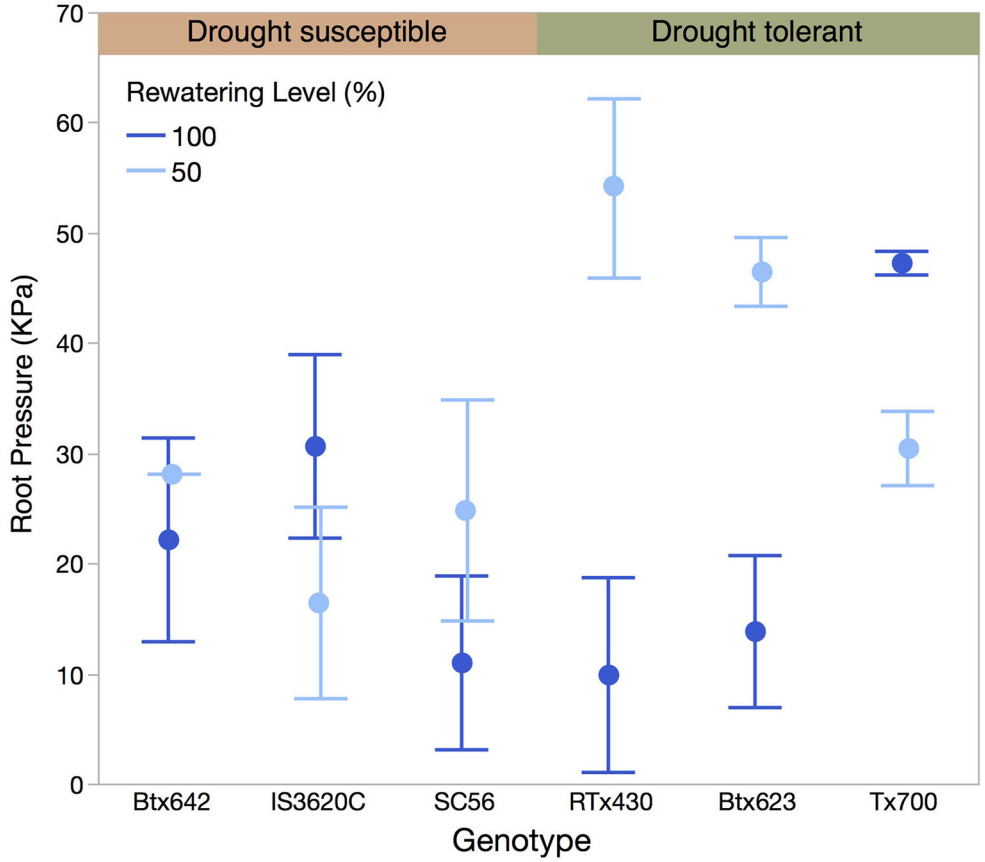


FIGURE 3 | Root pressure (KPa) by genotype in samples re-watered before measurement with 50 or 100% of daily evapotranspiration loss. Error bars represent standard error.

cell housekeeping functions, Deficit Low had three differentially expressed "drug transmembrane transport" genes (GO:0006855) in contrast to Control Low. Deficit Mid again showed enrichment in "drug transmembrane transport" genes, as well as "cell redox homeostasis" (GO: 0045454), compared to Deficit Low. Deficit Mid samples showed significant overexpression of pathogen defense responses compared to Control Low (GO:0050832, GO:0042742, GO:0006952, GO:0006032, GO:0016998).

DISCUSSION

The clearest result of this study is that sorghum requires prior exposure to drought to generate root pressure. Other studies have found that pre-exposure to drought increased root pressure (Stiller et al., 2003; Barrios-Masias et al., 2015) but in this study, re-watered individuals in the control group did not produce significant root pressure (> 5 kPa, **Figure 2**). This suggests that the experience of drought is a required trigger for the mechanisms that generate root pressure, at least in sorghum, although root pressure may still be constitutive or diurnal after priming by drought.

Interestingly, beyond partial re-watering following drought exposure, the magnitude of root pressure did not continue to increase with more re-watering across all genotypes (**Figure 3**). The significant interaction between genotype and re-watering level indicates that there could be genotype-specific responses depending on water availability, but root pressure is not consistently related to re-watering quantity after drought across different genotypes. Thus, soil water content either does not drive root pressure by a linear or exponential function in sorghum as it did for *Zea mays* in Gleason et al. (2017), or the threshold for re-watering is substantially lower either for sorghum in general or specifically in response to the treatments applied in this study. The lower root pressure in two drought tolerant genotypes in response to 100% re-watering compared to 50% re-watering is particularly notable, suggesting that the generation of root pressure was inhibited, and worth further study.

Interestingly, very few biometric and no physiological traits were correlated with root pressure magnitude. Root pressure was too variable, even within genotypes, to be statistically explained by re-watering amounts or root traits. There may be genotype-specific positive relationships between fine root allocation and root pressure, but these remain largely qualitative (**Figure 5**). An exception was the genotype SC56, which had very small relative fine root investment but produced root pressure magnitudes equal to those of much larger plants with higher

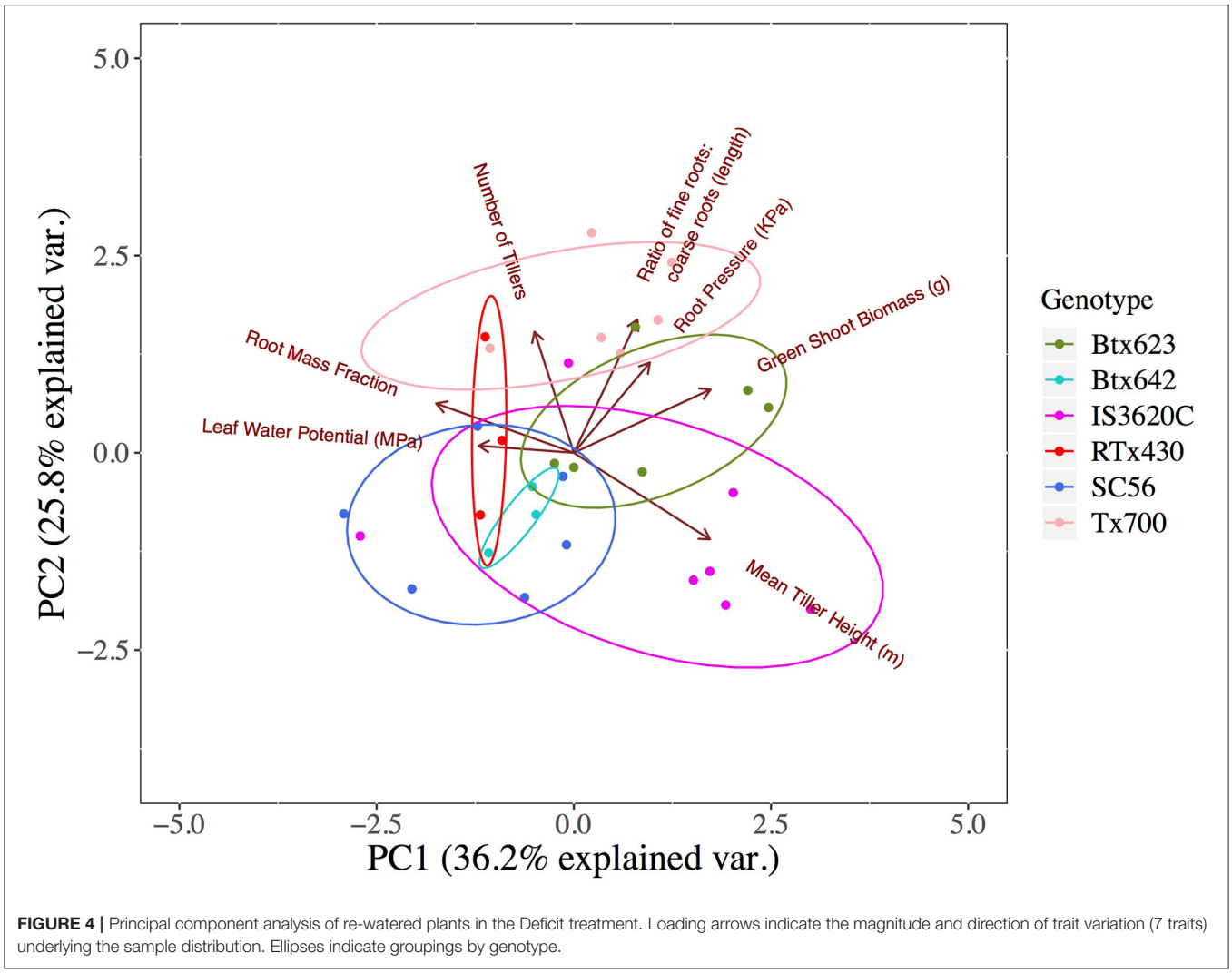


FIGURE 4 | Principal component analysis of re-watered plants in the Deficit treatment. Loading arrows indicate the magnitude and direction of trait variation (7 traits) underlying the sample distribution. Ellipses indicate groupings by genotype.

fine root allocation. Other studies have predicted that total bulk tissue quantity could contribute to maintenance of root, stem, or leaf pressure via tissue capacitance (Gleason et al., 2014; McCulloh et al., 2014). In this study, root pressure was significantly correlated with green shoot biomass, total shoot biomass, and total plant biomass but not root biomass, which is theoretically a major source of tissue water available to drive root pressure. The significant correlations of root pressure with total and aboveground green biomass, furthermore, suggests an agricultural yield benefit associated with increased root pressure under drought conditions (**Figure 4**, **Supplementary Figure 5**).

The specific adaptive function of root pressure in sorghum remains unclear. The magnitude of root pressures measured in the re-watered deficit treatment would be sufficient to pressurize a 6-m tall plant in the absence of transpiration, indicating that root pressure could refill daily embolisms in drought stressed plants (Comstock and Sperry, 2000). However, while photosynthetic rates measured prior to re-watering were correlated with leaf xylem embolism, the magnitude of root pressure did not correlate with either photosynthesis or the number of embolisms. Given the low variation in embolism counts (between 0 and 2 embolisms per leaf cross section) and the lack of difference between number of embolisms in the control and deficit treatments, it is possible that leaf xylem embolism is not a major issue for *S. bicolor*. It is also possible that deficit plants experienced greater numbers of embolisms prior to re-watering, and that 1 h at 50% ET constituted near-full refilling and recovery. It remains an important question whether root pressure is involved in embolism recovery in sorghum.

Exploratory transcriptomic analyses suggested a set of differentially-expressed genes between our three root pressure magnitude/watering treatments that could be involved in the creation of root pressure. The vast majority of these transcripts are of unknown function or code for cell housekeeping functions, pathogen defense, and synthesis of secondary metabolites. While drought is known to regulate expression of large and diverse suites of genes (Cohen et al., 2010; Kakumanu et al., 2012; Johnson et al., 2014), only a small set of genes in our differentially expressed subset had possible relevance to the creation and maintenance of root pressure. We found seven genes of interest

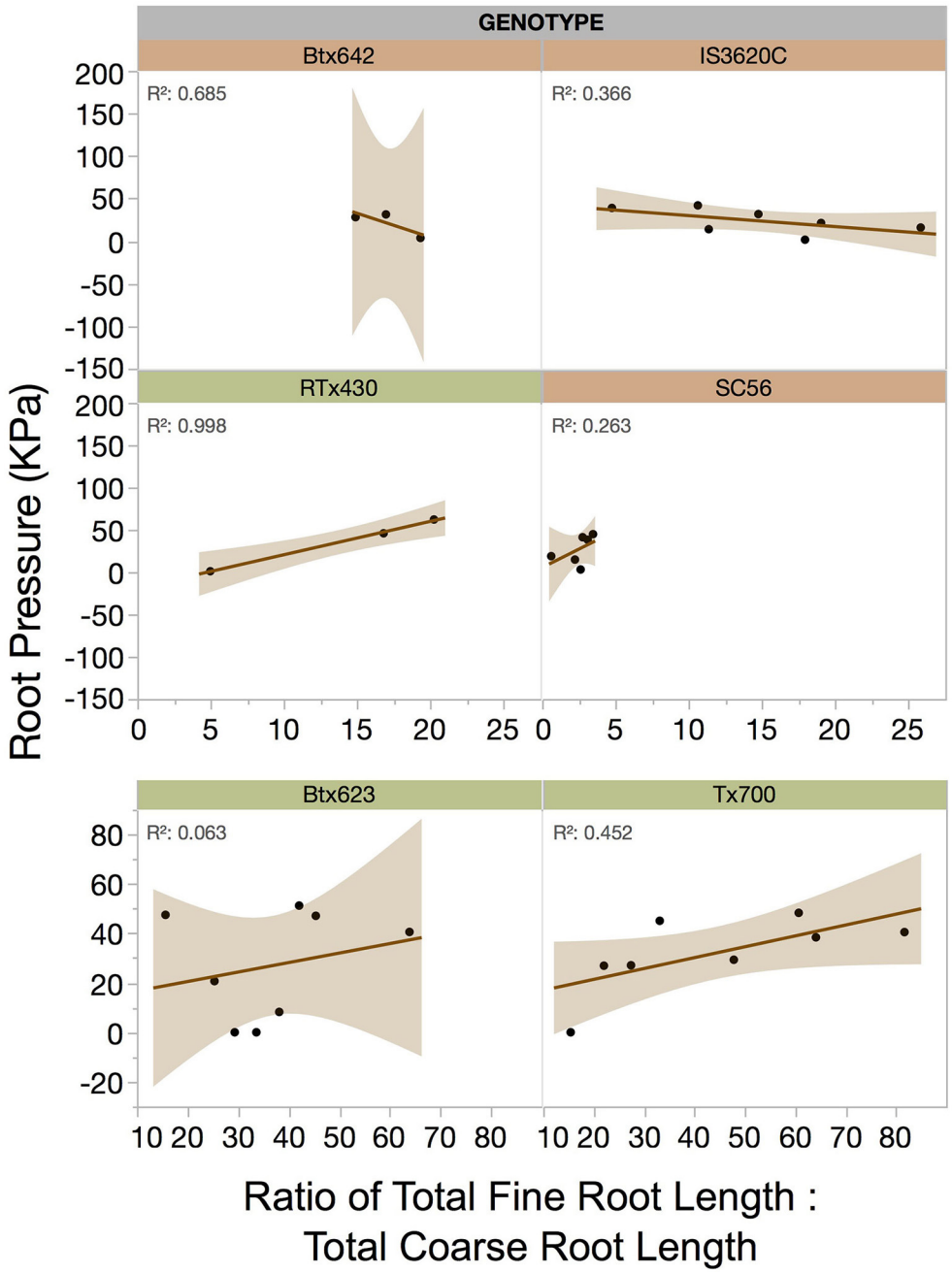


FIGURE 5 | Relationship between root pressure (KPa) and the root system's relative allocation to fine roots (ratio of total fine root length to total coarse root length, unitless), by genotype. Orange genotypes (Btx642, IS3620C, and SC56) are drought susceptible, and green genotypes (RTx430, Btx623, and Tx700) are drought tolerant. Note that Btx623 and Tx700 (bottom panels) have much higher proportions of fine roots than the other genotypes. Dotted regression lines indicate non-significant relationships.

whose expression involved significant up- or down-regulation in the Deficit Mid treatment.

Aquaporins

Two aquaporins were differentially expressed between the three treatments—PIP1;5 and NIP2;3. While PIPs are known efficient water transporting channels, NIPs tend to move other substrates, such as small organic solutes and minerals (Martre et al., 2002; Maurel et al., 2015). In this study, PIP1;5 is strongly down-regulated in the deficit treatments. Similarly, Liu et al. (2014) observed that while water uptake, hydraulic conductivity, root pressure, and most aquaporin expression increase in concert in *S. bicolor*, PIP1;5 does not. In *Hordeum vulgare*, aquaporin expression was up-regulated as root hydraulic conductivity was

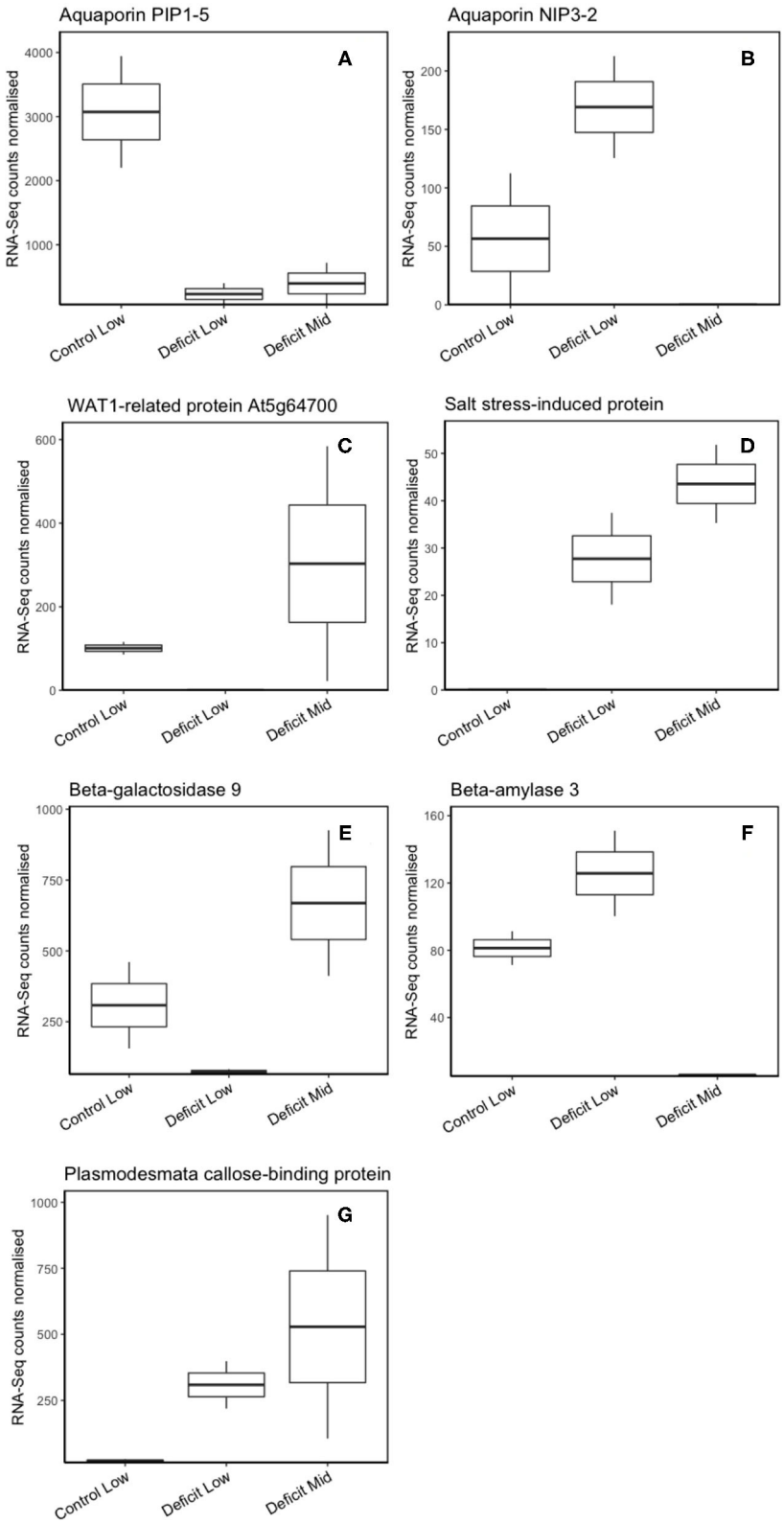


FIGURE 6 | Normalized RNA-Seq counts of gene transcripts in each of three treatment groups (Control Low, Deficit Low, and Deficit Mid) for the following differentially-expressed genes: **(A)** PIP1;5, **(B)** NIP2;3, **(C)** WAT1-related protein Atg64700, **(D)** Salt stress-induced protein, **(E)** Beta-galactosidase 9, **(F)** Beta-amylase 3, **(G)** Plasmodesmata callose-binding protein.

down-regulated, indicating that gene expression of aquaporins (as compared to gating or remobilization of aquaporins) may not always drive root hydraulic conductivity (Saini and Fricke, 2020). It is also possible that the down-regulation of PIP1;5 prevents flow of water back into the soil, supporting the buildup of root pressure, as opposed to facilitating water uptake from the soil. The second differentially expressed aquaporin, NIP2;3, is not clearly involved in root pressure generation: again, it is down-regulated in the Deficit Mid treatment (**Figure 6F**), and is known to transport arsenic, but not water, in rice and octopus (Chen et al., 2017). It should be noted that phenotypes resulting from differential aquaporin gene expression can be inconsistent between varieties of one species, and very often between species (Alexandersson et al., 2005; Grondin et al., 2016; Kadam et al., 2017).

Membrane Transport Proteins

The WAT1-related protein, a plasma membrane transporter also known as UmamiT11 in *A. thaliana*, is localized in the loading/unloading domains of the vasculature in direct contact with the protoxylem, companion cells, and sieve elements (Müller et al., 2015). Previous work on this protein has focused on its role in endosperm growth and amino acid transport, although WAT1 is an auxin transporter. It is up-regulated in the Deficit Mid treatment relative to the Low root pressure treatments and may play a role in setting up an osmotic gradient in the vascular bundles and parenchyma to draw in water from the soil (**Figure 6C**). Similarly, the salt stress-induced protein (saLT) is a plasma membrane transporter with a strong increase in expression in salt-stressed *O. sativa* and *A. thaliana*, and here is up-regulated in the Deficit Mid treatment (**Figure 6B**). It is a lectin that likely binds carbohydrates and plays a role in the regulation of cell osmotic potential (UniprotKB- Q0JMY8, Garcia et al., 1998).

Carbohydrate Metabolism

Carbohydrate metabolic enzymes strongly affect the osmotic potential of the cytosol and vacuole (Cram, 1976; Smeekens and Rook, 1997). We observed two significantly differentially expressed enzymes with opposite expression patterns—beta-amylase 3 and beta-galactosidase 4 (**Figures 6G,D**). Beta-amylase hydrolyzes starch to di- and monosaccharides, while beta-galactosidase catalyzes the hydrolysis of glycoproteins into monosaccharides. It is not clear why starch hydrolysis would cease while glycoprotein hydrolysis increases in plants with higher root pressure, but another study found that the gene expression of these two enzymes move counter to one another in the context of cold de-acclimation (Oono et al., 2006). It is possible that these enzymes are located in different cell types within our homogenized fine root samples and are somehow working additively to structure an osmotic potential gradient from soil to xylem.

Vascular Transport

The plasmodesmata callose-binding protein 2 (PCDB) is significantly up-regulated in the deficit treatments relative to the control (**Figure 6A**). In other studies, PCDB1 was observed to occlude plasmodesmata (the symplastic connections between plant cells) when up-regulated, while PCDB2 mutants did not, although both proteins are localized in the plasmodesmata and bind to callose *in vitro* (Simpson et al., 2009). While it is tempting to associate higher root pressure with increased symplastic flow, closure of plasmodesmata may play an important role in preventing leakage of water down the osmotic gradient and back into drying soil and may be required for the creation of root pressure (Schenk et al., 2021).

FUTURE DIRECTIONS

It will be critical to follow up on this study with diverse tools for investigating mechanisms involved with the recreation of root pressure. A larger, carefully replicated transcriptomic sampling of the same *S. bicolor* genotypes, or a subset therein would be valuable. Given the potential variability of mechanisms and transcriptomes between individuals, cultivars, and species in this and other studies, it may be difficult to rigorously pinpoint one set of mechanisms or genes that clearly drives, or responds to, root pressure generation. Moreover, as we have seen in many works studying evolutionary trade-offs in plant hydraulic traits, a wide variety of traits and phenologies can be variously adopted by different genotypes to achieve the same result, be it avoidance or tolerance of drought, or maintenance of an embolism-free hydraulic network (Watkins et al., 2010; Ocheltree et al., 2015; Han et al., 2017). The mechanisms and specific genes that regulate root pressure in *S. bicolor* may not bear resemblance to those that regulate root pressure in other species, such as *Zea mays*, although the creation of root pressure may achieve the same result of improved performance during drought.

DATA AVAILABILITY STATEMENT

The datasets presented in this study can be found in online repositories. The names of the repository/repositories and accession number(s) can be found below: https://www.ncbi.nlm.nih.gov/geo/, GSE152143; https://www.ncbi.nlm.nih.gov/geo/, GSM4604668; https://www.ncbi.nlm.nih.gov/geo/, GSM4604669; https://www.ncbi.nlm.nih.gov/geo/, GSM4604670; https://www.ncbi.nlm.nih.gov/geo/, GSM4604671; https://www.ncbi.nlm.nih.gov/geo/, GSM4604672; and https://www.ncbi.nlm.nih.gov/geo/, GSM4604673.

AUTHOR CONTRIBUTIONS

SD designed the experiments, collected data, analyzed data, and wrote the manuscript. LC designed the experiment, collected data, and edited the manuscript. NF designed the experiment and collected data. RB, JW, TP, JB, CJ, and SG collected data. JIC analyzed data. All authors contributed to the article and approved the submitted version.

FUNDING

TP was supported by USDA - NIFA National Needs Graduate Fellowship Program, Award no. 2014-38420-21801.

ACKNOWLEDGMENTS

The authors thank Dr. Evelyn Delfin for assistance with data collection, Dr. Jane Stewart for insight into experimental design, and Dr. Stephen Pearce and Kora Vyse for help with analysis and for editing the manuscript. This research was conducted with funds allocated to USDA-ARS NP211 project 3012-13000-007-00D.

SUPPLEMENTARY MATERIAL

The Supplementary Material for this article can be found online at: https://www.frontiersin.org/articles/10.3389/fpls.2021.571072/full#supplementary-material

REFERENCES

Alexandersson, E., Fraysse, L., Sjövall-Larsen, S., Gustavsson, S., Fellert, M., Karlsson, M., et al. (2005). Whole gene family expression and drought stress regulation of aquaporins. *Plant Mol. Biol.* 59, 469–484. doi: 10.1007/s11103-005-0352-1

Andrews, S. (2010). FastQC: *A Quality Control Tool for High Throughput Sequence Data*. Available online at: http://www.bioinformatics.babraham.ac.uk/projects/fastqc/

Barrios-Masias, F. H., Knipfer, T., and McElrone, A. J. (2015). Differential responses of grapevine rootstocks to water stress are associated with adjustments in fine root hydraulic physiology and suberization. *J. Exp. Bot.* 66, 6069–6078. doi: 10.1093/jxb/erv324

Boyer, J. S. (1982). Plant productivity and environment. *Science* 218, 443–448. doi: 10.1126/science.218.4571.443

Buchanan, C. D., Lim, S., Salzman, R. A., Kagiampakis, I., Morishige, D. T., Weers, B. D., et al. (2005). Sorghum bicolor's transcriptome response to dehydration, high salinity and ABA. *Plant Mol. Biol.* 58, 699–720. doi: 10.1007/s11103-005-7876-2

Chen, S., Zhou, Y., Chen, Y., and Gu, J. (2018). Fastp: an ultra-fast all-in-one FASTQ preprocessor. *Bioinformatics* 34, i884–i890. doi: 10.1093/bioinformatics/bty560

Chen, Y., Sun, S. K., Tang, Z., Liu, G., Moore, K. L., Maathuis, F. J. M., et al. (2017). The Nodulin 26-like intrinsic membrane protein OsNIP3;2 is involved in arsenite uptake by lateral roots in rice. *J. Exp. Bot.* 68, 3007–3016. doi: 10.1093/jxb/erx165

Choat, B., Brodersen, C. R., and McElrone, A. J. (2015). Synchrotron X-ray microtomography of xylem embolism in *Sequoia sempervirens* saplings during cycles of drought and recovery. *New Phytol.* 205, 1095–1105. doi: 10.1111/nph.13110

Clearwater, M. J., Blattmann, P., Luo, Z., and Lowe, R. G. (2007). Control of scion vigour by kiwifruit rootstocks is correlated with spring root pressure phenology. *J. Exp. Bot.* 58, 1741–1751. doi: 10.1093/jxb/erm029

Cohen, D., Bogeat-Triboulot, M. B., Tisserant, E., Balzergue, S., Martin-Magniette, M. L., Lelandais, G., et al. (2010). Comparative transcriptomics of drought responses in Populus: a meta-analysis of genome-wide expression profiling in mature leaves and root apices across two genotypes. *BMC Genomics* 11, 630-651. doi: 10.1186/1471-2164-11-630

Comstock, J. P., and Sperry, J. S. (2000). Theoretical considerations of optimal conduit length for water transport in vascular plants. *New Phytol.* 148, 195–218. doi: 10.1046/j.1469-8137.2000.00763.x

Cram, W. J. (1976). "Negative feedback regulation of transport in cells. The maintenance of turgor, volume, and nutrient supply," in *Transport in Plants II: Part A: Cells*, 284–316. doi: 10.1007/978-3-642-66227-0_11

Dahlberg, J. A. (2000). "Classification and Characterization," in *Sorghum: Origin, History, Technology, and production*, eds C. W. Smith and R. A. Frederiksen (John Wiley & Sons, Inc.), 99.

Doggett, H. (1988). *Sorghum*. New York, NY: Wiley.

Edgar, R., Domrachev, M., and Lash, A. E. (2002). Gene Expression Omnibus: NCBI gene expression and hybridization array data repository. *Nucleic Acids Res.* 30, 207–210. doi: 10.1093/nar/30.1.207

Enns, L. C., Canny, M. J., and McCully, M. E. (2000). An investigation of the role of solutes in the xylem sap and in the xylem parenchyma as the source of root pressure. *Protoplasma* 211, 183–197. doi: 10.1007/BF01304486

Evans, J., McCormick, R. F., Morishige, D., Olson, S. N., Weers, B., Hilley, J., et al. (2013). Extensive variation in the density and distribution of DNA polymorphism in sorghum genomes. *PLoS ONE* 8:e79192. doi: 10.1371/journal.pone.0079192

Ewers, F. W., Améglio, T., Cochard, H., Beaujard, F., Martignac, M., Vandame, M., et al. (2001). Seasonal variation in xylem pressure of walnut trees: root and stem pressures. *Tree Physiol.* 21, 1123–1132. doi: 10.1093/treephys/21.15.1123

Fiscus, E. L., and Kramer, P. J. (1975). General model for osmotic and pressure-induced flow in plant roots. *Proc. Natl. Acad. Sci. U.S.A.* 72, 3114–3118. doi: 10.1073/pnas.72.8.3114

Fisher, J. B., Ewers, F. W., and López-Portillo, J. (1997). Survey of Root Pressure in Tropical Vines and Woody Species. *Int. J. Plant Sci.* 158, 44–50. doi: 10.1086/297412

Garcia, A. B., De Almeida Engler, J., Claes, B., Villarroel, R., Van Montagu, M., Gerats, T., et al. (1998). The expression of the salt-responsive gene salT from rice is regulated by hormonal and developmental cues. *Planta* 207, 172–180. doi: 10.1007/s004250050470

Gleason, S. M., Blackman, C. J., Cook, A. M., Laws, C. A., and Westoby, M. (2014). Whole-plant capacitance, embolism resistance and slow transpiration rates all contribute to longer desiccation times in woody angiosperms from arid and wet habitats. *Tree Physiol.* 34, 275–284. doi: 10.1093/treephys/tpu001

Gleason, S. M., Wiggans, D. R., Bliss, C. A., Young, J. S., Cooper, M., Willi, K. R., et al. (2017). Embolized stems recover overnight in *Zea mays*: the role of soil water, root pressure, and nighttime transpiration. *Front. Plant Sci.* 8, 1–11. doi: 10.3389/fpls.2017.00662

Grondin, A., Mauleon, R., Vadez, V., and Henry, A. (2016). Root aquaporins contribute to whole plant water fluxes under drought stress in rice (Oryza sativa L.). *Plant Cell Environ.* 39, 347–365. doi: 10.1111/pce.12616

Grossenbacher, K. A. (1938). Diurnal Fluctuation in Root Pressure. *Plant Physiol.* 13, 669–676. doi: 10.1104/pp.13.4.669

Guo, D., Li, H., Mitchell, R. J., Han, W., Hendricks, J. J., Fahey, T. J., et al. (2008). Fine root heterogeneity by branch order: Exploring the discrepancy in root turnover estimates between minirhizotron and carbon isotopic methods. *New Phytol.* 177, 443–456. doi: 10.1111/j.1469-8137.2007.02242.x

Hales, S. (1727). *Vegetable Staticks: Or, an Account of Some Statical Experiments on the Sap in Vegetables: Being an Essay Towards a Natural History of Vegetation*. London: W. and J. Innys and T. Woodward.

Han, B., Umaña, M. N., Mi, X., Liu, X., Chen, L., Wang, Y., et al. (2017). The role of transcriptomes linked with responses to light environment on seedling mortality in a subtropical forest, China. *J. Ecol.* 105, 592–601. doi: 10.1111/1365-2745.12760

Hariprasanna, K., and Patil, J. V. (2015). "Sorghum: origin, classification, biology and improvement," in *Sorghum Molecular Breeding*, eds R. Madhusudhana, P. Rajendrakumar, and J. V Patil (New Delhi: Springer), 3–18. doi: 10.1007/978-81-322-2422-8

Heindl, J. C., Carlson, D. R., Brun, W. A, and Brenner, M. L. (1982). Ontogenetic variation of four cytokinins in soybean root pressure exudate. *Plant Physiol.* 70, 1619–25. doi: 10.1104/pp.70.6.1619

Henzler, T., Waterhouse, R. N., Smyth, a,. J., Carvajal, M., Cooke, D. T., a.R., et al. (1999). Diurnal varia- tions in hydraulic conductivity and root pressure can be

corre- lated with the expression of putative aquaporins in the roots of Lotus japonicus. *Planta C* 50–60. doi: 10.1007/s004250050653

Holbrook, N. M. (2001). In Vivo Observation of Cavitation and Embolism Repair Using Magnetic Resonance Imaging. *Plant Physiol.* 126, 27–31. doi: 10.1104/pp.126.1.27

Holmlund, H. I., Davis, S. D., Ewers, F. W., Aguirre, N. M., Sapes, G., Sala, A., et al. (2020). Positive root pressure is critical for whole-plant desiccation recovery in two species of terrestrial resurrection ferns. *J. Exp. Bot.* 71, 1139–1150. doi: 10.1093/jxb/erz472

Hölttä, T., Dominguez Carrasco, M. D. R., Salmon, Y., Aalto, J., Vanhatalo, A., Bäck, J., et al. (2018). Water relations in silver birch during springtime: how is sap pressurised? *Plant Biol.* 20, 834–847. doi: 10.1111/plb.12838

Johnson, S. M., Lim, F. L., Finkler, A., Fromm, H., Slabas, A. R., and Knight, M. R. (2014). Transcriptomic analysis of Sorghum bicolor responding to combined heat and drought stress. *BMC Genomics* 15, 1–19. doi: 10.1186/1471-2164-15-456

Kadam, S., Abril, A., Dhanapal, A. P., Koester, R. P., Vermerris, W., Jose, S., et al. (2017). Characterization and regulation of aquaporin genes of sorghum [*Sorghum bicolor* (L.) Moench] in response to waterlogging stress. *Front. Plant Sci.* 8:862. doi: 10.3389/fpls.2017.00862

Kakumanu, A., Ambavaram, M. M. R., Klumas, C., Krishnan, A., Batlang, U., Myers, E., et al. (2012). Effects of drought on gene expression in maize reproductive and leaf meristem tissue revealed by RNA-Seq. *PLANT Physiol.* 160, 846–867. doi: 10.1104/pp.112.200444

Knipfer, T., Cuneo, I., Brodersen, C., and McElrone, A. J. (2016). *In-situ* visualization of the dynamics in xylem embolism formation and removal in the absence of root pressure: a study on excised grapevine stems. *Plant Physiol.* 171, 1024–1036. doi: 10.1104/pp.16.00136

Knipfer, T., Eustis, A., Brodersen, C., Walker, A. M., and McElrone, A. J. (2015). Grapevine species from varied native habitats exhibit differences in embolism formation/repair associated with leaf gas exchange and root pressure. *Plant Cell Environ.* 38, 1503–1513. doi: 10.1111/pce.12497

Kramer, P. J. (2006). Soil moisture as a limiting factor for active absorption and root pressure. *Am. J. Bot.* 28, 446. doi: 10.1002/j.1537-2197.1941.tb10960.x

Kumar, R., Ichihashi, Y., Kimura, S., Chitwood, D. H., Headland, L. R., Peng, J., et al. (2012). A High-throughput method for illumina RNA-seq library preparation. *Front. Plant Sci.* 3:202. doi: 10.3389/fpls.2012.00202

Lee, S. H., Singh, A. P., Chung, G. C., Ahn, S. J., Noh, E. K., and Steudle, E. (2004). Exposure of roots of cucumber (*Cucumis sativus*) to low temperature severely reduces root pressure, hydraulic conductivity and active transport of nutrients. *Physiol. Plant.* 120, 413–420. doi: 10.1111/j.0031-9317.2004.00248.x

Liu, P., Yin, L., Deng, X., Wang, S., Tanaka, K., and Zhang, S. (2014). Aquaporin-mediated increase in root hydraulic conductance is involved in silicon-induced improved root water uptake under osmotic stress in Sorghum bicolor L. *J. Exp. Bot.* 65, 4747–4756. doi: 10.1093/jxb/eru220

Martre, P., Morillon, R., Barrieu, F., North, G. B., Nobel, P. S., and Chrispeels, M. J. (2002). Plasma membrane aquaporins play a significant role during recovery from water deficit. *Plant Physiol.* 130, 2101–2110. doi: 10.1104/pp.009019

Maurel, C., Boursiac, Y., Luu, D.-T., Santoni, V., Shahzad, Z., and Verdoucq, L. (2015). Aquaporins in plants. *Physiol. Rev.* 95, 1321–1358. doi: 10.1152/physrev.00008.2015

McCormack, M. L., Dickie, I. A., Eissenstat, D. M., Fahey, T. J., Fernandez, C. W., Guo, D., et al. (2015). Redefining fine roots improves understanding of below-ground contributions to terrestrial biosphere processes. *New Phytol.* 207, 505–518. doi: 10.1111/nph.13363

McCormick, R. F., Truong, S. K., Sreedasyam, A., Jenkins, J., Shu, S., Sims, D., et al. (2018). The Sorghum bicolor reference genome: improved assembly, gene annotations, a transcriptome atlas, and signatures of genome organization. *Plant J.* 93, 338–354. doi: 10.1111/tpj.13781

McCulloh, K. A., Johnson, D. M., Meinzer, F. C., and Woodruff, D. R. (2014). The dynamic pipeline: hydraulic capacitance and xylem hydraulic safety in four tall conifer species. *Plant Cell Environ.* 37, 1171–1183. doi: 10.1111/pce.12225

McCully, M. E. (1999). Root xylem embolisms and refilling. Relation to water potentials of soil, roots, and leaves, and osmotic potentials of root xylem sap. *Plant Physiol.* 119, 1001–1008. doi: 10.1104/pp.119.3.1001

McElrone, A. J., Bichler, J., Pockman, W. T., Addington, R. N., Linder, C. R., and Jackson, R. B. (2007). Aquaporin-mediated changes in hydraulic conductivity of deep tree roots accessed via caves. *Plant Cell Environ.* 30, 1411–1421. doi: 10.1111/j.1365-3040.2007.01714.x

Meng, D., Walsh, M., and Fricke, W. (2016). Rapid changes in root hydraulic conductivity and aquaporin expression in rice (*Oryza sativa* L.) in response to shoot removal – xylem tension as a possible signal. *Ann. Bot.* 118:mcw150. doi: 10.1093/aob/mcw150

Miller, S. B. (2018). *Phenotypic plasticity in the response of sorghum to water stress and recovery indicates pre-flowering drought tolerance* (Doctoral dissertation). Colorado State University, Fort Collins, CO, Uniteds States.

Müller, B., Fastner, A., Karmann, J., Mansch, V., Hoffmann, T., Schwab, W., et al. (2015). Amino acid export in developing arabidopsis seeds depends on UmamiT facilitators. *Curr. Biol.* 25, 3126–3131. doi: 10.1016/j.cub.2015.10.038

Ocheltree, T. W., Nippert, J. B., and Prasad, P. V. V. (2015). A safety vs efficiency trade-off identified in the hydraulic pathway of grass leaves is decoupled from photosynthesis, stomatal conductance and precipitation. *New Phytol.* 210, 97–107 doi: 10.1111/nph.13781

O'Leary, J. W. (1965). Root-pressure exudation in woody plants. *Bot. Gaz.* 126, 108–115. doi: 10.1086/336303

Oono, Y., Seki, M., Satou, M., Iida, K., Akiyama, K., Sakurai, T., et al. (2006). Monitoring expression profiles of Arabidopsis genes during cold acclimation and deacclimation using DNA microarrays. *Funct. Integr. Genomics* 6, 212–234. doi: 10.1007/s10142-005-0014-z

Panahi, B., Abbaszadeh, B., Taghizadeghan, M., and Ebrahimie, E. (2014). Genome-wide survey of alternative splicing in sorghum bicolor. *Physiol. Mol. Biol. Plants* 20, 323–329. doi: 10.1007/s12298-014-0245-3

Pickard, W. F. (2003). The riddle of root pressure. I. Putting Maxwell's demon to rest. *Funct. Plant Biol.* 30, 121–134. doi: 10.1071/FP02035

Priestley, J. (1920). The mechanism of root pressure. *New Phytol.* 19, 189–200. doi: 10.1111/j.1469-8137.1920.tb07326.x

Ranathunge, K., Steudle, E., and Lafitte, R. (2003). Control of water uptake by rice (*Oryza sativa* L.): role of the outer part of the root. *Planta* 217, 193–205. doi: 10.1007/s00425-003-0984-9

Reddy, P. S., Rao, T. S. R. B., Sharma, K. K., and Vadez, V. (2015). Genome-wide identification and characterization of the aquaporin gene family in *Sorghum bicolor* (L.). *Plant Gene* 1, 18–28. doi: 10.1016/j.plgene.2014.12.002

Rolland, V., Bergstrom, D. M., Lenné, T., Bryant, G., Chen, H., Wolfe, J., et al. (2015). Easy come, easy go: capillary forces enable rapid refilling of embolized primary xylem vessels. *Plant Physiol.* 168, 1636–1647. doi: 10.1104/pp.15.00333

Rosenow, D. T., Quisenberry, J. E., Wendt, C. W., and Clark, L. E. (1983). *Drought Tolerant Sorghum and Cotton Germplasm*. Amsterdam: Elsevier B.V. doi: 10.1016/0378-3774(83)90084-7

Saini, G., and Fricke, W. (2020). Photosynthetically active radiation impacts significantly on root and cell hydraulics in barley (Hordeum vulgare L.). *Physiol. Plant.* 170, 357–372. doi: 10.1111/ppl.13164

Schenk, H. J., Jansen, S., and Hölttä, T. (2021). Positive pressure in xylem and its role in hydraulic function. *New Phytol*. doi: 10.1111/nph.17085

Secchi, F., Gilbert, M. E., and Zwieniecki, M. A. (2011). Transcriptome response to embolism formation in stems of populus trichocarpa provides insight into signaling and the biology of refilling. *Plant Physiol.* 157, 1419–1429. doi: 10.1104/pp.111.185124

Secchi, F., and Zwieniecki, M. A. (2014). Down-regulation of plasma intrinsic protein1 aquaporin in poplar trees is detrimental to recovery from embolism. *Plant Physiol.* 164, 1789–1799. doi: 10.1104/pp.114.237511

Shi, Y., Zhang, Y., Han, W., Feng, R., Hu, Y., Guo, J., et al. (2016). Silicon enhances water stress tolerance by improving root hydraulic conductance in *Solanum lycopersicum* L. *Front. Plant Sci.* 7, 196. doi: 10.3389/fpls.2016.00196

Simpson, C., Thomas, C., Findlay, K., Bayer, E., and Maule, A. J. (2009). An arabidopsis GPI-anchor plasmodesmal neck protein with callose binding activity and potential to regulate cell-to-cell trafficking. *Plant Cell* 21, 581–594. doi: 10.1105/tpc.108.060145

Singh, S. (2016). "Root Pressure: Getting to the Root of Pressure," in *Progress in Botany 77*, eds. U. Lüttge, F. Cánovas, and R. Matyssek (Cham: Springer). doi: 10.1007/978-3-319-25688-7_3

Smeekens, S., and Rook, F. (1997). Sugar sensing and sugar-mediated signal transduction in plants. *Plant Physiol.* 115, 7–13. doi: 10.1104/pp.115.1.7

Sperry, J. S. (1983). Observations on the structure and function of hydathodes in *Blechnum lehmannii*. *Am. Fern J.* 73, 65–72. doi: 10.2307/1546852

Sperry, J. S., Holbrook, N. M., Zimmermann, M. H., and Tyree, M. T. (2008). Spring filling of xylem vessels in wild grapevine. *Plant Physiol.* 83, 414–417. doi: 10.1104/pp.83.2.414

Steudle, E. (2000). Water uptake by roots: effects of water deficit. *J. Exp. Bot.* 51, 1531–1542. doi: 10.1093/jexbot/51.350.1531

Stiller, V., Lafitte, H. R., and Sperry, J. S. (2003). Hydraulic properties of rice and the response of gas exchange to water stress. *Plant Physiol.* 132, 1698–1706. doi: 10.1104/pp.102.019851

Stiller, V., Sperry, J. S., and Lafitte, R. (2005). Embolized conduits of rice (Oryza sativa, Poaceae) refill despite negative xylem pressure. *Am. J. Bot.* 92, 1970–1974. doi: 10.3732/ajb.92.12.1970

Townsley, B. T., Covington, M. F., Ichihashi, Y., Zumstein, K., and Sinha, N. R. (2015). BrAD-seq: Breath Adapter Directional sequencing: a streamlined, ultra-simple and fast library preparation protocol for strand specific mRNA library construction. *Front. Plant Sci.* 6, 1–11. doi: 10.3389/fpls.2015.00366

Trapnell, C., Roberts, A., Goff, L., Pertea, G., Kim, D., Kelley, D. R., et al. (2012). Differential gene and transcript expression analysis of RNA-seq experiments with TopHat and Cufflinks. *Nat. Protoc.* 7, 562–578. doi: 10.1038/nprot.2012.016

Turner, M. F., Heuberger, A. L., Kirkwood, J. S., Collins, C. C., Wolfrum, E. J., Broeckling, C. D., et al. (2016). Non-targeted metabolomics in diverse sorghum breeding lines indicates primary and secondary metabolite profiles are associated with plant biomass accumulation and photosynthesis. *Front. Plant Sci.* 7, 1–17. doi: 10.3389/fpls.2016.00953

Tyree, M. T., Fiscus, E. L., Wullschleger, S. D., and Dixon, M. A. (2008). Detection of xylem cavitation in corn under field conditions. *Plant Physiol.* 82, 597–599. doi: 10.1104/pp.82.2.597

Vandeleur, R. K., Mayo, G., Shelden, M. C., Gilliham, M., Kaiser, B. N., and Tyerman, S. D. (2009). The role of plasma membrane intrinsic protein aquaporins in water transport through roots: diurnal and drought stress responses reveal different strategies between isohydric and anisohydric cultivars of grapevine. *Plant Physiol.* 149, 445–460. doi: 10.1104/pp.108.128645

Watkins, J. E., Holbrook, N. M., and Zwieniecki, M. A. (2010). Hydraulic properties of fern sporophytes: Consequences for ecological and evolutionary diversification. *Am. J. Bot.* 97, 2007–2019. doi: 10.3732/ajb.1000124

Wegner, L. H. (2014). Root pressure and beyond: Energetically uphill water transport into xylem vessels? *J. Exp. Bot.* 65, 381–393. doi: 10.1093/jxb/ert391

Wright, I. J., Westoby, M., Reich, P. B., Oleksyn, J., Ackerly, D. D., Baruch, Z., et al. (2004). The worldwide leaf economics spectrum. *Nature* 428, 821–827. doi: 10.1038/nature02403

Zhang, J., Zhang, X., and Liang, J. (1995). Exudation rate and hydraulic conductivity of maize roots are enhanced by soil drying and abscisic acid treatment. *New Phytol.* 131, 329–336. doi: 10.1111/j.1469-8137.1995.tb03068.x

Conflict of Interest: The authors declare that the research was conducted in the absence of any commercial or financial relationships that could be construed as a potential conflict of interest.

Copyright © 2021 Drobnitch, Comas, Flynn, Ibarra Caballero, Barton, Wenz, Person, Bushey, Jahn and Gleason. This is an open-access article distributed under the terms of the Creative Commons Attribution License (CC BY). The use, distribution or reproduction in other forums is permitted, provided the original author(s) and the copyright owner(s) are credited and that the original publication in this journal is cited, in accordance with accepted academic practice. No use, distribution or reproduction is permitted which does not comply with these terms.

frontiers in Plant Science

ORIGINAL RESEARCH
published: 05 February 2021
doi: 10.3389/fpls.2020.593207

Development of KASP Markers and Identification of a QTL Underlying Powdery Mildew Resistance in Melon (*Cucumis melo* L.) by Bulked Segregant Analysis and RNA-Seq

Yanyan Cao, Qiannan Diao, Youyuan Chen, Haijun Jin, Yongping Zhang and Hongmei Zhang**

Shanghai Key Lab of Protected Horticultural Technology, Horticultural Research Institute, Shanghai Academy of Agricultural Sciences, Shanghai, China

OPEN ACCESS

Edited by:
Magdalena Arasimowicz-Jelonek, Adam Mickiewicz University, Poland

Reviewed by:
Christina Cowger, Plant Science Research Unit (USDA-ARS), United States
Zhiyong Liu, Institute of Genetics and Developmental Biology, Chinese Academy of Sciences, China

***Correspondence:**
Yongping Zhang
zyp123944@126.com
Hongmei Zhang
zhanghongmei@saas.sh.cn

Specialty section:
This article was submitted to Plant Pathogen Interactions, a section of the journal Frontiers in Plant Science

Received: *10 August 2020*
Accepted: *28 October 2020*
Published: *05 February 2021*

Citation:
Cao Y, Diao Q, Chen Y, Jin H, Zhang Y and Zhang H (2021) Development of KASP Markers and Identification of a QTL Underlying Powdery Mildew Resistance in Melon (Cucumis melo L.) by Bulked Segregant Analysis and RNA-Seq. Front. Plant Sci. 11:593207. doi: 10.3389/fpls.2020.593207

Powdery mildew (PM), caused by *Podosphaera xanthii* (*Px*), is one of the most devastating fungal diseases of melon worldwide. The use of resistant cultivars is considered to be the best and most effective approach to control this disease. In this study, an F_2 segregating population derived from a cross between a resistant (wm-6) and a susceptible cultivar (12D-1) of melon was used to map major powdery mildew resistance genes using bulked segregant analysis (BSA), in combination with next-generation sequencing (NGS). A novel quantitative trait locus (QTL) named *qCmPMR-12* for resistance to PM on chromosome 12 was identified, which ranged from 22.0 Mb to 22.9 Mb. RNA-Seq analysis indicated that the *MELO3C002434* gene encoding an ankyrin repeat-containing protein was considered to be the most likely candidate gene that was associated with resistance to PM. Moreover, 15 polymorphic SNPs around the target area were successfully converted to Kompetitive Allele-Specific PCR (KASP) markers ($P < 0.0001$). The novel QTL and candidate gene identified from this study provide insights into the genetic mechanism of PM resistance in melon, and the tightly linked KASP markers developed in this research can be used for marker-assisted selection (MAS) to improve powdery mildew resistance in melon breeding programs.

Keywords: bulked segregant analysis, KASP markers, melon, powdery mildew, resistance gene

INTRODUCTION

Melon (*Cucumis melo* L.), which belongs to the Cucurbitaceae family, is an important horticultural and economic crop worldwide (Garcia-Mas et al., 2012). In view of its unique biological characteristics, such as a sweet fruit, unique aroma and rich nutritional value, melon is highly favored by consumers. Powdery mildew (PM) is a fungal disease that occurs commonly on leaves, petioles, and stems of most cucurbit crops in both field and greenhouse conditions (Perez-Garcia et al., 2009). This disease can result in a decrease in weight-based productivity and a reduction in fruit quality (Candido et al., 2014), thereby causing severe economic losses in many areas of the world (Romero et al., 2008).

Melon PM is often caused by *Podosphaera xanthii* (*Px*) and *Golovinomyces cichoracearum* (*Gc*) (Křístková et al., 2009; Li et al., 2017). These two fungi can be distinguished by observation of the pathogens' cleistothecia, conidia germination, microscopic morphology, and host identification (Liang et al., 2010; Liu et al., 2010). Both pathogens exist either as an asexual stage (conidia) or sexual stage (Cleistothecia); the morphological characteristics of the asexual stage are similar for the two pathogens, and the morphological distinction between them is based on whether fibrous bodies occur on the spore (*Px* spores possess fibrous bodies, whereas these are absent from those of *Gc*) (Wang et al., 2013). In China, *Px* is generally considered to be the main causal agent of PM in melon (Cheng et al., 2011; Zhang et al., 2013). Recent reports have shown that melon PM is caused by *Px* in Shanghai (Gu et al., 2010; Li et al., 2015). The five phases of the *Px* life cycle are separately germinating conidia, the formation of a primary germ tube, hyphae, conidiophores, and colonization (Wang et al., 2013). After a spore lands on the leaf cuticle, the interaction is initiated by the formation of a primary germ tube and is followed by the formation and maturation of an appressiorial germ tube; the next step involves haustorium formation within an attacked epidermal cell and fungal development proceeds via the formation of secondary hyphae and haustoria and terminates with sporulation (Wolter et al., 1993). *Px* can coexist with the diseased plants in the soil as hyphae, conidia and cleistothecia, or it can overwinter as hyphae on greenhouse plants, and when the temperature rises the subsequent year, the conidia are distributed by air or water to infect the plants (Zhang et al., 2007).

Currently, the main method applied to control powdery mildew is chemical prevention by the application of chemical fungicides, which is often time-consuming and labor-intensive (Chen, 2014). Furthermore, chemical control not only leads to the appearance of resistance and to mutations in PM, which therefore means that this treatment becomes ineffective, but it also increases the input costs and has a negative impact on the environment (McGrath, 2001; Hollomon et al., 2002). Therefore, breeding for disease resistance is a safe alternative or a complement to the chemical control of this disease (Perchepied et al., 2005). Marker-assisted selection (MAS) is a powerful genomic tool that assists phenotypic selection for the development of disease-resistant cultivars and can help breeders incorporate and pyramid resistance genes into breeding material, thereby reducing disease severity (Ribaut et al., 2002; Chen, 2013; Zhu et al., 2019). At present, MAS has been extensively applied to search for the molecular markers that are linked to a specific trait during the development of disease-resistant cultivars (Teixeira et al., 2008). To date, a variety of molecular markers have been developed, such as RFLPs, RAPDs, SSRs, InDels and SNPs, to detect allelic variation within different samples at the DNA level (Wang et al., 2015).

Bulked segregant analysis (BSA) is an important technique used to map quantitative trait loci (QTLs) and identify DNA markers. Compared with the traditional QTL mapping method, which is time-consuming and involves screening polymorphic markers and genotyping, BSA provides a convenient and rapid method with which to identify resistance genes by generating two DNA bulks with a contrasting target trait (Michelmore et al., 1991; Abe et al., 2012; Nie et al., 2015). Recently, due to the release of sequenced genomes and the significant reduction in the costs of next-generation sequencing (NGS), whole-genome resequencing has been coupled with BSA to map the genes of interest that are associated with a given phenotype. The combined application of BSA with NGS (BSA-Seq) has accelerated the identification of tightly linked markers for gene identification and QTL mapping (Zou et al., 2016). To date, BSA-Seq has been successfully used in mapping the traits of early flowering, flesh thickness and downy mildew resistance in cucumber (Lu et al., 2014; Xu et al., 2015; Win et al., 2017), cold tolerance and blast resistance in rice (Yang et al., 2013; Zheng et al., 2016), cotyledon color, and a high-sucrose and low-oil seed phenotype in soybean (Dobbels et al., 2017; Song et al., 2017).

At present, the availability of sequence information has facilitated the identification and development of single nucleotide polymorphism (SNP) markers, which have largely replaced simple sequence repeats (SSRs) as markers in crop species (Semagn et al., 2014). Because of the low assay cost, high genomic abundance, ease of documentation, locus specificity, co-dominant inheritance, the potential for high-throughput analysis, and relatively low genotyping error rates, the use of SNPs has emerged as a powerful approach for many genetic applications in areas such as germplasm characterization, quality control (QC) analysis, linkage mapping, linkage-based and linkage disequilibrium-based QTL mapping, allele mining, marker-assisted backcrossing (MABC), genomic selection (GS), and MAS (Rafalski, 2002; Schlotterer, 2004; Semagn et al., 2014). Kompetitive Allele-Specific PCR (KASP) is a high-throughput SNP genotyping platform. Due to its low cost and genotyping error rates, and its high reliability and reproducibility, KASP has evolved to become a global benchmark technology and has been widely used for genetic mapping and trait-specific marker development (He et al., 2014; Ertiro et al., 2015; Rasheed et al., 2016; Tan et al., 2017).

To date, several genes and QTLs that confer resistance to powdery mildew have been identified in melon, such as the genes of *Pm-w* from WMR 29 (Pitrat, 1991), *Pm-x* from PI 414723 and *Pm-y* from VA 435 (Périn et al., 2002), and *Pm-1* from the AF125^{Pm-1} Cantalupensis Charentais-type breeding line (Teixeira et al., 2008), and the QTLs of *PmV.1* and *PmXII.1* from PI 124112 (Perchepied et al., 2005), *Pm-R* from TGR-1551 (Yustelisbona et al., 2011) and *BPm12.1* from MR-1 (Li et al., 2017). In previous studies, many of these genes and QTLs have been found on chromosomes 2, 4, 5, and 12 (Pitrat, 1991; Périn et al., 2002; Fukino et al., 2008; Zhang et al., 2013; Li et al., 2017). Differing views exist concerning the genetic basis of PM resistance in melon. Some studies have indicated that PM resistance in melon is controlled by a single dominant gene (Epinat et al., 1992; Zhang et al., 2008; Wang et al., 2016; Li et al., 2017), whereas other research has reported that it is controlled by a recessive gene (McCreight and Coffey, 2011), by two dominant genes (Clements, 2014), or by one dominant and one recessive gene (Sun et al., 2010; Yuste-Lisbona et al., 2010). Moreover, it is also reported that resistance to PM in melon is controlled by different sets of QTL (Perchepied et al., 2005).

The melon cultivars wm-6 and 12D-1 are both high-generation inbred lines developed by our group and our previous study has shown that the melon cultivar wm-6 is highly resistant to PM, whereas 12D-1 is highly susceptible (Data not shown). In this study, we obtained an F_2 population from a cross between wm-6 (female) and 12D-1 (male). A major QTL that confers PM resistance on chromosome 12 was identified by BSA-Seq analysis, and a most likely candidate gene was predicted from RNA-Seq data in wm-6 melon. In addition, 15 suitable KASP markers were developed by the KASP SNP genotyping method. This will facilitate the cloning and functional validation of the candidate resistance gene and the linked markers will further provide a useful tool for MAS in melon breeding programs.

MATERIALS AND METHODS

Plant Materials, Growth Conditions and Inoculation With Powdery Mildew Fungus

Two inbred lines, wm-6 (P_1, resistant to PM) and 12D-1 (P_2, susceptible to PM), were used as parental lines to generate F_1 and F_2 populations for the QTL mapping of PM resistance in melon (*Cucumis melo* L.). The P_1, P_2, F_1 and F_2 individuals were all placed in a culture room at a temperature of 25/20°C (day/night) with a photoperiod of 14 h light and relative humidity of 50–75%. All the seeds used in this study were provided by the Shanghai Academy of Agricultural Sciences.

The PM fungus (*P. xanthii*) used in this study was isolated from leaves of diseased Cucurbitaceae plants according to the method of Nie et al. (2015). The plants were grown on the experimental farm of the Shanghai Academy of Agricultural Sciences, and the PM fungus was maintained by infection of susceptible melon cultivar plants. When the three true seedling leaves of melon plants were fully expanded, the fungus was collected and suspended in sterile distilled water containing 0.01% Tween 20 and was then used to inoculate plants at a concentration of 1×10^6 as previously described (Zhang et al., 2011).

Disease Evaluation for Resistance to Powdery Mildew

Phenotyping for powdery mildew resistance of melon was performed according to Zhang et al. (2013) with some modifications at 12-d post-inoculation (dpi), and each infected leaf was analyzed individually. Briefly, the disease grade of powdery mildew was categorized on a scale of 0–5 as follows: Class 0, no infection; Class 1, infection of less than 30% of the leaf; Class 3, infection of less than 70% of the leaf; Class 5, infection of approximately the entire leaf and coverage with heavy sporulation. The disease severity index (DSI) was calculated from the disease-rating scale using the following formula: DSI = $100 \times \Sigma$[(disease grade × number of plants in that grade)/(Total number of plants × maximum disease grade)]. For the inheritance study, lines with a DSI $\leq$ 20 were considered resistant and lines with a DSI $>$ 20 were considered susceptible. For the F_2 population, the same protocol was followed to identify resistant and susceptible plants. The phenotype of the two parental lines was analyzed at least three independent experiments with $>$15 seedlings examined in each experiment. The DSI of the two parental lines and the F_1 hybrid plants was separately measured three times for 20 seedlings in each measurement. The DSI of F_2 generation was calculated based on the phenotype of 193 F_2 plants. On the basis of the DSI scores, plants with a DSI of 0–1 were categorized as resistant, and those with a DSI of 3–5, as susceptible.

RNA Extraction, Library Construction and Sequencing

For RNA-Seq analysis, the two parental lines wm-6 and 12D-1 were separately treated with water (mock) or PM fungus. After 3 days, the leaves of wm-6 and 12D-1 plants (named wm-6K, wm-6P, 12D-1K, 12D-1P, respectively) were harvested, immediately frozen in liquid nitrogen and stored at −80°C before RNA extraction.

Total RNA was extracted using the Trizol reagent kit (Invitrogen, Carlsbad, CA, United States) according to the manufacturer's protocol. RNA quality was assessed on an Agilent 2100 Bioanalyzer (Agilent Technologies, Palo Alto, CA, United States) and analyzed using RNase-free agarose gel electrophoresis. Following total RNA extraction, eukaryotic mRNA was enriched by Oligo(dT) beads, whereas prokaryotic mRNA was enriched by removing rRNA with the Ribo-ZeroTM Magnetic Kit (Epicentre, Madison, WI, United States). The enriched mRNA was fragmented into short fragments using fragmentation buffer and reverse transcribed into cDNA with random primers. Second-strand cDNA was synthesized by DNA polymerase I, RNase H, dNTPs and buffer. The cDNA fragments were purified with a QiaQuick PCR extraction kit (Qiagen, Venlo, The Netherlands), and following end repair and the addition of poly(A), was ligated to Illumina sequencing adapters. The ligation products were selected according to size by agarose gel electrophoresis, amplified by PCR, and sequenced using Illumina HiSeq2500 by the Gene *Denovo* Biotechnology Company (Guangzhou, China).

Genomic DNA Extraction, Library Construction for Bulked Segregant Analysis and Whole-Genome Resequencing

Young leaves from the two parental lines, and from the F_1 and the F_2 populations were collected, and total genomic DNA was extracted using the CTAB method (Doyle, 1991). For bulked segregant analysis, four DNA pools were constructed, consisting of two parent bulks and two F_2 segregating bulks. The parent bulks were separately constructed from the female parent (wm-6) and male parent (12D-1), and the two F_2 segregating bulks were separately constructed by mixing an equal amount of DNA extracted from 25 extremely resistant (R-bulk) and 25 susceptible (S-bulk) F_2 plants. After the four sequencing libraries were prepared according to the standard protocol of Illumina, they were sequenced on an Illumina HisSeq platform (Illumina,

San Diego, CA, United States). Short reads obtained from the four bulks were aligned against the melon reference genome sequence to obtain the consensus sequence using BWA software. SNP calling was performed with GATK tools. The heterozygous alleles in both parents were filtered out during the process. The raw sequence reads are deposited in the NCBI Sequence Read Archive (SRA; Accession number: PRJNA655764).

Genetic Mapping

In this study, four methods (SNP-ratio, ED^4, G value and LOD) were used to map QTLs that underlay resistance to PM. The SNP-ratio (resistant alleles/sensitive alleles) of the R-bulk and S-bulk were calculated as described by Soyk et al. (2017) and the SNP-ratio of the R-bulk was then divided by the SNP-ratio of the S-bulk and plotted across the genomic regions that showed ratio peaks, which indicate the possible existence of the QTLs. The read depth for each allele at segregating allelic SNPs in 500-kb sliding windows was summed using a 100-kb step increment. The Euclidean distance of each SNP (ED-SNP) was calculated as described by Hill et al. (2013) and the ED was the sum of 100 ED-SNP values within a window of 100 consecutive SNPs. The ED^4 was calculated by raising ED to the fourth power. The G value averaged across neighboring SNPs was calculated according to Magwene et al. (2011). The LOD (logarithm of the odds) score was calculated as described by Zhang et al. (2019).

Development and Analysis of KASP Markers

The polymorphic SNPs identified around the target regions that associated with powdery mildew resistance were converted into KASP markers using PolyMarker software[1]. For each SNP, two allele-specific forward primers and one common reverse primer based on the flanking sequences around the variant position (SNP) were designed using Primer 3 software. The polymorphic SNP primers were converted to KASP markers to test their ability to differentiate the polymorphism by genotyping the two parents, and the KASP markers were then verified with the entire F_2 population. Each KASP reaction was carried out using a 3-μL reaction mixture consisting of 1.48 μL KASP 2 × reaction mix, 50 ng DNA template, 0.17 μM Hex forward primer, 0.17 μM FAM forward primer and 0.42 μM universal reverse primer. The cycling conditions were as follows: 94°C for 15 min followed by 10 touchdown cycles at 95°C for 20 s and 65°C for 60 s (dropping 0.8°C per cycle); after the final annealing temperature of 56°C was reached, 26 cycles were performed at 94°C for 20 s and at 57°C for 60 s. Thermocycling and fluorescence readings were performed on a Hydrocycler and PHERAstar of LGC SNPline platform. Genotyping data were viewed as a cluster plot by SNPviewer software supported from LGC Genomics[2]. The significance of the correlation coefficients between phenotype and genotype was determined with *t*-tests. Linkage groups were constructed using JoinMap 4.1.

RESULTS

Evaluation of Resistance to Powdery Mildew in wm-6 × 12D-1

The artificial inoculation results showed that the parental line wm-6 was highly resistant to *P. xanthii* (DSI = 8.0), whereas the other parental line 12D-1 (DSI = 94.0) was susceptible to the fungus (**Figure 1**, **Table 1** and **Supplementary Table 1**). The DSI of the F_1 plants was 68.0, which meant that the F_1 generation was susceptible to PM fungus (**Table 1** and **Supplementary Table 1**). The evaluation of infection by PM indicated that 58 F_2 plants showed PM resistance and 135 showed PM susceptibility, with a 1:3 segregation between resistant and susceptible individuals ($\chi^2 = 2.63$, $P = 0.11$) (**Table 1**). This indicated that resistance to *P. xanthii* in wm-6 was conferred by a single recessive gene.

[1]http://polymarker.tgac.ac.uk

[2]http://www.lgcgenomics.com

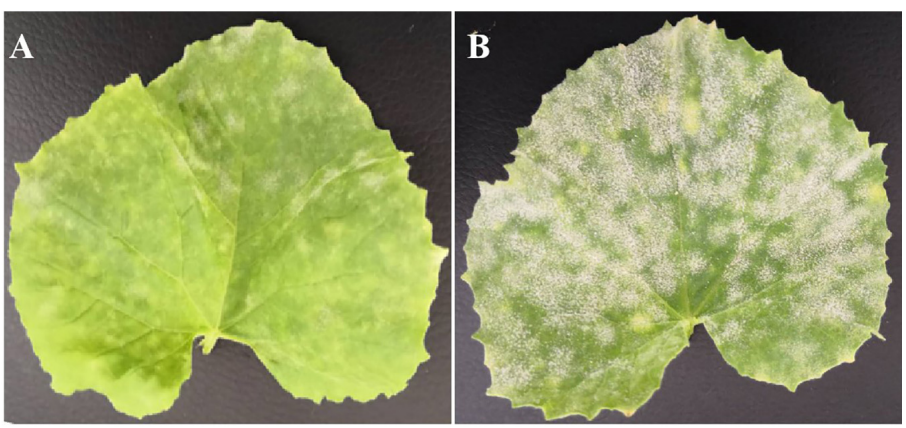


FIGURE 1 | Phenotype of resistant parent wm-6 and susceptible parent 12D-1, 12 days after inoculation with *P. xanthii*. **(A)** The phenotype of the resistant parent wm-6, 12 days after inoculation with *P. xanthii*. **(B)** The phenotype of the resistant parent 12D-1, 12 days after inoculation with *P. xanthii*. The experiments were repeated at least three times independently, with similar results.

TABLE 1 | Disease evaluation of powdery mildew in wm-6, 12D-1, F_1 and F_2 plants at 12 days post inoculation with *P. xanthii*.

Cross	Generation	Inoculation time	Disease rating[1]				Total	DSI
			0	1	3	5		
wm-6	P_1	2019	12	8	0	0	20	8
12D-1	P_2	2019	0	0	3	17	20	94
wm-6 × 12D-1	F_1	2019	0	5	6	9	20	68
wm-6 × 12D-1	F_2	2019	26	32	38	97	193	65.39

The disease severity index of the two parental lines and the F_1 hybrid plants were separately measured with 20 seedlings. The measurements were repeated three times independently with similar results, and the data of one representative experiment are shown.

[1]The DSI of leaves was rated on a 0–5 scale to determine the response of melon genotypes to powdery mildew, where 0 = immune, no symptom; 1 = highly resistant, infection of less than 30% of the leaf with low sporulation; 3 = moderately susceptible, infection of less than 70% of the leaf with moderate to high sporulation, and 5 = highly susceptible, infection of approximately the entire leaf with heavy sporulation.

Sequencing Data Analysis of Four DNA Bulks

BSA-Seq analysis was performed with the DNAs of four libraries (wm-6, 12D-1, R-bulk and S-bulk) using the Illumina HiSeq 2500 platform. In total, 60,401,327 and 57,755,318 clean reads for wm-6 and 12D-1, respectively, and 92,327,580 and 101,809,441 short reads for the R-bulk and S-bulk libraries, respectively, were generated. The GC content ranged from 36.76% to 37.1% and the Q20 and Q30 of each pool were over 98% and 93%, respectively. Over 95% of the reads were mapped to the melon reference genome, and the coverage rates were 95.78% in wm-6, 95.85% in 12D-1, 97.02% in R-bulk, and 97.05% in S-bulk, approximately resulting in a 23 × coverage depth for parental bulks and at least 35 × coverage for two F_2 progeny bulks (**Table 2**). These results indicated that the quantity and quality of the data were sufficient for further analysis.

QTL Mapping of PM Resistance

After alignment to the reference genome of melon, 2,624,079 SNPs were identified between the parental lines wm-6 and 12D-1, and the distribution of these SNPs on each chromosome is listed in **Supplementary Table 2**. The resistance-related candidate regions were identified by analyzing the resistant pool and the susceptible pool. Using four statistic methods, a 0.9-Mb region spanning 22.0–22.9 Mb on chromosome 12 was defined as the target region associated with PM resistance (**Figures 2A–D**), and the significant QTL was designated *qCmPMR-12*. Within the candidate region, a total of 4,033 SNPs showed polymorphisms, 115 of which were located within the 3′ UTR, 78 in the 5′ UTR, 547 in the downstream region, 397 in the exonic region, 2,243 in the intergenic region, 1,005 in the intronic region, and 735 in the upstream region (**Table 3**). In addition, the target region included 182 non-synonymous SNV, 3 stopgain, 1 stoploss and 211 synonymous SNV polymorphisms (**Table 4**). Moreover, the candidate region contained 476 small InDels, 29 of which were located within the 3′ UTR, 23 in the 5′ UTR, 199 in the downstream region, 28 in the exonic region, 892 in the intergenic region, 387 in the intronic region, and 298 in the upstream region (**Table 3**). The InDels included 9 frameshift deletions, 6 frameshift insertions, 8 non-frameshift deletions and 5 non-frameshift insertions (**Table 4**).

According to the melon gene annotation database[3], the target region contains approximately 126 annotated genes, and the specific information for these genes is listed in **Supplementary Table 3**.

RNA-Seq and Candidate Gene Analysis

To elucidate the changes in gene expression of resistant and susceptible melon lines after inoculation with *P. xanthii*, we performed an RNA-Seq analysis at 3 dpi. The dataset submitted to NCBI include the raw reads of the assembled transcriptome sequences from control and pathogen-treated melon plants. All transcriptome raw reads have been deposited in NCBI SRA[4] under the accession number PRJNA670091.

Analysis of the RNA-Seq results for the 126 annotated genes obtained by BSA-Seq indicated that the transcript levels of the two genes *MELO3C002434* and *MELO3C002477* ($|\log_2 FC| > 1$) were clearly up-regulated in the parental lines after inoculation with *P. xanthii*[5]. The two genes respectively encode an ankyrin repeat-containing (ANK) protein and a homeobox-leucine zipper

[3]https://www.melonomics.net/

[4]http://www.ncbi.nlm.nih.gov/sra

[5]https://submit.ncbi.nlm.nih.gov/subs/sra/SUB8336313/

TABLE 2 | Summary of sequencing data and the data aligned to the melon reference genome for the parental lines and the resistant and susceptible pools by BSA-Seq.

Sample name[1]	Clean reads[2]	Clean reads (%)	GC content (%)	Q20 (%)[3]	Q30 (%)[4]	Mapped reads (%)[5]	Coverage (%)[6]	Sequencing depth (×)
wm-6	60401327	95.86	36.80	98.02	93.17	95.80	95.78	23.34
12D-1	57755318	95.86	36.76	98.06	93.29	97.86	95.85	22.81
R-bulk	92327580	96.3	37.02	98.21	93.71	96.55	97.02	35.54
S-bulk	101809441	95.98	37.1	98.10	93.37	95.95	97.05	38.31

[1]wm-6, powdery mildew-resistant parent; 12D-1, powdery mildew-susceptible parent; R-bulk, powdery mildew resistance bulk; S-bulk, powdery mildew susceptible bulk.
[2]Number of reads after trimming and adapter removal.
[3]The percentage of base recognition accuracy above 99%.
[4]The percentage of base recognition accuracy above 99.9%.
[5]Alignment to the melon genome assembly V4.0 (www.melonomics.net/).
[6]Coverage (≥1 read).

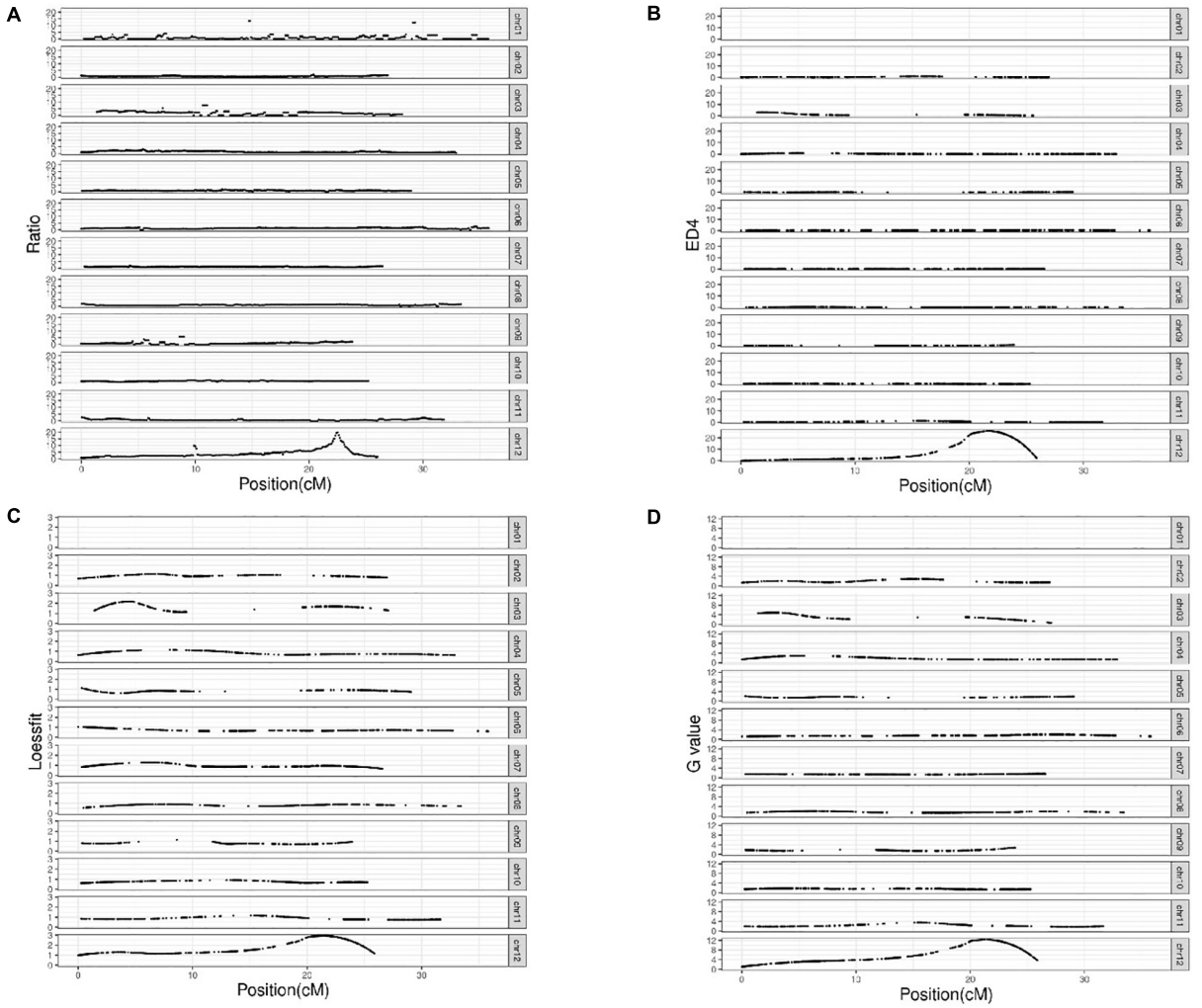


FIGURE 2 | BSA-Seq results. Analysis of the QTL location by **(A)** the SNP-Ratio method; **(B)** the ED[4] method; **(C)** the LOD method; **(D)** the G-value method.

protein (**Supplementary Table 3**). Further analysis showed that only the expression level of *MELO3C002434* was significantly higher in the resistant line wm-6 than in the susceptible line 12D-1 following PM infection. Notably, BSA-Seq showed that this gene contained 10 SNPs and 1 InDel (**Table 5**). Previous studies have shown that ANK proteins play important roles in regulating immune responses against various pathogens (Cao et al., 1997; Ryals et al., 1997; Yan et al., 2002; Li et al., 2013). Therefore, we speculated that *MELO3C002434* may confer PM resistance, or at least be a PM resistance-related gene in melon.

TABLE 3 | The chromosomal locations and numbers of SNPs and InDels in the target QTL region associated with powdery mildew resistance between the melon parental lines wm-6 and 12D-1.

Chromosomal location	3′ UTR	5′ UTR	Down-stream	Exonic region	Intergenic region	Intronic region	Upstream
SNP number	115	78	547	397	2243	1005	735
InDel number	29	23	199	28	892	387	298

KASP Marker Development and Physical Map Construction

KASP assays were designed for SNPs across the 20.0–23.9 Mb region on chromosome 12 and were tested on the F_2 population to determine which markers showed the highest association with PM resistance. In this region, thirty-seven chromosome-specific

TABLE 4 | The types and numbers of SNPs and InDels in the target QTL region associated with powdery mildew resistance between the melon parental lines wm-6 and 12D-1.

SNP type	SNP number	InDel type	InDel number
non-synonymous SNV[1]	182	frameshift deletion	9
stopgain	3	frameshift insertion	6
stoploss	1	non-frameshift deletion	8
synonymous SNV[1]	211	non-frameshift insertion	5

[1]*Single nucleotide variants.*

TABLE 5 | Analysis of SNPs and InDels present within the *MELO3C002434* gene in two parental melon lines.

Type	Position	Reference	Allele	wm-6	12D-1
SNP	22665882	C	T	1/1	0/0
SNP	22666490	A	G	1/1	0/0
SNP	22666491	G	A	1/1	0/0
SNP	22666786	A	G	0/0	1/1
SNP	22666869	G	A	0/0	1/1
SNP	22667081	C	G	0/0	1/1
SNP	22667159	T	C	0/0	1/1
SNP	22668006	A	C	0/0	1/1
SNP	22668100	T	C	0/0	1/1
SNP	22668300	T	C	0/0	1/1
InDel	22666219	C	CATT	1/1	0/0

0/0 means that the genotype of the inbred was the same as the reference, and 1/1 means that the genotype of the inbred was the same as the allele.

SNPs selected for conversion to KASP markers were used to screen the parents and bulks to confirm their polymorphisms, and 15 out of 37 markers successfully distinguished the parents and bulks (**Figure 3**), indicating that these KASP markers were suitable for use in MAS to improve the level of powdery mildew resistance in melon breeding. Specific information and the sequences of the polymorphic KASP markers are separately listed in **Supplementary Tables 4, 5**. The close-up view of QTL and KASP markers linked to the target regions is shown in **Figure 4**.

Using the 15 KASP markers, the genetic physical map and linkage map were constructed by JoinMap 4.1 (**Figures 5A,B**). As shown in the linkage map, the peak of the QTL was located in a 0.6-cM interval spanned by KASP markers KA002213 and KA002215 (**Figure 5B**).

DISCUSSION

The melon cultivar wm-6 is a high-generation inbred line developed by our group, which is highly resistant to powdery mildew (**Figure 1A**, **Table 1** and **Supplementary Table 1**). In this study, a genomic region ranging from 22.0 Mb to 22.9 Mb on chromosome 12 was identified using BSA-Seq technology. Similarly, Li et al. (2017) detected a major QTL for PM resistance on chromosome 12 and suggested that resistance to *P. xanthii* in MR-1 was controlled by a single dominant gene. However, in this study, the segregation ratio of the F_2 population indicated that the PM resistance in wm-6 was controlled by a single recessive gene, implying a different genetic basis of the PM resistance mechanisms between the melon cultivars wm-6 and MR-1. Other studies have also demonstrated that the genetic basis of resistance to PM differs depending on the tested melon material (Epinat et al., 1992; Zhang et al., 2008; Sun et al., 2010; Yuste-Lisbona et al., 2010; McCreight and Coffey, 2011; Wang et al., 2016).

To identify the PM resistance gene in wm-6, RNA-Seq analysis was performed with the melon lines wm-6 and 12D-1 in parallel. Combination of the results from BSA-Seq and RNA-Seq suggested that the *At3g12360*-like gene *MELO3C002434*, which encodes an ANK protein was the most likely candidate gene to confer PM resistance, because only this gene was significantly more highly expressed in the resistant line wm-6 than that in the susceptible line 12D-1 following infection with *P. xanthii*

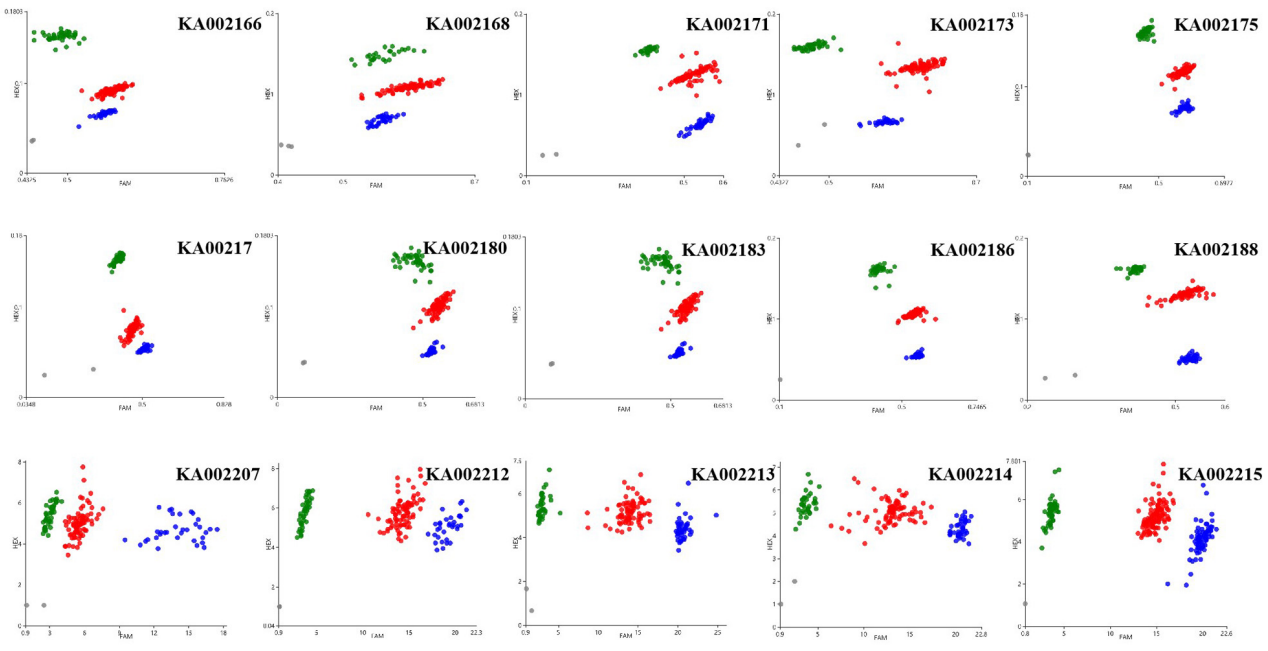


FIGURE 3 | Results of genotyping using the Kompetitive Allele Specific PCR (KASP) assay. Scatter plots for selected KASP assays showing clustering of varieties on the X- (FAM) and Y- (HEX) axes. The green and blue dots represent the homozygous F_2 lines and the red dot represents heterozygous F_2 lines from the mapping population of the wm-6 × 12D-1 cross. The gray dots represent the NTC (non-template control).

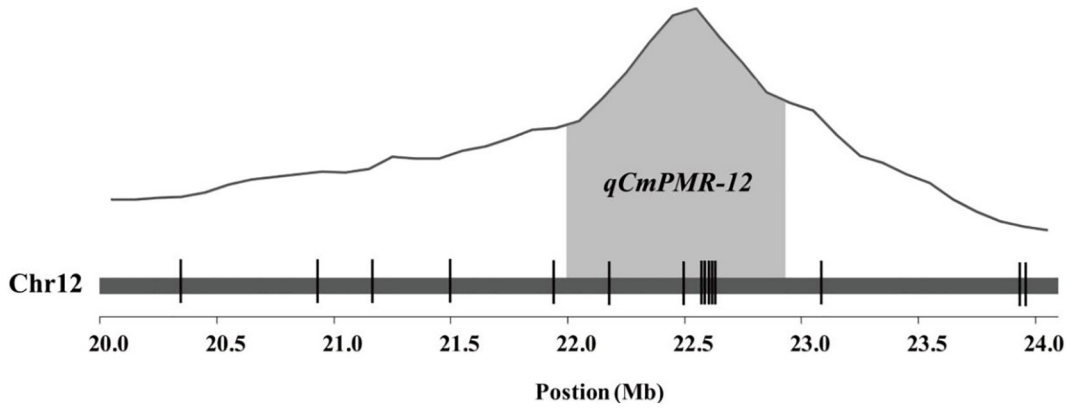


FIGURE 4 | Quantitative trait locus (QTL) analysis of resistance to powdery mildew and the distribution of KASP markers linked to the target region. The gray areas represent the QTL region. The positions of KASP markers are shown by vertical lines.

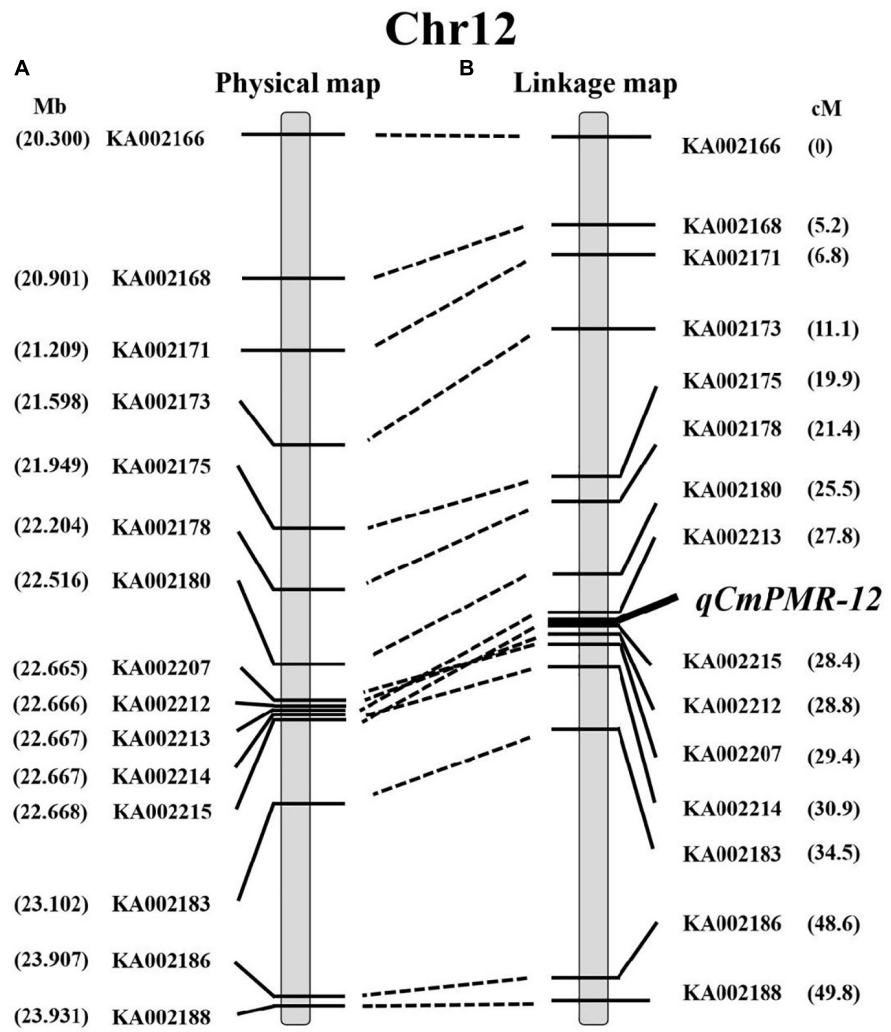


FIGURE 5 | The location of *qCmPMR-12* on melon chromosome 12. **(A)** The physical map around the region of *qCmPMR-12*; marker names are indicated to the left of the map. **(B)** The genetic linkage map of melon chromosome 12; map distances are shown on the right. The QTL region was identified by QTL mapping using phenotypic analysis and marker data from F_2 populations.

(see text footnote 5). Previous studies revealed that ANK proteins have critical functions in various biological processes of plant growth and development as well as in response to biotic and abiotic stresses (Albert et al., 1999; Yan et al., 2002; Ha et al., 2004; Hemsley et al., 2005; Garcion et al., 2006; Sakamoto et al., 2008; Shen et al., 2010; Li et al., 2013). It has been reported that the ANK protein NPR1 is important both in the SA-dependent immune response and in SA-independent resistance responses induced by the root-associated bacteria (Cao et al., 1997; Ryals et al., 1997); AKR2 functions in the oxidative metabolism of disease resistance and stress response in Arabidopsis (Yan et al., 2002); a plasma membrane-localized ANK protein, ACD6, is involved in SA-dependent signaling in defense responses and programmed cell death (Lu et al., 2003, 2005), and ectopic expression of the ANK protein *OsBIANK1* of rice confers enhanced disease resistance to *Botrytis cinerea* and *Pseudomonas syringae* in Arabidopsis (Li et al., 2013). Interestingly, the gene *MELO3C002434* contained 10 SNPs and 1 InDel (**Table 5**) and 5 out of 15 KASP markers that developed in this study were located within this gene (**Supplementary Table 5**). All of these results further implied that *MELO3C002434* is the most likely candidate gene associated with PM resistance in melon wm-6. In addition, the report of Li et al. (2017) suggested *MELO3C002434* to be one of the genes related to PM resistance in spite of the different genetic basis of the PM resistance mechanism in melon wm-6 and MR-1. Therefore, further genetic studies and more detailed analyses are required to confirm the role and molecular mechanism of action of *MELO3C002434* in the PM defense response.

In this study, 37 SNPs surrounding the candidate region were used to design KASP markers using the PolyMarker website and 15 of these were polymorphic among the bulk and parent populations. To the best of our knowledge, this is the first report that KASP markers have been developed and used in MAS to improve PM resistance in melon breeding, although several markers linked to resistance genes have been reported previously in melon (Ning et al., 2014; Han et al., 2015).

CONCLUSION

In this study, a major QTL that is associated with PM resistance was identified in a 0.9-Mb interval on chromosome 12 of melon using BSA-Seq technology. Additional RNA-Seq data suggested that an ankyrin repeat-containing gene within this region, *MELO3C002434*, was implicated to be the most important candidate gene. In addition, 15 suitable KASP markers that were tightly linked to the resistance phenotype were developed for the MAS of melon. These data can be used to improve PM resistance in breeding programs and to facilitate understanding of the molecular mechanisms that underlying PM resistance in melon.

DATA AVAILABILITY STATEMENT

The raw sequence reads produced by BSA-Seq are deposited in the NCBI Sequence Read Archive (SRA; Accession number: PRJNA655764).

AUTHOR CONTRIBUTIONS

YZ, YC, and HZ designed the research. YC and QD prepared the plant materials. YC performed the experiments, analyzed the data, and wrote the manuscript. YZ, YC, and HJ revised the manuscript. All authors contributed to the article and approved the submitted version.

FUNDING

This study was supported by the Shanghai Science and Technology Commission (20392000300), Shanghai Minhang Science and Technology Commission (2019MHC051), Excellent Team of Shanghai Academy of Agricultural Sciences (B-06), and Shanghai Melon and Fruit Industrial Technology System [(2020)1].

SUPPLEMENTARY MATERIAL

The Supplementary Material for this article can be found online at: https://www.frontiersin.org/articles/10.3389/fpls.2020.593207/full#supplementary-material

Supplementary Table 1 | Means, standard errors and ranges of DSI of the parents and F_1 plants at 12 dpi with *P. xanthii* in the year of 2019.

Supplementary Table 2 | The number of SNPs distributed on each chromosome of melon detected by BSA-Seq.

Supplementary Table 3 | The positions and annotations of candidate genes in the target region conferring powdery mildew resistance from 22.0 Mb to 22.9 Mb based on the melon reference genome (CM3.6.1).

Supplementary Table 4 | KASP primer sequences used for MAS in melon breeding programs.

Supplementary Table 5 | Genotypes and positions of the 15 KASP markers linked to powdery mildew resistance gene of melon.

REFERENCES

Abe, A., Kosugi, S., Yoshida, K., Natsume, S., Takagi, H., Kanzaki, H., et al. (2012). Genome sequencing reveals agronomically important loci in rice using MutMap. *Nat. Biotechnol.* 30, 174–178. doi: 10.1038/nbt.2095

Albert, S., Despres, B., Guilleminot, J., Bechtold, N., Pelletier, G., Delseny, M., et al. (1999). The EMB 506 gene encodes a novel ankyrin repeat containing protein that is essential for the normal development of Arabidopsis embryos. *Plant J.* 17, 169–179. doi: 10.1046/j.1365-313x.1999.00361.x

Candido, V., Campanelli, G., Viggiani, G., Lazzeri, L., and Camele, I. (2014). Melon yield response to the control of powdery mildew by environmentally friendly substances. *Entia Horticult.* 166, 70–77. doi: 10.1016/j.scienta.2013.12.008

Cao, H., Glazebrook, J., Clarke, J. D., Volko, S., and Dong, X. (1997). The Arabidopsis *NPR1* gene that controls systemic acquired resistance encodes a novel protein containing ankyrin repeats. *Cell* 88, 57–63. doi: 10.1016/s0092-8674(00)81858-9

Chen, X. M. (2013). High-temperature adult-plant resistance, key for sustainable control of stripe rust. *Am. J. Plant Sci.* 04, 608–627. doi: 10.4236/ajps.2013.43080

Chen, X. M. (2014). Integration of cultivar resistance and fungicide application for control of wheat stripe rust. *Can. J. Plant Pathol.* 36, 311–326. doi: 10.1080/07060661.2014.924560

Cheng, H., Kong, W., Su, Y., Liu, D., and He, Q. (2011). Identification on powdery mildew and physiological race of melon in china. *J. Changjiang Vegetables* 18, 1–5. doi: 10.29405/j.bes/411-104725

Clements, J. (2014). Powdery mildew resistance gene of ssr molecular markers linked to the 'wmr-29' strains of melon. *Northern Horticult.* 61, 347–357.

Dobbels, A. A., Michno, J. M., Campbell, B. W., Virdi, K. S., Stec, A. O., Muehlbauer, G. J., et al. (2017). An Induced Chromosomal Translocation in Soybean Disrupts a KASI Ortholog and Is Associated with a High-Sucrose and Low-Oil Seed Phenotype. *G3* 7, 1215–1223. doi: 10.1534/g3.116.038596

Doyle, J. (1991). DNA protocols for plants-CTAB total DNA isolation. *Mole. Techniq. Taxonomy* 43:25.

Epinat, C. M., Pitrat, M., and Bertrand, F. (1992). Genetic analysis of resistance of 5 melon lines to powdery mildews. *Acta Horticult.* 65, 135–144. doi: 10.1007/bf00022575

Ertiro, B. T., Ogugo, V., and Worku, M. (2015). Comparison of Kompetitive Allele Specific PCR (KASP) and genotyping by sequencing (GBS) for quality control analysis in maize. *BMC Genomics* 16:908. doi: 10.1186/s12864-015-2180-2

Fukino, N., Ohara, T., Monforte, A. J., Sugiyama, M., Sakata, Y., Kunihisa, M., et al. (2008). Identification of QTLs for resistance to powdery mildew and SSR markers diagnostic for powdery mildew resistance genes in melon (*Cucumis melo* L.). *Theoret. Appl. Genet.* 118, 165–175. doi: 10.1007/s00122-008-0885-1

Garcia-Mas, J., Benjak, A., Sanseverino, W., Bourgeois, M., and Baulcombe, D. C. (2012). The genome of melon (*Cucumis melo* L.). *Proc. Natl. Acad. Sci.* 109, 11872–11877.

Garcion, C., Guilleminot, J., Kroj, T., Parcy, F., Giraudat, J., and Devic, M. (2006). AKRP and EMB506 are two ankyrin repeat proteins essential for plastid differentiation and plant development in Arabidopsis. *Plant J.* 48, 895–906. doi: 10.1111/j.1365-313x.2006.02922.x

Gu, H. F., Zhang, X., Zhang, W. F., Jin, C. Y., Xu, L., Lu, X. L., et al. (2010). Identification of physiological races of watermelon and melon powdery mildew in shanghai. *Acta Agricult. Shanghai* 26, 155–158.

Ha, C. M., Jun, J. H., Nam, H. G., and Fletcher, J. C. (2004). BLADE-ON-PETIOLE1 encodes a BTB/POZ domain protein required for leaf morphogenesis in Arabidopsis thaliana. *Plant Cell Physiol.* 45, 1361–1370. doi: 10.1093/pcp/pch201

Han, Y., Lv, P., Hou, S., Li, S., Ji, G., Ma, X., et al. (2015). Combining next generation sequencing with bulked segregant analysis to fine map a stem moisture locus in sorghum (Sorghum bicolor L. Moench). *PLoS One* 10:e0127065. doi: 10.1371/journal.pone.0127065

He, C., Holme, J., and Anthony, J. (2014). SNP genotyping: the KASP assay. *Methods Mol. Biol.* 1145, 75–86. doi: 10.1007/978-1-4939-0446-4_7

Hemsley, P. A., Kemp, A. C., and Grierson, C. S. (2005). The TIP GROWTH DEFECTIVE1 S-acyl transferase regulates plant cell growth in Arabidopsis. *Plant Cell* 17, 2554–2563. doi: 10.1105/tpc.105.031237

Hill, J. T., Demarest, B. L., Bisgrove, B. W., Gorsi, B., Su, Y. C., and Yost, H. J. (2013). Mmappr: Mutation Mapping Analysis Pipeline for Pooled Rna-Seq. *Genome Res.* 23, 687–697. doi: 10.1101/gr.146936.112

Hollomon, D. W., Wheeler, I. E., Bélanger, R. R., Bushnell, W. R., Dik, A. J., and Carver, T. L. W. (2002). "The Powdery Mildews," in *A Comprehensive Treatise*, eds R. R. Bélanger, W. R. Bushnell, A. J. Dik, and T. L. W. Carver (Saint Paul, MN: APS Press), 249–255.

Křístková, E., Lebeda, A., and Sedláková, B. (2009). Species spectra, distribution and host range of cucurbit powdery mildews in the Czech Republic, and in some other European and Middle Eastern countries. *Phytoparasitica* 37, 337–350. doi: 10.1007/s12600-009-0045-4

Li, B., Zhao, Y., Zhu, Q., Zhang, Z., Fan, C., Amanullah, S., et al. (2017). Mapping of powdery mildew resistance genes in melon (Cucumis melo L.) by bulked segregant analysis. *Sci. Horticult.* 220, 160–167. doi: 10.1016/j.scienta.2017.04.001

Li, D., Wang, F., Liu, B., Zhang, Y., Huang, L., Zhang, H., et al. (2013). Ectopic Expression of Rice OsBIANK1, Encoding an Ankyrin Repeat-Containing Protein, in Arabidopsis Confers Enhanced Disease Resistance to Botrytis cinerea and *Pseudomonas* syringae. *J. Phytopathol.* 161, 27–34. doi: 10.1111/jph.12023

Li, P. F., Zhu, L. L., Yang, X. P., Xu, J. H., Liu, G., Yao, X. F., et al. (2015). Species and physiological race identification of melon powdery mildew fungus in Jiangsu, Zhejiang and Shanghai areas. *China Cucurbits Vegetables* 28, 16–20.

Liang, Q. L., Xu, B. L., and Yan, H. X. (2010). Hull-less pumpkin powdery mildew and its host range. *Mycosystema* 29, 636–643.

Liu, L. Z., Chen, Y. Y., Su, Z. H., Zhang, H., and Zhu, W. M. (2010). A sequence-amplified characterized region marker for a single, dominant gene in melon PI 134198 that confers resistance to a unique race of podosphaera xanthii in china. *Hortscience* 45, 1407–1410. doi: 10.21273/hortsci.45.9.1407

Lu, H., Lin, T., Klein, J., Wang, S., Qi, J., Zhou, Q., et al. (2014). QTL-seq identifies an early flowering QTL located near Flowering Locus T in cucumber. *Theor. Appl. Genet.* 127, 1491–1499. doi: 10.1007/s00122-014-2313-z

Lu, H., Liu, Y., and Greenberg, J. T. (2005). Structure-function analysis of the plasma membrane-localized Arabidopsis defense component ACD6. *Plant J.* 44, 798–809. doi: 10.1111/j.1365-313x.2005.02567.x

Lu, H., Rate, D. N., Song, J. T., and Greenberg, J. T. (2003). ACD6, a novel ankyrin protein, is a regulator and an effector of salicylic acid signaling in the Arabidopsis defense response. *Plant Cell* 15, 2408–2420. doi: 10.1105/tpc.015412

Magwene, P. M., Willis, J. H., and Kelly, J. K. (2011). Te Statistics of Bulk Segregant Analysis Using Next Generation Sequencing. *PLoS Comput. Biol.* 7:e1002255. doi: 10.1371/journal.pcbi.1002255

McCreight, J. D., and Coffey, M. D. (2011). Inheritance of resistance in melon PI 313970 to cucurbit powdery mildew incited by podosphaera xanthii race s. *HortScience* 46, 838–840. doi: 10.21273/hortsci.46.6.838

McGrath, T. M. (2001). Fungicide resistance in cucurbit powdery mildew: experiences and challenges. *Plant Dis.* 85, 236–245. doi: 10.1094/pdis.2001.85.3.236

Michelmore, R. W., Paran, I., and Kesseli, R. V. (1991). Identification of markers linked to disease resistance genes by bulked segregant analysis: a rapid method to detect markers in specific genomic regions by using segregating populations Proc. *Natl. Acad. Sci. U S A* 88, 9828–9832. doi: 10.1073/pnas.88.21.9828

Nie, J., He, H., Peng, J., Yang, X., Bie, B., Zhao, J., et al. (2015). Identification and fine mapping ofpm5.1: a recessive gene for powdery mildew resistance in cucumber (cucumis sativus L.). *Mole. Breed.* 35:7.

Ning, X., Wang, X., Gao, X., Zhang, Z., Zhang, L., Yan, W., et al. (2014). Inheritances and location of powdery mildew resistance gene in melon Edisto47. *Euphytica* 195, 1–9.

Perchepied, L., Bardin, M., Dogimont, C., and Pitrat, M. (2005). Relationship Between Loci Conferring Downy Mildew and Powdery Mildew Resistance in Melon Assessed by Quantitative Trait Loci Mapping. *Phytopathology* 95, 556–565. doi: 10.1094/phyto-95-0556

Perchepied, L., Marc, B., Catherine, D., and Pitrat, M. (2005). Relationship between loci conferring downy mildew and powdery mildew resistance in melon assessed by quantitative trait loci mapping. *Phytopathology* 95, 556–565. doi: 10.1094/phyto-95-0556

Perez-Garcia, A., Romero, D., Fernandez-Ortuno, D., Lopez-Ruiz, F., De Vicente, A., and Tores, J. A. (2009). The powdery mildew fungus Podosphaera fusca (synonym *Podosphaera xanthii*), a constant threat to cucurbits. *Mole. Plant Pathol.* 10, 153–160.

Périn, C., Hagen, L., Conto, V. D., Katzir, N., Danin-Poleg, Y., Portnoy, V., et al. (2002). A reference map of *Cucumis melo* based on two recombinant inbred line populations. *Theor. Appl. Genet* 104, 1017–1034. doi: 10.1007/s00122-002-0864-x

Pitrat, M. (1991). Linkage groups in *Cucumis melo* L. *Rep. Cucurbit Genetics Cooperative* 82, 406–411. doi: 10.1093/oxfordjournals.jhered.a111112

Rafalski, A. (2002). Applications of single nucleotide polymorphisms in crop genetics. *Curr. Opin. Plant Biol.* 5, 94–100. doi: 10.1016/s1369-5266(02)00240-6

Rasheed, A., Wen, W., Gao, F., Zhai, S., Jin, H., Liu, J., et al. (2016). Development and validation of KASP assays for genes underpinning key economic traits in bread wheat. *Theoret. Appl. Genet.* 129, 1843–1860. doi: 10.1007/s00122-016-2743-x

Ribaut, J. M., Banziger, M., Betran, J., Jiang, C., Edmeades, G. O., Dreher, K., et al. (2002). "Use of molecular markers in plant breeding: Drought tolerance

improvement in tropical maize," in *itor, Quantitative genetics, genomics, and plant breeding*, ed. M. S. Kang (Wallingford, UK: CABI Publishing).

Romero, D., Rivera, M. E., Cazorla, F. M., Codina, J. C., Fernandez-Ortuno, D., Tores, J. A., et al. (2008). Comparative histochemical analyses of oxidative burst and cell wall reinforcement in compatible and incompatible melon-powdery mildew (Podosphaera fusca) interactions. *J. Plant Physiol.* 165, 1895–1905. doi: 10.1016/j.jplph.2008.04.020

Ryals, J., Weymann, K., and Lawton, K. (1997). The Arabidopsis NIM1 protein shows homology to the mammalian transcription factor inhibitor I kappa B. *Plant Cell* 9, 425–439. doi: 10.1105/tpc.9.3.425

Sakamoto, H., Matsuda, O., and Iba, K. (2008). ITN1, a novel gene encoding an ankyrin-repeat protein that affects the ABA-mediated production of reactive oxygen species and is involved in salt-stress tolerance in Arabidopsis thaliana. *Plant J.* 56, 411–422. doi: 10.1111/j.1365-313X.2008.03614.x

Schlotterer, C. (2004). The evolution of molecular markers-just a matter of fashion? *Nat. Rev. Genet* 5, 63–69. doi: 10.1038/nrg1249

Semagn, K., Babu, R., Hearne, S., and Olsen, M. (2014). Single nucleotide polymorphism genotyping using Kompetitive Allele Specific PCR (KASP): overview of the technology and its application in crop improvement. *Mole. Breed.* 33, 1–14. doi: 10.1007/s11032-013-9917-x

Shen, G., Kuppu, S., Venkataramani, S., Wang, J., Yan, J., Qiu, X., et al. (2010). ANKYRIN REPEAT-CONTAINING PROTEIN 2A is an essential molecular chaperone for peroxisomal membranebound ASCORBATE PEROXIDASE3 in Arabidopsis. *Plant Cell* 22, 811–831. doi: 10.1105/tpc.109.065979

Song, J., Li, Z., Liu, Z., Guo, Y., and Qiu, L. (2017). Next-Generation Sequencing from Bulked-Segregant Analysis Accelerates the Simultaneous Identification of Two Qualitative Genes in Soybean. *Front. Plant Sci.* 8, 919–919. doi: 10.3389/fpls.2017.00919

Soyk, S., Lemmon, Z. H., Oved, M., Fisher, J., Liberatore, K. L., Park, S. J., et al. (2017). Bypassing Negative Epistasis on Yield in Tomato Imposed by a Domestication Gene. *Cell* 169, 1142–1155 e1112.

Sun, X. L., Liu, D., Zhang, H. Q., Huo, N. X., Zhou, R. H., and Jia, J. Z. (2010). Identification and mapping of two new genes conferring resistance to powdery mildew from aegilops tauschii (coss.) schmal. *J. Integr. Plant Biol.* 48, 1204–1209. doi: 10.1111/j.1744-7909.2006.00328.x

Tan, C., Assanga, S., Zhang, G., Rudd, J. C., Haley, S. D., Xue, Q., et al. (2017). Development and Validation of KASP Markers for Wheat Streak Mosaic Virus Resistance Gene Wsm2. *Crop Sci.* 57, 340–349. doi: 10.2135/cropsci2016.04.0234

Teixeira, A., Matosobarreto, A. P., and Aranha, L. E. (2008). An AFLP marker linked to the Pm-1 gene that confers resistance to *Podosphaera xanthii* race 1 in *Cucumis melo*. *Genet. Mol. Biol.* 31, 547–550. doi: 10.1590/s1415-47572008000300023

Wang, X. Z., Xu, B. Y., Wang, P., Luan, F. S., Ma, H. Y., and Ma, Y. Y. (2013). Identification of Powdery Mildew Pathogen and Ribosomal DNA-ITS Sequence Analysis on Melon. *J. Northeast Agricult. Univ.* 10, 18–97.

Wang, Y. H., Wu, D. H., Huang, J. H., Tsao, S. J., Hwu, K. K., and Lo, H. F. (2016). Mapping quantitative trait loci for fruit traits and powdery mildew resistance in melon (cucumis melo). *Botanical. Stud.* 57:19.

Wang, Y., Ning, Z., Hu, Y., Chen, J., Zhao, R., Chen, H., et al. (2015). Molecular Mapping of Restriction-Site Associated DNA Markers in Allotetraploid Upland Cotton. *PLoS One* 10:e0124781. doi: 10.1371/journal.pone.0124781

Win, K. T., Vegas, J., Zhang, C., Song, K., and Lee, S. (2017). QTL mapping for downy mildew resistance in cucumber via bulked segregant analysis using next-generation sequencing and conventional methods. *Theoret. Appl. Genet.* 130, 199–211. doi: 10.1007/s00122-016-2806-z

Wolter, M., Hollricher, K., Salamini, F., and Schulze-Lefert, P. (1993). The mlo resistance alleles to powdery mildew infection in barley trigger a developmentally controlled defence mimic phenotype. *MGG* 239, 122–128. doi: 10.1007/bf00281610

Xu, X., Lu, L., Zhu, B., Xu, Q., Qi, X., and Chen, X. (2015). QTL mapping of cucumber fruit flesh thickness by slaf-seq. *Scient. Rep.* 5:15829.

Yan, J., Wang, J., and Zhang, H. (2002). An ankyrin repeat-containing protein plays a role in both disease resistance and antioxidation metabolism. *Plant J.* 29, 193–202. doi: 10.1046/j.0960-7412.2001.01205.x

Yang, Z., Huang, D., Tang, W., Zheng, Y., Liang, K., Cutler, A. J., et al. (2013). Mapping of Quantitative Trait Loci Underlying Cold Tolerance in Rice Seedlings via High-Throughput Sequencing of Pooled Extremes. *PLoS One* 8:e68433. doi: 10.1371/journal.pone.0068433

Yustelisbona, F. J., Capel, C., Sarria, E., Torreblanca, R., Gomezguillamon, M. L., Capel, J., et al. (2011). Genetic linkage map of melon (Cucumis melo L.) and localization of a major QTL for powdery mildew resistance. *Mole. Breed.* 27, 181–192. doi: 10.1007/s11032-010-9421-5

Yuste-Lisbona, F. J., López-Sesé, A. I., and ómez-Guillamón, M. L. G. (2010). Inheritance of resistance to races 1, 2 and 5 of powdery mildew in the melon tgr-1551. *Plant Breed.* 129, 72–75. doi: 10.1111/j.1439-0523.2009.01655.x

Zhang, C., Ren, Y., and Guo, S. (2013). Application of comparative genomics in developing markers tightly linked to the Pm-2f gene for powdery mildew resistance in melon (*Cucumis Melo* L.). *Euphytica* 190, 1–12. doi: 10.12816/0011695

Zhang, H. Y., Su, F., Guo, S. G., Gong, G. Y., Yi, H. P., Wu, M. Z., et al. (2008). Genetic analysis and specific fragments linked to powdery mildew resistant gene Pm-2F in melon. *Acta Horticult. Sin.* 12, 1773–1780. doi: 10.16420/j.issn.0513-353x.2008.12.009

Zhang, H., Guo, S., Gong, G., Ren, Y., Davis, A. R., and Xu, Y. (2011). Sources of resistance to race 2WF powdery mildew in U.S. watermelon plant introductions. *Hortscience* 46, 1349–1352. doi: 10.21273/hortsci.46.10.1349

Zhang, H., Wang, X., Pan, Q., Li, P., Liu, Y., Lu, X., et al. (2019). QTG-Seq Accelerates QTL Fine Mapping through QTL Partitioning and Whole-Genome Sequencing of Bulked Segregant Samples. *Mol. Plant* 12, 426–437. doi: 10.1016/j.molp.2018.12.018

Zhang, S. X., Cui, J., Song, Y. Y., and Liu, S. Q. (2007). Occurrence and control of the melon cultivar. *Decid. Fruits* 39, 41–42.

Zhang, X. J., Ji, J., Zhai, W. Q., Li, M. H., Wang, H. J., and Yi, H. P. (2013). Identification of physiological races of powdery mildew on Cucumis melo ssp. melo in xinjiang. *Xinjiang Agricult. Sci.* 50, 1450–1455.

Zheng, W., Wang, Y., Wang, L., Ma, Z., Zhao, J., Wang, P., et al. (2016). Genetic mapping and molecular marker development for Pi65(t), a novel broad-spectrum resistance gene to rice blast using next-generation sequencing. *Theoret. Appl. Genet.* 129, 1035–1044. doi: 10.1007/s00122-016-2681-7

Zhu, H., Zhai, W., Li, X., and Zhu, Y. (2019). Two QTLs controlling clubroot resistance identified from bulked segregant sequencing in pakchoi (brassica campestris ssp. chinensis makino). *Scient. Rep.* 9:9228.

Zou, C., Wang, P., and Xu, Y. (2016). Bulked sample analysis in genetics, genomics and crop improvement. *Plant Biotechnol. J.* 14, 1941–1955. doi: 10.1111/pbi.12559

Conflict of Interest: The authors declare that the research was conducted in the absence of any commercial or financial relationships that could be construed as a potential conflict of interest.

Copyright © 2021 Cao, Diao, Chen, Jin, Zhang and Zhang. This is an open-access article distributed under the terms of the Creative Commons Attribution License (CC BY). The use, distribution or reproduction in other forums is permitted, provided the original author(s) and the copyright owner(s) are credited and that the original publication in this journal is cited, in accordance with accepted academic practice. No use, distribution or reproduction is permitted which does not comply with these terms.

frontiers in Plant Science

ORIGINAL RESEARCH
published: 09 February 2021
doi: 10.3389/fpls.2021.600371

Screening of Onion (*Allium cepa* L.) Genotypes for Drought Tolerance Using Physiological and Yield Based Indices Through Multivariate Analysis

Pranjali A. Gedam[1], A. Thangasamy[1], Dhananjay V. Shirsat[1], Sourav Ghosh[1], K. P. Bhagat[1], Onkar A. Sogam[1], A. J. Gupta[1], V. Mahajan[1], P. S. Soumia[1], Vanita N. Salunkhe[2], Yogesh P. Khade[1], Suresh J. Gawande[1], P. S. Hanjagi[3], R. Shiv Ramakrishnan[4] and Major Singh[1]*

[1] ICAR-Directorate of Onion and Garlic Research, Rajgurunagar, India, [2] ICAR-National Institute of Abiotic Stress Management, Baramati, India, [3] ICAR-National Rice Research Institute, Cuttack, India, [4] Jawaharlal Nehru Krishi Vishwa Vidyalaya, Jabalpur, India

OPEN ACCESS

Edited by:
Raul Antonio Sperotto, Universidade do Vale do Taquari–Univates, Brazil

Reviewed by:
Alireza Pour-Aboughadareh, Seed and Plant Improvement Institute, Iran
Ahmad Arzani, Isfahan University of Technology, Iran

***Correspondence:**
Pranjali A. Gedam
pranjali.ghodke123@gmail.com

Specialty section:
This article was submitted to Plant Abiotic Stress, a section of the journal Frontiers in Plant Science

Received: *29 August 2020*
Accepted: *18 January 2021*
Published: *09 February 2021*

Citation:
Gedam PA, Thangasamy A, Shirsat DV, Ghosh S, Bhagat KP, Sogam OA, Gupta AJ, Mahajan V, Soumia PS, Salunkhe VN, Khade YP, Gawande SJ, Hanjagi PS, Ramakrishnan RS and Singh M (2021) Screening of Onion (Allium cepa L.) Genotypes for Drought Tolerance Using Physiological and Yield Based Indices Through Multivariate Analysis. Front. Plant Sci. 12:600371. doi: 10.3389/fpls.2021.600371

Drought is a leading abiotic constraints for onion production globally. Breeding by using unique genetic resources for drought tolerance is a vital mitigation strategy. With a total of 100 onion genotypes were screened for drought tolerance using multivariate analysis. The experiment was conducted in a controlled rainout shelter for 2 years 2017–2018 and 2018–2019 in a randomized block design with three replications and two treatments (control and drought stress). The plant was exposed to drought stress during the bulb development stage (i.e., 50–75 days after transplanting). The genotypes were screened on the basis of the drought tolerance efficiency (DTE), percent bulb yield reduction, and results of multivariate analysis viz. hierarchical cluster analysis by Ward's method, discriminate analysis and principal component analysis. The analysis of variance indicated significant differences among the tested genotypes and treatments for all the parameters studied, viz. phenotypic, physiological, biochemical, and yield attributes. Bulb yield was strongly positively correlated with membrane stability index (MSI), relative water content (RWC), total chlorophyll content, antioxidant enzyme activity, and leaf area under drought stress. The genotypes were categorized into five groups namely, highly tolerant, tolerant, intermediate, sensitive, and highly sensitive based on genetic distance. Under drought conditions, clusters II and IV contained highly tolerant and highly sensitive genotypes, respectively. Tolerant genotypes, viz. Acc. 1656, Acc. 1658, W-009, and W-085, had higher DTE (>90%), fewer yield losses (<20%), and performed superiorly for different traits under drought stress. Acc. 1627 and Acc. 1639 were found to be highly drought-sensitive genotypes, with more than 70% yield loss. In biplot, the tolerant genotypes (Acc. 1656, Acc. 1658, W-085, W-009, W-397, W-396, W-414, and W-448) were positively associated with bulb yield, DTE, RWC, MSI, leaf area, and antioxidant enzyme activity under drought stress. The study thus identified tolerant genotypes with favorable adaptive traits that may be useful in onion breeding program for drought tolerance.

Keywords: onion, drought, genetic diversity, multivariate analysis, stress indices

INTRODUCTION

Bulb onion (*Allium cepa* L.) is an important vegetable crops, with nearly 98 million tones produced globally (FAOSTAT, 2019). With a production of 23.2 million tones and export of 1.58 million tones, India is the second-largest producer of bulb onion next to China[1]. In India, onions are grown under diverse climatic conditions. A substantial part of the area under onion cultivation is dependent on monsoon rainfall for its water demand, and therefore, the onion crop is vulnerable to climatic abberations such as drought. Frequent drought episode that are linked with climate change have led to approximately 30% decrement in global bulb production. Depending on the growing season, the onion crop requires approximately 45 lakh liters hectare^{-1} water during its growth period which is quite high. Therefore, developing drought-tolerant onion varieties with promising adaptive traits is crucial for enhancing its productivity in water-scare regions.

Drought stress affects plant growth by altering various morphological, physiological, and metabolic processes (Diaz et al., 2010). It causes major damages to plants by disturbing water relations, inducing cellular membrane damage and forming of reactive oxygen species in plant tissues (Sairam and Saxena, 2000). Prolonged dry spell leads to poor plant growth and photosynthesis, which ultimately results in heavy yield losses. Phenotyping is a significant approach for screening germplasm based on morpho-physiological, biochemical, and yield performance (Passioura, 2012). Phenotypic attribute is the best criterion used for identifying tolerant genotypes among different crops based on their promising adaptive traits under drought stress (Vaezi et al., 2010; Mwadzingeni et al., 2016). In cereals, traits namely the plant height, number of productive tillers, spikelet per spike, and days to maturity are some of the important yield traits used for screening genotypes under limited water supply (Blum, 2010). Thus largely diverse phenotypic responses have been reported among different crop genotypes due to alteration in various physiological, biochemical, and molecular responses (Fenta et al., 2014; Ramakrishnan et al., 2016; Aghaie et al., 2018). This indicates variation in genotypic difference among the genotypes in terms of their drought tolerance level. Therefore from the breeding perspective, effective screening techniques should be used to identify tolerant genotypes that can perform better under limited water supply than the other genotypes.

Bulb yield in the onion crop has been reported to be directly associated with the amount of water supply. Information regarding genetic diversity among genotypes and the correlation among different traits under different water regimes is limited. Bulb yield is the primary trait that needs to be considered while evaluating drought tolerance along with secondary indicators, namely plant water status, and physiological, and biochemical parameters. The extent of damage to bulb yield depends on the genotype and phenological stage at which drought stress occurrs (Ghodke et al., 2018). Typically, genotypes with better drought-adaptive traits and relatively higher yield under water stress conditions need to be identified. Screening of genotypes based on few phenotypic traits and identifying the best criterion or trait among them is the major challenge while a screening large germplasm pool. Thus numerous genotypes can be more precisely evaluated at the same time by using appropriate statistical tools and employing multiple phenotypic, physiological, biochemical, and yield traits.

Multivariate cluster analysis and principal component analysis (PCA) are reliable tools for grouping genotypes based on their performance under water stress. These tools also characterize the genetic divergence among the tested genotypes. Thus, selecting appropriate drought-tolerant onion genotypes from the available germplasm collection is a prime concern for developing improved varieties and hybrids. Thus, the present study screened and evaluated the response of 100 onion genotypes to drought stress at the bulb development stage. The identified tolerant genotype with drought-adaptive traits can significantly improve onion productivity in low rainfall areas and advance our understanding of the plant response to drought stress at physiological and biochemical levels.

MATERIALS AND METHODS

Plant Material and Experimental Site

A total of 100 onion genotypes were used as the plant material in the present study. All these genotypes were selected from the germplasm collection available at ICAR-Directorate of Onion and Garlic Research (ICAR-DOGR), Pune, India (N 18°84′, E 73°88′, and 553.8 m above mean sea level). The controlled experiment was conducted in an automated rain-out shelter at ICAR-DOGR following randomized block design after monsoon season (**Supplementary Figure 1**) from, November to April for two successive years (2017–2018 and 2018–2019). The soil of experimental plots was sandy loam in texture with 32–35% clay, 40% sand, and 20% silt with 7.9 pH. The recommended dose of potassium, phosphorus, and sulfur, and half dose of nitrogen were applied at the time of transplanting and remaining nitrogen was applied in splits doses at 30, 45, and 60 days after transplanting (DAT). At all stages of crop growth, recommended plant protection procedures and hand weeding were performed to combat weeds, pests, and disease.

Drought Treatment

Initially the seedlings for each genotypes were grown in the nursery on raised beds. Seeds were coated with fungicide (Thiram 1 g kg^{-1}) before sowing in the nursery to avoid fungal and soil-borne diseases. Six week healthy seedlings were transplanted in the rain-out shelter on raised bed of 1.2 m in width and 30 cm in height by maintaining a spacing of 15 cm row to row and 10 cm plant to plant in three replicates comprising of 15 seedlings in each replication. Regular water supply was maintained in both the plots (control and drought) until 50 DAT. To evaluate drought tolerance, two water regimes were maintained, namely well-watered condition

[1]http://agricoop.gov.in/

(control with 90% field capacity) and water-deficit stress (50% field capacity). For this, water supply was stopped in the drought plots for continuous 25 days during the bulb enlargement stage (50–75 DAT), whereas the plants in the control plots were maintained uninterruptedly hydrated as per their requirement. Gravimetric soil moisture content was measured by randomly collecting the soil sample from a depth of 55–60 cm on every alternate day during the stress period. The automated rain-out shelter protected the experiment from any possible seasonal rainfall. Data on all phenotypic and physiological traits were colleted from both the plots, and leaf samples were collected in liquid nitrogen and stored for biochemical analysis.

Morphological Traits

Morphological traits such as plant height, leaves per plant, and leaf area of well-watered and water-stressed plants were recorded on 50 and 75 DAT. Plant height was determined by measuring from the base to the tip of the longest leaves. The total number of leaves per plant was monitored after stress treatment. The leaf area of each genotype from both the water regimes was measured using a LICOR 3100 leaf area meter. All observations were recorded in replicates for each studied genotypes. The means of all the recorded parameters for 2 years were pooled (physiological, biochemical, and yield) and analyzed for screening, and evaluating genotypic performance under well-watered and water-deficit stress conditions.

Physiological Traits

Relative water content (RWC), membrane stability index (MSI), and total chlorophyll content were measured for each genotype and their means for 2 years were pooled from both the water regimes after relieving stress.

Relative Water Content

Leaf RWC was measured from a fully grown fourth leaf of each genotype. A fresh leaf sample of 0.5 g fresh weight (FW) was kept in distilled water for 4 h to record its turgid weight (TW). Turgid leaf samples were then kept for drying in a hot air oven at 70°C until the constant dry weight (DW) was attained. RWC was calculated using the formula given by Barrs and Weatherley (1962):

$$RWC = \frac{(FW - DW)}{(TW - DW)} \times 100$$

Membrane Stability Index

Drought-induced cellular membrane injury was monitored by measuring the MSI according to the procedure of Sairam et al. (1997). Leaves from both the treatments were collected, cut into small 2 cm discs, and washed with distilled water to remove debris if any from the leaf surface. MSI was estimated by taking 100 mg of the leaf disc in two test tubes each containing 10 mL of double-distilled water. The first test tube was heated at 40°C in a water bath for 30 min, and the electrical conductivity was measured on a conductivity bridge (C1). The second test tube was kept at 100°C for 10 min in a boiling water bath to record the conductivity on the conductivity bridge (C2). MSI was calculated in percentage by using the following formula as:

$$MSI = \left[1 - \frac{C1}{C2}\right] \times 100.$$

Total Chlorophyll

By using the non-maceration method (Hiscox and Israelstam, 1979), Total Chlorophyll was measured spectrophotometrically (UV-Visible Spectrophotometer, Thermo, United States) by incubating a leaf sample (0.05 g) in the test tubes containing 10 mL of dimethyl sulfoxide. The test tubes were placed in a water bath maintained at 60°C for 60 min. Absorbance was recorded at 645 and 663 nm after placing the tubes at room temperature for 30 min. Total chlorophyll was calculated using the following formula given by Arnon (1949):

$$\text{Total Chlorophyll} = \frac{(20.2 \times OD_{645} + 8.02 \times OD_{663}) \times \text{Voleme of extract} \times \text{Weight of sample}}{1000}$$

Where; OD_{663} is absorbance at 663 nm and OD_{645} is absorbance at 645 nm.

Biochemical Traits

Various biochemical traits namely phenol content, pyruvic acid, antioxidant enzyme activity, and total soluble solids (TSS) content were measured for each genotype and their means for years were pooled from both the water regimes after relieving stress.

Total Phenolic Content

The total phenolic content of the leaf sample was determined using the Folin-Ciocalteau (FC) reagent according to the method of Singleton and Rossi (1965) using gallic acid as the standard. The fresh leaf sample (1 g) was homogenized in 10 mL of 80% aqueous methanol and the homogenate was centrifuged at 5000 rpm for 10 min. A mixture of 200 μL supernatant and 1 mL FC reagent was incubated at room temperature for 5 min. After incubation, 800 μL of sodium carbonate was added to the reaction mixture and further incubated in dark at room temperature for 2 h. The absorbance was recorded at 765 nm. Phenol content was expressed as mg gallic acid equivalent g^{-1} dry weight.

Pyruvic Acid

Pyruvic acid was estimated spectrophotometrically through the method of Schwimmer and Weston (1961) using sodium pyruvate as the standard. The core of the bulb sample (1 g) was homogenized in 1 mL double distilled water and squeezed in a muslin cloth and allowed to settle at room temperature for 10 min. Then 0.5 mL of extract and 1.5 mL of 5% trichloroacetic acid were vortexed and diluted with 20 mL with double distilled water. The reaction mixture containing 1 mL extract, 1 mL double distilled water, and 1 mL dinitrophenylhydrazine reagent was incubated at 37°C in a water bath for 10 min and 5 mL of

0.6 M sodium hydroxide was added to this mixture. Absorbance was then recorded at 420 nm. Pyruvic acid was expressed as the μmole g^{-1} sample.

Antioxidant Enzyme Activity

The total antioxidant enzyme activity was determined spectrophotometrically through Ferric Ion Reducing Antioxidant Power (FRAP) assay as described by Stratil et al. (2006) by using ascorbic acid as the standard. The FRAP reagent was prepared freshly with 25 mL of 300 mM sodium acetate buffer, 2.5 mL of 10 mM 2,4,6-Tripyridile-S-Triazine, and 2.5 mL of 20 mM $FeCl_3$ prepared in 40 mM HCl and incubated at 37°C in a water bath for 10 min. An aliquot of 150 μL of the leaf extract was prepared in 80% aqueous methanol, mixed with 2850 μL of the FRAP reagent, and incubated in dark at room temperature for 30 min. The absorbance of the ferrous tripyridyltriazine complex was recorded at 593 nm against methanol as the blank. The FRAP value was expressed in μg g^{-1} dry weight of sample.

Total Soluble Solids

The TSS content of the bulb sample immediately after harvest was measured using a digital refractometer and the values are presented in Brix.

Bulb Yield and Drought Tolerance Indices

After more than 70% of the neck fall occurred at the end of the season, the bulbs were harvested separately for each genotype. Bulb yield was recorded separately from both the water regimes for each tested genotype, and their means for 2 years were pooled for further analysis. Bulbs were assessed visually to detect any sprouting or rotting losses caused by deficit irrigation. Drought tolerance indices based on bulb yield under the two water regimes were calculated as follows

- Drought tolerance efficiency (DTE %)

$$= \frac{\text{Yield under drought stress}}{\text{Yield under well watered}} \times 100;$$

(Fischer and Wood, 1981)

- Stress tolerance index (STI)

$$= \frac{\left(\text{Yield under drought stress} \times \text{Yield under well} - \text{watered}\right)}{\left(\text{Mean yield of all genotypes under well} - \text{watered}\right)^2};$$

(Fernandez, 1992)

- Drought susceptibility index (DSI)

$$= \frac{1 - \text{Yield under drought stress}/\text{Yield under well} - \text{watered}}{\text{Stress Intensity}}$$

Where,

$$\text{Stress Intensity} = \frac{1 - \text{Mean yield of all genotypes under drought}}{\text{Mean yield of all genotypes under well watered}};$$

(Fischer and Maurer, 1978)

- Mean relative performance (MRP)

$$= \frac{\text{Yield under stress}}{\text{Mean yield of all genotypes under stress}} + \frac{\text{Yield under well watered}}{\text{Mean yield of all genotypes under well watered}};$$

(Raman et al., 2012)

- Mean productivity (MP)

$$= \frac{\text{Yield under stress} + \text{Yield under well watered}}{2};$$

(Raman et al., 2012).

Analysis of Genetic Parameters

The data was subjected to analysis, the genotypic and phenotypic correlations were calculated by the technique given by Kwon and Torrie (1964) by following formula,

Genetic Variance (Vg) = Genotypic Mean Square (GMS)−Error Mean Square (EMS)/Number of Replications (r)

$$\textit{Environmental Variance} = \textit{Error mean Square}$$

$$\textit{Phenotype variance } (Vp) = Vg + Ve/r$$

The genotypic coefficient of variation (GCV) and phenotypic coefficient of variation (PCV) were calculated as per following formula,

Genetic coefficient of variation % = VgX×100

Phenotypic coefficient of variation % = VpX×100

The heritability (H^2) on entry mean basis was calculated by *t* formula,

$$\text{Heritability} = \frac{Vp}{Vg}$$

Statistical Analysis

Physiological, biochemical, and yield data for 2 years were analyzed using SAS software (Version 9.3; SAS Institute, Cary, NC, United States). Combined analysis of variance (ANOVA) and the least significance test were performed using SAS software to test the genotypic difference, drought stress effect and to compare the phenotypic value of the genotype for specific traits under both water regimes. The mean data (pooled) for the recorded traits for 2 years were used for calculating Pearson's correlation coefficient and the association between different traits under well-watered and water-deficit stress conditions by using SPSS software (Version 16.0). PCA and biplot PCA were performed for genotypes and traits under water-deficit stress by using SPSS and XLSTAT software to show the relationships among the tested genotypes based on different traits.

RESULTS

Effect of Drought Stress on Stress Indices

Eleven physiological traits and two stress indices were selected for screening 100 onion genotypes for their drought tolerance. The genotypes were classified into five groups according to 2 years pooled data of percent bulb yield reduction (**Table 1**). Yield decreased gradually in all genotypes exposed to drought stress during the bulb enlargement stage (50–75 DAT) irrespective of their year of planting. Eleven genotypes with less than 20% reduction in bulb yield were identified as highly tolerant to drought, whereas, 22 genotypes with 20–40% yield reduction as tolerant to drought. Twenty-three genotypes with 40–60% yield reduction were categorized as an intermediate group. Fourteen genotypes with yield reduction of more than 70% and poor plant stand were classified as a highly sensitive group whereas, 30 genotypes with a 60–70% yield reduction as a sensitive group. Another reliable stress index used to screen the genotypes under water stress was the drought tolerance efficiency (DTE). In total, 11 genotypes were identified with more than 80% DTE and hence categorized as highly tolerant to drought whereas, 22 genotypes with 60–80% DTE were grouped as tolerant. Likewise, 23 genotypes with 40–60% DTE were identified as an intermediate group. Fourteen genotypes recorded with less than 30% DTE were categorized as highly sensitive to drought whereas 30 genotypes with 30–40% DTE were grouped as sensitive genotypes (**Table 2**). Thus, based on DTE and bulb yield reduction, the genotypes were classified into different groups. Acc. 1656, Acc. 1658, W-009, and W-085 with more than 90% DTE and less than 20% yield reduction were identified as highly drought-tolerant genotypes. Two entries (Acc. 1627 and Acc. 1639) and three varieties (Bhima Raj, Bhima Light Red, and Phule Safed) with less than 20%, DTE and more than 80% yield reduction were identified as highly drought-sensitive genotypes. Thus, DTE and bulb yield can act as promising indicators of genotypes with improved drought tolerance.

Analysis of Variance

The combined ANOVA evaluated under well-watered and water-deficit stress conditions showed highly significant ($p \leq 0.05$) genotypic differences in the physiological parameters (plant height, leaves per plant, leaf area, RWC, MSI, and chlorophyll), biochemical traits (phenol, antioxidant enzyme activity, pyruvic acid, and TSS), yield components and all possible relationship among them (**Table 3**). The findings indicated the extent of differences among the genotypes that would be helpful in selecting promising genotypes with drought tolerance. Genotypes into environment interactions were also significant for the studied parameters, indicating that most genotypes performed contrastingly under different water regimes. Thus the significant variance among the genotypes, environment, and genotypes × environment indicated that the studied traits were greatly influenced by both genotypes and water stress conditions.

Association of Parameters Under Drought Stress

Correlation analysis was performed among the physiological, biochemical, and yield contributing traits of 100 genotypes under well-watered and water-deficit stress conditions, and Pearson's correlation matrix is presented in **Table 4**. Under drought stress conditions, a significant and strong positive correlation was observed between bulb yield and RWC (0.766**), chlorophyll (0.591**), MSI (0.642**), and antioxidant enzyme activity (0.347**) whereas the number of leaves (−0.298*) negatively correlated with bulb yield. Likewise, chlorophyll was significantly and positively associated with MSI (0.542**), RWC (0.697**), TSS (0.405**), antioxidant enzyme activity (0.247*), and phenol (0.496**) but negatively correlated with the number of leaves (−0.256*) under water stress. The promising phenotypic trait that is, leaf area, was positively associated with MSI (0.299*), RWC (0.200*), antioxidant enzyme activity (0.212*), and pyruvic acid (0.292*), whereas RWC with MSI (0.755**), antioxidant enzyme activity (0.392**), phenol (0.651**), TSS (0.230*), and pyruvic acid (0.244*) under limited water supply. Further, a significantly stronger association was observed between phenols and pyruvic acid (0.410**) under water stress. Under the well-watered condition, the yield was positively associated with leaf area (0.206*), whereas, pyruvic acid with phenols (0.386**) and antioxidant enzyme activity (0.303*). Chlorophyll content was negatively associated with pyruvic acid (−0.266*), antioxidant enzymes activity (−0.349*), and MSI (−0.236*), but positively correlated with TSS (0.366*). The drought stress indicator MSI was positively associated with antioxidant enzyme activity (0.302*) in the control group. Thus, the correlation matrix under water-deficit stress signifies the association of various physiological and biochemical traits with bulb yield. The correlation matrix among different yield indices showed a strong positive association among stress tolerance index (STI), DTE, Mean productivity (MP), and mean relative performance (MRP), whereas a negative association of these indices was observed with stress susceptibility index (SSI) (−0.757**) and bulb yield reduction (−0.924**) under water stress (**Table 5**). Further, as the water stress increased, SSI was strongly and positively associated with bulb yield reduction (0.853**). Taken together, strong negative and positive association was found between various parameters under water-deficit stress and these associations can be employed for identifying promising drought-responsive traits.

Descriptive Statistics

Descriptive statistics classified the 100 genotypes into five clusters using Ward's method of clustering, based on square Euclidean distance between different traits as presented in **Table 6**. Compared with the other three clusters, the mean value for important physiological parameters was higher in cluster II followed by cluster I. Genotypes of cluster II recorded significantly higher mean values for DTE (81.21), chlorophyll (5.96), MSI (73.86), RWC (71.99), antioxidant enzyme activity (3.16), and yield (31.07) than other genotypes in different clusters. The mean value of significant traits from cluster IV

TABLE 1 | Genotypes grouped based on yield loss due to drought stress.

Genotypes	Yield reduction (<20%)	Genotypes	Yield reduction (20–40%)	Genotypes	Yield reduction (40–60%)	Genotypes	Yield reduction (60–70%)	Genotypes	Yield reduction (>70%)
W 085	6.65	W 453	20.39	Acc. 1626	41.16	RGP-4	60.00	Acc. 1652	70.89
Acc. 1656	7.05	N-2-4-1	20.81	W 440	42.12	W 344	60.05	KH-M-4	74.41
W 009	7.73	W 419	20.89	Bhima Shweta	42.29	DOGR Hybrid-50	60.88	Acc. 1629	75.27
Acc. 1658	9.52	Acc. 1663	21.11	MS 100 × Bhima Shweta	43.08	DOGR Hybrid-5	61.14	KH-M-3	76.08
W 448	10.12	Acc. 1613	21.18	Bhima Shubhra	43.32	W 355	62.35	Acc. 1651	76.95
W 397	13.27	Acc. 1635	21.92	DOGR 1047	44.08	Acc. 1633	62.43	Acc. 1615	77.04
W 444	15.25	DOGR 1048	22.57	MS 100 × W-448	45.32	RGP-3	62.67	Acc. 1655	77.17
Acc. 1608	16.98	W 340	22.87	Acc. 1666	45.36	DOGR Hybrid-441	62.81	Acc. 1661	78.30
W 414	18.34	W 441	23.03	W 361	47.72	Bhima Red	63.00	Acc. 1668	80.04
Acc. 1622	18.72	Acc. 1649	23.31	MS 100 × W-361	49.76	Acc. 1669	63.06	Acc. 1627	83.11
W 439	19.29	W 396	23.35	DOGR Hybrid-1	51.95	DOGR Hybrid-6	63.53	Acc. 1639	84.05
		RGP-2	25.18	KH-M-2	53.96	Acc. 1664	63.76	Phule Safed	84.12
		Acc. 1609	25.69	DOGR 1050	54.51	KH-M-1	64.05	Bhima Light Red	84.29
		Acc. 1657	25.95	Acc. 1623	55.97	Acc. 1621	64.17	Bhima Raj	85.59
		DOGR 1044	27.30	Acc. 1632	56.66	Acc. 1700	64.41		
		W 408	35.27	Acc. 1612	56.75	Acc. 1694	64.94		
		Acc. 1630	35.33	Acc. 1617	56.91	Acc. 1660	65.20		
		W 043	35.65	DOGR 1172	57.08	P-1-3	65.46		
		W 394	36.24	DOGR Hybrid-7	57.69	Acc. 1637	66.29		
		DOGR Hybrid-8	37.91	Acc. 1636	58.04	W 132	66.76		
		546 DR	37.97	Acc. 1625	58.20	Bhima Safed	66.77		
		Bhima Kiran	38.08	DOGR Hybrid-2	58.22	Bhima Super	67.04		
				RGP-5	58.50	Bhima Shakti	67.57		
						W 306	67.72		
						Acc. 1646	67.80		
						Acc. 1619	68.30		
						W 172	68.52		
						RGP-1	68.53		
						Bhima Dark Red	68.90		
						W 504	69.46		

and cluster V was lower than that of respective parameters of other genotypes. Divergence analysis revealed that among the studied traits, DTE and percent yield reduction contributed maximum (15%) toward genetic divergence of the studied genotypes, followed by bulb yield (14.6%), RWC (13%), and MSI (11%) (**Table 7**), whereas, TSS contributed the least (0.7%). Thus, these traits can be exploited for identifying genetically diverse parents for a breeding program. The PCV, GCV, broad-sense heritability (h^2), and genetic advancement are presented as a percent of the mean for 12 traits. The value for the PCV was higher than that for the GCV for all the studied traits. The maximum estimated value for the PCV and the GCV was for DTE (479.98 and 477.97, respectively), followed by yield reduction (71.84 and 71.48, respectively), whereas, the minimum estimated value was for leaves per plant (0.38 and 0.12, respectively) and TSS (0.72 and 0.71, respectively). Heritability is the degree of influence of genotype and environment on the expression of the parameters. In our study, the estimated heritability values did not vary significantly among the traits except for leaves per plant (0.32), for the studied genotypes (**Table 8**).

Cluster Analysis

Cluster analysis performed using a dendrogram grouped the genotypes into five clusters based on the studied traits indicating the presence of greater genetic diversity among the genotypes in different clusters as represented by the rescaled Euclidean distance in **Figure 1**. The corresponding genotypes in each cluster are shown in **Table 9** and their characteristics are described as below:

Highly Tolerant Genotypes (Cluster II Group)

Twenty-six genotypes accounting for 26% of the total genotypes were placed in this group. These genotypes performed superiorly under water deficit stress with improved physiological and biochemical traits, especially higher plant water status, total chlorophyll, MSI, antioxidant enzyme activity, and photosynthetically active leaves that contributed to its higher bulb yield. Hence, these genotypes were identified as highly drought-tolerant genotypes (**Table 6**). Seven highly drought-tolerant genotypes of this group (Acc. 1656, Acc. 1658, W-009, W-448, W-444, W-397, and W-085) recorded less than 20% bulb yield reduction under drought stress (**Table 1**). These genotypes

TABLE 2 | Genotypes grouped based on drought tolerance efficiency (DTE %).

Genotypes	DTE (<30%)	Genotypes	DTE (30–40%)	Genotypes	DTE (40–60%)	Genotypes	DTE (60–80%)	Genotypes	DTE (>80%)
Bhima Raj	14.41	W 504	30.54	RGP-5	41.50	Bhima Kiran	61.92	W 439	80.71
Bhima Light Red	15.71	Bhima Dark Red	31.10	DOGR Hybrid-2	41.78	546 DR	62.03	Acc. 1622	81.28
Phule Safed	15.88	RGP-1	31.47	Acc. 1625	41.80	DOGR Hybrid-8	62.09	W 414	81.66
Acc. 1639	15.95	W 172	31.48	Acc. 1636	41.96	W 394	63.76	Acc. 1608	83.02
Acc. 1627	16.89	Acc. 1619	31.70	DOGR Hybrid-7	42.31	W 043	64.35	W 444	84.75
Acc. 1668	19.96	Acc. 1646	32.20	DOGR 1172	42.92	Acc. 1630	64.67	W 397	86.73
Acc. 1661	21.70	W 306	32.28	Acc. 1617	43.09	W 408	64.73	W 448	89.88
Acc. 1655	22.83	Bhima Shakti	32.43	Acc. 1612	43.25	DOGR 1044	72.70	Acc. 1658	90.48
Acc. 1615	22.96	Bhima Super	32.96	Acc. 1632	43.34	Acc. 1657	74.05	W 009	92.27
Acc. 1651	23.05	Bhima Safed	33.23	Acc. 1623	44.03	Acc. 1609	74.31	Acc. 1656	92.95
KH-M-3	23.92	W 132	33.24	DOGR 1050	45.49	RGP-2	74.82	W 085	93.35
Acc. 1629	24.73	Acc. 1637	33.71	KH-M-2	46.04	W 396	76.65		
KH-M-4	25.59	P-1-3	34.54	DOGR Hybrid-1	48.05	Acc. 1649	76.69		
Acc. 1652	29.11	Acc. 1660	34.80	MS 100 × W-361	50.24	W 441	76.97		
		Acc. 1694	35.06	W 361	52.28	W 340	77.13		
		Acc. 1700	35.59	Acc. 1666	54.64	DOGR 1048	77.43		
		Acc. 1621	35.83	MS 100 × W-448	54.68	Acc. 1635	78.08		
		KH-M-1	35.95	DOGR 1047	55.92	Acc. 1613	78.82		
		Acc. 1664	36.24	Bhima Shubhra	56.68	Acc. 1663	78.89		
		DOGR Hybrid-6	36.47	MS 100 × Bhima Shweta	56.92	W 419	79.11		
		Acc. 1669	36.94	Bhima Shweta	57.71	N-2-4-1	79.19		
		Bhima Red	37.00	W 440	57.88	W 453	79.61		
		DOGR Hybrid-441	37.19	Acc. 1626	58.84				
		RGP-3	37.33						
		Acc. 1633	37.57						
		W 355	37.65						
		DOGR Hybrid-5	38.86						
		DOGR Hybrid-50	39.12						
		W 344	39.95						
		RGP-4	40.00						

TABLE 3 | Combined ANOVA (mean square) for physiological, biochemical and drought stress indices under well-watered and stress condition.

Source	DF	MSI	Chl.	RWC	YLD	NL	LA	PH	PA	PHE	AOX	TSS
Environment	1	5460485**	41140.66**	162259**	23692.62**	984.04**	4067.78**	873.13**	28252.1**	253.08**	2096.11**	1637.64**
Rep (Env.)	4	7.54*	0.9922	2.86*	2.19	6.18*	1.39	2.15*	2.24	10.08*	2.71*	13.02*
Genotype	99	167.95**	75.41**	232.78**	141.72**	2.94**	31.33**	33.47**	995.13**	78.06**	842.63**	76.9**
Env.*Geno	99	160.88**	61.14**	224.48**	132.03**	2.43**	19.83**	8.4**	143.08**	46.64**	138.32**	8.41**
Error	396											
Total	599											

MSI, membrane stability index; Chl, chlorophyll; RWC, relative water content; YLD, bulb yield; NL, leaves Plant^{-1}; LA, leaf area; PH, plant height; PA, pyruvic acid; PHE, total phenols; AOX, antioxidant enzyme activity; TSS, total soluble solids; DF, degree of freedom.

**, ** significant at 5 and 1% level of significance, respectively.*

recorded considerable genetic diversity from the other tolerant genotypes as shown by the Euclidean distance in a dendrogram. Thus, these genotypes can be utilized in a breeding program to genetically improve this valuable crop for drought tolerance.

Tolerant Genotypes (Cluster I Group)

Sixteen genotypes were placed in this group, accounting for 16% of the total genotypes. These genotypes performed better under drought stress with improved physiological and biochemical traits and minimum bulb yield reduction (**Table 1**). The mean values for important traits, namely DTE (59.32), SSI (0.70), yield reduction (40.68), MSI (72.15), RWC (65.12), total chlorophyll (5.68), and leaf area (35.76) (**Table 6**). Therefore, these genotypes were identified as drought-tolerant genotypes with better phenotypic and biochemical traits.

TABLE 4 | Pearson's correlation matrix among the physiological and yield traits under well-water (Upper diagonal) and water-deficit stress condition (Lower diagonal).

Parameters	PA	TSS	PHE	AOX	MSI	RWC	CHL	LA	PH	NL	YLD
PA	0.767**	−0.034	0.386**	0.303*	0.163	0.104	−0.266*	−0.082	0.015	−0.028	−0.005
TSS	−0.100	0.800**	0.022	−0.295*	−0.164	−0.157	0.366*	0.094	0.079	0.000	0.060
PHE	0.410**	0.210*	0.263*	0.129	0.068	−0.058	−0.122	0.012	−0.056	0.037	0.056
AOX	0.458**	−0.065	0.422**	0.719**	0.320*	0.075	−0.349*	−0.226*	−0.011	−0.056	0.010
MSI	0.474**	0.157	0.588**	0.485**	0.164	0.027	−0.236*	−0.098	−0.095	0.078	−0.115
RWC	0.244*	0.230*	0.651**	0.392**	0.755**	0.079	−0.178	−0.129	−0.169	−0.183	0.184
CHL	−0.037	0.405**	0.496**	0.247*	0.542**	0.697**	0.413**	0.306*	0.060	0.015	0.098
LA	0.292*	0.082	0.154	0.212*	0.299*	0.200*	0.185	0.230*	−0.037	−0.054	0.206*
PH	−0.232*	0.428**	0.067	−0.037	0.113	0.182	0.380**	0.047	0.631**	0.232*	−0.159
NL	0.141	−0.092	0.015	0.052	−0.037	−0.079	−0.256*	0.063	0.131	0.104	0.021
YLD	0.090	0.057	0.484**	0.347*	0.642*	0.766**	0.591**	0.187	−0.021	−0.298*	0.060

PA, pyruvic acid; TSS, total soluble solids; PHE, total phenols; AOX, antioxidant enzyme activity; MSI, membrane stability index; RWC, relative water content; CHL, chlorophyll; LA, leaf area; PH, plant height; NL, leaves Plant^{-1}; YLD, bulb yield.
**, ** significant at 5 and 1% level of significance, respectively.*

TABLE 5 | Pearson's correlation matrix among yield indices under drought stress.

Parameters	STI	DTE	MP	MRP	SSI	YL%	GMP	HMP
STI	1	0.924**	0.973**	0.676**	−0.757**	−0.924**	0.910**	0.986**
DTE		1	0.830**	0.367*	−0.853**	−1.000**	0.994**	0.954**
MP			1	0.822**	−0.630**	−0.830**	0.807**	0.936**
MRP				1	−0.168	−0.367*	0.331*	0.583**
SSI					1	0.853**	−0.904**	−0.847**
YL%						1	−0.994**	−0.954**
GMP							1	0.956**
HMP								1

STI, stress tolerance index; YSI, yield susceptibility index; DTE, drought tolerance efficiency; MP, mean productivity; MRP, mean relative performance; SSI, stress susceptibility index; YL%, yield loss percentage; GMP, geometric mean productivity; HMP, harmonic mean productivity.
**, ** significant at 5 and 1% level of significance, respectively.*

TABLE 6 | Descriptive statistics for all traits of 100 onion genotypes under different clusters.

Parameters	Cluster I		Cluster II		Cluster III		Cluster IV		Cluster V		Total	
	Mean	SD	Mean	SD	Mean	SD	Mean	SD	Mean	SD	Mean	SD
DTE	59.32	4.06	81.21	6.16	39.00	4.73	20.27	3.98	32.58	2.85	46.48	4.35
SSI	0.70	0.12	0.24	0.09	1.64	0.33	4.37	1.28	2.13	0.20	1.82	0.40
YL%	40.68	4.06	18.79	6.16	61.00	4.73	79.73	3.98	67.42	2.85	53.52	4.35
TSS	13.84	0.69	13.14	0.85	13.41	0.94	12.96	0.40	12.61	0.65	13.19	0.70
AOX	3.18	1.28	3.16	0.95	2.95	1.11	1.68	0.46	1.79	0.77	2.55	0.91
MSI	72.15	1.44	73.86	1.92	72.17	1.81	66.22	1.41	65.95	1.63	70.07	1.64
RWC	65.12	3.47	71.99	3.75	65.20	2.52	56.81	2.44	57.70	1.75	63.36	2.79
CHL	5.68	1.24	5.96	1.16	4.78	1.07	2.70	1.08	3.03	1.23	4.43	1.16
LA	35.76	2.57	34.99	3.59	35.93	2.83	32.14	4.23	31.44	4.78	34.05	3.60
PH	46.17	6.17	44.65	5.87	47.68	7.06	42.99	4.23	41.37	4.56	44.57	5.58
NL	6.51	0.71	6.30	0.54	6.85	0.60	6.47	0.43	6.80	0.62	6.59	0.58
YLD	22.18	3.06	31.07	2.92	14.33	1.92	8.31	1.67	12.63	1.29	17.70	2.17
	Tolerant		Highly Tolerant		Intermediate		Highly Susceptible		Susceptible			

DTE, drought tolerance efficiency; SSI, stress susceptibility index; YL%, yield loss percentage; TSS, total soluble solids; AOX, antioxidant enzyme activity; MSI, membrane stability index; RWC, relative water content; CHL, chlorophyll; LA, leaf area; PH, plant height; NL, leaves plant^{-1}; YLD, bulb yield.

Intermediate Genotypes (Cluster III Group)

Thirty-six genotypes were placed in this cluster group forming 36% of the total genotypes. These genotypes are intermediate in their drought tolerance and sensitive in their performance for all the studied physiological and biochemical parameters. The mean values for important physiological traits, namely DTE

TABLE 7 | Contribution of different physiological, biochemical and yield traits toward genetic divergence in 100 onion genotypes.

Parameters	Contribution (%)
DTE	15.230
SSI	13.666
YL%	15.230
TSS	0.701
AOX	3.800
MSI	11.027
RWC	13.094
CHL	9.730
LA	1.508
PH	0.245
NL	1.108
YLD	14.659

DTE, drought tolerance efficiency; SSI, stress susceptibility index; YL%, yield loss percentage; TSS, total soluble solids; AOX, antioxidant enzyme activity; MSI, membrane stability index; RWC, relative water content; CHL, chlorophyll; LA, leaf area; PH, plant height; NL, leaves plant^{-1}; YLD, bulb yield.

TABLE 8 | Estimates of genetic parameters for 12 quantitative traits of 100 onion genotypes under drought stress condition.

Parameters	GCV	PCV	h^2 (Broad sense)	Genetic Advancement 5%	Genetic advancement as % of mean 5%
DTE	477.97	479.98	0.99	44.94	89.5
SSI	1.84	1.88	0.97	2.76	181.59
YL%	477.97	479.98	0.99	44.94	90.27
TSS	0.71	0.72	0.97	1.71	12.93
AOX	1.3	1.3	0.99	2.35	84.84
MSI	10.93	10.96	0.99	6.8	9.54
RWC	34.96	35.03	0.99	12.16	18.66
CHL	2.56	2.58	0.99	3.28	68.44
LA	13.06	13.69	0.95	7.27	20.92
PH	38.83	40.27	0.96	12.6	27.72
NL	0.123	0.38	0.32	0.41	6.22
YLD	71.48	71.84	0.99	17.37	91.43

DTE, drought tolerance efficiency; SSI, stress susceptibility index; YL%, yield loss percentage; TSS, total soluble solids; AOX, antioxidant enzyme activity; MSI, membrane stability index; RWC, relative water content; CHL, chlorophyll; LA, leaf area; PH, plant height; NL, leaves plant^{-1}; YLD, bulb yield; GCV, genetic coefficient of variance; PCV, phenotypic coefficient of variance; h^2, heritability.

(39.00), SSI (1.64), yield reduction (61.00), MSI (72.17), and RWC (65.20) (**Table 6**). Thus, these genotypes were identified as intermediate genotypes that performed according to the external environmental condition, particularly the water regimes.

Highly Sensitive Genotypes (Cluster IV Group)

Thirteen genotypes were placed in this cluster, accounting for 13% of the total genotypes. These genotypes were recorded with poor DTE and with the least performance for physiological and biochemical traits. Among these genotypes, the two most sensitive were Acc. 1627 and Acc. 1639. The mean values for crucial traits, namely DTE (20.27), SSI (4.37), yield reduction (79.73), MSI (66.22), RWC (56.81), total chlorophyll (2.70), and leaf area (32.14) (**Table 6**). Thus, these genotypes were categorized as highly sensitive genotypes.

Sensitive Genotypes (Cluster V Group)

Nine genotypes were placed in this cluster, accounting for 9% of the total genotypes. These genotypes were characterized as sensitive with low DTE and poor performance for physiological and biochemical traits. The mean values for important traits, namely DTE (32.58), SSI (2.13), yield reduction (67.42), MSI (65.95), RWC (57.70), total chlorophyll (3.03), and leaf area (31.44) (**Table 6**). These genotypes performed well with optimum irrigation and could recover from the water stress after subsequent irrigation. However, they failed to form good size bulbs after recovery and hence were classified as drought-sensitive genotypes.

Principal Component Analysis

The rotated component matrix presented in **Table 10** shows the percentage of total variance elucidated by different principal component groups and their correlation with the studied traits. The PCA resulted in three principal component groups having an eigenvalue of more than one, thus contributing 73.64% variability (**Figure 2**). The PC1, PC2, and PC3 groups contributed 48.94, 13.89, and 10.80% variability, respectively. Different parameters contributed both positively and negatively to different PC groups. In the PC1 group, DTE (0.390), yield (0.383), RWC (0.362), MSI (0.332), and chlorophyll (0.312) recorded the highest variability. By contrast, SSI, percent yield reduction, and the number of leaves contributed negatively to the PC1 group (−0.370, −0.390, and −0.105, respectively). Maximum variability was observed for plant height (0.645), TSS (0.602), and chlorophyll (0.317) in the PC2 group, whereas the number of leaves (0.656) recorded higher variability than the other traits in the PC3 group. Thus, PC1 group showed the highest variability (48.94%) for drought tolerance-contributing traits than the other groups.

The PCA further revealed the association between different parameters and genotypes as demonstrated by the principal component biplots (**Figure 2**) for drought stress. Genotypes × parameter biplots were created from a two-way matrix of 12 parameters and 100 onion genotypes for water-deficit stress conditions. A smaller angle between different parameters in the same direction indicated a high association between corresponding parameters for classifying genotypes. Genotypes superior for a particular parameter were plotted closer and along the vector line direction. Under the water deficit condition, the genotypes were mostly concentrated on the positive side of both, PC1 and PC2. The genotypes Acc. 1656, Acc. 1658, Acc. 1608, Acc. 1622, Acc. 1663, W-009, W-444, W-397, W-396, W-414, W-448, W-441, and RGP-2 were more inclined in the direction of bulb yield, DTE, RWC, MSI, leaf area, and antioxidant enzyme activity. The highly sensitive genotypes were categorized based on cluster analysis; Acc. 1639, Acc. 1627, Acc. 1629, Acc. 1615, Acc. 1668, Acc. 1651, Acc.1655, KH-M-3, KH-M-4, Bhima Raj, Bhima Light Red, and Phule Safed were clustered together in the direction of SSI and percent yield reduction. These genotypes showed inclination on the negative

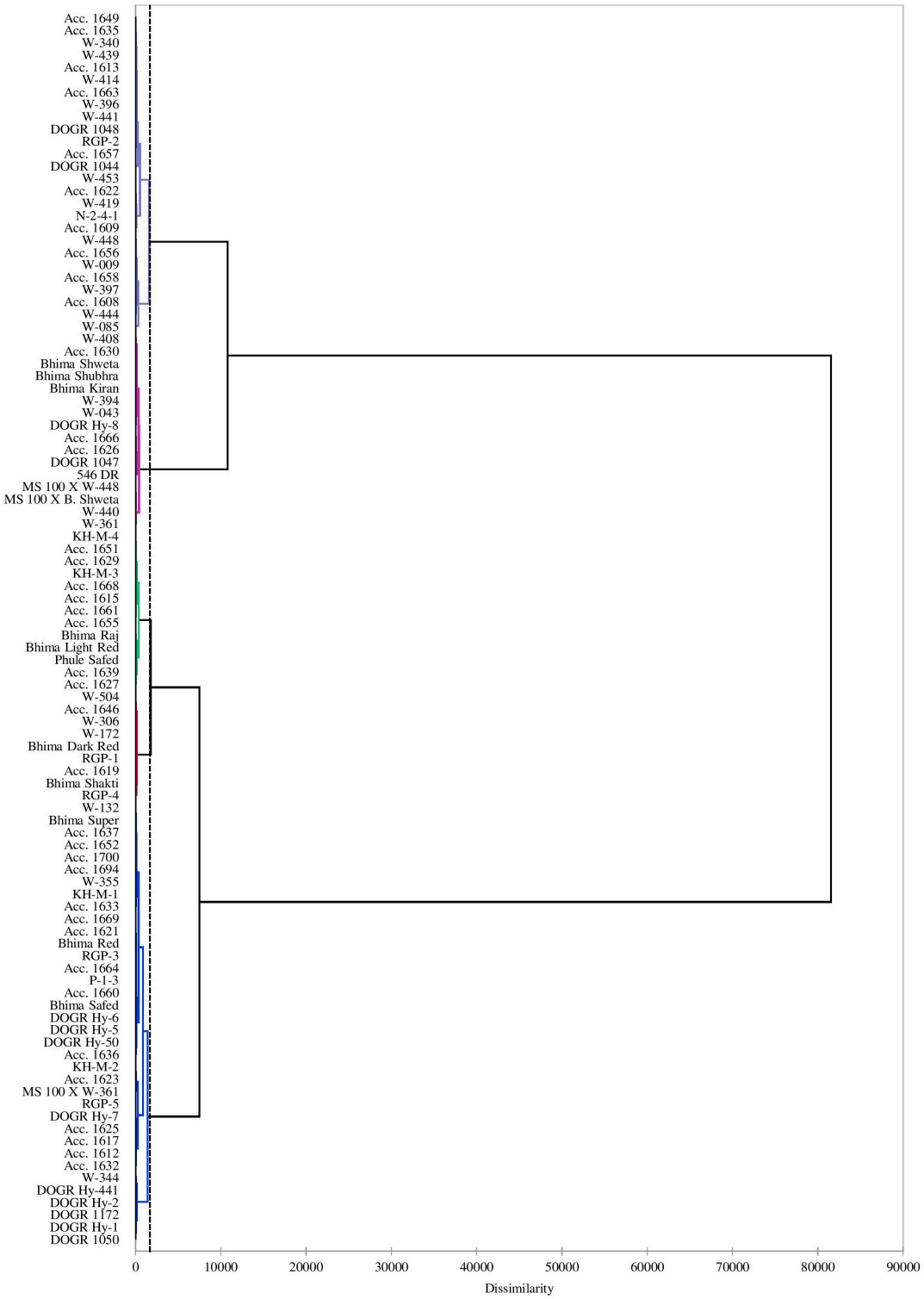


FIGURE 1 | Dendrogram using Ward's method presenting distribution of 100 onion genotypes under drought stress.

side ofPC1. The PCA thus confirmed that genotypes excelling in drought-adaptive traits namely RWC, MSI, total chlorophyll, antioxidant enzyme activity, and DTE, contributed maximum toward bulb yield under water stress than the other traits. Taken together, genotypes performing superior for these traits can thus be identified as drought-tolerant genotypes.

TABLE 9 | Grouping of 100 onion genotypes into six clusters based on Euclidean analysis.

Cluster group	No of genotypes	Name of genotypes
Cluster I	16	546 DR, Acc. 1626, Acc. 1630, Acc. 1666, W-043, W-361, W-394, W-408, W-440, DOGR 1047, DOGR Hybrid-8, MS 100 × Bhima Shweta, MS 100 × W-448, Bhima Kiran, Bhima Shubhra, Bhima Shweta
Cluster II	26	Acc. 1608, Acc. 1609, Acc. 1613, Acc. 1622, Acc. 1635, Acc. 1649, Acc. 1656, Acc. 1657, Acc. 1658, Acc. 1663, W-009, W-085, W-340, W-396, W-397, W-414, W-419, W-439, W-441, W-444, W-448, W-453, DOGR 1044, DOGR 1048, RGP-2, N-2-4-1
Cluster III	36	Acc. 1612, Acc. 1617, Acc. 1621, Acc. 1623, Acc. 1625, Acc. 1632, Acc. 1633, Acc. 1636, Acc. 1637, Acc. 1652, Acc. 1660, Acc. 1664, Acc. 1669, Acc. 1694, Acc. 1700, W-132, W-344, W-355, DOGR 1050, DOGR 1172, DOGR Hybrid-1, DOGR Hybrid-2, DOGR Hybrid-5, DOGR Hybrid-6, DOGR Hybrid-7, DOGR Hybrid-50, DOGR Hybrid-441, KH-M-1, KH-M-2, MS 100 × W-361, RGP-3, RGP-5, P-1-3, Bhima Red, Bhima Safed, Bhima Super
Cluster IV	13	Acc. 1615, Acc. 1627, Acc. 1629, Acc. 1639, Acc. 1651, Acc. 1655, Acc. 1661, Acc. 1668, KH-M-3, KH-M-4, Bhima Light Red, Bhima Raj, Phule Safed
Cluster V	9	Acc. 1619, Acc. 1646, W-306, W-504, W-172, RGP-1, RGP-4, Bhima Dark Red, Bhima Shakti

DISCUSSION

Drought stress differentially affected morpho-physiological, and yield attributes of the onion crop depending on the plant growth stage and genotype sensitivity (Pelter et al., 2004). Onion breeders mainly aim at screening effective germplasms by using phenotypic and drought indices for developing drought-tolerant varieties (Ghodke et al., 2020). To date, information regarding the screening of onion genotypes under drought stress is limited. To address this issue, 100 onion genotypes were screened on the basis of drought indices, and physiological, biochemical, and yield traits. In our study, drought stress severely altered the crop physiology and biochemical mechanisms, ultimately reducing the bulb yield in all the tested genotypes. The challenge was more pronounced during the bulb development stage. Based on DTE and percent yield loss the genotypes were classified as highly tolerant, tolerant, intermediate, sensitive, and highly sensitive. Genotypes with higher DTE had lower bulb yield reduction under drought stress than the other genotypes. The present study results are consistent with those of previous study, where 35 wheat genotypes were screened on the basis of DTE and tolerant genotypes with high DTE were identified (Ghodke et al., 2019). This stress indices might help the tolerant genotypes to adjust and sustain under stressful environments. Likewise, highly significant genotypic differences were observed for all the studied physiological, biochemical, and yield traits under drought stress, indicating that the tested genotypes had inherent genetic differences among themselves for the studied traits. Genotypes × environment interactions were also significant for various traits indicating that most of these traits were quantitatively inherited and differentially expressed in response to a diverse environment. A recent study in wheat also reported supportive findings for genotypes, treatments, replications, and their interaction effects (Mwadzingeni et al., 2016; Arifuzzaman et al., 2020). The findings thus revealed the huge genetic diversity exhibited by the studied genotypes that can be exploited in breeding programs.

TABLE 10 | Rotated component matrix for the principal components of 12 traits of 100 onion genotypes evaluated under drought stress.

Parameters	PC-1	PC-2	PC-3
DTE	**0.390**	−0.152	−0.118
SSI	−0.370	0.050	−0.032
YL%	−0.390	0.152	0.118
TSS	0.084	**0.602**	−0.171
AOX	0.195	−0.136	**0.464**
MSI	**0.332**	0.035	**0.246**
RWC	**0.362**	0.096	0.071
CHL	**0.312**	**0.317**	−0.137
LA	0.123	0.068	**0.440**
PH	0.050	**0.645**	0.047
NL	−0.105	0.121	**0.656**
YLD	**0.383**	−0.156	−0.124
Eigenvalue	**5.874**	**1.667**	**1.297**
Variability (%)	**48.947**	**13.891**	**10.808**
Cumulative variance%	**48.947**	**62.838**	**73.645**

DTE, drought tolerance efficiency; SSI, stress susceptibility index; YL%, yield loss percentage; TSS, total soluble solids; AOX, antioxidant enzyme activity; MSI, membrane stability index; RWC, relative water content; CHL, chlorophyll; LA, leaf area; PH, plant height; NL, leaves plant^{-1}; YLD, bulb yield; PC, principal component. Values in bold indicating maximum variability.

Effect of Genotypes and Drought Stress on Physiological Traits

Drought stress negatively influenced the plant phenotype by decreasing plant height, photosynthetically active leaves, and leaf area in all the employed genotypes. Plant height may be reduced due to a decline in cell growth and expansion that limits the overall plant architecture under drought stress. Similar changes in plant height, leaf area, and root growth were observed during the vegetative and reproductive phases of soybean crops under drought stress (Yan et al., 2020). Our previous findings in the onion crop support the present results, that drought stress severely affects plant height, leading to stunted growth (Ghodke et al., 2018). Further, drought stress significantly affects the photosynthesis apparatus and pigments that decrease the photosynthesis rate, light-harvesting mechanism, and assimilate partitioning in plants (Cornic and Massacci, 1996). Leaf senescence is a typical symptom under drought stress that increases with stress severity. Genotypes with higher chlorophyll content maintained their optimum

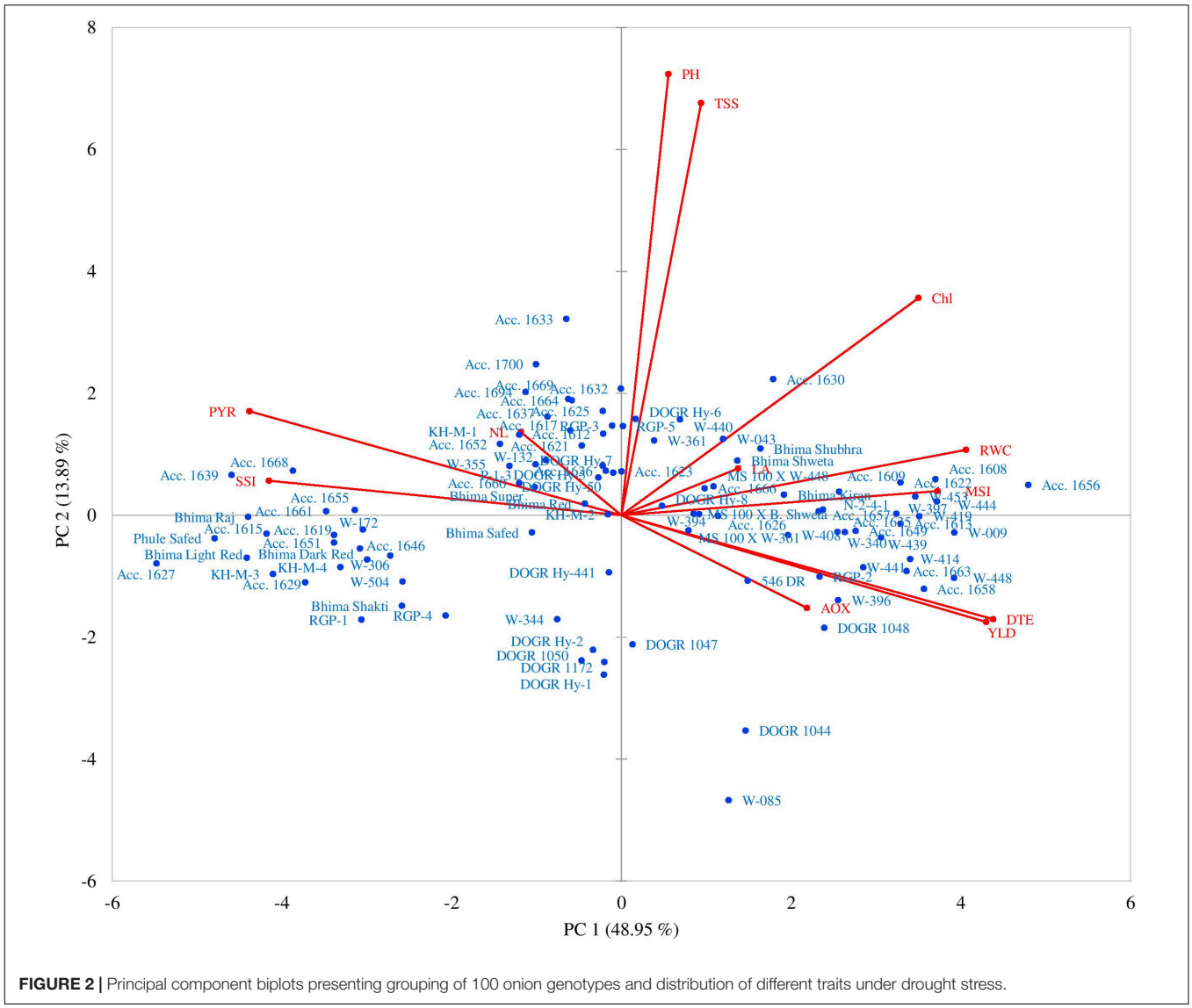


FIGURE 2 | Principal component biplots presenting grouping of 100 onion genotypes and distribution of different traits under drought stress.

photosynthesis rate to meet the crop requirement under limited water supply. Reduction in the number of leaves, and chlorophyll pigments, and a higher leaf senescence rate with a declined leaf area were found in the tested genotypes under water-deficit stress compared with well-watered conditions. These alterations in traits by defoliating functional leaves and reducing chlorophyll pigments adversely affect the overall photosynthesis process. Differential behavior was observed among the genotypes for these traits possibly due to their inherent divergence and tolerance mechanism under stress. Selective genotypes, namely Acc. 1656, Acc. 1658, W-009, W-448, and W-397, maintained their leaf area and chlorophyll pigments under both water regimes and were therefore categorized as drought tolerant. By contrast, few genotypes viz. Acc. 1627 and Acc. 1639, that exhibited a high leaf senescence rate and low chlorophyll with poor photosynthesis were designated as drought-sensitive. Several studies in other crops, such as wheat (Mwadzingeni et al., 2016), green gram (Baroowa et al., 2016), and black gram (Gurumurthy et al., 2019), have reported similar findings. In our study, genotypic variation in RWC was observed under drought stress in the tested genotypes. The tolerant genotypes with high RWC maintained cellular turgidity, which might have helped them to survive under stress through a desiccation tolerance mechanism. MSI is another important drought adaptive trait that is mostly over-expressed under the water-deficit stress condition compared with the well-watered condition. This trait is important in overcoming cellular injury or membrane damage caused by free radicals under water stress. The increasing MSI level was reported in most tolerant genotypes compared with the sensitive ones. The increase in MSI can directly be used for assessing stress-induced injury in numerous genotypes. Plants develop a complex defense mechanism (Enzymatic and Non-enzymatic antioxidant activity) to cope with oxidative stress induced by reactive oxygen species (Sairam et al., 1997). Antioxidant enzyme activity increases sharply under drought stress in crop such as leafy vegetables (Sarker and Oba, 2018),

tomato (Aghaie et al., 2018), and muskmelon (Ansari et al., 2017). All these previous reports have revealed that genotypes with high antioxidant enzyme activity perform better under drought stress. Phenolic compounds generally increases during water stress (Hodaei et al., 2018). In the tolerant genotypes levels of total phenol recorded increased as compaired to well-watered In our study, considerable genotypic variation was observed for these adaptive traits particularly, RWC, MSI, and antioxidant enzyme activity. Tolerant genotypes (Acc. 1656, Acc. 1658, W-009, and W-085) performed superiorly under drought stress by excelling in these traits as the stress increases. By contrast, sensitive genotypes (Acc. 1627, Acc. 1639, Bhima Raj, Bhima Light Red, and Phule Safed) with high SSI and poor yield responded negatively for these traits under drought stress. Our recent findings also support the results of the present study, where a drought-tolerant onion genotype had higher RWC, MSI, and antioxidant enzyme activity than the sensitive genotype (Ghodke et al., 2020). The findings were further supported by the study of Chaturvedi et al. (2019) in okra, where plant water status and cellular membrane stability decreased under drought stress during the crop vegetative and reproductive stage. The phenols are non-enzymatic antioxidants, and there accumulation reported in biotic and abiotic stress (Hodaei et al., 2018). Together, these traits can be believed to play an adaptive role in drought tolerance and can be used as a selection criterion for screening large germplasm pool for tolerant genotypes.

In our study, the value for the PCV was higher than that for the GCV for all the studied traits among the tested genotypes, signifying the influence of external environmental factors on various plant traits. The low heritability value further indicates the less genotypic variance among the tested genotypes. The higher influence of water deficit stress on the expression of adaptive traits might help in screening genotypes under the water stress environment.

Effect of Drought Stress on Yield and Its Contributing Traits

Previous studies have shown that drought stress significantly reduces onion bulb yield (Ghodke et al., 2018; Wakchaure et al., 2018). Variation was observed in the present study for bulb yield and its associated traits due to genetic divergence among the genotypes under the well-water and water-deficit stress conditions. The results of the pooled analysis for 2 years, revealed genotypes with optimum bulb yield under both water regimes with minimum yield reduction under water stress; these genotypes can be further employed in breeding programs. A significant yield difference was observed among the genotypes under the well-watered and water-deficit conditions, with most sensitive genotypes being severely affected by drought stress during the bulb development stage. Bulb yield reduction might be due to drought-induced reduction in leaf photosynthesis and the translocation process toward developing bulbs. Consequently, bulbs of small size and poor marketable quality were produced. Thus, unique tolerant genotypes with improved drought-adaptive traits can be useful for achieving the potential yield in different drought-prone areas. The results of various studies on different crops, such as maize, wheat (Webber et al., 2018), beans (Darkwa et al., 2016), and potato (Banik et al., 2016), where drought stress-induced yield losses are observed, support our findings.

Association Among Different Traits Under Drought Stress

The correlation analysis showed a significantly higher positive correlation between DTE and GMP and a negative association between DTE and SSI, indicating that genotypes with high DTE and low SSI have less bulb yield difference under the two water regimes. A strong positive association was also observed between bulb yield and physiological traits such as RWC, MSI, antioxidant enzyme activity, and total chlorophyll content under drought stress. Thus genotypes that maintained its water status, prevented membrane damage by enhancing antioxidant enzyme activity, and regulate its photosynthesis activity under limited water supply had a better drought tolerance mechanism than the other genotypes. These findings thus revealed the prominence of these traits and drought indices in selecting tolerant genotypes for drought stress. The present findings are supported by previous study results in wheat (Golabadi et al., 2006; Mohammadi, 2016; Ghodke et al., 2019) and safflower crop (Bahrami et al., 2014) under the drought environment.

Multivariate analysis further revealed the relationship between more than two traits at the same time through cluster analysis, descriptive statistics, and PCA. Cluster analysis produced a broad range of variability that helped in identifying tolerant genotypes. The cluster dendrogram was created using a Euclidean distance of 100 onion genotypes for drought conditions that grouped the genotypes into five clusters. Cluster II contained genotypes that exhibited more drought tolerance and less stress susceptibility with improved physiological and biochemical traits such as higher RWC, MSI, total chlorophyll, antioxidant enzyme activity, and leaf area. These genotypes were designated as highly drought-tolerant. Again, cluster I contained the tolerant genotypes that performed better for in terms of various physiochemical traits under limited water supply. Furthermore, genotypes with an intermediate performance for all physiological and yield traits were placed in cluster III. These genotypes, recorded good yield and growth behavior under the well-watered condition, whereas they failed to maintain their potential bulb yield under moderate to severe drought stress. The physiological traits, viz. RWC, MSI, and total chlorophyll, were severely affected due to water stress in genotypes of cluster IV. Poor bulb yield in genotypes of this group under water stress may be due to increased membrane damage, low plant water status, and altered enzyme activities which increased their sensitivity to drought. Likewise, genotypes of cluster V were categorized as sensitive as they performed relatively under mild stress and substantial yield reduction was observed under severe stress. This method of grouping genotypes based on their phenotypic traits and yield performance has been followed for many crops. In tomato crop, 14 cultivars were grouped into four clusters, with tolerant cultivars placed in cluster I with a high yield potential and proline

level, and sensitive and highly sensitive cultivars with a low proline level and severe membrane damage under moderate and severe drought stress were placed in cluster III and cluster IV, respectively (Aghaie et al., 2018). In our previous study, wheat genotypes were grouped into five clusters based on their drought tolerance and physiological performance under drought stress (Ghodke et al., 2019).

The PCA in the present study indicated that under drought stress, DTE, RWC, MSI, total chlorophyll, and antioxidant enzyme activity significantly influence bulb yield. Jan et al. (2018) showed that PC groups having an eigenvalue more than 1 exhibit greater variability than the PC group having an eigenvalue of less than 1, which supports our findings. According to this criterion, the first three PC groups contributed 73.64% of the total variability under drought stress, thereby clearly indicating the structure underlying the traits analyzed. In the PC1 group, maximum variability was observed for DTE, which indicates that this parameter can act as a promising trait for screening numerous onion genotypes under drought stress. Genotypes with high DTE performed superiorly with high yield and adaptive phenotypic responses under mild to severe drought stress. Arifuzzaman et al. (2020) showed that the maximum variability under drought stress was contributed by PC1 where leaf collar height of wheat genotypes accounted for the highest positive contribution, whereas the negative contribution of the chlorophyll content and root to shoot ratio was the highest. Similar findings were reported in a wheat crop, thus supporting our result for onion genotypes (Mwadzingeni et al., 2016).

A biplot created between PC1 and PC2 showed a clear pattern of grouping genotypes along the vector line. The outstanding performance of particular genotypes for a specific trait was plotted closer to the vector line. Genotypes and traits that lie far away from the origin have better breeding potential than the other genotypes. In this study, the genotypes Acc. 1656 and W-085 were at a considerable distance from the origin and hence can be utilized in onion breeding program as a tolerant genotype. Again, Acc. 1656 was close to the vector line and was associated with drought-tolerant characters (DTE, MSI, RWC, and antioxidant enzyme activity), and thus, it can be employed for developing a drought-tolerant onion variety. Similar findings in wheat were reported by Grzesiak et al. (2019) and Arifuzzaman et al. (2020) where drought-tolerant genotypes were plotted close to the drought adaptive promising traits and were found to be suitable for the wheat breeding program. These findings indicated that maintenance of high DTE contributes maximum (more acute angle) to bulb yield compared with other traits under drought stress. However, RWC, MSI, and antioxidant enzyme activity also contribute to bulb yield under drought stress by accelerating various adaptive physiological and biochemical mechanisms.

Overall, the findings suggested that drought indices, PCA, and hierarchical cluster analysis could be used as reliable methods for screening onion genotypes and classifying them into different categories based on the variation in phenotypic traits, and physiological, biochemical, and yield performance under drought stress. This approach can also be utilized for screening the onion germplasm for other biotic and abiotic stresses and for identifying the most contrasting genotypes for a particular stress. Here, the tolerant genotypes identified might carry genes for drought tolerance that may act as a useful tool in onion breeding program for drought tolerance. Further, these unique tolerant genotypes can be crossed with high yielding popular onion varieties to introgress the genes for drought tolerance in the variety without affecting its inherent yield potential under drought stress.

DATA AVAILABILITY STATEMENT

The original contributions presented in the study are included in the article/**Supplementary Material**, further inquiries can be directed to the corresponding author/s.

AUTHOR CONTRIBUTIONS

PG: project administration, resources, supervision, methodology, analysis, and writing original draft. AT: project administration, resources, supervision, and writing–original draft. DS: methodology, biochemical analysis, statistical analysis, writing–original draft, writing–review, and editing. SG: methodology, statistical analysis, and writing–original draft. KB: writing–original draft, and statistical analysis. OS: methodology, statistical analysis, writing–review, and editing. AG and VM: resources. PS: methodology and writing–original draft. VS and YK: methodology and analysis. SG: project administration, resources, supervision, writing–original draft, writing–review, and editing. PH and RR: methodology and statistical analysis. MS: project administration, resources, and supervision. All authors listed have made substential, direct and intellectual contribution to the work.

ACKNOWLEDGMENTS

The authors are grateful to Indian Council of Agricultural Research, New Delhi for supporting this research through the ICAR-National Innovations on Climate Resilient Agriculture and ICAR-Directorate of Onion and Garlic Research, Pune.

SUPPLEMENTARY MATERIAL

The Supplementary Material for this article can be found online at: https://www.frontiersin.org/articles/10.3389/fpls.2021.600371/full#supplementary-material

Supplementary Figure 1| Monthly temperature and rainfall patterns recorded during the experiment period for two constitutive years (2017–2018 and 2018–2019).

REFERENCES

Aghaie, P., Tafreshi, S. A. H., Ebrahimi, M. A., and Haerinasab, M. (2018). Tolerance evaluation and clustering of fourteen tomato cultivars grown under mild and severe drought conditions. *Sci. Hortic.* 232, 1–12. doi: 10.1016/j.scienta.2017.12.041

Ansari, W. A., Atri, N., Singh, B., and Pandey, S. (2017). Changes in antioxidant enzyme activities and gene expression in two muskmelon genotypes under progressive water stress. *Biol. Plant.* 61, 333–341. doi: 10.1007/s10535-016-0694-3

Arifuzzaman, M., Barman, S., Hayder, S., Azad, M. A. K., Turin, M. T. S., Amzad, M. A., et al. (2020). Screening of bread wheat (*Triticum aestivum* L.) genotypes under drought stress conditions using multivariate analysis. *Cereal Res. Commun.* 48, 301–308. doi: 10.1007/s42976-020-00039-8

Arnon, D. (1949). Estimation of total chlorophyll. *Plant Physiol.* 24, 1–15.

Bahrami, F., Arzani, A., and Karimi, V. (2014). Evaluation of yield-based drought tolerance indices for screening safflower genotypes. *Agron. J.* 106, 1219–1224. doi: 10.2134/agronj13.0387

Banik, P., Zeng, W., Tai, H., Bizimungu, B., and Tanino, K. (2016). Effects of drought acclimation on drought stress resistance in potato (*Solanum tuberosum* L.) genotypes. *Environ Exp. Bot.* 126, 76–89. doi: 10.1016/j.envexpbot.2016.01.008

Baroowa, B., Gogoi, N., and Farooq, M. (2016). Changes in physiological, biochemical and antioxidant enzyme activities of green gram (*Vigna radiata* L.) genotypes under drought. *Acta Physiol. Plant.* 38:219. doi: 10.1007/s11738-016-2230-7

Barrs, H. D., and Weatherley, P. E. (1962). A re-examination of the relative turgidity technique for estimating water deficits in leaves. *Aust. J. Biol. Sci.* 15, 413–428. doi: 10.1071/bi9620413

Blum, A. (2010). *Plant Breeding for Water-Limited Environments*. New York, NY: Springer Science and Business Media.

Chaturvedi, A. K., Surendran, U., Gopinath, G., Chandran, K. M., Anjali, N. K., and Ct, M. F. (2019). Elucidation of stage specific physiological sensitivity of okra to drought stress through leaf gas exchange, spectral indices, growth and yield parameters. *Agric. Water* Manag. 222, 92–104. doi: 10.1016/j.agwat.2019.05.041

Cornic, G., and Massacci, A. (1996). "Leaf photosynthesis under drought stress," in *Photosynthesis and the Environment*, ed. N. R. Baker (Dordrecht: Springer), 347–366. doi: 10.1007/0-306-48135-9_14

Darkwa, K., Ambachew, D., Mohammed, H., Asfaw, A., and Blair, M. W. (2016). Evaluation of common bean (*Phaseolus vulgaris* L.) genotypes for drought stress adaptation in Ethiopia. *Crop J.* 4, 367–376. doi: 10.1016/j.cj.2016.06.007

Diaz, P., Betti, M., Sanchez, D. H., Udvardi, M. K., Monza, J., and Marquez, A. J. (2010). Deficiency in plastidic glutamine synthetase alters proline metabolism and transcriptomic response in *Lotus japonicus* under drought stress. *New Phytol.* 188, 1001–1013. doi: 10.1111/j.1469-8137.2010.03440.x

FAOSTAT (2019). *Food and Agriculture Organization of the United Nations*. Rome: FAO.

Fenta, B. A., Beebe, S. E., Kunert, K. J., Burridge, J. D., Barlow, K. M., Lynch, J. P., et al. (2014). Field phenotyping of soybean roots for drought stress tolerance. *Agron* 4, 418–435. doi: 10.3390/agronomy4030418

Fernandez, G. C. J. (1992). "Effective selection criteria for assessing plant stress tolerance," in *Proceedings of the International Symposium on Adaptation of Food Crops to Temperature and Water Stress*, taiwan, 257–270.

Fischer, K. S., and Wood, G. (1981). "Breeding and selection for drought tolerance in tropical maize," in *Proceedings of an International Symposium on Principles and Methods in Crop Improvement for Drought Resistance with Emphasis on Rice* (Los Baños: IRRI).

Fischer, R. A., and Maurer, R. (1978). Drought resistance in spring wheat cultivars. I. Grain yield response. *Aust. J. Agric. Res.* 29, 897–912. doi: 10.1071/ar9780897

Ghodke, P., Khandagale, K., Thangasamy, A., Kulkarni, A., Narwade, N., Shirsat, D., et al. (2020). Comparative transcriptome analyses in contrasting onion (*Allium cepa* L.) genotypes for drought stress. *PLoS One* 15:e0237457. doi: 10.1371/journal.pone.0237457

Ghodke, P. H., Andhale, P. S., Gijare, U. M., Thangasamy, A., Khade, Y. P., Mahajan, V., et al. (2018). Physiological and biochemical responses in onion crop to drought stress. *Int. J. Curr. Microbiol. App. Sci.* 7, 2054–2062. doi: 10.20546/ijcmas.2018.701.247

Ghodke, P. H., Ramakrishnan, S., Shirsat, D. V., Vani, G. K., and Arora, A. (2019). Morphological characterization of wheat genotypes for stay green and physiological traits by multivariate analysis under drought stress. *Indian J. Plant Physiol.* 24, 305–315. doi: 10.1007/s40502-019-00458-8

Golabadi, M., Arzani, A. S. A. M., and Maibody, S. M. (2006). Assessment of drought tolerance in segregating populations in durum wheat. *Afr. J. Agric. Res.* 1, 162–171.

Grzesiak, S., Hordynska, N., Szczyrek, P., Grzesiak, M. T., Noga, A., and Szechynska-Hebda, M. (2019). Variation among wheat (*Triticum easativum* L.) genotypes in response to the drought stress: I–selection approaches. *J. Plant Interact.* 14, 30–44. doi: 10.1080/17429145.2018.1550817

Gurumurthy, S., Sarkar, B., Vanaja, M., Lakshmi, J., Yadav, S. K., and Maheswari, M. (2019). Morpho-physiological and biochemical changes in black gram (*Vigna mungo* L. Hepper) genotypes under drought stress at flowering stage. *Acta Physiol. Plant.* 41:42. doi: 10.1007/s11738-019-2833

Hiscox, J. D., and Israelstam, G. F. (1979). A method for the extraction of chlorophyll from leaf tissue without maceration. *Can. J. Bot.* 57, 1332–1334. doi: 10.1139/b79-163

Hodaei, M., Rahimmalek, M., Arzani, A., and Talebi, M. (2018). The effect of water stress on phytochemical accumulation, bioactive compounds and expression of key genes involved in flavonoid biosynthesis in *Chrysanthemum morifolium* L. *Ind. Crops Prods* 120, 295–304. doi: 10.1016/j.indcrop.2018.04.073

Jan, S. A., Shinwari, Z. K., Ali, N., and Rabbani, M. A. (2018). Morphometric analysis of Brassica Carinata elite lines reveals variation for yield related traits. *Pak. J. Bot*. 50, 1521–1524.

Kwon, S. H., and Torrie, J. H. (1964). Heritability of and interrelationships among traits of two soybean populations. *Crop. Sci.* 4, 196–198. doi: 10.2135/cropsci1964.0011183X000400020023x

Mohammadi, R. (2016). Efficiency of yield-based drought tolerance indices to identify tolerant genotypes in durum wheat. *Euphytica* 211, 71–89. doi: 10.1007/s10681-016-1727-x

Mwadzingeni, L., Shimelis, H., Tesfay, S., and Tsilo, T. J. (2016). Screening of bread wheat genotypes for drought tolerance using phenotypic and proline analyses. *Front. Plant Sci.* 7:1276. doi: 10.3389/fpls.2016.01276

Passioura, J. B. (2012). Phenotyping for drought tolerance in grain crops: when is it useful to breeders? *Funct. Plant Biol.* 39, 851–859. doi: 10.1071/fp12079

Pelter, G. Q., Mittelstadt, R., Leib, B. G., and Redulla, C. A. (2004). Effects of water stress at specific growth stages on onion bulb yield and quality. *Agric. Water* Manag. 68, 107–115. doi: 10.1016/j.agwat.2004.03.010

Ramakrishnan, R. S., Ghodke, P. H., Nagar, S., Vinoth, R., Kumar, B., Singh, V. P., et al. (2016). Genetic analysis of stay green trait and its association with morpho-physiological traits under water deficit stress in wheat. *Indian J. Plant Genet Res.* 29, 177–183. doi: 10.5958/0976-1926.2016.00025.5

Raman, A., Verulkar, S., Mandal, N., Variar, M., Shukla, V., Dwivedi, J., et al. (2012). Drought yield index to select high yielding rice lines under different drought stress severities. *Rice* 5, 31–42.

Sairam, R. K., and Saxena, D. C. (2000). Oxidative stress and antioxidants in wheat genotypes: possible mechanism of water stress tolerance. *J. Agron. Crop Sci.* 184, 55–61. doi: 10.1046/j.1439-037x.2000.00358.x

Sairam, R. K., Shukla, D. S., and Saxena, D. C. (1997). Stress induced injury and antioxidant enzymes in relation to drought tolerance in wheat genotypes. *Biol. Plant.* 40, 357–364. doi: 10.1023/a:1001009812864

Sarker, U., and Oba, S. (2018). Drought stress enhances nutritional and bioactive compounds, phenolic acids and antioxidant capacity of *Amaranthus* leafy vegetable. *BMC Plant Biol* 18:258. doi: 10.1186/s12870-018-1484-1

Schwimmer, S., and Weston, W. J. (1961). Enzymatic development of pyruvic acid in onion as a measure of pungency. *J. Agr. Food Chem.* 9, 301–304. doi: 10.1021/jf60116a018

Singleton, V. L., and Rossi, J. A. (1965). Colorimetry of total phenolics with phosphomolybdic-phosphotungstic acid reagents. *Am. J. Enol. Vitic.* 16, 144–158.

Stratil, P., Klejdus, B., and Kuban, V. (2006). Determination of total content of phenolic compounds and their antioxidant activity in vegetables evaluation of spectrophotometric methods. *J. Agr. Food Chem.* 54, 607–616. doi: 10.1021/jf052334j

Vaezi, B., Bavei, V., and Shiran, B. (2010). Screening of barley genotypes for drought tolerance by agro-physiological traits in field condition. *Afr. J. Agric. Res.* 5, 881–892.

Wakchaure, G. C., Minhas, P. S., Meena, K. K., Singh, N. P., Hegade, P. M., and Sorty, A. M. (2018). Growth, bulb yield, water productivity and quality of onion (*Allium cepa* L.) as affected by deficit irrigation regimes and exogenous application of plant bio-regulators. *Agric. Water Manag.* 199, 1–10. doi: 10.1016/j.agwat.2017.11.026

Webber, H., Ewert, F., Olesen, J. E., Müller, C., Fronzek, S., Ruane, A. C., et al. (2018). Diverging importance of drought stress for maize and winter wheat in Europe. *Nat. Commun.* 9:4929.

Yan, C., Song, S., Wang, W., Wang, C., Li, H., Wang, F., et al. (2020). Screening diverse soybean genotypes for drought tolerance by membership function value based on multiple traits and drought-tolerant coefficient of yield. *BMC Plant Biol.* 20:321. doi: 10.1186/s12870-020-02519-9

Conflict of Interest: The authors declare that the research was conducted in the absence of any commercial or financial relationships that could be construed as a potential conflict of interest.

Copyright © 2021 Gedam, Thangasamy, Shirsat, Ghosh, Bhagat, Sogam, Gupta, Mahajan, Soumia, Salunkhe, Khade, Gawande, Hanjagi, Ramakrishnan and Singh. This is an open-access article distributed under the terms of the Creative Commons Attribution License (CC BY). The use, distribution or reproduction in other forums is permitted, provided the original author(s) and the copyright owner(s) are credited and that the original publication in this journal is cited, in accordance with accepted academic practice. No use, distribution or reproduction is permitted which does not comply with these terms.

frontiers in Plant Science

ORIGINAL RESEARCH
published: 10 February 2021
doi: 10.3389/fpls.2021.613568

Oryza sativa cv. Nipponbare and *Oryza barthii* as Unexpected Tolerance and Susceptibility Sources Against *Schizotetranychus oryzae* (Acari: Tetranychidae) Mite Infestation

*Giseli Buffon[1], Édina Aparecida dos Reis Blasi[1], Thainá Inês Lamb[2], Janete Mariza Adamski[3], Joséli Schwambach[4], Felipe Klein Ricachenevsky[5], Amanda Bertolazi[6], Vanildo Silveira[6], Mara Cristina Barbosa Lopes[7] and Raul Antonio Sperotto[1,2]**

[1] Graduate Program in Biotechnology, University of Taquari Valley-Univates, Lajeado, Brazil, [2] Biological Sciences and Health Center, University of Taquari Valley-Univates, Lajeado, Brazil, [3] Graduate Program in Botany, Federal University of Rio Grande do Sul, Porto Alegre, Brazil, [4] Graduate Program in Biotechnology, University of Caxias do Sul, Caxias do Sul, Brazil, [5] Graduate Program in Molecular and Cellular Biology, Federal University of Rio Grande do Sul, Porto Alegre, Brazil, [6] Laboratory of Biotechnology, Bioscience and Biotechnology Center, State University of Northern Rio de Janeiro Darcy Ribeiro, Campos dos Goytacazes, Brazil, [7] Rice Research Institute (Instituto Rio-Grandense do Arroz), Cachoeirinha, Brazil

OPEN ACCESS

Edited by:
Jeremy Astier,
INRA UMR1347 Agroécologie, France

Reviewed by:
Sang-Wook Han,
Chung-Ang University, South Korea
Kanako Bessho-Uehara,
Tohoku University, Japan
Qian Qian,
Chinese Academy of Agricultural Sciences, China

***Correspondence:**
Raul Antonio Sperotto
rasperotto@univates.br;
raulsperotto@gmail.com

Specialty section:
This article was submitted to Plant Pathogen Interactions, a section of the journal Frontiers in Plant Science

Received: 02 October 2020
Accepted: 21 January 2021
Published: 10 February 2021

Citation:
Buffon G, Blasi ÉAR, Lamb TI, Adamski JM, Schwambach J, Ricachenevsky FK, Bertolazi A, Silveira V, Lopes MCB and Sperotto RA (2021) Oryza sativa cv. Nipponbare and Oryza barthii as Unexpected Tolerance and Susceptibility Sources Against Schizotetranychus oryzae (Acari: Tetranychidae) Mite Infestation. Front. Plant Sci. 12:613568. doi: 10.3389/fpls.2021.613568

Cultivated rice (*Oryza sativa* L.) is frequently exposed to multiple stresses, including *Schizotetranychus oryzae* mite infestation. Rice domestication has narrowed the genetic diversity of the species, leading to a wide susceptibility. This work aimed to analyze the response of two African rice species (*Oryza barthii* and *Oryza glaberrima*), weedy rice (*O. sativa* f. *spontanea*), and *O. sativa* cv. Nipponbare to *S. oryzae* infestation. Surprisingly, leaf damage, histochemistry, and chlorophyll concentration/fluorescence indicated that the African species present a higher level of leaf damage, increased accumulation of H_2O_2, and lower photosynthetic capacity when compared to *O. sativa* plants under infested conditions. Infestation decreased tiller number, except in Nipponbare, and caused the death of *O. barthii* and *O. glaberrima* plants during the reproductive stage. While infestation did not affect the weight of 1,000 grains in both *O. sativa*, the number of panicles per plant was affected only in *O. sativa* f. *spontanea*, and the percentage of full seeds per panicle and seed length were increased only in Nipponbare. Using proteomic analysis, we identified 195 differentially abundant proteins when comparing susceptible (*O. barthii*) and tolerant (Nipponbare) plants under control and infested conditions. *O. barthii* presents a less abundant antioxidant arsenal and is unable to modulate proteins involved in general metabolism and energy production under infested condition. Nipponbare presents high abundance of detoxification-related proteins, general metabolic processes, and energy production, suggesting that the primary metabolism is maintained more active compared to *O. barthii* under infested condition. Also, under infested conditions, Nipponbare presents higher levels of proline

and a greater abundance of defense-related proteins, such as osmotin, ricin B-like lectin, and protease inhibitors (PIs). These differentially abundant proteins can be used as biotechnological tools in breeding programs aiming at increased tolerance to mite infestation.

Keywords: osmotin, proline, protease inhibitors, proteome, resistance, wild species

INTRODUCTION

Rice (*Oryza sativa* L.) is extremely important for human nutrition, representing around 20% of the daily intake calories in the world. It is considered a staple food for over half of the world's population (Muthayya et al., 2014). To meet this nutritional demand, natural resources must be used efficiently, and crop production needs to be increased (Godfray et al., 2010). However, the search for new agricultural frontiers and the availability of natural resources is limited, exposing rice cultivation to several disturbances caused by biotic and abiotic stresses, which negatively impact grain yield (Palmgren et al., 2015). Among these important stresses that influence plant yield, the presence of arthropods (Oerke, 2006) impacts about 18–26% of annual crop production worldwide, causing losses of over US$ 470 billion (Culliney, 2014). Most of these losses (13–16%) occur in the field before harvesting, and losses are most often described in developing countries (Culliney, 2014). One of the arthropods that attack rice crops in Brazil, and has been reported in other South American countries, is *Schizotetranychus oryzae* Rossi de Simons mite species, which can cause more than 60% loss in rice grain yield (Buffon et al., 2018). An interesting strategy for reducing these losses is the search for mite-tolerant cultivars, as these plants tolerate mite infestation and maintain grain yield without the need to apply acaricides (Sperotto et al., 2018a).

Plant defense to herbivory includes both resistance (the ability of plants to escape attacking enemies) and tolerance (the ability of plants to withstand herbivory without any decline in yield) (Stenberg and Muola, 2017). Both defense strategies can be plant focused and can be useful to measure the plant's ability to defend from herbivores. Several molecular and physiological characteristics can be used to detect resistance/tolerance plant capacity, including expression of defense-related genes, levels of soluble protein/sugar, reactive oxygen species, lipid peroxidation, carotenoids/chlorophyll, photosynthetic efficiency, cell membrane damage, and others (Blasi et al., 2015).

The search for genetic variability in the *Oryza* genus is a shortcut to obtain resistant/tolerant rice genotypes and to develop cultivars that adapt to natural adversities (Menguer et al., 2017; Szareski et al., 2018). Several authors reported wild rice plants resistant/tolerant to biotic and abiotic factors (Brar and Khush, 2003). The use of wild rice species in breeding programs can facilitate adaptation to biotic and abiotic stresses, as well as meeting the demand for food security in the current scenario of rapidly growing world population (Henry, 2014). The *Oryza* genus is composed of 24 species, two cultivated (*O. sativa* and *Oryza glaberrima*) and other 22 wild species. These wild species represent between 15 and 25 million years of evolutionary diversification (Vaughan, 1994; Menguer et al., 2017).

Oryza barthii is an annual wild African species that is commonly known as the progenitor of *O. glaberrima*, the rice cultivated species grown in Africa. *O. barthii* is tolerant to several biotic and abiotic stresses (Khush, 1997), being adapted to more adverse ecological conditions, and resistant to multiple environmental restrictions (Sarla and Swamy, 2005). Weedy rice (*O. sativa* f. *spontanea*), which is the result of rice de-domestication process, also shows tolerance to environmental stresses. Therefore, the genetic background, morphology, and growth behavior are similar to cultivated rice (Qiu et al., 2017). However, differences in tolerance to stressful conditions may occur during de-domestication, e.g., weedy rice is tolerant to cold, high salinity and drought, and resistant to blast disease. Due to its greater stress tolerance/resistance, weedy rice has become one of the most feared and harmful weeds in rice producing regions worldwide (Dai et al., 2014). Nonetheless, interesting traits found in weedy rice can be eventually transferred to cultivated genotypes.

Aiming to identify novel resistance/tolerance mechanisms in rice plants exposed to *S. oryzae* mite infestation, we analyzed two African species (wild *O. barthii* and cultivated *O. glaberrima*), weedy rice (*O. sativa* f. *spontanea*) and cv. Nipponbare (*O. sativa* ssp. *japonica*). Although we expected wild rice species to show higher tolerance to mite infestation, we found unexpected results. According to our data, *O. barthii* and *O. glaberrima* are extremely sensitive to mite infestation, while cv. Nipponbare seems to be more tolerant. Therefore, we tried to understand the molecular and physiological mechanisms behind Nipponbare tolerance and African species susceptibility to this mite. Our results may be useful for future breeding programs aiming at resistance/tolerance to *S. oryzae* mite infestation.

MATERIALS AND METHODS

Plant Growth Conditions and Mite Infestation

Seeds of *O. sativa* cv. Nipponbare (hereafter "Nipponbare") were obtained from the seed bank Rice Genome Resource Center[1]. Seeds of weedy and African rice species are part of the International Rice Research Institute (IRRI) germplasm collection: *O. sativa* f. *spontanea* (IRGC 80590, hereafter "weedy rice"), *O. barthii* (IRGC 86524), and *O. glaberrima* (IRGC 103959). Seeds were surface sterilized and germinated for 4 days

Abbreviations: DAB, diaminobenzidine; EI, early infested; GA, gibberellin; JA, jasmonic acid; LI, late infested; PI, protease inhibitor.

[1]https://www.rgrc.dna.affrc.go.jp/

in an incubator (28°C) on paper soaked with distilled water. After germination, plantlets were transferred to vermiculite/soil mixture (1:3) for additional 14 days in greenhouse conditions, and then transferred to plastic buckets containing soil and water. Plastic buckets containing rice plants highly infested by *S. oryzae* were kindly provided by Instituto Rio-Grandense do Arroz (IRGA, Cachoeirinha, RS), and were used to infest rice plants in our experiment. Fifty plants (V10-13 stage, according to Counce et al., 2000) of each cultivar/species (five plants per bucket) were infested by proximity with the bucket containing the highly infested plants placed in the center of the other buckets. For greater homogeneity of infestation and contact, buckets of each cultivar/species were rotated at a 90° angle counterclockwise every 2 days. Ten plants of each cultivar were cultivated without infestation (control condition).

The level of damage caused by *S. oryzae* was analyzed from V10-13 stage until the plants reached the final stage of reproductive development (panicle maturity, R9 stage; Counce et al., 2000). Evaluation of damage in the abaxial and adaxial faces of leaves was based on a classification of four infestation levels: Level 1: control condition, without any sign of infestation; Level 2: early infested (EI) leaves, 10–20% of damaged leaf area, average of 168 h of exposure to the mite; Level 3: intermediate infested (II) leaves, 40–50% of damaged leaf area, average of 360 h; and Level 4: late infested (LI) leaves, more than 80% of damaged leaf area, average of 720 h, according to Buffon et al. (2018).

Plant Height and Tiller Number

Plant height and tiller number were evaluated ($n = 50$) during the vegetative stage (V10-13, before infestation) and during the last reproductive stage (R9, control and infested plants).

Chlorophyll *a* Fluorescence Transients

The chlorophyll *a* fluorescence transient was measured ($n = 10$) on the third upper leaves of control and infested plants in two different exposure times, 1 week (which correspond to EI) and 4 weeks (which correspond to LI), using a portable fluorometer (OS30p, Optisciences, United Kingdom). Before the measurements, plants were dark adapted for 20 min, and the fluorescence intensity was measured by applying a saturating pulse of 3,000 μmol photons m^{-2} s^{-1}. The resulting fluorescence of the chlorophyll *a* was measured from 0 to 1 s. The chlorophyll fluorescence intensity rises from a minimum level (the O level, F_O = 160 μs) to a maximum level (the P level, F_P = 300 ms), via two intermediate steps labeled J (F_J = 2 ms) and I (F_I = 30 ms) phases (Stirbet and Govindjee, 2011), also known as OJIP curve (Strasser et al., 2000).

Total Chlorophyll Concentration

Samples ($n = 3$) of leaves from rice plants submitted to control and LI conditions were collected, and total chlorophyll concentration was quantified. In brief, 100 mg of sample was sprayed in liquid nitrogen, homogenized in 1.5 mL of 85% (v/v) acetone, maintained in the dark for 30 min, and centrifuged at 12,000 *g* for 3 min. The supernatant was transferred to a new tube, and the process was repeated until complete discoloration of the plant tissue. Chlorophyll *a* and *b* were quantified by measuring absorbance at 663 and 645 nm, and the concentrations were calculated according to Ross (1974).

In situ Histochemical Localization of H_2O_2

In situ accumulation of H_2O_2 in control and LI leaves was detected by histochemical staining with DAB, according to Shi et al. (2010), with minor modifications. Leaves were excised and immersed in DAB solution (1 mg mL^{-1}, pH 3.8) in 10 mM phosphate buffer (pH 7.8) and incubated at room temperature for 8 h in the light until brown spots were visible, which are derived from the reaction of DAB with H_2O_2. Leaves were bleached in boiling concentrated ethanol to visualize the brown spots, which were kept in 70% ethanol for taking pictures with a digital camera coupled to a stereomicroscope.

Seed Analysis

Seeds of Nipponbare and weedy rice were collected in R9 stage, and the following agronomical parameters were evaluated: number of panicles per plant, number of seeds (empty + full) per panicle, percentage of full seeds per panicle, grain length, and weight of 1,000 full grains. Yield reduction caused by *S. oryzae* infestation in Nipponbare was calculated using the following equation, for each condition (control and infested): number of seeds (empty + full) per plant × percentage of full seeds × weight of one seed = seed weight per plant. Seeds from African rice species were not analyzed as these plants did not reach the reproductive stage.

Proline Quantification

Control and LI leaves of Nipponbare and weedy rice were collected, and proline accumulation was quantified ($n = 3$) according to Shukla et al. (2012). In brief, 250 mg of sample was sprayed in liquid nitrogen, homogenized in 2 mL of sulfosalicylic acid (3%), and centrifuged at 10,000 *g* for 30 min. Then, 1 mL of the supernatant was transferred to a new tube, and 1 mL of glacial acetic acid and 1 mL of ninhydrin (1.25 g of ninhydrin + 30 mL of glacial acetic acid + 20 mL of 6 M phosphoric acid) were added. The homogenized mixture was boiled in a water bath at 100°C for 30 min. Subsequently, the reaction was cooled on ice and 2 mL of toluene was added, mixing in the vortex for 30 s. The upper phase containing proline was measured on the spectrophotometer at 520 nm. The proline level (mmol g^{-1} fresh weight) was quantified using L-proline as standard. The standard curve was prepared from a stock solution of proline (5 mM) in sulfosalicylic acid for a concentration range between 10 and 320 mmol mL^{-1}. The free proline concentration of each sample was calculated from the linear regression equation obtained from the standard curve. The procedure for constructing the standard curve was the same as for free proline determination of the samples.

Plant Protein Extraction and Quantification

Three biological samples (250 mg of fresh weight) of control and EI leaves from *O. barthii* (mite-sensitive) and Nipponbare (mite-tolerant), each containing three leaves from three different plants,

were subjected to protein extraction using Plant Total Protein Extraction Kit (Sigma–Aldrich). The protein concentration was measured using 2-D Quant Kit (GE Healthcare, Piscataway, NJ, United States).

Protein Digestion

For protein digestion, three biological replicates of 100 μg of proteins from *O. barthii* and Nipponbare leaves were used. Before the trypsin digestion step, protein samples were precipitated using the methanol/chloroform methodology to remove any detergent from samples (Nanjo et al., 2012), followed by resuspension in urea 7 M and thiourea 2 M buffer in 50 mM ammonium bicarbonate. Right after, protein digestion was performed using the filter-aided sample preparation (FASP) methodology (Wiśniewski et al., 2009), with modifications described by Burrieza et al. (2019). In brief, after checking the integrity of the Microcon-30 kDa (Merck Millipore, Germany) filter units, protein aliquots were added to the filter units, washed with 200 μL of 50 mM ammonium bicarbonate (solution A), and centrifuged at 10,000 *g* for 15 min at 25°C (unless otherwise stated, all centrifugation steps were performed under this condition). This step was repeated once for complete removal of urea before reduction of proteins. Next, 100 μL of 50 mM DTT (GE Healthcare), freshly made in solution A, was added, gently vortexed, and incubated for 20 min at 60°C (1 min agitation and 4 min resting, at 650 r/min). Then, 200 μL of 8 M urea in 50 mM ammonium bicarbonate (solution B) was added, and centrifuged for 15 min. For protein alkylation, 100 μL of 50 mM iodoacetamide (GE Healthcare), freshly prepared in solution B, was added, gently vortexed, and incubated for 20 min at 25°C in the dark (1 min agitation and 19 min resting, at 650 r/min). Next, 200 μL of solution B was added and centrifuged for 15 min. This step was repeated once. Then, 200 μL of solution A was added and centrifuged for 15 min. This step was repeated twice. Approximately 50 μL of the sample should remain in the last washing. For protein digestion, 25 μL of 0.2% (v/v) RapiGest (Waters, Milford, CT, United States) and 25 μL of trypsin solution (1:100 enzyme:protein, V5111, Promega, Madison, WI, United States) were added, gently vortexed, and incubated for 18 h at 37°C (1 min agitation and 4 min resting, at 650 r/min). For peptide elution, the filter units were transferred to new microtubes and centrifuged for 10 min. Then, 50 μL of solution A was added and centrifuged for 15 min. This step was repeated once. For RapiGest precipitation and trypsin inhibition, 5 μL of 15% trifluoroacetic acid (Sigma–Aldrich) was added, gently vortexed, and incubated for 30 min at 37°C. Then, samples were centrifuged for 15 min, and the supernatants collected and vacuum dried. Peptides were resuspended in 100 μL solution of 95% 50 mM ammonium bicarbonate, 5% acetonitrile, and 0.1% formic acid. The resulting peptides were quantified by the A205 nm protein and peptide methodology, using a NanoDrop 2000c spectrophotometer (Thermo Fisher Scientific).

Mass Spectrometry Analysis

A nanoAcquity UPLC connected to a Synapt G2-Si HDMS mass spectrometer (Waters, Manchester, United Kingdom) was used for ESI-LC-MS/MS analysis. Runs consisted of injecting 1 μg of digested peptides from each biological replicate. During separation, samples were loaded onto the nanoAcquity UPLC 5 μm C18 trap column (180 μm × 20 mm) at 5 μL/min during 3 min and then onto the nanoAcquity HSS T3 1.8 μm analytical reversed phase column (75 μm × 150 mm) at 400 nL/min, with a column temperature of 45°C. For peptide elution, a binary gradient was used, with mobile phase A consisting of water (Tedia, Fairfield, OH, United States) and 0.1% formic acid (Sigma–Aldrich), and mobile phase B consisting of acetonitrile (Sigma–Aldrich) and 0.1% formic acid. Gradient elution started at 7% B, then ramped from 7% B to 40% B up to 91.12 min, and from 40% B to 99.9% B until 92.72 min, being maintained at 99.9% until 106.00 min, then decreasing to 7% B until 106.1 min and kept 7% B until the end of the experiment at 120.00 min. Mass spectrometry was performed in positive and resolution mode (V mode), 35,000 FWHM, with ion mobility, and in data-independent acquisition (DIA) mode; ion mobility separation ($HDMS^E$) using IMS wave velocity of 600 m/s, and helium and IMS gas flow of 180 and 90 mL/min, respectively; the transfer collision energy ramped from 19 V to 55 V in high-energy mode; cone and capillary voltages of 30 and 2750 V, respectively; and a source temperature of 70°C. In TOF parameters, the scan time was set to 0.5 s in continuum mode with a mass range of 50–2,000 Da. The human [Glu1]-fibrinopeptide B (Sigma–Aldrich) at 100 fmol/μL was used as an external calibrant and lock mass acquisition was performed every 30 s. Mass spectra acquisition was performed by MassLynx v4.0 software.

Proteomics Data Analysis

Spectral processing and database searching conditions were performed by ProteinLynx global server (PLGS; version 3.0.2) (Waters) and ISOQuant workflow software (Distler et al., 2014). The analysis used the following parameters: Apex3D of 150 counts for low energy threshold, 50 counts for elevated energy threshold, and 750 counts for intensity threshold; one missed cleavage, minimum fragment ion per peptide equal to three, minimum fragment ion per protein equal to seven, minimum peptide per protein equal to two, fixed modifications of carbamidomethyl (C), and variable modifications of oxidation (M) and phosphoryl (STY). The false discovery rate (FDR) for peptide and protein was set to a maximum of 1%, with a minimum peptide length of six amino acids. The analysis used the *O. sativa* ssp. *japonica* reference proteome from Uniprot[2] (48,903 protein sequences downloaded on 18 August 2018).

Comparative label-free quantification analysis was performed using ISOQuant software (Distler et al., 2014). Briefly, the analysis included retention time alignment, exact mass retention time (EMRT) and IMS clustering, as well as data normalization and protein homology filtering. ISOQuant annotates the resulting feature clusters by evaluating consensus peptide identifications and identification probabilities. Protein identification parameters in ISOQuant were set to FDR 1%, peptide score greater than six, minimum peptide length of six amino acids, and at least two peptides per protein. Label-free quantification was estimated using the TOP3 quantification approach (Silva et al., 2006),

[2]https://www.uniprot.org/proteomes/UP000059680

followed by the multidimensional normalization process implemented within ISOQuant (Distler et al., 2014). After data processing and to ensure the quality of results, only proteins present or absent (for unique proteins) in three out of three runs were accepted and submitted to differential abundance analysis. Data were analyzed using Student's *t*-test (two-tailed). Proteins with $P < 0.05$ were considered more abundant if the Log_2 of fold change (FC) was greater than 0.5 and less abundant if the Log_2 of FC was less than −0.5. All proteomics data were deposited to the ProteomeXchange Consortium (Deutsch et al., 2017) via the PRIDE repository[3] (Perez-Riverol et al., 2019) and can be accessed using the code PXD020940.

Statistical Analysis

Except for proteomics, data from other experiments were analyzed using the Student's *t*-test ($P \leq 0.05$ and 0.01) or one-way ANOVA followed by Tukey test ($P \leq 0.05$), using SPSS Base 23.0 for Windows (SPSS Inc., United States).

RESULTS

Different Responses of Rice Cultivars/Species to *S. oryzae* Infestation

Unexpectedly, we verified that African rice species (*O. barthii* and *O. glaberrima*) and weedy rice (*O. sativa* f. *spontanea*) presented high susceptibility to *S. oryzae* infestation, while *O. sativa* cv. Nipponbare showed low levels of leaf damage (**Figure 1**). After 4 weeks of infestation, leaves of *O. barthii* were dry and the leaf area was totally injured. The species *O. glaberrima* presented infestation level 4 (above 80% of the damaged leaf area), while Nipponbare presented level 2 (10–20% of damaged leaf area), and weedy rice revealed level 3 (40–50% of the damaged leaf area), as shown in **Figure 1**. Both African species died before reaching the reproductive stage, while both *O. sativa* were able to complete their life cycle and set seeds. Although the plant height was not negatively affected by mite infestation in any of the tested cultivars/species, tiller number decreased under infested conditions in all plants, except in Nipponbare (**Figure 2**).

Chlorophyll *a* fluorescence analysis showed that African rice species (*O. barthii* and *O. glaberrima*) and weedy rice presented a decrease in at least one of the OJIP curve-times. *O. barthii* seems to be the most affected species, with a decrease in all curve-times after four weeks of infestation (LI leaves), while *O. glaberrima* presented a decrease in J-I-P stages, and weedy rice in I-P stages. Nipponbare was the only one with no decrease during the entire OJIP curve under infested condition (**Figure 3**), suggesting that mite infestation triggers lower damage in Nipponbare photosynthetic apparatus than in the other tested cultivars/species. These results agree with total chlorophyll concentration analysis, where Nipponbare was the only tested cultivars/species with no decrease under infested conditions, while *O. barthii* presented the highest decrease comparing infested and control conditions (**Figure 4**). Also, histochemical staining assay using DAB indicated that

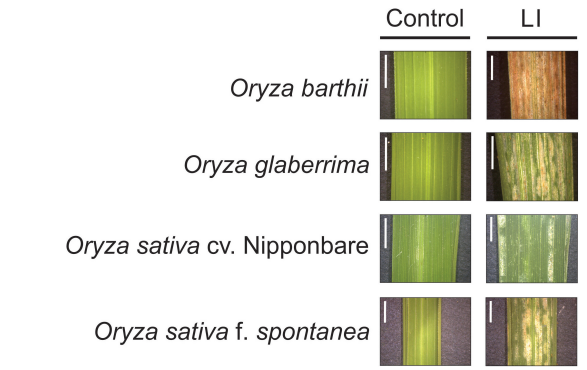


FIGURE 1 | Visual characteristics of leaves from control and late infested (LI) plants of *Oryza barthii*, *Oryza glaberrima*, *Oryza sativa* cv. Nipponbare, and weedy rice (*Oryza sativa* f. *spontanea*). Bars indicate 0.5 cm.

Nipponbare leaves accumulate lower levels of H_2O_2 than the other tested cultivars/species, especially when compared to *O. barthii* (**Figure 5**). Therefore, *S. oryzae* infestation differentially affects the generation of oxidative stress in LI leaves of the tested plants. Altogether, we suggest that *O. barthii* is extremely susceptible to *S. oryzae* infestation, while Nipponbare can be considered tolerant.

As African rice species were not able to reach the reproductive stage, seeds from Nipponbare and weedy rice were evaluated to verify whether *S. oryzae* infestation could impact seed production. Weedy rice presents higher number of panicles per plant than Nipponbare under both control and infested conditions (**Figure 6A**), even though the number of panicles per plant was affected by *S. oryzae* infestation only in weedy rice (**Figure 6A**). In Nipponbare, none of the analyzed parameters (number of panicles per plant— **Figure 6A**, number of seeds per panicle—**Figure 6B**, percentage of full seeds per panicle—**Figure 6C**, grain length—**Figures 6E,F**, and weight of 1,000 full grains—**Figure 6G**) was negatively affected by mite infestation. As seen in **Figure 6C**, 93% of the seeds produced by Nipponbare plants under infested condition were full, while in the same condition, weedy rice produced 87% of full seeds. Such difference, together with the higher number of panicles per plant in weedy rice than Nipponbare under infested condition (**Figure 6A**), probably explains the high number of empty seeds in weedy rice plants infested by *S. oryzae* (**Figure 6D**). Surprisingly, two parameters (percentage of full seeds per panicle—**Figure 6C** and grain length—**Figures 6E,F**) presented higher values in Nipponbare plants under infested than control condition, resulting in the maintenance of seed weight per plant (an estimate of yield) under infested condition (**Figure 7**). Therefore, Nipponbare reveals physiological characteristics of tolerance, since even during infestation, plants can maintain development, photosynthetic/antioxidant activities, and grain yield.

Overview of Proteomic Analysis

A total of 1,041 proteins were identified comparing control and infested conditions in *O. barthii* and Nipponbare, with 195

[3]https://www.ebi.ac.uk/pride/

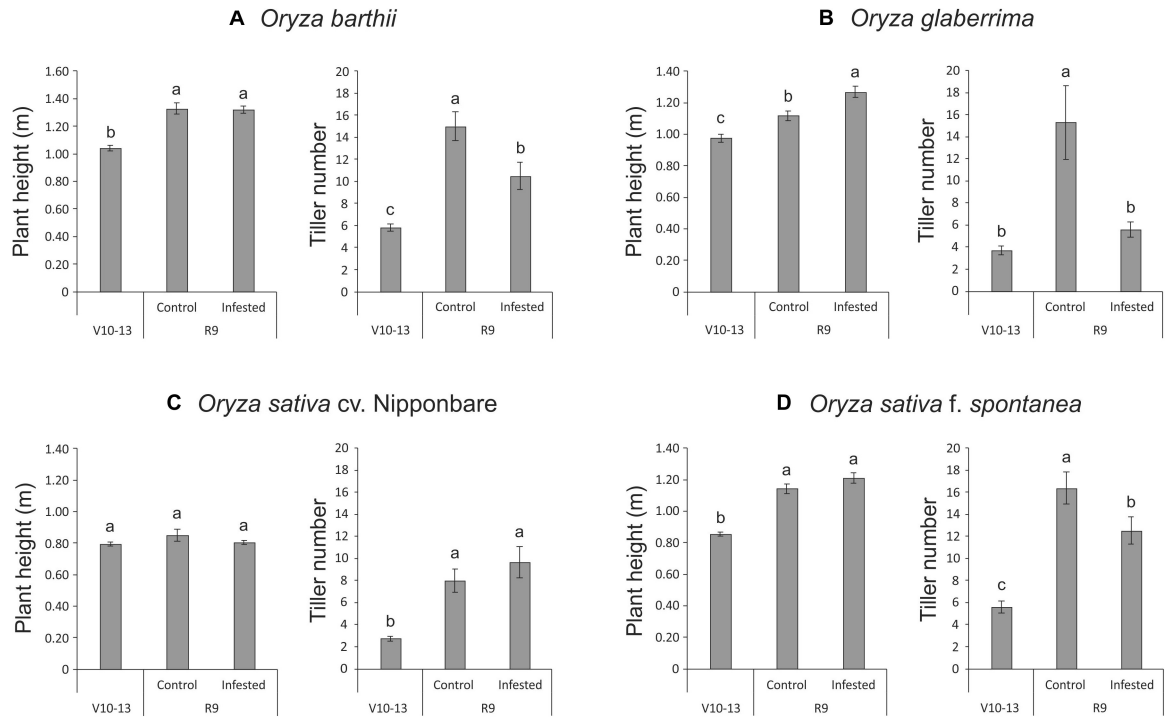


FIGURE 2 | Plant height (m) and tiller number of *Oryza barthii* **(A)**, *Oryza glaberrima* **(B)**, *Oryza sativa* cv. Nipponbare **(C)**, and weedy rice (*Oryza sativa* f. *spontanea*) **(D)** at the vegetative stage (no infestation, V10-13) and full maturity stage (control or infested conditions, R9). Represented values are the averages of 50 samples ± SE. Different letters indicate that the means are different by the Tukey HSD test ($P \leq 0.05$).

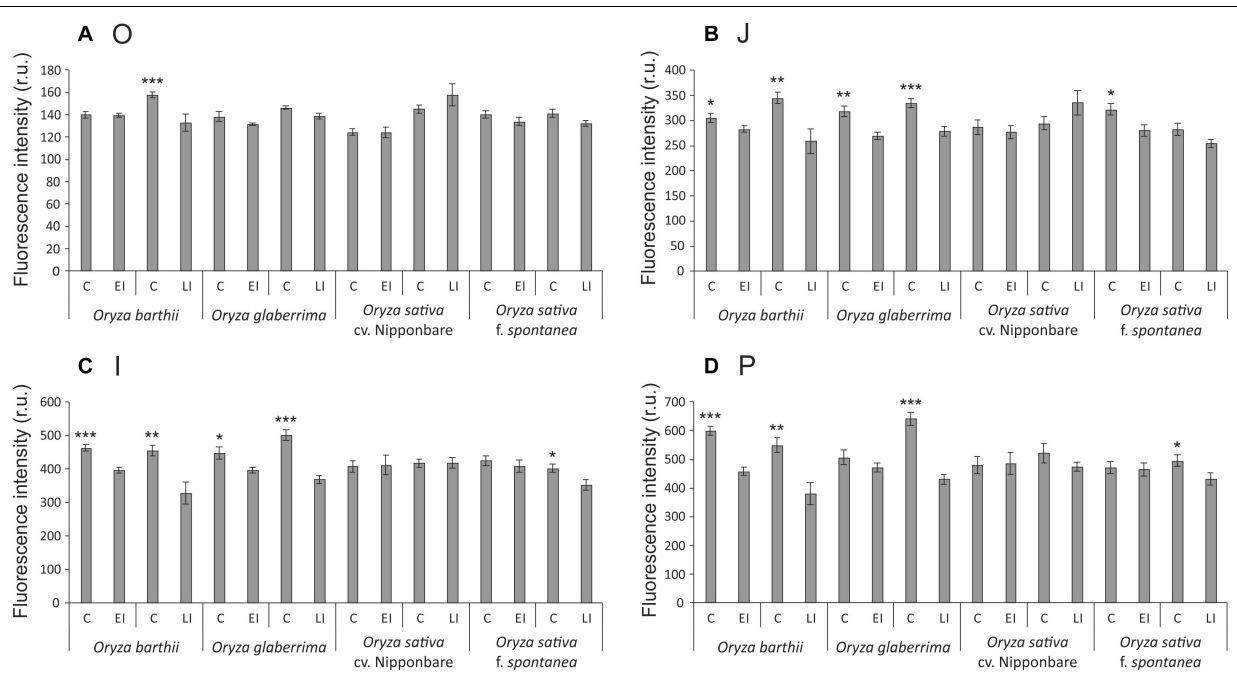


FIGURE 3 | OJIP-test parameters calculated from the chlorophyll *a* fluorescence transient in control (C), early infested (EI), and late infested (LI) leaves of *Oryza barthii*, *Oryza glaberrima*, *Oryza sativa* cv. Nipponbare, and weedy rice (*Oryza sativa* f. *spontanea*). **(A)** O; **(B)** J; **(C)** I; **(D)** P. Represented values are the averages of 10 samples ± SE. Mean values (from each species/cultivar and each exposure time: C × EI; C × LI) with one, two, or three asterisks are significantly different as determined by a Student's *t*-test ($P \leq 0.05$, 0.01, and 0.001, respectively). r.u., Raman units.

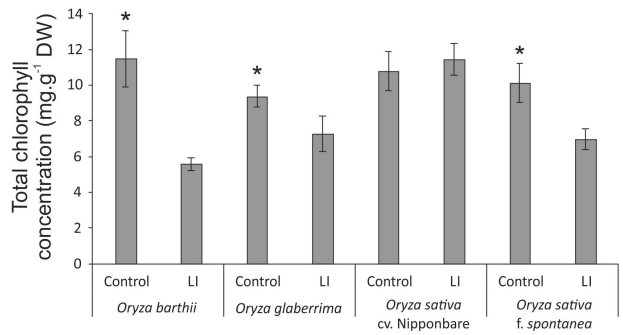


FIGURE 4 | Total chlorophyll concentration in control and late infested (LI) leaves of *Oryza barthii*, *Oryza glaberrima*, *Oryza sativa* cv. Nipponbare, and weedy rice (*Oryza sativa* f. *spontanea*) plants. Represented values are the averages of three samples ± SE. Mean values (from each species/cultivar: C × LI) with one asterisk are significantly different as determined by a Student's *t*-test (*p*-value ≤ 0.05). DW, dry weight.

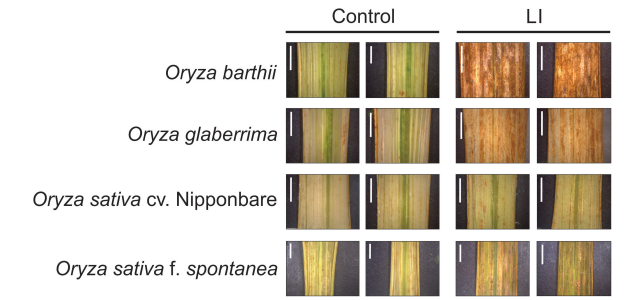


FIGURE 5 | Histochemical staining assay of H_2O_2 by diaminobenzidine (DAB) in control and late infested (LI) leaves of *Oryza barthii*, *Oryza glaberrima*, *Oryza sativa* cv. Nipponbare, and weedy rice (*Oryza sativa* f. *spontanea*). The positive staining (detected in higher levels on infested leaves) in the photomicrographs shows as bright images (brown-color). Bars indicate 0.5 cm.

(18.7%) proteins unique to or differentially abundant between treatments. As seen in **Figure 8**, comparing control and infested leaves of *O. barthii*, we detected 48 differentially abundant proteins, being two more abundant (and one unique) in control condition, and 44 more abundant (and one unique) in infested condition. We identified 147 differentially abundant proteins in control and infested conditions of Nipponbare, being 35 more abundant (and two unique) in control condition, and 104 more abundant (and six unique) in infested condition. Due to the different genetic background between *O. barthii* and *O. sativa*, we prefer not to compare the same conditions between species, in order to avoid the emergence of species-specific sequences that are not mite related.

The corresponding sequence of each identified protein was compared to NCBI BLASTp to identify specific domains, molecular functions, and protein annotations. Afterward, proteins were arbitrarily categorized in functional categories, according to the available literature and their putative molecular function. The lists of all unique or differentially abundant proteins identified in this work are presented in **Supplementary Tables 1**, **2**. In order to facilitate the overall understanding of the differential protein abundance in each functional category presented in **Supplementary Tables 1**, **2**, we summarize these data in **Table 1**. We detected four different patterns, based on the number of differentially abundant proteins: (1) most of the functional categories (antioxidant system, carbohydrate metabolism/energy production, general metabolic processes, hormone-related, lipid metabolism, protein modification/degradation, stress response, and others) were more represented in infested conditions, regardless the analyzed species; (2) four categories were differentially represented only in one species (amino acid metabolism in *O. barthii* under infested condition; cytoskeleton and transport in Nipponbare under control condition; and protease inhibitor (PI) also in Nipponbare, but under infested condition); (3) photosynthesis (over represented in *O. barthii* under infested condition, and in Nipponbare under control condition); and (4) translation, with no difference between control and infested conditions, regardless of the analyzed species.

Considering the tolerant Nipponbare, *S. oryzae* infestation seems to be less damaging and to generate a more complex defense response. It is interesting to highlight the higher diversity and expression level of antioxidant proteins in Nipponbare than *O. barthii* under infested conditions, which agrees with the lower oxidative stress seen in Nipponbare leaves (**Figure 5**), and also the higher diversity of proteins involved in general metabolic processes and carbohydrate metabolism/energy production, suggesting that Nipponbare can maintain the basal/primary metabolism more active than *O. barthii* under infested condition. This finding also agrees with our observation that photosynthesis is maintained in Nipponbare, whereas it is drastically affected in *O. barthii*. At the same time, Nipponbare seems more able to fight *S. oryzae* infestation than *O. barthii*, presenting higher diversity and/or representation level of PIs and proteins involved in stress response. As seen in **Figure 9**, we also detected enhanced proline levels only in Nipponbare leaves under infested condition, suggesting an active defense mechanism. Several proteins belonging to these functional categories are discussed in more detail below.

DISCUSSION

Our first screening of *Oryza* cultivars/species responses to *S. oryzae* infestation showed that none presents a classical resistance response involving antibiosis and antixenosis (Stenberg and Muola, 2017), since mite population increased over time for all cultivars/species, even though with different kinetics (**Figure 1**). Physiological analysis and agronomical parameters showed that *O. glaberrima* and especially *O. barthii* are extremely susceptible to *S. oryzae* infestation (being unable to reach the reproductive stage), while weedy rice and especially Nipponbare are less affected by mite infestation (**Figures 1–7**). Recently, we detected an *indica* rice cultivar able to maintain seed yield under *S. oryzae* infestation condition, which we characterized as mite tolerant (Buffon et al., 2018). Even though wild plant species have been widely recognized as valuable

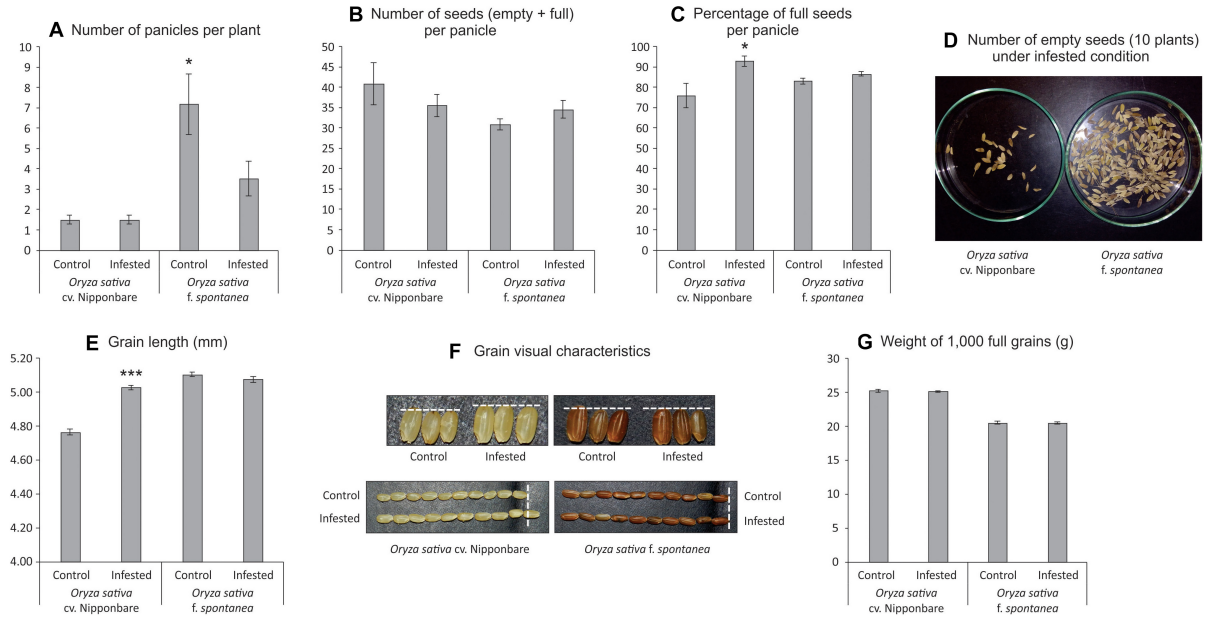


FIGURE 6 | Seeds analysis of *Oryza sativa* cv. Nipponbare and weedy rice (*Oryza sativa* f. *spontanea*). **(A)** Number of panicles per plant. **(B)** Number of seeds (empty + full) per panicle. **(C)** Percentage of full seeds per panicle. **(D)** Number of empty seeds (10 plants) under infested condition. **(E)** Grain length (mm). **(F)** Grain visual characteristics. **(G)** Weight of 1,000 full grains. Represented values are the averages of 50 samples ± SE. Mean values (from each cultivar: Control × Infested) with one or three asterisks are significantly different as determined by a Student's *t*-test ($P \leq 0.05$ and 0.001).

source of resistance genes for developing herbivore-resistant cultivars, Veasey et al. (2008) and Chandrasena et al. (2016) found no signs of mite resistance when different wild rice species were, respectively, tested against the infestation of *S. oryzae* and *Steneotarsonemus spinki*. These data differ from previously described ones, where *O. barthii* and *O. glaberrima* are recognized as resistant to diseases and pests (Khush, 1997; Linares, 2002). Still, our report is one of the first to test mite tolerance in wild and cultivated rice species.

Grain size is an important component trait of grain yield, which is frequently threatened by stress conditions (Lv et al., 2019; Dong et al., 2020). Interestingly, in our analysis, Nipponbare plants under infested condition presented higher seed length when compared to control condition (**Figures 6E,F**). Several studies have identified key grain size regulator genes, involved in different mechanisms (reviewed by Li et al., 2018). Even though none of the 43 genes cited by Li et al. (2018) as involved in rice grain size control code proteins differentially abundant in our proteomic analysis, it would be interesting to go deeper in such question, since we found similar results in a previous study with another mite-tolerant *indica* rice cultivar (IRGA 423—Buffon et al., 2018). Recent studies have identified molecular links between regulation of grain size and abiotic stress tolerance (Chen et al., 2016, 2019; Lv et al., 2019; Dong et al., 2020). However, as far as we know, any link between grain size regulation and biotic stress tolerance is unknown.

Recently, Sperotto et al. (2018b) hypothesized that mite-sensitivity presented by wild rice species could be explained, at least partially, by a presumable high GA:JA ratio in these plants, since most of the wild rice species are tall plants and

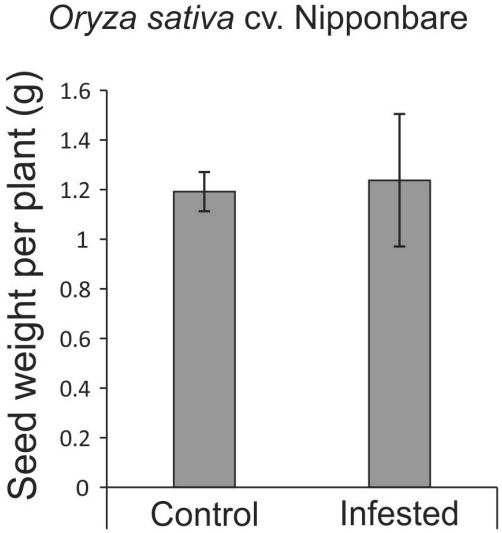


FIGURE 7 | Seed weight per plant (estimative of yield) of *Oryza sativa* cv. Nipponbare under control and infested conditions. Represented values are the averages of 10 samples ± SE.

probably present high GA levels. The roles of GA-JA in growth-defense conflicts during herbivory are not yet fully characterized. However, it is already known that plants need to prioritize GA- or JA-induced responses (Yang et al., 2019). Even though proteins related to GA biosynthesis have not been detected as differentially abundant in *O. barthii* or Nipponbare under infested conditions

TABLE 1 | Schematic representation of the functional categories differently represented in leaves of mite susceptible *Oryza barthii* and mite-tolerant *Oryza sativa* cv. Nipponbare plants under control and infested conditions.

	***Oryza barthii* (susceptible)**		***Oryza sativa* cv. Nipponbare (tolerant)**	
Functional categories	**Control**	**Infested**	**Control**	**Infested**
Amino acid metabolism	–	↑	↑↑	↑↑
Antioxidant system	↑	↑↑	↑	↑↑
Carbohydrate metabolism/energy production	–	↑↑	↑	↑↑
Cytoskeleton	↑	↑	↑↑	–
General metabolic processes	–	↑↑	↑	↑↑
Hormone-related	–	↑	–	↑↑
Lipid metabolism	–	↑↑	–	↑↑
Photosynthesis	–	↑↑	↑↑	↑
Protease inhibitor	–	–	–	↑↑
Protein modification/degradation	–	↑↑	↑	↑↑
Stress response	–	↑↑	↑	↑↑
Translation	↑	↑	↑↑	↑↑
Transport	–	–	↑↑	–
Others	↑	↑↑	↑	↑↑

Different shades of gray color represent the different patterns of response. Number of arrows (one or two) relates to the representation level, which is based on the number of differentially abundant sequences. (–): functional category not detected as differentially represented.

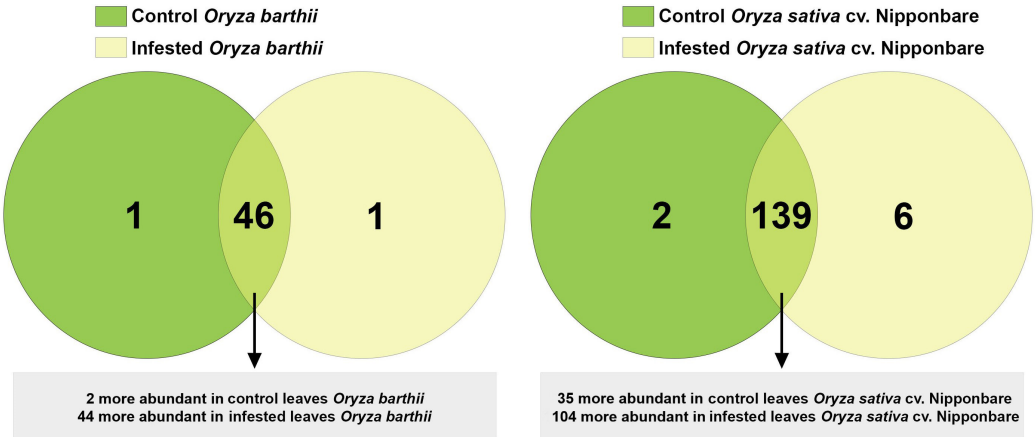


FIGURE 8 | Venn diagram showing the overlap of rice proteins identified in control and early infested (EI) leaves of mite susceptible *Oryza barthii* and mite-tolerant *Oryza sativa* cv. Nipponbare. Dark green circles: control leaves; yellow circles: EI leaves. Light green means overlap.

(**Supplementary Tables 1**, **2**), the height of these plants at full maturity stage is quite different (55% higher in *O. barthii*—**Figure 2**). It is important to highlight that *O. barthii* and Nipponbare plant heights are not affected by *S. oryzae* infestation (**Figure 2**), and this could explain the lack of differentially abundant proteins involved in GA biosynthesis when we compare control and infested conditions. Sperotto et al. (2018b) suggest short *Oryza* species (*O. minuta*, *O. meyeriana*, *O. neocaledonica*, and *O. schlechteri*) as primary sources of herbivory tolerance, including mites. According to these authors, plants with low GA level/sensitivity would probably amplify JA responses and drive plant resources toward defense instead of growth. Based on our data, the GA-based mechanism is not involved in the different tolerance level found in the tested species, although JA might play a role.

One of the most abundant proteins found in Nipponbare under infested condition is lipoxygenase (log2 FC 4.7), which is well known as a precursor of plant defense mechanisms. Once the herbivore feeds on plant tissues, polyunsaturated fatty acids are released from cell membranes, and accumulate at the wound site (Roach et al., 2015). Also, polyunsaturated fatty acids act as a substrate to lipoxygenase, leading to the production of several defense-related compounds, including different structures of JAs such as methyl jasmonate (MeJA) (Mochizuki et al., 2016; Yang et al., 2019). We detected a key enzyme related to JA biosynthesis, allene oxide cyclase (AOC), which converts allene oxide to 12-oxophytodienoic acid (Nguyen et al., 2020), more abundant in both species under infested conditions. However, the log2 FC is higher in Nipponbare than *O. barthii* (**Supplementary Tables 1**, **2**). Therefore, it is possible that Nipponbare presents

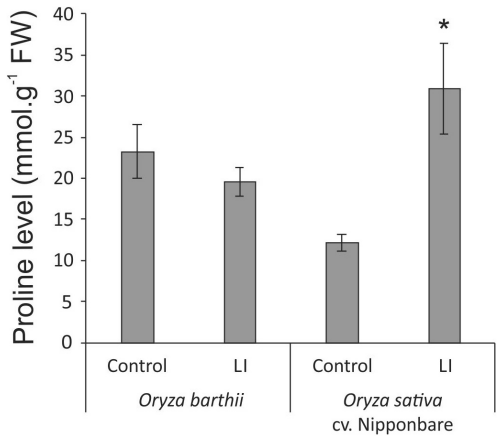


FIGURE 9 | Proline levels in control and late infested (LI) leaves of mite susceptible *Oryza barthii* and mite-tolerant *Oryza sativa* cv. Nipponbare. Represented values are the averages of three samples ± SE. Mean values with one asterisk are significantly different as determined by a Student's *t*-test ($P \leq 0.05$). FW, fresh weight.

a more active JA biosynthesis/signaling pathway, which can probably contribute to mite tolerance. Interestingly, MYB and WRKY transcription factors, which are involved in the activation of defense responses in plants, including JA signaling (Wang et al., 2014; Zhou and Memelink, 2016), were not detected as differentially abundant in our work, raising the possibility of new signaling/defense pathways in *O. barthii* and Nipponbare infested by *S. oryzae*.

The functional category most affected by *S. oryzae* infestation was antioxidant system, with 10 proteins more abundant in the mite susceptible *O. barthii* (**Supplementary Table 1**), and 22 in the mite-tolerant Nipponbare (**Supplementary Table 2**) under infested condition. This indicates that both species try to defend and maintain its redox homeostasis, since it is governed by the presence of large antioxidant pools that absorb and buffer reductants and oxidants (Foyer and Noctor, 2005). Considering the leaf damage (**Figure 1**), H_2O_2 accumulation (**Figure 5**), and the high diversity of differentially abundant proteins (**Supplementary Tables 1**, **2**), such strategy seems to be more efficient in the mite-tolerant Nipponbare than in *O. barthii*. Six proteins identified as more abundant under infested condition only in Nipponbare are ferredoxin, ferredoxin-$NADP^+$ reductase, thioredoxin H-type, peroxiredoxin, glutathione reductase, and superoxide dismutase (**Supplementary Table 2**). The stromal ferredoxin–thioredoxin system, a regulatory mechanism linking light to the activity of associated enzymes, is the best-characterized redox signal transduction system in plants, functioning in the regulation of photosynthetic carbon metabolism (Foyer and Noctor, 2005; Schürmann and Buchanan, 2008). Ferredoxin-$NADP^+$ reductase catalyzes the reduction of $NADP^+$ to NADPH, using the electrons provided by reduced ferredoxin (Cassan et al., 2005). Both NADPH and reduced ferredoxin are required for reductive assimilation and light/dark activation/deactivation of enzymes. Ferredoxin-$NADP^+$ reductase is therefore a hub, connecting photosynthetic electron transport to chloroplast redox metabolism (Kozuleva et al., 2016). Even though the precise mechanism remains unknown, a clear correlation between ferredoxin-$NADP^+$ reductase content and tolerance to oxidative stress is well established (Giró et al., 2006; Kozuleva et al., 2016).

Thioredoxins H-type are involved in the cellular protection against oxidative stress (Gelhaye et al., 2004), and function as electron donors to several antioxidant enzymes, such as peroxiredoxin and glutathione reductase (Rouhier et al., 2001). Plants over-expressing thioredoxin H-type genes show oxidative stress tolerance and lower levels of H_2O_2 accumulation (Sun et al., 2010; Zhang et al., 2011), similar to our findings with the mite-tolerant Nipponbare (**Figure 5**). Peroxiredoxins are abundant low-efficiency peroxidases that act as antioxidant and are involved in modulating redox-dependent signaling cascades (Dietz, 2003). Also, after being reduced by thioredoxin, peroxiredoxins reductively convert H_2O_2 to H_2O at the chloroplast (König et al., 2002), acting together with other peroxidase enzymes that use ascorbate as the electron donor. Ascorbate can be directly regenerated using photosynthetic electrons via reduced ferredoxin or using reduced glutathione (GSH). In the chloroplast, the oxidized glutathione (GSSG) is reduced by the glutathione reductase enzyme using NADPH (Kozuleva et al., 2016). It is important to highlight that very efficient scavenging mechanisms exist in chloroplasts to prevent oxidative damage, including the rapid conversion of superoxide radical ($O_2^{\bullet -}$, one of the dominant species produced during light excitation) to H_2O_2 by superoxide dismutase enzymes (Mubarakshina and Ivanov, 2010). This is the most likely explanation for the lack of differences in $O_2^{\bullet -}$ accumulation in the leaves of plants subjected to control and infested conditions (data not shown). Altogether, these data show that the mite-tolerant Nipponbare under infested condition can maintain the correct balance between rapid removal of damaging oxidative species and appropriate concentrations necessary to initiate signaling cascades.

We verified that all tested cultivars/species revealed a decrease in chlorophyll fluorescence parameters and total chlorophyll concentration, except the mite-tolerant Nipponbare (**Figures 3**, **4**). Increased photosynthesis is an important mechanism behind tolerance to herbivory (Thomson et al., 2003), and parameters of chlorophyll fluorescence (excess energy absorbed by chlorophyll that is reemitted as light) have been used to obtain quantitative information on the photosynthetic performance of plants (Maxwell and Johnson, 2000), since chlorophyll fluorescence curves allow to evaluate the physiological condition of photosystem II (PSII) components and photosynthetic electron transport chain (Kalaji et al., 2016), where ferredoxin protein acts. Recently, Madriaza et al. (2019) indicated that chlorophyll fluorescence is an accurate predictor of tolerance to herbivore damage, and claimed that this rapid methodology could be used to estimate plant tolerance to herbivory in natural populations.

Even though plant height was not affected by *S. oryzae* infestation in *O. barthii* and Nipponbare, the mite susceptible *O. barthii* presented a decrease in tiller number under infested condition, while Nipponbare maintained the same level found

in control condition (**Figure 2**), resulting in no yield losses (**Figure 7**). Reduction in tillering (and consequently in grain weight) was already seen in rice plants infested by the rice water weevil, *Lissorhoptrus oryzophilus* Kuschel (Zou et al., 2004), and also in IR22 (a rice variety susceptible to the brown planthopper, *Nilaparvata lugens*) (Horgan et al., 2018). It is important to highlight that planthopper damage to IR22 in field cages was severe, and plant death occurred in most of IR22 plants, similar to our findings with *O. barthii* and *O. glaberrima* under infested conditions. Both tillering and seed filling processes are expensive for the crop energy balance. As seen in **Supplementary Tables 1**, **2**, we verified a larger diversity of proteins involved in general metabolic processes and carbohydrate metabolism/energy production under infested condition in tolerant Nipponbare than in susceptible *O. barthii*, suggesting that general metabolism and energy production in Nipponbare are less affected by *S. oryzae* infestation.

Two proteins related to general metabolic processes were identified as more abundant under infested condition only in Nipponbare: CBS domain-containing protein (CBSX1) and cysteine synthase (**Supplementary Table 2**). In Arabidopsis, AtCBSX1 and AtCBX2 positively regulate thioredoxins, which then reduce target proteins, such as peroxiredoxin, which in turn reduce cellular H_2O_2 and regulate its level (Yoo et al., 2011). Recently, Kumar et al. (2018) overexpressed a rice Two Cystathionine-β-Synthase Domain-containing Protein (*OsCBSCBSPB4*) in tobacco. Transgenic seedlings exhibit delayed leaf senescence, profuse root growth, and increased biomass in contrast to the wild-type seedlings when subjected to salinity, dehydration, oxidative, and extreme temperature treatments, suggesting that OsCBSCBSPB4 is involved in abiotic stress response. As far as we know, this is the first time that a CBS protein is related to biotic stress tolerance in plants. The biosynthesis of cysteine is a limiting step in the production of glutathione, a thiol implicated in various cellular functions, including scavenging of reactive oxygen species and resistance to biotic stresses (Youssefian et al., 2001). At the same time, several studies have pointed out the function of cysteine-thiols and sulfur-based primary and secondary metabolites in basal defense responses to abiotic and biotic stresses (for a comprehensive review, see Tahir and Dijkwel, 2016). Even though herbivory resistance can employ metabolites containing cysteine such as glucosinolates (Guo et al., 2013), to the best of our knowledge, this is the first work that links the expression of cysteine synthase protein with mite tolerance.

Two proteins related to stress response were also identified as more abundant under infested condition only in Nipponbare: osmotin-like protein and ricin B-like lectin. Osmotin protein belongs to the PR-5 family of pathogenesis-related (PR) proteins, which are produced in response to various biotic and abiotic stresses. Osmotin can increase its own cytotoxic efficiency promoting changes in the cell wall structure and inhibiting defensive cell wall barriers, which in turn enables osmotin penetration into the plasma membrane (Hakim et al., 2018). Overexpression of genes encoding osmotins confers tolerance against biotic and abiotic stresses in different plant species (Barthakur et al., 2001; Xue et al., 2016; Chowdhury et al., 2017), besides stimulating the accumulation of proline, which functions as a compatible osmolyte useful in responding to abiotic stress, especially drought and salinity (Hakim et al., 2018). Proline also functions suppressing free radicals and preventing chlorophyll degradation in vegetative cells, in order to maintain the photosynthetic processes (Barthakur et al., 2001; Chowdhury et al., 2017). In the mite-tolerant Nipponbare, we detected higher levels of proline accumulation under infested condition when compared to control (**Figure 9**), along with maintenance of chlorophyll concentration (**Figure 4**) after mite infestation. This is the first time that expression of an osmotin protein is related to mite tolerance. Since the generation of transgenic plants overexpressing osmotin genes is being recommended as a biotechnological tool to generate stress tolerance, we are currently overexpressing and knocking out *OsOSM1* gene (LOC_Os12g38170) in rice plants.

Ricin B-like lectins, one of the most widespread families of carbohydrate-binding proteins (Lannoo and Van Damme, 2014), have been suggested to play a role in plant defense against pathogens (Vandenbussche et al., 2004) and insects (Wei et al., 2004; Shahidi-Noghabi et al., 2009). Since mutation of the carbohydrate-binding site can abolish or reduce the toxic effect, the entomotoxic properties of the proteins can be linked to their carbohydrate-binding activity (Shahidi-Noghabi et al., 2008). Our work is the first one that correlates a ricin B-like lectin expression with mite response/tolerance in plants. Curiously, it was shown that β-trefoil structure enables interactions between fungal ricin B-like lectins and PIs, and that these interactions modulate their biological activity (Žurga et al., 2015). It would be interesting to test whether the two PIs (putative Bowman Birk trypsin inhibitor) we found more abundant only in the mite-tolerant Nipponbare under infested condition (**Supplementary Table 2**) are able to interact with the ricin B-like lectins.

Among plant defenses, PIs have direct effects on herbivores, interfering with their physiology (Diaz and Santamaria, 2012; Martinez et al., 2016; Arnaiz et al., 2018). Once ingested by the arthropod, PIs inhibit proteolytic activities, preventing or hindering protein degradation (Terra and Ferreira, 2005). The first successfully overexpressed Bowman-Birk family PI gene in tobacco was the cowpea trypsin inhibitor (*CpTI*—Hilder et al., 1987). After, the *CpTI* gene was inserted into the genome of several plants, increasing the resistance to different herbivore species (Santamaria et al., 2012). Since then, different PIs have been obtained from cultivated plants such as rice, barley, soybean, sweet potato, and corn, and have been overexpressed in different plant species, conferring resistance to various pest insects (Clemente et al., 2019). Rice has seven Bowman Birk trypsin inhibitor genes, and overexpression of *RBBI2-3* in transgenic rice plants resulted in resistance to the fungal pathogen *Pyricularia oryzae*, indicating that PIs confer *in vivo* resistance against the fungal pathogen, and might play a role in the defense system of the rice plant (Qu et al., 2003). Recently, Arnaiz et al. (2018) verified that Kunitz trypsin inhibitors (KTI) participate in the plant defense responses against the spider mite *Tetranychus urticae*. Thus, our work is the first one to suggest that Bowman Birk trypsin inhibitors may be involved in the tolerance of rice plants to *S. oryzae* mite infestation.

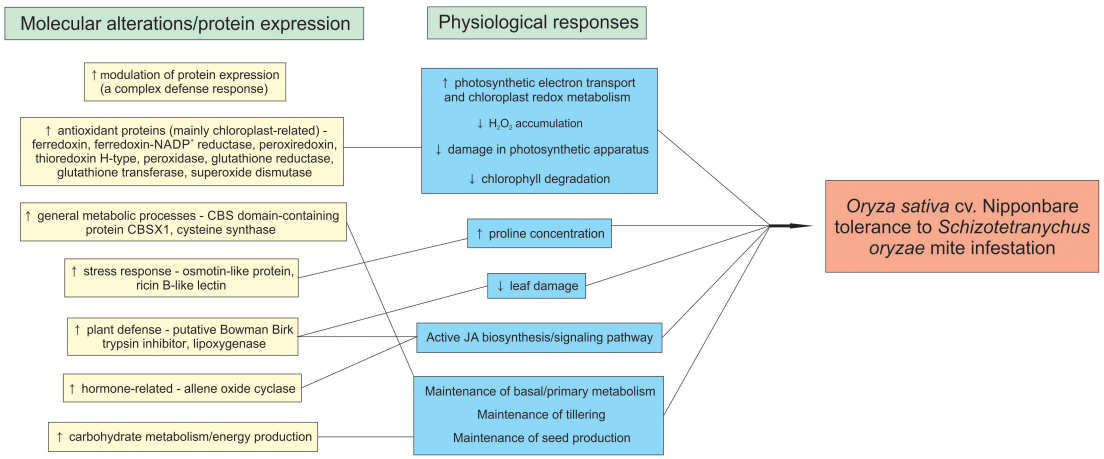


FIGURE 10 | Rice mechanisms employed by *Oryza sativa* cv. Nipponbare to tolerate *Schizotetranychus oryzae* mite infestation.

The model in **Figure 10** summarizes the rice tolerance mechanisms putatively employed by Nipponbare plants.

CONCLUSION

Tolerance is a sustainable pest management strategy as it only involves plant response, and therefore does not cause evolution of resistance in target pest populations (Peterson et al., 2017; Sperotto et al., 2018a). According to Gerszberg and Hnatuszko-Konka (2017), elucidation of the tolerance mechanisms at the biochemical, physiological, and morphological level remains one of the greatest challenges of contemporary plant physiology. Our physiological results showed that African rice species (wild *O. barthii* and cultivated *O. glaberrima*) and weedy rice (*O. sativa* f. *spontanea*) do not present tolerance to *S. oryzae* mite infestation. Still, we characterized *O. sativa* cv. Nipponbare as tolerant to mite infestation. Proteomic data showed that *O. barthii* presents a less diverse/efficient antioxidant apparatus under infested condition, not being able to modulate proteins involved in general metabolic processes and energy production, resulting in damage to its photosynthetic apparatus and development. On the other hand, Nipponbare presents more efficient antioxidant mechanisms that maintain cellular homeostasis and its photosynthetic capacity. Tolerant plants are able to modulate proteins involved in general metabolic processes and energy production, maintaining their development. In addition, these plants can modulate the expression of defense proteins, such as osmotin, ricin B-like lectin, and PIs, which may be used in future breeding programs for increasing rice tolerance to mite infestation.

DATA AVAILABILITY STATEMENT

All proteomics data were deposited to the ProteomeXchange Consortium (Deutsch et al., 2017) via the PRIDE repository (https://www.ebi.ac.uk/pride/; Perez-Riverol et al., 2019) and can be accessed using the code PXD020940.

AUTHOR CONTRIBUTIONS

JS, FR, and RS conceived and designed the research. GB, ÉB, TL, JA, and AB conducted the experiments. VS and ML contributed with analytical tools. GB, ÉB, JA, AB, VS, and RS analyzed the data. GB and RS wrote the manuscript. All authors read and approved the manuscript.

FUNDING

This research was supported by University of Taquari Valley–Univates, Fundação de Amparo à Pesquisa do Estado do RS (FAPERGS) and Conselho Nacional de Desenvolvimento Científico e Tecnológico (CNPq).

ACKNOWLEDGMENTS

The authors thank Instituto Rio-Grandense do Arroz (IRGA) for technical support. Pre-print of this manuscript at bioRxiv: https://doi.org/10.1101/2020.01.22.914184.

SUPPLEMENTARY MATERIAL

The Supplementary Material for this article can be found online at: https://www.frontiersin.org/articles/10.3389/fpls.2021.613568/full#supplementary-material

Supplementary Table 1 | Differentially abundant proteins in mite susceptible *Oryza barthii* (control × early infested condition).

Supplementary Table 2 | Differentially abundant proteins in mite-tolerant *Oryza sativa* cv. Nipponbare (control × early infested condition).

REFERENCES

Arnaiz, A., Talavera-Mateo, L., Gonzalez-Melendi, P., Martinez, M., Diaz, I., and Santamaria, M. E. (2018). Arabidopsis Kunitz trypsin inhibitors in defense against spider mites. *Front. Plant Sci.* 9:986. doi: 10.3389/fpls.2018.00986

Barthakur, S., Babu, V., and Bansa, K. C. (2001). Over-expression of osmotin induces proline accumulation and confers tolerance to osmotic stress in transgenic tobacco. *J. Plant Biochem. Biotechnol.* 10, 31–37. doi: 10.1007/bf03263103

Blasi, E. A. R., Buffon, G., da Silva, R. Z., Stein, C., Dametto, A., Ferla, N. J., et al. (2015). Alterations in rice, corn and wheat plants infested by phytophagous mite. *Int. J. Acarol.* 41, 10–18. doi: 10.1080/01647954.2014.988643

Brar, D. S., and Khush, G. S. (2003). "Utilization of wild species of genus *Oryza* in rice improvement," in *Monograph on Genus Oryza*, eds J. S. Nanda and S. D. Sharma (Enfield, NH: Science Publishers.), 283–309.

Buffon, G., Blasi, ÉA. R., Rativa, A. G. S., Lamb, T. I., Gastmann, R., Adamski, J. M., et al. (2018). Unraveling rice tolerance mechanisms against *Schizotetranychus oryzae* mite infestation. *Front. Plant Sci.* 9:1341. doi: 10.3389/fpls.2018.01341

Burrieza, H. P., Rizzo, A. J., Moura Vale, E., Silveira, V., and Maldonado, S. (2019). Shotgun proteomic analysis of quinoa seeds reveals novel lysine-rich seed storage globulins. *Food Chem.* 293, 299–306. doi: 10.1016/j.foodchem.2019.04.098

Cassan, N., Lagoutte, B., and Sétif, P. (2005). Ferredoxin-NADP+ reductase - Kinetics of electron transfer, transient intermediates, and catalytic activities studied by flash-absorption spectroscopy with isolated photosystem I and ferredoxin. *J. Biol. Chem.* 280, 25960–25972.

Chandrasena, G. D. S. N., Jayawardane, J. D. K. M., Umange, S. D., and Gunawardana, A. D. B. U. (2016). Host range of panicle rice mite *Steneotarsonemus spinki* smiley (Acari: Tarsonemidae) in Sri Lanka. *Univ. J. Agric. Res.* 4, 21–24. doi: 10.13189/ujar.2016.040104

Chen, C., Begcy, K., Liu, K., Folsom, J. J., Wang, Z., Zhang, C., et al. (2016). Heat stress yields a unique MADS box transcription factor in determining seed size and thermal sensitivity. *Plant Physiol.* 171, 606–622. doi: 10.1104/pp.15.01992

Chen, S., Zhang, N., Zhang, Q., Zhou, G., Tian, H., Hussain, S., et al. (2019). Genome editing to integrate seed size and abiotic stress tolerance traits in Arabidopsis reveals a role for DPA4 and SOD7 in the regulation of inflorescence architecture. *Int. J. Mol. Sci.* 20:2695. doi: 10.3390/ijms20112695

Chowdhury, S., Basu, A., and Kundu, S. (2017). Overexpression of a new osmotin-like protein gene (*SindOLP*) confers tolerance against biotic and abiotic stresses in sesame. *Front. Plant Sci.* 8:410. doi: 10.3389/fpls.2017.00410

Clemente, M., Corigliano, M. G., Pariani, S., Sánchez-López, E. F., Sander, V. A., and Ramos-Duarte, V. A. (2019). Plant serine protease inhibitors: biotechnology application in agriculture and molecular farming. *Int. J. Mol. Sci.* 20:E1345.

Counce, P. A., Keisling, T. C., and Mitchell, A. J. (2000). A uniform, objective, and adaptive system for expressing rice development. *Crop Sci.* 40, 436–443. doi: 10.2135/cropsci2000.402436x

Culliney, T. (2014). "Crop losses to arthropods," in *Integrated Pest Management*, eds D. Pimentel and R. Peshin (Dordrecht: Springer), 201–225. doi: 10.1007/978-94-007-7796-5_8

Dai, L., Dai, W., Song, X., Lu, B., and Qiang, S. (2014). A comparative study of competitiveness between different genotypes of weedy rice (*Oryza sativa*) and cultivated rice. *Pest Manag. Sci.* 70, 113–122. doi: 10.1002/ps.3534

Deutsch, E. W., Csordas, A., Sun, Z., Jarnuczak, A., Perez-Riverol, Y., Ternent, T., et al. (2017). The ProteomeXchange consortium in 2017: supporting the cultural change in proteomics public data deposition. *Nucleic Acids Res.* 45, D1100–D1106.

Diaz, I., and Santamaria, M. E. (2012). "Biotechnological approaches to combat phytophagous arthropods," in *Arthropod-Plant Interactions. Progress in Biological Control*, eds G. Smagghe and I. Diaz (Dordrecht: Springer), 159–176. doi: 10.1007/978-94-007-3873-7_6

Dietz, K. J. (2003). Plant peroxiredoxins. *Annu. Rev. Plant Biol.* 54, 93–107.

Distler, U., Kuharev, J., Navarro, P., Levin, Y., Schild, H., and Tenzer, S. (2014). Drift time-specific collision energies enable deep-coverage data-independent acquisition proteomics. *Nat. Methods* 11, 167–170. doi: 10.1038/nmeth.2767

Dong, N. Q., Sun, Y., Guo, T., Shi, C. L., Zhang, Y. M., Kan, Y., et al. (2020). UDP-glucosyltransferase regulates grain size and abiotic stress tolerance associated with metabolic flux redirection in rice. *Nat. Commun.* 11:2629.

Foyer, C. H., and Noctor, G. (2005). Redox homeostasis and antioxidant signaling: a metabolic interface between stress perception and physiological responses. *Plant Cell* 17, 1866–1875. doi: 10.1105/tpc.105.033589

Gelhaye, E., Rouhier, N., and Jacquot, J. P. (2004). The thioredoxin h system of higher plants. *Plant Physiol. Biochem.* 42, 265–271. doi: 10.1016/j.plaphy.2004.03.002

Gerszberg, A., and Hnatuszko-Konka, K. (2017). Tomato tolerance to abiotic stress: a review of most often engineered target sequences. *Plant Growth Regul.* 83, 175–198. doi: 10.1007/s10725-017-0251-x

Giró, M., Carrillo, N., and Krapp, A. R. (2006). Glucose-6-phosphate dehydrogenase and ferredoxin-NADP(H) reductase contribute to damage repair during the soxRS response of *Escherichia coli*. *Microbiology* 152, 1119–1128. doi: 10.1099/mic.0.28612-0

Godfray, H. C., Beddington, J. R., Crute, I. R., Haddad, L., Lawrence, D., Muir, J. F., et al. (2010). Food security: the challenge of feeding 9 billion people. *Science* 327, 812–818.

Guo, R., Shen, W., Qian, H., Zhang, M., Liu, L., and Wang, Q. (2013). Jasmonic acid and glucose synergistically modulate the accumulation of glucosinolates in *Arabidopsis thaliana*. *J. Exp. Bot.* 64, 5707–5719. doi: 10.1093/jxb/ert348

Hakim, Ullah, A., Hussain, A., Shaban, M., Khan, A. H., Alariqi, M., et al. (2018). Osmotin: a plant defense tool against biotic and abiotic stresses. *Plant Physiol. Biochem.* 123, 149–159. doi: 10.1016/j.plaphy.2017.12.012

Henry, R. J. (2014). Genomics strategies for germplasm characterization and the development of climate resilient crops. *Front. Plant Sci.* 5:68. doi: 10.3389/fpls.2014.00068

Hilder, V. A., Gatehouse, A. M. R., Sheerman, S. E., Barker, R. F., and Boulter, D. (1987). A novel mechanism of insect resistance engineered into tobacco. *Nature* 330, 160–163. doi: 10.1038/330160a0

Horgan, F. G., Peñalver Cruz, A., Bernal, C. C., Ramal, A. F., Almazan, M. L. P., and Wilby, A. (2018). Resistance and tolerance to the brown planthopper, *Nilaparvata lugens* (Stål), in rice infested at different growth stages across a gradient of nitrogen applications. *Field Crops Res.* 217, 53–65. doi: 10.1016/j.fcr.2017.12.008

Kalaji, H. M., Jajoo, A., Oukarroum, A., Brestic, M., Zivcak, M., Samborska, I. A., et al. (2016). Chlorophyll a fluorescence as a tool to monitor physiological status of plants under abiotic stress conditions. *Acta Physiol. Plant.* 38:102.

Khush, G. S. (1997). Origin, dispersal, cultivation and variation of rice. *Plant Mol. Biol.* 35, 25–34. doi: 10.1007/978-94-011-5794-0_3

König, J., Baier, M., Horling, F., Kahmann, U., Harris, G., Schürmann, P., et al. (2002). The plant-specific function of 2-Cys peroxiredoxin-mediated detoxification of peroxides in the redox-hierarchy of photosynthetic electron flux. *Proc. Natl. Acad. Sci. U.S.A.* 99, 5738–5743. doi: 10.1073/pnas.072644999

Kozuleva, M., Goss, T., Twachtmann, M., Rudi, K., Trapka, J., Selinski, J., et al. (2016). Ferredoxin: NADP (H) oxidoreductase abundance and location influences redox poise and stress tolerance. *Plant Physiol.* 172, 1480–1493. doi: 10.1104/pp.16.01084

Kumar, R., Subba, A., Kaur, C., Ariyadasa, T. U., Sharan, A., Pareek, A., et al. (2018). OsCBSCBSPB4 is a two cystathionine-β-synthase domain-containing protein from rice that functions in abiotic stress tolerance. *Curr. Genom.* 19, 50–59.

Lannoo, N., and Van Damme, E. J. M. (2014). Lectin domains at the frontiers of plant defense. *Front. Plant Sci.* 5:397. doi: 10.3389/fpls.2014.00397

Li, N., Xu, R., Duan, P., and Li, Y. (2018). Control of grain size in rice. *Plant Reprod.* 31, 237–251. doi: 10.1007/s00497-018-0333-6

Linares, O. F. (2002). African rice (*Oryza glaberrima*): history and future potential. *Proc. Natl. Acad. Sci. U.S.A.* 99, 16360–16365. doi: 10.1073/pnas.252604599

Lv, M. J., Wan, W., Yu, F., and Meng, L. S. (2019). New insights into the molecular mechanism underlying seed size control under drought stress. *J. Agric. Food Chem.* 67, 9697–9704. doi: 10.1021/acs.jafc.9b02497

Madriaza, K., Saldaña, A., Salgado-Luarte, C., Escobedo, V. M., and Gianoli, E. (2019). Chlorophyll fluorescence may predict tolerance to herbivory. *Int. J. Plant Sci.* 180, 81–85. doi: 10.1086/700583

Martinez, M., Santamaria, M. E., Diaz-Mendoza, M., Arnaiz, A., Carrillo, L., Ortego, F., et al. (2016). Phytocystatins: defense proteins against phytophagous insects and Acari. *Int. J. Mol. Sci.* 17, E1747.

Maxwell, K., and Johnson, G. N. (2000). Chlorophyll fluorescence: a practical guide. *J. Exp. Bot.* 51, 659–668. doi: 10.1093/jxb/51.345.659

Menguer, P. K., Sperotto, R. A., and Ricachenevsky, F. K. (2017). A walk on the wild side: *Oryza* species as source for rice abiotic stress tolerance. *Genet. Mol. Biol.* 40, 238–252. doi: 10.1590/1678-4685-gmb-2016-0093

Mochizuki, S., Sugimoto, K., Koeduka, T., and Matsui, K. (2016). Arabidopsis lipoxygenase 2 is essential for formation of green leaf volatiles and five−carbon volatiles. *FEBS Lett.* 590, 1017–1027. doi: 10.1002/1873-3468.12133

Mubarakshina, M. M., and Ivanov, B. N. (2010). The production and scavenging of reactive oxygen species in the plastoquinone pool of chloroplast thylakoid membranes. *Physiol. Plant.* 140, 103–110. doi: 10.1111/j.1399-3054.2010.01391.x

Muthayya, S., Sugimoto, J. D., Montgomery, S., and Maberly, G. F. (2014). An overview of global rice production, supply, trade, and consumption. *Ann. N. Y. Acad. Sci.* 1324, 7–14. doi: 10.1111/nyas.12540

Nanjo, Y., Skultety, L., Uvacìkova, L., Klubicova, K., Hajduch, M., and Komatsu, S. (2012). Mass spectrometry-based analysis of proteomic changes in the root tips of flooded soybean seedlings. *J. Prot. Res.* 11, 372–385. doi: 10.1021/pr200701y

Nguyen, T. H., Mai, H. T. T., Moukouanga, D., Lebrun, M., Bellafiore, S., and Champion, A. (2020). "CRISPR/Cas9-mediated gene editing of the jasmonate biosynthesis OsAOC gene in rice," in *Jasmonate in Plant Biology. Methods in Molecular Biology*, eds A. Champion and L. Laplaze (New York, NY: Humana Press), 199–209. doi: 10.1007/978-1-0716-0142-6_15

Oerke, E. C. (2006). Crop losses to pests. *J. Agric. Sci.* 144, 31–43. doi: 10.1017/s0021859605005708

Palmgren, M. G., Edenbrandt, A. K., Vedel, S. E., Andersen, M. M., Landes, X., Østerberg, J. T., et al. (2015). Are we ready for back-to-nature crop breeding? *Trends Plant Sci.* 20, 155–164. doi: 10.1016/j.tplants.2014.11.003

Perez-Riverol, Y., Csordas, A., Bai, J., Bernal-Llinares, M., Hewapathirana, S., Kundu, D. J., et al. (2019). The PRIDE database and related tools and resources in 2019: improving support for quantification data. *Nucleic Acids Res.* 47, D442–D450.

Peterson, R. K. D., Varella, A. C., and Higley, L. G. (2017). Tolerance: the forgotten child of plant resistance. *PeerJ* 5:e3934. doi: 10.7717/peerj.3934

Qiu, J., Zhou, Y., Mao, L., Ye, C., Wang, W., Zhang, J., et al. (2017). Genomic variation associated with local adaptation of weedy rice during de-domestication. *Nat. Commun.* 8:15323.

Qu, L. J., Chen, J., Liu, M., Pan, N., Okamoto, H., Lin, Z., et al. (2003). Molecular cloning and functional analysis of a novel type of Bowman-Birk inhibitor gene family in rice. *Plant Physiol.* 133, 560–570. doi: 10.1104/pp.103.024810

Roach, T., Colville, L., Beckett, R. P., Minibayeva, F. V., Havaux, M., and Kranner, I. (2015). A proposed interplay between peroxidase, amine oxidase and lipoxygenase in the wounding-induced oxidative burst in *Pisum sativum* seedlings. *Phytochemistry* 112, 130–138. doi: 10.1016/j.phytochem.2014.06.003

Ross, C. W. (1974). *Plant Physiology Laboratory Manual*. Belmont, CA: Wadsworth Publ. Comp. Inc.

Rouhier, N., Gelhaye, E., Sautiere, P. E., Brun, A., Laurent, P., Tagu, D., et al. (2001). Isolation and characterization of a new peroxiredoxin from poplar sieve tubes that uses either glutaredoxin or thioredoxin as a proton donor. *Plant Physiol.* 127, 1299–1309. doi: 10.1104/pp.010586

Santamaria, M. E., Cambra, I., Martinez, M., Pozancos, C., González-Melendi, P., Grbic, V., et al. (2012). Gene pyramiding of peptidase inhibitors enhances plant resistance to the spider mite *Tetranychus urticae*. *PLoS One* 7:e43011. doi: 10.1371/journal.pone.0043011

Sarla, N., and Swamy, B. P. M. (2005). Oryza glaberrima: a source for the improvement of *Oryza sativa*. *Curr. Sci.* 89, 955–963.

Schürmann, P., and Buchanan, B. B. (2008). The ferredoxin/thioredoxin system of oxygenic photosynthesis. *Antioxid. Redox Signal.* 10, 1235–1274. doi: 10.1089/ars.2007.1931

Shahidi-Noghabi, S., Van Damme, E. J. M., and Smagghe, G. (2008). Carbohydrate-binding activity of the type-2 ribosome-inactivating protein SNA-I from elderberry (*Sambucus nigra*) is a determining factor for its insecticidal activity. *Phytochemistry* 69, 2972–2978. doi: 10.1016/j.phytochem.2008.09.012

Shahidi-Noghabi, S., Van Damme, E. J. M., and Smagghe, G. (2009). Expression of *Sambucus nigra* agglutinin (SNA-I') from elderberry bark in transgenic tobacco plants results in enhanced resistance to different insect species. *Transg. Res.* 18, 249–259. doi: 10.1007/s11248-008-9215-2

Shi, J., Fu, X. Z., Peng, T., Huang, X. S., Fan, Q. J., and Liu, J. H. (2010). Spermine pretreatment confers dehydration tolerance of citrus *in vitro* plants via modulation of antioxidative capacity and stomatal response. *Tree Physiol.* 30, 914–922. doi: 10.1093/treephys/tpq030

Shukla, N., Awasthi, R. P., Rawat, L., and Kumar, J. (2012). Biochemical and physiological responses of rice (*Oryza sativa* L.) as influenced by *Trichoderma harzianum* under drought stress. *Plant Physiol. Biochem.* 54, 78–88. doi: 10.1016/j.plaphy.2012.02.001

Silva, J. C., Gorenstein, M. V., Li, G. Z., Vissers, J. P. C., and Geromanos, S. J. (2006). Absolute quantification of proteins by LCMSE: a virtue of parallel ms acquisition. *Mol. Cell. Proteomics* 5, 144–156. doi: 10.1074/mcp.m500230-mcp200

Sperotto, R. A., Buffon, G., Schwambach, J., and Ricachenevsky, F. K. (2018a). Crops responses to mite infestation: it's time to look at plant tolerance to meet the farmers' needs. *Front. Plant Sci.* 9:556. doi: 10.3389/fpls.2018.00556

Sperotto, R. A., Buffon, G., Schwambach, J., and Ricachenevsky, F. K. (2018b). Checkmite!? Is the resistance to phytophagous mites on short and stocky wild *Oryza* species? *Front. Plant Sci.* 9:321. doi: 10.3389/fpls.2018.00321

Stenberg, J. A., and Muola, A. (2017). How should plant resistance to herbivores be measured? *Front. Plant Sci.* 8:663. doi: 10.3389/fpls.2017.00663

Stirbet, A., and Govindjee. (2011). On the relation between the Kautsky effect (chlorophyll a fluorescence induction) and Photosystem II: basics and applications of the OJIP fluorescence transient. *J. Photochem. Photobiol. B* 104, 236–257. doi: 10.1016/j.jphotobiol.2010.12.010

Strasser, R. J., Srivastava, A., and Tsimilli-Michael, M. (2000). "The fluorescence transient as a tool to characterize and screen photosynthetic samples," in *Probing Photosynthesis: Mechanism, Regulation and Adaptation*, eds M. Yunus, U. Pathre, and P. Mohanty (London: Taylor & Francis), 443–480.

Sun, L., Ren, H., Liu, R., Li, B., Wu, T., Sun, F., et al. (2010). An h-type thioredoxin functions in tobacco defense responses to two species of viruses and an abiotic oxidative stress. *Mol. Plant Microbe Interact.* 23, 1470–1485. doi: 10.1094/mpmi-01-10-0029

Szareski, V. J., Carvalho, I. R., da Rosa, T. C., Dellagostin, S. M., de Pelegrin, A. J., Barbosa, M. H., et al. (2018). *Oryza* wild species: an alternative for rice breeding under abiotic stress conditions. *Am. J. Plant Sci.* 9:1093. doi: 10.4236/ajps.2018.96083

Tahir, J., and Dijkwel, P. (2016). β-Substituting alanine synthases: roles in cysteine metabolism and abiotic and biotic stress signalling in plants. *Funct. Plant Biol.* 43, 307–323. doi: 10.1071/fp15272

Terra, W. R., and Ferreira, C. (2005). "Biochemistry of digestion," in *Comprehensive Molecular Insect Science. Pergamon*, ed. L. I. Gilbert (Oxford: Elsevier), 171–204.

Thomson, V. P., Cunningham, S. A., Ball, M. C., and Nicotra, A. B. (2003). Compensation for herbivory by *Cucumis sativus* through increased photosynthetic capacity and efficiency. *Oecologia* 134, 167–175. doi: 10.1007/s00442-002-1102-6

Vandenbussche, F., Desmyter, S., Ciani, M., Proost, P., Peumans, W. J., and van Damme, E. J. M. (2004). Analysis of the *in planta* antiviral activity of elderberry ribosome-inactivating proteins. *Eur. J. Biochem.* 271, 1508–1515. doi: 10.1111/j.1432-1033.2004.04059.x

Vaughan, D. A. (1994). *The Wild Relatives of Rice: A Genetic Resources Handbook*. Los Baños: International Rice Research Institute, 137.

Veasey, E. A., da Silva, E. F., Schammass, E. A., Oliveira, G. C. X., and Ando, A. (2008). Morphoagronomic genetic diversity in american wild rice species. *Braz. Arch. Biol. Technol.* 51, 95–104.

Wang, Y., Kwon, S. J., Wu, J., Choi, J., Lee, Y. H., Agrawal, G. K., et al. (2014). Transcriptome analysis of early responsive genes in rice during *Magnaporthe oryzae* infection. *Plant Pathol. J.* 30, 343–354. doi: 10.5423/ppj.oa.06.2014.0055

Wei, G. Q., Liu, R. S., Wang, Q., and Liu, W. Y. (2004). Toxicity of two type II ribosome-inactivating proteins (cinnamomin and ricin) to domestic silkworm larvae. *Arch. Insect Biochem. Physiol.* 57, 160–165. doi: 10.1002/arch.20024

Wiśniewski, J. R., Zougman, A., Nagaraj, N., and Mann, M. (2009). Universal sample preparation method for proteome analysis. *Nature Met.* 6, 359–362. doi: 10.1038/nmeth.1322

Xue, X., Cao, Z. X., Zhang, X. T., Wang, Y., Zhang, Y. F., Chen, Z. X., et al. (2016). Overexpression of OsOSM1 enhances resistance to rice sheath blight. *Plant Dis.* 100, 1634–1642. doi: 10.1094/pdis-11-15-1372-re

Yang, J., Duan, G., Li, C., Liu, L., Han, G., Zhang, Y., et al. (2019). The crosstalks between Jasmonic Acid and other plant hormone signaling highlight the involvement of Jasmonic Acid as a core component in plant response to biotic and abiotic stresses. *Front. Plant Sci.* 10:1349. doi: 10.3389/fpls.2019.01349

Yoo, K. S., Ok, S. H., Jeong, B. C., Jung, K. W., Cui, M. H., Hyoung, S., et al. (2011). Single cystathionine β-synthase domain-containing proteins modulate development by regulating the thioredoxin system in *Arabidopsis*. *Plant Cell* 23, 3577–3594. doi: 10.1105/tpc.111.089847

Youssefian, S., Nakamura, M., Orudgev, E., and Kondo, N. (2001). Increased cysteine biosynthesis capacity of transgenic tobacco overexpressing an O-acetylserine(thiol) lyase modifies plant responses to oxidative stress. *Plant Physiol.* 126, 1001–1011. doi: 10.1104/pp.126.3.1001

Zhang, C. J., Zhao, B. C., Ge, W. N., Zhang, Y. F., Song, Y., Sun, D. Y., et al. (2011). An apoplastic h-type thioredoxin is involved in the stress response through regulation of the apoplastic reactive oxygen species in rice. *Plant Physiol.* 157, 1884–1899. doi: 10.1104/pp.111.182808

Zhou, M., and Memelink, J. (2016). Jasmonate-responsive transcription factors regulating plant secondary metabolism. *Biotechnol. Adv.* 34, 441–449. doi: 10.1016/j.biotechadv.2016.02.004

Zou, L., Stout, M. J., and Dunand, R. T. (2004). The effects of feeding by the rice water weevil, *Lissorhoptrus oryzophilus* Kuschel, on the growth and yield components of rice, *Oryza sativa*. *Agr. Forest Entomol.* 6, 47–54. doi: 10.1111/j.1461-9555.2004.00203.x

Žurga, S., Pohleven, J., Kos, J., and Sabotič, J. (2015). β-Trefoil structure enables interactions between lectins and protease inhibitors that regulate their biological functions. *J. Biochem.* 158, 83–90. doi: 10.1093/jb/mvv025

Conflict of Interest: The authors declare that the research was conducted in the absence of any commercial or financial relationships that could be construed as a potential conflict of interest.

Copyright © 2021 Buffon, Blasi, Lamb, Adamski, Schwambach, Ricachenevsky, Bertolazi, Silveira, Lopes and Sperotto. This is an open-access article distributed under the terms of the Creative Commons Attribution License (CC BY). The use, distribution or reproduction in other forums is permitted, provided the original author(s) and the copyright owner(s) are credited and that the original publication in this journal is cited, in accordance with accepted academic practice. No use, distribution or reproduction is permitted which does not comply with these terms.

frontiers in Plant Science

ORIGINAL RESEARCH
published: 15 February 2021
doi: 10.3389/fpls.2020.607869

A Comparative Study for Assessing the Drought-Tolerance of Chickpea Under Varying Natural Growth Environments

Anjuman Arif[1], Najma Parveen[2,3], Muhammad Qandeel Waheed[1], Rana Muhammad Atif[2,3], Irem Waqar[1] and Tariq Mahmud Shah[1]*

[1] Nuclear Institute of Agriculture and Biology (NIAB), Faisalabad, Pakistan, [2] Department of Plant Breeding and Genetics, University of Agriculture Faisalabad, Faisalabad, Pakistan, [3] Center for Advanced Studies in Agriculture and Food Security (CAS-AFS), University of Agriculture Faisalabad, Faisalabad, Pakistan

This study was planned with the purpose of evaluating the drought tolerance of advanced breeding lines of chickpea in natural field conditions. Two methods were employed to impose field conditions; the first: simulating drought stress by growing chickpea genotypes at five rainfed areas, with Faisalabad as the non-stressed control environment; and the second: planting chickpea genotypes in spring to simulate a drought stress environment, with winter-sowing serving as the non-stressed environment. Additive main effects and multiplicative interaction (AMMI) and generalized linear models (GLM) models were both found to be equally effective in extracting main effects in the rainfed experiment. Results demonstrated that environment influenced seed yield, number of primary and secondary branches, number of pods, and number of seeds most predominantly; however, genotype was the main source of variation in 100 seed weight and plant height. The GGE biplot showed that Faisalabad, Kallur Kot, and Bhakkar were contributing the most in the GEI, respectively, while Bahawalpur, Bhawana, and Karor were relatively stable environments, respectively. Faisalabad was the most, and Bhakkar the least productive in terms of seed yield. The best genotypes to grow in non-stressed environments were CH39/08, CH40/09, and CH15/11, whereas CH28/07 and CH39/08 were found suitable for both conditions. CH55/09 displayed the best performance in stress conditions only. The AMMI stability and drought-tolerance indices enabled us to select genotypes with differential performance in both conditions. It is therefore concluded that the spring-sown experiment revealed a high-grade drought stress imposition on plants, and that the genotypes selected by both methods shared quite similar rankings, and also that manually computed drought-tolerance indices are also comparable for usage for better genotypic selections. This study could provide sufficient evidence for using the aforementioned as drought-tolerance evaluation methods, especially for countries and research organizations who have limited resources and funding for conducting multilocation trials, and performing sophisticated analyses on expensive software.

Keywords: chickpea (*Cicer arietinum* L.), multi-environment, genotype environment interactions, genotype selection index (GSI), drought

OPEN ACCESS

Edited by:
Raul Antonio Sperotto, Universidade do Vale do Taquari – Univates, Brazil

Reviewed by:
Naeem Khan, University of Florida, United States
Sushil Kumar Chaturvedi, Rani Lakshmi Bai Central Agricultural University, India

****Correspondence:***
Anjuman Arif
arifanjuman@gmail.com

Specialty section:
This article was submitted to Plant Abiotic Stress, a section of the journal Frontiers in Plant Science

Received: *18 September 2020*
Accepted: *18 December 2020*
Published: *15 February 2021*

Citation:
Arif A, Parveen N, Waheed MQ, Atif RM, Waqar I and Shah TM (2021) A Comparative Study for Assessing the Drought-Tolerance of Chickpea Under Varying Natural Growth Environments. Front. Plant Sci. 11:607869. doi: 10.3389/fpls.2020.607869

INTRODUCTION

Drought is accepted as a serious threat to crops worldwide, more specifically to the areas where there is less rain fall. Grain yield is considered to be a determining factor of stress tolerance in crop plants as scarcity of water leads to reduced grain yield in cereal and legume crops. This has been indicated in a meta-analysis of more than 100 studies where chickpea stands on the seventh position among 13 legume species when categorized on the basis of drought-induced yield reduction (Daryanto et al., 2015).

Chickpea is the most important legume crop and a source of nutrition to millions of people globally due to its richness in protein, fiber, and minerals (Dadon Bar-El et al., 2017). It also re-mediates the soil by its ability to fix nitrogen in a symbiotic relationship with rhizobacteria upon nodulation. Pakistan is the third largest producer of chickpea in the world (FAOSTAT, 2015), and among all provinces, Punjab contributes 80% of chickpea production in Pakistan (Government of Pakistan [GOP], 2016). It is mainly cultivated in marginal lands, rainfed areas, and in sand dunes of the Thal desert (Rafiq et al., 2018; Nisa et al., 2020).

Besides, chickpea is a cool season crop and grown mainly in rainfed areas where it suffers terminal drought at the time of maturity and seed filling due to increase in temperature and reduced or no rainfall (if occurs), which causes drastic yield losses. Planting in spring rather than winter also exposed chickpea plants to face drought stress (Toker and Cagirgan, 1998; Richards et al., 2020).

High yielding genotypes when grown under limited water availability were used to be selected as drought tolerant varieties. Due to variations in weather conditions observed each coming year leads to variation in the pattern of onset of drought stress. Hence, selection on the basis of grain yield only seems not sufficient to produce high yielding drought tolerant varieties in the climate change scenario (Ludlow and Muchow, 1990; Blum, 1996).

Chickpea yield varies and is strongly influenced by environmental factors, i.e., photoperiod, temperature (Velu and Shunmugavalli, 2005), and it depends upon differential composition of soil type and available water, changing weather conditions on the same location (environment) in different years, or in multiple locations in one season or over years (Crossa, 1990; Purchase et al., 2000). This can be explained by genotype and environment (GE) interaction, which described that two genotypes in the same environment behave differently due to variations in their genetic makeup. Interactions can also be distinguished on the basis of whether they are repeatable or non-repeatable within the target genotype–environment system. Similarly, a specific environment can influence one genotype in a different way than other genotypes, or a single genotype behaves differently in different environments (Falconer, 1981; Misra et al., 2020; Nisa et al., 2020). However, genotypes with wider adaptability to a number of diverse environments without affecting their yield potential seems to be a better strategy, which needs extensive multi-location trials of genotypes under study consecutively for 2–3 years (Farshadfar et al., 2011).

The additive main effects and multiplicative interaction (AMMI) model has been used extensively in agriculture research for the evaluation of breeding lines prior to varietal approval. AMMI first applies analysis of variance (ANOVA) to partition the variation into genotype main effects (G), environment main effects (E), and genotype-by-environment interaction effects GE), and then it applies principal components analysis (PCA) by singular value decomposition to GE (Gauch, 1992, 2006; Yan et al., 2007; Gauch et al., 2008; Yang et al., 2009).

Generalized linear models (GLM) also used to measure variations contributed by genotypes, environment, and G × E interactions for each response variable by combined analysis of variance (ANOVA) and linear regression. GLMs relax the assumption about the dependent variables (Olsson, 2002).

The ability of crop cultivars to perform reasonably well in drought-stressed environments is paramount, and non-stressed environments can be used as an indicator to identify drought-resistant varieties in breeding for drought-prone environments. Several drought indices have been suggested on the basis of a mathematical relationship between yield under drought conditions and non-stressed conditions. These indices are based on either drought resistance or drought susceptibility of genotypes (Clarke et al., 1984).

In the context of ongoing international research on G × E interactions and the development of sustainable climate-resilient drought-tolerant chickpea genotypes, we realized the need for a large-scale cohesive study to evaluate the advanced breeding lines for drought tolerance based on the stability and yield prior to being subjected to the National Uniform Yield Trials, a pre-requisite of variety approval. We hypothesized that the breeders' lines coming from all over Pakistan from Government Agriculture Research Organizations for preliminary yield trials would be a good start. We planned the study keeping this in mind.

The objectives of this study were the assessment of yield potential, stability, and drought tolerance of chickpea genotypes under natural field conditions, and to identify discriminating environment-specific genotypes, and genotypes have wider adaptability for a range of environments.

MATERIALS AND METHODS

The germplasm used in the study were advanced breeding lines of chickpea. A set of 83 advanced breeding lines with commercial varieties as checks were acquired from the provincial and national uniform yield trials conducted at multiple locations across Pakistan (**Supplementary Table 1**) in the season of 2016–2017. In the next year (2017–2018), 80 genotypes were evaluated for drought tolerance, 50 from the previous year's trials and the rest were advanced breeding lines acquired from the Nuclear Institute for Agriculture and Biology (NIAB), Pakistan. In the third year of the study, 40 genotypes were selected from 80 genotypes tested in 2017–2018 on the basis of yield performance.

Experimental Design

The trials were laid out according to the randomized complete block design (RCBD), replicated four times with a plot size of

1.8 m^2 giving a plant density of approximately 25 plants per m^2. The harvesting and threshing were conducted manually.

Imposition of Field Drought Stress and Data Recording

The study was planned to evaluate the drought tolerance of advanced breeding lines of chickpea in natural field conditions. Two methods were employed to impose drought-stressed field conditions; Experiment 1, by growing chickpea genotypes at five locations in rainfed chickpea-growing areas (four of which were situated in the Thal desert of Pakistan) with only natural rainfall and no supplemental irrigation, and at an irrigated location, i.e., Faisalabad City of Pakistan, as the non-stressed environment. Descriptions of the planting environments are described in **Table 1**. Data were recorded, for observations, i.e., *Seed yield* (SY), *hundred-seed-weight* (100SW), *number of seeds* (NOS), *number of pods* (NOP), *number of primary branches* (NPB), *number of secondary branches* (NSB), and *plant height* (PH). Drought tolerance score (DRS) was estimated using a rating scale ranging from 1 (plants with 95–100% pod setting) to 9 (plants did not set any pods and dried out).

Experiment 2 involved the planting of chickpea genotypes in spring as simulating a drought stressed environment (S2), whereas winter-sowing was regarded as the non-stressed environment (S1). Five observations, i.e., *seed yield* (SY), *biological yield* (BY), *seed weight* (SW), *harvest index* (HI), and *plant height* (PH) were recorded under stressed and non-stressed conditions. The biological yield was recorded as shoot dry-weight (g) per plant, and the harvest index was calculated as described by El Naim et al. (2010). The formula is given below:

$$Harvest\ Index = \frac{\text{Seeds yield (g)}}{\text{Shoot dry weight (g)}}$$

Weather data was collected from *https://www.worldweatheronline.com/*. Soil texture and physical properties account for a major proportion in environmental characterization, and therefore, the soil types of six environments are listed in **Table 1**.

G × E Data Analyses

AMMI and GLM Models

Generally, genotype–environment interaction (GEI) is common when genotypes (G) are tested across a number of environments (E). The GE main effects were extracted using two statistical models, i.e., the AMMI and GLM.

The AMMI analysis has two parts. First, the analysis of variance of genotype (G), environment (E), and genotype–environment (GE) interactions (subdivided into principal components called interaction principal components or IPCAs) and AMMI main effect biplot in which GE means are plotted on the *x*-axis, while the IPCA1 scores are on the *y*-axis. Second is the genotype (G) and genotype–environment interaction (GEI) biplot (Yan and Tinker, 2006). There are several types of biplot options available in GenStat to plot GEI. On the other hand, GLM is basically analysis of variance and generalized linear regression without any principal component analysis. GenStat software was used for the AMMI and GGE biplot analysis, whereas MINITAB 14 was used for GLM analysis.

Genotype Selection Index

The AMMI stability value (ASV) was manually computed as per Purchase (2000); however, the IPCA sum of squares of interactions and IPCA1 and IPCA2 scores were used from the AMMI analysis using the GenStat software. The equation was as follows:

$$\text{AMMI Stability Value (ASV)} = \sqrt{\left[\frac{\text{IPCA1 Sum of Squares}}{\text{IPCA2 Sum of Squares}}(\text{IPCA1score})\right]^2 + [\text{IPCA2 score}]^2}$$

When computing ASV using Microsoft Excel, the following formula was used:

SQRT[(IPCA1 sum of squares/IPCA2 sum of squares*IPCA1 score)^2 + (IPCA2^2)].

The AMMI stability value (ASV) and the mean seed yield of individual genotypes across environments were used to derive another component of stability and yield-based selection of genotypes across environments as genomic selection index (GSI), described by Farshadfar (2008) and Pouresmael et al. (2018). We have modified its name to be "genotype selection index" rather than "genomic selection index." The genotype selection index (GSI) was calculated using the following formula:

$$GSI = RASV + RY$$

TABLE 1 | Environment types, soil properties, and geographic coordinates of environments.

Sr. #	Name	Type	Soil Type	Latitude, Longitude, Sea level
1	Karor	Rainfed	Calcareous, Sandy loam (light)	31.2301, 70.9475, 155 m
2	Bhakkar	Rainfed	Silt loam, Silty clay loam, Clay loam	31.6303, 71.0676, 169 m
3	Kallur Kot	Rainfed	Sandy loam	32.1567, 71.2724, 191 m
4	Bahawalpur	Rainfed	Silt loam, Silty clay loam, Clay loam	29.3946, 71.6638, 116 m
5	Faisalabad	Rainfed, Irrigated	Silt loam or very fine sandy loam	31.4126, 3.0551, 184 m
6	Bhawana	Rainfed	Silt loam or very fine sandy loam	31.5685, 72.6485, 172 m

Calcareous and clayey soils: potential productivity is high with adequate water and nutrients supply. Sandy loams: are capable of quickly draining excess water and usually deficient in micronutrients, especially zinc and iron. Silt soils: are fertile, light but moisture-retentive and easily compacted.

where RASV and RY are the rank of the AMMI stability value and the mean seed yield of a genotype, respectively. Ranking was performed with the lowest AMMI value and the highest mean seed yield ranked one. Lower ASV values indicate greater stability for a genotype; conversely, the less stable genotypes are those with close to maximum amounts of GSI. Therefore, GSI combines both mean yield and stability in a single criterion.

Drought Tolerance Indices

The mean yield of each genotype was recorded in stressed (Ys) and non-stressed (Yp) conditions and used to calculate eight drought stress tolerance indices to assess yield- and stability-based selections of genotypes under simulated stressed and non-stressed natural field conditions. Formulas are presented in **Table 2**. According to a classification by Fernandez (1992), he distributed the genotypes evaluated by drought tolerance indices into Group A consisting of genotypes with high seed yield under both drought stress and non-stressed conditions, Group B, comprised of genotypes with high yield only under non-stress conditions, Group C, genotypes could produce good yield only under stress conditions, whereas genotypes with poor yield performance under both conditions were categorized as Group D.

Graphics

Trellis plots and G × E plots were produced using GenStat software. R package "Corr," "Corrplot," and "Corrgram" were used for computing correlation matrix and graphics. However ggplot2 was used to produce boxplots.

RESULTS

Environmental and genetic factors impact certain metabolic processes that influence growth and yield in a crop, and quantitatively understanding the correlations between these factors and phenological development can help us predict crop yield. Emergence, flowering, pod set, and physiological maturity are defined as the four developmental stages of chickpea (*Cicer arietinum* L.). The last three stages are indeterminate and occur concurrently in different parts of the plant along with the vegetative growth (Summerfield and Wien, 1980; Saxena, 1984). Temperature, photoperiod, and available moisture are generally most influential to chickpea development (Soltani et al., 1999).

TABLE 2 | Drought tolerance indices, formulas, and references.

Index	Formula	References
Stress Tolerance	TOL = Yp–Ys	Rosielle and Hamblin (1981)
Mean Productivity	MP = (Yp + Ys)/2	Rosielle and Hamblin (1981)
Geometric Mean Productivity	GMP = $(Yp * Ys)^{0.5}$	Fernandez (1992)
Stress Susceptibility Index	SSI = [(1–(Ys/Yp)]/SI	Fischer and Maurer (1978)
Stress Index	SI = 1–(Ȳs/Ȳp)	Fischer and Maurer (1978)
Stress Tolerance Index	STI = $(Yp * Ys)/(Ȳp)^2$	Fernandez (1992)
Yield Index	YI = Ys/Ȳs	Gavuzzi et al. (1997)
Yield Stability Index	YSI = Ys/Yp	Bouslama and Schapaugh (1984)

Yp and Ys, seed yield of each genotype under non-stress and stress conditions, respectively. Ȳp and Ȳs, mean seed yield of all genotypes under non-stress and stress conditions, respectively.

Evaluation of Drought Tolerance Under Naturally Stressed and Non-stressed Environments

In this experiment, diverse chickpea genotypes were characterized for their drought stress tolerance on the basis of phenotypic traits through replicated yield trials (2017–2018) in five rainfed areas, which are referred to as *stressed environments*. Conversely, E5 was considered a non-stressed environment due to its soil type and irrigation system (**Table 1**).

The weather data of drought stressed environments were almost similar: dry with low rainfall, i.e., 16 mm at E3 and E2, 17 mm at E1, 8 mm at E4, and 27 mm at E6. The non-stressed environment E5, on the contrary, was very wet with 129 mm rainfall during the crop period (**Figure 1A**). The weather data recorded for Experiment 2 are shown in **Figure 1B**. The temperature from January to February was favorable for the chickpea plant, but these months were quite dry, as no rainfall was recorded after the spring sowing. Later, day and night temperatures rose in March and April, but these months had 82 mm rainfall, and decreased humidity due to the rise in temperature.

The average temperature at four environments was similar in these months but a rise in temperature of 1–2°C was noted in E1, and E4 in the months of October, February, and March. E4 had the highest average temperature among all six locations. The rainfall received was the least in E4 and the greatest in E5 (**Figure 1A**). It is suggested that E5 was found the most favorable and E4 with the most adverse soil characteristics among all six locations.

Estimation of Phenotypic Variations Among Environments

At large, trellis plots of environments described that environments have profound effects on individual observation. Environment influences GY, NPB, NSB, NOP, and NOS in the most predominant way; however, genotype was the main source of variation in 100 SW and PH. Genotype means of NPB and NSB was highest in Bhakkar, but Faisalabad was best for genotypes to attain maximum PH, NOP, NOS, and SY (**Figure 2**). DRS exhibited that the intensity of drought was minimum in Faisalabad, i.e., the non-stressed environment (**Figure 3**).

Correlation of Phenotypic Variations Among Environments

A correlation matrix of the mean data for NPB and NSB, PH, NOP, NOS, and SY showed a high positive correlation in NOP, NOS, and GY, and a strong positive correlation in PH, NOP, NOS, and GY. Increase in NSB also correlated with increases in NOP, NOS, and SY. NPB displayed a

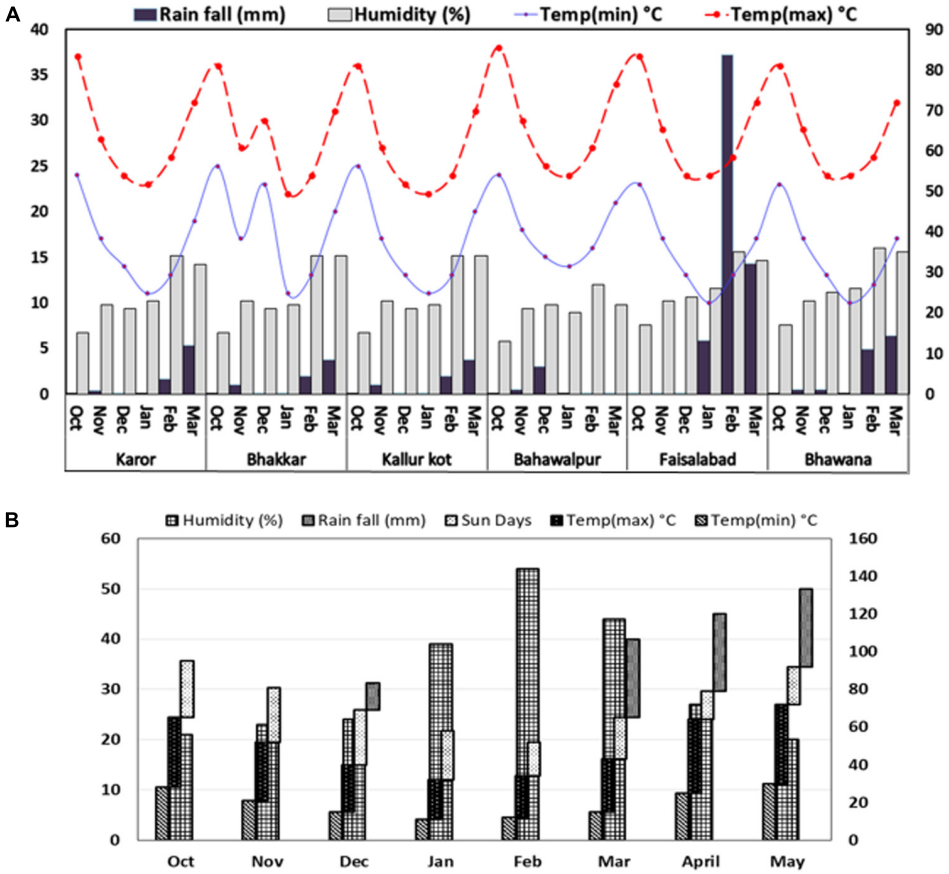


FIGURE 1 | Weather footprint describing monthly rainfall (mm), relative humidity *(%),* and extreme maximum and minimum temperatures °C in growth period of Chickpea genotypes grown under natural **(A)** drought stressed and non-stressed and **(B)** simulated drought stressed and non-stressed field conditions.

relatively low level of positive correlation with PH, NOP, NOS, 100 SW, and SY. NPB and NSB had moderately strong correlation. Drought score exhibited high negative correlation with SY and significant negative correlation with PH and NOS, whereas it showed no correlation with other traits (**Figure 4A**). A heat map provided a visual overview, and relative intensity of correlation values in a pair of observations demonstrated the extent and dimension of correlation. For instance, NOS, NOP, and SY shared a red colored grid of nine squares describing a strong positive correlation among them (**Figure 4B**).

Estimation of Genotypic Variations Among Environments

Trellis plots showing mean seed yield of individual genotypes clearly demonstrate that seed yield was higher in the non-stressed environment (E5) compared to the stressed environments (**Figure 5**). The trellis plots have shown that genotypes CH28/07 (G48) and CH10/08 (G49) performed well in most of the environments; however, DCD (G3) produced the highest mean seed yield at the non-stressed environment (E5). Similarly, some genotypes like CM616/10 (G41), TG12K10 (G45), and CH23/00 (G64) produced better mean seed yield in stressed environments.

Genotype × Environment Interaction

Genotype main effects: additive main effects and multiplicative interaction biplot

The AMMI main effects biplot helps to isolate the genotypes producing high yields and broadly (near the origin) or specifically (far from origin) adapted to nearby environments in biplot (**Figure 6A**). Genotypes like CH76/08 (G28), CH2/11 (G52), Bittle-2016 (G66), and AZC (G6) were plotted near the origin. This indicates that these were less sensitive to environmental interaction and broadly adapted with near average SY. However, G14 (D-13029), G16 (CM584/09), D-13036 (G8), D-13012 (G9), CH 39/08 (G2), CH28/07 (G48), and CH10/08 (G49) had a better mean seed yield than the mean of all genotypes and plotted far from the origin along the *x*-axis but close to the origin along the *y*-axis. These were suggested high-yielding and relatively insensitive to GEI. Similarly, CM877/10 (G40) and TG12K02 (G46) performed less than the grand mean yield, and plotted far from the origin on the x-axis but nearer to the *y*-axis, meaning that these were low-yielding genotypes and insensitive to GEI. DG-2017 (G31) and QG-1 (G32) genotypes belong to Province Sindh and were not able to adapt in Punjab. Moreover, ILC3279 (G65), a traditional cultivar acquired as germplasm from ICRISAT, produced very poor SY in comparison with the grand

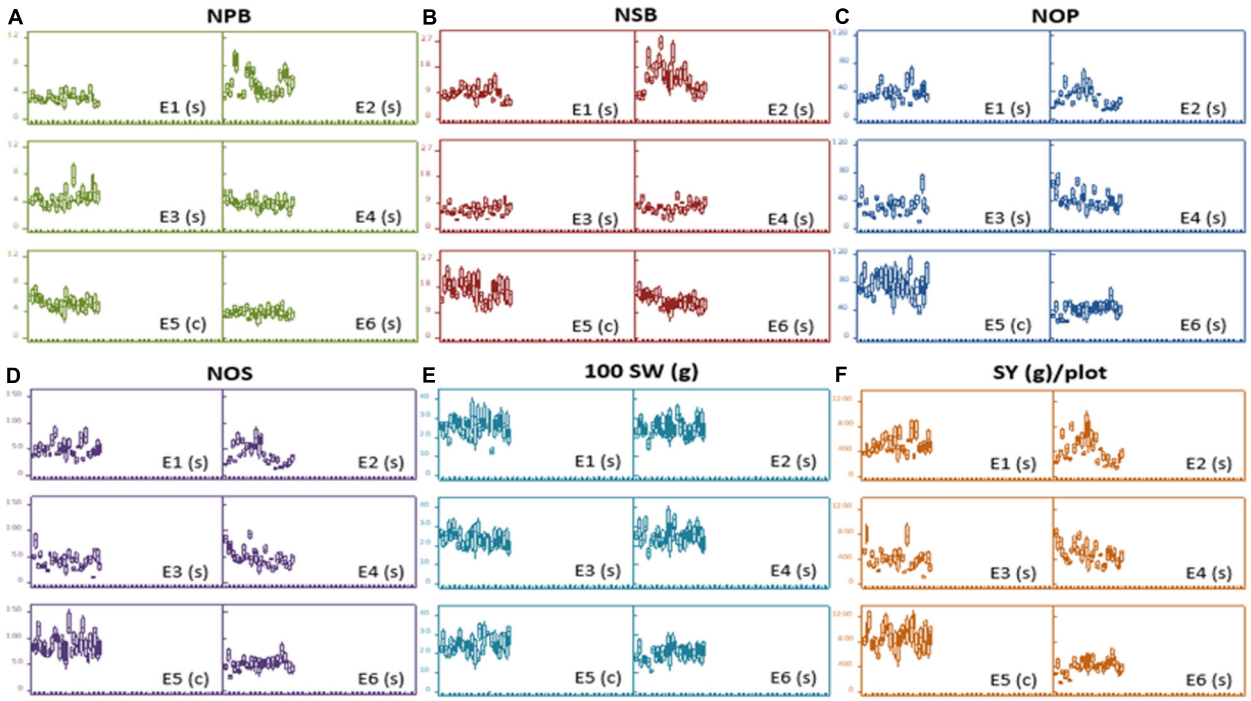


FIGURE 2 | Trellis plots exhibiting distribution of phenotypic data of different agronomic traits: **(A)** Number of primary branches (NPB). **(B)** Number of secondary branches (NSB). **(C)** number of pods (NOP), **(D)** number of seeds (NOS), **(E)** hundred-seed-weight [100SW(g)], and **(F)** seed yield [SY(g)/plot across six varying environments]. Each boxplot represents a data subset of genotypes with similar values in the data set instead of blurring the effect of each other in a single boxplot of each genotype.

mean. Similarly, environments near the origin along the *y*-axis with a lesser IPCA score contributed little in GEI, such as E4 and E6, while E1 and E2 elicited a moderate level of GEI, but E3 elicited strong interactive forces, and above all, E5 contributed most in terms of GEI as it was spotted farthest point on biplot. E5 also plotted from the origin along the *x*-axis and was the most productive environment in terms of producing SY, followed by E1, which had mean yield little better than average means. All other environments produced seed yields less than average where E2 was the least productive among all. Ranking of all genotypes according to AMMI estimates in all environments is presented in **Supplementary Table 2**. The first four AMMI selections in each environment and a hierarchical cluster analysis clustered genotypes according to the AMMI estimates (**Table 3**).

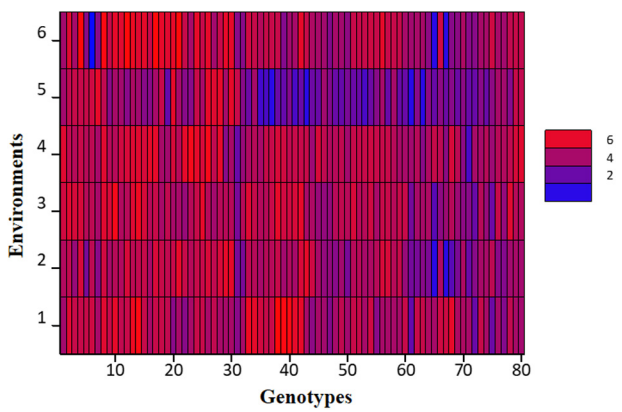


FIGURE 3 | Shade plot of drought tolerance scores of 80 chickpea genotypes across six environments.

Genotype main effects: analysis of variance (additive main effects and multiplicative interaction and generalized linear model)

As per good practice, GLM was applied to our data in addition to AMMI to compare analytical competitiveness of GLM with special software-based AMMI analysis. An analysis of variance revealed that both models produced the same results (**Table 4**). Both models revealed that the genetic makeup of genotypes contributed least in the phenotypic variations of all traits in comparison to the environment and GEI. However, it did have a significant influence when SW and DRS were taken into account. NSB, NOP, NOS, and SY were most influenced by environmental factors, whereas NPB, PH, 100 SW, and DRS were most affected by GEI. The number of secondary branches (NSB) produced were greatly influenced by the environment alone. Environment means and variances of SY showed that the non-stressed environment, i.e., Faisalabad elicited the highest interactive forces on genotypes than the stressed environments.

Genotype by environment interactions (GEIs) affect how well a genotype performs in different environments. The AMMI GGE

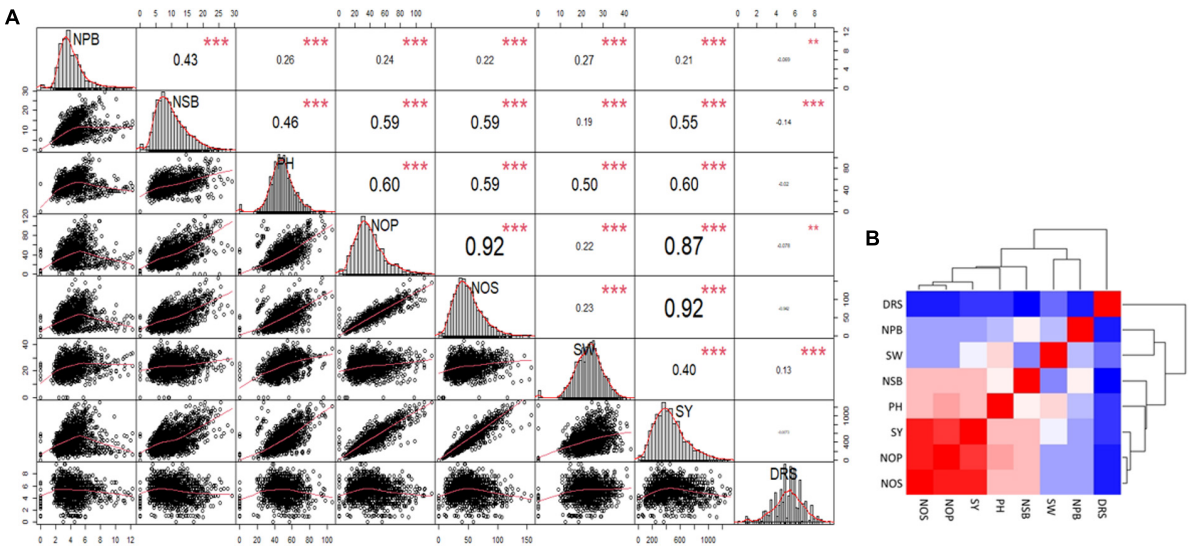


FIGURE 4 | (A) Correlation Matrix of the data for number of primary branches (NPB), number of secondary branches (NSB), plant height (PH), number of pods (NOP), number of seeds (NOS), hundred-seed-weight (SW), seed yield (SY), and Drought Tolerance Score (DRS). The distribution of each variable is shown on the diagonal. On the bottom of the diagonal: the bivariate scatter plots with a fitted line are displayed. On the top of the diagonal: the value of the correlation plus the significance level as stars. Color intensity and the size of the correlation values are proportional to the correlation coefficients. **(B)** Heat map and clustering of the correlation matrix, red color shows maximum correlation followed by pink then white and blue shows minimum or no correlation among the traits.

biplot, which is statistically a scatter plot, is summarized by the two interactive principal component (IPCA) axes. Axis 1 explains IPC1, axis 2 explains IPC2 and its origin represents no GEI. The scatter plot of seed yield data showed a positive correlation between all environments as indicated by an acute angle between them (**Figure 6B**). Genotypes D-14005 (G10), BRC-457 (G11), and CH15/11 (G73) clustered together, showing similar seed yields across environments and being influenced by GEI in a similar way. However, environments E4, E6, and E1 tended to cluster together influencing the genotypes in a similar way. Environments E4 and E6 close to the origin elicited weak interactive forces, whereas E5 was far from the origin and was suggested to elicit strong interactive forces. Genotypes CH28/07 (G48) and D-07509 (G63) were plotted far from the origin, and so were more prone to being influenced by GEI. G48 was plotted near E3 and was hence specifically adapted to E3, similarly D-14005 (G10), BRC-457 (G11), CH15/11 (G73), G18 (K-01216), and CH55/09 (G20) were specifically adapted and positively correlated to the non-stressed environment, i.e., E5.

Selection of Best Suitable Genotype and Environment

GGE plots can be improved by generating different types of biplots. Some are used here for creating better visuals of G × E analyses.

Which-won-where

A which-won-where view of the biplot helps to identify which genotypes performed best in each environment and in each mega environment. Our results revealed that the seed yield biplot contained three mega environments (ME): ME1, containing E1, E2, E3 (E3), E4, and E6; ME2, containing E2 and E4; and third; ME3 consisting of E5 only, which is a non-stressed and ideal environment as well (**Figure 6C**). As a general rule, genotypes that appear in the same sectors as a particular environment are the best performers in that environment, e.g., genotypes D-13012 (G9), D-14005 (G10), BRC-457 (G11), D-13029 (G14), and CH15/11 (G73) were located in the ME2 and are expected to produce maximum seed yield in these environments, whereas E5 was the most suitable for DCD (G3) and CH15/11 (G73) for producing maximum seed yield.

Comparison biplot

A comparison biplot is used to compare the performance of an environment with that of an ideal environment. In a comparison, E4 shares more attributes with E5 than with E2, E3 (E3), E6, and E1 (in decreasing order of common attributes). In addition, the smaller the circle containing a genotype, the greater is its stability and performance in an ideal environment. Genotypes DCD (G3), CH15/11 (G73), D-14005 (G10), BRC-457 (G11), K-01216 (G18), and CH55/09 (G20) are likely to be ideal genotypes in the ideal environment E5 in terms of achieving higher mean seed yield, good stability showing a low IPCA score (**Figure 6D**).

Ranking biplot

A ranking plot is a presentable method for showing the best performing genotypes in a specific environment and can also be used to show the best environment for a specific genotype. Genotypes DCD (G3), CH15/11 (G73), D-14005 (G10), BRC-457 (G11), K-01216 (G18), and so on are the best-performing genotypes in terms of seed yield in E5. Similarly **Figure 7** shows the ranking of all genotypes in each environment (A–E) on the basis of their yield performance.

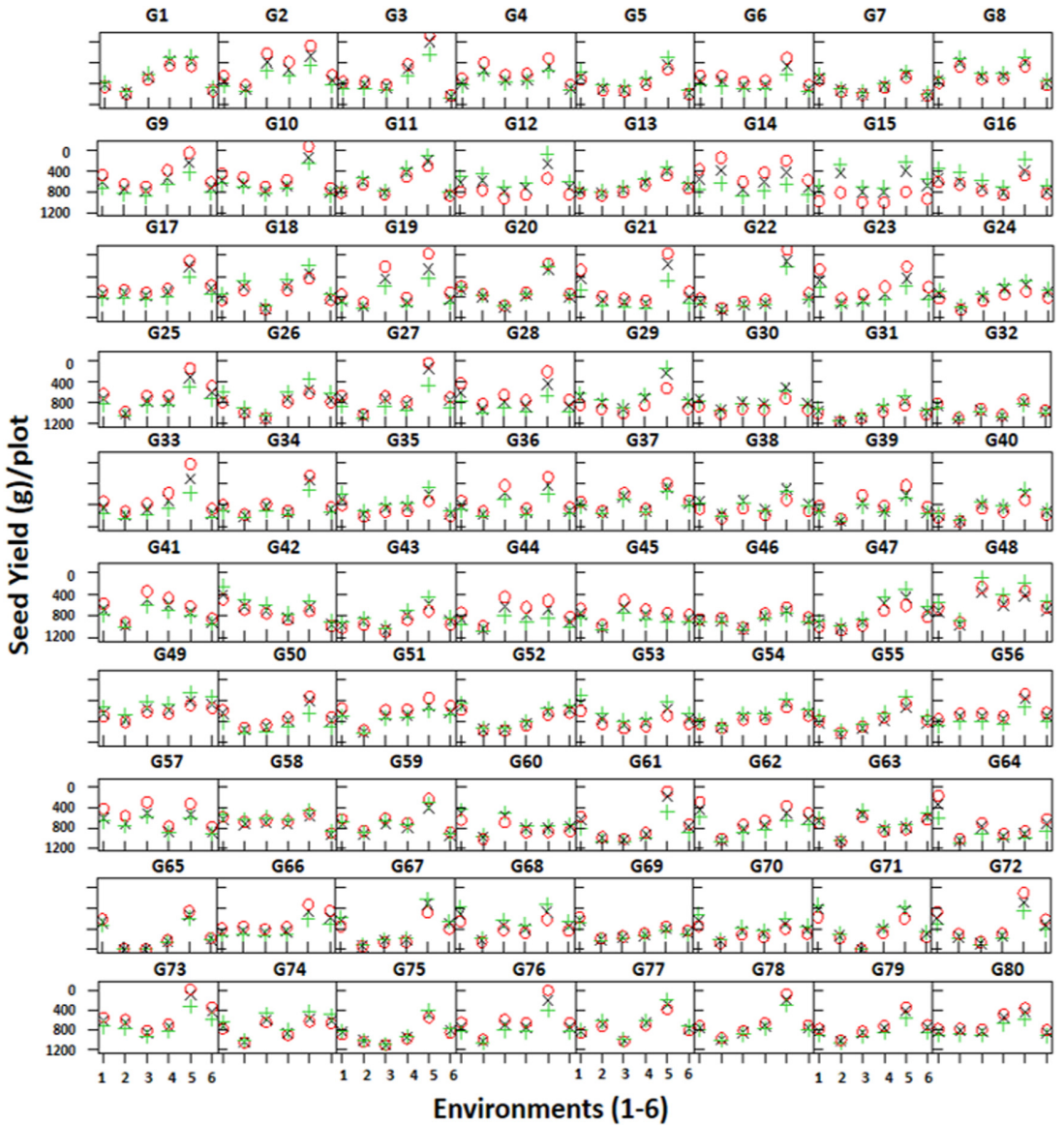


FIGURE 5 | Trellis plots showing mean seed yield (g/plot) of 80 genotypes across six environments. Genotypes are coded as G1–G80.

Genotypic Selections by Additive Main Effects and Multiplicative Interaction Model Based Indices

We found that on the basis of ASV, genotypes, for example, DG-2017 (G31), TG12K-07 (G25), CH76/08 (G28), and AZC (G6) were the top-most stable genotypes; however, based on yield performances, these were on the 80th, 28th, 44th, and 48th place in rankings (**Supplementary Table 3**). We identified that the GSI ranking is comparable to the AMMI model-based ranking (**Supplementary Tables 2**, **3**). Both identified DCD (G3), CH15/11 (G73), D-14005 (G10), BRC-457 (G11), K-01216 (G18), CH55/09 (G20), and CH28/07 (G48) as the few top-most stable and high-yielding genotypes in all environments. Similarly, both methods ranked the same genotypes, e.g., TG12K-07 (G25), K-01250 (G39), CM877/10 (G40), CH76/08 (G28), K-01302 (G38), K-01240 (G43), K-01308 (G34), K-01242 (G35), and K-01209 (G30) as low yielding in comparison to mean yield and relatively less stable in the list.

Evaluation of Drought Tolerance in Simulating Stressed and Non-stressed Environments

A box plot was used to differentiate the distinct values of mean data for observations, i.e., *seed yield* (SY), *biological yield* (BY), *seed weight* (SW), *harvest index* (HI), and *plant height* (PH) were recorded for 40 genotypes and quantified to assess their performance under the winter and spring sowings. The reduction observed in the mean GY, BY, SW, and PH of drought-stressed or spring-sown chickpea genotypes in comparison to

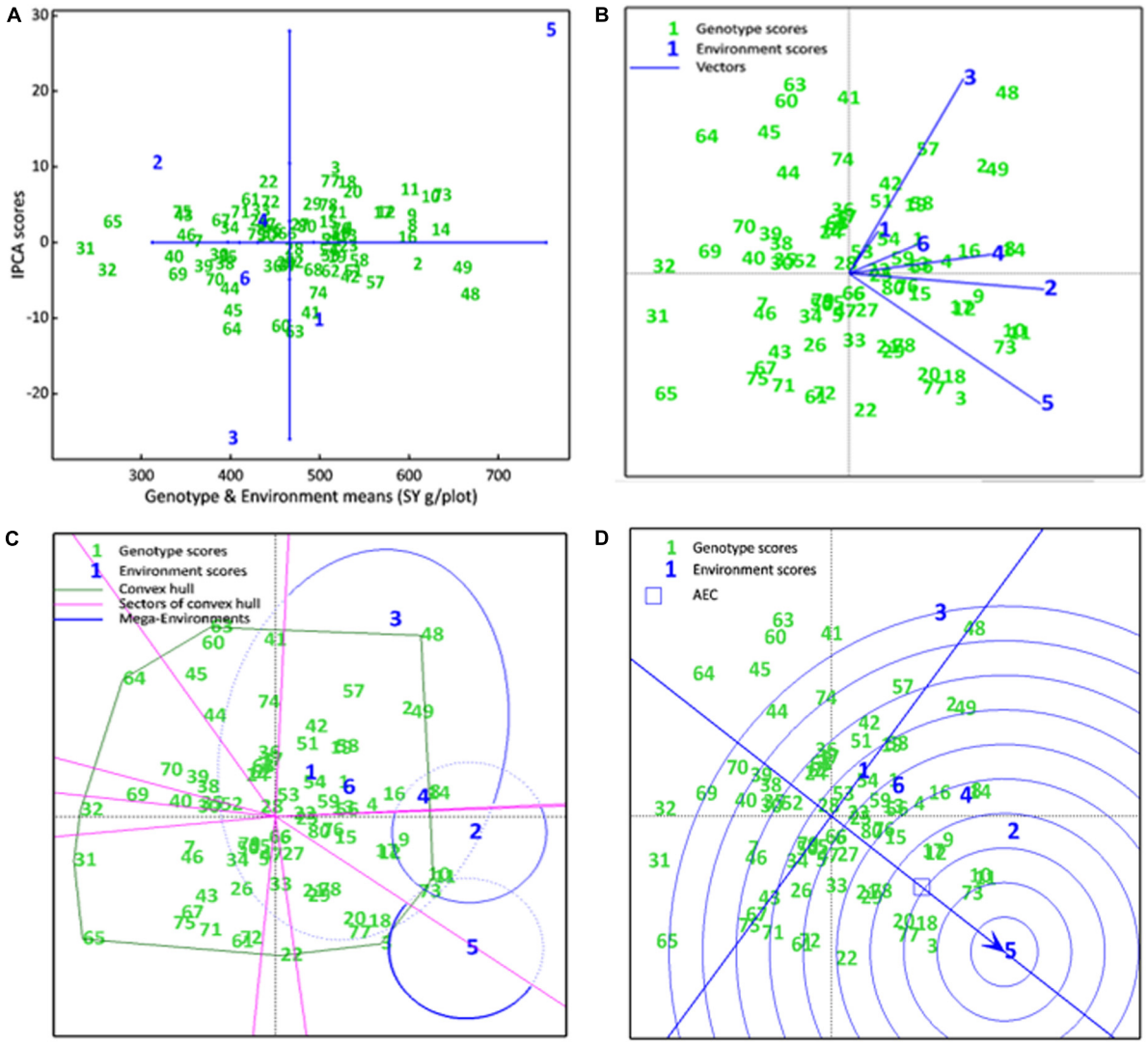


FIGURE 6 | (A) AMMI main effects biplot. SY of genotypes are plotted on the *x*-axis, while the IPCA1 scores are on the *y*-axis. The origin represents the average performance of all genotypes in each environment and there is zero GEL. Displacement along the *x*-axis shows differences in the main effects, whereas displacement along the *y*-axis reflects differences in the interaction effects. **(B)** The scatter plot of seed yield data of chickpea genotypes across six environments explained 58.52% of total variations. Axis 1 explains IPC1 (35.71%) along *x*-axis, axis 2 explains IPC2 (22.81%). **(C)** Which-won-where view of the biplot. A convex hull polygon around all genotypes scored has been drawn by connecting the farthest genotypes to form a polygon that encompasses all genotypes. Sectors draw lines from the origin perpendicular to each side of convex hull, that divide the biplot into sectors, while mega environments draw an ellipse around the environments that share the same sectors. **(D)** A Comparison biplot. Concentric circles plotted around ideal environment, the smaller the circle containing an environment, the more attributes it shares with ideal environment. The smaller circle containing a genotype, the greater is its stability and performance in an ideal environment

those that were non-stressed or winter-sown was 24, 86, 4, and 34%, respectively. On the contrary, HI increased by 80% in the stressed conditions due to less vegetative and more reproductive growth (**Figure 8**).

Analysis of Variance

Analysis of variance revealed that seed yield, biological yield, and plant height were more influenced by genotypic effects than by environment, and GEI indicates the germplasm tested was genetically diverse (**Table 5**). However, most of the variation in SY (58%) remained unexplained. The harvest index was mainly influenced by environment. Total variations measured in seed weight in two environments were 98% attributed to E and GEI (49% each).

Genotypic Selection by Drought Tolerance Indices

The calculation of drought tolerance indices listed the top 10 genotypes exhibiting the highest distinct values for MP, GMP, and STI as CH39/08 (G20), CH40/09 (G19), K-01211 (G12), DG-2017 (G17), K002-10 (G9), 09AG006 (G26), K-01241 (G1), D-13012 (G33), CH15/11 (G27), and K- K-01308 (G2). These are categorized as Group B

TABLE 3 | First four additive main effects and multiplicative interaction (AMMI) selections per environment with mean yield, variance, and score.

Environment	Mean	Variance	Score	1	2	3	4
E5	753.7	48,780	27.99	DCD (G3)	BRC-457 (G11)	CH15/11 (G73)	D-14005 (G10)
E2	312.5	34,556	10.45	CH15/11 (G73)	D-14005 (G10	D-13029 (14)	BRC-457 (G11)
E4	430.6	23,617	2.77	CH28/07 (G48)	CH39/08 (2)	CH10/08 (49)	BRC-457 (G11)
E6	410.2	19,273	-4.89	CH10/08 (49)	D-13029 (14)	CH28/07 (G48)	CH15/11 (G73)
E1	493.4	25,420	-10.34	CH23/00 (64)	*K-01219* (42)	CH3/11 (53)	CH2/11 (52)
E3	397.1	37,473	-25.99	CH28/07 (G48)	CH39/08 (2)	*CM616/10* (41)	CH10/08 (49)

genotypes, indicating that these are the best performers in a non-stressed environment. A ranking of genotypes according to all drought tolerance indices is presented in **Supplementary Table 4**.

On the other hand, the top 10 genotypes with low TOL and SSI were BRC-457 (G35), CM584/09 (G38), DG-2017 (G17), D-13012 (G33), K-01211 (G12), CH39/08 (G20), CH10/08 (G19), CH56/09 (G13), Noor2013 (G11), and CH55/09 (G10). These genotypes are suggested to be the best genotypes specifically adapted to be cultivated in drought-stressed environments with better yield performance, i.e., Group C. Genotypes common to groups B and C are CH39/08 (G20), CH10/08 (G19), K-01211 (G12), and DG-2017 (G17), and thus fit into Group A.

TG12K10 (G6), CM877/10 (G5), TG12K02 (G7), CH15/11 (G27), Pb2008 (G22), K-01248 (G4), D-13011 (G36), DCD (G21), CH61/09 (G14), TG12K-07 (G16), and Noor 2013 (G11) were showing highest TOL and SSI values indicated as the most drought-susceptible genotypes with poor yield performance in drought stress conditions. Among these, TG12K10 (G6), TG12K02 (G7), CH61/09 (G14), CM877/10 (G5), DCD (G21), and D-13011 (G36) showed 68, 47, 35, 49, 34, and 35% yield reduction, respectively, due to drought and ranked 40, 39, 35, 25, 27, and 21 in GMP and STI, and may fall in Group D with other genotypes ranked least in MP, GMP, and STI. Moreover, CH15/11 (G27), K-01248 (G4), and TG12K-07 (G16) showed 35, 35, and 30% yield reduction, in that order, but ranked as 10, 13, and 15 in the GMP ranking list. Listing is based on the yield performance; genotypes are listed as low performing in comparison to other lines in the tested genotypes.

Correlation Among Phenotypes

Evaluation of correlation coefficients showed a positive and significant correlation ($r^2 = 0.30$) between seed yield under non-stress (Yp) and stress (Ys) environments, but the correlation coefficient was very low. A positive and significant correlation of Yp was observed with BY2, HI1, SW1, PH2, MP, GMP, STI, TOL, SSI, and YI. Also noted, Ys had a significant positive correlation with HI2, MP, GMP, STI, YI, and YSI. The correlations of TOL and SSI with Ys were negative and highly significant. Indices MP, GMP, STI, and YI had positive and highly significant correlation with each other; similarly, TOL was positively correlated with SSI. The highest positive correlation was observed between Ys and YI, and the highest negative correlation was observed between SSI and YSI. Seed weight did not show any significant correlations with other phenotypic traits (**Figure 9A**).

Principal Component Biplot Analysis

The principal component analysis simplifies the complex data by transforming the number of correlated variables into a smaller number of variables called principal components.

The principal component biplot (**Figure 9B**) shows that STI, MP, and GMP have a strong positive correlation with Yp and Ys, which indicates that these indices can be used to select high yielding genotypes in both conditions. However YI, YSI had strong positive correlation with Ys only, and this can identify superior genotypes for stressed environments. A strong positive correlation was observed between SSI and TOL. Moreover, SSI and TOL indices revealed a positive correlation with Yp and had a low negative correlation with STI, MP, GMP, and a strong negative correlation with Ys, YI, and YSI. Genotypes far from the origin were those more selectively influenced by these indices, and genotypes near the origin were less likely to be influenced by these indices; for instance, Yp, Ys, and STI, MP, GMP, YI indices selected with more confidence the genotypes CH39/08 (G20), CH40/09 (G19), K-01211 (G12), DG-2017 (G17) as better performer. SSI and TOL identified TG12K10 (G6), G12K02 (7), and K-01216G5 (G8) as the most sensitive to drought.

Ranking of Drought Tolerant Genotypes in Natural and Simulating Stressed and Non-stressed Environments

Top 20 genotypes ranked in Experiments 1 and 2 for natural and simulating stressed and non-stressed environments are presented in **Table 6**. This can provide a broader view of the results obtained in this study and genotypes with consistent performance will be highlighted and selected for future use. Mostly genotypes ranked in both experiments have almost common places like CH39/08, CH40/09, and K-01211 were among the top genotypes in both experiments on the basis of seed yield. Similarly, genotypes TG12K10, TG12K02, and CM877/10 were found poor in producing seed yield in both experiments. Few genotypes behaved differently like DG-2017 was a low-yielding genotype in Punjab, due to severe infection by blight disease caused by *Ascochyta rabiei*, but ranked high in yield performance in Experiment 2.

TABLE 4 | Additive main effects and multiplicative interaction (AMMI) and generalized linear regression model (GLM) analysis of variance of the 80 chickpea genotypes tested across six environments.

Source	Number of primary branches				Number of secondary branches				Plant height (cm)				Number of pods			
	GLM	Var.	AMMI	Var.	GLM	Var.	AMMI	Var.	GLM	Var.	AMMI	Var.	GLM	Var.	AMMI	Var.
	SS	%	SS	%	SS	%	SS	%	SS	%	SS	%	SS	%	SS	%
Genotype (G)	464	12	468	12	2,832	9	2,878	9	33,961	13	33,901	13	51,230	10	50,959	10
Environment (E)	872	23	873	23	15,323	50	15,404	50	49,882	20	50,947	20	232,051	44	234,735	44
G × E	1,851	49	1,864	49	8,478	28	8,602	28	90,199	35	92,578	36	182,482	35	183,380	35
IPCA1	–	–	*1,123*	*29*	–	–	*3,948*	*13*	–	–	*37,984*	*15*	–	–	*67,113*	*13*
IPCA2	–	–	*400*	*10*	–	–	*1,709*	*6*	–	–	*27,496*	*11*	–	–	*43,912*	*8*
Residuals	–	–	*341*	*9*	–	–	*2,945*	*10*	–	–	*27,098*	*10*	–	–	*72,356*	*14*
Error	618	16	604	16	3,728	12	3,644	12	80,869	32	79,053	31	61,621	12	59,918	11
Total	3,804	100	3,822	100	30,362	100	30,612	100	25,4912	100	258,310	100	527,383	100	530,733	100
R-squared (%)	0.84	–	–	–	0.88	–	–	–	0.68	–	–	–	0.88	–	–	–
Source	**Number of seeds**				**100 grain weight (g)**				**Grain yield (g)**				**Drought Score**			
	GLM	Var.	AMMI	Var.	GLM	Var.	AMMI	Var.	GLM	Var.	AMMI	Var.	GLM	Var.	AMMI	Var.
	SS	%	SS	%	SS	%	SS	%	SS	%	SS	%	SS	%	SS	%
Genotype (G)	107,060	14	107,232	14	11,796	22	11,994	23	7,238	16	7,267	16	877	26	882	29
Environment (E)	313,954	40	315,338	40	4,036	8	4,067	8	17,309	38	17,432	38	368	11	399	13
G × E	275,354	35	276,180	35	18,383	35	18,795	35	15,620	34	15,689	34	1,334	39	1,259	41
IPCA1	–	–	*99,119*	*13*	–	–	*6,804*	*13*	–	–	*5,463*	*12*	–	–	*504*	*16*
IPCA2	–	–	*58,093*	*7*	–	–	*4,199*	*8*	–	–	*3,765*	*8*	–	–	*440*	*14*
Residuals	–	–	*118,968*	*15*	–	–	*7,792*	*15*	–	–	*6,461*	*14*	–	–	*316*	*10*
Error	92,680	12	90,561	11	18,284	35	17,880	34	5,291	12	5,153	11	853	25	539	17
Total	789,048	100	791,481	100	52,498	100	53,147	100	45,457	100	45,681	100	3,431	100	3,079	100
R-squared (%)	0.88	–	–	–	0.65	–	–	–	0.88	–	–	–	0.75	–	–	–

Var, variations; NPB, number of primary branches; NSB, number of secondary branches; PH, plant height; NOP, number of pods; NOS, number of seeds; SW, hundred-seed-weight; SY, seed yield; and DRS, drought tolerance score.

TABLE 5 | Analysis of variance (ANOVA) for biological yield (BY), seed yield (SY), harvest index (HI), seed weight (SW), and plant height (PH).

Source	Grain Yield		Biological Yield		Harvest Index		Seed Weight		Plant Height	
	SS	Var.%	SS	Var.%	SS	Var.%	SS	Var.%	SS	Var.%
Genotype (G)	3,504.64	18	4,660,202	75	3,693.39	8	105.063	2	60,098.5	52
Environment (E)	2,792.16	14	512,187	8	39,649.51	83	2,364.438	49	31,536.8	27
G × E	1,841.56	10	613,589	10	4,510.99	9	2,382.437	49	15,986.6	14
Error	11,202.8	58	462,429	7	0	0	0	0	7,606	7
Total	19,341.16	100	6,248,407	100	47,853.89	100	4,851.937	100	115,227.9	100

SS, sum of squares; Var.%, variation (%) of total variations.

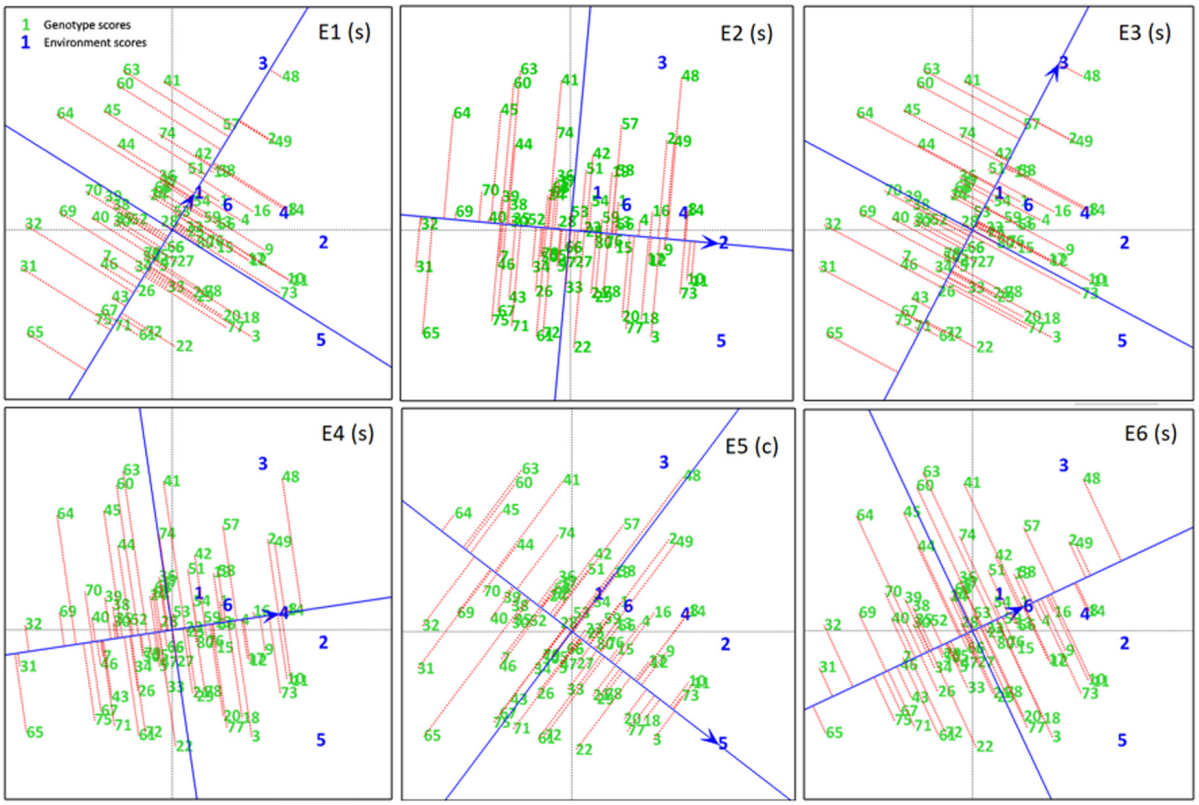
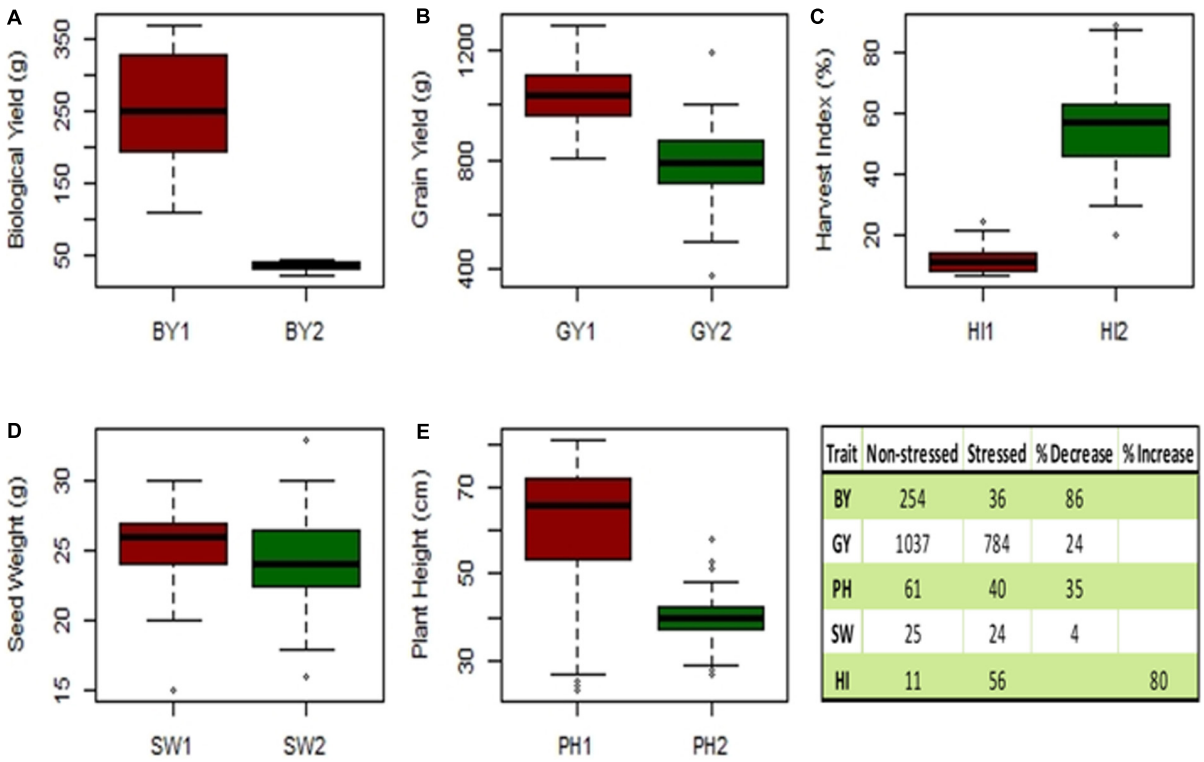


FIGURE 7 | Experiment 1: Ranking Plots of seed yield data of chickpea genotypes across six environments **(E1–E6)**. Arrows on the axis point in the direction of higher means performance of the genotype and consequently rank the genotypes with respect to their performance. Lines projected from the genotypes onto the axes to see that genotypes are ranked in descending order, the length of the line is a measure of genotype stability. Short lines indicate high stability, while long lines indicate low stability.

DISCUSSION

Drought Tolerance Evaluation of Advanced Breeding Lines Under Varying Natural Environments Should Be a Requirement Before Variety Approval

Drought-tolerance evaluation has been one of most studied traits in chickpea, as about 90% of chickpea is grown rainfed and dependent on left-over moisture from rainfall in the soil (Kumar and Abbo, 2001). Over a hundred studies done using drought-imposed yield reduction as a drought-tolerance measure showed significant variations in their results (Daryanto et al., 2015). Therefore, the selection of genotypes to be grown as cultivars needs to be evaluated for compliance with not only their yield under drought-stressed and non-stressed environments but also adaptation to their growing environments. Drought evaluation methods based on small-scale laboratory experiments in pots or tunnels are suitable for studying many drought-tolerance-related traits such as root architecture, vegetative growth rate, etc., but it is often seen that it is difficult, if not impossible, to reproduce laboratory results under field conditions. However, it is crucial to know how environments affect genotypes and, on this basis, to identify environment(s) unsurpassed for genotypes. Many



Trait	Non-stressed	Stressed	%Decrease	%Increase
BY	254	36	86	
GY	1037	784	24	
PH	61	40	35	
SW	25	24	4	
HI	11	56		80

FIGURE 8 | Experiment 2; Box plot of mean data traits of **(A)** *biological yield* (BY), **(B)** *seed yield* (SY), **(C)** *harvest index* (HI), **(D)** *seed weight* (SW), and **(E)** *plant height* (PH). Table has shown the reduction (%) observed in the mean of non-stressed (1) vs. drought-stressed genotypes (2).

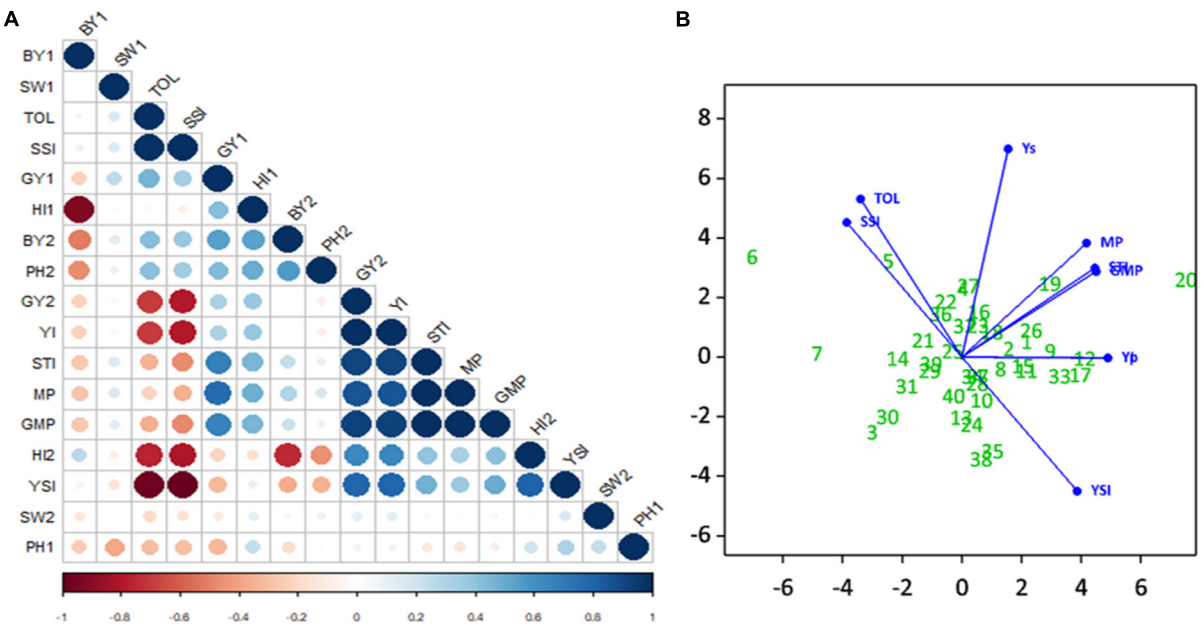


FIGURE 9 | Experiment 2; **(A)** Correlation Matrix of traits and drought stress indices i.e., *biological yield* (BY), *seed weight* (SW), Stress tolerance Index (TOL), Stress Susceptibility Index (SSI), *seed yield* (SY), *harvest index* (HI), Yield Index (YI), Stress Tolerance Index (STI), Mean Productivity Index (MP), and Yield Stability Index under non-stressed (1) and stressed (2) conditions. Positive **correlations** are displayed in blue and **negative correlations** in red color. Color intensity and the size of the circle are proportional to the **correlation coefficients.** In the right side of the **correlogram,** the legend color shows the **correlation coefficients** and the corresponding colors. **(B)** Principle Component Biplot of drought tolerance indices and seed yield under simulating stressed and non-stressed conditions.

TABLE 6 | Top 20 genotypes selected from 2 year's field conditioned drought stress experiments on the basis of AMMI selections, genotype selection indices (GSIs), and drought tolerance indices.

Experiment 1									Experiment 2					
Non-stress			Stress			GSI-Overall			Non-stress			Stress		
Rank	Code	Genotype	Rank	Code	Genotype	Rank	Code	Genotype	Rank	Code	Genotype	Rank	Code	Genotype
1	3	DCD	1	36	*TG12K10*	1	48	CH28/07	1	**20**	**CH39/08**	1	**6**	***TG12K10***
2	11	BRC457	2	37	*K01248*	2	2	CH39/08	2	19	CH40/09	2	5	*CM877/10*
3	73	CH15/11	3	41	K1221	3	11	BRC457	3	12	K-01211	3	7	*TG12K02*
4	10	D14005	4	44	*CM616/10*	4	73	CH15/11	4	17	DG-2017	4	22	Pb2008
5	18	K01216	5	45	K01338	5	3	DCD	5	9	K002-10	5	27	CH15/11
6	77	CH74/10	6	19	K00210	6	10	D14005	6	26	09AG006	6	36	D-13011
7	9	D13036	7	52	CH2/11	7	18	K01216	7	33	D-13012	7	14	CH61/09
8	20	CH55/09	8	54	CH13/11	8	20	CH55/09	8	1	*K-01241*	8	4	*K-01248*
9	22	CH56/09	9	62	PB2000	9	42	K01219	9	2	*K-01308*	9	21	DCD
10	17	D13030	10	64	CH23/00	10	77	CH74/10	10	27	CH15/11	10	16	TG12K-07
11	8	D13012	11	42	K01219	11	57	CH63/11	11	15	CH74/08	11	32	**Bittel-2016**
12	12	D13011	12	53	CH3/11	12	41	*CM616/10*	12	11	**Noor2013**	12	31	D-13036
13	78	BK2011	13	60	CH54/07	13	63	D07509	13	4	*K-01248*	13	39	D-13030
14	14	D13029	14	63	D07509	14	19	K00210	14	16	TG12K-07	14	23	CH49/09
15	29	CH77/08	15	68	CH2016	15	1	CH40/09	15	18	QG-1	15	29	AZC
16	2	CH39/08	16	51	CH1/11	16	49	CH10/08	16	23	CH49/09	16	25	CH28/07
17	76	BKK 2174	17	56	CH28/10	17	74	K850	17	8	K-01216	17	30	NIFA-1
19	1	CH40/09	18	57	CH63/11	18	12	D13011	18	32	**Bittel-2016**	18	3	*K-01242*
22	49	CH10/08	19	13	CH32/10	19	60	CH54/07	19	22	Pb2008	19	18	QG-1
24	56	CH28/10	20	48	CH28/07	20	21	K01211	20	36	D-13011	20	19	CH40/09
29	48	CH28/07	21	58	CH61/10	21	17	D13030	21	37	CH32/10	21	34	D-14005

*Low yielding and **cultivar check** genotypes are in italics and **bold**, respectively. GSI, genotypic selection index.*

studies have been carried out worldwide to evaluate genotype–environment interactions, e.g., Dehghani et al. (2010), Funga et al. (2017), Mohammadi et al. (2017), and Kaloki et al. (2019). In Pakistan. several research articles have been published on the subject, e.g., Arshad et al. (2003), Bakhsh et al. (2006), Atta et al. (2009), and Shah et al. (2020).

Evaluation of Drought Tolerance in Naturally Stressed and Non-stressed Environments

In this study, selected environments were situated in the chickpea growing areas, and most of the chickpea cultivation in Punjab is concentrated on the marginal lands in Thal and Cholistan desert regions. Crop season for chickpea is winter in this region, flowering initiate in February, and most of flowering completes in March and pod setting simultaneously. Weather and moisture conditions in these months are critical for chickpea plant development and determines final yield. Eighty diverse chickpea genotypes were characterized for their drought-stress tolerance in varying natural growth environments, (i) with multi-environment trials in five rainfed areas as the drought-stressed conditions, and irrigated environment as non-stressed conditions, (ii) the 40 best-performing genotypes from multi-environment trials along with checks were re-evaluated for their drought-tolerance in natural field conditions by a spring-sowing experiment as the stressed simulating environment and winter sowing, which is normal growing season in Pakistan as non-stressed environment.

Trellis plots and analysis of variance by both AMMI and GLM models equally established that phenotypic traits GY, NPB, NSB, NOP, and NOS showed significant variations among environments; however, 100 SW and PH were stable, which means that environmental effects were the lowest on these traits. The non-stressed environment fared the best among all, which revealed that rainfed environments have enforced ample drought stress on plants and, hence, hampered their growth. Moreover, drought score measured by visual scoring was also minimum in non-stressed environment (**Figure 3**), thus implying that the difference in phenotypic observations recorded in rainfed environments was due to plants experiencing drought stress; Hintsa and Abay (2013) and Erdemci (2018) also reported similar findings.

A strong high positive correlation in NOP, NOS, and SY was observed. Moreover, SY and NOS were reduced when drought score increased (**Figure 4A**). Seed yield (SY) produced by individual genotypes was higher in the non-stressed environment (E5) compared to the stressed environments (**Figure 5**). Some genotypes performed well in most of the environments; however, some produced the highest mean seed yield at the non-stressed environment (E5). Similarly, some genotypes produced better mean seed yield in stressed environments (**Figure 5**). Previous studies also show that genotype behavior varied across environments (Kendal et al., 2016).

GEI plays an important role in the variable performance of the same genotype in different environments. The presence of strong GEI leads to cross over interactions or reversal of genotype ranks for trait variable such as yield in different environment (Yan and Tinker, 2006). The main effects are changes in the relative response and interaction of the genotypes in different environments. The main effects for genotypes and environment were extracted with AMMI model, which combines standard analysis of variance (ANOVA) with principal component analysis. As per good practice, GLM was applied to our data in addition to AMMI to compare analytical competitiveness of GLM with special software-based AMMI analysis. Also we have used GLM to identify main effects as an alternative to AMMI model. It measures variations contributed by genotypes, environment, and G × E interactions for each response variable by combined ANOVA and linear regression. GGE biplots are useful visualization tools that help identify which genotypes perform best for specific environments, and also which genotypes are more broadly adapted.

Upon GEI analysis, genotypes produced similar yields across environments clustered together. However, environments E4, E6, and E1 shared similar attributes. Environments E4 and E6 elicited weak, whereas E5 (non-stressed environment) elicited strong interactive forces on genotypes. Genotypes CH28/07 (G48) and D-07509 (G63) were influenced by GEI at most. G48 was observed specifically adapted to E3; similarly, D-14005 (G10), BRC-457 (G11), CH15/11 (G73), G18 (K-01216), and CH55/09 (G20) were specifically adapted and positively correlated to the non-stressed environment, i.e., E5. The first four AMMI genotype selections in each environment extracted from the AMMI main effects biplot (**Figure 6A**) are presented in **Table 3**.

The which-one-where biplot of seed yield contained three mega environments (ME), where ME3 consists of only non-stressed environment (**Figure 6C**). The comparison biplot showed that E4 shared more attributes with E5 than with others. Genotypes DCD (G3), CH15/11 (G73), D-14005 (G10), BRC-457 (G11), K-01216 (G18), and CH55/09 (G20) are likely to be ideal genotypes in the ideal environment E5 in terms of achieving higher mean seed yield and good stability showing by low IPCA score (**Figure 6D**). Ranking biplot ranked genotypes in each environment by their yield performance.

There are other manual methods used to establish the stability and yield potential of genotypes in multi-location replicated yield trials. The AMMI stability value (ASV) is a measure to estimate genotype stability; a lower ASV shows how more stable is the genotype (Purchase et al., 2000). However, the stability value may not be the only criteria for selection because stable genotypes may not be performing well in the area of producing seed yield. It was then proposed by Kang (1993) to use a selection criterion that takes into account both yield and stability. The genomic selection index (GSI), proposed by Farshadfar et al. (2011) renamed as "genotype selection index (GSI)" is based on AMMI stability value derived from IPCA sum of squares and scores and can be manually calculated to evaluate genotypes for both yield and stability. A lower value of GSI indicates desirable genotypes with high mean yield and stability. We identified that the GSI ranking is comparable to the AMMI model-based ranking conducted by GenStat software, GenStat-VSN International (2020) (**Supplementary Tables 2**, **3**).

Both identified the same top-most stable and high-yielding genotypes in all environments and ranked the same genotypes as low-yielding in comparison to the mean yield and as relatively less stable.

The AMMI model-based analyses were conducted extensively around the globe. A few references from the past and present that exhibited similar findings are being reviewed here in order to support the work conducted in this study: Bhardwaj et al. (2017), Mohammadi et al. (2017), Maqbool et al. (2017), Mathobo and Marais (2017), Oral et al. (2017), Das et al. (2018), Erdemci (2018), and Oral (2018).

Evaluation of Drought Tolerance in Simulating Stressed and Non-stressed Environments

In Experiment 2, drought stress was imposed due to rise in temperature, decline in humidity, and increased day lengths in spring-sown chickpea. Winter and spring sowings were termed as non-stressed and stressed environments, respectively (Anwar et al., 2003). Winter-sown chickpea experienced a longer vegetative and reproductive period compared to spring-sown chickpea and, hence, produced larger leaf area and BY, which consequently resulted in the reduction in harvest index. Relatively, there are fewer reports about the comparison of chickpea growth in winter and spring sowings than drought-tolerance studies in winter. Our results endorsed the previous findings of Singh et al. (1987, 1998) and Toker et al. (2007).

Analysis of variance revealed that seed yield, biological yield, and plant height were more influenced by genotypic effects than by environment, and GEI indicates the germplasm tested was genetically diverse (**Table 5**).

It is established through many studies, e.g., Fischer and Maurer (1978) and Fernandez (1992), as the pioneer, and more recently, El-Hashash and Agwa (2018) that drought tolerance indices are the best criteria for the selection of discriminating, high-yielding drought-tolerant genotypes.

Results of many studies have also demonstrated that STI, GMP, and MP indices are the most relevant for the selection of drought-tolerant genotypes for both non-stressed and stressed environments as reported by Sanjari and Yazdansepas (2008) and Karimizadeh and Mohammadi (2011). Moreover, Golabadi et al. (2006) demonstrated that low SSI and TOL can also be used for the selection of superior genotypes for drought-prone areas, which can withstand drought stress better than other genotypes with a reasonable seed yield production. In this study, evaluation of correlation coefficients and principal component analysis showed that indices STI, MP, and GMP, due to strong positive correlation with Yp and Ys, can be used to select high-yielding genotypes in both conditions. However, YI and YSI had strong positive correlation with Ys only, and this can identify superior genotypes for stressed environments. The results obtained by principal component analysis confirmed the results obtained from drought-tolerance indices and correlation-based ranking of genotypes. El-Hashash and Agwa (2018) reported similar results.

CONCLUSION AND PROSPECTS

Drought evaluation in rainfed environments or in multi-location trials leads us to conclude that it is important to select superior genotypes with improved yield in a range of environments where these are going to be cultivated. We were able to categorize the genotypes under study into groups according to their performance. We identified genotypes performing differentially well in stressed and non-stressed environments, and those performed consistently well in both environments. Ranks in each environment and GSI will help breeders select genotypes of their choice for further use as variety or pre-breeding germplasm.

Drought stress evaluation in winter- and spring-sown chickpea genotypes proved that a high-grade drought stress was imposed on plants sown in spring, which leads to differentiate clearly the level of stress by looking into the change in growth parameters. Seed yield was set as the drought stress determinant, and we used various mathematical and statistical implications to extract the identification of genotypes performing well in non-stressed and stressed conditions. The results concluded that this strategy was very helpful in identifying high-yielding drought-tolerant genotypes because we found that a few top genotypes identified for each environment in multi-location trials were also on top in the spring-sown drought stress experiments. MP, GMP, and YI indices were more effective in identifying high-yielding cultivars in diverse water scarcity. It was observable that the chickpea germplasm in Pakistan has a reasonable level of genotypic diversity.

Regarding the technical evaluation for drought-tolerance in chickpea, we will recommend that spring-sown imposition of stress is effective in identifying drought-tolerant genotypes with high yield prior to testing them in multi-location trials, which were ultimately required for approving variety with broad and specific adaptability for growing environments. This will preserve the time and resources, which may be considered in a country of limited resources such as Pakistan. It can also be concluded that a breeder may apply a combination of statistical techniques for authentic genotype selection procedure. In the changing climatic scenario, this study provides useful information for agricultural planning, crop modeling, and research directions for development of drought-tolerant legume species to improve adaptation and resilience of agricultural systems in the drought-prone regions of the world.

DATA AVAILABILITY STATEMENT

The original contributions presented in the study are included in the article/**Supplementary Material**, further inquiries can be directed to the corresponding author/s.

AUTHOR CONTRIBUTIONS

AA carried out the planning, execution, and technical guidance of this study, and contributed to the data analysis, the interpretation of results, and the preparation and writing of this manuscript.

NP, MW, and IW contributed to the execution of field experiments, data recording, and analysis. TS provided the material used in this study, managed the out-station trials, and dispensed technical guidance throughout this study. RA contributed to the data analysis and the writing of the manuscript. All the authors contributed to the article and approved the submitted version.

FUNDING

This study was supported by the Agriculture Linkage Program (ALP) Endowment Fund as ALP Project CS-203 (2016-19) at the Pakistan Agricultural Research Council (PARC), Islamabad.

ACKNOWLEDGMENTS

We would like to express our great gratitude to the Pakistan Agriculture Research Council (PARC) and Pulses Research Institute, Faisalabad, Punjab, for sharing the seed material and data from the National and Co-operative Uniform Yield trials of chickpea lines developed by different research institutes from the Federal area (Islamabad) and provinces [Punjab, Khyber Pakhtunkhwa (KPK), and Sindh] with NIAB, Faisalabad, in the year 2016–2017. We are also grateful to the Agriculture Research Institutes, i.e., Adaptive Research Farms (ARF), Karor, District Layyah; Gram Breeding Research Sub-Station (GBRS), Kallurkot; Arid Zone Research Institute (AZRI), Bhakkar; Regional Agricultural Research Institute (RARI), Bahawalpur, and Hasan Mumtaz Research Farms, Bhawana, that graciously provided land and labor for the conduction of field experiments during the year 2017–2018.

SUPPLEMENTARY MATERIAL

The Supplementary Material for this article can be found online at: https://www.frontiersin.org/articles/10.3389/fpls.2020.607869/full#supplementary-material

REFERENCES

Anwar, M. R., McKenzie, B. A., and Hill, G. D. (2003). Water-use efficiency and the effect of water deficits on crop growth and yield of kabuli chickpea (*Cicer arietinum* L.) in a cool temperate sub humid climate. *J. Agric. Sci.* 141, 285–301. doi: 10.1017/s0021859603003630

Arshad, M., Bakhsh, A., Haqqani, A. M., and Bashir, M. H. (2003). Genotype-environment interaction for grain yield in chickpea (*Cicer arietinum* L.). *Pak. J. Bot.* 35, 181–186.

Atta, B., Shah, T. M., Abbas, G., and Haq, M. A. (2009). Genotype x environment interaction for seed yield in kabuli chickpea (*Cicer arietinum L.*) genotypes developed through mutation breeding. *Pak. J. Bot.* 41, 1883–1890.

Bakhsh, A., Arshad, M., and Haqqani, A. M. (2006). Effect of genotype x environment interaction on relationship between grain yield and its components in chickpea (*Cicer arietinum* (L.). *Pak. J. Bot.* 38, 683–690.

Bhardwaj, R. K., Gautam, S. S., and Saxena, R. R. (2017). Assessment of G X E interaction and adaptation of chickpea in chhattisgarh state using AMMI model. *Int. J. Curr. Microbiol. Appl. Sci.* 6, 834–844. doi: 10.20546/ijcmas.2017.607.102

Blum, A. (1996). Crop responses to drought and the interpretation of adaptation. *Plant Growth Reg.* 20, 135–148. doi: 10.1007/bf00024010

Bouslama, M., and Schapaugh, W. T. Jr. (1984). Stress tolerance in soybean. I: evaluation of three screening techniques for heat and drought tolerance. *Crop Sci.* 24, 933–937. doi: 10.2135/cropsci1984.0011183x002400050026x

Clarke, J. M., Towenley-Smith, T. M., McCaig, T. N., and Green, D. G. (1984). Growth analysis of spring wheat cultivars of varying drought resistance. *Crop Sci.* 24, 537–541. doi: 10.2135/cropsci1984.0011183x002400030026x

Crossa, J. (1990). Statistical analyses of multi-location trials. *Adv. Agron.* 44, 55–85. doi: 10.1016/S0065-2113(08)60818-4

Dadon Bar-El, S., Abbo, S., and Reifen, R. (2017). Leveraging traditional crops for better nutrition and health - the case of chickpea. *Trends Food Sci. Technol.* 64, 39–47. doi: 10.1016/J.TIFS.2017.04.002

Daryanto, S., Wang, L., and Jacinthe, P. A. (2015). Global synthesis of drought effects on food legume production. *PLoS One* 10:e0127401. doi: 10.1371/journal.pone.0127401

Das, C. K., Bastia, D., Naik, B. S., Kabat, B., Mohanty, M. R., and Mahapatra, S. S. (2018). GGE biplot and AMMI analysis of grain yield stability and adaptability behaviour of paddy (*Oryza sativa* L.) genotypes under different agroecological zones of Odisha. *ORYZA An Int. J. Rice* 55, 528–542. doi: 10.5958/2249-5266.2018.00076.0

Dehghani, H., Sabaghpour, S. H., and Ebadi, A. (2010). Study of genotype× environment interaction for chickpea yield in Iran. *Agron. J.* 102, 1–8. doi: 10.2134/agronj2009.0156

El Naim, A. M., Ahmed, M. F., and Ibrahim, K. A. (2010). 'Effect of irrigation and cultivar on seed yield, yield's components and harvest index of sesame (*Sesamum indicum* L.). *Res. J. Agric. Biol. Sci.* 6, 492–497.

El-Hashash, E. F., and Agwa, A. M. (2018). Genetic parameters and stress tolerance index for quantitative traits in barley under different drought stress severities. *Asian J. Res. Crop Sci.* 1, 1–16. doi: 10.9734/ajrcs/2018/38702

Erdemci, Ý (2018). Investigation of genotype × environment interaction in chickpea genotypes using AMMI and GGE biplot analysis. *Turk. J. Field Crops* 23, 20–26. doi: 10.17557/tjfc.414846

Falconer, D. S. (1981). *Introduction to Quantitative Genetics*, 2nd Edn. London: Longman Group Ltd, 1–133.

FAOSTAT (2015). Food and Agriculture Data FAOSTAT Provides Free Access to Food and Agriculture Data for over 245 Countries and Territories and Covers all FAO Regional Groupings from 1961 to the Most Recent Year Available. Available online at: http://faostat.fao.org (accessed January 2016).

Farshadfar, E. (2008). Incorporation of AMMI stability value and grain yield in a single non-parametric index (GSI) in bread wheat. *Pak. J. Biol. Sci.* 11, 1791–1796. doi: 10.3923/pjbs.2008.1791.1796

Farshadfar, E., Mahmodi, N., and Yaghotipoor, A. (2011). AMMI stability value and simultaneous estimation of yield and yield stability in bread wheat (*Triticum aestivum* L.). *Aust. J. Crop Sci.* 5, 1837–1844.

Fernandez, G. C. J. (1992). "Effective selection criteria for assessing stress tolerance," in *Proceedings of the International Symposium on Adaptation of VegeTables and Other Food Crops in Temperature and Water Stress*, ed. C. G. Kuo Tainan.

Fischer, R. A., and Maurer, R. (1978). Drought resistance in spring wheat cultivars. I: grain yield response. *Aust. J. Agric. Res.* 29, 897–907. doi: 10.1071/ar9780897

Funga, S., Tadesse, M., Eshete, M., Fikre, A., Korbu, L., Girma, N., et al. (2017). Genotype by environment interaction on yield stability of desi type chickpea (*Cicer arietinum* L.) at major chickpea producing areas of Ethiopia. *Aust. J. Crop Sci.* 11, 212–219.

Gauch, H. G. (1992). *Statistical Analysis of Regional Yield Trials: AMMI Analysis of Factorial Designs*. Amsterdam: Elsevier.

Gauch, H. G. (2006). Statistical analysis of yield trials by AMMI and GGE. *Crop Sci.* 46, 1488–1500. doi: 10.2135/cropsci2005.07-0193

Gauch, H. G., Piepho, H. P., and Annicchiarico, P. (2008). Statistical analysis of yield trials by AMMI and GGE: further considerations. *Crop Sci.* 48, 866–889. doi: 10.2135/cropsci2007.09.0513

Gavuzzi, P., Rizza, F., Palumbo, M., Campaline, R. G., Ricciardi, G. L., and Borghi, B. (1997). Evaluation offield and laboratory predictors of drought and heat tolerance in winter cereals. *Can. J. Plant Sci.* 77, 523–531. doi: 10.4141/p96-130

GenStat-VSN International (2020). *Genstat for Windows*. 21st Edn. Hemel Hempstead: VSN International. Web page: Genstat.co.uk

Golabadi, M., Arzani, A., and Maibody, S. A. M. (2006). Assessment of drought tolerance in segregating populations in durum wheat. *Afr. J. Agric. Res.* 5, 162–171.

Government of Pakistan [GOP] (2016). *Agricultural Statistics of Pakistan. Ministry of Food, Agriculture and Live Stock, Govt of Pakistan. Food and Agri. Divi (Planning unit) Islamabad*. Islamabad: Government of Pakistan.

Hintsa, G., and Abay, F. (2013). Evaluation of bread wheat varieties for their adaptability in wheat growing areas of Tigray region, northern Ethiopia. *J. Biodivers. Endanger. Species* 1, 12–18.

Kaloki, P., Trethowan, R., and Tan, D. K. (2019). Effect of genotype× environment× management interactions on chickpea phenotypic stability. *Crop Pasture Sci.* 70, 453–462. doi: 10.1071/cp18547

Kang, M. S. (1993). Simultaneous selection for yield and stability in crop performance trials: consequences for growers. *Agron. J.* 85, 754–757. doi: 10.2134/agronj1993.00021962008500030042x

Karimizadeh, R., and Mohammadi, M. (2011). Association of canopy temperature depression with yield of durum wheat genotypes under supplementary irrigated and rainfed conditions. *Aust. J. Crop Sci.* 5, 138–146.

Kendal, E., Sayar, M. S., and Tekdal, S. (2016). Assessment of the impact of ecological factors on yield and quality parameters in triticale using GGE biplot and AMMI analysis. *Pak. J. Bot.* 48, 1903–1191.

Kumar, J., and Abbo, S. (2001). Genetics of flowering time in chickpea and its bearing on productivity in semiarid environments. *Adv. Agron.* 72, 107–138. doi: 10.1016/s0065-2113(01)72012-3

Ludlow, M. M., and Muchow, R. C. (1990). A critical evaluation of traits for improving crop yields in water limited environments. *Adv. Agron.* 43, 107–153. doi: 10.1016/s0065-2113(08)60477-0

Maqbool, M. A., Aslam, M., and Ali, H. (2017). Breeding for improved drought tolerance in Chickpea (*Cicer arietinum* L.). *Plant Breeding.* 136, 300–318. doi: 10.1111/pbr.12477

Mathobo, R., and Marais, D. (2017). Evaluation of genotype x environment interaction using GGE-biplot on dry beans (*Phaseolus vulgaris* L.) in Limpopo province of South Africa. *Aust. J. Crop Sci.* 11, 506–515. doi: 10.21475/ajcs.17.11.05.p303

Misra, G., Joshi-Saha, A., Salaskar, D., Reddy, K. S., Dixit, G. P., Srivastava, A. K., et al. (2020). Baseline status and effect of genotype, environment and genotype× environment interactions on iron and zinc content in Indian chickpeas (*Cicer arietinum* L.). *Euphytica* 216, 1–16. doi: 10.1002/9781118912591.ch1

Mohammadi, R., Armion, M., Zadhasan, E., Ahmadi, M. M., and Amri, A. (2017). The use of AMMI model for interpreting genotype x environment interaction in durum wheat. *Exp. Agric.* 54, 670–683. doi: 10.1017/s0014479717000308

Nisa, Z. U., Arif, A., Waheed, M. Q., Shah, T. M., Iqbal, A., Siddiqui, A. J., et al. (2020). A comparative metabolomic study on desi and kabuli chickpea (*Cicer arietinum* L.) genotypes under rainfed and irrigated field conditions. *Sci. Rep.* 10:13919.

Olsson, U. (2002). *Generalized Linear Models – An Applied Approach*. Lund: Student literature.

Oral, E. (2018). Effect of nitrogen fertilization levels on grain yield and yield components in triticale based on AMMI and GGE biplot analysis. *Appl. Ecol. Environ. Res.* 16, 4865–4878. doi: 10.15666/aeer/1604_48654878

Oral, E., Çifçi, V., Kendal, E., and Doðan, Y. (2017). Some Chickpea (*Cicer arietinum* L.) Varieties Relations Betwen Features Correlation and Path Analysis.". *J. Institute Sci. Technol.* 7, 279–284. doi: 10.21597/jist.2017.186

Pouresmael, M., Kanouni, H., Hajihasani, M., Astraki, H., Mirakhorli, A., Nasrollahi, M., et al. (2018). Stability of chickpea (*Cicer arietinum* L.) landraces in national plant gene bank of Iran for drylands. *J. Agric. Sci. Technol.* 20, 387–400.

Purchase, J. L., Hattingh, H., and Van Deventer, C. S. (2000). Genotype × environment interaction of winter wheat (*Triticum aestivum* L.) in South Africa: II. Stability analysis of yield performance. *S. Afr. J. Plant Soil* 17, 101–107. doi: 10.1080/02571862.2000.10634878

Rafiq, C. M., Mahmood, M. T., Ahmed, M., Ali, I., Shafiq, M., Rasool, I., et al. (2018). Exploration of genetic divergence and performance of morpho-agronomic traits of chickpea. *Sci. Technol. Dev.* 37, 202–208.

Richards, M. F., Preston, A. L., Napier, T., Jenkins, L., and Maphosa, L. (2020). Sowing date affects the timing and duration of key chickpea (*Cicer arietinum* L.) growth phases. *Plants* 9:1257. doi: 10.3390/plants9101257

Rosielle, A. A., and Hamblin, J. (1981). Theoretical aspects of selection for yield in stress and non stress environments. *Crop Sci.* 21, 943–946. doi: 10.2135/cropsci1981.0011183x002100060033x

Sanjari, P. A., and Yazdansepas, A. (2008). Evaluation of wheat (*T. aestivum* L.) under pre and post anthesis drought stress conditions. *J. Agric. Sci. Technol.* 10, 109–121.

Saxena, N. P. (1984). "Chickpea," in *The Physiology of Tropical Field Crops*, eds P. R. Goldsworthy and N. M. Fisher (New Jersey, NJ: John Wiley & Sons Ltd.), 419–452.

Shah, T. M., Imran, M., Atta, B. M., Ashraf, M. Y., Hameed, A., Waqar, I., et al. (2020). Selection and screening of drought tolerant high yielding chickpea genotypes based on physio-biochemical indices and multi-environmental yield trials. *BMC Plant Biol.* 20:171. doi: 10.1186/s12870-020-02381-9

Singh, D. P., Chaudhary, B. D., Pannu, R. K., Singh, D., and Shawney, V. (1998). Agronomic, Physiological and breeding strategies for improving drought tolerance and productivity of dryland chickpea in North India. *Ann. Agri Bio Res.* 3, 71–86.

Singh, K. B., Malhotra, R. S., and Respana, B. L. (1987). Inheritance of yield and its components in chickpea, *Gicer arietinum* L. *Indian J. Heredity*. 19, 30–38.

Soltani, A., Ghassemi-Golezani, K., Rahimzadeh-Khooie, F., and Moghaddam, M. (1999). A simple model for chickpea growth and yield. *Field Crops Res.* 62, 213–224. doi: 10.1016/s0378-4290(99)00017-9

Summerfield, R. J., and Wien, H. C. (1980). "Effects of photoperiod and air temperature on growth and yield of economic legumes," in *Advances in Legume Science*, eds R. J. Summerfield and A. H. Bunting (Richmond: Ministry of Agriculture, Fisheries and Food) 17–36.

Toker, C., and Cagirgan, M. (1998). Assessment of response to drought stress of chickpea (*Cicer arietinum* L.) lines under rainfed conditions. *Turkish J. Agric. For.* 22, 615–621.

Toker, C., Canci, H., and Yildirim, T. (2007). Evaluation of perennial wild *Cicer* species for drought resistance. *Genet. Resour. Crop Evol.* 54, 1781–1786. doi: 10.1007/s10722-006-9197-y

Velu, G., and Shunmugavalli, N. (2005). *Genotype X Environment Interaction in Sesame (Sesamum indicum L.), Sesame and Safflower News*. 20, 1–5.

Yan, W., and Tinker, N. A. (2006). Biplot analysis of multi-environment trial data: principles and applications. *Can. J. Plant Sci.* 86, 623–645. doi: 10.4141/p05-169

Yan, W. K., Kang, M. S., Ma, B., Woods, S., and Cornelius, P. L. (2007). GGE biplot vs. AMMI analysis of genotype-by-environment data. *Crop Sci.* 47, 641–653.

Yang, J., Kloepper, J. W., and Ryu, C.-M. (2009). Rhizosphere bacteria help plants tolerate abiotic stress. *Trends Plant Sci.* 14, 1–4. doi: 10.1016/j.tplants.2008.10.004

Conflict of Interest: The authors declare that the research was conducted in the absence of any commercial or financial relationships that could be construed as a potential conflict of interest.

Copyright © 2021 Arif, Parveen, Waheed, Atif, Waqar and Shah. This is an open-access article distributed under the terms of the Creative Commons Attribution License (CC BY). The use, distribution or reproduction in other forums is permitted, provided the original author(s) and the copyright owner(s) are credited and that the original publication in this journal is cited, in accordance with accepted academic practice. No use, distribution or reproduction is permitted which does not comply with these terms.

frontiers in Plant Science

ORIGINAL RESEARCH
published: 18 February 2021
doi: 10.3389/fpls.2020.632919

Induction of Acquired Tolerance Through Gradual Progression of Drought Is the Key for Maintenance of Spikelet Fertility and Yield in Rice Under Semi-irrigated Aerobic Conditions

*V. S. Lekshmy[1], Preethi Vijayaraghavareddy[1,2], A. N. Nagashree[1], Vemanna S. Ramu[3], Venkategowda Ramegowda[1], Udayakumar Makarla[1] and Sheshshayee Sreeman[1]**

[1] Department of Crop Physiology, University of Agricultural Sciences, Bengaluru, India, [2] Department of Plant Sciences, Centre for Crop Systems Analysis, Wageningen University & Research, Wageningen, Netherlands, [3] Regional Centre for Biotechnology, Faridabad, India

Plants have evolved several adaptive mechanisms to cope with water-limited conditions. While most of them are through constitutive traits, certain "acquired tolerance" traits also provide significant improvement in drought adaptation. Most abiotic stresses, especially drought, show a gradual progression of stress and hence provide an opportunity to upregulate specific protective mechanisms collectively referred to as "acquired tolerance" traits. Here, we demonstrate a significant genetic variability in acquired tolerance traits among rice germplasm accessions after standardizing a novel gradual stress progress protocol. Two contrasting genotypes, BPT 5204 (drought susceptible) and AC 39000 (tolerant), were used to standardize methodology for capturing acquired tolerance traits at seedling phase. Seedlings exposed to gradual progression of stress showed higher recovery with low free radical accumulation in both the genotypes compared to rapid stress. Further, the gradual stress progression protocol was used to examine the role of acquired tolerance at flowering phase using a set of 17 diverse rice genotypes. Significant diversity in free radical production and scavenging was observed among these genotypes. Association of these parameters with yield attributes showed that genotypes that managed free radical levels in cells were able to maintain high spikelet fertility and hence yield under stress. This study, besides emphasizing the importance of acquired tolerance, explains a high throughput phenotyping approach that significantly overcomes methodological constraints in assessing genetic variability in this important drought adaptive mechanism.

Keywords: acquired tolerance traits, reactive oxygen species, gradual stress, rice, reactive carbonyls

OPEN ACCESS

Edited by:
Raul Antonio Sperotto, Universidade do Vale do Taquari – Univates, Brazil

Reviewed by:
Suriyan Cha-um, National Science and Technology Development Agency (NSTDA), Thailand
Kazuo Nakashima, Japan International Research Center for Agricultural Sciences (JIRCAS), Japan

***Correspondence:**
Sheshshayee Sreeman
msshesh1@uasbangalore.edu.in

Specialty section:
This article was submitted to Plant Abiotic Stress, a section of the journal Frontiers in Plant Science

Received: *24 November 2020*
Accepted: *22 December 2020*
Published: *18 February 2021*

Citation:
Lekshmy VS, Vijayaraghavareddy P, Nagashree AN, Ramu VS, Ramegowda V, Makarla U and Sreeman S (2021) Induction of Acquired Tolerance Through Gradual Progression of Drought Is the Key for Maintenance of Spikelet Fertility and Yield in Rice Under Semi-irrigated Aerobic Conditions. Front. Plant Sci. 11:632919. doi: 10.3389/fpls.2020.632919

INTRODUCTION

Rice (*Oryza sativa* L.), the most important staple cereal, accounts for more than half the water used in agriculture and represents a highly unsustainable practice in the face of climate change and water shortages (Basha et al., 2016; Kogan et al., 2019). Thus, cultivating rice with low water input to save water is quite essential, and it can only happen when the water requirement for a given yield potential is reduced (Foley et al., 2011). A strategic selection of relevant physiological traits for crop improvement and an appropriate agronomy of rice cultivation are needed to achieve the combined goal of sustaining productivity and saving irrigation water (Lambrecht et al., 2016; Sheshshayee et al., 2018). Semi-irrigated aerobic cultivation is one among several promising water-saving practices developed (Bouman et al., 2005; Nie et al., 2012). This method, with its periodic surface irrigation, has been shown to save around 50% of irrigation water. However, a water-limiting situation arises between episodes of irrigation, which reduces the yield potential despite the water saving advantage (Fereres and Soriano, 2007). Therefore, evolving appropriate rice cultivars well-suited to the aerobic conditions and with a sustained, if not increased, productivity is the most important need of the day.

Significant progress has been made in identifying specific relevant physiological traits that impart drought tolerance for improving productivity under water-limited conditions. The relevance of root traits (Abd Allah et al., 2010; Comas et al., 2013; Uga et al., 2015), water use efficiency (Richards et al., 2002; Sheshshayee et al., 2003; Blum, 2017; Dey et al., 2019), radiation use efficiency (Adeboye et al., 2016; Hao et al., 2016), etc. have been well established. However, lack of high throughput and accurate phenotyping options has often been quoted as one of the major reasons for the low pace of adoption of breeding for physiological traits. Furthermore, a comprehensive improvement in drought adaptation is possible only when several relevant traits are combined into the same genotype (Raju et al., 2014; Sheshshayee et al., 2018; Dharmappa et al., 2019). Three categories of traits operating at morphological, physiological, and cellular level would be needed for a comprehensive improvement in drought adaptation (Collins et al., 2008; Sheshshayee et al., 2018). While morphological and physiological traits such as canopy and root architecture, metabolic rates, biomass partitioning, reproductive growth, phenology etc. are constitutive and integral in nature (Haling et al., 2010; Sheshshayee et al., 2018), plants require several cellular level processes to maintain tissue turgor as well as metabolism collectively referred to as "adaptive" traits or "acquired tolerance" traits (Collins et al., 2008; Vijayaraghavareddy et al., 2020a). Most of the recent trait-based breeding efforts have so far attempted to improve or introgress constitutive traits. Although this strategy has great promise, combining these with acquired tolerance has greater relevance in achieving a comprehensive improvement in drought adaptation as well as productivity under water-limiting conditions.

Unlike constitutive traits, the acquired tolerance traits are expressed only upon exposure to stress (Sung et al., 2003; Senthil-kumar et al., 2007). Abiotic stresses, like soil moisture stress, develops progressively, and the rate of stress development generally depends on the prevailing weather conditions and soil texture (Ferrante and Mariani, 2018). Thus, plants initially experience a milder stress level, which can trigger the expression of acquired tolerance traits. This phenomenon would be extremely important, especially under rain-fed conditions. It is also known that significant genetic variability exists in the ability to respond to mild stress among several crop species (Clauw et al., 2016). That is, a genotype with greater propensity to respond to mild stress would have a higher level of adaptability subsequently if the stress level gets severe. Raju et al. (2014) demonstrated that genotypes with higher acquired tolerance in the background of sufficiently high constitutive traits showed a better field level adaptation.

Having recognized the importance of acquired tolerance traits, significant global initiatives led to the enumeration of several mechanisms and processes that govern them. Among several mechanisms, preventing the generation and scavenging the reactive oxygen species (ROS) and reactive carbonyl compounds (RCCs) appear to be the most prominent and relevant acquired tolerance response (Nisarga et al., 2017; Vemanna et al., 2020). Although under normal conditions also a low to moderate level of ROS and RCCs would be needed to maintain cellular signaling (Zhang et al., 2016), an imbalance between the production of ROS, RCCs, and their scavenging through antioxidant systems take center stage that determines the tolerance or susceptibility of a plant to stress (McCord, 2000; Vemanna et al., 2020). The ROS and RCC scavenging mechanisms are significantly upregulated when stress is mild, which protect cellular metabolism when stress becomes severe or lethal (Kumar et al., 1999; Senthil-kumar et al., 2003; Vidya et al., 2017). Based on the hypothesis that plants get primed during exposure to milder stress levels, a temperature induction response (TIR) technique was developed using germinated seedlings (Uma et al., 1995; Senthil-kumar et al., 2003; Vidya et al., 2017). However, capturing the variability in drought induction response has remained a challenge. The novel drought-simulator phenomics platform established at the Department of Crop Physiology, University of Agricultural Sciences, Bengaluru, India, with its automated transpiration-interfaced irrigation compliance, is capable of creating and maintaining a specific soil moisture status in the soil (Vijayaraghavareddy et al., 2020a).

Although these findings helped to understand acquired tolerance, lack of high throughput phenotyping made it difficult to validate this approach in different physiological phases of plants. Here, we standardize the methodology for capturing acquired tolerance traits at seedling phase in two contrasting genotypes of rice for drought using high throughput phenomics facility. Further, the role of oxidative stress management strategies associated with ROS and RCC scavenging mechanisms was examined as a potential measure of acquired tolerance in rice. We demonstrate a significant genetic variability in the acquired tolerance response to a gradually imposed stress protocol. Genotypes with superior acquired tolerance capacity maintain higher spikelet fertility and, hence, grain yields under drought stress.

MATERIALS AND METHODS

Plant Material and Stress Treatment

Maintaining similar moisture status for all genotypes, irrespective of differences in their transpiration rates, is a prerequisite for the phenotyping of acquired tolerance traits. To evaluate the acquired tolerance mechanisms in rice, two experiments were conducted at the drought-simulator phenomics facility established at the Department of Crop Physiology, University of Agricultural Sciences, Bengaluru, India (12°58′N, 77°35′E). The first experiment was to capture stress response of rapid and gradually stressed plants using two well-characterized contrasting rice genotypes for drought stress response, viz., drought-sensitive BPT 5204 and tolerant AC 39000 (Pushpa, 2016). In the second experiment, the drought responses and acquired tolerance were screened among 17 diverse genotypes at flowering phase.

Drought Imposition Protocol

The mini-lysimeter drought stimulator facility established at our center is designed to create gradual stress levels through the transpiration-interfaced automated irrigation system that mimics the natural environment condition. The facility is capable of gravimetrically determining the evapotranspiration of pot grown plants on a "real-time" basis. The automated irrigation system replenishes accurate volumes of water as and when the moisture status of soil decreases to 1.5% of the set field capacity (FC). A user-defined "dry-down" protocol ensures stress progression to mimic a real field-like situation (Vijayaraghavareddy et al., 2020a). The most prominent feature of this facility is its ability to ensure exactly the same level of soil moisture regime for plants irrespective of differences in leaf area and transpiration. Hence, this facility is most suited to capture acquired mechanisms at different growth phases.

EXPERIMENT 1: STRESS IMPOSITION AT SEEDLING STAGE IN CONTRASTING RICE GENOTYPES

Stress imposition was initiated on the 15th day after sowing for the two contrasting rice genotypes. Containers of 10-L capacity were filled with rooting mixture [red sandy loam soil and farm yard manure (FYM) in 3:1 ratio] were used for this study. Three treatments were created using phenomics platform:

1. Control: Plants were maintained at 100% FC throughout the experiment.

2. Rapid stress (RS): Rapid drought imposition was achieved by cessation of watering until the soil moisture reached to 50% FC.

3. Gradual stress (GS): The user defined protocol was tuned to reduce 5% of soil moisture per day.

After reaching 50% FC, both gradual and rapid stress plants were maintained at the same water status for a week (**Figures 1A–D** and **Supplementary Figure 1**). Four replicates were maintained per treatment, and all the pots were arranged in completely randomized design. Leaf samples were collected 5 days after stress level attained 50% FC for quantifying physiological traits.

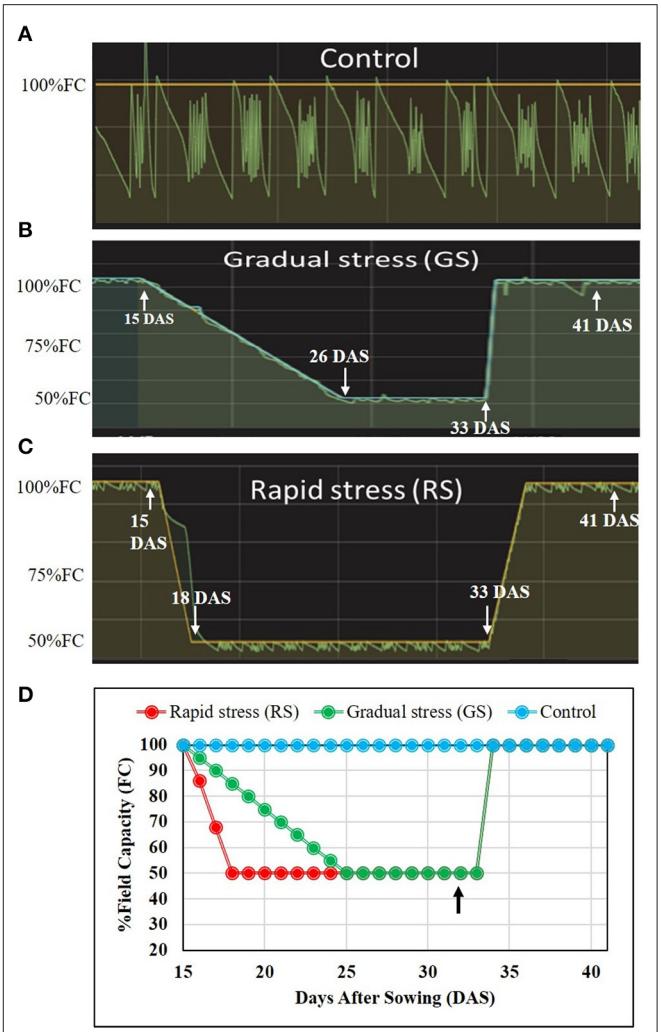


FIGURE 1 | Graphical representation of the dry down protocol for stress imposing protocol in two rice genotypes. Fifteen-day-old plants were subjected to drought stress using the transpiration interfaced mini-lysimeter facility. **(A)** Control, plants maintained at 100% field capacity (FC) throughout the experiment. **(B)** The gradual stress using the dry-down protocol with 5% reduction in FC per day to achieve 50% FC. **(C)** Rapidly stressed plants where stress reaches to 50% FC within 3 days. The soil moisture was elevated to 100% FC at 33 days after sowing (DAS). **(D)** Representation of all the three different treatments, with an arrow indicating point at which samples were collected from all the three treatments.

On the 7th day after stress reached 50% FC, soil water status was elevated to 100% FC, and plants were allowed to recover. Morphophysiological parameters such as total leaf area (TLA) and biomass were measured a week after recovery.

Relative Water Content (%)

Relative water content (RWC) at different stress levels were measured according to the method described by Tambussi et al. (2005). Fully expanded fresh leaves of equal size were weighed to record the fresh weight (FW). The leaves were immersed in deionized water and incubated for 5 h, and later, the saturation weight (SW) of the leaves was measured by removing the surface

water gently with a tissue paper. The samples were finally oven dried at 80°C to a constant dry weight (DW). RWC was calculated as:

$$\text{RWC}\,(\%) = \frac{(\text{FW} - \text{DW})}{(\text{SW} - \text{DW})} \times 100$$

Total Chlorophyll Estimation

Chlorophyll from the weighed leaf (0.1 g) was extracted by placing it in a known volume of acetone and dimethyl sulfoxide (DMSO) (1:1) solution until the tissue was fully decolorized. The absorbance of the solution was taken using a spectrophotometer at 645 nm and 663 nm with acetone/DMSO (1:1) as the blank (Arnon, 1949). Chlorophyll content was calculated using the following formula and expressed as mg g^{-1} fresh weight.

$$\text{Chl a} = \frac{(12.7\ \text{X A663}) - (2.54\ \text{X A645})}{\text{W} \times 1000} \times \text{V}$$

$$\text{Chl b} = \frac{(22.9\ \text{X A645})\ (4.68\ \text{X A663})}{\text{W} \times 1000} \times \text{V}$$

$$\text{Total chlorophyll} = \text{Chl a} + \text{Chl b}$$

where W is the weight of the leaf sample, V is the volume made, and A663 and A645 represents the absorbance measured at 663 and 645 nm.

Thermal Imaging

The leaf temperature was measured in control, gradual, and rapid stressed plants using the VarioCAM® high-resolution imaging system, long-wave infrared camera (spectral range of 7.5–14 μm), having a spatial resolution of 640 × 480 pixels, accuracy of ± 1.5 K (0–100°C) or ±2 of reading and temperature range from −40 to +1,200°C. All the measurements were made from the same distance. Images were analyzed using thermographic software IRBIS® remote 3.0* (Jenoptic, Germany). The leaf areas of interest from each image were outlined using imager's software for estimating average leaf temperature.

Quantification of Superoxide, Hydrogen Peroxide, and Hydroxyl Radicals

Quantification of superoxide (O_2^-) and hydrogen Peroxide (H_2O_2) was carried out using nitro blue tetrazolium chloride (NBT) and *diaminobenzedine* (DAB) staining assays, respectively, as described by Kumar et al. (2014). Deoxyribose assay (Aruoma, 1994) was adopted to quantify hydroxyl radicals ($^{\bullet}OH$). The concentration of these free radical was expressed as absorbance × 1,000.

Schiff Base Method for Quantifying Lipid Peroxidation

Aldehyde produced as result of lipid peroxidation was visualized using the Schiff base assay (Aswathi et al., 2018). Excised leaf tissues were immediate immersed into the test tube containing 5 ml of 10% (v/v) Schiff's reagent solution. The tissue samples dipped in Schiff's reagent were vacuum infiltrated for an hour and then rinsed with distilled water to remove the stain adhered to the tissue surface. For the proper visualization of the staining, the chlorophyll was removed using the bleaching solution [acetic acid/glycerol/ethanol (1:1:3, v/v/v) solution]. Further, samples were carefully mounted on the slide, and photographs were taken under a microscope at 10× magnification.

Extraction and Quantification of Malondialdehyde, Methylglyoxal, and Amadori Product

Plant samples (0.1 g) obtained from each of the stress and control replicates were immersed in liquid nitrogen. The samples were homogenized with 5% (w/v) trichloro acetic (TCA) and centrifuged at 12,000 rpm for 15 min at 4°C. The supernatant was used to determine malondialdehyde (MDA) concentrations using an ultraviolet–visible spectrophotometer using Nisarga et al. (2017) method. The concentration of methylglyoxal (MG) was calculated by homogenizing the plant sample into a known amount of distilled water in accordance with Nareshkumar et al. (2020). The Amadori products were measured according to the methods described by Nisarga et al. (2017).

Quantification of Membrane Damage by the Evans Blue Technique

Leaf samples collected from control and stress were immersed in 0.25 g Evans blue solution prepared in $CaCl_2$ (0.1 M, pH 5.6) and incubated for 1 h. To remove the unbound dye on the surface, the samples were rinsed thoroughly with water. Further, the samples were treated with 1% sodium dodecyl sulfate (SDS) to release the bound dye from the cell, and absorbance was recorded at 600 nm (Vijayaraghavareddy et al., 2017).

Quantification of Total Antioxidant Capacity

The total antioxidant capacity of the samples collected during the stress was quantified using the phosphomolybdenum method (Prieto et al., 1999). The fresh leaf sample (0.5 mg ml^{-1}) extracted in 50% ethanol was mixed with the reagent solution containing 0.6 M H_2SO_4, 28 mM sodium phosphate, and 4 mM ammonium molybdate in 1:3 ratios. After incubating at 95°C for 150 min, the mixture was cooled immediately to room temperature. The reagent solution (4 ml), without the sample extract, incubated at the same conditions, was used as blank. Total antioxidant capacity (TAC) was measured spectrometrically at A695 nm, and values were expressed as equivalents of tannic acid (TAE).

Quantification of Proline Content

Proline osmotic stress marker was estimated based on the protocol by Bates (1973). Leaf tissues (0.1 g) of both stressed and non-stressed seedlings were separately homogenized with 5 ml of 3% sulfosalicylic acid. Supernatants were collected by centrifugation at 12,000 rpm for 15 min for the estimation. To the 2 mL of supernatant, equal amounts of acid ninhydrin and glacial acetic acid were added. After boiling the mixture at 100°C for 1 h, samples were frozen in ice to terminate

the reaction. Toluene (4 ml) was added to this mixture and vortexed vigorously for a few seconds. The mixture was then allowed to settle, and absorbance of the colored upper layer was read at 520 nm. The proline content was calculated separately with the help of a standard curve and expressed as $\mu g\ g^{-1}$ fresh weight.

Morphophysiological Parameters

Total leaf area (TLA) was measured by specific leaf area (SLA) method. SLA was calculated by measuring leaf area of three representative leaves from the plants as described by Reddy et al. (2020). TLA was calculated by multiplying total leaf weight with SLA. Total biomass was measured a week after recovery. Stem, leaves, and roots were separated and oven dried at 80°C for 3 days. Total leaf, stem, and root weight was computed to arrive at total biomass.

RNA Extraction

To assess the expression levels of genes involved in scavenging mechanism, the total RNA was extracted from the leaves harvested from control, gradual, and rapidly stressed seedlings using the phenol–chloroform method (Datta et al., 1989). The quality and quantity of RNA was confirmed at A260/280 and A260/230 wavelength ratios using the NanoDrop® ND-1000 spectrophotometer. Complementary DNA (cDNA) was synthesized from the total RNA using oligo (dT) primers by M-MLV reverse transcriptase mediated reverse transcription. Quantitative RT-PCR reaction was carried out using iQ5 real-time PCR detection system (Bio-Rad) with a final volume of 20 µl using the TAKARA SYBR Green qPCR Kit. The PCR program was conducted with the following cycling conditions: 94°C for 3 min followed by a 25-cycle program (94°C, 30 s; 52–58°C, 30 s; 72°C, 40 s, and 72°C, 5 min per cycle). Ubiquitin was used as the endogenous reference gene to normalize the data. The relative expression of the scavenging genes (primer details are given in **Supplementary Table 1**) was estimated using $2^{-\Delta\Delta CT}$ method (Livak and Schmittgen, 2001; Yoo et al., 2017; Çelik et al., 2019; Rauf et al., 2019).

EXPERIMENT 2

Gradual moisture stress was imposed to 17 selected germplasm lines with similar phenology at flowering (85DAS) (**Supplementary Table 2**) during the Kharif season of 2019 to confirm the trait diversity, particularly for acquired tolerance traits. Phenotyping for acquired tolerance traits was carried out by raising the plants in mini-lysimeter drought-simulator platform. Experiment was carried out in 20-L capacity containers filled with red sandy loam soil and farm yard manure in 3:1 ratio. Three replicates each for control (100% FC) and gradual stress treatment were maintained per genotype, and all the pots were arranged in completely randomized design. A similar induction protocol, as described above, was followed with 5% reduction in soil moisture status per day. The dry down protocol was initiated at 5 days before flowering (80DAS) (during the booting stage). Plants reached 50% FC on the 10th day after stress imposition (90DAS). Plants were maintained at 50% FC for 1 week, and later, the stressed containers were brought back to 100% FC and continued till maturity. However, a set of plants were also raised in similar containers and maintained at 100% FC, as control. During stress, leaf samples from both stressed and control plants were collected and the ROS (superoxide, hydrogen peroxide), MDA content, total antioxidants, and proline content were quantified using the protocol described above. At harvest, shoot, leaves, and roots were separated and oven dried at 65°C for 3 days, and weighed values were computed to obtain the total biomass. The total numbers of filled grains and chaffy grains were counted manually to arrive at spikelet fertility.

$$\text{Spikelet fertility}\ (\%) = \frac{\text{number of filled grains}}{\text{total number of grains}} \times 100$$

Statistical Analysis

All data were analyzed to check for statistical significance using the software GENSTAT Ver. 12.1(http://www.genstat.co.uk/). To reveal differences between cultivars and between treatments, a two-way analysis of variance was carried out. Pearson's correlation coefficients were determined using r corr package in R version 4.0.3 (https://www.r-project.org/).

RESULT

Differences in Stress Response in Two Contrasting Rice Genotypes

The leaf relative water content (RWC) of both the contrasting genotypes, BPT 5204 and AC 39000, decreased significantly under stress (**Figure 2A**). Interestingly, the chlorophyll content marginally increased in both the genotypes under gradual stress treatment, while it significantly decreased in rapid stress treatment (**Figure 2B**). The moisture stress tolerant AC 39000 showed only a 15.7% reduction in total chlorophyll, while the corresponding reduction was 40.5% in BPT 5204 under RS compared to their respective controls (**Figure 2B**).

Leaf temperature increased significantly under stress in both the genotypes (**Figure 2C**), and the extent of increase in leaf temperature was less when the stress progressed gradually. Between the genotypes, the stress tolerant genotype, AC 39000, maintained a significantly cooler canopy, compared with BPT 5204.

Gradual Stress Primes the Plant for Better Management of ROS and RCCs Under Severe Stress

Levels of ROS such as H_2O_2, O_2^-, and $^{\bullet}OH$ radicals were significantly increased when plants were exposed to moisture stress. Increase in ROS levels was remarkably less when plants were gradually stressed (**Figures 3A–C**), indicating a better management of ROS levels when stress progressed gradually. The images of the staining procedure for quantification of ROS are given in **Supplementary Figure 2**. All ROS were significantly higher in the moisture stress-sensitive BPT 5204 compared with AC 39000. Similarly, the RCCs such as MDA, MG,

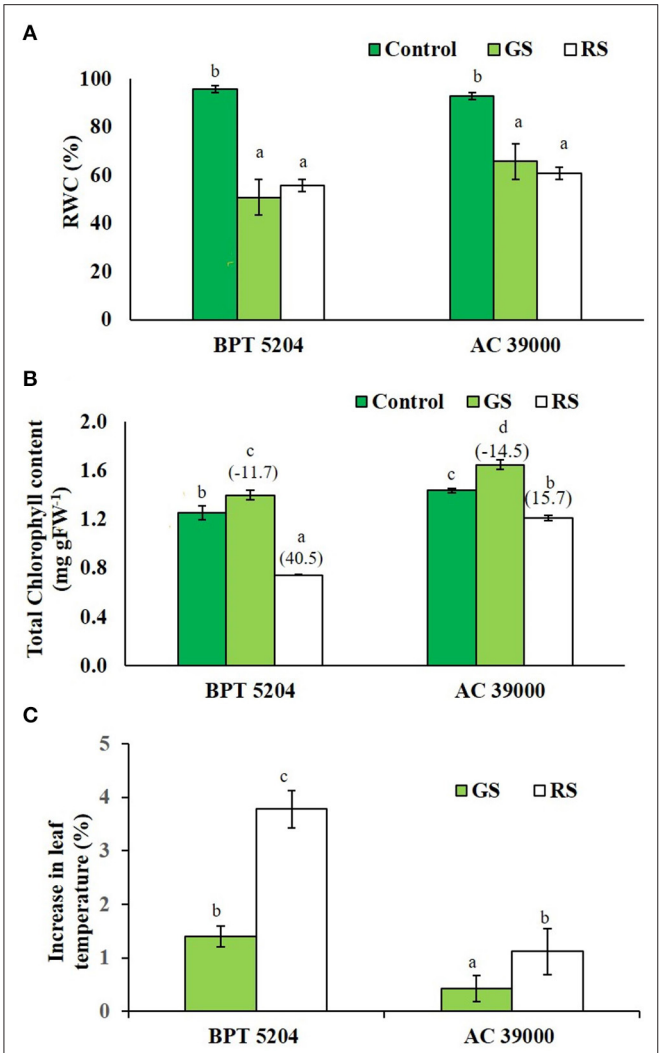


FIGURE 2 | Effect of moisture stress on **(A)** relative water content (RWC), **(B)** total chlorophyll, and **(C)** percent reduction in leaf temperature over control in two rice genotypes, BPT 5204 and AC 39000, in control, gradual stress (GS), and rapid stress (RS) conditions. Values are mean of three replicates. Values in parenthesis indicates percent reduction over control for mean. Different letters indicate significant different between genotypes and treatment at $P < 0.05$.

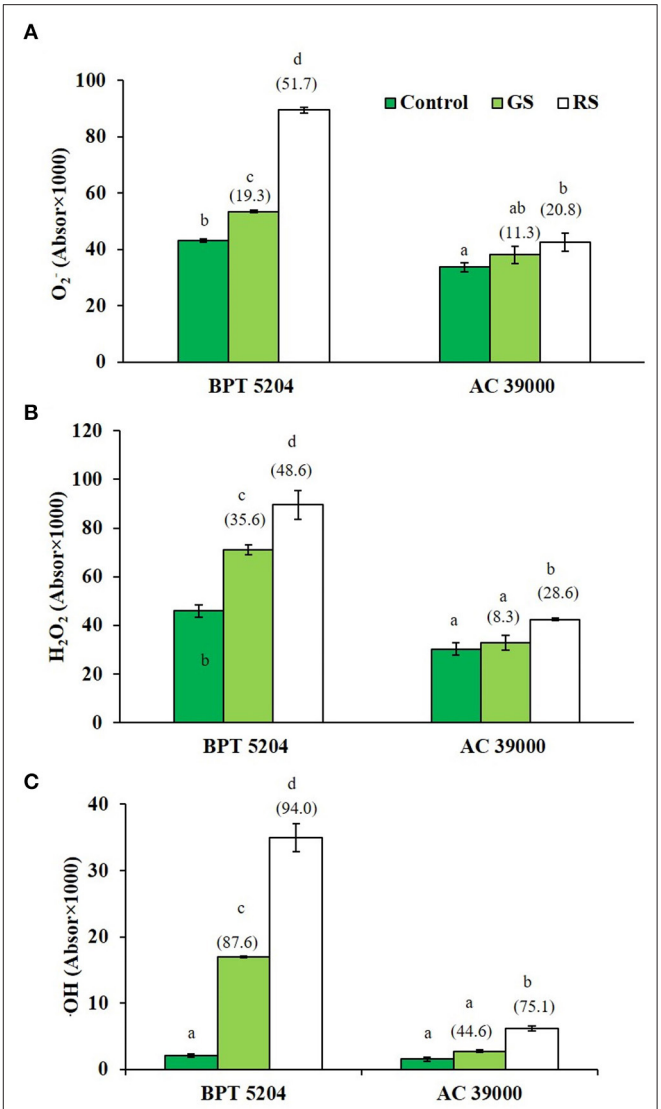


FIGURE 3 | Effect of moisture stress on reactive oxygen species production. **(A)** O_2^- using nitro blue tetrazolium chloride (NBT) staining, **(B)** H_2O_2 using diaminobenzedine (DAB) staining, and **(C)** •OH radical, in two rice genotypes, BPT 5204 and AC 39000, in control, gradual stress (GS), and rapid stress (RS) conditions. Values are mean of three replicates. Values in parenthesis indicates percent reduction over control for mean value. Different letters indicate significant different between genotypes and treatment at $P < 0.05$.

and Amadori compounds were higher in BPT 5204 under both gradual and rapid stresses compared with AC 39000 (**Figures 4A–C**). MG increased by 71 and 79% under gradual and rapid stress conditions, respectively, over control in the stress-sensitive BPT 5204 (**Figure 4B**), whereas MG increased by 53 and 68%, respectively, in gradual and rapid stress in AC 39000. Amadori compounds also showed a typically similar trend both between genotypes and between gradual and rapid stress progression representing a significant difference in RCC levels across genotypes as well as stress progression (**Figure 4C**).

ROS and RCCs would lead to destruction of cell membrane integrity, primarily through peroxidation of membrane lipids. The increased RCC levels were perfectly supported with the loss of cell membrane integrity as evidenced by a 54 and 74% increase in staining of Evan's Blue, respectively, under gradual and rapid stress treatments in BPT 5204 (**Figure 4D**). The corresponding values for loss of cell membrane integrity were 42 and 49% in AC 39000 under gradual and rapid stress progression (**Figure 4D**). The total antioxidant capacity also showed a similar trend between stress imposition protocol. The tolerant genotype, AC 39000, showed a much higher increase in total antioxidant capacity than BPT 5204 (**Figure 5A**). The moisture stress-tolerant genotype, AC 39000, accumulated noticeably lower

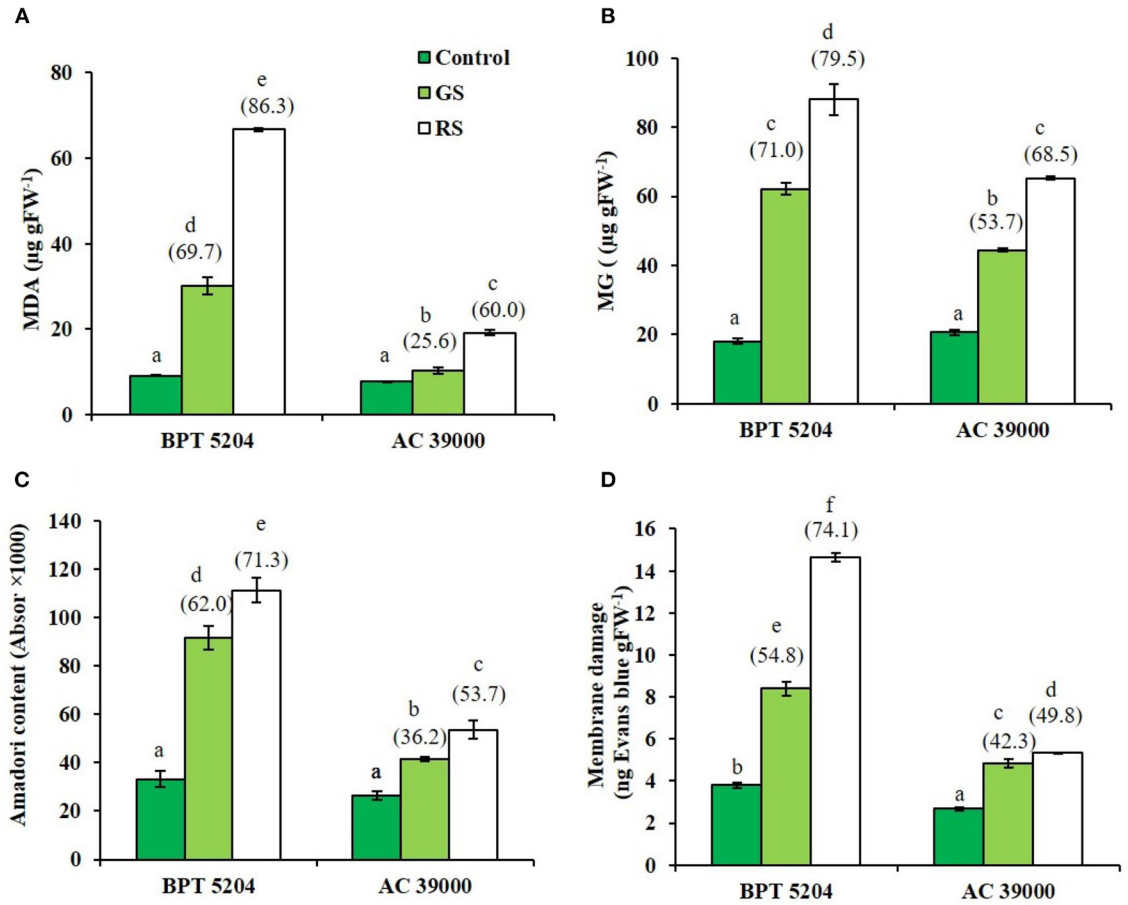


FIGURE 4 | Effect of moisture stress on production of reactive carbonyls and membrane damage. Measurements were made in control, gradual moisture stress (GS), and rapid moisture stress (RS) conditions at seedling stage. **(A)** Malondialdehyde (MDA), **(B)** methyl glyoxol (MG), **(C)** Amadori content, and **(D)** membrane damage using Evans blue staining. Values are mean of three replicates. Values in parenthesis indicate percent reduction over control for mean. Different letters indicate significant different between genotypes and treatment at $P < 0.05$.

proline content both in rapid and gradual stress treatments compared to BPT 5204 (**Figure 5B**).

Gradual Stress Induces ROS/RCC Scavenging Genes Better Than the Rapid Stress

Expression of genes involved in scavenging ROS and RCCs, viz., *ascorbate peroxidase (APX)*, *catalase (CAT)*, *superoxide dismutase (Fe-SOD)*, and *alcohol dehydrogenase 1 (ADH1)* showed significant genotypic and stress response. The differential expression of all the genes was significantly higher for AC 39000 compared with BPT 5204 (**Figure 6**). Among the gene expression examined, *APX* and *CAT* gene expressions were higher under gradual stress treatment in AC 39000. But for BPT 5204, only *Fe-SOD* gene expression responded to the rate of stress development, indicating a lack of propensity to respond to stress in the sensitive BPT 5204 (**Figure 6**). However, *ADH1* expression, although significantly high for AC 39000, did not respond to stress imposition protocols in either of the genotypes.

Seedling Growth vs. Stress Imposition Protocol

The reductions in leaf area and biomass accumulation were significantly high under rapid stress treatment in both genotypes. The moisture stress-sensitive genotype, BPT 5204, displayed significantly higher reduction in both leaf area and biomass than the tolerance AC 39000 under both moisture stress treatments (**Figures 7A,B**).

Genetic Variability in Acquired Tolerance Traits

Results from Experiment 1 clearly demonstrated that gradually progressing stress primed the upregulation of oxidative stress protective mechanisms. To examine if germplasm accessions differ in their propensity to respond, a set of 17 diverse rice germplasm accessions were screened for their response to gradual stress at the flowering phase.

The increase in O_2^- varied between 10.8 and 69.7% under stress among genotypes, and the percent increase in H_2O_2

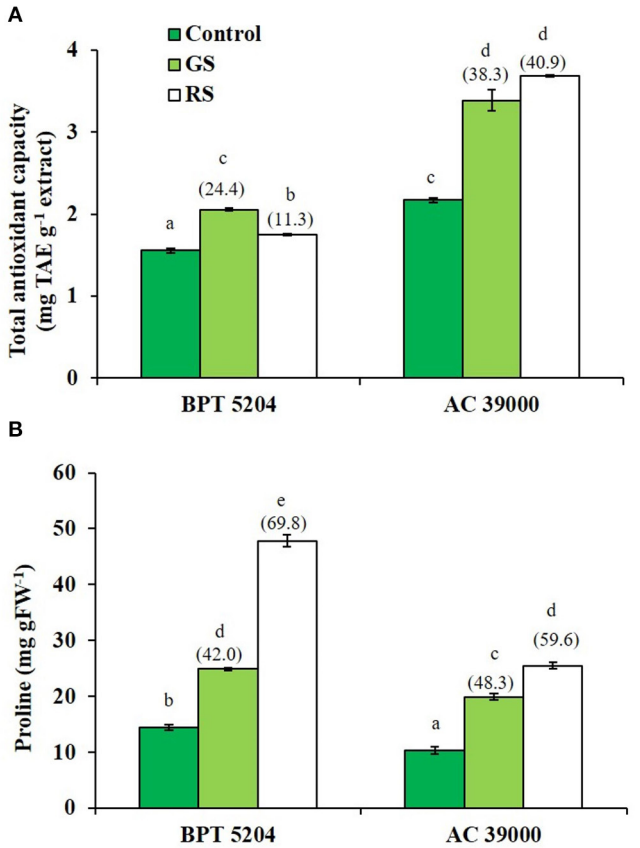


FIGURE 5 | Enhancement in the scavenging activity accompanying with gradual stress (GS) and rapid stress (RS) in terms of **(A)** total antioxidant content (TAC) calculated as tannic acid equivalence (TAE) and **(B)** proline content in two rice genotypes, BPT 5204 and AC 39000. Values are mean of three replicates. Values in parenthesis indicate percent reduction over control for mean value. Different letters indicate significant different between genotypes and treatment at $P < 0.05$.

ranged between 8.06 and 62.51%, representing a significant genotypic variability (**Table 1**). The values of all ROS and RCCs for all genotypes is presented in **Supplementary Tables 3, 4**. The increase in MDA content due to stress ranged from 5 to 34%. Stress-induced membrane damage also significantly increased in all the genotype ranging from 3.9 to 56.3% (**Table 1**). The upregulation of scavenging activity also showed significant variability of 4.9–54.8%. Similarly, the increase in proline content showed significant genotypic variability among the genotypes (11.2–79.4%). Genotypes GEN 224 and GEN 541 revealed lowest percent increase in ROS levels, lipid peroxidation, and a lower extent of membrane damage (**Supplementary Tables 3, 4**). Increased levels of TAC, which is an important component of acquired tolerance, closely matched with lower levels of ROS, RCC, and membrane damage in these genotypes (**Table 1** and **Supplementary Tables 3, 4**).

Spikelet fertility decreased under stress ranging from 12.11% in GEN 541 to 39.39% over control in GEN 484, representing a significant genotypic variability (**Table 2** and **Supplementary Table 5**). Similarly, percent reduction in biomass and yield per plant were also recorded, and its range in their respective reduction over control are given in **Table 2** and **Supplementary Table 5**.

Correlation Analysis for the Measured Parameters

A significant correlation was observed between O_2^- and H_2O_2 at $P < 0.01$. Similarly, lipid peroxidation end product also showed strong correlation with O_2^- and H_2O_2 (at $P < 0.001$ and $P < 0.05$, respectively). Membrane damage measured by Evans blue technique also showed significant positive correlation with O_2^- ($P < 0.001$), H_2O_2 ($P < 0.05$), and MDA ($P < 0.001$). TAC showed negative association with both the ROS and was significant only with H_2O_2 ($P < 0.05$). Similarly, spikelet fertility ($P < 0.01$), TDM ($P < 0.01$), and yield ($P < 0.05$) were also negatively correlated with TAC, whereas spikelet fertility and yield showed positive correlation with ROS, MDA, and membrane damage (**Figure 8**). Spikelet fertility was also strongly related to percent reduction in yield ($P < 0.001$) under stress (**Figure 8**), which explained around 75% of variability in yield loss (**Supplementary Figure 3**). These results emphatically illustrate the role of acquired tolerance traits associated with reduction in generation and/or improved scavenging of ROS, in regulating rice grain yield. Reduced ROS and RCC levels maintain grain yield through their influence on spikelet fertility. The two most stress tolerant genotypes GEN 541 and GEN 224 maintained significantly higher spikelet fertility and yield under stress compared with the two most sensitive genotypes, viz., GEN 484 and GEN 443. These two groups of genotypes significantly differed in their ROS and RCC levels (**Table 3**).

DISCUSSION

Plants cope with stresses through development of several adaptive strategies that can be generally classified as constitutive and acquired traits based on the pattern of their expression (Xin, 1998; Collins et al., 2008; Sheshshayee et al., 2018). While constitutive traits are time integrated, acquired tolerance traits/mechanisms are significantly upregulated only when plants experience milder levels of stress. Most of the abiotic stresses like drought progress gradually and prime plant responses by upregulating specific cellular mechanisms that provide decisive survival advantage during severe or even lethal levels of stress (Mittler, 2006; Galeano et al., 2019; Kollist et al., 2019; Zhang et al., 2020). Based on this premise, a simple temperature induction response technique was developed (Uma et al., 1995; Senthil-kumar et al., 2003; Vidya et al., 2017), which provided the initial screening option. The findings from these experiments on acquired ability to manage ROS and RCCs were done with young, germinated seedlings (heterotrophic stage). The skepticism about the validation of this approach in screening for acquired tolerance during more advanced phenological stages has been one of the reasons for the lack of keenness in adopting acquired tolerance traits in crop improvement.

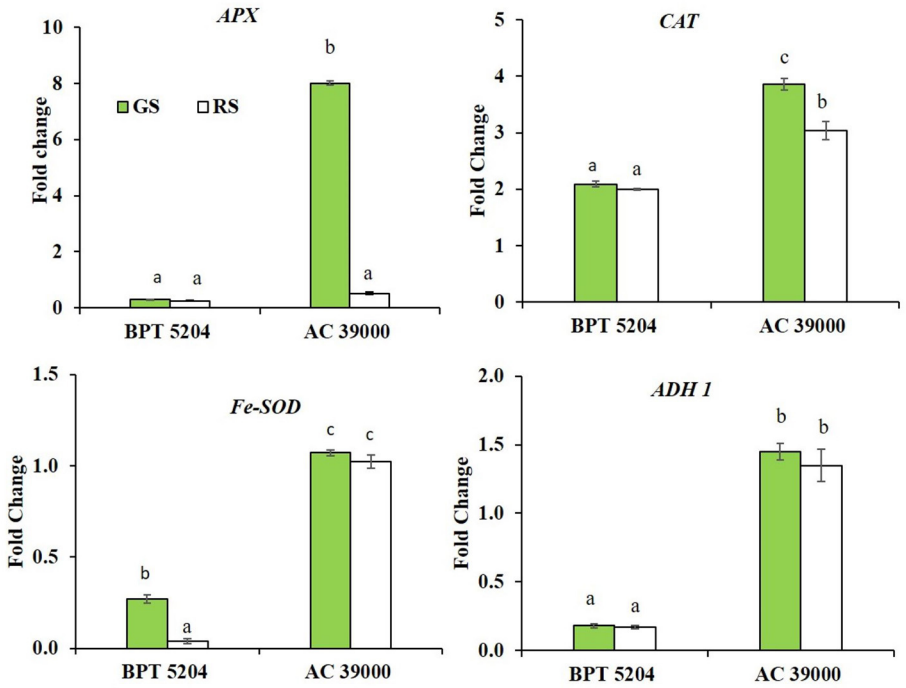


FIGURE 6 | Real-time quantitative RT-PCR analysis for genes associated with free radical scavenging in two rice genotypes BPT 5204 and AC 39000 under gradual stress (GS) and rapid stress (RS) conditions. Data represent the fold change in expression levels over control. Values are mean of three replicates. Different letters indicate significant different between genotypes and treatment at $P < 0.05$.

Screening for variability in induction response to drought stress in plants at advanced developmental stages, especially grand growth, flowering and anthesis, and grain filling periods, has been a challenge as methodology for imposing drought stress in a precisely controlled progression was not possible (Poorter et al., 2012; Manmathan and Lapitan, 2013). In container experiments, at phenological phases when canopy cover is maximum, withholding irrigation may lead to a rapid development of stress depending on soil texture and prevailing weather conditions. On the contrary, field-grown plants experience a gradual progression of soil moisture stress, which provides an opportunity for inducing acquired tolerance. However, differences in water mining abilities and transpiration rates between accessions creates variability in the tissue water relations and hence in acquired tolerance levels. Hence, research leads from rapid stress development in container experiments or field drought studies could not be translated for crop improvement, except for a few transcription activators (Snow and Tingey, 1985; Mishra et al., 2012; Marchand et al., 2013).

The transpiration-interfaced automated drought-simulator phenomics facility established at the Department of Crop Physiology, University of Agricultural Sciences, Bengaluru, India, significantly circumvents this lacuna (Vijayaraghavareddy et al., 2020a). The programmable "dry-down" protocol available in this facility is capable of developing a user-defined stress progression in containers, mimicking the field conditions and hence provide an excellent option to screen for plant response to gradually progressing stress (**Figures 1A–D** and **Supplementary Figure 1**).

In this study, we initially compared the plant response to rapid and gradual stress progression treatments using a drought tolerant and a sensitive cultivar of rice and analyzed the differences in acquired tolerance mechanisms. One of the most prominent *de novo* mechanisms of developing tolerance to stress is the management of oxidative burst. Production of ROS appears like an inevitable consequence when plants experience stress (Cruz de Carvalho, 2008). However, plants have also developed several mechanisms of scavenging these ROS and RCCs to manage the oxidative stress (Rogers and Munné-Bosch, 2016). Several of the known oxidative management strategies are induced only under stress and hence represent an important stress coping strategy. We examined the ROS and RCC levels under induced and uninduced seedlings and standardized the evaluation methodology. Subsequently, a set of diverse germplasm accessions was screened for oxidative response as a reflection of acquired tolerance under gradually progressing stress condition at flowering stage of the crop. We hypothesized that the induction of acquired tolerance in leaves would maintain the source activity and hence help in the spikelet growth and seed development.

Coping With Moisture Stress: Rapid vs. Gradual Stress

The first experiment revealed that the plants acquired tolerance when the stress progression was gradual, and the propensity to respond though was seen in both the genotypes; it was significantly higher in the tolerant AC 39000.

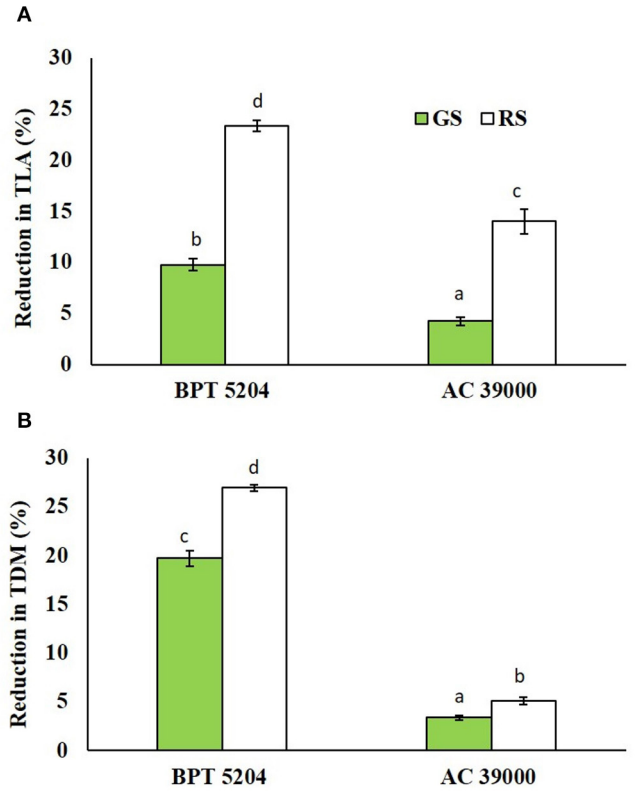


FIGURE 7 | Effect of the gradual stress (GS) and rapid stress (RS) in two rice genotypes (BPT 5204 and AC 39000) on **(A)** percent reduction in total leaf area (TLA) and **(B)** total dry matter (TDM) over control. Values are mean of three replicates. Different letters indicate significant different between genotypes and treatment at $P < 0.05$.

Leaf tissue water status determines the expression of mechanisms associated with acquired tolerance (Jones, 2007). Water mining associated with root traits generally determine the tissue water status. Hence, under field conditions, a deep-rooted plant often do not show water-deficient symptom even when the soil moisture content decreases (Yadav and Sharma, 2016). In the phenomics facility, the transpiration-interfaced automated irrigation system brings the soil moisture status to the same level irrespective of the differences in water mining and transpiration. This facility is hence quite suitable for capturing the genetic variability in acquired tolerances. The relative water content of the sensitive and tolerant genotype was comparable both at control and water-limited treatments. A significant difference in leaf temperature between the two genotypes was noticed with AC 39000 maintaining a much cooler canopy. This genotype apparently transpired more water during the same duration than IR64 both under control and water-limited conditions (data not shown). The thermal imaging system (VarioCAM®) used to measure the leaf temperature in this study was done by specifically selecting the leaf. This spot measurement was quite precise and did not require extensive background calibration for temperature measurements.

The automated irrigation combined with a predefined dry-down protocol of the drought-simulator phenomics facility facilitated the maintenance of comparable leaf tissue water relations between genotypes as well as between stress progression treatments irrespective of differences in total leaf area between the genotypes. Hence, the differential performance of the genotypes to stress levels would be almost entirely because of the ability to upregulate acquired traits under stress (**Figures 3–7**). The higher levels of TAC along with the levels of expression of free radical scavenging enzymes clearly illustrated that the drought tolerant AC 39000 displayed higher abilities to upregulate free radical management mechanisms and hence "acquired" higher levels of tolerance to drought stress (**Figures 5A**, **6**).

Genetic Variability in Acquired Tolerance Traits and Spikelet Fertility Under Gradually Imposed Moisture Stress

The relevance of acquired tolerance in plant stress adaptation has been well-accepted (Kumar et al., 1999; Sheshshayee et al., 2018). Yet, most of the investigations attempted the assessment of these acquired tolerance traits using young, germinated seedlings. Although some experiments provided evidences that the variability in acquired tolerance measured at the heterotrophic stage of germinated seedlings can reflect stress adaptation at an advanced autotrophic stage of the crop (Raju et al., 2014), such reports are not many. The mechanism(s) of stress adaptation could be highly variable between specific phenological phases of crop growth (Vijayaraghavareddy et al., 2020b). They reported that stress occurring at flowering stage can cause maximum damage to yield due to increased spikelet sterility. We hypothesized that genotypes with superior propensity to respond to milder stress would protect the spikelets from becoming sterile. This hypothesis was tested with a set of 17 diverse germplasm accessions of rice. A gradual stress protocol was adopted to coincide with the flowering phase of each genotype.

The yield of all the 17 germplasm lines showed a significant reduction under stress (**Table 2** and **Supplementary Table 5**). Stress during the flowering phase could have strong influence on anther dehiscence, pollen germination, stigmatic receptivity, extent of fertilization (Hedhly et al., 2003; Distefano et al., 2018; Matsui and Hasegawa, 2019), etc., leading to spikelet sterility. A strong association was also noticed between all the ROS and RCC levels with percent reduction in spikelet fertility (**Figure 8**). The TAC clearly revealed that a genotype that maintained ROS homeostasis through avoiding production and/or scavenging the ROS and RCCs would maintain higher grain yields under stress. The significant differential expressions of genes associated with ROS and RCC scavenging mechanisms indicate that phenotypic expression is strongly induced when plants experience mild stress and hence can be classified as acquired traits. Significant genotypic variability among germplasm accessions increases the possibility of using the best of genotypes as trait donor lines for improving acquired tolerance traits in crop improvement programs. Genotypes like GEN 224 and GEN 541 that maintained lower levels of ROS and RCCs and

TABLE 1 | Descriptive statistics for superoxide content (O_2^-), hydrogen peroxide (H_2O_2), malondialdehyde (MDA), membrane damage, total antioxidant capacity and total proline among 17 rice germplasm lines.

Plant trait	Treatment	Mean	Minimum (Percent change)	Maximum (Percent change)	SE	$LSD_{0.05}$	CV (%)
O_2^- (Absorb × 1,000)	Control (100% FC)	364.6	10.8	69.7	0.16	0.26	29.9
	Stress (50% FC)	693.4					
H_2O_2 (Absorb × 1,000)	Control (100% FC)	126.5	8.1	62.5	0.05	0.08	26.7
	Stress (50% FC)	233.0					
MDA ($\mu g g^{-1}$ FW)	Control (100% FC)	0.6	5.0	34.0	0.06	0.10	9.0
	Stress (50% FC)	0.7					
Membrane damage (ng Evans blue g^{-1} FW)	Control (100% FC)	14.6	3.9	56.3	3.31	5.54	17.7
	Stress (50% FC)	22.4					
Total antioxidant capacity (mg TAE g^{-1} extract)	Control (100% FC)	2.5	4.9	54.8	0.35	0.57	10.7
	Stress (50% FC)	3.5					
Total proline ($\mu g g^{-1}$ FW)	Control (100% FC)	8.7	11.2	79.4	2.17	3.52	13.7
	Stress (50% FC)	15.3					

$LSD_{0.05}$; least significant difference at 5%.

TABLE 2 | Descriptive statistics for total dry matter production (TDM), spikelet fertility (SF) and yield among 17 rice germplasm lines.

Plant trait		Mean	Minimum (percent change)	Maximum (percent change)	SE	$LSD_{0.05}$	CV (%)
TDM ($gpot^{-1}$)	Control (100% FC)	218.5	1.0	27.5	14.2	5.4	7.1
	Stress (50% FC)	187.0					
SF (%)	Control (100% FC)	88.7	12.11	39.4	3.6	1.4	4.7
	Stress (50% FC)	65.2					
Yield ($gpot^{-1}$)	Control (100% FC)	112.6	13.6	50	9.9	12.8	9.9
	Stress (50% FC)	76.4					

$LSD_{0.05}$; least significant difference at 5%.

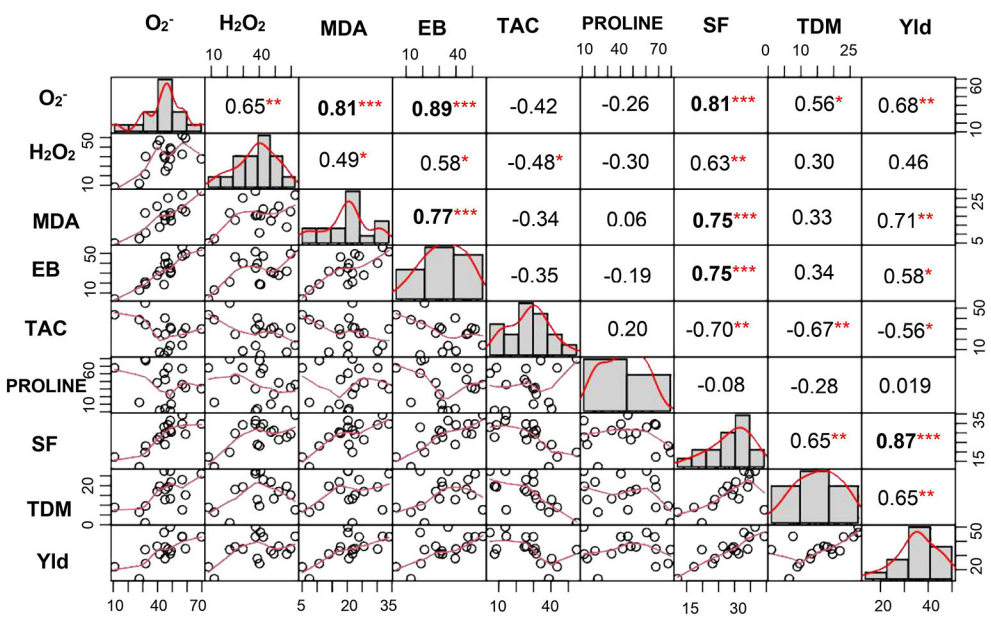


FIGURE 8 | Correlation coefficient matrix of percent change in various acquired and morphophysiological traits. In the diagonal panel, frequency of phenotypic traits is given as histograms. The lower panel is a scatter plot with a red line indicating the best fit. The upper panel represents the value of the Pearson correlation coefficient. *, **, and *** indicate significant correlations at $P < 0.05$, $P < 0.01$, and $P < 0.001$, respectively. O_2^-, superoxide content; H_2O_2, hydrogen peroxide content; EB, Evans blue; MDA, malondialdehyde; TAC, total antioxidant capacity; Yld, yield; SF, spikelet fertility; TDM, total dry matter among 17 lines of rice germplasm. All parameters were assessed at reproductive stage and correlation matrix was done for percent change over control.

TABLE 3 | Comparison of total yield and acquired tolerance traits in genotypes with maximum and minimum reduction in spikelet fertility (SF).

	Genotype	Yield (stress) (gpot^{-1})	O_2^- (%)	H_2O_2 (%)	Membrane damage (%)	MDA (%)	TAC (%)
Lowest reduction in SF	GEN 541	106.8 ± 3.2	27.6 ± 1.9	11.8 ± 0.5	12.9 ± 0.7	7.4 ± 0.6	38.8 ± 2.8
	GEN 224	105.7 ± 2.0	10.8 ± 1.7	8.1 ± 0.6	3.9 ± 0.2	5.0 ± 0.7	43.6 ± 0.7
Highest reduction in SF	GEN 484	59.7 ± 4.1	56.8 ± 0.9	62.5 ± 1.0	56.3 ± 1.3	31.8 ± 3.4	14.3 ± 0.5
	GEN 443	43.1 ± 1.0	48.6 ± 0.1	37.7 ± 0.0	35.3 ± 2.6	20.3 ± 3.5	13.8 ± 0.9

Percent increase in ROS and RCC (O_2^-,H_2O_2), membrane damage, malondialdehyde (MDA) and total antioxidant capacity (TAC) among selected four rice germplasm lines. (Note: Refer ***Supplementary Table 1*** *for the names of genotypes).*

hence cell membrane integrity and lowest percent reduction in spikelet fertility resulted in lower reduction in yield under stress (**Table 3** and **Supplementary Tables 3–5**).

CONCLUSIONS

This study demonstrated, for the first time, the relevance of precise stress imposition in capturing acquired tolerance traits. Significant upregulation of these traits were noticed only when the plants are gradually stressed. The mini-lysimeter (MLM)-based drought-simulator phenomic facility provided an excellent unique option to assess the drought stress response at a specific phenological phase of crop. The study revealed that the total antioxidant capacity was strongly related to maintenance of spikelet fertility, which led to a relatively higher grain yield. The genetic variability revealed in this study increases the optimism about breeding for enhanced acquired tolerance in rice to sustain yields, especially under water saving agronomic practices like semi-irrigated aerobic cultivation.

DATA AVAILABILITY STATEMENT

The original contributions presented in the study are included in the article/**Supplementary Material**, further inquiries can be directed to the corresponding author/s.

AUTHOR CONTRIBUTIONS

VL conducted all experiments, designed experimental methodology, analyzed the data, and developed the first draft of manuscript. PV designed the experimental methodology, conducted experiments, and edited the first draft. AN helped conduct all experiments in the drought-simulator phenomics platform. VSR provided useful inputs in developing methodology and edited the first draft. VR helped in conduct of phenomics experiments and edited the first draft. UM provided very useful discussions during the formation of this program and helped in the interpretation of data and discussions and edited the first draft. SS conceived the idea, directed the research, provided overall supervision, and provided funds for this investigation. All authors contributed to the article and approved the submitted version.

FUNDING

Fellowship to VL through DST-INSPIRE (03/2016/000206; IF160830) and a research grant support provided by Science and Engineering Research Board (SERB), Govt. of India to SS (EMR/2017/003802) are acknowledged.

ACKNOWLEDGMENTS

The authors thank Dr. Arvind Kumar, Director of IRRI South Asia Regional Centre (ISARC) and IRRI Representative—India, for sparing seeds of rice germplasm. We also thank M/s Spura Systems Pvt Ltd., Bangalore for establishing and maintaining the plant phenotyping platform.

SUPPLEMENTARY MATERIAL

The Supplementary Material for this article can be found online at: https://www.frontiersin.org/articles/10.3389/fpls.2020.632919/full#supplementary-material

REFERENCES

Abd Allah, A. A., Badawy, S. A., Zayed, B. A., and El-Gohary, A. A. (2010). The role of root system traits in the drought tolerance of rice (*Oryza sativa* L.). *J. Plant Prod.* 1, 621–631. doi: 10.21608/JPP.2010.86384

Adeboye, O. B., Schultz, B., Adekalu, K. O., and Prasad, K. (2016). Impact of water stress on radiation interception and radiation use efficiency of soybeans (*Glycine max L. Merr.)* in Nigeria. *Braz. J. Sci. Technol.* 3:15. doi: 10.1186/s40552-016-0028-1

Arnon, D. I. (1949). Copper enzymes in isolated chloroplasts. Polyphenoloxidase in beta vulgaris. *Plant Physiol.* 24, 1–15. doi: 10.1104/pp.24.1.1

Aruoma, O. I. (1994). Deoxyribose assay for detecting hydroxyl radicals. *Method Enzymol.* 233, 57–66. doi: 10.1016/S0076-6879(94)33008-5

Aswathi, J., Saha, B., Chowardhara, B., Devi, S., Borgohain, P., and Panda, S. (2018). Qualitative analysis of lipid peroxidation in plants under multiple stress through schiff's reagent: a histochemical approach. *Bio-Protocol* 8:e2807. doi: 10.21769/BioProtoc.2807

Basha, S. J., Basavarajappa, R., and Babalad, H. B. (2016). Crop performance and water use efficiency in aerobic rice (*Oryza sativa L.*) relative to irrigation schedule, planting geometry, and method of planting in northern transition zone of Karnataka, India. *Paddy Water Environ.* 15, 291–298. doi: 10.1007/s10333-016-0548-9

Bates, L. S. (1973). Rapid determination of free proline for water-stress studies. *Plant Soil* 39, 205–207. doi: 10.1007/BF00018060

Blum, A. (2017). Osmotic adjustment is a prime drought stress adaptive engine in support of plant production. *Plant Cell Environ*. 40, 4–10. doi: 10.1111/pce.12800

Bouman, B. A. M., Peng, S., Castañeda, A., and Visperas, R. M. (2005). Yield and water use of irrigated tropical aerobic rice systems. *Agric. Water. Manage* 74, 87–105. doi: 10.1016/j.agwat.2004.11.007

Çelik, Ö., Çakır, B. C., and Atak, C. (2019). Identification of the antioxidant defense genes which may provide enhanced salt tolerance in *Oryza sativa* L. *Physiol. Mol. Biol. Plants* 25, 85–99. doi: 10.1007/s12298-018-0618-0

Clauw, P., Coppens, F., Korte, A., Herman, D., Slabbinck, B., Dhondt, S., et al. (2016). Leaf growth response to mild drought: natural variation in arabidopsis sheds light on trait architecture. *Plant Cell* 28, 2417–2434. doi: 10.1105/tpc.16.00483

Collins, N. C., Tardieu, F., and Tuberosa, R. (2008). Quantitative trait loci and crop performance under abiotic stress: where do we stand? *Plant Physiol*. 147, 469–486. doi: 10.1104/pp.108.118117

Comas, L., Becker, S., Cruz, V. M. V., Byrne, P. F., and Dierig, D. A. (2013). Root traits contributing to plant productivity under drought. *Front. Plant Sci*. 4:442. doi: 10.3389/fpls.2013.00442

Cruz de Carvalho, M. H. (2008). Drought stress and reactive oxygen species: production, scavenging and signaling. *Plant Signal. Behav*. 3, 156–165. doi: 10.4161/psb.3.3.5536

Datta, S. K., Patel, H., and Berry, D. (1989). Extraction and purification of RNA from crop plants. *J. Exp. Bot*. 165:1252.

Dey, R., Lewis, S. C., Arblaster, J. M., and Abram, N. J. (2019). A review of past and projected changes in Australia's rainfall. *Wiley Interdiscip. Rev. Clim. Change* 10:e577. doi: 10.1002/wcc.577

Dharmappa, P. M., Doddaraju, P., Malagondanahalli, M. V., Rangappa, R. B., Mallikarjuna, N. M., Rajendrareddy, S. H., et al. (2019). Introgression of root and water use efficiency traits enhances water productivity: an evidence for physiological breeding in rice (*Oryza sativa* L.). *Rice* 12:14. doi: 10.1186/s12284-019-0268-z

Distefano, G., Gentile, A., Hedhly, A., and La Malfa, S. (2018). Temperatures during flower bud development affect pollen germination, self-incompatibility reaction and early fruit development of clementine (*Citrus clementina* Hort. ex Tan.*). Plant Biol*. 20, 191–198. doi: 10.1111/plb.12656

Fereres, E., and Soriano, M. A. (2007). Deficit irrigation for reducing agricultural water use. *J. Exp. Bot*. 58, 147–159. doi: 10.1093/jxb/erl165

Ferrante, A., and Mariani, L. (2018). Agronomic management for enhancing plant tolerance to abiotic stresses: high and low values of temperature, light intensity, and relative humidity. *Horticulturae* 4:21. doi: 10.3390/horticulturae4030021

Foley, J. A., Ramankutty, N., Braumann, K. A., Cassidy, E. S., and Gerber, J. S. (2011). Solutions for a cultivated planet. *Nature* 478, 337–342. doi: 10.1038/nature10452

Galeano, E., Vasconcelos, T. S., Novais de Oliveira, P., and Carrer, H. (2019). Physiological and molecular responses to drought stress in teak (*Tectona grandis* Lf). *PLoS ONE* 14:e0221571. doi: 10.1371/journal.pone.0221571

Haling, R., Simpson, R., Delhaize, E., Hocking, P., and Richardson, A. (2010). Effect of lime on root growth, morphology and the rhizosheath of cereal seedlings growing in an acid soil. *Plant Soil* 327, 199–212. doi: 10.1007/s11104-009-0047-5

Hao, B., Xue, Q., Marek, T. H., Jessup, K. E., Hou, X., Xu, W., et al. (2016). Radiation-use efficiency, biomass production, and grain yield in two maize hybrids differing in drought tolerance. *J. Agron. Crop Sci*. 202, 269–280. doi: 10.1111/jac.12154

Hedhly, A., Hormaza, J. I., and Herrero, M. (2003). The effect of temperature on stigmatic receptivity in sweet cherry (*Prunus avium* L.). *Plant Cell Environ*. 26, 1673–1680. doi: 10.1046/j.1365-3040.2003.01085.x

Jones, H. G. (2007). Monitoring plant and soil water status: established and novel methods revisited and their relevance to studies of drought tolerance. *J. Exp. Bot*. 58, 119–130. doi: 10.1093/jxb/erl118

Kogan, F., Guo, W., and Yang, W. (2019). Drought and food security prediction from NOAA new generation of operational satellites. *Geomat. Nat. Haz. Risk* 10, 651–666. doi: 10.1080/19475705.2018.1541257

Kollist, H., Zandalinas, S. I., Sengupta, S., Nuhkat, M., Kangasjärvi, J., and Mittler, R. (2019). Rapid responses to abiotic stress: priming the landscape for the signal transduction network. *Trends Plant Sci*. 24, 25–37. doi: 10.1016/j.tplants.2018.10.003

Kumar, D., Yusuf, M., A., Singh, P., Sardar, M., and Sarin, N. B. (2014). Histochemical detection of superoxide and H2O2 accumulation in *Brassica juncea* seedlings. *Bio-Protocol* 4:e1108. doi: 10.21769/BioProtoc.1108

Kumar, G., Krishnaprasad, B. T., Savitha, M., Gopalakrishna, R., Mukhopadhyay, K., Ramamohan, G., et al. (1999). Enhanced expression of heat shock proteins in thermotolerant lines of sunflower and their progenies selected on the basis of temperature induction response (TIR). *Theor. Appl. Genet*. 99, 359–367. doi: 10.1007/s001220051245

Lambrecht, S. C., Mahieu, S., and Cheptou, P. O. (2016). Natural selection on plant physiological traits in an urban environment. *Acta Oecol*. 77, 67–74. doi: 10.1016/j.actao.2016.09.002

Livak, K. J., and Schmittgen, T. D. (2001). Analysis of relative gene expression data using real- time quantitative PC and the 2–ΔΔCT method. *Methods* 25, 402–408. doi: 10.1006/meth.2001.1262

Manmathan, H., and Lapitan, N. L. (2013). Rapid induction of water stress in wheat. *Bio-Protocol* 3:e867. doi: 10.21769/BioProtoc.867

Marchand, G., Mayjonade, B., Vares, D., Blanchet, N., Boniface, M. C., and Maury, P., et al. (2013). A biomarker based on gene expression indicates plant water status in controlled and natural environments. *Plant Cell Environ*. 36, 2175–2189. doi: 10.1111/pce.12127

Matsui, T., and Hasegawa, T. (2019). Effect of long anther dehiscence on seed set at high temperatures during flowering in rice (*Oryza sativa* L.). *Sci. Rep*. 9:20363. doi: 10.1038/s41598-019-56792-2

McCord, J. M. (2000). The evolution of free radicals and oxidative stress. *Am. J. Med*. 108, 652–659. doi: 10.1016/S0002-9343(00)00412-5

Mishra, Y., Jänkänpää, H. J., Kiss, A. Z., Funk, C., Schröder, W. P., and Jansson, S. (2012). Arabidopsis plants grown in the field and climate chambers significantly differ in leaf morphology and photosystem components. *BMC Plant Biol*. 12:6. doi: 10.1186/1471-2229-12-6

Mittler, R. (2006). Abiotic stress, the field environment and stress combination. *Trends Plant Sci*. 1, 15–19. doi: 10.1016/j.tplants.2005.11.002

Nareshkumar, A., Subbarao, S., Vennapusa, A. R., Ashwin, V., Banarjee, R., Kulkarni, M. J., et al. (2020). Enzymatic and non-enzymatic detoxification of reactive carbonyl compounds improves the oxidative stress tolerance in cucumber, tobacco and rice seedlings. *J. Plant Growth Regul.* 39, 1359–1372. doi: 10.1007/s00344-020-10072-w

Nie, L., Peng, S., Chen, M., Shah, F., Huang, J., Cui, K., et al. (2012). Aerobic rice for water-saving agriculture. A review. *Agron. Sustain. Dev*. 32, 411–418. doi: 10.1007/s13593-011-0055-8

Nisarga, K. N., Vemanna, R. S., Chandrashekar, B. K., Rao, H., Vennapusa, A. R., Narasimaha, A., et al. (2017). Aldo-ketoreductase 1 (AKR1) improves seed longevity in tobacco and rice by detoxifying reactive cytotoxic compounds generated during ageing. *Rice* 10:11. doi: 10.1186/s12284-017-0148-3

Poorter, H., Fiorani, F., Stitt, M., Schurr, U., Finck, A., Gibon, Y., et al. (2012). The art of growing plants for experimental purposes: a practical guide for the plant biologist. *Funct. Plant Biol*. 39, 821–838. doi: 10.1071/FP12028

Prieto, P., Pineda, M., and Aguilar, M. (1999). Spectrophotometric quantitation of antioxidant capacity through the formation of a phosphomolybdenum complex: specific application to the determination of vitamin E. *Anal. Biochem*. 269, 337–341. doi: 10.1006/abio.1999.4019

Pushpa, A. D. (2016). *Molecular Characterisation of the Variability in Cellular Level Tolerance in Rice (Oryza sativa L.) an Analysis Based on Metabolomics Approach*. (Ph.D. thesis). University of Agricultural Sciences, Bangalore.

Raju, B. R., Beerasandra, A., Narayanaswamy, R., Malagondanahalli, A., Mohankumar, V., Sumanth, K. K., et al. (2014). Root traits and cellular level tolerance hold the key in maintaining higher spikelet fertility of rice under water limited conditions. *Funct. Plant Biol.* 41, 930–939. doi: 10.13140/RG.2.1.4994.4089

Rauf, M., Choi, Y. M., Lee, S., Lee, M. C., and Oh, S. (2019). Evaluation of anaerobic germinability in various rice subpopulations: identifying genotypes suitable for direct-seeded rice cultivation. *Euphytica* 215:19. doi: 10.1007/s10681-019-2341-5

Reddy, S. H., Singhal, R. K., DaCosta, M. V. J., Kambalimath, S. K., Rajanna, M. P., Muthurajan, R., et al. (2020). Leaf mass area determines water use efficiency through its influence on carbon gain in rice mutants. *Physiol. Plant* 169, 194–213. doi: 10.1111/ppl.13062

Richards, R. A., Rebetzke, G. J., Condon, A. G., and Van Herwaarden, A. F. (2002). Breeding opportunities for increasing the efficiency of water use and crop yield in temperate cereals. *Crop Sci*. 42, 111–121. doi: 10.2135/cropsci2002.1110

Rogers, H., and Munné-Bosch, S. (2016). Production and scavenging of reactive oxygen species and redox signaling during leaf and flower senescence: similar but different. *Plant Physiol*. 171, 1560–1568. doi: 10.1104/pp.16.00163

Senthil-kumar, M., Kumar, G., Srikanthbabu, V., and Udayakumar, M. (2007). Assessment of variability in acquired thermo tolerance: potential option to study genotypic response and the relevance of stress genes. Root and CLT traits improve spikelet fertility in rice. *Funct. Plant Biol*. 164, 111–125. doi: 10.1016/j.jplph.2006.09.009

Senthil-kumar, M., Srikanthbabu, V., Mohan Raju, B., Ganeshkumar, S. N., and Udayakumar, M. (2003). Screening of inbred lines to develop a thermotolerant sunflower hybrid using the temperature induction response (TIR) technique: a novel approach by exploiting residual variability. *J. Exp. Bot*. 54, 2569–2578. doi: 10.1093/jxb/erg278

Sheshshayee, M. S., Bindumadhava, H., Shankar, A., G., Prasad, T. G., and Udayakumar, M. (2003). Breeding strategies to exploit water use efficiency for crop improvement. *J. Plant Biol*. 30, 253–268. doi: 10.1093/jxb/erh277

Sheshshayee, M. S., Vijayaraghavareddy, P., Sreevathsa, R., Rajendrareddy, S., Arakesh, S., and Bharti, P., et al. (2018). Introgression of physiological traits for a comprehensive improvement of drought adaptation in crop plants. *Front. Chem*. 10:92. doi: 10.3389/fchem.2018.00092

Snow, M. D., and Tingey, D. T. (1985). Evaluation of a system for the imposition of plant water stress. *Plant Physiol*. 77, 602–607. doi: 10.1104/pp.77.3.602

Sung, D. Y., Kaplan, F., Lee, K. J., and Guy, C. L. (2003). Acquired tolerance to temperature extremes. *Trends Plant Sci*. 8, 179–187. doi: 10.1016/S1360-1385(03)00047-5

Tambussi, E. A., Nogués, S., and Araus, J. L. (2005). Ear of durum wheat under water stress: water relations and photosynthetic metabolism. *Planta* 221, 446–458. doi: 10.1007/s00425-004-1455-7

Uga, Y., Kitomi, Y., Ishikawa, S., and Yano, M. (2015). Genetic improvement for root growth angle to enhance crop production. *Breed. Sci*. 65, 111–119. doi: 10.1270/jsbbs.65.111

Uma, S., Prasad, T. G., and Udaya Kumar, M. (1995). Genetic variability in recovery growth and synthesis of stress proteins in response to polyethylene glycol and salt stress in finger millet. *Ann. Bot*. 76, 43–49. doi: 10.1006/anbo.1995.1076

Vemanna, S. R., Preethi, V., Nisarga, K. N., Srivastav, K. R., Sheshshayee, M. S., Mysore, K. S., et al. (2020). Carbonyl cytotoxicity affects plant cellular processes and detoxifying enzymes scavenge these compounds to improve stress tolerance. *J. Agric. Food Chem*. 68, 6237–6247. doi: 10.1021/acs.jafc.0c02005

Vidya, S. M., Laxman, R. H., and Bhatt, R. M. (2017). Temperature induction response technique: a screening tool for evaluation of banana cultivars for thermotolerance. *Ind. J. Plant Physiol*. 22, 79–84. doi: 10.1007/s40502-016-0273-9

Vijayaraghavareddy, P., Vanitha, P., Vemanna, R., Sheshshayee, M. S., and Makarla, U. (2017). Quantification of membrane damage/cell death using Evan's blue staining technique. *Bio-Protocol* 7:e2519. doi: 10.21769/BioProtoc.2519

Vijayaraghavareddy, P., Vemanna, R. S., Xinyou, Y. I. N., Struik, P. C., Udayakumar, M., and Sheshshayee, M. S. (2020a). Acquired traits contribute more to drought tolerance in wheat than in rice. *Plant Phenomics* 2020:5905371. doi: 10.34133/2020/5905371

Vijayaraghavareddy, P., Xinyou, Y. I. N., Struik, P. C., Makarla, U., and Sreeman, S. (2020b). Responses of lowland, upland and aerobic rice genotypes to water limitation during different phases. *Rice Sci*. 27, 345–354. doi: 10.1016/j.rsci.2020.05.009

Xin, Z. (1998). Eskimo mutants of Arabidopsis are constitutively freezing-tolerant. *Proc. Natl. Acad. Sci. U.S.A*. 95, 7799–7804. doi: 10.1073/pnas.95.13.7799

Yadav, S., and Sharma, K. D. (2016). "Molecular and morpho-physiological analysis of drought stress in plants," in *Plant Growth*, ed R. Everlon (London: IntechOpen), 149–173.

Yoo, Y. H., Nalini Chandran, A. K., Park, J. C., Gho, Y. S., Lee, S. W., An, G., et al. (2017). OsPhyB-mediating novel regulatory pathway for drought tolerance in rice root identified by a global RNA-Seq transcriptome analysis of rice genes in response to water deficiencies. *Front. Plant Sci*. 8:580. doi: 10.3389/fpls.2017.00580

Zhang, J., Wang, X., Vikash, V., Ye, Q., Wu, D., Liu, Y., et al. (2016). ROS and ROS- mediated cellular signaling. *Oxidative Med. Cell. Longev*. 2016:4350965. doi: 10.1155/2016/4350965

Zhang, X., Yang, Z., Li, Z., Zhang, F., and Hao, L. (2020). Effects of drought stress on physiology and antioxidative activity in two varieties of Cynanchum thesioides. *Braz. J. Bot*. 43, 1–10. doi: 10.1007/s40415-019-00573-8

Conflict of Interest: The authors declare that the research was conducted in the absence of any commercial or financial relationships that could be construed as a potential conflict of interest.

Copyright © 2021 Lekshmy, Vijayaraghavareddy, Nagashree, Ramu, Ramegowda, Makarla and Sreeman. This is an open-access article distributed under the terms of the Creative Commons Attribution License (CC BY). The use, distribution or reproduction in other forums is permitted, provided the original author(s) and the copyright owner(s) are credited and that the original publication in this journal is cited, in accordance with accepted academic practice. No use, distribution or reproduction is permitted which does not comply with these terms.

frontiers in Plant Science

ORIGINAL RESEARCH
published: 19 February 2021
doi: 10.3389/fpls.2021.629762

Low Soil Nutrient Tolerance and Mineral Fertilizer Response in White Guinea Yam (*Dioscorea rotundata*) Genotypes

Ryo Matsumoto, Haruki Ishikawa, Asrat Asfaw and Robert Asiedu*

International Institute of Tropical Agriculture, Ibadan, Nigeria

OPEN ACCESS

Edited by:
Raul Antonio Sperotto, Universidade do Vale do Taquari – Univates, Brazil

Reviewed by:
Vincent Lebot, CIRAD, Vanuatu
Valerie Hgaza Kouame, Swiss Centre for Scientific Research (Côte d'Ivoire), Côte d'Ivoire

***Correspondence:**
Ryo Matsumoto
r.matsumoto@cgiar.org

Specialty section:
This article was submitted to Crop and Product Physiology, a section of the journal Frontiers in Plant Science

Received: *15 November 2020*
Accepted: *28 January 2021*
Published: *19 February 2021*

Citation:
Matsumoto R, Ishikawa H, Asfaw A and Asiedu R (2021) Low Soil Nutrient Tolerance and Mineral Fertilizer Response in White Guinea Yam (Dioscorea rotundata) Genotypes. Front. Plant Sci. 12:629762. doi: 10.3389/fpls.2021.629762

Yam (*Dioscorea* spp.) is a major food security crop for millions of resource-poor farmers, particularly in West Africa. Soil mineral deficiency is the main challenge in yam production, especially with the dwindling of fallow lands for the indigenous nutrient supply. Cultivars tolerant to available low soil nutrients and responsive to added nutrient supply are viable components of an integrated soil fertility management strategy for sustainable and productive yam farming systems in West Africa. This study's objective was to identify white Guinea yam (*D. rotundata*) genotypes adapted to available low soil nutrients and responsive to externally added nutrient supply. Twenty advanced breeding lines and a local variety (Amula) were evaluated under contrasting soil fertility, low to expose the crop to available low soil nutrient supply and high to assess the crop response to added mineral fertilizer (NPK) input at Ibadan, Nigeria. The genotypes expressed differential yield response to low soil fertility (LF) stress and added fertilizer input. Soil fertility susceptibility index (SFSI) ranged from 0.64 to 1.34 for tuber yield and 0.60 to 1.30 for shoot dry weight. The genotypes R034, R041, R050, R052, R060, R100, and R125 combined lower SFSI with a low rate of reduction in tuber yield were identified as tolerant to LF stress related to the soil mineral deficiency. Likewise, the genotypes R109, R119, and R131 showed high susceptibility to soil fertility level and/or fertilizer response. Genotypes R025 and R034 had the tuber yielding potential twice of that the local variety under low soil nutrient conditions. Shoot dry weight and tuber yield showed a positive correlation both under low and high soil fertility conditions ($r = 0.69$ and 0.75, respectively), indicating the vigor biomass may be a morphological marker for selecting genotypes of white Guinea yam for higher tuber yield. Our results highlight genotypic variation in the tolerance to low soil nutrients and mineral fertilizer response in white Guinea yam to exploit through breeding and genetic studies to develop improved genotypes for low and high input production systems in West Africa.

Keywords: *Dioscorea*, low soil fertility tolerance, soil fertility susceptibility, West Africa, genotypic variation

INTRODUCTION

Yam (*Dioscorea* spp.) is an important tuber crop for human consumption. Yam is a common name of the various species in the genus *Dioscorea* with varying origins and distributions in the tropics, subtropics, and temperate regions (Darkwa et al., 2020). It is a highly valuable crop in the food and cultural systems of West Africa (Asiedu and Sartie, 2010), where 66.8 million tons (93%) of the global production occurs (FAOSTAT, 2020). Among the cultivated species, the white Guinea yam (*D. rotundata*) is the most planted, produced and consumed yam in West Africa (Asfaw et al., 2020). The yam production in West Africa has increased from 14.5 million tons in 1988 to 66.8 million tons in 2018. The annual rate of increase in total yam production was around 3.8% from 2000 to 2019 (FAOSTAT, 2020). The dramatic increases are associated with area expansion into the Savannas. However, chemical inputs are limited, and landraces are still frequently used in yam cultivation in West Africa (Degras, 1993; Scott et al., 2000). The fallow period traditionally lasted 20 years in the forest-savannah agro-ecological zone of West Africa. Recently, the fallow period's duration has decreased to less than five years because of population pressure and land competition from other crops and purposes (Ouédraogo, 2004; Asiedu and Sartie, 2010). A sharp decline in yam yield occurs when grown after a limited fallow of approximately 1–3 years (Watson and Goldsworthy, 1964). The yam yield has declined from 9.4 t ha^{-1} in 1988 to 8.4 t ha^{-1} in 2018 (FAOSTAT, 2020). Although there was productivity growth, it has been relatively marginal when compared to potato (FAOSTAT, 2020). This trend could be catastrophic unless steps are taken to change the situation (Manyong and Nokoe, 2003).

Several soil nutrient management technologies that enhance crop productivity have been developed, tested, and promoted in Africa's low-input farming systems (Kihara et al., 2020). However, there is little information on yam's input intensification technologies (Enesi et al., 2017). The results and recommendations of the few available soil fertility research on yams are variable and sometimes conflicting (Irving, 1956; Lugo et al., 1993; O'Sullivan and Ernest, 2008; Diby et al., 2009; Carsky et al., 2010; Enesi et al., 2017). Irving (1956) reported a positive tuber yield response of yam to N fertilizer application in eastern Nigeria. Likewise, Kpeglo et al. (1981) in southwest Nigeria and Lyonga (1981) in the northwest highlands of Cameron reported tuber yield increase with mineral fertilizer. In contrast, Carsky et al. (2010) reported no yield response to N mineral fertilizer application in Togo. However, their study showed tuber yield increases with K and tuber size increase with P application. Kang and Wilson (1981) also reported no significant chemical fertilizer effect on yam tuber yield. Diby et al. (2009) and Lugo et al. (1993) indicated a differential yield response to chemical fertilizer application in yam, depending on soil fertility conditions. The studies on the mineral fertilizer effect on yam were either used few cultivars or without creating nutrient-depleted plots to correctly assess the impact. However, fertilizer impact studies clearly highlighted promoted growth and yield of yam under low fertile soils (Diby et al., 2011).

Intensification of yam production through soil amendments, improved cultivars, and other inputs could bring yield increases per unit area. Cultivars tolerant to available low soil nutrients and responsive to external nutrient supply are the most effective and convenient way to improve productivity in low input smallholder farming systems. Cultivar tolerance to low soil nutrients supports sustainable crop production by reducing production costs and farmer dependence on fertilizers. On the other hand, cultivar responsive to mineral fertilizer application aids crop intensification to enhance production. However, studies on genetic variation to low and high soil fertility in yam crops in general and white Guinea yam are scarce. Genetic improvement efforts need to integrate high yields with high nutrient use efficiency (Asiedu and Sartie, 2010). Information on genetic variation within yam germplasm to low and high nutrient availability is a stepping stone to a selective breeding to improve yam for low and high input farming systems. Therefore, this study assessed genotypic differences among white Guinea yam (*D. rotundata*) genotypes for improved productivity under low and high soil nutrient conditions.

MATERIALS AND METHODS

Site and Soil Properties

The field experiments were conducted for two years (2018 and 2019 cropping seasons) at the low soil fertility (LF) experimental field at the International Institute of Tropical Agriculture (IITA), 7°31′ N and 3°54′ E, southwestern Nigeria. The LF condition was created by continuously cultivating high nutrient mining crops such as cassava, maize, and sorghum without fertilizer input from 2016 to 2018. Trial plots with the dimensions 100 m × 25 m were used. Cassava was grown from April 2016 to March 2017, followed by sorghum from April 2017 to January 2018, and then maize for four consecutive harvests from April 2017 to January 2018. The continuous planting of high nutrient mining crops in the same plot without additional nutrients successfully created LF or mineral nutrient-deficient soil conditions for our experiment.

Soil samples were collected in April 2016 and March 2018 at depths of 0 – 20 cm from thirty randomly selected spots in the plot. Samples were dried at 65°C before sifting (using a 2 mm sieve). Soil pH was determined by initially suspending the soil in water (at a 1:2.5 soil/water ratio). Exchangeable Ca^{2+}, Mg^{2+}, K^{+}, and available P were extracted according to the Mehlich-3 procedure (Mehlich, 1984). The cations were determined using an atomic absorption spectrophotometer (Accusys 211 Atomic Spectrophotometer, Buck Scientific, CT, United States). Phosphorus was assayed colorimetrically using Genesys 10S UV-Vis (Thero Scientific, MA, United States). Organic carbon was determined by chromic acid digestion with a spectrophotometric procedure using the Genesys 10S UV-Vis (Heanes, 1984). Total nitrogen was determined using the Kjeldahl method for digestion and colorimetric determination on a Technicon AAII Autoanalyzer (Seal Analytical, WI, United States) (Bremner and Mulvaney, 1982). The soil properties are presented in **Table 1**. In addition, the weather data for the experimental period

TABLE 1 | Soil chemical properties of the trial sites at IITA Ibadan, Nigeria.

Soil Properties	2016	2018
pH	5.93	6.41
Organic carbon (%)	1.23	0.15
Nitrogen (%)	0.13	0.03
Phosphorus (mg kg^{-1})	6.12	1.62
Calcium (Cmol[+] kg^{-1})	3.36	3.19
Magnesium (Cmol[+] kg^{-1})	0.46	0.90
Potassium (Cmol[+] kg^{-1})	0.59	0.27

was assessed using the data obtained from the Geographical Information System (GIS) unit of IITA.

Plant Materials and Trial Management

Twenty advanced genotypes from the IITA yam breeding program and a popular landrace cultivar (Amula) constituted the plant material for this study (**Supplementary Material 1**). All genotypes used for the field experiment were multiplied under uniform conditions at the IITA field in the 2017 cropping season to generate quality planting material. The plants with symptoms of virus disease such as yam mosaic virus were removed from field during the growing period. Visually assessed clean tubers with no sign of rot and pests were used as seed tuber material for planting the trials. Tubers weighing approximately 1 - 2 kg were cut horizontally to remove the head and tail components. The tuber's center component was cut into pieces of 50 ± 10 g to obtain uniform material for planting (yam setts). Yam setts were treated in a mixture of 70 g mancozeb (fungicide) and 75 mL chlorpyrifos (insecticide) in a 10 L volume of tap water for 5 min, and then the setts were dried for 20 h in the shade before planting for pre-sprouting. The yam setts were planted in plastic pots (12 cm diameter × 10 cm height) filled with topsoil. Plants with uniform sprouts were transplanted into the field with stakes 30 days after planting. In 2018 and 2019 trials, trial plots with dimensions 25 m × 25 m were prepared in LF soil plots for screening, respectively. The field experiment consisted of a split-plot in randomized block design replicated twice (Altman and Krzywinski, 2015). The main plot constituted two levels of fertilizer applications, nil as Low soil fertility condition and 90, 50, 75 kg N, P, and K ha^{-1} as high fertility soil condition (HF), while the subplot consisted of 21 genotypes. All plants in the main plot were at the planting density of 1 plant m^{-2}. Each subplot had 3 plants with a plot size of 3 × 1 m^2 without a border plant. The main plot size was 3 × 21 m^2 and replicated twice. There was three meters channel between replications. The ten meters channel was created between non-fertilized and fertilized plot (detail field design presented in **Supplementary Material 2**). Fertilizer was applied at 14 days after transplanting using the side dressing method. Weeds were removed manually whenever present to maintain weed-free plots throughout the experiment.

Data Collection

Shoot dry weight was evaluated using the non-destructive method described in Iseki and Matsumoto (2019) at 150 days after planting (150 DAP). This assessment correlated with yam's maximum aerial growth (Diby et al., 2011; Sartie et al., 2012). The normalized difference vegetation index (NDVI) was measured using a handheld sensor (GreenSeeker, Nikon Trimble, Tokyo, Japan) with a simultaneous plant height and green area measurement. Shoot dry weight was estimated by an equation using NDVI and plant height as explanatory variables. Shoot dry weight was evaluated for the three plants in each plot. In December, when the aerial parts were at full senescence, each plant's tubers were harvested at 230 DAP in the first-year and 232 DAP in the second-year. After harvesting, the fresh tuber weight was recorded. Biomass reduction in shoot dry weight at 150 DAP and tuber yield was calculated as

$$\text{Shoot biomass and tuber yield reduction rate (\%)} = \left(\frac{\overline{\text{xhf}} - \overline{\text{xlf}}}{\overline{\text{xhf}}}\right) \times 100$$

where $\overline{xlf}$ and $\overline{xhf}$ are the mean trait values of a given genotype under low and high soil nutrient environments, respectively.

The soil fertility susceptibility index (SFSI) was calculated using the following formula (Fischer and Maurer, 1978) and defined as

$$SFSI = \left(1 - \frac{\overline{xlf}}{\overline{xhf}}\right) / \left(1 - \frac{\overline{Ylf}}{\overline{Yhf}}\right)$$

where $\overline{xlf}$ and $\overline{xhf}$ are the mean trait values of a given genotype under low and high nutrients soil environments, respectively. $\overline{Ylf}$ and $\overline{Yhf}$ are the mean trait values of all genotypes under low and high soil nutrients environments, and $1-\overline{Ylf}/\overline{Yhf}$ is the soil fertility intensity (SI).

Data Analysis

Data were analyzed using the linear mixed model in lme4 package (Bates, 2010) in the R environment for statistical computing (R Core Team, 2018). To determine if there is a significant difference between the means value of trait obtained from LF and HF condition for each genotype, T-test was performed using R package ggplot2 (Kassambara, 2020). To compare the shoot growth and tuber yield performance of improved genotypes with local variety under LF condition, Dunnett's test was performed using multcomp R package (Hothorn et al., 2020). Person's correlation coefficients among traits were calculated using R package *corregram* (Wright, 2018).

RESULTS

Status of Soil Fertility and Meteorological Condition in the Experimental Field

The soil chemical property of the experimental field is presented in **Table 1**. Planting cassava, sorghum, and maize before yam planting depleted mineral nutrients and created low soil fertility stress for the yam experiment. The soil pH was 5.93 in 2016 and 6.41 in 2018. The organic carbon content was 1.23% in 2016. However, the organic carbon content was decreased to 0.15%

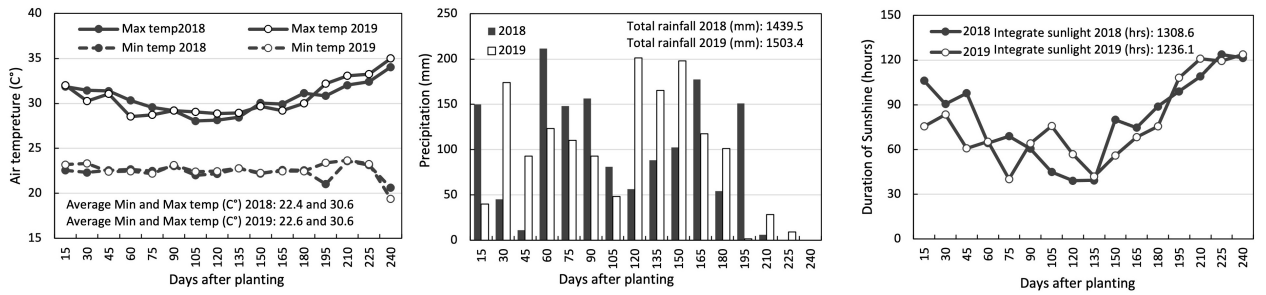


FIGURE 1 | Air temperature, precipitation, and duration of sunshine during the growth periods at IITA Ibadan, Nigeria. The air temperature (left box) includes solid lines and dashed lines representing maximum and minimum air temperature averages, respectively, for every 15 days after planting. For precipitation (center box) and sunshine duration (right box), data are cumulative values for every 15 days after planting.

when the field trial was set up for yam in 2018. The nitrogen content in 2018 (0.03%) was lower than in 2016 (0.13%). The available phosphorus content was 6.12 mg kg^{-1} in 2016, and it was reduced to 1.62 in 2018. The exchangeable Ca^{2+} and Mg^{2+} in 2016 were 3.19 Cmol[+] kg^{-1} and 0.46, Cmol[+] kg^{-1}, respectively. In 2018, the exchangeable Ca^{2+} and Mg^{2+} were 3.19 Cmol[+] kg^{-1} and 0.90 Cmol[+] kg^{-1}, respectively. The exchangeable Ca^{2+} in 2016 and 2018 was 3.19 and 3.97 Cmol[+] kg^{-1}, receptivity. The exchangeable Mg^{2+} was 0.46 Cmol[+] kg^{-1} in 2016 and 0.90 Cmol[+] kg^{-1} in 2018. Exchangeable K^{+} was 0.59 Cmol[+] kg^{-1} in 2016, which was higher than in 2018 (0.27 Cmol[+] kg^{-1}).

Figure 1 presents the meteorological conditions during the growth period, from planting to harvest (240 days after planting) for the trials. The total precipitation, average minimum/maximum temperatures, and integrated sunshine duration for this period were 1439.5 mm, 22.4/30.6°C, 1308.6 h in 2018, and 1503.4 mm, 22.6/30.6°C, and 1236.1 h in 2019.

Effect of Soil Fertility on Shoot Dry Weight and Tuber Yield

The main effects of genotype, soil fertility treatment, and year were significant for tuber yield and shoot dry weight (**Table 2**). The interaction effects were significant between a year and soil fertility treatments on shoot dry weight. The gap in shoot dry weight between LF and HF conditions was enormous in 2018 than in 2019. On the other hand, the interaction of genotype with soil fertility status was significant for tuber yield. Mean shoot dry weight and tuber yield were higher in 2018 than in 2019 (**Figure 2**). The overall mean shoots dry weight increased by 34.7% with HF condition, while such an increase was 51.9% for tuber yield.

Among the genotypes screened under two-variable soil fertility status, sixteen produced significantly higher tuber yield in HF condition than when grown with LF condition (**Table 3**). In contrast, five genotypes did not show significant tuber yield differences between the LF and HF conditions. The percent tuber yield reduction due to LF stress ranged from 33.4 (R125) to 69.8% (R119). The SFSI in tuber yield ranged from 0.64 to 1.34, with a mean of 0.98. The genotypes R034, R041, R050, R052, R060, R100, and R125 showed a lower SFSI than the local variety (0.87) (**Table 3**). On the other hand, R109, R119, and R131 showed a higher SFSI and larger reduction rate among tested genotypes. Tuber yield ranged from 367.5 (R131) to 1205.0 (R025) g $plant^{-1}$ under LF condition (**Figure 3**). The tuber yield of R025 and R034 were significantly higher than that of the local variety (199% and 187%, respectively) followed by R052 at LF condition.

The shoot dry weight of fourteen genotypes was significantly lower in LF than HF conditions (**Table 4**). On the contrary, seven genotypes showed non-significant differences in shoot dry weight between the LF and HF conditions (**Table 4**). Genotype R131 showed a 44.9% reduction in shoot dry weight in LF condition than the HF condition (averaged across the years). The lowest shoot dry weight reduction of 29.2% was recorded from the genotype R125 (**Table 4**). The soil fertility susceptibility index (SFSI) for shoot dry weight ranged from 0.64 (R125) to 1.30 (R131). The genotypes R041, R052, R101, R125, and R141 had lower SFSI values than the local variety (0.88).

TABLE 2 | Analysis of deviance (Type II Wald chi square tests for linear mixed model) of shoot dry weight and tuber yield in 21 white Guinea yam genotypes.

Shoot dry weight	Chisq	Df	Pr (> Chisq)	
Year (Y)	30.6	1	1.1E−12	***
Fertilizer treatment (T)	261.1	1	2.2E−16	***
Genotype (G)	63.5	20	8.0E−01	***
Y x T	20.9	1	54E−06	***
Y x G	17.7	20	1.00	
T x G	28.6	20	0.14	
Y x T x G	24.9	20	0.72	
Tuber yield				
Year (Y)	11.6	1	0.001	***
Fertilizer treatment (T)	183.9	1	2.2E−16	***
Genotype (G)	147.9	20	2.2E−16	***
Y x T	1.4	1	0.24	
Y x G	28.7	20	0.09	
T x G	67.3	20	0.5E−06	***
Y x T X G	16.8	20	0.67	

*** *Represents significant differences at* $p < 0.001$.

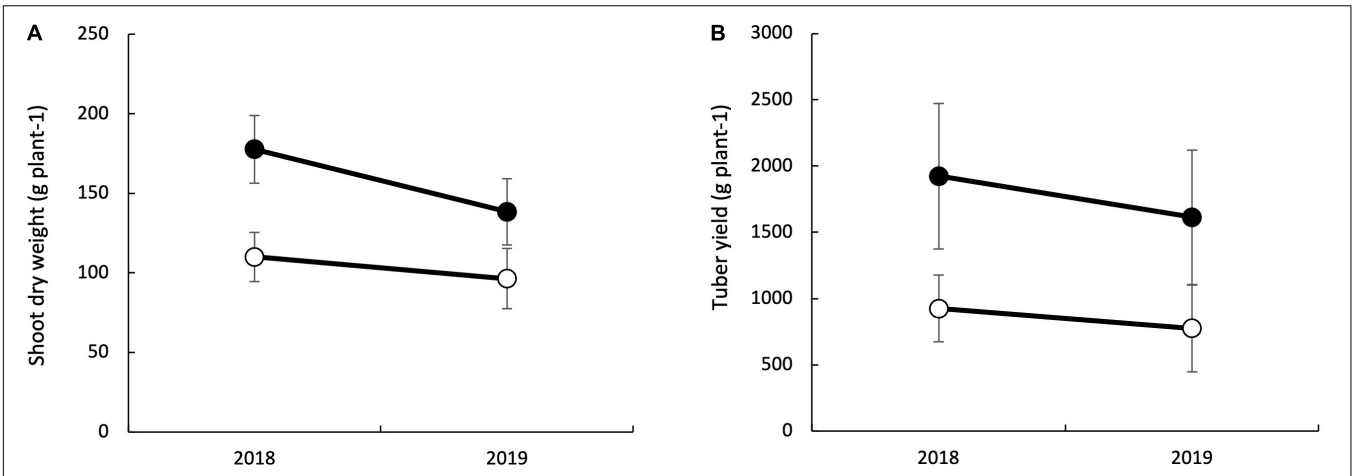


FIGURE 2 | Effects of fertilizer application on shoot dry weight at 150 days after planting **(A)** and tuber yield **(B)** of white Guinea Yam varieties. Bars indicate the standard deviation ($n = 21$).

Shoot dry weight had a positive and significant correlation with tuber yield in both LF ($r = 0.69$, $p = 0.0005$) and HF plots ($r = 0.75$, $p < 0.0001$) (**Figure 4**). Likewise, SFSI for shoot dry weight had a positive and significant correlation with SFSI for tuber yield ($r = 0.71$, $p = 0.0002$) (**Figure 5**).

TABLE 3 | Effect of genotype and soil fertility on tuber yield (gram per plant) in 21 white Guinea yam genotypes.

Genotype	Tuber yield (g plant^{-1})†				
	LF	HF	PR	*p*-Value	SFSI
R125††	908.3	1363.8	33.4	0.05	0.64
R052	1034.6	1604.2	35.5	0.10	0.68
R060	1003.3	1587.5	36.8	0.09	0.71
R041	1010.8	1652.5	38.8	0.08	0.75
R100	944.2	1639.2	42.4	0.18	0.82
R050	882.9	1545.0	42.9	0.04	0.83
R034	1124.2	2028.3	44.6	0.01	0.86
Local variety	602.9	1099.2	45.1	0.01	0.87
R133	891.7	1775.8	49.8	0.04	0.96
R069	707.5	1419.4	50.2	0.01	0.97
R120	780.0	1572.5	50.4	0.00	0.97
R101	893.3	1860.0	52.0	0.01	1.00
R141	851.7	1842.5	53.8	0.01	1.04
R117	800.0	1799.2	55.5	0.03	1.07
R028	863.8	1974.2	56.2	0.00	1.08
R025	1205.0	2756.7	56.3	0.00	1.08
R056	863.3	1992.5	56.7	0.01	1.09
R030	571.7	1461.7	60.9	0.00	1.17
R109	795.0	2506.7	68.3	0.00	1.32
R131	367.5	1160.0	68.3	0.01	1.32
R119	755.8	2500.0	69.8	0.01	1.34
Mean	850.4	1768.6	50.8		0.98

†*LF, low soil fertility; HF, high soil fertility; PR, present reduction due to LF; SFSI, Soil fertility susceptibility index; p-value was calculated using t-test between low soil fertility and high soil fertility condition. R means TDr1302 as IITA yam breeding code. Detail codes for the genotypes presented in* ***Supplementary Material 1****.*

DISCUSSION

This study assessed white Guinea yam genotypes' response to contrasting soil fertility levels, the LF and HF at field condition. The LF condition created by planting cassava, sorghum, and maize before yam planting was significant for assessing the yam's genetic variation at variable soil nutrients. Due to cassava, sorghum and maize cultivation from 2016 to 2018, the nitrogen, phosphorus and potassium contents decreased by 0.10%, 4.50% and 0.32 Cmol[+]kg^{-1}, respectively (**Table 1**). Cassava is heavy soil nutrient mining crop that could remove up to 86 - 177 kg ha^{-1} nitrogen, 70 - 104 kg ha^{-1} phosphorus and 70 - 104 kg ha^{-1} potassium from the soil during the growing period (Ezui et al., 2017). Likewise, Kumar et al. (2017) reported that sorghum plant could remove up to 107 - 290 kg ha^{-1} nitrogen, 62 -152 kg ha^{-1} phosphorus and 339 - 731 kg ha^{-1} potassium from the soil during growing period. Heckman et al. (2003) has quantified the nutrient removal by maize grain as 10.2 to 15.0 g kg^{-1} of nitrogen, 2.2 to 5.4 g kg^{-1} of phosphorus and 3.1 to 6.2 g kg^{-1} potassium. Soil mineral nutrient depletion by planting cassava, sorghum and maize in our experimental field was substantial. According to Chude et al. (2011), our experimental field (**Table 1**) had available low soil nutrients and could be inferred as close to a critical level for yam cultivation. Though the critical soil nutrient levels for yam cultivation has not yet established in West Africa, yam cultivation in soils containing < 0.1% nitrogen, < 10 mg kg^{-1} available P, and 0.15 Cmol[+] kg^{-1} of exchangeable K requires external fertilizer inputs (Carsky et al., 2010).

Yam tubers express variable sprouting time depending on the position or section of the tuber cut as a sett and used for planting. Seed tuber setts cut from the head section often sprouts earlier than that cut from the middle and tuber tail parts (Onwueme, 1973). The variation in sprout emergence time is the main cause

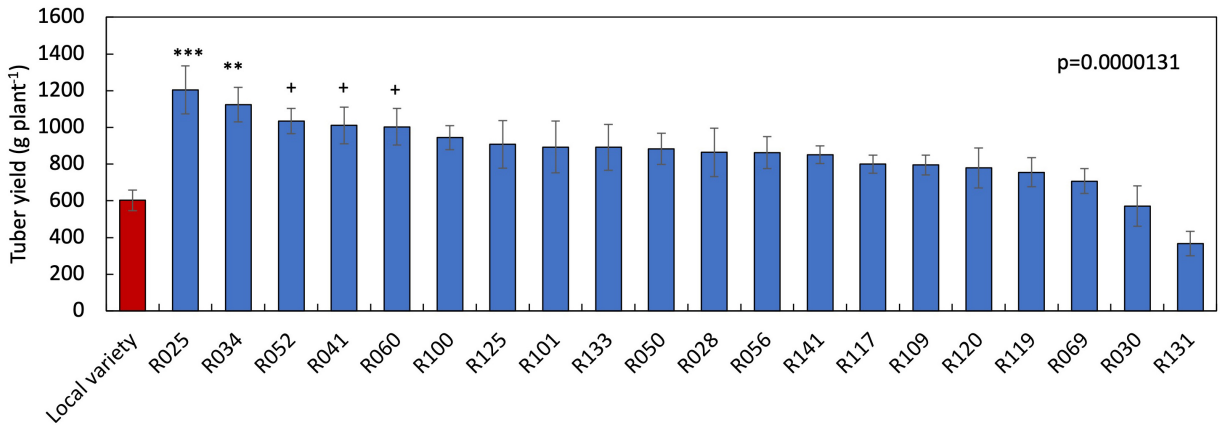


FIGURE 3 | Varietal differences in tuber yield in 21 white Guinea yam genotypes at low nutrients soil conditions. Data are the average of values obtained during a 2-year field experiment. Statistical significance was determined by Dunnett's test. ***($p < 0.001$), **($p < 0.01$) and + ($p < 0.1$) when compared with the local variety. Bars indicate standard error ($n = 12$). R means TDr1302 as IITA yam breeding code.

of variation in shoot biomass size and tuber yield within plot in yam trials (Cornet et al., 2014). Within plot tuber yield variation due to differential sprout emergence of the tuber setts originating from the different section of the tuber is a potential factor complicating the interpretation of the field experiment results in yam. To control such variability, this study used setts from the middle section tubers as planting material and pre-sprouted them to successfully establish uniform plants within plots in the field and assess genotypes response to low soil fertility stress and added fertilizer input.

We identified genotypes sensitive and tolerant to low nutrient soil stress using the susceptibility index values (**Tables 3**, **4**). The susceptibility index has been widely used to identify sensitive and tolerant genotypes for drought stress in wheat (Fischer and Maurer, 1978; Clarke et al., 1984; Winter et al., 1988; Clarke et al., 1992), maize, triticale (Kutlu and Kinaci, 2010; Grzesiak et al., 2013), and cassava (Oliveira et al., 2017) and soil fertility stress in common bean (Singh et al., 2003). Accordingly, R119, R109, and R131 combined higher SFSI values with tuber yield increase at HF condition were suitable candidates to maximize productivity under high input cultivation. Likewise, R034, R041, R050, R052, R060, R100, and R125 combined lower SFSI with a low rate of reduction in tuber yield were tolerant to low soil fertility stress. The genotype R025 and R034 had the tuber yielding potential twice of local variety under low nutrient soil stress (**Figure 3**). Besides, R025 has the yield potential of more than 1 kg of tuber plant^{-1} under the LF condition, which is higher than that has been reported in previous white Guinea yam study (Sartie et al., 2012).

There have been many conflicting reports on fertilizers' effect on yam production (Enesi et al., 2017). It is presumed that the variation in weather conditions and trial soil fertility status are the possible causes for these conflicting reports (Kang and Wilson, 1981; Lugo et al., 1993; Diby et al., 2011). Varietal differences in fertilizer responses and susceptibility to the low soil fertility might complicate the understanding of application of the fertilizer trial results in yam cultivation. Fertilizer response in yam seems genotype and growth context specific. Hence, genetic improvement efforts need to integrate high yields with high nutrient use efficiency at target farming system

TABLE 4 | Effect of genotype and soil fertility on shoot dry weight (gram per plant) in 21 white Guinea yam genotypes.

Genotype	Shoot dry weight (g plant^{-1})†				
	LF	HF	PR	*p*-Value	SFSI
R125	110.3	142.5	22.6	0.06	0.64
R101	107.4	139.0	22.7	0.16	0.66
R052	108.3	143.9	24.8	0.14	0.71
R041	127.0	172.6	26.4	0.06	0.76
R141	113.3	153.9	26.3	0.05	0.76
Local variety	104.1	150.4	30.8	0.06	0.08
R060	97.7	142.5	31.4	0.10	0.89
R120	101.9	152.2	33.1	0.03	0.95
R100	104.4	159.4	34.5	0.04	0.97
R028	113.1	171.7	34.1	0.00	0.99
R069	92.9	142.3	34.7	0.02	1.00
R025	116.4	177.9	34.6	0.05	1.00
R133	102.3	164.2	37.7	0.01	1.08
R117	100.9	162.3	37.8	0.03	1.09
R034	101.8	167.4	39.2	0.01	1.12
R050	98.6	163.6	39.7	0.02	1.14
R056	98.0	164.5	40.4	0.01	1.16
R119	99.3	170.6	41.8	0.04	1.20
R030	84.9	148.7	42.9	0.01	1.24
R109	106.3	188.1	43.5	0.00	1.25
R131	80.1	145.4	44.9	0.02	1.30
Mean	103.3	158.2	34.7		0.99

†*LF, low soil fertility; HF, high soil fertility; PR, present reduction due to LF; SFSI, Soil fertility susceptibility index. p-Value was calculated using t-test between low soil fertility and high soil fertility condition. R means TDr1302 as IITA yam breeding code. Detail codes for the genotypes presented in* ***Supplementary Material 1****.*

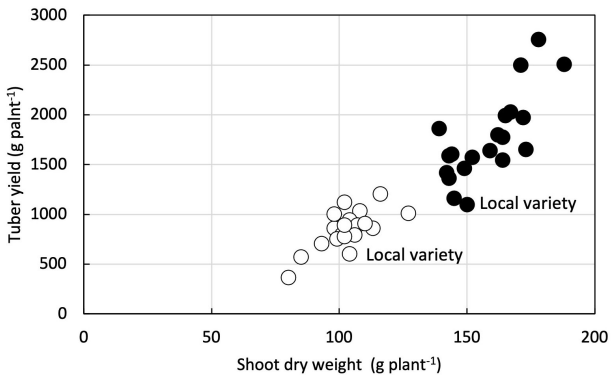


FIGURE 4 | Correlation between shoot dry weight and tuber yield under low nutrients soil fertility condition and high nutrient soil condition in 21 white Guinea yam genotypes.

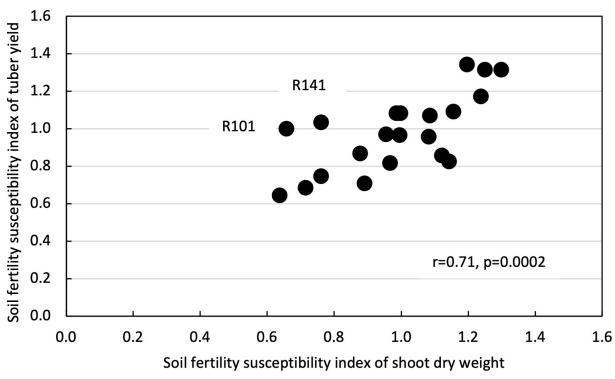


FIGURE 5 | Correlation between soil fertility susceptibility index of shoot dry weight and soil fertility susceptibility index of tuber yield in 21 white Guinea yam genotypes. R means TDr1302 as IITA yam breeding code.

(Asiedu and Sartie, 2010). The use of nutrient efficient genotypes should be maximized through breeding and genetic studies to establish environmentally friendly/sustainable agriculture in yam farming system.

We found that the breeding lines performed better than the local variety for low soil fertility tolerance and the added fertilizer response in our experiment. The observed superiority of improved genotypes compared to the local variety 'Amula' could be genetic or health status of the planting materials used. Seed degeneration due to virus infection/load is a critical problem with clonally propagated crops like yam. Yield reduction due to virus disease has been reported to be over 40% in yams (Kenyon et al., 2001). The local variety's viral load might be higher than breeding genotypes used in the experiment as local cultivar's chronological age is not well known. It has been cultivated and maintained in the field for several years by vegetative propagation, which could have caused the sub-optimal yield performance. The planting materials used in our trial, including the local variety, were visually selected disease-free tubers from disease-free plants. Work done in IITA on a positive selection with seed yam showed a significant decrease in virus incidence and disease severity score while maintaining reasonably good yields (Aihebhoria et al., 2017). However, we did not index the virus status of the planting materials in our trial and acknowledge the sub-optimal yield of local variety could be a confounded effect of the health status of the variety used in the trial.

We noticed an increase in shoot dry weight with added fertilizer, but the impact varied over the years (**Figure 2** and **Table 2**). The difference in fertilizer impact between 2018 and 2019 may be due to different meteorological conditions during field experiments (**Figure 2**). The temperature was identical in the two years, but the sunshine duration in 2018 was longer than in 2019, mostly from 30 to 90 days after planting when it was shoot growth phase in yam plants (Lebot, 2019). Since the total rainfall in 2019 was higher than in 2018, it could be considered that the utilization efficiency was low due to the outflow of fertilizer by the rain. However, detailed data of meteorological conditions were not recorded and also out of scope this study to quantify nutrient loss by leaching and surface run-off. Attempt was made to apply fertilizer in no rainy days to avoid the chance of excessive nutrient loss from the trial field. Therefore, further investigation is needed to determine type of meteorological factors that influence the fertilizer's impact on the shoot growth of white Guinea yam.

Our results revealed higher shoot biomass is critical for increased tuber yields in LF and HF conditions (**Figure 4**). Biomass accumulation and partitioning predicts the tuber yield in yam. Enhanced shoot biomass could support higher tuber yield through the genotype's efficiency for photosynthate accumulation and partitioning to the storage organ. The positive relationship between fresh tuber yield and shoot dry weight has also been reported (Akoroda, 1984; Sartie et al., 2012) and indicated that vigor biomass might be a morphological marker for selecting genotypes of white Guinea yam for high tuber yield (Sartie et al., 2012). On the other hand, it was suggested that SFSI of shoot growth alone as selection criteria for LF tolerance is not advocated. In genotypes, the SFSI in the shoot growth and the tuber yield was not consistent (**Figure 5**). Mineral fertilizer effect on yam shoot growth is greatly affected by the growth condition or environment. In contrast, the effect of fertilizer application on tuber yield was greatly affected by the genotypes used (**Table 2**). Our results, however, were based on limited sample size; hence the further analysis of a large population would provide a better understanding of SFSI of shoot and tuber yield in white Guinea yam. In addition, it has been reported that the predicted value of shoot dry weight using NDVI-based phenotyping method in *D. rotundata* is underestimated when shoot dry weight exceeds 200 g plant^{-1} (Iseki and Matsumoto, 2019). However, the predicted value of shoot dry weight rarely exceeded 200 g plant^{-1} even in HF condition. This is in agreement with the finding from the previous study on *D. rotundata* (Iseki and Matsumoto, 2019). In this sense, the method could also be useful to apply for field evaluation.

In this study, genotypic differences among white Guinea yam (*D. rotundata*) genotypes in response to low soil fertility and added fertilizer input (NPK) were investigated. Future research should include more physiological studies of yam, as there

is minimal information available currently. The present study revealed wide variations among the white Guinea yam genotypes for low soil fertility tolerance and added fertilizer response. The genotypes, R034, R041, R050, R052, R060, R100, and R125, were identified as low soil tolerance genotypes in this study. On the other hand, R119, R109, and R131 were susceptible to available low soil nutrient but responsive to mineral fertilizer input. Besides, R025 and R034 have a high potential to produce higher tuber yield than the local variety under LF conditions. The use of superior genotypes identified herewith should be maximized in breeding and genetic studies to develop improved varieties that enhance productivity under variable yam farming systems.

DATA AVAILABILITY STATEMENT

The original contributions presented in the study are included in the article/**Supplementary Material**, further inquiries can be directed to the corresponding author/s.

AUTHOR CONTRIBUTIONS

RM did the conceptualization, methodology and formal analysis, investigation and fieldwork, and writing-original draft preparation. HI, AA, and RA wrote, reviewed, and edited. HI did the project administration and funding acquisition. All authors read and agreed to the published version of the manuscript.

FUNDING

This research was supported by Ministry of Agriculture, Forestry and Fisheries through the "MAFF yam project".

ACKNOWLEDGMENTS

The authors wish to thank IITA for allowing us to use their facilities. We acknowledge IITA staff for their support. This study was performed with funds provided by the Ministry of Agriculture, Forestry, and Fisheries through the "MAFF yam project," for which the authors are grateful.

SUPPLEMENTARY MATERIAL

The Supplementary Material for this article can be found online at: https://www.frontiersin.org/articles/10.3389/fpls.2021.629762/full#supplementary-material

REFERENCES

Aihebhoria, D. O., Aighewi, B., and Balogun, M. O. (2017). The response of white Yam (*Dioscorea rotundata* Poir) tuber portions to positive selection for quality seed yam production. *Adv. Crop Sci. Technol.* 5:294. doi: 10.4172/2329-8863.1000294

Akoroda, M. O. (1984). Variability, repeatability, character correlation and path coefficient analyses in yellow yam. *Theor. Appl. Genet.* 69, 217–221. doi: 10.1007/BF00272898

Altman, N., and Krzywinski, M. (2015). Points of significance: split plot design. *Nat. Methods* 12, 165–166. doi: 10.1038/nmeth.3293

Asfaw, A., Aderonmu, D. S., Darkwa, K., De Keoyer, D., Agre, P., Abe, A., et al. (2020). Genetic parameters, prediction, and selection in a white Guinea yam early-generation breeding population using pedigree information. *Crop Sci.* 2020, 1–14. doi: 10.1002/cs2.20382

Asiedu, R., and Sartie, A. (2010). Crops that feed the world 1. Yams. Yams for income and food security. *Food Secur.* 2, 305–315. doi: 10.1007/s12571-010-0085-0

Bates, D. M. (2010). *R Package "lme4"*. Available online at: https://cran.Rproject.org/web/packages/lme4/lme4.pdf (accessed April 30, 2020).

Bremner, J. M., and Mulvaney, C. S. (1982). "Methods of soil analysis," in *American Society of Agronomy*, eds A. L. Page, R. H. Miller, and D. R. Keeny (Madison: Soil Science Society of America), 1119–1123.

Carsky, R. J., Asiedu, R., and Cornet, D. (2010). Review of soil fertility management for yam-based systems in West Africa. *Afr. J. Root Tuber Crops* 8, 1–17.

Chude, V. O., Olayiwola, S. O., Osho, A. O., and Daudu, C. K. (2011). *Fertilizer Use and Management Practices for Crops in Nigeria*. Abuja: Federal Fertilizer Department, Federal Ministry of Agricultural and Rural Development, 215.

Clarke, J. M., De Pauw, R. M., and Townley- Smith, T. W. (1992). Evaluation of methods for quantification of drought tolerance in wheat. *Crop Sci.* 32, 728–732. doi: 10.2135/cropsci1992.0011183X003200030029x

Clarke, J. M., Towenley-Smith, T. M., Mccaig, T. N., and Green, D. G. (1984). Growth analysis of spring wheat cultivars of varying drought resistance. *Crop Sci.* 24, 537–541. doi: 10.2135/cropsci1984.0011183X002400030026x

Cornet, D., Sierra, J., Tournebize, R., and Ney, B. (2014). Yams (*Dioscorea* spp.) plant size hierarchy and yield variability: emergence time is critical. *Eur. J. Agron.* 55, 100–107. doi: 10.1016/j.eja.2014.02.002

Darkwa, K., Agre, P., Olasanmi, B., Iseki, K., Matsumoto, R., Powell, A., et al. (2020). Comparative assessment of genetic diversity matrices and clustering methods in white Guinea yam (*Dioscorea rotundata*) based on morphological and molecular markers. *Sci. Rep.* 10:13191. doi: 10.1038/s41598-020-69925-9

Degras, L. (1993). *The Yam. A Tropical Root Crop*. London: Macmillan Press Ltd, 408.

Diby, L. N., Tie, T. B., Girardin, O., Sangakkara, R., and Frossard, E. (2011). Growth and nutrient use efficiencies of yams (*Dioscorea* spp.) grown in two contrasting soils of West Africa. *Int. J. Agron.* 2011:175958. doi: 10.1155/2011/175958

Diby, N. L., Hgaza, V. K., Tie, T. B., Assa, A., Carsky, R., Girardin, O., et al. (2009). Productivity of yams (*Dioscorea* spp.) as affected by soil fertility. *J. Anim. Plant Sci.* 5, 494–506.

Enesi, R. O., Hauser, S., Lopez-Montez, A., and Osonubi, O. (2017). Yam tuber and maize grain yield response to cropping system intensification in south-west Nigeria. *Arch. Agron. Soil Sci.* 64, 953–966. doi: 10.1080/03650340.2017.1404580

Ezui, K. S., Franke, A. C., Ahiabor, B. D. K., Tetteh, F. M., Sogbedji, J., Janssen, B. H., et al. (2017). Understanding cassava yield response to soil and fertilizer nutrient supply in West Africa. *Plant Soil* 420, 331–347. doi: 10.1007/s11104-017-3387-6

FAOSTAT (2020). Available online at: http://www.fao.org/faostat/en/#home (accessed May 7, 2020).

Fischer, R. A., and Maurer, R. (1978). Drought resistance in spring wheat cultivars. I. Grain yield responses. *Aust. J. Agric. Res.* 29, 897–912. doi: 10.1071/AR9780897

Grzesiak, M. T., Waligórski, P., Janowiak, F., Marcińska, I., Hura, K., Szczyrek, P., et al. (2013). The relations between drought susceptibility index based on grain yield (DSIGY) and key physiological seedling traits in maize and triticale genotypes. *Acta Physiol. Plant* 35, 549–565. doi: 10.1007/s11738-012-1097-5

Heanes, D. L. (1984). Determination of total organic carbon in soils by an improved chromic acid digestion and spectrophotometric procedure. *Comm. Soil Sci. Plant Anal.* 15, 1191–1213. doi: 10.1080/00103628409367551

Heckman, J. R., Sims, J. T., Beegle, D. B., Coale, F. J., Herbert, S. J., Bruulsema, T. W., et al. (2003). Nutrient removal by corn grain harvest. *Agron. J.* 95, 587–591. doi: 10.2134/agronj2003.5870

Hothorn, T., Bretz, F., Westfall, P., and Hothorn, M. T. (2020). *R Package 'Multcomp'*. Available online at: https://cran.Rproject.org/web/packages/multcomp/multcomp.pdf (accessed April 30, 2020).

Irving, H. (1956). Fertilizer experiments with yams in eastern Nigeria 1947-1951. *Trop. Agric. Trinidad* 33, 67–78.

Iseki, K., and Matsumoto, R. (2019). Non-destructive shoot biomass evaluation using a handheld NDVI sensor for field-grown staking yam (*Dioscorea rotundata* Poir.). *Plant Pro. Sci.* 22, 301–310. doi: 10.1080/1343943X.2018.1540278

Kang, B. T., and Wilson, J. E. (1981). Effect of mound size and fertilizer on white Guinea yam (*Dioscorea rotundata*) in Southern Nigeria. *Plant Soil* 61, 319–327. doi: 10.1007/BF02182013

Kassambara, A. (2020). *R package "Ggpubr"*. Available online at: https://cran.Rproject.org/web/packages/ggpubr/ggpubr.pdf (accessed April 30, 2020).

Kenyon, L., Shoyinka, S. A., Hughes, J. A., and Odu, B. O. (2001). "An overview of viruses infecting Dioscorea yams in sub-Saharan Africa," in *Proceedings of a conference on Plant Virology in Sub Saharan Africa,* (Ibadan) 432–439.

Kihara, J., Bolo, P., Kinyua, M., Nyawira, S. S., and Somer, R. (2020). Soil health and ecosystem services: lessons from sub-Sahara Africa (SSA). *Geoderma* 370:114342. doi: 10.1016/j.geoderma.2020.114342

Kpeglo, K. D., Obigbesan, G. O., and Wilson, J. E. (1981). "Yield and shelf life of white yam as influenced by fertilizer," in *Tropical Root Crops: Research Strategies for the 1980s. Proceedings of the First Triennial Root Crops Symposium of the International Society for Tropical Root Crops-Africa Branch*, eds E. R. Terry, K. A. Oduro, and F. Cavenes (Ottawa: International Development Research Centre).

Kumar, R., Mishra, J. S., Dwivedi, S. K., Kumar, R., Rao, K. K., Samal, S. K., et al. (2017). Nutrient uptake and content in sorghum cultivars (*Sorghum bicolor* L) under summer environment. *Ind. J. Plant Physiol.* 22, 309–315. doi: 10.1007/s40502-017-0306-z

Kutlu, I., and Kinaci, G. (2010). Evaluation of drought resistance indicates for yield and its components in three *Triticale* cultivars. *J. Tekirdag Agric. Faculty* 7, 95–103.

Lebot, V. (2019). *Tropical Root and Tuber Crops: Cassava, Sweet Potato, Yams and Aroids*. Crop Production Science in Horticulture Series 17. Wallingford, CT: CABI. doi: 10.1079/9781789243369.0000

Lugo, W. I. H. M., González, A., Rafols, N., and Almodóvar, C. (1993). Tillage and fertilizer rate effects on yam yields (*Dioscorea alata* L.). *J. Agric. Univ. P.R.* 77, 153–159. doi: 10.46429/jaupr.v77i3-4.4203

Lyonga, S. N. (1981). "The economics of yam cultivation in Cameroon," in *Tropical Root Crops: Research Strategies for the 1980s. in Proceedings of the First Triennial Root Crops Symposium of the International Society for Tropical Root Crops-Africa Branch*, eds E. R. Terry, K. A. Oduro, and F. Cavenes (Ottawa: International Development Research Centre).

Manyong, V. M., and Nokoe, S. K. (2003). "Modelling of yam production for effective policy formulation," in *Proceedings of the 8th Triennial Symposium of the International Society for Tropical Root CropsAfrica Branch (ISTRC-AB),* ed. M. O. Akoroda (Ibadan), 48–51.

Mehlich, M. (1984). Mehlich 3 soil test extractant: a modification of the Mehlich 2 extractant. *Commun. Soil Sci. Plant Anal.* 15, 1409–1416. doi: 10.1080/00103628409367568

Oliveira, E. J., Morgante, C. V., and de Tarso Aidar, S. (2017). Evaluation of cassava germplasm for drought tolerance under field conditions. *Euphytica* 213:188. doi: 10.1007/s10681-017-1972-7

Onwueme, I. (1973). The sprouting process in yam (*Dioscorea* spp.) tuber pieces. *J. Agric. Sci.* 81, 375–379. doi: 10.1017/S0021859600086408

O'Sullivan, J. N., and Ernest, J. (2008). *Yam Nutrition and Soil Fertility uanagement in the Pacific.* 143 Canberra: ACIAR.

Ouédraogo, E. (2004). *Soil Quality Improvement for Crop Production in Semi-Arid West Africa*. Tropical Resource Management Papers, vol. 51. Ph.D. thesis, Wageningen University, Wageningen.

R Core Team (2018). *R: A Language and Environment for Statistical Computing*. Vienna: R Foundation for Statistical Computing.

Sartie, A. M., Franco, J., and Asiedu, R. (2012). Phenotypic analysis of tuber yield- and maturity- related traits in water yam (*Dioscorea alata*). *J. Agric. Sci. Technol. B.* 1, 311–322. doi: 10.5897/AJB11.1292

Scott, G. J., Rosegrant, M., and Ringler, C. (2000). "Roots and tubers for the 21st century: trends, projections and policy options," in *Food, Agriculture and the Environment Discussion 31* (Washington, DC: International Food Policy Research Institute (IFPRI) and International Potato Center (CIP)).

Singh, S. P., Teran, H., Munoz, C. G., Osorno, J. M., Takegami, J. C., and Thung, M. D. (2003). Low soil fertility tolerance in landraces and improved common bean genotypes. *Crop Sci.* 43, 110–119. doi: 10.2135/cropsci2003.0110

Watson, K. A., and Goldsworthy, P. R. (1964). Soil fertility investigations in middle belt of Nigeria. *Emp. J. Exp. Agric.* 32, 290–302.

Winter, S. R., Musick, J. T., and Porter, K. B. (1988). Evaluation of screening techniques for breeding drought-resistance winter wheat. *Crop Sci.* 28, 512–516. doi: 10.2135/cropsci1988.0011183X002800030018x

Wright, K. (2018). *R Package "Plot a Correlogram"*. Available online at: https://cran.Rproject.org/web/packages/corrgram/corrgram.pdf (accessed April 30, 2020).

Conflict of Interest: The authors declare that the research was conducted in the absence of any commercial or financial relationships that could be construed as a potential conflict of interest.

Copyright © 2021 Matsumoto, Ishikawa, Asfaw and Asiedu. This is an open-access article distributed under the terms of the Creative Commons Attribution License (CC BY). The use, distribution or reproduction in other forums is permitted, provided the original author(s) and the copyright owner(s) are credited and that the original publication in this journal is cited, in accordance with accepted academic practice. No use, distribution or reproduction is permitted which does not comply with these terms.

frontiers in Plant Science

ORIGINAL RESEARCH
published: 26 February 2021
doi: 10.3389/fpls.2021.628960

Responses of Maize Internode to Water Deficit Are Different at the Biochemical and Histological Levels

*Fadi El Hage[1,2†], Laetitia Virlouvet[1], Paul-Louis Lopez-Marnet[1,3], Yves Griveau[1], Marie-Pierre Jacquemot[1], Sylvie Coursol[1], Valérie Méchin[1] and Matthieu Reymond[1]**

[1] Institut Jean-Pierre Bourgin, INRAE, AgroParisTech, Université Paris-Saclay, Versailles, France, [2] Ecole Doctorale n° 567: Science du Végétal: Du gène à l'écosystème, Université Paris-Saclay, Orsay, France, [3] Ecole Doctorale n° 581: ABIES, Paris, France

Maize feeding value is strongly linked to plant digestibility. Cell wall composition and structure can partly explain cell wall digestibility variations, and we recently showed that tissue lignification and lignin spatial distribution also contribute to cell wall digestibility variations. Although the genetic determinism of digestibility and cell wall composition has been studied for more than 20 years, little is available concerning that of tissue lignification. Moreover, maize yield is negatively impacted by water deficit, and we newly highlighted the impact of water deficit on cell wall digestibility and composition together with tissue lignification. Consequently, the aim of this study was to explore the genetic mechanisms of lignin distribution in link with cell wall composition and digestibility under contrasted water regimes. Maize internodes from a recombinant inbred line (RIL) population grown in field trials with contrasting irrigation scenarios were biochemically and histologically quantified. Results obtained showed that biochemical and histological traits have different response thresholds to water deficit. Histological profiles were therefore only modified under pronounced water deficit, while most of the biochemical traits responded whatever the strength of the water deficit. Three main clusters of quantitative trait locus (QTL) for histological traits were detected. Interestingly, overlap between the biochemical and histological clusters is rare, and one noted especially colocalizations between histological QTL/clusters and QTL for *p*-coumaric acid content. These findings reinforce the suspected role of tissue p-coumaroylation for both the agronomic properties of plants as well as their digestibility.

Keywords: maize internode, histological profile, cell wall biochemical composition, water deficit, quantitative trait locus

OPEN ACCESS

Edited by:
Raul Antonio Sperotto, Universidade do Vale do Taquari - Univates, Brazil

Reviewed by:
Rogelio Santiago, University of Vigo, Spain
Fa Cui, University of Chinese Academy of Sciences, China

***Correspondence:**
Matthieu Reymond
matthieu.reymond@inrae.fr

†Present address:
Fadi El Hage, Arvalis Institut du Végétal – Station Expérimentale HTPT – Route de Malesherbes, Boigneville, France

Specialty section:
This article was submitted to Crop and Product Physiology, a section of the journal Frontiers in Plant Science

Received: *13 November 2020*
Accepted: *22 January 2021*
Published: *26 February 2021*

Citation:
El Hage F, Virlouvet L, Lopez-Marnet P-L, Griveau Y, Jacquemot M-P, Coursol S, Méchin V and Reymond M (2021) Responses of Maize Internode to Water Deficit Are Different at the Biochemical and Histological Levels. Front. Plant Sci. 12:628960. doi: 10.3389/fpls.2021.628960

INTRODUCTION

Maize is nowadays a staple food in the world (Shiferaw et al., 2011). It not only provides carbohydrates, proteins, lipids, and vitamins for billions of people but also serves as an important energy resource for animal feed and biorefinery processes (Virlouvet et al., 2019). Its energy value is first related to its cell wall digestibility.

Maize stem represents up to 46% of the plant dry weight (Hansey et al., 2010) and is made of distinct tissues, distributed in the rind and the pith sections, which do not have the same levels of lignification, *p*-coumaroylation, and feruloylation (Lopez et al., 1993; Chesson et al., 1997; El Hage et al., 2018; Santiago et al., 2018) nor the same efficiency of enzymatic digestibility

(Lopez et al., 1993; Jung and Casler, 2006; El Hage et al., 2018). Therefore, spatial consideration of the maize stem will provide valuable knowledge to improve its utilization.

Recently, a non-lethal and cost-effective method has been proposed by puncture test (Seegmiller et al., 2020) to quantify rind thickness and stalk diameter on poison hemlock (*Conium maculatum*). Nevertheless, standardization of this method (for instance, puncturing probe geometry) is required to carry out meta-analysis of the results obtained by several groups (Cook et al., 2020). Other methods to quantify stem anatomy rely on the characterization of internode cross sections. An image processing software has been proposed to quantify rind thickness; pith area; vascular bundle number; and size in pith section of maize, sorghum, and other grass species (Heckwolf et al., 2015). Images are acquired on hand-cut cross section with a flatbed document scanner. The anatomical quantification rate required for genetic and physiological studies is therefore achieved. However, this method does not allow to demarcate the pith of the rind (Casto et al., 2018). In contrast, FASGA (abbreviation of Spanish names of fucsina, alcian blue, safranina, glicerina, and aqua) staining of internode cross sections (Tolivia and Tolivia, 1987) is a powerful approach that allows to distinguish highly lignified tissues and poorly lignified tissues. It was recently applied in sorghum (Perrier et al., 2017) and maize (El Hage et al., 2018; Vo et al., 2020) cross sections. Moreover, the advent of several plugins (Zhang et al., 2013; Legland et al., 2017) is allowing quantification of anatomical features from FASGA-stained cross sections, increasing the throughput of data analysis.

Variation of stem anatomical structure between genotypes has been revealed either by scoring visually the structure or by using the different quantification methods as described. For example, using a visual score, Casto et al. (2018) identified in different sorghum bi-parental populations a quantitative trait locus (QTL) on chromosome 6 that accounted for a large part of the variation in the amount of aerenchyma in these populations. Huang et al. (2016) similarly identified 16 QTL in a maize-teosinte population that accounted for 52% of the variation in the number of vascular bundle in the uppermost internode of that population. Using the protocol developed by Heckwolf et al. (2015); Mazaheri et al. (2019) also identified several candidate genes associated with maize stalk diameter, rind thickness, and vascular bundle density. However, to the best of our knowledge, no studies compare the position of QTL underlying biochemical trait variations to that of QTL underlying the variation of spatial distribution of lignified tissues.

In addition, severe episodes of drought are projected to become more frequent in the near future because of climate change (Harrison et al., 2014). We recently highlighted the impact of water deficit on cell wall digestibility and composition together with tissue lignification (El Hage et al., 2018; Virlouvet et al., 2019). Consequently, there is a need to elucidate the genetic determinism of lignin distribution in link with cell wall composition and digestibility for optimizing maize energetic value under water-limited conditions. To this end, the present study aimed at evaluating the biochemical and histological traits underlying the variation of cell wall digestibility in the maize stem and its plasticity in response to water deficit. A recombinant inbred line (RIL) population derived from the cross between F271 and Cm484 lines (Virlouvet et al., 2019) was evaluated during 2 years in the field under two contrasted irrigation scenarios. At final harvest, plant height, stem dry weight, biochemical composition, and tissue histology of the internode under the main ear were measured using high-throughput dedicated tools. A number of significant QTL for biochemical and histological traits were detected. Several colocalizations between histological QTL and QTL for PCAest were identified, supporting the major role of tissue *p*-coumaroylation for both the agronomic properties of plants as well as their digestibility.

MATERIALS AND METHODS

Plant Materials and Field Experiments

A RIL population consisting of 267 lines was developed at INRAE by single seed descent (SSD) for six generations from a cross between maize inbred lines F271 and Cm484 as described (Virlouvet et al., 2019). All the RILs were planted in a randomized augmented block design in open field trials at Mauguio (France). Four replicates were carried out over 2 years (2014 and 2015) under irrigated (I) and non-irrigated (NI) conditions as described (Virlouvet et al., 2019). Briefly, under the I scenario, the water was supplied with a mobile ramp of sprinklers twice a week (30 mm of water supplied every time). Under the NI scenario, water was no more supplied when plants reached the five-leaf collar stage until 14 days after all the RILs flowered. Parental lines were replicated in each block of the design in 2014.I, 2014.NI, 2015.I, and 2015.NI. In 2014.I and 2014.NI, 201 plots were divided into eight blocks. In each block, parental lines F271 and Cm484 were cultivated in one plot each. RILs were cultivated on the other plots. At silage stage, among the 201 plots cultivated in 2014.I, stovers were harvested from 170 plots and internodes from 175 plots, due to heterogeneity of plants within a plot or due to low number of plants present in some plots. In 2014.NI, stovers were harvested from 170 plots and internodes from 174 plots. In 2015.I and NI, 189 plots were divided into eight blocks. In each block, parental lines F271 and Cm484 were cultivated in one plot each. At silage stage, stovers were harvested on 180 plots and internodes on 183 plots in 2015.I and stovers and internodes on 147 plots in 2015.NI. In each plot, 36 seeds from the same inbred line were sown and only the first internode below the main ear was harvested among the grown plants at silage stage. On one side, 10 internodes below the main ear of 10 plants were harvested and pooled, dried (in a forced-air oven at 55°C during 72 h), and grinded (with a hammer mill—1-mm grid) for NIRS acquisition. On the other side, two internodes below the main ear were harvested from two others plants and stored in 70% ethanol for histological quantifications. Hence, only internodes below the main ear were harvested for biochemical and histological quantification, avoiding differences due to different tissue sampling between biochemical predictions and histological quantifications. Each line was grown in a single 4.20-m row with 0.80 m between rows and a planting density of 80,000 plants ha^{-1}.

Biochemical Analyses and Establishment of NIRS Predictive Equations

First, the NIRS predictive equations for the internode previously described (El Hage et al., 2018) were enriched with the results from wet biochemistry analyses of 56 samples from the RIL population collected in Mauguio in 2014 and 2015. The 56 samples were selected to cover the range of spectral variation obtained on all the samples collected in 2014 and 2015 in irrigated and non-irrigated conditions. To do so, we performed a principal component analysis (PCA) carried out on NIRS spectrum acquired on all the harvested internode samples, and we selected 56 samples that were evenly distributed on the PCA axes. Biochemical quantifications performed on the calibration samples set were the following (**Supplementary Table S1**): (1) cell wall content (CWR) was obtained with a water/ethanol extraction (Soxhlet); (2) lignin content in the cell wall (KL.CWR) was estimated using the Klason method (Dence, 1992); (3) the monomeric structure and composition of lignin (units bO4.S, bO4.G, and bO4.H) were obtained by thioacydolysis (Lapierre et al., 1986); (4) PCAest, FAest, and FAeth were obtained by alkaline hydrolysis (Morrison et al., 1994; Culhaoglu et al., 2011); (5) glucose, xylose, and arabinose contents were quantified by acidic hydrolysis (Updegraff, 1969; Harholt et al., 2006), and cellulose content was estimated by glucose content, and hemicellulose content has been obtained by adding xylose and arabinose; and (6) acidic pretreatment of DM and CWR followed by an enzymatic hydrolysis (Onozuka cellulase R10) bring the *in vitro* DM degradability (IVDMD) and cell wall degradability (IVCWRD), respectively, as described (Virlouvet et al., 2019). Second, 683 DM internode samples were scanned through a near-infrared reflectance spectrometer (Antaris II, Thermo Fisher Scientific). The biochemical traits were then estimated using the updated NIRS predictive equations.

Histological Analyses

Histological analyses have been carried out as described (Legland et al., 2017). Briefly, a 1-cm-long segment was sampled in the upper part of each internode 1.5 cm under the node. For each segment, one cross-section with a thickness of 150 μm was prepared. A total of 1,367 cross-sections were obtained using a sledge-microtome GSL1 (Gärtner et al., 2014) and stored in 70% ethanol. Sections were then stained for 24 h using a FASGA solution diluted in distilled water (1:8, *v*/*v*) and finally rinsed for 24 h with distilled water while stirring continuously. After two other successive washings during 5 min in MQ water, all the cross-sections were mounted in distilled water on slides and an image of each cross-section was acquired using a slide scanner piloted by the Metafer Scanning and Imaging Platform (MetaSystems GmbH, Altlussheim, Germany). Finally, each image was numerically analyzed on the ImageJ software to segment and quantify histological traits (Legland et al., 2017). The following nine histological traits were quantified:

- Stem_area, which is the area in square centimeter of the cross-section;
- Bundle_fraction, which is the percentage of the cross-section area occupied by the bundles;
- Bundle_number, which is the number of bundles in the pith of the cross-section;
- Lignified_fraction, which is the percentage of the cross-section area occupied by parenchyma stained by the safranin;
- Non-lignified_fraction, which is the percentage of the cross-section area occupied by parenchyma stained by the alcian blue;
- Rind_fraction, which is the percentage of the cross-section area occupied by the rind;

From all these traits quantified by the plugin, we calculated composite variables to synthetize the following information:

- Blue_parenchyma, which refers to the amount of blue intensity in the blue parenchyma;
- Red_parenchyma, which refers to the amount of red intensity in the red parenchyma;
- Red_rind, which refers to the amount of red intensity in the rind.

Statistical Analyses

All statistical analyses were performed using R software (R Core Team, 2014). To eliminate the block effect, single-plot values were corrected by a subtraction of the best linear unbiased prediction (BLUP) value of the block effect for each line, using the following mixed linear model (1):

$$Y_{\mathrm{ijkl}} = \mu + g_{\mathrm{i}} \times (1 - t_{\mathrm{i}}) + C_{\mathrm{i}} \times y_{\mathrm{i}} + e_{\mathrm{k}} + B_{\mathrm{jkl}} + g_{\mathrm{i}} + y_{\mathrm{i}} + g_{\mathrm{i}} + e_{\mathrm{k}} + y_{\mathrm{i}} + e_{\mathrm{k}} + E_{\mathrm{ijkl}} \quad (1)$$

where Y_{ijkl} is the phenotypic value of the ith recombinant inbred line in the jth year, in the kth irrigation scenario and located in the lth block. μ is the intercept. Effect of line i is considered as fixed and noted C_i if it was one of the two parental lines used as control and as random and noted g_i if i was a RIL. The parameter t_i was set to one for control lines or set to zero otherwise. The B_{jkl} block was considered as random effects, as well as the interaction between the g_i genetic and the y_j year or the e_k irrigation scenario effects. The interaction between the e_k irrigation scenario and the y_j year effects was considered as fixed effect. By using the parental replicates in each block, the parameter t_i was used to distinguish the RILs from the parental lines. On the corrected data set, another analysis of variance (ANOVA) was performed with the following linear model for each trait:

$$Y_{ij} = \mu + A_i + T_j + A_i \times T_j + R_{ij}$$

where Y_{ij} is the value of the year i under the condition j; μ = overall mean; A_i = the main effect of the year i; T_j = the main effect of the condition j; $A_i \times T_j$ = the interaction effect between the year i and the condition j; and R_{ij} = the random residual term. For each trait, heritabilities have been calculated over the years 2014 and 2015 either in I scenario or in NI scenario as the proportion of phenotypic variance explained by genotypic variance.

Principal Component Analysis

Principal component analysis (PCA) was carried out with the complete data set through all the years and treatments using FactoMineR, factoextra, ggplot2, and ggthemes.

QTL Detection

Genetic map of the population has been described previously (Virlouvet et al., 2019). Briefly, genomic DNA from 261 RIL was used for genotyping using the genotyping-by-sequencing (GBS) approach (Elshire et al., 2011). Initially, 955,720 markers were identified well-distributed on maize chromosomes 1–10. Among those, we selected 2,806 polymorphic markers between parental lines with less than 15% missing data among the RILs. These markers were then used to construct the linkage map using R scripts interacting with the CarthaGene software (de Givry et al., 2005), as described in Ganal et al. (2011). In total, 1,000 markers were retained. The total length of the framework map was 2,355 cM with an average spacing of around 2.4 cM. By looking *a posteriori* at singletons in the dataset, we verified that the increase of the genetic map length when saturating the scaffold with additional markers was not attributable to genotyping errors but more likely to the rather high level of missing data, which introduces a bias in the imputation procedure (EM algorithm) of CarthaGene as a result of genetic interference. QTL detection was performed using the multi-QTL mapping (MQM) method in the R/qtl package (Broman and Sen, 2009; Arends et al., 2010). The function mqmscan was used, setting the maximum cofactor marker number (number of individual minus 12, depending on the year and the condition), with a further processing by backward elimination. To quantify the explained variance, QTL above a LOD score at 3 (corresponding to approximately the 5% significance threshold using 1,000 permutations over all the quantified traits) were selected. The QTL detection by the MQM method was performed on the data corrected for the block effect per year and per irrigation scenario data. QTL confidence intervals were calculated as the genetic distance where LOD-1 from the QTL peak was reached.

RESULTS

Internodes of F271 Are Less Digestible, Have More Lignified Tissues in the Rind and the Pith, and Are More Sensitive to the Irrigation Scenario Than Those of Cm484

Agronomic traits were first evaluated for the two parental inbred lines F271 and Cm484. Under the I condition, plant height and biomass yield were higher in F271 than in Cm484 in both 2014 and 2015 (**Supplementary Table S2**). Under the NI scenario, these two agronomical traits decreased as expected, but less strongly in 2015 than 2014 (**Supplementary Table S2**). Furthermore, their decrease was more pronounced in F271 (reduction of 59.5 and 39% of biomass yield in 2014 and 2015, respectively, in the NI vs. I scenario; reduction of 32.7 and 9.3% of plant height in 2014 and 2015, respectively, in the NI vs. I scenario) than in Cm484 (reduction of 44.2 and 7.8% of biomass yield in 2014 and 2015, respectively, in the NI vs. I scenario; reduction of 25.9 and −0.6% of plant height in 2014 and 2015, respectively, in the NI vs. I scenario).

Quantification of cell wall biochemical traits in the internodes showed that IVDMD and IVCWRD were lower in F271 than in Cm484 whatever the year and the irrigation scenario (**Supplementary Table S2**). F271 internode contained also more lignin in the cell wall (KL.CWR) than Cm484 whatever the year and the irrigation scenario (**Supplementary Table S2**). However, for both years, the lignin content was more lowered in F271 than in Cm484 in response to the irrigation scenario. The same trend was observed for the PCAest content (**Supplementary Table S2**). Reduction of cellulose content in the cell wall was also higher in internodes of F271 than in those of Cm484 in both years studied. In contrast, hemicellulose content in the cell wall of F271 internode was similar to that of Cm484 internode and was not impacted by the different irrigation scenarios. Lignin structure (βO4 yield) was also similar for both parental lines whatever the year and the irrigation scenario.

Histological analyses showed that the cross section area of Cm484 was bigger than that of F271 in 2014 whatever the irrigation scenario (**Supplementary Table S2**). However, in 2015, F271 and Cm484 showed similar cross section area whatever the irrigation scenario. Additionally, F271 showed a greater rind section area than Cm484 whatever the year and the irrigation (**Supplementary Table S2**). The lignified fraction in the pith was also more important for F271 than for Cm484 whatever the year and the irrigation scenario, suggesting that the irrigation scenario did not impact the lignified fraction in the pith. The main difference between the two parental lines was that Cm484 showed mostly twice the amount of non-lignified fraction in the pith than F271 whatever the year and the irrigation scenario (**Supplementary Table S2**). In line with this observation, the Blue_parenchyma (i.e., the amount of blue intensity in the blue parenchyma) was always higher in Cm484 than in F271 (**Supplementary Table S2**). It is also noticeable than the Blue_parenchyma increased in F271 internode while it decreased in Cm484 internode in response to the NI scenario in 2015 (**Supplementary Table S2**). Bundle numbers were similar between the two parental lines whatever the year and the irrigation scenario (**Supplementary Table S2**). However, due to the decrease of the cross section area in response to the NI scenario, the bundle density increased in the two parental lines in response to the irrigation scenario, with the exception of Cm484 in 2015 (**Supplementary Table S2**).

Different Responses of Biochemical and Histological Traits to the Irrigation Scenario Among the F271 × Cm484 Progeny

The agronomic and cell wall-related traits were then evaluated in the F271 × Cm484 progeny, and PCA analysis was carried out for investigating these traits over the years under both irrigation scenarios (**Figure 1**). The first axis of the PCA explained 21.5% of the variation present in the data set. The traits that

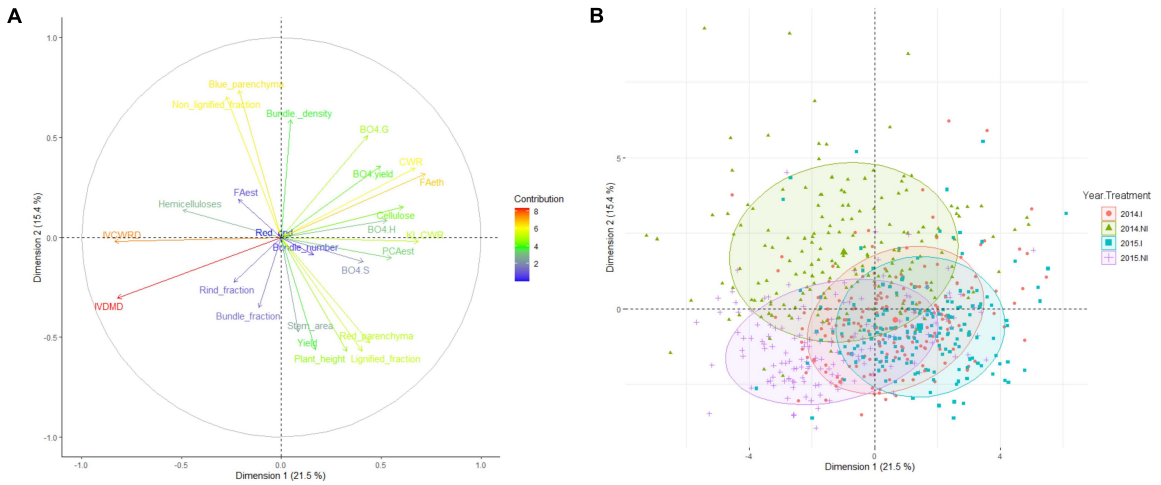


FIGURE 1 | PCA analysis including histological, biochemical, and agronomical traits quantified. **(A)** Representation of the contribution of each trait in dimension 1 (21% of the global variance) vs. dimension 2 (16.3% of the global variance). **(B)** Projection of each recombinant inbred line for each year and each irrigation scenario in dimension 1 and 2 area of the PCA analysis. Circles represent the area occupied by 70% of the RIL for each year and treatment combination.

contributed the most were IVCWRD and IVDMD on one side and FAeth, KL.CWR, CWR, cellulose, and PCAest on the other side (**Figure 1A** and **Supplementary Table S3**). Hence, this first ACP axis reflects the digestibility and the biochemical composition of the internode biomass. Internodes harvested under the I scenario in both 2014 and 2015 were located on the right side of this axis, whereas internodes harvested under the NI scenario in both 2014 and 2015 were located on the left side of this first PCA axis (**Figure 1B**). This reflects the fact that the digestibility and the biochemical composition of the internodes were modified by the NI scenario whatever the year. Under the NI scenario in both 2014 and 2015, IVCWRD increased while the lignin and PCAest contents in the cell wall decreased. Moreover, among the RIL population, the increase of IVCWRD in response to the NI scenario was similar in average for both years (**Supplementary Table S2**). The hemicellulose content in the cell wall increased slightly when internodes of the RILs were cultivated under the NI scenario in both 2014 and 2015, paralleled by a slight decrease of the cellulose content in 2014 and 2015.

The second axis of the PCA depicted 15.4% of the observed variability among the data set. The traits that contributed the most to this axis were the histological (Blue_parenchyma, Non-_lignified_fraction, and Bundle_density on one side and Lignified_fraction, Red_parenchyma, and Stem_area on the other side) and agronomical traits (Plant_height and yield) (**Figure 1A** and **Supplementary Table S3**). Internodes harvested when plant were cultivated under the I scenario in both 2014 and 2015 were located on the same position on this axis, while it was not the case for the internodes harvested under the NI scenario. Internodes harvested in 2015 were close to those harvested under the I scenario (**Figure 1B**). In contrast, internodes harvested under the NI scenario in 2014 were more distant than the others. This reflects the fact that the NI scenario in 2014 had a stronger impact on the histological and agronomical traits than the NI scenario in 2015 (**Supplementary Table S2**).

In accordance to the PCA results, comparing the correlations between traits within each field trials, the correlations obtained in 2014.NI differed from those obtained in 2015.NI (**Supplementary Table S4**). For instance, Blue_parenchyma is more strongly and significantly correlated to Red_rind and Red_parenchyma in 2014.NI than in the other field trials ($r = -0.26^{***}$ and $r = -0.70^{***}$, respectively, **Supplementary Table S4**). Bundle_density is significantly correlated to Non-_lignified_fraction and to IVCWRD only in 2014.NI on one side ($r = 0.21^{**}$ and $r = -0.21^{*}$, respectively, **Supplementary Table S4**) and it is also much less correlated to Bundle_number only in 2014.NI ($r = 0.20^{*}$; **Supplementary Table S4**). Correlation between lignified fraction and Rind_fraction is also weaker in 2014.NI than in the others field trials ($r = -0.16^{*}$; **Supplementary Table S4**). Blue_parenchyma, Non-_lignified_fraction, and Bundle_density are the traits that contributed the most to the second axis of the PCA. This reflects the fact that 2014.NI is located apart from the other field trials on the PCA and that histology of internodes responded more in 2014 to the NI scenario.

Taken together, the results suggest that the NI scenario led to internode modifications at the biochemical level of the same magnitude in 2014 and in 2015. However, changes in internodes at the histological levels were more pronounced in the NI scenario of 2014 than that of 2015.

QTL Mapping for Histological, Biochemical, and Agronomical Traits Under the Different Irrigation Scenarios

Consequently, QTL detection was performed for agronomical, histological, and biochemical traits for each year and each

irrigation scenario. For all year and scenario combinations (2014.I, 2014.NI, 2015.I, and 2015.NI), a total of 219 QTL involved in the variations of the quantified agronomical, biochemical, and histological traits were mapped (**Figures 2,3** and **Supplementary Table S5**).

For the biochemical traits, a total of 94 QTL were detected over the 2 years and the two irrigation scenario tested. Several colocalizations occurred at several loci between QTL for digestibility and/or QTL for composition/structure of the cell wall (**Figure 2** and **Supplementary Table S5**). Interestingly, among the 94 QTL detected, 30 mapped to four clusters. At cluster 2-Bioch (between 50 and 105 cM on the chromosome 2), one QTL for IVCWRD (2015.NI) colocalized with QTL for PCAest (2015.NI), hemicelluloses (2014.NI), and βO4 yield (2015.NI). At cluster 4-Bioch (between 73 and 117 cM on chromosome 4), a QTL for IVCWRD (2015.NI) colocalized with QTL for CWR (2015.I), KL.CWR (2015.I, 2014.NI and 2015.NI), PCAest (2014.I, 2015.I and 2014.NI), FAest (2015.I), hemicelluloses (2015.NI), and FAest (2014.NI). At cluster 5-Bioch (between 10 and 114 cM on chromosome 5), QTL for hemicelluloses (2014.I, 2015.I and 2014.NI) colocalized with QTL for PCAest (2014.I and 2015.NI), IVCWRD (2015.NI), and βO4 H (2014.NI). At cluster 6-Bioch (between 82 and 155 cM on chromosome 6), QTL for hemicelluloses detected in every condition colocalized with QTL for FAest (2015.I and 2014.NI) and βO4 yield (2014.I). If globally no locus seemed to be associated to the irrigation scenario, it is noteworthy that some QTL appeared exclusively under the NI scenario. This was the case at the top of the chromosome 6 (between 7 and 70 cM) and on chromosome 8 in which several biochemical QTL were detected only in 2014.NI and 2015.NI conditions (**Figure 2** and **Supplementary Table S5**).

For the histological traits, a total of 90 QTL were detected (**Figure 3** and **Supplementary Table S5**). The percentage of variation explained by each histological QTL was rather low and only six QTL explained more than 10% of the observed variation of the histological trait. Interestingly, among the 90 histological QTL identified, 25 mapped to three clusters (**Figure 3**). The 1-Hist cluster on chromosome 1 (between 250 and 290 cM) included 14 histological QTL detected whatever the year and the irrigation scenario. The 10-Hist cluster on chromosome 10 (between 80 and 105 cM) included seven QTL involved only in the variation of bundle-related traits (Bundle_number, Bundle_density, and Bundle_fraction) whatever the year and

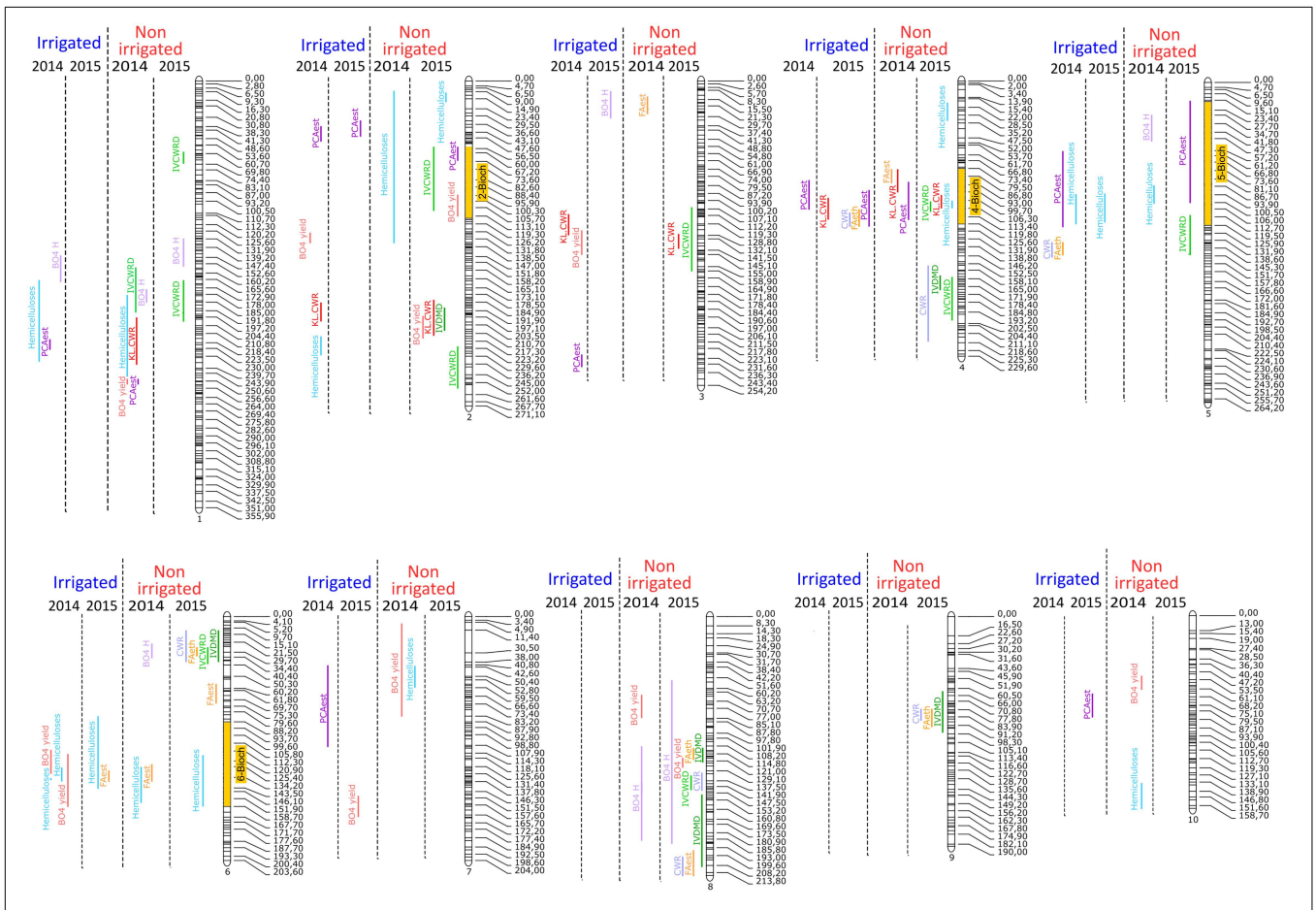


FIGURE 2 | Mapping of QTL involved in the variations of biochemical traits on the 10 chromosomes of maize genome for the four conditions: 2014 irrigated, 2015 irrigated, 2014 non-irrigated, and 2015 non-irrigated.

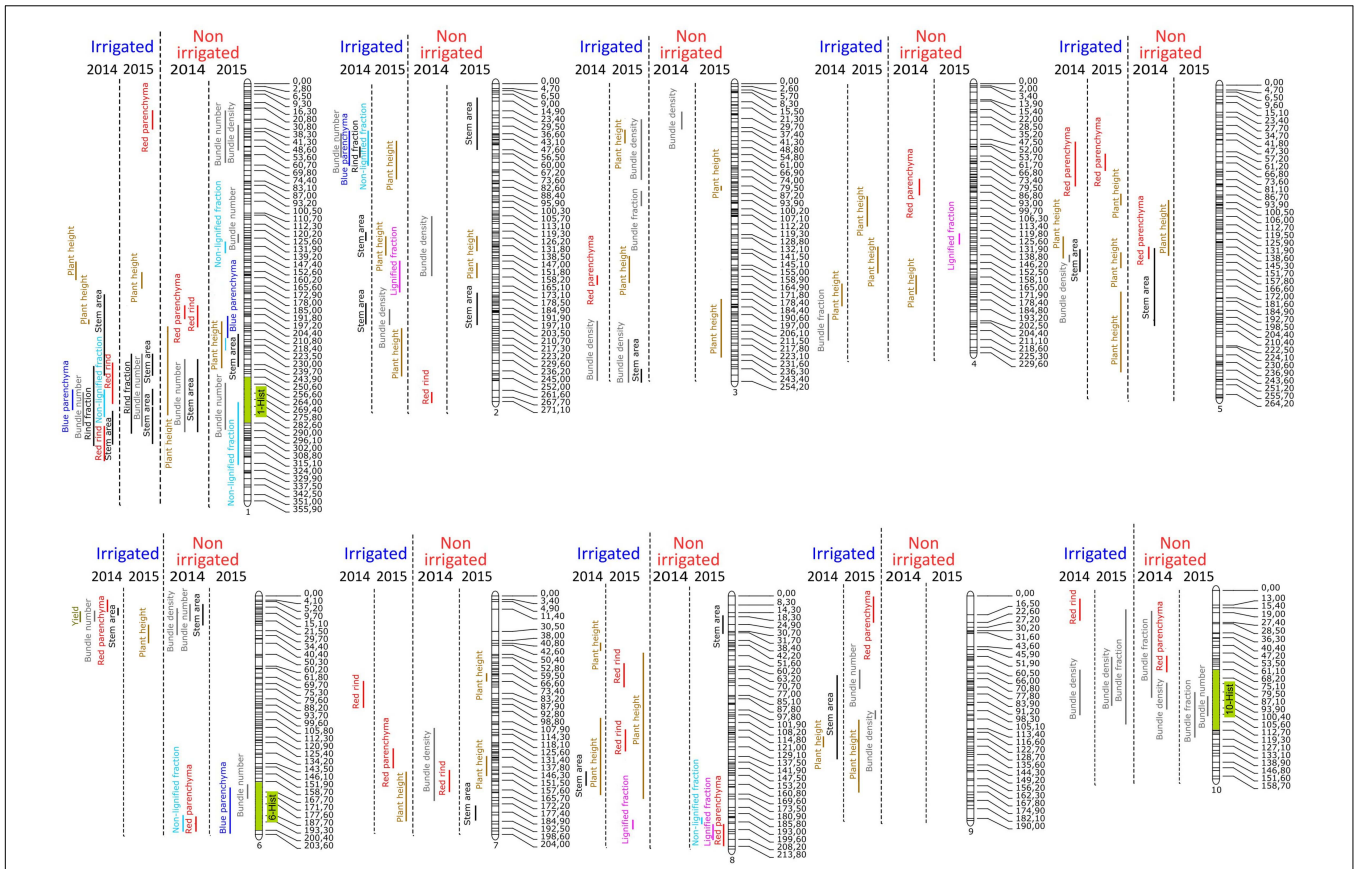


FIGURE 3 | Mapping of QTL involved in the variations of histological and agronomical traits on the 10 chromosomes of maize for the four conditions: 2014 irrigated, 2015 irrigated, 2014 non-irrigated, and 2015 non-irrigated.

the irrigation scenario. The 6-Hist cluster on the bottom of chromosome 6 (between 158 and 200 cM) included only four QTL for histological traits under the NI scenario in both 2014 and 2015. It did not overlap with the 6-Bioch cluster. Additionally, four QTL involved only in histological traits in the I scenario in both 2014 and 2015 were mapped on chromosome 9.

Finally, several colocalizations were observed between histological and biochemical traits. The 1-Hist cluster included two biochemical QTL (one QTL for PCAest and one QTL for βO4 yield) detected in 2014 in the NI scenario and one QTL for Plant_height detected as well in 2014 in the NI scenario. It is worth noting that QTL for PCAest content often colocalized with QTL involved in the variation of histological traits (**Figure 3**). Thus, at the top of chromosome 2, three QTL for PCAest (2014.I, 2014.NI, and 2015.NI) colocalized with three histological QTL (Rind_fraction, Blue_parenchyma, and Bundle_number) detected in 2014 under the I scenario. Similarly, at the bottom of chromosome 3, QTL for PCAest colocalized with QTL for Bundle_density detected in 2014 in the I scenario. On the chromosome 5, QTL for PCAest (2014.I and 2015.NI) also colocalized with QTL for Red_Parenchyma (2014.I and 2015.I). On chromosome 7, QTL for PCAest (2014.I) again colocalized with QTL for Red_rind detected under the same condition. Finally, on the chromosome 10, QTL for PCAest (2015.I) colocalized with the 10-Hist cluster.

DISCUSSION

Combining NIRS Predictions and Histological Profiling of Maize Internode to Decipher Biochemical and Histological Variations

Cm484 was previously reported to have a blue FASGA-stained parenchyma in the pith while F271 presented a much more reddish FASGA-stained parenchyma (Méchin et al., 2000; Méchin et al., 2005; Barrière et al., 2009). Based on these findings, a RIL population was developed from a cross between these two inbred lines. El Hage et al. (2018) recently characterized a set of maize inbred lines, including F271 and Cm484, and confirmed their biochemical differences. Surprisingly, Cm484 did not show a so intense blue FASGA-stained parenchyma anymore, making its histological profile much closer from that of F271. In the present study, Cm484 again did not exhibit an intense blue FASGA parenchyma. Nevertheless, we were still able

to highlight histological differences between the two parental lines, and we showed that indeed the Non-lignified_fraction of Cm484 was more present widespread in the parenchyma than that of F271. More importantly, transgression was observed for all agronomical-, biochemical-, and histological-quantified traits in the RILs, which allowed us to detect QTL for most of these traits. These quantifications were possible thanks to two high-throughput phenotyping tools. First, NIRS equations were established to accurately predict traits related to cell wall composition and structure as well as *in vitro* digestibilities (IVDMD and IVCWRD) in the internodes of the RIL population. Second, we used a high-throughput image analysis (Legland et al., 2017) to quantify histological traits from FASGA-stained maize internode cross sections. These two tools have enabled us to accurately characterize biochemical and histological traits in the mapping population. This is an important step compared to previous internode studies that only highlighted the link between the distribution of the lignification and cell wall degradability in maize (Jung and Casler, 2006; Boon et al., 2008; El Hage et al., 2018), sugarcane (Dos Santos et al., 2015), and sorghum (Perrier et al., 2017) using a small set of lines. A number of QTL for vascular bundle system or stem aerenchymas have been mapped in plants of agronomical interest such as in tomato (Coaker et al., 2002), wheat (Sang et al., 2010), rice (Sasahara et al., 1999; Zhang et al., 2002; Cui et al., 2003; Bai et al., 2012), and in sorghum (Casto et al., 2018). In maize, the genetic determinism of histological traits has also recently been investigated (Huang et al., 2016; Mazaheri et al., 2019; Zhang et al., 2020). Here, the use of FASGA-stained cross section allowed us to delimit the rind and the pith fractions and to differentiate level of lignification in the different fractions of maize internode.

Moreover, until now, no link was made between the variation of histological pattern and the variation of cell wall digestibility and composition.

Responses to Water Deficit Are Different When Considering Biochemical or Histological Traits

All lines were cultivated in field trials, where irrigation was either provided (I scenario) or stopped (NI scenario) in 2014 and 2015. The natural precipitation did not occur in the same way during the maize growing season in the 2 years: Indeed, a storm occurred on June 10th 2015, providing up to 80 mm of water under both I and NI conditions. The amount of water supply during this storm represented more water than all the rainfalls cumulated during the entire maize growing season in 2014. Thus, all the plants under the NI condition in 2015 benefited from a great water supply at the start of the onset of water stress. Plant height and biomass yield were less impacted in 2015 than in 2014 by the NI scenario, reflecting the differences between 2014 and 2015. Moreover, note that in the physiological development of the plant, the 10th of June coincides with the period of the development of the internode carrying the main ear. Consequently, the NI condition of 2014 and 2015 could not be considered similar at the internode level. This gives us the opportunity to compare the impact of two very different stress intensities. The significance of the year and treatment × year effects for most of the traits reflects this difference between 2014 and 2015.

We showed that most of the biochemical traits were impacted by the NI scenario in both years. These findings have already been reported in maize (El Hage et al., 2018; Virlouvet et al., 2019), sorghum (Luquet et al., 2019), and miscanthus (Van Der Weijde et al., 2017). Nevertheless, what is striking in the present analysis is that even if rainwater was supplied in large quantities from the onset of the stress period and of the development of the internode below the ear in 2015, biochemistry traits (such as PCAest and lignin contents) and *in vitro* digestibilities of the internodes were impacted similarly in 2014 and 2015, while the histological traits were not. Histological and agronomical traits contributed the most to the emergence of the second PCA axis, and only data from 2014 in the NI scenario were projected apart from the others on this second PCA axis, reflecting the fact that the NI scenario impacted histological pattern only in 2014 but not in 2015. According to El Hage et al. (2018), the histological responses observed in 2014 resulted in smaller internodes, with a smaller bundle area but greater density, and a proportionately larger non-lignified parenchyma area.

Distinct QTL Mapped for Biochemical and Histological Traits

Heritabilities on the un-replicated RIL field trials have been estimated either over the I scenario and the NI scenario carried out in 2014 and 2015 for biochemical and histological traits (**Supplementary Table S2**). Overall, for most of the traits, heritability in I scenario are higher than the ones in NI scenario. This corroborates with the fact that 2014_I and 2015_I trials are more similar than 2014_NI and 2015_NI trials (**Figure 1**). Moreover, heritability for most of the biochemical traits remained moderated (from 12.4 to 54.5%, except for FAest that reached only 7.6%). This maintenance of the value for heritability for most of the chemical traits goes along with the fact that biochemical traits responded similarly each year. Under I scenario, heritability of histological trait is in accordance with what is reported (rind thickness h^2 = 58% in Mazaheri et al., 2019; bundle-related traits h^2 from 12.8 to 83.6% in Zhang et al., 2020). However, histological traits were only impacted by NI scenario in 2014 but not in 2015 (see **Figure 1** and section "Discussion"). This leads to a pronounced reduction of estimated heritability for histological traits in NI scenarios, and it forced us to continue the identification of QTL trial by trial. Hence, the low heritability for some traits reported in **Supplementary Table S2** do not reflect the fact that we identify QTL for these traits under each field trial.

So far, numerous QTL studies have been reported on traits related to agronomic performance and cell wall composition and digestibility. The present study allows to map over 200 QTL for agronomical, biochemical, and histological traits under two contrasting water regimes in the field. It is noteworthy that the QTL for plant height identified on chromosomes 5 (2014.I and

2014.NI), 8 (2014.I and 2015.NI), and 9 (2014.I and 2015.I) colocalized with QTL for the same trait previously identified in a set of 800 maize inbred lines (Mazaheri et al., 2019). Furthermore, the QTL of stem area mapped on chromosomes 1 (2014.I), 2 (2014.I and 2015.NI), 5 (2014.NI), and 7 (2015.NI) colocalized with loci involved in stalk diameters measured on the third internode previously identified (Mazaheri et al., 2019). QTL involved in bundle numbers (chromosomes 1, 6, and 10 under 2015.NI) also colocalized with those previously identified in the uppermost internode of an 866 maize-teosinte BC2S3 RILs (Huang et al., 2016). In contrast, the QTL for Rind_fraction on chromosome 5 did not colocalize with the only association Mazaheri et al. (2019) reported for rind thickness. Additionally, the 1-Hist cluster colocalized with a locus involved in the variation of PCAest previously identified in the pith of the second internode below the main cob in a panel of 282 divers maize lines (López-Malvar et al., 2019). Moreover, at this position, a QTL for PCAest content has been also reported by Santiago et al. (2016). These authors also detected QTL for PCAest at the top of chromosome 2 and on chromosome 4, positions that colocalize with QTL for PCAest mapped in our study. The 1-Hist cluster did not colocalize with any association found by Zhang et al. (2020) using a panel of 482 lines and computed tomography (Du et al., 2016). Nevertheless, the QTL for Bundle_number on chromosome 1 at 61.4 Mb colocalized with some of their associations. These differences may be due to the fact that the studied internodes and the methods used differ.

At the biochemical level, four clusters of QTL were detected. It is noteworthy that only one them, the cluster 4-Bioch, encompassed QTL involved in the variation of both lignin content and *p*-hydroxycinnamic acid contents in the cell wall. Furthermore, three biochemical clusters (4-Bioch, 5-Bioch, and 6-Bioch) can be considered as constitutive since QTL for both years and irrigation scenarios have been detected at these loci. Interestingly, the clusters 4-Bioch and 6-Bioch colocalized with clusters of constitutive QTL detected on chromosome 4 and 6, respectively, at the whole-plant level (Virlouvet et al., 2019). In addition, QTL for biochemical traits identified only in the NI scenario (for instance on the bottom of chromosome 8) colocalized with responsive QTL mapped at the whole-plant level (Virlouvet et al., 2019). This suggests genetic links for cell wall biochemistry and its response to water deficit between the internode and whole-plant levels. Indeed, correlations for biochemical traits at the internode level and at the stover level (Virlouvet et al., 2019) have been calculated (**Supplementary Table S6**). For each field trial (2014.I, 2014.NI, 2015.I, and 2015.NI), correlations were significant for CWR, KL.CWR, FAest, PCAest, and for the *in vitro* digestibilities. This is in agreement with the correlation between digestibility of the stem and that of the stover previously reporter (Hansey et al., 2010; El Hage, 2018).

At the histological level, three clusters of QTL were detected. Among them, two (1-Hist and 10-Hist) included QTL detected whatever the year and the irrigation scenario. They are therefore constitutively involved in the variation of the histological profile of maize internode. On the other hand, the 6-Hist cluster was mapped only in the NI condition in both 2014 and 2015. It is worth noting that no overlap between histological and biochemical clusters occurred in this population. However, we frequently noticed colocalizations between QTL for PCAest content and QTL for histological variations mainly of rind and lignified parenchyma area and/or intensity. This is in accordance with the fact that these tissues are reported to be highly *p*-coumaroylated tissues (Lopez et al., 1993; Chesson et al., 1997; Barros-Rios et al., 2012).

CONCLUSION

We validated the feasibility of high-throughput tools developed to quantify biochemical and histological traits for QTL detection or for selection screening. Our work led to the identification of constitutive QTL, as well as QTL with an effect only in the NI condition, suggesting that the genetic determinism involved in cell wall development at the biochemical and histological levels are distinct from those involved under the NI scenario. Overall, our data highlighted the potential role of *p*-coumaroylation of maize stem in refining plant agronomic properties and digestibility.

DATA AVAILABILITY STATEMENT

The original contributions presented in the study are included in the article/**Supplementary Material**, further inquiries can be directed to the corresponding author/s.

AUTHOR CONTRIBUTIONS

MR, VM, and SC designed the study and supervised data collection. FEH, M-PJ, SC, VM, and MR collected the samples. FEH prepared the internode cross sections and quantified histological traits. YG, M-PJ, and VM carried out the biochemical traits quantification. YG established the NIRS predictive equations. FEH, P-LL-M, LV, and MR conducted the genetic study. FEH, P-LL-M, SC, VM, and MR wrote the manuscript. All authors contributed to the article and approved the submitted version.

FUNDING

This study was supported by the French Government Grant ANR-11-BTBR-0006 BIOMASS FOR THE FUTURE, managed by the French National Research Agency under an "Investments for the Future" program (Grant ANR- 11-IDEX-0003-02). This work has benefited from the support of IJPB's Plant Observatory technological platforms. The IJPB also benefits from the support of Saclay Plant Sciences-SPS (ANR-17-EUR-0007).

ACKNOWLEDGMENTS

We sincerely acknowledge the UE Diascope (Mauguio, France) for their precious contribution to field experiments.

SUPPLEMENTARY MATERIAL

The Supplementary Material for this article can be found online at: https://www.frontiersin.org/articles/10.3389/fpls.2021.628960/full#supplementary-material

Supplementary Table 1 | Characteristics of NIRS predictive equations developed for cell wall traits in maize internodes harvested at silage stage.

Supplementary Table 2 | Variations and heritabilities of each histological, biochemical, and agronomical trait observed for the parental lines and for the RILs cultivated in 2014 and 2015 in both I and NI scenarios. Different letters reported for the parental values indicated significant differences from a Tukey test.

Supplementary Table 3 | Cos2 and Pearson correlation of all the traits for the two first axes of the PCA.

Supplementary Table 4 | Pearson correlation table of all the biochemical and histological traits for the RILs in each field trial: 2014.I, 2014.NI, 2015.I, and 2015.NI.

Supplementary Table 5 | List of QTL detected for all the histological, biochemical, and agronomical traits. When the effect sign is positive, Cm484 alleles are responsible of the increase of the trait; when the effect sign is negative, the alleles from F271 are increasing the trait value.

Supplementary Table 6 | Correlations between the biochemical traits quantified at the internode and at the stover levels (Virlouvet et al., 2019).

REFERENCES

Arends, D., Prins, P., Jansen, R. C., and Broman, K. W. (2010). R/qtl: high-throughput multiple QTL mapping. *Bioinformatics* 26, 2990–2992. doi: 10.1093/bioinformatics/btq565

Bai, X., Wu, B., and Xing, Y. (2012). Yield-related QTLs and their applications in rice genetic improvementF. *J. Integr. Plant Biol.* 54, 300–311. doi: 10.1111/j.1744-7909.2012.01117.x

Barrière, Y., Méchin, V., Lafarguette, F., Manicacci, D., Guillon, F., Wang, H., et al. (2009). Toward the discovery of maize cell wall genes involved in silage quality and capacity to biofuel production. *Maydica* 54, 161–198.

Barros-Rios, J., Santiago, R., Malvar, R. A., and Jung, H. J. G. (2012). Chemical composition and cell wall polysaccharide degradability of pith and rind tissues from mature maize internodes. *Anim. Feed Sci. Technol.* 172, 226–236. doi: 10.1016/j.anifeedsci.2012.01.005

Boon, E. J. M. C., Struik, P. C., Tamminga, S., Engels, F. M., and Cone, J. W. (2008). Stem characteristics of two forage maize (*Zea mays* L.) cultivars varying in whole plant digestibility. III. Intra-stem variability in anatomy, chemical composition and in vitro rumen fermentation. *NJAS Wageningen J. Life Sci.* 56, 101–122. doi: 10.1016/s1573-5214(08)80019-x

Broman, K. W., and Sen, S. (2009). *A Guide to QTL Mapping with R/qtl*. New York, NY: Springer.

Casto, A. L., McKinley, B. A., Yu, K. M. J., Rooney, W. L., and Mullet, J. E. (2018). Sorghum stem aerenchyma formation is regulated by SbNAC_D during internode development. *Plant Direct* 2:e00085. doi: 10.1002/pld3.85

Chesson, A., Provan, G. J., Russell, W., Scobbie, L., Chabbert, B., and Monties, B. (1997). Characterisation of lignin from parenchyma and sclerenchyma cell walls of the maize internode. *J. Sci. Food Agric.* 73, 10–16. doi: 10.1002/(sici)1097-0010(199701)73:1<10::aid-jsfa697>3.0.co;2-e

Coaker, G. L., Meulia, T., Kabelka, E. A., Jones, A. K., and Francis, D. M. (2002). A QTL controlling stem morphology and vascular development in Lycopersicon esculentumx *Lycopersicon hirsutum* (Solanaceae) crosses is located on chromosome 2. *Am. J. Bot.* 89, 1859–1866. doi: 10.3732/ajb.89.12.1859

Cook, D. D., Meehan, K., Asatiani, L., and Robertson, D. J. (2020). The effect of probe geometry on rind puncture resistance testing of maize stalks. *Plant Methods* 16:35.

Cui, K., Peng, S., Xing, Y., Yu, S., Xu, C., and Zhang, Q. (2003). Molecular dissection of the genetic relationships of source, sink and transport tissue with yield traits in rice. *Theor. Appl. Genet.* 106, 649–658. doi: 10.1007/s00122-002-1113-z

Culhaoglu, T., Zheng, D., Méchin, V., and Baumberger, S. (2011). Adaptation of the carrez procedure for the purification of ferulic and p-coumaric acids released from lignocellulosic biomass prior to LC/MS analysis. *J. Chromatogr. B* 879, 3017–3022. doi: 10.1016/j.jchromb.2011.08.039

Dence, C. W. (1992). "The determination of lignin," in *Springer Series in Wood Science*, ed. W. Rupert (Berlin: Springer).

de Givry, S., Bouchez, M., Chabrier, P., Milan, D., and Schiex, T. (2005). $CAR_H{}^TA$ GENE: multipopulation integrated genetic and radiation hybrid mapping. *Bioinformatics* 21, 1703–1704. doi: 10.1093/bioinformatics/bti222

Dos Santos, A. B., Bottcher, A., Kiyota, E., Mayer, J. L. S., Vicentini, R., Dos Santos, et al. (2015). Water stress alters lignin content and related gene expression in two sugarcane genotypes. *J. Agric. Food Chem.* 63, 4708–4720. doi: 10.1021/jf5061858

Du, J., Zhang, Y., Guo, X., Ma, L., Shao, M., Pan, X., et al. (2016). Micron-scale phenotyping quantification and three-dimensional microstructure reconstruction of vascular bundles within maize stalks based on micro-CT scanning. *Funct. Plant Biol.* 44, 10–22. doi: 10.1071/fp16117

El Hage, F. (2018). *Impact du Déficit Hydrique sur la Dégradabilité, la Biochimie Pariétale et la Répartition des Tissus Lignifiés chez L'entrenoeud de Maïs et Déterminisme Génétique de ces Caractères*. Paris: Thèse de Doctorat, Biologie Université Paris-Saclay.

El Hage, F., Legland, D., Borrega, N., Jacquemot, M. P., Griveau, Y., Coursol, S., et al. (2018). Tissue lignification, cell wall p-coumaroylation and degradability of maize stems depend on water status. *J. Agric. Food Chem.* 66, 4800–4808. doi: 10.1021/acs.jafc.7b05755

Elshire, R. J., Glaubitz, J. C., Sun, Q., Poland, J. A., Kawamoto, K., Buckler, E. S., et al. (2011). A robust, simple genotyping-by-sequencing (GBS) approach for high diversity species. *PLoS One* 6:e19379. doi: 10.1371/journal.pone.0019379

Ganal, M. W., Durstewitz, G., Polley, A., Bérard, A., Buckler, E. S., Charcosset, A., et al. (2011). A large maize (Zea mays L.) SNP genotyping array: development and germplasm genotyping, and genetic mapping to compare with the B73 reference genome. *PLoS One* 6:e28334. doi: 10.1371/journal.pone.0028334

Gärtner, H., Lucchinetti, S., and Schweingruber, F. H. (2014). New perspectives for wood anatomical analysis in dendrosciences: the GSL1-microtome. *Dendrochronologia* 32, 47–51. doi: 10.1016/j.dendro.2013.07.002

Hansey, C. N., Lorenz, A. J., and de Leon, N. (2010). Cell wall composition and ruminant digestibility of various maize tissues across development. *Bioenergy Res.* 3, 28–37. doi: 10.1007/s12155-009-9068-4

Harholt, J., Krü Ger, Jensen, J., Sørensen, S. O., Orfila, C., Pauly, M., et al. (2006). Arabinan deficient 1 is a putative arabinosyltransferase involved in biosynthesis of pectic arabinan in arabidopsis. *Plant Physiol.* 140, 49–58. doi: 10.1104/pp.105.072744

Harrison, M. T., Tardieu, F., Dong, Z., Messina, C. D., and Hammer, G. L. (2014). Characterizing drought stress and trait influence on maize yield under current and future conditions. *Global Change Biol.* 20, 867–878. doi: 10.1111/gcb.12381

Heckwolf, S., Heckwolf, M., Kaeppler, S. M., de Leon, N., and Spalding, E. P. (2015). Image analysis of anatomical traits in stalk transections of maize and other grasses. *Plant Methods* 11:26.

Huang, C., Chen, Q., Xu, G., Xu, D., Tian, J., and Tian, F. (2016). Identification and fine mapping of quantitative trait loci for the number of vascular bundle in maize stem. *J. Integr. Plant Biol.* 58, 81–90. doi: 10.1111/jipb.12358

Jung, H. G., and Casler, M. D. (2006). Maize stem tissues: impact of development on cell wall degradability. *Crop Sci.* 46, 1801–1809. doi: 10.2135/cropsci2006.02-0086

Lapierre, C., Monties, B., and Rolando, C. (1986). Preparative thioacidolysis of spruce lignin: isolation and identification of main monomeric products. *Holzforschung* 40, 47–50. doi: 10.1515/hfsg.1986.40.1.47

Legland, D., El Hage, F., Méchin, V., and Reymond, M. (2017). Histological quantification of maize stem sections from FASGA-stained images. *Plant Methods* 13:84.

Lopez, S., Murison, S. D., Travis, A. J., and Chesson, A. (1993). Degradability of parenchyma and sclerenchyma cell walls isolated at different developmental

stages from a newly extended maize internode. *Acta Botanica Neerlandica* 42, 165–174. doi: 10.1111/j.1438-8677.1993.tb00693.x

López-Malvar, A., Butrón, A., Samayoa, L. F., Figueroa-Garrido, D. J., Malvar, R. A., and Santiago, R. (2019). Genome-wide association analysis for maize stem cell wall-bound hydroxycinnamates. *BMC Plant Biol.* 19:519.

Luquet, D., Perrier, L., Clément-Vidal, A., Jaffuel, S., Verdeil, J. L., Roques, S., et al. (2019). Genotypic covariations of traits underlying sorghum stem biomass production and quality and their regulations by water availability: insight from studies at organ and tissue levels. *GCB Bioenergy* 11, 444–462. doi: 10.1111/gcbb.12571

Mazaheri, M., Heckwolf, M., Vaillancourt, B., Gage, J. L., Burdo, B., Heckwolf, S., et al. (2019). Genome-wide association analysis of stalk biomass and anatomical traits in maize. *BMC Plant Biol.* 19:45.

Méchin, V., Argillier, O., Menanteau, V., Barrière, Y., Mila, I., Pollet, B., et al. (2000). Relationship of cell wall composition to in vitro cell wall digestibility of maize inbred line stems. *J. Sci. Food Agric.* 80, 574–580. doi: 10.1002/(sici)1097-0010(200004)80:5<574::aid-jsfa575>3.0.co;2-r

Méchin, V., Argillier, O., Rocher, F., Hébert, Y., Mila, I., and Pollet, B. (2005). In search of a maize ideotype for cell wall enzymatic degradability using histological and biochemical lignin characterization. *J. Agric. Food Chem.* 53, 5872–5881. doi: 10.1021/jf050722f

Morrison, T. A., Kessler, J. R., Hatfield, R. D., and Buxton, D. R. (1994). Activity of two lignin biosynthesis enzymes during development of a maize internode. *J. Sci. Food Agric.* 65, 133–139. doi: 10.1002/jsfa.2740650202

Perrier, L., Rouan, L., Jaffuel, S., Clément-Vidal, A., Roques, S., Soutiras, A., et al. (2017). Plasticity of sorghum stem biomass accumulation in response to water deficit: a multiscale analysis from internode tissue to plant level. *Front. Plant Sci.* 8:1516.

R Core Team (2014). *R: A Language and Environment for Statistical Computing*. Vienna: R Foundation for Statistical Computing. Available online at: https://www.R-project.org/

Sang, Y., Deng, Z. Y., Zhao, L., Zhang, K. P., Tian, J. C., and Ye, B. X. (2010). QTLs for the vascular bundle system of the uppermost internode using a doubled haploid population of two elite Chinese wheat cultivars. *Plant Breed.* 129, 605–610. doi: 10.1111/j.1439-0523.2009.01727.x

Santiago, R., López-Malvar, A., Souto, C., and Barros-Ríos, J. (2018). Methods for determining cell wall-bound phenolics in maize stem tissues. *J. Agric. Food Chem.* 66, 1279–1284. doi: 10.1021/acs.jafc.7b05752

Santiago, R., Malvar, R. A., Barros-Rios, J., Samayoa, L. F., and Butron, A. (2016). Hydroxycinnamate synthesis and association with mediterranean corn borer resistance. *J. Agric. Food Chem.* 64, 539–551. doi: 10.1021/acs.jafc.5b04862

Sasahara, H., Fukuta, Y., and Fukuyama, T. (1999). Mapping of QTLs for vascular bundle system and spike morphology in rice. *Oryza sativa* L. *Breed. Sci.* 49, 75–81. doi: 10.1270/jsbbs.49.75

Seegmiller, W. H., Graves, J., and Robertson, D. J. (2020). A novel rind puncture technique to measure rind thickness and diameter in plant stalks. *Plant Methods* 16:44.

Shiferaw, B., Prasanna, B. M., Hellin, J., and Bänziger, M. (2011). crops that feed the world 6. past successes and future challenges to the role played by maize in global food security. *Food Security* 3, 307–327. doi: 10.1007/s12571-011-0140-5

Tolivia, D., and Tolivia, J. (1987). Fasga: a new polychromatic method for simultaneous and differential staining of plant tissues. *J. Microsci.* 148, 113–117. doi: 10.1111/j.1365-2818.1987.tb02859.x

Updegraff, D. M. (1969). Semimicro determination of cellulose inbiological materials. *Anal. Biochem.* 32, 420–424. doi: 10.1016/s0003-2697(69)80009-6

Van Der Weijde, T., Huxley, L. M., Hawkins, S., Sembiring, E. H., Farrar, K., Dolstra, O., et al. (2017). Impact of drought stress on growth and quality of miscanthus for biofuel production. *GCB Bioenergy* 9, 770–782. doi: 10.1111/gcbb.12382

Virlouvet, L., El Hage, F., Griveau, Y., Jacquemot, M. P., Gineau, E., Baldy, A., et al. (2019). Water deficit-responsive QTLs for cell wall degradability and composition in maize at silage stage. *Front. Plant Sci.* 10:488.

Vo, L. T. T., Girones, J., Jacquemot, M.-P., Legée, F., Cézard, L., Lapierre, C., et al. (2020). Correlations between genotype biochemical characteristics and mechanical properties of maize stem - polyethylene composites. *Ind. Crops Prod.* 143:111925. doi: 10.1016/j.indcrop.2019.111925

Zhang, Y., Legay, S., Barrieìre, Y., Méchin, V., and Legland, D. (2013). Color quantification of stained maize stem section describes lignin spatial distribution within the whole stem. *J. Agric. Food Chem.* 61, 3186–3192. doi: 10.1021/jf400912s

Zhang, Y., Wang, J., Du, J., Zhao, Y., Lu, X., Wen, W., et al. (2020). Dissecting the phenotypic components and genetic architecture of maize stem vascular bundles using high-throughput phenotypic analysis. *Plant Biotechnol. J.* 1, 35–50. doi: 10.1111/pbi.13437

Zhang, Z.-H., Li, P., Wang, L.-X., Tan, C.-J., Hu, Z.-L., Zhu, Y.-G., et al. (2002). Identification of quantitative trait loci (QTLs) for the characters of vascular bundles in peduncle related to indica-japonica differentiation in rice (*Oryza sativa* L.). *Euphytica* 128, 279–284.

Conflict of Interest: The authors declare that the research was conducted in the absence of any commercial or financial relationships that could be construed as a potential conflict of interest.

Copyright © 2021 El Hage, Virlouvet, Lopez-Marnet, Griveau, Jacquemot, Coursol, Méchin and Reymond. This is an open-access article distributed under the terms of the Creative Commons Attribution License (CC BY). The use, distribution or reproduction in other forums is permitted, provided the original author(s) and the copyright owner(s) are credited and that the original publication in this journal is cited, in accordance with accepted academic practice. No use, distribution or reproduction is permitted which does not comply with these terms.

frontiers in Plant Science

ORIGINAL RESEARCH
published: 11 March 2021
doi: 10.3389/fpls.2021.647239

Identification of Candidate Genes Conferring Cold Tolerance to Rice (*Oryza sativa* L.) at the Bud-Bursting Stage Using Bulk Segregant Analysis Sequencing and Linkage Mapping

*Luomiao Yang†, Lei Lei†, Peng Li, Jingguo Wang, Chao Wang, Fan Yang, Jiahui Chen, HuaLong Liu, Hongliang Zheng, Wei Xin and Detang Zou**

Key Laboratory of Germplasm Enhancement, Physiology and Ecology of Food Crops in Cold Region, Ministry of Education, Northeast Agricultural University, Harbin, China

OPEN ACCESS

Edited by:
Felipe Klein Ricachenevsky, Federal University of Rio Grande do Sul, Brazil

Reviewed by:
Jieyun Zhuang, Zhejiang University, China
Yongzhong Xing, Huazhong Agricultural University, China

***Correspondence:**
Detang Zou
zoudtneau@126.com

† These authors have contributed equally to this work

Specialty section:
This article was submitted to Plant Abiotic Stress, a section of the journal Frontiers in Plant Science

Received: *29 December 2020*
Accepted: *22 February 2021*
Published: *11 March 2021*

Citation:
Yang L, Lei L, Li P, Wang J, Wang C, Yang F, Chen J, Liu H, Zheng H, Xin W and Zou D (2021) Identification of Candidate Genes Conferring Cold Tolerance to Rice (Oryza sativa L.) at the Bud-Bursting Stage Using Bulk Segregant Analysis Sequencing and Linkage Mapping. Front. Plant Sci. 12:647239. doi: 10.3389/fpls.2021.647239

Low-temperature tolerance during the bud-bursting stage is an important characteristic of direct-seeded rice. The identification of cold-tolerance quantitative trait loci (QTL) in species that can stably tolerate cold environments is crucial for the molecular breeding of rice with such traits. In our study, high-throughput QTL-sequencing analyses were performed in a 460-individual $F_{2:3}$ mapping population to identify the major QTL genomic regions governing cold tolerance at the bud-bursting (CTBB) stage in rice. A novel major QTL, *qCTBB9*, which controls seed survival rate (SR) under low-temperature conditions of 5°C/9 days, was mapped on the 5.40-Mb interval on chromosome 9. Twenty-six non-synonymous single-nucleotide polymorphism (nSNP) markers were designed for the *qCTBB9* region based on re-sequencing data and local QTL mapping conducted using traditional linkage analysis. We mapped *qCTBB9* to a 483.87-kb region containing 58 annotated genes, among which six predicted genes contained nine nSNP loci. Quantitative reverse transcription-polymerase chain reaction (qRT-PCR) analysis revealed that only Os09g0444200 was strongly induced by cold stress. Haplotype analysis further confirmed that the SNP 1,654,225 bp in the Os09g0444200 coding region plays a key role in regulating the cold tolerance of rice. These results suggest that Os09g0444200 is a potential candidate for *qCTBB9*. Our results are of great significance to explore the genetic mechanism of rice CTBB and to improve the cold tolerance of rice varieties by marker-assisted selection.

Keywords: ***Oryza sativa* L., cold tolerance, bulk segregant analysis sequencing, linkage mapping, bud-bursting**

INTRODUCTION

Rice (*Oryza sativa* L.) is an important food crop that has adapted to the tropical climate of the world. However, chilling injury of rice that occurs at high latitudes and high altitudes has severely restricted its production (Jena et al., 2012; Liu C. T. et al., 2019). Fast and uniform seed germination and vigorous seedling growth are essential for stable crop growth. The germination rate and early growth of seedlings after germination are the two main characteristics that are directly related to seedling vigor. Cold stress usually damages and delays germination and seedling growth of rice, leading to inferior stand establishment and uneven maturity, especially in areas where direct-seeded

rice and cultivation are performed under low local temperatures (Iwata and Fujino, 2010; Manangkil et al., 2013). Therefore, low-temperature sensitivity at the bud-bursting stage remains a major challenge for direct-seeded rice. Improved cold tolerance at the bud-bursting (CTBB) stage is an important agronomic characteristic of direct-seeded rice breeding programs.

Because of the complexity and polygenicity of cold tolerance, numerous efforts have been directed to the detection and mapping of quantitative trait loci (QTL). In the past 20 years, more than 550 QTLs have been reported for different growth stages (germination, seedling, and reproductive/booting stage) for low-temperature stress using molecular markers of different genetic backgrounds derived from bi-parental mapping populations and diverse genetic resources of rice accessions (Najeeb et al., 2020). For example, numerous double haploid lines, backcross-inbred lines, recombinant inbred lines (RIL), and near-isogenic lines have been developed, with cold-tolerant varieties such as Kunming Xiaobaigu (Dai et al., 2004), Lijiang Xintuanheigu (Shirasawa et al., 2012), Koshihikari (Endo et al., 2016), M202 (Andaya and Tai, 2006), Norin-PL8 (Saito et al., 2010), and a Chinese type of wild rice (Dongxiang wild rice) (Mao et al., 2015) as donors. These representative cold-tolerant germplasms have contributed valuable QTLs or genes for research on the cold tolerance of rice. However, fewer QTLs have been identified at the bud-bursting stage than at the other developmental stage. As of 2015, 29 QTLs related to CTBB were integrated into chromosomes through meta-analysis (Zhu et al., 2015). Among them, *qCTBP2*, *qCTBP4*, and *qCTBP7* were mapped using F_3 populations based on simple sequence repeat (SSR) markers (Qiao et al., 2005). Four QTLs on chromosomes 3, 7, and 12 were detected using 98 backcross-inbred lines (Yang et al., 2009). In total, four QTLs for CTBB were preliminarily mapped on chromosomes 5 and 7 using a set of 95 chromosome segment substitution lines (CSSLs) derived from indica rice 9311 and Japonica rice Nipponbare (Lin et al., 2010). In the past 5 years, five new QTLs have explained 4.17–6.42% of the total phenotypic variation explained during the bud-bursting stage based on an RIL derived from H335 and CHA-1 (Yang et al., 2020). The other two cold-tolerant QTLs (*qCTBB-5* and *qCTBB-6*) at the bud-bursting stage were mapped using single-segment substitution lines (Yang et al., 2016). These results indicate that the research on CTBB of rice is still in its infancy. Most QTLs lie within a range of 10–30 cM through primary populations, and it is difficult to perform molecular marker-assisted breeding. To date, only two QTLs have been cloned; *qLTG3-1* encodes a protein with unknown function, which might regulate the vacuolization of aleurone and epidermal cells, thereby causing relaxation of these tissues and enhancing the germination potential of seeds at low temperatures (Fujino et al., 2008; Fujino and Matsuda, 2010; Fujino and Sekiguchi, 2011), whereas *OsSAP16* encodes a zinc-finger domain protein and serves as the major causal gene for low-temperature germinability (Wang et al., 2018). These examples demonstrate that the molecular regulation of CTBB is extremely complex, and the aforementioned QTLs were identified by bi-parental cross-linkage mapping, which is a labor- and time-intensive method to map genotypes of a large number of individuals in a segregated population. Therefore, to obtain reliable QTLs, it is necessary to implement a fast and efficient method to identify QTLs.

Recently, with the rapid development of next-generation sequencing (NGS) technology, the combination of bulked segregant analysis with NGS has become an important path to mine QTLs and genes (Abe et al., 2012; Vikram et al., 2012; Kadambari et al., 2018; Wambugu et al., 2018). Compared with traditional linkage mapping, QTL-sequencing (Seq) can improve work efficiency and provide high-density variation. The efficiency of QTL-Seq has been successfully demonstrated in many plants, such as cucumber (Lu et al., 2014), soybean (Song et al., 2017), rice (Wambugu et al., 2018), and tomato (Wen et al., 2019). Although the technique allows for the quick identification of major QTLs, confidence interval (CI) resolution is still rough. Therefore, researchers have to combine QTL-Seq with fine-mapping (Zhang X. et al., 2018) and RNA-Seq (Park et al., 2019) to identify candidate QTL genes. For example, *CaqSW1.1* (Das et al., 2015) was mapped from 1.37 Mb to 35 kb by QTL-Seq and classical QTL mapping, and the final candidate genes were identified. In another case, four candidate genes (*SlCathB2*, *SlGST*, *SlUBC5*, and *SlARG1*) associated with heat tolerance were detected by QTL-Seq and RNA-Seq in tomato (Wen et al., 2019). Thus, the method of obtaining a major QTL interval by QTL-Seq combined with fine-mapping to mine target genes provides a new perspective.

In our study, two strategies, QTL-Seq followed by linkage mapping, were employed to identify the major QTL interval for CTBB in rice. An $F_{2:3}$ population derived from a cross between Dongnong430 (DN430, cold-sensitive variety) and Dongfu104 (DF104, strongly cold-tolerant variety) was used for QTL-Seq analysis. Furthermore, a linkage mapping strategy was considered to anchor major QTLs using a KASP marker. Furthermore, quantitative reverse transcription-polymerase chain reaction (qRT-PCR) and haplotype analysis were employed to verify the association between candidate genes and cold tolerance. The results obtained in this study are expected to help reveal the mechanism by which cold sensitivity changes into cold tolerance in rice at the molecular level and will improve the understanding of mechanisms underlying CTBB in rice.

MATERIALS AND METHODS

Plant Materials

In this study, two Japonica varieties, the cold-sensitive female parent Dongnong 430 (DN430) and the cold-tolerant male parent Dongfu104 (DF104), were used as the parental lines to develop the 460 $F_{2:3}$ lines. The materials mentioned previously herein were all obtained from Northeast Agriculture University in the northeast region of China.

Cold-Tolerance Evaluation at Bud-Bursting Stage

One hundred seeds of each $F_{2:3}$ family and two parental were incubated at 40°C for ∼36 h to break dormancy and were soaked in deionized water at 30°C for approximately 72 h for germination. Fifty 5-mm-long buds of the two parental seeds

were selected, washed with sterile water, and transferred to a petri dish with two layers of filter paper. In addition, 50 germinated seeds from 460 progeny lines were transferred to 96-well PCR plates. These 50 germinated seeds were then further subjected to a cold treatment at 5°C for 9 days in a growth chamber in darkness and were allowed to resume growth at 28°C for 3 days to investigate the severity of damage (SD). The SD of all 460 F2:3 lines and their parents was evaluated using the following scale: a cold score of 0 indicated that the seedling had normal leaf color and grew well with no damage, to a cold score of 7, which indicated that the germinated seed was dead with no green leaves, as described in previous studies (Zhang M. et al., 2018). The SD value of a plant represented the average score of 50 seeds. The seed survival rate (SR) was evaluated after 7 days of recovery of growth and was calculated as follows: SR (%) = (surviving seedlings/50) × 100 (Zhou et al., 2012). Three biological replicates were performed.

Construction of Segregating Pools

Young leaves of the 460 F_2 individuals were collected separately for total genomic DNA extraction using a minor modified cetyltrimethylammonium bromide (CTAB) method (Murray and Thompson, 1980). The genomic DNAs of 30 extremely cold-tolerant and 30 extremely cold-sensitive individuals were selected as two bulked pools according to the SR of the $F_{2:3}$ population, ranging from 0 to 100%. To simplify the following description, we abbreviate DF104 as T, DN430 as S, the cold-tolerant pool as the T-pool, and the cold-sensitive pool as the S-pool. Isolated DNA was quantified using a Nanodrop 2000 spectrophotometer (Thermo Scientific, Fremont, CA, United States). All DNAs from the T-pool and S-pool plants were quantified on a Qubit® 2.0 Fluorometer (Life Technologies, Carlsbad, CA, United States), and equal amounts of DNA from the T-pool and S-pool plants were mixed.

NGS Sequencing and QTL-Seq Analysis

Total genomic DNA was extracted from bulked pools, and at least 3 μg genomic DNA was used to construct paired-end libraries with an insert size of 500 bp using the Paired-End DNA Sample Prep kit (Illumina Inc., San Diego, CA, United States). These libraries were sequenced using the HiSeq X10 (Illumina Inc., San Diego, CA, United States) NGS platform at Genedenovo (Guangzhou, China). Quality trimming is an essential step in generating high confidence in variant calling; raw reads were processed to obtain high-quality clean reads according to three stringent filtering standards as follows: (1) reads with $\geq$ 10% unidentified nucleotides (N) were removed; (2) reads with $>$ 50% bases with a phred quality score of $\leq$ 20 were removed; and (3) reads were aligned to the barcode adapter.

To identify single-nucleotide polymorphisms (SNPs) and InDels, filtered reads were aligned to the Nipponbare reference genome sequence (International, 2005) using Burrows-Wheeler Aligner (BWA, v 0.7.16a-r1181) with parameter "mem -M"; -M is an option used to mark shorter split alignment hits as secondary alignments (Kumar et al., 2019). Variant calling was performed using the GATK UnifiedGenotyper (v3.5). SNPs and InDels were filtered using the GATK VariantFiltration function with proper standards (-Window 4, -filter "QD < 4.0 || FS > 60.0 || MQ < 40.0," -G_filter "GQ < 20"). All mutations were annotated for genes and functions, as well as genomic regions, using ANNOVAR (Wang et al., 2010). Association analysis was performed using the SNP-index (Abe et al., 2012), Δ(SNP-Index) (Takagi et al., 2013), calculation of G statistic (Magwene et al., 2011; Mansfeld and Grumet, 2018), Euclidean distance (ED) (Hill et al., 2013), and two-tailed Fisher exact test (Fisher, 1922) based on the SNPs. Finally, the overlapping interval of the four methods was considered the final QTL interval.

Development of KASP Markers and Linkage Mapping

To develop markers for validation of QTL-Seq results and narrow the candidate region, 26 non-synonymous SNPs (nSNPs) with significant peaks were found based on the CDS sequence of the two parents in the *qCSBB9* region under the four association analysis algorithms [Δ (SNP-Index), G-value, ED-value, and Fisher exact test] and were considered as further markers for linkage mapping. KASP primers were designed using Primer express 3.0.1[1]; the primers are listed in **Supplementary Table 1**. All markers were selected for polymorphism between parents, and genotyping of the 460 individuals was performed using the polymorphic markers, which were used to construct the linkage map and narrow the candidate region using the inclusive composite interval mapping (ICIM) module of QTL IciMapping 4.2[2] The threshold of the logarithm of odds (LOD) for declaring the presence of a significant QTL was determined by the permutation test with 1,000 repetitions at $P < 0.01$.

Prediction of Candidate Genes for the CTBB

To predict possible candidate genes for the CTBB, the following three strategies were comprehensively considered in this study. First, candidate gene prediction was performed to compare the DNA sequences of those genes within the QTL regions using the whole-genome DNA resequencing database of the parents. In the QTL regions, we focused on open reading frames with non-synonymous mutant SNPs between the two parents. For the second, the most possible candidate genes were reselected according to their functional annotations, screening the rice genome database[3]. For the third, gene functions were annotated by gene ontology (GO) (Ashburner et al., 2000) and Kyoto Encyclopedia of Genes and Genomes (KEGG) (Kanehisa et al., 2004) databases with BLAST software (Altschul et al., 1997). Finally, the candidate genes were obtained.

Verification of the Expression Level of Candidate Genes

Five-millimeter-long buds of DN430 and DF104 were collected at 2, 6, 12, 24, and 48 h after cold treatment for three repetitions, frozen in liquid nitrogen, and stored at −80°C for

[1]http://www.appliedbiosystems.com

[2]http://www.isbreeding.net

[3]http://rice.plantbiology.msu.edu/

total RNA extraction. Control plants were also collected and stored similarly. qRT-PCR was used to quantify the expression levels of candidate genes under cold treatment. Total RNA was extracted from rice tissues using TRIzol reagent (Thermo Fisher Scientific, Waltham, MA, United States) and treated with DNase I to eliminate any DNA contamination. RNA quality was assessed by electrophoresis, and the RNA was stored at −80°C until use. First-strand cDNA (10 μL) was synthesized according to the instructions for the PrimeScript^{TM} RT Master Mix [Takara Biomedical Technology (Beijing) Co., Ltd., Beijing, China]. Primers were designed with Primer Premier v. 5.0 (PREMIER Biosoft International, United States) and are listed in **Supplementary Table 2**. The housekeeping gene *Actin1* (Os05g36290) was used as an internal control (Siahpoosh et al., 2012), and qRT-PCR was performed using a Roche LightCycler 2.10 with a 2× SYBR Green I PCR Master Mix. qRT-PCR analysis was performed as previously described (Zhang Z. et al., 2018).

Haplotype Analysis of Candidate Genes

Here, we present one method of analyzing haplotypes of candidate genes, which are variants of candidate genes in the 30 T-pool, 30 S-pool, and 295 northern China Japonica rice strains (Li et al., 2019). Primer sequences were designed for candidate genes at SNP sites between parents, and the DNA fragments of the sequences in 60 lines were amplified by PCR to perform haplotype statistics on the distribution of target genes. All specific primer sequences are listed in **Supplementary Table 2**. The PCR reaction mixture had a total volume of 20 μL, containing 1.5 μL of forward primer (10 μm), 1.5 μL of reverse primer (10 μm), 2 μL of genomic DNA (50 ng/μL), 5 μL of ddH_2O, and 10 μL of Pfu master mix (Chinese Beijing cwbio), which included Taq DNA polymerase, PCR buffer, Mg^{2+}, and dNTPs. The PCR reaction was performed in an Eppendorf 5333 Mastercycler using the same protocol as that used for qRT-PCR (Zhang Z. et al., 2018). The products were examined by 1% agarose gel electrophoresis. Direct sequencing of PCR products was performed by BGI Life Technology Co., Ltd.

RESULTS

Phenotypic Analysis of the Parental Lines and $F_{2:3}$ Population

Two parental varieties, DN430 and DF104 (**Figure 1A**), along with their 460 $F_{2:3}$ lines (**Figure 1B**), were evaluated for two cold tolerance indices (SD and SR) at the bud-bursting stage at 5°C/9 days. The SR of the cold-tolerant variety DF104 was significantly higher than that of cold-sensitive DN430, indicating that DF104 had a stronger CT than DN430. In the $F_{2:3}$ population, SR exhibited continuous variation from 0 to 100% (**Figure 1C** and **Supplementary Table 3**), and SD showed variation from 0.00 to 7.00 (**Figure 1D** and **Supplementary Table 3**). Interestingly, the scatter plot revealed that all individuals with SD values of 0 or 1 had SR values between 90 and 100%, whereas lines with SD values of 5 or 7 had SR values distributed between 0 and 20% (**Figure 1E**). Correlation analysis showed that the correlation coefficient between SR and SD was −0.938 (P = 2.985E-213). **Figure 1C** shows that among the 460 lines, 30 cold-tolerant and 30 cold-sensitive lines were identified. These were then selected to prepare the T-pool and S-pool, respectively, which were then used for DNA re-sequencing.

Whole-Genome Re-sequencing and QTL-Seq Analysis

Illumina high-throughput sequencing generated 566.87 million raw reads; 562.53 million clean reads (99.20%) were obtained after filtering, and the four samples generated 84,033,193,174-bp bases. When compared with the "Nipponbare" reference genome, these four samples generated 23,53,180 SNPs and 4,16,850 Indels (**Supplementary Table 4**). These high-quality data provided a solid foundation for subsequent analysis.

For all obtained SNPs, using the association threshold of 95 and 99%, the values of Δ (SNP-Index) (**Figure 2A**), ED (**Figure 2B**), G′ value (**Figure 2C**), and Fisher's exact test (**Figure 2D**) were used to intercept the association interval for CTBB. There were four QTL regions to be identified, which mapped to chromosome 2, 3, 5, and 9 (**Table 1** and **Figure 2**). For chromosome 2, one genomic region (17.06–19.24 Mb) was obtained by the ED algorithm at the 95% significance level, which we designated *qCTBB2*. The other three genomic regions, namely, *qCTBB3* (16.32–22.58 Mb), *qCTBB5* (0–3.54 Mb), and *qCTBB9* (9.54–21.38 Mb) on chromosomes 3, 5, and 9 for CTBB at the 95% significance level were revealed. However, the highest peak-value could be seen on chromosome 9 in the four algorithms. Of note, only a single QTL, *qCTBB9*, was obtained when the cut-off CI value of 99% was applied. For Δ (SNP-Index), *qCTBB9* spanned 9.34 Mb intervals, and the ED algorithm completely included the result given by the Δ (SNP-Index) algorithm. The G′ value and Fisher's exact test similarly captured the results of the first two algorithms. Here, the ED, G-value, and Fisher's exact test identified a small QTL interval. Obviously, a larger peak-value was obtained at the 99% significance level than at the 95% significance level. Therefore, *qCTBB9* is considered the most significant target for CTBB; considering the overlap interval of the four calculation models, *qCTBB9* was narrowed to a region of 5.4 Mb, which contains 647 predicted genes. According to QTL-Seq analysis, for the *qCTBB9* coding region, 281 nSNPs and seven Indels were detected (**Supplementary Table 5**).

Fine Mapping of *qCTBB9*

Because the 5.4 Mb region still contained numerous genes, to fine-map *qCTBB9* based on the nucleotide polymorphism information of the 5.4 Mb it covers, the highly credible SNPs obtained by the four association algorithms were fully considered, and the SNPs with low credibility under some algorithms were filtered out. Finally, SNPs with a relative distance of less than 200 bp were eliminated, and 26 excellent nSNPs (**Supplementary Table 1**) were used to scan the genotypes of the 460 lines and were used to obtain a *qCTBB9* linkage map. A QTL was considered significant when the LOD value was equal to or larger than 3.0 (Zhao et al., 2018). The SR of the 460 lines under cold stress was analyzed by linkage mapping. *qCTBB9* was simultaneously linked with SR and anchored to the 483.87 kb interval between

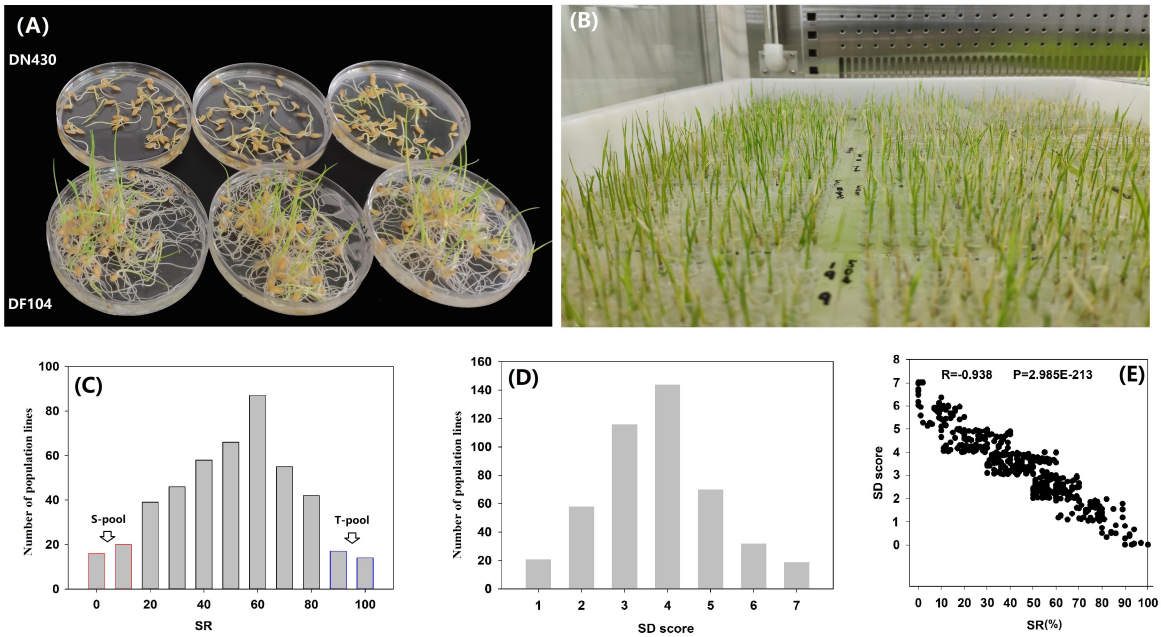


FIGURE 1 | Phenotypic analysis of cold tolerance in rice bud-bursting stage. **(A)** The performance of DN420 and DF104 under cold treatment (5°C/9 days). **(B)** Identification of cold tolerance of F_2 population in artificial climate chamber. **(C,D)** Frequency distribution of seed survival rate (SR) and severity of damage (SD) variation measured among 460 mapping individuals of $F_{2:3}$ populations. **(E)** Paired scatter plot analysis of SR and SD. T-Pool, DNA pool of cold-tolerant lines, S-pool, and DNA pool of cold-sensitive lines.

1,60,59,891 and 1,65,43,763 bp (**Figures 3A,B**); this explained 24.91% of the phenotypic variation in seed SR, and the peak-value for the LOD score was 14.01 (**Table 2**). The positive allele *qCTBB9* was contributed by DF104, and *qCTBB9* was optimized to a physical interval of 483.87 kb.

Putative Candidate Genes and Candidate SNPs in the Genomic Regions for CTBB

The 483.87 kb interval was intercepted through the annotation information of the Nipponbare genome[3], and 58 annotation genes were captured (**Supplementary Table 6** and **Figure 3C**). Some important genes or gene families related to cold tolerance in rice or other crops have been reported, such as cytochrome P450 (Su et al., 2010), a hypothetical protein (Zhao et al., 2017), a chromatin remodeling factor (Yang et al., 2019), an F-box domain (Saito et al., 2010), lipid metabolism genes (Zhang et al., 2019), a protein kinase (Ding et al., 2019), and a TATA-binding protein (Xu et al., 2020). Although similar genes or proteins were included in the list of 58 candidate genes, the 43 genes obtained from GO analysis were not annotated to the term response to cold. The most enriched terms of biological process, molecular function, and cellular component ontology were metabolic processes (i.e., GO:0006629, GO:0008152, and GO:0044237), activity (i.e., GO:0016491, GO:0003824, and GO:0016787), and cell (i.e., GO:0005575, GO:0005623, and GO:0044464), respectively (**Supplementary Table 7** and **Supplementary Figure 1**). Further, 483.87 kb on chromosome 9 had 240 effective SNPs between parental lines and a Δ (SNP−index), G-value, ED, and *P*-value of the two-tailed Fisher exact test higher than the statistical confidence at $P < 0.01$ (**Supplementary Table 6**). Of the 240 SNPs, 206 SNPs were intergenic and 34 SNPs were genic, including 16 intronic, nine non−synonymous, four synonymous, and five in UTRs. The nine nSNPs could be identified using both parents as a reference and affected six candidate genes encoding three hypothetical conserved genes (Os09g0436500, Os09g0443400, and Os09g0443700), one TATA-binding related factor domain containing protein (Os09g0443500), one similar to minus dominance protein (Os09g0444100), and one cholesterol acyltransferase family protein (Os09g0444200) (**Table 3**). As mentioned, these six types of genes might play an important role in responding to cold stress in plants. Of the six candidate genes, only Os09g0444200 was screened in the KEGG pathway (pathway ID K00679) (**Supplementary Table 7** and **Supplementary Figure 2**), which was involved in the glycerolipid metabolism, and glycerolipid is considered significantly related to plant cold sensitivity (Eriksson et al., 2011). Based on this, we identified the six final possible candidate genes through three approaches as follows: the possible relationship between gene response and cold stress, non-synonymous mutations in the gene coding region, and the participation of genes in specific metabolic pathways that affect cold tolerance.

Candidate Genes Verified by qRT-PCR and Haplotype Analysis

To identify strong candidate genes for *qCTBB9*, the expression levels of six genes under cold stress were further analyzed. The results showed that only Os09g0444200 showed strong induction

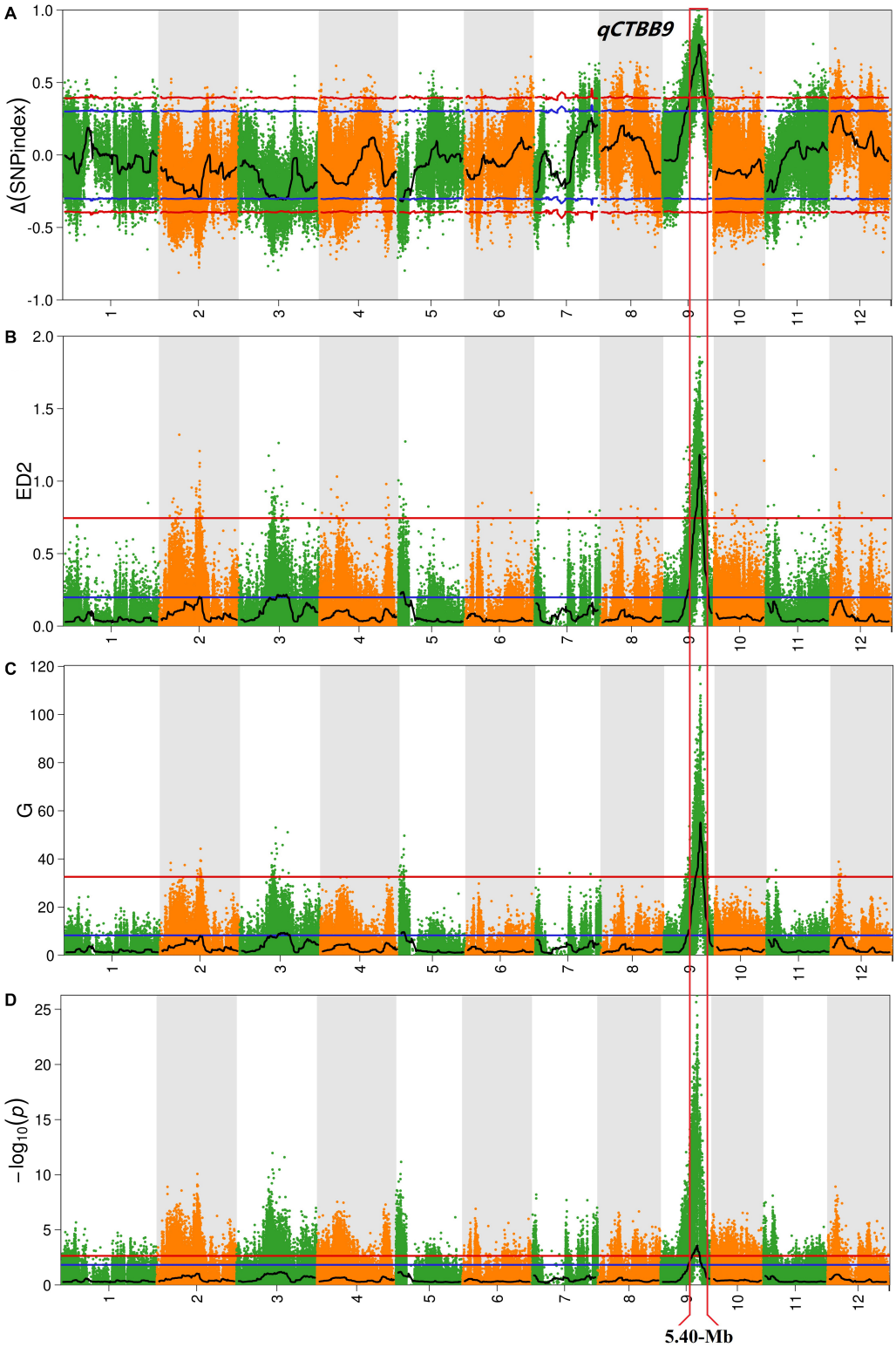


FIGURE 2 | Analysis of quantitative trait loci of cold tolerance at the bud-bursting stage based on QTL-Seq. **(A)** Manhattan plot shows the distribution of SNP-index and Δ (SNP-index) on chromosomes. **(B)** The Manhattan plot shows the distribution of the square of the Euclidean distance on the chromosomes. **(C)** The Manhattan plot shows the distribution of G′-Value on the chromosomes. **(D)** The Manhattan plot shows the distribution of $-\log_{10}$(P) value on the chromosomes based on Fisher exact test. The blue and red lines represent 95 and 99% confidence intervals, respectively.

TABLE 1 | QTLs conferring cold tolerance in four method identified using QTL-seq.

QTL names	Calculation models	CI	Chr	Start (bp)	End (bp)	Peak	Overlapping region (Mb)
qCTBB2	Euclidean distance	0.95	2	17,060,001	19,240,000	0.201677	17.06–19.24
qCTBB3	Δ(SNP-index)		3	16,320,001	22,580,000	−0.30825	16.32–22.58
	G′ value			16,140,001	23,600,000	9.325734	
	Euclidean distance			16,020,001	22,980,000	0.217969	
qCTBB5	Δ(SNP-index)		5	1	3,540,000	−0.3219	0–3.54
	G-statistic			1	3,660,000	9.641273	
	Euclidean distance			1	3,800,000	0.235656	
qCTBB9	Δ(SNP-index)		9	9,960,001	21,380,000	0.76226	9.54–21.38
	G′ value			9,580,001	21,500,000	55.11879	
	Euclidean distance			9,540,001	21,540,000	1.182111	
	Fisher's exact test			11,540,001	19,560,000	0.001811	
	Δ(SNP-index)	0.99	9	11,160,001	20,500,000	0.76226	13.38–18.74
	G-statistic			13,340,001	18,740,000	55.11879	
	Euclidean distance			13,380,001	18,740,000	1.182111	
	Fisher's exact test			13,200,001	18,740,000	0.001811	

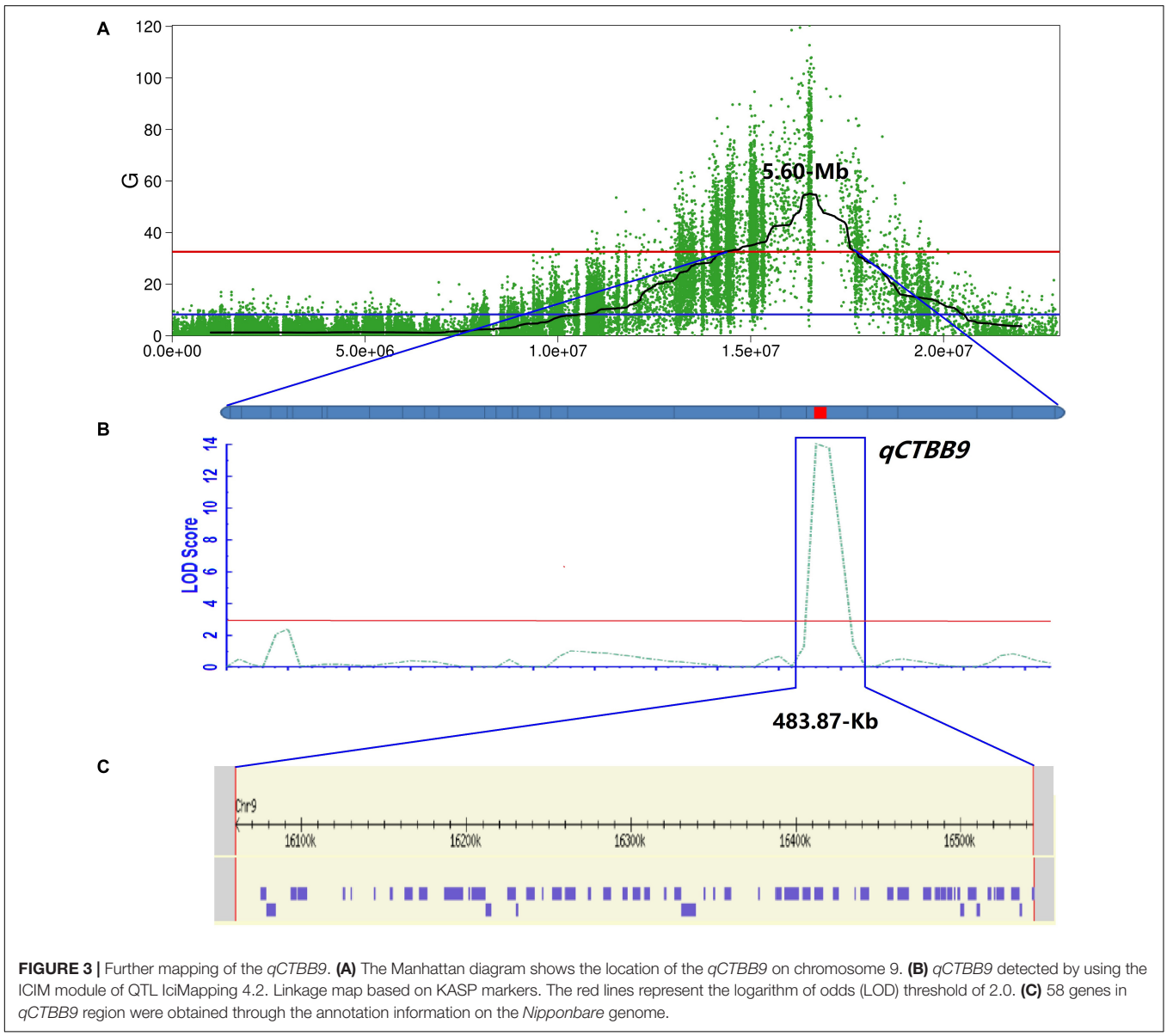


FIGURE 3 | Further mapping of the *qCTBB9*. **(A)** The Manhattan diagram shows the location of the *qCTBB9* on chromosome 9. **(B)** *qCTBB9* detected by using the ICIM module of QTL IciMapping 4.2. Linkage map based on KASP markers. The red lines represent the logarithm of odds (LOD) threshold of 2.0. **(C)** 58 genes in *qCTBB9* region were obtained through the annotation information on the *Nipponbare* genome.

TABLE 2 | Identification of *qCTBB9* for cold tolerance at bud-bursting stage by linkage analysis.

Trait	Position (cM)	LeftMarker	RightMarker	LOD	PVE(%)	Add	LeftCI	RightCI
SR	48	C9_16059891	C9_16543763	14.01	24.91	−4.09	47.5	49.5

TABLE 3 | Identification of SNPs in putative candidate genes for CTBB.

Gene ID	Position	DF-104 base	DN-430 base	T-pool base	S-pool base	Δ (SNP-index)	G-Value	ED	Fisher exact test	Structure_type	Function
Os09g0436500	16059891	A	C	A	C	0.92	118.55	1.68	2.21E-26	Exonic	Hypothetical conserved gene
Os09g0443400	16501770	A	G	A	G	0.30	6.07	0.18	1.56E-02	Exonic	Hypothetical conserved gene
	16501777	T	C	T	C	0.30	6.15	0.18	2.02E-02	Exonic	
	16501891	A	G	A	G	0.48	16.64	0.46	8.02E-05	Exonic	
Os09g0443500	16508612	G	T	G	T	0.89	57.80	1.60	2.84E-13	Exonic	TATA-binding related factor domain containing protein
Os09g0443700	16517219	G	C	G	C	0.86	86.30	1.46	1.36E-19	Exonic	Hypothetical conserved gene
Os09g0444100	16533992	T	C	T	C	0.67	41.01	0.89	6.13E-10	Exonic	Similar to minus dominance protein
	16535714	G	A	G	A	0.78	82.60	1.23	4.59E-19	Exonic	
Os09g0444200	16543763	A	G	A	G	0.86	91.09	1.48	1.14E-20	Exonic	Cholesterol acyltransferase family protein

of the cold stress response in parents with extremely strong CTBB (**Figure 4**), suggesting that Os09g0444200 is the most likely candidate gene for *qCTBB9*. In contrast, under normal conditions, all six candidate genes had no significant expression levels (**Supplementary Figure 3**). The strong correlation between RNA expression levels and SR in these 60 lines indicates the regulatory function of Os09g0444200 for CTBB (**Figure 5**). Based on these findings, we considered Os09g0444200 as a possible candidate CTBB gene based on *qCTBB9* for further analysis.

Os09g0444200 encodes lecithin–cholesterol acyltransferase. To reveal the significance of variations in the Os09g0444200 coding region, we selected 60 lines each from the T-pool and the S-pool and sequenced their Os09g0444200 genes by Sanger sequencing. Four SNPs were observed in the CDS sequence of Os09g0444200–SNP-16543710, SNP-16543763, SNP-16544225, and SNP-16546293. The four SNPs divided 460 $F_{2:3}$ genotypes into four haplotypes (HapI, *Hap*II, HapIII, and HapIV) (**Supplementary Table 8**). DN430 was classified as HapIII, and DF104 was classified as HapI. The 30 cold-tolerant and 30 cold-sensitive lines showed consistent isolation of the nSNP (1,654,225 bp), suggesting that this might lead to phenotypic differences in CTBB. We then referred to the data of the 3010 Rice Genomes Project and found that HapI (TAGT) and HapIII (CGAC) mainly exist in the genotype of Japonica rice (**Supplementary Table 9**). We subsequently analyzed the polymorphism types of Os09g0444200 in 295 China northern Japonica rice and found that HapI did not occur in the samples (**Supplementary Table 10**). It could thus be inferred that HapI is a rare natural variation. Therefore, it can be used as a special functional variation in DF104 to improve the CTBB of rice varieties. However, it cannot be ruled out that other Japonica Os09g0444200 markers might have similar SNPs.

DISCUSSION

Chilling injury events have been frequently observed in Northeast China in the past few years (Ma et al., 2017; Shen et al., 2019). The pre-germinated rice seeds directly planted in the soil are affected by the low temperature of air and/or irrigation water, which considerably reduces the germination rate and can lead to seed death (Fujino and Matsuda, 2010). Consequently, cold-tolerant rice varieties will contribute to food security and sustainable development. To locate the major QTLs of CTBB, in this study, we used several approaches to obtain the most reliable QTL interval. First, we used a large population to identify their phenotypes in low-temperature conditions, thereby obtaining accurate cold-tolerant phenotypes for each line. Second, two DNA pools with strict cold tolerance phenotypic differences were used to perform QTL-Seq analysis. Moreover, we used four bioinformatic analysis approaches to map QTL regions at the 99% significance level. Finally, only one highly significant peak (*qCTBB9*) was detected on chromosome 9 (**Table 1** and **Figure 2**), with the QTL mapped between 13.34 and 18.74 Mb. Some QTLs and genes for cold tolerance on chromosomes 9 have been reported in recent years. The QTL *qPGCG9-1* (Schlappi et al., 2017) was studied for the CTBB of rice, and according to the "Nipponbare" reference genome, was mapped to chromosome 9, at a position 6.83 Mb away from *qCTBB9*. *qLTS9* and *qCTS9-5* were associated with cold tolerance at the seedling stage (Lv et al., 2016), and they were located in the 22.701–22.887 and

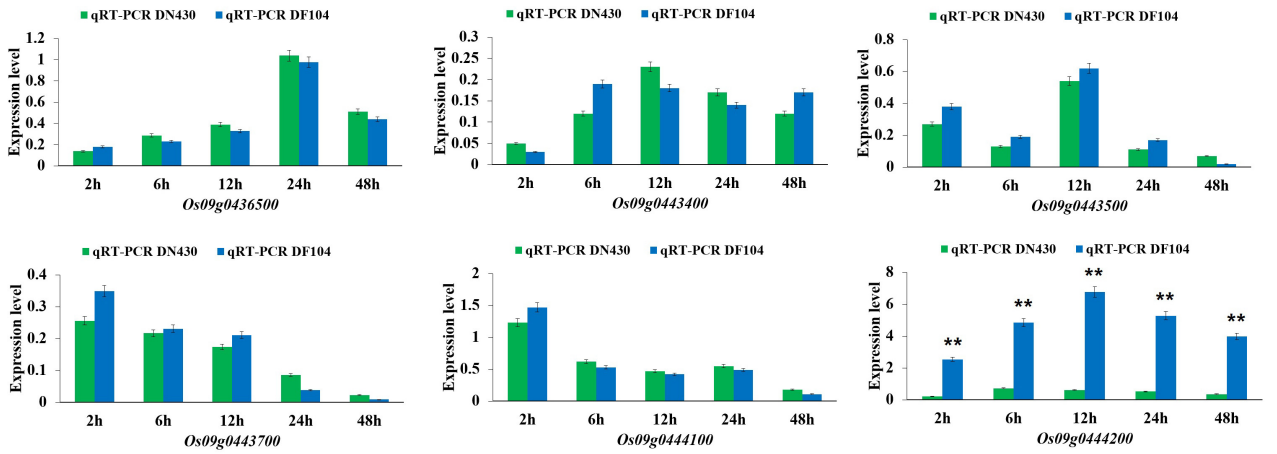


FIGURE 4 | Expression levels of the six candidate genes in DN430 and DF104 after cold stress measured by qRT-PCR. The results were statistically analyzed using Student's *t*-test (**$P < 0.01$).

4.304–4.488 Mb intervals on chromosome 9, respectively; their physical distances from the *qCTBB9* were 4.00 and 5.852 Mb, respectively. The location of *qCTBB9* in our study completely overlaps the previously reported region of *qCTS-9* (Zhao et al., 2017), which has been linked to cold tolerance at the seeding stage. Moreover, in the *qCTBB9* interval, *OsWRKY76* (Yokotani et al., 2013), *OsDREB1A*, and *OsDREB1B* (Ito et al., 2006) were involved in the regulatory mechanism of the rice cold-tolerance response. In addition, we did not find any cold-tolerance QTLs or genes related to the bud-bursting stage on chromosome 9. Notably, *qCTBB9* was associated with the only strong peak under the four calculation models (**Figure 2**). This shows that there is a significant difference in the allele ratio between the two mixed pools. Therefore, *qCTBB9* can be considered the most significant target for cold tolerance to explore candidate genes. Moreover, the other two QTL intervals, *qCTBB3* and *qCTBB5*, were detected by three approaches [Δ(SNP-index), G′ value, and ED] at the 95% significance level (**Table 1**); for *qCTBB3*, no existing cold-tolerance gene or QTL was found in its genome region, and in the *qCTBB5* interval, only *OsLti6b*, encoding a hydrophobic protein homologous, increased cold tolerance by overexpression (Kim et al., 2007). However, the peak of these two QTLs was less than one-third that of *qCTBB9* (**Table 1** and **Figure 2**). As suggested by previous studies, the causative genes underlying QTL probably reside in genomic regions with the highest peak-values (Win et al., 2017). Therefore, to identify genomic regions controlling CTBB with higher probability, we applied the $P < 0.01$ cutoff rather than $P < 0.05$.

In our study, several studies confirmed that combining QTL-Seq and traditional linkage mapping to uncover a very narrow candidate region is well suited for faster gene targeting (Feng et al., 2019; Liu G. et al., 2019). To screen potential candidate genes of the *qCTBB9* interval, based on the QTL-seq results, 26 nSNP markers were further used to perform genotype scanning on all 460 lines; using this approach, we reduced the number of candidate genes within the *qCTBB9* interval defined by QTL-Seq from 647 to 58 genes. Among these 58 genes, only six had nine functional base variations. Furthermore, the expression level of Os09g0444200 in the two parents showed that it was strongly induced after cold treatment. The expression analysis of Os09g0444200 in 60 lines with differences in extreme cold responses revealed a correlation between cold-tolerance and gene expression levels (**Figure 5**). Notably, there were four SNP differences between the two parents in the coding region of the Os09g0444200 gene, which directly led to the difference in the expression level of the Os09g0444200 gene under cold stress (**Figure 4**). Further haplotype analysis results show that the nSNP (1,654,225 bp) is responsible for the phenotypic difference (**Supplementary Table 8**). In addition, the 3010 Rice Genome Project database showed that the $Os09g0444200^{DF104}$ and $Os09g0444200^{DN430}$ haplotypes mainly exist in the genotype of Japonica rice (**Supplementary Table 9**). However, haplotype events did not occur in the 295 northern

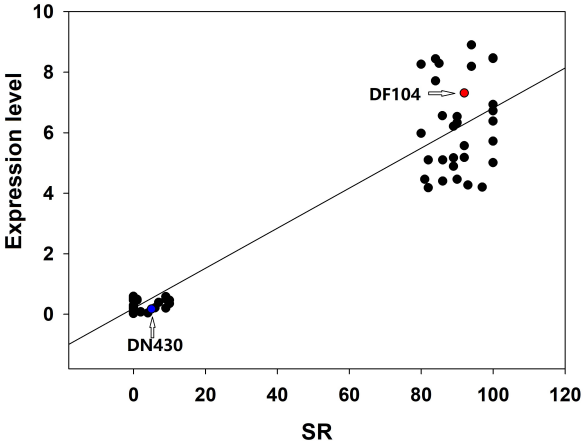


FIGURE 5 | Correlation between the expression level of *Os09g0444200* and seed survival rate in 30 cold-tolerant lines and 30 cold-sensitive lines after cold treatment.

cultivars (**Supplementary Table 10**). This means that the four SNPs in the DF104 coding region are rare variants of Japonica rice in northern China, which could serve as a genomic marker for improved CTBB. Moreover, the molecular mechanism of the interaction between Os09g0444200 and its cofactors needs to be investigated in future studies. Although we have found correlations between the nSNP in Os09g0444200 and the studied phenotypic traits, this is not enough to assign a certain tolerant phenotype to a single SNP. In contrast, we believe that a favorable allelic variant in one key gene is not sufficient to provide cold tolerance, and the final cold-tolerance phenotype of the plant should be considered a result of a combination of favorable allelic variations from different key genes.

Cold tolerance is a complex trait controlled by multiple genes (Zhang et al., 2014), and the genes that have been isolated thus far can be divided into two different types, those that regulate gene expression during stress responses, including signaling components and transcription factors (TFs) (Huang et al., 2012), and those that have specific functions and participate in systemic metabolism to defend against cold stress (Huang et al., 2012). For example, *OsLTPL159* enhances the cold tolerance of rice at the early seedling stage by decreasing the toxic effect of reactive oxygen species, enhancing cellulose deposition in the cell wall, and promoting osmolyte accumulation (Zhao et al., 2020). Moreover, *CTB4a*, as a leucine-rich repeat receptor-like kinase, positively regulates the activity and content of ATP under cold stress by interacting with the β subunit of ATP synthase, thereby increasing pollen fertility (Zhang et al., 2017). In our study, we observed that Os09g0444200 encodes a lecithin–cholesterol acyltransferase through the annotation information of the Nipponbare genome, and KEGG database annotation results revealed that Os09g0444200 is involved in the lipid metabolism pathway (ko01100//Metabolic pathways; ko00561//Glycerolipid metabolism) (**Supplementary Table 7**). For plants, chilling tolerance is closely related to the composition, structure, and metabolic processes of membrane lipids (Zhang et al., 2019), and plants can adjust membrane stability and fluidity by changing the unsaturation of fatty acids in membrane lipids, which is important for resisting cold stress (Karabudak et al., 2014). With the development of biotechnology, the genetic engineering of rice cold tolerance has considerably progressed. Several genes related to cold tolerance in fatty acid metabolism pathways have been cloned and transferred to plants for functional research (Nair et al., 2009; Cao et al., 2010); for rice, *qPSST6*, a major gene involved in the synthesis of long-chain fatty acids, was identified as a cold-tolerance gene at the booting stage of rice (Sun et al., 2018). However, whether Os09g0444200 regulates cold tolerance by participating in lipid metabolism requires further construction of transgenic rice for verification. Moreover, as a newly identified CTBB regulator, the signaling transduction system and the downstream pathways of Os09g0444200 are still unclear. The biological functions of Os09g0444200 and its associated genomic variations need to be further confirmed using gene editing and high-efficiency overexpression transformation systems.

DATA AVAILABILITY STATEMENT

The datasets presented in this study can be found in online repositories. The names of the repository/repositories and accession number(s) can be found below: NCBI (accession: PRJNA688381).

AUTHOR CONTRIBUTIONS

LY and DZ conceived and designed the research. LY, LL, and PL participated in data analysis. JW, HZ, CW, FY, JC, CW, and LL performed material development, sample preparation, and data analysis. LY wrote the manuscript. DZ corrected the manuscript. All authors read and approved the final manuscript.

FUNDING

This research was financially supported by the "Breeding of high-quality and resistant rice varieties" (Grant No. 2020ZX16B01), a major scientific and technological project of "Hundreds and Thousands" in Heilongjiang Province, China, and the China Postdoctoral Science Foundation (Grant No. 2019M651249).

ACKNOWLEDGMENTS

We thank Editage (www.editage.cn) for English language editing.

SUPPLEMENTARY MATERIAL

The Supplementary Material for this article can be found online at: https://www.frontiersin.org/articles/10.3389/fpls.2021.647239/full#supplementary-material

Supplementary Figure 1 | Clustering map of GO annotation of genes in 483.87 kb regions. The abscissa is the content of GO categories, and the left of the ordinate is the number of genes. This figure shows the gene classification of GO secondary functions in the context of all genes in the associated region.

Supplementary Figure 2 | Clustering map of KEGG annotation genes in 483.87 kb regions. The ordinate is the name of the KEGG pathway, and the abscissa is the number of genes annotated under the pathway.

Supplementary Figure 3 | Expression levels of the six candidate genes in DN430 and DF104 under normal condition measured by qRT-PCR. The results were statistically analyzed using Student's *t*-test (**$P < 0.01$).

REFERENCES

Abe, A., Kosugi, S., Yoshida, K., Natsume, S., Takagi, H., Kanzaki, H., et al. (2012). Genome sequencing reveals agronomically important loci in rice using MutMap. *Nat. Biotechnol.* 30, 174–178. doi: 10.1038/nbt.2095

Altschul, S. F., Madden, T. L., Schäffer, A. A., Zhang, J., Zhang, Z., Miller, W., et al. (1997). Gapped BLAST and PSI-BLAST: a new generation of protein database search programs. *Nucleic Acids Res.* 25, 3389–3402. doi: 10.1093/nar/25.17.3389

Andaya, V., and Tai, T. (2006). Fine mapping of the qCTS12 locus, a major QTL for seedling cold tolerance in rice. *Theor. Appl. Genet.* 113, 467–475.

Ashburner, M., Ball, C. A., Blake, J. A., Botstein, D., Butler, H., Cherry, J. M., et al. (2000). Gene ontology: tool for the unification of biology. *Nat. Genet.* 25, 25–29. doi: 10.1038/75556

Cao, Y. P., Shi, J. L., Li, Z., and Ming, F. (2010). Isolation of OsFAD2, OsFAD6 and FAD family members response to abiotic stresses in *Oryza sativa* L. *Hereditas* 32, 839–847. doi: 10.3724/SP.J.1005.2010.00839

Dai, L. Y., Lin, X. H., Ye, C. R., Ise, K., Saito, K., Kato, A., et al. (2004). Identification of quantitative trait loci controlling cold tolerance at the reproductive stage in Yunnan landrace of rice, Kunmingxiaobaigu. *Breed. Sci.* 54, 253–258. doi: 10.1270/jsbbs.54.253

Das, S., Upadhyaya, H. D., Bajaj, D., Kujur, A., Badoni, S., Laxmi, et al. (2015). Deploying QTL-seq for rapid delineation of a potential candidate gene underlying major trait-associated QTL in chickpea. *DNA Res.* 22, 193–203. doi: 10.1093/dnares/dsv004

Ding, Y., Shi, Y., and Yang, S. (2019). Advances and challenges in uncovering cold tolerance regulatory mechanisms in plants. *New Phytol.* 222, 1690–1704. doi: 10.1111/nph.15696

Endo, T., Chiba, B., Wagatsuma, K., Saeki, K., Ando, T., Shomura, A., et al. (2016). Detection of QTLs for cold tolerance of rice cultivar 'Kuchum'and effect of QTL pyramiding. *Theor. Appl. Genet.* 129, 631–640. doi: 10.1007/s00122-015-2654-2

Eriksson, S. K., Kutzer, M., Procek, J., Gröbner, G., and Harryson, P. (2011). Tunable membrane binding of the intrinsically disordered dehydrin Lti30, a cold-induced plant stress protein. *Plant Cell* 23, 2391–2404. doi: 10.1105/tpc.111.085183

Feng, X. X., Cheng, H. L., Zuo, D. Y., Zhang, Y. P., Wang, Q. L., Liu, K., et al. (2019). Fine mapping and identification of the fuzzless gene GaFzl in DPL972 (*Gossypium arboreum*). *Theor. Appl. Genet.* 132, 2169–2179. doi: 10.1007/s00122-019-03330-3

Fisher, R. A. (1922). On the interpretation of χ 2 from contingency tables, and the calculation of P. *J. R. Stat. Soc.* 85, 87–94.

Fujino, K., and Matsuda, Y. (2010). Genome-wide analysis of genes targeted by qLTG3-1 controlling low-temperature germinability in rice. *Plant Mol. Biol.* 72, 137–152. doi: 10.1007/s11103-009-9559-x

Fujino, K., and Sekiguchi, H. (2011). Origins of functional nucleotide polymorphisms in a major quantitative trait locus, qLTG3-1, controlling low-temperature germinability in rice. *Plant Mol. Biol.* 75, 1–10. doi: 10.1007/s11103-010-9697-1

Fujino, K., Sekiguchi, H., Matsuda, Y., Sugimoto, K., Ono, K., and Yano, M. (2008). Molecular identification of a major quantitative trait locus, qLTG3-1, controlling low-temperature germinability in rice. *Proc. Natl. Acad. Sci. U.S.A.* 105, 12623–12628. doi: 10.1073/pnas.0805303105

Hill, J. T., Demarest, B. L., Bisgrove, B. W., Gorsi, B., Su, Y. C., and Yost, H. J. (2013). MMAPPR: mutation mapping analysis pipeline for pooled RNA-seq. *Genome Res.* 23, 687–697. doi: 10.1101/gr.146936.112

Huang, G. T., Ma, S. L., Bai, L. P., Zhang, L., Ma, H., Jia, P., et al. (2012). Signal transduction during cold, salt, and drought stresses in plants. *Mol. Biol. Rep.* 39, 969–987. doi: 10.1007/s11033-011-0823-1

International, R. G. S. P. (2005). The map-based sequence of the rice genome. *Nature* 436, 793–800. doi: 10.1038/nature03895

Ito, Y., Katsura, K., Maruyama, K., Taji, T., Kobayashi, M., Seki, M., et al. (2006). Functional analysis of rice DREB1/CBF-type transcription factors involved in cold-responsive gene expression in transgenic rice. *Plant Cell Physiol.* 47, 141–153. doi: 10.1093/pcp/pci230

Iwata, N., and Fujino, K. (2010). Genetic effects of major QTLs controlling low-temperature germinability in different genetic backgrounds in rice (*Oryza sativa* L.). *Genome* 53, 763–768. doi: 10.1139/g10-060

Jena, K., Kim, S., Suh, J., Yang, C., and Kim, Y. (2012). Identification of cold-tolerant breeding lines by quantitative trait loci associated with cold tolerance in rice. *Crop Sci.* 52, 517–523. doi: 10.2135/cropsci2010.12.0733

Kadambari, G., Vemireddy, L. R., Srividhya, A., Nagireddy, R., Jena, S. S., Gandikota, M., et al. (2018). QTL-Seq-based genetic analysis identifies a major genomic region governing dwarfness in rice (*Oryza sativa* L.). *Plant Cell Rep.* 37, 677–687. doi: 10.1007/s00299-018-2260-2

Kanehisa, M., Goto, S., Kawashima, S., Okuno, Y., and Hattori, M. (2004). The KEGG resource for deciphering the genome. *Nucleic Acids Res.* 32, 277–280. doi: 10.1093/nar/gkh063

Karabudak, T., Bor, M., Ozdemir, F., and Turkan, I. (2014). Glycine betaine protects tomato (*Solanum lycopersicum*) plants at low temperature by inducing fatty acid desaturase7 and lipoxygenase gene expression. *Mol. Biol. Rep.* 41, 1401–1410. doi: 10.1007/s11033-013-2984-6

Kim, S. H., Kim, J. Y., Kim, S. J., An, K. S., An, G., and Kim, S. R. (2007). Isolation of cold stress-responsive genes in the reproductive organs, and characterization of the OsLti6b gene from rice (*Oryza sativa* L.). *Plant Cell Rep.* 26, 1097–1110. doi: 10.1007/s00299-006-0297-0

Kumar, S., Agarwal, S., and Ranvijay. (2019). Fast and memory efficient approach for mapping NGS reads to a reference genome. *J. Bioinformatics and Comput. Biol.* 17:1950008. doi: 10.1142/s0219720019500082

Li, N., Zheng, H., Cui, J., Wang, J., Liu, H., Sun, J., et al. (2019). Genome-wide association study and candidate gene analysis of alkalinity tolerance in japonica rice germplasm at the seedling stage. *Rice* 12:24. doi: 10.1186/s12284-019-0285-y

Lin, J., Zhu, W. Y., Zhang, Y. D., Zhu, Z., and Wang, C. L. (2010). Detection of quantitative trait loci for cold tolerance at the bud bursting stage by using chromosome segment substitution lines in rice (*Oryza sativa*). *Chin. J. Rice* 24, 233–236. doi: 10.3724/SP.J.1011.2010.01385

Liu, C. T., Schlappi, M. R., Mao, B. G., Wang, W., Wang, A. J., Chu, C., et al. (2019). The bZIP73 transcription factor controls rice cold tolerance at the reproductive stage. *Plant Biotechnol. J.* 17, 1834–1849. doi: 10.1111/pbi.13104

Liu, G., Zhao, T., You, X., Jiang, J., Li, J., and Xu, X. (2019). Molecular mapping of the Cf-10 gene by combining SNP/InDel-index and linkage analysis in tomato (*Solanum lycopersicum*). *BMC Plant Biol.* 19:15. doi: 10.1186/s12870-018-1616-7

Lu, H. F., Lin, T., Klein, J., Wang, S. H., Qi, J. J., Zhou, Q., et al. (2014). QTL-seq identifies an early flowering QTL located near *Flowering Locus T* in cucumber. *Theor. Appl. Genet.* 127, 1491–1499. doi: 10.1007/s00122-014-2313-z

Lv, Y., Guo, Z., Li, X., Ye, H., Li, X., Xiong, L., et al. (2016). New insights into the genetic basis of natural chilling and cold shock tolerance in rice by genome-wide association analysis. *Plant Cell Environ.* 39, 556–570. doi: 10.1111/pce.12635

Ma, Q. Y., Zhang, J. Q., Lai, Q., Zhang, F., Dong, Z. H., A, L. S., et al. (2017). Temporal and spatial variations of extreme climatic events in Songnen Grassland, Northeast China during 1960-2014. *J. Appl. Ecol.* 28, 1769–1778. doi: 10.13287/j.1001-9332.201706.002

Magwene, P. M., Willis, J. H., and Kelly, J. K. (2011). The statistics of bulk segregant analysis using next generation sequencing. *PLoS Comput. Biol.* 7:e1002255. doi: 10.1371/journal.pcbi.1002255

Manangkil, O. E., Vu, H. T. T., Mori, N., Yoshida, S., and Nakamura, C. (2013). Mapping of quantitative trait loci controlling seedling vigor in rice (*Oryza sativa* L.) under submergence. *Euphytica* 192, 63–75. doi: 10.1007/s10681-012-0857-z

Mansfeld, B. N., and Grumet, R. (2018). QTLseqr: an R package for bulk segregant analysis with next-generation sequencing. *Plant Genome* 11:180006. doi: 10.3835/plantgenome2018.01.0006

Mao, D. H., Yu, L., Chen, D. Z., Li, L. Y., Zhu, Y. X., Xiao, Y., et al. (2015). Multiple cold resistance loci confer the high cold tolerance adaptation of Dongxiang wild rice (*Oryza rufipogon*) to its high-latitude habitat. *Theor. Appl. Genet.* 128, 1359–1371. doi: 10.1007/s00122-015-2511-3

Murray, M., and Thompson, W. F. (1980). Rapid isolation of high molecular weight plant DNA. *Nucleic Acids Res.* 8, 4321–4326. doi: 10.1093/nar/8.19.4321

Nair, P. M. G., Kang, I.-S., Moon, B.-Y., and Lee, C.-H. (2009). Effects of low temperature stress on rice (*Oryza sativa* L.) plastid ω-3 desaturase gene, OsFAD8 and its functional analysis using T-DNA mutants. *Plant Cell Tissue Organ Cult.* 98, 87–96. doi: 10.1007/s11240-009-9541-y

Najeeb, S., Ali, J., Mahender, A., Pang, Y., Zilhas, J., Murugaiyan, V., et al. (2020). Identification of main-effect quantitative trait loci (QTLs) for low-temperature stress tolerance germination-and early seedling vigor-related traits in rice (*Oryza sativa* L.). *Mol. Breed.* 40:10. doi: 10.1007/s11032-019-1090-4

Park, M., Lee, J.-H., Han, K., Jang, S., Han, J., Lim, J. H., et al. (2019). A major QTL and candidate genes for capsaicinoid biosynthesis in the pericarp of Capsicum chinense revealed using QTL-seq and RNA-seq. *Theor. Appl. Genet.* 132, 515–529. doi: 10.1007/s00122-018-3238-8

Qiao, Y., Han, L., An, Y., Cao, G., Gao, Y., and Koh, H. J. (2005). Molecular mapping of QTLs for cold tolerance at the bud bursting period in rice. *Sci. Agric. Sin.* 38, 217–221.

Saito, K., Hayano Saito, Y., Kuroki, M., and Sato, Y. (2010). Map-based cloning of the rice cold tolerance gene Ctb1. *Plant Sci.* 179, 97–102. doi: 10.1016/j.plantsci.2010.04.004

Schlappi, M. R., Jackson, A. K., Eizenga, G. C., Wang, A., Chu, C., Shi, Y., et al. (2017). Assessment of five chilling tolerance traits and GWAS mapping in rice

using the USDA mini-core collection. *Front. Plant Sci.* 8:957. doi: 10.3389/fpls.2017.00957

Shen, X., Liu, B., Xue, Z., Jiang, M., Lu, X., Zhang, Q., et al. (2019). Spatiotemporal variation in vegetation spring phenology and its response to climate change in freshwater marshes of Northeast China. *Sci. Total Environ.* 666, 1169–1177. doi: 10.1016/j.scitotenv.2019.02.265

Shirasawa, S., Endo, T., Nakagomi, K., Yamaguchi, M., and Nishio, T. (2012). Delimitation of a QTL region controlling cold tolerance at booting stage of a cultivar,'Lijiangxintuanheigu', in rice, *Oryza sativa* L. *Theor. Appl. Genet.* 124, 937–946. doi: 10.1007/s00122-011-1758-6

Siahpoosh, M. R., Sanchez, D. H., Schlereth, A., Scofield, G. N., Furbank, R. T., van Dongen, J. T., et al. (2012). Modification of OsSUT1 gene expression modulates the salt response of rice *Oryza sativa* cv. Taipei 309. *Plant Sci.* 182, 101–111. doi: 10.1016/j.plantsci.2011.01.001

Song, J., Li, Z., Liu, Z., Guo, Y., and Qiu, L. J. (2017). Next-generation sequencing from bulked-segregant analysis accelerates the simultaneous identification of two qualitative genes in soybean. *Front. Plant Sci.* 8:919. doi: 10.3389/fpls.2017.00919

Su, C. F., Wang, Y. C., Hsieh, T. H., Lu, C. A., Tseng, T.-H., and Yu, S. M. (2010). A novel MYBS3-dependent pathway confers cold tolerance in rice. *Plant Physiol.* 153, 145–158. doi: 10.1104/pp.110.153015

Sun, J., Yang, L., Wang, J., Liu, H., Zheng, H., Xie, D., et al. (2018). Identification of a cold-tolerant locus in rice (*Oryza sativa* L.) using bulked segregant analysis with a next-generation sequencing strategy. *Rice* 11:24. doi: 10.1186/s12284-018-0218-1

Takagi, H., Abe, A., Yoshida, K., Kosugi, S., Natsume, S., Mitsuoka, C., et al. (2013). QTL-seq: rapid mapping of quantitative trait loci in rice by whole genome resequencing of DNA from two bulked populations. *Plant J.* 74, 174–183. doi: 10.1111/tpj.12105

Vikram, P., Swamy, B. P. M., Dixit, S., Ahmed, H. U., Cruz, M. T. S., Singh, A. K., et al. (2012). Bulk segregant analysis: "An effective approach for mapping consistent-effect drought grain yield QTLs in rice". *Field Crops Res.* 134, 185–192. doi: 10.1016/j.fcr.2012.05.012

Wambugu, P., Ndjiondjop, M. N., Furtado, A., and Henry, R. (2018). Sequencing of bulks of segregants allows dissection of genetic control of amylose content in rice. *Plant Biotechnol. J.* 16, 100–110. doi: 10.1111/pbi.12752

Wang, K., Li, M., and Hakonarson, H. (2010). ANNOVAR: functional annotation of genetic variants from high-throughput sequencing data. *Nucleic Acids Res.* 38:e164. doi: 10.1093/nar/gkq603

Wang, X., Zou, B., Shao, Q., Cui, Y., Lu, S., Zhang, Y., et al. (2018). Natural variation reveals that OsSAP16 controls low-temperature germination in rice. *J. Exp. Bot.* 69, 413–421. doi: 10.1093/jxb/erx413

Wen, J., Jiang, F., Weng, Y., Sun, M., Shi, X., Zhou, Y., et al. (2019). Identification of heat-tolerance QTLs and high-temperature stress-responsive genes through conventional QTL mapping, QTL-seq and RNA-seq in tomato. *BMC Plant Biol.* 19:398. doi: 10.1186/s12870-019-2008-3

Win, K. T., Vegas, J., Zhang, C., Song, K., and Lee, S. (2017). QTL mapping for downy mildew resistance in cucumber via bulked segregant analysis using next-generation sequencing and conventional methods. *Theor. Appl. Genet.* 130, 199–211. doi: 10.1007/s00122-016-2806-z

Xu, Y., Hu, D., Hou, X., Shen, J., Liu, J., Cen, X., et al. (2020). OsTMF attenuates cold tolerance by affecting cell wall properties in rice. *New Phytol.* 227, 498–512. doi: 10.1111/nph.16549

Yang, J., Li, D., Liu, H., Liu, Y., Huang, M., Wang, H., et al. (2020). Identification of QTLs involved in cold tolerance during the germination and bud stages of rice (*Oryza sativa* L.) via a high-density genetic map. *Breed. Sci.* 70, 292–302. doi: 10.1270/jsbbs.19127

Yang, J., Zhong, W., Wang, J., Chen, Z., and Cao, Q. (2009). Identification of QTL for rice plant cold tolerance at early seedling stage. *Genomics Appl. Biol.* 28, 46–50.

Yang, R., Hong, Y., Ren, Z., Tang, K., Zhang, H., Zhu, J. K., et al. (2019). A role for PICKLE in the regulation of cold and salt stress tolerance in Arabidopsis. *Front. Plant Sci.* 10:900. doi: 10.3389/fpls.2019.00900

Yang, T., Zhang, S., Zhao, J., Liu, Q., Huang, Z., Mao, X., et al. (2016). Identification and pyramiding of QTLs for cold tolerance at the bud bursting and the seedling stages by use of single segment substitution lines in rice (*Oryza sativa* L.). *Mol. Breed.* 36:96. doi: 10.1007/s11032-016-0520-9

Yokotani, N., Sato, Y., Tanabe, S., Chujo, T., Shimizu, T., Okada, K., et al. (2013). WRKY76 is a rice transcriptional repressor playing opposite roles in blast disease resistance and cold stress tolerance. *J. Exp. Bot.* 64, 5085–5097. doi: 10.1093/jxb/ert298

Zhang, H., Dong, J., Zhao, X., Zhang, Y., Ren, J., Xing, L., et al. (2019). Research progress in membrane lipid metabolism and molecular mechanism in peanut cold tolerance. *Front. Plant Sci.* 10:838. doi: 10.3389/fpls.2019.00838

Zhang, M., Ye, J., Xu, Q., Feng, Y., Yuan, X., Yu, H., et al. (2018). Genome-wide association study of cold tolerance of Chinese indica rice varieties at the bud burst stage. *Plant Cell Rep.* 37, 529–539. doi: 10.1007/s00299-017-2247-4

Zhang, Q., Chen, Q. H., Wang, S. L., Hong, Y. H., and Wang, Z. L. (2014). Rice and cold stress: methods for its evaluation and summary of cold tolerance-related quantitative trait loci. *Rice* 7:24. doi: 10.1186/s12284-014-0024-3

Zhang, X., Wang, W., Guo, N., Zhang, Y., Bu, Y., Zhao, J., et al. (2018). Combining QTL-seq and linkage mapping to fine map a wild soybean allele characteristic of greater plant height. *BMC Genomics* 19:226. doi: 10.1186/s12864-018-4582-4

Zhang, Z., Li, J., Tang, Z., Sun, X., Zhang, H., Yu, J., et al. (2018). Gnp4/LAX2, a RAWUL protein, interferes with the OsIAA3–OsARF25 interaction to regulate grain length via the auxin signaling pathway in rice. *J. Exp. Bot.* 69, 4723–4737. doi: 10.1093/jxb/ery256

Zhang, Z. Y., Li, J., Pan, Y., Li, J., Zhou, L., Shi, H., et al. (2017). Natural variation in CTB4a enhances rice adaptation to cold habitats. *Nat. Commun.* 8:14788. doi: 10.1038/ncomms14788

Zhao, J., Wang, S., Qin, J., Sun, C., and Liu, F. (2020). The lipid transfer protein OsLTPL159 is involved in cold tolerance at the early seedling stage in rice. *Plant Biotechnol. J.* 18, 756–769. doi: 10.1111/pbi.13243

Zhao, J., Zhang, S., Dong, J., Yang, T., Mao, X., Liu, Q., et al. (2017). A novel functional gene associated with cold tolerance at the seedling stage in rice. *Plant Biotechnol. J.* 15, 1141–1148. doi: 10.1111/pbi.12704

Zhao, M., Leng, Y., Chao, S., Xu, S. S., and Zhong, S. (2018). Molecular mapping of QTL for Fusarium head blight resistance introgressed into durum wheat. *Theor. Appl. Genet.* 131, 1939–1951. doi: 10.1007/s00122-018-3124-4

Zhou, L., Zeng, Y., Hu, G., Pan, Y., Yang, S., You, A., et al. (2012). Characterization and identification of cold tolerant near-isogenic lines in rice. *Breed. Sci.* 62, 196–201. doi: 10.1270/jsbbs.62.196

Zhu, Y., Chen, K., Mi, X., Chen, T., Ali, J., Ye, J., et al. (2015). Identification and fine mapping of a stably expressed QTL for cold tolerance at the booting stage using an interconnected breeding population in rice. *PLoS One* 10:e0145704. doi: 10.1371/journal.pone.0145704

Conflict of Interest: The authors declare that the research was conducted in the absence of any commercial or financial relationships that could be construed as a potential conflict of interest.

Copyright © 2021 Yang, Lei, Li, Wang, Wang, Yang, Chen, Liu, Zheng, Xin and Zou. This is an open-access article distributed under the terms of the Creative Commons Attribution License (CC BY). The use, distribution or reproduction in other forums is permitted, provided the original author(s) and the copyright owner(s) are credited and that the original publication in this journal is cited, in accordance with accepted academic practice. No use, distribution or reproduction is permitted which does not comply with these terms.

frontiers in Plant Science

ORIGINAL RESEARCH
published: 11 March 2021
doi: 10.3389/fpls.2021.595001

Cadmium-Tolerant and -Sensitive Cultivars Identified by Screening of *Medicago truncatula* Germplasm Display Contrasting Responses to Cadmium Stress

Vanesa S. García de la Torre[1], Teodoro Coba de la Peña[1,2], José J. Pueyo[1†] and M. Mercedes Lucas[1†]*

[1] Instituto de Ciencias Agrarias, Consejo Superior de Investigaciones Cientificas, Madrid, Spain, [2] Centro de Estudios Avanzados en Zonas Áridas, La Serena, Chile

Cadmium (Cd) pollution in soils is an increasing problem worldwide, and it affects crop production and safety. We identified Cd-tolerant and -sensitive cultivars by testing 258 accessions of *Medicago truncatula* at seedling stage, using the relative root growth (RRG) as an indicator of Cd tolerance. The factorial analysis (principal component analysis method) of the different growth parameters analyzed revealed a clear differentiation between accessions depending on the trait (tolerant or sensitive). We obtained a normalized index of Cd tolerance, which further supported the suitability of RRG to assess Cd tolerance at seedling stage. Cd and elements contents were analyzed, but no correlations with the tolerance trait were found. The responses to Cd stress of two accessions which had similar growth in the absence of Cd, different sensitivity to the metal but similar Cd accumulation capacity, were analyzed during germination, seedling stage, and in mature plants. The results showed that the Cd-tolerant accession (CdT) displayed a higher tolerance than the sensitive cultivar (CdS) in all the studied stages. The increased gene expression of the three main NADPH recycling enzymes in CdT might be key for this tolerance. In CdS, Cd stress produced strong expression of most of the genes that encode enzymes involved in glutathione and phytochelatin biosynthesis (*MtCYS*, *MtγECS*, and *MtGSHS*), as well as *GR*, but it was not enough to avoid a redox status imbalance and oxidative damages. Our results on gene expression, enzyme activity, antioxidant content, and lipid peroxidation indicate different strategies to cope with Cd stress between CdS and CdT, and provide new insights on Cd tolerance and Cd toxicity mechanisms in *M. truncatula*.

Keywords: heavy metal stress, cadmium, reactive oxygen species, nutrient content, *Medicago truncatula*, germplasm, metal tolerance, NADPH recycling enzymes

OPEN ACCESS

Edited by:
Felipe Klein Ricachenevsky, Federal University of Rio Grande, Brazil

Reviewed by:
Mirza Hasanuzzaman, Sher-e-Bangla Agricultural University, Bangladesh
Kamrun Nahar, Sher-e-Bangla Agricultural University, Bangladesh

***Correspondence:**
M. Mercedes Lucas
mlucas@ica.csic.es

† These authors have contributed equally to this work and share senior authorship

Specialty section:
This article was submitted to Plant Abiotic Stress, a section of the journal Frontiers in Plant Science

Received: *14 August 2020*
Accepted: *08 February 2021*
Published: *11 March 2021*

Citation:
García de la Torre VS, Coba de la Peña T, Pueyo JJ and Lucas MM (2021) Cadmium-Tolerant and -Sensitive Cultivars Identified by Screening of Medicago truncatula Germplasm Display Contrasting Responses to Cadmium Stress. Front. Plant Sci. 12:595001. doi: 10.3389/fpls.2021.595001

INTRODUCTION

Cadmium (Cd) is one of the most toxic substances for all living organisms, and its accumulation represents an increasing problem in agricultural soils due to anthropogenic activities, such as the extensive use of soil amendments and phytochemicals in agriculture, mining and industrial activities, transportation, uncontrolled dumping, and bad practices in waste treatment (Clemens et al., 2013). Plants are the main entry for Cd into the food chain (Peralta-Videa et al., 2009), presenting a risk both to the environment and to animal and human health. FAO is alerting of the hidden reality of soil pollution, especially in countries in development (Rodríguez-Eugenio et al., 2018). As an example, Cd levels in some areas of China have increased up to 250% in the last 30 years (Rodríguez-Eugenio et al., 2018), and in large cultivated areas, Cd accumulates to health-threatening levels in the so-called "cadmium rice" (Holdaway and Wang, 2018). Therefore, it is becoming of outmost interest the identification of crops and cultivars that are capable to tolerate moderate Cd stress and do not accumulate this heavy metal in their edible parts.

Legumes are together with cereals the main agricultural crops. They do not depend on nitrogen fertilization and are able to grow in poor and degraded soils, including heavy metal-polluted soils (Coba de la Peña and Pueyo, 2012). *Medicago truncatula* is a forage legume crop closely related to alfalfa, and a model legume plant. It constitutes an appropriate source for genetic improvement and an ideal model to study metal tolerance mechanisms in legumes. Cd-tolerant *M. truncatula* cultivars which do not accumulate Cd in the aerial part could be cultivated as a forage crop in moderately Cd-polluted soils, while cultivars with high metal accumulation could be used in phytoremediation of Cd-contaminated soils, due to its high biomass and good soil coverage. The identification of such cultivars in *M. truncatula* germplasm represents a potential tool to remediate the problems derived from Cd accumulation in both, arable lands and wild ecosystems. We have shown before the feasibility of identifying heavy metal-tolerant varieties in a *M. truncatula* germplasm by phenotyping a limited number of accessions (García de la Torre et al., 2013).

The effect of Cd stress on *M. truncatula* has been studied scarcely, mainly at the seedling stage (Aloui et al., 2009, 2011; Xu et al., 2010; Saeidi et al., 2012; Rahoui et al., 2014, 2015, 2017). Heavy metal tolerance and/or toxicity depend on the developmental stage of the plant, the metal concentration, and the time of exposure (Sanità di Toppi and Gabbrielli, 1999). In plants, Cd toxicity promotes growth reduction, macro and micronutrients uptake disturbance, and restriction in reserves mobilization at germination, among other detrimental effects (Benavides et al., 2005). Cd produces oxidative stress and lipid peroxidation (Romero-Puertas et al., 2012). In fact, the overproduction of reactive oxygen species (ROS) is considered the origin of the damage following Cd exposure (Cuypers et al., 2010). Cd does not take part in Fenton reactions for generating ROS but indirectly contributes to ROS formation by altering the antioxidant machinery of cells (Sharma and Dietz, 2009). Under Cd stress conditions, ROS play a dual role acting as toxic agents, but also as signal molecules, therefore the fine tuning of ROS homeostasis is crucial for the plant. The production of ROS and reactive nitrogen species with signaling functions are now considered strategies to avoid Cd toxicity (Romero-Puertas et al., 2019). Plants have several enzymatic and non-enzymatic antioxidant defense systems that allow ROS scavenging.

The first line of defense against ROS is the dismutation of O_2^- to H_2O_2 through superoxide dismutase enzymes (SODs) and then catalases and peroxidases detoxify H_2O_2. There are also important antioxidant enzymes of the ascorbate-glutathione (ASC-GSH) cycle that allow maintaining the redox state of the cell. Some of these reactions are NADPH-dependent, and this molecule has been described as a limiting factor for the plant antioxidant capacity (Foyer and Noctor, 2011). NADPH is mainly produced by three enzymes, glucose 6-phosphate dehydrogenase (G6PDH), 6-phosphogluconate dehydrogenase (6PGDH), and $NADP^+$-dependent isocitrate dehydrogenase (ICDH). Differential responses of these enzymes have been reported in stressed plants; and ICDH has been described as a key enzyme in NADPH recycling, and essential for the antioxidant defense under stress conditions (Marino et al., 2007). NADPH-recycling dehydrogenases are activated in response to Cd (Marino et al., 2013; Pérez-Chaca et al., 2014). There are several reports that study ROS production under Cd stress; however, most of them do not compare the differences between metal-tolerant and sensitive cultivars. Studies that analyze the antioxidant defense at different developmental stages are also scarce.

The aims of this work were to evaluate Cd tolerance in a *Medicago truncatula* germplasm, and to identify Cd-tolerant and Cd-sensitive genotypes. We also comparatively assessed Cd effects on tolerant and sensitive accessions at different developmental stages. Metal accumulation, nutritional status, and several markers for Cd tolerance, related with antioxidant defenses and Cd-induced oxidative stress, were analyzed. Our results suggest different strategies to cope with Cd stress depending on the Cd tolerance trait, and provide new insights on Cd response mechanisms in *M. truncatula*.

MATERIALS AND METHODS

Plant Material

Medicago truncatula cv. Parabinga was used to set up the experimental conditions for the tolerance assays. Two hundred and fifty-eight *M. truncatula* accessions obtained from the National Plant Germplasm System of the United States Department of Agriculture (ARS-USDA) were used for the Cd-tolerance screening.

Screening for Cadmium Tolerance

Seeds were scarified, sterilized, and germinated, and seedlings were transferred to a miniaturized hydroponic culture system containing modified Hoagland solution, pH 5.4, as previously described (García de la Torre et al., 2013). Seedlings were acclimatized during 24 h prior to Cd treatment.

Medicago truncatula cv. Parabinga seedlings were exposed to different Cd concentrations (0–40 μM $CdCl_2$) for 48, 72, and 96 h

under growth chamber conditions as described by García de la Torre et al. (2013). In subsequent experiments, seedlings of 258 *M. truncatula* accessions were exposed to 0 and 10 μM $CdCl_2$ for 48 h. Thus, seedlings were 3 days old at harvest. Ten to thirty seedlings per cultivar were analyzed per treatment (control or Cd stress). Seedling relative root growth (RRG) was calculated as previously described (Sledge et al., 2005; García de la Torre et al., 2013), and it was used as an indicator of tolerance.

Screening Validation in Growth Pouches

Two-day-old seedlings were acclimatized for 24 h prior to Cd exposure in growth pouches (CYG Seed Germination Pouches, Mega International, Minneapolis, MN, United States) containing 50 mL of nutrient solution. To set up the assay conditions, *M. truncatula* cv. Parabinga plantlets were grown in a range of Cd concentrations (0–200 μM $CdCl_2$) for 12 days, under growth chamber conditions (García de la Torre et al., 2013). Nutrient solution was changed every 48 h. In subsequent experiments, seedlings of four potentially Cd-tolerant and four potentially Cd-sensitive accessions were exposed to 0 or 100 μM $CdCl_2$ for 12 days. Thus, plants were 15 days old at harvest. Five to ten pouches, each containing five plants per cultivar and treatment, were analyzed. Root length, root and shoot fresh and dry weights, and number of leaves were measured, and relative parameters (RX) were calculated as follows: RX = (Parameter X_{Cd}/Parameter X_C) × 100.

Cadmium and Nutrients Content

The content of Cd and nutrients was analyzed. At harvest, plants were dipped in 10 mM Na_2EDTA, and then washed twice in ultrapure water. Roots and shoots were collected and stove-dried at 60°C for 3 days, and digested with nitric-perchloric acid (7:3). Contents of Cd and nutrients were determined using ICP-OES (Perkin-Elmer Optima 4300 DV). Three pouches, each containing five plants, per cultivar and treatment were analyzed.

Analysis of Two Genotypes With Contrasting Tolerance

The tolerant PI 516929 (CdT) and sensitive PI 660497 (CdS) genotypes were selected to study the Cd effect on the germination process, gene expression, glutathione content, SOD and catalase (CAT) activities, and lipid peroxidation.

Scarified and sterilized CdT and CdS seeds were transferred into Petri dishes with a sterile filter paper imbibed with 5 mL of sterile water or 5 mL 200 μM $CdCl_2$ for 72 h (25/19°C, 16/8 h) in the dark. Germination percentage was recorded on the third day. The seedlings radicles were removed and the cotyledons used in the α-amylase analysis. Four to six replicates (25 seeds per replicate) were assayed for each accession and treatment.

Three-day-old seedlings were transferred to the miniaturized hydroponic system for 72 h for acclimatization, prior to Cd treatment. Then, seedlings were exposed to 0 or 50 μM $CdCl_2$ for 12 h. Five to ten seedlings per cultivar and treatment were used for histochemical detection of lipid peroxidation and loss of plasma membrane integrity. The rest of the roots were used for the gene expression analyses and determination of glutathione content.

Finally, 3-day-old CdT and CdS germinated seedlings were acclimatized for 7 days in vermiculite pots (350 mL), and then exposed to 0 or 100 μM $CdCl_2$ for 15 days. Plants were 25 days old at harvest. Shoots and roots were analyzed for lipid peroxidation and CAT and SOD enzymatic activities. For each determination, four biological replicates per cultivar and treatment were analyzed.

Alpha-Amylase Activity

Cotyledons were ground in liquid nitrogen and homogenized (0.1 g FW mL^{-1}) in 2 mM imidazole-HCl buffer (pH 7.0). The homogenates were centrifuged (15,000 *g*, 1 h, at 0°C), and the supernatant was used to determine the α-amylase activity as described by Smith and Roe (1949). The reaction mixture (100 μL supernatant, 550 μL phosphate buffer, 0.9 μg μL^{-1} starch, and 0.5 M NaCl) was incubated during 30 min at 37°C, and the reaction was stopped with 80 μL of 1 N HCl. The remaining starch was stained with 700 μL of diluted lugol (1:6). A blank for each sample was prepared using 100 μL of supernatant, 650 μL of deionized water, and 700 μL of diluted lugol. The starch content was monitored at 620 nm. The α-amylase activity was expressed as μg hydrolyzed starch g^{-1} fresh weight min^{-1}.

RNA Isolation and Quantitative Real-Time PCR Analysis

Total RNA was isolated from seedling roots using the TRIZol (Invitrogen) method and treated with RNase-free DNase I (Thermo Fisher Scientific). RNA concentration was determined with a Nanodrop ND1000 spectrophotometer (Thermo Fisher Scientific). One microgram of DNA-free RNA was used for reverse transcription, using SuperScript® II Reverse Transcriptase (Invitrogen), and oligo-d(T)18 as primer. The cDNAs were diluted 10-fold before performing qPCR. The Primer3 software[1] was used to design specific primers for all genes tested (**Supplementary Table 1**).

Quantitative PCR reactions were run in a 7300 Real-Time PCR Sequence Detection System (PE Applied Biosystems). Each reaction contained 1 μL cDNA, 5 μL SYBR Green PCR master mix (PE Applied Biosystems), and 0.5 μM (final concentration) primer, in a total volume of 10 μL. Initial denaturing time (10 min, 95°C) was followed by 40 PCR cycles (95°C, 15 s; 60°C, 90 s; 72°C, 30 s), and a melting curve (95°C, 15 s; 60°C, 60 s; 95°C, 15 s). Relative gene expression was calculated according to the primer efficiency method (Pfaffl, 2001). Only fold-changes greater than two were considered as significant. Four biological replicates (10 roots each) per cultivar and treatment were analyzed.

Glutathione Determination

Reduced glutathione (GSH) and total glutathione (GSH + GSSG) were measured by means of the glutathione recycling assay (Floreani et al., 1997), essentially as described by Shvaleva et al.

[1]https://bioinfo.ut.ee/primer3-0.4.0/

(2010) with the following modifications: Roots were ground in liquid nitrogen and homogenized in 5% (w/v) sulfosalicylic acid (0.2 g FW mL^{-1}). Homogenates were centrifuged (15,000 *g*, 5 min, 4°C), and the supernatant was used for determination of total glutathione. Reaction mixture (1 mL) included 25 μL of supernatant, 80 mM TEA (pH 8), 0.6 mM 5,5′-dithio-bis (2-nitrobenzoic acid) (DTNB, Sigma), 0.21 mM NADPH (Sigma), and 1 unit glutathione reductase (Roche, Branchburg, NJ, United States). DTNB, NADPH, and glutathione reductase were dissolved or diluted in 150 mM K-phosphate buffer (pH 7.4), 6.3 mM EDTA. The 2-nitro-5-thiobenzoic acid (TNB) generation was monitored spectrophotometrically at 412 nm for 1 min at 25°C. For GSSG determination, GSH was derivatized by adding 6 μL of 2-vinyl-pyridine and 10 μL 1 M triethanolamine (pH 8.0) to 90 μL of supernatant, for 30 min. The final pH of the reaction was between 6.0 and 7.0. Derivatized samples were assayed as described above. GSH was determined as the difference between total glutathione and GSSG. Four biological replicates (10 roots each) per cultivar and treatment were analyzed.

Histochemical Analyses

Lipid peroxidation and loss of plasma membrane integrity detection were performed on intact seedling roots as described previously (Yamamoto et al., 2001). For lipid peroxidation, roots were stained for 20 min with Schiff's reagent, which detects aldehydes originated from lipid peroxides, and kept in a solution containing 0.5% (w/v) $K_2S_2O_5$ in 0.1 N HCl to retain the color.

The loss of plasma membrane integrity was detected by staining the roots with Evans blue solution [0.025% (w/v) Evans blue in 100 μM $CaCl_2$, pH 5.6] for 10 min and washed several times with 100 μM $CaCl_2$ (pH 5.6) until the dye no longer eluted from the roots.

The stained roots were observed under a stereomicroscope (Carl Zeiss Stemi 2000C, Fisher Scientific) with an attached digital camera (Leica DFC 420C). Color density was measured using the ImageJ software[2]. Five to ten seedlings per cultivar and treatment were analyzed.

Lipid Peroxidation

Assessment of malondialdehyde (MDA) was performed using the thiobarbituric acid method (Singh et al., 2007). Shoots and roots were ground in liquid nitrogen, homogenized in 1 mL of 0.1% TCA (0.1 g FW mL^{-1} for shoots and 0.25 g FW mL^{-1} for roots), and analyzed as described by Redondo et al. (2009). Four biological replicates per cultivar and treatment were analyzed.

Superoxide Dismutase and Catalase Activities

Shoots and roots (0.04 and 0.1 g FW mL^{-1}, respectively) were ground in liquid nitrogen and homogenized in 50 mM K-phosphate buffer (pH 7.8) containing 0.1 mM EDTA, 1% (w/v) PVP-10, and 0.1% (v/v) Triton X-100. After centrifugation (20,000 *g*, 4°C, 30 min), the supernatant was used for the spectrometric determination of SOD and CAT activities, as described by Redondo et al. (2009).

[2]http://imagej.nih.gov/ij/

Statistical Analyses and Tolerance Index

The statistical analyses were performed with the IBM SPSS Statistics 20 software (SPSS Inc., Chicago, IL, United States). The root lengths from the screening assay were analyzed by ANOVA ($p < 0.05$; $n \geq 10$). Cultivars that did not show significant differences or displayed a significantly higher root growth under Cd treatment than under control conditions were considered potentially Cd-tolerant. A Pearson's correlation analysis was performed comparing the results obtained here with those previously reported on mercury and aluminum tolerance for the same *M. truncatula* germplasm (Sledge et al., 2005; García de la Torre et al., 2013). The relative parameters, fresh weight root/shoot ratio, and elements content were analyzed by ANOVA ($p < 0.05$). Fisher LSD or Tukey HSD tests were applied for pair-wise comparison. Data were combined considering the different accessions as replicates of potentially tolerant or sensitive plants, and a factorial analysis (principal component analysis method, PCA) was conducted with the different relative parameters. The resulting components (PC1 and PC2) were plotted to check the associations. For each accession, a tolerance index was calculated and normalized (nTI) as described by García de la Torre et al. (2013). Germination percentage was analyzed by the Pearsons's chi-squared test. The glutathione content, lipid peroxidation, α-amylase activity, and SOD and CAT activities were analyzed by ANOVA ($p < 0.05$), and the Tukey HSD test was applied for pair-wise comparisons.

RESULTS

Medicago truncatula Germplasm Screening for Cd Tolerance

The appropriate Cd treatment (concentration and time) for the screening assays was determined based on the root growth response of *M. truncatula* cv. Parabinga, a Cd-sensitive cultivar (**Supplementary Figure 1**). The treatment with 10 μM $CdCl_2$ for 48 h had a clear effect on this cultivar without completely arresting root growth (RRG ≈ 30%), and it was selected for *M. truncatula* germplasm screening.

Seedlings of 258 *M. truncatula* accessions were tested for Cd tolerance. Root growth results are shown in **Supplementary Table 2**. The response to the metal of the different genotypes followed a normal distribution (**Figure 1**), suggesting that the number of tested accessions and the assay conditions were adequate. Most accessions displayed low RRG values, ranging from 10 to 50% (225 accessions), suggesting that *M. truncatula* is in general sensitive to Cd. Twenty-six accessions displayed values from 60 to 80%, and eight accessions exhibited RRG values above 80% (**Supplementary Table 2**). Cd had not a detrimental effect on the root growth of six of the accessions tested, as either there were not significant differences between control and Cd-treated seedlings, or the root growth values of Cd-treated seedlings were significantly higher than those of untreated seedlings (**Supplementary Table 2**).

Plants might have both metal-specific tolerance mechanisms and common mechanisms for different metals. A Pearson's

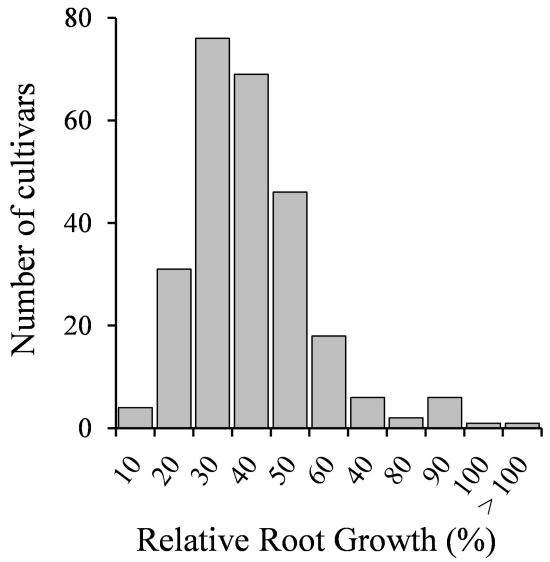


FIGURE 1 | Seedling relative root growth (RRG) distribution of 258 *M. truncatula* accessions grown in the absence or presence of Cd stress (10 μM $CdCl_2$, 48 h).

correlation analysis revealed no correlation between Al and Cd tolerances but a significant positive correlation between Cd and Hg tolerances ($r = 0.486$, $p < 0.01$) (**Figure 2**).

Validation of the Rapid Screening Method for Cd Tolerance

To determine the validity of the screening results, treatment with 100 μM $CdCl_2$ for 12 days in growth pouches was selected, as it was non-lethal but produced substantial differences in all growth parameters, in *M. truncatula* cv. Parabinga (data not shown).

Four potentially Cd-tolerant accessions (PI 660407, PI 660411, PI 516929, and PI 516933) with RRG values ranging from 66 to 90%, and four potentially Cd-sensitive accessions (PI 660497, PI 199257, PI 384634, and PI 516950) with RRG values ranging from 8 to 45% (**Supplementary Table 2**), were analyzed for morphological parameters. Results are shown in **Table 1**. No obvious phenotypic or anatomical differences were observed among accessions in the absence of Cd treatment. Root growth and root fresh weight were significantly affected in the presence of Cd in all accessions. While RRG and relative root fresh weight (RRFW) values of the potentially tolerant accessions were in general higher than those of the sensitive ones, two of the sensitive accession (PI 199257 and PI 660497) presented RRG values that were not significantly different from those of the tolerant accessions, and one tolerant accession (PI 516933) showed a similar RRFW value to those recorded for the sensitive varieties. No significant differences in relative root dry weight (RRDW) values were observed among varieties, and one sensitive accession (PI 660497) showed a significant reduction of the root dry weight after Cd treatment.

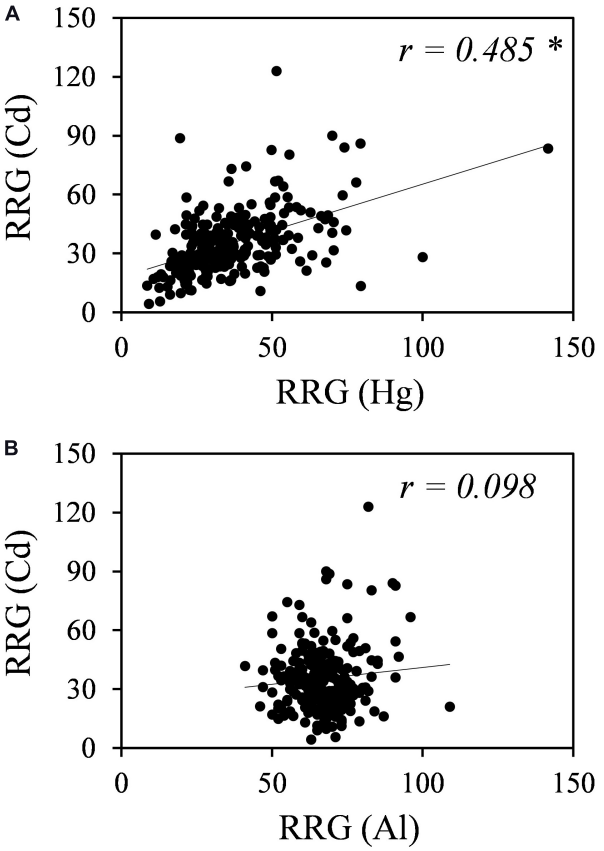


FIGURE 2 | Correlation analyses for Cd and Hg tolerances **(A)** and for Cd and Al tolerances **(B)**. RRG values for Hg were obtained from García de la Torre et al. (2013), and RRG values for Al were obtained from Sledge et al. (2005). * Indicates significant correlation at p-value < 0.01.

Regarding the Cd effect on the aerial part growth, the number of leaves decreased significantly in sensitive accessions following exposure to Cd, while non-significant differences were found for all potentially tolerant accessions. Tolerant accessions had relative number of leaves (RNL) values above 85%, and significantly higher than those of the sensitive accessions, which remained below 68%. Cd significantly affected the relative shoot fresh weight (RSFW) of accession PI 516933 (initially ranked as Cd-tolerant), while this parameter was not significantly affected for accession PI 516950 (initially ranked as Cd-sensitive). Only one potentially tolerant accession, PI 660407, presented an RSFW value that was significantly different from the potentially sensitive accessions. No significant differences were found between RSFWs for the potentially tolerant accessions PI 660407 and PI 5162929. Cd stress produced a significant decrease in the shoot dry weight of two sensitive accessions. Significant differences for relative shoot dry weight (RSDW) were found between the sensitive accession PI 660497 and the two tolerant accessions PI 660407 and PI 660411, which displayed the highest RSDW values. Cd significantly affected the root/shoot ratio (R/S) of all accessions, and accession PI 660407 showed the highest R/S ratio.

TABLE 1 | Relative growth parameters and normalized tolerance indices for selected *M. truncatula* accessions grown in hydroponic pouches with 0 or 100 μM $CdCl_2$ for 12 days.

Accession	RRG	RRFW	RRDW	RNL	RSFW	RSDW	R/S	nTI
PI 660407	41.46 ± 1.78^{*a}	59.04 ± 6.00^{*a}	91.95 ± 3.49^{a}	100.00 ± 0.00^{a}	100.36 ± 3.10^{a}	94.89 ± 6.68^{a}	73.94 ± 6.07^{*a}	1.00
PI 660411	42.50 ± 0.89^{*a}	46.60 ± 1.93^{*abc}	88.87 ± 0.53^{a}	100.00 ± 0.01^{a}	77.99 ± 4.76^{bc}	94.84 ± 6.57^{a}	60.24 ± 3.80^{*abc}	0.92
PI 516929	40.85 ± 1.59^{*a}	52.61 ± 3.64^{*ab}	83.38 ± 3.44^{a}	93.47 ± 2.66^{a}	87.73 ± 4.69^{ab}	79.62 ± 3.71^{ab}	62.80 ± 3.42^{*abc}	0.90
PI 199257	35.11 ± 0.80^{*ab}	42.06 ± 3.16^{*bc}	86.83 ± 8.93^{a}	64.58 ± 6.25^{*b}	70.72 ± 7.38^{*bcd}	79.83 ± 6.57^{*ab}	53.24 ± 3.19^{*bc}	0.78
PI 516933	40.34 ± 4.99^{*a}	38.63 ± 5.31^{*c}	74.94 ± 9.25^{a}	85.71 ± 7.65^{a}	60.26 ± 6.75^{*d}	76.26 ± 8.55^{ab}	68.06 ± 3.91^{*ab}	0.75
PI 516950	29.26 ± 1.61^{*b}	43.97 ± 6.21^{*abc}	80.75 ± 14.57^{a}	58.18 ± 8.39^{*b}	72.00 ± 11.27^{bcd}	76.96 ± 12.04^{ab}	57.03 ± 5.15^{*abc}	0.74
PI 660497	40.90 ± 1.77^{*a}	44.33 ± 3.30^{*bc}	72.70 ± 5.49^{*a}	67.74 ± 1.97^{*b}	64.22 ± 5.28^{*cd}	66.75 ± 8.27^{*b}	65.00 ± 3.45^{*abc}	0.72
PI 384634	30.55 ± 1.42^{*b}	33.64 ± 2.83^{*c}	70.33 ± 8.59^{a}	51.92 ± 5.76^{*b}	67.30 ± 4.44^{*cd}	79.83 ± 3.18^{ab}	49.35 ± 2.52^{*bc}	0.68

RRG, relative root growth; RRFW, relative root fresh weight; RRDW, relative root dry weight; RNL, relative number of leaves; RSFW, relative shoot fresh weight; RSDW, relative shoot dry weight; R/S, fresh weight root/shoot ratio relative to control conditions; nTI, normalized Cd tolerance index. Mean values and standard errors are indicated. Asterisks indicate significant differences between control and Cd treatment for each accession (ANOVA, $p < 0.05$, $n = 5$–10). Different letters indicate significant differences between accessions for each relative parameter (LSD test, $p \leq 0.05$).

A PCA analysis revealed two components that accounted for 83.42% of the total variance. PC1 accounted for 49.02% of the explained variance, with the following eigenvalues:

$$PC1 = RNL \times 0.46 + RRG \times (-0.076) + RRFW \times 0.568 + RRDW \times 0.887 + RSFW \times 0.875 + RSDW \times 0.921$$

The second component accounted for 34.40% of the total variance, with the following eigenvalues:

$$PC2 = RNL \times 0.749 + RRG \times 0.959 + RRFW \times 0.66 + RRDW \times 0.165 + RSFW \times 0.347 + RSDW \times 0.031$$

Plotting the values for each component one against another, two different groups were identified, corresponding to tolerant and sensitive categories (**Figure 3**). These groups were associated with both components, and the tolerant accessions exhibited higher values than the sensitive accessions for the PCs. The RSDW and RRDW for PC1 and the RRG for PC2 were the main contributors to the maximum principal component variation. A normalized index of Cd tolerance (nTI), ranging from 0 to 1, was generated and a ranking of tolerance for the analyzed accessions was obtained (**Table 1**). The nTI values for the initially ranked as Cd-sensitive accessions were lower than 0.80. PI 660407 was the most Cd-tolerant among the accessions tested, and PI 516929 and PI 660411 could be confirmed as Cd-tolerant. The nTI values for those three tolerant accessions ranged from 1.00 to 0.90. Accession PI 516933, which was initially classified as Cd-tolerant according to the screening, presented an nTI value below 0.80, and therefore it had to be re-classified as a sensitive accession.

To further characterize the eight selected accessions, Cd accumulation and nutrients content were determined in roots and shoots. Cd was mainly accumulated in roots and only low amounts of Cd were translocated to the shoots (**Figure 4**). Cd-tolerant accession PI 516929 accumulated the highest amount of Cd in roots (1802 mg kg^{-1}) and shoots (32 mg kg^{-1}), while Cd-tolerant accession PI 660407 had the lowest Cd content in roots (672 mg kg^{-1}) and high Cd content in shoots (29 mg kg^{-1}).

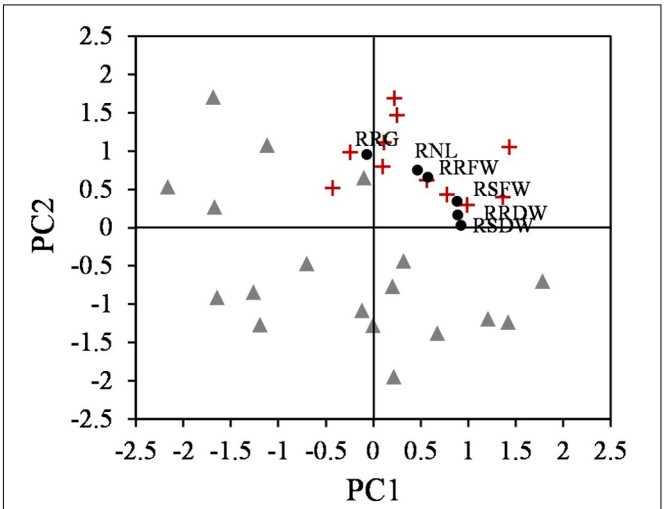


FIGURE 3 | Scatter plot of the two components obtained from PCA that differentiate two groups, tolerant (+) and sensitive (Δ) accessions ($n = 25$), and the relative parameters according to the eigenvalues (•).

Among the Cd-sensitive accessions, the highest Cd content in roots was found in PI 660497, which also had high Cd content in shoots. The lowest concentration of Cd in roots was observed in PI 516950, whose shoots showed the highest Cd content. Cd content in roots and shoots did not appear to correlate with the tolerance trait (Cd-tolerant or Cd-sensitive) and therefore, Cd accumulation cannot be considered as a suitable predictor for Cd tolerance.

The Cd effect on the macro and micronutrients contents in roots and shoots of the different tested accessions was diverse (**Tables 2**, **3**), but common features could be observed. In all accessions, Cd caused a significant decrease in Ca and S contents in shoots, and in Mn content in roots. The P content in roots and shoots was also decreased by Cd in all accessions, although it was not statistically significant for PI 660411 roots. Cd negatively affected the content of Mg in shoots of all accessions, although the decrease of Mg content was not statistically significant for PI 516929 and PI 384634. Following

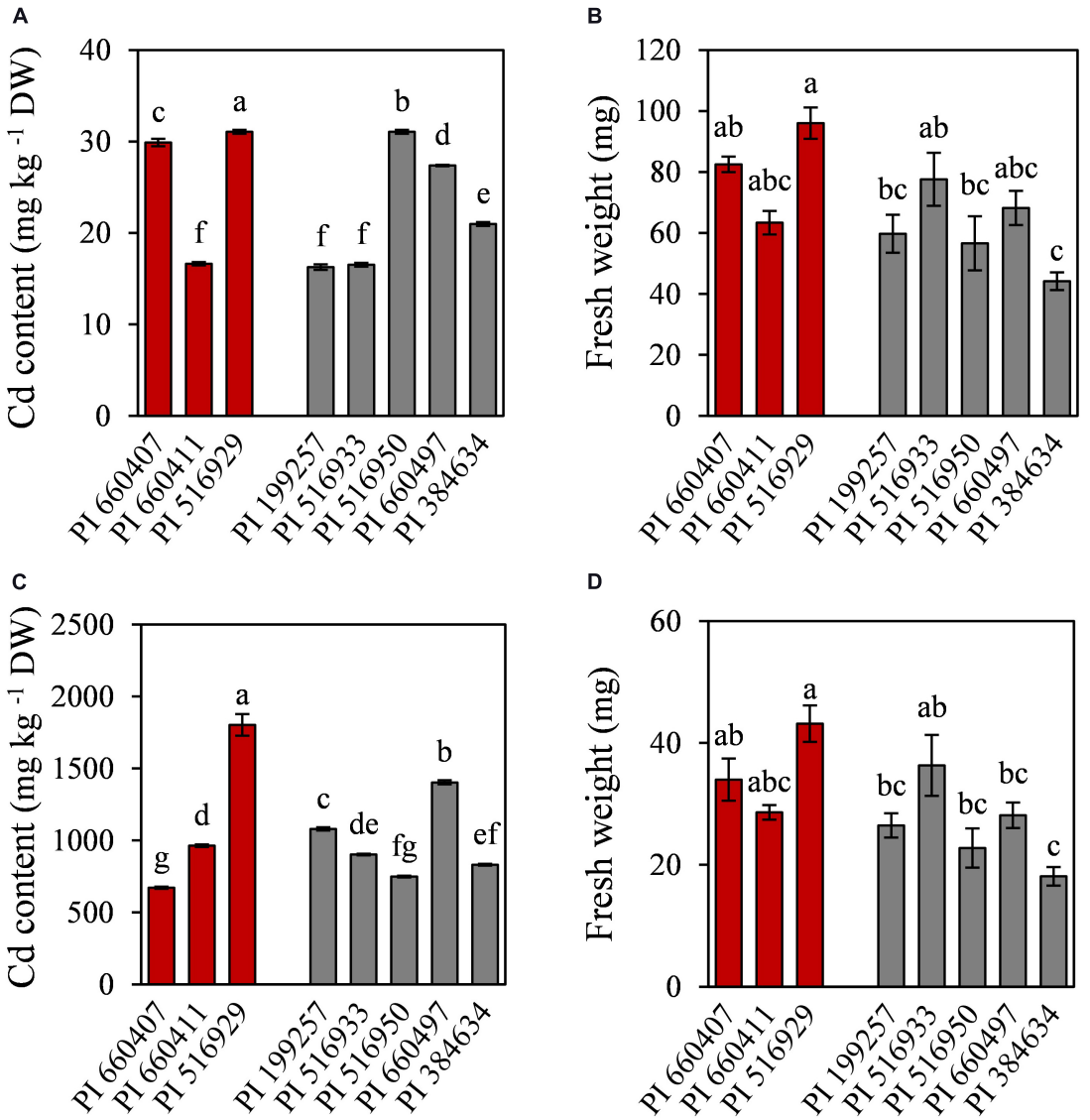


FIGURE 4 | Cadmium content and fresh weight of shoots **(A,B)** and roots **(C,D)** of tolerant (red) and sensitive (gray) *M. truncatula* accessions grown in hydroponic pouches under Cd stress (100 μM $CdCl_2$, 12 days). Mean values ± standard error are indicated, $n = 3$ for Cd content; $n = 5$–10 for fresh weight. Different letters indicate significant differences between cultivars (Tukey HSD test, $p \leq 0.05$).

Cd stress, S content increased significantly in roots of tolerant accessions as well as in the sensitive accession PI 199257, and it decreased or did not change in the roots of the rest of the sensitive accessions. For the rest of nutrients, the effect of Cd was quite heterogeneous and did not appear to correlate with tolerance.

Contrasting Responses to Cd Stress of Two Accessions With Different Sensitivity to Cd

The responses to Cd stress were analyzed in two accessions classified as Cd-tolerant (CdT; PI 516929) and Cd-sensitive (CdS; PI 660497), respectively. Both accessions were similar in size in the absence of Cd and presented similar accumulation of Cd in roots and in shoots following Cd exposure.

We analyzed the effect of Cd on germination and on the α-amylase activity in cotyledons, as an indicator of reserves mobilization. Cd promoted a significant reduction of CdS germination (23%), but it did not affect the germination of CdT (**Figure 5A**). In the absence of the metal, CdS was able to hydrolyze a significantly higher quantity of starch than CdT (**Figure 5B**). Cd induced a significant reduction in starch hydrolysis in both accessions, although this reduction was significantly higher in CdS (64%) than in CdT (26%).

To investigate the differences between CdT and CdS in the antioxidant defense response to Cd stress, the expression of

TABLE 2 | Macronutrients content in Cd-tolerant and Cd-sensitive accessions of *M. truncatula* grown in hydroponic pouches with 0 or 100 μM $CdCl_2$ for 12 days.

Accession		PI 660407		PI 660411		PI 516929		PI 199257	
Nutrient (μg g^{-1})	$CdCl_2$ (μM)	Root	Shoot	Root	Shoot	Root	Shoot	Root	Shoot
K	0	48148	72238	59248	68454	40749	66033	50577	83970
	100	42685*	44657*	51069*	60056*	44605	71336	54814	60665*
Ca	0	4174	3638	3095	3597	2648	4244	3637	4871
	100	5675*	263*	3013	1875*	2442*	2663*	3243*	2075*
Na	0	1809	595	1487	545	1348	517	1643	675
	100	2420*	505*	843*	517*	938*	500	978*	5106*
Mg	0	1399	1576	1036	1664	1206	1456	1211	2069
	100	1617*	831*	1083	1352*	1075*	1385	1228	1562*
P	0	3089	5956	3890	4377	3454	3944	5793	5143
	100	2848*	2230*	3689	3170*	2656*	3004*	5213*	3516*
S	0	1311	1963	880	1151	1757	2557	1174	1296
	100	2056*	1138*	1413*	951*	2330*	1329*	1546*	1028*
Accession		**PI 516933**		**PI 516950**		**PI 660497**		**PI 384634**	
Nutrient (μg g^{-1})	$CdCl_2$ (μM)	Root	Shoot	Root	Shoot	Root	Shoot	Root	Shoot
K	0	58245	79092	51150	74378	50838	56325	44575	64135
	100	52258*	71325	51131	56235*	44686*	53260	48576*	53056*
Ca	0	3375	5721	3191	3850	2517	4419	4123	2380
	100	3205*	2596*	3863*	1336*	3946*	2145*	2952*	822*
Na	0	1443	654	1535	610	1353	423	1983	597
	100	1106*	525*	1826*	886*	882*	417	1650*	562
Mg	0	1025	1672	1115	1757	1080	1697	1689	1347
	100	1204*	1499*	1484*	1600*	978*	1552*	1469*	1278
P	0	3856	5007	4798	5329	5570	5375	3015	5576
	100	3545*	4097*	2740*	3819*	4608*	4017*	2835*	3848*
S	0	2246	1870	2656	2690	1702	2176	2199	2327
	100	1754*	1163*	2027	1471*	1820	1036*	1526*	1393*

Asterisks indicate significant differences between treatments for each cultivar (ANOVA, LSD test, $p \leq 0.05$, $n = 3$).

some genes that codify for enzymes involved in the antioxidant machinery and PC biosynthesis was studied in seedling roots exposed to 0 or 50 μM $CdCl_2$ for 12 h.

In the absence of Cd, the two accessions showed different expression levels for some genes (**Figure 6A**). Different expression patterns were also observed in CdT and CdS after Cd exposure. The roots of Cd-treated CdT seedlings displayed enhanced expression of *MtCAT*, *MtγECS*, and *MtMR* and of the three genes encoding the NADPH-generating enzymes MtG6PDH, Mt6PGDH, and MtICDH, as compared to control unstressed seedling roots (**Figure 6B**). In contrast, Cd significantly reduced transcript accumulation of *MtCuZnSOD a* and *c* and *MtGalLDH* in CdS roots. Most of the players in GSH and phytochelatin biosynthesis strongly increased their expression in CdS roots (*MtCYS*, *MtγECS*, *MtGSHS*, *MtGR*, and *MtG6PDH*) (**Figure 6C**). The different Cd tolerance of the two accessions might be related to these variations in gene expression.

To obtain deeper insight into the redox state of the plants, oxidized glutathione (GSSG), reduced glutathione (GSH), and GSH/GSSG ratio were analyzed in CdT and CdS seedling roots (**Figure 7**). In the absence of Cd, the GSH/GSSG ratio was significantly higher in CdS roots. Cd promoted a significant reduction in glutathione content in both accessions, but the GSH/GSSH ratio increased significantly in Cd-treated CdT roots when compared with control roots, while the ratio did not change upon Cd stress in CdS roots.

We estimated the oxidative damage caused by Cd on CdT and CdS seedling roots by histochemical detection of lipid peroxidation and plasma membrane integrity. Cd promoted lipid peroxidation in both cultivars but with different intensity and localization (**Figures 8A,B**). In Cd-treated CdS roots, the staining was found along the entire root and was especially intense in the first 5 mm of the root apex, while in CdT-treated roots, lipid peroxidation was located on the first millimeter

TABLE 3 | Micronutrients content in Cd-tolerant and Cd-sensitive accessions of *M. truncatula* grown in hydroponic pouches with 0 or 100 μM $CdCl_2$ for 12 days.

Accession		PI 660407		PI 660411		PI 516929		PI 199257	
Nutrient (μg g^{-1})	**$CdCl_2$ (μM)**	**Root**	**Shoot**	**Root**	**Shoot**	**Root**	**Shoot**	**Root**	**Shoot**
Fe	0	225	225	102	71	73	51	116	69
	100	353*	80*	110*	55*	108*	52	80*	68
Mn	0	209	55	127	40	239	41	142	49
	100	45*	31*	93*	49*	80*	45*	85*	47
Zn	0	240	38	80	41	77	27	55	34
	100	110*	67*	46	47	62	30 *	70 *	24 *
Cu	0	206	27	106	35	38	14	57	31
	100	192*	64*	60*	29*	46*	26*	75*	15*
Accession		**PI 516933**		**PI 516950**		**PI 660497**		**PI 384634**	
Nutrient (μg g^{-1})	**$CdCl_2$ (μM)**	**Root**	**Shoot**	**Root**	**Shoot**	**Root**	**Shoot**	**Root**	**Shoot**
Fe	0	141	55	126	75	121	57	290	88
	100	401*	61*	477*	173*	105*	56*	126*	71*
Mn	0	189	45	239	50	267	48	204	61
	100	96*	48*	28*	61*	69*	40*	52*	42*
Zn	0	104	44	181	38	133	40	164	140
	100	117*	32*	299*	67*	79*	37*	173*	42*
Cu	0	136	27	126	75	71	21	208	75
	100	108*	17*	477*	173*	84*	25*	165*	23*

Asterisks indicate significant differences between treatments for each cultivar (ANOVA, LSD test, $p \leq 0.05$, $n = 3$).

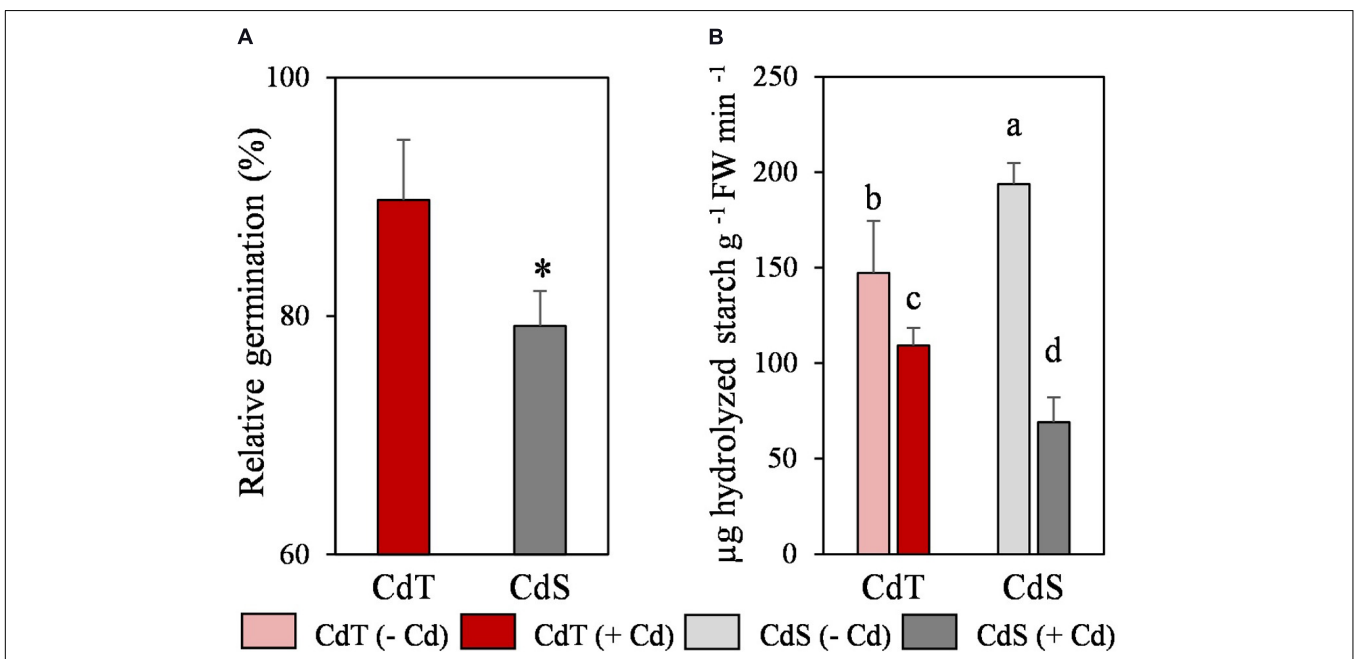


FIGURE 5 | Relative germination in the presence of Cd (200 μM $CdCl_2$, 72 h) **(A)** and α-amylase activity in cotyledons **(B)** of *M. truncatula* cultivars CdT (tolerant) and CdS (sensitive). Mean values ± standard deviation are represented. * Indicates significant differences between presence and absence of Cd for each accession [Pearsons's chi-squared test (χ^2), $n = 4$]. Different letters indicate significant differences between cultivars and treatments (Tukey HSD test, $p \leq 0.05$, $n = 4$–6).

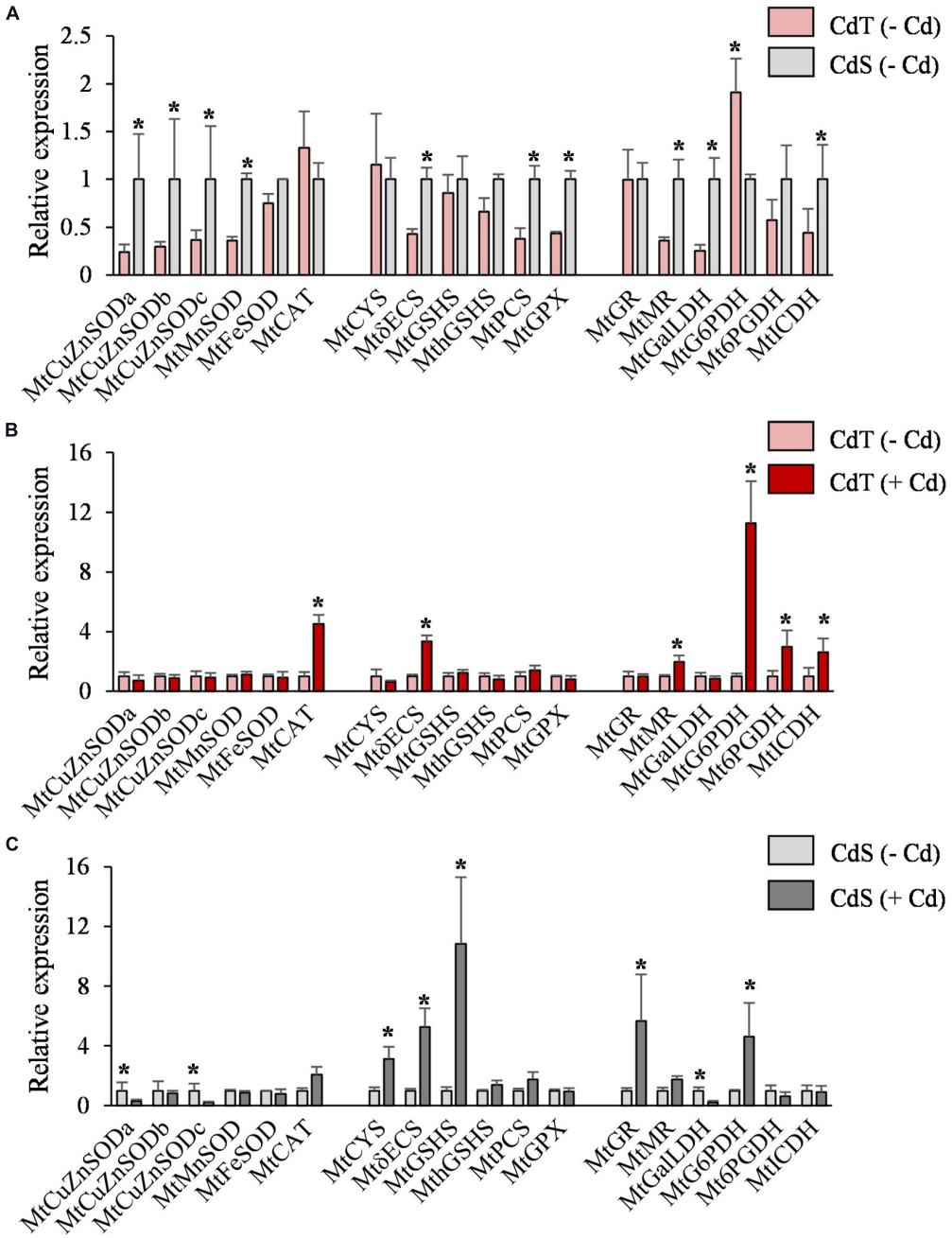


FIGURE 6 | Transcript accumulation of genes involved in the antioxidant machinery and NADPH biosynthesis in seedling roots of *M. truncatula* cultivars CdT (tolerant) and CdS (sensitive) grown in glass containers in the absence or presence of 50 μM $CdCl_2$ for 12 h. **(A)** Transcript accumulation for CdT and CdS in absence of Cd. **(B)** Effect of Cd on transcript accumulation in CdT roots. **(C)** Effect of Cd on transcript accumulation in CdS roots. Mean values ± standard deviation are represented (n = 4). * Denotes fold-changes greater than two.

of the root apex, suggesting lower oxidative damage than that observed in CdS roots. Cd also had a contrasting effect on the plasma membrane integrity of CdT and CdS seedling roots (**Figures 8C,D**). Cd-treated CdS roots showed loss of plasma membrane integrity along the whole root. Contrariwise, Cd-treated CdT roots displayed minimal loss of plasma membrane integrity along the root surface and the root apex was not affected (around 4 mm), suggesting again less oxidative damage produced by Cd in the roots of the tolerant cultivar.

To determine whether CdT and CdS presented differences in their response after a longer exposure to Cd, CdT and CdS plants were grown in the presence or absence of Cd stress for 15 days. Clear differences in plant growth were observed between both cultivars after Cd stress (**Figure 9**). The lipid peroxidation

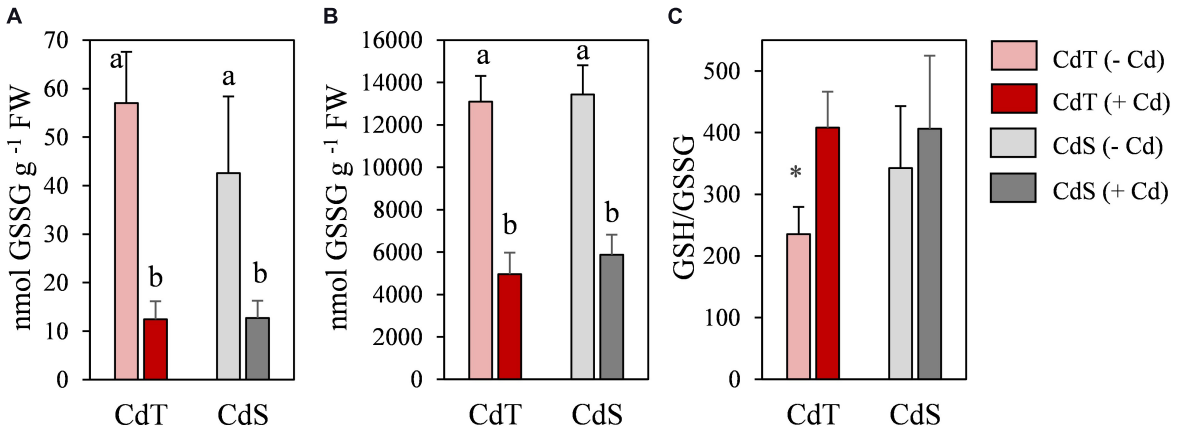


FIGURE 7 | Oxidized glutathione (GSSG) **(A)**, reduced glutathione (GSH) **(B)**, and GSH/GSSG ratio **(C)** in seedling roots of *M. truncatula* cultivars CdT (tolerant) and CdS (sensitive) grown in glass containers in the absence or presence of 50 μM $CdCl_2$ for 12 h. Mean values ± standard deviation are represented. Different letters indicate significant differences (Tukey HSD test, $p \leq 0.05$, $n = 4$). * Denotes significant differences between control and Cd treatment.

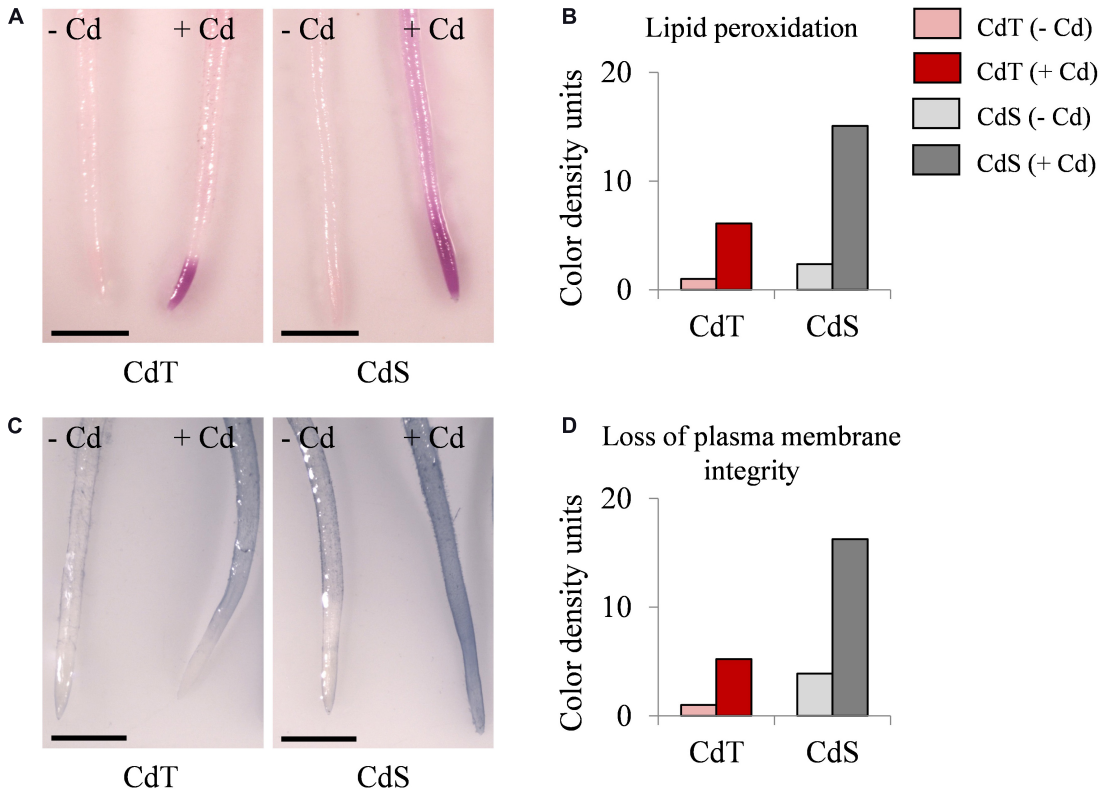


FIGURE 8 | Lipid peroxidation and loss of plasma membrane integrity in seedling roots of *M. truncatula* cultivars CdT (tolerant) and CdS (sensitive) grown in glass containers in the absence or presence of 100 μM $CdCl_2$ for 12 h. **(A)** Staining with Schiff's reagent for lipid peroxidation assessment. **(C)** Staining with Evans Blue for plasma membrane integrity assessment. Quantification of color developed with Schiff's reagent **(B)** and Evans Blue **(D)** on 1 cm root tips. Scale bar corresponds to 1 mm.

(MDA content) and the SOD and CAT enzymatic activities were analyzed in roots (**Figures 10A–C**) and shoots (**Figures 10D–F**). Cd induced a significant increase of MDA levels in roots of both cultivars. In the absence of Cd, CdS presented a significantly higher MDA content in shoots compared with CdT, and Cd caused a significant increase in MDA content only in CdS shoots.

In the absence of Cd, no significant differences were observed in SOD activity in roots between accessions, while in shoots, CdT presented a significantly higher SOD activity compared with

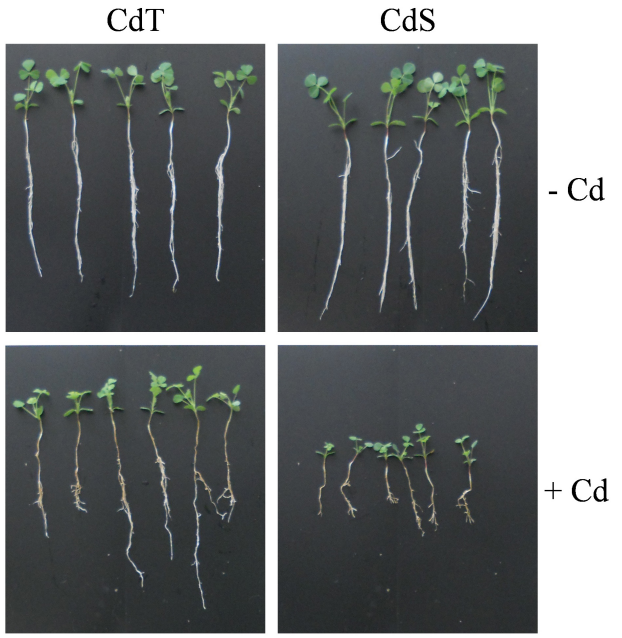


FIGURE 9 | Representative image of the plant growth *M. truncatula* cultivars CdT (tolerant) and CdS (sensitive) grown in pots containing vermiculite with 0 or 100 μM $CdCl_2$ for 15 days.

CdS. Cd induced a remarkable increase of the SOD activity in CdS roots and shoots, while CdT SOD activities were unaffected (**Figures 10B,E**).

In the absence of Cd, CAT activity was significantly higher in CdT roots than in CdS roots (**Figures 10C,F**). The Cd treatment induced a very significant CAT activity increment in CdS roots and CdT shoots and a significant decrease of CAT activity in CdS shoots (**Figure 10F**).

DISCUSSION

Cd toxicity is directly associated to cellular redox imbalance and ROS accumulation. Plant tolerance mechanisms and responses to Cd vary considerably among species and cultivars (Rizwan et al., 2017; Hasanuzzaman et al., 2019; Romero-Puertas et al., 2019). In this work, we evaluated Cd tolerance in a *M. truncatula* germplasm and identified tolerant genotypes. We analyzed several Cd toxicity and Cd tolerance markers in accessions displaying contrasted sensitivity to Cd. Relative root growth (RRG) has been described as a very suitable indicator of heavy metal tolerance (Sledge et al., 2005; Saeidi et al., 2012; García de la Torre et al., 2013; Rahoui et al., 2014). The screening of 258 *M. truncatula* accessions performed here showed a notable intraspecific variability in the response to Cd within *M. truncatula*, which suggests that cultivars with even higher tolerance could be detected by screening larger germplasm collections.

We focused our study on two *M. truncatula* accessions, CdT (tolerant) and CdS (sensitive) that presented similar growth in control conditions, and similar Cd accumulation in their roots and shoots, but remarkable differences in their growth under Cd stress. We analyzed the effect of Cd stress at two stages of plant development: seed germination and vegetative growth (seedlings and 25-day-old plants). Germination is considered a very Cd-sensitive process in comparison with other plant developmental stages (Rahoui et al., 2008), although large differences can exit among plant species and also cultivars (Huybrechts et al., 2019). During germination, reserves mobilization is required to allow plant emergence, and Cd may provoke changes in membrane composition, antioxidant status, and electrical conductivity that might promote nutrient leakages during germination (Sfaxi-Bousbih et al., 2010). Here we showed that both germination and reserves mobilization (starch hydrolysis) were more affected in CdS than in CdT under Cd stress. Significant restrictions in starch mobilization have also been observed in seeds of various Cd-sensitive legume cultivars (Mihoub et al., 2005; Rahoui et al., 2008). Rahoui et al. (2015) suggested that genotype-dependent negative effects of Cd on reserve mobilization, respiration recovery, and nutrient transport during seed germination might explain the different susceptibility to Cd in several lines of *M. truncatula*.

Cadmium uptake causes an imbalance in the nutrient metabolism (uptake, transport, and use) at the root level, probably by competition with the absorption and transport of essential elements, in particular Ca^{2+}, Fe^{2+}, Mg^{2+}, Mn^{2+}, Cu^{2+}, and Zn^{2+} (DalCorso et al., 2008; Loix et al., 2017; Ismael et al., 2019; Qin et al., 2020). Our results on nutrients contents suggest that Cd could be using different transporters, such as calcium, zinc, and/or iron transporters, as previously described (Thomine et al., 2000; Rodríguez-Serrano et al., 2009; Ismael et al., 2019). Stephens et al. (2011) reported that in *M. truncatula,* Zn uptake was inhibited by Cd. Sulfur is an essential macronutrient, key in protein synthesis, and an important structural component of many co-enzymes and thiol compounds that play important roles in stress tolerance (Ernst et al., 2008). The increase in S content under Cd stress found in CdT roots could contribute to its tolerance, as S assimilation activates the pathway leading to the synthesis of Cys, which is precursor of GSH and other thiol-containing compounds, and it is induced by Cd stress (Baig et al., 2019).

Antioxidant metabolism is critical in Cd tolerance (Terrón-Camero et al., 2020). SODs and CAT represent the first line of response to ROS to maintain the cell redox balance. Enhanced transcript accumulation of SODs after Cd treatment has been described in some *M. truncatula* cultivars, but also the contrary effect in a Cd-susceptible accession (Rahoui et al., 2014). In the present work, we observed repression of *MtCuZnSODa* and *MtCuZnSODc* in CdS seedlings, which could be related to the decrease in zinc content under Cd stress; SOD activity was not affected in CdT, and *CAT* expression was increased in CdT seedlings only. These results evidence differences in the response to Cd of both cultivars.

γ-ECS is a limiting enzyme for GSH synthesis; its activity is GSH regulated and dependent on Cys availability. It has been proposed that a high *γ ECS* expression could compensate GSH

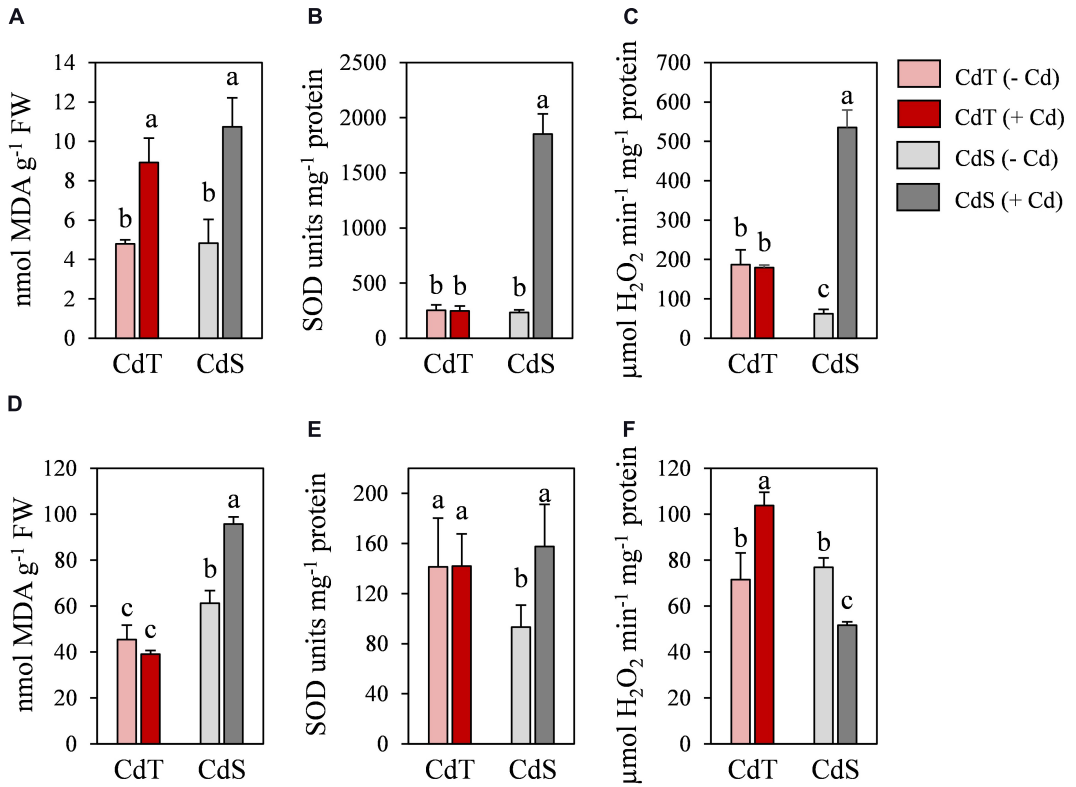


FIGURE 10 | Lipid peroxidation (MDA), and SOD and catalase activities in *M. truncatula* cultivars CdT (tolerant) and CdS (sensitive) grown in pots containing vermiculite with 0 or 100 µM $CdCl_2$ for 15 days. **(A–C)** Roots. **(D–F)** Shoots. Different letters indicate significant differences (Tukey HSD test, $p \leq 0.05$, $n = 4$).

deficiency under heavy metal stress (Sobrino-Plata et al., 2014). In CdT seedlings, Cd increased *MtγECS* transcript accumulation, but the rest of transcripts related to GSH and PCs biosynthesis (*MtCYS*, *MtGSHS*, and *MtPCS*) remained unaffected. On the contrary, in CdS, Cd provoked an increase in transcript accumulation of *MtCYS*, *MtγECS*, *MtGSHS*, as well as *MtGR*, which codes for a glutathione reductase, a significant enzyme in maintaining redox homeostasis via a correct GSH/GSSG ratio. This suggest that Cd tolerance is not so much dependent on phytochelatin quelation in tolerant plants, which is a common response to Cd stress in sensitive species as previously reported (Schat et al., 2002).

Glutathione plays a central role as chelator, antioxidant, and signaling molecule (Jozefczak et al., 2012). Cd caused a reduction in GSSG and GSH contents in the roots of both accessions and an increase in GSH/GSSG ratio in CdT, but not in CdS. These results are in agreement with the decrease in glutathione content without changes in GSH/GSSG ratio reported for a Cd-sensitive *M. sativa* cultivar (Sobrino-Plata et al., 2009).

NADPH is important in the defense against oxidative stress (Foyer and Noctor, 2011). It has been reported that Cd tolerance might be more dependent on NADPH availability than on its antioxidant capacity (León et al., 2002). The upregulation of gene expression and increased activities of NADPH-recycling dehydrogenases have been reported in *M. truncatula* nodules and soybean roots in response to Cd (Marino et al., 2013; Pérez-Chaca et al., 2014). The enhanced expression of the genes encoding three NADPH-recycling enzymes in CdT strongly suggests that it might represent an important defense mechanism, which appears to be absent in CdS.

Following Cd exposure, oxidative stress is considered as the origin of damage in plant tissues (Schützendübel et al., 2002; Rahoui et al., 2017). Cd-induced lipid peroxidation has been reported in *M. truncatula* (Sobrino-Plata et al., 2009; Rahoui et al., 2017). In CdS seedling roots, Cd produced higher lipid peroxidation and loss of cell membrane integrity than in CdT. Taken together, our results on seedlings indicate that Cd promoted a more severe oxidative damage in CdS than in CdT, which was able to better neutralize ROS production. In agreement with our results, a correlation between Cd tolerance and low oxidative stress at the seedling stage has been described in tolerant *M. truncatula* accessions (Rahoui et al., 2014).

Metal tolerance and/or toxicity also depend on the plant developmental stage. We analyzed the differences in tolerance of 25-day-old CdT and CdS plants after a long exposure to Cd. Lipid peroxidation (MDA content) and SOD and CAT activities were determined in roots and shoots. MDA content was unaffected in CdT shoots, and SOD activity was also not affected in CdT roots or shoots. Catalase activity significantly increased in CdT shoots, which could explain why lipid peroxidation did not increase in CdT shoots. In CdS roots, catalase activity increased, while a

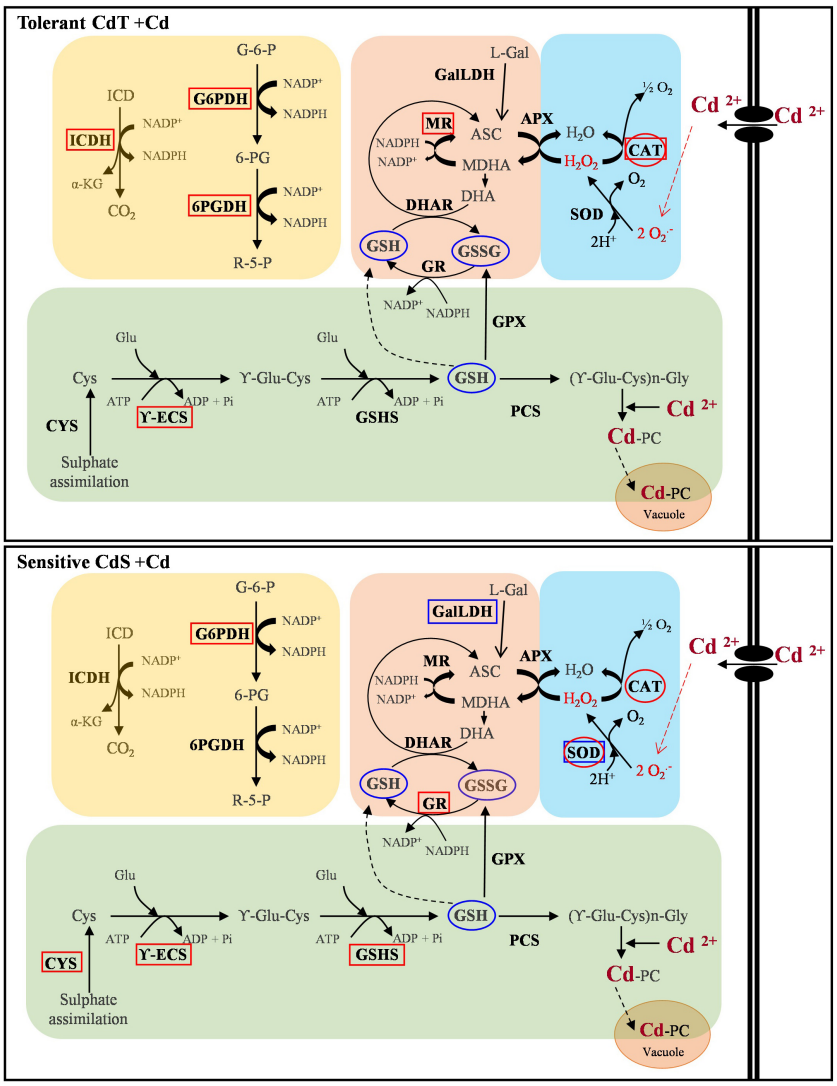


FIGURE 11 | Schematic overview of the contrasting responses observed in *M. truncatula* cultivars CdT (tolerant) and CdS (sensitive) upon Cd stress relative to gene expression, enzyme activity, and antioxidant content. Analyzed parameter is in bold letter. Rectangles denote a Cd effect on the expression of the gene encoding the enzyme. Ovals indicate a Cd effect on the enzymatic activity or content of non-enzymatic antioxidants. Red and blue colors denote increase and decrease, respectively, as compared with non-Cd treated plants. ASC, ascorbate; CAT, catalase; Cys, cysteine; CYS, cysteine synthase; DHA, dehydroascorbate; DHAR, dehydroascorbate reductase; GalLDH, galactono-1,4-lactone dehydrogenase; Glu, glutamic; G6P, glucose-6-phosphate; G6PDH, glucose-6-phosphate dehydrogenase; GPX, glutathione peroxidase; GR, glutathione reductase; GSSG, oxidized glutathione; GSH, reduced glutathione; GSHS, glutathione synthetase; ICD, isocitrate; ICDH, isocitrate dehydrogenase; L-Gal, L-galactono-lactone; MDHA, monodehydroascorbate; MR, monodehydroascorbate reductase; PCS, phytochelatin synthase; R5P, ribulose-5-phosphate; SOD, superoxide dismutase; 6PGDH, 6-phosphogluconate dehydrogenase; γ-ECS, γ-glutamyl-cysteine synthetase; α-KG, α-ketoglutarate.

decrease was observed in shoots. The consequent accumulation of H_2O_2 seems to be key in inducing growth reduction associated to Cd stress (Schützendübel et al., 2002).

Figure 11 summarizes our results on gene expression, enzyme activity, and antioxidant content. A contrasting behavior of the two cultivars can be observed.

In summary, CdT was more tolerant to Cd stress than CdS at all developmental stages studied. Both cultivars shared an increased CAT activity. In CdS, SOD increased in response to primary oxidative stress, while it did not seem to play a crucial role in CdT response. Their additional response mechanisms were different. CdT ensured availability of NADPH by increasing expression of NADPH-recycling enzymes, and, unexpectedly, presented no induction of the PC biosynthesis pathway. On the contrary, CdS upregulated the expression of three of the four genes involved in PC biosynthesis, but not those responsible for NADPH recycling. NADPH availability appears as the crucial factor in Cd tolerance in *M. truncatula*. PCs represent a common response to heavy metals, but depending on the stress level, they might not be sufficient. Conversely, when alternative factors are activated, PCs increase might not be necessary.

Our results point at the possibility of identifying highly tolerant cultivars with additional traits, such as high or low accumulation and translocation. The number of *M. truncatula* accessions available in different collections worldwide is above 6,000. Forage legumes present an important potential to be used in heavy-metal phytoremediation. Cultivars with high levels of the enzymes involved in NADPH production could be used to transfer the tolerance trait to cultivated *M. truncatula*, alfalfa, or other legumes. Additionally, a collection of *M. truncatula* mutant lines is available from the Noble Research Institute[2], and there are over 300 fully sequenced *M. truncatula* cultivars that can be obtained from the Medicago Hapmap Project Germplasm[4]. These resources will facilitate the identification and analysis of genes and loci involved in Cd tolerance and accumulation, and a better understanding of Cd tolerance and detoxifying mechanisms.

DATA AVAILABILITY STATEMENT

The original contributions presented in the study are included in the article and the **Supplementary Material**. Further inquiries can be directed to the authors.

AUTHOR CONTRIBUTIONS

VSGT, TCP, JJP, and MML conceived the experiments. VSGT performed the experiments and wrote the first draft. TCP contributed to the experimental part. JJP and MML supervised and contributed to the experiments. TCP, JJP, and MML wrote the last version of the manuscript. All authors read and approved the submitted version.

FUNDING

This work was supported by Comunidad de Madrid (Grant S2009/AMB-151 to MML, and a contract to TCP), MINECO (Grants AGL2013-40758-R to JJP and MML), AEI/FEDER-UE (Grant AGL2017-88381-R to JJP and MML), and Fundación Areces (Grant to JJP). VSGT was the recipient of an FPU fellowship from the Spanish Ministry of Education.

ACKNOWLEDGMENTS

We thank L. Barrios for her help with statistical analyses, and the National Plant Germplasm System, USDA for providing us with the *M. truncatula* accessions. We acknowledge support of 25% of the publication fee by the CSIC Open Access Publication Support Initiative through its Unit of Information Resources for Research (URICI).

SUPPLEMENTARY MATERIAL

The Supplementary Material for this article can be found online at: https://www.frontiersin.org/articles/10.3389/fpls.2021.595001/full#supplementary-material

[3] https://www.noble.org/

[4] http://www.medicagohapmap.org/

REFERENCES

Aloui, A., Recorbet, G., Gollotte, A., Robert, F., Valot, B., Gianinazzi-Pearson, V., et al. (2009). On the mechanisms of cadmium stress alleviation in *Medicago truncatula* by arbuscular mycorrhizal symbiosis: a root proteomic study. *Proteomics* 9, 420–433. doi: 10.1002/pmic.200800336

Aloui, A., Recorbet, G., Robert, F., Schoefs, B., Bertrand, M., Henry, C., et al. (2011). Arbuscular mycorrhizal symbiosis elicits shoot proteome changes that are modified during cadmium stress alleviation in *Medicago truncatula*. *BMC Plant Biol.* 11:75. doi: 10.1186/1471-2229-11-75

Baig, M. A., Ahmad, J., Ali, A. A., and Quresh, M. I. (2019). "Role of sulfur metabolism in cadmium tolerance," in *Cadmium Tolerance in Plants: Agronomic, Molecular, Signaling, and Omic Approaches*, eds M. Hasanuzzaman, M. N. V. Prasad, and K. Nahara (Amsterdam: Elsevier Inc), 335–365.

Benavides, M., Gallego, S. M., and Tomaro, M. (2005). Cadmium toxicity in plants. *Braz. J. Plant Physiol.* 17, 21–34. doi: 10.1590/S1677-04202005000100003

Clemens, S., Aarts, M., Thomine, S., and Verbruggen, N. (2013). Plant science: the key to preventing slow cadmium poisoning. *Trends Plant Sci.* 18, 92–99. doi: 10.1016/j.tplants.2012.08.003

Coba de la Peña, T., and Pueyo, J. J. (2012). Legumes in the reclamation of marginal soils, from cultivar and inoculant selection to transgenic approaches. *Agron. Sustain. Dev.* 32, 65–91. doi: 10.1007/s13593-011-0024-2

Cuypers, A., Plusquin, M., Remans, T., Jozefczak, M., Keunen, E., Gielen, H., et al. (2010). Cadmium stress: an oxidative challenge. *Biometals* 23, 927–940. doi: 10.1007/s10534-010-9329-x

DalCorso, G., Farinati, S., Maistri, S., and Furini, A. (2008). How plants cope with cadmium: staking all on metabolism and gene expression. *J. Integr. Plant Biol.* 50, 1268–1280. doi: 10.1111/j.1744-7909.2008.00737.x

Ernst, W., Krauss, G., Verkleij, J. A. C., and Wesenberg, D. (2008). Interaction of heavy metals with the sulphur metabolism in angiosperms from an ecological point of view. *Plant Cell Environ.* 31, 123–143. doi: 10.1111/j.1365-3040.2007.01746.x

Floreani, M., Petrone, M., Debetto, P., and Palatini, P. (1997). A comparison between different methods for the determination of reduced and oxidized glutathione in mamalian tissues. *Free Radic. Res.* 26, 449–445. doi: 10.3109/10715769709084481

Foyer, C. H., and Noctor, G. (2011). Ascorbate and glutathione: the heart of the redox hub. *Plant Physiol.* 155, 2–18. doi: 10.1104/pp.110.167569

García de la Torre, V. S., Coba de la Peña, T., Lucas, M. M., and Pueyo, J. J. (2013). Rapid screening of *Medicago truncatula* germplasm for mercury tolerance at the seedling stage. *Environ. Exp. Bot.* 91, 90–96. doi: 10.1016/j.envexpbot.2013.03.004

Hasanuzzaman, M., Prasad, M. N. V., and Nahara, K. (2019). *Cadmium Tolerance in Plants: Agronomic, Molecular, Signaling, and Omic Approaches*. Amsterdam: Elsevier Inc.

Holdaway, J., and Wang, W. (2018). From soil pollution to "cadmium Rice" to public health impacts: an interdisciplinary analysis of influencing factors and possible responses. *J. Resour. Ecol.* 9, 1–12. doi: 10.5814/j.issn.1674-764x.2018.01.001

Huybrechts, M., Cuypers, A., Deckers, J., Iven, V., Vandionant, S., Jozefczak, M., et al. (2019). Cadmium and plant development: an agony from seed to seed. *Int. J. Mol. Sci.* 20:3971. doi: 10.3390/ijms20163971

Ismael, M. A., Elyamine, A. M., Moussa, M. G., Cai, M., Zhao, X., and Hu, C. (2019). Cadmium in plants: uptake, toxicity, and its interactions with selenium fertilizers. *Metallomics* 11, 255–277. doi: 10.1039/c8mt00247a

Jozefczak, M., Remans, T., Vangronsveld, J., and Cuypers, A. (2012). Glutathione is a key player in metal-induced oxidative stress defenses. *Int. J. Mol. Sci.* 13, 3145–3175. doi: 10.3390/ijms13033145

León, A., Palma, J., Corpas, F., Gomez, M., Romero-Puertas, M., Chatterjee, D., et al. (2002). Antioxidative enzymes in cultivars of pepper plants with different sensitivity to cadmium. *Plant Physiol. Biochem.* 40, 813–820. doi: 10.1016/S0981-9428(02)01444-4

Loix, C., Huybrechts, M., Vangronsveld, J., Gielen, M., Keunen, E., and Cuypers, A. (2017). Reciprocal interactions between cadmium-induced cell wall responses and oxidative stress in plants. *Front. Plant Sci.* 8:1867. doi: 10.3389/fpls.2017.01867

Marino, D., Damiani, I., Gucciardo, S., Mijangos, I., Pauly, N., and Puppo, A. (2013). Inhibition of nitrogen fixation in symbiotic *Medicago truncatula* upon Cd exposure is a local process involving leghaemoglobin. *J. Exp. Bot.* 64, 5651–5660. doi: 10.1093/jxb/ert334

Marino, D., González, E. M., Frendo, P., Puppo, A., and Arrese-Igor, C. (2007). NADPH recycling systems in oxidative stressed pea nodules: a key role for the NADP+ -dependent isocitrate dehydrogenase. *Planta* 225, 413–421. doi: 10.1007/s00425-006-0354-5

Mihoub, A., Chaoui, A., and El Ferjani, E. (2005). Biochemical changes associated with cadmium and copper stress in germinating pea seeds (*Pisum sativum* L.). *C. R. Biol.* 328, 33–41. doi: 10.1016/j.crvi.2004.10.003

Peralta-Videa, J. R., Lopez, M. L., Narayan, M., Saupe, G., and Gardea-Torresdey, J. (2009). The biochemistry of environmental heavy metal uptake by plants: implications for the food chain. *Int. J. Biochem. Cell Biol.* 41, 1665–1677. doi: 10.1016/j.biocel.2009.03.005

Pérez-Chaca, M. V., Rodríguez-Serrano, M., Molina, A. S., Pedranzani, H. E., Zirulnik, F., Sandalio, L. M., et al. (2014). Cadmium induces two waves of reactive oxygen species in *Glycine max* (L.) roots. *Plant Cell Environ.* 37, 1672–1687. doi: 10.1111/pce.12280

Pfaffl, M. W. (2001). A new mathematical model for relative quantification in real-time RT-PCR. *Nucleic Acids Res.* 29, 2002–2007. doi: 10.1093/nar/29.9.e45

Qin, S. Y., Liu, H. E., Nie, Z. J., Rengel, Z., Gao, W., Li, C., et al. (2020). Toxicity of cadmium and its competition with mineral nutrients for uptake by plants: a review. *Pedosphere* 30, 168–180. doi: 10.1016/S1002-0160(20)60002-9

Rahoui, S., Ben, C., Chaoui, A., Martinez, Y., Yamchi, A., Rickauer, M., et al. (2014). Oxidative injury and antioxidant genes regulation in cadmium-exposed radicles of six contrasted *Medicago truncatula* genotypes. *Environ. Sci. Pollut. Res.* 21, 8070–8083. doi: 10.1007/s11356-014-2718-x

Rahoui, S., Chaoui, A., Ben, C., Rickauer, M., Gentzbittel, L., and El Ferjani, E. (2015). Effect of cadmium pollution on mobilization of embryo reserves in seedlings of six contrasted *Medicago truncatula* lines. *Phytochemistry* 111, 98–106. doi: 10.1016/j.phytochem.2014.12.002

Rahoui, S., Chaoui, A., and El Ferjani, E. (2008). Differential sensitivity to cadmium in germinating seeds of three cultivars of faba bean (*Vicia faba* L.). *Acta Physiol. Plant.* 30, 451–456. doi: 10.1007/s11738-008-0142-x

Rahoui, S., Martinez, Y., Sakouhi, L., Ben, C., Rickauer, M., El Ferjani, E., et al. (2017). Cadmium-induced changes in antioxidative systems and differentiation in roots of contrasted *Medicago truncatula* lines. *Protoplasma* 254, 473–489. doi: 10.1007/s00709-016-0968-9

Redondo, F. J., Coba de la Peña, T., Morcillo, C. N., Lucas, M. M., and Pueyo, J. J. (2009). Overexpression of flavodoxin in bacteroids induces changes in antioxidant metabolism leading to delayed senescence and starch accumulation in alfalfa root nodules. *Plant Physiol.* 149, 1166–1178. doi: 10.1104/pp.108.129601

Rizwan, M., Ali, S., Adrees, M., Ibrahim, M., Tsang, D. C. W., Zia-ur-Rehman, M., et al. (2017). A critical review on effects, tolerance mechanisms and management of cadmium in vegetables. *Chemosphere* 182:90e105. doi: 10.1016/j.chemosphere.2017.05.013

Rodríguez-Eugenio, N., McLaughlin, M., and Pennock, D. (2018). *Soil Pollution: A Hidden Reality*. Rome: FAO.

Rodríguez-Serrano, M., Romero-Puertas, M. C., Pazmiño, D. M., Testillano, P. S., Risueño, M. C., Del Río, L. A., et al. (2009). Cellular response of pea plants to cadmium toxicity: cross talk between reactive oxygen species, nitric oxide, and calcium. *Plant Physiol.* 150, 229–243. doi: 10.1104/pp.108.131524

Romero-Puertas, M. C., Ortega-Galisteo, A., Rodriguez-Serrano, M., and Sandalio, L. M. (2012). "Insights into cadmium toxicity: reactive oxygen and nitrogen species function," in *Metal toxicity in Plants: Perception, Signaling and Remediation*, eds D. K. Gupta and L. M. Sandalio (Berlin: Springer), 91–117.

Romero-Puertas, M. C., Terrón-Camero, L. C., Peláez-Vico, M. A., Olmedilla, A., and Sandalio, L. M. (2019). Reactive oxygen and nitrogen species as key indicators of plant responses to Cd stress. *Environ. Exp. Bot.* 161, 107–119. doi: 10.1016/j.envexpbot.2018.10.012

Saeidi, G., Rickauer, M., and Gentzbittel, L. (2012). Tolerance for cadmium pollution in a core-collection of the model legume, *Medicago truncatula* L. at seedling stage. *Aust. J. Crop Sci.* 6, 641–648.

Sanità di Toppi, L., and Gabbrielli, R. (1999). Response to cadmium in higher plants. *Environ. Exp. Bot.* 41, 105–130. doi: 10.1016/S0098-8472(98)00058-6

Schat, H., Llugany, M., Vooijs, R., Jeanette, H., and Bleeker, P. (2002). The role of phytochelatins in constitutive and adaptive heavy metal tolerances in hyperaccumulator and non-hyperaccumulator metallophytes. *J. Exp. Bot.* 53, 2381–2392. doi: 10.1093/jxb/erf107

Schützendübel, A., Nikolova, P., Rudolf, C., and Polle, A. (2002). Cadmium and H2O2 -induced oxidative stress in *Populus canescens* roots. *Plant Physiol. Biochem.* 40, 577–584. doi: 10.1016/S0981-9428(02)01411-0

Sfaxi-Bousbih, A., Chaoui, A., and El Ferjanim, E. (2010). Cadmium impairs mineral and carbohydrate mobilization during the germination of bean seeds. *Ecotoxicol. Environ. Saf.* 73, 1123–1129. doi: 10.1016/j.ecoenv.2010.01.005

Sharma, S. S., and Dietz, K. J. (2009). The relationship between metal toxicity and cellular redox imbalance. *Trends Plant Sci.* 14, 43–50. doi: 10.1016/j.tplants.2008.10.007

Shvaleva, A., Coba de la Peña, T., Rincón, A., Morcillo, C. N., García de la Torre, V., Lucas, M. M., et al. (2010). Flavodoxin overexpression reduces cadmium-induced damage in alfalfa root nodules. *Plant Soil* 326, 109–121. doi: 10.1007/s11104-009-9985-1

Singh, M., Singh, D., and Rai, M. (2007). Assessment of growth, physiological and biochemical parameters and activities of antioxidative enzymes in salinity tolerant and sensitive basmati rice varieties. *J. Agron. Crop Sci.* 193, 398–412. doi: 10.1111/j.1439-037X.2007.00267.x

Sledge, M. K., Pechter, P., and Payton, M. E. (2005). Aluminum tolerance in *Medicago truncatula* germplasm. *Crop Sci.* 45, 2001–2004. doi: 10.2135/cropsci2004.0673

Smith, B. W., and Roe, J. H. (1949). A photometric method for the determination of α-amylase in blood and urine, with use of the starch-iodine color. *J. Biol. Chem* 179, 53–59.

Sobrino-Plata, J., Meyssen, D., Cuypers, A., Escobar, C., and Hernández, L. E. (2014). Glutathione is a key antioxidant metabolite to cope with mercury and cadmium stress. *Plant Soil* 377, 369–381. doi: 10.1007/s11104-013-2006-4

Sobrino-Plata, J., Ortega-Villasante, C., Flores-Cáceres, M. L., Escobar, C., Del Campo, F. F., and Hernández, L. E. (2009). Differential alterations of antioxidant defenses as bioindicators of mercury and cadmium toxicity in alfalfa. *Chemosphere* 77, 946–954. doi: 10.1016/j.chemosphere.2009.08.007

Stephens, B. W., Douglas, R., Cook, D. R., and Grusak, M. A. (2011). Characterization of zinc transport by divalent metal transporters of the ZIP family from the model legume *Medicago truncatula*. *Biometals* 24, 51–58. doi: 10.1007/s10534-010-9373-6

Terrón-Camero, L. C., del Val, C., Sandalio, L. M., and Romero-Puertas, M. C. (2020). Low endogenous NO levels in roots and antioxidant systems are determinants for the resistance of *Arabidopsis* seedlings grown in Cd. *Environ. Pollut.* 256:113411. doi: 10.1016/j.envpol.2019.113411

Thomine, S., Wang, R., Ward, J. M., Crawford, N. M., and Schroeder, J. I. (2000). Cadmium and iron transport by members of a plant metal transporter family in *Arabidopsis* with homology to Nramp genes. *Proc. Natl. Acad. Sci. U.S.A.* 97, 4991–4996. doi: 10.1073/pnas.97.9.4991

Xu, J., Wang, W., Yin, H., Liu, X., Sun, H., and Mi, Q. (2010). Exogenous nitric oxide improves antioxidative capacity and reduces auxin degradation in roots of *Medicago truncatula* seedlings under cadmium stress. *Plant Soil* 326, 321–330. doi: 10.1007/s11104-009-0011-4

Yamamoto, Y., Kobayashi, Y., and Matsumoto, H. (2001). Lipid peroxidation is an early symptom triggered by aluminium, but not the primary cause of elongation inhibition in pea roots. *Plant Physiol.* 125, 199–208. doi: 10.1104/pp.125.1.199

Conflict of Interest: The authors declare that the research was conducted in the absence of any commercial or financial relationships that could be construed as a potential conflict of interest.

Copyright © 2021 García de la Torre, Coba de la Peña, Pueyo and Lucas. This is an open-access article distributed under the terms of the Creative Commons Attribution License (CC BY). The use, distribution or reproduction in other forums is permitted, provided the original author(s) and the copyright owner(s) are credited and that the original publication in this journal is cited, in accordance with accepted academic practice. No use, distribution or reproduction is permitted which does not comply with these terms.

frontiers in Plant Science

ORIGINAL RESEARCH
published: 08 April 2021
doi: 10.3389/fpls.2021.634237

Influence of Rootstock Genotype and Ploidy Level on Common Clementine (*Citrus clementina* Hort. ex Tan) Tolerance to Nutrient Deficiency

Julie Oustric[1], Stéphane Herbette[2], Raphaël Morillon[3,4], Jean Giannettini[1], Liliane Berti[1] and Jérémie Santini[1]*

[1] CNRS, Équipe de Biochimie et Biologie Moléculaire du Végétal, UMR 6134 SPE, Université de Corse, Corsica, France, [2] UCA, INRAE, PIAF, Clermont-Ferrand, France, [3] Equipe SEAPAG, CIRAD, UMR AGAP, Petit-Bourg, Guadeloupe, France, [4] AGAP, University of Montpellier, CIRAD, INRAE, Institut Agro, Montpellier, France

Nutrient deficiency, in particular when this involves a major macronutrient (N, P, and K), is a limiting factor on the performance of plants in their natural habitat and agricultural environment. In the citrus industry, one of the eco-friendliest techniques for improving tolerance to biotic and abiotic stress is based on the grafting of a rootstock and a scion of economic interest. Scion tolerance may be improved by a tetraploid rootstock. The purpose of this study was to highlight if tolerance of a common clementine scion (C) (*Citrus clementina* Hort. ex Tan) to nutrient deficiency could be improved by several diploid (2×) and their tetraploid (4×) counterparts citrus genotypes commonly used as rootstocks: Trifoliate orange × Cleopatra mandarin (C/PMC2x and C/PMC4x), Carrizo citrange (C/CC2x and C/CC4x), Citrumelo 4475 (C/CM2x and C/CM4x). The allotetraploid FlhorAG1 (C/FL4x) was also included in the experimental design. The impact of nutrient deficiency on these seven scion/rootstock combinations was evaluated at root and leaf levels by investigating anatomical parameters, photosynthetic properties and oxidative and antioxidant metabolism. Nutrient deficiency affects foliar tissues, physiological parameters and oxidative metabolism in leaves and roots in different ways depending on the rootstock genotype and ploidy level. The best known nutrient deficiency-tolerant common clementine scions were grafted with the doubled diploid Citrumelo 4475 (C/CM4x) and the allotetraploid FlhorAG1 (C/FL4x). These combinations were found to have less foliar damage, fewer changes of photosynthetic processes [leaf net photosynthetic rate (P_{net}), stomatal conductance (g_s), transpiration (E), maximum quantum efficiency of PSII (F_v/F_m), electron transport rate (ETR), ETR/P_{net}], and effective quantum yield of PSII [Y(II)], less malondialdehyde accumulation in leaves and better functional enzymatic and non-enzymatic antioxidant systems. Common clementine scions grafted on other 4× rootstocks did not show better tolerance than those grafted on their 2× counterparts. Chromosome doubling of rootstocks did not systematically improve the tolerance of the common clementine scion to nutrient deficiency.

Keywords: antioxidant, *Citrus*, nutrient deficiency, oxidative stress, photosynthesis, polyploidy, grafting

OPEN ACCESS

Edited by:
Felipe Klein Ricachenevsky, Federal University of Rio Grande do Sul, Brazil

Reviewed by:
Francisco Garcia-Sanchez, Spanish National Research Council, Spain
Nadia Bazihizina, University of Florence, Italy

****Correspondence:***
Julie Oustric
oustric_j@univ-corse.fr

Specialty section:
This article was submitted to Plant Abiotic Stress, a section of the journal Frontiers in Plant Science

Received: *27 November 2020*
Accepted: *22 February 2021*
Published: *08 April 2021*

Citation:
Oustric J, Herbette S, Morillon R, Giannettini J, Berti L and Santini J (2021) Influence of Rootstock Genotype and Ploidy Level on Common Clementine (Citrus clementina Hort. ex Tan) Tolerance to Nutrient Deficiency. Front. Plant Sci. 12:634237. doi: 10.3389/fpls.2021.634237

INTRODUCTION

Citrus fruit crops represent an important economic activity worldwide. In recent years, easy peeler fruits including mandarins and its related varieties such as clementines have acquired a special place in global citrus trade at the expense of oranges, lemons, and pomelos. Citrus fruit crops require a significant amount of fertilizer to ensure satisfactory production and good quality fruit. In the current context of agro-ecological transition, a move must be made toward sustainable agriculture by reducing the use of farm inputs (fertilizers, crop protection products). A more moderate use of fertilizers would make it possible to respond to two constraints, (i) the economic constraint of the high costs of farm inputs and (ii) the ecological constraint due to the negative impact on water and soil biodiversity of excess fertilizer products not assimilated by plants.

Essential nutrients can be divided into two groups; macro- (N, K, P, Ca, Mg, and S) and micro-nutrients (Zn, Cu, Fe, Mn, B, Mo, Cl, and Ni). These play many roles such as: (i) essential metabolites (e.g., proteins, enzymes and coenzymes, cell walls, and chlorophyll), (ii) enzyme activators or regulators of enzyme-associated processes and (iii) non-structural factors in physiological processes (i.e., membrane integrity, photosynthesis, stomatal movement and environmental signaling) (Marschner, 1995; Grusak, 2001). The lack of one of these nutrients unbalances mineral element homeostasis which is essential for plant growth and optimum development. Firstly, plant nutrient deficiency limits most of the factors determining plant performance in terms of production per hectare and food quality (Tewari, 2004). When the deficiency becomes more pronounced, visible symptoms appear on the leaves, fruits and roots, indicating plant malfunction (Ericsson, 1995; Srivastava, 2013).

To cope with nutrient deficiencies, the plant must detect nutrient levels in the surrounding soil and within its cells and regulate various processes such as uptake, metabolism, remobilization and sequestration that lead to nutrient accumulation in the cell (Schachtman and Shin, 2007; Ohkama-Ohtsu and Wasaki, 2010; Aibara and Miwa, 2014).

As for other environmental stresses, plants under nutrient deficiency must cope with an unbalanced redox status that disturbs physiological and biochemical processes and leads to a disruption of growth and development (Law et al., 2001; Tewari et al., 2007; Yu-Chuan et al., 2008; Oustric et al., 2019; Zhang et al., 2019; Gong et al., 2020; Patel et al., 2020). Cells suffer oxidative damage due to the accumulation of reactive oxygen species (ROS), including superoxide ($O_2^{\bullet -}$), singlet oxygen ($^1O_2$), radical hydroxyl ($OH^{\bullet}$) and hydrogen peroxide (H_2O_2). The highly reactive nature of these compounds causes severe damage to proteins and nucleic acids, as well as membrane leakage through lipid peroxidation (Mittler, 2002; Apel and Hirt, 2004; Mittler et al., 2004). Under environmental constraints, plants trigger the activity of antioxidant enzymes such as superoxide dismutase (SOD), catalase (CAT), ascorbate peroxidase (APX), or dehydroascorbate reductase (DHAR) and also the production of non-enzymatic compounds such as ascorbate and proline.

To improve tolerance to biotic and abiotic stresses, citrus cultivation relies on associations between a rootstock and a graft of economic interest. The roots store nitrogen and carbon reserves and absorb and assimilate nutrients from the soil before transferring them to the aerial parts via the xylem vessels. Nutrients and water uptake may increase in grafted plants due to the improved vigor of the rootstock root system which is one of the main reasons for the use of rootstocks in agriculture (Lee, 1994). These rootstock effects were also observed in citrus (Taylor and Dimsey, 1993; Lu et al., 2019).

Currently, most of the genetic resources of citrus rootstocks are diploid, i.e., they have two sets of chromosomes in their genetic heritage. Stress tolerance may be further improved by using tetraploid rootstocks. Indeed, much research has shown that the use of tetraploid rootstocks may be an effective way of improving stress tolerance in citrus trees, including water, salt and cold stress (Saleh et al., 2008; Allario et al., 2013; Oustric et al., 2017). Tetraploids (4×) resulting from incomplete mitosis of somatic embryos may occur naturally or artificially in seedlings with diploid (2×) apomictic genotypes (Cameron and Frost, 1968). Depending on the composition of their genomes and the mechanism of their formation, polyploids can be classified into two groups: autopolyploids that occur as a result of genome duplication or fusion of unreduced gametes ($2n$) within the same species, and allopolyploids formed by interspecific hybridization followed by chromosome doubling, fusion of unreduced gametes of two different species or spontaneous chromosomal doubling after hybridization, or by interspecific hybridization between two autotetraploid species.

Many *Citrus* genotypes used as rootstocks exist for clementine cultivation. Genotypes belong either to the *Citrus* volkameriana genus or are derived by hybridization between *Citrus* and *Poncirus* genus progenitors such as Citrumelo 4475, Carrizo citrange, and Trifoliate orange × Cleopatra mandarin. Volkameriana is widely used as it is adapted to dry, calcareous and saline soils and tolerant to tristeza, cachexia, and exocortis (Jacquemond et al., 2013). Citrumelo 4475 is used for its tolerance to tristeza and because it imparts cold tolerance to the graft (Jacquemond et al., 2013). Trifoliate orange × Cleopatra mandarin is adapted to calcareous, humid and saline soils and confers tolerance to several diseases including Tristeza and to cold conditions. Carrizo citrange is widely used in acidic and neutral soils and inherited Tristeza tolerance from its Trifoliate orange progenitor. Conversely, its poor performance in drought conditions limits its use in dry areas.

In a previous study, we compared the tolerance to nutritional deficiency of these 4 *citrus* seedling genotypes. In order to test the positive effect of polyploidization on the tolerance of seedlings to nutrient deficiency, their 4× counterparts were also

Abbreviations: 2×, diploid; 4×, doubled diploid; APX, ascorbate peroxidase; Asa, reduced ascorbate; Asa/DHA, redox status of ascorbate; C/CC2x, diploid Carrizo citrange; C/CC4x, doubled diploid Carrizo citrange; CAT, catalase; C/CM2x, diploid Citrumelo 4475; C/CM4x, doubled diploid Citrumelo 4475; C/FL4x, allotetraploid FlhorAG1; C/PMC2x, diploid Trifoliate orange × Cleopatra mandarin; C/PMC4x, doubled diploid Trifoliate orange × Cleopatra mandarin; DHA, oxidized ascorbate; ETR, electron transport rate; F_o, minimal chlorophyll a fluorescence; F_m, maximal fluorescence; F_m', actual light-adapted fluorescence; F_s, current fluorescence yield; F_v, variable fluorescence, F_v/F_m, maximum quantum efficiency of PSII; g_s, stomatal conductance; MDA, malondialdehyde; P_{net}, leaf net photosynthetic rate; ROS, reactive oxygen species; SOD, superoxide dismutase; Y(NPQ), non-photochemical quenching coefficient; Y(II), effective quantum yield of PSII.

studied (Oustric et al., 2019). The allotetraploid FlhorAG1, a somatic hybrid of Trifoliate orange and Willow leaf mandarin, was also included in the experimental design (Ollitrault et al., 2000). FlhorAG1 allotetraploid and Citrumelo 4475 doubled diploid appeared to be more tolerant than the other genotypes to prolonged nutrient deficiency, as shown by the lower reduction in photosynthesis parameters, and reduced accumulation of oxidation markers. This study was performed on seedlings and the value of these genotypes for the culture of citrus fruit requires studying their behavior as rootstocks.

The general working hypothesis that we wanted to check was that the use of a tetraploid rootstock could confer the scion a better tolerance under nutrient deficiency. Thus, the main objective of this paper was to highlight if several diploid and tetraploid citrus genotypes commonly used as rootstocks would improve the tolerance of a common clementine scion to nutrient deficiency. If so, technical itineraries requiring fewer inputs could be proposed taking into account the best scion/rootstock combination. The effect of nutrient deficiency was investigated on common clementine (C) (*Citrus clementina* Hort. ex Tan) grafted on 2× common rootstocks used in citrus cultivation and their 4× counterparts: the Trifoliate orange × Cleopatra mandarin hybrid (C/PMC2x and C/PMC4x), Citrumelo 4475 (C/CM2x and C/CM4x), Carrizo citrange (C/CC2x and C/CC4x). The allotetraploid FlhorAG1 (C/FL4x) was also included in the experimental design. The effects of nutrient deficiency on the clementine's tolerance were evaluated at root and leaf levels by investigating anatomical parameters, photosynthetic properties and oxidative and antioxidant metabolism.

MATERIALS AND METHODS

Plant Material and Growth Conditions

The experiment was carried out at the AREFLEC experimental station located in San Giuliano, Corsica (41° 47′ 27″N and 09° 23′ 40″E). Seedlings of 2× Trifoliate orange × Cleopatra mandarin (*Poncirus trifoliata* L. Raf. × *Citrus reshni* Hort. ex Tan.), Citrumelo 4475 (*Citrus paradisi* L. Macf. × *P. trifoliata* L. Raf.), Carrizo citrange (*Citrus sinensis* L. Osb. × *P. trifoliata* L. Raf.) and their three 4× counterparts were used as source materials. The FlhorAG1 (*Poncirus trifoliata* L. Raf. + *Citrus reticulata* Ten.), an allotetraploid form, was also included. For each of the seven genotypes, six plants were selected (giving a total of 42 plants) among seedlings made with seeds from trees maintained in the citrus germplasm collection (BCR NF 96-S-900 Citrus INRA/CIRAD) at San Giuliano, Corsica (France). The ploidy status of 2× and 4× seedlings was checked by 10-color flow cytometry (Partec I, Germany) as described by Froelicher et al. (2007). Clonal propagation by nucellar embryogenesis was verified by genotyping using SSR markers as described by Vieira et al. (2016). All 1-year seedlings were then grafted with a common clementine scion (*Citrus clementina* Hort. ex Tan; SRA 92) (**Table 1**) in 2013.

The 42 selected plants were potted in vermiculite and grown in a fertigation system in a tunnel greenhouse. Each scion/rootstock combination was then watered by two drippers (1 L/hr). The stock solution used for irrigation included 20-5-10 NPK + 2MgO fertilizer + trace components, in agreement with the recommendations of the local department of agriculture. The 42 plants were divided into two blocks treated by different levels of soil-less fertigation. A total of three plants of each variety was randomized by fertigation level. The two fertigation levels were the reference fertilization (control plants, 1 g/L) and irrigation water not supplemented with any nutrient inputs. The fertigation solutions were distributed by metering pumps. The vermiculite was washed for 48 h in order to eliminate all the nutritional reserves, prior to the start of the nutrient deficiency experiment. This avoided the latency phase that may have occurred if any fertilizer remaining in the vermiculite had been completely consumed by the plants.

According to a previous experiment of Oustric et al. (2019), samples and physiological measurements on leaves and roots were carried out from May 2018 to January 2019 at three different times (days): 0 (D0; control plant) and 210 (D210) days after

TABLE 1 | Description of scion/rootstock combinations.

Scion	Rootstock	Varieties	Abbreviations	Ploidy level
Citrus clementina Hort. ex Tan	*Poncirus trifoliata* L. Raf. × *Citrus reshni* Hort. ex Tan.	Trifoliate orange × Cleopatra mandarin	C/PMC	2×
				4×
	Poncirus trifoliata L. Raf. + *Citrus reticulata* Ten.	FlhorAG1	C/FL	4×
	Citrus paradisi L. Macf. × *Poncirus trifoliata* L. Raf.	Citrumelo 4475	C/CM	2×
				4×
	Citrus sinensis L. Osb. × *Poncirus trifoliata* L. Raf.	Carrizo citrange: Oranger whashington navel × Trifoliate orange	C/CC	2×
				4×

the start of nutritional deprivation, and after 30 days of recovery (30DR). Leaf measurements were made and samples taken from homogeneous plants comprising four branches with leaves that had reached full maturity. For the root samples, the genotypes were removed from their pots, rinsed with water and then primary and secondary roots were collected at the same time for each scion/rootstock combination.

Assessment of Leaf Damage

All the scion/rootstock combinations were ranked visually according to the degree of damage after 210 days of nutrient deficiency. Nutrient deficiency foliar tissue damage (chlorosis or shriveled leaves) was estimated on the five most representative and fully expanded leaves for each scion/rootstock combination (n = 15). Leaves were scored using a 0–3 rating scale, where 0 indicated the complete absence of symptoms, 1 light green leaves, 2 light green leaves with veins clearing and 3 shriveled yellow leaves.

Foliar Mineral Analysis

Nutrient contents were measured on three sample for each scion/rootstock combination, i.e., one per tree, obtained by pooling eight fully-expanded leaves (n = 3) collected between 10:00 and 11:00 am. The leaves were cleaned with deionized water, dried at 65 ± 10°C in an oven overnight and transferred into a desiccator until cool. The dehydrated leaves were then sent to a CIRAD laboratory (Montpellier, France) for analysis of macro- and micro-nutrients.

Nutrient contents (phosphorus (P), potassium (K), calcium (Ca), magnesium (Mg), and sodium (Na), iron (Fe), zinc (Zn), boron (B), copper (Cu), and manganese (Mn) in the leaves were studied using an Agilent 720 simultaneous ICP-OES after double calcination including silica removal by adding hydrofluoric acid.

Lead total nitrogen (N) content was determined by combustion using a Leco TruMac N determinator.

Gas Exchange Measurements

Leaf net photosynthetic rate (P_{net}), stomatal conductance (g_s) and transpiration rate (E) were measured using using a portable photosynthetic system (LCPro-SD, ADC Bioscientific, Hoddesdon, United Kingdom). The carbon dioxide concentration (CO_2) in the leaf chamber was 380 μmol.mol^{-1}, airflow rate was 500 μmol.s^{-1}, light intensity was 1,400 μmol.m^{-2}.s^{-1} and temperature 25°C. The measurements were made on three fully developed leaves for each scion/rootstock combination (n = 3) at between 7:00 and 11:00 am.

Measurements of Chlorophyll *a* Fluorescence

Chlorophyll *a* fluorescence parameters were monitored with an OS1p (Opti-Sciences, Inc., Hudson, NH, United States). Measurements were made on three fully developed leaves for each scion/rootstock combination (n = 3) at between 7:00 and 11:00 am. Leaves were dark-adapted for 30 min using lightweight leaf clips to measure the minimal level of fluorescence (F_o) followed by the maximal fluorescence (F_m) after 1 s of a saturating flash (3,000 μmol photon·m^{-2}·s^{-1}) by an array of three light-emitting diodes (650 nm). Maximum fluorescence [$F_v/F_m = (F_m - F_o)/F_m$] was calculated from these data according to Maxwell and Johnson (2000). Leaves were exposed to actinic light to evaluate the current fluorescence yield (F_s) and the actual light-adapted fluorescence (F_m'). The effective quantum yield of PSII [Y(II)], the electron transport rate (ETR) and the non-photochemical quenching coefficient [Y(NPQ)] were then calculated according to Baker (2008), using the following equations:

$$Y(II) = (F'_m - F_s)/F'_m \quad (1)$$

$$Y(NPQ) = (F_s/F'_m) - Y(NO) \quad (2)$$

The ETR thought PSII [ETR(II)] was calculated according to Schreiber et al. (1995), using the equation:

$$ETR(II) = Y(II) \times PAR \times 0.5 \times 0.84 \quad (3)$$

The ETR/P_{net} ratio was calculated to estimate the use of electrons in other processes not related to the photosynthetic CO_2 assimilation rate.

Determination of Oxidative Stress and Antioxidant Levels

Biochemical analyses were performed on three samples for each scion/rootstock combination, i.e., one per tree, obtained by pooling eight fully-expanded leaves (n = 3) and three samples for each scion/rootstock combination, i.e., one per tree, obtained by pooling an equal weight of primary and secondary roots collected (n = 3) between 10:00 and 11:00 am. Samples were immediately immersed in liquid nitrogen and then stored at −80°C. Immediately prior to biochemical analysis, each leaf and root sample was ground to a fine powder in liquid nitrogen.

Assays of malondialdehyde (MDA), ascorbate and antioxidant enzymes (SOD, CAT, APX and dehydroascorbate reductase) were performed as described by Santini et al. (2013).

Hydrogen peroxide (H_2O_2) was assayed using the PeroxiDetect kit (Sigma-Aldrich), which is based on the oxidation of ferrous (Fe^{2+}) to ferric (Fe^{3+}) ions at acidic pH. The subsequent reaction of Fe^{3+} ions forms a blue adduct with xylenol orange (3,3′-bis[*N*,*N*-bis(carboxymethyl)aminomethyl] *o*-cresolsulfonephthalein, sodium salt) visible at 560 nm. Proline content was measured as described by Oustric et al. (2019).

A V-630 spectrophotometer was used for all measurements (Jasco Inc., Tokyo, Japan).

Statistical Analyses

All statistical measurements were performed with R statistical software (v.2.12.1)[1] and the Rcmdr package. The qualitative factors studied were sampling date (days) (D0 and D210 after nutrient deficiency, and 30DR of recovery for leaves and roots),

[1]http://www.R-project.org

the common clementine scion grafted onto rootstocks and subjected to nutrient deficiency (C/PMC, C/FL, C/CC, and C/CM, for leaves and roots) and the ploidy level of nutrient stressed rootstocks (C/PMC2x and C/PMC4x, C/FL4x, C/CM2x and C/CM4x, C/CC2x and C/CC4x for leaves and roots). The impact of these three factors was analyzed using a two-way ANOVA followed by LSD test at $p < 0.05$.

The data for gas exchange, chlorophyll fluorescence, antioxidant parameters and oxidative markers obtained at D210 of nutrient deficiency and after 30DR of recovery for clementine scions grafted onto the seven rootstocks were analyzed by hierarchical group analysis and heatmaps generated by Heatmap.2 function of the gplot package 3.0.1 for Rstudio (v.1.3.1093)[2].

RESULTS

In order to minimize any effects due to changes in environmental conditions (photoperiod, temperature in the tunnel greenhouse, etc.) when comparing the responses to nutrient deficiency of different genotypes, results on stressed scion/rootstock combinations were expressed as ratios relative to the values obtained for controls. Thus, only the effect of the nutrient deficiency was taken into account.

Leaf Damage

The most representative level of leaf damage induced after 210 days of nutrient stress in each rootstock/scion combination is shown in **Figure 1**. Level 0 on our rating scale corresponded to the control with green leaves and no disease symptoms. Minimum foliar tissue damage (level l) was observed in C/CM4x and C/FL4x with light green leaves. C/PMC4x and C/PMC2x had light green leaves with yellow veins (level 2). Mean foliar tissue damage was higher in C/CM2x, C/CC2x and C/CC4x with yellow leaves (level 3).

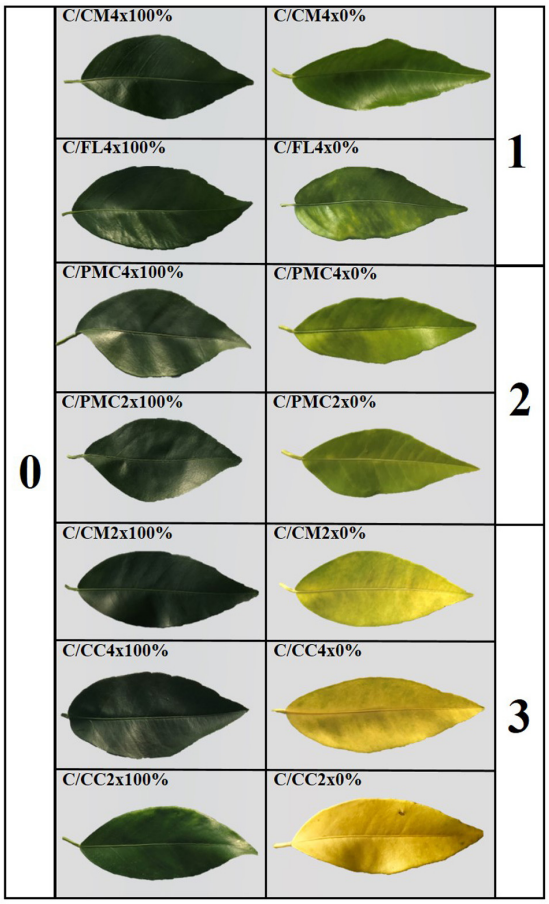


FIGURE 1 | Assessment of leaf damages after 210 days of total nutrient deficiency (0%) on clementine trees grafted onto the seven rootstocks compared to controls (100%). Genotypes are ranked based on the leaf symptoms from the lesser affected (1) to the more affected (3).

Change in Macro- and Micro- Nutrients

Overall after 210 days of nutrient stress, there was a decrease in foliar N, Fe (except C/CC4x), Cu (except C/PMC4x), Mn, and B of all scion/rootstock combinations (**Table 2** and **Supplementary Tables 1**, **2**). An increase or similar values was found for the P, K (except C/CC2x), Mg, Ca (except C/CC4x), Na (except C/PMC2x) and Zn (except C/CM4x, C/CC4x and C/CC2x) (**Table 2** and **Supplementary Tables 1, 2**).

After 30 days of recovery, N, Fe (except in C/CC4x and C/CM2x), Cu (except in C/CC2x), Mn (except in C/CM4x) and B contents were lower and P contents were higher than the control values in all scion/rootstock combinations. K, Ca, Mg (except C/CM4x) and Na contents were higher or similar than control values for all scion/rootstock combinations (**Table 2** and **Supplementary Tables 1**, **2**). Zn contents were similar in C/CC4x, C/CM2x and C/CM4x or lower in C/CC2x, C/PMC2x, C/PMC4x and C/FL4x than control values (**Supplementary Table 2**).

[2]https://rstudio.com

Physiological and Biochemical Responses of Scion/Rootstock Combinations to Nutrient Deficiency and Recovery

Based on photosynthesis and antioxidant parameters and oxidative markers visualized within the heatmap (**Figures 2A,B**), the seven scion/rootstock combinations could be separated into two groups.

After 210 days of nutrient deficiency, the first group comprised C/PMC4x, C/PMC2x, C/FL4x, C/CM4x and C/CM2x and the second group C/CC4x and C/CC2x. On the whole, the scion/rootstock combinations in group 1 were distinguished by a lower MDA and DHA content in leaves and H_2O_2 content in roots and a higher photosynthetic capacity [P_{net}, g_s, E, F_v/F_m, Y(NPQ)] (except for C/CM2x) and lower ETR/P_{net} than group 2.

After 30 days of recovery, C/CM2x and C/CC2x changed groups, respectively in groups 2 and 1. The first group comprised C/CC2x, C/PMC2x, C/FL4x, C/PMC4x and C/CM4x and the second group comprised C/CM2x and C/CC4x. The first group could be divided into 3 subgroups consisting of C/CC2x

TABLE 2 | Total leaf contents of macronutrient in common clementine scion grafted onto the seven rootstocks.

Parameters	Days	C/PMC4x	C/PMC2x	C/FL4x	C/CM4x	C/CM2x	C/CC4x	C/CC2x
N (%)	*D0*	*3.03 ± 0.25^{a}*	*2.94 ± 0.19^{a}*	*3.00 ± 0.16^{a}*	*3.91 ± 0.57^{a}*	*3.32 ± 0.04^{a}*	*3.40 ± 0.44^{a}*	*2.99 ± 0.15^{a}*
N (ratio)	D210	0.40 ± 0.02^{a}	0.37 ± 0.03^{ab}	0.35 ± 0.02^{ab}	0.43 ± 0.09^{a}	0.40 ± 0.02^{a}	0.40 ± 0.01^{a}	0.33 ± 0.02^{b}
	30DR	0.37 ± 0.01^{b}	0.38 ± 0.05^{ab}	0.35 ± 0.01^{b}	0.31 ± 0.08^{c}	0.34 ± 0.06^{b}	0.45 ± 0.01^{a}	0.40 ± 0.02^{ab}
P (%)	*D0*	*0.16 ± 0.09^{ab}*	*0.14 ± 0.01^{ab}*	*0.15 ± 0.01^{ab}*	*0.15 ± 0.01^{ab}*	*0.16 ± 0.01^{ab}*	*0.19 ± 0.01^{a}*	*0.15 ± 0.02^{ab}*
P (ratio)	D210	1.97 ± 0.15^{a}	1.27 ± 0.17^{b}	2.03 ± 0.15^{a}	1.30 ± 0.19^{b}	2.13 ± 0.15^{a}	1.53 ± 0.12^{b}	1.37 ± 0.07^{b}
	30DR	2.90 ± 0.13^{a}	1.71 ± 0.13^{b}	1.05 ± 0.26^{c}	1.59 ± 0.05^{b}	1.70 ± 0.08^{b}	2.18 ± 0.15^{ab}	2.03 ± 0.01^{ab}
K (%)	*D0*	*2.51 ± 0.02^{a}*	*2.15 ± 0.14^{ab}*	*2.53 ± 0.28^{a}*	*2.34 ± 0.22^{ab}*	*1.79 ± 0.08^{b}*	*2.21 ± 0.01^{ab}*	*2.60 ± 0.15^{a}*
K (ratio)	D210	1.16 ± 0.04^{b}	1.43 ± 0.04^{ab}	1.87 ± 0.02^{a}	1.56 ± 0.09^{ab}	1.46 ± 0.07^{ab}	1.14 ± 0.05^{b}	0.78 ± 0.15^{c}
	30DR	1.87 ± 0.05^{a}	1.01 ± 0.10^{c}	1.56 ± 0.02^{ab}	1.30 ± 0.01^{b}	1.41 ± 0.07^{ab}	1.55 ± 0.12^{ab}	1.58 ± 0.12^{ab}
Ca (%)	*D0*	*1.97 ± 0.05^{a}*	*2.20 ± 0.06^{a}*	*1.30 ± 0.13^{b}*	*1.60 ± 0.22^{ab}*	*1.67 ± 0.31^{ab}*	*1.32 ± 0.15^{b}*	*1.62 ± 0.12^{ab}*
Ca (ratio)	D210	1.19 ± 0.10^{ab}	1.03 ± 0.13^{b}	1.08 ± 0.06^{b}	0.91 ± 0.05^{b}	1.39 ± 0.01^{a}	0.84 ± 0.06^{bc}	0.96 ± 0.07^{b}
	30DR	1.15 ± 0.14^{b}	1.09 ± 0.08^{b}	0.98 ± 0.16^{b}	1.04 ± 0.02^{b}	1.50 ± 0.03^{a}	1.11 ± 0.06^{b}	1.16 ± 0.09^{b}
Mg (%)	*D0*	*0.68 ± 0.02^{b}*	*0.62 ± 0.05^{b}*	*0.66 ± 0.07^{b}*	*0.88 ± 0.02^{a}*	*0.54 ± 0.04^{b}*	*0.69 ± 0.07^{b}*	*0.62 ± 0.02^{b}*
Mg (ratio)	D210	1.15 ± 0.08^{b}	1.19 ± 0.03^{b}	1.17 ± 0.01^{b}	1.69 ± 0.05^{a}	1.63 ± 0.16^{a}	1.33 ± 0.09^{ab}	1.10 ± 0.11^{b}
	30DR	1.44 ± 0.07^{a}	1.48 ± 0.03^{a}	1.27 ± 0.07^{ab}	0.80 ± 0.03^{b}	1.47 ± 0.09^{a}	1.22 ± 0.09^{ab}	1.21 ± 0.16^{ab}
Na (%)	*D0*	*0.014 ± 0.001^{a}*	*0.019 ± 0.002^{a}*	*0.017 ± 0.001^{a}*	*0.018 ± 0.002^{a}*	*0.014 ± 0.002^{a}*	*0.014 ± 0.001^{a}*	*0.016 ± 0.002^{a}*
Na (ratio)	D210	0.980 ± 0.125^{d}	0.842 ± 0.100^{d}	4.464 ± 0.036^{a}	1.500 ± 0.178^{bc}	1.166 ± 0.066^{c}	4.119 ± 0.094^{a}	2.000 ± 0.121^{b}
	30DR	2.500 ± 0.179^{ab}	1.333 ± 0.209^{b}	1.307 ± 0.154^{b}	1.111 ± 0.101^{b}	1.409 ± 0.079^{b}	3.750 ± 0.120^{a}	2.526 ± 0.058^{ab}

Data shown at D210 and 30DR are means (n = 3 ± standard error) expressed as ratios with respect to the values obtained on control which have not been subjected to stress. For further informations, means values of control data (D0) (n = 3 ± standard error) were also included and indicated by italics characters. Data were analysed using ANOVA and Fisher LSD tests (P < 0.05). Different letters indicate significant differences between genotypes along the time course. D0, control, D210, 210 days after the start of nutritional deprivation, and 30DR, after 30 days of recovery.

associated with C/PMC2x, C/PMC4x with C/FL4x, and C/CM4x alone. C/CM4x were characterized by a higher photosynthetic capacity (P_{net}, g_s, E, chlorophyll, F_v/F_mratio, ETR) and lower foliar MDA content than C/CM2x and C/CC4x, whereas C/CC2x, C/PMC2x, C/FL4x and C/PMC4x had intermediate values for these variables. C/CM4x was distinguished by a higher Asa and SOD activity and higher DHA and H_2O_2 content in leaves and lower CAT and APX activities than the other scion/rootstock combinations.

Change in Photosynthetic Capacities

At D210, a smaller decline in P_{net}, g_s and E was observed in C/CM4x than in C/FL4x, C/PMC2x and C/PMC4x and, to a greater extent, in C/CM2x, C/CC2x and C/CC4x (**Tables 3**, **4** and **Supplementary Tables 3**, **4**). C/CM4x showed a better recovery of P_{net} at 30DR than C/PMC4x, C/FL4x and C/CC2x and, to a greater extent, C/CM2x, C/CC4x and C/PMC2x. The decrease in g_s and E content was lower in C/CM4x and C/PMC4x than in C/PMC2x, C/FL4x, C/CM2x, C/CC2x and C/CC4x at D210. C/CM4x showed a low decrease in g_s and E content at 30DR (**Table 3** and **Supplementary Table 3**). Concerning the decline in chlorophyll content, this was lower in C/CM4x and C/FL4x and C/PMC4x than in the other scion/rootstock combinations at D210 and 30DR, respectively (**Table 3** and **Supplementary Table 3**).

A smaller decrease in F_v/F_m was observed in C/CM4x, C/PMC2x, C/PMC4x and C/FL4x than in the other scion/rootstock combinations at D210 and in C/CM4x and C/PMC2x at 30DR (**Table 4** and **Supplementary Table 4**). Conversely to the other scion/rootstock combinations, ETR in C/CM4x remained below the control at D210 and 30DR (**Table 4** and **Supplementary Table 4**). Overall, ETR/P_{net} increased in all scion/rootstock combinations but this increase was greater in C/CM2x, C/CC2x and C/CC4x and in C/CC4x, C/PMC2x and C/CM2x than in the other scion/rootstock combinations at D210 and 30DR, respectively (**Table 4** and **Supplementary Table 4**). Although Y(II) remained stable in C/FL4x and C/CM4x, it decreased in the other scion/rootstock combinations and, in particular, in C/PMC2x at D210 (**Table 4** and **Supplementary Table 4**). However, Y(II) decreased in all scion/rootstock combinations, except in C/FL4x and C/CM4x and C/CM2x, where it remained stable at D210 and 30DR, respectively (**Table 4** and **Supplementary Table 4**). Y(NPQ) increased or stayed close to 1 in all scion/rootstock combinations except in C/CC2x at D210 and C/CC4x and C/PMC2x at 30DR (**Table 4** and **Supplementary Table 4**).

Change in Antioxidant Molecules

The Asa contents and Asa/DHA ratio increased or remained stable in all scion/rootstock combinations at D210 (**Table 5** and **Supplementary Table 5**). C/FL4x presented a larger increase Asa/DHA ratio than the other scion/rootstock combinations at D210. Asa content and Asa/DHA ratio decreased at 30DR in all scion/rootstock combinations or only in C/CC2x and C/CM4x, respectively.

The proline content was lower than the control in all scion/rootstock combinations at D210 and 30DR, but this

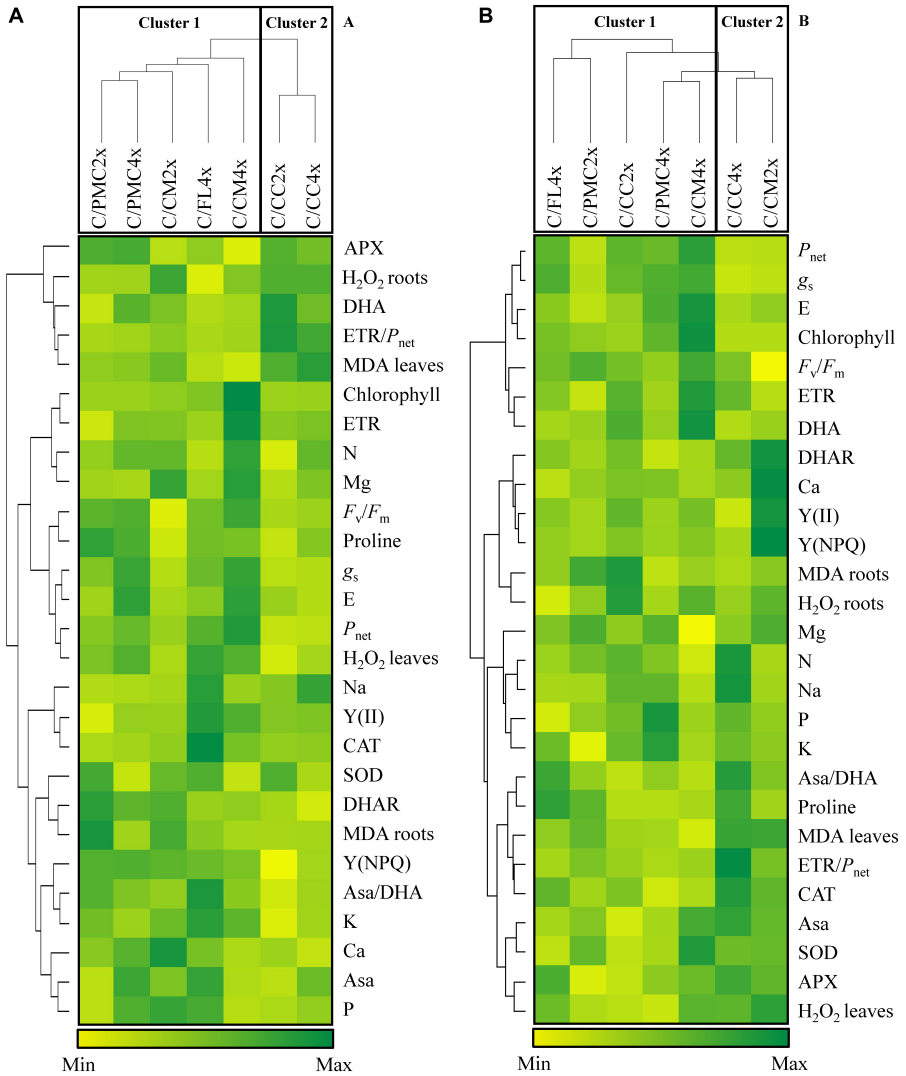


FIGURE 2 | Hierarchical cluster analysis and heatmap displaying mineral contents and parameters responding to nutrient deficiency in different scion/rootstock combinations after 210 days of nutrient deficiency (D210) **(A)** and after 30 days of recovery (30DR) **(B)**. Values are means of 3 independent (n = 3) measurements for each parameter. Hierarchical cluster analysis dispatches the seven scion/rootstock combinations based on the different parameters. The heatmap shows the differences between the seven scion/rootstock combinations and treatments for each parameter. Color scale shows the intensity of the normalized mean values of different parameters. Values are associated with color ranging from yellow (low) to dark green (high).

reduction was lower in C/CC2x at D210 and C/PMC4x and C/CC2x at 30DR (**Table 5** and **Supplementary Table 5**).

Change in Enzymatic Antioxidants

SOD and DHAR decreased in all scion/rootstock combinations at D210 and 30DR (**Table 5** and **Supplementary Table 5**). The decrease in SOD was greater in C/CM4x and C/PMC4x at D210 and in C/PMC4x, C/FL4x and C/CC2x at 30DR than in the other scion/rootstock combinations.

DHAR decreased more severely in C/CC4x, C/CC2x, C/CM4x and C/FL4x at D210 and in C/CM4x, C/PMC4x and C/PMC2x at 30DR in comparison to the other scion/rootstock combinations. CAT increased in C/FL4x and in lower extent in C/CM4x, whereas it decreased in the other scion/rootstock combinations at D210 (**Table 5** and **Supplementary Table 5**). Only C/PMC4x stayed below the control value at 30DR. APX was the only enzymatic activity to remain greater than 1 in all scion/rootstock combinations at D210 and 30DR (**Table 5** and **Supplementary Table 5**). APX activity was greater in C/PMC2x, C/PMC4x, C/CC2x and C/CC4x than in the other scion/rootstock combinations at D210, whereas there were no significant differences between the combinations at 30DR.

Change in Oxidative Markers in Leaves and Roots

At D210, the MDA content increased in leaves of all scion/rootstock combinations. On the contrary, no accumulation was observed for DHA content in leaves (except in C/PMC4x

TABLE 3 | Leaf photosynthetic parameters of the seven scion/rootstock combinations after 210 days of nutrient deficiency (D210) and 30 days of recovery (30DR).

Parameters	Day	C/PMC4x	C/PMC2x	C/FL4x	C/CM4x	C/CM2x	C/CC4x	C/CC2x
P_{net} (μmol CO_2.m^{-2} .s^{-1})	*D0*	*7.807 ± 1.077^{b}*	*9.247 ± 1.536^{ab}*	*9.343 ± 0.948^{ab}*	*10.368 ± 0.404^{a}*	*10.352 ± 0.225^{a}*	*9.482 ± 0.589^{a}*	*10.106 ± 0.445^{a}*
P_{net}(ratio)	D210	0.275 ± 0.004^{b}	0.197 ± 0.044^{bc}	0.319 ± 0.005^{ab}	0.447 ± 0.020^{a}	0.154 ± 0.019^{c}	0.065 ± 0.002^{d}	0.052 ± 0.004^{d}
	30DR	0.222 ± 0.001^{b}	0.051 ± 0.006^{c}	0.248 ± 0.021^{b}	0.350 ± 0.010^{a}	0.061 ± 0.043^{c}	0.056 ± 0.004^{c}	0.249 ± 0.081^{b}
g_s (mol CO_2.m^{-2} .s^{-1})	*D0*	*0.133 ± 0.033^{ab}*	*0.132 ± 0053^{ab}*	*0.165 ± 0.031^{a}*	*0.068 ± 0.019^{cd}*	*0.057 ± 0.005^{cd}*	*0.100 ± 0.019^{bc}*	*0.018 ± 0.015^{d}*
g_s(ratio)	D210	0.380 ± 0.034^{a}	0.214 ± 0.074^{b}	0.268 ± 0.029^{b}	0.387 ± 0.002^{a}	0.095 ± 0.008^{c}	0.098 ± 0.007^{c}	0.084 ± 0.008^{c}
	30DR	0.255 ± 0.005^{a}	0.092 ± 0.001^{b}	0.260 ± 0.056^{a}	0.278 ± 0.055^{a}	0.077 ± 0.002^{c}	0.060 ± 0.004^{c}	0.220 ± 0.074^{ab}
E (mmol H_2O.m^{-2} .s^{-1})	*D0*	*0.867 ± 0.084^{ab}*	*0.920 ± 0.007^{ab}*	*0.788 ± 0.176^{b}*	*0.904 ± 0.089^{ab}*	*0.344 ± 0.027^{c}*	*1.350 ± 0.148^{a}*	*1.140 ± 0.211^{a}*
E (ratio)	D210	0.472 ± 0.214^{a}	0.165 ± 0.017^{c}	0.221 ± 0.024^{b}	0.480 ± 0.005^{a}	0.145 ± 0.025^{cd}	0.112 ± 0.012^{d}	0.184 ± 0.024^{c}
	30DR	0.302 ± 0.012^{b}	0.079 ± 0.001^{d}	0.180 ± 0.023^{c}	0.406 ± 0.007^{a}	0.168 ± 0.025^{c}	0.119 ± 0.004^{cd}	0.156 ± 0.017^{c}
Chlorophyll (DUALEX units)	*D0*	*36.15 ± 2.855^{a}*	*40.883 ± 1.346^{a}*	*45.95 ± 9.758^{a}*	*45.133 ± 2.984^{a}*	*43.867 ± 6.323^{a}*	*45.217 ± 5.648^{a}*	*42.95 ± 5.687^{a}*
Chlorophyll (ratio)	D210	0.131 ± 0.066^{c}	0.130 ± 0.028^{c}	0.218 ± 0.023^{b}	0.628 ± 0.037^{a}	0.169 ± 0.096^{c}	0.142 ± 0.022^{c}	0.129 ± 0.058^{c}
	30DR	0.184 ± 0.009^{b}	0.143 ± 0.009^{c}	0.164 ± 0.019^{bc}	0.254 ± 0.043^{a}	0.114 ± 0.045^{d}	0.113 ± 0.017^{d}	0.133 ± 0.031^{cd}

Data shown at D210 and 30DR are means (n = 3 ± standard error) expressed as ratios with respect to the values obtained on control which have not been subjected to stress. For further informations, means values of control data (D0) (n = 3 ± standard error) were also included and indicated by italics characters. Data were analysed using ANOVA and Fisher LSD tests (P < 0.05). Different letters indicate significant differences between genotypes along the time course. D0, control, D210, 210 days after the start of nutritional deprivation, and 30DR, after 30 days of recovery.

TABLE 4 | Chlorophyll *a* fluorescence parameters of the seven scion/rootstock combinations after 210 days of nutrient deficiency (D210) and 30 days of recovery (30DR).

Parameters	Day	C/PMC4x	C/PMC2x	C/FL4x	C/CM4x	C/CM2x	C/CC4x	C/CC2x
F_v/F_m	*D0*	*0.825 ± 0.005^{a}*	*0.821 ± 0.007^{a}*	*0.82 ± 0008^{a}*	*0.825 ± 0.008^{a}*	*0.826 ± 0.003^{a}*	*0.771 ± 0.083^{a}*	*0.785 ± 0.044^{a}*
F_v/F_m (ratio)	D210	0.751 ± 0.060^{ab}	0.712 ± 0.040^{ab}	0.633 ± 0.023^{b}	0.820 ± 0.046^{a}	0.269 ± 0.018^{d}	0.492 ± 0.088^{c}	0.450 ± 0.029^{c}
	30DR	0.491 ± 0.040^{bc}	0.665 ± 0.012^{ab}	0.581 ± 0.021^{b}	0.712 ± 0.068^{a}	0.242 ± 0.065^{c}	0.552 ± 0.016^{b}	0.572 ± 0.011^{b}
ETR (μmol .e^{-1}.m^{-2} .s^{-1})	*D0*	*31.05 ± 2.936^{a}*	*28.667 ± 4.256^{a}*	*30.983 ± 6.126^{a}*	*31.05 ± 5.365^{a}*	*29.183 ± 8.800^{a}*	*25.367 ± 3.006^{a}*	*26.817 ± 6.963^{a}*
ETR (ratio)	D210	0.573 ± 0.025^{bc}	0.308 ± 0.118^{d}	0.470 ± 0.037^{c}	0.972 ± 0.022^{a}	0.567 ± 0.026^{bc}	0.587 ± 0.023^{bc}	0.537 ± 0.088^{bc}
	30DR	0.444 ± 0.012^{c}	0.263 ± 0.043^{d}	0.585 ± 0.012^{bc}	1.054 ± 0.005^{a}	0.325 ± 0.046^{d}	0.732 ± 0.011^{b}	0.792 ± 0.101^{b}
ETR/P_{net}	*D0*	*3.977 ± 0.442^{a}*	*3.100 ± 0.903^{ab}*	*3.316 ± 0.322^{ab}*	*2.995 ± 0.327^{ab}*	*2.819 ± 0.923^{ab}*	*2.675 ± 0.139^{b}*	*2.654 ± 0.721^{b}*
ETR/P_{net}(ratio)	D210	2.123 ± 0.173^{bc}	1.563 ± 0.053^{c}	1.473 ± 0.018^{c}	2.176 ± 0.112^{bc}	3.683 ± 0.002^{b}	9.026 ± 0.777^{a}	11.805 ± 0.593^{a}
	30DR	2.005 ± 0.237^{d}	5.157 ± 0.569^{b}	2.376 ± 0.020^{d}	3.011 ± 0.197^{c}	5.322 ± 0.118^{b}	13.066 ± 0.198^{a}	3.181 ± 0.464^{c}
Y(II)	*D0*	*0.624 ± 0.084^{a}*	*0.570 ± 0.041^{a}*	*0.616 ± 0.085^{a}*	*0.617 ± 0.106^{a}*	*0.580 ± 0.174^{a}*	*0.470 ± 0.113^{a}*	*0.558 ± 0.087^{a}*
Y(II) (ratio)	D210	0.574 ± 0.025^{c}	0.225 ± 0.103^{d}	1.192 ± 0.109^{a}	0.952 ± 0.034^{ab}	0.567 ± 0.026^{c}	0.707 ± 0.065^{bc}	0.674 ± 0.136^{bc}
	30DR	0.432 ± 0.031^{bc}	0.406 ± 0.054^{bc}	0.519 ± 0.140^{b}	0.587 ± 0.038^{b}	0.977 ± 0.029^{a}	0.250 ± 0.008^{c}	0.667 ± 0.025^{ab}
Y(NPQ)	*D0*	*0.186 ± 0.009^{a}*	*0.047 ± 0.003^{b}*	*0.055 ± 0.014^{b}*	*0.046 ± 0.005^{b}*	*0.052 ± 0.005^{b}*	*0.048 ± 0.010^{b}*	*0.047 ± 0.010^{b}*
Y(NPQ) (ratio)	D210	1.721 ± 0.221^{a}	1.684 ± 0.201^{a}	1.510 ± 0.272^{a}	1.383 ± 0.171^{a}	1.623 ± 0.035^{a}	1.074 ± 0.230^{a}	0.469 ± 0.062^{b}
	30DR	1.279 ± 0.038^{c}	0.819 ± 0.045^{d}	1.731 ± 0.251^{bc}	2.539 ± 0.504^{b}	10.329 ± 0.359^{a}	0.715 ± 0.151^{d}	2.846 ± 0.019^{b}

Data shown at D210 and 30DR are means (n = 3 ± standard error) expressed as ratios with respect to the values obtained on control which have not been subjected to stress. For further informations, means values of control data (D0) (n = 3 ± standard error) were also included and indicated by italics characters. Data were analysed using ANOVA and Fisher LSD tests (P < 0.05). Different letters indicate significant differences between genotypes along the time course. D0, control, D210, 210 days after the start of nutritional deprivation, and 30DR, after 30 days of recovery.

and C/CC2x) and MDA in roots (except C/PMC2x) and H_2O_2 in leaves (**Table 6** and **Supplementary Table 6**). H_2O_2 increased in roots of C/CM2x, C/CC4x and C/CC2x but decreased in the other scion/rootstock combinations.

At 30DR, only C/CM4x showed an increase in DHA content (**Table 6** and **Supplementary Table 6**). MDA accumulation in leaves was lower in C/CM4x than in C/PMC4x, C/CC2x and C/FL4x and much lower than in C/PMC2x, C/CM2x and C/CC4x. The H_2O_2 content in leaves increased in C/CM2x or stayed stable in C/FL4x, C/CM4x and C/CC4x whereas it decreased in the other scion/rootstock combinations at 30DR (**Table 6** and **Supplementary Table 6**). Unlike the other scion/rootstock combinations, C/PMC2x and C/CC2x showed an increase in MDA content in roots at 30DR (**Table 6** and **Supplementary Table 6**). H_2O_2 content increased in roots of C/CC2x, C/CM2x and C/CM4x and but

TABLE 5 | Antioxidant activities of the seven scion/rootstock combinations after 210 days of nutrient deficiency (D210) and 30 days of recovery (30DR).

Parameters	Day	C/PMC4x	C/PMC2x	C/FL4x	C/CM4x	C/CM2x	C/CC4x	C/CC2x
Asa (μmol .g^{-1} FW)	*D0*	*1.461 ± 0.096^{ab}*	*1.437 ± 0.106^{ab}*	*1.530 ± 0.037^{ab}*	*0.853 ± 0.322^{b}*	*1.398 ± 0.025^{ab}*	*1.674 ± 0.178^{a}*	*1.561 ± 0.087^{ab}*
Asa (ratio)	D210	3.852 ± 0.386^{a}	1.885 ± 0.229^{c}	3.978 ± 0.183^{a}	2.087 ± 0.086^{c}	2.833 ± 0.172^{b}	3.090 ± 0.142^{b}	1.881 ± 0.182^{c}
	30DR	0.507 ± 0.030^{a}	0.574 ± 0.059^{a}	0.503 ± 0.069^{a}	0.699 ± 0.147^{a}	0.639 ± 0.143^{a}	0.737 ± 0.056^{a}	0.416 ± 0.069^{a}
Asa/DHA	*D0*	*2.068 ± 0.157^{a}*	*2.810 ± 1.309^{a}*	*2.437 ± 0.067^{a}*	*1.356 ± 0.066^{a}*	*2.390 ± 0.303^{a}*	*2.189 ± 0.294^{a}*	*2.188 ± 0.219^{a}*
Asa/DHA (ratio)	D210	3.494 ± 0.428^{c}	4.756 ± 0.168^{b}	6.439 ± 0.052^{a}	3.158 ± 0.126^{c}	2.910 ± 0.302^{c}	2.536 ± 0.305^{cd}	1.086 ± 0.086^{d}
	30DR	1.511 ± 0.425^{ab}	1.416 ± 0.082^{ab}	3.364 ± 0.228^{a}	0.654 ± 0.053^{b}	1.832 ± 0.024^{ab}	3.862 ± 0.429^{a}	0.508 ± 0.009^{b}
Proline (μmol .g^{-1} FW)	*D0*	*12.986 ± 0.413^{c}*	*12.026 ± 0.570^{c}*	*15.217 ± 0.353^{a}*	*14.677 ± 0.231^{ab}*	*13.685 ± 0.275^{bc}*	*15.421 ± 0.576^{a}*	*13.487 ± 0.446^{bc}*
Proline (ratio)	D210	0.460 ± 0.078^{a}	0.506 ± 0.015^{a}	0.395 ± 0.010^{ab}	0.382 ± 0.010^{ab}	0.242 ± 0.006^{c}	0.363 ± 0.014^{b}	0.256 ± 0.003^{c}
	30DR	0.321 ± 0.129^{c}	0.479 ± 0.081^{ab}	0.563 ± 0.130^{a}	0.345 ± 0.009^{bc}	0.359 ± 0.023^{bc}	0.536 ± 0.097^{a}	0.319 ± 0.115^{c}
SOD (U .mg^{-1} protein)	*D0*	*3.734 ± 0.107^{c}*	*6.238 ± 0.186^{a}*	*3.773 ± 0.127^{c}*	*2.766 ± 0.023^{d}*	*2.996 ± 0.062^{d}*	*5.113 ± 0.211^{b}*	*3.097 ± 0.007^{cd}*
SOD (ratio)	D210	0.591 ± 0.019^{c}	0.750 ± 0.062^{a}	0.734 ± 0.021^{a}	0.594 ± 0.077^{c}	0.707 ± 0.038^{a}	0.624 ± 0.036^{b}	0.734 ± 0.021^{a}
	30DR	0.350 ± 0.016^{c}	0.476 ± 0.027^{b}	0.308 ± 0.019^{c}	0.597 ± 0.017^{a}	0.472 ± 0.001^{b}	0.458 ± 0.018^{b}	0.309 ± 0.019^{c}
CAT (μmol.min^{-1} protein)	*D0*	*1.309 ± 0.015^{ab}*	*1.052 ± 0.015^{b}*	*1.318 ± 0.213^{ab}*	*1.414 ± 0.004^{a}*	*1.010 ± 0.075^{b}*	*0.382 ± 0.003^{c}*	*0.941 ± 0.008^{b}*
CAT (ratio)	D210	0.479 ± 0.024^{c}	0.281 ± 0.003^{d}	3.538 ± 0.544^{a}	1.299 ± 0.109^{b}	0.818 ± 0.090^{bc}	0.890 ± 0.030^{bc}	0.778 ± 0.051^{bc}
	30DR	0.331 ± 0.004^{d}	1.157 ± 0.021^{c}	2.371 ± 0.325^{b}	0.951 ± 0.111^{c}	2.398 ± 0.330^{b}	3.566 ± 0.291^{a}	1.836 ± 0.112^{bc}
APX (μmol.min^{-1} protein)	*D0*	*1.742 ± 0.066^{a}*	*1.564 ± 0.083^{ab}*	*1.310 ± 0.009^{cd}*	*1.487 ± 0.003^{bc}*	*1.633 ± 0.006^{ab}*	*1.187 ± 0.009^{d}*	*1.161 ± 0.006^{d}*
APX (ratio)	D210	1.985 ± 0.053^{a}	1.934 ± 0.177^{a}	1.564 ± 0.050^{b}	1.118 ± 0.002^{c}	1.330 ± 0.063^{ab}	1.728 ± 0.016^{a}	1.898 ± 0.015^{a}
	30DR	2.442 ± 0.269^{a}	2.048 ± 0.112^{a}	2.778 ± 0.383^{a}	2.615 ± 0.316^{a}	2.664 ± 0.014^{a}	2.84 ± 0.233^{a}	2.173 ± 0.254^{a}
DHAR (μmol.min^{-1} protein)	*D0*	*43.744 ± 0.118^{b}*	*46.157 ± 0.323^{a}*	*22.757 ± 0.056^{c}*	*22.127 ± 0.677^{c}*	*19.18 ± 0.133^{d}*	*19.188 ± 0.366^{d}*	*21.455 ± 1.248^{cd}*
DHAR (ratio)	D210	0.581 ± 0.003^{b}	0.693 ± 0.025^{a}	0.452 ± 0.005^{c}	0.469 ± 0.014^{c}	0.610 ± 0.009^{b}	0.322 ± 0.019^{d}	0.420 ± 0.017^{c}
	30DR	0.371 ± 0.004^{b}	0.415 ± 0.019^{b}	0.453 ± 0.005^{ab}	0.410 ± 0.063^{b}	0.602 ± 0.010^{a}	0.495 ± 0.013^{ab}	0.476 ± 0.022^{ab}

Data shown at D210 and 30DR are means (n = 3 ± standard error) expressed as ratios with respect to the values obtained on control which have not been subjected to stress. For further informations, means values of control data (D0) (n = 3 ± standard error) were also included and indicated by italics characters. Data were analysed using ANOVA and Fisher LSD tests (P < 0.05). Different letters indicate significant differences between genotypes along the time course. D0, control, D210, 210 days after the start of nutritional deprivation, and 30DR, after 30 days of recovery.

decreased in the other scion/rootstock combinations (**Table 6** and **Supplementary Table 6**).

DISCUSSION

Comparison of the Sensitivity to Nutrient Deficiency of Clementine Scions Grafted on Different Rootstocks Genotypes Varying in Their Ploidy Level

Total nutrient deficiency induced chlorosis as shown by visual changes in color from yellow to light green in the whole plant of each scion/rootstock combination (**Figure 1**). Chlorosis is a characteristic symptom of nutritional deficiency, especially N deficiency, which is accompanied by the degradation of chlorophyll and the internal chloroplast structure altering the photosynthetic process (Lambers et al., 2008; Boussadia et al., 2010). Chlorosis was associated with a similar large decrease in N after 210 days of nutrient deficiency in all scion scion/rootstock combinations (**Figure 1** and **Table 2**) (Elavarasan and Premalatha, 2019). The increases in the P, K, and Mg contents in leaves of scion/rootstock combinations could be explained by a concentration effect due to the loss of nitrogen or their absorption from other anatomical parts of the plant (roots or leaves) (Tewari et al., 2007). This similar effect of nutrient deficiency on mineral contents cannot explain the differences in yellowing between scion/rootstock combinations. Yellowing variations might be related to a variation in chlorophyll oxidation as a consequence of an excess of ROS generated by nutrient deficiency (Praveen and Gupta, 2018; Qi et al., 2019). Depending on their genotype and level of ploidy, the rootstocks have different impacts on the regulation of oxidative stress rather than the regulation of minerals in the scion. To our knowledge, there are no data on the tolerance to total nutrient deficiency of the scion/rootstock combinations studied in this experiment.

In this study, scion/rootstock combinations were ranked according to their sensitivity to nutrient deprivation according to leaf damage and MDA content at D210 of nutrient deprivation (**Figure 1** and **Table 6**). Leaf symptom is a phenotypic response to nutrient deficiency used to rank plants (Srivastava, 2013; Oustric et al., 2019). C/CM4x and C/FL4x were ranked as "tolerant" and C/PMC2x and C/PMC4x as "moderately tolerant" because their leaves had level 1 and level 2 damage, respectively, with less MDA accumulation than the other scion/rootstock combinations. On the contrary, the level 3 leaf symptom and high MDA accumulation in C/CM2x, C/CC4x, and C/CC2x indicted their "sensitivity" to total nutrient deficiency.

TABLE 6 | Oxidative markers of the seven scion/rootstock combinations after 210 days of nutrient deficiency (D210) and 30 days of recovery (30DR).

Parameters	Day	C/PMC4x	C/PMC2x	C/FL4x	C/CM4x	C/CM2x	C/CC4x	C/CC2x
DHA (μmol .g^{-1} FW)	*D0*	*0.709 ± 0.067^{a}*	*0.571 ± 0.193^{a}*	*0.675 ± 0.012^{a}*	*0.631 ± 0.056^{a}*	*0.592 ± 0.082^{a}*	*0.792 ± 0.178^{a}*	*0.720 ± 0.100^{a}*
DHA	D210	1.248 ± 0.428^{ab}	0.387 ± 0.168^{d}	0.564 ± 0.052^{cd}	0.665 ± 0.126^{cd}	0.978 ± 0.302^{bc}	1.071 ± 0.305^{bc}	1.697 ± 0.086^{a}
	30DR	0.346 ± 0.070^{b}	0.337 ± 0.082^{b}	0.257 ± 0.228^{bc}	1.148 ± 0.053^{a}	0.335 ± 0.024^{b}	0.193 ± 0.088^{c}	0.795 ± 0.009^{ab}
MDA leaves (nmol .g^{-1} FW)	*D0*	*7.582 ± 1.324^{c}*	*3.093 ± 0.700^{c}*	*39.943 ± 5.297^{a}*	*20.478 ± 4.536^{b}*	*23.077 ± 2.643^{b}*	*21.622 ± 4.526^{b}*	*24.494 ± 5.424^{b}*
MDA leaves	D210	2.190 ± 0.033^{bc}	2.080 ± 0.286^{bc}	1.550 ± 0.202^{c}	1.242 ± 0.085^{d}	2.645 ± 0.146^{b}	3.530 ± 0.159^{a}	2.994 ± 0.080^{ab}
	30DR	0.885 ± 0.097^{c}	1.704 ± 0.085^{ab}	1.144 ± 002^{bc}	0.289 ± 0.052^{d}	2.180 ± 0.143^{a}	2.230 ± 0.250^{a}	0.922 ± 0.051^{bc}
H_2O_2 leaves (nmol .g^{-1} FW)	*D0*	*60.096 ± 3.086^{c}*	*64.293 ± 3.535^{bc}*	*62.605 ± 3.634^{bc}*	*79.600 ± 5.645^{a}*	*73.948 ± 3.085^{ab}*	*66.795 ± 3.667^{b}*	*79.524 ± 3.858^{a}*
H_2O_2 leaves	D210	1.008 ± 0.007^{a}	0.900 ± 0.050^{b}	1.080 ± 0.046^{a}	1.007 ± 0.175^{a}	0.777 ± 0.059^{bc}	0.789 ± 0.036^{bc}	0.671 ± 0.045^{c}
	30DR	0.563 ± 0.046^{d}	0.684 ± 0.103^{c}	0.991 ± 0.174^{b}	1.080 ± 0.07^{b}	1.278 ± 0.047^{a}	1.055 ± 0.039^{b}	0.631 ± 0.006^{c}
MDA roots (nmol .g^{-1} FW)	*D0*	2.818 ± 0.036^{c}	*3.256 ± 0.067^{bc}*	*5.724 ± 0.019^{b}*	*10.328 ± 0.846^{a}*	*5.946 ± 0.027^{b}*	*5.185 ± 0.110^{b}*	*5.272 ± 0.080^{b}*
MDA roots	D210	0.661 ± 0.034^{c}	1.313 ± 0.043^{a}	0.770 ± 0.001^{b}	0.620 ± 0.106^{c}	1.089 ± 0.070^{a}	0.633 ± 0.027^{c}	0.615 ± 0.051^{c}
	30DR	0.430 ± 0.171^{e}	1.452 ± 0.099^{ab}	0.784 ± 0.065^{bc}	0.748 ± 0.039^{c}	0.854 ± 0.086^{b}	0.589 ± 0.021^{d}	1.716 ± 0.128^{a}
H_2O_2 roots (nmol .g^{-1} FW)	*D0*	*22.271 ± 1.900^{b}*	*22.201 ± 4.466^{b}*	*31.459 ± 1.748^{a}*	*23.793 ± 1.347^{b}*	*23.425 ± 0.516^{b}*	*21.224 ± 0.949^{b}*	*11.536 ± 1.257^{c}*
H_2O_2 roots	D210	0.713 ± 0.021^{b}	0.703 ± 0.043^{b}	0.400 ± 0.089^{c}	0.866 ± 0.046^{b}	1.244 ± 0.017^{a}	1.134 ± 0.063^{a}	1.130 ± 0.046^{a}
	30DR	0.638 ± 0.178^{c}	0.801 ± 0.051^{b}	0.295 ± 0.046^{d}	1.227 ± 0.030^{ab}	1.200 ± 0.050^{ab}	0.752 ± 0.078^{b}	1.627 ± 0.058^{a}

Data shown at D210 and 30DR are means (n = 3 ± standard error) expressed as ratios with respect to the values obtained on control which have not been subjected to stress. For further informations, means values of control data (D0) (n = 3 ± standard error) were also included and indicated by italics characters. Data were analysed using ANOVA and Fisher LSD tests (P < 0.05). Different letters indicate significant differences between genotypes along the time course. D0, control, D210, 210 days after the start of nutritional deprivation, and 30DR, after 30 days of recovery.

What Are the Reasons for This Difference in Tolerance to Nutrient Deficiency Between Scion/Rootstocks Combinations?

The nutritional deficiency implemented for 210 days had a negative effect on all rootstock/scion combinations.

The decrease in N content would have affected photosynthetic capacity and chlorophyll *a* fluorescence (Terashima and Evans, 1988; Nunes et al., 1993; Amtmann and Armengaud, 2009; Jin et al., 2015). In fact, half of foliar N is allocated to the photosynthetic apparatus (Makino and Osmond, 1991). "Moderately tolerant" C/PMC2x and C/PMC4x and "tolerant" C/FL4x and C/CM4x (group 1) showed fewer changes of the photosynthetic process than "sensitive" scion/rootstock combinations, as evidenced by the lower decrease in P_{net}, g_s, E, F_v/F_m, ETR, ETR/P_{net}, and Y(II) (**Figure 2A** and **Tables 3**, **4**). P_{net} can be affected by stomatal and/or non-stomatal factors (Weng and Hsu, 2001). As indicated by the synergy and lower reduction in P_{net}, g_s, and E, "moderately tolerant" C/PMC2x and C/PMC4x and "tolerant" C/FL4x and C/CM4x (**Figure 2A** and **Table 3**) implement a more effective tolerance strategy than "sensitive" scion/rootstock, despite N decrease. This would be explained by a closure of stomata to limit transpiration and thus water loss at foliar level (Green and Mitchell, 1992; Fracheboud et al., 1999; Afrousheh et al., 2010; Feng et al., 2012; Marguerit et al., 2012). In addition, the higher P_{net} in "tolerant" C/CM4x and C/FL4x could be due to a lesser impact of N decrease in their chlorophyll content than in the other scion/rootstock associations (Fleischer, 1935). Their differences in P_{net} could be linked to a decrease in Rubisco concentrations and/or Calvin cycle enzyme also known to be affected during N deprivation (Ferrar and Osmond, 1986; Evans and Terashima, 1987).

A decrease in chlorophyll content associated with a disturbance in chlorophyll fluorescence parameters [F_v/F_m, ETR, ETR/P_{net}, and Y(II)] suggests that N decrease negatively influenced the efficiency of e^- capture (Evans and Terashima, 1987; Grassi et al., 2001; Kumar and Goh, 2002; Tikkanen et al., 2014; Cetner et al., 2017). The impact on the "tolerant" C/CM4x genotype was lower than for the other scion/rootstock combinations. The ETR/P_{net} ratio is indicative of increased electron consumption diverted to photorespiration or to alternative processes (Flexas et al., 1999, 2002). During electron transport, ROS are formed by the consecutive one-electron reduction of O_2 and by the concerted two-electron oxidation of H_2O on the PSII electron acceptor and donor sides, respectively (Pospíšil, 2009). In the heatmap at D210, ETR/P_{net} may have been associated with the increase in MDA (**Figure 2A** and **Tables 4**, **6**) which is a marker for oxidation. These results indicate that the formation of ROS is due to the excess of electrons for the carbon reduction process (Pan et al., 2006). Moreover, the decrease in photosynthetic capacity in all scion/rootstock combinations after D210 of nutrient deficiency is due to damage to the whole photosystem II complex and particularly to chloroplast structure following the action of oxidative molecules (Papadakis et al., 2004; Guerfel et al., 2009; Paparnakis et al., 2013). The synergy between Y(NPQ), Asa content and Asa/DHA ratio, with the increase Asa content and Asa/DHA ratio, may optimize protection against photoinhibition by enhancing non-photochemical quenching [Y(NPQ)] in all scion/rootstock combinations, except in the

"sensitive" C/CC2x (**Figure 2A** and **Tables 4**, **5**) (Talla et al., 2011; Karpinska et al., 2018).

After 30 days of recovery, C/CM4x (group 1) had higher values for photosynthesis parameters (P_{net}, g_s, E, F_v/F_m, and ETR) and a lower accumulation of MDA and H_2O_2 in leaves (**Figure 2B** and **Tables 3**, **4**, **6**). C/CM4x seemed to recover more rapidly with a better reversibility of the damage caused by nutrient deficiency compared to the other scion/rootstock combinations.

On the whole, rootstock autotetraploidization does not systematically improve the scion's tolerance to nutrient deficiency. C/CM4x is the only combination with a 4× rootstock that showed a significant improvement in tolerance compared to its homologous 2× rootstock after 210 days of nutrient deficiency and 30 days of recovery. These results are in agreement with those obtained by Oustric et al. (2019) who showed that ungrafted CM4x seedlings were more tolerant than CM2x seedlings. Conversely, C/PMC4x and C/PMC2x adapted better to nutrient deficiency than their non-grafted counterparts. The compatibility of the PMC rootstock with common clementine scion can be explained by their close genetic heritage (Jacquemond et al., 2013), as they both have the mandarin (*Citrus reticulata*) as parent. When considering allotetraploidisation, non-grafted FL4x showed a higher resistance than other non-grafted genotypes like CM4x in our previous study (Oustric et al., 2019). In the present study, C/FL4x appeared to present the same level of tolerance as C/CM4x when grafted.

Does the Antioxidant System Help Improve Tolerance to Nutrient Deficiency in Both Roots and Leaves?

The antioxidant capacity of the scion and rootstock during nutrient deficiency differed with rootstock genotype. Whatever the sensitivity of the rootstock/scion combination, DHAR and SOD activities did not seem to play a prominent role during nutrient deficiency (**Table 5**). These results did not agree with the large increases in SOD and DHAR activities observed in the same ungrafted rootstocks (Oustric et al., 2019). Although DHAR activity decreased, it appeared to be sufficient (except in C/PMC4x and C/CC2x) to maintain a lower or similar DHA content to the control while increasing the Asa/DHA ratio and Asa content after D210 (**Table 5**). Conversely, different changes in APX and CAT activity (**Table 5**) were observed. While CAT activity was only greater than controls in C/CM4x and C/FL4x, APX activity was greater than controls in all scion/rootstock combinations. The high APX activity is consistent with the large increase in Asa required for its function in all scion/rootstock combinations. The complementary metabolic role of CAT and APX suggested by their highly contrasted K_m for H_2O_2 (Mhamdi et al., 2012) would explain the low H_2O_2 and MDA values in "tolerant" C/CM4x and C/FL4x. Although proline decreased in all scion/rootstock combinations (**Tables 5**, **6**), it might be sufficient to complement the CAT activity in maintaining low H_2O_2 and MDA values in "tolerant" C/FL4x and C/CM4x (Kishor and Dange, 1990; Ozden et al., 2009). In the other scion/rootstock combinations, whatever their tolerance level, H_2O_2 contents were close to or below those of the control (**Table 6**) and were accompanied by a larger increase in MDA than in C/CM4x and C/FL4x. Unlike MDA, H_2O_2 is a transient molecule that accumulates over time to reveal different levels of oxidative damage between scion/rootstock combinations. These results suggest that APX activity is active on H_2O_2 but insufficient to prevent the formation of $OH^{\bullet}$ and therefore of compounds induced by lipid peroxidation such as MDA.

The high CAT and APX activity in "tolerant" C/CM4x and C/FL4x associated with a high ascorbate content indicates the importance of functional collaboration between enzymatic and non-enzymatic molecules for an effective antioxidant system (Blokhina et al., 2003). These results were consistent with their lower decrease in photosynthetic capacity (**Tables 3**, **4**).

At root level, MDA and H_2O_2 levels were similar or lower than the control values for all scion/rootstock combinations (**Table 6**) indicating an increase in the tolerance of the root system to nutrient deficiency regardless of the rootstock genotype and ploidy level. The root system appears to be less affected by mineral deficiency than the scion. Thus, differences in tolerance of scion/rootstock combinations appear to be due to the distinct influence of the rootstock depending on its genotype and ploidy level and on the performance of the scion.

During recovery, the activity of the antioxidant machinery was found to be similar in all scion/rootstock combinations. As during nutrient deficiency, SOD and DHAR activities were lower than controls but CAT and APX were similar or higher than controls depending on the scion/rootstock combination (**Table 5**). C/CC2x, C/PMC2x, C/PMC4x, C/FL4x and to a greater extent C/CM4x had lower MDA and H_2O_2 accumulation in leaves than C/CM2x and C/CC4x. This could be explained by their state of stress after D210 of nutrient deficiency (**Table 6**). C/CC2x seems to have a more effective antioxidant system than the "sensitive" C/CC4x and C/CM2x and this allows it to recover to a similar extent to the "tolerant" and "moderately tolerant" genotypes (**Figure 2B** and **Table 5**).

CONCLUSION

The experimental design of our study revealed differences in tolerance to nutrient deficiency in clementine scions depending on rootstock genotype and ploidy level.

Among the most tolerant scion/rootstock combinations, the doubled diploid Citrumelo 4475 and the allotetraploid FlhorAG1, both grafted with a common clementine scion, were characterized by less foliar damage, fewer alterations in photosynthetic processes, a reduction in oxidative markers and better functional enzymatic and non-enzymatic antioxidant systems. The other common clementine scion grafted on 4× rootstocks did not show better tolerance than their 2× counterparts. The fact that Citrumelo 4475 4× and FlhorAG1 4× rootstocks reduce the damage caused by nutrient deficiency in common clementine scion suggests that they could be used in citrus orchards.

A lower and more rationale use of fertilizers would have a positive impact on the economy and on soil and water ecology while conserving growth and development. In the future,

it would be interesting to test the impact of this 4× rootstock on growth, fruit production and clementine quality during nutrient deficiency. New emerging varieties such as triploids could also be tested. Recent citrus breeding programs have in fact mainly focused on these as they produce seedless fruit with a different maturity period and useful pomological, agronomical and organoleptic traits.

DATA AVAILABILITY STATEMENT

The raw data supporting the conclusions of this article will be made available by the authors, without undue reservation.

AUTHOR CONTRIBUTIONS

JO collected data, did the statistical analysis, interpreted the results, and drafted the manuscript. JS designed the study and drafted the manuscript. RM, SH, JG, and LB designed the study and helped to draft the manuscript. All authors contributed to the article and approved the submitted version.

FUNDING

This work was funded by the "Collectivité de Corse" as part of the "Innov'agrumes" research project (FEDER).

ACKNOWLEDGMENTS

We thank Jean-Claude Ribaut for hosting this study at the AREFLEC experimental station, and Gilles Paolacci and Paul Martin for installing and monitoring the fertigation system in the greenhouse.

SUPPLEMENTARY MATERIAL

The Supplementary Material for this article can be found online at: https://www.frontiersin.org/articles/10.3389/fpls.2021.634237/full#supplementary-material

Supplementary Table 1 Means of macronutrient contents in leaves of the seven scion/rootstock combinations.

Supplementary Table 2 | Means of micronutrient contents in leaves of the seven scion/rootstock combinations.

Supplementary Table 3 | Means of gas exchange parameters and chlorophyll content of the seven scion/rootstock combinations.

Supplementary Table 4 | Means of chlorophyll *a* fluorescence parameters of the seven scion/rootstock combinations.

Supplementary Table 5 | Means of antioxidant parameters of the seven scion/rootstock combinations.

Supplementary Table 6 | Means of oxidative markers of the seven scion/rootstock combinations.

REFERENCES

Afrousheh, M., Ardalan, M., Hokmabadi, H., and Afrousheh, M. (2010). Nutrient deficiency disorders in *Pistacia vera* seedling rootstock in relation to eco-physiological, biochemical characteristics and uptake pattern of nutrients. *Sci. Hort.* 124, 141–148. doi: 10.1016/j.scienta.2009.12.001

Aibara, I., and Miwa, K. (2014). Strategies for optimization of mineral nutrient transport in plants: multilevel regulation of nutrient-dependent dynamics of root architecture and transporter activity. *Plant Cell Physiol.* 55, 2027–2036. doi: 10.1093/pcp/pcu156

Allario, T., Brumos, J., Colmenero-Flores, J. M., Iglesias, D. J., Pina, J. A., Navarro, L., et al. (2013). Tetraploid Rangpur lime rootstock increases drought tolerance via enhanced constitutive root abscisic acid production. *Plant Cell Environ.* 36, 856–868. doi: 10.1111/pce.12021

Amtmann, A., and Armengaud, P. (2009). Effects of N, P, K and S on metabolism: new knowledge gained from multi-level analysis. *Curr. Opin. Plant Biol.* 12, 275–283. doi: 10.1016/j.pbi.2009.04.014

Apel, K., and Hirt, H. (2004). Reactive oxygen species: metabolism, oxidative stress, and signal transduction. *Annu. Rev. Plant Biol.* 55, 373–399. doi: 10.1146/annurev.arplant.55.031903.141701

Baker, N. R. (2008). Chlorophyll fluorescence: a probe of photosynthesis in vivo. *Annu. Rev. Plant Biol.* 59, 89–113. doi: 10.1146/annurev.arplant.59.032607.092759

Blokhina, O., Virolainen, E., and Fagerstedt, K. V. (2003). Antioxidants, oxidative damage and oxygen deprivation stress: a review. *Ann. Bot.* 91, 179–194. doi: 10.1093/aob/mcf118

Boussadia, O., Steppe, K., Zgallai, H., Ben, El Hadj, S., Braham, M., et al. (2010). Effects of nitrogen deficiency on leaf photosynthesis, carbohydrate status and biomass production in two olive cultivars 'Meski' and 'Koroneiki.'. *Sci. Hort.* 123, 336–342. doi: 10.1016/j.scienta.2009.09.023

Cameron, J., and Frost, H. (1968). "Genetics, breeding and nucellar embryony," in *The Citrus Industry*, Vol. II, eds L. B. Reuther and H. Webber (Berkeley: University of California Press), 325–370.

Cetner, M. D., Kalaji, H. M., Goltsev, V., Aleksandrov, V., Kowalczyk, K., Borucki, W., et al. (2017). Effects of nitrogen-deficiency on efficiency of light-harvesting apparatus in radish. *Plant Physiol. Biochem.* 119, 81–92. doi: 10.1016/j.plaphy.2017.08.016

Elavarasan, M., and Premalatha, A. (2019). A review: nutrient deficiencies and physiological disorders of citrus. *J. Pharmacogn. Phytochem.* 8, 1705–1708.

Ericsson, T. (1995). Growth and shoot: root ratio of seedlings in relation to nutrient availability. *Plant Soil* 168, 205–214. doi: 10.1007/978-94-011-0455-5_23

Evans, J. R., and Terashima, I. (1987). Effects of nitrogen nutrition on electron transport components and photosynthesis in spinach. *Funct. Plant Biol.* 14, 59–68. doi: 10.1071/PP9870059

Feng, X. P., Chen, Y., Qi, Y. H., Yu, C. L., Zheng, B. S., Brancourt-Hulmel, M., et al. (2012). Nitrogen enhanced photosynthesis of Miscanthus by increasing stomatal conductance and phosphoenolpyruvate carboxylase concentration. *Photosynthetica* 50, 577–586. doi: 10.1007/s11099-012-0061-3

Ferrar, P. J., and Osmond, C. B. (1986). Nitrogen supply as a factor influencing photoinhibition and photosynthetic acclimation after transfer of shade-grown Solanum dulcamara to bright light. *Planta* 168, 563–570. doi: 10.1007/BF00392277

Fleischer, W. E. (1935). The relation between chlorophyll content and rate of photosynthesis. *J. Gen. Physiol.* 18, 573–597. doi: 10.1085/jgp.18.4.573

Flexas, J., Bota, J., Escalona, J. M., Sampol, B., and Medrano, H. (2002). Effects of drought on photosynthesis in grapevines under field conditions: an evaluation of stomatal and mesophyll limitations. *Funct. Plant Biol.* 29, 461–471. doi: 10.1071/PP01119

Flexas, J., Escalona, J. M., and Medrano, H. (1999). Water stress induces different levels of photosynthesis and electron transport rate regulation in grapevines. *Plant Cell Environ.* 22, 39–48. doi: 10.1046/j.1365-3040.1999.00371.x

Fracheboud, Y., Haldimann, P., Leipner, J., and Stamp, P. (1999). Chlorophyll fluorescence as a selection tool for cold tolerance of photosynthesis in

maize (*Zea mays* L.). *J. Exp. Bot.* 50, 1533–1540. doi: 10.1093/jxb/50.338.1533

Froelicher, Y., Bassene, J.-B., Jedidi-Neji, E., Dambier, D., Morillon, R., Bernardini, G., et al. (2007). Induced parthenogenesis in mandarin for haploid production: induction procedures and genetic analysis of plantlets. *Plant Cell Rep.* 26, 937–944. doi: 10.1007/s00299-007-0314-y

Gong, X., Li, J., Ma, H., Chen, G., Dang, K., Yang, P., et al. (2020). Nitrogen deficiency induced a decrease in grain yield related to photosynthetic characteristics, carbon–nitrogen balance and nitrogen use efficiency in proso millet (*Panicum miliaceum* L.). *Arch. Agron. Soil Sci.* 66, 398–413. doi: 10.1080/03650340.2019.1619077

Grassi, G., Colom, M. R., and Minotta, G. (2001). Effects of nutrient supply on photosynthetic acclimation and photoinhibition of one−year−old foliage of Picea abies. *Physiol. Plant* 111, 245–254. doi: 10.1034/j.1399-3054.2001.1110217.x

Green, T. H., and Mitchell, R. J. (1992). Effects of nitrogen on the response of loblolly pine to water stress I. Photosynthesis and stomatal conductance. *New Phytol.* 122, 627–633. doi: 10.1111/j.1469-8137.1992.tb00090.x

Grusak, M. A. (2001). Plant macro- and micronutrient minerals. *Encycl. Life Sci.* 2001, 1–5. doi: 10.1038/npg.els.0001306

Guerfel, M., Ouni, Y., Boujnah, D., and Zarrouk, M. (2009). Photosynthesis parameters and activities of enzymes of oxidative stress in two young 'Chemlali' and 'Chetoui' olive trees under water deficit. *Photosynthetica* 47, 340–346. doi: 10.1007/s11099-009-0054-z

Jacquemond, C., Curk, F., and Heuzet, M. (2013). *Les Clémentiniers et Autres Petits Agrumes*. Versailles: Collection Savoir-Faire, 1–363.

Jin, X., Yang, G., Tan, C., and Zhao, C. (2015). Effects of nitrogen stress on the photosynthetic CO 2 assimilation, chlorophyll fluorescence and sugar-nitrogen ratio in corn. *Sci. Rep*. 5:9311. doi: 10.1038/srep09311

Karpinska, B., Zhang, K., Rasool, B., Pastok, D., Morris, J., Verrall, S. R., et al. (2018). The redox state of the apoplast influences the acclimation of photosynthesis and leaf metabolism to changing irradiance. *Plant Cell Environ.* 41, 1083–1097. doi: 10.1111/pce.12960

Kishor, P. B. K., and Dange, V. (1990). Sucrose metabolism in callus cultures of cotton during growth. *Indian J. Exp. Biol.* 28, 352–355.

Kumar, K., and Goh, K. M. (2002). Management practices of antecedent leguminous and non-leguminous crop residues in relation to winter wheat yields, nitrogen uptake, soil nitrogen mineralization and simple nitrogen balance. *Eur. J. Agron.* 16, 295–308. doi: 10.1016/S1161-0301(01)00133-2

Lambers, H., Chapin, F. S. III and Pons, T. L. (2008). *Plant Physiological Ecology*. New-York, NY: Springer Science. doi: 10.1007/978-1-4757-2855-2

Law, D. R., Crafts-Brandner, S. J., and Salvucci, M. E. (2001). Heat stress induces the synthesis of a new form of ribulose-1, 5-bisphosphate carboxylase/oxygenase activase in cotton leaves. *Planta* 214, 117–125. doi: 10.1007/s004250100592

Lee, J.-M. (1994). Cultivation of grafted vegetables I. Current status, grafting methods, and benefits. *HortScience* 29, 235–239. doi: 10.21273/HORTSCI.29.4.235

Lu, Z.-J., Yu, H.-Z., Mi, L.-F., Liu, Y.-X., Huang, Y.-L., Xie, Y.-X., et al. (2019). The effects of inarching *Citrus reticulata* Blanco var. tangerine on the tree vigor, nutrient status and fruit quality of *Citrus sinensis* Osbeck 'Newhall'trees that have *Poncirus trifoliata* (L.) Raf. as rootstocks. *Sci. Hort.* 256:108600. doi: 10.1016/j.scienta.2019.108600

Makino, A., and Osmond, B. (1991). Effects of nitrogen nutrition on nitrogen partitioning between chloroplasts and mitochondria in Pea and Wheat. *Plant Physiol.* 96, 355–362. doi: 10.1104/pp.96.2.355

Marguerit, E., Brendel, O., Lebon, E., Leeuwen, C. V., and Ollat, N. (2012). Rootstock control of scion transpiration and its acclimation to water deficit are controlled by different genes. *New Phytol.* 194, 416–429. doi: 10.1111/j.1469-8137.2012.04059.x

Marschner, H. (1995). *Mineral Nutrition of Higher Plants*, 2nd Edn. Orlando, FL: Academic Press, 889.

Maxwell, K., and Johnson, G. N. (2000). Chlorophyll fluorescence—a practical guide. *J. Exp. Bot.* 51, 659–668. doi: 10.1093/jexbot/51.345.659

Mhamdi, A., Noctor, G., and Baker, A. (2012). Plant catalases: peroxisomal redox guardians. *Arch. Biochem. Biophys.* 61, 4197–4220. doi: 10.1016/j.abb.2012.04.015

Mittler, R. (2002). Oxidative stress, antioxidants and stress tolerance. *Trends Plant Sci.* 7, 405–410. doi: 10.1016/S1360-1385(02)02312-9

Mittler, R., Vanderauwera, S., Gollery, M., and Van Breusegem, F. (2004). Reactive oxygen gene network of plants. *Trends Plant Sci.* 9, 490–498. doi: 10.1016/j.tplants.2004.08.009

Nunes, M. A., Ramalho, J. C., and Dias, M. A. (1993). Effect of nitrogen supply on the photosynthetic performance of leaves from coffee plants exposed to bright light. *J. Exp. Bot.* 44, 893–899. doi: 10.1093/jxb/44.5.893

Ohkama-Ohtsu, N., and Wasaki, J. (2010). Recent progress in plant nutrition research: cross-talk between nutrients, plant physiology and soil microorganisms. *Plant Cell Physiol.* 51, 1255–1264. doi: 10.1093/pcp/pcq095

Ollitrault, P., Froelicher, Y., Dambier, D., and Seker, M. (2000). Rootstock breeding by somatic hybridisation for the Mediterranean citrus industry. *Acta Hortic.* 535, 157–162. doi: 10.17660/ActaHortic.2000.535.18

Oustric, J., Morillon, R., Luro, F., Herbette, S., Lourkisti, R., Giannettini, J., et al. (2017). Tetraploid Carrizo citrange rootstock (*Citrus sinensis* Osb x *Poncirus trifoliata* L. Raf.) enhances natural chilling stress tolerance of common clementine (*Citrus clementina* Hort. ex Tan). *J. Plant Physiol.* 214, 108–115. doi: 10.1016/j.jplph.2017.04.014

Oustric, J., Morillon, R., Luro, F., Herbette, S., Martin, P., Giannettini, J., et al. (2019). Nutrient deficiency tolerance in citrus is dependent on genotype or ploidy level. *Front. Plant Sci.* 10:127. doi: 10.3389/fpls.2019.00127

Ozden, M., Demirel, U., and Kahraman, A. (2009). Effects of proline on antioxidant system in leaves of grapevine (*Vitis vinifera* L.) exposed to oxidative stress by H_2O_2. *Sci. Hort.* 119, 163–168. doi: 10.1016/j.scienta.2008.07.031

Pan, Y., Wu, L. J., and Yu, Z. L. (2006). Effect of salt and drought stress on antioxidant enzymes activities and SOD isoenzymes of liquorice (*Glycyrrhiza uralensis Fisch*). *Plant Growth Regul.* 49, 157–165. doi: 10.1007/s10725-006-9101-y

Papadakis, I., Dimassi, K., Bosabalidis, A., Therios, I., Patakas, A., and Giannakoula, A. (2004). Effects of B excess on some physiological and anatomical parameters of 'Navelina' orange plants grafted on two rootstocks. *Environ. Exp. Bot.* 51, 247–257. doi: 10.1016/j.envexpbot.2003.11.004

Paparnakis, A., Chatzissavvidis, C., and Antoniadis, V. (2013). How apple responds to boron excess in acidic and limed soil. *J. Soil Sci. Plant Nutr.* 13, 787–796. doi: 10.4067/S0718-95162013005000062

Patel, M., Rangani, J., Kumari, A., and Parida, A. K. (2020). Mineral nutrient homeostasis, photosynthetic performance, and modulations of antioxidative defense components in two contrasting genotypes of *Arachis hypogaea* L.(peanut) for mitigation of nitrogen and/or phosphorus starvation. *J. Biotechnol.* 323, 136–158. doi: 10.1016/j.jbiotec.2020.08.008

Pospíšil, P. (2009). Production of reactive oxygen species by photosystem II. *BBA Bioenerget.* 1787, 1151–1160. doi: 10.1016/j.bbabio.2009.05.005

Praveen, A., and Gupta, M. (2018). Nitric oxide confronts arsenic stimulated oxidative stress and root architecture through distinct gene expression of auxin transporters, nutrient related genes and modulates biochemical responses in *Oryza sativa* L. *Environ. Pollut.* 240, 950–962. doi: 10.1016/j.envpol.2018.04.096

Qi, D. U., Zhao, X. H., Le, X. I. A., Jiang, C. J., Wang, X. G., Yi, H. A. N., et al. (2019). Effects of potassium deficiency on photosynthesis, chloroplast ultrastructure, ROS, and antioxidant activities in maize (*Zea mays* L.). *J. Integr. Agric.* 18, 395–406. doi: 10.1016/S2095-3119(18)61953-7

Saleh, B., Allario, T., Dambier, D., Ollitrault, P., and Morillon, R. (2008). Tetraploid citrus rootstocks are more tolerant to salt stress than diploid. *Compt. Rend. Biol.* 331, 703–710. doi: 10.1016/j.crvi.2008.06.007

Santini, J., Giannettini, J., Pailly, O., Herbette, S., Ollitrault, P., Berti, L., et al. (2013). Comparison of photosynthesis and antioxidant performance of several *Citrus* and *Fortunella* species (Rutaceae) under natural chilling stress. *Trees* 27, 71–83. doi: 10.1007/s00468-012-0769-5

Schachtman, D. P., and Shin, R. (2007). Nutrient sensing and signaling: NPKS. *Annu. Rev. Plant Biol.* 58, 47–69. doi: 10.1146/annurev.arplant.58.032806.103750

Schreiber, U., Hormann, H., Neubauer, C., and Klughammer, C. (1995). Assessment of photosystem II photochemical quantum yield by chlorophyll

fluorescence quenching analysis. *Funct. Plant Biol.* 22, 209–220. doi: 10.1023/A:1006469809812

Srivastava, A. (2013). Nutrient deficiency symptomology in citrus: an effective diagnostic tool or just an aid for post –mortem analysis. *Agric. Adv.* 2, 177–194.

Talla, S., Riazunnisa, K., Padmavathi, L., Sunil, B., Rajsheel, P., and Raghavendra, A. S. (2011). Ascorbic acid is a key participant during the interactions between chloroplasts and mitochondria to optimize photosynthesis and protect against photoinhibition. *J. Biosci.* 36, 163–173. doi: 10.1007/s12038-011-9000-x

Taylor, B. K., and Dimsey, R. T. (1993). Rootstock and scion effects on the leaf nutrient composition of citrus trees. *Aust. J. Exp. Agric.* 33, 363–371. doi: 10.1071/EA9930363

Terashima, I., and Evans, J. R. (1988). Effects of light and nitrogen nutrition on the organization of the photosynthetic apparatus in spinach. *Plant Cell Physiol.* 29, 143–155. doi: 10.1093/oxfordjournals.pcp.a077461

Tewari, R. K. (2004). Role of mineral nutrient elements in Mulberry (*Morus alba* L.) Plants with particular reference to oxidative metabolism. *Tree Physiol.* 30, 68–77. doi: 10.1093/treephys/tpp093

Tewari, R. K., Kumar, P., and Sharma, P. N. (2007). Oxidative stress and antioxidant responses in young leaves of mulberry plants grown under nitrogen, phosphorus or potassium deficiency. *J. Integr. Plant Biol.* 49, 313–322. doi: 10.1111/j.1744-7909.2007.00358.x

Tikkanen, M., Mekala, N. R., and Aro, E. M. (2014). Photosystem II photoinhibition-repair cycle protects photosystem I from irreversible damage. *Biochim. Biophys. Acta* 1837, 210–215. doi: 10.1016/j.bbabio.2013.10.001

Vieira, D. D. S. S., Emiliani, G., Michelozzi, M., Centritto, M., Luro, F., Morillon, R., et al. (2016). Polyploidization alters constitutive content of volatile organic compounds (VOC) and improves membrane stability under water deficit in Volkamer lemon (*Citrus limonia* Osb.) leaves. *Environ. Exp. Bot.* 126, 1–9. doi: 10.1016/j.envexpbot.2016.02.010

Weng, J. H., and Hsu, F. H. (2001). Gas exchange and epidermal characteristics of Miscanthus populations in Taiwan varying with habitats and nitrogen application. *Photosynthetica* 39, 35–41. doi: 10.1023/A:1012483600367

Yu-Chuan, D., Chang, C.-R., Wen, L. U. O., Yan-Shou, W. U., Xiao-Li, R. E. N., Ping, W., et al. (2008). High potassium aggravates the oxidative stress inducedy by magnesium deficiency in rice leaves. *Pedosphere* 18, 316–327. doi: 10.1016/S1002-0160(08)60021-1

Zhang, S., Tang, D., Korpelainen, H., and Li, C. (2019). Metabolic and physiological analyses reveal that *Populus cathayana* males adopt an energy-saving strategy to cope with phosphorus deficiency. *Tree Physiol.* 39, 1630–1645. doi: 10.1093/treephys/tpz074

Conflict of Interest: The authors declare that the research was conducted in the absence of any commercial or financial relationships that could be construed as a potential conflict of interest.

Copyright © 2021 Oustric, Herbette, Morillon, Giannettini, Berti and Santini. This is an open-access article distributed under the terms of the Creative Commons Attribution License (CC BY). The use, distribution or reproduction in other forums is permitted, provided the original author(s) and the copyright owner(s) are credited and that the original publication in this journal is cited, in accordance with accepted academic practice. No use, distribution or reproduction is permitted which does not comply with these terms.

frontiers in Plant Science

ORIGINAL RESEARCH
published: 25 May 2021
doi: 10.3389/fpls.2021.599824

Acoustic Vulnerability, Hydraulic Capacitance, and Xylem Anatomy Determine Drought Response of Small Grain Cereals

Szanne Degraeve[1,2,3], Niels J. F. De Baerdemaeker[1,2], Maarten Ameye[1,3], Olivier Leroux[4], Geert Jozej Willem Haesaert[1] and Kathy Steppe[1,2]*

[1] Department of Plants and Crops, Faculty of Bioscience Engineering, Ghent University, Ghent, Belgium, [2] Laboratory of Plant Ecology, Department of Plants and Crops, Faculty of Bioscience Engineering, Ghent University, Ghent, Belgium, [3] Laboratory of Applied Mycology and Phenomics, Department of Plants and Crops, Faculty of Bioscience Engineering, Ghent University, Ghent, Belgium, [4] Department of Biology, Faculty of Sciences, Ghent University, Ghent, Belgium

Selection of high-yielding traits in cereal plants led to a continuous increase in productivity. However, less effort was made to select on adaptive traits, favorable in adverse and harsh environments. Under current climate change conditions and the knowledge that cereals are staple foods for people worldwide, it is highly important to shift focus to the selection of traits related to drought tolerance, and to evaluate new tools for efficient selection. Here, we explore the possibility to use vulnerability to drought-induced xylem embolism of wheat cultivars Excalibur and Hartog (*Triticum aestivum* L.), rye cultivar Duiker Max (*Secale cereale* L.), and triticale cultivars Dublet and US2014 (*x Triticosecale* Wittmack) as a proxy for their drought tolerance. Multiple techniques were combined to underpin this hypothesis. During bench-top dehydration experiments, acoustic emissions (AEs) produced by formation of air emboli were detected, and hydraulic capacitances quantified. By only looking at the AE_{50} values, one would classify wheat cultivar Excalibur as most tolerant and triticale cultivar Dublet as most vulnerable to drought-induced xylem embolism, though Dublet had significantly higher hydraulic capacitances, which are essential in terms of internal water storage to temporarily buffer or delay water shortage. In addition, xylem anatomical traits revealed that both cultivars have a contrasting trade-off between hydraulic safety and efficiency. This paper emphasizes the importance of including a cultivar's hydraulic capacitance when evaluating its drought response and vulnerability to drought-induced xylem embolism, instead of relying on the AE_{50} as the one parameter.

Keywords: acoustic emission, drought stress, hydraulic capacitance, small grain cereals, vulnerability curve, xylem anatomy, xylem embolism

OPEN ACCESS

Edited by:
Felipe Klein Ricachenevsky, Federal University of Rio Grande do Sul, Brazil

Reviewed by:
Mohsin Tanveer, University of Tasmania, Australia
João Paulo Rodrigues Marques, University of São Paulo, Brazil

****Correspondence:***
Szanne Degraeve
szanne.degraeve@ugent.be

Specialty section:
This article was submitted to Plant Abiotic Stress, a section of the journal Frontiers in Plant Science

Received: *28 August 2020*
Accepted: *12 April 2021*
Published: *25 May 2021*

Citation:
Degraeve S, De Baerdemaeker NJF, Ameye M, Leroux O, Haesaert GJW and Steppe K (2021) Acoustic Vulnerability, Hydraulic Capacitance, and Xylem Anatomy Determine Drought Response of Small Grain Cereals. Front. Plant Sci. 12:599824. doi: 10.3389/fpls.2021.599824

INTRODUCTION

Cereals, in particular rice, wheat, and maize, provide a major source of carbohydrates, proteins, vitamins, and minerals, and constitute more than 50% of the calories of the global population's diet (McKevith, 2004; Laskowski et al., 2019). During the green revolution, the selection of high-yielding traits in cereal plants led to a continuous increase in productivity.

However, historically less emphasis was given to adaptive traits, which are favorable in adverse and harsh environments, leaving crops at risk of failure under current climate change conditions (Choudhary et al., 2019). This impacts crop production, food access, price stability, and therefore food security in several regions of the world (Porter et al., 2014; FAO et al., 2018). Without the adaptation of current agronomic practices, this is expected to exacerbate as temperatures increase and climate extremes (e.g., droughts, floods, and storms) prevail more frequently and with higher intensity (IPCC, 2014). Drought in particular causes already more than 80% of the total climate-related damage and losses in agriculture. So, due to their importance, it is crucial to shift focus to the development of cereals resilient to current and future arid conditions, and to evaluate new tools for efficient selection. Different traits associated to drought tolerance exist in cereals. With a focus on plant survival, osmotic adjustment is an important mechanism by which plants postpone dehydration stress in dry environments (Farooq et al., 2009; Blum, 2014). Sustained turgor governed by active accumulation of solutes in the cytoplasm helps maintaining cell elongation and expansion and therefore plant growth and development. Cereals could also benefit from the ability to optimize root distribution and architecture dependent on soil water distribution. This guarantees a continuous water flow to the aboveground plant parts (Tricker et al., 2018). Vadez (2014) highlights the importance of water availability during the grain filling stage. Water extracted from the soil during grain filling almost fully contributes to grain growth since there is only limited vegetative growth after anthesis. In this regard, traits regulating the plant's water use efficiency, e.g., stomatal conductance, canopy development, and transpiration, are the most promising targets for breeding resilient new varieties (Vadez et al., 2013). However, when soil water supply becomes limiting during grain filling, drought tolerance will be dependent on the initial concentration of remobilizable carbohydrates in the stem and the efficiency of remobilization to the ear (Blum, 1998). Water soluble carbohydrates (WSCs) accumulated in the stem prior to flowering, and shortly after flowering, usually contribute for 10–20% of the grain yield, but under terminal dry conditions, they potentially account for 40–60% of the grain weight. Evidently, the ability of plants to regulate their water status requires a fully functional water transport system. Xylem is the tissue specialized in the long-distance transport of water, and according to the cohesion-tension theory (Dixon and Joly, 1895; Tyree and Zimmermann, 2002; Venturas et al., 2017), water is passively transported through the plant's vascular system. This passive transport originates in the evaporation of water in the substomatal cavities of the leaves (i.e., transpiration), resulting in a negative water potential, enabling the flow of water upward from the roots. However, an increasing evaporative demand and/or drying soil will result in decreasing water potential (more negative values) in the xylem conduits and may cause air nanobubbles entering the xylem vessels. When the nanobubbles coalesce, expand, and fill the entire conduit (Schenk et al., 2015), the water transport system is locally interrupted. Water from these embolized vessels may still contribute to the transpiration stream as water recedes into adjacent vessels via intervessel pit membranes (Venturas et al., 2017). These pit membranes additionally prevent the spread of air emboli throughout the vascular system by exerting strong capillary forces (Choat et al., 2008; Venturas et al., 2017). However, when negative pressure in the xylem vessels outpaces these capillary forces, nanobubbles can "seed" from one adjacent vessel to another, forming embolisms in the plant's entire hydraulic system and eventually leaving the plant to dehydrate to lethal levels (Tyree and Zimmermann, 2002).

The vulnerability of cereals to drought-induced xylem embolism could serve as a key trait for its drought tolerance (Choat et al., 2012). Assessing a species hydraulic safety is typically done by constructing a vulnerability curve (VC), in which the percentage loss of xylem hydraulic conductivity (PLC, %) is plotted against decreasing xylem water potential (Ψ_{xylem}, MPa) as indicator of increasing drought stress. Different methods to determine xylem hydraulic conductivity have been explored and reviewed (Cochard et al., 2013), including detection of acoustic emissions (AEs) produced by the formation of air bubbles (De Roo et al., 2016; Vergeynst et al., 2016), direct observations of the presence of air bubbles in the xylem (Choat et al., 2016; Brodribb et al., 2017; Johnson et al., 2018; Corso et al., 2020), and hydraulic detection of the decrease in xylem transport efficiency (Nolf et al., 2017). The water potential at which 50% loss of hydraulic conductivity occurs (P_{50} or AE_{50}, depending on the method used to determine hydraulic conductivity) is commonly used to interpret a species vulnerability. Such hydraulic parameters have been determined in several woody plants (Choat et al., 2012; Nolf et al., 2015; Epila et al., 2017), but despite their economic importance, few studies exist in cereal crops (Stiller et al., 2003; Gleason et al., 2017; Johnson et al., 2018; Corso et al., 2020). And if changes in hydraulic conductivity are determined, quantification of hydraulic capacitance, i.e., the amount of water released (ΔW; kg) for a given change in xylem water potential ($\Delta\Psi$; MPa) per unit of tissue volume (V; m^3) (Tyree and Ewers, 1991), is often lacking (Vergeynst et al., 2015a).

In this study, we assess the potential of using vulnerability to drought-induced xylem embolism as a proxy for drought resistance of different small grain cereals. Multiple techniques are therefore combined to apprehend the different aspects of xylem vulnerability to drought. (1) Through continuous measurements of AEs during bench-top dehydration, AE_{50} values are quantified and vulnerability to drought-induced xylem embolism assessed. (2) Hydraulic capacitance and capacitive water release during dehydration are derived from desorption curves (DC) after continuously weighing of samples. To corroborate these results, (3) xylem anatomical traits linked with a species' individual trade-off between hydraulic safety and efficiency (Hacke and Sperry, 2001; Sperry et al., 2008) are determined. This set of techniques is used to assess vulnerability of wheat (*Triticum aestivum* L.), triticale (*x Triticosecale* Wittmack), and rye (*Secale cereale* L.) to drought-induced xylem embolism. Wheat is included because of its economic importance and high productivity, rye because of its robustness to all kinds of abiotic stresses, and triticale, as a cross between the former ones, is believed to combine the best of both.

In this regard, we would expect AE_{50} values of rye and triticale to be highest.

MATERIALS AND METHODS

Plant Materials and Sampling Procedure

In this study, two spring wheat (*T. aestivum* L.) cultivars, Excalibur and Hartog, two spring triticale (*x Triticosecale* Wittmack) cultivars, Dublet and US2014, and one spring rye (*S. cereale* L.) cultivar, Duiker Max, were used (**Table 1**). For each cultivar, three 4-L pots, filled with potting soil (Jardino Basic, BVB Substrates, Netherlands), contained 10 seedlings. During the entire growing cycle, seedlings were well watered and grown in a climate chamber at 20°C and 12/12 h light/dark conditions (GRO-LUX SHP-TS 400W E40 SLV, Sylvania, Budapest, Hungary). Plants were fertilized with an NPK fertilizer (6/6/7 ratio) at the start of the elongation phase (Zadok Scale, Z30; Zadoks et al., 1974) and when the flag leaf appeared (Z40).

Plant material was collected at anthesis with the ear fully emerged (Z59). The day prior to the start of the experiment, eight uniform main shoots were tagged for the determination of VC_{AE} and hydraulic capacitances. At the same time, leaves of the remaining shoots were wrapped in aluminum foil to ensure equilibrium between leaf and stem water potential (Begg and Turner, 1970) at the start of the experiment (**Figure 1A**). The day of the experiment, selected shoots were excised just above the root zone while under water to avoid artificial embolism formation. The ends of the cut stems were covered with wet paper towel to prevent dehydration during installation. In addition, the cut stems were stripped of the ear and all leaves and wounds were covered with petroleum jelly (Vaseline, Unilever) to prevent water evaporating via the wounds. Sampling and installation occurred at room temperature (20°C) and under artificial green light to limit photosynthesis and transpiration.

Measurements During Bench Dehydration

To develop VC_{AE}s, four shoots were mounted in custom-built holders (**Figure 1B**) which ensured a fixed distance (80 mm) between the broadband point-contact AE sensor (KRNBB_PC, KRN Services, Richland, WA, United States) and the dendrometer (DD-S, Ecomatik, Dachau, Germany). To ensure good acoustic contact, a droplet of vacuum grease (High-Vacuum Grease, Dow Corning, Seneffe, Belgium) was added between the AE sensor and the sample. The pencil lead break test, as described in Vergeynst et al. (2015b), served as validation for the sensor functioning. The AE sensor and dendrometer were placed at the third and second internodes, respectively. Depending on the total length of the shoot, the distance between the end of the shoot and the dendrometer was 18.9 ± 3.5 cm on average and the distance between the end of the shoot and the AE sensor was 26.9 ± 3.5 cm on average. To obtain DCs, mass loss of the other four shoots was recorded continuously using weighing balances (DK 6200 with 0.01 g accuracy, Henk Maas, Veen, Netherlands; **Figure 1C**). The wet paper towel was removed from both the VC and the DC samples after finishing the experimental set-up. Bench dehydration occurred under laboratory conditions and artificial white light. Readings from balances and dendrometers were registered every minute by custom-built acquisition boards. AE signals were amplified by 35.6 dB (AMP-1BB-J, KRN Services, Richland, WA, United States) in order to acquire waveforms of 7168 samples length at 10 MHz sample rate. Signals were collected via two-channel PCI boards and redirected to the AEwin software (PCI-2, AEwin E4.70, Mistras Group BV, Schiedam, Netherlands). A 20–1000 kHz electronic band-pass filter was applied to only retain waveforms above the noise level of 28 dB_{AE} (Vergeynst et al., 2016).

The remaining shoots, with leaves wrapped in aluminum foil, were also excised under water and left to dehydrate under the same laboratory conditions (**Figure 1D**). The pressure chamber (PMS Instrument Company, Corvallis, OR, United States) was used to measure xylem water potential (Ψ_{xylem}, MPa). The frequency of Ψ_{xylem} readings was guided by the appearance of speed of AE signals, which were monitored in real time with the AEwin software program.

Processing Acoustic Emission Data Into Vulnerability Curves

The AE signals were translated into meaningful VC_{AE}s (Vergeynst et al., 2016; De Baerdemaeker et al., 2019a,b). AE signals per sample were cumulated and averaged over 5 min over the entire dehydration period. By calculating the first derivative over a time interval of 15 min, an AE activity curve was drafted. According to Vergeynst et al. (2016), the endpoint of the VC_{AE} (AE_{100}) was determined as the point at which the AE activity, following the AE activity peak, decreases most strongly, which mathematically corresponds to the local maximum of the third derivative. The time interval to calculate the third derivative is dependent on the

TABLE 1 | Different cultivars of wheat, triticale, and rye used in this study.

Cultivar	Species	Origin	Breeder	Source
Excalibur	*Triticum aestivum* L.	Australia	University of Adelaide, Roseworthy and South Australian Research and Development Institute	CIMMYT
Hartog	*Triticum aestivum* L.	Australia	Queensland Wheat Research Institute	CIMMYT
Dublet	x *Triticosecale* Wittmack	Poland	Danko	Danko
US2014	x *Triticosecale* Wittmack	South Africa	Stellenbosch University	Stellenbosch University
Duiker Max	*Secale cereale* L.	South Africa	Stellenbosch University	Stellenbosch University

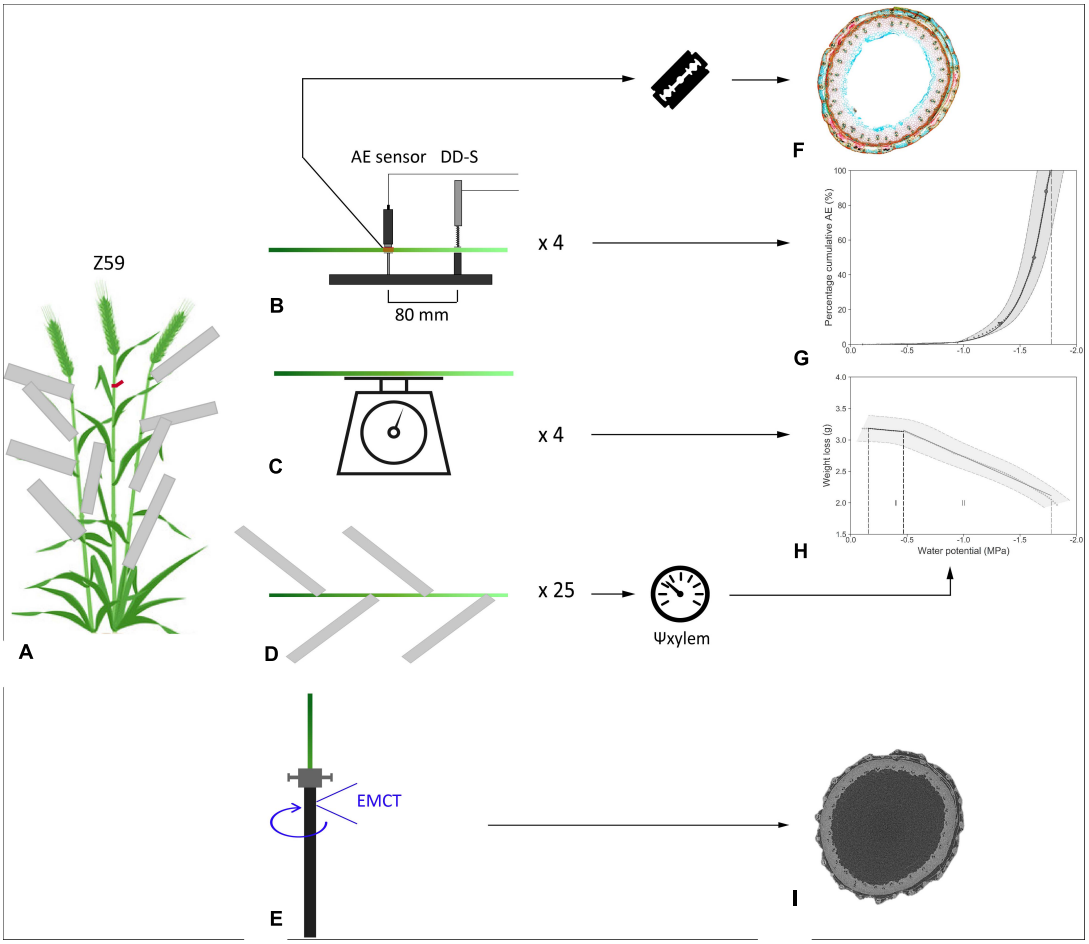


FIGURE 1 | Illustration of the workflow for **(A)** sampling and **(B–D)** measurements during bench dehydration, processing the data into **(G)** vulnerability and **(H)** desorption curves, **(F)** preparation of stem cross-sections, and **(E,I)** experimental setup of *T. aestivum* cultivar Excalibur in the EMCT.

duration of the bench-top dehydration period, the studied species, and the dehydration conditions (Vergeynst et al., 2016). For the species studied in this experiment, a time interval of 2–3 h was sufficient in order to obtain consistent results. Cumulative AE was rescaled from zero to the defined endpoint to obtain meaningful PLC (%). Values corresponding with the onset of xylem embolism (AE_{12}), 50% embolism-related AE (AE_{50}), 88% embolism-related AE (AE_{88}), and full embolism (AE_{100}) can be determined from the VC_{AE} (**Figure 1G**). Using a segmented-linear regression relationship between relative radial xylem shrinkage ($\Delta d/d_i$, $\mu m.mm^{-1}$), measured with the dendrometer, and point measurements of Ψ_{xylem} (MPa), a continuous *x*-axis (Ψ_{xylem}, MPa) for each VC_{AE} was realized.

Validation of the Acoustic Emission Measurements Using X-Ray Microcomputed Tomography

For *T. aestivum* cultivar Excalibur, one shoot in Z59 was excised under water, stripped of ear and leaves, and mounted on the rotation stage of the environmental microCT scanner (EMCT) (Dierick et al., 2014), a custom-built CT scanner at the Center for X-ray CT scanning of Ghent University (UGCT), Belgium. This scanner rotates around its mounting stage instead of having a rotating stage and allows several subsequent scans because a full rotation brings the scanner back to its starting position. The maximum resolution obtained with the EMCT is 5 μ m.

The shoot was fixed in a custom-built holder designed to prevent the shoot from vibrating during scanning, which would make it impossible to visualize the xylem vessels. The tube enclosing the shoot was made of carbon fiber, allowing easy penetration of X-rays (**Figure 1E**). During the experiment, as the shoot was dehydrating, we noticed shrinkage. As a result, the shoot was no longer tightly enclosed by the tube and started vibrating. Accordingly, Teflon was applied just above and below the scanning position, which was 180 mm from the end of the shoot (at the second internode) to eliminate vibration.

The shoot was scanned hourly from 11 a.m. until 6 p.m. and from 9 a.m. until 1 p.m. the next day. The tube voltage was 60 kV, the tube power was 6 W, and no additional filter was applied.

A rotation lasted 9 min, with 1801 projections taken per rotation. The approximated voxel size was 4.99 μm. Between each run, the shoot was removed from the carbon tube and left at the benchtop to dehydrate. Afterward, images were reconstructed (**Figure 1I**), using the Octopus reconstruction software package.

Desorption Curves and Hydraulic Capacitances

Mass loss, registered by the balances during dehydration, is a surrogate for overall change in water content (ΔWC, g) and was plotted against the continuous Ψ_{xylem}-axis (MPa, **Figure 1H**). The DC shows two interesting regions, separated by two defined breakpoints, calculated via the segmented R package (Muggeo, 2008). A first and a second breakpoint indicate the start and end of phase I, or the elastic shrinkage phase. Starting from the second breakpoint till AE_{100} is known as inelastic shrinkage phase (xylem embolism) or phase II (Vergeynst et al., 2015a). According to Vergeynst et al. (2015a), hydraulic capacitance (C, g MPa^{-1}) for both phases (C_{el} and C_{inel}, respectively) was calculated as the slope of the linear regression between mass loss and Ψ_{xylem}.

Microscopic Analysis

Segments of the third internode of approximately 3 cm, including the position where the AE sensor was positioned (26.9 ± 3.5 cm from the end of the shoot), were collected from all the shoots used for VC_{AE} measurements at the end of the dehydration period (**Figure 1B**, red square). These samples were stored in tubes containing a 20:40:40 ratio of 70% ethanol, glycerol, and distilled water. In addition, after finishing EMCT scanning, a segment of the stem at the scanning position was also collected and stored. After a pre-treatment in 2% (v/v) hydrofluoric acid and 0.5% (v/v) sulphuric acid for 48 h, samples were rinsed thoroughly in demineralized water and embedded in 8% (w/v) agarose. Agarose blocks containing the samples were glued onto the vibratome stage. Cross-sections of 70 μm thickness were produced with a vibration microtome (HM 650V, Thermo Scientific, Germany) and were stained with 0.5% (w/v) astra blue, 0.5% (w/v) chrysoidine, and 0.5% (w/v) acridine red to distinguish lignified (red) from cellulose (blue) cells (**Figure 1F**). Sections were finally mounted in Euparal (Carl Roth, Germany) and imaged using a Nikon Ni-U microscope equipped with a Nikon DS-Fi1c camera. The open source software Fiji was used for image analysis.

Both protoxylem and metaxylem were included in the analysis. Individual vessel areas (A_{ind}, μm^2; **Figure 2B** detail) and total vessel area (A_{total}, μm^2) were determined directly from the images and, assuming a circular vessel shape, individual vessel diameters (d, μm) were calculated. Hydraulic diameter (d_h, μm) was calculated as described by Steppe and Lemeur (2007):

$$d_h = \sqrt[4]{\frac{1}{n}\sum_{i=1}^{n} d_i^4}$$

Conduit wall reinforcement (CWR) was calculated by determining the double wall thickness (t) to conduit wall span (b) ratio (**Figure 2B** detail) as described in Hacke et al. (2001):

$$CWR = (t/b)_h^2$$

Vessel grouping index (V_g) was determined as the ratio of total number of vessels to total number of vessel groupings. The above were calculated separately for both stem and leaf sheath. In addition, area xylem parenchyma in the stem was derived from the images and allowed calculation of ratio xylem parenchyma to total stem area ($\%_{Xylem\ Parenchyma}$).

RESULTS

Acoustic Emissions by Drought-Induced Embolism and Hydraulic Capacitance

Acoustic emission measurements were taken to determine a cultivar's vulnerability to drought-induced xylem embolism (**Figure 3A**). Generally, AE_{50} values are used as a parameter to quantify vulnerability, with a more negative value indicating a more tolerant species. Acoustic vulnerability analysis showed the most negative AE_{50} value for wheat cultivar Excalibur (**Table 2**). Its AE_{50} value of −2.00 MPa is significantly more negative than the other cultivars tested. Triticale cultivars Dublet and US2014 had the highest AE_{50} values of −1.30 and −1.47 MPa, respectively. Values corresponding with the onset of xylem embolism (AE_{12}), 50% embolism-related AE (AE_{50}), 88% embolism-related AE (AE_{88}), and full embolism (AE_{100}) are indicated in **Figure 3A**. VC_{AE}s show that only a small decrease in xylem pressure is required to shift from onset of cavitation to full embolism, for all cultivars. For wheat cultivar Excalibur, xylem pressure ranged from −1.70 ± 0.07 MPa (AE_{12}) to −2.35 ± 0.09 MPa (AE_{100}) and for triticale cultivar Dublet, xylem pressure ranged from −1.16 ± 0.03 MPa (AE_{12}) to −1.38 ± 0.03 MPa (AE_{100}). The timespan necessary to reach full embolism ($t_{100\%}$, hours, **Table 2**) was longest for Duiker Max and Dublet (32.1 ± 5.9 and 32.0 ± 5.6 h, respectively) and shortest for Excalibur (21.0 ± 0.6 h). Nolf et al. (2015) hypothesized that the highest acoustic activity should occur when most embolism is forming within a narrow range of Ψ_{xylem} and therefore should be correlated to the AE_{50} value. We also found a positive linear correlation (R^2 = 0.928; $AE_{maxactivity} = 0.909 * AE_{50} - 0.174$) between the species' AE_{50} values and the Ψ_{xylem} at maximum AE activity ($AE_{max\ activity}$).

Continuously weighing of the stem samples led to quantification of the hydraulic capacitance and capacitive water release potential. The capacity of vascular plants to store water in its tissues and release of this water in the event that stress strains the hydraulic integrity could be a significant drought tolerance strategy. Hydraulic elastic (originating from living tissues) and inelastic (originating from xylem embolism) capacitances (**Table 2**) were significantly higher for triticale cultivar Dublet (C_{el}: 0.42 ± 0.10 g MPa^{-1} and C_{inel}: 2.48 ± 0.72 g MPa^{-1}), compared to the other cultivars in this experiment. **Figure 3B** shows that Dublet has the greatest capacitive water release per decreasing unit of xylem water potential.

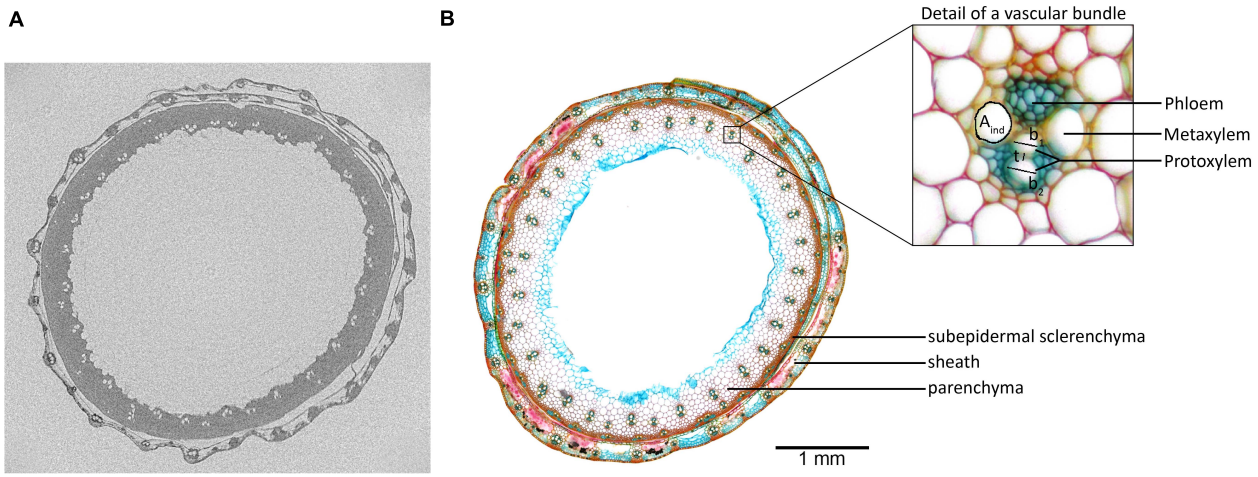


FIGURE 2 | (A) Reconstruction of the EMCT image of Excalibur, taken 26 h after onset of dehydration. From this exact scanning position, **(B)** a 70-μm-thick cross-section was made and stained with 0.5% (w/v) astra blue, 0.5% (w/v) chrysoidine, and 0.5% (w/v) acridine red. Individual vessel area (Aind), wall span (b), and wall thickness (t) are indicated on the detailed magnification of the vascular bundle.

The other cultivars showed no significant differences, with elastic capacitances ranging from 0.04 ± 0.07 to 0.20 ± 0.04 g MPa^{-1} and inelastic capacitances ranging from 0.57 ± 0.09 to 1.19 ± 0.32 g MPa^{-1}.

Validation of Acoustic Measurements Using X-Ray Microcomputed Tomography

Visual embolism detection on EMCT images closely corresponds to the micrograph of the same scanning position (**Figure 2**). The cross-section of the stem shows the vascular bundles arranged in two rings (**Figure 2B**). The ring of small vascular bundles is embedded in subepidermal sclerenchyma, while the second ring is composed of larger vascular bundles enclosed by parenchyma. Around the stem, the leaf sheath is present which also contains larger and smaller vascular bundles in alternating order. According to the EMCT image taken 26 h after onset of dehydration, all 33 large vascular bundles in the stem can be detected, which was not the case for the outer circle of smaller vascular bundles (**Figure 2A**). The maximum resolution of 5 μm likely explains why these bundles are invisible on the reconstruction image.

Comparison of visual embolism formation on EMCT images and AE detection for Excalibur (**Figure 4A**) shows a close correspondence. Seven hours after onset of dehydration, visual embolism detection is slightly higher, but still within the standard error margins of the mean cumulative AE curve. In the morning, when scanning started again, visual embolism detection was at the same level as the mean cumulative AE curve. **Figures 4B–D** show EMCT images of Excalibur with, respectively, 12, 50, and 88% of the vessels embolized.

Xylem Microscopic Analysis

Results from stem anatomy (**Table 3**) revealed that triticale cultivar Dublet had significantly higher A_{ind} (771 ± 120 μm^2) and d_h (34.8 ± 2.9 μm) compared to Excalibur and Duiker Max. Its average total stem area (A_{stem}) was also larger (5.04 ± 1.13 mm^2), though the difference between cultivars was not significant. V_g for Dublet (1.20 ± 0.035) was significantly higher than for Hartog (1.11 ± 0.026). On the other hand, Hartog had the highest CWR (0.0386 ± 0.0204) and the greatest area of stem occupied by vessels (2.61 ± 0.40%). Wheat cultivar Excalibur and rye cultivar Duiker Max had lowest values for A_{ind} (424 ± 103 and 457 ± 366 μm^2, respectively) and d_h (24.6 ± 3.2 and 26.6 ± 1.0 μm, respectively). The number of vessels ranged from 149 ± 9 for Duiker Max to 198 ± 20 for Excalibur, but differences between cultivars were not significant. The percentage of stem occupied by xylem parenchyma was greatest in Excalibur and smallest for triticale cultivars Dublet and US2014, although the difference between cultivars was not significant.

Anatomical analysis of the leaf sheath showed no significant differences between the cultivars for V_g and CWR. Duiker Max showed a significant smaller A_{ind} and d_h in the leaf sheath compared to the other cultivars. Duiker Max also had the lowest N_{vessel} and therefore also smallest $A_{vesseltotal}$. When combining stem and leaf sheath anatomical analyses, generally the same pattern was found as with stem anatomical analysis, except for N_{vessel}. Results for the leaf sheath and combined anatomical analyses are presented in **Supplementary Table 1**. **Supplementary Figure 1** shows, for every cultivar, a detail of the vascular bundles and the stem anatomy.

DISCUSSION

Using EMCT as validation technique, we can conclude that the measurements with the AE sensors correctly represent the course of embolism formation for the wheat cultivar Excalibur and by extension also for the other cultivars included in this study.

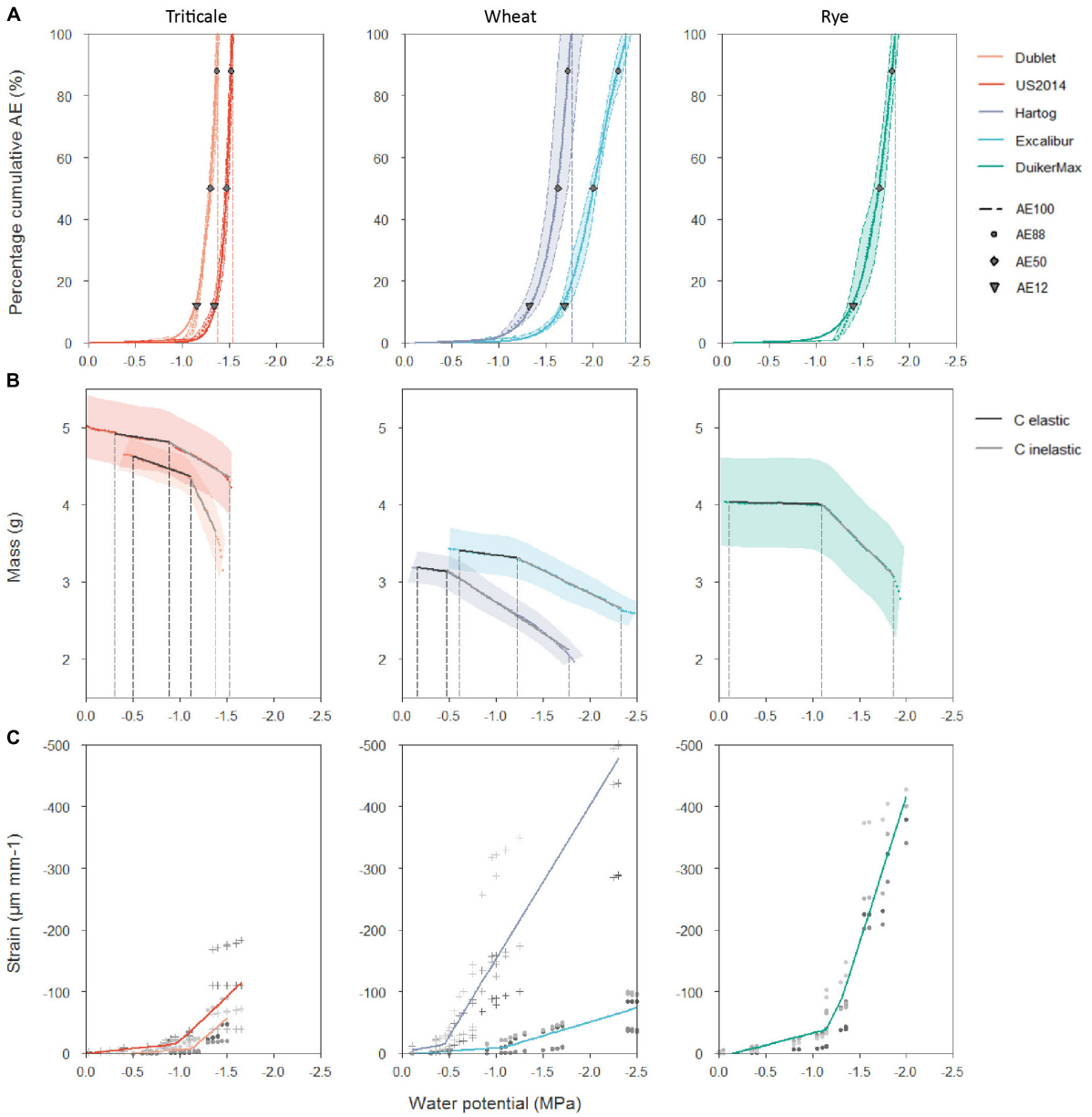


FIGURE 3 | (A) Averaged vulnerability curves (VCAEs) with standard error bands of triticale cultivars Dublet and US2014, wheat cultivars Hartog and Excalibur and rye cultivar Duiker Max. AE_{12}, AE_{50}, AE_{88}, and AE_{100} are indicated. **(B)** Averaged desorption curves (DCs) with standard error bands for the same cultivars. Elastic and inelastic shrinkage are delimited by vertical dashed lines, and the corresponding hydraulic capacitances (C, g MPa^{-1}) of both phases are calculated as the slope of the linear regressions. **(C)** General stress–strain relationship for all five cultivars. The different shade colors for or + indicate the different shoots for each cultivar.

The P_{50} or AE_{50} value is widely seen as relevant parameter to quantify a species' vulnerability to drought stress (Choat et al., 2012; Anderegg, 2015). The small grain cereals in this study have average AE_{50} values ranging from -1.30 ± 0.03 to -2.00 ± 0.07 MPa (**Table 2**). The few studies conducted on cereals show similar P_{50} values. Corso et al. (2020) explored the spread of embolism in leaves and stems of wheat (*T. aestivum* var. SY Mattis), using the optical technique and X-ray microCT. They found mean Ψ_{leaf}, at which 50% of the vessels were embolized, of -2.21 ± 0.17 MPa using the optical technique and similar values were observed for both leaf and stem with X-ray microCT. A study by Johnson et al. (2018) on wheat (*T. aestivum* var. Heron) used non-invasive imaging and found mean Ψ_{leaf} causing 50% xylem embolism of -2.87 ± 0.52 MPa. Gleason et al. (2017) measured losses of 50% of maximal hydraulic conductivity associated with Ψ_{leaf} values of -1.29 MPa in a greenhouse experiment with maize and Ψ_{leaf} values of -1.15 MP for field plants. In a field trail with up- and lowland rice varieties by Stiller et al. (2003), P_{50} values of -1.6 MPa were measured. When comparing our results with the P_{50} values

TABLE 2 | Water potential at which 12, 50, 88, and 100% loss of hydraulic conductivity occurs (AE_{12}, AE_{50}, AE_{88}, and AE_{100}), dehydration time till complete embolism formation ($t_{100\%}$), elastic capacitance (C_{el}), and inelastic capacitance (C_{inel}) for the different cultivars used in this study.

	Dublet	US2014	Hartog	Excalibur	Duiker Max
AE_{12} (MPa)	−1.16 ±0.03^{a}	−1.34 ±0.05^{a}	−1.32 ±0.18^{a}	−1.70 ±0.07^{b}	−1.40 ±0.13^{a}
AE_{50} (MPa)	−1.30 ±0.03^{a}	−1.47 ±0.04^{a,b}	−1.62 ±0.21^{b}	−2.00 ±0.07^{c}	−1.67 ±0.12^{b}
AE_{88} (MPa)	−1.37 ±0.03^{a}	−1.52 ±0.03^{a,b}	−1.73 ±0.22^{b,c}	−2.27 ±0.09^{d}	−1.81 ±0.08^{c}
AE_{100} (MPa)	−1.38 ±0.03^{a}	−1.54 ±0.03^{a,b}	−1.78 ±0.24^{b,c}	−2.35 ±0.09^{d}	−1.84 ±0.08^{c}
$t_{100\%}$ (hours)	32.02 ±5.63^{a,b}	27.34 ±3.90^{a,b,c}	22.58 ±1.96^{b,c}	20.95 ±0.63^{c}	32.14 ±5.90^{a}
C_{el} (g MPa^{-1})	0.42 ±0.10^{a}	0.20 ±0.04^{b}	0.15 ±0.08^{b}	0.17 ±0.07^{b}	0.04 ±0.07^{b}
C_{inel} (g MPa^{-1})	2.48 ±0.72^{a}	0.68 ±0.12^{b}	0.82 ±0.34^{b}	0.57 ±0.09^{b}	1.19 ±0.32^{b}

Values are mean ± standard deviation.
Letters (a, b, c, and d) indicate significant differences after a one-way ANOVA and Tukey test (p = 0.001).

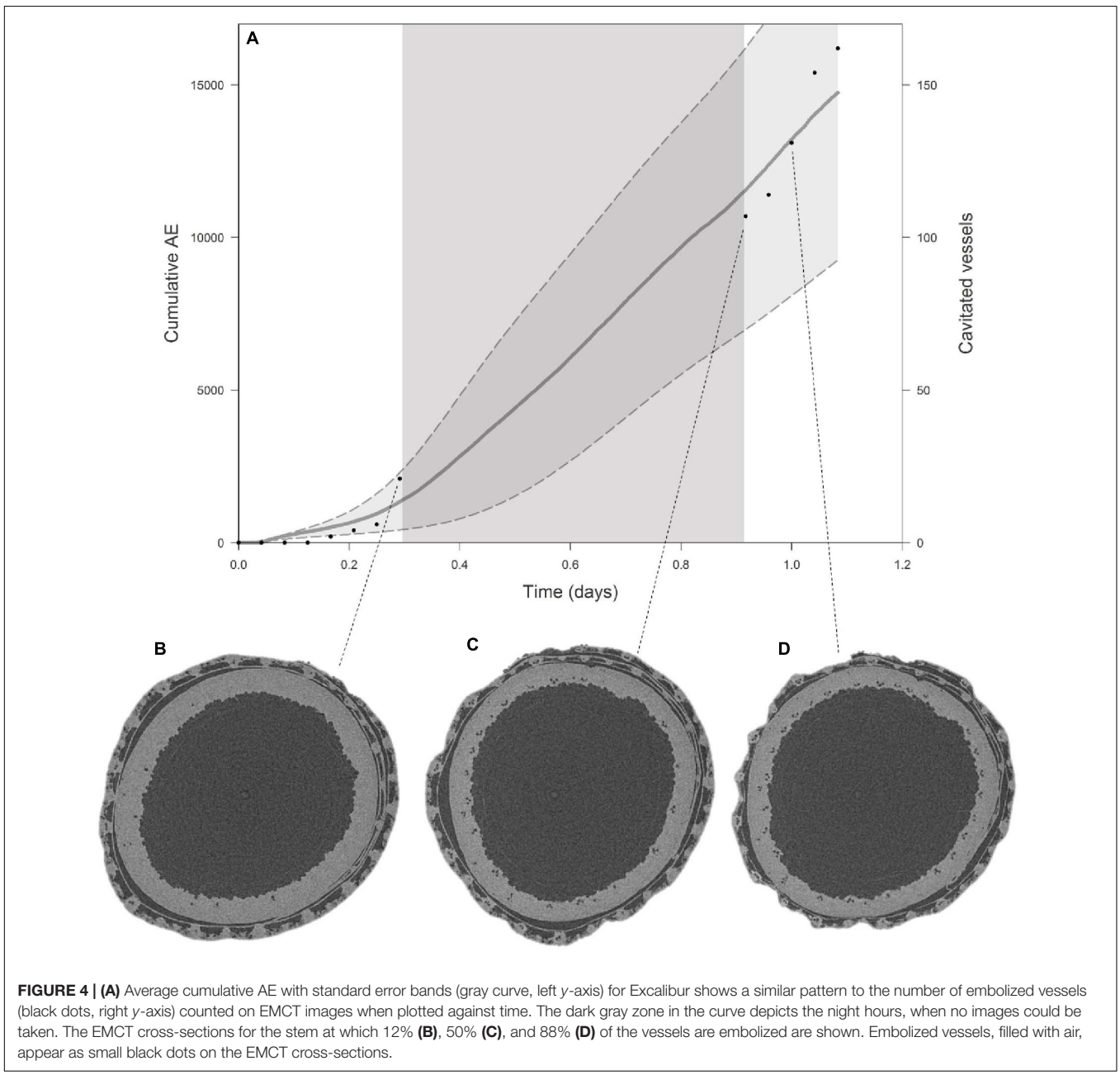


FIGURE 4 | (A) Average cumulative AE with standard error bands (gray curve, left *y*-axis) for Excalibur shows a similar pattern to the number of embolized vessels (black dots, right *y*-axis) counted on EMCT images when plotted against time. The dark gray zone in the curve depicts the night hours, when no images could be taken. The EMCT cross-sections for the stem at which 12% **(B)**, 50% **(C)**, and 88% **(D)** of the vessels are embolized are shown. Embolized vessels, filled with air, appear as small black dots on the EMCT cross-sections.

TABLE 3 | Stem anatomical parameters individual vessel area (A_{ind}), total vessel area (A_{total}), total stem area (A_{stem}), ratio xylem parenchyma to total stem area ($\%_{XylemParenchyma}$), hydraulic diameter (d_h), number of vessels (N_{vessel}), vessel grouping index (V_g), and conduit wall reinforcement (CWR) for the different cultivars in this study.

	Dublet	US2014	Hartog	Excalibur	Duiker Max
A_{ind} (μm^2)	771 ±120[a]	662 ±102[a,b]	594 ±185[a,b]	424 ±103[b]	457 ±366[b]
A_{total} (mm^2)	0.126 ±0.030[a]	0.119 ±0.011[a]	0.090 ±0.029[a,b]	0.086 ±0.028[a,b]	0.068 ±0.008[b]
A_{stem} (mm^2)	5.04 ±1.13[a]	4.67 ±0.18[a]	3.38 ±0.82[a]	4.27 ±1.09[a]	3.25 ±0.39[a]
$\%_{XylemParenchyma}$*	2.19 ±0.44 [a]	2.13 ±0.18[a]	3.24 ±1.11[a]	4.39 ±1.18[a]	3.92 ±1.76[a]
d_h (μm)	34.8 ±2.9[a]	31.2 ±2.1[a,b]	29.1 ±5.0[a,b]	24.6 ±3.2[b]	26.6 ±1.0[b]
N_{vessel}*	163 ±32[a]	182 ±21[a]	150 ±9[a]	198 ±20[a]	149 ±9[a]
V_g	1.20 ±0.035[a]	1.13 ±0.042[a,b]	1.11 ±0.026[b]	1.13 ±0.033[a,b]	1.16 ±0.042[a,b]
CWR	0.036 ±0.013[a]	0.033 ±0.006[a]	0.038 ±0.005[a]	0.035 ±0.009[a]	0.022 ±0.002[a]

Values are mean ± standard deviation.
Letters represent significant differences after a one-way ANOVA and Tukey test (0.05).
For parameters indicated with (*), a Welch correction and Dunnett T3 test (p = 0.05) were used.

of a wide range of mainly woody species studied by Choat et al. (2012), we can classify the cereals as being vulnerable to drought-induced embolism. The species in Choat et al. (2012) have P_{50} values ranging from −0.04 to −14.10 MPa and more than 60% have values lower than −2.00 MPa. Comparison of the cultivars in our study shows that Excalibur (*T. aestivum* L.) has the most negative AE_{50} value and could therefore, based on only this criterion, be classified as most tolerant to drought-induced xylem embolism, followed by Duiker Max (*S. cereale* L.), Hartog (*T. aestivum* L.), US2014, and Dublet (x *Triticosecale* Wittmack), respectively. Surprisingly, the timespan necessary to reach full embolism ($t_{100\%}$) was longest for Duiker Max and Dublet and shortest for Excalibur (**Table 2**). When including the DC analysis, Dublet has significantly higher C_{el} and C_{inel} compared to the other cultivars (**Table 2**). These results point out that Dublet has a greater ability to store water in its living tissue, to use this water to temporarily buffer or delay water shortage and to prolong its life span under drought stress. This clearly points to the importance of including a species' hydraulic capacitance when evaluating vulnerability to drought-induced xylem embolism. Also Körner (2019) argues that there is no need to attribute a critical role to xylem long distance transport capacity or its failure. Under severe drought, there is no or limited water supply but also limited demand (i.e., demand for water flux approaches zero because of stomatal closure). The remaining capacity of the transport system through the narrow non-embolized tracheids is able to cover this minimal demand. And when completely disconnected from any soil moisture, plants will rely on allocation of their own internal water reserves to the most essential tissues for survival. In this regard, it is assumed that the xylem transport activity could be restored after embolism formation and that living cells provide both water and energy to do so. Secchi and Zwieniecki (2010) found that changes in membrane water permeability during drought and refilling processes could be mediated by members of the PIP1 aquaporin subfamily. Meinzer et al. (2009) hypothesize that P_{50} may have no physiological relevance in the context of stomatal regulation of daily minimum xylem pressure and avoidance of hydraulic failure under non-extreme conditions. Their main results suggest that there is a reliance on different mechanisms which provide hydraulic safety under dynamic conditions. Species with low capacitances appear to rely mostly on xylem structural features to avoid embolism, whereas species with higher capacitances generally rely on transient release of stored water to constrain fluctuations in xylem tension and prevent the formation of air emboli. Analysis of the cultivars' xylem anatomy (**Table 3**) also supports the previous findings. Results revealed that Dublet has the highest A_{ind}, $A_{vesseltotal}$, A_{stem}, d_h, and V_g. Significantly lower A_{ind} and d_h are found for Excalibur and Duiker Max. These findings relate with a species individual trade-off between hydraulic safety and efficiency (**Figure 5**). Sperry et al. (2008) defined efficiency as the hydraulic conductivity per cross-sectional area, which is maximized when filled with fewer, though wider and longer vessels, free of internal obstructions. So Dublet's high individual vessel area (A_{ind}) and hydraulic diameter (d_h) illustrate that this cultivar is characterized by a higher hydraulic efficiency. This allows Dublet to maintain longer under conditions of drought stress. Excalibur, on the other hand, containing more but smaller vessels has a higher hydraulic safety allowing its water potential to become more negative before xylem embolism reaches lethal levels. In addition, Dublet's high individual vessel area (A_{ind}) combined with a higher vessel grouping index (V_g) makes it easier to allocate water from embolized to intact adjacent xylem vessels (which contributes to C_{inel}) and to allocate water stored in living tissue into the transpiration stream (which contributes to C_{el}). This contribution to the hydraulic capacity of Dublet explains the extended time span before lethal water potential levels are achieved compared to Excalibur. This contrasting response to drought stress in studied cereals is depicted in **Figure 5**.

Remarkable is the low C_{el} for Duiker Max, combined with a high C_{inel} and prolonged life span under stress. In this regard, it is worth noting that all cultivars have lower elastic and higher inelastic hydraulic capacitances (**Table 2**). In addition, the general stress–strain curves, representing the magnitude of elastic shrinkage of the stem in response to drought stress for all five cultivars, show a distinct breakpoint dividing the curves in two phases (**Figure 3C**). The first part shows a weak shrinkage for the strong decrease in Ψ_{xylem}, followed by a strong shrinkage per unit Ψ_{xylem}. The breakpoints in

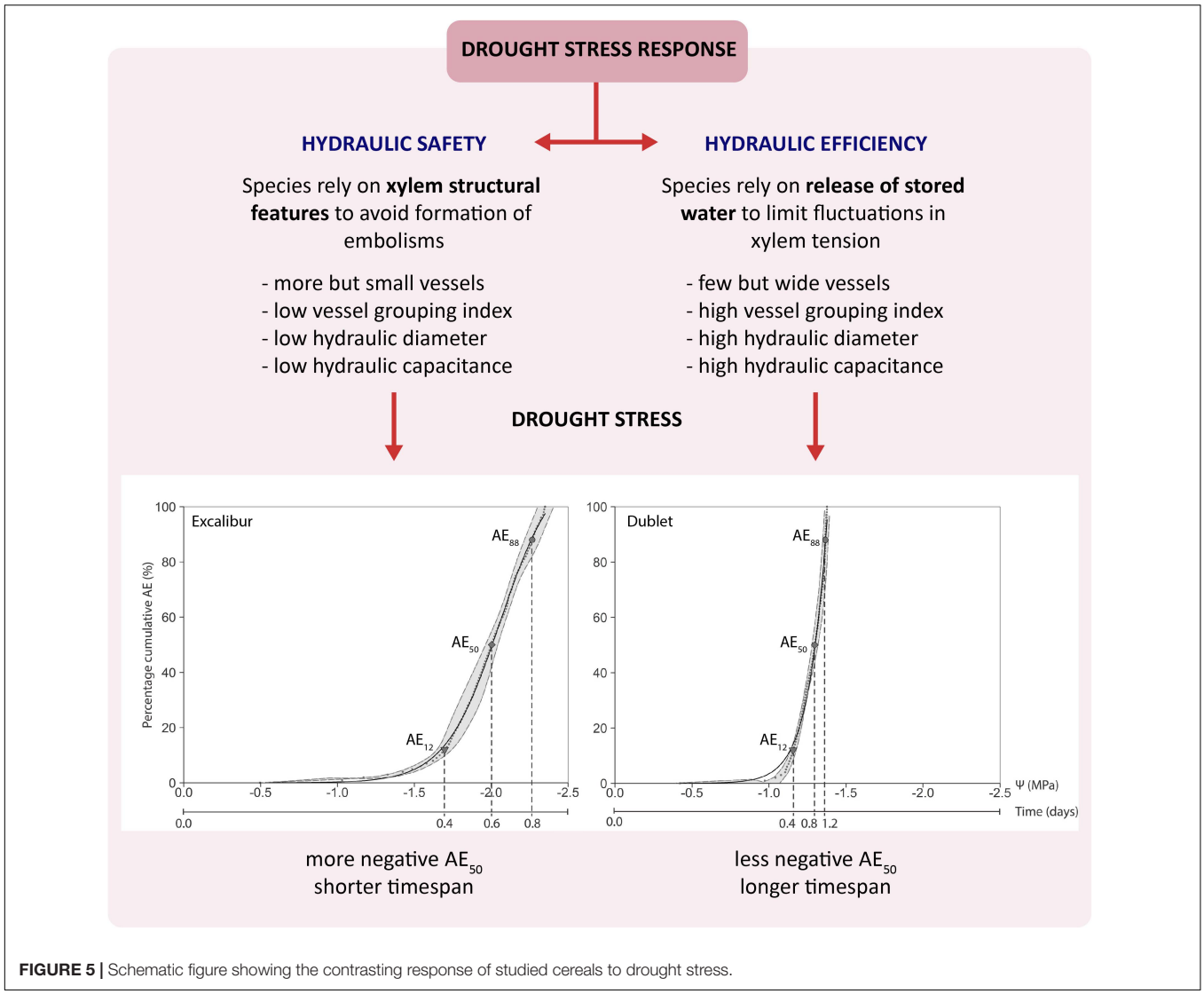


FIGURE 5 | Schematic figure showing the contrasting response of studied cereals to drought stress.

the stress–strain curves relate very well with the breakpoints in the DCs, indicating the shift from elastic to inelastic shrinkage. These results indicate that overall the elastic water storage in living tissue of small grain cereals is insufficient to buffer or delay decreases in Ψ_{xylem}, while water released from embolized vessels has a more significant contribution toward tempering and delaying xylem tension. These results also support the observations by Hölttä et al. (2009), Vergeynst et al. (2015a), and Epila et al. (2017) who declared that water from embolized vessels is released into the transpiration stream and significantly contributes to a species hydraulic capacitance under drought stress.

From the above, it is clear that AE_{50} values do not tell the entire story on vulnerability to drought-induced xylem embolism and that a sole parameter often does not provide a correct assessment of a species' overall drought stress response. The combination of methods proposed in this paper is necessary to

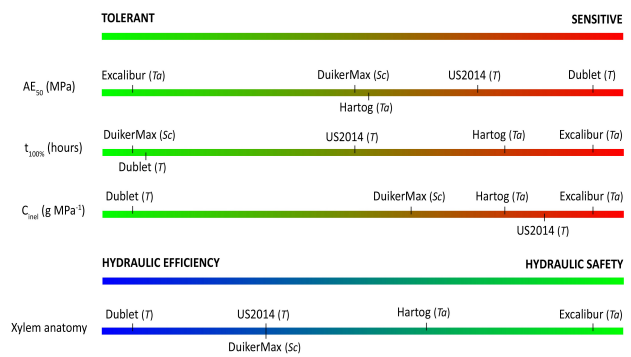


FIGURE 6 | Ranking of cultivars from tolerant to sensitive to drought stress, according to the different parameters explored in this study. Ta, T, and Sc indicate wheat (*T. aestivum* L.), triticale (x *Triticosecale* Wittmack), or rye (*S. cereale* L.).

get the full picture–from Ψ_{xylem} at which embolism formation occurs, over hydraulic capacitance and the ability to temporarily buffer or delay water shortage, to a species individual trade-off between hydraulic safety and efficiency—before postulating conclusions on this matter. So, keeping this message in mind and based on the aforementioned parameters, **Figure 6** shows our classification of the different cultivars from drought tolerant to drought sensitive per parameter.

DATA AVAILABILITY STATEMENT

The raw data supporting the conclusions of this article will be made available by the authors, without undue reservation.

AUTHOR CONTRIBUTIONS

SD, GH, and KS contributed to the design of the study. SD and NB carried out the experiments. OL provided his expertise on making, staining, and imaging the cross-sections. SD performed the data analysis and wrote the manuscript. All authors contributed to the article and approved the submitted version.

ACKNOWLEDGMENTS

Sincere gratitude goes to the seed suppliers of the cultivars used in this study: CIMMYT for Excalibur and Hartog, Zofia Banaszak, Head of breeding of Danko Hodowla Roslin SP. Z o.o., for Dublet, and Willem Botes from Stellenbosch University for Duiker Max and US2014. We also like to thank Geert Favyts (Laboratory of Plant Ecology) for manufacturing the carbon holder to fix the shoot into the EMCT, and Fran Lauriks and Linus De Roo (Laboratory of Plant Ecology) for their help during sampling and sensor installation. We wish to thank Jan Van den Bulcke (Laboratory of Wood Technology) and Ivan Josipovic (UGCT) with their help during the many hours of scanning and with their guidance during reconstructing the images.

SUPPLEMENTARY MATERIAL

The Supplementary Material for this article can be found online at: https://www.frontiersin.org/articles/10.3389/fpls.2021.599824/full#supplementary-material

Supplementary Figure 1 | Detail of a cross-section from the stem of **(A)** Dublet, **(B)** US2014, **(C)** Hartog, **(D)** Excalibur, and **(E)** Duiker Max. For each cultivar, phloem (ph), metaxylem (m), protoxylem (p), parenchyma (Pa), sclerenchyma (Sc), and lacunae (L) are indicated.

REFERENCES

Anderegg, W. R. L. (2015). Spatial and temporal variation in plant hydraulic traits and their relevance for climate change impacts on vegetation. *New Phytol.* 205, 1008–1014. doi: 10.1111/nph.12907

Begg, J. E., and Turner, N. C. (1970). Water potential gradients in field tobacco. *Plant Physiol.* 46, 343–346. doi: 10.1104/pp.46.2.343

Blum, A. (1998). Improving wheat grain filling under stress by stem reserve mobilisation (Reprinted from Wheat: Prospects for global improvement, 1998). *Euphytica* 100, 77–83. doi: 10.1023/a:1018303922482

Blum, A. (2014). The abiotic stress response and adaptation of triticale-a review. *Cereal Res. Commun.* 42, 359–375. doi: 10.1556/crc.42.2014.3.1

Brodribb, T. J., Carriqui, M., Delzon, S., and Lucani, C. (2017). optical measurement of stem xylem vulnerability. *Plant Physiol.* 174, 2054–2061. doi: 10.1104/pp.17.00552

Choat, B., Badel, E., Burlett, R., Delzon, S., Cochard, H., and Jansen, S. (2016). Noninvasive measurement of vulnerability to drought-induced embolism by x-ray microtomography. *Plant Physiol.* 170, 273–282. doi: 10.1104/pp.15.00732

Choat, B., Cobb, A. R., and Jansen, S. (2008). Structure and function of bordered pits: new discoveries and impacts on whole-plant hydraulic function. *New Phytol.* 177, 608–625. doi: 10.1111/j.1469-8137.2007.02317.x

Choat, B., Jansen, S., Brodribb, T. J., Cochard, H., Delzon, S., Bhaskar, R., et al. (2012). Global convergence in the vulnerability of forests to drought. *Nature* 491, 752–755. doi: 10.1038/nature11688

Choudhary, M., Wani, S. H., Kumar, P., Bagaria, P. K., Rakshit, S., Roorkiwal, M., et al. (2019). QTLian breeding for climate resilience in cereals: progress and prospects. *Funct. Integr. Genomics* 19, 685–701. doi: 10.1007/s10142-019-00684-1

Cochard, H., Badel, E., Herbette, S., Delzon, S., Choat, B., and Jansen, S. (2013). Methods for measuring plant vulnerability to cavitation: a critical review. *J. Exp. Bot.* 64, 4779–4791. doi: 10.1093/jxb/ert193

Corso, D., Delzon, S., Lamarque, L. J., Cochard, H., Torres-Ruiz, J. M., King, A., et al. (2020). Neither xylem collapse, cavitation, or changing leaf conductance drive stomatal closure in wheat. *Plant Cell Environ.* 43, 854–865. doi: 10.1111/pce.13722

De Baerdemaeker, N. J. F., Arachchige, K. N. R., Zinkernagel, J., Van den Bulcke, J., Van Acker, J., Schenk, H. J., et al. (2019a). The stability enigma of hydraulic vulnerability curves: addressing the link between hydraulic conductivity and drought-induced embolism. *Tree Physiol.* 39, 1646–1664. doi: 10.1093/treephys/tpz078

De Baerdemaeker, N. J. F., Stock, M., Van den Bulcke, J., De Baets, B., Van Hoorebeke, L., and Steppe, K. (2019b). X-ray microtomography and linear discriminant analysis enable detection of embolism-related acoustic emissions. *Plant Methods* 15:153. doi: 10.1186/s13007-019-0543-4

De Roo, L., Vergeynst, L. L., De Baerdemaeker, N. J. F., and Steppe, K. (2016). Acoustic Emissions to Measure Drought-Induced Cavitation in Plants. *Appl. Sci. Basel* 6:71. doi: 10.3390/app6030071

Dierick, M., Van Loo, D., Masschaele, B., Van den Bulcke, J., Van Acker, J., Cnudde, V., et al. (2014). Recent micro-CT scanner developments at UGCT. *Nucl. Instrum. Methods Phys. Res. Section B Beam Interactions Mater. Atoms* 324, 35–40. doi: 10.1016/j.nimb.2013.10.051

Dixon, H. H., and Joly, J. (1895). On the ascent of sap. *Philos. Trans. Royal Soc. London B* 186, 563–576.

Epila, J., De Baerdemaeker, N. J. F., Vergeynst, L. L., Maes, W. H., Beeckman, H., and Steppe, K. (2017). Capacitive water release and internal leaf water relocation delay drought-induced cavitation in African *Maesopsis eminii*. *Tree Physiol.* 37, 481–490. doi: 10.1093/treephys/tpw128

FAO, Ifad, Unicef, Wfp, and WHO (2018). *The State of Food Security and Nutrition in the World 2018. Building Climate Resilience for Food Security and Nutrition*. Rome: FAO.

Farooq, M., Wahid, A., Kobayashi, N., Fujita, D., and Basra, S. M. A. (2009). Plant drought stress: effects, mechanisms and management. *Agron. Sust. Dev.* 29, 185–212. doi: 10.1051/agro:2008021

Gleason, S. M., Wiggans, D. R., Bliss, C. A., Comas, L. H., Cooper, M., De Jonge, K. C., et al. (2017). Coordinated decline in photosynthesis and hydraulic conductance during drought stress in *Zea mays*. *Flora* 227, 1–9. doi: 10.1016/j.flora.2016.11.017

Hacke, U. G., and Sperry, J. S. (2001). Functional and ecological xylem anatomy. *Perspect. Plant Ecol. Evol. Syste.* 4, 97–115. doi: 10.1078/1433-8319-00017

Hacke, U. G., Sperry, J. S., Pockman, W. T., Davis, S. D., and McCulloch, K. A. (2001). Trends in wood density and structure are linked to prevention of xylem implosion by negative pressure. *Oecologia* 126, 457–461. doi: 10.1007/s004420100628

Hölttä, T., Cochard, H., Nikinmaa, E., and Mencuccini, M. (2009). Capacitive effect of cavitation in xylem conduits: results from a dynamic model. *Plant Cell Environment* 32, 10–21. doi: 10.1111/j.1365-3040.2008.01894.x

IPCC (2014). "Summary for policymakers," in *Climate Change 2014: Impacts,Adaptation, and Vulnerability. Part A: Global and Sectoral Aspects. Contribution of Working Group II to the Fifth Assessment Report of the Intergovernmental Panel on Climate Change*, eds C. B. Field, V. R. Barros, D. J. Dokken, K. J. Mach, M. D. Mastrandrea, T. E. Bilir, et al. (Cambridge: Cambridge University Press), 1–32.

Johnson, K. M., Jordan, G. J., and Brodribb, T. J. (2018). Wheat leaves embolized by water stress do not recover function upon rewatering. *Plant Cell Environ.* 41, 2704–2714. doi: 10.1111/pce.13397

Körner, C. (2019). No need for pipes when the well is dry-a comment on hydraulic failure in trees. *Tree Physiol.* 39, 695–700. doi: 10.1093/treephys/tpz030

Laskowski, W., Gorska-Warsewicz, H., Rejman, K., Czeczotko, M., and Zwolinska, J. (2019). How important are cereals and cereal products in the average polish Diet? *Nutrients* 11:679. doi: 10.3390/nu11030679

McKevith, B. (2004). Nutritional aspects of cereals. *Nutr. Bull.* 29, 111–142. doi: 10.1111/j.1467-3010.2004.00418.x

Meinzer, F. C., Johnson, D. M., Lachenbruch, B., McCulloh, K. A., and Woodruff, D. R. (2009). Xylem hydraulic safety margins in woody plants: coordination of stomatal control of xylem tension with hydraulic capacitance. *Funct. Ecol.* 23, 922–930. doi: 10.1111/j.1365-2435.2009.01577.x

Muggeo, V. M. R. (2008). Segmented: an r package to fit regression models with broken-line relationships. *R News* 8, 20–25.

Nolf, M., Beikircher, B., Rosner, S., Nolf, A., and Mayr, S. (2015). Xylem cavitation resistance can be estimated based on time-dependent rate of acoustic emissions. *New Phytol.* 208, 625–632.

Nolf, M., Beikircher, B., Rosner, S., Nolf, A., and Mayr, S. (2017). Visualization of xylem embolism by X-ray microtomography: a direct test against hydraulic measurements. *New Phytol.* 214, 890–898. doi: 10.1111/nph.14462

Porter, J. R., Xie, L., Challinor, A. J., Cochrane, K., Howden, S. M., Iqbal, M. M., et al. (2014). "Food security and food production systems," in *Climate Change 2014: Impacts, Adaptation, and Vulnerability. Part A: Global and Sectoral Aspects. Contribution of Working Group II to the Fifth Assessment Report of the Intergovernmental Panel on Climate Change*, eds C. B. Field, V. R. Barros, D. J. Dokken, K. J. Mach, M. D. Mastrandrea, T. E. Bilir, et al. (Cambridge: Cambridge University Press), 485–533.

Schenk, H. J., Steppe, K., and Jansen, S. (2015). Nanobubbles: a new paradigm for air-seeding in xylem. *Trends Plant Sci.* 20, 199–205. doi: 10.1016/j.tplants.2015.01.008

Secchi, F., and Zwieniecki, M. A. (2010). Patterns of PIP gene expression in Populus trichocarpa during recovery from xylem embolism suggest a major role for the PIP1 aquaporin subfamily as moderators of refilling process. *Plant Cell Environ.* 33, 1285–1297. doi: 10.1111/j.1365-3040.2010.02147.x

Sperry, J. S., Meinzer, F. C., and McCulloh, K. A. (2008). Safety and efficiency conflicts in hydraulic architecture: scaling from tissues to trees. *Plant Cell Environ.* 31, 632–645. doi: 10.1111/j.1365-3040.2007.01765.x

Steppe, K., and Lemeur, R. (2007). Effects of ring-porous and diffuse-porous stem wood anatomy on the hydraulic parameters used in a water flow and storage model. *Tree Physiol.* 27, 43–52. doi: 10.1093/treephys/27.1.43

Stiller, V., Lafitte, H. R., and Sperry, J. S. (2003). Hydraulic properties of rice and the response of gas exchange to water stress. *Plant Physiol.* 132, 1698–1706. doi: 10.1104/pp.102.019851

Tricker, P. J., ElHabti, A., Schmidt, J., and Fleury, D. (2018). The physiological and genetic basis of combined drought and heat tolerance in wheat. *J. Exp. Bot.* 69, 3195–3210. doi: 10.1093/jxb/ery081

Tyree, M. T., and Ewers, F. W. (1991). The hydraulic architecture of trees and other woody plants. *New Phytol.* 119, 345–360. doi: 10.1111/j.1469-8137.1991.tb00035.x

Tyree, M. T., and Zimmermann, M. H. (2002). *Xylem Structure and the Ascent of Sap. Springer Series in Wood Science*. Berlin: Springer-Verlag, 284. doi: 10.1007/978-3-662-04931-0

Vadez, V. (2014). Root hydraulics: the forgotten side of roots in drought adaptation. *Field Crops Res.* 165, 15–24. doi: 10.1016/j.fcr.2014.03.017

Vadez, V., Kholova, J., Zaman-Allah, M., and Belko, N. (2013). Water: the most important 'molecular' component of water stress tolerance research. *Funct. Plant Biol.* 40, 1310–1322. doi: 10.1071/fp13149

Venturas, M. D., Sperry, J. S., and Hacke, U. G. (2017). Plant xylem hydraulics: what we understand, current research, and future challenges. *J. Integr. Plant Biol.* 59, 356–389. doi: 10.1111/jipb.12534

Vergeynst, L. L., Dierick, M., Bogaerts, J. A. N., Cnudde, V., and Steppe, K. (2015a). Cavitation: a blessing in disguise? New method to establish vulnerability curves and assess hydraulic capacitance of woody tissues. *Tree Physiol.* 35, 400–409. doi: 10.1093/treephys/tpu056

Vergeynst, L. L., Sause, M. G. R., De Baerdemaeker, N. J. F., De Roo, L., and Steppe, K. (2016). Clustering reveals cavitation-related acoustic emission signals from dehydrating branches. *Tree Physiol.* 36, 786–796. doi: 10.1093/treephys/tpw023

Vergeynst, L. L., Sause, M. G. R., Hamstad, M. A., and Steppe, K. (2015b). Deciphering acoustic emission signals in drought stressed branches: the missing link between source and sensor. *Front. Plant Sci.* 6:494. doi: 10.3389/fpls.2015.00494

Zadoks, J. C., Chang, T. T., and Konzak, C. F. (1974). Decimal code for growth stages of cereals. *Weed Res.* 14, 415–421. doi: 10.1111/j.1365-3180.1974.tb01084.x

Conflict of Interest: The authors declare that the research was conducted in the absence of any commercial or financial relationships that could be construed as a potential conflict of interest.

Copyright © 2021 Degraeve, De Baerdemaeker, Ameye, Leroux, Haesaert and Steppe. This is an open-access article distributed under the terms of the Creative Commons Attribution License (CC BY). The use, distribution or reproduction in other forums is permitted, provided the original author(s) and the copyright owner(s) are credited and that the original publication in this journal is cited, in accordance with accepted academic practice. No use, distribution or reproduction is permitted which does not comply with these terms.

frontiers in Plant Science

ORIGINAL RESEARCH
published: 04 June 2021
doi: 10.3389/fpls.2021.646168

Night Temperature Determines the Interannual Yield Variation in Hybrid and Inbred Rice Widely Used in Central China Through Different Effects on Reproductive Growth

*Liying Huang[1,2], Fei Wang[3,4], Yi Liu[2] and Yunbo Zhang[2,4]**

[1]Engineering Research Center of Ecology and Agricultural Use of Wetland, Ministry of Education, Yangtze University, Jingzhou, China, [2]College of Agriculture, Yangtze University, Jingzhou, China, [3]Minister of Agriculture Key Laboratory of Crop Ecophysiology and Farming System in the Middle Reaches of the Yangtze River, College of Plant Science and Technology, Huazhong Agricultural University, Wuhan, China, [4]Hubei Collaborative Innovation Center for Grain Industry, Yangtze University, Jingzhou, China

OPEN ACCESS

Edited by:
Felipe Klein Ricachenevsky, Federal University of Rio Grande do Sul, Brazil

Reviewed by:
Manuela Silva, University of Lisbon, Portugal
Dongliang Xiong, Huazhong Agricultural University, China

***Correspondence:**
Yunbo Zhang
yunbo1022@126.com

Specialty section:
This article was submitted to Plant Abiotic Stress, a section of the journal Frontiers in Plant Science

Received: *25 December 2020*
Accepted: *26 April 2021*
Published: *04 June 2021*

Citation:
Huang L, Wang F, Liu Y and Zhang Y (2021) Night Temperature Determines the Interannual Yield Variation in Hybrid and Inbred Rice Widely Used in Central China Through Different Effects on Reproductive Growth. Front. Plant Sci. 12:646168. doi: 10.3389/fpls.2021.646168

Interannual variation in grain yield of rice has been observed at both farm and regional scales, which is related to the climate variability. Previous studies focus on predicting the trend of climate change in the future and its potential effects on rice production using climate models; however, field studies are lacking to examine the climatic causes underlying the interannual yield variability for different rice cultivars. Here a 6-year field experiment from 2012 to 2017 was conducted using one hybrid (Yangliangyou6, YLY6) cultivar and one inbred (Huanghuazhan, HHZ) cultivar to determine the climate factors responsible for the interannual yield variation. A significant variation in grain yield was observed for both the inbred and hybrid cultivars across six planting years, and the coefficient of variation for grain yield was 7.3–10.5%. The night temperature (average daily minimum temperature, T_{min}) contributed to the yield variability in both cultivars. However, the two cultivars showed different responses to the change in T_{min}. The yield variation in HHZ was mainly explained by the effects of T_{min} on grain filling percentage and grain weight, while the change in spikelets m^{-2} in response to T_{min} accounted for the yield variability in YLY6. Further analysis found that spikelets m^{-2} of YLY6 significantly and negatively correlated with T_{min} from transplanting to heading. For HHZ, the grain filling percentage and grain weight were significantly affected by T_{min} of the week prior to heading and from heading to maturity, respectively. Overall, there were differences in the response mechanism between hybrid and inbred cultivars to high night temperature. These will facilitate the development of climate-resilient cultivars and appropriate management practices to achieve a stable grain yield.

Keywords: rice, grain yield, climate variability, night temperature, grain filling percentage

HIGHLIGHTS

- Night temperature determines the inter-annual yield variation of hybrid and inbred cultivars.
- Hybrid and inbred cultivars showed different responses to the change in T_{min}.
- T_{min} affected spikelets m^{-2} of hybrid rice, and grain filling and grain weight of inbred rice.

INTRODUCTION

Rice is the staple food for more than half of the population in the world (Tao et al., 2014). China is the largest rice producer and consumer, producing 28.1% of the world rice output using 18.8% of the global rice-growing area (FAO, 2016). In the next decade, rice production must increase by 20% to meet the growing demand for food in China (Huang and Zou, 2018). As the arable land area decreases year by year due to the rapid development of urbanization, increasing rice yield per unit area has become an effective way to increase rice production (An et al., 2018). Yield potential is defined as the yield of a cultivar when grown in environments to which it is adapted, with nutrients and water nonlimiting and with pests, diseases, weeds, lodging, and other stresses effectively controlled (Evans, 1993). The maximum yield potential of irrigated rice reaches as high as 15.0 t ha^{-1} in China because of the development of super hybrid cultivars through the combination of interspecific heterosis and ideotype, and adopting the optimized management practices (Cheng et al., 2007; Peng et al., 2008; Sun et al., 2013). Nevertheless, yield gap analyses find that the current average Chinese rice yield is approximately 82% of the national yield potential, indicating that Chinese rice yields have been approaching their biophysical potential ceiling (Van Wart et al., 2013). The threshold of 80% is often used as an indicator for yield stagnation (Cassman et al., 2003), because there exists a fundamental constraint for further increasing yield, which appears to be the uncertainty in growing season weather (Lobell et al., 2009). Therefore, identifying the causal environmental factors contributing to the yield variation across planting years would provide the breeding target in the future to further reduce the yield gap in rice.

Variation in grain yield for the same cultivar has been widely observed across locations and planting years (Gravois and Helms, 1998; Wang et al., 2004; Gong et al., 2008; Blanche and Linscombe, 2009; Ma et al., 2011; Jaruchai et al., 2018). The fluctuation in the average yield at the regional scale was also observed; for example, the average yield of single-season rice is 8.27 and 7.95 t ha^{-1} in 2015 and 2016, respectively, in Hubei Province, China (National Bureau of Statistics, n.d.). Multiplying the planting area, the reduction in rice production of Hubei Province in 2016 is around 0.42 Mt, which corresponds to 41.2% of total rice production of the year in the United States (FAOSTAT).[1] Globally, the average rice yield variability (standard deviation) is about 0.5 tons ha^{-1} $year^{-1}$ (or 13% of average rice yields), and year-to-year climate variability explains about 32% of the rice yield variability (Ray et al., 2015). Among the environmental factors, understanding crop responses to temperature and the magnitude of regional temperature changes are two of the most important needs for the adaptation of agriculture to climate variability (Lobell and Burke, 2008). Projections using climate models suggest that both the increase in global mean temperature and the occurrence of extreme seasonal heat will cause significant damage to rice production (Lobell and Burke, 2008; Battisti and Naylor, 2009; Tao and Zhang, 2013; Zhao et al., 2017). In addition, precipitation and radiation also account for the year-to-year variability in rice yields (Peng et al., 2004; Lobell and Burke, 2008; Tao et al., 2013).

Rice grain yield is comprised of the number of spikelets m^{-2} (panicles m^{-2}×spikelets $panicle^{-1}$), grain filling percentage, and grain weight (Zhang et al., 2013). Among them, the number of spikelets m^{-2} is regarded as the most important factor affecting rice yield (Kropff, 1994). Genetic improvement in the yield potential of rice is mainly ascribed to the significant increase in the number of spikelets per panicle in China (Zhu et al., 2016). Newly developed hybrid and super hybrid cultivars have larger panicles and fewer tillers (Huang et al., 2011). In the tropics, the yield advantage of hybrid rice over inbred rice is also accounted for by the larger panicles (Bueno et al., 2010). However, the increased panicle size does not substantially improve yield if there is no sufficient substrate supply to fully satisfy the increased sink demand (Ohsumi et al., 2010). Previous studies indicate that anthesis and ripening are the most temperature-sensitive stages in rice, so spikelets per panicle, grain filling percentage, and grain weight are usually affected by the high temperature at these stages (Tashiro and Wardlaw, 1991; Matsui and Omasa, 2002; Peng et al., 2004; Mohammed and Tarpley, 2009; Sanchez et al., 2014). For example, by analyzing the relationship between rice yield and temperature using data from irrigated field experiments conducted at the International Rice Research Institute Farm from 1992 to 2003, Peng et al. (2004) found that grain yield declined by 10% for each 1°C increase in growing-season minimum temperature in the dry season of tropical rice. Therefore, to combat with the challenges of climate variability on rice production, it is necessary to ascertain the regional environmental factor responsible for interannual yield variability and its physiological mechanisms and then develop climate-resilient cultivars (Mittler and Blumwald, 2010).

Extensive studies have been conducted to predict the trend of climate change in the future and its potential effects on rice production using climate models and investigate the effects of environmental factors on rice yield in controlled environments. However, relatively fewer studies attempt to determine the relationship between the yield variation across years and the corresponding environmental conditions for different rice cultivars in field experiments. In the present study, a 6-year experiment from 2012 to 2017 was conducted with the representative inbred and hybrid rice cultivars in Central China.

[1]http://www.fao.org/faostat/en/#home

Rice production in this area accounts for 54% of national rice production in 2017 (National Bureau of Statistics, n.d.). The objectives of the study were to (1) determine the degree of interannual variation in grain yield for the inbred and hybrid cultivars, (2) identify the environmental factors contributing to inter-annual variation in rice grain yield in Central China, and (3) examine the agronomic traits that could be used for developing climate-resilient rice.

MATERIALS AND METHODS

Geographic Region Description

Field experiments from 2012 to 2017 were conducted in Wuxue County (29°51′ N 115°33′ E), Hubei Province, China. Wuxue County is located in the basin of the Yangtze River of Central China and represents a typical agricultural region of this region. The soil in the experimental field was a clay loam with pH of 5.2–5.5, organic C of 23.8–26.7 g kg^{-1}, total N of 1.80–2.10 g kg^{-1}, available P of 21.3–30.1 mg kg^{-1}, and available K of 118.6–158.3 mg kg^{-1}.

Experimental Design and Crop Management

In each growing season, Yangliangyou6 (YLY6) and Huanghuazhan (HHZ) were arranged in a randomized complete-block design with four replications. YLY6 is an *indica* hybrid variety developed by Lixiahe Institute of Agricultural Sciences with Guangzhan63-4 s as the female parent and Yangdao6 as the male parent using the two-line method. HHZ is an *indica* inbred variety developed using the pedigree method with Huangxinzhan as the female parent and Fenghuazhan as the male parent by the Guangdong Academy of Agricultural Sciences in 2007. YLY6 and HHZ are the representative and widely planted cultivars of hybrid and inbred cultivars for single-season rice in Central China, respectively. Pre-germinated seeds were sown and raised in wet seedbeds. Seedlings of 26–31 days were transplanted on 12 June 2012, 10 June 2013, 11 June 2014, 10 June 2015, 13 June 2016, and 17 June 2017, respectively. Hill spacing was 13.3 cm × 30.0 cm with two seedlings per hill in 6 experiment years. Plot size was 30 m^2 (5 m × 6 m). Nitrogen fertilizer of 180 kg N ha^{-1} as urea was applied in each plot at the basal, tillering, and panicle initiation stages at a ratio of 4:3:3. The amount of N applied by local farmers was 180–200 kg N ha^{-1} for single-season rice. P (40 kg P ha^{-1} as monocalcium phosphate), K (50 kg K ha^{-1} as potassium oxide), and Zn (5 kg Zn ha^{-1} as zinc sulfate) were applied and incorporated in all plots 1 day before transplanting. Additional 50 kg K ha^{-1} as topdressing was applied at the panicle initiation stage. Fertilizer management practices remained consistent from 2012 to 2017. The fields were flooded from transplanting until 10 days before maturity except that the water was drained at the maximum tillering stage to reduce unproductive tillers. Insects, weeds, and diseases were intensively controlled by chemicals to avoid biomass and yield loss. Detailed information about crop management is shown in **Supplementary Figure S1**.

Measurement of Grain Yield and Yield Attributes

Twelve hill plants from each plot were sampled at heading and mature stages. After recording the number of panicles, the plant samples were separated into leaves, stems (culm plus sheath), and panicles. The dry weights of each organ except for panicles at maturity were determined after oven-drying at 80°C to constant weight. Panicles at maturity were hand-threshed, and then filled spikelets were separated from unfilled spikelets by submerging them in tap water. After that, empty spikelets were separated from half-filled spikelets by winnowing. Three subsamples of 30-g filled spikelets and 2-g empty spikelets, and total half-filled spikelets were taken to quantify the number of spikelets per m^2. Dry weights of rachis and filled, half-filled, and empty spikelets were determined after oven drying at 80°C to constant weight. Total aboveground biomass was the summation of leaves, stems, rachis, and filled, half-filled, and empty spikelets dry weight. Spikelets per panicle, grain-filling percentage (100 × filled spikelets m^{-2}/total spikelets m^{-2}), sink size (total spikelets m^{-2} × grain weight), and harvest index (100 × filled spikelet weight/total aboveground biomass) were calculated. Grain yield was determined from a 5-m^2 sampling area in the center of each plot and adjusted to a standard moisture content of 0.14 g H_2O g^{-1} fresh weight.

Measurement of Climate Parameters

Climate parameters including daily minimum/maximum temperature and solar radiation were collected from the weather station located within 2 km of the experimental site. A data logger (CR800, Campbell Scientific Inc., Logan, Utah, United States) was used as the measurement and control module. A silicon pyranometer (LI-200, LI-COR Inc., Lincoln, NE, United States) and temperature/relative humidity probe (HMP45C, Vaisala Inc., Helsinki, Finland) were used to measure solar radiation and temperature, respectively.

Statistical Analysis

Analysis of variance was performed with Statistix 9.0, and means were compared based on the least significant difference (LSD) test at the 0.05 probability level. All figures were constructed using SigmaPlot 12.5.

RESULTS

Weather Conditions

The average daily maximum and minimum temperatures were 30.8 and 23.1°C for YLY6 and 31.5 and 23.9°C for HHZ during the rice-growing seasons from 2012 to 2017, respectively (**Figure 1**). The average annual mean solar radiation was 15.2 and 15.7 MJ m^{-2} d^{-1} for YLY6 and HHZ, respectively. The annual mean daily maximum and minimum temperatures and solar radiation of YLY6 ranged from 30.0 to 31.9°C, 22.0 to 24.3°C and 13.3 to 17.8 MJ m^{-2} d^{-1}, and the corresponding ranges of HHZ were 30.6 to 32.3°C, 22.8 to 24.8°C, and 13.3 to 18.2 MJ m^{-2} d^{-1} across years, respectively. The growing-season

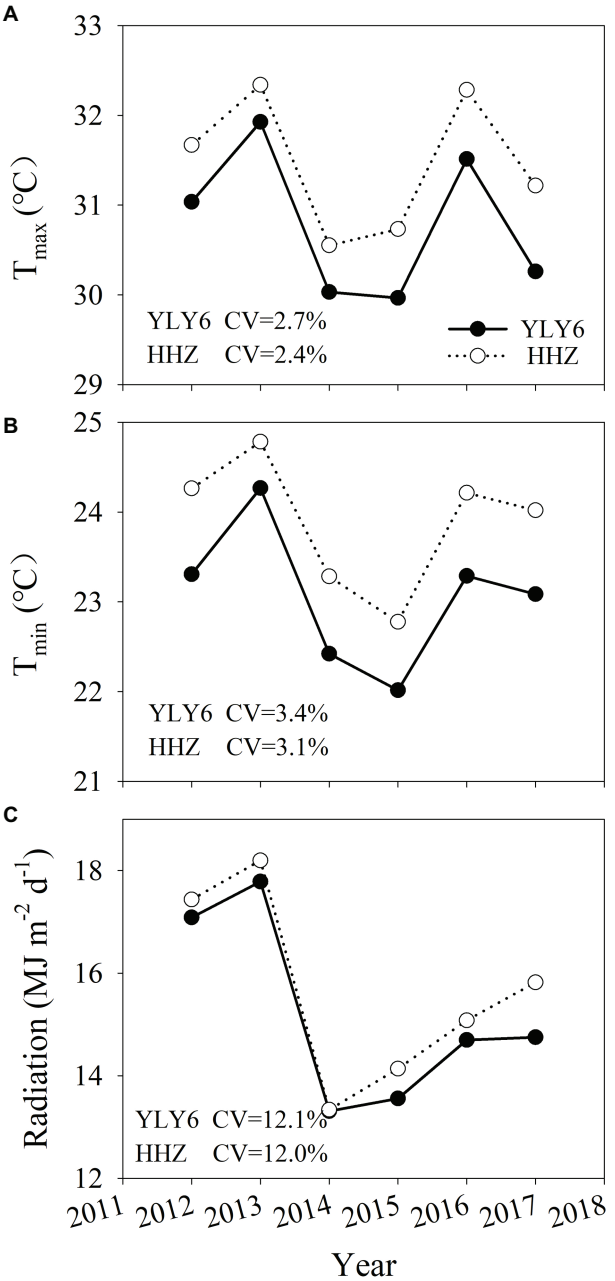


FIGURE 1 | The average daily maximum (T_{max}, **A**) and minimum temperature (T_{min}, **B**), and solar radiation **(C)** for YLY6 and HHZ during the rice-growing seasons (from transplanting to maturity) in Hubei Province, China, from 2012 to 2017. CV is the coefficient of variation.

average temperature and solar radiation were the highest in 2013 and relatively lower in 2014 and 2015. In general, HHZ experienced higher temperature and solar radiation than YLY6 during the rice-growing seasons from transplanting to maturity.

Growth Duration

Significant differences in days to heading and total growth duration were observed in YLY6 and HHZ from 2012 to 2017 (**Figure 2**). Averaged across 2012–2017, pre-flowering (from transplanting to heading), post-flowering (from heading to maturity), and total growth duration (from seeding to maturity) were longer in YLY6 than those in HHZ by 11, 6, and 18 days, respectively. Pre-flowering, post-flowering, and total growth duration of YLY6 ranged from 71 to 78, 34 to 48, and 140 to 149 days across years, respectively. The difference in total growth duration of YLY6 among experimental years was mainly due to the difference in post-flowering growth duration. The total growth duration of YLY6 was the longest in 2014, 2015, and 2017, but the shortest in 2013. The ranges of pre-flowering, post-flowering, and total growth duration of HHZ were 59–68, 33–39, and 126–130 days in 2012–2017, respectively. The total growth duration of HHZ was the highest in 2015, but the lowest in 2014 and 2016.

Grain Yield and Yield Components

Experimental year, cultivar, and their interaction significantly affected the grain yield and yield components, except for the effect of cultivar on grain filling percentage and the interactive effect on spikelets per panicle (**Table 1**). Averaged across all experimental years, the grain yield of YLY6 was significantly higher than that of HHZ by 7.1% (9.99 t ha^{-1} in YLY6 vs. 9.33 t ha^{-1} in HHZ). The yield difference between YLY6 and HHZ was explained by sink size (1181.4 g m^{-2} in YLY6 vs. 1031.0 g m^{-2} in HHZ), which was mainly due to the difference in the grain weight (26.9 mg in YLY6 vs. 18.8 mg in HHZ).

In 6 experiment years, the grain yield of YLY6 ranged from 9.20 to 11.22 t ha^{-1}, and the coefficient of variation (CV) was 7.3% (**Table 1**). The highest and lowest yields of YLY6 were achieved in 2015 and 2017, respectively. All yield components of YLY6 were the highest in 2015 among 6 experiment years, but the minimum value of each yield component was obtained in different years. The CV of yield components for YLY6 varied from 3.3 to 14.2%. Significant positive correlations between grain yield of YLY6 and its spikelets panicle^{-1}, spikelets m^{-2}, and sink size were observed during the experimental years, and the determinant coefficients (R^2) were 0.97, 0.91, and 0.86, respectively (**Figure 3**). The grain yield of HHZ varied from 7.97 to 10.63 t ha^{-1} in 2012–2017, and the CV was 10.5% (**Table 1**). HHZ produced more than 10 t ha^{-1} of grain yield in 2014 and 2015, but less than 8 t ha^{-1} in 2013. Yield components of HHZ were significantly affected by experiment years, and the CV of yield components ranged from 6.0 to 14.3%. The yield difference of HHZ was mainly explained by the differences in grain filling percentage (R^2 = 0.94) and grain weight (R^2 = 0.89) among experiment years (**Figure 3**).

Dry Matter Accumulation and Harvest Index

The total dry weight averaged across 2012–2017 was higher in YLY6 by 9.2% than that in HHZ (**Figure 4**). A significantly higher total dry weight of YLY6 was mainly attributed to its higher pre-flowering dry weight, since post-flowering dry weight was comparative between the two cultivars. In six experimental years, the total dry weights of YLY6 and HHZ ranged from 18.0 to 20.5 t ha^{-1} and from 15.3 to 21.7 t ha^{-1}, and the CV

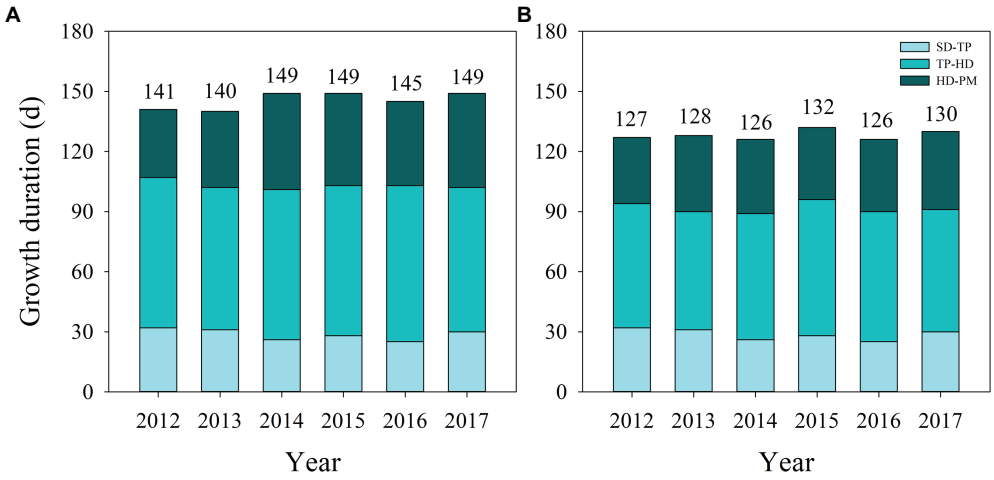


FIGURE 2 | Growth duration of YLY6 **(A)** and HHZ **(B)** from seeding to transplanting, transplanting to heading, and heading to maturity in Hubei Province, China, from 2012 to 2017. The numbers above the columns represent total growth duration from seeding to maturity. SD – seeding; TP – transplanting; HD – heading; PM – maturity.

TABLE 1 | Grain yield and yield components of YLY6 and HHZ from 2012 to 2017.

Variety	Year	Grain yield (t ha^{-1})	Panicles (m^{-2})	Spikelets (panicle^{-1})	Spikelets (×10^3 m^{-2})	Grain filling (%)	Grain weight (mg)	Sink size (g m^{-2})
	2012	9.49	229.5	185.9	42.7	75.8	27.3	1167.2
	2013	9.69	207.3	189.1	39.2	81.1	26.8	1052.0
	2014	10.39	229.3	202.4	46.4	76.5	27.2	1258.8
	2015	11.22	245.2	214.9	52.5	93.2	28.2	1478.6
YLY6	2016	9.96	220.8	195.6	43.3	74.9	25.5	1103.2
	2017	9.20	221.9	175.6	38.8	88.4	26.6	1028.9
	$LSD_{0.05}$	**0.54**	**23.3**	**26.1**	**6.1**	**7.1**	**1.0**	**147.9**
	Mean	**9.99 A**	**225.7 B**	**193.9 A**	**43.8 B**	**81.6 A**	**26.9 A**	**1181.4 A**
	CV (%)	**7.3**	**5.5**	**7.1**	**11.6**	**9.2**	**3.3**	**14.2**
	2012	9.51	290.1	167.0	48.4	84.5	19.4	939.6
	2013	7.97	293.0	183.7	53.7	75.3	17.6	943.0
	2014	10.08	355.3	189.1	67.0	84.7	19.8	1328.2
	2015	10.63	305.6	160.5	49.0	91.5	20.3	995.2
HHZ	2016	9.28	312.5	174.8	54.6	83.7	18.1	985.7
	2017	8.52	328.7	171.7	56.3	77.6	17.7	994.4
	$LSD_{0.05}$	**0.66**	**22.3**	**18.9**	**5.2**	**2.5**	**0.3**	**87.1**
	Mean	**9.33 B**	**314.2 A**	**174.5 B**	**54.9 A**	**82.9 A**	**18.8 B**	**1031.0 B**
	CV (%)	**10.5**	**7.8**	**6.0**	**12.3**	**6.9**	**6.3**	**14.3**
Analysis of variance								
Year (Y)		**	**	*	**	**	**	**
Variety (V)		**	**	**	**	ns	**	**
Y*V		**	**	ns	**	**	**	*

*Within a column, means followed by different letters are significantly different between YLY6 and HHZ at $p \leq 0.05$ according to LSD. ns, not significant at the 0.05 probability level; * and **, significant at the 0.05 and 0.01 probability levels, respectively. In statistical analysis using the "Least Significant Difference" method, LSD0.05 represents the LSD value of the data at P=0.05 probability level. Mean and CV represent the mean value and coefficient of variation of data from 2012 to 2017 for each parameter, respectively.*

was 5.0 and 13.8%, respectively. The harvest indexes (HI) of YLY6 and HHZ were 48.0 and 49.5% averaged across 2012–2017, respectively, and the difference in the average HI between YLY6 and HHZ was not significant. HI of YLY6 and HHZ varied from 45.1 to 54.2% and from 43.7 to 55.4%, and the CV was 6.6 and 8.5%, respectively. In terms of total dry weight and harvest index, HI rather than total dry weight explained the interannual variation in yield for both YLY6 and HHZ (**Figure 5**).

Correlations Between Yield Attributes and Climate Parameters

Grain yield and yield attributes were not related to the average daily maximum temperature (T_{max}) and solar radiation in YLY6 and HHZ ($p > 0.05$; **Figure 6**). Negative relationships between grain yield and the average daily minimum temperature (T_{min}) of the whole growing season were observed in both YLY6 and HHZ, but the correlation was statistically

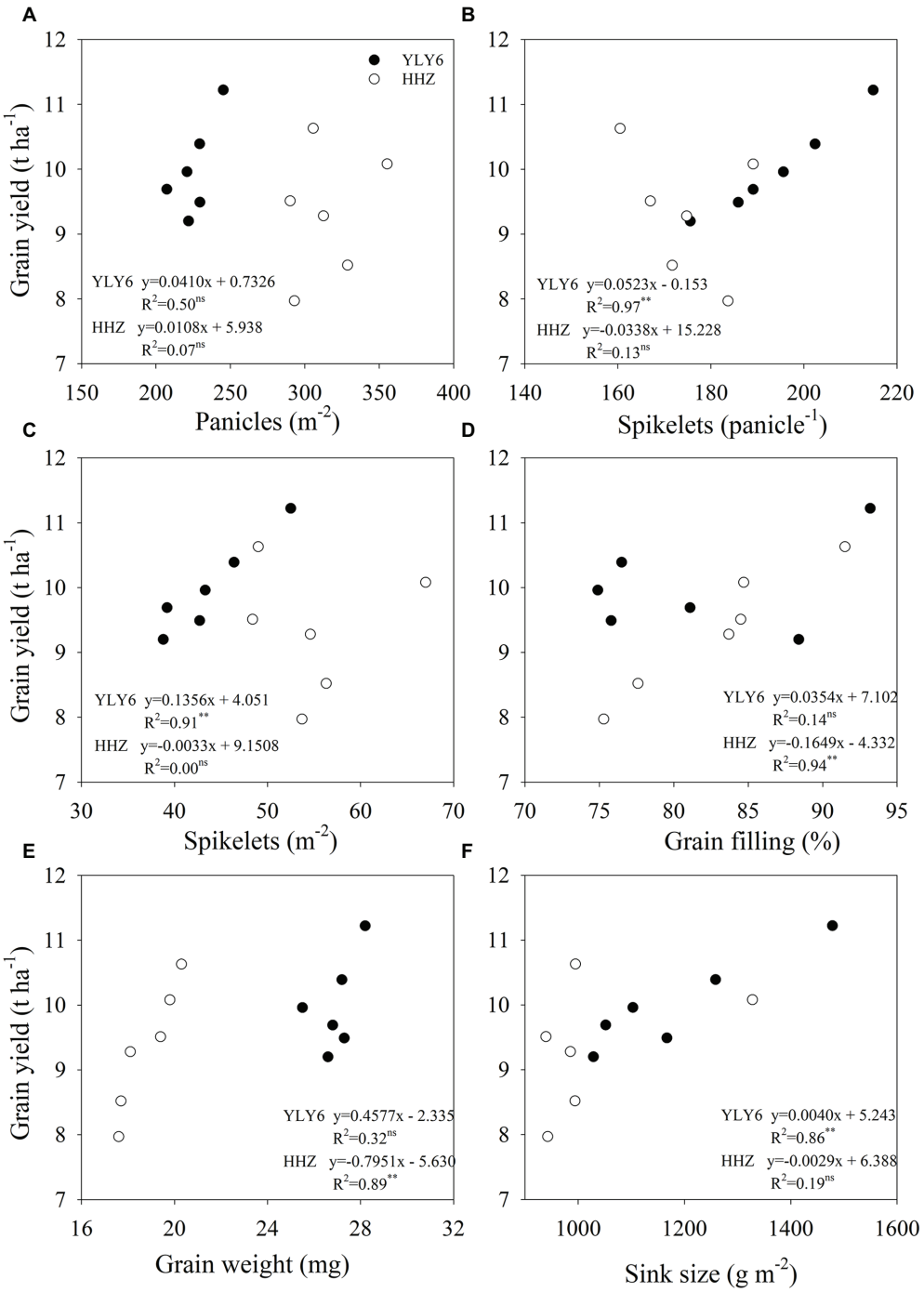


FIGURE 3 | Correlations of yield components (panicles m^{-2}, spikelets per panicle, spikelets m^{-2}, grain filling percentage, grain weight, and sink size) with grain yield **(A–F)** for YLY6 and HHZ (n = 6), respectively. ns and ** are not statistically significant at the $p \leq 0.05$ and significant at the $p \leq 0.01$ probability level according to the Student's t test, respectively.

significant only in HHZ ($p < 0.05$; **Figure 6G**). Around 79% of the interannual yield difference in HHZ was explained by growing-season T_{min}. The grain yield of HHZ decreased by 1.18 t ha^{-1} (≈12.6%) for each 1°C increase in the growing-season T_{min}. The partial-correlation coefficient between grain yield and minimum temperature with solar radiation held constant was −0.48 and −0.71 for YLY6 and HHZ, respectively. The partial-correlation coefficient between grain yield and solar radiation with minimum temperature held constant was 0.07 and 0.01 for YLY6 and HHZ, respectively (data not shown). The partial-correlation analysis shows that the increases in growing-season T_{min}, even small in range, had

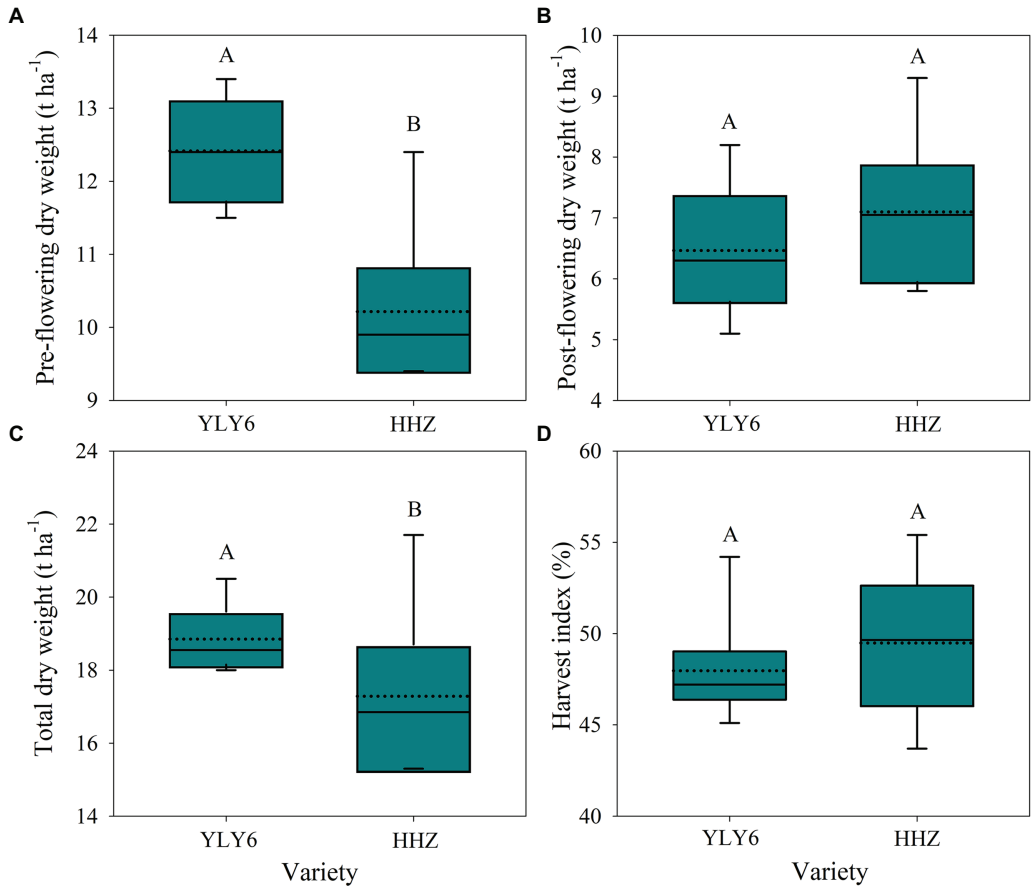


FIGURE 4 | Dry weight before flowering **(A)**, dry weight after flowering **(B)**, total dry weight at maturity **(C)**, and harvest index **(D)** for YLY6 and HHZ in Hubei Province, China, from 2012 to 2017. The box–whisker diagrams show the maximum (top of the vertical line), the 75th percentile (top of the box), the median (horizontal line within the box), the average (dotted lines within the box), the 25th percentile (bottom of the box), and the minimum (bottom of the vertical line) values (n = 6). The different letters represent means that are significantly different at the 0.05 probability level according to LSD.

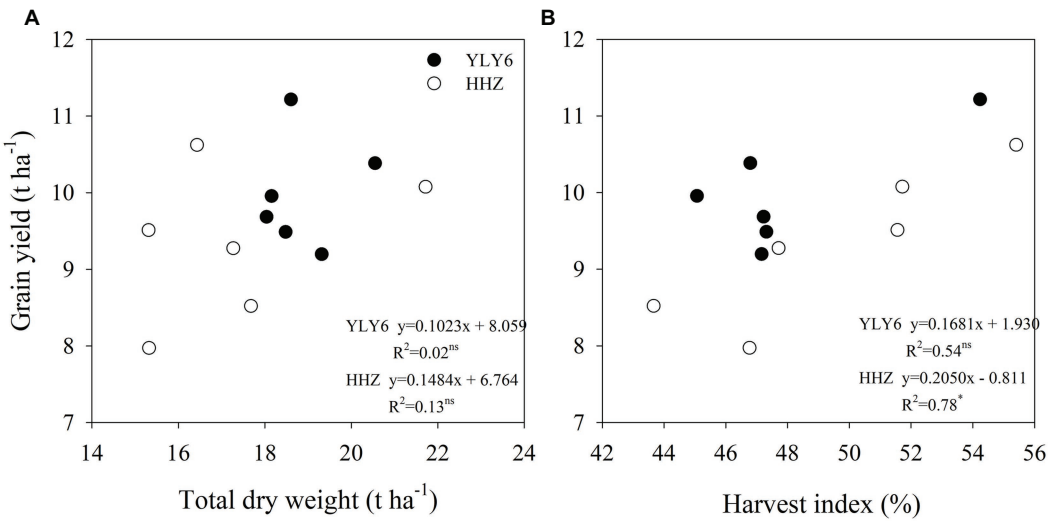


FIGURE 5 | Correlations of total dry weight **(A)** and harvest index **(B)** with grain yield for YLY6 and HHZ (n = 6), respectively. ns and * are not statistically significant and significant at the $p \leq 0.05$ probability level according to the Student's t test, respectively.

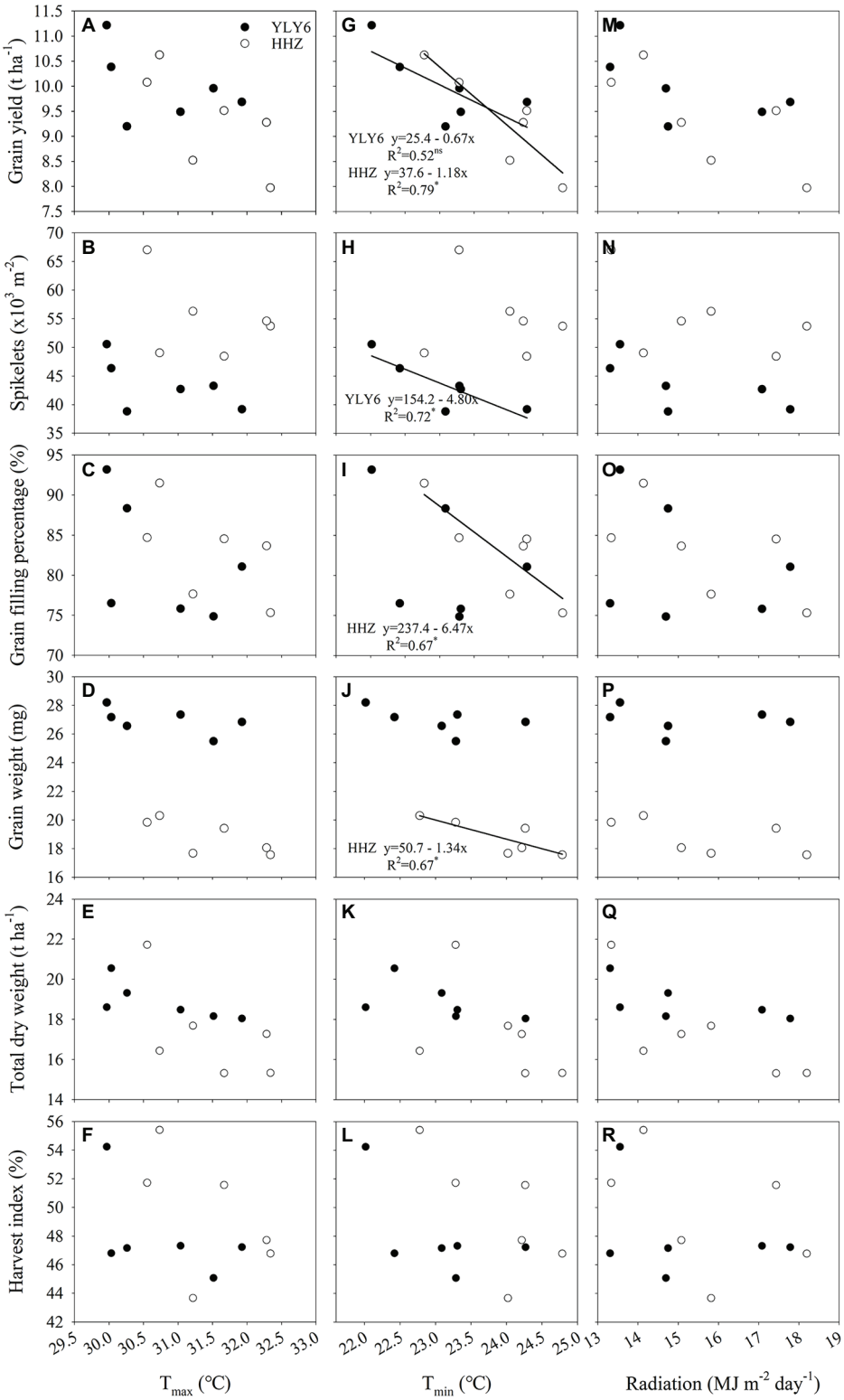


FIGURE 6 | The relationship between rice-yield attributes (grain yield, spikelets m^{-2}, grain filling percentage, grain weight, total dry weight, and harvest) and growing-season mean maximum temperature **(A–F)**, minimum temperature **(G–L)**, and radiation **(M–R)** for YLY6 and HHZ. Growing-season mean maximum and minimum temperature and radiation were calculated from daily values for the entire season from transplanting to harvest. ns and * are not statistically significant and significant at the $p \leq 0.05$ probability level according to the Student's *t* test, respectively. The regression equations are not shown in the graphs when the correlations are not significant. T_{max} – the growing-season mean maximum temperature; T_{min} – the growing-season mean minimum temperature.

a negative effect on the grain yield of YLY6 and HHZ, especially on HHZ, and that the effect was independent of solar radiation.

With the increase of growing-season T_{min}, spikelets m^{-2} declined linearly in YLY6 ($p < 0.05$; **Figure 6H**). Spikelets m^{-2} reduced by 13.7×10^3 (≈26.1%) from a 2.3°C increase in minimum temperature for YLY6. There were significant and negative relationships between grain filling percentage, grain weight, and the growing-season T_{min} in HHZ ($p < 0.05$; **Figures 6I,J**). The growing-season T_{min} explained 67% of the interannual variation in grain filling percentage and grain weight. Panicles m^{-2} were significantly and negatively related to the growing-season T_{min} only in YLY6 ($p < 0.05$), and spikelets $panicle^{-1}$ were not related to the growing-season T_{min} for both YLY6 and HHZ ($p > 0.05$; data not shown). Total dry weight and HI decreased with the increase of the growing-season T_{min}, but the correlation was not significant ($p< 0.05$; **Figures 6K,L**). The average T_{min} from transplanting to maturity was lower in YLY6 than in HHZ, which was mainly due to lower T_{min} from heading to maturity in YLY6 (**Supplementary Table S1**). Besides, the T_{min} of the week prior to heading and the week post heading were 1.3 and 1.7 lower in YLY6 than those in HHZ averaged across 6 years, respective (**Supplementary Table S1**). Further analysis found that spikelets m^{-2} of YLY6 significantly and negatively correlated with T_{min} from transplanting to heading. For HHZ, grain filling percentage and grain weight were significantly affected by T_{min} of the week prior to heading and from heading to maturity, respectively (**Figure 7**).

DISCUSSION

Rapid increases in minimum night temperature compared to maximum day temperature have been reported and are predicted to continue, posing a big challenge to rice production (Peng et al., 2004). Efforts are required to improve our understanding of the genotypic variation in response to night temperature, which will be conducive to achieving both high and stable yield through genetic improvement. In the present study, significant variation in grain yield was observed for both the inbred and hybrid cultivars across 6 planting years, and the CV for grain yield was 7.3–10.5% (**Table 1**). The hybrid cultivar YLY6 had a significantly higher and more stable grain yield than the inbred cultivar HHZ. Further analysis illustrated that variability in night temperature contributed to the yield variability in both cultivars despite the larger year-to-year variability in radiation (**Figure 6**). This is consistent with Wang et al. (2016), who found that the lower rice yield and radiation use efficiency in the tropical environment were mainly due to the higher temperature (instead of radiation) compared with the subtropical environment. By analyzing the historical yields and daily weather data in 1981–2010 on a global scale, Iizumi and Ramankutty (2016) found that over 21% of the yield variability change could be explained by the change in climate variability, especially the variability of temperatures exceeding the optimal range for yield formation. Ray et al. (2015) found that climate variation explained a third of global yield variability, and there were numerous regions where climate variability explained more than 60% of the yield variability in maize, rice, wheat, and soybean. Here we found that variability in night temperature explained around 80% of the interannual yield variability in rice (**Figure 6**).

Although it is well known that high night temperatures lead to yield loss, few studies focus on the genotypic variation of rice in response to high night temperature, especially in farmers' field conditions. In the present study, YLY6 (one hybrid cultivar) and HHZ (one inbred cultivar) are both the most widely planted cultivars in the last decades in Central China, which showed different responses to the change in T_{min} (**Figures 6, 7**). A significant negative correlation between grain yield and T_{min} was observed in HHZ, but not in YLY6 (**Figure 6**). Yang et al. (2017) reported that YLY6 performed better than HHZ in grain yield under daytime, nighttime, and all-day elevated-temperature treatments. Rehmani et al. (2014) found that Shanyou-63 was more susceptible to daytime warming, while Teyou-559 was affected more by nighttime warming. These studies suggested that significant genotypic variation exists among the elite hybrid and inbred rice cultivars in response to night temperature.

The yield variation in YLY6 was mainly explained by the effect of T_{min} on spikelets m^{-2}, but not on grain filling percentage and grain weight (**Figure 6**). For example, T_{min} was the highest in 2013 during the 6 years, and grain yield of YLY6 was higher than that of HHZ by 1.72 t ha^{-1} (21.6%) in this year (**Table 1**; **Figure 1**). Reduction in spikelets m^{-2} of YLY6 was compensated by a high grain filling percentage, which resulted in the high grain yield in 2013 (**Table 1**). T_{min} had a significant effect on the spikelets m^{-2} of YLY6, but not in HHZ, possibly because of the difference in their spikelets per panicle. YLY6, as a hybrid variety, had more spikelets per panicle than HHZ (**Table 1**), which might result in more spikelet abortion in YLY6 when exposed to heat stress. The spikelet fertility of rice was extremely sensitive to high temperature, and the adverse effect of high temperature on spikelet fertility was even higher at nighttime than at daytime (Fahad et al., 2018). Mohammed and Tarpley (2009) found that spikelet fertility was significantly reduced due to the reduction in pollen germination when night temperature during the reproductive growth was increased from 27 to 32°C in the greenhouse. The decrease of spikelet fertility in rice caused by high temperature mainly occurred at panicle initiation and flowering stages, which might be related to the development of reproductive organs, the process of anther dehiscence, powder dispersal, and pollen tube elongation (Cheng et al., 2009; Fahad et al., 2018; Hu et al., 2020). In the study, we also found that with the increase of T_{min} from transplanting to heading, the spikelets m^{-2} decreased significantly in YLY6, but not in HHZ (**Figure 7**). Peng et al. (2004) found that spikelets m^{-2} were significant reduced along with the increase in night temperature. The physiological mechanism of the different responses of spikelets m^{-2} to T_{min} between YLY6 and HHZ requires further investigation.

The change in grain filling percentage and grain weight in response to T_{min} also accounted for the yield variability in HHZ across 6 planting years (**Figure 6**). In field conditions, a near 2°C increase in night temperature during the reproductive growth resulted in a change in grain filling percentage by −12.2 to +2.7% (Shah et al., 2014). High-temperature exposure

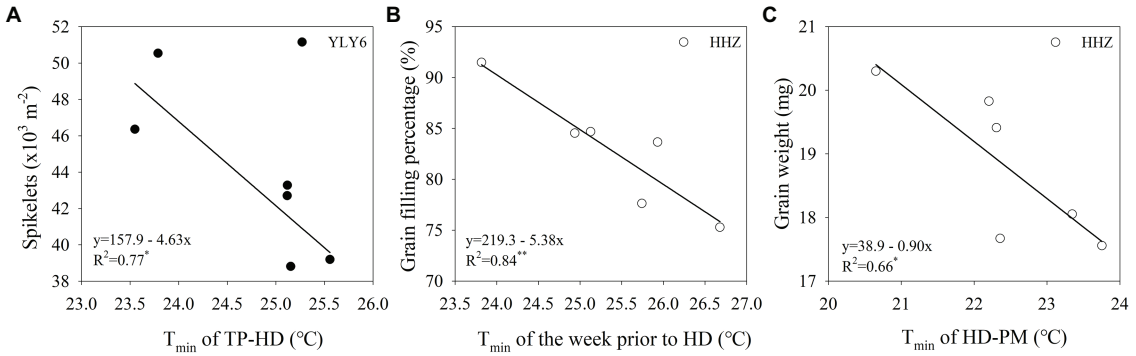


FIGURE 7 | The relationship between spikelets m^{-2} and T_{min} of transplanting (TP) to heading (HD) for YLY6 **(A)**, between grain filling percentage and T_{min} of the week prior to HD for HHZ **(B)**, and between grain weight and T_{min} of HD to maturity (PM) for HHZ **(C)**. * and ** are statistically significant at the $p \leq 0.05$ and $p \leq 0.01$ probability level according to the Student's *t* test, respectively. The regression equations are not shown in the graphs when the correlations are not significant. T_{min} – the growing-season mean minimum temperature.

during grain filling resulted in a decrease in grain weight due to the limited supply of assimilates and shortened grain-filling duration (Kobata and Uemuki, 2004; Shi et al., 2013). Morita et al. (2005) found that the adverse effect of high temperature on grain weight was greater at nighttime than at daytime. HHZ, as an inbred variety, had shorter post-flowering growth duration and total dry weight than YLY6, which might cause lower grain weight. Besides, high night temperature during the grain filling stage led to increased whole plant senescence and restricting translocation of dry matter from source to sink (Impa et al., 2021), which might have further reduced the grain filling percentage and grain weight in HHZ. Wu et al. (2016) also reported that yield reduction in HHZ was partly attributed to reduction in grain weight. Further analysis illustrated that grain filling percentage and grain weight for HHZ were significantly affected by T_{min} of the week prior to the heading and grain filling stages, respectively (**Figure 7**). The reproductive growth stage including panicle initiation, flowering, and grain filling is the most temperature-sensitive stage in rice. As a result, T_{min} affected the interannual yield variation in YLY6 and HHZ through different effects on reproductive growth. Despite the significant effect of high night temperature on yield variability through its effects on the development of spikelets and grain filling, the underlying physiological mechanisms are still obscure and need more attention.

Developing climate-resilient cultivars has been proposed and implemented by worldwide scientists to overcome the challenges of climate change (Mittler and Blumwald, 2010; Kole et al., 2015; Harfouche et al., 2019). Here we demonstrate the advantage of hybrid rice over inbred rice in both yield potential and yield stability (**Table 1**). It has been widely reported that the grain yield of hybrid rice is higher than that of inbred rice (Yuan et al., 1994; Peng et al., 1999, 2008). Given the different responses of grain yield and yield components of hybrid and inbred varieties to T_{min}, more attention should be paid to improving spikelet fertility of hybrid rice, and increasing grain filling and grain weight of inbred rice. Therefore, climate-resilient varieties and reasonable cultivation practices could be used to reduce yield loss caused by global warming, especially the increase of night temperature.

CONCLUSION

The present study found significant interannual variability in grain yield of hybrid and inbred cultivars in Central China, which was related to the variability in night temperature. The yield variation in HHZ was mainly explained by the effects of T_{min} on grain filling percentage and grain weight, while the change in spikelets m^{-2} in response to T_{min} accounted for the yield variability in YLY6. The genotypic difference was observed in the response of yield and yield components to the change in night temperature. There is a potential for genetic improvement in the yield potential and yield stability simultaneously in response to the increasing climate variability.

DATA AVAILABILITY STATEMENT

The original contributions presented in the study are included in the article/**Supplementary Material**, further inquiries can be directed to the corresponding author.

AUTHOR CONTRIBUTIONS

YZ conceived and designed the research. LH and YL conducted the experiments and collected the data. LH and FW analyzed the data and wrote the paper. YZ and FW commented and revised the paper. All authors contributed to the article and approved the submitted version.

FUNDING

This work was financially supported by the National Key Research and Development Program of China (2018YFD0301306),

Engineering Research Center of Ecology and Agricultural Use of Wetland, Ministry of Education (KF202011), the National Natural Science Foundation of China (32001467), and the grants from by the National Key Research and Development Program of China (2017YFD0301401-3 and 2016YFD0300208-03).

SUPPLEMENTARY MATERIAL

The Supplementary Material for this article can be found online at: https://www.frontiersin.org/articles/10.3389/fpls.2021.646168/full#supplementary-material

REFERENCES

An, N., Wei, W. L., Qiao, L., Zhang, F. S., Christie, P., Jiang, R. F., et al. (2018). Agronomic and environmental causes of yield and nitrogen use efficiency gaps in Chinese rice farming systems. *Eur. J. Agron.* 93, 40–49. doi: 10.1016/j.eja.2017.11.001

Battisti, D. S., and Naylor, R. L. (2009). Historical warnings of future food insecurity with unprecedented seasonal heat. *Science* 323, 240–244. doi: 10.1126/science.1164363

Blanche, S. B., and Linscombe, S. D. (2009). Stability of rice grain and whole kernel milling yield is affected by cultivar and date of planting. *Agron. J.* 101, 522–528. doi: 10.2134/agronj2008.0160x

Bueno, C. S., Pasuquin, E., Tubana, B., and Lafarge, T. (2010). Improving sink regulation, and searching for promising traits associated with hybrids, as a key avenue to increase yield potential of the rice crop in the tropics. *Field Crop Res.* 118, 199–207. doi: 10.1016/j.fcr.2010.04.004

Cassman, K. G., Dobermann, A., Walters, D. T., and Yang, H. (2003). Meeting cereal demand while protecting natural resources and improving environmental quality. *Annu. Rev. Environ. Resour.* 28, 315–358. doi: 10.1146/annurev.energy.28.040202.122858

Cheng, S. H., Cao, L. Y., Zhuang, J. Y., Chen, S., Zhan, X. F., Fan, Y. Y., et al. (2007). Super hybrid rice breeding in China: achievements and prospects. *J. Integr. Plant Biol.* 49, 805–810. doi: 10.1111/j.1744-7909.2007.00514.x

Cheng, W. G., Sakai, H., Yagi, K., and Hasgawa, T. (2009). Interactions of elevated [CO2] and night temperature on rice growth and yield. *Agric. For. Meteorol.* 149, 51–58. doi: 10.1016/j.agrformet.2008.07.006

Evans, L. T. (1993). *Crop Evolution, Adaptation and Yield*. Cambridge: Cambridge University Press.

Fahad, S., Ihsan, M. Z., Khaliq, A., Daur, I., Saud, S., Alzamanan, S., et al. (2018). Consequences of high temperature under changing climate optima for rice pollen characteristics-concepts and perspectives. *Arch. Agron. Soil Sci.* 64, 1473–1488. doi: 10.1080/03650340.2018.1443213

FAO (2016). FAOSTAT Database: Agriculture Production. Available at: http://faostat.fao.org/site/291/default.aspx (Accessed October 25, 2020).

Gong, W. G., Hu, M. Z., Hua, Q. X., and Lu, J. X. (2008). Reason analysis of rice yield fluctuation in recent years. *Shanghai Agric. Sci. Technol.* 4:34. doi: 10.3969/j.issn.1001-0106.2008.04.025

Gravois, K. A., and Helms, R. S. (1998). Seeding date effects on rough rice yield and head rice and selection for stability. *Euphytica* 102, 151–161. doi: 10.1023/A:1018344615296

Harfouche, A. L., Jacobson, D. A., Kainer, D., Romero, J. C., Harfouche, A. H., Mugnozza, G. S., et al. (2019). Accelerating climate resilient plant breeding by applying next-generation artificial intelligence. *Trends Biotechnol.* 37, 1217–1235. doi: 10.1016/j.tibtech.2019.05.007

Hu, Q. Q., Yan, N., and Cui, K. H. (2020). High temperature injury on spikelet fertility and its regulation in rice. *Plant Physiol. J.* 56, 1177–1190. doi: 10.13592/j.cnki.ppj.2019.0223

Huang, M., and Zou, Y. B. (2018). Integrating mechanization with agronomy and breeding to ensure food security in China. *Field Crop Res.* 224, 22–27. doi: 10.1016/j.fcr.2018.05.001

Huang, M., Zou, Y. B., Jiang, P., Xia, B., Ibrahim, M., and Ao, H. J. (2011). Relationship between grain yield and yield components in super hybrid rice. *J. Integr. Agric.* 10, 1537–1544. doi: 10.1016/S1671-2927(11)60149-1

Iizumi, T., and Ramankutty, N. (2016). Changes in yield variability of major crops for 1981-2010 explained by climate change. *Environ. Res. Lett.* 11:034003. doi: 10.1088/1748-9326/11/3/034003

Impa, S. M., Raju, B., Hein, N. T., Sandhu, J., Prasad, P. V. V., Walia, H., et al. (2021). High night temperature effects on wheat and rice-current status and way forward. *Plant Cell Environ.* doi: 10.1111/pce.14028 [Epub ahead of print]

Jaruchai, W., Monkham, T., Chankaew, S., Suriharn, B., and Sanitchon, J. (2018). Evaluation of stability and yield potential of upland rice genotypes in North and Northeast Thailand. *J. Integr. Agric.* 17, 28–36. doi: 10.1016/S2095-3119(16)61609-X

Kobata, T., and Uemuki, N. (2004). High temperatures during the grain-filling period do not reduce the potential grain dry matter increase of rice. *Agron. J.* 96, 406–414. doi: 10.2134/agronj2004.0406

Kole, C., Muthamilarasan, M., Henry, R., Edwards, D., Sharma, R., Abberton, M., et al. (2015). Application of genomics-assisted breeding for generation of climate resilient crops: progress and prospects. *Front. Plant Sci.* 6:563. doi: 10.3389/fpls.2015.00563

Kropff, M. J. (1994). "Quantitative understanding of yield potential," in *Breaking the Yield Potential*. eds. K. G. Cassman, S. B. Peng, R. B. Mathews and T. L. Setter (Los Baños, Philippines: International Rice Research Institute (IRRI)), 21–38.

Lobell, D. B., and Burke, M. B. (2008). Why are agricultural impacts of climate change so uncertain? The importance of temperature relative to precipitation. *Environ. Res. Lett.* 3:34007. doi: 10.1088/1748-9326/3/3/034007

Lobell, D. B., Cassman, K. G., and Field, C. B. (2009). Crop yield gaps: their importance, magnitudes, and causes. *Annu. Rev. Environ. Resour.* 34, 179–204. doi: 10.1146/annurev.environ.041008.093740

Ma, L., Yang, L. Z., Shen, M. X., Xia, L. Z., Li, Y. D., Liu, G. H., et al. (2011). Study on crop yield stability in a typical region of rice-wheat rotation based on long-term fertilization experiment. *Trans. Chinese Soc. Agric. Eng.* 27, 117–124. doi: 10.3969/j.issn.1002-6819.2011.04.020

Matsui, T., and Omasa, K. (2002). Rice (*Oryza sativa* L.) cultivars tolerant to high temperature at flowering: anther characteristics. *Ann. Bot.* 89, 683–687. doi: 10.1093/aob/mcf112

Mittler, R., and Blumwald, E. (2010). Genetic engineering for modern agriculture: challenges and perspectives. *Annu. Rev. Plant Biol.* 61, 443–462. doi: 10.1146/annurev-arplant-042809-112116

Mohammed, A. R., and Tarpley, L. (2009). High nighttime temperatures affect rice productivity through altered pollen germination and spikelet fertility. *Agric. For. Meteorol.* 149, 999–1008. doi: 10.1016/j.agrformet.2008.12.003

Morita, S., Yonemaru, J. I., and Takanashi, J. I. (2005). Grain growth and endosperm cell size under high night temperatures in rice (*Oryza sativa* L.). *Ann. Bot.* 95, 695–701. doi: 10.1093/aob/mci071

National Bureau of Statistics (n.d.). Available at: http://www.stats.gov.cn/tjsj/

Ohsumi, A., Takai, T., Ida, M., Yamamoto, T., Arai-Sanoh, Y., Yano, M., et al. (2010). Evaluation of yield performance in rice near-isogenic lines with increased spikelet number. *Field Crop Res.* 120, 68–75. doi: 10.1016/j.fcr.2010.08.013

Peng, S. B., Cassman, K. G., Virmani, S. S., Sheehy, J., and Khush, G. S. (1999). Yield potential trends of tropical rice since the release of IR8 and the challenge of increasing rice yield potential. *Crop Sci.* 39, 1552–1559. doi: 10.2135/cropsci1999.3961552x

Peng, S. B., Huang, J. L., Sheehy, J. E., Laza, R. C., Visperas, R. M., Zhong, X. H., et al. (2004). Rice yields decline with higher night temperature from global warming. *Proc. Natl. Acad. Sci. U. S. A.* 101, 9971–9975. doi: 10.1073/pnas.0403720101

Peng, S. B., Khush, G. S., Virk, P., Tang, Q. Y., and Zou, Y. B. (2008). Progress in ideotype breeding to increase rice yield potential. *Field Crop Res.* 108, 32–38. doi: 10.1016/j.fcr.2008.04.001

Ray, D. K., Gerber, J. S., MacDonald, G. K., and West, P. C. (2015). Climate variation explains a third of global crop yield variability. *Nat. Commun.* 6, 1–9. doi: 10.1038/ncomms6989

Rehmani, M. I. A., Wei, G. B., Hussain, N., Ding, C. Q., Li, G. H., Liu, Z. H., et al. (2014). Yield and quality of two *indica* rice hybrids to post-anthesis asymmetric day and night open-field warming in lower reaches of Yangtze River delta. *Field Crop Res.* 156, 231–241. doi: 10.1016/j.fcr.2013.09.019

Sanchez, B., Rasmussen, A., and Porter, J. R. (2014). Temperatures and the growth and development of maize and rice: a review. *Glob. Chang. Biol.* 20, 408–417. doi: 10.1111/gcb.12389

Shah, F., Nie, L. X., Cui, K. H., Shah, T., Wu, W., Chen, C., et al. (2014). Rice grain yield and component responses to near 2°C of warming. *Field Crop Res.* 157, 98–110. doi: 10.1016/j.fcr.2013.12.014

Shi, W. J., Muthurajan, R., Rahman, H., Selvam, J., Peng, S. B., Zou, Y. B., et al. (2013). Sourcesink dynamics and proteomic reprogramming under elevated night temperatures and their impact on rice yield and grain quality. *New Phytol.* 197, 825–837. doi: 10.1111/nph.12088

Sun, Y. F., Liang, Y. M., Wu, G. M., Yang, Q. Q., Chen, J. H., and Lou, W. P. (2013). Evaluation of the maximum grain yield of Yongyou12 over 1000 kg per 667 m^2. *China Rice* 19, 94–96.

Tao, Y. Y., Qu, H., Li, Q. J., Gu, X. H., Zhang, Y. N., Liu, M. J., et al. (2014). Potential to improve N uptake and grain yield in water saving ground cover rice production system. *Field Crop Res.* 168, 101–108. doi: 10.1016/j.fcr.2014.08.014

Tao, F. L., and Zhang, H. (2013). Climate change, high-temperature stress, rice productivity, and water use in Eastern China: a new superensemble-based probabilistic projection. *J. Appl. Meteorol. Climatol.* 52, 531–551. doi: 10.1175/JAMC-D-12-0100.1

Tao, F. L., Zhang, Z., Shi, W. J., Liu, Y. J., Xiao, D. P., Zhang, S., et al. (2013). Single rice growth period was prolonged by cultivars shifts, but yield was damaged by climate change during 1981-2009 in China, and late rice was just opposite. *Glob. Chang. Biol.* 19, 3200–3209. doi: 10.1111/gcb.12250

Tashiro, T., and Wardlaw, I. (1991). The effect of high temperature on kernel dimensions and the type of occurrence of kernel damage in rice. *Aust. J. Agric. Res.* 42, 485–496. doi: 10.1071/AR9910485

Van Wart, J., Kersebaum, K. C., Peng, S. B., Milner, M., and Cassman, K. G. (2013). Estimating crop yield potential at regional to national scales. *Field Crop Res.* 143, 34–43. doi: 10.1016/j.fcr.2012.11.018

Wang, D. P., Laza, M. R. C., Cassman, K. G., Huang, J. L., and Peng, S. B. (2016). Temperature explains the yield difference of double-season rice between tropical and subtropical environments. *Field Crop Res.* 198, 303–311. doi: 10.1016/j.fcr.2016.05.008

Wang, B. S., Lu, D. M., Liu, W. Y., and Du, X. L. (2004). Reason analysis of rice yield fluctuation in Jiangxi province and its corresponding solutions. *Jiangxi Meteorol. Sci. Technol.* 27, 25–27. doi: 10.3969/j.issn.1007-9033.2004.02.007

Wu, C., Cui, K. H., Wang, W. C., Li, Q., Fahad, S., Hu, Q. Q., et al. (2016). Heat-induced phytohormone changes are associated with disrupted early reproductive development and reduced yield in rice. *Sci. Rep.* 6:34978. doi: 10.1038/srep34978

Yang, Z. Y., Zhang, Z. L., Zhang, T., Fahad, S., Cui, K. H., Nie, L. X., et al. (2017). The effect of season-long temperature increases on rice cultivars grown in the central and southern regions of China. *Front. Plant Sci.* 8:1908. doi: 10.3389/fpls.2017.01908

Yuan, L. P., Yang, Z., and Yang, J. (1994). "Hybrid rice in China," in *Hybrid Rice Technology: New Developments and Future Prospects*. ed. S. S. Virmani (Los Banos, Philippines: International Rice Research Institute), 143–147.

Zhang, H., Chen, T. T., Liu, L. J., and Wang, Z. Q., Yang, J. C, and Zhang, J. H. (2013). Performance in grain yield and physiological traits of rice in the Yangtze river basin of China during the last 60 yr. *J. Integr. Agric.* 12, 57–66, doi: 10.1016/S2095-3119(13)60205-1.

Zhao, C., Liu, B., Piao, S. L., Wang, X. H., Lobell, D. B., Huang, Y., et al. (2017). Temperature increase reduces global yields of major crops in four independent estimates. *Proc. Natl. Acad. Sci. U. S. A.* 114, 9326–9331. doi: 10.1073/pnas.1701762114

Zhu, G. L., Peng, S. B., Huang, J. L., Cui, K. H., Nie, L. X., and Wang, F. (2016). Genetic improvements in rice yield and concomitant increases in radiation- and nitrogen- use efficiency in middle reaches of Yangtze river. *Sci. Rep.* 6:21049. doi: 10.1038/srep21049

Conflict of Interest: The authors declare that the research was conducted in the absence of any commercial or financial relationships that could be construed as a potential conflict of interest.

The reviewer DX declared a shared affiliation, with no collaboration, with one of the authors FW to the handling editor at the time of the review.

Copyright © 2021 Huang, Wang, Liu and Zhang. This is an open-access article distributed under the terms of the Creative Commons Attribution License (CC BY). The use, distribution or reproduction in other forums is permitted, provided the original author(s) and the copyright owner(s) are credited and that the original publication in this journal is cited, in accordance with accepted academic practice. No use, distribution or reproduction is permitted which does not comply with these terms.

frontiers in Plant Science

ORIGINAL RESEARCH
published: 11 June 2021
doi: 10.3389/fpls.2021.628167

The Resistance of Oilseed Rape Microspore-Derived Embryos to Osmotic Stress Is Associated With the Accumulation of Energy Metabolism Proteins, Redox Homeostasis, Higher Abscisic Acid, and Cytokinin Contents

Milan O. Urban[1], Sébastien Planchon[2], Irena Hoštičková[3], Radomira Vanková[4], Peter Dobrev[4], Jenny Renaut[2], Miroslav Klíma[1] and Pavel Vítámvás[1]*

[1] Crop Research Institute, Plant Stress Biology and Biotechnology, Prague, Czechia, [2] Luxembourg Institute of Science and Technology, "Environmental Research and Innovation," (ERIN) Department, Belvaux, Luxembourg, [3] Department of Plant Production and Agroecology, University of South Bohemia in Ceské Budějovice, Ceské Budějovice, Czechia, [4] Laboratory of Hormonal Regulations in Plants, Institute of Experimental Botany of the Czech Academy of Sciences, Prague, Czechia

OPEN ACCESS

Edited by:
Felipe Klein Ricachenevsky, Federal University of Rio Grande Do Sul, Brazil

Reviewed by:
Vivek Kumar Pandey, University of Kentucky, United States
Rogerio Margis, Federal University of Rio Grande Do Sul, Brazil

***Correspondence:**
Milan O. Urban
m.urban@cgiar.org

Specialty section:
This article was submitted to Crop and Product Physiology, a section of the journal Frontiers in Plant Science

Received: *12 November 2020*
Accepted: *20 May 2021*
Published: *11 June 2021*

Citation:
Urban MO, Planchon S, Hoštičková I, Vanková R, Dobrev P, Renaut J, Klíma M and Vítámvás P (2021) The Resistance of Oilseed Rape Microspore-Derived Embryos to Osmotic Stress Is Associated With the Accumulation of Energy Metabolism Proteins, Redox Homeostasis, Higher Abscisic Acid, and Cytokinin Contents. Front. Plant Sci. 12:628167. doi: 10.3389/fpls.2021.628167

The present study aims to investigate the response of rapeseed microspore-derived embryos (MDE) to osmotic stress at the proteome level. The PEG-induced osmotic stress was studied in the cotyledonary stage of MDE of two genotypes: Cadeli (D) and Viking (V), previously reported to exhibit contrasting leaf proteome responses under drought. Two-dimensional difference gel electrophoresis (2D-DIGE) revealed 156 representative protein spots that have been selected for MALDI-TOF/TOF analysis. Sixty-three proteins have been successfully identified and divided into eight functional groups. Data are available *via* ProteomeXchange with identifier PXD024552. Eight selected protein accumulation trends were compared with real-time quantitative PCR (RT-qPCR). Biomass accumulation in treated D was significantly higher (3-fold) than in V, which indicates D is resistant to osmotic stress. Cultivar D displayed resistance strategy by the accumulation of proteins in energy metabolism, redox homeostasis, protein destination, and signaling functional groups, high ABA, and active cytokinins (CKs) contents. In contrast, the V protein profile displayed high requirements of energy and nutrients with a significant number of stress-related proteins and cell structure changes accompanied by quick downregulation of active CKs, as well as salicylic and jasmonic acids. Genes that were suitable for gene-targeting showed significantly higher expression in treated samples and were identified as phospholipase D alpha, peroxiredoxin antioxidant, and lactoylglutathione lyase. The MDE proteome profile has been compared with the leaf proteome evaluated in our previous study. Different mechanisms to cope with osmotic stress were revealed between the genotypes studied. This proteomic study is the first step to validate MDE as a suitable model for follow-up research on the characterization of new crossings and can be used for preselection of resistant genotypes.

Keywords: microspore, 2D-DIGE, osmotic stress, *Brassica napus*, screening, RT-qPCR

INTRODUCTION

Plant breeding is focused on the permanent increase of crop production to meet the needs of an ever-growing world population, improving food quality to ensure long and healthy life, and to address the problems of global warming and environmental pollution, together with the challenges associated with developing novel biofuel sources. A combination of different approaches (mechanistic physiological understanding, -omics, association mapping, envirotyping, gene editing, and other tools) need to be utilized to improve significantly the abiotic stress resistance of crops in the field (Mittler and Blumwald, 2010). It is worthy to study contrasting genotypes and search for proteins potentially correlated with abiotic stress adaptability and acclimation in order to characterize the responsiveness of individual genotypes to multiple environmental parameters (Frenck et al., 2011; Claeys et al., 2014).

Brassica napus (winter oilseed rape), the second most-grown oil crop in the world, is the major oilseed crop in temperate regions of Europe and China (Hu et al., 2011). Several proteomics articles and reviews on stress-treated plants from the *Brassicaceae* family have been published (Subramanian et al., 2005; Devouge et al., 2007; Zhu et al., 2010, 2012; Bandehagh et al., 2011; Demartini et al., 2011; Fernandez-Garcia et al., 2011; Gan et al., 2013; Chu et al., 2015; Shen et al., 2015), including integrated proteomic/transcriptomic approach (Kubala et al., 2015; Shokri-Gharelo and Noparvar, 2018; Zhang et al., 2019; Schiessl et al., 2020). However, despite the importance of oilseed rape worldwide, between the years 2005 and 2021, only four drought-focused comparative proteomic studies were aimed at *B. napus* [seedling roots (Mohammadi et al., 2012), 20-day-old seedlings (Koh et al., 2015), and mature plants (Wang et al., 2016; Urban et al., 2017)]. NaCl and PEG solution proteomic analysis on 15-day-old seedlings of one cultivar was studied by Luo et al. (2015).

Microspore embryogenesis (the formation of embryos from immature pollen grains) is a unique system that speeds up breeding programs and, in the context of developmental biology, provides an excellent tool for embryogenesis to be investigated in greater detail. For some species, isolated microspore culture protocols have been well-established and are routinely used in laboratories for developing new varieties as well as for basic research areas, such as genomics, gene expression, and genetic mapping (Ferrie and Caswell, 2011). The last few years have provided ample evidence that has allowed researchers of Brassica to markedly increase their understanding of the molecular and subcellular changes underlying the early events of totipotency that permit microspores to develop into embryos and facilitate their transformation (Ahmadi et al., 2018). Isolated plant microspores can be diverted from their normal gametophytic pathway toward sporophytic development and used also in stress-responsive studies. In this shift transformation, the osmolality of growth media plays a significant role (Yadollahi et al., 2011), besides other stresses such as heat or cold (Prem et al., 2012) shock, starvation (Najafabadi et al., 2015), or endogenous auxin biosynthesis (Rodriguez-Sanz et al., 2015).

More than 340 and 78 article topics and titles, respectively, focused on "*B. napus* + microspore," were published in the 2005–2020 period (Web of Science). Recently, Kitashiba et al. (2016) have identified loci associated with embryo yield in microspore culture of *Brassica rapa*. Daurova et al. changed microspore-derived embryos (MDE) fatty acid composition (Daurova et al., 2020). Genes associated with the induction and the establishment of embryogenesis in isolated microspores were studied by Malik et al. (2007), and Tsuwamoto et al. (2007). The potential involvement of specific ROP GTPases in early-stage microspore culture responses was studied by Chan and Pauls (2007). By comparing intervarietal substitution lines, eight genomic regions containing genetic factors controlling the rate of a direct embryo to plant conversion in rapeseed were identified by Kampouridis et al. (2016). *Via* label-free proteomics, Su et al. studied proteomic variations on cabbage embryo induction after short-term heat shock treatment (Su et al., 2020). Whittle et al. presented comparative transcriptional profiles of ovule, microspores, and pollen in *B. napus* (Whittle et al., 2010). Microspore embryogenesis constitutes a convenient system for studying the mechanisms underlying cell reprogramming and embryo formation. However, a comparative proteomic study aimed at already developed MD embryos and, besides, individual microspores in *B. napus* is missing.

In *B. napus,* doubled haploid (DH) production was first described in 1975 by Thomas and Wenzel (1975). DH production is a valuable technology in modern plant breeding of oilseed rape (Cegielska-Taras et al., 2008; Kaczmarek et al., 2008; Germana, 2011). Only a small part of Brassica MDEs will regenerate to the functional DH plants; therefore, the possibility of early, concise, and relevant detection of resistant genotypes can increase the effectivity of the whole process. Rapeseed DHs, which are haploids that have undergone chromosome duplication, represent an attractive biotechnological method to accelerate plant breeding by the production of entirely homozygous lines.

The novelty of this study is that the osmotic stress responses of two contrasting genotypes (their MDEs) are compared on different levels. The main aim of this study is to screen for proteins in oilseed rape MDE that are differentially regulated under osmotic stress, to characterize embryo hormonal profiles, and to explore in detail the mechanism of this response to low water potential in the growing medium during the MDE development. To date, this is the first proteomic study on PEG-influenced MDE. Different mechanisms to cope with osmotic stress were revealed between the genotypes studied. The wish of authors is to revalidate the MDE system as a suitable screening tool for early/mass selection of resistant DH embryos (e.g., using real-time quantitative PCR, RT-qPCR, from one cotyledon while the rest is cultivated later on). The comparison of MDE proteomic results with our previous leaf proteomic study (Urban et al., 2017) is also presented.

MATERIALS AND METHODS

Samplings and Measurements

Seeds of two winter oilseed rape (*B. napus*. L.) cultivars (cvs.), Cadeli (D), and Viking (V) were germinated, and plants were cultivated under controlled conditions according to protocol

described by Urban et al. (2017). After vernalization, plants were cultivated until the flower-bud stage as described below. For detailed information about cultivars, refer **Supplementary Table 1**.

Microspore Culture Treatment With Antimitotic Agents

Microspore cultures were prepared according to the basic protocol of Klima et al. (2008). In short: young flower buds with microspores at mid-uninucleate and late-uninucleate developmental stages were collected from donor plants grown under controlled conditions in a culture chamber (light intensity, 84 μmol m^{-2} s^{-1}; at 22/20°C, day/night; and photoperiod, 16/8 h). Microspores were isolated from flower buds after the microspore developmental stage observation. Freshly isolated and purified microspores were resuspended in the NLN liquid medium (Klima et al., 2008), supplemented with corresponding amounts of particular doubling agent stock solutions to get the final concentration of trifluralin 10 μmol/dm^3. Microspores in 60 mm plastic Petri dishes containing 6 cm^3 of suspension were incubated for 18 h at 30°C in the dark. After incubation, the microspores were purified by centrifugation, resuspended in a fresh NLN medium, and cultivated in the dark at 30°C with an antimitotic agent. After 3 weeks, embryos at the torpedo and early cotyledonary stage (at least 2 mm in length) were on the Petri dishes placed on a shaker (70 rpm) under continuous light at 22°C until embryos started growing and turned green. To lower the medium water potential (for treated medium), sterile aqueous PEG 4000 30% w/v (Sigma-Aldrich, 95904) solution was poured on the top of the solid differentiation medium (DM; Klima et al., 2008) with benzyl amino purine (0.2 mg/dm^3), indole-3-acetic acid (0.2 mg/dm^3), and 2% sucrose, solidified by 0.8% agar and then poured out after 24 h, according to protocol described by Verslues et al. (2006). Only traces of PEG are present in the final DM. That way prepared PEG is inert, non-ionic solutes able to decrease the osmotic pressure of tissues or media. The media low-water potential is stable for over a month (data not shown). The control DM was not treated. The pH of DM and PEG solution was adjusted to pH 5.8 just after autoclaving. Cotyledonary embryos of at least 4 mm in length were then transferred to a solid PEG-free treated (osmotically activated plates) or non-treated DM and maintained at 22/20°C, with photoperiod 10/14 h, and a light intensity of 300 $\mu molm^{-2}s^{-1}$. After 1 day (for transcriptomic and hormonal study, C1 for control and S1 for a treated variant, respectively), and 7 days (for transcriptomic, hormonal, and proteomic studies, C2 for control and S2 for a treated variant, respectively), of cotyledonary embryo cultivation at control DM or PEG-treated DM, one-third of the bulked embryos was cleaned from media, weighed, and frozen immediately in liquid nitrogen for further protein extraction; then, two-third was cleaned, weighed, and frozen in liquid nitrogen for transcriptomic and hormonal study; and the last part was used for biomass accumulation. Only embryos similar in shape, color, and size were carefully selected and used for the study. Three independent biological replicates (MDE cultures established individually in time) with five technical repetitions (Petri dishes) were performed for each treatment. To prevent any possible osmotically-driven differences between dishes, we used half of each dish for both cultivars. MDE weight gain was calculated as a fresh weight difference from each repetition between the first and the last days of the treatment after MDE was cleaned from the medium. From each repetition (Petri dish), ∼2 g of fresh MDE was used for further analyses. The repetitions were bulked together (after previous shape/size/stage verification) as one biological replicate. Each replicate (in total 10 g from five repetitions, fresh weight) was then immediately divided into three parts for further analyses.

Protein Extraction and Two-Dimensional Difference Gel Electrophoresis (2D-DIGE) Analysis

Total soluble proteins were extracted from embryos as described in Wang et al. (2003), with some modifications as described in detail in Urban et al. (2017). Dry protein pellets were resolved in a lysis buffer according to GE Healthcare manual for 2D-DIGE analysis, pH of the solution was adjusted to 8.5 by 50 mM NaOH, and protein concentration was determined by 2D Quant kit (GE Healthcare; Sigma-Aldrich GE80-6483-56). The protein samples (15 μg) were labeled with CyDye® minimal dyes (GE Healthcare; Sigma-Aldrich GE25-8008-61) according to the instructions of the manufacturer. Samples were run on 11 cm IPG strips with a pI range of 5–8. Image capture of 1 mm thick gels was done using the PharosFX Plus (Bio-Rad) at a resolution of 600 dpi. Densitometric analysis of scanned images was carried out using PDQuest Advanced 8.0.1 (Bio-Rad). Protein spot normalization was carried out using the local regression model, and spot manual editing was carried out using a group consensus tool. The differentially abundant protein spots (characterized as those with at least a 2-fold change; $p < 0.05$ determined by Student's *T*-test) were chosen for spot excision (ExQuest Spot Cutter; Bio-Rad) and identification from preparative gels (2-DE of 200 μg of an internal standard sample) stained by Bio-Safe Coomassie G-250 stain (Bio-Rad; Sigma-Aldrich B0770). Each of three biological replicates of protein samples was created as bulk from five technical repetitions. Samples of control Viking (VC) and treated Cadeli (DS) were dyed four times and samples of control Cadeli (DC) and treated Viking (VS) were dyed six times. Cy3- and Cy5-labeled samples were randomly combined, and the Cy2-labeled internal standard was added to form a mixed sample for loading onto an IPG strip.

The MS-Based Spot Identification and Database Search

For protein identification, the excised proteins were processed as described in Guerra-Guimaraes et al. (2015). Briefly, each sample was washed initially in 50 mM ammonium bicarbonate solution, containing 50% (v/v) methanol and dehydrated using 75% (v/v) acetonitrile (ACN) solution. Proteins were then digested in 8 μL of trypsin Gold (Promega; 5 ng/μL trypsin in 20 mM ammonium bicarbonate). After extraction with 50% (v/v) ACN, containing. 0.1% (v/v) trifluoroacetic acid (TFA), the peptides were dried at 50°C and spotted on MALDI-TOF target plates.

A volume of 0.7 mm^3 of 7 mg/cm^3 α-cyano-4-hydroxycinnamic acid in 50% (v/v) ACN, containing 0.1% (v/v) TFA was added. A MALDI peptide mass spectrum was acquired using the AB Sciex 5800 TOF/TOF (AB Sciex, Foster City, CA, USA), and the 10 most abundant peaks, excluding known contaminants, were selected and fragmented. The ProteinPilot™ software 4.0.8085 was used for database searches with an in-house MASCOT platform (version 2.3, Matrix Science, www.matrixscience.com, London, UK). All proteins were identified by a search against NCBInr database 20151110 (76068736 sequences; 27,658,295,194 residues) with the taxonomy Viridiplantae (http://www.ncbi.nlm.nih.gov) containing 3,269,297 sequences and downloaded on November 15, 2016. All searches (combined MS and 10 MS/MS spectra) were carried out using a mass window of 100 ppm for the precursor and 0.5 Da for the fragments. During the different searches, the following parameters were defined: maximum two missed cleavages, fixed carbamidomethylation of cysteine, variable oxidation of methionine or tryptophan, and tryptophan to kynurenine or double oxidation to N-formylkynurenine, an unrestricted protein mass, and mass value set to monoisotopic. The 980 spots were found on each gel on average. Out of all differentially abundant protein spots (894 normalized spots, Boolean union of all normalized spots, revealing at least a 2-fold change at a 0.05 level determined by Student's *T*-test), just 212 spots were assessed by PDQuest with quantitative change of at least ± 2-fold. From these, those present in at least 80% of gels and revealing <50% variability in their SD density values relative to the mean sample values have been selected for protein spot excision (156 spots). All identification was manually validated, and extra precursors were selected for fragmentation if the obtained data were judged as insufficient. When high-quality spectra were not matched to sequences, a sequence was determined manually, and, in the current data set, it could be linked to the identified protein by allowing for more missed cleavages, semitryptic peptides, or specific modifications. At least three peptides with a score > 20, or at least two peptides with a score > 30, or at least one peptide with a score > 50 and 1 > 20, or, finally, a single peptide with a score > 90 were considered as significant ($p < 0.05$). Only the spots with a single (unique) and significant protein identification were considered for further bioinformatics analyses. The spots with multiple protein identification were not considered in the study and were all discarded.

RNA Isolation and RT-qPCR

Samples for studying the expression of genes identified to encode osmotically induced proteins were collected as a bulk of three replicates (three biological replicates per five technical repetitions) and were stored at −80°C. Total RNA was extracted using the RNeasy plant mini kit (Qiagen) according to the instructions of the manufacturer. Contaminating DNA was removed using the DNA-free™ DNA Removal Kit (Ambion; ThermoFisher Scientific AM1906). RNA was quantified using spectrophotometric measurements (OD260), and sufficient quality was assessed (OD260/280 ratio and OD260/230 ratio) by BioSpec Nano (Shimadzu). Total RNA was stored at −80°C. Complementary DNA templates were prepared using Standard Reverse Transcription Protocol (Promega) and stored at −20°C. The RT-qPCR was performed on the QuantStudio™ 6 Flex Real-Time PCR System (Applied Biosystems) using Power SYBR® Green PCR Master Mix (Applied Biosystems; ThermoFisher Scientific 4368708) in a 96-well reaction plate using parameters recommended by the manufacturer (2 min at 50°C, 10 min at 95°C, and 40 cycles of 15 s 95°C, 1 min of 60°C, 15 s at 95°C, 1 min at 60°C, and 15 s at 95°C). The three replicates and no-template controls were included. The specificity of amplification was determined by dissociation curve analyses. A comparative threshold cycle method was applied to determine relative concentrations of mRNA. The primers used are shown in SI 5 (Excel **Supplementary Data**). All the gene expression levels were normalized to Actin gene expression (BnAct), as a reference gene, and the obtained data were normalized to BnAct using the ΔΔCT method according to Livak and Schmittgen (2001). The reference gene was selected by using geNorm (Vandesompele et al., 2002). CT value of the Catalase gene (CAT4) in C1—cultivar D was used as a calibrator sample.

Hormone Analysis

Embryo samples were purified and analyzed according to protocols described by Dobrev and Kaminek (2002) and Dobre and Vankova (2012). Samples were homogenized with a ball mill (MM301, Retsch) and extracted in pre-cold (−20°C) methanol/water/formic acid (15/4/1 v/v/v). The extracted samples were left at −20°C overnight. The following labeled internal standards (10 pmol/sample) were added: $^{13}C_6$-IAA, $^2H_2$-OxIAA (Cambridge Isotope Laboratories); $^2H_4$-SA (Sigma-Aldrich); $^2H_3$-PA (phaseic acid), $^2H_3$-DPA (dihydrophaseic acid), $^2H_4$-7OH-ABA, $^2H_5$-ABA-GE (ABA-glucosyl ester) (NRC-PBI), $^2H_6$-ABA, $^2H_5$-JA, $^2H_5$-transZ, $^2H_5$-transZR, $^2H_5$-transZ7G, $^2H_5$-transZ9G, $^2H_5$-transZOG, $^2H_5$-transZROG, $^2H_5$-transZRMP, $^2H_3$-DHZ, $^2H_3$-DHZR, $^2H_3$-DZRMP, $^2H_7$-DZOG, $^2H_3$-DHZ9G, $^2H_7$-DZOG, $^2H_6$-iP, $^2H_6$-iPR, $^2H_6$-iP7G, $^2H_6$- iP9G, and $^2H_6$-iPRMP (Olchemim). The extract was centrifuged (17,000 *g*, 4°C, 20 min) to remove solid debris. It was then concentrated using an Alpha RVC vacuum centrifuge (Christ; 40°C, 15 mbar, 1.5 h). Extracts were purified using a mixed-mode reverse-phase–cation exchange SPE column (Oasis-MCX, Waters) at room temperature. Two hormone fractions were sequentially eluted: (1) fraction A, eluted with methanol containing auxins, ABA, IAA, SA, JA and (2) fraction B, eluted with 0.35-M NH_4OH in 60% methanol containing cytokinins. Hormone metabolites were analyzed using HPLC (Ultimate 3000, Dionex), coupled to a hybrid triple quadrupole/linear ion trap mass spectrometer (3200 Q TRAP, Applied Biosystems). Quantification of hormones was done using the isotope dilution method with multilevel calibration curves (R_2 >0.99). Data processing was carried out with Analyst 1.5 software (Applied Biosystems). Data are presented as means ± SE. Three biological replicates were analyzed.

Bioinformatic Analysis of Proteins and Biological Functions of Identified Proteins

Molecular functions of proteins were searched in AgBaseGORetriever (McCarthy et al., 2006) (http://agbase.

msstate.edu/cgi-bin/tools/goretriever_select.pl). For Gene Ontology annotation (GO), GOSlimViewer (http://www.agbase.msstate.edu/cgi-bin/tools/goslimviewer_select.pl) was used to characterize general cellular components, biological functions, and biological processes (Ag Base version 2.00; Select GOSlim set: Plant). Only the original identified sequences were used for these analyses.

GOModeler is a tool that enables researchers to conduct hypothesis-based testing of high throughput datasets using the GO (http://agbase.msstate.edu/cgi-bin/tools/GOModeler.cgi). All information necessary for understanding the program processes is covered by Manda et al. (2010). The net effect is a product of quantitative value (logarithm of protein abundance expressed as stress density/control density) with qualitative value (+1, 0, or −1; assessed by GOModeler according to GO annotation of each protein). Program inputs: GOModeler settings used in this article are as follows [for details, refer Urban et al. (2017)]:

Gene Information Input Type: Uniprot Accession
Expression Values Input Type: Log10 (Treatment/Control)
Species: *Arabidopsis*
Default Effect of Unsigned GO Terms Positive
Default Method for Conflict Resolution for Contradictory GO Terms: Positives Override

Proteins were sorted into clusters according to their mode of accumulation using Permut Matrix (Caraux and Pinloche, 2005) (version 1.9.4.) on the basis of Z-score standardization of protein density data. In order to draw Venn diagrams, we used "Venn Diagram Plotter," available on http://omics.pnl.gov/software/venn-diagram-plotter. For data used to characterize "unnamed proteins," the protein accession versions were blasted to *Arabidopsis* (*taxid: 3701*) in NCBI blastp (https://blast.ncbi.nlm.nih.gov) and manually searched for a gene locus in TAIR (www.arabidopsis.org). Blastp search Database: Non-redundant UniProtKB/SwissProt sequences; Molecule Type: Protein; Update date: 2016/12/11; Number of sequences: 465,342; *Arabidopsis* (*taxid:3701*); and Matrix: BLOSUM62.The mass spectrometry proteomics data have been deposited to the ProteomeXchange Consortium *via* the PRIDE partner repository with the dataset identifier PXD024552.

Statistical Analysis of Differentially Accumulated Physiological, Biochemical, and Protein Data

Exploratory data analysis (EDA) was used to determine statistically important features of the measured dataset. A combination of statistical tests, together with diagnostics graphs, was used for descriptive statistics (mean, variance, etc.), verification of normality and homogeneity of the data, and detection of the outliers. Linear dependence of the parameters of interest was determined by correlation and regression analyses. For a deeper understanding of the relationship between measured characteristics, principal components analysis (PCA) was used. The same method was also applied to a protein dataset. Diagnostic indicators, such as the Scree plot, loading plot, and the total amount of explained variability, were used to find an optimal model. All statistical tests were computed in STATISTICA ver.12 (StatSoft, Inc.). Cluster analysis of the final protein spot relative abundances has been carried out using Permut Matrix software (Caraux and Pinloche, 2005) (version 1.9.4). For all cluster analyses, the Z-score transformation of data was carried out. Euclidean distances (dissimilarity) and Ward's criteria (rows linkage rule) were used for the analysis. For every Permut Matrix analysis, the highest rows and columns objective functions (R) and a sum of all pairwise distances of neighboring rows or columns (S; shortest path length) were chosen to describe patterns within genotypes and treatments.

RESULTS AND DISCUSSION

Two cultivars of winter oilseed rape differing in their drought-adaptation strategies (detailed description in **Supplementary Table 1**) were included in this analysis. According to our previous study (Urban et al., 2017), D is a drought-resistant water-saver, and V is drought-susceptible water-spender. The cv. V is considered an early and cv. D as intermediate/late cv. (Urban et al., 2017). Embryos, derived from microspores, were placed in the control and PEG-activated media and harvested after 24 h and after 7 days.

Biomass Accumulation and Other Physiological Characteristics Revealed Better Adaptation of D to PEG-Infused Media

The responses of MDE to steady low osmotically activated plates (Petri dish) were observed after 24 h (acute response) and after 7 days (long-term + recovery response). The MDE fresh weight changes 1 day after stress (DAS; C1 and S1) and 7 DAS (C2 and S2) are shown in **Figure 1**. The osmotic potential of aqueous PEG 4000 solution (30 g w/v) was measured by vapor pressure deficit osmometer WESCOR Psypro, and its value was −1.05 MPa at 25°C. The osmotic potential of solid media in control conditions was −1.11 MPa at 25°C. This potential changed after it was osmotically activated by PEG solution to −1.55 MPa at 25°C. No statistical difference between MDE biomass accumulation was detected until 7 DAS of PEG treatment, making this system reliable for further use (additionally, the osmotic potential of well-sealed media in Petri dishes without plants did not change even after 3 months; data not shown). Biomass accumulation in PEG-treated D was significantly higher (3-fold) than in the case of V. The increase of biomass in PEG-treated cultivation media agrees with the water-saver behavior of D. The cv. D MDE seems to be better adapted and then able to acclimate and grow under increased osmotic potential (or osmolality). We can only hypothesize whether this reflects the observed field phenotype (published earlier) or not. The D biomass increase is similar to its growth under control conditions. V slightly decreased its MDE weight (not significant; **Figure 1**) after 7 days in the control medium. The other explanation may be a higher and rapid

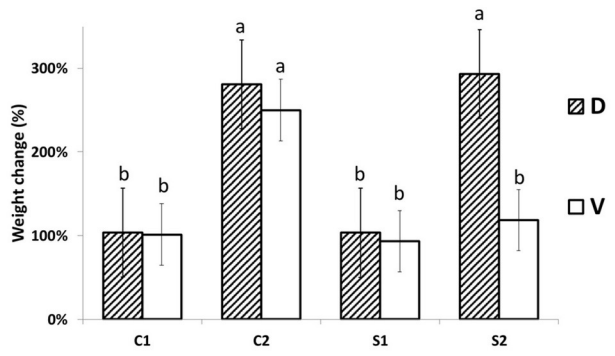


FIGURE 1 | MDE growth changes. MDE relative (%) fresh weight changes (the day after stress +1/day after stress 0) are significantly lower in Viking (V) in comparison to Cadeli (D) only after 7 days of cultivation under stress (S2). Controls and treated samples (C1 and S1, respectively), for the first sampling (24 h after stress); C2, S2 arecontrols and treated samples seven DAS, respectively. Homogeneous groups above the error bars indicate significant changes between cvs. by the Student's *t*-test ($p < 0.05$). Only different letters show significantly different values.

accumulation of osmolytes in D vs. V, which further stabilizes MDE cytosol against PEG-driven dehydration.

The observed MDE growth results agree with previous reports and show that even only data of MDE growth on osmotically activated media can be used as a screening tool to select resistant cultivars. In addition, the stability of the system suggests the non-significant artifact effect of cultivation technique on growth characteristics (**Supplementary Figure 1**). However, further study needs to be conducted to verify the stability of MDE derived from different cultivars regressed to their actual field-observed phenotypes.

Proteomic Analysis of V Embryos Showed a High Number of Accessions Changed in Stress/Defense-Related Processes

Two genotypes of winter oilseed rape cultivars (D and V) exhibit contrasting levels of drought resistance, and two different treatments (control and PEG-induced drought simulation) were compared after 7 DAS in the 2D-DIGE proteomic experiment. Despite the same age of embryos, PEG-treated MDE of both cvs. was slightly dwarfish (likely because of low water tissue content upon osmotic; **Supplementary Figure 1**), however, without discoloration (suggesting no mineral deficiency).

The representative 2D-DIGE gel of MDE with highlighted 156 spots, showing protein resolution, is shown in **Figure 2**. All normalized protein spots (894 spots) and these chosen for identification (156) protein spots across the gels were included in two separate PCAs to identify sample outliers and to group samples from different stages of treatment for each cultivar (SI 1). Two PCAs were prepared: (1) analysis based on all raw protein abundances of all individual gels (**Supplementary Figure 2**) and (2) analysis based on averaged values of protein abundances of individual samples (DC, DS, VC, and VS; **Supplementary Figure 3**). PCA based on all values (**Supplementary Figure 2**) distinguished both genotypes in all factors 1–3 and may explain almost 33% of data variability. PCA based on averages of abundances (**Supplementary Figure 3**) distinguishes between controls samples from treated samples between cultivars, despite the fact DC+VS and DS+VC were projected closer to each other. This result is caused by the fact that these groups share high numbers of similarly oriented (down- or up-accumulated) proteins (refer **Figure 3**) and it is supported also by PermutMarix clustering analysis. Factors 1–2-based projection of **Supplementary Figure 3** data may explain almost 66% of data variability. The protein spots belonging to 156 chosen spots are placed in the center of the plots of the PCA, which revealed that spots exhibit contradictory accumulation patterns within genotypes (and ergo the mean is centered close to zero).

The heat map (**Figure 4**) was created on the basis of standardized protein abundance of 156 chosen protein spots (standardization by Z-score values) in Permut Matrix. All differently accumulated spots (156 spots) showed clustering into nine main clusters according to their accumulation pattern in controls and treated genotypes (**Supplementary Table 2**; or graphs in SI 1). These nine clusters were divided according to genotypes and treatments as follows: Cluster 1, proteins accumulated mainly in DC; cluster 2, proteins accumulated mainly in DS; cluster 3, proteins with generally higher abundance in cv. D; cluster 4, proteins accumulated in VC; cluster 5, proteins mainly accumulated in VS; cluster 6, proteins with generally higher abundance in cv. V; cluster 7, proteins accumulated mainly in controls; cluster 8, proteins accumulated mainly in treated samples; and cluster 9, proteins with mixed patterns of accumulation.

Some proteins (e.g., cobalamin-independent methionine synthase, glyceraldehyde-3-phosphate dehydrogenase) have been found in more protein spots; however, they belong to different accumulation clusters. It refers to one of the main advantages of the gel/based method—the possibility to visualize and quantify different gene products and/or posttranslational modifications of the same protein that could have different or opposite accumulation under the same growth condition.

Generally, cv. D showed a high number of proteins changed in the amino acid (AA), protein, and energy metabolism (protein clusters 1 and 3) category. Cv. V showed a high number of proteins changed in AA, protein, and energy metabolism and stress/defense-related processes (clusters 1, 3, and 5). Interestingly, both treated cvs. (cluster 8) showed an enhanced accumulation of proteins involved in energy metabolism and redox homeostasis, ROS, and signaling (clusters 3 and 4).

According to Venn diagrams (**Figure 3A**; additional graphs in SI 2b, 2c), D showed the highest number of unique spots differently up- or down-accumulated in controls and a treated variant. On the other side, cv. V showed a high number of genotype-related variants. This result can partially be explained by different growth rates in control and PEG-treated conditions (**Figure 1**). In contrast to the data shown in **Figure 3A**, when the S/C protein ratio was used in a treatment-based variant (**Figure 3B**), significantly, more proteins were down-accumulated in the VS/VC ratio. In DS/C, only 5 and

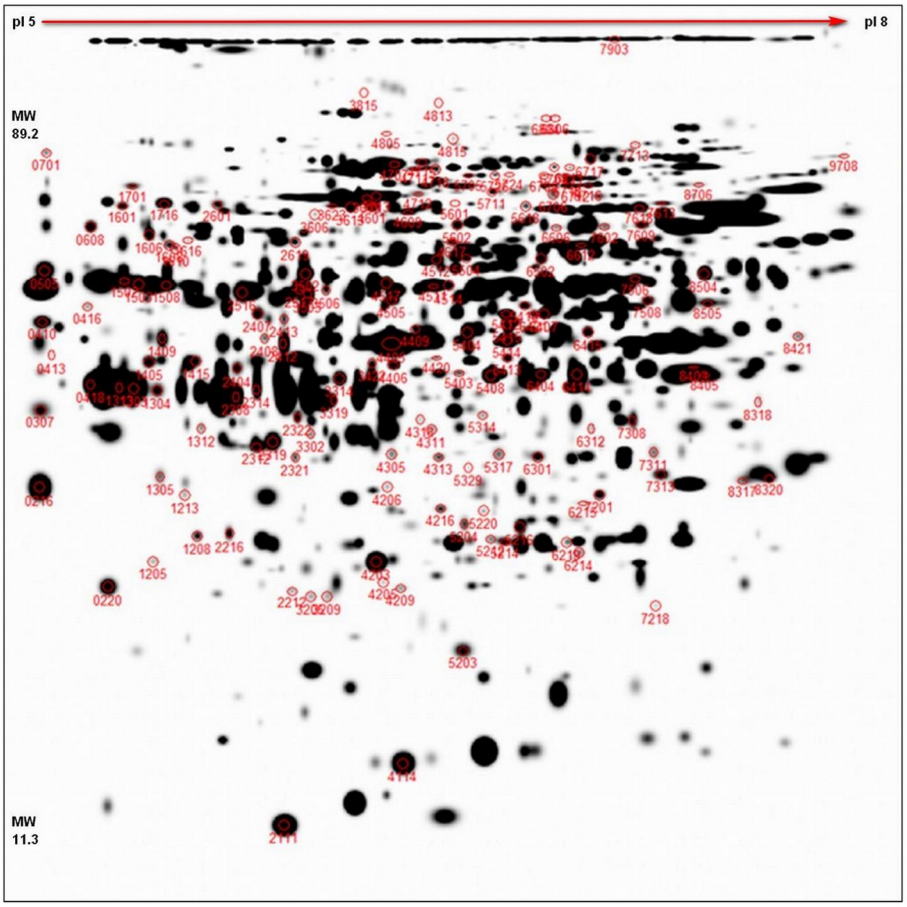


FIGURE 2 | 2D-DIGE representative proteome map. Representative proteome map of total MDE proteins of winter oilseed rape, separated by 2D-DIGE. At least two times up- or down-accumulated proteins ($p < 0.05$, 11 cm IPG strip, pI 5–8, 1 mm thick gel) are marked with the corresponding spot numbers. In total, 156 spots chosen for cutting and identification are shown in red circles.

13 were down- and up-accumulated, respectively. For VS/C, 25 and 16 were down- and up-accumulated, respectively. This result showed that cv. V was more influenced by changes in cultivation conditions and that its homeostasis was disturbed. In conclusion, the protein abundance is likely the cause of the different growth rates (genotype behavior described in **Supplementary Table 1**), not a consequence.

Eleven spots were not sufficiently identified, probably due to a lack of sequence similarity or low abundance; nevertheless, these spots were included in Permut Matrix clusters and PCA analysis. The table of identified proteins (SI 2a) contains all 63 successfully identified spots. The search for identified protein spots with large changes in protein abundance (more than ± 3-fold; $p < 0.05$) has revealed seven protein spots (aspartate aminotransferase, AT2G47510-fumarate hydratase 1, rubisco, peroxiredoxin antioxidant, peroxidase 12, jasmonate inducible protein, and elongation factor EF-2-like protein). Highly accumulated proteins belong mostly to protein and energy metabolism, and stress/defense-related proteins.

Functional Categories of Drought-Responsive Proteins Highlighted Eight Functional Groups

Detailed information about protein identification *via* the NCBI database is presented in SI 3. The biological functions of individually differently accumulated proteins were determined by GO Retriever output in the domain of biological processes according to their NCBI Accession version (SI 4). To investigate the functional and biological process-based identity of the individually identified differentially accumulated proteins (DAP), the 63 identified spots were categorized into eight groups (**Figure 5**; details in SI 2a) based on their putative biological processes: (1) Amino acid, nitrogen, and sugars metabolism/protein metabolism (13 DAP); (2) ATP interconversion (1 DAP); (3) energy metabolism (glycolysis, gluconeogenesis, TCA pathway, respiration, and photosynthesis) (24 DAP); (4) Redox homeostasis, ROS, and signaling (7 DAP); (5) stress/defense-related/detoxification (8 DAP); (6) transcription (DNA/RNA processing and binding)/protein

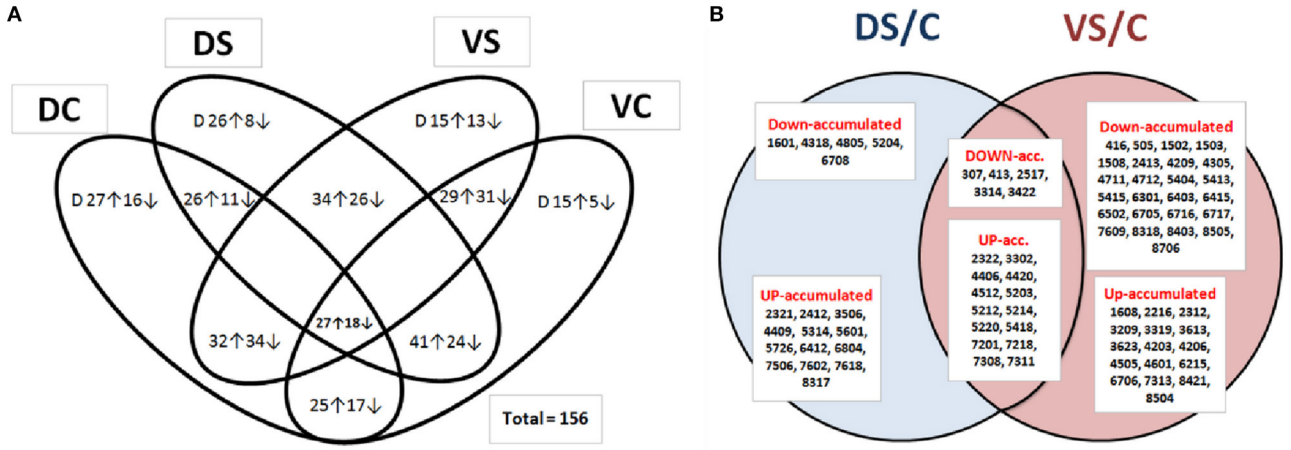


FIGURE 3 | Venn diagram of protein abundances. Venn diagram of identified and non-identified spots **(A)**, showing all differentially abundant protein spots (at least 2-fold change at $p < 0.05$ and SD ≤ 0.5; $n = 156$), revealing differential abundance between PEG-treated and control samples (DC, Cadeli control; DS, Cadeli stress; VC, Viking control; VS, Viking stress). Venn diagram **(B)** showing SSPs of unique identified protein spots (at least ± 2-fold change at $p < 0.05$ and SD ≤ 0.5; $n = 63$), revealing differential abundances between PEG-treated and control samples among genotypes. DS/C, Cadeli-treated/control, 18 SSPs; VS/C, Viking-treated/control, 41 SSPs and its union (19 SSPs). ↑ The arrow means increased abundance with respect to a ratio, while ↓ means decreased abundance with respect to a ratio. Letter "D" in **Figure 3A** inside ovals means a change of protein spot density just over the background of DIGE gels (at least 2-fold change; $p < 0.05$ and SD ≤ 0.5) because they do not have a comparison to other treatment.

synthesis (2 DAP); (7) protein destination and storage, proteolysis (5 DAP); (8) cell structure (1 DAP).

GOModeler output of functional groups (**Figure 6**) reveals groups with higher estimated effects (net effect) in controls (e.g., AA, sugar/protein metabolism; stress/defense-related; and cell structure) and higher importance of energy metabolism, ROS/redox, and protein destination groups in treated plants. Interestingly, when cultivars were GOModeler compared (**Supplementary Figure 4**), higher importance of AA, sugar/protein metabolism, ATP, stress/defense-related with protein destination for V was observed. A significantly higher net effect in D was observed in energy metabolism, ROS/redox, and protein synthesis groups.

According to these eight functional groups, we designate these groups most affected by PEG-related osmotic stress in studied winter oilseed rape MDEs. Differences found in the numbers of proteins responsible for the individual biological processes influenced by osmotic stress indicate the existence of diverse response strategies to osmotically-driven drought between the selected contrasting genotypes. This conclusion was also proved in drought-related differential leaf proteomics of four cvs. in Urban et al. (2017).

Generally, a significant decrease in the accumulation of proteins could be explained by the reduction of a growth rate and/or different development of strategy under osmotic stress conditions.

Functional Groups Regarding *B. napus* MDE Specific Response to Osmotic Stress

All differentially abundant proteins, which were successfully identified, and their distribution into functional groups with detailed information are available in SI 2a, with details from NCBI identification in SI 3.

Amino Acid, Nitrogen, and Sugars Metabolism/Protein Metabolism

The proteins in this group are involved in the chemical reactions and pathways concerning organic or inorganic compounds that contain nitrogen and sulfide interconversion with sugars and protein metabolism. Sugars play a central regulatory role in many vital processes besides serving the energetic function and are considered important signals that regulate plant metabolism and development (Kosova et al., 2015). This group represents the second biggest part of an identified protein. In the *Brassicaceae* family, the nitrogen and sulfide compounds are important from point of view of metabolism (thiols, glucosinolates, brassinosteroids) and biotic and/or abiotic stress adaptation (Sehrawat and Deswal, 2014). *B. napus* genotypes with high sulfur- and nitrogen-use efficiency are more resistant to PEG-induced osmotic stress (Limami et al., 2008). This functional category includes proteins that are significantly down-accumulated in DC vs. VC (e.g., isocitrate dehydrogenase, glutamine synthase, sucrose synthase, and glyoxalase). Some proteins are only accumulated in treated D vs. V (aspartate aminotransferase, cobalamin-independent methionine synthase, and nodulin).

Energy Metabolism (Glycolysis, Gluconeogenesis, TCA Pathway, Respiration, and Photosynthesis)

To maintain sufficient energy and balanced carbohydrate production belong to one of the most important pathways in all plants as sessile organisms. In contrast to Urban et al. (2017),

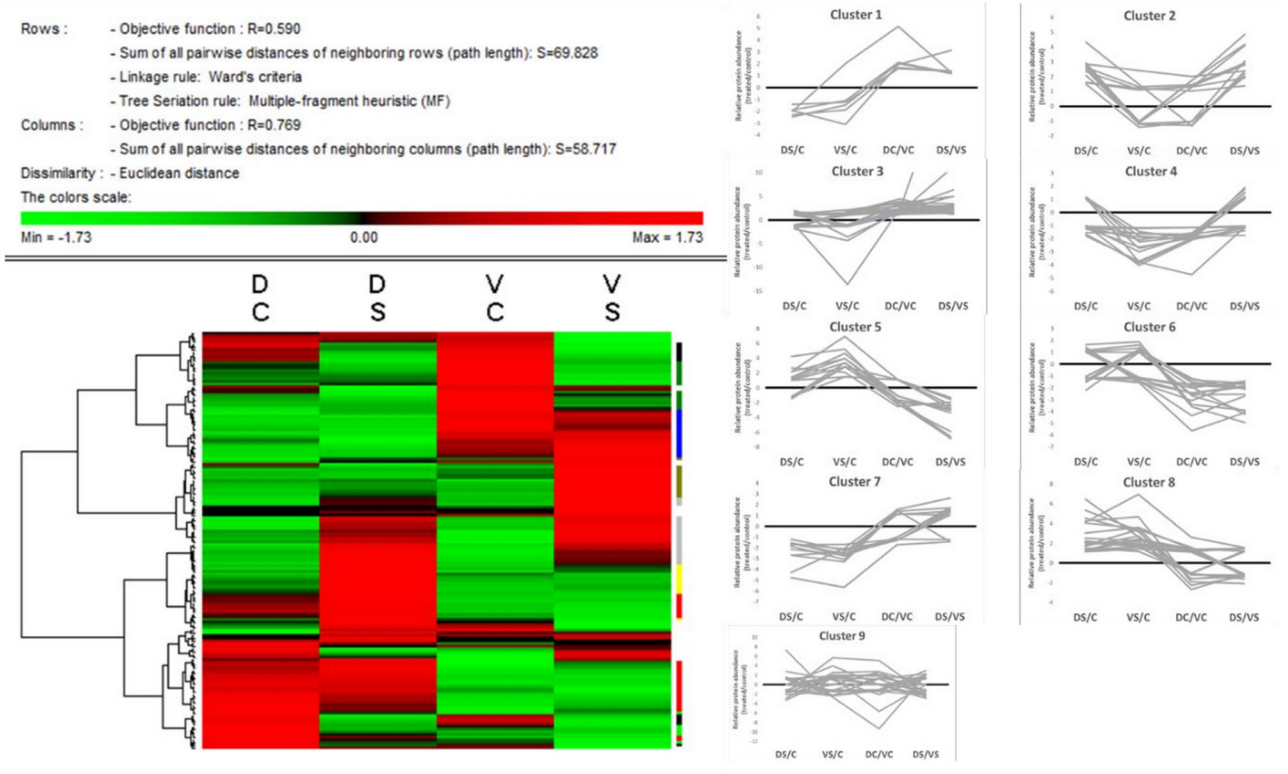


FIGURE 4 | Heat map + protein clusters. The compacted version of the heat map (Permut Matrix 1.9.3) of all 156 protein spot abundances, clustered according to the row Z-score values using Euclidean distance and Ward's minimum criteria, calculated from protein spot abundances. The red values mean higher protein spot abundance in the samples; the green values mean lower protein abundance in the sample according to the variant (DC, Cadeli control; DS, Cadeli stress; VC, Viking control; VS, Viking stress). On the right side, the tiny color marks show nine different clusters, revealing information about the protein accumulation patterns. Clusters: 1, light green, higher in DC; 2, light yellow, higher in DS; 3, red, higher in both DC and DS; 4, green, higher in VC; 5, dark yellow, higher in VS; 6, blue, higher in both VC and VS; 7, black, higher in both controls; 8, gray, higher in both treated samples; and 9, white, miscellaneous patterns.

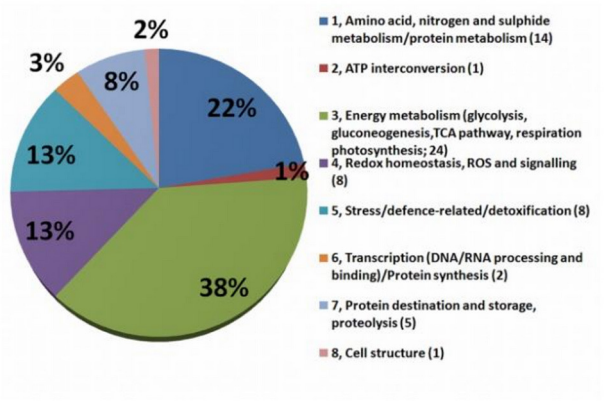


FIGURE 5 | Graph of functional groups. The functional classification of MDE proteins differentially accumulated after 7 days after stress ($n = 65$). The numbers in brackets are numbers of proteins involved in each process.

energetic metabolism-related proteins and photosynthesis-related ones were joined together into one group. The ability of plants to adapt and/or acclimate to adverse environments is related to the plasticity and resilience of photosynthesis, which, in combination with other processes, determines plant growth and development (Abreu et al., 2013). This group represents the biggest part of identified proteins (**Figure 5**). Some carbon/nitrogen metabolism-related proteins identified (e.g., malate dehydrogenase), show increased energy demand as well as enhanced cellular activities in the root tissues of rapeseed upon drought (Mohammadi et al., 2012).

Most protein spots were up-accumulated in cv. D in comparison with cv. V. Also, between treatments (S/C of individual genotypes), most proteins were significantly changed in cv. V (e.g., glyoxysomal beta-ketoacyl-thiolyase, fumarate hydratase 1, FBA, phosphoenolpyruvate carboxykinase). These changes support the link between the growth (**Figure 1**) and energy metabolism proteins. cv. D grew significantly more in treated conditions than cv. V, probably because of its enhanced levels of proteins involved in energy metabolism under stress.

Unfortunately, no clear consensus has been achieved that would reveal stress-resistant genotypes according to their changes in energy metabolism-related proteins. More DAPs were accumulated in cv. D (both in controls and treated samples).

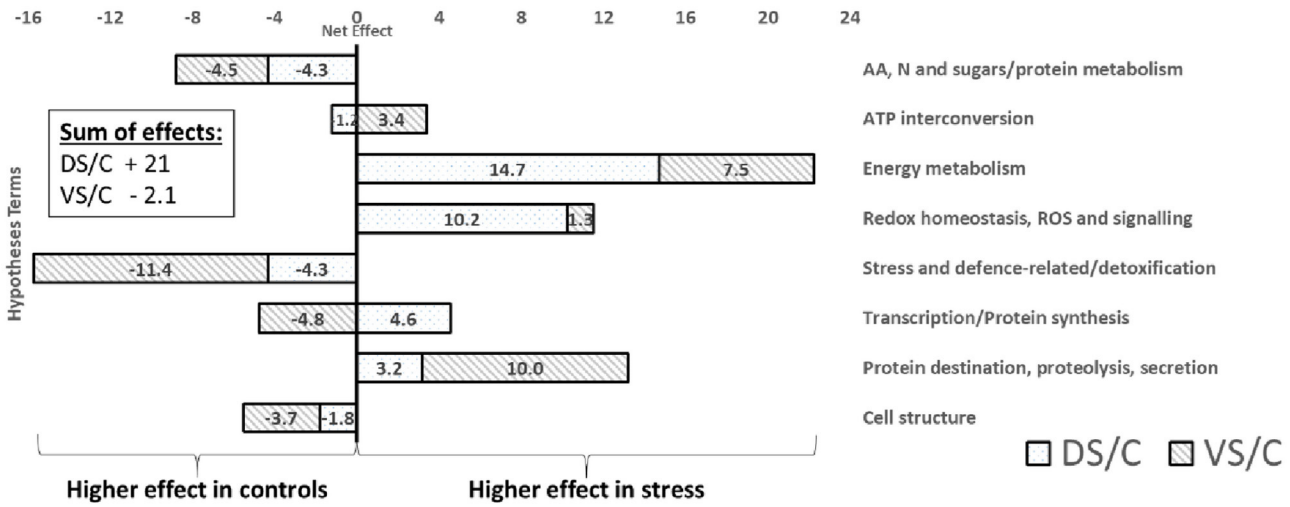


FIGURE 6 | GOModeler output. The GOModeler-based graphical summary of proteome net effects for each of eight chosen hypotheses terms (right side), showing net effects on treated protein accumulation (protein abundance change). The net effect is a product of quantitative value (logarithm of protein abundance expressed as stress density/control density) with qualitative value (+1, 0, or −1; assessed by GOModeler according to GO annotation of each protein). In the corner, the sum of all net effects for individual combinations is calculated. A positive value (right side of the graph) means higher protein net effect in treated plants; negative values mean higher net effect importance in controls.

Nevertheless, this is only a quantitative point of view; several proteins play an important qualitative role, too.

Redox Homeostasis, ROS, and Signaling

Together with stress/defense-related proteins, this category contains the third most abundant protein pool. The cellular redox homeostasis is significantly affected by the stress-induced production of ROS, which also serves as a signal for the synthesis of defense enzymes and other antioxidant systems. Together with the photosynthesis and stress proteins, the redox homeostasis and signaling are likely to integrate all stresses into the cellular response with a stress-adaptive program (Fernandez and Strand, 2008). Spots found in this study show that the antioxidant system and ROS production play a crucial role in MDE resistance and should be further examined to contribute to the selection of adaptable rapeseeds. An increase in several ROS scavenging enzymes was reported practically in all proteomic studies dealing with plant stress responses, as the imbalance in energy metabolism during stress treatments is associated with an enhanced risk of oxidative stress (Kosova et al., 2011). Proteins in this category showed up-accumulation in both treated cvs. Interestingly, several proteins showed higher accumulation in controls of V in comparison to lower accumulation in D (e.g., alcohol dehydrogenase class III, S-nitrosoglutathione reductase, peroxiredoxin antioxidant, etc.). A similar trend was clearly visible in the leaf proteome study of cv. V in comparison with other cvs. (Urban et al., 2017) but in contrast to drought-related transcriptomic study, where higher ROS were joined to tolerant rapeseed genotypes (Schiessl et al., 2020).

Stress and Defense-Related Proteins

Half of the proteins in this group showed down-accumulation in treated vs. control samples. Only MLP-like protein 329 (SSP 4114) was accumulated in treated samples in both cvs. cv. D generally showed a lower accumulation of stress and defense-related proteins than cv. V. In the DS/VS ratio, only catalase, and ABA-modulated tyrosine-phosphorylated proteins were more accumulated.

Transcription, Protein Synthesis/Protein Storage/Cell Structure

This is an artificial category, jointing the remaining three small functional groups together (6–8). Proteins in DNA/RNA processing and binding/protein synthesis showed higher accumulation in treated D vs. treated V. The cruciferin cru 2/3 subunit significantly increased in both treated cvs., while tubulin decreased.

High ROS, Protein Turnover, and Cell Trafficking System With Available Energy-Related Pathways Support D Resistance

The highest number of proteins accumulated significantly in D vs. V (clusters 1–3; 9) belongs to energy metabolism, redox homeostasis + signaling, transcription, protein destination, storage, and proteolysis. Cv. D showed effective energy-related pathways, higher sensing of ROS-related changes in cell compartments, higher protein turnover, and/or synthesis and, also, an increase in cell trafficking system. Selected proteins with a changed abundance in D are listed.

Aspartate biosynthesis is mediated by the enzyme aspartate aminotransferase (de la Torre et al., 2014a) (SSP 1405, 2404); both its cytosolic and plastid forms play a central role in nitrogen metabolism and its storage (de la Torre et al., 2014b). The enzyme activity increases after infection with a necrotrophic pathogen

(Brauc et al., 2011). One gene product (isoform) of aspartate aminotransferase is accumulated in cv. D (SSP 2404), the other in cv. V (SSP 1405). In the chloroplasts and in non-green plastids, aspartate serves as the precursor for the biosynthesis of different amino acids and derived metabolites that play distinct and important roles in the regulation of plant growth, reproduction, development, or defense. This protein probably plays a dual role in both somatic embryogenesis and stress responses, as proposed by Almeida et al. (2012).

Proteins fluG-like (SSP 5705, 5724, and 5726) were searched by Blastp and proved similar to nodulin/glutamate-ammonia ligase-like proteins (NodGS). NodGSs belong to the glutamine synthetase family. Recent studies highlight the importance of nodulin-like proteins for the transport of nutrients (especially nitrogen), solutes, amino acids, or hormones and for major aspects of plant development (Denance et al., 2014). Some of the nodulins showed aquaporin activity (Katsuhara et al., 2014), facilitating water, hydrogen peroxide, and even arsenite transports out of the cytosol. Doskocilova et al. (2011) pointed the role for NodGS in root morphogenesis and microbial elicitation. However, the role of NodGS in abiotic stress response is still unknown. NodGS proteins (SSP 5705, 5724) were accumulated significantly more in DS (in comparison to VS). SSP 5726 was highly accumulated in both treated cultivars in comparison with its controls.

AT4g37510/F6G17_160 (SSP 5601; NDH-1) is a subunit of the mitochondrial membrane respiratory chain NADH dehydrogenase (Complex I) and functions in the transfer of electrons from NADH to the respiratory chain (Klodmann and Braun, 2011). NDH-1 belongs to Quinone reductases (QRs), which are flavoproteins that protect organisms from oxidative stress. The function of plant QRs has not been as yet addressed *in vivo* despite biochemical evidence for their involvement in redox reactions (Heyno et al., 2013).

The AT2G47510 (SSP 416, FUM1) is recognized as fumarase 1, which is a mitochondrial-localized protein and plays an important role in the tricarboxylic acid cycle (TCA). FUM1 was down-accumulated in both treated samples; however, it was generally much more accumulated in cv. D in contrast to V.

Among the other energy metabolism-related proteins with significantly higher accumulation in treated samples of cv. D (DS/DC) is UDP-glucose 6-dehydrogenase (SSP 3506). UDP-glucose dehydrogenase (UGD) plays a key role in the nucleotide sugar biosynthetic pathway, as its product UDP-glucuronic acid is the common precursor for many sugar residues found in the cell wall (Klinghammer and Tenhaken, 2007). The importance of UDP GlcA for plant primary cell wall formation was also shown by Reboul et al. (2011).

Two proteins from the redox homeostasis, ROS, and signaling group were accumulated only in DS: S-nitrosoglutathione reductase (SSP 2412, GSNOR) and mitogen-activated protein kinase 4 (SSP 5403, MAPK4). Nitric oxide (NO) may react with glutathione (GSH) to form GSNO, which is considered the main reservoir of NO in cells (Silveira et al., 2016). The redox-active molecule NO is known to modulate plant responses to stressful conditions, plant immunity (Thalineau et al., 2016), cross talk in salt resistance (Fatma et al., 2016), photosynthetic apparatus protection and to improve shoot and root growth upon drought in sugarcane (Silveira et al., 2016), etc.

The MAPK is a generally important factor in the regulation of signal transduction in response to biotic and abiotic stresses (Yanagawa et al., 2016). Gawronski et al. (2014) and others concluded that MAPK4 is a complex regulator of chloroplast retrograde signaling related to photosynthesis, growth, and immune defense in *Arabidopsis*. MAPK4 is also recognized as a salicylic acid-independent regulator of growth (Gawronski et al., 2014), expression of brassinosteroid-related genes in rice (Duan et al., 2014), and general abiotic/biotic stress response in barley (Abass and Morris, 2013).

The peroxiredoxin antioxidant (SSP 5214) and hydroxyacylglutathione hydrolase 3 (SSP 5220) were significantly accumulated in both treated cvs. This result is in accordance with Urban et al. (2017). Peroxiredoxins (Prx) are known to play an important role in combating the reactive oxygen species generated at the level of electron transport activities in plants exposed to different types of biotic and abiotic stresses. Kim et al. (2012) suggested that in Brassicaceae Prx isotypes play time- and issues-specific roles in the cells, but that they also cooperate with each other to protect the plants. Hydroxyacylglutathione hydrolase 3 (SSP 5220; ETHE) is also called "persulfide dioxygenase" and is located in mitochondria. ETHE catalyzes the oxidation of persulfides in the mitochondrial matrix and is essential for early embryo development in *Arabidopsis* (Holdorf et al., 2012; Krussel et al., 2014).

Surprisingly, no protein from the stress-related group was significantly up-accumulated in DS. Ascorbate peroxidase (SSP 5204; APX) exhibited an enhanced DC/VC ratio, and catalase (SSP 1502), with ABA-modulated tyrosine-phosphorylated protein (SSP 4216), was elevated in stressed D (high DS/VS ratio). APX was found to be specifically required for the resistance of *Arabidopsis* plants to drought and heat stress combination (Mittler and Blumwald, 2010). In the thylakoid lumen, APX is essential for photo protection as a cofactor of violaxanthin de-epoxidase, the key enzyme in non-photochemical quenching. It has to be mentioned that H_2O_2 plays a signaling function in the modulation of plant phenotype (Huener et al., 2012); therefore, the APX is a powerful part of a complex response to any biotic and/or abiotic stresses.

Also, transcriptional factor Pur ALPHA-1 (SSP 5314; PurA) involved in RNA processing showed accumulation in DS. PurA is a single-stranded DNA-binding protein that plays a role in cell growth and differentiation by modulating both transcriptional and translational controls of gene expression.

SSP 4711 was blasted to elongation factor EF-2-like protein LOS1 (SSP 4711; EF2). This spot was significantly reduced in VS and accumulated in DS. The DS/VS ratio was more than 11. LOS1 encodes a translation elongation factor 2-like protein that is involved in cold-induced translation; however, more importantly, LOS means "low expression of osmotically responsive genes."

Three protein spots belonged to protein destination and a storage group: 26S proteasome ATPase subunit, cruciferin cru2/3 subunit, and Clp ATPase. 26S proteasome ATPase subunit (SSP 2407) belongs to AAA+ (ATPases associated with a wide variety

of cellular activities). This superfamily represents an ancient group of ATPases. Members of the AAA+ ATPases function as molecular chaperons, ATPase subunits of proteases, helicases, or nucleic-acid stimulated ATPases. This protein showed a significant ratio in DC/VC.

Clp ATPase (SSP 6710) belongs also to AAA+. This protein is sometimes called "HSP93-III" and is involved in protein import into chloroplast stroma. This protein showed an increased value in the DS/VS ratio.

Higher Abundance in ATP Interconversion Pathways With Stress/Defense Proteins Shows the Higher Vulnerability of V

The proteins exhibiting an enhanced relative abundance in cv. V (clusters 4–6; 9) belong to four functional groups: AA, nitrogen, and protein metabolism; ATP interconversion; stress and defense-related/detoxification; and cell structure. This fact supports the idea about the higher need for ATP and nutrient (re)utilization, deeper stress impact, and increased stress-related cell structure changes. This is also in agreement with slower MDE growth (**Figure 1**). Selected proteins with significant changes in V are described below.

Glutamine synthetase precursor (SSP 5408; EC 6.3.1.2; GS) decreased in VS and also in relation to DC/VC. GS is an ATP-dependent plastid enzyme that plays an essential role in the metabolism of nitrogen and in photorespiration where it is a key enzyme. According to studies (Doskocilova et al., 2011; Orsel et al., 2014), plants with low GS isoform 2 have reduced capacity for photorespiration and decreased resistance to light stress, so they are photo inhibited more severely by high light compared with control plants. GS accumulation can directly protect plants from drought-related photo-inhibition, so D could probably photo-acclimate better because of the lower decrease of GS in treated conditions.

Glyoxalases are known to be differentially regulated under stress conditions, and their overexpression in plants confers resistance to multiple abiotic stresses (Kaur et al., 2014). The glyoxalase system is a set of at least two enzymes (glyoxalases 1 and 2) that carry out the glutathione-dependent detoxification of methylglyoxal and the other reactive aldehydes that are produced by cellular metabolism even under optimal conditions. Putative lactoylglutathione lyase (synonym: glyoxalase 1; SSP 7201) in both treated genotypes was significantly accumulated, as also shown in Urban et al. (2017). The same pattern is shown in the RT-qPCR result (**Figure 7C**).

ChloroplastatpA gene product, also called "NADH dehydrogenase" (SSP 8504; ATPA), produces ATP from ADP in the presence of a proton gradient across the membrane. ATP production is significantly higher in VS (VS/VC ratio) while no change was observed in DS/DC. This protein was accumulated in treated V samples and was highly suppressed in DS in comparison to VS (−6.6-fold), which suggests a higher energy need of V. This accumulation pattern is contradictory to Urban et al. (2017).

In the energy-related protein category, glyceraldehyde-3-phosphate dehydrogenase (SSP 418) and chloroplast beta-carbonic anhydrase like 1 (SSP 1208; CA1), together with malate dehydrogenase 2 (SSP 2312), F21D18.28 (blasted pyridine nucleotide-disulfide oxidoreductase or dihydrolipoamide dehydrogenase; SSP 3502; PYROXD), and fructose-bisphosphate aldolase (SSP 3319) were uniquely accumulated in VS. CAs are ubiquitous enzymes involved in fundamental processes like photosynthesis, respiration, pH homeostasis, and ion transport. CAs proteins are involved in the CO_2 signaling pathway, which controls gas exchange between plants and the atmosphere by modulating stomatal movements (Ferreira et al., 2008; Rowlett, 2010). CA promotes water use efficiency by influencing the internal conductance (Warren, 2008; Cui et al., 2012) and is phosphorylated, which has been found important for drought-tolerant rapeseeds (Wang et al., 2016).

Cobalamin-independent methionine synthases (SSP 3619 and 3713; MetE) were found to have mixed accumulation. The predicted function of the cobalamin-independent methionine synthase isozyme is closely related to ethylene biosynthesis (Wang et al., 2014) and then in stress-related signaling. SSP 3619 showed highly significant accumulation in VC; SSP 3713 was accumulated in treated D. Each MetE, however, belongs to different genes (SSP3713 is likely connected to different phenotypes of D).

Phosphoglucomutase 1 (SSP 5602, PGM1) catalyzes the bidirectional interconversion of glucose-1-phosphate (G-1-P) and glucose-6-phosphate (G-6-P) *via* a glucose 1,6-diphosphate intermediate. PGM1 shows higher accumulation in both VC and VS.

MLP-like protein 329 (SSP 4114, NP_565265.1; MLP329) is a pathogenesis-related protein with still no clear function within plants and predicted location in the nucleus and/or chloroplast (Cerny et al., 2013). In both cvs., MPL329 was increased in treated conditions. Interestingly, this protein was accumulated more than 3-fold than in D. Its possible role in cytokinin signaling was mentioned in Cerny et al. (2013) and is discussed in the hormonal profile below.

Glutathione S-transferase (SSP 4203; gi|87294807; GST) is a cytosolic dimeric protein involved in cellular detoxification by catalyzing the conjugation of glutathione (GSH) with a wide range of endogenous and xenobiotic-alkylating agents. GST showed increased abundance only in VS (in opposite to gene expression in **Figure 7G**). GST is a part of the plant protection mechanisms against toxic oxygen intermediates, together with superoxide dismutases, catalases, ascorbate peroxidases, and glutathione peroxidases (Abreu et al., 2013). Other results suggest that a decrease of the glutathione redox status during embryo development may represent a metabolic switch needed for the elevation of the endogenous levels of ABA contents, which is required for successful completion of the developmental program (Belmonte et al., 2006).

Jasmonate inducible protein (SSP 6717) containing a jacalin-like lectin domain is a lectin. Its accumulation is significantly lower in VS in comparison to VC, which is, however, in comparison with DC 4.7 higher (also supported by gene expression analysis in **Figure 7F**). Jacalin-like lectins have sugar-binding protein domains mostly found in plants, e.g., salt stress-induced in rice (Zhang, 2014) or wheat cold-regulated (Kosova

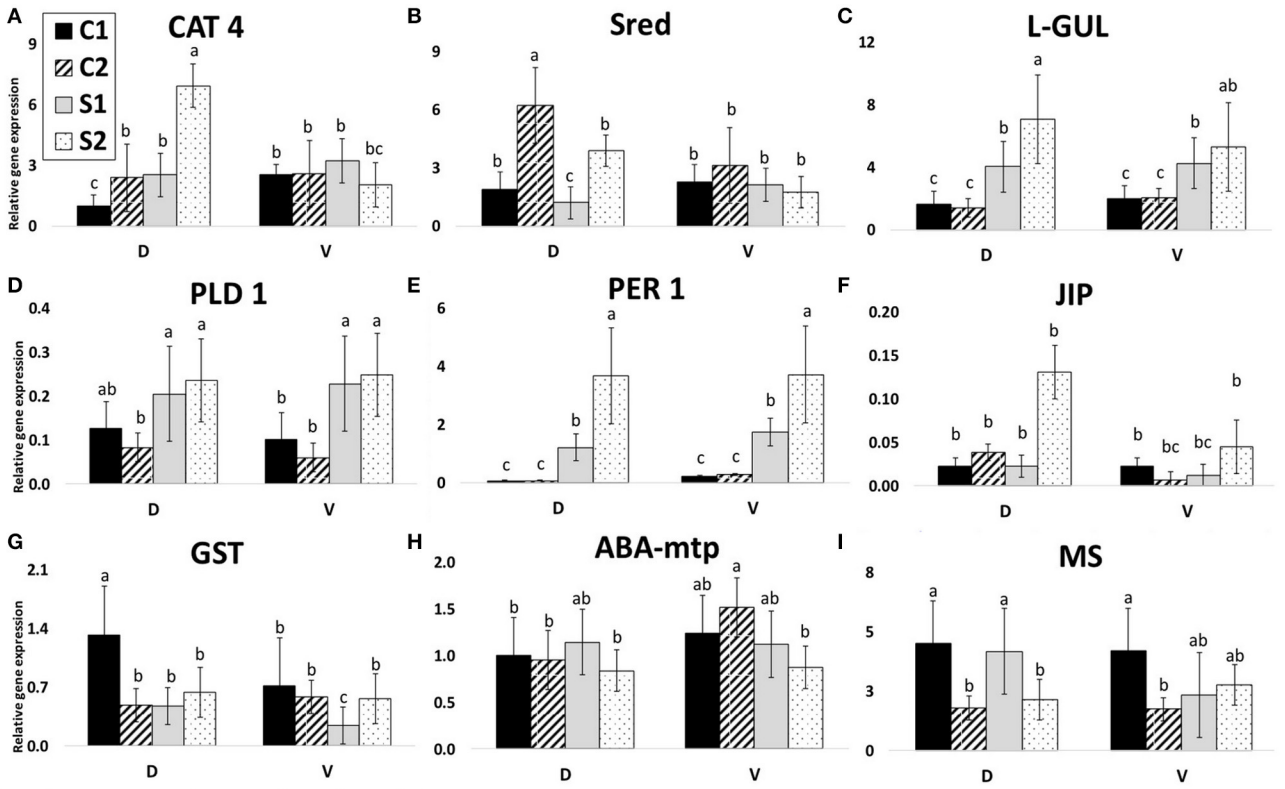


FIGURE 7 | Gene expressions. Relative gene expressions of nine selected genes according to protein identification. C1, control after 24 h after transfer to solid medium; S1, treated samples after 24 h after transfer; C2, control after 7 days after transfer; and S2, treated samples after 7 days after transfer. Gene expression was calculated according to the $2^{-\Delta\Delta CT}$ method. Means with the same letter within each gene are not significantly different at 5% probability. Error bars denote three technical replications. **(A)** CAT 4, catalase; **(B)** Sred, sultite reductase; **(C)** L-GUL, putative lactoylglutathione lyase; **(D)** PLD 1, phospholipase D alpha 1; **(E)** PER 1, peroxiredoxin antioxidant; **(F)** JIP, jasmonate inducible protein; **(G)** GST, glutathione S-transferase; **(H)** ABA-mtp, ABA-modulated tyrosine-phosphorylated protein; **(I)** MS, 5-methyltetrahydropteroyltriglutamate-homocysteine methyltransferase.

et al., 2013). More importantly, lectins are involved in the regulation of plant development (e.g., the transition of SAM from vegetative to the reproductive stage).

Cruciferin cru 2/3 (SSP 5203; CRU) is a storage protein (also called "11S globulin") localized on a rough endoplasmic reticulum. CRU principal function appears to be the major nitrogen source for developing plants. Cruciferins can be classified on the basis of their structure into different families. This family is a member of the "cupin" superfamily on the basis of its conserved barrel domain. Gabrisova et al. (2016) showed that an increased abundance of cupin fragments in radium-contaminated flax contributed to growth and reproduction. CRU showed low relative accumulation in DC and high in VS. However, both cvs. showed significant CRU up-accumulation upon stress.

Phospholipases and Rubisco Precursor—Proteins Accumulated Mainly in Controls or Treated Samples Support Results From Hormonal Profiling

Proteins in cluster 7 did not show differences between treatments but differential accumulation in controls or upon stress (cluster 8). However, some of them show a mixed pattern of their gene products (isoforms; cluster 9). Therefore, they were similarly up- or down-accumulated despite treatments in both cvs. However, to understand all proteome changes and have deeper insight, these data are discussed to share the complexity of the MDE answer to PEG-related osmotic stress.

Rubisco ssu precursor (SSP 2111) showed a very high increase in DS/DC (seven times) and a significant decrease in the VS/VC ratio. However, VC showed nine times the higher accumulation of Rubisco SSU precursor (ssp 2111) than in DC but, interestingly, higher accumulation in DS in contrast to VS.

Fructose-bisphosphate aldolase 3 (SSP 2322 and 3319; EC 4.1.2.13; FBA) catalyzes the reversible cleavage of fructose-1,6-bisphosphate to glyceraldehyde 3-phosphate and dihydroxyacetone phosphate. Glycolysis uses this forward reaction, while gluconeogenesis and the Calvin cycle, which are anabolic pathways, use the reverse reaction. However, these reactions are not possible under energy deficit. The level of FBA was found to decline under salt stress in most of the plant species studied [reviewed by Abreu et al. (2013)]. Yin et al. (2008) found FBA important in maintaining plant physiological functions during wound response in leaves of *B. napus*. Aldolase has also been implicated in many non-catalytic functions based upon its

binding affinity for multiple other proteins, including tubulin and phospholipase D, which were found in this study (decreased in both treated samples).

Malate dehydrogenase (SSP 2312 and 2319; EC 1.1.1.37; MDH) reversibly catalyzes the oxidation of malate to oxaloacetate using the reduction of NAD+ to NADH. This reaction is a part of many metabolic pathways, including the citric acid cycle and gluconeogenesis. MDH showed mixed abundance in stressed plants, which cannot support an idea about its important role in water transport and the need for NADPH reduction power, as was postulated in our previous study (Urban et al., 2017).

The phospholipases D alpha 1 (PLD 1; SSP 6705 and 6712; refer to in **Figure 7D**), phospholipase D alpha 2 (SSP 6716), catalase (SSP 1502; also in **Figure 7A**), ABA-modulated tyrosine-phosphorylated protein (SSP 4216; also in **Figure 7H**), both transcription-related proteins (SSP 4711 and 5314), and Clp ATPase (SSP 6710) showed increased protein abundance in DS vs. VS (gene expression of mentioned proteins is shown in **Figure 7**; mentioned increase in DS is valid for catalase only). Phospholipase D alpha 1 (SSP 6705, 6712) and phospholipase D alpha 2 (SSP 6716; PLD 2) are important enzymes of phospholipid metabolism. Phospholipases D (PLD) and their products, phosphatidic acids, are now considered to be one of the key elements of numerous physiological processes in plants, including the salicylic acid-signaling pathway (Janda et al., 2015). Distefano et al. (2015) showed that pld *Arabidopsis* mutants were more tolerant to severe drought than wild-type plants. This finding suggests that, in wild-type plants, PLD disrupts membranes in severe drought stress and, in the absence of the protein (PLD knockout), might drought-prime the plants, making them more tolerant to severe drought stress. Thus, in contrast to cultivar characteristics and treatment, all PLDs proteins decreased in treated samples, however, D vs. V comparison showed always higher abundance of PLDs in D. These data are in contrast to the PLD 1 gene expression data (**Figure 7D**) where there is significant increase in all treated samples. However, in V, the SA content (**Figure 8E**) decreased in treated samples and increased in S2 of D.

The Comparison Between Leaf Proteome Under Drought and MDE Proteome Under Osmotic Stress

The osmotic stress-affected MDE-derived proteome was compared with the drought-stressed leaf proteome (in the stem-prolongation stage) and analyzed in our previous study (Urban et al., 2017). C vs. D and V were used in both cases. The reason for this comparison has been to reveal possible associations between these two different studies and distinct developmental stages with the aim to evaluate the possible role of MDE in the early selection of more adaptable rapeseed cultivars.

In a simplified way, a comparison of the number of proteins in each functional category between MDE and leaves may reveal a significant increase in protein turnover in MDE. Some protein functional categories, e.g., "protein destination" and "cell structures," are missing in leaf proteomes. On the other side, ATP interconversion, redox homeostasis, and protein synthesis are higher in the leaf proteome of these two cvs. If we compare individual numbers of increased proteins in each genotype, similarities between MDE and leaf proteome in ATP interconversion and redox homeostasis can be seen in V. Comparison of decreased proteins in individual genotypes for each functional category shows similarities between MDE and leaves proteomes for both cvs., especially in "redox homeostasis" and "stress/defense proteins."

Some proteins are similar or even identical in both studies (heat map **Supplementary Figure 5**): glutamine synthetase, lactoylglutathione lyase (glyoxalase), atpA gene product, carbonic anhydrase, malate dehydrogenase 1, oxygen-evolving enhancer protein 1-2, L-ascorbate peroxidase, and glutathione S-transferase. Unfortunately, none of these proteins showed similar patterns in protein accumulation. Interestingly, in MDE, only one small chain RuBisCO (CAA30290.1; SSP 2111; rubisco ssu precursor) was found in contrast to five rbcL (ribulose-1,5-bisphosphate carboxylase/oxygenase large subunit) and nine activases (chloroplast ribulose-1,5-bisphosphate carboxylase/oxygenase activase) in leaves. This can be attributed to the high sugar content (2%) presented in the DM.

Even though drought can be primarily manifested also as osmotic stress (low water potential of soil, increasing xylem sap potential, etc.), a simple relationship between in-pot substrate dry-down and in-sterile cultivation vapor-saturated media is definitely not obvious. Also, at the proteome level, we cannot easily compare these two cultivation methods and developmental stages. Generally, we can conclude that proteome response at the MDE and leaf levels is very different from mean abundances in each category or in comparison of Z-scores. The information about individual protein behavior has already been described in the text above. In this study, the MDE biomass accumulation (higher in D) significantly shows adaptability to osmotic stress at a non-proteomic level. In Urban et al. (2017) study, cultivar D revealed a middle-drought-resistant water-saver strategy in contrast to the drought-susceptible water-spender strategy of cultivar V.

Comparison/Correlation of Selected Protein Abundance With Relative Gene Expression

The mRNA expression values have provided a lot of information in a broad range of applications, including the diagnosis and the classification of diseases. These results are almost certainly only correlative rather than causative. Most probably, the concentration of proteins and their interactions are the true causative forces in the cells; therefore, the corresponding protein quantities ought to be studied (Greenbaum et al., 2003).

Nine proteins were selected according to their interesting accumulation pattern across genotypes and treatments (**Figure 7**). The chosen proteins were as follows (SSP, name): 1502, catalase (CAT 4; **Figure 7A**); 7201, putative lactoylglutathione lyase (L-GUL; **Figure 7C**); 6705 and 6712, phospholipase D alpha 1 (PLD 1; **Figure 7D**); 5214,

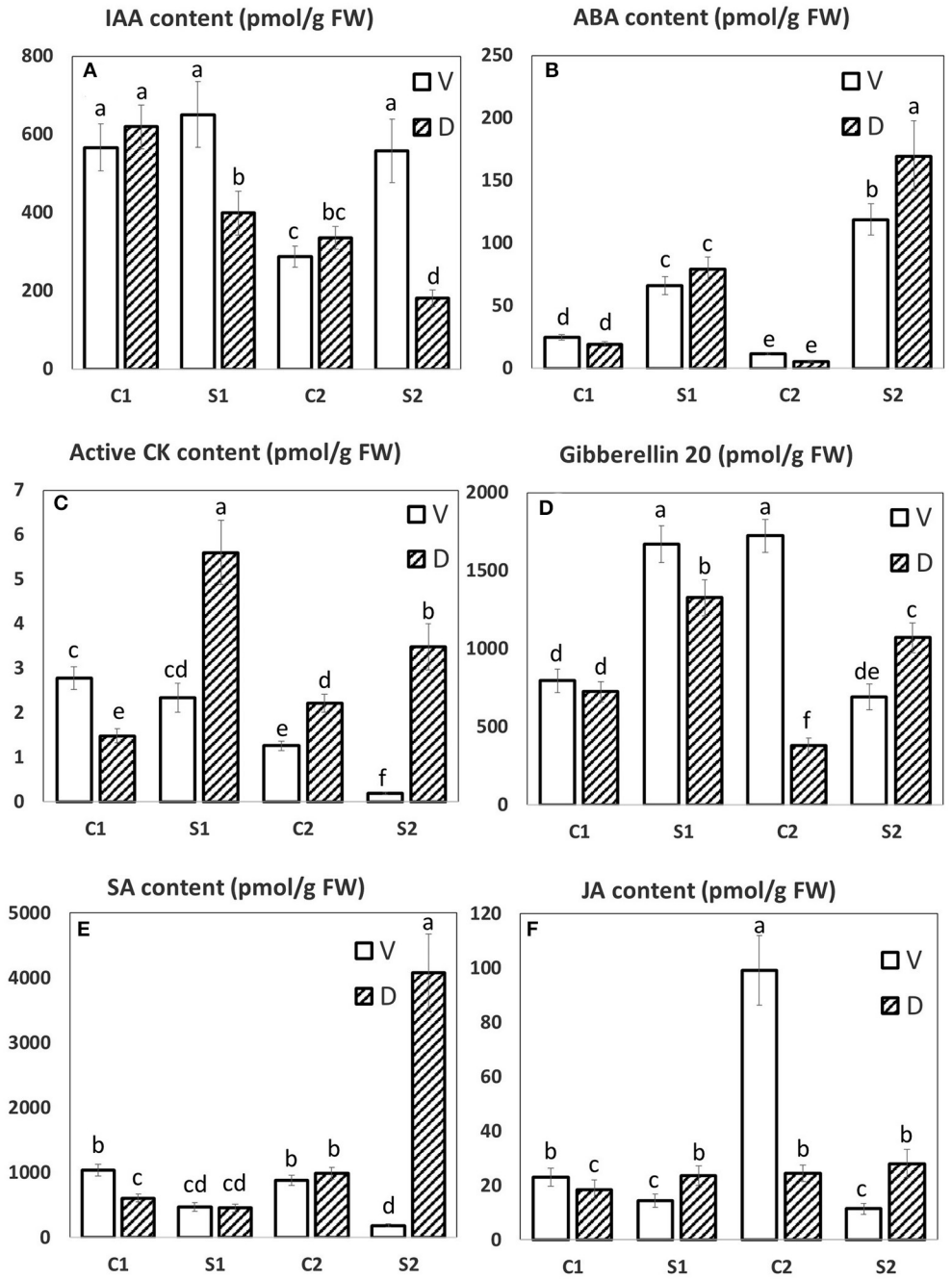


FIGURE 8 | The hormonal profile of MDE. The LC/MS hormonal profile of six selected hormones. **(A)** IAA, indole-3-acetic acid; **(B)** ABA, abscisic acid; **(C)** active CK, active cytokinins; **(D)** Gibberellin 20, Gb_{20}; **(E)** SA, salicylic acid; **(F)** JA, jasmonic acid. Means with different letters show significantly different values between treatments at 5% probability. Error bars denote SD.

peroxiredoxin antioxidant (PER 1; **Figure 7E**); 6717, jasmonate inducible protein (JIP; **Figure 7F**); 4216, ABA-modulated tyrosine-phosphorylated protein (ABA-mtp; **Figure 7H**); 1608, sulfite reductase (found N.S. in this study; Sred; **Figure 7B**); 4805, 5-methyltetrahydropteroyltriglutamate-homocysteine methyltransferase (MS 1; **Figure 7I**); and 4203, glutathione S-transferase (GST; **Figure 7G**). Expression patterns of individual transcripts are shown in **Figure 7** and data in SI 6.

Three of the expression profiles (7DAS) are very similar to protein abundance profiles (7DAS): CAT 4, PER 1, L-GUL (**Figures 7A–E**).

The other gene expression profiles are not similar to protein accumulation patterns. There is a clear opposite reaction (gene

expression vs. protein abundance) visible for Sred, both PLD's, JIP, GST, ABA-mtp, and, partially, also MS 1.

Two of these gene-relative expression profiles (7 DAS) are similar to protein abundance profiles (7 DAS): PER1 and L-GUL. L-GUL acts with Glyoxalase II and detoxification of highly cytotoxic metabolite methylglyoxal accumulated in plant cells due to drought stress (Hasanuzzaman et al., 2017; Askari-Khorasgani and Pessarakli, 2019). Gene expression of L-GUL was upregulated in both cultivars, but D showed a higher level of transcripts (opposite to protein). The accumulation level of L-GUL protein was higher in both treated samples of both cultivars. Protein accumulation of PER1 was accumulated in both cultivars after 7 DAS significantly. This enzyme plays a crucial role in extreme drought stress resistance (Shaikhali et al., 2008; Chen et al., 2016). This corresponds to the gene expression level of PER1. Expression of this gene was upregulated after 7 DAS as well as after 1 DAS. Relative gene expression of this gene in controls was five times higher in the V line in comparison to D (the trend similar in protein accumulation too). Similarly, after 1 DAS, higher levels of PER1 transcript accumulation were found in the V line. After 7 DAS, the level of PER1 transcript accumulation was even increased and was almost the same in both lines. This enzyme is important in the degradation of the reactive oxygen species generated in plants exposed to different types of biotic and abiotic stresses (Tripathi et al., 2009). Generally, lower levels of transcripts in D could indicate a more efficient prevention system of reactive oxygen species generation during early drought stress conditions. Expression of this gene can be thus one of the potential markers for the early selection of more adaptable rapeseed cultivars. Gene expression of PLD 1 increased after 7 DAS as well as after 1 DAS in both lines D and V. In V, accumulation of this protein decreased after 7 DAS (similar decrease observed in VS vs. VC for SSP 6705; SSP 6712 was even missing in VS). This gene is important in the ABA-signaling pathway (Janda et al., 2015; Zhao, 2015). Decreased accumulation of this protein in intolerant V shows that the accumulation efficiency of expressed proteins can be an important part of drought tolerance. The other gene expression profiles are not similar to protein accumulation patterns.

According to Greenbaum et al. (2003), in the case of the lack of obvious correlation between mRNA and protein data, both quantities could be used as independent sources of information for machine-learning algorithms, for example, to predict protein interactions. On this basis, these three genes (L-GUL, PER 1, and PLD 1) can be postulated as suitable for gene-targeting and, also, for early selection of embryos in regard to their osmotic stress adaptability. All genes, PLD 1, PER 1, and L-GUL can be used for early MDE selection as they are stress-related proteins, possibly increasing the adaptability of MDE to osmotic stress (**Figures 7C–E**). However, CAT 4 and JIP (**Figures 7A,F**) can be used for characterizing resistant vs. sensitive cultivars.

Hormonal Analyses Reveal That ABA and Active Cytokinins Play a Crucial Role

The hormonal profile of selected hormones is presented in **Figure 8**. The complete hormonal profile of PEG-treated MDE upon 1 and 7 DAS can be found in SI 11.

Abscisic acid (ABA) is the most important hormone-controlling plant water loss and, hence, water status and performance in water-limited conditions (Cutler et al., 2010). ABA induces closure of stomata, the crucial water regulation site, as well as stimulates substantial transcription changes, associated with growth suppression and activation of defense. ABA is the key hormone in the responses to abiotic stresses associated with dehydration, not only to drought but also to osmotic stress and cold. The growth on PEG resulted in both MDE tissues, D, and V in early stimulation of ABA content. During the stress progression, ABA levels were further elevated to a significantly higher extent in D line (**Figure 8B**). ABA elevation was at the early response (after 1 DAS), associated with diminished content of ABA catabolites (DPA, PA, and ABA-GE). During the stress progression, ABA biosynthesis was upregulated to such an extent that catabolite contents increased to maintain ABA at the optimal level.

During abiotic stress responses, ABA exhibits an intensive cross-talk with other plant hormones. For example, jasmonic acid (JA) activates synergistically several branches of the ABA-signaling pathway [especially MYC/MYB and ANAC transcription factors; (de Ollas and Dodd, 2016)]. JA plays an important role, e.g., in the dehydration of desiccation-tolerant plants (Djilianov et al., 2013). Under controlled conditions, D exhibited lower JA content than V (**Figure 8F**); however, upon PEG treatment, cv. D exhibited significantly higher JA content in comparison to cv. V already after 1 day of stress. After 7-day treatment, D exhibited significant elevation of the active JA conjugate—JA-Ile, while in V content of this compound substantially dropped.

The participation of the other stress hormone—salicylic acid (SA) in drought response may be deduced from the elevation of this hormone during drought stress as well as by the positive effect of exogenous SA application on plant tolerance [(Miura and Tada, 2014); **Figure 8E**]. Both lines exhibited low SA levels after 1 DAS. During prolonged stress, the D line showed profound SA increase, in contrast to V, which showed SA downregulation. Interestingly, the JA and SA levels in stressed V were almost always lower than control values, opposite to the situation in D.

Also, hormones preferentially associated with stimulation of cell division and growth—auxins and cytokinins (CKs)—were found to participate significantly in stress responses. They affect the growth rate, which is generally diminished upon stress, in order to reallocate the energy sources to defense activation. Regulation of auxin content and transport in osmotic stress response was recently described by Rowe et al. (2016). Auxin (indole-3- acetic acid, IAA, **Figure 8A**) levels were found to stay low in controls in both cultivars. V cv. maintained relatively high IAA levels during the stress response, while D downregulated IAA content in stress, especially after 7 DAS. The IAA precursor IAN was downregulated in both cultivars at stress conditions. The content of irreversibly inactivated IAA conjugates IAA-Asp correlated with IAA levels (PEG-induced downregulation in D and upregulation in V, respectively). In contrast, the IAA drop was associated with an increase of its deactivation product oxIAA.

CKs affect not only plant growth but also stabilize the photosynthetic system (Boonman et al., 2007; Honig et al., 2018). V diminished significantly the levels of active CKs (trans-zeatin, dihydrozeatin, isopentenyladenine, and cis-zeatin; **Figure 8C**) during the stress progression, which might indicate "quiescent" stress strategy (diminishing of the energy requirements by growth suppression). A similar strategy was observed, e.g., in plants over-expressing the main CK-degrading enzyme cytokinin oxidase/dehydrogenase (Mackova et al., 2013). In contrast, the D line transiently increased active CK levels, and, even after prolonged stress, it maintained relatively high levels of active CKs, which might have positive effects on the photosynthetic rate and plant metabolism. This result is supported by a high abundance of Rubisco ssu precursor (SSP 2111) and fructose-bisphosphate aldolase 3. This approach has been observed in plants over-expression of CK biosynthetic enzyme isopentenyl transferase under the control of senescence, inducible promoter (Rivero et al., 2007). CK biosynthesis was transiently promoted in both genotypes (after 1 DAS), being diminished after 7 DAS. Downregulation of active CKs in V was accompanied by a stronger increase of CK deactivation products, CK N-glucosides.

Hormonal profiles clearly indicate that D exhibits higher osmotic resistance, which was associated with higher levels of stress hormones ABA, SA, JA, and GA_{20}, as well as of active CKs under stress conditions, both from absolute (D vs. V) as from relative (treated vs. control tissues) points of view. In contrast, V quickly downregulates active CK content, which might represent an advantage in case of long-term stress.

CONCLUSIONS

Fertile plants from doubled haploid embryos derived from microspores are both a challenging task and an interesting method to address and understand the effects of abiotic or biotic stress treatments. The likely upcoming new-generation breeding strategies (epigenetic breeding, stress-memory-based breeding, gene editing, associative mapping, etc.) are looking for stable but wide genetic variability within established crops. The MDE seem to be one of the appropriate ways to manage this goal. The technique itself is not easy and far from being used extensively; however, it has already been established for several crops. This proteomic study is among the first steps to demonstrate that MDE is a suitable model for follow-up research aimed at the characterization of new crossings. MDE methodology can likely be used for phenotype-based selection of genotypes resistant to other disrupting effects (other abiotic stresses and their combinations), even though such an effort needs to be confirmed by upcoming studies, including more cultivars or quick selection using biochemical assays.

Cultivar D showed an enhanced biomass accumulation under osmotic stress reflected by the high number of proteins, which belong to energy metabolism (especially glycolysis), redox homeostasis + signaling (phospholipases, MAPK4), transcription, and, also, protein destination, storage, and proteolysis functional categories. Simultaneously, D revealed a unique hormonal profile, high contents of ABA, CKs, SA, JA, and GA_{20} that reflect processes during acclimation of D embryos.

Cultivar D also showed a higher number of unique energy-related proteins and a lower number of down-accumulated proteins compared with V, better ability for protein synthesis, and adjunctive communication between compartments. On the other hand, the V protein profile showed a high need for energy (ATP) and an increased need for nutrients with a significant number of stress-related proteins and cell structure changes. Also, an enhanced number of proteins involved in anaerobic metabolism (e.g., alcohol dehydrogenase) were found in V. In addition, more proteins were generally down-accumulated in sensitive V, which may be connected with the rapid depletion of energy molecules. A similar trend for V was observed also in its leaf proteome upon drought in our previous study Urban et al. (2017).

From a gene expression point of view, we highlighted three genes, which show an interesting pattern of accumulation, and these patterns were in relation to their protein abundances: L-GUL, PLD 1, and PER 1.

Taking these findings together, cv. D showed quick adaptation to osmotically activated PEG-infused cultivation media, while cv. V showed an alert-based response with clear signs of damage. Maintenance of the primary metabolism, oxidative stress response, and signaling seems to be a strategy for D osmotic resistance. On the other hand, susceptibility might be related to the maintenance of the energy-consuming homeostatic equilibrium in V.

DATA AVAILABILITY STATEMENT

The mass spectrometry proteomics data have been deposited to the ProteomeXchange Consortium via the PRIDE partner repository with the dataset identifier PXD024552.

AUTHOR CONTRIBUTIONS

MU: conceptualization, validation, writing of the original draft, reviewing, and editing of the draft. SP: methodology development, protein analysis data, review, and editing of the draft. IH: methodology development, RT-qPCR data, validation of the review, and editing of the draft. RV: methodology development, hormonal analysis, validation, review, and editing of the draft. PD: methodology development and hormonal analysis of data. JR: methodology, review, and editing of the draft. MK: MDE methodology development, validation, supervision, and review of the draft. PV: 2D-DIGE methodology development, validation, supervision, review, and editing of the draft. All authors contributed to the article and approved the submitted version.

FUNDING

The work was supported by the Czech Ministry of Agriculture, MZe QJ 1510172 and Ministry of Education, Youth and

Sports of CR from European Regional Development Fund, Project Center for Experimental Plant Biology: No. CZ.02.1.01/0.0/0.0/16_019/0000738.

ACKNOWLEDGMENTS

The authors thank Dr. Herman Kopecek and Dr. Jana Krtkova for their linguistic editing of the whole manuscript. MU is grateful for support from the German Center for International Migration and Development (CIM).

SUPPLEMENTARY MATERIAL

The Supplementary Material for this article can be found online at: https://www.frontiersin.org/articles/10.3389/fpls.2021.628167/full#supplementary-material

REFERENCES

Abass, M., and Morris, P. C. (2013). The Hordeum vulgare signalling protein MAP kinase 4 is a regulator of biotic and abiotic stress responses. *J. Plant Physiol.* 170, 1353–1359. doi: 10.1016/j.jplph.2013.04.009

Abreu, I., Farinha, A., Negrao, S., Goncalves, N., Fonseca, C., Rodrigues, M., et al. (2013). Coping with abiotic stress: proteome changes for crop improvement. *J. Proteom.* 93, 145–168. doi: 10.1016/j.jprot.2013.07.014

Ahmadi, B., Ahmadi, M., and da Silva, J. A. T. (2018). Microspore embryogenesis in Brassica: calcium signaling, epigenetic modification, and programmed cell death. *Planta* 248, 1339–1350. doi: 10.1007/s00425-018-2996-5

Almeida, A. M., Parreira, J. R., Santos, R., Duque, A. S., Francisco, R., Tome, D. F., et al. (2012). A proteomics study of the induction of somatic embryogenesis in Medicago truncatula using 2DE and MALDI-TOF/TOF. *Physiol. Plantarum* 146, 236–249. doi: 10.1111/j.1399-3054.2012.01633.x

Askari-Khorasgani, O., and Pessarakli, M. (2019). Manipulation of plant methylglyoxal metabolic and signaling pathways for improving tolerance to drought stress. *J. Plant Nutr.* 42, 1268–1275. doi: 10.1080/01904167.2019.1589502

Bandehagh, A., Salekdeh, G. H., Toorchi, M., Mohammadi, A., and Komatsu, S. (2011). Comparative proteomic analysis of canola leaves under salinity stress. *Proteomics* 11, 1965–1975. doi: 10.1002/pmic.201000564

Belmonte, M. F., Ambrose, S. J., Ross, A. R. S., Abrams, S. R., and Stasolla, C. (2006). Improved development of microspore-derived embryo cultures of Brassica napus cv Topaz following changes in glutathione metabolism. *Physiol. Plantarum* 127, 690–700. doi: 10.1111/j.1399-3054.2006.00707.x

Boonman, A., Prinsen, E., Gilmer, F., Schurr, U., Peeters, A. J. M., Voesenek, L., et al. (2007). Cytokinin import rate as a signal for photosynthetic acclimation to canopy light gradients. *Plant Physiol.* 143, 1841–1852. doi: 10.1104/pp.106.094631

Brauc, S., De Vooght, E., Claeys, M., Hofte, M., and Angenon, G. (2011). Influence of over-expression of cytosolic aspartate aminotransferase on amino acid metabolism and defence responses against Botrytis cinerea infection in Arabidopsis thaliana. *J. Plant Physiol.* 168, 1813–1819. doi: 10.1016/j.jplph.2011.05.012

Caraux, G., and Pinloche, S. (2005). PermutMatrix: a graphical environment to arrange gene expression profiles in optimal linear order. *Bioinformatics* 21, 1280–1281. doi: 10.1093/bioinformatics/bti141

Cegielska-Taras, T., Pniewski, T., and Szala, L. (2008). Transformation of microspore-derived embryos of winter oilseed rape (*Brassica napus* L.) by using *Agrobacterium tumefaciens*. *J. Appl. Genet.* 49, 343–347. doi: 10.1007/BF03195632

Cerny, M., Kuklova, A., Hoehenwarter, W., Fragner, L., Novak, O., Rotkova, G., et al. (2013). Proteome and metabolome profiling of cytokinin action in Arabidopsis identifying both distinct and similar responses to cytokinin down- and up-regulation. *J. Exp. Bot.* 64, 4193–4206. doi: 10.1093/jxb/ert227

Chan, J., and Pauls, K. P. (2007). Brassica napus Rop GTPases and their expression in microspore cultures. *Planta* 225, 469–484. doi: 10.1007/s00425-006-0362-5

Chen, H. H., Chu, P., Zhou, Y. L., Ding, Y., Li, Y., Liu, J., et al. (2016). Ectopic expression of NnPER1, a Nelumbo nucifera 1-cysteine peroxiredoxin antioxidant, enhances seed longevity and stress tolerance in Arabidopsis. *Plant J.* 88, 608–619. doi: 10.1111/tpj.13286

Chu, P. Y. G., Yang, Q., Zhai, L. N., Zhang, C., Zhang, F. Q., and Guan, R. Z., (2015). iTRAQ-basedquantitative proteomics analysis of Brassica napus leaves reveals pathwaysassociated with chlorophyll deficiency. *J. Proteomics*. 113, 244–259. doi: 10.1016/j.jprot.2014.10.005

Claeys, H., Van Landeghem, S., Dubois, M., Maleux, K., and Inze, D. (2014). What is stress? Dose-response effects in commonly used *in vitro* stress assays. *Plant Physiol.* 165, 519–527. doi: 10.1104/pp.113.234641

Cui, S., Hu, J., Guo, S., Wang, J., Cheng, Y., Dang, X., et al. (2012). Proteome analysis of Physcomitrella patens exposed to progressive dehydration and rehydration. *J. Exp. Bot.* 63, 711–726. doi: 10.1093/jxb/err296

Cutler, S. R., Rodriguez, P. L., Finkelstein, R. R., and Abrams, S. R. (2010). Abscisic acid: emergence of a core signaling network. *Annu. Rev. Plant Biol.* 61, 651–679. doi: 10.1146/annurev-arplant-042809-112122

Daurova, A., Daurov, D., Volkov, D., Karimov, A., Abai, Z., Raimbek, D., et al. (2020). Mutagenic treatment of microspore-derived embryos of turnip rape (*Brassica rapa*) to increase oleic acid content. *Plant Breeding* 139, 916–922. doi: 10.1111/pbr.12830

de la Torre, F., Canas, R. A., Pascual, M. B., Avila, C., and Canovas, F. M. (2014a). Plastidic aspartate aminotransferases and the biosynthesis of essential amino acids in plants. *J. Exp. Bot.* 65, 5527–5534. doi: 10.1093/jxb/eru240

de la Torre, F., El-Azaz, J., Avila, C., and Canovas, F. M. (2014b). Deciphering the role of aspartate and prephenate aminotransferase activities in plastid nitrogen metabolism. *Plant Physiol.* 164, 92–104. doi: 10.1104/pp.113.232462

de Ollas, C., and Dodd, I. C. (2016). Physiological impacts of ABA-JA interactions under water-limitation. *Plant Mol. Biol.* 91, 641–650. doi: 10.1007/s11103-016-0503-6

Demartini, D. R., Jain, R., Agrawal, G., and Thelen, J. J. (2011). Proteomic comparison of plastids from developing embryos and leaves of *Brassica napus*. *J. Proteome Res.* 10, 2226–2237. doi: 10.1021/pr101047y

Denance, N., Szurek, B., and Noel, L. D. (2014). Emerging functions of nodulin-like proteins in non-nodulating plant species. *Plant Cell Physiol.* 55, 469–474. doi: 10.1093/pcp/pct198

Devouge, V., Rogniaux, H., Nesi, N., Tessier, D., Gueguen, J., and Larre, C. (2007). Differential proteomic analysis of four near-isogenic *Brassica napus* varieties bred for their erucic acid and glucosinolate contents. *J. Proteome Res.* 6, 1342–1353. doi: 10.1021/pr060450b

Distefano, A. M., Valinas, M. A., Scuffi, D., Lamattina, L., ten Have, A., Garcia-Mata, C., et al. (2015). Phospholipase D delta knock-out mutants are tolerant to severe drought stress. *Plant Signal. Behav.* 10:1089371. doi: 10.1080/15592324.2015.1089371

Djilianov, D. L., Dobrev, P. I., Moyankova, D. P., Vankova, R., Georgieva, D. T., Gajdosova, S., et al. (2013). Dynamics of endogenous phytohormones during desiccation and recovery of the resurrection plant species haberlea rhodopensis. *J. Plant Growth Regul.* 32, 564–574. doi: 10.1007/s00344-013-9323-y

Dobre, P., and Vankova, R. (2012). Quantification of abscisic acid, cytokinin, and auxin content in salt-stressed plant tissues. plant salt toler. *Methods Mol. Biol.* 913, 251–261. doi: 10.1007/978-1-61779-986-0_17

Dobrev, P., and Kaminek, M. (2002). Fast and efficient separation of cytokinins from auxin and abscisic acid and their purification using mixed-mode solid-phase extraction. *J. Chromatogr.* 950, 21–29. doi: 10.1016/S0021-9673(02)00024-9

Doskocilova, A., Plihal, O., Volc, J., Chumova, J., Kourova, H., Halada, P., et al. (2011). A nodulin/glutamine synthetase-like fusion protein is implicated in the regulation of root morphogenesis and in signalling triggered by flagellin. *Planta* 234, 459–476. doi: 10.1007/s00425-011-1419-7

Duan, P. G., Rao, Y. C., Zeng, D. L., Yang, Y. L., Xu, R., Zhang, B. L., et al. (2014). SMALL GRAIN 1, which encodes a mitogen-activated protein kinase kinase 4, influences grain size in rice. *Plant J.* 77, 547–557. doi: 10.1111/tpj.12405

Fatma, M., Masood, A., Per, T. S., Rasheed, F., and Khan, N. A. (2016). Interplay between nitric oxide and sulfur assimilation in salt tolerance in plants. *Crop J.* 4, 153–161. doi: 10.1016/j.cj.2016.01.009

Fernandez, A. P., and Strand, A. (2008). Retrograde signaling and plant stress: plastid signals initiate cellular stress responses. *Curr. Opin. Plant Biol.* 11, 509–513. doi: 10.1016/j.pbi.2008.06.002

Fernandez-Garcia, N., Hernandez, M., Casado-Vela, J., Bru, R., Elortza, F., Hedden, P., et al. (2011). Changes to the proteome and targeted metabolites of xylem sap in Brassica oleracea in response to salt stress. *Plant Cell Environ.* 34, 821–836. doi: 10.1111/j.1365-3040.2011.02285.x

Ferreira, F. J., Guo, C., and Coleman, J. R. (2008). Reduction of plastid-localized carbonic anhydrase activity results in reduced Arabidopsis seedling survivorship. *Plant Physiol.* 147, 585–594. doi: 10.1104/pp.108.118661

Ferrie, A. M. R., and Caswell, K. L. (2011). Isolated microspore culture techniques and recent progress for haploid and doubled haploid plant production. *Plant Cell Tissue Organ Culture* 104, 301–309. doi: 10.1007/s11240-010-9800-y

Frenck, G., van der Linden, L., Mikkelsen, T. N., Brix, H., and Jorgensen, R. B. (2011). Increased CO_2 does not compensate for negative effects on yield caused by higher temperature and O-3 in *Brassica napus* L. *Eur. J. Agronomy* 35, 127–134. doi: 10.1016/j.eja.2011.05.004

Gabrisova, D., Klubicova, K., Danchenko, M., Gomory, D., Berezhna, V. V., Skultety, L., et al. (2016). Do cupins have a function beyond being seed storage proteins?. *Front. Plant Sci.* 6:1215. doi: 10.3389/fpls.2015.01215

Gan, L., Zhang, C.-Y., Wang, X.-D., Wang, H., Long, Y., Yin, Y.-T., et al. (2013). Proteomic and comparative genomic analysis of two brassica napus lines differing in oil content. *J. Proteome Res.* 12, 4965–4978. doi: 10.1021/pr4005635

Gawronski, P., Witon, D., Vashutina, K., Bederska, M., Betlinski, B., Rusaczonek, A., et al. (2014). Mitogen-activated protein kinase 4 is a salicylic acid-independent regulator of growth but not of photosynthesis in arabidopsis. *Mol. Plant* 7, 1151–1166. doi: 10.1093/mp/ssu060

Germana, M. A. (2011). Gametic embryogenesis and haploid technology as valuable support to plant breeding. *Plant Cell Rep.* 30, 839–857. doi: 10.1007/s00299-011-1061-7

Greenbaum, D., Colangelo, C., Williams, K., and Gerstein, M. (2003). Comparing protein abundance and mRNA expression levels on a genomic scale. *Genome Biol.* 4:117. doi: 10.1186/gb-2003-4-9-117

Guerra-Guimaraes, L., Tenente, R., Pinheiro, C., Chaves, I., Silva, M. D., Cardoso, F. M. H., et al. (2015). Proteomic analysis of apoplastic fluid of Coffea arabica leaves highlights novel biomarkers for resistance against Hemileia vastatrix. *Front. Plant Sci.* 6:478. doi: 10.3389/fpls.2015.00478

Hasanuzzaman, M., Nahar, K., Hossain, M. S., Al Mahmud, J., Rahman, A., Inafuku, M., et al. (2017). Coordinated actions of glyoxalase and antioxidant defense systems in conferring abiotic stress tolerance in plants. *Int. J. Mol. Sci.* 18:200. doi: 10.3390/ijms18010200

Heyno, E., Alkan, N., and Fluhr, R. (2013). A dual role for plant quinone reductases in host-fungus interaction. *Physiol. Plantarum* 149, 340–353. doi: 10.1111/ppl.12042

Holdorf, M. M., Owen, H. A., Lieber, S. R., Yuan, L., Adams, N., Dabney-Smith, C., et al. (2012). Arabidopsis ETHE1 encodes a sulfur dioxygenase that is essential for embryo and endosperm development. *Plant Physiol.* 160, 226–236. doi: 10.1104/pp.112.201855

Honig, M., Plihalova, L., Husickova, A., Nisler, J., and Dolezal, K. (2018). Role of cytokinins in senescence, antioxidant defence and photosynthesis. *Int. J. Mol. Sci.* 19:4045. doi: 10.3390/ijms19124045

Hu, Z.-Y., Hua, W., Huang, S.-M., and Wang, H.-Z. (2011). Complete chloroplast genome sequence of rapeseed (*Brassica napus* L.) and its evolutionary implications. *Genet. Resour. Crop Evol.* 58, 875–887. doi: 10.1007/s10722-010-9626-9

Huener, N. P. A., Bode, R., Dahal, K., Hollis, L., Rosso, D., Krol, M., et al. (2012). Chloroplast redox imbalance governs phenotypic plasticity: the "grand design of photosynthesis" revisited. *Front. Plant Sci.* 3:255. doi: 10.3389/fpls.2012.00255

Janda, M., Jezkova, L., Novakova, M., Valentova, O., Burketova, L., and Sasek, V. (2015). Identification of phospholipase D genes in *Brassica napus* and their transcription after phytohormone treatment and pathogen infection. *Biol. Plant.* 59, 581–590. doi: 10.1007/s10535-015-0513-2

Kaczmarek, Z., Adamska, E., Cegielska, T., and Szala, L. (2008). The use of statistical methods to evaluate winter oilseed rape doubled haploids for industrial purposes. *Industrial Crops Products* 27, 348–353. doi: 10.1016/j.indcrop.2007.11.012

Kampouridis, A., Ziese-Kubon, K., Nurhasanah, and Ecke, W. (2016). Identification and evaluation of intervarietal substitution lines of rapeseed (*Brassica napus* L.) with donor segments affecting the direct embryo to plant conversion rate of microspore-derived embryos. *Euphytica* 211, 215–229. doi: 10.1007/s10681-016-1732-0

Katsuhara, M., Sasano, S., Horie, T., Matsumoto, T., Rhee, J., and Shibasaka, M. (2014). Functional and molecular characteristics of rice and barley NIP aquaporins transporting water, hydrogen peroxide and arsenite. *Plant Biotechnol.* 31, 213–U173. doi: 10.5511/plantbiotechnology.14.0421a

Kaur, C., Ghosh, A., Pareek, A., Sopory, S. K., and Singla-Pareek, S. L. (2014). Glyoxalases and stress tolerance in plants. *Biochem. Soc. Trans.* 42, 485–499. doi: 10.1042/BST20130242

Kim, S. Y., Jung, Y. J., Shin, M. R., Park, J. H., Nawkar, G. M., Maibam, P., et al. (2012). Molecular and functional properties of three different peroxiredoxin isotypes in Chinese cabbage. *Mol. Cells* 33, 27–33. doi: 10.1007/s10059-012-2166-8

Kitashiba, H., Taguchi, K., Kaneko, I., Inaba, K., Yokoi, S., Takahata, Y., et al. (2016). Identification of loci associated with embryo yield in microspore culture of Brassica rapa by segregation distortion analysis. *Plant Cell Rep.* 35, 2197–2204. doi: 10.1007/s00299-016-2029-4

Klima, M., Vyvadilova, M., and Kucera, V. (2008). Chromosome doubling effects of selected antimitotic agents in *Brassica napus* microspore culture. *Czech J. Genet. Plant Breed.* 44, 30–36. doi: 10.17221/1328-CJGPB

Klinghammer, M., and Tenhaken, R. (2007). Genome-wide analysis of the UDP-glucose dehydrogenase gene family in Arabidopsis, a key enzyme for matrix polysaccharides in cell walls. *J. Exp. Bot.* 58, 3609–3621. doi: 10.1093/jxb/erm209

Klodmann, J., and Braun, H.-P. (2011). Proteomic approach to characterize mitochondrial complex I from plants. *Phytochemistry* 72, 1071–1080. doi: 10.1016/j.phytochem.2010.11.012

Koh, J., Chen, G., Yoo, M.-J., Zhu, N., Dufresne, D., Erickson, J. E., et al. (2015). Comparative proteomic analysis of brassica napus in response to drought stress. *J. Proteome Res.* 14, 3068–3081. doi: 10.1021/pr501323d

Kosova, K., Vitamvas, P., Planchon, S., Renaut, J., Vankova, R., and Prasil, I. T. (2013). Proteome analysis of cold response in spring and winter wheat (*Triticum aestivum*) crowns reveals similarities in stress adaptation and differences in regulatory processes between the growth habits. *J. Proteome Res.* 12, 4830–4845. doi: 10.1021/pr400600g

Kosova, K., Vitamvas, P., Prasil, I. T., and Renaut, J. (2011). Plant proteome changes under abiotic stress - Contribution of proteomics studies to understanding plant stress response. *J. Proteom.* 74, 1301–1322. doi: 10.1016/j.jprot.2011.02.006

Kosova, K., Vitamvas, P., Urban, M. O., Klima, M., Roy, A., and Prasil, I. T. (2015). Biological networks underlying abiotic stress tolerance in temperate crops-a proteomic perspective. *Int. J. Mol. Sci.* 16, 20913–20942. doi: 10.3390/ijms160920913

Krussel, L., Junemann, J., Wirtz, M., Birke, H., Thornton, J. D., Browning, L. W., et al. (2014). The mitochondrial sulfur dioxygenase ethylmalonic encephalopathy protein1 is required for amino acid catabolism during carbohydrate starvation and embryo development in arabidopsis. *Plant Physiol.* 165, 92–104. doi: 10.1104/pp.114.239764

Kubala, S., Garnczarska, M., Wojtyla, L., Clippe, A., Kosmala, A., Zmienko, A., et al. (2015). Deciphering priming-induced improvement of rapeseed (*Brassica napus* L.) germination through an integrated transcriptomic and proteomic approach. *Plant Sci.* 231, 94–113. doi: 10.1016/j.plantsci.2014.11.008

Limami, A. M., Glevarec, G., Ricoult, C., Cliquet, J. B., and Planchet, E. (2008). Concerted modulation of alanine and glutamate metabolism in young Medicago truncatula seedlings under hypoxic stress. *J. Exp. Bot.* 59, 2325–2335. doi: 10.1093/jxb/ern102

Livak, K. J., and Schmittgen, T. D. (2001). Analysis of relative gene expression data using real-time quantitative PCR and the 2(T)(-Delta Delta C) method. *Methods* 25, 402–408. doi: 10.1006/meth.2001.1262

Luo, J. L., Tang, S. H., Peng, X. J., Yan, X. H., Zeng, X. H., Li, J., et al. (2015). Elucidation of cross-talk and specificity of early response mechanisms to salt and PEG-simulated drought stresses in brassica napus using comparative proteomic analysis. *PLoS ONE* 10:138974. doi: 10.1371/journal.pone.0138974

Mackova, H., Hronkova, M., Dobra, J., Tureckova, V., Novak, O., Lubovska, Z., et al. (2013). Enhanced drought and heat stress tolerance of tobacco plants with ectopically enhanced cytokinin oxidase/dehydrogenase gene expression. *J. Exp. Bot.* 64, 2805–2815. doi: 10.1093/jxb/ert131

Malik, M. R., Wang, F., Dirpaul, J. M., Zhou, N., Polowick, P. L., Ferrie, A. M. R., et al. (2007). Transcript profiling and identification of molecular markers for early microspore embryogenesis in Brassica napus. *Plant Physiol.* 144, 134–154. doi: 10.1104/pp.106.092932

Manda, P., Freeman, M. G., Bridges, S. M., Jankun-Kelly, T. J., Nanduri, B., McCarthy, F. M., et al. (2010). GOModeler- A tool for hypothesis-testing of functional genomics datasets. *Bmc Bioinform.* 11:29. doi: 10.1186/1471-2105-11-S6-S29

McCarthy, F. M., Wang, N., Magee, G. B., Nanduri, B., Lawrence, M. L., Camon, E. B., et al. (2006). AgBase: a functional genomics resource for agriculture. *Bmc Genomics* 7:229. doi: 10.1186/1471-2164-7-229

Mittler, R., and Blumwald, E. (2010). Genetic engineering for modern agriculture: challenges and perspectives. *Annu. Rev. Plant Biol.* 61, 443–462. doi: 10.1146/annurev-arplant-042809-112116

Miura, K., and Tada, Y. (2014). Regulation of water, salinity, and cold stress responses by salicylic acid. *Front. Plant Sci.* 5:4. doi: 10.3389/fpls.2014.00004

Mohammadi, P. P., Moieni, A., and Komatsu, S. (2012). Comparative proteome analysis of drought-sensitive and drought-tolerant rapeseed roots and their hybrid F1 line under drought stress. *Amino Acids*‘43, 2137–2152. doi: 10.1007/s00726-012-1299-6

Najafabadi, F. P., Shariatpanahi, M. E., Ahmadi, B., Sima, N. K., Alizadeh, B., and Oroojloo, M. (2015). Effects of heat shock and 2, 4-D treatment on morphological and physiological characteristics of microspores and microspore-derived doubled haploid plants in *Brassica napus* L. *Iran. J. Biotechnol.* 13, 31–38. doi: 10.15171/ijb.1148

Orsel, M., Moison, M., Clouet, V., Thomas, J., Leprince, F., Canoy, A.-S., et al. (2014). Sixteen cytosolic glutamine synthetase genes identified in the *Brassica napus* L. genome are differentially regulated depending on nitrogen regimes and leaf senescence. *J. Exp. Bot.* 65, 3927–3947. doi: 10.1093/jxb/eru041

Prem, D., Solis, M. T., Barany, I., Rodriguez-Sanz, H., Risueno, M. C., and Testillano, P. S. (2012). A new microspore embryogenesis system under low temperature which mimics zygotic embryogenesis initials, expresses auxin and efficiently regenerates doubled-haploid plants in *Brassica napus*. *Bmc Plant Biol.* 12:127. doi: 10.1186/1471-2229-12-127

Reboul, R., Geserick, C., Pabst, M., Frey, B., Wittmann, D., Luetz-Meindl, U., et al. (2011). Down-regulation of UDP-glucuronic acid biosynthesis leads to swollen plant cell walls and severe developmental defects associated with changes in pectic polysaccharides. *J. Biol. Chem.* 286, 39982–39992. doi: 10.1074/jbc.M111.255695

Rivero, R. M., Kojima, M., Gepstein, A., Sakakibara, H., Mittler, R., Gepstein, S., et al. (2007). Delayed leaf senescence induces extreme drought tolerance in a flowering plant. *Proc. Natl. Acad. Sci. U.S.A.* 104, 19631–19636. doi: 10.1073/pnas.0709453104

Rodriguez-Sanz, H., Solis, M. T., Lopez, M. F., Gomez-Cadenas, A., Risueno, M. C., and Testillano, P. S. (2015). Auxin biosynthesis, accumulation, action and transport are involved in stress-induced microspore embryogenesis initiation and progression in *Brassica napus*. *Plant Cell Physiol.* 56, 1401–1417. doi: 10.1093/pcp/pcv058

Rowe, J. H., Topping, J. F., Liu, J. L., and Lindsey, K. (2016). Abscisic acid regulates root growth under osmotic stress conditions via an interacting hormonal network with cytokinin, ethylene and auxin. *New Phytol.* 211, 225–239. doi: 10.1111/nph.13882

Rowlett, R. S. (2010). Structure and catalytic mechanism of the beta-carbonic anhydrases. *Biochim. Biophys. Acta-Proteins Proteomics* 1804, 362–373. doi: 10.1016/j.bbapap.2009.08.002

Schiessl, S. V., Quezada-Martinez, D., Orantes-Bonilla, M., and Snowdon, R. (2020). Transcriptomics reveal high regulatory diversity of drought tolerance strategies in a biennial oil crop. *Plant Sci.* 297:110515. doi: 10.1016/j.plantsci.2020.110515

Sehrawat, A., and Deswal, R. (2014). S-nitrosylation analysis in brassica juncea apoplast highlights the importance of nitric oxide in cold-stress signaling. *J. Proteome Res.* 13, 2599–2619. doi: 10.1021/pr500082u

Shaikhali, J., Heiber, I., Seidel, T., Stroher, E., Hiltscher, H., Birkmann, S., et al. (2008). The redox-sensitive transcription factor Rap2.4a controls nuclear expression of 2-Cys peroxiredoxin A and other chloroplast antioxidant enzymes. *Bmc Plant Biol.* 8:48. doi: 10.1186/1471-2229-8-48

Shen, Y., Zhang, Y., Zou, J., Meng, J., and Wang, J. (2015). Comparative proteomic study on Brassica hexaploid and its parents provides new insights into the effects of polyploidization. *J. Proteomics* 112, 274–284. doi: 10.1016/j.jprot.2014.10.006

Shokri-Gharelo, R., and Noparvar, P. M. (2018). Molecular response of canola to salt stress: insights on tolerance mechanisms. *Peerj* 6:4822. doi: 10.7717/peerj.4822

Silveira, N. M., Frungillo, L., Marcos, F. C. C., Pelegrino, M. T., Miranda, M. T., Seabra, A. B., et al. (2016). Exogenous nitric oxide improves sugarcane growth and photosynthesis under water deficit. *Planta* 244, 181–190. doi: 10.1007/s00425-016-2501-y

Su, H. N., Chen, G., Yang, L. M., Zhang, Y. Y., Wang, Y., Fang, Z. Y., et al. (2020). Proteomic variations after short-term heat shock treatment reveal differentially expressed proteins involved in early microspore embryogenesis in cabbage (Brassica oleracea). *Peerj* 8:23. doi: 10.7717/peerj.8897

Subramanian, B., Bansal, V. K., and Kav, N. N. V. (2005). Proteome-level investigation of Brassica carinata-derived resistance to Leptosphaeria maculans. *J. Agric. Food Chem.* 53, 313–324. doi: 10.1021/jf048922z

Thalineau, E., Truong, H. N., Berger, A., Fournier, C., Boscari, A., Wendehenne, D., et al. (2016). Cross-regulation between N metabolism and nitric oxide (NO) signaling during plant immunity. *Front. Plant Sci.* 7:472. doi: 10.3389/fpls.2016.00472

Thomas, E., and Wenzel, G. (1975). Embryogenesis from microspores of *Brassica-Napus*. *J. Plant Breed.* 74, 77–81.

Tripathi, B. N., Bhatt, I., and Dietz, K. J. (2009). Peroxiredoxins: a less studied component of hydrogen peroxide detoxification in photosynthetic organisms. *Protoplasma* 235, 3–15. doi: 10.1007/s00709-009-0032-0

Tsuwamoto, R., Fukuoka, H., and Takahata, Y. (2007). Identification and characterization of genes expressed in early embryogenesis from microspores of *Brassica napus*. *Planta* 225, 641–652. doi: 10.1007/s00425-006-0388-8

Urban, M. O., Vasek, J., Klima, M., Krtkova, J., Kosova, K., Prasil, I. T., et al. (2017). Proteomic and physiological approach reveals drought-induced changes in rapeseeds: Water-saver and water-spender strategy. *J. Proteom.* 152, 188–205. doi: 10.1016/j.jprot.2016.11.004

Vandesompele, J., De Preter, K., Pattyn, F., Poppe, B., Van Roy, N., De Paepe, A., et al. (2002). Accurate normalization of real-time quantitative RT-PCR data by geometric averaging of multiple internal control genes. *Genome Biol.* 3:research0034.1. doi: 10.1186/gb-2002-3-7-research0034

Verslues, P. E., Agarwal, M., Katiyar-Agarwal, S., Zhu, J. H., and Zhu, J. K. (2006). Methods and concepts in quantifying resistance to drought, salt and freezing, abiotic stresses that affect plant water status. *Plant J.* 45, 523–539. doi: 10.1111/j.1365-313X.2005.02593.x

Wang, L. L., Zhang, P., Qin, Z. W., and Zhou, X. Y. (2014). Proteomic analysis of fruit bending in cucumber (*Cucumis sativus* L.). *J. Integrat. Agri.* 13, 963–974. doi: 10.1016/S2095-3119(13)60406-2

Wang, L. M., Jin, X., Li, Q. B., Wang, X. C., Li, Z. Y., and Wu, X. M. (2016). Comparative proteomics reveals that phosphorylation of beta carbonic anhydrase 1 might be important for adaptation to drought stress in *Brassica napus*. *Sci. Rep.* 6:39024. doi: 10.1038/srep39024

Wang, W., Scali, M., Vignani, R., Spadafora, A., Sensi, E., Mazzuca, S., et al. (2003). Protein extraction for two-dimensional electrophoresis from olive leaf, a plant tissue containing high levels of interfering compounds. *Electrophoresis* 24, 2369–2375. doi: 10.1002/elps.200305500

Warren, C. R. (2008). Stand aside stomata, another actor deserves centre stage: the forgotten role of the internal conductance to CO(2) transfer. *J. Exp. Bot.* 59, 1475–1487. doi: 10.1093/jxb/erm245

Whittle, C. A., Malik, M. R., Li, R., and Krochko, J. E. (2010). Comparative transcript analyses of the ovule, microspore, and mature pollen in Brassica napus. *Plant Mol. Biol.* 72, 279–299. doi: 10.1007/s11103-009-9567-x

Yadollahi, A., Abdollahi, M. R., Moieni, A., and Danaee, M. (2011). Effects of carbon source, polyethylene glycol and abscisic acid on secondary embryo induction and maturation in rapeseed (*Brassica napus* L.) microspore-derived embryos. *Acta Physiol. Plantarum* 33, 1905–1912. doi: 10.1007/s11738-011-0738-4

Yanagawa, Y., Yoda, H., Osaki, K., Amano, Y., Aono, M., Seo, S., et al. (2016). Mitogen-activated protein kinase 4-like carrying an MEY motif instead of a TXY motif is involved in ozone tolerance and regulation of stomatal closure in tobacco. *J. Exp. Bot.* 67, 3471–3479. doi: 10.1093/jxb/erw173

Yin, H., Li, S., Zhao, X., Bai, X., and Du, Y. (2008). Isolation and characterization of an oilseed rape SKP1 gene BnSKP1 involved on defense in *Brassica napus*. *J. Biotechnol.* 136, S227–S227. doi: 10.1016/j.jbiotec.2008.07.480

Zhang, J. (2014). Salinity affects the proteomics of rice roots and leaves. *Proteomics* 14, 1711–1712. doi: 10.1002/pmic.201400289

Zhang, Y. T., Ali, U., Zhang, G. F., Yu, L. Q., Fang, S., Iqbal, S., et al. (2019). Transcriptome analysis reveals genes commonly responding to multiple abiotic stresses in rapeseed. *Mol. Breed.* 39:158. doi: 10.1007/s11032-019-1052-x

Zhao, J. (2015). Phospholipase D and phosphatidic acid in plant defence response: from protein-protein and lipid-protein interactions to hormone signalling. *J. Exp. Bot.* 66, 1721–1736. doi: 10.1093/jxb/eru540

Zhu, M., Dai, S., Zhu, N., Booy, A., Simons, B., Yi, S., et al. (2012). Methyl jasmonate responsive proteins in brassica napus guard cells revealed by iTRAQ-based quantitative proteomics. *J. Proteome Res.* 11, 3728–3742. doi: 10.1021/pr300213k

Zhu, M., Simons, B., Zhu, N., Oppenheimer, D. G., and Chen, S. (2010). Analysis of abscisic acid responsive proteins in Brassica napus guard cells by multiplexed isobaric tagging. *J. Proteomics* 73, 790–805. doi: 10.1016/j.jprot.2009.11.002

Conflict of Interest: The authors declare that the research was conducted in the absence of any commercial or financial relationships that could be construed as a potential conflict of interest.

Copyright © 2021 Urban, Planchon, Hoštičková, Vanková, Dobrev, Renaut, Klíma and Vítámvás. This is an open-access article distributed under the terms of the Creative Commons Attribution License (CC BY). The use, distribution or reproduction in other forums is permitted, provided the original author(s) and the copyright owner(s) are credited and that the original publication in this journal is cited, in accordance with accepted academic practice. No use, distribution or reproduction is permitted which does not comply with these terms.

frontiers in Plant Science

ORIGINAL RESEARCH
published: 25 June 2021
doi: 10.3389/fpls.2021.628687

Genome Wide Association Mapping of Root Traits in the Andean Genepool of Common Bean (*Phaseolus vulgaris* L.) Grown With and Without Aluminum Toxicity

*Daniel Ambachew and Matthew W. Blair**

Department of Agricultural and Environmental Sciences, Tennessee State University, Nashville, TN, United States

Common bean is one of the most important grain legumes for human diets but is produced on marginal lands with unfavorable soil conditions; among which Aluminum (Al) toxicity is a serious and widespread problem. Under low pH, stable forms of Al dissolve into the soil solution and as phytotoxic ions inhibit the growth and function of roots through injury to the root apex. This results in a smaller root system that detrimentally effects yield. The goal of this study was to evaluate 227 genotypes from an Andean diversity panel (ADP) of common bean and determine the level of Al toxicity tolerance and candidate genes for this abiotic stress tolerance through root trait analysis and marker association studies. Plants were grown as seedlings in hydroponic tanks at a pH of 4.5 with a treatment of high Al concentration (50 μM) compared to a control (0 μM). The roots were harvested and scanned to determine average root diameter, root volume, root surface area, number of root links, number of root tips, and total root length. Percent reduction or increase was calculated for each trait by comparing treatments. Genome wide association study (GWAS) was conducted by testing phenotypic data against single nucleotide polymorphism (SNP) marker genotyping data for the panel. Principal components and a kinship matrix were included in the mixed linear model to correct for population structure. Analyses of variance indicated the presence of significant difference between genotypes. The heritability of traits ranged from 0.67 to 0.92 in Al-treated and reached similar values in non-treated plants. GWAS revealed significant associations between root traits and genetic markers on chromosomes Pv01, Pv04, Pv05, Pv06, and Pv11 with some SNPs contributing to more than one trait. Candidate genes near these loci were analyzed to explain the detected association and included an Al activated malate transporter gene and a multidrug and toxic compound extrusion gene. This study showed that polygenic inheritance was critical to aluminum toxicity tolerance in common beans roots. Candidate genes found suggested that exudation of malate and citrate as organic acids would be important for Al tolerance. Possible cross-talk between mechanisms of aluminum tolerance and resistance to other abiotic stresses are discussed.

Keywords: abiotic stress, citrate and malate transporters, hydroponic culture, root traits, single nucleotide polymorphism markers

OPEN ACCESS

Edited by:
Felipe Klein Ricachenevsky, Federal University of Rio Grande do Sul, Brazil

Reviewed by:
Harsh Raman, New South Wales Department of Primary Industries, Australia
Enéas Ricardo Konzen, Federal University of Rio Grande do Sul, Brazil

***Correspondence:**
Matthew W. Blair
mblair@tnstate.edu

Specialty section:
This article was submitted to Plant Abiotic Stress, a section of the journal Frontiers in Plant Science

Received: *12 November 2020*
Accepted: *13 April 2021*
Published: *25 June 2021*

Citation:
Ambachew D and Blair MW (2021) Genome Wide Association Mapping of Root Traits in the Andean Genepool of Common Bean (Phaseolus vulgaris L.) Grown With and Without Aluminum Toxicity. Front. Plant Sci. 12:628687. doi: 10.3389/fpls.2021.628687

INTRODUCTION

Common bean (*Phaseolus vulgaris*) is one of the most important grain legumes for human diets (Blair, 2013). The legume is produced on marginal lands in many parts of the globe where unfavorable soil factors constrain yield potential (Eticha et al., 2010; Yang et al., 2013). Among these factors, soil acidity is an important problem of crop production in the humid and semi-humid sub-tropical or tropical regions of bean production (Rangel et al., 2010). These acid soils represent 30–50% of the world's arable land (Hede et al., 2001; Kochian et al., 2004). Under low pH stable forms of Aluminum (Al) are solubilized into phytotoxic Al^{3+} ions (Bojórquez-Quintal et al., 2017). Therefore, Al toxicity is one of the major problems of common bean production in low pH soils typical of Latin America and African production zones (Rangel et al., 2010). Additionally, nutrient deficiencies, and other proton and mineral toxicities are the important factors limiting crop production on acidic soils (Eticha et al., 2010; Zhou et al., 2011).

Al is the most abundant metal in earth's crust (Arunakumara et al., 2013; Gupta et al., 2013)and as mentioned is one of the major constraints to crop production on most acidic soils (Barceló and Charlotte, 2002). Under acidic conditions, when the soil pH is below 4.5, Al dissolves rapidly into soil solution and becomes a positive ion $[Al\ (H_2O)_6]^{3+}$, generally referred to as soluble aluminum (Al^{3+}) (Delhaize et al., 1993; Kochian et al., 2005). High concentration of Al^{3+} is highly toxic to plants and primarily inhibit root growth and function (Arunakumara et al., 2013; Mendoza-Soto et al., 2015). Al toxicity causes 30 – 60% yield reduction and substantial economic loss in common bean (Horst et al., 2009; Rangel et al., 2010). Even a micro-molar concentration of Al^{3+}, can interfere with many physiological and cellular processes in susceptible plants (Hede et al., 2001; Kochian et al., 2004).

Aluminum toxic conditions inhibit the growth and function of roots when the Al^{3+} ions injure the root apex, which in turn affects the function of other plant parts (Rangel et al., 2007, 2010; Yang et al., 2013, 2011). While primary physiological response is at the root level Al toxicity results in strong yield reduction (Gupta et al., 2013). Poor root growth, changed root morphology, stunted plant growth, thicker lateral and taproots, browning of roots, inefficient water and nutrient uptake, and accumulation of Al and other toxic ions (Mugai et al., 2000; Bartoli et al., 2017), are symptoms of Al toxicity induced in susceptible lines of common bean (Rao et al., 2008, 2016).

Tolerant plants can be developed by different mechanisms of response to Al toxicity (Bojórquez-Quintal et al., 2017). The reaction of Al tolerance has been studied in many plant species and external and internal mechanisms have been identified (Hede et al., 2001). An external tolerance mechanism is where plants exclude Al^{3+} from the root apex using selective permeability of the plasma membrane or by exudation of organic acids, root mucilage or free phosphate to bind the Al ions. The internal tolerance mechanisms that confer the ability to tolerate Al in the plant symplasm use Al binding proteins (Gupta et al., 2013). Both mechanisms are related to mitochondrial metabolism and acid transport (Nunes-Nesi et al., 2014). Though rehabilitation is only on the thin upper layer of the soil surface, Al toxicity and soil acidity can be corrected with the bulk application of lime or gypsum (Neto et al., 2020). This type of soil amelioration will restrict the plant roots from growing deeper which limits their ability to access and extract water from deeper soils and make plants prone to drought stress. Long-term sustainable agricultural production requires the use of Al tolerant genotypes improved through plant breeding combined with the application of adapted agronomic practices.

Sources of genetic resistance/tolerance to Al toxicity in common beans are multiple: Blair et al. (2009), identified common bean genotypes from an Andean gene pool that are tolerant to a higher level of (20 μM) Al concentration. Butare et al. (2011) reported on inter-specific lines combining Al^{3+} and drought resistance/tolerance from a set 11 bean genotypes from *P. vulgaris*, *P. coccineus*, and *P. acutifolius*. Butare et al. (2012) developed recombinant inbred lines (RILs) for Al^{3+} tolerance from the interspecific cross between SER16 (sensitive) and G35246-Q (tolerant). SER16 is common bean breeding line with ability to remobilize photosynthate while G35246-Q is an accession of *P. coccineus* tolerant to Al toxicity. Most research was with Mesoamerican small-seeded beans like SER16. However, Al tolerance mechanisms were also characterized using a cross of Al-tolerant Andean genotype ICA Quimbaya and Al-susceptible Mesoamerican genotype, VAX-1 (Yang et al., 2013). Al tolerance in common beans involves Al-activated exudation of organic acids with malate, citrate and oxalate anions differentially produced in Al tolerant versus sensitive genotypes (Miyasaka et al., 1991; Mugai et al., 2000; Yang et al., 2000; Eticha et al., 2010; Rangel et al., 2010).

Common bean plants have evolved various additional adaptive strategies to alleviate and recover from the adverse effects of Al stress or other abiotic stresses. Root system architecture is very responsive to soil elements and enables the plants to avoid environmental challenges and abiotic stresses by sensing and responding to them (Pandey et al., 2017). Root metabolites (Eticha et al., 2010; Rangel et al., 2010), root growth rate, the average root diameter, total root length and density of primary and lateral roots are phenotypes frequently used to measure the effects on roots of Al toxicity, drought or salinity stress and phosphorous deficiency (Yan et al., 2004; Beebe et al., 2006; Ochoa et al., 2006; Asfaw and Blair, 2012).

The genetic control and inheritance of Al resistance have not been well studied in common beans except for bi-parental QTL mapping (López-Marín et al., 2009). That pioneering study tried to understand the genetic architecture of Al resistance and showed the polygenic inheritance of Al resistance in common beans. The authors reported 9 and 7 Quantitative Trait Loci (QTLs), respectively, for root traits from the evaluation of RILs derived from the cross between DOR364 and G19833 in Al-treatment and control growth conditions. Relative traits were also calculated from comparison of +/− Al. In this population, DOR364 was a Mesoamerican small seed red bean and G19833 was a large-seeded Andean, but both parents were tolerant to Al toxicity. The same study reported that the identified QTLs were distributed all over the genome except chromosome Pv10 and QTLs with major effect resided on Pv09.

In a later study, Njobvu et al. (2020), identified eight QTLs for root length and root dry weight from the evaluation of 150 F4:5 recombinant inbred lines (RILs) derived from a cross between Solwezi, a landrace, with type IV growth habit and resistant to Al toxicity and AO-1012-29-3-3A, a determinate Andean dark red kidney variety with susceptibility to Al toxicity. The QTL identified by this group resided on Pv02, Pv04, Pv06, Pv07, Pv09, and Pv10. Colocalization of QTL for Al resistance and tolerance to phosphorous deficiency was also reported suggesting the cross link in bean roots between the two conditions of acidic soils (López-Marín et al., 2009). Most other studies of Al toxicity tolerance in common beans have been physiological in nature (Rangel et al., 2007; Mimmo et al., 2009) but some have looked at germplasm screening (Blair et al., 2009).

Association mapping exploits the linkage disequilibrium (LD) present among individuals from natural populations or germplasm collections to dissect the genetic basis of complex trait variation (Myles et al., 2009). Germplasm collections generally contain more genetic diversity than segregating progenies and, since association mapping exploits all the recombination events that have occurred in the evolutionary history of the association panel, a much higher mapping resolution is expected (Ingvarsson and Street, 2011). In addition, the number of QTLs that can be mapped for a given phenotype is not limited to the segregation products in a specific cross, but rather by the number of QTLs underlying the trait and the degree to which the studied population captures the genetic species-wide diversity (Yano et al., 2016).

Recently, a number of genome wide association studies (GWAS) have been conducted on common beans for diseases like *Rhizoctonia solani* (Oladzad et al., 2019b); angular leaf spot (Perseguini et al., 2016); common bacterial blight (Shi et al., 2011), nematodes (Wen et al., 2019); anthracnose (Zuiderveen et al., 2016); heat and drought stresses (Oladzad et al., 2019a), agronomic traits (Kamfwa et al., 2015a,b; Moghaddam et al., 2016; Raggi et al., 2019), cooking time and culinary quality traits (Cichy et al., 2015b) using diversity panels either from one or both the Mesoamerican and Andean genepool. One neglected area of study is the root traits of diverse genotypes and this is especially the case for Al toxicity effects on legumes such as common bean, the leading pulse for direct human consumption.

The major goal of this study was to identify candidate genes associated with Al tolerance in early stages of development in common beans. Our hypothesis was that in a hydroponic system with careful control of aluminum stress levels we could find repeatable phenotypic differences of high heritability for the root traits measured which would allow the identification of candidate genes through a genome wide association study approach. We used common bean seedlings, heritability estimates and repeated measures to accommodate and study the large number of genotypes of an Andean genepool panel, as this class of large-seeded common beans has been less well studied for Al toxicity tolerance but is grown in many regions of the world where low pH soils are prevalent, such as East and Southern Africa. Seedlings present the first response to the serious soil challenge of high Al concentrations and are critical for plant establishment.

MATERIALS AND METHODS

Plant Materials

A subset of 227 genotypes from the Global Andean bean diversity panel (ADP) of 278 cultivars (**Supplementary Table 1**), were phenotyped for root traits using a hydroponic system described below. The ADP consisted of cultivated genotypes only. The geographic sources of the varieties were Africa and North America. The panel was assembled mainly from public and private breeding programs, including varietal releases, elite lines, and land races (Cichy et al., 2015a). The ADP represented different market classes, seed size and three growth types (I, II, and III). For each genotype, seeds were surface sterilized for 1 min with 70% alcohol, 2% sodium hypochlorite (NaClO) and rinsed with deionized water and dried with a sterilized paper towel. Seeds were then scarified using scalpel just on the opposite side of the seed micropyle to ensure uniform germination of the genotypes from the panel. After scarification, the seed were transferred to a sterilized magenta box with a sterile paper towel in it. Deionized water was added to moisten the paper.

Hydroponic System

After germination at three days, seedlings with uniform length were transferred and planted into a hydroponic system with a standard protocol for Al toxicity testing and plant nutrient solution based on previous studies (Rao et al., 2008; Butare et al., 2011). Plants were grown as seedlings in hydroponic tanks at a pH of 4.5 with a treatment of high Al concentration (50 μM) compared to a control (0 μM). The seedlings were individually placed into 5 cm diameter × 5 cm deep net plastic pots and suspended over 30.2 cm deep, 65.4 cm long × 43.8 cm wide, 50-liter Sterilite® black plastic tanks. Each tank was set up with a continuous aeration system with two eight port Hydrofarm ActiveAqua^{TM} air pumps and the constant pumping of nutrient solution with 172 GPH EcoPlus® Adjustable flow submersible water pumps to ensure water agitation and avoid sedimentation. The experimental setup was as shown in **Supplementary Figure 1** for arrangement of hydroponic tanks in the control and Al treatments along with recirculating pumps and chambers as well as aeration system. The number of tanks used per treatment is also shown as well as the method for sensing solution electrical conductivity (EC), its pH and temperature.

Nutrient Solution

The standard nutrient solution was the same for the two treatments except in concentration of Al (50 μM versus 0 μM) added as Al chloride ($AlCl_3$). The remaining nutrients were 286 μM $CaSO_4.2H_2O$, 300 μM KNO_3, 150 μM NH_4NO_3, 2.5 μM $NaH_2PO_4.H_2O$, 150 μM $MgCl_2.6H_2O$, 14 μM $CaCl_2.H_2O$, 5 μM $FeCl_3.6H_2O$, 5 μM $Na_2EDTA.2H_2O$, 1 μM $MnCl_2.4H_2O$, 1 μM $ZnCl_2$, 0.2 μM $CuCl_2.2H_2O$, $6H_3BO_3$, 5 μM $NaSiO_3.9H_2O$, 0.001 μM $NaMoO_4.2H_2O$, 57.5 μM NaCl (Rao et al., 2008). The pH, Electrical conductivity (EC) and temperature of the hydroponic tank system and around the roots were monitored in real time using a Supervisory Control and Data Acquisition (SCADA) system designed by

indoor grower's world, Nashville, TN. The system consisted of a master site controller and two reservoir remote terminal units (RTUs). A randomized balanced design was used with three replicates, reusing the same hydroponic tanks over three planting times, with bleach sterilization (7.5% Sodium Hypochlorite) between uses.

Greenhouse Conditions

A glass-roofed greenhouse at the Tennessee State University Agricultural Research and Extension Center (AREC) was the site of the benches used to hold the hydroponic system 1.5 m above a gravel floor. Temperature conditions were set to 23 $\pm$3°C (day) / 20 $\pm$ 3°C (night) with relative humidity (RH) between 70 and 80%. The greenhouse temperature and relative humidity was monitored with *WADSWORTH*® step up control system, and when heating was needed it was provided by a natural gas heater with winter shade cloth for heat retention. Fans were used for air circulation. The first replication of the experiment was planted in September, the second in October and the third replication was planted in November 2018. Each replication took 15 days from seeding to root image acquisition. Upon planting, each tank was covered with a 5 cm thick Styrofoam floating sheet cut to the size of the tank and able to carry 49 seedlings in a 5 × 10-hole design where one of the holes was used to insert air sones, hydroponic solution control system probes.

Root Phenotyping

Phenotypic data were measured on the seedlings growing as described above in the hydroponic tanks. The small plants were carefully removed from the tank and the float collar and the root systems scanned with a flatbed EPSON perfection V850 pro scanner (Seiko EPSON Corporation, Japan). The following traits were measured: (1) Average root diameter (AvgD), (2) Number of root forks (NRF), (3) Number of root tips (NRT), (4) Number of root links (NRL), (5) Root surface area (RSA), (6) Root volume (RV), (7) Root surface area (RSA), and (8) Total root length (TRL), were recorded by. Scanned images of the harvested seedling roots were analyzed using a software program WinRHIZO pro V 2008b (Regent Instruments, Inc., Quebec, Canada). The root images were acquired in a gray scale to a resolution of 800 dots per inch (dpi). The analysis was done on the root morphology by setting the rough edge and noise removal to higher level, and dark root on white background measurement option.

Analyses of Variance and Adjusted Means Estimates

Analyses of variance was conducted on the recorded root data on each treatment; Al and control treatment using mixed models in SAS 9.3 (SAS Institute Inc, 2011), using the following equation:

$$Y_{ij} = \mu + Tt_i + bj + e_{ij};$$

where *Yij* is a response variable of genotypes the ith genotype in jth replication, μ and T_i are fixed parameters such that the mean for the ith genotype is $\mu_i = \mu + T_i$, b_j is the random effect associated with the jth replication and e_{ij} is the random error associated with the genotypes in each replication. All the datasets were filtered for outlier genotypes that violate the assumption of the ANOVA even after data transformation. To estimate the adjusted means based on best linear unbiased estimation, we fit the genotypes as fixed and replication as random effects in the model. The variance components and the adjusted means based best linear unbiased estimation were estimated by fitting genotypes and replication as random in the mixed model. Heritability of traits was calculated for each treatment and combined data using the method described in Holland et al. (2003). The adjusted means from the best linear unbiased estimates were then used to calculate the percent change in the traits from control treatment and Al -treatment using the following formula:

$$\text{Percent change } y_i = \left(\frac{(\text{YCi} - \text{YAi treatment})}{\text{YCi}}\right) \text{x } 100\%$$

where Y_i is the percent change of a trait of the ith genotype, YC_i is the mean value of a trait for the ith genotype, and YA is the mean value of a trait for the ith genotype in the Al treatment. The percent change of means of traits were used for genome wide association. Similarly, the adjusted means based of prediction were used for genomic prediction analysis.

Genotyping Quality Control

Previous genotypic data on the ADP including 31K SNPs found by ApeKI genotyping-by-sequencing (GBS) method described by Elshire et al. (2011) optimized for common beans by Hart and Griffiths (2015). The associated HapMap file of the SNP dataset were publicly available at the feed the future website[1]. After filtering for missingness > 10%, SNPs with missing data were imputed using the LD KNNi imputation method (Money et al., 2015) plugin of TASSEL software (Bradbury et al., 2007) with the default parameters. Two SNP data sets were generated from the original 31K SNP dataset. the first dataset (DATASET1) was a set of 13906 SNPs and 227 genotypes which were retained after SNPs with MAF < 0.05, heterozygosity > 0.02 and SNPs with more than two alleles were filtered out. The second dataset (DATASET2). A set of 2286 SNP markers and 227 genotypes were kept from DATASET1 after removing markers in strong disequilibrium (R^2 > 2). Linkage Disequilibrium (LD) pruning was done using PLINK software (Purcell et al., 2007). Data were converted from HapMap to numerical format using GAPIT3 software (Wang and Zhang, 2018) in R. DATASET1 was used in GWAS while DATASET2 was used to perform principal component analysis using "prcomp" function of "stats" package in R (R Core Team, 2020).

Marker–Trait Association Tests and Candidate Gene Identification

Genome wide association analyses were performed with TASSEL software using Mixed linear model (MLM). The first three

[1]http://arsftfbean.uprm.edu/bean/?p=472

principal components calculated from LD pruned SNP dataset were included as a covariate in the MLM model to control for population structure. The MLM equation used in the analysis was:

$$Y = X\alpha + P\beta + K + \varepsilon$$

Where: Y is the phenotype of a genotype; X is the fixed effect of the SNP; P is the fixed effect of the population structure; K is the random effect of the relative kinship; ε is the error term and is assumed to be normally distributed with a mean of zero. Percent change datasets calculated from BLUPs of traits measured under control and Al treatment trials were used as a phenotype input for the association analysis. Kinship matrix was also calculated using EMMA algorithm (Kang et al., 2010) and included in the model in addition to the PCs when using MLM in TASSEL. Manhattan plots and QQ plots were generated using the "CMPlot" R package (Lin-Yin, 2020) and significance levels were established using a Bonferroni correction at $p < 0.05$ based on the effective number of independent tests determined via SimpleM (Gao et al., 2008). We also used an exploratory significance cutoff at $p < 0.0001$. When reporting significant SNPs from each GWAS analysis, the SNP with the lowest p-value was chosen to represent each locus of interest. The significant SNPs were positioned to the *Phaseolus vulgaris* v.1 reference genome (G19833) using Jbrowse on Phytozome v.1.3 (Goodstein et al., 2012) to assess candidate genes in $\pm$ 100 k window positioning the significant SNP at the center. Gene annotation was done using mainly Phytozome v.1.3 but also other databases including TAIR, Pfam, KEGG, KOG, EXPASY, PANTHER were used to capture the maximum number of gene models. Literature was also consulted in addition to gene annotations to evaluate the function of the candidate genes.

RESULTS

Differential Response of Genotypes to Al Treatment

The analysis of variance (ANOVA) was done on 227 genotypes remained after outlying genotypes were filtered out. The resulting analysis indicated the presence of significant variations ($p < 0.001$) among the genotypes for all traits under Al treated and control treatment experiments (**Table 1**). The small variance values of replication of treatments over time indicated that replication had little effect on the expression of each trait. This is because the greenhouse condition and the root zone conditions were monitored and maintained at similar conditions throughout the experiment (**Supplementary Figure 2**).

Broad sense heritability for all traits were high in both experiments of Al and non-Al treatments ($h^2 > 0.7$) except for root volume (RV) in Al which was slightly lower ($h^2 = 0.67$) and average root diameter (AvgD) in control ($h^2 = 0.57$). Average total root length (TRL) (290.07 cm) was higher in control treatment while the range was narrower in Al treatment (7.7 to 200.7 cm) compared to the control treatment (11.9 to 638.3 cm). Similar trends were observed for root surface area (RSA), RV, number of root tips (NRT) and number of root forks (NRF). Unlike other traits, average AvgD (0.92 mm) was higher in Al treatment with narrow range (0.49 to 1.2) in control treatment compared to Al treatment (0.53 to 1.41 mm).

The treatment with aluminum had a pronounced effect in the quantitative traits measured. Higher average percent reduction was recorded for TRL (−75.18), RV (−64.96), RSA (−70.76), NRF (−73.56), NRT (−70.74), and NRL (−73.91) under Al treatment while percent increase was recorded on AvgD (+21.05) (**Table 1** and **Figure 1**). In general, the heritability of traits in both treatments were high indicating the good repeatability of the hydroponic evaluation of traits. High heritability made the use of the averages for these traits as suitable for GWAS analysis. Also, treatment with aluminum had a pronounced effect on all the quantitative traits measured.

GWAS and Candidate Gene Identification

The broad sense heritability of each trait was high indicating the root traits measured in this study were suitable for GWAS analysis. The first two principal components accounted for 28.2% of the total variation (**Figure 2**) and were included as a covariate in GWAS analysis. GWAS associations identified multiple genomic regions associated with the six root traits (AvgD, NRF, NRL, RV, RSA, and TRL). Fifteen significantly associated SNPs resided on five chromosomes: Pv01, Pv04, Pv05, Pv06, and Pv11 at p-value = 1×10^{-5} Bonferroni corrected p-value for independent number of tests (**Figure 3** and **Table 2**). The strongest association was found for NRF and NRL with S1_38584873 and S1_25957702 resided on chromosome Pv01. For AvgD, five significant signals were identified on chromosome Pv01 and Pv06 and all explained 70% of the phenotypic variation.

The largest number of significant signals (8 SNPs) were found for NRL on chromosomes Pv01, Pv04, and Pv11. However, most of them (5 SNPs) were from Pv01. Collectively, the eight SNP loci accounted for 91% of the variation in NRL. Same signals (7 out of 8 SNPs) were also found for NRF, where they explained 98% of phenotypic variation. For RSA, four significant SNP signals were located on chromosomes Pv01 and Pv06. Similarly, two SNP loci on Pv06 were significant for RV. Two of the significant SNP (S6_6504245 and S6_3698197) signals on chromosome Pv06 were common for AvgD, RSA and RV. For TRL, five significant SNPs were identified on three chromosomes (Pv01, Pv05, and Pv11) where they accounted for 57% of the phenotypic variation. From this description we saw that there were several SNPs associated with more than one trait. The list of significant SNP loci and their association level, the phenotypic variation explained by significant markers are indicated in **Table 2** and visualized in **Figure 2**.

Based on significant GWAS hits and the sequence of the common bean reference genome (G19833) scanned with $\pm$100 kb window from each SNP, we identified 192 gene regions of interest. The gene ID, Phytozome-annotated function of the gene, genomic position, and top or bottom chromosomal strand direction of the gene on the genome are presented in **Supplementary Table 2**. The function of these genes fell in the categories of regulation of plant development, signal transduction and reception, carbohydrate metabolism, integral components of membranes, binding protein and other processes.

TABLE 1 | Mean, Minimum (Min), Maximum (Max), genotypic variance (σ2g), replication variance (σ^2r) error variance (σ^2e) and heritability values of traits measured for the root phenotypes of 227 common bean genotypes from the Andean Diversity Panel (ADP) grown under Al treated and control hydroponic conditions.

Treatment	Trait	Mean	Min	Max	σ^2g	σ^2r	σ^2e	H^{2a}‡	Mean %Δ†	Min %Δ†	Max %Δ†
Al treatment	AvgD	0.92***	0.53	1.41	0.013	9.41×10^{-5}	0.003	0.87	22.78	0.37	105.56
	NRF	363.86***	40	887	20986	6.19	1799.33	0.92	−66.43	−2.78	−97.22
	NRL	593.68***	82	1342	50931	1.2×10^{-6}	2038.8	0.96	−67.83	−0.65	−97.25
	NRT	68.83***	9	153	437.21	0.55	65.99	0.87	−6.58	−94.69	−65.52
	RSA	20.45***	4.16	68.25	54.32	0.822	18.14	0.75	−65.27	−2.61	−93.24
	RV	0.47***	0.09	1.69	0.036	0.001	0.02	0.67	−56.58	−2.44	−93.03
	TRL	72.89***	7.73	200.7	699.44	0.122	788.4	0.89	−70.4	−0.92	−96.05
Control treatment	AvgD	0.76***	0.49	1.2	0.008	7.2×10^{-4}	0.006	0.57			
	NRF	1366.45***	4	3519	365396	0.00	30730	0.92			
	NRL	2275.72***	11	5639	988320	0.00	52187	0.95			
	NRT	230.11***	4	550	7932.15	0.00	1296.2	0.86			
	RSA	69.48***	3.3	158.58	620.68	10.59	118.29	0.84			
	RV	1.36***	0.05	4.07	0.29	0.01	0.12	0.71			
	TRL	290.07***	11.9	638.31	11293	0.879	1043.34	0.92			

AvgD, average root diameter (mm); NRF, number of root forks; NRT, number of root tips; NRL, number of links; RSA, root surface area (cm^2); RV, root volume (mm^3); TRL, total root length (cm);

‡*Broad sense Heritability calculated using the formula explained in Holland et al., 2003.*

†*Percent change of traits in aluminum treatment from control treatment. ***Means a significance level at $p < 0.001$.*

Each significant marker produced multiple hits of coding regions making identification of genes difficult. For the sake of simplicity, we report genes that were meaningful with regards to Al stress tolerance rather than all genes in the GWAS window.

Nearly half (48%) of the identified genes were associated with seven significant markers on chromosome Pv01. AvgD was associated with two SNP loci (S1_30086531 and S1_1396792) on chromosome Pv01. These two loci were linked with many candidate genes. Among these, *Phvul.01G117300* which was found ∼100 kb downstream of the significant SNP S1_30086531. Another gene associated with same marker and found 38 kb downstream was *Phvul.01G117800*. Four genes were found in close vicinity of the second SNP substantially associated with AvgD. While *Phvul.001G017000,* and *Phvul.001G017400* were located 72 and 39 kb downstream, *Phvul.001G017800,* and *Phvul.001G018000* were located upstream at 29 and 35.5 kb, respectively, of the SNP S1_1396792.

Four root traits namely, NRF, NRL, RSA, and TRL were significantly associated with two SNP loci (S1_22164004 and S1_38584873) on chromosome Pv01. The SNP S1_38584873 was a highly significant marker explaining 20, 20, 14, and 15% of the phenotypic variation in NRF, NRL, RSA, and TRL, respectively. We found 16 genes located 100 kb up and downstream of S1_38584873. Among these genes, *Phvul.001G141900* and were involved in abiotic stress tolerance. *Phvul.001G141900* was found 98.5 kb downstream and *Phvul.001G142750* was found in the region containing the significant marker itself. Another five genes (*Phvul.001G139000, Phvul.001G139100, Phvul.001G139200, Phvul.001G139250, Phvul.001G139400,* and *Phvul.001G139600*) were also found within 91 kb distance downstream of SNP S1_38162226, a significant SNP associated with NRF and NRL.

Fewer candidate genes were found on other chromosomes apart from Pv01 and we reported them in consecutive order. On chromosome Pv04, NRF and NRL were associated with two significant SNP loci; S4_45347157 and S4_1455630. Two genes *Phvul.004G150600* and *Phvul.004G151200* were located downstream at 81 and 35 kb, respectively, of SNP S4_45347157. Another SNP, S4_1455630, was surrounded by multiple genes which encode leucine-rich repeat-containing protein. On chromosome Pv05, 10 genes encoding leucine-rich protein kinase related proteins and leucine-rich repeat containing proteins were found surrounding only one significant SNP (S5_39203550). This SNP is significantly associate with TRL and accounted 10% of the total phenotypic variation explained in TRL. Chromosome Pv06 had one candidate gene, *Phvul.006G014600,* 63.5 kb upstream, 59 kb upstream of a significant SNP S6_6644197 which was significantly associated with three traits; AvgD, RSA, and RV, encoding a Zinc-binding protein. Finally, on chromosome Pv11, we found only one significant SNP associated with TRL. A total of 16 functional genes were identified near the significant SNP S11_44269. Among these genes, *Phvul.011G000700* and *Phvul.011G001300* were located 2 and 65 kb upstream of the significant SNP.

DISCUSSION

The root systems of beans are the major interface between these plants and numerous biotic and abiotic factors and enables them to avoid these environmental challenges by sensing and responding to them (Rao et al., 2008). Roots are used by plants to absorb water and nutrients from the soil, to store food or nutrients and used as architecture to anchor plants to the ground (Kochian et al., 2004). Therefore, roots must be protected from stresses such as rhizotoxicity of Al which causes inhibition of root growth and function

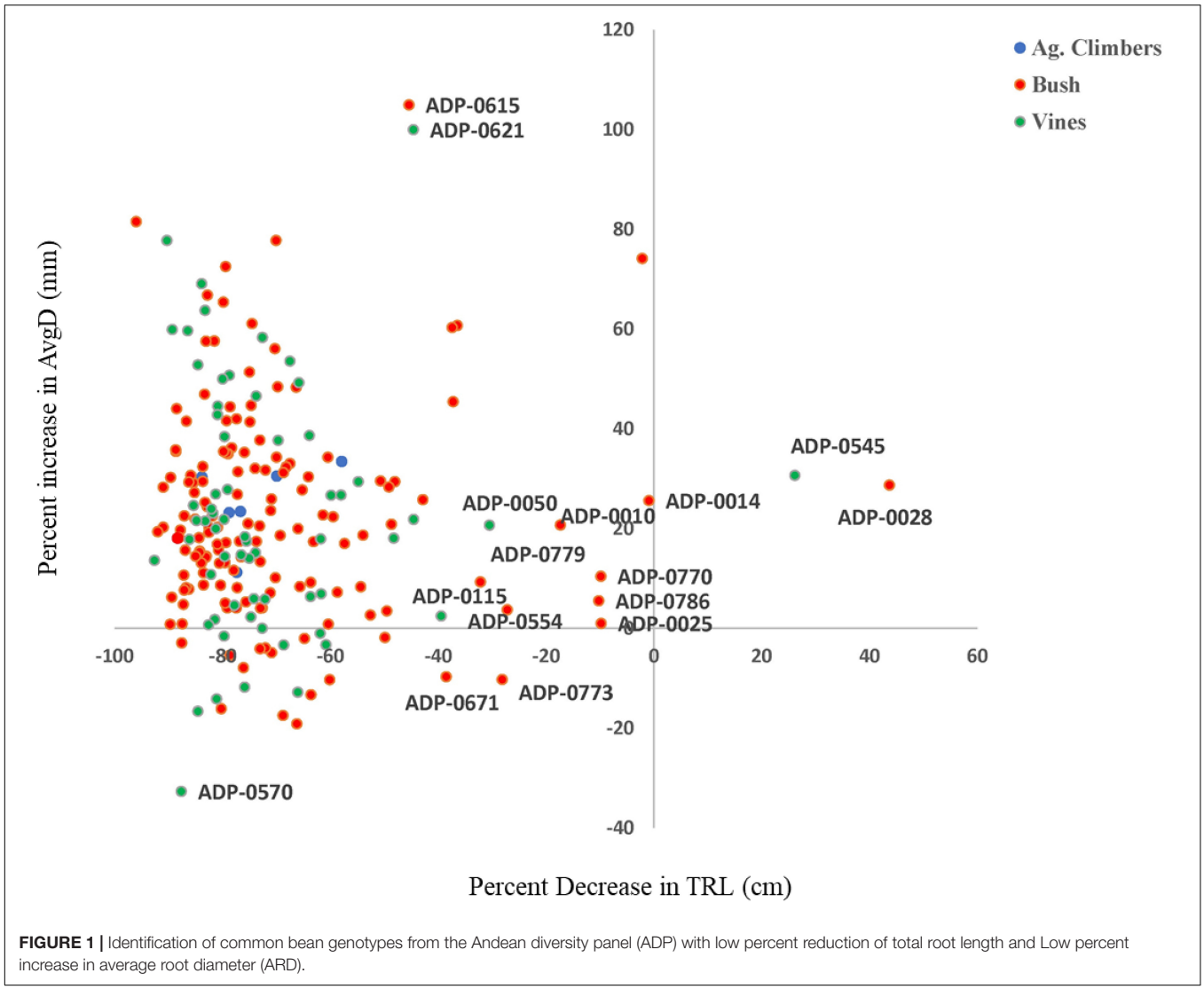


FIGURE 1 | Identification of common bean genotypes from the Andean diversity panel (ADP) with low percent reduction of total root length and Low percent increase in average root diameter (ARD).

(Horst et al., 2009). Genetic and environmental factors impact both the structure and functions of roots under Al stress (Rangel et al., 2010). Understanding the pattern and magnitude of traits relations, identifying breeding objectives, assessing the available genetic diversity, and identifying candidate genes are the most important tasks of a breeding program when considering root improvement in beans.

Andean beans are important components of agri-food system in Africa and Latin America where they are preferred by consumers because of their large seeds and colors. Andean beans are produced by small holder farmers on marginal lands where acidic soils are more prevalent (Blair et al., 2009) and productivity is constrained by Al toxicity and other abiotic stressed including drought. Andean beans are characterized by narrower genetic diversity (Cichy et al., 2015a) and their genetic improvement has lagged behind Mesoamerican bean improvement. Some promising results show that it is possible to improve aluminum tolerance in Andean beans (Blair et al., 2009; López-Marín et al., 2009).

The use of hydroponics to study aluminum resistance in plants is an option to complement field evaluations. Screening in hydroponics has advantages over field experiments in allowing the evaluation of large number of genotypes and providing precise control over the timing and concentration of nutrient supply and Al stress (Butare et al., 2011). Evaluation of genotypes in hydroponics experiments has been used for determining aluminum tolerance expression traits in many plants; including, barley (Ma et al., 1997), wheat (Sasaki et al., 2004, 2010; Furuichi et al., 2010), sorghum (Magalhaes et al., 2004), soybeans (Bianchi-Hall et al., 2000), and common beans (Butare et al., 2011).

Our study assessed the genetic variation in root traits of 227 Andean common bean genotypes under contrasting Al toxicity treatments (control with no Al treatment versus 50 μM Al toxicity treatment) which produced additional insights helpful for the development of new improved varieties with greater adaptation to problematic Al toxic soils. The greenhouse conditions of tank temperature, electrical conductivity, and pH around the root of the bean seedlings were monitored

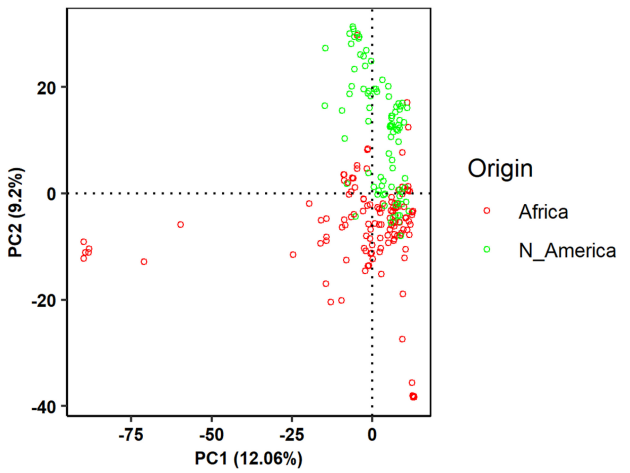


FIGURE 2 | Principal component analysis for common bean genotypes from the Andean diversity panel (ADP) based on the single nucleotide polymorphism (SNP) dataset pruned for the criteria of non-linkage disequilibrium (LD).

in real time and kept constant to avoid external variation (**Supplementary Figure 1**). The Al toxicity concentration used was ideal for revealing genotypic differences for root traits considered in this study. A higher percentage of reduction was observed in all root traits measured under Al toxicity treatment except average root diameter which showed an increase (23% on average) but with a wide range in variation (0.37 to 105.56%). Previous hydroponic studies with common bean created consistent levels of Al toxicity for germplasm screening as we did here; however, we added a level of precision in temperature and pH control through constant, real-time, in-tank monitoring.

The higher percentage reduction in root traits other than average diameter indicated that inhibition of root elongation, lateral root initiation and outgrowth and increased root diameter are important effects of Al toxicity in common beans. The increase in average root diameter and reduction in total root length under Al- toxicity treatments were also reported by various authors (Blair et al., 2009; Butare et al., 2012). Studies suggested that genotypes with lower percent inhibition of total root length and percent increase of average root diameter were most Al tolerant (Rao et al., 2016, 2008). Several genotypes (e.g., ADP-014, ADP-028, and ADP-545) had an increased percentage of total root length and average root diameter (up to 40%) and considered as moderately tolerant to Al toxicity. Blair et al. (2009) and Butare et al. (2012, 2011) identified common bean genotypes from an Andean gene pool and interspecific inbred lines of *Phaseolus* species that are tolerant to a higher level of Al concentration.

The Al tolerance we reported in this study could be due to different reasons. Tolerant plants developed two different physiological mechanisms to Al toxicity. The mechanisms of Al toxicity tolerance studied in many plant species identified both external and internal plant mechanisms (Hede et al., 2001). The external mechanism is where plants exclude Al from the root apex using selective permeability of the plasma membrane, exudation of chelating organic acids, production of root mucilage and exudation of root phosphate. The internal tolerance mechanisms that confer the ability to tolerate Al in the plant symplasm usually involves Al binding proteins (Gupta et al., 2013). These

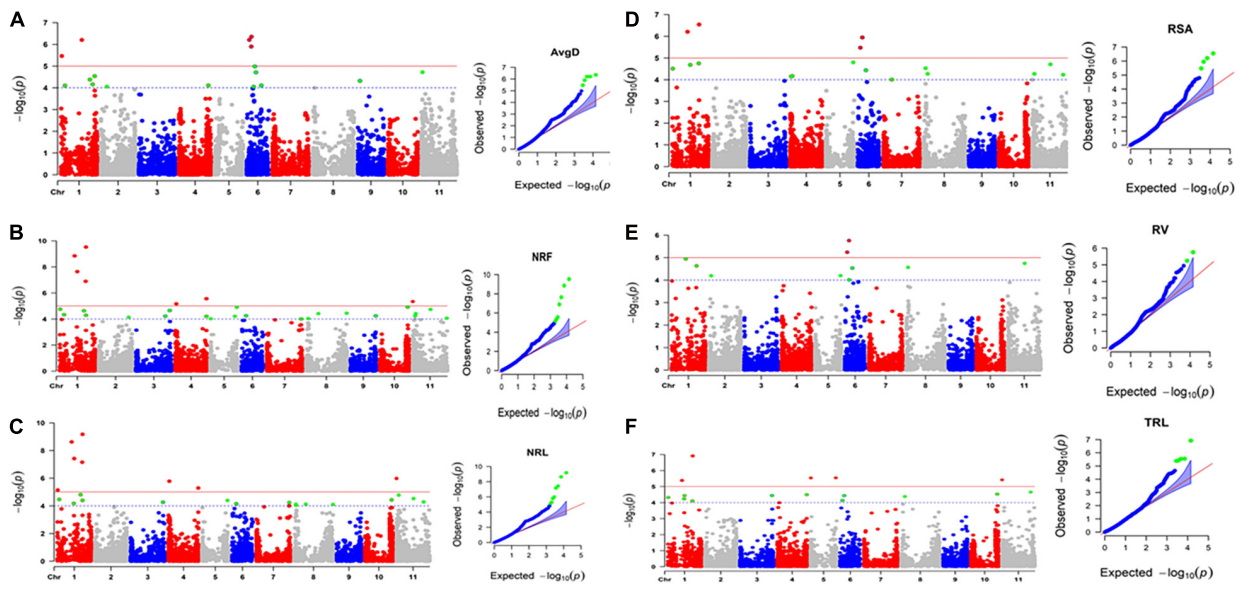


FIGURE 3 | Manhattan and QQ plots of genome wide association study (GWAS) results of Average root diameter **(A)**, Number of root forks **(B)**, number of root links **(C)**, Root surface area **(D)**, Root volume **(E)**, and Total root length **(F)**, where single nucleotide polymorphism (SNP) loci are ordered by physical position and grouped by chromosome. The black dash line indicates the genome wide significance threshold. The SNP loci highlighted in red were significant with a given trait at *p*-values lower than the Bonferroni corrected significance cut-off value for number of independent tests which was $p = 1 \times 10^{-5}$.

TABLE 2 | List of significant SNP markers detected for root traits evaluated for the common bean Andean Diversity Panel (ADP) showing physical position, association level (*p*-value), phenotypic variation (R^2) explained by the locus, additive SNP effect and minor allele frequencies (MAF).

Trait	SNP	Chr.	SNP-Position	*p*-value	R^2	SNP effect	MAF
AvgD	S1_30086531	Pv01	30086531	6.25E-07	0.15	−0.57	G (0.41)
AvgD	S1_1396792	Pv01	1396792	3.43E-06	0.14	0.81	G (−0.44)
AvgD	S6_6644197	Pv06	6644197	4.43E-07	0.13	−5.87	T (0.09)
AvgD	S6_3698197	Pv06	3698197	6.19E-07	0.14	−6.45	G (0.11)
AvgD	S6_6504245	Pv06	6504245	1.27E-06	0.14	−3.75	T (0.11)
NRF	S1_38584873	Pv01	38584873	2.99E-10	0.2	−11.23	T (0.15)
NRF	S1_22164004	Pv01	22164004	1.41E-09	0.19	7.18	C (0.17)
NRF	S1_25957702	Pv01	25957702	2.30E-08	0.16	11.09	A (0.19)
NRF	S1_38162226	Pv01	38162226	1.27E-07	0.13	−11.16	G (0.15)
NRF	S4_45347157	Pv04	45347157	2.76E-06	0.1	0.75	T (0.08)
NRF	S4_1455630	Pv04	1455630	6.82E-06	0.1	−3.33	T (0.34)
NRF	S11_44269	Pv11	44269	4.52E-06	0.1	−3.12	G (0.13)
NRL	S1_38584873	Pv01	38584873	6.67E-10	0.2	−10.36	T (0.15)
NRL	S1_22164004	Pv01	22164004	2.36E-09	0.19	6.64	C (0.17)
NRL	S1_25957702	Pv01	25957702	3.77E-08	0.16	10.17	A (0.19)
NRL	S1_38162226	Pv01	38162226	6.96E-08	0.13	−10.57	G (0.15)
NRL	S1_908352	Pv01	908352	7.20E-06	0.1	3.84	G (0.12)
NRL	S4_1455630	Pv04	1455630	1.65E-06	0.11	−4.1	T (0.34)
NRL	S4_45347157	Pv04	45347157	5.10E-06	0.1	1.78	T (0.08)
NRL	S11_44269	Pv11	44269	1.04E-06	0.12	−4.36	G (0.13)
RSA	S1_38584873	Pv01	38584873	2.87E-07	0.14	−7.32	T (0.15)
RSA	S1_22164004	Pv01	22164004	6.21E-07	0.14	3.8	C (0.17)
RSA	S6_6504245	Pv06	6504245	1.13E-06	0.14	3.52	T (0.11)
RSA	S6_3698197	Pv06	3698197	3.35E-06	0.12	1.58	G (0.11)
RV	S6_6504245	Pv06	6504245	1.75E-06	0.14	4.77	T (0.11)
RV	S6_3698197	Pv06	3698197	5.74E-06	0.12	2.03	G (0.11)
TRL	S1_38584873	Pv01	38584873	1.22E-07	0.15	−7.18	T (0.15)
TRL	S1_22164004	Pv01	22164004	4.12E-06	0.12	3.92	C (0.17)
TRL	S5_39203550	Pv05	39203550	2.84E-06	0.1	0.84	T (0.28)
TRL	S5_736525	Pv05	736525	2.88E-06	0.1	2.92	G (0.31)
TRL	S11_44269	Pv11	44269	3.80E-06	0.1	−1.44	G (0.13)

TRL, total root length (cm); RSA, root surface area (cm^2); RV, root volume (mm^3); AvdG, Average root diameter (mm); NRT, number of root tips; NRF, number of root forks; NRC, number of root crosses; NRL, number of links.

mechanisms are related to mitochondrial metabolism and acid transport (Nunes-Nesi et al., 2014).

Generally, common bean is relatively poor at adapting to Al stress conditions (Rao et al., 2008). However, studies reported that some Al tolerant common bean genotypes display Al activated exudation of citrate and Al chelating organic compound (Mugai et al., 2000; Eticha et al., 2010; Rangel et al., 2010) which is much smaller in the Al sensitive genotypes than in tolerant ones (Miyasaka et al., 1991). The exudation of citrate and Al chelating organic compounds help the plant to exclude Al from their root system. Recent advances in physiological, biochemical and molecular studies also revealed that the modification of the binding properties of the root apoplast contributes to Al tolerance (Horst et al., 2010). Testing of top lines from the hydroponic trials for analysis of organic acid exudation *in vitro* or on acid soils, would be useful.

Genome wide association study exploits the linkage disequilibrium (LD) present among individuals from natural populations or germplasm collections to dissect the genetic basis of complex quantitative trait variation with a powerful resolution as compared to studying a biparental mapping population. Our GWAS study allowed us to identify 15 significant SNP loci associated with six root traits on five common bean chromosomes Pv01, Pv04, Pv05, Pv06, and Pv11. Seven of the 15 significant markers for all traits other than RV were located on chromosome Pv01. Furthermore, the majority of Al stress tolerance related genes were also on Pv01. This suggested that Pv01 be considered for targeted study to further understand the mechanism of Al tolerance and associated metabolic pathways and network of genes in common beans. We found no significant SNP associated with any of the trait studied on chromosome Pv09. In contrary López-Marín et al. (2009) found Al responsive QTL (*Trl9.1*) on this chromosome derived from G19833 which was not included in the current study. Njobvu et al. (2020) identified Al tolerance QTLs on chromosomes Pv02, Pv07, Pv09, and Pv10, chromosomes on which we did

not find significant SNP markers. However, they positively identified QTLs on chromosomes Pv04, Pv05, and Pv 06, where we found many functional genes associated with plant responses against Al toxicity.

Related to the QTLs, the candidate genes identified in this study can be classified in to the following categories: genes encoding malate transporters, MATE transporters, protein kinases, receptors, and growth regulators, or pentatricopeptide proteins (PPRs). One of the most important genes identified was *Phvul.01G117300* which encoded an Al activated malate transporter homologous to the gene *ALMT1* (Hoekenga et al., 2006), a protein involved in malate exudation (Liu et al., 2012; Kobayashi et al., 2013, 2007). This gene was found on chromosome Pv01 and had similar sequence to *Phvul.007G025900,* a gene found on chromosome Pv07 found influencing Al tolerance in common bean by Njobvu et al. (2020). A homolog from Al tolerant wheat lines, also encoding membrane protein (*TaALMT1*) and facilitating malate efflux was reported to be highly expressed in this cereal's root apices (Ryan et al., 2009). This confirmed work in Arabidopsis, where *AtALMT1* was identified as critical for Al tolerance (Hoekenga et al., 2006). Study of association of aluminum tolerance candidate genes in beans with the balance of organic acids released by roots could be done through gene and metabolic expression profiles.

Secondly, a multidrug and toxic compound extrusion *(PvMATE)* membrane protein gene, (*Phvul.001G017400*) was identified for Al tolerance in bean. The MATE efflux proteins are important to Al tolerance (Wu et al., 2019) and *HvMATE* was first described as a candidate for controlling Al tolerance in barley by Wang et al. (2007). Ryan et al. (2009) showed correlation between the expressed sequence for *TaMATE* and citrate efflux in Al tolerant wheat cultivars describing organic acid exudation as an important mechanism of Al tolerance along with genes involved in Al detoxification through iron translocation. The *PvMATE* gene we found is a functional homolog of genes characterized in sorghum (Magalhaes et al., 2004, 2007), barley (Zhou et al., 2013), maize (Maron et al., 2010) and soybean (Liu et al., 2016). Successful cloning of Al tolerance QTL was reported using this gene in sorghum and barley (Liu et al., 2014). Among other genes identified for Al tolerance was *Phvul.01G117800*, encoding a homolog of phosphatidylinositol 4-kinase gamma 1 (PI4K), which in Arabidopsis activates early Al signaling and regulates the process of Al-induced malate transport by *AtALMT1*. *Phvul.001G142750* was another gene which encoded a cation efflux protein, involved in transmembrane transport of cations that confer metal tolerance (Mäser et al., 2001; Singh et al., 2016).

A third group of genes we found involved in Al tolerance were classified for signal reception and growth regulation (*Phvul.001G017000* and *Phvul.001G018000*). Two genes encoded threonine protein kinases which are central in signal transduction from receptors that sense environmental conditions into appropriate outputs such as shifts in metabolism, gene expression, and cell growth or division (Hardie, 1999). *Phvul.004G151200* was another candidate gene identified by this study, which encoded a mitogen-activated protein kinase, also for signaling and DNA repair during and after Al-induced nuclear damage thus providing an adaptive response in root cells (Panda and Achary, 2014). Many additional genes were further candidates which encoded leucine-rich repeat (LRR)-containing proteins on chromosome Pv04 and 05 (**Supplementary Table 2**). These genes could be important in the elongation zone of root meristem and involved in cellular proliferation, plant growth and stress tolerance (Jones and Jones, 1997; Lorenzo et al., 2009; Zhao et al., 2018). Additionally, we found *Phvul.001G017800*, a gene encoding a cytochrome P450 enzyme that might be important to abiotic stress responses (Pandian et al., 2020) and *Phvul.001G141900*, a gene for a zinc finger CCCH domain-containing proteins, found to be involved in salt and drought tolerance (Sun et al., 2007; Bogamuwa and Jang, 2016).

Finally, a fourth class of genes were PPPs, whose involvement in Al tolerance is probably new to plant science. Genes *Phvul.011G000700* and *Phvul.011G001300* were examples of this class. These genes are likely to encode pentatricopeptide repeat (PPR) proteins known to be involved in post-transcriptional regulation of gene expression (Kosová et al., 2018) during abiotic stresses like drought and salinity (Xing et al., 2018; Sertse et al., 2019). The finding was supported by the fact that we also found many genes associated with salt and drought tolerance. This showed the possible cross talk and links of tolerance mechanisms between different abiotic stresses. Similar reports support this result in common bean for abiotic stresses of the acid soil complex of Al toxicity plus low P availability (López-Marín et al., 2009; Njobvu et al., 2020). In general, Al tolerance in common beans is complex and governed by coordination of many genes involved in many metabolic pathways from signal transduction (Canonne et al., 2011; Panda and Achary, 2014) to transcription and translation, post-transcriptional regulation of gene expression (Kosová et al., 2018), transmembrane transport of metabolites (Liu et al., 2016; Singh et al., 2016), and cell proliferation and plant growth regulation (Lorenzo et al., 2009).

In conclusion, this study identified sources of genetic variation for Al tolerance, estimated heritability of root characteristics in response to Al stress, and explained complexity of root reactions to Al in common beans. Significant association between SNP markers and root traits were found with multiple QTL explaining polygenic inheritance involving four chromosomes. Putative candidate genes related to malate and citrate exudation were encountered near significant SNP loci. Similar studies in wheat also showed complex nature of Al tolerance (Ryan et al., 2009, 2010; Raman et al., 2010). Further to this work we identified a number of candidate genes, whose regulation and detailed function in associated pathways could be studied in the future as they relate to Al tolerance. The utilization of germplasm sources, genetic diversity and genes identified in this research will hopefully permit the improvement of common bean varieties tolerant to Al toxicity and other related abiotic stresses. The positive GWAS loci and flanking SNP markers will enable common bean breeding programs to make rapid genetic gains for a difficult to assess root trait that would be underground or would require hydroponic growth systems for phenotyping. Candidate genes found in this study could be converted into direct gene markers for the specific traits of interest after thorough examination of the nucleotide variation at their location and implications for marker development in bean germplasm.

DATA AVAILABILITY STATEMENT

The original contributions presented in the study are included in the article/**Supplementary Material**, further inquiries can be directed to the corresponding author.

AUTHOR CONTRIBUTIONS

MB and DA planned the study, setup the experiment, took data, and wrote the manuscript. DA organized and analyzed the data and prepared graphs and tables. Both authors contributed to the article and approved the submitted version.

FUNDING

The sources of funding included Evans Allen project TENX-07 to Tennessee State University and a Capacity Building Professional Training grant (No. 2018-38821-27731) from the United States Department of Agriculture (USDA), providing a Ph.D. student assistantship for DA as well as research funds for MB. We also acknowledge additional funds for this project to MB research program on legumes from the Bill and Melinda Gates Foundation via a subgrant through Evolutionary Genomics Thirsty Planet Inc., TSU funds for farm work was also gratefully recognized.

ACKNOWLEDGMENTS

We are grateful to Michigan State University and USDA for providing the Andean Diversity Panel germplasm used in this study. We are grateful to TSU staff involved in AREC (Agricultural Research and Education Center) at TSU's farm facility. We acknowledge advice from W. Messier of Thirsty Planet Inc., and J. Ehlers from Gates Foundation.

SUPPLEMENTARY MATERIAL

The Supplementary Material for this article can be found online at: https://www.frontiersin.org/articles/10.3389/fpls.2021.628687/full#supplementary-material

REFERENCES

Arunakumara, I. U., Buddhi, C. W., and Min, H. Y. (2013). Aluminum Toxicity and Tolerance Mechanism in Cereals and Legumes - A Review. *J. Korean Soc. Appl. Biol. Chem.* 56, 1–9. doi: 10.1007/s13765-012-2314-z

Asfaw, A., and Blair, M. W. (2012). Quantitative trait loci for rooting pattern traits of common beans grown under drought stress versus non-stress conditions. *Mol. Breed.* 30, 681–695. doi: 10.1007/s11032-011-9654-y

Barceló, J., and Charlotte, P. (2002). Fast Root Growth Responses, Root Exudates, and Internal Detoxification as Clues to the Mechanisms of Aluminium Toxicity and Resistance: A Review. *Environ. Exp. Bot.* 48, 75–92. doi: 10.1016/S0098-8472(02)00013-8

Bartoli, G., Sanità di, T., Andreucci, A., and Ruffini, M. C. (2017). Aluminum Effects on Embryo Suspensor Polytene Chromosomes of *Phaseolus Coccineus* L. *Plant Biosyst.* 3504, 1–9. doi: 10.1080/11263504.2017.1359213

Beebe, S. E., Rojas-Pierce, M., Yan, X., Blair, M. W., Pedraza, F., Muñoz, F., et al. (2006). Quantitative Trait Loci for Root Architecture Traits Correlated with Phosphorus Acquisition in Common Bean. *Crop Sci.* 46, 413–423. doi: 10.2135/cropsci2005.0226

Bianchi-Hall, C. M., Carter, T. E., Bailey, M. A., Mian, A. R., Rufty, T. W., Ashley, D. A., et al. (2000). Aluminum Tolerance Associated with Quantitative Trait Loci Derived from Soybean PI 416937 in Hydroponics. *Crop Sci.* 40, 538–545. doi: 10.2135/cropsci2000.402538x

Blair, M. W. (2013). Mineral Biofortification Strategies for Food Staples: The Example of Common Bean. *J. Agricult. Food Chem.* 64, 6383–6396. doi: 10.1021/jf400774y

Blair, M. W., López-Marín, H. D., and Rao, I. M. (2009). Identification of Aluminum Resistant Andean Common Bean (*Phaseolus Vulgaris* L.) Genotypes. *Brazi. J. Plant Physiol.* 21, 291–300.

Bogamuwa, S., and Jang, J. C. (2016). Plant Tandem CCCH Zinc Finger Proteins Interact with ABA, Drought, and Stress Response Regulators in Processing-Bodies and Stress Granules. *PLoS One.* 11:e0151574. doi: 10.1371/journal.pone.0151574

Bojórquez-Quintal, E., Escalante-Magaña, C., Echevarría-Machado, I., and Martínez-Estévez, M. (2017). Aluminum, a Friend or Foe of Higher Plants in Acid Soils. *Front. Plant Sci.* 8, 767. doi: 10.3389/fpls.2017.01767

Bradbury, P. J., Zhang, Z., Kroon, D. E., Casstevens, T. M., Ramdoss, Y., and Buckler, E. S. (2007). TASSEL: Software for Association Mapping of Complex Traits in Diverse Samples. *Bioinform. Appl.* 23, 2633–2635. doi: 10.1093/bioinformatics/btm308

Butare, L., Rao, I. M., Lepoivre, P., Cajiao, C., Polania, J., Cuasquer, J., et al. (2012). Phenotypic Evaluation of Interspecific Recombinant Inbred Lines (RILs) of *Phaseolus* Species for Aluminium Resistance and Shoot and Root Growth Response to Aluminium-Toxic Acid Soil. *Euphytica* 186, 715–730. doi: 10.1007/s10681-011-0564-1

Butare, L., Rao, I. M., Lepoivre, P., Polania, J., Cajiao, C., Cuasquer, J., et al. (2011). New Genetic Sources of Resistance in the Genus *Phaseolus* to Individual and Combined Aluminium Toxicity and Progressive Soil Drying Stresses. *Euphytica* 181, 385–404. doi: 10.1007/s10681-011-0468-0

Canonne, J., Froidure-Nicolas, S., and Rivas, S. (2011). Phospholipases in Action during Plant Defense Signaling. *Plant Sign. Behav.* 6, 13–18. doi: 10.4161/psb.6.1.14037

Cichy, K. A., Porch, T. G., Beaver, J. S., Cregan, P., Fourie, D., Glahn, R. P., et al. (2015a). A *Phaseolus Vulgaris* Diversity Panel for Andean Bean Improvement. *Crop Sci.* 55, 2149–2160. doi: 10.2135/cropsci2014.09.0653

Cichy, K. A., Wiesinger, J. A., and Mendoza, F. A. (2015b). Genetic Diversity and Genome-Wide Association Analysis of Cooking Time in Dry Bean (*Phaseolus Vulgaris* L.). *Theoret. Appl. Genet.* 128, 1555–1567. doi: 10.1007/s00122-015-2531-z

Delhaize, E., Ryan, P. R., and Randall, P. J. (1993). Aluminum Tolerance in Wheat (*Triticum Aestivum*). *Plant Physiol.* 103, 695–702. doi: 10.1104/pp.103.3.695

Elshire, R. J., Glaubitz, J. C., Sun, Q., Poland, J. A., Kawamoto, B. K., and Mitchell, S. E. (2011). A Robust, Simple Genotyping-by-Sequencing (GBS) Approach for High Diversity Species. *PLoS One* 6:e19379. doi: 10.1371/journal.pone.0019379

Eticha, D., Zahn, M., Bremer, M., Yang, Z., Rangel, A. F., Rao, I. M., et al. (2010). Transcriptomic Analysis Reveals Differential Gene Expression in Response to Aluminium in Common Bean (*Phaseolus Vulgaris*) Genotypes. *Anna. Bot.* 105, 1119–1128. doi: 10.1093/aob/mcq049

Furuichi, T., Sasaki, T., Tsuchiya, Y., Ryan, P. R., Delhaize, E., and Yamamoto, Y. (2010). An Extracellular Hydrophilic Carboxy-Terminal Domain Regulates the Activity of TaALMT1, the Aluminum-Activated Malate Transport Protein of Wheat. *Plant J.* 64, 47–55. doi: 10.1111/j.1365-313X.2010.04309.x

Gao, X., Starmer, J., and Martin, E. R. (2008). A Multiple Testing Correction Method for Genetic Association Studies Using Correlated Single Nucleotide Polymorphisms. *Genet. Epidemiol.* 32, 361–369. doi: 10.1002/gepi.20310

Goodstein, D. M., Shu, S., Howson, R., Neupane, R., Hayes, R. D., Fazo, J., et al. (2012). Phytozome: A Comparative Platform for Green Plant Genomics. *Nucleic Acids Res.* 40, 1178–1186. doi: 10.1093/nar/gkr944

Gupta, N., Gaurav, S. S., and Kumar, A. (2013). Molecular Basis of Aluminium Toxicity in Plants?: A Review. *Am. J. Plant Sci.* 4, 21–37. doi: 10.4236/ajps.2013.4.12A3004

Hardie, D. G. (1999). PLANT PROTEIN SERINE/THREONINE KINASES: Classification and Functions. *Annu. Rev. Plant Physiol. Plant Mol. Biol.* 50, 97–131.

Hart, P. J., and Griffiths, P. D. (2015). Genotyping-by-Sequencing Enabled Mapping and Marker Development for the Potyvirus Resistance Allele in Common Bean. *Plant Genome* 8:eplantgenome2014.09.0058. doi: 10.3835/plantgenome2014.09.0058

Hede, A. R., Skovmand, B., and López-Cesati, J. (2001). Acid Soils and Aluminum Toxicity. *Appl. Physiol. Wheat Breed.* 1995, 172–182.

Hoekenga, O. A., Maron, L. G., Piñeros, M. A., Cançado, G. M., Shaff, J., Kobayashi, Y., et al. (2006). *AtALMT1*, Which Encodes a Malate Transporter, Is Identified as One of Several Genes Critical for Aluminum Tolerance in Arabidopsis. *Proc. Natl. Acad. Sci. U. S. A.* 103, 9738–43. doi: 10.1073pnas.0602868103

Holland, J. B., Nyquist, W. E., and Cervantes-Martínez, C. T. (2003). "Estimating and Interpreting Heritability for Plant Breeding: An Update," in *Plant Breeding Reviews*, ed. J. Janick (Hoboken, NJ: John Wiley & Sons, Ltd), 9–112. doi: 10.1002/9780470650202.ch2

Horst, W. J., Rangel, A. F., Eticha, D., Ischitani, M., and Rao, I. M. (2009). "Aluminum Toxicity and Resistance in Phaseolus Vulgaris," in *International Symposium on Plant-Soil Interactions at Low pH*. (Ithaca, NY: USABoyce Thompson Institute).

Horst, W. J., Wang, Y., and Eticha, D. (2010). The Role of the Root Apoplast in Aluminium-Induced Inhibition of Root Elongation and in Aluminium Resistance of Plants: A Review. *Anna. Bot.* 106, 185–197. doi: 10.1093/aob/mcq053

Ingvarsson, P. K., and Street, N. R. (2011). Association genetics of complex traits in plants. *New Physiol.* 189, 909–922. doi: 10.1111/j.1469-8137.2010.03593.x

Jones, D. A., and Jones, J. D. G. (1997). The Role of Leucine-Rich Repeat Proteins in Plant Defences. *Adv. Bot. Res.* 24, 89–167. doi: 10.1016/S0065-2296(08)60072-5

Kamfwa, K., Cichy, K. A., and Kelly, J. D. (2015a). Genome-Wide Association Analysis of Symbiotic Nitrogen Fixation in Common Bean. *Theoret. Appl. Genet.* 128, 1999–2017. doi: 10.1007/s00122-015-2562-5

Kamfwa, K., Cichy, K. A., and Kelly, J. D. (2015b). Genome-Wide Association Study of Agronomic Traits in Common Bean. *Plant Genome* 8:lantgenome2014.09.0059. doi: 10.3835/plantgenome2014.09.0059

Kang, H. M., Sul, J. H., Service, S. K., Zaitlen, N. A., Kong, S. Y., Freimer, N. B., et al. (2010). Variance Component Model to Account for Sample Structure in Genome-Wide Association Studies. *Nat. Genetics* 42, 348–354. doi: 10.1038/ng.548

Kobayashi, Y., Hoekenga, O. A., Itoh, H., Nakashima, M., Saito, S., Shaff, J. E., et al. (2007). Characterization of AtALMT1 Expression in Aluminum-Inducible Malate Release and Its Role for Rhizotoxic Stress Tolerance in Arabidopsis. *Plant Physiol.* 145, 843–852. doi: 10.1104/pp.107.102335

Kobayashi, Y., Lakshmanan, V., Kobayashi, Y., Aasai, Iiuchi, M. S., Kobayashi, M., et al. (2013). Overexpression of *AtALMT1* in the Arabidopsis Thaliana Ecotype Columbia Results in Enhanced Al-Activated Malate Excretion and Beneficial Bacterium Recruitment. *Plant Signal. Behav.* 8:565. doi: 10.4161/psb.25565

Kochian, L. V., Hoekenga, O. A., and Piñeros, M. A. (2004). How Do Crop Plants Tolerate Acid Soils? Mechanisms of Aluminum Tolerance and Phosphorous Efficiency. *Annu. Rev. Plant Biol.* 55, 459–493. doi: 10.1146/annurev.arplant.55.031903.141655

Kochian, L. V., Piñeros, M. A., and Hoekenga, O. A. (2005). The Physiology, Genetics and Molecular Biology of Plant Aluminum Resistance and Toxicity. *Plant Soil* 274, 175–195. doi: 10.1007/s11104-004-1158-7

Kosová, K., Vítámvás, P., Urban, M. O., Prášil, I. T., and Renaut, J. (2018). Plant Abiotic Stress Proteomics: The Major Factors Determining Alterations in Cellular Proteome. *Front. Plant Sci.* 9:122. doi: 10.3389/fpls.2018.00122

Lin-Yin, L. (2020). *Package ' CMplot*. 1–8. Available online at: https://github.com/YinLiLin/CMplot (accessed on Jun 6, 2020).

Liu, J., Li, Y., Wang, W., Gai, J., and Li, Y. (2016). Genome-Wide Analysis of *MATE* Transporters and Expression Patterns of a Subgroup of *MATE* Genes in Response to Aluminum Toxicity in Soybean. *BMC Genomics* 17:223. doi: 10.1186/s12864-016-2559-8

Liu, J., Luo, X., Shaff, J., Liang, C., Jia, X., Li, Z., et al. (2012). A Promoter-Swap Strategy between the *AtALMT* and *AtMATE* Genes Increased Arabidopsis Aluminum Resistance and Improved Carbon-Use Efficiency for Aluminum Resistance. *Plant J.* 71, 327–337. doi: 10.1111/j.1365-313X.2012.04994.x

Liu, J., Piñeros, M. A., and Kochian, L. V. (2014). The Role of Aluminum Sensing and Signaling in Plant Aluminum Resistance. *J. Integr. Plant Biol.* 56, 221–230. doi: 10.1111/jipb.12162

López-Marín, H. D., Rao, I. M., and Blair, M. W. (2009). Quantitative Trait Loci for Root Morphology Traits under Aluminum Stress in Common Bean *(Phaseolus Vulgaris L.). Theoret. Appl. Genet.* 119, 449–458. doi: 10.1007/s00122-009-1051-0

Lorenzo, L. D., Merchan, F., Laporte, P., Thompson, R., Clarke, J., Sousa, C., et al. (2009). A Novel Plant Leucine-Rich Repeat Receptor Kinase Regulates the Response of Medicago Truncatula Roots to Salt Stress W. *Plant Cell* 21, 668–680. doi: 10.1105/tpc.108.059576

Ma, J. F., Zheng, S. J., Li, X. F., Takeda, K., and Matsumoto, H. (1997). A Rapid Hydroponic Screening for Aluminium Tolerance in Barley. *Plant Soil* 191, 133–137. doi: 10.1023/A:1004257711952

Magalhaes, J. V., Garvin, D. F., Wang, Y., Sorrells, M. E., Klein, P. E., Schaffert, R. E., et al. (2004). Comparative Mapping of a Major Aluminum Tolerance Gene in Sorghum and Other Species in the Poaceae. *Genetics* 167, 1905–1914. doi: 10.1534/genetics.103.023580

Magalhaes, J. V., Liu, J., Guimarães, C. T., Lana, U. G. P., Alves, V. M. C., Wang, Y. H., et al. (2007). A Gene in the Multidrug and Toxic Compound Extrusion (*MATE*) Family Confers Aluminum Tolerance in Sorghum. *Nat. Genet.* 39, 1156–1161. doi: 10.1038/ng2074

Maron, L. G., Piñeros, M. A., Guimarães, C. T., Magalhaes, J. V., Pleiman, J. K., Mao, C., et al. (2010). Two Functionally Distinct Members of the *MATE* (Multi-Drug and Toxic Compound Extrusion) Family of Transporters Potentially Underlie Two Major Aluminum Tolerance QTLs in Maize. *Plant J.* 61, 728–740. doi: 10.1111/j.1365-313X.2009.04103.x

Mäser, P., Thomine, S., Schroeder, J. I., Ward, J. M., Hirschi, K., Sze, H., et al. (2001). Phylogenetic Relationships within Cation Transporter Families of Arabidopsis. *Plant Physiol.* 126, 1646–1667. doi: 10.1104/pp.126.4.1646

Mendoza-Soto, A. B., Naya, L., Leija, A., and Hernández, G. (2015). Responses of Symbiotic Nitrogen-Fixing Common Bean to Aluminum Toxicity and Delineation of Nodule Responsive MicroRNAs. *Front. Plant Sci.* 6:587. doi: 10.3389/fpls.2015.00587

Mimmo, T., Sciortino, M., Ghizzi, M., Gianquinto, G., and Gessa, C. E. (2009). The Influence of Aluminium Availability on Phosphate Uptake in *Phaseolus Vulgaris* L. and *Phaseolus Lunatus* L. *Plant Physiol. Biochem.* 47, 68–72. doi: 10.1016/j.plaphy.2008.09.009

Miyasaka, S. C., Buta, J. G., Howell, R. K., and Foy, C. D. (1991). Mechanism of Aluminum Tolerance in Snapbeans: Root Exudation of Citric Acid. *Plant Physiol.* 96, 737–743. doi: 10.1104/pp.96.3.737

Moghaddam, S. M., Mamidi, S., Osorno, J. M., Lee, R., Brick, M., Kelly, J., et al. (2016). Genome-Wide Association Study Identifies Candidate Loci Underlying Agronomic Traits in a Middle American Diversity Panel of Common Bean. *Plant Genome* 9:lantgenome2016.02.0012. doi: 10.3835/plantgenome2016.02.0012

Money, D., Gardner, K., Migicovsky, Z., Schwaninger, H., Zhong, G. Y., and Myles, S. (2015). LinkImpute: Fast and Accurate Genotype Imputation for Nonmodel Organisms. *G3* 5, 2383–2390. doi: 10.1534/g3.115.021667

Mugai, E. N., Agong, S. G., and Matsumoto, H. (2000). Aluminium Tolerance Mechanisms in *Phaseolus Vulgaris* L.: Citrate Synthase Activity and TTC Reduction Are Well Correlated with Citrate Secretion. *Soil Sci. Plant Nutr.* 46, 939–950. doi: 10.1080/00380768.2000.10409159

Myles, S., Peiffer, J., Brown, P. J., Ersoz, E. S., Zhang, Z., Costich, D. E., et al. (2009). Association Mapping: Critical Considerations Shift from Genotyping to Experimental Design. *Plant Cell Online* 21, 2194–2202. doi: 10.1105/tpc.109.068437

Neto, J. S., Delfini, J., Silva, T. W., Hirose, A. A., Novais, J. M., Gonçalves, L. S. A., et al. (2020). Response of Common Bean Cultivars and Lines

to Aluminum Toxicity. *Agronomy* 10, 1–15. doi: 10.3390/agronomy10020296

Njobvu, J., Hamabwe, S. M., Munyinda, K., Kelly, J. D., and Kamfwa, K. (2020). Quantitative Trait Loci Mapping of Resistance to Aluminum Toxicity in Common Bean. *Crop Sci.* 60, 1294–1302. doi: 10.1002/csc2.20043

Nunes-Nesi, A., Brito, D. S., Inostroza-Blancheteau, C., Fernie, A. R., and Araújo, W. L. (2014). The Complex Role of Mitochondrial Metabolism in Plant Aluminum Resistance. *Trends Plant Sci.* 19, 399–407. doi: 10.1016/j.tplants.2013.12.006

Ochoa, I. E., Blair, M. W., and Lynch, J. P. (2006). QTL Analysis of Adventitious Root Formation in Common Bean under Contrasting Phosphorus Availability. *Crop Sci.* 46, 1609–1621. doi: 10.2135/cropsci2005.12-0446

Oladzad, A., Porch, T., Rosas, Juan, C., Moghaddam, S. M., Beaver, J., et al. (2019a). Single and Multi-Trait GWAS Identify Genetic Factors Associated with Production Traits in Common Bean under Abiotic Stress Environments. *G3* 9, 1881–1892. doi: 10.1534/g3.119.400072

Oladzad, A., Zitnick-Anderson, K., Jain, S., Simons, K., Osorno, J. M., McClean, P. E., et al. (2019b). Genotypes and Genomic Regions Associated With *Rhizoctonia Solani* Resistance in Common Bean. *Front. Plant Sci.* 10:956. doi: 10.3389/fpls.2019.00956

Panda, B. B., and Achary, V. M. (2014). Mitogen-Activated Protein Kinase Signal Transduction and DNA Repair Network Are Involved in Aluminum-Induced DNA Damage and Adaptive Response in Root Cells of Allium Cepa L. *Front. Plant Sci.* 5:256. doi: 10.3389/fpls.2014.00256

Pandey, P., Irulappan, V., Bagavathiannan, M. V., and Senthil-Kumar, M. (2017). Impact of Combined Abiotic and Biotic Stresses on Plant Growth and Avenues for Crop Improvement by Exploiting Physio-Morphological Traits. *Front. Plant Sci.* 8:537. doi: 10.3389/fpls.2017.00537

Pandian, B. A., Sathishraj, R., Djanaguiraman, M., Prasad, P. V., and Jugulam, M. (2020). Role of Cytochrome P450 Enzymes in Plant Stress Response. *Antioxidants* 9:454. doi: 10.3390/antiox9050454

Perseguini, J., Oblessuc, P. R., Rosa, J., Gomes, K. A., Chiorato, A. F., and Carbonell, S. (2016). Genome-Wide Association Studies of Anthracnose and Angular Leaf Spot Resistance in Common Bean (*Phaseolus Vulgaris* L.). *PLoS One* 11:150506. doi: 10.1371/journal.pone.0150506

Purcell, S., Neale, B., Todd-Brown, K., Thomas, L., Ferreira, A. R., Bender, D., et al. (2007). PLINK: A Tool Set for Whole-Genome Association and Population-Based Linkage Analyses. *Am. J. Hum. Genet.* 81, 559–575. doi: 10.1086/519795

R Core Team (2020). *A Language and Environment for Statistical Computing*. Austria: R Foundation for Statistical Computing.

Raggi, L., Caproni, L., Carboni, A., and Negri, V. (2019). Genome-Wide Association Study Reveals Candidate Genes for Flowering Time Variation in Common Bean (*Phaseolus Vulgaris* L.). *Front. Plant Sci.* 10:962. doi: 10.3389/fpls.2019.00962

Raman, H., Stodart, B., Ryan, P., Delhaize, E., Emberi, L., Raman, R., et al. (2010). Genome wide association analyses of common wheat (*Triticum aestivum* L) germplasm identifies multiple loci for aluminium resistance. *Genome* 53, 957–966.

Rangel, A. F., Rao, I. M., Braun, H. P., and Horst, W. J. (2010). "Aluminum Resistance in Common Bean (*Phaseolus Vulgaris* L.) Involves Induction and Maintenance of Citrate Exudation from Root Apices. *Physiol. Plant.* 138, 176–190. doi: 10.1111/j.1399-3054.2009.01303.x

Rangel, A. F., Rao, I. M., and Horst, W. J. (2007). Spatial Aluminium Sensitivity of Root Apices of Two Common Bean (*Phaseolus Vulgaris* L.) Genotypes with Contrasting Aluminium Resistance. *J. Exp. Bot.* 58, 3895–3904.

Rao, I. M., Miles, J. W., Beebe, S. E., and Horst, W. J. (2016). Root Adaptations to Soils with Low Fertility and Aluminium Toxicity. *Anna. Bot.* 118, 593–605. doi: 10.1093/aob/mcw073

Rao, I. M., Vélez, A. A., Miles, J. W., Watanabe, T., Shinano, T., Osaki, M., et al. (2008). Advances in developing screening methods and improving aluminum resistance in common bean and Brachiaria. *Rev. Brasil. Agroc.* 14, 1–7.

Ryan, P. R., Raman, H., Gupta, S., Horst, W. J., and Delhaize, E. (2009). A second mechanism for aluminum resistance in wheat relies on the constitutive efflux of citrate from roots. *Plant Physiol.* 149, 340–351.

Ryan, P. R., Raman, H., Gupta, S., Sasaki, T., Yamamoto, Y., and Delhaize, E. (2010). The multiple origins of aluminium resistance in hexaploid wheat include *Aegilops tauschii* and more recent cis mutations to *TaALMT1*. *Plant J.* 64, 446–455.

SAS Institute Inc (2011). *Base SAS® 9.3 Utilities: Reference*. Cary, NC: SAS Institute Inc. ISBN 978-1-60764-905-2

Sasaki, T., Mori, I. C., Furuichi, T., Munemasa, S., Toyooka, K., Matsuoka, K., et al. (2010). Closing Plant Stomata Requires a Homolog of an Aluminum-Activated Malate Transporter. *Plant Cell Physiol.* 51, 354–365. doi: 10.1093/pcp/pcq016

Sasaki, T., Yamamoto, Y., Ezaki, B., Katsuhara, M., Ahn, S. J., Ryan, P. R., et al. (2004). A Wheat Gene Encoding an Aluminum-Activated Malate Transporter. *Plant J.* 37, 645–653. doi: 10.1111/j.1365-313X.2003.01991.x

Sertse, D., You, F. M., Ravichandran, S., and Cloutier, S. (2019). The Complex Genetic Architecture of Early Root and Shoot Traits in Flax Revealed by Genome-Wide Association Analyses. *Front. Plant Sci.* 10:1483. doi: 10.3389/fpls.2019.01483

Shi, C., Navabi, A., and Yu, K. (2011). Association Mapping of Common Bacterial Blight Resistance QTL in Ontario Bean Breeding Populations. *BMC Plant Biol.* 11:52. doi: 10.1186/1471-2229-11-52

Singh, S., Parihar, P., Singh, R., Singh, V. P., and Prasad, S. M. (2016). Heavy Metal Tolerance in Plants: Role of Transcriptomics, Proteomics, Metabolomics, and Ionomics. *Front. Plant Sci.* 2015:143. doi: 10.3389/fpls.2015.01143

Sun, J., Jiang, H., Xu, Y., Li, H., Wu, X., Xie, Q., et al. (2007). The CCCH-Type Zinc Finger Proteins AtSZF1 and AtSZF2 Regulate Salt Stress Responses in Arabidopsis. *Plant Cell Physiol.* 48, 1148–1158. doi: 10.1093/pcp/pcm088

Wang, J., and Zhang, Z. (2018). GAPIT Version 3:An Interactive Analytical Tool for Genomic Association and Prediction. preprint. https://github.com/jiabowang/GAPIT3.

Wang, J. P., Raman, H., Zhou, M. X., Ryan, P. R., Delhaize, E., Hebb, D. M., et al. (2007). High-resolution mapping of the Alp locus and identification of a candidate gene *HvMATE* controlling aluminium tolerance in barley (*Hordeum vulgare* L.). *Theoret. Appl. Genet.* 115, 265–276.

Wen, L., Chang, H. X., Brown, P. J., Domier, L. L., and Hartman, G. L. (2019). Genome-Wide Association and Genomic Prediction Identifies Soybean Cyst Nematode Resistance in Common Bean Including a Syntenic Region to Soybean Rhg1 Locus. *Horticult. Res.* 6, 1–12. doi: 10.1038/s41438-018-0085-3

Wu, L., Sadhukhan, A., Kobayashi, Y., Ogo, N., Tokizawa, M., Agrahari, R. K., et al. (2019). Involvement of Phosphatidylinositol Metabolism in Aluminum-Induced Malate Secretion in Arabidopsis. *J. Exp. Bot.* 70, 3329–3342. doi: 10.1093/jxb/erz179

Xing, H., Fu, X., Yang, C., Tang, X., Guo, L., Li, C., et al. (2018). Genome-Wide Investigation of Pentatricopeptide Repeat Gene Family in Poplar and Their Expression Analysis in Response to Biotic and Abiotic Stresses. *Scient. Rep.* 8, 1–9. doi: 10.1038/s41598-018-21269-1

Yan, X., Liao, H., Beebe, S. E., Blair, M. W., and Lynch, J. P. (2004). QTL Mapping of Root Hair and Acid Exudation Traits and Their Relationship to Phosphorus Uptake in Common Bean. *Plant Soil* 265, 17–29. doi: 10.1007/s11104-005-0693-1

Yang, Z. B., Eticha, D., Rotter, B., Rao, I. M., and Horst, W. J. (2011). Physiological and Molecular Analysis of Polyethylene Glycol-Induced Reduction of Aluminium Accumulation in the Root Tips of Common Bean (*Phaseolus Vulgaris* L.). *N. Phytol.* 192, 99–113. doi: 10.1111/j.1469-8137.2011.03784.x

Yang, Z. B., Rao, I. M., and Horst, W. J. (2013). Interaction of Aluminium and Drought Stress on Root Growth and Crop Yield on Acid Soils. *Plant Soil* 372, 3–25. doi: 10.1007/s11104-012-1580-1

Yang, Z. M., Sivaguru, M., Horst, W. J., and Matsumoto, H. (2000). Aluminium Tolerance Is Achieved by Exudation of Citric Acid from Roots of Soybean (Glycine Max). *Physiol. Plant.* 110, 72–77. doi: 10.1034/j.1399-3054.2000.110110.x

Yano, K., Yamamoto, E., Aya, K., Takeuchi, H., Lo, P., Hu, L., et al. (2016). Genome-Wide Association Study Using Whole-Genome Sequencing Rapidly Identifies New Genes Influencing Agronomic Traits in Rice. *Nat. Genet.* 48:927. doi: 10.1038/ng.3596

Zhao, C., Zayed, O., Yu, Z., Jiang, W., Zhu, P., Hsu, C. C., et al. (2018). Leucine-Rich Repeat Extensin Proteins Regulate Plant Salt Tolerance in Arabidopsis. *Proc. Natl. Acad. Sci. U. S. A.* 115, 13123–13128. doi: 10.1073/pnas.1816991115

Zhou, G., Delhaize, E., Zhou, M., and Peter, R. (2011). Biotechnological Solutions for Enhancing the Aluminium Resistance of Crop Plants. *Abiot. Stress Plants* 72:187. doi: 10.5772/25187

Zhou, G., Delhaize, E., Zhou, M., and Ryan, P. R. (2013). The Barley MATE Gene, HvAACT1, Increases Citrate Efflux and Al3+ Tolerance When Expressed in Wheat and Barley. *Anna. Bot.* 112, 603–612. doi: 10.1093/aob/mct135

Zuiderveen, G. H., Padder, B. A., Kamfwa, K., Song, Q., and Kelly, J. D. (2016). Genome-Wide Association Study of Anthracnose Resistance in Andean Beans (*Phaseolus Vulgaris* L.). *PLoS One* 11:e156391. doi: 10.1371/journal.pone.0156391

Conflict of Interest: The authors declare that the research was conducted in the absence of any commercial or financial relationships that could be construed as a potential conflict of interest.

Copyright © 2021 Ambachew and Blair. This is an open-access article distributed under the terms of the Creative Commons Attribution License (CC BY). The use, distribution or reproduction in other forums is permitted, provided the original author(s) and the copyright owner(s) are credited and that the original publication in this journal is cited, in accordance with accepted academic practice. No use, distribution or reproduction is permitted which does not comply with these terms.

frontiers in Plant Science

ORIGINAL RESEARCH
published: 11 August 2021
doi: 10.3389/fpls.2021.641087

Association Analysis Revealed That *TaPYL4* Genes Are Linked to Plant Growth Related Traits in Multiple Environment

Yinghong Xue[1,2†], Jingyi Wang[2†], Xinguo Mao[2], Chaonan Li[2], Long Li[2], Xi Yang[1], Chenyang Hao[2], Xiaoping Chang[2], Runzhi Li[1] and Ruilian Jing[2]**

[1] College of Agronomy, Shanxi Agricultural University, Jinzhong, China, [2] National Key Facility for Crop Gene Resources and Genetic Improvement, Institute of Crop Sciences, Chinese Academy of Agricultural Sciences, Beijing, China

OPEN ACCESS

Edited by:
Magdalena Arasimowicz-Jelonek, Adam Mickiewicz University, Poland

Reviewed by:
Samanta Zelasco, Council for Agricultural and Economics Research (CREA), Italy
Yong Zhao, Agricultural University of Hebei, China
Anna Nadolska-Orczyk, Plant Breeding and Acclimatization Institute, Poland

***Correspondence:**
Runzhi Li
rli2001@126.com
Ruilian Jing
jingruilian@caas.cn

† These authors have contributed equally to this work

Specialty section:
This article was submitted to Crop and Product Physiology, a section of the journal Frontiers in Plant Science

Received: *13 December 2020*
Accepted: *20 July 2021*
Published: *11 August 2021*

Citation:
Xue Y, Wang J, Mao X, Li C, Li L, Yang X, Hao C, Chang X, Li R and Jing R (2021) Association Analysis Revealed That TaPYL4 Genes Are Linked to Plant Growth Related Traits in Multiple Environment. Front. Plant Sci. 12:641087. doi: 10.3389/fpls.2021.641087

Abscisic acid (ABA), one of phytohormones, plays an important regulatory role in plant growth and development. ABA receptor *PYL4* (pyrabactin resistance 1-like 4) was previously detected to be involved in plant response to a variety of stresses. *TaPYL4* overexpression could enhance wheat (*Triticum aestivum*) drought resistance. In order to further investigate TaPYL4's role in regulating development of other major agronomic traits in wheat, genes of *TaPYL4-2A*, *TaPYL4-2B,* and *TaPYL4-2D* were cloned from wheat, respectively. Polymorphism analysis on *TaPYL4* sequences revealed that encoding regions of the three genes were highly conserved, without any SNP (single nucleotide polymorphism) presence. However, nine SNPs and four SNPs were identified in the promoter regions of *TaPYL4-2A* and *TaPYL4-2B*, respectively. Functional molecular markers were developed based on these polymorphisms, which were then used to scan a natural population of 323 common wheat accessions for correlation analysis between genotype and the target phenotypic traits. Both *TaPYL4-2A* and *TaPYL4-2B* markers were significantly correlated with plant growth-related traits under multiple environments (well-watered, drought and heat stress treatments). The additive effects of *TaPYL4-2A* and *TaPYL4-2B* were verified by the combinational haplotype (*Hap*-AB1∼*Hap*-AB4) effects determined from field data. *Cis*-acting elements were analyzed in the promoters of *TaPYL4-2A* and *TaPYL4-2B*, showing that a TGA-element bound by ARFs (auxin response factors) existed only in *Hap*-2A-1 of *TaPYL4-2A*. Gene expression assays indicated that *TaPYL4-2A* was constitutively expressed in various tissues, with higher expression in *Hap*-2A-1 genotypes than in *Hap*-2A-2 materials. Notably, TaARF4 could act as *TaPYL4-2A* transcription activator in *Hap*-2A-1 materials, but not in *Hap*-2A-2 genotypes. Analysis of geographic distribution and temporal frequency of haplotypes indicated that *Hap*-AB1 was positively selected in wheat breeding in China. Therefore, *TaPYL4-2A* and *TaPYL4-2B* could be a valuable target gene in wheat genetic improvement to develop the ideal plant architecture.

Keywords: association analysis, functional molecular marker, ABA receptor, *TaPYL4*, plant growth related-traits, wheat

INTRODUCTION

Wheat (*Triticum aestivum*) is one of the most important food crops in the world, and also the main grain crop in China. The global demand of food is increasing greatly with social development and human population growth. Enhancement of wheat yield plays an important role in ensuring world food security. To increase wheat grain yield, gene mining and innovation of germplasm with superior agronomic traits are always the key research fields in wheat breeding. During the "Green Revolution" of 1960s, the discovery of semi-dwarf genes led to a dramatic increase in wheat yields (Peng et al., 1999; Saville et al., 2012). Despite many regulator genes of plant height were reported such as *TaCOLD1*, *Rht18*, and *Rht12* (Van De Velde et al., 2017; Dong et al., 2019; Buss et al., 2020; Tang et al., 2020), other important genes associated with wheat plant height remain to be identified. Combined with previous findings, exploiting the excellent genetic resources of wheat is the most economical and effective way to breed new varieties with higher grain yields.

Abscisic acid (ABA) is a key factor in balancing the metabolism of endogenous hormones and growth-related active substances in plants (Li et al., 2012). Early studies evidence that ABA can bind to ABA receptor, and such binding causes PP2Cs (clade A type 2C protein phosphatases) to lose phosphatase activity. The inhibition of PP2Cs enables activation of SnRK2s (sucrose non-fermenting 1-related protein kinase 2s) which consequently direct phosphorylation of downstream transcription factor AREB/ABFs (ABA-responsive element-binding factors) to induce the expression of ABA-responsive genes in the ABA signal transduction pathway (Fujii et al., 2009; Li et al., 2013; Vishwakarma et al., 2017; Zhao et al., 2020). Thus, ABA receptor plays a crucial role in the ABA signal transduction pathway (Park et al., 2009; Dittrich et al., 2019).

In *Arabidopsis*, the pyrabactin resistance 1 (PYR1)/PYR1-like (PYL)/regulatory components of the ABA receptor (RCAR) family of proteins contains 14 proteins (PYR1 and PYL1-13) with highly homologous sequences and structures (Nakashima et al., 2009; Zhao et al., 2018). The properties, structures and functions of PYLs have been extensively studied (Ma et al., 2009; Klingler et al., 2010; Hao et al., 2011b). There is increasing evidence that PYLs have a variety of functions in plant species such as *Arabidopsis*, rice and tomato. For instance, among the six PYL members expressed in the guard cells, PYL4 and PYL5 are involved in CO_2 response (Dittrich et al., 2019). PYL9 could improve drought resistance and promote leaf senescence in *Arabidopsis* and rice (Zhao et al., 2016). PYL1, PYL4 and PYL6 in rice play a particularly important role in regulating plant growth (Miao et al., 2018). PYL5 in rice could increase drought tolerance and concurrently retard plant growth (Kim et al., 2014). Moreover, a recent report indicated that *TaPYL4* was highly acted in wheat tolerance to drought (Mega et al., 2019). However, the role of TaPYL4-mediated plant growth and development remains to be explored.

Candidate-gene association study (CGAS) is a kind of analysis based on the sequence of candidate genes. CGAS includes identification of the sequence polymorphism in the target gene and a correlation analysis between the polymorphism and the phenotypic traits, aiming to obtain the allelic variation affecting the target traits. Particularly, CGAS is used to analyze the correlation between different haplotypes and phenotypes to identify the excellent haplotype combinations responsible for the traits (Su et al., 2018). This tool is also used to excavate the excellent alleles with positive contribution to the target traits in germplasm resources. Functional markers can be directly used in detecting allele types of target genes, distinguishing different alleles and predicting phenotypic traits (Wang et al., 2019a). Moreover, functional markers can be used as the ideal molecular markers in marker-assisted breeding (Wang et al., 2020). With the development of functional genomics and genetic engineering, many functional molecular markers have been developed, providing abundant genetic markers for wheat molecular breeding.

In this study, gene sequencing was employed to examine polymorphism within *TaPYL4* locus (*TaPYL4-2A*, *TaPYL4-2B*, and *TaPYL4-2D*) in a populations consisting of 32 widely varied wheat germplasm. Functional markers were developed for *TaPYL4-2A* and *TaPYL4-2B* based on the *TaPYL4* polymorphism. These markers were then used to scan a natural population of 323 common wheat accessions for correlation analysis between genotypes and phenotypic traits. *TaPYL4-2A* and *TaPYL4-2B* were identified to be significantly correlated with plant growth-related traits. Furthermore, the additive effects of *TaPYL4-2A* and *TaPYL4-2B* were detected. Distribution of these haplotypes among the population consisting of wheat varieties from China was also examined, showing that *Hap*-AB1 was positive selected in wheat breeding. This work provides theoretical basis for wheat genetic improvement to obtain the ideal plant architecture, benefiting our understanding of ABA receptor upstream signaling network in plant morphogenesis.

MATERIALS AND METHODS

Plant Materials

A common wheat (*Triticum aestivum*) variety, the Chinese Spring, was used for cloning of *TaPYL4* gene sequences. Thirty-two wheat accessions (**Supplementary Table 1**) with wide variation screened by 209 SSR markers (Zhang et al., 2013) were used to get gene sequences for detecting SNPs of *TaPYL4s*.

Three wheat populations were employed in this research. Population 1 (323 accessions) (Wang et al., 2019a) was used for agronomic character analysis. This population consisting of 275 modern cultivars, 36 advanced lines, and 12 landraces was also employed for association analysis. Population 2 and Population 3 consisted of 157 landraces and 348 modern cultivars (Zhang et al., 2002), respectively. The latter two populations were mainly from a Chinese wheat microcore germplasm, accounting for more than 70% of the genetic diversity of the whole Chinese wheat germplasm resources (Hao et al., 2011a). Haplotype frequencies among 10 wheat-producing areas in China were determined using Population 2 and Population 3 (Zhang et al., 2002).

Management of Growth Conditions and Determination of Agronomic Traits

Population 1 was planted in 2015–2017 in Shunyi (40°23′N; 116°56′E) and Changping (40°13′N; 116°13′E) field experiment stations of the Institute of Crop Sciences, Chinese Academy of Agricultural Sciences, Beijing. Field water management was divided into two conditions: rain-fed (drought stressed, DS) and well-watered (WW). DS referred to that no artificial irrigation was given in the whole growing season of wheat, and the growth was completely fed by rain. WW was designed to irrigate the field with 750 m^3ha^{-1} (75 mm) water at pre-wintering, jointing, flowering, and grain-filling stages, respectively. Moreover, a heat stress experiment (HS) was applied to wheat plants of 1-week post-anthesis by placing a plastic film supported by steel frames over the plots in the field at Shunyi. Wheat phenotypic data under 16 environments (E1-E16) were obtained. E1-E16 represented the environments at Shunyi in 2015 under DS + HS, DS, WW + HS and WW, at Shunyi in 2016 under DS + HS, DS, WW + HS and WW, at Changping in 2016 under WW and DS, at Shunyi in 2017 under DS + HS, DS, WW + HS and WW, at Changping in 2017 under DS and WW (Li et al., 2019a), respectively (**Supplementary Table 2**).

The agronomic traits including plant height (PH), spike length (SL), peduncle length (PLE), length of penultimate node (LPN), number of spikes per plant (NSP), number of spikelet per spike (NSS), number of grains per spike (NGS), and 1,000-grain weight (TGW) were measured under 16 environments. Population 2 and 3 were grown at Luoyang (36°61′N; 112°45′E) in Henan Province in 2002 and 2005, and also grown at Shunyi (40°23′N; 116°56′E) in Beijing in 2010 (Zhang et al., 2017). In all cases, each variety was planted on a 2-m, 4-row plot with 30 cm row spacing of 40 seeds in each row. Phenotypic sampling was performed for 5 plants grown in the middle of each plot at maturity.

TaPYL4 Gene Cloning and Construction of a Phylogenetic Tree

The reference sequence (Accession number MG273654 in the NCBI database) of *TaPYL4* was obtained according to Mega's research (Mega et al., 2019). Genome-specific primers 2A-F1/R1, 2B-F1/R1, and 2D-F1/R1 were designed to amplify the promoter and coding region sequences of Chinese Spring wheat using Primer Premier 5.0 software (**Supplementary Table 3**). MEGA7 software was used to construct a neighbor joining phylogenetic tree.

Sequence and Single Nucleotide Polymorphism Analysis of *TaPYL4s*

All genomic DNA used in this study was extracted from the wheat by CTAB method (Stewart and Via, 1993). Gene promoter and coding region sequences of *TaPYL4s* were amplified from the 32 diverse wheat accessions (Li et al., 2019b), and subsequently ligated into pEASY-Blunt vector, respectively (Trans Gen Biotech, Beijing). Positive clones were randomly selected, and the plasmid from each clone was extracted for sequencing.

According to the sequence information of *TaPYL4-2A*, *TaPYL4-2B,* and *TaPYL4-2D*, genome-specific sequencing primers CX-A-R1/R2, CX-B-R1/R2, and CX-D-F1/R1 (**Supplementary Table 3**) were designed by Primer 5 and using a 3730 XI DNA Analyzer (ABI) sequencing. Seqman software in DNASTAR Lasergene 7.1 package was used for sequence splice and assembly. Meg Align software was used for sequence polymorphism analysis.

Development of Functional Molecular Markers for *TaPYL4-2A* and *TaPYL4-2B*

According to the two polymorphic sites detected, two molecular markers (TaPYL4-2A-dCAPS and TaPYL4-2B-dCAPS) were established at A genome −1635 bp (G/A) and B genome −1146 bp (G/C) upstream of the ATG translation start site, respectively. These dCAPS primers were designed with an available program dCAPS Finder 2.0. The primers were named 2A-*Sal*I-F/R and 2B-*Bam*HI-F/R, respectively (**Supplementary Table 3**). The first PCR product obtained with A genome-specific primers and B genome-specific primers, respectively, were served as the template for the second round of PCR. The annealing temperature and elongation time were determined by primer pairs and lengths of the expected PCR products. The PCR products were digested with the appropriate restriction enzyme at 37°C for 1.5 h and further separated on 4% agarose gel electrophoresis.

Association Analysis

Genotype scanning was performed on the Population 1 using the molecular markers (*TaPYL4-2A*-dCAPS and *TaPYL4-2B*-dCAPS) developed. Population 1 was performed on Wheat 660 K SNP Array, which consisted of 630,517 SNPs (Li et al., 2019b). By removing nucleotide variations with missing rates $\geq$ 0.2 and minor allele frequency (<0.05), 395,681 SNPs were eventually used to detect the structure of population 1 by software STRUCTURE 2.3.4 (Li et al., 2019a). Using the general liner model (GLM) of TASSEL (Version 5.2.51) software and population structure (Q) as covariable, correlation analysis was conducted for phenotypic traits and genotypes of *TaPYL4-2A* and *TaPYL4-2B*. Associations were considered as significant at $P < 0.05$. Analysis of variance by SPSS (version 19.0) software was used to detect different effects of haplotype on the agronomic traits.

Prediction of *Cis*-Acting Element in Promoter of *TaPYL4-2A* and *TaPYL4-2B*

Based on the above sequencing results, analysis of *cis*-acting element in Plant CARE[1] was employed to predict the *cis*-acting element in the promoter region of around 2,000 bp upstream of *TaPYL4-2A* and *TaPYL4-2B* genes, respectively.

Expression of *TaPYL4-2A* in Wheat

The expression pattern of *TaPYL4-2A* was analyzed using the wheat accession Chinese Spring. The spatiotemporal expression patterns of *TaPYL4-2A* were examined for different tissues (shoot and root at seedling stage, flag leaves, spikes, penultimate nodes,

[1]http://bioinformatics.pAet.ugent.be/webtools/plantcare/html

root bases, and root at heading stage). Twelve accessions of two different haplotypes were randomly selected from Population 1 (**Supplementary Table 4**). The gene expression levels were evaluated in shoot (St) for 20 d-old seedlings. Three biological replications were performed with each repeat at least three technical duplications.

Yeast One-Hybrid Assays

Yeast one-hybrid assays were employed to verify the binding of TaARF4 to *TaPYL4-2A* in different haplotype promoter regions. *Not*I was used to digest the pB42AD vector to obtain *TaARF4* fragment with a restriction enzyme site. Next, the *TaARF4* was cloned into the vector with seamless clonal enzyme. Two fragments of different haplotype promoter regions of *TaPYL4-2A* (−1890 to −1440 bp) were cloned into pLacZi as the reporter gene plasmid, respectively. The plasmid of pB42AD carrier with *TaARF4* was co-transformed into EGY48 in yeast with 2 reporters by standard yeast transformation method, respectively (Lin et al., 2007). The yeast was grown on SD/-Trp/-Ura medium with x-gal. LacZ staining was used to detect the interaction between TaARF4 and promoter fragments (Wang et al., 2016). This experiment was conducted in triplicate.

Dual-Luciferase Assays of Transformed Tobacco Leaves

Primers TaARF4-1,300-F/R (**Supplementary Table 3**) were used to amplify *TaARF4* full-length cDNA. The cDNA was further cloned into effector vector pCAMBIA1300 driven by CaMV35S. *TaPYL4-2A* promoter fragments of different haplotypes were amplified by primers PYL4-LUC-F1/R1 (**Supplementary Table 3**) and then cloned into the reporting vector pGreenII0800-LUC. The plasmid of pCAMBIA1300 vector with *TaARF4* and different reporter genes were separately transformed into GV3101 cells containing pSoup. The *Agrobactium* GV3101 containing the recombinant vector was used to transform tobacco leaves of 4 weeks by co-osmosis. The luciferase activity of firefly luciferase (LUC) and Renilla luciferase (REN) were determined at 48 h after osmosis using a Dual Glo® Luciferase Assay System (E2920, Promega) with a multimode reader (TriStar^{2}S LB942). The ratio of LUC to REN was used to calculate promoter activity.

RESULTS

Cloning and Molecular Characterization of *TaPYL4s* in Common Wheat

Three sub-genomic sequences of *TaPYL4* gene were isolated from a wheat accession, the Chinese Spring, namely as *TaPYL4-2A*, *TaPYL4-2B,* and *TaPYL4-2D*, respectively. The gene coding regions from A, B, and D sub-genomes are 654, 654, and 645 bp in length, respectively. Like other PYL family members, TaPYL4 proteins were highly conserved (**Supplementary Figure 1A**). The phylogenetic tree showed that the *TaPYL4s* were more similar to OsPYL4 (**Supplementary Figure 1B**).

[2]http://bioinformatics.psb.ugent.be/webtools/plantcare/html

SNPs of *TaPYL4s* and Functional Molecular Markers Developed for *TaPYL4-2A* and *TaPYL4-2B*

In the present study, SNPs in the coding and promoter regions of *TaPYL4-2A*, *-2B*, and *-2D* genes were detected by sequencing 32 diverse wheat accessions. No SNP was identified in the coding regions of *TaPYL4-2A* and *TaPYL4-2B.* However, nine SNPs were observed in *TaPYL4-2A* promoter region while two SNPs existed in *TaPYL4-2B* promoter region. For *TaPYL4-2D,* neither coding sequence nor promoter region was detected to have SNP. Therefore, no further investigation was on *TaPYL4-2D* in this study. According to the SNPs in *TaPYL4-2A* (**Figure 1A**) and *TaPYL4-2B* (**Figure 2A**) promoter regions, two haplotypes were identified for *TaPYL4-2A* (*Hap*-2A-1 and *Hap*-2A-2) and *TaPYL4-2B* (*Hap*-2B-1 and *Hap*-2B-2), respectively.

To accurately distinguish two haplotypes of *TaPYL4-2A*, a molecular marker (dCAPS) was developed based on the SNP (G/A) at −1635 bp of the gene, namely as *TaPYL4-2A*-dCAPS. The marker included two mismatches (AC/TT) in the downstream primer that generated the recognition site for the restriction enzyme *Sal*I (**Figure 1B**). In a similar way, a dCAPS marker was also developed with restriction enzyme *Bam*HI based on *TaPYL4-2B,* namely as *TaPYL4-2B*-dCAPS (**Figure 2B**).

Association Analysis of *TaPYL4-2A* Haplotypes With Agronomic Traits

Association analysis was conducted on agronomic characters of Population 1 under 16 environments in three growth seasons. For *TaPYL4-2A*, *Hap*-2A-1 accounted for 48.9% in the Population 1 (**Supplementary Figure 2**). The association analysis of *TaPYL4-2A* haplotypes and agronomic traits revealed that *TaPYL4-2A* was significantly associated with SL, PLE, and PH (**Table 1**). The statistical analysis showed that the SL of *Hap*-2A-1 was significantly shorter than that of *Hap*-2A-2 under 16 environmental conditions (**Figure 3A**). Under 14 environmental conditions, the PLE of *Hap*-2A-1 was significantly shorter than that of *Hap*-2A-2 (**Figure 3B**). Under eight environmental conditions, the PH of *Hap*-2A-1 was significantly shorter than that of *Hap*-2A-2 (**Figure 3C**). In summary, the values measured for plant growth related traits of *Hap*-2A-1 were lower than that of *Hap*-2A-2.

Association Analysis of *TaPYL4-2B* Haplotypes With Agronomic Traits

For *TaPYL4-2B*, *Hap*-2B-1, and *Hap*-2B-2 accounted for 75.5 and 24.5% in Population 1 (**Supplementary Figure 2**), respectively. Significant association between *TaPYL4-2B* haplotypes and PH was identified under 13 environments (**Table 2**). The PH of *Hap*-2B-1 was significantly shorter than that of *Hap*-2B-2 (**Figure 4A**). Similarly, *TaPYL4-2B* haplotypes were associated with PLE. *Hap*-2B-1 had significantly shorter PLE compared with *Hap*-2B-2 in 14 environments (**Figure 4B**). According to the description above, the values measured for plant growth related traits of *Hap*-2B-1 were lower than that of *Hap*-2B-2.

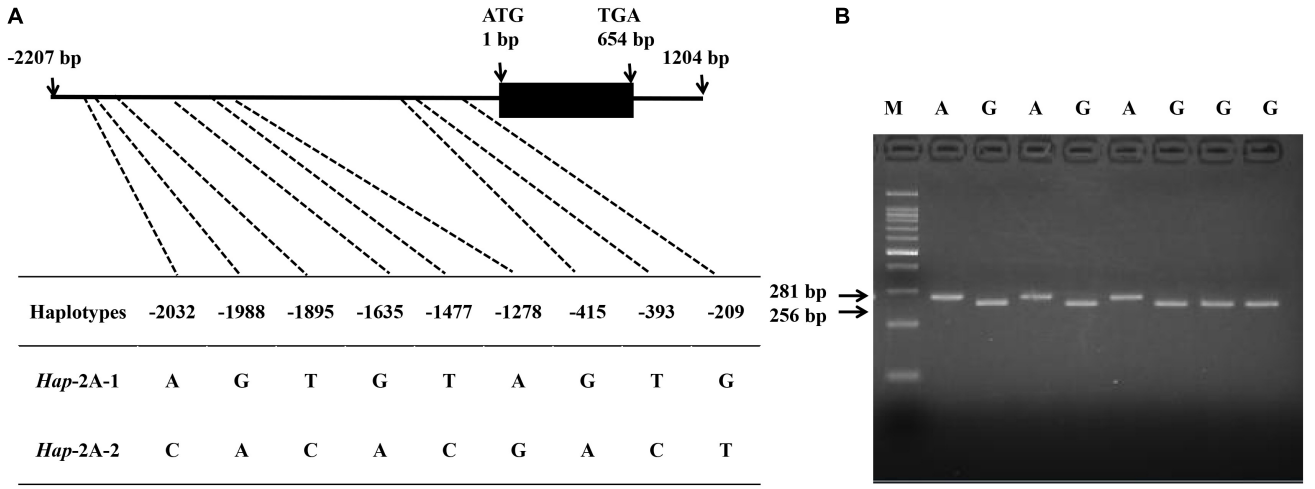


FIGURE 1 | Nucleotide polymorphisms and development of a molecular marker in wheat *TaPYL4-2A*. **(A)** Nine single nucleotide polymorphisms (SNPs) were detected in the promoter region of *TaPYL4-2A*. **(B)** dCAPS marker was developed based on the –1635 bp single-nucleotide polymorphism (G/A) with restriction endonuclease *Sal*I, which cleaved the sequence only when the site was G. M, 100-bp DNA ladder.

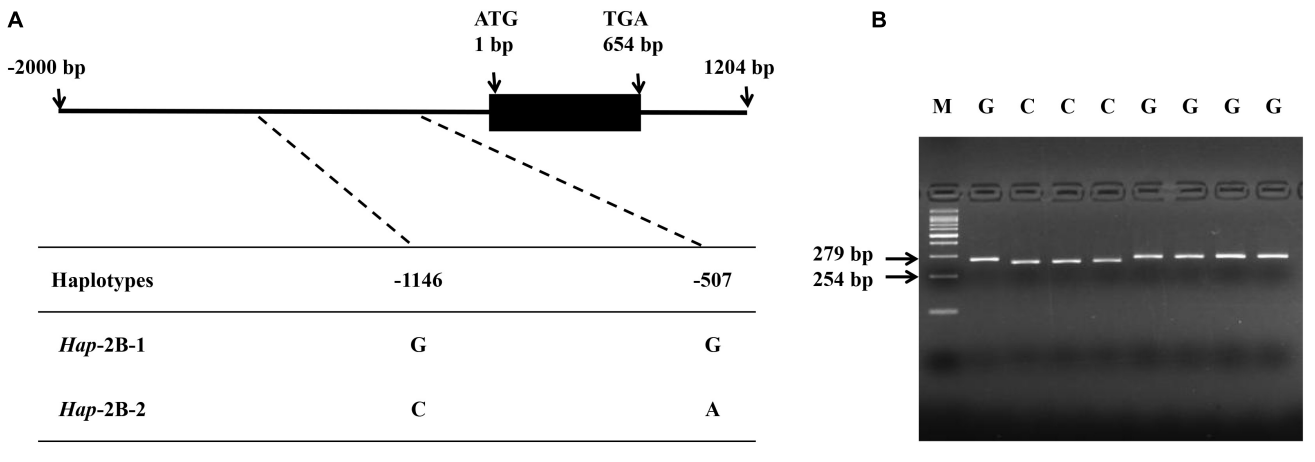


FIGURE 2 | Nucleotide polymorphisms and development of a molecular marker in wheat *TaPYL4-2B*. **(A)** Two single nucleotide polymorphisms (SNPs) were detected in the promoter region of *TaPYL4-2B*. **(B)** dCAPS marker was developed based on the –1146 bp SNP (G/C) with restriction endonuclease *Bam*HI, which cleaved the sequence only when the site was C. M, 100-bp DNA ladder.

TABLE 1 | *TaPYL4-2A* haplotypes associated with agronomic traits across 16 environments.

Environment	SL	PLE	PH	Environment	SL	PLE	PH
	P-value	*P*-value	*P*-value		*P*-value	*P*-value	*P*-value
2015-SY-WW-HS	0.00253**	0.00967**	n.s	2015-SY-DS-HS	6.21E-05***	0.03124*	n.s
2015-SY-WW	0.00859**	0.02429*	0.03729*	2015-SY-DS	0.00150**	0.02430*	0.01396*
2016-SY-WW-HS	2.76E-04***	0.02109*	n.s	2016-SY-DS-HS	0.00442**	0.00876**	0.02804*
2016-SY-WW	4.39E-04***	0.00569**	0.03819*	2016-SY-DS	0.00214**	7.60E-04***	0.02648*
2016-CP-WW	2.39E-04***	0.01006*	n.s	2016-CP-DS	4.01E-04***	0.00855**	0.04638*
2017-SY-WW-HS	0.00196**	0.01231*	n.s	2017-SY-DS-HS	0.00847**	n.s	n.s
2017-SY-WW	0.00253**	0.01257*	0.03924*	2017-SY-DS	0.00145**	0.00926**	0.01551*
2017-CP-WW	5.70E-04***	0.01732*	n.s	2017-CP-DS	0.00806**	n.s	n.s

*SY, Shunyi; CP, Changping; DS, drought stress; HS, heat stress; WW, well-watered; SL, spike length; PLE, peduncle length; PH, plant height; n.s, not significant. *P < 0.05, **P < 0.01, and ***P < 0.001.*

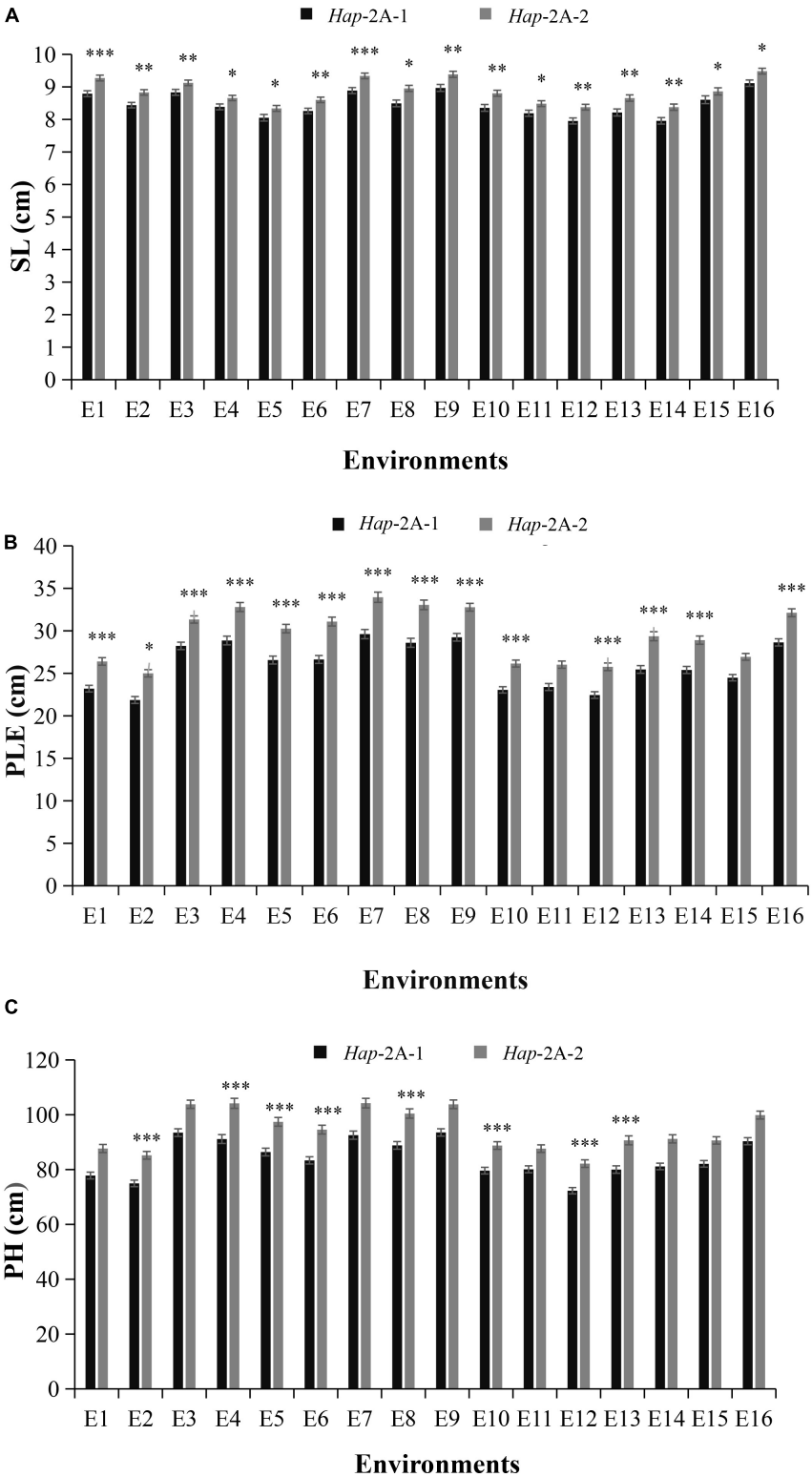


FIGURE 3 | Comparisons of agronomic traits in the two wheat *TaPYL4-2A* haplotypes *Hap*-2A-1 and *Hap*-2A-2. SL: spike length **(A)**; PLE: peduncle length **(B)**; PH: plant height **(C)**. E1–E16 indicated the environments of 2015-SY-DS-HS, 2015-SY-DS, 2015-SY-WW-HS, 2015-SY-WW, 2016-SY-DS-HS, 2016-SY-DS, 2016-SY-WW-HS, 2016-SY-WW, 2016-CP-WW, 2016-CP-DS, 2017-SY-DS-HS, 2017-SY-DS, 2017-SY-WW-HS, 2017-SY-WW, 2017-CP-DS, 2017-CP-WW, respectively. SY, Shunyi; CP, Changping; DS, drought stress; HS, heat stress; WW, well-watered; $^{*}P < 0.05$, $^{**}P < 0.01$, and $^{***}P < 0.001$, respectively. Error bars denote ± SE.

TABLE 2 | *TaPYL4-2B* haplotypes associated with agronomic traits across 16 environments.

Environment	PH	PLE	Environment	PH	PLE
	***P*-value**	***P*-value**		***P*-value**	***P*-value**
2015-SY-WW-HS	0.00141**	0.01614*	2015-SY-DS-HS	0.00734**	0.00340**
2015-SY-WW	n.s	n.s	2015-SY-DS	0.03998*	0.01702*
2016-SY-WW-HS	0.00136**	0.00721**	2016-SY-DS-HS	0.01330*	0.00412**
2016-SY-WW	0.00217**	0.00134**	2016-SY-DS	5.49E-04***	0.00172**
2016-CP-WW	0.01378*	0.00758**	2016-CP-DS	n.s	0.00792**
2017-SY-WW-HS	7.38E-04***	1.54E-04***	2017-SY-DS-HS	0.03369*	0.00205**
2017-SY-WW	0.00479**	9.98E-04***	2017-SY-DS	0.01239*	0.00214**
2017-CP-WW	0.04709*	0.00571**	2017-CP-DS	n.s	0.00913**

*SY, Shunyi; CP, Changping; DS, drought stress; HS, heat stress; WW, well-watered; SL, spike length; PLE, peduncle length; PH, plant height; n.s, not significant. *P < 0.05, **P < 0.01, and ***P < 0.001.*

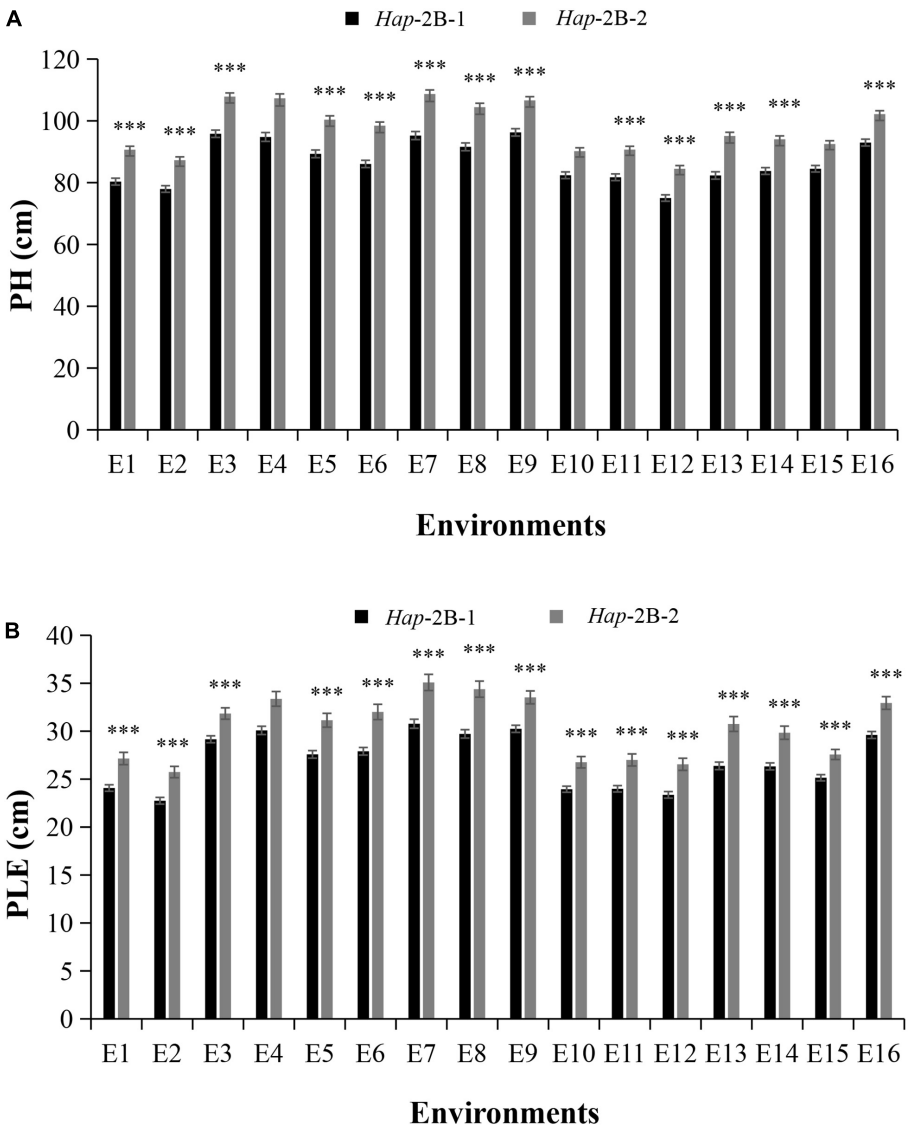


FIGURE 4 | Comparisons of agronomic traits in the two wheat *TaPYL4-2B* haplotypes *Hap*-2B-1 and *Hap*-2B-2. Agronomic traits included PH **(A),** PLE **(B)**. See footnote to **Figure 3** for abbreviations. ***$P < 0.001$. Error bars denote ± SE.

TaPYL4-2A and *TaPYL4-2B* Haplotypes Have Additive Effects on Plant Growth Related Traits

Since both *TaPYL4-2A* and *TaPYL4-2B* were associated with plant growth related traits (PH and PLE), we speculated that the *TaPYL4-2A* and *TaPYL4-2B* haplotypes may have a combinational effect on plant growth related traits. The present association studies showed that both *TaPYL4-2A* and *TaPYL4-2B* haplotypes can be divided into low PH and PLE haplotypes (*Hap*-2A-1 and *Hap*-2B-1) and high PH and PLE haplotypes (*Hap*-2A-2 and *Hap*-2B-2). Wheat accessions presenting these four combinations were divided into groups of low-/ low-, low-/ high-, high-/ low-, and high-/high-PH and PLE haplotypes, which were named as *Hap*-AB1, *Hap*-AB2, *Hap*-AB3, and *Hap*-AB4 (**Supplementary Table 5**), respectively. Among the four combinations, *Hap*-AB1 was associated with the lowest PLE (**Figure 5A**) and PH (**Figure 5B**) in Population 1, while *Hap*-AB4 associated with the highest PH and PLE. The plant growth related traits of *Hap*-AB2 was lower than that of *Hap*-AB3. These results demonstrated the *TaPYL4-2A* haplotypes had a larger contribution to plant growth related traits than the *TaPYL-2B* haplotypes' effects. Furthermore, an additive effect of the *TaPYL4-2A* and *TaPYL4-2B* haplotypes was detected to work on the regulation of plant growth.

Cis-Acting Element Analysis of Promoters of Two Different Haplotypes in *TaPYL4-2A* and *TaPYL4-2B*

Cis-acting elements in promoter region could reflect the function and regulatory mechanism of the genes. In order to further clarify the influence of polymorphic sites located in *TaPYL4-2A* and *TaPYL4-2B* promoter region, we used Plant CARE[2] to analyze the *cis*-acting elements in promoters of two haplotypes detected for *TaPYL4-2A* and *TaPYL4-2B,* respectively. Interestingly, an ARF binding site, TGA-element (AACGAC), was detected at −1635 bp upstream of the ATG translation starting point of *Hap*-2A-1. This *cis*-acting element was absent in the promoter of *Hap*-2A-2 due to a nucleotide variation (**Supplementary Figure 3**). However, in the promoter regions of two haplotypes of *TaPYL4-2B,* there was no difference in

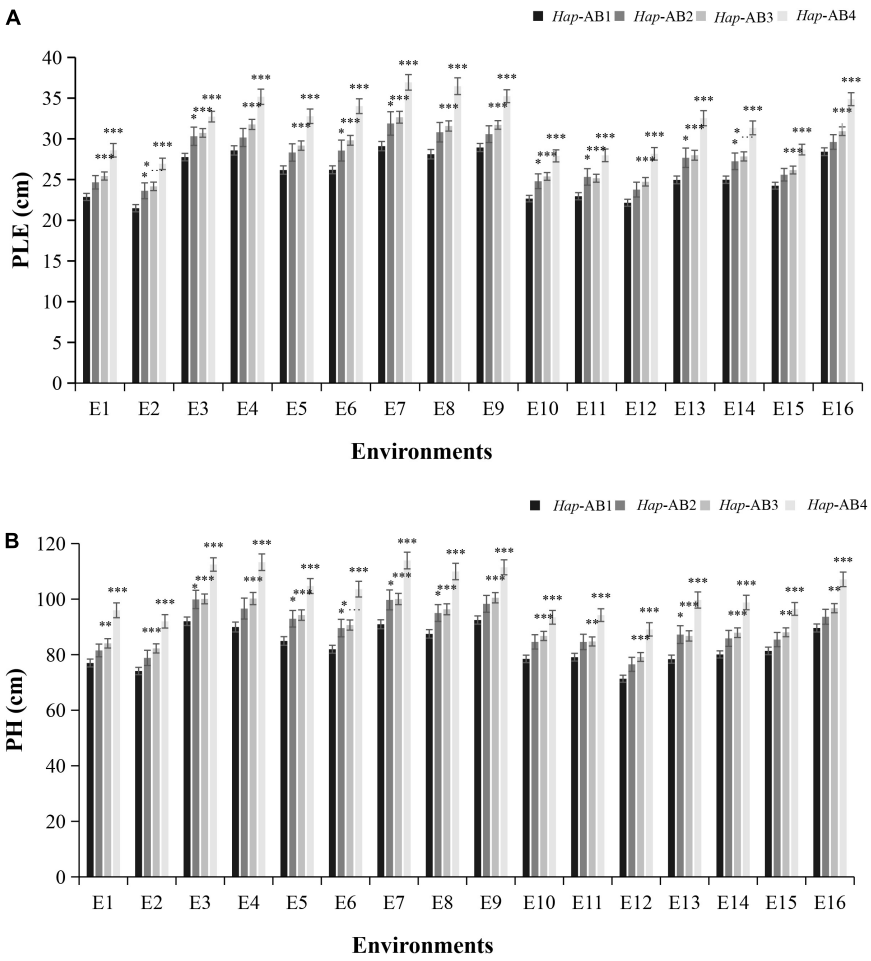


FIGURE 5 | Combination of the *TaPYL4-2A* and *TaPYL4-2B* haplotypes with different effects in plant growth. Association of combinational haplotypes (*Hap*-AB1∼*Hap*-AB4) with PH **(A)** and PLE **(B)** in Population 1. $^{*}P < 0.05$, $^{**}P < 0.01$, and $^{***}P < 0.001$, respectively. Error bars denote ± SE.

cis-acting elements related to plant growth and development (**Supplementary Figure 4**).

Expression Pattern of *TaPYL4-2A* in Various Wheat Tissues

Since the nucleotide variation site is located in the *TaPYL4-2A* promoter region, we further examined the impacts of this variation on the gene expression. The expression pattern of *TaPYL4-2A* gene was identified by real-time PCR at different stages of growth, showing that *TaPYL4-2A* was constitutively expressed in various tissues tested (**Figure 6A**).

The 12 wheat accessions representing two haplotypes of *TaPYL4-2A* were randomly selected from Population 1 and planted in the field. After 20 days of growth, shoot samples were taken for measuring the expression of *TaPYL4-2A*. Notably, the expression level of *TaPYL4-2A* in *Hap*-2A-1 wheat accessions was higher than that in *Hap*-2A-2 wheat accessions (**Figure 6B**).

Association analysis and expression patterns indicated that the expression level of *TaPYL4-2A* was high in *Hap*-2A-1 wheat accessions with shorter SL and PLE as well as shorter PH. On the contrary, the low expression of *Hap*-2A-2 was detected in the accessions with longer SL and PLE as well as taller PH. Therefore, *TaPYL4-2A* gene expression might be negatively correlated with plant growth-related traits.

TaARF4 Regulates *TaPYL4-2A* Expression by Binding to the Promoter Region

Previous reports showed that ARF7 and ARF19 could be bound to the TGA-element in *Arabidopsis* (Huang et al., 2018).

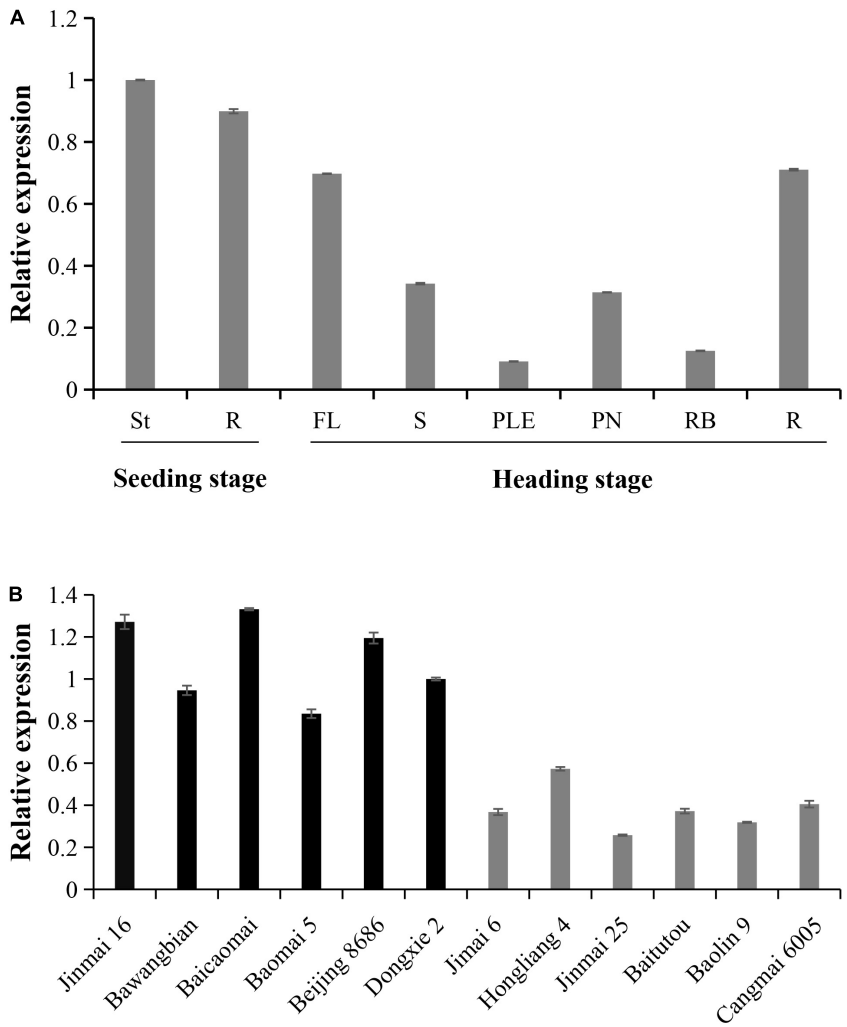


FIGURE 6 | Expression patterns of the wheat *TaPYL-2A* haplotypes *Hap*-2A-1 and *Hap*-2A-2. **(A)** Tissue expression patterns of *TaPYL4-2A* were detected in the Chinese Spring by real-time PCR. St, shoot; R, root; at seedling stage. FL, flag leaves; S, spikes; PN, penultimate nodes; RB, root bases; R, root; at heading stage. The values were relative to St, which was set as 1. Error bars denote ± SE. **(B)** Expression pattern of *TaPYL-2A* in two genotype accessions at seedling stage. Jinmai 16, Bawangbian, Baicaomai, Baomai 5, Beijing 8686, and Dongxie 2 belong to *Hap*-2A-1. Jimai 6, Hongliang 4, Jinmai 25, Baitutou, Baolin 9, and Cangmai 6005 belong to *Hap*-2A-2. The values were relative to Dongxie 2, which was set as 1. Error bars denote ± SE.

TaARF4 was related to plant height in wheat (Wang et al., 2019b). Therefore, we speculated that *TaARF4* may regulate the expression of *TaPYL4-2A*. Yeast one-hybrid assays were carried out to determine whether TaARF4 binds to the promoter region of *TaPYL4-2A*. The *TaARF4* DNA binding region was cloned into pB42AD vector. The promoter regions of the haplotype

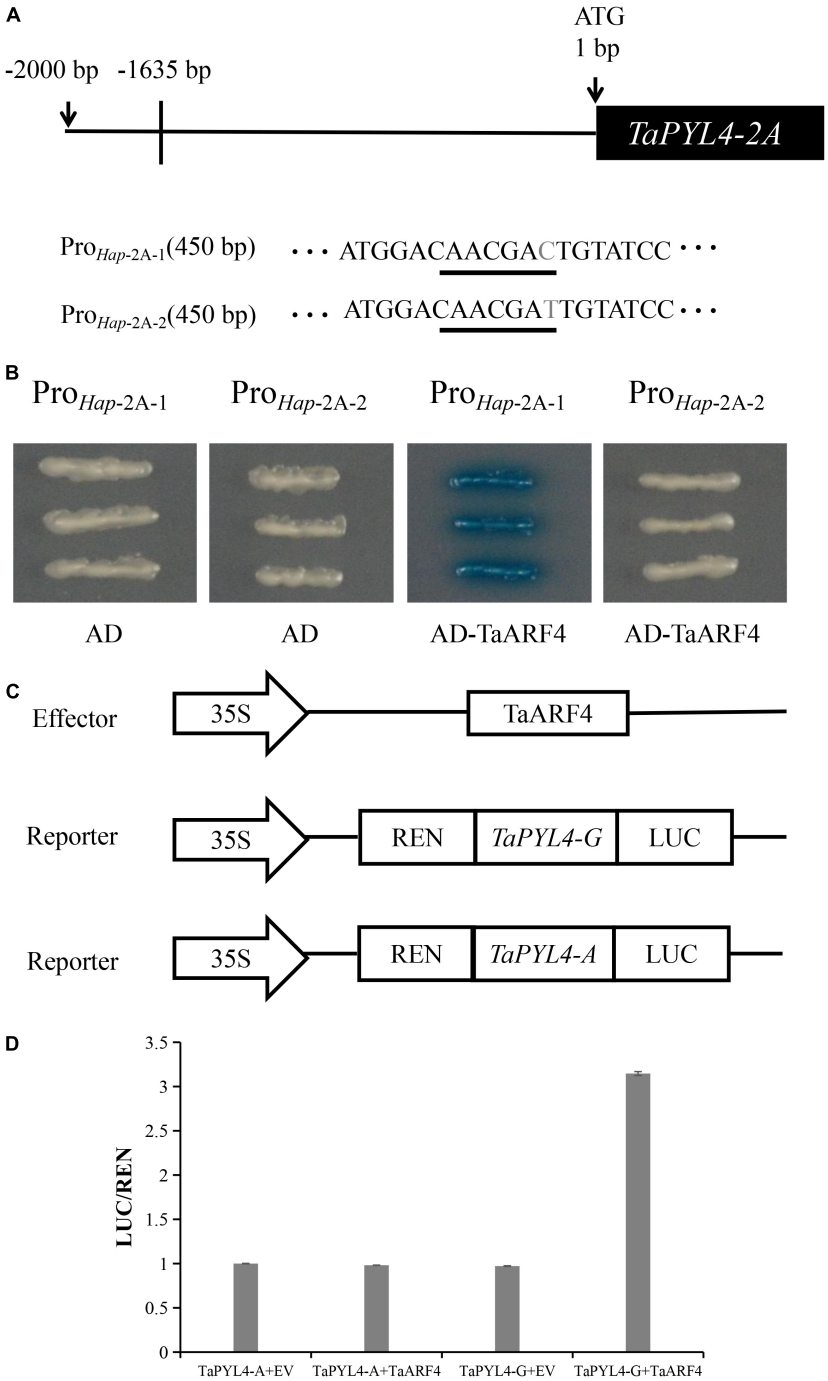


FIGURE 7 | TaARF4 binds to the wheat *TaPYL4-2A* of *Hap*-2A-1 promoter region. **(A)** Schematic diagram of *Hap*-2A-1 of *TaPYL4-2A*. Underlined letters indicated the TGA-element. Letter in gray was the single-nucleotide polymorphism site (G/A). **(B)** Yeast one-hybrid assays of TaARF4 and *TaPYL4-2A* two haplotype promoters. **(C)** Dual-luciferase assay of transformed tobacco leaves to detect the interaction between TaARF4 and the *TaPYL4-2A* promoter. Schematic diagrams of the effector and reporter constructs are performed. *TaARF4* was cloned into the effector construct pCAMBIA1300 and the *TaPYL4-2A* two haplotype promoters were inserted into the reporter vector pGreen II 0800-LUC. Agrobacterium combine with vector pSoup containing reporter and effector or with empty carrier (EV) after transformation, infiltrate into leaves together. **(D)** Promoter activities were shown as the ratio of LUC to REN. Data are means (± SE) of three biological replicates.

TaPYL4-2A with and without the TGA-element were cloned into the pLacZi, separately (**Figure 7A**). In order to identify the interaction between promoters and TaARF4, the plasmid containing each of these 2 promoter regions was transformed into yeast EGY48 with *TaARF4* plasmid, respectively. Positive yeast EGY48 cells were cultured on the selective medium of x-gal without Ura and Trp. In the presence of TGA-element in *Hap*-2A-1 of *TaPYL4-2A*, TaARF4 were successfully bound to the promoter to activate the expression of LacZ reporter gene. However, in the absence of TGA-element in *Hap*-2A-2 of *TaPYL4-2A*, TaARF4 could not bind the promoter to activate the LacZ reporter gene (**Figure 7B**). The results indicate that due to the difference of A/G at −1635 bp upstream of ATG translation starting point, TaARF4 could bind to the promoter region of *Hap*-2A-1, but not to the promoter region of *Hap*-2A-2.

We also performed a LUC experiment for further verification. Dual luciferase assays illustrated that LUC activity was higher than that of the negative control in the presence of TaARF4 effector and *TaPYL4-2A* promoter containing TGA-element (**Figures 7C,D**). On the contrary, LUC activity was similar to that of the negative control in the presence of TaARF4 effector and *TaPYL4-2A* promoter without the TGA-element. These results again indicated that TaARF4 functions as a transcription activator for *Hap*-2A-1, but not for *Hap*-2A-2.

Geographical and Temporal Distribution of *TaPYL4-2A* and *TaPYL4-2B* Haplotypes Among the Wheat Varieties Cultivated in China

According to the regional climate characteristics, topography, cultivation characteristics, sowing and maturity stage, Chinese wheat planting regions were divided into 10 major ecological areas (Zhang et al., 2002). From Chinese landraces to modern cultivars, the proportion of *Hap*-AB1 was increased significantly in regions I, II, VI, and IX, but not significantly changed in wheat regions III, IV, and V (**Figures 8A,B**). The mean PH in modern wheat varieties released in China from the 1940s to the 1990s has been reduced from 121.50 cm to 80.08 cm, and this change was associated with the increasing of proportion of haplotype *Hap*-AB1 from 16.70 to 72.41% (**Figure 8C**). To sum up, *Hap*-AB1 was selected by wheat breeders in the past decades, showing a considerable utilization potential in wheat genetic improvement.

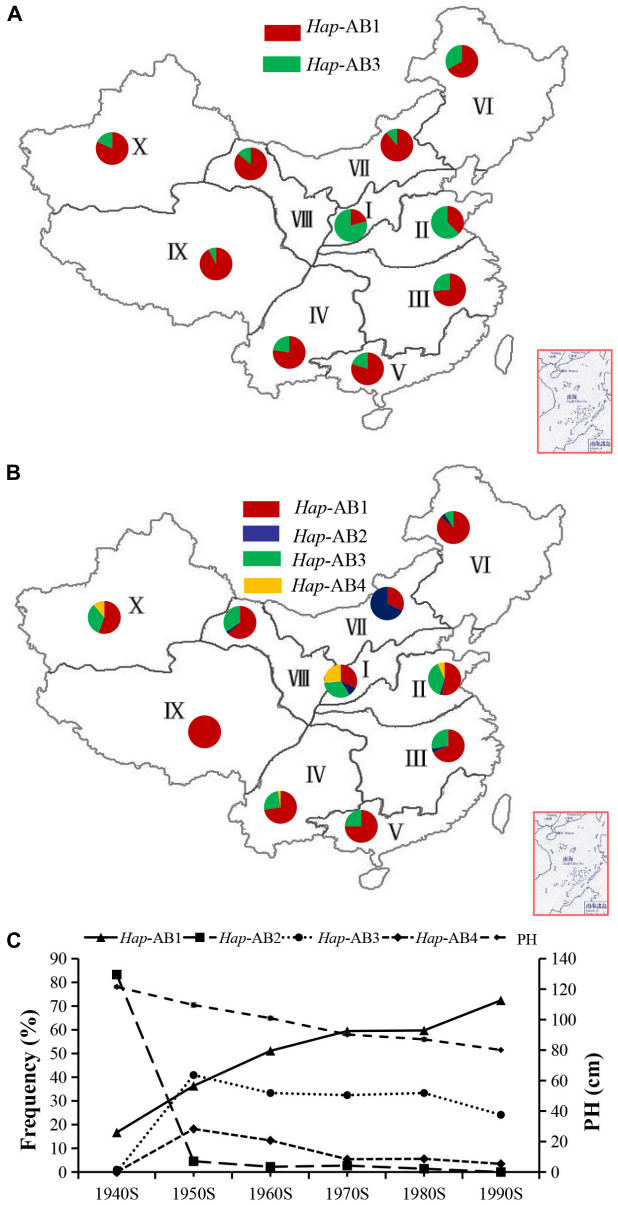


FIGURE 8 | Haplotype distribution and frequency change of *TaPYL4-2A* and *TaPYL4-2B* in 10 wheat-producing regions across China. **(A)** Distributions of *TaPYL4-2A* and *TaPYL4-2B* haplotypes (*Hap*-AB1∼*Hap*-AB4) in 157 Chinese landraces. **(B)** Distributions of *TaPYL4-2A* and *TaPYL4-2B* haplotypes (*Hap*-AB1∼*Hap*-AB4) in 348 modern cultivars. I, Northern winter wheat region; II, Yellow and Huai River valley winter wheat region; III, Low and middle Yangtze River valley winter wheat region; IV, Southwestern winter wheat region; V, Southern winter wheat region; VI, Northeastern spring wheat region; VII, Northern spring wheat region; VIII, Northwestern spring wheat region; IX, Qinghai-Tibet spring-winter wheat region; X, Xinjiang winter-spring wheat region. **(C)** Haplotype frequency and PH (cm) change of *Hap*-AB1∼*Hap*-AB4 in 348 modern cultivars of Chinese major wheat zones. The data for PH (cm) are from Hao et al. (2011a).

DISCUSSION

Since the Green Revolution, breeders have been trying to develop the ideal plant architecture to increase wheat yield. As a consequence, it is vitally significant to reveal the molecular mechanism of the plant development. In the present study, we found that *TaPYL4-2A* and *TaPYL4-2B* contributed to the growth-related traits such as spike length (SL), peduncle length (PLE) and plant height (PH) in wheat. No polymorphism was detected for *TaPYL4-2D* among the wheat accessions tested. It is unclear whether *TaPYL4-2D* affects plant height, which needs further study. Our data demonstrated that TaARF4 could activate

expression of *Hap*-2A-1 of *TaPYL4-2A* by binding to the *cis*-acting element in the promoter. Therefore, *TaPYL4* might play an important role in controlling the growth and development of plants.

ABA receptors are important signaling molecules in plant ABA signaling pathways. They could activate transcription factors in downstream of signaling pathways and regulate the expression of the related genes, thus participating in plant growth and stress responses (Tian et al., 2015). Previously, *Arabidopsis* plants overexpressing *PYL9/RCAR1*, *PYL5/RCAR8,* or *PYL8/RCAR3* were reported to have a significant increase in drought tolerance and more sensitive to ABA during seed germination, vegetative growth, stomatal movement and other physiological processes (Fujii et al., 2009; Santiago et al., 2009). In rice, *OsPYL4* and *OsPYL/RCAR5* were identified to play important roles in plant development (Kim et al., 2014; Miao et al., 2018). In wheat, *TaPYL4*-overexpressed lines showed significant increase in grain yield compared to the control under the condition of insufficient water (Mega et al., 2019). More importantly, our study indicated that *TaPYL4* functions in the morphogenesis of plant growth-related traits, suggesting that *TaPYL4* can balance wheat stress resistance and plant growth.

ABA is a versatile hormone. For example, ABA and auxin could co-regulate root growth to adapt to the changing environment (De Smet et al., 2003; Overvoorde et al., 2010; Zhao et al., 2014). Auxin enhanced ABA signaling through ARF10 and ARF16-mediated activation of *ABI3* expression in regulating lateral root formation and seed dormancy (Brady et al., 2003; Liu et al., 2013). AtPYL8 was revealed to regulate lateral root growth by enhancing transcription of auxin responsive genes (Zhao et al., 2014). Recently, ARF7 and ARF19 transcription factors were examined to bind to TGA-element to regulate the expression of downstream genes (Huang et al., 2018). TaARF4 were linked to plant height (Wang et al., 2019b). Thus, it could be inferred that auxin response factors were related to ABA receptors. Our data demonstrated that TaARF4 could bind to the promoter region of *Hap*-2A-1 of *TaPYL4-2A* to activate the expression of *TaPYL4-2A* (**Figure 7**). In wheat materials having *Hap*-2A-1, *TaPYL4-2A* expression was high, but plant growth-related traits were low. On the contrary, *TaPYL4-2A* expression in *Hap*-2A-2 was low whereas plant growth-related traits were high (**Supplementary Figure 5**). These studies revealed that TaARF4 regulates *TaPYL4-2A* gene expression to affect plant growth-related traits. However, whether TaARF4 and TaPYL4-2A affect the content of ABA and auxin is still unclear. Further study needs to focus on this regard.

Association analysis showed that *TaPYL4-2B* gene was also closely related to PLE and PH. Additive effects were detected for *TaPYL4-2A* and *TaPYL4-2B*. However, no difference in *cis*-acting elements of two *TaPYL4-2B* haplotype's promoters was found to be related to plant growth and development. More studies are needed to clarify the molecular mechanism underlying plant growth and development of *TaPYL4-2B*. At present, no polymorphism was detected for *TaPYL4-2D*, and this gene function has not been elaborated. Furthermore, *TaPYL4-2D* was structurally conservative, implying that its function may be important to other traits.

Marker-assisted selection is recognized as an efficient method to accelerate wheat breeding process (Liu et al., 2012). Here, we analyzed polymorphisms in *TaPYL4-2A* and *TaPYL4-2B*, and consequently developed the functional molecular markers to identify different haplotypes associated with plant growth-related traits. Therefore, these markers could be used in marker-assisted selection to breed wheat varieties with more suitable plant architecture despite the frequency of the favorable *Hap*-AB1 allele was increased from 16.70 to 72.41% in modern wheat varieties.

In conclusion, the coding sequence of *TaPYL4* gene (*TaPYL4-2A*, *TaPYL4-2B*, and *TaPYL4-2D*) is highly conserved. Nucleotide variations were identified in *TaPYL4-2A* and *TaPYL4-2B*'s promoter regions. Based on the SNP at position−1635 (G/A) of *TaPYL4-2A* and −1146 (G/C) of *TaPYL4-2B*, two haplotypes were detected, respectively. TaARF4 could activate the expression of *TaPYL4-2A* by binding to the promoter region of *Hap*-2A-1 of *TaPYL4-2A*. Remarkably, the combinational haplotype *Hap*-AB1 was positively associated with low PH. This *Hap*-AB1 haplotype was broadly selected in wheat breeding during the last decades. The functional marker developed for *Hap*-AB1 can be used in wheat genetic improvement to develop the ideal plant architecture with high grain yield.

DATA AVAILABILITY STATEMENT

The authors acknowledge that the data presented in this study must be deposited and made publicly available in an acceptable repository, prior to publication. Frontiers cannot accept a manuscript that does not adhere to our open data policies.

AUTHOR CONTRIBUTIONS

RJ, JW, and RL conceived the idea and revised the manuscript. YX, JW, XM, CL, XC, and XY performed the experiments. YX, JW, LL, XM, CH, and RJ analyzed the data. YX wrote the manuscript. All authors contributed to the article and approved the submitted version.

FUNDING

This research was supported by the National Key R&D Program of China (2017YFD0300202) and the Shanxi Province Key Projects of Coal-based Science and Technology (FT-2014-01).

SUPPLEMENTARY MATERIAL

The Supplementary Material for this article can be found online at: https://www.frontiersin.org/articles/10.3389/fpls.2021.641087/full#supplementary-material

REFERENCES

Brady, S. M., Sarkar, S. F., Bonetta, D., and McCourt, P. (2003). The ABSCISIC ACID INSENSITIVE 3 (ABI3) gene is modulated by farnesylation and is involved in auxin signaling and lateral root development in *Arabidopsis*. *Plant J.* 34, 67–75. doi: 10.1046/j.1365-313x.2003.01707.x

Buss, W., Ford, B. A., Foo, E., Schnippenkoetter, W., Borrill, P., Brooks, B., et al. (2020). Overgrowth mutants determine the causal role of GA2oxidaseA13 in Rht12 dwarfism of wheat. *J. Exp. Bot.* 71, 7171–7178. doi: 10.1093/jxb/eraa443

De Smet, I., Signora, L., Beeckman, T., Inze, D., Foyer, C. H., and Zhang, H. (2003). An abscisic acid-sensitive checkpoint in lateral root development of *Arabidopsis*. *Plant J.* 33, 543–555. doi: 10.1046/j.1365-313x.2003.01652.x

Dittrich, M., Mueller, H. M., Bauer, H., Peirats-Llobet, M., Rodriguez, P. L., Geilfus, C. M., et al. (2019). The role of Arabidopsis ABA receptors from the PYR/PYL/RCAR family in stomatal acclimation and closure signal integration. *Nat. Plants* 5, 1002–1011. doi: 10.1038/s41477-019-0490-0

Dong, H., Yan, S., Liu, J., Liu, P., and Sun, J. (2019). TaCOLD1 defines a new regulator of plant height in bread wheat. *Plant Biotech. J.* 17, 687–699. doi: 10.1111/pbi.13008

Fujii, H., Chinnusamy, V., Rodrigues, A., Rubio, S., Antoni, R., Park, S. Y., et al. (2009). In vitro reconstitution of an abscisic acid signalling pathway. *Nature* 462, 660–664. doi: 10.1038/nature08599

Hao, C., Wang, L., Ge, H., Dong, Y., and Zhang, X. (2011a). Genetic diversity and linkage disequilibrium in Chinese bread wheat (*Triticum aestivum* L.) revealed by SSR markers. *PLoS One* 6:e17279. doi: 10.1371/journal.pone.0017279

Hao, Q., Yin, P., Li, W., Wang, L., Yan, C., Lin, Z., et al. (2011b). The molecular basis of ABA-independent inhibition of PP2Cs by a subclass of PYL proteins. *Mol. Cell* 42, 662–672. doi: 10.1016/j.molcel.2011.05.011

Huang, K. L., Ma, G. J., Zhang, M. L., Xiong, H., Wu, H., Zhao, C. Z., et al. (2018). The ARF7 and ARF19 transcription factors positively regulate PHOSPHATE STARVATION RESPONSE1 in *Arabidopsis* roots. *Plant Physiol.* 178, 413–427. doi: 10.1104/pp.17.01713

Kim, H., Lee, K., Hwang, H., Bhatnagar, N., Kim, D. Y., Yoon, I. S., et al. (2014). Overexpression of PYL5 in rice enhances drought tolerance, inhibits growth, and modulates gene expression. *J. Exp. Bot.* 65, 453–464. doi: 10.1093/jxb/ert397

Klingler, J. P., Batelli, G., and Zhu, J. K. (2010). ABA receptors: the START of a new paradigm in phytohormone signalling. *J. Exp. Bot.* 61, 3199–3210. doi: 10.1093/jxb/erq151

Li, L., Mao, X., Wang, J., Chang, X., Reynolds, M., and Jing, R. (2019a). Genetic dissection of drought and heat-responsive agronomic traits in wheat. *Plant Cell Environ.* 42, 2540–2553. doi: 10.1111/pce.13577

Li, L., Peng, Z., Mao, X., Wang, J., Chang, X., Reynolds, M., et al. (2019b). Genome-wide association study reveals genomic regions controlling root and shoot traits at late growth stages in wheat. *Ann. Bot.* 124, 993–1006. doi: 10.1093/aob/mcz041

Li, W., Wang, L., Sheng, X., Yan, C., Zhou, R., Hang, J., et al. (2013). Molecular basis for the selective and ABA-independent inhibition of PP2CA by PYL13. *Cell Res.* 23, 1369–1379. doi: 10.1038/cr.2013.143

Li, Y., Xiao, J., Wu, J., Duan, J., Liu, Y., Ye, X., et al. (2012). A tandem segmental duplication (TSD) in green revolution gene Rht-D1b region underlies plant height variation. *New Phytol.* 196, 282–291. doi: 10.1111/j.1469-8137.2012.04243.x

Lin, R., Ding, L., Casola, C., Ripoll, D. R., Feschotte, C., and Wang, H. (2007). Transposase-derived transcription factors regulate light signaling in *Arabidopsis*. *Science* 318, 1302–1305. doi: 10.1126/science.1146281

Liu, X., Zhang, H., Zhao, Y., Feng, Z., Li, Q., Yang, H. Q., et al. (2013). Auxin controls seed dormancy through stimulation of abscisic acid signaling by inducing ARF-mediated ABI3 activation in *Arabidopsis*. *Proc. Natl. Acad. Sci. U.S.A.* 110, 15485–15490. doi: 10.1073/pnas.1304651110

Liu, Y., He, Z., Appels, R., and Xia, X. (2012). Functional markers in wheat: current status and future prospects. *Theor. Appl. Genet.* 125, 1–10. doi: 10.1007/s00122-012-1829-3

Ma, Y., Szostkiewicz, I., Korte, A., Moes, D., Yang, Y., Christmann, A., et al. (2009). Regulators of PP2C phosphatase activity function as abscisic acid sensors. *Science* 324, 1064–1068. doi: 10.1126/science.1172408

Mega, R., Abe, F., Kim, J. S., Tsuboi, Y., Tanaka, K., Kobayashi, H., et al. (2019). Tuning water-use efficiency and drought tolerance in wheat using abscisic acid receptors. *Nat. Plants* 5, 153–159. doi: 10.1038/s41477-019-0361-8

Miao, C., Xiao, L., Hua, K., Zou, C., Zhao, Y., Bressan, R. A., et al. (2018). Mutations in a subfamily of abscisic acid receptor genes promote rice growth and productivity. *Proc. Natl. Acad. Sci. U.S.A.* 115, 6058–6063. doi: 10.1073/pnas.1804774115

Nakashima, K., Fujita, Y., Kanamori, N., Katagiri, T., Umezawa, T., Kidokoro, S., et al. (2009). Three Arabidopsis SnRK2 protein kinases, SRK2D/SnRK2.2, SRK2E/SnRK2.6/OST1 and SRK2I/SnRK2.3, involved in ABA signaling are essential for the control of seed development and dormancy. *Plant Cell Physiol.* 50, 1345–1363. doi: 10.1093/pcp/pcp083

Overvoorde, P., Fukaki, H., and Beeckman, T. (2010). Auxin control of root development. *Cold Spring Harbor Perspect. Biol.* 2:a001537. doi: 10.1101/cshperspect.a001537

Park, S. Y., Fung, P., Nishimura, N., Jensen, D. R., Fujii, H., Zhao, Y., et al. (2009). Abscisic acid inhibits type 2C protein phosphatases via the PYR/PYL family of START proteins. *Science* 324, 1068–1071. doi: 10.1126/science.1173041

Peng, J., Richards, D. E., Hartley, N. M., Murphy, G. P., Devos, K. M., Flintham, J. E., et al. (1999). 'Green revolution' genes encode mutant gibberellin response modulators. *Nature* 400, 256–261. doi: 10.1038/22307

Santiago, J., Rodrigues, A., Saez, A., Rubio, S., Antoni, R., Dupeux, F., et al. (2009). Modulation of drought resistance by the abscisic acid receptor PYL5 through inhibition of clade a PP2Cs. *Plant J.* 60, 575–588. doi: 10.1111/j.1365-313X.2009.03981.x

Saville, R. J., Gosman, N., Burt, C. J., Makepeace, J., Steed, A., Corbitt, M., et al. (2012). The 'Green Revolution' dwarfing genes play a role in disease resistance in *Triticum aestivum* and *Hordeum vulgare*. *J. Exp. Bot.* 63, 1271–1283. doi: 10.1093/jxb/err350

Stewart, C., and Via, L. E. J. B. (1993). A rapid CTAB DNA isolation technique useful for RAPD fingerprinting and other PCR applications. *Biotechniques* 14, 748–750.

Su, Q., Zhang, X., Zhang, W., Zhang, N., Song, L., Liu, L., et al. (2018). QTL detection for kernel size and weight in bread wheat (*Triticum aestivum* L.) using a high-density SNP and SSR-based linkage map. *Front. Plant Sci.* 9:1484. doi: 10.3389/fpls.2018.01484

Tang, T., Botwright Acuna, T., Spielmeyer, W., and Richards, R. A. (2020). Effect of GA sensitive Rht18 and GA insensitive Rht-D1b dwarfing genes on vegetative and reproductive growth in bread wheat. *J. Exp. Bot.* 72, 445–458. doi: 10.1093/jxb/eraa481

Tian, X., Wang, Z., Li, X., Lv, T., Liu, H., Wang, L., et al. (2015). Characterization and functional analysis of pyrabactin resistance-like abscisic acid receptor family in rice. *Rice* 8:28. doi: 10.1186/s12284-015-0061-6

Van De Velde, K., Chandler, P. M., Van Der Straeten, D., and Rohde, A. (2017). Differential coupling of gibberellin responses by Rht-B1c suppressor alleles and Rht-B1b in wheat highlights a unique role for the DELLA N-terminus in dormancy. *J. Exp. Bot.* 68, 443–455. doi: 10.1093/jxb/erw471

Vishwakarma, K., Upadhyay, N., Kumar, N., Yadav, G., Singh, J., Mishra, R. K., et al. (2017). Abscisic acid signaling and abiotic stress tolerance in plants: a review on current knowledge and future prospects. *Front. Plant Sci.* 8:161. doi: 10.3389/fpls.2017.00161

Wang, H., Wang, S., Chang, X., Hao, C., Sun, D., and Jing, R. (2019a). Identification of TaPPH-7A haplotypes and development of a molecular marker associated with important agronomic traits in common wheat. *BMC Plant Biol.* 19:296. doi: 10.1186/s12870-019-1901-0

Wang, J., Li, Q., Mao, X., Li, A., and Jing, R. (2016). Wheat transcription factor TaAREB3 participates in drought and freezing tolerances in *Arabidopsis*. *Int. J. Biol. Sci.* 12, 257–269. doi: 10.7150/ijbs.13538

Wang, J., Wang, R., Mao, X., Li, L., Chang, X., Zhang, X., et al. (2019b). TaARF4 genes are linked to root growth and plant height in wheat. *Ann. Bot.* 124, 903–915. doi: 10.1093/aob/mcy218

Wang, J., Wang, R., Mao, X., Zhang, J., Liu, Y., Xie, Q., et al. (2020). RING finger ubiquitin E3 ligase gene TaSDIR1-4A contributes to determination of grain size in common wheat. *J. Exp. Bot.* 71, 5377–5388. doi: 10.1093/jxb/eraa271

Zhang, B., Shi, W., Li, W., Chang, X., and Jing, R. (2013). Efficacy of pyramiding elite alleles for dynamic development of plant height in common wheat. *Mol. Breed.* 32, 327–338. doi: 10.1007/s11032-013-9873-5

Zhang, B., Xu, W., Liu, X., Mao, X., Li, A., Wang, J., et al. (2017). Functional conservation and divergence among homoeologs of TaSPL20 and TaSPL21, two SBP-box genes governing yield-related traits in hexaploid wheat. *Plant Physiol.* 174, 1177–1191. doi: 10.1104/pp.17.00113

Zhang, X. Y., Li, C. W., Wang, L. F., Wang, H. M., You, G. X., and Dong, Y. S. (2002). An estimation of the minimum number of SSR alleles needed to reveal genetic relationships in wheat varieties. I. Information from large-scale planted varieties and cornerstone breeding parents in Chinese wheat improvement and production. *Theor. Appl. Genet.* 106, 112–117. doi: 10.1007/s00122-002-1016-z

Zhao, H., Nie, K., Zhou, H., Yan, X., Zhan, Q., Zheng, Y., et al. (2020). ABI5 modulates seed germination via feedback regulation of the expression of the PYR/PYL/RCAR ABA receptor genes. *New Phytol.* 228, 596–608. doi: 10.1111/nph.16713

Zhao, Y., Chan, Z., Gao, J., Xing, L., Cao, M., Yu, C., et al. (2016). ABA receptor PYL9 promotes drought resistance and leaf senescence. *Proc. Natl. Acad. Sci. U.S.A.* 113, 1949–1954. doi: 10.1073/pnas.1522840113

Zhao, Y., Xing, L., Wang, X., Hou, Y. J., Gao, J., Wang, P., et al. (2014). The ABA receptor PYL8 promotes lateral root growth by enhancing MYB77-dependent transcription of auxin-responsive genes. *Sci. Signal.* 7:ra53. doi: 10.1126/scisignal.2005051

Zhao, Y., Zhang, Z., Gao, J., Wang, P., Hu, T., Wang, Z., et al. (2018). *Arabidopsis* duodecuple mutant of PYL ABA receptors reveals PYL repression of ABA-Independent SnRK2 activity. *Cell Rep.* 23, 3340–3351.e3345. doi: 10.1016/j.celrep.2018.05.044

Conflict of Interest: The authors declare that the research was conducted in the absence of any commercial or financial relationships that could be construed as a potential conflict of interest.

Publisher's Note: All claims expressed in this article are solely those of the authors and do not necessarily represent those of their affiliated organizations, or those of the publisher, the editors and the reviewers. Any product that may be evaluated in this article, or claim that may be made by its manufacturer, is not guaranteed or endorsed by the publisher.

Copyright © 2021 Xue, Wang, Mao, Li, Li, Yang, Hao, Chang, Li and Jing. This is an open-access article distributed under the terms of the Creative Commons Attribution License (CC BY). The use, distribution or reproduction in other forums is permitted, provided the original author(s) and the copyright owner(s) are credited and that the original publication in this journal is cited, in accordance with accepted academic practice. No use, distribution or reproduction is permitted which does not comply with these terms.

frontiers in Plant Science

ORIGINAL RESEARCH
published: 07 September 2021
doi: 10.3389/fpls.2021.629776

Laccase Directed Lignification Is One of the Major Processes Associated With the Defense Response Against *Pythium ultimum* Infection in Apple Roots

Yanmin Zhu[1†], Guanliang Li[2†], Jugpreet Singh[3†], Awais Khan[3], Gennaro Fazio[4], Melody Saltzgiver[1] and Rui Xia[2*]*

[1] Tree Fruit Research Laboratory, USDA-ARS, Wenatchee, WA, United States, [2] College of Horticulture, South China Agricultural University, Guangzhou, China, [3] Plant Pathology and Plant-Microbe Biology Section, Cornell University, Geneva, NY, United States, [4] Plant Genetic Resources Unit, USDA-ARS, Geneva, NY, United States

OPEN ACCESS

Edited by:
Magdalena Arasimowicz-Jelonek, Adam Mickiewicz University, Poland

Reviewed by:
Mickael Malnoy, Fondazione Edmund Mach, Italy
Laura Ellen Rose, Heinrich Heine University Düsseldorf, Germany
Sophie De Vries, Heinrich Heine University Düsseldorf, Germany, in collaboration with reviewer LR

***Correspondence:**
Yanmin Zhu
yanmin.zhu@ars.usda.gov
Rui Xia
rxia@scau.edu.cn

[†] These authors have contributed equally to this work

Specialty section:
This article was submitted to Plant Pathogen Interactions, a section of the journal Frontiers in Plant Science

Received: 15 November 2020
Accepted: 09 August 2021
Published: 07 September 2021

Citation:
Zhu Y, Li G, Singh J, Khan A, Fazio G, Saltzgiver M and Xia R (2021) Laccase Directed Lignification Is One of the Major Processes Associated With the Defense Response Against Pythium ultimum Infection in Apple Roots. Front. Plant Sci. 12:629776. doi: 10.3389/fpls.2021.629776

Apple replant disease (ARD), incited by a pathogen complex including *Pythium ultimum,* causes stunted growth or death of newly planted trees at replant sites. Development and deployment of resistant or tolerant rootstocks offers a cost-effective, ecologically friendly, and durable approach for ARD management. Maximized exploitation of natural resistance requires integrated efforts to identify key regulatory mechanisms underlying resistance traits in apple. In this study, miRNA profiling and degradome sequencing identified major miRNA pathways and candidate genes using six apple rootstock genotypes with contrasting phenotypes to *P. ultimum* infection. The comprehensive RNA-seq dataset offered an expansive view of post-transcriptional regulation of apple root defense activation in response to infection from *P. ultimum*. Several pairs of miRNA families and their corresponding targets were identified for their roles in defense response in apple roots, including miR397-laccase, miR398-superoxide dismutase, miR10986-polyphenol oxidase, miR482-resistance genes, and miR160-auxin response factor. Of these families, the genotype-specific expression patterns of miR397 indicated its fundamental role in developing defense response patterns to *P. ultimum* infection. Combined with other identified copper proteins, the importance of cellular fortification, such as lignification of root tissues by the action of laccase, may critically contribute to genotype-specific resistance traits. Our findings suggest that quick and enhanced lignification of apple roots may significantly impede pathogen penetration and minimize the disruption of effective defense activation in roots of resistant genotypes. The identified target miRNA species and target genes consist of a valuable resource for subsequent functional analysis of their roles during interaction between apple roots and *P. ultimum*.

Keywords: apple root, soilborne pathogens, defense activation, plant resistance, small RNA profiling, degradome sequencing, post-transcriptional regulation

INTRODUCTION

Apple replant disease (ARD) is defined by the stunted growth or possible death of newly planted trees in replant sites, where continuous cultivation of apples or closely related species leads to pathogen inoculum accumulation. ARD form a soilborne pathogen complex that includes necrotrophic soilborne oomycetes (*Phytophthora* and *Pythium*) and fungi (*Ilyonectria* and *Rhizoctonia*) (Jaffee et al., 1982; Mazzola, 1998), has been a serious threat for the establishment of economically viable orchards. *Pythium ultimum* is a major component of this pathogen complex in orchard soils worldwide (Mazzola, 1997; Tewoldemedhin et al., 2011). Management of ARD depends almost exclusively on pre-plant fumigation of orchard soils to eradicate ARD pathogens, which also inadvertently eliminates other beneficial soil microbiota. Use of these chemical fumigants is under increasing regulatory restriction due to environmental and human health concerns. Maximized exploitation of host resistance through investigation of the molecular regulation controlling defense responses of apple roots, and thereafter development and deployment of resistant apple rootstocks can offer a cost-effective, environment friendly and durable strategy for ARD management (Zhu et al., 2014; Zhu and Saltzgiver, 2020).

To uncover the molecular mechanisms regulating apple roots resistance responses toward *P. ultimum* infection, two previous transcriptome analyses have provided the first panoramic description of genome-wide transcriptional networks during defense activation (Shin et al., 2016b; Zhu et al., 2017, 2019). The peak transcriptomic changes in apple roots in response to *P. ultimum* infection were shown to be at 48 hpi (hour post inoculation) when about 2% of the protein-encoding genes were differentially regulated (Shin et al., 2016b). A recent comparative transcriptome analysis identified a large number of differentially expressed genes between a *P. ultimum* resistant G.935® and a susceptible B.9 rootstock genotype (Zhu et al., 2019). The candidate genes, which may crucially contribute to resistance traits, include those with annotated function of pathogen perception, hormone signaling, secondary metabolite production, and resistance proteins (Zhu et al., 2017, 2019). Overall, it appears that an earlier and stronger molecular-level defense activation occur in the roots of resistant genotypes as they are challenged by *P. ultimum*. In contrast, deficient detoxification, weakened effector-triggered immunity (ETI), or existence of a susceptibility (*S*) gene may contribute to a disrupted defense activation process in the roots of the susceptible genotype. Parallel to these transcriptome analyses, a systematic phenotyping effort has recently identified a panel of apple rootstock germplasm with contrasting and reliable resistance traits against *P. ultimum* infection (Shin et al., 2016a; Zhu et al., 2018a,b). Besides the expression patterns of the protein coding genes, elucidating post-transcriptional control of genotype-specific defense responses may facilitate the identification of key genes underpinning apple roots resistance traits.

Plant endogenous small RNAs (sRNAs) are a class of short (∼21–25 nucleotides) non-coding single-stranded RNAs, which are ubiquitous in most cellular processes including plant-microbe interactions (Bartel, 2004; He and Hannon, 2004; Eckardt, 2012; Borges and Martienssen, 2015; Weiberg and Jin, 2015). sRNAs can be divided into two major categories based on their distinct biogenesis pathways, i.e., microRNAs (miRNAs) and small interfering RNAs (siRNAs) (Axtell, 2013). sRNAs are generated by DICER or DICER-like (DCL) endoribonucleases, and the mature sRNAs are loaded into Argonaute (AGO) proteins to induce silencing of genes with complementary sequences (Rogers and Chen, 2013; Borges and Martienssen, 2015), which is generally referred to as RNA interference (RNAi). By base-pairing to the target mRNAs of protein coding genes, sRNAs modulate gene expression through either translational repression or post-transcriptional silencing. Accumulating evidence indicates that plant miRNAs play a pivotal role in controlling plant immune responses to pathogen infection through numerous cellular processes (Katiyar-Agarwal and Jin, 2010; Fei et al., 2013, 2016; Bologna and Voinnet, 2014; Chen et al., 2018). For example, the NBS-LRR-miR482/2118 regulatory network has been demonstrated to have a role in fine-tuning the timing and intensity of defense responses in tomato-*Phytophthora infestans* pathosystem (Jiang et al., 2018; Hong et al., 2019). On the other hand, pathogens can hijack the host RNA silencing system to reduce plant defense responses (Weiberg and Jin, 2015; de Vries et al., 2018b, 2019). Profiling miRNAs during interaction between apple roots and necrotrophic oomycete pathogen *P. ultimum*, as well as identifying their corresponding target genes by degradome sequencing (German et al., 2008), should provide critical insights into regulation of resistance in apple roots to this pathogen.

The objective of this study was to identify key miRNA families and their specific target genes in apple roots during interaction with *P. ultimum* using high-throughput RNA sequencing analysis. Six apple rootstock genotypes showing contrasting phenotypes against *P. ultimum* infection were included in this study to identify genotype-specific patterns in miRNA expression and the identities of miRNA-targeted genes.

MATERIALS AND METHODS

Apple Rootstock Genotypes and Plant Maintenance

Based on the results from a systematic phenotyping study (Zhu et al., 2018b), six apple rootstock genotypes, i.e., three resistant (or R group: R-#58, R-#161, and R-#164) and three susceptible genotypes (or S group: S-#106, S-#115, and S-#132), were identified and included in this study. These genotypes originated from an "Ottawa 3" × "Robusta 5" (O3R5) apple rootstock F1 population developed in the mid-1970s. Individual plants for each apple rootstock genotype and mock-inoculation controls were produced using synchronized plant tissue culture or micro-propagation procedures, as described previously (Zhu et al., 2018a). Shoot propagation and root induction/elongation required 6 weeks and 4 weeks, respectively. Individual plants with enough root system were transferred to pots containing autoclaved artificial soil consisting of construction sand, vermiculite and perlite in 1:1:1 ratio for a 1-week "in-soil acclimation" before pathogen infection assays

and root tissue collection. For tissue culture generated root system, the in-soil acclimation is a critical step to allow further differentiation of root tissues and to fully express the inherent resistance traits. To minimize the effects of transplanting shock on plants, especially in roots from culture medium to soils in pots, a transparent 7′ vented humidity dome (Greenhouse Megastore, Danville, IL, United States) was used to cover the flat tray holding the pots to retain humidity. The temperature in the growth room was approximately 22 ± 1°C at night and 25 ± 1°C during daytime with 12 h light/dark photoperiod regime.

Inoculation of Apple Roots With *Pythium ultimum* and Root Tissue Collection

The *Pythium ultimum* isolate (#1062) used in this study was originally isolated from the roots of "Gala"/M.26 apple grown at Moxee, WA, United States. Inoculum of *P. ultimum* was prepared as previously described (Shin et al., 2016b). Briefly, the inoculum of *P. ultimum* was prepared by cultivation in potato-carrot broth (20 g of carrots and 20 g of peeled potatoes in 1 L of water boiled for 30 min) with two drops of wheat germ oil added per L of medium. The *P. ultimum* cultures were grown in potato-carrot broth in 9-cm petri dishes at 22°C for 4–6 weeks. Oospores and mycelium from the resultant hyphae mat were collected and ground in 0.5% methyl cellulose solution using a household electric blender for 30 s. The oospores and hyphal fragments were resuspended in 0.5% methyl cellulose to give a final concentration of approximately 2,000 oospores per milliliter (mL). The inoculation of seedlings with *P. ultimum* was performed by dipping the root system in the inoculum solution for 5 s. Inoculated plants were immediately transplanted into pots with autoclaved soils and watered thoroughly. Control plants were mock inoculated with 0.5% methyl cellulose solution and maintained similarly to the *P. ultimum* inoculated plants. All plants were maintained in an environmental growth room as specified above. Root tissues were collected at 48 hpi (hour post inoculation) by excising the roots after excavating plant from pot and quick rinsing off attached soil medium. Three independent biological replicates were set for each sample (genotype/treatment), and each replicate included the pooled root tissues of five plants. Tissues were store in −80°C freezer until RNA isolation.

Plant Survival Rate and Microscopic Root Necrotic Patterns

A detailed description of the resistance phenotypes for included six genotypes has been reported previously (Zhu et al., 2018b). Briefly, inoculated plants were allowed to grow for 4 weeks in autoclaved potting mix. Plant survival rate for each genotype was recorded at 3, 7, 10, 14, and 28 dpi (days post inoculation), although overall plant survival rate for most of the tested genotypes was stabilized after 7 dpi. Infection assays were repeated at least three times. For microscopic observation, plants were carefully excavated from the soil to minimize mechanical damage to the roots from 2 to 7 dpi. Residual soil along the root branches was gently removed under running tap water. Roots for both mock-inoculated control and *P. ultimum* inoculated plants were kept separately in 100-mL beakers filled with water until microscopic examination within 2 h. Individual root branches were carefully separated from each other, and a glass slide was used to hold the roots in petri dish filled with autoclaved water. A minimum of six plants per genotype from control and *P. ultimum* treated were examined with the assistance of a dissecting microscope (Olympus SXZ12). Images of healthy or necrotic root tissues were obtained using a DP73 digital camera installed on Olympus SXZ12 and the associated software suite of Celsense (Olympus, Center Valley, PA, United States). Digital images were only processed for resizing, cropping and adjusting overall brightness using a publicly available software FastStone Image Viewer 5.5.[1]

RNA Isolation, Sequencing, Target Genes Identification and phasiRNA Analysis

Total RNA was isolated as previously described (Zhou et al., 2018). Thirty-six libraries were constructed to represent six genotypes, two treatments (mock-inoculation and *P. ultimum* inoculation), and three independent biological replicates for each sample (genotype/treatment). Each biological replicate included the pooled root tissues from five plants. Frozen root tissue samples were ground to a fine powder in liquid nitrogen, and RNA quantity was determined using a NanoDrop spectrophotometer (ND-1000, Thermo Fisher Scientific). The quality of total RNA used for RNA-seq passed the required standard of RNA integrity number (RIN) $x \geq 8$, which was evaluated using an Agilent 2100 Bioanalyzer. Total RNAs (∼2 μg for each sample) were gel purified and fragments within the 18–30 nucleotide length range were selected to construct a library. Thirty-six sRNA libraries were prepared and sequenced at the Center for Genome Research and Biocomputing in Washington State University using an Illumina HiSeq2500™ (Illumina Inc., San Diego, CA, United States). Clean sequence reads were obtained after removal of the low-quality tags, 3′ adapter null, insert null, 5′ adapter contaminants, poly A reads and reads shorter than 18 nt. The apple miRNAs were annotated as described previously (Xia et al., 2012, 2015). The total number of reads in a given library that perfectly matched the *Malus* × *domestica* genome was used for the normalization of read abundance. Each miRNA was normalized to 10 million reads. *Malus* × *domestica* genome sequences (*Malus* × *domestica* HFTH1 Whole Genome v1.0) were downloaded from the GDR.[2] The microRNA sequence data was deposited in SRA (Sequence Read Archive) at the NCBI website under the accession number SRP295189.[3] Statistical analysis of measured expression values between genotypes or treatments was performed using Mann–Whitney *U* test.

To identify which specific apple genes are targeted by miRNA-directed degradation after *P. ultimum* infection, three degradome libraries were sequenced and resulted sequence tags were annotated and quantified (German et al., 2008). First library (L1) was constructed using pooled total RNAs from roots of all

[1] www.faststone.org

[2] https://www.rosaceae.org/species/malus_x_domestica_HFTH1/genome_v1.0

[3] ncbi.nlm.nih.gov/sra/review/SRP295189

mock-inoculation controls, second library (L2) from pooled total RNAs from infected root tissues of all three resistant genotypes, and third library (L3) from pooled total RNAs from root tissues of all three susceptible genotypes. Identification of miRNA target genes was conducted by analyzing three degradome libraries with CleaveLand (version 4) pipeline for degradome analysis (Addo-Quaye et al., 2009). Identification of PHAS loci is based on *P*-value calculation, which was developed and modified in previous studies (De Paoli et al., 2009; Xia et al., 2013). PHASMinerCLI from an in-house software "sRNAminer" was used to predict PHAS loci and TargetSoPipe from sRNAminer was used to identify the trigger miRNA of PHAS loci. The degradome *p*-adjusted value < 0.05 is adopted in assigning the identity of target genes.

The expression patterns of three laccase genes were examined using RT-qPCR as previously described (Zhu et al., 2019). The same set of total RNA samples for small RNA-seq were used for RT-qPCR analysis. The total RNA was treated with DNase I (Qiagen, Valencia, CA, United States) and then purified with RNeasy cleanup columns (Qiagen, Valencia, CA, United States). Two micrograms of DNase-treated RNA were used to synthesize first-strand cDNA using SuperScript II reverse transcriptase (Invitrogen, Grand Island, NY, United States) and poly dT (Operon, Huntsville, AL, United States) as the primer. The expression values of target genes were normalized to that of a previously validated internal reference gene (MDP0000095375) specific for gene expression analysis in apple roots $2^{-\Delta\Delta CT}$ method (the comparative Ct method) (Livak and Schmittgen, 2001). The gene sequences were retrieved from GDR.[4] Forward and reverse primers were designed using web-based Primer3Plus[5] and IDT OligoAnalyzer.[6] Where possible, an optimum annealing temperature of 60°C, a GC content of 40–60%, an amplicon length of 150–180 bp, and a primer length of 20 bp were applied. The primer sequences of three laccase genes and a reference gene were listed in **Table 1**.

Genomic Location of miR397a and Variant Analysis

A *de novo* genome of "Robusta 5" parent was assembled using long-read PacBio sequences to identify the genomic location of miR397a precursors. The raw sequence quality cleaning and genome assembly was performed as per Canu assembly pipeline parameters with default settings (Koren et al., 2017). The miR397 sequences were aligned to the assembled "Robusta 5" genome to identify corresponding matching sequences using "Blastn" in the National Center of Biotechnology Information (NCBI) Blast software (Johnson et al., 2008). A 20 kb sequence around miR397a genomic locus on matching "Robusta 5" contigs was extracted using a custom script. Coding regions across these sequences were annotated by comparing them with the Golden Delicious double haploid (GDDH13 v1.1) genome (Daccord et al., 2017). In addition, a nucleotide blast search was conducted using online NCBI Blast tool (Johnson et al., 2008) to further annotate the miR397 matching sequences of "Robusta 5." To identify nucleotide variants across the miR397a matching regions, sequence reads from "Ottawa 3" parent, and six *P. ultimum* susceptible and resistant genotypes were used for SNP (Single Nucleotide Polymorphism) variant calling as described earlier (Singh and Khan, 2019). First, sequence reads from individual genotypes were quality cleaned using the Trimmomatic software (Bolger et al., 2014) with parameters: leading:20, trailing:20, slidingwindow:4:15, avgqual:20, minlen:25. Read sequences below threshold quality of 20 were also removed. Remaining high-quality reads were aligned against the 20 kb miR397 matching sequences of "Robusta 5" as a reference using burrows-wheeler aligner (BWA) with default parameters (Li and Durbin, 2009). The alignment files were used as input to call SNP variants using Genome Analysis Toolkit (GATK version 3.8.0) (McKenna et al., 2010). SNP variant files for each sample were recorded in genotype variant call format (gVCF) with the HaplotypeCaller plugin in GATK. The sample-specific gVCF files were combined to obtain total SNP variants across all samples using the Genotype GVCF plugin in GATK. A final set of SNP variants supported by minimum 10 read sequences were retained using VCFtools software (Danecek et al., 2011).

[4]http://www.rosaceae.org

[5]www.bioinformatics.nl/cgi-bin/primer3plus/primer3plus.cgi

[6]www.idtdna.com/analyzer/Applications/OligoAnalyzer/

RESULTS

Resistance Phenotypes and Overall Experimental Design

Six apple rootstock genotypes included in this study were previously identified to have contrasting resistance traits based on repeated root infection assays with *P. ultimum*, as shown in **Figure 1A** (Zhu et al., 2018a,b). In addition to remarkable differences of plant survivability, microscopic observation revealed necrosis progression patterns and the intensity of pathogen hyphae growth along infected root that were distinguishable between resistant and susceptible apple

TABLE 1 | Primer sequences of laccase and reference genes used for qRT-PCR analysis to study their expression patterns in apple roots in response to *Pythium ultimum* infection.

Gene IDs	Gene description	Primers F/R (5′-3′)
MD03G1056400	Laccase-3	F-5′ CAACCCCAGAACAGATCCAG 3′ R-5′ AAACCCAGGAAGAGATGTGC 3′
MD01G1159400	Laccase-5	F-5′ TGGGCAGTCATTCGATTTGT 3′ R-5′ AACAAAGAGGCAGATCCACC 3′
MD16G1147100	Laccase-7	F-5′ TAATCCGCAAGTACGCAACA 3′ R-5′ CAGATCAAGTGGTGGTGGAG 3′
MD02G1221400	Reference gene	F-5′ ATGGAGAGATGGAATGGCAAAG 3′ R-5′ GTGAGCATCGGATCCCATTTAG 3′

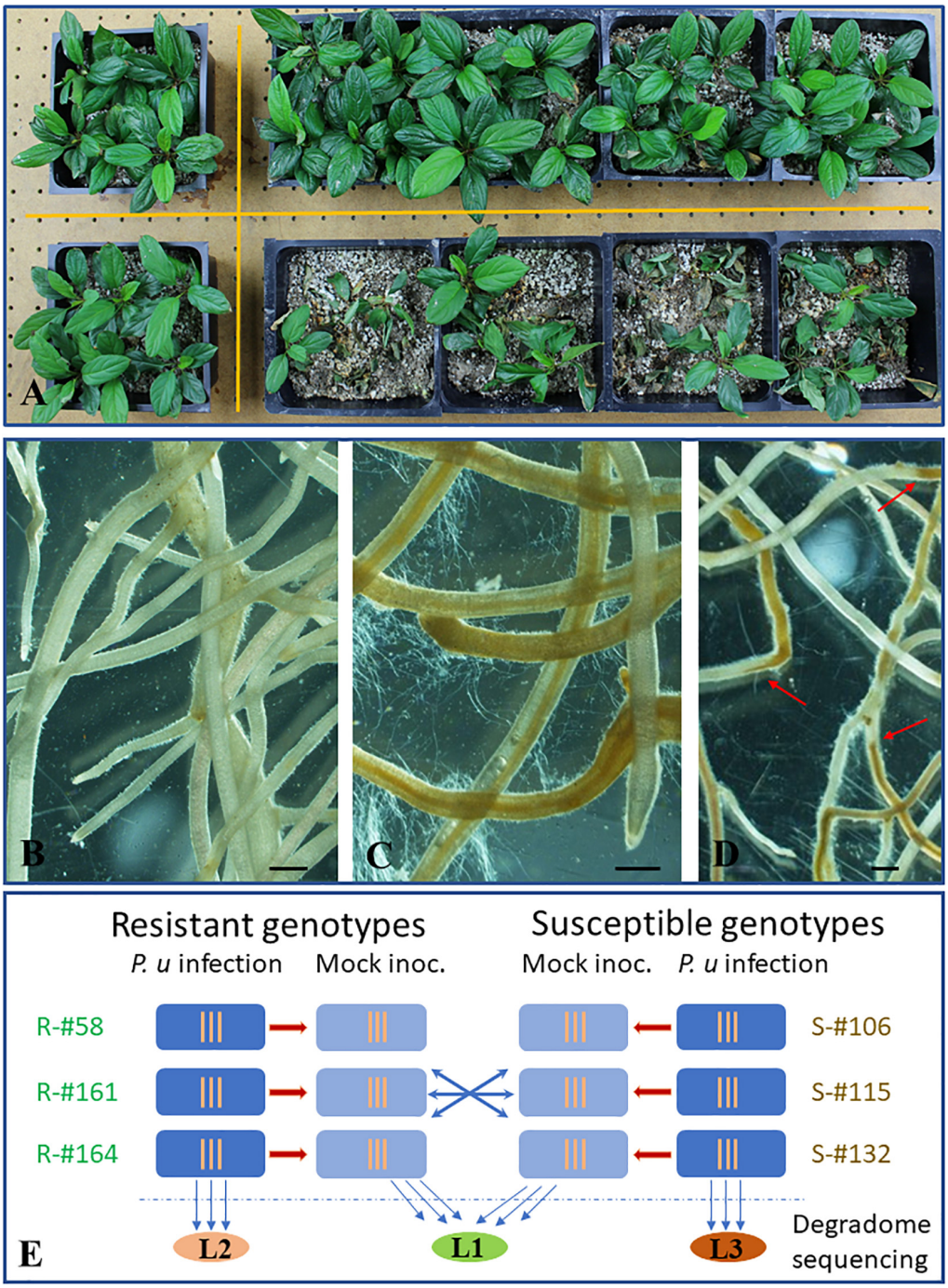


FIGURE 1 | Resistance phenotypes of apple rootstock in response to infection from *Pythium ultimum* and the experimental design for miRNA profiling and target gene identification. **(A)** Plant survival rates between a resistant (top, R-#58) and a susceptible (bottom, S-#106) genotype which were simultaneously inoculated with the same preparation of pathogen inoculum. Plants in the left column were the mock-inoculated control for each genotype. **(B)** Representing image of a mock-inoculated apple root system at 48 hpi; **(C)** Representing image of apple root branches of a susceptible rootstock genotype (S-#132) inoculated with *P. ultimum* at 48 hpi, showing profuse hyphae growth and widespread tissue necrosis and collapses. **(D)** A representing image of apple root branches for a susceptible rootstock genotype (R-#161) inoculated with *P. ultimum* at 48 hpi, showing abrupt necrosis arrest, with distinct lines separating healthy and necrotic sections along infected roots. Bars represent 300 μm. **(E)** Experimental design for microRNA profiling analysis and degradome sequencing. Root tissues at 48 hpi from three resistant (R-#58, -#161, and -#164) and susceptible genotypes (S-#106, -#115, and -#132) were used for small RNA library construction and subsequent high-throughput sequencing. Normalized read counts were compared within and between genotypes. Three vertical lines indicate three biological replicates for each sample (specific genotype/treatment combination). Three colored oval shapes represent three pooled samples for degradome libraries and sequencing analysis, where L1 stands for combined mock-inoculated root tissues (from both resistant and susceptible genotypes), L2 for combined root tissues consisting of infected resistant genotypes, and L3 for combined root tissues consisting of infected susceptible genotypes. Red arrows indicate the defined lines separating healthy and necrotic sections.

rootstock genotypes. Compared to the white and intact tissue of mock-inoculated apple roots (**Figure 1B**), the sweeping spread of necrotic tissues and profuse growth of pathogen hyphae along the infected roots was frequently associated with the root system of inoculated susceptible genotypes (**Figure 1C**). In contrast, within the infected root system of the resistant genotypes, the defined lines separating healthy and necrotic sections (**Figure 1D**, red arrows) were commonly observed, suggesting an effective impediment of pathogen progression. For genotype-specific analysis of miRNA expression profiles and identification of miRNA target genes, three resistant (or R group: R-#58, R-#161, and R-#164) and three susceptible genotypes (or S groups: S-#106, S-#115, and S-#132) were directly compared at the critical stage of defense activation at 48 hpi (hour post inoculation) (**Figure 1E**).

Overview of miRNA Sequencing Statistics in Apple Roots in Response to *P. ultimum* Infection

A total of ∼2.8 billion reads were generated by Illumina HiSeq2500 from 36 sequenced small RNA libraries. An average of 47% of clean reads among the thirty-six libraries were mapped to the apple genome (Zhang et al., 2019)[7] according to an established protocol (Xia et al., 2012; **Supplementary Table 1**). The relative similarity of total read numbers from each sample indicated that neither sampling procedure, library construction, nor sequencing processes created significant bias or errors (**Figure 2A**). A similar distribution pattern of the size of identified sRNA from thirty-six libraries was observed, with 24 nt (nucleotide) sRNAs being the most abundant, followed by 23, 21, and 22 nt (**Figure 2B**). A total of 233 (including 50 novel) candidate miRNA species, belonging to 48 known and 39 novel miRNA families were mapped to the apple genome (Zhang et al., 2019; **Figure 2C**). The complementary miRNA* sequences for each novel candidate miRNA were also detected, even though most were present at lower copy levels than their corresponding mature miRNAs. The family size ranged from 1 to 22 species among identified miRNA families. Unsurprisingly, the expression levels, as expressed by reads per 10 million, showed vast differences from single digits to 10^6 of normalized read counts among miRNA species (**Supplementary Table 1**).

[7]https://www.rosaceae.org/analysis/162

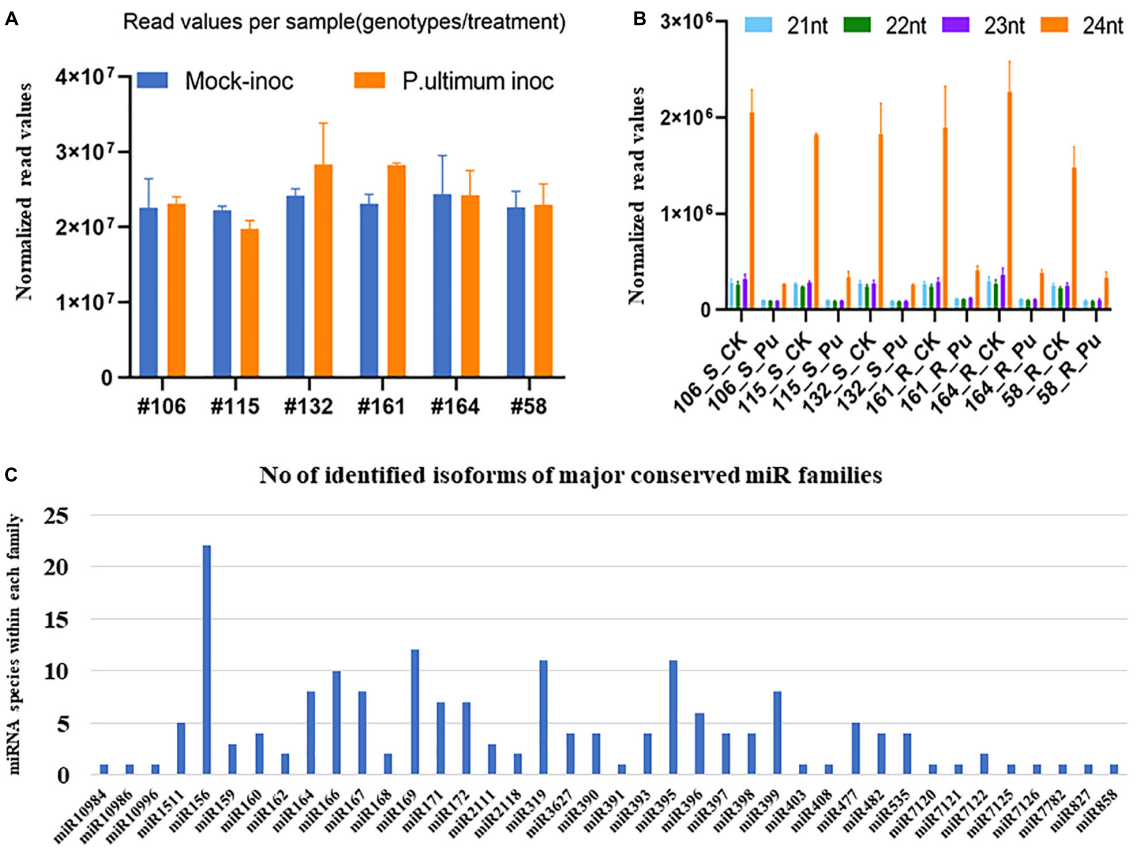


FIGURE 2 | Overall statistics of identified miRNAs in apple roots. **(A)** The average numbers of sequence reads from three replicates for each sample (genotype/treatment). **(B)** Size distribution of small RNAs based on number of unique sequence reads. **(C)** Size of family of major miRNA in apple roots.

Expression Patterns of miRNA Families in Response to *P. ultimum* Infection

Among 43 major known miRNA (miR) families, most demonstrated downregulated expression in response to *P. ultimum* infection for all six genotypes, with rare exceptions, while only five miRNA families were upregulated in both resistant and susceptible genotypes, with a few more families specifically in infected root tissue of resistant genotypes (**Table 2**). Three upregulated miRNA families, miR160, miR167, and miR393 directly participate in auxin signaling, which may represent one of the significant transitions of cellular pathways from normal growth to defense responses in response to *P. ultimum* infection. Seven miRNA families (**Table 2**) showed differential regulation patterns between resistant and susceptible genotype groups, and five of them were upregulated in resistant genotypes; only the miR3627 family showed the opposite. Majority of the 43 known miRNA families exhibited low to medium levels of expression across the six genotypes, as judged arbitrarily by the normalized read counts at the level of 2–4 digits (**Table 2**). The remaining six families were highly expressed at the level of 10^5 to 10^6 normalized read counts.

miRNA Families Regulating Apple Root Immune Responses to *P. ultimum* Infection

Several miRNA families appeared to be directly linked to plant immunity based on their target genes. Although these miRNA families all showed downregulated expression in response to *P. ultimum* infection, subtle variations in the level of downregulation existed between resistant and susceptible groups. Laccase-targeting miR397 showed the consistent and substantial levels of reduced expression. For example, compared to values of mock-inoculation controls, infection from *P. ultimum* resulted in significant reduction of detected read counts for miR397a across all genotypes (**Figure 3A**). More interestingly, even between the mock-inoculated controls, the resistant genotypes (except R#58) demonstrated strikingly lower levels of miR397a expression compared to those of susceptible genotypes. This observation suggests that a high level of laccase activity (from lower miRNA level) may also function as a part of the pre-formed defense system even before pathogen challenge. The targets of miR398 family include the genes encoding superoxide dismutase (SOD). Together with laccase and other groups, SODs belong to copper proteins, and their roles in early immune responses have been well elucidated (Pilon, 2017; Hong et al., 2019). The expression of miR398 in apple roots were uniformly downregulated upon pathogen inoculation (**Figure 3B**). However, miR398 had a slightly higher expression level in mock-inoculated tissues of resistant genotypes and a slightly stronger downregulation in infected root tissues of the susceptible genotypes. The regulatory mechanisms of miR398-SOD and their contribution to resistance traits of apple roots deserve further investigation.

Members of the miR482/miR2118 super family are well-documented for their role in targeting specific NBS-LRR encoding genes (Fei et al., 2016; Islam et al., 2018). The entire miR482/miR2118 super family showed uniform downregulation in response to *P. ultimum* infection (**Figures 3C,D** and **Supplementary Table 1**), but a closer examination, both miR482a/b as the examples, indicated a subtle variation at the levels of downregulation between resistant and susceptible genotypes. A more substantial (>1x) downregulation was observed for all resistant genotypes, but in comparison, only one out of three susceptible genotypes showed a comparable level in response to pathogen infection. The minor variation, observed at miRNA level, could lead to amplified effect, through phasiRNA generation, on genotype-specific resistance trait toward *P. ultimum* infection.

miRNA Families Targeting Plant Hormone Signaling and TFs Involved in Defense Activation

Three miRNA families (miR160, miR167, and miR393) that target auxin signaling showed mostly upregulated expression upon *P. ultimum* infection (**Table 3**). Some members of miR160 family demonstrated differential expression patterns between R and S genotypes. Compared to the consistent upregulation of miR160b in all three susceptible genotypes, its downregulation was observed for two out of three resistant genotypes (R-#58 and R-#164) due to pathogen infection. miR172a, which targets *AP2* and therefore potentially affects ethylene signaling, also demonstrated differential expression between resistant and susceptible genotypes, though its overall expression level was low. While miR172a was downregulated in the roots of all three susceptible genotypes, two out of three resistant genotypes (R-#58 and R-#161) showed upregulated expression. Five miRNA families, i.e., miR396, miR319, miR159, miR858, and miR164, are known to target various TF families including WRKY, TCP, MYB, and NAC that are implicated in JA biosynthesis and secondary metabolism under biotic or abiotic stress conditions (**Table 3**; Curaba et al., 2014; Liu and Axtell, 2015; Zhang, 2015). However, the overall comparability of their regulation patterns between R and S genotype groups suggested that their post-transcriptional regulations are unlikely the critical factor differentiating resistance and susceptibility, though they are the essential components of defense responses in apple roots. Notably, the targets of these miRNA families, such as those for TFs and hormone signaling, were the commonly identified genes from previous transcriptome analyses (Shin et al., 2016b; Zhu et al., 2019).

Degradome Sequencing Identified Key Target Genes Due to *P. ultimum* Infection

Degradome sequencing identified a relatively wide, but generally expected, range of categories of target genes specific to this pathosystem between apple roots and *P. ultimum* (**Table 4** and **Supplementary Table 2**). Most of the identified target genes fell into the typical spectrum of reported gene targets for a known miRNA family, although novel targets for several miRNA families were also identified. For example, "betaine aldehyde dehydrogenase" and "cation/calcium exchanger" were

TABLE 2 | Genotype-specificity of miRNA regulation in apple roots in response to *Pythium ultimum* infection.

miRNA family	Expression level	Known targets	Genotype-specific regulation			Color code
			Rep member	S	R	
miR10984	4		10984	↓	↓	
miR10986	3	Polyphenol oxidase	10986	↓	↓	
miR10996	3		10996	↓	↓	
miR11014	2		11014	↓	↓	
miR1511	5		1511d	↓	↓	
miR1526	2		1526	↓	↑	
miR156	4	Squamosa-promoter binding protein-like gene (SPL)	156h	↓	↓	
miR159	5	MYB	159a	↓	↓	
miR160	3	Auxin response factor (ARF)	160a, d	↑	↑	
miR162	4	Dicer-like gene (DCL1)	162a	↓	↓	
miR164	3	NAC	164a	↓	↓	
miR166	6	Class III homeodomain leucine zipper TF	166b	↓	↓	
miR167	3	Auxin response factor (ARF)	167a	↑	↑	
miR168	4	Argonaute 1 (AGO1)	168a, b	↓	↓	
miR169	4	Nuclear factor Y (NF-Y)	169d	↓	↓	
miR171	3	Scarecrow-like proteins (SCL)	171a	↓	↓	
miR172	2	APETALA 2 (AP2)	172a	↓	↑	
miR2111	2		2111a	↓	↓	
miR2118	4	NB-LRR	2118a, b	↓	↓	
miR319	5	TCP, JA biosynthesis/MYB	319a, f	↓	↓	
miR3627	2		3627b	↑	↓	
miR390	3	TAS3	390a	↓	↓	
miR391	2		391	↓	↓	
miR393	3	Toll-like receptors (TIR)	393b	↑	↑	
miR395	2	Sulfate transporter	395a	↓	↓	
miR396	5	Growth regulating factor	396e	↓	↓	
miR397	4	Laccase (LAC)	397a	↓	↓	
miR398	5	SOD/Copper superoxide dismutase (CSD)	398b	↓	↓	
miR399	3	Phosphate over accumulator (PHO)	399a	↓	↑	
miR403	3	Argonaute 2 (AGO2)	403a	↓	↓	
miR408	4	UCL (Uclacyanin)	408a	↓	↓	
miR477	3	GRAS domain-containing protein	477a	↓	↑	
miR482	4	Nucleotide binding site-leucine-rich repeats (NB-LRR)	482c	↓	↓	
miR5139	2		5139	↓	↑	
miR535	4	Squamosa-promoter binding protein-like gene (SPL)	535d	↓	↓	
miR7120	3		7120	↓	↓	
miR7121	3		7121	↓	↓	
miR7122	4	Pentatricopeptide repeat-containing (PPR) gene	7122b	↓	↑	
miR7125	3		7125	↑	↑	
miR7126	4		7126	↓	↓	
miR7782	3		7782	↓	↓	
miR827	3	Phosphate transporter 5 (PHT5)	827	↓	↓	
miR858	3	MYB	858	↑	↑	

Column 1 lists known miRNA families identified from current RNA-seq analysis; Column 2 shows the relative expression levels expressed by a heatmap based on the normalized read values per 10 million reads, the numbers indicate the highest exponent of detected maximum count values among the samples (genotype/treatment); Column 3 denotes referred target gene with annotated functions; Column 4 indicates the representing (rep) member from an individual family; Columns 5 and 6 demonstrate the regulation direction due to P. ultimum infection, based on the values of corresponding controls and infected tissues, for a specific miRNA family (as exampled by the selected); Column 7 exhibits the visual representation of genotype-specific regulation patterns using "color code": red for upregulation in P. ultimum infected tissues, yellow for differential expression between S and R group (opposite directions); light blue for uniformly downregulation with less than 1x difference comparing to values of control tissue, and darker blue for those with uniformly downregulated expression but with larger than 1x downregulation comparing to values of control tissue. Lower case letters denote various species in the same microRNA families.

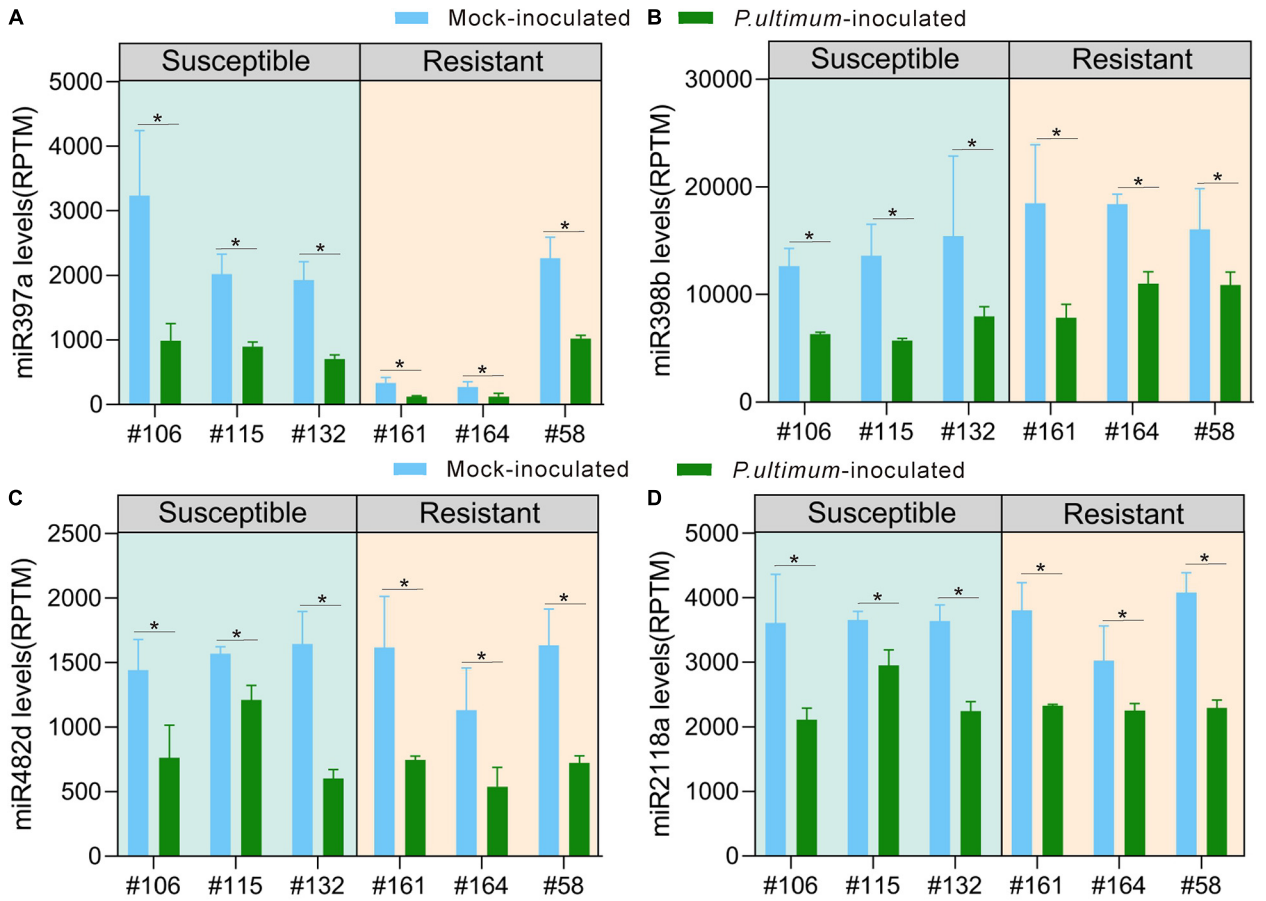


FIGURE 3 | Genotype-specific expression patterns for representing members in selected miRNA families potentially participating in apple roots resistance responses. **(A)** miR397a; **(B)** miR398b; **(C)** miR482d; **(D)** miR2118a. The numbers on *Y* axis represent the average values of the normalized read counts from three biological replicates. Genotype/treatment are aligned along *X* axis; with CK representing mock-inoculation control and "Pu" representing root samples inoculated using *P. ultimum*. Error bars are the standard deviation (SD) of count values within three biological replicates. Error bars represent SE of three independent biological replicates. Asterisks denote statistically significant differences in a one-tailed Mann–Whitney *U* test (*$P < 0.05$).

TABLE 3 | Genotype-specific expression patterns for miRNA families regulating hormone signaling and TFs in secondary metabolisms in apple roots in response to *Pythium ultimum* infection.

miRNA family	No of members	Primary target	Representing member	*P. ultimum-inoculation* vs. mock-inoculation					
				S-106	S-115	S-132	R-58	R-161	R-164
160	4	Auxin response factor (ARF)	160b	**1.4**	**1.7**	**1.4**	0.7	**1.2**	0.9
167	8	Auxin response factor (ARF)	167a	**1.8**	**1.7**	**1.4**	**1.5**	**2.5**	**1.8**
393	4	Toll-like receptor (TLR)	393b	**1.1**	**1.1**	0.5	0.9	**1.3**	**1.3**
396	6	Growth regulation factor	396b	0.8	0.8	0.8	0.7	0.8	0.6
319	11	TCP/MYB, JA biosynthesis	319a	0.4	0.7	0.4	0.5	0.5	0.5
172	7	Apetala 2 (AP2)	172a	0.9	0.5	0.3	**1.9**	**1.7**	0.4
159	3	MYB	159a	0.5	0.8	0.4	0.5	0.5	0.4
858	1	MYB	858	**2**	**1.4**	0.8	**1.4**	**1.3**	**1.4**
164	8	NAC	164a	0.5	0.3	0.6	0.3	0.5	0.4

Expression patterns were expressed by the ratio of normalized read counts of P. ultimum infected root tissues over those of corresponding mock-inoculated tissues. The values of larger than 1.0 denote the upregulated expression in response to pathogen infection; Conversely, the values smaller than 1.0 indicate the downregulation due to pathogen infection. The absolute values of the ratio reflect the level of upregulation or downregulation per genotype and miRNA family. Those with upregulated patterns are in bold. The values were calculated using the averages of three biological replicates. Lower case letters denote various species in the same microRNA families.

TABLE 4 | Identified target genes, their functional annotations and detected tag abundance in apple roots in response to *Pythium ultimum* infection.

Member(s) of miRNA	Target gene	Functional annotation of identified target genes	Tag abundance		
			L1	L2	L3
miR10984	HF07668	ASC1-like protein	N/A	5	N/A
miR10986	HF12097	Polyphenol oxidase, chloroplastic	92	N/A	N/A
	HF12099		1417	1426	724
	HF12100		1390	1493	739
	HF12105		146	N/A	43
	HF17936		105	139	154
	HF17941		3	N/A	N/A
miR156a, c, d, e,	HF26180	Squamosa promoter-binding-like protein 12	47	44	21
f, l, k, l, n, o, u, v	HF35297		56	36	N/A
	HF42804		N/A	46	N/A
	HF41242	Betaine aldehyde dehydrogenase 1, chloroplastic	N/A	N/A	12
	HF42782	U-box domain-containing protein 6	N/A	2	2
	HF42611	Optineurin	N/A	N/A	3
	HF05261	Probable polyribonucleotide nucleotidyltransferase 1	10	N/A	N/A
	HF30813	Cation/calcium exchanger 4	N/A	14	N/A
	HF26192	Teosinte glume architecture 1	75	77	27
miR159a-c	HF17403	Transcription factor GAMYB	6	N/A	N/A
	HF06666*		119	N/A	N/A
	HF34775	Patellin-3	N/A	13	N/A
	HF03195	Protein SPEAR1	32	N/A	11
	HF03914*		42	20	N/A
	HF12011	Receptor-like protein kinase HSL1	6	N/A	N/A
miR160a, d	HF06172*	Auxin response factor 18	47	N/A	6
	HF40525*		48	43	N/A
	HF01570		65	64	27
	HF04836		N/A	59	N/A
	HF24306*		N/A	47	15
	HF25001*		69	N/A	N/A
	HF04836		64	N/A	34
	HF44485*	Auxin response factor 17	N/A	818	N/A
	HF07133*		N/A	869	426
	HF00444	Solute carrier family 25 member 44	12	N/A	N/A
miR162a, b	HF05621*	Endoribonuclease Dicer homolog 1	N/A	66	27
	HF20945	ATP-dependent zinc metalloprotease FTSH	N/A	7	N/A
miR164a, d, h	HF09293*	NAC domain-containing protein 100	653	N/A	112
	HF24823*		642	488	N/A
	HF27440	Methionine aminopeptidase 1D	N/A	N/A	3
	HF16100	U-box domain-containing protein 35	5	N/A	N/A
	HF11267	NAC domain-containing protein 21/22	588	438	116
	HF22809		559	419	118
miR166a, j	HF00268*	Homeobox-leucine zipper protein ATHB-15	174	N/A	100
	HF28547*		N/A	196	100
	HF12939*	Homeobox-leucine zipper protein ATHB-8	N/A	174	N/A
	HF21765*		174	195	N/A
	HF40749	Glucan endo-1,3-beta-glucosidase 14	19	N/A	N/A
	HF06176*	Homeobox-leucine zipper protein REVOLUTA	N/A	170	111
	HF40517*		446	N/A	N/A
	HF11732*	Homeobox-leucine zipper protein HOX32	N/A	118	N/A
	HF23204		114	113	54
miR167a, f, j, h	HF32107*	Auxin response factor 8	620	N/A	402
	HF37005*		N/A	651	375
	HF11771*	Auxin response factor 6	95	86	N/A
	HF34014		95	N/A	48
	HF18290*		N/A	77	57
	HF29114		78	74	41

(Continued)

TABLE 4 | Continued

Member(s) of miRNA	Target gene	Functional annotation of identified target genes	Tag abundance		
			L1	L2	L3
miR168a, b, d	HF09608*	Protein argonaute 1	N/A	299	166
	HF13064	Mannose-P-dolichol utilization defect 1 protein homolog 2	N/A	N/A	3
	HF36007	Thaumatin-like protein 1	5	N/A	N/A
miR169d	HF19226	Pentatricopeptide repeat-containing protein At2g17670	2	N/A	N/A
miR171a, b, c, e, g	HF27082*	Scarecrow-like protein 6	990	N/A	474
	HF37501*		N/A	21	N/A
	HF01470*		N/A	20	7
	HF00464	Phosphopentomutase	4	N/A	N/A
	HF07177	Nodulation-signaling pathway 2 protein	12	25	8
	HF44555		11	10	N/A
	HF44340	Sugar transport protein 5	N/A	N/A	8
	HF10118	Alkylated DNA repair protein alkB homolog 8	4	N/A	N/A
	HF24442	Interleukin-3 receptor class 2 subunit beta	N/A	4	N/A
miR172a, d, f, g	HF40428*	Ethylene-responsive transcription factor RAP2-7	453	N/A	193
	HF06289*		N/A	481	205
	HF24247*		N/A	88	N/A
	HF25060*		N/A	57	22
	HF01637	Floral homeotic protein APETALA 2	18	N/A	7
	HF27401*		7	N/A	7
	HF04766*		N/A	4	N/A
	HF31388		13	11	N/A
miR2111a, c	HF32972*	F-box/kelch-repeat protein At3g27150	N/A	58	35
miR2118a, b	HF17618	Protein MARD1	7	N/A	N/A
	HF44440		N/A	N/A	6
	HF07401	Protein JINGUBANG	3	N/A	N/A
miR319a, c, f	HF03499*	Transcription factor MYB101	N/A	8	4
	HF16566	Transcription factor GAMYB	118	119	64
miR395a, b, e, h, k	HF01798*	ATP sulfurylase 1, chloroplastic	223	293	N/A
	HF13989*		105	N/A	96
	HF07090	Low affinity sulfate transporter 3	3	N/A	N/A
	HF09045*	Probable pectate lyase 22	N/A	3	N/A
	HF41418		N/A	N/A	5
	HF35421*	Sulfate transporter 2.1	12	17	N/A
	HF34432	Mitochondrial uncoupling protein 1	N/A	N/A	2
miR396a-f	HF00473	Growth-regulating factor 5	2	N/A	N/A
	HF30789		73	70	9
	HF19000*		N/A	23	9
	HF07761	Caffeoylshikimate esterase	21	N/A	N/A
	HF21477	Growth-regulating factor 6	170	142	82
	HF13165		201	215	129
	HF27291	Growth-regulating factor 1	113	88	35
	HF31510*		N/A	95	N/A
	HF42039	Dynein light chain, cytoplasmic	3	3	2
	HF00333	LRR receptor-like serine/threonine-protein kinase	N/A	2	N/A
	HF13870	Probable ATP-dependent DNA helicase CHR12	N/A	N/A	6
	HF08723	Growth-regulating factor 8	24	17	5
	HF41682*		5	N/A	N/A
	HF26054*	Growth-regulating factor 7	2	N/A	N/A
	HF27171*	Growth-regulating factor 12	20	15	N/A
	HF36486*	Growth-regulating factor 4	244	N/A	120
	HF19974*		N/A	21	10
	HF02750*	60S ribosomal protein L18-2	42	22	N/A
	HF10798	E3 ubiquitin-protein ligase CHIP	14	N/A	N/A
	HF41728	Transcription factor LHW	4	N/A	2

(Continued)

TABLE 4 | Continued

Member(s) of miRNA	Target gene	Functional annotation of identified target genes	Tag abundance		
			L1	L2	L3
miR397b	HF23917	Laccase-5	2	11	N/A
	HF26400	Laccase-7	30	N/A	N/A
	HF27792		45	N/A	82
	HF40034	Laccase-3	15	N/A	N/A
miR398a-d	HF42086	Multicopper oxidase LPR2	24	20	7
	HF30403	Umecyanin	N/A	1442	1135
	HF25617*	Copper transporter 6	110	58	N/A
	HF06452		92	71	19
	HF01373	Copper chaperone for superoxide dismutase	283	298	129
	HF08261		290	293	181
	HF29451	Dehydration-responsive element-binding protein 2A	12	7	N/A
	HF40618	Superoxide dismutase [Cu-Zn], chloroplastic	17	15	N/A
	HF41261	LIM domain-containing protein WLIM1	64	N/A	46
	HF31034	Serine/threonine-protein phosphatase PP1 isozyme 4	N/A	N/A	4
miR399c, e, g	HF05992	Heme-binding protein 2	N/A	11	N/A
	HF38390	GRF1-interacting factor 1	N/A	4	N/A
miR408	HF17186	Basic blue protein	2	N/A	3
	HF20292	Nudix hydrolase 23, chloroplastic	3	N/A	N/A
miR477a, b	HF05240	DTW domain-containing protein 2	7	7	6
	HF41450	DELLA protein GAI1	3	3	N/A
miR482a, c, d	HF37161	Disease resistance protein RPM1	N/A	N/A	112
	HF43810	Disease resistance protein At4g27190	9	N/A	5
	HF01646	Putative disease resistance protein RGA1	4	N/A	6
	HF04762	Putative disease resistance protein RGA3	11	N/A	N/A
	HF40153	Putative disease resistance protein At1g50180	4	N/A	7
	HF07514	Probable apyrase 6	16	N/A	N/A
	HF40855	Pro-apoptotic serine protease nma111	N/A	6	N/A
	HF00026	Chaperone protein dnaJ 8, chloroplastic	194	200	276
	HF32497		191	197	251
miR5225a	HF20446	Putative disease resistance protein RGA4	N/A	N/A	2
miR535b, d	HF02059	Ribosome maturation factor RimM	2	N/A	N/A
	HF32583	Pyrophosphate-energized vacuolar membrane proton pump	17	N/A	N/A
miR7122a, b	HF44234	Pentatricopeptide repeat-containing protein At1g12700	N/A	187	162
miR7125	HF11513	Zinc transporter 1	189	133	121
miR7126	HF16036	E3 ubiquitin protein ligase DRIP2	N/A	N/A	4
miR7782	HF21767	Thioredoxin-related transmembrane protein 2	8	9	8
miR858	HF00466	Transcription repressor MYB4	56	166	103
	HF28765		35	108	57
	HF08482	Transcription factor MYB26	3	N/A	N/A
	HF13276	Anthocyanin regulatory C1 protein	62	182	117
	HF18993		41	87	93
	HF21423		63	150	77
	HF13279	Transcription factor MYB3	49	72	81
	HF16086	Transcription factor MYB15	18	60	68
	HF21717	Transcription factor MYB44	15	36	31
	HF24028	Transcription factor MYB1	4	4	10
	HF29485	Transcription factor MYB102	2	N/A	N/A
	HF30785	Transcription factor TT2	44	88	76
	HF05712	Transcription factor MYB7	N/A	40	47

*L1 represent for the degradome libraries constructed from pooled root tissues of mock-inoculation including both resistant and susceptible genotypes, L2 for the degradome libraries constructed from pooled root tissues of P. ultimum-inoculation resistant genotypes, and L3 for the degradome libraries constructed from pooled root tissues of P. ultimum-inoculation susceptible genotypes. *After individual gene ID indicates the individual gene ID was targeted by another miRNA species from the same family. Refer to* ***Supplementary Table 2*** *detailed information, such as the P value and degradome value for each gene ID, and the cleavage site sequence. Lower case letters denote various species in the same microRNA families.*

identified as the targets of miR156, in addition to its primary known targets of SPLs for this miRNA family. Similarly, "glucan endo-1,3-beta-glucosidase" was among the targets beyond the commonly predicated targets of "homeobox-leucine zipper protein" encoding genes for miR166, and "probable pectate lyase 22" as the target for miR395 (**Table 3** and **Supplementary Table 2**). More practically, this experimental approach allowed the pinpointing of a small number of specific genes from a large gene family, which are specific to this pathosystem. For example, only five NBS-LRR encoding genes out of potentially a few hundred in the apple genome were identified as targets for miR482 from this pathosystem. On the other hand, only two ARF genes were shown to be the targets for miR160 out of several dozens of likely ARF family members. Great variation of the detected "tag abundance" existed per gene/miRNA species/library, from a single digit to over a thousand (HF12099, polyphenol oxidase), although this value can be dependent on the expression levels of both the target gene and miRNA. For some genes, such as those encoding laccases, it appeared the cleavage activity was reduced in *P. ultimum* infected tissues for both resistant and susceptible genotypes (L2 and L3, respectively), as compared with the mock-inoculation control tissue (L1). For other genes such as those encoding MYBs targeted by miR858, an elevated cleavage activity was observed for most target genes. In many cases, more than one member of the same miRNA family were shown to target the same gene ID, such as those genes encoding "growth regulating factors" that were targeted by miR396 species and genes encoding "auxin response factor" targeted by miR167 species. In contrast, many other genes showed a strict one (miRNA species) to one (gene ID) interaction pattern, such as those genes encoding laccase and targeted by miR397 species and R genes targeted by miR482 species. These identified target genes consist of valuable candidates for subsequent functional analysis to define their specific contribution to apple roots resistance to *P. ultimum*.

Three laccase encoding genes (laccase −3, −5, and −7), the target genes of miR397b based on degradome sequencing analysis, showed mostly upregulated expression patterns in response to *P. ultimum* infection (**Figure 4**). Among them, laccase-7 appeared to be more responsive to *P. ultimum* infection especially for resistance genotypes. For example, the detected transcript level of laccase-7 was increased three-fold in the infected root tissues of the resistant genotype #161, as compared to the mock-inoculated control tissue. The upregulated expression of these target genes corresponded to the downregulated expression of miR397b in response to *P. ultimum* infection. The observation of upregulated expression of these apple laccase genes in *P. ultimum* infected apple root tissues is consistent with the findings from a previous comparative transcriptome analysis between a resistant genotypes G.935 and a susceptible genotype B.9, which showed a peak response at 48 hpi and with stronger induction in the roots of the resistant genotype (Zhu et al., 2019). Therefore, the expression profiles of these laccase encoding genes are consistent with the findings from degradome sequencing, i.e., the reduced expression of miR397b and attenuated cleavage events likely contributed to the

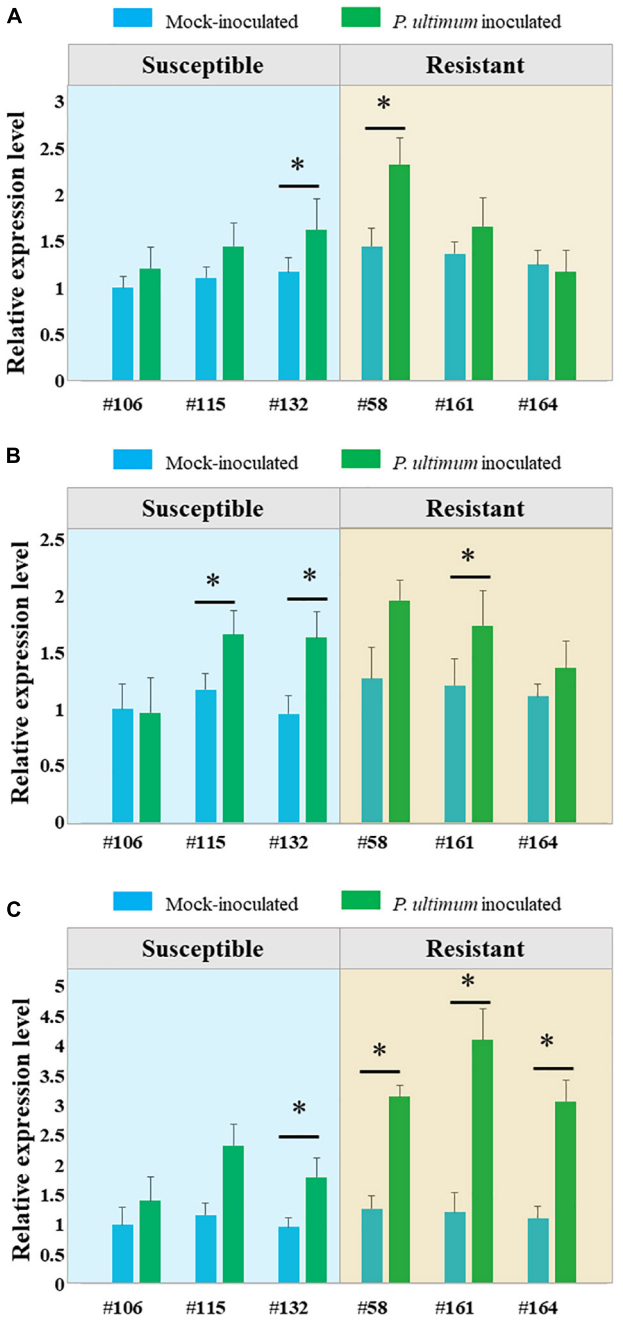


FIGURE 4 | Genotype-specific expression patterns of three laccase encoding genes in apple roots in response to *Pythium ultimum* infection. **(A)** Laccase-3; **(B)** Laccase-5 and **(C)** Laccase-7. The expression levels of these genes were measured by qRT-PCR. Genotypes are listed along *X* axis, with susceptible genotypes grouped at the left panel, and resistant genotypes grouped at right panel. Blue bar represents value of mock-inoculated root tissue and green bar represents the value of *P. ultimum* inoculated root tissue for each genotype. The values on *Y* axis represent the fold change of detected transcript level after normalizing to a reference gene (MD02G1221400) and calibrating by values of mock inoculated root tissue of the susceptible genotype #106. The values are the average of three biological replicates, and error bars are the standard deviation (SD) of fold changes. Error bars represent SE of three independent biological replicates. Asterisks denote statistically significant differences in a one-tailed Mann–Whitney *U* test (*$P < 0.05$).

TABLE 5 | The genotype-specific expression of miR397b and target genes in response to *Pythium ultimum* infection of apple roots.

Genotype-specific expression: miR397b-known-5p-mature						
Susceptible genotypes						
	Control			***P. ultimum* infected**		
#106	962.179	1088.28	1174.93	511.3	491.7	548.6
#115	864.0	945.8	1100.5	604.4	593.9	608.5
#132	977.9	1491.3	1115.1	300.2	416.5	398.1
	Ave (S_CK) = [a]1080.0			**Ave (S_Pu) = [b]497.0**		
Resistant genotypes						
	Control			***P. ultimum* infected**		
#58	802.8	1392.7	777.4	600.5	448.1	541.7
#161	583.8	528.8	590.2	248.8	244.5	261.3
#164	475.9	341.7	534.1	335.7	339.5	306.6
	Ave (R_CK) = [a]669.7**			**Ave (R_Pu) = [b]369.6***		

The identified target genes based on degradome sequencing: Laccase-5 OS = *Arabidopsis thaliana* GN = LAC5 PE = 2 SV = 1 (also, laccase-3 and laccase-7) (*P*-value = 0)

Cleavage site	**Target site sequence**	**Tag abundance**		
		L1	L2	L3
713	AGUCAUCAACGCUGCACUCAA	2	11	N/A
662	CCUAAUCAACGCUGCACUCAA	30	N/A	N/A
647	CCUAAUCAACGCUGCACUCAA	45	N/A	82
779	AGUCGUCAACUCUGCACUCAA	15	N/A	N/A

*The values in the top section of the table, are the normalized read counts for each replicate per genotype/treatment. The average values are calculated for individual group (R vs. S), and under either mock-inoculation or P. ultimum infection. Different letters (a or b) in front of the average values indicate the significant difference between treatments (mock-inoculation and P. ultimum inoculation). Asterisks denote statistically significant differences in a one-tailed Mann–Whitney U test (*P < 0.05) between genotype-groups (resistant and susceptible) of the same treatment (mock-inoculation or P. ultimum inoculation).*

upregulated expression of these laccase genes in the infected apple root tissues.

Genotype-Specific Expression of Selected miRNAs and Their Target Cleavage Activity

MiR397b-known-5p-mature is one of the four members from this family abundantly expressed in apple roots, and its cleavage activity on target (laccase) genes was only detected for miR397b (**Tables 4**, **5**). One of the notable features regarding the genotype-specific miR397b expression, similar to miR397a (**Figure 2**), was that it expressed at a significantly lower level in mock-inoculated root tissues of resistant genotypes (except R-#58) compared to that of the susceptible genotypes. In response to *P. ultimum* infection, its expression was downregulated for all genotypes. Nevertheless, the lowest average value of read counts was detected in the infected root tissues of the resistant genotypes. The data from degradome sequencing indicated that three laccase encoding genes that are homologous to *Arabidopsis thaliana* laccase −3, −5, and −7, were the targets of miR397b. Furthermore, a substantially higher cleavage activity was observed in the infected root tissues of susceptible genotypes (L3), compared to that in resistant genotypes (L2). Taken together, the reduction of miR397b may result in less cleavage of laccase target mRNA, which could lead to higher laccase enzyme activity, possibly contributing to the observed resistance to *P. ultimum* infection.

Resistance protein encoding genes, or R genes, are evidently the key players during plant-pathogen interactions. The differential expression patterns of miR482 between R and S genotypes and specifically identified targeted R genes by degradome sequencing were among the key findings from the current study (**Table 1** and **Supplementary Table 1**). For example, miR482c-known-3p-mature is one of the three members in miR482 family which showed intriguing expression patterns among six genotypes and in response to *P. ultimum* infection (**Table 6**). In response to *P. ultimum* inoculation, the levels of miR482c were downregulated in both R and S genotypes, but with slightly larger reduction (>1x) in R group than that of S groups (<1x). The degradome sequencing identified the target of miR482c-known-3p-mature is Arabidopsis RPM1 homolog encoding gene, with two cleavage sites. Based on the detected values of tag abundance in three different libraries, it appeared that a more active cleavage activity occurred in susceptible genotypes than in resistant genotypes. Notably, the same RPM homolog gene was identified as one of the downregulated R genes specifically in susceptible B.9 plants from a previous comparative transcriptome

analysis (Zhu et al., 2019). Therefore, at transcriptional or post-transcriptional levels, a consistent regulation scheme seemed to corroborate each other.

The expression of miR10986 was generally detected at a low to moderate level in apple roots (**Table 7**), but a relatively large variation at read count values (2–3x) were observed among genotypes within the same R or S groups, or even within replicates for a given sample (genotype/treatment). Such uncommon variation among genotypes (within the same genotype group) probably indicated that its expression is also prone to certain abiotic stress conditions. In response to *P. ultimum* infection, downregulation was observed in all genotypes, but the degree of downregulation was more substantial (>1x) in resistant genotypes compared to that of susceptible genotypes. Similar to the regulation features for miR397, miR10986 also showed the lower basal expression in mock-inoculated tissues of R group as compared to that in susceptible genotypes. Degradome analysis indicated a polyphenol oxidase (PPO) is the cleavage target of miR10986. The overall cleavage activity on these PPO genes (for example, HF12100) was one of the strongest among the observed miRNA-target pairs from this dataset. However, a clear trend was missing, as the stronger cleavage activity was on either library L2 or L3 depending on the choices of cleavage sites. Therefore, the role of miR10986-PPO regulation during interaction between apple root and *P. ultimum* deserves future investigation.

Both the mature and star forms of miR7122a were detected with comparable abundance in apple roots (**Table 8**). In susceptible genotypes, their expression levels were slightly downregulated due to *P. ultimum* infection (<25% for both mature and star form). In contrast, variable regulation patterns were exhibited among resistant genotypes, i.e., slight upregulated for its mature form (∼5%) and substantially downregulated (47.8%) for its star form. Analysis of degradome sequencing data demonstrated that a homolog to the "putative pentatricopeptide repeat (PPR)-containing protein At1g12700" was the target of miR7122a. Slightly elevated cleavage activities on this target gene occurred in the resistant genotypes (L2). The roles of PPR proteins in plant immunity have been reported (Schmitz-Linneweber and Small, 2008; Barkan and Small, 2014) in other pathosystems, the definitive contribution of this miR-target pair in shaping up the resistance traits in apple roots to *P. ultimum* infection deserve subsequent research.

PhasiRNA Analysis for miRNA390 and miRNA482/2118

PhasiRNAs are another main class of small RNAs in plants. Interestingly, we found that overall production of phasiRNAs was significantly lower in the *P. ultimum*-inoculated root tissues for both susceptible and resistant materials, suggesting that phasiRNA pathway contributes to the defense to *P. ultimum*.

TABLE 6 | The genotype-specific expression of miR482c and target genes in response to *Pythium ultimum* infection of apple roots.

Genotype-specific expression: miR482c-known-3p-mature						
Susceptible genotypes						
	Control			***P. ultimum* infected**		
#106	1041.2	1291.5	1424.5	541.1	697.0	413.4
#115	1393.7	1260.4	1173.9	916.5	846.5	825.6
#132	1281.1	2224.9	1455.1	714.4	798.6	671.0
	Ave (S_CK) = [a]1394			**Ave (S_Pu) = [b]713.8**		
Resistant genotypes						
	Control			***P. ultimum* infected**		
#58	1341.2	1628.7	1368.5	560.3	724.2	585.8
#161	898.0	1054.3	1482.5	598.5	622.8	538.5
#164	1121.1	583.5	719.2	523.1	443.3	332.6
	Ave (R_CK) = [a]1133.0			**Ave (R_Pu) = [b]547.7***		

The identified target genes based on degradome sequencing: Disease resistance protein RPM1 OS = *Arabidopsis thaliana* GN = RPM1 PE = 1 SV = 1 (*P*-value = 4.67E-100)

Cleavage Site	**Target site sequence**	**Tag abundance**		
		L1	L2	L3
655	GGAAUGGGAGGCAUAGGCAAGA	9	N/A	5
3391	GGAAUGGGAGGAAUGGGGAAGA	N/A	N/A	112

*The values in the top section of the table, are the normalized read counts for each replicate per genotype/treatment. The average values are calculated for individual group (R vs. S), and under either mock-inoculation or P. ultimum infection. Different letters (a or b) in front of the average values indicate the significant difference between treatments (mock-inoculation and P. ultimum inoculation). Asterisks denote statistically significant differences in a one-tailed Mann–Whitney U test (*P < 0.05) between genotype-groups (resistant and susceptible) of the same treatment (mock-inoculation or P. ultimum inoculation).*

TABLE 7 | The genotype-specific expression of miR10986 and target genes in response to *Pythium ultimum* infection of apple roots.

Genotype-specific expression: miR10986 probable 5p mature						
Susceptible genotypes						
	Control			***P. ultimum* infected**		
#106	65.9	67.8	65.6	31.9	81.2	17.6
#115	208.1	267	271.5	138.7	157.3	161
#132	170.5	630.4	278.2	261.7	139.6	141.6
		Ave (S_CK) = 225			**Ave (S_Pu) = 125.6**	
Resistant genotypes						
	Control			***P. ultimum* infected**		
#58	223	260.7	232.1	101.4	111.4	108.3
#161	189.6	167.3	111.8	80	42.2	67.3
#164	68.8	58	50	39	42.2	34.1
		Ave (R_CK) = [a]151.3			**Ave (R_Pu) = [b]69.5***	

The identified target genes based on degradome sequencing: Polyphenol oxidase, chloroplastic OS = *Malus* × *domestica* PE = 2 SV = 1 (*P*-value = 0)

Cleavage site	**Target site sequence**	**Tag abundance**		
		L1	L2	L3
1692	UUGGUGGUGACUUUGGUGCCG	92	N/A	N/A
1692	UUAGUGGUGACUUUGGUGCCA	1417	1426	724
930	UUGGUGGUGACUUUGGUGCCA	1390	1493	739
1686	UUGGUAGUGACUUUGGUGCCG	146	N/A	43
1752	CGUGGUGGUGACUUUGGUGCCC	105	139	154
1767	UGUGGUGGUGACUUUAGUGCCC	3	N/A	N/A

*The values in the top section of the table are the normalized read counts for each replicate per genotype/treatment. The average values are calculated for individual group (R vs. S), and under either mock-inoculation or P. ultimum infection. Different letters (a or b) in front of the average values indicate the significant difference between treatments (mock-inoculation and P. ultimum inoculation). Asterisks denote statistically significant differences in a one-tailed Mann–Whitney U test (*P < 0.05) between genotype-groups (resistant and susceptible) of the same treatment (mock-inoculation or P. ultimum inoculation).*

miR390 triggers the production of trans-acting siRNA3 (TAS3)-derived tasiRNAs to repress auxin responsive factor 2/3/4 (ARF2/3/4) genes, critical for auxin signaling; these tasiRNAs are known as tasiARFs. In plants, 5′ proximal miR390 target site on TAS3 is non-cleavable while 3′ proximal target site is sufficient for miR390-directed slicing, leading to a "two-hit, one-cleavage" model (Xia et al., 2017). In this study, the expression levels of miR390, tasiARF and all siRNAs from TAS3 transcripts were all significantly downregulated in *P. ultimum*-inoculated root tissues (**Figure 5A**), indicating that auxin signaling module regulated by the miR390-TAS3-ARF pathway were turned down by the *P. ultimum* infection. Detailed examination of the mapping profile of a *TAS3* gene revealed that the miR390 cleavage site set the phase of the phasiRNA production, and indeed the abundance of sRNAs in mock-inoculated sample was much higher than that in *P. ultimum*-inoculated sample (**Figure 5B**).

MiR482/2118 is a well-known miRNA family important for disease resistance. All miRNA members of this family, including both miR482 and miR2118 variants are 22-nt long, and are capable to target NBS-LRR genes to trigger phasiRNAs biogenesis (Cuperus et al., 2010; Shivaprasad et al., 2012). In this study, a significant reduction on the expression levels of miR482, miR2118, and siRNAs from NBS-LRR transcripts were found in the *P. ultimum*-inoculated root tissues (**Figure 5C**), elucidating that miR482-mediated silencing of NBS-LRR genes was released in root tissues upon *P. ultimum* inoculation to activate defense. Detailed examination of the mapping profile of a NBS-LRR gene (R protein RPM1 homolog, HF37161) revealed that the miR482 cleavage site set the phase of the phasiRNA production and the abundance of phasiRNAs was greatly decreased in *P. ultimum*-inoculated roots (**Figure 5D**). These results regarding phasiRNAs suggested that apple trees turned down the endogenous sRNA silencing pathway to promote quick resistance response to the infection of *P. ultimum*. This kind of responses is likely widely present in plants.

Genomic Location of miR397a in Apple Genome

A comparison of miR397a precursor sequences against Robusta 5 *de novo* genome assembly identified four contig sequences (**Figure 6A**); two of which aligned to the same regions of chromosome 5 and chromosome 10, respectively, of the Golden Delicious Double Haploid genome (Daccord et al., 2017). The

TABLE 8 | Genotype-specific expression of miR7122a-known-5p-mature, 3P-star, and identified target genes in apple roots in response to *Pythium ultimum* infection.

Genotype-specific expression: miR7122a-known-5p-mature and 3p-star							
Susceptible genotypes							
		Control			***P. ultimum* infected**		
#106	5p-mature	462.5	734.0	485.2	637.0	498.1	558.4
	3p-star	415.1	336.8	447.9	308.9	397.7	284.1
#115	5p-mature	1247.3	841.1	791.6	919.0	784.5	1216.9
	3p-star	698.1	638.5	568.4	802.6	673.7	803.2
#132	5p-mature	730.7	1022.6	760.6	236.0	414.2	402.2
	3p-star	774.8	1077.2	652.2	308.2	572.1	552.0
		Ave (S_CK) = 786.2 (m)			**Ave (S_Pu) = 629.6 (m)**		
		Ave (S_CK) = 623.2 (s)			**Ave (S_Pu) = 522.5 (s)**		
Resistant genotypes							
		Control			***P. ultimum* infected**		
#58	5p-mature	824.2	1604.0	817.0	1015.4	930.1	875.9
	3p-star	1261.9	1393.5	763.8	686.5	670.9	672.1
#161	5p-mature	945.4	891.1	1081.8	1127.4	1154.1	1139.6
	3p-star	634.6	635.0	835.3	521.9	511.9	477.6
#164	5p-mature	886.7	910.0	733.2	870.5	823.2	1189.3
	3p-star	688.0	546.7	545.0	513.3	453.8	431.6
		Ave (R_CK) = 965.9 (m)*			**Ave (R_Pu) = 1013.9 (m)**		
		Ave (R_CK) = [a] 811.5 (s)**			**Ave (R_Pu) = [b]548.9 (s)**		

The identified target gene based on degradome sequencing: Putative pentatricopeptide repeat-containing protein At1g12700, mitochondrial OS = *Arabidopsis thaliana* GN = At1g12700 (*P*-value = 2.19E=-10)

Cleavage site	**Target site sequence**	**Tag abundance**		
		L1	L2	L3
281	CGGCCGUGAUUUCUUUGUAUAA	N/A	187	162

*The values in the top section of the table are the normalized read counts for each replicate per genotype/treatment. The average values are calculated for individual groups (R vs. S), and under either mock-inoculation or P. ultimum infection. Lower case letter "m" and "s" indicate the mature and star form of the miR7122a. Different letters (a or b) in front of the average values indicate the significant difference between treatments (mock-inoculation and P. ultimum inoculation). Asterisks denote statistically significant differences in a one-tailed Mann–Whitney U test (*P < 0.05) between genotype-groups (resistant and susceptible) of the same treatment (mock-inoculation or P. ultimum inoculation).*

two overlapping contigs on same chromosomes represented the distinct haplotypes of the heterozygous apple genome. In addition, the regions of chromosomes 5 and 10 represent paralogs that were differentiated from a single ancestral chromosome through ancient whole genome duplication of the apple genome (Velasco et al., 2010). Annotation of 20 kb sequences around miR397a genomic loci identified a zinc-finger domain protein, an unknown protein, and a major facilitator superfamily protein. The unknown protein sequence appeared to match the promoter region of a miR397a gene from *Pyrus pyrifolia* (NCBI blast identifier: KY438936.1). Further comparison of Robusta 5 and Ottawa 3, across the miR397a targeted 20 kb genomic regions, identified 1,278 variants between them (**Figure 6B**). Co-linear contigs on chromosome 5 had relatively more variants than on chromosome 10 between Robusta 5 and Ottawa 3 on these regions. An alignment of *P. ultimum* susceptible (S) and resistant (R) genotype groups against Robusta 5 contigs resulted in 27 and 33 unique variants specific to each group, respectively (**Figure 6B**). A higher coverage of these regions with more sequencing reads can likely identify more variants in these regions.

DISCUSSION

Upon pathogen infection, plants activate a sophisticated defense system that initiates massive reprogramming of global gene expression. As an integral part of the host transcriptome themselves, sRNAs are versatile and important post-transcriptional regulators of gene expression in almost all cellular processes including plant-pathogen interactions (Staiger et al., 2013; Weiberg et al., 2014; Yang and Huang, 2014; Chaloner et al., 2016). These sRNAs negatively regulate gene expression by binding and cleavage of their specific target

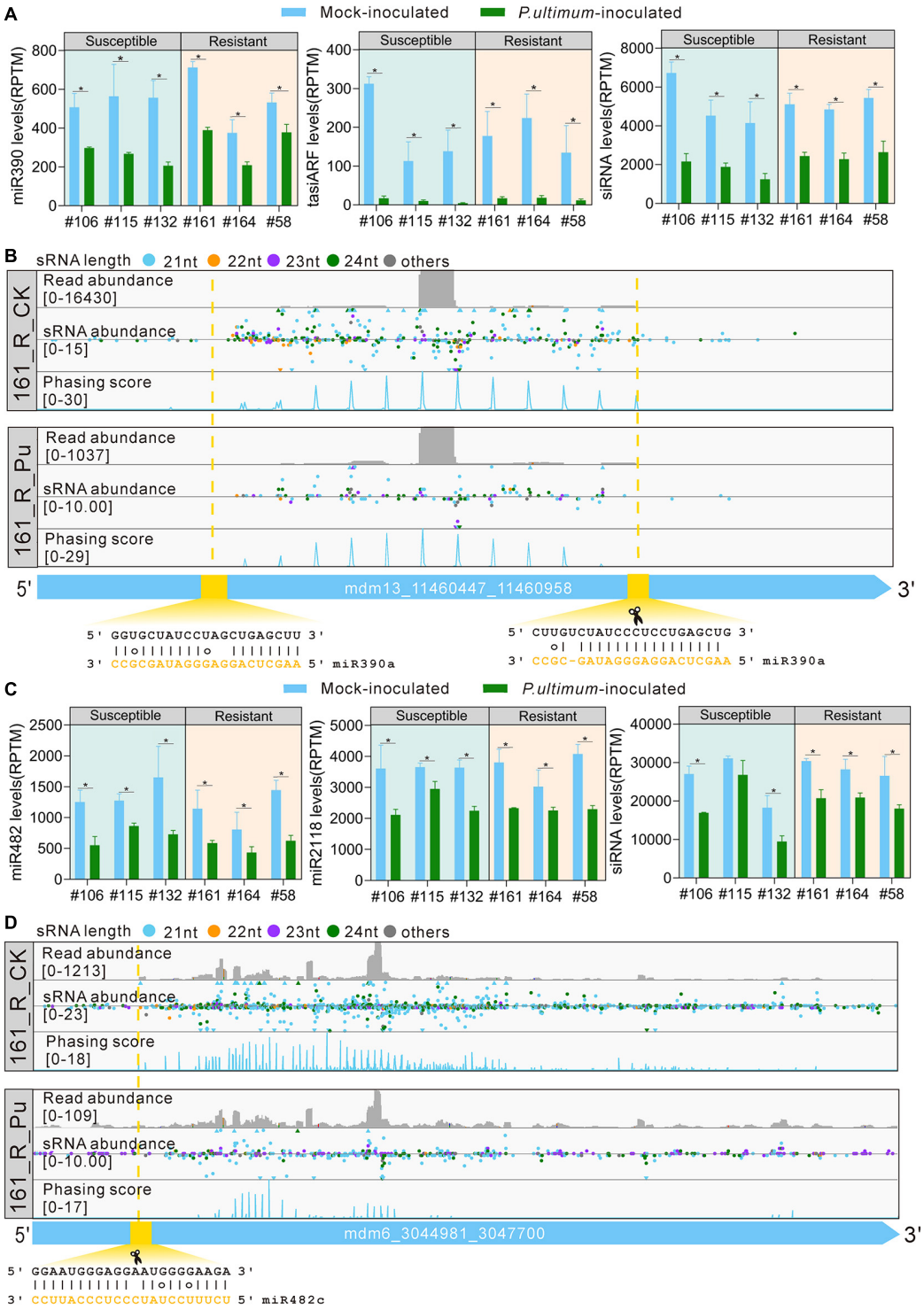


FIGURE 5 | miRNA triggers phasiRNA biogenesis in response to *P. ultimum* inoculation. **(A)** The expression levels of miR390, tasiARF, and siRNA from TAS3 transcripts in mock-inoculated (blue bars) and *P. ultimum*-inoculated (green bars) root issues. **(B)** Read abundance, sRNA abundance and phasing score distribution of a TAS3 locus in mock-inoculated and *P. ultimum*-inoculated root issues were viewed in IGV-sRNA. The yellow dashed lines and rectangle indicate the target site and slicing site of miR390a. **(C)** The expression levels of miR482, miR2118, and siRNA from NBS-LRR transcripts (HF37161) in mock-inoculated (blue bars) and *P. ultimum*-inoculated (green bars) root tissues. **(D)** Read abundance, sRNA abundance, and phasing score distribution of a representative PHAS locus in mock-inoculated and *P. ultimum*-inoculated root tissues were viewed in IGV-sRNA. The yellow dashed lines and rectangle indicate the target site of miR482c. Phasing score was calculated based on the mapping results of 21-nucleotide siRNAs (Xia et al., 2013). Error bars represent SE of three independent biological replicates. Asterisks denote statistically significant differences in a one-tailed Mann–Whitney *U* test (*$P < 0.05$).

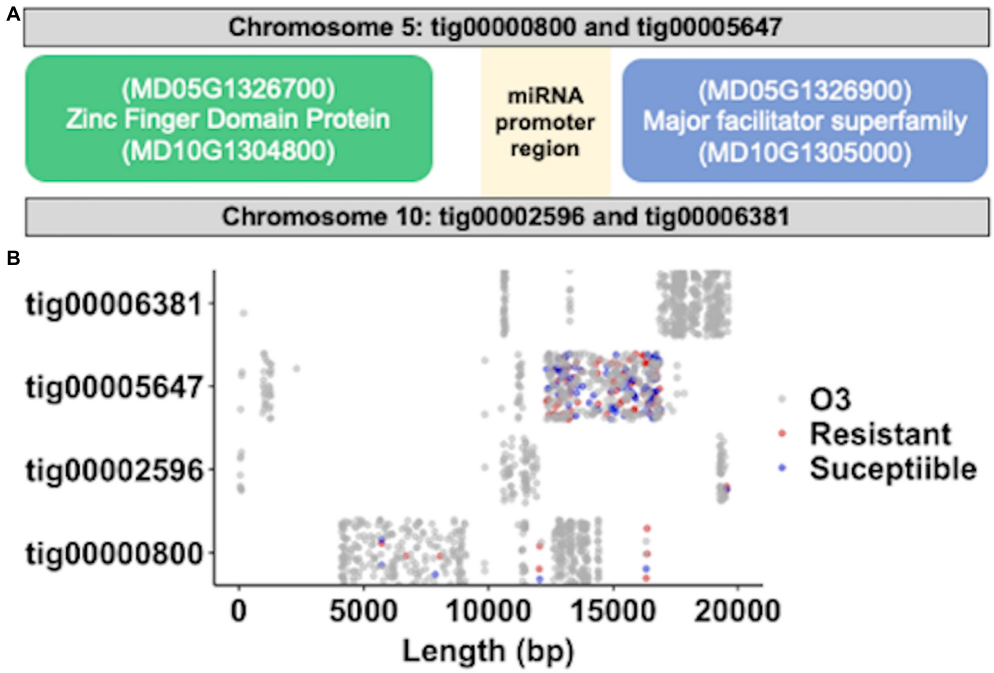


FIGURE 6 | Genomic location of miR397a, expression variant analysis. **(A)** Illustration of physical map around MIR397a. The two regions on chromosome 5 and 10 that matches MIR397a containing contigs are shown. The relative upstream and downstream sequences from MIR397a position was used to identify the annotated genes including zinc finger domain protein and a major facilitator superfamily protein on the two apple chromosomes. **(B)** Distribution of variants across the four MIR397a matching "Robusta 5" contigs after its comparison with the "O3" parent (gray dots), resistance (red dots), and susceptible (blue dots) genotypes.

mRNAs, or repressing the translation process (Bartel, 2004; Axtell and Bowman, 2008). The current study is part of an integrated effort to define the resistance mechanisms in apple roots to infection from *P. ultimum*, through the identification of key miRNA families and their corresponding targets.

The majority of identified miRNA families exhibited downregulated expression patterns in response to *P. ultimum* infection, although variable degrees of downregulation existed between resistant and susceptible genotypes. It is apparent that most of these target genes positively regulate defense activation in apple roots, and upon pathogen infection the reduced or attenuated cleavage activities from corresponding miRNAs lead to elevated defense activation. On the other hand, there is a possibility that the pathogen-derived effectors, toxins, or even mobile sRNAs, effectively and non-selectively sabotaged host miRNA pathways and many other cellular processes (Qiao et al., 2013; de Vries et al., 2017; Hou et al., 2019). Therefore, existence of non-host (or passive) resistance, or certain forms of preformed defense systems, such as the chemo/physical barrier impeding the initial pathogen penetration, may be a critical contributor to resistance to this necrotrophic pathogen. The microscopic features of necrosis progression or arrested necrotic progression could partially owe to the enhanced tissue fortification which impede pathogen hyphae penetration at the initial stage of infection and enhance the plant survivability for those resistant genotypes (Zhu et al., 2018b).

In response to pathogenic pressure, an increased level of tissue fortification such as lignin deposition has been hypothesized as a fundamental resistance mechanism (Vance et al., 1980; Bhuiyan et al., 2009; Miedes et al., 2014; Yang et al., 2018). In this dataset, four miRNA families which belong to copper (Cu) microRNAs (Pilon, 2017), i.e., laccase-targeting miR397, *SOD*-targeting miR398, nudix hydrolase-targeting miR408, and *PPO*-targeting miR10986, were markedly downregulated in infected root tissue. The targets of these miRNAs are known to directly participate in abiotic and biotic stresses through increased H_2O_2 generation, enhanced lignin content and modified cell wall composition (Lu et al., 2013). The levels of downregulation for both miR397 and miR10986 were more obvious in resistant genotypes, than in susceptible genotypes. Interestingly, even in mock-inoculated root tissues of resistant apple rootstock genotypes, much lower levels of miR397a/b and miR10986 were observed. The elevated activities of laccase and PPO appear to exist prior to pathogen exposure in resistant genotypes, which likely function as a preformed defense mechanism. Upon pathogen challenge, the stronger downregulation of laccase-targeting miRNA was observed in resistant genotypes, possibly leading to a quicker and stronger tissue fortification for an effective impediment of pathogen progression at the initial stages of infection. As an important part of the inducible defense mechanisms, production of secondary metabolites such as phenolics from phenylpropanoid pathway and the formation of lignin are believed to be responsible for delay or stop of the establishment of pathogen infection in many pathosystems (Danielsson et al., 2011; Oliva et al., 2015). Gene expression regulation such as that from MYB TFs and microRNAs as

well as biochemical feature such as secondary metabolites from phenylpropanoid pathway and defense phytohormones appear to be evolutionarily conserved from non-flowering land plants and even streptophyte algae to angiosperms (Overdijk et al., 2016; de Vries et al., 2018a; Carella et al., 2019). Future studies are needed to define the detailed functional roles of Cu-miRNAs in shaping up resistance traits in apple roots to *P. ultimum* infection.

Post-transcriptional regulation of R genes is known to be a crucial aspect of plant immune response (Staiger et al., 2013; Weiberg et al., 2014; Liu et al., 2017; Islam et al., 2018). The roles of miR482/2118 on the expression of NBS-LRRs in tomato (*Solanum lycopersicum*) during infection by *Phytophthora infestans* infection are well investigated; and overexpression of mir482c was shown to induce enhanced susceptibility to late blight in tomato (de Vries et al., 2018b; Jiang et al., 2018; Canto-Pastor et al., 2019; Hong et al., 2019). Interestingly, in addition to a decreased expression of target NBS-LRR genes, the transgenic tomato plants overexpressing miR482c also showed lower peroxidase (POD), superoxide dismutase (SOD), and phenylalanine ammonia-lyase (PAL) activities, indicating the interconnected immune responses (Hong et al., 2019). Our data revealed a consistent downregulation of miR482/miR2118 superfamily across genotypes, which indicated that regulation of R gene expression, through miRNA function, is essential for the resistance traits of apple roots to *P. ultimum* infection. A slightly higher level of downregulation appeared to be the case in infected roots of resistant genotypes. In many plant species, including perennial woody plants, the miRNA–NB-LRR interactions result in the production of phased, secondary small interfering (phasi)RNAs, which function in both *cis* and *trans*, to amplify the regulatory effects across additional members of the target gene family (Katiyar-Agarwal and Jin, 2010). Therefore, it is likely that the subtle variation of expression of miR482/miR2118 leads to amplified effect on phasiRNA biogenesis, which may become an important factor differentiating apple roots resistance vs. susceptibility.

Hormone signaling and their interactions with corresponding transcription factors (TFs) are the integrated modules regulating plant defense response, and both elements are the preferred targets of miRNA regulation (Curaba et al., 2014). At the same time, both miRNAs and TFs are the primary regulators of gene expression, often for the same target genes at transcriptional and/or post-transcriptional levels (Li et al., 2014; Samad et al., 2017). The complicated interactions among these regulatory components (miRNA-TF-hormone signaling) are the common theme in many pathosystems (Balmer and Mauch-Mani, 2013; Weiberg and Jin, 2015; Chaloner et al., 2016; Liu et al., 2017). From our dataset, miR393, miR160, and miR167, all of which target auxin signaling, were among a few of the identified miRNA families with mostly upregulated expression upon *P. ultimum* infection. Interestingly, miR160 showed partially differential regulation between R and S groups, where two out of three resistant genotypes exhibited downregulated expression in response to *P. ultimum* infection. Results from previous transcriptome analyses also identified regulatory components related to JA, auxin, WRKY, MYB, and NAC, which are largely consistent with the findings in the current study; (Shin et al., 2016b; Zhu et al., 2017, 2019). The role of these regulatory components in secondary metabolites including monolignols or the precursors of lignin deserves further investigation.

The identification of *bona fide* targets of a given miRNA species represents one of the fundamental aspects of small RNA research. Plant miRNAs can target multiple non-paralogous but functionally related genes (Djami-Tchatchou et al., 2017; You et al., 2017), which are often from a large gene family. Utilizing powerful degradome sequencing, a few target genes specific to this pathosystem were experimentally identified (rather than by *in silico* prediction). For example, three miRNA families (miR159, miR319, and miR858) are known to target a large number of MYB TFs in the apple genome, this approach pinpointed less than a dozen of MYB TF encoding genes which are potentially essential in this pathosystem. As an extreme example, only a single SPL encoding gene was identified as the target of miR156. In addition, novel targets were identified beyond the "commonly" established spectrum of genes functioning in this pathosystem such as those genes encoding PPRs (pentatricopeptide repeat-containing proteins). Most plants contain several hundred PPRs, the RNA-binding proteins with proposed functions of RNA editing, RNA splicing, RNA cleavage and translation within mitochondria and chloroplasts (Barkan and Small, 2014; Park et al., 2014) which has been linked to plant resistance response (Schmitz-Linneweber and Small, 2008; Barkan and Small, 2014). Moreover, the quantified "tag abundance" also provides the estimated miRNA cleavage activities between resistant or susceptible genotype groups. For example, the detected tag abundance for two target gene IDs "HF12099-RA and HF12100-RA" (polyphenol oxidase) were about 50% in infected susceptible root tissues (L3), compared to the values of mock-inoculated control tissues (L1), or infected resistant root tissues (L2). These identified target genes constitute a focused candidate gene list, which may significantly contribute to apple root resistance traits through post-transcriptional regulations.

As part of the integrated effort to uncover the underpinned molecular mechanism controlling apple roots resistance to *P. ultimum*, the current dataset of miRNA profiling and degradome sequencing offers a unique perspective on its post-transcriptional regulation. The identified "miRNA-target gene" pairs likely represent the crucial components functioning in apple root defense activation to *P. ultimum* infection. As examples, genotype-specific expression patterns for miR397-laccse, miR10986-PPO, and miR398-SOD appeared to link with apple root resistance vs. susceptibility. Cell wall fortification through the function of copper protein encoding genes could be a key strategy to defend apple roots against this necrotrophic pathogen. Young apple roots, as a primary organ for taking up water and nutrients, lack effective protection layers such as cuticle or wax in aerial parts of a plant to deter or impede penetration from pathogen like *P. ultimum*. Winning the chemical war at the early stage of infection is crucial to thwart disruptive arsenals of effectors and toxins from this fast-growing necrotrophic pathogen. Therefore, quick and effective cell wall modification through the function of these Cu-miRNAs

(Pilon, 2017) can significantly determine the outcome between the apple roots and *P. ultimum*. Such initial defense reactions are likely "buying the time" for a steady and robust defense activation to be developed. Inclusion of multiple genotypes with contrasting resistance phenotypes enhanced the reliability of this comprehensive dataset from this study. Those miRNA families targeting R genes, hormonal signaling, and various TFs represent the core regulation circuits for this pathosystem. Noticeably, many of the identified target genes in the current study are consistent with the results from previous transcriptome analyses (Shin et al., 2016b; Zhu et al., 2017, 2019). As an example, the same RPM1 homolog gene was also identified from a susceptible genotype B.9 with downregulated expression (Zhu et al., 2019). In summary, the identified miRNA species and their corresponding target genes constitute a valuable resource for subsequent functional analysis to define their detailed roles in shaping up the resistance traits in apple roots against *P. ultimum* infection. The findings from this study significantly contribute to the effort for deciphering the molecular mechanisms controlling defense responses for this less explored pathosystem between apple roots and a necrotrophic pathogen.

DATA AVAILABILITY STATEMENT

The datasets presented in this study can be found in online repositories. The names of the repository/repositories and accession number(s) can be found in the article/**Supplementary Material**.

AUTHOR CONTRIBUTIONS

YZ, RX, AK, and GF participated in the experimental design, data analysis, interpretations, and manuscript writing. MS performed most of the experiments of phenotyping and RNA preparation. GL and JS analyzed the dataset and contributed to the manuscript preparation. All authors contributed to the article and approved the submitted version.

FUNDING

This work was supported by the USDA-ARS base fund.

ACKNOWLEDGMENTS

The authors would like to thank India Amy Cain for language editing and reviewing the manuscript.

SUPPLEMENTARY MATERIAL

The Supplementary Material for this article can be found online at: https://www.frontiersin.org/articles/10.3389/fpls.2021.629776/full#supplementary-material

REFERENCES

Addo-Quaye, C., Miller, W., and Axtell, M. J. (2009). CleaveLand: a pipeline for using degradome data to find cleaved small RNA targets. *Bioinformatics* 25, 130–131. doi: 10.1093/bioinformatics/btn604

Axtell, M. J. (2013). Classification and comparison of small RNAs from plants. *Annu. Rev. Plant Biol.* 64, 137–159.

Axtell, M. J., and Bowman, J. L. (2008). Evolution of plant microRNAs and their targets. *Trends Plant Sci.* 13, 343–349.

Balmer, D., and Mauch-Mani, B. (2013). Small yet mighty–microRNAs in plant-microbe interactions. *MicroRNA* 2, 73–80.

Barkan, A., and Small, I. (2014). Pentatricopeptide repeat proteins in plants. *Annu. Rev. Plant Biol.* 65, 415–442.

Bartel, D. P. (2004). MicroRNAs: genomics, biogenesis, mechanism, and function. *Cell* 116, 281–297.

Bhuiyan, N. H., Selvaraj, G., Wei, Y., and King, J. (2009). Role of lignification in plant defense. *Plant Signal. Behav.* 4, 158–159.

Bolger, A. M., Lohse, M., and Usadel, B. (2014). Trimmomatic: a flexible trimmer for Illumina sequence data. *Bioinformatics* 30, 2114–2120.

Bologna, N. G., and Voinnet, O. (2014). The diversity, biogenesis, and activities of endogenous silencing small RNAs in *Arabidopsis*. *Annu. Rev. Plant Biol.* 65, 473–503. doi: 10.1146/annurev-arplant-050213-035728

Borges, F., and Martienssen, R. A. (2015). The expanding world of small RNAs in plants. *Nat. Rev. Mol. Cell Biol.* 16:727.

Canto-Pastor, A., Santos, B. A., Valli, A. A., Summers, W., Schornack, S., and Baulcombe, D. C. (2019). Enhanced resistance to bacterial and oomycete pathogens by short tandem target mimic RNAs in tomato. *Proc. Natl. Acad. Sci. U.S.A.* 116, 2755–2760. doi: 10.1073/pnas.1814380116

Carella, P., Gogleva, A., Hoey, D. J., Bridgen, A. J., Stolze, S. C., Nakagami, H., et al. (2019). Conserved biochemical defenses underpin host responses to oomycete infection in an early-divergent land plant lineage. *Curr. Biol.* 29, 2282.–2294. doi: 10.1016/j.cub.2019.05.078

Chaloner, T., van Kan, J. A., and Grant-Downton, R. T. (2016). RNA 'Information Warfare'in pathogenic and mutualistic interactions. *Trends Plant Sci.* 21, 738–748. doi: 10.1016/j.tplants.2016.05.008

Chen, C., Zeng, Z., Liu, Z., and Xia, R. (2018). Small RNAs, emerging regulators critical for the development of horticultural traits. *Horticult. Res.* 5, 1–14. doi: 10.1038/s41438-018-0072-8

Cuperus, J. T., Carbonell, A., Fahlgren, N., Garcia-Ruiz, H., Burke, R.T., Takeda, A., et al. (2010). Unique functionality of 22-nt miRNAs in triggering RDR6-dependent siRNA biogenesis from target transcripts in Arabidopsis. *Nat. Struct. Mol. Biol.* 17, 997–1003. doi: 10.1038/s41438-018-0072-8

Curaba, J., Singh, M. B., and Bhalla, P. L. (2014). miRNAs in the crosstalk between phytohormone signalling pathways. *J. Exp. Bot.* 65, 1425–1438.

Daccord, N., Celton, J.-M., Linsmith, G., Becker, C., Choisne, N., Schijlen, E., et al. (2017). High-quality de novo assembly of the apple genome and methylome dynamics of early fruit development. *Nat. Genet.* 49:1099. doi: 10.1038/ng.3886

Danecek, P., Auton, A., Abecasis, G., Albers, C. A., Banks, E., DePristo, M. A., et al. (2011). The variant call format and VCFtools. *Bioinformatics* 27, 2156–2158.

Danielsson, M., Lundén, K., Elfstrand, M., Hu, J., Zhao, T., Arnerup, J., et al. (2011). Chemical and transcriptional responses of Norway spruce genotypes with different susceptibility to *Heterobasidion* spp. infection. *BMC Plant Biol.* 11:154. doi: 10.1186/1471-2229-11-154

De Paoli, E., Dorantes-Acosta, A., Zhai, J., Accerbi, M., Jeong, D.-H., Park, S., et al. (2009). Distinct extremely abundant siRNAs associated with cosuppression in petunia. *RNA* 15, 1965–1970. doi: 10.1261/rna.1706109

de Vries, S., de Vries, J., and Rose, L. E. (2019). The elaboration of miRNA regulation and gene regulatory networks in plant–microbe interactions. *Genes* 10:310. doi: 10.3390/genes10040310

de Vries, S., de Vries, J., von Dahlen, J. K., Gould, S. B., Archibald, J. M., Rose, L. E., et al. (2018a). On plant defense signaling networks and early land plant evolution. *Commun. Integr. Biol.* 11, 1–14.

de Vries, S., Kukuk, A., von Dahlen, J. K., Schnake, A., Kloesges, T., and Rose, L. E. (2018b). Expression profiling across wild and cultivated tomatoes supports the

relevance of early miR482/2118 suppression for *Phytophthora* resistance. *Proc. R. Soc. B* 285:20172560. doi: 10.1098/rspb.2017.2560

de Vries, S., von Dahlen, J. K., Uhlmann, C., Schnake, A., Kloesges, T., and Rose, L. E. (2017). Signatures of selection and host-adapted gene expression of the *Phytophthora* infestans RNA silencing suppressor PSR2. *Mol. Plant Pathol.* 18, 110–124. doi: 10.1111/mpp.12465

Djami-Tchatchou, A. T., Sanan-Mishra, N., Ntushelo, K., and Dubery, I. A. (2017). Functional roles of microRNAs in agronomically important plants—potential as targets for crop improvement and protection. *Front. Plant Sci.* 8:378. doi: 10.3389/fpls.2017.00378

Eckardt, N. A. (2012). A microRNA cascade in plant defense. *Plant Cell* 24:840. doi: 10.1105/tpc.112.240311

Fei, Q., Xia, R., and Meyers, B. C. (2013). Phased, secondary, small interfering RNAs in posttranscriptional regulatory networks. *Plant Cell* 25, 2400–2415.

Fei, Q., Zhang, Y., Xia, R., and Meyers, B. C. (2016). Small RNAs add zing to the zig-zag-zig model of plant defenses. *Mol. Plant Microbe Interact.* 29, 165–169. doi: 10.1094/MPMI-09-15-0212-FI

German, M. A., Pillay, M., Jeong, D.-H., Hetawal, A., Luo, S., Janardhanan, P., et al. (2008). Global identification of microRNA–target RNA pairs by parallel analysis of RNA ends. *Nat. Biotechnol.* 26:941. doi: 10.1038/nbt1417

He, L., and Hannon, G. J. (2004). MicroRNAs: small RNAs with a big role in gene regulation. *Nat. Rev. Genet.* 5:522. doi: 10.1038/nrg1379

Hong, Y.-H., Meng, J., He, X.-L., Zhang, Y.-Y., and Luan, Y.-S. (2019). Overexpression of MiR482c in tomato induces enhanced susceptibility to late blight. *Cells* 8:822. doi: 10.3390/cells8080822

Hou, Y., Zhai, Y., Feng, L., Karimi, H. Z., Rutter, B. D., Zeng, L., et al. (2019). A Phytophthora effector suppresses trans-kingdom RNAi to promote disease susceptibility. *Cell Host Microbe* 25, 153–165 e155. doi: 10.1016/j.chom.2018.11.007

Islam, W., Qasim, M., Noman, A., Adnan, M., Tayyab, M., Farooq, T. H., et al. (2018). Plant microRNAs: front line players against invading pathogens. *Microb. Pathog.* 118, 9–17. doi: 10.1016/j.micpath.2018.03.008

Jaffee, B., Abawi, G., and Mai, W. (1982). Fungi associated with roots of apple seedlings grown in soil from an apple replant site. *Plant Dis.* 66, 942–944.

Jiang, N., Meng, J., Cui, J., Sun, G., and Luan, Y. (2018). Function identification of miR482b, a negative regulator during tomato resistance to *Phytophthora infestans*. *Horticult. Res.* 5, 1–11. doi: 10.1038/s41438-018-0017-2

Johnson, M., Zaretskaya, I., Raytselis, Y., Merezhuk, Y., McGinnis, S., and Madden, T. L. (2008). NCBI BLAST: a better web interface. *Nucleic Acids Res.* 36(suppl_2), W5–W9. doi: 10.1093/nar/gkn201

Katiyar-Agarwal, S., and Jin, H. (2010). Role of small RNAs in host-microbe interactions. *Annu. Rev. Phytopathol.* 48, 225–246.

Koren, S., Walenz, B. P., Berlin, K., Miller, J. R., Bergman, N. H., and Phillippy, A. M. (2017). Canu: scalable and accurate long-read assembly via adaptive k-mer weighting and repeat separation. *Genome Res.* 27, 722–736. doi: 10.1101/gr.215087.116

Li, H., and Durbin, R. (2009). Fast and accurate short read alignment with Burrows–Wheeler transform. *Bioinformatics* 25, 1754–1760.

Li, J., Reichel, M., Li, Y., and Millar, A. A. (2014). The functional scope of plant microRNA-mediated silencing. *Trends Plant Sci.* 19, 750–756. doi: 10.1016/j.tplants.2014.08.006

Liu, Q., and Axtell, M. J. (2015). Quantitating plant microRNA-mediated target repression using a dual-luciferase transient expression system. *Methods Mol. Biol.* 1284, 287–303. doi: 10.1007/978-1-4939-2444-8_14

Liu, S. R., Zhou, J. J., Hu, C. G., Wei, C. L., and Zhang, J. Z. (2017). MicroRNA-mediated gene silencing in plant defense and viral counter-defense. *Front. Microbiol.* 8:1801. doi: 10.3389/fmicb.2017.01801

Livak, K. J., and Schmittgen, T. D. (2001). Analysis of relative gene expression data using real-time quantitative PCR and the $2-\Delta\Delta CT$ method. *Methods* 25, 402–408.

Lu, S., Li, Q., Wei, H., Chang, M.-J., Tunlaya-Anukit, S., Kim, H., et al. (2013). Ptr-miR397a is a negative regulator of laccase genes affecting lignin content in *Populus trichocarpa*. *Proc. Natl. Acad. Sci. U.S.A.* 110, 10848–10853. doi: 10.1073/pnas.1308936110

Mazzola, M. (1997). Identification and pathogenicity of *Rhizoctonia* spp. isolated from apple roots and orchard soils. *Phytopathology* 87, 582–587. doi: 10.1094/PHYTO.1997.87.6.582

Mazzola, M. (1998). Elucidation of the microbial complex having a causal role in the development of apple replant disease in washington. *Phytopathology* 88, 930–938. doi: 10.1094/PHYTO.1998.88.9.930

McKenna, A., Hanna, M., Banks, E., Sivachenko, A., Cibulskis, K., Kernytsky, A., et al. (2010). The Genome Analysis Toolkit: a MAPREDUCE framework for analyzing next-generation DNA sequencing data. *Genome Res.* 20, 1297–1303. doi: 10.1101/gr.107524.110

Miedes, E., Vanholme, R., Boerjan, W., and Molina, A. (2014). The role of the secondary cell wall in plant resistance to pathogens. *Front. Plant Sci.* 5:358. doi: 10.3389/fpls.2014.00358

Oliva, J., Rommel, S., Fossdal, C., Hietala, A., Nemesio-Gorriz, M., Solheim, H., et al. (2015). Transcriptional responses of Norway spruce (*Picea abies*) inner sapwood against *Heterobasidion parviporum*. *Tree Physiol.* 35, 1007–1015. doi: 10.1093/treephys/tpv063

Overdijk, E. J., De Keijzer, J., De Groot, D., Schoina, C., Bouwmeester, K., Ketelaar, T., et al. (2016). Interaction between the moss *Physcomitrella patens* and *Phytophthora*: a novel pathosystem for live-cell imaging of subcellular defence. *J. Microsc.* 263, 171–180. doi: 10.1111/jmi.12395

Park, Y. J., Lee, H. J., Kwak, K. J., Lee, K., Hong, S. W., and Kang, H. (2014). MicroRNA400-guided cleavage of pentatricopeptide repeat protein mRNAs renders *Arabidopsis thaliana* more susceptible to pathogenic bacteria and fungi. *Plant Cell Physiol.* 55, 1660–1668. doi: 10.1093/pcp/pcu096

Pilon, M. (2017). The copper microRNAs. *New Phytol.* 213, 1030–1035.

Qiao, Y., Liu, L., Xiong, Q., Flores, C., Wong, J., Shi, J., et al. (2013). Oomycete pathogens encode RNA silencing suppressors. *Nature Genet.* 45, 330–333.

Rogers, K., and Chen, X. (2013). Biogenesis, turnover, and mode of action of plant microRNAs. *Plant Cell* 25, 2383–2399.

Samad, A. F., Sajad, M., Nazaruddin, N., Fauzi, I. A., Murad, A., Zainal, Z., et al. (2017). MicroRNA and transcription factor: key players in plant regulatory network. *Front. Plant Sci.* 8:565. doi: 10.3389/fpls.2017.00565

Schmitz-Linneweber, C., and Small, I. (2008). Pentatricopeptide repeat proteins: a socket set for organelle gene expression. *Trends Plant Sci.* 13, 663–670. doi: 10.1016/j.tplants.2008.10.001

Shivaprasad, P. V., Chen, H.-M., Patel, K., Bond, D. M., Santos, B. A., and Baulcombe, D. C. (2012). A microRNA superfamily regulates nucleotide binding siteâĂŞleucine-rich repeats and other mRNAs. *Plant Cell* 24, 859–874. doi: 10.1016/j.tplants.2008.10.001

Shin, S., Lee, J., Rudell, D., Evans, K., and Zhu, Y. (2016a). Transcriptional regulation of auxin metabolism and ethylene biosynthesis activation during apple (*Malus*× *domestica*) fruit maturation. *J. Plant Growth Regul.* 35, 655–666.

Shin, S., Zheng, P., Fazio, G., Mazzola, M., Main, D., and Zhu, Y. (2016b). Transcriptome changes specifically associated with apple (*Malus domestica*) root defense response during *Pythium ultimum* infection. *Physiol. Mol. Plant Pathol.* 94, 16–26.

Singh, J., and Khan, A. (2019). Distinct patterns of natural selection determine subpopulation structure in the fire blight pathogen, *Erwinia amylovora*. *Sci. Rep.* 9, 1–13. doi: 10.1038/s41598-019-50589-z

Staiger, D., Korneli, C., Lummer, M., and Navarro, L. (2013). Emerging role for RNA-based regulation in plant immunity. *New Phytol.* 197, 394–404. doi: 10.1111/nph.12022

Tewoldemedhin, Y. T., Mazzola, M., Botha, W. J., Spies, C. F., and McLeod, A. (2011). Characterization of fungi (*Fusarium* and *Rhizoctonia*) and oomycetes (*Phytophthora* and *Pythium*) associated with apple orchards in South Africa. *Eur. J. Plant Pathol.* 130, 215–229.

Vance, C., Kirk, T., and Sherwood, R. (1980). Lignification as a mechanism of disease resistance. *Annu. Rev. Phytopathol.* 18, 259–288.

Velasco, R., Zharkikh, A., Affourtit, J., Dhingra, A., Cestaro, A., Kalyanaraman, A., et al. (2010). The genome of the domesticated apple (*Malus*× *domestica* Borkh.). *Nat. Genet.* 42:833.

Weiberg, A., and Jin, H. (2015). Small RNAs—the secret agents in the plant–pathogen interactions. *Curr. Opin. Plant Biol.* 26, 87–94. doi: 10.1016/j.pbi.2015.05.033

Weiberg, A., Wang, M., Bellinger, M., and Jin, H. (2014). Small RNAs: a new paradigm in plant-microbe interactions. *Annu. Rev. Phytopathol.* 52, 495–516. doi: 10.1146/annurev-phyto-102313-045933

Xia, R., Meyers, B. C., Liu, Z., Beers, E. P., Ye, S., and Liu, Z. (2013). MicroRNA superfamilies descended from miR390 and their roles in secondary small

interfering RNA biogenesis in eudicots. *Plant Cell* 25, 1555–1572. doi: 10.1105/tpc.113.110957

Xia, R., Xu, J., Arikit, S., and Meyers, B. C. (2015). Extensive families of miRNAs and PHAS loci in Norway spruce demonstrate the origins of complex phasiRNA networks in seed plants. *Mol. Biol. Evol.* 32, 2905–2918. doi: 10.1093/molbev/msv164

Xia, R., Zhu, H., An, Y.-Q., Beers, E. P., and Liu, Z. (2012). Apple miRNAs and tasiRNAs with novel regulatory networks. *Genome Biol.* 13:R47. doi: 10.1186/gb-2012-13-6-r47

Xia, R., Xu, J., and Meyers, B. C. (2017). The emergence, evolution, and diversification of the miR390-TAS3-ARF pathway in land plants. *Plant Cell* 29, 1232–1247. doi: 10.1186/gb-2012-13-6-r47

Yang, C., Liang, Y., Qiu, D., Zeng, H., Yuan, J., and Yang, X. (2018). Lignin metabolism involves Botrytis cinerea BcGs1-induced defense response in tomato. *BMC Plant Biol.* 18:103. doi: 10.1186/s12870-018-1319-0

Yang, L., and Huang, H. (2014). Roles of small RNAs in plant disease resistance. *J. Integr. Plant Biol.* 56, 962–970. doi: 10.1111/jipb.12200

You, C., Cui, J., Wang, H., Qi, X., Kuo, L.-Y., Ma, H., et al. (2017). Conservation and divergence of small RNA pathways and microRNAs in land plants. *Genome Biol.* 18:158.

Zhang, B. (2015). MicroRNA: a new target for improving plant tolerance to abiotic stress. *J. Exp. Bot.* 66, 1749–1761. doi: 10.1093/jxb/erv013

Zhang, L., Hu, J., Han, X., Li, J., Gao, Y., Richards, C. M., et al. (2019). A high-quality apple genome assembly reveals the association of a retrotransposon and red fruit colour. *Nat. commun.* 10, 1–13. doi: 10.1038/s41467-019-09518-x

Zhou, Z., Tian, Y., Cong, P., and Zhu, Y. (2018). Functional characterization of an apple (*Malus* x *domestica*) LysM domain receptor encoding gene for its role in defense response. *Plant Sci.* 269, 56–65. doi: 10.1016/j.plantsci.2018.01.006

Zhu, Y., and Saltzgiver, M. (2020). A systematic analysis of apple root resistance traits to Pythium ultimum infection and the underpinned molecular regulations of defense activation. *Horticult. Res.* 7:62. doi: 10.1038/s41438-020-0286-4

Zhu, Y., Fazio, G., and Mazzola, M. (2014). Elucidating the molecular responses of apple rootstock resistant to ARD pathogens: challenges and opportunities for development of genomics-assisted breeding tools. *Horticult. Res.* 1:14043. doi: 10.1038/hortres.2014.43

Zhu, Y., Saltzgiver, M., and Zhao, J. (2018a). A phenotyping protocol for detailed evaluation of apple root resistance responses utilizing tissue culture micropropagated apple plants. *Am. J. Plant Sci.* 9:2183.

Zhu, Y., Shao, J., Zhou, Z., and Davis, R. E. (2017). Comparative transcriptome analysis reveals a preformed defense system in apple root of a resistant genotype of G.935 in the absence of pathogen. *Int. J. Plant Genomics* 2017:8950746. doi: 10.1155/2017/8950746

Zhu, Y., Shao, J., Zhou, Z., and Davis, R. E. (2019). Genotype-specific suppression of multiple defense pathways in apple root during infection by *Pythium ultimum*. *Horticult. Res.* 6:10. doi: 10.1038/s41438-018-0087-1

Zhu, Y., Zhao, J., and Zhou, Z. (2018b). Identifying an elite panel of apple rootstock germplasm with contrasting root resistance to *Pythium ultimum*. *J. Plant Pathol. Microbiol.* 9, 1–8. doi: 10.4172/2157-7471.1000461

Conflict of Interest: The authors declare that the research was conducted in the absence of any commercial or financial relationships that could be construed as a potential conflict of interest.

Publisher's Note: All claims expressed in this article are solely those of the authors and do not necessarily represent those of their affiliated organizations, or those of the publisher, the editors and the reviewers. Any product that may be evaluated in this article, or claim that may be made by its manufacturer, is not guaranteed or endorsed by the publisher.

Copyright © 2021 Zhu, Li, Singh, Khan, Fazio, Saltzgiver and Xia. This is an open-access article distributed under the terms of the Creative Commons Attribution License (CC BY). The use, distribution or reproduction in other forums is permitted, provided the original author(s) and the copyright owner(s) are credited and that the original publication in this journal is cited, in accordance with accepted academic practice. No use, distribution or reproduction is permitted which does not comply with these terms.

Advantages of publishing in Frontiers

OPEN ACCESS
Articles are free to read for greatest visibility and readership

FAST PUBLICATION
Around 90 days from submission to decision

HIGH QUALITY PEER-REVIEW
Rigorous, collaborative, and constructive peer-review

TRANSPARENT PEER-REVIEW
Editors and reviewers acknowledged by name on published articles

Frontiers
Avenue du Tribunal-Fédéral 34
1005 Lausanne | Switzerland

Visit us: www.frontiersin.org
Contact us: frontiersin.org/about/contact

REPRODUCIBILITY OF RESEARCH
Support open data and methods to enhance research reproducibility

DIGITAL PUBLISHING
Articles designed for optimal readership across devices

FOLLOW US
@frontiersin

IMPACT METRICS
Advanced article metrics track visibility across digital media

EXTENSIVE PROMOTION
Marketing and promotion of impactful research

LOOP RESEARCH NETWORK
Our network increases your article's readership